

AD-A213 198

**Second  
International Conference  
on  
Case Histories in  
Geotechnical Engineering**

(2)

**June 1-5, 1988**

**DTIC  
ELECTE  
OCT 10 1989  
S Dg D**

**DISTRIBUTION STATEMENT A**  
Approved for public release;  
Distribution Unlimited

**University of Missouri-Rolla  
Rolla, Missouri**

**89 10 10148**

## REPORT DOCUMENTATION PAGE

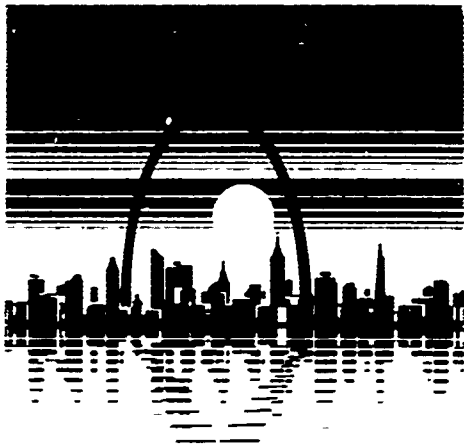
|  |       |   |  |   |                    |
|--|-------|---|--|---|--------------------|
| 1a. REPORT SECURITY CLASSIFICATION<br><b>Unclassified</b>  |       |   | 1b. RESTRICTIVE MARKINGS   |   |                    |
| 2a. SECURITY CLASSIFICATION AUTHORITY  |       |   | 3. DISTRIBUTION/AVAILABILITY OF REPORT<br><br>Approved for public release;<br>distribution unlimited.  |   |                    |
| 2b. DECLASSIFICATION/DOWNGRADING SCHEDULE  |       |   |  |   |                    |
| 4. PERFORMING ORGANIZATION REPORT NUMBER(S)  |       |   | 5. MONITORING ORGANIZATION REPORT NUMBER(S)<br><br>ARO 25645.1-GS-CF   |   |                    |
| 6a. NAME OF PERFORMING ORGANIZATION<br><br>Univ. of Missouri at Rolla  |       | 6b. OFFICE SYMBOL<br>(If applicable)        |  | 7a. NAME OF MONITORING ORGANIZATION<br><br>U. S. Army Research Office   |                    |
| 6c. ADDRESS (City, State, and ZIP Code)<br>Rolla, MO 65401-0149  |       |   | 7b. ADDRESS (City, State, and ZIP Code)<br>P. O. Box 12211<br>Research Triangle Park, NC 27709-2211  |   |                    |
| 8a. NAME OF FUNDING/SPONSORING ORGANIZATION<br><br>U. S. Army Research Office  |       | 8b. OFFICE SYMBOL<br>(If applicable)        |  | 9. PROCUREMENT INSTRUMENT IDENTIFICATION NUMBER<br><br>DAAL03-87-G-0129 |                    |
| 8c. ADDRESS (City, State, and ZIP Code)<br>P. O. Box 12211<br>Research Triangle Park, NC 27709-2211  |       |   | 10. SOURCE OF FUNDING NUMBERS  |   |                    |
|  |       |   | PROGRAM ELEMENT NO.  | PROJECT NO.   | TASK NO.           |
| 11. TITLE (Include Security Classification)<br><br>Second International Conference on Case Histories in Geotechnical Engineering<br>Volume I   |       |   |  |   |                    |
| 12. PERSONAL AUTHOR(S)<br>Shamshear Prakash  |       |   |  |   |                    |
| 13a. TYPE OF REPORT<br>Final   |       | 13b. TIME COVERED<br>FROM 1/1/88 TO 6/30/89 |  | 14. DATE OF REPORT (Year, Month, Day)                                   |                    |
|  |       |   |  | 15. PAGE COUNT<br>885   |                    |
| 16. SUPPLEMENTARY NOTATION<br>The view, opinions and/or findings contained in this report are those of the author(s) and should not be construed as an official Department of the Army position, policy, or decision, unless so designated by other documentation.   |       |   |  |   |                    |
| 17. COSATI CODES   |       |   | 18. SUBJECT TERMS (Continue on reverse if necessary and identify by block number)  |   |                    |
| FIELD  | GROUP | SUB-GROUP                                   | Geotechnical Engineering, Case Histories, Soil Dynamics, Rock Mechanics, Earthquake Engineering, Dams, Embankments, Slopes, Radioactive Waste, Hazardous Waste, Soil Structure |   |                    |
|  |       |   |  |   |                    |
|  |       |   |  |   |                    |
| 19. ABSTRACT (Continue on reverse if necessary and identify by block number)<br><br>The conference papers and state-of-the-art reports have been printed in two volumes which will be issued before the conference. The third volume containing reports, discussions, authors' replies, speeches and special programs, will be issued after the conference. The first volume contains 136 papers, and the second volume contains 100 papers and six state-of-the-art papers. |       |   |  |   |                    |
| 20. DISTRIBUTION/AVAILABILITY OF ABSTRACT<br><input type="checkbox"/> UNCLASSIFIED/UNLIMITED <input type="checkbox"/> SAME AS RPT. <input type="checkbox"/> DTIC USERS   |       |   | 21. ABSTRACT SECURITY CLASSIFICATION<br>Unclassified   |   |                    |
| 22a. NAME OF RESPONSIBLE INDIVIDUAL  |       |   | 22b. TELEPHONE (Include Area Code)   |   | 22c. OFFICE SYMBOL |



**Second  
International Conference  
on  
Case Histories in  
Geotechnical Engineering**

**June 1-5, 1988**

---



Geotechnical Engineering  
St. Louis 1988

**Vol. I**

**Editor: Shamsheer Prakash**

---

**University of Missouri-Rolla  
Rolla, Missouri**

## **Disclaimer**

"The views, opinions, and/or findings contained in these proceeding volumes are those of the author(s) and should not be construed as an official Department of the Army or University of Missouri-Rolla position, policy, or decision, unless so designated by other documentation."

## Preface

The University of Missouri-Rolla had hosted a very successful International Conference on Case Histories in Geotechnical Engineering in May 1984. The Second Conference in the series was planned in 1985, and a Call for Papers was issued in December 1986. The conference has been co-sponsored and partially funded by the U.S. Army Department of Research. It has been organized in cooperation with the International Society for Soil Mechanics and Foundation Engineering, International Association of Earthquake Engineering, Earthquake Engineering Research Institute, Association of Engineering Geologists, United States Committee on Large Dams, United States National Committee for Rock Mechanics, Transportation Research Board, American Society of Civil Engineers—Mid-Missouri Section, Association of Soil and Foundation Engineers, and Engineering Geology Division of the Geological Society of America.

The Call for Papers was issued in December 1986 and papers were contributed from 47 countries: Australia, Austria, Brazil, Bulgaria, Canada, China, Denmark, Egypt, France, Germany, Ghana, Greece, Hong Kong, India, Indonesia, Iraq, Ireland, Israel, Italy, Japan, Jordan, Kenya, Korea, Libya, Mexico, Netherlands, New Zealand, Nigeria, Norway, Pakistan, Panama, Peru, Portugal, Puerto Rico, Romania, Saudi Arabia, Singapore, South Africa, Sri Lanka, Sweden, Taiwan, Turkey, United Kingdom, United States, U.S.S.R., Vietnam, and Yugoslavia, making this conference a truly international one. The large number of papers received were reviewed by a panel of 12 international experts.

The conference papers and state-of-the-art reports have been printed in two volumes which will be issued before the conference. The third volume containing reports, discussions, authors' replies, speeches and special programs, will be issued after the conference. The first volume contains 136 papers, and the second volume contains 100 papers and six state-of-the-art papers.

The organizing committee was always ready to assist in matters of organization. In the initial stages of planning, guidance was obtained from W.D. Liam Finn, E. D'Appolonia, Norbert O. Schmidt, and Allen W. Hatheway. The University of Missouri-Rolla staff has been very cooperative throughout, especially personnel of the Engineering Continuing Education unit. In addition, our secretaries, particularly Janet Pearson, worked hard to keep pace with the paperwork associated with such a venture. Their work is especially appreciated since everyone knows how difficult it would be to handle such a monumental work without the active cooperation of these people.

The timely printing of the proceedings has been made possible through the efforts of personnel at UMR Centralized Printing Office. Without the expertise and technical assistance of these individuals, the proceedings would not exist in their present form.

We now look forward to a successful conference in St. Louis during the week of June 1-5, 1988.

JANUARY 3, 1988

Shamsher Prakash, Editor  
and Conference Chairman

|                  |                                     |
|------------------|-------------------------------------|
| Accession For    |                                     |
| NTIS             | <input checked="" type="checkbox"/> |
| CR&I             | <input checked="" type="checkbox"/> |
| DTIC             | <input type="checkbox"/>            |
| Tab              | <input type="checkbox"/>            |
| Unannounced      | <input type="checkbox"/>            |
| J. L. ...        |                                     |
| By ...           |                                     |
| Date ...         |                                     |
| No. of ... Cases |                                     |
| DA               | ...                                 |
| A-1              |                                     |



## Table of Contents

cont'd  
Partial Contents of Volume I include:

### Session I

#### Case Histories of Geotechnical and Hydrological Management of Solid, Hazardous, and Radioactive Wastes

cont'd pg. vi  
Page No.

|   |  |    |
|---|--|----|
| W.C.B. Gates<br>(USA)   | Use of Deeply Weathered Rock as Landfill Cover Material,<br>Patacon Landfill, Republic of Panama. 1.05 .....       | 1  |
| D. Raghu<br>H.N. Hsieh<br>(USA)   | Disposal of Phenolic Waters from a Producer Gas Plant. 1.06 .....  | 7  |
| D. McGrane<br>(USA)   | Complementing Radiologic Data with Geology—A Case History. 1.07 .....  | 13 |
| W.M. Kilkenny<br>(England)  | A Low-Rise Hospital Development on Restored Opencast Fill. 1.08 .....  | 19 |
| J.A. Caldwell<br>R.E. Rager<br>L. Coons<br>(USA)                              | Geotechnical and Groundwater Site Characterization on the<br>Umtra Project. 1.09 .....                             | 25 |
| D.E. Mills<br>D.A. Cordell<br>(USA)   | Evaluation of Remedial In-Waste Leachate Head Reduction. 1.10.....   | 35 |
| H. Dezfulian<br>(USA)   | Site Assessment and Remediation of an Oil-Producing Property. 1.11 .....   | 43 |
| D. Raghu<br>R.J. Van Orden<br>(USA)   | Failure and Reconstruction of a Waste Containment Pond Slope. 1.13 .....   | 51 |
| M.D. Huag<br>J. Atwater<br>R.B. Knight<br>P. Kozicki<br>A. Lissey<br>(Canada) | Implementation of Remedial Measure to Contain a PCB Spill. 1.14 .....  | 55 |
| P.J. Bosscher<br>T.B. Edil<br>(USA)   | Performance of Lightweight Waste Impoundment Dikes. 1.17 .....   | 63 |
| G.H. Cramer<br>(USA)  | A Study of Contamination Migration at a Hazardous Waste Facility<br>in Louisiana. 1.21 .....                       | 71 |
| R.V. Sarsby<br>(England)  | Control of Uplift from Ground Water. 1.22 .....  | 75 |
| A.S. Burgess<br>M.S. Leonard<br>G.S. Laird<br>(USA)                           | Design and Construction of a Soil Bentonite Slurry Wall Around an<br>Operating Facility Superfund Site. 1.23 ..... | 81 |

|   |   |    |
|---|---|----|
| G.S. Laird<br>A.M. Gurevich<br>W.B. Lozier<br>(USA) | A Modified Field Infiltrometer Test for Clay Liners. 1.25 ..... | 89 |
|---|---|----|

|                     |  |    |
|---------------------|--|----|
| S.M. Testa<br>(USA) | Hazardous Waste Disposal Site Hydrogeologic Characterization. 1.26 ..... | 97 |
|---------------------|--|----|

Cont'd

## Session II

### Case Histories in Geological Engineering and Rock Mechanics *Cont'd page IX*

|                         |  |     |
|-------------------------|--|-----|
| S.C. Bandis<br>(Greece) | Engineering Design of Rock Slope Reinforcement Based on<br>Non-Linear Joint Strength Model. 2.03 ..... | 107 |
|-------------------------|--|-----|

|                         |   |     |
|-------------------------|---|-----|
| J. Pitts<br>(Singapore) | Stability of a Rock Slope at Bukit Batok New Town Singapore. 2.07 ..... | 115 |
|-------------------------|---|-----|

|  |  |     |
|--|--|-----|
| J.K.P. Kwong<br>(USA)<br>L.J. Endicott<br>(Hong Kong)<br>A.C. Lumsden<br>(England) | Slope Stability Evaluation for an Existing Steep Cut in Weathered<br>Volcanics Hong Kong. 2.08 ..... | 123 |
|--|--|-----|

|                       |  |     |
|-----------------------|--|-----|
| N.M. Patel<br>(India) | Distress in a Hill and Remedial Measures. 2.11 ..... | 127 |
|-----------------------|--|-----|

|                                    |   |     |
|------------------------------------|---|-----|
| Z.Q. Wang<br>R.X. Zhang<br>(China) | Case Study—Ground Failures and Ruptures in Xian City. 2.12..... | 131 |
|------------------------------------|---|-----|

|                    |   |     |
|--------------------|---|-----|
| G.A. Hu<br>(China) | On a New Problem of High Speed Landslides. 2.13 ..... | 137 |
|--------------------|---|-----|

|  |  |     |
|--|--|-----|
| K.D. Weaver<br>D.J. Gross<br>L.T. Bauer<br>(USA) | Slope Stabilization Measures for Kirkwood Penstock, Early Intake<br>California. 2.14 ..... | 143 |
|--|--|-----|

|  |   |     |
|--|---|-----|
| B. Prabhakar<br>J.L. Jethwa<br>B. Singh<br>(India) | A Case History of Tehri Tunnels. 2.15 ..... | 147 |
|--|---|-----|

|  |   |     |
|--|---|-----|
| C. Rodriguez-Perez<br>L. Vazquez Castillo<br>C. Rodriguez-Molina<br>A. Vazquez Castillo<br>(Puerto Rico) | A Study of a Road Landslide in Puerto Rico. 2.16..... | 151 |
|--|---|-----|

|                        |   |     |
|------------------------|---|-----|
| Z.R. Fattohi<br>(Iraq) | Simultaneous Velocity Measurements with Uniaxial Loading on<br>Weak Sandstone from Iraq. 2.18 ..... | 159 |
|------------------------|---|-----|

|   |  |     |
|---|--|-----|
| A.C. Van Besien<br>N.B. Aughenbaugh<br>(USA)            | Johnston City School, Mine Subsidence or Shallow Foundation Problem. 2.19 .....  | 163 |
| L. Jiayou<br>M. Jianyun<br>(China)                      | The Successful Construction of a High Gravity Dam on Complex Rock Formations. 2.20 .....                                 | 167 |
| M.G. Karfakis<br>B.A. Suprenant<br>(USA)                | Ground Failure Investigation Over Abandoned Coal Mines: A Case Study. 2.21 .....   | 173 |
| R.K. Goel<br>J.L. Jethwa<br>B. Singh<br>(India)         | Case History of Maneri—Uttarkashi Power Tunnel. 2.22 .....   | 177 |
| J.G. Cabrera<br>(USA)                                   | Foundation Investigation and Treatment for the Main Dam, Itaipu Project. 2.23 .....                                      | 185 |
| D. Raghu<br>D.A. Antes<br>J.L. Lifrieri<br>(USA)        | Grouting a Water Tower Foundation in a Carbonate Formation. 2.24 .....   | 195 |
| R.D. Prager<br>G.S. Grainger<br>R.L. Butts<br>(USA)     | Rock Response in a 12-M Tunnel Through a Zone of Low Strength. 2.25 .....  | 201 |
| P.S. Khare<br>S.G. Kulkarni<br>S.L. Mokhashi<br>(India) | Stability Check of Escarpment Using Finite Element Method. 2.28 .....  | 207 |
| A.K. Dube<br>B. Singh<br>(India)                        | Rock Mass Behaviour Assessment for Large Cavern in Rock. 2.29 .....  | 211 |
| J.A. Larson<br>(USA)<br>D.P. Richards<br>(Turkey)       | Support Over Cavities of Unknown Depth for Underground Facility. 2.34 .....  | 215 |
| R.C. Ilsley<br>S.B. Fradkin<br>E.F. Shorey<br>(USA)     | Evaluation of the Site Investigation and Construction Related Aspects of the Milwaukee Crosstown Deep Tunnel. 2.36 ..... | 221 |
| J.M. Descour<br>R.J. Miller<br>(USA)                    | Microseismic Activity in an Open Pit Lignite Mine. 2.37 .....  | 229 |
| A.O. Erol<br>A.W. Dhowian<br>(Saudi Arabia)             | Foundation Failures Associated with Salt Rock and Surrounding Coastal Plain. 2.39 .....                                  | 237 |

|   |  |     |
|---|--|-----|
| G.S. Mehrotra<br>R.K. Bhandari<br>(India)                 | A Geological Appraisal of Slope Instability and Proposed Remedial Measures at Kaliasaur Slide on National Highway Garhwal Himalaya. 2.40 ..... | 245 |
| Y.P. Chugh<br>K. Chandrashekar<br>R. Missavage<br>(USA)   | Subsidence Movements and Structural Damage Related to an Abandoned Coal Mine. 2.41 .....   | 253 |
| T. Ramamurthy<br>V.M. Sharma<br>(India)                   | Performance of Some Tunnels in Squeezing Rocks of Himalayas. 2.42 .....  | 263 |
| B. Hasan<br>(Pakistan)                                    | Effects of Geology and Geotechnical Properties of Rocks for the Selection of Type of Dams. 2.44 .....  | 271 |
| A.M. Jokhyo<br>(Pakistan)                                 | Slopes in Weak Rocks. 2.46 .....   | 279 |
| K.K. Kapoor<br>S.C. Patodiya<br>(India)                   | Construction of a Hydel Power House in Weak Rocks. 2.47 .....  | 285 |
| M.C. Betournay<br>C. Mirza<br>K.C. Lau<br>(Canada)        | Coring of Soft Soil-Like Rock Materials. 2.49 .....  | 291 |
| K. Anguelov<br>(Bulgaria)                                 | The Great Landslides in the East-Maritza Open-cast Mines (Bulgaria)—A Theoretical Paradox in the Engineering Geology. 2.50 .....               | 299 |
| H.C. Nainwal<br>Y.P. Sundriya<br>C. Prasad<br>(India)     | Study of Some Debris Avalanches in Garhwal Himalaya, India. 2.52 .....   | 305 |
| R.S. Mithal<br>(India)                                    | Lithotectonic Landslides and Hazards in Parts of Garhwal-Kumaon Himalaya. 2.55 .....   | 311 |
| M.A. El-Sohby<br>S.O. Mazen<br>(Egypt)                    | Geotechnical Characterization of Subsoil Deposits at Cairo. 2.56 .....   | 321 |
| D.M. Pancholi<br>K.E. Modhwadia<br>P.H. Vaidya<br>(India) | Geo-Engineering Problems in the Spillway Foundations and Their Treatment at Guhai Reservoir Project in Gujarat, India. 2.58 .....              | 327 |
| R.K. Bhandari<br>(India)                                  | A Novel Low Cost Drum Diaphragm Wall for Landslide Control in The Himalaya. 2.60 .....   | 333 |
| M. Christos<br>(Greece)                                   | Prevision of the Bearing Capacity of Superficial Foundation on Jointed Rock. 2.61 .....  | 337 |
| K. H. Earley<br>D. Rudenko<br>(USA)                       | Use of Geophysical Methods in a Geotechnical Investigation. 2.64 .....   | 341 |

~~Cont'd~~  
**Session III**  
**"Case Histories of Dams, Embankments, and Slopes"**

Cont'd pg. Xiii →  
 Page No.

|  |   |     |
|--|---|-----|
| D. Abolhassani<br>F. Bahrami-Samani<br>(Iran)<br>R.P. Brenner<br>(Switzerland) | Unusual Behaviour of An Earth-Rockfill Dam. 3.01 .....                                    | 347 |
| J.W. Erwin<br>G.R. Baer<br>(USA)   | Seepage Incident, St. Stephen Powerhouse, St. Stephen, S.C. 3.04 .....                    | 355 |
| T.K. Natarajan<br>A.V.S.R. Murty<br>D. Chandra<br>(India)                      | Control of Surficial Slides by Different Erosion Control Techniques. 3.05 .....           | 361 |
| T.K. Natarajan<br>P.J. Rao<br>(India)  | Restoration of the Stability of Retaining Wall. 3.06 .....                                | 365 |
| Z.V. Solymar<br>G.C. MacTavish<br>W.G. Matthews<br>(Canada)                    | Some Design Aspects and Performance of an Embankment Dam. 3.08 .....                      | 369 |
| K. Kogure<br>K. Matsuo<br>(Japan)  | Settlement Measurements of Peat Deposits as Embankment Foundation.<br>3.09 .....          | 377 |
| L. Knuppel<br>F. McLean<br>A. Roodsari<br>(USA)                                | Underseepage Control Measures at Painted Rock Dam. 3.10 .....                             | 383 |
| R.B. Smith<br>W.O. Yandell<br>(Australia)                                      | Prediction and Field Performance of an Instrumented Road. 3.11 .....                      | 395 |
| R.C. Findlay<br>(USA)  | Hydrostatic Pressure at a Soil-Structure Interface. 3.12 .....                            | 401 |
| V.K. Singh<br>B.D. Baliga<br>B. Singh<br>(India)                               | Openpit Mine Slope Stability—A Case Study. 3.13 .....                                     | 407 |
| H.J. Von M. Harmse<br>F.A. Gerber<br>(South Africa)                            | A Proposed Procedure for the Identification of Dispersive Soils. 3.14 .....               | 411 |
| Z.J. Ke<br>C.H. Yong<br>Y.H. Chang<br>(China)                                  | Failure and Repair of the Slope of Railway Embankments and<br>Expansive Soils. 3.15 ..... | 417 |



|  |  |     |
|--|--|-----|
| M.C. Goel<br>(India)<br>D. Mudjihardjo<br>(Indonesia)                      | Performance Evaluation of Rarem Dam. 3.16 .....                            | 423 |
| M.C. Goel<br>(India)<br>A. Zainiko<br>J.L. Surabaya<br>(Indonesia)         | Colbond Drains for Rapid Consolidation at Manggar Besar Dam. 3.17 .....    | 433 |
| K.V. Rupchang<br>(India)   | Problems and Behaviour of a Dam Founded on a Weak Zone. 3.18 .....         | 437 |
| D.G. Anderson<br>J.G. Dehner<br>T.B. King<br>(USA)                         | Performance of a Harbor Embankment. 3.20 .....                             | 443 |
| T. Smith<br>C.E. Deal<br>(USA)   | Cracking Studies at Sand H Basin by the Finite Element Method. 3.21 .....  | 451 |
| J. Christodoulis<br>H. Giannaros<br>(Greece)                               | Failure of Railway Embankment. 3.22 .....                                  | 457 |
| H. Hejazi<br>(USA)   | Construction Problems with an Earth and Rockfill Dam. 3.24 .....           | 461 |
| J. Alberro<br>G. Macedo<br>L. Montanez<br>F. Gonzalez-Valencia<br>(Mexico) | Penitas Dam—In Situ Stress-Strain Characteristics of Materials. 3.26 ..... | 467 |
| M.D. Scott<br>R.C. Lo<br>E.J. Klohn<br>K.K. Lum<br>(Canada)                | Overview of Highland Valley Tailings Storage Facility. 3.27 .....          | 479 |
| B. Bailey<br>E. Bloom<br>T.R. West<br>J.A. Mundell<br>(USA)                | Excessive Seepage Losses at Westwood Lake Dam. 3.29 .....                  | 489 |
| D.R. East<br>J.W. Ransone<br>W.A. Cincilla<br>(USA)                        | Testing of the Homestake Mine Tailings Deposit. 3.30 .....                 | 495 |
| J.R. Lambrechts<br>E.B. Kinner<br>(USA)                                    | The Great Salt Lake Causeway—A Calculated Risk Revisited. 3.31 .....       | 503 |

|  |   |     |
|--|---|-----|
| J. Binquet<br>U. Zappi<br>(France)                                 | Wadi Qattarah Dams Case History. 3.32 .....   | 511 |
| J.L. Llopis<br>C.M. Deaver<br>D.K. Butler<br>S.C. Hartung<br>(USA) | Comprehensive Seepage Assessment: Beaver Dam, Arkansas. 3.33 .....                            | 519 |
| R.K. Katti<br>D.R. Katti<br>A.R. Katti<br>(India)                  | Remedial Measures to Seepage and Instability Aspect of a Dam<br>Near Bombay. 3.34 .....       | 527 |
| R.J. Termaat<br>E.O.F. Calle<br>R.O. Petschl<br>(The Netherlands)  | The Probability of Failure of an In Stages Constructed Embankment<br>on Soft Soil. 3.37 ..... | 533 |
| J.A. van Herpen<br>J. de Pee<br>(The Netherlands)                  | Dike Reconstruction Polder Oudendijk. 3.38 .....  | 541 |
| J. Dekker<br>(The Netherlands)                                     | Evaluation of the Failure of an Important Dike in the Netherlands. 3.39 .....                 | 547 |
| R.C. Chaney<br>D.C. Tuttle<br>(USA)                                | Coastal Bluff Retreat at Big Lagoon, California. 3.40 .....                                   | 555 |
| P.L.R. Pang<br>Y.C. Chan<br>(Hong Kong)                            | Investigation of Settlements of a Trunk Road Embankment in<br>Hong Kong. 3.41 .....           | 559 |
| W.R. Stroman<br>R.R.W. Beene<br>P.D. Thornhill<br>(USA)            | Kerrville Ponding Dam, Guadalupe River, Texas. 3.42 .....                                     | 567 |
| Z. Shixuan<br>(China)  | A Case Study of Success to Structures Founded on Expansive Soils. 3.44 .....                  | 575 |
| T. Sivapatham<br>(Sri Lanka)                                       | Behaviour of Inginimitiya Embankment Dam. 3.45 .....  | 581 |
| T. Mathur<br>R. Willis<br>(USA)                                    | Performance of an Instrumented Earth Dam With Fat Clay Core. 3.46 .....                       | 587 |
| B.D. Leonard<br>J.M. Olsen<br>(USA)                                | A Finite Element Analysis of the Utah "Thistle" Failure. 3.48 .....                           | 593 |

*Session III continued*

Page No.

|   |  |     |
|---|--|-----|
| F. Colleselli<br>P. Simonini<br>M. Soranzo<br>(Italy)                       | Improvement of Mechanical Properties of Soft Soils by Use of a<br>Pre-Loading Embankment. 3.51 ..... | 599 |
| T. Ramamurthy<br>S.L. Jain<br>(India)                                       | Deformation Response of Some Earth and Rockfill Dams. 3.52 .....                                     | 607 |
| B.V.K. Lavanaia<br>(India)  | History of Tehri Rockfill Dam Design. 3.53 .....   | 615 |
| B.V.K. Lavanaia<br>(India)  | Treatment of Left Bank Slopes of Ichari Dam. 3.54 .....  | 621 |
| A.J.T. Gilchrist<br>(United Kingdom)  | Design and Construction of Geocell Mattress as Embankment<br>Foundation. 3.56 .....                  | 627 |
| N.H. Wade<br>L.F. Wei<br>L.R. Courage<br>R.A. Keys<br>(Canada)              | Performance of an Earthdam and Cut-off Through Deep Alluvium. 3.57 .....                             | 635 |
| K.B. Agarwal<br>(India)   | An Undrained Failure in the Foundation of an Earthdam. 3.58 .....                                    | 645 |
| J.R. Schneider<br>R.W. Lindquist<br>(USA)<br>G.K. Sammy<br>(West Indies)    | Design and Performance of Arena Dam. 3.59 .....  | 651 |
| K.K. Kapoor<br>S.C. Patodiya<br>(India)                                     | Case History of a Partially Underground Power House. 3.60 .....                                      | 657 |
| I.I. Corda<br>(Romania)   | Iron Gates II: Design and Performance of Dams—<br>Geotechnical Considerations 3.63 .....             | 663 |
| St. Christoulas<br>E. Gassios<br>N. Kalteziotis<br>G. Tsiambaos<br>(Greece) | Slope Stability Problems Related to a Semi-Bridge Construction. 3.65 .....                           | 671 |
| J.A. Posse<br>R.P. Hermosilla<br>J.M.M. Santamaria<br>(Spain)               | Monitoring of the Canales Dam and Its Control During<br>Construction Period. 3.66 .....              | 677 |
| D.C. Cowherd<br>V.G. Perlea<br>A. Coulson<br>(USA)                          | Performance of a Coal Refuse Embankment. 3.68 .....  | 683 |

|   |   |     |
|---|---|-----|
| R. Azevedo<br>L.A. Santos<br>(Brazil)                 | Field Observation and Finite Element Analysis of a Subway Excavation. 3.70 ....                       | 689 |
| A. Marsland<br>(England)                              | Failure of Flood Banks Due to Under Seepage. 3.72 .....   | 695 |
| J.D. Nelson<br>(USA)<br>B.P. Wrench<br>(South Africa) | Construction of Road Embankments Over Very Soft Soils<br>Using Band Drains and Preloading. 3.73 ..... | 699 |
| Izhar-ul-Haq<br>(Pakistan)                            | Seepage Problems and Remedies—Hub Dam. 3.77 .....   | 705 |
| A.I. Harsulescu<br>(Romania)                          | The Behaviour in Time of Ripa Albastra Dam Impervious<br>Bentonitic Core. 3.78 .....                  | 711 |
| F. J. Gichaga<br>F.S. Atibu<br>B.K. Sahu<br>(Kenya)   | Horizontal and Vertical Movements of Red Clay Highway<br>Embankments. 3.79 .....                      | 717 |

cont'd  
at

## Session IV

**Case Histories of Geotechnical Earthquake Engineering and Soil Dynamics.** *Keywords: Soil Structure, (AW)*

|   |  |     |
|---|--|-----|
| Y. Koga<br>O. Matsuo<br>(Japan)                   | Stability Analysis of Seismically Damaged Embankments. 4.01 .....                              | 721 |
| S. Chonggang<br>(China)                           | Some Experiences from Damages of Embankments During Strong<br>Earthquakes in China. 4.03 ..... | 729 |
| I. Rosenthal<br>M. Itskowitch<br>(Israel)         | Vibration Response of Railway Bridge Piers to Nearby Pile Driving.<br>4.04 .....               | 737 |
| P. Fulan<br>(China)                               | Theory and Experiment of Hammer Foundation Vibration. 4.05 .....                               | 743 |
| T. Zhen-Yu<br>T. Fang-Fu<br>(China)               | Stress Field Under a Reservoir and Its Induced Earthquake. 4.06 .....                          | 749 |
| W. Xikang<br>(China)                              | On Properties of Damping of Bases. 4.07 .....  | 755 |
| W. Xikang<br>D. Shiwei<br>Y. Xianjinan<br>(China) | On Propagation of Elastic Surface Wave in Soil. 4.08 .....                                     | 759 |

|   |  |     |
|---|--|-----|
| Q. Taiping<br>L. HuiShan<br>(China)                                 | Influence of Piling on Characteristics of Liquefiable Soils. 4.10 .....  | 765 |
| W. Yuqing<br>(China)  | The Simplified Formulas for Predicting Seismic Liquefaction of Saturated Clayey Silt Site. 4.11 .....                            | 769 |
| D. Shiwei<br>(China)  | The Effect of Foundation Shape on Dynamic Parameter of Bases. 4.12 .....   | 773 |
| L.S. Srivastava<br>(India)  | Landslides in Rock Slopes During January 19, 1975 Kinnaur Earthquake in Himachal Pradesh, India. 4.14 .....                      | 779 |
| T.F. Wolff<br>G.L. Hempen<br>M.M. Dirnberger<br>B.H. Moore<br>(USA) | Probabilistic Analysis of Earthquake-Induced Pool Release. 4.15 .....  | 787 |
| M. Lew<br>J.C. Bowman, Jr.<br>(USA)                                 | Case History of Seismic Base Isolation of a Building—The Foothill Communities Law and Justice Center. 4.16 .....                 | 795 |
| K.V. Rodda<br>C.W. Perry<br>R.E. Tepel<br>(USA)                     | Upgrading the Seismic Resistance of Stevens Creek Dam. 4.18 .....  | 801 |
| M.B. Ray<br>D.K. Ghosh<br>(India)                                   | Seismic Response Analysis of Forebay Structure for C.W. Pump House of a Nuclear Power Project. 4.20 .....                        | 807 |
| G. Maurath<br>D. Amick<br>(USA)                                     | Characterization of Liquefaction Sites/Features in the Charleston, S.C. Area. 4.21 .....   | 811 |
| P. Kvasnicka<br>T. Ivsic<br>A. Kirichenko<br>(Yugoslavia)           | Analysis and Measurement of Foundation Vibrations at Two Compressor Stations in Yugoslavia. 4.23 .....                           | 819 |
| A. Bapat<br>(India)   | Seismosedimentation and Lives of Reservoirs. 4.24 .....  | 825 |
| R.C. Lo<br>W.G. Milne<br>E.J. Klohn<br>G.T. Handford<br>(Canada)    | Seismic Assessment of Syncrude Tailings Dyke. 4.26 .....   | 829 |
| S. Bandyopadhyay<br>M.K. Gupta<br>A.S. Arya<br>(India)              | Reliability of the Wave Equation Analysis in the Estimation of Static Bearing Capacity of Vertical Pile—a Case Study. 4.27 ..... | 837 |

*Session IV continued*

|  | Page No.  |
|--|---|
| M.D. Gillon<br>(New Zealand)   | The Observed Seismic Behavior of the Matahina Dam. 4.29 ..... 841   |
| P.S. Seco e Pinto<br>(Portugal)  | Soil Liquefaction Potential of a Highway Bridge Foundation. 4.31 ..... 849  |
| P. Srinivasulu<br>N. Lakshnaman<br>K. Muthumani<br>B.S. Sarma<br>(India) | A Study of Dynamic Pile-Soil Interaction. 4.33 ..... 855  |
| P.M. Byrne<br>H. Vaziri<br>U. Atukorala<br>D. Fraser<br>(Canada)         | Model Tests on Seismic Stability of an Approach Fill Embankment,<br>Annacis Island Bridge Project Vancouver, Canada. 4.34 ..... 863 |
| V.D. Miglani<br>(India)  | In-Situ Determination of Dynamic Properties of Soil for<br>Foundation of a Turbo-Generator. 4.36 ..... 871                          |
| F. Ciuffi<br>(Italy)   | Geotechnical Services for a Bridge in a Seismic Area. 4.40 ..... 877  |
| Author Index .....   | 883   |

## Volume II

### Session V

#### "New Solutions to Traditional Geotechnical Problems [Case Histories]"

|  | Page No.   |
|--|--|
| H. Grice<br>E.T. Mosley<br>R.M. Berry<br>(USA)                               | Vertical Excavation Below Footing Solved by Compaction Grouting.<br>5.01 ..... 885   |
| T.V. Nhiem<br>(France)   | Recent Examples of Cut and Fill Reinforcement on A41-Highway in<br>France. 5.02 ..... 889  |
| B. Wietek<br>(Austria)   | Drainage Walling as Excavation Support. 5.03 ..... 905   |
| T.J. Lyman<br>M.J. Robison<br>D.S. Lance<br>(USA)                            | Compaction and Chemical Grouting Phoenix Drain Tunnels. 5.04 ..... 911   |
| R.P. Kummerle<br>(USA)<br>J.C. Dumas<br>(Canada)                             | Soil Improvement Using Dynamic Compaction for the Bristol<br>Resource Recovery Facility. 5.05 ..... 921                            |
| G.E. Blight<br>(South Africa)  | Effects of Collapse Settlement of Fill on Reinforced Earth Walls. 5.06 ..... 929   |
| H.O. Chukweze<br>(Nigeria)   | Pavement Failure Caused by Soil Erosion. 5.10 ..... 935  |
| T.B. Celestino<br>O.A. Ferrari<br>C.T. Mitsuse<br>L.C. Dominique<br>(Brazil) | Progress in the Use of NATM for the Sao Paulo Subway. 5.12 ..... 941   |
| C. Mastrantuono<br>A. Tomioio<br>E. Arcangeli<br>(Italy)                     | Effectiveness of Sand Drains in Peaty Soil in a Case of Differential<br>Settlement Recovering. 5.13 ..... 947                      |
| H. Meissner<br>G. Borm<br>(Germany)  | Construction of a Double Tunnel with Ground Windows. 5.14 ..... 953  |
| W. Yuqing<br>Z. Weiquan<br>Q. Taiping<br>(China)                             | Evaluation of the Effect of Saturated Silty and Fine Sand Foundation<br>Improved by Vibroflotation in Seismic Area. 5.15 ..... 963 |
| B. Song<br>(Korea)<br>M. Gambin<br>(France)                                  | Dynamic Compaction—An Unusual Application. 5.16 ..... 969  |

|   |   |      |
|---|---|------|
| L.W. Franks<br>J.M. Duncan<br>S.A. Collins<br>J. Fowler<br>J.F. Peters<br>V.R. Schaefer<br>(USA)      | Use of Reinforcement at Mohicanville Dike No. 2. 5.17 .....                                     | 977  |
| C.T. Yih<br>R.P. Khera<br>(USA)   | Slurry Wall Instrumentation and Monitoring in Taipei. 5.18 .....                                | 985  |
| L.D. Johnson<br>(USA)   | Deformation Behavior of Wilford Hall Hospital Mat. 5.19 .... ..                                 | 989  |
| J.E. Laier<br>R.M. Mattox<br>(USA)  | Oversteepened Slopes Reinforced with Tensar Geogrid. 5.21 .....                                 | 993  |
| S.J. Kravits<br>H.C. Harrel<br>(USA)  | Demonstrating Borehole Drilling Accuracy at the Navajo Dam. 5.23 .....                          | 997  |
| S. DeFour<br>A.S. Judge<br>P. Lafleche<br>(Canada)  | Design and Monitoring of Earth Embankments over Permafrost. 5.25 .....                          | 1001 |
| W. Schubert<br>(Austria)<br>T.L. Richardson<br>(USA)  | Soft Ground Tunneling on the Seoul Subway Using NATM. 5.27 .....                                | 1011 |
| J.R. Davie<br>M.R. Lewis<br>L.W. Young<br>(USA)   | Accelerated Consolidation of Soft Clays Using Wick Drains. 5.29 .....                           | 1019 |
| J.C. Neyer<br>K.M. Swaffar<br>H.R. Price<br>(USA)   | Tunnel Repair Using Cement-Stabilized Flyash. 5.30 .....  | 1025 |
| M.D. Boscardin<br>(USA)   | Impact of Tunneling on Two Brick-Bearing-Wall Structures. 5.31 .....                            | 1029 |
| G. Guatteri<br>(Brazil)<br>J.L. Kauschinger<br>(USA)<br>A.C. Doria<br>(Brazil)<br>E.B. Perry<br>(USA) | Advances in the Construction and Design of Jet Grouting Methods in<br>South America. 5.32 ..... | 1037 |



|   |   |      |
|---|---|------|
| W. Fan<br>M. Shi<br>Y. Qiu<br>(China)                           | Ten Years of Dynamic Consolidation in China. 5.33 .....   | 1047 |
| N. Ghosh<br>M.M. Tabba<br>(England)                             | Experience in Ground Improvement by Dynamic Compaction and<br>Preloading at Half Moon Bay—Saudia Arabia. 5.35 ..... | 1055 |
| R.L. Curtis<br>V.E. Chouery-Curtis<br>D.A. Miller<br>(USA)      | Geogrid Reinforced Soil Retaining Wall on Compressible Soil. 5.35 .....   | 1063 |
| R.D. Charles<br>(USA)   | Performance of Prefabricated Drains in Soft Soils. 5.36 .....   | 1069 |
| K.R. Darye<br>M.R. Madhav<br>(India)                            | Case Histories of Foundations with Stone Columns. 5.37 .....  | 1075 |
| D.J. Hardin<br>M.L. Byington<br>S.V. Mills<br>(USA)             | The Rehabilitation of Terminal 2—A Case History. 5.40 .....   | 1087 |
| B.R. Christopher<br>A.B. Wagner<br>(USA)                        | A Geotextile Reinforced Embankment for a Four Lane Divided<br>Highway U.S. Hwy 45 West Bend, Wisconsin. 5.42 .....  | 1093 |
| T. Matsui<br>K.C. San<br>T. Amano<br>Y. Otani<br>(Japan)        | Field Measurement on a Slope Cutting With Tensile Inclusions. 5.43 .....  | 1099 |
| D.L. Jones<br>G.J. Macdonald<br>M.H. Golder<br>(United Kingdom) | The Performance Behaviour of a Grain Silo Foundtion in Jeddah<br>Supported on Stone Columns. 5.44 .....             | 1107 |
| K.Y.C. Chung<br>(USA)   | Designing Geotextile Support for Submarine Power Cables. 5.45 .....   | 1113 |
| K.S.A. Rahim<br>A.W. Dhowian<br>(Saudi Arabia)                  | Foundations on Stone Columns Resting on Coral Limestone. 5.46 .....   | 1117 |
| D.A. Bruce<br>F. Gallavresi<br>(Italy)                          | Special Tunnelling Methods for Settlement Control:<br>Infilaggi and Premilling. 5.48 .....                          | 1121 |
| J. Paul<br>(United Kingdom)                                     | Reinforced Soil in the Repair of Embankment and Cutting<br>Slip Failures. 5.51 .....                                | 1127 |

*Session V continued*

Page No.

|  |   |      |
|--|---|------|
| M.L. Ohri<br>A. Singh<br>G.R. Chowdhary<br>(India)     | Distribution of Contact Pressure and Stresses Under Skirted Footings. 5.53 .....              | 1133 |
| D. Cazzuffi<br>A. Pagotto.<br>P. Rimoldi<br>(Italy)    | Behaviour of a Geogrid Reinforced Embankment Over Waste Material. 5.55 .....                  | 1137 |
| E.R. Farrel<br>T.L.L. Orr<br>T. O'Donovan<br>(Ireland) | Performance of LPG Storage Tanks on Ground Improved by Stone Columns. 5.56 .....              | 1145 |
| H.D. Sharma<br>P. Kozicki<br>(Canada)                  | The Use of Synthetic Liner and/or Soil-Bentonite Liner for Groundwater Protection. 5.61 ..... | 1149 |
| R.F. Reed<br>P. Wright<br>(USA)                        | Long Term Building Performance Over An Injected Subgrade. 5.64 .....                          | 1159 |
| A.V. Shroff<br>D.P. Amin<br>D.L. Shah<br>(India)       | Epoxy Resin Grout System for Solutions to Traditional Geotechnical Problems. 5.66 .....       | 1165 |

**Session VI****"Case Histories of Soil Structure Interaction"**

|   |  |      |
|---|--|------|
| P.D. Long<br>N. Van Quang<br>(Vietnam)<br>B. Berggren<br>(Sweden) | Partial Underpinning of a Five-Storey Building. 6.02 .....   | 1169 |
| A. Ghinelli<br>G. Vannucchi<br>(Italy)                            | Damage to Masonry Structures in the Historic Center of Arezzo (Italy) Following the Excavation of Sewer Tunnel. 6.05 ..... | 1173 |
| A.H. Wu<br>(USA)  | Structural Damage Arrested by Stabilization of Landfill. 6.06 .....  | 1179 |
| R.B. Seed<br>C.Y. Ou<br>(USA)                                     | Compaction-Induced Distress of a Long-Span Culvert Overpass Structure. 6.10 .....  | 1183 |
| L.W. Abramson<br>W.H. Hansmire<br>(USA)                           | Three Examples of Innovative Retaining Wall Construction. 6.11 .....   | 1191 |
| J.J. Grosch<br>K.S. Al-Yahyai<br>(Saudi Arabia)                   | Anchored Bulkhead Failure on the Arabian Gulf. 6.13 .....  | 1201 |

|  |   |      |
|--|---|------|
| R. Cameron<br>C.A. Carr<br>(Canada)              | The Influence of Thin Clay Layers on the Design and Performance of a Flexible Cantilever Retaining Wall. 6.16 .....                         | 1209 |
| S.I. Tsien<br>(China)                            | Some Case Histories in Urban and Rural Geotechnical Engineering. 6.20 .....   | 1219 |
| W. Yiji<br>(China)                               | Treatment of KARST Subgrade by Deep Drilled Pile Foundations. 6.24 .....  | 1225 |
| G.E. Barnes<br>(United Kingdom)                  | Diagnosis of Structural Damage and Movement Due to More Than One Cause. 6.25 .....  | 1229 |
| M.R. Lewis<br>M.M. Blendy<br>(USA)               | Pressure-Injected Footings—a Case History. 6.26 .....   | 1233 |
| V.K. Garga<br>(Canada)                           | Anchor Failures at a Deep Excavation. 6.27 .....  | 1239 |
| S. Dovnarovitch<br>Y. Ivanov<br>(USSR)           | The Failure of Oil Storage Tanks and Their Control. 6.28 .....  | 1245 |
| J.M. Keaveny<br>P.M. Aas<br>F. Nadim<br>(Norway) | GBS Platform Evaluation Using Field Instrumentation. 6.29 .....   | 1249 |
| T.K. Kiu<br>C. Soydemir<br>M.P. Mitsch<br>(USA)  | Underpinning of an 11-Storey Building in Boston—A Case Study. 6.31 .....  | 1257 |
| R. Riker<br>D. Dailer<br>(USA)                   | Design, Construction, and Performance of a Deep Excavation in Soft Clay. 6.32 .....   | 1263 |
| A.V. Chummar<br>(India)                          | Failure of an Oil Storage Tank. 6.33 .....  | 1271 |
| C.J.F.P. Jones<br>(United Kingdom)               | The Effects of Mining Subsidence on a Motorway Bridge. 6.35 .....   | 1275 |
| H.O. Chukweze<br>(Nigeria)                       | Correlation Between the Actual and Predicted Settlements of Structures on Tropical Soil Foundation. 6.36 .....                              | 1279 |
| X. Sheng-sun<br>(China)                          | Bearing Capacity of Pile Foundation. 6.37 .....   | 1285 |
| J.K. Jain<br>R.K. Khare<br>(India)               | Stress Analysis of Gravity Dam Founded on Rock Mass Having Horizontal Seam (A Case Study of Bargi Dam in Madhya Pradesh, India). 6.39 ..... | 1289 |
| W.B. Ferguson<br>E.F. Glynn<br>(USA)             | A Foundation Failure in Philadelphia. 6.42 .....  | 1293 |

|   |   |      |
|---|---|------|
| R.J. Finno<br>(USA)<br>D.K. Atmatzidas<br>(Greece)<br>S.M. Nerby<br>(USA) | Ground Response to Sheet Pile Installation in Clay. 6.43 .....                        | 1297 |
| S.A. Bucher<br>R.J. Krizek<br>(USA)<br>D.K. Atmatzidis<br>(Greece)        | Full-Scale Load Test of Caisson on Chicago Hardpan. 6.44 .....                        | 1303 |
| J.R. Davie<br>M.R. Lewis<br>(USA)   | Settlement of Two Tall Chimney Foundations. 6.45 .....                                | 1309 |
| M.A. Gouda<br>I.W. Lippincott<br>D. Raghu<br>(USA)                        | Distress to Structures on Loose Ash and Cinders Fills. 6.49 .....                     | 1315 |
| N.P. Angeles<br>U.W. Stoll<br>(USA)                                       | Design and Field Monitoring of 70-Foot High Tied Anchor<br>Retaining Wall. 6.50 ..... | 1319 |
| D.P. Gado<br>G.P. Kelley<br>J.J. McElroy<br>(USA)                         | Performance of Foundations and Retaining Structures. 6.51 .....                       | 1327 |
| S. Hansbo<br>(Sweden)   | Common-Sense Foundation Design. 6.54 .....  | 1337 |
| S.S.M. Cheng<br>S.A. Ahmad<br>(Canada)                                    | Dynamic Testing Versus Static Load Test: Five Case Histories. 6.55 .....              | 1343 |
| R.C. Hepworth<br>J. Langfelder<br>(USA)                                   | Settlement and Repairs to Cement Plant in Central Utah. 6.56 .....                    | 1349 |
| K.D. Tucker<br>(USA)  | Performance Evaluation of Pile Foundation Using CPT Data. 6.58 .....                  | 1355 |
| D. Sharma<br>(India)  | Foundation Failure of the St. Thomas Church, New Delhi. 6.59 .....                    | 1365 |
| Z.S. Zhang<br>D.Z. Luan<br>X.X. Zhang<br>(China)                          | The Case Record of Ba-Yu-Quan Anchor Slab Retaining Wall. 6.60 .....                  | 1371 |
| T.L. Cooling<br>J.B. Hummert, Jr.<br>(USA)                                | Drilled Pier Load Test, Fort Collins, Colorado. 6.61 .....                            | 1375 |

|   |   |      |
|---|---|------|
| B.R. Christopher<br>C.N. Baker, Jr.<br>(USA)            | Caisson Load Test and Instrumentation Program—Sohio Corporate Headquarters. 6.62 .....  | 1383 |
| C.N. Baker, Jr.<br>S.B. Steinberg<br>W. Lam<br>(USA)    | Building Design and Construction Over Organic Soil. 6.63 .....  | 1389 |
| M.R. Lewis<br>J.R. Davie<br>C.L. Weaver<br>(USA)        | Differential Settlement of Nuclear Power Plant Foundations. 6.64 .....  | 1395 |
| G. Hannink<br>(The Netherlands)                         | Reconstruction of the Settlement History of Buildings. 6.67 .....   | 1403 |
| G. Hannink<br>A.F. van Tol<br>(The Netherlands)         | Large Horizontal Displacements of Houses in Rotterdam. 6.68 .....   | 1409 |
| K.M. Chua<br>L.J. Petroff<br>(USA)                      | Predicting Performance of Large-Diameter Buried Flexible Pipe:<br>Learning from Case Histories. 6.72 .....  | 1417 |
| J.C. Li<br>H.L. Yao<br>L.P. Shi<br>B.I. Shy<br>(Taiwan) | Behavior of Ground Anchors for Taipei Sedimentary Soils. 6.73 .....   | 1421 |
| A.J. Nicholson, Jr.<br>J.R. Wolosick<br>(USA)           | Post-Tensioned Caissons Permit Interstate Construction:<br>A Case History. 6.74 .....   | 1425 |
| A.S. Stipho<br>(Saudi Arabia)                           | Model Test of Reinforced Earth Retaining Wall. 6.76 .....   | 1433 |
| S. Abdel-Salam<br>M. Mashhour<br>(Egypt)                | Repair and Rehabilitation of a Residential Building at Nile River<br>in Cairo. 6.77 .....   | 1437 |
| Y.S. Kim<br>P.Y. Thompson<br>(USA)                      | Behavior of Buried Concrete Box Culvert. 6.79 .....   | 1443 |
| R.H. Borden<br>W.J. Sullivan<br>W. Lien<br>(USA)        | Settlement Predictions in Residual Soils by Dilatometer,<br>Pressuremeter and One-Dimensional Compression<br>Tests: Comparison with Measured Field Response. 6.83 ..... | 1449 |
| M.P. Luong<br>(France)                                  | Collapsing Peak up of a Large Highway Steel Pipe-Arch. 6.88 .....   | 1455 |
| A. Kropp<br>(USA)                                       | Existing Pile Load Capacity Evaluation. 6.89 .....  | 1471 |

|   |   |
|---|---|
| R. Azevedo<br>N. Consoli<br>(Brazil)                                    | Comparisons Between Field and Analytical Behavior of an<br>Experimental Excavation. 6.90 ..... 1465 |
| D.C. Cowherd<br>S.M. Thrasher<br>V.G. Perlea<br>J.O. Hurd<br>(USA)      | Actual and Predicted Behavior of Large Metal Culverts. 6.92 ..... 1471                              |
| E.A. Nowatzki<br>(USA)<br>B.P. Wrench<br>(South Africa)                 | Geotechnical Investigation into Causes of Failure of a Gabion<br>Retaining Wall. 6.96 ..... 1477    |
| S.V. Nathan<br>(USA)  | Two Case Histories: Performance of Shallow Foundations on Sand. 6.97 ..... 1483                     |
| P.K. Jain<br>B. Singh<br>G.C. Nayak<br>(India)                          | Geotechnical Studies of Foundation of a Tilted Tank at<br>Parikshatgarh, India. 6.98 ..... 1489     |
| R.J. Rapp<br>J.S. Schwenk<br>(USA)                                      | Lock and Dam No. 26 R, Lock Cofferdam, Construction Sequencing.<br>6.99 ..... 1495                  |
| X.H. Zhao<br>Y.A. Yin<br>Y.P. Qian<br>J.G. Dong<br>W.Y. Shen<br>(China) | A Study of 15 Cases of Soil-Structure Interaction in China. 6.100 ..... 1501                        |
| I. Houssamy<br>M.M. Daman<br>(USA)                                      | Simulation of Drilled Pier Behavior Under Three-Dimensional<br>Loading. 6.101 ..... 1505            |
| G. Ranjan<br>S.K. Kaushik<br>V.K. Gupta<br>(India)                      | Health of Ammonia Horton Spheres and Foundations—a Case Study.<br>6.102 ..... 1509                  |

## State-of-the-Art Papers

|                           |  | Page No. |
|---------------------------|--|----------|
| B.B. Broms<br>(Singapore) | Design and Construction of Anchored and Strutted Sheet Pile Walls<br>in Soft Clay. ....              | 1515     |
| C.S. Desai<br>(USA)       | Case Studies Through Material Modelling and Computation. ....  | 1551     |
| G.F. Sowers<br>(USA)      | Movement in the Powerhouse Excavation Saguling Project, Indonesia. ....                              | 1567     |
| J. Ramage<br>(USA)        | Lipari Landfill: Lechate Containment System—Geotechnical<br>Considerations. ....                     | 1577     |
| W.D.L. Finn<br>(Canada)   | Case Histories in Seismic Response Analysis. ....  | 1585     |
| G.W. Clough<br>(USA)      | Review of River Bank Stability Processes in Stabilizing Measures. ....                               | 1597     |
| M.L. Silver*<br>(USA)     | Lessons Learned from Case History Performance of Earth Dams,<br>Embankments and Natural Slopes. .... | 1609     |
| Author Index .....        |  | 1609     |

\*To be printed in Volume III

## **Session I**

# **“Case Histories of Geotechnical and Hydrological Management of Solid, Hazardous, and Radioactive Wastes”**



## Use of Deeply Weathered Rock As Landfill Cover Material, Patacon Landfill, Republic of Panama

W.C.B. Gates

Captain, United States Army Environmental Hygiene Agency,  
Aberdeen Proving Ground, Maryland

**SYNOPSIS:** Under normal conditions weathered rock provides poor landfill cover because of its permeable nature. However, a recent hydrogeological investigation conducted by the US Army Environmental Hygiene Agency (AEHA) of the Patacon Landfill in the Republic of Panama revealed the contrary. The operators were using weathered rock from the surrounding saprolitic outcrops of the Panama formation and Tertiary andesite intrusions for landfill cover. The AEHA selected samples of the weathered rock from the borrow sites for engineering tests at their soils engineering lab at Aberdeen Proving Ground, Maryland. The following are test results. Water induces the weathered rock to slake very quickly to a gravely silt. Compaction of the samples yielded an average Proctor density of  $1.74 \text{ gm/cm}^3$  at 19 percent optimum moisture content. The lab achieved a low permeability of  $6 \times 10^{-7} \text{ cm/sec}$  on the compacted samples. The test results suggest that properly prepared weathered rock will substitute as borrow material for landfill cover.

### INTRODUCTION

The Republic of Panama owns and operates the Patacon Sanitary Landfill. The facility has been in operation since May 1985, when the Government of Panama closed the Panama Viejo dump.

The location of the facility is 2 km north of the Panama Canal (Figure 1). The site occupies a tropical intermontane valley between Rios Mocambo and Guanabano, respectively. In addition, it is west of Cerro Patacon and south of

the Continental Divide. The land upon which the facility lies was formerly the Panama Canal Zone property. The United States later deeded the property to the Republic of Panama as a result of the 1977 Panama Canal Treaty.

Because of the potential for surface and ground-water contamination from the Patacon Landfill, the US Army Garrison in Panama requested the AEHA review the operations and management of the landfill and attendant hydrogeology and water quality.

I conducted the study in two phases. Phase I, the initial hydrogeological investigation of the Patacon Landfill and vicinity, occurred during June 1986 (Gates, 1986). During Phase I, I preselected locations for installation of downgradient monitoring wells. In addition, I reviewed the operation and management of the Patacon Landfill.

While conducting the initial study, I observed one thing which grasped my interest as a geological engineer. The operators were using weathered rock as landfill cover. Usually, ripped, weathered rock provides poor landfill cover because it is very permeable. To see if this borrow material was viable as a source of landfill cover, I obtained two samples for testing at the AEHA Soils Lab. The initial test results of the mechanical properties suggested that weathered rock would provide good cover. This prompted additional geotechnical investigations. Therefore, in November 1987, I returned to collect additional rock samples from three primary borrow sites for geotechnical testing.

This paper does not discuss the analytical results of the Phase II ground-water study. Rather, the purpose of this paper is to analyze the merits of the unique landfill cover material employed by the Patacon operators.

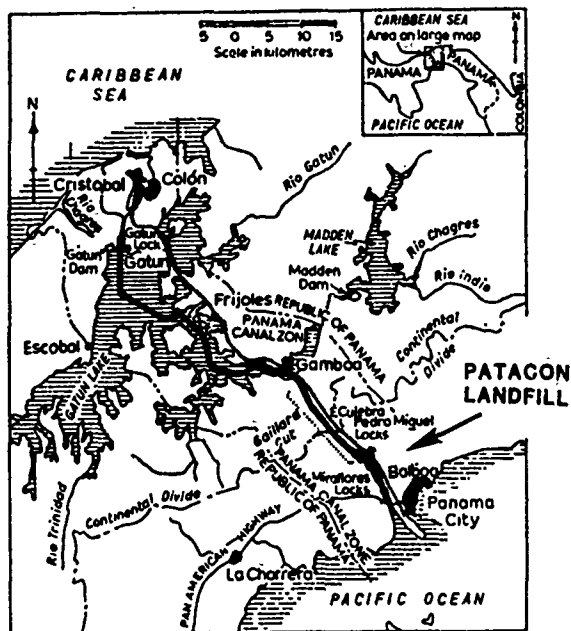


Fig. 1 Location of the Patacon Landfill

## ENGINEERING GEOLOGY

For an in-depth review of the geology of Panama refer to Woodring (1957), the Stewarts' (1980), and Weyl (1980). The local engineering geology surrounding Patacon Landfill follows.

### Stratigraphy

Surficial deposits around Patacon Landfill are largely red clay laterites overlying silty saprolites formed by weathering of the underlying parent bedrock.

The Panama formation (Early to Late Oligocene) is the principal bedrock unit surrounding the landfill (Figure 2). This rock unit is an agglomerate of angular to subangular blocks of differentially weathered andesite, widely scattered in a matrix of fine-grained tuff (Woodring, 1957; Stewart and Stewart, 1980). Because of deep weathering from the tropical environment, this unit slakes readily to small friable cobbles, chips and mud. Fresh chunks of the Panama formation break easily with both hand and hammer.



Fig. 2 Outcropping Weathered Rock of the Panama Formation Used for Borrow Landfill Cover

Intrusive andesites (Oligocene and Miocene) surround the landfill site (Figure 3). The exposed, outcropping portion of the rock units have weathered to a coarse, friable saprolite. Because of the deep weathering, the rock is very easy to rip with a hammer.

### Structure

According to Woodring (1957) and the Stewarts' (1980), the Panama formation exhibits an apparent gentle dip of 7 degrees southwest towards the canal.

Distinct fracture tectonics dominate the Canal Zone (Weyl, 1980). In general, faults trend on

a north bearing. Woodring (1957) and the Stewarts' (1980) have identified the Miraflores and the Rio Pedro Miguel faults 3 km west of the landfill. Both form major drainage pathways. Although not identified as faults, the northern trends of Rios Guanabano and Mocambo, also, suggest fracture zones. There is no evidence of active faulting within the study area.



Fig. 3 Weathered Andesite Outcrop Used for Borrow Cover Material

### Hydrogeology

Patacon Landfill is hydraulically upgradient of Fort Clayton and adjacent to a potential recharge area. Recharge occurs along the geologic contact of the andesite intrusions and the Panama formation. The ground water flows down dip and along fracture zones towards the Panama Canal. A semi-confined ground-water zone occurs approximately 40 feet below the surface (PCC, 1961; Patacon Well Log 2, 1985; Allinger and Gates, 1988). A shallow aquifer, approximately 20 feet below the surface, ties into the alluvial aquifer bordering Rios Guanabano and Mocambo (CONAMA, 1985; Allinger and Gates, 1988). Because there is a direct hydraulic link between the aquifer and the streams, the aquifer fluctuates with the seasonal discharge of the stream. In addition, the shallow aquifer reflects the pollution of the stream. For instance, Allinger and Gates (1988) found total coliform bacteria colonies in the streams and ground water that were too numerous to count. They concluded, the coliform bacterial pollution comes directly from the landfill via runoff.

## PATACON LANDFILL

### Operation

The site location for the Patacon Landfill is excellent, if managed properly. The engineers from the University of Panama developed a detailed engineering plan for the landfill site (CONAMA, 1985). There is sufficient acreage and borrow material for the landfill to expand. The engineers estimate that the maximum size of the facility will approach 300 hectares. At the time of the June 1986 survey (Gates, 1986), the City landfilled about 900 tons of solid waste per day by the modified trench-area fill method (Figure 4).



Fig. 4 Operators Employ the Area/Trench Fill Method at Patacon Landfill

During the first trip, I noted the operators attempted to follow the engineering plans for the landfill as closely as possible. However, during the second visit, the rainy season was at its height. Because of the poor road maintenance and the heavy rain, travel to the disposal site was at a standstill. The roads were impassable. Because the operators could not get to the borrow sites for landfill cover, nearly 12 hectares, 3 meters high of uncompacted, uncovered solid waste lay exposed to the elements. The rain had thoroughly saturated the solid waste. The surface of the landfill bubbled and hissed from escaping methane gas and other organic products. The operators had not controlled the surface runoff and leachate, rather the effluent drained into Rios Guanabano and Mocambo. Turkey vultures covered and defecated on the surface of the landfill (Figure 5). The turkey vultures were the primary source of the coliform pollution of the streams.



Fig. 5 Patacon Landfill (Note vulture problem)  
Cover Material

To cover the landfill, the engineering plans called for a simple cut and fill operation. That is, the operators filled the natural topographic-low depressions with partially compacted solid waste. Once they had spread and compacted the waste with bulldozers, they covered it with borrowed weathered rock from the adjacent outcrops and hills. Of note, surrounding the landfill are sufficient quantities of lateritic clay to use as cover. However, the operators chose not to use this material.

Under normal conditions, we, as geotechnical engineers, would not select weathered rock for landfill cover material because it would be too permeable. Intermediate and final cover should be clay-like, near impermeable material that will reduce influent percolation of fluids and prevent subsequent leachate production. My first impression of the cover material that the Panamanian engineers selected was that it was totally inadequate. However, on closer inspection, I noted that the cover had characteristics of a low permeable clay-like material. This is atypical of crushed rock.

The borrow sites selected by the landfill operators were outcrops of rock within the boundaries of the landfill. The rock units were the Panama formation (Tp) and Tertiary andesite (Ta) intrusions (Figures 2 and 3). The operators excavated the rock material by ripping with a front-end loader or bulldozer. After removing the rock from the borrow pit, they spread and compacted it on the surface of the landfill with a bulldozer.

I noted two things while visiting the site during the dry and rainy season. During the rainy season, the crushed rock weathers very quickly to a sticky mud if the moisture exceeds the optimum. During the dry season, there was just enough rain to bring the cover to optimum moisture. This eased the trafficability.

Daily precipitation facilitated the rock to slake to a soil-like material which aided in mechanical compaction. Where the operators compacted the cover material, the permeability appeared very tight because water pooled on the surface.

## GEOTECHNICAL TESTING

### General

After observing the Panamanian operators, I noted the most important aspect in locating weathered rock for landfill cover material was the ability to distinguish the durable from the nondurable rock. The operator needs to locate the nondurable material that will react as soil and compact easily.

Several authors have suggested various mechanical tests to evaluate the durability of shale or weak rock (Chapman, 1975; Strohm and others, 1978; ASTM D 4644-87; Franklin, 1983). Geotechnical engineers employ these tests to distinguish weak rock from more durable material. The simple slaking tests provide easy identification of weathered rock and shales that are relatively soft and nondurable (Strohm and others, 1978). Other weathered rock that is mechanically hard and durable is recognizable by its resistance to weathering in the field, density, and ringing when struck by a hammer or its unchanged nature after a slake-durability test.

To evaluate the mechanical adequacy of the cover material selected by the Panamanian engineers, I chose to use the slake tests in reverse. That is, I wanted to know how well the rock slaked to a soil-like material rather than how durable it was. I chose the following slake tests described by Strohm and others (1978): Jar-slake test, rate of slaking test and slake test (substituted for the slake-durability test). In addition, I investigated other physical characteristics of the cover material such as Grain size, Atterberg limits, Proctor densities, moisture contents (natural, saturated, and optimum) and the permeabilities achievable at Proctor density. The following is a discussion of the test methods and analytical results.

### Sample Sites

I selected three, 110 kg, representative weathered rock samples from the active borrow sites. Two came from the Panama formation (Tp1, Tp2) and one from the andesite (Ta) outcrop.

### Jar-slake Test

The jar-slake test is a simple quick qualitative test which describes six descriptive degrees of slaking (Strohm and others, 1978). The investigator determines the degrees of slaking by observing the reaction of oven-dried samples immersed in water. I used this test during the first trip, as a quick indicator of the durability of both rock units. All rock samples (Panama formation and weathered andesite) reacted immediately to the jar-slake test. Since the Panama formation is an

agglomerate, the individual clasts slaked differentially, based on the degree of weathering. The andesitic samples reacted slower because they were apparently more durable. The test provided useful information on the behavior and hardness of the water-soaked rock samples. Some of the clasts which did not slake immediately, broke apart between the thumb and fingers. In general, the Jar-slake index for these samples ranged from 2.5 to 3.5. The implication of this is the samples break down rapidly to form few to many chips mixed with flakes and mud.

### Rate of Slaking Test

Chapman (1975) and Strohm and others (1978) discuss the rate of slaking test. This test is a useful supplement performed in conjunction with the Jar-slake test. The rate of slaking is a function of the change in liquidity index. The liquidity index is the difference between the in situ water content and soaked water content divided by the plastic index of the sample. The average change in liquidity index for all samples exceeded 1.25. Therefore, the borrow material slakes very fast.

### Slake Test

The American Society for Testing and Materials (ASTM) considers the slake-durability test (ASTM 4644-87) the primary test for weak rocks and shales. The slake-durability index ( $I_d$ ) measures the percent of the rock material retained at the completion of the test. Conversely, the slake test is a measure of the total material lost during the test. The slake test is an alternative to the slake-durability test since the slake index is equal to  $100 - I_d$  (Chapman, 1975; Strohm and others, 1978). The slake-durability index, based on the slake index for the samples, ranged from 66 to 87 percent. The material retained on the sieve consisted of a mixture of hard clasts, large and small, intermixed with soil-like nondurable material. The ASTM classification is Class II (ASTM D 4644-87).

### Proctor Density

Since I was evaluating the weathered rock as landfill cover, I employed the 15-blow compaction test to determine Proctor density. The 15-blow compaction test approximates field compactions expected of cover over a spongy solid waste landfill (Lutton, 1980). It differs from the standard 25-blow test because the technician uses less compactive effort. This results in lower maximum densities and higher optimum moisture contents (Lutton and others, 1979; US Army, 1980).

Figure 6 depicts the combined Proctor density test results. The results show that under ideal laboratory conditions, one can compact the weathered rock to an average Proctor density of  $1.74 \text{ gm/cm}^3$  at an optimum moisture content (OMC) of 19 percent.

PROCTOR DENSITY RESULTS, PANAMA & ANDESITE UNITS  
PATACON LANDFILL, REPUBLIC OF PANAMA

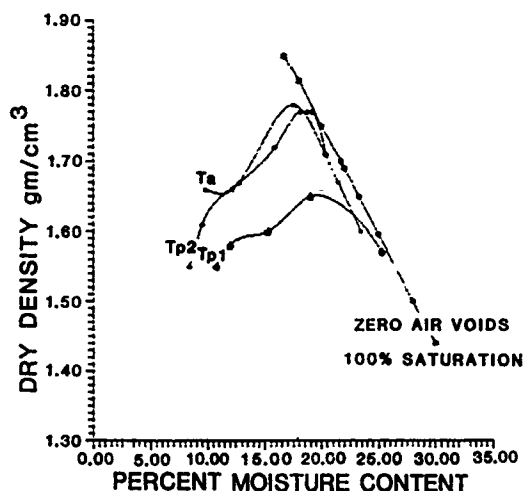


Fig. 6 Consolidated Proctor Density Results  
Permeability

We conducted constant head permeabilities on all compacted samples. The following are the laboratory permeability results on the compacted samples. For the Panama formation (Tp1 and Tp2), we achieved an average permeability of  $9 \times 10^{-7}$  cm/sec at an OMC of 20 percent and a Proctor density of 1.72 gm/cm³. Similarly, for the weathered andesite (Ta), we achieved a permeability of  $2 \times 10^{-8}$  cm/sec at an OMC of 18 percent and a Proctor density of 1.78 gm/cm³.

#### DISCUSSION

The tropical climate has reduced the rock to a weathered saprolite. Both rock units slake readily to a combination of durable clasts of cobbles and gravel mixed with nondurable clasts and soil-like material. The Panama formation reacts faster because of its agglomeratic nature. However, overall the rate of slaking for both is very fast. Based on the slake test, the rock durability is moderate. The reason for this is the differential weathering of the rock. Thus, some clasts are more durable than others.

For the weathered rock to work properly as landfill cover, the operators must mechanically rework both rock units. A goal that the Panamanian operators should strive for when compacting the cover layers is 95 percent of Proctor density at optimum moisture based on the 15-blow compaction test. At these conditions, the operator can achieve a permeability of approximately  $6 \times 10^{-7}$  cm/sec, also. According to Lutton (1980), one can approach this goal by six passes with an intermediate-size dozer or similar on soil cover over municipal solid waste.

#### AREAS FOR RESEARCH

Using weathered rock as an alternative to clay-like soil for landfill cover is an area for additional geotechnical research. The researcher should obtain many samples from a variety of geologic formations and geographical areas for testing. Since the texture of the weathered rock is more coarse than soil, the researcher should select larger compaction molds and permeameters. This will reduce error and more approximate field conditions. The slake-durability test should include the slake-durability apparatus as a primary testing device. In addition, the investigator should investigate problems attendant to compaction and hydraulic conductivity which may cause errors. The following are problem areas identified by the EPA (1984) for research on soil cover which is, also, applicable to weathered rock cover: (1) effects of moisture content on compactions; (2) the maximum size of soil aggregates; (3) cause and effect of deleterious substances, such as rocks and roots; (4) methods of compaction and compactive effort; (5) effects of air in the samples; (6) effects of excessive hydraulic gradients; and (7) permeameter and sample size.

#### CONCLUSIONS

The Patacon Landfill, if properly operated, is an excellent site for a landfill. The CONAMA developed excellent and viable landfill engineering design plans. The problem noted, however, was the operators follow the design plans sporadically.

The results of the engineering tests suggest that weathered rock from the Panama formation and the andesite intrusions will work well as landfill cover when properly prepared and applied. The weathered rock reacts readily to slaking tests. Laboratory permeabilities of the cover material of  $6 \times 10^{-7}$  cm/s are achievable at 15-blow Proctor densities of 1.74 gm/cm³.

#### ACKNOWLEDGEMENTS

I extend thanks to the following individuals in the Waste Disposal Engineering Division for their editorial, laboratory and clerical support: Steve Curran, geologist; Keith Hoddinott, soil scientist; Mark Farro and Duane Maners, engineering technicians; Esther Webb, editor; and Lynne Griest, typist.

#### REFERENCES CITED

- Allinger, Richard J. and William C. B. Gates (1988), Phase II, Ground-water Consultation No. 38-26-0930-87, Potential Impact of the Patacon Landfill on the Ground Water Beneath Fort Clayton, 193d Infantry Brigade, Republic of Panama, 3-10 November 1987, US Army Environmental Hygiene Agency, Aberdeen Proving Ground, Maryland.
- ASTM D 4644 - 87 (1987), "Standard Test Method for Slake Durability of Shales and Similar Weak Rocks," Annual Book of Standards, Vol. 14.02, 1-5.

Chapman, D. R., (1975), "Shale Classification Tests and Systems: A Comparative Study." MSCE Thesis and Joint Highway Research Project No. 75-11, Purdue University, West Lafayette, IN, 90.

CONAMA (1985), Republica de Panama, Diseno de Ingenieria Para el Proyecto Relleno Sanitario de la Ciudad de Panama en: Mocambo, Comision Nacional del Medio Ambiente (CONAMA).

EPA (1984), "Soil Properties, Classification, and Hydraulic Conductivity Testing," Draft Technical Resource Document for Public Comment (SW-925), Office of Solid Waste and Emergency Response, US Environmental Protection Agency, Washington D.C., 39-52.

Franklin, J. A. (1983), "Evaluation of Shales for Construction Projects - An Ontario Shale Rating System," Ministry of Transportation and Communications, Research and Development Branch, Downsview, Ontario, 99.

Gates, William C. B. (1986), Phase I, Groundwater Consultation No. 38-26-0930-87, Potential Impact of the Patacon Landfill on the Ground Water Beneath Fort Clayton, 193d Infantry Brigade, Republic of Panama, 9-18 June 1986, US Army Environmental Hygiene Agency, Aberdeen Proving Ground, Maryland.

Lutton, R. J. (1980), Evaluating Cover Systems for Solid and Hazardous Waste, Interagency Agreement No. EPA-IAG-D7-01097, Municipal Environmental Research Laboratory, Office of Research and Development, US Environmental Protection Agency, Cincinnati, Ohio, 28-32.

Lutton, R. J., G. L. Regan, and L. W. Jones (1979), Design and Construction of Covers for Solid Waste Landfills, Interagency Agreement No. EPA-IAG-D7-01097, Municipal Environmental Research Laboratory, Office of Research and Development, US Environmental Protection Agency, Cincinnati, Ohio, 22-24 and 41-48.

Patacon Well Log (1985), Pozo #2, Patacon Landfill, Republic of Panama.

PCC (1961), Geological Field Log, Chiva-Chiva Receiver Station, Panama Canal Company, Engineering and Construction Bureau.

Stewart R. H. and Stewart J. L. (1980), "Geologic Map of the Panama Canal and Vicinity, Republic of Panama," Miscellaneous Investigation Series, US Geological Survey.

Strohm, W. E., G. H. Bragg and T. W. Ziegler, (1978), "Design and Construction of Compacted Shale Embankments; Volume 5, Technical Guidelines," US Army Waterways Experiment Station, Geotechnical Laboratory, Vicksburg, MS.

US Army (1980), EM 1110-2-1906, Laboratory Soils Testing, Department of the Army,

Office of the Chief of Engineers, 30 November 1970.

Woodring, W. P. (1957), "Geology and Paleontology of Canal Zone and Adjoining Parts of Panama," US Geological Survey Professional Paper 306-A.

Weyl, Richard (1980), Geology of Central America, Geologisch-Palaontologisches Institut der Universität Giehep.

## Disposal of Phenolic Waters from a Producer Gas Plant

**Dorairaja Raghu**

Civil Engineering Department, New Jersey Institute of Technology,  
Newark, New Jersey

**Hsin-Neng Hsieh**

Civil Engineering Department, New Jersey Institute of Technology,  
Newark, New Jersey

**SYNOPSIS:** Phenolic waters are generated in a producer gas plant in India. Since harmful environmental effects can result even with low concentrations of phenol in water, its disposal poses a problem. Four options for disposal were considered. One of these options considered involves disposal in a earthen pond situated close to a river. In order to avoid river pollution by possible seepage of phenolic waste, geotechnical aspects have to be considered. For each option, cost analysis is performed. This paper discusses as to how the final disposal technique is decided taking into account all the relevant aspects of the problem.

### INTRODUCTION

Industrial development is occurring all over the world. Such activity generates certain substances that are to be disposed off in an environmentally accepted manner. Phenol is one such chemical. In this paper, a case history involving the disposal of phenolic waters and slag will be presented to illustrate as to how phenolic compounds can be safely disposed.

### STATEMENT OF THE PROBLEM

Phenol is generated in several processes (Forney, 1974; Luthy, 1981; Keating, et al., 1979). In the case history cited herein, phenol is produced in a producer gas plant in India. Producer gas is manufactured by the destructive distillation of coal. Three types of phenolic waters are produced in the various units of the gas producer plant. They are:

1. First type: phenol is produced during the contact between the gas and water in scrubbers. Its concentration ranges from 20 to 30 mg/l. It has been estimated that on completion of the final stage of the project, a quantity of 14,600 m<sup>3</sup>/day of this type of water will be generated.

2. Second type: High concentration phenolic waters (ranging from 9 to 10 g/l) are produced by the condensation of water vapors while passing through gas coolers and electrostatic filters. Upon completion of the project cited here, it is estimated that a quantity of 216 m<sup>3</sup>/day of this type of phenolic waters will be produced.

3. Third Type: Phenolic waters with concentrations ranging from 10 mg/l to 3 g/l are also discharged from various operational units into water seals. The quantity of these waters in comparison with those of the first and the second types is small and variable. Hence this is considered to fall under the category of the second type. No further discussion of this type will be presented in this paper.

### DISPOSAL OF PHENOLIC WATERS

#### First Type:

The first type of phenolic waters produced in the scrubbers have a concentration ranging from 20 to 30 mg/l. This concentration is less than the maximum admissible concentration of 50 mg/l of phenolic waters that can enter the central sewage treatment plant. Hence these phenolic waters do not pose any major disposal problems. This is based on the premise that the scrubbers are considered to operate with the fresh process water and that no recirculation is taken into consideration.

From the point of view of economy, reduction in the consumption of process water with consequent reduction in the capital expenditure on the treatment plant is desirable and recirculation of water is considered a necessity. As a consequence of this, the phenolic waters will have concentrations greater than 20 to 30 mg/l. In this case, if a circulation system were to be adopted, the average concentration of phenols of these waters works out to be about 85 mg/l.

The quantity of wastewater with high concentration of phenol entering the treatment plant can be regulated in the circulation system according to the requirements of the treatment plant. It may also be noted that the circulation cooling system provides for the lowering of concentration due to oxidation by atmospheric oxygen. For this reason, average phenol quantities mentioned above can be considered as maximum and the probable quantities of phenol entering the treatment plant as not exceeding the lower limit (20 mg/l).

#### Second Type:

These waters have concentrations from 9 to 10 g/l. They contain an average of 70% phenols and 30% substituted phenols. These waters have to be treated separately as they can not be handled by the central sewage treatment plant.

At the time of disposal, the concentration of phenol has to be reduced to that below the tolerable limits. In the following sections, a discussion on this topic will be presented.

#### TOLERABLE LIMITS FOR PHENOLIC WATERS

Phenol and other phenolic compounds are either toxic or lethal to fish at relative low concentration and impart objectionable tastes to drinking water. McKee and Wolfe (1963) following a review of world literature concluded that phenol in a concentration of more than 0.001 mg/l would interfere with the domestic water supplies, 0.2 mg/l would interfere with fish and aquatic life and 1000 mg/l would interfere with stock watering. Chlorinated phenols also present problems in drinking water supplies because phenol is not efficiently removed by conventional water treatment and can be chlorinated during the final water treatment process to form persistent odor-producing compounds. Hence it was decided to adopt a method of disposal that result in no pollution of river waters by the flow of phenolic waters from the slag pond.

#### TREATMENT OPTIONS CONSIDERED

For the treatment of the second type of phenolic waters, four different options were considered. These will be discussed in detail in the subsequent sections.

##### METHOD 1 Hydraulic Transport of Slag with High Concentration Phenols as the Carrying Medium

Daily, 14,600 m<sup>3</sup> of the first type of phenolic waters with a concentration of 85 mg/l will be mixed with 216 m<sup>3</sup> of the second type of phenol with a concentration of 10 g/l. This will result in a total quantity of phenolic water of 14,816 m<sup>3</sup>/day with a concentration of 230 mg/l. Slag produced by the burning of coal in the producer gas plant along with the phenolic water will be transported hydraulically to an open air slag pond. This pond is proposed to be constructed outside the plant area.

The treatment proposed in this option consists of the following:

1. Adsorption of the highly concentrated phenolic waters by slag.
2. Effect of atmospheric oxygen on slag saturated with phenolic waters in the proposed slag pond.

In this chemical process, some of the phenols gradually change to harmless humus substances and the rest remain combined with water in the slag, which according to the preliminary tests conducted show a high degree of saturation. To achieve maximum contact between phenolic waters and slag particles from producer gas plant and boiler house, the slag will be hydraulically conveyed utilizing the high concentration phenols as the medium to a proposed slag dump pond outside the plant area.

#### Details of the Slag Dump Pond

The slag dump pond will be situated southwest of the plant adjacent to the left bank of a river. For the construction of the bottom and the sides of the pond, it is proposed to utilize the locally available soils. The banks must be above the level of the surrounding area in order to check monsoon storm water coming into the area. It is also necessary to provide an intercepting trench around the pond to prevent flooding of the pond by torrential rain water from outside and to prevent the leakage of phenolic water from the inside of the pond into the river so as not to cause river pollution. The pumping station for return water is built near the pond. This water is to be pumped back into the gas producer plant wherein it will be mixed with highly concentrated phenolic waters and slag and from there it will be led again to the pond.

Figure 1 shows the layout of the pond with respect to the plant. An existing railway embankment forms on one side of the pond. The other enclosures will be provided by a curvilinear embankment as shown. An intercepting trench all around the embankment is provided on the outer side. The purpose of this trench is two fold: (1) to collect water seeping out of the pond and (2) to monitor the quality of water seeping out in order to take suitable mitigating measures in time.

#### Soil Conditions at Site

Preliminary borings and test pits were performed for investigating the in-situ conditions. The soil conditions comprise of a layer of top soil about 0.5 meters thick on top of a 10 meter thick layer of silty clay. This is underlain by a layer of clayey silt, 6 meters thick. Soil Samples were obtained for testing. Relevant standards of the American Society for Testing and Materials referred to as A.S.T.M. were utilized for testing procedures.

#### Geotechnical Properties of In-situ Soils

Index tests were conducted to classify the soils. The liquid limits for the silty clay and the clayey silt were determined to be respectively 65 and 38. Corresponding plastic limits were 32 and 22 respectively. Modified proctor compaction tests were conducted on these materials with a view to utilizing these materials for embankment. Optimum moisture contents for the above two materials were 15 % and 12%, respectively. Maximum dry densities corresponding to these optimum moisture contents were 123 lbs/cubic foot and 110 lbs/cubic foot respectively. From a compaction point of view, the locally available material did not pose any problems.

#### Permeability Tests

In order to prevent any seepage of water from inside the pond to the river, the foundation material has to be sufficiently impervious. Otherwise, suitable liner systems or slurry walls have to be provided with imported



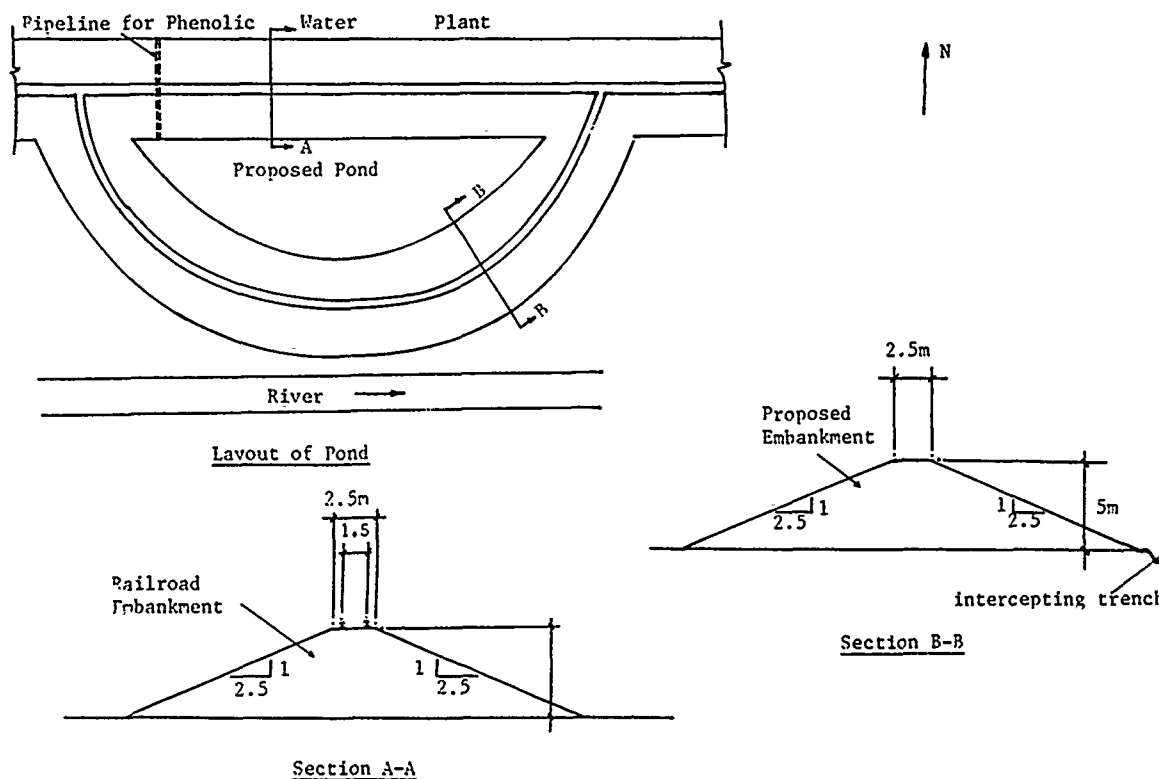


FIGURE 1

soils and geotextiles. So permeability tests were conducted for this purpose on the in-situ materials. Several types of tests are available to determine the permeability of soils. A review of available literature indicates that the conductivity is affected by the type of test (Daniel, et al., 1985). Mitchell and Madsen (1987) feel that the consolidometer permeability test is potentially the most useful one due to the versatility of the equipment. Hence, the use of consolidation tests for determining the permeability of silty clays in this paper can be justified.

For imperviousness, compaction on the wet side of the optimum is required (Daniel 1984). Hence, consolidation tests to determine permeabilities of local soils were conducted at dry densities corresponding to 95 percent maximum proctor dry densities on the wet side of optimum. These tests indicate that the silty clay and the clayey silt have average coefficients of permeability respectively  $7.3 \times 10^{-7}$  cm/sec and  $1.1 \times 10^{-6}$  cm/sec. Consolidation tests conducted on in-situ undisturbed silty clay foundation materials indicated that the average coefficient of permeability was of the order of  $10^{-7}$  cm/sec.

#### Effect of Phenolic Waters on the Hydraulic Conductivity

The permeability determinations referred to above were made with water as conducting fluid. It is well known that hydraulic conductivity is

susceptible to changes with time or exposure to chemicals. Mitchell and Madsen (1987) recommend that the permeant used for testing to be of the same composition as to that to which the foundation material will be subjected in the field. Since, in this project, phenolic waters will be seeping through the foundation material of the dam, the possibility of conducting permeability tests on silty clay with phenolic waters as permeant was considered. As stated earlier, the concentration of phenolic waters will be 230 mg/l. But, due to oxidation in pond, only 32% of phenols will remain, thus reducing the concentration of phenolic waters reaching the bottom of pond to 76 mg/l.

A review of literature regarding the effect of phenols on the hydraulic conductivity was made. For this project, it can be stated that the hydraulic conductivity of silty clays will not be affected by phenols of the concentration produced in this plant, based on the following:

1. It appears that concentrations of organic solutions at or below the solubility limit have no effect of hydraulic conductivity of clay soils irrespective of the test methods (Mitchell and Madsen, 1987). The solubility of phenol in water is 86 g/l (Mitchell Et. al, 1987), whereas the concentration of phenol in the case history cited in this paper is 74 mg/l.

2. Acar et al. (1985), observed from flexible wall tests that in a compacted soil with 0.1 % concentration phenol the hydraulic

conductivity did not change appreciably. The concentration of phenolic waters from the producer gas plant is 74 mg/l and thus it is less than 0.1%.

Hence, it was decided not to perform hydraulic conductivity tests on native clay with phenol as permeant.

Based on the foregoing discussions, it can be assumed that a coefficient of permeability value of the order of  $10^{-7}$  cm/sec would be admissible. Thus, it can be inferred that the native foundation soil has sufficient imperviousness to retain the phenol without polluting the river, eliminating the need for cutoff walls or special lining systems.

If this option were to be implemented, besides the storage pond, approach roads, pipe bridges, pumping stations for pumping water from peripheral trenches are to be constructed. Basalt coated pipes are needed for the hydraulic transport of phenol to prevent abrasion due to the slag. These pipes have to be imported from abroad, costing valuable foreign exchange.

The major disadvantage of this method is that very strict quality control measures for compaction have to be adopted to make the dam impermeable to prevent river pollution.

#### METHOD 2 Treatment of Phenol in an Independent Treatment Plant

In this option, the slag is transported hydraulically by the phenolic waters of low concentration obtained by the treatment of high concentration phenols by a special process. As part of this technique, high concentration phenol waters are diluted with 5 times low concentration waste to give an effluent of 1,296 m<sup>3</sup>/day of concentration 1,525 mg/l. Depending on the condition of the diluted effluent, it may be necessary to adjust pH value between 7 to 10 prior to treatment. Nutrients are added to obtain a concentration in the diluted effluent of 75 mg/l nitrogen and 15 mg/l of phosphorus.

An aeration tank is provided for the biological treatment of wastewater. This tank is fitted with mechanical aerators to supply oxygen and with an anti-foam dosing device which will operate automatically in the event of a build-up of foam occurring. A settling tank is also provided to separate the sludge from clarified effluent. This 16 ft diameter concrete settling tank is fitted with mechanical sludge scraper. The settled biological sludge will be recycled by means of pump to the aeration tanks to maintain a constant concentration of microorganisms in the aeration tank and the clarified treated effluent will overflow from the settling tanks to the drain. The treated effluent has a concentration of only 10 mg/l. This can be handled by the central sewage treatment plant.

The advantages of this method are:

1. Construction of earthen dam is avoided.

2. Load on central sewage treatment plant will be reduced.
3. Neither change nor alteration in the mechanical equipment for which orders are already being placed.

#### Method 3 Biological Treatment of Phenol and storage of sludge only in the pond

In this method, uncrushed slag delivered by conveyor belt falls in the truck and transported to a storage pond. For access to the pond, an underbridge below the railway line will be built. High concentration phenol water will be treated separately by the special process explained in the above option. The effluent will be allowed to enter the sanitary sewer leading to the central sewage treatment plant.

Advantages claimed are:

1. River pollution is totally avoided.
2. Trucks manufactured in India can be utilized avoiding costly foreign exchange.
3. Crushers, pumps, basalt-coated pipes and pipe bridge are unnecessary and hence savings in foreign exchange can be realized.
4. Disposal of slag into a particular place is not necessary. The whole area can be used. capital and operating costs are less.

#### METHOD 4

This option differs from the Method 3 in that the mode of transportation of uncrushed slag is by aerial ropeway. Spreading of slag is accomplished by human labor.

Advantages are the same as those for method 3. Disadvantage is the aerial ropeway that would impede with height clearances and air rights.

#### COST ANALYSES

For each option, capital costs, operations costs and working costs were estimated and presented in the form of tables. Costs were worked out for a period of operation of 25 years. In arriving at working costs, annual maintenance, operation and depreciation for such items whose life is shorter than 25 years and are to be replaced by new ones are considered. In order to aid in the process of comparison, the costs are shown in units and not in any currency.

A comparison of the four different methods discussed above can be made from the figures in Table I:

TABLE I  
COST COMPARISON

| Item                      | Method 1   | Method 2   | Method 3   | Method 4   |
|---------------------------|------------|------------|------------|------------|
| Capital cost              | 17,091,380 | 7,826,170  | 2,150,880  | 12,537,380 |
| Working cost per year     | 1,848,006  | 2,372,482  | 735,560    | 1,272,140  |
| Working cost for 25 years | 46,200,150 | 59,312,050 | 18,390,000 | 31,803,500 |
| Total Cost (Add A and C)  | 63,291,530 | 67,138,220 | 20,540,880 | 44,340,880 |

#### Basis For Selection Of Disposal Technique

From the above table, it appears that the methods 2 and 3 have respectively the highest and the lowest working costs for 25 years. The capital costs for option 1 are the highest of all. Method 2 was rejected on the basis of high costs. It was decided to adopt method 3 since it costs the least. But due to the existing problems regarding the import of equipments, it was anticipated that there will be a 2-year delay in obtaining the required equipment. Hence it was decided to adopt option 1 in the interim (for a period of two years).

Phenolic waters will be pumped into the pond through a pipeline and the slag will be transported by trucks. In the meanwhile orders will be placed for basalt-coated cast iron pipes from abroad. These pipes will be used for the hydraulic transport of phenolic waters and slag.

#### CONCLUSIONS

As the avoidance of river pollution is the main technical concern, the scheme that satisfies this requirement in addition to being the cheapest in respect of the total cost was the one chosen. Thus it can be shown as to how geotechnical aspects such as pollution control and other environmental aspects control the final solution to the problem.

#### REFERENCES

- Acar, Y.B., Hamidon A., and Scott, L., "The Effect of Organic Fluids on the Hydraulic Conductivity of Compacted Kaolinite", *Hydraulic Barriers in Soils and Rock*, ASTM STP 874, 1985, pp. 171-187.
- Daniel, D.E., "Predicting Hydraulic Conductivity of Clay Liners", *Jour. of the Geotechnical Engineering Division, ASCE*, Vol. 110, No. GT2, February 1984.
- Daniel, D.E., Anderson, D.C., and Boynton, S.S., "Fixed-Wall vs. Flexible Wall Permeameters", *Hydraulic Barriers in Soils and Rock*, ASTM STP 874, 1985, pp. 107-126.
- Forney, A. J. et al., "Analysis of Tars, Chars, Gases, and Water in Effluents from the Synthane Process," *U.S. Bureau of Mines Tech. Progress Report 76*, Pittsburgh Energy Research Center, Pittsburgh, PA, 1974.
- Keating, et al., E.J., et al., "Phenolic Problems Solved with Hydrogen Peroxide Oxidation," *Proceeding of the 33rd Industrial Waste Conference*, Purdue University, Ann Arbor Science Publishers, Ann Arbor, MI, 1979, pp.464-470.
- Luthy, R.G., "Treatment of Coal Coking and Coal Gasification Wastewaters," *Jour. Water Poll. Control Fed.*, Vol. 53, 1981, pp. 325-339.
- McKee, J.E., and Wolfe, H.W., "Water Quality Criteria", *State Water Quality Control Board*, Sacramento, California, Pub-3A, 1976.
- Mitchell, J.K., and Madsen, F.T., "Chemical Effects on Hydraulic Conductivity", *Geotechnical Practice for Waste Disposal '87*, *Proceedings of a Specialty Conference Sponsored by the Geotechnical Division of ASCE*, *Geotechnical Special Technical Publication No. 13*, Ann Arbor, Michigan, June 1987, pp. 87-116.
- Quality Criteria For Water: U.S. Environmental Protection Agency, Washington., D.C., 1976.

# Complementing Radiologic Data with Geology—A Case History

Dennis McGrane

Geologist, Bechtel Civil Inc., San Francisco, California

**SYNOPSIS:** The goal in characterizing radioactively contaminated soil is to quantify the degree of contamination and its parameters. A cost effective, small scale characterization is done by performing a surface radiological survey with subsurface data coming from boreholes augered in a tight grid pattern. Confidence in the between-hole extrapolations depends on the grid size. However, at the widely contaminated site in Maywood, New Jersey a grid width of 100 feet was the only economical choice. Accurate contamination parameters were determined despite the wide hole spacings once geologists and health physicists learned how local geologic conditions controlled the contamination's location and extent. The contamination pathway was found to be fluvially dependent, and various logged soil types could be confirmed by their distinctive radiologic signatures. With this knowledge, grid drilling was abandoned. Drillhole sites were individually selected based on geologically supported, between-hole extrapolations thereby eliminating many costly boreholes.

## HISTORY, LOCATION, AND DESCRIPTION

The 1984 Energy and Water Appropriations Act authorized the Department of Energy (DOE) to conduct a decontamination research and development project at the former Maywood Chemical Works (now owned by the Stephan Company) and its vicinity properties. DOE now owns 11.7 acres of the land just west of the Stepan Company and has constructed the Maywood Interim Storage Site (MISS) there. The MISS lies in a highly developed area in the Borough of Maywood and the Township of Rochelle Park, New Jersey. Contaminated residential properties lie further south in the Borough of Lodi (FIG 1).

From 1916 through 1956, the Maywood Chemical Works processed monazite sand (thorium ore) for industrial products. During this time, slurry containing process wastes from the thorium operations was pumped to diked areas west of the plant. Historical aerial photographs show these tailings ponds were located in former swampy areas, the headwaters for the southward flowing Lodi Brook. In 1932, New Jersey Route 17 was built through this disposal area, leaving contaminated material isolated on what is now known as the Ballod property, west of the MISS. During this time, process wastes were removed from the Maywood Chemical Works for use as mulch and fill on nearby commercial and residential properties, thereby contaminating them with radioactive thorium and its daughters (some elevated concentrations of Uranium-232 and its daughters are also present). Maywood Chemical Works stopped processing Thorium in 1956. Construction of vicinity commercial properties began in 1960. At this time 80-90% of Lodi Brook leaving the MISS area was confined to a concrete conduit and buried. Above this conduit, commercial and residential development occurred during the next 27 years.

The goal of this project is to define all contamination parameters and remediate all those areas exceeding DOE guidelines. During a previous phase of this project, 25 residential properties in Rochelle Park, Lodi and Maywood, and a portion of the Ballod property were characterized and underwent remedial action. The low level radioactive soil removed from these areas is now being stored at the MISS. The project phase discussed here involved the characterization of the MISS, portions of the Stepan site, seven commercial properties (Sears, Desaussure, Hunter Douglas, Federal Express, Sunoco, Gulf, and Bergen Cable), 27 Lodi properties, the New Jersey Vehicle Inspection Station (NJVIS) and the Lodi Municipal Park.

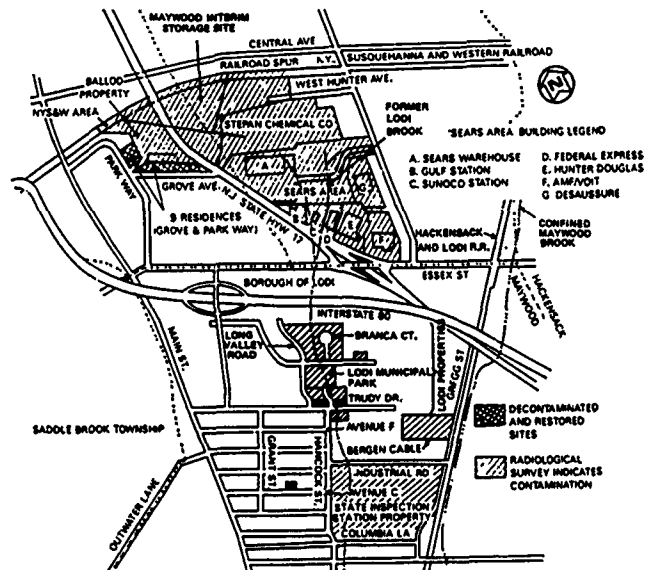


FIGURE 1—MAYWOOD INTERIM STORAGE SITE AND VICINITY PROPERTIES

## SITE CHARACTERIZATION PLAN

The first step in the characterization involved establishing a 50 foot grid tied into the New Jersey State grid system, allowing the grid to be easily reestablished during any remedial action. Next, cone-shield gamma measurements were taken 12 inches from the ground, 10 feet apart throughout all designated properties. Once locations exceeding the DOE guideline of 5 pCi/g were found, surface soil samples were collected and analyzed for thorium-232, radium-226, and uranium-238. Subsurface borehole locations were established at 100 foot intervals on the MISS and commercial properties. Borehole locations on residential properties were to be designated by the geologist, but it was believed that a grid pattern with shorter between-hole spacings would be the most logical hole site selection plan. Subsurface (downhole) measurements were conducted using a 2 inch by 2 inch sodium iodide gamma scintillation detector. This instrument was calibrated so that a count rate of 40,000 cpm was approximately equal to the 15-pCi/g DOE subsurface guideline for thorium-232. Because of the possible volatile chemical hazard, hole locations were first scanned using a metal detector (to detect buried drums and utilities), and then continuously monitored during drilling using an environmental monitor (ENMET).

## GEOLOGY AND HYDROGEOLOGY

Successfully carrying out the subsurface augerings depended on the geologist's ability to discriminate between various local geologic units. The thin alluvial topsoil in this area of northern New Jersey is underlain by the deltaic Brunswick sandstone (Triassic age). The Brunswick is a moderately hard, mostly fine grained argillaceous formation with occasional rounded gravel and cobbles; it is often interbedded with thin, discontinuous organic lenses. The relatively flat topography and temperate climate enables a residual soil to develop in more elevated, nonsaturated areas. Typically, the soil horizons here can be described as a thin (5-1.0 ft.), moderate brown (5 YR 3/4) organic horizon over a 3.0-8.0 foot dark yellowish brown (10 YR 4/2) decomposed layer which grades into competent, dark reddish brown (10 YR 3/4) Brunswick sandstone (FIG II). Typically, competent rock lies at a depth between 12 and 15 feet, with depths at the NJVIS ranging from outcroppings to greater than 20 feet.

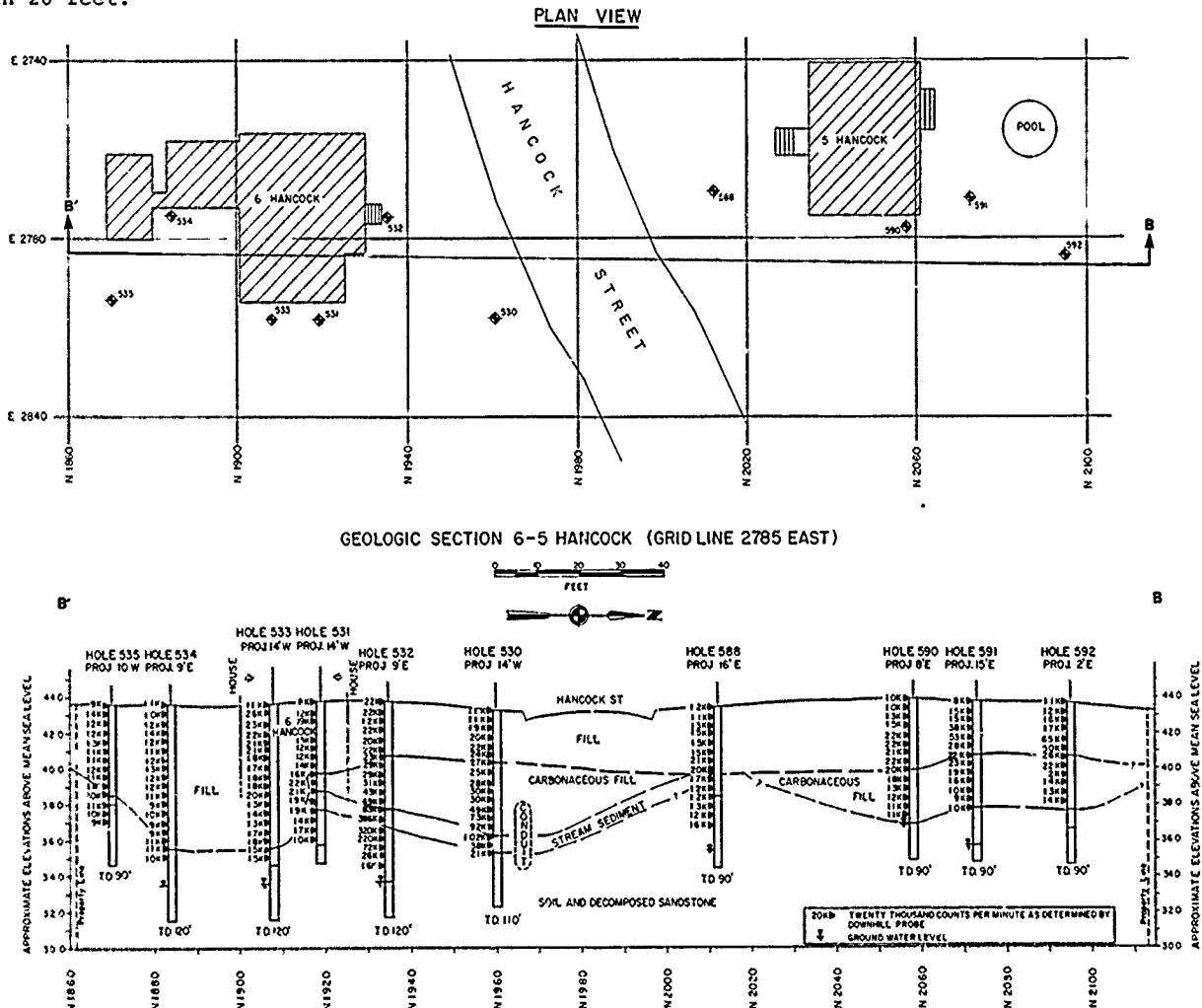


FIGURE II - PLAN VIEW AND CROSS SECTION OF 6-5 HANCOCK STREET

In and adjacent to the low lying dendritic drainages of the Lodi Brook watershed (namely the commercial property areas), saturated conditions permit the development of a silty organic cumuloose soil. This black silt sequence originated through seasonal floodwater deposition and is subsequently very mobile. The silts presence helped identify areas of floodwater deposition in Lodi Brook, indicate former intermittent tributary streams, and quantify the width of the Lodi Brook floodplain.

Knowing ground water conditions was important in understanding surface transport mechanisms. Because the summertime ground water level is shallow (typically 7.0-9.0 feet below the ground surface), saturated conditions leading to surface runoff are quickly reached during heavy rains. Knowing this, we were not surprised to find large amounts of stream flow transported contamination extending far downstream and well out to either side of the main stream channel.

Subsurface contaminant transport by groundwater was not a problem owing to the insolubility of Thorium-232. However, documenting precise groundwater levels and local gradients was important to identify potential chemically contaminated plumes, especially at the Sears site. Accurate ground water levels were also needed to explain radiation flux attenuation in holes that do penetrate below the water table. For remedial action purposes, accurate seasonal ground water levels were also necessary to support excavation planning.

#### INITIAL ASSUMPTIONS

At the start of this characterization, Lodi Brook was not known to be a major contaminant transport mechanism. In 1984, six Lodi properties underwent remedial action, but only two of these homes were located over the former Lodi Brook floodplain. Contamination around the four homes was explained by human residential backfilling. No explanation could be made for the deep contamination on the other two properties because Lodi Brook was not visually present, and because a geologist was not present to identify the contaminant-bearing media as stream sediment.

During this early segment of the characterization, contaminant location was also not assumed to be environmentally dependent. On the former Maywood Chemical Works site (MISS, Ballod, and Stepan), the expectation was to find thick sequences of radioactive material where it had been interpreted that former tailings ponds had been located, based on historical aerial photographs. Moreover, expectations were to encounter lenses of contaminated tailings below fill extending onto the commercial properties. Another expectation was to find contamination in fill used to level each commercial area before construction. South of the commercial properties (excluding Bergen Cable), contamination location had not been deemed environmentally dependent, but was also wrongfully assumed to also be mechanically deposited by humans.

The initial characterization drill plan was based solely on the above assumptions. Excluding former tailings pond areas, the contaminant transport mechanism seemed random and unpredictable. Therefore, the correct drill plan selected would most logically be a grid pattern.

#### CHARACTERIZATION OF MISS AND ADJACENT COMMERCIAL PROPERTIES

The surface and subsurface of the MISS and Sears sites were characterized according to the previously discussed guidelines. Hole locations were only displaced from grid points if overhead or below ground utilities or suspected buried drums made it necessary. Drilling on the grid pattern provided adequate coverage of the large buried tailings pond areas. It is also provided the precise locations where fill was placed before commercial property construction. Drilling on a set grid pattern did not allow the flexibility to better define contaminated areas with additional holes. We also may have missed penetrating some smaller contaminated areas because of the 100 foot grid interval. On the whole though, grid pattern drilling at Sears and the adjacent commercial properties was effective to adequately quantify contamination extent and depth.

In topographically elevated areas the drilling results were consistent with our assumption that contamination would be found in the disturbed, uppermost residual soil sequence. There, determining the boundary between contaminated and clean materials could only be done by radiological means. Visual identification of white Thorium Oxide was impossible in almost all cases for drillholes outside the tailings areas because the contaminant was masked by darker, fine grained host materials. In tailings ponds areas, a thick sequence of white radioactive tailings was found above clean natural material (mostly black organic silt). Downward migration of Thorium into the silt was prevented by Thorium's insolubility. In the southern part of the Sears and other commercial properties, Lodi Brook headwaters end and a slightly incised channel begins. This is also where no tailings ponds were located. Here we found that the contamination began to extend into the native black silt sequence. In some holes contamination extended only into the uppermost portions of the silt, while in others the entire black silt soil horizon was contaminated. This can be explained by the theory that spilled, released, or eroded radioactive materials from the tailings ponds were mixed into silt mobilized by high water. Forty years of such mixing is enough to account for contamination throughout thick natural sequences in Lodi Brook's downstream channel and partial contamination of its adjacent floodplain. This theory had not yet been developed while this drilling occurred. Instead, the randomness of contamination depth and extent, along with the myriad of hosting materials, all pointed to mechanical backfilling as the primary contaminant spreading mechanism.

The discovery of buried metal drums proved useful in defining low-lying portions of Lodi Brook and will aid in any subsequent remedial action. In two sites on the Sears property, buried chemical-filled drums were discovered, and the detection of suspicious metal objects in other locations

resulted in displaced drillholes. The map locations of drums and other metallic objects correlates precisely with the former channel of Lodi Brook. This formerly depressed area is logically a good place for dumping, eliminating the need to dig a waste pit. Knowing this relationship, when remedial action occurs, the excavator may encounter chemical-laden drums throughout the former stream channel on the Sears property.

#### CHARACTERIZATION OF LODI PARK AND BERGEN CABLE

The characterization of the Lodi Municipal Park was also done on a grid pattern; in this case a 75 foot grid spacing provided the best coverage. It was here, almost one half mile downstream from the MISS, that the Lodi Brook conduit was first encountered. With this discovery came the first conscious correlation between contamination and fluvially transported black silt.

At this time, the extent of floodplain contamination was not known. Lodi Brook was thought to have been merely a small stream, not one capable of spreading contaminated silt 75 feet from its channel. The few boreholes drilled into the floodplain were enough to establish a silt/contamination correlation, but their wide spacings on the grid prevented the attainment of a good cross-sectional channel profile.

On both sides of the conduit, black organic silt was identified as originating from floodplain deposition and not as wetland cumuloose soil like that which had developed at the brook's headwaters (MISS and Sears). Since we were out of Lodi Brook's swampy headwaters and onto its former meandering channel, our drilling should have been directed specifically towards defining the lateral extent of the contaminated floodplain. This could have been done by drilling lines of holes perpendicular to stream flow and noting the lateral extent of contaminated black floodplain sediment. Instead, initial volume estimates were made based on inadequate and ineffective borehole locations possibly resulting in imprecise conclusions. More precise volume estimates could have been made with a more geologically sensitive drill plan.

South of the buried conduit in Lodi Park another important correlation between a geologic material and contamination was established. A 2-6 foot thick black, coal ash lense was found just below the sandy topsoil fill and above decomposed Brunswick sandstone. This coal ash revealed a radiological signature above DOE guidelines and appeared as a black, sandy, fine-course grained material similar in appearance to the contaminated black stream sediment. The only major difference was in its much lower density. If only radiological data were used for contamination volume estimates, this material would have been falsely classified as material originating from MISS. More radioactive coal ash was subsequently found under some Lodi residential properties where it had been used as fill around housing foundations.

Subsurface drilling at Bergen Cable was done on a 100 foot grid pattern. Before drilling, surface scan measurements revealed contamination in the site's southeastern corner. Downhole probe readings in boreholes within the contaminated area failed to quantify any contaminated zones because of the minute thickness of the contaminated topsoil. Because this area is completely out of the Lodi Brook drainage basin, fill emplacement seems to be a logical mode of contaminant transport. It is also possible that nearby (less than 100 feet) Maywood Brook also transported contaminants, but from a different source.

#### CHARACTERIZATION OF THE LODI RESIDENTIAL PROPERTIES

The characterization of a single residential property requires full hole-coverage if the mode of contamination transport is unknown or random. Because contaminated fill was still believed to be the cause of contamination, individual homes were characterized as if contamination could be anywhere and at any depth. Drillhole site locations were conservatively chosen to provide total coverage. Holes were located around the property's perimeter and house foundation, and in all "hot-spots" delineated by the surface cone shield survey.

While characterizing the first few residential Lodi properties, understanding the site's geologic and radiologic relationships grew to the point where drill plan modifications were deemed necessary. Plotted and contoured cone-shield data first led to the realization that contamination coincided precisely with the extent of the Lodi Brook floodplain. Cone-shield data in the nonfill covered backyards of 18, 20, and 22 Long Valley Road showed a linear contamination boundary paralleling the former stream channel 75 feet away. This distance agreed with the interviewed residents who stated that before confinement, Lodi Brook floodwaters once extended over a hundred feet wide.

As more holes were drilled along the conduit, a definite correlation developed between the black stream sediment and contamination. Rough geological sections revealed a black silt lense approximately 150 feet across which deepened and thickened in the center and tapered outwards to higher elevations - the classic graded stream and floodplain profile. Since contamination was fluvially deposited by a graded stream, the following suppositions could be made: 1) contamination could be expected at higher elevations farther away from midchannel; 2) contamination thickness would be greater in the channel due to bed load transport; 3) contamination would be under a house if the house is located on the floodplain and only then if the excavated foundation did not penetrate the contaminated lense; 4) the lateral subsurface contamination boundaries could be projected up and downstream because of the gradual directional changes which characterize a graded stream; 5) contamination may be only at the surface of the floodplain sediment, and it may not extend as far away from the stream as the extent of black silt since silt deposition probably began long before the contamination was introduced; and 6) the lateral boundary of contamination may suggest low lying areas such as intermittent tributaries. Evidence of this last observation can be seen at the NJVIS (FIG III). There, the undulating boundary reflects numerous smaller tributaries and former topographical variances.

With these depositional theories in mind, a new drill strategy was developed to take advantage of contamination predictability. From this time on, drillhole locations were selected by the field geologist based on existing drilling and radiologic data and knowledge of shallow geologic conditions. Hole frequencies were increased in areas on top of the former floodplain and decreased outside the high water depositional boundary. Holes were not completely eliminated outside the floodplain due to the fact that contaminated fill was always a possibility. Hole locations were

staggered to provide better coverage for cross-sections perpendicular to stream flow. Fewer holes were needed at each residence because contamination boundaries could be projected down or upstream. And, during drilling, the radiologic logs of each drillhole complimented the geologic logs by helping the geologist better define the contacts between the "hot" black silt sandwiched between clean surface fill and natural decomposed sandstone. This gave us assurance in the field that all contamination had been penetrated.

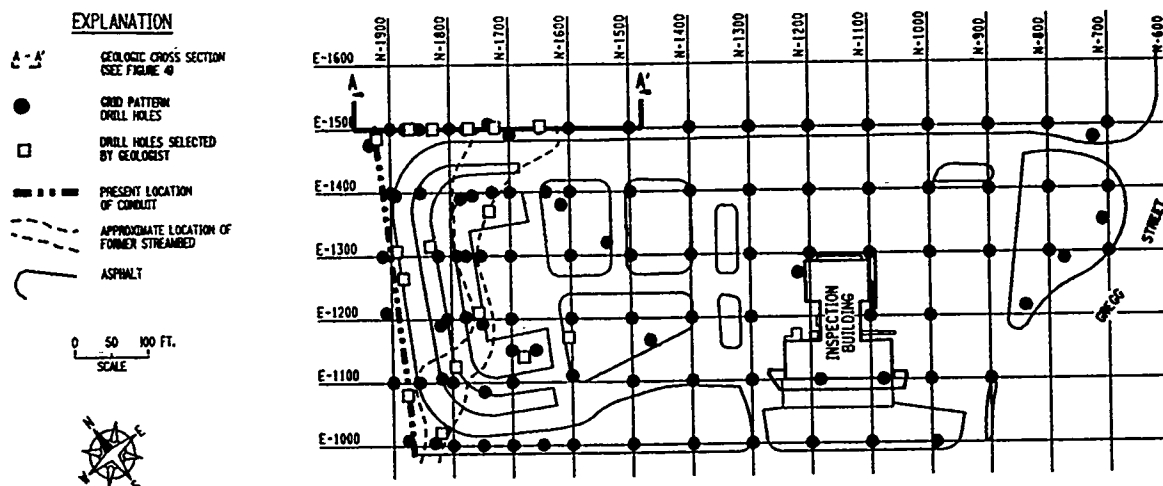


FIGURE III - BOREHOLE LOCATIONS AT THE NEW JERSEY VEHICLE INSPECTION STATION PROPERTY

South of the Lodi Municipal Park, the geologist and health physicist worked closely together to identify the radiologic signature of coal ash surrounding many designated home foundations. Often this ash lies directly above black contaminated stream sediment. Knowing the coal ash to be physically less dense and having a lower radiation flux (20,000 - 30,000 cpm), it was possible to discriminate between it and Thorium-contaminated black silt. Again, this discrimination was usually done by the juxtaposition of geologic and radiologic logs (FIG II). Any geologic contact discrepancies were usually explained by the alpha-attenuating affects of ground water.

Knowing the radiologic signatures of various geologic materials, it was possible to compare existing radiologic and geologic data from Lodi Park to better define the limits of Thorium contaminant as opposed to the coal ash fill. The geologist's ability to discriminate between the two radioactive materials encountered at Lodi Park and many residential properties was essential; otherwise, the volume estimate of Thorium-232 contaminated materials, based solely on radioactive readings, would have been far too high.

#### NEW JERSEY VEHICLE INSPECTION STATION (NJVIS)

The NJVIS was first characterized after drilling at Lodi Park was completed. At that time, Lodi Brook was not known to be the main contamination transport mechanism, and drilling was proceeding on a strict 100 foot grid pattern. Predrill surface cone shield measurements showed contamination in the northern property reaches, but south of the buried Lodi Brook conduit. With this information alone, there was no reason to question the belief that transported fill was the principle mode of contamination.

Just as at Lodi Park, the grid drilling plan did not adequately characterize the former creek channel. Drilling data showed only two holes with significant contamination at depth. If the final contamination volume estimate had been based only on this information, the result would have been too low. Outside the channel, in the southern NJVIS property, a more cost effective drill strategy would have simply been to drill boreholes on hot spots delineated by the surface cone shield survey or in areas where fill was known to be thick.

After characterizing the Lodi properties, confidence was lost in the effectiveness of the original NJVIS characterization. Personnel returned to the NJVIS thinking that a contaminated lense of stream sediment existed below the buried conduit just as had been found on the Lodi properties. Additional drilling proved this theory false. The additional drilling was intentionally done in a linear fashion perpendicular to the stream channel (FIG II). Information from these drillholes helped define the former floodplain width and channel depth without additional holes between drill lines.

The results of the second drill session showed the former channel near the surface and south of the conduit (FIG IV). Contaminated fill was also found around the conduit in the northwestern



corner of the property. Our revised drilling technique provided the information needed for an accurate volume estimate without excess holes. Every hole was used to either define contamination extent and/or depth. Most importantly, the former creek channel was found to be south of the existing conduit, meaning the conduit leaves the former channel somewhere between the southernmost designated Lodi property and the NJVIS. This is valuable information for determining the next properties to be designated for characterization.

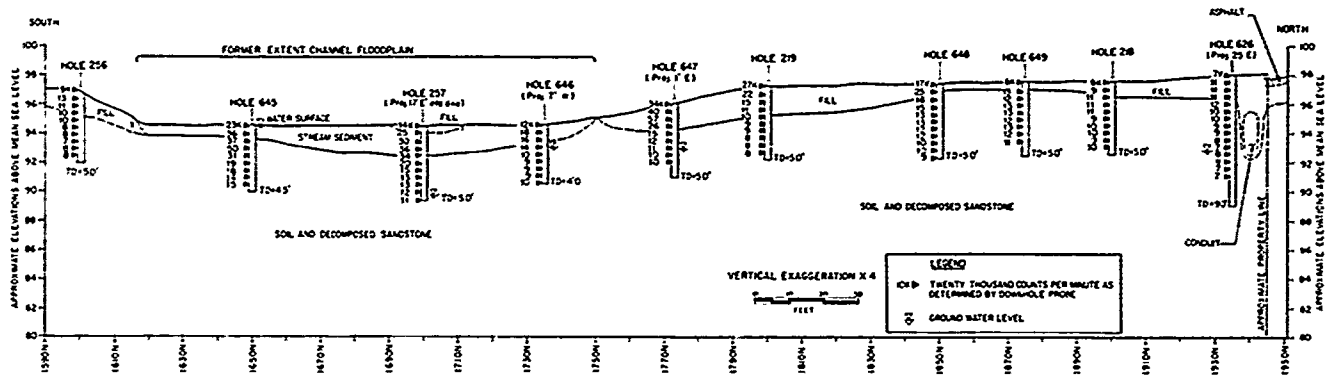


FIGURE IV - GEOLOGIC SECTION GRID LINE 1500E (NEW JERSEY VEHICLE INSPECTION STATION)

## CONCLUSION

Many important ideas were developed throughout this characterization which will expedite further work of this kind. Most importantly, knowing the mode of contamination transport is essential in developing an investigation plan. As the MISS (excluding tailing pond areas) and Lodi properties, it was initially believed the contamination was in randomly placed fill material. The most logical drill plan for random contamination is a grid. At the MISS and commercial sites a grid plan proved an appropriate method, but along the former Lodi Brook channel the continued use of a grid could have resulted in an inaccurate contaminated soil volume estimate. The geologist's ability to recognize natural deposition and predict trends was crucial in evolving geologically sensitive drilling strategies.

It also became evident that a great amount of information can be gathered before drilling by interviewing knowledgeable parties, in this case long-time residents. For this project, time budgeted for predrill site research, including the use of aerial photographs, would have been much more cost effective than deciphering the site history through a subsurface investigation.

The cone-shield surface survey proved extremely helpful in selecting potential drillhole locations, finding the lateral extent of contamination, and revealing geologic trends. And lastly, the juxtaposition of drillhole radiologic and geologic logs was invaluable for determining the contamination's vertical dimensions and defining geologic contacts.

## A Low-Rise Hospital Development on Restored Opencast Fill

W.M. Kilkenny

Senior Lecturer in Geotechnical Engineering, University of Newcastle  
upon Tyne, England

**SYNOPSIS:** An extensive low-rise hospital development has taken place since 1982 on a former opencast coal mining site 30 years after working and restoration. The clay and shale fill some 20 metres deep was placed without systematic compaction. Five separate site investigations have been carried out at different times during the last 20 years and a detailed engineering geological mapping exercise was completed in 1977. Drainage works and the main buildings in Scheme 1 and 2 have been monitored during and after construction. Significant settlements have occurred requiring some remedial work. A surcharge and inundation trial has been undertaken prior to the design and construction of Scheme 3. The response of the buildings and the drainage to ground movement is described and design recommendations made for future development.

### INTRODUCTION

Opencast coal mining began in earnest in the United Kingdom in 1942. Early developments were slow due to inexperience and the absence of suitable plant. Operations were often restricted to around 20 metres depth. Plant and technical assistance were provided by the United States and some 43 million tons were extracted in the 5 year period 1942-1947. United Kingdom opencast coal mining has often taken place in areas of past deep mine activity in or around population centres. The opencast mines in the United Kingdom are characterised by multiple thin seams giving overburden/coal ratios up to 20, excavation frequently below the water table requiring dewatering and backfilling without systematic compaction. The geology is commonly stiff glacial till overlying the sandstones, shales and mudstones of the Upper Carboniferous Coal Measures. The overburden is excavated either by dragline and cast to one side or where face shovels are used, loaded into trucks and end tipped in high lifts. Superficial soils are usually removed using scraper equipment and stored on site until restoration. Occasionally coal washing plant and associated lagoons or settlement ponds for general site drainage alter groundwater conditions locally. While all opencast sites are restored for agricultural purposes it is only recently that controlled compaction in layers for all or part of the fill has been adopted for specific sites. Elsewhere the vertical restored profile can be expected to show large variations in material type, grading, density and moisture content. There have been many modest commercial, industrial and residential structures with their associated roads and services constructed on uncompacted fills up to 60 metres deep since the late 1950's. Most of this development has been trouble free and where it has not the response of the clay/shale/sandstone backfill to increasing moisture content has been the most probable source of

settlement-related damage. The prediction and control of the post-construction groundwater regime is the most challenging aspect of developing these sites.

### SETTLEMENT OF OPENCAST FILL: GENERAL

There are three main components of settlement

- A. Settlement due to self-weight at original moisture content.
- B. Settlement due to building loads.
- C. Settlement due to wetting-up.

While A always occurs first, B and C may occur in any order or contemporaneously.

A. Most settlement due to self-weight occurs rapidly as the fill is dumped. This primary compression is therefore of little interest long term. Measurements of surface movements on backfilled opencast sites have shown that settlement continues but the rate of settlement of the ground surface decreases rapidly with time and often appears to be negligible several years after backfilling, Kilkenny, W.M. (1968), Leigh, W.J.P. and Rainbow, K.R. (1981). This long-term compression due to self-weight may be defined by the creep compression rate parameter,  $\alpha$ , which is the percentage vertical compression of the fill that occurs during a  $\log_{10}$  cycle of time from one to ten years after restoration. Typical values of  $\alpha$  for opencast fill lie in the range 0.5-1.0 per cent reflecting the proportion of weak rocks to superficiais in the backfill and the predominant rock type e.g. sandstones or limestones as opposed to shales or mudstones. These values relate to unsaturated conditions. Modest heave has been recorded where a location has been pre-loaded by a spoil heap.

B. Most settlement due to building loads will occur as the load is applied.

This immediate settlement may be estimated by the use of the constrained vertical drained modulus  $E_v = \frac{1}{m_v}$ . The compressibility of open-cast fills without pre-compaction or wetting-up may vary from  $E_v = 2000-6000 \text{ KN/m}^2$  and a value of  $E_v = 4000 \text{ KN/m}^2$  is often recommended for preliminary design [Building Research Establishment (1983)]. The long-term creep settlement under building loads may be estimated using the creep compression rate parameter with zero time taken at completion of the building.

C. Significant additional settlement can be caused by an increase in the moisture content of the opencast backfill, Charles, J.A., Naismith, W.A., Burford, D. (1977). This increase may be caused by precipitation, surface ponding, ingress of water from flooded surface or near surface construction such as drainage trenches, broken services or by a general restoration of the water table. Episodic exposure to relatively small quantities of water, e.g. precipitation, has a modest effect on overall settlement. The settlement of recent fill has been observed to accelerate during the winter. However, inundation from surface or groundwater sources has caused initial collapse compression of up to 6 per cent. The creep compression rate is enhanced following inundation but generally the fill is less susceptible to dramatic settlement thereafter.

#### PROJECT DESCRIPTION

The North Tyneside District General Hospital is situated in Tyne & Wear, England, (National Grid Reference NZ 342703). The hospital site covers an area of about 13 hectares which formed part of the larger Whitley Bay opencast coal site on which work began in 1948 and which was fully restored in 1952. The hospital consists of single and two-storey buildings of load-bearing brick and blockwork cavity wall construction on flexible reinforced concrete rafts which incorporate the strip footings for internal and external walls as ground beams in a composite foundation. The buildings are divided into smaller structures by movement joints. The complex stormwater and separate foul drainage systems use concrete and clayware pipes ranging from 100-700mm diameter with rubber ring joints laid at shallow gradients with backdrops to brick manholes cast on reinforced concrete slabs. The first two phases of construction are complete, Scheme 3 is at the design stage. This paper reviews the ground conditions, the settlements and the structural response of a sub-section of the buildings, Area 39 and the site drainage, Figure 1.

#### GROUND CONDITIONS

Mining records show that in addition to the opencast coal operations which worked the Yard seam, 0.79 metres thick, five other coal seams exist within 155 metres of the surface. The closest to the pavement of the restored opencast working is the Bensham seam, 1.38 metres thick, which lies some 26 metres below it. This seam was extensively worked using deep mine techniques up till 1929. The old workings in this seam, together with the bed separation associated with them allows underdrainage to take place drawing down the groundwater level such that no positive porewater pressures have

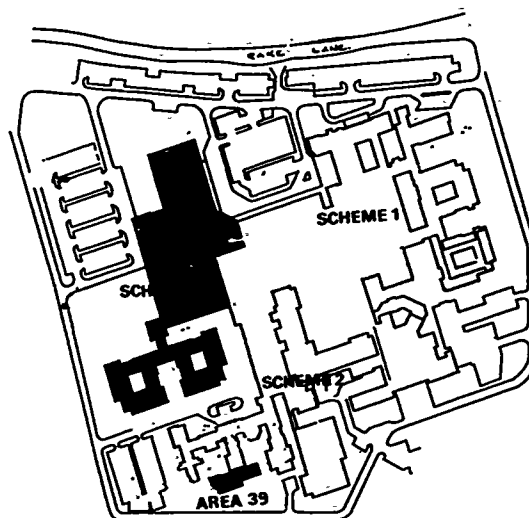


Fig. 1 Site Plan

been observed in the backfill. Interconnected old workings appear to drain to the adjacent North Sea and River Tyne causing permanent drawdown. At different times, some 5 site investigations have been carried out together with an engineering geological mapping exercise, Dearman, W.R. et al (1977), which has defined accurately the position, extent and depth of the opencast workings, Figure 2.

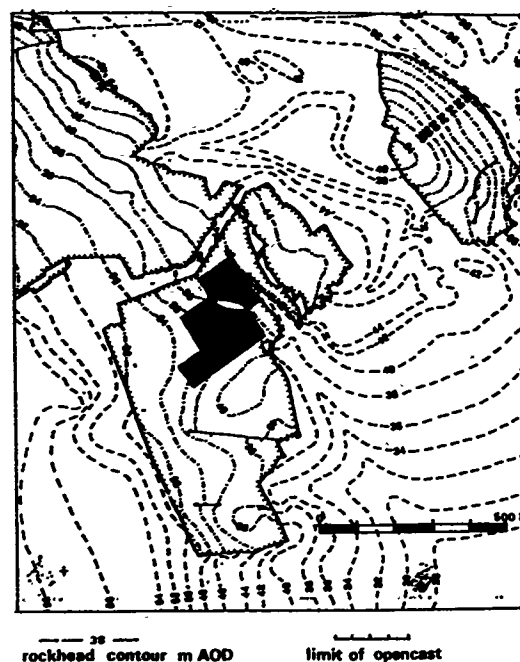


Fig. 2 Rockhead Contours

The low point in the excavation and accordingly the deepest fill, some 26 metres, lay on the Western boundary of the opencast site decreasing to 6 metres on the Eastern boundary. The 'average' depth of fill under Scheme 1 and 2 are 10 and 15 metres respectively. The opencast excavation was not continuous over the whole area but mining factors and the modus operandi combined to leave a ridge and a spur of undisturbed ground running in a NW-SE direction immediately to the East of Scheme 1 across which the site drainage ran. The commercial site investigations variously describe the backfill as "grey shale fill", "stiff grey clay with boulder and mudstone fragments" and "clayey sandy mudstone and shales". The compressibility of the opencast fill in its present condition has been assessed by in-situ testing using the Standard Penetration Test, Figure 3, by laboratory consolidation tests on undisturbed 75mm diameter samples of the finer grained material and on 250mm diameter samples recompacted at in-situ moisture content to field densities, Table 1. Field densities recorded on samples from two 75mm diameter cored holes ranged from 1884-2285 Kg/m<sup>3</sup> and the degree of saturation from 45-95 per cent.

| Sample Size mm    | Initial Moisture Content % | Bulk Density Kg/m <sup>3</sup> | Constrained Modulus, E <sub>v</sub> MN/m <sup>2</sup> | Effective Stress Range KN/m <sup>2</sup> |
|-------------------|----------------------------|--------------------------------|---|--|
| 75 (Undisturbed)  | 10-14                      | 2000-2220                      | 4.8-6.6   | 50-400                                   |
| 250 (Recompacted) | 8-14                       | 1970-2220                      | 12.0-20.0   | 135-570                                  |
|                   | 8-12                       | 1800                           | 1.4-5.0   | 68-375                                   |

Table 1 Laboratory Compressibility Determination

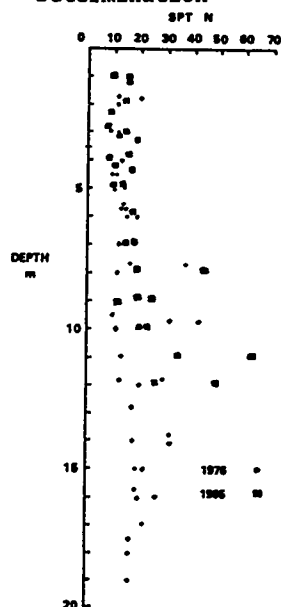


Fig. 3 Standard Penetration Test 'N' v Depth

A surcharge trial has been undertaken involving the construction of three trial embankments, each 20 metre square and 2, 4 and 6 metres high respectively, in the area of the proposed Scheme 3. Magnetic extensometers enabled the settlement at the surface and at 2, 3, 5, 7, 10, 13 and 16 metres below ground level to be determined. Values of constrained vertical modulus were computed by estimating the stress levels at the mid-height of each layer after Giroud and dividing by the observed vertical strain, Table 2. The response of the fill to inundation has been measured in the field by flooding a granular blanket under the 4 metre high embankment after near equilibrium had been established under the surcharge load in the dry conditions. This resulted in collapse compressions occurring but only in the previously identifiable zone of high compressibility between 5 and 13 metres below the surface, Figure 4.

| Embankment Height Metre | Depth Metre | Constrained Modulus E <sub>v</sub> MN/m <sup>2</sup> | Effective Stress Range KN/m <sup>2</sup> |
|-------------------------|-------------|--|--|
| 2                       | 0-5         | 52.8   | 52-95                                    |
|                         | 5-7         | 19.4   | 126-165                                  |
|                         | 7-10        | 10.6   | 178-210                                  |
|                         | 10-20       | 40.5   | 315-335                                  |
| After Inundation        |             |  |  |
| 4                       | 0-5         | 35.9   | 52-139                                   |
|                         | 5-7         | 2.1  | 126-203                                  |
|                         | 7-10        | 1.6  | 178-236                                  |
|                         | 10-13       | 4.0  | 253-302                                  |
|                         | 13-20       | 7.9  | 346-376                                  |
| 6                       | 0-5         | 101.2  | 52-174                                   |
|                         | 5-7         | 70.4   | 126-232                                  |
|                         | 7-10        | 4.2  | 178-252                                  |

#### Inundation beneath 4 metre embankment

| Depth metres | Collapse Compression per cent |
|--------------|-------------------------------|
| 0-5          | 0.18                          |
| 5-7          | 0.5                           |
| 10-13        | 2.0                           |
| 13-20        | 0.14                          |

Table 2 Field Compressibility Determination

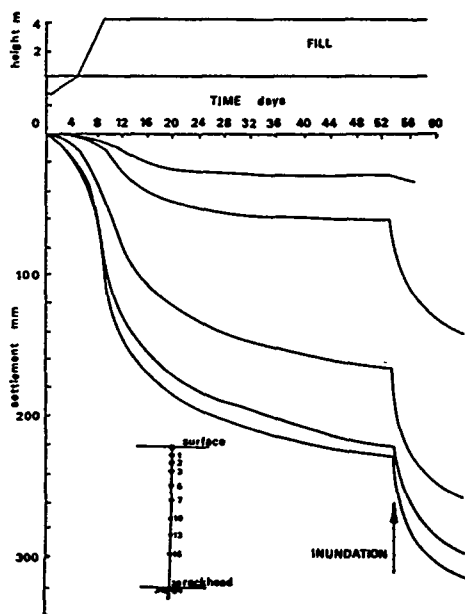


Fig. 4 4m Embankment, Settlement v Time

#### SETTLEMENT, DIFFERENTIAL SETTLEMENT AND STRUCTURAL RESPONSE

##### Buildings

The modest building loads transferred to the opencast backfill through the flexible raft foundations are of the order of 30-50 kN/m<sup>2</sup>, Figure 5. Some slight cracking has occurred in places throughout Scheme 1 and 2 which may be settlement related but this has not required remedial work. Observed settlements due to initial structural loads varied from 25-70mm. Some significant additional movement was first noticed in the summer of 1985 after completion of the structural frame, across the movement joint between Area 36/39 and along the South wall of Area 39. Monitoring pins were installed at dam proof course level throughout Scheme 2. Settlement in Area 39 proceeded rapidly initially and then continued at a diminishing rate, Figure 6. The relationships between the maximum total settlement 161mm at W34 and minimum total settlement 23mm at W23, giving a maximum differential settlement of 138mm which plots well outside quoted limits for building on raft foundations. The relative rotation across the building is much higher than load bearing walls would be expected to accommodate, Table 3.

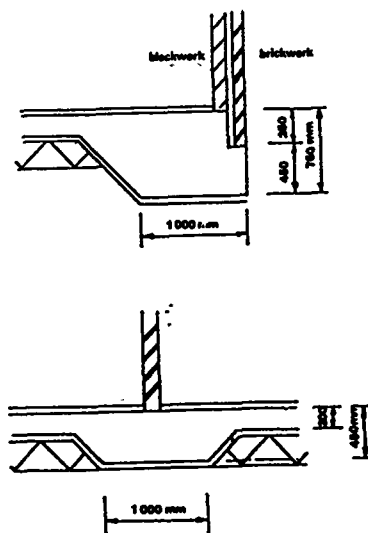


Fig. 5 Foundation Details

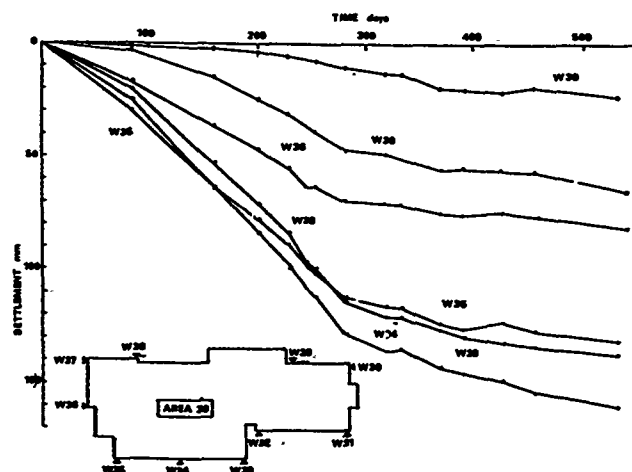


Fig. 6 Area 39: Settlement v Time

| Scheme 2 : Area 39 |     |                                |                 |
|--------------------|-----|--------------------------------|-----------------|
| Section            | L/H | $\frac{\Delta}{L} \times 10^3$ | Settlement Mode |
| W35/W37            | 4.2 | 6.6                            | Hogging         |
| W33/35             | 6.1 | 1.3                            | Sagging         |
| W31/32             | 6.2 | 4.2                            | Hogging         |

Table 3 Deflection Ratios

Internally, some minor cracks have appeared in the plaster finish of the long corridor walls at floor level adjacent to doors and windows and along the south elevation at the locations indicated, Figure 7.

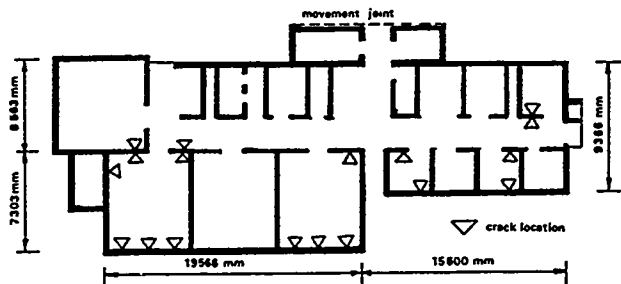


Fig. 7 Area 39: Crack Locations

Openings reduce wall stiffness and act as stress concentrators. No cracking has been observed in the external brickwork other than hairline cracks in the mortar bed joints around the windows on the south elevation. This reactivation of settlement under constant load has been attributed by the Author to wetting-up of the opencast fill from an, as yet, unidentified source. Because the foundation raft is relatively flexible it is the configuration and stiffnesses of the walls which control redistribution of contact stress, differential settlement and resulting crack patterns. This subject forms a continuing area of research at the University of Newcastle upon Tyne.

#### Drainage

Light linear structures such as pipelines are vulnerable to settlement damage particularly where they pass from undisturbed ground to fill, from a supported position within a structure to fill, or from a stressed condition under a structure to an unstressed condition outside. As early as 1980, during installation of the drainage on this site movements of manholes and foul and stormwater sewers were reported. A level survey in November 1982 suggested that manholes and associated drainage on the western and southern boundary of the site had settled up to 150mm. Pipeline inspections, prior to handover, revealed a number of bending and shear failures in the 100-250mm diameter clayware pipes of the foul drainage and back falls and changes of gradient in the larger diameter concrete pipes, together with manhole settlement.

Five categories of failure were identified which were settlement related and associated with the high compressibility of the opencast backfill and its sensitivity to moisture content changes.

(i) Pipe and pipe joint failure immediately adjacent to or under loaded structures due to shear forces and stress related settlement.

(ii) Pipe failures caused by differential movement at manhole connections. Both through pipes and backdrops were affected.

(iii) Backfalls and pipe failures due to bending stresses at trench crossings caused by localised settlements in trench backfill or trench formations.

(iv) Backfalls and pipe failures at boundaries between fill and undisturbed ground.

Records and on-site inspection showed ample evidence of precipitation causing collapse of trench backfill, groundwater movement through the site backfill and groundwater movement within the granular trench bedding. While most of the installed drainage has performed satisfactorily, considerable expense was incurred in reinstatement of failed sections.

#### CONCLUSIONS

The upper layers of opencast fill on this site appear to have relatively low compressibility which is probably due to the precompaction caused by landscaping operations and precipitation causing volume reduction in the near surface zone by wetting-up. The majority of the fill below this level is of medium to high compressibility and is the seat of settlement at existing in-situ moisture content as well as being the zone most susceptible to collapse settlement. The acceleration of settlements at constant stress which have been observed on this site can only be attributed to wetting-up. Any design should recognise the limitations of uncompacted opencast backfill sites and seek to provide and appropriate structure and sufficient flexibility in the drainage to accommodate settlements and differential settlements of the order experienced here without significant damage or loss of serviceability. On this site the flexible raft used on Scheme 1 and 2 has to a large extent achieved this. Surcharging such sites prior to construction will reduce total settlements, reduce variability and hence differential settlements and reduce but not eliminate susceptibility to wetting-up. Drainage design should incorporate steeper gradients rather than shallow gradients and backdrops, increased flexibility or sleeving where pipes exit from building foundations or manholes and where pipes pass closely under loaded areas. Increasing the bending strength of the pipes and the pipe diameter beyond that necessary for hydraulic design would also reduce the incidence of failures.

## REFERENCES

- Kilkenny, W.M. (1968), "A Study of the Settlement of Restored Opencast Coal Sites and their suitability for Building Developments", Bulletin 38, Department of Civil Engineering, University of Newcastle upon Tyne.
- Leigh, W.J.P. and Rainbow, K.R. (1981), "Observations of the Settlement of Restored Backfill of Opencast Sites", Conference on Urban and Industrial Fills, University of Birmingham.
- Charles, J.A., Naismith, W.A. and Burford, D. (1977), "Settlement of Backfill at Horsley Restored Opencast Coal Mining Site", Building Research Establishment, Watford, England. Current Paper CP46/77.
- Building Research Establishment (1983), "Fill", Building Research Establishment, Digest 274, Watford, England.
- Dearman, W.R., Money, M.S., Coffey, J.R., Scott, P. and Wheeler, M. (1977), "Engineering Geological Mapping of the Tyne and Wear Conurbation", Quarterly Journal Engineering Geology, Volume 10, pp 145-168.

## Geotechnical and Groundwater Site Characterization on the UMTRA Project

**J.A. Caldwell**

Technical Assistance Contractor, Albuquerque, New Mexico

**R.E. Rager**

Technical Assistance Contractor, Albuquerque, New Mexico

**L. Coons**

Technical Assistance Contractor, Albuquerque, New Mexico

**SYNOPSIS:** Reclamation of 24 inactive uranium mill tailings piles involves remedial work to stabilize the piles for 1000 years. Site characterization of geotechnical and groundwater conditions at each site is undertaken prior to remedial action design. This paper describes the approach to UMTRA Project site characterization. A case history, Green River, is described. Details of site characterization costs for most sites are provided.

### INTRODUCTION

The Uranium Mill Tailings Remedial Action (UMTRA) Project involves the construction of remedial action to stabilize and reclaim 24 inactive uranium mill tailings piles in 10 states. An important part of the planning and design of remedial action is site characterization. This paper describes the UMTRA Project site characterization program. Details of site characterization at the Green River, Utah, site are discussed in order to provide a complete overview and a specific case history of UMTRA Project approaches and methods, as well as the end product.

Site characterization work at UMTRA Project sites, discussed in this paper, includes the following: geological investigations; field drilling and test pitting; collection of tailings, soil, rock, and surface-water and groundwater samples; laboratory testing of tailings, soils, rocks, and water; and the compilation of site characterization reports describing the site stratigraphy, groundwater regime, and the properties of the in-place and construction materials. Site characterization work performed at UMTRA Project sites, but not discussed in this paper, includes: archaeological surveys; plant and animal surveys; radiological and other waste characterization work; and climatological and surface-water characterization.

### THE UMTRA PROJECT

The UMTRA Project is managed by the U.S. Department of Energy (DOE) in terms of the Uranium Mill Tailings Remedial Control Act (UMTRCA) of 1983. Site characterization, design, and construction are performed by contractors to the DOE.

In terms of UMTRCA, the U.S. Environmental Protection Agency (EPA) sets the standards for the remedial action. The U.S. Nuclear Regulatory Commission (NRC) and affected states and tribes review and concur in the design of the remedial action works.

The EPA standards require, among other things, that the remedial action be effective for at least 1000 years, to the extent practical, and at least for 200 years. Remedial action must be designed and constructed to prevent dispersal of the tailings and other contaminated materials, and must prevent inadvertent use of tailings by man. Remedial actions should not rely for their efficacy on maintenance, although in practice, maintenance and surveillance programs are planned at all sites.

To date, construction is complete at: Canonsburg, Pennsylvania; Shiprock, New Mexico; and Salt Lake City, Utah. Construction work is in progress at: Durango, Colorado; Mexican Hat, Utah; and Lakeview, Oregon. Site characterization is complete, or significantly advanced at the remaining sites, with the exceptions of Gunnison and Naturita, Colorado, where alternate site selection studies are in progress. In terms of Federal legislation, the Project is scheduled to be complete by 1993.

### THE TECHNICAL APPROACH DOCUMENT AND CONTRACTUAL PROCEDURES

#### Technical Approach

The technical approach to site characterization at UMTRA Project sites is described in a Technical Approach Document (TAD). The TAD, which was compiled in close discussion with the EPA, NRC, and affected states and tribes, sets out in detail the methods and approaches employed to characterize the following aspects of tailings piles and new disposal sites: geology; groundwater; site and regional seismicity; subsurface soils and rocks and their geotechnical and hydrogeochemical properties; tailings and their geotechnical and radiological properties; and the geotechnical and radon attenuation properties of potential construction materials (soils and rocks that will be used to construct and cover the reshaped or relocated tailings pile and associated contaminated materials). A later section of this paper discusses some of the technical approaches in detail.



Detailed site characterization procedures are documented in the Standard Operating Procedures of the various contractors to the DOE on the UMTRA Project.

#### Performance of Site Characterization Work

The UMTRA Project is managed from the DOE Albuquerque Operations Office in Albuquerque, New Mexico. The Technical Assistance Contractor (TAC) is located with the DOE. The TAC is contracted to the DOE to provide, among other services: site characterization work; conceptual designs; and the compilation of Environmental Impact Statements/Environmental Assessments (EIS/EAs) and Remedial Action Plans (RAPs). TAC staff perform geological site characterization work as well as planning, control, interpretation, and compilation of field programs and their results for geotechnical and groundwater characterization work.

Due to the fact that the 24 sites are scattered across a wide geographic area, TAC subcontractors are employed to perform site characterization work. This work involves drilling, geotechnical sampling, and in-situ testing (i.e., with a piezocone). Laboratory testing of soils, rocks, and water is done in commercial facilities subcontracted to the TAC.

Because of the technical expertise required, groundwater sampling is done by a team of TAC staff who travel from site to site with specially-equipped vehicles.

#### Scopes of Work

When subcontract work is required at a site, the usual procedure is for the TAC to call for bids from qualified subcontractors. The number of bidders varies significantly depending on the site location and the nature of the work required. Once bids have been issued, there is usually a site meeting at which salient aspects of the terrain as well as the work required are discussed with prospective subcontractors. Bids are reviewed upon receipt in Albuquerque in accordance with standard government contract procedures. Normally, the contract is awarded to the lowest bidder. (This has, unfortunately, not always led to the employment of the better, more competent contractors.)

The technical work to be performed by the subcontractor is described in the bid in the Scope of Work. This is the only part of the bid and contract compiled by the TAC technical staff. A typical Scope of Work incorporates a description of the site, a detailed listing of the work to be done, and technical specifications.

#### Site control

During subcontractor performance of site characterization work, technical staff from the TAC are present. A full-time site person, the

Field Technical Representative (FTR), is empowered to: monitor the contractor; observe that proper work is performed; confirm that required operating procedures are observed; and request that specific work (e.g., in-situ testing) be done at appropriate times. The FTR is not empowered to control or direct the subcontractor's work. The FTR keeps a daily diary that is used as the basis for agreeing to and paying bills submitted by the subcontractor.

#### GEOTECHNICAL SITE CHARACTERIZATION - TECHNICAL APPROACH

Geotechnical site characterization includes geologic, geomorphic, subsurface investigations, and seismic studies.

Geologic site characterization of UMTRA Project sites is an integral part of the overall design effort. This characterization consists of a summary of the regional geologic setting, local site geology, regional and local structures, Quaternary geology of the site region, and the local distribution of surficial units. The in-depth geologic studies are presented in the Site Characterization Report section of the Remedial Action Plan (RAP).

The purpose of the geomorphic hazard assessment is to identify the geomorphic processes that affect the site, to estimate the probability of their occurrence, and to evaluate the possible magnitude of their effects during the life of the reclamation. The general approach used to accomplish these goals involves three steps: (1) identify past geomorphic processes and estimate their rates from the geomorphic and stratigraphic records (post-glacial time, roughly 10,000 years); (2) identify present geomorphic processes and estimate their rates from historic records and field observations (typically less than 80 years); and (3) predict future geomorphic processes and rates.

The purpose of subsurface characterization of UMTRA Project sites is to define the geotechnical conditions of existing tailings piles, foundation soils, and proposed borrow sources. The stratigraphy and physical properties of materials composing the stratigraphic units are characterized. Stratigraphy is determined by using information logged in boreholes and test pits. Piezocone probings or seismic field studies may also be used to define stratigraphy. Material properties are determined by laboratory and field tests.

The nature and material properties of the tailings piles must be determined in order to decide if stabilization in place can be accomplished without recompacting or otherwise consolidating the pile. In addition, the behavior and stratigraphy of the foundation soils must be determined in order to assess the stability of the pile. An initial exploratory program consisting of a series of piezocone penetration tests similar to the static cone penetration test described in the ASTM D3441 are performed at a minimum density of one per

acre to cover the tailings pile. Each test penetrates the entire depth of the pile and extends into the foundation soils until stiff or dense soils are encountered. Data from these probes are used to: (1) define the stratigraphy of the pile (e.g., locate significant layers, zones, and pockets of slimes within the embankment); (2) determine the rate of dissipation of induced pore pressures (the rate of pore water pressure dissipation is used to estimate the tailings hydraulic conductivity and consolidation parameters); (3) obtain the penetration resistance of the tailings and their strength and bearing capacity; and (4) determine the groundwater level.

The stratigraphy interpreted from the piezocone data is considered in determining the location of additional boreholes conducted in the second phase of field work. These borings are performed to obtain undisturbed and disturbed samples for laboratory testing and to verify the stratigraphy defined by the piezocone data. Sufficient borings are conducted to verify the information from the piezocone. At least one of the borings is taken 20 feet into bedrock or up to 250 feet below the tailings-soil interface if foundation stratigraphy and material properties permit.

Borings with sampling are also conducted adjacent to the piles in order to identify variability of the near-pile foundation soils. Test pits are excavated on the pile to obtain representative sand, sand-slime, and slime tailings samples for laboratory testing. Test data are used to determine the geotechnical properties of the tailings when placed as fills.

For separate disposal areas, borings are required in order to determine the foundation soil and bedrock characteristics at a disposal site. The density of borings is approximately one for every three acres. A sufficient area is covered to allow repositioning of the pile within the general area of interest. These borings extend at least 20 feet below grade; at least two borings extend up to 50 feet below grade, or to a minimum of 20 feet, into bedrock. One of the borings may extend as deep as 250 feet if the soil at the site is deep.

Borrow areas are identified by performing a borrow assessment. For radon cover material, a limited number of areas are investigated by excavating eight to 12 test pits at each area. Both large and small bulk samples are obtained in order to perform classification and material properties tests.

For rock armoring material, one or more areas are investigated in order to define the limits and quality of rock armor borrow material. For gravel sites, six to eight test pits are conducted at each area. Both large and small bulk samples are obtained. For bedrock sites, samples are obtained from rock outcrop areas.

Laboratory tests are performed on tailings, foundation, fill, and soil borrow sources in order to determine appropriate material properties needed for design. These include strength, compressibility, compaction, permeability, capillary moisture, radon

diffusion coefficient, and correlative property tests. Rock samples are tested for durability using petrographic, LA abrasion, absorption, sodium sulfate soundness, and specific gravity tests. Other types of soil and rock tests are performed if needed.

As part of the design of reclamation work at UMTRA Project sites, studies are conducted to define the seismic hazard. These evaluations result in a seismotectonic characterization of each site and provide a set of earthquake design parameters. These parameters include: the design earthquake magnitude; on-site peak horizontal ground acceleration; the distances to, and lengths of, capable faults; and the types of capable fault displacement. During the seismic investigation, the potential for on-site fault rupture is analyzed.

Once the acceleration has been determined for a site using methods outlined in the previous sections of this chapter, the impact of stratigraphy upon the acceleration is evaluated. The site is classified as having shallow or deep soils. Based upon this classification, modification to the site acceleration is as follows:

- o For shallow soil sites having less than 30 feet of overburden above bedrock, the site surface acceleration used in liquefaction and slope stability analyses is considered to be the same as the acceleration derived from the seismic study.
- o Deep soil sites require adjustment to the on-site acceleration derived from the seismotectonic site characterization. The acceleration must be modified for attenuation to amplification through the soil in order to derive the surface acceleration used as input into liquefaction and stability analyses.

In order to assess the long-term stability of the tailings piles, the long-term static and earthquake loading conditions are determined. Natural slopes, which may affect the long-term performance of the embankment, are also analyzed for static and earthquake loading conditions. In addition, short-term static and seismic loading of the embankment and construction slopes must be analyzed to assess the suitability of the proposed designs.

Settlement of the reconstructed tailings piles at UMTRA Project sites is assessed in order to evaluate long-term stability. Settlement can occur within the reclaimed tailings embankment and in the foundation soils upon which the embankment is constructed. The absolute and differential settlement depend on the distribution of different types of materials, the compressibility of each soil type, and the stresses on specific soil layers. Settlement, especially differential settlement, can lead to surface-water runoff flow concentrations which could erode the pile cover and/or lead to cracking of the radon cover.

In order to evaluate the long-term stability of tailings piles at UMTRA Project sites, the liquefaction potential of the pile and foundation soils under design earthquake conditions is assessed. The liquefaction potential of a site is determined by the soil properties, depositional history, depth to groundwater, and characteristics of the earthquake motion to which it is subjected.

#### GROUNDWATER SITE CHARACTERIZATION

Subsurface investigations are performed at each former mill processing site and potential tailings disposal site to define the presence and extent of groundwater-bearing (hydrostratigraphic) units. The ultimate objective of these investigations is to develop the appropriate remedial action plan for water resources protection and a cost-effective remedial action plan for cleanup of the inactive mill sites. Aquifer hydraulic and geochemical characteristics are defined for each hydrostratigraphic unit to aid in determining the amount and extent of present and potential contamination by the mill tailings operations.

Groundwater site characterization begins with an inventory and review of existing hydrogeologic literature and water well records in the vicinity of the site. An early assessment is made to: (1) identify water users within a two-mile radius of the site; (2) estimate the extent of contamination; (3) identify possible sources of contamination near the mill site other than mill tailings; and (4) to identify potential disposal sites. Field testing, drilling and monitor well installation, water sampling, soil sampling, and aquifer-hydraulic testing are completed in phases.

Key elements in the groundwater characterization for each site include the following:

- o Definition of the contaminant source.
- o Characterization of representative background water quality for each hydrostratigraphic unit of concern and for surface water.
- o Definition of presence and extent of contaminant plumes, as well as discharge of plumes to surface water.

The contaminant source term is characterized by collecting and analyzing tailings solids and pore water samples. Saturated and unsaturated hydraulic conductivities of undisturbed tailings samples may be determined. To estimate the rate of movement of leachate through the tailings at the disposal site, the hydraulic conductivity of one or more remolded and compacted tailings samples is determined. Contaminant sources other than mill tailings are identified and may be characterized if it is determined that contamination from that source may affect, or in any way bias, the characterization of the tailings pile or the disposal site hydrogeology.

Background groundwater quality is determined by establishing representative values for constituents from water samples obtained from wells upgradient of the tailings pile. These background wells must be sufficiently upgradient so that the groundwater is unaffected by tailings seepage. Existing springs and wells may be used, or it may be necessary to install monitor wells specifically to determine background water quality. Where six or more sample analyses are available, the background concentration range is assumed to be the arithmetic mean (or possibly the geometric mean, depending upon the distribution of the data) plus or minus two standard deviations. For less than six samples, the background concentration range is assumed to be equal to the observed range of data. Obvious outliers in the data set are eliminated and an explanation for doing so is provided for reviewers.

The vertical extent of contamination in the groundwater system is determined by installing a group or "nest" of monitor wells at specific locations on the site, and downgradient and crossgradient from the site. Each well in this nest is screened within a discrete interval which is different in depth below the surface from all other wells in the nest. The deepest well showing no impact from tailings seepage defines the lower limit of contamination. The lateral extent of contamination is determined by installing monitor wells progressively away from the contaminant source(s) until water-quality analyses from the outermost wells show that there is little or no contamination. At many of the UMTRA Project sites, the lateral extent of contamination is defined by one or more groundwater discharge points such as springs, intermittent drainages, or rivers.

As solvents and other chemicals were used at some of the UMTRA Project sites during the milling processes, an EPA Priority Pollutant scan is conducted at one or more of the monitor wells, usually on the site or immediately downgradient from the site. Then, at several of the other wells at each site, organic contamination is screened by analyzing for total organic carbon (TOC) and total organic halogens (TOX).

#### CASE HISTORY: GREEN RIVER

Green River, Utah, is one of the 24 UMTRA Project sites at which remedial action work will be undertaken. The following sections describe the site characterization work completed at the Green River site. Final designs have been prepared for the remedial action work; and construction is scheduled to begin in the summer of 1988.

#### Green River Site Description

The Green River inactive uranium mill site is in Grand County, Utah, approximately one mile southeast of the city of Green River and 0.5 mile south of U.S. Highway 6 & 50. The 48-acre site is in Sections 15 and 22, Township 21 South, Range 16 East, Salt Lake Meridian, and is bordered by the mainline track of the Denver and Rio Grande Western (D&RGW) Railroad on the north and the recently completed Interstate 70 on the south.

The 48-acre designated site consists of the tailings pile (eight acres), the mill yard and ore storage areas (23 acres), four main buildings, a water tower, and several small buildings. The buildings are all structurally sound and marginally contaminated.

Dispersion of tailings by wind and water erosion has contaminated approximately 30 acres. The total volume of contaminated materials, including the tailings and underlying soils, is estimated to be 185,000 cubic yards (cy).

In order to stabilize the tailings and meet the EPA standards, the tailings and other contaminated materials will be consolidated into a disposal cell out of Brown's Wash approximately 500 feet south and 50 feet higher in elevation than the existing mill site. The site occupies a level area that is dissected by a shallow, ephemeral stream. This stream drains to the northwest around the mill site. Bedrock is exposed in the bottom of drainage near the mill site. The site surface is formed of pediment sand and gravel and is covered by sagebrush and wild forbs. A power line crosses the site area.

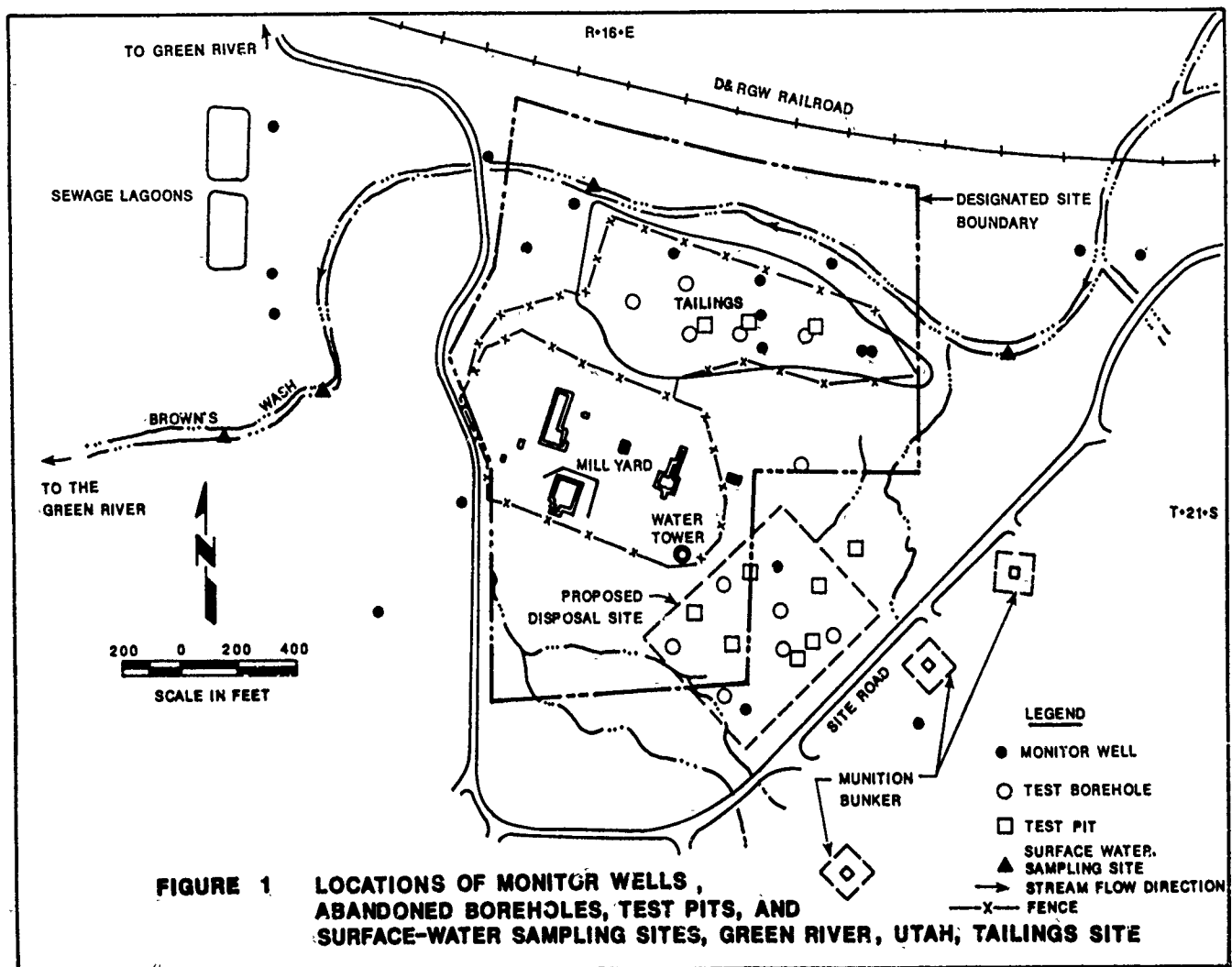
## Geotechnical Site Characterization

The Green River site is in the northern part of the Canyon Lands section of the Colorado Plateau Physiographic Province, an area of low historic seismicity. The site region is drained by the Green River which passes 0.5 mile west of the site. The tailings pile rests on the bank of Brown's Wash, intermittent tributary with a watershed of 85 square miles. The peak horizontal acceleration at the site is 0.21g.

## Subsurface Investigation

The Green River tailings pile was characterized by drilling five borings and excavating three test pits on the pile. The locations of these boreholes and test pits are presented in Figure 1.

Tailings are divided into three categories according to the size of the particles. The three designations are: sand; sand-slime; and slime. At Green River, the slimes were removed for upgrading at Rifle, Colorado, leaving only



the sand tailings. Sand tailings, as used here, refers to those tailings with up to 30 percent passing the No. 200 sieve. Most of the Green River pile contains less than 20 percent passing the No. 200 sieve. The Unified Soil Classification System (USCS) classifies the material as silty or clayey sand: SP-SM, SP-SC, SM, and SC.

Moisture contents within the tailings pile range from 1.2 to 6.4 percent. Blow counts from SPT tests range from four to 16, which correlates with a loose to medium-dense consistency. Groundwater was not encountered within the tailings.

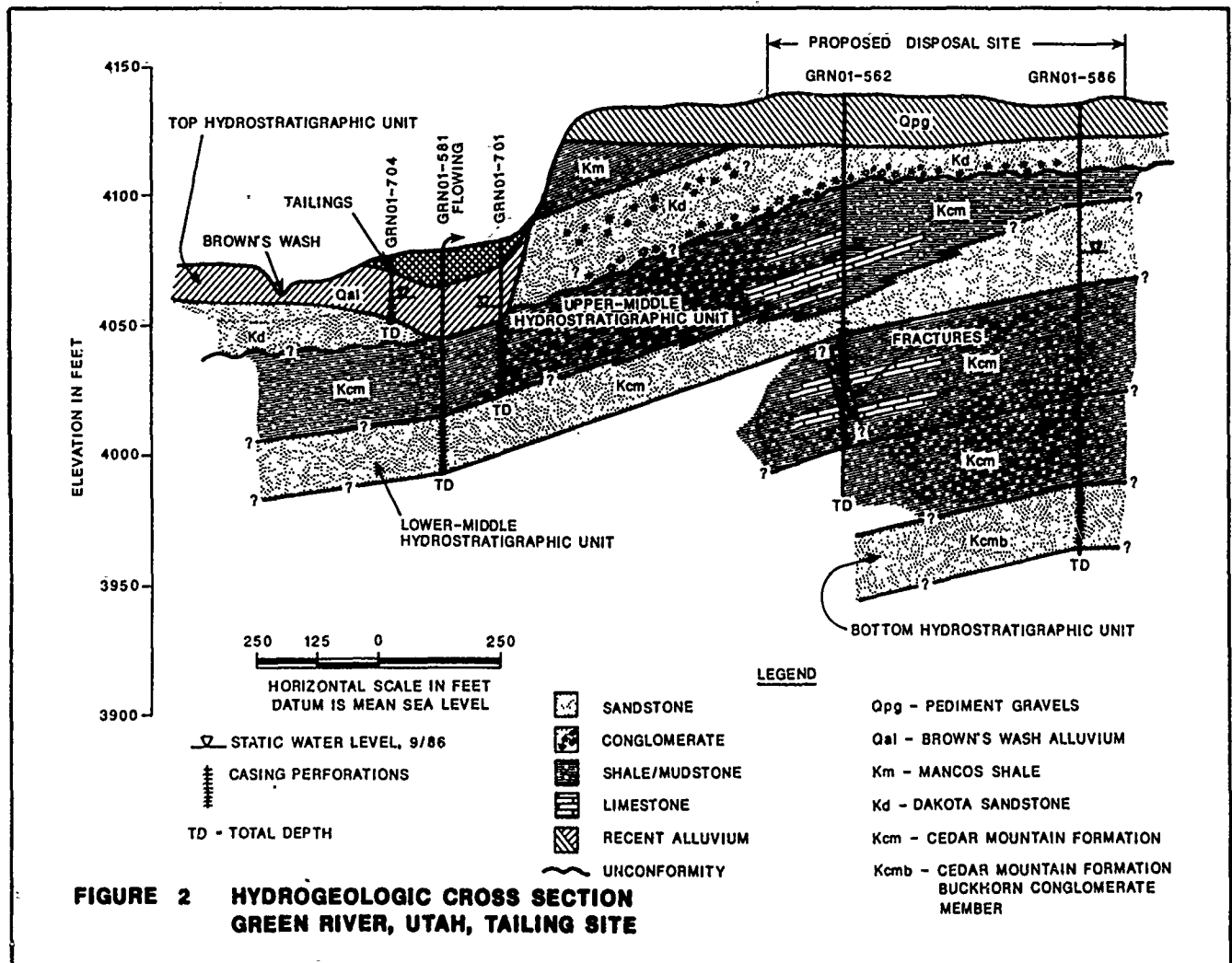
The Green River disposal area was characterized by drilling eight borings and excavating seven test pits as shown on Figure 1. In addition, information obtained from many of the 34 monitor well drill holes was used to define subsurface stratigraphy.

The soils underlying the site consist of between five and 16 feet of loose to dense silty or clayey sand alluvium. Large lenses of clay are contained within the layer. Dense to

very dense sand and gravel alluvium underlies these near-surface soils. The soils in turn overlie bedrock of coarse conglomerate sandstone of the Dakota Sandstone and shales of the Cedar Mountain Formation. These near-surface soils lie within the area of windblown contamination and are considered representative of this material. Groundwater was not encountered within the soils at the site.

Geologic cross sections were developed from outcrop and borehole information. A typical cross section is shown on Figure 2. The conditions at the site reflect the regional bedrock configuration of shallow dipping beds of Mancos Shale overlying a thin and discontinuous layer of Dakota Sandstone which in turn overlies the Cedar Mountain Formation.

Geotechnical testing of the site soils and tailings included standard penetration tests, moisture content and dry densities, gradation tests, Atterberg Limits, compaction tests, remolded and undisturbed consolidation, triaxial shear, permeability, and capillary moisture tests.



## Groundwater Site Characterization

Thirty four monitor wells, three well points, and six surface-water sampling sites (Figure 1) were used to characterize the shallow groundwater system at the Green River site. Eight of the wells were installed by previous investigators in 1982 to characterize the tailings pile and the alluvium beneath and peripheral to the pile. The remaining wells, well points, and surface-water sites were installed by the TAC and were used to characterize three distinct Cretaceous-age bedrock units.

Depth to groundwater in the alluvium beneath the tailings surface ranges from 11 to 16 feet; the base of the tailings is above the water table. At the proposed disposal site south of the present pile (see Figure 2), groundwater is first encountered at an approximate depth of 60 feet below the surface. The general direction of groundwater flow in the alluvium and bedrock aquifers is west toward the Green River.

Background water-quality analyses indicate that the total dissolved solids (TDS) contents of the alluvial aquifer and the two shallow-most bedrock aquifers range from 4000 milligrams per liter (mg/l) to 7000 mg/l; the bottom bedrock unit contains groundwater of significantly better quality (TDS near 1900 mg/l). The EPA and State of Utah Secondary Drinking Water Standard for TDS is 500 mg/l. Contamination from tailings seepage was detected in the alluvium beneath the pile and in the shale and siltstone bedrock unit immediately beneath the

alluvium. The lateral contamination (nitrate, ammonium, uranium, and manganese) is restricted to the area beneath the pile. Downgradient from the pile, some contamination discharges from the alluvial aquifer into Browns Wash, a small intermittent tributary of the Green River. Contamination in the underlying bedrock aquifer disperses downgradient and flows preferentially in some areas through interconnected fractures visible in outcrops and core samples. The bottom sandstone unit is protected from tailings seepage by strong upward vertical hydraulic gradients. Three of the wells completed in this unit flow at the land surface during certain times of the year.

Preliminary estimates of contaminant migration and future contamination were made for the two contaminated aquifers beneath the present tailings pile. These estimates assume dispersion (non-point discharge) in the bedrock unit and discharge of contaminated water from the alluvium into Brown's Wash 400 feet west (downgradient) of the tailings. To reduce nitrate concentrations as  $\text{NO}_3$  to 44 mg/l, the EPA primary drinking water standard for nitrate, calculations show a natural flushing time of 90 years is needed for the alluvium; 30 years is needed for the bedrock aquifer. Uranium concentrations will be reduced to the EPA health advisory level of 0.015 mg/l (10 picocuries per liter (pCi/l)) in 160 years in the alluvium, and in 260 years in the bedrock aquifer. These two contaminants represent the most mobile and one of the most retarded contaminants at the Green River site, respectively.

TABLE 1 COMPARISON OF SITE CHARACTERIZATION COSTS FOR THREE UMTRA SITES

|                                       |                         |         |           |                       |         |           |
|---------------------------------------|-------------------------|---------|-----------|-----------------------|---------|-----------|
| SITE ID:                              | AMBROSIA LAKE           |         |           | GREEN RIVER           |         |           |
| REMEDIAL ACTION COST:                 | 21.2                    |         |           | 7.1                   |         |           |
| TOTAL SITE COST:                      | 29.5                    |         |           | 16.8                  |         |           |
| ITEM                                  | NUMBER                  | FOOTAGE | COST/ITEM | NUMBER                | FOOTAGE | COST/ITEM |
| GEOTECHNICAL BOREHOLES                | 42                      | 1192    | 28550     | 12                    | 277     | 20955     |
| TEST PITS                             | 25                      | 250     | 1527      | 24                    | 240     | 1365      |
| MONITOR WELLS,LYSIMETERS & STANDPIPES | 23                      | 4050    | 76942     | 35                    | 1047    | (W/GEOT)  |
| GEOPHYSICAL LOGGING                   | 23                      | 4050    | 10998     | 35                    | 1047    | (W/GEOT)  |
| PIEZOCONE                             | 126                     | 3668    | 33652     | N/A                   | N/A     | N/A       |
| WATER ANALYSIS                        | N/A                     | N/A     | 14883     | N/A                   | N/A     | 11202     |
| SOIL ANALYSIS                         | N/A                     | N/A     | 23314     | N/A                   | N/A     | 22482     |
| TOTAL                                 |                         |         | 189866    |                       |         | 56004     |
| SITE ID:                              | RIFLE (PROCESSING SITE) |         |           | RIFLE (DISPOSAL SITE) |         |           |
| REMEDIAL ACTION COST:                 | 48.1                    |         |           |                       |         |           |
| TOTAL SITE COST:                      | 73.7                    |         |           |                       |         |           |
| ITEM                                  | NUMBER                  | FOOTAGE | COST/ITEM | NUMBER                | FOOTAGE | COST/ITEM |
| GEOTECHNICAL BOREHOLES                | 29                      | N/A     | (OTHERS)  | 11                    | 755     | 150777    |
| TEST PITS                             | 5                       | N/A     | (OTHERS)  | 16                    | 170     | 4061      |
| MONITOR WELLS                         | 85                      | 4830    | 299731    | 10                    | 1180    | (W/GEOT)  |
| LYSIMETERS & TENSIMETER               | N/A                     | N/A     | N/A       | 12                    | 228     | (W/GEOT)  |
| GEOPHYSICAL LOGGING                   | 85                      | 4830    | 23715     | 10                    | 1180    | 8783      |
| WATER ANALYSIS                        | N/A                     | N/A     | 8568      | N/A                   | N/A     | 0         |
| SOIL ANALYSIS                         | N/A                     | N/A     | 5609      | N/A                   | N/A     | 18950     |

## SITE CHARACTERIZATION COSTS

Table 1 lists details of the costs of geotechnical and groundwater site characterization work at three UMTRA Project sites. In particular, the costs of work involved in the Green River case history are provided. Table 2 gives a summary of site characterization costs at the remaining UMTRA Project sites.

Also shown on Table 1 are the remedial action costs and the total site costs. The remedial action cost is the cost of constructing remedial works at the site. It includes the costs of site preparation, decontamination, relocation, cover, erosion protection, restoration, and construction management. The total site cost includes the costs of: planning and design development; engineering; site acquisition, surveillance and maintenance; and technical and management support. The cost for the Rifle processing and disposal sites is given as a single combined cost as all tailings will be consolidated at one facility.

## CONCLUSION

This paper has described the work to be performed in order to characterize geotechnical and groundwater conditions at the 24 sites that

constitute the UMTRA Project. The case history of the Green River site characterization has been discussed in detail. Costs for the site characterization work have been provided.

Complete site characterization is an essential first step in preparing cost-effective remedial action plans for engineering works that must remain stable for 200 to 1000 years. As shown in both the project and site case histories described in this paper, complete site characterization is a multifaceted undertaking that involves skill, cost, and site-specific approaches.

## ACKNOWLEDGEMENTS

The Technical Assistance Contractor to the U.S. Department of Energy is a joint venture of: Jacobs Engineering Group Inc.; Roy F. Weston; and Sergeant, Hauskins and Beckwith. The authors acknowledge the work and contributions of all their colleagues on the UMTRA Project: in particular Marie Lucero who compiled the cost data is to be especially thanked. The authors also wish to thank DOE for permission to publish this paper.

TABLE 2 SITE CHARACTERIZATION SUMMARY

|                        |                        |                  |                  |                        |
|------------------------|------------------------|------------------|------------------|------------------------|
| SITE ID:               | OUR (PROC & DISP SITE) | MEXICAN HAT      | TOMA CITY        | GRJ (PROC & DISP SITE) |
| REMEDIAL ACTION COST:  | 36.5                   | 25.0             | 12.1             | 67.5                   |
| TOTAL SITE COST:       | 61.2                   | 36.6             | 20.3             | 169.5                  |
| ITEM                   | NUMBER COST/ITEM       | NUMBER COST/ITEM | NUMBER COST/ITEM | NUMBER COST/ITEM       |
| GEOTECHNICAL BOREHOLES | 25 38130               | 39 289535        | 17 32610         | 48 214533              |
| TEST PITS              | 28 1425                | 14 930           | 18 2000          | 80 5314                |
| MONITOR WELLS          | 25 (W/GEOT)            | 11 (W/GEOT)      | 19 174926        | 42 19770               |
| LYSIMETERS             | N/A N/A                | N/A N/A          | N/A N/A          | N/A N/A                |
| GEOPHYSICAL LOGGING    | N/A N/A                | N/A N/A          | N/A N/A          | N/A N/A                |
| PIEZOCONE              | N/A N/A                | 40 12015         | 26 (W/GEOT)      | N/A N/A                |
| WATER ANALYSIS         | N/A 15347              | N/A 8787         | N/A 25263        | N/A 1170               |
| SOIL ANALYSIS          | N/A 15449              | N/A 17309        | N/A 15998        | N/A 24911              |
| TOTAL                  | 70351                  | 328576           | 254799           | 265698                 |
| SITE ID:               | BELFIELD/BOWMAN        | FALLS CITY       | MINORANT VALLEY  | LEV (PROC & DISP SITE) |
| REMEDIAL ACTION COST:  | 5.4                    | 18.6             | 9.8              |                        |
| TOTAL SITE COST:       | 19.8                   | 32.2             | 18.0             |                        |
| ITEM                   | NUMBER COST/ITEM       | NUMBER COST/ITEM | NUMBER COST/ITEM | NUMBER COST/ITEM       |
| GEOTECHNICAL BOREHOLES | 72 (OTHERS)            | 138 (OTHERS)     | 0 N/A            | 36 82570               |
| TEST PITS              | 30 (OTHERS)            | 20 2845          | 5 800            | 16 2940                |
| MONITOR WELLS          | 18 36690               | 40 93062         | 23 145830        | 28 (W/ GEOT.           |
| LYSIMETERS             | 11 (W/MON)             | N/A N/A          | N/A N/A          | N/A N/A                |
| GEOPHYSICAL LOGGING    | 11 4798                | 40 14000         | N/A N/A          | N/A N/A                |
| PIEZOCONE              | N/A N/A                | 222 26750        | N/A N/A          | N/A N/A                |
| WATER ANALYSIS         | N/A 12840              | N/A 10800        | N/A 30234        |                        |
| SOIL ANALYSIS          | N/A 15079              | N/A 26750        | N/A 13200        |                        |
| TOTAL                  | 69407                  | 174207           | 190064           | 85510                  |
| SITE ID:               | RIVERVIEW              | SHIPROCK         | SLICK ROCK       | MAYBELL                |
| REMEDIAL ACTION COST:  | 15.8                   | 11.8             | 16.0             | 16.1                   |
| TOTAL SITE COST:       | 27.3                   | 20.0             | 26.7             | 26.0                   |
| ITEM                   | NUMBER COST/ITEM       | NUMBER COST/ITEM | NUMBER COST/ITEM | NUMBER COST/ITEM       |
| GEOTECHNICAL BOREHOLES | 47 80134               | 69 (OTHERS)      | 11 5985          | 33 9396                |
| TEST PITS              | 19 3000                | 24 1282          | 23 1173          | 10 1050                |
| MONITOR WELLS          | 32 (W/GEOT.)           | 34 14365         | 22 44172         | 15 107975              |
| LYSIMETERS             | N/A N/A                | N/A N/A          | N/A N/A          | N/A N/A                |
| GEOPHYSICAL LOGGING    | N/A N/A                | N/A N/A          | 5 1000           | 15 5900                |
| PIEZOCONE              | N/A N/A                | N/A N/A          | 12 1929          | 40 14779               |
| WATER ANALYSIS         | N/A 5330               | N/A 4882         | N/A 9590         | N/A 28794              |
| SOIL ANALYSIS          | N/A 3184               | N/A 11590        | N/A 19466        | N/A 18285              |
| TOTAL                  | 91648                  | 32119            | 83315            | 186179                 |
| SITE ID:               | SLC (PROC & DISP SITE) | SPOOK            | LOWMAN           |                        |
| REMEDIAL ACTION COST:  | 44.9                   | 2.8              | 4.4              |                        |
| TOTAL SITE COST:       | 67.1                   | 9.9              | 12.7             |                        |
| ITEM                   | NUMBER COST/ITEM       | NUMBER COST/ITEM | NUMBER COST/ITEM |                        |
| GEOTECHNICAL BOREHOLES | 97 (OTHERS)            | 1 890            | 21 26000         |                        |
| TEST PITS              | 6 600                  | 20 2165          | 16 2187          |                        |
| MONITOR WELLS          | 36 97000               | 10 28686         | 12 983           |                        |
| LYSIMETERS             | N/A N/A                | N/A N/A          | 6 36598          |                        |
| GEOPHYSICAL LOGGING    | N/A N/A                | 10 10302         | N/A N/A          |                        |
| PIEZOCONE              | N/A N/A                | N/A N/A          | N/A N/A          |                        |
| WATER ANALYSIS         | N/A 4882               | N/A 5817         | N/A 2126         |                        |
| SOIL ANALYSIS          | N/A 11597              | N/A 6945         | N/A 15675        |                        |
| TOTAL                  | 114079                 | 54605            | 83569            |                        |



## Evaluation of Remedial In-Waste Leachate Head Reduction

Denise E. Mills

Hydrogeologist, Sweet, Edwards and Assoc., Inc., Redmond,  
Washington

Donald A. Cordell

Associate Geologist, Sweet, Edwards and Assoc., Inc., Kelso,  
Washington

**SYNOPSIS:** Water quality monitoring at Cedar Hills Regional Landfill, in King County, Washington has indicated that shallow ground water perched in lodgement till has been impacted by solid waste disposal. A leachate mound to 50 feet in thickness was identified in the refuse which overlies the low permeability till. The leachate head over the till is sufficient to cause downward flow of leachate through the till to shallow ground water, and may contribute to water quality impacts at the site. Lowering the leachate head, therefore, may reduce the potential for impacts on water quality. A study was conducted to obtain estimates of the hydraulic properties of solid waste and to determine if lowering the leachate head using horizontal drains and vertical extraction wells is feasible. This paper discusses the findings of the investigation.

### INTRODUCTION

The Cedar Hills Regional Landfill is a 920 acre site in King County, Washington which currently accepts 3,500 tons of refuse per day. It has been operated by King County since 1964. The landfill is located approximately 9 miles southeast of the town of Issaquah (Figure 1). It is situated on the east side of the Puget Sound lowlands, at the foothills of the Cascade Mountains. The Puget Sound lowlands consist of a structural trough between the Cascade Range on the east and the Olympic Mountains to the west. Knowledge of the deep structural geology and pre-glacial history is limited due to over 350 feet of glacial sediments overlying bedrock in the region (Sweet, Edwards and Assoc., Inc., 1984).

The landfill is underlain by Vashon till and undifferentiated pre-Vashon glacial sediments (Livingston, 1971; Rosengreen, 1965; and Vine, 1962). Vashon till was deposited in the Puget Sound region roughly 13,500 years ago during the final stage of the Fraser Glaciation. Glacial deposits identified at the site include up to 70 feet of lodgement till of Vashon age, underlain by over 300 feet of advance outwash sands and gravels deposited during the advance of the Fraser ice sheet and younger ice-contact deposits.

Several historic solid waste disposal areas exist at the site, but the majority of waste received by the County has been deposited on the Main Hill solid waste pile, denoted in Figure 2. The Main Hill refuse area is over 5,000 feet in length along the north-south axis and it is about 1,600 feet wide (Figure 2). The refuse thickness in the Main Hill disposal area has been found to be over 140 feet near the center, and it directly overlies the low permeability lodgement till.

Monitoring of ground water quality has indicated that shallow ground water perched in the low permeability lodgement till has been impacted by solid waste disposal activities at Cedar Hills.

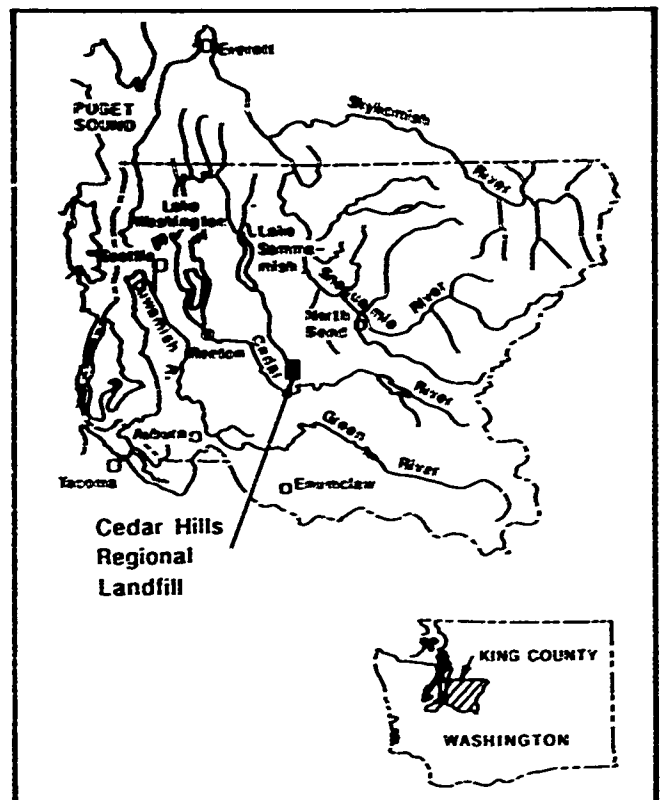


Figure 1. Map of western Washington showing location of Cedar Hills Regional Landfill

Documented leachate seepage on the slopes of the Main Hill refuse area suggested that leachate was mounding in the refuse. The

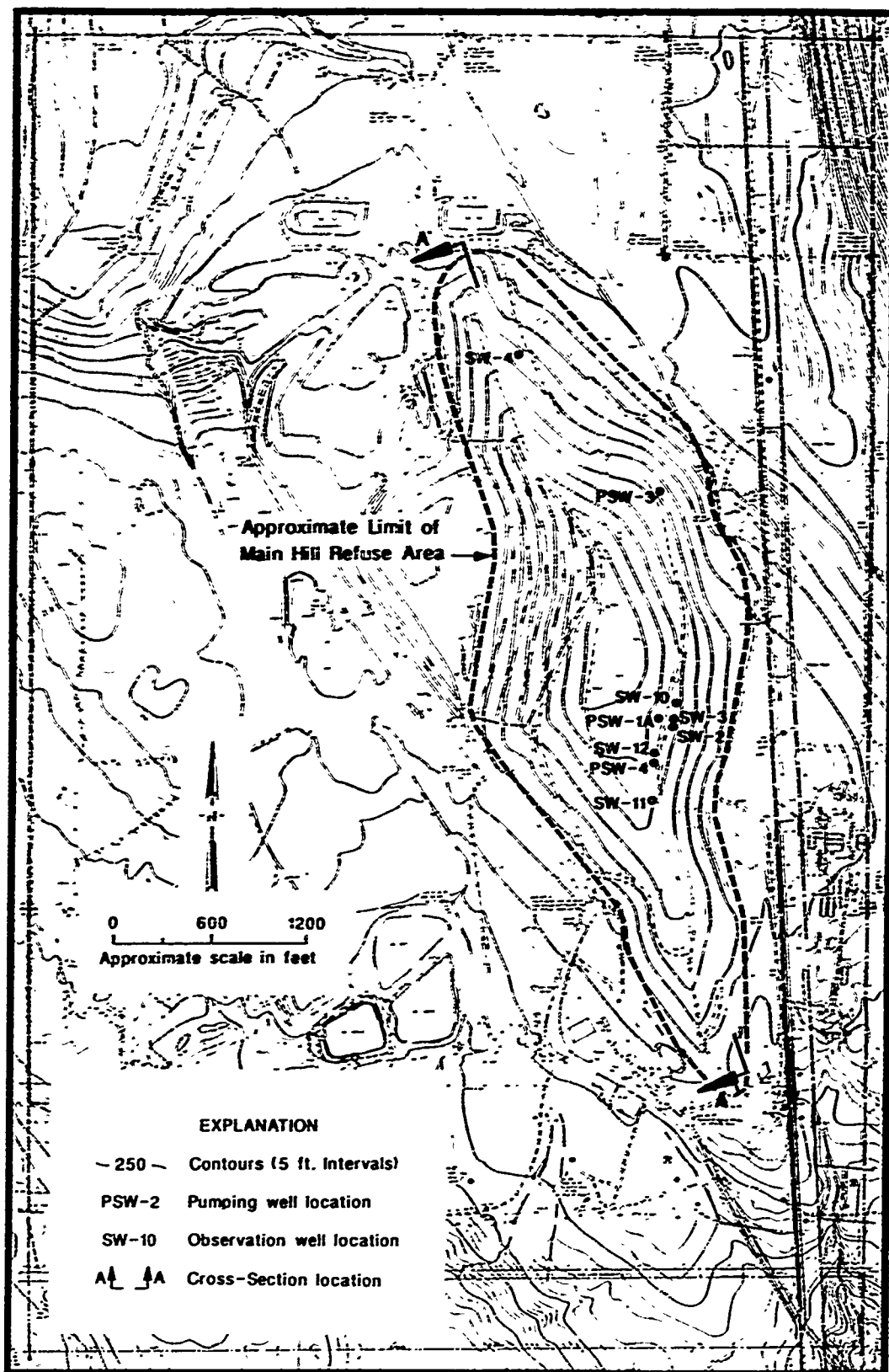


Figure 2. Map of Cedar Hills Regional Landfill

leachate mound over the till may contribute to water quality impacts as a result of percolation through imperfections in the till, particularly if leachate heads are high. If the leachate heads acting on the till can be lowered, the potential for leachate impacts on shallow ground water may be decreased significantly.

#### PREVIOUS INVESTIGATIONS

In 1985, an investigation was conducted to verify the existence of a leachate mound in the refuse (Sweet, Edwards and Assoc., Inc., 1985). Three borings were advanced through the Main Hill refuse into original ground and 2-inch diameter leachate monitoring wells (SW-2, SW-3, and SW-4, Figure 2) were completed in each boring. A leachate mound, ranging in thickness from 12 feet at SW-4 to 30 feet at SW-2, was identified in all three wells; and landfill gas pressures to 7 psig were measured.

A 4-hour pumping test was conducted on SW-2 to obtain preliminary estimates of the hydraulic characteristics of the saturated refuse. From the pump test data, the hydraulic conductivity was calculated at  $3.4 \times 10^{-4}$  ft/min ( $1.7 \times 10^{-4}$  cm/sec), and the storage coefficient was found to be  $3.7 \times 10^{-4}$  suggesting the mound is acting as a partially confined "aquifer" due to the lack of a true confining stratum. The confining conditions are believed attributable to both the compacted layering or "stratification" in the waste as well as high gas pressures which encourage stratification and simulate pressure head (Sweet, Edwards and Assoc., Inc., 1985).

In general, the distribution of the well-compacted or loosely-compacted refuse interlayered with fine- or coarse-grained cover soils was found to be random.

#### PROJECT OBJECTIVES

In 1987, a comprehensive investigation of the hydraulic properties of the solid waste comprising the Main Hill refuse area was completed to evaluate the feasibility of in-waste leachate head reduction using horizontal drains and vertical extraction wells.

#### FIELD INVESTIGATIONS

For the feasibility study, three 6-inch diameter wells (PSW-1A, PSW-3, and PSW-4, Figure 2) and three additional 2-inch diameter wells (SW-10, SW-11, and SW-12) were completed in the Main Hill refuse. The wells were installed to conduct long duration pump tests in the saturated refuse and verify previously calculated hydraulic parameters of the solid waste. These data are required to determine the performance of horizontal drains and vertical extraction wells for remedial in-waste leachate head reduction.

#### LEACHATE MOUND MORPHOLOGY

Monitoring of leachate levels and landfill gas prior to testing indicated that the leachate mound thickness varies areally and fluctuates daily. At PSW-1A (Figure 2), the leachate thickness varied from 45 to 50 feet. During the same period, the leachate thickness in SW-

12 varied from 5 to 11.7 feet. Gas pressures also fluctuated daily at some locations. For example, gas pressures measured in PSW-1A varied from 5 to 11 psig during the initial monitoring period, while the pressure in PSW-4 generally remained at 5 psig.

Figure 3 shows the approximate configuration of the leachate mound. Along the north-south axis, the mound is roughly 3,450 feet in length. The extent of the mound along the east-west axis is unknown. The leachate mound is thin toward the north perimeter of the Main Hill and toward SW-11. Several perched leachate production zones were observed during drilling, however the quantity of leachate in these zones appeared small.

#### PERMEABILITY TESTING

To assess the feasibility of dewatering of the Main Hill refuse area as a remediation option, drawdown and recovery hydraulic conductivity tests were conducted on wells PSW-1A and PSW-4 (Figure 2). Wells SW-2, SW-3, SW-10, SW-11, and PSW-4 were monitored as observation wells while pumping PSW-1A; and SW-2, SW-3, SW-10, SW-12, and PSW-1A were monitored while pumping PSW-4.

Following well installation and development, leachate foam (a mixture of leachate and landfill gas) was observed in the wells and rose up to 75 feet above the static liquid level. In addition, leachate typically blew out of SW-10 about 4 feet above the top of the well casing, and leachate foam blew out of SW-12 about 12 feet above the well casing. As a result of the leachate foam, pressure transducers were required to obtain reliable leachate measurements during testing. Leachate levels were therefore recorded during pumping and recovery periods using a TERRA8 computerized data logger system.

One criterion used to obtain representative leachate levels from each well during drawdown and recovery periods was that constant gas pressures be maintained in each well. To achieve this, pressure-tight well head caps were affixed to each well. The pressure was regulated using a ball valve attached to the well head. On wells PSW-1A and PSW-4, pressure-tight fittings were used for the discharge pipe and electrical and transducers cables. The well head caps on the observation wells included pressure-tight fittings for the transducer cables. In addition, a pressure gauge was attached to a sealed outlet in each well head.

The wells were pumped using an electric submersible pump. Discharge during pumping was regulated using a flow restrictor valve, and pumped leachate was directed to the onsite leachate collection system for treatment and disposal.

Well PSW-1A was pumped for 6-1/2 hours initially at a rate of 2 gpm, but the rate decreased gradually to 0.5 gpm 280 minutes after pumping started. The total observed drawdown was 19.90 feet. No change in leachate level was measured in the observation wells. Prior to testing, the gas pressure in well PSW-1A was measured at 12.5 psig. An effort was

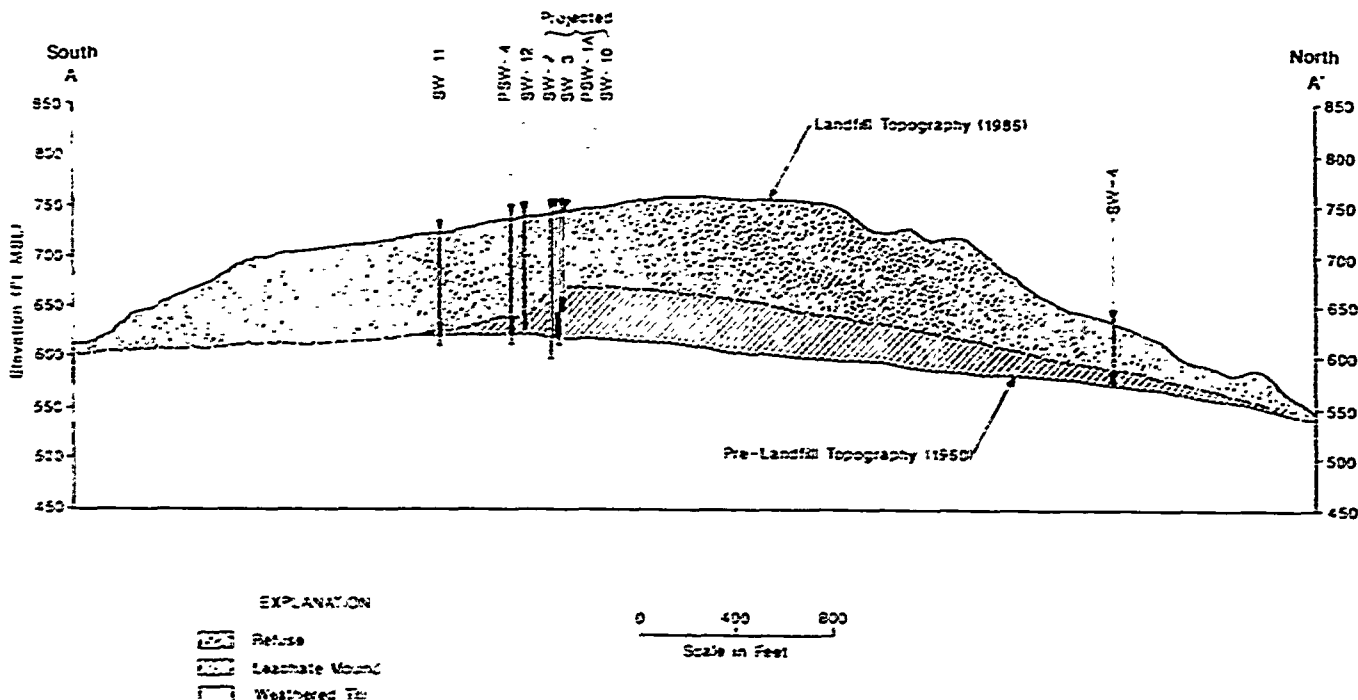


Figure 3. Cross-Section A-A'

made to maintain the gas pressure in all the wells at 2 psig, but roughly 4 hours into the pump test pressures had dissipated to zero at all locations.

Well PSW-4 was pumped for 14 hours at a rate of 2 gpm. During the last hour, the rate decreased to 1 gpm. The total measured drawdown was 4.50 feet. In well SW-12, located 52.8 feet north of PSW-4, 1.96 feet of drawdown was measured.

#### HYDRAULIC PROPERTIES OF THE LEACHATE MOUND

The hydraulic conductivity and transmissivity of the refuse (summarized in Table 1) were calculated from drawdown and recovery data from wells PSW-1A, PSW-4, and SW-12 using several methods. As noted previously, PSW-1A was pumped at a decreasing discharge rate. The methods used to evaluate drawdown data from this well (Papadopolus-Cooper and Cooper-Jacob, Table 1) account for non-steady state conditions. Methods used to evaluate data from PSW-4 and SW-12 require steady state conditions.

The hydraulic conductivities calculated ranged from  $1.6 \times 10^{-3}$  to  $1 \times 10^{-2}$  ft/min ( $8.1 \times 10^{-4}$  to  $5.1 \times 10^{-3}$  cm/sec). The average hydraulic conductivity estimate was  $4.7 \times 10^{-3}$  ft/min ( $2.4 \times 10^{-3}$  cm/sec). The storage coefficient was calculated from leachate level measurements made in SW-12, and was found to be  $6.9 \times 10^{-4}$ . These results agree well with the preliminary estimates found during the 1985 investigation.

It is emphasized that the permeabilities found from these pump tests represent horizontal permeabilities. Vertical permeabilities are expected to be one to two orders of magnitude lower than the reported values.

#### ANALYSIS OF IN-WASTE LEACHATE HEAD REDUCTION

In general, investigation of the occurrence of leachate in solid waste at Cedar Hills identified a combined liquid head and head due to landfill gas pressures totaling up to 75 feet in the vicinity of PSW-1A, with leachate heads and gas pressures decreasing toward the perimeter of the landfill. The combined liquid head and gas pressure exerted by landfill gas on the upper surface of the till unit may be sufficient to force leachate flow through the till to ground water perched in the low permeability unit. Lowering the leachate head in the refuse pile is expected to reduce the rate of leachate percolation through the till.

For the feasibility study, three scenarios for in-waste leachate head reduction were examined:

1. Horizontal drains,
2. A combined system of horizontal drains and vertical extraction wells,
3. Vertical extraction wells.

The in-waste head reduction analyses are based on achieving a 50 percent head reduction of the leachate mound. For the evaluation, an average leachate head of 29 feet was assumed. A 50 percent reduction of the head, therefore would yield an average head of 14.5 feet and should significantly reduce the potential for impacts on water quality in the vicinity of the landfill. A hydraulic conductivity of  $6.0 \times 10^{-3}$  ft/min was assumed. Additional assumptions include:

- The landfill gas pressure is 0 psig and remains at steady state;
- The refuse is homogenous and isotropic;
- There is constant recharge to the leachate mound;
- The hydraulic properties of leachate are similar to ground water.

Table 1

Summary of Aquifer Parameters for Refuse Using  
Several Methods of Data Analysis

| Well No | Method used         | Transmissivity<br>(gpd/ft) | Hydraulic Conductivity<br>(ft/min) | Conductivity<br>(cm/sec) | Storage<br>Coefficient |
|---------|---------------------|----------------------------|------------------------------------|--------------------------|------------------------|
| PSW-1A  | Papadopoulos-Cooper | 1069                       | $5 \times 10^{-3}$                 | $2.5 \times 10^{-3}$     | -                      |
| PSW-1A  | Cooper-Jacob        | 377                        | $1.8 \times 10^{-3}$               | $9.1 \times 10^{-4}$     | -                      |
| PSW-4   | Distance-Drawdown   | 960                        | $8.9 \times 10^{-3}$               | $4.5 \times 10^{-3}$     | -                      |
| PSW-4   | Jacob (Drawdown)    | 108                        | $1 \times 10^{-3}$                 | $5.1 \times 10^{-4}$     | -                      |
| PSW-4   | Jacob (Recovery)    | 170                        | $1.6 \times 10^{-3}$               | $8.1 \times 10^{-4}$     | -                      |
| SW-12   | Theis               | 1089                       | $1 \times 10^{-2}$                 | $5.1 \times 10^{-3}$     | $8.4 \times 10^{-4}$   |
| SW-12   | Jacob (Drawdown)    | 960                        | $5.3 \times 10^{-3}$               | $2.7 \times 10^{-3}$     | $4.3 \times 10^{-4}$   |
| SW-12   | Jacob (Recovery)    | 680                        | $3.8 \times 10^{-3}$               | $1.9 \times 10^{-3}$     | $7.9 \times 10^{-4}$   |

The last assumption is particularly important. It is recognized that the hydraulic properties of leachate and water are dissimilar. Consistency, specific gravity, viscosity, temperature, gas saturation, and composition all influence the hydraulic properties of leachate and prevent direct comparison with water.

#### Horizontal Drain Analysis

The effectiveness of removing leachate from the refuse by a system of horizontal drains was examined using a drain spacing of 475 feet, indicating that 7 drains would be required along the north-south axis of the mound. A graphical relationship between drawdown, drain spacing, aquifer parameters, and dewatering time developed by the U. S. Bureau of Reclamation (USBR, 1978) was used to estimate the time required to lower the leachate head 50 percent. According to this method, a 50 percent reduction of the leachate head by 7 drains can be achieved in approximately 1 month (Sweet, Edwards and Assoc., Inc., 1987).

As a result of drilling limitations, the length of the drains is expected to range from 200 to 400 feet, with the average length of completed drains being approximately 300 feet. Initial discharge from the system was estimated at 227 gpm, and it is expected to decrease to 76 gpm following 50 percent head reduction.

Several factors may affect the projected performance of horizontal drains in the refuse. The most significant of these include the presence of high landfill gas pressures and the physical characteristics of layered refuse. First, landfill gas pressures up to 12.5 psig may provide sufficient head to increase the rate of leachate flow to the drains, and should effectively improve the drain efficiency. As the leachate mound decreases, however, gas pressures should decrease, as observed locally while pumping well PSW-1A. If the gas pressure

exerted of the leachate mound is reduced to 0 psig, the drains are expected to perform within the predicted theoretical efficiencies (Sweet, Edwards and Assoc., Inc., 1987).

Secondly, as previously mentioned, the refuse is interlayered with low permeability cover material and compacted, resulting in "stratification" of the refuse. Hence, it is almost certainly heterogenous and anisotropic to some degree. This anisotropy may impede vertical flow of leachate to drains installed near the base of the landfill, effectively reducing the drain efficiency. A horizontal drain field alone, therefore, may not be sufficient to dewater the refuse.

#### Combined Horizontal Drain and Vertical Well Analysis

King County has constructed an impermeable liner system as part of active refuse disposal areas on much of the west side of the refuse pile. Eventually the liner will extend to the top of the hill on the west and north sides. Installation of a system of horizontal drains for leachate collection in the waste, therefore, is limited to the south and east side of the waste pile. In addition, the maximum length of successful boring completion will probably be 400 feet. These factors limit the area where horizontal drains can be completed to a small portion of the landfill whose maximum width is about 1,600 feet (Figure 2). Considering these limitations, the performance of a system of horizontal drains for reducing the leachate mound can be enhanced by a network of large-diameter vertical extraction wells.

The number of vertical wells required to supplement the horizontal drainage system was computed by first estimating the total discharge capacity expected to occur from a well field completed in the leachate mound. The following well theory formula (modified

from Powers, 1981) was used:

$$Q_T = \frac{7.5 K (2Hh_0 - h_0^2)}{\ln (R/r)} \quad (1)$$

where:  $Q_T$  = Total discharge from the well field

$K$  = Average hydraulic conductivity

$H$  = Average head prior to dewatering

$h_0$  = Average head after dewatering

$r$  = Radius of the entire area to be dewatered with vertical wells

$R$  = Radius of influence

Equation (1) was developed for dewatering analyses for an island where recharge occurs laterally from all points and is modified from the basic well theory formula (Cedergren, 1967):

$$Q_T' = \frac{7.5 K (H^2 - h^2)}{\ln (R/r)} \quad (2)$$

which accounts for recharge from a line source. The island calculation was selected for Cedar Hills because it provides a conservative discharge value particularly when the aquifer thickness is unknown or variable.

The radius of influence for the refuse was found to be 238 feet using Sichart's formula (Powers, 1981; TM 5-818-5/NAVFAC P-418/AFM 88-5, 1971, p. 150):

$$R = 3 (H-h) K \quad (3)$$

The approximate radius of the portion of the leachate mound to be reduced using vertical wells,  $r$ , was calculated at 1241 feet. This value assumes that the mound extends through out the refuse.

From equation (1), the estimated discharge from a system of vertical extraction wells,  $Q_T$ , is 508 gpm; and, given an estimated discharge of 76 gpm from 7 horizontal drains completed in the remaining portion of the leachate mound, the total estimated leachate flow from a combined dewatering system is 584 gpm.

Assuming the vertical wells are 24 inches in diameter, the expected yield is 1.5 gpm per foot of saturation if the hydraulic conductivity is  $6 \times 10^{-3}$  cm/sec. Therefore for an average saturated thickness of 14.5 feet during leachate extraction, the average yield per well would be 21.8 gpm. From this, 23 vertical wells can theoretically remove leachate from the areas where drains are not completed, and the leachate mound can be reduced to an average thickness of 14.5 feet in less than 5 months.

It is important to note that placement of a final cover over the landfill and the use of an impermeable liner system for current and future development will reduce leachate generation and recharge to the landfill. Decreased leachate generation will enhance the effectiveness of the leachate removal system.

## Vertical Extraction Well Analysis

The feasibility of in-waste leachate head reduction using a dewatering system comprised entirely of vertical wells was also evaluated. The parameters for the analysis are identical to those used for the combined system except the radius of the area to be dewatered,  $r$ , is increased to the radius of the entire leachate mound, 1,350 feet. The total discharge estimate for a network comprised entirely of vertical wells is 549 gpm. If a yield of 21.8 gpm per well is achievable, 25 wells can theoretically reduce the leachate head to an average of 14.5 feet in approximately 5 months.

## CONCLUSIONS

Based on the hydraulic parameters calculated from "aquifer" testing conducted in the saturated refuse, it appears that two alternatives for in-waste leachate head reduction are technically feasible. First, a dewatering system consisting of 7 horizontal drains and 23 large-diameter vertical extraction wells may be able to reduce the average leachate head from 29 feet to 14.5 feet in less than six months, with a total estimated discharge of 584 gpm.

Second, a dewatering system comprised solely of 25 vertical wells is also feasible. From the hydraulic analysis, a system of this design may be capable of reducing the average head 50 percent in approximately 5 months with an estimated discharge of 549 gpm.

The existing leachate collection system has a limited capacity for leachate treatment and disposal which restricts the quantity of leachate that can be removed daily from the Main Hill refuse area. If the horizontal drains are as efficient as predicted by theoretical analysis, it will be necessary to have flow controls on each drain outlet. If flow to the drains is high, risk of blowouts at the slope face is increased when flow from the drains is restricted. Thus potential maintenance problems are associated with completion of horizontal drains. In addition, vertical extraction wells may allow more complete leachate head reduction in the refuse, particularly where the underlying topography is variable. For example, borings for vertical wells can be advanced until native ground is encountered and the well screens can be placed at the till/refuse interface. Less topographic, hence, less complete head reduction, can be achieved when installing horizontal drains. Hence, horizontal analysis of lowering the leachate head in the refuse suggests that the most flexible and effective method for leachate removal is the vertical extraction well system.

## ACKNOWLEDGEMENTS

This project was completed for the King County Solid Waste Division under subcontract to CH<sub>2</sub>M HILL Northwest, Inc. and we wish to thank them for their support. We are also indebted to Larry West for his assistance in the preparation of the original work and to Gerritt Rosenthal for reviewing the manuscript.

## REFERENCES

- Cedergren, H.R. (1967), Seepage, Drainage, and Flow Nets, John Wiley and Sons, Inc., New York.
- Powers, J.P. (1981), Construction Dewatering: A Guide to Theory and Practice, John Wiley and Sons, Inc., New York.
- Sweet, Edwards and Associates, Inc. and Herrera Environmental Consultants (1987), "Cedar Hills Site Development Plan, Task 45 - Investigation of the Feasibility of In-waste Leachate Head Reduction", Report to CH<sub>2</sub>M HILL Northwest, Inc.
- Sweet, Edwards and Associates, Inc. (1985), "Cedar Hills Site Development Plan, Task 13, Subtask 13.3 -- Investigations of Leachate in Solid Waste", Cedar Hills Regional Landfill, Phase 2 - Site Development Plan, CH<sub>2</sub>M HILL Northwest, Inc.: Report to King County Solid Waste Division.
- U.S. Bureau of Reclamation (1978), Drainage Manual, U.S. Government Printing Office, Washington D.C.: 143-149.
- U.S. Department of the Army, the Navy and the Air Force (1971), Dewatering and Ground Water Control for Deep Excavations: TM 5-818-5 /NAVFAC P-418/AFM 88-5, Chap. 6: U.S. Government Printing Office, Washington D.C.

# Site of an Oil-Producing Property

H. Dezfulian

Woodward-Clyde Consultants, Santa Ana, California

**SYNOPSIS:** An assessment of a 6.78-acre parcel of oil-producing land with one active, seven idle, and two abandoned oil wells was performed. Following the collection and review of site data, an evaluation was made of the toxic properties of on-site soils for the presence of hazardous substances. Soil samples were collected by advancing boreholes at eight locations. These locations were selected on the basis of the results of an aerial photographs review, a geophysical survey, and statistical sampling design techniques. An analytical program was conducted to test for chemicals that would likely be present from the oil field operations.

It was concluded that the on-site soils are not hazardous. However, soils contaminated with petroleum hydrocarbons were identified. A soil gas survey was performed to evaluate the presence of methane and other hazardous gases. Based on the results of the survey, recommendations for reducing the adverse effects of such gases were developed, which were incorporated into the design of the building foundations. A soil remediation plan was developed and approved by the regulatory agencies. The contaminated soils were excavated, blended with clean soils, and recompact under areas to be paved. The existing oil wells were abandoned, and the previously abandoned wells were re-abandoned in accordance with the applicable standards.

## INTRODUCTION

A site assessment was conducted for a property, 6.78 acres in area, located in the city of Santa Fe Springs, California. The location of the site is shown in Figure 1. The site is located within the Santa Fe

Springs Oil Field. At the time of the investigation, the site was being considered for development of eight two-story industrial buildings.

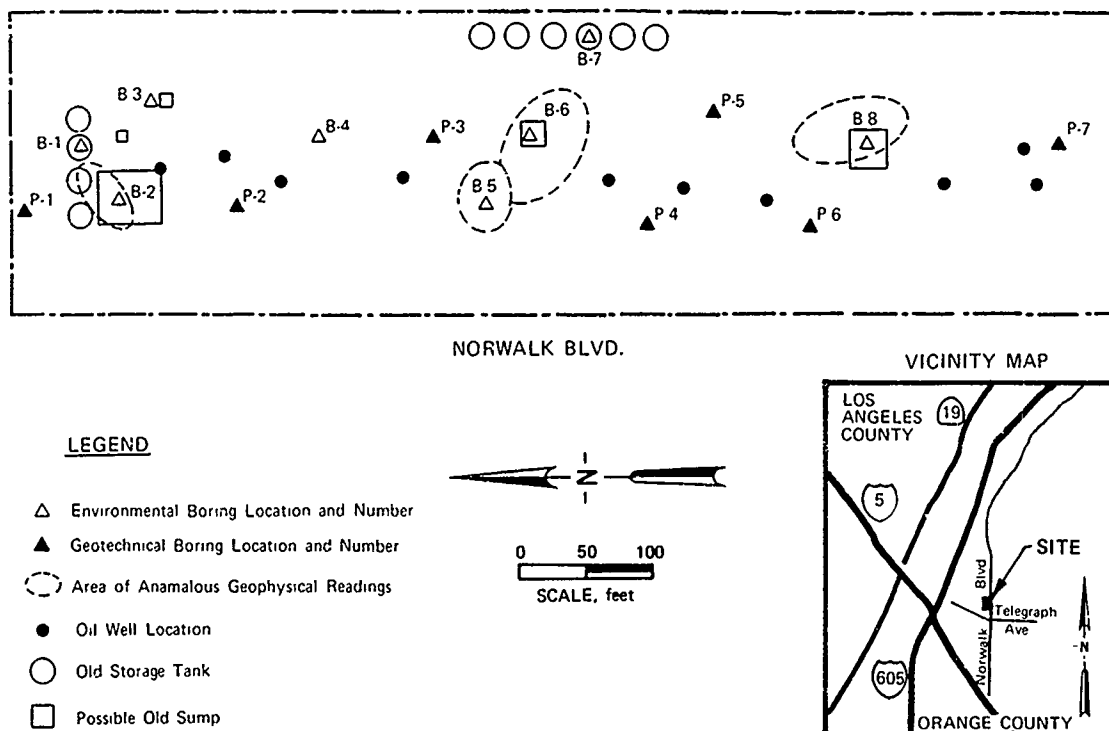


FIGURE 1 - SITE AND BORING LOCATION PLAN



Geologically, the area is underlain by about 7,000 feet of Pleistocene sediments and sedimentary rocks, below which the Miocene units occur. The upper 200 to 300 feet of the sediments are generally sand and gravel with some clay underlain by hard shale and boulders. The shallow materials, revealed in borings drilled on-site to a depth of 46 feet, generally consist of sand, silty sand, sandy silt, and some clayey materials in the upper 20 feet underlain by generally dense gravelly sand and fine gravel.

The depth to ground water is about 60 feet in a well maintained by the City of Santa Fe Springs, located about one-half mile northeast of the site. The depth to ground water in three wells located about one mile south of the site reportedly ranges from 92 to 100 feet.

At the time of the investigation, there were no buildings at the site. The site was leased to a major oil company for production and storage of crude oil. Oil storage tanks did not remain on the site. There were eight visible oil wells at the site. Seven of these were idle, with the oil production facilities dismantled and the well heads capped above ground. The Santa Fe Springs Oil Field Map (California Division of Conservation, Department of Oil and Gas, Sheet No. 102, 1985) indicated that there were two abandoned oil wells on-site. The approximate locations of the oil wells are shown in Figure 1. Several abandoned and active pipelines crossed the site.

#### METHODOLOGY

The site assessment was comprised of the following three phases:

- Phase I: Environmental site appraisal
- Phase II: Site characterization and assessment
- Phase III: Development of remedial measures

The objective of the Phase I study was to identify areas within the site that may be contaminated. Accordingly, the scope of the Phase I study was planned to respond to the following question:

Considering the past land-use history, are there likely to be hazardous materials at the site and, if so, within which areas of the site?

The objective of the Phase II investigation was to study the characteristics of the site materials for the presence of hazardous materials at areas within the site identified in the Phase I study. It was considered cost-effective to conduct the Phase IIa investigation in two sub-phases. Using this approach, the scope of initial Phase II investigation was designed to respond to the following question:

Are the materials in the investigated areas hazardous or non-hazardous as defined under the applicable laws?

If hazardous materials were discovered during the initial Phase IIa effort, a supplementary Phase IIb sampling and analysis would be required to address the following additional issue:

What are the nature and lateral and vertical extent of contamination?

Developing mitigation measures, consisting of in-situ, on-site, and/or off-site remedial alternatives would be part of the Phase III investigation, if mitigation was required.

#### ENVIRONMENTAL SITE APPRAISAL

The environmental site appraisal included the following efforts:

- Site visits;
- Interviews with staff of the oil company leasing the site;
- Review of oil well records;
- Review of historical aerial photographs;
- Performing a geophysical survey; and
- Preparing a Phase II work plan.

A literature search showed that the Santa Fe Springs Oil Field was discovered in 1919 (Ybarra, 1957). Intensive drilling campaigns were undertaken in 1921-23 and again in 1928-29. The wells were drilled with rotary drilling equipment. The site history review showed that the site was used as a chicken farm prior to 1920, but environmental impairment was not suspected from that activity. No commercial or industrial uses other than normal oil field and crude oil storage operations were suspected.

Available historical aerial photographs were reviewed. Two old above-ground storage tank areas and several features appearing to be sumps were identified. The locations of these features are shown in Figure 1.

#### Geophysical Survey

A geophysical terrain conductivity survey was conducted to identify areas within the site exhibiting anomalous conductivity values. A region of anomalous values is generally associated with unusual soil conditions, such as the presence of petroleum products. The presence of metallic conductors, such as buried tanks, pipelines or metallic debris would also cause distinctive anomalous values. The results of this type of survey are generally useful in locating areas underlain by metallic objects or previously used as sumps.

A Geonics EM-31 conductivity meter was used to conduct the survey. The Geonics EM-31 is a one-man, portable instrument, and has a depth of penetration of about 19 feet. Measurements were taken continuously and, due to the freedom from wires and direct ground contact, the technique provided a rapid means of site evaluation.

Initial reconnaissance at the site revealed several underground pipelines and metallic debris. Four geophysically anomalous areas, shown in Figure 1, were identified.

#### Site Investigation Work Plan

Based on the site's land-use history, on-site chemical contaminants were believed to include drilling fluids, spilled crude oil, metals from paint or tank oxidation, and tank-bottom sludges. A preliminary evaluation of possible sources of soil contamination at the site identified oil wells, above-ground storage tank sites, old sumps, and oil pipelines as areas of suspected environmental hazards.

A Phase II investigation plan (work plan) was developed. The scope of the investigation was designed only with respect to soil contamination, and not for evaluating the possibility of ground water contamination, as the possibility of ground water contamination does not appear to be great. Data from existing water wells located less than one mile from the site show the ground water to be at depths ranging between about 60 and 100 feet below ground surface.

The numbers and locations of the soil borings were selected on the basis of the following considerations:

- ° Areas identified on historic aerial photographs as possible old sumps;
- ° Areas identified in the geophysical survey as exhibiting anomalous conductivity values; and
- ° Statistical sampling design techniques, which allowed assigning confidence levels to the results of the sampling program.

The work plan included the following information:

- ° Location and depth of soil samples;
- ° Sampling procedures, including drilling and sampling methods, sample collection procedures, auger and sampling equipment decontamination, documentation and chain-of-custody procedures, procedures for handling of drill cuttings and steam cleaning waste water, and backfilling of boreholes;
- ° Chemical analyses procedures and criteria for selection of chemical analyses and soil samples to be analyzed;

- ° Quality Assurance/Quality Control (QA/QC) procedures; and
- ° Health and safety precautions during field activities.

#### FIELD AND LABORATORY INVESTIGATION

The field investigation program consisted of drilling boreholes, collecting soil samples, and performing laboratory analyses. For selecting the sampling locations, it was noted that if the site is clean, then none of the collected soil samples would show contamination. In contrast, if the site is actually contaminated, some of the collected samples may not detect contamination. Realizing this uncertainty in results, it was decided to design a sampling program that was likely to provide a 95 percent confidence in results. With this stipulation, it was calculated that eight borings were needed to detect contamination. Consequently, eight boring "sites" were selected in areas of the property identified as possible sources of soil contamination: four in the old sump areas, two in the old storage tank areas, one in proximity of oil wells, and one in the oil pipeline areas. Within each boring "site," the boring location was obtained by randomization.

The locations of the eight borings are shown in Figure 1. Two of the borings, B-2 and B-6, were advanced to a depth of 46 feet, and the remaining six to a depth of 22.5 feet. Drilling was performed using an 8-inch outside diameter hollow-stem auger. Soil samples were collected using a modified California split-spoon sampler that contained four brass tubes. All borings were sampled at depths of 1, 5, 13, and 21 feet. The two deeper borings were additionally sampled at 29, 37, and 45 feet.

Fifteen surface samples were collected from locations selected based on oil staining, discoloration, and/or odor. The samples were collected by scooping soil from a depth of 6 to 12 inches using a stainless steel trowel. The samples were placed in glass jars.

As part of the geotechnical investigation program (performed subsequent to the site assessment investigation), seven borings, designated in Figure 1 as P-1 through P-7, were drilled. During the drilling of Boring P-3, hydrocarbon odor was noticed at depths between about 3 and 20 feet. Soil samples from these depths were analyzed in the laboratory for total petroleum hydrocarbons.

The soil samples collected as part of the site assessment investigation were screened for laboratory analysis on the basis of visual observations, odor or field readings obtained on the Organic Vapor Meter (OVM) or HNu. Composite samples were prepared in the laboratory by combining approximately equal volumes of soil taken from the brass tubes or glass jars containing field samples. Compositing of subsurface samples was limited to samples collected from the same boring.

The analytical parameters were selected considering the requirements of Article 11, Chapter 30, Title 22 of the California Administrative Code for assessment of hazardous properties of on-site materials, as described below under Assessment Methodology. Since the land-use history review had indicated that no materials from other than oil production and storage operations were likely to be found at the site, it was assumed that the only hazardous property of concern is toxicity. Therefore, the program was designed to identify hazardous materials on the basis of toxicity. The analytical program did not test for other physical and chemical characteristics like corrosivity, ignitability or reactivity.

The test samples were analyzed for:

- Total petroleum hydrocarbons using infrared spectrometry, EPA Method 418.1;
- Total metals (arsenic, barium, cadmium, total chromium, copper, lead, mercury, nickel, vanadium, and zinc) using Inductively Coupled Plasma/Mass Spectrometry (ICP/MS);
- Extractable metals using 48-hour citric acid extraction by California Waste Extraction Test (WET);
- Volatile and semi-volatile (base-neutral/acid extractable) organic priority pollutants by Gas Chromatography/Mass Spectrometry (GC/MS) using EPA Methods 8240 and 8270, respectively;
- Head space vapor analysis (for inhalation toxicity) by GC/MS using EPA Method 5020; and
- Aquatic (fish) toxicity using California Waste Assessment Bioassay procedures.

#### QUALITY ASSURANCE/QUALITY CONTROL (QA/QC)

A quality assurance program, was followed throughout the investigation. The QA/QC procedures followed in the field included calibration of the OVM and HNu, standard sample handling, and standard quality control documentation procedures. Chain-of-custody forms, labels, data forms, and field logbooks were used.

The QA/QC program performed in the chemical laboratories consisted of the following procedures:

- Initial calibration of instruments;
- Periodic recalibration of instruments during analytical work;
- Analysis of preparation blanks;
- Analysis of interference check samples;
- Analysis of spiked samples;

- Analysis of duplicate samples; and
- Performance of standard QA/QC procedures.

#### ASSESSMENT METHODOLOGY

In California, the Hazardous Waste Control Law (Health and Safety Code, Chapter 5.6, Division 20) and hazardous waste regulations (Chapter 30, Division 4, Title 22 of the California Administrative Code) provide for a program to ensure safe handling, storage, use, processing, and disposal of hazardous wastes, and recovery of resources from hazardous wastes. The California Administrative Code (CAC), as supplemented by the California Administrative Register, is an official publication of the State of California. The California Department of Health Services uses Chapter 30 (Minimum Standards for Management of Hazardous and Extremely Hazardous Wastes), Division 4 (Environmental Health), Title 22 (Social Security) of CAC for identification of hazardous materials. For evaluations made in the present site assessment, current revisions to the CAC were considered.

A "hazardous material" is defined in Chapter 30, Title 22 of the CAC as:

" . . . a substance or combination of substances which, because of its quantity, concentration, or physical, chemical or infectious characteristics, may either; (1) cause, or significantly contribute to an increase in mortality or an increase in serious irreversible, or incapacitating reversible, illness; or (2) pose a substantial present or potential hazard to human health or environment when improperly treated, stored, transported or disposed of or otherwise managed."

Criteria utilized for identification of hazardous materials include toxicity (including persistent and bioaccumulative properties), corrosivity, ignitability, and reactivity. Acute toxicity is considered in terms of the lethal dose and concentration for 50 percent of a population of specified laboratory animals (LD<sub>50</sub> and LC<sub>50</sub>, respectively). According to Kenaga (1986), dosage is the amount of chemical applied directly to an organism. The LD<sub>50</sub> is the dosage of a chemical that will cause 50 percent mortality in a given test species. A concentration applied to a given medium, such as water, soil or food, results in uptake of a certain amount by an organism. The LC<sub>50</sub> is the concentration in the medium that results in 50 percent mortality of a given test species of test organism. Toxicity values are commonly expressed in terms of milligrams of chemical per kilogram of body weight of the organism tested. To arrive at this toxicity value, LD<sub>50</sub> values do not need conversion. However, LC<sub>50</sub> values must be converted by such values as the bioconcentration factor or dietary intake rate to calculate milligrams of toxicant per kilogram of body weight (Kenaga, 1986).

According to the criteria specified in Article 11, Chapter 30, Title 22 of the CAC, a waste, or a material, is toxic and hazardous if it:

- ° Has an acute oral LD<sub>50</sub> less than 5,000 mg/kg; or
- ° Has an acute dermal LD<sub>50</sub> less than 4,300 mg/kg; or
- ° Has an acute inhalation LC<sub>50</sub> less than 10,000 ppm as a gas or vapor; or
- ° Has an acute aquatic 96-hour LC<sub>50</sub> less than 500 mg/l; or
- ° Contains any of the 16 organic substances listed at a single or combined concentration equal to or exceeding 0.001 percent by weight; or
- ° Has been shown through experience or testing to pose a hazard to human health or environment because of its carcinogenicity, acute toxicity, chronic toxicity, bioaccumulative properties or persistence in the environment; or
- ° Is listed in 40 CFR 261 (Code of Federal Regulations, 1982) as a hazardous waste.

For persistent and bioaccumulative toxic substances, two threshold limit values are specified. The higher value is the Total Threshold Limit Concentration (TTLC), and the lower value is the Soluble Threshold Limit Concentration (STLC). Lists of specified STLCs and TTLCs for 20 inorganic and 16 organic persistent and bioaccumulative toxic substances (metals, pesticides, and PCBs) are provided in Article 11. A waste listed in Article 11 is considered hazardous if its total concentration exceeds its specified TTLC or its soluble concentration exceeds its STLC.

#### RESULTS OF SITE ASSESSMENT

The results of total petroleum hydrocarbons analyses showed that five soil samples contained concentrations exceeding 1,000 mg/kg up to 6,400 mg/kg. These samples were collected from depths between 13 and 21 feet in Boring B-6 and from depths between 3 and 15 feet in Boring P-3.

The total concentrations of the ten metals analyzed were below the TTLCs of the metals. One composite sample exceeded the STLC of arsenic and three other composite samples exceeded the STLC of lead. The discrete samples making these composite samples were analyzed by the California Waste Extraction Test (WET) for extractable (soluble) concentrations of arsenic and lead. The soluble concentrations were below the STLCs of arsenic and lead (5.0 mg/l).

Test samples were analyzed for the presence of volatile and semi-volatile organic compounds.

Volatile organic compounds were also measured in the head space vapor of the test samples for inhalation toxicity assessment. Organic chemicals found in the test samples and their maximum concentrations in ppm were: ethylbenzene (0.7), fluorene (0.9), 2-methylnaphthalene (11.0), naphthalene (4.3), phenanthrene (1.7), toluene (13), and xylenes (111). The analytical data also indicated the presence of undifferentiated C9-35 aliphatic hydrocarbons at concentrations up to 1,000 ppm and C9 aromatic hydrocarbons at concentrations up to 168 ppm.

For the organic chemicals identified in the test samples, published oral and dermal acute toxicity estimates derived from laboratory tests on mammals were obtained from Tatken and Lewis (1983), Lewis and Sweet (1984), Clayton and Clayton (1979), Sax (1979), and Union Oil Company (1982). Using the published oral and dermal acute toxicity values and the waste mixture formula given in Article 11, Title 22 of the CAC, the lowest calculated oral and dermal LD<sub>50s</sub> were found to be greater than 5,000 and 4,300 mg/kg, respectively.

Concentrations of the materials in the head space vapor of the test samples were calculated, and were compared to published acute inhalation toxicity estimates obtained from the literature cited in the preceding paragraph. The results showed that the materials in the head space vapor of the test samples had acute inhalation LD<sub>50s</sub> greater than 10,000 ppm.

Aquatic toxicity tests were performed on selected test samples. Fish mortality was not observed during the exposure periods.

Following the assessment criteria described under Assessment Methodology, it was concluded that the materials contained in the test samples are not hazardous. However, it was recommended that soils with concentrations of total petroleum hydrocarbons exceeding 1,000 mg/kg be excavated and remediated on-site, as described under Soil Remediation.

#### SOIL GAS SURVEY AND METHANE GAS MITIGATION

Since the fire and explosion incidence, which occurred in March 1985 in Ross Stores of the Fairfax area of Los Angeles, and, which is believed to have been caused by gas seeping from a natural accumulation of gas from the soil, there has been increased concern in southern California regarding the accumulation of methane and other hazardous gases within oil fields. As noted by GeoScience Analytical, Inc. (1986), gas accumulation can be the result of seepage from abandoned wells, natural petroleum or gas seeps or shallow biogenic gas (resulting from bacterial activity). Methane can also be the result of thermogenic (heating) processes and can resemble biogenic gas in composition.

To investigate the presence of methane at the site, a soil gas survey was conducted. The soil gas survey technique is based on the

premise that many Volatile Organic Compounds (VOCs) will volatilize from contaminated soils. VOCs move as vapors (gas phase) by molecular diffusion away from source areas, toward regions of lower concentration in the overlying and surrounding soil profile. They also move in response to pressure gradients, to the extent these exist in the soil column. As the VOCs degrade, other biogenic byproducts such as methane may also be generated. Soil gas survey is used in an attempt to identify areas of high soil gas concentration as a means of broadly delineating the zones of soils containing volatile constituents.

Soil gas probes were installed at seven locations. The locations were selected to cover the site area underlying the proposed buildings. At the time of the survey, the subsurface soils appeared to be wet. At each probe location, a probe was driven to depths of about 4, 8, and 12 feet. The probes are 1/2-inch galvanized steel pipes, perforated over the bottom 9 inches. The probes were driven using a post-driver and a compressor.

A suction pump removed subsurface soil vapor through the probes. The removed vapors were monitored using a Century System Model 128 Organic Vapor Analyzer (OVA) with a flame ionization detector. The OVA is capable of detecting most VOCs encountered in the field. The range of the measurement of the OVA is 0 to 1,000 ppm.

OVA readings were taken generally after pumping periods of 1, 5, and 10 minutes for the 4-, 8-, and 12-foot probe depths, respectively. These periods approximately correspond to the lengths of time required to remove equal volumes of gas from the probes.

The results of the OVA readings indicated that except for one probe, the OVA readings at all depths were 20 ppm or lower. At one probe, installed at a location half-way between Borings B-5 and P-3, the readings were in excess of 1,000 ppm at the 4- and 12-foot depths and about 360 ppm at the 8-foot depth. No trend of increasing or decreasing gas concentrations with depth is indicated by the data. These readings are considered to be relatively high, although it should be noted that gas accumulation rates can vary significantly depending on soil's moisture content, temperature, changes in paved surfaces, and changes in conditions of oil wells (e.g., abandonment).

Based on the results obtained and considering the requirements of the County of Los Angeles and the City of Santa Fe Springs, it was recommended that measures to mitigate the potential hazards from accumulation of methane and other hazardous gases at the site be included in the development of the site. The mitigative measures described below were performed prior or during the construction of the buildings:

1. Unabandoned oil wells were abandoned and previously abandoned oil wells were re-abandoned in accordance with current

re-abandonment requirements of the California Department of Conservation, Division of Oil and Gas.

2. On-site pipelines were removed. Soil adjacent to the pipelines observed to be contaminated on the basis of discoloration, oil-staining or odor was excavated. The excavated soil was treated according to the remediation procedure described in the following section.
3. To minimize accumulation of methane and other hazardous gases in the buildings, the following methane gas mitigation measures were implemented:

- ° The foundations were sealed with 30-mil layers of reinforced chlorinated polyethylene below the concrete slab-on-grade; and
- ° Perforated 4-inch diameter vent pipes, laid in gravel trenches, were installed to collect and vent the accumulated gases from beneath the sealed foundations.

#### SOIL REMEDIATION

Soils containing high concentrations of total petroleum hydrocarbons were remediated following the preparation of a soil remediation plan. This plan was approved by the California Department of Health Services and implemented by the oil company leasing the on-site oil wells. The remediation operations were directed, observed, and documented by Woodward-Clyde Consultants.

The general procedure described below was followed in remediating the oil-contaminated soils:

1. A pit measuring approximately 85 by 150 feet in area and 15 to 25 feet deep was excavated in the general area surrounding Borings B-6 and P-3. Soil excavation stopped when concentrations of total petroleum hydrocarbons, as measured by EPA Method 418.1, were below 1,000 mg/kg.
2. Excavated soil was aerated by spreading it on the ground for several hours and plowing it a few times. This process was found to be helpful in reducing the concentration of petroleum hydrocarbons.
3. Aerated soil was blended with clean soil excavated from on-site areas to further reduce the concentration of petroleum hydrocarbons.
4. Blended soil was stockpiled on-site and was mixed and aerated periodically.

5. Stockpiled soil was placed in areas of the site designated for paved street and parking. Prior to placement, samples of the stockpiled soil were analyzed by an on-site mobile laboratory to verify reduction of total petroleum hydrocarbons to below the 1,000 mg/kg cleanup action level.
6. The excavated pit was backfilled and compacted. Prior to backfilling, soil samples were collected from the bottom and walls of the pit and analyzed to verify that they did not contain total petroleum hydrocarbon concentrations in excess of 1,000 mg/kg. Clean on-site soil was used for backfilling those parts of the pit underlying the areas designated for the buildings. Stockpiled (treated) soil was used for backfilling areas of the site designated for paved street and parking.

The excavation, aeration, blending, and mixing operations were accomplished using one CAT 613B scraper, one J.D. 860B scraper, one IH D50C track-mounted loader, and one IH D-20 dozer. All excavated soils were continuously sprayed with a 1,000-gallon water truck to minimize dust. Compaction was performed by a rubber-tire roller and/or by track rolling using the scrapers or the loader.

#### CONCLUSIONS

As available land for development becomes scarce, potentially contaminated sites within oil fields become attractive for development. These sites are generally used for production and storage of crude oil only; however, a historical evaluation of the site should confirm this. A site assessment investigation needs to be performed to investigate the presence of hazardous substances. A remediation plan that addresses mitigation of hazardous materials, oil contaminated soil, and sump materials, if present, should be prepared and implemented. The potential for accumulation of methane and other hazardous gases should be minimized by implementing appropriate measures.

#### REFERENCES

- California Department of Conservation, Division of Oil and Gas (1985), "Santa Fe Springs Oil Field, Map 102, Scale 1 in. = 500 ft."
- Clayton, D. C., and F. E. Clayton (1982), "Patty's Industrial Hygiene and Toxicology," John Wiley, Three Volumes, Third Revised Edition.
- Code of Federal Regulations (1982), "Protection of Environment: Title 40, Part 261."
- GeoScience Analytical, Inc. (1986), "A Study of Abandoned Oil and Gas Wells and Methane and Other Hazardous Gas Accumulations," prepared for the California Department of Conservation, Division of Oil and Gas, October 10.
- Lewis, R. J., and D. V. Sweet (1984), "1983 Supplement to the Registry of Toxic Effects of Chemical Substances," NIOSH, U.S. Department of Health and Human Services, Cincinnati, Ohio, Two Volumes, October.
- Sax, N. I. (1979), "Dangerous Properties of Industrial Materials," Van Nostrand Reinhold Company, N.Y., Fifth Edition.
- Tatken, R. L., and R. J. Lewis (1983), "Registry of Toxic Effects of Chemical Substances," 1981-82 Edition. NIOSH, U.S. Department of Health and Human Services, Cincinnati, Ohio, Three Volumes, June.
- Union Oil Company (1982), "Premanufacturing Notice: Full Range Dewaxed Shale Oil," November.
- Woodward-Clyde Consultants (1985), "Ross Stores Corporation - Fairfax District Investigation," prepared for Manchester, Welling & Leland - Attorneys at Law, August 13.
- Ybarra, R.A. (1957), "Recent Development in the Santa Fe Springs Oil Field," in Summary of Operations, California Oil Fields, Forty-third Annual Report of the State Oil and Gas Supervisor, Department of Natural Resources, Division of Oil and Gas, Vol. 43, No. 2, pp. 39-45.

# Failure and Reconstruction of a Waste Containment Pond Slope

Dorairaja Raghu

Civil & Environmental Engineering Department, New Jersey Institute of Technology, Newark, New Jersey

Robert J. Van Orden, P.E.

Partner, Melick-Tully and Associates, Inc., South Bound Brook, New Jersey

**SYNOPSIS:** A portion of a slope of a subsurface waste containment cell failed. It is believed that this failure could be attributed to a sudden drawdown condition caused by the pumping of treated wastewater effluent stored inside the cell prior to construction of the permanent liner. This conclusion seems to be in agreement with the results of a stability analysis conducted utilizing post-failure slope profile data. A discussion of the analysis of the failure and the reconstruction of the slope is presented in this paper.

## INTRODUCTION

The waste containment cell referred to in this paper is located somewhere in the northeastern United States. The purpose of this earthen containment is to store hazardous solid wastes. Figure 1 shows a typical cross section of this structure. The bottom and the sides of the containment cell are lined with a 2 foot thick soil liner consisting of compacted glacial till (clay), and a 10 mil thick impervious membrane liner.

## GEOLOGY AND SUBSURFACE CONDITIONS

The surficial deposits in the area are of glacial and glacio-fluvial origin. They are reported to be about 50 to 60 feet thick and are underlain by bedrock, which is a shale formation. The glacial soils are comprised of a dense glacial till of sufficient shear strength to be stable under the 2:1 slope configuration of the containment structure. Occasional lenses of varved silts and silty clays of low shear strength known as glacio-fluvial clays have been encountered within the till deposit. In the area of the containment structure, borings performed prior to construction indicated that glacio-lacustrine clays were

encountered at or below the level of the bottom of the containment cell.

## SEQUENCE OF EVENTS PRIOR TO FAILURE

The sequence of events preceding the failure of the slope is presented in Table 1.

TABLE 1

| Elapsed Time<br>(months) | Event   |
|--------------------------|---|
| 0                        | Excavation for containment commenced  |
| 6                        | Excavation for containment completed  |
| 6                        | Treated wastewater effluent was temporarily ponded to a maximum depth of 15 feet in the unlined containment cell excavation |
| 12                       | Ponded liquid pumped out very quickly   |
| 13                       | Liner installed   |
| 14                       | Solid waste placed in center of containment cell  |
| 17                       | Limited slope movement observed by maintenance personnel  |
| 18                       | Treated wastewater effluent ponded again inside the containment cell to a maximum depth of 6 feet                           |
| 24                       | Ponded liquid pumped out quickly  |
| 25                       | Failure of slope observed by on-site personnel  |

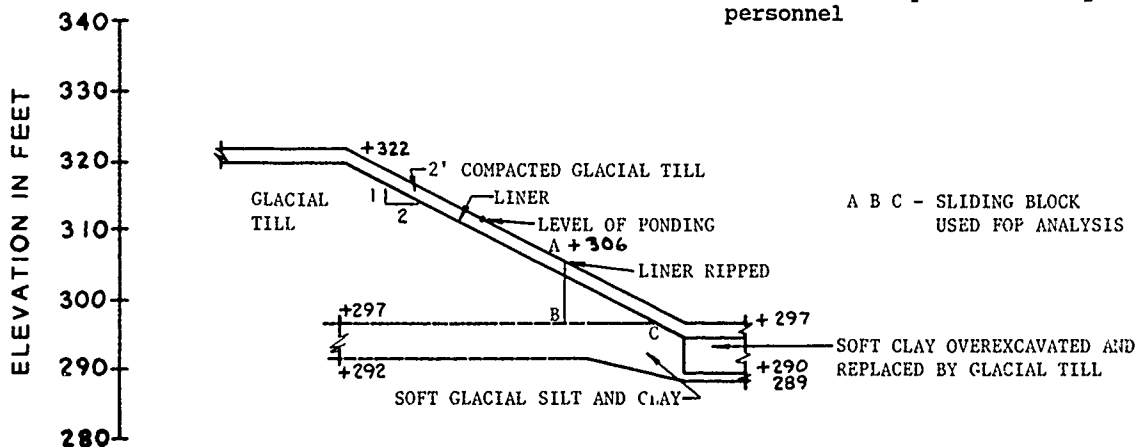


FIGURE 1- CROSS SECTION OF NORTH SLOPE

## POST-FAILURE INVESTIGATIONS

In order to determine the cause of failure and to design remedial work to be performed on the slope, a post-failure investigation of the slope was undertaken. This consisted of: 1. Field investigations to survey and observe the conditions after failure and to determine the nature and the extent of failure; 2. Testing to determine the properties of the embankment and liner soils; and 3. Stability analysis of the slope.

## FIELD INVESTIGATIONS

These consisted of several site visits to the site by the authors, surveyors and other technical personnel. Figure 2 shows the details of conditions observed. Two test pits and several hand-excavated holes were excavated in the vicinity of failure to observe the soils and expose the liner. Soil samples from the liner materials and underlying natural soils were obtained for testing. Some undisturbed tube samples of soft clay were obtained from locations in the vicinity of failure. At selected stations along the north-central slope, survey cross sections of the slope were obtained. A typical post-failure slope profile is shown in Figure 3.

NOTE: DIMENSIONS SHOWN ARE TENTATIVE. THE EXACT EXTENT OF THE AREA OF REMEDIAL WORK IS TO BE ADJUSTED BASED ON FIELD CONDITIONS.

- EXISTING SLOPE EDGES
- APPROXIMATE BOUNDARIES OF REPAIR AND ADDITIONAL FILL
- LONGITUDINAL FOLD IN HYPALON LINER
- TEST PITS AT LOCATION OF UPHEAVED SOIL AND RIPPED LINER

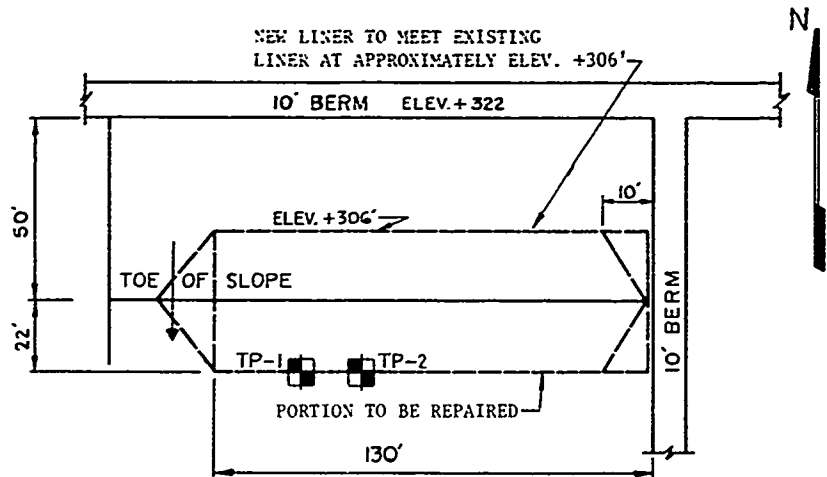


FIGURE 2- PLAN VIEW OF THE CENTRAL PORTION OF THE NORTH SLOPE SHOWING CONDITIONS AND THE EXTENT OF REMEDIAL WORK TO BE DONE.

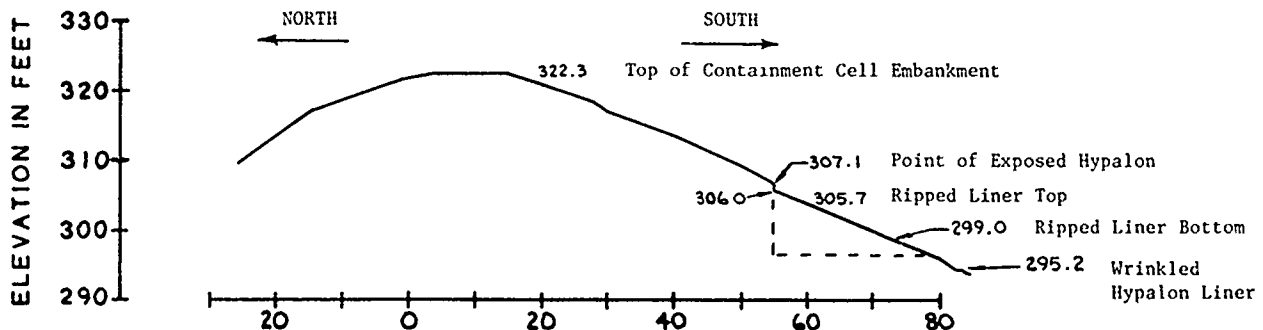


FIGURE 3- TYPICAL POST-FAILURE SLOPE PROFILE

## OBSERVATIONS BASED ON FIELD INVESTIGATIONS

Based on the above investigations, the following observations were made:

1. The soil above and 6 inches below the membrane liner was saturated.
2. The membrane liner separated along a seam near the top of the slope approximately in an east-west direction and no rips were noted near the top of the slope.
3. The membrane liner was ripped at an elevation approximately 8 to 10 feet above the bottom of the landfill cell.
4. The bottom of the cell adjacent to the toe of the slope heaved to a distance of 15 feet horizontally from the initial toe of slope.
5. In the region near the bottom of the cell, the underlying natural clays heaved up over the compacted glacial till liner soils.
6. The slope moved horizontally in the region between the elevation where the membrane liner ripped and the bottom of the containment cell slope.



7. Some secondary laminar movement of the slope above the elevation where the liner ripped was also observed.

#### PROPERTIES OF SOFT SOILS

Index tests and unconfined compression tests were performed on the undisturbed tube samples recovered from the site. The average Liquid Limits and Plastic Limits were 30% and 15%, respectively. Natural water contents were close to the plastic limit. The materials exhibited characteristics of a silty clay. Average unconfined compressive strengths in the undisturbed and remolded conditions were determined to be 460 psf and 110 psf, respectively.

#### STABILITY ANALYSIS

From the boring logs, there is evidence that a soft layer of glacio-lacustrine silt and clay underlies the surficial glacial till. Test pits made at two locations, shown in Figure 2, indicate that the contact between the soft layer and the till occurs at an elevation of approximately +297 feet. At this elevation, the liner was observed to have displaced horizontally. Hence it was presumed that failure occurred along the glacial till-soft soil contact.

A sliding block analysis for a sudden drawdown condition (assuming no internal friction) as recommended in the literature (Taylor 1959, Sherard et. al. 1963, and Lambe and Whitman 1964) was performed. Since data regarding pore pressures at the time of failure was not available, a total stress approach was utilized. Cohesion required in the soft clay for stability of the base was determined to be about 330 psf, whereas the soft soil had an unconfined compressive strength of 110 psf in the remolded condition.

#### CAUSE AND MECHANISM OF SLOPE FAILURE

Based on the analysis, it was concluded that the lower portion of the slope above the soft clay-glacial till contact slid horizontally. This caused a portion of the glacial till above this contact to drop. In this process, the membrane liner along the slope sheared. The limited failure of the liner near the toe in

the bottom of the containment could be attributed to localized upward and horizontal movement of the soft clays from under the slope to the toe causing shearing of the membrane liner. It is felt that the slope would not have failed if: 1. the unlined containment cell had not been flooded with treated effluent prior to installation of the liner; and 2. the toe of the north slope had been restrained by waste fill materials soon after construction of the liner. The remaining portions of the containment cell where waste fill was placed soon after installation of the liner experienced no slope movements.

#### RECOMMENDATIONS FOR REMEDIAL CONSTRUCTION

Two alternates were proposed for the remedial construction of the slope. The details of the first alternate are shown in Figure 4. In order to reconstruct the limited portion of the north slope to its original configuration, the disturbed soft clay soils within the area of the toe of the slope would have to be removed. A stable slope configuration, as initially constructed, would require overexcavation and replacement of soft clay soils to a depth of approximately six feet at the toe of the slope, as well as up the side of the slope, to the contact with the overlying glacial till. The overexcavation work would require that limited areas be excavated and filled with suitable compacted material in order to minimize potential slope failure during remedial earthwork.

Details of the second alternate proposed are shown in Figure 5. Implementation of this solution would require that the disturbed soft clay soils be removed to the initial slope configuration and a layer of compacted glacial till at least 4 to 5 feet in thickness be placed above the toe of the north slope prior to replacing the membrane liner. This solution would flatten the final slope in the region of the disturbed soft clays, and would provide a blanket of compacted fill above the in-place soft clay soils to minimize the effects of future settlements due to consolidation of the underlying soft clays. It is felt that this alternate would provide a suitable base for the reconstruction of the liner without creating potential safety hazards during remedial construction which would be involved with any

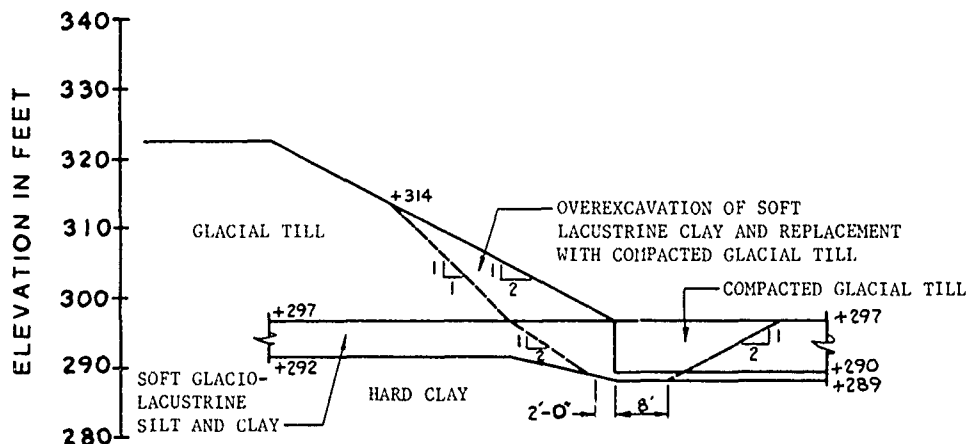


FIGURE 4- NORTH SLOPE REMEDIAL WORK - ALTERNATE NO. 1

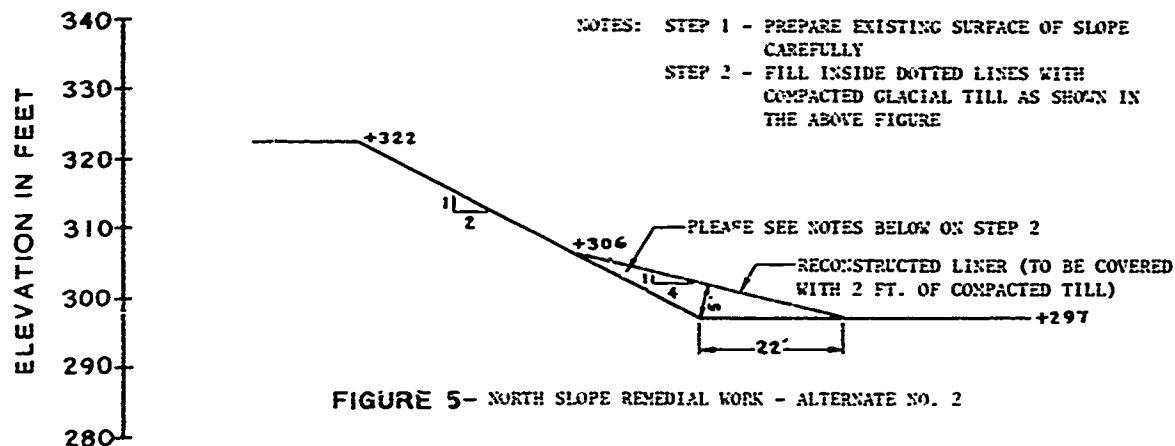


FIGURE 5- NORTH SLOPE REMEDIAL WORK - ALTERNATE NO. 2

extensive overexcavation of the soft clays. Hence, this alternate was selected for the remedial construction.

#### OTHER DETAILS OF REMEDIAL WORK

The following are some other relevant details of remedial work:

1. The soft disturbed glacial till materials should be excavated to the initial slope configuration within the area to be repaired.
2. Following the removal of the disturbed soils, glacial till material should be spread in loose lifts approximately 12 inches in thickness.
3. Each lift of fill should be compacted to at least 90% of its maximum dry density (ASTM D-1557).
4. The compacted glacial till should be placed within the limits shown on Figure 2 to the slope configuration shown on Figure 5.
5. Upon completion of the placement of the compacted glacial till, the membrane liner should be reconstructed on the top of the glacial till and sealed to the existing membrane liner around the perimeter of the area to be repaired.
6. A final 2 feet thick layer of compacted glacial till should be constructed above the new liner in accordance with the original design plans.
7. It is suggested that the final exposed layer of glacial till be moisture conditioned as

required to avoid shrinkage cracks prior to burial within the cell. The exposed glacial till layer beyond the limits of the liner repair may also require moisture conditioning and/or recompaction.

The work was completed according to the above specifications and the containment structure has performed satisfactorily without additional slope movements.

#### CONCLUSIONS

From the post-failure investigation, it can be concluded that the slope of the containment cell failed due to a sudden drawdown type of condition caused by the pumping of the liquid wastewater effluent. This failure could have been avoided, if the inside of the pond were lined prior to ponding of treated wastewater effluent, and/or if the containment cell were filled with solid waste soon after the construction of the liner. This case history demonstrates the importance of developing an operations manual for waste facilities at the time of design and construction.

#### REFERENCES

- Lambe, T.W. and R.V. Whitman, "Soil Mechanics", John Wiley and Sons, New York, 1969.
- Sherard, J.L., R.J. Woodward, S.F. Gizienski and W.A. Clevenger, "Earth and Rockfill Dams", John Wiley and Sons, New York, 1963.
- Taylor, D.W., "Fundamentals of Soil Mechanics", John Wiley and Sons, New York, 1959.

## Implementation of Remedial Measures to Contain a Spill of PCBs

**M.D. Huag**

Professor and Head, Department of Civil Engineering, University of Saskatchewan, Saskatoon, Saskatchewan, Canada

**J. Atwater**

Professor, Department of Civil Engineering, University of Saskatchewan, Saskatoon, Saskatchewan, Canada

**R.B. Knight**

Knight and Piesold, Ltd., Vancouver, British Columbia, Canada

**P. Kozicki**

Ground Engineering Ltd., Saskatchewan, Canada

**A. Lissey**

MLM Groundwater and Engineering Ltd., St. Albert, Alberta, Canada

**SYNOPSIS:** A large spill of Polychlorinated Biphenols (PCB's) occurred at Federal Pioneer Limited's Regina Plant in 1976. The City of Regina is underlain by a relatively shallow aquifer which supplies a significant proportion of its drinking water. A remedial measures plan was developed to contain this spill within the boundaries of the site and clean up any contamination which had spread to adjacent property. The remedial measures plan developed involved limiting or reversing the normal downward hydraulic gradient. The three principle measures introduced to accomplish this reversal included the construction of a cutoff wall around the site, installation of a thick surface seal over the entire surface and active dewatering. The performance of these measures was monitored by an extensive network of piezometers and sampling well. Monitoring over the past seven years has produced no evidence of further downward migration of PCB's.

### INTRODUCTION

The development of remedial measures to contain and control the spread of hazardous waste is one of the most challenging tasks in waste management. Many of these wastes are chemically active, present a threat to uncontaminated groundwater and must be contained for considerable lengths of time. This paper presents a case history of the development, installation, monitoring and analysis of remedial measures designed to control a spill of liquid PCB. It describes the background of the spill and development of the remedial measures plan. The installation of the remedial measures and problems encountered during the installation are also presented. This paper also describes the monitoring system set up to measure the effectiveness of the system, and presents an analysis of monitoring results over the past seven years. This analysis shows that the system has been effective in preventing further downward migration of PCB's and should remain effective as long as the remedial measures are adequately maintained.

### BACKGROUND

In 1976, Canada's first major known spill of PCB's occurred at Federal Pioneer Limited's Regina Plant. This plant used a non-destructive oil containing 70 percent PCB's and 30 percent tri- and tetra- chlorobenzenes (TCB's) in the manufacture of transformers. The oil was stored in an outside tank and pumped to the plant through an underground line. The exact date this line ruptured is not known, and the total quantity of PCB's released is also not known. However, a review carried out by the National Research Council of Canada (NRCC, 1980) estimated that up to 21,000 litres of oil was involved. At the time of the spill little was known about the health hazards of PCB's or their threat to the environment. Even less was known on how to effectively contain such a spill. The manufacturer responded to the spill by drilling some shallow holes to pump off free oil, and had a thin asphalt seal placed over the PCB saturated soil.

In 1977 the Canadian Government prohibited the use of PCB's for most applications. This increased awareness of the potential problems associated with PCB's and in 1978 public concern was expressed over the security of the city of Regina's drinking water. The reason for this concern was the presence of an important aquifer under the site which supplies approximately one-third of the city's drinking water. These concerns eventually lead to the formation of an *ad hoc* panel of scientist under the umbrella of the National Research Council of Canada. This panel was requested to evaluate information on the nature and consequences of the spill, and prepare a public report. The report (NRCC, 1980) identified the major areas of contamination and recommended that all of the contaminated soil under the plant be eventually removed and deposited in a hazardous waste facility.

The major areas and the depths of contamination identified in the NRC study are shown in Figure 1. The manufacturing plant is located on a lot approximately 105 m wide and 190 m long. Old concrete pads at the rear of the lot mark the location of a previous plant which burned in 1974. The natural slope of the site changes near the rear of the plant, with water draining to the north and south. The location of heaviest concentrations of PCB's were found at the north-east corner of the plant near the location of the buried underground line. PCB's migrated out from this location to the west along an underground power line trench, south along the east limit of the building and east to an old transformer oil sump. Other areas of contamination were found near the railroad tracks where the oil was unloaded.

The high costs associated with the removal of the contaminated soil and the lack of a suitable facility in the Province of Saskatchewan to deposit such waste forced the company to look for more economically acceptable alternatives. Thus, in 1980 a team of waste management and environmental specialists headed by Ground Engineering Ltd. of Regina was engaged to develop a set of remedial measures to secure the site and enable the company

to continue operations.

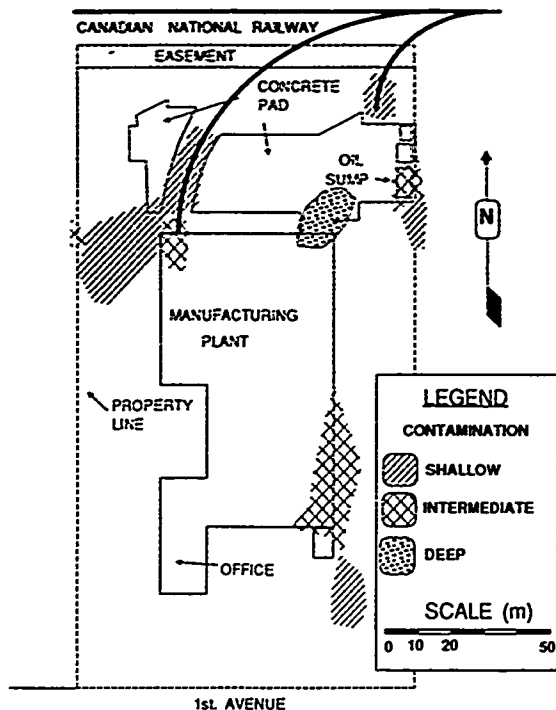


Fig. 1 Location of Major Areas of Contamination

#### PHYSICAL ENVIRONMENT OF THE SITE

Christiansen (1979) carried out an investigation to determine the geology and stratigraphy underlying the site. This information is presented in Figure 2. It shows a north-south cross section through the site. The surface of the site is covered with approximately 1 m of fill. Underlying this fill is a weathered clay referred to as Regina Clay. This highly plastic clay was formed in a large glacial lake during the recession of the last ice age. Its depth varies from 7.3 to 8 m. under the site. Prolonged periods of drying have resulted in severe desiccation of this clay, significantly increasing its permeability. The clay is underlain by 3 to 7 m of silt. The silt is underlain by 1 to 5 m of soft till, which is underlain in turn by 5 to 6 m of hard till. Underlying the till is a deposit consisting of from 16 to 22 m of interglacial silts and sands. The Regina Aquifer is located in this zone, approximately 35 m below the surface of the site.

At least three different water tables underly the site. The first is a perched water table located in the fill. The second is located on top of dense silt underlying the weathered clay. A third water table was located further down in the silt.

#### DEVELOPMENT OF THE REMEDIAL MEASURES PLAN

The objective of the remedial measures plan was to develop a less costly and more practical alternative to the excavation and removal solution proposed by the NRC panel. This alternative was to also permit the plant to continue operations. With these requirements as a guideline a strategy was developed to contain the spill within the boundaries of the site and to prevent further

downward migration of PCB's.

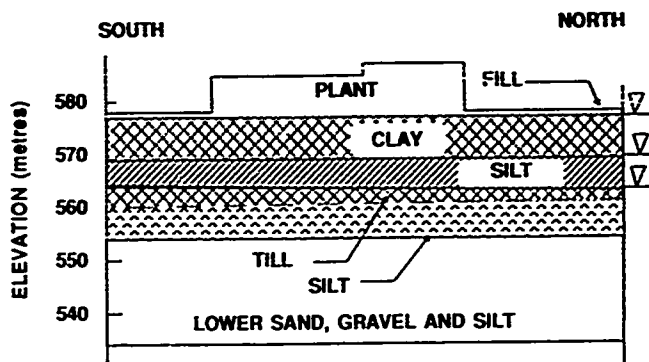


Fig 2 Geological Stratigraphy of the Site

The fundamental principle on which this strategy involved severely limiting and possibly reversing the hydraulic gradient in the fill and clay beneath the site. Since the supply of PCB's had been cut off the primary downward driving force was the natural downward movement of moisture through the clay. This downward movement is driven by water in the fill replenished by precipitation through the year. The goal of the remedial measures plan was to seal the surface of the site preventing the recharging of the perched water table and forcing a reversal of the hydraulic gradient. To aid in this reversal, the perimeter of the site was ringed with a cutoff wall extending down through the clay to the silt. Shallow sumps were installed to dewater the fill. Figure 3 shows an east west cross section through the zone of deepest contamination. This figure conceptually illustrates how the cutoff wall, surface seal and dewatering combined to enhance the containment strategy.

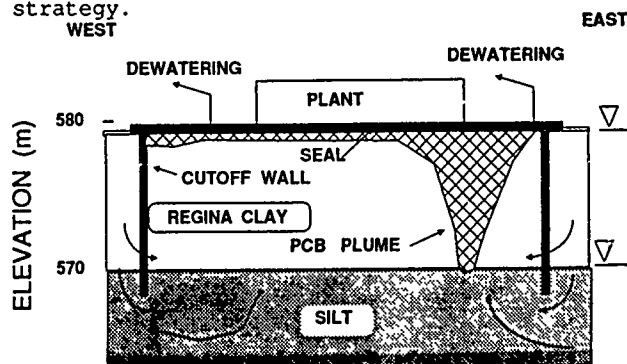


Fig. 3 Conceptual Sketch of Containment System

The remedial measures plan also involved excavation of contaminated soil on the fringe and outside the boundaries of the site. Soil containing more than 50 ppm PCB's was excavated in this process. The contaminated soil was transported to an interim storage facility established on the east side of the plant. It was intended that this facility would hold the contaminated soil until a permanent facility was constructed for such purposes.

The effectiveness of these measures was monitored with a network of piezometers spread over the site. The volume of water collected in the sumps

was recorded and its PCB concentration checked periodically. In addition, the movement of the deepest contamination was monitored with a deep hole drilling and sampling program.

#### IMPLEMENTATION OF REMEDIAL MEASURES

On September 15, 1980 Saskatchewan Environment formally gave approval to proceed with the remedial measures plan. The first step in implementing the remedial measures involved further drilling and sampling to determine the exact extent of the contamination off site. At the time this was proceeding contract documents were drawn up and discussions commenced with various contractors. The principle areas of work involved excavation of the contaminated soil, construction of the cutoff wall, placement of the surface seal and installation of the dewatering and monitoring network. Negotiations were also commenced with government agencies responsible for workers health and safety, to ensure smooth implementation of the remedial measures.

#### Excavation of Contaminated Soil From Off Site

The primary locations of excavation of contaminated soil are shown in Figure 4. The soil excavated from these areas was transported to the Interim Storage Facility. The initial estimation of the quantity of contaminated soil of the site was 300 m<sup>3</sup>. However, this increased substantially as the excavation proceeded. It was estimated that the contamination in these areas would vary in depth from 0.3 to 3 m. The contractor was directed to excavate the contaminated soil by advancing excavation equipment towards areas of greatest concentration, without backing equipment over contaminated soil and back on to uncontaminated soil. The contractor was instructed to take precautions to ensure that contaminated soil did not spill while being transported to the Interim Storage Facility. Water found in the excavation as a result of rainfall or seepage was treated as contaminated, and pumped into special containers. These containers were numbered and stored for later treatment or disposal.

Area "A" was located on the western boundary of the site near a electrical power facility serving the plant. The PCB's apparently migrated along the north wall of the plant and over to this facility through an underground concrete service conduit. Excavation in this area was delayed until the electrical power facility was moved. Area "B" was located outside an old Askarel sump on the eastern boundary of the site. This unlined sump contained high levels of PCB's and some had migrated down slope to the east.

Area "C" was located near the rail oil unloading facility in the north-east corner of the site. The depth of contamination in this area was initially considered shallow. However, soil sampling and testing following excavation continued to show high levels of PCB's. Figure 5 shows a hydraulic excavator attempting to reach the lowest levels of contamination, near the base of the weathered clay. In addition to these areas some minor contamination at the south end of the site was also excavated for storage in the Interim Storage Facility. Following excavation these areas were backfilled and compacted with uncontaminated soil.

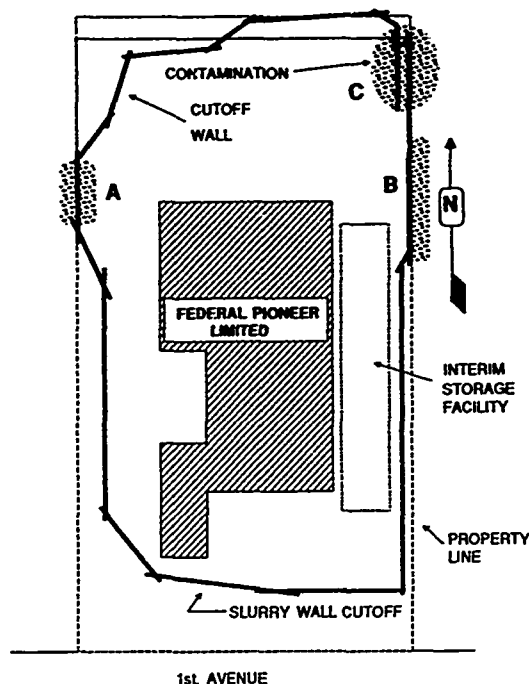


Fig. 4 Location of Areas of Off Site Contamination and Route of Slurry Trench Cutoff Wall



Fig. 5 Excavation of Zone of Deep PCB Contamination

#### Interim Storage Facility

The Interim Storage Facility was designed to receive contaminated soil from off the site. It was constructed in the weathered clay on the east side of the plant. This area was flooded with PCB's during and shortly after the pipe line break. Thus, the PCB concentrations in these soils were carefully monitored during excavation. Uncontaminated soil was separated from contaminated soil for future use, and contaminated soil was placed back in the completed facility. The depth of the facility varied from approximately 1 m at the south end to 2 m at the north end. The facility covered an area approximately 12 m wide by 37 m long. This was later increased to approximately 14 m by 64 m for the above ground level storage. The

base and sides of the excavation were lined with compacted 5 percent lime-modified clay. Lime was used to inhibit the swelling characteristics of the highly plastic clay. The base of the facility consisted of two 150 mm lifts of lime modified clay compacted to 98 percent of standard Proctor density. Following compaction the lime modified clay was covered with a liquid asphalt seal coat.

Special provisions were made for the placement of the contaminated soil in the Interim Storage Facility. This soil was placed in a loose layer of approximately 150 mm in thickness. The contaminated soil was mixed with 2 percent lime by weight and compacted to 95 percent of standard Proctor density. Figure 6 shows the contaminated soil placement and compaction operation in progress. The final step in the construction of this facility involved the installation of a surface seal. This seal consisted of 300 mm of lime modified contaminated clay, covered with a 150 mm hot mix sand-asphalt base course.



Fig. 6 Placement of Soil in Interim Storage Facility

#### Washdown Facility

A temporary washdown facility was constructed immediately north of the Interim Storage Facility. This shallow washdown area consisted of 200 mm of 95 percent standard Proctor density compacted clay. A medium curing liquid asphalt was sprayed over the compacted clay to further improve the seal. The final layer of protection consisted of a polyethylene geomembrane.

This facility proved difficult to maintain and a more permanent installation was constructed. This facility was established over a concrete sump located at the rear of the plant (Figure 7). This sump was turned into a washdown facility by installing a heavy steel channel iron grate capable of supporting large construction equipment.

All equipment used to excavate or handle contaminated soil was washed in these facilities. Washing consisted of alternately spraying the equipment with acetone and hexane. These facilities were also used to decontaminate drilling and sampling equipment.



Fig. 7 Decontamination of Construction Equipment at Washdown Facility.

#### Installation of Cutoff Wall

A key element of the containment strategy was the installation of a cutoff wall around the site. The location of this cutoff wall is shown in Figure 4. The length of the wall was approximately 550 m, and extended down to a depth of 10.5 m. A vibrated beam cutoff wall was chosen because it can be used to install a wall through potentially contaminated soil without excavating additional soil. This reduced the volume of soil requiring storage in the Interim Storage Facility and decreased the risk of further contamination.

The thin cutoff wall was constructed using a vibrating beam having a web depth of 500 to 825 mm, and a flange width of 250 to 375 mm. An attempt was made to ensure that the beam was plumb to within plus or minus 1 percent. A minimum overlap of 1 m of wall was constructed at all changes in direction.

Figure 8 show the installation of the cutoff wall. The wall was constructed from a mixture of sodium bentonite, fly ash and soda ash in water. Special attention was given to the seal between the cutoff wall and the surface seal.

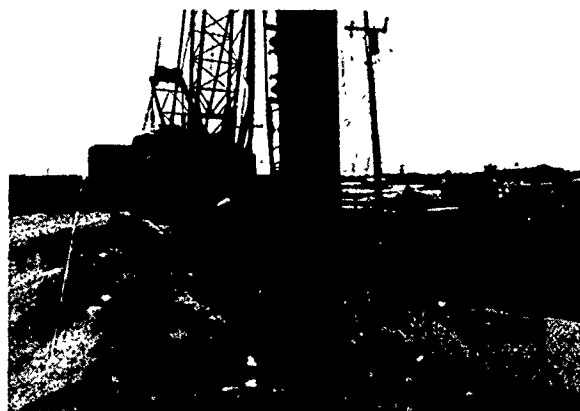


Fig. 8 Installation of Vibrated Beam Cutoff Wall

## Surface Seal

The installation of the surface seal was a critical element in the overall containment strategy. A significant effort was made to minimize infiltration. This involved the construction of a continuous seal capable of draining precipitation from the site. However, the site contained a number of areas requiring special attention. Some of these areas consisted of old cracked and weathered concrete from the previous plant. The concrete at the rear of the plant was also at the same elevation as the floor of the plant and restricted positive drainage off the site. Manholes leading to abandoned sewer lines, space adjacent railway tracks, transformer enclosures and other such facilities also presented problems. To accommodate these variations, the nature, type and quality of surface seal varied considerably from location to location. In addition special measures had to be taken to ensure that continuity existed between the different seals.

In unsurfaced areas, the general approach used was to excavate the subgrade, mix this soil with lime and compact. The thickness of this lime modified clay base varied up to 450 mm. Prior to compaction the soil was pulverized and dry lime was added at a rate of 5 percent by weight of soil. The lime was mixed with the soil with a rotary mixer and water added in the field.

The lime modified clay was covered and brought to grade with an asphalt seal. This seal consisted of a hot sand-asphalt base mix overlain by a hot asphalt concrete surface course. The thickness of these layers varied from 0 up to 50 mm for surface course material and up to 100 mm for base.

The old concrete at the rear of the plant was handled in different ways. The large concrete pad at the rear of the plant was covered with asphalt concrete. The old concrete pad west of the railroad was covered with a new layer of concrete. The new lift of concrete was placed back from the edge of the existing concrete to improve its seal with the adjacent asphalt overlay seal. Concrete was required to provide the plant with structures capable of supporting heavy transformers. For this reason some additional concrete was poured in area outside the north-east corner of the plant and at the north east corner of the site.

## Installation of Dewatering and Monitoring Equipment

The location of the shallow dewatering sumps used to dewater the fill are shown in Figure 9a. This figure also shows the location of the storage tank used to hold the water removed from the sumps. In addition, a purge well was located at the center of the PCB plumb near the location of the pipe line break. A total of 13 sumps were installed. Three of these sumps are located inside the plant. Sump 6 is the concrete lined sump used to decontaminate excavation equipment. Sump 8 is an old Askarel sump.

The location of the most frequently recorded piezometers is shown in Figure 9b. A total of 73 piezometers have been installed on this site. Most of these piezometers were read on a weekly basis since completion of the remedial measures.

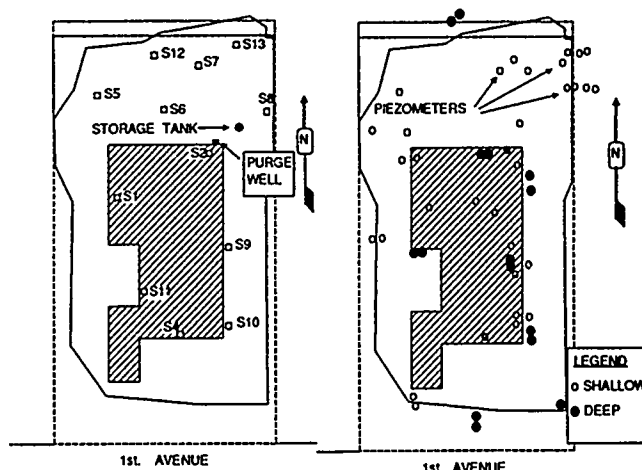


Fig 9a. Location of Dewatering Sumps

Fig 9b. Location of Piezometers

## PRELIMINARY EVALUATION OF REMEDIAL MEASURES

The remedial measures were completed in the summer of 1981, when monitoring was commenced. The sumps were dewatered when sufficient water was available to enable them to be pumped. The piezometers were recorded weekly, except during the winter when the water was frozen. The initial dewatering rates were surprisingly high. During the first year sumps dewatering the perched water table in the fill were quite active, producing approximately 20,000 liters of water. In 1981, the first full year of operation, their yield increased to approximately 110,000 liters. In 1982 this value dropped somewhat to near 90,000 liters. However, in 1983 it increased again to near 125,000 liters, when it was recognized that the majority of the water being removed was due to infiltration of precipitation. This conclusion was based on the close comparison between dewatering and precipitation.

A review of the initial remedial measures found a number of potential sources of infiltration. The first was the general lack of continuity and adequate grade at the rear of the site. The second was the presence of open or poorly sealed areas along the railway tracks and around a large complex of transformers adjacent the outside north wall of the plant. In addition, considerable water was being discharged onto the rear of the site from the roof of the plant itself. Based on this review a second phase of remedial measures was initiated.

The second phase of the remedial measures introduced to correct the deficiencies in the first program were carried out in the summer of 1984. These measures included: a) resurfacing the site with asphalt to provide a minimum grade off the site of 1 percent, b) raising concrete slabs 60 mm above the asphalt surface, c) re-sealing the perimeter of all concrete slabs, d) constructing an asphalt berm around the building to prevent the backup of water e) raising the tops of the sumps and piezometer so that they were higher than the surface seal, f) regrading the remaining railway track so that the grade sloped off the site, h) constructing a lean-to-roof over the transformer area to prevent rain from entering the fill in that area, and i)

re-directing runoff from the plant roof.

The majority of this work was completed in 1984. Only the addition of flashing around the building adjacent to its contact with the asphalt pavement was left until 1985 for installation.

#### PERFORMANCE EVALUATION OF THE REMEDIAL MEASURES

The performance of the remedial measures has been monitored over the past seven years. The goal of the remedial measures was to strictly limit or reverse the normal downward hydraulic gradient under the site. If successful the level of dewatering of the fill should drop significantly. A second measure of the performance is given by the variation in water levels of the piezometers. However, these levels are also influenced by lateral movement of water under the site and reflect general trends rather than precise determinations. A third measure of the performance is given by the volume of PCB's removed from the purge well and the location and levels of contamination reported in the deep hole drilling monitoring in the vicinity of the purge well.

#### Piezometers

A typical piezometer profile over the past six years is presented in Figure 10. This piezometer is located inside the north wall of the plant. The base of the piezometer is located in sand lenses in the silt. This piezometer was flooded in 1982 to measure its response. Since that time the water level has been dropping yearly to its 1981 value of 570.3 m. This and some of the other deep piezometers have shown a tendency to drop slightly during summer as a result of the dewatering, and increase in elevation during the winter.

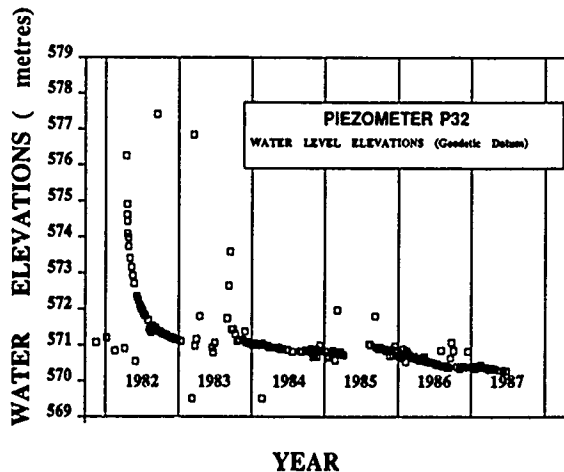


Fig. 10 Variation in Water Elevation with Time for Deep Piezometer No. 32

#### Sump Dewatering

The volume of water removed from the sumps has shown a considerable decrease since the installation of the remedial measures. Figure 11 shows the cumulative yield from these sumps for the past seven years. The cumulative yield values start in January and end in December as the 12th month. The second phase of the remedial measures was carried out in 1984. The volume of water

extracted from the sumps has fallen every year since, to near one-third of its 1984 level by 1986. The 1987 values indicate further improvement.

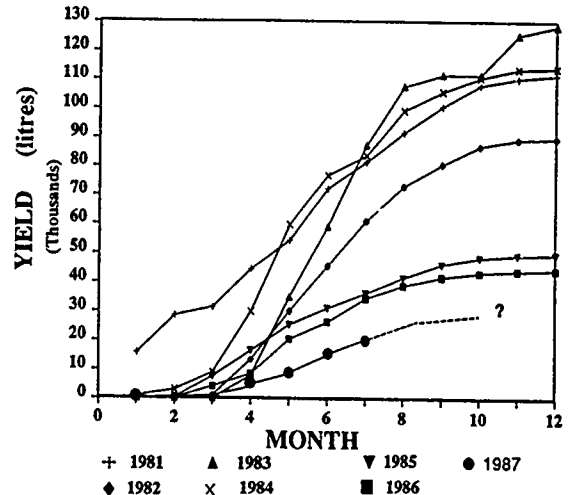


Fig. 11 Cumulative Yield From Dewatering Sumps From 1981 to 1987.

Another illustration of the improvement in the surface seal is shown in Figure 12. It presents a comparison of the ratio of sump yield in litres to precipitation in mm. The figure clearly illustrates the connection between precipitation and infiltration. It also demonstrates the effectiveness of the 1984 remedial measures in lowering infiltration through the surface seal.

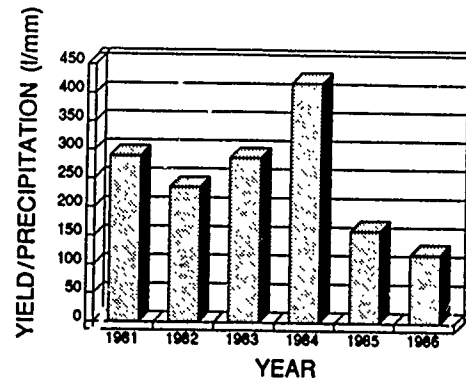


Fig. 12 Variation in Yield Versus Precipitation

Figures 11 and 12 clearly show that further improvements in restricting inflow are possible. However, most of the obvious sources of infiltration were dealt with in the 1984 improvements. The one source of possible infiltration causing some concern and not dealt with at that time was the quality of the seal over the Interim Storage Facility. Sump 8 located a short distance north of this facility has consistently been the leading source of water. In addition the height and geometry of this facility made placement and compaction of the asphalt surface seal very difficult. As a result cracks of up to 100 mm opened every spring along the sides and top of this facility. These cracks were sealed with various asphaltic compounds on a regular basis. However, the cracks still re-opened. A number of attempts were made to check the possible influence of this facility by placing



die in the crack. Unfortunately no trace of the die was found at any of the sumps.

A further analysis of the present situation can be made by examining the cumulative yield versus precipitation relationships for sumps located near a far away from the Interim Storage Facility (Figure 13). This figure shows that the ratio of yield to precipitation is considerably higher for the sumps located near the Interim Storage Facility.

The information obtained from the purge well and deep drilling and sampling program in the vicinity of the purge well has found some free PCB's in the clay. It also found some evidence of lateral migration in the clay above the silt. However, it showed no evidence of any downward migration of PCB's.

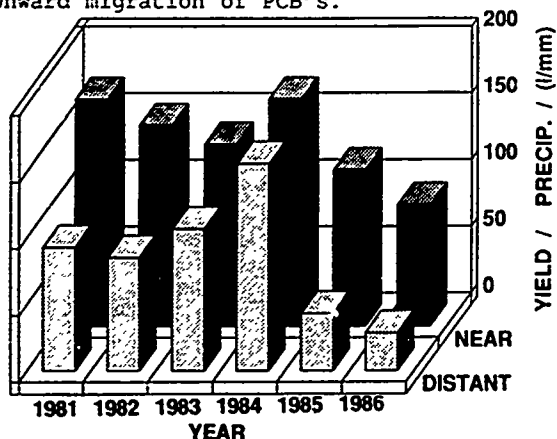


Fig. 13 Comparison of Yield Versus Precipitation Ratios for Sumps Located Near and Far Away From The Interim Storage Facility

#### CONCLUSION

Information obtained from the ongoing monitoring and surveillance program has shown that the remedial measures and containment strategy developed have been effective. No evidence has been found of further downward migration of PCB's. The monitoring data also shows that water entering the fill has been considerably reduced, thus minimizing the potential for downward movement of PCB's. The piezometers have also shown evidence of the effectiveness of the dewatering program.

While these measures have been effective to date, there is also evidence that the remedial measures must be adequately maintained to ensure a continued successful performance of the containment system. For this reason it is essential that a permanent monitoring and surveillance system be set up and maintained for such system.

A review of the measures used and effort expended on this project to completely seal the surface and dewater the fill demonstrates the difficulties of such a task. It also demonstrates the increased effort and attention to detail required to move towards a "perfect" surface seal.

#### ACKNOWLEDGEMENTS

The successful installation of these remedial measures would not have been possible without the

cooperation and conscientious attitude of Mr. Ken Booth and the Management of Federal Pioneer Limited. In addition, the assistance, patience and guidance of Dr. Victor Chang and Saskatchewan Environment is appreciated.

#### REFERENCES

Christiansen, E.A. (1979), "Regional Geology of the PCB Spill Site Regina, Saskatchewan", Saskatchewan Environment Report No. 0031-002,

NNCR (1980), "A case Study of a Spill of Industrial Chemicals-Polychlorinated Biphenyls and Chlorinated Benzenes", National Research Council of Canada Publication No. 17586.

# Performance of Lightweight Waste-Impoundment Dikes

Peter J. Bosscher

Assistant Professor of Civil and Environmental Engineering,  
University of Wisconsin-Madison, Madison, Wisconsin

Tuncer B. Edil

Professor of Civil and Environmental Engineering, University of  
Wisconsin-Madison, Madison, Wisconsin

**SYNOPSIS:** The containment dikes of two sludge disposal lagoons were founded on low strength, highly compressible wetland soils in Madison, Wisconsin. These lagoons, constructed in 1942 and 1967 respectively, encompass 130 acres of digested sludge produced at the sewage treatment plant. The dikes have experience two previous failures in 1970 and 1973. A dike rehabilitation program was initiated in 1976 to prevent additional failures. New dikes were built using wood chips as a lightweight fill. Non-woven synthetic filter fabric was used to prevent soil intrusion into the chips and to provide resistance to lateral spreading. An investigation was initiated in 1984 to assess the current and long term stability and settlement of the dikes, to determine the fate of the wood chip fill, and to develop recommendations for ways to stabilize the dikes, if necessary. This paper presents the results of the stability and settlement analyses, and the attendant interpretations. The investigation indicated better than marginal stability, predicted minor loss of freeboard between 1987 and the year 2000, and found only minor changes in the wood chips after 10 years of service.

## INTRODUCTION

Wood chips have been used to rehabilitate sludge lagoon dikes constructed over wetland soils in Madison, Wisconsin. The previous dikes required rehabilitation because of two dike failures. The Madison Metropolitan Sewerage District authorized rehabilitation work to be carried out in two phases because of the risk involved. A 600-ft long demonstration project was built and successfully completed in August, 1976. The remaining rehabilitation was done in 1977. Because of site constraints, rehabilitation had to be made near the alignment of existing dikes. The dike rehabilitation program was described by Schneider and Roth (1977). A light-weight fill was made using wood chips from diseased elm trees and a non-woven filter fabric to prevent soil intrusion into the wood chips and to provide restraint against lateral spreading. A soil cover was provided to protect the wood chips and to retain the sludge. This paper describes the evaluation of the state of stability of the dikes nearly 10 years after their rehabilitation. The evaluation program was designed to answer the following questions:

1. What is the state of stability of the dikes 10 years after rehabilitation? Is shear failure similar to the previous failures likely to take place?
2. Is there a significant deterioration of the dike constructed of wood chips? What is the projected dike competency?
3. What is the projected settlement of the dikes? Where is the current procedure of maintaining freeboard leading to in terms of additional settlements and dike stability?

## BACKGROUND

The two lagoons are located on the western edge of Nine Springs Marsh, an extensive grass-sedge wetland area, and east of the Madison Metropolitan Sewerage District (MMSD) Nine Springs sewage treatment plant as shown on Figure 1. Lagoon 1 is a 45-acre lagoon constructed in about 1942 and Lagoon 2 is an 85-acre lagoon installed in 1967. Digested sludge produced at the treatment plant is currently discharged and held in these two lagoons.

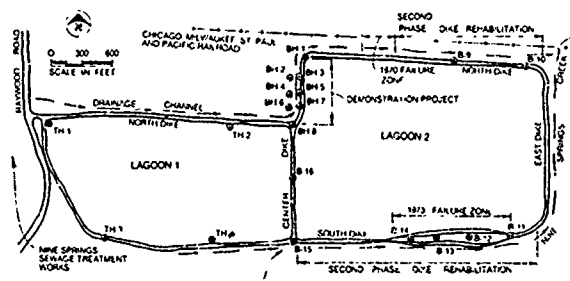


Figure 1. General Plan of the Dikes (from Schneider and Roth, 1976).

Soils underlying the lagoons are of glacial drift and post glacial drift origin. Surface soils are organic and range in thickness from about 10 to 40 feet. The organic soils overlie silt, sand, and gravel till. The till extends to depths of approximately 250 ft where sandstone bedrock is found. Since the water table lies at about the ground surface, the wetland area is often subject to flooding during spring runoff.

Nine Springs Creek flows along the south and east perimeter of the lagoons, and the drainage channel is located along the north edge of the lagoons. They converge at the northeast corner of Lagoon 2 and flow together about one-half mile to the Yahara River. The Chicago, Milwaukee, St. Paul, and Pacific Railroad crosses Nine Springs Marsh just north of the lagoons on a railroad embankment installed in 1854 using displacement methods.

The dikes for Lagoon 1 were built with fill hauled in over a 10-year period. The dikes of Lagoon 2 were constructed by drag-lining peat from the wetland to form embankments around the lagoon area. As the dikes consolidated and displaced the wetland soils, miscellaneous fill consisting mainly of silty sand and gravel, was periodically imported and placed to maintain embankment heights. Existing embankments ranged from 5 to 7 ft in height, with crest widths of 15 to 22 ft and side slopes ranging from 1:1 to 1.5:1.

Dikes around Lagoon 1 have been relatively stable although they require periodic maintenance to compensate for settlement. Dikes surrounding Lagoon 2, however, require continual maintenance and have failed twice since construction. The two areas of embankment failure are shown on Figure 1. Both failures were similar in nature beginning with relatively rapid subsidence of portions of the embankment. As the dikes settled, imported fill was placed to try to maintain freeboard and prevent discharge of supernatant into the

adjacent surface waters. The dikes generally continued to settle rapidly, and mud waves formed on both inboard and outboard sides. The failure zones spread longitudinally along the dikes as repair filling proceeded. The failure zone at the north dike eventually extended approximately 300 ft; the failure zone at the south dike extended approximately 1,300 ft.

At the time the north dike failed, sludge and supernatant escaped into the drainage channel. After this failure, more fill was placed and the failure zone eventually stabilized. A similar failure occurred in 1973 in the south dike. The dike crest settled below lagoon level, but the associated mud waves rose high enough to prevent discharge of supernatant.

Presently, both sludge lagoons are essentially filled to capacity. In order to permit continued discharge of sludge to the lagoons, settled sludge is excavated from the lagoons and applied to farmlands. To maintain freeboard, supernatant is also returned to the plant. Disposal of the liquid sludge produced at the treatment works and of the sludge currently held in the lagoons was studied as part of a pollution control facilities plan for MMSD. This study proposed emptying the sludge from Lagoon 2 and the eastern half of Lagoon 1 over a period of 9 to 14 years. The western half of Lagoon 1 would be kept operable for seasonal sludge storage, but the remainder of the lagoons would be abandoned after the sludge was removed. Based on past performance, it was apparent that rehabilitation of the unstable dikes would be necessary to minimize risk of failure until the sludge was completely removed.

Several significant constraints were placed on the design of the rehabilitation of the dikes including the inability to empty the sludge, the inability to construct new dikes on the inboard side without increasing dike height, and the inability to expand the lagoons by building new dikes on the outboard side because of the proximity of Nine Springs Creek, the drainage channel, and the railroad. For these reasons, it was necessary to design the dike rehabilitation as closely as possible to the existing dike alignments. Based on a field exploration and laboratory testing program, Schneider and Roth (1977) evaluated the existing conditions and possible rehabilitation schemes. The rehabilitation methods selected by them use wood chips from trees infected with Dutch elm disease. The City of Madison, working with an independent contractor, was starting to reduce the logs of diseased elm trees to wood chips. The presence of this regularly available supply of wood chips made dike rehabilitation with the wood-chip fill economically attractive. Use of the light-weight wood chips reduced loads to a sufficiently low level so that excess settlement and ultimate general shear failure caused by placement of additional fill could be avoided. Non-woven synthetic filter fabric was used to provide restraint against spreading failures and to prevent intrusion of soil into the wood-chip fill.

In 1979, the Madison Metropolitan Sewerage District initiated an active program of applying the sludge to farmland as a fertilizer. However, this program, which was aimed at removing the sludge from the lagoons, was retarded by the discovery of PCB's in portions of the sludge and by regulatory restrictions on the allowable concentration of PCB's in the farmland fertilizers. Therefore, it is expected that the lagoons could be holding sludge for another 15 to 20 years, nearly doubling the initial design life of the rehabilitated dikes. Since another uncontrolled release of sludge and supernatant caused by continued subsidence of existing dikes and/or shear failure is not acceptable, an evaluation of the current status of stability of the dikes was undertaken nearly 10 years after their construction.

## SUBSURFACE CONDITIONS AND SOIL PROPERTIES

Twenty test borings were drilled at various locations around the lagoons by Schneider and Roth (1977) as shown in Figure 1. Based on results of those explorations, the general soil conditions at the sludge lagoons were determined to be as given in Figure 2. Three new boreholes and a number of cone penetrometer soundings were made initially as part of the current evaluation program. Another 8 boreholes were made later as part of the installation of instrumentation for the field monitoring program. The subsurface conditions revealed in these boreholes generally supported the subsurface conditions described in Figure 2.

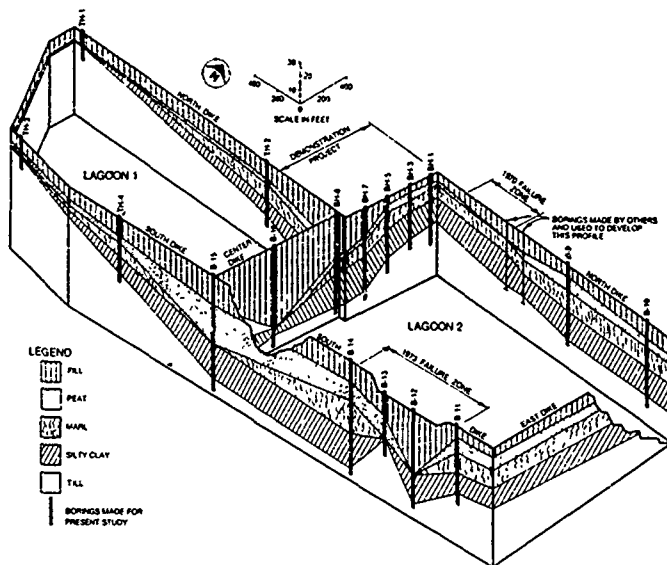


Figure 2. Subsurface Fence Diagram (from Schneider and Roth, 1976).

Some of the boreholes were made very close to the boreholes made in the investigation of Schneider and Roth. For instance, a new borehole located near boring B-14 (see Figure 1) in the 1973 failure zone revealed the presence of 7 ft of new fill of gravel/wood chips combination underlain by 14 ft of old fill material consisting of gray-brown sandy-silty material. The native material below the fill is a high organic content (89%) peat with water contents of up to 400%. The thickness of the peat was 11.5 ft in the recent boring compared to 13 ft in boring made by Schneider and Roth. Under the peat, an organic material with lower water contents (about 200 to 300%) and a lower organic content (28%) was encountered. This 22.5 ft thick layer corresponds, perhaps, to the 24 ft thick deposit referred to as "silt, brownish-gray with occasional shell fragments" in B-14 of Schneider and Roth. This layer was underlain with another peat deposit of lower organic content (44%) compared to the upper fibrous peat. This is referred to as "amorphous peat" herein. This deposit is about 5 ft thick. At a depth of 55 ft there is a gray silty clay of lower water content (about 68%). This latter material is classified as a "highly plastic silt" according to the Unified Soil Classification System. It has a low organic content of about 5%. The thickness of the peat in the underlying organic material is about 1.5 ft less than the values given in the boring of 1975, perhaps indicating the amount of compression of the layers within the last 10 years.

Laboratory tests were performed to characterize the wetland soils and to determine the shear strength and compressibility of the subsurface materials. The testing program included 11 consolidated-undrained triaxial compression tests with pore pressure measurements on undisturbed samples of the old fill, peats, and organic silt. Additionally, 4 consolidated-drained direct shear tests on samples of wood chips obtained from depth of 2.5 ft and 9 ft, respectively, were performed to provide a comparison of the strengths of the young and old wood chips. Laboratory consolidation tests were performed on samples from the major compressible soil units encountered, i.e., the peat, the organic soil called "marl", and the silty clay. These tests provided an updating of the extensive laboratory tests performed by Schneider and Roth (1977).

## Strength Properties of Wood Chips and Soils

The effective strength parameters of the various soil units were estimated based on the recent tests and compared with the values reported and used by Schneider and Roth.

### Wood Chips

The direct shear tests performed on wood chip samples retrieved from 2.5 and 9 ft depths, indicated friction angles of 53° to 57° as compared to 49° reported by Schneider and Roth. This may be a result of the difference in densities as specimens were reconstituted in the laboratory. The most recent specimens were denser than the Schneider and Roth specimens. The insitu density was determined from an undisturbed Shelby tube sample first, and the chips were reconstituted at this density for the strength test. Furthermore, the higher friction angles were determined using a drained direct shear test, whereas Schneider and Roth performed triaxial tests.

An interesting observation is the difference of 4° in the friction angles of the wood chips obtained from 2.5 ft and 9 ft. The deeper (older) wood chips exhibited the lower friction angles. Apparently, some degradation due to decomposition has taken place, but not to a great extent over 10 years. It is believed that there has not been a major change in the source of wood chips during this time. The older wood chips have smaller size than the younger wood chips.

### Old Fill

The low plasticity silty clay material found in the old fill of the north bank indicated an effective friction angle of about 29° which compared well with the values in the analysis by Schneider and Roth. There is an effective cohesion intercept of about 400 lb/ft<sup>2</sup>.

### Organic Soils

The tests of the top fibrous peat gave an effective friction angle of 53°, which is decidedly higher than 40.5° reported by Schneider and Roth. The stability of the dikes was checked with both 42° and 53° in the analyses. A cohesion intercept of 200 lb/ft<sup>2</sup> was also measured.

It was noticed that the 22.5 feet of soil under the fibrous peat revealed in the boring is a rather complex material with a range of organic contents. The first 17.5 feet of this material consists of "organic silt with shell fragments". The 2 samples fitting this description were tested giving 40° for the effective friction angle with a cohesion intercept of 400 lb/ft<sup>2</sup>. Schneider and Roth reported two tests of friction angles of 36° to 38° for this material. However, they chose to use 29° in their stability analyses.

The bottom 5 ft of this organic layer is an amorphous peat, which gave an effective friction angle of 5.5° and a cohesion intercept of about 830 lb/ft<sup>2</sup>. These values are considered somewhat unusual. However, they did not influence stability analyses since most of the critical failure surfaces were confined to the zone above this layer.

### Highly Plastic Silt

This is a deposit of very low organic content encountered in the recent borings as well as the borings of Schneider and Roth. There were no strength tests on samples from this layer. Most failure surfaces were confined to the weak peat deposits above this layer in the analyses.

### Compression Properties of Soils

The marl had an organic content of about 28% and exhibited a compression behavior very similar to that of the peat samples (organic content 23% to 89%). The silty clay had a markedly lower organic content (about 5%) and exhibited much less compressibility compared to the others as shown in Figure 3. This figure also implies that the soils encountered had been compressed under a stress of about 1,000 lb/ft<sup>2</sup> or less. The one-dimensional laboratory compression versus time curves were represented using an equation first proposed by Gibson and Lo (1961) and applied to peats and organic soils by Edil and Dhowian (1979). This equation has been found to be quite useful in representing the compression of peats from numerous sites and has the following form:

$$\epsilon(t) = \Delta\sigma \left\{ a + b \left[ 1 - e^{-\left(\frac{\lambda}{b}\right)t} \right] \right\} \quad (1)$$

where  $\epsilon(t)$  = vertical strain,

$\Delta\sigma$  = stress increment,

$t$  = time,

$a$  = primary compressibility,

$b$  = secondary compressibility,

$\lambda/b$  = rate factor for secondary compression.

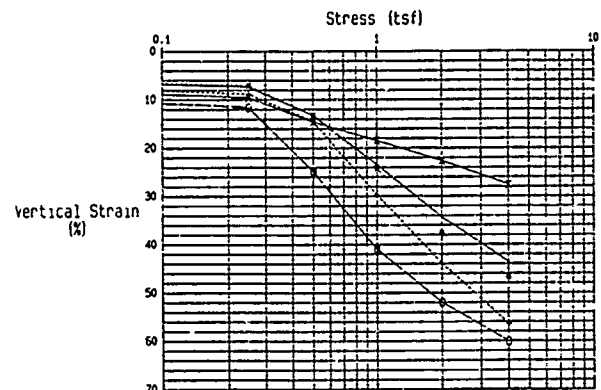


Figure 3. Compression Curves of Wetland Deposits

A convenient method of analysis of a given set of either laboratory or field vertical strain versus time data was described by Edil and Dhowian (1979). This method is used in determining the empirical compression parameters ( $a$ ,  $b$ , and  $\lambda/b$ ). The settlement is calculated by multiplying the vertical strain by the initial thickness of the soil (in the laboratory or in the field). The compression parameters depend on the type of peat and the stress level. Often there is a difference between the measured laboratory values and those seen to be governing the field compression.

The laboratory compression curves (vertical strain versus time) under different increments of stress have been evaluated using the compression equation given above to obtain the parameters resulting in the best possible fit of the equation to the measured data. Figures 4 and 5 provide a plot of parameters  $a$  and  $b$  as a function of the stress level used in the laboratory tests. These curves show trends noted before for similar soils from other sites (Edil and Mochtar, 1984). There is a decrease of compressibility with increasing stress. Figure 6 shows the rate factor for secondary compression ( $\lambda/b$ ) as a function of the average strain rate ( $\dot{\epsilon}$ ). Average strain rate is defined as the final measured strain divided by the lapsed time under a given increment of stress applied.

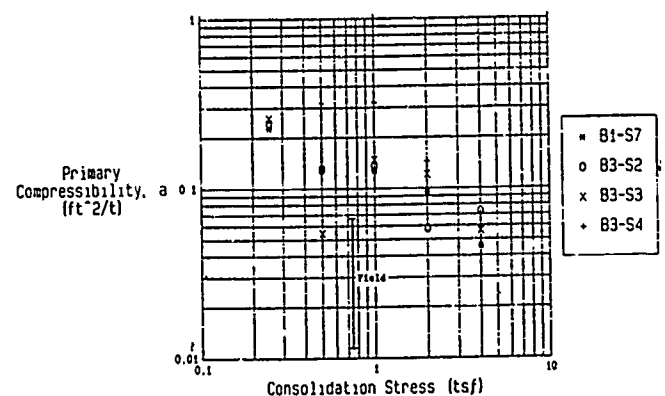


Figure 4. Primary Compressibility versus Consolidation Stress

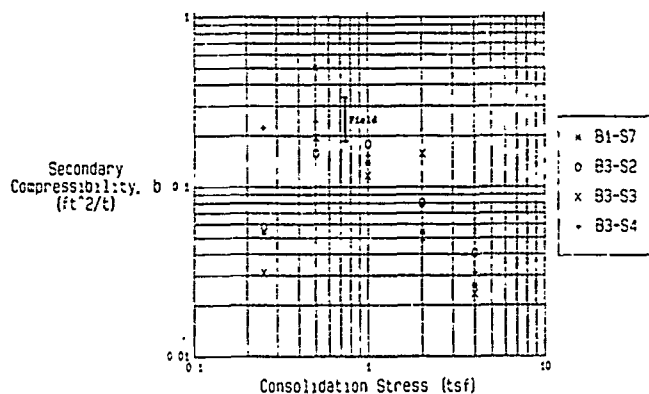


Figure 5. Secondary Compressibility versus Consolidation Stress

10 MOST CRITICAL OF SURFACES GENERATED  
MINIMUM FACTOR OF SAFETY = 1.19572

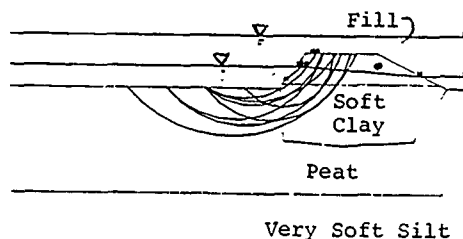


Figure 7. Stability Analysis Section and Critical Failure Surfaces

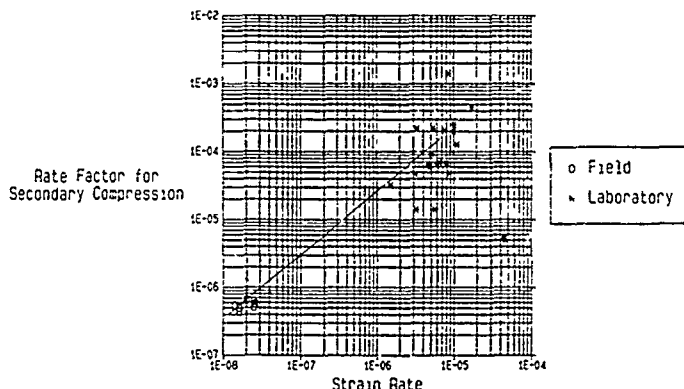


Figure 6. Rate Factor for Secondary Compression versus Strain Rate

## STABILITY ANALYSES

A series of stability analyses for a cross section (see Figure 7) through the south dike of Lagoon 2 near the west end of the 1973 failure zone was performed. This section was considered to be a critical section based on the thicknesses of the soft soil deposits and the geometry of the embankment. Furthermore, the most detailed account of soil properties and the stratigraphy was available at this location. Initially, it was assumed that all of the excess pore pressure in the peat underlying the fill had completely dissipated. In effect, the pore pressures in the underlying soils were set equal to the hydrostatic pressures produced by the lagoon and canal water elevations. Other analyses were made in which the pore pressures in the peat were higher than the hydrostatic pressure. There were also analyses performed in which the soil properties were varied within the perceived range of uncertainty. All of the analyses used an effective stress approach and were performed using the STABL computer program (Siegel, 1975) which is based on the limiting equilibrium method of slices for circular and non-circular failure surfaces. A summary of safety factors as a function of amount of excess pore water pressure assumed in the peat layer (0, 100, and 200  $\text{lb/ft}^2$ ) is given in Figure 8 for different assumptions about the soil properties and the choice of analysis. These analyses indicated the following (Edil and Bosscher, 1985):

- 1 Under the hydrostatic pore pressure regime, the cross section was quite stable.
- 2 The slope on the lagoon side was found to be more unstable than the slope on the canal side.
- 3 The presence of excess pore pressures in the underlying peat layer is very significant relative to stability.
- 4 All of the critical failure surfaces were confined basically to the upper peat layer.

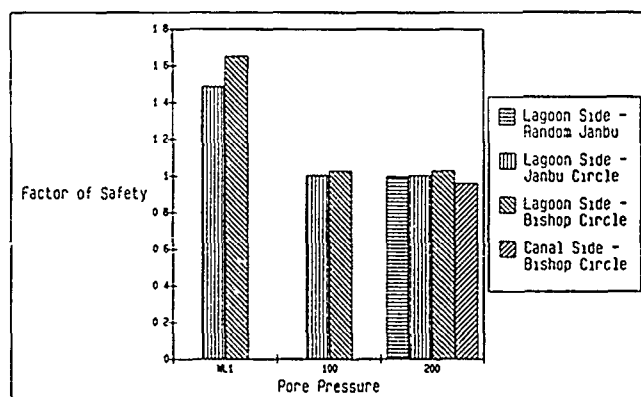


Figure 8. Safety Factors for Different Pore Pressures  
[WL1=Hydrostatic Pressure; 100,200=Excess Pore Pressure ( $\text{lb/ft}^2$ )]

It is clear from this analysis that the presence of residual excess pore pressures induced by the weight of the fill (dike material) and additional pore pressures due to upward ground water discharge can reduce the stability of the dike slope to near critical levels. Since the lagoons lie within a groundwater discharge zone (as indicated in the previous studies), upward seepage should be investigated relative to stability.

Since it is clear that the dike stability is dependent on the magnitude of the excess pore water pressure in the underlying soils, it became imperative to make an assessment of the amount of excess pressure. For this purpose, a piezometer and a well were installed near boring B-14. The porous tip of piezometer was at a depth of 25 ft below the top of the dike and sealed in the underlying peat deposit. A cased open well was placed in the middle of the dike crest at the same location and extended 15 ft into the fill material. The water levels observed in the piezometer indicated that the peat deposit is not experiencing higher pore pressures than would be expected. It is, however, higher than the level indicated in the open well in the dike material. This may be due to the lag in water level response to the changes in the water levels of both the lagoon and the nearby stream channel. Using this new information, additional stability analyses were performed. These analyses indicated better than marginal stability of the dike under present conditions of strength and pore water pressure. However, because of the limited hydrologic record, further periodic observations of the pore water pressures was needed to ensure the maintenance of this stability.

## SETTLEMENT ANALYSES

During construction, settlement plates were installed under the reconstructed dikes, six settlement plates were placed under the southeastern half of Lagoon 2 dikes in 1977, another 3 settlement plates were installed later along the southwestern half of Lagoon 2 dikes and settlement plates along the northeastern portion in 1979. Some of the settlement plates were damaged due to traffic on the dikes and the data related to them was discarded. However, there were about 7 settlement plates giving useful data. These 7 sets of settlement data were analyzed by assuming a stress increase of 420 lb/ft<sup>2</sup> (corresponding to a 7 ft high wood-chip embankment above water) and estimating the compressible layer thickness from the borings. The field settlement data collected by the MMSD personnel over the years since the rehabilitation of the dikes was evaluated using the same compression equation given above (equation 1). A range of values for parameters a and b as obtained from the field settlement data are also marked on Figures 4 and 5 at a stress level of 0.75 ton/ft<sup>2</sup> (estimated to be the average stress level in the field). The field values of  $\lambda/b$  are plotted at the field average strains on Figure 6. The grouping of the field and laboratory  $\lambda/b$  values and difference between them is noted. This conforms with the observations made at other sites (Edil and Mochtar, 1984).

An interpretation of the laboratory and the field measured compression values provides some insight into the settlement behavior of the dikes in the future. Table 1 gives the average values and the ranges of the three compression parameters as obtained from the field and the laboratory data. The estimated average values from the empirical curves reported by Edil and Mochtar (1984) based on numerous case records are also listed. It should be noted here that there are some uncertainties in the field analysis of the data stemming from the assumed equal stress increase of 420 lb/ft<sup>2</sup> at each settlement plate and the assumed compressible layer thicknesses. Furthermore, all compressible layers are combined in the back analysis of the field settlement data. The field settlement records, themselves, could be suspect as damage to the settlement plates is likely due to the traffic on the dikes. Nevertheless, some trends do emerge from an examination of all sources of information available.

Table 1. Compression Parameters

| Parameter              | Field Measured<br>Average | Field Measured<br>Range    | Lab Measured<br>Average                                    | Lab Measured<br>Range      | From Empirical Curves<br>(Edil and Mochtar, 1984) |
|------------------------|---------------------------|----------------------------|--|----------------------------|---|
| a (rc <sup>2</sup> /t) | 0.0263                    | 0.0113-0.0473              | $\frac{\Delta t}{\Delta e} = 0.5 \frac{t}{rc^2}$<br>0.1583 | 0.1256-0.3158              | 0.2735  |
|                        |                           |                            | $\frac{\Delta t}{\Delta e} = 1.0 \frac{t}{rc^2}$<br>0.1828 | 0.1271-0.3209              | 0.0940  |
| b (rc <sup>2</sup> /t) | 0.2492                    | 0.1911-0.3259              | $\frac{\Delta t}{\Delta e} = 0.5 \frac{t}{rc^2}$<br>0.2739 | 0.1577-0.5008              | 0.0874<br>(0.2466)*                               |
|                        |                           |                            | $\frac{\Delta t}{\Delta e} = 1.0 \frac{t}{rc^2}$<br>0.1471 | 0.1164-0.1794              | 0.0536<br>(0.4824)*                               |
| $\lambda/b$ (1/day)    | $7.9 \times 10^{-8}$      | $(6.4-9.3) \times 10^{-8}$ | $1.8 \times 10^{-7}$                                       | $(1.4-6.5) \times 10^{-7}$ | $5.5 \times 10^{-8}$                              |

\* Corrected to the field as recommended by Edil and Mochtar (1984).

The laboratory measured values of parameter a are higher than the field values. The empirical values provide a range comparable to the laboratory and field values of a, depending on the stress level. The higher laboratory values of a will make the prediction of field settlements larger than given by the settlement plates. However, the rate of settlement after a number of years would not be affected as much by the value of parameter a as by the values of b and  $\lambda/b$ . The values of parameter b are quite consistent between the field and the laboratory. The empirical values corrected to the field as suggested by Edil and Mochtar (1984) also compare well with the Nine Springs values. It is noted here that the type of laboratory/field corrections suggested by Edil and Mochtar is not required for the Nine Springs data. The values of  $\lambda/b$  in the field are much lower than obtained in the laboratory. This is a well-established trend. The value given by the empirical curves for the average field strain is very comparable to the average value of  $\lambda/b$  obtained directly from the field data.

The presence of uncertainties and unresolved inconsistencies, i.e., discrepancy between the field and laboratory a values, and the lack of the expected discrepancy between the field and the laboratory b values, precludes highly conclusive predictions of future settlements. However, an attempt can be made in establishing some bracketing values.

If we assume that the settlement plate data are a reliable indicator of the actual settlement trends, we can use the lowest and highest combinations of the compression parameters obtained from the field data and estimate upper and lower bounds of future settlements. Table 2 presents such a prediction using the compression equation. The compressible layer thicknesses used were 34 and 23 ft for the upper and lower bounds estimates, respectively. The settlement data as given by the settlement plate SP2 is also included in Table 2. This settlement plate gave the largest settlement of all the plates considered to be undamaged. At the site of this plate, which is near boring B-14, the compressible layers are perhaps the thickest, measuring about 34 ft. The upper bound estimates compare well with the SP2 record. Extrapolation of the settlement plate data to the present (3,010 days) and to the year 2,000 (8,054 days) indicates that less than 2 inches of additional settlement is to be expected.

Table 2. Settlement Prediction

| Date       | Time<br>(days) | Settlement<br>Upper Bound |                | Estimate<br>Lower Bound |                | Settlement at SP2 |                |
|------------|----------------|---------------------------|----------------|-------------------------|----------------|-------------------|----------------|
|            |                | Magnitude<br>(ft)         | Change<br>(in) | Magnitude<br>(ft)       | Change<br>(in) | Magnitude<br>(ft) | Change<br>(in) |
| 12/12/1977 | 0              |                           |                |                         |                |                   |                |
| 4/12/1978  | 121            | 0.73                      |                | 0.11                    |                | 0.55              |                |
| 11/16/1979 | 704            | 1.60                      | 10.4           | 0.34                    | 2.8            | 1.46              | 10.6           |
| 6/18/1980  | 919            | 1.82                      | 2.6            | 0.40                    | 0.7            | 1.70              | 2.9            |
| 6/1/1983   | 1997           | 2.44                      | 7.4            | 0.62                    | 2.6            | 2.46              | 9.1            |
| 3/10/1986  | 3010           | 2.67                      | 2.8            | 0.73                    | 1.3            | 2.82              | 4.3            |
| 1/1/2000   | 8054           | 2.81                      | 1.0            | 0.85                    | 1.4            |                   |                |

If estimates for settlement are based on the largest values of parameters a, and b, considering both the field and the laboratory data, 4 inches of settlement between now and the year 2,000 can be expected. These estimates, while not very firm, are quite encouraging with respect to future settlement performance of the dikes. Either of these estimates results in a minor loss of freeboard and is quite tolerable.

## DIKE INSTRUMENTATION

### Justification

Based on this evaluation of the rehabilitated dikes nearly 10 years after their construction (Edil and Bosscher, 1986), the following observations could be made:

1. The stability analyses indicate better than marginal stability of the dikes under present conditions of strength and pore water pressure. However, because of the limited nature of the hydrologic record collected, further periodic observations of the pore water pressures are needed to ensure the maintenance of the stability.
2. Wood chips placed in the dikes 10 years ago seem to exhibit strength properties close to those recently placed indicating relatively low amounts of degradation. Based on a careful survey of the literature, common estimates of useful life of wood chips are found to extend to at least 15 years (Nelson and Allen, 1974; Jackson, 1979). No published studies of chip durability have extended these estimates beyond 15 years even though it is expected that wood chips could provide acceptable performance for longer periods.
3. Settlement estimates indicate a minor loss of freeboard can be expected between the present and year 2000. These estimates, while not very firm, are quite encouraging with respect to future settlement performance of the dikes.

Based on these observations, the Madison Metropolitan Sewerage District was advised as follows:

1. No evidence has been found to warrant additional major construction to improve dike stability. This recommendation is based, however, on an adoption of a continual monitoring program relative to dike settlement and stability.
2. The monitoring program should consist of multilayer settlement and piezometric measurements. In addition, any regrading or other significant construction activity should be noted and evaluated for the potential effect on dike stability.
3. The levels of supernatant in the lagoon and the water level in the stream channels should be recorded periodically. The levels of these fluids are important relative to the stability of the dikes. Safe levels for these fluids may be established, with any variation outside of these levels to be allowed only after an evaluation of the effect on dike stability.

Following these recommendations, Madison Metropolitan Sewerage District authorized installation of an instrumentation system during the Fall of 1986. The instrumentation system was designed to monitor the following elements of the lagoon dikes:

1. The settlement under the weight of dike fill materials of various compressible layers in the dike foundation.
2. The lateral movements within relatively soft and weak soil layers.
3. The excess pore water pressures in the substrata created by dike fill.
4. The phreatic water levels within the dike due to the levels of supernatant in the lagoon and water in channels outside the dikes.

#### Field Instrumentation

The Sondex settlement system and the slope indicator system by Slope Indicator Company were chosen to monitor settlement and lateral movements at various depths in the substrata below the dike fill materials. The settlement system consists of 3 inch I.D. flexible corrugated plastic pipe with metal rings attached at 5 ft intervals. An electrical probe is used to determine the vertical location of the metal rings within  $\pm 0.01$  feet. A 2.75 inch O.D. grooved plastic casing, used for the inclinometer system, was typically installed inside the Sondex plastic pipe. The inclinometer, when lowered into the casing and oriented with the casing grooves, provides a rapid means of assessing the deviations of the casing from vertical as a function of depth. These readings may then be compared with readings taken at an earlier time to determine the amount of lateral movement as a function of depth and time.

Geonor M206 piezometers were used to monitor total pore pressures (hydrostatic plus excess) for this project. The piezometer point consists of a hollow stem approximately 1-ft long with 3 bronze filters mounted on the stem. Plastic tubing (1/4 in.-I.D.) is attached to the porous point and threaded first through a 5 ft length of E-rod and then through a 1 inch diameter steel water pipe. After the piezometer is pushed or driven into the ground, the water level in the plastic tubing is measured with a small diameter water level indicator especially designed for this purpose. Phreatic water levels in the lagoon dikes were measured using conventional groundwater monitoring wells consisting of 2-in diameter, Schedule 40 PVC slotted well screen and riser pipe. The 10 ft screens were enclosed by No. 30 flint sand to be used as filter material around the screen and as backfill. A seal of dry granular bentonite was placed over the sand to prevent surface water infiltration. Water levels are measured with a conventional electronic water level indicator.

Eight locations along the dikes were chosen for the placement of instrumentation clusters (Weber, 1987). These positions are located at sites circling Lagoon 2 and at other points near Lagoon 1. Criteria used in determining the instrument locations included:

1. areas of observed prior dike failures,
2. areas of known deep wetland soils based on early investigations,
3. areas of unknown subsurface conditions or gaps in the soil profile, and
4. budget constraints.

At 7 of the 8 cluster locations, the Sondex and inclinometers were installed in the same borehole. At each cluster location settlement instrumentation, a lateral movement instrumentation, multiple piezometers, and a well were installed. In all, 8 Sondex and inclinometer systems, 6 monitoring wells, and 10 piezometers were installed. Instrument depths were established by review of an initial boring at each cluster location which was sampled at 2.5-ft intervals in the upper 10 ft, and at 5-ft intervals thereafter with a split-spoon sampler using standard penetration test (SPT) procedures and extended on the order of 5 to 10 ft into sand soil below the compressible wetland deposits. Additional boreholes within a cluster were drilled to permit instrument installation without additional sampling. The drilling methods included 4-in diameter continuous flight augering and rotary wash boring.

Since the completion of the installation of the instrumentation system by the end of 1986, a program for periodic measurement of the instruments was initiated. A computer program for the database management, reduction and presentation of the data was developed.

#### FIELD MONITORING DATA

The data obtained from the field consists of:

1. water levels in the open wells and the piezometers,
2. depths of the Sondex rings, and
3. inclinometer readings.

The data has been collected since late February, 1987 upon completion of the instrument installation. The water level data has been used to support the assumptions made in the dike stability analysis. The results as obtained from the monitoring instrumentation near boring B-14 are presented in Figure 9. The measured piezometric levels are similar to the values assumed during the analysis phase. It can also be noted that the previous assumptions of the region being a groundwater discharge zone is substantiated (see piezometric levels in Piezometers 2 and 3 compared to the surface well). The dramatic dip in the piezometric levels around early August in Piezometers 2 and 3 is due to pumping of these piezometers to determine the response of the system. It should also be noted that the surface well water elevation lies between the creek elevation and the sludge elevation, the two boundary elevations.

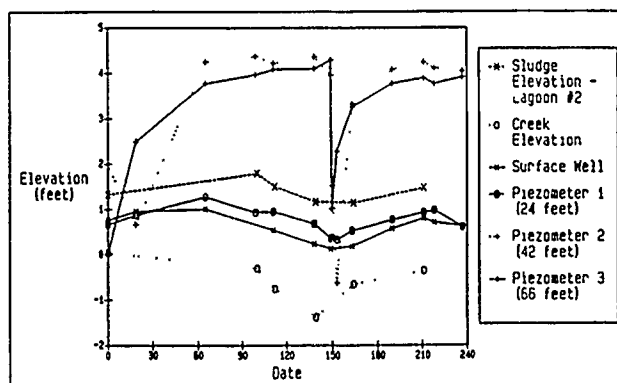


Figure 9. Ground Water Level and Pore Pressure Measurements

The settlement data has been reduced and plotted in Figure 10. This figure indicates the small amount of settlement which can be measured using the Sondex system. The data is presented with the amount of settlement assumed to be zero at the time of installation. Even with only 240 days of settlement, the results show that the settlement is zero in the mineral soils at +68 feet, and the settlement occurring mainly in the soils in the 40-68 ft depths. Additional settlement can be seen in the 15-20 ft depth. The Sondex pipe was riveted to the inclinometer pipe at

the ground surface which is thought to account for the reduction in measured settlement at the ground surface. Based upon the measured rate of 0.07 feet occurring in 240 days, the additional total settlement expected between now and the year 2000 is under 1.5 inches assuming a logarithmic decline in the settlement rate. This value compares well with the previous prediction of less than 2.0 inches.

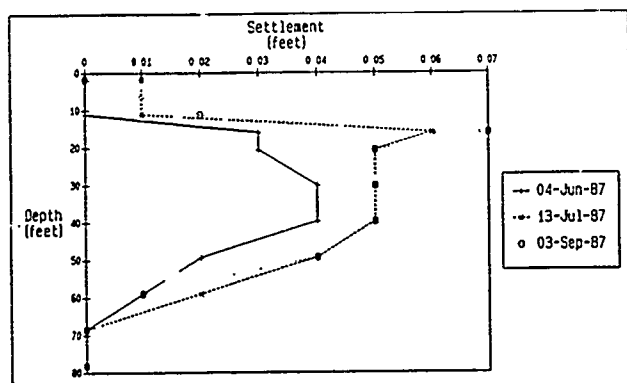


Figure 10. Settlement Measurements

The inclinometer data indicated negligible movements in the tubes since installation. This supports the stability analyses which indicated that the dikes should be stable in their present configuration.

Further monitoring of this site is continuing on an ongoing basis. The level of effort in data acquisition will likely taper off as the data is analyzed and annual trends in data are noted and shown to support the previous conclusions.

## CONCLUSIONS

Sludge lagoon dikes rehabilitated using wood chips and founded on highly compressible and weak wetland deposits have provided satisfactory performance over the past 10 years in a difficult environment for the use of conventional stabilization techniques. The present evaluation of stability and settlement based both in analysis and field data collected to date indicates that the dikes are likely to continue to provide satisfactory service for another 15 to 20 years. Due to rather marginal stability of the dikes and the environmental risks associated with a dike failure, a field monitoring program has been initiated. This program has provided an initial verification of certain assumptions used in the analyses. The instrumentation is expected to serve as a continuing control and warning system during the service life of the dikes.

## ACKNOWLEDGEMENTS

The authors wish to express their appreciation to the Madison Metropolitan Sewerage District and Mr. James L. Nemke, Director, for their support of this work. CH2M Hill Engineers designed the dike rehabilitation and Warzyn Engineering, Inc. installed the field monitoring instrumentation. Messrs. N. Paschke and G. Sachs made the field measurements. Mr. N. H. Severson's help in the field and the laboratory is gratefully acknowledged.

## REFERENCES

- Edil, T.B. and P.J. Bosscher, (1985), "Geotechnical Investigation of Nine Springs Sludge Lagoon Dikes," An Interim Report to the Madison Metropolitan Sewerage District, Madison, Wisconsin.
- Edil, T.B. and P.J. Bosscher, (1986), "Geotechnical Investigation of Nine Springs Sludge Lagoon Dikes," The Final Report to the Madison Metropolitan Sewerage District, Madison, Wisconsin.
- Edil, T.B. and A.W. Dhowian, (1979), "Analysis of Long-Term Compression of Peats," Geotechnical Engineering, Southeast Asian Society of Soil Engineering, Vol. 10, No. 2, p.159-178.
- Edil, T.B. and N.E. Mochtar, (1984), "Prediction of Peat Settlement," Proc., Sedimentation/Consolidation Models, American Society of Civil Engineers, p.411-424.
- Gibson, R.E. and K.Y. Lo, (1961), "A Theory of Soils Exhibiting Secondary Compression," Acta Polytechnica Scandinavica, CI 10296, p.1-15.
- Jackson, N.C., (1979), "A Summary of the Use of Sawdust for Highway Fills," Materials Office Report No. 157, Washington State Department of Transportation.
- Nelson, D.S. and W.L. Allen, Jr., (1974), "Sawdust as Lightweight Fill Material," Report No. FHWA-RD-74-502, Federal Highway Administration, Offices of Research and Development, Washington, D.C.
- Schneider, J.R. and L.H. Roth, (1976), "Geotechnical Investigation Sludge Lagoon Dike Rehabilitation, Phase II," CH2M Hill Report L-9617.7 to Madison Metropolitan Sewerage District, Madison, Wisconsin.
- Schneider, J.R. and L.H. Roth, (1977), "Dike Rehabilitation Using Wood Chips," Proc. Conference on Geotechnical Practice for Disposal of Solid Waste Materials, American Society of Civil Engineers, Ann Arbor, Michigan, p.661-679.
- Siegel, R.A., (1975), "STABL User Manual," Joint Highway Research Project JHRP-75-9, Purdue University and Indiana State Highway Commission, West Lafayette, Indiana.
- Weber, R.H., (1987), "Sludge Lagoon Dike Instrumentation," Warzyn Engineering Inc. Report C12764 to Madison Metropolitan Sewerage District, Madison, Wisconsin.



## A Study of Contamination Migration at a Hazardous Waste Facility in Louisiana

George H. Cramer, II

Administrator, Ground Water Protection Division, Department of  
Environmental Quality, Baton Rouge, Louisiana

**SYNOPSIS:** Traditionally clay soils have been regarded as being relatively impermeable to the migration of water and contaminants. Recent studies in Louisiana are beginning to show, however, that laboratory permeability tests are not true indicators of the ability of an in-situ soil to retain or transmit fluids. Both the depositional and post-depositional environment of a soil can greatly alter its in-situ permeability. In particular, post-depositional structural fractures provide preferential pathways for contaminant migration at rates that far exceed those predicted by using laboratory permeability values.

Difficulties in field identification of these pathways reduces modeling of their effect on site hydrology to very basic terms. Since their distribution is not yet predictable, the net increase in permeability caused by their presence at a site can not be factored into any hydrologic models, except as gross estimates.

### INTRODUCTION

For many years clay has been regarded as an impermeable barrier to the migration of all fluids. Landfills and impoundments constructed in clay were regarded as the safest place to dispose of hazardous and solid wastes. Recent studies are showing that the clays themselves are not immune to attack by chemicals. In addition, in Louisiana, contaminate studies at quite a few facilities are showing that laboratory permeability tests are not giving an accurate indication of the ability of a particular soil layer to retain or transmit fluids. Factors introduced by both the depositional and the post-depositional environments have a significant influence on the in-situ permeability of at least the Pleistocene, and perhaps older, soils. In particular, post-depositional structural features provide pathways for the migration of fluids, most importantly organic compounds. These pathways are not being found or predicted by laboratory testing. Thus, false assumptions have been used in determining the siting of disposal facilities and in the design of these facilities due to overly-optimistic values of permeability obtained for local soils.

The site that first confirmed this situation in Louisiana is located in Calcasieu Parish (county). Originally the site of an oil and gas well with ancillary impoundments, it was later expanded to accept wastes from other oil fields and from the petrochemical industry in nearby Lake Charles. Liquid wastes were accepted into several large surface impoundments which were constructed by excavating a trench around the desired area and using the spoil material to build a levee. In early 1977, the site received a permit to convert the oil and gas well to a Class I (hazardous waste) injection well. Thereafter, new receiving basins were constructed which were lined with five feet of recomacted clay. The old impoundments were closed out by pumping the liquids down the injection well, solidifying the sludges with cement fly ash, and capping with recomacted clay. Most of the sludges were left in-place; however, sludges from three impoundments were placed in several of the landfill cells that were constructed at the site.

### GEOLOGY

The site is located on unconsolidated deposits of Pleistocene Age known as the Prairie Formation or Prairie Terrace. The formation consists of clay interbedded with clayey silt and sandy clay. Underlying the terrace deposits, so named because of the terrace effect caused by erosion, at a depth of 50 to 70 feet, is the Montgomery Formation, also of Pleistocene Age. This formation is the uppermost member of the regional Chicot Aquifer System and contains a thick sequence of sands at the top, known as the "200 Foot Sand" - named after the depth of this unit at the pumping center in Lake Charles (Jones, 1954). Beneath the Montgomery Formation are the Bentley and Williana Formations, also of Pleistocene Age, which contain the "500 Foot Sand" and the "700 Foot Sand" respectively, and compose the remaining units of the Chicot Aquifer. The sands grade from fine sand at the top to coarse sand and gravel at the base. They are separated by leaky confining units of clays and silt. The Chicot Aquifer had been declining for many years, however, after the completion of the Sabine River Diversion Canal in 1981, industrial pumping declined and the water levels in the aquifer began to rise.

The eastern edge of the site dips down into the flood plain of the Little River, a tributary of the Calcasieu River. Here deposits of Recent Alluvium overlie the Pleistocene formations. Periodic flooding from Little River inundates this area, and in time past, has overtopped the impoundment levees.

The site hydrogeologic conditions have been extensively studied. Since 1977 over 257 borings, totaling over 17,480 linear feet, have been drilled on or adjacent to the facility. Fifty-three monitoring wells and thirty-two piezometers have been installed to monitor the ground water. In addition, four large diameter (36 inch) wells and five 4 inch wells are recovering contaminated ground water at a rate of over 7,000 gallons per day. More hydrogeologic work is currently being done at the site.

The earliest engineering studies (DEQ, unpublished data) state that the permeabilities of the soils at the site range from  $1 \times 10^{-9}$  cm/sec in the clays to  $1 \times 10^{-5}$  cm/sec in the silts and clayey sands. The site was generally characterized as having four "zones" or layers, except at the eastern edge where the depositional patterns of the Little River imposed a different regime. The upper 50 feet of soil is composed of stiff to very stiff clays and silty clays. This stratum of thin layers of overlapping and interfingering soils is typical of surficial Pleistocene deposits in southern Louisiana. Beginning at 40-50 feet below ground surface is a layer of silt and clayey sand, varying between five and eight feet thick, labeled the "50-foot pervious zone". This is the first water bearing stratum at the site, although the overlying clays approach saturation.

Beneath the "50-foot pervious zone" is another clay layer varying from 0-10 feet in thickness. This immediately overlies the 200 foot sand of the Chicot Aquifer. Throughout the years of study, the extent of interconnection between the "50-foot pervious zone" and the 200 foot sand has been disputed. A recent study of water levels and stratigraphy at the site (Hebert, unpublished) concluded that the area of interconnection extends over the eastern half of the site. Earlier studies have confined this area to the southeastern portion of the site. This difference plays a significant role in determining effective corrective measures for ground water contamination at the site.

#### SITE CONTAMINATION

The first systematic investigation of contamination at the site began in early 1983. The extension of landfill cell 7 at the site (figure 1) was infiltrated by volatile organics contaminants shortly after being excavated. The subsequent investigation determined that the excavation had come close to the downward pathway of migration for these contaminants, allowing them to seep into the cell. The contamination at the site is composed of a variety of volatile organics, notably dichloroethane, dichloroethylene, trichloroethane, trichloroethylene, methylene chloride and vinyl chloride, in the part per million range.

The investigation concluded that waste migrated from the old impoundments while they were active by a variety of mechanisms. From observations in the side wall of the cell, it was readily apparent that the waste was migrating through a series of structural cracks in the clay, called "Slickensides". This preference was so strong that the waste would migrate through rather than into silt lenses and thin layers within the clay. Contaminates were found down to the top of the "50-foot pervious zone" but did not penetrate the zone as a distinct phase. Dissolved constituents were found in the water of that zone, apparently coming from the floating contaminants. The extent of the dissolved phase was eventually determined to cover most of the center of the site, and to extend slightly off-site in the downgradient direction.

By calculating the length of time that the contaminants were available for transport versus the actual distance of migration, a relative permeability of about  $1 \times 10^{-5}$  cm/sec can be derived. This is opposed to the measured laboratory permeabilities in the  $1 \times 10^{-7}$  and  $1 \times 10^{-8}$  cm/sec range. This increase in the vertical permeability of two to three orders of magnitude was observed at this site to be due to migration through the slickensides. Slickensides are fractures in the cohesive soils of the Gulf Coast region which were produced by the elastic rebounding of soils when stress was removed. During Pleistocene time a large volume of sediment was deposited in the Gulf Coast area. The weight of the overlying sediments introduced a large amount of stress on the buried soil layers. When this overburden was removed by subsequent erosion, the pressure acting on the soil was released causing a rebounding effect within the soils. This produced a pressure relief fracture called a slickenside. The slickensides are not extensive in length, but they form a prevalent pattern in all of the Pleistocene soils. This network of fractures allows fluids to migrate much more rapidly than if they had had to pass totally through the actual clay fabric.

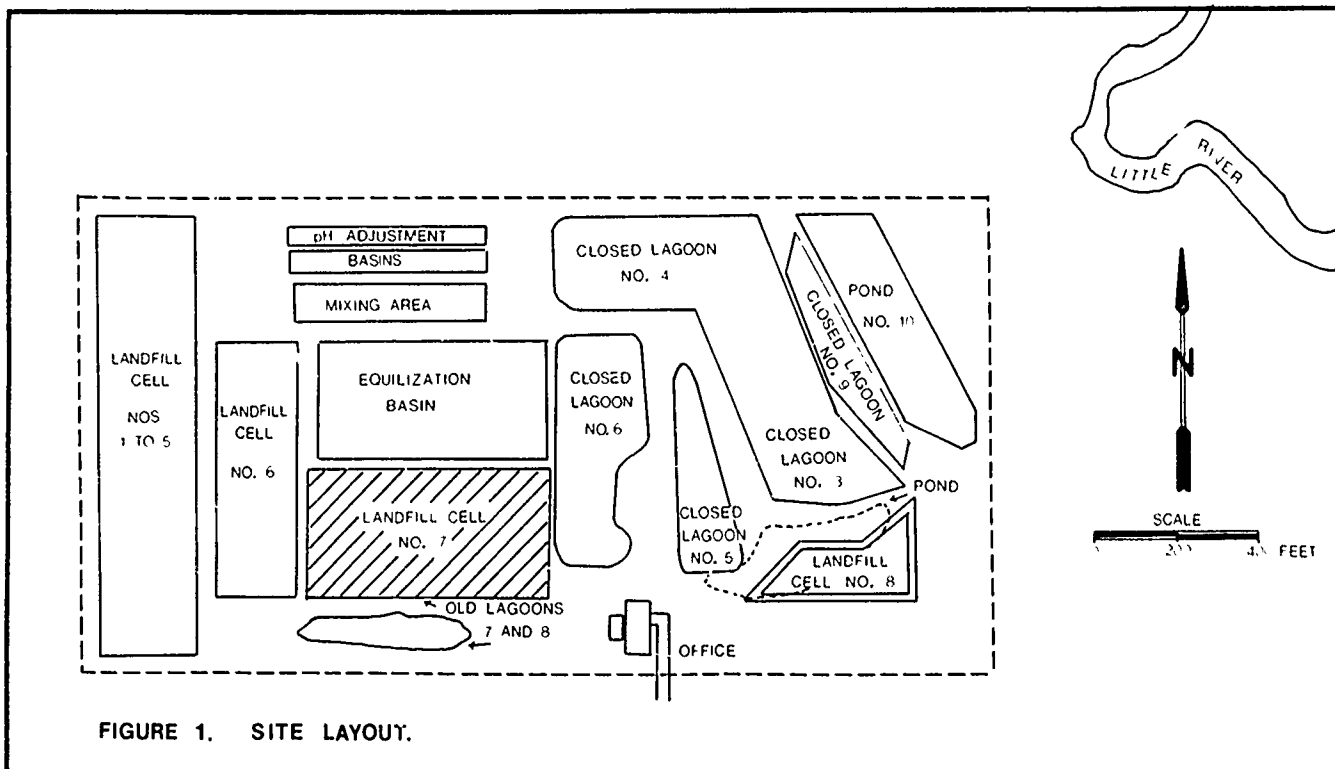


FIGURE 1. SITE LAYOUT.

Other pathways also exist at the site, although they were not directly observed to have influenced the migration of contamination. The site was originally covered with pine timber. When the lagoons were first excavated, the timber was not cut. As the trees decayed a path for migration down the decaying tap root of the tree was introduced. These tap roots can extend 20 to 35 feet deep in some places.

Animal burrows can likewise provide pathways for migration of contaminants. In southern Louisiana, crawfish burrows are common in open ground. Crawfish burrows have been measured as deep as twenty feet in some areas, since they burrow down to reach the water table. These burrows even when subsequently abandoned and collapsed, leave a disturbed area behind which is more permeable than the surrounding soil.

#### OTHER STUDIES

These potential pathways for contaminant migration are not being adequately identified during sampling, nor are they being accounted for in the testing of soils for geotechnical purposes. An extensive study of sample handling was conducted by Louisiana State University (Arman, 1977). They intensively studied disturbances to soil samples caused by the normal sampling procedures used in Louisiana and many of the southern states. The most common method is to use a rotary drill for advancing the boring, and a thin-walled Shelby Tube for taking the sample. The soil sample is brought to the surface and mechanically extruded with a hydraulic ram. The sample is then scraped of excess mud, classified, and approximately 18 inches is kept as a representative sample, while the rest is discarded.

All of the steps described above introduce disturbances in the sample. The report draws the following conclusions regarding the effect of these disturbances on permeability:

"Permeability is affected by changes in density and void ratios caused by structural disturbance. Estimates concerning settlement rates deviate drastically from the performance in the field if tests are conducted on samples with excessive disturbance.

"Soils composed primarily of platy or flakey grains develop anisotropy with respect to permeability depending on the grain orientation. Minor disturbances can rearrange these grains to change permeability by several orders of magnitude while making only fractional change in other engineering properties."

Even minor disturbances in clay samples can significantly alter the measured permeability of a sample without changing the other properties and thus alerting the geologist or engineer that the sample is not giving an accurate reading.

Slickensides and thin silt or sand interbeds are features that are often not representatively sampled. If the slickenside or interbed extends through the core, the sample, upon extrusion, will often break along that line. Rather than attempting to include the feature in the retained sample, so that its effect can be measured, the break is most often used as the place to trim the sample and so the effect of this feature on the permeability is not measured.

Slickensides and interbeds that do not extend through the core are often masked by the sample handling technique. The scraping of the drilling fluids from the core will smear the sides of the sample to some extent. This will seal small silt or sand interbeds, and to some extent the slickensides as well.

#### CONCLUSIONS

The only recognition of the potential pathways described above is usually a minor note in the driller's log of a boring. No systematic studies of the distribution of slickensides have been done. Silt lenses and animal burrows are impossible to statistically described for a given location. Since these features cannot be described statistically, they cannot be factored into a model except in general terms. Field permeability tests will give the closest approximation to the actual in-situ permeability of a site. Even these tests may under-rate the permeability of the soils at a site due to the placement of the boring for the test.

At the current time the only accurate way to calculate the effect of these pathways on soils at a site is to measure the extent of contamination and determine the net permeability of the soil. This factor can then be introduced into any flow models used to evaluate corrective measures for clean-up of a site.

#### REFERENCES

- Arman, A. and McManis, K. L. (1977), "The Effects of Conventional Soil Sampling Methods of the Engineering Properties of Cohesive Soils in Louisiana", Engineering Research Bulletin No. 117, Baton Rouge, Louisiana
- Harder, A. H. (1960), "The Geology and Ground-Water Resources of Calcasieu Parish Louisiana", Geological Survey Water-Supply Paper 1488, Washington, D.C.
- Hebert, J. H. (1987), DEQ unpublished study
- Jones, P. H., et al (1954), "Geology and ground-water resources of southwestern Louisiana", Louisiana Department of Conservation, Geological Survey Bulletin 30

# Control of Uplift from Ground Water

R.V. Sarsby

Reader in Civil Engineering, Bolton Institute of Higher Education,  
Bolton, England

**SYNOPSIS:** This paper relates to the conversion of a disused water reservoir into a landfill site for domestic and industrial refuse. The reservoir was initially subdivided into four cells (by using earth bunds) and three of the cells have been successfully prepared and filled. The fourth cell is the largest and presents the greatest number of geotechnical problems, the major one being the problem of ensuring that leachate does not escape into the groundwater.

The first owner of the site removed natural clay from various parts of the reservoir base to seal the first three cells. In doing so he exposed water-bearing sandstones, mudstones and badly-shattered shales and ground water is now issuing freely from these strata. Standpipes in the base of the completed cells indicate a significant artesian pressure in the groundwater and sealing of the exposed rocks in cell 4 represents a major problem. In an attempt to form a low permeability seal with compacted clay temporary pressure relief drains have been installed to connect with the water bearing rocks. However closure of these drains may lead to excessive uplift pressure and rupture of the seal and so the relief drains will be left open, whilst waste is placed, until they can be safely closed.

## THE SITE

The site is a disused water reservoir which is being converted into a disposal area for domestic and industrial refuse - a general plan of the location is shown in figure 1. The reservoir lies in a natural valley with the ground falling generally from North to South. When the reservoir was no longer required it was drained and the dam, which consists of a puddle clay core with boulder clay shoulders, was breached.

Although there are no records of the construction of the reservoir a deep well was sunk (at position W) to supplement the natural inflow into the catchment. During the boring of this hole the observed ground stratigraphy was 4.5ft (1.37m) of soil and clay overlying water-bearing bands of fissured shale, sandstone and gritstone. A limited hand auger survey in the basin of the site confirmed that the ground profile consisted of a relatively-thin layer of clay overlying water bearing shattered shale and fissured sandstone. The thickness of the clay varied from 2.5 ft (0.76m) in the bottom of the valley to 12.8ft (3.9m) at the edges. Both the ground level and the underlying rocks rise from South to North and to the North of the site the fissured sandstone forms the bed of the stream which fed the reservoir. The foothills of the Pennines are approximately 2 miles (3.2km) North of the site. The auger holes revealed an artesian pressure in the shale and sandstone and groundwater issues were visible at several locations in cell 4.

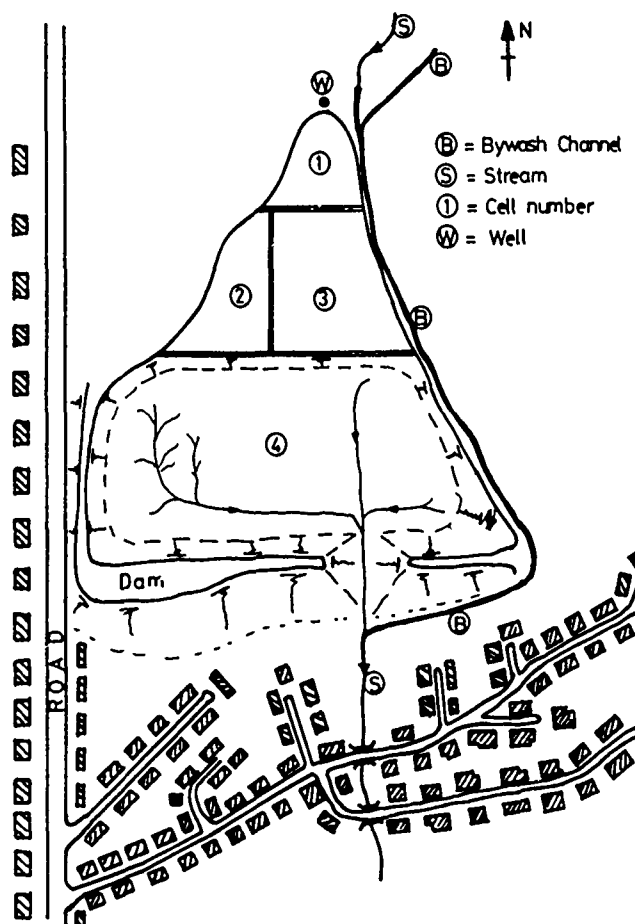


Fig. 1 Site Plan

To develop the site for refuse disposal the local authority required that the basin of the reservoir should be sealed by the establishment of either an impermeable membrane or a low permeability clay liner. The clay liner has to have a minimum thickness of 1m and a permeability of not greater than  $10^{-7}$  cm/sec. Falling head permeability tests showed that for certain areas of the site the naturally-occurring clay had a sufficiently-low permeability to act as a partial sealing layer. In addition compaction permeameter tests confirmed that clay was available on site which could be compacted to achieve the requisite permeability. The first owner of the site opted to install a clay liner for two reasons:

- i) There was sufficient, suitable clay on site - in fact in some parts there was a naturally-occurring partial clay liner.
- ii) The clay liner option was very much cheaper than installing an impermeable membrane which would itself have to be contained within low-permeability clay layers.

#### INITIAL SITE DEVELOPMENT

The initial development of the site was undertaken by a person who had no experience of waste management or earthworks and as described in an earlier paper (Sarsby 1987) his first attempts at forming a clay liner had resulted in much good quality clay being contaminated and wasted. Cells 1 to 3 were eventually lined and filled with waste but in the process the problems associated with cell 4 (by far the largest cell) were greatly exacerbated. The problems were:

- 1) Partial loss of naturally occurring clay seal. To line cell 3, and to form containment bunds, clay was removed indiscriminantly from cell 4's basin so that the thickness of the natural clay seal varied randomly over the site and in many places its thickness was reduced well below the necessary one metre. In addition earthmoving had taken place whatever the weather and the wheels of the plant had created deep ruts which had penetrated through the clay, thus creating leakage points.
- 2) Exposure of underlying water-bearing strata. The underlying shales and sandstone had been uncovered and groundwater issues created (as indicated in figure 2) due to removal of clay for use in cell 3 and due to 'rutting' and 'bogging-down' of earth moving plant. These issues created large ponds and miniature stream courses at many locations within the basin of cell 4.
- 3) Clay could not be placed and compacted to the required degree where there was standing or running water. The natural moisture content of the in-situ clay was significantly greater than the optimum value and adding water and

then kneading the soil (as in field compaction) rapidly causes the clay to degenerate to mud - as discovered by the site developer. The North-West of England has a damp climate which severely restricts the times when earthworks can be undertaken. Even during the drier parts of the year the numerous ground issues meant that there was always a lot of standing water on the site.

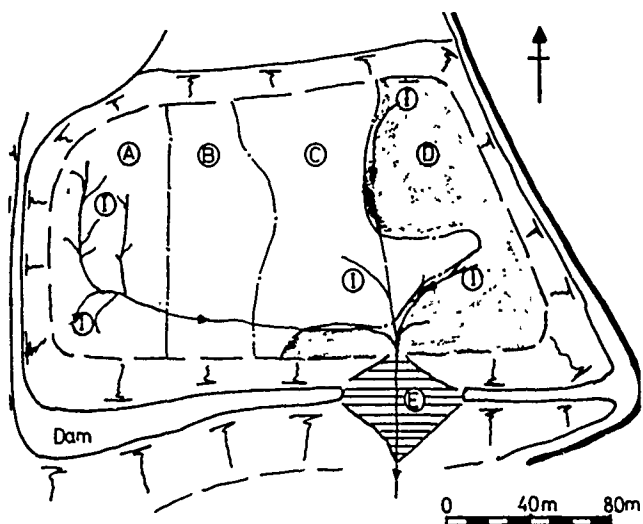
- 4) The development of high uplift pressure from the groundwater. Extrapolation of the pumping data from well W indicated that the steady-state water level in the borehole would be close to the ground surface - the top of the well being approximately 12m above the lowest point of cell 4. A standpipe had been installed to measure the development of head in the shales underlying cell 3. When this cell was sealed the water level in the standpipe rose to 2.8 ft (0.86m) above the lowest part of the clay seal, i.e. 6.8 ft. (2.07m) above original ground level. This head rise had occurred despite the fact that issues in cell 4 were acting as pressure relief points. With cell 4 sealed it was estimated that the underlying head could rise to 8m above ground level. If there was insufficient weight on top of the seal at this stage then uplift and consequential fracture of the liner would occur.
- 5) There appeared to be insufficient clay on site for the completion of the liner in cell 4. Importation of material would be very costly since there was no suitable source in the immediate vicinity and the use of an impermeable liner would be even more costly (even if such a liner were only used over part of the area). Even if an impermeable membrane were used then sealing clay would need to be placed above and below it as a 'fail-safe' measure against puncture of the membrane.

Shortly after the Writer commenced an investigation of the extent of the natural liner and the availability of additional clay on site the developer went bankrupt. The new owner then requested a feasibility plan to be drafted for the the completion of cell 4 using on-site materials if at all possible.

#### TREATMENT OF CELL 4

##### Availability of clay

The first thing to be done was to identify the zones where there was already an adequate natural liner (low permeability clay not less than 1m thick) and the zones where additional clay was required - as shown in figure 2. This investigation was undertaken by hand auger. "Undisturbed" samples of clay were taken using a 4" (102mm) diameter cutter driven into the ground to obtain a plug of soil approximately 4½" (114mm) long which was then subjected to a falling head permeability test. All of the samples tested had permeabilities in the range  $0.10$  to  $0.60 \times 10^{-7}$  cm/sec. so that this material would satisfy the local authority requirements for



Zone A: Natural liner = 0 to 0.5m thick - more clay needed  
 Zone B: " " = 0.5 to 1.0m " " "  
 Zone C: " " = 1.0 to 1.5m " - satisfactory  
 Zone D: " " = greater than 1.5m thick - source of suitable clay  
 Zone E = Dam breach I = Groundwater issue

Fig. 2 Cell 4

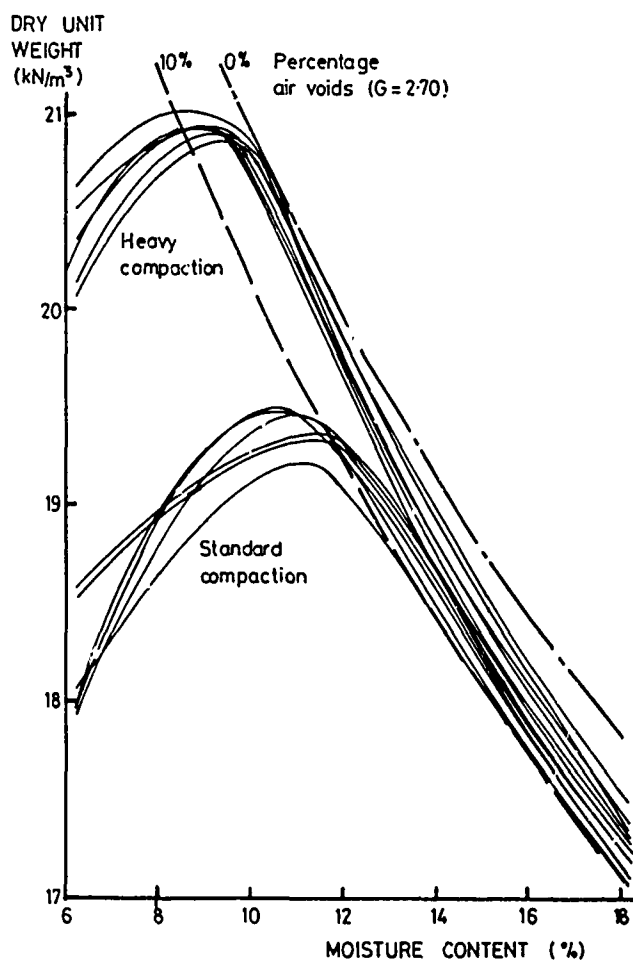


Fig. 3 Compaction Curves

sealing clay. Furthermore it was estimated that the volume of suitable clay was just sufficient for the completion of a 1m thick sealing blanket over the whole cell and the construction of a clay core within the dam breach. This balancing of volumes would only apply if; (a) clay could be excavated from one part of the cell and then be compacted elsewhere, to achieve a maximum permeability of  $10^{-7}$  cm/sec, and; (b) there was no further wastage of suitable clay material.

#### Compaction/Permeability Control

Random samples were taken from the 'borrow' areas of the site and were subjected to compaction and permeability tests to provide both a specification for placement of the clay and a rapid means of checking that the liner would have the requisite permeability. Dry density/moisture content relationships were established in accordance with the procedures contained in BS 1377 (1976). For each sample relationships were derived for both standard compaction (Proctor) and heavy compaction (modified A.A.S.H.O. test). The resultant compact curves are shown in figure 3. For each type of test the six soil samples gave very similar compaction curves. The effect of increased compactive effort is to increase the maximum dry density and reduce the optimum moisture content. However on the 'wet side' of optimum there is close correspondence between the data obtained from the two types of test. The natural moisture content of the clay ranged from 13.5 to 17.6%, i.e. wet of optimum and in the region where both standard and heavy compaction gave virtually identical dry unit weight values.

Since the compaction curves for the samples were very similar it was decided to establish the variation of permeability with compaction state for only one clay (sample 1) using both standard and heavy compaction. For the other samples the coefficient and permeability was only determined for optimum and natural moisture content under both standard and heavy compaction. The permeability was determined using compaction permeameters into which the clay was compacted, at a specific moisture content, in accordance with the requirements of BS 1377. To saturate the samples gentle vacuuming was employed so that water was drawn up through a specimen.

The results from the permeability test programme, which are presented in figure 4, agree with the trends reported by Daniel (1984). The data show several important points:

- i) On the 'dry side of optimum' the coefficient of permeability (k) increases rapidly as moisture content and dry unit weight decrease.
- ii) Minimum permeability is obtained when the clay is compacted slightly 'wet of optimum'.
- iii) On the 'wet side of optimum' the permeability is virtually independent of moisture content (at preparation) or dry unit weight.
- iv) Increased compactive effort decreases the permeability - in this case by a

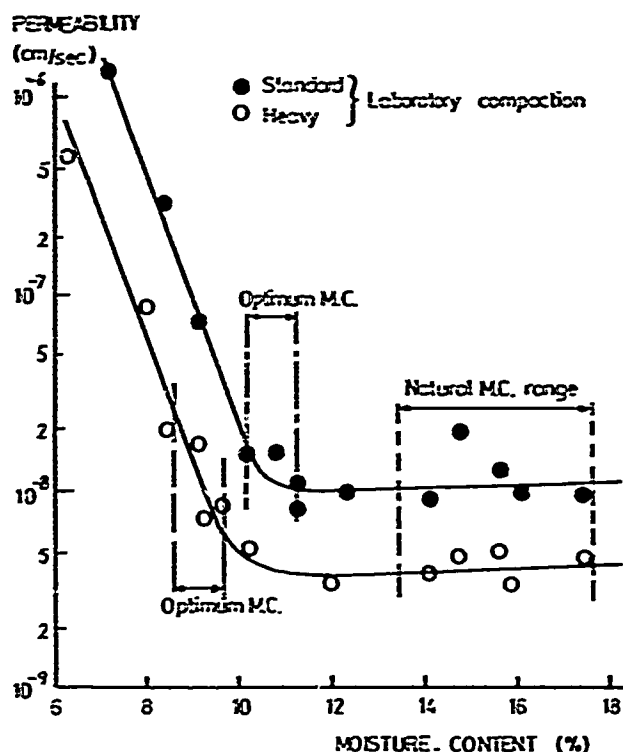


Fig.4 Effect of Moisture Content on Permeability

factor of approximately 3 in going from standard to heavy compaction.

- v) Clay compacted at natural moisture content had a permeability less than 10<sup>-7</sup> cm/sec.

As a consequence of the preceding findings it was agreed with the Local Authorities that quality control of the liner (as regards permeability) would be undertaken by monitoring the dry density and moisture content of the compacted clay. To be acceptable the material would have to be wet of Proctor optimum and have a dry unit weight not less than that obtained from standard compaction at that moisture content. In addition samples of the compacted clay would be taken for permeability testing (as each part of the cell was prepared).

#### Groundwater control

To be able to place the clay liner satisfactorily standing and running water had to be eliminated from the cell. The easiest way to do this would be to collect the groundwater within relief drains, discharge the water from site, and compact the clay liner over the drains. However the Local Authorities will not accept permanent underdrainage to a refuse site in case the liner leaks and hence pollutes groundwater and stream courses. Unfortunately any relief drains could not be closed immediately after preparation of the liner as the induced uplift

from the ground water would fracture the clay seal - the clay was only 1m thick and the anticipated uplift head was about 9m maximum. To overcome these problems the following method of operation was proposed:

- i) Connect all issues to relief drains and lead these to a central collection point (the freshwater chamber). Water is then discharged from this point to a stream to the South of the site.
- ii) Complete the clay liner while the groundwater is being discharged freely.
- iii) Test the integrity/impermeability of the liner by applying an excess head to the groundwater, i.e. raise the level of the outlet from the relief drains. The head to be applied (0.5m above ground level) is insufficient to lift the liner and has to be maintained for a minimum of 28 days. If leaks develop in the liner these should be eliminated (with the excess head removed) and then the whole liner should be re-tested for 28 days and so on until no leakage occurs.
- iv) Commence reinstatement of the breached dam so that the fill in the breach is at least 3m above the floor level of cell 4.
- v) When the liner has passed the pressure test install leachate drains and commence construction of the leachate chimney.
- vi) Place waste in the cell and simultaneously raise the level of the outlet in the freshwater chamber so that the groundwater head is always 0.5m above the surface of the refuse. Check the purity of the water in the chamber and if it is clean discharge it into the stream to the South of the site.
- vii) Once the level of water in the outlet pipe becomes static, i.e. there is no further overflow of groundwater, close the relief drains off and seal the freshwater chamber. The cell can then be completed in the usual manner.

The proposal was accepted by the authorities for several reasons :-

- a) It enables the whole of the clay liner to be pressure tested for leaks and imperfections.
- b) The groundwater pressure is controlled so that it never exceeds the overburden thus preventing lift and fracture of the liner.
- c) The groundwater pressure will always be greater than the pressure in the leachate inside the cell (due to regular pumping from the leachate chimney) so that there will be no tendency for leachate to flow out of the cell if the liner becomes porous.
- d) During filling of the cell the purity of the groundwater is checked so contamination would be quickly detected.
- e) If the groundwater does ever become polluted then the problem can be contained by opening the outlet pipe in the freshwater chamber. This chamber will consist of a permanent manhole built into the dam just downstream of the central clay core. If the outlet pipe is opened at its lowest level, i.e. the bottom of the manhole, and the

chamber is pumped out then groundwater will flow to the chamber since it is the lowest point in the system. Thus polluted water would be drawn to the outlet from whence it would be taken for treatment.

#### WORK UNDERTAKEN

Figures 5 and 6 show general views of cell 4 after completion of clay lining. In figure 5 the original dam is in the right-hand-side of the picture. The breach is approximately half-way along the embankment and has a shallow bund in front of it so that reinstatement of the dam can be commenced. The upstream slope of the dam is currently 1 on 2½ but this will be cut back to 1 on 2 to provide fill for the breach. Figures 5 and 6 show the proximity of the site to residential properties. The view in figure 6 was taken from the South-East corner of the dam with the bund between cell 3 and 4 being on the right-hand-side of the picture. The water in the basin of cell 4 is not from ground water issues but is due to rainfall (Manchester and the North-West being a notoriously damp part of England).

Data from tests on the compacted clay of the liner are presented in figure 7. The earthworks were undertaken using an 'end-result specification', i.e. acceptability of the work is based on the end result rather than on strict adherence with a specified method of working. Quality control was undertaken by specifying that the clay should be compacted in accordance with the relevant Department of Transport specification (1976) as regards weight of compaction plant, number of passes of the roller, etc. Quality assurance was achieved by checking that the compacted clay had the appropriate moisture content and density values (as stated previously) together with a limited number of permeability tests and pressure testing of the completed liner. After placement all of the material was well wet of Proctor optimum with dry unit weight values close to the theoretical curve for 100% saturation - the compacted clay was generally denser than the laboratory samples formed using either standard or heavy compaction. The permeability of the field specimens is in keeping with the laboratory data obtained for heavy compaction and is well below the requisite  $10^{-7}$  cm/sec. These data vindicated the method used for the quality assurance/control of the clay liner.

To collect all of the ground water issues 3 major relieve drains had to be installed. At the location of each weep a perforated section of pipe was inserted into the line and was covered with a granular filter. Clay was then compacted by hand around the drains before they were covered by the full clay liner. The pipes were brought to a common junction in the basin of the cell from where the single 4 ins (102 mm dia)



Fig.5 Cell 4 - Looking to the South-East



Fig.6 Cell 4 - Looking Westwards

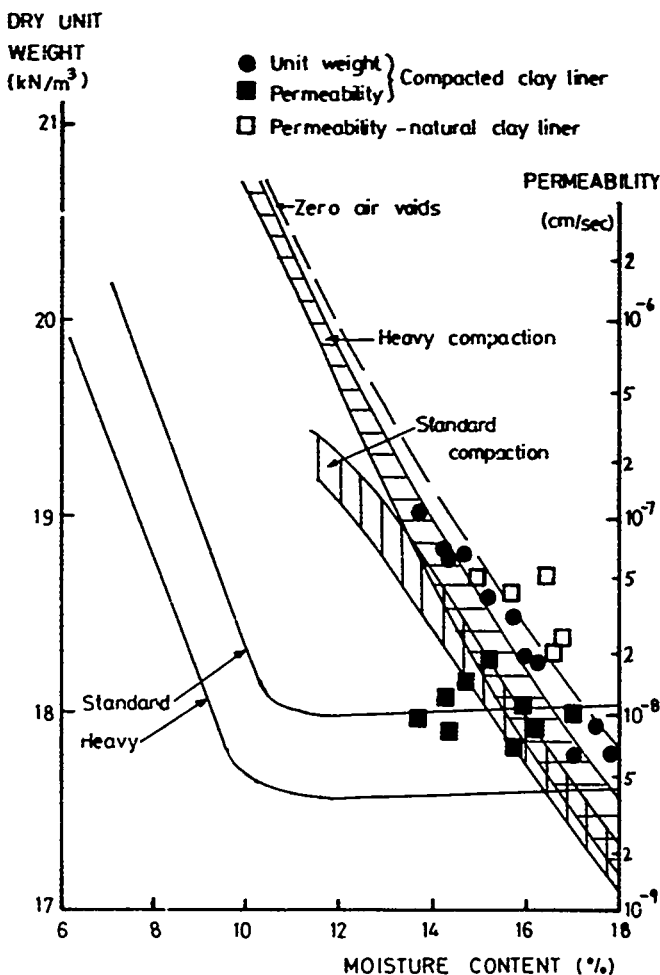


Fig.7 Properties of the Clay liner





Fig. 8 Relief Drain Connection



Fig. 9 Outlet of Relief Drains

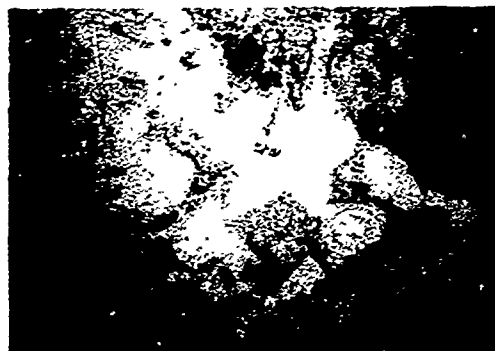


Fig. 10 Leaks through the liner

drain pipe shown in figure 8 carried the water out of the site via the breach in the dam. Figure 8 shows a section of the outfall relief pipe in between the clay seal and the temporary bund (on the right-hand-side) and a temporary access across the breach (on the left-hand-side).

The temporary outlet of the relief drains, set to induce an excess head of 1.6 ft (0.5m) above the clay liner, is shown in

figure 9. The left-hand picture shows the drain emerging from a protective steel pipe under the temporary access across the breach. The other view shows the outflow from the relief drain which at this stage was approximately 0.6 litres/second (about 480 gallons/hour). When the outlet was first raised and the liner was pressure tested a few leaks were detected - as indicated by the bubbles in figure 10. At these locations the liner was dug out completely and carefully recompacted. For the past six weeks the clay has been under pressure and no further leaks have been detected. Work is now starting on the sealing and reinstatement of the dam breach and it is anticipated that tipping of refuse will commence in about four weeks - during the whole of this time the liner will be left under test.

#### CONCLUSIONS

A method of forming a clay liner (for a land fill site) has been devised to overcome uplift induced by groundwater issues at a particular site. The method has two major benefits; the integrity of the completed liner is checked and; leakage of leachate from the landfill is inhibited by the positive groundwater pressure which will act on the exterior of the liner once the site is filled. Control of the placement of the clay liner (to achieve the requisite low permeability) was undertaken by a simple specification based on bulk unit weight and moisture content as a result of the data obtained from an extensive laboratory programme of permeability testing.

#### REFERENCES

- Anon (1976) "Methods of Testing Soils for Civil Engineering Purposes", BS1377, British Standards Institution, London.
- Anon (1976) "Specification for Road and Bridge Works", Fifth Edition, Dept. of Trans., HMSO, London.
- Daniel, D.E. (1984) "Predicting Hydraulic Conductivity of Clay Liners", Proc. A.S.C.E., Jn. of Geot. Eng. vol.110, No. 2.
- Sarsby, R.W. (1987) "Conversion of a Reservoir into a Landfill Site", A.S.C.E. Geot. Special Publ. No. 13, Proc. of a Speciality Conf. on Geot. Practice for Waste Disposal, Michigan, June.

## Design and Construction of a Soil Bentonite Slurry Wall around an Operating Facility Superfund Site

A.S. Burgess

Principal, Golder Associates, Inc., Redmond, Washington

M.S. Leonard

Senior Geotechnical Engineer, Golder Associates, Inc., Redmond, Washington

G.S. Laird

Project Hydrologist, Golder Associates, Inc., Redmond, Washington

**SYNOPSIS:** A soil bentonite slurry wall was designed for an NPL site to stop further migration of chemicals in a complex aquifer system, and to facilitate the removal of possible chemical sources from saturated zones beneath the site. Pumping from within the slurry wall will maintain inward and upward hydraulic gradients and thus stop further lateral or vertical migration of chemicals from the contained area. The slurry wall was constructed under an exceptionally detailed Quality Assurance/Quality Control review by the Contractor and two independent consulting firms. Ground movements, vibration levels and opacity of dust produced during construction were monitored for compliance with design specifications. It was made a condition of the contract that no hazardous material could leave the site. Federal regulations required all persons involved in site work to have health and safety training. Careful planning and close liaison between the Owner, Engineer and Contractor has enabled the slurry wall to be constructed in a business park environment around an operating manufacturing facility without disruption to production.

### INTRODUCTION

A soil bentonite slurry wall was constructed around the perimeter of a facility belonging to the Raytheon Company Semiconductor Division (Ellis Street site), Mountain View, California (Owner) between June and October, 1987.

Although a large number of soil bentonite slurry walls have been installed in the past for dam cut-offs and deep open excavations, this soil bentonite wall was unique in that the wall was constructed in a business park environment around an operating facility. This setting required considerable foresight in the preparation of contract documents and in coordination between the Contractor and the Owner in order to avoid delays to either party during construction of the slurry wall. Pumping from within the slurry wall will maintain inward and upward hydraulic gradients and thus stop any further vertical or lateral migration of chemicals from the contained area. Wall construction was accompanied by an exceptionally detailed Quality Assurance/Quality Control (QA/QC) review performed by the Contractor and two consulting firms.

### SITE DESCRIPTION

The site is situated in Mountain View, California, ("Silicon Valley"), between San Francisco and San Jose, and was placed on the National Priorities List (NPL), owing to the presence of chemicals in the ground and ground water. The site is at approximately fifty feet above sea level, with a drop in grade of approximately nine feet between the south west and north east corners. The site measures approximately 1000 feet by 840 feet, and is shown on Figure 1.

The Ellis Street facility is a one story building where semiconductor products are

manufactured. The building contains equipment sensitive to vibrations and dust, and the facility is supplied with several underground and overhead utilities. Access to the Ellis Street facility was by three entrances from Ellis Street, and an interbuilding access from an adjacent Raytheon plant on Middlefield Road to the south of the Ellis Street site. Two other buildings exist on the south side adjacent to the Ellis Street site, and a soil bentonite wall forty feet deep had previously been installed on a neighboring property, at a distance of approximately twenty feet from the west property line. A multistory building exists along most of the length of the north boundary. Immediately in front of and along the sides of the Ellis Street facility the area is paved. The western half of the Raytheon property is an undeveloped open area.

### SUBSURFACE CONDITIONS

The site had been thoroughly investigated by Raytheon, by drilling over 200 boreholes and installing over 100 monitoring or extraction wells to characterize the soil and ground water from a hydrogeological and chemical point of view. Most of the investigations were oriented to chemical identification, and sampling was performed with a 3.0 inch O.D. California drive sampler, to provide six inch long samples for chemical analysis using an on-site gas chromatograph. The chemicals detected were essentially volatile organic compounds (VOC), in concentrations less than 37 parts per million (ppm) in the soil in the vicinity of the slurry wall and less than 200 mg/l in the ground water (Golder Associates, 1987). The chemicals detected most frequently were trichloroethylene (TCE) and 1,2-dichloroethylene (1,2-DCE).

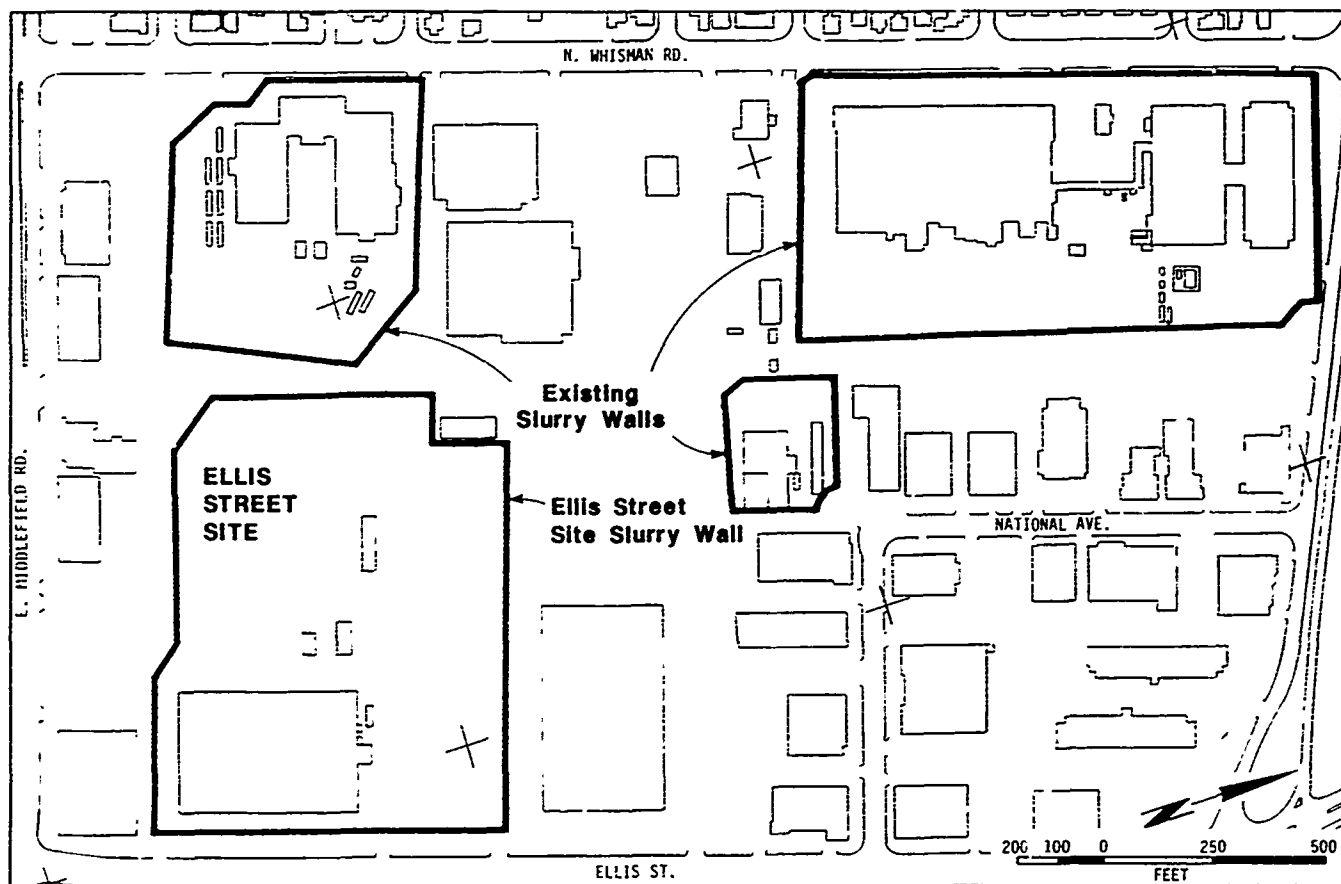


FIGURE 1. Site Vicinity Map

Investigations at the Ellis Street site and at neighboring facilities show the area to be underlain by a complex succession of medium dense to dense interbedded clays, silts, sands and gravels.

The grain size distribution of soil samples have a  $D_{60}$  (the grain size diameter larger than 60 percent of a soil sample by weight) between 30 and 0.02 mm and a  $D_{10}$  between 0.5 and less than 0.0006 mm. The fine grain samples have Atterberg limits above the "A" line.

A typical interpreted soil section through the site is presented in Figure 2. The continuity, thickness, and areal extent of the strata are highly variable, with many units thinning or pinching out. In general, the soils beneath the site can be categorized into five major water bearing zones; A, B1, B2, B3, and C (Figure 2).

Prior to construction, the groundwater surface was approximately twenty feet below ground surface with the horizontal hydraulic gradient generally to the north in all aquifer zones. The vertical gradients were upward within the A and B aquifer zones, but downward across the B/C aquitard due to pumping for water supply from the C aquifer. With the possible exception of the B/C aquitard, all other

aquitards are considered to show some degree of interconnection and leakage.

#### SLURRY WALL DESIGN

Based upon the results of the extensive investigations at the site, a number of alternatives were evaluated for Interim Remedial Action, including excavation, groundwater control, and slurry wall with pumping from within the contained area. The installation of a slurry wall, together with pumping to maintain inward and upward hydraulic gradients was considered the best alternative to satisfy the objective of stopping further migration of chemicals from the site, protecting underlying aquifers and facilitating removal of possible chemical sources in saturated soils beneath the site. An additional important requirement was that the plant remain operational during all stages of construction and operation.

Conventionally, slurry walls have been tied in to a less permeable horizon for containment. After reviewing and assessing the site data, it was decided that this would not meet the remedial objectives. A novel concept was therefore developed in which the wall would be constructed to a predetermined depth around the site to act as a curtain within which pumping would accentuate inward and upward

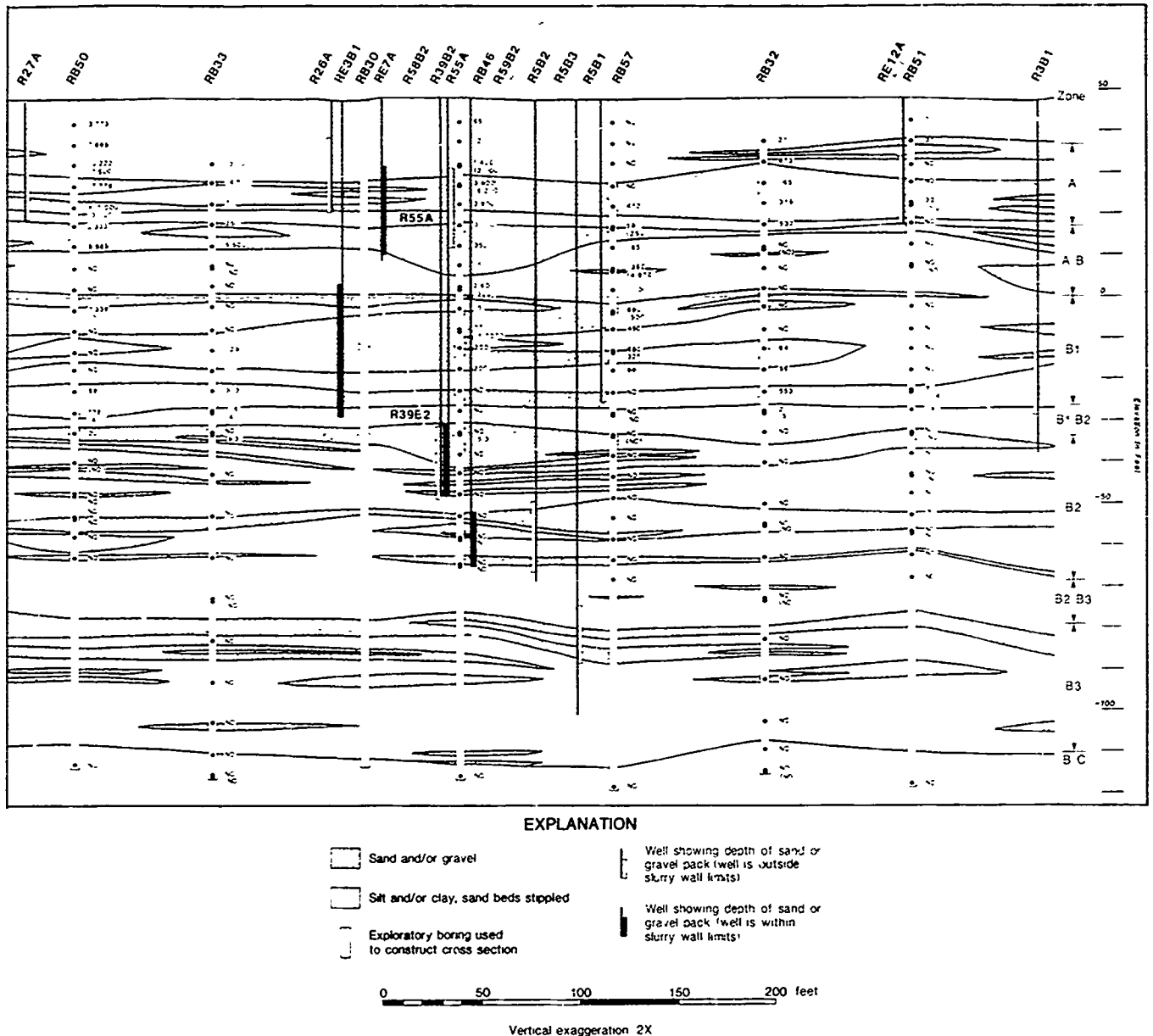


FIGURE 2. Typical Geological Cross Section (Along North Property Line)

hydraulic gradients and so stop further offsite migration of chemicals within the impacted zones (Figure 3).

Extensive design studies were undertaken, including 2-D and 3-D computer modeling of groundwater flow to confirm the utility of the novel design concept and to determine the optimum wall depth. To ensure that the wall would accentuate upward gradients across the aquitards beneath the site, it was determined that a maximum hydraulic conductivity of  $1 \times 10^{-7}$  cm/sec was required.

#### Utilities

Twenty six utilities were identified that would be affected by wall construction. In addition to water, sewerage, and storm water

drainage, the Ellis Street facility is supplied with piped hydrogen, nitrogen and de-ionized water, and underground data cables linked it to an adjacent Raytheon building.

It was decided to perform utility diversions before the start of the slurry wall construction, under a contract separate from the slurry wall contract. Underground utility diversions were designed to withstand accidental impact from the slurry wall excavation equipment. Overhead utility diversions were to provide enough clearance for normal site and Contractor truck traffic, and to be demountable to allow the passage of large excavating equipment.

Potential contractors were consulted on the feasibility of utility protection. A 15 feet clearance under a utility bridge on the south

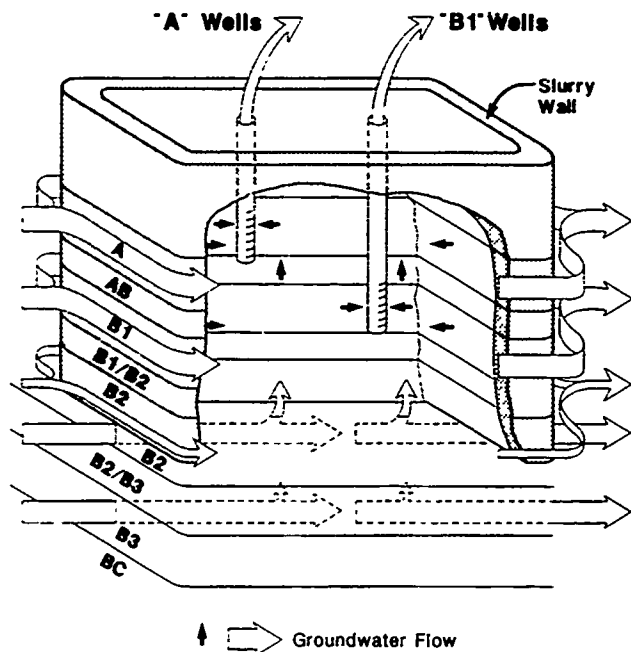


FIGURE 3. Slurry Wall Schematic

side of the site was provided, and underground utilities across the slurry trench alignment were encased in reinforced concrete sleeves. The utility conduits were consolidated to minimize separate crossings of the slurry wall. The slurry wall was located about 30 feet from the property boundary to leave enough space between construction equipment and overhead electric lines in a public utility easement around the site.

The site also contained a large number of extraction and monitoring wells that had to function during slurry wall construction. The slurry wall construction was responsible for protecting all wells or instrumentation more than ten feet from the edge of the slurry wall. Wells within ten feet of the slurry wall alignment were abandoned by grouting in accordance with the requirements of the Santa Clara Water District.

#### Specifications

A considerable amount of effort went into the preparation of the specifications for the slurry wall construction particularly as there was no published precedent for slurry wall construction in constraints of the kind at the Ellis Street facility. It was decided from the outset that wall construction should be carried to a minimum performance specification for the wall materials, and that the Contractor would be responsible for providing a detailed and thorough QA/QC program.

The bentonite slurry in the trench was specified to have a minimum density of 70 pounds per cubic foot (pcf) instead of the usual 65 pcf in order to reduce potential ground movements during excavation. Bentonite was to be stored in two lined ponds, so that it would be easier to clean out the ponds at the end of the work.

Prior to the issue of the final bid documents, tests were performed to demonstrate that it was possible with the materials on site to provide a mix meeting the maximum permeability requirement of  $10^{-7}$  cm/sec. The specifications defined a minimum bentonite content of two percent for the final soil bentonite mix, but gave the Contractor the responsibility for the mix composition to meet the specified maximum permeability. The wall width was defined as a minimum of three feet, to a depth of 100 feet. The wall had to be horizontally continuous, and the specifications required excavation and backfilling operations to be separated by a distance of at least 50 feet. The specifications allowed the Contractor the freedom to decide on equipment, although it was anticipated that he would use a backhoe and clamshells. Backfill was specified to be placed from the surface, which is usual for this kind of slurry wall.

The contract documents required that only excavated soil with VOC concentrations less than 0.5 ppm could be used in the backfill. This was to avoid the potential for introducing chemicals below the areas currently affected. The extensive investigations undertaken prior to wall design, with boreholes as close as 75 feet and samples and chemical analyses every 5 feet, provided the designers with a comprehensive picture of the vertical and lateral distribution of chemicals along the wall alignment. There was also provision in the contract documents for field checking by the Engineer, using an organic vapor analyzer (OVA).

The Engineer's method to evaluate VOC content involved mixing prescribed volumes of soil and distilled water in a glass jar. The head space above the mixture was sampled with the OVA and injected into the gas chromatograph (GC). A strip chart recorder provided the signatures of the chemicals in the soil sample which were then compared to chromatograms of standard solutions of TCE and 1,2-DCE. Actual soil concentrations were calculated by peak height comparison with these standards. Before actual excavation began, a field program was performed, with samples tested with the OVA and at an independent laboratory using the EPA method 8010 for independent confirmation.

In view of the sensitive equipment installed in the Ellis Street facility and other buildings, the specifications set maximum vibration levels at the buildings that were not to be exceeded. Vibrations were monitored for construction activities that took place approximately 100 feet away from the sensitive buildings. The maximum allowable vibration levels are given below:

| Frequency   | Acceleration               |
|-------------|----------------------------|
| > 500 Hz    | 2.0 g.                     |
| 50 - 500 Hz | 1.0 g.                     |
| 5 - 50 Hz   | 0.2 g.                     |
| shocks      | 2.0 g. for 10 milliseconds |

Concern was expressed for the problems that could arise from dust produced by construction. After considerable research, it was decided to adopt the Environmental

Protection Agency (EPA) opacity standards used for smoke stacks, with a maximum intensity of 20 percent.

One of the most important practical consequences of the site being on the NPL was that the wall construction would be under 29 CFR Part. 1910, which requires health and safety training for all persons involved in site work. The specifications required all persons on site to have level D safety protection, with equipment available for all persons to wear level C protection. Each employer was made responsible for the health and safety of his own staff.

It was made a condition of the contract that no hazardous material could leave the site. Although the work would be performed in summer, when rainfall was usually negligible, allowance had to be made to contain run off from an exceptional storm. Calculations were made to estimate the surface run-off from a storm with a 25 year recurrence interval. The potential for run-off led to the requirement to isolate the site with a earthen berm three feet high. The design therefore included sums for stormwater collection, with a pumping system to transfer the water to lined ponds with a total capacity of approximately 3,900 cubic yards. Provision was made for the collected water to pass through settlement tanks and be aerated to remove any VOC before being discharged into the sewer system. As it turned out, the summer was dry, and no run-off had to be collected.

## Quality Assurance

The specifications defined the minimum QA/QC testing to be performed by the Contractor. The Engineer reviewed the Contractor's QA/QC test results and independently verified these results by performing separate tests. Another consultant reviewed the test results of the Contractor and the Engineer and performed additional permeability tests.

No acknowledged QA/QC program existed for EPA Superfund sites (JRB Associates, 1984), and therefore a high testing frequency for monitoring workmanship and material properties, particularly permeability was required. The minimum QA/QC requirements are shown in Table 1. For the first two weeks of excavation and backfilling, the materials testing frequencies were doubled. The philosophy was to be able to identify any non-compliant materials or workmanship as early as possible, and have records available to show where any such materials may have been placed.

Before excavation could begin, the Contractor had to provide a detailed QA/QC plan defining testing and remedial actions for non-compliant materials. The Engineer also provided a QA/QC plan that was reviewed by the independent consultant. The Contractor was required to provide a qualified person, specifically for the QA/QC and his qualifications were to be approved by the Engineer. The Engineer had four employees on site to observe the construction.

TABLE 1. Slurry Wall Quality Assurance/Quality Control Testing Specifications

| SOIL BENTONITE WALL                       |           |                             |  |   |
|---|-----------|-----------------------------|--|---|
| Subject                                   | Standard  | Type of Test                | Frequency                                      | Specified Values  |
| M<br>A<br>T<br>E<br>R<br>I<br>A<br>L<br>S | Water     | -----                       | pH   | As required to properly hydrate bentonite with approved additives |
|   |           |                             | Total Hardness                                 |   |
|   | Bentonite | API 13A                     | All tests needed to show compliance to API 13A | Premium grade sodium catopm montmorillonite                       |
|   | Clay      | ASTM D1140 (modified)       | % Passing #200                                 | As measured   |
|   |           | ASTM L.L. D423<br>P.L. D424 | Plasticity Index                               | As measured   |
| S<br>L<br>U<br>R<br>R<br>Y                | Ponds     | API Std. 13B                | Viscosity                                      | Min. 40 sec. Marsh @ 68F  |
|   |           |                             | Unit Weight                                    | Max. 85 lb/cu. ft.<br>Min. 63 lb/cu. ft.                          |
|   |           | API Std. 13B                | Filtrate Loss                                  | Loss <25 cc in 30 min.<br>@ 100 psi                               |
|   | Trench    | API Std. 13B                | Viscosity                                      | Min. 40 sec. Marsh  |
|   |           | API Std. 13B                | Unit Weight                                    | Max. 85 lb/cu. ft.<br>Min. 70 lb/cu. ft.                          |

TABLE 1 (Continued)

## SOIL BENTONITE WALL

| Subject                         | Standard             | Type of Test                 | Frequency  | Specified Values                         |
|---------------------------------|----------------------|------------------------------|--|--|
| Trench                          | See Section 2.9.2    | Permeability (laboratory)    | 1 per 500 cy, at least once per shift  | $10^{-7}$ cm/sec                         |
| B<br>A<br>C<br>K<br>F<br>I<br>L |                      | Permeability (field)         | 10 in situ tests plus one lab test on sample taken from each in-situ test location | $10^{-7}$ cm/sec                         |
| Trench                          | ASTM C-143           | Slump                        | 1 per 200 cy and at least once per shift   | 3" minimum - 7" maximum                  |
| Trench                          | See Section          | Bentonite Content            | 1 per 200 cy and at least once per shift   | 2½ dry weight of backfill                |
| Trench                          |                      | Unit Weight                  | 1 per 200 cy at least twice per shift  | 15 lb/cu. ft. slurry unit weight         |
| Trench                          | See Section 2.9.2(D) | Slope                        | 1 per week   | No irregularities which are not backfill |
| T<br>R<br>E<br>N<br>C<br>H      | Profile              | Depth measurment             | Per 10 LF of excavation  | Min. specified key depth                 |
| C<br>H                          | Continuity           | Movement of excavation tools | Each Panel   | Continuous trench                        |
|                                 | Key                  | Examine cuttings             | Continuous during key  | Competent aquaclude material             |

The Contractor established an on site laboratory, equipped to perform all the tests in Table 1. Most of the tests were standard for the permeability tests the consolidation pressure, hydraulic gradient, apparatus type, and permeant were specified. The Engineer maintained an independent, fully equipped on site laboratory, and performed testing at approximately one half the frequency required of the Contractor.

Slurry trench depths were verified at ten feet horizontal intervals. The Contractor maintained a large scale elevation drawing of the wall, showing excavation and backfilling progress on a daily basis to enable any materials found later as non-compliant to be located.

The specification provided a list of reporting items, to be provided in weekly reports. Any non-compliant items were discussed at daily progress meetings with the Owner, Engineer and Contractor.

#### Instrumentation

Three inclinometers; accelerometers for vibration monitoring in the x, y, and z directions; and a number of settlement points were installed around the site. To assess the ground movement around neighboring buildings, the inclinometers were placed inside the

slurry wall equidistant from the wall as the buildings of concern or in between the wall and the building. The first inclinometer was placed near the starting point, in order to have early information on ground movements. The inclinometers were read as part of the Owners QA/QC, and the results were reviewed by the Engineer.

The inclinometers were of the Sinco type, with 10 foot long casings 3 inches in diameter. The inclinometers went to a depth of 150 Feet, and were surrounded by a grout mix approved by the Santa Clara Water District, for imperfect sealing could lead to communication between the aquifers.

#### SLURRY WALL CONSTRUCTION

Slurry wall construction began in June 1987, and the wall was completed by the end of October. The Contractor used a backhoe with an extended boom to excavate the trench to a depth of approximately 50 feet. Two 200 ton Manitowoc cranes were used with the 12 ton clamshells, to excavate the trench to a depth of 100 feet. The wall perimeter measured over 3400 feet.

Backfill was mixed in a mixing pit, by placing a volume of excavated soil that had been mixed with slurry in a pit of known volume. The bentonite was added from sacks submerged in

the pit, which considerably reduced the problems associated with dust. The backfill was mixed in the pit with a backhoe, which was also used to load the final mix into trucks. The trucks then transported the backfill to the slurry trench, where it was end dumped onto the exposed backfill already in the trench. This caused the backfill to enter the trench by continuous failure of the backfill slope, and thus minimized segregation and the chance for incorporating slurry pockets in the backfill. This method of handling the excavated soil and backfill kept the site relatively clean. Tarpaulins were placed over the facades of adjacent buildings, and no complaints were received from the public on site cleanliness. At the end of wall construction, the excess soil was stockpiled and the slurry was left in the lined ponds.

Construction of the slurry wall beneath the buried utilities was performed carefully, and it is to the Contractor's credit that not one utility was damaged. After the start of construction, the sequence of excavation was changed at the request of the Owner. This required the Contractor to use bulkheads of soil to support different elevations of slurry in the trench across the site where there was a difference in grade of more than four feet. Actual wall construction led to the phasing shown in Figure 4. The excavation sequence

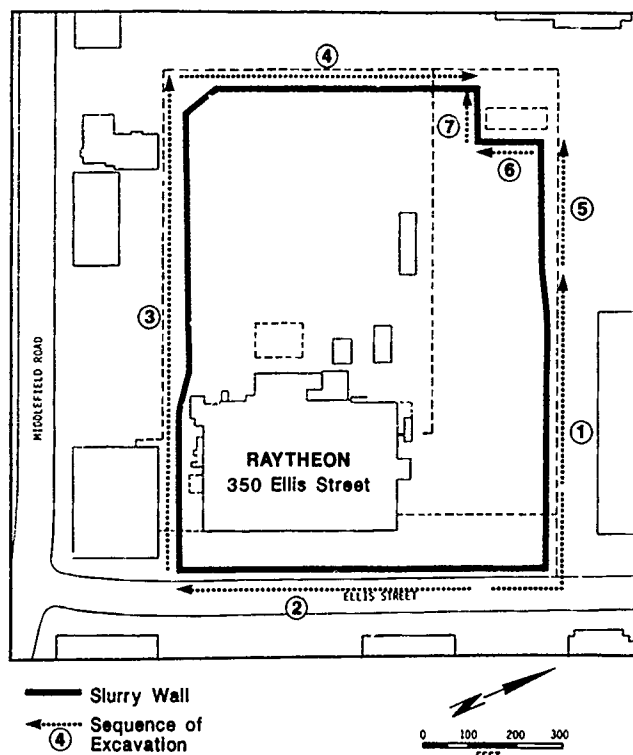


FIGURE 4. Slurry Wall Excavation Sequence

required considerable coordination between the Contractor and the Owner to ensure the facility with all of its traffic could remain in operation. Construction was completed on time and within budget, with no major breakdowns or mishaps.

The results of the QA/QC showed that no non-compliant material was in the wall backfill. All the permeability test results, which are shown on Figure 5, were well below the required maximum.

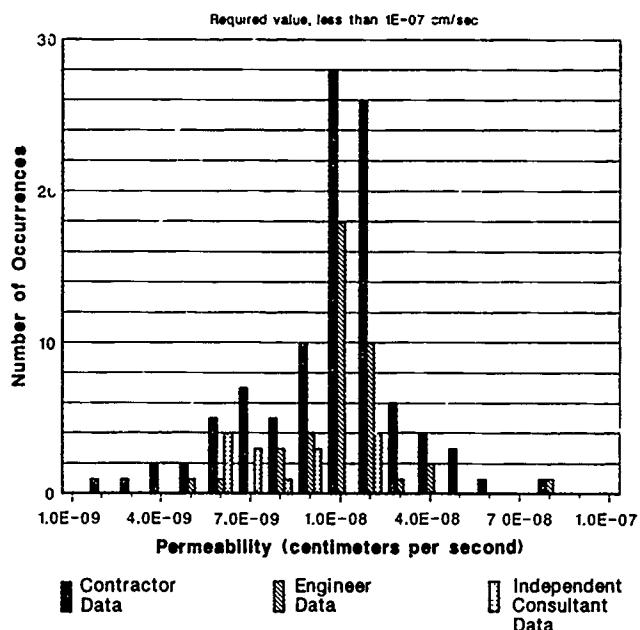


FIGURE 5. Histogram of Permeability Test Results by Laboratory

Measurements of actual soil VOC content, as performed on the excavated soil, showed an excellent correlation with the anticipated concentrations based upon boreholes along the wall alignment. Airborne VOC levels were monitored for health and safety purposes, and level C protection was not required at any time.

Inclinometer movements showed up to 0.8 inches of movement towards the trench during excavation, followed by an outward movement below 20 feet depth after placing the backfill. Inclinometers have shown movement towards the trench subsequent to placing the backfill.

#### Slurry Wall Effectiveness

The effectiveness of the slurry wall was demonstrated during the construction, based upon water level measurements in the monitoring wells. Deep well pumping continued during wall construction, and water levels in the pumped aquifers within the contained area dropped as soon as the wall was near completion.

#### CONCLUSIONS

Extensive QA/QC testing has indicated that the slurry wall meets the specified maximum permeability requirements, and will prevent further offsite migration of chemicals in groundwater. Careful planning and close liaison between the Owner, Engineer and Contractor has enabled slurry wall technology, usually applied in a less restrictive setting, to be used around an operating manufacturing facility, without disruption to production.



#### Acknowledgements

The successful result of the project is due to excellent co-operation between the Owner, Raytheon Semiconductor Company; the Engineer, Golder Associates, Inc.; the Owner's QA/QC engineer, Harding Lawson Associates; and the Contractor, GKN-Hayward Baker. The views expressed in this paper are those of the authors, and do not represent those of the above mentioned organizations.

#### References

- Golder Associates, Inc., (March 1987),  
"Interim Remedial Measures, 350 Ellis  
Street, Mountain View, California, Final  
Report", Vol. I and II.
- JRB Associates, Incorporated, (1984), "Slurry  
Trench Construction for Pollution  
Migration Control", U.S. Environmental  
Protection Agency (EPA), EPA-540/2-84-001.

## A Modified Field Infiltrometer Test For Clay Liners

G.S. Laird

Project Hydrologist, Golder Associates, Inc., Redmond, Washington

A.M. Gurevich

District Engineer, Chemical Waste Management, Inc., Newark, California

W.B. Lozier

Project Hydrologist, Golder Associates, Inc., Redmond, Washington

**SYNOPSIS:** Regulatory agencies are looking more frequently to in situ field hydraulic conductivity tests for the assessment of a liner's compliance to a specified hydraulic conductivity. Most field tests have evaluated hydraulic conductivity by measuring the infiltration rate of the liner. The infiltration rate can be used to arrive at a hydraulic conductivity value if the hydraulic boundary conditions of the test can be identified or if the head loss at different depths can be measured.

A test fill of a clay liner was evaluated for its saturated vertical hydraulic conductivity. This paper discusses the use of eight tensiometers to measure soil suction at four depths beneath a double ring infiltrometer. The hydraulic conductivity results using the tensiometer data displayed good consistency and agreed well with laboratory test results.

### INTRODUCTION

Hydraulic barriers of compacted soil are widely used for covering waste disposal facilities and for lining solid waste landfills, liquid storage ponds, and other impoundments. These soil barriers are generally made of naturally clayey soil or a soil/bentonite mixture. The materials used for these clay covers/liners may have to conform to a design specification such as a certain plasticity index or a minimum bentonite content, however, most often the design specification will require that these barriers must have a hydraulic conductivity not exceeding a specified value.

The determination of the hydraulic conductivity of a clay liner is most often made from laboratory hydraulic conductivity tests, but, recently, regulatory agencies are looking more frequently to field hydraulic conductivity tests for the assessment of a barrier's compliance to a specified impermeability. Field tests may be receiving more attention because it has been suggested that laboratory hydraulic conductivity tests underestimate in situ hydraulic conductivity (Daniel, 1984), because field tests may be better at accounting for any hydraulic defects in the in situ barrier (Stewart and Nolan, 1987), and/or because field tests evaluate hydraulic conductivity on the scale more representative of the hydraulic barrier (Day and Daniel, 1985b).

Most field tests have evaluated hydraulic conductivity by measuring the infiltration rate for the hydraulic barrier. The infiltration rate can be used to arrive at a hydraulic conductivity value if the hydraulic boundary conditions of the test can be identified or if the head loss at different depths can be measured (Daniel and Trautwein, 1986).

The purpose of this paper is 1) to describe the use of tensiometers with an infiltrometer test for evaluating the hydraulic condition of soil

suction (soil tension), 2) to discuss options utilizing the tensiometers, and 3) to describe a recent field test where an infiltrometer test using tensiometers was conducted with success. Before proceeding, a clarification of terms is necessary. The terms permeability and hydraulic conductivity are often used interchangeably. Strictly speaking, permeability is a property of the soil independent of the fluid. However, the data collected from field tests is often a measure of the hydraulic conductivity, which is a property of the soil and the fluid passing through it. Therefore, the term hydraulic conductivity is used in this report.

### Infiltration Test

There are three broad categories of infiltration tests: the borehole or percolation test, the single ring infiltrometer, and the double ring infiltrometer. Advantages and disadvantages of each type of infiltration test are well documented (Day and Daniel, 1985b; Daniel and Trautwein, 1986). All of these tests measure the loss of water to the soil as infiltration. The borehole test uses the change in the water level in an uncased or cased hole. A single ring infiltrometer pools the water above the barrier to be tested and reduces the effects of lateral infiltration by being at least as wide as the barrier is thick. The double ring infiltrometer minimizes the effects of lateral infiltration by having two pools of water. A large pool of water, surrounding an inner pool of water, is the source of all water affected by lateral infiltration. The loss of water through the inner ring is used to determine the infiltration.

### Description of Test Apparatus

As an extension of the double ring infiltrome-

ter described above, a sealed double ring infiltrometer featuring a covered inner ring that eliminates evaporation as a flux term, has been developed by Trautwein Soil Testing Equipment of Houston, Texas. The apparatus consists of two rings: a fiberglass rectangular ring approximately five feet to the side (inner ring) which is positioned in the center of a second rectangular aluminum ring that is approximately twelve feet long on the side (outer ring). Two sets of the Trautwein apparatus were used. A schematic of the test layout and a cross-section are shown in Figure 1. Both rings are filled with water, and the loss of water from the inner ring is measured periodically by weighing a flexible bag that is the reservoir of water for the inner ring (Figure 1). This water loss is the amount of water that has infiltrated the test fill beneath the inner ring. The water level in the outer ring is maintained at a level slightly above the top of the inner ring. The head of water in the inner ring is equal to the outer ring by placing the flexible bag in the water of the outer ring. Submerging the inner ring reduces the effects of temperature changes on measurements of water volume lost through the inner ring.

Initially, the water from the inner ring enters a clay cover/liner which is unsaturated. The water is forced through the barrier by the head of water in the rings and by the soil suction caused by capillary tension. Eventually, the

soil beneath the ring will become saturated, and the infiltration rate will approach steady state. If a drainage layer (vented to the atmosphere) is provided beneath the barrier, it would be possible to measure the outflow through the barrier. When the outflow is equal to the inflow, steady state conditions are said to exist. Under these saturated steady state conditions, the boundary condition below the barrier can be easily identified. To arrive at the hydraulic conductivity of the barrier from a measured infiltration rate, either the boundary conditions beneath the barrier must be known, or the head loss between different soil depths must be measured.

Previous application of the Trautwein apparatus (Daniel and Trautwein, 1986) and of single ring infiltrometers (Day and Daniel, 1985b; Stewart and Nolan, 1987) have not measured pore water pressure (soil suction). When the soil barrier is saturated and steady state conditions exist, as verified with a free draining layer underlying the barrier, pore water pressure can be assumed to be zero. However, clay liners with low hydraulic conductivity may take several months to saturate if thicker than a couple of feet.

#### Theory

The seepage of water into the test fill is driven by the hydraulic gradient caused by the

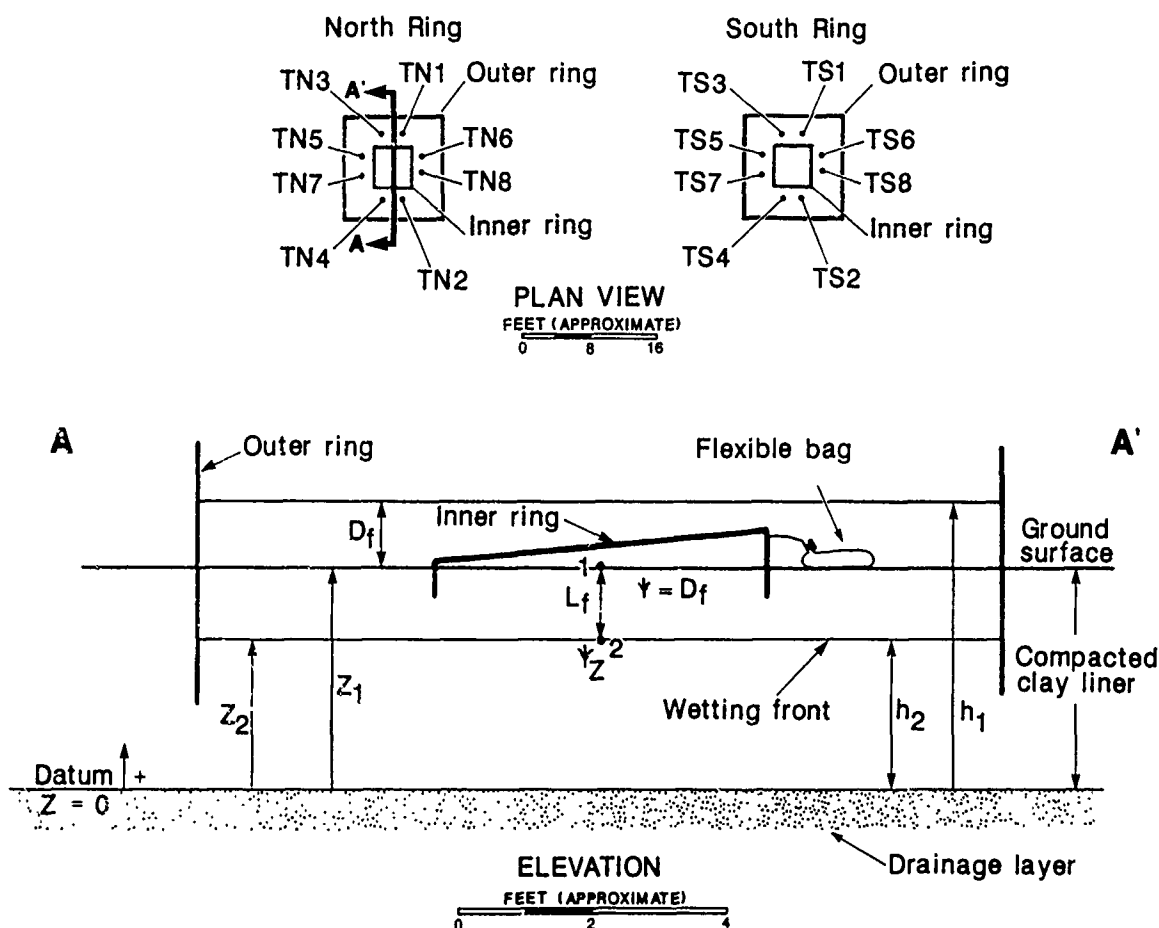


Figure 1. Infiltrometer Test Schematic

ponded water depth and soil suction (tension). The saturated hydraulic conductivity can be computed using a form of Darcy's Law which includes terms for the total hydraulic gradient. The governing equation that describes the flow of water into the compacted clay is developed below. Illustration of the terms and sign convention is shown in Figure 1.

According to Darcy's Law, and by observation of Figure 1 (the flow direction is in the negative Z-direction, downward):

$$q = -K \frac{\Delta h}{\Delta L} \quad (1)$$

where,

$q$  = flow rate per unit area (L/T)

$K$  = saturated hydraulic conductivity (L/T)

$\frac{\Delta h}{\Delta L}$  = total hydraulic gradient (L/L)

Recognizing that,  $\Delta h = h_1 - h_2$  and  $\Delta L = Z_1 - Z_2$  between points 1 and 2 (see Figure 1) taken at ground surface and immediately below the wetting front, respectively, Equation 1 becomes:

$$q = -K \left[ \frac{(Z_1 + \psi_1) - (Z_2 + \psi_2)}{(Z_1 - Z_2)} \right] \quad (2)$$

where,

$\psi$  = pressure head

$Z$  = elevation head, and

$h = \psi + Z$ .

Rewriting:

$$q = -K \left( \frac{\psi_1}{L_f} - \frac{\psi_2}{L_f} + 1 \right) \quad (3)$$

where,

$$L_f = Z_1 - Z_2.$$

By reviewing Figure 1, it can be seen that at point 1 the pressure head is equal to the depth of flooding, or  $\psi_1 = D_f$ . Also, since the clay fill is unsaturated, the in situ pressure head at point 2 will be negative and can be designated simply as  $\bar{\psi}$ , i.e.,  $\bar{\psi} = -\psi_2$ .

Substituting into Equation 3:

$$q = -K \left( 1 + \frac{D_f}{L} + \frac{\bar{\psi}}{L_f} \right) \quad (4)$$

The minus sign indicates that flow is in the negative Z direction (downward).

Equation 4 is time dependent. That is, the flow rate per unit area (infiltration rate,  $q$ ) and the depth of the wetting front ( $L_f$ ) are interrelated and vary with time. As the wetting front advances, Equation 4 can be used to calculate hydraulic conductivity at various wetting front depths, provided values of soil tension ( $\bar{\psi}$ ) are measured at these depths using tensiometers.

The position of the wetting front at a point in time is evidenced by the soil tensiometer readings falling to zero. In Equation 4, the length of the wetting front ( $L_f$ ) is known by

noting the depth at which the tensiometer was installed. The depth of flooding ( $D_f$ ) is taken

as an average value. The soil suction ( $\bar{\psi}$ ) is set equal to the average soil tension preceding the passage of the wetting front. The infiltration rate ( $q$ ) is determined by weighing the flexible bag (Figure 1) periodically to determine the volume of water lost. The change in volume is then divided by the area of the inner ring and the elapsed time over which the volume change occurred. The values of  $q$ ,  $L_f$ ,  $L$ , and  $\bar{\psi}$ , are then used to back calculate  $K$  from

Equation 4. In addition, it is possible to evaluate  $K$  for individual layers of the clay fill, i.e., zero to 6 inches, 6 inches to 12 inches, zero to 12 inches, etc.

The test procedure and analysis methodology described above, is based on the assumptions Darcy's law applies, the test fill is homogeneous and isotropic, the flow from the infiltration ring is vertically downward, and a discrete and well defined wetting front exists between the saturated soil and the partially saturated soil. The assumption of the well-defined wetting front is valid at early stages of the test, but may not be totally valid at subsequent times since a transition zone between the saturated and partially saturated soil is likely to exist. The errors which could be introduced by the possible limited validity of the assumptions, all result in hydraulic conductivity values which will be too high. Consequently, the test results are conservative.

The other method used to analyze the infiltrometer test is suggested by the manufacturer of the test apparatus in their technical literature. This method assumes that steady state conditions exist and soil tension does not contribute to the hydraulic gradient. In this method, Equation 4 is evaluated using the same values as used above, but setting soil tension equal to zero. The depth of the saturated zone will be identified by the depth of the tensiometer which reads zero soil suction (i.e., complete saturation).

#### CASE HISTORY

A test fill was constructed between August 19 and September 4, 1986 on a site just outside of Chemical Waste Management, Inc., Kettleman Hills, California facility. The test fill is approximately 140 feet long by 50 feet wide at the surface, with a depth between three and three and one half feet.

The test fill was underlain with a drainage layer of geonet and geotextile. Prior to hauling soil to the test fill each day, the admix stockpile was moisture conditioned to maintain a moisture content of approximately 30 percent. The admix was placed in approximately eight inch loose lifts. Compaction consisted of wheel rolling by the routing of the scrapers used to haul the soil, and two complete passes with a sheepsfoot compactor.

After the compactor made its last pass, the lift was tested to assure the lift had the proper water content and density, and samples

were obtained for laboratory hydraulic conductivity tests. At the end of each day the test fill was wheel rolled to seal the surface and minimize the moisture lost from the soil. Before a new lift was applied, the underlying lift was scarified and moisture conditioned as a method to improve the bonding between lifts.

#### Field Measurements

After placement and compaction of each lift, a series of field measurements were conducted. The field measurements consisted of nuclear density tests and sand cone density tests for each lift. In addition, samples of admix at each nuclear density test location were obtained for laboratory water content tests and undisturbed shelly tube samples were also obtained from select lifts for laboratory hydraulic conductivity tests. Occasionally, pocket penetrometer tests were also conducted to determine the undrained shear strength of the compacted admix.

#### Laboratory Tests

Laboratory tests were conducted on bulk samples of the admix stockpile to determine the relationship between the degree of compaction, water content and hydraulic conductivity. Tests included index tests, compaction tests and hydraulic conductivity tests.

Shelby tube samples were taken from select lifts of the test fill. Portions of the shelly tubes were then tested to determine the hydraulic conductivity of each lift. The results of these tests are tabulated in Table 1.

TABLE 1. Test Fill Permeability Results

| Tested Depth | Dry Density*<br>(lb/ft <sup>3</sup> ) | Water Content*<br>(percent) | K<br>(cm/sec)      |
|--------------|---------------------------------------|-----------------------------|--------------------|
| lift 1       | 89.0                                  | 30.2                        | 4x10 <sup>-9</sup> |
| lift 2       | 90.0                                  | 30.7                        | 1x10 <sup>-9</sup> |
| lift 3       | 92.5                                  | 29.5                        | 4x10 <sup>-9</sup> |
| lift 4       | 87.8                                  | 31.2                        | 7x10 <sup>-9</sup> |
| lift 5       | 94.2                                  | 26.5                        | 1x10 <sup>-8</sup> |
| lift 6       | 97.6                                  | 24.3                        | 2x10 <sup>-8</sup> |
| lift 7       | 92.7                                  | 30.7                        | 2x10 <sup>-9</sup> |

\* Density and water contents from lift near permeability sample.

$$1 \text{ lb/ft}^3 = 16.02 \text{ kg/m}^3$$

#### INFILTRMETER TEST

##### Site Preparation and Installation

The test fill was prepared for the infiltrometer by using a motor grader and a vibratory drum roller to level and smooth the test fill's surface. The surface was lightly sprayed with water and then covered with a black plastic tarp.

The outer rings for both sets of infiltrometers were positioned on the tarp and their outlines were marked on the tarp to locate the trenches for the rings. The outer rings trenches were

cut with a Ditch Witch, series 1420, to a depth of 18 inches. The inner rings were positioned in the center of the outer rings and their outlines marked. The five inch deep trenches for the inner rings were cut by hand using mason's hammers.

The outer ring trenches were sealed with bentonite pellets while the outer ring was in the trench. The trenches for the inner rings were sealed with a thin layer of bentonite pellets in the bottom of the trenches and the remainder of the depth filled with a viscous Voclay grout. The inner rings were placed in their trenches during the grouting process.

The inner ring was checked for leaks by adding a little water to it. The outer ring was flooded until the inner ring was slightly submerged, then the inner ring was partially filled. The outer ring was filled to its final depth and the inner ring was topped off. The bags and hoses for the measurement of water infiltrating through the inner rings were attached, the inner ring was purged of air, and the tests began.

#### Data Collection

Each inner ring has a heavy duty flexible bag of water connected to it in order to provide a volume of water to replace that water which infiltrated the test fill beneath the inner ring. The bags were fitted with no volume change valves to allow new (refilled) bags to be exchanged after the original bags were depleted without any water loss. The difference in the initial and final weight of the bag is the amount of infiltration that occurred over that particular time period. During the first days of the test, several bags of water were needed each day. In less than a week, each bag was changed once a day.

In addition to the amount of infiltration, data collected daily for each ring included: depth of water in the outer ring, temperature of the water, and tensiometer values. Notes about the condition of the water (i.e., algae growth) and the test fill, and the weather were recorded when deemed relevant. Periodically, the inner rings were purged of any air which may have collected in the inner rings. The air volume was measured and the the accumulative infiltration adjusted to include this volume. In general, the volume of air purged from the system was very small compared to the volume of water infiltrating on a daily basis.

#### Results Based on Using Tensiometers

Both the North and South Rings have two tensiometers, each at the depths of 6, 12, 18, and 24 inches (a total for both rings of 16 tensiometers). The tensiometers register the passage of the wetting front by displaying a soil tension of zero. All of the tensiometers went to zero at different times; therefore, the values used to solve for the hydraulic conductivity are different for each of the tensiometers. Figures 2 and 3 present the accumulated infiltration as a function of time for the North and South Rings. Figure 4 presents two examples of the soil tension versus time. The values used

in Equation 4 are listed in Table 2.

Figure 2. Accumulative Infiltration Versus Time (North Ring)

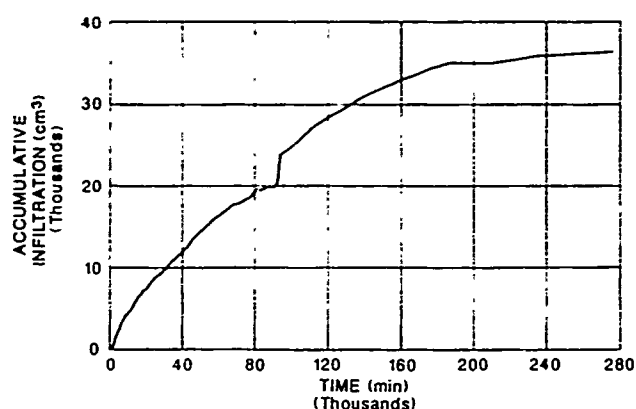


Figure 3. Accumulative Infiltration Versus Time (South Ring)

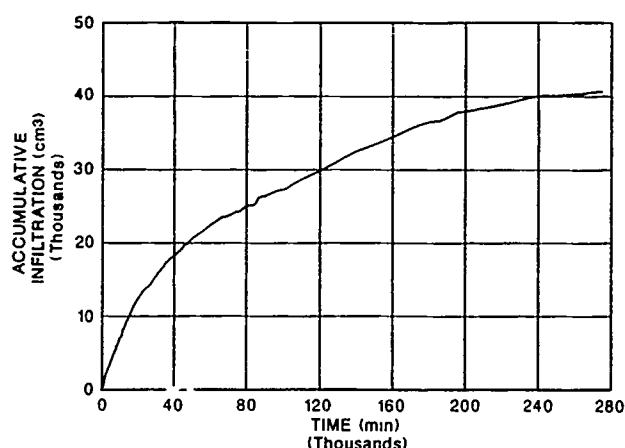


Figure 4. Soil Tension Versus Time at 24 Inch Depth (North Ring)

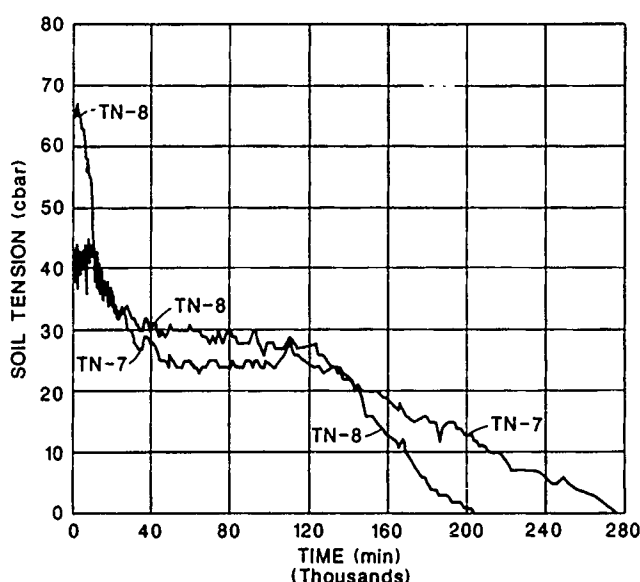


TABLE 2. Infiltrometer Test Values

| Tensiometer | q<br>(cm/sec)          | D <sub>f</sub><br>(in) | L <sub>f</sub><br>(in) | ψ<br>(in) |
|-------------|------------------------|------------------------|------------------------|-----------|
| TN-1        | 3.1 x 10 <sup>-7</sup> | 11.1                   | 6                      | 60.3      |
| TN-2        | 2.3 x 10 <sup>-7</sup> | 11.1                   | 6                      | 100.5     |
| TN-3        | 1.1 x 10 <sup>-7</sup> | 11.4                   | 12                     | 76.4      |
| TN-4        | 1.6 x 10 <sup>-7</sup> | 11.4                   | 12                     | 76.4      |
| TN-5        | 9.9 x 10 <sup>-8</sup> | 11.5                   | 18                     | 92.5      |
| TN-6        | 1.3 x 10 <sup>-7</sup> | 11.4                   | 18                     | 100.5     |
| TN-7        | 4.1 x 10 <sup>-8</sup> | 11.5                   | 24                     | 56.3      |
| TN-8        | 5.5 x 10 <sup>-8</sup> | 11.4                   | 24                     | 56.3      |
| TS-1        | 4.3 x 10 <sup>-7</sup> | 10.8                   | 6                      | 112.6     |
| TS-2        | 4.2 x 10 <sup>-7</sup> | 10.8                   | 6                      | 74.4      |
| TS-3        | 1.5 x 10 <sup>-7</sup> | 10.8                   | 12                     | 60.3      |
| TS-4        | 1.9 x 10 <sup>-7</sup> | 10.8                   | 12                     | 48.2      |
| TS-5        | 8.7 x 10 <sup>-8</sup> | 10.9                   | 18                     | 56.3      |
| TS-6        | 8.6 x 10 <sup>-8</sup> | 10.9                   | 18                     | 30.2      |
| TS-7        | 6.4 x 10 <sup>-8</sup> | 10.9                   | 24                     | 68.3      |
| TS-8        | 8.0 x 10 <sup>-8</sup> | 10.9                   | 24                     | 64.3      |

NOTE: ψ (in) = ψ (cbar) x 4.02

1 in = 2.54 cm

The hydraulic conductivity for the soil between two particular depths is the geometric mean of the separate values for that range of depth. Applying the values given in Table 2 to Equation 4, the range of hydraulic conductivity for the soil of depths for each six inch thickness of soil is presented in Table 3.

TABLE 3. Summary of Infiltrometer Test Accounting for Soil Tension

| Soil Depths<br>(in) | Range in<br>Permeability<br>(cm/sec)        | Geometric<br>Mean<br>(cm/sec) |
|---------------------|---|-------------------------------|
| 0 - 6               | 1 x 10 <sup>-8</sup> - 3 x 10 <sup>-8</sup> | 2 x 10 <sup>-8</sup>          |
| 6 - 12              | 1 x 10 <sup>-8</sup> - 3 x 10 <sup>-8</sup> | 2 x 10 <sup>-8</sup>          |
| 12 - 18             | 1 x 10 <sup>-8</sup> - 3 x 10 <sup>-8</sup> | 2 x 10 <sup>-8</sup>          |
| 18 - 24             | 1 x 10 <sup>-8</sup> - 2 x 10 <sup>-8</sup> | 1 x 10 <sup>-8</sup>          |

1 in = 2.54 cm

The composite hydraulic conductivity for the soil from zero to twenty four inches deep is calculated by applying to Equation 5, the mean hydraulic conductivity for the different ranges of depth.

Applying the geometric means given in a preceding paragraph, the equivalent hydraulic conductivity for the depths from zero to twenty four inches is 2x10<sup>-8</sup> cm/sec.

#### Results Without Considering Soil Suction

An alternative methodology suggested for analysis of the test provided by the manufacturer is based upon the assumption that soil suction is not a factor in the hydraulic gradient. This assumption is valid only when steady state is reached. Assuming steady state is attained when and where the soil is saturated, Equation

4 may be applied if the soil suction term is set to zero. The resulting hydraulic conductivity ranges are shown in Table 4.

Applying these values to Equation 5, the equivalent hydraulic conductivity for the depths from zero to twenty four inches is

$6 \times 10^{-8}$  cm/sec.

$$K = \frac{D}{\frac{d_{0-6}}{K_{0-6}} + \frac{d_{6-12}}{K_{6-12}} + \frac{d_{12-18}}{K_{12-18}} + \frac{d_{18-24}}{K_{18-24}}} \quad (5)$$

where  $K$  = equivalent hydraulic conductivity (L/T)

$D$  = total depth (L) (= 24 in)

$d_{a-b}$  = depth of the zone a to b (L) (= 6 in)

$K_{a-b}$  = hydraulic conductivity of the zone a to b (L/T)

TABLE 4. Summary of Infiltrometer Test Without Accounting for Soil Tension

| Soil Depths (in) | Range in Permeability (cm/sec)        | Geometric Mean (cm/sec) |
|------------------|---------------------------------------|-------------------------|
| 0 - 6            | $8 \times 10^{-8} - 2 \times 10^{-7}$ | $1 \times 10^{-7}$      |
| 6 - 12           | $6 \times 10^{-8} - 1 \times 10^{-7}$ | $8 \times 10^{-8}$      |
| 12 - 18          | $5 \times 10^{-8} - 8 \times 10^{-8}$ | $6 \times 10^{-8}$      |
| 18 - 24          | $3 \times 10^{-8} - 6 \times 10^{-8}$ | $4 \times 10^{-8}$      |

1 in = 2.54 cm

#### Discussion of Results

The tensiometers had different values and registered zero soil suction at different times for the same depth. This is expected for a material that had different moisture contents when placed. In the North Ring, one of the tensiometers at the 18 inch depth measured zero soil suction after one of the 24 inch tensiometers on the opposite side of the North Ring had measured zero. This could be the result of different moisture contents and compactive efforts of the placed material causing a greater hydraulic conductivity on one side of the infiltrometer. Tensiometers TN-3, TN-5, and TN-7 all recorded zero soil suction after their counterparts. A review of the field data for the density and moisture content of the soil from 12 to 18 inches revealed one test on the south side of the North Ring which had a low density and a high moisture content. This moisture/density relationship may result in a higher hydraulic conductivity, but the true effect can not be quantified.

The scale of the infiltrometer tests appears to be evaluating the overall hydraulic conductivity of the test fill rather than the hydraulic

conductivity of discrete samples, which is accomplished in laboratory tests. The hydraulic conductivity results of the infiltrometer tests utilizing the tensiometers are consistent between the North and South Rings and between the soil at different depths.

The infiltrometer test results, which accounted for soil tension, compared well with the laboratory results for hydraulic conductivity. The geometric mean of the laboratory results is

$5 \times 10^{-9}$  cm/sec, and the geometric mean of the infiltrometer tests is  $2 \times 10^{-8}$  cm/sec. The difference between the means of less than an order of magnitude is considerably better than previous investigations (Day and Dannel, 1985a). The good results in the field tests underscore the importance of quality control during construction of the test fill and installation of the infiltrometer.

The analysis of the infiltrometer data without accounting for soil tension reveal that the differences between the infiltrometer and the laboratory results may be as much as two orders of magnitude. If the full thickness of the test fill were considered saturated when only the first six inches were saturated, the gradient would be  $1.31$  ( $1 + D_f/L_f = 1 + 11/36$ ). The resulting hydraulic conductivity would

range from  $2 \times 10^{-7}$  cm/sec to  $3 \times 10^{-7}$  cm/sec. Clearly this method of analysis gives an overly conservative upper bound of the hydraulic conductivity of the material.

At the end of the test, the system can be assumed to be saturated through its entire depth. No water was noted to drain out the underlying drainage layers. Since the system drains to the edge of the test fill, any water draining from the system would be hard to notice because of the high evaporation of the site and low flow rates. Using the last infiltration rates for the two infiltrometer

sets ( $1.5 \times 10^{-8}$  cm/sec and  $1.6 \times 10^{-8}$  cm/sec), and assuming steady state, the hydraulic conductivity would be  $1 \times 10^{-8}$  cm/sec.

The test fill took over 200 days to be saturated through the first two feet. To shorten the time to conduct the test, the tensiometers could have been used to identify the saturated depth. If the analysis included the use of the tensiometers to identify the depth of saturation without accounting for the soil tension, the hydraulic conductivity results after the first six inches of the test

fill were saturated would only be  $8 \times 10^{-8}$  cm/sec to  $2 \times 10^{-7}$  cm/sec. The first six inches took just over 21 days to be completely saturated. Therefore, use of the tensiometers just to note the saturated depth does not improve the results significantly, while using the tensiometers to quantify soil suction does improve the analysis significantly.

#### CONCLUSIONS

An in situ hydraulic conductivity test using two sets of sealed double ring infiltrometers

was conducted with the soil suction measured by tensiometers. The infiltrometer tests have worked to adequately characterize the in situ hydraulic conductivity of the clay liner. The results display good consistency between the North and South Rings and between the soil at different depths. In addition, the laboratory hydraulic conductivity tests conducted on samples of the test fill correlate well with the results from the infiltrometer. Using the tensiometers and accounting for soil tension could reduce the testing time by approximately a factor of ten. Using the tensiometers merely to identify the saturated thickness may improve the correlation between the laboratory and field hydraulic conductivity tests, but not improve it significantly.

#### References

- Daniel, D.E., (1984), "Predicting Hydraulic Conductivity of Clay Liners", Journal of Geotechnical Engineering, Proceedings of the ASCE, Vol. 110, No. 2, 285-300.
- Daniel, D.E., and S.J. Trautwein, (1986), "Field Permeability Test for Earthen Liners", Proceedings of In Situ '86, Geotechnical Special Publication No. 6, 146-160.
- Day, S.R. and D.E. Daniel, (1985a), "Hydraulic Conductivity of Two Prototype Clay Liners", Journal of Geotechnical Engineering, Proceedings of the ASCE, Vol. 111, No. 8, 957-970.
- Day, S.R. and D.E. Daniel, (1985b), "Field Permeability Test for Clay Liners", Hydraulic Barriers in Soil and Rock, ASTM STP 874, A.I. Johnson, R. K. Frobels, N.J. Cavalli, and C.B. Pettersson, Eds., American Society for Testing and Materials, Philadelphia, 276-288.
- Stewart, J.P., and T.W. Nolan, (1987), "Infiltration Testing for Hydraulic Conductivity of Soil Liners", Geotechnical Testing Journal, GTJODJ, Vol. 10, No. 2, 41-50.



## Hazardous Waste Disposal Site Hydrogeologic Characterization

S.M. Testa

Vice President, West Coast Operations, Engineering Enterprises, Inc.,  
Long Beach, California

**SYNOPSIS:** A major hazardous waste disposal facility near Arlington, Oregon serving the Pacific Northwest, Canada, and Alaska maintains numerous favorable environmental characteristics for siting of a hazardous waste disposal facility.

The risk of contamination as a result of potential leakage from a waste management unit via primary pathways to surface water, groundwater or by direct contact and/or ingestion is thus reasonably low. However, these same characteristics which make the site most suitable for hazardous waste disposal often conflict with: 1) the demonstration of the groundwater monitoring system's ability to adequately perform immediate leak detection monitoring as mandated under the Resource Conservation and Recovery Act (RCRA), 40 CFR Part 264, part F, and, 2) the level of demonstration required for the site to be "properly characterized."

### INTRODUCTION

An extensive field investigative program to characterize existing site geologic and hydrogeologic conditions was conducted during the period from December, 1983 through November, 1986 in support of a Part B Application under RCRA (Dames & Moore, 1983). This program has included:

- o Detailed geologic mapping including trenching to evaluate and characterize faults;
- o Drilling of over 102 boreholes and installation of over 120 wells/piezometers to depths ranging to 363 feet below ground surface to evaluate subsurface hydrogeologic conditions and the groundwater flow regime;
- o Collection of undisturbed samples for detailed laboratory evaluation and testing;
- o Performance of both pumping/packer and slug tests to assess in-situ hydraulic characteristics and possible intercommunication between the uppermost aquifer and the underlying basalts;
- o Performance of both surface and borehole geophysics;
- o Performance of analytical testing of groundwater samples to evaluate general water chemistry and water quality, including the presence of tritium to assess recent recharge; and
- o Development of a groundwater detection monitoring network.

The results of the site characterization, specifically, the site geology, and the existing groundwater recharge-discharge regime, and the implication to site suitability and groundwater detection monitoring are discussed herein.

### SITE DESCRIPTION

The Arlington facility is located 6.5 miles south of the Columbia River and 7.5 miles southwest of the town of Arlington in Gilliam County, Oregon (Figure 1). The facility site is situated on a 640-acre parcel, of which 320 acres (eastern tract property) are currently used for waste management operations (Figure 2). The property is bounded on the south by the east-west trending Alkali Canyon at an elevation of approximately 700 feet (site datum). The upland plateau is at an elevation of approximately 850 to 995 feet. Waste management activities are limited to that area above 920 feet on the eastern tract property. In the southern portion of the property bounded by Alkali Canyon, the relief between the valley floor and the upland plateau is approximately 280 feet.

Adjacent tracts to the north, east, south, and west of the site are owned by others. Portions of the tract to the east of the Chem-Security site are under cultivation and are irrigated. The facility is remote from any residential, commercial, or industrial developments. The nearest residence is approximately one mile by road west of the western site boundary.

### FACILITY LAYOUT AND OPERATION

The Arlington facility was opened in 1976 and provides hazardous waste treatment, storage, and disposal services primarily to the Pacific Northwest, Alaska, and Hawaii, although it also receives hazardous wastes from other western states and Superfund-related activities. The Arlington facility presently operates under RCRA Part A Interim Status authorization, and a Hazardous Waste Disposal Site License from the Oregon State Department of Environmental Quality (DEQ License No. HW-1). PCB wastes regulated under the Toxic Substances Control Act (TSCA) are accepted at the site under authorization from EPA Region X and are stored, treated, and

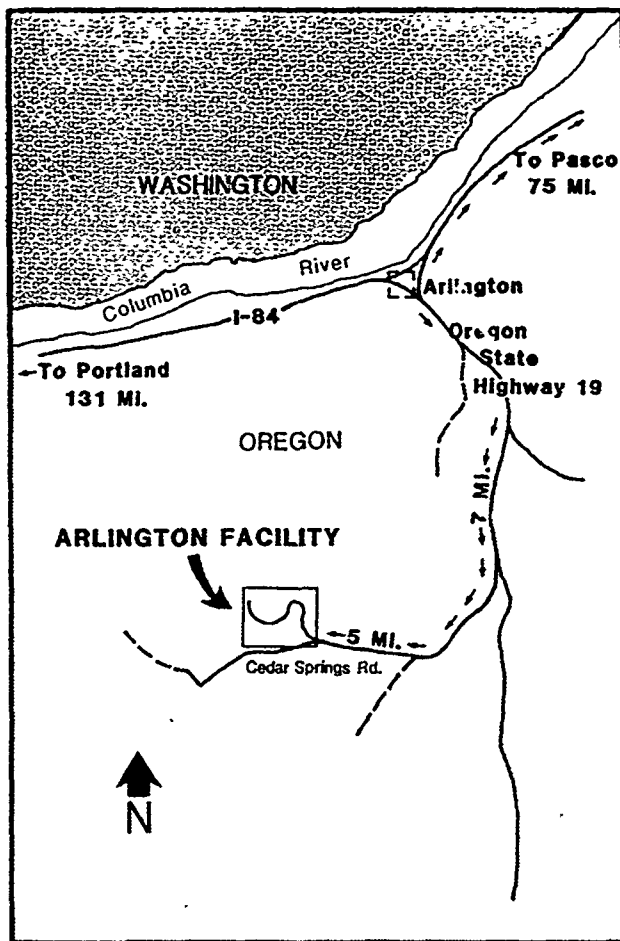


Figure 1 Site Location Map

disposed of separately from the RCRA-regulated wastes. The facility does not accept explosive, radioactive, or infectious wastes. Wastes that cannot be treated or disposed of at the facility, or that can be reused or recycled are temporarily stored at the facility and then shipped elsewhere for treatment, recycling, disposal, or beneficial use.

The existing waste management units that require groundwater monitoring under RCRA at the Arlington facility include surface impoundments, reactive solids hydrolysis, and landfills (of which four are complete), seven container storage areas and four storage tanks comprise the existing major RCRA waste management units at the site; although additional facilities are planned for the future. A liquid waste solidification system and a truck-wash operation are also in use. The layout of the existing waste management units of most importance at the facility shown in Figure 2.

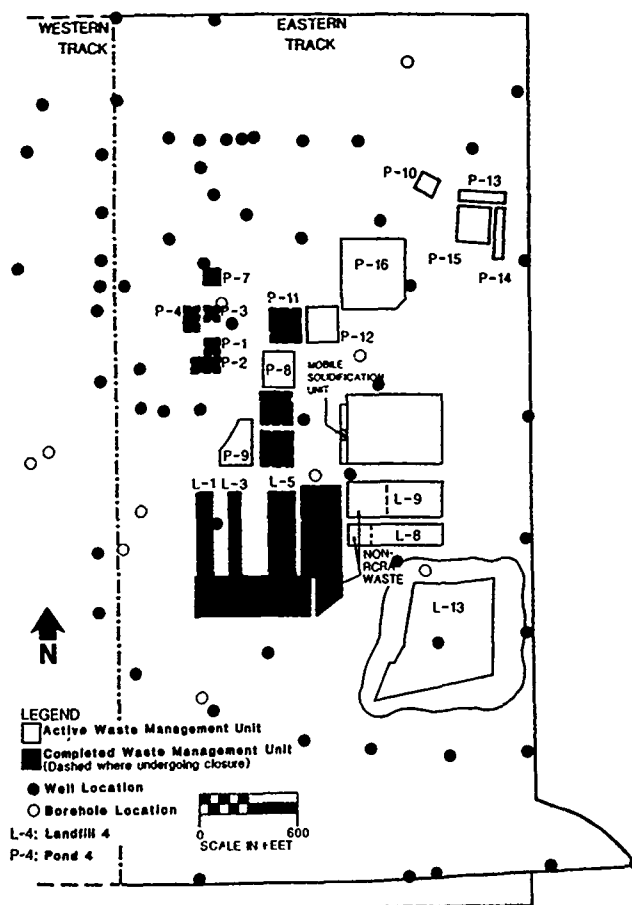


Figure 2 Facility Layout Map Showing Major Waste Management Units

#### GEOLOGIC SETTING

The Arlington facility is located in the south-central portion of the Columbia Plateau physiographic province within the Deschutes-Umatilla Plateau (Dicken, 1955). The area is characterized by upland areas of sandy deserts separated by relatively wide, deep to moderate ephemeral stream drainages such as the Alkali Canyon which borders the south side of the property. In addition to the semi-arid climate, several factors account for the physiography of the area and include the presence of extensive flood-basalt bedrock, subsurface geologic structure, and catastrophic floods of glacial meltwater.

The subsurface geology of the facility and surrounding areas consists of a thick, accretionally layered sequence of basalt flows and sedimentary interbeds, collectively known as the Columbia River Basalt Group. The basalt flows are part of the Columbia Plateau geological flood-basalt province (Fenneman, 1931) of Miocene to lower Pliocene age (8 to 17 million years old). This sequence is unconformably overlain by younger intercalated and suprabasalt sedimentary units of Miocene to Holocene age.

Within the site area the formations which comprise the Columbia River Basalt and the Ellensburg Formation include several members of regional extent. These are the Frenchman Springs and Priest Rapids Members of the Wanapum Basalt, the Pomona Member of the Saddle Mountains Basalt, and the Selah and Rattlesnake Ridge Members of the Ellensburg Formation. In addition to these formal stratigraphic units, several informal units useful to comprehension of site structure and stratigraphy are defined. These include several unnamed interbeds within the Priest Rapids Member, and an areally extensive vitric tuff which occurs at the top of the Selah Member. In addition to the informal units are several facies of local extent. These include three facies of different lithology within both the Selah Member of the Ellensburg Formation and the Dalles Formation. A generalized stratigraphic column is shown in Figure 3. A discussion of the underlying geologic units, oldest to youngest, is presented below:

#### Grand Ronde Basalt

The Grande Ronde Basalt is the oldest formation within the Columbia River Basalt group in the site area. In the site area, thickness of the Grande Ronde Basalt is not known although it is suggested to be probably 3,000 to 4,000 feet thick based on review of well records and regional outcrops (Rockwell Hanford Operations, 1979). Because these large flows advanced to the limits of the Plateau and then cooled while ponded, they form nearly continuous sheets of competent, black, glassy, fine-grained, columnar-jointed basalt, which are separated by vesicular to rubbly flow breccias which occur at the top of most of the flows. Only a few thin discontinuous sediments occur as interbeds within the Grande Ronde. This unit was not penetrated by on-site borings.

#### Vantage Member of the Ellensburg Formation

The Vantage Member of the Ellensburg Formation is an arkosic sandstone deposited by the ancestral Columbia River on top of the Grande Ronde Basalt. In most areas of the Plateau the Vantage sandstone is absent; however, a well developed saprolitic soil generally considered to be part of the member occurs at its stratigraphic position on top of the Grande Ronde. This unit was also not penetrated by on-site borings but is about 22 feet in thickness as noted in a boring drilled about six miles southeast of the facility (Foundation Sciences, Inc., 1980a).

#### Priest Rapids Member

The Priest Rapids Member of the Wanapum Basalt consists of two to six large and several smaller basalt flows. In the site area, the member is comprised of two flows which are laterally contiguous with the Priest Rapids Member north of the Columbia River (Schminke, 1964) and generally separated by an interbed. A thickness of 136 feet is inferred from a geophysical log of the onsite water supply well.

| PERIOD   | EPOCH       | AGE                   | STRATIGRAPHIC UNIT                | GEOLOGIC UNIT (Common Name)       | LITHOLOGY   |
|----------|-------------|-----------------------|-----------------------------------|-----------------------------------|---|
| Tertiary | Quaternary  | Recent                |                                   | Loess                             | Silt and sand of Eolian origin  |
|          |             |                       |                                   | Alluvium                          | Sand gravel and silt water-laid   |
|          |             |                       |                                   | Colluvium                         | Slope wash-silt, sand & rock frag   |
|          | Pleistocene | 1.6 mil years         |                                   | Flood Gravels                     | Sand and gravel, some silt, some caliche  |
|          |             |                       |                                   | Channel unit                      | Poorly sorted silty gravel  |
|          | Neogene     | 1.6-5.3 million years | Dalles Foundation                 | Upper Tuff Unit                   | Tan to light green, massive, very soft  |
|          |             |                       |                                   | Conglomerate Unit                 | Poorly to moderately indurated conglomerate   |
|          |             |                       |                                   | Rattlesnake Ridge Member          | Weathered tuff  |
|          |             |                       | Ellensburg Formation              | Pomona Basalt                     | Dark grey, very hard, massive, fine grained occasionally vesicular                        |
|          |             |                       | Saddle Mountains Basalt Formation | Vitric Tuff Unit                  | Light buff to cream, very soft  |
|          |             |                       | Ellensburg Formation              | Selah Member                      | Tuffaceous siltstone (some clay and sand interbeds), light olive green, very soft to soft |
| Neogene  | Miocene     | 13.6 million years    | Wanapum Formation                 | Priest Rapids Basalt (Upper Flow) | Dark grey, massive, fine grained, occasionally vesicular, very hard                       |
|          |             |                       |                                   | Priest Rapids Interbed            | Tuffaceous vitric to lithic tuff, light olive green very soft to soft                     |
|          |             |                       |                                   | Priest Rapids Basalt (Lower Flow) | Dark grey, massive fine grained occasionally vesicular, very hard                         |
|          |             |                       |                                   | Frenchman Springs Basalt Member   | Dark gray, massive, fine grained, occasionally vesicular, very hard                       |
|          |             |                       |                                   | Grande Ronde Fm                   | Grande Ronde Basalt   |

LEGEND "-----" Unconformity

Figure 3 Generalized Stratigraphic Column

The upper part of the lower Priest Rapids flow and the Priest Rapids interbed are exposed in several outcrops in the vicinity of the site, and were reached in several onsite boreholes. The lower flow is approximately 45 feet thick. It is very similar to the upper flow with respect to petrography, jointing, and joint linings; however, in most of the boreholes the lower flow has a flow-top breccia. This breccia consists of ash to block-size fragments of scoria and vesicular basalt that is often loose; however, in some places it is slightly welded to form a relatively competent rock. Open voids are typical of this interval. In some boreholes, the voids are infilled with fine-grained sedimentary material which effectively reduces the permeability of the breccia.

The Priest Rapids interbed varies from two-to-twelve feet thick in boreholes at the site and is characterized as a tuffaceous siltstone; however, it is quite variable in lithology and includes clayey silt, silty clay, weathered hyaloclastite, and clayey silty sandstone.

The upper Priest Rapids flow at the site generally consists of hard, dark gray to greenish gray basalt. The upper few feet of the flow consist of vesicular basalt, flow breccia, or scoria that is moderately weathered or decomposed. The weathered basalt consists of soft to

medium hard rock with the consistency of a clayey, sandy siltstone because of alteration.

The upper Priest Rapids flow varies from approximately 60 to 95 feet in thickness at the site. In outcrops in Alkali Canyon southwest of the site, the upper Priest Rapids flow is characterized by well developed columnar jointing ranging from four to eight feet in diameter and rise from the base of the flows for two-thirds to three-fourths the total thickness. Nearly vertical and roughly hexagonal in cross section, these columns are cut into sections by subhorizontal cross-joints with highly variable spacing (0.5 to 10 feet). Randomly oriented joints frequently extend through the upper part of the colonnade. These random joints increase in density upwards, creating a brickbat jointing pattern which forms the upper one-third to one-fourth of the flow. A generalized schematic diagram showing the structure of a typical basalt flow is shown in Figure 4.

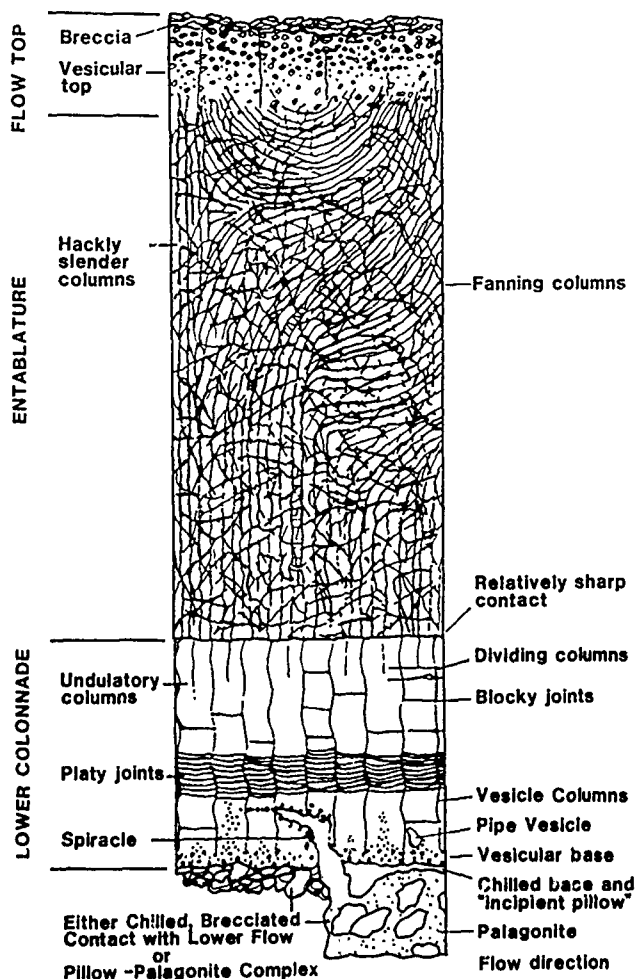


Figure 4 Generalized Schematic Diagram Showing Structure of a Basalt Flow

#### Selah Member

The Selah Member of the Ellensburg Formation (Schminke, 1967) occurs as an interbed between the Priest Rapids Member and the Saddle Mountains Member. Deposited directly on the underlying Priest Rapids Basalt, it is the most prominent interbed in the vicinity and is comprised of weathered tuffs and fluviolacustrine tuffaceous sediments that accumulated during the volcanic hiatus between extrusion of the Priest Rapids and Pomona Basalts. The thickness of the Selah varies from approximately 115 to 160 feet in boreholes at the site where the top has not been eroded in channels of Dalles or glaciofluvial gravel. The uneroded Selah averages approximately 138 feet in thickness.

The Selah contains three facies which are readily distinguishable on geophysical logs. Due to severe weathering, and zeolitic and clayey alteration of the member, they are not as discernable in outcrop or borehole samples. The facies include: 1) a lower facies comprised primarily of flood plain deposits derived from the Columbia Plateau and adjacent areas, but also containing three to four airfall tuff units; 2) a middle facies similar to the lower, but containing large amounts of silicic-volcaniclastic material derived from volcanic areas; and, 3) an upper or channel facies which results, in part, from reworking of the lower two facies.

The lower facies of the Selah is distinguished from the overlying middle and upper channel facies by generally lower density and higher porosity, and from the middle facies by lower potassium content as indicated by the gamma gamma, neutron neutron, and natural gamma logs, respectively. Where the middle facies overlies the lower facies a marked decrease in natural gamma occurs at the boundary. Samples of the lower lithologies have textures which range from yellow-green massive clayey siltstone to laminated sandy siltstone, and yellow-brown to blue-green silty sandstone. Bedding is generally preserved in the sandy layers but obscured by weathering and possibly by bioturbation in silty claystone and clayey siltstone intervals. Tuff layers in the lower member are altered to massive silty claystone; their origin is indicated only by their high natural gamma and the presence of accretionary lapilli. In many of the boreholes, a blue-green, fine-grained sandstone occurs at the base of the Selah. The thickness and distribution of the sandstone are variable. Thickness variations of the lower facies suggest that the east-west trending anticline initiated development during deposition of the lower facies of the Selah. This is demonstrated by non-deposition of the lower facies in the north-central portion of the site at the approximate location of the axial trace of the structural high, and systematic thickening to the north and south. Variations of the lower facies of the Selah, therefore, appears to account for most of the variation in the total thickness of the Selah Member, except in localized areas where the Dalles Channel exist.

The middle facies of the Selah consists of soft to medium hard yellow green to brown, tuffaceous, silty claystone and clayey siltstone. It is characterized by higher natural gamma, higher density, and lower porosity than the lower facies. Samples of the middle facies from boreholes frequently contain finely laminated, weathered tuffs.

Locally, the middle or highly tuffaceous facies of the Selah Member appears to contain broad shallow channels filled with flood plain deposits range from clayey siltstone to fine sandy siltstone. These channel-fill sediments have low natural gamma similar to the lower facies. However, unlike the lower facies, they are dominantly weathered tuff that has the consistency of clayey siltstone.

Two of the test trenches excavated at the site exposed the top of the Selah member and provide excellent exposures of the middle facies. In both trenches the Selah consists of weathered tuffs that have the consistency of clayey siltstone and silty claystone. At natural moisture content they appear massive; however, upon drying fine laminations are locally visible.

#### Vitric Tuff Bed of the Selah Member

A gray, dacitic, vitric tuff attaining a maximum thickness of about 30 feet occurs at the top of the Selah Member of the Ellensburg Formation. Geologic mapping in the area indicates that the ash most likely originated from eruptions in the Cascades Range (Schminke, 1964). Texturally, the vitric tuff is soft to medium hard, gray, medium-grained sandstone (tuff) which is well-sorted and massive in the central 20 to 24 feet of the deposit. The lower one to five feet consist of soft to medium hard, gray to dark gray, laminated, silty sandstone (tuff) and sandy siltstone (tuff). The finer laminae are weathered to soft, clayey siltstone or silty claystone. The upper three to eight feet consist of silty, fine to medium, vitric sandstone that occurs as cross-laminated and/or thinly graded beds. These fine-grained layers consisted of weathered clayey silt/silty clay similar to the bottom laminated portion. Development of an open-pit pozzalana mine and explorations for its development have provided nearly continuous exposure of the vitric tuff in the southern part of the site.

#### Rattlesnake Ridge Member of the Ellensburg Formation

Overlying the vitric tuff in the north part of the site is a tan, fine-grained tuff which varies from zero to about eight feet thick. It averages four to six feet in thickness in areas where it was not scoured away prior to deposition of the overlying Dalles conglomerate. In the south part of the site, the tan tuff rests directly on the underlying vitric tuff and has a sharp, conformable contact with it. The tuff typically consists of weathered to decomposed fine volcanic ash and has the texture of a plastic, silty clay or clay which is largely montmorillonitic. The tuff is generally massive; however, locally the top and bottom few inches have thin laminae of carbonaceous material.

#### Pomona Member

The Pomona flow is restricted to the northern portion of the site and consists of very hard, black, fine-grained to glassy porphyritic basalt. Maximum thickness is about 40 feet while the average thickness is about 20 feet. The Pomona onsite exhibits its characteristic jointing habit of lower colonnade, entablature and upper colonnade (Figure 4). However, where the flow is thin (25 feet thick) the flow top consists of three to five feet of platy jointed, vesicular basalt with little columnar development. Also, development of the distinctive fans of joints in the entablature is attenuated where the flow is thin.

#### Dalles Formation

The Dalles Formation overlies the Columbia River Basalt and Ellensburg Formation throughout the site area. It consists of fluvial gravel, conglomerate, sandstone, fluviolacustrine siltstone, tuffs, and loess. Many fossil soil horizons represented by zones of caliche are present in the Dalles, and local unconformities are common.

Two facies of different origin are present throughout most of the site area: a basal cemented sandstone and conglomerate facies, and an overlying tuffaceous siltstone facies. In addition to these two facies, a third facies consisting of poorly sorted silty, sandy gravel occupies a channel which meanders across the site and is cut to the top of the Selah Member.

#### Surficial Materials

Pleistocene glaciofluvial, slackwater, torrential flood, colluvial, alluvial and Holocene eolian deposits locally mantle the bedrock units.

#### Structural Geology

The geologic structure of the site is relatively simple. The site lies partially astride one of several small east-west anticlinal folds that interrupt the floor of the required Dalles-Umatilla synclinorium. The overall trend of this small anticline is east-west; however, it is somewhat sinuous in detail. The strike of the anticline varies from about N 70 W in the north-east part. North and south of the anticline, the bedrock units dip relatively uniformly to the north and south, respectively, toward adjacent synclines.

Structure contours of the top of the Priest Rapids Member define the shape and amplitude of folding that has occurred in the site area since extrusion of the member approximately 15 million years before present. Maximum amplitude of the fold in the Priest Rapids Basalt is approximately 130 feet between the local culmination on the anticline in the northwest corner of the site and synclinal axis south of the site in Alkali Canyon. Average dip of the Priest Rapids Basalt is about 1.5 degrees although higher dips occur along the anticlinal axis (1.5 to 5 degrees), and lower dips occur in the south part of the site (0.5 to 1 degrees). Folding of the east-west anticline is slightly disharmonic, in that the folding of the Priest Rapids, Selah, and Pomona was not perfectly concentric.

Folding of the anticline was accompanied by minor faulting along the fold axis. Faults and related shears on the Selah are typically characterized by gouge zones consisting of remolded, plastic clay and clay and thus appear to be of relatively lower permeability than the small thrust faults are typically open or filled with loose glaciofluvial deposits and thus appear to be of relatively higher permeability than that of the Selah.

Evidence developed during investigations of the site and nearby areas indicates a lack of Holocene deformation (i.e., since the Spokane flood, 10,000 to 13,000 years ago). This evidence includes: 1) that developed by geologic mapping which shows that unfaulted glacial flood deposits cover the small faults onsite and in the western tract where no waste management activities presently exist and, 2) by relationships exposed in excavated trenches whereas the fault zones exposed are truncated by unfaulted glacial flood deposits.

#### HYDROGEOLOGIC SETTING

Within the Columbia Plateau, groundwater recharge is derived mainly from incident precipitation and surface runoff; however, a small percentage may also be derived from irrigation and irrigation water diversions from the Columbia River (Pacific Northwest River Basins Commission, 1970). The climate of the Arlington area is arid to semi-arid; consequently, potential rates of groundwater recharge from precipitation are low in comparison with those for the more-humid areas such as the Blue Mountains south of the site. According to National Weather Bureau statistics, the mean annual precipitation at Arlington, Oregon is less than ten inches, mostly occurring between October and March. The low annual precipitation and high summer evapotranspiration (40 to 55 inches) is evidenced by the sparse vegetation consisting of prairie grasses, low flowering plants, sage brush and occasional junipers. Phreatophytes, including some deciduous trees, mostly brought in by early settlers, are found along the steam valleys, near springs, and in other areas where the groundwater table is at moderate to shallow depths (Dickens, 1955).

The principal aquifers within the Arlington area are associated with the interflow zones between basalt flows. The principal interflow aquifers in the site area are within and between the Priest Rapids, Frenchman Springs, and the upper part of the Grande Ronde Basalt. Of these, the Frenchman Springs is the principal aquifer developed locally for irrigational purposes. The use of this aquifer has decreased in recent years due to the reduction in yields as a result of overpumping.

Within the site area, the uppermost basalt aquifer of regional importance occurs within the interbed zone between the two Priest Rapids basalt flows at an elevation of 620 to 640 feet (site datum). The static water level in test wells completed within the Priest Rapids interflow zone is 100 feet or more above that reported for wells completed in the Frenchman Springs. The Priest Rapids has also been severely depleted in recent years because of overpumping. The Grande Ronde, which underlies the Priest Rapids and Frenchman Springs, is tapped by the city of

Arlington for its water supply and by several irrigation wells south of the Arlington facility.

Recharge to the basalt interflow aquifers occurs mainly along outcrops and through fractures which provide hydraulic communication to the surface. The principal areas of groundwater recharge to the Priest Rapids, Frenchman Springs, and Grande Ronde aquifer systems are south of the Arlington facility, where the edge of north dipping basalt flows is exposed and precipitation is comparatively higher. Additionally, the Priest Rapids and Frenchman Springs are exposed locally along the major drainages south of the site which are local areas of groundwater flow within the Columbia River Basalts in the Arlington area is to the north toward the Columbia River.

The interflow aquifers within the Columbia River Basalts typically have high to very high permeability and low storativity because of the open nature, but limited volume, of joints and fractures. Furthermore, because of the generally impervious nature of the intervening tuffaceous sediments and dense basalt, stratigraphically isolated interflow zones may be hydraulically isolated over large geographic areas. This physical and hydraulic separation is commonly reflected by differences in both piezometric levels and water quality between adjacent interflow aquifers.

#### Groundwater Occurrence

The hydrogeologic conditions at the Arlington facility were evaluated by installation of over 120 perimeter and interior wells and/or piezometers at the locations shown in Figure 2. These conditions encountered are complex, consisting of multiple zones of saturation with varying degrees of interconnection (Figure 5). The uppermost zone of saturation beneath the Arlington facility is at the base of the Selah, 100 to 200 feet beneath the existing ground surface. This zone of saturation at the base of the Selah is the first detectable zone encountered during drilling capable of yielding even small quantities of water to an open borehole and it is, therefore, the uppermost zone capable of being monitored. Because of stratification and marked permeability contrasts that exist within and between the overlying Dalles Formation, Pomona Basalt, Vitric Tuff, and the Selah, it is reasonable to expect that isolated, perched zones of saturation could exist above the base of the Selah. However, no such zones have been detected. Furthermore, no perched zones of saturation were identified from the downhole geophysical logs although variation in soil moisture content with depth is evident.

Groundwater occurs under water table conditions at the base of the Selah. It also occurs under both water table and partially confined conditions within the upper Priest Rapids flow above the interbed between upper and lower flows, and within the interflow zone between the two Priest Rapids basalt flows. Barometric efficiency tests were performed to assess whether there were measurable fluctuations in water levels as a result of changes in atmospheric pressure. The test indicated that water level fluctuations in the uppermost aquifer within the lower portion of the Selah on the order of 0.25 foot, and that these fluctuations are in part of a function of varia-

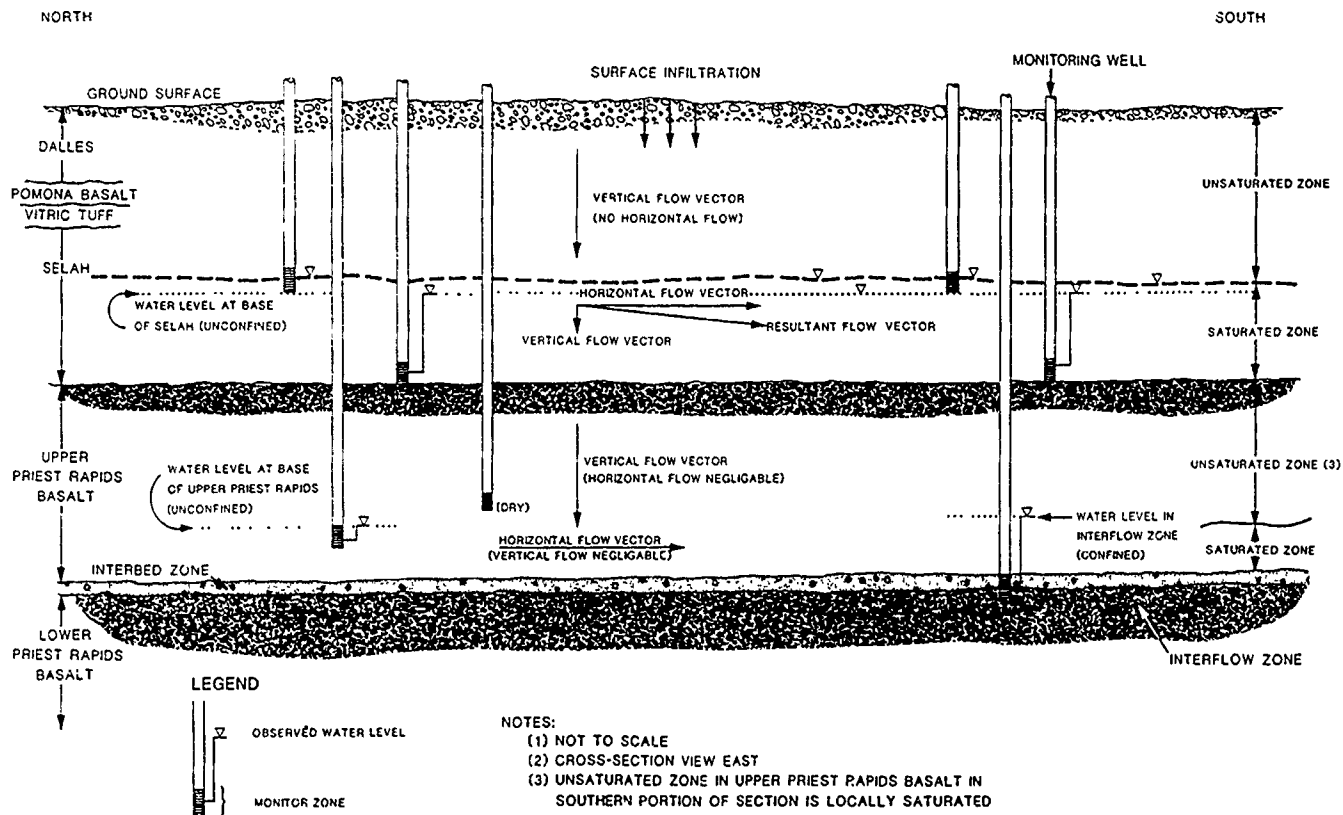


Figure 5 Conceptual Flow Model Showing Flow Vectors in Relationship to Observed Water Levels

tions in atmospheric pressure. Thus, the uppermost aquifer is partially confined and therefore responds to changes in atmospheric pressure; although these fluctuations are minimal.

The uppermost zone of saturation is located physically within the Selah and above the top of the Priest Rapids Basalt. This saturated zone is continuous across the southern two-thirds of the site (north of Alkali Canyon) where waste management activities occur. It is either thin or absent beneath the northwestern corner and in the north-central part of the site. Groundwater that would otherwise be present in these areas is believed to flow downward from the Selah into the Priest Rapids, in contrast to other areas of the site where groundwater is perched on top of the Priest Rapids and forms a continuous saturated zone.

Beneath the northern two-thirds of the site and along its southern margin, an unsaturated zone exists within the upper part of the upper Priest Rapids basalt flow. The thickness of this unsaturated zone ranges from a few feet near the southern boundary of the property to greater than 80 feet in the northern portion of the site. The lower portion of the upper Priest Rapids basalt flow is saturated. In the southeastern portion of the site, continuous saturation appears to exist from the base of the Selah downward to the top of the interbed. The existence of the saturated zone within the Selah is thus a manifestation of the anisotropic nature of the Selah as well as the existence of a low permeability zone(s) at the Selah/Priest Rapids interface.

Groundwater also occurs under both confined and water table conditions within the interflow zone at the top of the lower Priest Rapids basalt flow. Groundwater within the interflow zone beneath the south-central portion of the site, in general, is confined or partially confined. In the northern portion of the site where the interbed rises toward the anticline, groundwater within it exists under water table or unconfined conditions.

#### Groundwater Regime

The groundwater regime within the uppermost zone of saturation within the lower portion of the Selah was evaluated by installation of wells which discretely screened the top of the zone of saturation (on the water table), at or near the base of the Selah and occasionally intermediate between the water table and the base of the Selah. Groundwater flow is predominantly lateral from the groundwater divide in the northwest corner of the site to the south and southeast, and toward Alkali Canyon (Figures 6 and 7). Groundwater movement appears to be principally horizontal, although available piezometric data indicate that there is also a vertical (downward) hydraulic gradient within the zone of saturation. This indicates recharge from the Selah to the Priest Rapids, albeit at a slow rate. The observed pressure head distribution within the Selah suggests the existence of a low hydraulic conductivity zone at the base of the Selah/top of the Priest Rapids. Evidence of the presence of such a layer was found in rock core samples from the Selah/Priest Rapids interface. In these core samples, the fractures and

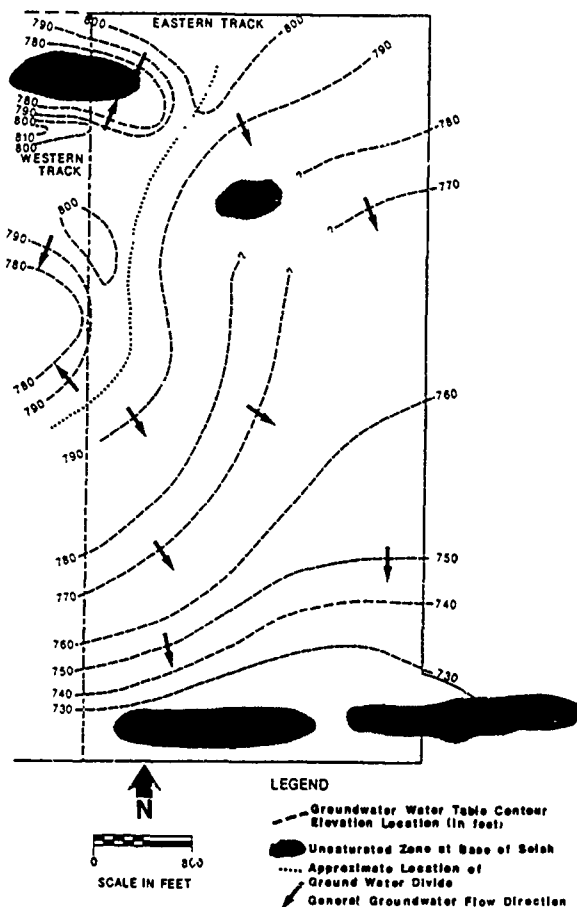


Figure 6 Generalized Groundwater Table Contour Map of Uppermost Aquifer at Base of Selah

vesicles within the top several inches of Priest Rapids were infilled with secondary weathering products (clay and silt).

Comparison of the water table contour map and the piezometric contour map for the base of the Selah compares favorably although the piezometric contours at the base of the Selah more closely reflects the configuration of the top of the Priest Rapids than do the water table contours (Figures 6 and 7). The piezometric head at the base of the Selah is also lower than that of the water table. This reflects the geologic control on groundwater occurrence and the flow regime within the Selah.

Kriging analysis, a statistical technique for estimating quantitative values for spatial (geographic) variables based on the results of sampling at discrete points, was performed to assess the degree of confidence in relation to predicted groundwater flow directions at the site (Wolf and Testa, 1985). The Kriging analysis performed was consistent with and support the regularity and predictability of the groundwater contours (i.e., low variance from a reasonable model) within the active portion of the site. Kriging is limited in that it does not account for geologic and hydrogeologic factors which could reduce the level of uncertainty (i.e., underlying erosional surfaces which may substantially alter the occurrence and

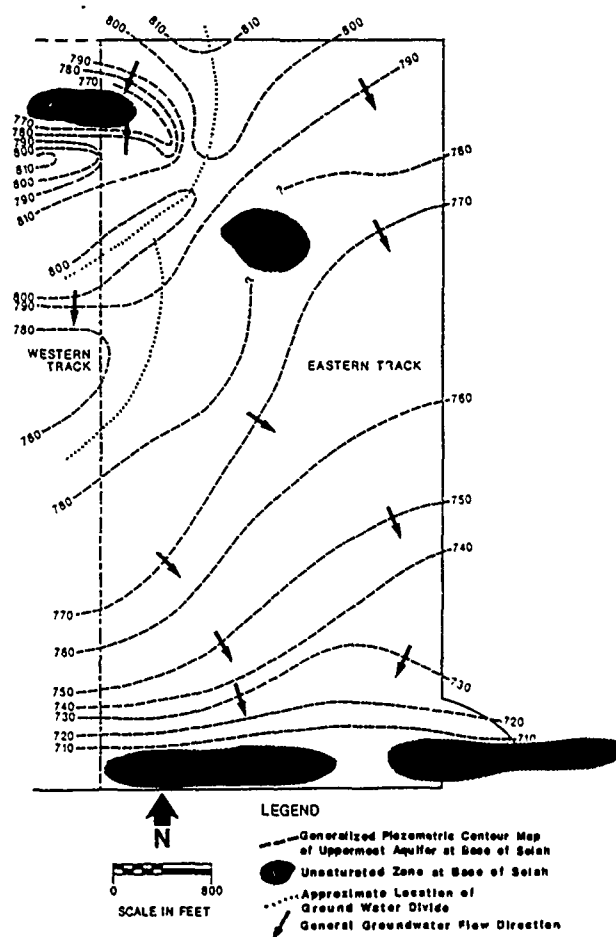


Figure 7 Generalized Piezometric Contour Map of Uppermost Aquifer at Base of Selah

movement of groundwater, or vertical gradients). However, Kriging was used to assess whether the level of uncertainty or variability within the site area is small compared to the overall hydrogeological constraints -- specifically, the boundary condition of the saturated zone and the configuration of the potentiometric surface (Wolf and Testa, 1985).

Recharge to the saturated zone at the base of the Selah is believed to be from direct infiltration of incident precipitation across the site and ponded surface runoff. In this regard, the closed depressions in the northern portion of the site and the silty gravel-filled Dalles channel are believed to be preferential areas for groundwater recharge. Groundwater discharge is to Alkali Canyon as evapotranspiration, as lateral inflow to the glaciofluvial deposits in the canyon and by vertical recharge to the underlying Priest Rapids Basalt. The water table at the base of the Selah is depressed below the top of the Priest Rapids Basalt along the extreme southern boundary of the site. This depression of the water table coincides with a groundwater mound within the upper Priest Rapids basalt indicating recharge from the Selah to the Priest Rapids. Tritium analysis indicates that groundwater within the lower portion of the Selah predates 1953.



## Aquifer Characteristics

The existence of a zone of saturation at the base of the Selah directly overlying an unsaturated zone within upper Priest Rapids Basalt suggests either a permeability contrast between the Selah and the Priest Rapids or the presence of a lower hydraulic conductivity layer or zone. The latter hypothesis is consistent with the observed pressure head distribution within the Selah.

In-situ falling head permeability (slug) tests in open boreholes terminated at the base of the Selah/top of the Priest Rapids indicate that the horizontal hydraulic conductivities at the base of the Selah range over two orders of magnitude from about  $1 \times 10^{-6}$  to  $1 \times 10^{-4}$  cm/sec. Laboratory tests on undisturbed cores from the saturated zone at the base of the Selah indicate that the vertical hydraulic conductivity, which ranges from  $1 \times 10^{-8}$  to  $1 \times 10^{-5}$  cm/sec, is one to several orders of magnitude less than the horizontal hydraulic conductivity as determined from slug tests. The apparent difference between field horizontal hydraulic conductivity may be attributed in part to the difference in measurement techniques.

Packer tests conducted within the Priest Rapids Basalt indicate wide variations in hydraulic conductivity of the Priest Rapids Basalt is generally of the same order of magnitude as that within the basal portion of the Selah.

To assess their hydraulic characteristics and degree of hydraulic connection, pumping tests were conducted in the Selah and the Priest Rapids. The Selah pump tests entailed pumping from the base of the Selah and monitoring the response to pumping at the base of the Selah, at an intermediate depth between the base and the water table, and at the water table. Two locations were selected and pumped at rates 0.25 and 0.167 gpm, respectively, which resulted in full drawdown in the pumping wells. The Selah pump tests were, however, of limited duration because of the low permeability of the Selah.

The calculated horizontal hydraulic conductivity of the Selah for the Jacobs nonequilibrium (Lohman, 1972), and the Theis (Lohman, 1972) analytical methods ranges from  $1 \times 10^{-6}$  to  $1 \times 10^{-4}$  cm/sec. These values are based on the time-drawdown responses, which closely follow the Theis curve predictions. Because of the limited duration of the tests, the calculated results were considered order-of-magnitude estimated only.

The Priest Rapids pump test had dual objectives: 1) the assessment of the aquifer characteristics within the Priest Rapids interflow zone and 2) the assessment of possible interaquifer communication between the Priest Rapids interflow zone, the upper Priest Rapids basalt flow, and the saturated zone at the base of the Selah. Observation wells/piezometers were installed at three levels: within the saturated zone at the base of the Selah, within the upper Priest Rapids basalt flow and within the Priest Rapids interflow zone. The Priest Rapids interflow zone was pumped at a constant rate of 0.5 to 1 gpm, which was the maximum sustainable pumping rate over the planned duration of the tests.

The Theis and Jacobs analyses were applied on the assumption that the observation wells partially penetrate an anisotropic, unconfined aquifer composed of the Selah, the upper Priest Rapids basalts, and the interflow zone. These analyses, however, would not be applicable if an unsaturated zone existed between the base of the Selah and the interflow zone. An unsaturated zone would provide an effective discontinuity between the saturated zone at the base of the Selah and the pumping zone within the Priest Rapids, and hence mask any response. The area in which the Priest Rapids pump test was conducted is the only known area on the site that is fully saturated from the base of the Selah to the interflow zone. The drawdown response of several of the observation wells indicates that the interflow zone in this area is hydraulically connected with the saturated zone at the base of the Selah.

The transmissivity calculated on the basis of the Priest Rapids pump test ranges from 0.3 to 19.1 ft/day. Assuming an average saturated thickness of approximately 7.5 feet for the interflow zone, the horizontal hydraulic conductivity of the interflow zone is estimated to be  $1 \times 10^{-5}$  to  $9 \times 10^{-4}$  cm/sec. Due to the limited duration of the test, and the mathematical limitation of the Theis and Jacobs analyses, the calculated pump test results are considered order-of-magnitude estimates.

An analysis by Witherspoon (et al, 1967) for aquitard response to pumping in an aquifer has also been applied on the assumption that the Selah, the upper Priest Rapids basalt, and the interbed zone are an aquitard and the interflow zone is an aquifer. In this analysis, the observed drawdown responses in the aquitard are used to estimate the vertical hydraulic conductivity of the aquitard. The estimated vertical hydraulic conductivity of the aquitard estimated on this basis ranges from  $1 \times 10^{-7}$  to  $2 \times 10^{-7}$  cm/sec, although these values may be an underestimate due to the time lag response to the piezometers.

## DISCUSSIONS AND CONCLUSIONS

Geologic and hydrogeologic characterization of the Arlington facility to the extent necessary to proceed with development of a detection groundwater monitoring system was approved by the Environmental Protection Agency Region 10 in November, 1986. The studies performed addressed criteria established under 40 CFR 264, Subpart F and included identification of the uppermost aquifer and aquifers hydraulically interconnected thereto beneath the waste management area, evaluation of their respective groundwater flow rates and direction, and the basis for such identification. These studies have also demonstrated that the geologic and hydrogeologic conditions at the Arlington facility make it environmentally favorable for hazardous waste disposal. The favorable environmental characteristics include:

- o Semi-arid climate;
- o Low precipitation;
- o High evapotranspiration;
- o Low rate of infiltration;
- o Deep water table (uppermost zone of saturation);

- o Thick vadose zone;
- c Abundant low permeability and moisture deficient soils;
- o Low population density; and
- o Lack of nearby surface water bodies.

These favorable conditions at the site; however, have been very difficult to demonstrate in an unequivocal manner due to tenuous reliability of testing methods available for use under the site conditions described herein.

For the purpose of designing a detection monitoring network, each regulated waste management unit at the facility was considered to be a discrete entity with its own point of compliance. Thus, a primary monitoring network within the saturated zone at the base of the Selah was prepared for each unit. However, in designing a groundwater monitoring system to detect the "immediate" potential release of contaminants from a particular waste management unit, such favorable environmental characteristics warrant consideration of and conflicts with site-specific factors such as:

- o Heterogeneous mixture of waste types;
- o Complex stratigraphic depositional environments;
- o Identification of hydrostratigraphic units;
- o Complex groundwater movement regimes within the vadose and saturated zones;
- o Infeasibility to use conventional unsaturated zone monitoring techniques which reflect low permeable and moisture deficient soils; and
- o Level of demonstration versus level of risk to site integrity.

#### REFERENCES

- Dames & Moore, 1983. Report of subsurface investigation and monitoring well installation, CSSI Arlington facility, Arlington, Oregon. Unpublished report prepared for Chem-Security System, Inc., Bellevue, Washington (December 5).
- Dicken, S.N., 1955. Oregon geography. Eugene, Oregon, 127 pp.
- Fenneman, M.M., 1931. Physiography of western United States. New York: McGraw-Hill Book Company, Inc., 534 pp.
- Foundation Sciences, Inc., 1980a. Geologic reconnaissance of parts of the Walla Walla and Pullman, Washington and Pendleton, Oregon, 1 x 2 AMS quadrangle. Prepared for USACE, Seattle District, Contract No. DACW 67-80-C-0125.
- Lohman, S.W., 1972. Groundwater hydraulics. US. Geol. Survey Prof. Paper 708. 70 pp.
- Mackin, J.H., 1961. A stratigraphic section in the Yakima basalt and the Ellensburg formation in south-central Washington. Washington DOE, 45 pp.
- Rockwell Hanford Operations, 1979. Geologic studies of the Columbia Plateau -- a status report. Report No. RHO-BWI-ST-4.
- Schminke, H.U., 1964. Petrology, paleocurrents, and stratigraphy of the Ellensburg formation and interbedded Yakima basalt flows, south-central Washington. Ph.D. dissertation, John Hopkins University, 426 pp.

- Swanson, D.A., T.L. Wright, P.R. Hooper, and R.D. Bentley, 1979a. Revisions in stratigraphic nomenclature of the Columbia River basalt group. U.S. Geol. Survey Bull. 1457-G, 59 pp.
- Witherspoon, P.A., I. Javandel, S.P. Neuman, and R.A. Freeze, 1967. Interpretation of aquifer gas storage conditions from water pumping tests. American Gas Association, Inc., New York, N.Y.
- Wolf, F.G. and S.M. Testa, 1985. Kriging: A Geostatistical Technique for Evaluating Groundwater Monitoring Networks; Proceedings of the National Conference on Hazardous Wastes and Environmental Emergencies, May 14-16, Cincinnati, Ohio.

**Session II**  
**“Case Histories in Geological Engineering and Rock Mechanics”**

# Engineering Design of Rock Slope Reinforcement Based on Non-Linear Joint Strength Model

Stavros C. Bandis

Lecturer of Geotechnical Engineering, Dept. of Civil Engineering,  
Faculty of Engineering, Aristotelian University, Thessaloniki, Greece

**SYNOPSIS.** Optimum dimensioning of bolts or anchors for the reinforcement of slopes in jointed rock masses, requires compatible strength-deformation data, for both the rock joints and the reinforcing elements. Most types of rock joints behave in non-linear fashion and, thus, realistic modelling can have serious implications in the design, both from the economical and the technical standpoints. This paper will present, briefly, the principles of a constitutive model of joint shear behaviour and a method for optimum bolt or anchor design. The implications of non-linear joint behaviour will be demonstrated with numerical examples. Finally, a case study of slope stabilization, in which the method was adopted, will be reported.

## INTRODUCTION

Statics show, that the minimum tensioning force for the support of a rock mass resting on an inclined plane, requires, if moments are neglected, an optimum angle of installation ( $\beta$ ) w.r.t. the failure plane, given by:

$$\tan \beta = (1/F) * \tan \varphi \quad (1)$$

where  $\varphi$  is the friction angle along the contact interface and  $F$  is the safety factor. Depending upon the desired stiffness of the reinforcing system to be installed, the choice of the design value of  $\varphi$ , must be made in accord with the amount of shear deformation, which the reinforcing element would be capable of tolerating.

In some rock slope engineering problems, it may prove advantageous to allow a certain amount of deformation, thus dissipating a portion of the excavation induced shear stress. In addition, shearing may also initiate an efficient self-draining process within the rock mass, effected by the opening of dilating joints. By implication, the designer should be able to quantify the changes in shear behaviour at corresponding stages of joint deformation.

The non-linear constitutive model for the shear behaviour of joints reported by Bandis et al. (1981), Barton & Bandis (1982), Barton et al. (1985), and Barton and Bandis (1987), offers the basis for a convenient method for bolt design. The method has been described by Barton and Bakhtar (1983) and Bandis et al. (1985) and is based on a concept of "mobilized" friction, by which the shear strength available at various stages of shear deformation, can be quantified.

## NON-LINEAR MODEL OF JOINT SHEAR BEHAVIOUR

The shear behaviour of a singly jointed rock block is largely determined by the effective

normal stress ( $\sigma_n'$ ) and the length of the joint ( $L_n$ ). The variations observed in the shear properties of different joint types are attributed to differences in the geometric and strength properties of the joint surfaces, i.e. roughness, aperture, wall strength and basic friction.

Four key-indices are required, to fully model the shear behaviour of an unfilled joint:

- (i) the Joint Roughness Coefficient (JRCo), a dimensionless number ranging from 0 for planar-smooth to 20 for undulating - rough joints;
- (ii) the Joint Compressive Strength (JCSo), which is the uniaxial compressive strength of the rock material at the joint wall;
- (iii) the Angle of Residual Friction ( $\varphi_r$ ) or Basic Friction ( $\varphi_b$ ) - if the joint is completely fresh, and,
- (iv) the Mechanical Aperture ( $E_o$ ).

Simple index tests have been devised to measure JRCo (tilt, pull or push tests), JCSo (Schmidt hammer tests),  $\varphi_r$  or  $\varphi_b$  (combination of tilt and S.H. testing) and  $E_o$  (flow tests in the field or the lab). The subscript (o) is used to denote the joint length ( $L_o$ ), which was index tested. Details of the measuring techniques appear elsewhere (Barton and Choubey, 1977, Barton et al., 1985). Extrapolation of the measured indices to field scale (length  $L_n$ ), require appropriate scaling conversions:

$$JRC_n \approx JRC_o (L_n/L_o)^{-0.02 * JRC_o} \quad \dots\dots (2)$$

$$JCS_n \approx JCS_o (L_n/L_o)^{-0.03 * JRC_o} \quad \dots\dots (3)$$

The peak shear strength ( $T_{peak}$ ) of a joint can be predicted from Barton's (1973) criterion:

$$T_{(peak)} = \sigma_n' * \tan \left[ JRC_n * \log_{10} \left( \frac{JRC_n}{\sigma_n'} \right) + \varphi_r \right] \quad \dots\dots (4)$$

The latter is attained at a peak shear displacement,  $\Delta h$  (peak):

$$\Delta h(\text{peak}) = \frac{Ln}{500} \left[ \frac{JRCn}{Ln} \right]^{-0.33} \dots (5)$$

The shear strength mobilized at any given displacement,  $\Delta h$  can be expressed by:

$$T(\text{mob}) = \alpha_n' \tan \left[ JRCn(\text{mob}) * \log_{10} \left( \frac{JRCn}{\alpha_n'} \right) + \Phi_r \right] \dots (6)$$

$$\text{or } \Phi(\text{mob}) = JRC(\text{mob}) * \log_{10} \left( \frac{JRCn}{\alpha_n'} \right) + \Phi_r \dots (7)$$

The model illustrated in Fig. 1 simulates the following fundamental features of joint shear behaviour:

- (i) mobilization of the basic frictional resistance, upon initiation of shear
- (ii) the amount of initial shear for roughness mobilization is scale dependent ( $\approx 0.3 * \Delta h_{\text{peak}}$ ).
- (iii) dilation begins when roughness is mobilized.
- (iv) peak shear strength is reached at  $JRC(\text{mob})/JRC(\text{peak})=1.0$  and  $\Delta h/\Delta h(\text{peak})=1.0$ . The peak shear displacement,  $\Delta h(\text{peak})$ , corresponds to 1% of the joint length. A value of  $\Delta h/\Delta h(\text{peak})=2$  has been adopted for relatively smooth and planar joints ( $JRC < 5$ ).
- (v) the contribution of roughness declines in the post - peak region, owing to surface mismatch and wear.
- (vi) the residual state ( $JRC \text{ mob}=0$ ) is reached after large shear displacements ( $\Delta h/\Delta h_{\text{peak}}=100$ ).

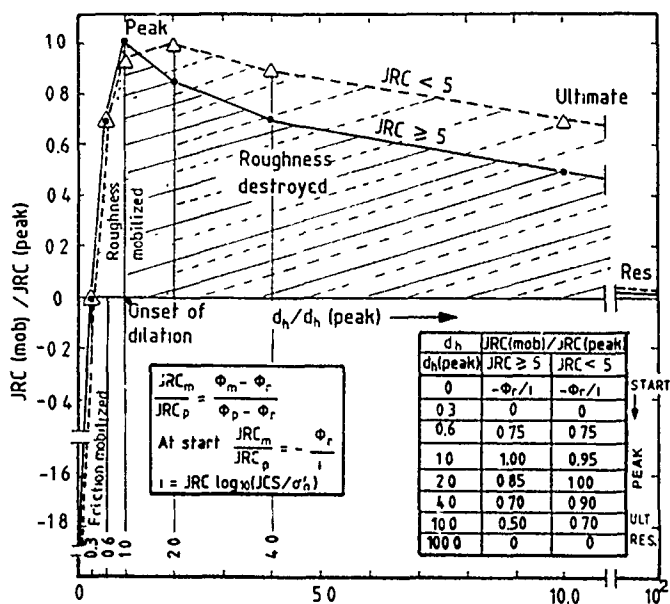


Fig. 1. Dimensionless model of joint shear behaviour (from Barton & Bandis, 1987).

Dilation can be modelled utilizing an expression quite similar to (4):

$$dn^\circ(\text{mob}) = 1/2 JRC(\text{mob}) * \log_{10} \left( \frac{JCS}{\alpha_n'} \right) \dots (8)$$

The increase of the mechanical aperture ( $E_o$ ) associated with dilation can be calculated from:

$$\delta E_o = \delta(\Delta h) * \tan dn^\circ(\text{mob}) \dots (9)$$

Numerical examples of model application are given in Fig. 2

#### BOLT DESIGN BASED ON NON-LINEAR JOINT MODEL

Barton and Bakhtar (1983) suggested a graphical solution for optimum bolt design, utilizing normal stress and scale dependent values of  $\Phi$  (mobilized). The technique essentially combines the appropriate "mobilized" strength envelope, with a conventional force diagram.

From the T- $\Delta h$  plots in Fig. 2a, values of  $JRC(\text{mob})$  can be back-calculated at any shear displacement,  $\Delta h$ , e.g.  $\sim 4.0\text{mm}$  (at peak),  $20.0\text{mm}$  and  $80\text{mm}$ . Those values of  $JRC(\text{mob})$  are then used to derive the corresponding mobilized strength envelopes. Combination of the latter with the force polygon for a simple slope problem is demonstrated in Fig. 3. It is seen, that the frictional resultants  $R_1, R_2, R_3$ , which are perpendicular to the minimum bolt forces  $T_1, T_2, T_3$ , intersect the envelopes at different levels of normal stress. The design  $\Phi(\text{mob})$  value corresponds to an effective normal stress, which incorporates the normal component of the force T, in addition to the forces N, V and U.

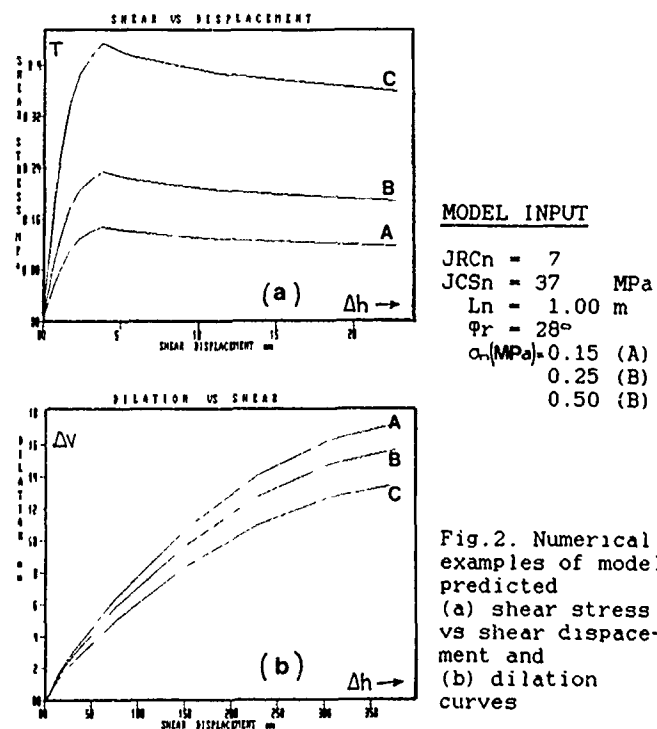


Fig. 2. Numerical examples of model predicted (a) shear stress vs shear displacement and (b) dilation curves

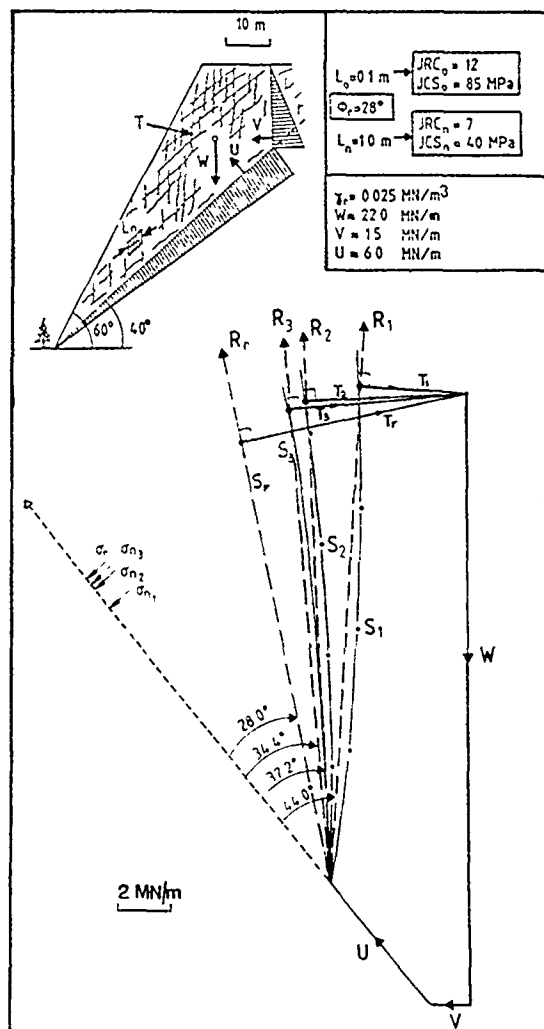


Fig. 3. Example of graphical solution for optimum bolt design using normal stress and scale dependent values of  $\Phi$  (mobilized) (from Bandis et. al. 1985).

The engineering implications in bolt/anchor design, if the non-linearity in joint shear behaviour is neglected, can readily be demonstrated. In the hypothetical problem illustrated in Fig. 4, it is assumed that the rock mass structure favours translational sliding along a potential failure surface, consisting of segments with variable inclination. The slope system can be analyzed assuming transfer of loads by superposition from the active to the passive blocks. Joint strength indices were assigned to the failure surface, as listed in Fig. 4.

A computer programme containing a subroutine for the JRC-JCS model was used for the analyses. The computing procedure was to calculate the normal force component acting on each segment of the failure surface and, then, determine the normal stress dependent values of friction ( $\Phi$ ) through an iterative procedure.

The calculations gave for dry slope :  
 Safety Factor (SF) = 1.06  
 Predicted  $\Phi$ (Bottom) = 45°  
 $\Phi$ (Top) = 49°  
 $\Phi$ (Middle) = 38.5°

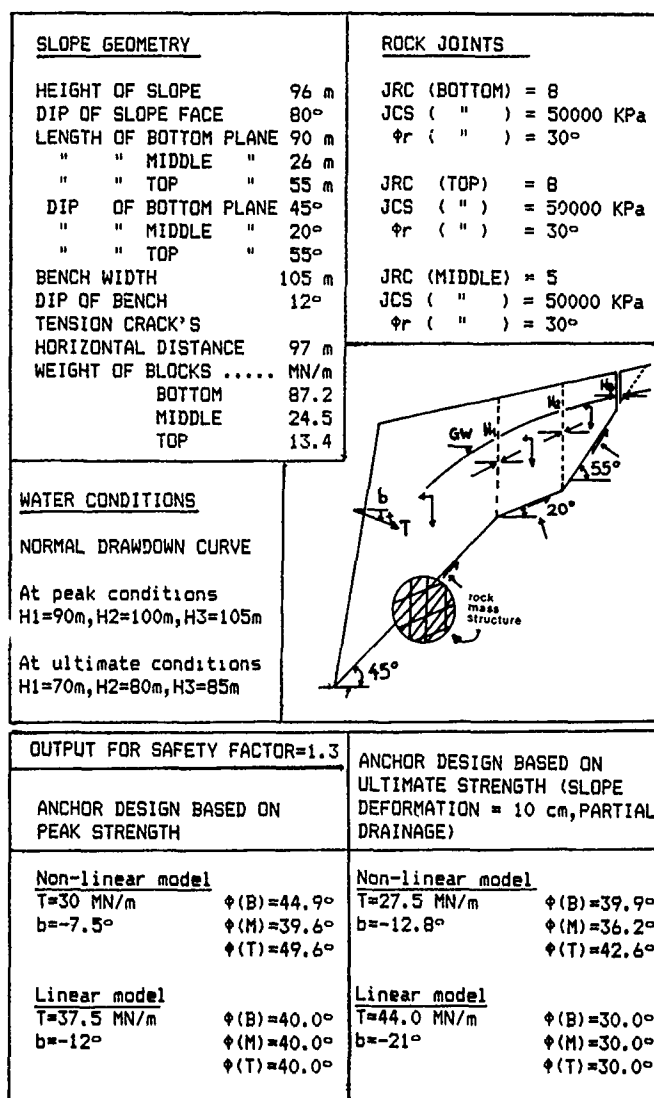


Fig. 4. Comparison of calculated anchor forces for a hypothetical slope problem, utilising the non-linear JRC/JCS model and Coulomb's linear concept of joint behaviour.

In a simplified approach, a constant value of  $\Phi=40^\circ$ , equal to the mean inclination of the potential failure surface, might be adopted. For the water pressures assumed in Fig. 4, an external anchoring force, T is required for stability. It can be shown, that the inclination, w.r.t. horizontal of a minimum force (T) for safety factor, (SF) is given by:

$$\tan b = \frac{(\tan \Phi_{\text{bottom}} / \text{SF}) - \tan \gamma_p}{(\tan \Phi_{\text{bottom}} / \text{SF}) \tan \gamma_p + 1} \dots (10)$$

where  $\gamma_p$  = inclination of the bottom segment of the failure surface.

For the case of design based on peak strength and safety factor of 1.3 :

$T = 30.0 \text{ MN/m}$   
 $b = -7.5^\circ$  | ..... non-linear model

and  $T = 37.5 \text{ MN/m}$   
 $b = -12^\circ$  | ..... linear model

For the case of design based on ultimate strength, the following were assumed:

$\Delta h = 100 \text{ mm}$  (slope deformation)  
 $L_n = 1.0 \text{ metre}$  (in-situ block length)  
 $\left. \begin{array}{l} \text{JRC(mob) BOT} = 5.5 \\ \text{JRC(mob) TOP} = 5.5 \\ \text{JRC(mob) MIDD} = 3.5 \end{array} \right\} \text{ non-linear model in Fig. 1.}$

The calculated anchor force for  $SF=1.3$  and water conditions as originally :

$T = 37.0 \text{ MN/m}$                        $b = -12^\circ$

If we assumed that the normal drawdown GW curve was lowered by 20% due to self-draining, then :

$T = 27.5 \text{ MN/m}$                        $b = -21^\circ$

Finally, if the deformed slope was assigned a conservative residual friction angle  $\Phi=30^\circ$ , then :

$T = 44.0 \text{ MN/m}$                        $b = -21^\circ$

The above examples indicate a conservative over-estimation of  $T$  between 25 and 40%, depending on the mode of joint behaviour and the conditions assumed.

## CASE STUDY OF ROCK SLOPE REINFORCEMENT

### Background information.

In November 1985 and during the excavation of a new slope face in a drydock at Stavanger, Norway, problems of instability were encountered in the form of translational sliding failures (Figure 5). The slope (0.0-12.0 in height and ~50.0 in length) had a major functional role, bearing the foundation loads of a back-filled sheet-pile wall, which acted as sea-water barrier. Figure 6 presents a vertical section along the final slope line, as appeared in the "good for construction" plans.

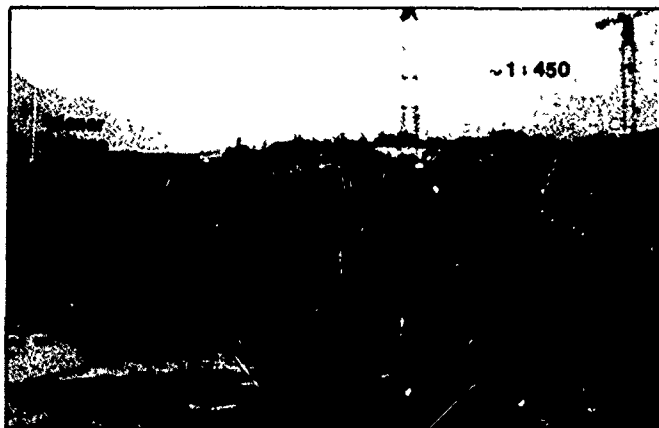


Fig. 5. General view of preexisting slope and new excavation (R. H. half).

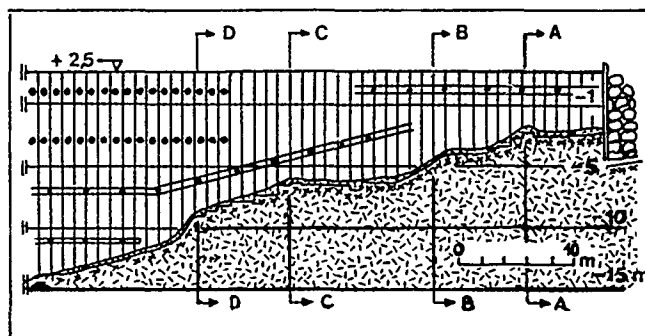


Fig. 6. Vertical section of seawater barrier along the final slope line. A - A, etc. indicate sections of different geometry, which were analyzed.

Under the pressure of circumstances, the contractor proceeded with immediate installation of anchors along a line at the crest of the slope, at a small distance behind the final excavation line, as shown in Fig. 11. Prestress loads were calculated by adopting a constant  $\Phi$  value of  $43^\circ$  along potential failure planes inclined by  $45^\circ$  w.r.t. horizontal.

Following geotechnical control of the undertaken measures, it was concluded, that the eccentric line-loading along the crest, could create, in addition to undesirable moments, a tensile zone in the central part of the slope. It was also argued, that the use of a constant value of  $\Phi$ , would prohibit optimization of the anchor tensioning forces, causing under- or over- loading of certain sections, due to the variable slope geometry.

Reevaluation of the design parameters was made, by using normal stress and scale dependent estimates of the friction angle, calculated according the non-linear JRC/JCS model. The design values of  $\Phi$ , thus obtained, ranged between  $39^\circ$  and  $45^\circ$ , instead of the initial constant value  $\Phi=43^\circ$ , thus allowing for the changing geometry of the slope. The prestress loads had to be modified accordingly. In addition, since any instability of the lower part of the slope could threaten the integrity of the whole structure, additional reinforcement by bolting of the lower slope half was designed.

## INVESTIGATION OF THE FIELD CONDITIONS

### Rock material

The rock type was a slightly to moderately weathered phyllite, with well-developed foliation. The uniaxial compression strength ranged between 50-60MPa ( $\perp$ ) and 20-30MPa ( $\parallel$ ).

### Rock mass structure

The direction/amount of dip of the foliation was  $N80^\circ - 95^\circ / 40^\circ - 45^\circ$ . Foliation joints of similar orientation appeared frequently, spaced 0.5-1.0m apart and with lengths of up to several metres. No other systematic jointing was observed.

Occasional stress relief joints were of no practical importance, due to the relatively gentle dip. Scarcely distributed subvertical joints were also found.

#### Stability conditions

It was evident, that the persistent foliation joints could provide with potential failure planes. Several of them "daylighted" at the slope face. Considering the climatic condition in the area and a maximum water head of 16.0m, the slope could be expected to sustain significant hydraulic loading. Severe seepage was observed at several locations at the slope face. The part of the slope in need of reinforcement comprised the new excavation (between section A-A and D-D) and a potentially unstable block at the middle part (section E-E) as indicated in Fig. 5.

#### EVALUATION OF JOINT SHEAR STRENGTH

The exposed failure plane at the rightmost end of the slope (Fig.5), was quite accessible for direct measurements of the surface roughness. Detailed line-profiling along section 2-2 in Fig.8(a) gave the trace presented in Fig.9.

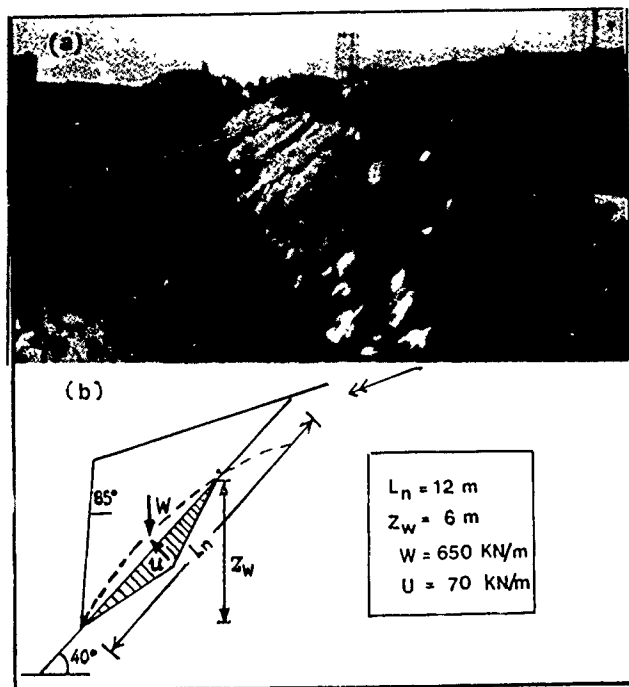


Fig.8 (a) Persistent joint surface along which translational failure took place.  
(b) Conditions assumed for back-analysis of failure.

The value of JRCn characterizing a particular surface, represents an approximate measure of the roughness amplitude ( $a$ ) divided by the length ( $L_n$ ) of the profile. From analyses of a large volume of data, Barton (1982) arrived at the nomogram of Fig.10.

The length of profile in Fig.9 is  $L_n \approx 11.0$  m and  $a \approx 150$  mm. Then, a value of JRCn 6-7 is predicted from the nomogram. The independently derived JRCn value was used to back-calculate the drained friction angle, which was mobilized along the failure plane, as shown in Fig.8:

$$\phi' = \text{JRCn} * \log_{10} \frac{\text{JCS}}{\sigma_n} + \phi_r \dots \dots (11)$$

where: JRCn = 6  
JCSn = 30 MPa  
 $\phi_r = 22^\circ - 24^\circ$   
 $\sigma_n' = 0.032$  MPa  
 $\sigma_n' = (4W \cos 40^\circ - Z_w^2 \gamma_w \cos 40^\circ) / 4L_n$   
 $W = 650$  kN/m  
 $L_n = 12.0$  m  
 $Z_w = 6.0$  m

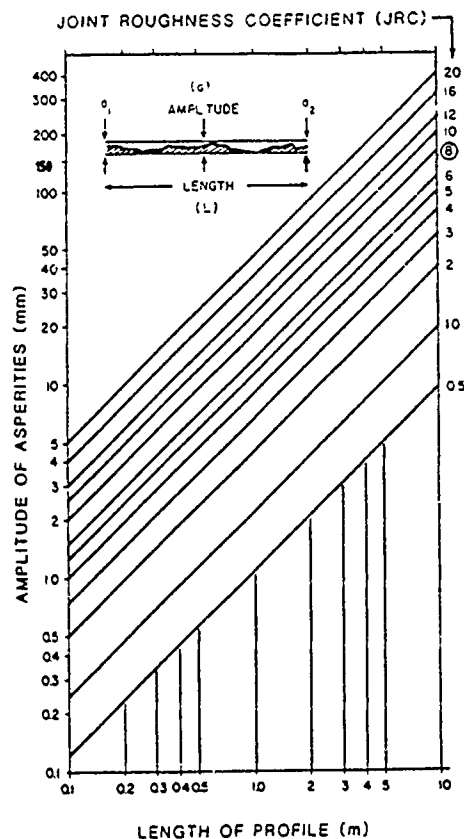


Fig. 10. Joint roughness characterization according to the amplitude of asperities and length of profile. (Barton, 1982).

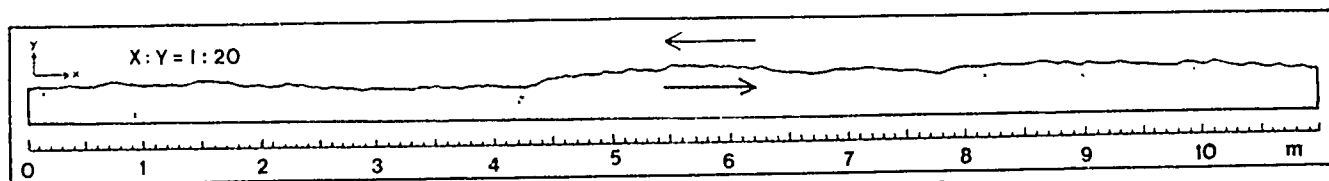


Fig. 9. Roughness profile along section 2-2 in Fig. 8(a).



The calculated value of  $\Phi=40^\circ-42^\circ$  clearly complied with the conceptual limit equilibrium condition of  $\Phi=\gamma_p$  (inclination of failure surface) for planar sliding.

Several more foliation joint planes  $\sim 1.0$  metre in length were profiled and characterized according to the nomogram in Fig.10. The conclusion from the field observations was that foliation joints invariably contained undulating features of various sizes. Wavelengths ranged from a few cm's to  $>5.0$  m and the amplitudes from some mm's to  $>10$  cm. In general, high JRC values (15-18) were assigned to joint lengths up to 1.0 m. The latter represented the JRC<sub>0</sub> and L<sub>0</sub> value for scaling extrapolations to JRC<sub>n</sub> according to eqn(2)

#### STATIC ANALYSES-PRESTRESS LOAD CALCULATIONS

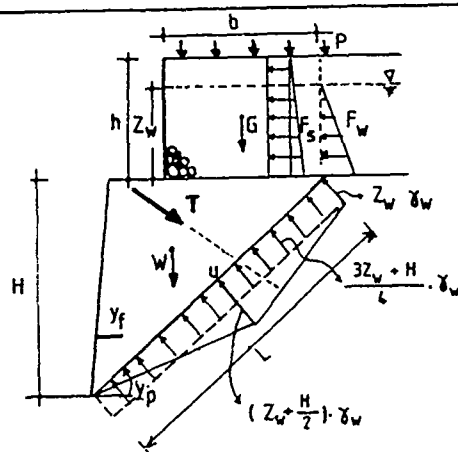
A typical slope section (B-B according to Fig.6) is contained in Fig.11, with all information concerning the assumed distribution and calculation of forces.

Table 1 summarizes the geometrical data, the joint plane indices, the operating  $\Phi$  values and the calculated prestress loads for limit equilibrium at the corresponding sections A-A, etc. (see Fig.6 for positions of analyzed sections). The angle of anchor installation w.r.t. horizontal was  $25^\circ$  (not optimum, but imposed from practical constraints and the fact that most of the holes had been drilled). The tensioning force was in each case determined graphically, by locating the common intersection between the vectors of force T and frictional resultant R, and the appropriate strength envelope (also refer to previous Fig.3).

For purposes of comparison, the T values calculated for constant  $\Phi=43^\circ$  have been included in Table 1. It is worth noting, that, despite the same angle of anchor installation,

TABLE 1. Input parameters and calculated anchor prestress loads at limit equilibrium.

| Section                |                         | A-A                                 | B-B                                 | C-C                                 | D-D                                 | E-E                                 |
|------------------------|-------------------------|-------------------------------------|-------------------------------------|-------------------------------------|-------------------------------------|-------------------------------------|
| Input                  |                         |                                     |                                     |                                     |                                     |                                     |
| GEOMETRY               | H(m)                    | 12.5                                | 10.5                                | 8.5                                 | 5.5                                 | 12.0                                |
|                        | h(m)                    | 4.5                                 | 6.5                                 | 8.5                                 | 11.5                                | -                                   |
|                        | b(m)                    | 7.6                                 | 5.5                                 | 4.5                                 | 3.5                                 | -                                   |
|                        | Z <sub>w</sub> (m)      | 3.6                                 | 5.6                                 | 7.6                                 | 10.6                                | 12.0                                |
|                        | Y <sub>p</sub>          | ----- 45° -----                     |                                     |                                     |                                     |                                     |
|                        | Y <sub>f</sub>          | ----- 85° -----                     |                                     |                                     |                                     |                                     |
| FAILURE PLANE INDICES  | Ln(m)                   | 18.0                                | 15.0                                | 12.0                                | 8.0                                 | 18.0                                |
|                        | JRC <sub>n</sub>        | 6.5                                 | 7.0                                 | 7.5                                 | 8.5                                 | 6.5                                 |
|                        | JCS <sub>n</sub>        | ----- 30 MPa -----                  |                                     |                                     |                                     |                                     |
|                        | $\Phi_r$                | ----- 22° -----                     |                                     |                                     |                                     |                                     |
| PRESTRESS LOADS (KN/m) | $\Phi=43^\circ$         |                                     |                                     |                                     |                                     |                                     |
|                        | $\beta=25^\circ$        | 1190                                | 1198                                | 1450                                | 964                                 | 585                                 |
|                        | $\Phi=f(\sigma_n, L_n)$ | 1400                                | 1350                                | 1450                                | 750                                 | 730                                 |
|                        | $\beta=25^\circ$        | $\Phi=39^\circ$                     | $\Phi=41^\circ$                     | $\Phi=43^\circ$                     | $\Phi=45^\circ$                     | $\Phi=39^\circ$                     |
|                        | Optimum                 | 1200                                | 1100                                | 1260                                | 660                                 | 850                                 |
|                        |                         | $\beta=-7^\circ$<br>$\Phi=38^\circ$ | $\beta=-2^\circ$<br>$\Phi=43^\circ$ | $\beta=-1^\circ$<br>$\Phi=44^\circ$ | $\beta=+3^\circ$<br>$\Phi=48^\circ$ | $\beta=-7^\circ$<br>$\Phi=38^\circ$ |



#### CALCULATION OF FORCES

Surcharge load (P) :  $P = P_N \cdot 1.6 \cdot b$   
(where  $P_N = 30 \text{ kN/m}^2$  and 16 is a safety factor)

Load of backfill (G) :  $G = b \cdot h \cdot \gamma_f \text{ (dry)}$

Weight of rock wedge (W) :  $W = \frac{1}{2} \cdot H^2 \cdot \gamma_r$

Uplift force (u) :  $u = \frac{1}{4} \cdot (3Z_w + H) \cdot \gamma_w \cdot L$   
(assuming uniform distribution as illustrated)

Lateral forces on sheetpile wall :

- due to pore water ( $F_w$ ) :  $F_w = \frac{1}{2} \cdot Z_w^2 \cdot \gamma_w$

- due to earth pressure and surcharge load ( $F_s$ ) :  $F_s = \left[ (P_N \cdot 1.6 \cdot K) + \right.$

$\gamma_f$  = unit weight of earth fill  
dry =  $20 \text{ kN/m}^3$   
sat =  $10 \text{ kN/m}^3$

$\gamma_w$  = unit weight of water  
=  $10 \text{ kN/m}^3$

$\gamma_r$  = unit weight of rock  
=  $27 \text{ kN/m}^3$

K = coefficient of active earth pressure = 0.35

Fig. 11. Diagrammatic illustration of analyzed cross-section and of the assumed forces distribution.

significant differences in the prestress loads were found, particularly for the shortest slope sections.

As expected, the optimum anchor force (T vector to frictional resultant) gave lower T values for a range of  $\beta$  angles from  $-7^\circ$  to  $+3^\circ$  (the minus symbol indicates angle above the horizontal).

#### DESIGN OF THE BOLT REINFORCEMENT

For the reasons already referred to, a rock bolting system was designed to secure the lower

part of the slope, at the final excavation line. Limiting equilibrium analyses were conducted for the slope sections A-A to D-D, by assuming a tension crack at the zone of potential relaxation and perpendicular to the failure plane, as illustrated in Fig.12(a).

Depending upon the geometry of the slope section, the calculated minimum bolting forces at equilibrium ranged between 510 KN/m (A-A) and 64 KN/m (D-D). The corresponding design  $\phi$  values were between  $45^\circ$  and  $54^\circ$  and the optimum installation angles  $\beta$  were  $0^\circ$ – $9^\circ$  (see Fig. 12b).

Fully-grouted, untensioned bolts of 250 kN capacity ( $\phi 24\text{mm}$ ) were recommended for installation in a pattern with similar lateral and vertical spacing ( $2 \times 2\text{ m}$ ). A total of > 50 bolt units were installed (Fig. 13). Drainage holes were also drilled during bolt installation, horizontally spaced at 5–6 metres and drilled at two different levels.

Finally, the photograph in Fig.14 shows the anchor reinforced unstable block in the middle of the slope (section E-E in Fig. 5). Since completion of the reinforcing measures, the slope has presented with no further problems.



Fig. 13. Rock slope face at the final excavation line reinforced with bolts.

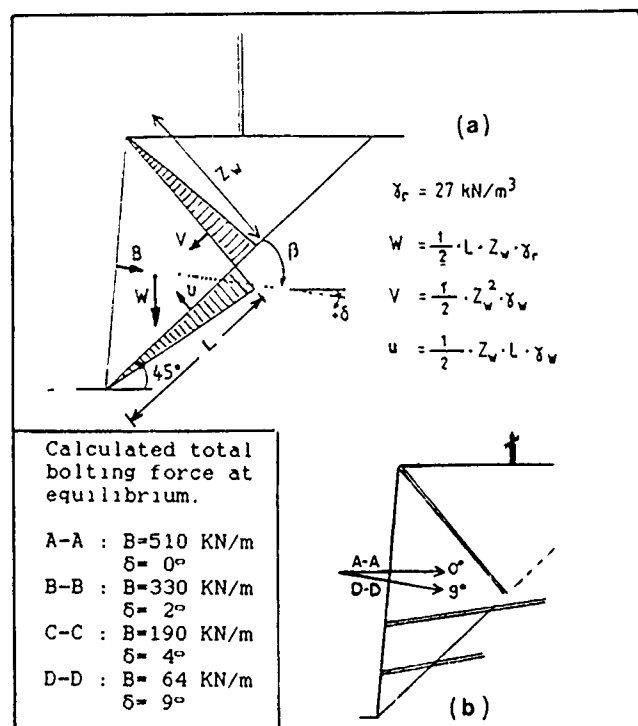


Fig. 12. Illustration of (a) assumed slope geometry forces for bolt design (active pressure from upper slope-half considered equal to zero); (b) recommended bolt direction and position of drainage holes

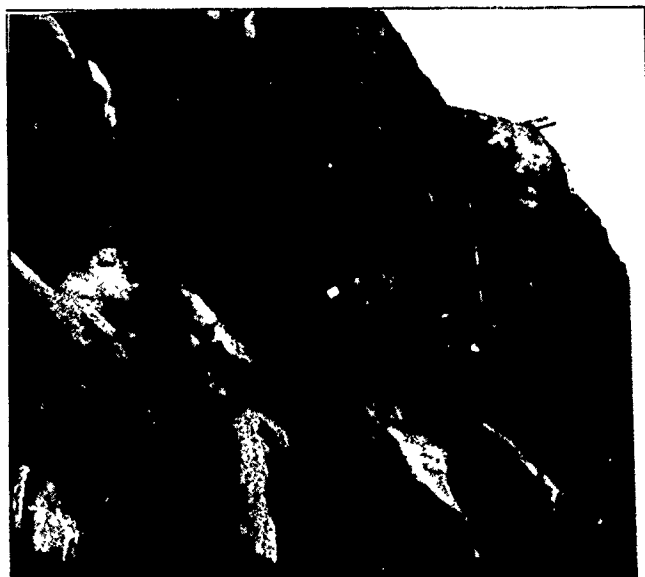


Fig. 14. Anchor reinforced unstable block in section E-E.

#### CONCLUDING REMARKS

1. The choice of linear or non-linear model for the shear behaviour of joints, has significant implications upon the design of reinforcing systems for unstable rock slopes.

2. A constitutive non-linear model based on simple indices ( JRC, JCS,  $\phi_r$  ), can be used to calculate the optimum angle of installation for a minimum prestress load.

3. The model predicted value for  $\phi$  depends upon the normal stress, the scale of joints and the amount of shear deformation. The effects of all applied forces can be allowed for, by using either a graphical solution or an iterative numerical technique for relatively complex failure surface geometry.

4. The reported case study of slope reinforcement revealed good agreement between model predicted and back-calculated friction values of a failed slope section. Comparisons between conventional anchor design and the suggested method, indicate potential over- or under-loading, if non-linearity is ignored.

#### ACKNOWLEDGMENTS

The case history included in this paper was part of NGI Contract Project No. 85060-1/1986. Permission to publish the material is acknowledged with appreciation.

#### REFERENCES

- Bandis, S.C., Lumsden, A.C. and N. Barton (1981): Experimental studies of scale effects on the shear behaviour of rock joints. Int.J. Rock Mech. Min. Sci. & Geom. Abstr., 18: 1-21.
- Bandis, S.C., Barton, N. and M. Christianson (1985): Application of a new numerical model of rock joint behaviour to rock mechanics problems Proc. Intern. Symp. on Fundamentals of Rock Joints, Bjorkliden, Sweden : 345-355.
- Barton, N.R. 1973. "Review of a new shear strength criterion for rock joints", Engineering Geology 7 :287-332.
- Barton, N. and V. Choubey (1977): The shear strength of rock joints in theory and practice. Rock Mechanics, 10 : 1-54.
- Barton, N. and Bandis S.C. (1982): Effects of block size on the shear behaviour of jointed rock. Keynote Lecture, 23rd U.S. Symposium on Rock Mechanics, Berkeley, California.
- Barton, N. and K. Bakhtar (1983): Bolt design based on shear strength. Proc. Intern. Symp. on Rock Bolting, Abisko, Sweden : 367-376.
- Barton, N., Bandis, S.C. & K. Bakhtar (1985): Strength, deformation and conductivity coupling of rock joints. Int.J. Rock Mech. Min. Sci & Geom. Abstr., 22(3):121-140.
- Barton, N. and S.C. Bandis (1987): Rock joint model for analyses of geological discontinua. 2nd Int. Conf. on Constitutive Laws for Engineering Materials: Theory and Applications Tuscon, Arizona.

## Stability of a Rock Slope at Bukit Batok New Town, Singapore

John Pitts

Head of Geotechnical Services, Harry Stanger Limited, Elstree, U.K.

**SYNOPSIS:** The stability of a deep rock cutting is discussed, the face of which mainly corresponded to a bedding surface. The slope failed during heavy rain. Analyses show that either surface roughness or cohesion along the failure surface accounts for the initial stability, and mobilisation of these was necessary during failure.

### INTRODUCTION

As part of the major re-housing programme instigated by the Government of Singapore, several new towns have been built. One of these, Bukit Batok is situated in the west-central area of Singapore Island (Figure 1). As a part of the development of Bukit Batok New Town, a series of major cuttings have been excavated, and it is the stability of one of these which is to be described. The cutting in question (Figure 2) is along Bukit Batok Avenue 6 and was excavated in 1983 by deepening an existing col which originally rose to over 45m in height between two hills over each 60m high.

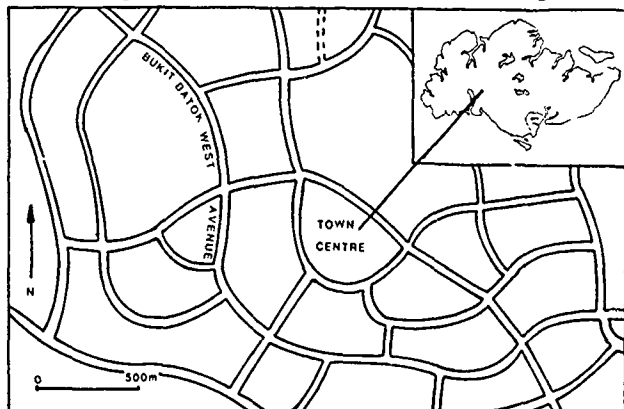


Fig. 1 Location Map



Fig. 2 The unfailed cutting

The slope is over 30m high, the lower 23m sloping at about 45° with a 3.7m sub-vertical toe (Figure 3).

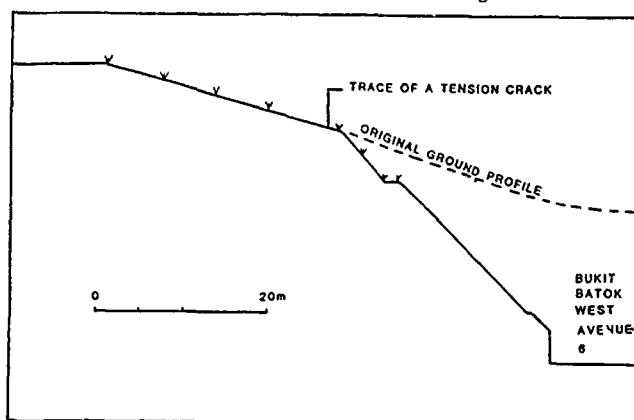


Fig. 3 Profile of the cutting slope

The slope failed initially on or about October 3rd, 1985 (Figure 4), and coincided with a storm which resulted in 53.5m of rainfall, as measured at the nearest gauging station. The preceding month had been unseasonably wet, with 230mm of rain having been recorded at the same meteorological station. This represents a figure some 33% higher than the September average for that station. During a further wet period between 8th and 11th January 1986, coinciding with the northeast monsoon, a further movement occurred (Figure 5). A new failure also developed in the slope immediately to the south (Figure 6).



Fig. 4 First phase failure of October 4th 1985

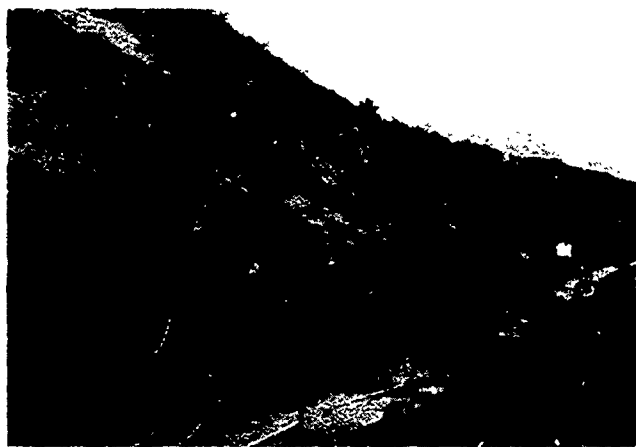


Fig. 6 Failure of adjacent slope in January 1986

#### GEOLOGICAL SETTING

The geological setting of the Bukit Batok area is shown in Figure 7. It is composed of siliciclastic rocks of the Jurong Formation (PWD, Singapore 1976; Pitts, 1984 (a) & (b)). The slope in question is part of a sequence conglomerates, sandstones and mudrocks and is composed mainly of partially recrystallised quartz sandstones (orthoquartzites) with muddy intercalations, lenses and interbeds. The muddy material is usually clay rich, although is occasionally silty and contains abundant diagenetic muscovite. In the main part of the slope, the muddy sediments infill what appear to be potholes scoured on the bedding surfaces of the orthoquartzites (Figure 8). However, it is clear from the cutting on the opposite side of the road that within some parts of the orthoquartzite sequence, the muddy sediments are much more persistent, and eventually develop into full beds in the higher part of the unit.

The slope itself was excavated by blasting, and has been cut back so that it is roughly coincident with a bedding surface. However, some beds daylight in the steep toe section of the slope. The rock mass possesses a blocky structure, and signs of weathering and discolouration were originally confined to discontinuity surfaces. The rock mass was therefore showing Grade II weathering, (Anon, 1977). The discontinuity surfaces did show rapid deterioration once exposed to the vagaries of the equatorial climate of Singapore. The rapid colonisation of these surfaces and of the slope surface itself by algae and lichens

resulted in a rapid disaggregation of the surface, so that a loose, fine sandy residue was quickly formed. In addition, a certain amount of stress relief occurred following the blasting which was manifested as surface loosening with dislodged small blocks sliding down the slope surface.

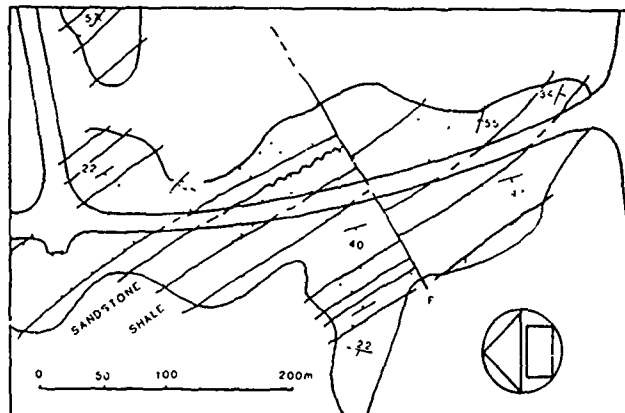


Fig. 7 The geological setting

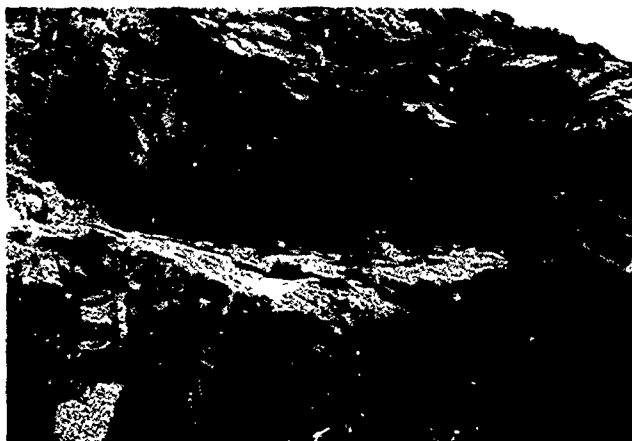


Fig. 8 Scours infilled with muddy sediments

The slope forms part of the eastern limb of an open syncline. The geological structure of the rock mass forming the slope is summarised in the stereographic projection, Figure 9. The plotting of poles of normals to planes was carried out on an equatorial equal area net, and the poles were contoured using a Denness Type B counting net (Denness, 1972). Pole concentration A represents the bedding. There are about fifty readings of bedding, and some scatter in the results was experienced. The reasons for this are probably two fold. Firstly, along the length of the face measured, there was a very gradual change in the strike of the bedding by a few degrees, indicating that the fold was either periclinal, or had been re-folded. Secondly, the roughness of parts of some of the bedding surfaces, seemingly as a result of localised penecontemporaneous erosion, also led to variations in orientation at that scale of measurement. Pole concentrations B and C are joint sets, each one sub-vertical in nature.

Also included on the stereographic projection are cyclographs of the more important sets of discontinuities with respect to the slope failure. Cyclograph D represents the joint set which formed the release surface at the northern limit of the slide; E

is a wrench fault (Figure 7) which formed the release surface at the southern limit; F is the joint set mainly responsible for the backscar, although G and H were also involved, and I is the cyclograph of the average dip and dip direction of the bedding from the nearly fifty bedding readings taken. However, because of the gradual change in strike as the toe of the failed part of the slope is approached, this is rather misleading, and there is closer coincidence of the dip direction of the bedding and the slope at this point. The main structures controlling the slide can therefore be seen to come from the master joint sets and the bedding.

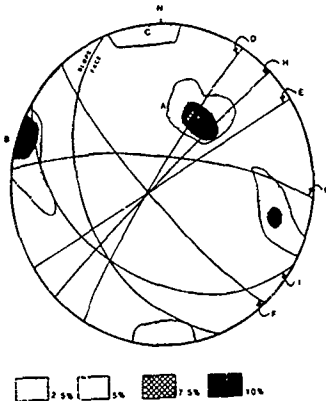


Fig. 9 Stereographic projection of main geological structures

The bedding surfaces vary from smooth, with first order waviness producing an angle  $i$  (Patton, 1966) of  $2^\circ$  to  $10^\circ$ , with a wavelength of 200mm to 300mm, to rough, with second order asperities producing roughness angles of up to about  $23^\circ$ , (Figure 10) but also including some backslipping elements of  $10^\circ$  to  $15^\circ$ . However, the morphology of the bedding surface is further complicated by the inclusion of the muddy intercalations and lenses. Although the bedding plane scours are important elements of roughness, they are infilled with material of an inherently weak nature. The muddy infill is also shaly, fissured or even sheared in parts, and it is therefore unlikely that the roughness contributes very much to the shearing resistance of the bedding in the areas occupied by muddy sediments.

#### MORPHOLOGY OF THE SLIDE

The failed slope involved up to about  $5000\text{m}^3$  of rock. It forms three distinct zones which give some impression of the detailed mode of failure of the slope. The toe block moved forward by up to one metre, and remained in an essentially intact state. The sliding surface did not daylight in the slope, but in a backfilled trench at the toe. The block extended upslope by only a few metres and was terminated behind by its own backscar controlled mainly by joint set G. A block of rock behind the toe then also moved forward in response to the removal of toe support.

However, the extent of movement was limited and the tension crack which opened up as a result of movement of the toe block was only partially closed. Small blocks of rock failed along muddy bedding partings and fell into the tension crack. The crack remained open to the extent of about one metre at the toe to less than 0.3m at the crest of the toe block. The rearmost and by far the largest portion of the slope then failed. The results is a very complex area of movement indicative of sudden, rapid, and wholesale failure

(Figure 11). The backscar is clearly defined and has a deep, chasm-like space in front of it occupied by random blocks which have dropped from the backscar itself and from the rear of the slipped mass in front.

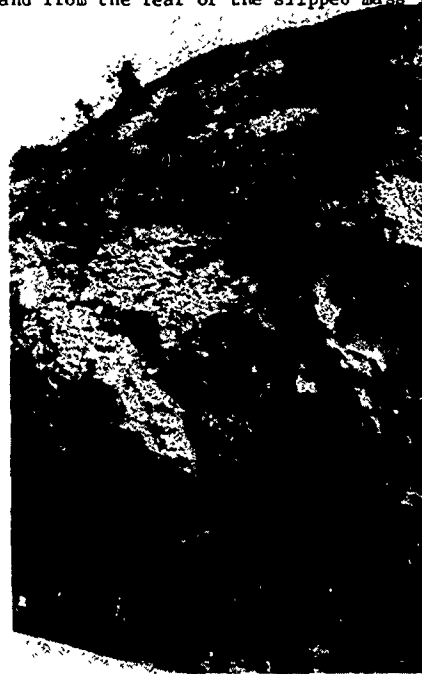


Fig. 10 Contrasting morphology of discontinuity surfaces



Fig. 11 Rear, complex crest area of slide

The sliding mass constitutes a partially disintegrated block, where additional failures by sliding on clean, fairly smooth bedding surfaces has occurred. Also of importance is toppling, and a second "low spot" in front of the rearmost block is infilled with small columns of sandstone which have toppled forward into it. The front area of this main sliding mass shows clear upthrusting over the top of the rear of the second toe block (Figure 12). Some of the upthrust masses are now sub-vertical but clearly display the original lichen-covered slope surface. The whole area behind the two toe blocks is generally heavily disturbed and very irregular with large disintegrating blocks separated by deep depressions or chasms, partly infilled with blocks.

Disruption in front of the toe of the slope resulting from the first stage of failure was remarkably little because the main energy of the failure, generated by the rearmost mass, has been absorbed by the two intact



Fig. 12 Over-riding of toe block by slipped material from rear part of slide.

toe blocks. A deep, reinforced concrete-lined culvert at the toe appears to be intact, and the lining may well have acted as a retaining structure limiting the movement of the toe block. It may however have been pushed forward 'en masse'. The failure surface was just below the ground and forward movements along it were clearly limited by the culvert. Leading to the culvert but trending at right angles to it from the road were scupper drains. These have remained essentially rigid and have translated the forward motion of the rock slope to the kerb line of the road. Where the scupper drains meet the kerb, the kerbstones have been pushed forward. The scupper drains themselves have heaved up so that a gap now exists between the concrete bed of the drains and the courses of bricks beneath.

Some additional movements took place during the rains of 8th to 11th January 1986, particularly along the toe. At the southern edge of the slide, a toe block shows additional movement of 0.25m (Figure 13), and debris from the block now fouls part of one of the covers of the main culvert. Toe blocks have collapsed and disintegrated along bedding and joint surfaces. Some of the bedding contains mudshale partings and joints are frequently iron stained. All of the larger blocks show clear structural control of faces, although some blocks have disintegrated to form gravel and cobble sized debris.

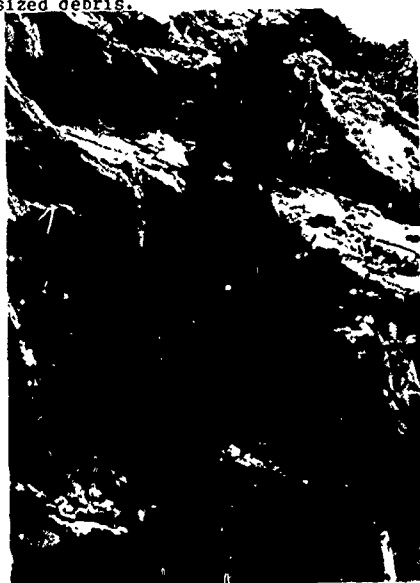


Fig. 13 Opening of large fissure between first and second toe blocks after January 1986 movements.

At the northern edge of the rockslide, a block has toppled forward from the front edge of the block behind the toe block. This is now aligned vertically and is jammed in the crack between the toe and second blocks.

All four of the drains leading from the toe of the slide to the road are cracked and heaved. Some minor repair work where mortar had been placed to infill earlier cracks is itself cracked (Figure 14). The heave has produced vertical and horizontal gaps. The kerbstones at the end of the drains at the road are more severely cracked (Figure 15), have been pushed further out (Figure 16) and there is now a clear gap between the kerbline and the soil of the verge behind. The displacement of the kerbline varies from 10 to 30mm.

Immediately downhill of the main rockslide, there has been a major collapse of a mainly shallow nature, occupying the slope from the crest downwards. It is a debris slide, with total disintegration of blocks (maximum size 0.5m) and much debris reduced to sand size. A long debris slope has formed over the intact in situ bedrock. Minor secondary failures of originally slipped blocks have, with the addition of much water, produced mudflows. Subsequently, water has washed down the slope and has formed a series of sandy alluvial fans at the toe which contain braided rivulets. The fans have formed across the footpath. At the road side of the footpath, the soil has collapsed and a hole has formed against the wall of the main drain.



Fig. 14 Cracking of repair mortar in scupper drain



Fig. 15 Cracked kerbstone at end of scupper drain



Fig. 16 Forward translation of kerbstone

The backscar is clean, sandy, iron stained and fresh and is now continuous over 15m from the edge of the main rock slide. The scar is formed mainly at the crest of the slope, above which there is a berm. Sandy lithologies are most obvious, although there is some obvious purple staining more associated with the interbedded mudrocks. The scar is occasionally ill-defined and irregular, although is clearly fresh.

The toe area is formed of a competent block of sandstone showing no disintegration. The block has cracked irregularly along intersecting joints. The crack varies in width from 20 to 30mm in the higher parts of 50 to 100mm at the toe, is totally controlled by the joints, and is rarely vertical. The block has moved forward only a small amount and has rucked up the sandy fill at the toe over a distance of 7.0m. There is no sign of damage to the main culvert, to feeder drains or to the kerb of the road, and so horizontal movement is limited. Between the rock toe and the sandy fill is ponded water about 0.25m deep.

The terminating side shear of this slipped block is formed along two parallel joint lines. The width of the zone in between is about 0.75m. The inside shear is controlled by joints in the orthoquartzite whereas the outside feature reveals large amounts of grey and purple mudrock in the scar, and is less regular and clearly defined. The downward movement is obviously slight but has caused minor breakage of the rock within the zone, which increases downslope.

The scar is slightly irregular in that there is a small amount of displacement downslope from the midslope berm, and then the main scar is up to 2m below that on the face. The backscar is steep and even overhanging in some places. The gap between the base of the scar and the rear of the main intact slide block is fully 2m, although the gap is infilled by a slab of the original slope which has collapsed into it and now produces a sub-horizontal surface. The failure of this slope slab was along a joint, and it collapsed into the gap left by the original forward motion of the main block.

Immediately downhill soil slumps 5.0m wide with about 1.0m of downslope movement have later been complicated by secondary mudflows. The downhill termination is against sandstone and some sandstone is exposed in the backscar.

Adjacent to the slump in the downhill direction is a toe slip about 3m in height, formed within a very mixed soil of clayey matrix with angular gravel and cobble sized fragments of sandstone. This is terminated in turn by a large "boss" of sandstone showing minor spalling along bedding planes many of which show the grey mudshale lining. A block failure some 3-4m wide and 1-1.5m high has failed along a bedding plane at one of the purple-grey mudrock partings.

A geomorphological map of the slope failure to the south of the main rockslide is shown on Figure 17.

#### STRENGTH CHARACTERISTICS

Pock strengths were obtained both in the field and in the laboratory. Schmidt Hammer (N Type) rebound tests were performed on the discontinuity surfaces in the field. For saturated joint surfaces and a rock unit weight of  $24.6 \text{ kN/m}^3$ , the equivalent uniaxial compressive strength was  $27 \text{ MN/m}^2$ . For dry surfaces, the equivalent uniaxial compressive strength was  $33.6 \text{ MN/m}^2$ . Uniaxial compressive strength tests on samples of the fresh sandstone gave results in the range of  $150\text{--}200 \text{ MN/m}^2$ , which suggests that weathering on the discontinuity surfaces was well developed.

Shear strengths of discontinuities were determined from large block samples using a tilt table. The blocks were obtained from the toe portion of the slope where the bedding was generally smooth and wavy.

The average tilt angle obtained for these samples was  $44^\circ$ . Rough sawn blocks were also tested in the portable field shear box apparatus (Ross-Brown and Walton, 1975), in order to determine the basic friction angle (Barton and Choubey, 1977). These produced results of  $\phi_b = 32^\circ$ .

Barton and Choubey (1977) suggested the following equation for estimating peak shear strength:

$$\tau_p = \sigma_n \tan (\text{JRC} \log_{10} \text{JCS}/\sigma_n + \phi_r) \quad \dots\dots\dots (1)$$

where  $\tau_p$  = peak shear strength, back calculated from Barton's (1973) empirical equation  
 $\tau = \sigma_n \tan (\phi + \text{JRC} \cdot \log_{10} \sigma_j/\sigma)$

$\sigma_n$  = normal stress due to self weight of overlying blocks

JRC = Joint Roughness Coefficient

JCS = Joint Compressive Strength

$\phi_r$  = Residual angle of shearing resistance

Fairly small errors in estimating the value of JRC when visually comparing joint profiles could result in serious errors in estimating the peak shear strength, especially if the ratio  $\text{JCS}/\sigma_n$  was large. Bandis et al (1981) suggested that accurate estimates of JRC can be conveniently obtained from the tilt angle ( $\alpha^\circ$ ) by:



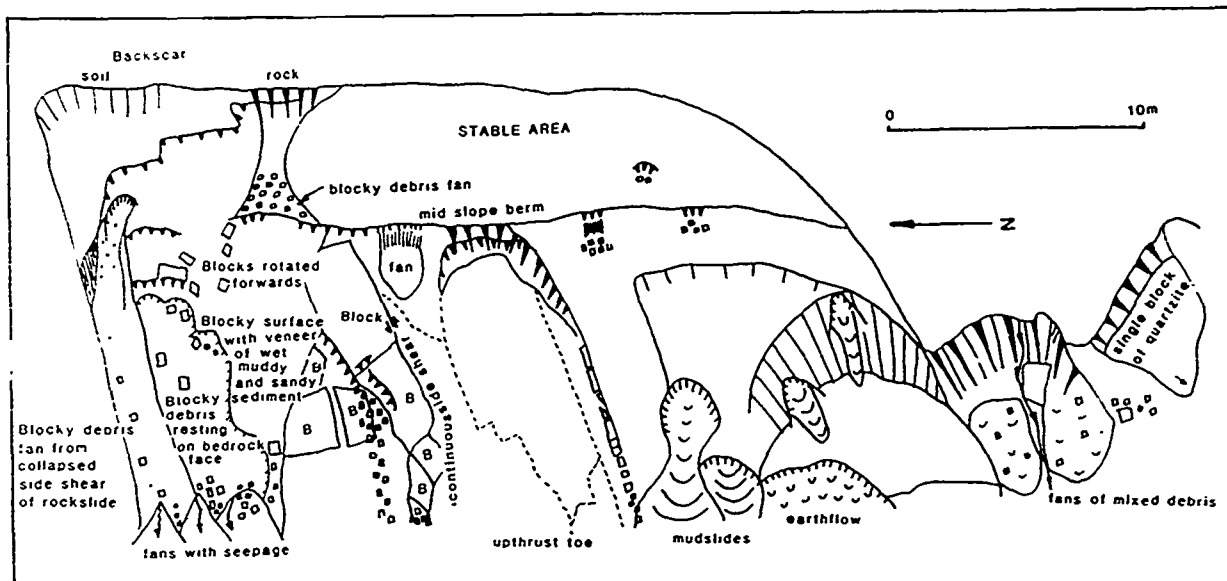


Fig. 17 Geomorphological Map of Slope Failure

$$JRC = \frac{\alpha^\circ - \phi_r}{\log_{10} \frac{JCS}{\sigma_{no}}} \dots\dots\dots (2)$$

Where  $\sigma_{no}$  is the normal stress due to the self weight of the overlying block.

The joint wall compressive strength and  $\phi_r$  can be estimated by using a Schmidt Hammer:

$$\phi_r = (\phi_b - 20) + 20 (r/R)$$

where  $\phi_b$  = basic friction angle  
 $r$  = rebound number of a saturated joint wall  
 $R$  = rebound number of a dry unweathered surface

From the laboratory and field tests, and applying equation (3),  $\phi_r = 28.8^\circ$ . From equation (2),  $JRC = 4.7$ , and from equation (1)  $\tau_p = 41^\circ$ .

#### ANALYSIS OF FAILURE

The analysis of the rock slope failure was carried out using the method for planar failure detailed in Hoek and Bray (1981). Back analyses were also performed in an attempt to define the combination of shear strength parameters mobilised at failure. This was done in a manner similar in principle to the secant method (Nguyen, 1984). For the back analyses, three different cases were considered:

- Case 1. Bedding plane dry.
- Case 2. Bedding plane filled with water.
- Case 3. Water-filled tension crack present.

The results of the sensitivity analyses for the three cases are shown in Figures 18, 19 and 20.

#### DISCUSSION

Intuitively, if a peak friction angle of  $41^\circ$  is used in an analysis, the factor of safety of the slope will be less than unity for a range of bedding plane angles from  $42.5^\circ$  to  $45^\circ$ . The stability of the slope therefore depends upon the roughness of the bedding plane, and possibly, the apparent cohesion that can be derived from the crushing of the partially crystalline structure of the quartzite.

The persistence of the rough asperities was difficult to determine accurately, as they were superimposed on waviness. Some asperities were, however, found to be dipping into the slope. It was found that decompositional weathering was occurring rapidly following the initial excavation, and as well as the Schmidt Hammer results, obvious surface softening and loosening was taking place on all exposed surfaces. It is therefore open to question as to what mode of failure is most likely to have occurred. In the light of the low levels of normal stress on the failure surface, sliding predominantly by over-riding of asperities might be expected. However, in view of the rapid softening of the surface, significant shearing through of the asperities may have occurred, with a cohesion being mobilised at failure. Unfortunately, no part of the failure surface was exposed in order that the more likely of the two solutions may be identified.

Stress relief may have occurred along the bedding planes at shallow depths with ingress of water accelerating the softening along the failure surface.

#### CONCLUSIONS

The slope has now been stabilised by a combination of re-grading and rock bolting. The lithological and structural complexities of the site when combined with excavation led to a quasi-stable slope being established. Heavy rains were the trigger of the rockslide and of the complex failure in the adjacent slope. The cause of failure may well however relate to stress relief and extremely rapid softening under an equatorial climate in the period following excavation.

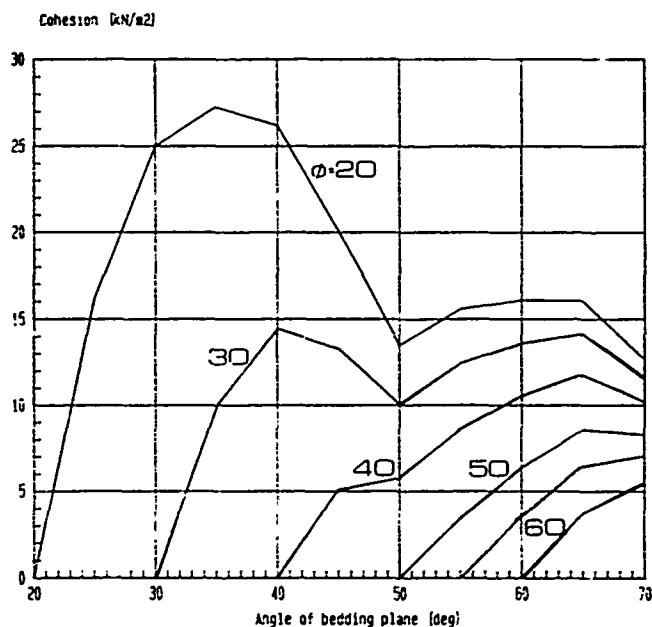


Fig. 18 Results of Stability Analyses. Case 1

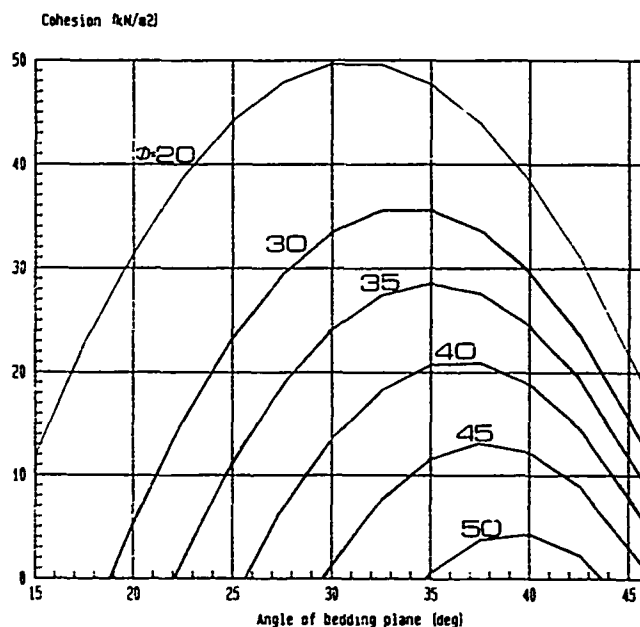


Fig. 20 Results of Stability Analyses. Case 3

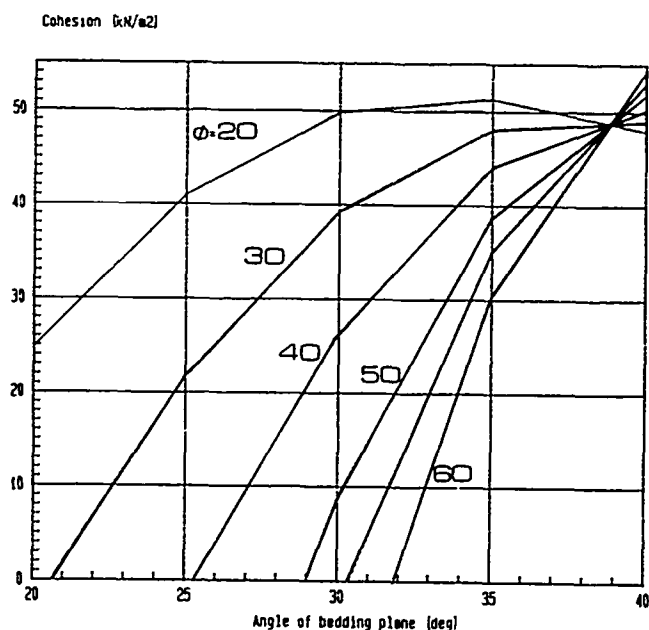


Fig. 19 Results of Stability Analyses. Case 2

#### REFERENCES

- Anon, 1977, "The description of rock masses for engineering purposes." Quarterly Journal of Engineering Geology, 10, 355-388.
- Bandis, S., Lumsden, A.C. and Barton, N.R. 1981, "Experimental studies of scale effects on the shear behaviour of rock joints." International Journal of Rock Mechanics and Mining Science, 18, 1-21.
- Barton, N.R. & Choubey, V. 1977, "The shear strength of rock joints in theory and practice." Rock mechanics, 10, 1-54.
- Denness, B. 1972, "A revised method of contouring stereograms using variable curvilinear cells." Geological Magazine, 109, 157-163.
- Hoek, E. and Bray, J. 1981, "Rock Slope Engineering." Institution of Mining and Metallurgy, London, 3rd Edition.
- Nguyen, V.U. 1984, "Back calculation of slope failures by the secant method". Geotechnique, 34, 423-426.
- Patton, F.D. 1966, "Multiple modes of shear failure in rock." Proceedings, 1st International Congress of Rock Mechanics, 1, 509-513.
- Pitts, J. 1984, "A review of geology and engineering geology in Singapore." Quarterly Journal of Engineering Geology, 17, 93-101.
- Pitts, J. 1984, "A survey of engineering geology in Singapore." Geotechnical Engineering, 15, 1-20.
- Public Works Department, Singapore, 1976, "Geology of the Republic of Singapore." Public Works Department, Singapore. p.79.
- Ross-Brown, D.M., & Walton, G. 1975, "A portable shear box for testing rock joints." Rock Mechanics, 17, 129-153.

#### ACKNOWLEDGMENTS

Thanks go to C.Y. Shun, Lee Yow Jinn and Lim Peng Heng who have assisted with this work throughout the period of investigation. Catherine Mac Groarty typed the manuscript and John Anketell-Jones assisted with the illustrations. Dr. GSP Thomas of Liverpool University kindly provided the geological map of the site.

## Slope Stability Evaluation for an Existing Steep Cut in Weathered Volcanics, Hong Kong

J.K.P. Kwong  
Presently Dames & Moore, Honolulu, Hawaii

L.J. Endicott  
Dames & Moore, Hong Kong

A.C. Lumsden  
University of Leeds, England

**SYNOPSIS :** This case study concerns an investigation of a major existing soil slope. It is a 60m (197 ft) high cutting slope, at 40 degrees to 60 degrees to the horizontal, exhibiting a considerably greater degree of stability than was obtained by a series of geotechnical investigations and analyses.

The common practice of correlation between widely spaced borings is shown to be inappropriate at this site because of the highly variable ground conditions. Rather, the comprehensive geological comprehensive engineering investigation carried out has enabled a detailed appreciation of the distribution and nature of weathered materials at the site. Transitional materials with soil-like appearance and weak rock properties have been identified. Based on this information, slope stability evaluation was carried out with more realistic results and with greater confidence.

### INTRODUCTION

Due to the steepness of the hilly terrain and intensive development of Hong Kong there are many large steep slopes in close proximity to occupied high rise buildings. Analysis of these slopes is important because of the severe consequences if they were to fail. Investigation is often costly due to difficult access and size of the slopes involved. Such has been the demand for development that even the steep slopes themselves may be considered as development sites. These circumstances are further complicated when an investigation obtains factors of safety of below unity for commonly occurring conditions and with no signs of imminent collapse.

### PREVIOUS EXPLORATORY PROGRAMS

Considerable borehole data for the site existed prior to this study due to the many attempts by successive owners to obtain permission to develop the upper part of the site. In addition, in 1978 an investigation of the slope was carried out following which horizontal drains were installed in the lower portion of the slope (Tong and Maher 1975), (Figure 1). The next investigation primarily consisted of 30 borings and the hand excavation of a caisson shaft which permitted the installation of a series of tensiometers which were used to measure pore water suction in the ground at various depths (Sweeney 1982). Research into the effects of unsaturation on shear strength was carried out (Fredland 1981) in order to reconcile the observed stability of the slope with the low factors of safety obtained previously.

### PRELIMINARY EVALUATION

The unusually large number of borings already drilled prior to this study facilitated to the early development of a geological model of the complex subsurface conditions. From the interpretation of aerial photographs, geological site surface mapping, and review of existing borehole data and ground water level monitoring, three major zones of deep weathering were considered to extend across this area (Figure 2). Correlation of field mapping and borehole data suggested that these zones of deeper weathering were probably shear or fracture zones in the rock mass.

The deeper zones of weathering also exhibited permanent ground water. Horizontal drains installed along the deeper zones of weathering, and the drains which intercept these zones at depth were found to yield a permanent flow of

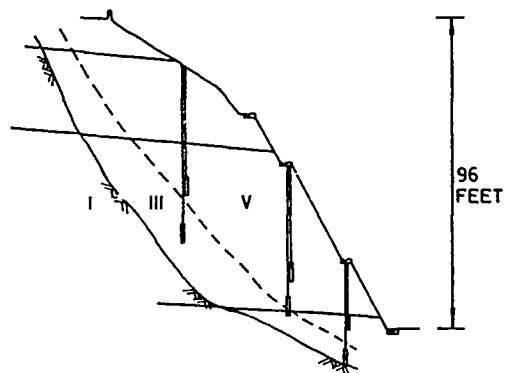


Fig. 1 Lower Slope Section Showing Horizontal Drains and Piezometers



Fig. 2 Site Plan Showing Zones of Deep Weathering

ground water during dry seasons. The presence of these deeper zones of weathering and fracturing and their inferred attitudes indicates that they serve as preferred paths where ground water from both regional and local sources could be concentrated. In areas associated with these zones, a seasonal rise of ground water is evident from both piezometer monitoring and from seepage stains beneath horizontal drains.

Elsewhere on site there is a general lack of ground water both at the relatively higher soil to rock interface and within the bedrock.

Samples remaining from some of the previous borings were re-logged in greater detail, and it was suspected that a transitional zone, not recognised previously, exists between the grade V and the grade IV weathered volcanic rock. Classification of the grades of weathering is given in Table 1.

Based on the findings of this preliminary evaluation, geological factors relevant to slope stability evaluation at the site include:-

- The highly variable rockhead and weathered profile, which may be the result of differential weathering along shear zones and granite/volcanics contact areas.
- The presence of a significantly thick but variable transitional zone of weak rock material at the soil to rock interface.
- The weak rock material is sensitive to sampling disturbance.
- The occurrence of ground water, which was found to be associated with geological structures.

TABLE 1 : Weathering Classification

| Grade | Degree of weathering | Typical Diagnostic Features   |
|-------|----------------------|---|
| VI    | Residual             | Soil, original rock fabric destroyed.   |
| V     | Completely Weathered | Soil, discolouration, original rock fabric is mainly preserved.                                   |
| IV-V  | Transition Material  | Soil-like to rock-like, highly variable, rock fabric preserved.                                   |
| IV    | Highly Weathered     | Rock weathered, discoloured throughout, variable, weak rock, alteration of primary minerals.      |
| III   | Moderately           | Partially weathered, discoloured, joints stained to altered, some alteration of primary minerals. |
| II    | Slightly Weathered   | Rock slightly discoloured, particularly adjacent to discontinuity.                                |
| I     | Fresh                | No stains along joints, no alteration of minerals.  |

A detailed exploratory program was planned to test the geological model, to better interpret the ground conditions, and to provide more realistic geotechnical engineering parameters.

#### EXPLORATION FIELDWORK

Additional fieldwork was carried out for this study. 12 vertical and 4 horizontal drillholes were each selected for a specific purpose such that the geological features of the site can be defined. During the course of the field exploration, the locations of some of the later holes and test pits were revised as a result of the information obtained from the first few holes and test pits. Core samples of soil, transitional material and rock were obtained using a Mazier retractable triple tube core barrel. Block samples of weathered rocks were collected from trial pits and exposed areas on the existing cut slope. Grades of weathering were classified by visual examination and a pocket penetrometer modified for testing strong materials was used to provide a quantitative index strengths of materials which had undergone different degrees of weathering (Figure 3), (Kwong et al., 1984).

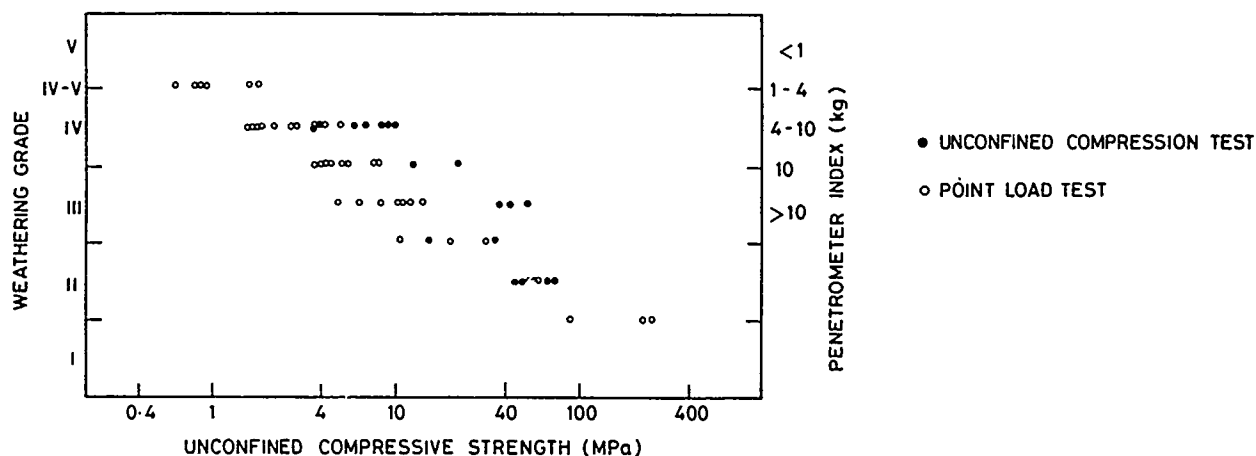


Fig. 3 Index Strength Test Results (After Kwong 1985)

#### DETAILED EVALUATIONS

The volcanic and granite rock mass at depth is generally grade III. Except along major stream courses, to either side of the site, a weathering mantle capped by thin colluvium covers the study area. In most areas, where a soil to rock interface exists, the rock is grade III to IV. The soil to rock interface is a transitional zone comprised of grade IV to V material. The transitional materials usually have high SPT "N" values ( $N=80$  to  $>200$ ) and when soaked in water, only the disturbed part of the sample disintegrates. A layer of grade V volcanic soil generally overlies this transitional zone (Figure 4).

The thickness of the materials in the weathering profile varies across the study area. The transitional zone is thickest in the area of deep weathering associated with closely spaced fracturing and shearing of the rock mass.

The zones of the slope classified previously as soil were found to consist primarily of grade IV, transitional, and grade V weathered volcanic rock. The deeper weathering profile is believed to be controlled by a very complex geological condition. Detailed logging of recovered rock cores and petrographic examination of thin sections prepared from rock samples indicated that the welded tuff was

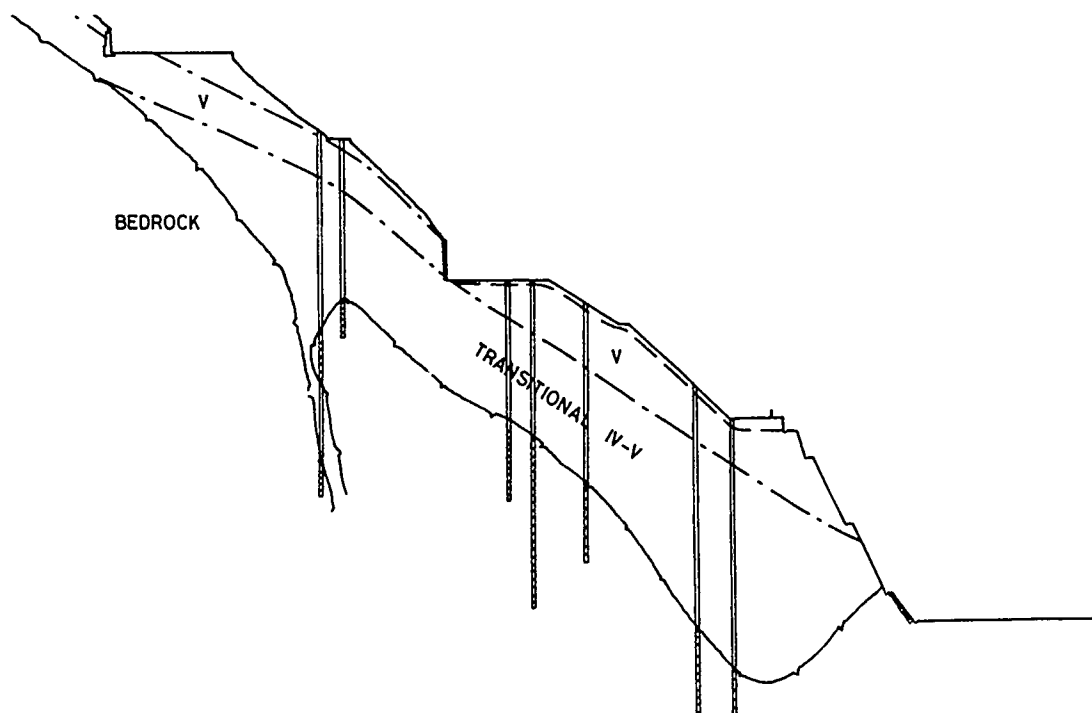


Fig. 4 Cross Section of Slope

affected by the younger granite intrusion, and was tectonically fractured. Alteration to the otherwise unweathered volcanic rock is believed to be mainly due to chemical weathering, as the degree of weathering appears to be associated with openings or fractures in the parent material, and in general, the degree of weathering also decreases with depth.

Differentiation between grade V, transitional and grade IV materials was further studied with the use of a scanning electron microscope for purposes of examining the microfabric. In parallel the mineral content of specimens of each material was determined by the use of X-ray diffraction techniques. The transitional material was classified as a soil-like but weak rock which still retains a skeletal framework of physical and chemical bonds between partially weathered feldspars and quartz crystals. These bonds contribute to a cohesion of the material and prevent slaking of a soaked sample. However the bonds are weak and can be broken by sampling disturbance (Kwong 1985).

For grade V materials, significantly high values for cohesion have not been found; although there is evidence of strength reduction around the periphery of carefully taken Mazier samples (Kwong, 1985).

The strength parameters for grade V, transitional, and grade IV materials were obtained by performing consolidated drained triaxial tests on Mazier samples (Figure 5), Table 2. Point load strength tests and unconfined compression tests were carried out using NX size cores, (Figure 3).

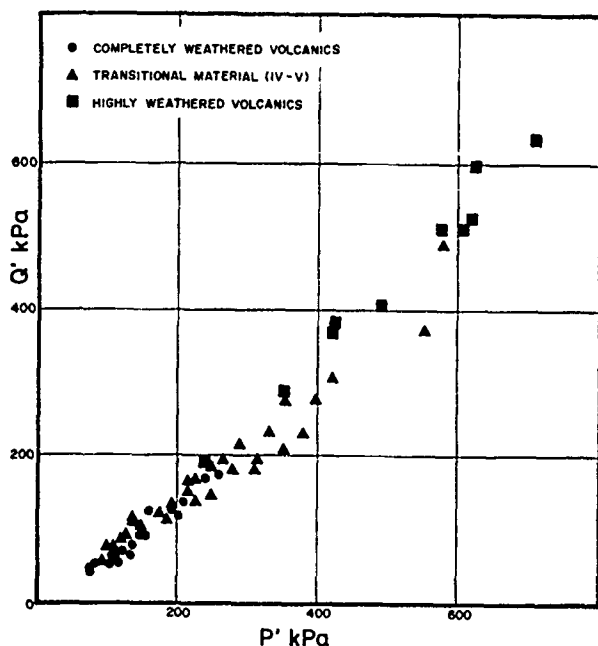


Fig. 5 Triaxial Strength Test Results

Slope stability calculations, carried out as part of this investigation, obtained factors of safety close to 1.4 for deep seated failure

surfaces under designed conditions relating to 10 year return period rainstorms. Shallow slip surfaces of the steeper areas, above the predicted water table, obtained factors of safety of as low as 1.0 under saturated (no suction) conditions. Whereas slope stability calculations carried out previously obtained factors of safety as low as 0.55 initially for deep seated failures, rising to above 1.0 on the basis of selective use of triaxial test strength data and allowing for an increase of strength with depth.

TABLE 2 : Strength Parameters

| Type         | c' (kPa) | $\phi'$ (deg.) |
|--------------|----------|----------------|
| Grade V      | 9        | 37             |
| Transitional | 18       | 39             |
| Grade IV     | 34       | 42.5           |

## CONCLUSIONS

This case study shows that vertical and lateral changes in the degree of weathering and in the soil to rock interface can be difficult to interpolate between vertical borings. An understanding of the conditions confirmed by appropriate field work is essential.

Recognition of transitional materials, between grade IV and V, with a soil-like appearance and a weak rock microfabric is important. Its strength can contribute significantly to the stability of slopes. Failure to recognise this material can lead to unrealistically low assessment of stability.

The transitional material is sensitive to disturbance. Very careful sampling and testing is required.

## REFERENCES

- Fredlund, D.G., 1981. The shear strength of unsaturated soils and its relationship to slope stability problems in Hong Kong. H.K. Engineer, Vol. 9, No. 4, pp. 37-45.
- Hencher, S, 1987. Private communication.
- Kwong, J.K.P., 1985. Effects of geological and environmental factors on the engineering properties of weathered igneous rocks in Hong Kong. Ph. D. Thesis, University of Leeds.
- Kwong, J.K.P., Lumsden, A.C., Endicott, L.J., and Smalley, I.J., 1984. Engineering Geology and Slopes Stability Problems in Chemically Weathered Terrain, Proc. 27th Int. Geol. Conf., 1984, Moscow.
- Sweeney, D.J., 1982. Some in-situ soil suction measurements in Hong Kong's residual soil slopes. Proc. 7th South East Asian Geotechnical Conference, Nov. 1982, Hong Kong, Vol. 1, pp. 91-106.
- Tong, P.Y.L. and Maher, R.O., 1975. Horizontal drains as a slope stabilising measure. Hong Kong Engineer, Vol. 3, No. 1, pp. 15-27.

## Distress in a Hill and Remedial Measures

**N.M. Patel**

Assistant Professor, Civil Engineering Dept., Delhi College of Engineering, India

**SYNOPSIS:** The paper presents a case study of a hill which developed signs of distress in 1979-80. Retaining and breast walls provided at many locations on the hill had been damaged and laterally shifted, indicating some movement in the hill. It created anxiety since big water tanks were supported on top of the hill. The distress in the hill were attributed to poor drainage of hill water, weaker sections of walls, dumping of loose lateritic material on the slopes, formation of erosion gullies etc. The hill was stabilised by removing these signs of distress with suitable remedial measures which are functioning satisfactorily over last 5-6 years. Systematic photographic presentation of different portions/features of the hill which showed signs of distress and then of different remedial measures which proved satisfactory makes the case study very interesting.

### INTRODUCTION

It is a case of a 50m high hill having two water tanks constructed at its top. The site is situated about 5 km away from Dharampur on way from Kalka to Simla in Himalayas (India). The tanks store water brought from distant springs through pipes and it is then pumped to higher level localities. So the complex on the hill consists of two big tanks and a large pumping station.

Alarming signs of distress were observed in the hill in 1979-80. They were of two types. Firstly, some of the retaining/breast walls of the approach road had cracked, bulged out and laterally shifted. Secondly, some part of the hill was constantly being eroded by rain water leading to formation of deep gullies.

All these created anxiety because the hill was supporting tanks on it. So factors contributing to distress in the hill were investigated and certain remedial measures were adopted in 1981. Since then there is no difficulties with the slopes and walls on the hill.

The paper reports details of signs of distress, their analysis and suggested remedial measures which have proved to be satisfactory.

### STUDY OF DAMAGES

#### Damaged Walls

A breast wall constructed at the foot of the hill on the main Simla road was damaged as shown in Fig.1. The damages were in the form of bulging out of the wall in the middle of its height and stones coming out of it at many locations. These signs indicated development of heavy earth pressures which might be partly due to lateral outward movement of the hill and partly due to accumulation of hill water in the backfill.

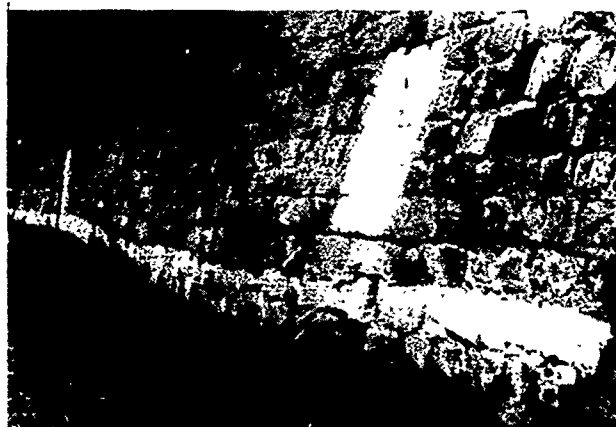


Fig.1: Damaged Wall at the foot of the Hill.

The complex with water tanks located at top of the hill was approachable through a Jeepable road. Certain portion of this approach road was damaged as shown in Fig.2. Originally the road



Fig.2: Sinking Side of Approach Road.

on curve was provided with outer edge at a higher level than the inner edge. But the figure shows sinking of the outer edge below the inner edge by more than 30 cm and cracking of the road surface. This happened since the retaining wall supporting the outer side of the road had experienced large outward shifting and rotation. It also resulted in movement of soil in certain lower portions of the hill. The breast wall reported in Fig.1 was in the lower portion of the hill.

The breast wall seen by the side of the road in Fig 2 had also cracked. A close-view of the damaged wall is seen in Fig.3. The cracks were so wide that in certain patches the wall had become almost ineffective.



Fig.3: Cracked Breast Wall.

The worst damage to the breast wall is seen in Fig.4. The wall had failed, rubbles had rushed out and a big opening was formed in the wall.



Fig.4: Completely Failed Wall.

#### Causes of Damages:

The damages to the wall shown in Fig.1 to 4 were on account of the following three main reasons:

1. In certain portions, the strength of the wall was not adequate, viz. either the wall was relatively thin in section or the quality of mortar used was poor. The bulging of wall along its height shown in Fig.1 is partly due to inadequate thickness of the wall. The cracking and opening out of the joints shown in the wall of Fig.3 is partly due to poor quality of mortar.

2. The portion of the hill below the approach road shown in Fig.2 had relatively steeper slope. Stability analysis of the slope gave a factor of safety of 1.03 which indicates state of critical equilibrium. Probably this resulted in the lateral shift of the wall supporting the approach road and cracking of the road surface.

3. There were two small natural streams of water in the hill. Their free flow was hindered by the transverse walls. Collection of water in the backfill increased the earth pressure and damaged the wall. The wall in Fig.4 is broken open by the water collected at its back. The rubbles carried by the gushing water were deposited in the front of the wall. Fig.1 also shows collection of such water which had seeped through the damaged wall. This poor drainage of hill water was another major cause of damages to the walls.

#### Erosion Gullies

Another cause of anxiety was the constant erosion of the soil in the eastern part of the hill. It resulted into deeper and wider erosion gullies as shown in Fig.5. One of the water tanks is



Fig.5: Eastern- side View of the Hill.

also seen on the left side in the back ground of the figure. The soil excavated during the construction of this partly under ground tank was deposited on the slopes of the hill with an idea that it would increase stability. But the soil so deposited did not support any plant-life and constant erosion of it under rain water led to formation of erosion gullies. Another close view of it is shown in Fig.6.





Fig.6. Close-view of Active Erosion-Gulley.

#### Causes of Erosion

The hill was made of lateritic soil. Grain size analysis of the freshly excavated soil revealed that it was a well-graded mixture of 40% gravel-sand, 47% silt and 13% clay which if compacted in proper wet condition could form a stable slope. But the soil when left loose and subjected to weathering, got converted into stiff angular grained material which with dry sieve analysis was classified as gravelly coarse sand.

The soil excavated out during construction of the partly underground tank was deposited on the hill. And on weathering, it had changed into gravelly coarse sand like material as shown in Fig.7. The grains of the deposit had become

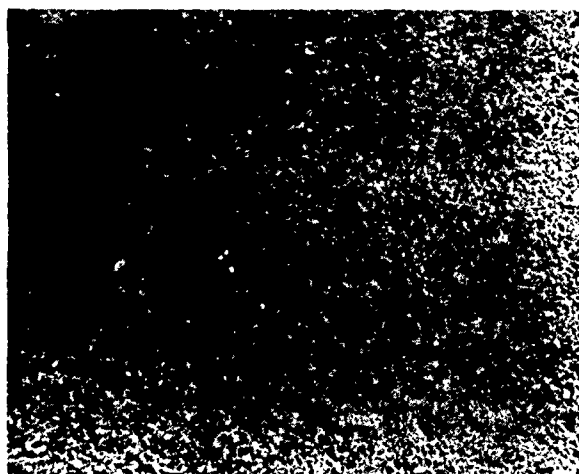


Fig.7: Weathered Granular Material

stiff, angular in shape. The material was non-cohesive and its grains used to roll down the slope even with scanty rain fall. So it resulted in as low an angle of repose as  $35^\circ$  as seen in Fig.8.

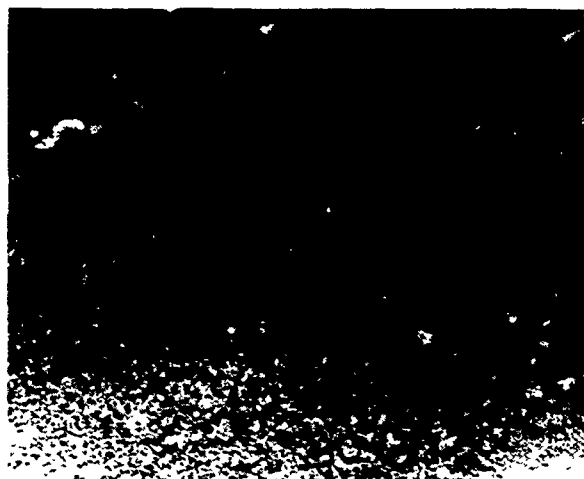


Fig.8: Slopes of Banks of Erosion Gullies.

Another reason of such eroding embankments of the hill was the inorganic nature of the loose deposit. It did not promote growth of vegetation cover which was essential for arresting erosion of such material.

#### REMEDIAL MEASURES

As reported earlier, in the portion between the foot of the hill and the approach road, the slope was in a critical condition. Hence the slope was regraded, the approach road was realigned and the section of the foot wall was improved. The measures stabilised the slope and the reconstructed foot wall showed no sign of distress over last 5-6 years. A recent picture of the wall is shown in Fig.9. Its comparison with Fig.1 speaks of satisfactory functioning of the remedial measures.

The damaged breast wall reported in Fig.3 and 4 was also reconstructed with wider section after adopting necessary measures for proper drainage of the hill water. It is also functioning very satisfactorily now.



Fig. 9: Reconstructed Foot Wall.

The other important remedial measure which effectively arrested the signs of distress was the wall planned scheme of drainage of seepage water from all parts of the hill. Along the main erosion gully formed on the hill which was shown in Fig.6, a drain was constructed as shown in Fig.10. It was of adequate section to carry the maximum rain water discharge and had adequate longitudinal slope to allow uninterrupted flow of water

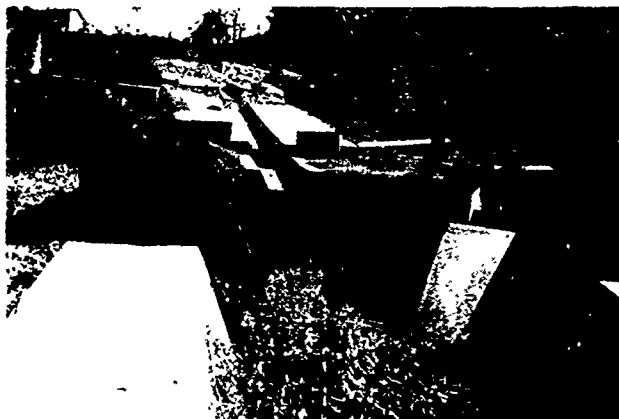


FIG. 10: Main Drain.

in all seasons. Also for matching the bed level of the drain with the natural topography of the hill, falls of heights of 1 to 2.5 m were constructed at suitable intervals along its length. Also the rain water of the areas adjoining to the drain was made to flow towards the drain by suitable landscaping with construction of transverse walls as shown in Fig.11. These walls form



Fig.11: Another View of the Main Drain.

part of the fall-structure and also support the ground above them. The soil in between these walls was protected from erosion either by properly compacting it and then growing grass on it or by covering the surface with a bituminous premix carpet,. Fig.12 shows one such transverse wall with a premix carpet cover in the front of it and vegetation cover on the surface of the slope at the back of it.



Fig. 12: A Transverse Wall

## CONCLUSIONS

Generally instability of an embankment is studied by considering equilibrium of an earth mass over an assumed potential slip surface and under action of disturbing and restoring forces. But this approach is not suitable for natural hills of Himalayas which are made of non-homogeneous and heterogeneous materials and since the approach cannot consider the role of different agencies causing distress at different parts of the hill ( Bhandari. R.K., 1986). Some of the agencies found active in the present case study were (i) presence of inorganic deposit on the hill which did not promote growth of protective vegetation cover, (ii) presence of lateritic material which on weathering changed into easily erodable loose granular material, (iii) inefficient drainage of natural hill water causing development of excessive earth pressures on retaining walls and (iv) development of critical equilibrium state in certain slopes subjected to constant erosion.

The remedial measures which proved successful in removing the distress from the hill were (i) regrading of the slopes which were in critical equilibrium state, (ii) compacting loose earth masses of the hill, (iii) preparing vegetation cover on barren surfaces with special measures like introducing manure, watering it and protecting it manually or by using geogrids, (iv) covering erosion-susceptible surfaces with bituminous premix carpets, (v) providing suitable retaining and breast walls, (vi) providing longitudinal and transverse drains with suitable cross-falls etc.

## Acknowledgement

For the case-study reported in the paper, the opportunity was provided by the Central Building Research Institute, Roorkee ( India ).

## References:

- Bhandari, R.K. ( 1986), "Slope Instability in the Fragile Himalaya and Strategy for development", 9th IGS Annual Lecture delivered at IG C-86 Conference held at I.I.T., New Delhi, December.

## Case Study—Ground Failures and Ruptures in Xian City

Wang, Zhong-Qi

Professor, Comprehensive Institute of Geotechnical Investigation & Surveying (CIGIS), Beijing, China

Zhang, Rong-Xiang

Engineer, Comprehensive Institute of Geotechnical Investigation & Surveying (CIGIS), Beijing, China

**SYNOPSIS.** Xian city, the most well known ancient city of China for her incredible Terra Cotta Warriors and so forth, has been suffered from ground fracture for years. Surface ruptures and "faultings" encountered in strips all over the city. Hundreds of buildings were severely destroyed and many of them even have been demolished. Ground failures wide-spread and enlarged from time to time, especially right from Tangshan earthquake of July 28, 1976. Therefore serious concerns and suspicious of being associated with major earthquakes have arisen. Thus it has been a problem of both engineering and social influence.

Like many other cities in China and even in the world such as Houston, Texas, USA, surface faulting or surface rupture often caused many guess-works and arguments among different engineers, geologists and seismologists. In turn, many projects either underway or to be undertaken will be seriously lagged out due to discrepancies of different assessment and measures of mitigation.

The authors have been deeply involved in surface faulting and ruptures as a background for exploring the mechanism and predicting its possible effects from the engineering point of view.

In this paper, the authors introduce their systematic case study on Xian ground failures towards this end, including site investigations, typical damages assessment, numerical analysis on fracture mechanism, model tests in laboratory and comprehensive evaluations etc. Conclusions were drawn not only for this particular ancient city but also provided a referential real case for the like in the world.

### 1. INTRODUCTION

Early from 1950s, ground subsidence took place in Xian city. Meanwhile, surface ruptures encountered around the same area and finally developed into five major rupture belts with a total length of 26.3km. All the rupture belts tend to strike in N-E direction (Fig. 1). Buildings and many other constructions on the ground or underground were severely destroyed as shown in plate (1) and (2). This problem seemed to be more and more serious after the disastrous Tangshan earthquake ( $M = 7.8$  July 28, 1976), because many people terribly worried about that their development would be associated with any seismic event to come. Consequently, the occurrence of ground ruptures not only cause great loss in construction, but also form a social problem which affected people psychologically, and make the city planners much confused.

This problem has been investigated by many relevant professional agencies and quite different conclusions have been drawn. One conclusion is that the ground ruptures are the extension of the active fault in the deep bedrock which is about several hundred meters below the ground surface. Another conclusion insisted in thinking of the consequence of excess draw-down of ground water table due to over pumping in recent thirty years. However, either of the two could not convince the other with sufficient reasons. Therefore, further research work is required to verify the actual mechanism of the ground ruptures in Xian city.

Ground rupture is a general term describing the discontinuity on which covers surface faultings of any kind. The case history in Xian city is one of the numerous similar events in China and other countries like that in Houston and Shan-xi province of China. Controversy often arises based on various view points. But as a practical problem in geotechnical engineering, the following questions should be answered definitely:

- (1) Whether or not the ground ruptures used to be or will be closely related to a strong earthquake.
- (2) Whether or not the occurrence of ground ruptures can be predicted and prevented. This is also a common problem somewhere in the world like Houston, Texas [1], San Joaquin valley, CA. [2] and south-central Arizona [3] even though some factors differ from place to place.

### 2. PRELIMINARY DISCUSSION ON THE MECHANISM OF GROUND RUPTURES

Research work began with evaluating the stand-points of the two different theories as mentioned above.

The tectonic theory put emphasis on the background of the fault in the bedrock and any evidence showing the link between ground rupture and causative fault. It has been examined and

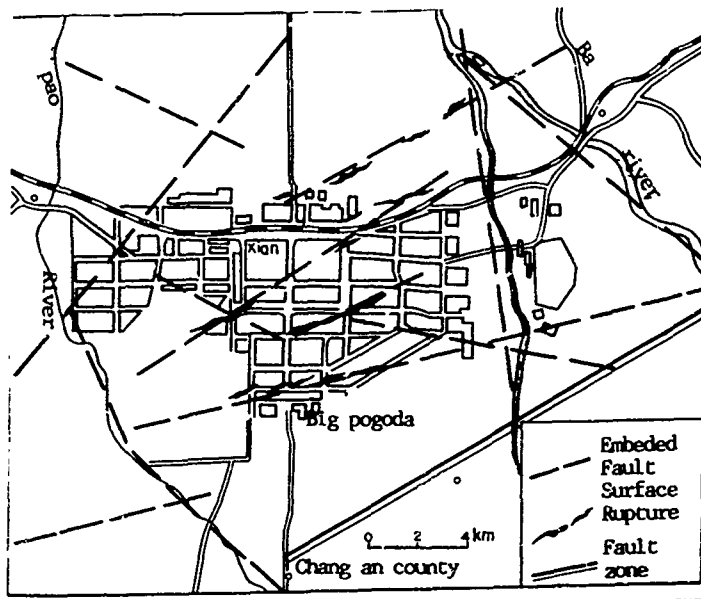


Fig. 1. Distribution of surface ruptures over Xian urban area



Plate 2. Damages on buildings caused by composite ground ruptures

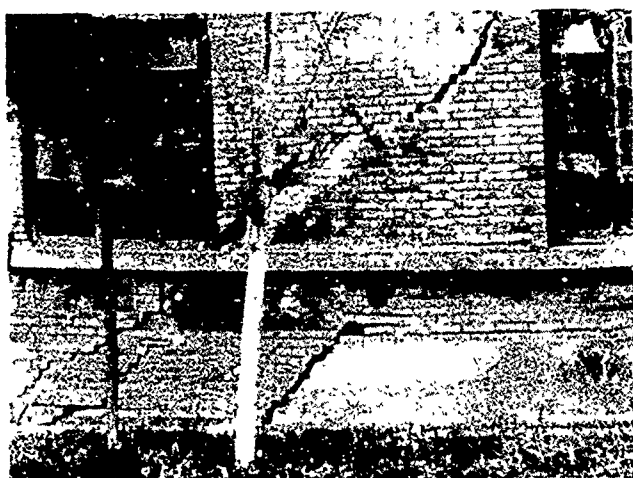


Plate 1. Damages on buildings caused by composite ground ruptures

verified that:

- (1) Ground rupture belts are basically in the same direction as the regional tectonic fault;
- (2) Ground ruptures basically coincide with major tectonic faults;

However, discrepant phenomenon still exists which will be pointed out in the following. The over pumping theory stressed out that:

- (1) Ground subsidence did occur in good conformity with the occurrence of ground rupture;
- (2) The center of subsidence cone coincides with the drawn down center of ground water Fig. 2;
- (3) Ground ruptures used to match up with the

change of ground water level in time.

However, the distribution of ground ruptures didn't follow the border of conic subsidence. Therefore anyone of the above theories can not give satisfactory answer alone.

In order to figure out comprehensively the actual behavior and mechanism of the ground rupture, the following work was carried out in detail:

- (1) Detail exploration and inspection on the rupture characteristics and behavior;
- (2) Laboratory modelling to trace out the propagation geometry of rupture itself under the law of similarity;
- (3) Numerical modelling by finite element method to verify the laboratory modelling result and the criteria of rupture propagation.

Conclusion was finally drawn that the mechanism of ground rupture in Xian possesses a double feature of both tectonic faulting and ground subsiding due to over pumping. A particular term was suggested to be given -- composite rupture which is explained separately as follows.

### 3 SITE VERIFICATION OF GROUND RUPTURE BEHAVIOR

Obvious characteristics were examined and proved by surveying and monitoring. It was found that:

- (1) Only vertical dislocation can be visible with the rupture, and no horizontal dislocation at all;
- (2) New ruptures appeared at the very position of the ancient ruptures -- an illustrative evidence showing the recurrence of ground rupture;
- (3) Ground ruptures seemed to be activated by both lowering of ground water table and the ground subsidence due to over pumping;
- (4) Ground rupture extended down to certain depth in the soil formation and vanished

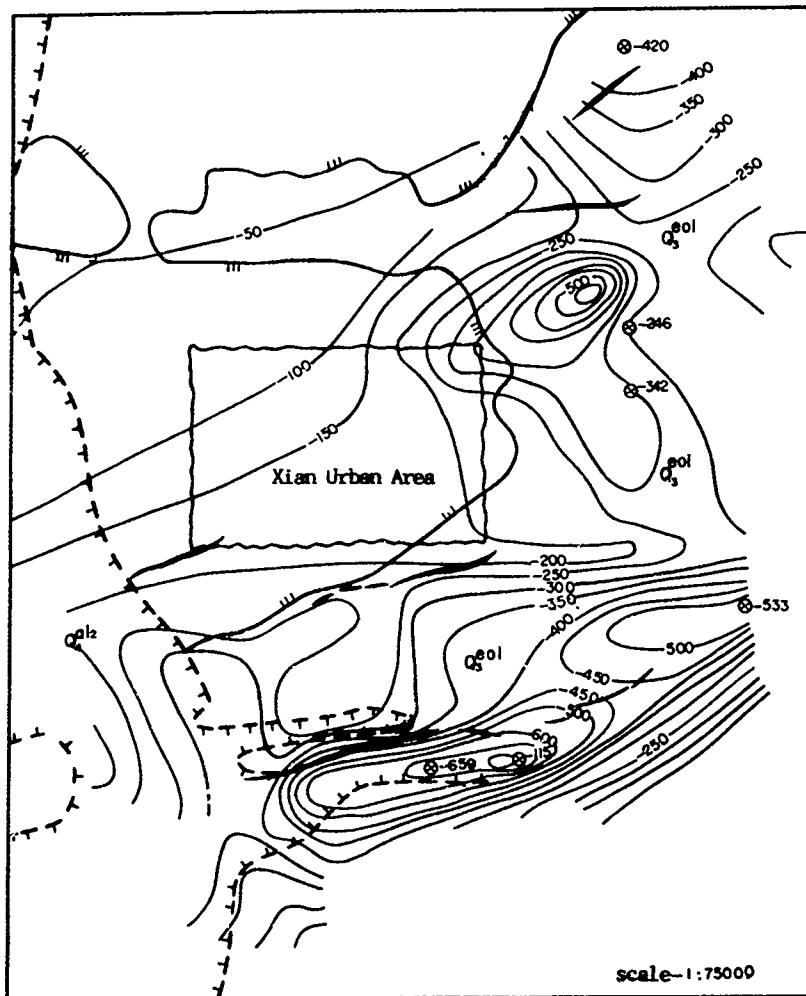


Fig. 2 Surface ruptures and land subsidence

with increasing depth(Fig. 3);

(5) All the ground ruptures distributed within the scope of ground subsidence. The most active ruptures are directly associated with the drawn-down of ground water(Fig. 4);

(6) The cracks of ground surface are the secondary effect of the activity of the underlying ancient ruptures in the sense of both manner and time;

(7) Ground ruptures have a very strong seismic background. Evidence verified the historical record that major earthquakes around Xian like Hua-xian earthquake in 1556 ( $I_0 = 11$ ) excited strong motion in Xian to an intensity  $I = 9$ . As the ground encountered in good conformity with the tectonic stress field.

#### 4. LABORATORY MODELLING

The purpose of laboratory modelling is to simulate the mechanism of ground ruptures and consequently to specify the propagation criteria of the bedrock dislocation up to the ground

surface so as to clarify whether and how the ruptures in bedrock may extend to the ground surface.

Model test was so designed that the law of similarity should be satisfied with the following assumptions:

- (1) The overlying soil is both homogenous and isotropic halfspace;
- (2) The contact between overlying soil and the bedrock is a rigid interface, the tectonic stress exerted is the subsequent transferring effect of the dislocation in bedrock;
- (3) The length of rupture in bedrock is theoretically infinite, and no attenuation of displacement in both longitudinal and transverse direction;
- (4) The constitutive behavior of soil is elasto-plastic;
- (5) When any creep occurs, the stress in the soil can be considered as pseudo-static;
- (6) The rupture induced in soil can be treated

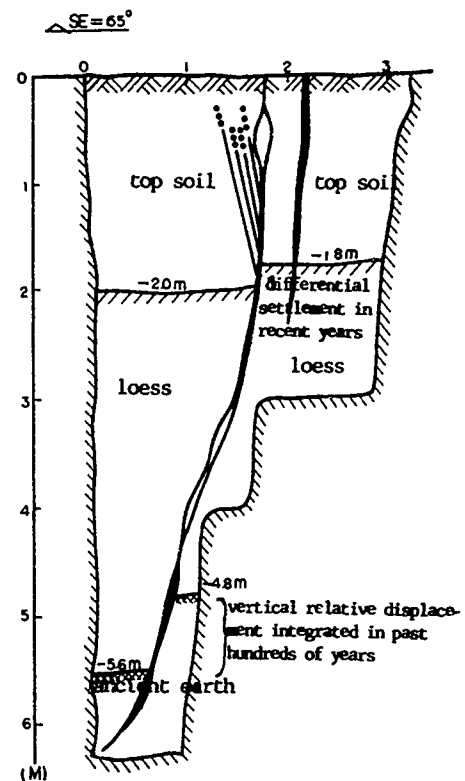


Fig. 3 Profile of a testing pit

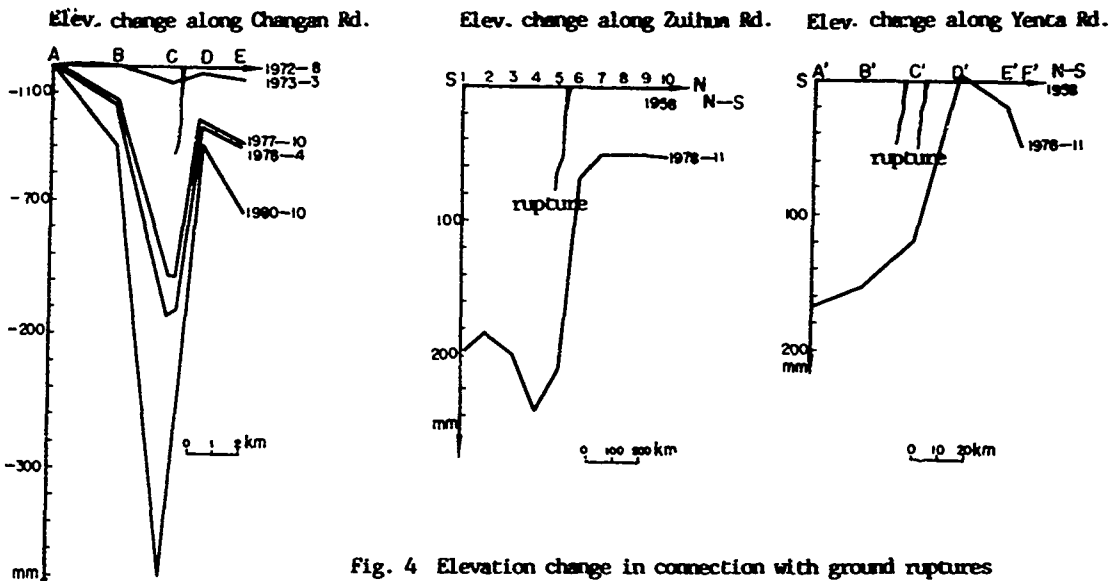


Fig. 4 Elevation change in connection with ground ruptures

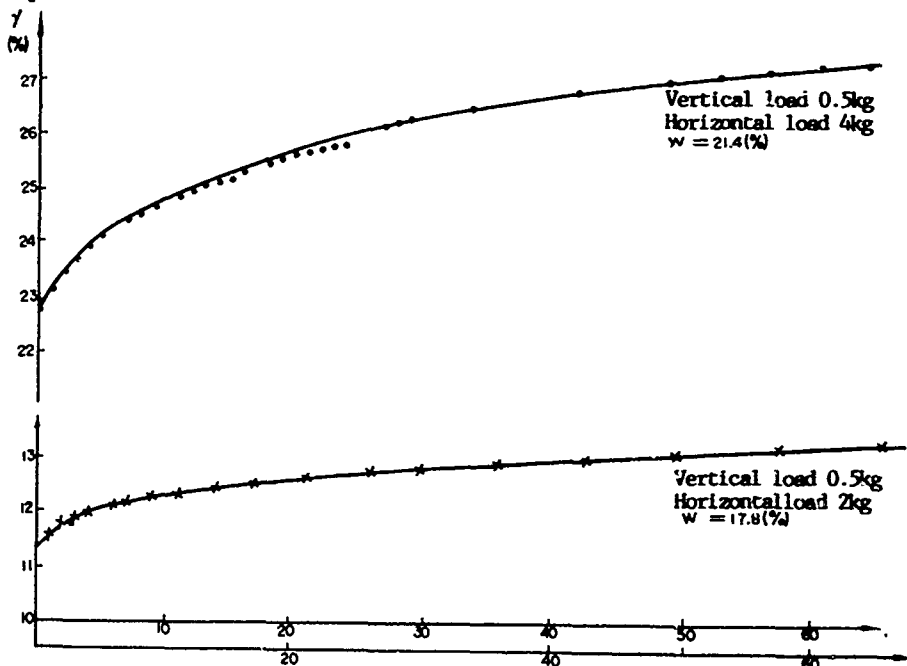


Fig. 5 Shear strain versus time of the material used for the model test

as macroscopic yield in soil mass.  
By the law of similarity, the model test should simulate the strain behaviors of the quaternary soil. And the model test should satisfy the following similarity conditions:

For motion,  $C_\sigma \cdot C_x / C_t = 1$

For boundary displacement,  $C_{u_0} / C_u = 1$ ,

$C_t / C_{u_0} = 1$ ,  $C_{u_0}' \cdot C_t / C_{u_0} = 1$ ,

For boundary stress,  $C_\sigma / C_r = 1$ ,

For stress-strain,  $C_v = 1$ ,  $C_r / C_\sigma = 1$ ,  $C_t' / C_r = 1$ ,  $C_\sigma = 1$

Where  $C_\sigma$  constant for stress similarity,  
 $C_t$  constant for geometric similarity,  
 $C_x$  constant for volume weight similarity,  
 $C_u$  constant for displacement similarity,  
 $C_t'$  constant for time similarity,  
 $C_\sigma'$  constant for strain similarity,  
 $C_\sigma$  constant for elastic modulus,

$C_r$  constant for boundary stress similarity,  
 $C_{u_0}$  constant for boundary displacement similarity,  
 $C_{u_0}'$  constant for boundary displacement similarity.

Thus, a silt clay was adopted to make the sample and further behavior specified as follows:

- (1) Stress-strain relationship looked like parabolic type;
- (2) Change of confined pressure may have big influence on stress-strain path;
- (3) The horizontal to vertical load ratio and the water content have bigger influence on the rheological properties of soil.

A number of test results show that:

- (1) When the horizontal displacement of the

base becomes greater than 1/2 of the sample thickness, micro rupture on the surface began to occur;

(2) As the base dislocated horizontally, ruptures in soil began from the bottom to the top. when the base dislocation extended about 1/2 of the thickness, ruptures comes thro out of the sample;

(3) Ruptures on the sample have quite different figures on the real ground surface.

## 5. NUMERICAL ANALYSIS

An elastoplastic finite element analysis program was used to figure out the mechanism of the rupture. It has a big variety of elements which lead soil mechanics into plasticity. To modify the soil properties, Cap-model was first put into consideration. Since this model is actually composed of both a cap and a Drucker-Prager yield plane (Fig. 6 A), and the stress path mainly goes along  $f_1$ , and  $f_2$  will become a minor factor, so Drucker-prager model was finally used for simplicity which yielding plane is as shown in Fig. 6 B.

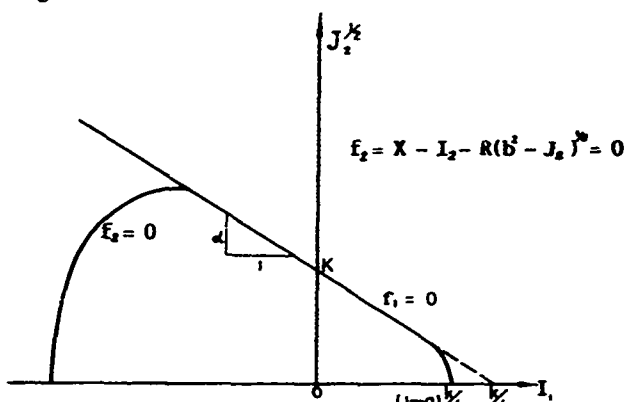
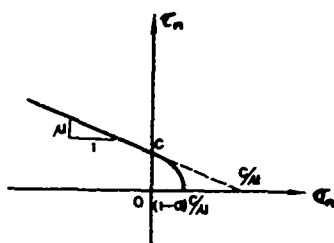


Fig. 6 (A) Cap model



(B) Drucker - prager model

Fig. 6 Numerical model and its parameters

In addition, the loess in Xian behaves as a weak work-hardening or even work-softening material as shown in Fig. 7.

In calculation, the boundary elements were used to facilitate the displacement calculation at the boundary under loading. Besides, infinite elements to deal with integration problem -- i.e. Gauss-Legendre integral and Gauss-Laguerre integral were used in tangential direction and radial direction separately. To simulate the dislocation in bedrock, joint element was used.

Based on surface faulting and rupture pattern over observed triangular elements were adopted to input displacement or load. The result shows:

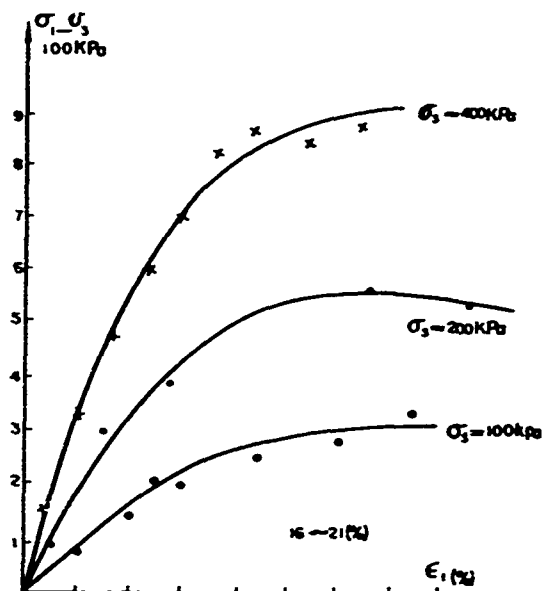


Fig. 7 Stress-strain relationship of the materials used for the model test

(1) When the ratio of vertical dislocation of bedrock to the thickness of overlying soils is 1/20 (Fig. 8 A) no rupture extends to ground surface until the ratio reaches 1/10 (Fig. 8 B); (2) When dislocation reaches 3/5 of the thickness of overlying soil, the rupture in the soil extend downward, and finally rupture in soil goes thro out the soil layer;

Referring to the geological data in Xian, the thickness of overlying soil is 600 - 700 m, and dislocation of bed rock is about 2000 - 3000 m. The vertical dislocation of bedrock necessary to cause the 2000 m thick soil layer to break must be at least 200 m. When the horizontal dislocation is over 1000 m, the 2000 m thick of soil layer to begin break thoroughly.

## 6. CORRELATION BETWEEN GROUND RUPTURE AND ANCIENT FRACTURES IN SOIL

By visual observation in exploration trenches at many localities over Xian city, many ancient fractures embedded with top soil at a depth 0.7 - 0.3 m below ground surface were found which were caused by tectonic movement of ground in historical event [4]. Fig. 3 is an example where an ancient fracture belt striking in N 65°-70° E, about 5 - 6 m wide, embedded at 2m depth by top soil. The fractures vanish downward at a depth of 6.5 m. It was verified that the fractures were caused tectonically by Hua-xian earthquake in 1556. It was also noticed that most of the ground ruptures lay on the ancient fractures which were normally filled by the materials from top layer. Very important evidence is that there existed micro-fractures in the top soil directly above the ancient fracture. Since the ground rupture is partially the sequel of ancient fracture in the soil, it is easy to locate the ground rupture by simply digging trenches and identifying whether ancient fracture exist or not.

## 7. CONCLUSIONS

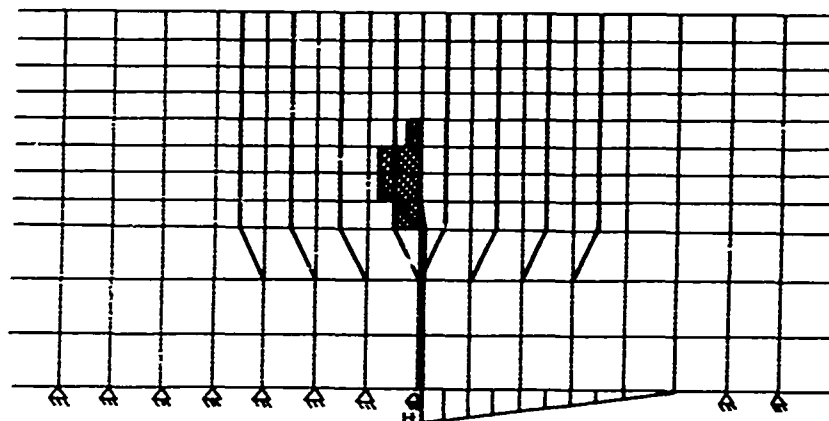


Fig. 8 (A)

H: Displacement input

H = 1/20 of soil thickness

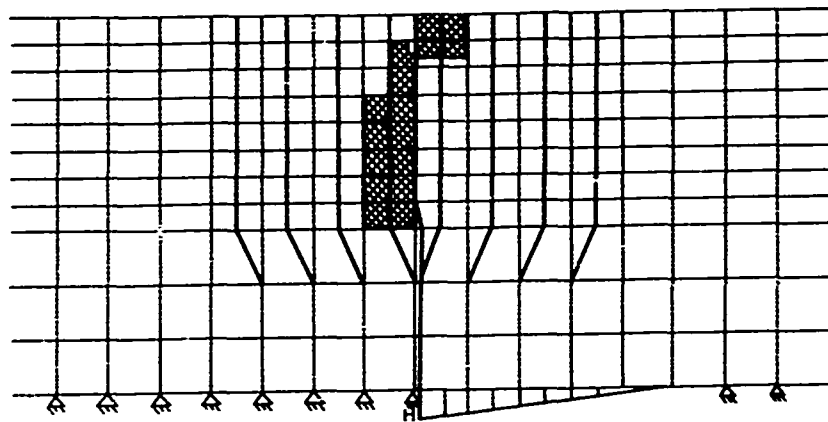


Fig. 8 (B)

H = 1/10 of soil thickness

Fig. 8 Ground rupture propagation from the bedrock by numerical analysis

(1) The ground ruptures or "surface faulting" in Xian is a particular type of composite mechanism which characterized in 6 points as follows:

- (1) Orientation - all the ruptures are oriented into five alignments which strike 75-85°NE. Therefore it reveals common tectonic nature;
- (2) In series - each alignments is composed of a series of ruptures which are in good coordination with each other;
- (3) In coincidence with land subsidence - all the ruptures occurred within the boundary of subsiding area, where the more the ground settled, the more the rupture took place;
- (4) Ruptures vanishing downward - since ruptures are the result of ground shaking, its size varies inversely with depth and finally diminishes to invisible degree at relatively shallow depth;
- (5) Vertical displacement only - all ruptures were caused by differential vertical displacement without any horizontal one. This is because the ruptures were activated only by gravitational force of the soil mass;
- (6) Coincidence with ancient underground rupture - ancient tectonic ruptures in soil are the origin of the composite ruptures. Normally the former extends to the latter.

(2) On one hand, lots of ancient fractures in

soil overspread in Xian caused by strong historical earthquakes, which provides the geological background of the ground rupture.

(3) On the other hand, the ancient fractures in soil have been activated by ground subsidence due to over pumping of ground water.

(4) Therefore, the mechanism of ground ruptures consists of two major factors: (1) the ancient fractures; (2) the ground subsidence due to drawn down of ground water.

(5) When siting a project in an area like Xian, a very practical way to evaluate the possible occurrence of ground ruptures is to make trench exploration and conduct visual verification.

#### REFERENCE

- [1] Houston Geological Society (1981) Faults in the Houston Metropolitan area, Texas "Houston Area Environmental Geology".
- [2] Heizer, T.L. (1981) Faulting Caused by Groundwater Level Declines, San Joaquin Valley, CA "Water Resources Research" Vol.16 No.16.
- [3] Schuman, H.H. & Tostine, D.T. (1984) Occurrence & Prediction of Earth Fissure Hazards Caused by Groundwater Depreciation in South-central Arizona "3rd International Conf. on Land-Subsidence".
- [4] Wang Zhong-Qi et al (1983) Surface Displacement in Relation to Shallow Surface Fractures & Deep Faulting "Canadian Geotechnical Journal Vol.20".



## On a New Problem of High-Speed Landslides

Hu Guangtao

Professor of Engineering Geology, Xian Geology College, Xian,  
China

**ABSTRACT:** This paper has discussed the problem proposed about multiple stroke of high-speed landslides its multiple strokes, change of energy, and overstepping gas billows spattered with mud.

### INTRODUCTION

This paper for the first time puts forward the problem of multiple-stroke and high-speed landslides in bedrock, and the problem of overstepping gas billows spattered with mud and made theoretical discussion about them so that much attention should be paid to protected slope environments from the point of view of engineering geology and to improving its quality to prove landslides in theory and take appropriate measures for prevention and management.

### PROBLEM PROPOSED IN THIS PAPER

Leng-shui-gou, Shi-jia-po landslide in Sang-su-wan village in Ning-qiang county is a typical one first proposed with multiple-stroke, , intensely-moving and high-speed. Shi-jia-po multiple-stroke, intensely-moving and high-speed landslide lies on the left bank(Shi-jia-po) of Leng-shui-gou branch of upper reaches of JIANG HAN River. The place near Leng-shui-gou is very dangerous. At about 10 o'clock at that night, on 23, August, 1981, rock soil of bulk 480,000 m<sup>3</sup> in all on the left bank of the slope rapidly and intensively dived and slid down from the elevation of 925 m., accompanied by boom and great noise, suddenly stopping up rivers. And the body slide under enormous impulsive forces crossed the valley floor in length if 50-100 m., and upthrust valley slope on the right bank, lifting up the 40m.. What is more, in the front part of the landslide took place the secondary slide bed plane which dived and slid down from the elevation of 40m. to the opposite direction and after turning to the former left bank, upthrust lifting up to 20m.. From here, it mixed with large amount of stream water and rains, continuously made up three moving strokes in the form of fluids from the left to the right, and then from the right to the left, and stopped in the regions Shantand-su and Long-wang-miao. The whole course is about 1,060m. long, which spent less than 10 minutes sliding. It is emphasized that damages made by Shi-jia-po multiple-stroke landslide is rare in our country. At the left bank of down stream which is 600 m. away from the starting place landslides overturned a mountain to a farmer household in the village Qing-gang-su-wan and thirteen farmers were died of sliding fluids and no one is alive.

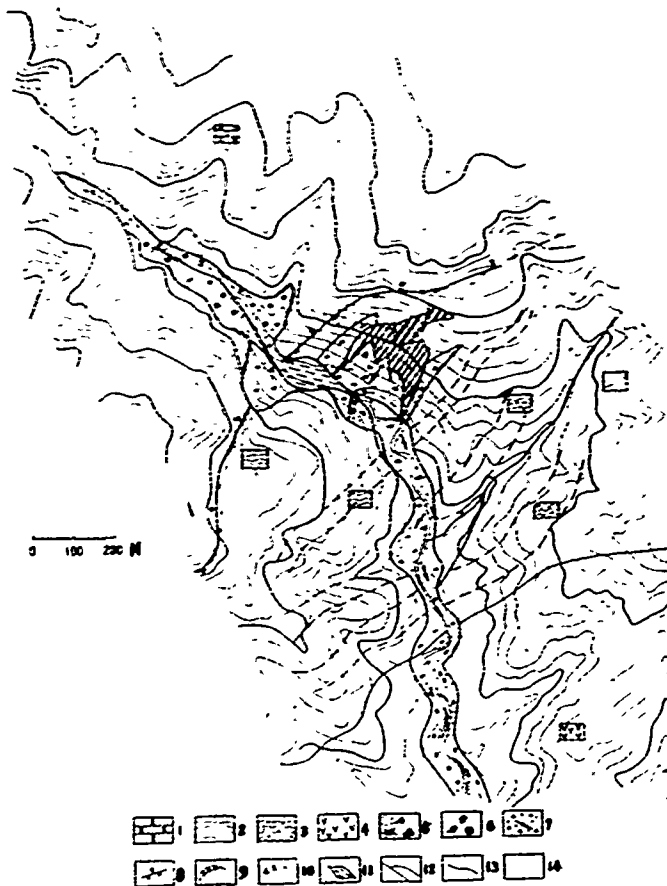


Fig. 1. A geological map of Shi-jia-po section in Ning-qiang county, Shaanxi Province  
1. quartzite, 2. phyllite, 3. chlorite-schist,  
4. basalt-andesite, porphyrite, 5. slope wash,  
6. alluvial soil, 7. sliding accumulation,  
8. fault.

## MULTIPLE STROKES

High-speed landslides in the southern part of Shaanxi Province have been well known for a long time. However, Shi-jia-po landslide is a typical and multiple-stroke and high-speed landslide. From the beginning of sliding, in a matter of several minutes, there appear five grades of strokes in the whole sliding course as long as 1,060 m., each having more or less double strokes—"dive" and "upthrust", that, a pair of strokes which dive from higher places to lower, and then from lower to higher. The first two strokes are typical sliding ones of body slides, while the last three strokes are moving ones appeared under particular conditions of that time (Fig. 1, 2).

The first grade stroke (A) of Shi-jia-po landslide—Shi-jia-po—begins from the left bank of Lengsu-gou river in Shi-jia-po where landslides take place (TABLE 1). This grade stroke is the consequent sliding stroke of front dive and upthrust. The secondary grade stroke (B) of Shi-jia-po landslide—Shui-jing-wan stroke—occurs upon the front slope bodies (sliding tuquer) of the former stroke of landslides. This is a especial and interesting problem about motive forces of land slides. This grade stroke is a contrary sliding stroke of reverse dive and upthrust.

The third grade stroke (C) of Shi-jia-po—Tong-guan-wan stroke—also happens on the front edge of sliding bodies of the former stroke, but this stroke is different from the former stroke in features of motive forces and changed greatly. After Shi-jia-po landslides, there appear one month's rainy days and flood, so the level of river bed rises high enough to make larger discharge. In the first grade stroke, because its front edge (sliding tuquer) is mixed with large amount of rains and water of river, sliding bodies having fragments in a moist saturated state and mixed with sticky soil further disintegrate and break out. This stroke is a turned and consequent moving stroke of dive and upthrust.

The fourth grade stroke (D) of Shi-jia-po landslide is a Shan-tang-su stroke. This stroke is also a turned and consequent moving stroke of dive and upthrust.

The last—the fifth—stroke (E) of Shi-jia-po landslide is a Long-wang-miao stroke near Sha-tang-su village, the characters of which are similar to those of the former. In this case, Shi-jia-po multiple-stroke landslide has finished its activities if five grades of strokes in all. It may take several minutes to finish the whole process of sliding.

Table 1 The situation of "dive" and "upthrust" Shi-jia-po multiple-stroke landslide (elevation of the back edge 925 m.)

| stroke                  | the lowest elevation (m) |
|-------------------------|--------------------------|
| A Shi-jia-po stroke     | 800                      |
| B Shui-jing-wan stroke  | 800                      |
| C Tong-guan-wan stroke  | 775                      |
| D Sha-tang-su stroke    | 767                      |
| E Long-wang-miao stroke | 757                      |

| the highest elevation (m) | the direction of stroke | dive (m) | upthrust (m) | angle of intersection with the former | distance | remark         |
|---------------------------|-------------------------|----------|--------------|---------------------------------------|----------|----------------|
| 940                       | SW225°                  | 125      | 40           |                                       | 300      | sliding stroke |
| 820                       | SW102°                  | 40       | 20           | 123°                                  | 100      | sliding stroke |
| 745                       | SW155°                  | 45       | 10           | 50°                                   | 200      | moving stroke  |
| 775                       | SW206°                  | 14       | 4            | 51°                                   | 200      | moving stroke  |
| 763                       | SW143°                  | 10       | 0            | 63°                                   | 100      | moving stroke  |

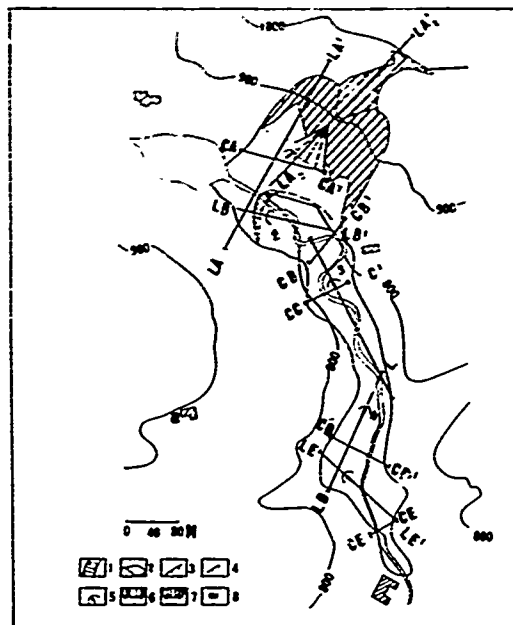


Fig. 2 A plane of multiple-stroke landslide of Shi-jia-po in Ming-qiang county, Shaanxi Province  
1. landslide, 2. lake and river, 3. the first landslide, 4. the secondary landslide, 5. the direction of sliding, 6. longitudinal profile, 7. cross profile, 8. village.

Changes of energy in multiple-stroke landslides should be studied from a complete stroke (dive, upthrust). For this reason, first, a typical energy system of multiple-stroke landslides must be chosen (Fig. 3) — just as "ABCDE" system. It must be stated that it is difficult in proving clearly, generally such a complex theory in practice without some supposition, imagination and simplification providing that this may not affect changes of energy studied in this paper. Therefore about forms of the slide bed plane on the land-

slide profile introduced in the paper we will not discuss.

This is not significant for the problem discussed in the paper. There only according to the lines of basic slide bed planes ( $A_1B_1C_1D_1$ ) which are existing in Shi-jia-yo multiple-stroke landslide and their developing characters, slide bed plane may be properly repaired and simplified. So they are introduced to be well-known slide bed planes ( $A_1B_1C_1D_1$ ) in a form of circle and are lines which may generally correspond to most conditions and actually accepted by scientists. Actual slide bed planes ( $A_1B_1C_1D_1$ ) are essentially similar to simplified slide bed planes ( $A_2B_2C_2D_2$ ). The section  $A_1B_1$  is quite different from the section  $A_2B_2$ . But in fact the section (slide walls) is rebuilt from the original slide bed plane by bursting apart (to form  $EB_1F$  colluvium). So it must be much steeper and closer to the section  $A_2B_2$ . Otherwise, in spite of deviation, section  $EB_2C_2$  are close to  $EB_1C_1$ . Reversed and turned-back body slides ( $A_2B_2C_2F$ ) are in the states of body slides deformed after sliding. Although they do not entirely correspond to lines of the former terrain before sliding, they are approximate to each other. Besides, it is supposed to be a problem of plane and this means that in different planes and during the whole sliding process, the strength of shear-resistance of slide bed planes is equal and unchanged, the whole slide bodies at a definite speed. This may not affect the essence of problems discussed in this paper.

At any time ( $t$ ) in sliding of high-speed landslides, the parts beyond sliding bed planes should be taken as an energy balance system while the others do not belong to it. When taking point M as the centre of conversion, slide bodies slide at a definite speed ( $V$ ), the interior energy of this system is regarded as potential energy ( $EP$ ) of slide bodies. Slide bodies in motion possess sliding kinetic energy ( $EK$ ). Besides, for overcoming shear-resistant strength of rock masses beyond the system energy wasted by friction and resistance in interior bodies and other resistance (such as air resistance) and ect. ( $t$ ) for doing work is considered to be negative outer energy  $Ee$ . Therefore, according to relative elevation 0 line—basic line—shown in the Fig. and energy balance principles, we suppose the total weight of slide bodies to be  $W$ , and can clearly see all kinds of energy stated above:

$$EP = HW \quad (1)$$

$$EK = \frac{WV^2}{2g} \quad (2)$$

$$Ee = \tau L \xi \quad (3)$$

where:  $L$  = the total length of a slide bed plane ( $A_2B_2C_2D_2$  or  $B_2C_2D_2$ );

$\xi$  = the distance of sliding ( $C_2D_2$ );  
The shortened thickness is equal to 1. On the basis of energy law of thermodynamics or the law of conversion of energy and from formulas (1), (2), (3), we may make energy balance formulas of whole processes of dive and upthrust in high-speed and intensively-moving landslides, but outer energy is usually regarded as negative outer energy ( $-Ee$ ):

$$EP + Ee + EK = U \quad (4)$$

$$HW + \tau L \xi + \frac{WV^2}{2g} = U \quad (5)$$

the total energy ( $U$ ) of slide bodies system in sliding keeps some balance. In the same way, at the moment when body slides have just started or will stop, we may write the following formulas:

$$W(H_1 - H_2) = \tau L(\xi_1 - \xi_2) = -\frac{W}{2g}(V_1^2 - V_2^2) = 0 \quad (6)$$

Therefore, in order to prove in detail or partly to investigate the relationship of energy conversion among slide bodies we may divide slide bodies into many strips in definite size and make up formulas for energy balance in complete dive and upthrust processes of high-speed and intensively-moving landslides. From formulas (1), (2), (3), we may write the following formulas:

$$\sum_{n=1}^{i+1} W_n h_n + b_1 \sum_{n=1}^{i+1} \tau \Delta L \xi + \frac{WV_1^2}{2g} = U \quad (7)$$

$$\sum_{n=1}^{i+1} W_n h_n + b_2 \sum_{n=1}^{i+1} \tau \Delta L \xi + \frac{WV_2^2}{2g} = U \quad (8)$$

$$\sum_{n=1}^{i+1} W_n (h_{1n} - h_{2n}) + (b_1 - b_2) \sum_{n=1}^{i+1} \tau \Delta L \xi + \frac{W}{2g} (V_1^2 - V_2^2) = 0 \quad (9)$$

From basic formulas of energy balance (6) and (9), it is not difficult in seeing that in the total energy of slide bodies potential energy, kinetic energy and negative outer energy may convert to each other in the whole dive and upthrust process of high-speed and intensively-moving landslides, or straightly speaking, the energy is completed by arranging and converting the difference of elevation of gravity centre, the speed of sliding and the difference of migration of sliding. There is a clear and strict conversion relationship among them.

According to the former formula and formulas

stated above, it is not different in proving laws of energy conversion of multiple-stroke landslides (Fig. 4, 5).

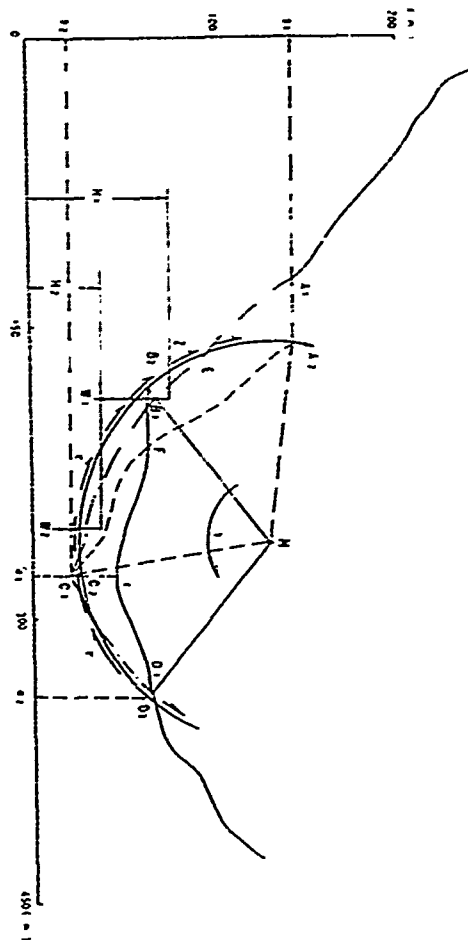


Fig. 3 An analysis map of energy balance of Shi-jia-po landslide

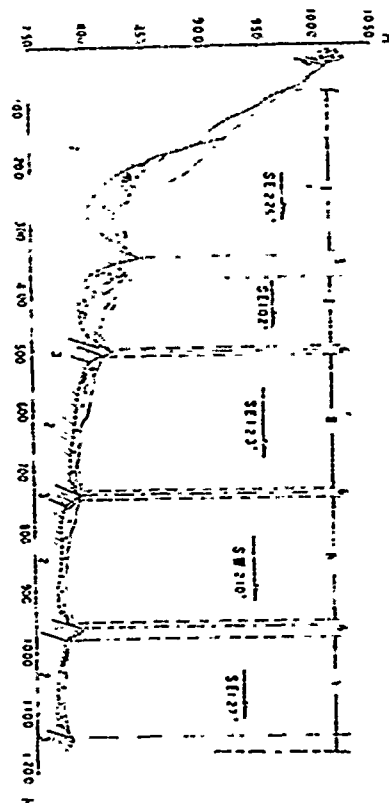


Fig. 4 A process map of multiple-stroke dive and upthrust of Shi-jia-po landslide  
I. the first (sliding) stroke, II. the second (sliding) stroke, III. the third (moving) stroke, IV. the fourth (moving) stroke, V. the fifth (moving) stroke, 1. quartzite, 2. sericite, 3. chlorite-schist, 4. fault, 5. line of former terrains, 6. links.

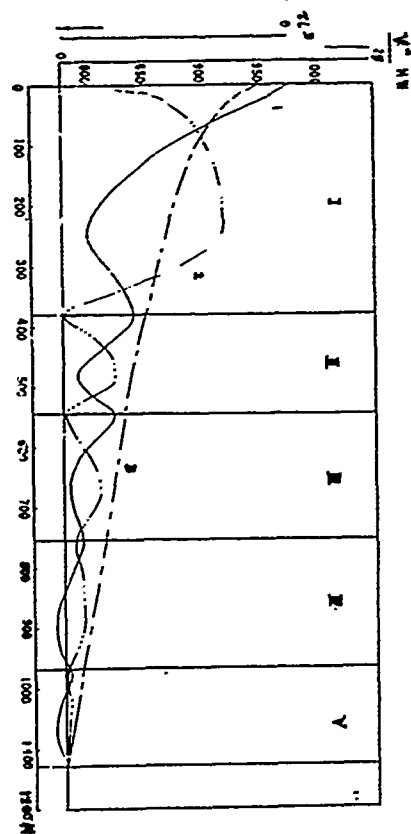


Fig. 5. An inferred map of energy conversion of multiple-stroke Shi-jia-po landslide  
1. curve of potential energy, 2. curve of kinetic energy, 3. curve of energy wasted by friction and resistance.

#### OVERSTEPPING GAS BILLOWS SPATTERED WITH MUD

Shi-jia-po landslide has its own characters and a new phenomenon different from that of common landslides. This is overstepping gas billows spattered with mud of active slide bodies. They may bring us extraordinary disasters that are difficult in imagining. Overstepping gas billows spattered with mud may damage building and installation, break trees, burst the surface soil and even may break and lift quite far objects away. For forming overstepping gas billows spattered with mud, it is necessary to have sufficient high speed. Slide bodies at high speed have enormous kinetic energy, thus causing gasses in front parts of body slides to press swiftly, expand and then suddenly burst out under proper conditions. If in a region there may exist a suitable distance, very different rocks—soft and hard, a proper fracture belt in structure or the combination of the former two, there would be formed wide or narrow, and winding river valleys, obvious projected mountain spur and whetstones which can stop slide bodies to turn. Therefore, it makes parts of kinetic energy of body slides be changed into an enormous impulse. So this is important objective conditions under which overstepping gas billows spattered with mud are formed (Fig. 6, 7). The projected mountain spur must have steep slopes (about  $45^{\circ}$ – $75^{\circ}$ ) so as to cause parts of pressed air and converted enormous impulse to break out swiftly and violently, thus forming the maximum height ( $h_{max}$ ) and distance ( $l_{max}$ ) of gas billows spattered with mud. Obviously, slide bodies at a high speed must possess sufficient weak rock masses and developed fractures (weathered rocks or low-strength rocks) or loose soil for rapidly disintegrating, breaking out and grinding. In this way, the front or the side part can be changed into mud. This is material conditions for making up gas billows spattered with mud. At last, there must be large amount of underground water and surface water to take part in forming overstepping gas billows spattered with mud. The humid weather, rains, especially, flood season provide enough materials for overstepping gas billows spattered with mud.

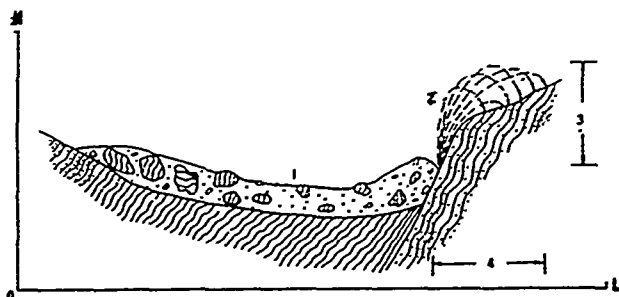


Fig. 6 A sketch map of overstepping gas billows spattered with mud of Shi-jia-po landslide  
1. body slide, 2. overstepping gas billows spattered with mud, 3. the maximum height of spattering ( $h_{max}$ ), 4. the maximum dis-

tance of spattering.

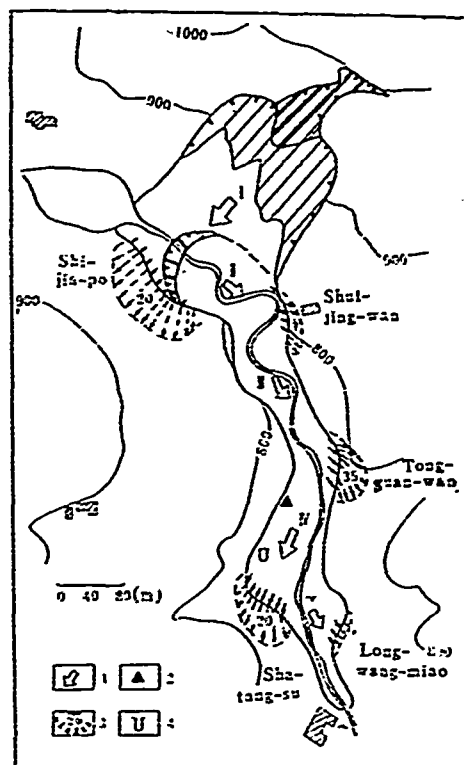


Fig. 7. Overstepping gas billows spattered with mud of Shi-jia-po landslide  
1. sliding, moving stroke and its direction, 2. overstepping gas billows spattered with mud and their height (m), 3. houses damaged (thirteen people were buried) 4. boulder (stone tablet overturned)

#### REFERENCES

- Hu Guang-tao, (1980), "Energy Equilibrium and Superstability of Intensively-moving Slope Basement of Landslides", Learned Journal of Xian Geology College, Xian Geology College Press.
- Hu Guang-tao and ect., (1984), "Engineering Geology", Geological Publishing House.
- Hu Guang-tao, (1984), "Problems of Engineering Geology in Basin Environments in the Region Han-Zhong", "Environmental Science", Environmental Science Publishing House.
- Hu Guang-tao, (1985), "Changes in Imbalance during Natural Processes in Developing River Beds in Han-Zhong Basin", Environmental Science Publishing House, Scientific Publishing House.

## Slope Stabilization Measures for Kirkwood Penstock, Early Intake, California

K.D. Weaver

Staff Consultant, Woodward-Clyde Consultants, Oakland, California

D.J. Gross

Senior Associate, Woodward-Clyde Consultants, Oakland, California

L.T. Bauer

Civil Engineer, Hetch Hetchy Water and Power, San Francisco, California

**SYNOPSIS:** Kirkwood Penstock, located in a deep, steep-sided canyon near Yosemite National Park, California, is an integral part of the Hetch Hetchy system, which conveys water from the Sierra Nevada mountains to the city of San Francisco, California. A heavy rainfall approximately 17 years following construction of the facility triggered settlement of the foundation. Measures undertaken to arrest this settlement included consolidation grouting, construction of facilities to divert surface runoff away from the penstock, and installation of a geomembrane to prevent infiltration of rainfall and snow melt in the vicinity of the penstock. No evidence of further settlement has been detected since completion of the remedial work.

### INTRODUCTION

Kirkwood Penstock is a 1955-foot-long, 8-foot-diameter facility located in a deep, steep-sided canyon near Yosemite National Park, California. It is an integral part of the Hetch Hetchy system, which conveys water from the Sierra Nevada mountains to the city of San Francisco, California. Construction in 1966 was preceded by geologic and geophysical investigations that were interpreted to indicate that the penstock would be located on weathered or decomposed in-place granitic bedrock beneath the surface talus (Woodward-Clyde-Sherard and Associates, 1964). The penstock was protected from rockfalls by concrete walls and was secured in place by use of anchor blocks and 60-foot-long anchor cables.

The penstock performed satisfactorily until January 1984, when a Dresser coupling at the top of the penstock and immediately downslope from an anchor block founded on rock was found to have undergone an extension of 1 3/4 inches. Settlement of the concrete foundation slab and walls was also found to have occurred. It was inferred that the settlement had been triggered by heavy rainfall that occurred during December 1983. However, the underlying cause of the settlement was not evident. Therefore, geologic studies to ascertain the cause were undertaken. These studies included geologic mapping, drilling exploratory borings, and installing and monitoring slope indicator casings (Woodward-Clyde Consultants, 1985). Additionally, extensometers were installed on the penstock and a program of frequent surveys was instituted so as to detect any further displacement.

Extremely difficult drilling conditions were encountered in the exploratory holes, delaying accumulation of sufficient data to confidently assess the cause of the settlement. Due to the importance of the Kirkwood Penstock to the Hetch Hetchy Water and Power System, a decision was made to leave the penstock in service and to institute stabilization measures prior to completion of the exploratory work. The measures undertaken were based upon an assumption that loose talus was present beneath the penstock; they included consolidation grouting, diversion of surface flow originating upslope, and covering the affected portion of the slope with an impervious membrane. Stairs and a foot bridge were constructed to facilitate access for long-term

measurements in the slope indicator casings.

### INFERRED GEOLOGIC CONDITIONS

#### Preliminary Working Hypothesis

A crude stair-step morphology, in which roughly parallel steep bluffs of granitic rock are separated by intervening areas of talus and deeply weathered rock, exists in the site area. It was inferred at the outset of the studies leading to the design of remedial treatment that the "stair-steps" were related to regional jointing. Because the observed settlement of the concrete support system for the Kirkwood penstock took place in one of the talus-filled areas between bedrock bluffs, it was hypothesized that the settlement was the result of water-induced migration of fine particles into the interstices of coarser talus deposits and into open joints and fractures. The fact that continuous intact rock was not encountered in the core borings that subsequently were made was ascribed to weathering along joints. The initial minor movements shown in the inclinometer readings were inferred to be the result of snifting of casing backfill material and possibly also related to movement in the water-eroded talus materials contained in a subsurface bedrock trough.

#### Block Sliding Hypothesis

Consideration was given, both during the initial field reconnaissance and the subsequent subsurface studies, to the possibility that the settlement of the penstock was related to landslide movement. One important purpose of the core borings, as well as of the inclinometers, was to examine this possibility. The borings appeared to show the existence of a relatively deep bedrock trough that might conceivably represent a pull-apart feature between in-place bedrock and the main mass of a block slide. However, neither the inclinometer data nor the results of frequent surveys disclosed any conclusive evidence of slide movement.

## Ridge-Spreading Hypothesis

It ultimately was concluded that the morphology and apparent subsurface physical characteristics of the site are the result of large-scale gravitational spreading and fracturing processes. These processes, which we will refer to here as ridge-spreading, entail dilation of a ridge along fractures, joints, foliation, or other structural weaknesses as a result of gravity-induced tensional stresses. Such structural weaknesses may become opened to considerable depth. According to Radbruch-Hall and others (1976), the usual topographic expression of this type of gravitational movement, which occurs in many different types of rock, consists of horizontal linear trenches and uphill-facing (anti-slope) scarps on steep slopes and ridge crests.

One implication that can be drawn from this hypothesis is that the penstock may cross an extremely deep crevasse-like opening that is choked with blocks and masses of granitic rock. This condition would account for the large "takes" of thick, mortar-like grout that were experienced during the remedial treatment program. If this condition actually exists, one would expect infiltrating rainfall to tend to flush fine-grained materials into adjacent open zones, leading to readjustment and settling of the larger blocks and masses of material.

## SUBSURFACE TREATMENT

### Design Approach

The possible need for subsurface drainage measures was assessed. However, on the basis of habitual loss of circulation in all of the exploratory holes, and a finding that the water table depths were in the range of 100 to 150 feet or more, it was decided that no benefits would be derived from a drainage tunnel or drainage borings. As the available data indicated that readjustment of loose talus was the most probable cause of settlement of the penstock, it was concluded that some type of consolidation grouting should be done. It was evident that a conventional slurry grout would travel too far beyond the penstock foundation, so a compaction grouting approach was selected. It was inferred that the grout alone would not be able to bind the presumed talus mass together to the optimum extent, so Dywidag reinforcing bars were placed in each grout hole. In order to provide optimum distribution of grout, one row of holes was drilled and grouted on each side of the penstock. The maximum hole spacing was 10 feet.

### Grout Hole Drilling

The drilling and grouting operations were performed with the aid of a steel platform that was mounted on the penstock wing walls, and moved up and down the slope by means of manually-operated grip-hoists. The holes were drilled with a ROC-601 rotary percussion drill that could be shifted along slots in the deck of the platform. NW casing, with an outside diameter of 3 1/2 inches, was advanced above a 4-inch-diameter bit until the planned depth of 60 feet was reached or until there was reason to believe that bedrock had been reached. The drill string was then extracted, the bit removed, and the casing driven back into place. The casing was then cleaned out preparatory to grouting. The rates of penetration ranged

from nearly instantaneous where the drill "string" dropped through voids to a few hundredths of a foot per minute in fresh, hard rock.

## Grouting Procedures

The grout was batched in a horizontally-mounted paddle-type mixer. The typical content of a 5-cubic-foot batch was 25 shovels full of silty sand, 2 bags of cement, one gallon of prehydrated bentonite, and sufficient water to produce a six-inch slump at the pump. Depending upon the pumping pressure, loss of water at the delivery line couplings dropped the slump to 3 1/2 to 5 inches at the injection point. It did not prove feasible to pump at a pressure sufficient to deliver and inject a thicker grout. As the grout was more fluid than anticipated, the injection quantity was arbitrarily limited to 4 cubic feet per foot of stage length after reaching an injection pressure of 100 psi. Injection of grout was stopped when the pressure exceeded 10 psi per foot of stage depth if the volume criterion was not met. In general, injection was performed in one-foot increments, with the casing being raised following completion of each increment.

## Summary of Results

Twenty eight holes were drilled an aggregate depth of 1700 feet, and 4000 cubic feet of grout were injected into the 60-foot-deep zone being treated. An additional 250 cubic feet of grout were injected into an inclinometer hole that extended 85 feet below that zone. In general, relatively large grout takes occurred in the lowest injection stages, where a relatively thin grout was used. Grout takes exceeded 20 cubic feet at intermediate depths in 10 holes. The largest volume injected in a single stage was 59.5 cubic feet; the injection pressure in this stage didn't exceed 140 psi.

The injection pressure commonly would build up to two or more peaks during the grouting of an interval, and then would drop off before building back up again. This behavior, an example of which is presented on Figure 1, is ascribed to the grout pushing loose talus blocks aside and exposing additional voids. These pressure peaks were not necessarily high as compared to the refusal pressure for the stage; as is shown on Figure 2, injection of intervals deeper than about 20 feet was more commonly halted on the basis of grout take than of excessive pressure.

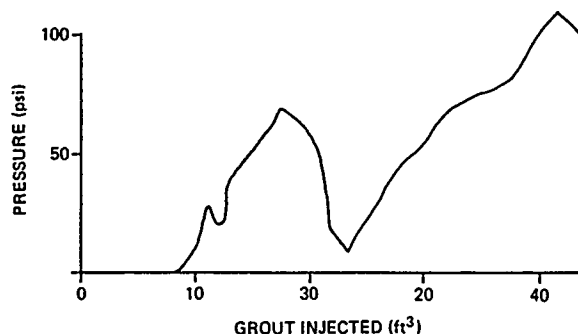


Figure 1. Pressure Behavior at Constant Injection Rate

There was no noteworthy reduction in take between primary holes and secondary holes. Therefore, supplementary holes were drilled and grouted beneath the Dresser coupling that had exhibited evidence of settlement.

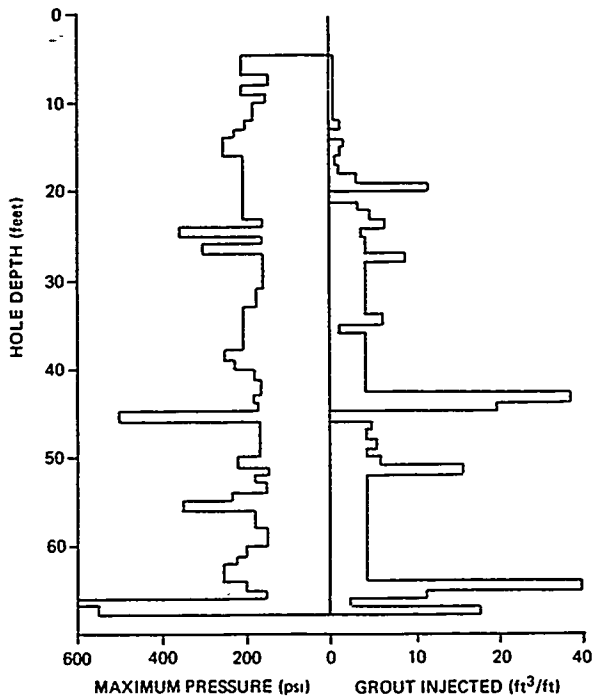


Figure 2. Injection Pressure - Volume Relationship for Typical Hole

These holes, which extended beneath an anchor block immediately upslope from the coupling, took relatively little grout. Contact grout holes drilled through the concrete slab on which the penstock is located also took very little grout. However, the mobile platform was left in place as a precautionary measure in case further grouting is decided to be needed.

#### SURFACE TREATMENT MEASURES

##### Surface Drainage

The existing surface drainage facilities were improved and supplemented to divert surface runoff around and away from the vicinity of the penstock. Due to the steep, irregular, brush-covered topography, much of this work had to be accomplished by hand labor. The work performed included the following:

1. An existing interceptor trench was extended and lined, and was provided with outfall pipes to divert the runoff 200 to 300 feet to the sides of the problem area.
2. The access road to the top of the penstock was regraded and paved to divert surface runoff to a new drop inlet and outfall pipe leading away from the penstock.
3. Additional outfall facilities were constructed at the downslope end of the slope area that was covered with a geomembrane.

The ground surface area extending about 200 feet downslope from the valve house at the top of the penstock and about 150 feet to each side of the penstock was covered with a geomembrane for the purpose of preventing direct infiltration of rainfall and snow melt water into the problem area. Preparation of the ground surface for placement of the geomembrane consisted of clearing of brush and trees, trimming of numerous large protruding rocks, laying and pinning wire mesh to "smooth out" a few irregular areas, and hand-excavating ditches in which to tuck-in and secure the outside edges of the membrane. The area was then covered with a layer of 18-ounce Trevira geotextile. This geotextile is a continuous-spun polyester fabric, and is approximately 235 mils thick. Its function is to provide a tear-resistant foundation for the geomembrane, protecting it from direct exposure to puncturing by sharp protruding rocks.

The geotextile was covered with Shelter-Rite XR-5, style 8130, which is a 30-mil-thick polymer-coated membrane that is extensively used as a pond lining. This material was installed in panels ranging up to 50 feet by 160 feet in size. These panels were heat-welded together to form a continuous waterproof membrane. The membrane was fastened to the concrete foundation of the penstock, to a newly-constructed concrete stairway at the top edge of the western panel, and to a rock outcrop cliff along the eastern side, using galvanized battens and expansion bolts. The outside and downslope edges were tucked into hand-excavated ditches that were then backfilled to tie down the membrane. Finally, sandbags were placed at numerous locations on the membrane to provide resistance to uplifting wind forces.

Small concrete dams were constructed at the lower end of the groins formed by the penstock wingwalls and the geomembrane-covered surfaces that slope toward the penstock. These dams divert concentrated flows into CMP pipes that convey these flows to a pre-existing outfall that collects water from an underdrain system beneath the penstock foundation slab.

#### POST-TREATMENT MONITORING

Slope indicator readings have been performed weekly during the rainy season and monthly during the dry season since completion of the slope stabilization measures. The data obtained have indicated no continuing or renewed movement.

#### CONCLUSIONS

The absence of evidence of further settlement following completion of the slope stabilization measures is inferred to indicate that the grouting operations produced a coherent wedge that bridges the underlying opening that is believed to be present. It is further concluded that influent moisture is unlikely to trigger further settlement. However, the geologic mechanism involved in ridge-spreading at the site is too poorly understood to allow a confident conclusion to be reached concerning the long-term stability of the penstock. Therefore, consideration is being given to alternatives for replacing it.



## REFERENCES

- Radbruch-Hall, D. H., D. J. Varnes, and W. Z. Savage  
(1976), "Gravitational spreading of steep-sided  
ridges ("Sackung") in western United States",  
Bulletin of the International Association of  
Engineering Geology, No. 14, 23-35.
- Woodward-Clyde Consultants (1985), "Geologic report on  
special treatment area, Kirkwood Penstock, Early  
Intake, California", Consultant's report prepared for  
Utilities Engineering Bureau, City and County of San  
Francisco.
- Woodward-Clyde-Sherard & Associates (1964)  
"Investigations for the proposed Canyon Penstock,  
Tuolumne County, California", Consultant's report  
prepared for the Power and Utilities Engineering  
Bureau, City and County of San Francisco.

## A Case History of Tehri Tunnels

**B. Prabhakar**

Scientist, Central Mining Research Station Unit, Nagpur, India

**J.L. Jethwa**

Assistant Director, Central Mining Research Station Unit, Nagpur, India

**B. Singh**

Director, Central Mining Research Station Unit, Nagpur, India

**SYNOPSIS :** Tehri Dam Project, a multi purpose river valley project, is being constructed in Garhwal, Himalaya. The project consists of a 260 m high earth and rock fill dam with a clay core, four diversion tunnels each of 11 m finish diameter, four head race tunnels each of 8.5 m finish diameter and two underground powerhouses cavities each measuring 180 m long, 49.5 m high and 21.5 m wide. The project is located near the district headquarters of Tehri in the state of Uttar Pradesh. The rock masses in the project area are fragile, tectonically active and geologically disturbed. The terrain is rugged and inaccessible and therefore precludes thorough geotechnical investigations for the design of the cavern. The diversion and the head race tunnels were therefore used to conduct geotechnical investigations with the purpose of collecting geotechnical data for the design of two caverns. Goodman Jack tests were used to estimate the modulus of deformation of the rock masses. Load cells and tape extensometers were used to monitor the support pressure and the tunnel closures. The modulus of deformation varied from 0.18 to 0.32 kg/cm.sq.  $\times 10^5$ . Tunnel closures were about 0.3% of the tunnel size. The support pressure stabilized within three months of excavation and the measured support pressures varied between 0.16 and 1.14 kg/cm.sq. This geotechnical data indicate that the rock masses behaviour was elastic in nature and the cavern could be designed without much difficulties.

### INTRODUCTION

The Tehri project is the first multi-purpose development scheme being constructed in the Garhwal Himalayas for utilising the surplus monsoon waters of river Bhagirathi, a principal tributary of the mighty Ganga. The project, located in Tehri district of the state of Uttar Pradesh, envisages the construction of a 260 m high earth and rock fill dam with a claycore and an underground powerhouse of 2000 MW capacity to be built in two stages with an installed capacity of 1000 MW in the first stage. The layout plan of the Tehri dam project has been shown in figure 1. The first stage complex shall have conventional turbines and the second stage shall have reversible machines housed in a separate cavity at a comparatively lower setting. A balancing reservoir shall be created by constructing a 85 m high Koteshwar dam, about 20 km downstream of the Tehri dam project.

The project when completed will create a live storage of 2615 million cubic meters and provide irrigation to 270 thousand hectares of land and generate 2900 million units of power annually at 90% water availability, besides other benefits like moderation of floods, development of tourism and generating employment opportunities. The estimated cost of the first stage is Rs.1066 crores as on January, 1983.

The underground works mainly comprise of four diversion tunnels of 11.00 m diameter (two on each bank), four head race tunnels of 8.5 m diameter on the left bank of the river Bhilangana and the underground powerhouse complex. The diversion tunnels of 11.00 m diameter

horseshoe shape are designed to pass a construction stage flow of nearly 7,500 cumecs and flood discharge of 7300 cumecs corresponding to a flood discharge of 12850 cumecs for a 1000 year return period. The two right bank diversion tunnels of 1298 and 1429 m length have already been constructed and the two left bank diversion tunnels of 1778 and 1774 m length are in an advanced stage of construction. The four head race tunnels of horseshoe shape take off at the left flank of the reservoir. Two head race tunnels will convey the water to the four machines of stage I powerhouse and the other two head race tunnels will convey the water to the stage II machines. Construction of the machine hall cavities has not begun yet. The paper describes the geology of the project area, the details of various underground excavations, details of instrumentation results and the geotechnical investigations. Estimated values of tunnel deformations from elastic analysis have been compared with measured values in the field.

### GEOLOGY

The rock formations encountered in the tunnels are the phyllites of Chandpur series. The phyllites are generally banded in appearance, the bands composed of argillaceous materials. Based on the lithological character of the rock masses and the varying magnitude of tectonic deformation suffered by them, these have been broadly classified as phyllites of grades I, II and III. The rock masses of grade I are the most competent. These are predominantly arenaceous, massive in character and distinctly

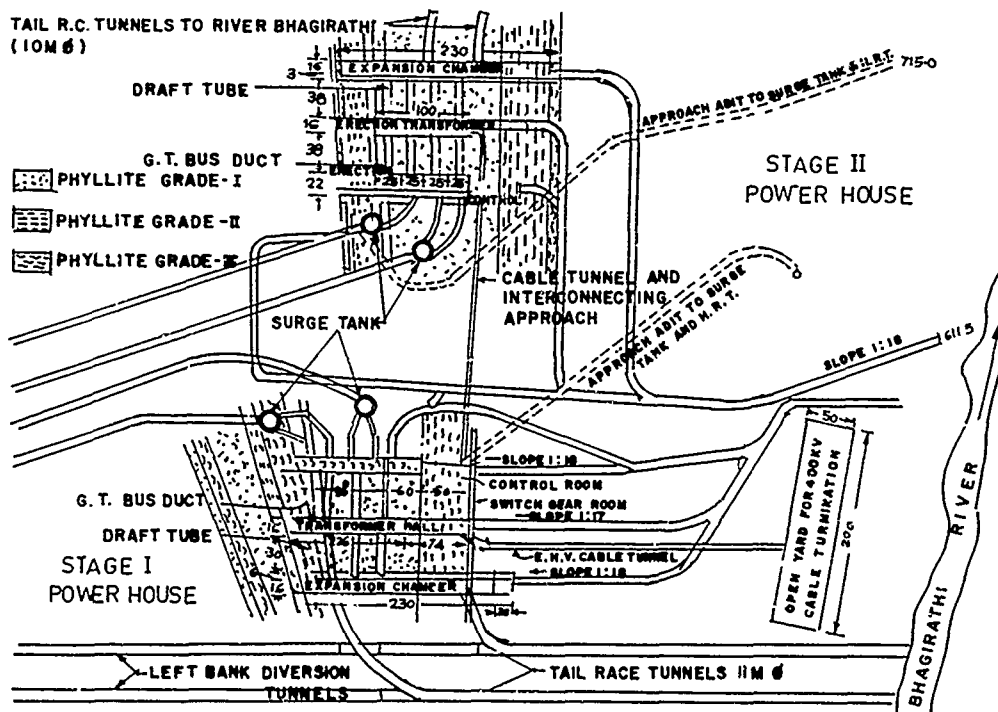


Fig. 1 Layout Plan of Tehri Dam Project

jointed. Rock masses of grade II are banded due to rapid alteration of arenaceous and argillaceous materials. The rock masses of grade III are the weakest formations and are mainly composed of the argillaceous component with lesser amount of arenaceous material. The three grades of the phyllites are interbanded and show gradual change from one grade to another along the strike direction.

#### GEO-TECHNICAL INVESTIGATIONS

The geo-technical investigations are being conducted to study the behavioural aspects of the different rock units, their probable mode of interaction with various engineering structures and the state of stability of the underground structures vis-a-vis the geological defects.

The process of geotechnical investigations had been initiated since the inception of the project and is being carried out contemporaneously with the construction of the various structures such as diversion tunnels, head race tunnels and approaches to the powerhouse cavern. The following studies are being conducted in the different underground openings of the project complex.

#### Geo-technical Tests

The Geo-technical studies consist of determination of shear strength parameters, permeability and groutability tests, deformation modulus tests and laboratory tests to find out the tensile, the shear and the compressive strength and Poisson's ratio.

Deformation modulus has been determined by both direct tests and by the rock mass classification approach. For direct tests, plate jack and Goodman jacks are commonly employed. Plate jacking test has been used to determine the deformation modulus in exploratory drifts. This technique has been found to be inferior in relation to the Goodman jack test method. The latter has therefore been used recently to determine the deformation modulus values from tests conducted in the tunnels. The tests were conducted in the NX size bore holes. The pressure was applied in cycles of 100, 200, 250, 500 and 700 kg/cm<sup>2</sup>. Pressures-deformation characteristics are given in figure 2.

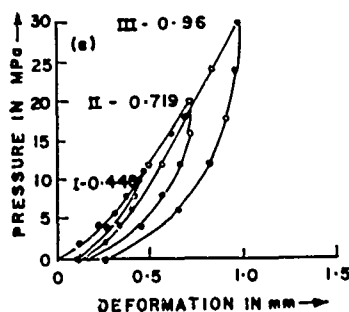


Fig. 2 Load Deformation Characteristic in a Typical Goodman Jack Test in HRT-1, ch.223.07 m, phyllites

#### Rock Mass Behaviour and Support Pressure

Bieniawski (1973) proposed a rock mass classification for predicting rock mass behaviour and

Table I

Deformation Modulus by Various Techniques in  $\text{Kg/Cm}^2 \times 10^5$ 

| Sl.No. | Type of Rock | Plate Jack Test  | Goodman Jack       | Rock Mass Classification | Recommended Value |
|--------|--------------|------------------|--------------------|--------------------------|-------------------|
| 1.     | Grade I      | 0.68             | 0.06-0.570 (0.32)  | 1.30                     | 0.30              |
| 2.     | Grade II     | 0.18-0.57 (0.38) | 0.046-0.385 (0.21) | 0.43                     | 0.20              |
| 3.     | Grade III    | 0.10-0.39 (0.25) | 0.025-0.345 (0.18) | 0.18                     | 0.15              |

Note : Figures in bracket give average values.

Table II

Comparison of Estimated and Observed Support Pressure in  $\text{Kg/Cm}^2$ 

| Sl.No. | Type of Rock Mass | Estimated Support Pressure         |                        |      |              | Observed Support Pressure (40 days) | Recommended value (Kg/Cm <sup>2</sup> ) |
|--------|-------------------|------------------------------------|------------------------|------|--------------|-------------------------------------|---|
|        |                   | Terzaghi's Rock Load Tables (L.T.) | Barton's Approach L.T. | S.T. | Wedge Theory |                                     |   |
| 1.     | Grade I           | 0.0-1.4                            | 0.80                   | 0.40 | -            | 0.16-0.42                           | 1.0                                     |
| 2.     | Grade II          | 0.0-2.8                            | 2.10                   | 1.30 | 1.75-2.00    | 0.52-1.14                           | 1.5                                     |
| 3.     | Grade III         | -                                  | -                      | -    | -            | Not available                       | -                                       |

a relationship between rock material and rock mass deformation modulus. The deformation modulus with the help of this technique has been determined on the basis of the information available so far. Table I gives the range of values of deformation modulus determined by different techniques.

Various techniques are applied for the determination of support pressure. Empirical approaches of Terzaghi (1946) and Barton et al (1974) have been used for the determination of support pressure for tunnels. Sometimes a wedge of rock which may get loosened in the crown and may sit on the supports. Support pressure has also been estimated from the Wedge theory. Estimated and observed support pressures have been shown in Table II.

#### SEQUENCE OF CONSTRUCTION AND SUPPORT SYSTEM

##### Left Bank Diversion Tunnels

Excavation of diversion tunnels T-1 and T-2 were planned from both inlet and outlet ends. The inlet portal was established in October 1979. However, the hill slopes at the outlet portal were very unstable and the work was delayed due to a huge landslide near the outlet portal which occurred in the year 1980. The outlet portal therefore could be established only in 1981.

The excavation has been done by heading and bench method employing the conventional drilling and blasting technique. The pull varied from 2.0 m to 2.5 m. The consumption of explosive was of the order of 0.7 kg/cum of the excavated rock mass. Steel sets of ISMB 300 mm supported on wall brackets placed at springing level were used where the site conditions warranted the use of permanent supports.

##### Right Bank Diversion Tunnels

The invert of diversion tunnels T-3 and T-4 at the outlet are at RL 600 m and 603 m respectively. Thus these tunnels negotiate a drop of 6 m. Tunnel T-3 is straight in its entire length, while the tunnel T-4 traverses a horizontal curve of  $78^\circ$  after being straight in the first 28 m length. The remaining length of the tunnel is straight. For the early completion of these tunnels, the construction was taken up from both ends. The supporting system consisted of RSJ 300 x 140 steel ribs 600 mm centre to centre and M75 concrete backfill. The redistribution of stresses in the rock mass around the excavated cavity in this zone has taken place within about 3 months of the blasting and then a state of equilibrium had been reached. A record progress of about 800 cubic metre of excavation per day was obtained.

##### DEFORMATION MODULUS

The data collection process is going on with the construction of various components of the project. The deformation modulus of all the three grades of the rock masses have been determined by different techniques (Table I). The plate jacking test seems obsolete and the data collected may not be used for design purposes. Results of the Goodman jack tests have been accepted for design. About 130 tests have been performed, mostly in the tunnels (under pressures varying between 80 to 600  $\text{kg/cm}^2$ ). The design pressures may not be more than 40  $\text{kg/cm}^2$  hence the values were calculated at this pressure.

##### INSTRUMENTATION

Construction stage instrumentation was undertaken in the tunnels to monitor the behaviour

of the rock masses surrounding the cavities by the Central Mining Research Station, Dhanbad. Load cells had been installed to measure support loads. Tape Extensometer was used to measure tunnel closures. For this purpose closure bolts had been installed in all the tunnels randomly. At a few selected test-sections both closure bolts and load cells were installed.

In the right bank diversion tunnel T-4, one test-section was established between chainages 614.50 m and 615.30 m with mechanical type of load cells. In the left bank diversion tunnel T-1, one test-section at ch. 083-84 m was established. Mechanical type load cells were installed. In the head race tunnel T-3, one test-section was installed at ch. 828-829 m. Vibrating wire and mechanical type load cells were installed. Typical closure-time and load-time graphs are shown in figures 3 to 4 respectively for this test-section. The theoretical values are also shown in these figures.

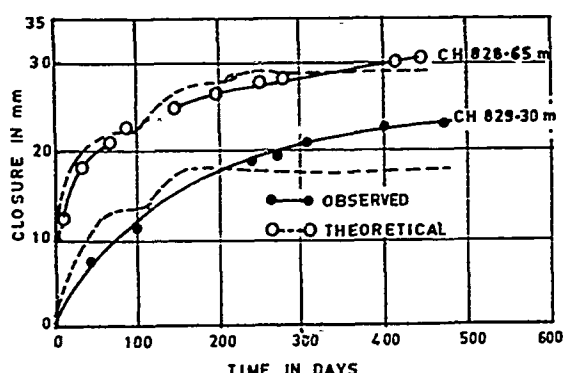


Fig. 3 Closure-Time Relation in HRT-3 (Grade III phyllites)

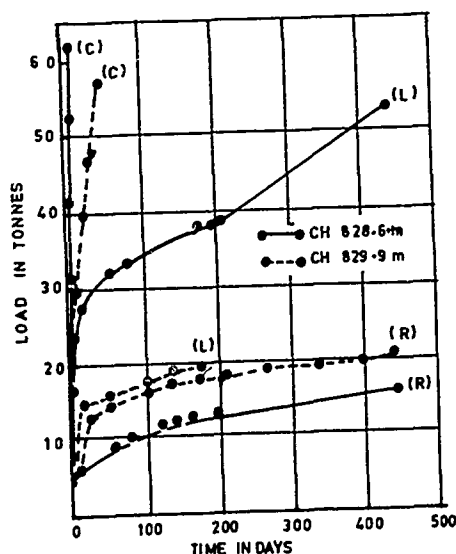


Fig. 4 Load-Time Relation in HRT-3 (Grade - III phyllites)

## Tunnel Closures

The measured tunnel closures are close to the predicted values (Fig.3). The maximum value of about 30 mm works out to the only 0.3 per cent of the tunnel size and is considered due to the elastic relaxation of the rock mass surrounding the tunnel openings.

## Support Pressure

Support pressures calculated by the wedge theory, Terzaghi's rock load table and Barton's method have been compared with measured values (Table II). The support pressures are very low. It can be seen that the short-term support pressure estimated by Barton's approach are close to the measured values.

## CONCLUSIONS

The instrumentation data has shown that both the tunnel closures and the support pressures are very low. These can be considered due to elastic relaxation of the rock mass surrounding the tunnel openings. Grade I and grade II phyllites can, therefore, be considered competent to locate the powerhouse cavern.

The measured support pressures for 40 days compares favourably with the short-term values estimated by Barton's method. This would suggest that the short-term support pressure for the cavern may be calculated by this approach provided that the Q values are estimated from the full sized cavern.

## REFERENCES

- Barton, N. Lien, J. and Lunde, J (1974), "Engineering Classification of Rock Masses for the Design of Tunnel Supports" Rock Mech. Vol.6, pp 189-256.
- Bieniawski, Z.T. (1973) "Engineering Classification of Jointed Rock Masses", Trans. S. Afr. Instn., Civil Engineers, Vol.15, pp 335 - 342.
- Bieniawski, Z.T. (1974), "Geomechanics Classification of Rock Masses and its Application in Tunnelling" Proc. 3rd. Int. Cong. Rock Mech., ISRM, Denver, Vol. IIA, pp 27-32.
- Jethwa, J.L. Dube, A.K. and Singh, B. (1978), "Rock Mechanics Instrumentation for Tunnels in India" Tunnels and Tunnelling, Sept, pp 63-66.
- Terzaghi, K (1946), "Tunnelling with steel supports" Commercial Shearing and Stamping Co. Youngstown, Ohio, USA.

## A Study of a Road Landslide in Puerto Rico

**C. Rodriguez-Pérez**

Project Engineer, Vázquez Agrait, Vázquez Castillo & Associates,  
Puerto Rico

**L. Vázquez Castillo**

Partner, Vázquez Agrait, Vázquez Castillo & Associates, Puerto Rico

**C. Rodriguez-Molina**

Engineering Geologist, Vázquez Agrait, Vázquez Castillo &  
Associates, Puerto Rico

**A. Vázquez Castillo**

Partner, Vázquez Agrait, Vázquez Castillo & Associates, Puerto Rico

**SYNOPSIS:** Numerous landslides have plagued the construction of a 1.3 mile road sector in the mountainous region of central Puerto Rico. The area is underlain by a sequence of landslide deposits overlying a muddy limestone and hard overconsolidated clayey soils. Landslides have occurred in both cuts and fills that have delayed the road construction for a period of more than two years, bringing as a result, great economic losses for the Puerto Rico Highway Authority. The landslide trigger mechanism has been intimately related to high rainfall, commonly observed in this region. The geotechnical and geological studies performed previous to the construction of this road sector were few and meager. These studies did not recognize the presence of unstable deposits along the road sector alignment. As a result, several large slope failures developed during construction that halted the completion of the road. For investigating the slope failures, detailed geological and geotechnical studies were performed, including monitoring of groundwater levels, rainfall, and slope movements followed by laboratory and slope stability analyses. Remedial measures have been provided in the form of excavation, drainage, and stability berms. Renewal of the road construction with the remedial measures is prompt to start.

### INTRODUCTION

Numerous landslides have plagued the construction of a 1.3 mile road sector in the mountainous region of central Puerto Rico. The area is underlain by a sequence of landslide deposits overlying a muddy limestone and hard overconsolidated clayey soils. Landslides have occurred in both cuts and fills that have delayed the road construction for a period of more than two years, bringing as a result, great economic losses for the Puerto Rico Highway Authority. The landslide trigger mechanism has been intimately related to high rainfall, commonly observed in this region.

The road sector alignment runs parallel to a high limestone scarp which rises at steep angles to elevations of up to 400 feet above the road level. North of the scarp is a cone-karsted terrain characterized by north-south and east-west trending limestone ridges, sinkholes and inter-ridge valleys. The proposed road grade follows a 300 to 600 feet wide bench along the base of the scarp. The bench is underlain by an 80 ft. thick sequence of landslide deposits, hard overconsolidated clayey soils and volcanic rock. The ground surface south of the bench steepens considerably toward a river running 430 feet below. Figure 1 shows a schematic cross section drawn at the road sector.

The geotechnical and geological studies performed previous to the construction of this road sector were few and meager. These studies did not recognize the presence of unstable deposits along the road sector alignment. As a result, several large slope failures developed during construction that halted the completion of the road.

The study of a single slide that occurred in a 40 ft. high cut in the previously mentioned road sector is presented herein. The slide involved a large ground mass of about 1150 feet along the road, 350 feet wide normal to the road, and 40 feet deep (Fig. 2). The landslide consisted of a combined slump lateral spreading slide with rotational characteristics and graben/horst structures. The failure developed during a heavy rainfall period in the area after the 40 ft. high cuts were performed.

For investigating this slope failure, a detailed geological and geotechnical study was performed. Several deep borings were drilled at and around the sliding mass. Inclined meters and piezometers were installed and monitored for a period of six months. Laboratory testing was conducted on recovered undisturbed soil samples to determine their engineering characteristics. A detailed engineering geologic reconnaissance was performed and slope stability analyses were carried out.

### SITE GEOLOGY

The route alignment runs nearly east-west at an elevation of about 1050 ft. above sea level. It is located upon a gently sloping to locally irregular bench 300 to 600 ft. wide which is bounded on the south by the moderately steep, heavily vegetated valley slope of Rio Grande River of Arecibo, which flows about 430 ft.

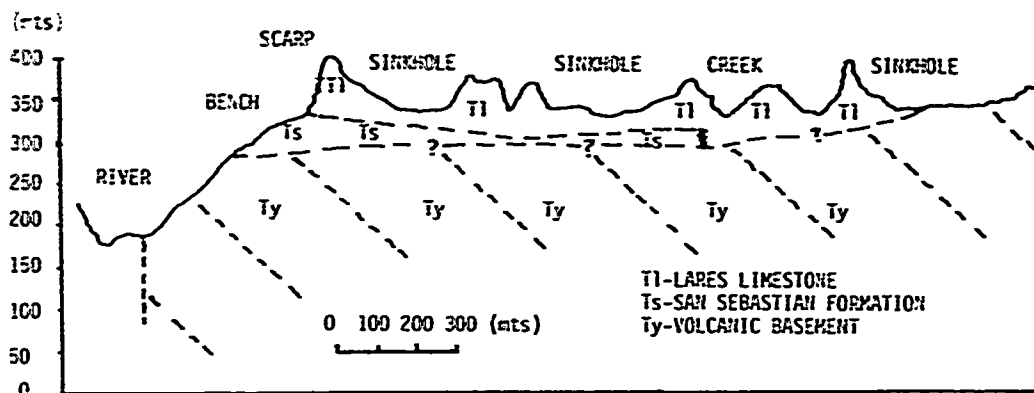


Fig. 1 Schematic Cross Section in a North-South Direction

below, and on the immediate north by the steep rock escarpment (cuesta scarp) of the Lares limestone plateau which extends another 150 to 300 ft. higher (Figure 1). This position places the route alignment right along a precarious condition of a plateau margin (Deere et al. 1987), as shown in Fig. 1.

For most of its alignment, the road sector is underlain by landslide deposits (Q1), a muddy limestone unit of the Lares Limestone Formation (T1), hard overconsolidated clayey soils called the San Sebastian Formation (Ts), and a generalized volcanic rock basement (Ty, Ka). Figure 2 shows a typical profile in the failed road sector.

The Lares limestone, which constitutes the northern plateau, consists of a mid-Tertiary upper unit of hard, white to tan, massive to bedded limestone (recrystallized chalk and calcarenite) of 250 to 330 ft. thick, and a 80 ft thick lower unit of softer, thick to medium bedded, tan marly, muddy limestone containing coral beads and calcareous algal fragments. The upper unit has undergone extensive dissolution with many small to large cavities and an elaborate karstic surface with isolated rock cones, steep ridges, and columns separated by elongated and circular sinkhole depressions (Fig. 3).

The Lares limestone (T1) is underlain conformably by the San Sebastian Formation (Ts), also of mid-Tertiary age, which consists of hard interbedded and lenticular masses of varicolored hard clay, silty clay, and clayey silt with some weathered gravel at the base. This gravel is probably the weathered surface of the underlying volcanic rocks. Some thin lignitic zones occur near the top of the sequence. The San Sebastian formation ranges in thickness from 0 to 6 ft. on the east to about 80 ft on the west end of the studied section.

The above described formations are the two bedrock formations that enter into the construction problem, the resistant Lares limestone at the cuesta scarp and the weaker San Sebastian deposits which underlie and support the limestone at the scarp and beneath the plateau. The bench has been formed in the San Sebastian formation

with the limestone having been removed by solutioning, erosion, and ancient landsliding.

The San Sebastian formation rests unconformably on the weathered surface of the volcanic rock basement of early Tertiary age.

The most recent geologic unit is the Quaternary landslide deposits (QL) or colluvium that have accumulated at the base of the limestone scarp and on the bench of the San Sebastian formation over the last few hundred to thousands years. These deposits consist of a heterogeneous mixture of limestone blocks that have fallen or toppled from the scarp, clay and weathered limestone fragments washed out of the limestone joints, and slide debris from block creep, block slides, and rock slumps which contain both limestone blocks and disturbed clays and silts from the underlying San Sebastian formation.

Old slide scarps can be recognized in the field and on aerial photographs in the colluvium, many of which coalesce giving a scalloped appearance to the escarpment. Further weathering and high rainfall have resulted in additional deterioration of the colluvium causing local, small and large debris flows and earth flows, the latter involving the greenish clay from the upper part of the San Sebastian formation which was softened and squeezed out from below the escarpment or which was brought to the surface by rotational slumps.

#### HYDROGEOLOGY

The general area of road sector is humid and tropical with an average annual rainfall of about 6 ft, most of which falls from May to November. Most of the rain that falls on the karstic limestone plateau on the north is collected through the sinkhole system into an internal drainage network. Part of this water emerges as springs from open joints or cracks along the base of the escarpment. A few springs appear on the south side of the bench at the colluvium, at the contact of the

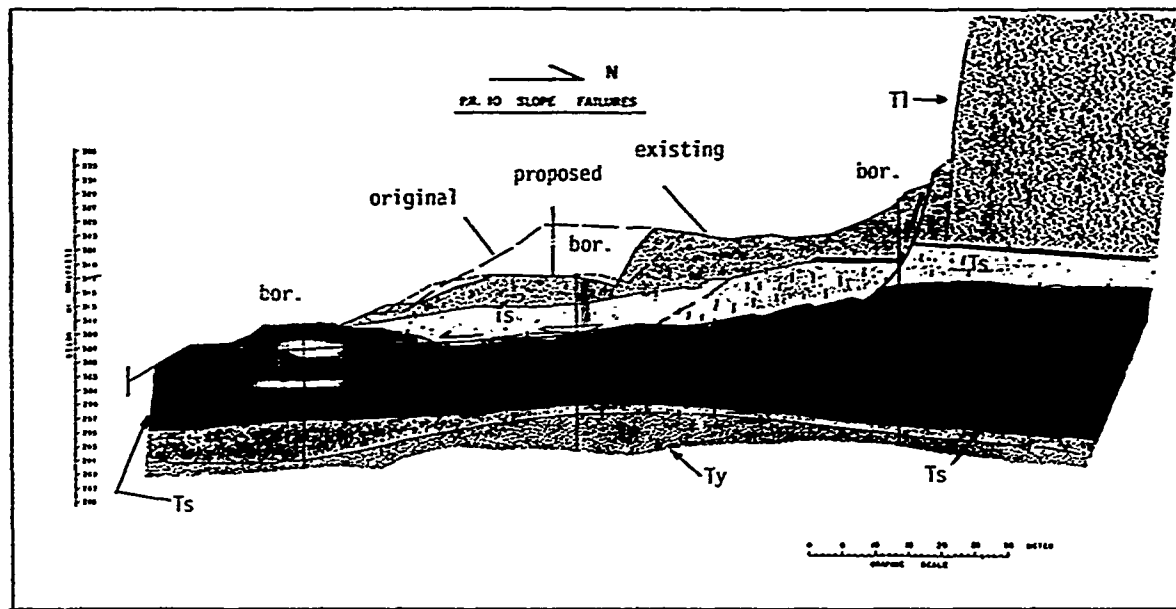


Fig. 2 Soil Profile and Slide Surface at Station 192+10

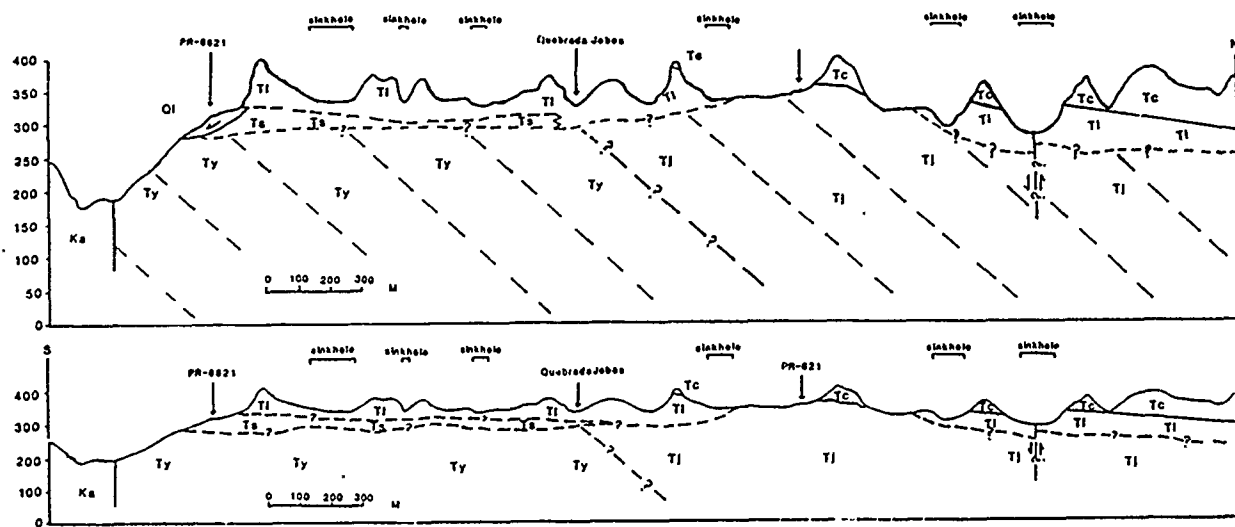


Fig. 3 Schematic Geologic Cross Section in a North-South Direction



colluvium and the San Sebastian formation, and at the contact of the weathered gravelly San Sebastian and the weathered volcanic bedrock. Part of the water seeps down and along the contact with the San Sebastian clays, giving an opportunity to the clays to absorb water, swell, and soften under the reduced stress beneath and outside the limestone scarp.

The combination of colluvium mixed with clay, resting on a clayey foundation, and of a steady inflow of seepage water from the limestone plateau becomes particularly unfavorable for the sector stability and has been the main cause of the slides developed during construction. Some of the northern sinkholes appear to be partially plugged allowing the development of shallow lakes in them during the wet season. These lakes slowly drain and feed the underground water supply. A small creek runs north of the scarp. The creek has been dammed by a small dike for local use. The resulting small lake may also be an additional source of water for the internal drainage network.

The complex geological and groundwater conditions observed at the project area place this site in a hazardous geological environment.

#### SLIDE MORPHOLOGY

An engineering geologic mapping and air photo analysis were performed along the road sector alignment and within areas lying north and south. The results of these analyses helped to identify the physical characteristics of the sliding mass and its surroundings. Figure 4 schematically shows these characteristics. The

slide consisted of a combined slump-lateral spreading slide with rotational characteristics (near the head) and graben-horst structures. The main body of the slide moved in a horizontal translatory fashion with a horizontal off-set estimated at 10 ft. The slide main scarp, 1150 ft. long and 10 to 15 ft. high, was located near the escarpment of the Lares limestone. Secondary scarps and tension cracks were observed within the moving mass and the slide toe was located about 350 ft. south of the main scarp. The toe was characterized by bulging (10 ft. high) and overriding ground. Several springs were observed emerging at the slide toe and green silty clay with high water content (90%) was oozing out and slowly flowing away.

The air photo analysis showed that an old large landslide existed at the road sector before the road construction. The development of this old slide may be associated with the same geologic condition described before. The construction and grading operations for the road, where 40 ft. high cuts were performed, reactivated this old slide with the physical characteristics mentioned above.

#### GEOTECHNICAL EVALUATION

A detailed geotechnical evaluation was conducted. Several deep borings were drilled at and around the sliding mass. The resulting soil profiles were consistent with the anticipated sequence of geologic strata described before. Figure 2 shows a typical profile of the sliding road sector. For the borings located near the base of the limestone scarp, the upper soil samples could belong to the lower unit of the Lares limestone or to the colluvium accumulated down-slope.

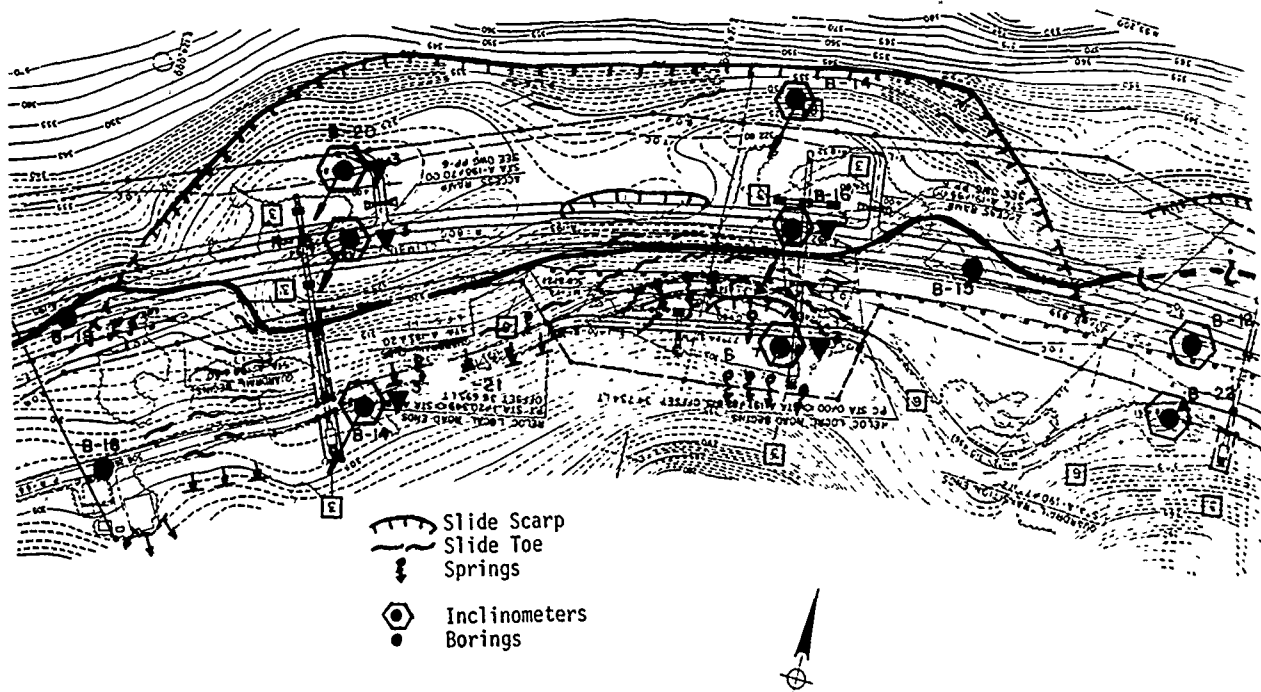


Fig. 4 Slide Physical Characteristics at Station 192+10

The standard penetration N-values for this material were usually in the range of 25 to 50 blows/ft (higher values were associated with hard inclusions or limestone blocks). The borings also found a clear contact of the colluvium with the upper part of the San Sebastian formation marked by a lignite layer overlying 35 ft. or so of hard, green to dark gray, organic clayey silt to silty clay (N-values of 100 bpf or more and natural water contents of 25 to 35%, classification of CL to CH).

The borings in about the middle of the bench did not show the lignite and the underlying green organic clayey silt, both of which were probably removed by erosion or old landsliding. Instead, a layer of calcareous, light to dark brown, clayey silt was found with volcanic and limestone inclusions. This layer was softer and wetter than the organic green layer at the edge of the scarp (N-values ranging from 5 to 30 bpf, natural water contents of 35 to 50%).

Figure 2 shows that the upper part of the San Sebastian formation is underlain by the "typical" San Sebastian formation, which consists of purple, green, brown, and gray clayey silt to silty clay with faint to partially decomposed clasts. The typical layer is hard, with N-values greater than 100 bpf, unconfined compressive strengths of 4.5 tsf or greater and moisture contents of about 20 to 30%. The average liquid limit and plasticity index are 50 and 30%, respectively. The typical San Sebastian soil has lower N-values of 30-50 bpf when sampled below the bench, particularly in the uppermost part where swelling has been more important. The soil samples of the formation showed the characteristics of stiff fissured clays of shiny luster and slickensides and polished faces when broken.

The clasts in this formation are less weathered with depth as the volcanic basement is approached (leading to difficulty in distinguishing between the San Sebastian deposit and any gravelly saprolite developed on the volcanic breccia). At this contact, the soil matrix was wetter, perhaps from being in contact with water from the bedrock joints. The transition gravel zone is about 6 ft. thick with some clay matrix.

Ten piezometers and eight inclinometers were installed and monitored for a period of six months for determining groundwater levels and depths of active sliding surfaces. The inclinometers were installed during a relatively dry period where the movements measurements were small (Fig. 5). It is during the period of heavy rains that the rate of movement increased, reaching large displacements in excess of 1 inch where shearing off of some of the inclinometers casings developed (Fig. 5).

The depth and shape of the sliding surface was determined with the inclinometer data and the field characteristics of the moving mass. The sliding surface starts at the head scarp and follows the contact between the organic and "typical" layers of the San Sebastian formation. The depth of the sliding surface as determined by the off-sets in the inclinometers was about 40 ft. The sliding mass included the base of the muddy limestone, the colluvium and the underlying overconsolidated clays. The sliding mass has a volume of about 0.6 million cubic yards. Figures 2 and 6 show two profiles indicating the position of the sliding surface and the observed groundwater levels.

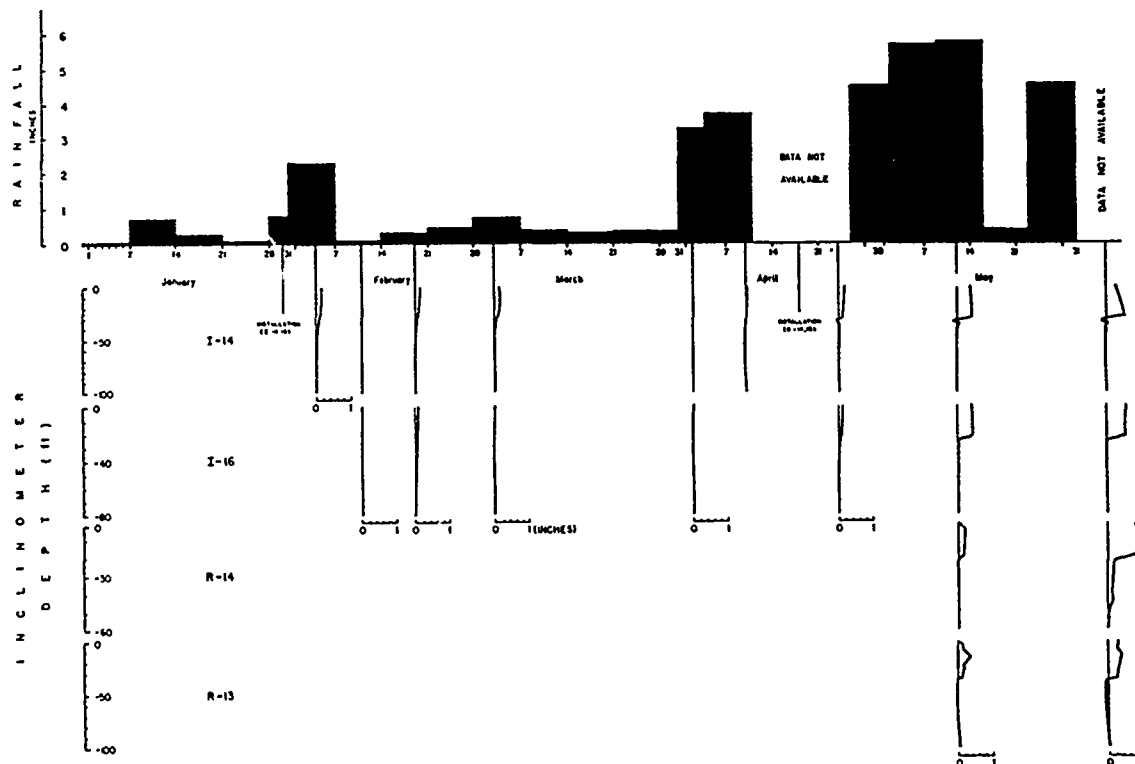


Fig. 5 Rainfall versus Displacements at Inclinometers

## STABILITY EVALUATION

To evaluate the stability conditions of the slide, back-calculating and parametric analyses were performed varying the position of the water levels, the depth of the sliding surface, and strength parameters. The back analyses used the residual friction value along the sliding surface. Results from direct shear tests on the San Sebastian deposits indicated a residual friction angle of 16 to 18 degrees. An assumption was made in these analyses that during the heavy rainfalls at the time of failure the water levels rose near the surface. Although reasonable, the assumption was not confirmed by the piezometers, as difficulties were encountered to measure during the rain. However, large quantities of water were observed seeping at several sectors of the existing ground surface at higher elevations than the slide toe. By using this information, the assumed water levels were defined.

The conclusions of the stability evaluation indicated that the causes in reactivating the old slide were the following:

- 1) The performance of large cuts (40 ft-high) to reach the desired road grading. These cuts deprived the sliding mass of resisting weight.
- 2) The geologic conditions and strength characteristics of the ground mass, particularly the combination of colluvium resting on an overconsolidated clayey foundation and the presence of the old landslide.

3) The presence of large amount of water seeping into the sliding mass as a result of heavy rainfall and the development of high water pressures associated with the nearby sinkhole system.

A detailed geological and geotechnical study previous to the road construction would have helped in defining the steps required to avoid the reactivation of the old slide. Such steps could consist of smaller cuts, incorporation of drainage schemes, and possible relocation of the road.

## REMEDIAL MEASURES

The results of the stability evaluation and the field information were used to draw the remedial measures needed to stabilize the sliding mass and proceed with the road construction.

The recommended solution alternatives involve several forms of subsurface drainage, improvement of the soil conditions at the slide toe area, and incorporation of a weighting berm (to increase the resisting forces and reduce the effect of the large cuts for grading operations). The following remedial alternatives have been proposed for this project (Fig. 7):

- a. Stabilizing drainage key
- b. Solution (a) with upslope drainage trenches
- c. Solution (b) with 8 ft. high berm
- d. Solution (c) with horizontal drains
- e. Drainage galley with horizontal drains
- f. Permanent wells with horizontal drains
- g. Combination of some of the above

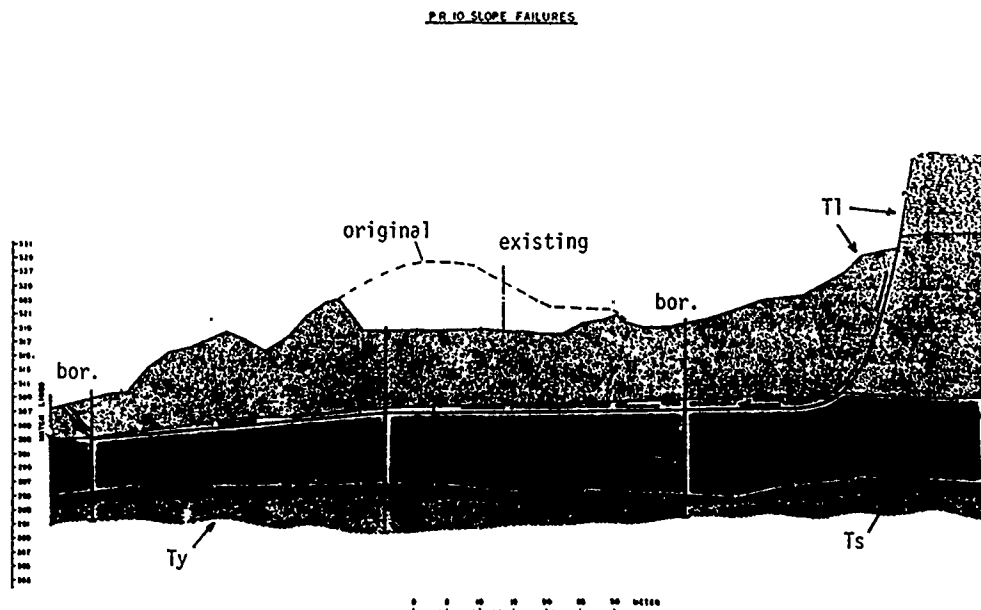


Fig. 6 Soil Profile and Slide Surface at Station 193+65

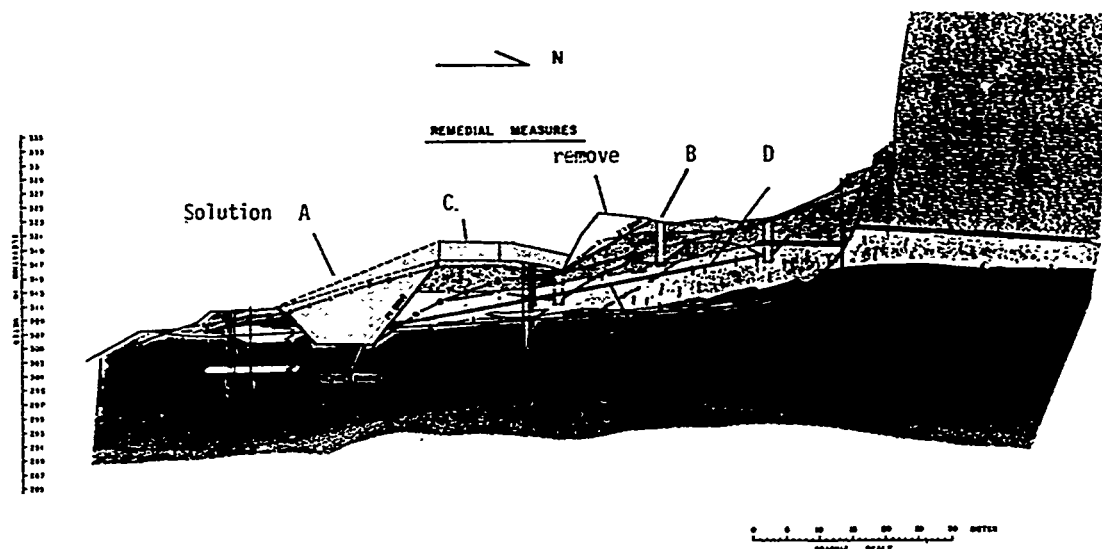


Fig. 7 Remedial Measures for Landslide at Station 191 to 195

The major stabilizing element will be the "stabilization drainage key", an excavated drainage ditch near the toe of the slide and to the downslope side of the new highway. The proposed key is up to 50 ft. deep, backfilled with gravel and with a filter fabric lining (Fig. 7). The key will extend a few meters below the determined sliding plane and will increase the factor of safety from 1.0 (rainy season potential condition) to about 1.4. Prior to building the key, it is required to lower the existing water level, considering the disturbed and fissured nature of the slide mass. Studies are presently being made of two procedures for lowering of the water level: (1) parallel small, drainage trenches or ditches (labeled B in Fig. 7) at two or three locations between the new highway and the scarp (excavated and backfilled in small lengths), or (2) 10 ft. to 13 ft. diameter drainage wells (or shaft) near the scarp with horizontal drain holes drilled from the shaft at all wet zones. Also, borings are presently being made in the karstic northern limestone to evaluate the possibility of partially draining the sinkhole system to reduce the feeding of water to the lower colluvium and the San Sebastian formation.

The remedial measure of shifting the alignment either to the right or left of the bench is considered difficult to carry out due to the presence of the large cuesta scarp (on the north) and the steep sloping ground (on the south). Also, previous construction operations performed at other road sectors restrain the realignment of this road sector to its present location.

In conclusion, this case history illustrates the difficulty of road construction in a hazardous geological environment such as this, where the presence of an old slide and colluvium resting on clayey

foundation make the road sector a very unstable area. For locations as this, a detailed preliminary evaluation of the area is mandatory and appropriate geological and geotechnical studies previous to road construction are necessary to define the proper construction scheme required to avoid the reactivation of existing old landslides. The use of field instrumentation should not be overlooked and the evaluation of the general area surrounding the troublesome location shall also be included.

#### REFERENCES

- Deere, D., P. Jimenez, and D. Hernandez, (1987), "Complex Landslides at Plateau Margins with an Example from Puerto Rico", Proc., Peck Symposium, Urbana.
- Vazquez-Agrait, Vazquez-Castillo & Associates, (1986), "Report Subsoil Exploration, PR-1081, Utuado, Puerto Rico", Submitted to Highway Authority, Commonwealth of Puerto Rico, San Juan, P.R.

# Simultaneous Velocity Measurements with Uniaxial Loading on Weak Sandstone from Iraq

Zuhair Rammo Fattohi

Assistant Prof. in Rock Mechanics and Engineering Geology,  
University of Baghdad, Engineering College, Baghdad, Iraq

**SYNOPSIS :** Transit pulse wave times through a weakly cemented sandstone rock being measured on prismatic specimens with and without initial plane of weakness, which is uniaxially loaded at different stages. The velocity, Elastic moduli bulk compressibility, and vertical strain were calculated for each loading level. Results have shown , that such rock properties have changed dramatically. Thus they should be considered thoroughly for any engineering evaluation in such rock type.

## INTRODUCTION

Many large engineering projects have been initiated recently in the country, among such project is the construction of the western international high way running mostly in desertic and semidesertic climatic area, Figure 1. The area is covered by loose sands, laid out physiographically on a flat surfaces except in few places where sand dunes of Barchan type occurs or when rock layers exposed to the surface. Main rock layers being recognized at the site of Abughar-Nasiriyah, consequently from top-down ward were the following: calcareous breccia, Mudstone, Sandstone, conglomeratic ( fragmental ) sometimes dolomitic limestone. These layers are interbedded with each other making facies like structure, Figure 2. Surficial layers are highly effected by heat and eolian weathering which characterized by the eolian ripple marks and many fractures formed on the external surfaces of the calcareous breccia. A drilling programme including 30 bore holes were performed in the studied area. It was realized from the investigated holes that good quality rocks are occurred at depth exceeded 10 m, Alezie etal,(1985). The present work mainly intended to evaluate the engineering behaviours of weakly cemented and weathered sandstone layer under normally



Fig. 1 Landscape For The Studied Area .



Fig. 2 Insitu Lithologic And Structural Relation.

increased load. Both the static and dynamic properties of this rock type were considered for each loading stage using a portable ultrasonic device. Rock axial strain and bulk compressibility were measured at different levels of load too, using a prismatic shaped samples. Many authors like Fatt (1958 b ) , Brace ( 1965 a ), King (1969), Chilingarian and Wolf (1975), Gregory ( 1977 ), and many others have tackled such properties for different rock types. However it is noticed that data published on sandstone rock material behaviour is not as much

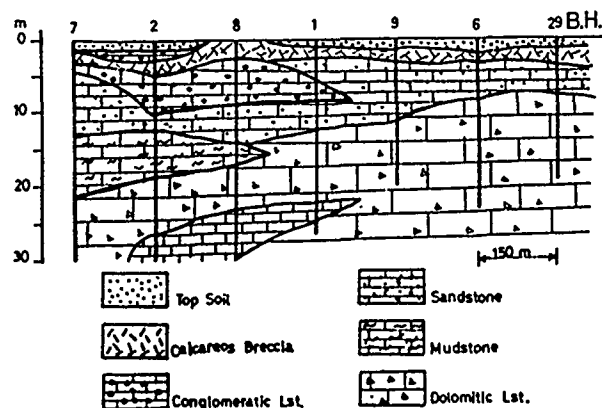


Fig.3 Boreholes Profile Showing Rock Types

as was thought to be . These data are of prime importance to engineering design.

#### INSITU ROCK CONDITION

A typical site locality was selected for this work , it lies on the boundary between the structural stable and unstable zone, Fattohi (1986 b) . Geologically this zone is characterized by calcareous deposits and evaporites, mainly composed of horizontal layers . 30 bore holes ranges indepth from 10 to 30 m were accomplished by the construction company (Dromex Co. of Poland, 1980) . Across sectional profile was constructed using data obtained from 7 Bore holes to explain the vertical and lateral lithologic contacts for the subsurface horizons in the investigated area as its illustrated in Figure 3.

#### EXPERIMENTAL APPROACH AND RESULTS

The sandstone rock layers, medium to coarse grained ( 2-0.6 mm) were selected for this paper. This sandstone rock material having bulk density = 2.4 g/cm<sup>3</sup> and fractional porosity  $\phi = 27.5\%$ , but with moderately high permeability  $K = 90.5$  md. Such rock material was expected to be effected by contineous normal and possibly to vibrated stresses. Prismatic samples of (9.5 x 4.5 x 5 cms) were prepared using rotary diamond pregated saw machine without a water flushing system , to avoid rock disintegration during preparation. Testing programme included two type of tests :  
Test (1) , was performed to study the effect of heterogeneity (either bedding plane or horizontal plane of fracture ) of the rock material by putting two prismatic specimens having surface area  $A = 45.4$  cm<sup>2</sup> one above the other and then loaded at right angle to its longest axis as illustrated in Figure 4. Sonic velocity (V.m/s) for each stage of loading ( normal compaction) was then calculated using the transit pulse wave time (  $\mu$ s ) and the specimen length . The axial deformation interm of vertical strain,  $\epsilon_v$  , ( using mechanical dial gauges up to 0.001 mm), and bulk compressibility ( $C_b$ ) were predicted for each stage of loading.

Test (2) , was performed on single prismatic shaped sample with its longest axis parallel to the direction of loading ( See Fig. 4). The static ( $E_s$ ) and dynamic ( $E_d$ ) constants as well as bulk compressibility ( $C_b$ ) values were found, using the conventional method adopted by Chilingarian and Wolf (1975 ) as follows :

$$C_b = \frac{1}{V_b} \frac{dV_p}{dP} \quad (1)$$

Where :  $C_b$  = Bulk Compressibility

$V_b$  = Bulk volume for prismatic specimen  
= 410.6 cm<sup>3</sup> for test 1, = 185.9 cm<sup>3</sup> for test 2

$P$  = Normal pressure applied

In test 1, the normal load ( $P$ ) increased gradually from 0Kgs. upto failure load at 3470kgs. (vertical stress ,  $S = 76.5$  kg/cm<sup>2</sup>) and upto

2150 kgs ( $S = 109$  kg/cm<sup>2</sup>) for test 2. The above rock measurements were plotted as it is seen in Figures 5., 6., 7. respectively. Variation of sonic velocity ( $V$ ) with loading level ( $P$ ) for both tests are shown in Figure 5a and 5b. which is a plot of polynomial relations of the form :

$$y = a + bx + cx^2 + dx^3 + ex^4 \quad (2)$$

where  $y$  = sonic velocity ( $v$ ) m/s

$x$  = loading level ( $P$ ) kgs

$a, b, c, d, e$  are the polynomial constants

upto 4<sup>th</sup> degree least square fit. The maximum sonic velocity reached in test 1 is 2212 m/s corresponding to loading level  $P = 3000$  kgs. ( $S = 66.2$  kg/cm<sup>2</sup>), and for test 2, the maximum

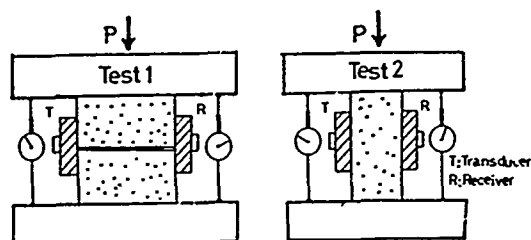


Fig. 4 Schematic Diagram For Test Procedure

value of ( $V$ ) , reached was 1739 m/s at loading level of  $P = 1500$  kgs. After these maximum values the velocity decrease to 1521 m/s while the applied vertical load is still increasing up to 3470 kgs in test 1 and to 1559 m/s at loading level of 2150 kgs in test 2. Values for static ( $E_s$ ) and dynamic modulus ( $E_d$ ) of elasticity at each loading stage are shown in Figure 6a and 6b . which also represent the best fit upto 4<sup>th</sup> polynomial as below :

Where  $y$  = Modulus of elasticity ,  $E_s$  and  $E_d$

$x$  = Loading level  $P$  ( kgs ).

$a, b, c, d, e$  are the polynomial constants

The highest contrast between the two moduli were found at 2500 kgs to be  $7.3 \times 10^4$  kg/cm<sup>2</sup> for test 1 and  $6.4 \times 10^4$  kg/cm<sup>2</sup> at 250 kgs.

loading level for test 2. It appears that the increasing rate of ( $E_s$ ) values having more linear form than for ( $E_d$ ) values, this is possibly due to the isotropic effects in the rock material it self.

Figure 7. showing the ( $C_b$ ) variation with the vertical stress ( $S$ ) . It is clear from the diagram that ( $C_b$ ), for both tests were decreased with increasing vertical stresses, as the ( $C_b$ )

values was decreased from  $7.395 \times 10^{-4}$  ( $\text{kg}/\text{cm}^2$ )<sup>-1</sup> at  $S=11 \text{ kg}/\text{cm}^2$  to  $2.694 \times 10^{-4}$  ( $\text{kg}/\text{cm}^2$ )<sup>-1</sup> at  $76.5 \text{ kg}/\text{cm}^2$  in test 1 and from  $8.8 \times 10^{-4}$  ( $\text{kg}/\text{cm}^2$ )<sup>-1</sup> at  $S=12.7 \text{ kg}/\text{cm}^2$  to  $2.1 \times 10^{-4}$  ( $\text{kg}/\text{cm}^2$ )<sup>-1</sup> at  $S=109 \text{ kg}/\text{cm}^2$  in test 2. Saturation effect was carried out on other prism of ( $9.5 \times 7.0 \times 5 \text{ cm}$ ), which is loaded from 0 up to 750 kgs. The pulse wave velocity has increased from 100 m/s to 1305.6 m/s, while porosity of rock decreased from 27.5% to 14.3%.

## DISCUSSION AND CONCLUSION

It appears from Figure 5. that the longitudinal pulse wave transit through the sample was increased by 16 % in test 1 when the load have increased from 0 to 3000 kgs, and by 6.4 % in test 2 when the load increases from 0 to 1500 kgs. This fact was mentioned in the pioneer work of wyllie et al. (1958) and confirmed by Warren (1973) as well as by the recent work of Masayasu (1981) on his study concerning the relation of uniaxial compressive strength and elastic waves for soft rock. In other hand he concluded that this relation is rather very poor. However, the velocity increases at high pressure which is followed by increases in  $C_b$ ,  $E_s$  and  $E_d$  too, may results from changes in intrinsic properties of the rock such as the compaction and the reduction of the pore space caused by the contact occurs between Particles during loading. Thus the rapid increases of velocity at low pressure may be attributed to these effects. It was suggested that velocity

may reduces sharply just before the maximum bearing capacity reached. In one way or another this fact looks to agree with results obtained in Figure 5. It can be traced from results also that ratio  $E_d/E_s$  was decreased by increasing the normal pressure (Figure 6) from 4 at 500 kgs. to 2.5 at 3000 kgs. for test 1 and from 3.5 at 500 kgs. to 1.4 at 1500 kgs in test 2. However this ratio was found to approach unity at higher level of loading. According to King (1969) the  $E_d/E_s$  ranging from 1 to 3 for most rock type. Although the compressibility ( $C_b$ ) results (Figure 7) were almost identical for test 1 and test 2, but it does show the effect of heterogeneity, plane of weakness on rock deformability when subjected to normal loading. Brace (1965) mentioned that linear compressibility on a number of rocks with preferred orientations dependent upon the orientation of grains and pressure and is different in different direction. Fattohi, 1986 a, found out that the particle reorientations and

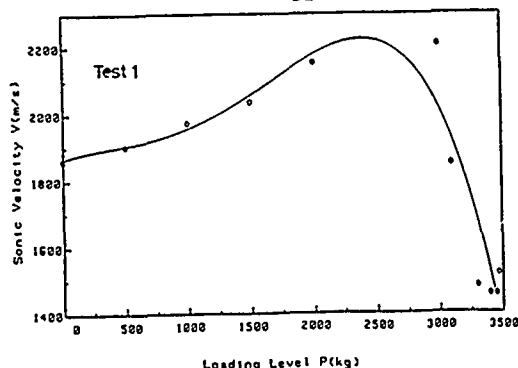


Fig. (5a) Variation of loading level with sonic velocity

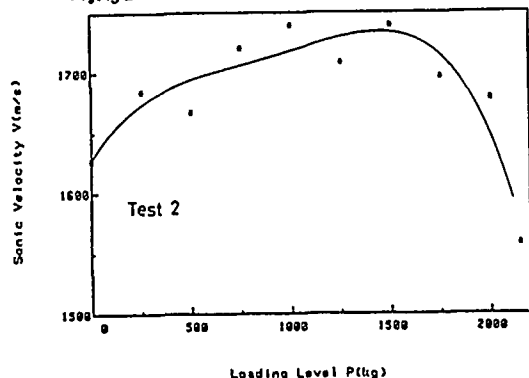


Fig. (5b) Variation of loading level with sonic velocity

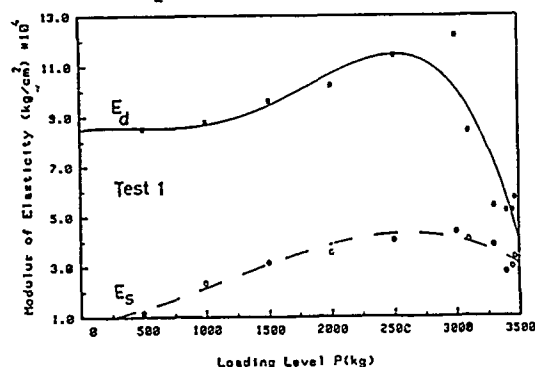


Fig. (6a) Changes of static and dynamic moduli values with loading level

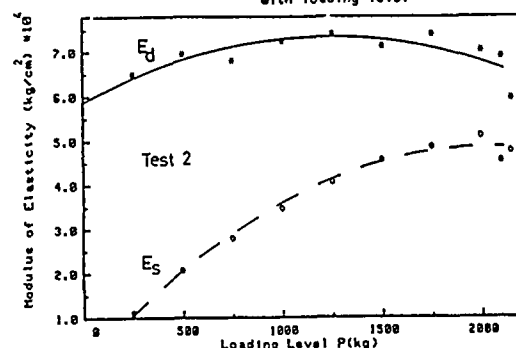


Fig. (6b) Changes of static and dynamic moduli values with loading level

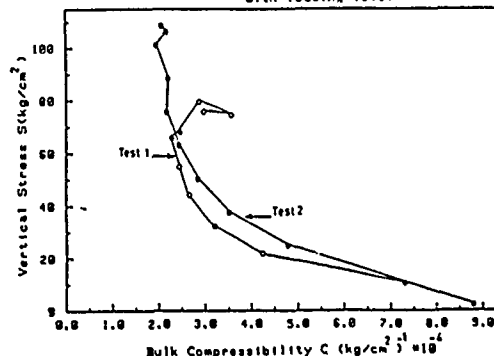


Fig. (7) Bulk compressibility Vs. vertical stress

displacement, which may take place during compaction have changed the bulk compressibility of soft sandstone. Lama and Vitukuri (1978) have also confirmed the effects of grain, pores and cracks on such rock property. For a more clear picture of these effects, Figure 8, is a plot of vertical strain ( $\epsilon_v$ ) and stress. It is clear that ( $\epsilon_v$ ) for test 2 is more linear and having a brittle form than the curve for test 1 because of the initial fracture occurrence.

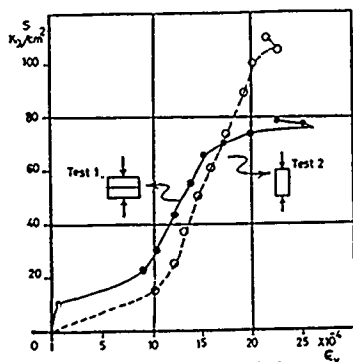


Fig. 8 Stress-Strain Relation

#### REFERENCES

- Brace, W.F. (1965a) Some New Measurements of linear compressibility of Rocks, J. Geophys. Res. Vol. 70.
- Chilingarian, G.V. and K.H. WOLF, (1975) Compaction of Coarse-Grained Sediment, I Elsevier Scientific Pub. Comp. (Development in Sedimentology 18 A).
- Dromex-Co. Poland (1980), Site Investigation Report of Abu-Ghar Quarry-Iraq (Personal use).
- Elizzi, A.S., Z. R. Fattohi, A.H. Maha Wish (1985), Evaluating the use of Crushed Rocks in Concrete Production (Southern Part of Iraq. Abu-Ghar Area), Journal of Building Research (Research Council) Vol. 4. No.1, 1-24, IRAQ.
- Fatt, I., (1958b) Compressibility of Sandstone at low to Moderate Pressures, AAPG Bull Vol. 42, 1924 - 1957.
- Fattohi, Z.R. (1986 a), Particle Displacements and the Changes of Sandstone Rock Properties From Southern Iraq. Int. Symp. on Large Rock Caverns, Vol.2, Bl.10, 961-970 Helsinki, Finland, Pergamon Press.
- Fattohi, Z.R. (1986 b), The Engineering Behaviours of Rocks From Different Tectonic Regions In Iraq. Proc. of the Int. Symp. on Engr. In Complex Rock Formation, 309-317, Beijing-China.
- Gregory, A.R., (1977), Aspect of Rock Physics from Laboratory and Log Data that are Important to Seismic Interpretation. AAPG, Memoir 26, Ed. by Payton, C.E., Tulsa Oklahoma, U.S.A.
- King, M.S. (1969), Static and Dynamic Moduli of Rocks under Pressure, 11th Symp. on Rock Mech., Berkeley Calif.) 35 P.
- Lama, R.D. and V.S. Vitukuri, (1978), Handbook On Mechanical Properties of Rocks, Vol. II, Trans Tech. Pub.
- Masayasu, I. and M. Ohmi, (1981), Relation between Uniaxial Compressive Strength and Elastic-Wave Velocity of Soft Rock, Int. Symp. on Weak Rock. Tokyo, Japan.
- Warren, N. and O.L. Anderson, (1973), Elastic Properties of granular materials under Uniaxial Compaction Cycles, Jour. of Geoph. Research, Vol. 78 No. 29 6911- 6925.
- Wyllie, M.R.J., and G.H.F. Gardner, (1958), An Experimental Investigation of Factors affecting elastic wave velocities in Porous Media. Geophysics Vol. 23 1429-493.

#### ACKNOWLEDGMENTS

The author expresses his gratitude to the Eng. College, University of Baghdad, and to People helped in this work in Particular to Kowthar. W. . My deepest appreciations paid to Sonia, V. Aziz for tracing some diagrams.



## Johnston City School, Mine Subsidence or Shallow Foundation Problem?

Alphonse C. Van Besien

Dept. of Geology & Geological Engineering, University of Mississippi, USA

Nolan B. Aughenbaugh

Dept. of Geology & Geological Engineering, University of Mississippi, USA

**SYNOPSIS:** Johnston City, a small community in southern Illinois, lies above the Herrin (Illinois No. 6) coal seam. The community has experienced sporadic episodes of surface subsidence due to the collapse of underground mines since the 1930's. Although the mining company left a large block of coal beneath the town's elementary school to prevent subsidence damage to the structure, large cracks appeared in the school building in December, 1971. After the building was razed, construction of a new school was initiated in 1974. Approximately six months after the start of construction, new evidence of structural distress was observed in the still-uncompleted structure. Construction was suspended indefinitely while site investigations were conducted. These investigations, along with recent air photo studies, indicate that renewed mine collapse and the resulting downward displacement of the surface, were the cause of this second incident of structural distress.

### INTRODUCTION

Johnson City is a community of approximately 4000 population, located 85 miles (140 km) southeast of the St. Louis metropolitan area (Figure 1). Situated near the northern boundary of Williamson County, Johnson City is in the center of what was once widely known as the "Quality Circle", a portion of Illinois famous for the thickness and high quality of its coal seams. Mining of the Herrin (Illinois No. 6) coal seam, which here is eight feet (2.4 metres) thick, provided the economic life-blood of the community during the early years of this century. The Lake Creek Mine, which underlies most of the town, was closed in 1929, and surface subsidence, caused by collapse of portions of the mine workings, was observed almost immediately and at irregular intervals ever since. In 1971, the town's elementary school was damaged by what was believed to be mine subsidence, and was subsequently razed. In 1974, construction of a replacement school building was initiated on the same site. New evidence of structural distress was observed even before the replacement building was completed, and construction was suspended indefinitely. Physical evidence at the site indicates that the second episode of damage was caused by renewed collapse of the mines below Johnston City.

### GEOLOGY

#### Stratigraphy

Johnston City is situated in the Till Plains Section of the Central Lowlands Physiographic Province. The Pleistocene deposits of this area are the Equality Formation of Wisconsin age and the Glasford Formation of Illinoian age (William and Frye, 1970). The Equality Formation is composed of lacustrine deposits of calcareous, silty, and sometimes sandy, clay representing the Periglacial Muddy Lake of Wisconsin age. The Equality clays are usually brown or yellow-brown in color. The Glasford Formation is made up of ground moraine tills of Illinoian age. In the Johnston City area, these Pleistocene materials have a combined thickness of from 50 to 100 feet (15 to 30 metres).

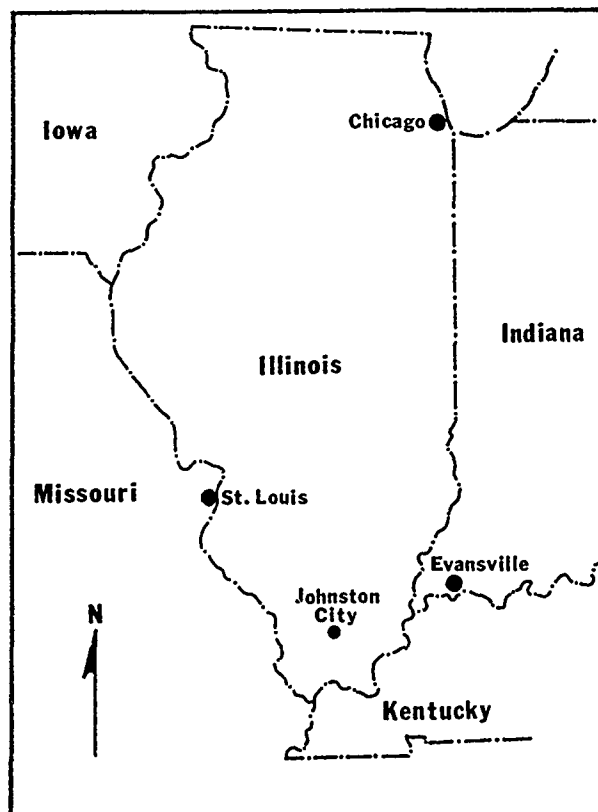


Figure 1. Location Map.

Being located near the southern boundary of the Illinois Coal Basin, Johnston City is underlain by some of the oldest formations of the Pennsylvanian System in Illinois. Most important for this study is the Carbondale Formation of the Kewanee Group. This formation includes the Herrin coal seam and extends upward to the Danville (Illinois No. 7) coal seam. The Herrin seam is usually underlain by the Energy Shale which consists primarily of a medium-gray, poorly laminated, silty shale (Damberger et al, 1960).

The Carbondale Formation is the uppermost of the Kewanee Group, and is in turn overlain by the Modesto Formation of the McLeansboro Group.

### Structural Geology

The most important structural feature in the vicinity of the site is the Cottage Grove Fault System (Figure 2) which interrupts the slight regional dip to the north, trends WNW-ESE and has been characterized as a right-lateral strike-slip fault with a displacement of less than one mile (Nelson and Krausse, 1981). Numerous minor faults are associated with the system; most are normal, but reverse and oblique-slip faults have been described. Vertical displacements of up to 200 feet (60 metres) are associated with these minor faults. Subsidiary anticlines with limbs dipping up to 15 degrees have been reported in association with the Cottage Grove Fault

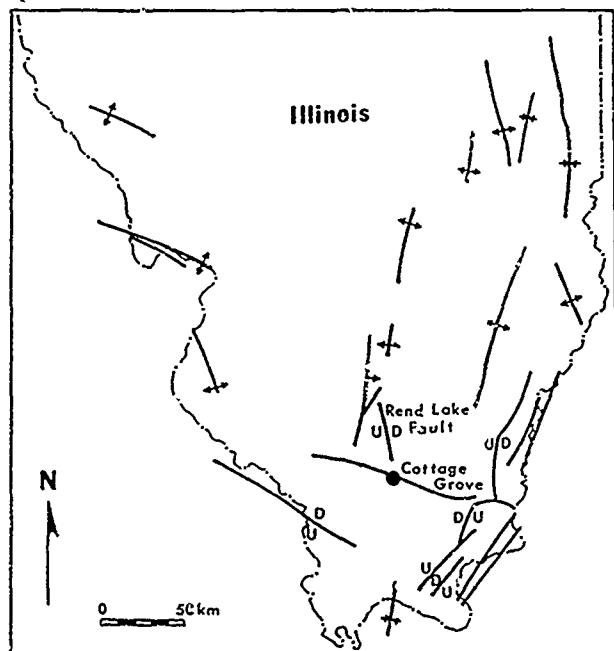


Figure 2. Structural features of southern Illinois.

System. In the eastern part of Williamson County, approximately 15 miles (25 kilometres) southeast of Johnston City, peridotite dikes have been reported, intruded along minor faults (Clegg, 1955). Both faults and intrusions are dated only as post-Pennsylvanian in age.

### MINING HISTORY

Coal was mined in Williamson County as early as 1850, with the first shipping mine being opened in 1872 by the Carbondale Coal and Coke Company (Peltier, 1912). Mechanical mining was introduced into the area as early as 1891, although successful mechanization was delayed until 1920, when it was utilized by the Egyptian Coal and Mining Company. Room-and-Pillar mining methods were used throughout this area, with rooms 20 feet (6 m.) wide and pillars 14 feet (4.3 m.) wide. Rooms were generally 200 to 250 feet (60 to 75 m.) in length, with cross-cuts being driven at intervals of 60 feet (18 m.). The mining method produced frequent incidents of surface subsidence (Young, 1916).

The Lake Creek Coal Mine, which underlies Johnston City,

was active at the turn of the century and continued in operation until 1929. Mine layout was typical of the area with the room and pillar dimensions previously cited. Company personnel left an irregular block of coal, approximately 160 feet (43 m.) square, to provide, what was believed would be permanent protection for the elementary school against mine subsidence. In 1927, the mine encountered a Grove Fault system, which trended NNW-SSE and had a vertical displacement of approximately 60 feet (18 m.). Like most mines in the area, the Lake Creek Coal Mine experienced some problems with groundwater. Drilling performed in conjunction with these studies in the 1970's indicated that the mine was flooded.

### SUBSIDENCE HISTORY

#### Pre-1971 Subsidence

Sporadic incidents of mine subsidence have been reported in Johnston City ever since the Lake Creek Coal Mine was abandoned. In the 1930's, the town's high school was damaged by subsidence, as were the football field and the community's baseball park. In the 1940's, two residential blocks northeast of the elementary school experienced subsidence damage. Another baseball park developed a dish-shaped subsidence depression, three feet (1 m.) deep, in 1964. In June 1965, several more homes suffered severe cracking of basement walls and foundations; cracks were also visible in the ground surface. Subsidence eventually affected so much of the town that one resident indicated, with some exaggeration, that there wasn't a house in the town where a pencil could be laid on a table without having it roll off.

#### 1971 Subsidence

The initial subsidence damage to Johnston City's Washington Elementary School was first observed during the Christmas school holidays. Janitors working during this break discovered cracks in the walls and ceilings of eight school rooms (Figure 3). Door frames were misaligned (Figure 4) and large fractures were visible on outside foundations, sidewalks, and school playgrounds (Figure 5). Damage was so extensive that the building was declared unsafe and was demolished shortly thereafter.

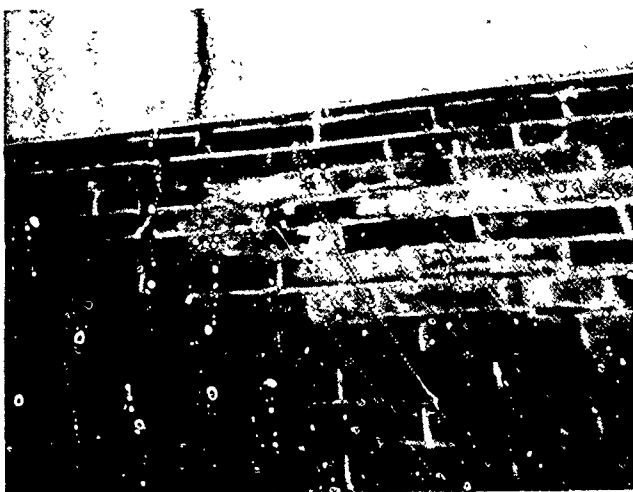


Figure 3. Cracks in classroom walls and ceilings.



Figure 4. Misaligned door frames.

#### 1974 Subsidence

In the belief that the mine subsidence was completed, construction of a replacement elementary school was initiated on the same site, in the summer of 1974. In October of that year, the contractor reported damage to the building under construction. The damage was in the form of dislocated and misaligned structural members. Construction was suspended indefinitely.



Figure 5. Crack in playground.

A damage survey of the area indicated that a number of residences were damaged, and that several water-main breaks occurred simultaneously with the damage to the new school building. Eight breaks were reported in the water-mains in the six blocks to the east and southeast of the school, with five occurring in the southeast. Thirty-three homes were reported to have been damaged during the suspected subsidence incident; again, most of the damage incidents were reported in the area to the southeast of the school.

Surveys accomplished during October and November of 1974 established that the center of the subsidence zone was south of the school, although the exact magnitude of the settlement could not be determined. Displacements within the school amounted to approximately 4 inches (10 centimetres). Extended observation of settlement monuments indicated that the rate of subsidence was slowing, and that, by the end of November, downward

displacement had practically ceased.

Ten borings were drilled in the vicinity of the school during these investigations. Two of the borings encountered coal, while eight borings encountered collapsed, or partially collapsed, mine workings. Where the mine was partially collapsed, openings ranging in height from 6 inches to 2.2 feet (0.2 to 0.7 m.) were encountered. Boring B-2 (Figure 6) followed a vertical fracture from near the surface to a depth in excess of 190 feet (58 metres).

Recently, air photos taken of the site in May, 1960, and December, 1974, were examined for evidence of subsidence. No evidence of subsidence was observed in the 1960 air photos (Figure 7). Digital image processing applied to the 1974 air photos revealed a lineament trending NE-SW and corresponding generally with the reported water-main breaks (Figures 6 and 8). The light-colored lineament is interpreted as a narrow zone of soil which has dried, and become lighter in color, due to the presence of an underlying fracture in the bedrock. The fracture is believed to be a tension fracture associated with the mine subsidence. Once the lineament was observed in the enhanced image, it could be observed in the original 1974 photo, although only very faintly.

Studies of mine subsidence in the United States indicate that the angle of draw, the angle between the vertical and a line drawn from the edge of the collapsing mine opening to the outer limit of surface displacement caused by subsidence, ranges from 20 to 35 degrees. With the Lake Creek Coal Mine lying at a depth of 240 to 280 feet (73 to 85 m.) below the surface, the coal Pillar was not large enough to prevent subsidence damage to the school, if the area of mine collapse was near the school.

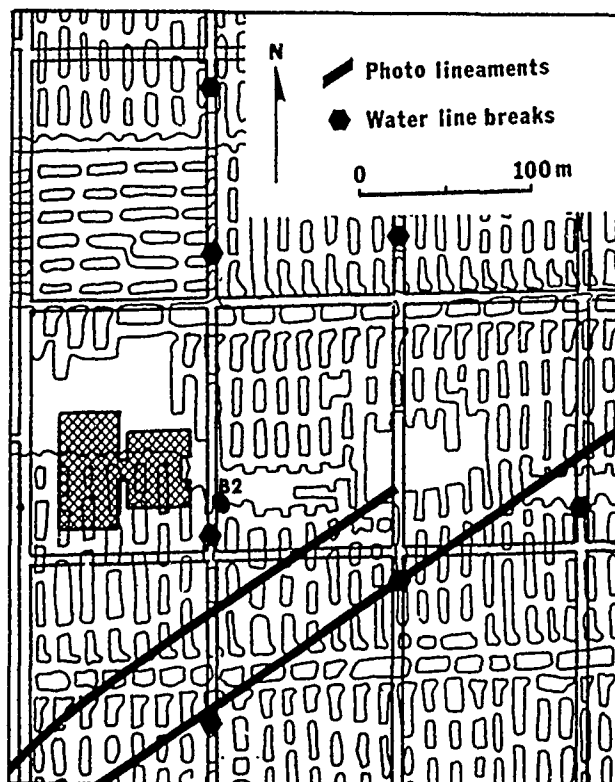


Figure 6 Mine layout and indications of subsidence.

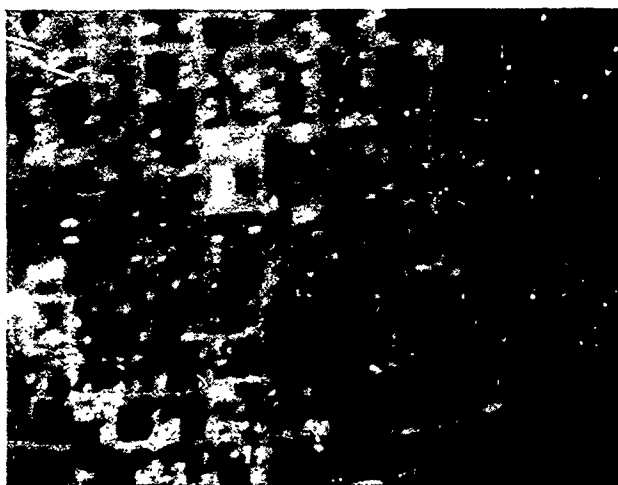
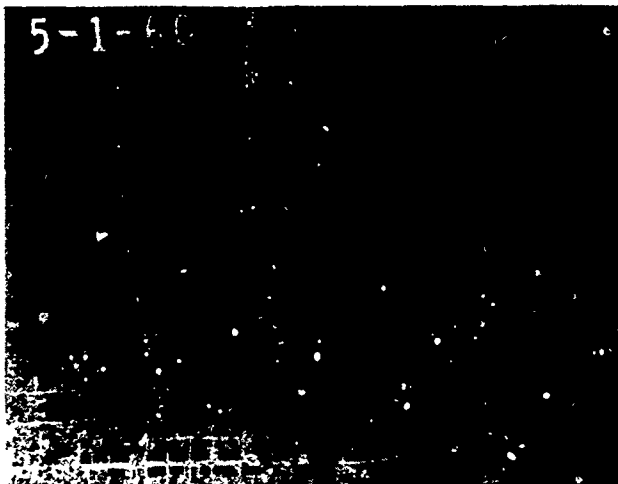


Figure 8. Air photo of Johnston City in 1974.

#### CONCLUSIONS

Although other explanations have reportedly been offered for the damage to the Johnston City elementary school buildings, there can be little doubt that both damage incidents were caused by mine subsidence. The occurrence of only-partially-collapsed mine openings in the immediate vicinity of the school, coupled with water-main ruptures, damage to private residences, surveyed displacements of the ground surface and the fractures observed in the ground surface at the time of the original damage to the old school building, are strongly indicative of subsidence damage. The lineaments observed in the digitally enhanced air photos, taken after the damage of the replacement school building, and generally coinciding with water-main ruptures, are consistent with subsidence-related ground displacements. The presence of only-partially-collapsed mine openings near the school after the second subsidence incident, indicates that additional subsidence, although probably of lesser magnitude, was possible after 1974.

#### REFERENCES

- Anonymous, 1940, Mining methods and mechanical loading, southern Illinois deep mines: Coal Age, Vol. 45, No. 10, p. 76-88.
- Clegg, K. E., 1955, Metamorphism of coal by peridotite dikes in southern Illinois: Illinois State Geological Survey, Report of Investigations 178, 18p.
- Damberger, H. H., Nelson, W. J., and Krausse, H. F., 1980, Effect of geology on roof stability in room-and-pillar mines in the Herrin (No. 6) coal of Illinois: Proceedings first conference on ground control problems in the Illinois coal basin, Illinois University at Carbondale, p. 14-32.
- Hunt, C. B., 1974, Natural regions of the United States and Canada: W. H. Freeman and Company, San Francisco, 725p.
- Nelson, W. J., and Krausse, H. F., 1981, The Cottage Grove fault system in southern Illinois: Illinois State Geological Survey, Circular 522, 65p.
- Peltier, M. F., 1912, Mining methods in Illinois: Coal Age, Vol. 1, No. 23, p. 732-735.
- Willman, H. B., and Frye, J. C., 1970, Pleistocene stratigraphy of Illinois: Illinois State Geological Survey, Bulletin 94, 204p.
- Young, L. E., 1916, Surface subsidence in Illinois resulting from coal mining: Illinois State Geological Survey, Cooperative Coal Mining Investigation Series Bulletin 17, 225p.

# The Successful Construction of a High Gravity Dam on Complex Rock Formations

Lu Jiayou

Institute of Water Conservancy and Hydroelectric Power Research,  
Beijing, China

Mei Jianyun

Institute of Geophysics, Academia Sinica, Beijing, China

**SYNOPSIS:** This paper presents an analysis of the stability against sliding of a gravity dam built on a layered rock formation. During the design of this dam, detailed studies of the dam foundation were carried out from a viewpoint of rock mechanics, including laboratory and in-situ tests of the mechanical properties of rocks, calculations by the theory of limit equilibrium and FEM, as well as model tests. Based on these studies, the dam type was selected.

## INTRODUCTION

The dam of Zhuzhuang reservoir is a stone masonry gravity dam. Its original designed height was 110m. The rock at the dam site is a layered silicarenite consisting of nine thick layers in total. The bedding surface dips downstream at an angle of  $6-8^\circ$ . There are many layers of weak intercalations among which intercalations II-5 and Cn72 (Fig.1) are rather unfavourable to the sliding-resistance and hence the controlling layers for the dam foundation stability. In design, not only the safety factor for the stability against sliding of the foundation was calculated by the traditional theory of limit equilibrium, but also the foundation stability was studied by model tests and the stress in the foundation computed by FEM. Based on the result of model tests and consulting the results of limit equilibrium and FEM analysis, the dam type was selected and a dam height of 95m was determined. In model tests and FEM computation, the effect of fault  $F_4$  which traverses the dam foundation was taken into consideration. The Zhuzhuang dam was completed in 1976 and has worked in a good state for more than 10 years.

to various limitations such as the constructional operation etc., studies were carried out more by static methods than by dynamic ones and more on the surface than in the depth.

The static modulus of elasticity was measured in an adit with a jack and typical stress-deformation curves for loading-unloading cycles are shown in Fig. 2.

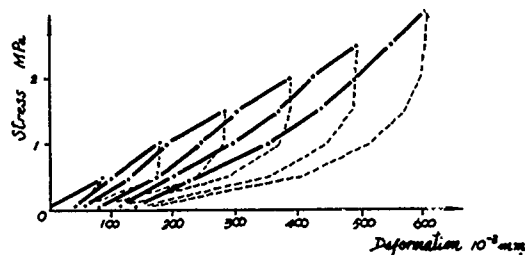


Fig. 2 Stress-deformation curves for rockmass

With the requirement for analysing the stress of the foundation in mind, deformations were measured not only in the vertical but also in the horizontal direction in the test.

Test results showed that for the silicarenite and striped sandstone, every loading-unloading cycle caused an obvious incremental residual deformation. The modulus of elasticity was calculated for each loading-unloading cycle. It was found that the higher the loading stress, the smaller the value of  $E$  was, and that the modulus of deformation was much lower than the modulus of elasticity for the same loading level. To the maximum, they may differ by a factor of 3. This was more conspicuous in the horizontal than in the vertical direction. The values of  $E$  in the horizontal direction were mostly greater than those in the vertical, and the degree of anisotropy decreased with increasing stress. The anisotropy of the rockmass was mainly brought about by the effects of the occurrence of various discontinuities, the state of fractured zones and the properties of fill-in materials.

Virgin specimens  $50 \times 50 \text{ cm}$  and  $15 \times 15 \text{ cm}$  in size were used in-situ and in laboratory respectively to determine

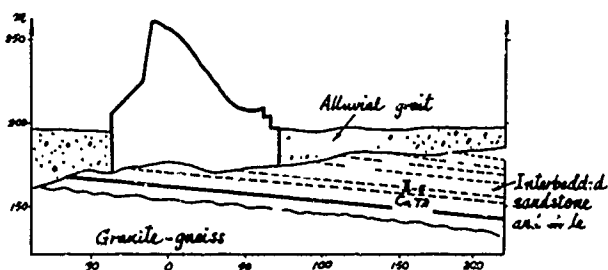


Fig. 1 Rock formation of the dam site.

## MECHANICAL PROPERTIES OF THE ROCKMASS

In order to assess the stability against sliding of the dam foundation, the deformability of the rock mass and the shear strength of weak intercalations were studied experimentally. The modulus of elasticity of the rockmass was measured by both static and dynamic methods. Owing

the shear strengths of weak intercalations. Besides, some disturbed soil was collected from the clayey intercalations No. III to VI and remoulded specimens with controlled water content were prepared and tested by consolidated quick shear tests in direct shear apparatus. 14, 16 and 106 groups of tests were conducted respectively for the three kinds of tests mentioned above.

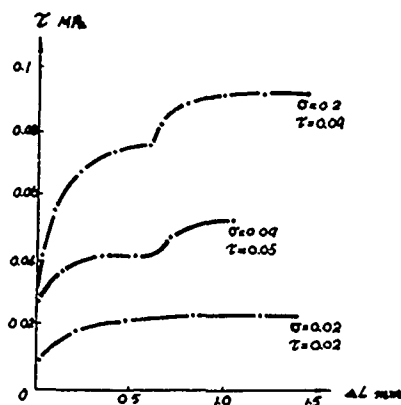


Fig. 3 Typical stress-displacement curves for clayey intercalation NO. II-5.

Typical stress-deformation curves for the clayey intercalation II-5 are shown in Fig. 3. It was found from the test result that the clayey intercalation was characterized by large deformation and low strength. Its shear strength depended on the roughness of the interface and the thickness of intercalation. Four different cases were identified. First, when the interface was smooth and the intercalation thickness was greater than the interface fluctuation, the shear strength was very low since shear fracture took place along the weak interface between the rock and intercalation. Second, when the intercalation thickness was smaller than the interface fluctuation, the shear strength was controlled by the interlocking between the rock surfaces and had a higher value. Third, when the intercalation was locally lacking, the shear strength was increased significantly by the friction between rock surfaces. Finally, when the rock had a zigzag surface, a portion of it was sheared off and thus the shear strength was greatly increased.

The shear strengths of intercalations obtained by laboratory tests on 15x15cm specimens and by in-situ tests were close to each other, while those by geotechnical tests were generally lower than both of them. When the rock surfaces above and below the intercalation were smooth or only had a small fluctuation, the laboratory data were close to or slightly greater than the in-situ data.

According to the yield limit criterion, the peak strength of intercalations II-5 and Cn72 were multiplied by a reduction factor of 0.7 and  $f=0.29$ , 0.22 and  $C=0$  were taken for these two layers respectively.

#### APPLICATION OF THE THEORY OF LIMIT EQUILIBRIUM

The weak intercalation dipping downstream was assumed as a sliding plane (BE) when using the theory of limiting equilibrium to analyze the stability against sliding in design. It was also assumed that there was a vertical shear fracture plane CE (Fig. 4) in the dam site. Since the most developed fracture perpendicular to the river bed in the dam site has a high dip angle of  $80^\circ$ , this assumption seems to be a reasonable approximation of the reality. By assuming that the rockmass behind the dam fractures along plane CD when the sliding plane has

reached its limiting state and making use of limit equilibrium analysis, the force R transferred to the downstream rockmass can be obtained as

$$R = \frac{\sum H \cos \theta + (\sum V + G_1) \sin \theta - f_1 [\sum V + G_1] \cos \theta - \sum H \sin \theta}{\cos(\varphi - \theta) - f_1 \sin(\varphi - \theta)} \quad (1)$$

Then by assuming that the fracture plane CD in the rockmass behind the dam makes an angle with the horizontal, K can be obtained from

$$K = \frac{f_2 [R \sin(\varphi + \alpha) + G_2 \cos \alpha]}{R \cos(\varphi + \alpha) - G_2 \sin \alpha} \quad (2)$$

A series of  $\alpha$  values were assumed for trial calculation and the one which gives the least value of K was used to determine the plane CD. That K value so obtained was considered as being the safety factor of stability against sliding. In the above expressions,  $\sum V$  is the sum of the vertical forces above the calculation plane AE;  $G_1$  the dead weight of rockmass ABCE;  $G_2$  the dead weight of rockmass CDE;  $f_1$ ,  $f_2$  and  $f_3$  the coefficients of friction for the weak intercalation, the first and second fracture planes respectively, among which  $f_1$  was obtained experimentally while  $f_2$  and  $f_3$  were assumed;  $\theta$  and  $\alpha$  are the angles which the weak intercalation and the first fracture plane make with the horizontal; while  $\varphi$  gives the direction of R (the angle it makes with the horizontal) and is taken to be  $\varphi = \arctan f_3$  here.

In some sections, e. g., the overflow dam section, cut-off were excavated on the upstream side. The concrete of the dam body there is in direct contact with the sandstone below the weak intercalation. For those sections,  $f=0.55$  and  $C=0$  were used in calculation. Since the coefficient of friction for the sliding plane varies from section to section, the total load was distributed to the subsections according to the vertical stresses calculated by the mechanics of materials.

Even if the safety factor was high enough to fulfill the requirement of design specifications, the problem was still not ultimately solved for the theory of limit equilibrium was too simplified to reflect the mechanical behaviour and failure mechanism of a loaded formation so complex as in Zhuzhuang reservoir. For this reason, model tests and finite element computation were also used in design to assess further the stability against sliding of the dam foundation.

#### APPLICATION OF STRUCTURAL MODEL TESTS

This item was mainly carried out in relation to the selection of dam type. Five schemes in total were made for comparison. Only the two intercalations II-5 and Cn72 and the fault  $F_4$  were simulated in our tests.

There are two independent scale factors in the law of similarity for static model tests.

They are:

- (1) the length ratio

$$C_L = \frac{L_p}{L_M} \quad (3)$$

and

- (2) the stress ratio

$$C_\sigma = \frac{\sigma_p}{\sigma_M} \quad (4)$$

where L and  $\sigma$  represent the geometrical dimension and stress while the subscripts "P" and "M" refer to prototype and model respectively. The volume weight of solid and liquid materials has a dimension of  $[\rho] = [\sigma][L^{-1}]$  and hence its scale factor is

$$C_\rho = \frac{\rho_p}{\rho_M} = \frac{\sigma_p L_p^{-1}}{\sigma_M L_M^{-1}} = \frac{C_\sigma}{C_L} \quad (5)$$

Since the problem to be solved in this test was that of the shear failure in weak intercalation and surrounding rock, the condition of strength similarity should be

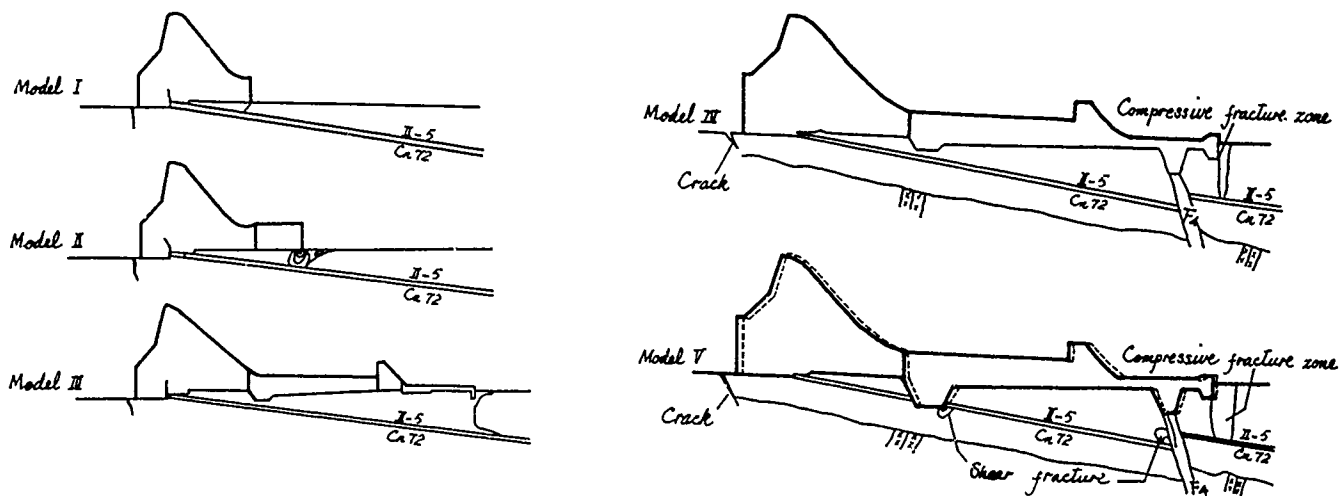


Fig. 5 The mechanism of failure of test models

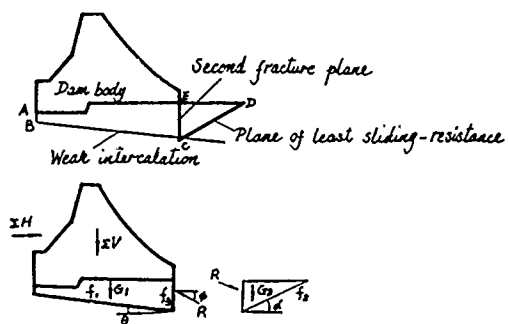


Fig. 4 The force system for limit equilibrium calculation

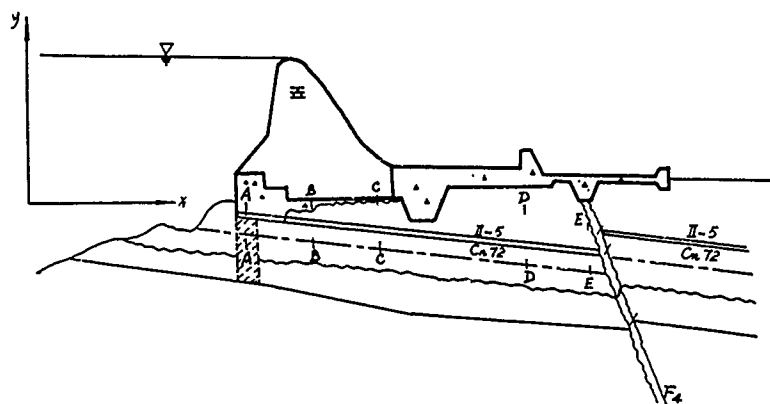


Fig. 7 A schematic diagram showing the sections for computation

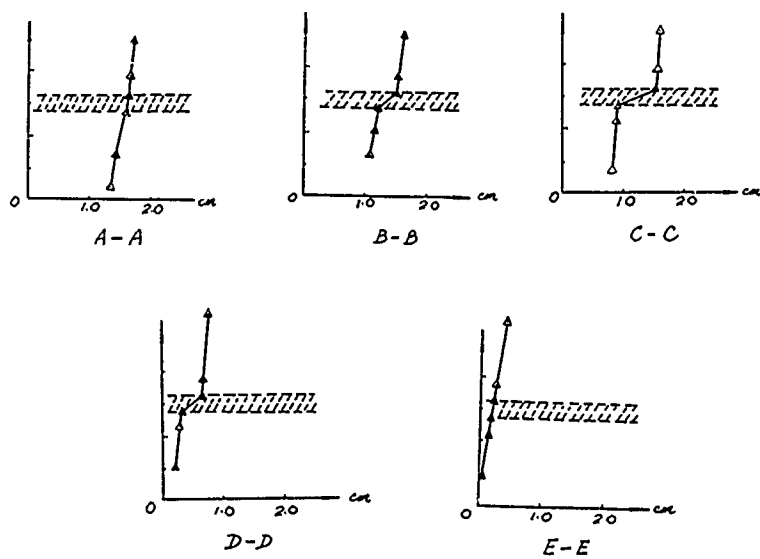


Fig. 8 Displacement distribution in the intercalation along sections A-A, B-B, C-C, D-D, and E-E, where shaded areas show the position of intercalations II-5 and Ca 72

satisfied. The strength ratio is just  $C\sigma$ , i. e., all the compressive, tensile and shear strengths must have a ratio of  $C\sigma$ . The model of Zhuzhuang dam only simulated the shear strength of weak intercalations.

The values of  $C$  for intercalations II-5 and Cn72 obtained from in-situ tests were very small and hence were taken to be zero in the model. Furthermore, since  $f$  is dimension-less, the law of similarity can be satisfied by the shear strength of intercalations provided  $f_p = f_M$ .

$$[\tau] = C + f.$$

The strength of the host rock and the deformability of the intercalation were not simulated. The lower and upper limit safety factors  $K_1$  and  $K_2$  were obtained from the overload capacities for the initial sliding and limiting state. Among them,  $K_1$  had a higher level of approximation than  $K_2$ .

Five models were made. They were (see Fig. 5): Model I: in the foundation of the dam type originally designed before finding II-5 and Cn72, cut-off passing through these two intercalations was excavated in front of the dam; Model II: the same as model I except that the dam back was thickened; Model III: underflow-overflow scheme; Model IV: developed from model III with fault  $F_4$  stabilized by fault plugs and shallow cut-off excavated at the heading part of the apron; Model V: it differed from model IV in that a deep cut-off cutting out the two intercalations was excavated at the heading part of the apron.

The degrees of safety for the five schemes mentioned above are listed in Table 1 where the safety factor is the ratio of the actual to the design load and the lower and upper limit safety factors refer to the overload factors when the intercalation begins to slide and reaches its limiting state respectively.

Table 1 Safety factors for the five models

| Test scheme | Lower limit safety factor $K_1$ | Upper limit safety factor $K_2$ | $K_2/K_1$ |
|-------------|---------------------------------|---------------------------------|-----------|
| I           | 0.84                            | 1.72                            | 2.25      |
| II          | 0.96                            | 2.56                            | 2.69      |
| III         | 1.49                            | 5.08                            | 3.41      |
| IV          | 1.79                            | 5.97                            | 3.34      |
| V           | 1.84                            | 10.01                           | 5.44      |

Both the lower limit safety factors for model I and II were less than 1. Cracks appeared at the dam heel of both models. The crack was vertical in model I while slightly inclined downstream in model II. Vertical cracks developed in the dam body at the cut-off, i. e., where the host rock changes its shape abruptly. The crack in model II was deeper. The downstream rockmass above the weak intercalation ruptured completely.

Models III to V were all underflow overflow schemes. Model III did not simulate the fault  $F_4$ , while models IV and V lowered the dam height by 10m. The lower limit safety factors for all these three models were greater than 1 and model V showed the highest potential safety.

In model III, a vertical upward crack first developed in the dam body where the host rock changes abruptly, then cracking took place at the dam toe and finally the host rock above the intercalation ruptured at the end of the apron.

The modes of failure of models IV and V are shown in Fig. 5. In model V, obvious overall movement of the host rock between the middle cut-off and fault  $F_4$  was observed

when ultimate failure took place. This indicated that by excavating a deep cut-off at the middle part to cut out the two intercalations, the integrity of the rockmass above II-5 was increased and hence a greater portion of horizontal thrust was transmitted downstream by the rockmass below Cn72. It was found from the model deformation measured at the heel (Tab. 2) that the deformation of model V was less than that of model IV. In Tab. 2,  $P_0$  denotes the design load and  $P$  the load actually applied to the model during test. In the elastic range, deformations in the two models were very close to each other. However, after the primary cracking, the difference between the deformations in two models was not proportional to their load increments. In a certain extent, this was related to the nonlinearity of materials, but the main reason was that the fracture surfaces in two models propagated in different manners after initiation.

Table 2 Displacements at the dam heel of models IV and V

| Model | $P/P_0$ | Heel displacement (mm) | Remark           |
|-------|---------|------------------------|------------------|
| IV    | 1.00    | 0.034                  | Primary cracking |
|       | 1.79    | 0.060                  |                  |
|       | 2.42    | 0.123                  |                  |
|       | 2.93    | 0.177                  |                  |
|       | 3.79    | 0.802                  | Ultimate failure |
|       | 5.97    | 2.000                  |                  |
| V     | 1.00    | 0.032                  | Primary cracking |
|       | 1.84    | 0.054                  |                  |
|       | 2.73    | 0.103                  |                  |
|       | 3.52    | 0.175                  |                  |
|       | 6.03    | 0.473                  | Ultimate failure |
|       | 10.01   | 5.000                  |                  |

#### APPLICATION OF FEM

Triangular elements were used for the dam foundation. The weak intercalations II-5 and Cn72 were treated as layered media, i. e., in the normal direction of the layer, only compressive stress can be transmitted whilst tensile stress can not exist and the shear stress transmitted by the clayey intercalations can not exceed  $|f\sigma_n|$ .

The elastic stress field  $\{\sigma_0\}^e$  was computed first by considering the layered media as being homogeneous and elastic. Then the result was compared with the strength criterion of the clayey intercalation. There were three possible cases, namely,

(1)  $\sigma_{oy}' > 0$ , the intercalation was broken by tension and thus lost its ability of transmitting shear stress;

(2)  $\sigma_{oy}' < 0$  and  $|\tau_{ox'y'}| < -f\sigma_{oy}'$ , the layered medium was in its elastic range and the result of first computation gave the solution of the problem.

(3)  $\sigma_{oy}' < 0$  and  $|\tau_{ox'y'}| > -f\sigma_{oy}'$ , the shear stress was higher than the limit value and was actually impossible. The actual state of stress ought to be

$$\{\sigma_t\} = \begin{Bmatrix} \sigma_{ox}' \\ \sigma_{oy}' \\ |f\sigma_{oy}'| \end{Bmatrix} \quad (6)$$

In this case, adjustment of the difference between the computed and actual stresses

$$\{\sigma\}^e = \{\sigma_0\}^e - \{\sigma_t\}^e \quad (7)$$

was necessary.

Using the initial stress method for solving nonlinear problems, linear equations

$$\{\delta_i\} = [K]^{-1} \{R_i\} \quad (i=0, 1, 2, \dots) \quad (8)$$



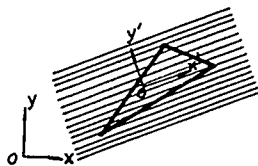


Fig. 6 Coordinate systems for finite element analysis

were solved first.  $\{\delta_0\}$  was obtained using actual applied load  $\{R_0\}$ ,

$$\{\delta_0\} = [K]^{-1} \{R_0\} \quad (9)$$

and the elastic stress  $\{\sigma_0\}$  was computed. The calculated  $\{\sigma_0\}$  was compared with the above-mentioned judging standard and the corresponding stress difference  $\{\sigma'_0\}$  was obtained. Then the unbalanced equivalent nodes forces were computed by

$$\{F_0\} = \int [B]^T \{\sigma_0\} t dx dy \quad (10)$$

and iteration was repeated using the same procedure by

$$\{\delta_1\} = [K_0]^{-1} \{R_0 + F_0\} \quad (11)$$

until

$$\{\delta_n\} = [K_0]^{-1} \{R_0 + F_n\} \quad (12)$$

resulted in a displacement difference

$$\{\delta_n\} - \{\delta_{n-1}\}$$

less than the permissible deviation.

In computation, 11 materials of different properties were used and some 900 elements were divided (Fig. 7) which were the main part of the computed region. It was known from the result of computation that horizontal tensile stress occurred in most elements within in the dam heel zone. Owing to the low tensile strength of the rockmass, cracks with high dip angles developed especially in the dam foundation. Therefore, in the first adjustment, cracking along a certain interface between elements was assumed (cracking along a vertical interface at the dam heel was assumed in actual computation). Along that interface, original nodes were replaced by twin-nodes while the interface was considered as a free boundary.

By using the above two methods to treat the intercalations and the dam heel zone in tension, stress distributions in the dam foundation for a number of load combinations were computed. The occurrence of tensile stress at the dam heel was consistent with the cracking in test models. As for the slip in intercalations, no complete data were available for comparison. In computation, the initial slip often occurred between the dam heel and toe. The location of initial slip was not recorded in model tests. According to the modes of ultimate failure, it seemed that the slip in intercalations was greater in the upstream side than in the downstream. The result of stress computation showed that the deformation of the weak intercalation was greater in its upper part than in the lower part. In particular, the slip between the upper and lower parts in section C-C was the greatest (see Figs. 7 and 8). On the curtain (A-A in Fig. 8) and near the fault F4, the deformation in the upper and lower parts of the weak intercalation varied linearly. This fact implied that no slip took place there. The result of computation indicated that for the calculated sections (corresponding to model IV in Fig. 5), the dam foundation was in a stable state under the action of design load.

The stress field computation by FEM is very beneficial to the selection of dam site and directive for the dam foundation treatment. However, when using it to analyze

the stability of against sliding of dam foundations, there are still some problems need to be studied further. At present, the criterion for judging the stability against sliding has not been well established yet. Some ones use the ratio of the total sliding-resistance capability ( $\sum f\sigma + LC$ ) and total sliding force ( $\sum T$ ) to determine the safety factor, while others use the vertical and horizontal loads regardless whether the weak intercalation slides or not. For the Zhuzhuang reservoir, its stress field was computed by the above-mentioned nonlinear FEM while its stability against sliding was still assessed by the ratio of the total sliding-resistance to the total sliding force.

According to the result of model tests, the safety factor of the stability against sliding for the dam type of model III was high enough to fulfill the design requirement. However, after a comprehensive consideration based upon the analyses of limit equilibrium and FEM stress computation, the dam type of scheme IV was decided with its dam height 5m lowered, i. e., the actual dam height for the finally selected scheme was 95m.

#### DISCUSSION ON THE SAFETY FACTOR OF AGAINST SLIDING STABILITY

The overloading factor was used as the safety factor in model tests.  $K_1$  is an overloading factor for the clayey intercalation to slide, or the lower limit safety factor; and  $K_2$  is an overloading factor for the foundation to lose its load-bearing capacity due to failure, or the upper limit safety factor.

In principle, according to the theory of limit equilibrium, values of  $C$  and  $f$  should be determined from the ultimate strength criterion. The safety factor estimated from them is the upper limit safety factor  $K_2$ . Though  $K=1.1-1.0$  ( $K=1.0$  is allowable for some special load combination) has been specified in the design specifications of China, it is insufficient to insure the safe operation of the dam foundation and hence the strength parameters have to be modified. In our design, values of  $C$  and  $f$  were determined from the yield criterion. In addition to the yield criterion, there are also many other prevailing criteria for evaluating  $C$  and  $f$ , such as these of the proportional limit, residual strength, test body uplift, maximum displacement, rheological strength, etc.. So many methods of evaluation have caused serious difficulty and confusion for the choice of strength parameters.

The FEM is a powerful tool for stress analysis. However, it has not yet been brought into full play in assessing the stability against sliding. In fact, it has become possible to determine the lower limit safety factor  $K_1$  from stress distribution. With increasing understanding about the process of sliding failure of layered rock formation and with the establishment of proper mechanical models, it will also be possible to calculate the upper limit safety factor  $K_2$  which can reflect the actual status better than limit equilibrium analysis.

In view of the permissible working conditions of the foundation, it is relatively reasonable to control the shear stress in the clayey intercalation so that slip can not take place in it. Meanwhile, since the failure mechanism of the dam toe is still not very clear, to use the lower limit safety factor  $K_1$  can avoid the disadvantage of assuming a failure mechanism arbitrarily. In the future, even when the upper limit safety factor can be computed rather accurately and reliably by simulating the failure process step by step, the lower limit safety factor will still be one of the basic parameters for assessing the safety of dam foundation.

Since the limit equilibrium method is the recommended method in design specifications of gravity dam in China, its reasonable use should be limited to the determination of the upper limit safety factor  $K_2$ . A question arising here is that when a certain stress leading to the initial sliding of the clayey intercalation is used to calculate the lower limit safety factor  $K_1$ ,

$$K_1 = \frac{f(\sigma_n - u) + c}{\tau} = 1.1 - 1.0, \quad (13)$$

what a value should be assigned to  $K_2$  so that it can match  $K_1$ ? In eq. (13),  $\sigma_n$  and  $\tau$  denote the normal and shear stresses in the claysy intercalation and  $u$  the water pressure in cracks. It was the model test which gave us some inspiration. Table 1 gives the overloading factors for initial sliding and ultimate failure of the five dam types. It can be seen that  $K_1 < 1$  and  $K_2/k_1 > 2$  in dam type II while  $K_1 > 1$  and  $K_2/K_1 > 3$  in dam type III. Inferring from these limited preliminary results,  $K_2$  should lie around 3 when  $K_1$  is taken to be 1.1 - 1.0.

Therefore,  $K_2$  can be considered as being in the range of 4 - 2, i. e.,

$$K_2 = \frac{f(W - U) + CA}{H} = 4 - 2, \quad (14)$$

where  $W$  and  $H$  are the vertical and horizontal components of the total load,  $U$  the buoyant force and  $A$  the area of clayey intercalation.

Owing to the limited data of model tests and to the lack of systematic data concerning the strengths for initial fracture and ultimate failure in direct shear tests, taking  $K_2 = 4 - 2$  was only based on our understanding at that time.

#### CONCLUSIONS

For analyzing the stability against sliding of dam foundations, the limit equilibrium method is simple and straightforward but too simplified to take many complicated geological factors into consideration. Model tests can provide directly visible phenomena and are convenient for studying the possible modes of failure and load-bearing capacity of dam foundations. However, because the stress-strain relationship of the weak intercalations was not simulated in our models, the test result was still an approximation. The FEM can be used to compute the stress field and to examine the relative shear deformation in weak intercalation, but there are still some difficulties when using it to assess the stability against sliding of dam foundations. For the dam discussed in the present paper, various schemes of the dam type were compared through model tests, the safety factors for stability against sliding were determined by limit equilibrium analyses and stress and deformation of the dam foundation were computed by the FEM. On these bases, the dam type and height were decided and the safety of stability against sliding of the dam foundation was insured. The dam has worked in a good state for 10 years.

#### REFERENCES

- Zienkiewicz, O. C. et al., "The Finite Element Method in Engineering Science" McGraw-Hill, 1971.
- Lu Jiayou, "Some problems related to stability analysis of a dam on layered rock foundation" Chinese Journal of Geotechnical Engineering, V. 2, NO.1, 1980.
- "Collected Research Papers for Application of Computer in Hydropower Engineering" Water Resources and Electric Power Press, 1977.

# Ground Failure Investigation over Abandoned Coal Mines: A Case Study

**Marlo G. Karfakis**

Assistant Professor of Mining Engineering, University of Wyoming,  
Laramie, Wyoming

**Bruce A. Suprenant**

Associate Professor of Civil Engineering, University of South Florida,  
Tampa, Florida

**SYNOPSIS:** The slurry backfill operation for the Rock Springs subsidence control project is briefly described. The extent of ground failure and building damage is presented. The scope of the ensuing geotechnical investigation to indicate any possible cause and effect relationship between the pumped slurry backfill operation and observed damage is described. The general and specific findings regarding the damaged area are discussed. Conclusions from the investigation are presented.

## INTRODUCTION

Development of the City of Rock Springs, Wyoming, as a coal mining community began in the 1860's with the westward expansion of the Union Pacific Railroad through Southern Wyoming. What were once coal mine camps, built over or near abandoned coal mines, is the community of Rock Springs. Approximately 900 acres within the Rock Springs city limits were undermined by room-and-pillar coal mining, between 1869 and 1934, to meet the railroad's demand for coal. This method, compounded by the later removal or "robbing" of pillars, left insufficient support for the mine roof in many areas, which has resulted in the collapse and upward migration of mine voids (Karfakis et.al., 1987). Historical records indicate that subsidence has occurred in Rock Springs from the start of mining to the present day (Case, 1986). Collapse of these abandoned workings has caused extensive damage.

Rock Springs mine subsidence problems qualify for the highest priority of funding under the Surface Mine Control of Reclamation Act of 1977, in that they constitute extreme danger to public health, safety and properties. In order to stabilize the undermined areas and reduce the probability of further mine subsidence, a large scale backfill project was undertaken. The Rock Springs Subsidence Control Project began in March, 1985. In mid-September, during the slurry injection, ground movement and building damage was reported. A geotechnical investigation was undertaken to evaluate and establish the potential cause or causes of damage to the residences and indicate any possible cause and effect relationship between the pumped slurry backfill operation and observed damage.

## PUMPED-SLURRY BACKFILLING OPERATION

The method used to backfill the mine voids in the Rock Springs Subsidence Control Project was the pumped-slurry method of hydraulic backfilling (Colaizzi and Bithell, 1986; Colaizzi, et.al., 1981). In this process, a homogeneous mixture (slurry) of water and granular material is pumped from a remote plant site to the injection hole. The free falling slurry moves through a vertical steel casing to be deposited in subsurface voids (Fig. 1).

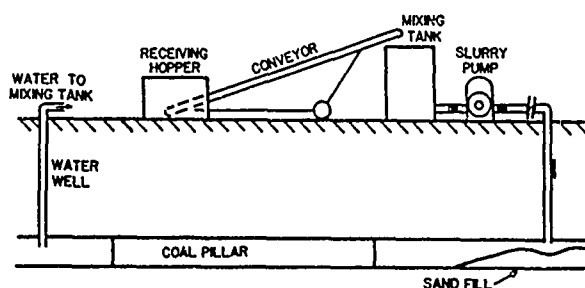


Fig. 1 Slurry Pumping System (Colaizzi et.al., 1985).

The degree of void filling is a function of the velocity of the slurry flow at the mine level. As the slurry first enters the mine void from the injection borehole, its velocity is greatly reduced due to the increased cross sectional area of the transporting conduct (Fig. 2). This

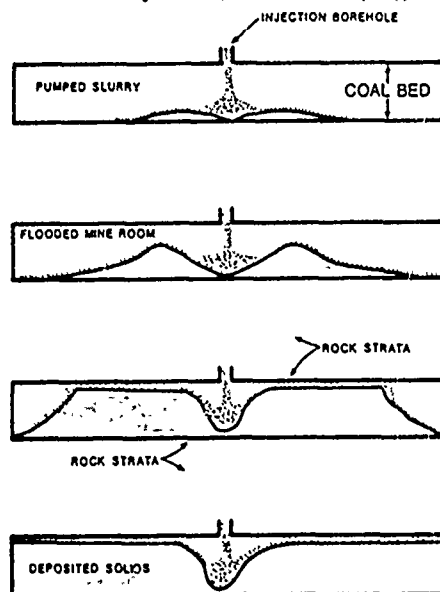


Fig. 2 Section View of Slurry Deposition (Colaizzi and Bithell, 1986).

rapid drop in velocity causes the solid particles to be deposited to form a doughnut-shaped mound on the mine floor. As the height of the mound approaches the mine roof, the velocity of the slurry increases through the narrowing channels, and the solid particles are transported to the outer limits of the mound. At the boundary of the mound, the velocity decreases abruptly and the solids are deposited on the advancing face of the pile. The process continues until the energy required to maintain the flow of the suspended particles becomes greater than the energy supplied by the available gravity head.

The Rock Springs Subsidence Project began in March 1985, with exploratory and water well drilling. In the following three months, the slurry plant was erected, pipelines were laid, and injection wells were drilled and cased. In mid-June, the slurry injection began. In mid-September, during the slurry injection, ground movement and damage to residential buildings were reported in the Adams Avenue area.

### SURFACE DAMAGE

The Adams Avenue residences exhibited architectural damage and some moderate to severe structural damage. The architectural damage usually consisted of vertical and diagonal cracking at window and door openings and at sheetrock joints; horizontal stairwell cracking of plaster covering wood sill plates; and mis-aligned doors and cabinets.

The structural damage was usually concentrated at basement level. The most common problem being vertical, horizontal and diagonal foundation wall cracking. A few cracks were as wide as 1 1/2 inches. Most of the observed foundation wall cracking was less than one-quarter inch wide.

The damage at the Adams Avenue area was evaluated to indicate possible causes. Most of the damage at the Adams Avenue residences was consistent with a downward movement of the structure.

Cracks in buildings caused by settlement are found predominantly at the basement of one story homes. This is because floors, roofs and walls interact to decrease crack widths in upper stories. By contrast, cracks due to construction practices and poor materials tend to increase with the structure height. More and wider cracks were observed in the basements, also supporting the conclusion of downward movement.

### GEOTECHNICAL INVESTIGATION

Rather than evaluating pre-conceived ideas or thoughts as to the cause of surface damage at Adams Avenue, it was deemed preferable to evaluate each potential cause of vertical movements.

Vertical ground movements can be the result of surface erosion, frost action, collapsible soils, shrinking and swelling soils, fluid extraction and consolidation, densification by vibration, bearing capacity failures, settlement under surface loads and mining subsidence (GAI Consultants, Inc. 1983).

Positive identification of the mode of ground movement could be helpful in identifying its source. Subsurface exploration, ground surveys, instrumentation and testing may be required. Also, it is important to recognize that due to the complexities of soil structure interaction, the building movement is not necessarily the same as that of the ground.

An investigation was undertaken to evaluate and establish the potential cause or causes of damage to the residences and indicate any possible relationship to the pumped slurry backfill operation.

The extent of surface damage was assessed. Crack movements were monitored and measured. Surface ground cracks were surveyed and mapped (Fig. 3). Rotary and core drilling was performed around the affected area and the residences reporting damage. Boreholes were inspected with a video camera. Soil and rock samples from coring were tested.

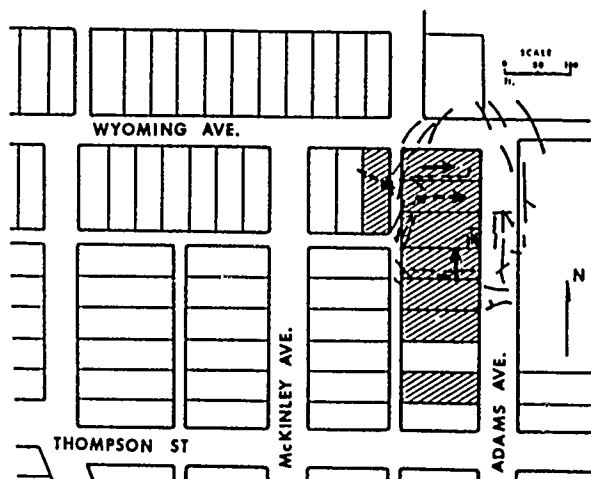


Fig. 3 Surface Damage Adams Avenue Area.

In light of all the information gathered, except for mine subsidence, all possible sources of ground movement were eliminated as the cause of the observed surface damage. The evidence obtained from the investigation indicate that the most conceivable cause of movement at Adams Avenue was mine subsidence (University of Wyoming, Suprenant, 1985).

The area surrounding the Adams Avenue area is undermined at a depth of approximately 90 ft. This mine is in a coal seam which is seven to eight feet thick, dipping at 6°, and was mined by the room-and-pillar method. The mine map in this area is ambiguous, showing only that the area is mined out. Nevertheless, based on data collected through drilling, video camera interpretation, and study of the mine map, it is believed that the area of Adams Avenue overlies a room-and-pillar section. The extent of mining in this pillar section probably varies from 60% extraction to near total extraction.

Subsidence above abandoned room-and-pillar mine workings is either chimney or through subsidence (Karfakis 1987). In the Adams Avenue area, it

was determined that subsidence was a through subsidence (University of Wyoming, Abel, 1985).

Through subsidence develops when several pillars fail in the underlying workings. Normally, pillars of sufficient size are left during room-and-pillar mining to prevent their failure. However, pillar failure may occur as the result of long-term pillar deterioration, increased pillar height accompanying roof collapse, or as the result of load redistribution due to boundary condition changes.

The Adams Avenue subsidence event developed a nearly classic mining induced subsidence trough, i.e. an ovaloidal surface fracture pattern (Fig. 3). The size of the ovaloid defined by tensile surface cracking indicates a pillar failure area in the mine approximately 100 ft. wide and 260 ft. long.

Using the NCB (1975) and the Abel and Lee (1984) method, room and pillar subsidence strain predictions were performed (University of Wyoming, Abel, 1985). The predicted maximum super critical vertical surface subsidence was 12.4%, corresponding to 1.0 ft. vertical displacement, and the maximum predicted tensile strain was 7220  $\mu\text{E}$ .

The predictions appear reasonable in terms of the Adams Avenue observations and measurements.

The next task of the investigation was to determine if a reasonable interpretation of all factors indicate a cause and effect relationship between the slurry backfill operation and the subsidence event.

#### CAUSE AND EFFECT RELATIONSHIP

The backfilling operation in the vicinity of Adams Avenue stopped on September 17, 1985. The first damage report was made two days later on September 19, 1985.

The first step in assessing a cause and effect relationship between the slurry backfill operation and the subsidence event is to determine first, whether the slurry was present under the affected area and second, how the slurry may have triggered the subsidence.

The slurry injection hole location with respect to the subsidence site is critical to slurry backfill reaching that location.

The nearest injection hole to the Adams Avenue site is SI-8A (Fig. 4). The injection hole is located over a NW-SE entry across the fault pillar. The south side of the fault pillar has about 40 ft. of upthrow. The mine floor elevation at this location is approximately at 6320 ft. This injection hole received 32,439 tons of slurry.

As the slurry is released, the solid particles will be deposited equally in all directions until the energy required to maintain the flow of the suspended particles becomes greater than the energy supplied by the available gravity head (Colaizzi et.al. 1981).

The pressure at the base of hole SI-8A, approximately 90 ft. below the surface, was about 39 psi during active slurry injection.

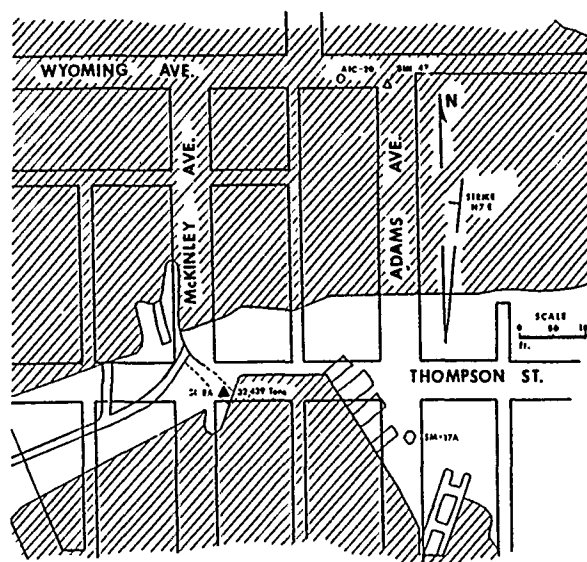


Fig. 4 Mine Workings Overlay.

This pressure is more than sufficient to push slurry 20 ft. vertically, which corresponds to 140 ft. horizontally in the updip direction.

Reports from the pilot backfill project conducted by the Bureau of Mines (Colaizzi et.al. 1981), indicated that flow can occur in a single channel updip over long distances after fill material is deposited up to roof level. Furthermore, hydraulic model studies support the observations made in the field (Carlson, 1975). In the model studies, as deposited, backfill material reached the quantity and pattern to build up back pressure in the injection system, one final break out may occur. A channel would be formed along on unobstructed corridor between rows of pillar. Fill material is carried along this channel in suspension or as bedload according to basic sediment transport principles. With the full flow of the injection pipe discharging along a channel, an equilibrium condition develops for sediment transport. Fill material deposits at intersections to essentially block side corridors and confine the flow along the one channel. Deposits build in the channel until the cross-sectional area reduces and the velocity increases to cause critical transport conditions. In all sloping mine floor models, the breakout channels formed updip. In a dipping mine floor, backfill material will fill up to the roof more rapidly in the downdip direction, presenting greater resistance to channel breakout.

From the above discussion, it is evident that slurry and/or water from the slurry can reach the Adams Avenue area. The next step is to determine the path the slurry and/or water followed to reach the mine workings under Adams Avenue.

As the slurry discharges, in the NW-SE entry, solids would be deposited equally in the downdip and updip direction. On the south side of the fault pillar, the slurry can easily reach the area where blocked entries are shown on the mine map. Based on the drilling experience in the

region, the mine maps proved to be inaccurate. It is possible to have one of these entries crossing the fault pillar to the north side under the Adams Avenue area. Mine floor elevation at the entry on the south side would be at 6330-6340 ft. and on the north side at 6300 ft. updip from the Adams Avenue area. Following this path, it would be possible to have slurry and/or water from the slurry in the mine workings under the area reporting subsidence damage. The inspection hole SMI-47 at the intersection of Adams Avenue and Wyoming Street, which was dry before the start of backfilling, had six feet of water above mine level immediately after the first damage report.

The next question is, what are the mechanisms by which the presence of slurry or water from the slurry could induce subsidence?

The most probable scenario is that collapse chimneys had occurred and stabilized by bulking prior to the introduction to slurry water. When slurry water was introduced, the bulked rubble supporting the roof was softened. Low durability shales and other argillaceous rocks would, under stress, tend to fall apart when water was added. The low durability rock fragment would weaken in water and be crushed under the same stress they were able to carry before water was introduced. The finer fragments produced would tend to filter down into the underlying rubble pile, filling voids between more durable sandstones. This process would shift load onto the coal pillars, potentially triggering pillar failure and subsidence. This appears to be a possible scenario for the Adams Avenue subsidence event in view of the slake durability tests run on the overburden and the presence of rubblized zone in the mine.

Slake durability tests were run on 12 different shale samples recovered from coreholes. One sample exhibited very low durability, five low durability, three medium durability, two medium high durability, and one high durability.

The drill logs before and after the subsidence event indicate the presence of rubble in the Adams Avenue area.

It can be stated that some of the rock formation present in the overburden would tend to deteriorate if stressed or agitated in water and that collapsed roof rock was present. The resulting load transfer could trigger a pillar failure and thereby a surface subsidence event.

The result of the detailed analysis indicate the possibility that the slurry backfilling operation caused the subsidence event at the Adams Avenue site.

## CONCLUSION

The architectural and structural damage exhibited by residences in the Adams Avenue has been caused by mine subsidence. It is possible that the mine subsidence has been triggered by

the water from the slurry. Nevertheless, there is no evidence to prove or disprove the chain of events hypothesized above.

During the investigation, water from inspection hole SMI-47 after the subsidence event should have been analyzed to determine its origin. Furthermore, exploratory drilling should have been done to determine if additional entry ways across the fault pillar were present. These two tasks would have helped in the assessment of cause and effect relationships between the slurry backfill operation and the subsidence event of Adams Avenue.

## REFERENCES

- Abel, J. F., Jr., and Lee, F. T., (1984), "Lithologic Control on Subsidence", Trans. SME-AIME, V. 274.
- Carlson, E. J., (1975), "Hydraulic Model Studies for Backfilling Mine Counties", Bureau of Reclamation, REC-ERC-75-3
- Case, J. C., (1986), "Overview of Coal Mine Subsidence in Wyoming", Proceedings of the Governor's Workshop on Mine Subsidence, ed. M. G. Karfakis, University of Wyoming, Laramie, WY, October.
- Colaizzi, G. J., and Bithell, L.M., (1986), "Methods of Controlling Abandoned Mine Subsidence", Proceedings of the Governor's Workshop on Mine Subsidence, University of Wyoming, Laramie, WY, October.
- Colaizzi, G. J., Whaite, R. H., and Donner D. L., (1981), "Pumped-Slurry Backfilling of Abandoned Coal Mine Workings for Subsidence Control at Rock Springs, Wyoming", USBM, IC 8046.
- GAI Consultants, Inc., (1984), "Survey of Ground Surface Conditions Affecting Structural Response to Subsidence", Bureau of Mines Open File Report 12-84.
- Karfakis, M. G., (1987), "Subsidence Over Abandoned Coal Mines - Mechanisms and Prediction", Proceedings of the 23rd Symposium on Engineering Geology and Soil Engineering, Logan, Utah, April.
- Karfakis M. G., Beach, G., and Case, J., (1987), "Subsidence Problems in Wyoming and Their Social Impact", Proceedings of the 1987 National Symposium on Mining, Hydrology, Sedimentology and Reclamation, Springfield, Illinois, December.
- NCB, (1975), "Subsidence Engineer's Handbook", National Coal Board, Mining Department, England.
- University of Wyoming, (1985), Suprenant, B. A., Karfakis, M. G., Edgar, T. V., Basham, K. D., Abel, J. F., Jr., "Investigation of Residential Damage in Rock Springs, WY", DEQ - State of Wyoming, December.

## Case History of Maneri-Uttarkashi Power Tunnel

R.K. Goel

Scientist, Central Mining Research Station, Nagpur, India

B. Singh

Director, Central Mining Research Station, Nagpur, India

J.L. Jethwa

Assistant Director, Central Mining Research Station, Nagpur, India

**SYNOPSIS :** A 8.56 km long circular tunnel of 4.75 m diameter has been constructed under Maneri hydel project on the river Bhagirathi. The tunnel passes alternatively through quartzitic and metabasic rock formations of the young Himalayan terrain. Tunnel excavation was started from four faces, one at the upstream end at maneri, two from an intermediate adit at Heena, and one at the downstream end near Uttarkashi where a 80 MW surface powerhouse is located.

In excavating the tunnel from different faces, the problems of tunnel face collapse with or without heavy ingress of water, cavity formations and large tunnel closures leading to buckling of steel ribs on account of squeezing ground conditions were encountered. In the paper the approach of combating these problems has been dealt in detail.

The predicted values of support pressure obtained from Terzaghi, Barton et al and CMRS approaches have been compared with the observed values of support pressure. The CMRS approach shows promise for better results in both squeezing and the elastic ground conditions.

### INTRODUCTION

A large number of tunnels have been located to tap the vast power potential of rivers flowing from the Himalayas. The Himalayan mountain ranges contain rock formations of different ages and represent a mixed lithology and tectonic activity. This bounty of nature is therefore associated with several tunnelling problems e.g. sudden inrush of water, roof collapses, occurrence of methane gas, squeezing and swelling ground conditions etc.

A 8.56 km long circular tunnel of 4.75 m finished diameter has been constructed through such a geological set-up under Maneri-Bhali Hydel Scheme Stage-I on the river Bhagirathi, a tributary of the mighty Ganga to utilise a head of 184 m for generating 80 MW of power. The tunnel passes alternatively through quartzitic and metabasic (chlorite-schist) rock formations of the young Garhwal-Himalayan terrain. The tunnel excavation was started from four faces, one at the upstream end at Maneri, two from an intermediate adit at Heena, and one at the powerhouse end near Uttarkashi, a place of pilgrimage.

### REGIONAL GEOLOGY, TUNNELLING PROBLEMS AND REMEDIAL MEASURES

#### Regional Geology

The regional geology of the area has been described by Jain et al (1976). The rocks exposed in the area are quartzites, quartzites interbedded with thin bands of slate, chlorite schists, phyllites, metabasics and basic intrusives belonging to the Garhwal group. Towards

the north and north-east of the project area, the formations of the Garhwal group have a thrust contact (main central thrust). Similarly the Srinagar thrust (north Almora thrust) separates these formations from the Chandpur group towards the south and south-west.

The general strikes of the rock masses in different locations are variable. However, some generalisations are made below :

Maneri area : Strike N15° to 20° - S15° to 20°E; dip 25° to 35° towards S70° to 75° W directions

Heena area : Strike N40°E - S40°W; dip 30° to 45° in S 50° W direction

Tiloth end : Strike N20°W - S20°E to N20°E - S20°W; dip 35° to 45° in NE to SE direction

The surface geological mapping of the area between Heena and Tiloth has been done by Jain et al (1976). The individual rock units as observed in the area from north to south are described below :

|                                   |               |
|-----------------------------------|---------------|
| Quartzites                        |               |
| Metabasics                        | Garhwal Group |
| Quartzites with minor slate bands |               |

These lithounits have been intensely folded and faulted due to high tectonic disturbance. The tectonic activity in the area has developed close joints, brecciation and shearing even in quartzites, which are considered competent.

The longitudinal geological cross-section along the original straight alignment and along the alternative alignment No.2 between Heena and

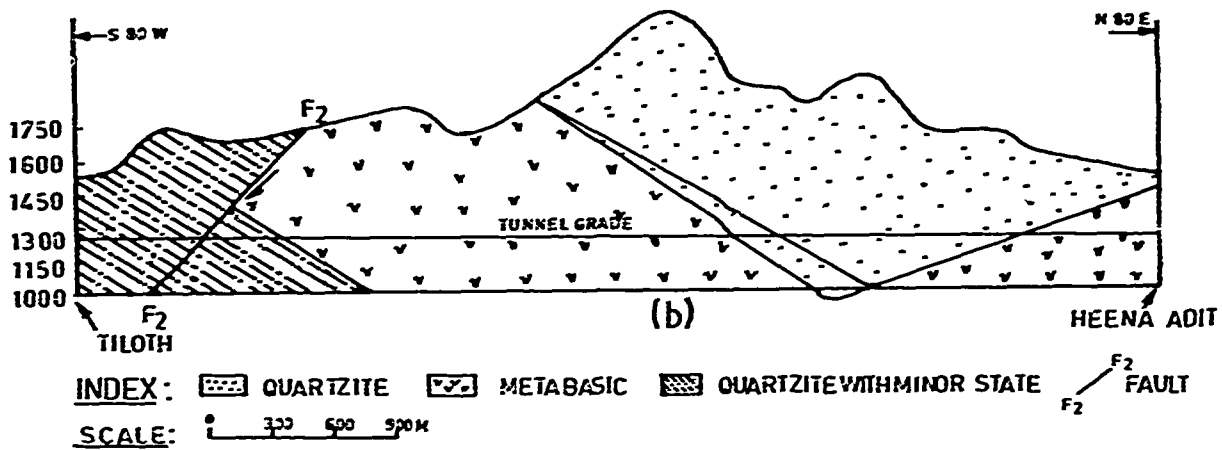
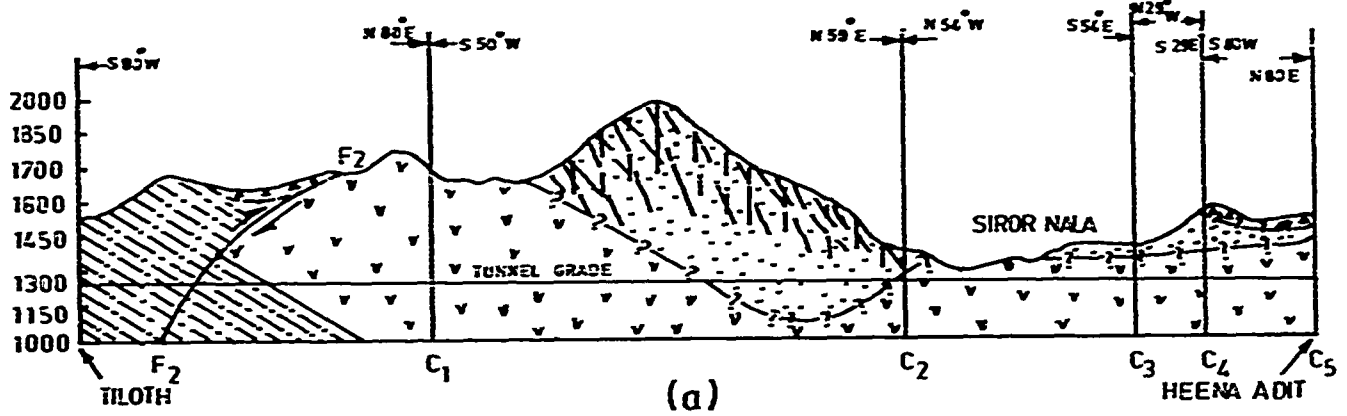


Fig.1 Geological Sections Between Heena and Tiloth along (a) Alternative Alignment No.2 and (b) The Straight Tunnel Alignment (after Jain et al, 1976)

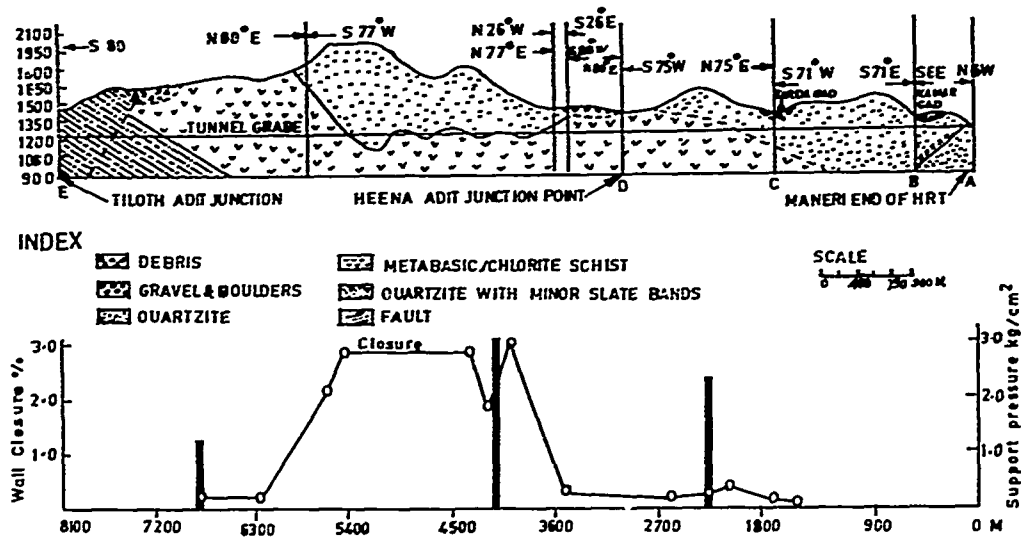


Fig.2 Longitudinal Geological Cross-Section Along the Power Tunnel (after G.S.I.)



Tiloth has been shown in Fig.1, while the longitudinal section along the final alignment has been shown in Fig.2.

#### Tunnelling Problems and Remedial Measures

In excavating the tunnel from different faces, a number of problems were encountered. The major problems were tunnel face collapses with or without heavy ingress of water, cavity formations and large tunnel closure leading to buckling of steel ribs on account of squeezing ground conditions.

#### Water inrush, ch.3549 m

During tunnel driving on the downstream side of the intermediate adit at Heena, the tunnel face collapsed suddenly at ch 3549 m on October 19th, 1974 with a fall of about 300 cum of loose rock with heavy inrush of water at a rate of 6 cusecs. This was followed by sliding of 200 cum of muck exactly two months later on 18th December. The ingress of water, which started at a rate of 6 cusecs in October 1974, stabilised at a rate of 1.28 cusecs in February 1975.

The tunnel passes through basic-metabasic-chlorite-schist type of rocks upto ch 3530 m. Beyond this place the tunnel passed through jointed and blocky quartzites folded in a synclinal form Fig.2. The quartzites occurring in the core of the syncline were bounded by relatively impervious metabasic chlorite-schist formations on both the sides. The quartzites occurring in the syncline were, thus, heavily charged with water, the water head being 80 m. Two cross shear zones of about 40 cm width were intersecting close to the crown of the tunnel (Fig.3). The presence of these two shear zones, their intersections at the tunnel grade and the presence of a water reservoir inside the hill triggered the collapse of the tunnel face and the sliding of a huge quantity of muck with heavy inrush of water. The washings of the drill holes indicated that the material in the shear zones was not groutable with ordinary portland cement.

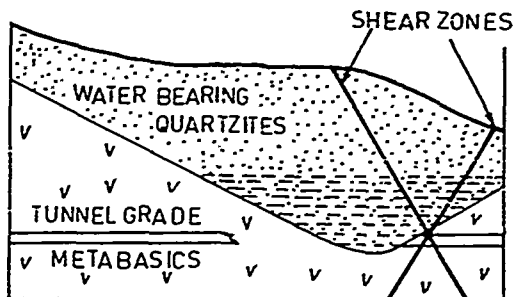


Fig.3 Detailed Sketch Showing the Causes of Water Inrush

It was decided to divert the tunnel alignment slightly to the right side at a distance of about 50 m behind the collapsed face, i.e. ch 3495 m, with an objective to keep the tunnel alignment through the metabasic chlorite schists parallel to the contact plane and then to investigate by deep drilling a suitable place to enter into the quartzite zone and follow the original alignment. It was ascer-

tained that after driving parallel to the contact plane for a distance of about 75 m the quartzites would be suitable for taking grout. It was considered that the tunnel could be driven by umbrella grouting in the crushed quartzite charged with water. The tunnel was, therefore, turned towards the original alignment and the tunnel excavation was continued cautiously with advance probe holes ahead of the tunnel face (Fig 4). When the face reached 5 m from the contact plane, umbrella grouting was done through 16 numbers of 20 m deep and 75 mm diameter drill holes along the periphery of the tunnel face. These holes were inclined at 10° upwards to the tunnel axis. Perforated pipes of 50 mm dia were inserted in the drill holes and the 20 m deep zones around the tunnel was grouted with cement in stages using packers, at a pressure of 35 kg/cm<sup>2</sup> (Fig 5). The probe holes made after grouting indicated that the grouted zone had become a solid mass and there was no in-rush of water through the holes. The tunnel was then driven without difficulty leaving a bulkhead of 5 m in front. While grouting the first group of 16 holes, it was found that the holes in the bottom half

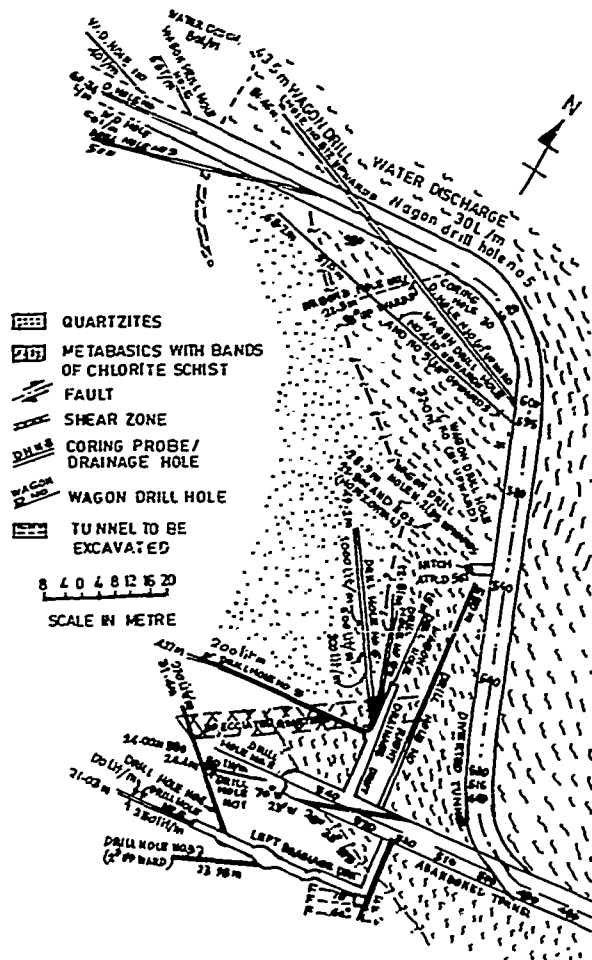
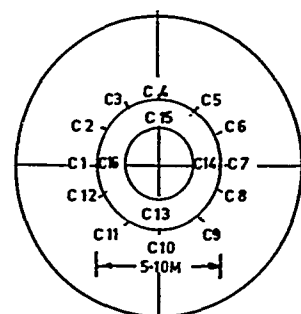
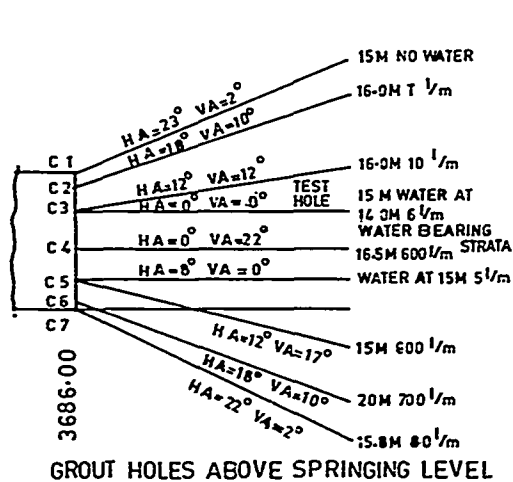


Fig.4 Plan at EL 1266 m Showing the Details of Exploration Work



POSITION OF WASON DRILL HOLES

| DETAILS OF GROUTING |                |
|---------------------|----------------|
| HOLE NO             | CEMENT IN BAGS |
| C 1                 | 14             |
| C 2                 | 1              |
| C 3                 | 5              |
| C 4                 | 36             |
| C 5                 | 100            |
| C 6                 | 26             |
| C 7                 | 37             |
| C 8                 | 16             |
| C 9                 | 20             |
| C 10                | 8              |
| C 11                | 6              |
| C 12                | 2              |
| C 13                | 10             |
| C 14                | 11             |
| C 15                | 8              |
| C 16                | 9              |
| TESTHOLE            | 3              |

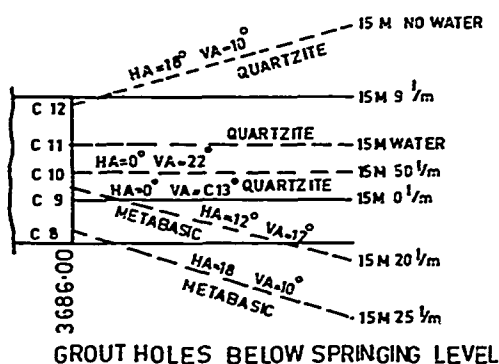


Fig.5 Pattern of Grout Holes

section did not take any grout. Holes only in the top half section of the tunnel were, therefore, drilled and grouted in the subsequent phases of the umbrella grouting operations.

#### Alternate alignments

The tunnelling operations were stopped beyond ch. 3530 m downstreams of Heena because of sudden in-rush of water and loose rock fall. Despite the continuous efforts for six months, the excavation work at this face remains standstill. It was decided to change the tunnel alignment by diverting the tunnel towards the right side from ch 3530 m.

Three alternate alignments (as shown in Fig.6) for diverting the tunnel towards the right side were proposed with the objective of maximising the rate of tunnelling through a safe and better tunnelling media, i.e. through the meta-basic formations. The length of the tunnel in the process increased by 0.47 to 1.85 km but the tunnel length through the highly water charged and fractured quartzites could be reduced by about 280 to 680 m in the case of alternatives I & III and completely avoided in alternative II.

The total tunnel length and the length through water charged quartzites in different alternate

proposal are given in Table-I.

The added advantage in alternatives I & II was that two additional working faces could be obtained.

#### Cavity formation, ch.5038-5055 m

A number of small and big cavities were formed during the excavation of the tunnel. A major cavity was formed during excavation between ch. 5038 - 5050 m. The tunnel grade at ch 5050 crossed a shear zone of crushed quartzites heavily surcharged with water. The total volume of the cavity was estimated as 813 cum. Mucking had to be stopped because of continuous inflow of the muck from the top of the muck pile.

The face was sealed after fore-poling with rolled steel joists. Drainage holes were provided on both sides of the tunnel to drain the seepage water. The cavity above the forepoles was then filled with concrete and grouting was done to control the flow of water and to consolidate the muck. The quantities of concrete and grouting were about 67 cum and 3295 cement bags (each of 50 kg.) respectively. This attempt did not prove effective and, therefore, a side drift was excavated on the left side of the tunnel for draining the seepage water to

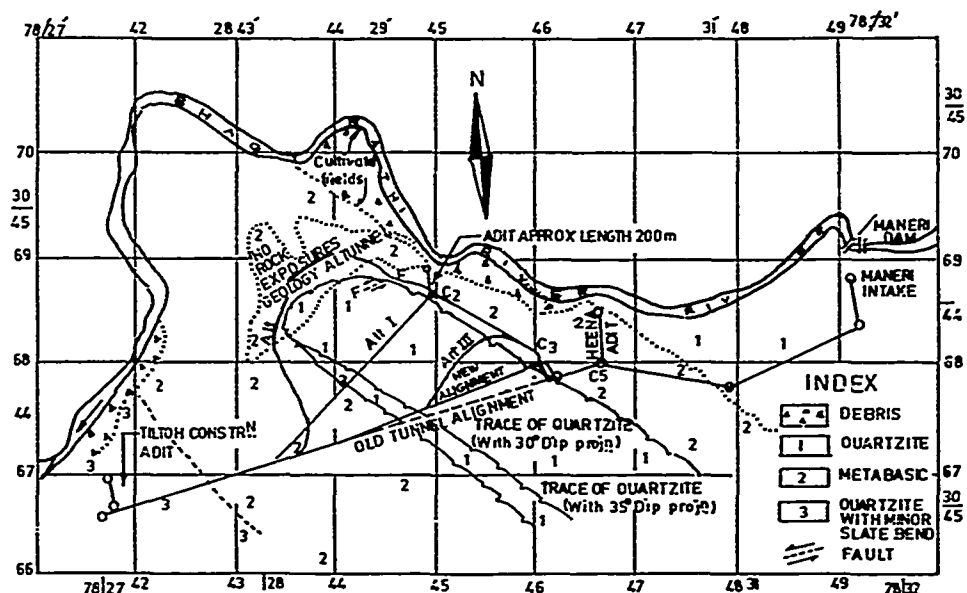


Fig.6 Plan at EL 1250 m Between Maneri and Tiloth Showing Alternative Tunnel Alignments

Table I

| Sl. No. | Proposed layout | Total Tunnel length between Heena and Tiloth, m | Tunnel length through water charged Quartzites, m | Increase in tunnel length, m |
|---------|-----------------|---|---|------------------------------|
| 1.      | Original        | 5065  | 1200  | -                            |
| 2.      | Alternative I   | 5940  | 920   | 875                          |
| 3.      | Alternative II  | 7170  | -   | 2105                         |
| 4.      | Alternative III | 5535  | 920   | 470                          |

the possible extent. This drift met the centre line of the tunnel at ch 4036 m beyond the shear zone where good metabasic rock mass was encountered. The bulkhead at the face was then opened and excavation started in the heading. But, this attempt did not succeed due to inflow of crushed material with water. The face was, therefore, sealed again and some drainage pipes were provided through this bulk head. The muckpile was then grouted. Tunnel construction in this reach was now accomplished by the multi-drift method from the two opposite ends.

#### Squeezing problems, ch.5250-5550 m

Tunnelling activities at depths varying from 700 to 900 m between ch 5550 m and 5250 m through partially wet and thinly foliated metabasics were beset with high squeezing ground conditions. The tunnel was supported by ISMB 150 mm x 150 mm ribs spaced at 810 mm to 965 mm. Blocking concrete was done upto the outer flange of these ribs. No problem was faced during the excavation or the supporting of this tunnel section. However, after a period of 5-6 months, it was observed that the blocking concrete started cracking and the ribs started deforming due to squeezing pressure as shown in Figs.7(a) and 7(b).

For solving the problem of cracking of blocking

concrete and deformation of steel ribs in the squeezing ground the ribs were strengthened with laggings of ISMB 150 mm x 75 mm and blocking concrete was done upto the inner flanges of the ribs. The treatment proved helpful in controlling further deformations of the ribs. However, at the time of providing the final concrete lining in this reach in November-December 1982, nearly three years later, it was found that most of the ribs in this reach had twisted and deformed to such an extent that their removal was considered necessary to obtain the required finished bore. The invert heave was as much as 80 cms. The twisted ribs and the blocking concrete were removed and the rock mass was trimmed and resupported by 150 mm x 150 mm ribs spaced 750 mm apart for obtaining the required finished diameter. This rectification job was completed in the most of the affected length but while removing the twisted ribs between ch 5509 m and 5517 m, there was a heavy rock fall from the roof. A cavity of 430 cum was formed. This cavity was tackled by putting forepoles of 40 mm dia bars, 13 to 15 m long at a spacing of 300 mm centre to centre and grouting the muck above the forepoles at a pressure of 5 kg/cm<sup>2</sup>, thus forming a concrete ring as roof support. Thereafter the tunnel in this portion was reexcavated and supported by ISMB 150 mm x 150 mm ribs spaced 60 cm centre to centre.

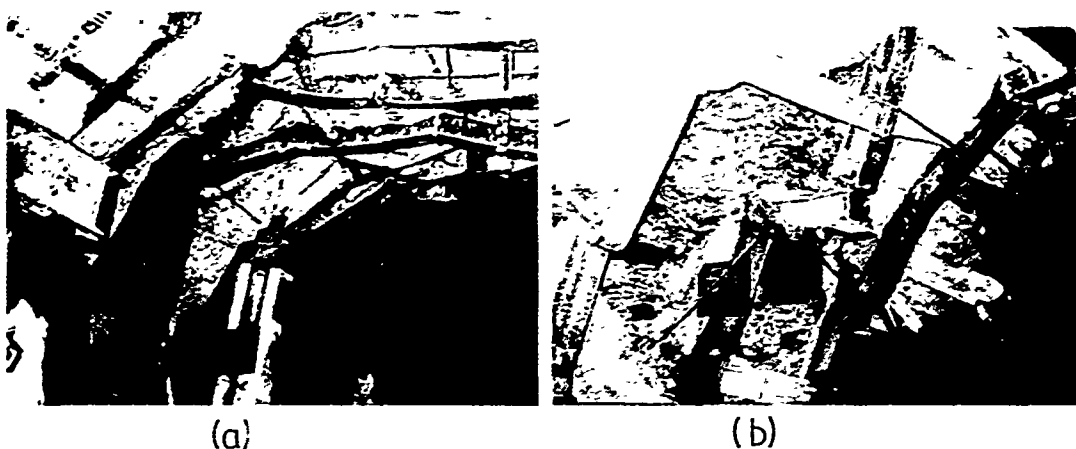


Fig.7 (a) and (b) Buckling of Steel Ribs and Damage to the Blocking Concrete

#### PREDICTION OF TUNNEL BEHAVIOUR

Rock mass classification systems proposed by Terzaghi (1946) and Deere (1969), are based upon qualitative assessment of rock masses. These are at best applicable to hard and fractured rock masses at shallow depths only.

In recent years, efforts have been made to include various other geomechanical factors and to describe the rock masses in quantitative terms. Consequently, a few quantitative classifications have been developed. Notable amongst these classification systems are those of Bieniawski (1973) and Barton et al (1974).

Some modifications in the Barton's classification have been made by incorporating the effects of overburden and tunnel closure, the two factors important in squeezing conditions. A quantitative classification is a useful tool in assessing the quality of rockmass in quantitative terms and hence it is not only possible to compare the probable engineering behaviour, but also to predict the support pressure. However, the reliability of the predictions will depend on the reliability of the geological information. The approaches of Terzaghi, Deere et al, Barton et al and CMRS (Jethwa, 1986) have been used to predict the support pressures and the predictions have been compared with the measured values in Table II.

TABLE II : PREDICTED AND MEASURED SUPPORT PRESSURE (after Jethwa et al, 1981)

| Rock Description  | Predicted Support Pressure, kg/cm <sup>2</sup> |                |                |                | Observed Support Pressure<br>Kg/cm <sup>2</sup> |
|---|--|----------------|----------------|----------------|---|
|   | Tenzaghis                                      | Barton et al   |                | CMRS approach  |   |
|   | P <sub>v</sub>                                 | P <sub>v</sub> | P <sub>h</sub> | P <sub>v</sub> |   |
| 1. Moderately fractured quartzites                      | 0.3<br>to                                      | 1.3<br>to      | 0.8<br>to      | 1.23           | -   |
| a=2.4 m, h=225 m, γ=2.5gm/cc                            | 0.7  | 1.5            | 1.0            |                |   |
| QD=75%, Q=3.6, U <sub>a</sub> /a=0.06%                  | (0.5)  | (1.4)          | (0.9)          |                |   |
| 2. Foliated metabasics                                  | 0.3<br>to                                      | 1.0<br>to      | 0.8<br>to      | 1.56           | 1.22  |
| a=2.4 m, h=550 m, Y=2.5 gm/cc                           | 0.7  | 1.4            | 1.0            |                |   |
| RQD=82%, Q=3.4-6.8, U <sub>a</sub> /a=0.05%             | (0.5)  | (1.2)          | (0.9)          |                |   |
| Thinly laminated foliated and wet metabasics(squeezing) | 5.02<br>to                                     | 1.34<br>to     | 0.99<br>to     | 3.46           | 4.36*   |
| a=2.4 m, h=800 m, Y=2.5 gm/cc                           | 10.8   | 1.69           | 1.24           |                |   |
| RQD=60%, Q=1.64-3.28, U <sub>a</sub> /a=17%             | (7.91)   | (1.51)         | (1.11)         |                |   |
| 3. Sheared metabasics                                   | 0.8<br>to                                      | 1.6<br>to      | 1.0<br>to      | 2.37           | 2.36  |
| a=2.4 m, h=340 m, Y=2.5 gm/cc                           | 2.6  | 3.0            | 2.4            |                |   |
| RQD=60%, Q=0.3-3.3, U <sub>a</sub> /a=0.4%              | (1.7)  | (2.3)          | (1.7)          |                |   |

a = radius of tunnel opening; h = thickness of cover,  $\gamma$  = unit weight of rock mass, RQD = Rock Quality Designation, Q = Barton's rock mass Quality,  $U_a$  = observed tunnel wall displacement,  $p_v$  = roof support pressure,  $p_h$  = wall support pressure, \* = estimated from support capacity; average values of the predicted pressures are shown in brackets.

## OBSERVED TUNNEL BEHAVIOUR

A tunnel instrumentation programme was adopted to evaluate the predicted support pressures and to modify the support as per actual requirements during construction of the tunnel. The instrumentation programme consisted of measuring hoop load on the steel arches by hydraulic load cells and "tunnel closure", defined as reduction in the size of the tunnel opening, by closure meter to an accuracy of  $\pm 0.1$  mm.

The instruments installed were designed and developed at the Central Mining Research Station, Dhanbad (India). The closure bolts and load cells were installed at a few locations as shown in Fig.2.

The data analysis shows that the maximum closure was of the order of 430 mm (8.9 percent) in 600 days at the synclinal contact of metabasics and quartzites at ch. 4180 m (Fig.8). At other locations, the closure varies from 10 mm to 20 mm (0.2 to 0.4 percent) except at ch. 5510 m, where the total closure observed in 100 days was about 105 mm (2.18 percent) at a depth of 750 m (Fig 9). It is clear from Fig.9 that the wall closure increased in stages. This is due to the buckling of the steel ribs. Support pressure estimated from the load-cell data varies from  $1.22 \text{ kg/cm}^2$  at ch.6760 to  $3.05 \text{ kg/cm}^2$  at ch.4140 m (please see Fig.2).

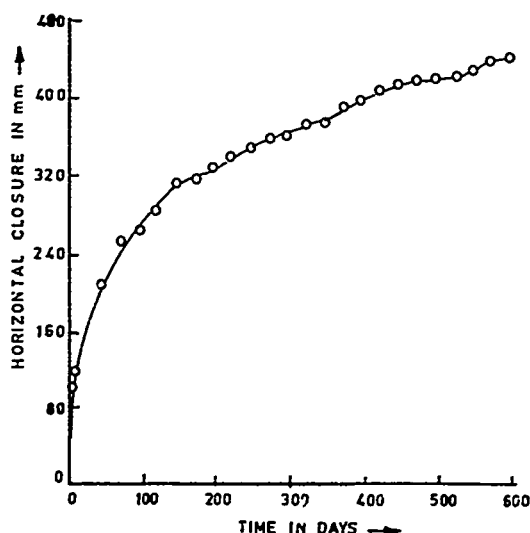


Fig.8 Closure-Time Relation at ch.4180 m

The support pressure of  $3.05 \text{ kg/cm}^2$  could not be predicted because of the complex geological conditions and the presence of an inferior rock mass were not known at the design stage.

The comparison of predicted and observed support pressure (Table II) shows that the predicted values by Barton et al and CMRS approach are more or less equal to the observed values for non-squeezing ground conditions. Unfortunately, no instruments were installed at ch. 5500 m, where the squeezing problems were encountered. However, the back calculation from the

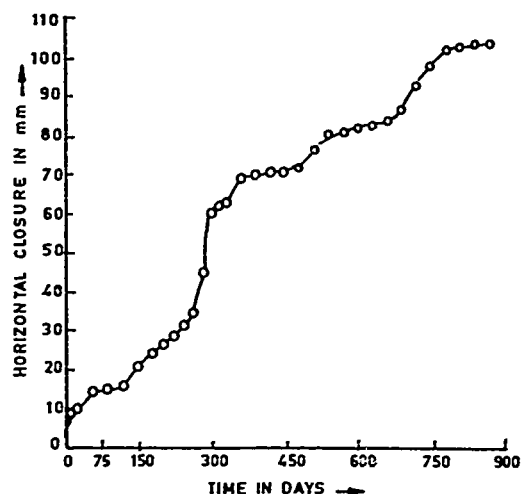


Fig.9 Closure-Time Relation at ch.5510 m

supports shows that the predicted values of support pressure from CMRS approach is nearer to the design pressure for uniform loading (Table II) while Terzaghi's approach is conservative. Buckling of ribs may have occurred due to a possible non-uniform pressure distribution around the ribs.

## CONCLUSIONS

From the case-history of the power tunnel of the Maneri Hydel Project, Stage I and its instrumentation, the following conclusions are drawn :

- i) Inadequate surface and sub surface investigations have been responsible for wrong planning of the tunnel alignment.
- ii) The classification method of Barton et al leads to reliable predictions for non-squeezing conditions only. On the other hand, the CMRS approach leads to more reliable predictions for both squeezing and non-squeezing ground conditions. However, the data is limited to draw generalised conclusions.

## REFERENCES

- Barton, N., Lien, R. and Lunde, J. (1974), 'Engineering Classification of Rock Masses for the Design of Tunnel Supports', Rock Mechanics, Vol.6, No.4, pp 189-236.
- Bieniawski, Z.T. (1973), 'Engineering Classification of Jointed Rock Masses', Trans. S. Afr. Instn. Civil Engrs., Vol.15, pp 335-342
- Deere, D.U., Peck, R.B., Monsees, J.W. and Schmidt, B (1969), Design of Tunnel Liner and Support System, Univ. of Illinois, Report Prepared for the Office of High Speed Ground Transportation, U.S. Department of Transport, Contract No.3-0152.

Jain, M.S., Jaitle, G.S., Sondhi, S.N. and Rajagopalan, G. (1976), Geotechnical Note on the Alternative Alignments Between Heena and Tilothe Adits, Memo., XIV meeting, Board of consultants, Maneri Stage I Project.

Jethwa, J.L. (1981), Evaluation of Rock Pressure in Tunnels Through Squeezing Ground in Lower Himalayas, Ph.D. Thesis, Deptt. of Civil Engg., University of Roorkee, India.

Jethwa, J.L. (1986), Indian Contribution on Rock Mechanics Problems of Tunnels, Proc. All India Seminar on Underground construction, Nagpur.

Singh, R.I. (1986), Tunnelling Problems in Young Himalayan Rocks, Proc. Research-Industry meet on Rock Mechanics in Tunnels, New Delhi.

Terzaghi, K. (1946), Rock Defects and Load on Tunnel Supports, Introduction to Rock Tunneling with Steel Supports by Proctor, R.V. and White, T.L., Commercial Shearing and Stamping Co, Youngstown, Ohio, U.S.A.

## Foundation Investigation and Treatment for the Main Dam, Itaipu Project

John G. Cabrera

Consulting Engineering Geologist, Las Cruces, New Mexico

**SYNOPSIS:** After selection of the site for this major hydroelectric project on the Upper Paraná River, initial borings in the river bed revealed an extremely fractured zone near the base of the dense basalt flow on which the main dam would be founded. This zone was later seen to correspond to intersecting faults beneath the river bed, therefore upon dewatering the river channel several exploratory tunnels were driven parallel and perpendicular to the dam axis, foreseeing their incorporation into an elaborate "shear key" system to prevent renewed movements of the shear zones. The tunnel grid was backfilled with concrete through holes drilled from the foundation surface and grouted at low pressures.

### INTRODUCTION

Itaipu, the world's largest hydroelectric project, is situated on the Paraná River, between Brazil and Paraguay, approximately 14 km upstream from the bridge joining the two countries (Figs. 1 and 2) and consists of a concrete dam and spillway 2,610 m long flanked by embankments totaling 5,150 m in length (Fig. 3). The maximum height of the hollow gravity main dam across the river gorge is 196 m, and over 56 million cubic meters of earth and rock were excavated for the project. The total cost is presently estimated at close to 18.6 billion U.S. dollars.

The Itaipu project is a binational undertaking established by Brazil and Paraguay in accordance with a treaty signed by the two governments in 1973 and the statutes of an entity created a year later, known as "Itaipu Binacional", which determine equal sharing of generated power (Cotrim et al, 1977).

The engineering consortium selected to carry out the feasibility studies, a joint venture of International Engineering Co., U.S.A., and Electroconsult of Italy, began the study of the stretch of the Paraná River between Guaira Falls and the mouth of the Iguacu River with a regional geologic appraisal to characterize the basalt flows and select viable dam sites. This work was aided by the interpretation of satellite imagery and aerial photos to determine the principal structural lineaments and to differentiate soil and rock types.

A general study of various alternatives for locating the dam was made by means of borings and geophysical profiling; this resulted in the selection of a reach of the Paraná in which the project could be situated. More detailed investigations followed to determine the best axis within the reach, considering river channel configuration, proximity of abutments and the lithologic and structural conditions of the

basalt sequence at the various sites. Thereafter an axis was defined by closer-spaced borings and short adits in which rock mechanics tests were made, followed by the sinking of a deep shaft and more detailed in situ tests of the principal discontinuities.

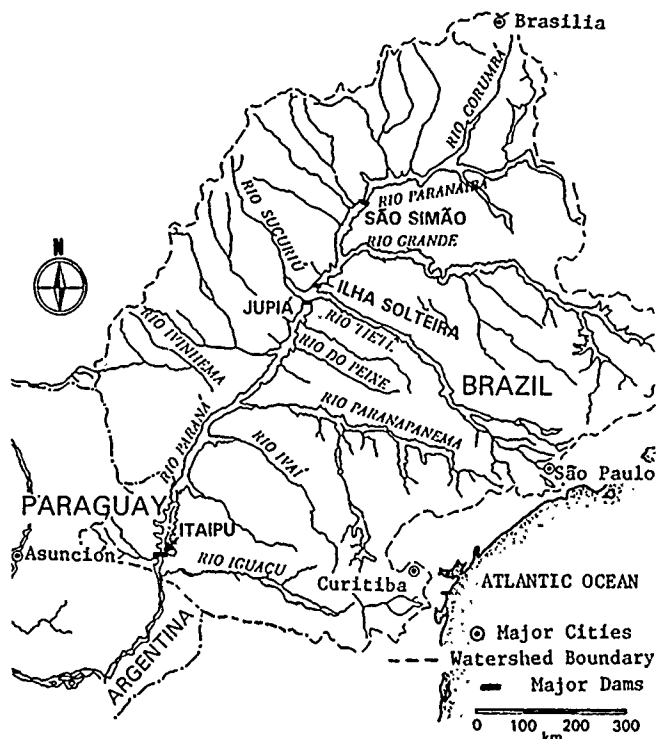


Fig. 1 Site Location Map.

During the construction phase, a program of exploratory tunneling was followed to investigate shear zones encountered beneath the river bed.

From this program an elaborate treatment plan of shear key tunnels was developed to prevent renewed movement along the shear zones.

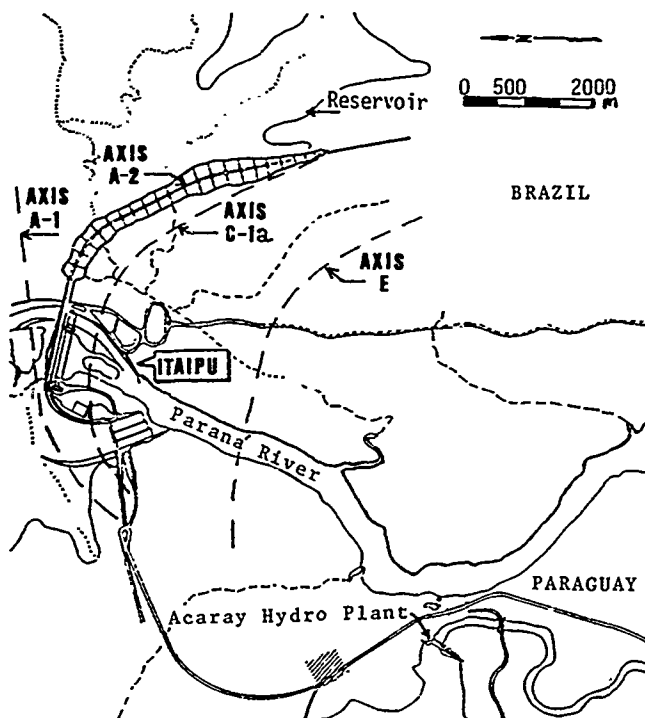


Fig. 2 Locations of Alternative Dam Axes.

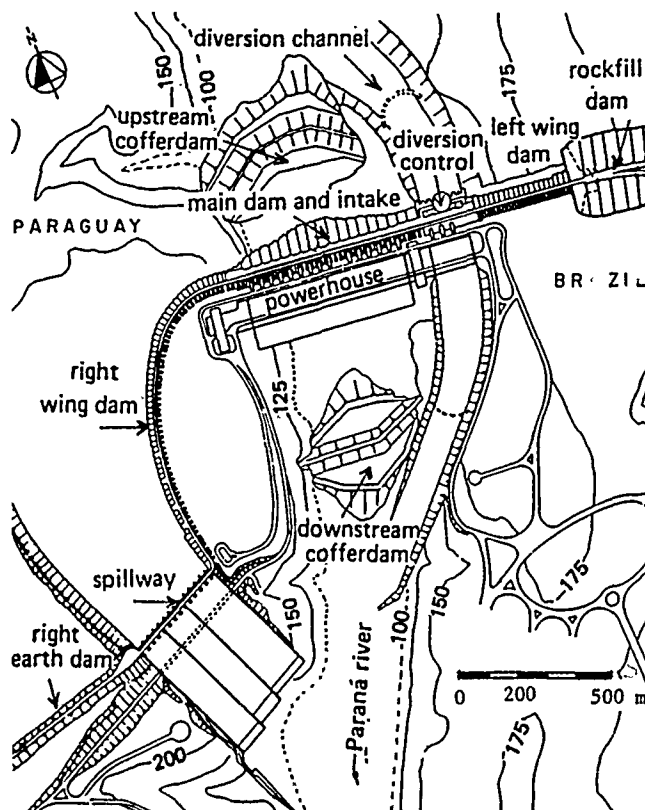


Fig. 3 General Layout of the Itaipu Project.

## SELECTION OF DAM AXIS

Starting at first with eight alternative layout axes, the preliminary borings and geophysical profiles narrowed down the choice to four, namely Axis A-1, just downstream from Itaipu Island, Axis A-2, 300 m farther downstream, Axis C-1a, 800 m downstream from A-1 and Axis E, 3,100 m downstream from A-1 (Fig. 2). The information obtained from pre-feasibility investigations made at or near the four axes indicated that Axis E had the best geological conditions beneath the river bed. However, that axis had the disadvantage of requiring that the spillway chutes be located close to an existing hydroelectric plant in Paraguay, which could be affected by high discharges. It would also have adversely affected the location for the future river navigation facility.

Of the three upstream axes, Axis A-2 was shown to be preferable, chiefly because of a much better river cross section and spillway location.

## SITE INVESTIGATIONS

### Preliminary Investigations - Phase 1

Investigations of the foundation area for the high dam within the deep channel carved by the Parana River began with some preliminary conventional borings in the banks, abutments and on the shallow Itaipu Island itself. The first stage of the studies called for only a few borings and seismic refraction traverses to define rock types at several alternative dam axes. Five basalt flows with interflows of sedimentary breccia were identified during this stage and named, from the bottom up, flows A through E (Fig. 4).

Initially borings were made in 1973 using only a double tube core barrel, consequently, recovery of core in zones of closely-jointed or highly fractured rock was low. It soon became apparent that more accurate drilling methods had to be employed, specially within the river channel itself. Most of the initial river borings encountered difficulties such as:

- Flow velocities of 2 to 3 meters/second, which tended to shift the drilling barge and bend or break casing.
- An average depth of water of 50 m (164 ft) and 10 m to 15 m of relatively loose alluvium at the bottom.
- Sudden variations of water level, which snapped anchoring and guy cables.
- Dense morning mist during the winter months (June-September) which would last until 10 A.M.
- Extreme fracturing of the top of rock in the river bed.
- Strong winds funneled along the narrow valley.

All of the above contributed to slowing down and decreasing the efficiency of borings made in the section for the main dam.



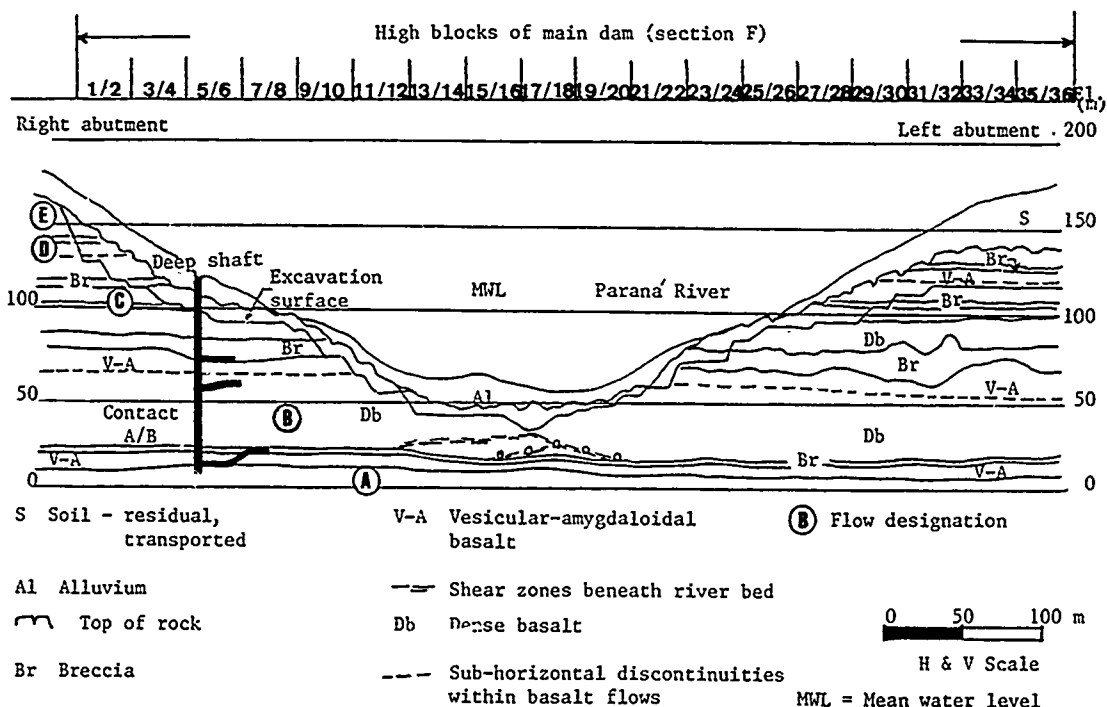


Fig. 4 Itaipu Dam Site. Geologic Section across the River Valley.

#### Investigations - Phase II

Once the axis was selected, a more intense phase of investigations for the feasibility report proceeded. Small adits were driven into inter-flow sedimentary breccia B, overlying flow B, and determinations of elastic moduli and direct shear tests were made to characterize this horizon of relatively weak rock, having an average thickness of 10 m. The new phase of core borings consisted of wireline N diameter holes drilled using double tube core barrels with core lifter sleeves (M series). This improved core recovery somewhat, but not enough to recover soft, altered rock.

Drilling within the river took on a more thorough approach, benefiting from the earlier attempts. The drilling barge had more anchoring points and an 8 inch (20.3 cm) outer casing, well-guyed to the barge's hull, protected a 5 inch (12.7 cm) casing that penetrated the alluvium and in which H and N casings were used during wireline core drilling.

Due to the high degree of fracturing of the uppermost dense basalt in the river bed (flow B) pressure tests gave inordinately high water loss readings, but this was primarily due to difficulties in properly seating the packers as the drill string rocked to and fro with the barge.

The river borings carried out to below flow B revealed a continuous zone of highly fractured rock near or at the base of that flow. It was speculated that this signified the presence of a zone of lamellar jointing. Although core recovery techniques were still not adequate to retrieve all of the material in that zone, it became possible to drill some borings in excess of 200 m depth and determine the conditions of five additional flows below flow A.

#### Investigations - Phase III

It was then decided to drill several integral core borings at both banks to define the fractured zone at the base of flow B and the condition of the open contact with flow A. These were among the deepest borings (100 m) made up to that date (1975) using that technique of core reinforcing. Nevertheless, at the considerable depths where the zone of fragmented rock occurred, binding of the fragments could not be efficiently achieved with cement grout, even using quick setting additives. It was only by using a fast-setting epoxy resin that some core of the weak seams was recovered.

The in situ or residual stresses within the basalt sequence were determined near the location of the main dam by several borings in which overcoring strain measurements were made using a stress tensor gauge (Rocha et al., 1974). It was surprising to find that horizontal stresses had been relieved in proximity to the river channel, whereas normal stresses remained moderately high (to 4.41 MPa).

#### Investigations - Phase IV

A fourth, more intensive phase of investigations was decided upon. This included a deep shaft in the right bank, with short tunnels radiating from it to investigate and test the principal adverse features in situ. The shaft, 4 meters in diameter, was excavated from El. 120 m to El. 7 m and tunnels driven at El. 70 m, 59 m and 12 m. From the latter drift, an upward-sloping tunnel reached the contact between flows A and B, approximately at El. 20 m.

The tunnel at El. 70 m was made to study breccia B and carry out plate jacking and grouting tests. The results indicated an average modulus of elasticity of 6,800 MPa. A part of this

breccia had been grouted from holes made before initiating the shaft and the results could be verified. There was an extremely low grout acceptance in the compact breccia, classified as type I.

The drilling program had revealed the existence of a zone of closely-spaced, parallel fractures in basalt flow B, between elevations 55 and 62 m. The gallery at El. 59 m was raised somewhat and a test niche made at El. 62 m to carry out a series of direct shear tests on blocks measuring 1 m on the side. The discontinuity (named "B") consisted of parallel joints, well-cemented in some areas by calcite or silica, and the average angle of shearing resistance was found to be 35°, with a cohesion of 0.5 MPa.

The most important feature revealed by the deep shaft and the tunnel at El. 20 m was the zone of crushed rock at the base of flow B. This was determined to be a shear zone filled with a mylonite gouge. The zone could only be observed within the short length of the tunnel, which was not continued fearing it could intercept one of the borings made in the river channel, that was not plugged with cement. Therefore, it was decided that a crash program of subsurface investigation would be carried out by tunneling after unwatering the river channel in the foundation area for the main dam.

Three direct shear tests were made at the base of flow B where the sheared basalt could be cut into blocks with a diamond saw without disintegrating it. The angles of shearing resistance obtained were  $\phi = 25.1^\circ$ ,  $26.1^\circ$ , and  $29.2^\circ$ . It should be emphasized that this was a highly fractured, blocky, dense basalt with some clay filling the fractures, not the basalt entirely reduced to a mylonite, (Cabrera and Barbi, 1981).

#### Final Investigations - Phase V

After unwatering and excavating the thick alluvium in the foundation area for the main blocks of the dam, five shafts were sunk to elevations 8 m to 10 m above sea level, that is, 1 m to 9 m below the contact between basalt flows A and B. A sixth shaft was made in the downstream part of the area between the stems of double block F15/16 to investigate and treat a local concentration of highly sheared zones.

In all of the shafts one or two zones of closely-spaced open fractures filled with clay were found. In shaft 13, situated just downstream from the head of double buttress F-15/16, a very thick zone of weathered and highly fractured dense basalt, with oxidized, open fractures filled with clay, was found between elevations 38 m and 31 m.

The river thalweg was being excavated in the powerhouse foundation area at the same time and a zone of lamellar, weathered basalt was found dipping approximately 20° E-SE. This zone was followed upstream along its nearly N-S strike, by ripping and light blasting, and the suspicion that it coincided with the zone encountered in shaft 13 was confirmed. Its extent was further verified by two short tunnels that followed the ascending shear zone westward from shafts 9 and 12. It soon became apparent that several intersecting shear zones traversed the remnant of

flow B in the river channel. While various solutions were being sought, an accelerated program of borings was initiated to determine the distribution and extent of the shear zones. In addition, it was decided to follow those zones, to permit direct observations and more accurate appraisal of the geomechanical parameters by tunneling parallel and perpendicular to the dam axis whenever possible (Fig. 5).

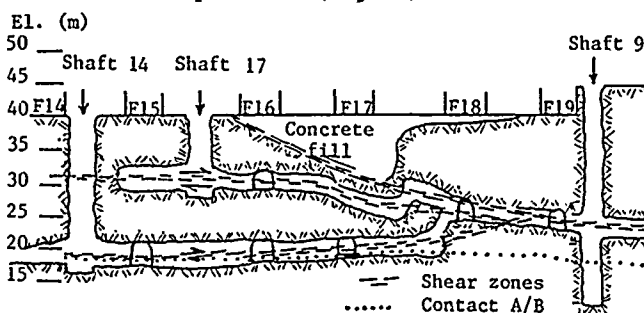


Fig. 5 Section along Axis of Main Itaipu Dam Showing Principal Shear Zones below Foundation Level Followed and Intercepted by Tunnels.

#### DESCRIPTION OF THE SHEAR ZONES BELOW THE RIVER CHANNEL

The borings made from the foundation level and the exploratory tunnels eventually permitted a three dimensional visualization of the relationship among the shear zones within the foundation area for the high concrete dam. When the investigations were completed it was possible to differentiate the zones as follows (Fig. 6):

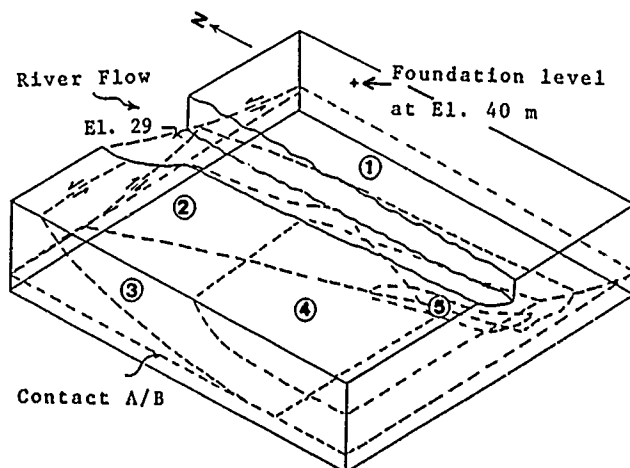


Fig. 6 Block Diagram Indicating Relative Locations of Shear Zones below River Channel.

1. Eastward-dipping shear zone. This is the uppermost shear zone and the first to be exposed along the deepest portion of the river, following the stem of half block F-17. It intercepts the originally proposed foundation level of El. 40 m at the head of half-block F-15, dips  $15^\circ - 20^\circ$  E-SE and varies from very weathered, with a filling consisting mostly of clay at higher elevations, to almost a rock to rock contact of lamellar slabs at the lower levels, close to the contact between flows A and B. Slickensides on the surface of this zone indicated that the rock mass above it was thrust westward, towards Paraguay.
2. Westward-dipping zone. This zone is tangential to contact A/B on the west side of the river channel, as seen in the deep, right bank shaft and the tunnel at El. 20 m. It rises at a low angle until it is intercepted by the eastward-dipping zone. Shear displacements could not be observed on the west side, probably because of a high degree of weathering and considerable clay. Eastward updip displacements of as much as 30 cm were measured.
3. Upstream southward-dipping zone. This zone has the main disadvantage that it dips downstream. It was initially located in shaft 14 at El. 29.5 m. In a downstream direction it tends to become tangential to contact A/B. It consists mostly of crushed rock, with some clay filling between fragments. Proper investigation of this shear zone required an additional shaft (No. 17) from which a short drift followed it eastward to a N-S tunnel that ramped down to the A/B contact.
4. Downstream southward-dipping zone. This zone, with an approximate area of only 40 m by 50 m, was found during the final phase of investigations of the foundation area. Core drilling in an area nearly 46 m south of shaft 17 had revealed another zone of lamellar fragments with a low clay content. As it progresses downstream from El. 35 m and El. 30 m to lower levels, it tends to narrow down and disappear, forming a fault slice imbricated upon the upstream south-dipping zone described above.
5. A fifth, less important shear zone was found at the downstream portion of the high dam foundation area.

#### GEOMECHANICAL PROPERTIES OF THE SHEAR ZONES

The various forms in which the shear zones beneath the river bed occur were differentiated into five classes, based on detailed observations, measurements on the tunnel walls and the results of laboratory direct shear tests on 20 cm cubes. The principal factors considered in the following classification are the amount and type of clay filling.

1. Fracture zone with rock-to-rock contact; the angle of shearing resistance  $\phi = 35^\circ$ . This form of occurrence is generally restricted to greater depths or close to where the

fracture pinches out.

2. Zone of subhorizontal rock fragments, with clay coating or partial clay filling ( $\phi$  between  $25^\circ$  and  $30^\circ$ ).
3. Zone of crushed rock (mylonite) with small, angular rock fragments and a small percentage of clay ( $\phi < 30^\circ$ ).
4. Open zone with well-defined borders, filled principally with clay gouge and angular fragments of sound or slightly-weathered basalt ( $\phi \approx 25^\circ$ ).
5. Zone filled principally with highly plastic clay ( $\phi < 25^\circ$ ). As the shear zones approach the original river bottom level the clay filling is mostly an orange-tan, very plastic, colloidal clay that appears to have been introduced by infiltrating river water.

#### PROPOSED TREATMENT

The 1974 cost estimate in the feasibility report included a sum of \$20 million for special treatment of breccia zones, thought at the time to be the weakest features in the foundation. This treatment was described as "removal of weaker breccia from certain strata of the foundation and replacement by concrete to improve the shear strength of the foundation for the dam".

Once the program of exploratory tunnels following the shear zones at various levels was well underway, it became apparent that treatment or elimination of the fractured seams was necessary in order to have the required factor of safety. Initially, several alternatives were considered, including: excavating part of the foundation area to below contact A/B; hydraulic excavation of the material filling the shear zones using high pressure jets; a series of trenches filled with concrete; concreted tunnels acting as shear keys. Of these, lowering of the downstream third of the foundation area and concrete shear keys along the fault zones and contact A/B were analyzed in detail. Although both of these solutions would yield equivalent safety factors, an open excavation would have required nearly 7 months to remove the rock by controlled blasting, then backfill with concrete from El. 20 m to El. 40 m, which would have seriously delayed the construction schedule. The second alternative would permit underground treatment while the high blocks of the main dam were poured to a safe limiting height (El. 90 m) and would be 20% less costly, in view of the smaller amounts of excavation and concrete required, (Caric et al., 1982).

Based on these considerations, the alternative of underground treatment by shear keys was selected. Already in 1978, before the river channel foundation area was unwatered, a comparative study of subsurface treatment methods carried out at other projects (e.g. Green Peter Dam, Oregon, New Bullards Dam, California) had been made. Conventional limiting equilibrium stability analyses against shear failure, utilizing very conservative assumptions, showed that

to obtain an adequate factor of safety the minimum area to be treated by concrete keys had to be approximately 25% of the general foundation area under the four main double blocks of the dam (Itaipu Binacional, 1981).

Finite element analyses were used to determine the proper orientation of the concreted tunnels to serve as shear keys. It was found that with keys only parallel to the dam axis (transverse to the applied load) there was a tendency to concentrate the stresses in the upstream rows of keys in a manner that could cause progressive failure. On the other hand, keys aligned in an upstream-downstream direction and located directly under each stem of the blocks would provide a continuous, effective shearing resistance over the whole foundation width, even bridging over unexcavated areas of the foundation.

In order to include the best elements of both orientations and increase the area of treatment, it was decided to have a grid of 8 tunnels parallel to and 12 perpendicular to the dam axis, surrounded by peripheral drainage tunnels. Such a grid would have the advantage of a more uni-

form stress distribution, reducing the concentration in the shear keys across the river (Fig. 7).

The grid beneath the high central blocks in the river channel consisted of tunnels 3.5 m wide and 2.5 m high, totaling 2,600 m in extent, which were filled with approximately 30,000 m<sup>3</sup> of concrete and then grouted.

The shear keys are not at a uniform elevation. Practically all the keys parallel to the dam's axis rise from either extreme towards the area beneath the stems of double block F-17/18, where two of the shear zones intersect. The upstream-downstream key tunnels are somewhat more regular in elevation. A separate grid was designed around shaft 17 in order to cope with the south-dipping shear zones at approximately El. 30 m. In addition, short stub tunnels were driven upstream under the heads of half blocks F-16, F-17 and F-18 and westward in the area beneath the stems of F-17 and F-18, where the existence of very soft mylonitic gouge was a source of concern with respect to settlement.

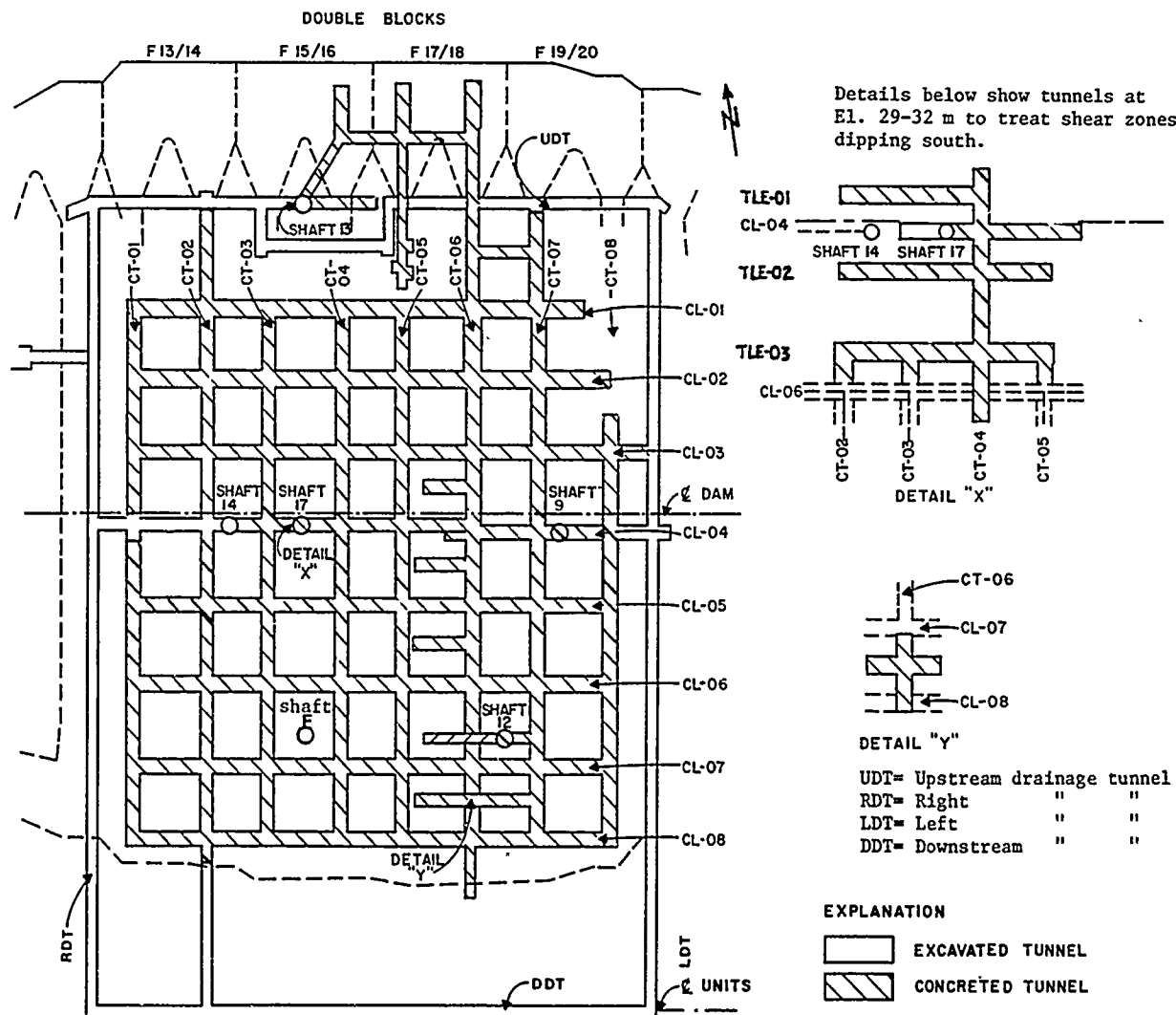


Fig. 7 Itaipu Dam. Grids of Tunnels under River Bed for Concrete Shear Keys and Drainage.

## SHEAR KEY TUNNEL GRID CONSTRUCTION

Excavation of the tunnels for the shear keys was carried out with extreme care to prevent damage to the sound foundation rock, always controlling the blasts so that the concrete rising above the area would not be affected. Blasting vibrations were very carefully monitored. The maximum advance for each round of blasting was 1 to 6 m, after which scaling was done with special lances and the muck removed with a miniloader. Where two or more shear zones occurred close above one another it was necessary to heighten the tunnel, excavating it by benches to a vault 8 to 10 m high. These chambers were concreted as soon as possible to reduce stand up time, in spite of the use of tensioned rock bolts and wire mesh. The use of gunite together with rock bolts and wire mesh was very effective in some areas where shear zones overlapped and a larger excavation was required.

Prior to concrete placement, the tunnel surfaces were thoroughly washed with air/water jets to remove all loose material and all surface clay was removed from the shear zones to guarantee good concrete adhesion. Detailed geologic mapping of the tunnel walls and roof was carried out, indicating all the important lithologic and structural features. This was done with reference to station and elevation marks placed by the surveyors.

The concrete used to backfill the tunnels was generally of a specified compressive strength of 27.4 MPa (3,973 psi) after one year, with a maximum aggregate size of 3.8 cm (1.5 inch). However, for the stub tunnels beneath the heads of the blocks, 34.3 MPa (4,973 psi) strength was specified. In order to distribute the concrete thoroughly within the tunnels it was fed through 6 inch holes bored from the foundation surface with "down the hole" percussion drills on 4 m to 6 m centers.

Up to a certain height within the tunnels, concrete was vibrated by a crew positioned upon a platform made of rebars. This was followed by some vibration from the ends of the section being concreted and by lowering vibrators down the placement holes. The last 50 cm of tunnel height were filled with concrete containing an expansion agent.

Grouting of the concreted shear key tunnels was carried out from the surface through holes drilled at 2 m centers to fill any voids left due to concrete shrinkage, insufficient filling of the irregularities of the rock surface or to opening of joints by blasting at nearby continuations of the grid system.

Grout pressures were limited to 0.6 times the height of the overlying rock and the slurry generally consisted of a 1:1 water-cement ratio. When grouting was completed, core borings were made to verify grout penetration and pressure tests carried out to determine if the fractures had been filled.

## FOUNDATION INSTRUMENTATION

To monitor the behavior of the rock mass in the

foundation area of the high blocks, instruments were installed even before backfilling the shear key tunnels. The most successful type of instrument has been the multiple-position borehole extensometer. The behavior of these instruments showed that the beginning of excavation was characterized by continuous deformations, specially at the heads of double blocks F-15/16 and F-17/18, which reached 1 mm/month during the opening of the stub tunnels under those blocks. After the tunnels were back-filled with concrete and grouted, the rate of settlement decreased to 0.7 - 0.4 mm/month, then stabilized. Tangential movements were determined by triorthogonal gages installed along contact A/B in the peripheral drainage gallery and the water pressures developed during reservoir filling measured by a series of Casagrande type piezometers and open wells that permitted piezometric measurements at any point along the hole. Permission to continue pouring concrete above El. 90 m on the high blocks depended on the settlement rates measured by the extensometers. As tunneling progressed while the main blocks rose from the foundation, the behavior of the rock mass subjected to increased loading became critical, specially in areas where chambers had to be excavated and the overlying rock burden was decreased. The instruments monitoring these areas indicated higher deformations and thus they were the first tunnel sections to be concreted.

## REMEDIAL MEASURES IN OTHER AREAS WITH FOUNDATION STRUCTURAL DEFECTS

Following is a brief account of the principal problems encountered in basalt flows at progressively higher elevations due to the presence of discontinuities, and the measures taken to remedy them within the area of the main dam.

### Discontinuity B

This is the imbricate series of fractures that was tested at El. 61.5 m in a niche excavated beside the gallery leading from the deep shaft at El. 59 m, within the upper portion of the dense basalt of flow B.

Shortly after the river was diverted in October 1978, this discontinuity was investigated by tunnels into both abutments. It soon became evident that on both sides its shear strength is high, for it consists principally of a zone of closely-spaced, subhorizontal joints cemented by calcite and/or silica. It was, however, found that some seepage along it could cause uplift pressure once the reservoir was filled, therefore the exploratory adits were converted into drainage tunnels extending 165 m at El. 60 m in the right abutment and 210 m at El. 55 m within the left flank.

### Contact C/D

A shear key tunnel grid similar to that beneath the river bed, but of much smaller dimensions, was required to treat the foundation of blocks F-1, E-6, E-5 and E-4, the E blocks being simple buttresses on top of the right abutment. In that area the contact between flows C and D, approximately at El. 112, was found to be filled

with a highly plastic orange-tan clay derived from the river when it flowed at much higher levels in the past. In the left abutment contact C/D is tightly cemented, with no clay filling. In comparison to the main grid, this smaller one consists only of four upstream-downstream tunnels and three tunnels parallel to the dam axis, having the same cross section as the river tunnels. The upstream-downstream tunnel coincident with block E-6 turns sharply east under the head of block E-6 and passes under the heads of half blocks F-1 and F-2. Access to the grid was through a shaft downstream from the stem of block E-6. The three tunnels parallel to the dam's axis were extended westward to below the stem of buttress E-2 in order to make certain that the contact had progressively greater rock to rock contact in that direction. The total length of tunnels is nearly 600 m and filling them required approximately 6,000 m<sup>3</sup> of concrete.

#### Discontinuity D

This is one of the most extensive discontinuities present at the Itaipu site. It became apparent not only in borings made on the left side of the river but in road cuts and the sides of the Diversion Canal excavation. In that area it developed within a band of expansive clay minerals concentrated in the upper third of flow D and is filled with colloidal clay derived from the river and even some small pockets of fine, uniform sand.

The concrete dam foundation on the east (left) side of the Diversion Canal was 20 m to 34 m above Discontinuity D, with sound, dense basalt in the intervening thickness. The first two concrete blocks adjacent to the Diversion Structure on the east side of the canal were changed from single buttresses to massive gravity blocks for greater stability. With the dam founded at higher elevations to the east, the load imposed upon the rock would be distributed over a considerable area at the depth of the fracture.

Originally it was intended to found the uppermost double buttress blocks of the main dam at El. 125 m on the left abutment, but in that area Discontinuity D, which had evidence of shear displacement, bifurcated into two branches approximately at elevations 117 m and 115.5 m. In addition to being open and clay-filled, it was affected by blasting vibrations during canal excavation, so that the rock mass above it underwent stress relief and some movement. Consequently, the foundation level had to be lowered below the fracture to El. 115 m.

In the right abutment, Discontinuity D was followed for over 120 m by a tunnel excavated at El. 125 m and was found to have enough areas with rock to rock contact to yield an estimated friction angle  $\phi$  of 35°. Only the foundation of half-block F-1 had to be lowered from El. 125 m to El. 123 m due to the occurrence of a branch of the discontinuity observed exposed on the cut slope between the foundation berms of buttresses F-1 and F-2. This exploratory tunnel was left as a drainage tunnel after adequate roof supporting treatment.

#### FOUNDATION GROUTING AND DRAINAGE OF THE MAIN DAM

Prior to curtain grouting, consolidation grouting was carried out under the heads of the double buttress blocks in vertical holes 3 m deep and on 6 m centers, just after the first lift of concrete was poured. The main purpose of this grouting was to seal any fractures that could open near the foundation surface due to excavation blasting.

Contact grouting was carried out from the upstream berm of the blocks in two rows of inclined holes extending about 6 m below the block foundation level and with a spacing of 3 m.

The main grout curtain is situated upstream of the dam blocks and is connected by means of lateral curtains in the abutments with the downstream grout curtain of the powerhouse. Thus the entire foundation area of the main dam in the river channel is surrounded by a grout curtain to reduce seepage to a minimum and the shear key grid within this area is encircled by a drainage tunnel system with drains and weirs to collect and measure what little infiltration passes through the encircling curtain.

The upstream grout curtain consists of 3 rows of vertical holes drilled from the upstream platform of the blocks. It would have been preferable to initiate the curtain directly under the buttress heads but, by doing so, concreting would have been delayed. Moreover, calculations showed that a grouting gallery across the blocks would have weakened them.

The grouting sequence consisted of primary holes on 6 m centers, secondary ones at half-spacing and tertiary and quaternary holes at split-spacing, depending on grout absorption. The first line to be grouted was the one nearest the drainage curtain. Grout absorptions greater than 12.5 kg/meter would dictate the need to grout tertiary or higher orders of grout holes. The depths of grout holes reached 40 m below the foundation rock surface in the river channel area.

All the grout holes were drilled with percussion equipment. It was found that the "down the hole" type of air drill produced faster, straighter holes than those drilled with a rotary rig and cuttings could be readily flushed out. Rotary borings drilled with diamond drill bits tended to produce much fine-grained "rock flour" slurry that could be forced into the very fractures that had to be sealed with cement grout. Furthermore, the cost of percussion drilling was considerably less than diamond drilling.

Pressure increase during grouting observed the following specifications:

| Depth    | Maximum Effective Pressure (pressure at level being grouted) |                                  |
|----------|--|----------------------------------|
| 0 to 5 m | not greater than   | 1 kgf/cm <sup>2</sup> (98 KPa)   |
| 6 m-20 m | 0.3 x depth  | kgf/cm <sup>2</sup> (98 KPa)     |
| 20 m     | 6 + 0.75(depth-20)   | kgf/cm <sup>2</sup> (98 KPa)     |
|          | to a maximum surface gauge pressure of                       | 50 kgf/cm <sup>2</sup> (4.9 MPa) |

## SALIENT FEATURES OF THE INVESTIGATION AND SELECTION OF THE ITAIPU DAM SITE

1. Core drilling in the river channel had to be done in nearly 50 m of water.
2. The dam axis was chosen by giving point ratings to essential features, for example, width of site, geological conditions in the river bed, necessary height of embankments, etc.
3. Although downstream site E was found to have a relatively unfractured thick basalt (flow A) as a foundation for the main dam, it was not selected primarily because spillway discharges from it, and probably the powerhouse discharge as well, would affect the small Acaray project which develops a stream of the same name a short distance downstream from that site, on the right side of the river (Fig. 2). It also received a low rating for the location of future navigation facilities.
4. After the five basalt flows that influence the selected site were investigated by core borings and defined as flows A through E from the bottom up, deeper borings were made and five additional underlying flows were characterized.
5. A sum of 20 million dollars was included in the construction estimate to cover the cost of any radical foundation treatment program.
6. The core borings made before the foundation area of the main dam was unwatered did not reveal the true character of the shear zones in the lower part of flow B. The first confirmation of the nature of these zones was obtained in a tunnel advanced from the bottom of the deep shaft on the right bank.
7. All the basalt flows in the area have a sub-horizontal discontinuity, generally in the upper third of the flow's thickness. Some of these discontinuities developed in horizons of expansive clay mineral concentration. The clays in turn appear to have formed due to deuteric alteration of volcanic glass along a horizon controlled by the cooling rate of the flow (Cabrera, 1985).
8. The results of the detailed investigations of the shear zones below the river bed near the base of flow B, indicate that they occurred due to unloading by rapid downcutting of the river and consequent high horizontal stresses, which buckled and overthrust the remaining thickness of flow B (Cabrera, 1986).

## CONCLUSIONS

The foregoing account of the selection and investigation of the Itaipu dam site can illustrate the fact that the input from the engineering geologist is often not sufficient to prevail over other factors that influence the location of a dam's axis. At site E, farther downstream, the river eroded down to flow A, which investigations showed did not have zones of frag-

mented and comminuted rock corresponding to shear zones.

In the area of the axis finally selected for the dam (Axis A-2) it appears likely that as basalt flow B was eroded by rapid river downcutting to nearly 20 m from its base, the decrease of normal load in the valley allowed the high residual horizontal stresses to cause buckling and shearing of the remainder of the flow.

No evidence of shear displacement was found on the surfaces of contact A/B, only filling by colloidal clay, probably transported by water infiltrating from the river. Directly under the river thalweg the contact is more open, probably separated by an arching effect.

## ACKNOWLEDGMENTS

The investigations for site selection, and the feasibility and design stages of the Itaipu Project were directed by IECO-ELC, an engineering consortium consisting of International Engineering Co. (IECO) of San Francisco, USA and Electroconsult (ELC) of Milan, Italy. IECO-ELC was also made responsible for the design of the canal and all structures required for river diversion and the rockfill embankment of the left (East) side of the river. Eventually it became the coordinator of all engineering design carried out by consortia of Brazilian and Paraguayan firms. The writer was principal Engineering Geologist for IECO from 1975 to 1981.

Most of the final investigations for the treatment of the shear zones under the river channel and other major discontinuities affecting the foundation of the main dam were carried out by Itaipu Binacional's Division of Geology, Rock Mechanics and Instrumentation, headed by Engineering Geologist Adilson L. Barbi.

## REFERENCES

- Cabrera, J. G. (1986), "Buckling and Shearing of Basalt Flows Beneath Deep Valleys", Proceedings, Fifth International Congress of the International Association of Engineering Geology, Buenos Aires, Vol. 2, Theme 5, 589-594.
- Cabrera, J. G. (1985), "Development of Some Major Discontinuities in Basalt Flows", Bulletin of the Association of Engineering Geologists, Vol. XXII, no. 1, 114-117.
- Cabrera, J. G. and A. L. Barbi, (1981), "Engineering Geology of Dam Foundations on Basalt Flows of the Upper Paraná Basin, Brazil". In F. H. Kulhawi (editor) Recent Developments in Geotechnical Engineering for Hydro Projects: American Society of Civil Engineers, New York, N.Y., 177-191.
- Caric, D. M., L. P. Eigenheer, J. Uriarte, A. Szpilman, A. Gallico and G. S. Sarkaria, (1982), "The Itaipu Hollow Gravity Dam", Water Power and Dam Construction, Vol. 34, no. 5, May, 30-44.

Cotrim, J. R., H. W. Krauch, J. G. Da Rocha, A. Gallico, and G. S. Sarkaria, (1977). "The Binational Itaipu Hydropower Project", Water Power and Dam Construction, Vol. 29, no. 10, October, 40-47; Vol. 29, no. 11, November, 44-52.

Itaipu Binacional, (1981), "The Itaipu Hydroelectric Project - 12,600 MW, Design and Construction Features", Published by Itaipu Binacional, Rio de Janeiro, 536.

Rocha, M., A. Silverio, J. Pedro and J. Delgado, (1974), "A New Development of the LNEC Stress Tensor Gauge", Proceedings, Third Congress of the International Society of Rock Mechanics, Denver, Vol. 2A, 464-467.



## Grouting a Water Tower Foundation in a Carbonate Formation

**Dorairaja Raghu**

Civil Engineering Department, New Jersey Institute of Technology,  
Newark, New Jersey

**David Antes**

Vice President, Paulus, Sokolowski and Sartor, Inc., Warren,  
New Jersey

**Joseph J. Lifrieri**

Senior Associate, Paulus, Sokolowski and Sartor, Inc., Warren,  
New Jersey

### SYNOPSIS

Grouting the cavities in cavernous carbonate formations is one of the techniques employed to achieve reliable bearing support for structures founded in and on such rock units. For this purpose, conventional exploration methods, such as test borings and geophysical measurements, can be employed to obtain the necessary subsurface data; but, they are usually limited in extent, expensive, time consuming, and can be misleading. These limitations can be overcome by employing percussion probing techniques. A case history is cited wherein percussion probing was successfully employed.

### INTRODUCTION

Carbonate formations are rock units that contain limestones and dolomites. These units possess varying degrees of solubility in water, depending upon its acidity. Due to this, cavities form resulting in structural weakness of the rock formation. Sound rock above these openings tend to bridge or arch. If these bridges are not strong enough to span these openings and/or if they are weakened by natural phenomenon, such as jointing or weathering, or other causes, they can collapse.

### Foundation Support in Cavernous Carbonates

The ability of the foundation material to support foundations in, on, and within the soil above these formations is affected by the location and extent of cavities within these rocks and the thickness and quality of rock between the cavities and the foundation. In some cases, it may be necessary to improve the quality of the rock mass to obtain the required strength. Several methods of improving foundation response and reliability within these formations have been reported in the literature (Wagener, 1984, Depman and Backe, 1976). A case history where grouting was performed to improve the foundation support will be presented in this paper.

### Geology of Case History Cited

The project cited in this paper is located in central New Jersey and comprised a portion of a major corporate headquarters building complex. A literature review pertaining to the geology of the site was conducted. The site is located on the southeastern edge of the Highlands physiographic province and extends west into the adjacent Triassic Lowlands (Widmer, 1964). Regional bedrock mapping (New Jersey Department of Environmental Protection, 1974)

indicated that four formations occurred at the site region, exhibiting evidence of Cambrian through Mesozoic Tectonic events which controlled the region's geologic development. From the oldest to the youngest, the formations found were: Hardyston Formation, Leithsville and Allentown Formations (all Cambrian), and the Border Conglomerate of the Brunswick Formation (Triassic). Basement rock is Precambrian Byram Gneiss.

The Leithsville Formation, which underlies the immediate vicinity of the project, is a dolomite rock. At least two members of this formation are believed to be present at the site (Markiewicz, et. al., 1981). The major member present is fine grained and thinly bedded with interbedded residual clay layers (the Hamburg member). A coarse grained and massively bedded, crystalline dolomitic limestone, which weathered in a pinnacled configuration, is the other member (the Califon member). The site is intensely folded and faulted. In addition, the literature indicated the bedrock contains cavities of varying sizes, some of which were found to have been filled with soil (Wheeler and Myers, 1976).

### Subsurface Explorations Performed Prior to Grouting

Conventional subsurface explorations performed revealed the presence of a cavity under the proposed structure. In order to determine the exact location, extent, and configuration of this cavity, several conventional subsurface exploration techniques can be employed. Borings with rock coring tend to be slow and expensive, especially when performed at each proposed foundation location. Interpretation of subsurface conditions from more widely

spaced, less frequent borings tend to be extremely misleading. Geophysical methods do not yield absolute subsurface information and frequently detect at best only the largest cavities. It is thus desirable to employ a technique, that would be more reliable than the geophysics, and more rapid and less expensive than the borings for performing the additional investigations necessary for grouting. This was accomplished by utilizing a closely spaced grid of percussion probes correlated to site conditions.

#### Percussion Probes

Percussion probes, commonly known as "Air Track Probes" were utilized to conduct detailed investigations of the location and the extent of the cavity below the proposed water tower. In this country, such probes have been used to verify the adequacy of the bearing stratum of caissons in carbonate formations. These probes have also been successfully utilized in South Africa in cavernous regions (Wagener, 1984). But at the time the authors employed this technique, they were not aware of the use of percussion probes for determining the extent of cavities.

The air track probe rig utilized for these investigations was a Crawlair ECM-350, equipped with VL-140 valveless drifter. Of the various drill bits tested, the 3-inch bit size was selected for use since it provided penetration rates that were easier to record but rapid enough to be economical. To provide the necessary compressed air, an Ingersoll Rand Spiro Flo DXL 750P compressor, delivering 750 cubic feet of air per minute at 125 psi was used. This equipment does not yield representative samples; but, it is possible to record the rates of penetration through different subsurface materials, as the probes penetrate through them. More details of the equipment used for percussion probing can be obtained from literature (Lifrieri and Raghu, 1982).

#### Basis for Interpreting the Probe Data

A site specific correlation was developed between percussion probe penetration rates and the type of material encountered for this project site. For this purpose, a test area was selected where borings were previously drilled. Probes were advanced adjacent to borings. Penetration data obtained from these probes were compared with the materials recovered from the borings. Based on this, a preliminary correlation could be established between the observed probe penetration rates and the quality of the subsurface materials, especially the rock. Utilizing these results, a judgement regarding the bearing strength of the material could be made.

As explorations progressed further for the complex, it became evident that these preliminary correlations had to be modified based on a visual inspection of the material penetrated in order to obtain quantitative data regarding the quality of the subsurface materials. To accomplish this, a probe rig was set up at the top of a slope of a near

vertical excavation exposing rock and soil of various quality. Probes were advanced immediately behind the face of the slope. The quality of the rock exposed in the excavation could then be visually inspected and compared to the corresponding penetration rates observed during probing operations. Thus, a final and more realistic correlation was established between the penetration rates and the strength of the subsurface materials penetrated. This correlation is presented in Table 1. More details of these correlations, the limitations and interpretation of data based on a term called "Foundation Quality Index" are reported elsewhere (Lifrieri and Raghu, 1982).

Table 1

| <u>Penetration Rate<br/>of the Percussion<br/>Probe<br/>(Seconds per Foot)</u> | <u>Type of<br/>Material</u> | <u>Symbol</u> |
|--|-----------------------------|---------------|
| 0 - 2  | Void/Soil<br>Filled Cavity  | V             |
| 2 - 5  | Loose Soil                  | S             |
| 5 - 15   | Residual Soil               | RS            |
| 15 - 30  | Decomposed Rock             | DR            |
| Above 30   | Sound Rock                  | R             |

#### Probing Program

Forty-five percussion probes were drilled at several locations around the perimeter of this structure which measured only 25 feet square (see Figure 1). Also shown in Figure 1 is the layout of the original proposed foundation for the structure. The penetration rates were recorded for each foot of each probe. The percussion probes were generally terminated upon penetrating at least 15 feet into competent bedrock free of cavities. A typical probe log is presented in Figure 2.

It should be noted that all 45 probes were drilled in only four days at a total cost, including inspection, of approximately \$4,500. Since the overburden soil cover is relatively thin, detailed subsurface exploration by borings would involve a significant footage of rock coring. It was estimated that the cost to obtain, by means of test borings, similar information regarding the extent of the cavity beneath the structure would have been about fifteen times greater and would have required fifty to eighty rig days to complete.

The percussion probes indicated that the overburden soils were relatively thin and that the bedrock contained a large, continuous cavity beneath the entire plan area of the proposed structure. A typical subsurface cross section depicting the subsurface stratigraphy before grouting, as inferred from probing, is shown in Figure 3. For these conditions, several foundation design alternatives were considered.

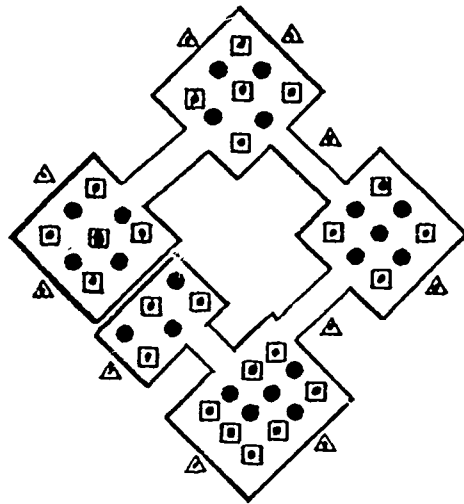


FIGURE 1 - LAYOUT PLAN OF STRUCTURE

PROBE LOG  
-----

|   |  |                   |  |
|---|--|-------------------|--|
| PROJECT: Proposed Corporate Headquarters                |  | PROBE 1 of 1      |  |
| CLIENT:   |  | SHEET 1 of 1      |  |
| GROUNDWATER:  |  | JOB NO.:          |  |
| EQUIPMENT DETAILS: Bit - Carbide,<br>Diameter - 3 in.   |  | GROUND ELEVATION: |  |
| HAMMER: Type - VL140, Rating - 100 psi @ 750 cfm.       |  | DATE:             |  |
| RIG: Type - Crawler ECM 350, Rods - Steel               |  | INSPECTOR:        |  |
| COMPRESSOR: Type - IRDL750, Rating - 125 psi @ 750 cfm. |  | DRILLER:          |  |

| DEPTH (Feet) | PENETRATION (Seconds/ft.) | SKETCH | IDENTIFICATION OF STRATA                    | REMARKS |
|--------------|---------------------------|--------|---|---------|
| 0            | 8                         |        | Residual soil and decomposed rock fragments |         |
| 5            | 6                         |        |   |         |
| 10           | 43                        |        | Gray dust, rock fragments (gray dolomite)   |         |
| 15           | 55                        |        |   |         |
| 20           | 8                         |        |   |         |
| 25           | 100                       |        |   |         |
| 30           | 120                       |        |   |         |
| 35           | 125                       |        |   |         |
| 40           | 125                       |        |   |         |
| 45           | 125                       |        |   |         |
| 50           | 125                       |        |   |         |
| 55           | 125                       |        |   |         |
| 60           | 125                       |        |   |         |
| 65           | 125                       |        |   |         |
| 70           | 125                       |        |   |         |
| 75           | 125                       |        |   |         |
| 80           | 125                       |        |   |         |
| 85           | 125                       |        |   |         |
| 90           | 125                       |        |   |         |
| 95           | 125                       |        |   |         |
| 100          | 125                       |        |   |         |
| 105          | 125                       |        |   |         |
| 110          | 125                       |        |   |         |
| 115          | 125                       |        |   |         |
| 120          | 125                       |        |   |         |
| 125          | 125                       |        |   |         |
| 130          | 125                       |        |   |         |
| 135          | 125                       |        |   |         |
| 140          | 125                       |        |   |         |
| 145          | 125                       |        |   |         |
| 150          | 125                       |        |   |         |
| 155          | 125                       |        |   |         |
| 160          | 125                       |        |   |         |
| 165          | 125                       |        |   |         |
| 170          | 125                       |        |   |         |
| 175          | 125                       |        |   |         |
| 180          | 125                       |        |   |         |
| 185          | 125                       |        |   |         |
| 190          | 125                       |        |   |         |
| 195          | 125                       |        |   |         |
| 200          | 125                       |        |   |         |
| 205          | 125                       |        |   |         |
| 210          | 125                       |        |   |         |
| 215          | 125                       |        |   |         |
| 220          | 125                       |        |   |         |
| 225          | 125                       |        |   |         |
| 230          | 125                       |        |   |         |
| 235          | 125                       |        |   |         |
| 240          | 125                       |        |   |         |
| 245          | 125                       |        |   |         |
| 250          | 125                       |        |   |         |
| 255          | 125                       |        |   |         |
| 260          | 125                       |        |   |         |
| 265          | 125                       |        |   |         |
| 270          | 125                       |        |   |         |
| 275          | 125                       |        |   |         |
| 280          | 125                       |        |   |         |
| 285          | 125                       |        |   |         |
| 290          | 125                       |        |   |         |
| 295          | 125                       |        |   |         |
| 300          | 125                       |        |   |         |
| 305          | 125                       |        |   |         |
| 310          | 125                       |        |   |         |
| 315          | 125                       |        |   |         |
| 320          | 125                       |        |   |         |
| 325          | 125                       |        |   |         |
| 330          | 125                       |        |   |         |
| 335          | 125                       |        |   |         |
| 340          | 125                       |        |   |         |
| 345          | 125                       |        |   |         |
| 350          | 125                       |        |   |         |
| 355          | 125                       |        |   |         |
| 360          | 125                       |        |   |         |
| 365          | 125                       |        |   |         |
| 370          | 125                       |        |   |         |
| 375          | 125                       |        |   |         |
| 380          | 125                       |        |   |         |
| 385          | 125                       |        |   |         |
| 390          | 125                       |        |   |         |
| 395          | 125                       |        |   |         |
| 400          | 125                       |        |   |         |
| 405          | 125                       |        |   |         |
| 410          | 125                       |        |   |         |
| 415          | 125                       |        |   |         |
| 420          | 125                       |        |   |         |
| 425          | 125                       |        |   |         |
| 430          | 125                       |        |   |         |
| 435          | 125                       |        |   |         |
| 440          | 125                       |        |   |         |
| 445          | 125                       |        |   |         |
| 450          | 125                       |        |   |         |
| 455          | 125                       |        |   |         |
| 460          | 125                       |        |   |         |
| 465          | 125                       |        |   |         |
| 470          | 125                       |        |   |         |
| 475          | 125                       |        |   |         |
| 480          | 125                       |        |   |         |
| 485          | 125                       |        |   |         |
| 490          | 125                       |        |   |         |
| 495          | 125                       |        |   |         |
| 500          | 125                       |        |   |         |
| 505          | 125                       |        |   |         |
| 510          | 125                       |        |   |         |
| 515          | 125                       |        |   |         |
| 520          | 125                       |        |   |         |
| 525          | 125                       |        |   |         |
| 530          | 125                       |        |   |         |
| 535          | 125                       |        |   |         |
| 540          | 125                       |        |   |         |
| 545          | 125                       |        |   |         |
| 550          | 125                       |        |   |         |
| 555          | 125                       |        |   |         |
| 560          | 125                       |        |   |         |
| 565          | 125                       |        |   |         |
| 570          | 125                       |        |   |         |
| 575          | 125                       |        |   |         |
| 580          | 125                       |        |   |         |
| 585          | 125                       |        |   |         |
| 590          | 125                       |        |   |         |
| 595          | 125                       |        |   |         |
| 600          | 125                       |        |   |         |
| 605          | 125                       |        |   |         |
| 610          | 125                       |        |   |         |
| 615          | 125                       |        |   |         |
| 620          | 125                       |        |   |         |
| 625          | 125                       |        |   |         |
| 630          | 125                       |        |   |         |
| 635          | 125                       |        |   |         |
| 640          | 125                       |        |   |         |
| 645          | 125                       |        |   |         |
| 650          | 125                       |        |   |         |
| 655          | 125                       |        |   |         |
| 660          | 125                       |        |   |         |
| 665          | 125                       |        |   |         |
| 670          | 125                       |        |   |         |
| 675          | 125                       |        |   |         |
| 680          | 125                       |        |   |         |
| 685          | 125                       |        |   |         |
| 690          | 125                       |        |   |         |
| 695          | 125                       |        |   |         |
| 700          | 125                       |        |   |         |
| 705          | 125                       |        |   |         |
| 710          | 125                       |        |   |         |
| 715          | 125                       |        |   |         |
| 720          | 125                       |        |   |         |
| 725          | 125                       |        |   |         |
| 730          | 125                       |        |   |         |
| 735          | 125                       |        |   |         |
| 740          | 125                       |        |   |         |
| 745          | 125                       |        |   |         |
| 750          | 125                       |        |   |         |
| 755          | 125                       |        |   |         |
| 760          | 125                       |        |   |         |
| 765          | 125                       |        |   |         |
| 770          | 125                       |        |   |         |
| 775          | 125                       |        |   |         |
| 780          | 125                       |        |   |         |
| 785          | 125                       |        |   |         |
| 790          | 125                       |        |   |         |
| 795          | 125                       |        |   |         |
| 800          | 125                       |        |   |         |
| 805          | 125                       |        |   |         |
| 810          | 125                       |        |   |         |
| 815          | 125                       |        |   |         |
| 820          | 125                       |        |   |         |
| 825          | 125                       |        |   |         |
| 830          | 125                       |        |   |         |
| 835          | 125                       |        |   |         |
| 840          | 125                       |        |   |         |
| 845          | 125                       |        |   |         |
| 850          | 125                       |        |   |         |
| 855          | 125                       |        |   |         |
| 860          | 125                       |        |   |         |
| 865          | 125                       |        |   |         |
| 870          | 125                       |        |   |         |
| 875          | 125                       |        |   |         |
| 880          | 125                       |        |   |         |
| 885          | 125                       |        |   |         |
| 890          | 125                       |        |   |         |
| 895          | 125                       |        |   |         |
| 900          | 125                       |        |   |         |
| 905          | 125                       |        |   |         |
| 910          | 125                       |        |   |         |
| 915          | 125                       |        |   |         |
| 920          | 125                       |        |   |         |
| 925          | 125                       |        |   |         |
| 930          | 125                       |        |   |         |
| 935          | 125                       |        |   |         |
| 940          | 125                       |        |   |         |
| 945          | 125                       |        |   |         |
| 950          | 125                       |        |   |         |
| 955          | 125                       |        |   |         |
| 960          | 125                       |        |   |         |
| 965          | 125                       |        |   |         |
| 970          | 125                       |        |   |         |
| 975          | 125                       |        |   |         |
| 980          | 125                       |        |   |         |
| 985          | 125                       |        |   |         |
| 990          | 125                       |        |   |         |
| 995          | 125                       |        |   |         |
| 1000         | 125                       |        |   |         |

FIGURE 2 - TYPICAL PROBE LOG

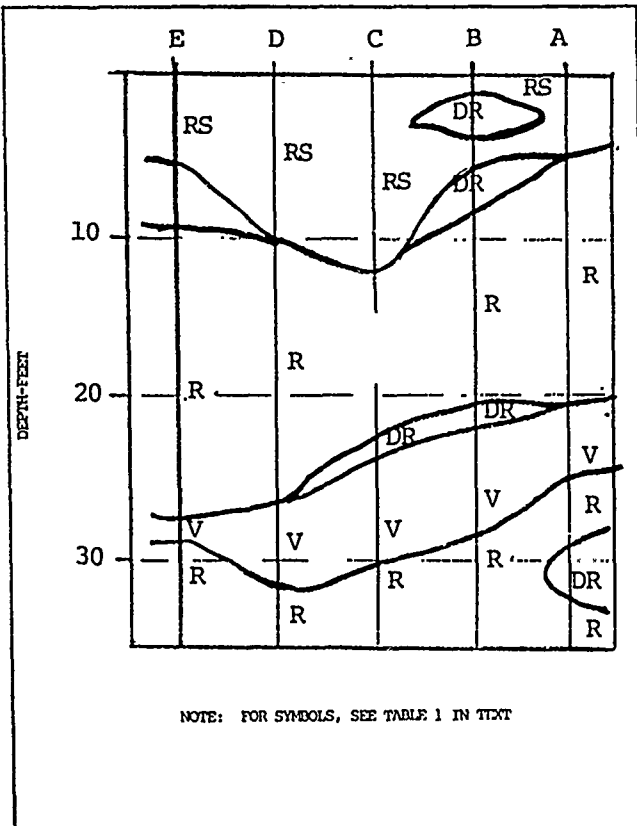


FIGURE 3 - SUBSURFACE STRATIGRAPHY AS INFERRED FROM PROBING

## Foundation Design Scheme

It was determined that construction of a spread footing foundation system or a large mat foundation on the upper bedrock layer over the cavity could eventually lead to a potential settlement problem of the proposed structure. Economic analyses indicated that there would be a significant cost savings (over \$50,000) if, rather than pre-drilling holes through the upper bedrock layer and driving steel H-piles to competent bedrock beneath the cavity, the cavity was to be filled with a cement grout and a mat foundation then constructed on the surface of the upper bedrock after the overburden soils were removed. Accordingly, it was decided to proceed with a grouting program.

### Details of the Grouting Program

The grouting program required the use of 3½ inch diameter grout holes placed in a grid pattern. The locations of the grout holes are shown in Figure 1. To reduce costs, many of the original percussion probe holes, which had been drilled with a 3-inch diameter bit, were over-reamed to the required diameter for grouting. Three inch diameter perforated grout pipes were inserted in the grout holes that extended through the cavities into the competent bedrock below. Cement-bulk filler grout was pumped into each hole under varying pressures until there was no more grout take (refusal). Provisions were made to perform secondary and tertiary grouting operations, if deemed necessary.

### Rock Mass Quality After Grouting

After grouting, probes were advanced adjacent to the grout holes to determine rock mass quality and the extent of any remaining cavities. A comparison of the results of probes showing the rock mass qualities and extent of cavities before and after grouting is presented in Figure 4. It can be seen from this comparison that there was only a slight improvement in rock quality due to grouting. This was attributed to the fact that the grout was not able to displace the soil present in the cavities. It was decided to abandon plans to proceed with additional grouting. The grout pipes which had been in place were relied on to act as "needle piles" to help transfer the foundation load below the cavities into the competent bedrock below. The structure has not experienced any settlement since it was constructed several years ago. Hence, it may be concluded the limited benefit of the grouting program together with the beneficial support of the "needle piles" was effective in solving the problem presented by the cavities at this site. However, without the additional data obtained by post-grouting percussion probes, the need to incorporate the "needle piles" into the foundation would not have been known and the structure would probably have been subjected to unacceptable and perhaps objectionable movements.

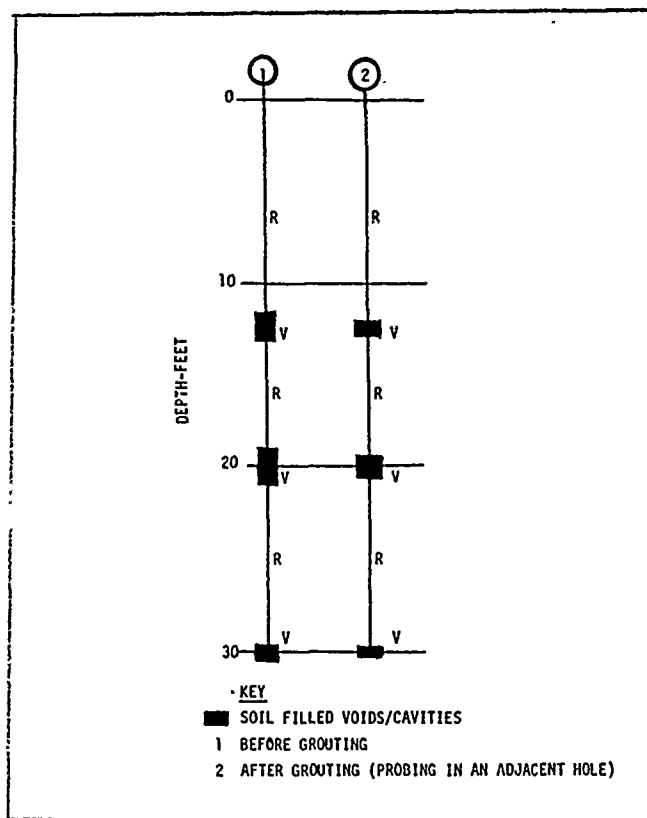


FIGURE 4 - ROCK MASS QUALITY BEFORE AND AFTER GROUTING

### Conclusions

Some of the limitations and drawbacks involved in grouting cavernous carbonate formations have been presented in this paper. The need for determining the improvement of rock mass quality after grouting is also clearly demonstrated. A new technique based on percussion probe penetration rates to obtain the required subsurface information for grouting was developed. Also it was shown that this technique can be also employed to verify the effectiveness of grouting. This technique is shown to be superior to the conventional subsurface investigation in terms of accuracy, cost and speed.

## References

Depman, A.J., and Backé, H.A., 1976, "Typical Problems and Solutions in Urban Areas", Proceedings of a Conference on "Engineering, Construction and Maintenance Problems in Limestone Regions", Lehigh University, Bethlehem, Pennsylvania, pp. 35-50.

Lifrieri, J.J., and Raghu, D., 1982, "Development of a Foundation Quality Index for Foundations in Solution-Prone Carbonate Formations", Bulletin of the Association of Engineering Geologists, vol. xix., No. 1, pages 35-47.

Markewicz, F.J., Dalton, R., and Canace, R., 1981, "Stratigraphy, Engineering and Geohydrologic Characteristics of the Lower Paleozoic Carbonate Formations of Northern New Jersey", Proceedings of the Conference on the Design and Construction of Foundations on the Carbonate Formations of New Jersey and Pennsylvania, New Jersey Institute of Technology, New Jersey, March 1981, Pages 3-42.

New Jersey Department of Environmental Protection, 1984, Bureau of Geology, "Atlas Sheet Series, Number 25, Geologic Overlay".

Wagener, F. Von M., 1981, "Engineering Construction on Dolomite", Printed and Distributed by the Geotechnical Division of the South African Institute of Civil Engineers, P.O. Box 210, Marshalltown 2107, Johannesburg.

Wheeler, James R., and Myers, Paul B., "Carbonate History and Foundation Problems in Carbonate Rocks of the Lehigh Valley", Proceedings of a Conference on "Engineering, Construction and Maintenance Problems in Limestone Regions", Lehigh University, Bethlehem, Pennsylvania, pp. 51-77.

Widmer, K., 1974., "The Geology and Geography of New Jersey", Volume 19., The New Jersey Historical Society, Van Nostrand Company, Inc., Princeton, New Jersey.

## Rock Response in a 12-M Tunnel through a Zone of Low Strength

**R.D. Prager**

Senior Geotechnical Engineer, Southern Electric International,  
Birmingham, Alabama

**G.S. Grainger**

Supervisor Engineering Geology, Southern Electric International,  
Birmingham, Alabama

**R.L. Butts**

Engineering Geologist, Southern Electric International, Birmingham,  
Alabama

**SYNOPSIS:** At the Rocky Mountain Pumped Storage Project a 12 meter diameter power tunnel was excavated through sedimentary rock for 760 meters. Approximately 10% of this tunnel was through Pennington shale that is described as a dark gray massive organic shale. This paper will describe the methods of testing and rock characterization, the results of instrumentation and monitoring, and the post-construction testing program for the excavation, and conclude with a discussion of the observed rock response in relation to the measured strength and deformation properties. This particular zone of the tunnel required the addition of longer rockbolts, and a discussion of that supplemental rock reinforcement will be included.

### INTRODUCTION

The Rocky Mountain Project is a pumped storage facility rated at approximately 800 megawatts of peaking energy. The project is located approximately 16 km (10 m) northwest of Rome, Georgia, in the Valley and Ridge Physiographic Province.

Construction of the project required the excavation of a 12-m (39.5-ft) tunnel, 640-m (2,100-ft) long. Construction also included the placement of a 10.7-m (35-ft) diameter reinforced concrete liner in the tunnel. The construction of the water tunnel has been completed.

The zone of anticipated low strength occurred along a 111.3-m (365-ft) stretch of the tunnel starting approximately 193.5-m (635-ft) upstream from the portals.

The investigative program included geological mapping, rock borings, geophysical testing, laboratory and field testing of core samples, construction of an exploratory adit and test chamber.

Design of the excavation and rock reinforcement will be discussed. During the excavation representatives from engineering mapped the geological conditions, observed the rocks response to excavation, and monitored rock movements with instrumentation of the excavated surfaces.

Field tests of in-situ rock properties were made during the excavation of the tunnel.

### INVESTIGATION PROGRAM

From 1977 through 1979, a series of borings were drilled along the tunnel alignment to determine the geological conditions. Geophysical data were acquired using crosshole velocity measurements, uphole velocity surveys and downhole measurements (sonic

velocity, gamma radiation and borehole verticality). Water pressure testing was conducted in selected borings.

An exploratory adit was excavated during 1978-1979 above the centerline of Penstock no. 2. A test chamber, the same diameter as the upper half of the planned tunnel, was constructed at the end of the exploratory adit to provide information on the behavior of the rock during and after excavation. This test chamber also revealed additional rock exposure for the measurement of structural features and geological conditions.

During the fall of 1980, a detailed field and laboratory program was undertaken to define the rock mass properties for use in the design of the tunnel and shaft. Two additional core holes were located off the tunnel centerline and carefully oriented and angle-drilled to: 1) obtain rock conditions in the bifurcation area, 2) intersect steeply-dipping joints at an angle that was appropriate for lab testing, and 3) assess the frequency and spacing of steeply-dipping joint sets. Detail line surveys were conducted to determine fracture extent, spacing, opening, and orientation. Seismic refraction surveys were conducted along the walls of the exploratory-drainage adit to determine the in situ velocity, elastic modulus, and thickness of loosened zones.

During the excavation of the tunnel, plate jacking tests and cross-hole and downhole geophysical tests were conducted in shale and siltstone units from the upper bench excavation to determine in-situ rock properties.

### LOCAL GEOLOGY

#### Stratigraphy

Paleozoic rocks of Pennsylvanian and Mississippian age occurred along the shaft and tunnel alignment and were identified as 17 distinct units. The zone of interest is a

25.9-m (85-ft) thick layer of moderately-hard, massive-bedded, organic shale with very thin sandstone laminae and siderite layers (unit 16). Below the zone is a 100-m (330-ft) thick very-hard, massive bedded, medium- to coarse-grained, fossiliferous crystalline limestone (unit 17). Above the zone is a 19.8-m thick (65-ft) moderately-hard, thin- to medium-bedded, clayey siltstone (unit 15).

### Structure

The strength and stability of a rock mass is highly affected by the discontinuities: bedding, joints, faults, and shear zones. Measurements indicated that bedding in unit 16 at tunnel grade would strike N72°E and dip 13° to the northeast (perpendicular to the tunnel axis). Jointing occurred in two sets: 1) a predominant set with a strike of N 60-70°E and dipping 70-75°NE and 2) an infrequent set with a strike of N 30-40°E and dipping 30°NE. The investigation program did not indicate possible faults or shear zones.

### Ground Water

The ground-water conditions for the tunnel are topographically, lithologically, and structurally controlled. Water pressure testing of the shale, unit 16, indicated very low permeabilities with no measurable water take. The overlying siltstone, unit 15, had a permeability of approximately  $5.0 \times 10^{-5}$  cm/sec.

## ROCK PROPERTIES

Rock properties from field and laboratory testing are presented in Table 1.

### DESIGN

The design criteria for the tunnel excavation was to provide a stable opening during and after construction for the placement of the concrete lining. The design was also intended to minimize the disturbance of the surrounding rock mass so that it would be able to resist excessive deformation of the tunnel lining upon internal pressurization. The excavation was stabilized for loadings due to gravity, blasting vibrations, hydrostatic forces due to ground water in joints and bedding planes, and additional loads caused by destressing the rock as the excavation proceeded. The rock stabilization designs take these conditions into account, while retaining the flexibility required to handle unexpected rock conditions.

Excavation of the tunnel was divided into a top heading and bench operations to limit raveling of the excavation face along the N60-70°E joint set. The philosophy of design was that by using rock reinforcement the rock became self supporting. Rock stabilization design was based on average conditions for two groups of rock, classified simply as soft rocks and hard rocks. A primary bolt pattern was designed for each group. Bolt length and spacings were chosen using standard rules of

TABLE 1

| Property                                     | Design Values          |                        | Excavated Values |                   |
|--|------------------------|------------------------|------------------|-------------------|
|  | Unit 16-Shale          | Unit 15-Siltstone      | Unit 16-Shale    | Unit 15-Siltstone |
| Point load-diam.                             | 8.89 MPa               | 7.72 MPa               |                  |                   |
| Point load-axial                             | 30.06 MPa              | 62.1 MPa               |                  |                   |
| Brazilian tensile strength                   | 5.14 MPa               | 5.16 MPa               |                  |                   |
| Uniaxial compressive strength                | 52.54 MPa              | 57.02 MPa              |                  |                   |
| Triaxial compressive strength @ 300psi       | 46.45 MPa              | 66.97 MPa              |                  |                   |
| Direct shear strength @ 300psi               | 1.56 MPa               | 1.97 MPa               |                  |                   |
| Density                                      | 2.67 Mg/m <sup>3</sup> | 2.67 Mg/m <sup>3</sup> |                  |                   |
| Dilation                                     | 0.15 cm                | 0.26 cm                |                  |                   |
| Cohesion                                     | 5.51 MPa               | 9.31 MPa               |                  |                   |
| Angle of friction                            | 38.5°                  | 51°                    |                  |                   |
| Youngs modulus-lab                           | 14.06 GPa              | 17.65 GPa              |                  |                   |
| "P" velocity-field cross-hole                | 5,212 m/s              | 4,840 m/s              | 4,460 m/s        | 4,175 m/s         |
| "S" velocity-field cross-hole                | 2,150 m/s              | 2,360 m/s              | 1,900 m/s        | 2,209 m/s         |
| "P" velocity-uphole                          | 3,800 m/s              | 4,200 m/s              | 3,505 m/s        | 4,511 m/s         |
| Youngs modulus-dynamic from cross-hole       | 30.68 GPa              | 37.16 GPa              | 23.96 GPa        | 34.06 GPa         |
| Youngs modulus of intact rock-seismic        | 7.67 GPa               | 9.29 GPa               | 5.99 GPa         | 8.51 GPa          |
| Youngs modulus of loosened zone-seismic      | 1.92 GPa               | 2.32 GPa               | 1.50 GPa         | 2.13 GPa          |
| Youngs modulus of loosened zone-jacking test | --                     | --                     | 2.76 GPa         | 4.14 GPa          |
| Blast loosened zone                          | 0.91-1.52 m            | --                     | 0.30-0.60 m      | 0.0-0.30 m        |
| Rock mass rating                             | 47                     | 43                     | 55-67            | 54-68             |
| Rock mass strength determination             | --                     | --                     | 180-500          | 500-580           |

thumb. Checks were then made to assure that the design would reinforce joints against shear movement, prevent wedge failure in the roof, and restrain the loosened zone around the opening. A supplemental bolt pattern was designed for both support systems for use in problem areas.

For the section of tunnel discussed, the primary bolt pattern was installed on a 1.7-m (5.5-ft) spacing radially through the upper 300°. However, in the crown the bolts were installed into the walls 45° above the horizontal. The bolts were 3.7-m (12-ft), No. 11, Grade 60 reinforcing bars that were fully-resin-grouted. Shotcrete and mesh was placed to 30° below the springline. When necessary, the bolts in the supplemental pattern were placed between the primary pattern reinforcing. In addition spot bolts were placed as necessary. During construction the reinforcing pattern was modified to decrease the reinforcing cycle.

#### RESPONSE TO EXCAVATION

Initial inspections of the low strength shale zone indicated low permeabilities, thus only minor water flow was anticipated into the excavation. However, as the excavation progressed, wet conditions were noted along the shale bedding. The wet conditions generally reduced the efficiency of shotcrete application to the rock surface and increased the frequency of air slaking along bedding.

Excavation confirmed that bedding and the N60°-70°E joint set were the dominant structural discontinuities in the low strength shale zone. Fractures present within the zone were commonly masked due to blast shattering along bedding of the fissile shale. The separations along bedding and the N60°-70°E joint set locally resulted in flat breakage in the crown and quarter arches, reducing the natural stability offered by an arch geometry. In several areas continued unravelling of the rock yielded steeple-shaped overbreaks which ranged up to 1.5-m (5-ft) beyond the designed excavation limits.

The contractor had difficulty installing the specified rockbolts, wiremesh and shotcrete in the required eight hours. The excavation blast rounds were shortened by the contractor to 2.4 meter (8.0-ft) rounds in lieu of 3.0 meter (10.0-ft) rounds. Continued slaking and spalling of the low strength shale zone eventually required the shortening of blast rounds to 1.5 meters (5.0-ft). In order to increase the efficiency of the tunnel advance and the need for immediate sealing of the rock surface a phased shotcrete application was recommended with 3.0 meter blast rounds. The phased shotcreting required the immediate application of two inches of shotcrete after excavation and rock bolting. Then, following rockbolt and wiremesh installation, a final two inch coat of shotcrete was added. To facilitate continued excavation, lagging of the wire mesh and second shotcrete application was allowed in areas of the shale zone where more stable ground was encountered.

Cracking and sagging of the shotcrete was common throughout the low strength shale zone. One major problem with the shotcrete was its failure to obtain a quick initial set, resulting in inadequate bonding to the rock surfaces. It was also difficult to achieve the application of a wet-shotcrete mix on to an already wet rock surface. Shooting the wet shotcrete to the crown and quarter arches often resulted in a 20-40 percent rebound of the mix. Slaking of the rock after shotcrete application commonly resulted in cracking of the shotcrete. To provide a method of measuring continued cracking and sagging spackling compound was applied to shotcrete cracks and periodically inspected to evaluate the extent and rate of movement.

To alleviate overbreak, pre-blast support spiling-bolts were installed at low angles to the crown and quarter arch surfaces. In general the spiling bolts were only partially effective in the shale zone and some were shot out with the next blast round. Finally, in two locations, continued unravelling of rock and shotcrete spalling required the installation of channel-iron mine straps for support along the crown.

#### INSTRUMENTATION

For safety and to verify the design assumptions, the tunnel was instrumented during construction to monitor the behavior of the rock mass. The instrumentation needed to be simple to install, durable, and allow rapid data collection and interpretation. The instrumentation also had to be sophisticated enough to allow differentiation between various types of deformation.

The instrumentation system originally planned utilized two types of instruments; convergence points and extensometers. Due to problems with loss of convergence points their use was discontinued.

The second type of instrument used was the borehole extensometer. The single point borehole extensometers installed in the tunnel consisted of a No. 8, Grade 60 reinforcing bar, with a grouted anchor up to 0.6 m (2-ft) long installed in a 0.04 m (1 1/2 in) diameter hole, with a collar grouted to the rock at the wall of the tunnel. Measurements of the relative movement between the collar and the bar were taken using a depth micrometer. Borehole extensometers were originally intended to be installed in the crown and quarterarches at approximately 61 m (200-ft) intervals along the main tunnel axis. Each location was to have 2 borehole extensometers installed, one 1.5 m (5-ft) deep and one 4.6 m (15-ft) deep. However, in order to allow the phased shotcrete application to lag behind the advancing face, additional instrumentation was required to more closely monitor ground behavior. To achieve this requirement, borehole extensometers were installed 4.6 m (15-ft) deep in the crown and arches at 15.2 m (50-ft) intervals along the tunnel, in addition to the originally designed dual installations



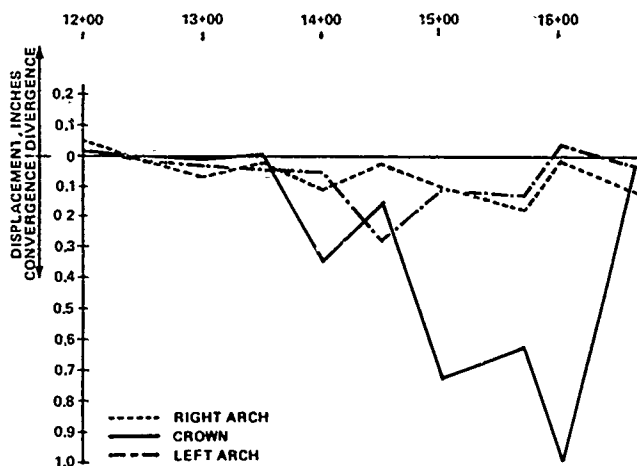
every 61 m (200-ft). Before the bench was excavated, 4.6 m (15-ft) long borehole extensometers were installed in the springlines, at the same stations as the crown and arch instruments.

The schedule for reading the extensometers was daily until the face had advanced a distance of 2 tunnel diameters past the instrument locations, weekly until the movements appeared to have ceased, and monthly after apparent stabilization, or as often as necessary to confirm the stability of the rock mass. This monitoring program was continued until the lining was placed. After each reading was taken, it was compared to previous readings. If a large difference was noted, the reading was immediately checked. In some extensometers blast-induced disturbances of the reference collars indicated false movement. If a discrepancy persisted, readings were taken every shift until the problem was resolved or explained. Plots of deformation versus time were primarily used to evaluate the instrument data. Other plots, such as deformation versus depth and deformation versus distance from the working face, were used as necessary to complete the picture.

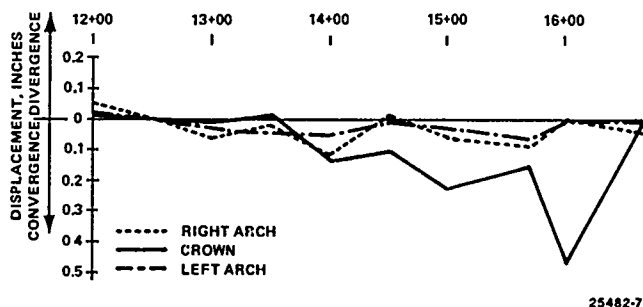
Based on calculations as well as professional judgement, it was decided that wall movements (relative to the 4.6 m (15-ft) deep extensometer anchor) of up to 5.1 mm (0.2 in) would be considered allowable, and those over 7.6 mm (0.3 in) would be considered a sign of possible instability and excessive loosening. In areas where the movements exceeded 7.6 mm (0.3 in), treatment was based on a thorough analysis of the cause of the movements.

As shown in the figures, the movements recorded at instrumented stations in the shale were some of the largest observed anywhere along the tunnel. At station 16+00 the total movement in the crown was slightly over 25 mm (1.0-in). Approximately one half of this movement occurred during the excavation of the top heading. As the bench was excavated past station 16+00, the movements were again triggered and convergence proceeded at an undesirable rate. Station 16+00 was located at the interface between the shale and siltstone. When excavated, this area was very blocky and wet. The data indicated that significant movements took place at depths greater than 1.5 m (5-ft) from the excavated surface and possibly deeper than 4.6 m (15-ft). These movements were probably the result of loosening and moving of rock blocks, especially in the crown area. This movement may have been partially driven by water pressure in the rock. Nine meter (30-ft.) long tensioned rock bolts were installed in the converging area, and were successful in stabilizing it.

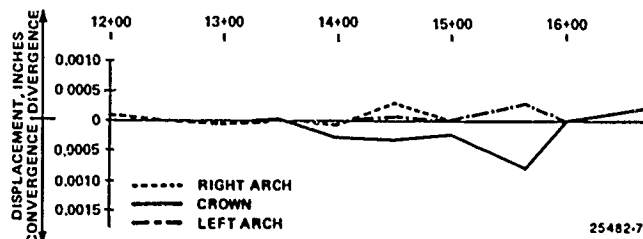
In general, the springline instruments showed that very little movement took place as the bench was excavated. Measurements of convergence that were recorded were determined to be the result of loosening of very near surface rock slabs or shotcrete.



TOTAL DEFORMATIONS MEASURED AT 15 FOOT DEEP EXTENSOMETERS



DEFORMATIONS MEASURED AT 15 FOOT DEEP EXTENSOMETERS AFTER BENCH EXCAVATION



DEFORMATION VELOCITY MEASURED AT 15 FOOT DEEP EXTENSOMETERS

## DISCUSSION

The results of the pre-construction exploration indicated that the shale would be the weakest material encountered in driving the tunnel. It was felt, based on the test chamber in the adit and the measured rock properties that if the top heading could be reinforced with the specified rockbolts, wiremesh, and 10 cm (4-in) of shotcrete in the required 8 hours there would not be a problem in excavating through the shale. If problem areas were encountered the supplemental pattern of bolts and spot bolts could be used.

The contractor had difficulty installing the rock reinforcing within the specified 8 hours after blasting. This resulted in a loosening of the crown and slabbing of the shale. The contractor elected to shorten the advance rounds to meet the 8 hour requirement for installation of reinforcement.

The shortened round impacted the schedule and the design was modified to allow installation of rockbolts and 5 cm (2-in) of shotcrete within 8 hours of blasting. The application of wiremesh and the remaining 5 cm (2-in) of shotcrete would lag behind the advance. This modification in design was allowed only with an increase in instrumentation to monitor rock movement. If movement occurred the wiremesh and remaining shotcrete was to be applied immediately.

In general, the shale behaved as anticipated. The problems encountered, rock convergence and additional tensioned bolt support, may have been avoided if quality shotcrete, controlled blasting and timely reinforcement could have been achieved. It was unfortunate that the weakest material of the tunnel was one of the first encountered. The designer, contractor, and owner were still learning to work together.

As a result of the movements that occurred, post-excavation testing was performed. The two main parameters of concern were the deformation modulus of the rock and the depth of the loosened zone. The results of this testing is presented in Table 1 and was within the required limits used in the tunnel lining design. The tunnel was lined in 1984 and no distress has been observed since that time.

## SELECTED REFERENCES

- Bakhtar, K. and Barton, Nick., (1986) "In Situ Rock Deformability Tests at the Rocky Mountain Pumped Storage Project," Proceedings, SME-AIME, 27th U.S. Symposium on Rock Mechanics-Tuscaloosa, AL., 949-953.
- Bieniawski, Z. T., (1976) "Rock Mass Classification in Rock Engineering," Proc. Symposium of Exploration for Rock Engineering, Johannesburg, Vol. 1, 97-106.
- Grainger, G. S., Butts, R. L., Cummings, R. A. Kendorski, F. S. (1986), "The Rock Mass Characteristics of the Rocky Mountain Pumped Storage Project Hydroelectric Tunnel," Proceedings, SME-AIME, 27th U.S. Symposium on Rock Mechanics-Tuscaloosa, AL., 961-967.
- Kendorski, F. S., (1980), "Field and Laboratory Assessment of Rock Mass Strength for Tunnel Design with Allowance for Dilation," Underground Rock Engineering Special Vol. 22, Canadian Institute of Mining and Metallurgy, Montreal, P.Q., 162-167.
- Prager, R. D., Kendorski, F. S., and Lundell, C. M., (1986), "The Design of the Excavation For The Underground Works At The Rocky Mountain Pumped Storage Project," Proceedings, SME-AIME, 27th U.S. Symposium on Rock Mechanics-Tuscaloosa, AL., 968-974.

## Stability Check of Escarpment Using Finite Element Method

P.S. Khare

Research Officer, Central Water and Power Research Station,  
Khadakwasla, Pune, India

S.L. Mokhashi

Additional Director, Central Water and Power Research Station,  
Khadakwasla, Pune, India

S.G. Kulkarni

Assistant Research Officer, Central Water and Power Research  
Station, Khadakwasla, Pune, India

**SYNOPSIS:** The valve house of the Tons Hydel Project, Madhya Pradesh, India is located just adjacent to a steep escarpment. The stability analysis of scarp near the valve house was made by the Central Water and Power Research Station, using finite element method. The problem was treated as a plain strain case. The analysis under self weight and with seepage forces indicated tensile stresses less than  $4 \text{ kg/cm}^2$  in the scarp. A proposal by the project authorities namely removing rock in the area

above R.L.230 m at 74 degrees and filling lean concrete below the overhang was found to provide a stable condition. The state of stress in the scarp near the valve house was obtained under different conditions. The finite element method thus proved to be a very useful tool in analysing problem

### INTRODUCTION

Bansagar-Tons hydel project is located at a distance of about 45km, from Rewa town, in Madhya Pradesh, India, shown in fig. 1. The rivers Tons and Beehar, after their confluence, flow into the Gangetic plains. Downstream of the confluence there are a series of Cascade falls within a short reach of 8 kms. Use is made of this natural topography which provides a gross

head of 180 m for the generation of power. However, there are no suitable sites on rivers Beehar and Tons for storage reservoirs and during postmonsoon periods sufficient water is not available for power generation. To overcome this difficulty water from Bansagar multipurpose project (on Sone river) is diverted into the Tons-Beehar valley. This accumulated water at

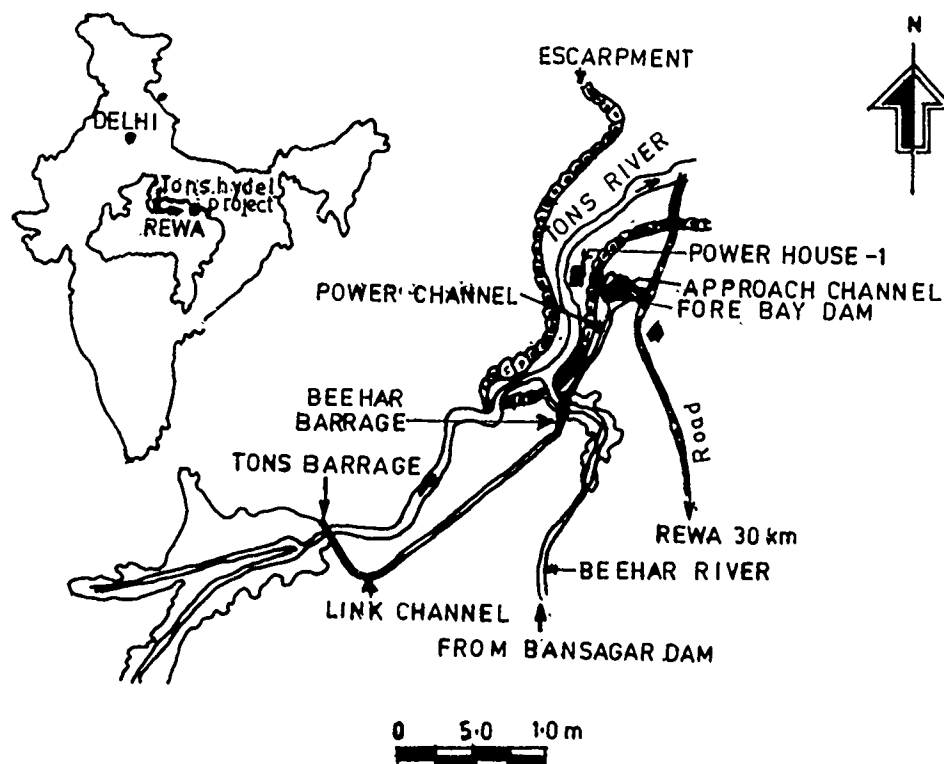


Fig 1 : Index Map of Tons Hydel Project, Madhya Pradesh, India.

Beehar barrage and water from Tons river is taken through 9.4 km long power channel to Forebay dam and from here regulated discharge is released through a 310 m long power tunnel trifurcating into three steel lined penstocks leading to valve house located at the foot of the Rewa scarp. In order to ensure the safety of the valve house against any rock fall, the stability of the escarpment was investigated.

#### Geology of Rewa Scarp (Ref.1)

Rewa scarp lying on the northern gentle limb of Rewa syncline, exposing Rewa formation of the Upper Vindhyan group, overlooking Tons valley at valve house consists of unusual 'Concave slope' segment at crown and pronounced overhang with 'acute convex segment association' of magnitude of about 15 m. The scarp is composed of blocky rock mass of sandstone belonging to Rewa formation of Upper Vindhyan group. This sandstone at places rests on shale formation.

The unusual morphology of the scarp with concave slope close to crown, is attributed to the occurrence of swallow/absorption points along joints. The scarp is under process of active erosion, the factors causing this process are fractures, phenomenon of valley relief, runoff, infiltration and seepage, chemical weathering of heterogeneous cross beds, etc. There were broadly three rock zones in the scarp vide fig. 2 which could be assigned values of modulus of elasticity (E) based on the strength rating (Ref.1)

a) Massive coarse grained sandstone with large scale cross stratifications having through spatulate confining beds and heterogeneous fine grained lithology with open joints,

$$E = 0.1 \times 10^6 \text{ kg/cm}^2$$

b) Moderately bedded, medium grained sandstone with flat beddings and lenticular intercalations

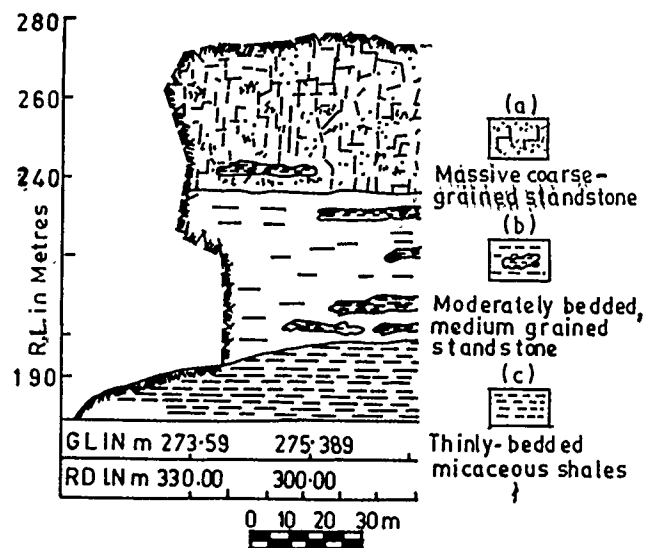


Fig.2 Geological Section of Escarpment

of shale

$$E = 0.8 \times 10^5 \text{ kg/cm}^2$$

c) Thinly bedded, reddish brown, chocolate and greenish grey coloured micaceous shales with massive silt stone units and lenticular bands of sand stone.

$$E = 0.4 \times 10^5 \text{ kg/cm}^2$$

#### ANALYSIS OF THE PROBLEM

The problem was studied by finite element method (Ref 3) treating it as plain strain case, using eight noded isoparametric elements. The escarpment structure was discretized into 160 elements incorporating 533 nodes. The detailed idealised model incorporating the extent of scarp near the valve house is shown in fig.3.

While the Young's Modulus values for the three zones were adopted as indicated earlier, density of rock for all the layers was assumed to be  $0.0025 \text{ kg/cm}^3$  and Poisson's ratio was taken to be 0.2. The studies were carried out for the following loading conditions

- i) Scarp under self weight
- ii) Scarp under self weight with seepage forces

From results of the above cases it is seen that the maximum tension is of the order of

$4 \text{ kg/cm}^2$ . It was also observed that the effect of seepage was insignificant. However, since valve house is an important component in power generation system where discharge is controlled, its failure would seriously affect the power generation. As such an alternative proposal was suggested by the project authorities. This proposal envisaged removal of some overhanging rock at 74 degrees above R.L.230 m and concrete filling below overhang as shown in fig 4. This modified proposal was also investigated. The variation of tensile stresses on the outer face of the scarp near overhang, under existing condition and with the proposal by project authorities is shown in fig.5. The idealised model of this proposal is shown in fig.6. The results obtained for all these cases are shown in table below.

| Details of cases studied   | Max. Tensile Stress $\text{kg/cm}^2$ | Max. shear Stress $\text{kg/cm}^2$ |
|--|--------------------------------------|------------------------------------|
| 1. Escarpment under self weight  | 3.97<br>(Element 71)<br>Fig-3        | 8.59<br>(Element 61)<br>Fig-3      |
| 2. Escarpment with concrete filling below overhang and removal of some of the portion of the overhang at 74 degree | 1.95<br>(Element 62)<br>Fig-5        | 4.18<br>(Element 10)<br>Fig-5      |

#### Sliding Stability Check

The above check (Ref.3) for the escarpment was made from the principal stresses obtained by finite element analysis and assuming plane of failure 45, 60 and 74 degrees with the

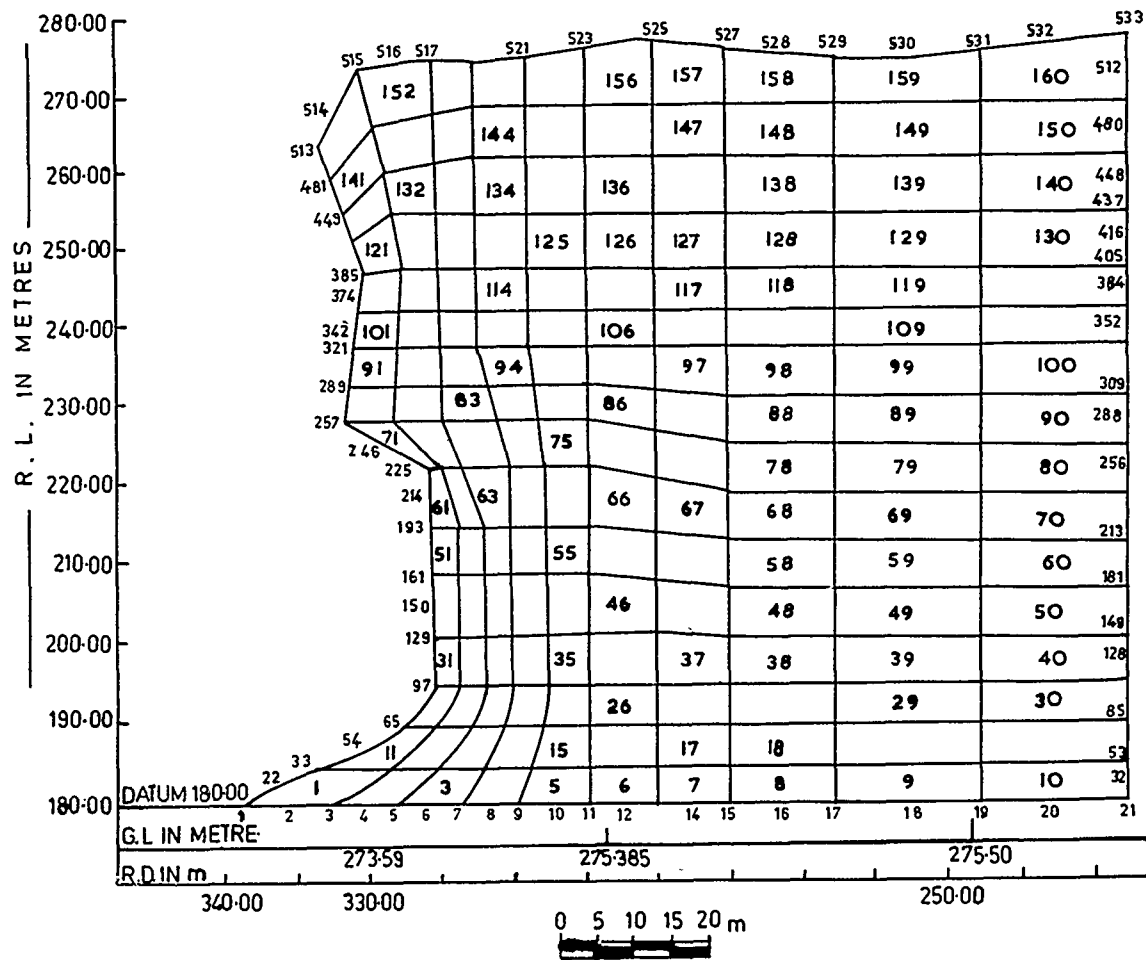


Fig.3 Finite Element Idealisation For Escarpment Near Valve House

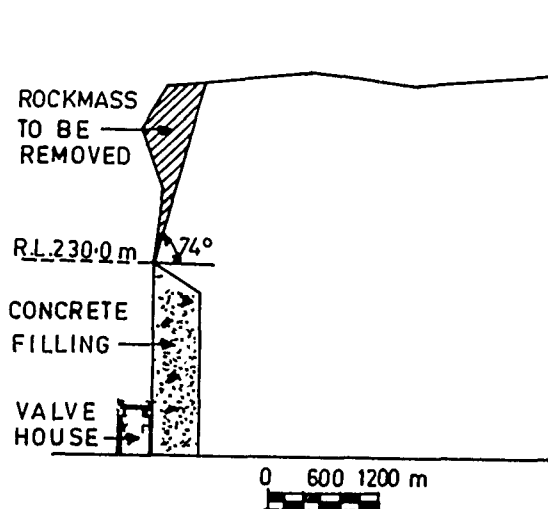


Fig.4 A Proposal by Project Authorities

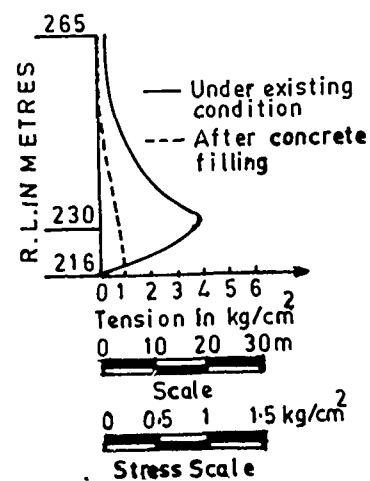


Fig.5 Variation of Tensile Stresses at The Outer Face of Scarp near Overhang.

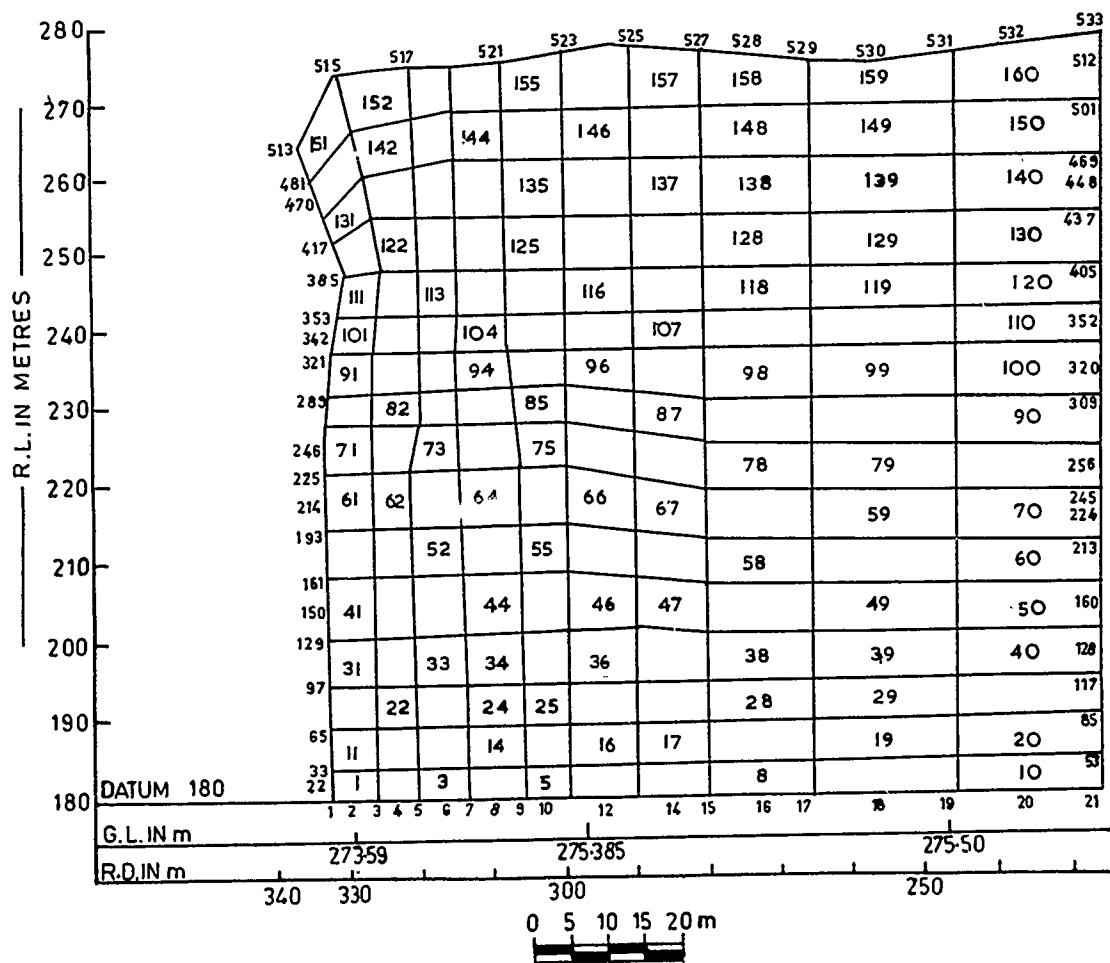


Fig.6 Finite Element Idealisation For Escarpment (Near Valve House) with Concrete Filling below Overhang

horizontal. The ratio of shear strength/shear stress obtained for all the cases was more than one indicating that there will not be any sliding failure.

#### DISCUSSION OF RESULTS

The results are presented in table. Studies indicate that the values of tensile stresses under different conditions are small. The effect of seepage on the state of stress in the scarp is also insignificant. Stability of the escarpment was examined from the point of sliding stability along the different assumed planes of failure i.e. 45, 60 and 74 degrees. For all these conditions factor of safety obtained was more than 1.5 for the assumed value of angle of friction equal to 45 degree and cohesion 5 kg/cm<sup>2</sup>. The shear and tensile stresses are further reduced for the case where some of the overhanging portion of the rock is removed and concrete filled under the overhang.

#### REMEDIAL MEASURES

In order to ensure the stability of the scarp, the proposal as suggested by the project

authorities, of removing the rock above R.L.230 m at 74 degrees was found to provide quite a stable condition for the scarp. It was also recommended that shallow anchoring by few rock bolts above R.L.230 m would be effective to prevent any local rock fall on the valve house. Further to reduce the effects of seepage forces suitable drainage system for diverting the surface runoff through the stream draining the scarp area was suggested. It was also advised to make ample provision for draining the interface of concrete and rock for releasing water pressure behind the concrete.

#### CONCLUSION

The two dimensional analysis using finite element method helped in understanding stability of the scarp and suggesting strengthening measures.

#### REFERENCES

- Desai C.S. & Abel (1972) 'Introduction to the finite element Method', Litton Educational Inc.
- Mishra P.S. (1982) 'A report on Geotechnical Investigations in valve house'.
- Timoshenko S.P., and Goodier J.N. (1951) 'Theory of elasticity', McGraw Hill Publishing Co. N.Y.

## Rock Mass Behaviour Assessment for Large Cavern in Rock

A.K. Dube

Assistant Director, Central Mining Research Station, Dhanbad, India

B. Singh

Director, Central Mining Research Station, Dhanbad, India

**SYNOPSIS:** A large power house cavern (22mx50mx250m) is proposed to be excavated for installing a 1000 MW hydroelectric power plant for Tehri Dam Project. The gorge chosen for the dam is very narrow and the topography is rugged and inhospitable. This dampened the process of preconstruction investigations. A number of tunnels were constructed for various project structures in the vicinity of the cavern. This provided an excellent opportunity to study the rock mass behaviour. Tunnel closure and rock loads were monitored with the help of instruments. Deformation moduli were also determined for different rock grades with the help of various techniques. A voluminous data had been obtained. This data had been analysed thoroughly and values of various parameters had been suggested for the final design of underground cavern and the supporting structures.

### INTRODUCTION

Tehri Dam Project (TDP) is a major multipurpose river valley project presently under construction. Figure 1 gives general layout of the project. So far, four diversion tunnels (11m dia) four head race tunnels (8m dia) and a number of approach adits had been constructed. Not much of investigations could be conducted to ascertain the subsurface geology due to adverse topography and inaccessibility. The construction of various underground structures mentioned above provided an excellent opportunity to generate additional informations about the rock mass behaviour and to use it for refining the criteria for the design of tunnel supports. Experiments were conducted in various tunnels to determine the deformation modulus, rock pressure on supports and closure. The experiment locations were so dispersed as to cover statistically all grades of rocks and their variations. Besides the above experimental studies, modern rock mass classifications have also been used to assess the rock mass behaviour.

### GENERAL GEOLOGY

The Geological Survey of India (GSI) conducted extensive geological studies in the area and identified the main geological features found in and around the Tehri Gorge. These phyllites are banded in appearance. The bands are constituted of argillaceous and arenaceous materials. The degree of the presence of these materials and the magnitude of the tectonic deformation suffered by the rocks constituted the basis for grouping the rocks in three main grades i.e. I, II and III. Grade I rocks are predominant and constitute 45% of the gorge however, Grade II and III account for 25% and 35% respectively. Grade I rocks are predominantly arenaceous, massive in character and distinctly jointed. The band width varies between a few millimetres to about a metre. Grade II phyllites are thinly banded and are considerably impregnated

with quartz veins, both along and across the foliation planes. The thickness of individual bands varies from a few to 100 millimetres. Grade III rocks are characterised by thin foliations impregnated by quartz veins. Closely spaced foliation planes, cleavages and joints transverse the rock mass and minor folds had also been seen.

### EXPERIMENTAL STUDIES

As already mentioned, the various tunnels while construction provided excellent opportunities for instrumentation. Many tests had been done and additional data was generated which helped in understanding the rock mass behaviour. Closure bolts had been installed in all the tunnels randomly and regular observations were taken. At a few selected locations test sections were made where closure bolts and loadcells were installed simultaneously. Deformation moduli were also determined at various locations in the tunnels and exploration drifts with the help of various techniques.

Periodic monitoring of these instrument as per a well defined scheme was done. Figure 2 gives a typical closure-time relation and figure 3 depicts rock pressure-time graph.

The deformation modulus of the rockmass at various places was determined with the help of flat jack and Goodman Jack. It had also been back worked out from the observed closure for various rocks. Rock pressures were also estimated with the help of Barton's approach and were compared with those observed with the help of loadcells.

### DATA ANALYSIS

The data analysis had been done on the basis of prevailing theories and practices. These theories are dependent upon various idealisations and assumptions. Such

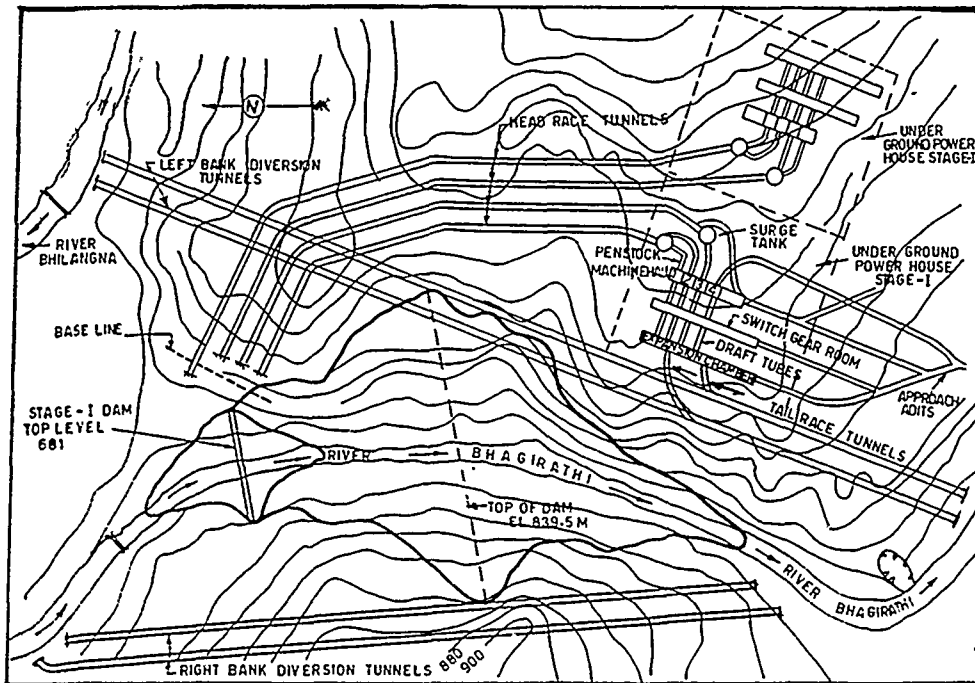


Fig. 1 General Layout Plan of Tehri Dam Project

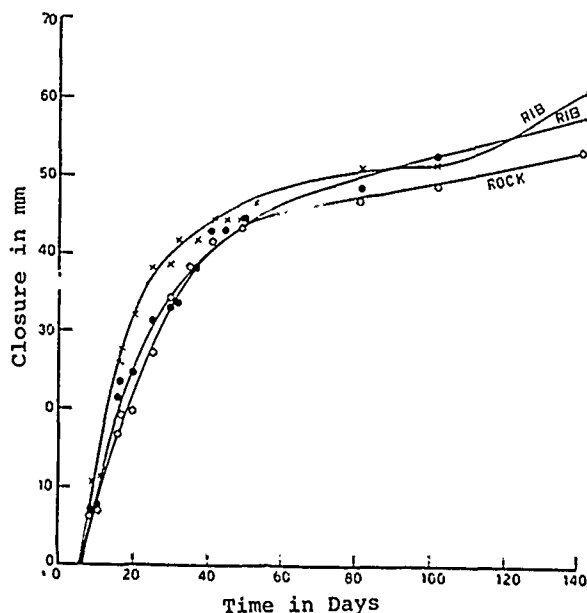


Fig. 2 Closure-Time Relation for Rock and Rib Closure

idealisations are not always true in the field conditions. The data so obtained is never the most true value, however, it approaches the reality. The rock is a heterogeneous material and various structural defects make it more varied in nature. The test results conducted on such a material may have a very high degree of scatter. The degree of scatter depends upon the intensity of various rock defects, such as joints, joint conditions and the water content of rock mass. It is not possible to prescribe a limit for the scatter. Reviewing

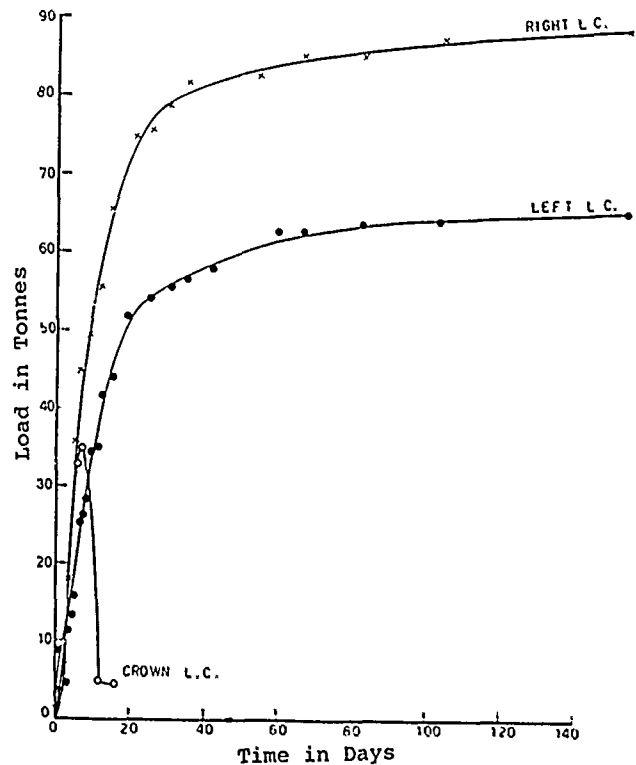


Fig. 3 Load-Time Relation for Mechanical Type Load Cells in Grade II Phyllites

the results we may observe that the ratio between the lowest and the highest value of deformation modulus is 1:30 (scatter ratio) in case of values derived by Bieniawski's (1973) geomechanical approach, however, it reduces to 1:2 in case of values back worked from closure observations (see Table I). The deformation modulus had been determined at



Table I Comparison of Deformation Modulus Determined by various Techniques  
in  $\text{kg/cm}^2 \times 10^5$

| Rock                | Flat Jack |         | Goodman Jack |         | Geomechanical Approach |         | Assessed from tunnel Closure |         |
|---------------------|-----------|---------|--------------|---------|------------------------|---------|------------------------------|---------|
|                     | Range     | Average | Range        | Average | Range                  | Average | Range                        | Average |
| Phyllites Grade I   |           | 0.68    | 0.06-0.57    | 0.18    | 0.10-3.05              | 1.57    | 1.98-4.01                    | 2.99    |
| Phyllites Grade II  | 0.02-0.50 | 0.29    | 0.04 -0.38   | 0.17    | 0.10-0.35              | 0.22    | 0.21-2.04                    | 1.12    |
| Phyllites Grade III | 0.08-0.39 | 0.23    | 0.02 -0.34   | 0.16    | 0.10-0.35              | 0.22    | 0.21-2.12                    | 1.16    |

a number of locations by Goodman Jack test method also. The scatter ratio for Grade I, Grade II and III phyllites was found to be 1:9.5, 1:8.3 and 1:13.8 respectively at the testing stress level of  $40 \text{ kg/cm}^2$  (the average expected stress level during operation as well as at present).

During the investigation period, some flat jack tests were also done in the drifts. These drifts may not be close to the tunnels presently under construction but had been driven in similar rock formations, Very scanty data is available. Only one test was done in Grade I phyllites and the deformation modulus was found to be  $0.68 \times 10^5 \text{ kg/cm}^2$ . Grade II had a range of  $0.02-0.05 \times 10^5 \text{ kg/cm}^2$  and the range for Grade III was  $0.08-0.39 \times 10^5 \text{ kg/cm}^2$ . The scatter ratio for Grade II and III is thus 1:27 and 1:5.

The values obtained by various techniques are compared in Table I. The scatter is large and it is possible to narrow it down by statistical treatment.

Estimation of rock pressure had been done with the help of Barton's approach. About 30 sets of estimates were done at various locations for different grades of rocks. The observed pressures are different for different grades of rocks. The ratio between the lowest and the highest observed rock pressure is 1:8.4. This ratio in case of estimated pressures is as high as 1:17.5. Table II gives these results.

#### DISCUSSION OF RESULTS

It is a difficult task to formulate and implement investigation scheme for a major project lying within inhospitable terrain, fragile and tectonically active rock formations. The investigation process was therefore not a continuous one as it had to be undertaken whenever an opportunity was available. The preliminary investigations were done through drifts and some deformation modulus tests with the help of flat jack were conducted. With the start of the construction phase, the diversion tunnels were made first and with that started the

Table II. Comparison of Observed and Estimated Vertical Rock Pressure in  $\text{kg/cm}^2$

| Sl No. | Rock                | Observed Pressure |      | Estimated Pressure |      |
|--------|---------------------|-------------------|------|--------------------|------|
|        |                     | Range             | Av.  | Range              | Av.  |
| 1.     | Phyllites Grade I   | 0.25-0.56         | 0.40 | 0.05-0.45          | 0.25 |
| 2.     | Phyllites Grade II  | 0.16              | 0.16 | 0.08-0.81          | 0.45 |
| 3.     | Phyllites Grade III | 0.32-0.42         | 0.37 | 0.99-2.51          | 1.75 |

process of detailed investigations which concluded with the construction of head race tunnels.

The above tunnels were excavated through Grade I, II and III rocks. As already mentioned, these tunnels were instrumented at a few selected locations to determine rock loads and deformation modulus. The locations of these tunnels were different, the different grades of rocks were exposed in the tunnels at different locations. Such a situation helped in increasing the scatter of the data obtained for various grades of rock masses. This scatter may be attributed to the variations within the rock mass, the errors in conducting the experiments and not very correct assessment of rock mass parameters. It is difficult to eliminate these sources of errors and there is no process available to separate them. The occurrence of scatter is thus a reality of geotechnical instrumentation.

Statistical treatment of large data may help in reducing the scatter to some extent. An attempt had been made in this case also and Table III and IV give narrowed down ranges with respective confidence limits.

After the above analysis a range is suggested which may be considered for design purposes.

Table III. Range of Deformation Modulus after Statistical Treatment

| Sl No | Rock Type           | Range in $10^5 \text{kg/cm}^2$ | Percent Confidence |
|-------|---------------------|--------------------------------|--------------------|
| 1.    | Phyllites Grade I   | 2.004 - 3.246                  | 83.85              |
| 2.    | Phyllites Grade II  | 0.711 - 1.391                  | 84.42              |
| 3.    | Phyllites Grade III | 0.568 - 1.444                  | 84.20              |

Table IV. Range of Rock Pressure in  $\text{kg/cm}^2$  After Statistical Treatment

| Sl No | Rock Type           | Range       | Percent Confidence |
|-------|---------------------|-------------|--------------------|
| 1.    | Phyllites Grade I   | 0.21 - 0.50 | 52.05              |
| 2.    | Phyllites Grade II  | 0.63 - 0.94 | 52.05              |
| 3.    | Phyllites Grade III | 0.80 - 1.93 | 52.05              |

It is suggested that the upper bound value may be taken for design purpose with factor of safety as unity.

The study and its results have helped in arriving at a sound engineering judgement in selecting the design values. Some thoughts having practical overtones, have also emerged through this process of data analysis and discussions. It had been seen that the surrounding rocks were largely intact and the stresses induced due to tunnelling were low and well within the competence of rock mass. There had been less shattering and joint opening within the surrounding rock mass. This had been inferred from the nature of closure-time curves and the magnitudes of the observed closures. The pressures were thus largely due to relaxation of surrounding rock mass and marginal loosening. There had been no indications of squeezing ground conditions any where in the tunnels studied so far. Such rocks may not need any type of consolidation grouting. The lining reinforcement may also be eliminated whenever sufficient rock cover is available to counteract the internal water pressure.

The tunnels are fairly stable and the presently installed supports are more than adequate in most of the situations.

The suggested rock pressures have been generated through instrumentation of tunnels as large as 11m dia. Whether this value would

be appropriate for an opening as large as 22m is a wide open question. It is reassuring to note that Barton's criteria suggests that rock pressures do not increase with the increase in the size of opening.

#### CONCLUSIONS

Preliminary design of supports and lining may be based on the suggested data, however, additional data may be generated during the construction phase to optimise the support requirements. The closures are low and the surrounding rocks are intact and this has resulted in low rock pressures. The stability of the large cavern can be improved further by employing smooth blasting technique.

#### REFERENCES

- Barton, N., Lien, J and Lunde, J.(1974), Engineering classification of rock masses for the design of tunnel support, Rock Mech., Vol.6, No.4, pp. 189-236.
- Bieniawski, Z.T. (1973), Engineering classification of jointed rock masses, Trans. S.Afr. Instn. Civil Engrs. Vol.15, pp. 335-342.
- Dube, A.K., Singh, B., Prasad, V.V.R., Saini, G.S., and P. Kumar (1987), Report on Assessment of Rock pressure and deformation modulus in the tunnels of Tehri Dam Project (unpublished CMRS Report).

## Support over Cavities of Unknown Depth for an Underground Facility

**James A. Larson**

Senior Project Manager-Geotechnical, Sverdrup Corporation,  
St. Louis, Missouri

**Donald P. Richards**

Geotechnical Manager-Parsons Brinckerhoff International, Ankara,  
Turkey  
Formerly with CRS, Saudi Arabia

**SYNOPSIS:** Rock excavation for a 7,200-square-meter building site in Saudi Arabia intercepted a large cavity underlying approximately half the site. Relocation was impossible; therefore, a grouting program was selected to modify the site to accept the allowable design load of 2.1 mega pascals. Due to the extreme depth of the cavity, the modification was limited to a depth of 25 meters under the building.

### INTRODUCTION

A new facility for the Royal Saudi Air Force (RSAF) required a building area of 7,200 square meters (8,600 square yards) to be excavated to a depth of 22 meters (72 feet). The subsurface data obtained from borings for site selection indicated that the excavation in limestone bedrock contained very small cavities, tubes and vugs of insignificant size. These would not create problems or difficulties during excavation.

Excavation, however, was interrupted at 13 meters (43 feet) depth when a collapse in the 2.5-meter (8-foot) thick rock roof over a cavity partially swallowed a D9 dozer. During this pause in excavation, a probe hole investigation was initiated to determine how extensive this cavity or a system of cavities may be. Problems during drilling limited the hole depth to final excavation grade. These 220 holes did not reveal any indication of significant voids. A ground probing radar survey followed the borehole investigation, but it was ineffective. The collapsed hole was filled with rock to provide support of the roof rock and a safer condition in the area of collapse.

Cautiously, the excavation continued over the entire site until final grade was reached. The final excavation depth defined the collapse as a vertical annulus which was dubbed "the doughnut."

Another boring program was planned along load bearing walls with 15 borings to be advanced to 15 meters (49 feet) depth and 101 borings to 8 meters (26 feet) depth. Around one of the deeper borings, which revealed a cavity south of the collapse, a group of 13 borings were drilled to determine the cavity extent. All penetrated into the cavity.

The annulus was cleaned of rubble fill which permitted visual observation. The collapse had occurred directly above the apex of a large dome of rubble rock. The vertical space over the dome was relatively uniform at about 1 meter in the east, north and west directions. The height of vertical space to the south was about 0.5 meter (1.6 feet) or less. A trench was dug from the annulus southward to where the rubble pile steepened

and it opened into a large chamber up to 7 meters (23 feet) in vertical space. Its main axis started at the east end and extended to mid-point of the south excavation limit. Normal to this were two more long chambers extending southward beyond the excavation. All three chambers had long flat ceilings and near vertical sides.

After visual examinations, it was established that one continuous cavity extended underneath approximately half the area of excavation.

### BACKGROUND

In recent years, cavities have often been encountered in eastern Saudi Arabia but have not been documented in literature. Lack of documentation has failed to forewarn designers and contractors of the widespread and frequent problem. Recent articles indicate that progress is being made to alert engineers of cavities and their relationship to regional and structural geology.

Prior to the design and construction of the RSAF facility, other organizations had been assigned the task of finding a location for the building. With known loading conditions, they selected a site on the King Abdulaziz Air Base in Dhahran. They planned and administered the initial subsurface investigation program of borings which indicated limestone bedrock to full excavation depth in the Rus formation without any significant cavities.

The building would exert an average dead load of 2.1 mega pascals (MPa) (22 tons per square foot, TSF) under interior and perimeter continuous bearing walls. Half of this load is a true dead load, the remainder could possibly come from a dynamic type load which may come in the life of the facility. The full allowable load would approach uniformity at about 13 to 17 meters (45 to 56 feet) into the underlying materials.

Following several boring programs and the completion of excavation, the project was at a new threshold where we started our study. Direct contact and visual observations were used to evaluate the cavity. Until these

were made, it was difficult to visualize a cavity of the magnitude that was observed.

Time constraints did not permit relocation of the facility to another site. The problem was to adapt this site to support the very high loading conditions to be placed over this cavity.

#### SITE GEOLOGY

The King Abdulaziz Air Base is located in the Interior Platform Section of the eastern Arabian Shelf. This structural division consists of sedimentary rocks ranging from Precambrian to Quaternary in age, with the area surrounding the site consisting of Paleocene and early Eocene marl, chalky limestone, dolomite, shale and geodal quartz. The site is located near the southern end of the Damman Dome, a broad 14 km by 10 km (8.5 by 6 mile) elliptically-shaped structure oriented N30°W and which rises to an elevation of approximately 150 meters (492 feet) above sea level. It is generally thought that the Damman Dome is the result of a deep-seated salt dome intruding the overlying sedimentary rocks (J. J. Grosch, F. T. Touma, and D. P. Richards).

The RSAF site is underlain by calcarenite and calcarenitic limestones of the Rus and Damman Formation. Logs of exploratory borings drilled at the site indicate an upper unit of light gray-brown fine calcarenitic limestone exhibiting abundant solution pitting. The limestone units contain numerous small solution cavities and vugs which are generally filled with calcite near the surface and iron-stained with greater depth.

The carbonate rocks of the entire Damman Dome region are characterized by solution cavities and karstic features. In general, solution channels have developed along the major joint system oriented tangential or radially to the dome structure. Case histories of cavity sites in the Dhahran area by Grosch, Touma and Richards indicate a reasonable agreement of cavity orientations with respect to the rock structure of the dome and location to each other.

#### GROUND WATER

Ground water was encountered at the base of the cavity chamber underlying the excavation and was recorded in borings. The water surface elevation is in agreement with the elevation recorded in surrounding wells. Samples of the water were obtained and analyzed in a laboratory to determine its compatibility or limitations with the grout to be used. The temperature of water and cavity were determined to be uniformly 85°F.

All exposed surfaces in the cavity, excepting those covered with dust and rock from the collapse, were an intense black. Slight

variations in the color intensity continued at the same elevation throughout the cavity. Ground water was lowered through the cavity in the early 1950's. The hydrocarbons are believed to have been deposited on the surfaces at that time. Using this phenomenon as a guide, there was no evidence of disturbance since the deposition.

#### PROBABILITY OF CAVITY DETECTION

Detection and evaluation of cavities by means of a standard boring program is very difficult and usually impossible. Because the borings are limited in coverage, the number needed would depend on the size, depth and location of cavities that would be critical for the project. Once a cavity is detected, the best assessment is by visual observation in person or by means of downhole cameras or boroscopes.

Considering the site and cavity size on this project, the initial and subsequent boring programs could have revealed cavity information; however, the borings were not deep enough. Drilling problems limited depths in some borings and greater depths were not deemed feasible or cost-effective. A ground penetrating radar survey also proved ineffective.

Previous experience in Riyadh, Saudi Arabia using electrical resistivity and seismic geophysical methods demonstrated that especially the seismic method had potential of locating possible cavities. The boring program that followed investigated the locations indicated by seismic to be cavities and proved there were some cavities at shallow depth. More experience is needed to substantiate the effectiveness of the method.

#### DESCRIPTION OF TREATMENT

Before entry into and having direct contact within the cavity, it was apparent that the cavity should be filled. Inside observations revealed a flat ceiling spanning a space on the order of 26 meters (84 feet) under the south edge of the excavation. The ceiling warped into a dome in a northerly direction going from a relatively flat dome to a rather abrupt dome in the area of the collapse. Computations proved the cavity roof needed support. Filling of the cavity would transfer load to the rock fall material in the floor of the cavity. Since none of the boring programs had provided information on material and conditions underlying the cavity, 21 additional borings were advanced to a depth of 50 meters (164 feet) below final excavation grade using rock coring methods.

Core boring was difficult. A mud-rotary drilling method was used to stabilize the hole, remove cuttings, and cool and lubricate the drill bit. There was no return of drill-

ing fluid below about 12-meter depth. At different depths in each hole, the rock conditions required use of a casing fitted with a cutting shoe to advance the boring. To facilitate recovery of rock cores, various types of core barrels were used.

Loose fine-grained material was encountered in some of the various sized cavities. Adequate quantities were obtained in seven samples for sieve analysis which revealed a gradation of silty sand and limestone fragments. Comparable materials were observed in the space between rubble rock pieces in the south end of the cavity floor as well as in the area of the original collapse and a partial roof fall nearby.

Unconfined compression tests on twenty-four representative rock cores yielded results between 6.8 and 100.5 MPa (71 and 1,045 TSF) which averaged 50 MPa (520 TSF). These strength test results suggest the rock be classified as relatively weak to strong. The complex stratigraphy based on poor rock recovery and quality of rock made it difficult to correlate between the deep boreholes.

Cavities were detected by observing the rate of penetration, drop of the rods and pressure exerted during the drilling operations. This procedure allowed detection of vertical cavity size from 50 mm (2 inches) and larger.

Treatment necessary to adapt this site for support of the facility had to consider the following:

- o The roof rock over the cavity needed support.
- o Filling the cavity would provide roof support and apply load to cavity floor.
- o Conditions in the cavity indicated that large masses of rock had dropped many meters, some only a matter of a few cm.
- o There was no sign of rock fall in the cavity since deposition of the hydrocarbons.
- o Large rubble rock in the chamber area had been bonded at contact points by calcite. The bonding suggests long-term inactivity in rock fall.
- o The cause or origin of the cavity was very deep seated. If originating in the edge of the salt dome, it could be hundreds of meters deep.
- o The nature of the rock falls observed in the cavity led to the belief that large rock masses had dropped.
- o All voids below 15-meter depth would be water-filled.
- o The true void space in material underlying the major cavity was not known.

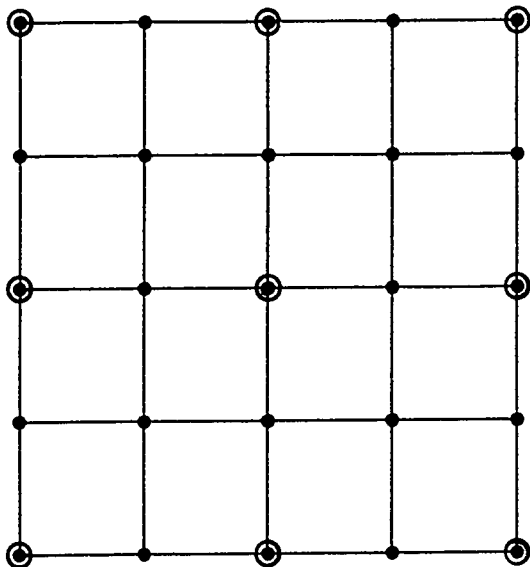
It was hypothesized that the originating cause of the cavity was very deep-seated and that a remedial program to provide needed support would be limited to a relatively shallow depth. It was decided that the most effective solution for stabilizing the ground support for the facility was to fill the original cavity (the doughnut) with concrete and to grout the cavities and fragmented rock. For safety reasons, the "doughnut" was filled with concrete under a separate existing contract, prior to development of recommendations for the grouting program.

The purpose of the grouting program was to fill openings, though not all the small interstices, in the rock down to a 25-meter depth and out to a boundary extending from the edge of the excavation at 45 degrees. This grouted mat would distribute the load and prevent the possible loss of material into underlying cavities. The primary activities included in the grouting program were as follows:

1. Drilling southern perimeter barrier grout holes.
2. Placement of southern perimeter barrier grout.
3. Drilling mass cavity fill holes.
4. Placement of mass cavity fill.
5. Drilling primary grout holes.
6. Placement of primary grout.
7. Drilling secondary (verification) grout holes.
8. Placement of secondary (verification) grout.

The initial phase of the subsurface stabilization program consisted of placement of perimeter barrier grout at the southern end of the excavation in the large horizontal chamber. Following completion of the perimeter barrier grout placement, mass cavity filling began. Shortly thereafter, vertical placement hole drilling was initiated in the northern portion of the site. This drilling was performed concurrently with the mass cavity filling operation. These holes provided additional information on rock conditions to 25-meter depth.

Exploratory borings and observations inside the cavity indicated that the southern and eastern portions of the site contained the most extensive voids; therefore, the primary grouting work was initially concentrated in the southeastern corner of the site. A test area was located in this corner. A first pass grout injection pattern was developed as shown on Figure No. 1. Approximately 30% of the total number of primary holes were grouted in the first pass. Injection in the remaining 70% of the primary holes (second pass) indicated that the 30% pattern was insufficient to insure adequate ground stabi-

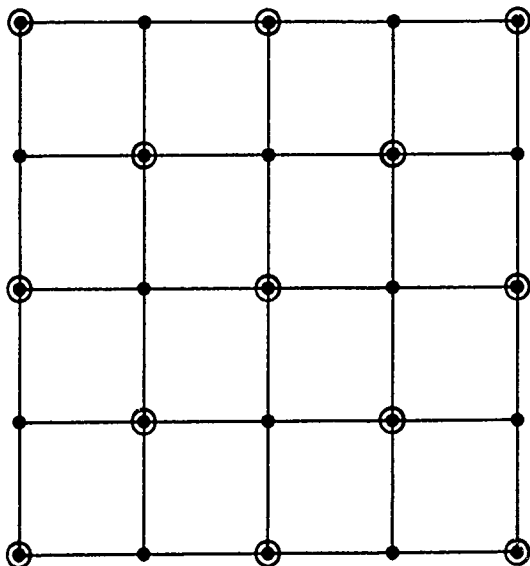


**Legend:**

- Primary Holes on 3.2m centers
- ⊙ Injection Holes in the first pass (30% of the Pattern)

Pattern shown typical of Contractor's Grid Pattern

**Figure 1 Plan of First Pass Injection Holes**



**Legend:**

- Primary Holes on 3.2m centers
- ⊙ Injection Holes in the first pass (50% of the Pattern)

Pattern shown typical of Contractor's Grid Pattern

**Figure 2 Plan of Modified First Pass Injection Holes**

lization. Therefore, a modified first pass grout injection pattern was developed and used thereafter. This pattern is shown in Figure No. 2 and utilizes 50% of the full primary pattern in each pass.

The data obtained in the test area was extremely useful in assessing grouting results throughout the remainder of the site. Table No. 1 contains tabulation of partial grouting data from the test area. The quantities in this table are the recorded grout quantities placed in the test area, broken down by stage (pass) of grouting.

Significant grout takes were realized during first pass grouting in the 12.5 meters of depth immediately below the facility foundation and in the 12.5 to 25-meter depth zone. Second pass grout takes were considerably less for the upper 12.5 meters than the lower 12.5 meters.

#### GROUTING WITHIN THE BUILDING LIMITS

The program emphasized grouting in the vicinity of the known large cavity in the southeastern portion of the site to gain experience and to establish grouting guidelines. As grouting progressed toward the northwestern portion of the site, it was possible to identify two separate areas with differing ground conditions and differing grout takes. The line of demarcation between these two areas was quite distinct and was as shown on Figure No. 3. Segment No. 1 contained the large horizontal void and a system of smaller cavities; Segment No. 2 contained in general only small cavities and fractured rock. Grout takes in Segment No. 1 were relatively large and erratic while in Segment No. 2 they were relatively small and consistent.

In general, five conditions were utilized in the evaluation of the effectiveness of the ground stabilization and the determination of the extent of grouting required: grout quantity, location of grout quantity, grout take correlation between nearby grout holes, time required for grouting each hole, and logs of investigative borings and grout holes.

Conditions encountered in Segment No. 1 required the full verification grouting program. Several grout mixes, covering a wide range of viscosity, were evaluated for use in verification grouting and were tested in Segment No. 1. The primary grout mix was concluded to be appropriate for all primary and verification grouting.

In one portion of Segment No. 1 (lines 52 to 62, Lines A to I), a number of verification grout takes were high. Careful evaluation of the data indicated that ground stabilization was accomplished in the upper 12.5 meters during the primary grouting. Some minor voids remained to be filled by the verification grouting below the 12.5-meter depth.

Use of the full primary grouting pattern in the northeastern corner of Segment No. 2 per-

**TABLE 1**  
**TEST SECTION GROUTING DATA**

|                                   | <u>No. of<br/>Grout<br/>Borings</u> | <u>Total<br/>Grout<br/>Quantity</u> | <u>Average<br/>Grout<br/>Quantity<br/>Per Boring</u> | <u>Percent of<br/>Total Grout<br/>Injected in<br/>Test Area</u> |
|-----------------------------------|-------------------------------------|-------------------------------------|--|---|
| First Pass<br>Top 12.5 meters     | 30                                  | 529.49m <sup>3</sup>                | 17.65m <sup>3</sup>                                  | 31.8%   |
| First Pass<br>Bottom 12.5 meters  | 30                                  | 426.19m <sup>3</sup>                | 14.21m <sup>3</sup>                                  | 25.6%   |
| Second Pass<br>Top 12.5 meters    | 69                                  | 119.12m <sup>3</sup>                | 1.73m <sup>3</sup>                                   | 7.2%  |
| Second Pass<br>Bottom 12.5 meters | 69                                  | 588.09m <sup>3</sup>                | 8.52m <sup>3</sup>                                   | 35.4%   |
|                                   |                                     | 1662.89m <sup>3</sup>               |  | 100.0%  |

mitted evaluation of the effectiveness of first pass injection. First pass grouting was sufficient throughout Segment No. 2 and was verified by selected verification grout holes.

#### GROUTING OUTSIDE THE BUILDING LIMITS

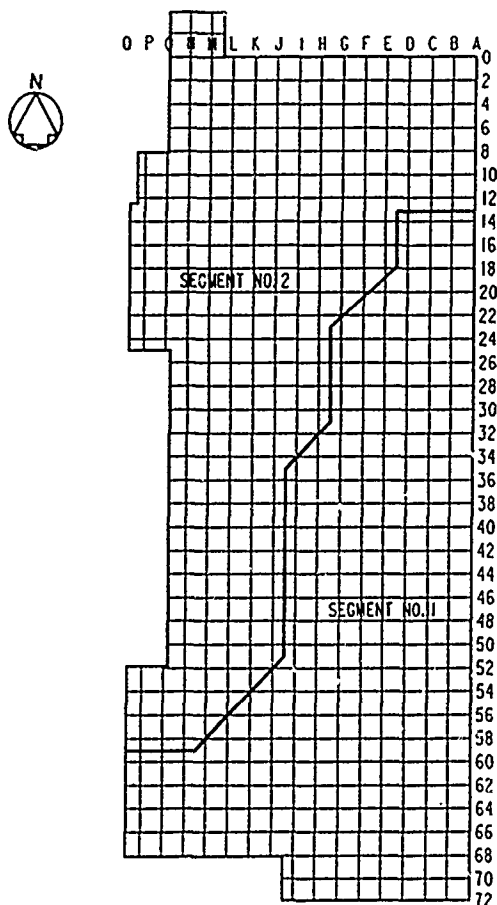
Grout take data for the inclined borings was evaluated in the same manner as indicated above for the interior of the site, taking into consideration the difference in spacing at 25-meter depth. The inclined borings were at the ends of the grouting grid lines and the cluster of borings were drilled at pre-determined angles. At various locations, verification borings were directed in order to substantiate ground stabilization.

An area of high grout take was encountered along the southern boundary of the site during placement of grout in the inclined holes. Full verification grouting was directed in this area and ground stabilization was indicated by the verification grouting.

#### COMPLETION OF PROGRAM

The subsurface grouting stabilization program began in early August of 1986 and was completed in a timely manner on February 2, 1987. The following quantities of grout had been placed:

|  |                                |
|--|--------------------------------|
| Perimeter Barrier Grout                  | 65.20 m <sup>3</sup>           |
| Mass Cavity Fill (Concrete Not Included) | 3,322.44 m <sup>3</sup>        |
| Primary Grout                            | 7,009.62 m <sup>3</sup>        |
| Secondary Grout                          | 618.39 m <sup>3</sup>          |
| <b>TOTAL Grout Quantity</b>              | <b>11,015.65 m<sup>3</sup></b> |



**NOTE:** Numbers and Letters Indicate Contractor's Grid Pattern on 3.2m spacing.

Test Section Was Inside Grid Lines 52 to 72 and A to I.

**Figure 3 Plan of Segments 1 and 2**

The grouting program was completed according to the design plan and procedure.

#### CONCLUSION

The grouting work has bonded together a rock mass 2½ meters thick. This very stiff mat bridges the unstable area and provides for a relatively uniform load distribution into underlying rock fall and the more stable surrounding bedrock. Drilling and observation data indicates that the conditions causing the cavity and displaced bedrock has been inactive and stable for a long period of time.

This project demonstrates the need for an awareness of possible cavities in eastern Saudi Arabia, especially those not encountered during excavation. After assessing the size and depth of a cavity that would be critical to a project, one must select an exploratory method(s) to detect critical cavities under a building site.

#### REFERENCES

- Grosch, J. J., Touma, F. T. and Richards, D. P., (undated), "Solution Cavities in the Limestone of Saudi Arabia"; paper presented at Faculty Engineering, University of Petroleum and Minerals, Dhahran. Unpublished.
- Powers, R. W., Ramirez, L. R., Redmond, C. O. and Elberg, E. L., (1963), "Geology of the Arabian Peninsula - Sedimentary Geology of Saudi Arabia." USGS Professional Paper No. 560-D.



## Evaluation of the Site Investigation and Construction Related Aspects of the Milwaukee Crosstown Deep Tunnel

**R.C. Ilsley**  
Principal Engineering Geologist, STS D'Appolonia, Ltd., USA

**E.F. Shorey**  
Senior Engineering Geologist, CH2M Hill, Inc., USA

**S.B. Fradkin**  
Project Geologist, STS D'Appolonia, Ltd., USA

**SYNOPSIS:** The excavation of the 21,300 foot long, 32.33 foot diameter Crosstown Phase I Tunnel was completed by tunnel boring machine at an average rate of 108 feet per 3 shift day. No geologic conditions were encountered which were sufficiently adverse to impede the work. The geotechnical report combined with contract provisions prevented the unusual conditions encountered from becoming issues that delayed the work. It is probable that the monetary aspects related to these unusual conditions can be equitably resolved using the geotechnical data "base line" portrayed in the geotechnical report.

### INTRODUCTION

The 21,300 foot long, 32.33 foot bored diameter Crosstown Phase I Interceptor is required for sewage storage and transport as part of the \$2.2 billion Milwaukee Water Pollution Abatement Program (MWPAP). The tunnel with two 25 foot diameter construction shafts is located in Silurian Age dolomites of the Niagara Group. The tunnel was excavated down a 0.1 percent gradient with a Robbins tunnel boring machine. The excavation began in October 1985 and was completed in September 1986, the only significant delay being a 4 week period when a main bearing was replaced (Santacroce 1987). The work was done on a 3 shift 5 days a week basis.

The tunnel alignment is primarily beneath the Menomonee River Valley (Figure 1), which is also a pre-glacial valley, thereby resulting in up to 220 feet of glacial and post-glacial sediments with the water table level at about 5 feet below the existing ground surface, except at the west end of the alignment. Here the alignment moves out of the pre-glacial valley with correspondingly thinner soil cover resulting. The depth of the tunnel ranges between 275 and 345 feet. The bedrock cover over the tunnel crown is typically about 100 feet, but ranges from a minimum thickness of 18 feet to about 200 feet. The minimum thickness occurs in a depression of the bedrock surface within the pre-glacial valley as described above. The depressed area has been termed the "bedrock valley area". A series of 15 foot long probe holes into the tunnel crown in this area during construction did not encounter the bedrock surface.

### EXPLORATION PLAN

The exploration was done in three phases. These phases may be broadly described as the study area exploration, corridor exploration and the potential problem or geological hazard exploration. Borehole spacing ranged from 200 feet centers in the potential problem areas to a maximum of 2,500 feet along the alignment.

The geotechnical report relied upon the vertical boreholes to recover core for logging, water pressure testing and for placement of piezometers. In addition, local tunnels (within 10 miles) and quarries were mapped and three pump tests performed. A laboratory test program to characterize rock material properties, including direct shear tests of discontinuities was performed. This information was combined to describe the rock mass characteristics. Angled boreholes were considered but given the perceived technical difficulties were not used. Also, the use of geophysical methods for fault location was not used because the potential offsets in formation boundaries were considered insignificant.

### ROCK CONDITIONS

#### Lithology

The tunnel is in dolomite and is located primarily within the upper part of the Mayville Formation and the Waukesha Formation, mostly the latter (Figure 2). Along its length the tunnel penetrates almost the full thickness of the Waukesha Formation. The principal features used to subdivide the formations were: the presence of chert; zones of shale partings; and the presence and size of vugs. The lithologic descriptions of the formations developed from the geologic mapping of the excavated tunnel are consistent with the descriptions provided in the geotechnical report included with the contract documents. There are no differences of note. In addition, the location of the formation contacts encountered in the tunnel conformed closely to those predicted in the geotechnical report.

#### Rock Structure

**Bedding** - The bedding is defined by horizontal shale layers that range from very thin partings to layers about 2 inches in thickness. The thickness is generally variable along a single bedding plane. Ninety eight percent of the bedding planes logged from the core indicated shale fillings with an average thickness of approximately 0.05 inches and clay typically

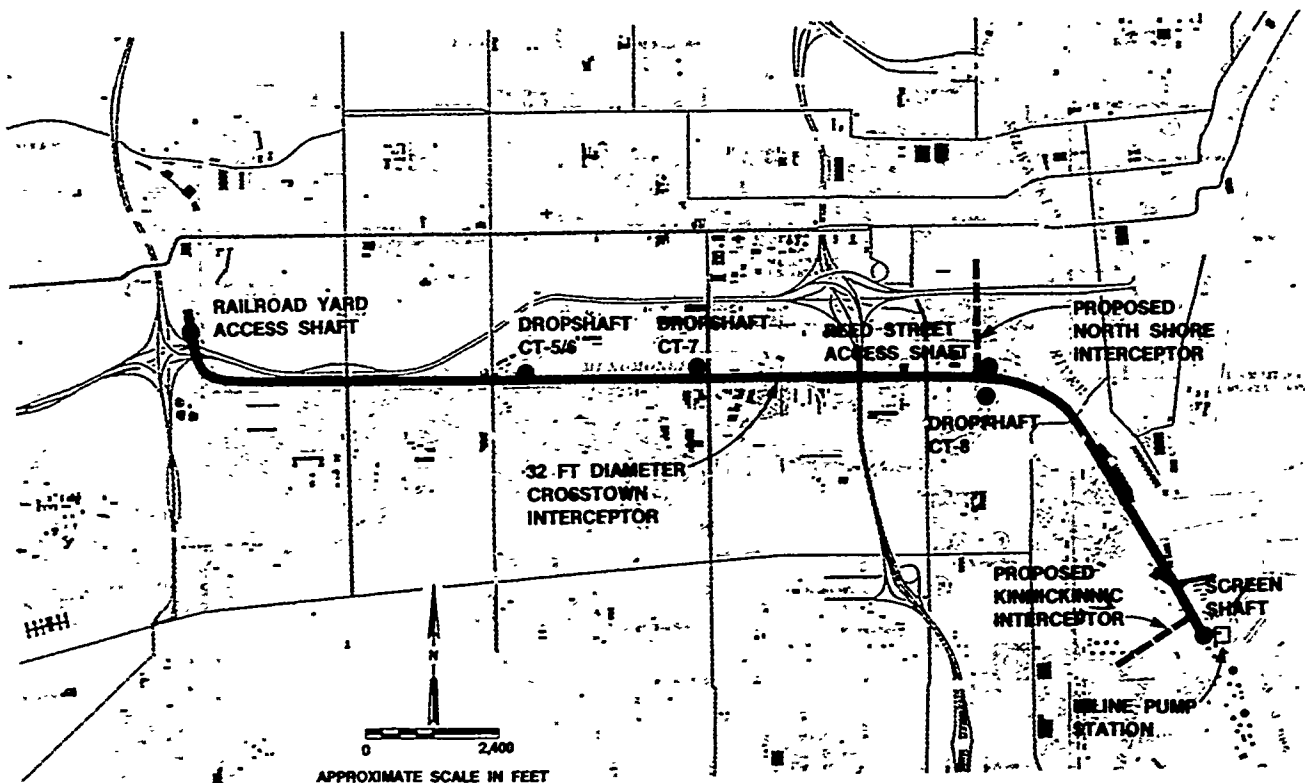


Figure 1. Vicinity Map: Crosstown Interceptor and Shafts.

0.25 inches. The gradient of the tunnel with respect to the dip of the beds was such that it cut downwards through the bedding planes at a very slight angle. Because of the circular tunnel shape, the limited slaking effects on the bedding plane fillings and the placement of rock reinforcement behind the TBM cutter head, no significant failure of thin bedding slabs was experienced, either short or long term.

**Joints** - For the site investigation, mapping of area tunnels and quarries during the exploration phase provided the orientation data for the joints (Ilsley '83). Logging of rock core provided the joint characteristics on a site specific basis. The principal part of the mapping effort was the detailed engineering geological mapping of an 8 foot diameter tunnel (excavated by TBM) in the Waukesha Formation, located about 10 miles from the project site. Determination of the preferred joint orientations in the Milwaukee area were made by plotting this data on stereograms. Joint spacing data were compiled from the tunnel maps and presented in tabular form in the geotechnical reports (Ilsley '84).

The geologic conditions in the excavated Crosstown Phase I tunnel were recorded on graphic and descriptive logging forms by engineering geologists.

The following general conclusions are based upon a comparison of the geotechnical report data and that from the geological mapping.

- The majority of joints are steeply dipping and belong to two major sets, one striking NW-SE and one striking NE-SW as predicted by the geotechnical report.
- The predominant joint set is the NW set; the table of joint spacings included in the geotechnical report inferred this was the case but not to the degree actually found.
- About 70 percent of the joints logged are either clay or shale filled. This is about three times more than indicated in the geotechnical report.

The most probable reason that the indicated percentage of clay or shale filled joints was greater was because the average joint aperture logged in the core was very small (in the range of 0.01 inch to 0.25 inch), whereas in the tunnel the significant joints logged had an average thickness of 1.25 inch. We would therefore recommend that when logging core for such facilities only discontinuities with an aperture greater than 0.10 inch be logged.

True spacings (measured perpendicular to joint strike) of the joints are tabulated for each joint set below for the whole length of tunnel.

#### TRUE JOINT SPACINGS

| Joint Set(ft.) | Minimum (ft.) | Maximum (ft.) | Median (ft.) | No. of Joints |
|----------------|---------------|---------------|--------------|---------------|
| NW             | 1 (6)         | 370 (>100)    | 34 (24)      | 198           |
| NE             | 1 (9)         | 3,200 (>100)  | 50 (75)      | 105           |

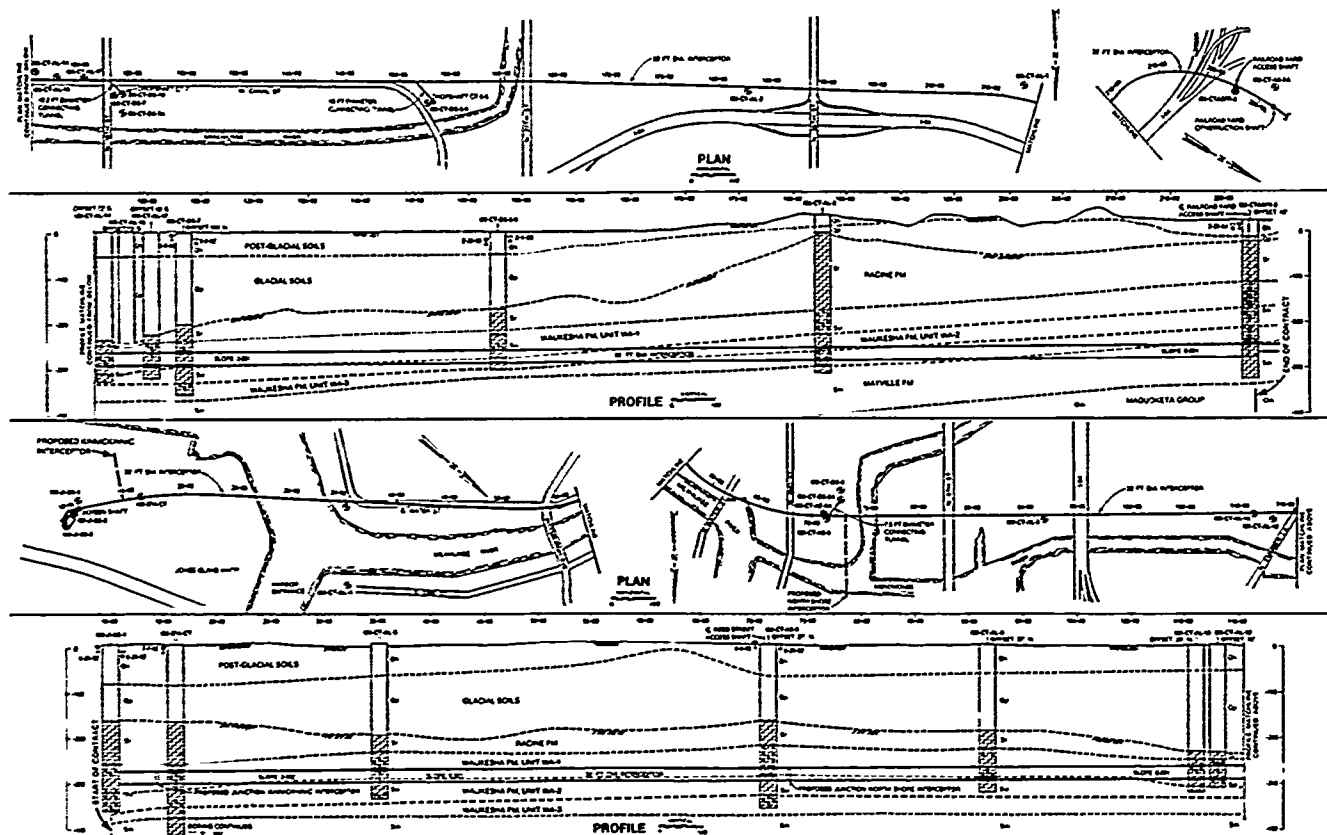


Figure 2. Plan and Geologic Profile.

The values in parentheses in the above table are those presented in the geotechnical report. The data presented in the table indicate that the observed joint spacings compare favorably with the values presented in the geotechnical report.

However, in the section of tunnel beneath the "bedrock valley" (station 108+00 to 121+00) the joint spacings were less than those presented in the geotechnical report.

**Faults** - The geotechnical report describes the type of fault that may be intersected as having a true width of 5 feet or less and having gouge or crushed rock zones. Also indicated is a possibility of encountering one or more faults of this size per mile of tunnel.

Most of the 126 faults mapped are features with relatively narrow width that are similar in character to the observed joints in the tunnel. About 80 percent of the observed faults have widths less than 0.1 foot; only about 5 percent have widths greater than 0.5 foot. In most cases the rock adjacent to the fault is undisturbed. About 80 percent of the observed faults have clay and/or shale fillings, occasionally with crushed rock (breccia) or secondary mineral deposition. The remaining faults typically have fillings of crushed or sheared rock, or mineral deposits.

All of the wider faults occur in the "bedrock valley" area between station 117+50 and 120+50.

Five (5) faults occur in this section. They have maximum widths of 1 to 4 feet, but in all cases they narrow to about 1 inch or less in the tunnel crown. These features have apparent vertical displacements of 1 to 3 feet, but the total apparent vertical displacement across the zone is only about 2 feet. As the rock was continuous in the crown, no delays were experienced by the TBM.

Steel ribs and lagging were used to construct forms at the tunnel surface and across the faults which were then filled with grout.

#### Rock Strength

The average unconfined compressive strength for the Waukesha Formation, was 26,640 psi with a range of 6,750 to 45,100 psi. Unconfined compression tests on samples of weathered rock from boreholes within the "bedrock valley" area (station 108+00 to 121+00) gave values of 5,429 and 6,709 psi. The tunnel maps contain general qualitative descriptions of the rock fabric, including references to solutioning and weathering from station 110+50 to 119+50. This was the only tunnel section where the rock was weaker, however, the rate of TBM advance was somewhat greater than the average. It appears that the presence of chert did not affect the rate of TBM penetration or the disc-cutter replacement rate.

## Initial Support

A 5 by 5 foot pattern of dowels with 9 dowels per station was required and paid for in the contract. This pattern of dowels functioned as both the minimum initial support and minimum final support. The dowels are 1.125 inch diameter rebar, encapsulated with polyester resin. The top five bolts are 10 feet long and the remainder 12 feet. The dowels were closed up to a 3 feet longitudinal spacing in the "bedrock valley" area where the rock cover was known to be thin. Other occasional spot reinforcement with dowels was used, sometimes with steel straps or wire mesh. These additional dowels were also paid for under the contract and numbered some 45,000 lineal feet (about 10 percent more than required for the 5 by 5 foot pattern). Steel straps and wire mesh were not paid for.

The top 5 dowels were placed directly behind the cutter head through slots cut in the trailing partial steel shield. The remaining 4 dowels were placed at a point some 75 feet behind the cutter head.

## Final Support

The contract required about 700 feet of reinforced concrete lining at junctions with shafts and connecting tunnels. There was also a provision for 3,500 feet of lining to be placed at the engineer's direction. The evaluation of data collected during the tunnel mapping was the basis of determination of which parts of the tunnel should be lined. The general criteria used were:

- . Greater than normal frequency of jointing.
- . Increased number and/or thickness of clay, shale and/or gypsum fillings in joints and bedding planes.
- . Juxtaposition of joints from different sets that may delineate wedges, blocks or slabs with potential for fall out.
- . The presence of weathered zones which could be eroded or deteriorate with time.

In general, lining was recommended for tunnel sections in which joint and bedding characteristics, in terms of the criteria listed above, combine in a manner that gives potential for deterioration of the rock mass over time. Such deterioration is expected to be limited to minor spalling or raveling of the rock surface and to washout or solutioning of thicker joint fillings which could lead to new sources of groundwater inflow. The potential for washout and/or solutioning of isolated joints is recognized by specifying "dental treatment" for such features. This involves removing the joint filling to a depth proportional to the width and backfilling with shotcrete. A total of about 5,500 feet of engineer directed lining has been specified, some 25 percent of the total tunnel length.

## GROUNDWATER CONDITIONS

### Introduction

The dolomite bedrock through which the tunnel was excavated is a semi-confined aquifer. The underlying Maquoketa Group is a leaky aquitard and the overlying glacial soils provide recharge. Recharge also occurs to the west of Milwaukee where the dolomite outcrops or is close to the surface. The aquifer characteristics were estimated during the exploration phase by water pressure testing in the boreholes and three pump tests at different locations. The pump tests yielded flows of 34, 150, and 508 gpm and transmissivities of 470, 1300 and 5000 gpd/ft. The permeability coefficient

measured ranged from  $>1 \times 10^{-3}$  cm/sec to  $<1 \times 10^{-7}$  cm/sec with most values less than  $1 \times 10^{-5}$  cm/sec. Piezometric levels of the dolomite are generally within 10 to 20 feet of the ground surface. However, there is a 2 mile diameter cone of depression centered on the Red Star Yeast high capacity well which is offset about 600 feet to the north of station 165+00.

The soils aquifer along the tunnel alignment within the Menomonee River Valley, ranges from 150 to 220 feet thick. The soil stratigraphy is generally as follows; glacial soils (usually till) on bedrock, overlain by glacial lacustrine clays, outwash, alluvial soils, estuarine (marsh) deposits and fill. Observation wells open in the upper 30 feet or so show a water table generally about 5 feet below ground level. Piezometers placed in the alluvial zone indicate a semi-confined aquifer with piezometric levels a few feet higher than those placed at the soil/rock interface or within the bedrock.

It was recognized that dewatering of the alluvial layer might induce significant consolidation related settlements of the overlying estuarine deposits. Hence no dewatering at the Reed Street Access construction shaft was permitted. The possibility of connection between the dolomite bedrock and the upper alluvial aquifer was judged to be minimal and probably balanced by recharge from the river. However, provision was made in the contract to place a series of piezometers directly over the tunnel alignment, sensing the alluvial soil layer.

### Water Inflows to the Tunnel

Sources of Inflow - The geologic mapping indicates that most inflows to the tunnel are from joints. Bedding planes are a minor inflow source. Also, some inflows are from zones of interconnected vugs.

Roughly one half of the northwest joints and one third of the northeast joints produced flowing water. Another approximate 15 percent of the joints in each set produced small amounts of water inflow that were described as dripping. Significant groundwater inflows into the tunnel did not begin until mid-March 1986 (Figure 3) at which time the TBM entered the "bedrock valley" area at about station 121+00.

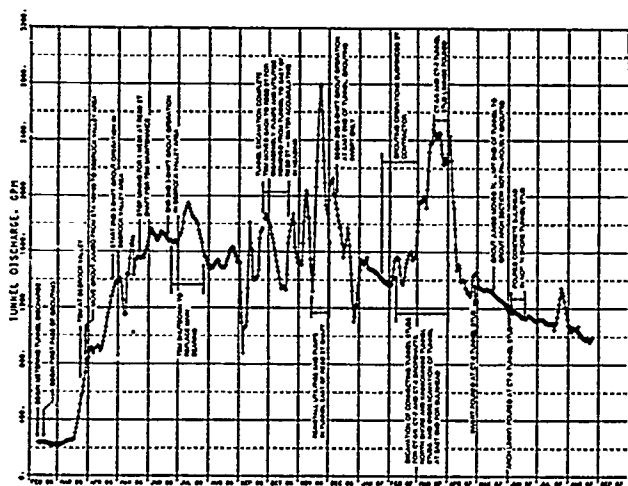


Figure 3. Estimated Inflows to Tunnel.

The next 1300 feet yielded total inflows of about 700 gpm and further tunnel excavation, raised this to a maximum of about 1,800 gpm. The geotechnical report indicated a total flow of about 1,500 gpm for the tunnel whereas the actual ungrouted flow (estimated from tunnel maps) was 2,300 gpm.

The "bedrock valley" area initially was, and remains, one of the wettest tunnel sections (Figure 4). The zone of wider faults (see "Joints and Faults") between station 117+50 and 120+50, the western end of the "bedrock valley" area, combined with the section from station 115+00 to 117+50, which includes four narrower faults, account for somewhat more than one third of the groundwater inflow estimated for the "bedrock valley" area.

**Measurement of Inflow** - Groundwater inflows have been indirectly measured using the amount of water being discharged by the contractor's pumping system (corrected for the amount of service water introduced) as an estimate of the amount of groundwater flowing into the tunnel. A plot of metered tunnel discharge with time is provided in Figure 3. The plot represents a 7-day term moving average through the data; i.e., the data point plotted for each day is the average of the discharge for that day plus the three preceding and three subsequent days.

Figure 3 contains a number of annotations of events in the tunnel which have likely affected the amount of water being discharged from the tunnel at specific points in time.

A review of Figure 3 indicates that the overall trend of the water inflows to the tunnel has been, and continues to be, downward from the peak inflows of June 1986. The current (late August 1987) water inflow rate of just less than 1,000 gpm is slightly more than half of the peak inflow rate of June 1986, and is less than half (about 45 percent) of the estimated initial ungrouted inflow rate for the whole tunnel of approximately 2,300 gpm.

Inflow monitoring within the tunnel has been conducted over nearly 80 percent of the tunnel length. Measurements were made between 20 January 1987 and 10 April 1987. The results

are summarized in Table 1, and are compared graphically to the estimated initial inflows (based on the geologic mapping) in Figure 4.

A review of Figure 4 indicates that for a number of tunnel sections the groundwater inflows to the tunnel have been reduced significantly as a result of cementitious grouting. In a number of tunnel sections, significant inflow reductions have been achieved with one pass of grouting. However, for a number of sections in the west half of the tunnel, one pass of grouting has produced marginal results. An as yet unknown amount of grouting remains to be done in the invert in the western half of the tunnel (see "Grouting"), and it is expected that this additional grouting will result in further inflow reductions.

For a few sections, however, the dye dilution measurements appear to indicate that inflows have increased from the initial rates (Figure 4). The probable reason for these apparent increases is that the initial estimates were visual and were probably low. In general, these sections have relatively small inflows.

#### Contractual Provisions

**Pumping of Inflows** - Items in the contract bid provided graduated payments for pumping of the groundwater inflows beginning when flows exceeded 1,500,000 gpd. Measurement of these pumped flows by meters must take into account the water added by the contractor's operations. Also, the meters should be calibrated using a method such as the dye dilution method of flow measurement.

**Grouting** - Because the design aimed at minimizing the amount of tunnel to be lined, the control of groundwater by grouting was specified to be at the direction of the engineer. Bid items were provided for drilling grout holes, water pressure testing the grout hole and connecting the grout pump to the drill hole (connections), sacks of cement and cubic feet of grout placed. At the end of August, 1987 essentially two tunnel passes of cement grouting have been done. The quantities used are shown in Table 2. Although the contract has provision for chemical grouting (silica), none has been done at this time. The grouting plan was essentially feature grouting beginning with mixes based upon initial single water pressure test takes of the grout hole. Increases in grouting pressures signaled the use of progressively thicker mixes. The starting grout mix ratio was usually 10 to 1, water to cement by weight (Coon 1987) with 2 percent by weight of bentonite.

#### Piezometric Levels

Piezometric levels in soil and rock aquifers were drawn down as a result of groundwater inflows into the Crosstown Phase I tunnel and into Crosstown dropshaft excavations. The significant drawdowns occurred as the tunnel excavation passed into and through the "bedrock valley" area.

Numerous piezometers are located along the tunnel alignment. These piezometers have

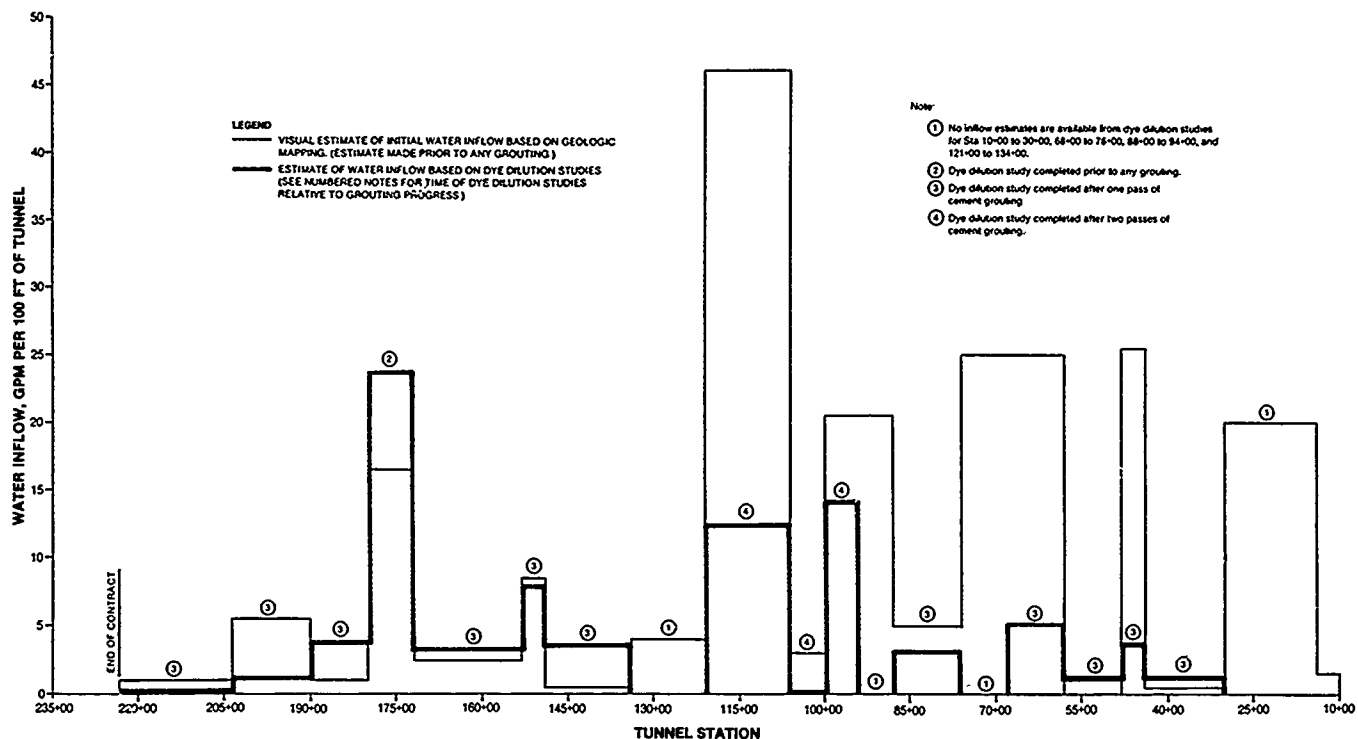


Figure 4. Water Inflows by Tunnel Section.

sensing zones in the alluvial, lacustrine and dolomite aquifers which underlie the estuarine deposits in the lower Menomonee River Valley. Piezometers with sensing zones within or above the estuarine deposits generally sense the water table aquifer; which was not drawn down. The measured piezometric levels in the alluvial soil aquifer are recovering from the low levels recorded in 1986. The recoveries as a percentage of the maximum drawdown are in the range of 20 to 40 percent. The measured piezometric levels in the dolomite aquifer are also recovering from the low levels recorded in 1986. Recoveries as a percentage of the maximum drawdown are in the range of 50 to 60 percent.

Table 1. Measured Water Inflows.

Note: W and D denote measurement by weir and dye dilution.

| Stations         | Test Method | Inflow (GPM) | Test Date |
|------------------|-------------|--------------|-----------|
| 219+85 to 174+00 | D           | 239          | 4-10-87   |
| 174+00 to 153+25 | D           | 64           | 4-9-87    |
| 157+25 to 148+00 | W           | 65           | 3-2-87    |
| 146+50 to 129+00 | D           | 193          | 4-2-87    |
| 123+00 to 110+00 | W           | 300          | 3-6-87    |
| 120+50 to 97+75  | D           | 214          | 4-8-87    |
| 98+75 to 94+00   | D           | 62           | 2-20-87   |
| 88+00 to 78+00   | D           | 25           | 2-20-87   |
| 67+75 to 27+75   | D           | 110          | 1-20-87   |

Table 2. Grout Quantities.

Notes: (1) Grouting suspended by contractor.  
(2) Not a bid quantity.

| Month                         | Station                              | No. of Holes | Lineal Ft. of Drilling | Bags of Cement | Cu. Ft. Grout |
|-------------------------------|--------------------------------------|--------------|------------------------|----------------|---------------|
| February, 1986                | 211+45 to 201+04                     | 74           | 778                    | 206            | 814           |
| March                         | 200+50 to 180+55                     | 85           | 1,002                  | 278            | 1,168         |
| April                         | 121+00 to 117+40                     | 117          | 2,557                  | 972            | 2,558         |
| May                           | 121+00 to 108+00                     | 202          | 8,302                  | 5,357          | 17,711        |
| June                          | 119+00 to 93+00                      | 122          | 4,407                  | 4,424          | 24,437        |
| July                          | 99+35 to 73+55                       | 190          | 5,501                  | 3,666          | 17,268        |
| August                        | 70+00 to 58+50                       | 185          | 6,645                  | 6,234          | 19,651        |
| September                     | 66+00 to 24+50                       | 169          | 5,743                  | 2,932          | 11,750        |
| October                       | 93+57 to 58+50                       | 170          | 6,867                  | 5,148          | 24,186        |
| November                      | 89+95 to 98+34                       | 155          | 7,094                  | 2,560          | 15,392        |
| December                      | 98+00 to 108+85<br>10+85 to 18+50    | 122          | 4,251                  | 2,042          | 9,961         |
| January, 1987                 | 125+00 to 174+00<br>18+65 to 25+50   | 155          | 5,242                  | 4,191          | 17,430        |
| February (1)                  |                                      | —            | —                      | —              | —             |
| March                         | 149+00 to 157+50<br>108+00 to 111+00 | 189          | 7,877                  | 3,963          | 14,840        |
| April                         | 111+00 to 120+00<br>173+00 to 180+00 | 279          | 10,224                 | 3,183          | 10,592        |
| May                           | 10+30 to 17+00                       | 57           | 2,506                  | 2,410          | 7,445         |
| June                          | 17+00 to 24+00                       | 180          | 8,093                  | 5,551          | 21,019        |
| July                          | 24+00 to 29+00<br>45+00 to 60+00     | 163          | 7,554                  | 3,131          | 12,768        |
| August                        | 60+00 to 70+00                       | 205          | 9,177                  | 2,310          | 13,464        |
| Totals through 28 August 1987 |                                      | 2,819        | 103,820                | 58,558         | 242,454       |
| Bid Quantities                |                                      | 2)           | 200,000                | 20,000         | 250,000       |

## SUMMARY

A most successful aspect of the geotechnical exploration was the planned phasing of the work into the study area, corridor and problem or geological hazard exploration. This allowed the investigation to focus on the areas requiring further study and provided current geotechnical information for the facilities planning and design.

The spacing of exploratory boreholes along the alignment (maximum of about 2,500 feet) was adequate. The recognition of the potential for a "bedrock valley" came from topographic bedrock surface maps drawn using data from the first two phases. This prompted a final phase (problem area borings) of exploration which defined the extent of the depression, the increased joint frequency and the presence of weathering. However, no faults were intersected and none specifically inferred in this area because there were no apparent displacements across well defined formation contacts. The depression in the top of rock in itself indicated the probability of preferred erosion but without other corroborating factors it was judged that speculation on the presence of faults in this section was not appropriate. As it turned out, the thinning of the faults to joint dimensions through the crown enabled the TBM to continue excavation without delay. The volumes of water encountered in the "bedrock valley" were not predicted specifically in the geotechnical report. However, the contract provisions for pumping of this water and for grouting it off have prevented the inflows from being an issue.

The significant drawdown in the piezometric surface of the dolomite was related to the large inflows from the "bedrock valley" which in turn induced large drawdowns in the alluvial layer. This connection was unexpected as was the areal extent of the effect (about 2 miles in total length). Four recharge wells were setup and operated with some success in equalizing the levels. At the same time grouting efforts were doubled in the "bedrock valley" area. Recovery is underway in both the alluvial and dolomite aquifers. An optical survey of settlement points set up on sensitive structures within the affected area show settlements thus far to be generally less than 0.30 inch.

In hindsight, it would appear that having a shotcrete option for final lining support of the tunnel arch would have given more flexibility in choice of permanent support types. This would have been an intermediate choice between the pattern of dowels and a full circle, unreinforced concrete liner. Also, the specified nine bolt pattern could have safely been reduced to five, with the remaining four as optional depending upon the encountered rock conditions.

In conclusion it may be said that the geotechnical report was generally accurate when predicted and encountered conditions are compared. The phased approach to the exploration worked well. The important areas of initial support and groundwater inflows did not become issues because of provisions made elsewhere in the contract documents as previously described.

## REFERENCES

Coon R.F., Shorey E.F., and Fradkin S.B., "Grouting for Groundwater Control, Milwaukee Inline Project" (1987), RETC Proceedings. Vol. 1 p. 435, New Orleans.

Ilsley R.C. and Costello M.J., "Discontinuity Characterization for Underground Openings in the Milwaukee Water Pollution Abatement Program" (1983), Underground Space, Vol. 7 pp. 214-220.

Ilsley R.C., Fradkin S.B. and McBee J.J., "Characterization of Rock Conditions for the Deep Tunnel Project in Milwaukee" (1984), Proceedings of 25th Rock Mechanics Symposium.

Santacroce P.U. and Meinholz J.H., "Tunnel Boring Machine Experience in the Milwaukee Program" (1987) RETC Proceedings, Vol. 2 p. 684.

# Microseismic Activity in an Open Pit Lignite Mine

J.M. Descour

Research Associate, Colorado School of Mines, Golden, Colorado

R.J. Miller

Associate Research Professor, Colorado School of Mines, Golden, Colorado

**SYNOPSIS:** An increased level of horizontal stress related to tectonic forces is often held responsible for unexpectedly strong mining induced seismicity. The authors use the Belchatow open pit lignite mine in central Poland to show that this seismicity can be explained without tectonic forces as well. The presented approach should offer affordable ways of detecting the problem before it occurs, and either preventing it or controlling its scale.

## INTRODUCTION

Mining induced seismicity is common in many coal and hard rock mines. Mining induced seismicity associated with open pit mining is rarely observed.

Development of the opening cut for the Belchatow open pit lignite mine in central Poland started in 1976. The depth of the opening cut reached approximately 90 m (meters) when the first tremor of magnitude 3.6 occurred in August 1979. It was sensed by the crew on the dispatcher tower (Fig. 1), which experienced a series of swinging movements. Ground movements were also strong in a small building occupied by the mine hydrogeological team (Fig. 1). The spilling of a tea on the table marked the direction of

the horizontal displacement (generally to the southwest). In addition, cracks showed up in the walls inside the southern portion of the building. Ground motion also was sensed in the management building (Fig. 2), and by the residents of the nearby villages.

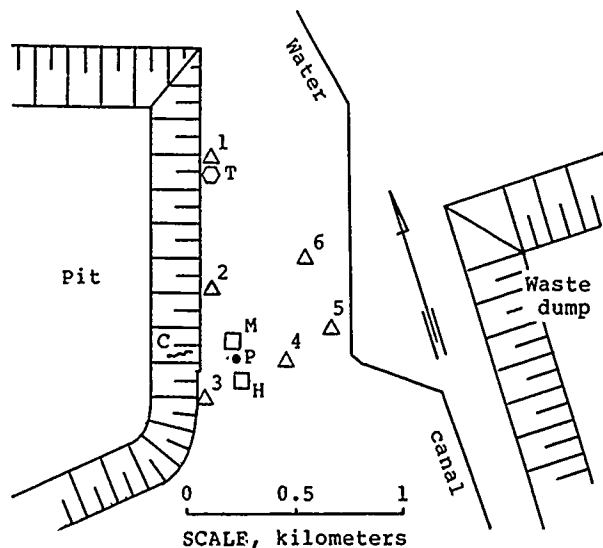


Fig. 1. Mining Situation and Elements Related to the Study on Seismic Activity. T-tower, M-monitoring station, P-piezometer, H-building, C-crack in slope, 1,2,3-geophones.

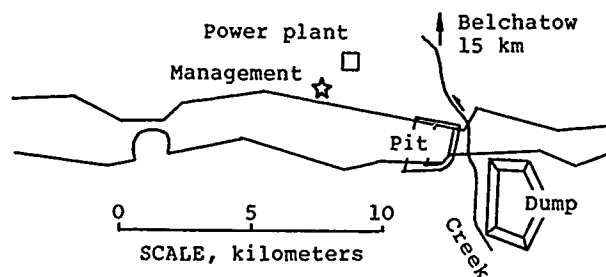


Fig. 2. Lignite Deposit in the Belchatow Trench.

The shock triggered concern about the nature of the activity, and a possible threat to the turbines of the power plant being constructed near the perimeter of the mine (Fig. 2).

The interpretation of the Belchatow case was published by Gibowicz et al. (1981, 1982), and Kijko (1983). This interpretation considered mining as responsible for disturbing an equilibrium in a "tectonically unstable, pre-stressed" horizontal stress system in the mine area. The interpretation was based on data from seismological observatories in Poland, Czechoslovakia, and a few central and northern European countries. These observatories were located more than 100 kilometers from the mine. Their ground movement recording instruments were designed for monitoring earthquakes in a frequency range below singular hertz.

Microseismic equipment was installed at the Belchatow mine site and the monitoring of microseismic activity began in the Fall of 1979. Location of the geophone array (Fig. 1) was selected based on:



- information collected from the witnesses of the first tremor,
- location of the opening pit and the waste (overburden) dump with respect to the local geological conditions,
- anomalies in the water table and vertical displacements of the ground adjacent to the pit contour.

Part-time monitoring and a number of breakdowns of the system resulted in incomplete recording or missing 11 out of 12 seismic events (magnitudes 2 and above) which occurred in 1980-81 (Gibowicz et al., 1981, 1982). All the weaker events often recorded by the system were not of seismic origin (sonic booms from jets). The epicentral location of the event of April 1980 (Fig. 1, magnitude 3.5) confirmed that the selection of the site for the geophone array was correct. It also was consistent with the model of the mining induced deformation process held responsible for the seismic events. Discussion of this model was presented to the Annual International Symposium on Geophysical Investigations in Mines held in Poland in September 1980.

The content of this paper relies on the author's recollection of his presentation and the experience at the Belchatow seismicity investigation. Study of published materials related to the subject also was helpful. The intention of this paper is to present another point of view as to the cause of the seismicity in the Belchatow case. It also emphasizes the importance of running an extensive dynamic analysis of the deformation and stress concentration process (induced by mining, in particular, geological conditions) for providing a reliable explanation of the observed seismic activity. This type of analysis is superior to considering seismic activity alone, with geological and mining situations as a static background. In each case, the choices of the monitoring equipment and array are fundamental for comprehensive study and reliable interpretation of data from mining induced seismicity.

#### GEOLOGICAL CONDITIONS

The Belchatow lignite deposit is located in the Belchatow tectonic trench approximately 15 km (kilometers) south of the town of Belchatow. The trench, 1.5 to 2 km wide and approximately 0.5 km deep, stretches east-west for over 40 km (Fig. 2). Southern walls of the trench are nearly vertical, and formed of limestone with karst (Upper Jurassic formation, Fig. 3). Cretaceous rocks, mostly sandstones and marls, border the trench from the north. Parallel faults shape these rocks into a series of steps gently dipping to the south. The bottom of the trench is lined with siltstones and claystones sometimes clayey sandstones of Lower Jurassic cut by a few parallel faults. The lignite deposit up to 150 m thick is covered by 100 to 200 m of overburden, mostly fine sands and argils with

lenses of boulder clays and silts (Fig. 3). Similar materials form the bedding sediments

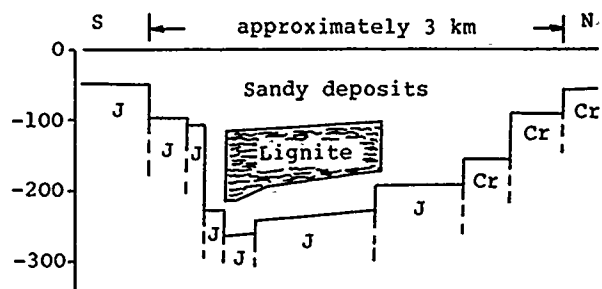


Fig. 3. Cross-section of the Belchatow Trench near the Area of Mining. J-Jurassic rock, Cr-Cretaceous rock.

down to the bottom of the trench. The deposit, 1.5 km wide in the area where the mining started, comes close to the southern wall of the trench. The northern edge of the deposit is separated from the northern side of the trench by a 0.5 to 1 km wide strip of Quaternary sands (Fig. 3). A map showing contours of the trench in the area of mining (reconstruction) is presented in Figure 4.

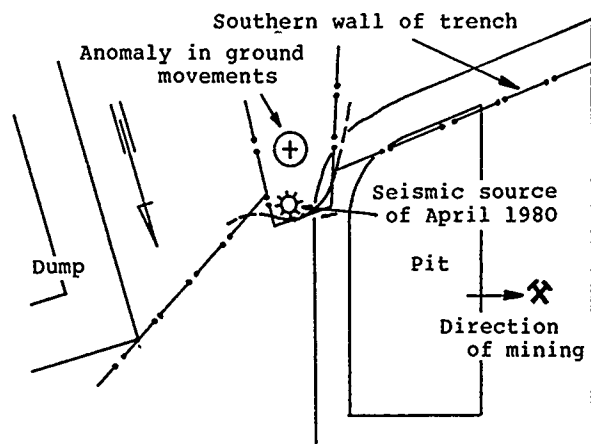


Fig. 4. Mining Situation with Respect to the Trench Morphology and Deposits.

Note the dislocation of the southern wall of the trench toward the north in front of the southeastern corner of the opening pit. Part of this wall adjacent to the pit contour is probably separated by a fault. It forms an uplifted limestone pillar with the top close (30-50 m) to the ground surface.

Permeability of the sandy sediments provides good hydraulic connections between all water reservoirs.

#### SEISMICITY AND INDICATIONS OF TECTONIC FORCES

Poland is situated far away from the tectonic hot spots of the globe. This does not exclude the presence of slowly varying weak or very uniform horizontal stress fields referred to as tectonic forces. The country sits over the transition zone between the Eastern European Precambrian platform to the northeast, and the Paleozoic platform to the southwest. Mountains along the southern border belong to two different orogenic formations. Local (in the scale of the globe) concentrations of tectonic forces are held responsible for rare and weak natural earthquakes in some locations along the southern border, and (much less) in central and north-eastern parts of the country (Olczak, 1962; Pagaczewski, 1972).

No earthquakes were reported in the Belchatow area in historic times. Based on the study of the vertical movements of the ground in Poland prior to 1975, the ground in the Belchatow area was sinking at 1 mm per year (Kielbasiewicz et al., 1982). Besides this information, the authors have no knowledge of any experimental data allowing assessment of the true level of the horizontal stress underground in Poland.

#### MINING SITUATION

The perimeter of the future mining (Fig. 2) follows the shape of the deposit. Dewatering in the mine area down to the lignite seam level started in 1975. The fine sands of the bedding deposits were left saturated with water. Figure 4 illustrates the contours of the opening pit and a part of the base of the waste (overburden) dump in 1979-80. Of the four slopes of the pit, the two parallel to the trench and the eastern slope were cut to the final angle of approximately 30 degrees. The slopes were formed mostly of sandy material. Only the bottom part of the southern slope was in the Jurassic limestone. There were no plants or grass cover which would provide any stabilizing action to the slopes. This also prevented masking surface failures as they occurred. The western slope was cut in wide steps as part of the advancing process of overburden removal. The bottom of the pit nearing the top of the lignite deposit in 1979-80 was from 90 to 110 m deep, approximately 1.5 km wide and 0.8 km

long (with respect to the trench orientation). Anomalous characteristics of slower subsidence next to the southern part of the eastern slope of the pit was related to the local bedrock structure (limestone pillar; Fig. 4). As remembered, the water table indicated a similar anomaly. There were no measurements of horizontal displacements at that time.

Dewatering of overburden probably resulted in removing water from many karst caves and tunnels in the limestone walls of the trench. In some cases, it could turn a hydraulic pressure into a depression. In each case, it should disturb the balance in a local stress system.

#### MICROSEISMIC MONITORING SYSTEM

A geophone array of six accelerometers was installed on the ground in front of the eastern slope of the pit (Fig. 1). A short period seismometer was installed side by side with the accelerometer (No. 3) for covering lower frequencies of the wave spectrum routinely recorded by seismological instruments. All transducers were oriented to respond to vertical components of the ground motion.

Accelerometers were installed in shallow holes; each was mounted on the top of a 1 m long fiberglass rod driven vertically to the full length into the ground for coupling. The seismometer was partially buried in the ground. Each hole was covered with a steel bucket, its bottom flush with the ground and capped with turf to reduce the noise from the strong winds. Signals from accelerometers were conditioned by preamplifiers and transmitted through shielded cables to the central multichannel FM magnetic tape recorder. Signals from the seismometer were transmitted directly to the recorder. Power for preamplifiers was provided from a car battery through an additional wire in each transmission cable. A loudspeaker allowed continuous audible monitoring of recorded signals. Magnetic tapes were replayed audibly and selected fragments of the record were reproduced with a stripchart oscillograph for the final data analysis.

Recording and reproducing equipment was adjusted for the frequency range from 0.5 to 375 hertz, with accelerometers covering from 10 to 3,000 hertz and the seismometer covering 0.5 to 30 hertz. An average sensitivity of the transducers was 0.015 V/m/s<sup>2</sup> for accelerometers and 400 V/m/s (volt per meter per second) for the seismometer. Dynamic range of recorded waves was limited by the tape recorder to 46 dB. The standard precision of the time reading was 0.5 ms (millisecond).

## MICROSEISMIC EVENTS AND RELATED OBSERVATIONS

A number of weak events were recorded by the system. They were generated by sonic booms from jets. Double impulse character of their waveforms and uniform frequency were detected by accelerometers. These features were filtered to singular, low frequency, weak signals on records from the seismometer. Lack of small natural seismic events between strong tremors suggested a simple stress system and a uniform stress concentration process.

The epicentrum of the event of April 1980 (magnitude 3.5) was located over the uplifted limestone pillar (Fig. 4). The dominant wave frequency detected by accelerometers was approximately 60 hertz. The dominant frequency recorded by the seismometer was approximately 12 hertz. The event was accompanied by a crack in the eastern slope of the pit almost matching to the source location. In addition, the bottom of the piezometer well near the epicenter (Fig. 1) was damaged.

Moreover, the ground deformation associated with tremors was of concern in our study of the Belchatow case. Based on published materials (Kielbasiewicz, 1982), the deformation of the ground which accompanied the first tremor was interpreted as a superposition of two types of deformation (Fig. 5a, b):

- Loose material flow toward the pit as a result of a stress relief both in vertical and horizontal direction. This flow was controlled by the trapezoidal shape of the pit and the shape of the trench.
- A powerful displacement of loose material below the lignite seam directed to the northwest. This displacement resulted in relative sinking of the ground adjacent to the southeastern corner of the pit, and strong upheaval around the northwestern corner.

## DISCUSSION

The common product of an investigation of mining induced seismicity is a retrospective model of the deformation process which has led to structural failures accompanied by seismic phenomena. While developing the model, all available data and observations allowing reconstruction of significant steps in the deformation process should be considered. The model should allow reliable prediction of the trend in the development of seismic activity, and should give clues as to how the problem can be corrected if necessary.

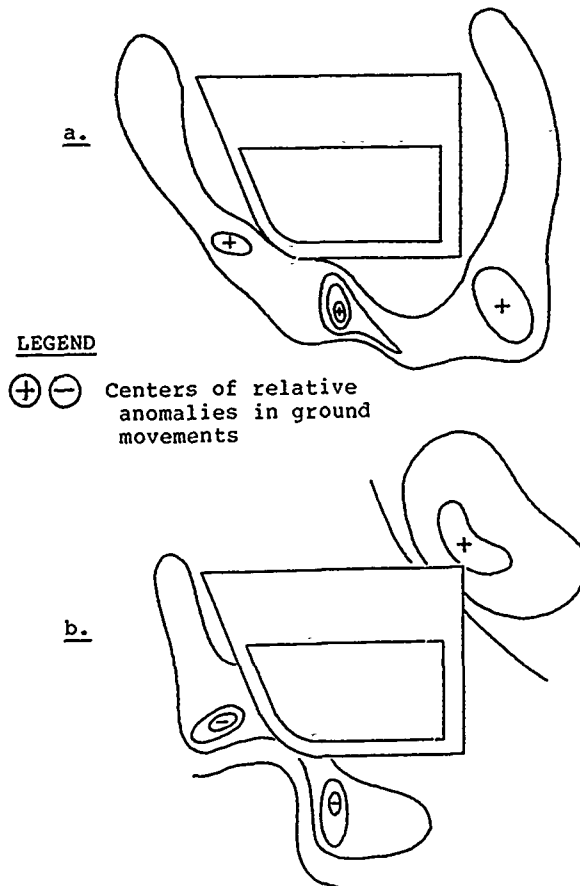


Fig. 5. Idealized Anomalies in Increments of Ground Vertical Movements: a. forced by stress relief in the trench; b. after a tremor.

## The Nature of Mining Induced Seismicity - A Model

Dewatering of overburden around the pit resulted in a thicker layer of drained but still wet sands above the water table, and a drop in hydrostatic pressure in the remaining water saturated sands down to the bottom of the trench (Fig. 6). The subsequent shift from plastic toward elastic behavior improved the stability of loose material in the trench as a result of higher cohesion, and an increase of effective stress. A reduction of the load caused by dewatering upon the trench bottom and walls was considered insignificant.

Removing large amounts of overburden from the opening pit and storing them on the waste dump resulted in a substantial change in the distribution of vertical load.

An increase of load from the waste dump outside the trench (Figs. 2,4) should not affect deposits in the trench directly. However, some concentration of horizontal stress in

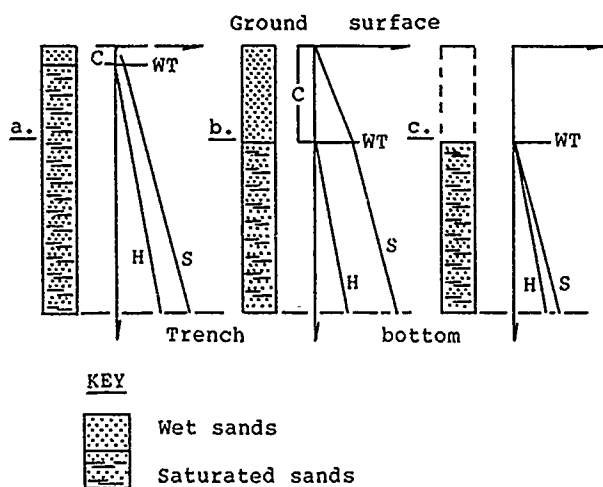


Fig. 6. Changes in Vertical Stress, Hydraulic Pressure, and Cohesion Zone in Loose Materials (a) as caused by Dewatering (b), and Overburden Removal (c). C-cohesion zone, H-hydrostatic pressure, S-effective stress, WT-water table.

the trench caused by the load from the dump could not be excluded. Nevertheless, the overburden removal was considered the major factor controlling both the vertical and the horizontal stresses within loose materials in the trench.

Horizontal stress relief should force a horizontal deformation of the surrounding material toward the pit. Flow of the material toward the pit should result in a concentration of stress, and possibly an upheaval of the ground surface in front of the pit corners and along the arch shaped zones facing each slope. The effect should be seen as anomalies in the vertical ground movements (Fig. 5a). Also, a general upheaval of the entire pit area should be expected. The upheaval phenomenon was observed since 1979 reaching the pace of up to 6 mm per year (Kielbasiewicz et al., 1982).

Mining operations inside the trench and the configuration of the pit with respect to the trench, should cause additional nonuniformities in stress. Flow of the materials from the west toward the pit should be relatively uniform, being continuously disturbed by mining advancing toward west at 400 m/year. The limestone pillar on the eastern side reduced a portion of the eastern slope exposed to the loose material flow from the east. This and the stationary character of the eastern slope resulted in developing a relatively stable stress zone in the loose materials east of the pit. This zone kept loose materials of the eastern part of the trench from flowing toward the pit. The stress zone was resting on the trench bottom and had relatively uniform support in loose

materials from the north (Fig. 7). The highest level of stress concentration (high shear stress) developed in the limestone pillar. Local centers of the stress concentration within this pillar and in the adjacent portion of the southern wall of the trench were expected to develop earlier as a result of draining water from karst caves and tunnels.

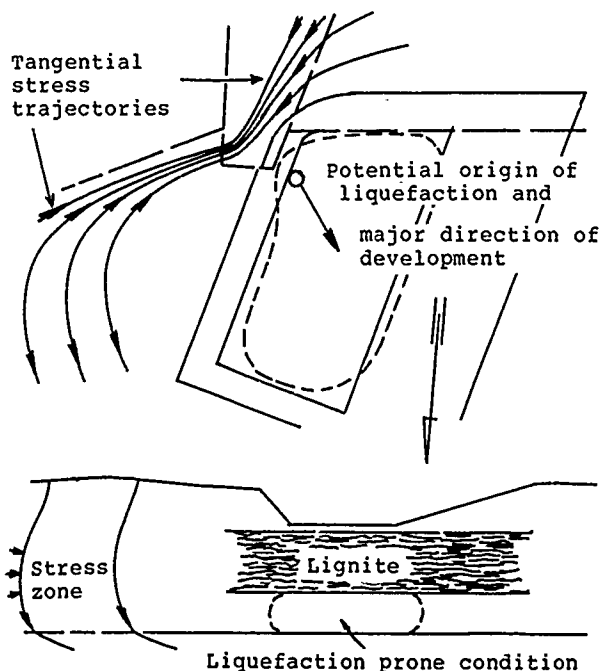


Fig. 7. Stress Zones and Liquefaction Prone Area Developed Around the Pit.

The stress concentration meant that even for a low average disturbance of stress caused by mining and dewatering operations at the pit, a local horizontal stress in the limestone pillar could reach considerable levels (Fig. 7). This could cause either collapse of individual caves or a shear failure within the pillar itself. Location of the event in April 1980 indicated the limestone pillar as the center of the stress concentration (Fig. 4). Failure in the piezometer well (Fig. 1) adjacent to the epicentral location was considered as related to the event occurrence.

Overburden removal gradually reduced a direct load upon the lignite seam and the bedding sands below the pit. Effective stress between grains dropped, while a free inflow of water maintained the hydrostatic pressure on a steady level. In the area around the lignite pillar, the obstructed flow of loose material from the east magnified the effect of the stress relief between sand grains, resulting in a condition prone to liquefaction (Fig. 7).

The energy released by any failure in the pillar should be absorbed by the stress concentration zone east of the pit. Considering

properties of the material, the large portion of this zone also should fail, resulting in a sudden massive load upon the liquefaction prone area. A hydraulic impact developing horizontally off the pillar area should force large amounts of loose materials to make a short (few centimeters) but powerful move toward the stress relief zone under the pit and up the slope of the northern wall of the trench. This should result in a strong secondary seismic effect (a phenomenon similar to the gas outbursts in coal mines). The ground surface around the pillar should drop while the upheaval of the ground surface adjacent to the northwestern corner of the pit should be expected (Fig. 5b).

Effects of this kind, with ground displacements on the order of a centimeter, were observed after the shock of August 1979 (Kielbasiewicz et al., 1982). Macroseismic effect from the strongest tremor which occurred in September 1980 (Gibowicz et al., 1982) also was directed to the northwest. In addition, the location of the crack in the eastern slope after the event of April 1980 (Fig. 4) was consistent with the surface effects expected to follow a failure in the pillar and a deformation which triggered a liquefaction.

#### Evaluation of the Total Energy as Dependent on Monitoring Equipment

According to the presented model, the stress system developed in response to the stress relief should be shallow and simple. A local stress concentration within the limestone pillar was directly attributed to the potential primary failure. When a failure occurred, the local stress structure absorbed part of the released energy. This resulted in seismic waves of proportional energy, and of frequency inversely proportional to the size of the stress structure and the wave velocity in the limestone (Brune, 1970). The size of the stress structure in the limestone during the event of April 1980 was estimated between 10 and 20 m (based on records from accelerometers). The frequency of 60 hertz was well above the range covered by seismological instruments.

A portion of energy released during a failure in the limestone pillar should be absorbed by the stress zone in loose materials next to the failure area. The large portion of the energy released when the loose material failed should contribute to the development of liquefaction. The liquefaction phenomenon should convert most of its energy into a powerful secondary seismic event. Large amounts of this energy should be radiated in the frequency range covered by seismological instruments. Consequently, proportions between the total energy involved during seismic event and the energy carried by seismic waves (frequencies below singular hertz) should be reduced from 100:1 (McGarr et al., 1979) to less than 10:1 (Duvall et al., 1967). This approach should result in a

considerable reduction of the estimated total energy released during each seismic event. Consequently, the energy disturbance caused by mining should be sufficient to justify the level of seismicity in the Belchatow mine.

#### CONCLUSIONS

The model presented in this paper gives another explanation of the nature of mining induced seismicity in the Belchatow mine. The explanation takes under consideration all available information regarding local conditions. This approach dictates largely qualitative character of the analysis in which relative increments are predominantly used.

The model does not require any high and unstable tectonic stress as a condition for seismic events of the observed magnitude to occur. This is consistent with the fact of no seismic activity in this area before the mining started.

According to this model, the conditions which contributed to the mining induced seismicity in the Belchatow case were:

- Fine and uniform sands of overburden as well as bedding deposits.
- Saturation of bedding deposits with water along with a partial sealing effect provided by the lignite deposit from the top and along the southern wall of the trench.
- Location of the lignite deposit in the tectonic trench formed of strong rock formations.
- Lowering the triggering level of liquefaction in bedding deposits as a result of an effective stress relief below the pit and within the limits of the protective stress concentration zone formed around the pit.
- Presence of the limestone pillar (possibly karstified) in front of the eastern slope of the opening pit.

All these factors formed a unique environment in which:

- the mining induced loading and unloading system destabilized the stress in the bedding sand deposits,
- stress concentration in the pillar resulted in local failures,
- waves generated by each failure triggered a massive failure in loose materials adjacent to the pillar,
- subsequent rapid increase of load triggered liquefaction below the lignite deposit,
- developing liquefaction resulted in a hydraulic impact polarized predominantly northwest toward the opening pit.

The scale and horizontal orientation of the hydraulic impact and its shallow location

were held responsible for very strong macroseismic intensity and its northwest orientation.

Seismic activity in the Belchatow area was interpreted as a temporary phenomenon related to mining in contact with the eastern slope of the pit. This activity should cease after the mining reaches the bottom of the lignite seam and moves to the west. In the meantime, a periodic blasting in the limestone pillar at the location where seismic events originated should force more uniform flow of loose material from the east toward the pit. The blasting should eliminate subsequent major seismic events, or lessen their magnitude.

Testing the stress and pressure in which sands become liquefaction-prone should provide information confirming the presented model.

Regarding the instrumentation part of this study, the selection of microseismic monitoring equipment (widened frequency range) is considered fundamental for the comprehensive study on any mining induced seismicity. This is particularly true for shallow and open pit mining operations, and other engineering projects dealing with slopes.

#### REFERENCES

- Brune, J.N. (1970), "Tectonic Stress and the Spectra of Seismic Shear Waves from Earthquakes," *Journal of Geophysical Research*, Vol. 75, No. 26, 4997-5009.
- Gibowicz, S.J., Z. Droste, B. Guterch, and J. Hordejuk (1981), "The Belchatow, Poland, Earthquakes of 1979 and 1980 Induced by Surface Mining," *Engineering Geology*, 17, 257-271, Amsterdam.
- Gibowicz, S.J., B. Guterch, H. Lewandowska-Marciniak, L. Wyoskiński (1982), "Seismicity Induced by Surface Mining: the Belchatow, Poland, Earthquake of 29 November 1980," *Acta Geophysica Polonica* (Quarterly), Vol. XXX, 3, 193-219, Warsaw.
- Kielbasiewicz, W. and N. Malinowski (1982), "Interpretation of Vertical Displacements Connected with Seismic Tremors in an Open Mine," *Proc.: Third International Symposium on Deformation Measurements by Geodetic Methods*, Budapest.
- Kijko, A. (1983), "Seismic Risk in the Belchatow Area," *Acta Geophysica Polonica*, Vol. XXXI, 4, 331-341, Warsaw.
- McGarr, A., S.M. Spottiswoode, N.C. Gay, and W.D. Ortlepp (1979), "Observations Relevant to Seismic Driving Stress, Stress Drop, and Efficiency," *Journal of Geophysical Research*, Vol. 84, No. B5, 2251-2260.
- Obert, L. and W.I. Duvall (1967), Rock Mechanics and the Design of Structures in Rock, Wiley, New York.
- Olczak, T. (1962), "Seismic Phenomena on the Territory of Poland During the Period 1901-1950," (in Polish with English Summary), *Acta Geophysica Polonica*, Vol. X, 1, 3-9, Warsaw.
- Pagaczewski, J. (1972), "Catalogue of Earthquakes in Poland in 1000-1970 Years," *Publications of Institute of Geophysics, Polish Academy of Sciences*, 51, 3-36, Warsaw.

# Foundation Failures Associated with Salt Rock and Surrounding Coastal Plain

A. Orhan Erol

Civil Engineering Department, King Saud University, Riyadh, Saudi Arabia

Abdulmohsin W. Dhowian

Civil Engineering Department, King Saud University, Riyadh, Saudi Arabia

**SYNOPSIS:** A detailed investigation has been conducted to study the causes of severe and widespread damages in a town situated on a salt dome. The study includes a thorough assessment of ground conditions in the coastal plain surrounding the salt dome for possible utilization of the plain as redevelopment areas. Major geological features in the study area comprised of collapsible windblown sands which are underlain by salt rock in the old town and soft/loose sabkha deposits in the proposed redevelopment zones. It has been found that the extensive damages in the buildings and roads are primarily due to subsidence phenomenon associated with the dissolution of salt rock. The properties of the sabkha sediments and anticipated geotechnical problems have been described.

## INTRODUCTION

A detailed investigation has been conducted to study the causes of the severe and widespread structural damages in the city of Jazan, situated in a coastal plain on southwest of Saudi Arabia. In the city more than 120 buildings are damaged beyond repair. The problem would have been more apparent if large tracts of severely damaged or collapsed buildings had not been demolished. The investigation program consisted of an extensive drilling program, laboratory testing, field load tests, survey of damaged buildings and, geological and geophysical studies. It has been found that the dramatic damages in the town is primarily associated with the unusual ground conditions prevailing in the region. This paper presents an assessment of ground conditions, with reference to typical engineering geological features of the region and their implications in identifying the major geotechnical factors which have contributed to the failures of the structures.

## GEOLOGICAL FEATURES

The town of Jazan is situated on an elevated terrain underlain by a salt dome measuring 4 sq. kms in area and reaching about 50m. above the sea level. The salt dome is surrounded by a coastal plain in the southwest corner of Saudi Arabia. The coastal plain which is planned as the redevelopment area in the region, stretches north and south for approximately 190 kms. A schematic geological cross section of the region is shown in Fig. 1.

The salt dome is the predominant structural feature in the coastal plain. It protrudes about 50m above the surrounding sabkha flats. Throughout the geologic time since the formation of salt deposits and its burial, the salt dome gradually pierced through the overlying country rocks. This

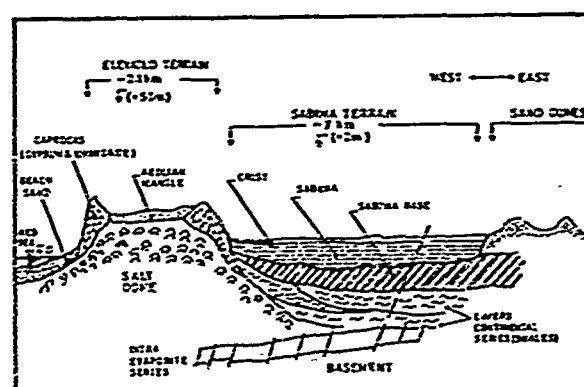


Fig. 1 Representative cross section of Jazan region

movement is probably due to the lower density of the salt as compared to the surrounding country rocks. As the salt dome reaches to the surface, most of the overlying country rock and caprock are subsequently removed by erosional processes. There are few outcrops of the salt body and the thickness of the soil underlain by salt rock varies over a range 6m to 15m in the town. The topography of the rock surface exhibits considerable variations within short distances. Highly irregular surface of the salt dome is an evidence of active erosion of the salt through dissolution processes.

An aeolian sand mantle overlies the salt dome. The sand has uniform grain sized distribution, typical for windblown deposits and its relative density varies from medium dense to very dense depending on the depth, water content and degree of cementation.

The caprocks which are formed upon the rising salt dome come in contact with ground

water, appear as high ridges, as shown in Fig. 1. The gypsum and anhydrite hills enclose the low lying area which is covered by sand dune deposits. This topographic feature can be attributed to a long term collapse mechanism associated with the dissolution of salt rock by groundwater (Al-Mutairi, 1985).

The area surrounding the elevated terrain (salt dome) is essentially flat, and is covered by thick sediments of soft/loose organic saline soils which are referred to as sabkha deposits in published literature (Akili et al, 1981). In the sabkha terrain three zones comprise the soil profile: i. sabkha crust; ii. compressible sabkha complex and; iii. sabkha base. The sabkha crust has an average thickness of 1.5m and is a mixture of fine sand and silt size particles encrusted by precipitations of soluble salts resulting from evaporation of saline groundwater. The middle zone is composed of soils varying from non-plastic fine sands to highly plastic organic clays. Variety of materials, mutually interlayered at random, occur in sabkha complexes without exhibiting any real stratification. The distinct feature of sabkha deposits is their poor mechanical properties and heterogeneous nature. Their highly variable compressibilities coupled with significantly low bearing resistances often give rise to serious geotechnical problems (Jullie et al, 1983; Khan et al, 1981; Akili, 1981). The plasticity characteristics of the sabkhas from Jazan region, shown in Fig. 2., reflect the variable nature of the sediments.

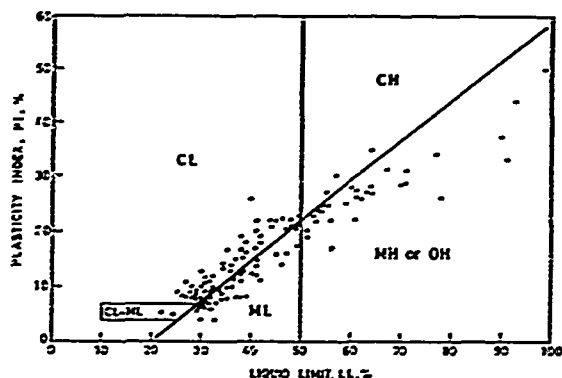


Fig. 2 Consistency limits of sabkha sediments

#### GEOTECHNICAL PROBLEMS

##### Subsidence in the Salt Dome Region:

The most populated part of the city is situated on the elevated terrain which is underlain by the salt dome. In this section of the city numerous buildings have been damaged beyond repair. The distribution of existing damaged structures are shown in Fig.3. Typical extent of damages observed in the distressed buildings are illustrated in Fig. 4. In some heavily damaged buildings the ground movements caused

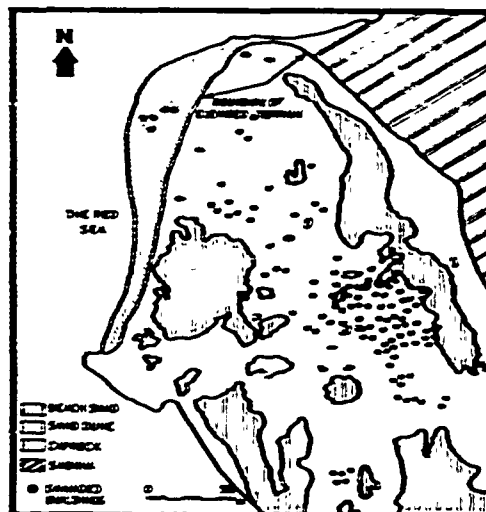


Fig. 3 The distribution of damaged structures in the old town



Fig. 4 Damaged school building and ice factory in the salt dome region



displacements of foundations in the order of meters. Excessive differential movements have been observed even under fence walls and pavements, as shown in Fig. 5, where the foundation loading is not significant. Such magnitude of ground movements can not be attributed to compressibility of foundation soils. Evidently the case is a typical subsidence problem arising from the dissolution of the salt rock.



Fig. 5 Damages in the fence wall and pavement

Halite or salt rock is known as highly soluble in water and numerous case histories associated with the failure of structures due to dissolution and subsequent subsidence of salt rock has been reported in published literature (James et al., 1980; Durie et al., 1964; Drescher, 1984). The ground subsidence observed in the location of damaged structures appeared as local sinkhole type depressions as well as linear depressions associated with solution channels. It is noted that the occurrence of damaged zones in the city is erratic. Occasionally stable or slightly distressed zones can be found nearby the heavily damaged buildings.

Other field evidences reflecting the occurrence of subsidence phenomenon were the followings: i. highly irregular surface of the salt body which is an indication of solution features; ii. loss of drilling fluid near the top of the salt rock in boring operations.

In order to ascertain that the dissolution of salt rock is the primary cause of the damages, some field measurements were taken in the site of an deserted factory buildings. The movements at the ground level were monitored while the site was artificially inundated. The displacements measured upon wetting of the site are shown in Fig. 6. It is interesting to note that the elapsed time of 4 weeks which corresponds to noticeable acceleration of settlements in Fig. 6, coincides with a heavy rainfall which lasted few hours in the city. Almost immediate response of the ground to the artificial wetting and the

rainfall confirms that the salt dissolution and subsequent ground subsidence is the principal contributor to the damages.

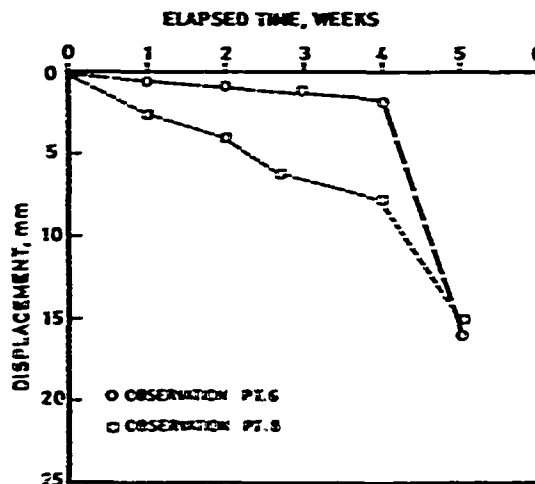


Fig. 6 Ground movements observed in the inundated site

#### Collapsible Nature of Windblown Sands:

The study revealed that the second major geotechnical problem in the salt dome region arises from collapse potential of the windblown sand mantle. In the study area, the ground water table is at the boundary of rock surface with the overlying soils. It has been found that the groundwater has significantly high salt concentration because of dissolution of the salt rock. Capillary rise of salty groundwater and its rapid evaporation due to hot and arid climatic conditions prevailing in the region, lead to precipitation of water soluble salts at shallow depths. The evaporite contents of the sand deposit at shallow depths is given in Fig. 7. The data shown in Fig. 7 indicate that the soluble chlorides and sulfate contents are in the range of (1.0-2.5) and (0.25-0.75) percent, respectively. Evidently these salts together with the capillary stresses provide a temporary bonding among the soil grains. The temporary cementation loses its effectiveness on soaking and consequently the soil is weakened and is susceptible to collapse (Dudley, 1970).

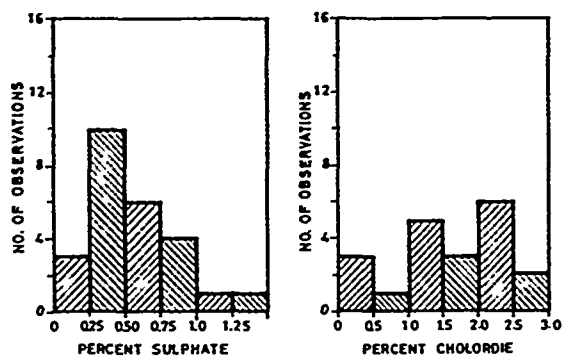


Fig. 7 Evaporite contents in windblown sand

The results of double oedometer tests on cemented sand specimens indicated that collapse severity of the sand fall into "moderate trouble" to "trouble" categories according to the collapse classification criteria proposed by Knight (1963). The studies on collapse behaviour of the windblown sands included in-situ plate load tests which are performed in natural and inundated state. The load-displacement curves obtained from plate load tests, in Fig. 8, confirm the relatively high collapse potential of the soils predicted by the double oedometer tests. Thus it is believed that some of the damages in the region may be attributed to the collapse of the windblown sands due to wetting of the ground following the occupation of the land. However, collapse phenomenon can not solely account for the unprecedented magnitude of the ground movements experienced in the region. The subsidence phenomenon is to be considered as the major contributor to ground displacements.

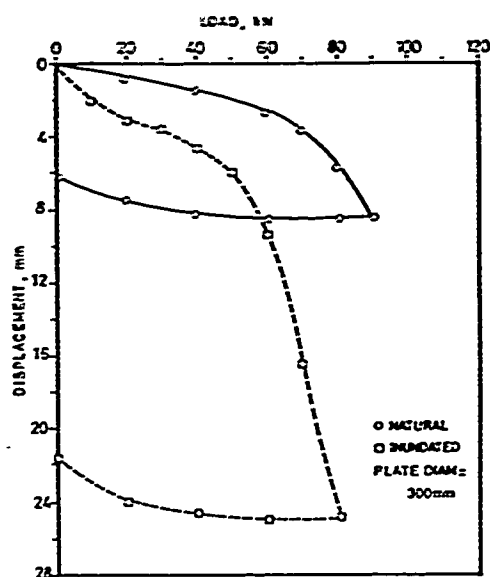


Fig. 8 Typical plate load test data reflecting the collapsing nature of windblown sands.

#### Problems with Sabkha Sediments:

Due to intolerable property losses and high risks involved in building on salt dome terrains, utilization of the sabkha plains as residential areas have been considered. The site investigation program was extended into sabkha plains to determine the subsoil conditions in the proposed development areas. The study revealed that sabkha soils present series of engineering problems associated with their variable nature, poor mechanical properties and high evaporite and organic contents. Although development of sabkha deposits and their material properties are well documented in the published literature, limited information is available concerning the nature and range of construc-

tional problems that may be encountered on sabkha plains (Ellis, 1973; Kinsman et al. 1971; Johnson et al. 1978).

From geotechnical engineering point of view, sabkha sediments are highly variable in lateral and vertical extent. Variations have been noted in terms of layering, soil composition, cementation, organic content and mineral constituent. Lateral variation appears to depend on proximity with respect to shore line, whereas vertical variation arises from development sequence of sabkha sediments, prevailing depositional environment, and subsequent diagenesis (Akili et al. 1981). The borehole profiles given in Fig. 9 from an area measuring 40x40 sqm in the sabkha terrain reflect the heterogeneity of the sabkha profiles. The heterogeneous character of the deposits lead to difficulties and uncertainties in the analysis of sabkha behaviour.

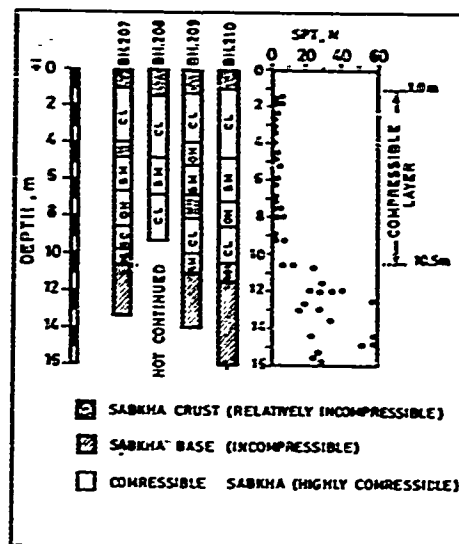


Fig. 9 Variations in sabkha subsurface profiles

Another distinguishing feature of sabkha flats is the presence of highly saline ground water table which lies within two meters from the surface. The salts precipitate at or near the surface as a result of evaporation and dessication and form a relatively hard crusty surfaces. The salt encrusted surfaces are sufficiently strong and durable. However they become impassible upon wetting due to rainfall or storm tides. The salt encrustations are readily visible with their puffy appearance as shown in Fig. 10. Unstable nature of sabkha crusts and their corrosive attack on foundation materials create serious constructional problems.

The range of undrained shear strengths measured on sabkha deposits are shown in Fig. 11. The undrained shear strengths obtained from field vane tests, which are referred to as peak and remolded strengths in Fig. 11, and various laboratory tests

vary over a range from 5 to 40 KPa at shallow depths. This magnitude of soil strength is not adequate to support most of the common engineering structures through conventional shallow foundation systems. Thus either special foundation systems and/or ground improvement techniques are to be considered to avoid possible failures of foundations. Presently the phase of the study which concerns with selection of the most appropriate foundation methodology for the particular ground conditions is under consideration.



Fig. 10 Appearance of sabkha crust

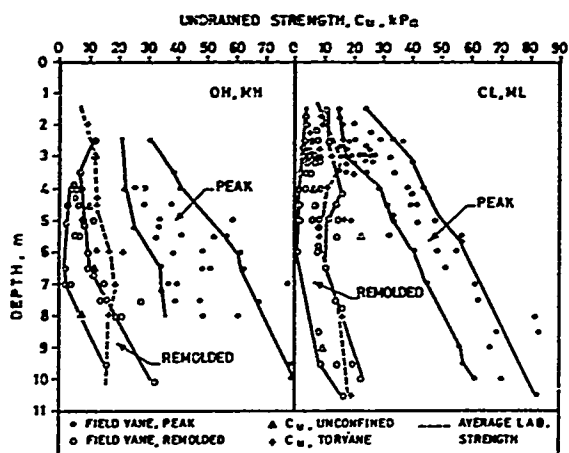


Fig. 11 Shear strength characteristics of sabkha sediments

Laboratory and field investigations were carried out to study the compressibility characteristics of the sabkhas in the region. Laboratory studies included numerous oedometer tests on undisturbed samples. An instrumented test embankment was constructed to investigate the in-situ compressibility behaviour of sabkha profiles. The range of compression indices of different soil types obtained from oedometer tests are shown in Fig. 12. Compression

indices,  $C_c$  vary over a wide range (i.e. from 0.1 to 1.0) depending on predominant soil type in the stratum, and correlates well with the reciprocal of dry density. Relatively high magnitudes of  $C_c$  clearly reflects the compressible nature of the sabkhas. This observation is confirmed by the settlements monitored in the instrumented test section where a total settlement of about 200 mm were measured under an embankment loading of 48.6 KPa. This magnitude of settlements under moderate loading conditions is beyond the permissible range for most engineering structures. Moreover, potential variation of compressibility characteristics of sabkha sediments may lead to excessive differential settlements and subsequent failures.

Additional settlement problems are to be anticipated due to potential secondary compression associated with the relatively high organic content of sabkha sediments. The sabkhas encountered in the region, contain appreciable organic matter (i.e. from 3% to 9%).

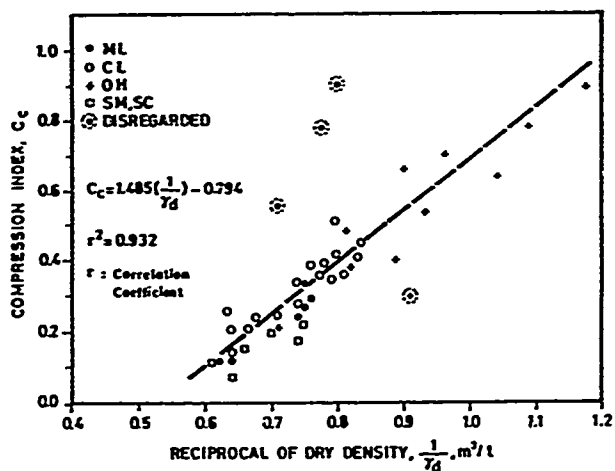


Fig. 12 Compressibility characteristics of sabkha sediments

The in-situ measurements indicated that field settlements extend out on to a secondary consolidation phase within a relatively short period of time. The settlement log-time plots given in Fig. 13 are represented by two straight lines which are typical for organic soils and taken to indicate primary and secondary compression ranges (Long et al. 1984). The secondary consolidation problem which is usually overlooked in routine geotechnical investigations appears to be a serious problem in sabkha sediments since secondary compression may reach to significant magnitudes as evidenced by the field data.

The comparison coefficient of consolidation,  $C_v$ , obtained from laboratory tests with those determined from in-situ time-settlement behaviour of the test embankment revealed that the average ratio of field to laboratory  $C_v$  is in the order of 55. This

discrepancy can be attributed to a more efficient than anticipated subsurface drainage system due to presence of thin permeable sublayers. It is conceivable that the inclusion of permeable sublayers into the sabkha complex serve to accelerate the consolidation processes. The comparison of

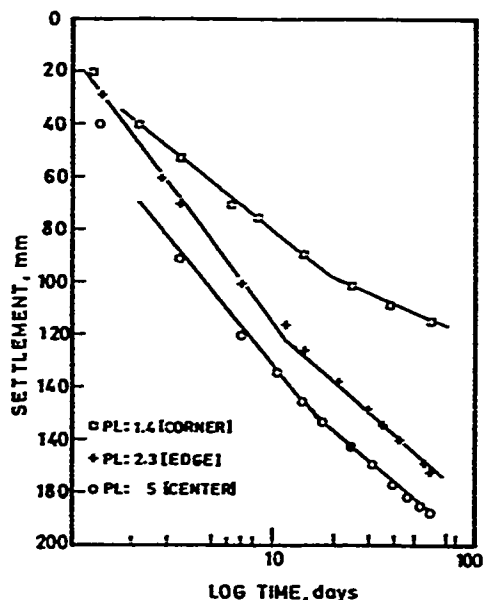


Fig. 13 In-situ settlements versus log-time plots showing the secondary consolidation effects

the observed and predicted settlements given in Fig. 14 indicate that despite the primary consolidation settlements can be predicted from laboratory determined parameters within acceptable limits, time-settlement predictions are far from being realistic. This observation stresses the fact that the routine sampling and laboratory testing methods are not adequate for heterogeneous and complex subsoil profiles to represent the in-situ conditions. Large scale loading tests with the measurement of in-situ para-

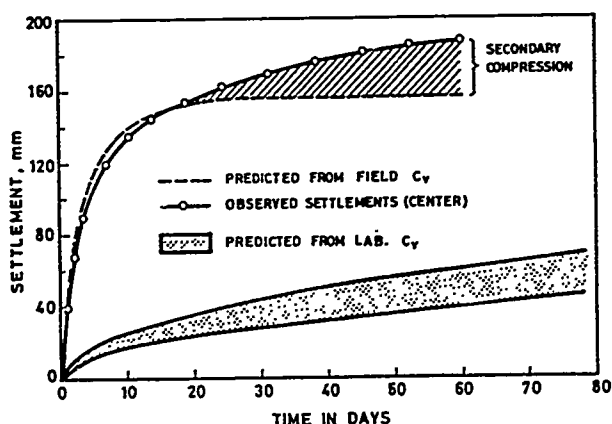


Fig. 14 Comparison of measured and predicted time settlement behaviour

meters are essential to achieve reliable predictions of time-settlement behaviour particularly if preloading schemes are employed to improve the ground conditions.

## CONCLUSIONS

A comprehensive subsurface exploration program has been undertaken to investigate the causes of severe and widespread damages in a town situated on the southwest coast of Saudi Arabia. The scope of the investigation was to identify the factors contributing to the structural damages, and to propose an urban development scheme for new residential areas. The existing town is situated on a salt dome which is covered by an aeolian mantle. The salt dome is surrounded by salt bearing recent sediments, known as sabkha. The study has revealed that the ground conditions present the following geotechnical and constructional problems.

1. The structural damages are primarily due to subsidence phenomenon associated with the dissolution of rock salt.
2. Evaporative pumping processes in desert environment are responsible for the accumulation of evaporite minerals at shallow depths. The collapse potential of the aeolian mantle is attributed to the weak cementation of soil grains by the evaporites; and to be considered as a major geotechnical problem in the region.
3. Sabkha sediments are highly compressible materials with low bearing resistances and serious foundation instability problems are to be expected upon the utilization of sabkha plains for urban development.
4. Analysis of sabkha behaviour is complicated by the composite and heterogeneous nature of sabkha profiles with respect to soil composition and stratification. Relatively high organic content of sabkhas and existences of salt encrusted surfaces present potential engineering problems.
5. Measures must be taken to protect the construction materials from highly corrosive effect of the salts present in sabkhas, as well as wind blown sands overlying the salt dome.

## ACKNOWLEDGEMENT

The study described in this paper is supported by a research grant from King Abdulaziz City for Science and Technology, Saudi Arabia; Grant No. KACST-8-106. Part of the field data presented is published with the kind permission of the Ministry of Municipal and Rural Affairs.

## REFERENCES

- Akili, W. 1981 "On sabkha sands of Eastern Saudi Arabia", Symp. on Geotechnical Problems in Saudi Arabia, Vol. 2, pp. 775-793.
- Akili, W., J.K. Torrance, 1981 "The development and geotechnical problems of sabkha, with preliminary experiments on the static penetration resistance of cemented sand" Q.J. of Engnr. Geology, Vol. 14, No. 1, pp. 59-74.
- Al-Muhendis, 1985, "Jazan Town Planning and Structural Engineering Studies", Unpublished Report, Ministry of Municipal and Rural Affairs, Kingdom of Saudi Arabia.
- Drescher, G.J. 1984 "Underground problems in the subsidence area of Luenenburg city", X. ICSMFE, Vol. 3, pp. 83-87, Stockholm.
- Dudley, J.H. 1970, "Review of collapsing soils" ASCE, Journal of Soil Mechanics and Foundations Division, Vol. 96, No. SM3, pp. 925-947
- Durie, R.W., F.W. Jessen 1964 "Mechanism of the dissolution of salt in the formation of underground salt cavities", Soc. Pet. Eng. J. Vol. 4, pp. 183-190.
- Ellis, C.I., "Arabian salt bearing soil (sabkha) as an engineering material", Transp. Rd. Res. Lab. Report. LR 523 Crowthorne, Berkshire, U.K., 1973.
- James, A.N., I.M. Kirkpatrick, 1980, "Design of foundations of dams containing soluble rocks and soils", Quarterly Journal of Engineering Geology, Vol. 13, pp. 189-198.
- Johnson, D.H., Kamal, M.R., Pierson, G.O. and Ramsay J.B., "Sabkhas of Eastern Saudi Arabia", In: Al-Sayyari, S.S. and Zotl, J.G. (ed.), Quaternary period in Saudi Arabia, Springer-Verlag, 84-93, 1978.
- Juillie, Y., D.E. Sherwood, 1983, "Improvement of Sabkha soils of the Arabian Gulf Coast", Improvement of Ground, Proc. of 8th European Conf. on SMFE, pp. 781-788.
- Khan, I.H., S.I. Hasnain, 1981, "Engineering properties of Sabkha soils in the Bengazi plain and construction problems", Engineering Geology, Vol. 17, pp. 175-183.
- Kinsman, D.J.J., Park, R.K., and Patterson, R.J., "Sabkhas: studies in recent carbonate sedimentation and diagenesis, Persian (Arabian) Gulf, Abs. Geol. Soc. Am., Annual Meetings, 1971.
- Knight, K., 1963, "The origin and occurrence of collapsing soils", 3rd, Regional Conference for Africa on Soil Mechanics and Foundation Engineering, Vol. 1, pp. 127-130.
- Long, R.P., W.H. Hover, 1984, "Performance of sand drains in a tidal marsh", Int. Conf. on Case Histories in Geotechnical Engineering, Vol. 3, pp. 1235-1244.

# A Geological Appraisal of Slope Instability and Proposed Remedial Measures at Kaliasaur Slide on National Highway, Garhwal Himalaya

G.S. Mehrotra  
Central Building Research Institute, Roorkee, India

R.K. Bhandari  
Central Building Research Institute, Roorkee, India

## SYNOPSIS

For over six decades Kaliasaur landslide (Lat.  $30^{\circ} 14' 30''$  N, Long.  $78^{\circ} 55' 50''$  E) is a nightmare on the Hardwar-Badrinath road in the Garhwal Himalaya. Located on a sharp bend on the left bank of river Alaknanda, it has emerged as a multi-tier repetitive major landslide, retrogressive in nature. Both surficial and deep seated movements have been monitored. The sliding in the upper layers have been predominantly in the colluvium but where interfaces of quartzite and shale participates, the sliding surfaces have been better defined and discrete.

In the present paper, the authors have highlighted the geological, geomorphological and morphometric parameters to diagnose the factors responsible for instability of slope and the magnitude of the problems involved. A scheme of remedial measures which include modification of existing drainage pattern, timber piling for stitching of debris cover on to the slope, construction of retaining walls and putting back the vegetation on the slope are recommended for control of the landslide.

## INTRODUCTION

The Kaliasaur landslide located at km 147 in the Garhwal Himalaya has been a major problem to the communication and safety of road users for over six decades (Fig.1).

The slope forming material consists of weathered, loose, crushed and pulverised rockmass mainly of quartzites and shales. The slide is constantly on the move particularly during the monsoon season (June-September) when the debris flow and rock fall are quite severe. These mass-movements are caused mainly by heavy precipitation and consequent development of hydrostatic pressure build up in the colluvium in highly fractured and jointed rock mass. In addition, extensive toe erosion by meandering Alaknanda river also cause progressive failure of the overlying materials (Fig. 2).



FIG.1 - KALIASAUR LANDSLIDE ON HARDWAR-BADRINATH ROAD



FIG. 2 - CONTOUR MAP SHOWING THE LOCATION OF KALIASAUR LANDSLIDE

The uphill slope of the slide area is steep being around  $45^{\circ}$  to  $70^{\circ}$ . The slide has advanced over 165m above the road and it is still advancing during the period of monsoon each year. The paper highlights the mechanism responsible for occurrence of multi-tier slides and a scheme for control measures based on the findings of investigation. It also reports on the experiences with timber piling and low cost retaining wall construction.

### HISTORY OF THE LANDSLIDE

The Geological Survey of India records declare location km 147 on Hardwar-Badrinath road as the landslide area since 1920. Further occurrences of moderate to heavy landslides in 1952, 1963, 1964 and 1965 are reported. A major landslide at this location, however, occurred on 19th September, 1969 blocking nearly three fourth of the river about 100 m below the road level. A 300 m stretch of the road was badly damaged and got dislocated both vertically and laterally by about 2.5 - 3.0 m. The slide is reported to have remained active till 23rd September, 1969. During 1970, 1971 and 1972 repeat of moderate to heavy landslides occurred disrupting the communication system and each time, a new formation width had to be cut. During September, 1984, following heavy rainfall, a major landslide occurred and damaged the road considerably, extending the rear scar of the slide retrogressively. The most recent slide was in August, 1986. The total area of the slide above and below the road level together measure 86000 m<sup>2</sup>. Nearly one lac cu.m of landslide produced rock debris have gone into the river since the origin of the landslide.

### GEOLOGY OF THE AREA

The rock formation in the landslide area belongs to the Garhwal Group of rocks namely white and light green quartzites interbedded with maroon shales.

Geological mapping of the area was carried out on a 1:2500 scale and the area included the surroundings of the landslide zone. Three traverses were taken i.e. along the main road, along the river and along the Khankra-Chhantikhil road (Fig. 3).

Observations along the road and along the river suggest the presence of two types of quartzites. One is of light green colour with thin beds of maroon shales, and the other is massive and well jointed yellowish white quartzite. On the western side of the slide zone the quartzite are light green with shale bands having a general southward dip with amounts ranging from  $25^{\circ}$  to  $60^{\circ}$ . These quartzites end up abruptly along a scree zone beyond which massive yellowish quartzites dipping southeast with amounts  $30^{\circ}$  to  $40^{\circ}$ , are exposed. It appears that the scree zone conceals a fault zone trending NE-SW and extending across the river. The massive quartzites continue upto the western flank of the slide zone where they end up against the slide debris. On the eastern side of the slide zone the quartzites exposed have maroon shales with a south eastern dip and amounts varying from  $30^{\circ}$  to  $60^{\circ}$ . These quartzites continue along the river bed. It appears that another fault zone trending NW-SE may be present somewhere within the slide zone.

### LEGEND:

- SLICE BOUNDARY
- ▤ DRAINAGE
- ▥ TENSION CRACKS
- ▧ MODERATELY WEATHERED QUARTZITE
- ▨ HEAVILY WEATHERED QUARTZITE
- ▩ SLIDE DEBRIS
- ROCK COVERED WITH VEGETATION
- ▬ SHEAR ZONE
- ▮ COMPACT QUARTZITE
- F-1 FAULT

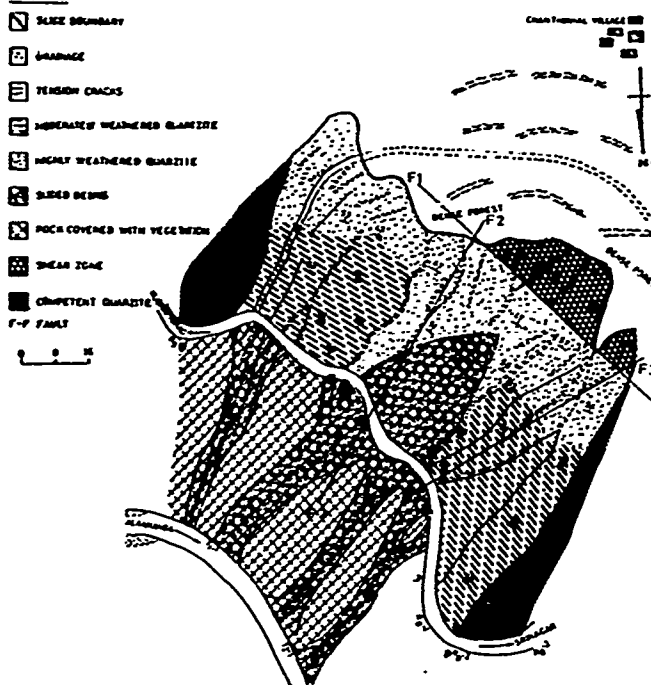


FIG. 3 - GEOLOGICAL MAP OF KALIASAUR LANDSLIDE ON HARDWAR-BADRINATH ROAD

The geological succession in this area appears to be as follows :

Massive yellowish white quartzites

Greenish quartzites interbedded with maroon shales and Metabasics

Greenish grey phyllites and shales  
Dolomitic limestone

The rocks appear to have been folded into a plunging overturned anticline on the western side of the slide zone with a plunge towards north-east. Another anticline appears to be on the eastern side of the slide zone with plunge towards south. There appears to be a number of fault zones in this area. A major fault appears to be along roughly East-West trend. This fault zone passes through the crest of the slide zone and separate the metabasics from the quartzites. Two other faults with trends roughly NE-SW exist in this area. They all appear to be high angled and one of these passes through the main slide zone. All these faults merge into Chhantikhil fault.

### GEOMORPHOLOGY

The geomorphological mapping was carried out on scale 1:3125. In this area Alaknanda occupies a deep sinuous gorge with the crest of sinuosity located near the slide zone.

The slopes on the left side of the river are steep whereas they are rather gentle on the right side. Slide zone is located on the left side of the river, where the main road is passing through. This area contains a number of smaller scree zones, along with exposures of

quartzites. There appears to be a significant escarpment running east-west below the Chhantikhali village. This escarpment continues upto the river bed. The lower part of this escarpment is occupied by colluvium resting nearly at its angle of repose. The middle part exposes quartzites and on the top there are cultivated fields. Above this escarpment, there is a dense forest.

There are a number of small streamlets flowing over the escarpment and meeting the river at high angles. Two such streamlets are reported to pass through the landslide zone.

The profile of first streamlet towards the eastern part of slide zone is very smooth and is concave upward characterising the profile of stabilised repose slope. The profile of second streamlet in the slide zone indicated the upper part of the slope to be gentle and slightly convex possibly due to the accumulation of talus. In the middle part, the slopes become highly convex with exposed free faces of quartzites. The tension cracks varying in length from 1 m to more than 50 m were present at several locations above the crown of the slide. The lower part of this profile is slightly concave having accumulation of talus material. It appears that the slopes are generally unstable above the road and are currently under the process of severe mass wasting.

#### MORPHOMETRIC PARAMETERS

The morphometric parameters studied in this area can be classified (a) Drainage Basin Morphometry and (b) Landslip Morphometry Parameters.

##### Drainage Basin Morphometry :

Seventeen second order basins present in this area were analysed and studied in details. The mean values of various parameters studied are given in Table I.

TABLE I. Stream Morphometry Parameters (Mean Values)

| Basins       | Area<br>(Sq. km) | Shape<br>(km) | Stream<br>(km) | Drainage<br>(km <sup>2</sup> ) | Relief<br>(m) | Drainage<br>(km) |
|--------------|------------------|---------------|----------------|--------------------------------|---------------|------------------|
| Eastern Part | 2.58             | 0.41          | 2.45           | 0.42                           | 1.95          | 1.10             |
| Slide Zone   | 0.74             | 0.22          | 5.86           | 0.60                           | 2.72          | 3.62             |
| Western Part | 1.62             | 0.38          | 2.46           | 0.36                           | 1.91          | 1.05             |

The data clearly indicate that the longer and larger basins are located in the eastern part of the slide zone whereas shorter and smaller basins are present in the slide area. The parameters like stream frequency, drainage density, relief and drainage texture etc. have maximum values for slide zone. All these facts suggest that the slide zone is full of newly emergent streams and is highly dissected with an active process of erosion. Due to the presence of porous scree material in slide zone only few streams can be seen. This, however, shows that there must be many concealed underground streams active in the slide zone.

#### Landslip Morphometry Parameters :

The landslide parameters were analysed on the basis of stream profiles, classification index, and dilation index values.

The distribution of these parameters are given in Table II.

TABLE II. Landslip Morphometry Parameters (Mean Values)

| Area         | Classification Index | Dilation Index | Type of Mass Wasting                   |
|--------------|----------------------|----------------|--|
| Eastern Part | 9.5                  | 14.8           | Debris Avalanche/<br>Rotational Slides |
| Slide Zone   | 7.5                  | 9.8            | Planar Slides                          |
| Western Part | 4.5                  | 4.7            | Flow and Creep                         |

The values of classification index for the slide zone and eastern parts of the area suggest failure mainly by planar slides by the process of debris avalanche whereas in the western side of slide zone the classification index values depict failure by erosion only. The values of dilation index show the possibility of rotational slides involving the movement of bed rocks along with planar slides in the eastern part of the slide zone. In slide zone only planar slides are possible through debris avalanche. All these data clearly indicate that the eastern part of the slide area may be potential slide zone and the present slide zone may get extended eastwards by future landslides and mass movements.

#### INSTRUMENTATION AND MONITORING

The landslide was monitored for its surface as well as crustal movement behaviour.

For measurements of slope movement a scheme was drawn for locating markers for tape extensometer and geodetic triangulation observations. Grid map of the slide area was used for locating the positions of monuments and pedestals (Fig. 4). To facilitate measurements of relative surface displacements between points, 65 pedestals (markers) were installed. Measurements were made through tape extensometer and clinometer. Additionally 50 RCC pillar/monuments (markers) anchored up to 2 - 3 m depth were monitored through triangulation and high precision methods.

Monitoring of surface movements were started before the onset of the monsoon in 1986. During rainy season fortnightly observations were taken. About 1000 observations have been taken so far. Some of the typical time displacement observations are shown in Fig. 5. The analysis of the data clearly indicated two directional movements - north eastern and north western - in the eastern and western sides of the slide zone (Fig. 6). The extent of the lateral movement of pedestals towards the eastern side varied from 0 - 117.8 cm whereas the pedestals on western side showed movement 0 - 76.1 cms indicating thereby that the eastern part of the slide area is more unstable.



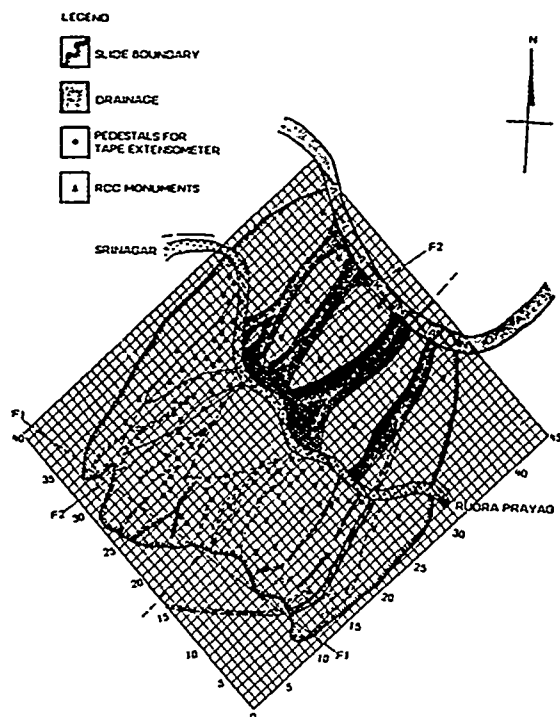


FIG. 4 - SCHEME FOR MONITORING OF SURFACE MOVEMENTS OF SLOPES AT KALIASAUR LANDSLIDE

The crustal movement studies pertaining to movement of the underlying slope material were carried out with the help of Electronic Distance Meter (EDM). The observations were taken before monsoon, during rainy season and thereafter till April 1987. The analysis of the data have shown significant lateral movement towards north east direction ranging from 0-22.5cm. The lateral movement towards north-west direction varied

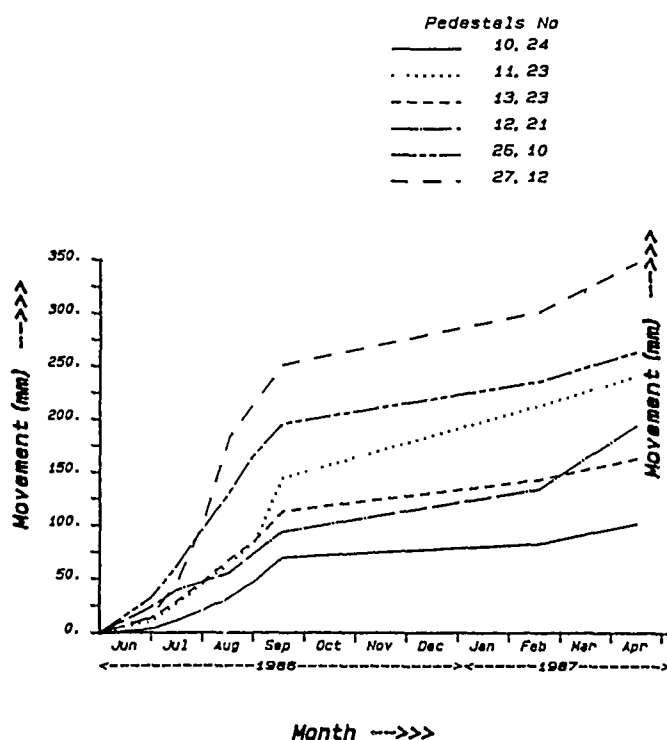


FIG. 5 - LATERAL MOVEMENT OF PEDESTALS BY TAPE EXTENSOMETER

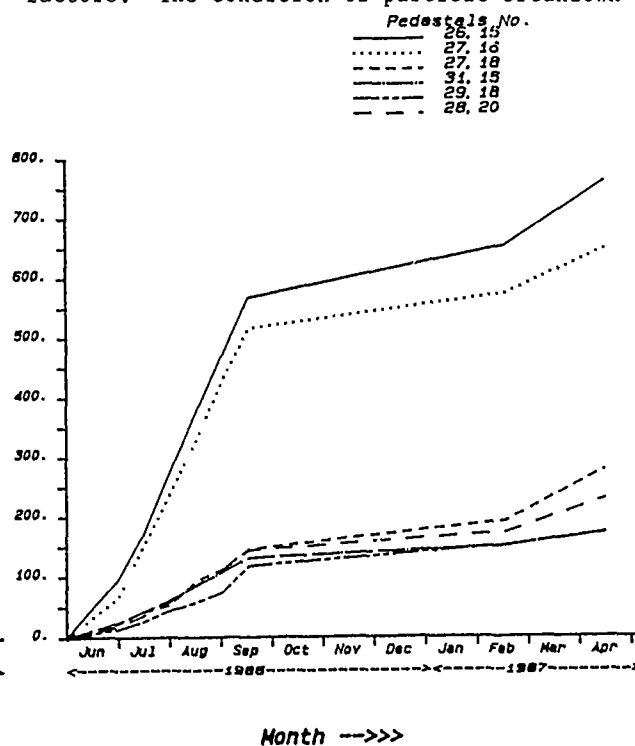
from 0-17.6 cm.(Fig. 7). The results further indicated movement in vertical direction ranging from 0-6.9 cm.

The study has thus clearly indicated that the eastern side of the slide area is a zone of intensive landslide movements involving both deep seated and surface movements. In the central and western sides of the slide area, the movement is conferred predominantly to surface debris.

#### MECHANISM OF KALIASAUR LANDSLIDE

Kaliasaur landslide is essentially a multi-tier, retrogressive landslide in a complex rock formation with clear evidences of fault planes revealing intense tectonic activity in the geological past. Evidences of sliding at the interface of quartzites and maroon shales must presumably have been the starting point. Road construction activity in general and repeated back cutting required for restoring the road width, year after year, poor drainage, recurring debris slides in the colluvium cover on the slope robbing it of the vegetative cover and river action at the slope toe have all been responsible to develop the landslide to it's formidable size obtaining today. A typical slide cross-section is shown in Fig. 8.

A very large number of point load tests on quartzite specimens reveal uniaxial compressive strength of the order of 1800 kg/cm<sup>2</sup>. The samples of maroon shale were however found to be so soft that even undisturbed sampling was difficult to achieve. During dry weather, samples were found to readily crumble into powder. Large displacements have, however, been inferred due to presence of polished surfaces. The characteristics of polished surfaces and genesis of their formation were therefore important factors. The condition of particle breakdown at



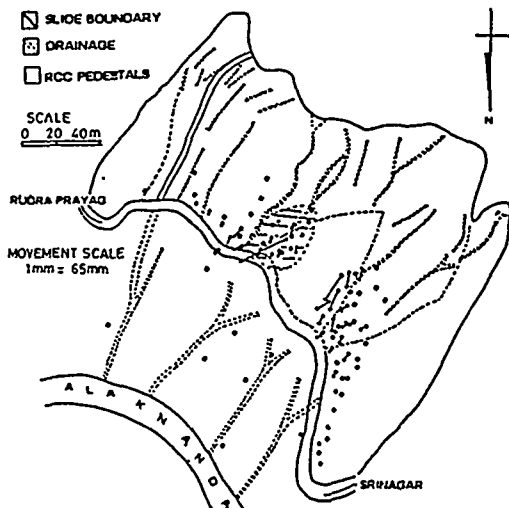


FIG. 6 - SURFACE MOVEMENT PATTERN OF KALIASAUR LAND SLIDE

the shale surface was simulated in the laboratory by subjecting the surface to artificially created abrasion effect for different intervals of time and determining particle size in laser particle Analyser. The results, clearly indicate that initially because of break down of bigger particles proportion of the clay size fraction at the boundary tends to decrease but later on clay fraction records marked increase, as could be expected corresponding to large movements. Well graded character of material at slide boundary is seen to turn into very nearly a single size fraction. The angle of shearing resistance is of the order of  $28^\circ$  but it's residual value corresponding to very large strains is yet to be studied in the light of the above observation though post peak values of shearing resistance may lie in the range  $18^\circ$ - $22^\circ$ , Bhandari (1987).

Debris accumulation on the slope is excessive. Plentiful supply of water during the monsoon season combines with it to cause debris flow. Rockfalls are also very frequent.

Field studies have also shown that outlet of some concealed flow channels below the existing road level are responsible for undercutting of road resulting into its subsidence.

#### CONTROL MEASURES

As a result of detailed investigation, the following measures were recommended and are under various stages of implementation :

1. Grading of the slope uphill of the road.
2. All tension cracks and fissures in the rocks to be sealed.
3. Timber piling for stitching of the slope.
4. Construction of anchored drum diaphragm retaining wall along the road to control the slide mass overlooking the road.
5. Construction of anchored stone masonry wall towards other side of road to check the undercutting of road due to palaeo channels.

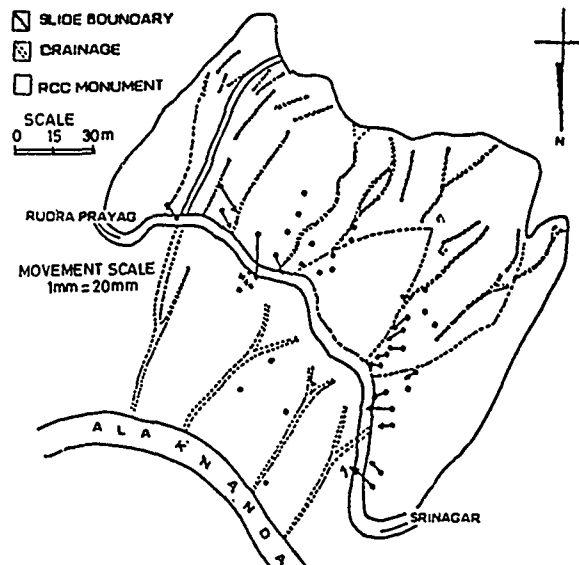


FIG. 7 - CRUSTAL MOVEMENT PATTERN OF KALIASAUR LAND SLIDE

6. Vegetating the slope.

7. A toe wall in masonry at the junction of the slope down hill of the road with the river. This wall is to be designed to withstand the scour of the river.

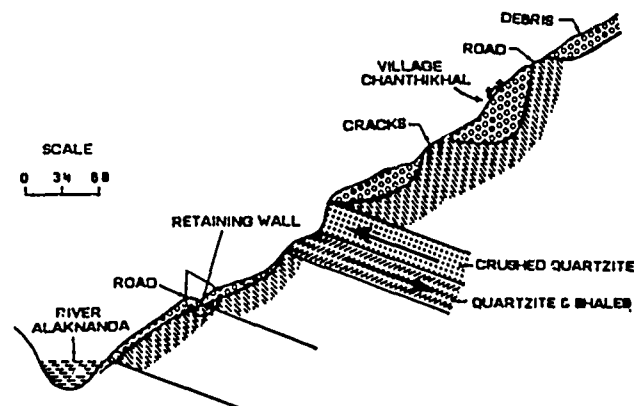


FIG. 8 - CROSS SECTION OF KALIASAUR LANDSLIDE

Of the above recommendations, the drum retaining wall as a concept is described by Bhandari (1987). The stitching of debris on slope and vegetative turfing are briefly described below.

#### Stitching of Debris on Slopes

Timber piling or bally cribbing is sometimes being used for arresting surficial movements in the slope cover so that vegetation and drainage facilities are not harmed and hazards due to debris flow could be minimised. Driving of timber piles result in densification of loose and shallow granular slide prone carpet on the slope and provide 'stitch action' that helps to hold the earth mass. Such piles are usually stiffened laterally by horizontal runners of timber. For example some 60,000 ballies of 12.5 - 15 cm diameter, 3 m long were driven to depths ranging from 1.5 to 2.0 m to stabilise Padamchen

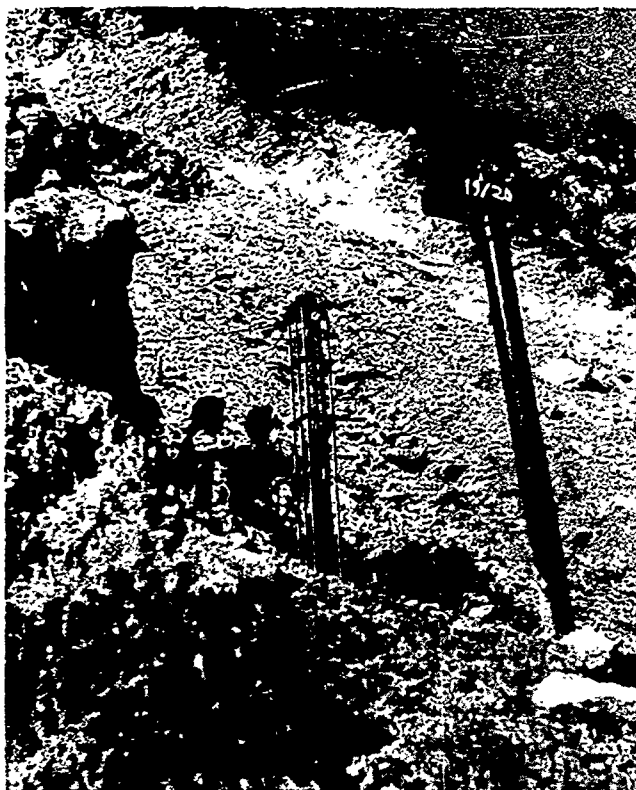


FIG. 9 - STITCHING OF COLLUVIUM ON THE SLOPE AT KALIASAUR BY A SIMPLE PILING MACHINE

Slide in Sikkim. After stiffening the ballies laterally, the space (in between) was filled up and the vertical parts were tied with each other by 8 SWG binding wire. The bally cribbing and terracing were also used to stabilise a shallow landslip at the rear slopes of Idgah sub station building in Simla, Bhandari (1973). After intensive field trials, 20 cm diameter, 3 m long ballies were driven to a depth of about 2 m using a 30 kg hammer, about a metre apart. These ballies were braced on the uphill side by means of 15 cm diameter, 3 m long ballies in three tiers using dogs, nails and 8 SWG wire.

Difficulties of timber piling have now been largely overcome by a new, lowcost portable timber piling machine developed at the Central Building Research Institute, (Fig. 9). Timber piles 10 cm square from Deodar, Sheesham and Eucalyptus wood were driven in lengths of 1.5 m each suitably spliced, at six locations on the Kaliasaur slide using the portable machine requiring only one man to operate. The 30 kg hammer used earlier is now being replaced by 50 kg hammer to achieve higher orders of driving energy.

#### **Vegetative Turfing on the Slope**

The corrective measure appropriate for stabilising this slide after stitching the slope with timber piles comprise erosion control by establishing vegetation on the slopes. The resulting dense network of root system, penetrating about one metre into the slope anchors the soil adequately so as to render it resistant to erosional control. Slope treatment by vegetation is considered an important a maor corrective

measure in surficial slides whereas in multi-tier slide like Kaliasaur the vegetation by itself will not be meaningful unless used in conjunction with other remedial measures.

#### **CONCLUDING REMARKS**

The slide at km 147 on Hardwar-Badrinath road has been a major problem to the road users. The past treatments given to this slide area have met with little success. The slide is constantly on the move during the monsoon each year. The present detailed investigation has led to better understanding of the nature and cause of the slide.

Based on the study corrective measures have been suggested with a view to stabilise the slide mass. The corrective measures include construction of retaining walls to check the under cutting of the road, a masonry toe wall to withstand the scour of the river, grading of slope, timber piling,, vegetation turfing and a system of surface and trench drains.

As a part of the landslide control programme, a drum diaphragm wall 100 m in length and 2.15 m high has already been constructed. Stabilisation of surface colluvium by timber piling has been partially accomplished. The total success could however be expected only after all other control measures are completed. The stage has already been set for the total completion of the programme in early 1988.

#### **REFERENCES**

- Barata, F.E. (1969), "Landslide in Tropical Region of Rio de Janeiro", Proceedings International Conference on Soil Mechanics and Foundation Engineering, Mexico, 2 : 507-516.
- Bhandari, R.K. (1973), "Instability of Idgah Sub station Building at Simla, CRRI Report (unpublished) Furnished to Simla Municipal Corporation, Simla.
- Bhandari, R.K. & S.C. Sharma (1975), "Mechanics and Control of Rockfalls", Journal of Institution of Engineers, 57 : 14-23.
- Bhandari, R.K. (1977), "Some Typical Landslides in the Himalaya", Proc. Second International symposium on Landslides, Tokyo, 1-32.
- Bhandari, R.K. and V. Sreenivasulu (1980), "Some New Instruments For Landslide Studies", Proc. International Symposium on Landslides, New Delhi, 1 : 343-348.
- Bhandari, R.K. (1981), "Landslides in Himalaya, Causes and Curves", Proc. International Seminar on Landslides and Mud Flows and the Prevention of Their Negative Impact on the Environment, Alma Ata, USSR.
- Bhandari, R.K. (1984), "State-of-the-Art-Report on Simple and Economical Instrumentation and Working Systems for Landslides and Other Mass Movements", Proc. Fourth International Symposium on Landslides, Toronto, 251-273.
- Bhandari, R.K. and Mehrotra, G.S. (1985), "Hill Roads and Himalayan Landslides", Proc. Indian Road Congress Seminar on Road Construction in Hill Areas, Nainital, V : 123-141.

Bhandari, R.K. and Mehrotra, G.S. (1985), "Slope Monitoring of the Musscorie-Chamba Bypass Landslide", Proc. Indian Road Congress Seminar on Road Construction in Hill Areas, Nainital, V : 143-160.

Bhandari, R.K. (1987), "Slope Instability in the Fragile Himalaya and Strategy for Development", Ninth Indian Geotechnical Society Annual Lecture, Indian Geotechnical Journal, 1.

Brown, C.B. and M.S. Shen (1975), "Effects of Deforestation on Slope", Journal of Geotechnical Engineering Division, ASCE, 101 : 147-165.

Chandra, H. (1975), "Landslides in Teesta Valley", Proc. Seminar on Landslides & Toe Erosion Problems with Special Reference to Himalayan Region, Gangtok, 147-165.

Chansarkar, R.A. (1975a), "Geotechnical and Geomorphic Factors in Landslide Investigations", Proc. Seminar on Landslide and Toe Erosion Problems with Special Reference to Himalayan Region, Gangtok, 54-66.

Chopra, B.R. (1977), "Landslides and Other Mass Movements Along Roads in Sikkim & North Bengal", Proc. Symposium on Landslides and Other Mass Movements, Prague, 16 : 162-166.

Fukuoka, M. (1980), "Instrumentation, Its Role in Landslide Prediction and Control", Proc. Second International Symposium on Landslides, New Delhi, (II) : 139-153.

Ganseer, A. (1964), "Geology of Himalayas", Interscience Publishers, New York.

Krishnaswamy, V.S. (1980), "Geological Aspects of Landslides With Particular Reference to the Himalayan Region", Proc. International Symposium on Landslides, New Delhi, 2 : 61 - 71.

Natarajan, T.K. & Gupta, S.C. (1980), "Technique of Erosion Control for Surficial Landslides", Proc. International Symposium on Landslides, New Delhi, 3 : 413-417.

Wadia, D.N. (1957), "Geology of India", Macmillan and Company Limited, London.

# Subsidence Movements and Structural Damage Related to an Abandoned Coal Mine

Y.P. Chugh

Professor, Department of Mining Engineering, Southern Illinois University-Carbondale, Carbondale, Illinois

K. Chandrashekhar

Department of Mining Engineering, Southern Illinois University-Carbondale, Carbondale, Illinois

R.J. Missavage

Department of Mining Engineering, Southern Illinois University-Carbondale, Carbondale, Illinois

**SYNOPSIS:** An area in southwestern Illinois has been experiencing surface and subsurface movements with associated damage to surface structures. The area is underlain by an abandoned, partially extracted room-and-pillar underground coal mine. Instrumentation included TDR (Time Domain Reflectometry), inclinometers, Sondex, Tiltplates, and precision land surveys. This paper presents the results of a 16-month cooperative study between the Department of Mining Engineering at SIUC and a local coal company.

## INTRODUCTION

Surface subsidence movements related to underground coal mining in southwest Illinois have been known to cause property damage ever since mining was begun in the region in the late 19th century. Records of mapping areas of subsidence date back as early as 1934. Underground mining of coal, with associated surface subsidence movements, is continuing in the region. Partial extraction room-and-pillar mining method has been the primary mining system in the region, and most mining has been done at less than 60 m (200 ft.) depth. Until about mid 1940's, mining layout and geometry was generally irregular (Figure 1) because of manual loading techniques. Rooms were generally 12 m (40 ft.) or more wide and 60 m (200 ft.) or more long with local extraction ratios exceeding 65%.

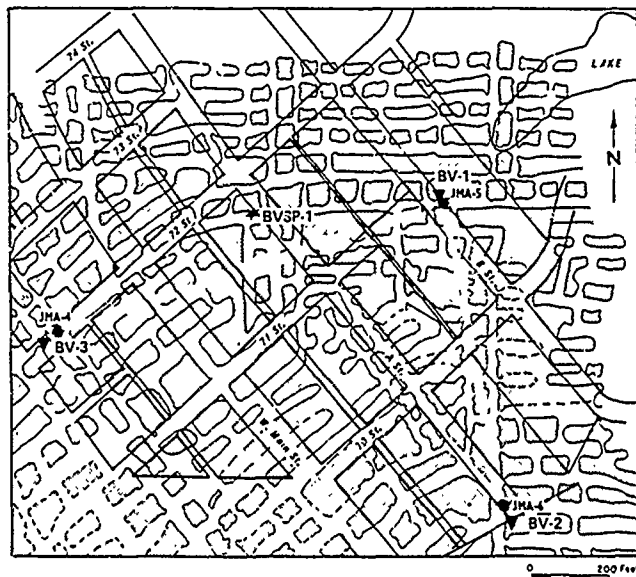


Figure 1. Irregular Mine Workings Prior to 1940, (from DuMontelle, 1978)

Over the last 30 years or so, continuous mining machines have been utilized for coal extraction and the mining layout is more regular (Figure 2). Entry widths are generally restricted to less than 6 m (20 ft.) and roof bolting is used as the primary artificial support.

In spite of a long history of subsidence in the region, very few engineering studies of mine

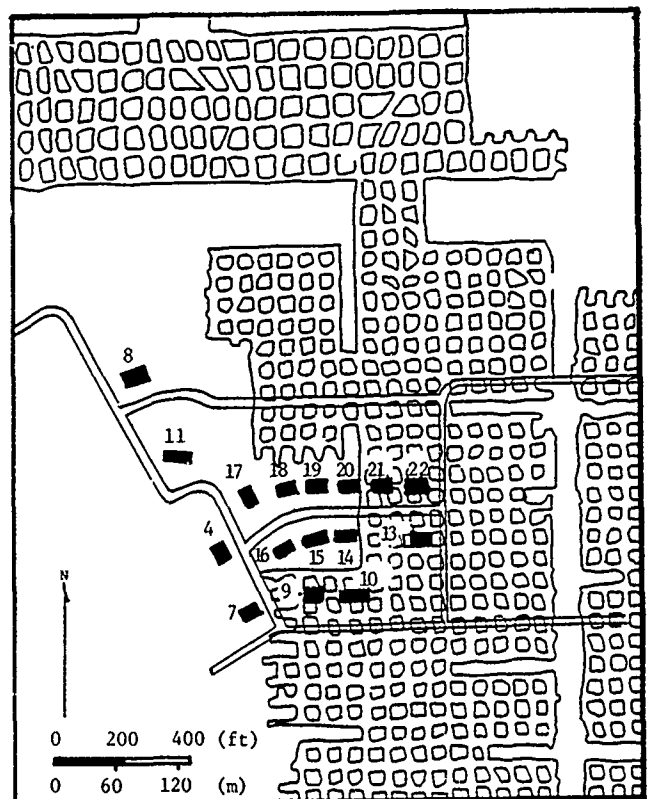


Figure 2. Mine Workings and Surface Structures

subsidence have been conducted in the area. To the best of the authors' knowledge the study conducted by the Illinois State Geological Survey (DuMontelle, 1978) in cooperation with the Bureau of Mines of the U.S. Department of the Interior, is the only study which provides details on geology and hydrogeology of the area, engineering properties of surficial as well as bedrock materials, and progressive subsidence movements. Due to irregular layout of mine workings in the area and limited instrumentation, very few specific conclusions were drawn in this study.

In August 1983, the Department of Mining Engineering signed a 16-month cooperative agreement with a coal company to undertake a detailed study of the causes, mechanisms, and characteristics of surface and subsurface subsidence movements and associated possible damage to surface structures in a 30,000 m<sup>2</sup> (75 acre) area overlying workings mined in late 1970's using continuous mining equipment. Subsidence movements, with associated damage to surface structures, have been experienced in the area since 1977. A detailed discussion of the history of subsidence in the area is provided elsewhere (Chugh et al, 1985). This study area is located about 25 km (15 miles) south of the above mentioned study area.

#### SPECIFIC OBJECTIVES OF THE STUDY

- 1) Determine the extent to which surface and subsurface movements are complete in the area,
- 2) Determine the influence of geology and hydrology of the area on subsidence movements,
- 3) Identify the mechanism(s) of subsidence in the area,
- 4) Characterize the extent of damage and monitor possible progressive damage to selected surface structures, and
- 5) Develop recommendations to (a) minimize further damage to surface structures in the area, (b) identify future areas that may be affected by these movements and (c) modify mining systems to minimize these movements.

#### MINE AND AREA DESCRIPTION

The area covers approximately 30,000 m<sup>2</sup> (75 acres) with a relief of less than 6 m (20 ft.) in surface topography and has 30 residential houses. The area overlies a 540 m x 280 m (1800 ft. x 840 ft.) panel (Figure 2) at a depth ranging from 30-45 m (100-150 ft.). Mining thickness ranged 1.8-2.4 m (6-8 ft.) with pillars at 18 m (60 ft.) centers and 6 m (20 ft.) wide entries and an extraction ratio of about 60%.

Surficial overburden thickness in the area varies from 17-27 m (50 to 80 ft.) and primarily consists of glacial silts and clays (Figure 3). The rocks overlying the coal seam consist of interbedded limestones, sandstones and shales and vary in thickness from 11.7-13.3 m (35-40 ft.). Claystone forms the immediate floor of the coal seam and its thickness varies from 0.3-1.7 m (1-5 ft.). It is underlain by

interbedded shales and limestones of varying thickness.

Previous regional hydrological studies (Buchler, 1971) have categorized the study area in the low probability region for large volume water wells. The Mississippian formation lying well below the coal seam, is the best source for bedrock groundwater supplies. Sand and gravel lenses have been found locally but prediction of their presence or extent is difficult.

#### DESCRIPTION OF THE RESEARCH STUDY

Twenty two (22) boreholes were drilled in and around the study area to study geology and hydrology of the area. Data were collected on surficial as well as bedrock overburden thickness, sequence and thickness of different beds in consolidated overburden, claystone thickness below the coal seam, change in lithology, charge and recharge zones, thickness of impermeable strata and other variables which may influence surface and subsurface movements in the area.

Four (4) boreholes were sampled for surficial overburden and five (5) boreholes for bedrock overburden to characterize overburden geotechnical properties. Soil samples were obtained with shelly tubes and were studied for natural moisture content, Atterberg limits, unconfined compressive strength and shear strength. Rock sampling consisted of core drilling, over mine openings and coal pillars, 54 mm (2 1/8 in.) diameter boreholes below the bedrock surface to about 3 m (10 ft.) below the coal seam. The objective of the boreholes over

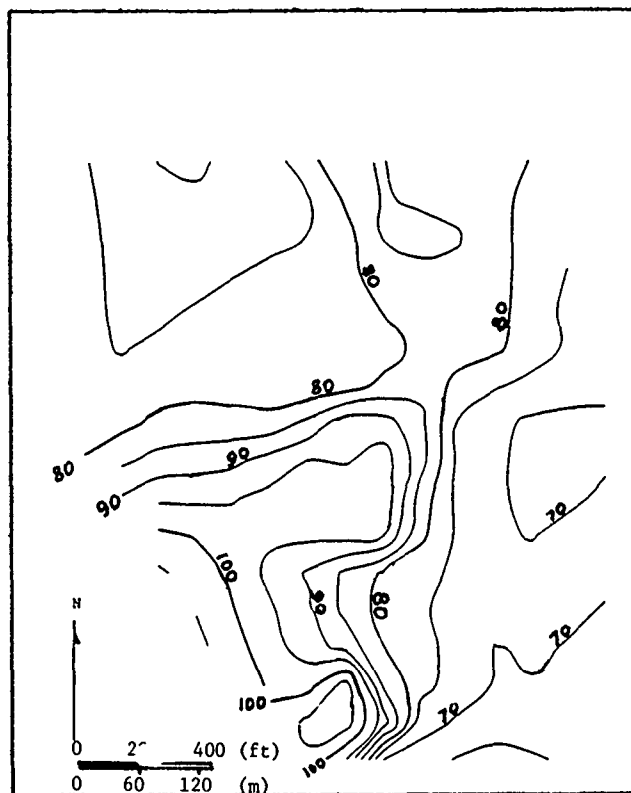


Figure 3. Unconsolidated Overburden Contours

mine openings was to study the extent of fracturing in rock strata above the coal seam due to subsidence movements and also to determine the height of remaining open cavities and extent to which mine openings had been filled by roof falls. Several boreholes were drilled over coal pillars to obtain relatively undisturbed cores of roof strata, coal seam, and claystone below the coal seam. Unconfined compressive strength, indirect tensile strength, slake durability, swelling strain index, water content, Atterberg limits, and clay mineral composition tests were conducted on cores (Chandrashekhar, 1985).

Surface subsidence movements were monitored along six (6) lines consisting of 152 monuments (Figure 4) located at about 18 m (60 ft.) intervals. Subsidence monuments were designed to minimize freeze-thaw associated movements. The monuments were surveyed for vertical and horizontal movements with standards for Second order class II accuracy.

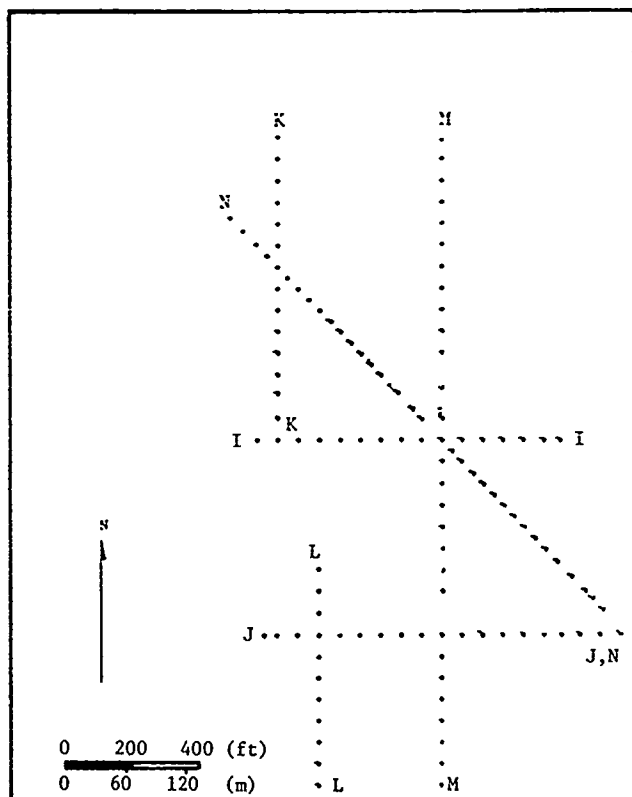


Figure 4. Survey Monuments Along the Subsidence Monitoring Grid Lines

Subsurface vertical and horizontal subsidence movements were monitored using an inclinometer and time domain reflectometry (TDR) instrumentation. Three (3) inclinometer-sondex holes, two through coal pillars and one at an intersection, were instrumented. The casing was installed from the surface to about 6 m (20 ft.) below the coal seam. Five (5) TDR boreholes were located at the center of mine openings.

A total of thirteen (13) tiltplates on foundation walls were installed in four (4) houses critically located with respect to underground

mine workings. In addition, carpenter levels ( $\pm 0.5$  deg) were also installed in houses to determine large movements in the upper structure of the houses.

Ground water levels and flows in surficial (soil) and bedrock (rock) overburden were monitored in six (6) surficial wells and four (4) bedrock wells including the one monitoring the mine pool level. Details on instrumentation and test procedures for these wells are given elsewhere (Chugh et al, 1985). All instrumentation was monitored at intervals of 2-4 weeks.

Selected boreholes in the study area were observed with a borehole TV camera. The borehole walls in bedrock overburden and underground mine workings were carefully inspected with the camera. This was done to determine the 1) amount of overburden fracturing above the coal seam, 2) condition of coal pillars, (intact, sloughing) and mine openings (floor heave, roof falls, presence or absence of water etc.) and 3) height of remaining cavities above roof falls.

#### STATE OF SURFACE AND SUBSURFACE MOVEMENTS IN THE STUDY AREA

Typical crosssection and contour plots of vertical surface subsidence movements over the study area are shown in Figures 5 and 6. Based on an estimated precision of 7 mm (0.3 in.) in elevation surveys, two types of subsidence movements are identified: (1) gradual relatively uniform subsidence of the entire study area, and (2) localized areas (A, B, C, in above figures) of large movements in the form of a trough over a 60-60 m (200-250 ft) area. Movements appear to occur very rapidly in some cases for latter type of subsidence events. Most of the localized subsidence events appear to occur in areas of a bedrock valley (Figure 7) where the proportions of the surficial to bedrock overburden are very large (100:30, 110:20, 120:10 etc.).

#### MECHANISMS OF SUBSIDENCE

Two mechanisms are hypothesized in the study: 1) slow compressional settlement of coal pillars in the panel over weak claystone floor leading to development of relatively uniform sag subsidence, and 2) localized subsidence events initiated by roof failure over one or more entries or intersections. A brief description of each with evidence from geotechnical studies justifying the hypothesis is given below.

1. Vertical surface subsidence movement data (Figure 5) show gradual downward movement with time over the entire area. Surface movements over mine openings and coal pillars are approximately the same except near the barrier pillars where movements are somewhat smaller. Subsurface vertical movement data from Sondex instrumentation in boreholes over the coal pillars (Figure 8) also show downward movement in lower portions of the pillar near the claystone floor. Over the 16-month study period, approximately 12 mm (0.5 in.) of compressional settlement is noted in the area.

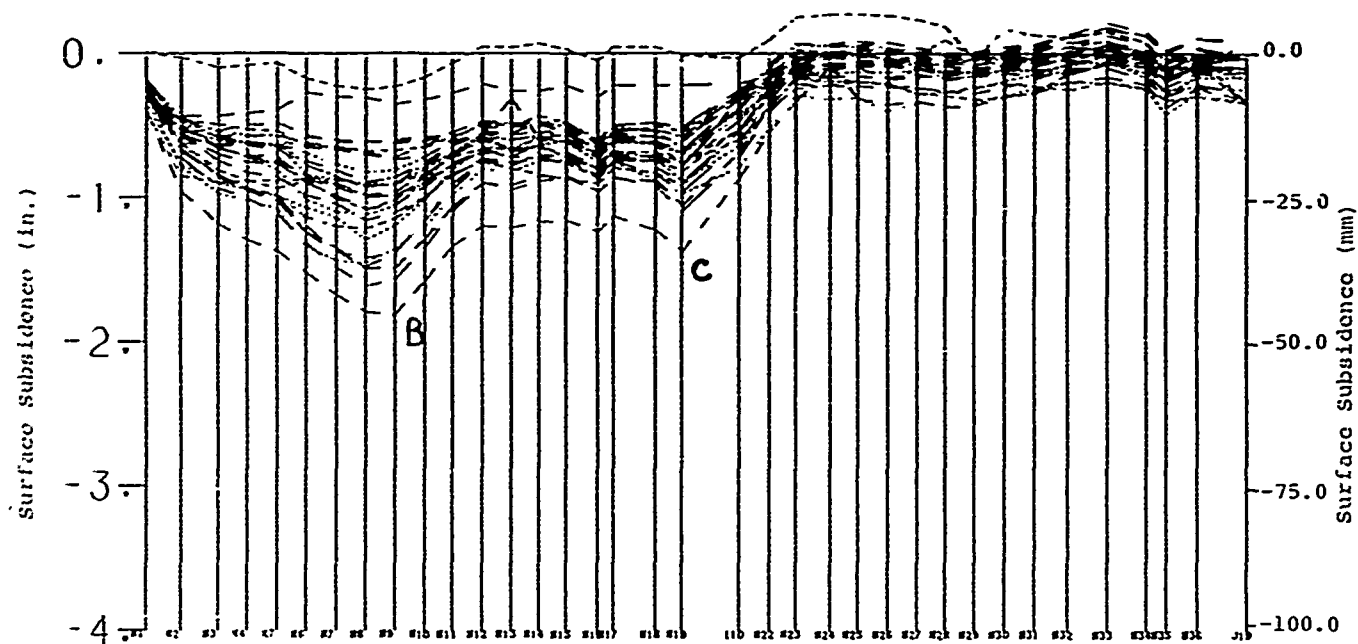


Figure 6. Surface Subsidence Cross Section  
Along N Grid

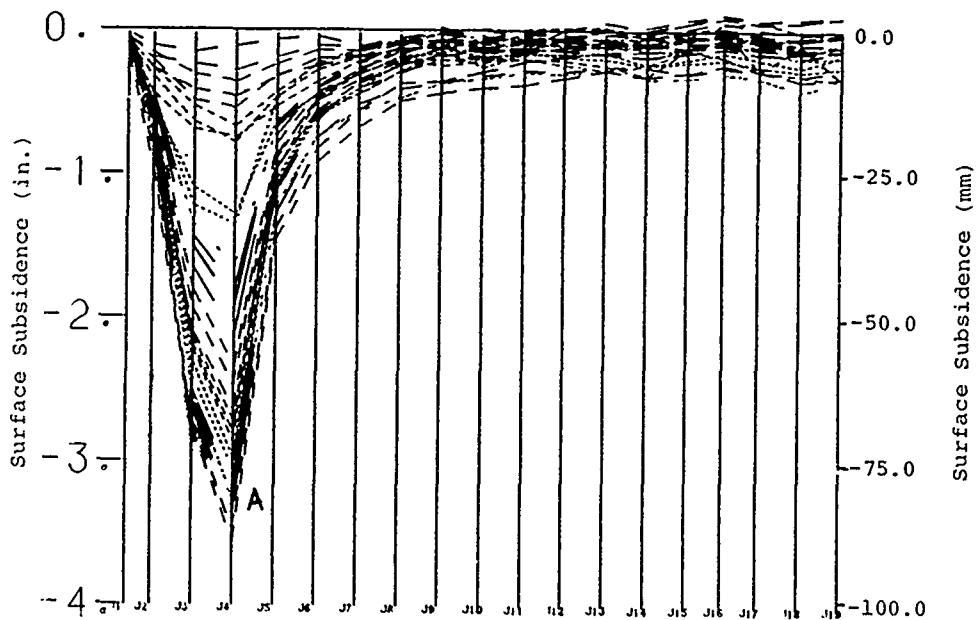


Figure 5. Surface Subsidence Cross Section  
Along J Grid



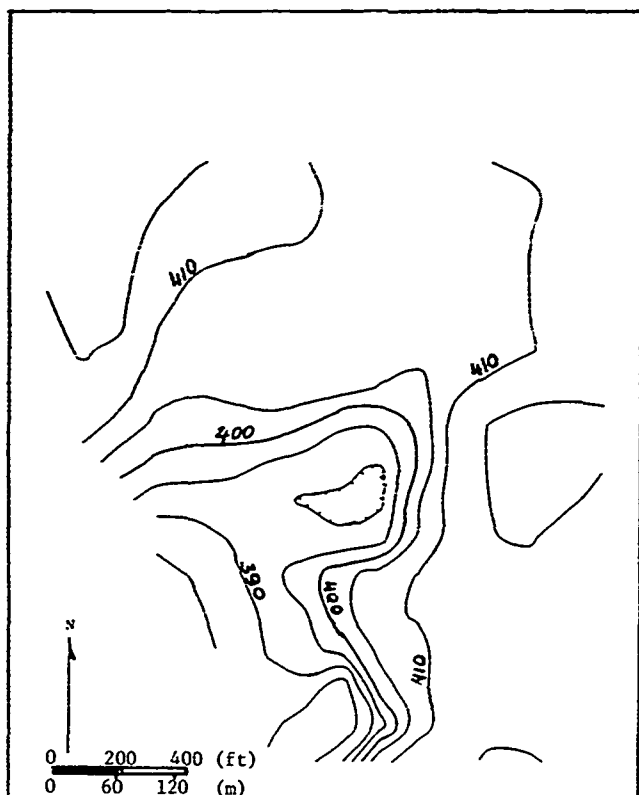


Figure 7. Bedrock Structural Elevation

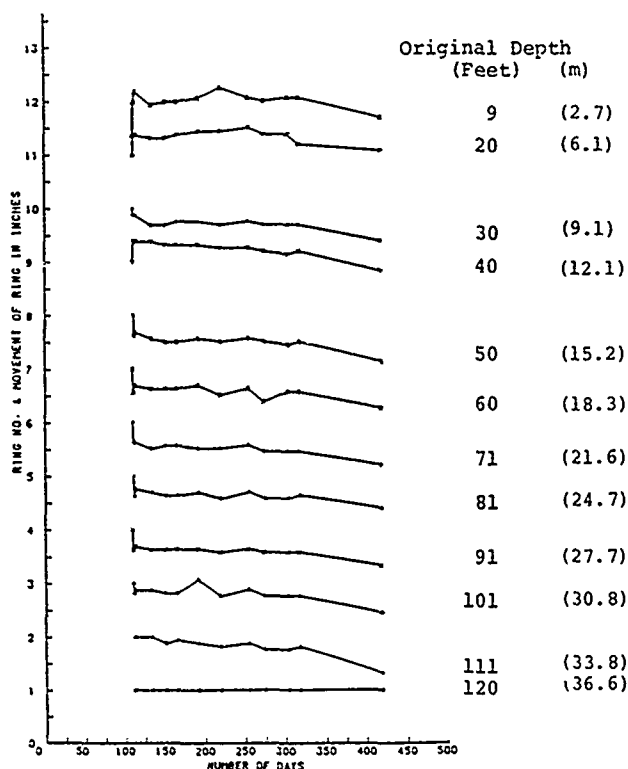


Figure 8. Subsurface Vertical Movements Sondex Hole IS2

The settlement is continuing even after a decade of mining although its rate seems to be decreasing (Figure 9). The expected vertical settlements due to this mechanism will depend upon claystone thickness, overburden pressure, percent extraction, and deformability of claystone. Over a long period of time, these movements may be large enough to cause differential coal pillar settlements and roof falls leading to surface subsidence. Consolidation and compression of claystone floor may be enhanced by the presence of water. In this mechanism, surficial overburden which is at or above its plastic limit (Figure 10) moves downward slowly as pillars settle. No extension strains are expected in the overburden since settlement rates are very small.

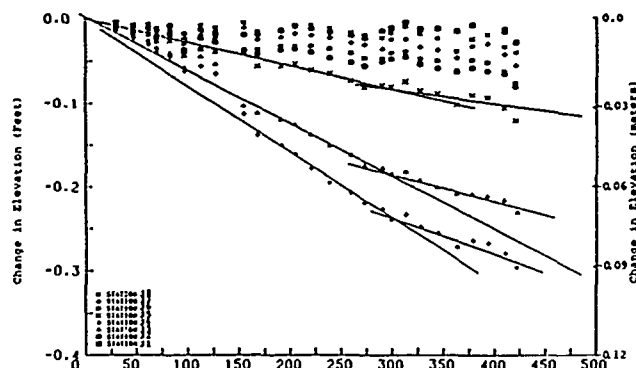


Figure 9. Subsidence Rate of Selected Stations on J Grid Line

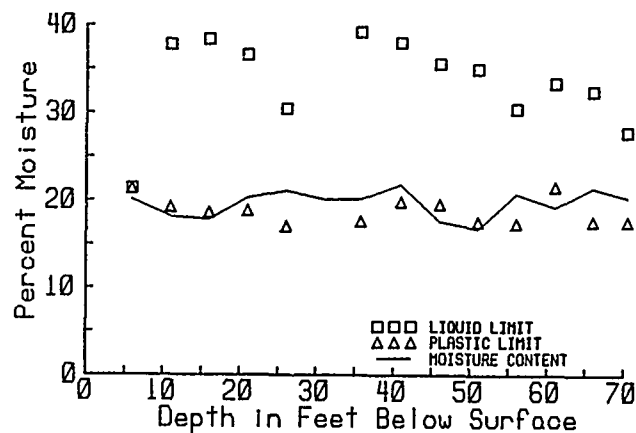


Figure 10. Comparison of Moisture Content, Liquid Limit, and Plastic Limit

2. Fracturing of immediate roof strata due to wide intersections, discontinuities in the immediate roof, and/or prolonged excessive loading of thinly layered and weak overburden may cause the soil overburden to flow into mine voids causing surface subsidence (Figure 11). Differential settlements of pillars on weak claystone floor may also cause initiation or development of such subsidence movements. At least three or four such events (A, B, C, D) with vertical movements ranging from 25-90 mm (1.0-3.5 in.) were observed during the study period. At one such site where access was possible after the subsidence event occurred,

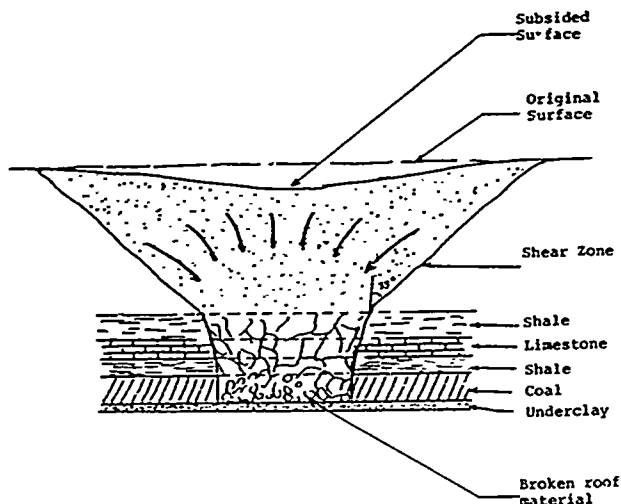


Figure 11. Schematic of Subsidence Mechanism 1

underground mine observations by the Coal Company staff showed flow of surficial overburden into mine voids. No cracks are expected on the surface or subsurface in the surficial overburden in this mechanism also since its moisture content is at or above its plastic limit.

Settlement rate due to sag subsidence appears to vary 5-7 mm (0.2-0.3 in.) per month and shows slightly decreasing trends (Figure 9) over the last six months of the study period. Borehole T.V. camera observations in several of these areas showed relatively intact roof, floor, and coal pillars. It is difficult to predict the maximum possible amount of settlement and the rate at which it will occur. Both will be enhanced in the presence of water. Since there are no indications of floor heave or otherwise filling up of void areas underground, additional subsidence movements are possible. These may or may not, however, result in damage to structures on the surface since movements are small and should occur very slowly in the absence of water. If the area was to get flooded, the magnitude and rates of these movements may result in damage to surface structures.

Borehole TV camera observations in the area of localized subsidence events showed roof falls in entries with dripping water, partially or completely flooded mine workings and highly fractured immediate roof strata. The open cavities above roof falls are common indicating that additional movements in the area are likely to occur. Based on association developed between the presence of the bedrock valley and localized subsidence events observed in this study, it is expected that additional movements of this nature may occur in future and may cause damage to surface and subsurface structures.

#### EFFECT OF GEOLOGY AND HYDROLOGY

Contours of surface topography, unconsolidated overburden thickness and structural elevation on the top of the bedrock surface (Figure 7) were prepared based on all available data (boreholes drilled during this study and those drilled prior to this study). Pertinent observations are:

1. A bedrock valley approximately 9 m (30 ft) deep is observed in the area (Figure 7). The thickness of the bedrock overburden in this valley is only 3-11 m thick (10-35 ft) while the thickness of the surficial overburden varies 24-34 m (80-110 ft). A cross-sectional map of the boreholes revealed the absence of the Bankston Fork Limestone in the bedrock valley. Thinly bedded immediate roof strata and the absence of the competent limestone bed in the roof together form favorable conditions for roof falls and localized rapidly occurring subsidence events such as A, B, C, and D.

Roof instability may also be induced by differential pillar settlements, prolonged dead load of soil overburden on roof rock and weakening of immediate roof shales due to high swelling strain potential (5-15%).

2. A 1.2-1.8 m (4-6 ft) thick sand bed/sand lens was found at a depth varying from 4.5-7.5 m (15-25 ft) below the ground surface in several soil exploration holes. No trends as to the presence of these confined sand beds were discernible based on available data. Considerable amount of water under low pressure 20-28 kPa (3-4 psi) was observed. Based on available data on water levels in surficial wells and the nearby lake was the east side of the study area it was concluded that the lake was not a water source for the sand bed. Underground roof falls and associated movements in soil overburden may eventually intercept these sand beds. Water from these beds may significantly affect the weak claystone floor because its swelling potential is high. Flow of water from sand lenses sometimes prevented borehole TV camera observations in the bedrock overburden.

- 3) About 1.8 m (6 ft) of rock below the bedrock surface was highly fractured (RQD < 50%) with a rating of poor to very poor. There is not enough data to verify whether this condition existed prior to mining due to movement of glaciers or resulted from subsidence movements.

- 4) The immediate roof strata generally had low RQD values (<30%) and high moisture content (8%). The presence of weak thinly layered roof strata would favor localized subsidence events.

- 5) Immediate claystone floor stratum has high moisture content (10-15%) and contains considerable amount of expandable clay minerals (Table I). Wetting of immediate floor strata may considerably reduce its strength and deformation modulus which may increase total and differential pillar settlements, and may lead to roof falls.

- 6) Surficial overburden is above its plastic limit, it has an average moisture content of about 20% and it is relatively independent of the depth below the surface (Figure 10). Unconfined compressive strength of soil overburden varies from 75-925 kPa (11-134 psi) and it generally increases with depth below the surface. An elastic-perfectly plastic material behavior is indicated by stress-strain curves.

#### HYDROLOGICAL STUDIES

Data from monitoring of surficial and deep water

wells were compared with the local water table, surface drainage and the water level in the nearby pool.

1) There is no evidence of a hydraulic connection among the surficial wells, bedrock wells and the mine water pool. The water levels appear to follow the local ground elevation and the water table levels follow the local surface drainage pattern.

2) The pressures due to observed water levels in surficial wells are small to be significantly contributing to ground movements in the study area.

3) There is no evidence that a) hydrology in the area has affected mine subsidence and 2) subsidence has had any long-term effects on hydrology.

#### EXTENT OF DAMAGE TO SURFACE STRUCTURES

The first report of subsidence occurred in late December of 1977. A circular depression formed on the surface bisecting house (Figure 12) in the study area. Even though mining was terminated and supports were installed underground, subsequent surface settlements continued to occur and house 9 had to be moved due to damage to the foundation. Houses 7 and 10 also showed tension cracks in the foundations which were repaired in 1983. To monitor progressive movements of both these houses, tiltplates were installed in the Fall of 1983. In house 7, 3 tiltplates were installed on the foundation walls to monitor the movement on both sides of the major cracks in the foundation and floor. Based on the tiltplate data with a precision of

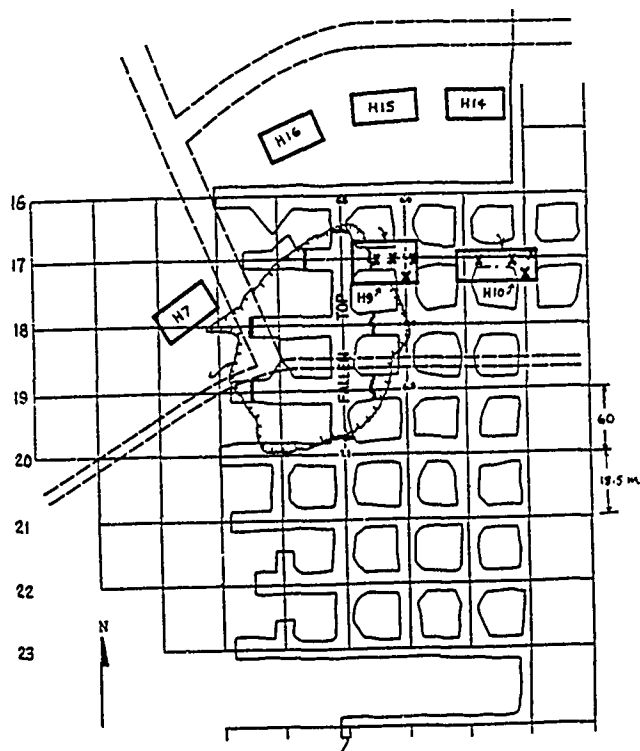


Figure 12. Limits of Surface Cracking from First Report of Subsidence, Dec. 1979

$\pm 4$  seconds, the southern portion of the house is tilting most to the southeast, toward the center of the first depression, while the north side of the house is tilting toward the east but its magnitude is less than that of the southern portion of the house. A typical plot of the tilt is shown in Figure 13. A maximum horizontal displacement 2 mm (0.08 in.) is observed in the foundation since the tiltplates were installed. In house 10, 3 tiltplates were installed; one on the west side and two on the east side. The largest movement occurred on the west side of the house, with a tilt of 46 seconds to the west. This corresponds to a horizontal displacement of about 8 mm (0.32 in.).

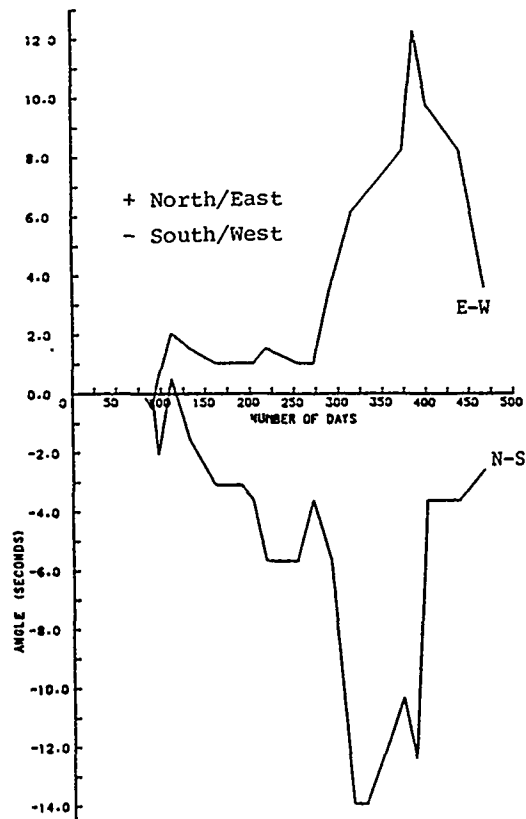


Figure 13. Angular Displacement of Tiltplate H20TP4.

TABLE I. Clay Mineral Analyses

| SAMPLE | ILLITE | KAOLINITE | CHLORITE | SMECTITE | *MIXED LAYER | **RATIO S:I | †TOTAL CLAY |
|--------|--------|-----------|----------|----------|--------------|-------------|-------------|
| C      | 46     | 18        | --       | --       | 36           | 37:63       | 38.0        |
| D      | 34     | 2         | --       | 6        | 58           | 30:70       | 33.6        |
| E      | 14     | 1         | 1        | 37       | 47           | 30:70       | 35.1        |
| F      | 12     | tr        | 1        | 60       | 27           | 33:67       | 32.4        |

\* Percentage of mixed-layer illite/smectite present

\*\*Ratio of smectite to illite within the mixed-layer fraction

In addition to the tiltplates, an inclinometer/sondex instrumented hole was located to the south of house 7 to measure the subsurface movements. The maximum horizontal movement 6.8 mm (0.27 in.) in the N 77° E correlates well with the horizontal movement measured from the tiltplates for house 7 since the inclinometer was much closer to the center of the depression than house 7.

Movement in and around houses 7 and 10 are also consistent with the surface subsidence data for survey lines J and L. Since the movements are continuing and decrease only gradually with distance from the center of the depression, it is expected that the tension cracks in both houses will continue to occur for some time in the future.

House 20 had 5 tiltplates installed on the basement walls. Two tiltplates were on opposite sides of a major crack in the north wall. A comparison of the movements in the two tiltplates indicate a twisting of the house along an E-W axis. The movement in this house is complex and indicates probable roof falls to both the north and east causing an overlapping movement.

#### SUMMARY OF RESEARCH FINDINGS

1) A bedrock valley is located in the study area. At the base of this valley, the thickness of surficial overburden increases to about 34 m (110 ft) and the thickness of bedrock overburden decreases to about 3 m (10 ft).

2) A large number of subsidence events in the past seem to be associated with this bedrock valley. Additional events in the future may also be associated with it.

3) Hydrology of the area does not appear to have either significantly affected or been affected by surface and subsurface movements in the area.

4) The surficial overburden behaves like modeling clay based on its moisture content and plastic limit. Most of the weight of the soil overburden has to be supported by relatively weak and thin rock overburden overlying the coal seam.

5) The immediate floor claystone, 0.3-1.2 m (1-4 ft) thick, is weak and highly moisture sensitive. The mineralogy of the claystone shows high percentage of expandable clay minerals and high clay size content.

6) Strength of the coal is adequate for the mining depth and percentage extraction practiced at the mine.

7) Localized areas on the surface are continually undergoing subsidence (Figure 14). Most subsidence is observed adjacent to House 7 with a total vertical movement of about 89 mm (3.5 in.).

8) Inclinometer-Sondex data show subsurface movements in the surficial and bedrock overburden which correlate quite well with those measure by precise land surveys.

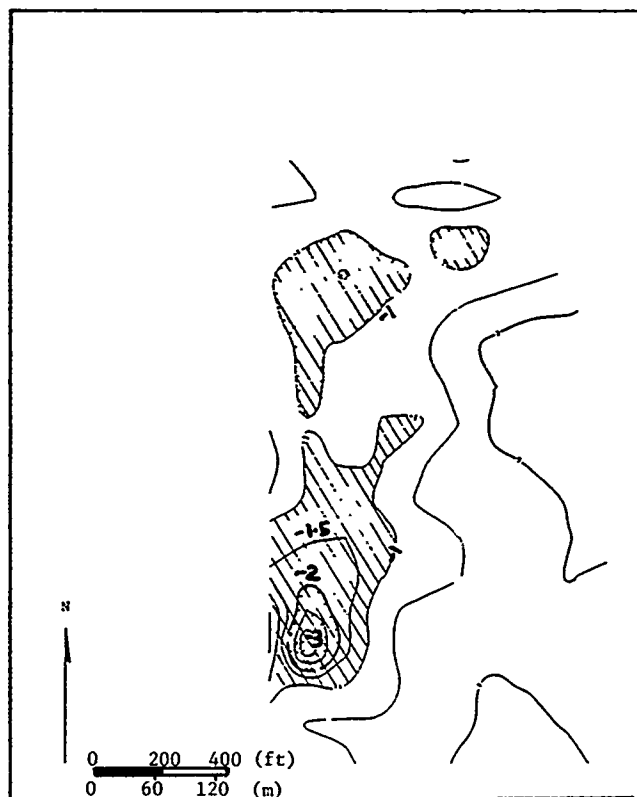


Figure 14. Localized Areas Currently Subsiding

9) Borehole TV camera observations in 10 boreholes show a) the northwest corner of the panel partially filled with water, b) roof falls in two areas around boreholes with open cavities 1.2-1.5 m (4-5 ft) high, c) relatively intact immediate roof, roof bolts and cap blocks, d) little or no pillar sloughing and floor heave, and e) highly fractured rock overburden overlying the coal seam.

10) The major subsidence mechanism causing damage in the area appears to localize roof falls with soil overburden flowing into mine workings. The differential settlement of pillars on weak claystone floor may only be a small contributory factor in causing roof falls and associated surface movements.

11) Residential structures in the study area are undergoing progressive movements and may suffer additional damage. The structures of concern are houses 7, 20, 14, and 10. Over a long period of time, houses 19, 18, 17, and 12 may also be affected.

12) Subsidence in the area is not complete. Slow settlement of the entire study area and localized subsidence events may be anticipated in the future.

13) An angle of draw of 55° in surficial overburden is noted. Based on the angle of draw, a 55 m (180 ft) barrier pillar between two panels is not adequate to eliminate surface subsidence movements on the surface.

14) Maximum tension in a structure appears to occur at about 18-28 m (60-90 ft) away from the edge of mine workings. Major cracks may be anticipated in these areas observed in garages of house 20, house 14, and house 7.

15) Tiltmeters appear to correctly predict direction of vertical movements in relationship to the position of mine structural workings.

16) Slow settlement of pillars on weak clay-stone floor has been continuing since mining was started in the area almost ten (10) years ago. The authors think that most of the future subsidence events will be related to localized roof falls rather than slow compressive settlement.

17) The influx of water into abandoned mine workings through any source could significantly increase compressive settlement rate, incidence of roof falls and associated surface subsidence.

#### RECOMMENDATIONS

1) Active mine workings should consider reducing width of mine openings and developing three way intersections wherever possible. The size of the coal pillars may also be reduced.

2) The minimum safe distance to locate a surface structure is 45-60 m (150-200 ft) from the edge of mine workings where similar geology and mining conditions are found.

3) Surface and subsurface movements are not complete. Analysis of current data indicates that houses 7, 10, 14 and 20 may have to be relocated or structurally modified if they are to sustain additional subsidence movements.

4) Areas that may be affected by subsidence movements in the future have been outlined in Figure 14. Monitoring of these and other areas should continue at regular intervals to develop a stronger database for future subsidence studies.

5) Future design of mine workings should consider geological and geotechnical data for overburden and immediate floor strata.

6) To minimize damage to surface structures, a study of different methods of stabilization against planned subsidence with high extraction ratios is also recommended.

#### ACKNOWLEDGEMENTS

The authors sincerely appreciate the interest, cooperation and technical support of the coal company management and staff in conducting the study. Without their assistance this study would not have been possible.

Thanks are also due to Ms. Katherine Mann, Mr. Abdullah Godah and Mrs. Wilma Reese for preparing the manuscript.

#### REFERENCES

Buchler, J. E., Geologic Report on the Groundwater Conditions for a Municipal Supply in Sections 13,14,23,26,27,33, and 34, T.1S R.7W, St. Clair County, Illinois, Illinois Geological Survey, July 8, 1971.

Chandrashekhar, K., (1985), "An Analysis of Subsidence Movements and Structural Damage Related to an Abandoned Room-and-Pillar Coal Mine", Masters Thesis, Dept. of Mining Engineering, Southern Illinois University - Carbondale, Carbondale Illinois, 62901.

Chugh, Y. P., Missavage, R., Chandrashekhar, K., Ober, S., (1985), "An Analysis of Surface and Sub-Surface Movements Around the Saturn Terrace Subdivision", Field Report vol. 2, Laboratory and Field Studies, Results and Discussion, Recommendations.

DuMontelle, P., (1978), "Geologic Studies for Mine Backfilling Projects, Southwestern Illinois," First Annual Report for the U.S. Bureau of Mines, U.S. Department of the Interior, Contract No. JO177076.

# Performance of Some Tunnels in Squeezing Rocks of Himalayas

**T. Ramamurthy**

Professor, Department of Civil Engineering, Indian Institute of Technology, New Delhi, India

**V.M. Sharma**

Joint Director, Central Soil and Materials Research Station, New Delhi, India

**SYNOPSIS:** Data regarding the performance of three tunnelling projects in the Himalayan region has been collected. It is seen that rock loads or deformations calculated on the basis of Barton, Bieniawski or RMR approach do not match the field data. A mathematical model has been developed incorporating modifications in the approach of Brown et.al of rock-support interaction, using elastic-strain softening-plastic ground characteristics. A non-linear relationship between radial and tangential strains around the tunnel has been considered and the method of calculation of stresses and deformations altered to incorporate exact integration of the governing differential equation for a thin cylindrical annulus replacing finite difference approximation. It is seen that a closer match and a more rational explanation of the observed data from the tunnelling project is provided by the mathematical model.

## INTRODUCTION

There are two main approaches for estimation of rock loads and deformations of underground openings. The first approach is analytical and mostly utilises continuum mechanics principles making certain simplifying assumptions regarding ground behaviour, yield criterion and volume changes, etc. The second approach is empirical in nature and is based on statistical analyses of observed behaviour of underground openings in different geologic environments. Both the methods have their own relative advantages and are applicable with varying degrees of reliability for several different categories of rock masses ranging from massive to heavily jointed. However, none of the approaches seem to work for tunnels through squeezing grounds.

In an attempt to predict rock loads and deformations of tunnels through squeezing grounds, the approach of Brown et al(1983) of rock support interaction has been modified using elastic-strain softening-plastic ground characteristics. A non-linear relationship between radial and tangential strains around the tunnel has been considered and the method of calculation of stresses and deformations has been altered to incorporate exact integration of the governing differential equation for a thin cylindrical annulus replacing finite difference approximation.

The model developed has been tried for the calculation of rock loads and deformations of three tunnelling projects in the Himalayan region.

## THE MATHEMATICAL MODEL

Literature survey reveals that there are three main considerations which distinguish one mathematical model from the other. The first consideration concerns the yield criterion for the strength of the rock mass. Most of the earlier researchers have used Coulomb's or

Mohr-Coulomb's criterion. Some others have used the second order parabolic criterion of Fairhurst. In the more recent past, the non-linear criterion of Hoek and Brown has gained popularity, and the same has been used in the present work. The second consideration is regarding the stress-strain behaviour of the ground. Whereas closed form solutions are available for elasto-plastic and elastic-brittle-plastic materials a step by step procedure can be used for elastic-strain softening-plastic material. The third consideration that matters is concerning the change in volume of rock as it yields. Here again, different researchers have used different assumptions starting from no volume change to the ones following flow rules.

## Use of Non-linear Relationship between Strains

It is seen from the results of experiments described above that the relationship between axial and radial strains of rock samples after failure is non-linear. The rate of increase of radial strain is large initially as the material yields but it decreases as the axial strain further increases.

A similar relationship between the radial and tangential strains of yielding rock around the circular tunnel can be anticipated. If the initial slope of  $\epsilon_\theta - \epsilon_r$  curve be  $h_1$  and if  $h_2$  be the amount by which the secant slope of curve reduces as the major principal strain increases from an initial value  $\epsilon_{\theta 0}$  to infinity, the secant slope  $h$  of the curve corresponding to any intermediate value of  $\epsilon_\theta$  is given by

$$h = h_1 - h_2 \left(1 - \frac{\epsilon_{\theta 0}}{\epsilon_\theta}\right) \quad (1)$$

where  $h$  is ratio of radial strain  $\epsilon_r$  to axial strain  $\epsilon_\theta$  at any stage, such that  $\epsilon_r = -h\epsilon_\theta$ ,  $h_1$  is the initial tangent of  $\epsilon_\theta - \epsilon_r$  curve, and  $(h_1 - h_2)$  is the corresponding secant slope as

$\epsilon_{\theta}$  goes to infinity.

$\epsilon_{oe}$  is the major principal elastic strain at which the rock yields and goes from elastic to a plastic behaviour. The assumed relationship between the two strains is shown in the Fig.1.

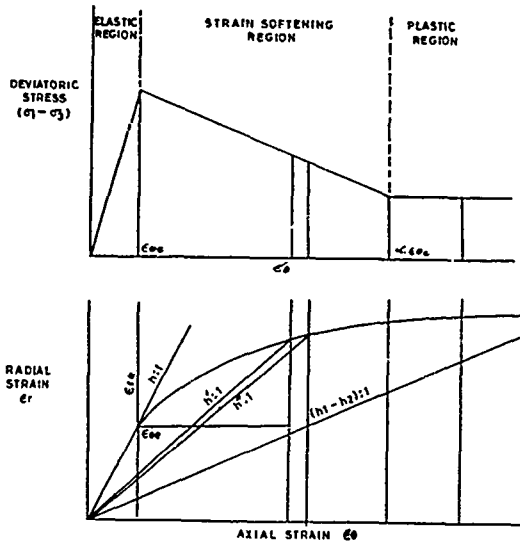


Fig.1 Assumed Material Behaviour Model

#### Use of Integration

The entire rock mass surrounding the tunnel is divided into a number of thin concentric annular rings. The radius, stresses and strains at one surface of any ring are known. For the calculation of corresponding radii, stresses and strains at the other surface of the ring, Brown et.al(1983) have used a finite difference method. It is, however, possible to replace the finite difference approximation by actual integration of the differential equation for the thin annulus and thus use an approach which is part integration and part finite-difference.

From the conditions of axial symmetry, we know that

$$\epsilon_{\theta} = -\frac{u}{r} \quad (2)$$

$$\epsilon_r = -\frac{du}{dr} \quad (3)$$

where  $\epsilon_{\theta}$  and  $\epsilon_r$  are the tangential and radial strains,  $u$  is the radial displacement at a radius  $r$ .

As the  $\epsilon_{\theta}$ - $\epsilon_r$  relationship is non-linear, an average value of  $h$  is assumed for the thin annulus between radius  $r_1$  and  $r_2$ , such that

$$\epsilon_r = -h \epsilon_{\theta} \quad (4)$$

If the radial and tangential strains at the elastic-plastic boundary ( $r = r_e$ ) are given by  $\epsilon_{re}$  and  $\epsilon_{\theta e}$  respectively

$$(\epsilon_r, -\epsilon_{re}) = -h_1(\epsilon_{\theta, -\epsilon_{\theta e}}) \quad (5)$$

$$\text{and } (\epsilon_r - \epsilon_{re}) = -h_2(\epsilon_{\theta 2} - \epsilon_{\theta e}) \quad (6)$$

where  $\epsilon_{r1}$ ,  $\epsilon_{r2}$  and  $h_1$ ,  $h_2$  are the radial strains and the value of parameter  $h$  at the two surfaces of the annulus respectively. Combining these equations we have

$$\frac{du}{dr} = -h \frac{u}{r} - (h-1) \epsilon_{\theta e} \quad (7)$$

where  $h$  is the average value of  $h_1$  and  $h_2$ . Integrating the equation yields

$$u = -\frac{(h-1)}{(h+1)} r \epsilon_{\theta} + C_1 r^{-h} \quad (8)$$

The constant  $C_1$  can be evaluated by using the condition  $u = -r_e \epsilon_{\theta e}$  when  $r = r_e$ .

$$\epsilon_{\theta} = -\frac{u}{r} = \left\{ (h-1) + 2 \left( \frac{r_e}{r} \right)^{h+1} \right\} \frac{\epsilon_{\theta e}}{(h+1)} \quad (9)$$

Applying this equation to the annulus with radii  $r_1$  and  $r_2$  and on re-arranging

$$r_2 = \frac{r_1}{\left\{ \frac{(h+1) \epsilon_{\theta 2}}{2 \epsilon_{\theta 1}} - \frac{(h-1)}{2} \right\}^{\frac{1}{h+1}}} \quad (10)$$

This equation can be used to get the radius of the second surface  $r_2$ .

#### COMPLETE STEPWISE PROCEDURE

To summarise, the complete procedure for calculation of radial convergence is enumerated in the following steps.

1. The following data are required

$E$  = Modulus of deformation of rock mass

$\mu$  = Poisson's ratio.

$p_0$  = In-situ hydrostatic stress

$\sigma_c$  = Uniaxial compressive strength of rock material

$m, s$  = Constants describing the peak strength of rock mass.

$m_r, s_r$  = Constants describing the residual strength of failed rock mass.

$h_1, h_2$  = Constants relating radial strain to the tangential strain,

$r_1$  = Radius of the tunnel.

2. Three different zones are assumed to exist around the tunnel (Fig.2).

a) an elastic zone remote from the tunnel

b) an intermediate plastic zone in which the stresses and strains are associated with the strain softening portion of Fig.2.

c) an inner plastic zone in which the

stresses are limited by the residual strength of the rock mass.

3. The yield criterion of Hoek and Brown (1980) has been used, which gives the peak strength as

$$\sigma_1 = \sigma_3 + (m \sigma_c \sigma_3 + s \sigma_c^2)^{1/2} \quad (11)$$

where  $\sigma_1$  = major principal stress

$\sigma_3$  = minor principal stress

$\sigma_c$  = uniaxial compressive strength of the rock material

$m, s$  = constants which depend upon the nature of rock mass and the extent to which it is broken before it is subjected to stresses  $\sigma_1$  and  $\sigma_3$ .

4. It is assumed that in the broken zone the parameters  $m$  and  $s$  will be reduced to  $m_r$  and  $s_r$ , and the residual strength of the rock mass will be given by

$$\sigma_1 = \sigma_3 + (m_r \sigma_c \sigma_3 + s_r \sigma_c^2)^{1/2} \quad (12)$$

5. The rock mass is assumed to be linearly elastic with Young's modulus  $E$  and Poisson's ratio  $\mu$ , until the initial strength for the appropriate value of  $\sigma_3$  is reached. Thereafter the strength gradually drops with increasing strain as shown in Fig. 3. Strength reduction from the peak and continued deformation at residual strength are accompanied by plastic dilation. Some elastic volume increase may also occur when the stresses are reduced. These aspects are covered in the appropriateness of constants  $\alpha$ ,  $h_1$  and  $h_2$ .

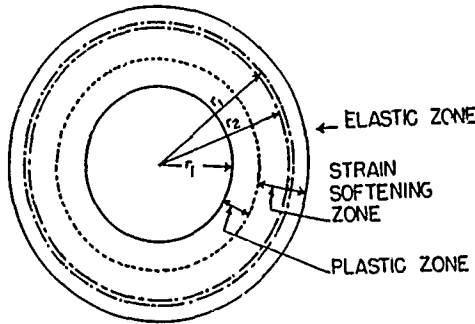


Fig.2 Assumed Zones Around the Tunnel

6. To start with, the initial value of the radius of the plastic zone i.e. the boundary of elastic-plastic region is calculated using the closed-form solution. The radial and tangential strains and the stresses at the boundary are also calculated using the closed-form solution for elastic brittle plastic case. The relevant equations are reproduced,

i) radius of broken zone

$$r_e = r_i \exp \left\{ N - \frac{2}{m_r \sigma_c} (m_r \sigma_c p_i + s_r \sigma_c^2)^{1/2} \right\} \quad (13)$$

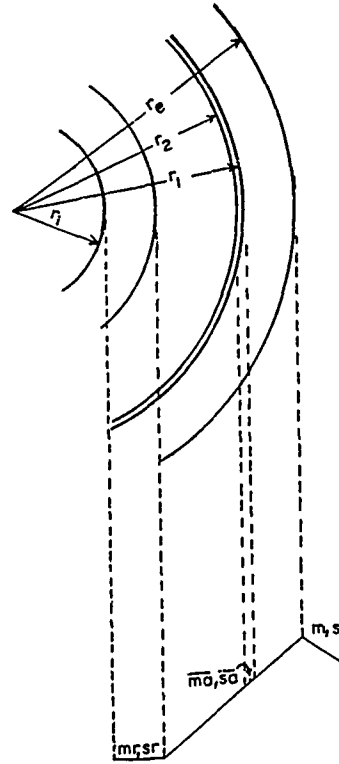


Fig.3 Interpolation for the Values of  $m$  and  $s$  in the Strain-Softening Region.

where  $N = \frac{2}{m_r \sigma_c} (m_r \sigma_c p_0 + s_r \sigma_c^2 - M m_r \sigma_c^2)^{1/2} \quad (14)$

ii) Strains

$$\epsilon_{\theta e} = \frac{M \sigma_c}{2G}, \quad \epsilon_{re} = -\frac{M \sigma_c}{2G} \quad (15)$$

where  $\epsilon_{\theta e}$  = major principal strain corresponding to yielding stress

$\epsilon_{re}$  = minor principal strain corresponding to yielding stress and

$$G = \frac{E}{2(1+\mu)} \quad (16)$$

iii) Stresses

The radial stress at the boundary of the broken zone is given by

$$\sigma_{re} = p_0 - M \sigma_c \quad (17)$$

7. The entire plastic zone including the strain-softening portion is divided into a number of thin concentric annular rings. The tangential strain is increased by an amount  $d\epsilon_{\theta}$  as we move from one ring to the next adjoining one. The new values of the tangential and radial strains are calculated with the help of material behaviour model as shown in Fig. 3. If



the values corresponding to two-surface of annular ring are subscripted by 1 and 2 respectively, we know  $\epsilon_{r1}$ ,  $\epsilon_{\theta1}$ ,  $\epsilon_{r2}$ ,  $\epsilon_{\theta2}$  and  $r_1$ . The corresponding radius  $r_2$  can be calculated from the equation

$$r_2 = \frac{r_1}{\left\{ \frac{(h+1)\epsilon_{\theta2}}{2\epsilon_{\theta1}} - \frac{(h-1)}{2} \right\}^{\frac{1}{h+1}}} \quad (18)$$

where  $h = \frac{(h' + h'')}{2}$

$$h' = h_1 - h_2 \left\{ 1 - \frac{\epsilon_{\theta c}}{\epsilon_{\theta 1}} \right\}$$

$$h'' = h_1 - h_2 \left\{ 1 - \frac{\epsilon_{\theta c}}{\epsilon_{\theta 2}} \right\}$$

8. Once the radius of the annular ring is known, the radial stresses may be calculated from the equation

$$\sigma_{r2} = b - \sqrt{b^2 - a} \quad (19)$$

where  $a = \sigma_{r1}^2 - 4k \left\{ \frac{1}{2} \bar{m}_a \sigma_c \sigma_{r1} + \bar{s}_a \sigma_c^2 \right\}$

$$b = \sigma_{r1} + k \bar{m}_a \sigma_c$$

and  $k = \left\{ \frac{r_1 - r_2}{r_1 + r_2} \right\}^2$

9. The above mentioned procedure is continued till we reach the strain exceeding which implies that we are in the plastic region. The value of constants  $m$  and  $s$  in the strain softening region  $\bar{m}_a$ ,  $\bar{s}_a$  which are calculated by linear interpolation, are taken as  $m_p$  and  $s_p$  in the plastic region. The process of calculation is further continued till we reach a value of radius  $r_2$  for which  $\sigma_r$  equals the internal pressure  $p_i$ .
10. This value of  $r_2$  is made equal to the given radius of tunnel  $r_i$  and all the other values of  $r_2$  and  $r$  are reduced in the same proportion.
11. The axial strain at the tunnel boundary when multiplied with the radius  $r_i$  gives the convergence  $u_i$ .

It is seen that by making these changes, the iterative procedure converges faster and the results for a particular case of elastic-brittle-plastic rock are closer to those obtained from closed-form solutions (Sharma 1985, Sharma and Ramamurthy, 1986, Ramamurthy 1986).

#### FIELD STUDIES

The response of the rock mass during and after tunnelling was observed on three tunnelling projects in the Himalayan region. The salient features of the projects along with response data are briefly described below :

##### Giri Hydro-Electric Project

The first stage of the Giri hydro-electric project (Himachal Pradesh, India) has an installed capacity of 2 units of 30 MW each. Besides a 160m long barrage and an intake regulator, the

water conductor system of the project comprises a concrete-lined tunnel of 7.4 km. length, (3.66 m. diameter finished) through the ridge separating the valleys of the Giri and the Bata. In addition, it has access adits of about 0.8km. length, bringing the total tunnelling work in the project to over 8 kms.

##### Geology of the Tunnel Areas

The tunnel passes through an area which is geologically very complex. The most important feature from engineering geology view point is the occurrence of three major thrusts lying in close proximity of one another. Rocks of different ages have come together as a result of large scale movements resulting in folding, faulting and cutting up by numerous joints and occasional crushing. The alignment crosses two major regional thrusts viz. Krc1 and Nahan.

From the inlet heading, the tunnel initially traverses rock formations of Bailani series of carboniferous age for a length of about 1500m. The bailanis are dark grey black quartzitic slates containing angular to round pebbles and boulders firmly embedded in a clay-silt matrix. The boulders vary in size and show great variation in the density of their distribution and very often the matrix is without any boulders. The rock formations show extensive jointing and shearing at places and tunnel alignment generally follows the strike.

In between, along the tunnel alignment, the strata changes to claystones and siltstones which are highly jointed and deteriorate on saturation. The material in the vicinity of the faults is highly saturated, soft and plastic. Towards the outlet of the tunnel, the strata generally comprises sandstones with occasional thin bands of claystone and siltstones. The rock is jointed but generally competent, except when moisture is present and claystone bands are present.

##### Rock Behaviour during Construction

The initial support system was part circular section of rolled steel joints 150 mm x 79 mm x 19 kgs., placed at a spacing of 1 metre centre to centre, and back-filled with lean concrete laid over reinforced concrete laggings. The initial collapse in the inlet tunnel indicated the possibility of the section being inadequate. The support system in these reaches was then modified to 150 mm x 150 mm x 37.5 kg. steel section at the spacing of one metre centre to centre. After some time it was noticed that even these ribs began exhibiting signs of distress by opening joints and twisting. These supports were strengthened by additional steel. As the movements became more pronounced, the spacing was reduced to  $\frac{1}{2}$  metres centre to centre. The following observations were made at the site.

- i) The supporting system comprising heavy steel sections of 150 mm x 150 mm x 37.5kg. @  $\frac{1}{2}$  m. c/c showed evidence of twisting and buckling even where the space between the rock and the ribs had been completely back-filled with lean concrete. The phenomenon was observed a few weeks after the erection of the support system.

- ii) wherever the rock mass was exposed the rock had intruded into the space between the supports. This intrusion has been considerable, even as much as 15-20 centimetres. The intrusion was observed all around the diameter and the flowing rock was good even after two years and had not detached from the parent rock mass.
- iii) The full circular steel rings, though considered better in resisting the rock pressure, showed evidence of much worse twisting and buckling as compared to the deformation noticed in the adjacent D-type ribs. In both the cases, the ribs were of the same size and placed at the same spacing. In the case of D-type ribs, some deformation was absorbed in the inward movement of the sides, which were free to move at the bottom, causing relaxation in loads.
- iv) In an experimental reach, the ribs were completely embedded in pneumatically placed concrete of 10 MPa compressive strength. The distortion of ribs was much worse in this zone. The concrete showed evidence of cracks at numerous places and had bulged out by as much as 15-20 centimetres, without showing any signs of detachment from the parent rock mass with which it had developed a bond.
- v) The phenomenon of the opening up of the ribs was observed at a number of locations. In some cases, the bottom segment had absolutely detached from the rib but the arch was still in position. In case, the loads were due to loosening, the ribs should have failed or collapsed due to sustained load over it. It shows that the load manifested only when the deformation was resisted. Once the rock created room for deformation, by the failure of the joints and the twisting of the ribs, the loads were 'shed' to the surrounding strata and hence even the ribs without significant bottom support were standing.

In the back-ground of the above, it was decided to use compressible back-fill in the space available between the rock face and the rib. This gave some relief to the support system, but it was only a matter of time, when the closure caught up with the empty space, and thereafter, even the back-filled sections were equally affected.

#### Time Closure Observations

The horizontal closure of the ribs was observed daily with respect to the day of the installation. The average closure was found in the range of 25-30 centimetres, the maximum being of the order of 50 centimetres. The tunnel showed appreciable closures in all reaches, irrespective of the type of the support and the type of backfill.

The rate of closure was very high in the first 20-30 days of the installation of the ribs. Typically, the closure was 26 centimetres at the end of 20 days in the case of the concrete back-filled ribs, which rose to 28 centimetres at the end of 75 days.

In the case of reaches with loose back-fill, the closures took place more gradually, in a more uniform manner, though the ultimate magnitudes were of the same order.

In some reaches, the closures continued even after 300 days, though at a much reduced rate. Figs.4 shows typical closure observations with respect to time, for reaches with loose packing.

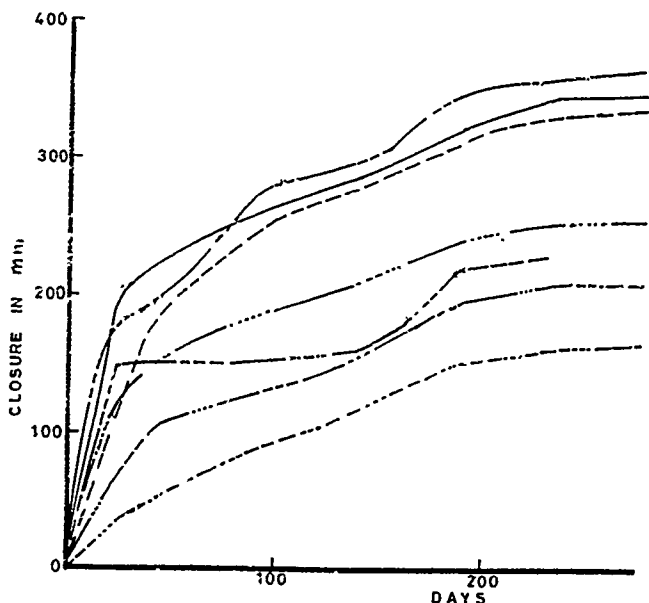


Fig.4 Giri Project - Closure vs. Time for a Zone with Loose Packing

#### Analysis of Data

Using the Rock Mass Classification Systems and the correlations that go with them, the following magnitudes of rock loads are calculated:

- i) Terzaghi's Theory, rock load = 2.31 to 4.41 kg./cm<sup>2</sup>.
- ii) Bieniawski's RMR System, RMR = 34, rock load = 0.71 kg./cm<sup>2</sup>
- iii) Barton's System,  $Q = 0.6875$ , rock load = 4.5 kg./cm<sup>2</sup>.
- iv) Using the mathematical model described above, the rock load corresponding to a radial deformation of 28.55 cms; = 1.9 kg./cm<sup>2</sup>.
- v) Actually observed load = 2.0 - 2.4 kg./cm<sup>2</sup>.

#### YAMUNA HYDRO-ELECTRIC PROJECT

##### General Features

Yamuna Hydro-electric Project located in the foot-hills of the Himalayas in Uttar Pradesh is being constructed in four stages. The Stage II, Part II of this scheme envisages the utilisation of 64m. drop available between tail race of Chhibro underground powerhouse and Khodri Powerhouse. A 7.5m. dia (finished) and 5.6 km. long tunnel has been constructed

for carrying water from Chhibro to Khodri Powerhouse. The excavation of the tunnel has been done through i) a shaft at Chhibro which goes down to about 40m. below the river bed, ii) an approach adit at Khodri and iii) through an inclined adit at Kalawar which was initially excavated for the purpose of investigation of intra thrust zone material characteristics.

#### Geology of the Head-race Tunnel

According to earlier geological investigations, the tunnel was to pass through bands of sandstones, siltstones and claystones on the downstream side, and quartzites and slates on the upstream side. In between, these two formations, an intra-thrust zone of about 300 metre width, bounded by Krol and Nahan thrusts, comprising sheared red shales and 'sabathu' clays was to be met with along the tunnel alignment.

As the work of excavation of the tunnel progressed, the red shales of intra-thrust zones were encountered again and again due to tear faulting which had uplifted the 'Sabathu' shales along the tunnel alignment.

#### Ground Behaviour in the Intra-thrust Zone

The Kalawar inspection gallery was excavated for the investigation of intra-thrust zone material. It was later used as an adit for excavation. The gallery starts in Nahan sandstones, where the steel supports of 152mm x 152mm sections with 175 mm x 90 mm channel lagings were provided with wooden struts for back packing. The Nahan thrust was exposed in the gallery at chainage 164 to chainage 240. Twisting and inward displacement of ribs was reported from this region after a period of about about a month and a half. The supports were strengthened initially by providing struts, and later by changing the shape of supports to a circular one and adding heavier sections to increase their moment of inertia. In certain reaches 152mm x 152 mm H sections with steel plates of 20mm thickness welded on its flanges have been placed at a spacing of 400 mm, centre to centre.

#### Field Measurements in Red Shales

The Central Mining Research Station, Dhanbad, carried out measurements of load on steel supports, closure of tunnel surface and borehole extension in a 3.0m diameter section of the head race tunnel in red shale at chainage 15m, towards Chhibro, from the junction of Kalawar adit and head race tunnel.

The load cells recorded an equivalent pressure of 2.3 - 4 kg./cm<sup>2</sup>. A maximum closure of 94mm. along vertical axis and 45mm along horizontal axis at this section was recorded. It was observed that the time-load and time-closure curves were somewhat identical in nature. This prompted them to plot the load-closure curve and give a linear relationship between load and closure.

$$y = 0.2 x + 1.75 \quad (20)$$

where y is the load in tonnes and x is the closure in cms.

The borehole extensometers showed an extension of about 30mm. The depth of anchors was only 3 metres in this study which is just equal to the tunnel diameter, hence a limitation. Fig.5 shows time-closure relationship.

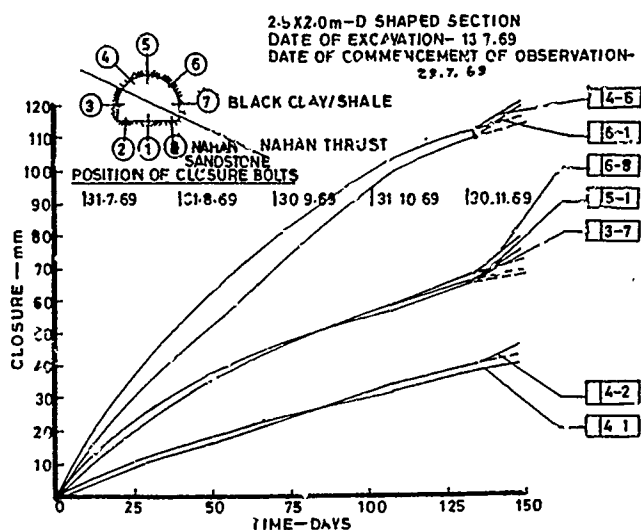


Fig.5 Yamuna Project : Time-Closure Relationship

#### Rock Mass Properties

TIWAG radial jacking test was conducted in red shales in the 3.0m diameter tunnel. Pressures of 3.0, 5.0 and 7.0 kg/cm<sup>2</sup> were applied in the increasing order. Somewhat erratic deformations on the sides were observed. The average modulus of the deformation of the rock mass on the basis of the test was worked out as 0.1x10<sup>5</sup> kg/cm<sup>2</sup>.

Flat jack tests were conducted in the cross cut portion of the gallery in black clay portion of the formations. These clays are similar to shales in their behaviour and properties. The modulus of deformation obtained from this test was 9.061 x 10<sup>5</sup> kg./cm<sup>2</sup>.

Other properties of red shales are as follows (Jethwa 1981).

- i) Unit weight 2.73 g/cc
- ii) Unconfined compressive strength 21.0 kg/cm<sup>2</sup>
- iii) Shear strength  $c = 1.0 \text{ kg/cm}^2$ ;  
 $\phi = 8.40^\circ$

#### Rock Loads and Closures

- i) Terzaghi's Rock Load Theory ; rock load = 3.3 to 7.4 kg/cm<sup>2</sup>
- ii) Rock Mass Rating = 34; rock load = 1.34 kg/cm<sup>2</sup>
- iii) Barton Rock Mass Quality,  $Q = 0.033$  ; Rock load = 3.12 kg/cm<sup>2</sup>.

iv) On the basis of mathematical model the rock load corresponding to 97.5mm = 3.73 kg/cm<sup>2</sup>.

v) Actually measured load = 4.0 kg/cm<sup>2</sup>.

## MANERI BHALI PROJECT

### General Features

Maneri Bhalī Hydro-electric Scheme Stage I, harnesses the power potential of water flowing down the river Bhagirathi between Maneri and Uttar Kashi. The project works included the construction of a 8.63 km long, 4.75m diameter circular concrete lined tunnel, besides a concrete dam, an intake cum sedimentation chamber and a powerhouse. The tunnel passes through complex geological formations under rock covers of 30m to 900m.

### Regional Geology

Rocks encompassed by the project area are Quartzites, Quartzites interbedded with thin slate bands, chloritic schists and phyllites, metabasics and basic intrusives belonging to the the Garhwal group of rocks. Towards the north and north-east of the project area, the rocks of the Garhwal group have a thrust contact (Main Central thrust) with the Central crystallines. Similarly towards the south and south west of the area, the Srinagar thrust (North Almora thrust) separates the two rocks from the Chandpur group.

The metabasics are bright green or greyish green in colour and are interbedded with phyllitic and sericitic quartzite which varies in thickness from 10 cms to 25 m. The bedding in the rocks is demarcated by lithological variations (argillaceous and arenaceous components). The metabasics are in a highly folded condition. A major asymmetrical anticline is exposed at the top. The resident geologist at the site had prepared three-dimensional logs of the geology of the tunnel as actually revealed. Taking the orientation of joints from these logs and using stereographic projection techniques, poles have been plotted to see if the weaknesses have any preferred orientation. The strike of most of the weakness planes is nearly the same, but the dips are different. This is what would be expected in a folded stratum of this nature.

### Properties of Rock Material and Rock Mass

A number of plate jacking and flat jack tests have been conducted in the drift. The average modulus of the rock mass (secant value) is of the order of  $0.5 \times 10^5$  kg/cm<sup>2</sup>. The laboratory test: on rock samples have given a modulus of elasticity of  $3.6 \times 10^5$  kg/cm<sup>2</sup> and a poisson's ratio of 0.17. The unconfined compressive strength of the rock material was 316 kg/cm<sup>2</sup> and triaxial shear tests on rock material have shown  $c = 75$  kg/cm<sup>2</sup> and  $\phi = 43.5^\circ$ .

### Ground Behaviour on Tunnelling

The tunnel is constructed by the conventional drilling and blasting technique. Steel supports of 150mm x 150 mm H Section have been provided at a spacing of 0.3m, 0.5m and 1.0m depending upon the judgement of the engineer at the site. Precast concrete laggings have been provided

in between and the remaining space has been filled back with lean concrete. The system started showing distress in course of time when the steel supports started twisting and buckling. As the foundation provided for the steel girders was nominal, not much resistance was offered to the converging movement. At some places a horizontal strut was welded to increase its stiffness. These girders got sheared off in course of time.

Closures and rock loads have been measured at a number of locations; for the present purpose, we would consider a reach in metabasics which is located between chainages 1000-1200 from Heena adit. The observed closures are plotted and shown in Fig. 6. It is seen that even after a closure of about 380 mm, the system has still not stabilised. A rock pressure of the order of 4 kg/cm<sup>2</sup> has been recorded.

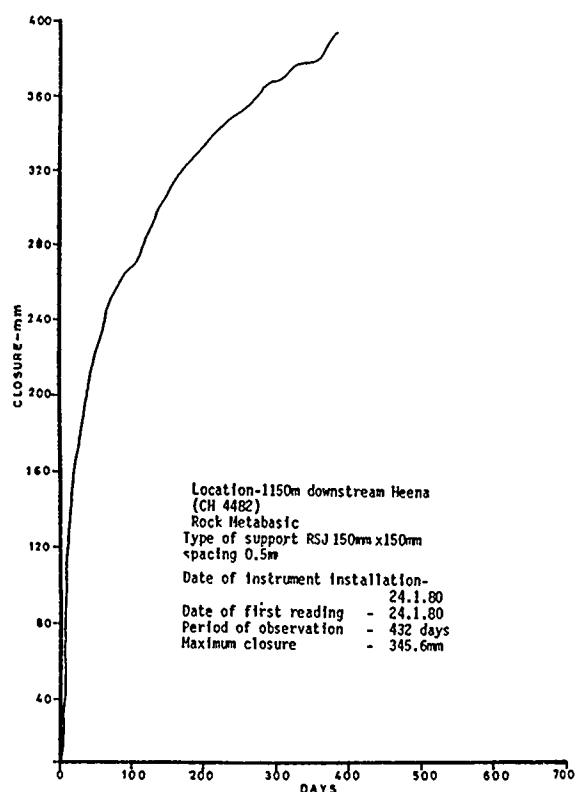


Fig.6 Maneri Bhalī Project - Closure Observations at Chainage 1150

### Rock Loads & Closures

i) Terzaghi's theory,

$$\text{rock load} = 2.64 \text{ kg/cm}^2$$

ii) Rock Mass Rating = 39, rock load =  $0.8 \text{ kg/cm}^2$

iii) Barton's Rock Mass Quality,  $Q = 0.5$ ,  
rock load =  $1.26 \text{ kg/cm}^2$ .

iv) Using the mathematical model, the rock load corresponding to convergence of 380 mm =  $7.9 \text{ kg/cm}^2$ .

- v) Actually measured rock load 4.0 kg/cm<sup>2</sup>  
(with convergence continuing)

## CONCLUSIONS

Comparison of data regarding performance of three tunnels through squeezing grounds, shows that convergence-confinement method offers a better choice in the estimation of radial closures and rock loads. With appropriate modifications the existing methods of evaluation of ground convergence characteristics can be made more effective.

## REFERENCES

- Brown, E.T., Bray, J.W., Ladanyi, B. & Hoek, E. (1983), "Ground Response Curves for Rock Tunnels", Journal of the Geotechnical Engineering Division, ASCE, Vol. 109, No. 1, pp15-39.
- Hoek, E. and Brown, E.T. (1980), "Empirical Strength Criterion for Rock Masses", Journal of the Geotechnical Engineering, ASCE, vol.106, No. GT9, Proc. Paper 15715, pp 1013-1035.
- Jethwa, J.L.(1981), "Evaluation of Rock Pressures in Tunnels through Squeezing Grounds in Lower Himalayas", Ph.D. Thesis, University of Roorkee, India.
- Sharma, V.M.(1985), "Prediction of Closure and Rock Loads for Tunnels in Squeezing Grounds", Ph.D. Thesis, Indian Institute of Technology, Delhi, India.
- Sharma, V.M., and Ramamurthy, T.(1986), "Ground Convergence Curves for Tunnels through Elastic Strain Softening Plastic Ground", Asian Regional Symposium on Geotechnical Problems and Practices in Foundation Engineering, Colombo, Sri Lanka, pp 338-344.
- Ramamurthy, T. (1986), "Stability of Rock Mass", 8th Annual Lecture, Indian Geotechnical Jnl., 16:1:1-74.

# Effects of Geology and Geotechnical Properties of Rocks for the Selection of Type of Dams

**Baqir Hasan**

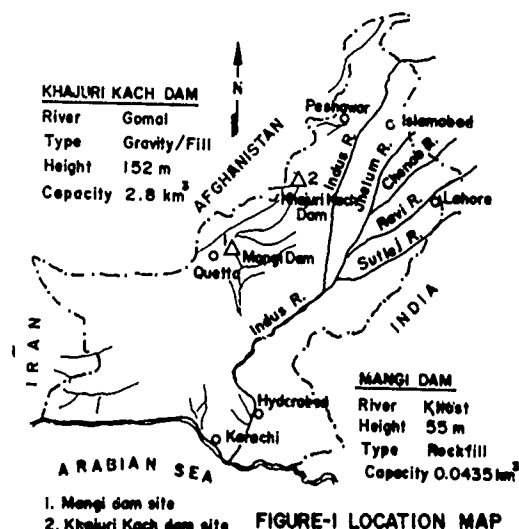
Chief Geologist, Dams Review Cell, Water & Power Development Authority, WAPDA, Lahore, Pakistan

**SYNOPSIS:** The topography, geology, foundation conditions and geotechnical properties of the rock units play a dominant role in the selection of type of a dam. It is usually difficult to determine initially, what particular type of dam is technically feasible and economically viable, for a particular dam site. In selecting the most suitable type of dam, a thorough consideration is given to the characteristic of each type of dam. Before the final selection of the type of dam, detailed evaluation is made of location, topography, geology, foundation condition, geological structure, seismicity, depth of the overburden in the valley section, geotechnical properties of various rock units etc. The paper deals only with the geological problems and geotechnical properties of rock of Khajuri Kach and Mangi Dam in Pakistan. It has been demonstrated, as to how far the geology and geotechnical features of rock units have effected the selection of the type of the dam for these two dam sites.

## INTRODUCTION

The topography, geology, foundation conditions and geotechnical properties of rock play a dominant role in the selection of type of a dam. The shape and geomorphologic features of the gorge, depth of the bed rock in river valley, structural geological features of the area, not only effect the type of the dam, but also determine its dimensions. It is usually difficult to determine initially what particular type of dam is technically feasible or most economical for a particular dam site. In selecting the most suitable type of dam, a thorough consideration is given to the characteristic of each type of dam. Evaluation is made of location, topography, geology, foundation conditions, geological structure, depth of overburden in the valley section, seismicity, availability of suitable construction material, geotechnical properties of the rock units, glaciation, hydrological regime of the catchment and constraints by environmental consideration etc. In the selection of dam site, some time the accessibility of the site, spillway discharges, limitation of outlet works and diversion of the river during construction etc. have an important bearing on the type of the dam. The final selection of the type of dam is generally made after careful considerations of the above factors, which differ from site to site. However, the economics and technical viability of the project, is usually the prime factor in determining and selecting the type of dam.

The geology and geotechnical properties of various rock units of Khajuri Kach and Mangi Dam sites have been described and discussed in this paper briefly, for location of sites refer Fig. 1. It shall be demonstrated as to how the different geological and geotechnical aspects have effected the selection of type of dam for these two dams.



## KHAJURI KACH DAM SITE

From topographic and morphologic point of view, the proposed Khajuri Kach dam site, on river Gomol is one of the finest in Pakistan refer Fig. 2. The project has been investigated upto project planning stage. Considerable amount of surface and sub-surface investigations have already been completed which has given quite good insight of the geotechnical properties of the various rock units.

## INVESTIGATIONS

Detailed investigations include detailed surface geological mapping, together with sub-surface explorations including drilling, aditting and pitting etc. refer Fig. 3. Moreover the foundation rock; limestone was subjected to the

detailed grout test, in-situ modulus of elasticity tests and microseismic tests.



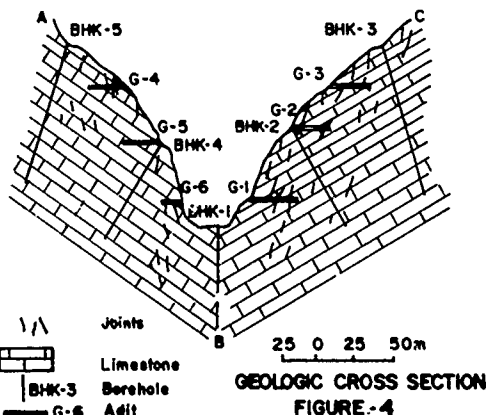
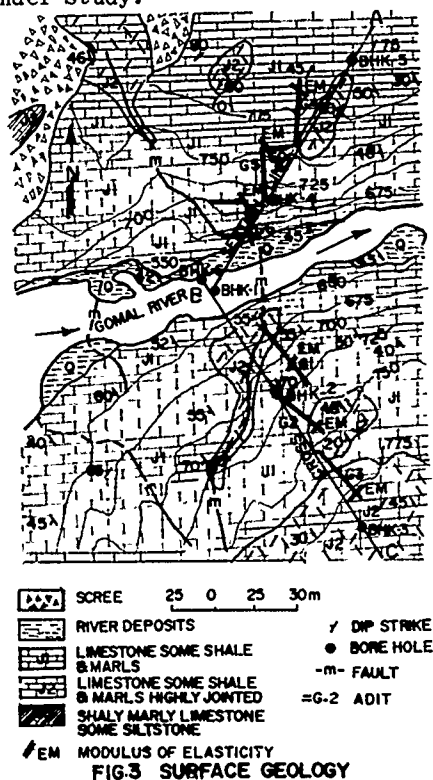
Fig. 2-A General view of the main gorge of Khajuri Kach dam site.

#### GEOLOGIC FEATURES OF THE DAM SITE

The canyon forming the dam site is about 152 m deep, with steep bank slopes on the left side  $75^\circ 1/4 : 1$  and on the right side  $65^\circ 1/2 : 1$  reducing to  $45^\circ 1 : 1$  at the top. The gorge near the dam site area has a width of about 30 m at the bottom increasing to about 213 m at the top. The dam site foundations basically consist of thinly bedded Jurassic limestone which is dark grey, hard, and more or less free from caverns and solution channels refer geologic map Fig. 3 and cross section Fig. 4. The microscopic examination indicates that the limestone consists predominantly of calcite (about 95 to 98%). Other minerals consist of quartz, graphite, biotite, pyrite and gypsum etc. Traces of gypsum occur along the joint planes. The limestone rock unit has some intercalations of argillaceous limestone, marly limestone and shale. The limestone is mostly thin bedded with lot of calcite veins refer Fig. 5.

Outside the gorge, towards west, black sandy shales are exposed, while towards east, grey-yellow or reddish shales are present. The limestone is thin bedded and strike generally in a direction perpendicular to the valley line and dip upstream  $30^\circ$  to  $80^\circ$ . Some deposits of sands and gravels are also met within the gorge along the alignment, but these are superficial and only 2.5 to 4 m deep. The dam foundations substantially protected from seepage by impermeable shale interbeds with an average ground level at about 116 m. These shale intercalations appear to be continuous

but for their main dislocation at their intercalations with the 'm' fault. These formations at the dam site are a part of a limb of a major anticline, the apex of which is far from the area under study.



However, the rocks at the dam site have been subjected to considerable tectonic forces and have suffered extensive jointing and fracturing due to lateral thrusts and over stresses. These rocks also experienced stress release and associated jointing etc. The tectonic forces also produced near the dam site, few faults of small throw and associated shear surfaces have been noted and evaluated. The traceable faults have been mapped and plotted on the map refer Fig. 3. Among the faults only the 'm' fault, is important. The fault generally dips towards downstream and cuts the dam foundations near the right abutment but this is comparatively a minor fault. Five sets of open joints were produced by the above



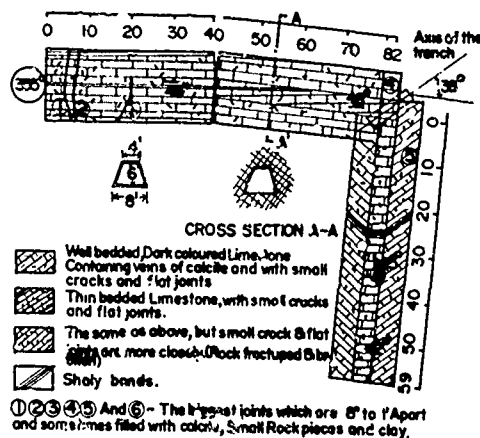
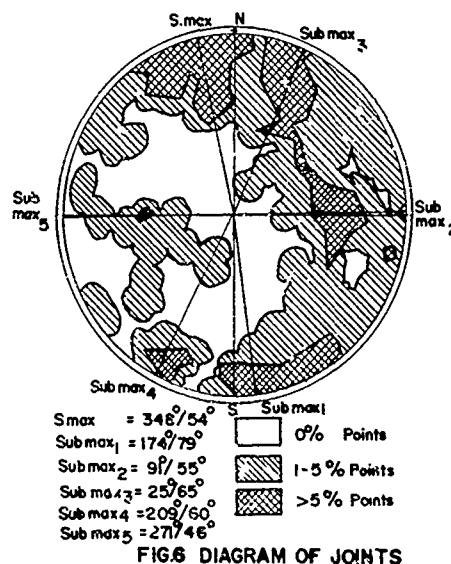
Fig. 5 Thinly bedded limestone at Khajuri Kach dam site.

forces, one along the bedding planes, second at right angles to the strike line i.e. parallel to the valley walls, third parallel to the fault system, and two other sets in other directions. These joint systems have loosened the bed rock forming the dam foundations to an unusual extent. The 8 to 25% openings of the joints with a width of 2 to 3 mm 'rarely' upto 5 mm' form, as much as, 6 to 9% voids in the rock. However these joints and fissures are comparatively open but generally filled with clayey or silty material. At the surface the joints, fissures and cracks are intensive, regular and generally open but with increasing depth these are found to be comparatively tight. The joints are more intensive on the right bank as compared to the left bank and the central portion of the gorge. The limestone bedrock blocks surrounded by the surfaces of joints etc., however, have not suffered any damage by the tectonic forces and are found to possess quite good engineering properties. Their specific gravity is 2.65 to 2.70, water absorption is 0.2 to 1.2%, compressive strength is 750 to 1500 kg/cm<sup>2</sup>, and their modulus of elasticity is as high as 800,000 to 950,000 kg/cm<sup>2</sup>.

#### JOINT SYSTEM

The foundation rock of limestone is highly jointed. The detailed mapping of these joints have been carried out, particularly in the exploratory adits. Some of the joints are quite open and wide, while others are tight and filled by calcite and clay. Joints are well exposed in the galleries, but mostly filled with clay. Crushed and brecciated zones are present in the galleries. The geological

mapping of the joints in the galleries has indicated that joints and fractures are mainly of tectonic origin, and that only a small number of minor joints may have been caused by external force. On the basis of the detailed mapping of these joints hystorograms has been prepared which give the lineation and orientation of these joints refer Fig. 3, 6 and 7.



In addition to the bedding joint there are four well developed joint systems, having different orientation. As a result of these joints the rock has become highly fractured and comparatively weak.

Although the geological map of the dam site shows several faults, their throw is small or negligible. Some of them are important and require special consideration, however there is no surface evidence of these faults being active.

Fault 'm' is the most important tectonic feature at the dam site and requires special attention. In the abutments it is more pronounced. Its extent is not so pronounced



in the valley section. In the area not covered in the Fig. 3, the throw of the fault is calculated to be 1.5 m to 3 m. In the vicinity of the river, the limestone on both abutments are correlatable where suggest that the river is not following any fault zone. The river seem to have cut along the pronounced joint pattern.

The fault 'm' is a reverse type dipping east  $65^\circ$  to  $80^\circ$ . The eastern block has moved upwards in relation to western block.

#### FOUNDATION CONDITION

The evaluation of the exposed rock, drilling data and condition of the rock in adits indicate that the limestone is thinly bedded, highly jointed and may not be good foundation for rigid type of dam without improving it by grouting. The final selection of rigid type of dam, depends on the effectiveness of consolidation grouting. The water pressure tests reveal that permeability of the bed rock forming the dam foundations is fairly high specially in the top layers. There is non-homogeneity as well as an isotropy in the permeability of the foundation rock. Permeability of the bed rock at the right abutment is considerably higher than that at the left abutment and at the central gorge. The competent limestone bed rock forming the dam foundations has suffered much reduction in strength due to the joint systems, fracture, shearing and minor faulting. Some of the joints are tight and filled with clays, others are quite open, however the limestone is devoid of any major solution cavities as revealed by drilling and adits. Using modulus of elasticity 'E' as a yardstick for comparing inherent quality and strength of various foundation materials and taking into account that 'E' for average concrete is of the order of  $150,000 \text{ kg/cm}^2$ , the following figures of 'E' for the bed rock forming the dam foundations may be considered. As against the figures of  $800,000$  to  $950,000 \text{ kg/cm}^2$  for 'E' of the unfractured blocks of foundation limestone the modulus of deformation 'Ed' of the jointed bed rock is as low as  $2000$  to  $10,000 \text{ kg/cm}^2$  in regions near the faults is slightly better i.e.  $20,000$  to  $25,000 \text{ kg/cm}^2$  in other regions of the dam foundations. These figures have been obtained on the actual field tests performed in various limestone zones of the abutments. In the conducted load tests practically no deformation of the highly strong bed rock blocks take place and therefore the strains, on basis of which 'Ed' of the jointed rock is calculated, are almost entirely due to the closing and tightening of the open joints system, under the applied load. It is, therefore, very aptly said that the measured 'Ed' of the jointed and fractured bed rock can better be described as "Squeeze ratio" of the joints, fractures and other weak zones.

There is non-homogeneity, as well as, anisotropy in the strength of the bed rock forming the dam foundations. The 'Ed' of the bed rock in the left bank is higher than at the right bank, and the 'Ed' of the rock under the control gorge is substantially greater than that for the rock at the flanks. The

bed of the foundation rock dip upstream at angles upto  $80^\circ$  and therefore the major component of the stresses applied in the tests acts on the side of the beds where the strength of the rock will be at its maximum. The strength of the foundation rock under maximum stresses caused during the operation of the dam will therefore be some-what better than that shown by the load and this is a favourable situation.

The only way to reduce higher permeability and seepage through the open joints and fractures and to improve the strength of bed rock to the desired level is by grouting. Consolidation grouting is a universally accepted measure to seal off the open joints and fractures and improve weak zones of the foundation rock. But to use the consolidation grouting to improve whole scale the bed rock strength will be very expensive proposition. The foundation rock is highly fractured and jointed limestone, and the joints are filled with clayey or silty material. It may be very difficult to clean the joints and fracture completely from the clay material, before consolidation grouting, as such the proper effectiveness of the grouting for improvement of permeability and consolidation has been doubted. It has been observed by some experts that with modern techniques, it may be possible to clean up the filled joints with clay and proper and effective grouting would be possible, however, other experts feel that in the clay filled joints proper consolidation grouting may not be fully effective.

#### INFLUENCE OF GEOLOGY ON TYPE OF DAM

Khajuri Kach dam site is a classical example where geology and geotechnical properties of the rock units have influenced extensively on the selection of type of dam. The topographic and morphologic feature of the area at the first sight indicate that the site is ideally suited for any type of dam including an arch type. However, after the initial investigations, it was inferred that the jointed and fractured limestone foundation rock, would not be competent enough for an arch type of dam. Afterwards extensive investigation including the grout tests were conducted to see if the site would be suitable for concrete gravity dam or not? Even the international experts deferred as to which type of dam is suited at this location. The main differences of opinion is about the successful groutability of the jointed and fractured limestone foundation rock. It is apprehended that it might not be possible to grout the thin bedded jointed limestone, when the joints are filled by clayey material. However, some expert feel that specialised grouting conducted under supervision of grout experts will turn the bed rock at site into a competent foundation for a concrete gravity dam or even for the arch type. Here the main purpose of the grouting will be to achieve uniformity rather than increase the strength of abutments and foundations. However, other experts feel that it is difficult to grout the clay filled joints and the foundation cannot be improved uniformly throughout the whole foundation area, as such a concrete gravity dam may not be feasible and for this

reason they proposed a rock fill dam. Due to topographic features, spillway for a fill type of dam, at this location would be very expensive. The controversy is still going on. More comprehensive investigations, grouting tests and insitue rock mechanic tests may finally settle the issue.

#### MANGI DAM PROJECT

The Mangi Dam site, is located about 100 km north east of Quetta on the Khost river. This proposed dam site has been investigated in detail for the drinking water supply of the major town of Quetta by lifting the water for more than 122 m in 3 stages.

In confirmity with the modern engineering practice in the dam construction, appropriate attention was given to the appreciation and understanding of the geology of Mangi dam project. For the effective understanding of the geological aspects and influence thereof on the engineering requirement assumption, investigation plans were formulated and executed. For the accomplishment of the investigation objectives, standard techniques and tools were deployed which includes surface geological mapping on regional and local basis and sub-surface exploration-drilling of 31 boreholes to a total 1372 m and excavation of pits, to a total length of 76 m digging out trenches and adits, geophysical studies were also undertaken, for resolving one of the complex seepage and groundwater problems, recently developed techniques such as radio isotope studies were also carried out and experimented. The radio isotope studies were conducted mostly to evaluate the groundwater conditions, particularly its directional movement and its possible effect.

#### REGIONAL GEOLOGY

The predominant rock units exposed in the immediate project area are limestone and shales. Sandstone and shale are exposed mostly towards west which extend beyond the limits of regional map.

The most striking aspects of the structure are the alternating, well developed anticlines and synclines, which are oriented in east-west direction. Limbs of both of the anticlines are formed by Brewery limestone, while the synclinal basin is comprised of Ghazij shale. The southern anticline, on which the dam site is located plunges towards the west refer Fig. 8.

There are a number of major and minor faults many of regional distributions, which can be traced for long distances. At places major faults have clearly shifted the axes of the anticlines. Several regional faults are traceable on both anticlines and, therefore probably cross the synclinal basin also.

The limestone is jointed, fractured and sheared to varying degree. Apparently the regional structure has influenced the north-south orientation of many narrow gorges which appear to have been developed along prominent north-south joint pattern.

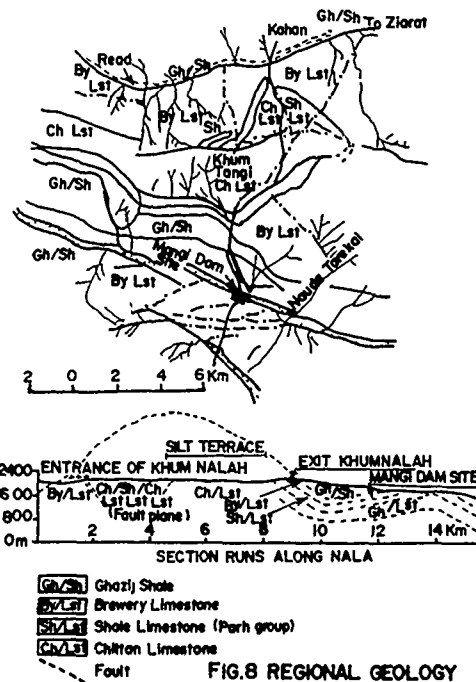


FIG.8 REGIONAL GEOLOGY

Many perennial springs have been observed in the Brewery limestone of the northern anticline. They are particularly prominent in the Khum Tangi refer Fig. 8.

A number of perennial springs also exist in the Brewery limestone of the southern anticline downstream of the dam axis refer Fig. 9. The evaluation of regional geology and the investigations to date, suggest that these springs are being generally fed from regional ground water which follows the regional geological structures.

The regional ground water movements in the area are extremely complex. The stream flow entering the Khum nala in the upstream anticline, supplemented by spring flows from within the gorge, often disappears entirely into the alluvium in the gorge. This phenomenon occurs as the water passes the downstream dipping limb of the anticline. All the evidences available indicate that at least some of this water seeps into the Brewery and Chiltan limestones and possibly passes beneath the reservoir under the syncline. A portion of it emerges in the form of spring downstream of the dam site. This may indicate the possibility of a sizeable groundwater potential existing within the Mangi basin. A programme using radio isotopes as tracer element was utilized to determine the direction of the movement of groundwater. Radio isotope injection in bore holes indicated that the ground water at the abutment is connected with the springs at the abutments.



Fig. 9 showing location of spring in the Brewery limestone.

#### DAM SITE GEOLOGY

The dam site is located on the northern limb of the downstream anticline on the Khost river. For a masonry dam, the axis would be located about 122 m downstream of the confluence of three tributaries refer Fig. 10. At this axis the width of the gorge at river level is only about 25 m with vertical side walls and many over hangs. For a fill type of dam, the axis would be shifted further upstream on to the dip slopes of the anticline.

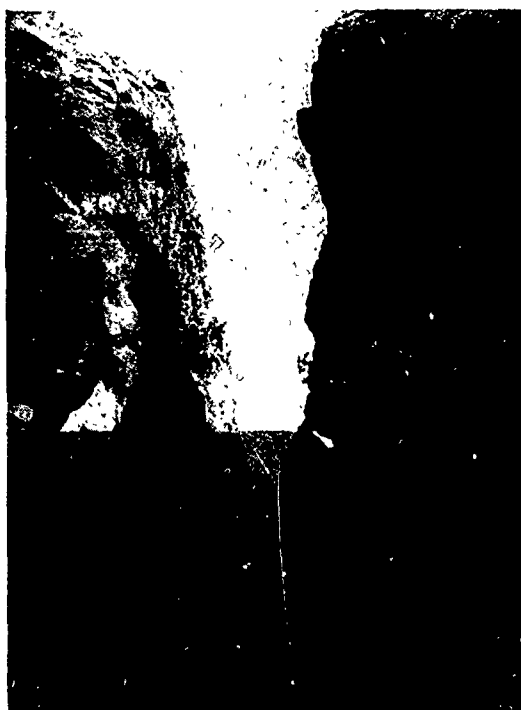
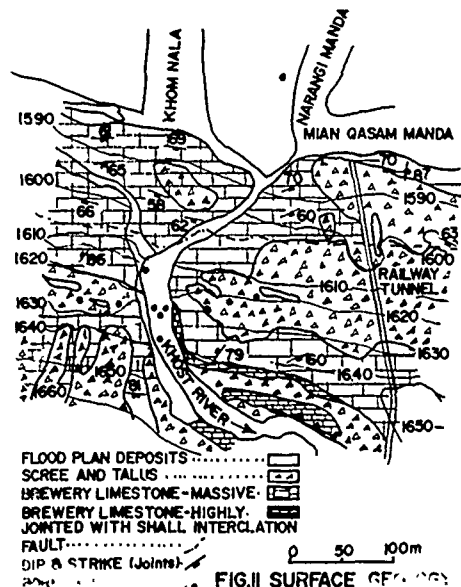


Fig. 10 General view of the gorge of Mangi dam site.

The rock exposed at both the masonry or fill dam sites is Brewery limestone. It is hard, massive to thin bedded, with shale intercalation at lower elevations. At the axis of the masonry dam the limestone can be divided into two units; upper massive limestone and lower highly jointed limestone, with thin intercalations of shale. At the axis for the fill dam, only the massive limestone is exposed on a dip slope refer Fig. 11.



The bore hole Nos. MRS-13, 18 & 21 including twenty four pits near the upstream toe of the limestone slope have revealed that shale is exposed at a shallow depth, which varies from 0.9 to 4.5 m. The shale is generally soft and splintery at surface but hard at greater depths and obviously impermeable.

The geologic structure at the dam site is not complicated. The limestone dip uniformly about  $24^\circ$  to the north west i.e. towards upstream and strike  $N85^\circ E$  approximately parallel to the axis of the dam. There appears to be no offset between the abutments, which suggests that there is no apparent fault in the valley section of the gorge. However, a gravity type fault crosses the two abutments in a nearly east-west direction about 41 m upstream of the masonry dam axis. A fault with apparently a small displacement can also be traced across the left abutment near the railway tunnel. There are a number of additional faults further downstream of the axis along which some of the downstream springs emerge.

The limestone is highly jointed with the most prominent joints striking 'a'  $N 85^\circ W$  and dipping  $60^\circ$  to  $70^\circ$  south west and 'b'  $N 50^\circ W$  with a dip of  $75^\circ - 85^\circ$  towards south west. These joints are generally spaced about 0.6 to 1.2 m apart. Two less prominent sets have the following strikes and dips.

1.  $N 40^\circ W, 45^\circ SW$
2.  $N 45^\circ E, 77^\circ SE$

All sets of joints are exposed on the abutment slopes and have been shown on figure 7. The prominent joint sets near the dam axis are quite open and will play an important role in the stability of the slopes and seepage loss through the abutment.

The valley in the gorge is filled by alluvium, composed of silt, sand, gravel and big boulders. The narrowness of the gorge and the steepness of the stream gradient, gives the impression that the gorge may have been formed along a fault plane, but the detailed study of the stratigraphy and correlatable beds on the two abutments does not support this theory and suggest that the gorge has probably developed along a major joint pattern refer figure 12 and 13. Nine boreholes drilled in the valley section of the gorge 'three on the masonry dam axis' indicate the bed rock to be within 7.6 m of the surface and thus eliminate the possibility of the existence of buried channel within the valley.

#### FOUNDATION EVALUATION AND GEOTECHNICAL PROPERTIES

The information obtained from sub-surface exploration indicates that the condition of the limestone improve with depth. However, the rock at depth is moderately to highly jointed. Some of the joints are quite open. This condition contributes to the appreciable water loss during pressure testing and shows that the limestone is quite permeable. The maximum water loss recorded on the right abutment is 53.68 litres/metre/minute at 689 kilo pascals. On the left abutment the maximum water loss is 52.19 litres/metre/minute at 689 kilo pascals. The water losses vary from place to place, depending upon the intensity and openness of the joints. The valley section bore hole data indicates comparatively less water loss. This may be due to the presence of thin shale layer in the limestone.

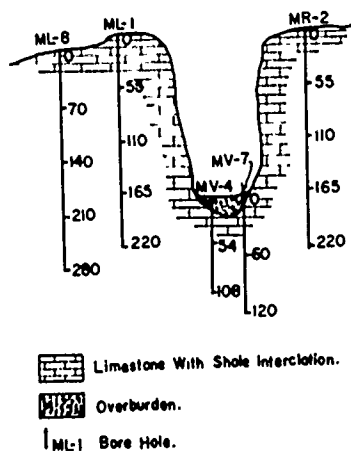


FIG.12 GEOLOGICAL SECTION

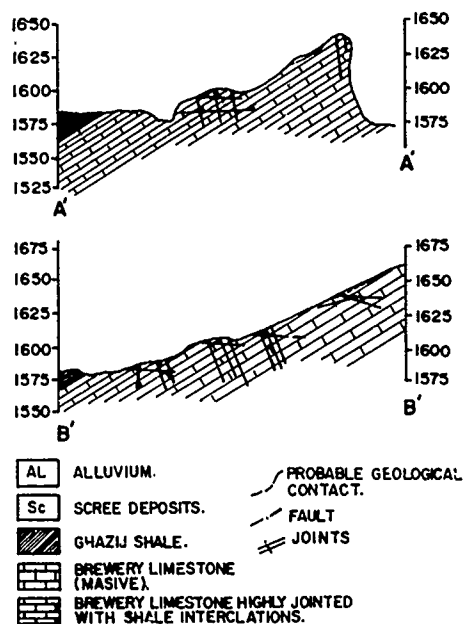


FIG.13 GEOLOGICAL SECTIONS

In-situ or laboratory tests have not yet been performed to determine the bearing capacity of the limestone. However the good core recovery and freshness of the core suggests that the limestone would be quite competent to support either a masonry, or a concrete gravity structure or a fill type of structure of the proposed height. Elaborate bearing pressure tests are, therefore, not essentially required. Due to topography as well as highly jointed nature of the rock, an arch dam is not feasible; enough rock mass is not available behind the left abutment to withstand the thrust from the arch section.

The dam site and reservoir area is punctuated by number of minor and major faults. There is no evidence that these faults are active. However, since this area lies in active seismic zone, the effect of the severe earthquake would probably be concentrated along these comparatively weak planes. It is, therefore, necessary that while designing the dam and appurtenant structures, due consideration factor should be given for adequate seismic factor.

#### SEEPAGE LOSS

This being a predominantly limestone area, water loss through seepage merits very careful consideration. Appreciable water loss in the borehole during pressure tests, highly jointed nature of the limestone and existence of numerous springs in both the anticlines strongly underline the highly permeable nature of the limestones.

Ground water elevation in the bore holes on the abutments and in the valley has been regularly observed. The record indicates that the ground elevation ranges between 1564 and 1567 m. The ground water elevation is influenced by

the climatic conditions in the region and the ground water table slopes from upstream of the dam axis. Even during the fluctuations the ground water table has maintained the downward slope. The groundwater which lies within the limestone is recharged from the regional groundwater and is not directly connected with the stream flow in the Mangi Basin overlain with thick shale mass.

After the dam is built, a large column of water would be standing against the highly permeable limestone of the anticline. This could contribute significant amount of water to the water table below, which may increase the flow of existing springs and or create new ones downstream of the dam. If such a condition occurs a substantial quantity of water may be lost. The dam site anticline plunges towards the west and may direct the seepage flow in that direction away from the reservoir. This water may be irrecoverably lost.

The most potential seepage area is on the left abutment. The distance between the full reservoir level and the scarp face downstream is only about 41 m. This distance is inadequate. Seepage water, almost under full reservoir head, would exert pressure, and could, besides seepage loss, create serious stability problem, for highly jointed limestone ledge. The critical area extends to a distance of about 183 m from the left gorge wall. Special drainage and protective measures shall have to be taken in this area.

The expected excessive seepage through the limestone abutments, the valley section and the limestone periphery will require extensive protective measures. The seepage can be reduced to acceptable levels, by a well planned grouting programme or blanketing of the slopes with impervious materials.

The total length of the limestone, which will be in contact with reservoir water will be about 2591 m. In case, a masonry dam is constructed, grouting of the whole limestone periphery would be prohibitively costly. However, it may be possible, to grout the foundations of the structure only to the extent of 61 to 91 m, on the right abutment and about 183 m on the left. The remainder of the limestone periphery could be blanketed with impervious material. It may, however, be essential to excavate drainage galleries at several elevations in both the abutments.

In case of fill dam it is possible to remedy the seepage problem, by blanketing the entire limestone abutments and periphery by impervious material. The impervious core of the dam could be tied into the reservoir shale, which is at shallow depth and covers the entire reservoir floor. This will provide more or less a continuous impervious cut-off and will minimize the seepage problem. The extensive costly grouting would be considerably reduced or possibly entirely eliminated. Drainage galleries at proper elevations will probably be required for a fill dam also.

#### INFLUENCE OF GEOLOGY AND GEOTECHNICAL PROPERTIES OF ROCK FOR THE SELECTION OF TYPE OF DAM.

Narrowness of the gorge obviously competent looking exposed rock suggests an arch type of dam. However, the detailed investigation revealed the highly jointed nature of the limestone foundation rock, coupled with the fact that due to the falling away of a part of the left abutment downstream of the dam axis, enough rock mass is not available to withstand the thrust for the arch section makes such a dam unfeasible.

Alternatively the topography and the foundation conditions evidently suggest a masonry or concrete gravity structure and that is what it was initially proposed. However, investigation revealed acute seepage problem both due to the regional and local geological aspects. Mangi Dam site is one of the rare project, where regional geological aspect has contributed substantially in the seepage problem at and near the dam site. The regional and local excessive seepage and danger of more excessive seepage after the construction of the dam has effected considerably on the selection of the type of dam. The remedial measures against excessive seepage concrete or masonry dam a very costly proposition.

For this project, which faces acute water deficiency, seepage control is the most important aspect. In case of rigid structure both extensive and costly grouting and blanketing all along the limestone ridge would not only be extremely costly, but the tie in of the blanket, will be artificial unless and until it is tied with due comparatively impervious shale of the reservoir basin. In case of fill dam, the impervious shale covering the reservoir thus providing a better seepage control. Since enough rock is available at and near the dam site, rock fill section will be comparatively cheaper and earthfill structure. A rockfill dam would, however, require a separate and bigger spillway whereas a masonry dam itself would function as such. Addition of a spillway would, therefore, add to the cost of the fill structure. The peripheral blanketing would be common to the both. For fill structure most of the excavated material from the spillway, the diversion and the site preparation could be used in the body of the dam.

In ultimate analysis, it would be the economics which would decide the issue. From the geological and seismic point of view and in the light of the information now available, a fill type of structure is preferable.

## Slopes in Weak Rocks

Ali Mohammad Jokhyo

Assistant Professor, Department of Geology, University of Sind,  
Jamshoro, Pakistan

**SYNOPSIS:** During the construction of high way along Albaha-Descent (Saudi Arabia) through schistose rocks, unexpected engineering problems arose due to geo-mechanical defects of the rocks. The original design of the highway had to be altered at many places after re-examination of the properties of the rocks, for the safety of the road.

Following stability analysis various slope protection measures including rock anchorage dywidage bars and rock nails with expansion heads, were taken. The results were very promising and indicated that it was possible to construct roadways in very weak rocks within practical limits of safety and stability.

### INTRODUCTION

Road work in weak schistose rocks present difficult stability problems particularly in high cuts. Not unexpectedly many road cuts fail due to defective primary design. The protection works check temporarily the full operational capability of the rock mass, but it remains susceptible and threatening.

It is also costly to deal with weak rock slopes. At many cut slope sections the comparative study was made between slope reinforcement and flattening of the slopes in many such cases the justification was for the slope protection measures in terms of economy, time space and for technical, environmental as well as archeological reasons. The case history mentioned below aims at highlighting the problems encountered in weak rocks which necessitate design modification and measures resorted to, to ensure road stability and safety.

### GEOLOGY OF THE AREA

The area of Albaha road descent project Saudi Arabia lies at an elevation of about 2300 meters above sea level; on the western margin of red sea trough where the rocks are mainly, pre-Cambrian to pre-Permian metamorphics dissected by complicated faults system and intruded by basic rocks (As per Technical report of the project by Ital Consult Rome 1980.)

Geomorphologically the form and trend of the surface is quite rugged terrain, consisting of ridges of stiff green schist rocks and wadis that are natural drainage channels. The depressions and wadis generally contain alluvial deposits of cobbles, gravel sand silt with some clay having thickness of 2-10 meters

Natural agents of weathering and erosion have been acting for long time giving rise to rather stable slopes of mountains, talus deposits, soils and alluvial deposits.

Lithologically the most commonly appearing rocks are green-schists, green stones, slates argilla-

ceous schists (containing phyllites and chlorite schists) intruded by basic igneous rocks.

Structurally the strike of these formations is generally NNW-SSE, and dip varying ( $40^{\circ}$  to  $70^{\circ}$ ) at various degrees to NW and SE direction. These schistose rocks are slightly to highly fractured. The geological observations of strike and dip directions on sites suggest that main tectonic force was at right angle to N-S clearly the red sea trend from West.

### DESIGN CRITERIA:

The soil geological investigation was carried out by M/s. Ital Consult Rome, Italy, initially based on Photogeological interpretation due to rugged terrain. The metamorphosed rocks were schematized into various groups. The mechanical and Physical characteristics assigned, were deduced by direct inspection of the material from technical literature and the results of laboratory tests on samples from these areas. A minimum safety factor of 1.5 was adopted to allow for variability.

The geotechnical parameters established by the designers were based on the degree of fracturing state of decompression of the rock and dip of schistosity planes as these mainly govern the shearing strength along the surface of discontinuity. Accordingly, following internal friction and cohesion values were given

| Unit weight | Angle $\phi$                | C                      | Rock type |
|-------------|-----------------------------|------------------------|-----------|
| 2.6         | $30^{\circ}$ - $35^{\circ}$ | 12-15 t/m <sup>2</sup> | A         |
| 2.3         | $30^{\circ}$ - $35^{\circ}$ | 7-10 t/m <sup>2</sup>  | B, H, N.  |
| 2.1         | $25^{\circ}$ - $30^{\circ}$ | 5-7 t/m <sup>2</sup>   | E         |
| 2.2         | $35^{\circ}$ - $40^{\circ}$ | 3-5 t/m <sup>2</sup>   | Z         |
| 2.1         | $35^{\circ}$ - $50^{\circ}$ | 1-3 t/m <sup>2</sup>   | D         |

Where angle  $\phi$  = Angle of internal friction  
C = Cohesion along the failure plane

## HISTORY OF THE CUT OPERATION

The excavation of the area was started as per designed cross section. The rocks exposed were highly fractured and badly weathered green schists upto the berm. On the either sides of the tunnel two small valleys existed. After a week as a result of rain the rock material fell down and tension cracks developed at the top of the cut. Therefore the rocks characters were studied again. The (8) samples of the rocks with a portable shear machine were tested, the shearing strength of potential failure surface showed the average cohesion in failure plane of 3 tons/m<sup>2</sup> instead of 7 tons/m<sup>2</sup> as per design. The specific (unit) weight of the particular rocks were taken again; the average of 10 samples gave 2.1 t/m<sup>3</sup> instead of 2.3 t/m<sup>3</sup> which was corrected for stability calculations.

Site investigations of the rock defects revealed that weathering had effected the rocks to a depth of 8m to 15m. The fractures were found in 3 sets, the dominant one was parallel to the strike of the plane of schistosity. Other one is perpendicular to this set and the third set is in a plane perpendicular to both. The main fractures are spaced 5-20 cms apart and other two sets are spaced 10-30cms apart. In most of the area the fractures are filled with clayey material.

Once this slope above the crown of the tunnel was protected with rock anchorages (as discussed later) and gunite with mesh, the actual tunnel portal excavation started. The progress of the portal cutting was also hampered by bad geomechanical rock conditions, those changed from poor to worst, where the rock mass was completely decomposed. Consequently extra safety measures were used, by rock bolting and concreted portal that was reinforced by rock nails with expansion head. These rock nails were 6meter long and given 10 ton tension to increase the friction within the rock mass and help the stability of the portal (see the frontal view of the cut) Fig.2.

The dywidag rock anchorages were retested after one month for the detensioning if any, and found within limits of elongation. As such the global stability of slope was achieved by rock strengthening.

### DESIGN HYPOTHESIS FOR SLOPE STABILITY.

(See design model Fig. 1)

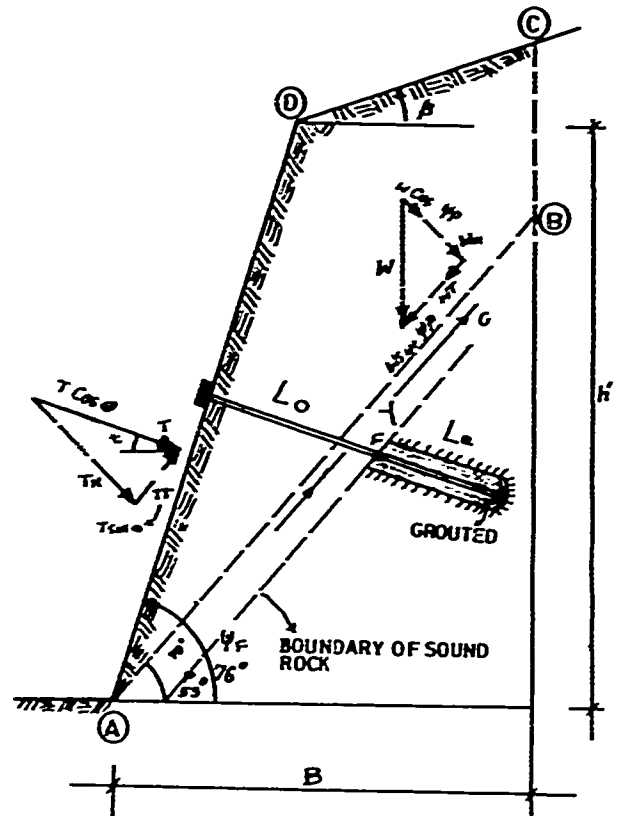
It is assumed that there is no water inside the tension crack or along the failure plane. The calculation ignores all resistance along the surface of the tension crack. The calculations are carried out for 1m wide mass of rock. The total height of the cut was 30 meters. A berm of 2 meters was given at 12 meters, (4 m above the tunnel crown). Again, a cut slope of 18m, h' above the berm was given, with  $\beta$  the angle being less than 45°.

### STABILITY ANALYSIS

Mechanical Datas.

Specific weight  $\gamma = 2.1 \text{ t/m}^3$   
 Angle of internal friction  $\phi = 30^\circ$   
 Cohesion along the failure plane = 3 t/m<sup>2</sup>

## DESIGN MODEL FOR ROCK-ANCHORAGE



## EQUILIBRIUM CALCULATION FOR ROCK MASS A-B-C-D. MECHANICAL PARAMETERS FOR THE ROCK

$\gamma$  = Unit Weight [t/m<sup>3</sup>]

$P_i$  = Angle of internal friction [ $\phi$ ]

$C_i$  = Cohesion [t/m<sup>2</sup>]

A-B = Most dangerous sliding plane ( $\gamma P$ )

B-C = Most dangerous vertical crack (B)

$F_{stab} = T + F + C$

$F_{slid} = W \cdot r$

$f = \frac{F_{stab}}{F_{slid}} \geq 1.5$  (factor of safety against slide)

FIG.1

DESIGN MODEL FOR ROCK ANCHORAGE.

### Geometric Data.

Height of cut  $h' = 18\text{m}$   
 Grade of cut slope (4V: 1 H)  $\psi = 76^\circ$   
 Grade of most dangerous sliding plane  $\psi_P = 53^\circ$   
 $\psi_P = 1/2 (\psi + \theta)$   
 Distance of most dangerous sliding plane  $B = 7.8\text{m}$

$$\beta = H \sqrt{1/\tan^2 \psi_P + 1/\tan^2 \psi}$$

Area of sliding plane.

$$A = \gamma \times \frac{k^2}{2} \times \left\{ \left[ 1 - \left( \frac{z}{k} \right)^2 \right] \tan \psi_P - \frac{1}{2} \left[ \frac{BC - L'}{k} \right] \tan \beta \right\}$$

Equilibrium calculation of rocks

Weight of sliding mass  $W = 125.9 \text{ ton}$

Sliding force ( $W \sin \psi_P$ )  $F_s = 99.7 \text{ ton}$

Friction Force ( $W \cos \psi_P$ )  $F_f = 43.2 \text{ ton}$

Cohesion force ( $C \times A$ )  $F_c = 39.0 \text{ ton}$

$$\text{Factor of safety. } F = \frac{F_f + F_c}{F_s} = 0.82$$

Note:- This factor of safety is less than the required. Therefore the cut-slope should be supported with Rock-anchorage. As a better rock is assumed behind the fracture zone.

### Need for Anchorages

It is considered that there is a resultant force  $T$  which acts on the surface of the slope, and is attributable to the presence of one or more anchors. Under these circumstances when the failure plane passes through the foot of the slope, the factor of safety expression can be given as follows.

$$SF = \frac{CXA + (W \cos \psi_P + T \cos \theta) \tan \theta}{W \sin \psi_P + T \sin \theta} = 1.5$$

where  $\theta = \psi_P + 10^\circ$

The resultant force ' $T$ ' per linear meter of the slope length will be:

$$T = \frac{W(1.5 \cos \psi_P - \cos \psi_P \tan \theta) - CA}{\cos \theta \tan \theta + 1.5 \sin \theta}$$

$$= \frac{125 (1.5 \times .798 - .601 \times .577) - 39}{.453 \times .577 + 1.5 \times .891} = 42 \text{ ton}$$

### DIMENSIONAL DESIGN OF ANCHORAGES

(see design model Fig.1.)

If ' $T$ ' the resultant force per linear metre of slope length, ' $i$ ' is the spacing of the anchorages, and  $n$  = the number of anchorages in a vertical row, then the force on the anchorages is

$$T_0 = \frac{T \times i}{n}$$

$$\text{or } n = \frac{42 \times 25}{45} = 2.3, \text{ say } 2 \text{ rows}$$

If  $l_a$  indicate the length of the active part of the anchorage and  $D$  the diameter of hole with ' $C$ ' the cohesion of the rock, and ' $a$ ' the friction co-efficient, then the resisting force per unit of active length is

$$\frac{T_r}{l_a} = a \times C \times \pi \times D$$

For 32 Dia,  $T_o = 45 \text{ ton}$  anchorage  
 Assuming  $C = 35 \text{ ton per metric square}$   
 $a = 0.8$  and  $D = 0.15 \text{ m}$  then active length would be

$$l_a = \frac{T_r}{a \times c \times \pi \times D} = 5.8 \text{ m}$$

Having fixed the spacing of anchors, on the basis of consideration concerning the degree of fracturing of the rock, the number of anchorages  $n$  and the active length of  $l_a$ , it will be established to ensure the following condition.

$$n = \frac{T_r}{T_o} \geq 2, \quad T_r = 2 \times T_o$$

as after certain length the resisting force does not increase linearly with length  $l_a$ , also the low values are not very effective. With the anchorage set at height ' $x$ ' above the foot of the slope, the passive length  $l_p$  will be

$$l_p = l_o + Y$$

Where  $l_o$  (free length) can be checked from (site, stability analysis, from the charts of the design) and  $Y$  is the distance of the boundary of the sound rock from the critical failure plane.

The total length of each anchorage will thus be

$$L = l_a + l_o + Y$$

$$= 6.8 + 4 + 4.2 = 15 \text{ m}$$

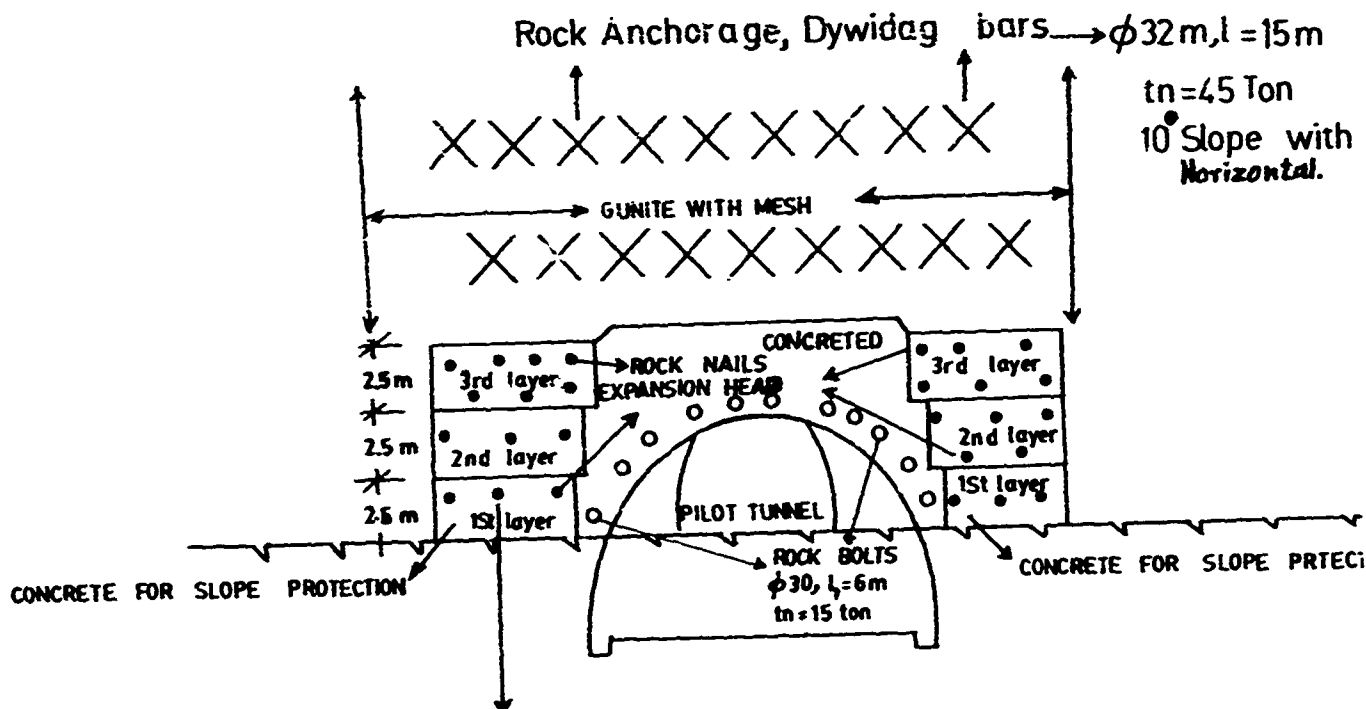
### DISCUSSION:

The amount of geomechanical defects must be taken into consideration by design engineer for high cuts in roadways.

For example, the cut slope of 4/1 ( $76^\circ$ ) in high cuts require a very strong rock with fairly constant rock character. Where a highly weathered and decomposed zone crosses the cut face, the global stability can not be achieved by ordinary means.

Selection of parameters used in the design formulae basically depends on the experience gained from the past work in similar area. In tectonically intensely disturbed areas, the geomechanical character of the rock vary greatly from place to place along the roadway and as such no single parameter can be evolved





ROCK NAILS  $\phi 26, l=6m, t_n=15 \text{ ton}$ . EXPANSION HEAD.

## FRONTAL VIEW: OUT-LET TUNNEL NO:2 SLOPE & PORTAL PROTECTION WORKS

NOTE:- DYWIDAG BARS ONLY AFTER PILOT TUNNEL IS EXCAVATED.

Frontal View of the Cut Fig.2.

for application through out the cut. Judgement should be made about their values clearly by the designer. Hence it is basically a result of knowledge of the in-situ rock qualities and stresses, combined with experience.

In order to increase design perfections cut-slope rock indices should be determined by using rock mass classification system and orientation of major fractures / joints sets with respect to the cut be established. In addition to this, effects of other workings should also be included in the analysis.

### CONCLUSIONS:

Main conclusions from the case history can be summerised as under:-

- Construction of highways in weak rocks need special attention to have a safe and economic design

- The depth of weathering and rock quality variation should be precisely marked and surveyed for different type of cuts.
- Correlation between designed and predicted parameters of rocks should be taken into consideration before starting a particular rock slope cut.

### ACKNOWLEDGEMENTS:

The author would like to thanks Doctor of Engineering Guesseps Depra, Resident Engineer of Albaha, Descent Project, Saudi Arabia for his encouragement and to all the colleagues who contributed to the compilation of this paper.

#### REFERENCES:

Dywidag Post tensioning Systems. (1979)  
Report No.30,  
Unter schleissheim/ Munchen.

Grouted Rock bolts for support of underground  
works (1963) Research report no.1726 by  
Pender, Hosking & Mattner  
submitted by Snowy Mountains Hydroelectric  
Authority.

Technical Report, Soil Survey (1980) and Design  
and Specification Albaha-Descents Road Pro-  
jects. Tihamma- Descents Projects.  
M/s. Ital Consult, Rome, Italy.

## Construction of Hydel Power House in Weak Rocks

**K.K. Kapoor**

Deputy Chief Engineer (Civil), Mahi Hydel Project, R.S.E.B.,  
Banswara, India

**S.C. Patodiya**

Executive Engineer (Civil), R.S.E.B., Jaipur, India

**SYNOPSIS :** Geological uncertainties have always played an important role in planning of a hydel power house. This paper presents case study of a power house which was subjected to major revisions in its planning due to inherent instabilities in rock slopes. Initially the power house was planned with service bay and other facilities on its left hand side, but the weak and instable slopes and sliding of large rock masses necessitated its thorough revision by bringing service bay and other facilities to its right hand side alongwith addition of many new features and flattening of slopes. There were many alternatives under consideration and final selection was based on techno-economic balance of the project.

### INTRODUCTION

The power house-I of Mahi Hydel Project, Banswara (India) is an indoor type surface power house located in 64 m deep open excavated pit with installed capacity of 2x25 MW generated through 40 m head of water. The lowest foundation level is at El-217.0 m whereas general ground level of the area is at El-281.0 m. Location of this power house is latitude : 23° 32'30" North and longitude : 74° 28' 00" East.

### GEOLOGICAL DETAILS

Geological investigations of the area were made prior to starting the excavation work. It was revealed that power house pit lies in pre-Aravali gneisses and schists. The country rocks are granite, gneisses, schists, amphibolites and pegmatite veins associated at places with graphite schists all moderately to steeply dipping towards south with foliation striking from North West-South East and overlain by horizontal basaltic lava flow and a thin layer of residual and transported soil.

### EXCAVATION OF PIT

The excavation of power house pit was started in Oct. 76. Excavation plans, pit slopes, berms etc. were designed on the basis of geological findings and functional requirements. It was suggested to excavate the pit in a slope of 1/4 : 1 from top upto El-240.0 m and in 1/8 : 1 below El-240.0m. However, the Geologist had warned in the early stages to excavate with great care in view of extreme metamorphism and alterations of heterogeneous assemblage of rock types.

The pit in the course of excavation showed signs of distress in the slopes. It was feared that presence of unfavourable discontinuity surfaces dipping at an angle of 50°-60° towards free face on the right hand side may not allow excavated slopes to remain stable. Situation was further aggravated due to occurrence of heterogeneous

rock masses consisting of mixed gneisses with graphite schists.

Finally in the month of May, 1980, when the pit had been excavated upto El-235.0m, the northern slopes failed and there was a major rock slide on the right hand side of pit between 'C' line and 'A' line.

### MAIN FEATURES OF INITIAL LAYOUT

On the basis of available geological details and other technical requirements, the initial layout plans for the power house complex were prepared. Fig. 1 and 2 shows the plan & section of power house as per this planning. Main features of this initial planning were as under.

(a) Erection bay was placed at El-247.5 m on left hand side of power house.

(b) Approach to erection bay at El-247.5 m was arranged from main highway at El-281.0 m by means of a service road located along surge pool in a regular slope of 15:1. This service road was to come down over berms of tail pool area.

(c) Pit slopes were prepared in a slope of 1/4 : 1 from top upto El-240.0 m and in a slope of 1/8:1 from El -240.0 m to El-218.0m.

(d) A counterfort retaining wall was provided on RHS from El-235.0m to protect the right side of power house.

(e) Intake dam was placed 54.50m upstream of power house with penstock length of 82 m. But in the very early stage, the intake dam was shifted towards RHS by 12 metres due to geological constraints. This shifting resulted in increase of penstock length to 92 m. Fig. 1 shows later position of penstock.

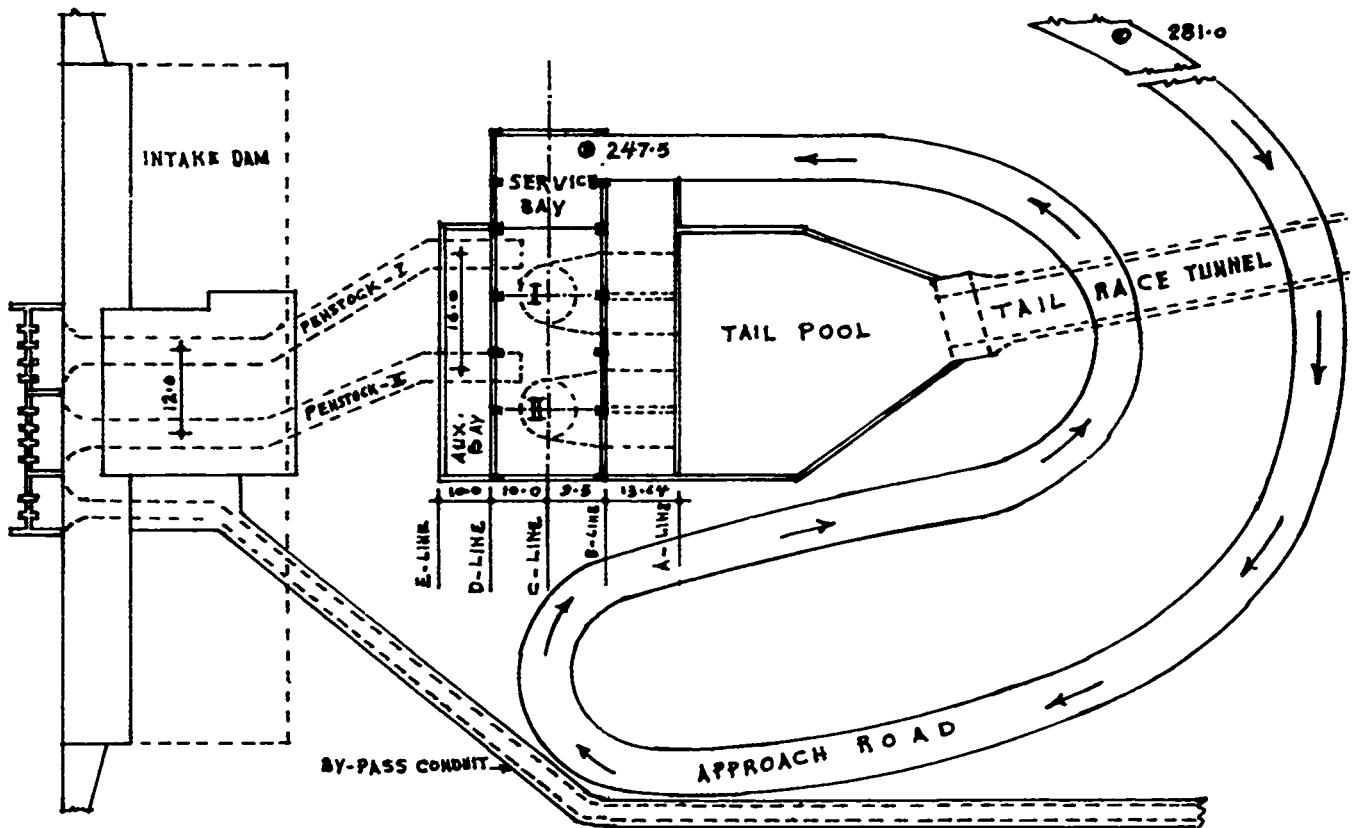


Fig. 1 Original layout plan of power house complex.

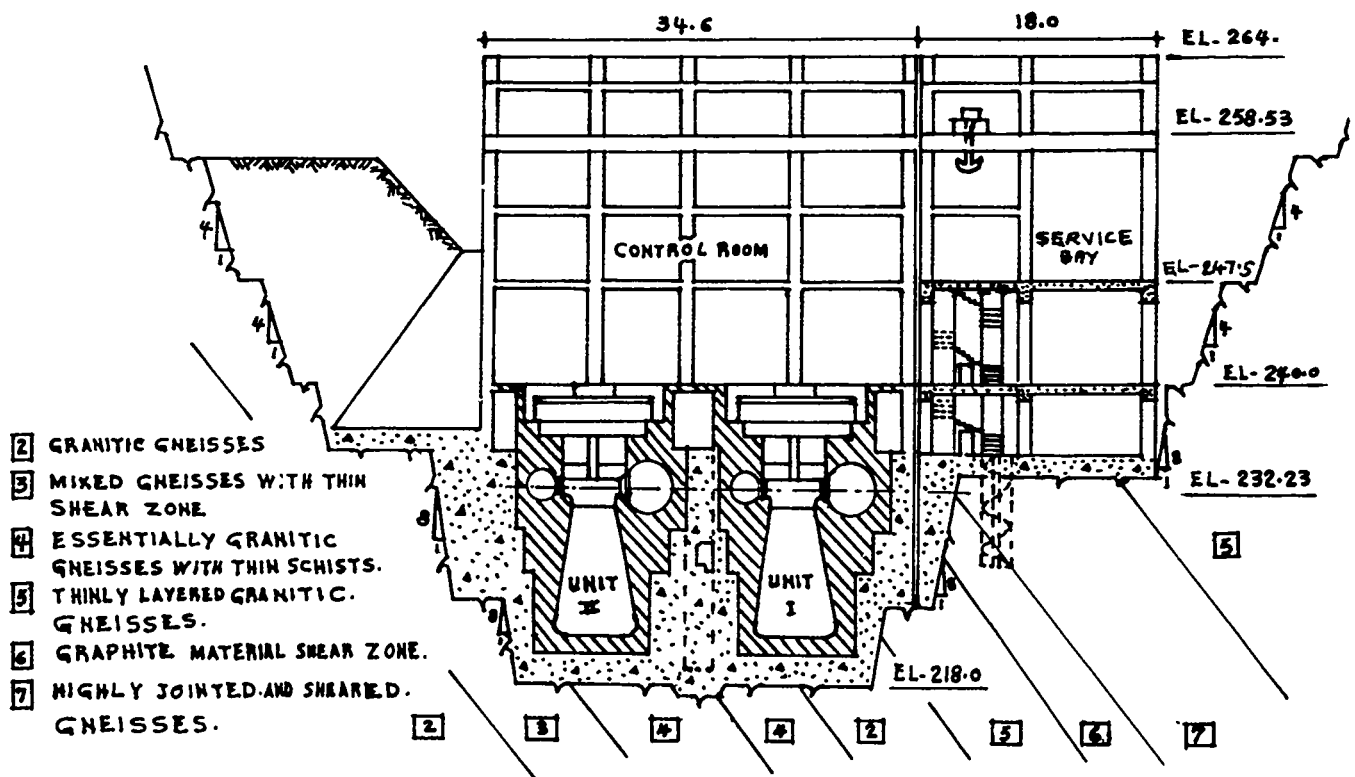


Fig. 2 Section of power house as per original plan.



Fig. 3 Photo showing rock slide

#### DEFFICULTIES ENCOUNTERED

Excavation as per initial planning had been started but in May, 1980 there was a major rock slide and this failure of rock slopes raised many doubts about the future of this power house and its safety. Further, in this rock slide, a large portion of approach road collapsed indicating unsafe approach to the power house. Due to this mishap, an attempt was made to again examine the whole area geologically. It was revealed that country rocks are deeply weathered and decomposed upto a considerable depth. Rocks above El-250.0 m were found to be highly weathered and upto El-235.0 m slightly to moderately weathered. The fresh rock configuration was found to be highly irregular between El-225.0 m to El-240.0 m due to structural peculiarities which controlled the extent of weathering.

It was also revealed that on the RHS of the pit and in tail pool area there is a thick graphite inter-calated zone and as such the area is unstable and unsafe for carrying approach road. It necessitated for finding some alternative to the earlier planned road for reaching upto erection bay.

At that stage it was not possible to relocate this power house at any other place and therefore it became a main challenging task to construct this power house in such weak rocks. Due to such weak condition of rocks, Geologist suggested for flattening of the rock slopes with provision of berms at suitable interval. At one stage it was advised to reshape the pit slopes in 1:1 gradient but this would have involved very heavy increase in excavation quantities, excessive expenditure and delay in completion of the project. Therefore, it was essential to find a safe and economical proposal for replanning the whole power house complex suitably.

#### MAIN FEATURES OF REVISED LAYOUT

Failure of power house pit slopes compelled for making major revisions in the layout of power house. The revisions mainly based on techno-economic balance of the whole scheme. Following are the main features of revised layout.

(a) First and fore most necessity was to stabilise the rock slopes. For this purpose several alternatives were available such as deep anchoring of slopes, grouting of rock masses, adequate flattening of pit slopes etc. It was opined that unstable and weak rocks of power house pit should not be taken care by short term measures such as anchoring or grouting etc. Only flattening of pit slopes was considered useful & effective. Accordingly pit slopes were reshaped in 1:1 gradient from top upto El-240.0 m and in 1/2:1 gradient below El-240.0 m. This reshaping of slopes was more essential for right hand side face. The left hand side slopes were comparatively more stable due to their favourable dip inside the rocks.

(b) At that stage when all other connected works had also started, it was not possible to change or shift power units as this change would have involved change in position of intake dam, penstocks and tail race tunnel also. Further due to favourable dip of rocks on left hand side, it was felt not to disturb or do least excavation on that side. As such the erection bay and other facilities on left hand side were shifted to right hand side without effecting the position of power units.

(c) Most important point to be decided was to provide approach to the erection bay floor level through service road. Adverse geological features of tail pool area did not allow to bring down service road along berms of tail pool. Therefore, efforts were made to replan the service road through other route, but it was not possible without making excessive excavations to bring down the service road upto El-247.5 m i.e. the floor level of erection bay.



Fig.4 Photo showing power house pit during initial stage of construction.

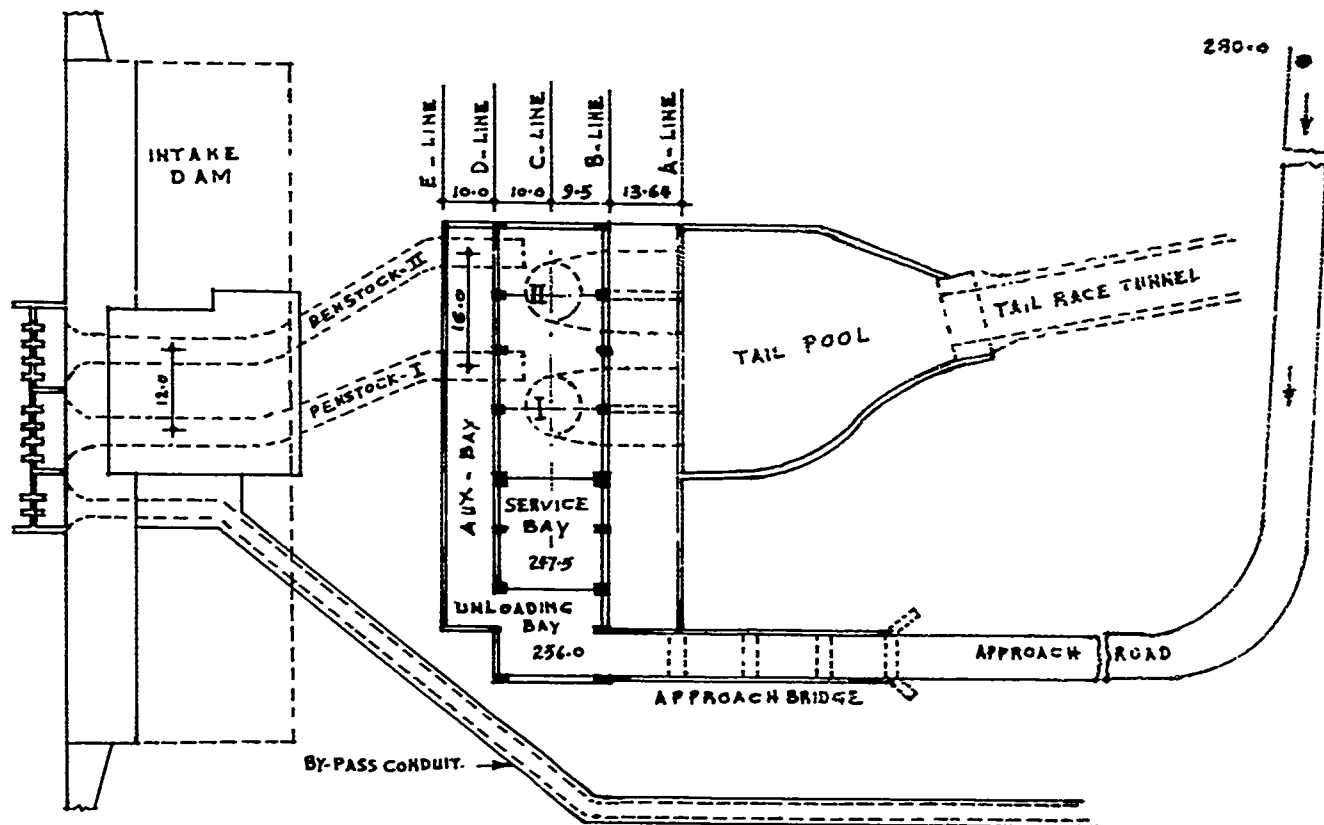


Fig. 5 Revised layout plan of power house complex.

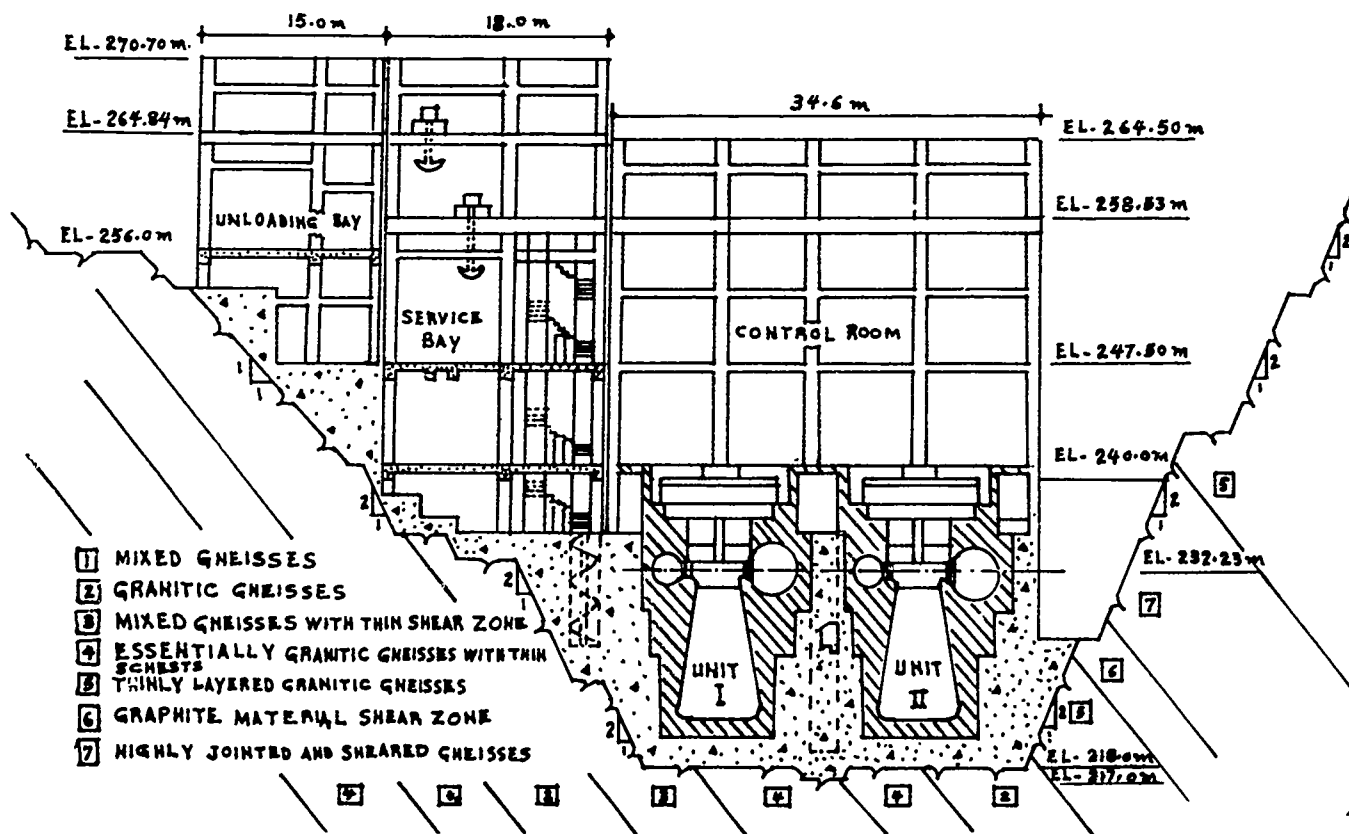


Fig. 6 Section of power house as per revised plan.



Fig. 7 General view of Power House.

Since direct access upto this level was practically not possible, idea of two level service bay was conceived and one additional floor 10 m wide at El-256.0 m was proposed to work as unloading bay. Service road from main highway was arranged upto this unloading bay at El-256.0 m by locating it along by-pass channel. Earlier only one E.O.T. crane was sufficient for this power house but now due to addition of unloading bay at higher level, it became necessary to provide one more E.O.T. crane to operate between unloading bay and service bay. The roof of the power house had also to be arranged in two levels.

(d) Approach portion of service road to unloading bay at El-256.0 m was earlier located on a gravity retaining wall curved in plan and having its foundation at El-240.0 m. The approach portion was to be provided on its back fill. But the geological advice restrained from adding so much load of gravity retaining wall and its back fill on the right hand side rocks. Then the idea of approach bridge with 4 spans of 8.8 m each was adopted and the service road was connected with unloading bay through this approach bridge. Foundations of this approach bridge piers were placed on El-240.0 m. Later on again on geological grounds the position of approach bridge was further shifted to right hand side by 5.0 m so that the rocks on which its foundations rested do not get daylighted in tail pool. This resulted in increase in the width of unloading bay by 5.0 m, thus making it total 15.0 m.

(e) Earlier provision was kept of counterfort retaining wall on the right hand side between 'B' line and 'D' line, but to expedite the construction work of service bay and unloading bay, it was replaced with mass concrete filling. Thus the right hand side slopes were supported with mass concrete filling for the main power house building portion.

(f) The shape of the tail pool was revised to semi circular mainly to minimise the rock cutting work in this area. This was done without affecting the total capacity of the tail pool.

#### CONCLUSION

Many problems were faced in construction of this power house due to unstable slopes and complex and critical geological conditions at the site. Revisions as stated above resulted into appreciable increase in the quantities of concrete and excavation, but the challenge of constructing this power house in such weak rocks was successfully met with. The power house was commissioned within reasonably good period without much cost overruns. It is generating power since Feb., 86 and working without problems. A constant watch has been kept on the stability of rock slopes around power house complex and so far nothing adverse has been noticed.

## Coring of Soft Soil-Like Rock Materials

Marc C. Bétournay

Project Leader, Canada Centre for Mineral and Energy Technology (CANMET), Ottawa, Ontario, Canada

C. Mirza

Principal, Strata Engineering Corp., Don Mills, Ontario, Canada

K.C. Lau

Director of Research, Strata Engineering Corp., Don Mills, Ontario, Canada

**SYNOPSIS:** A new coring technique is described for the sampling of highly altered rock. This and an innovative field survey method were developed to supply valid and representative data for numerical modelling of openings in this soil-like material. The results were not only reflective of in situ behaviour, but successful enough to be adopted for the sampling and modelling of other highly altered surface crown pillar masses, mining structures in need of better design methods.

### INTRODUCTION

In Canadian hard rock mines, the stability of surface crown pillars (the rock mass separating the uppermost underground opening from surface) is a pressing problem (Bétournay et al., 1987). The safe design of such pillars requires an understanding of near surface conditions and material behaviour. Demands are growing for numerical modelling techniques to enable parametric and detailed design studies to be carried out. The results and implications of a near surface rock mass evaluation drilling program, excerpted from a CANMET sponsored and industry supported research study, are presented in this case history.

Rock mass characterization is often necessary and vital in advance of creating safe and economic underground openings. The traditional method has been and continues to be extraction of high quality rock cores for determination of rock quality and rock mass characterization, aided by in situ mapping during excavation, shaft sinking, and the like. In strong rocks, the traditional techniques of diamond core drilling are often satisfactory. However, in weaker rock masses, traditional techniques have led to poor rock core recovery and even loss of core through wash outs and erosion during the drilling process.

### SITE AND GEOLOGY

The minesite, Les Mines Selbaie, is a 1500 tonnes per day underground copper mine located some 80 km north of Joutel, Québec (See Figure 1).

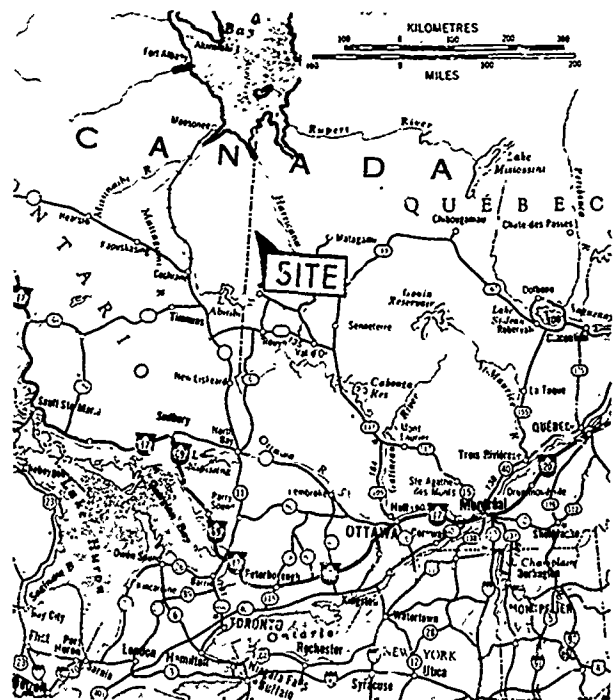


Figure 1. Location of Les Mines Selbaie

The overburden at the mine site is thick and averages about 45 m, consisting primarily of fine grained very dense tills and till-like sediments. The native rock consists of a series of tuffs and breccias, bedded chert-pyrite and volcanoclastic debris occurring within a plutonic complex (Deptuck et al., 1982).



The ore zone (dipping about 50°) consists of quartz-sulfide vein systems up to 200 mm in width. These veins occur within several elongate lenses of heavily fractured rock, (as much as 30 m in width) caused by and lying above a major fault.

The enrichment of original ore values to depths of 200 m within the fault zone has been attributed to supergene alteration (Sinclair and Gasparrini, 1979). Supergene alteration is made possible by descending meteoric waters through the fault zone. The chalcopyrite in this zone has been altered to sooty chalcocite, bornite, limonite and relatively high quantities of native copper, all of which occur within a sugary quartz and kaolin gangue. As a result, the rock mass is not only severely fractured, but is also surrounded by and/or consists of kaolinized and other gangue-like materials.

The richest ore values at the mine are found nearest the surface, at about the 50 to 60 m level immediately below the overburden. The uppermost working level of the mine is located at a depth of 55 m below prevailing ground surface. Mining safety regulations require a surface crown pillar thickness of 15 m or more. However, at this site, special dispensation has been received to reduce that thickness to 7.5 m based on the richness of ore values in this zone.

Some of the facilities at the mine site, primary ore processing facilities, office buildings, and a dormitory are located above actively mined stopes.

#### SCOPE OF STUDY

The research study into modelling and verification of surface crown pillar behaviour in the weak rock mass at Les Mines Selbaie was divided into three phases - material characterization (drilling, sampling and laboratory testing), numerical modelling, and verification of predictions.

The first phase - drilling, sampling and laboratory testing - was completed in August 1986 (C. Mirza Engineering Inc., 1986), and the second phase, numerical modelling, was completed in late 1987 (Strata Engineering Corp., 1987). Results of field verification are presently being evaluated.

The scope of the first phase included drilling and sampling of both the overburden and the upper rock mass, down to the level of the surface crown pillar. The geographical remoteness of the site made it necessary to utilize the on-site, resident, production type drilling contractor, rather than experienced geotechnical drilling contractors.

The field work in the first phase included the coring of the weak soil-like rock mass at three borehole locations, MT-10, MT-11 and MT-12, Figure 2. The overburden drilling and sampling experiences are omitted from this paper. Since

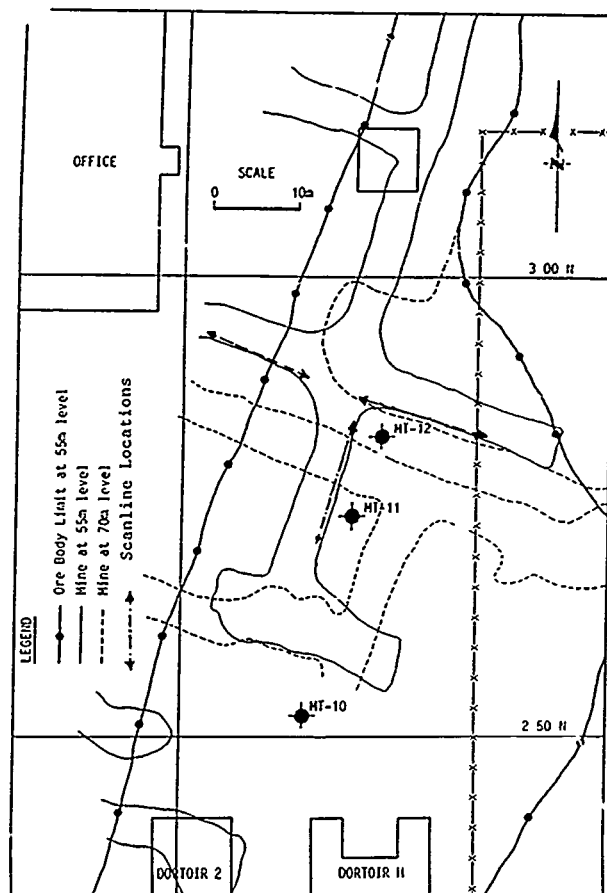


Figure 2. Borehole and Scanline Locations (C. Mirza Engineering Inc., 1986)

surface drill coring for rock mass characterization in remote locations is necessarily expensive, the scope of the study was expanded to rock mass characterization by means of underground scanline surveys, covered in a subsequent section of this paper. By correlating scanline results with those of laboratory tests on the recovered cores, it is hoped to reduce the requirements for additional high quality (and therefore expensive) rock coring for the design of future surface crown pillars. To this end, the study has proven to be successful, due mainly to excellent core recoveries made possible by a simple modification to the traditional rock coring techniques normally used in hard rock, production coring.

#### ROCK DRILLING AND CORING

All soil and rock drilling, sampling and coring was performed by resident drillers without the expense in either soil or rock drilling for sampling purposes. The machine available at the mine site was a skid-mounted Inspiration III drill rig. The drilling program commenced on October 22 and ended on November 26, 1986, totalling approximately 165 m of soil and rock

sampling/coring, for an average production rate of about 7 m/day, with ranges between 1 m/day to 15 m/day. A work-day averaged about 8 hours, from dawn to dusk, typical for that time of the year. At the end of the drilling program, the weather turned extremely cold, and daily production rates dropped dramatically due to frozen lines, pump and rig starting problems, and the like.

MT-11 was the first borehole to be drilled. Core recoveries were generally very poor (less than 30 per cent) due to an unusually weak and soil-like rock mass immediately below the overburden contact. The techniques used to recover cores included:

1. using a double tube bit on a triple tube core barrel;
2. alternating between face-discharge and standard bottom hole discharge bits;
3. double tube core barrel.

Only tap water was used as the drilling fluid in this borehole.

None of these variations in rock coring techniques had any significant influence on core recoveries. The recovered core pieces were from harder rock material.

The next borehole drilled was MT-10. The first few core runs met with the same lack of success as at MT-11. Subsequently, a small amount of Polydrill R, a polymer mud, was added, which improved the core recoveries from 30 per cent to 60 per cent, on average in a few of the core runs. In order to improve the recoveries even further, a variant of a technique first reportedly used in England (Hughes, 1982) for very soft friable rocks was tried. The techniques of creating a foam at the bit is well known in the water well drilling industry (Driscoll, 1986).

An air compressor was connected by a T-Joint to the drill stem water swivel, and air pumped under pressure along with reduced water flow from the water supply pump was reduced. Immediate success was noted, not only in progress of the coring operation, but also in core recoveries. Average core recoveries increased to over 90 per cent in the weakest rock zones being drilled. Large cores of kaolinitic materials, finely disintegrated siliceous dacite tuff breccia in a clayey silt matrix, highly fractured sooty chalcocite and sounder rocks were all recovered intact from the double tube core barrel. The final weak soil-like rock core recovery in MT-10 was over 95 per cent subsequent to the use of compressed air.

The original terms of reference for this research program were to drill only boreholes MT-10 and MT-11. The huge success achieved at MT-10, for the first time in the mine's history of coring operations, prompted the initiation of an extra borehole, MT-12, to verify the validity of the compressed air injection technique.

Tri-coring to a depth of 30 m was done in MT-12 to save time. The dense nature of the overburden had prevented thus far obtaining decent

and meaningful undisturbed samples of the soil immediately above the rock contact. Therefore, an attempt was made to try the air-water mixture technique for coring of the overburden materials. Unfortunately, the compressor broke down and the validity of the technique for coring dense, almost cohesionless, tills and similar finer grained soils could not be verified. When the borehole drilling reached the bedrock contact area, the compressor had been repaired, and excellent core recoveries were obtained until the compressor broke down once again, at which time core recoveries immediately dropped to values equivalent to those obtained earlier at MT-11.

The results of the rock coring operations, with and without introduction of air into the drill fluid stem, are summarized in Table 1, for various rock types in the surface crown pillar. Core recoveries in a weak, soil-like rock mass, can be improved if a polymer based drilling mud is used in conjunction with compressed air by drilling in an N-size double tube core barrel fitted with a face-centred discharge diamond bit.

Adding air to the drilling fluid permitted the use of less water for lubrication, cooling, and lifting of cuttings, and hence less erosion of the soil-like rock core, while keeping wear on the diamond bits to a minimum. Best results were obtained with a bit advance rate of about 2 m/hr, and a water/air pressure ratio of between 10 and 15.

#### UNDERGROUND SCANLINE SURVEYS

For realistic modelling of the surface crown pillar, it was necessary to carry out detailed underground surveys of the orebody formation. Three scanline surveys were carried out at the 55 m level, shown in Figure 2. Detailed photomosaics were taken along each scanline. All contracts, faults and joints greater than 500 mm in dimension were noted, along with continuity, orientation, joint resistance factors, and infilling type. Pocket penetrometer tests were carried out along with torvane shear tests on the soil-like components of the scanned lines.

The visible rock mass was classified in accordance with the ranking scheme shown in Table 2. A rank of 1 to 6 was chosen to represent the rock-line material, and a rank of 7 to 11 to represent the soil-like material. This simple classification, aided by the scanline survey results, and correlated with laboratory test results on the recovered cores, gave an excellent overall representation of the rock mass characteristic, and in particular, the relative proportion of soil-like rock volume to the total volume of rock (last column of Table 2).

The orebody rock consists of moderately to highly kaolinized Dacitic Tuff Breccia with zones and seams of limonization, silty clay infillings, finely ground sooty chalcocite and native copper. Kaolinization is particularly

Table 1. Rock Coring Results With or Without Air Pressure (C. Mirza Engineering Inc. 1986)

| ROCK TYPE   | WITHOUT AIR PRESSURE               |   |                     | WITH 0.14 MPa AIR PRESSURE         |   |                     |
|---|------------------------------------|---|---------------------|------------------------------------|---|---------------------|
|   | Optimum Range Water Pressure (MPa) | Optimum Range Penetration Rate (mm/sec) | Average Recovery ** | Optimum Range Water Pressure (MPa) | Optimum Range Penetration Rate (mm/sec) | Average Recovery ** |
| Slightly Kaolinized Dacite Tuff Breccia   | 3.4 - 7.0                          | 0.6 - 2.0                               | 100                 | 1.7 - 7.0                          | 0.4 - 3.0                               | 100                 |
| Moderately Kaolinized Dacite Tuff Breccia   | 2.8 - 3.5                          | 0.6 - 1.3                               | 95                  | 1.7 - 7.0                          | 0.4 - 1.0                               | 98                  |
| Highly Kaolinized Dacite Tuff Breccia   | 2.5 - 3.0                          | 0.6 - 1.3                               | 70                  | 1.7 - 2.5                          | 0.4 - 0.6                               | 90                  |
| Pieces of Rock in Silty Clay to Clayey Silt matrix, finely fractured sooty chalcacite | 2.5 - 3.0                          | 0.6 - 1.3                               | 60                  | 1.7 - 2.5                          | 0.4 - 0.6                               | 95                  |

\*\* Must use Face-Centred Discharge Bits and POLYDRILL® to obtain these Recoveries.

Table 2. Rock Mass Ranking Scheme and Average Volume of Each Rock Type, Underground Scanline Surveys (C. Mirza Engineering Inc., 1986)

| RANK | CHARACTERIZATION  | FIELD METHOD OF DETERMINING RELATIVE STRENGTH | AVERAGE VOLUME (%) |
|------|-------------------|---|--------------------|
| 1    | Very Strong       | > 1 hammer blow to break                      | 9.7                |
| 2    | Strong            | 1 hammer blow to break                        | 17.4               |
| 3    | Moderately Strong | 5 mm indentations with pick                   | 12.4               |
| 4    | Moderately Weak   | Cannot be cut by hand                         | 6.3                |
| 5    | Weak              | Crumbles under firm blows with pick           | 14.1               |
| 6    | Very Weak         | Broken in hand with difficulty                | 9.4                |
| 7    | Very Stiff        | Indented by fingernail                        | 6.6                |
| 8    | Stiff             | Cannot be moulded in fingers                  | 5.7                |
| 9    | Firm              | Difficult to mould in fingers                 | 7.2                |
| 10   | Soft              | Easily moulded in fingers                     | 10.4               |
| 11   | Very Soft         | Can be squeezed between fingers               | 0.8                |

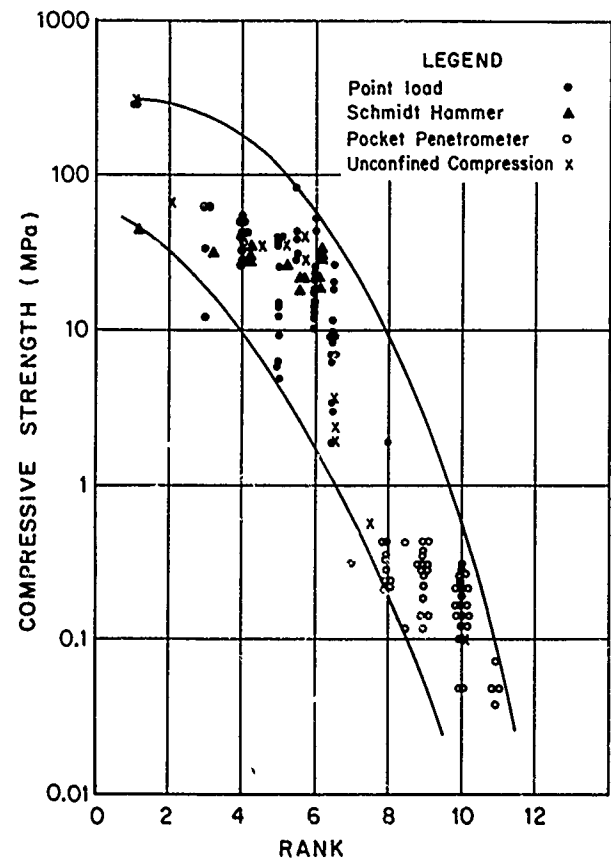


Figure 3. Unconfined Compressive Strength Versus Rank of Material From Scanline Surveys (C. Mirza Engineering Inc., 1986)

extensive in the ore-enriched zones, and increases in intensity towards the surface.

The degree of kaolinization varies from a bleached tuff breccia to pure kaolinitic clay. In the worst areas this altered rock mass can be described as soft, soil-like with small irregularly spaced remnant rock pieces.

#### LABORATORY TESTING

Several types of laboratory tests were carried out on the different types of rock materials recovered from the coring operations, as well as on bulk samples obtained from the 55 m level during the scanline surveys. These included: index property testing (moisture content, Atterberg limits, unit weights, grain size distribution) of both the soil-like rock and joint infill materials, slake durability, point load, Schmidt rebound hammer, and both unconfined and triaxial type compression tests (on those specimens which could be lifted intact from the core box), as well as direct shear tests on both undisturbed and reconstituted samples.

A protocol for storage and handling of the fragile rock samples was developed during the field work at the mine site, and proved to be invaluable in preservation of the integrity of the samples both in storage and upon subsequent transportation by vehicle to the laboratory across a distance of over 1000 km.

The results of the point load and Schmidt tests were converted to approximate compressive strength values (Bieniawski, 1974,; Deere and Miller, 1966). Results of the correlation between the ranking of Table 2 and compressive strengths derived by various test methods are shown on Figure 3. A statistical method using the Hoek and Brown failure criterion for rock (Hoek and Brown, 1980) was used to approximate the material constants for the failure envelope derived from triaxial tests. The moduli of deformation for the rock-like materials were determined using correlations with the Schmidt hammer R values and the stress-strain curves from unconfined compression tests. The tangential modulus of deformation was approximated from calibration curves developed for the Schmidt hammer rebound number (Deere and Miller, 1966). The stress-strain curves from unconfined compression tests were used to determine the tangential and scant moduli of deformation at 50 per cent of peak strength.

Some key results of the laboratory testing program are given in Table 3.

#### APPLICATIONS TO NUMERICAL MODELLING

The ability to extract cores from soil-like rock formations near the orebody-overburden contact zone, and laboratory tests and correlations with scanline information, enabled

Table 3. Summary of Laboratory Test Results  
(C. Mirza Engineering Inc. 1986)

| Property Tested                               |  | Competent Rock | Soil-Like Rock | Kaolin Zones |
|---|--|----------------|----------------|--------------|
| Moisture Content (%)                          |  |                | 5 - 25 (12)    | 15 - 24 (18) |
| Liquid Limit (%)                              |  |                | 28 - 35        | 18 - 25      |
| Plastic Limit (%)                             |  |                | 20 - 23        | 15 - 18      |
| Plasticity Index (%)                          |  |                | 8 - 12         | 3 - 7        |
| Gravel Size (>4.75 mm) (%)                    |  |                | 20 - 67        |              |
| Sand Size (<2.0 mm) (%)                       |  |                | 25 - 56        |              |
| Silt & Clay (<75µm) (%)                       |  |                | 6 - 13         |              |
| Unit Weight - General (kN/m <sup>3</sup> )    |  | 24 - 30        | 19 - 26        |              |
| Unit Weight - Chalcocite (kN/m <sup>3</sup> ) |  |                | 26 - 40 (33)   |              |
| Slake Durability, I <sub>2</sub> (%)          |  |                | 69 - 98        |              |
| Compressive Strength:                         |  |                |                |              |
| Point Load (I <sub>50</sub> ) (MPa)           |  | 106 - 288      | 3 - 48         |              |
| Schmidt Hammer R (MPa)                        |  |                | 30             |              |
| Unconfined Compression (MPa)                  |  |                |                | 0.1 - 0.6    |
| Angle Internal Friction, φ (°)                |  |                | 41             | 33           |
| Cohesion Intercept, c (kPa)                   |  |                | 45             | 5            |
| Modulus of Deformation:                       |  |                |                |              |
| Unconfined Compression (GPa)                  |  | 12 - 32        | 1 - 10         |              |
| Point Load (GPa)                              |  | (23)           | 12 - 24        |              |

Note: Numbers in brackets refer to average values

the construction of a numerical model for the prediction of surface crown pillar stability. In essence it was concluded from the first phase of the study that the crown pillar rock formation comprised approximately 70 per cent rock-like materials and 30 per cent soil-like materials. Probex pressuremeter/dilatometer tests were carried out in boreholes MT-11 and MT-12 to obtain in situ values of the deformation moduli in both the overburden and the orebody. Prior information was already available on in situ stresses obtained by overcoring with a CSIRO hollow inclusion triaxial strain cell (Arjang, 1984).

To assist with realistic modelling, the Mine was asked for their proposed or preferred method of mining of the surface crown pillar. The stope size beneath the surface crown pillar is generally 22 m long in the strike direction. In weaker ground, this width is cut in half along the strike direction. In the weakest ground (soil-like rock mass), the surface crown pillar is mined in 5.5 m wide panels. The mine is totally depressurized with respect to ground water.

The numerical model chosen was a multi-dimensional finite element program capable of accepting Mohr-Coulomb type elements, with a 'birth' and 'death' option for each element. Two dimensional modelling was found to be inadequate, and all subsequent modelling was three dimensional. The failure mechanism adopted, based on the authors' previous experience and research (Bétournay, 1980), was as follows. The soil-like mass is held together around an opening by negative pore pressure, induced by the creation of the opening. With time this condition dissipates at the boundary leading to tensile failure, a mechanism which progresses upward. In order to

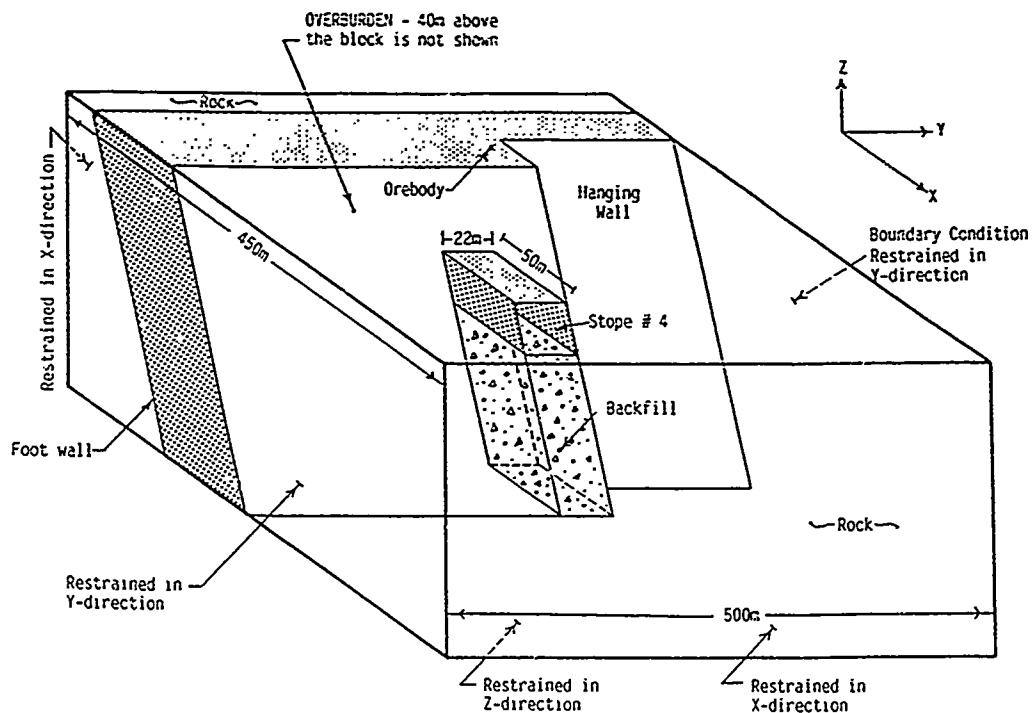


Figure 4. Numerical Model Layout, to Simulate Stope 4 Cave-in (Strata Engineering Corp., 1987)

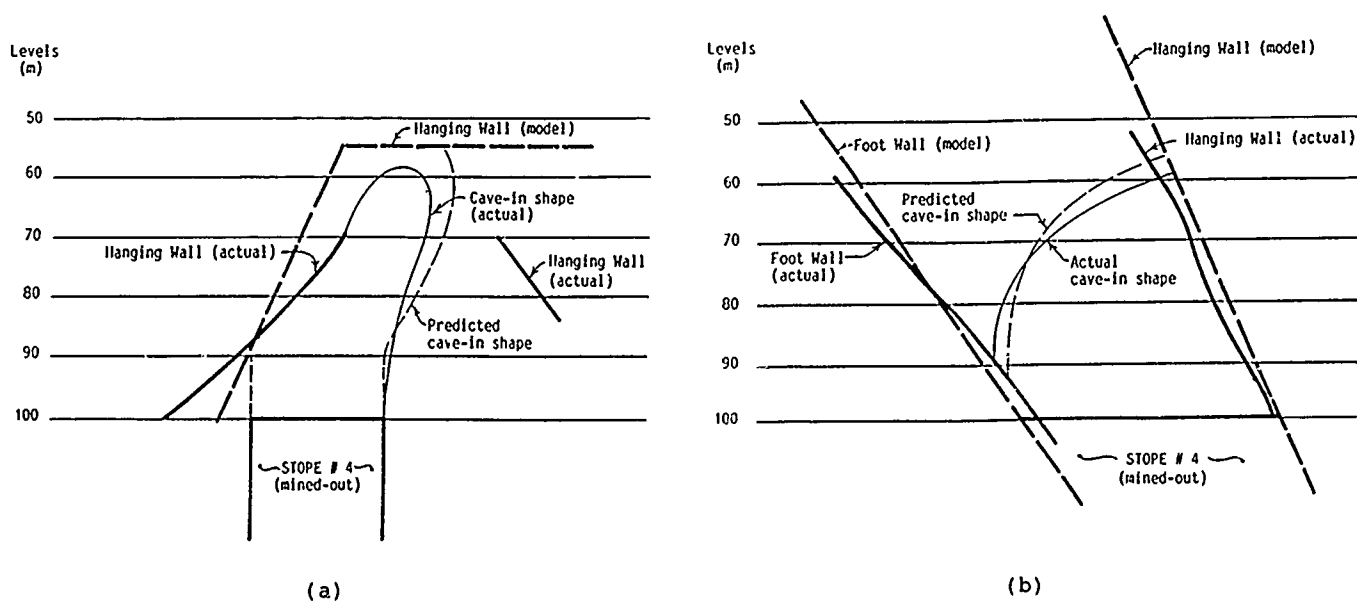


Figure 5. Numerical Model Prediction of Stope 4 Failure vs. Actual Failure  
(a) Along Strike, (b) Normal to Strike (Strata Engineering Corp., 1987)

accommodate tensile failure, gravitational forces were applied in ten computational steps, which enabled the analysis to be halted as to eliminate all tensile failed elements (by changing the status of the failed elements into unborn elements), and the analysis was continued until full gravity loading was reached. The remnant rock pieces were too small to affect the stability as failure mechanism of the soil-like material.

A schematic of the model layout is shown in Figure 4 for back calculations of a 1983 cave-in which occurred in Stope 4 at Les Mines Selbaie. Approximately 9,000 tonnes of material was involved. The cave-in commenced at the 100 m level and progressed upward to the 60 m level in a total period of about 6 to 8 months. A comparison of the predicted versus actual failure surfaces is given in Figure 5a and 5b.

The good quality of comparison reflects favourably on the choice of rock mass characteristics used in the numerical model, and proves the worthiness of good field data to predict or substantiate observations of geotechnical behaviour.

## CONCLUSIONS

The successful prediction of an actual cave-in by numerical modelling techniques based on high quality field information and understanding of material behaviour shows the feasibility of designs of surface crown pillars in weak, altered rock masses.

This case history shows that quality objectives for field geotechnical data can be met using ordinary, available mine site machines, tools and personnel despite site remoteness or drill-crew inexperience. In this study, the lack of core recovery using standard rock coring techniques arose due to the presence of a soil-like rock mass in the surface crown pillar below the overburden. The problem was overcome by the introduction of compressed air at the water swivel to allow reduction of water pressure and flow, so as to minimize core erosion and washouts, while at the same time allowing the lifting up of cuttings and prevention of premature diamond bit wear. The coring and scanline surveys are new techniques to obtain geotechnical parameters from materials hitherto difficult to quantify.

## ACKNOWLEDGEMENTS

The field drilling program was supervised by John A. Blair, P.Eng., ably assisted by Messrs: Dean Cutting and Luc Closset of Les Mines Selbaie. The assistance and cooperation provided by Mine staff and management during this study is gratefully acknowledged. Technical guidance throughout the study was provided by Dr. Adrian M. Crawford of the

University of Toronto.

## REFERENCES

- Arjang, B. (1984), "Field Stress Determination at Selbaie Mine, Québec", Division Report 84-55(TR), CANMET, Ottawa.
- Bétournay, M.C. (1980), "A Study of Two Decayed Monzonite Dykes from Mt. Royal, Montréal". Unpublished paper.
- Bétournay, M.C., Nantel, S. and Lessard, D. (1987), "Summary of Twenty Four Surface Crown Pillar Case Studies", CIM, Eighty-ninth Annual General Meeting, Toronto, paper #44.
- Bieniawski, Z.T. (1974), "Geomechanics Classification of Rock Masses and its Application in Tunnelling", Proc., Third International Congress on Rock Mechanics, vol. IIA, 27-32.
- C. Mirza Engineering Inc. (1986), "Weak Rock Mass Model for Support of Crown Pillar. Phase I-Drilling, Sampling and Laboratory Testing", Report submitted to CANMET/EMR under DSS File: 15SQ.23440-5-9017, vols. 1 and 2, Toronto.
- Deere, D.U. and Miller, R.P. (1966), "Engineering Classification and Index Properties for Intact Rock", Technical Report No. AFNL-TR-65-116,, Air Force Weapons Laboratory, New Mexico.
- Deptuck, R.H., Squaid, H.J., and Wierzbicki, V. (1982), "Geology of the Detour Zinc-Copper Deposits, Brouillon Township, Québec. Special Paper No. 25, Precambrian Sulphide Deposits, H.S. Robinson Memorial volume, Geological Association of Canada, Ed. R.W., Hutchinson.
- Driscoll, F.G. (1986), "Groundwater and Wells", Johnson Division, St. Paul, Minnesota, 1108 pp.
- Hoek, E. and Brown, E.T. (1980), "Underground Excavation in Rock", Inst. Mining and Metallurgy, 527 pp.
- Hughes, P.M. (1982), "The Techniques of Diamond Coring with Stable Foam", Geodrilling, No. 18, 10-17.
- Sinclair, I.G.L., and Gasparrini, E., (1980), "Textural Features and Age of Supergene Mineralization in the Detour Copper-Zinc-Silver Deposit, Québec, Economic Geology, vol. 75 #3,470-477.
- Strata Engineering Corp., (1987), "Weak Rock Mass Model for Support of Crown Pillar at Les Mines Selbaie, Phase II-Model Development and Calibration", Draft Report submitted to CANMET/EMR under DSS File: 15SQ.23440-9017, Toronto.

## The Great Landslides in the East-Maritza Open-Cast Mines (Bulgaria)— A Theoretical Paradox in the Engineering Geology

Kiril Anguelov

Associate Professor in Engineering Geology, Higher Institute of  
Mining and Geology, Sofia, Bulgaria

**SYNOPSIS:** The exploitation of the opencast mines in the East-Maritza coal basin was proceeded of detailed explorations and analysis of the engineering geological conditions. Nevertheless, one of the greatest landslides in the engineering geological practice occurred within the period of 1966 - 1968. The volume of the sliding masses reached  $30 - 75 \times 10^6 \text{ m}^3$ . These landslides made questionable some of the classic formulations of the soil mechanics and engineering geodynamics, as for instance:

- the possibility of formation of sliding surfaces with inclination opposite to the direction of sliding;
- the validity of the Coulomb-Navier's law in conditions of high confining pressure;
- the existence of the so called "pore pressure" within the sliding zones during the deformation process.

In the present paper, there could be found certain experimental data and interpretations on some of the above mentioned questions.

### INTRODUCTION

The East-Maritza coal basin is situated near the town of Stara Zagora and is one of the main energy supplying sources in Bulgaria. At the moment two open-pit mines "Trojanovo-North" and "Trojanovo-South" provide 2.5 million tons per year. The coal seams are with total thickness about 20 m, with almost horizontal occurring /  $0^\circ - 2^\circ$  slope/ and at a depth of 60 - 120 m (fig. 1).

Right from the initial stages of the coal exploitation different in character and volume landslides, which affected different parts of the open-cast mines took place. The greatest and deepest ones (about  $30 - 75 \cdot 10^6 \text{ m}^3$ ) occurred within the period of 1966 - 1968. They affected the working (fig. 2) and non-mining boards of the mines although there were carried out great preliminary engineering geological prospecting and stability estimations. These landslides caused numerous scientific disputes. Further detailed investigations were carried out as a result of which there were established some very interesting features of the geological structure of the basin and engineering geological paradoxes.

### PECULIARITIES OF THE ENGINEERING-GEOLOGICAL CONDITIONS IN THE EAST-MARITZA COAL BASIN

The sediment coal field consists mainly of clays, where the mixed layers minerals (montmorillonite-mica ones in their composition) are prevailing. The clays interlaying the coal seams are with increased contents of hydrophilic organics, mainly from the group of the humine acids [2]. That fact determines the higher contents of montmorillonite sheet units in the composition of the clay minerals and some paradoxes in the changing of the physical, strength and deformation properties of the clays depending on the depth of occurrence /i.e. with increasing of the geologic load/:

1. Water contents /  $W_n$  / of the clays increases (fig. 1).

2. Unit weight /  $\gamma_n$  / of the clays decreases (fig. 1);

3. The axial strength of the clays is quite variable with a tendency towards decreasing in the clays of the coal seams complex (fig. 1).

4. The type of structural bonds also changes - from transitional (atomic) coagulation in the top laying clays to coagulation ones in the clays from the coal complex (fig. 3).

These peculiarities in the variations of the engineering geological conditions in the East-Maritza coal basin are determined from a multi-layered unstable medium, where the strongest coal seams are interlayered by weak unconsolidated clays with coagulation contacts between the particles and clearly expressed plastic properties. Special attention must be paid to the greyish-black clays in which hydrophilic organic matter is dispersed mainly between the clay clusters. From the obtained SEM images, it becomes clear that highly dispergated clay minerals and amino-acids form a water saturated system, where the water is in absorbed condition (fig. 4a,b). For this reason, the classic geotechnical models for the description of the strength and deformation properties of soils are not valid for these clays.

The same clays were as a medium of formation on the main sliding surfaces of the great landslides were an object of special detailed investigations (fig. 2).

### THE GREAT LANDSLIDES IN EAST MARITZA BASIN - A THEORETICAL PARADOX IN ENGINEERING GEOLOGY

For the designing of the open-cast mines, there were used all classical ideas of soil mechanics about the deformation behaviour of the clays from the coal field. The Fp method of Maslov was used for determining the stable slope of the boards as a method of higher reserve of security. Nevertheless, right from the beginning of mines exploitation landslides of Earth block slide type occurred under the action of the so called "active prisms" / 10/.

| Geological<br>int. nos. | Geologic<br>section | Depth, m | Name of Geological Complexes                             | Physical & Mechanical properties |     |     |     |     |           |     |     |                |                                |
|-------------------------|---------------------|----------|--|----------------------------------|-----|-----|-----|-----|-----------|-----|-----|----------------|--------------------------------|
|                         |                     |          |  | 0,2                              | 0,4 | 0,6 | 0,8 | 1,0 | 2,2       | 2,4 | 2,6 | $\sigma$ , MPa | $\sigma_n$ , g/cm <sup>3</sup> |
|                         |                     |          |  | 20                               | 30  | 40  | 50  | 60  | $w_n$ , % |     |     |                |                                |
|                         |                     |          |  | 1,4                              | 1,5 | 1,6 | 1,7 | 1,8 |           | 1,9 | 2,0 |                |                                |
| Qal                     |                     | 0-1      | 1. Deluvial and aluvial clays                            |                                  |     |     |     |     |           |     |     |                |                                |
| N2                      |                     | 1-1,5    | 2. Yellow and Brown Clays                                |                                  |     |     |     |     |           |     |     |                |                                |
|                         |                     | 1,5-3    | 3. Bluish-green Clays                                    |                                  |     |     |     |     |           |     |     |                |                                |
| N2                      |                     | 3-4,5    | 4. Dark gray Clays                                       |                                  |     |     |     |     |           |     |     |                |                                |
|                         |                     | 4,5-5    | 5. First and Second Coal Seams                           |                                  |     |     |     |     |           |     |     |                |                                |
|                         |                     | 5-6      | 6. Plastic Layered Clays                                 |                                  |     |     |     |     |           |     |     |                |                                |
|                         |                     | 6-7      | 7. Third coal seam                                       |                                  |     |     |     |     |           |     |     |                |                                |
|                         |                     | 7-8      | 8. Dark-gray Plastic Clays                               |                                  |     |     |     |     |           |     |     |                |                                |
|                         |                     | 8-9      | 9. Grayish-green Clays                                   |                                  |     |     |     |     |           |     |     |                |                                |
|                         |                     | 9-10     | 10. Silty Clays with Sand Layers                         |                                  |     |     |     |     |           |     |     |                |                                |
| J                       |                     | 10-16    |  |                                  |     |     |     |     |           |     |     |                |                                |
| T                       |                     | 16-20    |  |                                  |     |     |     |     |           |     |     |                |                                |
| Pz                      |                     | 20-60    |  |                                  |     |     |     |     |           |     |     |                |                                |
|                         |                     | 60-80    | 11. Silty Clays Grading in Depth to Gravels              |                                  |     |     |     |     |           |     |     |                |                                |
|                         |                     | 80-100   | 12. Crystal Shists, Limestones, Sandstones and Andesites |                                  |     |     |     |     |           |     |     |                |                                |

$\sigma$ -Axial Strength  
 $w_n$ -Water Contents  
 $\sigma_n$ -Unit Weight

Fig. 1. Engineering Geological Section of the East-Maritza Basin

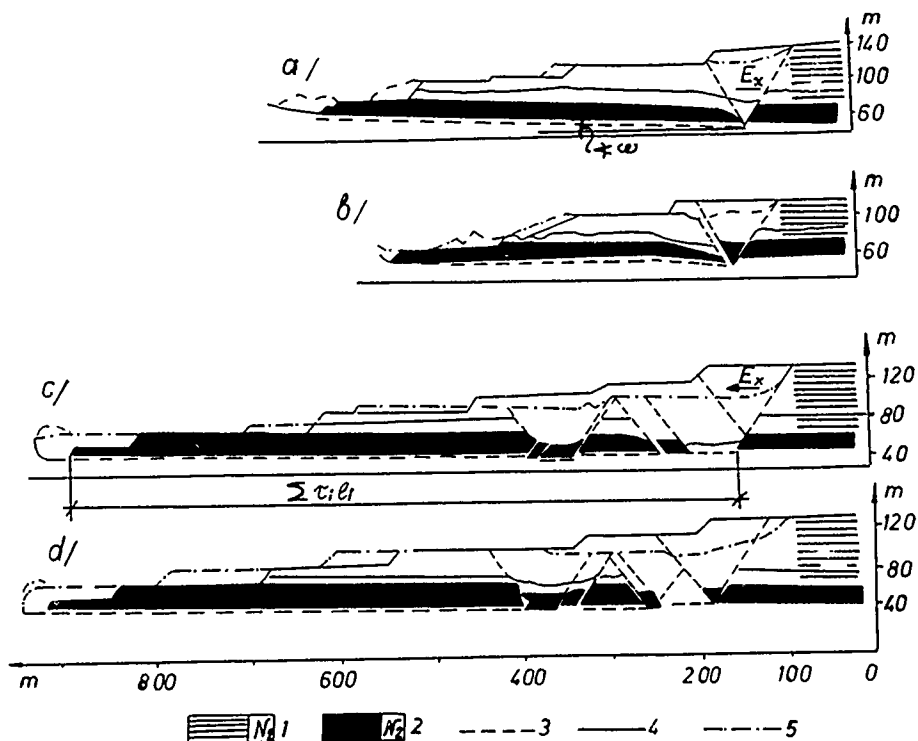


Fig. 2. Schematic Profiles of the Great Landslides in the East-Maritza Open-cast Mines in 1966 ( a, b) and in 1968 ( c, d)  
1- Pliocene Clays; 2- Coal Seams; 3- Landslide Surface; 4- Line of the Profiles of Flanks before the Landslides; 5 - Line of the Profiles of Flanks after the Landslides.



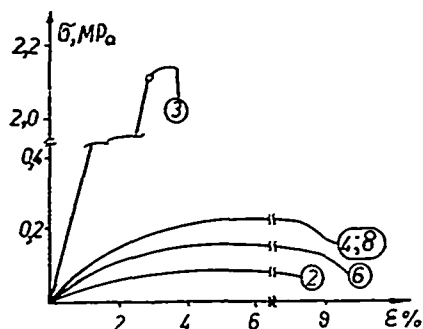


Fig. 3. Relationships "stress-strain" for the clays of the East-Maritza basin (the numbers of the curves correspond to the Numbers of the clays from fig. 2).

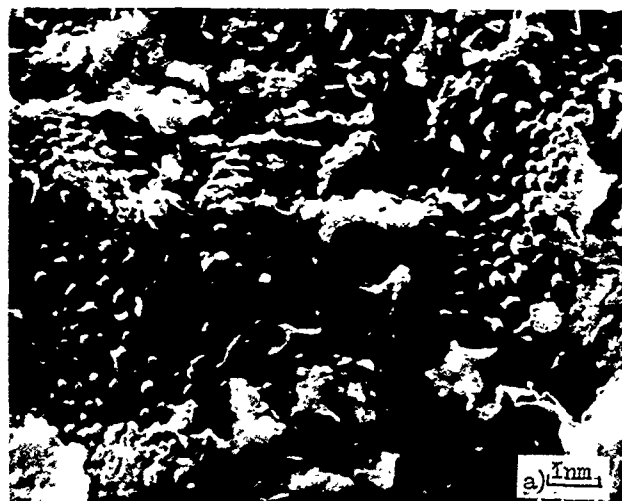


Fig. 4. SEM images of clays from the sliding surfaces

- a/ a general view of the clay minerals and humine acids
- b/ Humine acids

Without discussing the numerous details of originating and development of the sliding processes some essential paradoxes will be mentioned:

1. Landslides originated not only when the dip of the major sliding surface was  $0 - 2^\circ$

towards the toe of the board (fig. 2 b, c, d) but also when dip was  $2-30^\circ$  towards the massif (fig. 2a).

2. The following computations of the initial stability of the sliding zones show that the horizontal force resulting from active prism weight  $/E_i/$  is about twice lower than the sum of the resistance forces from the main sliding surface  $/\sum \tau_i l_i/$  determined through the classical methods of soil mechanics, i.e. landslides should not occur.

3. Numerous investigations at site and laboratory show that engineering geological conditions are approximately the same in both mines. Frequently however boards with equal general slopes are more stable in Troyanovo-South mine than in Troyanovo-North.

In our opinion, these paradoxes are determined from the paradoxal strength and deformation properties of the clays from the major sliding surfaces - i.e. the most weak unconsolidated greyish-black clays interlayering the coal seams (fig. 1, 2, 4). If the maximum values of the deviator stresses  $(\sigma_1 - \sigma_3)_{\max}$  or the plane shear stresses  $(\tau_{\max})$  are used for plotting the relationship  $\tau = f(\sigma)$  the following results are obtained (fig. 5).

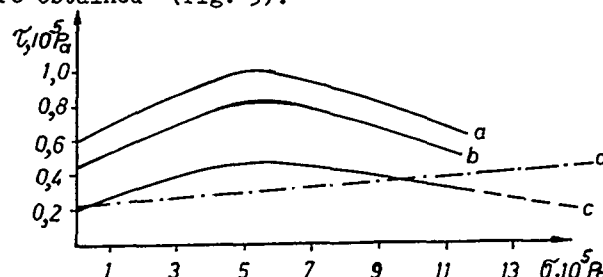


Fig. 5. Relationships "shear stress - normal stress" for greyish-black clays from the main sliding surfaces, obtained from:

- a/ maximum deviator stresses
- b/ ultimate deviator stresses
- c/ allowable deviator stresses
- d/ back analysis of initial landslides stability

The obtained results show that after applying normal stresses  $\sigma = 5 \cdot 10^5 \text{ Pa}$ , the values of  $\tau_{\max}$  decrease  $/1,5/$ . That experimental fact contradicts to the Coulombs theory and similar results are accepted as incorrect or paradoxal as the values of the angle of internal friction  $(\psi)$  could not be negative.

Moreover, most of the pore pressure measurement during triaxial tests were unsuccessful, i.e. the pore pressure  $u = 0$ . These results were rejected by the designers of the open-cast mines and the strength parameters of the clays from the main sliding surfaces were determined through the method of back analysis based on the great landslides, which originated in different stages of mines exploitations (fig. 2). Unfortunately, similar empiric solutions are usually applied in the practice not only in Bulgaria. And what is more, in many cases they are the only ones for slopes stability computations.

In our opinion, in such cases, a detailed analysis of the strength and deformation behaviour of the clays of the sliding zones should be carried out and some classic ideas of soil mechanics should be corrected. For instance, if the SEM images of the greyish-black clays are examined once again (fig. 4), it will become clear that the pore pressure during triaxial

testing should be  $u = 0$ , as the water between the clay and organic particles is in absorbed condition. Under confining pressure  $2 - 15 \cdot 10^5$  Pa that water could not filtrate through the micropores. The adsorption of water is due to the composition and high dispersion of the particles, building the clay structure. As a confirmation to that fact it is considered the following: the value of the clay permeability is not precisely determined and is accepted to be  $k_f < 10^{-9}$  m/24 h.

Analysing the microfabric and physical properties of these clays with close coagulation contacts, it was ascertained that they should be considered as a special structural and mechanical type, for which the classic ideas of soil mechanics are not valid. We gave up using the traditional strength parameters  $\varphi$  and  $c$  as characteristics of strength properties of these clays. Instead of them, there were accepted the so called "allowable"  $\tau_a$ , ultimate  $\tau_u$  and maximum shear stresses  $\tau_{max}$  obtained through the analysis of the relationships  $(\sigma_1 - \sigma_3) = f(\epsilon)$  in logarithmic scale (fig. 6).

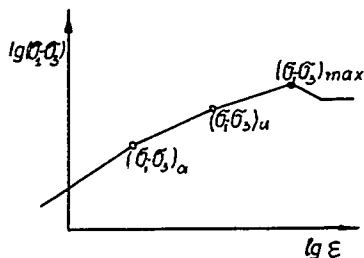


Fig. 6. Relationships "stress-strain" for clays from sliding zones

According to the contemporary views of the comparatively new science - physico-chemical mechanics (Georgiev G., 1981, Osipov V., 1975, Osipov V., V. Babak, V. Zuev, 1979, Rebinder P.A. 1958, Van Olphen, Z., 1963.) and the numerous analysis of the obtained results, it is considered that to the first linear section correspond processes of reorientation of clay particles around their contacts without failure of the structural bonds. To the second linear section correspond prevailing plastic equilibrium processes of failure of coagulation bonds and formation of new ones and to the third - progressive intensification of the process of collapse of structural bonds. The boundaries which mark that processes determine the allowable  $\tau_a$ , the ultimate  $\tau_u$ , and the maximum shear stresses.

#### ANALYSIS OF THE OBTAINED RESULTS

The analysis of the experimentally obtained relationships  $\tau = f(\sigma)$  /fig. 5 a, b, c/ and the relationship /fig. 5, d/ received through back analysis could hardly explain the mentioned paradoxes in originating of landslides in East-Maritza open-cast coal mines:

1. The values of the allowable shear stresses /fig. 5c/ are close to the values of the shear stresses obtained through back computations /fig. 5, d/ and are about twice lower than the maximum ones /fig. 5 a/. That fact, as well as the ideas for the character of deformation of the contacts unambiguously show that for the analysis of slopes stability there should be used the

the allowable shear stresses  $\tau_a$ . When the horizontal force of the weight of the active prisms  $E_x$  (fig. 2) gets over the sum of the available resistance forces  $\sum \tau_{a,i}$  in the major sliding surface (not the maximum  $\sum \tau_{max,i}$ ) plastic deformations leading to land sliding and formation of secondary prisms take place.

2. The obtained experimental relationships  $\tau = f(\sigma)$  with maximum values of  $\sigma$  corresponding to about  $5 \cdot 10^5$  Pa explain why is it so that with one and the same general slopes of the boards the deeper mine Troyanovo-North has less stable boards than Troyanovo South. Obviously, it is due to the lower resistance forces in the greyish-black clays as the values of the allowable shear stresses ( $\tau_a$ ) decrease with the increasing of the normal stresses. (fig. 5c).

3. The numerous mine surveying and investigations in site proved that the active prisms are the prime cause for originating the sliding processes and they always form at the highest outcropping levels or on terrain, i.e. where the values of normal stresses are higher and the corresponding shear stresses lower. That is why if the horizontal sliding forces of the active prisms overcome the resistance forces within the massif landslides could take place even with the sliding surface dipping towards the massif.

#### PROPOSALS FOR APPLYING THE OBTAINED RESULTS

Having ascertained, that the experimental results regarding the strength properties of the sliding zone clays (though incorrect to Mohr-Coulombs theory) could explain a number of engineering geological paradoxes of the landslides in East-Maritza open-cast coal mines there should be discussed the question concerning their rational using for board projecting /6/. The outcropping levels determining normal stresses about  $5 \cdot 10^5$  Pa were proposed to be broader and those under which the resistance forces are lower to be more narrow (fig. 7). So, the sum of resistance forces in the main sliding surface will remain constant but the general length of the boards shortens. There general form also changes from convex to "s" shaped one (fig. 8). If the obtained "s" shaped form of the boards is discussed, it is of interest to note that such a profile is near to the profile of stabilised old landslides, so the board could be projected with that form.

#### CONCLUSION

The detailed analysis of mineral composition and physico-mechanical properties of the clays interlayering the coal seams could allow to examine the numerous engineering geological paradoxes in originating and development of landslides in East-Maritza open-cast mines. The coagulation structural bonds and adsorbed around the particles water determine the decreasing of shear stresses with the increase of normal stresses. Further these lower resistance forces determine the development of active pressure prisms and great landslides. That analysis shows once again that the experimental results should never be rejected even when they do not confirm some classical views of well known theories.

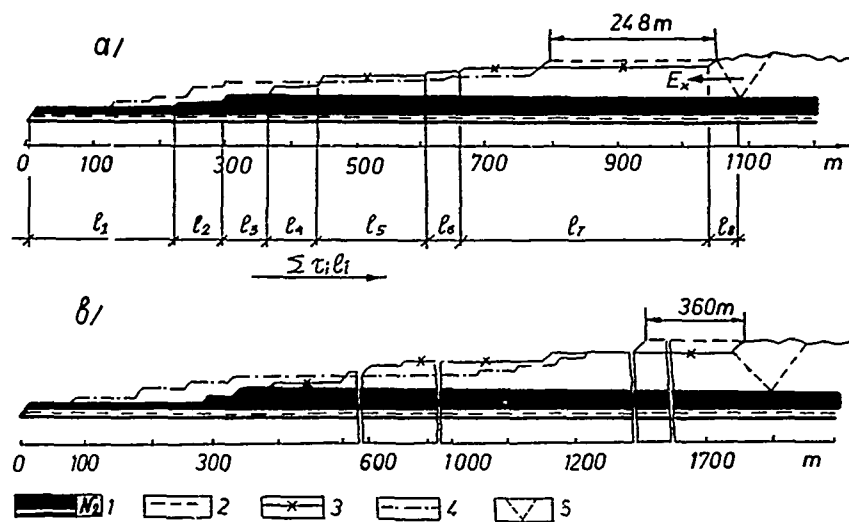


Fig. 7. Technological Profiles of the Working Flanks in the Troyanovo-South Opencast :  
 a) profile III - second quarter of 1981  
 b) profile 43 - second quarter of 1981  
 1 - coal seams; 2 - shear planes for which the pit edge stability is determined;  
 3 - line of working flanks along which the coal winning is done; 4 - line of the  
 S profile; 5 - zone of active pressure

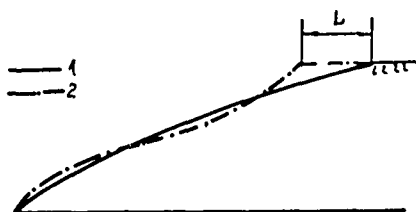


Fig. 8. General form of the slopes  
 1 - convex shape;  
 2 - "S" - shape profile

## REFERENCES

1. Anguelov K., and P. Mechkarski. 1982. A new Approach for Determining the Working Flanks in the Opencast Mines of SMEK "Maritza- East", Bulletin "Coal", No. 5, pp. 12-16, (in Bulgarian)
2. Demirev, An., K. Anguelov. 1979-1980. Structural Features of Clays from the Maritza-East Basin as a Factor in Slope Deformation, Annual of the HIMG, v. XXVII, Section II, pp. 171-189, (in Bulgarian)
3. Georgiev G., 1972. On the Character of Deformations in the Zones of Prisms of Active Pressure in the Maritza-East Coal Basin, Coal Journal, No. 1 (in Bulgarian)
4. Georgiev G., 1976. Analysis of the State-of-the-art of Landslide Phenomena and the Problem of Pit Edge Stability of Open Casts and Slopes of Spoil Banks in the Maritza East Coal Basin, Ministry of Energetics, Minproject (in Bulgarian)
5. Georgiev G. et al. 1981. Methodical Handbook for Stability Calculations of Working Packed and Unpacked Non-Mining Flanks and Spoil Bank Slopes in the Maritza-East Basin, Archives of Minproject
6. Mechkarski, P., K. Anguelov, T. Iliev, 1985. Designing and Controlling the State of Pit Edges in Open Casts of the Maritza-East Energy Complex Pros. with Int. Conf. ISMS Harrogate . v. 2, 733-741.
7. Osipov V. 1975. Structural Bonds and the Properties of Clays . Bulletin of the International Association of Engineering Geology No. 12, pp. 3-11
8. Osipov V., V. Babak, V. Zuev. 1979. A Physico-Chemical Approach in Studying the Mechanical Properties of Clayey Soils. "Engineering Geology". Nauka, M., No. 4 , pp. 15-27 (in Russian)
9. Rebinder, P.A. 1958. Physico-chemical Mechanics- New Field of Study (in Russian) Moscow.
10. Schuster R., R. Krizek, 1978. Landslides. Analysis and Control. National Acad. of Sciences, Washington
11. Van Olphen, H. 1963. An Introduction to Clay Colloid Chemistry. Interscience Publ. N.Y.

## Study of Some Debris Avalanches in Garhwal Himalaya, India

**H.C. Nainwal**

Lecturer, Department of Geology, Garhwal University, Srinagar (Garhwal), U.P., India

**Y.P. Sundriyal**

Lecturer, Department of Geology, Garhwal University, Srinagar (Garhwal), U.P., India

**C. Prasad**

Professor and Head, Department of Geology, Garhwal University, Srinagar (Garhwal), U.P., India

**ABSTRACT:** This study was carried out in the Alaknanda - Dhāuliganga catchment area, located in the north and north-east of Joshimath in the Garhwal Himalaya. The snow fields, cirques and the related glaciers are located above the altitude approximate 4000 meters, while the river valley have a mean altitude of around 2000 meters.

The strategic roads viz. Joshimath-Badrinath and Joshimath-Nitipass pass through this area with a number of villages along with their cultivated land are located along the roads. These roads are often blocked on huge debris avalanches not only damage the road, but also the cultivated land and forests.

The geological studies has indicated the presence of a major thrust viz, Main Central Thrust (M.C.T.) in this area, with highly deformed rocks. Most of the zones with frequent debris avalanches do not follow the thrust zones etc.

The glaciers have been studied on the basis of aerial photographs and landset imageries. It appears although most of the glaciers are slowly receding back, are located in the crest of Badrinath is apparently static and many crevasses etc., are formed and slumpping is taking place. The slumped mass of Ice is pushing the moraines down in the valley and large scale debris avalanches are causes on the Joshimath-Badrinath road.

### INTRODUCTION

The study area is located in catchment area of Alaknanda-Dhāuliganga rivers. It is situated in north and north-east of Joshimath, bounded by longitude  $79^{\circ}30'-79^{\circ}45'$  and latitude  $30^{\circ}30'-30^{\circ}45'$  in Chamoli district of Uttar Pradesh, India (Fig.1). The area has a high seismic intensity along with frequent landslides, debris avalanches etc., are the regular features happened there. Due to these features, two important strategic roads viz, Joshimath-Badrinath and Joshimath-Nitipass are effected regularly.

The study was taken in order to identify the processes of debris avalanches, landslides. Studies of the position of the glaciers indicate the state of glacial retreat. The retreat in case of the Juma and Tipra glaciers is found to be greater than other glaciers lying on the north-west in area. The western part's glaciers of the area (above the Badrinath) is apparently static and many crevasses etc., are formed. The slumpping are regular feature in this area, pushing the moraines down in the valley slope and large scale debris avalanches are caused on the roads of strategic importance.

Cotter and Brown (1907) were the first to survey some of the glaciers of Kumaon and Garhwal Himalayas. The other workers are Heim and Gansser (1936) Jangpangi and Vohra (1958,62), Gopendra Kumar, Syed Hyder Mehdi and Gyan Prakash (1964).

### GEOLOGY

#### Structure and Rock Types

The greater Himalaya is situated in between two great thrusts viz, the Main Central Thrust (MCT) and the Tethyan Thrust (T.T). This is indicated by the metamorphic rock which are gradually increase in metamorphism northwards and intruded by granite batholiths. The tectonic plane of Main Central Thrust

dips at an angle of  $45^{\circ}$  to  $15^{\circ}$  towards the North-east. The term Main Central Thrust was first proposed by Heim and Gansser (1936). Valdiya (1980) while redefining the Main Central Thrust proposed another name, farther north and called it the Vaikrita Thrust. The Main Central Thrust is clearly definable on the surface in the mountain slope and deep cut river gorges of Alaknanda. Sinha-Roy(1982) defines the Main Central Thrust as the basal thrust of the crystalline nappe sequence either rooted or detached from the Central Crystalline zone. It could be inferred that activity along the Main Central Thrust started in the Palaeogene (Krishnaswamy, 1981 and Sinha, 1982).

The general trend of strike of the rocks in the area is E-W. Descending to the gorge at Vishnuprayag, where the gneiss is exposed. It is overlain by highly metamorphic mica schist and paragneiss. The succession is overlain by highly metamorphic sedimentary series (Fig.2)

#### Geomorphology

North of Vishnuprayag the gorge of Alaknanda is not only continuous but also more tremendous. The view from Joshimath to north, Convex Valley sides are tremendous showing no more place for the rivers, as if they had been caused by a fault collapse. It may be assumed that these transverse gorge is also exclusively formed on river erosion.

When river meets to moraines the valley become widens, as from Pandukeshwar. The low gradual terraces are on both flank of the river. The Lateral moraines are following both side along the river. The villages are lies just below the moraine wall near Pandukeshwar.

The topography of a Great Himalaya, which is an enormous curvilinear, arch, is highly rugged with horned peaks, surrected crest of ridges, cirques and hanging wall valley with glaciers causing cascades of gushing

icy water through deep canyons (Fig.3). In beginning of this sector, the ridges are rapidly rise then the river and afterwards it run parallel to it. The river is narrower in lower elevation, while it is wider in upper one. Rivers has a very low gradient at higher elevation as in the case of Alaknanda, has a very low gradient of 5.5% from Badrinath to Mana village, while below the Badrinath the gradient is 15% (Heim and Gansser 1936).

Epigenetic gorges are abundant in higher elevation with numerous hanging valley. The terraces of higher elevation are covered by the moraines. The widened valley of Alaknanda is filled with recent mounting slide material and fan deposits. Which came down from both sides covering the older moraines and gravel deposits. The glacial striations are well preserved within the rocks. Inter glacial and interstadial lake deposits are also there. (Fig.4,5 and 6).

#### GLACIERS AND THEIR DEPOSITS

As given in the map (Fig.3), there are two main cirques in this area viz. the Juma and Rajbank. Their cirques shoot out a number of the glaciers, of which the two main glaciers are Tiprabank, originating from Rajbank and the Kagbhusandi, originated from Juma glacier. These glaciers in turn shoot out their glacial streams.

The following table gives the altitudinal position of the glaciers, along with position of snow, the zone of accumulation and ablation (Fig.7).

TABLE I. Altitudinal Zones

| Glaciers            | Glacial streams | Altitudes in meters  |                  |
|---------------------|-----------------|----------------------|------------------|
|                     |                 | zone of accumulation | zone of ablation |
| Tiprabank           | Bhuindar Nadi   | 4000                 | 3600             |
| Kagbhusandi glacier | Laxman ganga    | 4100                 | 3360             |

The morphometric parameters of these glaciers were calculated on the basis of the technique suggested by Prasad (1987), which is based on the general observations that an advancing glaciers has a wider snout, and a relatively larger area than a retreating glaciers. Moreover a retreating glacier will have more rugged appearance viz. higher relief ratio.

The following table gives the values of various glacial morphometric parameters.

TABLE II Glacial Morphometric Parameters

| Glacier     | Area Index | Relief Ratio | Snout ratio |
|-------------|------------|--------------|-------------|
| Tiprabank   | 0.63       | 0.72         | 2.2         |
| Kagbhusandi | 0.34       | 0.84         | 1.4         |

In addition to the glacial morphometric parameters, the drainage parameters of the glacial streams were also calculated, which are summarised in the following tables.

TABLE III Drainage Morphometry of Glacial Streams

| Drainage    | Mean Altitude | Area      |
|-------------|---------------|-----------|
| Kagbhusandi | 3600-4400     | 0.43-2.39 |
| Laxmanganga | 3400-4200     | 0.69-2.83 |
| Bhuindar    | 3380-4280     | 0.54-1.83 |

TABLE IV Drainage Morphometry of Glacial Streams

| Drainage    | Shape     | Bifurcation Ratio | Drainage Density |
|-------------|-----------|-------------------|------------------|
| Kagbhusandi | 0.21-0.52 | 2-4.1             | 0.97-3.1         |
| Laxmanganga | 0.17-0.66 | 2.6-4.6           | 3.3-26.2         |
| Bhuindar    | 0.47-0.77 | 2.5-4.5           | 7.14-15.19       |

The glacial moraines consisting of Boulder-clay etc., are found deposited in the zone of ablation upto following altitude in the valleys

TABLE V Altitudinal Position of the Moraines

| Glacials   | Altitudes of moraines | Type of Moraines                            |
|------------|-----------------------|---|
| Tiprabank  | 3200                  | Boulder clay                                |
| Kagbusandi | 2400                  | Boulder clay alongwith gravel and sand beds |

#### MASS MOVEMENTS

Various morphometric parameters, alongwith field observations aided by the study of aerial photographs suggests that the zone of ablation is larger in case of the Kagbhusandi glacier which is retreating. The Kagbhusandi and Laxmanganga streams have wider basins with greater bifurcation ratio and drainage density, suggesting relatively greater erosion done by the streams existing in zone of ablation for the Kagbhusandi glacier.

On the otherhand, in case of the Tipra bank glacier the zone of ablation is narrow and mass movements is mainly debris avalanche.

## DISCUSSION AND CONCLUSIONS

As already pointed out the zone of ablation in case of the Kagbhusandi glacier is larger than that of Tiprabank. Kagbhusandi glacier shoot out the streams of Home Gadhera and the Kagbhusandi.

The stream profiles of these streams (Fig.7) shows that the zone ablation is only 500 meters thick in case of Home Gadhera, but is 1400 meters thick in case of Kagbhusandi. On the other hand, in case of streams originated from Tiprabank viz, Laxmanganga the zone of ablation is only 200 meters thick.

The profile of Laxmanganga is concave upwards, convex in the middle and again concave downwards but concavity is very feable in the Uppar part. The profile of Home Gadhera is also very similar but the concavity is more in the upper part. Whereas incase of the Kagbhusandi, the profile is convex in the upper part and is concave in the lower part.

The mass movement is generally controlled by the type of the slope profile (Small 1970). The more steaper profile of Kagbhusandi indicates the presence of debris avalanche followed by the debris flow, whereas in case of Laxmanganga and Home Gadhera the mass movement is mainly by debris flow. This fact is supported by the drainage morphometric parameters, which suggest a greater intensity of erosion in case of Kagbhusandi Nadi, than in Laxmanganga.

Therefore, it can be concluded that since the Kagbhusandi glacier is retreating more in comparison to the Tiprabank glacier. The mass movement are in case of rapid debris avalanche here. Because of the debris avalanche the slope are more unstable in the southern part of the area, which contain the ablation for the Kagbhusandi glacier.

## ACKNOWLEDGEMENT

First author, H.C. Nainwal is thankful to Council of Scientific and Industrial Research, New Delhi, India, for financial assistance. Our sincere thanks goes to Professor S. Prakash of University of Missoorie Rolla, U.S.A. for warm encouragement, in preparation of this paper.

## REFERENCES

- Cotter, G.DE.P. and J.C. Brown (1907), Note on certain glaciers of Kumaon, India. Record Geological Survey of India. Volume 35, 148-157.
- Gansser, A., (1964), Geology of the Himalaya, Interscience Publishers, London.
- Gopendra, K., S.H. Mehdi and G.Prakash(1968). Observations of some Glaciers of Kumaon Himalaya, India. Record Geological Survey of India. Volume 106, Part 2:231-239.
- Heim, A. and A. Gansser(1939), Central Himalayan Geological observations of Swiss expedition,1936. Reprint Hindustan Publishing Corporation Delhi,India.
- Jangpangi, B.S. (1958), Study of some of the Central Himalayan glaciers, Journ. Sc. Ind. Res., Vol.17A, No.12, Supplement: 91-93.
- Jangpangi, C.P. Vohra (1962), The retreat of Shunkalpa (Ralam) glaciers in Central Himalaya, Pithoragarh District, U.P., India, Union Geodseique Et Geophysique Internationale, Commission Des Neiges Et Des Glaces, Colleeue D'obergurgl, Publication No 58 : 234-238.
- Krishnaswamy, V.S. (1981), Status report of the work carried out by Geological Survey of India in the framework of International Geodynamics Project. In H.K.Gupta and F.M. Delany (Editors), Zagros Hindukush Himalaya-Geodynamic evolution. Geodyn. Ser., Am. Geophys. Union, Volume 3\_ 169-188.
- Nainwal, H.C. M.P.S. Bisht C. Prasad (1987), Studies on mass movement of the Kaliasaur Landslide area district Pauri Garhwal, U.P., India, JOHSARD, Garhwal University Srinagar (Garhwal), India, Volume 9 & 10: 77-81.
- Prasad, C.(1987), Studies in morphometry of a glaciaded terrain. Proceeding of International Seminar on Geomorphology, Allahabad, India.
- Sinha, A.K. (1982), Tectonic framework and Geological evolution of Higher Central Himalaya, D.Sc Thesis, state University Moscow.
- Sinha, A.K. (1987), Tectonic Zonation of the Central Himalaya and the crustal evolution of collision and Compressional belts. Tectonophysics,134:59-74.
- Sinha-Roy, S.(1982), Himalayan Main Central Thrust and its implication for Himalayan inverted metamorphism. Tectonophysics, 84:197-224.
- Small,R.J. (1970), Study of landforms, Cambridge University, London.
- Valdiya, K.S.(1980), Geology of the Kumaon Lesser Himalaya Wadia Institute of Himalayan Geology, Dehradun, India.

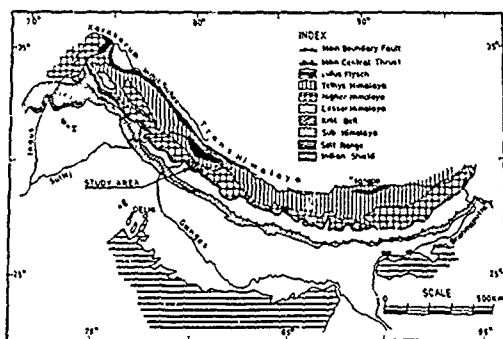


Fig. 1- STRUCTURAL MAP OF HIMALAYA SHOWING  
LOCATION OF THE STUDY AREA

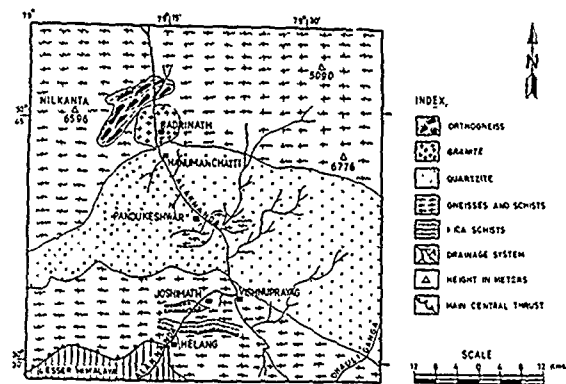


Fig. 2- GEOLOGICAL MAP OF THE STUDY AREA  
(MODIFIED AFTER A.K. SINHA 1987)

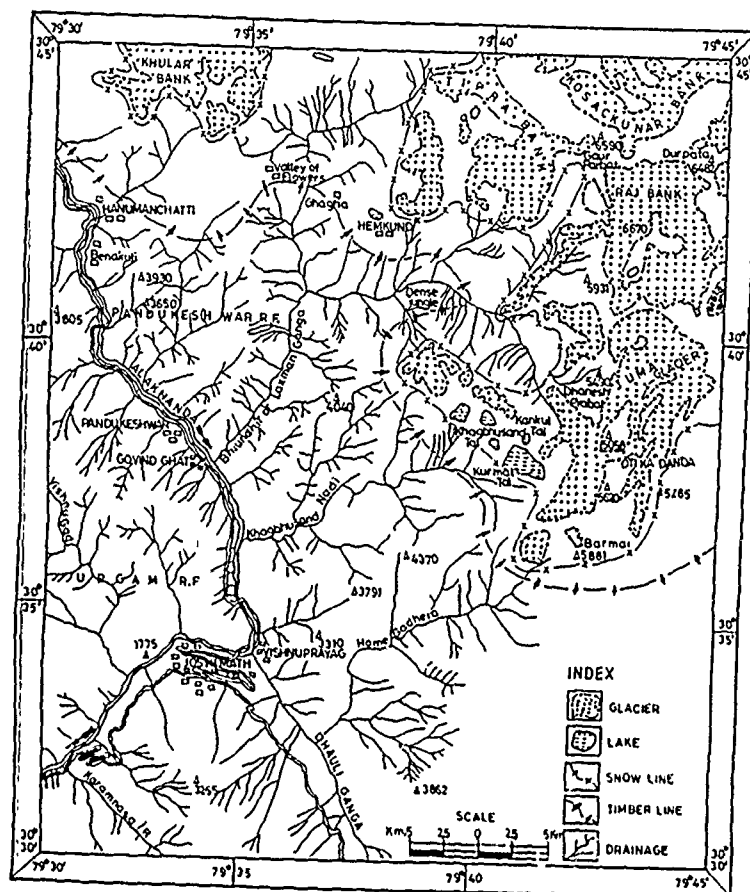


Fig. 3- PHYSIOGRAPHIC MAP OF THE NORTH OF JOSHIMATH GARHWAL  
HIMALAYA INDIA



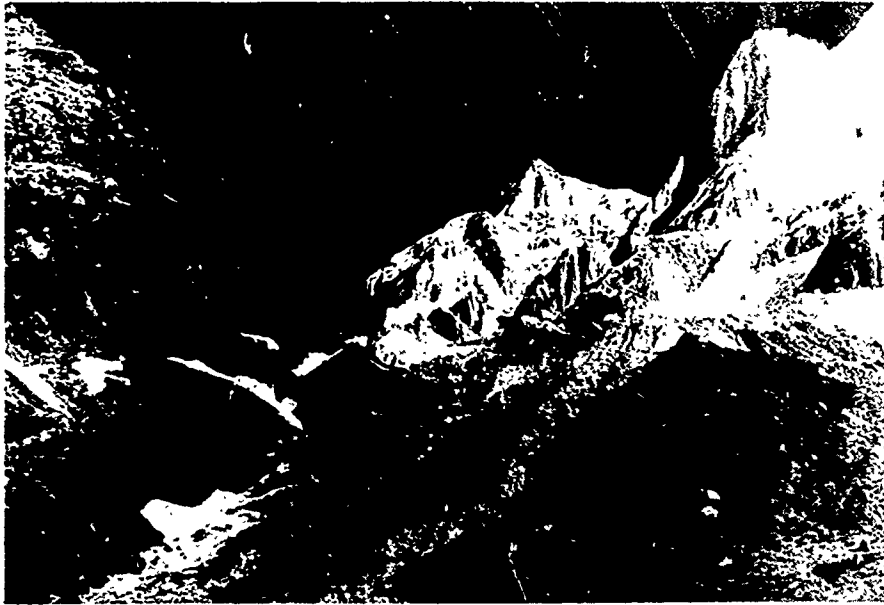


Fig.4 Glacial valley alongwith the Lateral moraines  
Garhwal Himalaya, India.

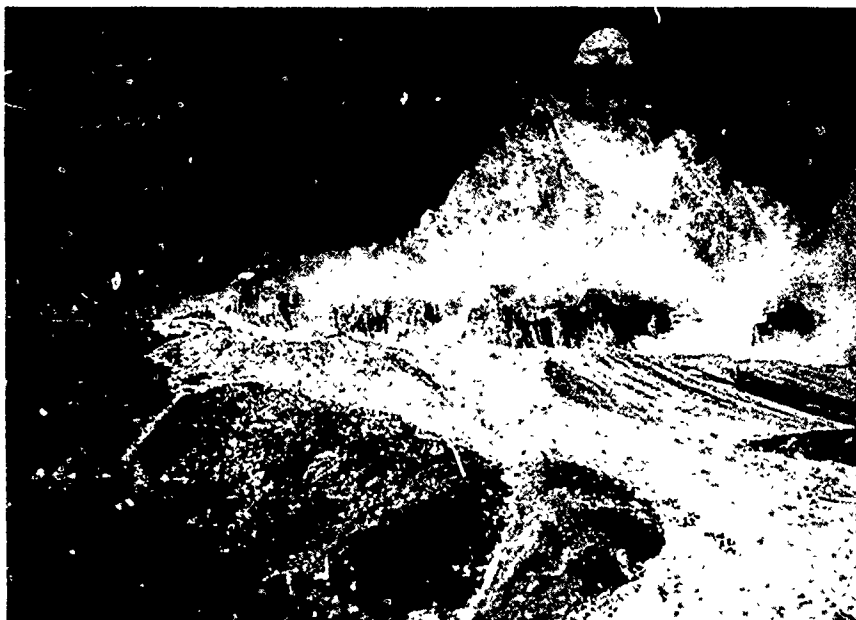


Fig.5 Part of the Cirque and the shooting out glaciers, Garhwal Himalaya  
India.

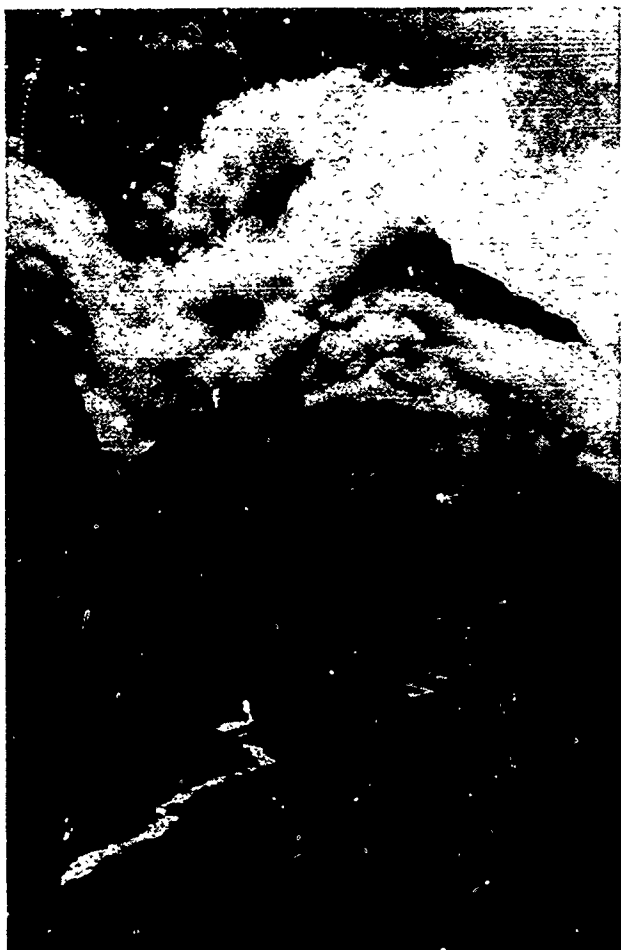


Fig.6 Glaciated Valley, glacial streams in the zone of ablation, Garhwal Himalaya, India.

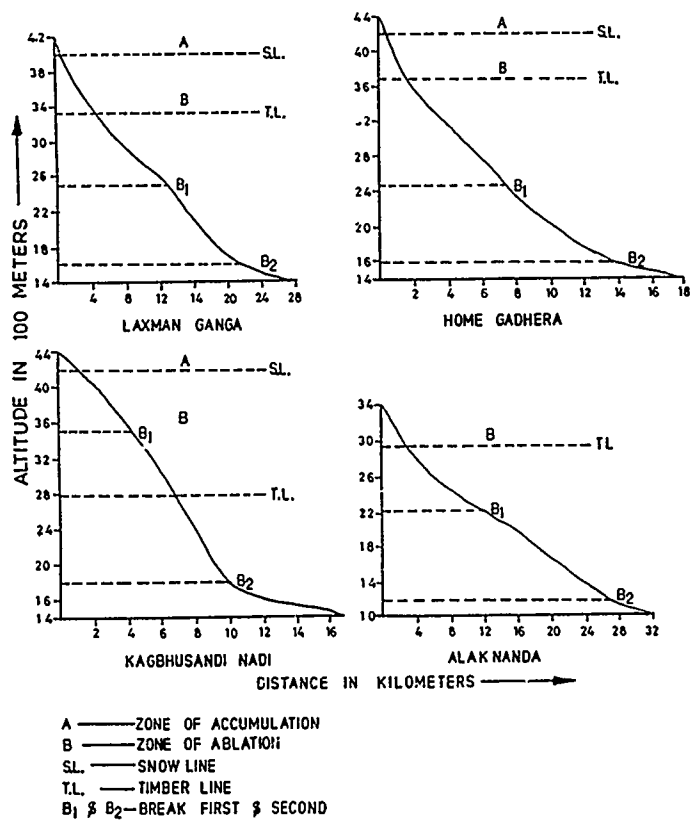


Fig.7—SLOPE PROFILES OF THE RIVERS

## Lithotectonic Landslides and Hazards in Parts of Garhwal-Kumaon Himalayas

R.S. Mithal

Emeritus Professor, Earth Sciences, University of Roorkee, Roorkee, India

### SYNOPSIS

Landslides produce an awesome picture of the hill sides with steep scarred, hollowed and gullied geomorphic features devoid of vegetation particularly between the major thrust zones. A look on the tectono-stratigraphic map of the region with marked major tectonic features like the Main Central Thrust (MCT), North Almora Thrust (NAT) and South Almora Thrust (SAT) indicates that the region is highly prone to landslides and is affected by repeated tectonic and orogenic processes. These factors with the nature of the rocks, climate and the heavy monsoon rains are responsible for sculpturing the region. The mountain features and the valley slopes thus indicate the influence of the activities and the dynamic forces at a particular locality and time. Many times developmental activities have also contributed towards the degradation of the environs due to disturbance of the already stabilized slopes and the angles of repose e.g. along the Rishikesh - Badrinath Road, where a new alignment has been given, sometimes overlapping the old pilgrim route.

### INTRODUCTION

In India, the awareness of the effects of landslides is hardly two decades old. Though the phenomenon has been going on, the importance of their occurrence and the resultant losses had been recognised only after the Belakuchi disaster in 1970 due to flash floods. As a result the whole Alaknanda valley got flooded, caused innumerable landslides in its course, dammed the river, formed new terraces in the wider valleys, breached the existing lakes and reservoirs, pulled down lines of communications and transmission, washed out roads and by-passed the existing bridges, wiped out a number of hamlets and habitations and road side shops etc. killed at least 17 people and lots of 23 vehicles, silted up the existing canals, changed the river courses and by-passed the bridges, washed off miles of road sections thus disrupting the life and livelihood of the people.

In fact, even this was being forgotten, when another similar catastrophe occurred close to Ganganani in July 1978 on the Uttarkashi Gangotri road another pilgrim route. Due to this calamity another 8 vehicles got lost and a number of pilgrims died with more than 2km road on the right bank washed away and a girder bridge by-passed. Later, a new alignment on the left bank had to be laid and cut through almost vertical precipices. This is still not stabilized and a team of workers with bulldozers are posted to keep the passage open.

Landslides are ambiguous processes of catastrophic events of which the most important and direct effects on mankind are loss of life and property, damage to natural resources, disturbance in the ecosystem and environment. Recently a number of papers have appeared

on the Himalayan slides but not much has been said on their relationship to the geological and tectonic set up and the hazards caused (in the region), particularly with a view to civil works. Barring a few, the accounts portray only the events, though most of them, as major disturbances have disrupted the life of the local people and caused hazards to the developmental activities in the region. Majority of these slides chiefly lie in a belt nearly 30 to 50km in width and extend from a general level of 150m to nearly 2,750m.

The slope failures are largely due to rock falls, debris flow, slumps, creep flow, earth flows and certain complex mass failures including the rock avalanche types. Many a time massive and temporary blockages occur due to sudden inflow of waste debris forming small reservoirs, lakes or lakelets in the courses of rivers. However, the latter and sudden bursts or breaches of these lakes are often observed to have caused unimaginable havoc and catastrophes in the lower reaches of the catchment area. Of these, floods of years 1880, 1924, 1971, 1978 coupled with large scale slides are still memorable. The creation of Gohna Tal in 1893 and its later obliteration in 1971 due to high monsoon rains or flash floods is one of the most important events in the landslide history of the region.

Along the Rishikesh-Badrinath road and many other new excavations and cuts, landslides are more common now and numerous as old angles of repose have been disturbed. In brief, the horrendous topography with inhospitable terrain full of complex geomorphic features, all make the region most hazardous to the people, the locality as well as for any developmental activities.

## GEOTECTONIC SUBDIVISIONS OF HIMALAYA

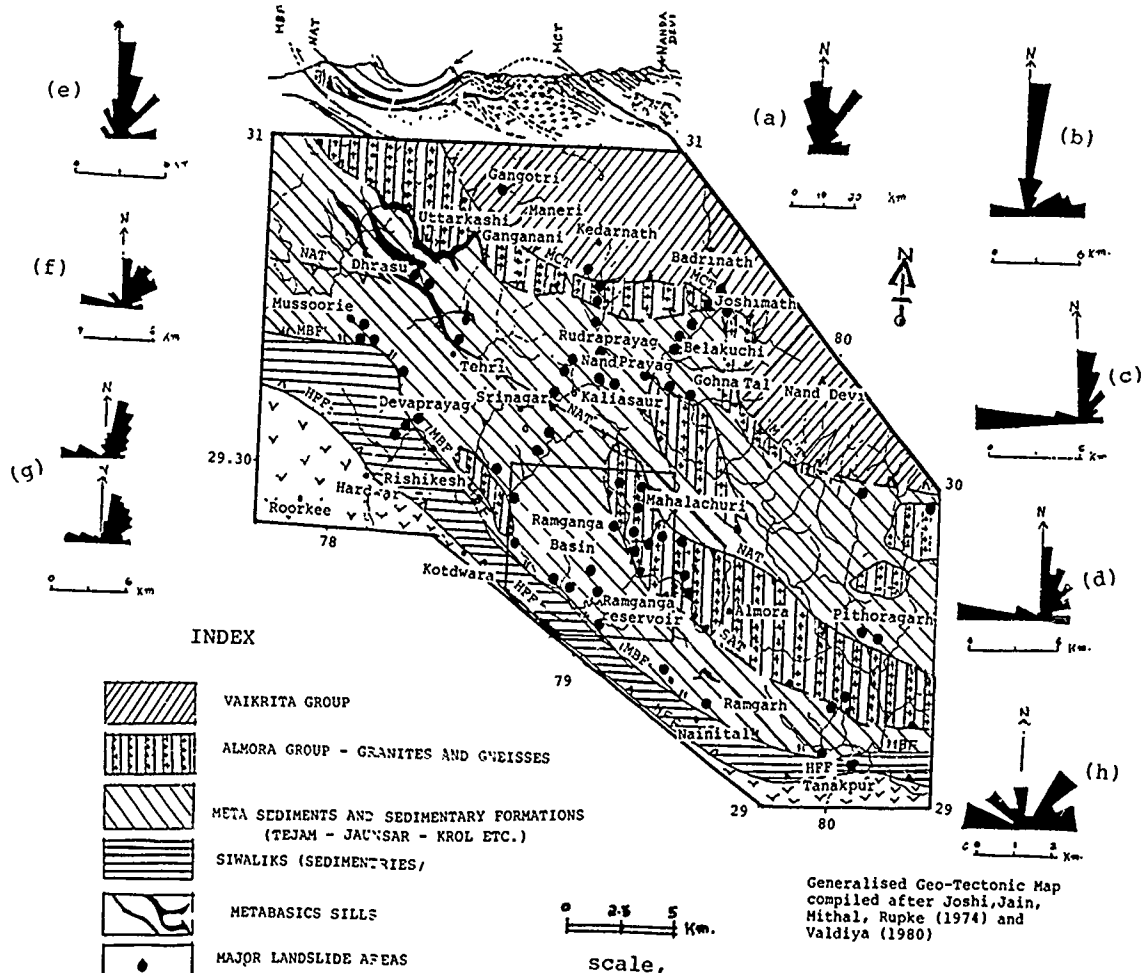
Gansar (1964) gave a four fold longitudinal geotectonic division of Himalaya - (i) Sub-Himalaya (Siwaliks), (ii) Lower or Lesser Himalaya, (iii) Higher/Greater or Central Himalaya and (iv) Tibetan or Tethys Himalaya. Broadly, the Garhwal-Kumaon Himalaya are a part of the same geo-tectonic frame and could also be sub-divided and placed into smaller similar morphotectonic units. These are marked by distinct geological formations of different tectonic style and frame work producing characteristic geomorphic features.

## GEOLOGY AND STRUCTURE

Geologically, the Garhwal-Kumaon Himalaya generally trend in NW-SE direction and are

made up of highly crystalline schists, gneisses and massive quartzites (Klippe) on top of the mountains, which in turn are underlain and surrounded by the less altered unmetamorphosed arenaceous and argillaceous or calcareous rock units including minor metabasics and basic sheets and dykes along with some nummulitic limestones dipping into the older ones. The Main Central Thrust (MCT) separates the older formations. The North Almora Thrust and the South Almora Thrust (NAT and SAT) divide the Garhwal-Kumaon rocks from the Dudatoli/Kumaon-Almora groups of rock formations, which are again separated from the younger formations by the Krol Thrust or the Main Boundary Fault (MBF) (Fig.1).

Fig. 1 GEO-TECTONIC MAP OF GARHWAL-KUMAON HIMALAYA SHOWING IMPORTANT LANDSLIDE AREAS



## FRACTURE PATTERNS

- (a) Lineament Pattern - Garhwal - Kumaon Region, (b) Tehri Sector, (c) Dharasu - Uttarkashi Sectors, (d) Mussoorie Area, (e) Rishikesh Sector, (f) Hardwar Sector, (g) Devaprayag - Srinagar Sectors, (h) R. Ramganga Basin Slides and Fracture Patterns (Mean)

In addition, numerous faults and minor thrusts trending in NW-SE and N-S directions also dissect the region along with many sets of joints, fractures, cleavages and lineaments and other discontinuities in almost all directions of azimuth. Of these, weak structures in NE-SW, NNE-SSW and N-S (in order) directions are prominent and fully responsible for the fragile nature of the rocks involved. Thus the rock units are highly vulnerable to erosion and even to other minor disturbances prevalent in this mountainous terrain.

Structurally, the rocks are more complex and complicated due to several tectonic episodes. In addition to the major thrusts, nappe sheets and klippen etc. at least three to four phases of tectonic and neo-tectonic events are recognisable and established in the field. The neotectonic activity appears to be spasmodic (Mithal 1968) as evidenced by the recent level disturbances and the most recent episodes in the river terraces along the valleys of the major rivers and the frequent seismic tremors felt in the area.

From the location of landslides or the potential zones of mass movements, the Garhwal-Kumaon groups of rocks are more susceptible to landslide activity (Table 1) and the major landslide zones are mainly confined to these formations.

#### LITHOLOGY AND TECTONIC UNITS

The sub-himalayan zone comprises of Neogene molasse sediments (Siwaliks) and the lower Tertiary Subathu formations, north of which lie the MBF or the Krol Thrust and in the south these formations are overlain by the thick Indo-Gangetic alluvium. Structurally this zone is affected by NW-SE running asymmetrical folds bounded by large scale high angled reverse faults also cutting the axes. In the lesser Himalaya, unfossiliferous Pre-cambrian to Tertiary sediments of low grade metamorphism are predominant and are delimited by the MBF-Krol Thrust (in the south) and the Main Central Thrust in the north. These are highly folded and deformed due to multiple folds, faults and thrusts many times in association of meta-basic sills or sheets. Thus they produce a highly complex structure with at least three subtectonic divisions: (i) Autochthonous Pre-cambrian low grade sediments in the inner or the northern parts, (ii) the middle Krol Nappe (including the Nagthar quartzites, Chandpur Phyllites, Blaini and Infra Krol formations, Krol limestone and Tal and Subathu formations), (iii) Rocks of the Almora or Garhwal Nappe of low to high grade metamorphics. These litho-tectonic units are highly complex since these also are affected by many thrusts and faults with associated imbricate structures and shears in both transverse and longitudinal directions. Many of these features also appear to be still active. Many other minor features like joints, cleavages and fractures also affect these rock units. As such the massive competent rocks are crumpled and crushed while the non-competent types are foliated and have developed fissility. Likewise, the metabasics in thinner bodies are also foliated and fissile, while the thicker massive sills or dykes behave

both as competent and incompetent bodies in the area, e.g. at Kaliasaur, Dunda, Nakuri etc. in Garhwal and Ramgarh etc. in Kumaon.

TABLE I. Tectonic Succession and its Correlation in the Garhwal-Kumaon Himalaya

| FORMATION            |                                  | LITHOLOGY  |
|----------------------|----------------------------------|--|
| Garhwal Kumaon Group | Amri Formation                   | Phyllite, quartz-mica schist, mica schist, garnetiferous mica schist, granite-gneiss |
|                      | Thrust                           |  |
|                      | Raitpur Formation                | Muddy boulder bed, shale, limestone  |
|                      | NAT or Garhwal Thrust            |  |
| Subathu Group        |                                  | Shale, sandstone, fossiliferous limestone  |
|                      | Unconformity                     |  |
| Tal Group            | Upper Tal                        | Oolitic limestone, sandstone   |
|                      | Middle Tal                       | Ortho-quartzite, shale, limestone, siltstone   |
|                      | Lower Tal                        | Shale, siltstone, phosphorite  |
| Krol Group           | Krol formation                   | Massive limestone, dolomite, shale and red shale                                     |
|                      | Infra Krol formation             | Shale, slate, limestone  |
|                      | Blaini formation                 | Muddy boulder bed, limestone, sandstone, shale                                       |
|                      | Unconformity                     |  |
| Jaunsar Group        | Nagthar formation                | Sandstone, quartzite, quartz schist, grit, conglomerate, phyllite                    |
|                      | Chandpur formation               | Quartzite, phyllite, shale   |
|                      | Mandhali formation               | Quartzite, conglomerate, slate, limestone  |
|                      | Krol Thrust/Main Boundary Thrust |  |
|                      | Subathu Formation                |  |
|                      | Main Boundary Fault              |  |
|                      | Siwalik Group                    |  |
|                      | Foot-hill Fault                  |  |
|                      | Indo-Gangetic Plain              |  |

The rocks of the Higher (Central) or Tethyan Himalaya are 10 to 20km thick, dip northwards and are highly metamorphosed with associated tertiary granites. To the north, the Central Himalayan metamorphics grade into the fossiliferous, gently deformed Cambrian-Ordovician sedimentary sequence of the Tethys. The Siwaliks are comprised of NW-SE striking typical sandstones and sands - the latter being predominant in the upper and the clays and claystones in the lower succession. The folds are repeatedly faulted at their crests with steep strike faults and gently dipping thrusts at 25° to 30° to the north east. These all are responsible for steep south facing fault scarps and 'cuesta' type landforms with gentle bedding slopes to the north.

#### PHYSIOGRAPHY

Physiographically, the Himalaya are divisible into four sub-zones which are also concordant with the litho-tectonic units of the Lesser Himalaya, i.e. the Siwalik belt, the Krol Nappe Zone, the Almora Nappe and the Autochthonous zone. A study of their cross profiles indicates a close relationship and control between geomorphology, geology, lithology, tectonics and structure on the one hand and rainfall, climate fauna and flora on the other.

As stated earlier the Himalayan region is very fragile due to tectonically folded, faulted and crumbled rock formations in the various thrust sheets. Secondly, the region is subjected to sporadic earthquakes and seismic activity. These have played a great role in the configuration and carving of the present topography of the region. Thirdly most parts of the terrain experience heavy monsoon rains followed by long severe winters and long summers. Fourthly, many areas are devoid of forest cover and lastly the indiscriminate grazing and construction activity of roads etc. have all been responsible for the degradation of the slopes and the valleys.

Morphologically, only two types of land forms (a) Erosional and (b) Depositional are predominant in the area. The hills and peaks are generally isolated, conical in shape and appear to be only the linear extensions of the crests of ridges which also form water divides. The valleys on the other hand vary from small ravines to deep gullies, narrow or wide valleys. Deep gorges are mostly controlled by the tectonic features of the litho units and the rock formations, for example, the valleys of Rivers Ramganga, Bhagirathi, Alaknanda and many others are generally controlled by the geology and tectonics. The control is mainly due to dislocations and fault zones. At many places the valleys are wide due to excessive erosion and mass wasting of the slided slopes. Some valleys, particularly in the Lesser Himalaya, e.g. in Siwaliks are homoclinal, i.e. controlled by the strike of the rocks, while others follow the fold axes of the antiforms or the synforms.

#### SLOPES AND THEIR DEVELOPMENT

As has been made out from the Survey of India topographic sheets, the aerial photographs and the actual field observations, the hill slopes in the region are very variable and seem to be controlled with the nature of the rock formations, the tectonics and the competency of the rock masses alongwith the climate of the region. These slopes could be classed as: (1) gentle - with an inclination of < 30° best developed in gneisses, schists and phyllites of the Lesser Himalaya and in the shales and unconsolidated sediments of the upper Siwaliks, (2) Moderate - with an inclination of 20° - 45° predominantly in schists, phyllites, crushed quartzites, gneisses and limestones of the Middle Himalaya, (3) Steep Slopes - with an inclination of 45° - 70° are common in the hard, compact and well jointed quartzites, limestones of Central Himalaya and even in the coarse massive sandstones of the Siwaliks, (4) Scraps with inclination of >75° due to differential erosion and deep cutting streams (5) Topographic Flats - with sub-horizontal surfaces are predominant in the stable zones, as a result of erosion of the gently dipping thick massive sedimentary formations. In the granitic regions, rounded or sub-rounded mounts are also noteworthy in the Middle Himalaya. In brief, it may be concluded that the hill forms, the slopes and the valleys in the region are products of the lithology, tectonics, dip failures, and structural deformations and discontinuities coupled with the variations in the climate and the erosive activity of waters along the weak planes and toe erosion.

#### LANDSLIDE AND LITHOLOGY

On an over view and evaluation of the land failures activity, it is noted that the clastic rock units of the Siwaliks are less susceptible to landslide activity. It may be due to the easy weathering of soft rocks producing good soils for luxuriant vegetation. The Nagthar quartzites, Krol limestones etc. and the low grade metamorphics (phyllites, schists and slates etc.) being well jointed, well foliated are less vegetated and show an higher incidence of landslide activity. The rocks of higher grade metamorphics and the crystallines i.e. granites, gneisses and quartzites alongwith the massive krol limestone (not influenced by weak characters) are comparatively less prone and affected by landslides only at few localities close to the major tectonic features like the NAT, MBF or MCT. However, the massive crushed, fractured and foliated rocks suffer of rock falls, rock debris, in the neighbourhood of the tectonic features/shears or weak zones, particularly when associated with meta-basics or epidiorites, (Table II, Fig.2).

Almost all thrust faults and shear zones are evidenced by the presence of breccia, crushed and gouged materials. Such characters are best observed particularly along the recent and Neotectonic (?) features. Along the other weak zones meta-basics or their weathering products are invariably present, e.g. Almora-Dubautoli-Bijnath thrust sheet in Kumaon; Main

TABLE II. Characters of some Important Thrusts and Landslides Zones along Bhagirithi Valley in Garhwal Himalaya

(Modified and compiled after Jain, 1972)

|           |       | CHARACTERS OF THRUSTS |                                     | CHARACTERS OF LANDSLIDE  |   |
|-----------|-------|-----------------------|-------------------------------------|--|---|
| TECTONISM | OLDER | NORTH<br>(Sainj)      | Main Central Thrust (MCT)           | Impersistant chlorite schist, increase in metamorphic effects towards top of Gamri quartzites near thrust; development of foliations, mica lineation and quartz sericite schist. | Intensely crushed, 3-5km wide zone on the sub-thrust side, zone of intense landslide, e.g. Sainj landslide.                                       |
|           |       |                       | Uttarkashi Thrust                   | Persistent metabasics, metamorphic effects maximum, wherever metabasics are absent development of foliation, mica lineation and schistose quartzite.                             | Highly crushed and friable zone of 1.5 to 3km in width landslide zone with flowing highly crushed material e.g. Netala landslide.                 |
|           |       |                       | Dunda Thrust                        | Persistent metabasics, metamorphic effect minimum wherever metabasics are thick  | Highly crushed zone of 1 to 2.5km width, metabasic blocks in flowing debris.  |
|           |       |                       | Singuni Thrust                      | Impersistent mylonites, increasing metamorphic effects towards the sole of the thrust in Gamri quartzites, development of foliation, mica lineation and quartz schist.           | Highly crushed limestone zone along Tehri-Dunda Road crushed zone upto 1.5 to 2km wide e.g. Khattukhal slides.                                    |
|           |       |                       | Srinagar/ North Almora Thrust (NAT) | Impersistent metabasics, increased metamorphic effects in Dharasu formation along thrust zone, crushing of rocks   | Intermediate width (upto 1.5 km landslide zone of angular blocks and crushed rocks in flowing slide zone, e.g. Nail slide north of Dharasu        |
|           | NEWER | SOUTH<br>(Rajpur)     | Tons Thrust                         | Fault breccia and crushed slate, lack of metamorphism  | Narrow zone of crushed rock material, also rock slides, 150 to 200m wide one, e.g. Nagun slide.   |
|           |       |                       | Basul Thrust                        | Sericite quartz schist and schistose quartzites in thrust zone, increase in metamorphic effects, development of foliation and mica lineation.                                    | Localised landslides zones along less significant thrust faults, e.g. Jakh slide on the Tehri Chamba road.  |
|           |       |                       | Krol Thrust                         | Fault breccia, crushed Chandpur phyllite, friable carbonaceous matter, lack of metamorphism, typical of other thrusts in foothills   | 100 to 200m wide landslide zone of crushed and massive rock materials persistent, evidence of holocene movements, e.g. Rajpur Toll Barrier slide. |
|           |       |                       | Main Boundary Fault (MBF)           | Fault breccia, crushed and powdered material.  | Narrow, intermittent landslide zones of crushed rock material dip-slip slopes more problematic.   |
|           |       |                       |                                     |  |   |

PROBABLE SHALLOWING AND YOUNGING OF THRUST

INNER LESSER HIMALAYA

LESSER HIMALAYA

POSSIBILITY OF INCREASE IN SLIDE NUMBERS AND FREQUENCY.

POSSIBILITY OF INCREASE IN SLIDE NUMBERS AND FREQUENCY.

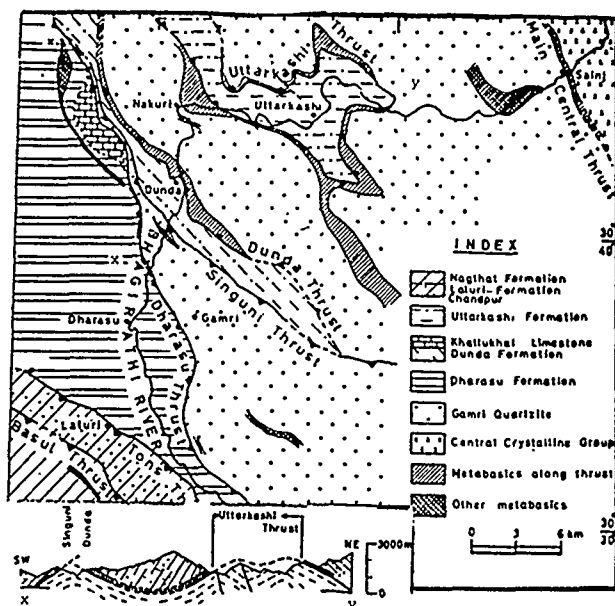


Fig. 2(a) GEOLOGICAL MAP AND CROSS SECTION ALONG X-Y SHOWING DISTRIBUTION OF METABASICS IN UTTARKASHI AREA

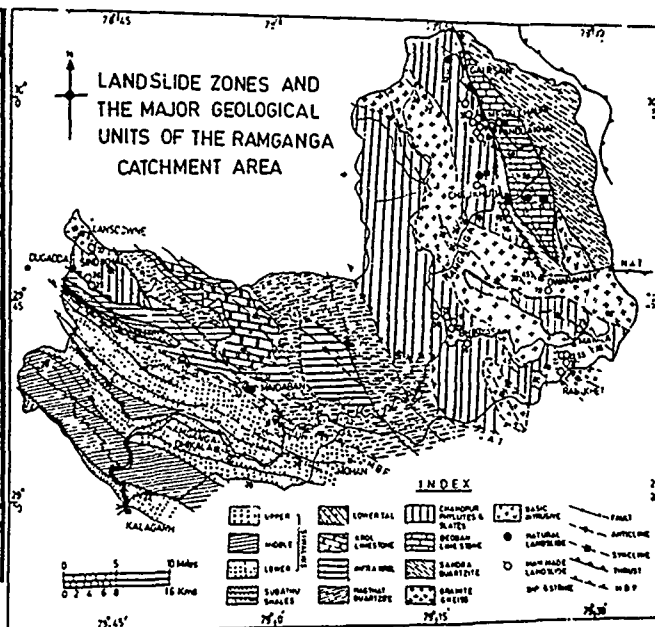


Fig. 2(b) MAN MADE SLIDES IN RAMGANGA BASINS

Central Thrust, Uttarkashi Thrust, Singuni and North and South Almora Thrusts in the Kumaon-Garhwal region and Uttarkashi, Singuni, Tons, Srinagar, Krol thrusts etc. in the Garhwal area. These metabasics are highly prone to weathering and erosion. They give rise to brownish clays - very similar to the 'bole' overlying the Deccan traps. This bole clay is expensive and rich in montmorillonite types of clay minerals. It flows on wetting, sometimes carrying huge blocks of massive competent rocks during rains or even later as at Kaliasaur on the Badrinath road or near Dunda etc. localities on the Tehri - Uttarkashi road. Similar flowing brownish clayey mass has also been observed in a tunnel being excavated (August-Sept. 1987) for the Maneri (Stage II) Hydro power scheme, a little north of Uttarkashi.

Following the postulations of Reed (1964) for the correlations of metabasics and their characters along the Alpine faults in New Zealand, the marked occurrence of brecciated and mylonitised or weathered meta-basics (in Garhwal-Kumaon Himalaya) may also lead in deciphering their depths and the deepening or shallowing of the faults and thrusts. The main characters of certain important thrusts and the associated landslide features are shown in Table II.

On considerations of the morphology, lithology and tectonics of the Garhwal-Kumaon region it may be suggested that the estimation of the depth of slip surfaces and crown cracks should form essential aspects of the investigations of landslides in the Himalayan terrain before any preventive measures for their control are adopted.

#### DISTRIBUTION OF LANDSLIDES

As a sample for discussion, the Ramganga basin is chosen as an example. On a study of more than 500 landslides, it is concluded that in the (four sub-basins) the number of recent slides is comparatively more, where certain developmental activities are in progress. Similar phenomena are also observed along the pilgrim routes of Rishikesh-Badrinath-Rudraprayag-Kedarnath and Rishikesh-Uttarkashi-Gangotri roads etc. Wherever the new alignments occupy the old sections of these roads the sliding activity is almost absent or the slopes are least affected.

#### LANDSLIDE SIZE AND PERCENTAGE OF ACTIVITY

It has been noted that the recent slides are many times more in number and are mainly medium in size. Very large or giant sized slides are almost absent in the region, while the smaller ones are innumerable and not taken into consideration for this discussion. Table III shows the percentage of the mapped slides (522 Nos) in Ramganga Basin both in the field and on the aerial photographs:

In addition to the above, the major slide zones lie in the sparsely vegetated areas followed by in the agricultural strips of lands (irrigated and unirrigated) and maximum in the deforested and barren slopes. The deciduous forests suffer the least while the coniferous zones are appreciably more afflicted with medium slides.



TABLE III. Percentages of Recent and Old Slides (After Joshi 1987)

| Type                                   | Recent   | Old and Recent | Remarks  |
|--|----------|----------------|--|
| Giant size 100,000m <sup>2</sup>       | Absent   | 2.7%           | The giant size slides appear to be historic  |
| Very large 70-100,000m <sup>2</sup>    | 0.4%     | 4.1%           | Comparatively old and large sized slides may be due to repetitive failures till the angle of repose is reached.                    |
| Large 35-70,000m <sup>2</sup>          | 2.6%     | 24.6%          | Majority of these slides occur in low grade metamorphics followed by Infra Krol slates, shales, quartzites, granites and gneisses. |
| Medium-Small 5000-35,000m <sup>2</sup> | 97.0%    | 68.5%          | Some of the smaller and medium slides appear to have been washed out in time.  |
| <b>SHAPE</b>                           |          |                |  |
| Elongated                              | 24-26.5% | 24-26%         |  |
| Equidimensional                        | > 70%    | > 60%          |  |
| Elliptical                             | 3-14%    | 8-15%          |  |

#### LANDSLIDE ACTIVITY AND NEARNESS TO TECTONIC CONTACTS

Of the over 500 landslides, the majority of these occur within short distances of 1-1.5km from the tectonic contacts. Further away the number of failures gradually decrease. From this, it is inferred that the slide zones lie close to the tectonic features (regional thrusts and faults or even to the local faults). A review of the litho-tectonic units (Tables I and II) in the area also support such an inference, from which it is noted that the maximum number of hazardous slides occur in the belt (Fig.1) between the MBF - Srinagar thrust or the NAT and SAT and the MCT coupled with the minor and local structures affected by Neotectonics, e.g. near Dhrasu, Maneri, Ganganani etc. on the Tehri-Gangotri road, while along the Rishikesh-Badrinath road active zones are observed close to Pipalkoti, Joshimath, confluence of Patalganga and Alaknanda, the middle reaches of R. Birehi Ganga and near Mandprayag etc. etc. From the frequent slides and the percentage of landslides, it is also easily inferred that the dynamic forces are still active.

As a result of the landslides the morphology of the region has become rugged and exhibits

an awesome picture of the barren mountain slopes, the hill sides or even in the once forested valleys. The hill sides are steeply scared, hallowed and gullied, devoid of vegetation and serve important clues for the identification and recognition of the major tectonic and thrust zones on the aerial photographs. From Table III (recent and old slides) it is evident that the new and recent slides far outnumber the older ones. Human activities (including agriculture) coupled with deforestation, road and bridge constructions etc. on the fragile hill slopes are equally responsible for the degradation of the unstable slopes mainly due to the disturbances of the angles of repose. To sum up, Table IV gives the relationship of the geo-environments and landslides.

TABLE IV. Geo-Environmental Factors commonly Associated with Landslide Zones (Based on the study of the four selected sub-basins of Ramganga - after Joshi, 1987)

| Geo-Environmental Factor | Landslides more Common   | Landslides less common  |
|--------------------------|--|---|
| Rock types               | Massive quartzites, slates, shale, Phyllite and Schists              | Limestone, dolomite, gneisses.                                  |
| Land use type            | Barren or sparsely vegetated areas.                                  | Forests, agricultural lands                                     |
| Azimuth directions       | North-east, South-West and West facing slopes.                       | North, North-West South, South-East and East facing slopes      |
| Proximity to shear zones | Areas lying within the range of 3kms distance from the shear contact | Areas lying away by 3kms distance from the shear contacts.      |
| Relief of the area       | Areas of higher relief and steep slopes                              | Areas of low relief and gentle slopes                           |
| Ruggedness of the area   | Areas of the lower ruggedness and less developed drainage network    | Areas of higher ruggedness and well developed drainage network. |

From the above, it is considered that the Nagthat quartzites, Infra Krol slates, shales and siltstones and the low grade metamorphics of the region are relatively moderate to landslide activity, while the other formations are comparatively less prone. Whereas when these lie close or are affected by a tectonic feature they are highly susceptible to slides or rock falls. In the inner higher parts of Himalaya particularly close to the MCT the massive jointed rocks or the crystallines and gneisses with steep slopes are more prone to the rock falls. These are thus highly hazardous for road and bridge works or for any other developmental activities.

## HAZARDS AND ECONOMIC LOSSES

The economic implications of landslides in the region are manifold. The important and direct effects on the mankind are: (i) loss of life and property, (ii) economic losses due to (a) loss of forest wealth, (b) broken roads, canals, bridges and sometimes even the habitations, (c) damage to other means of transportation and transmission lines etc. (d) loss of fisheries and other sites of sports etc. Of the indirect, the most important effects are the higher rates of erosion and devastation of forests on the hill sides and slopes, falls of shooting rocks, sedimentation and silting of lakes and reservoirs and last but not the least, formation of crevasses and slumps on ground surfaces.

As a result, the pace of development in the region is comparatively slow. As such, the human activities like the growth in agriculture, exploitation of minerals and other natural resources, construction activities of roads, defence establishments, tourists centres and spas and sports complexes etc. are very limited and few. From what has been discussed in these pages the landslides, the nature of rocks and tectonism, it is evident that the Himalayan mountains in this region are not so strong. There is a constant dynamic change going on intertwined with the climate, geology, hydrology and the forest cover. In this change the part of human activity could also be included as another factor, since almost sixty to seventy percent slides are thought to have been reactivated due to improper road alignments and uncontrolled excavations solely dictated by the local political and 'economic' factors without caring of the geotectonic considerations - no matter what happened in future to the 'developmental activity'. On consideration of the geo-environmental factors in Table IV and losses during the recent years and the magnitude of the problems involved, the hazards and losses could easily be estimated from the few examples of immediate past events as noted below:

### Examples of losses

#### Loss of Life and Property

- (a) Belakuchi disaster in 1970.
- (b) Ganganani calamity and falls of 1978
- (c) Gohna slides of 1893 and 1894.

#### Economic Losses:

- (a) Civil works and constructions

Belakuchi, Kaliasaur, Ganganani,  
Pipalkoti, Joshimath, Devprayag,  
Nainital, Mussoorie, Kalagad (Rajpur)  
and on Pithoragarh-Dharchula road etc.

- (b) Canals: Ganga canal in 1970, Belakuchi- and Gohna slide on R. Birehiganga in 1893 and 1894 later siltation of the reservoir and its breach in 1970 also

contributed in the siltation of the century old canal upto Bahadarabad near Roorkee.

Total damage to the barrage at Tanakpur in 1880.

- (c) Roads and Bridges: Belakuchi in 1970 and R. Birehi ganga slides and floods breached off 3km long stretch of road and bypassed a girder bridge. Ganganani slips and slides caused similar havoc in 1978, left a bridge hanging washed off the road for more than 4km length.
- (d) Village: Belakuchi shops on the road side.
- (e) Other properties: 23 vehicles at Belakuchi in 1970; 8 vehicles at Ganganani in 1978.
- (f) Life: 17 persons in Belakuchi and at least 8 persons in Ganganani.
- (g) Electric lines etc. near Belakuchi.

Fishery etc. Obliteration of Gohna Tal in 1970.

Higher Erosion and Deforestation: Patalganga floods in 1970. Slides on the banks of Birehi-Ganga in 1893, 1894, 1970, 1971 and in 1974. Slides at Ganganani in 1978.

Formation of lakes: Gohna Tal in 1893, 1894, Blockade of Rishiganga near Reni in 1968.

Sedimentation and Silting of lakes and reservoir: Gohna Tal-sedimentation during 1893-1970 made the lake totally extinct. Ramganga reservoir getting silted up at the rate of 0.158 Hect m per sq.km per mts. Siltation of Tarag Tal. Bhogwali Pokhar in Ramganga basin etc.

Cracks Crevices and Falls: Kaliasaur slides and falls almost every year since 1964 or may be earlier, Mussoorie, Rajpur, Mahalachuri etc. etc.

## CONCLUSIONS

1. The Garhwal Group of Rocks are more susceptible to landsliding and the major slides zones are mainly confined to a 30-50km wide belt between the major thrust zones, i.e. MCT, NAT/SAT and MBF.
2. The Himalaya are typeified by a complex land morphology, controlled to a large extent by the geologic set-up, structural deformations, rock discontinuities and lineaments.
3. Mass wasting and sliding mainly occurs during the monsoons or due to cloud bursts. Rain water on percolation along the weak zones in hard rocks ensure the slides through an increase of the hydrostatic pressures.
4. An increase in gravity due to massive loadings and decrease in shearing strength acting together or even independently, generally cause landsliding. The phenomena is enhanced by the associated weathered

meta-basics or its weathered product 'bole' clay.

5. In order to visualise the magnitude, the calamitic effects and hazards caused by a particular landslide, attempt must be made to determine the depth of the slip circle and the amount and passage of percolation.
6. While treating a landslide zone, the original angle of repose of the rock or debris mass should be maintained as far as possible.
7. Large scale toe erosion is responsible for feeding the large number of rivers with huge amounts of sediment loads, and is a major cause of siltation in the river channels/reservoirs and even on the flood plains.
8. The dynamic activity is still continuing as indicated by recent disturbances affecting the collovium and terrace deposits along the river channels.

#### ACKNOWLEDGEMENT

The author is grateful to Drs A.K.Jain, H.Sinvhal, R.P.Gupta of the University of Roorkee and G.S.Mehrotra of CBRI, Roorkee and B.C.Joshi, Senior Research Fellow, Dept. of Earth Sciences, University of Roorkee for their critical discussions and suggestions. The author has freely made use of the thesis and dissertations of his past students and published or unpublished works and his personal unpublished materials, data and reports on the topic collected during the past more than a quarter of a century. He is much obliged to Dr.S.Prakash for inviting him to write this article. Thanks are also due to Mr.P.N.Zutshi, a close friend for going through the manuscript and Shri K.V.Gangadharan for assistance in the preparation of the paper.

#### REFERENCES

- Auden, J.B. (1934), "Structure of the Himalaya in Garhwal", Recd. Geol. Surve. Ind., Vol.71, pp.407-433.
- Gansser, A (1964), "Geology of the Himalayas", Interscience Publishers, London.
- Gaur, G.C.S. (1974) - Ph.D. Thesis (unpublished), "Geology and Magnesite Deposits of Chamoli Garhwal Himalayas", Dept. of Geology and Geophysics, University of Roorkee, Roorkee, U.P.
- Jain, A.K. (1972) - "Overthrusting and Emplacement of basic rocks in Lesser Himalaya, Garhwal", U.P. Jour. Geol. Soc. Ind., Vol.13, No.3.
- Jain, A.K. (1987) "Kinematics of transverse lineaments, regional tectonics and holocene stress field in the Garhwal Himalaya", Jour. Geol. Soc. Ind., Vol.30, No.3.
- Joshi, B.C. (1987) - Ph.D. Thesis (unpublished), "Geo-environmental studies in parts of Ramganga catchment, Kumaon Himalaya", Dept. of Earth

Sciences, University of Roorkee, Roorkee, U.P., India.

Joshi, B.C., Gupta, R.P. and Mithal, R.S. (1987), "Landslide studies and hazard zoning in Ramganga catchment, Kumaon Himalaya" Com. to Indian Journal of Earth Sciences.

Krishnaswami, V.S. and Jain, M.S. (1975) "A review of some of the major landslides in northern and north-eastern Himalaya", Seminar on Landslides and Toe Erosion Problems, Him. Region, ISEG, Sikkim (India).

Mithal, R.S. (1968), "The physiographical and structural evolution of the Himalaya", Chapter III in Mountains and Rivers of India, Ed. B.C. Law, 21st Int. Geog. Cong., India, 1968.

Mithal, R.S. (1984), "The physical impact of the Rihand and Ramganga Dam Project on the drainage basin and their catchment areas", Emeritus Scientist Scheme - Report completed during 1.1.1983 to 31.12.1985. Extra Mural Research Division, C.S.I.R., New Delhi-12.

Mithal, R.S., Chandsarkar, R.A. and Gaur, G.C.S. (1972) - "Geomorphic Studies of the R.Birehi Ganga, Garhwal Himalaya, Him. Geology, Vol.2

Pandey, I.C. (1949), "A note of the epidiorite sills of Ramgarh area, Dist. Nainital, Q.J.M.M.S., India, Vol.21,

Reed, J.J. (1964), "Mylonites cataclastics and associated rocks along the Alpine faults, South Island, New Zealand, Jour. Geol. and Geophy., Vol.7, pp.645-684.

Valdiya, K.S. (1980), "The two Intra crustal boundary thrusts of the Himalaya", Tectonophysics, Vol.66

Valdiya, K.S. (1980), "Geology of Kumaon Lesser Himalaya", Wadia Instt. of Himalayan Geology, Dehradun, India.

Valdiya, K.S. (1985), "Accelerated erosion and landslides prone zones in the Central Himalayan region", Environmental Regeneration in Himalaya, Central Himalayan Environmental Assoc., Nainital.

Valdiya, K.S. (1986), "Neotectonic activities in the Himalayan belt, Int. Symp. on Neotectonics in South Asia, Survey of India, Dehradun (India)

Varnes, D.J. (1978), "Slope movement types and processes in landslides, analysis and control", Spl. Report, Ed. Schuster, R.L. and Krizek, R.J., Transportation Resch. Board, Nat. Acad. Sc., Washington, D.C., U.S.A.

Wadia, D.N. and West, W.D. (1964), "Structure of the Himalaya", Int. Geol. Cong., 22nd Sess, India. pp. 1-30.

## Geotechnical Characterization of Subsoil Deposits at Cairo

**Mohamed A. El-Sohby**

Professor, Civil Engineering Department, University of Al-Azhar,  
Madinet Nasr, Cairo, Egypt

**S. Ossama Mazen**

Senior Researcher, General Organization for Housing, Building and  
Planning Research, Dokki, Cairo, Egypt

**SYNOPSIS:** As a result of considering the historical aspects in Cairo subsoil at different stages of its development, soil deposits in the alluvial plain in Cairo area could be identified and classified on their origin into limited number of major types. Their distribution could be produced on maps on which classes of engineering significance are recognized. The boundaries between map units have been drawn separating areas of equal origin and characteristics. Verification of soil profile from field investigation indicated complete agreement with the previous characterization based on theoretical considerations.

### INTRODUCTION

Cairo is one of the few great symbolic cities with their extended history and current vitality. In all probabilities, the earliest development of civilization had took place near to this strategic site and, as a capital of Egypt, Memphis of the Pharaoh, in the vicinity of Cairo antedates almost every other human conglomerate larger than a village. The parade of historical monuments preserved in and around Cairo span a period of more than five thousand years and express the entire civilization of the country. There is no one epoch of history which had not left within it numerous and precious traces.

The wonder of Egypt is not only in its history but also in its site. At the meeting point of the three big continents of the ancient world, Europe, Asia and Africa lies Egypt. Here also two waterways meet, important in history and commerce of the world: The Mediterranean and the Red Sea. The former brings Egypt in direct contact with the West, while the latter joins it with the Far East. And just as Egypt stands astride East and West, so, Cairo, its capital stands astride Egypt linking, as well as dominating, the two subregions - Upper Egypt to its South and Lower Egypt to its North. Its dominance is challenged only by The Nile, the river that bisects both Cairo and the nation but paradoxically unifies as it divides.

Its location is 30° 4' North latitude and 31° 17' East longitude 20 kilometers to the South of the point where the Nile divides into the Rosetta and Damietta branches. To the East, Cairo reaches the Mokattam Hills, announcing the Eastern Desert, in the West it crosses the Nile into Giza to the Western Desert which eventually extends to the Libyan Desert.

Cairo today, home for more than 10 million inhabitants, presents, to the geotechnical engineer, primary problems and enormous challenge. It is a city with a pressing problem of

land use inefficiencies. Most good building sites have already been exploited and more use will have to be made of sites with less favorable conditions. Many structures will have to go underground and installation of services beneath existing building will necessitate tunneling.

As a result, a great volume of routine investigation has been carried out and still going on by several public bodies, private companies and consultants for different important projects such as Cairo Underground Metro, and Greater Cairo Sewerage Plan.

Because boring records and reports for each site or project are generally very detailed and no or a little exchange of information has been experienced, soil deposits in Cairo give the impression that they are of extreme complexity and countless variety. Therefore duplication of effort is likely to be extensive.

The primary aim of the present work is to improve that situation by making clear the ground formation in Cairo area. This would develop the knowledge of subsoil conditions, help in recognizing potential soil problems; and guide in good planning of site investigation work. Thus the time and effort donated to field work and laboratory testing can be greatly reduced.

The implicit goal is to extract a form or a pattern from what appears to be capricious disorder. However, if order is to be found, more than the traditional methods must be employed to uncover the hidden framework.

Geology and history, envisaged to be of relevance of the present work, were used to separate the accidental from the essential and to trace the chains that binds present with past and links part with whole. This to uncover the orderly patterns and sequences in Cairo's growth and development that yielded the present soil formations and have given rise to its particular characteristics.

## GEOGRAPHY

Egypt may be divided into four geographical regions: The Eastern Desert, The Western Desert, The Nile River and Delta, and the Sinai Desert. Cairo covers portions of the first three regions (see Fig. 1).

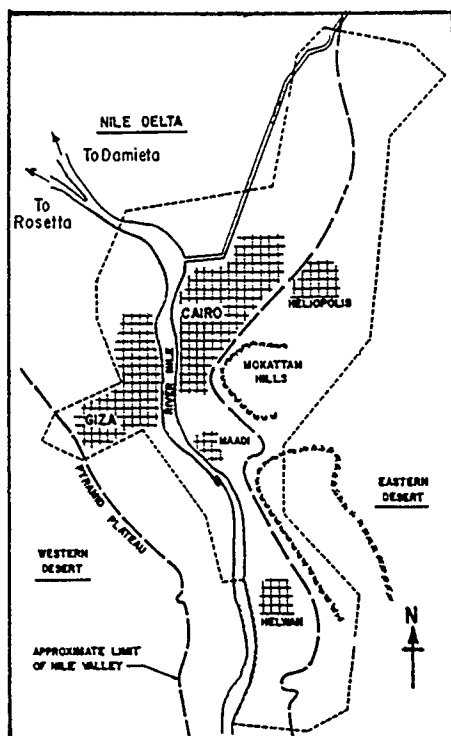


Fig. 1 Greater Cairo Area & Topographic Features

The Nile is a perennial stream which flows South to North and divides Egypt into the Eastern and Western Deserts. The relatively flat alluvial plain and the gently sloping terraces to the higher desert areas form the Nile Valley. At the site of Cairo the Nile Valley is 10 to 15 kilometers wide.

Through Cairo area, the Nile passes by the high Mukattam Plateau of the Eastern Desert. On the Western side, beyond the valley, the cliffs are lower and form the Pyramids Plateau. Just downstream from Cairo, the valley widens and forms a large delta tributary to the Mediterranean sea. Two branches of the Nile meander through the delta area; the western branch enters the Mediterranean Sea at Rosetta and the eastern branch at Damietta.

The general slope of the Nile flood plain is to the North. Elevations along the river flood plain range, from 22 m at the South end of Cairo area to 13 m at the Northern end. The highest elevation of the Mukattam Hills on the Eastern side of the river is 213 m at point Southeast of the Citadel. To the North, but Southeasterly from Heliopolis, elevations in the 200 to 218 m range are found.

## GEOLOGICAL ASPECTS

The geological formations at the site of Cairo have the features of hill-slopes which appear as wall bordering the valley and filled with deposits. These deposits which comprise the valley fill within the area of the bordering Eocene limestone are fluvial sediments ranging from Pliocene to Recent.

The geology of Cairo has been studied intensively by many researchers, as far as the older formations are concerned (Beadnell, 1902; Barron, 1907; Cuvillier, 1924; Hume, 1925; Lawson, 1927; Shukri, 1953; Attia, 1954; Said and Youssef, 1964; Youssef, 1968; Abu Al-Izz, 1971; Said, 1981). However, the fluvial sediments of the Nile Valley have been treated lightly. The most thorough treatment of the latter deposits was done by El-Sohby and Mazen (1985). Their study depended on information received from boreholes, detailed records, wells and excavations that penetrate the formations.

According to El-Sohby and Mazen (1985), the fluvial sediments comprises of alluvium and diluvium. Alluvium are soil deposits laid down in recent times by flood waters while diluvium are deltaic soil deposits formed at earlier stages of river developments.

## HISTORICAL ASPECTS

Because Cairo is a very old city, historical elements dictated the city pattern of growth and they are the key to the pattern of formation of deposits in alluvial plain. Therefore, in the following, the telescopic lense of history is used in studying the Cairo subsoil at different stages of its development. Three main elements are considered in the study; they are: 1) the geographic features of the site; 2) the River Nile and its changes; 3) Man's occupation of the area. Although the history of Cairo spans more than 7000 years, the more recent history with impact upon subsoil and relevance in explaining soil conditions can be traced from the founding AD 641 of Al-Fustat which lies towards the Southern boundary of the existing city.

The references consulted for historical information were numerous. However, we relied heavily on three notable original sources. They are: 1) the Khittat of Al-Maqrizi; 2) Description de l'Egypte of the French Expedition; and 3) Al-Khittat Al-Tawfiqiah Al-Gadida by Mubarak.

### Geographic Features in the Seventh Century

At the site of Cairo, the boundary of the Nile flood plain is fixed by two sudden escarpments of the Mukattam Hills on the East and the Pyramids plateau on the West. The ridge which divides valley from desert on the Eastern side is nearest to the river at the site of Qasr Al-Shama before it pivots Northeast until it disappears when the valley opens at the site of Al-Fustat; then it becoming increasingly broader to the North. Furthermore, in the seventh century the Eastern border was farther to the East than it does now. Therefore, the flood plain area on the East bank was much narrower.

### The River Nile and its Changes

From verbal description of early historians (Al-

Magrizi, Al-Muqddassi, Ali Ibn Moussa, Al-Qalaqshandi, Al-Baladhury, Al-Baghdadi; Al-Gabarti) and from previous research work in history (Casanova, 1913; Creswell, 1918; Haswell, 1922; Tousseun, 1923, 1925, 1926; Clerget, 1934; Ahmed, 1939; Abd Al-Tawwab, 1963; Volkoff, 1970; Zaki, 1979; Mubarak, 1980), the Nile border at different stages of Cairo development could be traced. Successive recessions and transgressions of the Nile border are shown in Figs. (2-6).

The figures show that most of contemporary Cairo is built on land which lay either permanently or periodically submerged under the river in the seventh century. In later centuries the land that came into existence due to gradual recession of the Nile was the result of: natural silting, diversion of flood waters through a system of canals and lakes; and complex dam storage upstream.

#### Man's Occupation of the Area

Man's occupation of the area has given rise to considerable deposits of human debris to overlie the alluvial Nile plain.

Firstly, the destruction of Al-Qataie (Capital of Tulunids) in AD 905 and the burning of Al-Fustat in AD 1163 caused a big area of land to be abandoned. This included Al-Qataie, and a big portion of Al-Askar (Capital of Abbassids). Since that date and down to the present day, this area has been the site of rubbish. And with progressive accumulation of filling on the ruin mounds it became one connected area of rubbish heap that cover the entire terrain where Al-Fustat, Al-Askar, and Al-Qataie once stood.

Secondly, during the time of Mohamed Ali (1805-1848), changes in the city were directed toward cleaning up the abuses which had rendered the city less habitable. Among the changes introduced were the leveling of the rubbish mounds on the Western edge of the city and filling in the lakes, ponds depressions and swamps.

#### ROLE OF HISTORICAL ASPECTS IN CHARACTERISATION OF SOIL DEPOSITS IN ALLUVIAL PLAIN

As a result of considering the previously mentioned historical aspects in subsoil development, soil deposits in alluvial plain could be classified on their origin and mode of formation into a limited number of major types. Their distribution could be produced on a map on which classes of engineering significance are recognized. The boundaries between map units have been drawn separating areas of equal origin and characteristics (Fig. 7). They are: 1) Terrace Alluvium; 2) Flood Silting; 3) Channel Deposition; 4) Island Formation; and 5) Fill or Made Ground.

##### 1) Terrace Alluvium

This unit represent the older flood deposits or the last Nile terrace. It exists on both sides of the Nile and is bounded on one side by the geological boundaries and on the other side by the Nile border in the seventh century (AD 641).

After transposition of the Nile course and shift of river bed in historical times, flood waters began to fill the land left by the receding Nile allowing the coarser grains to settle first. Therefore a layer of fine sand overlain by stiff silty clay (old deposits) is conceivable.

##### 2) Flood Silting

It is the land that came into existence after the seventh century due to gradual recession of the Nile and successive flooding and sedimentation. This unit occurs only on the East bank of the Nile. It is bounded on the East by the Nile border in AD 641 and on the West by the Nile border at the time of the French Expedition (AD 1800).

In this unit, a sequence of layers similar to the previous unit is conceivable due to the similarity in sedimentation mechanism. However, this type is relatively modern Nile deposits when compared to the previous type. Therefore upper clay layer, had not been consolidated as the previous type, it is expected to be soft to medium.

##### 3) Channel Deposition

It is the land formed on both sides of the Nile banks in the nineteenth century after forcing the main flow of the river to its present course. This was done by filling up the Western channel in the area between the Nile border in AD 1800 and the present one; and strengthening the Eastern level of the Nile.

The sites of this unit is near the river banks and the main deposits expected are silts and fine sands overlying the coarse sand and gravel which had previously formed the bed of the river channel.

##### 4) Island Formation

This unit comprises all the lands that came into existence in the form of islands. They are Geziret Al-Rowdah (Al-Rowdah); Geziret Al-Fil (Shoubra); Geziret Bulaq (Boulaq); and Geziret Arwy (Zamalek).

Due to sedimentation mechanism encountered in island formation, a considerable layer of silt is expected at a depth near to ground surface followed by fine sand overlying the coarse sand and gravel. After the island had been formed and the velocity of water flow became slower, the clay particle would be allowed to settle particularly in the middle and in the upstream. Therefore, a top clay layer as well as clayey intercalations in the upstream of the island are expected to occur.

##### Fill or Made Ground

This unit varies from place to place. It is the heritage of urban development in Cairo area throughout its history. On the East bank of the Nile, the occurrence of fill deposits and their thicknesses must be remarkably significant when compared with the West bank. They are the product of old channels (Khalig), lakes (Birkah) and ruin mounds of early settlements. It is worth-noting that some areas in Cairo are still known by their early land marks such as: Al-Azbakiya; Birket El-Fil, and Birket El-Ratli; They were previously lakes.

The old channels and lakes were filled in the nineteenth century with near by mounds. The site of old channels (e.g. El-Khalig El-Masri),

[illegible]

This topographic map depicts the Tula region in Mexico. The Tula River flows from the north towards the south, passing through the town of Tula. To the east of the river is the Tlaxcala region, featuring the Tlaximilco area. The map shows various settlements, including Tula, Tlaxcala, and Tlaximilco. The terrain is characterized by numerous hills and mountains, with elevations ranging from 1,000 to 2,000 meters. A scale bar indicates a distance of 5 kilometers. A north arrow is located in the upper right corner of the map.

[illegible][illegible]

**LEGEND:-**

- Terrace Alluvium
- Flood Silting
- Channel Deposition
- Island Formation
- FBI or Made Ground
- Pleistocene
- Pliocene
- Oligocene
- Upper Miocene
- Middle Eocene

0 1 2 Km

820 815 810

835 840 845

810 815 820

835 840 845

GEOLOGICAL MAP HISTORICAL



must therefore, form at present on elongate basin of fill underlying Port Said street with a depth of about 10 m as that of El-Khalig. Similarly the depth of fill at the site of old lakes must range between 5 and 10 ms.

The filling on ruin mounds of early settlements had began to form just South the Mosque of Ibn Tulun. According to chronology and description of historical events, the ruin segment must had got a triangular slope with the mosque of Ibn Tulun as apex and one side striking South parallel to El-Khalifah cemetery and the other side striking South-West parallel to Qasr-Al-Shama and Mosque of Amr.

Another segment of fill must exist extending parallel to Muqattam edge to the North-East where it had served for a long time as a rubbish mound.

## CONCLUSION

- 1- As a result of considering the historical aspects in Cairo subsoil at different stages of its development, soil deposits in alluvial plain could be identified and classified on their origin and mode of formation into five major types. They are 1) Terrace Alluvium; 2) Flood Silting; 3) Channel Deposition; 4) Island Formation; and 5) Fill or Made Ground. their distribution could be produced on maps on which classes of engineering significance are recognized. The boundaries between map units were drawn separating areas of equal origin and characteristics.
- 2- Borings and subsoil sections passing through different types of alluvial deposits have been in complete agreement with the characterization based on the consideration of historical aspects.
- 3- An analysis of the experience of the present work for the city of Cairo can be taken as a model for study of other old cities whose growth and development were affected by historical aspects.

## REFERENCES

- Abu Al-Izz, M.S. (1971) "Landforms of Egypt", The American Univ. in Cairo, pp. 281.
- Abd El-Tawab, Abd El-Rahman (1963) "Our Waterway Constructions Throughout History", Dar El-Qalam, Cairo.
- Ahmed, Mahmoud (1939) "Concise Guide to the Principal Arabic Monuments in Cairo" Government Press, Cairo.
- Al-Baladhury, Ahmed Ibn Yahya (1966) "The Origin of Islamic State-Kitab Futuh Al-Buldan", Philip Hitti Trans., Khayyats Publ., Beirut.
- Al-Gabarti, Abd Al-Rahman (1875) Aga'eb Al-Athar fi Al-Taragim Wa Al-Akhbar", Bulaq Press, 4 Vols.
- Al-Maqrizi, Taqi El-Din Ahmed Ibn Ali (1911-1927), "Al-Mawa'iz wa Al-I'tibar fi Zikr Al-Khitat wa Al-Athar", 4 Vols, edited by M. Gaston Wiet (in Arabic), Memoire de l'Institut Francaise D'Archeol. Orientale du Caire, Cairo.
- Al-Muqaddassi, Mohammad Ibn Ahmed (1906) "Ahsan Al-Taqasim fi Ma'rifat Al-Aqalim" (The Best Divisions in the Knowledge of the Countries), edited by M.J. De Goeje (in Arabic), Brill Publ., Leiden, 1966, pp. 193-215.
- Al-Qalaqshandi, Abu Al-Abbas Ahmed (1913) "Subh Al-Aasha" Dar Al-Kutub Al-Khediwiyyah Government Press, 9 Vols., Cairo.
- Al-Baghdadi (1884) "Extrait de l'auto biographie d'Abd el Latif", trans. Baron Mac Guckin de Slane, Academie des Inscriptions et Belles Lettres, Historiens Orientaux, Vol. III, Paris.
- Atia, M.I. (1954) "Deposits in the Nile Valley and the Delta", Mines and Quarries Dept. Geol. Surv. Egypt, Cairo, pp. 356.
- Barron, T. (1907) "The Topography and Geology of the District between Cairo and Suez", Egypt Surv. DEpt., Cairo, pp. 133.
- Casanova, Paul (1913) "Essai de reconstitution topographique de la ville d'al Fostat ou Misr". L'Imprimerie de l'Institut Francais d'Archeologie Orientale, Cairo.
- Clerget, Marcel (1934) "Le Caire; Etude de geographic urbaine et d'histoire economique", 2 Vols. Imprimerie E & R. Shindler, Cairo.
- Creswell, K.A.C. (1919) "Brief Chronology of the Muslim Monuments of Egypt" Bull. de l'Institut Francais d'Archeologic Orientale, XVI, Cairo.
- Cuvilier, J. (1924) "Contribution a l'etude geologique du Muqattam", Bull. Inst. Egypt, Vol. 6 (New Ser.), pp. 95-102.
- Description de l'Egypte (1809-1813) "Text and Plates", 20 Vols, Imprimerie Imperial, Paris.
- El-Sohby, M.A. and Hazen, S.O. (1985) "Geological Aspects in Cairo Subsoil Development", Proc., XI International Conference on Soil Mechanics and Foundation Engineering, Vol. 4, San Francisco, pp 2401-2405.
- Haswell, C.I.R. (1922) "Cairo Origin and Development. Some Notes on the Influence of the River Nile and its Changes", Bulletin de la Societe Royale de Geographie d'Egypte, Vol. XI, Nos. 3 & 4, pp. 171-176.
- Hume, W.F. (1925) "Geology of Egypt", Geological Survey Department, Cairo, Vol. 1, pp. 408.
- Lawson, A.C. (1927) "The Valley of the Nile". Univ. Calif. Chronicles, Vol. 29, Berkeley, pp. 235-259.

## Geo-Engineering Problems in the Spillway Foundations and Their Treatment at Guhai Reservoir Project in Gujarat, India

**D.M. Pancholi**

Superintending Engineer (Geology), Central Designs Organisation,  
Irrigation Department, Gandhinagar, Gujarat, India

**K.E. Modhwadia**

Superintending Engineer, Central Designs Organisation, Irrigation  
Department, Gandhinagar, Gujarat, India

**P.H. Vaidya**

Geologist (Senior), Central Designs Organisation, Irrigation  
Department, Gandhinagar, Gujarat, India

**SYNOPSIS:** During the initial stage of construction of a 23 m high composite dam across the Guhai river, the downstream dipping sedimentary rock sequence of conglomerate, sandstone and shale resting unconformably over quartzite and schist was encountered as a surprise during the excavation of the foundation. Besides, an 8 to 8.5 m wide major fault zone along with three minor faults running across the dam axis were also noticed. Extensive subsurface investigations to study the nature and characteristics of sedimentary rocks, fault zones, etc. met with in the foundations were undertaken concurrently with the construction activity. As a result, the construction schedule was greatly affected.

The paper discusses the detailed evaluation of the geological flaws by thorough investigation and foundation treatment evolved to safeguard the structure.

### INTRODUCTION

Guhai Reservoir Project located about 90 km NE of Ahmedabad city in Gujarat State of India is under construction since 1980 and on completion it would create irrigation facilities to 7111 hectares of land of Sabarkantha district.

The project includes the construction of a composite dam across the Guhai river. The construction of a 23 m high zoned earth dam on the left bank is in progress and the river section is kept open till the construction of a 34.57 m high spillway and N.O.F. structures located on the right side of the river, is over. When completed, the dam will impound 62.34 Mm<sup>3</sup> of water at F.R.L. 173 m. Based on the hydrological study, an 88.72 m long spillway has been provided to negotiate the designed discharge of 4384.92 m<sup>3</sup>/s through six radial gates of 6.09 x 9.14 m size.

Geological setting at the dam site is intricate and had played a pivotal role in effecting modifications in design and layout of the project. At the project site, quartzite interbedded with schist belonging to Delhi System is seen intruded by quartz porphyry of post Delhi age. Except the left and right abutment rocky hills, the entire area of the main dam including the river channel is covered with alluvium and sand.

It was only during the construction stage that a sedimentary rock sequence (Cretaceous ?) with a low downstream dip resting unconformably over the Delhi formation and affected by an 8 to 8.5 m wide steep angle fault zone running across the dam axis, was noticed in the foundation. The unconformity is marked by the presence of conglomerate predominantly consisting of pebbles of quartzite and occasional quartz. Unusual geological setting could not be detected during the investigation stage due to the absence of exposures of sedimentary rocks around the dam site and inadequate subsurface exploratory data. Detailed investigations divulged the occurrence of conglomerate, sandstone and shale beds with a low downstream dip associated with clay filled bedding joints and fault zones. Geological setting posed the integrated problems of sliding, settlement as well as seepage and led to the modification in design of masonry dam and proper treatment to weak features encountered.

### INVESTIGATIONS

The project was conceived as back as 1954. The details of the core drilling done are given in table 1.

TABLE 1. Details of Core Drilling

| Period  | No. of holes Drilled | Depth Drilled (m) |
|---------|----------------------|-------------------|
| 1958    | 2                    | 21.59             |
| 1971-72 | 8                    | 149.34            |
| 1980-81 | 6                    | 143.47            |
| 1981-82 | 23                   | 554.20            |
| 1982-83 | 19                   | 727.23            |
| 1983-84 | 4                    | 71.20             |
|         | 62                   | 1667.03           |

### GEOLOGY OF MASONRY DAM FOUNDATIONS

The spillway with a non overflow section on the right side has been located hugging the right bank. At the dam site, igneous, metamorphic and sedimentary rocks are met with. The rocks encountered in the masonry dam foundations are quartzite and schist of Delhi System intruded by quartz porphyry of post Delhi age. During the initial stage of construction, when the foundations of the spillway were being excavated an unanticipated sedimentary rock sequence was observed which lies unconformably over quartzites and schists. The unconformity is marked by the presence of conglomerate (Fig. 1). The description of rock types is given hereunder.

#### Quartzite and Schist

Quartzite and schist occur as alternate bands. Quartzite bands vary in thickness from 1 to 2 m whereas schist occurs as thin bands having thickness of 5 to 30 cm. These bands strike in N20°-40°E - S20°-40°W direction with downstream dips varying from 45° to 50° towards S50°-70°E direction.

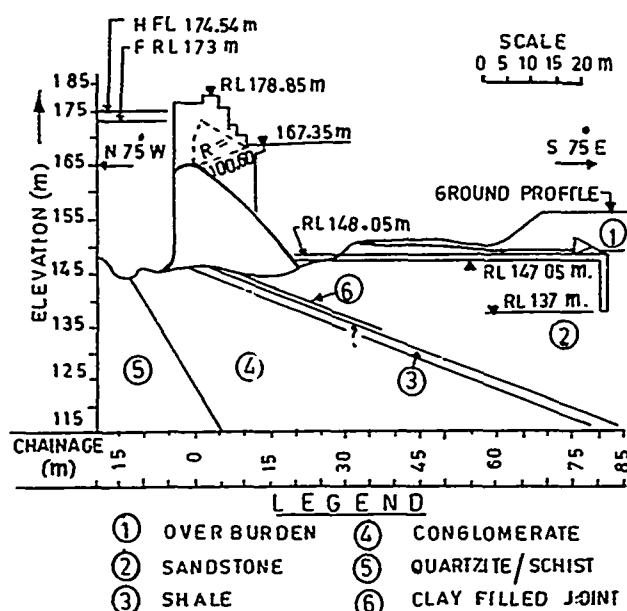


FIG.1: GEOLOGICAL CROSS SECTION

Quartzite is fresh, hard and resistant while schist is comparatively soft. These beds are intruded by quartz porphyry which is not met with in the masonry dam foundations.

#### Conglomerate

Conglomerate marks the unconformity between metamorphics below and sedimentaries above. Conglomerate seems to have been deposited over the pre-eroded surface of quartzite and schist. It mainly consists of rounded pebbles and gravels of quartzite and at times of quartz having 25 to 40 cm size. The matrix is siliceous. Thin ferruginous coating is seen along the boundaries of pebbles and gravels. The matrix of conglomerate is somewhat weakened in the close proximity of the faults. Pebbles are sharply cut along the sets of joints developed sympathetic to the faults. At the foundation level and even below it, conglomerate is fresh and hard. The thickness of conglomerate amplifies towards the downstream being more than 45 m at 70 m downstream as compared to 15 m at the dam axis.

#### Sandstone

Sandstone is fresh and sparsely jointed. However, a few 0.5 to 1.5 cm thick low downstream dipping clay filled bedding joints are observed within sandstone. The interface of sandstone and conglomerate is also marked by the presence of clay at a few spots. Sandstone associated with thin shale beds and lenticular beds of conglomerate is seen deposited over conglomerate. Dip of these beds varies from 25° to 30° towards the downstream.

#### GEO-ENGINEERING PROBLEMS

During the course of investigation and foundation excavation, certain geo-engineering problems cropped up which stalled the progress of work for a considerable period.

Since the sedimentary rock sequence could be seen only in the river bed during excavation of the foundations, a thorough subsurface investigation became imperative

to assess its nature, characteristics, extent, etc. more so because of conglomerate as it is normally known for its pervious and incompetent nature. Extensive subsurface exploration was, therefore, undertaken concurrently with the construction activities (Fig. 2). The exploration revealed the following.

- (i) Thin clay beds associated with sandstone and at the interface of conglomerate and sandstone having low downstream dip of 25°.
- (ii) Occurrence of conglomerate which was apprehended for its weak and pervious nature.
- (iii) One major and three minor faults running across the dam axis with steep to vertical dips (Table 2).
- (iv) Discovery of palaeo river channel occupied by 30 to 33 m thick sand between Ch. 630 and 730 m (Fig. 3).

TABLE 2. Details of Faults

| Location (m)                          | Attitude    |                                | Width at foundation level (m) | Description of the material   |
|---------------------------------------|-------------|--------------------------------|-------------------------------|---|
|                                       | Strike      | Dip                            |                               |   |
| Ch. 835 (Monolith 2)                  | N75°W-S75°E | 80° on either side to vertical | 0.1 to 0.5                    | Clay with sheared rock pieces   |
| Ch. 861 (Monoliths 3 and 4)           | N65°W-S65°E | 75° due S25°W                  | 0.2 to 1.0                    | Predominantly clay with rock pieces   |
| Ch. 871.5 to 880 (Monolith 5)         | N75°W-S75°E | 80° due N15°E                  | 8.0 to 8.5                    | 4.0 m thick yellow clay and 2.4 to 4.4 m thick zone of sheared conglomerate |
| Ch. 921 to 922 (Monolith 8-Right NOF) | E-W         | 80° due North                  | 0.3 to 1.5                    | Gougy material with crushed rock pieces                                     |

#### INFLUENCE OF GEOLOGY ON LAYOUT AND DESIGN

In view of the integrated effects of the geological flaws, the following modifications in design and layout of the spillway were warranted for its better performance.

Three alternative spillway locations were studied besides the one originally contemplated between Ch. 806.52 and 895.24 m. This study revealed that from all considerations the original spillway location was suitable, hence finally accepted.

At the finally selected spillway location, the sloping cum horizontal apron has been designed and provided instead of roller bucket. This design would shift the scour much away from the toe. Moreover, deeper excavation through rock is avoided which has provided adequate safety against sliding along clay/shale beds.

Earlier five spillway gates of 14.93 x 10.67 m were proposed.

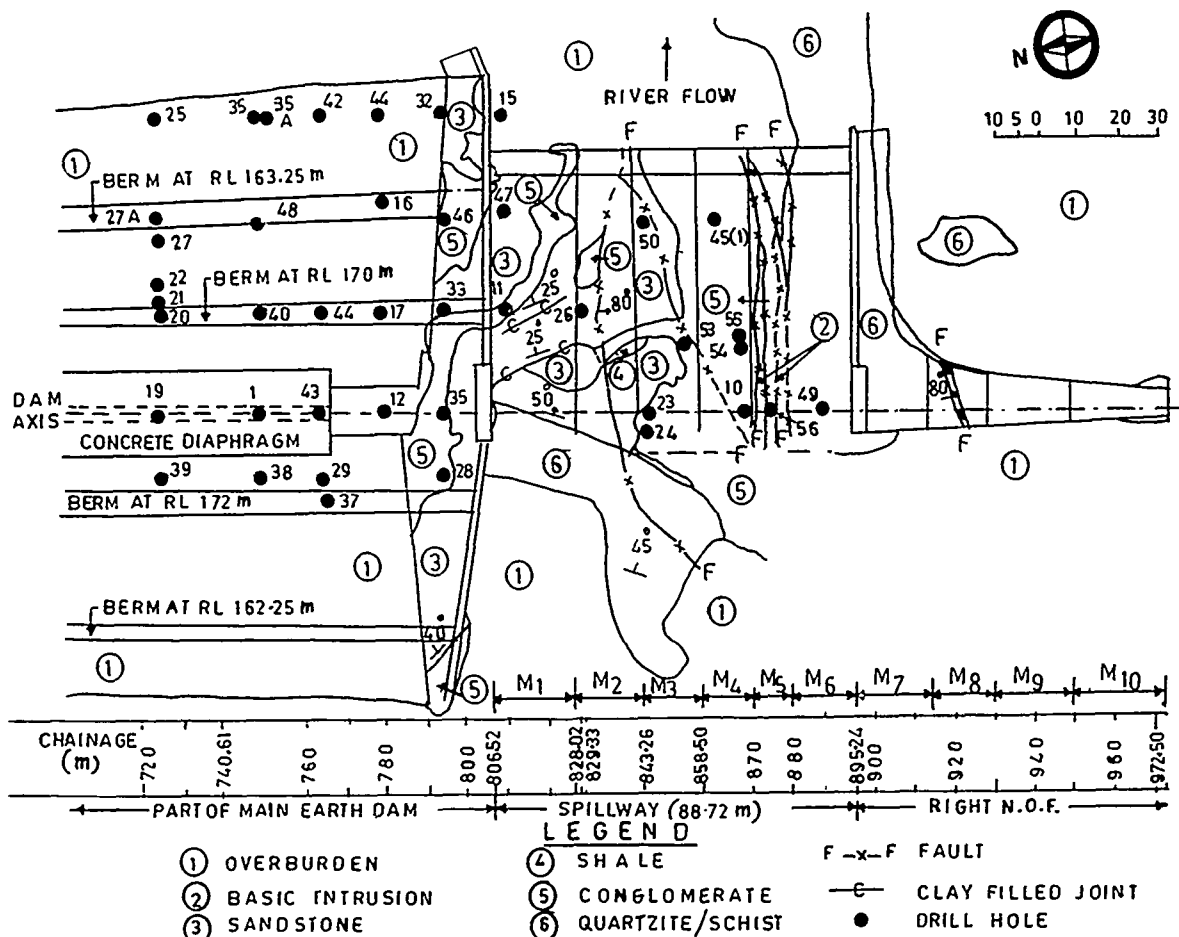


FIG. 2 GEOLOGICAL MAP OF MASONRY DAM

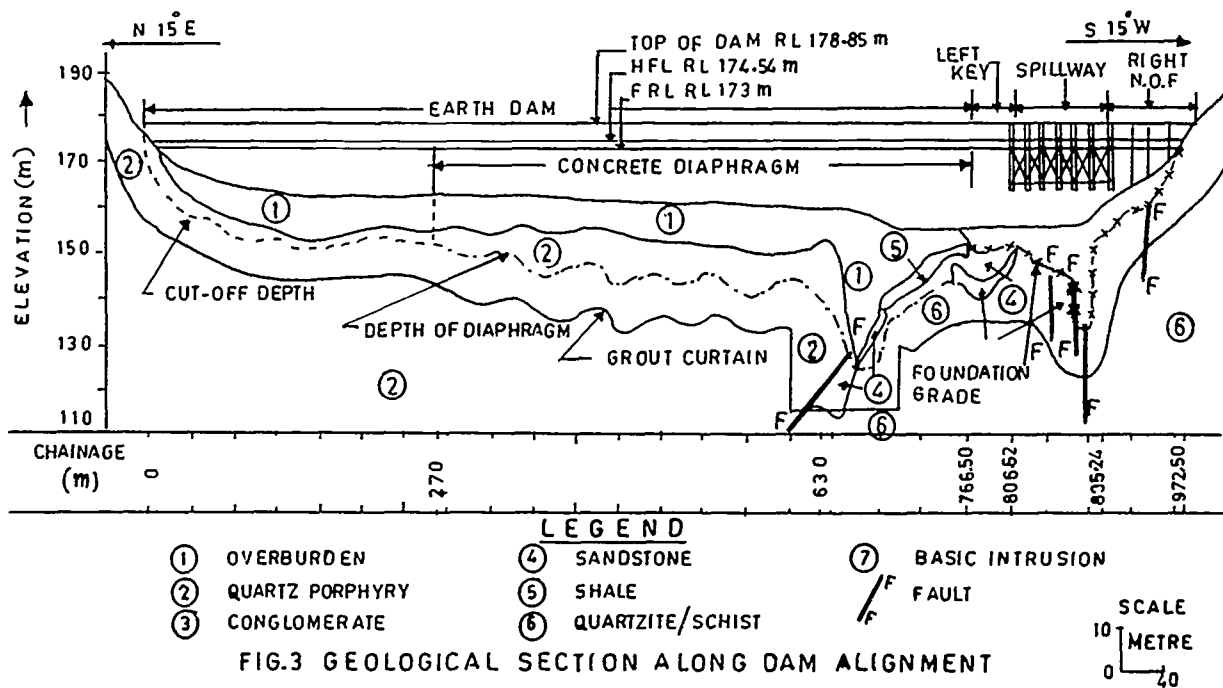


FIG.3 GEOLOGICAL SECTION ALONG DAM ALIGNMENT

Apprehending the weak nature of conglomerate, the number and size of the gates were modified to six of 12.5x8.23 m which reduced the discharge intensity from 76.18 m<sup>3</sup>/s/m to 58.53 m<sup>3</sup>/s/m.

Earlier a separate monolith for the major fault zone had been designed to avoid any differential settlement but later on contraction joints between monoliths 4 and 5 and that between 5 and 6 have been eliminated to have a bridging effect.

#### PHYSICAL CHARACTERISTICS OF FOUNDATION ROCKS

Physical characteristics of the rocks encountered in the masonry dam foundations have been evaluated for their anticipated behaviour after impounding of the reservoir. The details are enumerated in table 3.

TABLE 3. Physical Characteristics of Rocks

| Rock Type                        | Conglomerate    | Sandstone       | Quartzite |
|----------------------------------|-----------------|-----------------|-----------|
| Specific Gravity                 | 2.5 to 2.7      | 2.62 to 2.73    | 2.71      |
| % Water Absorption               | 0.064 to 0.73   | 0.26 to 2.13    | 0.21      |
| Compressive Strength (Wet) (MPa) | 65.36 to 147.70 | 28.56 to 171.44 | 71.64     |
| % Core Recovery                  | 47 to 100       | 52 to 100       | 50 to 100 |
| Penetration Rate (m/hour)        | 0.30            | 0.40            | 0.24      |
| Permeability (Lugeon)            | 1 to 60         | 1 to 57         | 1 to 66   |

Physical characteristics of conglomerate fairly match with those described by F.P. Pettijohn for ortho quartzitic conglomerate (oligomict). Such conglomerates normally belong to Lower Cambrian age. It is possible to deduce from the above that conglomerate formation occurring at the project site must have been formed during the early geological time (Delhi formation ?) and has attained thorough induration and compaction.

Moreover, the data given in table 3 indicate that the properties of conglomerate, sandstone and quartzite are quite comparable. Thin shale beds occurring within the sandstone are soft to moderately hard in nature.

#### FOUNDATION TREATMENTS

In view of the foregoing foundation problems, the following curative measures to safeguard the structure have been evolved.

##### Treatment to the Low Downstream Dipping Clay Bed and Clay Filled Bedding Joints

Low angle (25° to 30°) downstream dipping clay filled bedding joints/shale beds in sandstone were encountered in the spillway monolith 1 and in a part of monolith 2. The mechanical analysis and shear parameters of clay were determined in the laboratory to carry out the stability analysis of monoliths 1 and 2 (Table 4).

TABLE 4. Mechanical Analysis and Shear Parameters of Clay

| Location (m)                   | Grain Size Analysis (%) |      |      |      | Box Shear |        | Triaxial Shear |        |
|--------------------------------|-------------------------|------|------|------|-----------|--------|----------------|--------|
|                                | Gravel                  | Sand | Silt | Clay | C (MPa)   | $\phi$ | C (MPa)        | $\phi$ |
| Ch. 828 to 829, down-stream 10 | 05                      | 38   | 35   | 22   | 0.015     | 21°    | 0.02           | 22°    |

The stability analysis for monolith 1 was carried out on the low dipping clay filled joints taking into consideration the shear parameters  $C=0$  and  $\phi=20^\circ$ . The values of the sliding and shear friction factors obtained after considering the passive resistance available from the downstream side rock ledge are acceptable.

##### Treatment to Conglomerate

Conglomerate was apprehended for its weak and permeable nature. Laboratory test results of conglomerate and sandstone samples indicated that the minimum compressive strength in saturated condition is 65.36 and 28.56 MPa respectively which is about 29 times higher than the maximum stress of 0.98 MPa that will be developed after the completion of the spillway. Thus, their relative deformability would also be similarly less in the light of the maximum stress considered in design of the structure.

Usually, the value of bond between good rock and masonry is considered as 0.686 MPa, but due to weak nature of rock this value is considered as 0.49 MPa. Thereby, the values of shear friction factor for all conditions of loading are satisfied. Moreover, to achieve better bond with the foundation rock where conglomerate is exposed a 50 cm thick bottom layer of M 20 (20 N/mm<sup>2</sup>) strength concrete has been provided and masonry work was started when concrete was green. Some bond stones have also been inserted in the bottom concrete to have proper bond with masonry. This treatment has been provided in monoliths 3 and 4. Adequate curtain and consolidation grouting has been done to minimise the seepage and to further improve the modulus of deformation of foundation rocks including conglomerate.

##### Treatment to Fault Zones

(a) The foundations of the spillway monoliths 2 to 5 and 8 are traversed by four steep angle faults (Table 2).

Before finalising the treatment, an in-depth geological investigation of the fault zone in monolith 5 by sinking two inclined and one vertical drill holes to ascertain its thickness, nature of the material, etc. were undertaken. Data obtained from these drill holes indicated that (i) the width of the clay zone below RL 115.85 m reduced and (ii) the fault zone narrowed down at depth and towards the downstream.

Of these faults, those met with in the monoliths 2 to 4 and 8 were minor ones and were given the usual dental treatment. While excavating the trench along the fault zone in monoliths 3 and 4 for dental treatment from 7 to 13 m downstream, the width of the fault gouge increased to 2.1 m as against 0.3 to 1.0 m observed in the rest of the area. Further, the condition of conglomerate constituting the foundations of these monoliths beyond 7 m downstream is also somewhat weakened due to effect of faulting. Keeping in view the above conditions, a concrete plug of M 20 strength was provided in the fault zone trench and due to the increase in the width of the fault zone from 7 to

13 m downstream, a 1 m thick concrete raft spanning the entire block has been provided to guard against any local differential settlement.

(b) Fault zone encountered in monolith 5 being a major one, elaborate treatment was considered imperative. Because of an 8 to 8.5 m wide fault zone traversing across the dam axis, a separate monolith had been provided. By adopting the Shasta formula for the plug treatment, the depth of excavation worked out to 6 m from the general foundation level at RL 143.5 m. Accordingly, the fault zone material was excavated down to RL 137 m where it was revealed that the clayey gauge was the decomposed product of basic intrusive along the fault zone. The excavated trench has been plugged with M 15 (15 N/mm<sup>2</sup>) strength concrete. To transfer the load to the competent shoulders, arch shaped concrete has been done. Hammock reinforcement of 32 mm diameter deformed bars placed at 30 cm both ways has been provided to take care against any settlement. This has been extended upto RL 143.5 m. Above this and upto RL 146 m concreting is done (Fig. 4).

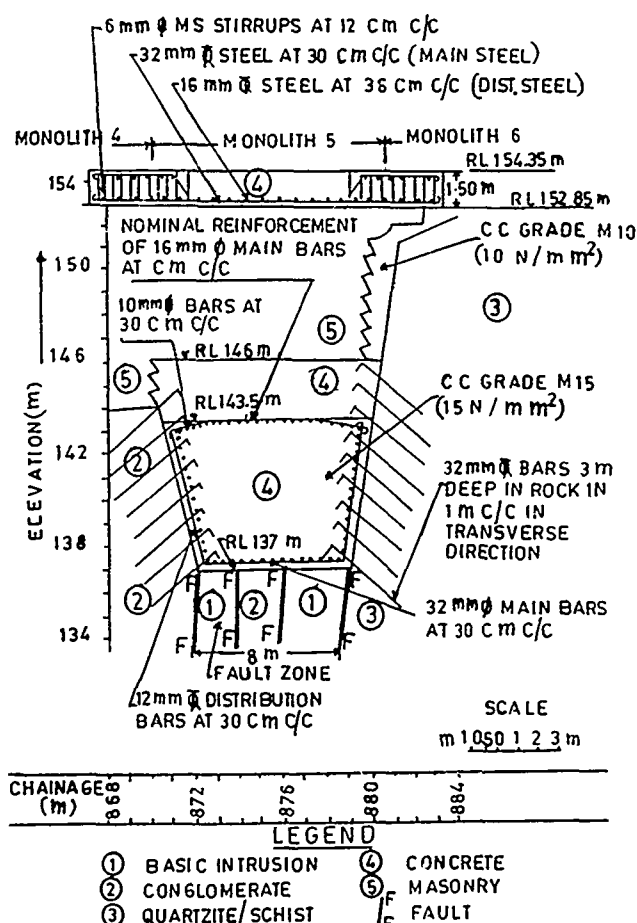


FIG. 4: FAULT ZONE TREATMENT IN MONOLITH 5

The left shoulder of the fault zone trench is formed by conglomerate whereas the right one is made up of competent quartzite interbedded with thin schist bands. The sides of the trench were roughened to have proper bond between the concrete and the rock. Contact grouting has also been done to take care against shrinkage, etc.

Plasticity index of the gauge material was more than 15 hence piping is not apprehended. However, to have adequate path of percolation through the fault zone, a 5 m wide upstream cut-off to a depth of 3 m (RL 134 m) below the bed of the trench has been provided. To achieve the desired path of percolation, the plug treatment was extended upto 36 m downstream. The bottom of the trench from 30 to 36 m downstream was kept at RL 139.5 m to avoid dewatering problem (Fig. 5).

Since the horizontal apron beyond the fault zone concrete was to rest on comparatively softer strata, differential settlement was likely. To obviate this possibility, a longitudinal joint with water stop arrangement has been provided in the apron portion of monolith 5 itself.

At the final excavation level of the trench, conglomerate in 2 m width occurred in the central portion of the foundation. It is bounded on both sides by basic rock intrusion of 2 and 3 m width. Basic intrusive rock is highly weathered while conglomerate is slightly weathered and jointed due to the effect of faulting. The contacts between basic intrusion/conglomerate and basic intrusion/quartzite and schist are marked by the presence of a thin layer of clay.

The spillway monoliths 4 to 6 posed unique problems because of - (i) differential foundation levels in monolith 4 (RL 144 m), monolith 5 (RL 137 m) and monolith 6 (RL 152 m), (ii) coincidence of pier location exactly over the contact of monoliths 5 and 6 and (iii) FEM analysis indicated differential settlement of 1.75 cm of the fault zone material at RL 137 m.

Considering these points, R.C.C. slab beam above the fault zone in monolith 5 had been designed and constructed. This raft is 1.5 m thick and provided between RL 152.85 and 154.35 m and has been extended by 2.75 m on either side of the monoliths 4 and 6, thereby affording an adequate bearing to the raft on either side of monolith 5. All the three monoliths have been combined to reduce the load intensity on the foundation rocks (Fig. 4 and 5).

## CONCLUSION

For safe and sound design as also timely execution of any irrigation project, thorough prognostications are imperative.

## REFERENCE

Pettijohn, F.J. (1957), "Sedimentary Rocks", Oxford Book & Stationery Company, Calcutta.

## ACKNOWLEDGEMENT

The authors are highly indebted to Mr. J.F. Mistry, Secretary, Irrigation Department, Government of Gujarat and Mr. M.U. Purohit, Chief Engineer (Irrigation Projects) and Joint Secretary, Irrigation Department, Government of Gujarat for inspiring to write the paper. The help rendered by

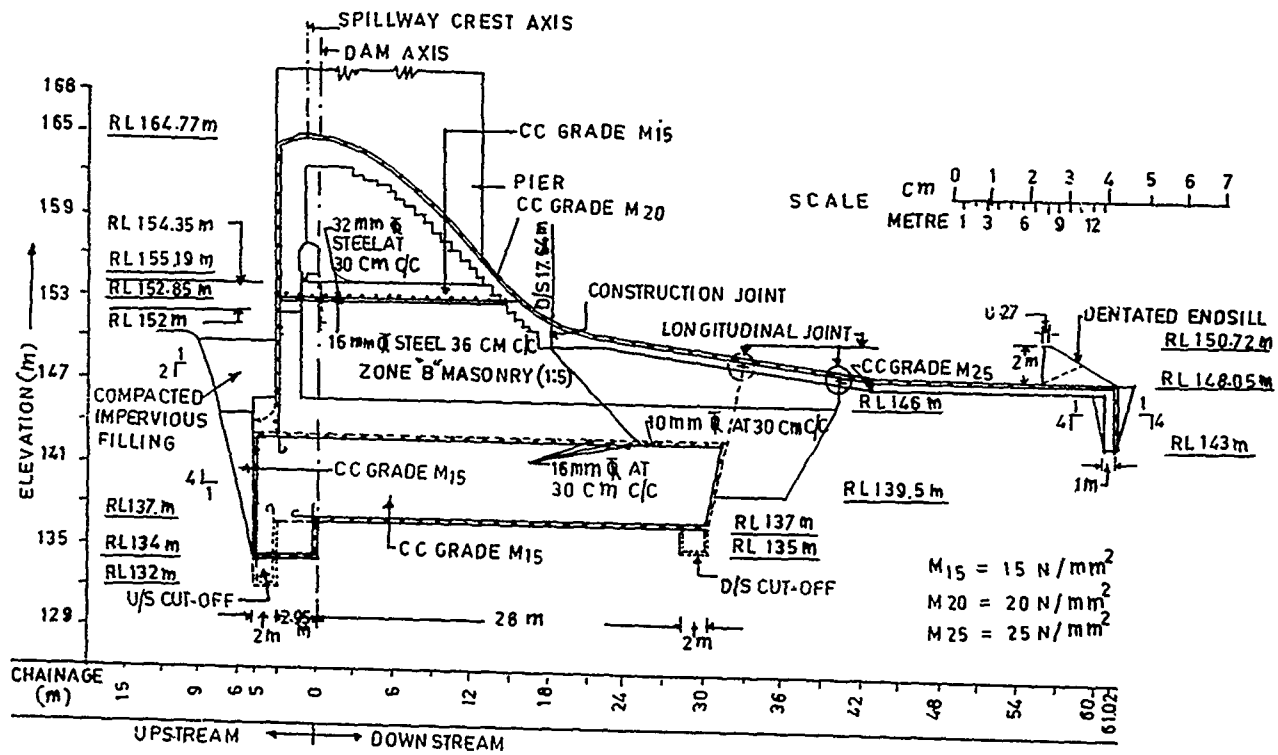


FIG. 5 SECTION OF FAULT ZONE TREATMENT IN MONOLITH 5

Mr. J.P. Vora, Deputy Executive Engineer, Central Designs Organisation, Mr. J.J. Thakor, Geologist, Himatnagar Irrigation Project Circle and Mr. J.K. Nathani, Geologist, Central Designs Organisation in the preparation of this paper is also gratefully acknowledged.

## A Novel Low Cost Drum Diaphragm Wall for Landslide Control in the Himalaya

R.K. Bhandari

Director, Central Building Research Institute, Roorkee, India

### SYNOPSIS

Construction of masonry and reinforced cement concrete retaining walls are common as a measure of landslide control in the Himalayan region. They are usually very expensive and call for import of cement, steel, stones, sand and water from long distances. The paper spotlights a novel technology of constructing anchored drum diaphragm retaining walls which make use of slope waste material itself for wall construction, saving to the tune of 40 per cent in cost. Utilisation of slope debris in turn minimises hazards due to debris flow, rockfalls etc and other mass movements.

### INTRODUCTION

Himalayan landslides generate staggering amount of debris most of which are eventually swept away by its mighty river system capable of carrying incredibly large amount of sediment. Satellite pictures taken in 1974 dramatically reveal that eroded debris carried by the Himalayan rivers have indeed created a new land mass about 50,000 sq.km in area extending well beyond 700 km into the sea. With the vast slopes of Nepal, Western Sikkim, Kumaon, Garhwal Kashmir and several other hilly regions getting robbed of their vegetal cover particularly due to indiscriminate deforestation, the gravity of slope erosion and consequent landloss may become even more alarming. As the population grows, more and more of human settlement, dams, tunnels, water reservoirs and roads would be added. The current experience highlights that the network of 40,000 km of hill roads in the Himalaya is already prone to heavy landsliding involving on an average 5,000 tonne of debris and slope waste on every major landslide spot each year. Every kilometre of road when constructed could be expected to generate 1 to 2 lac tonne of debris right at the time of construction. If effective methods of landslide control are to be found, the enormous slope waste material must be put to effective use. By doing so, not only the hazards associated with debris flow and rock falls would reduce but a tremendous economy in building materials and construction costs of control measures would seem possible.

The usual package of landslide control measures for Himalayan landslides inter alia include construction of gravity retaining walls, gabion type walls, timber piling for stitching debris perched on slopes, prestressed anchoring of sliding masses, vegetating of the problematic slopes and provision of surface and subslope drainage systems. The construction of retaining walls normally require large quantities of cement, steel, stones, sand and water to be transported usually from long distances at a very heavy expense. It is for this reason that the idea of making effective use of landslide debris and slope waste was pursued at the

Central Building Research Institute and the technology of drum anchored diaphragm walls was evolved through design and field trial. Such a construction technology makes the fullest use of landslide generated debris and costs only 60 per cent of the cost of conventional retaining walls.

### DRUM ANCHORED DIAPHRAGM WALL

A simple to do, low cost technology for construction of retaining wall to stabilise slopes has been developed by the author Bhandari (1987), which promotes extensive use of slope waste and landslide debris. The system of drum anchored diaphragm walling consists of empty bitumen drums interconnected vertically and laterally, filled up with wasteful debris to achieve gravitational effect and suitably anchored at the slope foundation as well as on to the slope retained. It is basically a dry system of construction. Besides promoting utilisation of slope waste and enhanced speed of construction in difficult hilly terrains, the system offers following advantages :

- Effective utilisation of wasteful slope debris, thereby saving scarce building materials and their long distance transportation.
- Partial elimination of expensive and dangerous excavations for foundation associated with conventional types of retaining walls.
- Effective use of wasteful empty bitumen drums available in abundance through road construction agencies.
- Dry construction technology, which does not require water otherwise difficult to get particularly in the hilly areas.
- Self draining system thus relieving excess hydrostatic pressures behind the retaining wall.
- Easy construction that does not require heavy equipment for construction.



- Speed of construction is usually high and need for skilled personal is generally low.

### SPECIAL FEATURES

The system of retaining wall makes use of empty bitumen drums to serve as containers. The top and bottom portions of drums are removed and only the cylindrical shell is utilised. In an actual construction, these were arranged at Kaliasaur landslide (Fig. 1) in two rows, one behind the other.



FIG. 1 KALIASAUR LANDSLIDE

The rear row was of 2 1/2 drums height and the front row was of 2 drums height. The drums were interconnected in both vertical and horizontal direction by m.s. plates and bolts to ensure continuity and were filled with debris to give weight and impart stability. The drum wall was anchored at the base and also to the back-fill to attain further stability against sliding and tilting. Details of the wall are shown in Fig. 2. The contact surface between the two adjoining drums being irregular allows free flow of water, which also flows between the drums and that should relieve the unbalanced hydrostatic pressures on the wall. The rain water that accumulates inside the drums also drains out through the drum bottom.

### DESIGN CONSIDERATIONS

A retaining wall of above description constructed from slope waste can be analysed for its

stability by Finite Element Method assuming it as a plane strain problem. A typical drum diaphragm wall is built of slope waste placed into empty bitumen drums which are anchored using 25 mm dia mild steel bars grouted into the foundation to a depth of 0.6 m. The diaphragm is anchored to the slope with the help of 50 x 6 mm m.s. flat at 2 m centres 2.5 m into the slope.

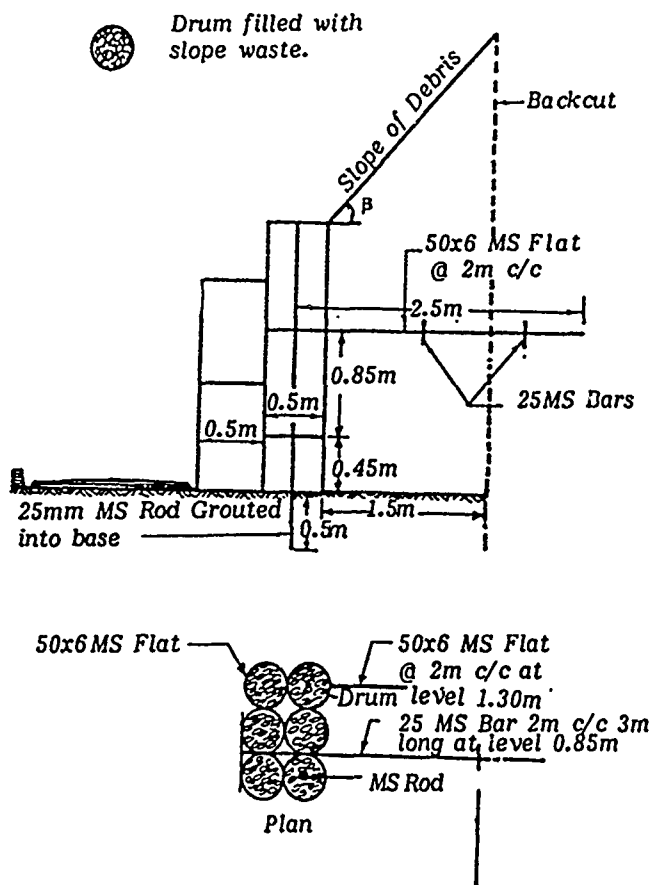


FIG. 2 ANCHORED DRUM DIAPHRAGM WALL BUILT OF SLOPE WASTE AND EMPTY BITUMEN DRUMS

Tsui and Clough (1974) have examined the validity of assuming the condition of plane strain for the anchored walls. It has been demonstrated that most anchored walls have a tie back spacing that is close enough to justify the assumption of plane strain. They have defined the earth pressure as dimensionless parameter  $I_p$  which equals  $l_0^2 p/P$ , where  $l_0$  is the characteristic length of the slab,  $p$  the earth pressure, and  $P$  the prestress load. The maximum deviation of the plane strain pressure from the three-dimensional pressures works out to be only 15 per cent. In the general case, the deviation of three-dimensional pressures from a plane strain distribution was defined in terms of the soil stiffness, the wall stiffness and the tie back spacing. The results showed that stiffer the wall, the closer the tie back spacing and the softer the soil, the more accurate is the assumption of plane strain condition. In this case the anchors were ordinarily grouted and

there was no prestress. As such, the assumption of plane strain condition for the drum diaphragm wall appears to be justified.

The analysis of the diaphragm wall with the retained earth has been carried out by discretizing the continuum by 8-noded isoparametric element. The continuum has been extended to be 7 m below the diaphragm wall and also on either side of it. The following material properties for the retained disintegrated soft rock mass have been adopted in the analysis.

$$E = 250 \text{ kg/cm}^2; \nu = 0.30; \gamma = 1800 \text{ kg/m}^3; \phi = 30^\circ$$

For the slope wastefill inside the bitumen drum, the following material properties have been taken :

$$E = 1500 \text{ kg/cm}^2; \nu = 0.30; \gamma = 2000 \text{ kg/m}^3; \phi = 35^\circ$$

Fig. 3 shows the distribution of horizontal earth pressure, Fig. 4 the horizontal displacement of the drum diaphragm wall obtained by the finite element analysis and the same has been compared with that obtained by Coulomb's theory. The slope of surcharge of the retained material has been taken as  $30^\circ$ .

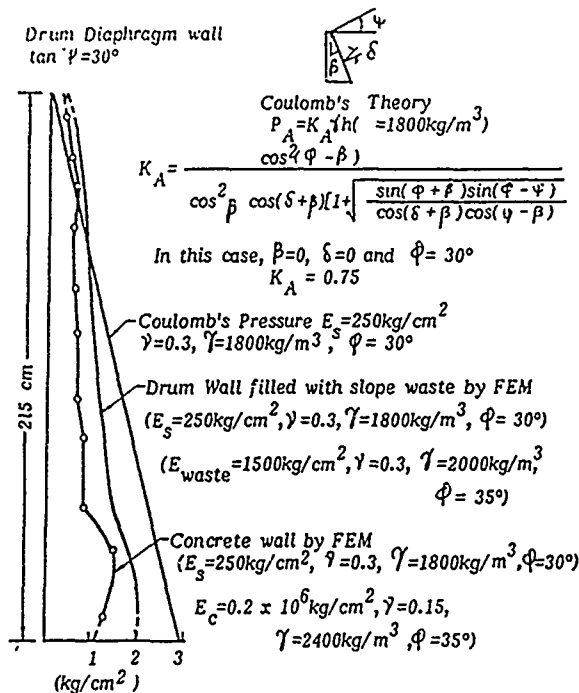


FIG. 3 EARTH PRESSURE DISTRIBUTION

## CONSTRUCTION

The alignment of the retaining wall is first marked on a prepared level base on the slope. Holes are drilled using a suitable compressor to a minimum depth of 60 cm at predetermined positions, 1 m apart, to accommodate 25 mm dia m.s. rods. The rods are driven into these holes. About 15 cm wide and 45 cm deep pit is made around these rods and the pit is filled with 1:3:6 cement concrete. The rods serve as vertical anchors at the base and do provide a high degree of resistance against sliding. The drums are then assembled and bolted in the sequence shown in Fig. 5. Alternate vertical

rods in the rear row are supported at 1.3 metre level with the help of 50 mm x 6 mm m.s. flat which is taken into debris accumulated over the slope. The flats are held in position by two 25 mm dia m.s. bars driven vertically into the debris; this helps preventing tilting of the retaining wall.

As the construction of drum wall continues, the already completed portion of the wall is filled with debris which provides mass to the wall. The space behind the retaining wall is filled with debris. A 50 mm x 6 mm flat having a 28 mm dia hole at the centre is held against two drums of the front row. An L-shaped 25 mm dia, 3 m long m.s. rod is inserted into the hole and driven into the debris. This system is provided at 2 m centres to keep it in a proper alignment and to provide additional stability.

Based on this technology, about a 100 metre long and 2.15 m high wall has been constructed at Kaliasaur landslide area, 18 km east of Srinagar (Garhwal) on Rishikesh-Badrinath road. A view of the wall after construction in August 1986, at a time when debris flow in the slope cover was at its peak, is shown in Fig. 6. Even when a lot of debris rolled down from the top of the slope and covered the wall, it has stood stable.

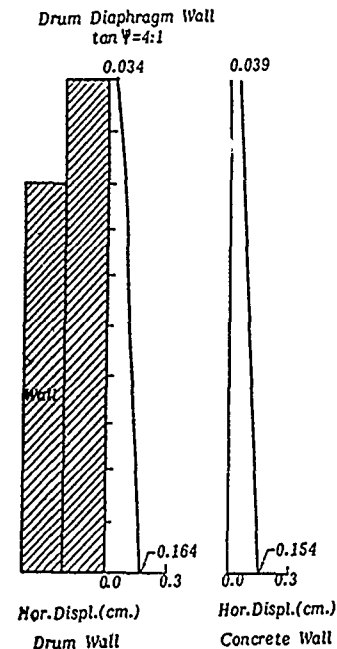


FIG. 4 HORIZONTAL DISPLACEMENT OF WALL

The alignment of the wall, monitored so far has not indicated any significant displacements. Observations are continued to monitor the performance of wall. In addition to the drum retaining wall provided at the toe of the slope, other measures like slope drainage and slope vegetation are also being implemented to enhance slope stability.

The materials used for a typical 100 m long wall are given below :

1. Empty bitumen drum - 50 cm dia = 900 Nos.  
(available from Road Construction Deptt. as Waste Material)

2. 12 mm dia, 7.5 cm long bolts = 250 kg with nuts
3. M.S. flat 50 mm x 6 mm = 3570 kg
4. M.S. rod 25 mm dia = 2770 kg
5. Debris for filling drums = 160 cu.m (available in plenty at site as waste material)

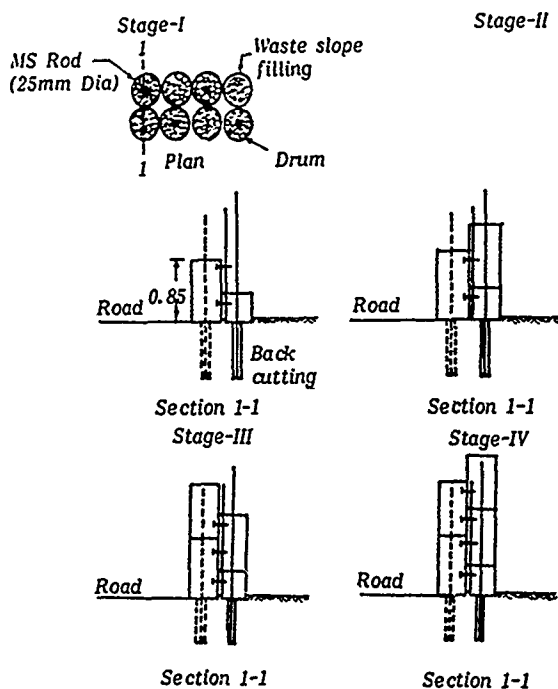


FIG. 5 SEQUENCE OF CONSTRUCTION OF ANCHORED DRUM DIAPHRAGM WALL



FIG. 6 DRUM DIAPHRAGM RETAINING WALL ON KALIASAUR LANDSLIDE

#### FIELD MONITORING

The wall was monitored using EDM surveys and the displacements over a period of 18 months were found to be negligible. Prediction of displace-

ments were made using FEM and the correspondence between the prediction and performance was, so far, found to be satisfactory.

#### CONCLUSION

It can be concluded that the drum diaphragm retaining wall built at the Kaliasaur landslide in Garhwal-Himalaya has been successful. The technique could safely be recommended to provide effective and economical substitute for stone masonry or concrete retaining walls elsewhere in the Himalaya. They may ultimately workout to be much cheaper and safer than even the conventional wire-netted sausage walls and gabion walls. The greatest advantage appears to be that the material of construction is available in-situ eliminating need for import.

#### ACKNOWLEDGEMENT

The author would like to thank Dr. G.S. Mehrotra and Shri B.K. Jindal for carrying out most of the field work. Thanks are due to Dr. S.C. Chakraborti for assistance in analysis.

#### REFERENCES

- Bhandari, R.K. (1987), Slope Instability in the Fragile Himalaya and Strategy for Development, Journal of IGS, Vol. 17, No. 1, pp 1-78.
- Tsui, Y., Clough, G.W. (1974), Plane Strain Approximations in Finite Element Analysis of Temporary Walls, Proc. Bi-Annual ASCE Geotech. Conf., Austin, Texas, June, 1974.

# Prevision of the Bearing Capacity of Superficial Foundation on Jointed Rock

Marangos Christos

Dr. Ing. Lecturer of the Geotechnical Engineering Department,  
University of Thessaloniki, Greece

**SYNOPSIS:** The article describes the application, in Greece, of an approximate resolution of the prevision of the superficial foundation bearing capacity of a school building group on jointed granite. The method is based on the mechanics of the discontinuous media. On a sufficient number of a canvas points which is situated on the critical section under the foundation, the developing shear stresses are defined, based on the elastic theory, and they are compared with the variable -into the various directions- shear strength of the jointed rock. The resulted data conduct to the setting of boundaries of plastic zones which allow the approach of the failure form and of the sliding body. The limited load value is defined by successive approximations.

## 1. INTRODUCTION. PROBLEM SETTING

There are sufficient solutions that calculate the bearing capacity in soil mechanics. This happens because of the homogeneous and isotropic character of the soil and of the easy way to define its mechanical characteristics.

The problem is not simple in case of jointed rock. The difficulties result because:

- The mechanical behavior depends mainly on the tectonic fabric of the rock mass. The joints divide the material and constitute low strength surfaces. Therefore, the failure form for a given loading, will be different from the form that is defined by the state of stress for a continuous-isotropic medium. So, according to the kind of the fabric and to the orientation of the main normal stresses, the failure tracks will follow partly or thoroughly the already existing joint surfaces and consequently the resistance will be differentiated to friction strength along the joint surfaces and to resistance of proper shear strength of the intact rock.

The approach of this "residual" strength pre-supposes the statistical measurement of the rock fabric and the knowledge of the stress distribution.

- The joints will have a great influence on the development of the shear fields that will result from the external loads. Deviations and local stress assemblies, till the failure limit, will appear in the stress paths with consequence the development of new stress fields in these places, which will conduct to progressive failure phenomena. The estimation of the fabric influence on the stress distribution meets insuperable difficulties practically, if we take into account the uncertainty that exists with reference to the orientation and the values of the pre-existing main stresses.

- The necessary mechanical characteristics for

a bearing capacity calculation, and the quantitative parameters which characterize the fabric, require expensive investigation work.

Of course, we expect almost always that the bearing capacity of a jointed rock to be greater than a soil mass. But the problem is to find the permissible soil pressure as a magnitude that results from calculations in which to be able to take under consideration as much as possible the parameters from whom it depends.

The problem is complex in its origins and its approach seems to be possible only with assumptions.

Very simplified methods, where the jointed rock is characterized by a mean angle of friction and a mean cohesion, don't take into account the important influence of the joints on the rock behavior, conduct to great uncertainty regarding the value of the safety factor and they must be used with great prudence.

An approximate method for the study of the loading rock slopes has been proposed by Müller and Pacher. In this method for the determination of the stress distribution, the assumption of the elastic-isotropic semi-space is made but on the various points of the critical section the shear stress is getting under dependence from the orientation of the stress field and the orientation of the discontinuities that characterize the rock.

This article describes the application, in Greece, of an approximate resolution of the prevision of the foundation bearing capacity of a school building group on jointed granite, based on the principle of the method of Müller and Pacher. The great extension of the buildings, about 23.000 sq.m., obliges to take advantage of the rock resistance for economy reasons.

## 2. GEOTECHNICAL DATA OF THE REGION

The rock that exists at the region is a strongly jointed granite. The determination of the fabric data is based only on the measurement of the dips of the joints which have been observed in the cores of conventional coring boreholes of about 300 meters in total depth (core recovery about 100%). The statistical study of the joint planes conducted to the following fabric data. The rock mass is characterized by three joint sets J1, J2, J3 with dips  $\alpha$  and frequencies  $f$  ( $f$  = number of joints per meter) equal to: J1:  $\alpha=0^\circ$ ,  $f=4,0 \text{ m}^{-1}$ , J2:  $\alpha=30^\circ$ ,  $f=2,5 \text{ m}^{-1}$ , J3:  $\alpha=65^\circ$ ,  $f=2,0 \text{ m}^{-1}$ . The joints are filled by clay material at the majority of the areas with deverse mechanical characteristics.

### 3. PREVISION OF THE BEARING CAPACITY

In the adapted method, the assumption that the joint sets can have the most unfavourable combination of strikes - that lies on the safety side - is made. Hence, it is based on the statistical measurement only of the dips of the joint planes, abolishing the costly sampling of orientated core.

The investigation is focussed in the determination of the limit load which in case of its application can give a sliding body able to move.

This method follows the following steps:

- Determination -for various loads successively-

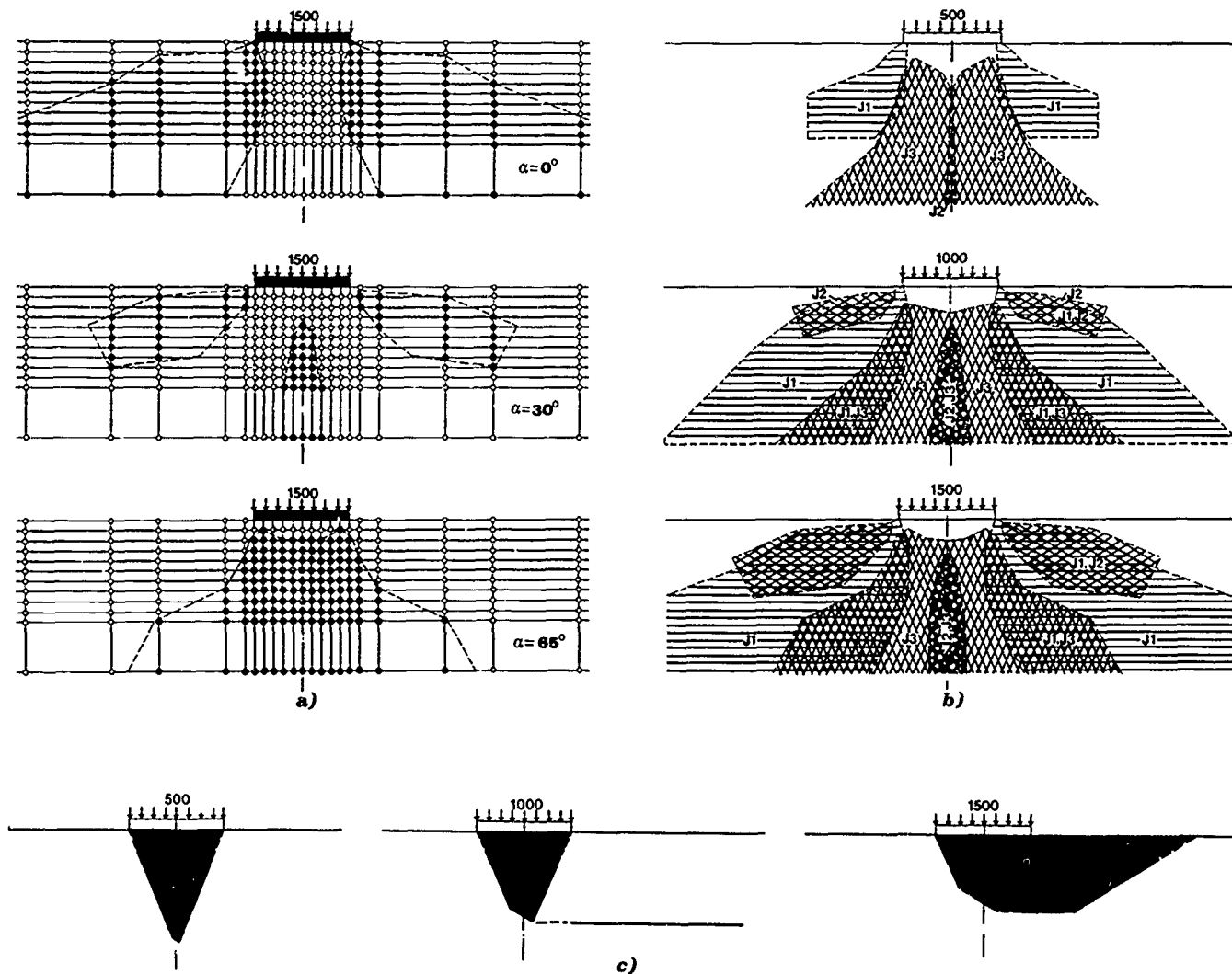


Fig. 1. Static analysis of the superficial foundation bearing capacity on jointed rock.

a) Partial safety factors  $R=t/\tau$  and plastic zones, separately for each of the joint sets J1, J2, J3 in points of canvas situated on the critical section for load  $p = 1.500 \text{ kN/m}^2$ .  $\bullet = R \leq 1,0$ ,  $\circ = R > 1,0$ . b) Plastic zones, under the footing of all the joint sets J1, J2, J3 for loads  $p = 500, 1.000, 1.500 \text{ kN/m}^2$ . c) Approximation of the limit load. Failure form and sliding body. --- = progressive failure.

Geotechnical data: Jointed granite. Fabric: three joint sets: J1:  $\alpha=0^\circ$ ,  $f=4,0 \text{ m}^{-1}$ , J2:  $\alpha=30^\circ$ ,  $f=2,5 \text{ m}^{-1}$ , J3:  $\alpha=65^\circ$ ,  $f=2,0 \text{ m}^{-1}$ . Joint sets filled by clay filling material with parameters  $\phi=17^\circ$ ,  $c_f = 45,0 \text{ kN/m}^2$ . Form data: Rigid strip footing,  $B = 2,80 \text{ m}$  in width. Superficial foundation.

of the state of stress that results from the self weight and from the transported loads on a sufficient number of points of a canvas that is situated on the critical section under the footing, with the assumption that the rock consists elastic-isotropic semi-space. That is, we don't take into account deviations that result from the fabric in the development of the shear fields.

- Calculation on the points of the canvas of the shear strength  $t$  and of the shear loading  $\tau$  along all the joint sets and comparison between the shear stress and shear strength. The resulting stability factors  $R = t/\tau$  -they are also called partial safety factors- conduct to the setting of the boundaries -for every load and every joint set separately- of zones where the shear strength along the joint set will be exceeded. The position and the extension of these critical zones (plastic zones) give information regarding to the form of the sliding body and the moving possibilities and allow the determination of the limit load.

The state of stress has been determined for canvas points with distances equivalent to the statistical mean value of the distance of the horizontal joints, that is 0,25 meters. The calculation has been made for the case of the plane strain state (strip footing = the most unfavourable case). The shear strength has been calculated for the three joint sets for the case where the joints are filled by clay material or not, respectively, by the relations:

$$t = c_f + \sigma \cdot \tan \phi_f \quad \text{and} \quad t = \sigma \cdot \tan \phi_R,$$

where  $c_f$ ,  $\phi_f$  = the cohesion and the angle of friction of the filling clay material of the joints,  $\phi_R$  = the angle of friction of the rock,  $\sigma$  = the normal stress on the joint plane.

The following cases are investigated:

- The joints don't contain filling material. The angle of friction of the jointed granite was determined -by triaxial tests- equal to  $\phi_R = 240.000$  kN/m<sup>2</sup>.

- The joints are filled by clay material 1-3 cm in thickness. The strength characteristics, in the various areas, are illustrated in the figures 1-3.

The results of the calculations of the examined cases are given in the figures 1-3.

The zones of the joint sets, where exceeding of the shear strength is observed, have been plotted in the figures for various loads. They have been plotted based on the values of the partial safety factors  $R$  and contain all the points of the section where  $R \leq 1,0$ . The critical zones for every joint set are characterized by delineation with the same dip as the dip of the concerned joint set. The lack of the strike values of the discontinuities imposes the assumption that the joint sets can have as dips  $\alpha^0$  and  $\alpha+90^0$ . The number of joints which will fall in the critical zones will depend on the statistical mean value of the joint distance of every joint set.

We observe the increase of the extensions of the

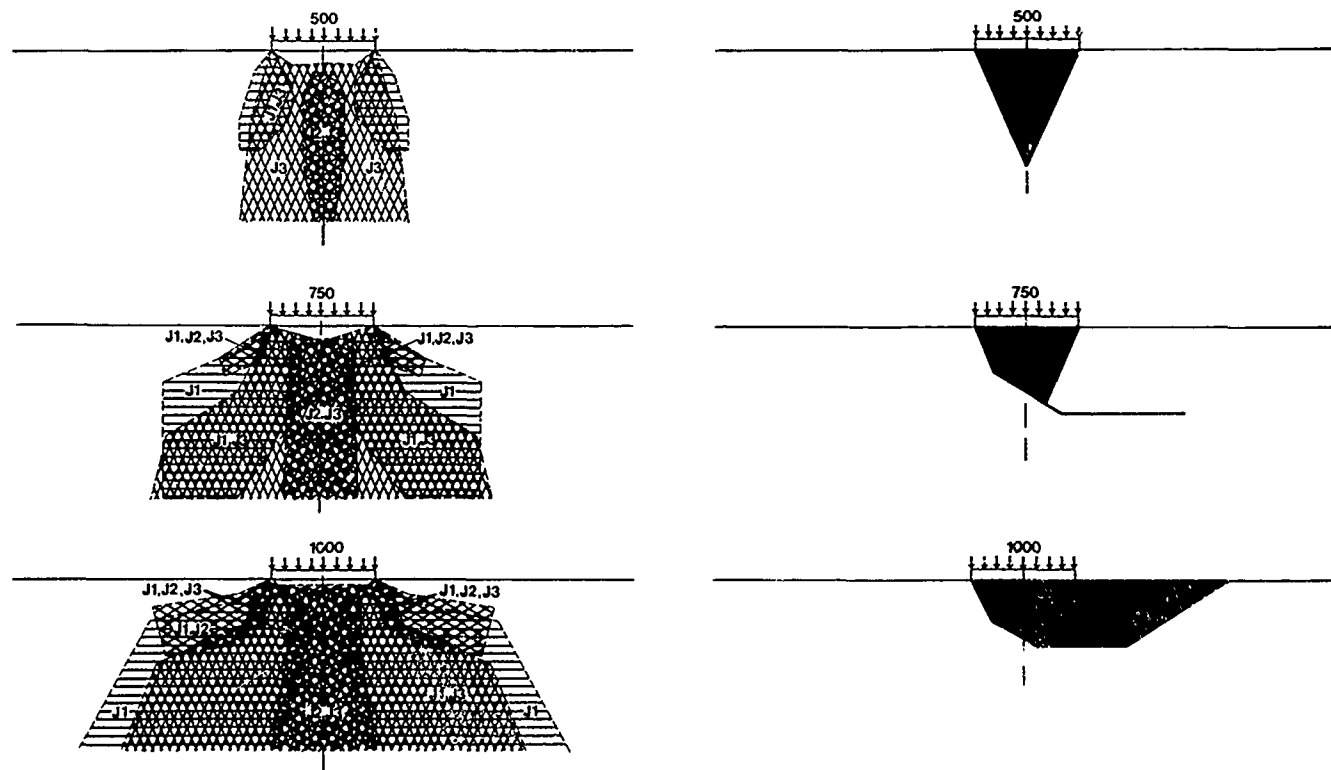


Fig. 2. Plastic zones of joint sets in the critical section. Failure form and sliding body. The joint sets are filled by clay filling material with mechanical parameters  $\phi_f = 0$ ,  $c_f = 95,0$  kN/m<sup>2</sup>.

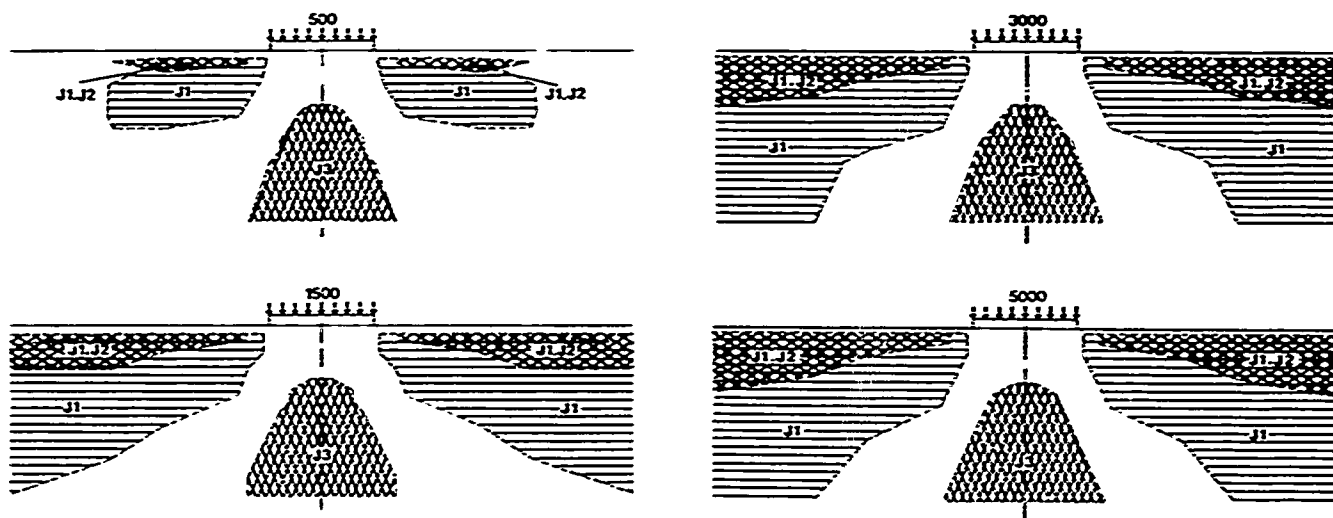


Fig. 3. Plastic zones in case where the joints of rock mass don't contain clay filling material.

plastic zones with the size of the load in the figures. Plastic zones, which have common areas, are developed for relatively bigger loads for the two or for the three joint sets (Fig. 2). The further load increase conducts finally to unfavourable combination of the plastic zones of the joint sets with consequence the creation of a sliding body and the failure of the foundation.

The limit state would be determined considering that the bearing capacity is getting exhausted for the load for which a continuous failure surface is created. The shear stresses must have the moving direction along all the parts of this failure surface.

The partial safety factors  $R$  have been computed for the state of stress which is caused by the foundation loads. It is certain that the creation of wedges under the footing will conduct to more unfavourable loading conditions of the lateral parts with consequence the development of additional stresses on these and of progressive failure phenomena which have to be taken under consideration for the evaluation of the limit load. The failure forms and the limit loads that are illustrated in the figures have been estimated according to the above.

#### 4. CONCLUSIONS

The following general conclusions are resulted from the carried out investigation:

- The bearing capacity decreases considerably for the same strength parameters with the increase of the number of joint sets. The control of the bearing capacity is judged as necessary in case where the rock is characterized by more than two joint sets which are filled by clay filling material.
- The presence of clay filling material of the joints conducts to a considerable decrease of the bearing capacity, until more than ten times.

- The presence of only one joint set, independently of joint density and filling material, doesn't decrease considerably the rock resistance, because in this case the high shear strength of the intact rock will considerably contribute in the bearing capacity.

#### 5. REFERENCES

- Döring, T. (1967), "Über den Einfluss der Klüftung auf die Spannungsverteilung im Fels", Felsmech. u. Ingen.-Geologie, Suppl. III.
- Jäger, J.C. (1969), "Behaviour of Closely jointed Rock", Proc. Eleventh Symp. on Rock Mechanics, Berkeley, California.
- Müller, L. (1963), "Die Standfestigkeit von Felsböschungen als spezifisch geomechanische Aufgabe", Felsmech. u. Ing.-Geol. 1.
- Pacher, F. (1967), "Zur messtechnischen Kontrolle des Gründungsfelsens von Bogenstaumauern", Rock Mechanics and Engineering Geology, Supplementum III.
- Pacher, F. (1978), "Der Begriff der Sicherheit bei Speziellen Aufgaben des Felsbaues", Felsmechanik Kolloquium Karlsruhe 1978. Trans Tech. Publications.
- Rocha, M. (1964), "Some Problems on Failure of Rock Masses", Felsmech. u. Ingen. Geologie, Suppl. I, 1.

## Use of Geophysical Methods in a Geotechnical Investigation

K.H. Earley

Geologist, NTH/Russell Associates, West Chester, Pennsylvania

D. Rudenko

Geophysicist, Vibra-Tech Engineers, Inc., Hazleton, Pennsylvania

**SYNOPSIS** This paper describes a case study in which a geotechnical investigation encountered complex subsurface conditions requiring geophysical methods to supplement test boring data. Electromagnetic (EM) and seismic refraction methods were used to model subsurface conditions at the site of a proposed three-story office building. The three investigative techniques used in this study all revealed bedrock to be at a shallow depth. The test borings provided vertical resolution while the EM and seismic studies yielded lateral resolution. Good correlation was achieved when comparing the results of each method. The EM and seismic methods in conjunction with a test boring program can provide a better understanding of subsurface conditions than can be obtained by any single technique.

### INTRODUCTION

A geotechnical investigation was undertaken at a four-acre site located in Chester County, Pennsylvania. The objective of the study was to collect subsurface information at the proposed building site for recommendations pertinent to the design and construction of foundations for a 11,520 sq. m., three-story office building.

Near-surface pinnacles and solution activity were suspected at this site, based on previous geotechnical reports from the area and the known geology. Deep cuts were required to achieve finished floor elevations; therefore it was very important to accurately define the limits of shallow rock. The significant costs associated with rock excavation would be estimated based on the subsurface investigation. When irregular conditions were observed during the test boring program as anticipated, geophysical methods were chosen to supplement the boring data.

### GEOLOGY

The area of study lies in the Piedmont physiographic province, comprised of gently sloping uplands. The rocks in this region are found in vertical or steeply-inclined positions, evidence of severe compression. The site is located in the long, narrow Chester Valley Syncline, a prominent geologic and topographic feature enclosing Cambrian and Ordovician limestones and renowned for its shallow rock.

The Elbrook Formation (upper-Cambrian) reportedly contacts with the Conestoga Formation (Ordovician) in a east-west orientation south of the site. Both formations are described as impure limestones with the Conestoga containing phyllite members. Both formations weather to a clayey, residual soil overburden as the carbonates are dissolved by infiltrating surface water, however, intact limestone pinnacles are not uncommon.

Aerial photographic review and field observations have confirmed sinkhole activity in the study area. The site has discernable remnants of surface cavities resulting from solution activity in the underlying shallow limestone. A relationship is known to exist between fracture traces and zones of incipient sinkhole development in this region. Based on the aerial photographs, fracture lineaments are oriented sub-perpendicular to bedrock strike in the local area. These traces along with the proposed building footprint, study area and site and geologic features are shown in Figure 1.

### TEST BORING METHODS

Thirty-four test borings and twelve auger probes were drilled as part of the initial site evaluation and the final building investigation. The boring locations were chosen to provide an overview of the subsurface conditions with an emphasis on the building pad area. Soil samples for identification and laboratory analysis were taken at 0.9 to 1.5 m. intervals at the test boring locations. Six to ten inches of topsoil was encountered throughout the site. The investigation did not encounter any existing fills on the site. The character and condition of the intact limestone was examined by coring rock in four test borings. The test boring locations are shown in Figure 2. Major soil/rock horizons defined by the test boring program are described below in the general order of their occurrence.

#### Residual Soils

The residual soils showed the highest degree of limestone decomposition, with none of their original rock structure being retained. A stiff to very stiff red-brown silty clay grading to clayey silt with limestone fragments covers the site with an irregular thickness. The irregularities result from differential weathering along the bedding surfaces and fractures. The strength and consistency of the soils reflected



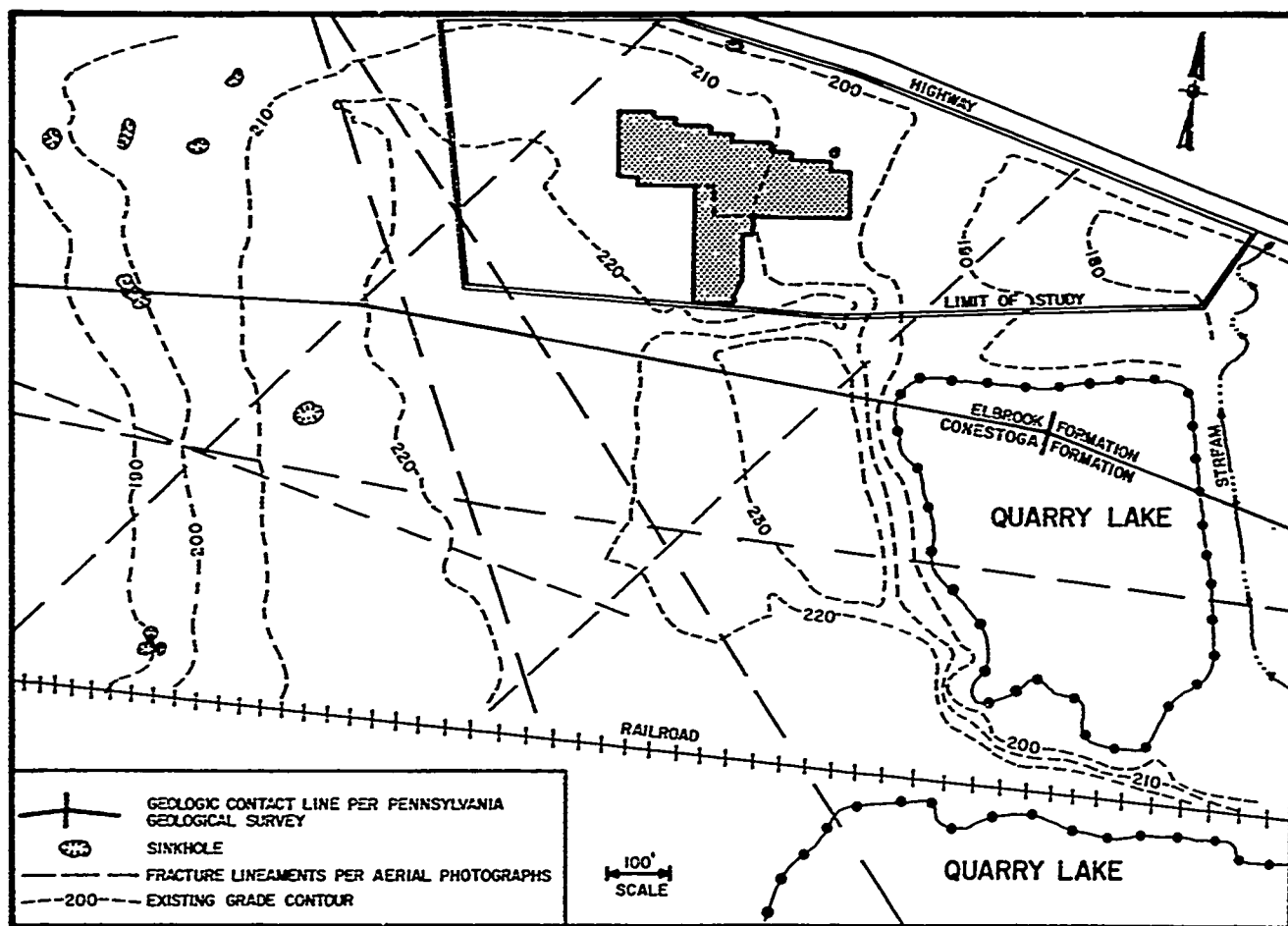


FIGURE 1 SITE CONDITIONS PLAN

in the Standard Penetration Resistance (SPR) values indicate a gradual increase in strength with depth. Some low readings were documented in the lower 20 percent of the profile and are attributed to a loss of strength in the overburden due to solution activity.

#### Decomposed Limestone

The residual soil overburden and intact limestone interface is very irregular and is characterized by discontinuous zones of limestone fragments and sand intermixed with residual soils. The decomposed limestone soils tend to be less plastic than the overlying clayey residual soils.

#### Intact Limestone

Rock cores identified the bedrock immediately underlying the proposed building footprint as a hard to very hard, fractured limestone with occasional clay seams. Some voids and soil infilled cavities were also identified. The investigation identified a rugged rock pinnacle interface located primarily along the northern portion of the building footprint. The ridge of weathered resistant limestone appeared to be aligned with strike at N80°E. Deep weathering and solutioning typically occurred along the steep dipping beds and in fracture joints per-

pendicular to strike. Phyllite was encountered in eleven borings as a member of the Conestoga Formation, moving the contact previously mapped north at least 90 meters.

In summary, the test boring program identified steeply dipping, near-surface pinnacles with deep overburden troughs. Based on the test boring program, Figure 2 infers zones where shallow rock (less than 3 meters) may be encountered. Experience indicates that additional limestone pinnacles may occur anywhere on site. Based on the data obtained and the poor lateral resolution test borings offer, geophysical methods were needed to supplement the data.

#### SEISMIC REFRACTION METHODS

A seismic refraction survey was performed at the site to further delineate areas of possible shallow bedrock, and evaluate compressional wave velocities in the soils and bedrock. The test boring program previously identified a ridge of near-surface limestone pinnacles. The seismic refraction method was useful in determining orientation and limits of the fractured bedrock on site.

A total of 6,630 linear feet of seismic pro-

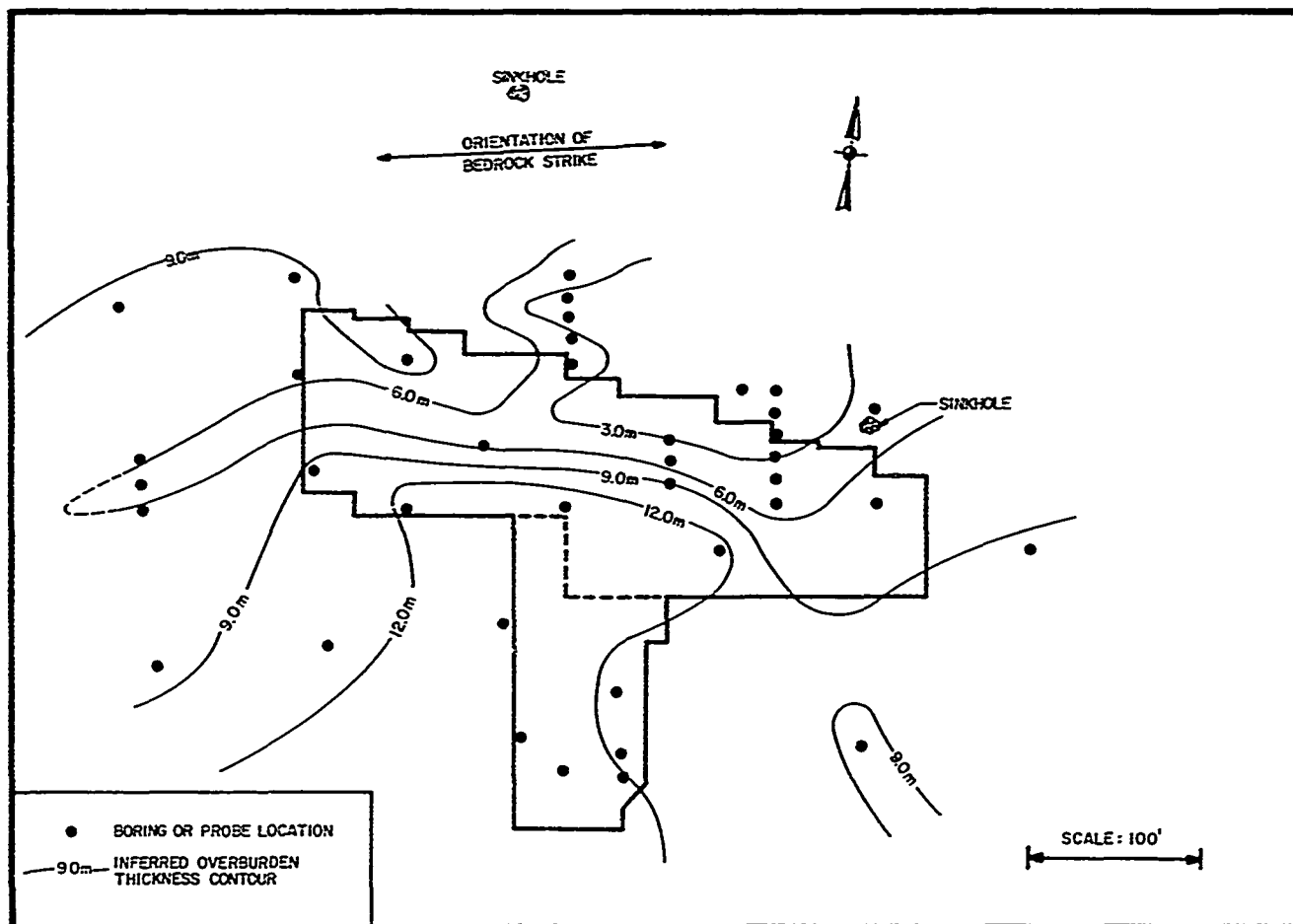


FIGURE 2 TEST BORING LOCATION AND OVERBURDEN ISOPACH

filing was completed using standard shallow seismic refraction techniques. A grid system of traverse lines was laid out perpendicular to bedrock strike. Three traverses also ran parallel to strike, as shown in Figure 3. Spreads of twelve geophones, with 10 ft. or 20 ft. spacing between geophones, were placed along the ground surface.

Because of the way seismic energy travels through the earth it is possible to determine two parameters, depths to materials of increasing velocity and compressional seismic wave velocities. The seismic velocity is a direct measure of the strength, hardness and degree of compaction of the material. Unconsolidated soil overburden would have a low velocity (1000-2000 ft./sec.), whereas hard, unweathered bedrock would have a high velocity (10,000 ft./sec.).

The seismic data indicated a ridge of shallow, intact limestone (3 meters deep or less) running parallel to strike along the northern section of the proposed building. The intact limestone surface dips steeply to the south at 60 to 80 degrees and is in contact with a more deeply weathered, softer phyllite.

Differential weathering of the limestone has created pinnacles aligned parallel to bedrock

strike (N80°E). This was made more apparent by the fact that the seismic velocities calculated from the data collected in the east-west direction were higher than the velocities calculated with the data from the north-south lines. The reason for this discrepancy is that the seismic refraction method uses the seismic energy traveling the minimum time path from the explosive source to each geophone location. For geophones aligned east-west, the minimum time path to each geophone would be along the high-velocity, east-west trending rock pinnacles. The seismic energy traveling in the north-south direction was slower because it travelled through a series of pinnacles and troughs or high velocity and low velocity zones respectively. The anisotropic seismic wave velocities are a direct result of the differential weathering of the underlying calcareous rock and the geologic structure.

Some travel time delays were also observed in the seismic data. A travel time delay is caused by the seismic energy being slowed down crossing a fracture system or a zone that has a lower compressional wave velocity than the material on either side of it. The most prominent time delay was noted at the interface between the shallow, intact limestone ridge on the north end of the site and the softer, deeply weathered

phyllite to the south. It is likely that this is a zone of more severe solution activity. Several smaller travel time delays were also noted on other traverse lines. These delays are interpreted to represent fracture zones traversing across bedrock strike and are roughly parallel to other lineaments in the area. Depth to bedrock has been calculated and an overburden isopach is shown, along with areas containing travel time delays in Figure 3.

#### ELECTROMAGNETIC METHODS

The purpose of the electromagnetic (EM) survey was to identify conductivity anomalies within the limit of study and correlate the findings with the results of the boring program and seismic survey to produce lateral limits of major subsurface conditions. The primary objective was to attempt to locate shallow rock and weak compressible soils associated with sinkholes.

The EM field survey was conducted utilizing an EM-34 Terrain Conductivity meter manufactured by Geonics, Ltd. The instrument uses a magnetic induction method to measure apparent conductivity in millimhos/meter (mmho/m). The EM-34

operates with two coils that can be spaced at 10, 20 or 40 meters apart for successively greater penetration. The effective penetration is about .75 times the intercoil spacing in the horizontal dipole position, and 1.5 times the spacing in the vertical position. Two people are required to operate the instrument.

Approximately 12 hours were needed to adequately cover the four-acre site. The same grid used for the seismic study was used for the EM survey. Over two hundred readings were taken at 10 and 20 meter spacings. Several readings with the 40 meter spacing were attempted, but yielded fluctuating values of less than 1.0 mmho/m. Most readings were measured in the horizontal dipole (HD) orientation since vertical dipole (VD) measurements are more time consuming and prone to coil misalignment.

Variations in terrain conductivity are influenced by several factors including near-surface bedrock, soil porosity and soil moisture. Intact fractured bedrock is a relatively poor conductor in comparison to clayey overburden soils; therefore low conductivity may be indicative of shallow rock.

The 10 meter spacing in the HD mode produced conductivity values ranging from 1.9 mmho/m to

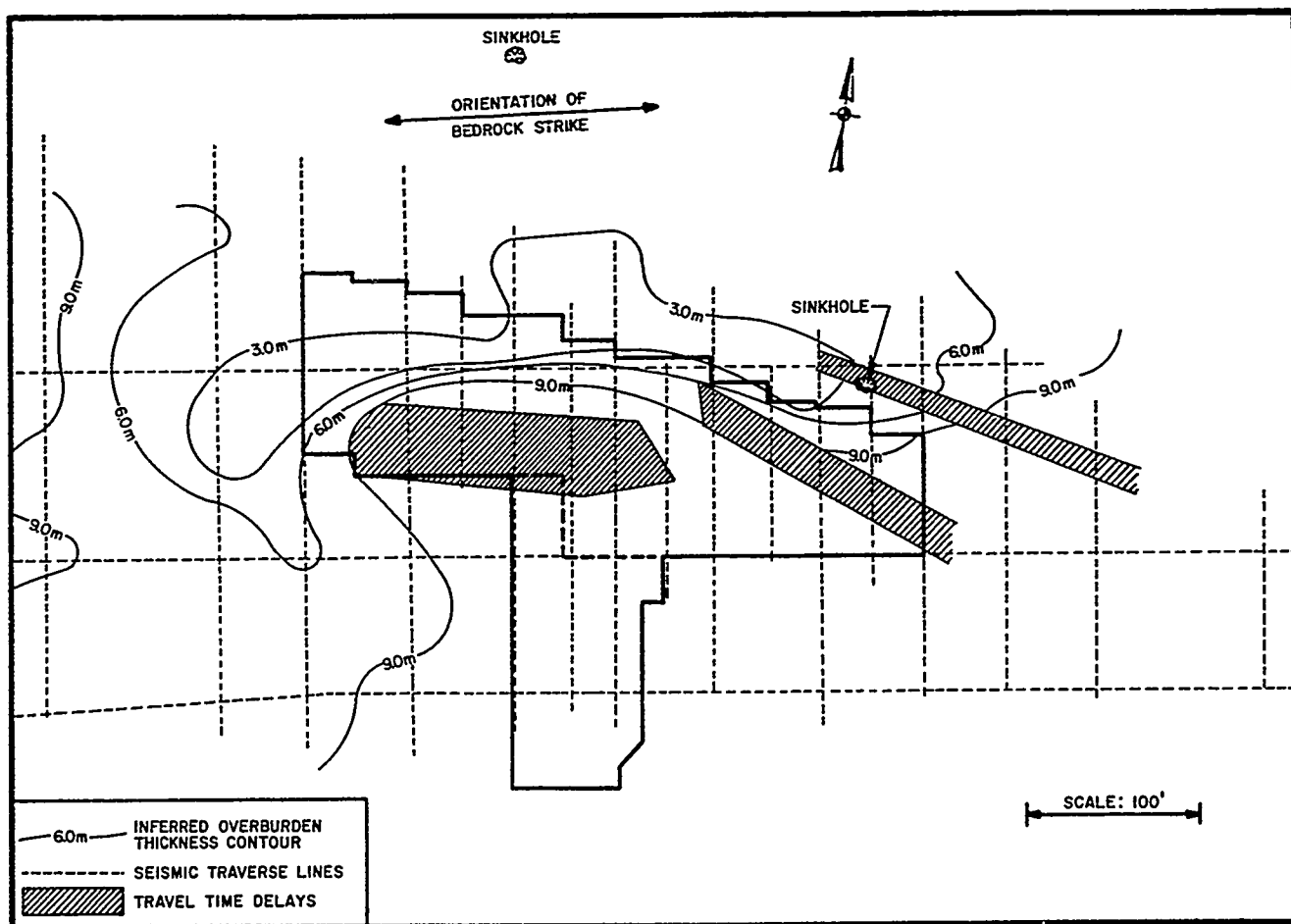


FIGURE 3 OVERBURDEN ISOPACH BASED ON SEISMIC SURVEY

7.6 mmho/m across the site. The data generated is contoured and presented in Figure 4. The 20 meter spacing in the HD mode produced conductivity values ranging from 1.0 mmho/m to 5.1 mmho/m across the site. The contoured data is similar to the 10 meter results, with 20 meter conductivity values reduced overall due to the greater penetration and therefore increase in bedrock effects, shown in Figure 5.

When utilizing information obtained from the test borings, interpretation of the conductivity data allows for several inferences. Since results from the 20 meter spacing confirm the orientation of trends and are not as representative of the overburden, interpretation is based on the more contrasting data provided by the 10 meter spacing. Based on test boring data, zones of near-surface bedrock or pinnacles less than 3 meters below the ground surface occur in areas with conductivity values less than 2.5 mmho/m. Conductivity values greater than 3.5 mmho/m represent a thicker overburden associated with a more easily weathered phyllite. This contact is relatively parallel to bedrock strike except to the east where groundwater effects raise the composite conductivity. A relatively high conductivity anomaly (greater than 4.5 mmho/m) located in the southern portion of the proposed building footprint may represent a fracture zone or lineament that has been infilled with soil. Another conductivity trend in the northeast corner of the site is aligned with observed surface cavities and is parallel to the anomaly to the

south. These features are both parallel to other lineaments in the study area (shown in Figure 1).

#### CORRELATION OF TECHNIQUES

By comparing the results of the test boring program, seismic refraction survey and electromagnetic survey, a high degree of confidence was achieved when interpreting subsurface conditions. Test boring data immediately identified the complexity of conditions when offsets indicated gross overburden thickness variations. However, the data provided an unclear picture of the exact nature of near-surface pinnacles and deep troughs, the lateral limits of which were poorly defined. When comparing EM data with known overburden thicknesses, an empirical correlation was made between apparent terrain conductivity and depth to bedrock. This allowed for delineation of trends and lineaments as well as the limits of shallow rock.

The seismic survey provided a well defined picture of overburden thickness, along with orientating and delineating subsurface features. Of significant importance was the identification of travel time delays representing fracture zones. These lineaments correlated well with other known lineaments in the area. Apparent conductivity data, primarily using the 10 meter coil spacing, generally correlated to those

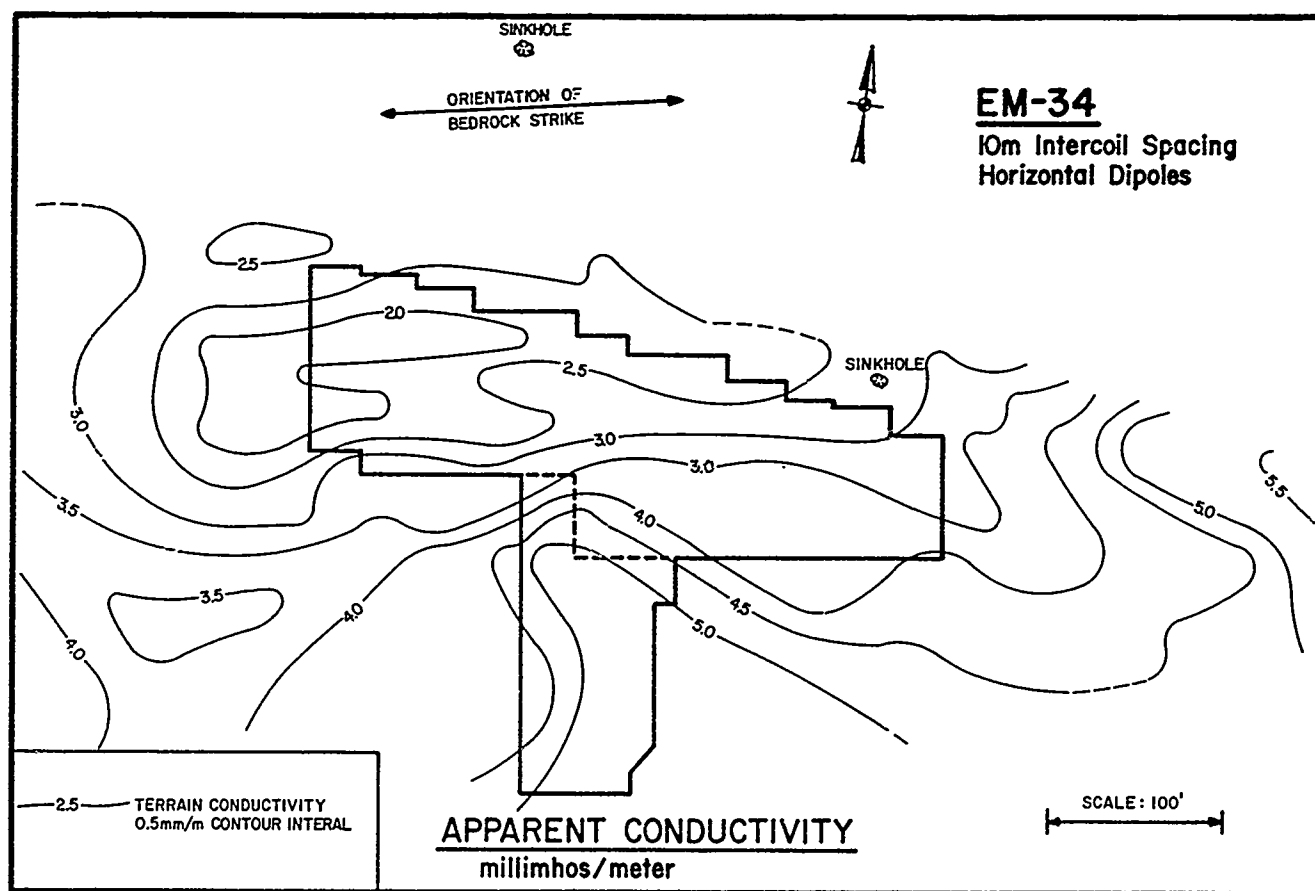


FIGURE 4 ELECTROMAGNETIC SURVEY PLAN

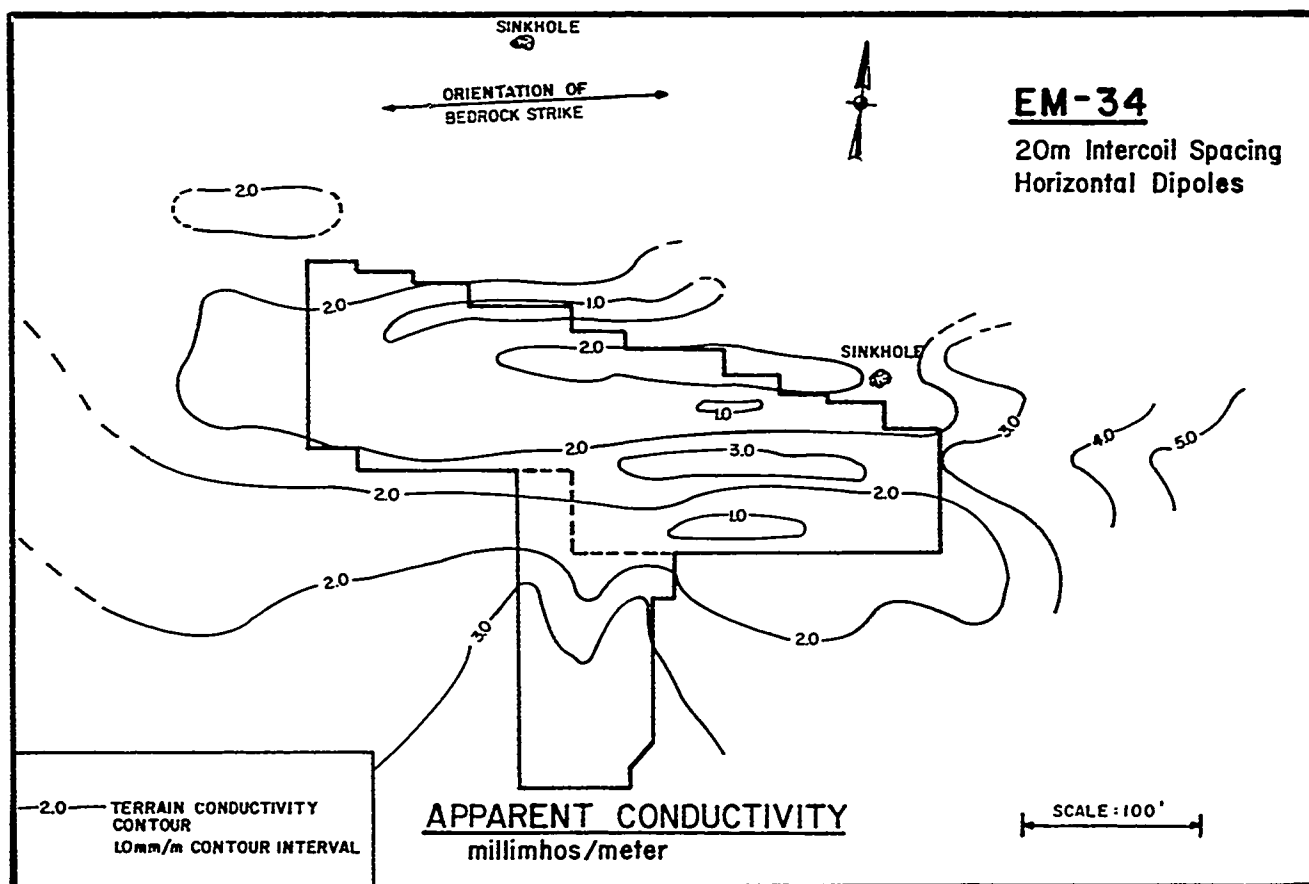


FIGURE 5 ELECTROMAGNETIC SURVEY PLAN

features. Travel time delays aligned with elevated or rapidly changing conductivity values due to either an increase in soil moisture content or a dramatic increase in overburden thickness. This did not hold true to the east, where groundwater effects raised the composite terrain conductivity. Overburden thickness calculations compared well with test boring data except when rock was very shallow (less than 2.0 m.); then overburden thicknesses were slightly overestimated.

In comparing the results of the three techniques shown in Figures 2, 3 and 4, it is clear that each method generally inferred similar subsurface conditions. Although each technique has limitations, the combination of techniques can enhance the interpretation.

#### CONCLUSIONS

It should be noted that neither test borings nor geophysical methods alone can be expected to provide all the information that an engineer may need in a subsurface investigation. However, the combination of the two can provide the lateral and vertical resolution needed in complex environments. A great deal of 'traditional' subsurface investigations are done based on a systematic examination of strata as determined by evenly spaced test borings located at the corners of a proposed building. This method may

be adequate for smaller buildings situated over thick, uniform alluvial deposits or flat-lying, homogenous rock strata. However, in more complex conditions, the geotechnical engineer is left to infer conditions based on limited knowledge of actual conditions. Engineers would ideally like to cost-effectively locate "smart" test boring locations. The use of non-destructive geophysical methods, such as EM or seismic refraction, prior to a test boring program will not only assist in the proper location of borings, but will provide additional resolution to enhance inferred subsurface conditions.

At this site the geologic complexities warranted extensive drilling. However, the investigation demonstrates the use of geophysical methods as a supplemental, cost-effective technique in subsurface investigations; in many cases, the number of test borings required can be reduced by judicious use of geophysical methods.

#### REFERENCES

- Meiser & Earl, Inc. (1985), "Fracture Trace Investigation," unpublished report.
- NTH/Russell Associates (1986), "Geotechnical Assessment Study," unpublished report.
- Vibra-Tech Engineers, Inc. (1987), "Seismic Refraction Report," unpublished report.

## **Session III**

# **“Case Histories of Dams, Embankments, and Slopes”**

## Unusual Behaviour of an Earth-Rockfill Dam

**D. Aboihassani**

Geotechnical Engineer, Mahab-Ghodss Consulting Engineers,  
Tehran, Iran

**F. Bahrami-Samani**

Engineering Geologist, Mahab-Ghodss Consulting Engineers,  
Tehran, Iran

**R.P. Brenner**

Principal Geotechnical Engineer, Electrowatt Engineering Services  
Ltd., Zürich, Switzerland

**SYNOPSIS:** The post-construction behaviour of a 47.5 m high and 700 m long earth-rockfill dam, located in northwestern Iran, is described. The embankment dam is founded on Tertiary rock on both abutments, but in the river channel it rests on alluvial deposits of variable composition and thickness. Since the first impoundment, the dam has undergone large deformations, both in vertical and in horizontal directions. These have resulted in unusual differential settlements, visible along the crest, and have produced wide longitudinal cracks in the asphalt pavement of the crest road. The principle features of the dam are described and selected monitoring results of the crest movements for a sixteen year period are presented. Based on the analysis of the available data and taking into account the geotechnical characteristics of the foundation and the fill materials, an interpretation of the unusual behaviour has been attempted.

### INTRODUCTION

Behaviour control of large fill dams is of great importance to both the dam (geotechnical) engineer and the dam owner. For the dam engineer every large dam usually constitutes a unique experience, because dam geometry, subsurface conditions, construction materials, and construction procedures are never the same, and continuous observation of the behaviour of a constructed facility will show whether the design was successful. For the dam owner, on the other hand, safety, efficient operation and serviceability are the main concerns. Past experience has shown that good site investigation practice and adequate instrumentation are key factors in successfully predicting the future behaviour of a dam. Prediction in turn, forms the basis for implementing appropriate measures during construction to guarantee a satisfactory performance during the dam's service life.

In this paper, the unusual deformation behaviour of Mahabad dam will be presented. After first describing the principal features of the dam and its foundation, selected data on the present condition of the structure and its performance during the past 16 years of operation will be given. Finally, an attempt will be made to interpret the data in the light of subsurface conditions and properties of the fill materials and to give possible causes for the deformations observed.

### PRINCIPAL PROJECT DATA

The Mahabad earth-rockfill dam, located in northwestern Iran, forms part of a multipurpose project which provides irrigation for some 20,000 ha of agricultural land. Furthermore, it generates power from a small plant for Mahabad Town and the villages in the irrigation area, and finally, it

stores potable water for Mahabad Town. The dam was completed in 1970 and filling of the reservoir started subsequently. A layout of the facility is shown in Fig. 1.

#### Embankment Dam and Reservoir

The dam has a maximum height of 47.5 m, a slightly curved, 700 m long crest, and a base width at the valley floor of 221.5 m. A typical cross-section is displayed in Fig. 2. The fill volume is about 1.5 million m<sup>3</sup>. The maximum normal operating water level of the reservoir is at 1358.5 and the minimum at 1333.0. This gives a useful storage of 180 million m<sup>3</sup>.

The dam has a rather narrow central clay core with a slight inclination in the lower 2/3 of its height. The width at the top is 4.0 m and at the bottom 11.0 m. The other material zones can be seen from Fig. 2. The surface of the D/S (downstream) face is covered by a placed top soil layer with planted grass.

#### Engineering Geology and Foundation Conditions

Lithostratigraphy. - Basically, the dam site consists of Cretaceous rocks underlying Neogene deposits which in turn are overlain by Quaternary deposits. The original width of the river plain was about 250 m. Figure 3 shows a cross-section through the valley and dam abutments along the dam axis.

On the left abutment the dam rests first on Cretaceous bedrock for some 50 m. The Cretaceous series consists mainly of shales and slates which are intercalated by limestone beds. For the following 150 m the foundation consists of Neogene rocks of variable thickness and compressibility, but supposedly well consolidated. These are conglomerates and siltstones, but in the only borehole drilled in this section, they are described as "silty clay with lenses of sandy clay and some

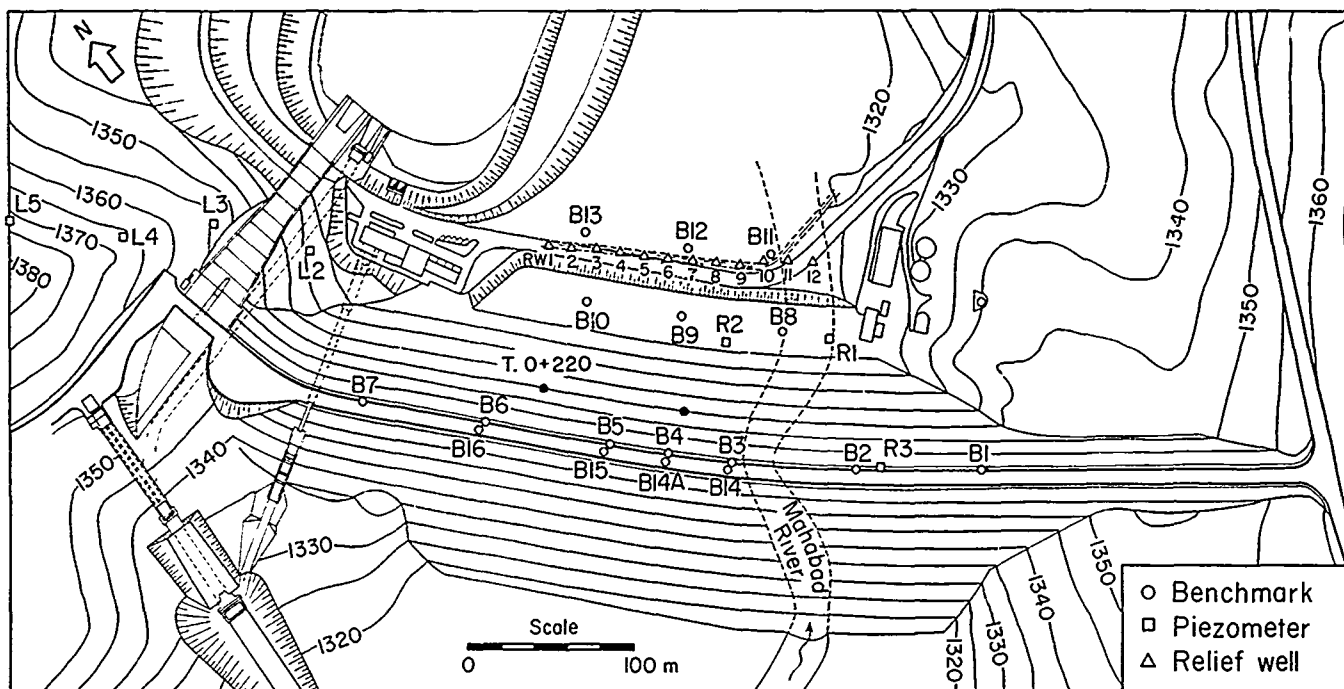


Fig. 1 Layout of Marabad dam showing locations of available monitoring facilities

pebbles" reaching a depth of 29 m.

In the river channel, the Cretaceous formation occurs at a depth of 45 to 48 m. It is overlain by Neogene, Pleistocene and Holocene deposits. The Neogene consists of siltstone, silty sand with lenses of gravel and pebbles, and the thickness of the beds varies from about 25 m on the left side to 8 m on the right side of the valley. The Pleistocene beds are composed of silty clay, sand and silty gravel. The Holocene at the top has an average thickness of about 6 m and contains predominantly silt, sand and gravel. The alluvial fill is very heterogeneous and does not show a continuous stratification.

On the right abutment the supporting rock consists of a thick body of travertine which has formed from (still active) mineral springs between chainage 0+440 and 0+610. It lies partly on the weathered surface of the Cretaceous shales and slates and partly on a thin, lenticularly-shaped remnant of Neogene rock. Further up the right abutment there are again Neogene deposits in the form of clay, silty clay, sand and gravel at the bottom and breccia at the top. They are overlain by a thin mantle of Quaternary silty clay and sand.

Properties of foundation materials. - During the final design phase, the subsurface was inve-

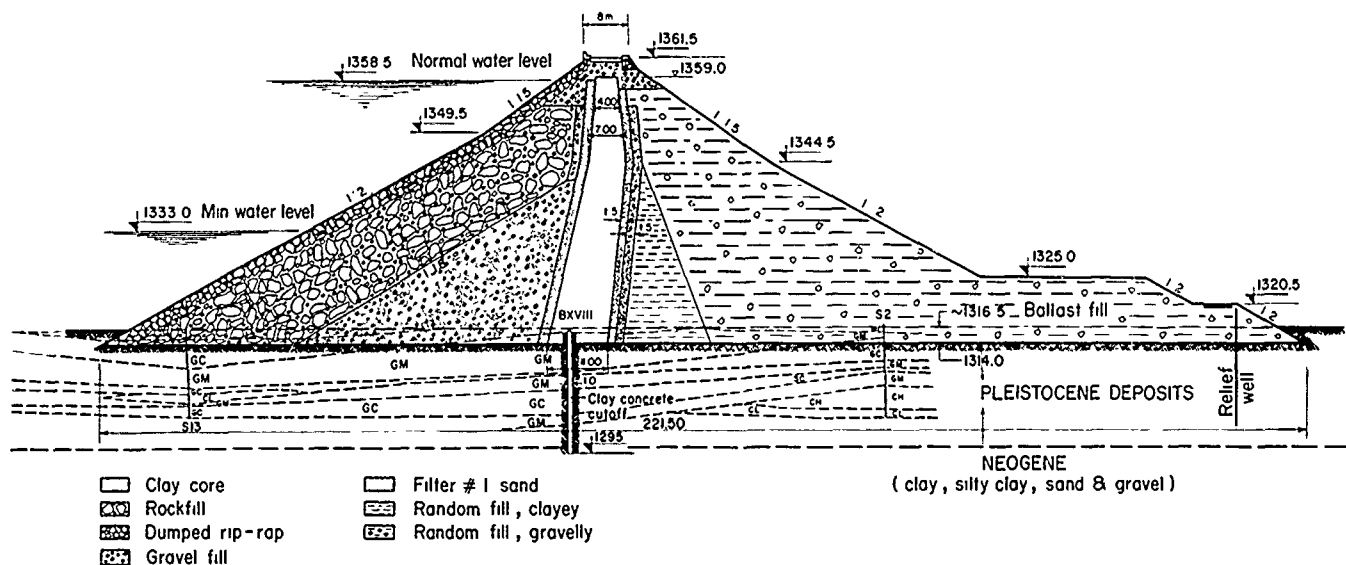


Fig. 2 Cross-section of dam showing material zones



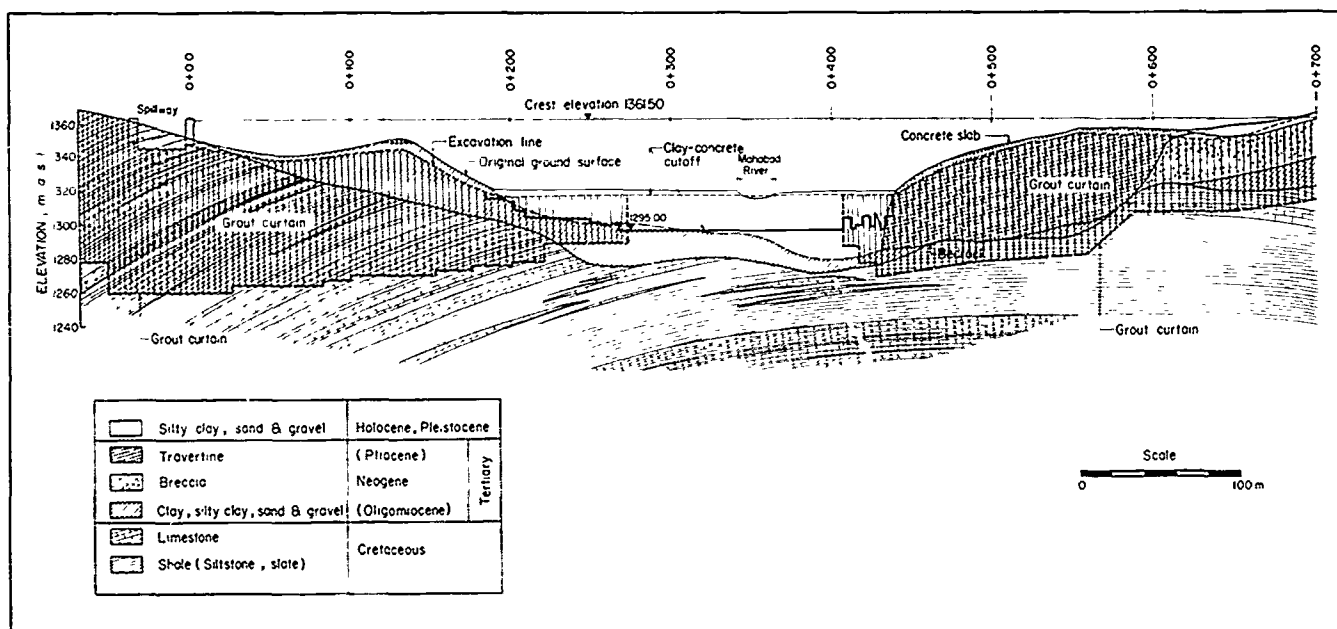


Fig. 3 Longitudinal section along dam axis (looking D/S) showing geology, grout curtain and cutoff

stigated by more than 50 boreholes. Most of these were drilled to shallow depths (15-30 m), but a few also reached down as far as 100 m. The logs revealed the very erratic character of the subsoil. Silty sands, clayey and silty gravel and low-plastic clays were abundant; high-plastic clays, on the other hand, were less common.

In many boreholes standard penetration tests (SPT) were conducted and typical blow counts in the upper 15 m of the alluvium were around 30 with minimum values of about 15. Blow counts varied irregularly and increased as well as decreased with depth in the same borehole.

Permeability tests revealed that there were surprisingly many zones with a  $k$ -value of less than  $10^{-6}$  cm/s or between  $10^{-3}$  and  $10^{-6}$  cm/s. This indicated that the subsoil may actually have been finer-grained than inferred from the boring logs. It is possible that with the drilling method employed some of the fine material had been washed out.

Except for grain size analyses, only few laboratory tests were carried out. Of interest here are oedometer tests on CL and CH soils. For CL soils, the compression index,  $C_c$ , of samples taken from as deep as 40 m typically varied from 0.17 to 0.40 ( $e_0 = 0.40-0.75$ ) when the load increased from 0.8 to 1.6 MPa. CH soils gave higher  $C_c$ -values, e.g. in a borehole 45 m D/S of the dam axis at about chainage 0+250, a sample from 12 m depth had  $C_c$ -values of 0.65 to 0.70 ( $e_0 = 1.45$ ).

#### Seepage Control

Means employed for the control of seepage and to prevent piping were a grout curtain in the abutments and a continuous clay-concrete diaphragm wall along the central part of the dam (see Fig. 3). The diaphragm wall was 20 m deep and 3 m wide. It

cut off fairly pervious Holocene deposits and penetrated into less permeable Pleistocene layers. In the abutments the cutoff was continued as shallow trench excavated through the weathered bedrock. In travertine, the excavation was about 3 m deep and the bottom of the trench was lined with a concrete slab.

An additional control feature which was thought necessary was a row of twelve relief (bleeder) wells, spaced 15 m apart, which are located at the edge of the D/S berm (see Figs. 1 & 2). The top of the relief well is at El. 1320.5. The water level in these wells, however, always remains below the ground elevation.

#### Embankment Fill Materials

Engineering properties of the embankment fill materials are summarized in Table I.

The core material was compacted with a Dynapac CF 44 vibrating sheepsfoot roller in lifts of 30 cm with 6 passes. Field compaction results showed that the field compaction curve was between the standard Proctor and the modified Proctor curves and test results plotted mainly on the wet side with respect to the field compaction curve. Frequency curves of compaction test results demonstrated that 100% of all dry density values were above 95% of the standard Proctor maximum dry density and about 70% were higher than 100% Proctor standard. The most frequent values were between 16.4 and 16.6 kN/m<sup>3</sup>. About 60% of the tests were drier than the standard Proctor optimum water content. The fill water contents varied between about  $\pm 3\%$  with respect to the optimum value which was around 20%.

The random fill and the ballast fill were spread in layers of 30 to 50 cm and compaction was effected by two passes of a 5.4 t vibratory roller.

TABLE I Material properties

| Material type | Granulometry<br>Dis<br>Des<br>(mm) | $\gamma_d$<br>(kN/m <sup>3</sup> ) | $c'$<br>(kPa) | $\phi'$<br>(°) | k<br>(cm/s)       |
|---------------|------------------------------------|------------------------------------|---------------|----------------|-------------------|
| Core          | 0.004<br>0.025-0.2                 | 15.8-17.0                          | 70-140        | 27-30          | $5 \cdot 10^{-8}$ |
| Filter I      | 0.02- 0.1<br>0.5 - 2.0             | 14.7-16.7                          | -             | -              | $10^{-4}$         |
| Filter II     | 0.4 - 2.0<br>15 - 40               | 17.7-18.6                          | -             | -              | -                 |
| Random        |                                    | 18.6-19.6                          | -             | -              | -                 |
| Rockfill      | > 8<br>> 127                       | 18.6-19.6                          | -             | 42             | -                 |
| Gravel fill   |                                    | 19.6-20.6                          | -             | -              | $10^{-3}$         |

Gravel fill was densified in layers of 50 cm with two passes of a 4.6 t vibratory roller. A relative density of 70-75% could be achieved.

The rockfill of the U/S (upstream) shell was placed in lifts of 1.5 m and compacted with four passes of a 15 t vibratory roller. Bulk densities of 19.6 to 21.1 kN/m<sup>3</sup> could be achieved.

Finally, the rip-rap was placed in its full-course thickness.

#### Construction History of the Embankment

Construction of the embankment started in June '68 with fill placement to the left of chainage 0+340 (which was the edge of the river). It continued until October and reached El. 1346. The slope of the fill towards the river (in the direction of the dam axis) was rather steep, probably as much as 1V:1H. Filling was resumed in June 1969 when the river had been diverted through the bottom outlet tunnel. First the breach on the right hand side of the valley was filled and then placement proceeded over the entire length of the embankment. The final elevation was reached in December 1969.

#### Instrumentation and Monitoring Facilities

Facilities to assess embankment performance, both during construction and after putting the dam into service, have been limited to the observation of surface movements and water levels. The following devices and installations are presently available (see Figs. 1 & 4):

##### (1) for deformation measurements:

- Seven target points (or benchmarks) B1 to B7, located on the D/S curbstone of the crest between chainage 0+100 (B7) and 0+485 (B1).
- Three benchmarks, B8, B9 & B10 on the D/S

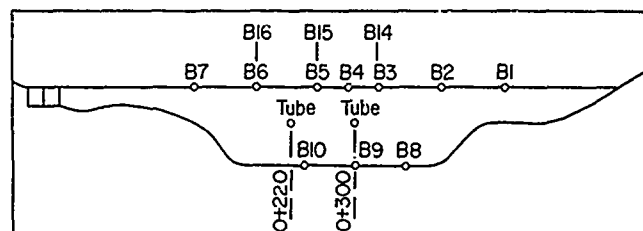


Fig. 4 Longitudinal section showing locations of benchmarks and settlement tubes

berm of the embankment.

- Three benchmarks B11, B12 & B13 located 15m D/S of the foot of the berm.

All these benchmarks could be used to monitor both vertical and horizontal displacements (with azimuth).

- Four benchmark shafts B14, B14A, B15 & B16 along the dam axis on the crest to monitor the vertical and horizontal movements of the top of the clay core. They consist of a 0.4 m ID steel pipe inside a concrete-lined shaft placed on the clay core. Inside the pipe there is a  $\phi$  35 mm steel bar, about 1.5 m long, pushed into the clay such that its top, which is used as a reference, is 0.5 m above the top of the core (installed at the end of 1973).

- Two pipes with a steel plate at the foundation level (approx. El. 1314), 31 m D/S from the dam axis at chainages 0+220 and 0+300. Vertical movements are measured at the top of the pipe (installed in June 1968).

- Twenty-four points (marked by paint) on the U/S curbstone and seventeen points on the D/S curbstone (in addition to the benchmarks) for the measurement of vertical displacements (settlement).

##### (2) for the measurement of pore water and uplift pressures:

- Three open standpipe piezometers R1, R2 and R3 in the D/S foundation of the embankment on the right side of the valley, and four piezometers in the left abutment, i.e. L2 to L5.

- Twelve relief wells, RW1 to RW12, located along the edge of the D/S berm (see Fig. 1).

##### (3) for the measurement of seepage water or leakage through the dam:

- a grouting gallery in the right abutment
- a ditch with V-notch weir located at the foot of the dam on the right side of the valley (near to the water treatment plant).

Data from piezometers and relief wells, as well as from seepage, will not be discussed here; the limited records do not indicate unusual behaviour.

# PRESENT CONDITION AND AVAILABLE DATA ON DEFORMATION BEHAVIOUR

## Dam Crest

The constructed width of the crest was 8.32 m and consisted of a 6 m wide asphalt road and concrete curbstones, 0.30 m high, on both sides. On the D/S side the 0.82 m wide curbstone is supported by dry rubble fill which slopes with 0.8H:1V. It has provision for seating lamp posts and also contains the geodetic target points. The 1.50 m wide U/S curbstone is seated on about 1 m of dry rubble fill with a similar slope as on the D/S side. It contains 0.7 m high masonry wall segments connected by a continuous guard rail. The crest road had an initial camber of 1.0 m.

The present condition of the crest clearly shows that the dam has undergone a complex pattern of differential movements. Figure 5 shows a map of the crest with some of the more prominent features of distress. The most striking ones are the wavy edge of the D/S curbstone, longitudinal cracks in the asphalt pavement, and a tilting of the crest towards U/S. In the following some more details on the appearance of the crest are given:

- Transversal cracks appear around chainage 0+110 and also from 0+450 to about 0+500. These cracks occur because of differential settlements between the abutments and the valley part and are a common phenomenon for dams on com-

pressible foundations (Blinde, 1987).

- Longitudinal cracks appeared between chainage 0+120 and 0+250 and again between 0+335 and 0+370. (A crack opened for the first time close to the D/S curbstone on May 1, 1972, when the reservoir level rose to El. 1357.5 for the first time). Some of the cracks had widths of up to 15 cm, and some also showed a vertical offset of the asphalt by as much as 10 cm, whereby the U/S part settled with respect to the D/S part. The cracks were later filled in with sand and mortar and most of them have remained closed since.
- Between chainage 0+265 and 0+325 the D/S curbstone has buckled forming an arch over the underlying rubble fill with an uplift of about 30 cm.
- At about chainage 0+400 compressive forces have sheared the U/S curbstone and guard rail and produced an overlap of the sheared parts.
- There is a considerable tilt of the road pavement towards U/S. The positions of the leveling points on the D/S and U/S curbstones are shown in Fig. 6, together with the original elevation, for June 1986. The largest differential settlement (tilt) between the two curbstones occurs at 0+226, and on June 14, 1986 it had reached 64 cm. (To get the pavement elevation, the height of the curbstone, usually 30 cm, must be subtracted). The camber at this

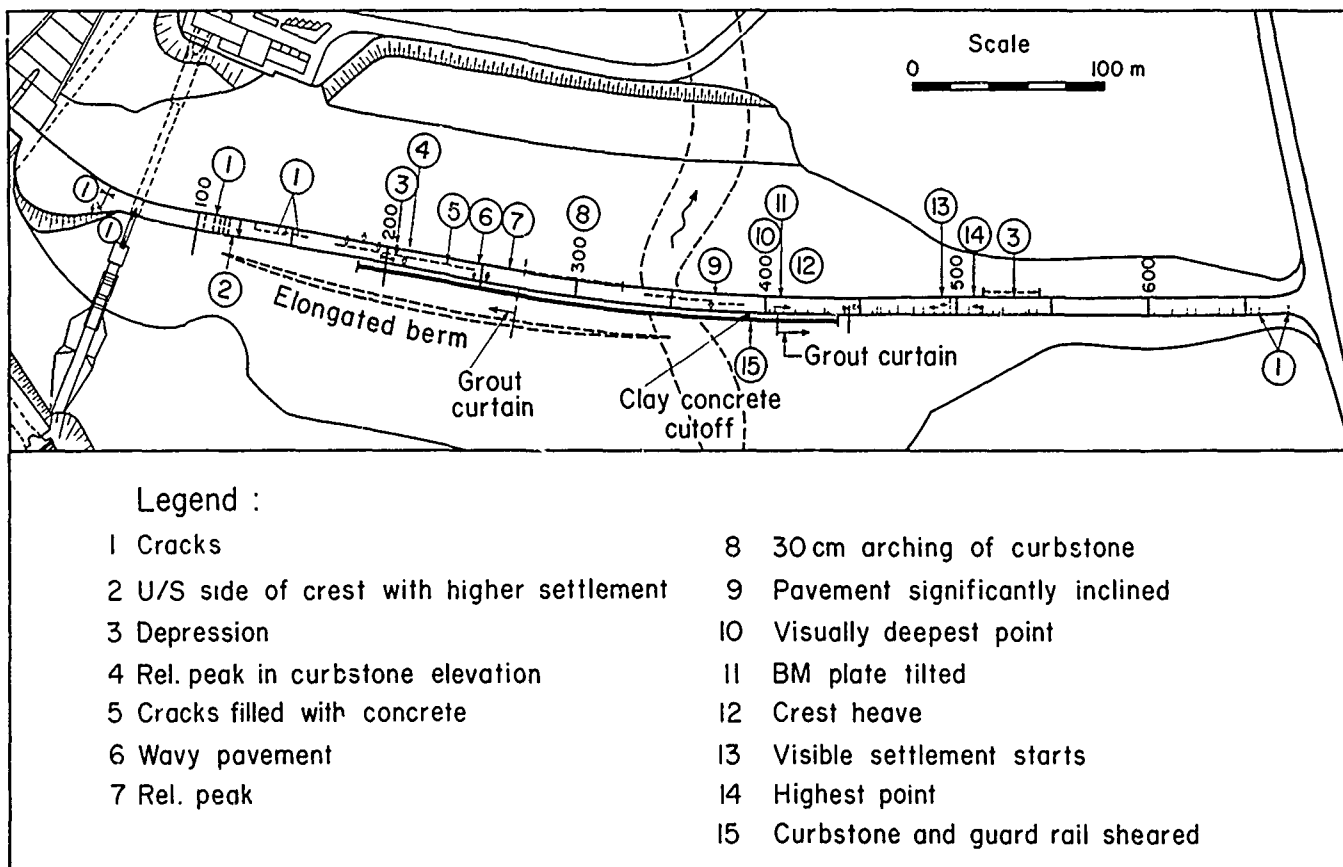


Fig. 5 Crest map showing some of the distress features

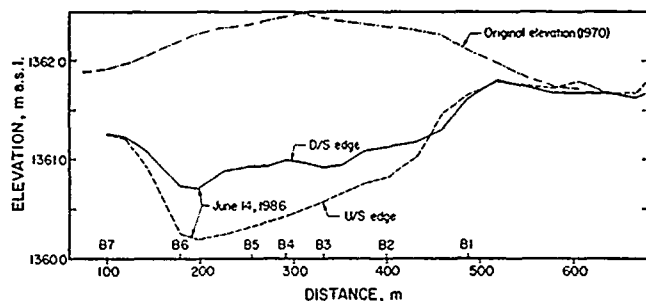


Fig. 6 Differential settlements of U/S and D/S curbstones along dam crest

section was originally 0.85 m and hence the settlement at the centerline of the pavement amounts now to more than 2 m.

#### Vertical Displacements

The time variation of vertical displacements, i.e. the vertical components of the displacement vectors, of crest benchmarks B3, B5, B6 & B7 and of core benchmarks B14, B15 & B16 are shown in Fig. 7. Also shown are the rates of settlement of the ground surface plates (tubes) at 0+220 and 0+300. The positions of these curves are, however, arbitrary. The value of the total settlement (since June 1968) is obtained by adding 700 mm to the settlement value shown by tube 0+220 and 950 mm to that of tube 0+300. The reliability of these ground settlements is, however, questionable, because there is no sleeve provided between the settlement pipe and the fill material.

During the first phase of fill placement to El. 1346, the settlements of tubes 0+220 and 0+300 were 520 and 830 mm respectively. The corresponding stress increase was approximately 0.55 MPa.

During the following eight months of no fill placement, the settlements increased by 90 and 120 mm respectively. When fill placement was completed in December 1969, additional settlements of 130 and 340 mm respectively had taken place with an estimated stress increase of 0.12 MPa. From these data the constrained modulus of the foundation can roughly be estimated as 10 to 20 MPa (assuming a compressible layer thickness of about 20 m).

For the vertical movements the first four filling and drawdown cycles are of particular interest. During the first year of impounding (1971) the reservoir level reached a peak of 1351. Settlement rates started to increase when the level had reached 1342.5. They decreased soon after the peak had been exceeded. During the second reservoir peak in 1972, settlement rates started to increase when the reservoir level reached El. 1353, and decreased again when it receded to El. 1355. Interestingly, an increase also took place during the very deep drawdown in winter 1972/73. Benchmarks B8, B9 & B10, on the other hand, showed a slight rebound of about 2 cm. No increase in the rates of settlement was observed during the following reservoir peak in spring 1973 which attained only El. 1353. A further increase occurred in summer 1974, especially also with the newly installed core benchmarks B14 to B16. It started when the reservoir level reached about El. 1345. Another increase in settlement rates can be noticed in 1976, but since then settlement rates have decreased steadily without showing a strong relationship with reservoir level fluctuations.

Settlement rates at benchmarks B8 to B13 remained quite small and were not affected by the reservoir level. Tubes 0+220 and 0+300 had a much reduced settlement rate when compared with B3 to B6

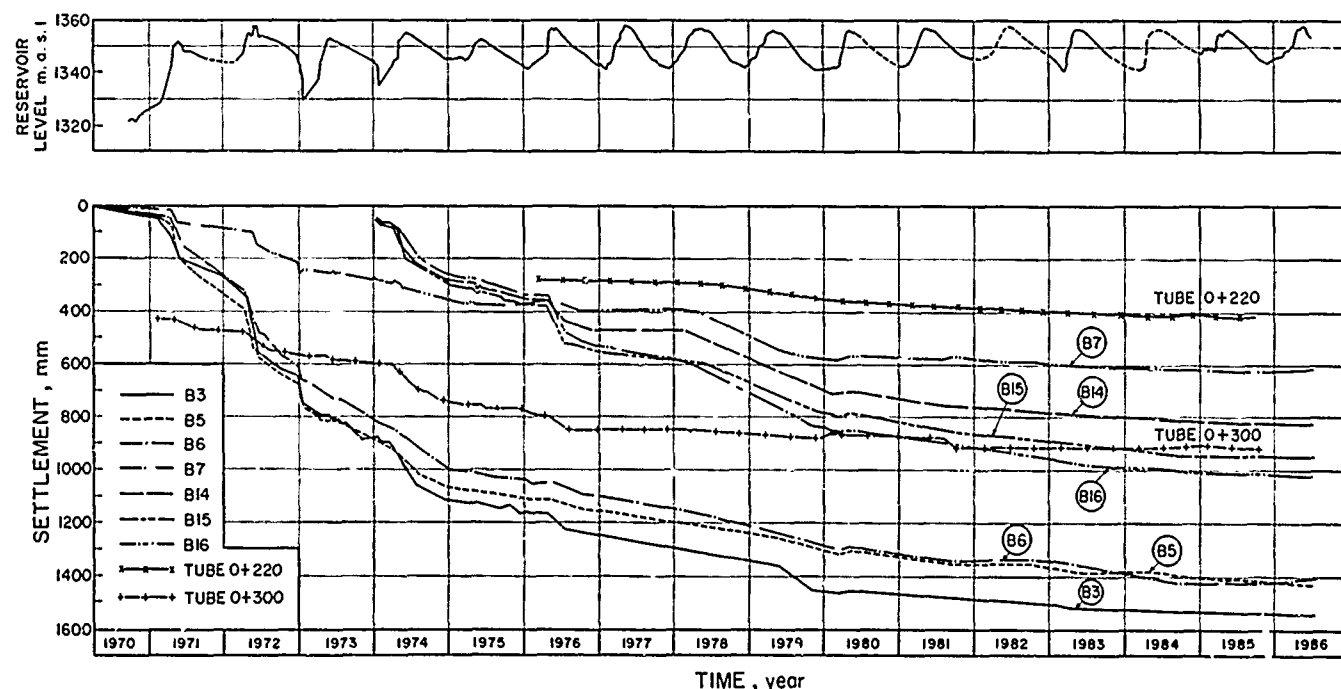


Fig. 7 Vertical components of displacement vectors (settlement) of selected points

and were not very sensitive to the water load imposed.

The rates of settlement of the top of the clay core, as observed by the shaft benchmarks B14 to B16, were higher than those of the corresponding curbstone benchmarks. For example, since installation at the end of 1973, B16 has settled 1020 mm while B6 has settled only 610 mm. This is because of the rigidity of the curbstone which may cause arching.

The distribution of the vertical displacements between B1 and B7 is more or less symmetric with respect to B4, i.e. the center of the valley.

#### Horizontal Displacements

Figure 8 shows the time variation of horizontal displacements (i.e. the components of the displacement vectors perpendicular to the longitudinal axis of the dam) of benchmarks B3, B5, B6, B7 and of B14, B15 & B16. It can be seen that during the first filling cycle in 1971, the crest points moved first towards U/S. Only after the peak had been exceeded, i.e. about 4 months after start of impounding, the movements reverted to the D/S direction. Benchmarks on the D/S berm, B8 to B10, on the other hand, always moved towards D/S, but at a much smaller rate.

The time variations of the horizontal displacements are similar to those of the vertical components (settlement), i.e. accelerations in the movements can be noticed when the reservoir level reached 1353 during the 2nd filling in 1972 and again when it reached 1345 during the 4th cycle in 1974. During the deep drawdown in winter 1972/73 there was a small rebound and the crest moved U/S by about 3 cm.

In a horizontal plane the displacement vectors point to the center of the valley, i.e. B1 to B4 move to the left, while B5 to B7 follow a path turning to the right. The displacement pattern with respect to the valley is not symmetric; the largest horizontal displacement has occurred at B6.

#### DISCUSSION

Large settlements of dams on compressible foundations are as such not unusual. In the case history presented here, the unusual behaviour refers to the underestimation of the settlements and the relatively large horizontal displacements and tilting of the crest.

An analysis of the deformations Mahabad dam has

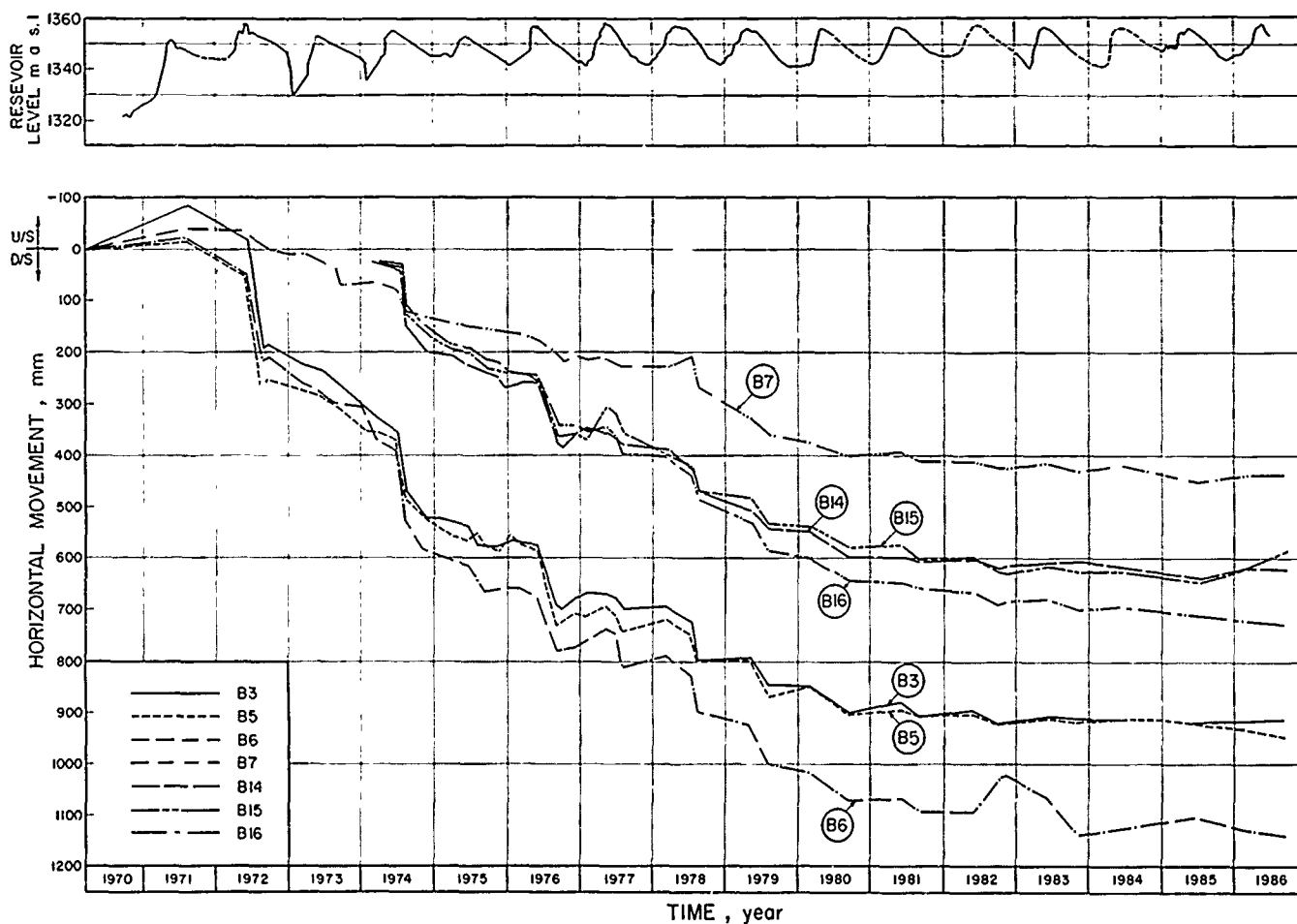


Fig. 8 Horizontal components of displacement vectors of selected benchmarks

experienced must involve some speculations because the data now available are not sufficient to find out the true mechanism with certainty. The main factors which have most likely contributed to the unpredicted differential movements are: (1) a foundation which was more compressible than anticipated from site investigation, and (2) a strength decrease (weakening) with time of the U/S rockfill under submerged conditions or under wetting and drying cycles. In the following, a possible mechanism is put forward which would explain the phenomena observed.

During the first filling, the U/S shell settled partly because of the wetting of the rockfill, which caused a strength decrease, and partly from the compression of the relatively impervious lake bottom U/S of the dam axis, which was wetted for the first time, under the water load. This produced a tilt of the crest towards U/S with a horizontal displacement component in the same direction. The importance of the compressible foundation in contributing to this mechanism has actually been verified by physical model and finite element studies (Alberro et al, 1976). During the 2nd filling, the water load was considerably larger than in the previous year (it increases with the square of the depth of the impounded water) and the rather plastic core was pushed on the D/S shell causing the crest to move in D/S direction (compare also with the analysis given by Nobari & Duncan, 1972). In addition, the steeper U/S part of the U/S shell became submerged for the first time; its settlement produced additional tilting. The settlement of the U/S shell in combination with the D/S movement of the crest produced longitudinal cracks which became visible in the rigid asphalt pavement. These cracks were probably also associated with a sliding movement. The D/S curbstone which originally had not been divided into segments buckled as a result of the compressive forces developed by the D/S movement. The settlement of the D/S shell remained small, as evidenced from benchmarks B8 to B10 and also from the foundation settlement plates (e.g. tube 0+300).

When the dam was subjected to a deep drawdown in winter 1972/73, the U/S shell, for the first time after about 1 1/2 years of submergence, experienced an increase in effective stress leading to additional settlements. It must also be assumed here that parts of the rock in the rockfill have been weakened during soaking. This hypothesis can be substantiated by the facts that also in the rip-rap (for which rock of the highest available quality was employed) some large blocks show now a splitting up along numerous fissures. In the quarry from which the rockfill had been obtained, the rock is often highly fissured and in some places also platy. Tests on these rocks also showed that after wetting the compressive strength was reduced to one half or even less.

It is believed that most of the settlement observed after the dam was completed was due to the weak foundation which was more clayey than originally inferred from site investigation and indicated in the foundation of Fig. 2. The dam was well-built according to the monthly construction reports and usually a dam of this height does not settle more than about 20 cm if it were

founded on rock (max. 0.3% of its height according to Dascal, 1987). The rate of settlement and also that of horizontal movement have steadily decreased and it can be concluded that primary consolidation has now been completed. Further settlement will be due to creep.

## CONCLUSIONS

The case history presented here demonstrates first the importance of instrumentation in large dams. Had the dam been properly instrumented, especially with respect to settlements and lateral movements, in both the foundation and the dam body, it would have been possible to predict future settlements after completion of construction fairly accurately and an appropriate camber could have been provided. It also would have been possible to clearly separate the settlements taking place in the foundation from those occurring in the dam body.

Second, the benefit of a good quality site investigation which is able to identify the true characteristics of the subsurface strata, must be emphasized. Layers with low permeabilities, even if coarse materials appear to make up the bulk, will not complete their consolidation during construction and will be a source of long-term movements.

## ACKNOWLEDGEMENTS

The work presented herein forms part of an ongoing study on the monitoring facilities and safety of Iranian dams carried out by Mahab-Ghodss Consulting Engineers, Tehran, in association with the Joint Venture Stucky-Electrowatt, Lausanne, Zürich. Much of the data given here has been compiled from numerous reports and records stored in the archives at the dam site and the provincial water board. The cooperation of the staff of Mahabad dam site in making these sources of information available is gratefully acknowledged.

## REFERENCES

- Alberro, A.J., A. Arenas D. and J. Flores N. (1976), "Requena Dam", in: Behavior of Dams built in Mexico, pp. 41-61.
- Blinde, H. (1987), "Staudämme und ihr Untergrund", Felsbau, 5(3): 138-143.
- Dascal, O. (1987), "Postconstruction deformations of rockfill dams", J. of Geotechnical Engineering, 113(1): 46-59.
- Nobari, E.S. and J.M. Duncan (1972), "Movements in dams due to reservoir filling", Proc. Conf. Performance of Earth and Earth-Supported Structures, Lafayette Indiana, 1:797-815.

# Seepage Indicent, St. Stephen Powerhouse, St. Stephen, S.C.

**J.W. Erwin**

Ph.D., Supervisory Geologist, U.S. Army Engineer Division,  
South Atlantic

**G.R. Baer**

P.E., Geotechnical Engineer, U.S. Army Engineer Division,  
South Atlantic

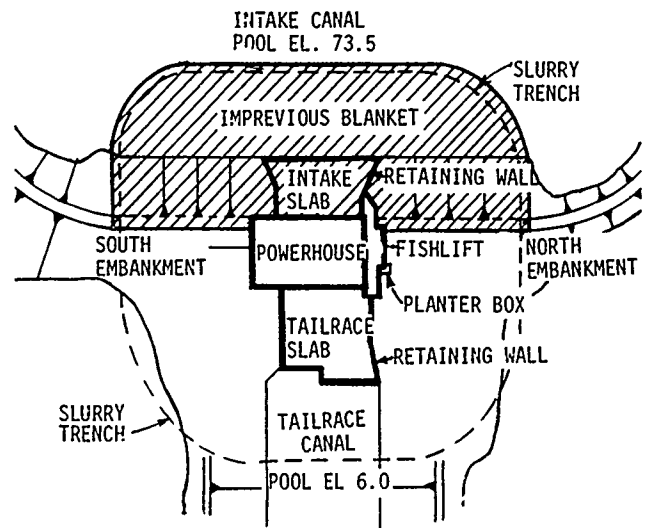
**SYNOPSIS:** On 4 November 1983 during the initial filling of the upper pool for the St. Stephen Powerhouse an emergency seepage condition developed in the north embankment immediately adjacent to the powerhouse and fishlift. At the time of the incident there was approximately 67 feet of head across the structure. A carefully planned investigative excavation of the north embankment was conducted to expose the conditions involved in the seepage incident. An Investigative Panel concluded that there were four design related physical factors which contributed to the development of the seepage. Fragmentation of responsibility for the design and construction of the St. Stephen Powerhouse was a major contributing factor to the development of the physical factors which led to the seepage incident. Excavation of the embankment also indicated serious construction deficiencies, which although not directly related to the seepage incident, would in the opinion of the Investigative Panel have ultimately led to a seepage problem.

## INTRODUCTION

The St. Stephen Powerhouse is part of the U.S. Army Corps of Engineers' Cooper River Rediversion Project near Charleston, South Carolina. It is located in a canal which connects Lake Moultrie and the Santee River. The project purpose is to reduce dredging in Charleston Harbor. This has been accomplished by diverting a large portion of the flow of the Santee River which flowed through Lakes Marion and Moultrie and down the Cooper River back into the Santee River. The flow in the Cooper River caused excessive siltation in Charleston Harbor. The powerhouse was constructed to take advantage of the hydropower potential available in the diversion canal and to replace the energy lost at the Pinopolis Powerhouse on the Cooper River because of the rediversion.

The powerhouse is tied into a system of levees on each side of the canal by a north and south embankment (reference Figure 1). The embankments are zoned fills with a crest elevation of 86. The invert of the intake canal is elevation 50 and the tailrace canal is elevation 0.0. With a normal pool at elevation 75 the embankments are subjected to a head differential of approximately 69 feet. A fishlift is incorporated into the north side of the powerhouse.

Reservoir filling was initiated on 1 November 1983 and was within 1.5 feet of normal pool on 4 November when an emergency seepage condition developed in the north embankment adjacent to the powerhouse and fishlift. The first manifestation of the problem was flow from the north tailrace retaining wall weep holes located at elevation 6.0 at 0830 hours. Later that afternoon around 1300 hours water was observed coming through the bottom of a large planter box placed about midway in the downstream slope of the embankment adjacent to



PLAN VIEW-POWERHOUSE AND APPURTENANT STRUCTURES

FIGURE 1

the powerhouse and fishlift wall. Within four to five minutes, water was overflowing the top of the planter box which was at elevation 64, or just 9.5 feet below the upper pool. Initial flow was calculated to be approximately 1700 gpm. By 1400 hours flow from the planter box ceased and at 1500 hours a sink hole was discovered on the upstream slope a few feet from the crest of the embankment. At 1530 hours flow from the tailrace weep holes increased and became muddy. The flow was strong enough to cause turbulence in the tailrace surface out a distance of 25 feet. The flow from the weep holes subsequently cleared.

The Contractor and Corps' Resident Engineer and staff worked throughout the evening of 4 November to ensure that the problem was under control. The first action was to dump sacks of dry bentonite into the lake around the upstream retaining wall. The bentonite was later observed in the water coming through the bottom of the planter box. A surcharge fill was also placed on the upstream slope to choke the seepage intake. After a few hours the seepage rate declined significantly. Initially, this was attributed to the placement of the surcharge fill, however, it was later determined that the internal filters within the dam functioned to the extent that they clogged and blocked the seepage paths. In a separate action an earthen plug was placed across the canal upstream of the powerhouse to prevent the potential loss of Lake Moultrie. By the end of the day the emergency seepage condition was under control and drawdown of the pool upstream of the powerhouse was initiated.

A ten member Investigative Panel from within the Corps was convened to investigate the causes related to the development of the seepage. The Panel closely evaluated all aspects of the design and construction of the project which may have contributed to the seepage incident. The north embankment adjacent to the powerhouse was carefully excavated and examined. Some of the findings of the Panel are unique to this specific project, others, however, have a much wider application.

#### EMBANKMENT SEEPAGE CONTROL

In the plans and specifications the seepage control immediately adjacent to the powerhouse consisted of a 30 feet wide impervious core extending from the top of the embankment, elevation 86, to the bottom of the structural excavation. A sheet pile wall then extended through the overburden materials to the top of a clay shale unit at approximately elevation -23. The combination core/sheet pile cutoff tied into a slurry trench constructed around the perimeter of the site for the purpose of construction dewatering. The zonation in the remaining portion of the embankment was somewhat complicated due to the structural configuration of the powerhouse and connecting fishlift on the north side, as well as the intake and tailrace retaining walls. Immediately downstream of the core, however, was zone II material (silty and clayey sand).

Upstream of the core at the lower elevation was a "select backfill" material consisting of a crushed rock which served as the foundation of the intake retaining walls. This material was overlain by a very open "pervious fill". A modification to the contract added a zone of filter material upstream of the impervious core to separate it from the "pervious fill".

As a result of anticipated problems with the installation of the steel sheet piling cutoff, the contractor submitted a Value Engineering Change Proposal (VECP) to alter the seepage control features of the embankment. The VECP eliminated the sheet piling cutoff and the impervious core below elevation 45. It replaced these features with a five feet thick upstream impervious blanket which tied into the impervious core, the structure, and the construction dewatering slurry trench that encircled the structure. Below elevation 45, the impervious core material was replaced with zone I material which was a silty to clayey sand (refer to Figures I and II). Since the impervious blanket encompassed the intake retaining walls, waterstops were also required between monolith joints as a result of the VECP.

#### PANEL INVESTIGATION

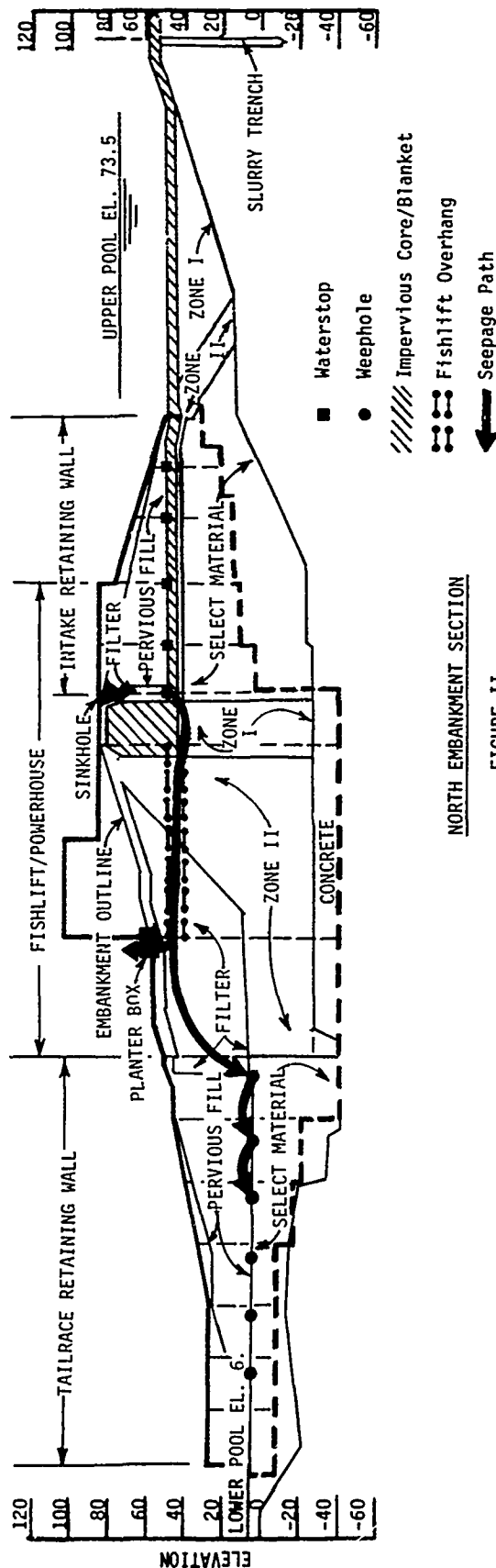
The Investigative Panel was composed of nine senior engineers and one engineering geologist from within the Corps. Over a period of approximately two months the Panel performed an in-depth evaluation of the circumstances and events leading to the seepage incident. The following is a summary of the Panel's findings on the more pertinent items.

#### Excavation and Exploration of the Embankment.

A carefully planned investigative excavation of the north embankment was begun on December 8, 1983 to expose the conditions involved in the emergency seepage problem. The investigative excavation was methodical and detailed. The records obtained and the observations made as it progressed were invaluable to the Investigative Panel in furnishing factual information relative to the seepage incident.

The excavation revealed that the path of the seepage flow began through and around the waterstop located in the monolith joint between the upstream retaining wall and the powerhouse (reference Figure II). This waterstop was added as a part of the VECP. The monolith joint is 16 feet upstream of the centerline of the embankment at the approximate contact of the core and the upstream filter. The flow breached the upstream impervious blanket at the waterstop and caused the development of a sinkhole in the embankment above the lake level. There were numerous deficiencies associated with both the design and construction of the waterstop. The flow traveled through the joint and into the select fill (pervious crushed rock) beneath the upstream impervious blanket. This allowed full reservoir head to act on the silty and clayey sands of the zone I fill immediately beneath the impervious core





NORTH EMBANKMENT SECTION

FIGURE II

of the dam.

A concrete overhang on a 45 degree slope between elevations 42 and 49.83 was constructed as part of the fishlift on the north face of the structure. This overhang extended from 9 feet downstream of the centerline of the embankment to 105 feet downstream. The overhang actually extended six feet into the core section of the embankment which at that point is approximately 30 feet wide. As previously stated the bottom of the core was at elevation 45. A void developed beneath this overhang due to settlement of the embankment fill.

The path of seepage flow extended in a downstream direction by either piping the zone I fill underlying the core into the void beneath the overhang or by hydraulically fracturing and eroding the zone I fill or, by a combination of these. The extension of the seepage path between the waterstop and the overhang was beneath the contact of the impervious core and zone I. A considerable portion of the path was at the contact of zone I and the fishlift wall. The seepage path followed the void beneath the overhang thus extending downstream approximately 96 feet. The seepage path divided at this location. One path went vertically up the concrete and embankment interface and exited through the planter box, the bottom of which was located immediately above the downstream end of the overhang. The other continued downstream to the tailrace retaining wall weepholes. It, too, followed the interface of the concrete and the embankment.

The waterstop between the powerhouse and first intake retaining wall monolith consisted of a split faced PVC waterstop. The split side was attached to the face of the powerhouse with mastic and bolted into the concrete with 1-1/4 inch long expansion bolts through a 1/4 inch steel strap. The other half of the waterstop was encapsulated in the concrete of the retaining wall. This waterstop failed by being pulled from the powerhouse due to opening of the joint, probably due to normal shrinkage and thermal contraction. The waterstop was also deficient in other respects. For one, it depended upon a seepage path through the upstream impervious blanket which was only as long as the thickness of the waterstop membrane to resist the full hydraulic head acting across the impervious blanket. The waterstop also lacked approximately 1-1/2 inches of extending to the outer edge of the concrete which permitted an open gap between the end of the waterstop and the edge of the impervious blanket.

A 25 foot wide structural notch in the fishlift wall which the impervious core ties into was also believed to have contributed to the seepage incident. The notch is formed by the two sides of the main fishlift structure and partially by the first upstream retaining wall on the third side. The problem with the notch, which almost entirely encompasses the core, is two-fold. First, the notch interfered with machine compaction and required considerable hand compaction in what is one of the most critical sections for

seepage control in the dam. Secondly, the core in contact with the notch, specifically on the downstream and south sides, had the potential of causing a reduction in compressive stresses in the core at the lower elevations due to arching of the fill. The potential reduction of compressive stresses within the core was an invitation for hydraulic fracturing and subsequent piping, particularly when it is considered in combination with the overhang.

From the investigative excavation the Panel determined that the seepage incident occurred due to four design deficiencies: (1) the overhang on the fishlift which protruded into the embankment fill and resulted in the development of a void when settlement occurred in the embankment, (2) the upstream retaining wall waterstop, designed as a part of the VECP, which failed to act as a seepage barrier, (3) the fishlift notch which presented an obstruction to machine compaction and magnified the tendency for fill to arch in contact with a steep abutment such as was formed by the concrete structure, thereby facilitating hydraulic fracturing and piping and (4) replacement of impervious core material with zone I material below elevation 45 which placed more pipeable and erodible material in the path of seepage than would have existed under the original design.

In addition to the design deficiencies, the excavation also revealed a number of construction deficiencies. Extensive interfingering or overlapping of the embankment zones were noted. There were locations where the zone II fill downstream of the core was interfingering into the impervious core as much as 7.5 feet. Unsuitable material was also found in the core section between elevation 48+ and 49+. In addition, in most density tests above elevation 54, the materials encountered in excavating the impervious core section failed to meet the specified density. Excavation of a trench across the tie-in of the impervious blanket and the slurry trench in one area indicated a blanket thickness varying from 0.2 to 4.0 feet. The thickness was specified as 5.0 feet. Although these construction deficiencies were not directly related to the seepage incident, it was the opinion of the Panel that these deficiencies could have led to a future seepage problem.

#### Embankment and Structural Design and Design Review Process

The design process for the St. Stephen Powerhouse Project was complicated in that 3 Corps districts and an Architect Engineer firm were involved in the design. This factor made it impossible to isolate the responsibility for the design deficiencies. Late in the design stage, in an effort to accommodate requests from the U.S. Fish and Wildlife Service, significant changes were made in the outside configuration of the powerhouse structure. The changes were (1) the introduction of the fishlift overhang that protruded into the impervious core and (2) the provision for the structural notch which the impervious core tied into. The effects of

these changes were not fully considered. The district which accomplished the original embankment design was not involved in these changes or given the opportunity to review the final design or plans and specifications which were developed by an AE. In fact, there was a significant lack of geotechnical involvement during the final design on the part of the Corps as well as the AE. Of ten review and approval meetings conducted during the final design, only one was attended by a Corps' geotechnical engineer, and he was young and lacked experience in dam design.

Review at both the district and division levels within the Corps of the embankment plans and specifications as presented by the AE indicated inadequacies, particularly with the embankment plans. Emphasis placed on meeting the scheduled advertising date for the project, however, dictated that only revisions be made rather than completely redoing the embankment plans. These revisions were performed primarily by the Corps since the AE had displayed a lack of geotechnical expertise. Although the embankment sections added to the final plans and specs by the Corps helped clarify the embankment zoning, they failed to identify the impact the overhang and notch had on the embankment. In the opinion of the Panel, considering the condition of the plans and specs received from the AE and the time restraints imposed for review and revisions, the district responsible for the revisions did the best they could.

The primary problem during the overall design process was the failure to "marry" the embankment design by the Corps with the final powerhouse design of the AE. The Panel found that this can be attributed to (1) the failure to involve the original district responsible for the embankment design in the final design, (2) the lack of geotechnical expertise committed to the project by the AE, and (3) the lack of geotechnical involvement by the Corps during the A-E's final design. The Panel was also of the opinion that once the inadequacies of the geotechnical portions of the plans and specifications as received from the AE were identified, it would have been prudent to have taken the time necessary to ensure a quality product.

#### Constructibility Review

A detailed constructibility review of the embankment plans and specifications was not performed. It appears that there were two reasons for this. First, there was no construction division in the district which was responsible for the construction of the powerhouse. A special field construction office had been set up for this project. Consequently, the responsibility for the constructibility review fell on the Resident Engineer's office which had limited capability to perform such a review. The other reason was that the earthwork plans and specifications which were received from the AE required significant revisions by the Corp's designers to get them into acceptable condition to advertise. These revisions consumed most of the time that was available for such a review.

## Construction Management and Supervision

The evaluation of the construction management and supervision centered on the construction deficiencies which were observed during the excavation of the north embankment which indicated that the Contractor Quality Control (CQC) and the Corps Quality Assurance (QA) programs were not effective for the embankment. In general, it was determined that there was an absence of consistent CQC inspection of the embankment construction. The CQC effort focused on testing rather than inspection. Testing is not quality control; it is quality verification. The Corps' quality assurance program suffered from a number of factors which made it less effective than was necessary. Lack of full time inspection coverage of the embankment construction was a major failing. But to retain proper perspective, it is worth noting that the QA personnel are not responsible for the instances of noncompliance with the contract specifications; the Contractor holds the entire responsibility to ensure that his work is in compliance, regardless of the right of government inspection. The CQC was not effective in achieving acceptable quality of the embankment construction.

## Value Engineering Contractor Proposal Design Change

The Value Engineering Contractor Proposal as stated previously, resulted in a major change to the seepage control features of the embankment. The Panel found that certain features of the VECP changes contributed directly to the emergency seepage problems as they occurred. These features were the design of the waterstop and the replacement of the impervious clay core material with more erosive zone I fill below elevation 45. The VECP was submitted in a conceptual form only, and the contractor indicated that the government would bear all responsibility for design if accepted. The VECP was evaluated and accepted by the Corps and revisions to contract plans and specification were made by the Construction Project Office with guidance from engineering. The Panel was of the belief that the design efforts required by the revisions exceeded the capability and responsibility of the Construction Project Office. Further, there appeared to be insufficient coordination between engineering and construction during the revision process, particularly concerning the waterstop details. It was the opinion of the panel that the time and effort expended on the evaluation of the VECP was not sufficient to evaluate the full impact of the VECP changes or to develop adequate details for implementation. The changes resulting from VECP constituted a significant departure from the approved design and their development should have warranted effort consistent with effort for an original design.

## CONCLUSIONS

### Mode of Seepage

The Panel found the seepage incident to initiate with water which was able to bypass a

failed waterstop in the monolith joint between the powerhouse and the first upstream retaining wall monolith. This allowed the water to flow beneath the upstream impervious blanket and bring full reservoir head against the pipeable zone I fill beneath the impervious core section in the embankment. The zone I material was piped into the void which resulted from settlement of the fill beneath the fishlift overhang. A structural notch which the impervious core tied into increased the tendency for possible hydraulic fracturing and piping in the zone I fill. The seepage path followed the void to the downstream end of the overhang and then branched into two paths. One path went vertically up the fishlift and exited the bottom of a planter box. The planter box actually worked similar to a sandbag loop which is typically used to stabilize boils. The other seepage path continued downstream at the contact of the fishlift wall and the downstream filter until it exited the north tailrace retaining wall weep holes.

## Factors Contributing to the Emergency Seepage Problem

The Panel concluded that there were four physical factors which were directly related to the seepage failure. In order of significance these were: (1) the fishlift overhang, (2) the inadequate waterstop, (3) the structural notch, and (4) zone I material beneath the impervious core.

In addition, the fragmentation of responsibility for design and construction between the three Corps' Districts and the Architect Engineer was a factor which must be accorded considerable responsibility for the development of the physical factors which led to the seepage incident.

## Major Factors Unrelated to the Seepage Incident but Significant to Note

There were a number of significant factors discovered during the investigation which are significant to note but could not be directly related to the seepage incident by the investigation. These factors were: (1) extensive overlapping of embankment zones, (2) low densities of embankment fill, (3) questionable compatibility of filter zones, (4) unsuitable material found in the impervious core section, (5) thin impervious blanket section at slurry trench tie-in, (6) absence of full time QA inspection, (7) lack of CQC inspection, and (8) the lack of a constructibility review.

The Panel found that the immediate causes of the seepage problem were all design deficiencies, however, the construction deficiencies discovered during the investigation were sufficiently severe that in the opinion of the Panel these deficiencies could have eventually lead to a seepage problem.

## Lessons Learned

There are a number of significant lessons which can be learned from this experience and

applied to other projects. In the opinion of the Panel many of the problems that existed at this project also frequently occur to varying degrees in other projects. The more important lessons learned were: (1) designers involved in a critical feature of a project during early phases should maintain involvement throughout, (2) the design/review process for major projects should involve interdisciplinary teams comprised from all involved disciplines to ensure that design interfaces are properly considered, (3) when significant inadequacies are recognized during the latter stages of designs, time should be taken to reanalyze and to correct the inadequacies. Commitment to schedules for advertising and award must not be allowed to override design quality. (4) continuous, full-time quality assurance inspection is necessary during all earth dam construction, (5) CQC specifications should emphasize the requirement for inspection, (6) additional staffing should be provided to a Resident Office in a district which does not have a construction division, in order to provide the technical and administrative resources required by this increased self-reliance, and (7) there appears to be a general tendency throughout the Corps to devote insufficient time and effort to the development of design changes and VECP changes during construction.

## Control of Surficial Slides by Different Erosion Control Techniques

T.K. Natarajan

Deputy Director, Central Road Research Institute, New Delhi, India

A.V.S.R. Murty

Central Road Research Institute, New Delhi, India

Deep Chandra

Central Road Research Institute, New Delhi, India

### SYNOPSIS

Many natural and embankment slopes fail due to the erosion of the top surficial soil mantle. Denudation of vegetation from soil slopes combined with the further steepening of slopes due to natural and man-made causes such as cuts result in such a type of failure. Essentially, the corrective measures appropriate for stabilizing these slopes comprise erosion control by establishing vegetation on the slope. The methods of vegetative turfing include asphalt mulch, coir/jute netting, geogrids and stone apron techniques. The paper sets forth the case history giving details of some of the relatively new techniques for erosion control on a hill road in India and evaluates the relative performance and the relative economics of these methods.

### INTRODUCTION

Landslides are difficult to analyse due to the complexity of geologic settings and variation in the type of materials involved. Landslides can occur slowly or suddenly, with or without apparent provocation.

External disturbances such as undercutting the foot of an existing slope or digging an excavation with unsupported sides can cause slides. Some times slopes which are stable for a long time, suddenly fail due to deterioration in the strength of the soil or a temporary increase in run-off water on the surface or an increase of seepage water into the soil mantle. The increased weight of soil from an increased degree of saturation owing to heavy rainfall often starts a slide in humid regions.

Most 'surficial landslides' occur as a result of denudation of vegetation on the hill slopes. Vegetative turfing represents one of the most important corrective measures in either case of landslides caused by run-off water or by seepage of water into the soil mantle causing a deep seated landslide (Ref. 1). In hill roads bristling with actual or potential landslide problems, there is a strong case for undertaking systematic treatment of all denuded soil slopes along the hill road with a view to establishing vegetative turfing. Based on experience with several field trials carried out by the Central Road Research Institute, the above technique has been developed and sponsored for the treatment of erodible slopes as part of landslide corrective measures to be used either singly or in combination with other techniques.

The CRRI had undertaken a field trial using this technique in combination with other techniques of surface drainage at one of the landslide spots in the Nilgiri hills in Tamilnadu in South India. The paper attempts to bring out the effectiveness of the different techniques vis-a-vis their relative costs for a proper evaluation of their techno-economic benefits.

### SITE INVESTIGATION

The Nilgiris in the Western Ghats are known to be susceptible to landslides. Many landslides occurred in this region during 1978-79. The landslides in the Nilgiri district in 1978-79 caused heavy damages in the District. Extensive field studies

conducted in this area have shown that the rocks in the Nilgiris area are of deep-seated metamorphic origin (Ref. 2). The bed rocks comprise mainly chlorites with lateritic soil forming a thick cover over them. Field observations indicated a build-up of excess hydrostatic pressure within the slope at certain places due to heavy rains. The causes include seepage of excess rain water into the soil mass combined with deforestation of the hill slopes. After a careful study of the failure mechanism, it was concluded that if the excess hydrostatic pressure built-up in the soil mass is relieved and the phreatic surface maintained at an acceptable level, the slope would remain stable. In order to reduce seepage of rain water, vegetative turfing by coir/jute netting and asphalt mulch technique or stone apron were considered suitable in combination with horizontal drains to drain out the excess subsoil water that had already seeped into the body of the slope. A brief description of the techniques are given in the following paragraphs.

### SLOPE TREATMENT BY COIR/JUTE NETTING

The Slope area proposed to be treated (Fig.1) is demarcated and graded to a uniform slope by raking the top soil for about 2 to 5 cm. The root stumps and sharp objects are removed from the area to be treated so that the netting gets a proper seating on the soil surface. Then the first seeding @ 5 kg per acre is done and dibbling of root slips of the locally available grass (willow grass) is also done. The root slips are planted, 15cm apart, in both directions, on a square pattern. The tops of the root slips are removed before dibbling. After this operation, tamping by wooden rammers is done to obtain a smooth surface and achieved appropriate compaction of the seed and the root slips and to ensure even sowing. Thereafter, coir/jute netting of 2.54 cm square openings having a width 1.22m is laid on the prepared surface firmly in the direction of flow (Fig. 2). The different widths of coir netting already rolled out are secured against displacement by making them overlap by 8 cm and pegging them down into the slope with hair-pin-shaped steel staples. The top and bottom ends of coir/jute netting are firmly anchored in 30 cm deep trenches fully stretched. The net provides innumerable miniature "check dams" absorbing the impact and the kinetic energy of the falling rain. The soil, seeds and root slips are kept in their respective place without being dislodged. The coir/jute netting disintegrate after the first rainy season and adds to the humus content of the soil. The



Fig.1:Preparation of the Slope for Erosion Control Measure.



Fig 2: Coir netting in position on the hill slope.

seeded and sprigged vegetation (Fig.3) forms a turf covering the hill slope and serves to protect the slope from subsequent erosion.



Fig. 3: Growth of Vegetation on the hill slope.

As in the earlier method, the proposed area to be treated is prepared in to vast seed beds. The root slips of the most promising local grass (willow grass) is dibbled, 15 to 20 cm apart from root to root and row to row, taking care to see that no tufts or clumps are dibbled. An asphalt-emulsion (mulch) of a specified grade is then spread by a suitable sprayer (Fig. 4) so that the emulsion is sprayed

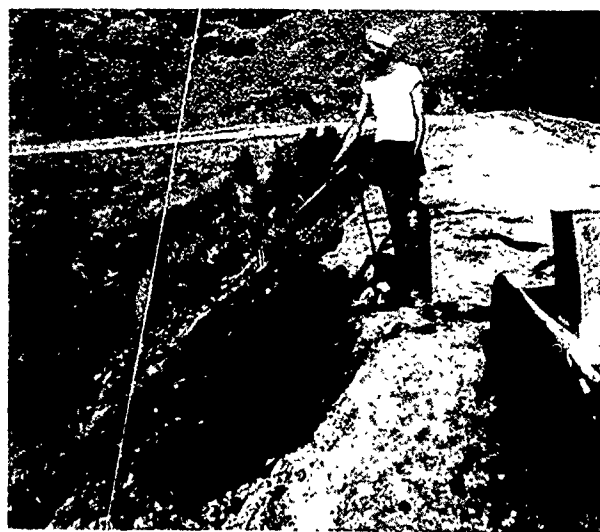


Fig. 4: Spraying of Bituminous Emulsion on the Slope.

gently and uniformly all over the treated area. The optimum rate of application of emulsion coating is about 0.90 ltr. per sq.m. so that a thin layer (film) is formed over the entire treated area. This optimum rate of emulsion spraying is maintained as the thicker application would tend to retard the growth of the vegetation.

The emulsion film gradually disintegrates and its place

is as gradually taken up by a green vegetative carpe (Fig. 3). The emulsion film acts as an immediate cover for the slope and retain the soil moisture till the vegetation takes root. To augment the lack of nutrients in the soil and to reduce the acidic nature of the soil, calcium ammonium nitrate is applied to the soil at the rate of 50 kg per 1000 sq.m. (Ref. 2 & 3), if at all considered necessary.

#### PROVISION OF STONE APRON FOR EROSION CONTROL

Erosion control on the hill slope can also be achieved by

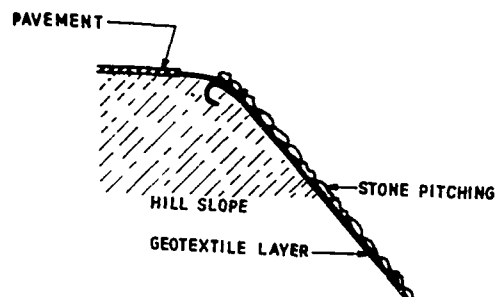


Fig. 5 : Protection of Hill Slope by Stone Apron

providing a stone apron on the soil slope to be protected.

The apron consists of a geogrid or geotextile providing a protective cover over the slope subjected to run off. The fabric due to its high filtration characteristics allows the water to flow out, while at the same time retaining the soil. In situations where a continuous sheet of flowing water is involved, fabric protection of the underlying soil by itself, is not sufficient. The current involved will eventually undercut the soil beneath the fabric and tend to dislodge it, rendering the soil base exposed and making it susceptible to erosion. In most cases, stone pitching is required over the fabric to keep the fabric in place, Fig. 5 to improve the efficiency of the controlling measures. When the velocity of run off water is not very high, slope erosion can be controlled by mere stone pitching without the fabric. When a geotextile is used, proper precautions should be taken to protect the geotextile from damages before and after laying, (Ref. 4).

#### DISCUSSION

The above mentioned erosion control measures are invariably applied for controlling surficial erosion of slopes, both natural and man-made. These measures are to be conjointly supplemented by other remedial measures such as providing surface & subsurface drainage systems when the job is one of the controlling deep-seated slides.

Erosion control measures including both the asphalt mulch technique and the coir netting technique have been tried out on a large scale for the control of surficial slides in the Nilgiri hills. Experience with these methods has shown growing a vegetative turfing of willow grass to be more effective than the mere planting of big trees. The willow grass tends to cover the surface more uniformly and anchors down the soil mantle more firmly. The cost aspects of the different methods of treatment tried out in the Nilgiri hills are set out in Table I.

An analysis of the experience gained from these field trials involving different methods of slope treatment together

TABLE I  
COMPARATIVE COST DATA OF DIFFERENT EROSION CONTROL TECHNIQUES

| S.No. | Technique                | Area<br>Sqm. | Cost of<br>material<br>Rs. | Labour<br>Charges<br>Rs. | Over-<br>head<br>charges<br>Rs. | Total<br>cost<br>Rs. | Remarks if<br>any |
|-------|--------------------------|--------------|----------------------------|--------------------------|---------------------------------|----------------------|-------------------|
| 1.    | Asphalt Mulch Technique  | 100          | 500/-<br>(\$41)            | 1000/-<br>(\$83)         | 500/-<br>(\$41)                 | 2000.00<br>(\$167)   |                   |
| 2.    | Coir Netting             | 100          | 550/-<br>(\$46)            | 1000/-<br>(\$83)         | 100/-<br>(\$8)                  | 1650/-<br>(\$137)    |                   |
| 3.    | Jute Netting             | 100          | 650/-<br>(\$54)            | 1000/-<br>(\$83)         | 100/-<br>(\$8)                  | 1750/-<br>(\$145)    |                   |
| 4.    | Netlon                   | 100          | 5800/-<br>(\$483)          | 1000/-<br>(\$83)         | 100/-<br>(\$8)                  | 6900/-<br>(\$574)    |                   |
| 5.    | Apron without geotextile | 100          | 1500<br>(\$125)            | 1300/-<br>(\$108)        | 200/-<br>(\$17)                 | 3000/-<br>(\$250)    |                   |
| 6.    | Apron with geotextile    | 100          | 3500/-<br>(\$292)          | 1300/-<br>(\$108)        | 200/-<br>(\$17)                 | 5000/-<br>(\$417)    |                   |

Note: Cost of each technique is approximate, based on Indian CPWD & other market rates as in August, 1987.  
(Exchange rate at 12 Indian Rupees per US Dollar)

with the cost data as reflected by Table 1 point to the following conclusions:

### CONCLUSIONS

1. Vegetative turfing is an effective tool for the treatment of surficial slides. However, for deep-seated slides, it would prove effective only when used in combination with other measures (like surface drainage and subsurface drainage) designed to control the landslides.
2. In India, where coir/jute is plentifully available and are relatively inexpensive, coir/jute netting techniques deserve to be used extensively, for purposes of erosion control.
3. From the point of view of limits of application of the different techniques, it would seem that the asphalt mesh technique would suffice for erosion control problems obtaining in areas of moderate rainfall whereas the technique of coir/jute netting would be more suitable for tackling problems of erosion control in areas of heavy rainfall. It logically follows that geogrids made of polypropylene can always be used instead of coir/jute netting in many situations, provided it proves to be cost-effective.

### ACKNOWLEDGEMENT

This paper is published with the kind permission of the Director, Central Road Research Institute, New Delhi-110020.

### REFERENCES

1. Mehra, S.R. Natarajan, T.K. (1966): Handbook on Landslide Analysis and Correction.
2. CRRI (1931) Report 'Field Trials on the Installation of Horizontal Drains near Ooty in Nilgiris.
3. Natarajan, T.K. Gupta S.C. (1980) "Techniques of Erosion Control for surficial Landslides" Proc. International Symposium on Landslides" New Delhi-India.
4. Natarajan, T.K., Murty, AVSR (1985) "Geotextiles in Erosion Control Works for Landslide Correction" Seminar on Construction of Roads in Hill Areas: Nainital, India.



# Restoration of the Stability of Retaining Wall

**T.K. Natarajan**

Deputy Director, Central Road Research Institute, New Delhi, India

**P. Jagannatha Rao**

Head, Geotechnical Engineering Division, Central Road Research Institute, New Delhi, India

## SYNOPSIS :-

The paper sets out the salient features concerning the failure of a retaining wall on a sloping ground. The retaining wall experienced a displacement of about 1.50m both in the downward and outward directions without experiencing any tilt or structural distress. The stability analysis of the slope on which the retaining wall was located, established that the failure was caused by inadequate drainage of the fill resulting in a build up of pore pressures. Four more such retaining wall sections were also analysed.

The remedial measures consist of providing adequate drainage using a geotextile - covered filter drain, use of light weight saw dust back fill to reduce the disturbing moments, in the case of the retaining wall that experienced movement. In the other sections, suitable regrading of the slope in front of the retaining walls along with a slight reduction in the height of the backfill was found to be the most economical solution available.

## INTRODUCTION

A large level area was required to be developed at a location where the natural ground consists of a gently sloping hillside near sea shore. Five retaining walls, ranging in height from 3 to 5 meters, were built along the periphery of the area whose level was to be raised. These retaining walls are identified as PQ, QR, RS, ST and TU. Backfilling was started behind the retaining wall TU and soon reached the full height. Shortly thereafter, a heavy and sustained rainfall occurred for about 3-4 days. During this period, the wall was noticed to be moving and over a period of four days, the total movement experienced by the wall was observed to be 1.60m in lateral direction and 1.50m in the vertical direction. It was found that the displacements experienced by the retaining wall were of the rigid body type. The retaining wall did not undergo any structural damage. In the displaced position, the wall remained vertical with no tilt.

In order to reduce the active earth pressure behind the retaining wall TU, action was initiated to remove the backfill. Surface drainage was also improved. The movement of the wall ceased following these measures.

Fig. 1 shows the retaining wall TU in the displaced position. The other retaining wall sections, behind which no backfill was placed, are also seen in the same figure.

In the following section, the causes for the displacement experienced by the retaining wall are brought out. Remedial measures to keep the regraded slope stable over entire area are also described.

## GEOTECHNICAL INVESTIGATIONS

Geotechnical investigations were conducted in two phases. In the first phase 5 boreholes were made in the vicinity of retaining wall TU, which had undergone displacement and the adjoining slope area. The results from these investigations are summarised Table 1.



Fig. 1 General View of the Slope

Table 1. Properties of Subsoil in Slope area TU.

|         | LL | PI | Shear Strength Parameters |                    |
|---------|----|----|---------------------------|--------------------|
|         |    |    | c'<br>kPa                 | $\phi'$<br>degrees |
| Layer 1 | 30 | 14 | 0                         | 28                 |
| Layer 2 | 48 | 23 | 10                        | 20                 |

Fig.2. shows the stratification of soil in this area. A relatively softer pocket of soil was found to be present in the slope area TU.

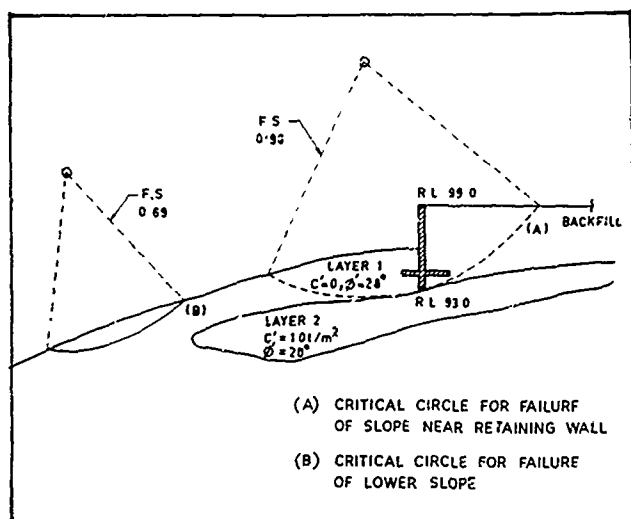


Fig.2, Soil Stratification and location of Critical Failure Surfaces.

In the second phase, soil investigations were carried out in the slope area behind the retaining walls PQ, QR, RS, ST. The results from these investigations are summarised in Table 2. While soil type in both the areas is broadly similar i.e. sand-silt-clay mixture with some gravel, the gravel content was found to be relatively higher in this part of the slope. Accordingly a wider variation in the shear strength value was noticed.

Table: 2 Subsoil Properties.

| Retaining Wall section | Depth. m below G.L. | LL. | PI. | Shear Strength Parameters |                |
|------------------------|---------------------|-----|-----|---------------------------|----------------|
|                        |                     |     |     | c' kPa                    | $\phi$ degrees |
| PQ                     | 3.0                 | 30  | 12  | 0                         | 41             |
|                        | 3.5                 | 29  | 11  | 24                        | 28             |
|                        | 2.0                 | 35  | 15  | 10                        | 31             |
| QR                     | 2.0                 | 41  | 18  | 10                        | 27             |
|                        | 3.0                 | 34  | 16  | 4                         | 34             |
|                        | 3.3                 | 36  | 15  | 16                        | 34             |
| RS                     | 2.0                 | 34  | 15  | 0                         | 38             |
| ST                     | 2.0                 | 58  | 29  | 0                         | 20             |
|                        | 3.0                 | 36  | 16  | 24                        | 33             |

#### RESULTS OF STABILITY ANALYSIS

The stability of the slope containing the retaining walls was evaluated using Bishop's method of analysis. Computer programme developed at CRRRI was utilised for this purpose.

#### STABILITY OF SLOPE AREA TU.

The profile used in stability analysis for this part of slope is shown in Fig.2. The results of stability analysis for varying piezometric levels are shown in Table. 3.

Table: 3. Restuls of Stability Analysis for Slope Area TU.

| Fill Level | Piezometric Level | Factor of Safety |
|------------|-------------------|------------------|
| RL 99.0 m  | G.L.              | 0.98             |
| RL 99.0 m  | 0.5 m below GL.   | 1.19             |
| RL 99.0 m  | 1.0 m below GL    | 1.39             |
| RL 99.0    | 1.5 m below GL.   | 1.57             |
| RL 99.0 m  | 3.0 m below GL    | 2.13             |

These results clearly bring out that the stability of the slope is highly sensitive to changes in piezometric level and a rapid increase in the factor of safety occurs when the water level goes down. The slope is likely to fail when the water table is at RL 99.0m i.e. at the top of the fill. As shown the critical failure surface is located just below the retaining wall and is tangential to the softer layer found in the region.

It has been concluded on the basis of the above analysis and field evidence that the natural slope on which the retaining wall was located, experienced failure along a circular surface. The primary cause of the failure is identified as overloading at the head of the slide due to fully saturated fill. As the soil mass experienced an outward movement, the retaining wall was also carried along with the moving soil mass. Since the rate of movement was slow, no structural damage or tilt had occurred. It seems that the retaining wall has in all possibility slid along the failure surface and came to rest at the lower most position. This displacement has an outward and an downward component each of the order of about 1.5m each.

#### REMEDIAL MEASURES

In order to keep the piezometric level low in the fill area inspite of long and sustained duration of rain storms, two rubble drains, one inclined and the second vertical are provided as shown in Fig. 3. The rubble drains are covered with permeable geotextile layer that would serve as a separation barrier. These drains are located such that they nearly form the boundary of the mass susceptible to failure. Thus the mass is kept in a well drained condition, thereby limiting the driving forces to a minimum.

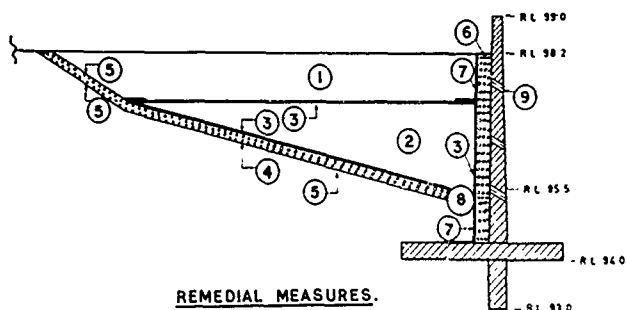
#### USE OF SAW DUST IN THE BACKFILL.

Driving forces can be reduced further by the use of saw dust as backfill. Saw dust was available as a waste product at the local timber mills. It is easy to compact. It is protected against any changes in moisture content since an impermeable geomembrane has been provided as envelope. Further, in this area, temperature changes, both seasonal and diurnal, are limited in magnitude. The chances of saw dust decomposing are very minimal.

The factors of safety of the slope area TU. for different ambient conditions are given in table 4.

#### STABILITY ANALYSIS OF AREAS PQ, QR, RS, ST.

Stability analysis was carried out for the rest four sections viz. PQ, QR, RS, ST as well. The slope profiles are shown in Figs. 4,5,6 and 7. The factor of safety of these slope areas assuming piezometric level to be at RL 99.0m are



### LEGEND

1. 1m SOIL FILL.
2. COMPACTED SAW DUST ENCAPSULATED IN IMPERMEABLE GEOMEMBRANE. (2 LAYERS PVC SHEETING)
3. IMPERMEABLE PVC SHEET OR GEOMEMBRANE.
- 4, 6. RUBBLE FILTER DRAINS.
- 5, 7. PERMEABLE GEOTEXTILE.
8. COLLECTOR DRAIN WITH LONGITUDINAL SLOPE TO THE NATURAL NALLA.
9. WEEPHOLES.

R.L. 99.0 IS ASSUMED TO CORRESPOND TO THE TOP OF THE RETAINING WALL IN THE PRESENT POSITION.

Fig. 3. Remedial Measures.

Table 4. Factor of Safety of Slope area TU with Remedial Measures.

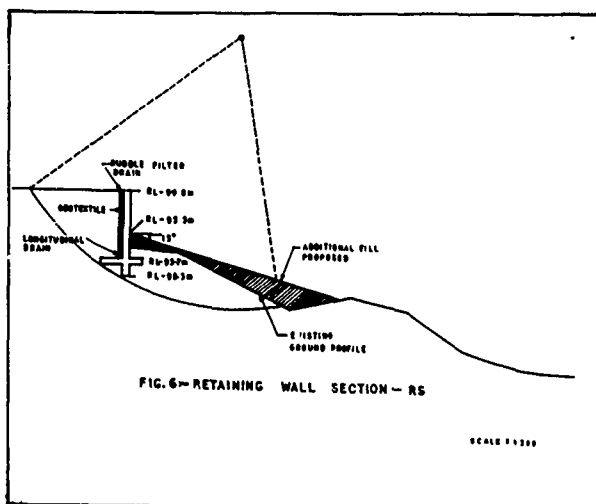
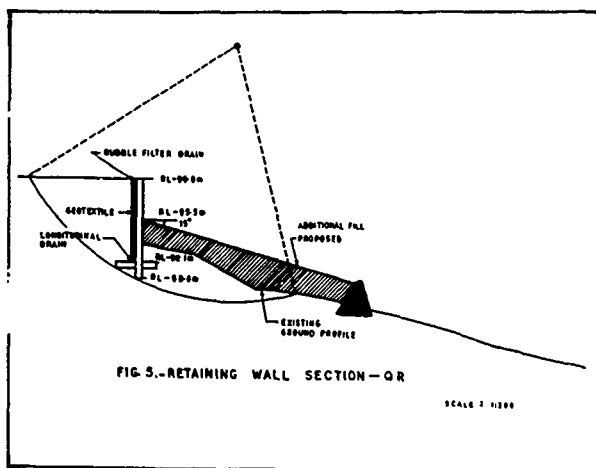
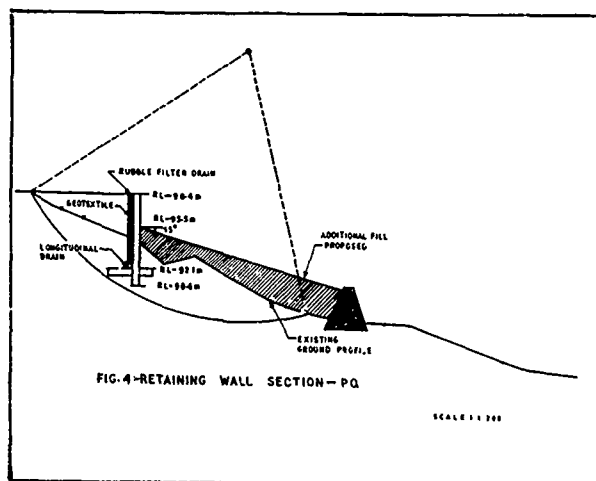
| Fill Level | Piezometric   | Backfill      | Factor of Safety |
|------------|---------------|---------------|------------------|
| 98.2 m     | G.L.          | Soil+Saw dust | 1.17             |
| 98.2 m     | 0.5m below GL | Soil+Saw dust | 1.47             |
| 98.2 m     | 1.0m below GL | Soil+Saw dust | 1.75             |
| 98.2 m     | 1.5m below GL | Soil+Saw dust | 2.00             |

given in Table 5.

Table 5. Factors of safety of Slope Areas PQ, QR, RS, ST.

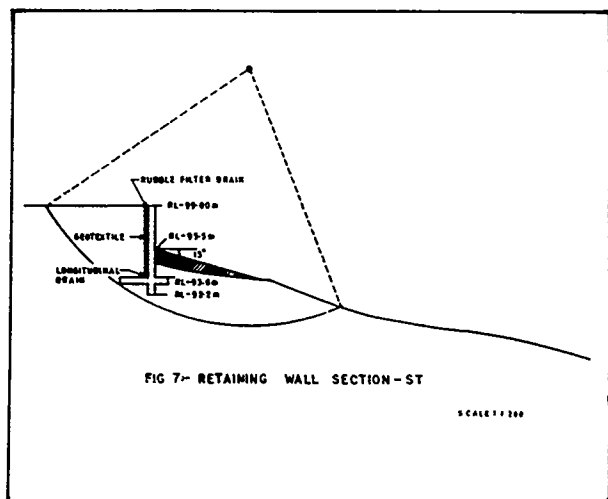
$$c' = 10 \text{ kPa}, \phi = 30^\circ$$

| Slope area near wall section | Factor of Safety |
|------------------------------|------------------|
| PQ                           | 0.95             |
| QR                           | 0.95             |
| RS                           | 1.07             |
| ST                           | 1.42             |



### REMEDIAL MEASURES FOR SLOPE AREA PQ, QR, RS, ST.

Stability analysis have clearly shown that the slope is liable to fail when the backfill is fully saturated i.e. with piezometric level at the top of the fill. Simple and inexpensive method of improving the stability of slopes by regulating the height of backfill has been considered the most feasible



backfill have occurred due to the undissipated pore pressure following heavy rains. In order to keep the slope and the retaining wall stable, adequate drainage measures have been provided for. These consist of graded filter at the back of the retaining wall singly or in combination with inclined filter as shown in fig. 3. It has also been found economical to ensure safety of the slope by resorting to appropriate regradation both at back and front of retaining wall. The proposed use of saw dust as backfill is yet another novel feature. Saw dust which is at present considered a waste material has been found to be a suitable light-weight fill material because of its good compactability and good shear strength.

#### ACKNOWLEDGEMENTS

Shri O.P. Yadav, Shri D.Mukerjee, Shri V.L.Gokhale, Shri S.Saha rendered assistance in different aspects of the work. The same is thankfully acknowledged. The paper is published with the permission of Director, Central Road, Research Institute, New Delhi.

method of improving the overall slope stability for these areas. The factor of safety with different levels of the backfill proposed and addition of fill material in the front of the retaining wall (designated as lower slope) are summarised in table 6. Piezometric level is assumed to be at the top of the fill.

Table 6. Factors of Safety of Sections PQ, QR, RS, ST with Remedial Measures.

| Back fill | Lower Slope Configuration                                    | Factor of Safety |                  |
|-----------|--|------------------|------------------|
|           |  | Sections PQ & QR | Sections RS & ST |
| RL 98.5 m | Lower Slope dressed to 15° and starts at RL 95.5 m of walls. | 1.49             | 1.48             |
| RL 99.0 m | Lower Slope dressed to 15° and starts at RL 96.0 m of walls. | 1.50             | 1.50             |

To ensure that the fill material is well drained, in addition to weep holes, a vertical rubble drain consisting of clean well graded gravel is provided between the backfill and the retaining wall with permeable geotextile fabric at the interface between rubble and the backfill. Additional provision has been made for draining out the water collected in the gravel drain at levels below RL 95.5 m by providing a porous drain pipe running along the length of the retaining walls and discharging water so collected to a suitable natural outlet in the vicinity.

#### CONCLUSION

The mechanism by which the retaining wall resting on a gently sloping ground has experienced an outward and downward displacement is analysed. Such type of failure as discussed in the paper where the retaining wall itself experienced no tilt or any structural damage but has undergone rigid body displacement has only been rarely reported in literature.

Analysis have shown that the failure of the slope with the

# Some Design Aspects and Performance of an Embankment Dam

**Z.V. Solymar**

Geotechnical Engineer, formerly with Monenco Consultants Ltd.,  
Canada

**G.C. Mactavish**

Project Manager, Monenco Consultants Ltd., Indonesia

**W.G. Matthews**

Resident Engineer, Monenco Consultants Ltd., Papua New Guinea

**SYNOPSIS:** The Jebba Main Dam is a zoned embankment dam founded on river alluvium. The deformation of the dam/foundation system under the various applied loading conditions was determined by finite element analysis. Series of in situ and analytical tests were performed to evaluate the coefficient of permeability of the riverbed sediments. Computer solution provided results of seepage quantities, velocity of the groundwater flow, and total head occurring throughout the defined finite element mesh.

Results of instrumentation permit comparison between the actual deformations and those determined by analysis. The flow from pressure relief wells can be utilized in connection with pore pressure measurements to calculate the bulk coefficient of permeability of the foundation materials and total discharge under the dam.

## INTRODUCTION

The Jebba Hydroelectric Development is located on the Niger River about 400 km north of Lagos, Nigeria. The Main Dam is an earth and rockfill structure with a maximum height of 42 m, crest length of 650 m, and a volume of 2.89M m<sup>3</sup> including an impervious blanket extending 550 m upstream from the centre line of the dam. The powerhouse contains six 90 MW units. In addition, there are two earth and rockfill auxiliary dams, one saddle dam, two concrete auxiliary dams, two spillways and one navigation lock.

Construction of the development commenced in March 1979 and reservoir impoundment began in August 1983. The first unit began operation in December 1983.

## SUBSURFACE CONDITIONS

The Main Dam forms the closure of the present day Niger River channel. Locally, steep rock slopes characterize both the right bank and the buried bedrock surface in the river bed.

The alluvial foundation underlying the Main Dam and impervious blanket comprises mostly uniformly graded fine to coarse grained, clean quartzitic sands with traces of fine gravel of low to medium high density. It is primarily the result of water and/or wind deposition and has a maximum depth of some 30-70 m.

The densities of the river sands throughout the foundation for the Main Dam and the adjoining upstream and downstream areas were established by standard, dynamic and static cone penetration tests. Fig. 1 shows some typical contours of equivalent relative density in plan at el. 65 m and in section along the centreline of the Main Dam.

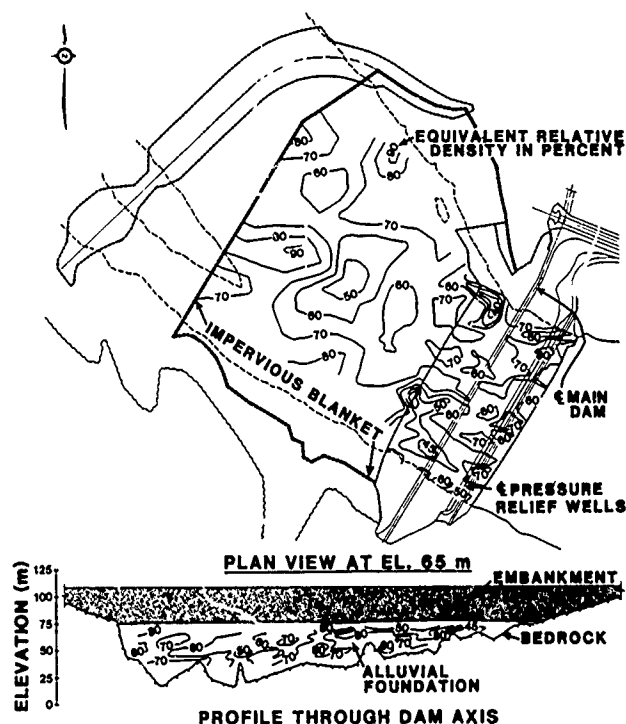


Fig. 1 Relative Density Contours

It was evident from these results that the densities vary appreciably in both the vertical and horizontal directions. These variation densities indicated that differences in compressibility might exist, which could result in unacceptable differential settlement.

The design called for in-situ compaction of the alluvial foundation of the Main Dam and portions

of the blanket to prevent any such occurrence. To achieve desired densities, the Contract specified that compaction below 25 m would be done by blasting and the top 25 m compacted by vibrocompaction (Fig. 2). Details of the densification program are presented elsewhere (Solymar et al 1984a, Solymar 1984b and Mitchell 1986).

mold and trimmed to triaxial specimen dimensions of 37 mm diameter and 76 mm in length. The triaxial tests were conducted using confining pressures of 211, 352 and 563 kPa.

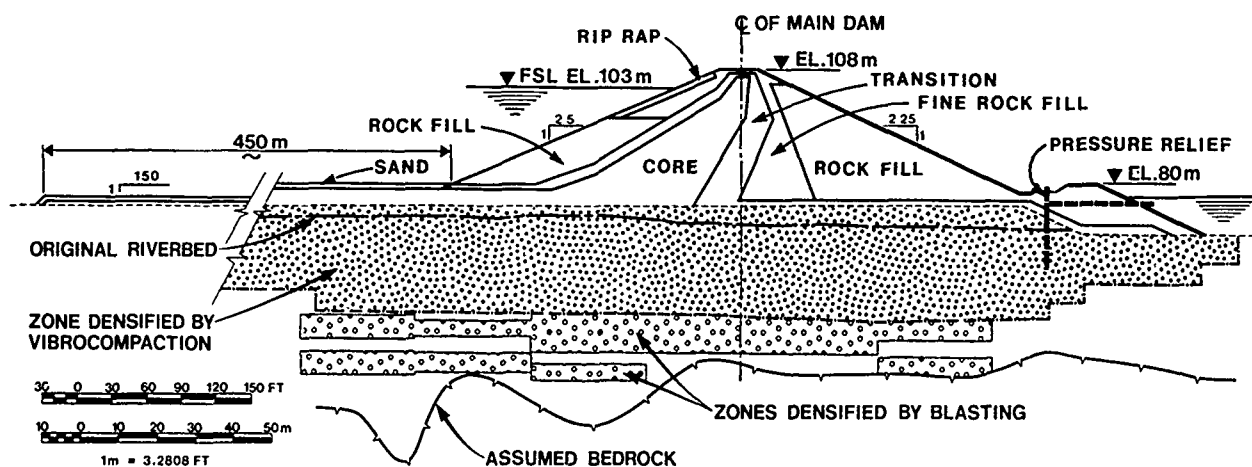


Fig. 2 Main Dam Cross Section

Series of in-situ and analytical tests were performed to evaluate the coefficient of permeability of the riverbed sediments. The study involved falling head tests, pumping tests on screened wells with observation piezometers, Lefranc Mandel tests at a number of depths in cased boreholes, slug tests in piezometers, computer model simulating aquifer response to river fluctuation, and coefficient of permeability calculations based on grain size distribution of sand samples.

#### LABORATORY TEST RESULTS

Grain size analyses and tests for specific gravity and maximum/minimum density were routinely performed to samples of the river sands, while representative samples were subjected to direct shear, consolidation, triaxial and permeability testing. Such representative foundation sand samples were mixed to simulate depths of 0-10 m, 10-20 m and 20-30 m (Fig. 3). Six series of three triaxial tests each were performed, three at 70% relative density and three at 40% relative density. Since the foundation treatment was required to achieve densification of the sand to 70%, 60% and 50% relative density ( $D_r$ ), interpolations of the results of the 70% and 40% relative density tests were required to obtain the 60% and 50% values. Table I is a summary of the consolidated drained triaxial shear strength parameters for the foundation sands.

The triaxial tests on the impervious core material were performed with a back pressure (saturation) of approximately 270 kPa and resulting pore pressure parameter equal to approximately 0.95. The samples used were compacted to a maximum modified Proctor density at an optimum water content in a 150 mm Proctor

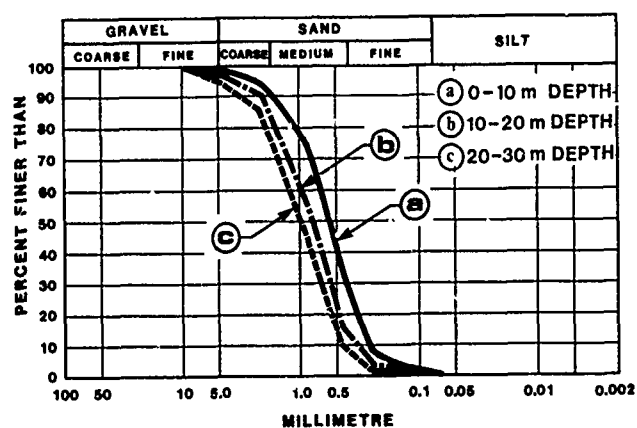


Fig. 3 Grain Size Envelopes

TABLE I

Drained Shear Strength Parameters of River Sand

| Relative Density | Strength Parameter | Sample a<br>Depth<br>0-10 m | Sample b<br>Depth<br>10-20 m | Sample c<br>Depth<br>20-30 m |
|------------------|--------------------|-----------------------------|------------------------------|------------------------------|
| 70%              | Friction angle     | 37°                         | 38°                          | 39°                          |
| 40%              | Friction angle     | 33°                         | 35°                          | 35.5°                        |

Note  $c' = 0$  for all

## DEFORMATION ANALYSIS

The computer program used for the stress-strain deformation analysis on the Main Dam and its foundation is entitled "Finite Element Non-Linear analysis for Two Dimensional Problems (FENA 2D)" by Krishnayya.

This computer program was developed for an analysis of the cracking of earth dams during construction and at the end of construction with full impoundment. The non-linear analysis of soils is performed by using the stress-strain relationships obtained from the conventional triaxial tests. Since an isotropic elastic theory with piece wise linearity is assumed in the analysis, the dilatancy effect of soils is neglected. The triaxial test data are supplied to the program in a digital form by specifying the deviator stress or volumetric strain with a corresponding axial strain and the confining stress.

It was not practicable to perform triaxial tests on rockfill and transition materials. Accordingly relationships of non-linear stress-strain and volumetric-axial strain curves for the rockfill and the transition materials were developed according to the method presented by Duncan and Chang (1970). The parameters required by these stress-strain relationships were based on Jebba rockfill characteristics and supplemented with some values taken from studies of stress deformation of the Oroville Dam as documented by Kulhawy and Duncan (1972). This is an important consideration when actual settlements are compared with the predicted. The confining pressures used for the theoretical results of the shell material triaxial tests were 0, 211, 422 and 632 kPa.

The cross-sections used in this analysis extend 120 m upstream and 120 m downstream from the centre line. The profile along the centre line of the dam is 565 m in length and extends from station 1 + 20 to station 6 + 85. Table II lists the various parameters for all materials used in the computer study.

TABLE II

Material Properties for Finite Element Analysis

| Material                     | Dry Density<br>(kg/m <sup>3</sup> ) | Cohesion<br>(kPa) | Friction Angle<br>(degrees) |
|------------------------------|-------------------------------------|-------------------|-----------------------------|
| Impervious fill <sup>1</sup> | 1900                                | 37                | 25.2                        |
| Rockfill and transition      | 1800                                | 0                 | 38.0                        |
| Sand ( $D_r = 70\%$ )        | 1779                                | 0                 | 37.9                        |
| Sand ( $D_r = 60\%$ )        | 1749                                | 0                 | 36.8                        |
| Sand ( $D_r = 50\%$ )        | 1718                                | 0                 | 35.7                        |

<sup>1</sup> Based on samples prepared at maximum modified Proctor density

The results representing the end of construction and full reservoir impoundment for stations 1 + 70 and 2 + 00 are shown (Fig. 4).

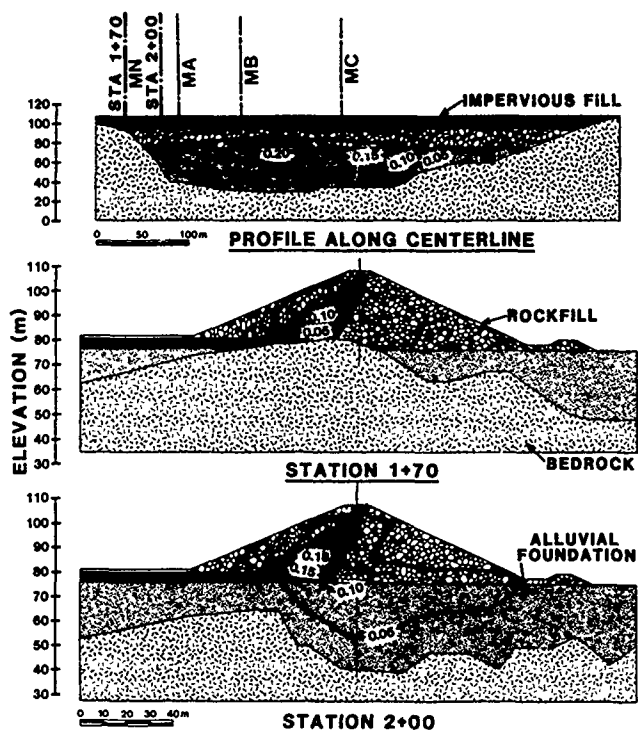


Fig. 4 Material Zones Used in Analysis and Computed Settlements

## SEEPAGE ANALYSIS

The control of seepage through the alluvial foundation of the Main Dam is accomplished by the provision of an impervious blanket extending upstream from the base of the impervious core. A row of relief wells is also provided along the downstream toe to further ensure that seepage pressures in the toe area are of an acceptably low magnitude.

A computer study to analyze the underseepage behaviour for a wide range of assumptions corresponding to all conceivable conditions of the blanket/dam/foundation system was undertaken.

The analyses were performed employing the finite element method in a computer program developed by Verruijt, entitled "Plane Flow with Sources and Sinks - Program LM4", which provides solutions for problems of two dimensional steady groundwater flow in a homogeneous isotropic medium. This program requires the idealization to be divided into a mesh consisting of triangular elements to which effective or weighted coefficients of permeability are assigned.

A typical section was selected to model the conditions of seepage for all analyses. The profile of the riverbed foundation was taken through the centre of the dam and was extended perpendicularly some 900 m and 300 m upstream and downstream respectively. All irregularities in the elevations of the underlying bedrock were corrected to obtain a smooth linear profile on which the finite element mesh was superimposed.

Bedrock was thus taken to lie 30-40 m beneath the riverbed surface. The width of core contact on the riverbed surface is approximately 50 m. Relief wells located 68 m downstream from the dam axis were included in the general model.

Seepage through the main dam itself was not taken into account, the core was considered to be completely impervious and therefore the nodes situated along the core contact surface were assumed to be impermeable. The underlying bedrock was considered in the same manner and its boundary nodes were defined accordingly. The end and surface nodes were assigned appropriate heads corresponding to the reservoir and tail water levels.

Since the purpose of the computer analyses was also to provide seepage behaviour for the most probable occurrence of cracking in the blanket, two cases were selected, one with a crack at 130 m and one with a crack at 70 m upstream from the main dam axis. The effects that cracking in these locations would have on seepage were determined for all assumed foundation permeabilities. In the event that cracks do form after filling of the reservoir, it is anticipated that this would be a temporary condition that would tend to correct itself. Openings in the blanket would eventually be sealed by infiltrating particles from the sand layer placed on top of the blanket (Fig. 2), and by the filtering action of the sandy alluvium on which the blanket is founded. The coefficients of permeability and foundation conditions assumed for the computer analyses are presented in Table III.

Computer solutions provided results for seepage quantities, velocity of groundwater flow and total head loss occurring throughout the defined finite element mesh. Flow nets were also drawn, facilitated by plots of total head. This enabled computation of seepage pressure potentials along the foundation surface and at selected points within the foundation. Results of the computer studies indicated that seepage quantities and hydraulic exit gradients were substantially reduced due to the presence of the sand infill in the cracks as compared to seepage quantities (Table III) and gradients obtained for the open crack conditions.

TABLE III

Summary of Computer Solutions and Seepage Discharges

| Case                                 | $k_s$<br>( $\times 10^4$<br>m/s) | $k_h$<br>$\frac{k_h}{k_v}$ | Discharge ( $m^3/s$ ) with |      |      |                      |
|--------------------------------------|----------------------------------|----------------------------|----------------------------|------|------|----------------------|
|                                      |                                  |                            | $k_f =$                    | 50   | 4    | $0.5 \times 10^{-4}$ |
| No crack                             | 4                                | 1                          | 0.23                       |      |      |                      |
|                                      | 4                                | 4                          | 0.47                       |      |      |                      |
|                                      | 4                                | 9                          | 0.61                       |      |      |                      |
|                                      | 2.5                              | 1                          | 1.30                       |      |      |                      |
|                                      | 2.5                              | 4                          | 2.28                       |      |      |                      |
| Crack in blanket<br>(130 m upstream) | 4                                | 1                          | 2.39                       | 0.71 | 0.39 | 0.28                 |
|                                      | 2.5                              | 1                          | 4.57                       | 2.53 | 1.42 | 1.29                 |
|                                      | 2.5                              | 4                          | 7.95                       | 3.04 | 2.40 | 2.34                 |
| Crack in blanket<br>(70 m upstream)  | 4                                | 1                          | 4.04                       | 0.61 | 0.43 | 0.28                 |
|                                      | 4                                | 9                          | 4.95                       | -    | 0.81 | 0.70                 |

$k_s$  = weighted coefficient of permeability =  $k_h k_v$  of foundation materials (m/s)  
 $k_h$  = coefficient of horizontal permeability of foundation materials (m/s)  
 $k_v$  = coefficient of vertical permeability of foundation materials (m/s)  
 $k_f$  = weighted coefficient of permeability of in-fill sand (m/s)

## INSTRUMENTATION

Finite element analyses have shown that the deformations within the Main Dam embankment and sand foundation will not be significant. However, to permit comparison between the actual deformations and those determined by analysis, the dam/foundation system was instrumented extensively. Monitoring would confirm that the system is behaving as expected or would help to detect, at an early stage, any anomalies that may occur so that measures can be implemented to ensure continued safety of the structures.

Settlement monuments used for measurements of vertical movement are installed along the upstream edge of the dam crest and along the upstream edge of the crest of the downstream berm. They are also installed along the upstream and the downstream slopes (Fig. 2).

Measurements of internal displacements which are required to detect possible differential movement of the core, are made with inclinometer probe units lowered down initially vertical access tubes. These inclinometer tubes are located along the centre line of the dam and along the downstream slope. From this system, the distribution of settlement and horizontal movements within the dam can be determined.

Full piezometer instrumentation has been installed along three cross sections, MA, MB and MC (Fig. 4), to monitor the seepage pressures on the alluvial foundation sands and within the impervious core and transition zones.

The flow from pressure relief wells can be utilized in connection with pore pressure measurements to calculate the bulk coefficient of permeability of the foundation materials and total discharge under the dam.

## PERFORMANCE

Settlements in the foundation have been very much as anticipated. The maximum settlement recorded during construction was 160 mm. Construction of the embankment resulted in a compression of 0.19 to 0.27% of the alluvial foundation. The impounding of the reservoir resulted in an additional maximum compression of 0.04%. Compression of the foundation with depth was fairly uniform, indicating that the densification program achieved its aim. The surface and embankment settlements are less than those predicted by the finite element analysis, except in the transition zones. The largest differential settlement within the core is 30 mm and occurred between Sections MN and MA and the largest differential strain is 0.06 percent. These are half of the predicted values (Fig. 5).



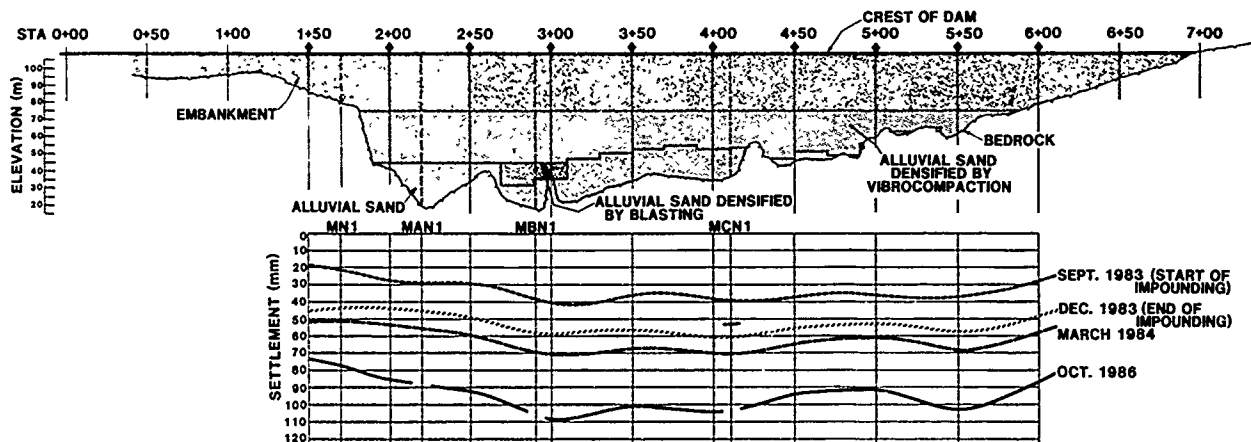


Fig. 5 Settlement of the Crest

The settlement behaviour of the rockfill and the transition zones at inclinometer locations MN1, MBN1, MBN2 and MCN1 (Fig. 6) varied quite significantly, which was contrary to the assumptions made in the analysis. This is surprising since the filter material was well compacted and the average relative density obtained from 685 field tests was 84%. Only 7 of the tests indicated lower than the specified 70% relative density.

It can be concluded from the comparison between predicted and measured deformations that the finite element, non-linear analysis is a useful tool for predicting settlements as long as the input parameters are correct. This was the case for the alluvial sand and the core material, where the stress-strain relationships obtained from triaxial tests on small samples were representative for in-situ behaviour of the materials. Comparison of curves for rock fills discloses only slight differences in deformability of these materials as compacted in the embankment, which is in agreement with experimentally and theoretically derived results.

The principal observations for monitoring the performance of the impervious blanket are (1) the readings from the foundation piezometers and (2) the flows from the relief wells.

A comparison between theoretical and observed potentials with time are shown in Fig. 7. Generally, at the beginning, piezometric levels followed the head difference between reservoir level and tail water. At approximately 8 m head differential the piezometric levels started to lag. A further sharp reduction in potential occurred just prior to completion of the impounding. The change in potential indicates extension of the blanket by natural siltation or reduction of permeability due to filtration of silt into the sand foundation. The result is the same. In effect, the length of the blanket was extended by approximately 150 percent or the average coefficient of permeability reduced by the same percentage.

This phenomenon can be explained by observing the difference in clarity of the water between the reservoir and the discharge from the downstream relief wells. The water in the reservoir is loaded with fine, clay size soil particles while the discharge from the relief wells is clear. The sand foundation under the dam works as a filter and the clay size particles become trapped in the pores between sand grains. Gradually the pores are filled and the permeability is reduced. The net effects are reduced pressure under the blanket and reduced seepage.

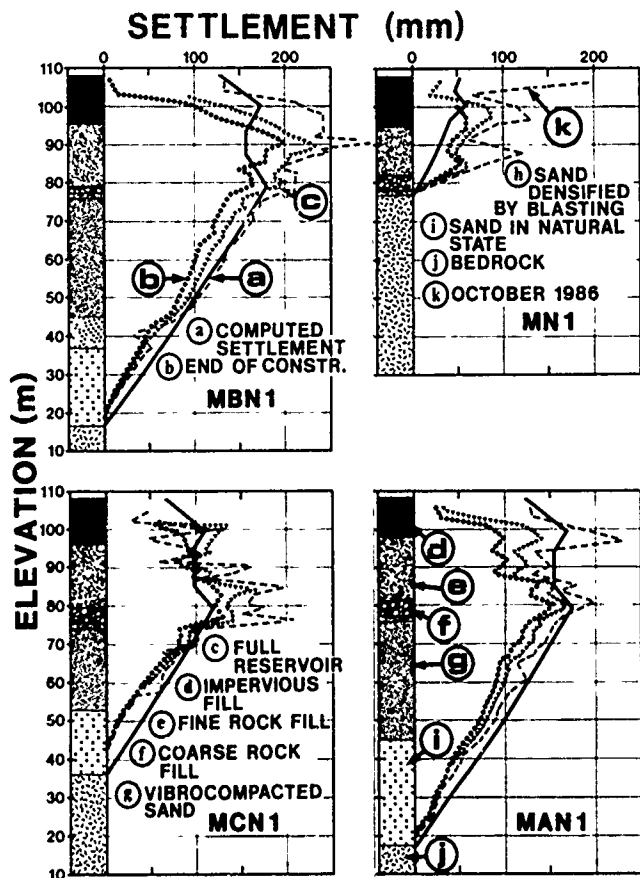


Fig. 6 Foundation and Embankment Settlement

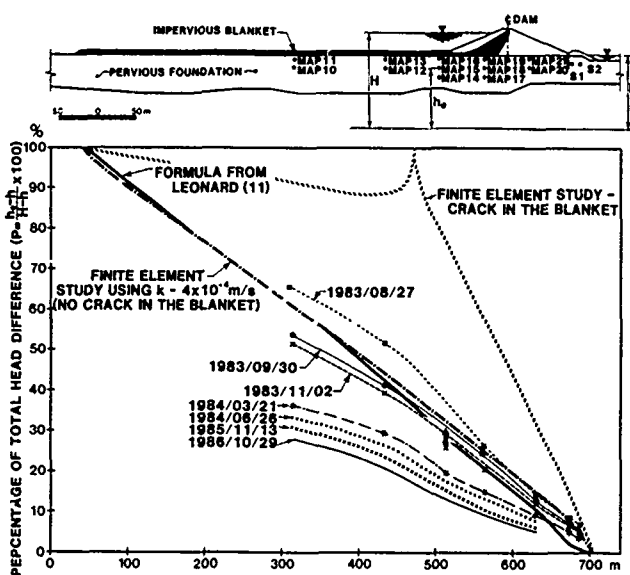


Fig. 7 Comparison Between Calculated and Observed Potentials

The piezometric head can also be plotted directly (Fig. 8). The latest readings again indicate lower pore pressures in the foundation than those assumed in the design. The pressure above the blanket equals that of a full reservoir and, since the pressure underneath the blanket is much smaller the resulting differential pressure will cause some settlement of the blanket. Where the differential pressure is greatest, near the upstream toe of the dam, the foundation was compacted to the same depth as underneath the dam. Therefore differential settlement or cracking of the blanket is not expected to occur and piezometer readings would immediately detect any such cracking.

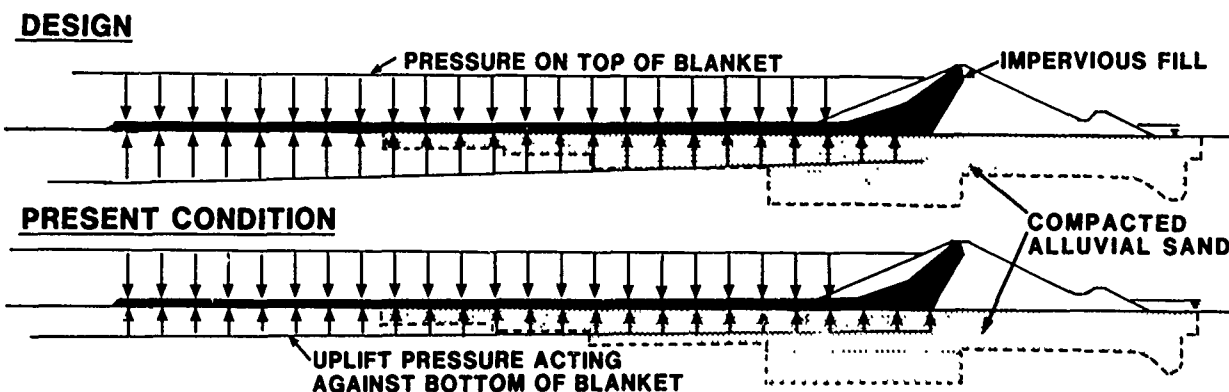


Fig. 8 Pressure Acting on the Impervious Blanket and Depth of Compaction

Flow from relief wells has stabilized at a value of about  $0.06 \text{ m}^3/\text{s}$  per well. Total flow under the dam calculated from the upstream gradients is about  $0.2 \text{ m}^3/\text{s}$ , which is slightly less than the predicted lowest value.

The average gradient under the dam/blanket system after 3 years operation is 0.021 compared

to 0.031 calculated after the first 8 months, which is very favourable. The exit gradient near the downstream toe (between the last row of standpipe piezometers and tailwater) is 0.15 which gives a factor of safety greater than 5 against piping.

The calculated coefficient of permeability ranges from  $2.3 \times 10^{-4}$  to  $1.1 \times 10^{-3}$  m/s along the instrumented sections for a weighted average of  $5.4 \times 10^{-4}$  m/s. A comparison between coefficient of permeability determined from in-situ tests and from flow and piezometer data obtained impounding is shown in Fig. 9.

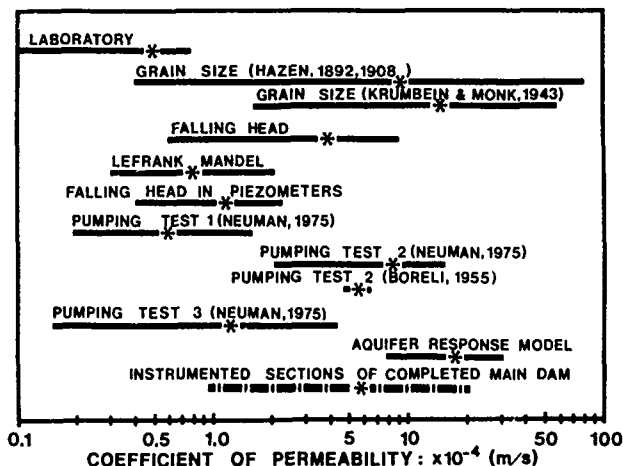


Fig. 9 Summary of Coefficient of Permeability

Piezometers installed in the upstream transition zone reacted instantaneously and are following reservoir level. The reservoir has not yet affected the piezometric levels at the piezometers installed in the impervious fill, which are yielding small pressures within the expected zero reading fluctuations. It is now estimated that the coefficient of permeability

of the compacted impervious core is less than  $1 \times 10^{-9}$  m/s. The coefficient of permeability used in the design analyses of the core and blanket was conservatively chosen as  $1 \times 10^{-7}$  m/s, so observations have now confirmed that the core is 100 times less pervious than assumed in the design.

## CONCLUSIONS

The Jebba Main Dam is founded on river alluvium and is constructed of earth/rockfill zones around an inclined impervious core which extends to an impervious blanket 450 m long on the upstream side. The deformations of the dam/foundations system under the various applied loading conditions were determined by finite element analysis.

Series of in-situ and analytical tests were performed to evaluate the coefficient of permeability of the riverbed sediments. Computer solution provided results of seepage quantities, velocity of the groundwater flow, and total head occurring throughout the defined finite element mesh. The flow from pressure relief wells can be utilized in connection with pore pressure measurements to calculate the bulk coefficient of permeability of the foundation materials and total discharge under the dam.

Settlements in the foundation have been very much as anticipated. The maximum settlement recorded during construction was 160 mm. Construction of the embankment resulted in a compression of 0.19 to 0.27% of the alluvial foundation. The impounding of the reservoir resulted in an additional maximum compression of 0.04%. Compression of the foundation with depth was fairly uniform, indicating that the densification program achieved its aim. The surface and embankment settlements are about the same as those predicted by finite element analysis, except in the transition zones. The largest differential settlement within the core is 30 mm and the largest differential strain is 0.06 percent.

Generally, at the start of impounding, piezometric levels followed the head difference between reservoir level and tail water. At approximately 8 m head difference the piezometric levels started to lag. A further sharp reduction in potentiail occurred just prior to completion of the impounding. The change in potential indicates extension of the blanket by natural siltation or reduction of permeability due to filtration of silt into the sand foundation. The result is the same. Total flow under the dam calculated from the upstream gradients is about 0.2 m<sup>3</sup>/s, which is slightly less than the predicted lowest value.

The gradual reduction in permeability of the foundation materials due to siltation resulted in lowering the uplift pressures under the blanket. Since the pressure above the blanket equals that of full reservoir, the resulting differential pressure increased since impounding and it is considerably greater than the value assumed in the design. As a result of this, the deformation of the dam and its foundation continue, even if at a very small rate. Extension of the foundation densification upstream of the dam prevented development of large differential settlements and cracking of the blanket-core contact.

Comparing measured bulk coefficient of permeability values obtained from piezometer readings and relief well discharges with values obtained from laboratory and field tests it is concluded that laboratory tests results are low

by a magnitude of 100 and Lefranc-Mandel and falling head tests in piezometers by a magnitude of 4-10. The upper range of the results from the falling head tests in cased holes and the pump test results have been the most reliable. The simulation of aquifer response to river fluctuation gave values that were higher than those found with the prototype during operation of the reservoir. The analytically derived results using the Hazen formula show a great scatter. More than 430 samples were analyzed and the average varied from borehole to borehole. The overall average ( $8.67 \times 10^{-4}$  m/s) is remarkably close to the weighted average ( $5.4 \times 10^{-4}$  m/s) obtained during operation. The selection of the constant C in the Hazen formula introduces a great unknown. It is not suggested that the results obtained using the Hazen formula are used for design; however, if a large number of samples is taken, the grain size is useful in indicating the wide range of permeabilities to be expected.

## ACKNOWLEDGEMENT

Consulting engineering services for the Jebba Hydroelectric Development were provided by Monenco Consultants Limited. The main civil contract was awarded to Jeddah Company Fougerolle Nigeria. The Owner is National Electric Power Authority (NEPA).

## REFERENCES

- Boreli, M. (1955), "Free-Surface Flow Toward Partially Penetrating Wells", Trans. Am. Geophys. Un. 36, No. 4, pp. 664-672.
- Clough, R.W. and Woodward, R.J. (1967), "Analysis of Embankment Stresses and Deformations", J. Soil Mech. Found. Div., ASCE, Vol. 93, No. SM4.
- Duncan, J.M. and Chang, C.Y. (1970), "Non-Linear Analysis of Stress and Strain in Soils", J. Soil Mech. Found. Div., ASCE, Vol. 96, No. SM5, Proc. Paper 7513.
- Hazen, A. (1892), "Experiments Upon the Purification of Sewage and Water at the Lawrence Experiment Station", 23rd Annual Report, Massachusetts State Board of Health.
- Hazen, A. (1908), "The Filtration of Water Supplies", Wiley, New York.
- Krishnayya, A.V.G., "Finite Element Non-Linear Analysis for two Dimensional Problems (FENA 2D)", User's Manual, Soil Mechanics No. 19, Dept. of Civil Engineering, University of Alberta, Edmonton, Canada.
- Krumbein, W.C. and Monk, C.D. (1943), "Permeability as a Function of the Size Parameters of Unconsolidated Sand", Trans. Am. Inst. Min. Metall. Engrs. 151, pp 153-163.
- Kulhawy, F.H. and Duncan, J.M. (1972), "Stresses and Movements in Oroville Dam", J. Soil Mech. Found. Div., ASCE, Vol. 98, No. SM7, Proc. Paper 9016.

- Neumann, S.P. (1975), "Analysis of Pumping Test Data from Anisotropic Unconfined Aquifers Considering Delayed Gravity Response", Wat. Resour. Res. 11, No. 2, pp 329-342.
- Solymar, Z.V. (1984), "Compaction of Alluvial Sand by Deep Blasting", Can. Geotech., J 21, No. 2, pp 305-321.
- Solymar, Z.V., Iloabachie, B.C., Gupta, R.C. and Williams, L.R. (1984), "Earth Foundation Treatment at Jebba Dam Site", J. Geotech. Engrg. Div., ASCE, 110, No. 10, pp 1415-1430.
- Solymar, Z.V. and Mitchell, J.K. (1986), "Blasting Densifies Sand", Civil Engineering, ASCE, March.
- Solymar, Z.V. and Iloabachie, B.C. (1986) "Permeability Determined in an Alluvial Dam Foundation", Geotechnique, 36, No. 1, pp 95-108.
- Verruijt, A. (1970), "Plane Flow with Sources and Sinks", Program LM4, Ottawa.

## Settlement Measurements of Peat Deposits as Embankment Foundation

**K. Kogure**

Department of Civil Engineering, The National Defense Academy,  
Yokosuka, Kanagawa, Japan

**K. Matsuo**

Department of Civil Engineering, The National Defense Academy,  
Yokosuka, Kanagawa, Japan

**SYNOPSIS:** A low test embankment have been constructed on a soft and fibrous peat deposits. The thickness of the soft peat layer is about 2.5 m. Under the peat layer, there is silty clay deposit with thickness of about 13 m. The site investigations were performed for both the layers. The laboratory soil tests on undisturbed samples obtained from both the layers were carried out. The settlement of foundation deposits was predicted by the one dimensional consolidation theory using the soil parameters obtained from laboratory soil tests. The results of field observations were compared with the calculated results by the conventional theory. The results of observations and caluculation do not agree. If the settlement of foundation deposits under embankment loading is predicted by a monitoring method, it appears that a lot of case records of settlement give the conclusion that the agreement of the prediction and the field observation is favourable.

### INTRODUCTION

In recent years, peaty ground is often utilized as the foundation of embankment such as road, residential district and others. It is known that peat deposit is highly compressible compared with most mineral soils. The general condition of peaty ground is typically very high in water content and is usually of extremely low bearing capacity. The major involvement of peat in engineering work is in its use as a foundation material. In this role, the high compressibility of peat stands out as a most significant engineering property. The consolidation settlement of peat will now be considered as the total compression resulting from volume change under a vertical load.

One of the most striking differences in the compression of peat deposit as compared to mineral soils is the long-term compression which appears to be an almost continuous process. The most part of the continuous settlement have shown a straight-line relation with the logarithm of time [Hanrahan, 1964, Molisz et al., 1973].

In applying the conventional theory to the consolidation of peat, there are two major deviations from the usual assumptions, that is, the compressibility of solids and the change in permeability under applied load [Matsuo, 1986].

These two anomalies are believed to account for the significant differences in consolidation behaviour between peat and mineral soils. Settlement behaviour of peat under embankment loading has reported [Noto, 1987, Lefebvre, 1984]. However, the prediction of settlement remain difficult owing to the heterogeneity of peat deposit.

A test embankment was recently built on peat deposit to study the settlement of low embankment. The site where the test embankment was constructed is located in Saitama prefecture, Japan. The peat layer is about 2.6m thick. There is underlying silty clay layer about 13 m thick. The water level in the peat layer was about 40 cm below the ground surface. The peat and underling silty clay samples were obtained before the construction at the location of the test embankment. Various identification tests and one-dimensional consolidation tests were conducted on the samples.

The fill thickness is 2.0 m. Two test section were built. In the first test section, the sand mat in thickness of 50 cm was laid between the ground surface and the bottom of the fill. In the second test section, the sand mat was not laid. The wide and length of the fill is 45 m and 120 m respectively. The instrumentation consisted of settlement plates, inclinometers, displacement piles and pore-water pressure cells. All instruments were put in place

before and during the construction. The results of settlement observations were compared with the results calculated by the conventional one-dimensional consolidation theory using the soil parameters obtained from laboratory tests. The field observation give slower settlement than the predicted ones by the laboratory tests for peat layer. However, the field observations give faster settlement than the predicted ones for the silty clay layer.

If the settlement of the peat layer under the low embankment loading is predicted by a monitoring method, it appears that a lot of case records of settlement give the conclusion that the agreement of the prediction and the field observation is favourable.

## OUTLINE OF EMBANKMENT CONSTRUCTION

### Soil Profile of Foundation Deposits

The low test embankment was constructed in Saitama prefecture. The area consists of the terrace ranging from +12 m to 14 m above sea level and alluvial valley which eroded the terrace. The terrace is diluvial deposit and called "Kanto loam". The Kanto loam is volcanic sedimentary soil. The alluvial deposit is featured with cohesive soil of drowned valley fill and the upper peat soil as shown in Figure 1.

The low test embankment was constructed on the alluvial deposits. From the site investigations, the alluvial deposits were classified into two layers. That is,

- upper peat layer
- underlying silty clay layer.

In this study, the upper peat layer and the underlying silty clay layer is called Pt layer and Sc layer respectively. The thickness of the alluvial deposits in the embankment area is almost constant with the depth of about 13 m on north-south direction. The thickness of the alluvial deposits on east-west direction varies from 7 to 16 m.

In soil exploration practice drilling and sounding have been made to the embankment area at required interval in both the north-south and the east-west directions. Figure 2 shows the soil profile and the other soil properties.  $N$  and  $q_c$  value was obtained by the standard penetration test and the Dutch cone penetration test respectively. The natural water content  $w_n$  and the wet density  $\rho_t$  was measured from the sample obtained by thin-wall piston sampler. The unconfined compression test was carried out for the undisturbed sample and the unconfined compression strength  $q_u$  was also shown in Figure 2.

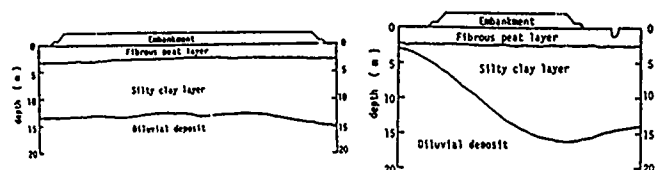


Figure 1 (a) Cross-section of north-south direction of foundation deposits

Figure 1 (b) Cross-section of east-west direction of foundation deposits

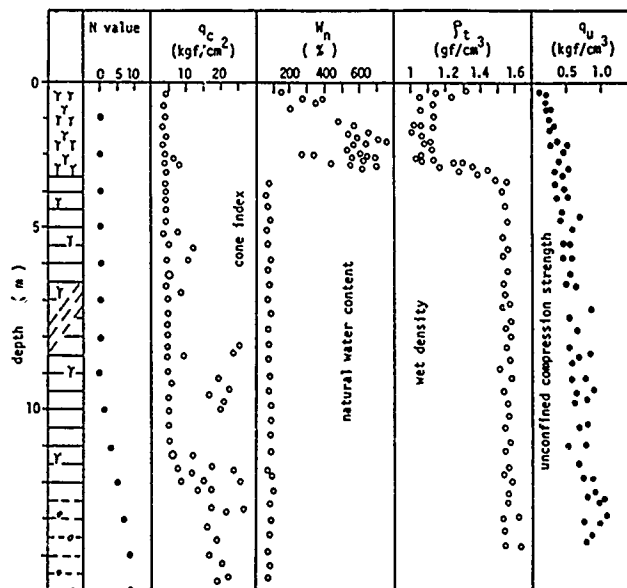


Figure 2 Soil profile and others of foundation deposits

### Mechanical Properties of Deposits

The undisturbed samples of peat and silty clay were obtained by the thin-wall piston sampler before the embankment construction. Figure 3 shows the variation of the preconsolidation pressure  $p_c$  in relation to depth.

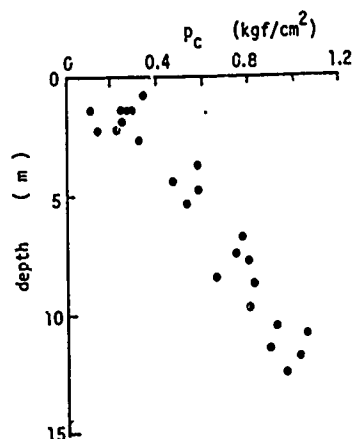


Figure 3 Variation of preconsolidation pressure in relation to depth

It is observed from Figure 3 that the preconsolidation pressure  $p_c$  of the peat is in the range between 0.1 and 0.35 kgf/cm<sup>2</sup> and the average value is 0.25 kgf/cm<sup>2</sup>. The value is considerably larger than the effective overburden pressure and it is noticed that the peat layer is overconsolidated. The overconsolidation of surface layer in this case is attributed to desiccation. The preconsolidation pressure  $p_c$  of the silty clay is in the range between 0.32 and 1.05 kgf/cm<sup>2</sup>. In the silty clay layer,  $p_c$  is also considerably larger than the effective overburden pressure.

The relationships between the coefficient of volume compressibility  $m_v$  and the consolidation pressure  $p$  were shown in Figure 4. It is found that the relationships are almost linear for values beyond the preconsolidation

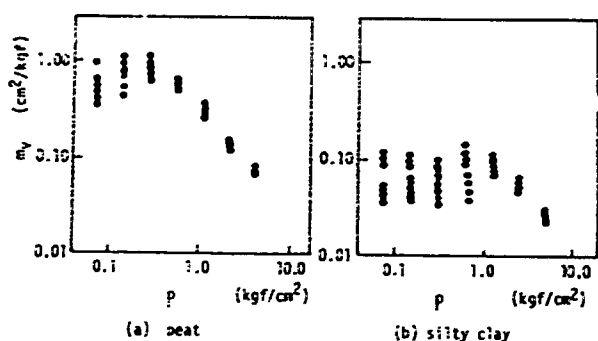


Figure 4 Relationships between volume compressibility  $m_v$  and consolidation pressure  $p$

pressure. Figure 5 shows the relationships between the coefficient of consolidation  $c_v$  and the consolidation pressure  $p$ . The final settlement and the time-settlement relation was calculated by using the results shown in Figures 4 and 5.

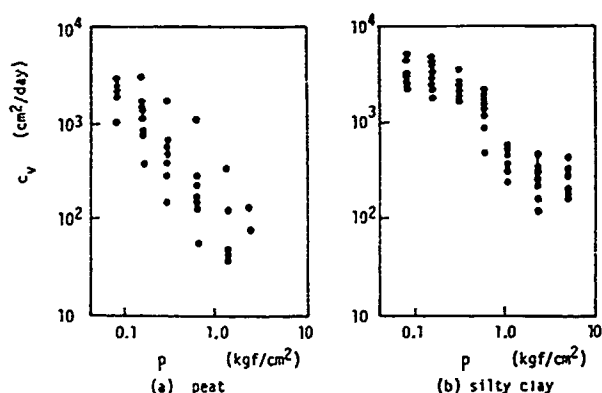


Figure 5 Relationship between coefficient of consolidation  $c_v$  and consolidation pressure

## Low Test Embankment

The plan of the low test embankment was shown in Figure 6. The gauge arrangement was also shown in Figure 6. The embankment can be divided into two sections. In this study, the section of left hand side in Figure 6 is called section 1. In the section 1, the sand mat with 50 cm thick was laid between the ground surface and the bottom of fill. The section of right hand side in Figure 6 is called section 2 and the sand mat was not laid in the section 2.

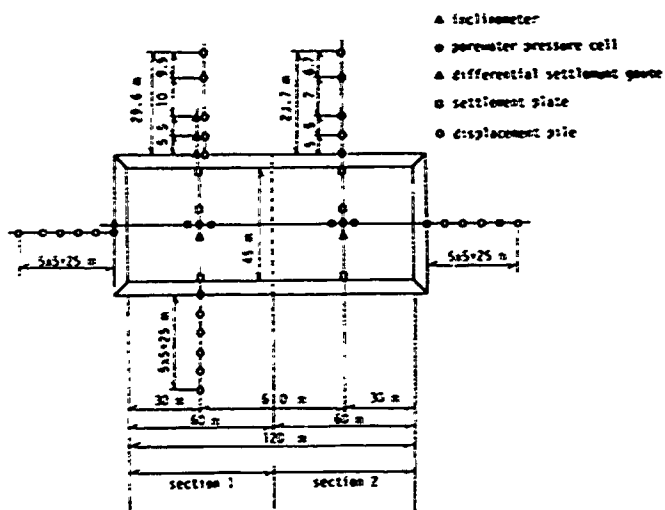


Figure 6 Plane of embankment and arrangement of instruments

## FIELD OBSERVATIONS

All the instruments were put in place before and during the construction. The arrangement of instruments was shown in Figure 6. The settlements of the foundation deposits at the center and periphery of the sections 1 and 2 were observed using the settlement plates. Using the differential settlement gauge, the settlements of the peat and underlying silty clay layers were separated. The settlement observations separated were carried out at the center of the sections 1 and 2. The ground surface movements due to the embankment loading were surveyed using the displacement piles in the area from the toe of embankment to about 25 m outside. The lateral displacements at from the surface to the depth of 20 m in the foundation deposits were measured using the inclinometers in the area from the toe of embankment to 10 m outside. The porewater pressures in the peat and the silty clay were measured by the porewater pressure cells. At the center of sections 1 and 2, the groundwater level were measured by the stand-pipe with strainer.

## PREDICTION OF SETTLEMENT

Prediction methods of settlement can be classified in two categories. The first is theoretical: Settlement is predicted by theoretical calculation using soil parameters obtained from soil tests and boundary conditions obtained from soil investigations. The conventional one dimensional consolidation theory, the analysis by finite element method(FEM) and others fall in the category. The second is monitoring method: Settlement is predicted according to the field observations.

For the first, the next conditions have to be satisfied:

(1) Accurate soil parameters are obtained, (2) accurate boundary conditions are obtained, (3) theory is reasonably established. For analysis by FEM, the determination of soil parameters is very difficult. From the reasons mentioned above, the overestimation of FEM have to be examined oneself[Shibata,1983]. The methods in the second category, that is, monitoring methods are useful to examine the adequacy on the initial design and to revise it. From the facts mentioned above, the prediction by the conventional theory is compared with the field observations and the prediction by the monitoring method.

The hyperbolic curve method and others have been proposed as the monitoring method[Krizek et al,1977, Hoshino,1962, Asaoka,1978, Monden,1963]. For the accuracy of these monitoring methods, a interesting results have been reported[Yoshikuni et al,1981]. That is, if the final settlement is predicted using the observations after the degree of consolidation of about 70 and 60 %, the range of the prediction error is in about 10 and 20 % regardless of the monitoring methods used, respectively. The hyperbolic curve method is used in this report.

The hyperbolic curve method is based on the assumption that the rate of settlement is represented by a hyperbolic curve. It is assumed that the relationship between settlement  $S$  and time  $t$  is schematically represented by a hyperbolic curve as shown in Figure 7(a).

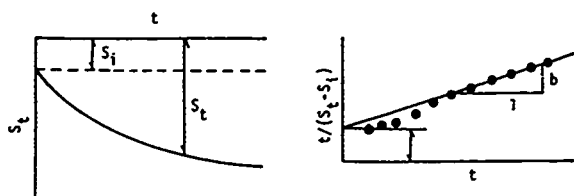


Figure 7 Schematically representation of hyperbolic curve method

The hyperbolic curve is expressed as follow:

$$S_t = S_i + \frac{t}{a + bt} \quad (1)$$

where,  $S_t$  is settlement at time  $t$ ,  $S_i$  is initial settlement,  $a$  and  $b$  are constants obtained from observations.

Equation (1) is written as follow:

$$\frac{t}{S_t - S_i} = a + bt \quad (2)$$

The relationship between  $t/(S_t - S_i)$  and  $t$  can be plotted by a straight line as shown in Figure 7(b). The slope of the straight line gives the value of  $b$  and the interception of  $t/(S_t - S_i)$  axis gives the value of  $a$ . The final settlement  $S_f$  is given as the value of  $S_t$  when  $t \rightarrow \infty$  and is written as follow:

$$S_f = S_i + \frac{1}{b} \quad (3)$$

## RESULTS OF OBSERVATIONS AND DISCUSSIONS

### Stability of Foundation Deposits

To examine the stability of foundation deposits during construction, the diagram for construction control of embankment have been proposed[Matsuo et al,1978]. It is very convenient that the stability of foundation deposits is examined using this diagram. It was confirmed that the foundation deposits under the low embankment loading was stable to failure.

### Final Settlements

The results of settlement observations were shown in Figures 8 (a) and 9(a). The relationships between  $t$  and  $t/(S_t - S_i)$  are plotted in Figures 10 and 11.

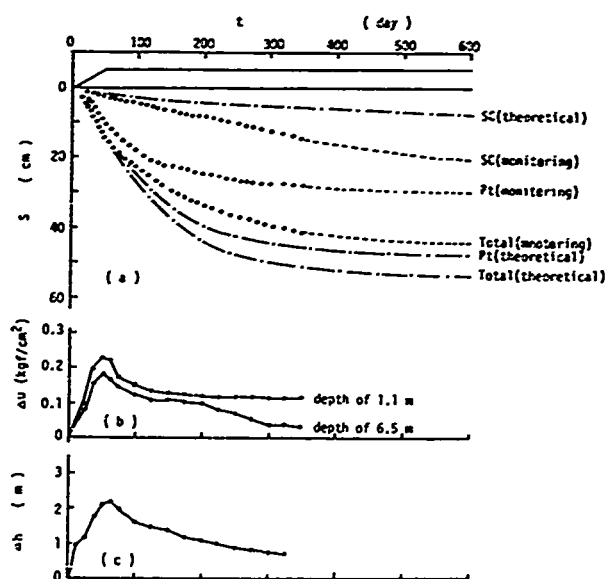


Figure 8 Settlement  $S$ , porewater pressure  $\Delta u$  and groundwater level  $\Delta h$  at center in section 1



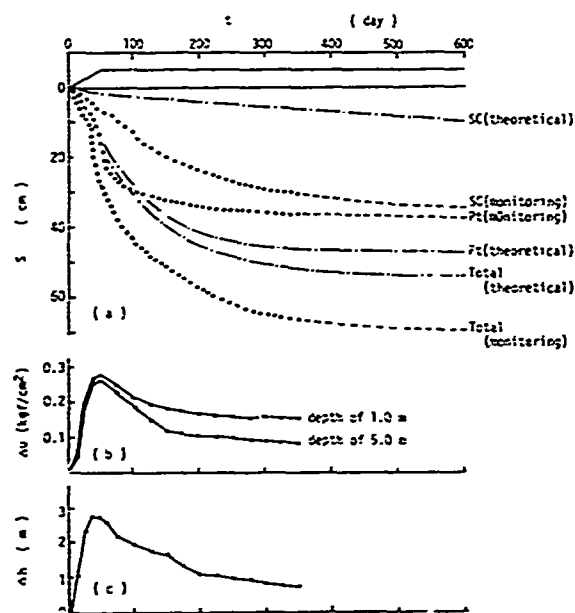


Figure 9 Settlement  $S$ , porewater pressure  $\Delta u$  and groundwater level  $\Delta h$  at center in section 2

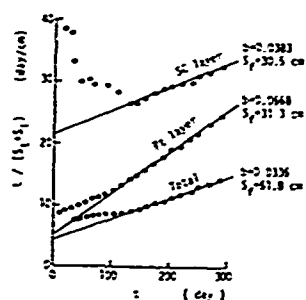


Figure 10 Prediction of settlement by hyperbolic curve method (section 1)

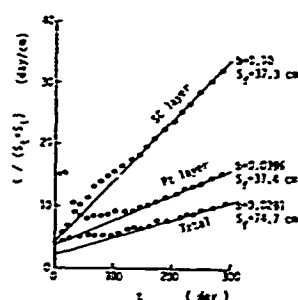


Figure 11 Prediction of settlement by hyperbolic curve method (section 2)

The regression lines can be obtained from the plots shown in Figures 10 and 11. The constants  $a$  and  $b$  can be obtained from the regression line and are shown in Figures 10 and 11. The final settlement  $S_f$  can be calculated from equation (3) and the values of  $S_f$  calculated are also shown in Figures 10 and 11.

The final settlements of the sections 1 and 2 calculated by the theoretical method ( $m_v$  method) are shown in Table 1 with the results by the hyperbolic curve method.

Table 1 Comparison of final settlement

|           |            | final settlement $S_f$ (cm)           |                                   |         |
|-----------|------------|---------------------------------------|-----------------------------------|---------|
|           |            | theoretical<br>( $m_v$ method)<br>(1) | monitoring<br>(hyperbolic)<br>(2) | (2)/(1) |
| section 1 | peat       | 46.1                                  | 31.3                              | 0.68    |
|           | silty clay | 21.5                                  | 30.5                              | 1.41    |
|           | total      | 67.6                                  | 61.8                              | 0.91    |
| section 2 | peat       | 46.8                                  | 37.3                              | 0.80    |
|           | silty clay | 24.2                                  | 37.4                              | 1.56    |
|           | total      | 71.0                                  | 74.7                              | 1.05    |

For Pt layers, the final settlements by theoretical method indicate the results larger than these by the hyperbolic curve method. On the other hand, for the SC layers, the final settlements by the hyperbolic curve method are larger than these by the theoretical. The prediction of final settlement by the theoretical was found to be far from satisfactory. Better prediction can be expected if more accurate values of  $m_v$  and boundary condition are employed.

#### Time-Settlement Relations

To simplify the calculation of rate of consolidation for the multi-layered foundation, the two strata were converted to a single stratum by the method previously proposed [Palmer et al, 1957]. Figures 8(a) and 9(a) show the comparisons between the observed and predicted settlements. For the SC layers, the observed settlements are far larger than predicted ones. On the other hand, for the Pt layers, the predicted settlements are larger than observed ones.

The degree of consolidation  $U_{350}$  at 350 days after the beginning of construction is calculated and shown in Table 2. In Table 2,  $S_{350}$  is the settlement at 350 days after the beginning of construction. For Pt layers,  $U_{350}$  is more than about 90 %. However, the

Table 2 Comparison of degree of consolidation  $U_{350}$  at 350 days after beginning of construction

|           |            | theoretical |           |           | hyperbolic |           |           |
|-----------|------------|-------------|-----------|-----------|------------|-----------|-----------|
|           |            | $S_f$       | $S_{350}$ | $U_{350}$ | $S_f$      | $S_{350}$ | $U_{350}$ |
| section 1 | peat       | 46.1        | 45.2      | 98 %      | 31.3       | 28        | 89 %      |
|           | silty clay | 21.5        | 5.6       | 26 %      | 30.5       | 14        | 46 %      |
|           | total      | 67.6        | 50.8      | 75 %      | 61.8       | 42        | 68 %      |
| section 2 | peat       | 46.8        | 46.2      | 99 %      | 37.3       | 36        | 97 %      |
|           | silty clay | 24.2        | 6.4       | 26 %      | 37.4       | 31        | 83 %      |
|           | total      | 71.0        | 52.6      | 74 %      | 74.7       | 66        | 88 %      |

\* measured value

degree of consolidation of SC layers is lower than these of the Pt layers. There is a considerable difference between the degrees of consolidation by the theoretical and hyperbolic methods.

#### Porewater Pressures and Groundwater Levels

The variation of the porewater pressure  $\Delta u$  in the Pt and SC layers under the center of the sections 1 and 2 are shown in Figures 8(a) and 9(b). It is seen that the maximum porewater pressure occurs at the end of construction and the values are from 0.19 to 0.29  $\text{kgf/cm}^2$ . On the other hand, the increment load by the embankment is 0.35  $\text{kgf/cm}^2$ . The maximum porewater pressure occurred in foundation deposits are smaller than the increment load. For both the sections 1 and 2, the dispersion of porewater pressure in SC layer is faster than it in Pt layer. The maximum porewater pressure in the section 1 is smaller than it in the section 2 due to the effect of the sand mat.

The groundwater level in the stand pipe at the center of the sections 1 and 2 were shown in Figures 8(c) and 9(c). The maximum groundwater level in the section 1 is lower than it in the section 2. The groundwater levels approximately correspond to the porewater pressures. The degrees of consolidation  $U_{350}$  at 350 days calculated from the porewater pressure measured were shown in Table 3.

Table 3 Degree of consolidation obtained from porepressure at 350 days after beginning of construction

|           |            | depth | porewater pressure at 350 days $u_p$ (kgf/cm <sup>2</sup> ) | maximum porewater pressure $u_m$ (kgf/cm <sup>2</sup> ) | theoretical porewater pressure $u_{th}$ (kgf/cm <sup>2</sup> ) | degree of consolidation $U_{350}(\%)$ |
|-----------|------------|-------|---|---|--|---------------------------------------|
| section 1 | peat       | 1.2   | 0.286   | 0.274   |  | 77                                    |
|           | silty clay | 6.5   | 0.070   | 0.19  |  | 81                                    |
|           | silty clay | (8.0) | (0.050)   | (0.19)  | 0.37   | (89)                                  |
| section 2 | peat       | 1.0   | 0.161   | 0.286   |  | 62                                    |
|           | silty clay | 5.0   | 0.104   | 0.277   |  | 72                                    |
|           | silty clay | (8.0) | (0.100)   | (0.270)   | 0.37   | (73)                                  |

$U_{350} = 1 - \frac{u_p}{u_m}$

#### Movements of Foundation Deposits

Figures 12 and 13 show the horizontal movements measured by the inclinometer located at the foot of the slope edge

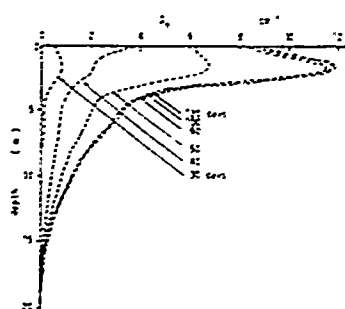


Figure 12 Horizontal displacement  $U_h$  at toe of embankment (section 1)

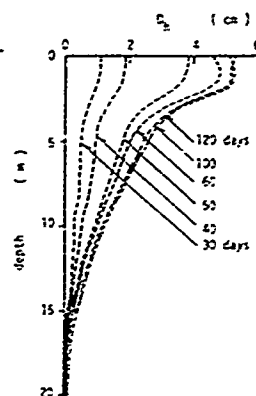


Figure 13 Horizontal displacement  $U_h$  at 5 m away from toe of embankment (section 1)

and 5 m away from it in the section 1 respectively. At the end of the measurements, the maximum displacement measured was about 12 cm at the toe of slope and about 5 cm at 5 m away from it. It is noted that the horizontal displacement is considerably small.

Figure 14 shows the vertical movements measured by the displacement piles located at from the foot of the slope edge to 23 m away it in the section 1. At the toe of the slope, a considerable settlement occurred, but the vertical displacement do not nearly occurred at from 5 m to 20 m away it.

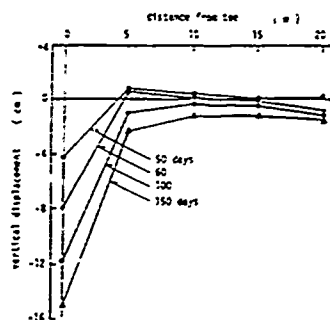


Figure 14 Vertical displacement at from toe of embankment to 20 m (section 1)

#### SUMMARY

In this report, the measured results of the settlement and others of the soft foundation deposits due to the low embankment were shown. The observations are presently continuing. Therefore, the final conclusion can not be obtained. From the observations until the present, the followings can be summarized.

The final settlement by theoretical method do not agrees with it by the monitoring method. The rate of settlement by the conventional theory do not also agrees with the field observations. The theoretical prediction must be used as the probable value at the initial design and the prediction during and after construction must be corrected by the monitoring method.

We would like to express our thanks to the Japan Hosing Corporation for having made available their observed data for inclusion in this report.

#### REFERENCES

- Asaoka, A. (1978), "Observational Procedure of Settlement Prediction", *Soils & Foundations*, Vol. 18, No. 4, pp. 87-101.
- Hanrahan, E. T. (1964), "A Road Failure on Peat", *Geotechnique*, Vol. 14, pp. 185-201.
- Hoshino, K. (1962), "Recent Problems on Foundations," *Proc. of JSCE*, Vol. 47, No. 7, pp. 63-67.
- Krizek, R. J., Corotis, R. B. and El-Moursi, H. H. (1977), "Probabilistic Analysis of Predicted and Measured Settlement," *Canadian Geotechnical Journal*, Vol. 14, pp. 17-33.
- Lefebvre, G., Langlois, P., Lupien, C. and Lavallee, J. G. (1984), "Laboratory Testing and In-Situ Behaviour of Peat as Embankment Foundation," *Canadian Geotechnical Journal*, Vol. 21, pp. 322-337.
- Matsuo, K. (1986), "Relationship between Physical Properties and Compression Index Arranged by Logarithmic Strain," *Jour. of JSSMFE*, Vol. 26, No. 4, pp. 177-185.
- Matsuo, M. and Kawamura, K. (1978), "Diagram for Construction Control of Embankment of Soft Ground," *Tsuchi to Kiso*, Vol. 26, No. 7, pp. 5-10.
- Holisz, R., Baran, L., Najder, J. and Werno, M. (1973), "Field Studies of Embankment over Peat," *Proc. of 8 th ICSMFE*, Moscow, Vol. 2-2, pp. 139-143.
- Monden, H. (1963), "A New Time-Fitting Method for the Settlement Analysis of Foundation on Soft Clay," *Memoir Faculty of Engrg, Hiroshima Univ.*, 2-1, pp. 21-29.
- Noto, S. (1987), "Prediction of Settlement for Peaty Soft Ground," *Jour. of JSSMFE*, Vol. 27, No. 2, pp. 107-117.
- Palmer, L. A. and Brown, P. P. (1957), "Settlement Analysis for Areas for Continuing Subsidence," *Proc. 4 th ICSMFE*, pp. 395-398.
- Shibata, T. (1983), "Actual State and Prediction of Settlement and Deformation, Text of the Recent Problems on Soils and Foundations," *JSSMFE*, pp. 19-27.
- Yoshikuni, H., Inoue, T., Sumioka, N. and Hara, H. (1981), "On the Characteristics of Settlement Prediction Methods by Monitoring," *Tsuchi to Kiso*, Vol. 29, No. 8, pp. 7-13.

## Underseepage Control Measures at Painted Rock Dam

### L. Knuppel

Geotechnical Engineer, Ohio River Division, USACE, Cincinnati, Ohio; previously Chief, Soil Section, Los Angeles District, USACE, Los Angeles, California

### F. McLean

Chief, Division of Research & Laboratory Services, USBR, Denver, Colorado; previously Chief, Geotechnical & Materials Branch, South Pacific Division, USACE, San Francisco, California

### A. Roodsari

Chief, Soils Section, Los Angeles District, USACE, Los Angeles, California

**SYNOPSIS:** Painted Rock Dam, a 181 ft (55.2 m) high, zoned earth embankment detention structure near Gila Bend, Arizona, retained approximately 2.3 million acre ft ( $2.8 \times 10^9 \text{ m}^3$ ) of water for an extended period during the winter of 1978-1979.

Several areas of seepage developed over major portions of the downstream valley and in a minor area on the right abutment. These areas were monitored while instrumentation was installed and investigations made to determine the nature of the seepage and provide the basis for evaluation of structural performance and design of necessary relief and control measures.

Construction of seepage relief and control measures and stabilizing berms was accomplished in the fall of 1979. Performance of the project has been evaluated during subsequent storage periods through 1986, with the conclusion that the control measures are functioning satisfactorily, and in general accordance with design concepts. Site conditions, original design and construction, seepage observations, instrumentation, investigations, evaluations, and design and construction of remedial measures are summarized and lessons learned are presented.

### PROJECT DESCRIPTION

Painted Rock Dam is a compacted, zoned earth embankment, flood control structure located on the Gila River about 22 miles (35.4 km) northwest of the Gila Bend, Arizona. Construction of the project was initiated in 1957 and was completed in November 1959, Figure 1. The length of the dam is 4796 ft (1461.8 m), with a maximum height of 181 ft (55.2 m) (Elev 705 ft msl) above the streambed and the crest width is 20 ft (6.09 m). The 25 ft (7.6 m) diameter gated outlet structure has a discharge capacity of 30,500 cfs (863.8  $\text{m}^3/\text{s}$ ), while the 610 ft (185.9 m) wide, ungated, broadcrested weir, rock spillway has a discharge capacity of 405,000 cfs (11,469.6  $\text{m}^3/\text{s}$ ). The reservoir capacity is 2,491,700 acre ft ( $3.1 \times 10^9 \text{ m}^3$ ) at spillway crest (Elev 661) and 4,825,000 acre ft ( $5.9 \times 10^9 \text{ m}^3$ ) at maximum water surface (Elev 696.4).

The authorized operation plan for Painted Rock Dam was established to reduce peak flood flows by retaining water for only short durations (several months at most). During nonflood periods the reservoir was intended to be dry. Unfortunately, the unimproved downstream channel of the Gila River has a relatively small, nondamaging flow capacity, approximately 5,000 cfs (141.6  $\text{m}^3/\text{s}$ ). To prevent damages and hardship, releases have been considerably less than the original design intended.

#### Site Conditions

The geologic setting of the site is volcanic, with alluvial deposits in valley sections, Figure 2. The complex foundation is composed of several rock units, and complicated by faulting. Three faults were exposed in the main stream channels and two on the left abutment saddle, with shear zones existing in all units at various locations across the site.

The pink rhyolite is generally hard and massive with steeply dipping joints oriented in an intersecting pattern near north-south and east-west. Most of the joints along the dam axis are relatively tight and spaced

an average of about one foot apart. However, several open, near-horizontal fractures were noted in the upper portion of the left abutment saddle. The tuff and agglomerate units vary from porous and friable to moderately hard and dense, and are generally massive with occasional vertical joints. The rhyolitic andesite is hard and dense, but deeply weathered where vertical flow bands intersect the surface, with a contorted, platy structure due to flow banding. Joints are more widely spaced than in the rhyolite, and tend to strike north-south with near vertical dips. These joints are especially prominent in the left stream channel and the adjoining steep left abutment ridge.

The alluvium consists of recent and older units with the recent deposits occurring only in the Gila River streambed, where it was 60 ft (18.3 m) deep in the right channel and 80 ft (24.4 m) deep in the left channel at the dam axis. Under the dam the alluvium consists of clean coarse material, including sand, gravel and cobbles with irregular lenses of open gravel, which become more coarse with depth.

The older alluvium is composed primarily of terrace deposits containing silts, sands, gravels and talus, and occurs only in the left abutment saddle. In the central portion of the left abutment saddle the older alluvium was sufficiently cemented with caliche to be classified as rock.

#### Design

In light of the short duration of planned storage, it was not felt that steady-state seepage conditions would be fully developed during project operation. Consistent with contemporary practice and the purpose of the project, the only instrumentation designed into the project were surface settlement monuments.

To accommodate the site conditions it was decided to



Figure 1. Aerial view of Painted Rock Dam as seen from approximately 1/2 mile (0.8 k) east of the right abutment.

carry the impervious and transition zones through the pervious alluvium to rock, Figure 3. The pervious shells were to be founded on prepared alluvium. Materials for all zones, except the impervious, were to come from a downstream borrow area, while the source for impervious materials was approximately 2 miles (3.2 k) upstream of the dam. Foundation preparation and treatment was performed in accordance with the state of practice at the time. A single grout line was used to provide for a final indication of the quality of the foundation rock, with a split-spacing process and expansion of lines planned if considered necessary during construction.

#### Construction

Construction proceeded largely as envisioned during the design. Excavation of the cutoff trench was in the dry, but dewatering measures were required in the recent alluvium of the left and right stream channels, including the installation of gravel filled collection trenches in the rock immediately upstream and downstream of the impervious zone in several areas.

Several borings and exploration trenches were made during construction to confirm the condition of the foundation and the extent of treatment required in local areas. The single grout line was constructed beneath the impervious zone, approximately along the centerline of the section, with an average take of 0.3 sacks per linear ft (0.3 m) in holes ranging from 10 to 60 ft (3 to 18.3 m) in depth. Early in the program borings were made to evaluate grout penetration, which was found to be good. One grout hole in the right abutment (Sta 16+95) took 173 sacks with no surface leaks, and was bracketed with additional holes to attain closure.

Rock in the cutoff trench and the abutment was prepared for fill placement by removing all loose and objectionable material to obtain suitable foundation conditions. Vertical and overhanging rock ledges were removed from the abutments and mid-valley rock ridge. Dental concrete was required only in scour channels and

pockets in the bedrock of the left stream channel cutoff trench.

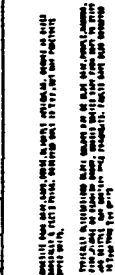
The alluvium was prepared for embankment placement by removing unsuitable materials in the sidewalls of the cutoff trench and on the surface underlying the embankment. Stripping to a depth of several feet was required, with excavation to the existing water table elevation at several locations in the stream channels. The alluvium was proof rolled prior to placing fill.

The moisture content of fill materials was adjusted by prewetting and mixing in the borrow areas. These materials were hauled and placed in accordance with the specifications, although rapid surface drying of the impervious materials due to summer sun and wind necessitated a change of procedures. The resulting construction met specification requirements with regard to both moisture content and material gradation.

#### THE OCCURRENCE OF SEEPAGE

After a prolonged period of water storage at about Elev 583, on December 20, 1978, reservoir inflows of up to 70,000 cfs (1,982.4 m<sup>3</sup>/s) caused a rapid rise of reservoir surface elevation, which reached a record high of Elev 613 on December 26, 1978. On January 2 and 8, 1979, the dam operations staff noticed isolated seeps in the valley downstream of the toe, Figure 4. As seeps occurred they were numbered sequentially and monitored for quantity and sediment. Visual monitoring of the seeps was intensified, and on about January 19, 1979, the reservoir began rising again. Seepage rates increased with almost no time lag and four additional seeps developed over the next two weeks, Table 1. During this period foot patrols and monitoring efforts were increased using additional staff temporarily assigned to the project. The reservoir reached Elev 634.6 on February 7, and subsequently dropped and then raised to the maximum peak of Elev 642.3 on April 17, 1979.

Since the early seepage carried no sediment, it was



385

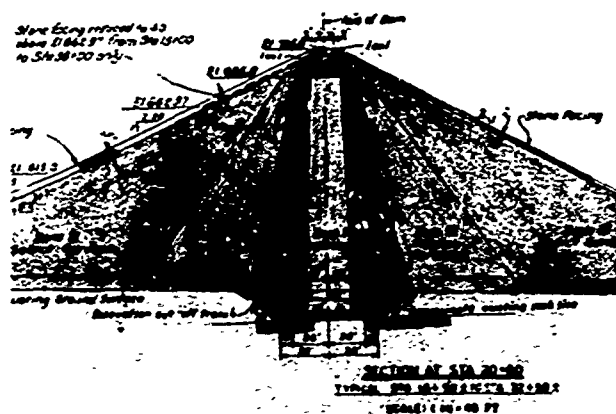


Figure 3. Cross-section of dam at Sta 20+00.

decided to leave the areas free of any temporary relief or control measures so that visual monitoring of the exit conditions could be maintained while investigations and studies were carried out to determine the physical basis for the seepage and provide a rationale for the design of permanent relief and control measures. This decision did not preclude the installation of temporary measures, and arrangements were made for quick availability of construction personnel, equipment and materials, should they have been needed. As the reservoir reached the higher levels, Seeps 1 and 2 were blanketed with gravel wrapped in filter cloth and weighted with a surcharge berm as a preventive measure.

#### INVESTIGATIONS AND STUDIES

Due to the dispersed seeps and the apparent complexity of the situation, it was decided to execute a comprehensive program of complementary investigations. The possible urgency of the situation dictated that the most expedient methods be used as quickly as possible, to be followed by programs requiring borings or more time consuming installations. Table 2 summarizes the types of investigations, while Figure 5 shows locations of instruments and surveys. Several of the investigations occurred concurrently in the January-February time period, and some were completed prior to the high water conditions in early February. These results contributed to decisions governing operations made during that period.

#### Seepage Collection and Measurement

As soon as seeps developed the water was collected at points where monitoring of quantity and sediment could occur. An attempt was made to maintain this capability throughout the study period, although later activities necessitated combining several flows. Temperature readings were taken and, later, samples for chemical analysis obtained. This effort contributed to the early decision process and provided continuous information on response times to reservoir changes and piping potential.

#### Observations Wells

Corps of Engineer staff quickly installed a total of 22 well points in the valley alluvium and fill downstream of the toe. Eleven of these were placed in the general area

of Seep 1, between Sta 43+75 and Sta 49+80. The balance were placed in the vicinity of Seeps 3, 4 and 5, between Sta 6+00 and Sta 30+00. In addition to observing water levels, these wells were also pumped to gain an indication of permeability.

#### Electrical Resistivity

During the period of January 19 to 26, 1979, electrical resistivity surveys were performed in the vicinity of Seeps 1, 2 and 3. The use of Wenner and Bristow arrays resulted in interpreted seepage paths under the dam associated with the rock ridge near Seeps 2 and 3, and in the foundation near Seep 1, where several shallow seepage paths appear to converge.

#### Geothermal Monitoring

Thermistors were installed in 10 ft (3 m) deep holes as follows: (1) 20 along the crest of the dam at 200 ft (61 m) intervals, (2) 13 along the lower access road at 100 ft (30.5 m) intervals, and (3) 12 along the access ramp at 100 ft (30.5 m) intervals. They were allowed to stabilize, and readings were initially taken on January 23, 1979. Three other sets of readings were made between January 26 and February 4, 1979. Interpretation of the temperature anomalies resulted in identification of six zones of potential seepage, Figure 5. Temperature surveys, accomplished in the deep borings made for piezometer installations, indicated the seepage paths to be in the foundation rock.

#### Aerial Imagery

On January 28, 1979, two flights were made, at 0755 and 1040 hours, to obtain color, color infrared and thermal infrared images. The intent was to take advantage of thermal differentials to confirm the location of seeps already discovered, possibly locate seeps as yet undiscovered by the extensive foot patrols, and to extend the area of coverage beyond that possible by foot. Temperatures of Seeps 1 and 2 were determined to be 6 to 8° F higher than the reservoir, while the balance of the detected areas were nearly the same temperature as the reservoir. No seeps were discovered outside of the immediate region of the dam. Existing seeps were largely confirmed and two seeps, Seeps 7 and 8, were discovered before surface seepage was observed.

#### Refraction Seismic

Refraction seismic surveys were performed during the period of February 2 to 8, 1979. The objective was the expedient profiling of subsurface conditions to use in the evaluation of seepage and the selection and design of relief and control measures. In particular, preliminary design of the relief well systems was based on these results, confirmed by some boring data.

#### Chemical Analyses

On April 20, 1979, a long term program of measuring reservoir temperature and water chemistry (dissolved solids) was initiated for comparison with concurrent evaluations of seepage water temperature and chemistry. In the seeps a broad range of total dissolved solids, 2,090 to 31,770 ppm, was measured compared with 400 to 650 ppm for the water in the reservoir. The higher values are associated with the cooler water in Seep 6. By August 14, the concentrations had dropped in all areas, ranging from 1,500 to 7,740 ppm, the higher values remaining associated with Seep 6. The interpretation of shorter seepage paths resulting in less dissolution of salts from the geologic units was consistent with the physical conditions at the site, and the reduction overall indicated that the development of solution channels was improbable.



Figure 4. Plan view of Painted Rock Dam showing sequentially numbered seeps in their order of occurrence.

TABLE 1  
Summary of Seepage Areas

| Number | Location   | Surface Elev., msl | Depth to Rock          | Remarks   |
|--------|--|--------------------|------------------------|---|
| 1A     | Sta 47+00 at base of downstream access ramp.                         | 600                | 15-20 ft (4.6-6 m)     | Natural topographic low with rock outcrop as one boundary.              |
| 1B     | Sta 47+00, 200 ft (61 m) north of Area 1A.                           | 600                | 15-20 ft (4.6-6 m)     | Natural topographic low with rock outcrop as one boundary.              |
| 2      | Sta 31+00 at downstream of lower access road.                        | 560                | 0                      | On face of mid-valley rock ridge; north-south joints.                   |
| 3      | 200 ft (61 m) north of Area 2.                                       | 565±               | 0                      | On face of mid-valley rock ridge; north-south joints.                   |
| 4      | In remote spillway, 200 ft (61 m) downstream of crest.               | 600                | 0                      | Fractured rhyolitic andesite.   |
| 5      | Sta 17+00 at right abutment and lower access road.                   | 555±               | 0                      | Rhyolitic andesite with joints.   |
| 6      | Sta 54+00 at downstream toe.   | 615±               | 6 ft (1.8 m)           | Thin alluvium.  |
| 6A     | Sta 54+00 at downstream toe.   | 615±               | 6 ft (1.8 m)           | Thin alluvium.  |
| 7      | Sta 47+00 to 51+00 at about 200-1000 ft (61-305 m) downstream of toe | 600                | 4 ft (1.2 m)           | Rock ridge; exposed contact of tuff-agglomerate and rhyolitic andesite. |
| 8      | Sta 20+00 at 600 ft (183 m) downstream of toe.                       | 531                | 60-80 ft (18.3-24.4 m) | Main channel; foundation rock faulted.                                  |

#### Piezometers

Multipoint piezometers, a Casagrande and two pneumatic, were installed in each of nine borings ranging from 41.4 to 150 ft (12.6 to 45.7 m) in depth during the period February through June 1979. The Casagrande device was generally installed in or near rock, with the two pneumatics above. In three of the borings all three devices were placed in rock. Borings made from the crest of the dam were angled downstream to avoid the impervious zone and surveyed to determine location. Initial readings indicated that all piezometers were operational, except for two of the pneumatic devices.

#### EVALUATION OF SEEPAGE CONDITIONS AND STABILITY

Examination of the design exploration data, geologic information collected during construction, and results of the various investigations confirmed that the complex site conditions gave rise to erratic seepage paths. There was general agreement between the data and investigations regarding the location of seepage paths, correlating to the joint systems in the foundation rock. No evidence was found to indicate seepage through the embankment, although quasi-steady state conditions could possibly develop during long storage durations.

In addition to evaluation of seepage and stability at each defined seepage zone by Corps staff, an independent evaluation was commissioned. Both evaluations concluded that seepage pressures developed under the dam, in areas of shallow alluvium, would give rise to conditions of marginal stability, i.e., a safety factor near 1.0 for pool elevations of about 650 and long term storage, while

in areas of deeper alluvium pressures would be dissipated in the foundation alluvium without endangering the embankment. This conclusion was based on flownets adjusted to piezometer and well point data and stability analyses. The decision was made to construct relief, control and collection systems and stability berms in the downstream seepage areas.

#### DESIGN AND CONSTRUCTION OF CONTROL MEASURES

Based on the determination that the seepage was under-seepage in the rock foundation rather than seepage through the embankment, the decision was made to incorporate three distinct components into the downstream relief and control system. (1) A series of relief wells drilled into rock and angled to intercept the maximum number of joints in the foundation rock. A separate collector and discharge system, designed to accommodate over 200 gpm (0.1 m<sup>3</sup>/s) per well while only flowing one-half full, was provided for each group of wells. (2) Graded toe drains with drainage blankets over the seep areas where exit gradients were calculated to exceed 2, to prevent the possibility of fines being piped and provide for controlled discharges. (3) A drained surcharge berm over the toe/blanket drains and embankment toe to provide additional stability at high pool levels.

The required capacity of relief wells was evaluated by installing three wells in seep areas 1 and 1A, and pumping to observe drawdown and flow conditions. A capacity of at least 200 gpm (0.1 m<sup>3</sup>/s) was required to effect the desired amount of relief. Due to construction considerations, the design configuration of the installed



TABLE 2  
Summary of Investigations

| Name   | Objective  | Date                                     | Results   |
|--|--|--|---|
| Observation Wells<br>(welipoints)                              | Early and continued monitoring of conditions in the vicinity of seeps and in the valley section.   | 1/79                                     | Provided indication of subsurface flow conditions, time lags, and permeability (when pumped).   |
| Electrical Resistivity   | Early identification and location of seepage paths, Areas 1, 2 and 3 only. Wenner & Bristow arrays.  | 1/19/79-1/26/79                          | Identified possible seepage paths contributing to Areas 1, 2 and 3.   |
| Geothermal:<br>- 10 ft deep<br>- deep profiles                 | Early identification of seepage paths from crest and access roads by thermal anomalies. Vertical surveys in deep piezometer borings indicated elevations.                    | 1/20/79-2/4/79, and continuing into 1980 | Identified possible seepage paths for Areas 1, 2, 3, 5 and 8.   |
| Aerial Imagery:<br>- Thermal IR<br>- Color Photo<br>- Color IR | Early identification or verification of seepage locations over a broad area, taking advantage of wide daily thermal variations and possible water temperature differentials. | 1/28/79                                  | Verified seeps 1, 2, 3 and 4. Detected seeps 7 & 8 before visual detection. Did not detect seeps 5 & 6. Indicated seeps 1 & 2 to be 6-8° F warmer than reservoir. |
| Refraction Seismic   | Locate depth to rock across broad area to aid in design of piezometer and relief well systems.   | 2/2/79-2/8/79                            | Provided top of rock data. Partially saturated flow conditions negated ability to locate paths.   |
| Thermal & Chemical   | Early and continued evaluation of seepage and reservoir temperature and quality to aid in identification of seepage conditions.  | 4/79 into 1980                           | Provided comparison of temperature and dissolved solids for incorporation into seepage evaluations.   |
| Piezometers  | Long-term monitoring of seepage conditions in the embankment and foundation. Installation based on visual observations, electrical resistivity and geothermal surveys.       | 4/79 to present                          | Monitored pressure response and lag time for original seepage condition and to evaluate remedial construction effectiveness.                                      |

drainage blankets was calculated to have 100 to 300 percent of the capacity required for satisfactory performance. Design of the stability berms conservatively assumed that relief systems were ineffective, a desirable and relatively inexpensive approach in light of the complex seepage conditions.

Seeps were grouped to form three areas, identified as Areas A, B, and C in Figure 6. Typical cross-sections for the systems constructed in each area are shown in Figures 7 and 8.

Area A, encompassing the right abutment contact and extending to Sta 17+35, contained Seep 5 and had eight wells drilled at least 40 ft (12.2 m) into rock on 20 ft (6 m) centers along the contact. The contact was blanketed with a drain extending over the abutment and embankment 15 ft (4.6 m) in each direction, and a 15 ft (4.6 m) thick stability berm constructed over the area. Drainage discharge was routed through a headwall located on the downstream side of the access road at the toe, Figure 9.

Area B included the embankment-rock ridge contact at the left side of the main valley, extending from Sta 30+72 to 32+76 and encompassing Seeps 2 and 3. The system is the same as described for Area A, with nine wells installed along the contact.

Area C extends from Sta 40+00 to 54+70 and contains Seeps 1 and 6. It was considered the most critical area due to the shallowness of the foundation alluvium and a contained basin in the rock surface at depth. Four gravel packed relief well systems were installed in this area, totaling 40 wells drilled 40 ft (12.2 m) into rock at 20 ft (6 m) spacing. Wells were deleted when the alluvium exceeded the 15 to 20 ft (4.6 to 6 m) depth. Discharge from each group of wells was routed into a manhole which contains silt basins and provisions for measuring flow quantities. From the manholes the flow is routed to a headwall for discharge. The area was covered with a drainage blanket and stability berm extending onto the embankment, Figure 8.

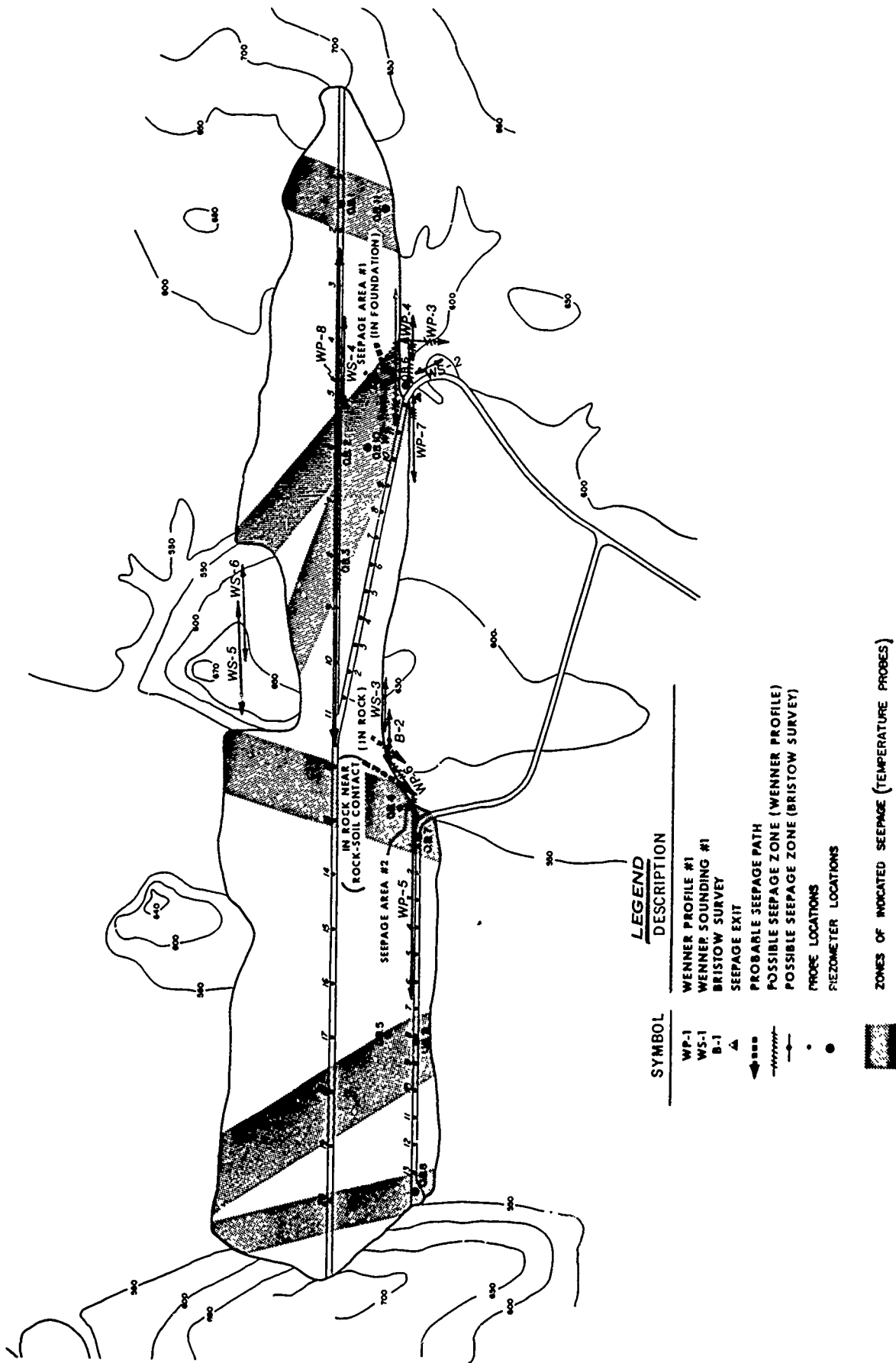


Figure 5. Plan view showing locations of instruments and surveys used to study seepage. Also shown are the probable seepage paths inferred from the various methods.

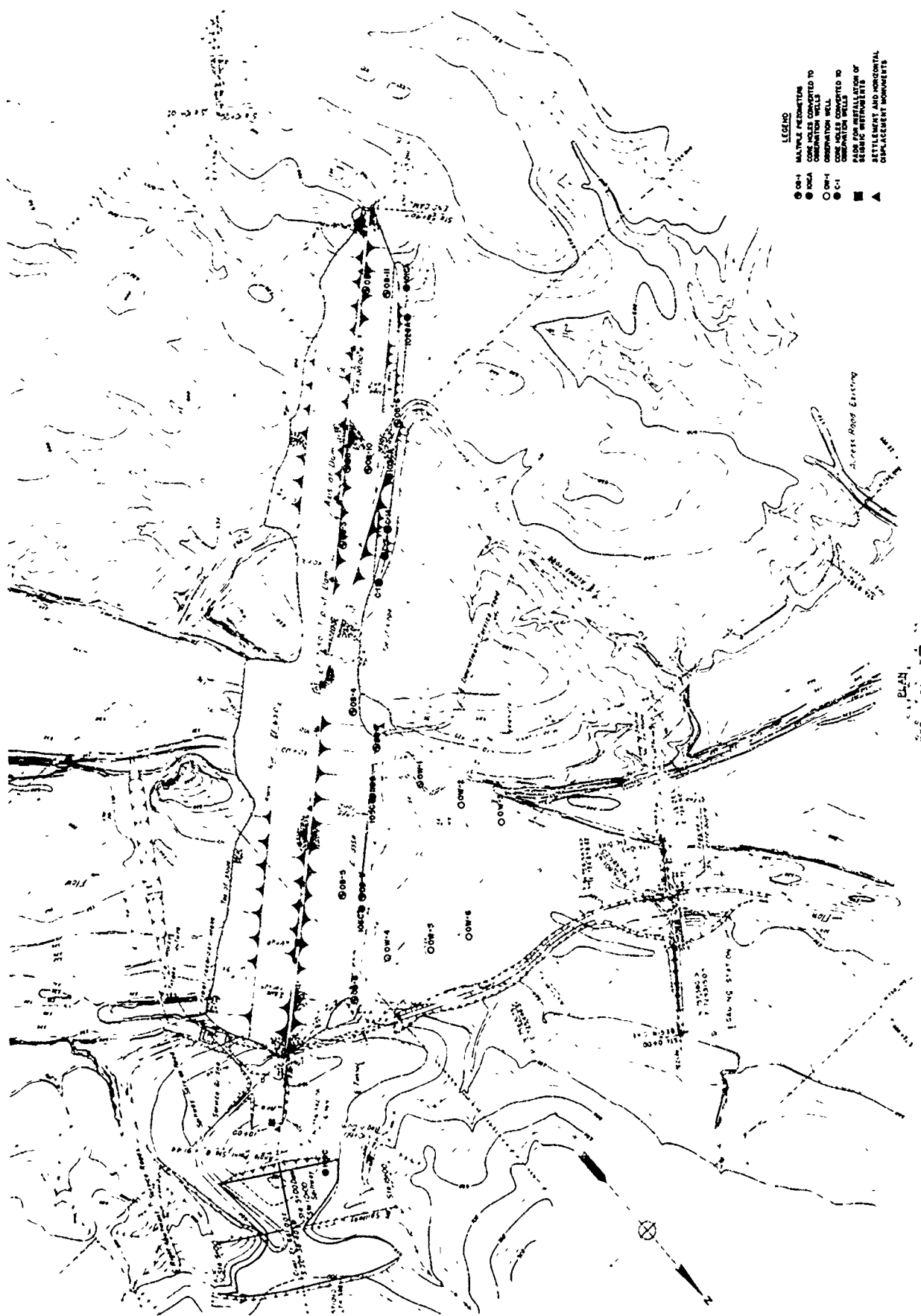


Figure 6. Plan view showing areas of remedial measures and all instrumentation which is presently installed and operating.

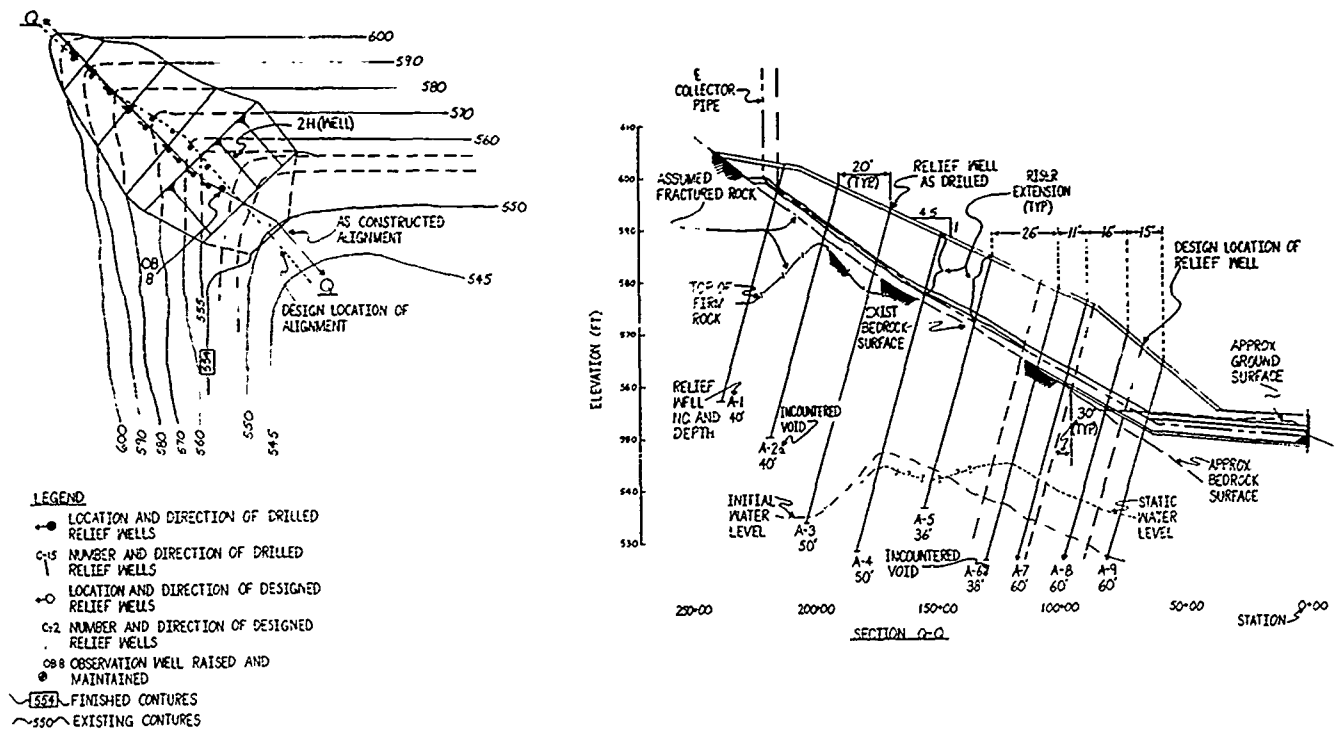


Figure 7. Plan and section of seepage control systems and stability berm constructed in Areas A and B.

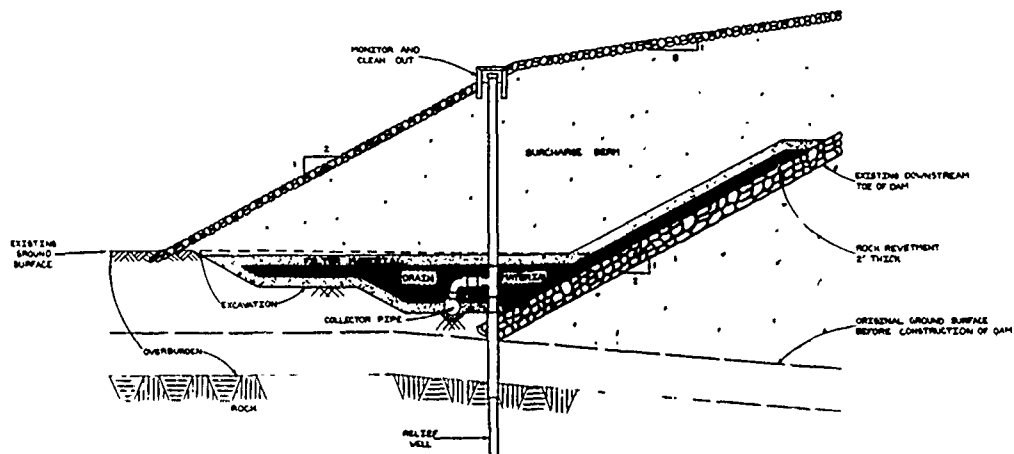


Figure 8. Section of seepage control systems and stability berm construction in Area C.



Area B



Area C

Figure 9. Completed headwalls in Areas B and C. The weephole discharge is from the gravel drainage blankets and the discharge from the larger pipes is from the relief wells.

#### POST CONSTRUCTION PERFORMANCE

Large inflows in February and March of 1980 resulted in a new record high pool at Elev 647.7 on March 6, 1980. Relief wells in Area C started flowing on February 25, followed by well flows in Areas A and B on February 27. Depth to the gravel pack was measured in Area C wells, and three wells were observed to have had some consolidation of the pack.

Seeps appeared on the right abutment downstream of Area A, on the rock ridge downstream of Area B, and downstream of the headwall in Area C on March 3, 1980. Additional seepage appeared in Area C on March 4, expanding downstream in a linear fashion a distance of about 35 ft (10.7 m), see Figures 10, 11 and 12.

Piezometer readings indicated general relief of pressures in rock, but one was artesian, demonstrating that flow in the complex foundation warranted the conservatism exercised in the design of relief and control measures. Overall performance of the relief, control and stability measures was satisfactory to assure safe performance of the structure at design pool elevations, but the relief wells were not as effective as anticipated, due largely to flow occurring in foundation joints which were not intercepted by wells.

#### LESSONS LEARNED

1. Continued awareness must be maintained for changes which may compromise the original design intent and, hence, safe performance of a project.
2. As many investigative methods as needed and reasonably possible should be used to obtain information in complex situations so that confidence can be developed regarding existing conditions and proposed solutions.
3. Geothermal monitoring can be an effective diagnostic tool for locating complex seepage paths.
4. A measure of conservativeness should be maintained in the design of remedial measures to accommodate unknowns and inaccuracies.

#### ACKNOWLEDGEMENTS

The work covered herein was the result of a high level of cooperation between several organizations and the dedicated effort of many individuals. Coordination and direction of the work was done by Hugo Kraythoff, project engineer. The investigation, design and construction of these measures within essentially one year attests to the success of their efforts.

#### REFERENCES

- Design Memorandum No. 3, Dam and Appurtenances for Painted Rock Reservoir, Gila River, Arizona, March 1955. U.S. Army Corps of Engineers, Los Angeles District.
- Design Memorandum No. 6, Dam and Appurtenances for Painted Rock Reservoir, Gila River, Arizona, November 1956. U.S. Army Corps of Engineers, Los Angeles District.
- Report on Construction Control and Embankment Construction, Painted Rock Reservoir, Dam and Appurtenances, Gila River, Arizona, U.S. Army Corps of Engineers, Los Angeles District.
- Painted Rock Dam, Arizona, Study of Seepage Conditions - 1979 Filling, H.R. Cedergren, January - July 1979.
- Thermal Monitoring of Painted Rock Dam, Maricopa County, Arizona. Geothermal Surveys, Inc., February 1979.
- Remote Sensing Study, Painted Rock Dam, Arizona. Fugro, Inc., March 1979.
- Piezometer Installations, Painted Rock Dam, Arizona, Fugro, Inc., March 1979.
- Painted Rock Dam, Part I: Surface Resistivity Studies, and Part II: Refraction Seismic Surveys. U.S. Army Engineer Waterways Experiment Station, February 1979.
- Seepage Control Measures, Painted Rock Dam, Gila River Basin, Arizona, October 1981. U.S. Army Corps of Engineers, Los Angeles District.



Figure 10. Area A completed. Flow along toe of surcharge berm is from observation well OB-8 which became artesian with high reservoir elevation and a small seep in the abutment rock.



Figure 11. Area B completed. Damp spot in center is from seepage exiting through fractures in the bedrock.

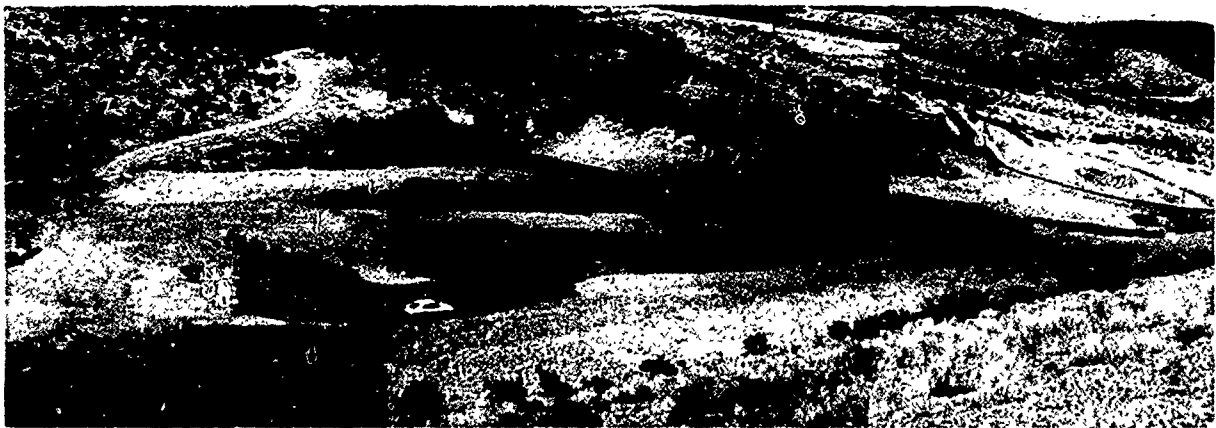


Figure 12. Area C completed. Nuisance surface flow exists along what could be a fault zone. Seepage expanded downstream in a linear fashion along this line.

## Prediction and Field Performance of an Instrumented Road

Robert Brian Smith

Senior Scientific Officer, Department of Main Roads—New South Wales, Parramatta, New South Wales, Australia

William Otho Yandell

Senior Lecturer, University of New South Wales, Kensington, New South Wales, Australia

**SYNOPSIS:** Performance of a surface-treated crushed rock pavement, 250 mm thick and placed over a weak subgrade, is predicted using mechano-lattice analysis and the results are compared with actual performance after the passage of the equivalent of 800 000 standard axles. Input is in terms of the deformation characteristics determined from repeated loading triaxial testing. Performance is measured in terms of pavement profile, roughness and permanent deformation or rutting. Predicted straight-edge rutting was within the range of values measured in the field. The measured profile index and roughness count were consistent with a pavement showing little deformation over its initial six years of service. Considering the possible field variation of material properties over the evaluation period and the single set of input data the results indicate the applicability of the mechano-lattice method for the prediction of the performance of crushed rock flexible pavements.

### INTRODUCTION

The mechano-lattice method of analysis has been described extensively by Yandell and his co-workers (eg Yandell 1971a,b; Smith and Yandell 1986a,b, 1987). The method was developed by Yandell to investigate hysteretic sliding friction, and to predict the behaviour of elasto-plastic roads during repeated rolling.

Space precludes a detailed description of the analysis. The method is a type of finite element method but, unlike other available methods, it utilises the elasto-plastic properties of the constituent materials rather than elastic behaviour only, as do most other methods such as VESYS. It takes into account the loading and unloading moduli of the various materials.

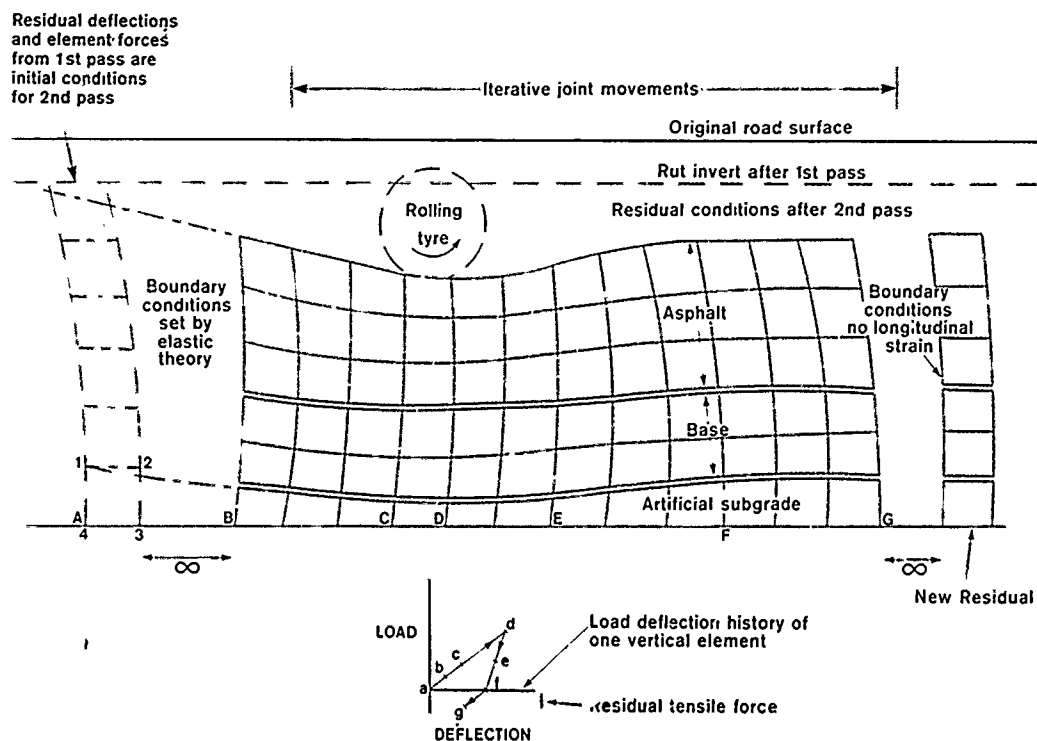


Fig. 1 Diagrammatic Longitudinal Section of the Three Dimensional Pavement Analysis Showing Boundary Conditions, and Computational Process (after Smith and Yandell, 1986a)

A longitudinal section of a mechano-lattice simulation of a pavement is given in Fig. 1. The hysteresis loop at the bottom of the figure was formed by plotting sequential load-deflection values through positions A,B,C,D,E,F and G of a vertical element in one particular unit. A similar but more complex task is performed by the computer after each cycle of element length-load calculations. The forces at each joint are resolved into vertical, longitudinal and lateral components, and the joint is then moved in a damped manner in the direction of the unbalanced forces. The calculation damping factor is proportional to the largest force that is instantaneously out of balance at any free joint. This process is continued until all out of balance forces at free joints become insignificant. This now generally occurs after around 400 computational cycles. After convergence, and after stresses have been calculated, the wall of units on the right of Fig. 1 is used to give the initial condition for the next simulation wheel pass. The above process is then repeated until a total of 32 load-deflection histories is followed for each mechano-lattice unit.

#### THE PAVEMENT

The pavement consisted of 250 mm of crushed rock overlying an imported subgrade having a nominal 4-day soaked CBR value between 2% and 4%. The latter material was imported because the natural subgrade was too variable and it was considered that a 200 mm layer of material having a uniformly low CBR would be more appropriate for evaluation purposes. The full construction details and an evaluation of the initial service life of the pavement, after the passage of the equivalent of 250 000 standard axles (esa), have been given by Smith (1984, 1985, 1986).

The 130 m long pavement was constructed in 1981 as one of six experimental pavements. Electrical resistance strain gauges were installed to measure longitudinal strain under the transient load (8.2t standard axle) but they failed after the passage of the equivalent of 40 000 standard axles. The pavement was assessed periodically using a profilograph, NAASRA roughness meter, and visual assessment. Rutting (permanent deformation) was determined using a 1.2 m straight-edge and by level surveys.

The evaluation reported in this paper covers the period from construction in 1981 to the completion of an estimated 800 000 esa in mid-1987.

The climate in the area is temperate with warm to hot summers and mild winters.

#### MATERIAL PROPERTIES

The crushed rock was tested at 4.5% moisture content and 95% of maximum dry density using standard compactive effort. These conditions approximated the field conditions at compaction and were considered to represent the service condition over the ensuing six years. Long-term load/deformation behaviour was determined under repeated loading conditions using a vertical

stress of 450 kPa and a lateral stress of 150 kPa with a 3 sec loading cycle. The permanent deformation was found to be 0.12 mm after 22 000 cycles in a 200 mm high specimen (Fig. 2).

The imported subgrade was tested at 95% of maximum dry density using standard compactive effort which was close to the construction figure. The long-term load/deformation data were determined at a vertical stress of 85 kPa and a constant lateral stress of 30 kPa. Testing was carried out at two moisture contents, namely 9.2% which was probably lower than the field moisture content, and 14% which was close to the moisture content at compaction in the field. Because of poor drainage in the area it is considered that the field condition approximated the higher moisture content and remained fairly constant over the six year evaluation period. The long-term load/deformation behaviour was 0.07 mm in 36 000 cycles for material compacted at a moisture content of 9.2% and 0.60 mm in 22 000 cycles for material compacted at a moisture content of 14% (Fig. 3). Specimens were 100 mm high.

Whilst the natural subgrade was not modelled in the computer simulation its behaviour is presented here for completeness. It was also compacted at 95% of maximum dry density using standard compactive effort as this approximated the field condition. Long-term load/deformation data were determined at a vertical stress of 66 kPa and a static lateral stress of 30 kPa. Testing was carried out at a moisture content of 11.6% which was close to the expected service moisture content. The permanent deformation was found to be 0.35 mm in 40 000 cycles in a 100 mm high specimen (Fig. 4).

The deformation data were then plotted on a log/log plot and extended to the estimated number of wheel passes to the date of evaluation. Appropriate unloading moduli were assumed based on the relative plasticities of the pavement materials. In this case the mechano-lattice input data were those used to predict performance after the passage of 250 000 esa (see Smith and Yandell, 1986c). Appropriate values were also assumed for use in the model for the semi-infinite layer - in this case the imported subgrade. Such a calculation expedient is used to keep the computer time to a minimum without affecting the overall accuracy of the predictions. The mechano-lattice input data are presented in Table I.

TABLE I. Mechano-lattice Input Data (after Smith and Yandell, 1986a)

| Material          | Moisture Content (%) | Poisson's Ratio | Loading Modulus (MPa) | Unloading Modulus (MPa) |
|-------------------|----------------------|-----------------|-----------------------|-------------------------|
| Crushed Rock      | 4.5                  | 0.30            | 202                   | 204                     |
| Imported Subgrade | 14.0                 | 0.20*<br>0.45†  | 43                    | 207                     |

\* top 50 mm; † next 50 mm.



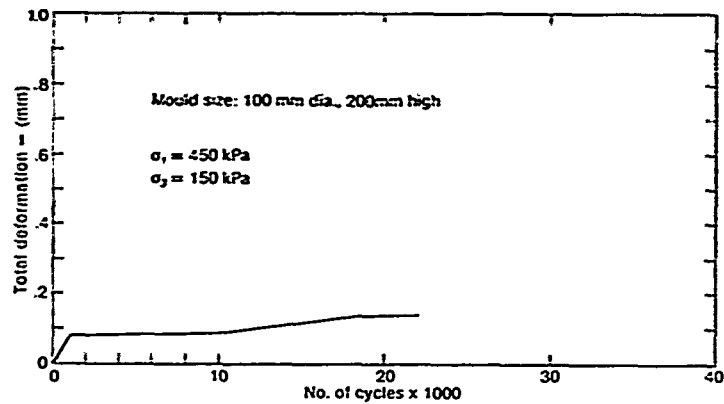


Fig. 2 Total Deformation versus Loading Cycles for Crushed Rock (after Smith and Yandell, 1986a)

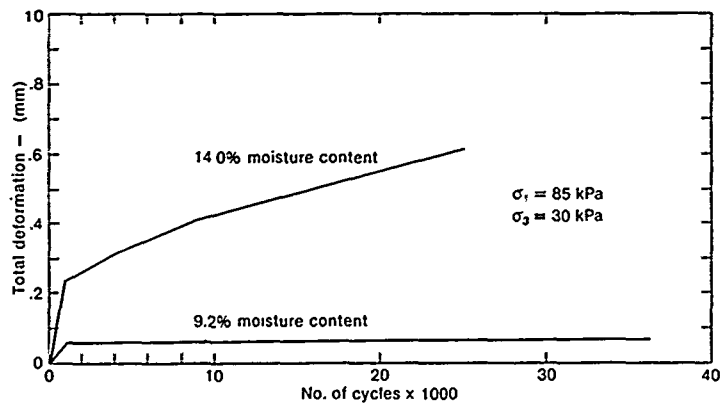


Fig. 3 Total Deformation versus Loading Cycles for Imported Subgrade (after Smith and Yandell, 1986a)

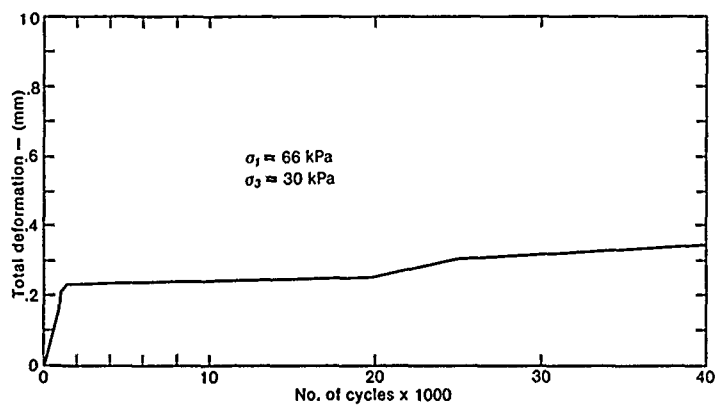


Fig. 4 Total Deformation versus Loading Cycles for Imported Subgrade (after Smith and Yandell, 1986a)

## FIELD PERFORMANCE

Field performance was measured in terms of profile index, NAASRA roughness, visual assessment, and rut depth based on survey level data and 1.2 m straight-edge values. The two methods of rut depth prediction both provide a measure of the depth of the rut in the wheelpath relative to the untrafficked part of the pavement. In the case of the 1.2 m straight-edge any deformation (such as heaving or shoving) within the length of the straight-edge is incorporated in the measurement. In the case of the survey data the datum for each day of measurement was the mean of the values at the centre-line and and of the values on the pavement 300 mm from the pavement edge. The mean value for each of the wheelpaths was then subtracted from the datum. These values were then used to determine the progress of rutting over time. This method is unlikely to include permanent deformation other than the gradual decrease in the level of the wheelpath unless shoving in the wheelpaths becomes quite significant and affects the values used in determining the datum.

On most occasions the visual assessment was performed at the same time as the roughness survey. The initial visual assessments included measurement of the rut depth to the nearest mm. Later surveys only included band widths because of the difficulty of accurately measuring a rut depth, particularly over a chip seal surface. In the latter case the minimum band was 0 to 10 mm. Roughness data are presented in Table II.

TABLE II. NAASRA Roughness

| Date   | Roughness<br>(C/km) |
|--------|---------------------|
| 160981 | 62                  |
| 050783 | 53                  |
| 211283 | 60                  |
| 110286 | 26                  |
| 150786 | 57                  |

When the first visual assessment was performed in July 1983 (250 000 esa) the average 1.2 m rut depth was 2 mm in the outer wheelpath (standard deviation [sd] = 2.0) and 4 mm in the inner wheelpath (sd = 2.4). The roughness had dropped slightly from an initial value at construction of 62 Counts/km (C/km) to 53 C/km. Little change was observed up to December 1983 (300 000 esa) although there was a perceived drop in 1.2 m rut depth in both the outer (mean = 0.4 mm; sd = 0.6 mm) and inner (mean = 2 mm; sd = 1.5 mm) and a slight increase in the roughness to 60 C/km.

Visual surveys were also carried during 1985, 1986 and the last in September 1987 (approximately 800 000 esa). Each time it was reported that the pavement was in good condition with 100% rutting 0 to 10 mm deep in each wheelpath. No pot-holes, cracking or other signs of

distress other than slight bleeding of the seal were found. Two further roughness surveys were conducted. In February 1986 an abnormally low value of 26 C/km was recorded whilst in July 1986 (650 000 esa) the count was 57 C/km.

Three profilograph surveys were undertaken and confirmed the initial 1.2 m rut depth surveys in that the values in the outer wheelpath were lower than those in the inner wheelpath. The values remained fairly low throughout the period. At construction the average profile index was 308 mm/km in the inner wheelpath and 285 mm/km in the outer wheelpath. After the passage of the equivalent of 110 000 esa the average profile index was 474 mm/km in the inner wheelpath and 252 mm/km in the outer wheelpath. After the final survey at 510 000 esa the index was 323 mm/km in the inner wheelpath and 192 mm/km in the outer wheelpath.

The rut depths calculated from the survey data were somewhat difficult to interpret. This is considered to be partially due to the swelling nature of both the imported subgrade and the heavy clay subgrade and the fact that the measured differences in the levels over time were almost within the order of accuracy of the survey in which levels were measured to the nearest 1 mm. The results indicated that the increase in rutting was very gradual and for the passage of at least the first 500 000 esa rutting of 2 to 4 mm was experienced in both wheelpaths. Data are too incomplete to attempt to determine change in the rut depth over the ensuing 300 000 esa.

These assessments all show that whilst rutting and deformation are no doubt occurring the degree of deformation is relatively minor and the pavement has considerable service life left. This is reinforced by the fact that the roughness even after the passage of the equivalent of 650 000 was at level of the order of the desirable initial roughness required of a heavy duty pavement.

## COMPARISON BETWEEN PREDICTED AND FIELD BEHAVIOUR

### Rut Depth

In the mechano-lattice analysis the rut depth is calculated by plotting the predicted rut depths after each calculation rolling pass and extending the line through these points (a log/log plot was appropriate in this case) until the point corresponding to the required number of standard axles is reached (800 000 in this case). The point is determined from the residual strain (R) from the loading and unloading modulus used as input in the model, and the calculated cumulative strain (S) extrapolated from the repeated loading test. The number of calculation passes to reach 800 000 esa is then determined by dividing the residual strain by the cumulative strain (ie S/R). In this case the appropriate number of calculation passes was 90. The prediction for the absolute rut depth is given in Table III. It had been ascertained by plotting the rut profile after the third calculation rolling pass that the 1.2 m straight-edge was only 75% of the absolute rut depth as the pavement was calculated to drop 0.1 mm after the third calculation rolling pass.

TABLE III. Determination of Absolute Rut Depth at 800 000 esa

| Calculation Rolling Pass | Calculated Absolute Rut Depth (mm) |
|--------------------------|------------------------------------|
| 1                        | 0.2                                |
| 2                        | 0.3                                |
| 3                        | 0.4                                |
| 90*                      | 3.5                                |

\*equivalent to 800 000 esa (see text)

The absolute rut depth predicted after the passage of the equivalent of 800 000 esa (3.5 mm) was only 0.5 mm greater than that after the passage of the equivalent of 250 000 esa indicating that the progress of rutting was very gradual. The 1.2 m straight-edge rutting was found to be between 2 mm and 4 mm at 250 000 with a predicted value of around 2 mm. At the equivalent of 800 000 esa the predicted value is around 2.6 mm. Although the field observations provided a 0 to 10 mm rutting bandwidth in the observations during the latter part of the evaluation period, the consistent roughness and profile values over the service life would indicate that the rutting and deformation had not increased markedly over the life of the pavement to date. In line with this it is considered that the 1.2 m straight-edge values would be at no more than the middle of the band width (ie no more than 5 mm).

#### Transient Longitudinal Strain

The strain gauges failed after the passage of the equivalent of 40 000 esa so it is not possible to make comparisons later in the service life. Smith and Yandell (1986b,c) compared the results at the time of failure with predicted values after the passage of the equivalent of 250 000 esa. Results are presented in Table IV. All values are in tension.

TABLE IV. Predicted and Measured Transient Longitudinal Strain under Loading (after Smith and Yandell, 1986b,c)

| Gauge Depth (mm) | Field Values at 40 000 esa (microstrain) |     | Predicted Values at 250 000 esa (microstrain) |
|------------------|--|-----|---|
|                  | mean                                     | sd  |   |
| 125              | -1290                                    | 61  | -400  |
| 250              | -1915                                    | 650 | -750  |

As can be seen the mechano-lattice analysis predicted that the tension at the mid-height of the crushed rock layer would be approximately half that at the interface between the crushed rock and the imported subgrade. Because of the

relatively consistent roughness and rutting results it is considered that the strain results would remain fairly consistent over the evaluation period.

#### Rebound Deflections

For a discussion of the predicted rebound deflections at 250 000 esa the reader is referred to Yandell and Smith (1986c). Smith and Hewitt (1984) discuss the problem of applying correction factors for cyclic variations in deflection measurements, in the general area of the study, even where accurate rainfall and evaporation data are available.

#### DISCUSSION

The significance of these predictions is not so much in the fact that they were close to the field results but rather that they predicted a very slow deterioration in pavement performance and, that this relatively thin pavement placed over a weak imported subgrade would have a long service life. It is doubtful whether anyone who was involved with the design and construction of the experimental pavements would have predicted that it would have provided in excess of six year's service and be successfully subjected to the passage of at least 800 000 esa. Even after the passage of the equivalent of 250 000 esa one would have been considered to be optimistic in predicting a long service life for this pavement.

No doubt the accuracy of the predictions can be improved by using a greater range of input data and taking account of moisture variation in the subgrade. One could also perform a sensitivity analysis to ascertain the impact of the variation of the material properties on the predictions. In this case it is considered that further runs are not warranted as the results are probably for a "worst" case situation and as they predict a long service life further analyses are not warranted. Such is not the case for the thin (100 mm) crushed rock pavement reported by Smith and Yandell (1986b,c) where the mechano-lattice rut depth predictions were significantly higher than the measured values. In that case further refinements of the input data would be warranted.

#### CONCLUSIONS

In this study the mechano-lattice method of analysis has been shown to accurately predict the rutting of a relatively thin (250 mm) crushed rock pavement placed over a weak subgrade. More importantly the mechano-lattice analysis predicted that pavement performance would only reduce very slowly and would still be providing good service after the passage of the equivalent of 800 000 esa. The predictions were confirmed by the field measurements.

#### ACKNOWLEDGEMENTS

The authors wish to thank Mr B.G. Fisk, Commissioner for Main Roads, New South Wales for

permission to publish this paper and to the staff of the Department's Materials Section, and Parramatta and Blacktown Divisional Offices who performed testing and carried out visual assessment tasks. The opinions expressed are those of the authors and not necessarily those of the Department of Main Roads, New South Wales.

#### REFERENCES

- Smith, R.B. (1984), "Comparison of Predicted Performance of Two Full Scale Crushed Rock Experimental Pavements Using Mechano-lattice Analysis with Field Performance During Initial Service Life", unpublished Master of Engineering Science dissertation, University of New South Wales.
- Smith, R.B. (1985), "Rooty Hill Field Trial: Construction Report for Crushed Rock Pavements", unpublished Report, Department of Main Roads, NSW.
- Smith, R.B. (1986), "Evaluation of Early service Life of Two thin Crushed Rock Pavements", Australian Road Research, vol. 16, no. 2 117-127.
- Smith, R.B., and J.W. Hewitt, (1984), "Seasonal Variation in Pavement Deflection Measurements in the Sydney Metropolitan Area", Australian Road Research, vol. 14, no. 3 133-141.
- Smith, R.B., and W.O. Yandell, (1986a), "Use of Mechano-lattice Analysis in Prediction of Pavement Performance", Australian Road Research, vol. 16, no. 1 10-17.
- Smith, R.B., and W.O. Yandell, (1986b), "Prediction of Surface Deformation in a Full Scale Test Pavement", Computers and Geotechnics, vol. 2, no. 1 23-41.
- Smith, R.B., and W.O. Yandell, (1986c), "Predicted Performance of Two Crushed Rock Pavements in Initial Service Life", Proc. 13th Australian Road Research Board/5th REAAA Conference, vol. 13, no. 5 193-205.
- Smith, R.B., and W.O. Yandell, (1986c), "Predicted and Field Performance of a Thin Asphalt Pavement Placed Over a Weak Subgrade", Proc. 6th International Conference on Structural Design of Asphalt Pavements, Ann Arbor, vol. 1, 443-454.
- Yandell, W.O. (1971a), "A New Theory of Hysteretic Sliding Friction", Wear, vol. 17, 229-244.
- Yandell, W.O. (1971b), "Prediction of the Behavior of Elastoplastic Roads During Repeated Loading Using the Mechano-Lattice Analogy", Highway Research Record, no. 374, 29-41.

## Hydrostatic Pressure at a Soil-Structure Interface

R. Craig Findlay

Senior Geotechnical Engineer, E.C. Jordan Co., Portland, Maine

**SYNOPSIS:** A case history of hydrostatic pressure development along the soil-structure interfaces of a water retaining structure is discussed in this paper to illustrate the use of instrumentation to verify expected performance during construction. For the project described, the development of hydrostatic pressure along the soil-structure interface during and after head pond watering was monitored using pneumatic piezometers. Monitoring of the piezometers detected a high hydrostatic pressure caused by a leaky contraction joint seal. Subsequent repair of the seal reduced water levels along the interface to expected levels, resulting in successful operation of the facility.

### INTRODUCTION

The recently completed Pontook Hydroelectric Project is located north of Berlin, New Hampshire on the Androscoggin River. The project was designed by E.C. Jordan Company and was constructed by C-E Hydro Power Systems, Inc. the project turnkey contractor. The project included construction of:

- o an 800 foot (244 m) long timber crib and earthen embankment dam retaining a head of about 10 feet (3 m);
- o a concrete canal headworks structure;
- o a 6,000 foot (1,829 m) long unlined power canal consisting of an earth cut up to 70 feet (21 m) deep as well as side hill diked portions at the headworks and at the approach to the powerhouse penstock intake structure;
- o a concrete penstock intake structure which trains water from the diked canal into three short steeply sloped 8-foot (2.5 m) diameter penstocks; and
- o a concrete powerhouse containing 3 CE/Neyrpic tubular turbines with a total installed capacity of approximately 10 MW.

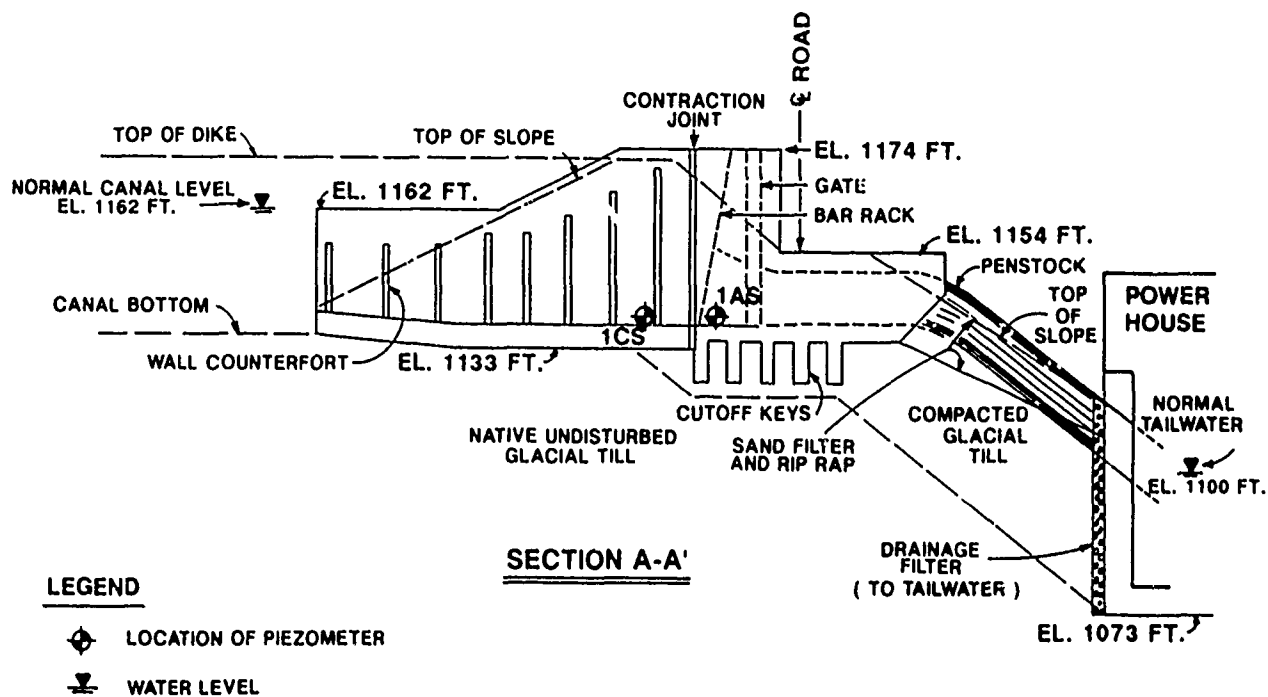
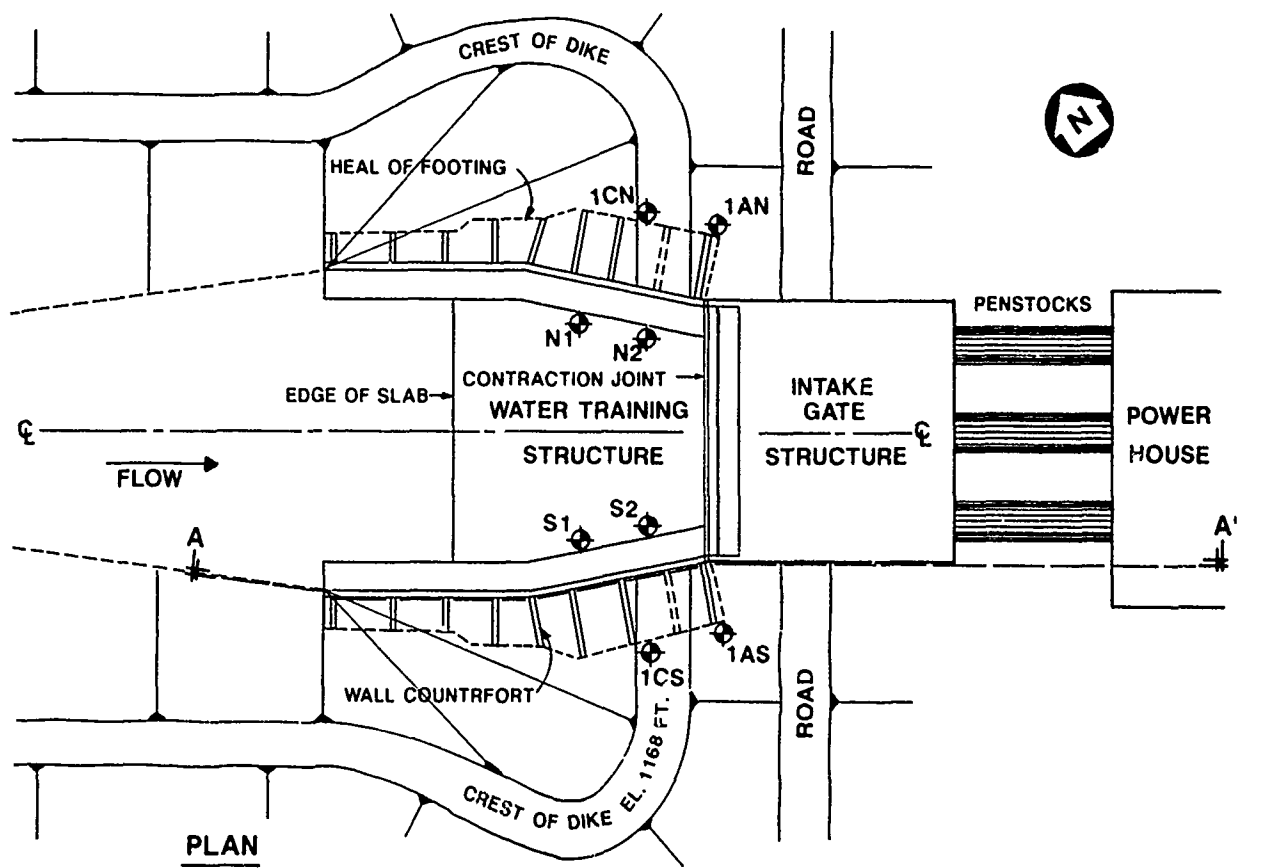
This article focuses on the development of the hydrostatic pressure along the soil-structure interface between the canal dikes and the penstock intake structure. A schematic plan and sectional view depicting the configuration of the soil-structure interface along the penstock intake structure are presented as Figure 1.

### SITE AND PROJECT DESCRIPTION

The Pontook Project is situated in the Androscoggin River Valley, located in northern New Hampshire. The area is a mountainous region characterized by northeast trending

bands of metamorphic rocks lying in tight folds, produced by past mountain building events. The most significant of those events was the collision of the North American and European crustal plates, some 350 million years ago. More recently, during the Wisconsin glaciation, regional ice flow was sustained in the Pontook project area, with outwash accumulating further downstream. The ice eventually retreated in this valley and left sequences of stratified ice contact, outwash, and glacial till deposits above bedrock. Borings made for site development indicated the penstock intake area was underlain by a thick deposit of glacial till which was interbedded with braided gravel outwash deposits of up to a few feet in thickness. Bedrock was encountered over 150 feet (46 m) below the existing ground surface by exploratory borings.

The glacial till at the site was found to be a non-plastic, unsorted mixture of silt, sand, gravel, cobbles, and boulders which was widely graded with from 25 to 35 percent by weight passing the No. 200 sieve and had a coefficient of uniformity of more than 10. Although the native deposits of the glacial till contained some boulders greater than one cubic yard (1 cu. m) in size, no particles over eight-inches (20 cm) in diameter were permitted in the glacial till which was reused for construction of dikes and structural fills. Testing of the glacial till included a long term (two month) constant head permeability test in a fixed wall permeameter done on a remolded sample, the results of which indicated the glacial till had a hydraulic conductivity (permeability to water) of about  $5 \times 10^{-4}$  centimeters per second ( $1 \times 10^{-7}$  ft/min.) at a dry density of about 125 pounds per cubic foot ( $1,204 \text{ Kg/m}^3$ ) or about 92 percent of maximum dry density. Other testing included pinhole dispersion testing, which indicated the till to be non-dispersive (not highly piping susceptible), however, observations on site indicated the till would generally ravel and erode when unconfined, until a self-



**LEGEND**

- LOCATION OF PIEZOMETER
- WATER LEVEL

NOTE: DRAWING NOT TO SCALE

Fig. 1 Plan and Section of Penstock Intake Structure

armoring of till stones prevented further erosion.

The penstock intake consists of two parts. These two parts are a water training structure and a gate structure. The training structure consists of two 25-foot (8m) high reinforced concrete retaining walls and a base slab which act as a transition from the earth-dike portion of the canal to the intake gate structure. The gate structure is also constructed of reinforced concrete, and in addition to providing gate control of the downstream terminus of the canal, it also acts to channel water from the training structure into three 8 foot (2.5 m) diameter penstocks. The training and gate portions of the penstock intake structure retain a 25 foot (8 m) of water. The two portions were designed structurally separate using a contraction joint to reduce adverse stresses which could develop in an otherwise monolithically constructed single structure. This contraction joint was designed to be water tight, using fused center bulb water stops and special caulking. By design, it is imperative that the joint not leak because of the relatively large retained head of water and the short distance, about 10 to 50 feet (3 to 15 m) from the contraction joint to the downstream side of the abutting dike slope. If significant leakage were to occur, the potential for piping along the soil structure interface would be significantly increased, with the possible result of a breach of the canal dike. As a result, it was determined that careful monitoring of the hydrostatic pressure development along the soil-structure interface during, and after canal filling was necessary.

The penstock intake structure was constructed on undisturbed and recompacted glacial till as shown on Figure 1. The canal dikes were constructed of recompacted glacial till excavated from the cut areas of the 6,000 foot (1829 m) long canal which channels water to the penstock intake. These dikes directly abut the penstock intake forming a soil-structure interface. The penstock intake was designed to have piping resistance by counterforting the structure side walls and provision of cut off keys along the base of the structure (see Figure 1), thus providing a serrated interface with the dike and base soils and effectively increasing the seepage path. Because of concern for piping potential along the soil-structure interface and the large head drop (62 feet or 19 meters) between the canal and tailwater, four pneumatic piezometers (two on each side of the intake structure, as located on Figure 1, denoted as 1CN, 1AN, 1CS, and 1AS) were installed to monitor the development of the hydrostatic pressure across the soil-structure interface during and after initial canal watering. The piezometers were the double tube type, with a pressure range of 0 to 60 pounds per square inch (0 to 4.2 Kg/cm<sup>2</sup>), actuated and monitored using dry nitrogen gas from a portable indicator box.

## CONTRACTION JOINT SEAL

The penstock intake was constructed in numerous concrete pours during the late summer and early fall of 1986. After concrete placement for the training walls and intake structure had been completed and form work stripped, inspection of the contraction joint revealed that the fused center bulb water stop had apparently slipped out of position during concrete placement, having been cast parallel to the contraction joint rather than across the joint. This slippage of the water stop resulted in a non-positive seal against water passage through the joint. To rectify the situation, an exterior seal was designed and retrofitted on the water side of the contraction joint. The retrofit seal was composed of a Hyplon strip which covered the joint, held against the concrete and the joint by adhesive and plate metal strips which were through-bolted into the concrete. A protective steel shielding was secured over the seal to protect from abrasion by waterborne debris and the teeth of an adjacent trash rack cleaning rake.

## INITIAL FILLING

After placement of the retrofit seal, the training walls and gate structure were partially filled with water for the first time. This initial filling was done without filling the entire canal by constructing an earthen cofferdam across the canal just upstream of the intake structure. The canal area between the cofferdam and intake structure was thus a relatively smaller, confined head pond of water for initial watering of the intake which could be drawn down rapidly if need be. This confined headpond area was filled with water to elevation 1156 feet (normal canal level is 1162 feet) over a period of about 36 hours. Elevation 1156 feet is equivalent to about 17.5 feet (5 m) of water in the headpond. As the headpond was filled, pneumatic piezometers outside of and adjacent to the contraction joint (piezometers 1AN and 1AS) registered pore pressure readings equivalent to the rising headpond level. Because of the potential of piping which could otherwise have occurred if the head condition were allowed to continue, the decision was made to immediately empty the confined headpond area and inspect the contraction joint rather than to continue filling the head pond to proposed normal levels. During drawdown of the headpond, which was dewatered at a rate of about 1 foot per hour (0.3 m/hr), the piezometers indicated a direct response with the decreasing water level. At all times during filling and dewatering, the other piezometers (piezometers 1CN and 1CS) registered pore pressures well below the headpond level, indicating seepage along the sides of the structure were not likely responsible for the high readings of piezometers 1AN and 1AS. After dewatering the headpond, careful inspections were made of the seal in an attempt to determine the cause of the apparent leakage. The inspections indicated that areas where the concrete surface was irregular, including the corners where the retaining walls meet the base of the

structure, were not adequately sealed. Dye was injected on the soil side of the seal in an effort to see if the zones of leakage could be positively identified. The dye came through the seal in numerous locations indicating an inadequate seal. Prior to identifying the leaky seal, there was concern that underseepage below the structure may have occurred, contributing to the high measured pore pressures. Down stream drains and ditches located at the toes of the canal dikes were inspected to see if and observable piping had taken place. No evidence of such piping was noted. Further investigation of underseepage was done utilizing pump tests. These tests were conducted by digging sump pits at the upstream edge of the water training structure base slab, followed by continuous pumping of the pits. The piezometers were monitored before, during and after the pumping to see if a response of the piezometers could be observed, which would indicate that underseepage might have occurred. The tests indicated no response. Based on all the observations, it was concluded that the cause of the high measured pore pressure adjacent to the contraction joints was leakage of the contraction joint.

The retrofitted seal was redesigned and repaired to accommodate the difficult sealing conditions. The revised seal was essentially identical to the original retrofit seal except that a 1/4-inch (0.6 cm) thick hydrophylic membrane material was placed behind the steel plate strips. This material swelled to almost double its original size in the presence of water, forming a positive seal between the concrete, Hyplon and the metal strips. To monitor potential development of hydraulic pressure which could be an indication that underseepage below the structure may have developed, four additional piezometers (numbered N1, N2, S1, and S2) were installed through the base slab of the training structure, located as shown on Figure 1, to measure hydrostatic pressure below the structure.

#### HEADPOND REFILLING

After the modifications to the retrofit seal were made, the canal was refilled at an average rate of about 1.5 feet per hour (0.5 m/hr) to an elevation of about 1156 feet. During this refilling, the piezometers readings were monitored about once per hour, however, piezometers 1CN and N1 were malfunctioning and did not provide usable data. Readings of the functioning piezometers during the first 500 hours are presented on Figure 2. During the refilling, hydrostatic pressures as indicated by the piezometers remained below headpond level. Piezometer 1CS registered a head unexpectedly less than 1AS and 1AN, probably due to its somewhat more isolated location within the glacial till beside the structure and away from the flow path of least resistance which is likely to be along the bottom of the water training structure and then along the sides of the gate structure. After filling the confined headpond to elevation 1156 feet, refilling was terminated and the

elevation of the headpond was monitored with time over a 40 hour period. During this hold period, the piezometers initially indicated continued increase in the hydrostatic pressure at the soil-structure interface, generally followed by a leveling off or decrease in pressure. Also during the hold period, the headpond level decreased by 1.8 feet (0.5 m). The volume of water lost as indicated by the headpond level reduction was of the same magnitude as would be expected by the estimated normal gate leakage, so it appeared that leakage through the contraction joint had been substantially eliminated, reducing the previous concern that underseepage and piping may have developed during initial filling. After the hold period, head pond filling continued to about elevation 1162 feet, which was achieved about 100 hours after refilling of the headpond began. At this time, the cofferdam across the canal was removed.

The piezometers were closely monitored until it became apparent that steady state conditions had been achieved and that the contraction joint was not leaking. The hydrostatic pressure along the soil-structure interface, as indicated by the piezometers, appeared to come into equilibrium (indicating steady state flow) about 400 hours (17 days) after the headpond was filled, except for piezometer 1CS, which continued to rise for about 1100 hours, finally equilibrating about a foot or so in hydrostatic head above 1AN and 1AS. The final equilibrium levels of the hydrostatic pressure were at the approximate elevations predicted by steady-state seepage through an earthen embankment of similar profile to the soil-structure interface, however, this equilibrium occurred many magnitudes faster than would be indicated by the measured laboratory permeability (about  $10^{-4}$  centimeters per second), indicating the permeability along the soil-structure interface is likely about  $10^{-3}$  to  $10^{-4}$  centimeters per second ( $2 \times 10^{-3}$  to  $2 \times 10^{-4}$  ft/min). The piezometer readings were monitored frequently for a six month period to assure the steady state conditions remained constant, and that seal leakage did not restart. Currently monitoring is done on a seasonal basis by the station operators with no change from the expected steady state conditions as yet observed.

#### CONCLUSIONS

The following conclusions were made as a result of the experience of the Pontook penstock intake structure:

- o water retaining structures with joints requiring mechanical seals and whose stability is sensitive to piping should be equipped with a means of determining if such seals are functioning as designed;
- o such seals should be initially tested under controlled circumstances (a situation where drawdown can be implemented quickly, if necessary, is desirable);



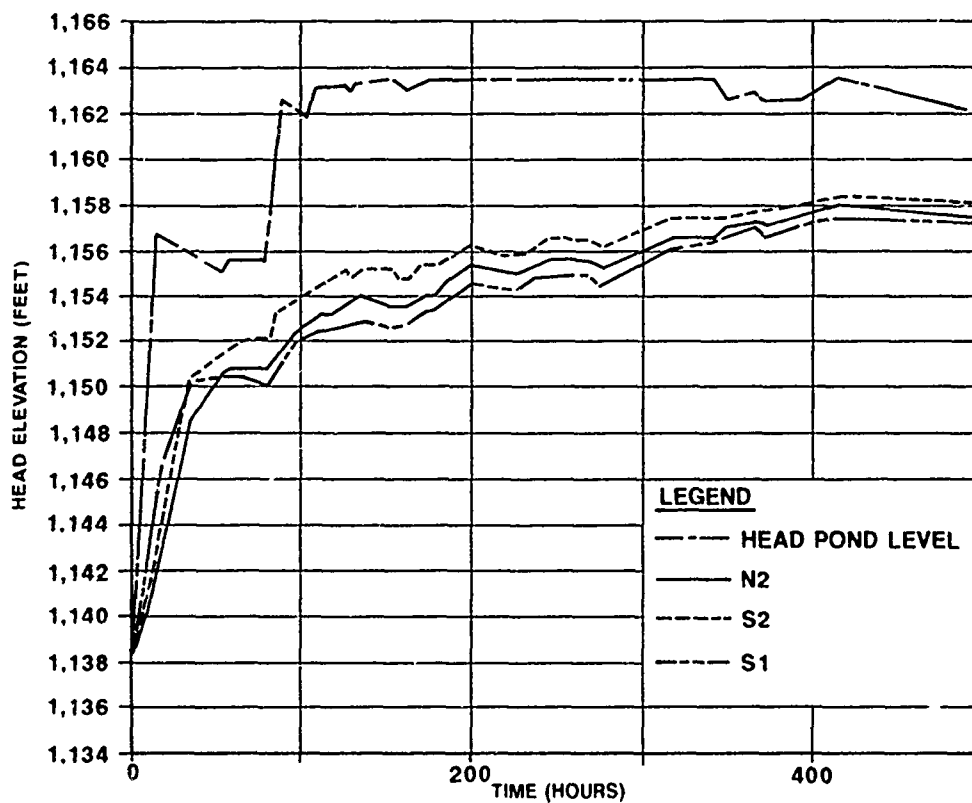
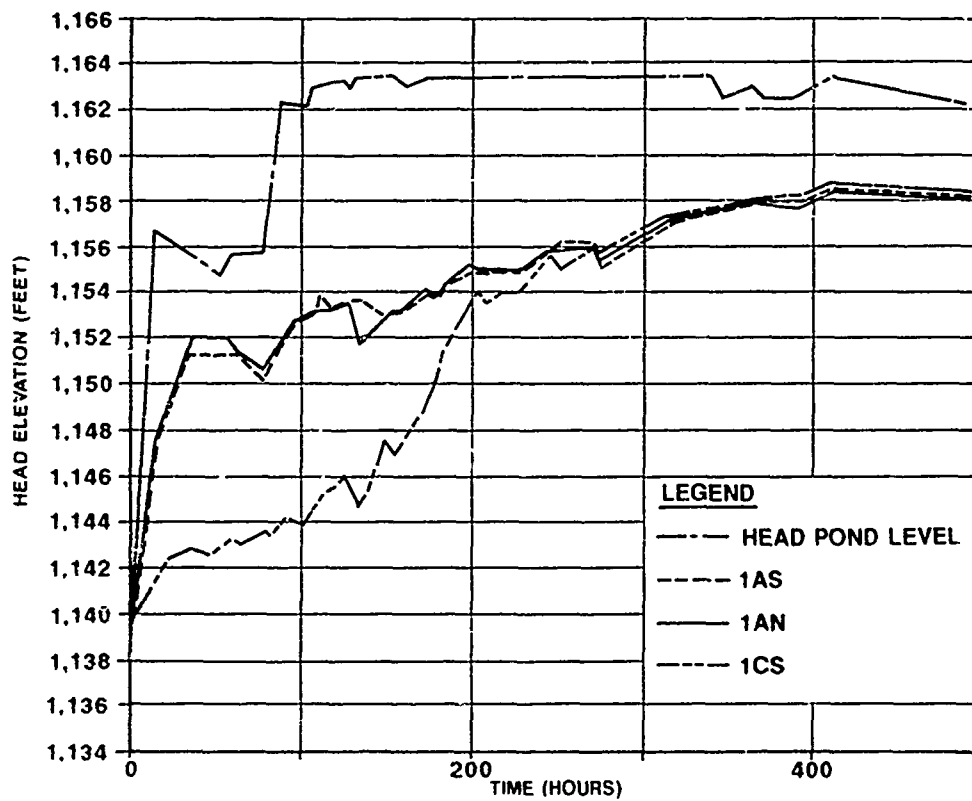


Fig. 2 Piezometer Response vs Head Pond Level  
After Final Seal Repair

- o adequate redundancy in instrumentation (Piezometers, in this case) should be provided as a safe guard against inevitable malfunctions; and
- o under normal circumstances (no leakage at the contraction joint) the development of the hydrostatic pressure at the penstock intake along a soil-structure interface appears to develop significantly faster than would be indicated by the permeability of the soil placed at the interface.

## Openpit Mine Slope Stability—A Case Study

V.K. Singh

Scientist, Central Mining Research Station, Dhanbad, India

B. Singh

Director, Central Mining Research Station, Dhanbad, India

B.D. Baliga

Asst. Director, Central Mining Research Station, Dhanbad, India

**SYNOPSIS:** For profitability steep overall slope angle is essential for openpit mines without endangering the safety for the life time of the pit. Openpits have been designed to depths of 150 to 200 metres. For optimum slope angles of the footwall and the hanging wall of a rock phosphate mine, near Udaipur, Rajasthan, geotechnical investigation covering discontinuity mapping, analysis of data, testing of geo-mechanical properties in laboratory and in in-situ condition were conducted. Slope monitoring was done by precise surveying instruments to give advance warning of impending ground movement. On the basis of geotechnical studies the mine has been designed with an overall slope angle of 33 degrees upto 200 metres depth.

### INTRODUCTION

Growing depths and increase in overburden rock handling have become recent characteristic features of openpit mining. The slope angle of an openpit is the most important factor influencing the profitability of deep mines. Data pertinent to rock discontinuities, rock mass strength and ground water pressure should be collected and analysed while recommending optimum slope angle.

The rock phosphate mine near Udaipur in Rajasthan is hill side mine proposed to operate above the water table for the major part of the life. The deposit extends over a strike length of about 16 kms. For the sake of convenience in mining the deposit has been divided into 12 blocks viz. A, B, C, D, E, F, G, H, I, J, K, L. Block - D constitutes the most important in respect of length, width, quality of the ore body. The present case study is limited to this block only which extends to a strike length of 1500 metres and average width of 20 metres. Dip of the ore body varies from 30 to 50 degrees. At present the depth of the block is 100 metres with top reduced level of 580 metres. The predominant rock type is dolomitic limestone. The paper describes the geotechnical study conducted for determining the optimum slope angle.

### GEOLOGY OF THE AREA

The area shows a succession of geosynclinal sediments deposited during precambrian period over an uneven surface of banded gneissic complex. The rocks of the block are of Pre-Aravalli and Aravalli system. Geological succession of rocks in the area is as follows :

|  |   |
|--|---|
| Aravalli System  | Dolomitic and silicified limestone, Phosphorite, Dolomitic, ferruginous, and siliceous limestone, Quartzites. |
|  | --- Uncoformity ---   |
| Pre-Aravalli   | Banded gneissic complex   |
| Dolomitic limestone is a predominant lithounit in the area and as such constitutes the bulk of |   |

the overburden. This unit is important due to the fact that it contains a thick bed of phosphorite. At places silicification has taken place in dolomitic limestone.

### GEO-MECHANICAL PROPERTIES

For slope stability analysis geo-mechanical properties of the slope forming rocks must be known. In-situ shear tests were conducted in the footwall and hanging wall side of the mine by a specially fabricated equipment. Typical test values of shear strength have been presented in Table- 1.

TABLE 1. Shear Strength Parameters for the Dolomitic Limestone

| Sl. No. | In-Situ Shear Strength Parameters |                               |
|---------|-----------------------------------|-------------------------------|
|         | Cohesion<br>KPa                   | Friction Angle<br>( Degrees ) |
| 1       | 9.807                             | 30                            |
| 2       | 11. 77                            | 31                            |
| 3       | 12. 75                            | 32                            |
| 4       | 11. 77                            | 35                            |
| 5       | 15. 70                            | 28                            |
| 6       | 11. 77                            | 30                            |

Till now no failure has taken place in block-D mine, but few small (bench) failures in dolomitic limestone in block -B and E has taken place. So, to check the reliability of in-situ shear strength tests conducted in block - D, back analysis of the small failures in block- B and E has been done. It was found that the cohesion and friction angle comes to be 5.2 to 9.8 KPa and 24 degrees to 28 degrees respectively. Although dolomitic limestone is highly weathered in block- B and E, while in block - D it is not weathered to that extent. So, the

most appropriate value of cohesion and friction angle of dolomitic limestone for block-D of rock phosphate mine was considered to be 9.8 KPa and 30 degrees respectively, which was used for slope stability analysis. The unit weight of dolomitic limestone was measured in laboratory, which comes to be 24.52 KN/m<sup>3</sup>.

The histogram of compressive strength of dolomitic limestone (Fig. 1) of the block show high strength to low strength rock (Bieniawski, 1973).

#### GEOTECHNICAL STUDY CONDUCTED

Data pertinent to rock structures of the mine were collected from field to evaluate the type of failure which is likely to take place during the life of the mine.

Around three hundred joint data were recorded during field work. Joint poles were plotted on equatorial equal-area stereonet and then contoured to get contourplot of the joint poles (Fig. 2). It shows the existence of four joint sets in D-block. The dip amount and dip direction of different sets which are identified from this plot is presented in Table- 2.

TABLE 2. Joint Sets with Dip Amount and Direction

| Joint Set No.  | Dip Amount (Degrees) | Dip Direction (Degrees) |
|----------------|----------------------|-------------------------|
| J <sub>1</sub> | 74                   | N 172                   |
| J <sub>2</sub> | 40                   | N 055                   |
| J <sub>3</sub> | 66                   | N 245                   |
| J <sub>4</sub> | 80                   | N 301                   |

All these joint sets have been analysed with respect to different slope angles to recognise joint sets likely to cause failure (Fig. 3). For this analysis slope direction for the foot-wall and hanging wall was taken to be N 30 degrees E and S 30 degrees W respectively.

#### Wedge Failure Analysis

The essential condition for the wedge failure is - the inclination of the slope face should always be more than the dip of the intersection line of the two joint planes, forming the wedge, which in turn should always be more than the angle of internal friction of the rock in which the wedge has been formed.

From Fig. 3 it is clear that total six wedges have been formed (W<sub>1</sub> to W<sub>6</sub>) with four joint sets, mentioned in table 1. The only wedge fulfilling the essential condition for the wedge failure is W<sub>1</sub>, i.e., it is unfavourably oriented in the slope, rest of the five wedges are favourably oriented in the slope and failure along them are unlikely.

Wedge failure analysis of W<sub>1</sub> wedge has been done separately (Fig. 4) and the calculation has been presented below.

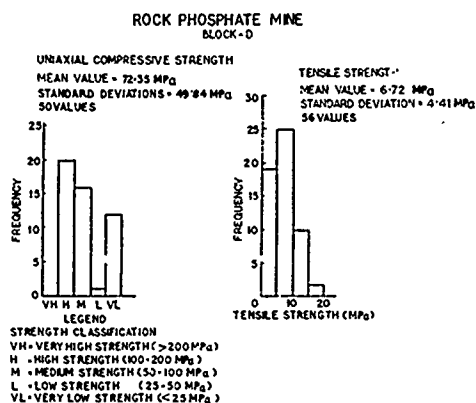


FIG 1 HISTOGRAM FOR COMPRESSIVE AND TENSILE STRENGTH OF DOLOMITIC LIMESTONE

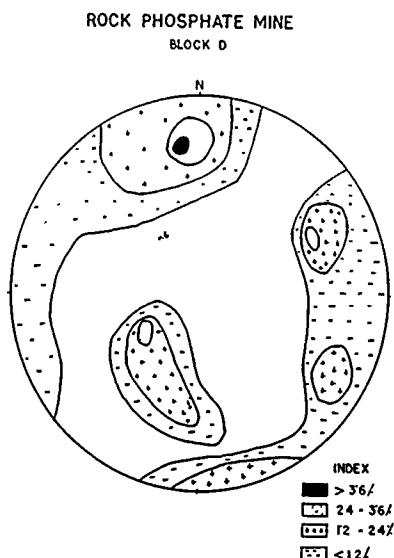


FIG 2 STEREOCONTOUR PLOT OF JOINT POLES

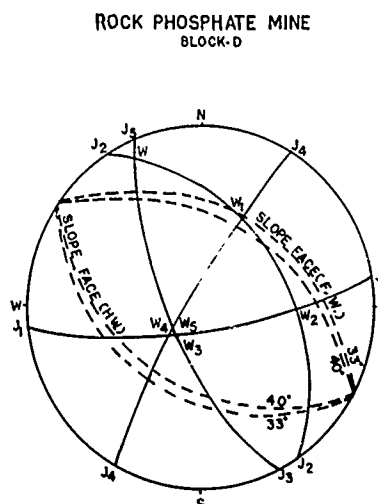


FIG 3 STEREO PLOT FOR THE ANALYSIS OF TYPE OF FAILURE

Input data available from fig. 4 are -

$$\begin{aligned}\psi_a &= 40^\circ, \psi_b = 80^\circ, \psi_5 = 36^\circ, \psi_{na.nb} = 88^\circ, \\ \theta_{2.4} &= 28^\circ, \theta_{4.5} = 24^\circ, \theta_{2.na} = 90^\circ, \theta_{1.3} = 76^\circ, \\ \theta_{3.5} &= 60^\circ, \theta_{1.nb} = 74^\circ.\end{aligned}$$

Input data available after testing of geo-mechanical properties of dolomitic limestone are -

$\phi = 30^\circ$ ,  $\gamma = 24.52 \text{ KN/m}^3$ ,  $C = 9.8 \text{ KPa}$   
Factor of Safety (F) (Hoek and Bray, 1981) is-  
For Wet Slope -

$$F = \frac{3C}{\gamma H} (X + Y) + \left( A - \frac{\gamma_w}{2\gamma} X \right) \tan \phi + \left( B - \frac{\gamma_w}{2\gamma} Y \right) \tan \phi \quad (1)$$

For Dry Slope -

$$F = \frac{3C}{\gamma H} (X+Y) + \tan \phi (A+B) \quad (2)$$

where:

$$A = \frac{\cos \psi_a - \cos \psi_b \cdot \cos \theta_{na.nb}}{\sin \psi_5 \cdot \sin^2 \theta_{na.nb}}$$

$$B = \frac{\cos \psi_b - \cos \psi_a \cdot \cos \theta_{na.nb}}{\sin \psi_5 \cdot \sin^2 \theta_{na.nb}}$$

$$X = \frac{\sin \theta_{2.4}}{\sin \theta_{4.5} \cdot \cos \theta_{2.na}}$$

$$Y = \frac{\sin \theta_{1.3}}{\sin \theta_{3.5} \cdot \cos \theta_{1.nb}}$$

- Note: (1) na and nb are poles of plane  $J_2$  and  $J_4$  respectively, which form  $W_1$  wedge.  
(2)  $\psi_a, \psi_b$  and  $\psi_5$  are dip amount of plane  $J_2, J_4$  and the line of intersection of  $J_2$  and  $J_4$  planes respectively.

From equation 1 and 2 the factor of safety of  $W_1$  wedge in wet condition comes to be 0.4 at an overall slope angle of 40 degrees and in dry condition (when slope is fully drained) it comes to be 0.9.

So, the overall slope angle of 40 degrees is not safe, even if the slope is fully drained. The only solution to the problem is to go for a flatter slope. From fig. 3 it can be seen that for overall slope angle of 35 degrees the line of intersection of  $W_1$  wedge does not daylight in the slope face and also does not fulfill the essential condition for wedge failure.

For 35 degrees slope angle  $W_1$  wedge is no more unstable and the slope is free from any wedge failure. So, 35 degrees overall slope angle comes to be safe for the 200m depth of the mine, from this analysis. To account for weathering effect and damage due to production blasting it was decided to have 33 degrees overall slope angle.

## ROCK PHOSPHATE MINE

BLOCK D

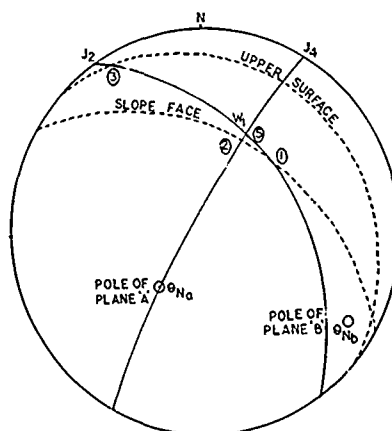


FIG 4-STEREOPLOT FOR THE ANALYSIS OF WEDGE FAILURE ALONG  $W_1$  WEDGE

### Plane Failure Analysis

It occurs along a single discontinuity plane which strikes parallel to the slope face and dips in to the excavation at an angle greater than the angle of friction. From fig. 3 it is clear that not a single discontinuity fulfils the above mentioned criteria. So, for an overall slope angle of 33 degrees plane failure is unlikely.

### Toppling Failure Analysis

Steeply dipping joint sets ( $J_1$  &  $J_4$ ) either alone or in combination with the shallow dipping joints may cause toppling failure. Blasting vibration and water pressure behind the joints may assist in getting the blocks loose from the slope. The only remedy of this instability is periodic loose dressing of slope faces to get rid-off loose hanging blocks.

### BENCH SLOPE AND OVERALL SLOPE

Rock phosphorite is a low cost mineral, Economics dictates steep slopes from the starting stage to that of ultimate slopes. The design of pit slopes and bench slopes is dictated by the Indian Mines Regulation during the major part of the operations. Before 1976 the phosphorite had been mined for 50 to 60m without cutting any benches in the footwall and the benching of the footwall was insisted upon.

The individual benches were designed according to the predominant joint dip and the maximum digging height of shovel employed. The height, width and slope angle of individual bench were adopted to be 10m, 6m and 75-80 degrees respectively.

This pattern gives an overall slope angle of 45 degrees. To reduce the overall slope angle, as deciphered after analysis of geological data, bench width has been increased to 10-12 metres after every 30 metres for safety berms or transport berms to get 33 degrees overall slope angle.

Experiments are being carried out with steep bench slopes as the rock discontinuity in the footwall dips predominantly vertical. It has also been planned to experiment with double benching at the final stage of mining.

#### INSTRUMENTATION AND MONITORING

Slope monitoring should be done at all stages of mining for ensuring the stability of the pit. It can establish the position of the slipping surface, the rate of displacement of individual parts of the deforming mass, and the effect of climatic and hydrogeological conditions on increased speed of displacement.

Slope monitoring of the footwall slopes was (hill side) done by using Wild DI 4 Electronic Distance measuring (EDM) instrument and Wild NA2 Precise level. One year intensive monitoring did not show any movement.

Inclinometers are likely to be installed in drill holes below 500m R.L. to know subsurface movements. Installation of Piezometers in drill holes below 500m R.L. have been planned to establish water pressure and to monitor change in level of ground water during mining.

#### CONCLUSION

The rock phosphate mine, near Udaipur in Rajasthan has been designed to 200 metres depth after extensive geotechnical studies. Geomechanical properties of rocks were determined in laboratory and in in-situ condition, and collection of geological data related to slope stability of the pit. The results obtained from geotechnical study were utilized for slope stability analysis to get maximum safe slope angle for the openpit, which come, to be 33 degrees for 200 metre depth.

Slope monitoring work was also done to ensure the stability of slopes by very precise surveying instruments. Till date no failure has taken place in the pit. At present the depth of the pit is 100 metres. Slope monitoring should be continued with growing depth of the pit. It is recommended that proper drainage pattern should be adopted in and around the pit so that no water should enter in the slope which is very detrimental to the slope stability. Drainage as well as blasting pattern should also be suitably modified time to time depending upon the requirements as the pit goes to greater depth. Periodically loose dressing of the slope face should also be done to ensure the safety from toppling or sliding of loose hanging blocks in slope face.

#### ACKNOWLEDGEMENT

The generous grants from the Ministry of Mines and Steel, New Delhi has enabled us to in depth geotechnical study of the mine. So the authors are thankful to ministry also.

The first author is highly thankful to Director, for giving permission to publish the paper and for his valuable suggestions and guidelines given during the preparation of the paper.

#### REFERENCES

- Bieniawski, Z.T. (1973), "Engineering Classification of Jointed Rock Masses", Trans. S. Afr. Inst. Civil Eng., 15:335-343.
- Herget, G. (1977) "Pit Slope Manual" Chapter 2 - Structural Geology, 123p, CANMET.
- Hoek, E. and Bray, J.W. (1981) "Rock Slope Engineering", Institution of Mining and Metallurgy, London.
- Mines Safety Manual (1979), Third Edition, DGMS, India.
- Rensburg Van, P.W.J. (1970), Proc., Planning Openpit Mines, South African Inst. of Mining and Metallurgy, Johannesburg.

## A Proposed Procedure for the Identification of Dispersive Soils

H.J. Von M. Harmse

Professor of Pedology, University of Potchefstroom for Christian  
Higher Education, Potchefstroom, South Africa

F.A. Gerber

Hydrologist, Department of Water Affairs, Pretoria, South Africa

**ABSTRACT:** The piping failure of the Senekal dam and many other small dams in South Africa, despite the use of apparently sound material and good control during construction, emphasizes the need for a method to unambiguously identify dispersive soils. Physical and chemical tests of one hundred and seventy soil samples were evaluated against the double hydrometer method, after removal of free salts. The chemical methods based on characterization of the exchange complex (CEC and ESP) gave consistently more reliable results than the physical tests, such as the pinhole, crumb and sticky point tests and even the double hydrometer test when free salts are not removed.

### INTRODUCTION

The Senekal dam, an off-channel storage reservoir, is situated in the Sand River approximately 3 km upstream from the town of Senekal in the Orange Free State, South Africa.

The country rock underlying the alluvium, which is also the parent material of the soils used for construction, comprises mustones and arkosic sandstones of the Adelaide Subgroup (Beaufort Group), of the Karoo Sequence. The foundations are situated on alluvial soils and the wall was constructed using the B-horizon and subsurface horizons of a solonchic soil excavated from a borrow pit 500 m away. The material was blended and the moisture content and density were checked at regular intervals during construction (Wagner, *et al*, 1981).

The earth wall which has a maximum height of 8 m, is 1100 m long and contains a reservoir of approximately 19 ha with a capacity of

$1.4 \times 10^6 \text{ m}^3$  (Wagner, *et al*, 1981).

Filling of the reservoir commenced in November 1974 by pumping water into the dam, but was stopped a week later when leaks were detected on the downstream toe of the embankment. The water level was about 3 m above the floor. The flow increased rapidly and failure through piping occurred approximately four days later (Wagner, *et al*, 1981). A detailed geotechnical investigation to determine the cause of failure was initiated by Jones and Wagner during 1975. The results of the geotechnical investigation are described in detail by Wagner, *et al*, (1981). After an initial physical, chemical and physical-chemical analysis of 9 samples from the core (Table 1) it was con-

cluded that the cause of failure was dispersive clays. Subsequent and earlier investigations confirmed that piping failure in small dams and the soil erosion associated with dispersion is of widespread occurrence in South Africa (Donaldson, 1973; Harmse, 1973). The piping failure of the Senekal dam and many other small dams, as well as the influence of dispersion on the erodibility of soils, emphasized the need for a method to identify soils which may be susceptible to dispersion unambiguously.

### DISPERSION

Although the behaviour and characteristics of dispersive soils are reasonably well understood and adequately explained by the double layer theory (Bolt and Bruggenwert, 1976), a satisfactory and analytical method for the identification of dispersive soils remains a problem. This is probably mainly due to the fact that dispersion is a physical manifestation of chemical and mineral-dependent physico-chemical properties of soils (Greenland and Hayes, 1978). The relative influences of these factors has not been considered in the past, especially the influence of the clay mineralogy.

The clay mineralogy of soils is the result of several factors acting upon the parent material, such as climate and associated intensity of weathering. Accumulation and loss of the products of weathering within soil profiles are often related to their position in the landscape, vegetation and the duration of these weathering influences.

Only for a limited number of combinations of conditions do soil forming factors and processes have a uniquely determining effect on

the clay mineralogy. The clay mineralogy of soils therefore depends only rarely upon the direct influence of the parent material from which it developed. Most of the physical properties of mineral soils, including dispersion, hydraulic conductivity, swelling and erodibility, can be related to the interaction between the composition of the soil solution and the clay mineralogy (Low, 1968; Bolt and Bruggenwert, 1976).

from broken edges and protonization of exposed oxygen and OH-groups.

3. Oxides, hydrous oxides and hydroxides of iron and aluminium of tropical areas with low net negative charge or cation

exchange ( $1-5 \text{ me}100\text{g}^{-1}$  of clay). Dispersion is expected to be virtually non-existent in natural soils containing

TABLE 1. Average physical and chemical properties of 19 Samples from the core of the Senekal dam

|                  | Chemical Properties |         |           | Index Properties |      | Grading |       |
|------------------|---------------------|---------|-----------|------------------|------|---------|-------|
|                  | pH                  | EC<br>* | ESP<br>** | LL               | PI   | Silt%   | Clay% |
| Avarage          | 8,3                 | 14,6    | 24,8      | 42,5             | 26,5 | 31      | 53    |
| Std. Deviation   | 0,4                 | 50,4    | 12,5      | 10,1             | 7,7  | 5,1     | 9,8   |
| Coeff. Deviation | 0,06                | 0,35    | 0,50      | 0,24             | 0,29 | 0,16    | 0,19  |

\* EC = Electric conductivity in  $\text{mSm}^{-1}$   
 \*\* ESP =  $\frac{\text{Exchangeable sodium}}{\text{CEC}} \times 100$

In general, soil clays are mixtures of mineralogically related clay components.

Some of these clay components, however, have an irregular structure that makes unique identification in terms of the mineralogical components difficult. Furthermore, identification of the minerals in the clay fraction of the soil requires complex procedures and expensive equipment. It cannot be applied for routine analysis of large numbers of samples, especially in semi-arid countries where mixed layer minerals and dispersive soils are widespread. The cation exchange

capacity CEC, expressed in  $\text{me}100\text{g}^{-1}$  of clay), or net negative charge on the colloidal fraction of mineral soils may, however, be used to define broad categories within which certain minerals in the soil could be expected to have related properties (Dixon and Weed, 1977). This can be applied during routine analysis for the positive identification of dispersive soils. These categories are:

1. The 2:1 types of phyllosilicates which include hydromica, vermiculite, chlorites and smectites. The CEC ( $40-150 \text{ me}100\text{g}^{-1}$  clay) of these clay minerals is mainly derived from ionic substitution in either the octahedral or tetrahedral layer, or both.
2. The 1:1 types of phyllosilicates, such as kaolinite and halloysite, with intermediate to low CEC-values ( $5-40 \text{ me}100\text{g}^{-1}$  of clay). The negative charges of these clays are pH dependent and arise mainly

these minerals as dominant components of the clay fraction.

This case history reports on an investigation of the phenomena of dispersion to determine an unambiguous method for the positive identification of dispersive soils.

The approach adopted was to apply and evaluate the results of various dispersion tests in order to investigate the interaction of soil properties. This approach resulted in a reduction of the number of tests and led to the selection of a limited number of reliable methods which give consistent results for the identification of dispersive soils. The results of these tests are also indispensable for the determination of the amount of gypsum required for the reclamation of dispersive soils.

#### METHODS AND MATERIALS

One hundred and seventy soil samples ranging in CEC  $100\text{g}^{-1}$  clay from 5 to 140, and in ESP values from 0 to 20 per cent, were selected and prepared and subjected to both physical and chemical methods of evaluation. Cation exchange capacity, exchangeable cations, particle-size distribution and electric conductivity were determined by standard procedures (Hess, 1971).

The results of nine physical and five chemical dispersion tests were evaluated.



From these fourteen methods, four were selected on the basis of consistency of the results (Gerber and Harmse, 1986).

The four methods chosen were:

1. The sodium concentration in a saturated paste (Sherard, Dunningan and Decker, 1972).
2. The percentage exchangeable sodium (ESP method) (Sherard, Decker and Ryker, 1972).
3. The ESP + PEMg method (PEMg = percentage exchangeable magnesium) (Harmse, 1980).
4. The percentage dispersion or double hydrometer method (Anderson, 1951; van Zyl, 1973) was used as a criterium for dispersion after removal of free salts. This method was selected because of the fact that the amount of clay in suspension in distilled water is a measure of dispersion (Anderson, 1951) and because of the consistency of the results.

## RESULTS AND DISCUSSION

During the re-evaluation of 67 of the samples, 46 of which were dispersive (Table 2) and 21 non-dispersive (Table 3) by the double hydrometer method, attention was also given to the influence of clay content, CEC value, phosphate, pH, electric conductivities and type of cation adsorbed on the exchange complex. The curves shown in Figure 1 were established from these results. The influence of free salts in the soil solution on the flocculation of dispersive soils is shown in figure 2. The threshold values of free salts at which flocculation occurs are also clearly dependent upon the clay mineralogy as manifested in the  $\text{CEC } 100\text{g}^{-1}$  clay.

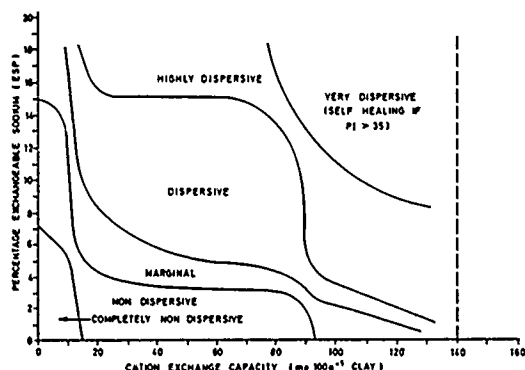


FIGURE 1. Diagram illustrating the influence of composition of the clay fraction as manifested in  $\text{CEC } 100\text{g}^{-1}$  of clay and ESP on dispersion (according to all four methods evaluated).

From figure 1 it is evident that variation

in clay mineralogy ( $\text{CEC } 100\text{g}^{-1}$  of clay) influences the ESP values at which total dispersion will occur. All samples with ESP values above 15 per cent were dispersive (Figure 1).

Soils with low cation exchange values of 15

$\text{me } 100\text{g}^{-1}$  of clay were completely non-dispersive at ESP-values of 6 (Figure 1). Soils with high CEC-values and plasticity indices greater than 35 (PI), swell to such an extent that the influence of dispersion on the stability of structures are expected to be insignificant. This explains why these soils can be used for hydrosealing if judiciously placed. From the research it became evident that the results of the physical methods, namely the pinhole, double hydrometer, sticky point and crumb tests, will be invalid if the water quality is not considered, or if the soil solution contains soluble free salts. This is due to the influence of free salts in the soil and water on dispersion (Bolt and Bruggenwert, 1976) (Figure 2). The inability of these methods to identify dispersive soils unambiguously was proven in all instances where free salts were present, which is more often than not the case with sodium saturated natural soils (Gerber and Harmse., 1986).

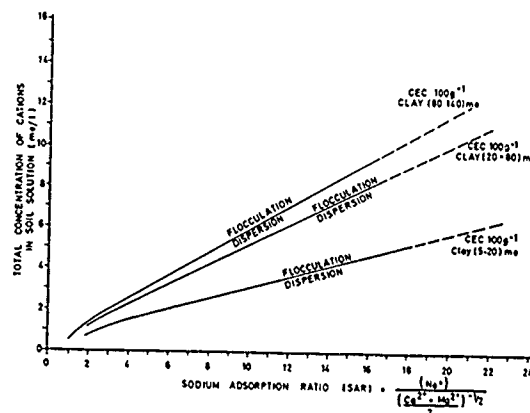


FIGURE 2. The influence of free salts with a high sodium content on flocculation and dispersion as influenced by the composition of the colloidal fraction of mineral soils.

Determination of CEC by the summation of extractable cations (Sherard, Dunningan and Decker, 1972) may lead to conflicting results. This method can be invalid if soluble salts occur in the soil solution or if the base saturation of the soil is less than 100 per cent. Application of the results represented in figures 1, 2 and 3 enables easy

TABLE 2. Analytical data of soils with a percentage dispersion of more than 25% according to the double hydrometer method (free salts removed)

| Sample No | pH H <sub>2</sub> O | EC   | CEC  | ESP  | Clay % (me) | CEC (me 100g <sup>-1</sup> ) Clay | Dispersion % * |
|-----------|---------------------|------|------|------|-------------|-----------------------------------|----------------|
| A3573     | 8,1                 | 5,3  | 21,4 | 9,6  | 59          | 36                                | 26,8           |
| A4767     | 7,2                 | 6,5  | 16,7 | 14,6 | 60          | 28                                | 27,1           |
| A4813     | 8,3                 | 22,8 | 26,6 | 11,9 | 63          | 42                                | 28,5           |
| A4773     | 7,8                 | 22,5 | 10,9 | 14,2 | 65          | 29                                | 29,1           |
| A2514     | 7,8                 | 10,0 | 11,4 | 12,7 | 68          | 17                                | 29,6           |
| A3770     | 8,6                 | 11,5 | 27,6 | 8,1  | 44          | 63                                | 32,7           |
| A3731     | 7,1                 | 7,7  | 17,9 | 17,2 | 46          | 39                                | 33,0           |
| A2472     | 6,8                 | 2,7  | 9,4  | 8,2  | 44          | 21                                | 33,5           |
| A3204     | 8,0                 | 8,4  | 25,3 | 11,6 | 62          | 41                                | 36,7           |
| A2744     | 7,1                 | 6,3  | 29,0 | 13,1 | 36          | 81                                | 38,5           |
| A4753     | 8,4                 | 24,0 | 24,8 | 12,0 | 65          | 38                                | 39,0           |
| A4594     | 8,3                 | 28,3 | 23,3 | 13,6 | 65          | 36                                | 39,4           |
| A1565     | 7,2                 | 5,4  | 9,0  | 7,6  | 53          | 17                                | 41,9           |
| A3946     | 8,2                 | 15,5 | 25,6 | 6,9  | 43          | 60                                | 43,0           |
| A4729     | 7,4                 | 11,9 | 18,7 | 7,4  | 64          | 29                                | 43,8           |
| A3289     | 6,8                 | 3,2  | 21,4 | 7,6  | 54          | 40                                | 43,9           |
| A3633     | 8,8                 | 8,6  | 18,7 | 7,6  | 36          | 52                                | 44,0           |
| A4688     | 7,5                 | 19,0 | 22,4 | 10,9 | 61          | 37                                | 49,5           |
| A1654     | 9,1                 | 10,5 | 28,0 | 8,1  | 44          | 64                                | 49,5           |
| A3005     | 7,7                 | 4,4  | 27,1 | 4,8  | 45          | 60                                | 50,0           |
| A1535     | 8,2                 | 13,9 | 25,6 | 11,1 | 60          | 43                                | 52,8           |
| A3908     | 8,2                 | 10,6 | 37,3 | 7,9  | 63          | 59                                | 54,8           |
| A2884     | 7,3                 | 4,3  | 17,2 | 19,0 | 65          | 26                                | 56,3           |
| A2754     | 7,8                 | 8,5  | 30,9 | 5,0  | 45          | 69                                | 57,9           |
| A3184     | 8,31                | 6,1  | 24,1 | 5,7  | 46          | 52                                | 59,3           |
| A2804     | 6,8                 | 5,3  | 20,0 | 16,5 | 50          | 40                                | 59,8           |
| A3755     | 9,0                 | 10,8 | 26,1 | 15,5 | 55          | 48                                | 60,1           |
| A4793     | 7,7                 | 17,5 | 22,0 | 17,6 | 55          | 40                                | 60,8           |
| A3514     | 8,4                 | 10,5 | 35,4 | 14,9 | 49          | 72                                | 63,6           |
| A1592     | 9,2                 | 40,6 | 41,6 | 11,6 | 65          | 64                                | 64,9           |
| A3603     | 8,1                 | 18,9 | 18,3 | 16,5 | 64          | 29                                | 66,7           |
| A2674     | 6,9                 | 8,7  | 20,0 | 18,7 | 52          | 38                                | 69,2           |
| A1655     | 9,1                 | 13,0 | 31,8 | 6,7  | 42          | 76                                | 69,7           |
| A3425     | 8,7                 | 20,4 | 28,6 | 15,0 | 58          | 49                                | 70,9           |
| A4744     | 7,8                 | 10,5 | 13,4 | 11,0 | 53          | 25                                | 74,6           |
| A2524     | 8,8                 | 8,8  | 24,7 | 11,7 | 41          | 60                                | 80,0           |
| A2764     | 7,4                 | 8,5  | 14,2 | 22,4 | 57          | 25                                | 86,2           |
| A4693     | 8,1                 | 17,8 | 18,7 | 20,0 | 61          | 31                                | 86,2           |
| A1595     | 9,3                 | 64,5 | 21,2 | 36,6 | 65          | 33                                | 93,9           |

EC - Electrical conductivity in mSm<sup>-1</sup>  
 CEC - Cation exchange capacity (me100g<sup>-1</sup> soil)  
 ESP - Exchangeable sodium percentage  
 CEC 100g<sup>-1</sup> clay - Cation exchange capacity per 100g of clay (me 100g<sup>-1</sup>)  
 \* - Percentage dispersion (double hydrometer method, free salts removed)

and unambiguous determination of the dispersive potential of a soil, even in water containing free salts. The following procedure should be followed:

1. With the aid of figure 3 determine if the soil is dispersive.
2. Determine the degree of dispersivity with the aid of figure 1.

The presence of lithium on the adsorption complex can be expected to have the same in-

fluence as sodium. The effect of magnesium alone and of magnesium with sodium on dispersion has not been quantified successfully nor has the influence of organic material been researched but should receive further attention.

TABLE 3. Analytical data of soils with a percentage of dispersion according to the double hydrometer method (free salts removed) of less than 25%

| Sample No | pH H <sub>2</sub> O | EC * | CEC * | ESP * | % Clay * | CEC 100g <sup>-1</sup> clay * | % Dispersion * |
|-----------|---------------------|------|-------|-------|----------|-------------------------------|----------------|
| A5740     | 4,9                 | 3,0  | 6,1   | 4,9   | 35       | 17                            | 12,3           |
| A5750     | 5,8                 | 7,9  | 20,1  | 2,2   | 47       | 43                            | 12,8           |
| A1670     | 7,2                 | 4,5  | 17,5  | 3,2   | 47       | 37                            | 14,2           |
| A3268     | 5,6                 | 5,4  | 17,4  | 2,5   | 60       | 29                            | 14,4           |
| A3428     | 6,4                 | 7,5  | 23,0  | 1,7   | 45       | 51                            | 14,8           |
| A3368     | 5,9                 | 8,7  | 15,2  | 3,1   | 46       | 33                            | 15,1           |
| A3313     | 5,7                 | 2,7  | 17,2  | 2,4   | 62       | 28                            | 16,7           |
| A2391     | 7,3                 | 4,0  | 22,7  | 2,5   | 30       | 76                            | 20,0           |
| A2715     | 6,8                 | 14,5 | 28,4  | 2,8   | 62       | 43                            | 18,4           |
| A3549     | 6,5                 | 6,3  | 19,8  | 2,2   | 60       | 33                            | 18,9           |
| A2854     | 6,5                 | 9,6  | 23,0  | 2,3   | 68       | 34                            | 19,0           |
| A2391     | 7,9                 | 10,0 | 23,4  | 2,9   | 32       | 73                            | 17,5           |
| A3134     | 7,4                 | 6,5  | 22,2  | 2,4   | 31       | 72                            | 20,0           |
| A2300     | 6,6                 | 5,2  | 23,1  | 2,4   | 40       | 58                            | 20,9           |
| A3613     | 6,0                 | 9,5  | 25,6  | 2,0   | 51       | 50                            | 21,8           |
| A3444     | 6,4                 | 8,4  | 18,8  | 2,3   | 69       | 27                            | 22,4           |
| A5749     | 6,6                 | 7,9  | 10,0  | 3,7   | 41       | 24                            | 24,2           |
| A2726     | 6,2                 | 8,0  | 17,6  | 2,4   | 58       | 30                            | 25,0           |
| A3074     | 7,2                 | 8,0  | 19,2  | 3,4   | 60       | 32                            | 25,6           |
| A2814     | 6,3                 | 5,5  | 21,1  | 1,8   | 54       | 39                            | 26,2           |

\* For explanation of abbreviations see Table 2.

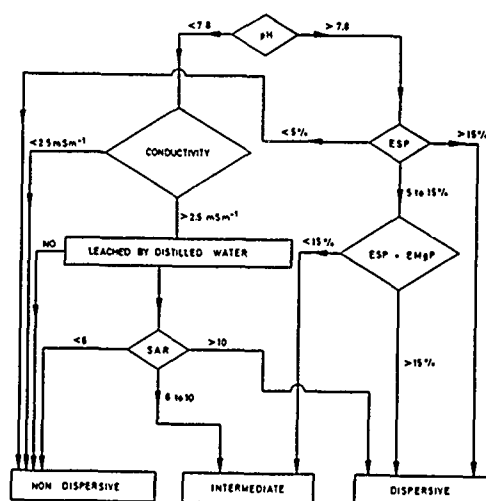


FIGURE 3. Proposed procedure for identification of dispersive soil from which free salts were not removed (Harmse, 1980).

## CONCLUSION

Dispersion is a phenomenon which is mainly controlled by the chemical and mineralogical composition as well as the free salt content

of soils. It is therefore logical that these factors be considered in evaluating the potential of soils to disperse to the degree where it would render earth structures unsafe. The results of the analytical procedures proposed in this study, lead to the conclusion that the tendency for the potential of soils to disperse, especially those containing free salts, may be evaluated more consistently with the aid of physical-chemical methods. The results should enable investigators to identify potentially dispersive soils with greater reliability and to determine the amount of gypsum required for reclamation of dispersive soils readily.

## ACKNOWLEDGEMENTS

The facilities of the Hydrological Research Institute, Department of Water Affairs were used for this research. This paper is published with the permission of the Department of Water Affairs.

## REFERENCES

- Anderson, H.W. 1951. Physical characteristics of soils related to erosion Soil cons. J. 13. pp 129-133. Bolt, G.H. and Bruggenwert, M.G.G. 1976. Soil chemistry.

- Basic elements. Elsevier Sci. Amsterdam.
- Dixon, J.B. and Weed, S.B. 1977. Minerals in the soil environment. Soil Sci. Soc. of America, Madeson.
- Donaldson, G.W. 1973. Piping failures in small earth dams in South Africa. Symposium. Transportation and the environment, Durban. Ann. S.A. Inst. of Civil Eng.
- Gerber, F.A. 1983. Evaluering van die fisies-chemiese eienskappe van dispersiewe grond en die metodes vir identifisering van dispersiewe grond. M.Sc. Thesis, 1983, PU for CHE (Unpublished), pp 127.
- Gerber, F.A. and Harmse, H.J. von M. 1986. n Evaluering van die fisies-chemiese eienskappe van dispersiewe grond en die metodes vir identifisering van dispersiewe grond. Technical report no. TR 123. Dept. of Water Affairs, pp 136.
- Greenland, D.J. and Hayes, M.H. 1978. The chemistry of soil constituents. Wiley Interscience, New York.
- Harmse, H.J. Von M. 1973. Die invloed van die tipe geadsorbeerde katione en die grondoplossing op die erodeerbaarheid van gronde. Symposium Transportation and the environment, Durban. Ann. S.A. Inst. of Civil Eng.
- Harmse, H.J. von M. 1980. Dispersiewe grond, hul ontstaan, identifikasie en stabilisasie. Ground Profile No. 22, pp 10-31.
- Hesse, P.R. 1971. A textbook of soil chemical analysis. John Murray Publs. London.
- Jones and Wagner. 1975. Geotechnical investigation on dam failure at Senekal. Consulting Engineers report to Cahi & Gertenbach, J. & W. report No. G2/2/75.
- Low, P.F. 1968. Mineralogical requirements in soil physical investigations. Special Pub. No. 4, SSSA.
- Sherard, J.L., Decker, R.S. and Ryker, N.L. 1972. Piping in earthdams of dispersive clay. Proceedings of the speciality conference on the performance of earth and earth supported structures. Purdue University. Published by ASCE.
- Sherard, J.L., Dunningan, L.P. and Decker, R.S. 1972. Identification and nature of dispersive soils. Geot. Eng. Div. J. 162 pp 278-301.
- van Zyl, D.J.A. 1973. Gronderosie deur water: n Fisiese proses. Annale van die vyfjaarlikse konvensie van die Suid-Afrikaanse Instituut vir Siviele Ingenieurs. Vervoerwese en Omgewing, pp 16-25.
- Wagner, F. von M., Harmse, H.J. von M., Stone, P. and Ellis, W. 1981. Chemical treatment of a dispersive clay reservoir. Proc. of the 10<sup>th</sup> Conf. on Soil Mechanics-sand Found. Eng., Stockholm, pp 285-291.

# Failure and Repair of the Slope of Railway Embankments and Expansive Soils

Zun Jing Ke

Professor of Civil Engineering, Guangxi University, Nanning, Guangxi, China

Chao-Hai Yong

Lecturer of Engineering Geology, Guangxi University, Nanning, Guangxi, China

Yun-Huang Chang

Lecturer of Civil Engineering, Guangxi University, Nanning, Guangxi, China

**SYNOPSIS:** This paper mainly discusses the stability of the slope of the four sections of railway embankments of expansive soils, describes their basic condition and the properties of the soil materials, analyzes the types and causes of slope failures, discusses the repair of such slopes, and the remedial measures to prevent recurrent of the slides, and sums up experience of using expansive soils to construct railway embankments.

## PREFACE

In China, there are extensive deposits of expansive clays. It is almost impossible to avoid using them to construct railway embankments. It is estimated that at present there are many hundreds of kilometers of railway embankments constructed of this soil, which is particularly susceptible to sliding. Railway traffic is endangered or delayed, and sometimes there are accidents caused by the slides.

The repair of such slopes, and the remedial measures to prevent recurrence of the slides is the topic of this paper. Four case histories illustrate the problem and solutions.

### THE XIANG-YU RAILWAY K317+280 - K317+366

An 86 meter long, 24m high section of a long embankment was constructed with a local expansive clay fill. Its properties were:

LL = 45.3%, PL = 17.4%, PI = 27.9,  
SL = 10.2%

<5 $\mu$  soil particle content  $X_5$  = 47.5%,

<2 $\mu$  soil particle content  $X_2$  = 38.0%,

free swell of disturbed sample FS = 65.0%,  
percent of volume change from saturation

to air-dry  $\delta_m$  = 26.2%, swelling pressure  
 $p_s$  = 150KPa.

The shear strength parameters of the compacted soil ( $w = w_{op}$ ,  $\gamma_d = \gamma_{dmax}$ ):

undrained shear test:  $c = 50\text{KPa}$ ,  $\phi = 12^\circ$ ;

saturated undrained shear test:  $c = 25\text{KPa}$ ,  
 $\phi = 8^\circ$ .

There are three sets of tracks on the embankment, which was completed in 1973. The upper approximately ten meters of the embankment at 1v:1.5h are steeper than the lower portion at 1v:1.75h. Transverse 2.5m wide stone-filled drains have been placed in the slope, spaced at approximately 8 meters. The drains are approximately 1.5 to 2.0m deep. Between them are arch-shaped drains. A retaining wall was constructed at the foot of the slope.

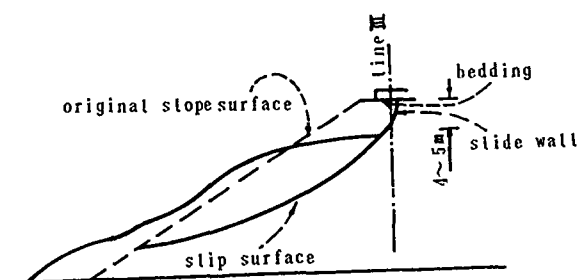


Figure 1

The rainy season in the region of the embankment is from July to September. On the 11th of October, 1980 a slide occurred on the slope of the embankment. See Fig. 2. The slide was about 50m wide, and about 4 to 5m thick. The slide scarp was about 0.3m on the 12th, 2.0m on the 19th, and was about 4 to 5m high by the 21st of October. The drains on the slope and the retaining wall at the foot of the slope were damaged, and the rails were suspended from their ends, due to the removal of support by the embankment.



Figure 2

Reasons for the failure:

1. It is unstable to construct such a high embankment with the expansive soil with a slope of 1:1.5 to 1:1.75. A stability analysis based on the saturated undrained shear strength shows that the factor of safety is less than 1.

2. Since there was poor drainage on the surface of the embankment, water accumulated under the ballast bedding. Such accumulation seeped into the embankment, softening the soil.

3. Water accumulation under the ballast bedding softened the embankment and allowed penetration of ballast into the bedding, causing a ballast pocket. See Fig. 3. In turn, this pocket became a reservoir for further accumulation of water and fed the water into the embankment.

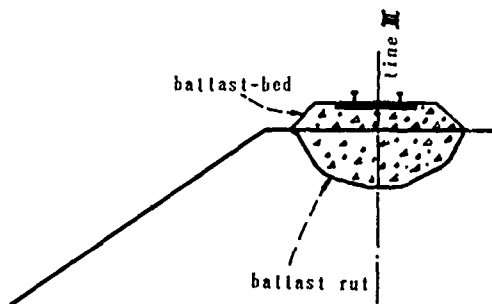


Figure 3

4. The original density of the embankment was low and not uniform, since compaction had been attempted with earth-hauling machinery, and probably without proper rolling. Moreover the slope surface was not well protected so that shrinkage cracks formed in the dry season, with rain infiltrating these cracks during the rainy season.

5. The rock drains on the slopes were apparently too shallow.

The main repair measures that were adopted are shown in Fig. 4.

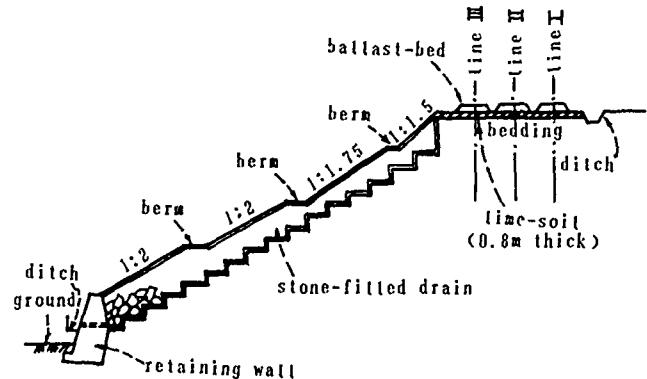


Figure 4

1. A lime-soil mixture with a ratio of lime to sand to soil of 1:5:10 was used as a 0.8 meter thick bedding just below the ballast. A longitudinal ditch was set on the embankment to drain surface water.

2. After removing the slide materials, local expansive soil was mixed with 25% sand and recompact, with overall slope steepness reduced and three small berms introduced.

3. Nine transverse rock drains, 2m wide, and spaced 8m apart were built to extend one-half meter below the slip surface. Between the transverse drains, rock arch-drains were constructed. See Fig. 5.

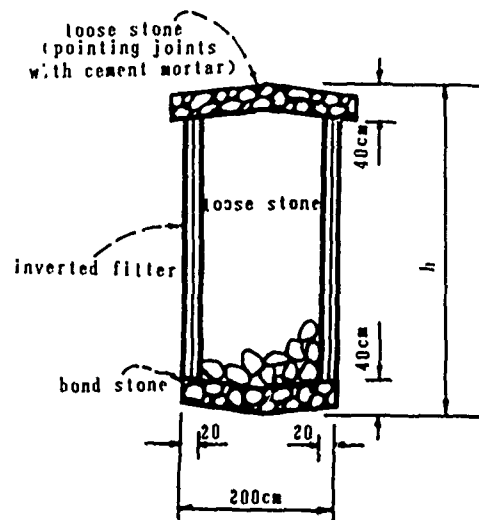


Figure 5

4. A seven to eight meter high retaining wall with a base width of 3.8m was built at the foot of the slope.

The embankment was repaired in November 1983. Since that time the slope has been stable and the embankment has been completely serviceable.

#### THE XIANG-YU RAILWAY K310+325 TO 310+480

This embankment is 155m long, with a maximum height of 26.7m. The upper six meters of the embankment has a slope of 1v:1.5h; from 6 to 18m below the crest the slope is 1v:1.75h; and where the embankment is higher than 18 meters, all below that height is 1v:2h. There was no slope protection built into the embankment in 1973, when it was constructed of local expansive clays. The properties of this clay were:

LL = 43.6%, PL = 18.5, PI = 25.1,  
SL = 11.0%,  
X<sub>S</sub> = 48.3%, X<sub>2</sub> = 35.3%,  
FS = 68.0%,  $\gamma_m$  = 27.4%,  $p_s$  = 120KPa.

The shear strength parameters of the compacted soil ( $W = W_{op}$ ,  $\gamma_d = \gamma_{dmax}$ ):

undrained shear test:  $c = 55.0\text{KPa}$ ,  $\phi = 10.5^\circ$ ,  
saturation undrained shear test:  $c = 36.0\text{KPa}$ ,  
 $\phi = 7.6^\circ$ .

The failure consisted of multiple shallow slides in the middle sections of the slope during the rainy season of 1974. These slides covered more than half the area of the slope between the above referenced stations. The slides initially took the shape of a horse's hoof, and were relatively small in area. See Fig. 6. The individual slides were about 10-20m wide, and 0.8-2.0m thick. As they developed, several of the slides joined and overrode one another, and then continued to expand up the slope. It was anticipated that if not repaired promptly, sliding would result in the rails losing support.



Figure 6

It was evident that this failure resulted from a shallow layer of the slope becoming saturated due to water seepage, rapidly reducing the shear strength of the soil. Specifically:

1. The rainy season of 1974 was long and rainfall was heavy.

2. Compaction of the embankment had been done using hauling equipment rather than with rollers, and the compaction was poor and non-uniform.

3. Shrinkage cracks had appeared before the rainy season, and had not been repaired at the time of the rains.

4. The slope was too steep. Soil tests on a sample which had been permitted to swell in water gave shear parameters of  $C = 10\text{KPa}$  and  $\phi = 4$  degrees. A stability analysis was made with the assumption that the slip surface was a plane, and the factor of safety of the slope was determined to be less than one.

Measures to repair the slope were as follows:

1. Fifteen transverse stone drains were constructed on the slope at 10m spacing. The drains were 1.5m wide and 2m deep. Between the transverse drains arch-drains were constructed as shown in Fig. 7.

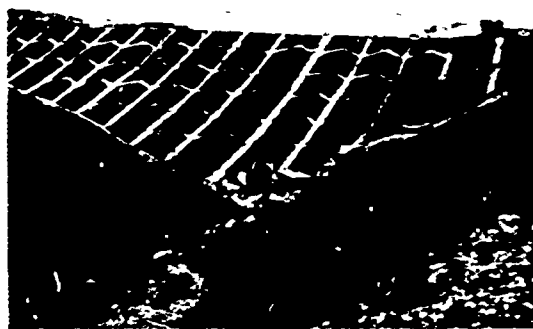


Fig. 7

2. Between the drains were planted a bush called False Indigos which has roots that can reach 2-3m deep. These bushes were expected to reinforce the slope.

3. A longitudinal ditch was built at the foot of the slope.

Repairs were completed in 1977. In the intervening ten years the slopes have remained in good condition and there has been no evidence of sliding or distress.

#### THE JIAO-ZHI RAILWAY K703+700 TO K704+300

The embankment is 600m long with a height of 8-14m. The upper 10m of the slope are at 1v:1.5h, and below this 1v:1.75h. The fill is local expansive soil without slope protection. Two soils were used, a gray clay and a brown clay. Their properties are given in tables 1 and 2.

The embankment was completed in 1970. The slopes began to fail during the rainy season during the first year that it was open to traffic.

The failures appeared chiefly in the form of shallow slides. Generally these slides were limited to the top two-thirds of the embankment with a width of 10-30m and usually about 1 to 1.5m in thickness. Slide scarps were generally 1.0-1.5m in height. Fig. 8 shows details.

There were very many slides along the slopes of the embankment.

Table 1. Basic Properties of the Soil Materials

| soil type  | LL   | PL   | PI   | $X_s$ | $X_c$ | FS   | SL   | $\delta_m$ | $p_s$ |
|------------|------|------|------|-------|-------|------|------|------------|-------|
|            | %    | %    | —    | %     | %     | %    | %    | %          | KPa   |
| gray clay  | 58.7 | 18.3 | 32.4 | 49.5  | 39.8  | 45.8 | 11.2 | 44.5       | 150   |
| brown clay | 46.5 | 19.4 | 27.1 | 49.2  | 28.5  | 65.8 | 19.7 | 27.9       | 90    |

note:  $X_s$ —<5 $\mu$  soil particle content;

$X_c$ —<2 $\mu$  soil particle content;

$\delta_m$ —percent of volume change from saturation to air-dry;

$p_s$ —swelling pressure.

Table 2. Shear Strength Properties of the Compacted Soil

| soil type  | undrained shear |            | saturation undrain shear |            |
|------------|-----------------|------------|--------------------------|------------|
|            | $c$ (KPa)       | $\phi$ (°) | $c$ (KPa)                | $\phi$ (°) |
| gray clay  | 58.5            | 8.0        | 31.5                     | 5.9        |
| brown clay | 90.0            | 19.2       | 49.0                     | 6.0        |

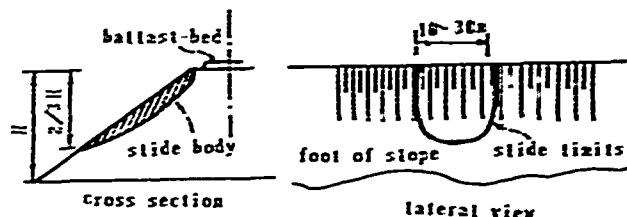


Fig. 8

It was obvious that the failures of the slopes were the results of poor compaction of the slopes, lack of protection for the slope surface, and surface water seeping into the slope through shrinkage cracks or hollows in the slope and shoulder of the crest. In some cases water had accumulated in ballast pockets, and was aggravating the problem.

As shown in Fig. 9, at some places the surface water caused successive shallow slides which eventually undermined the track at the top of the embankment.

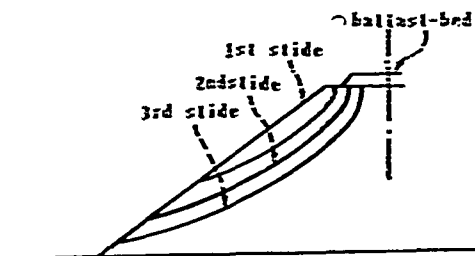


Fig. 9

In addition, slides occurred with slide scarps 2-3m high beneath the tracks, with slide bodies 30-40m in width and 2-3m thick. These formed because the saturated ballast pockets 1-1.5m deep were squeezed outwards under the loading of the trains. Both surface water and water that had accumulated in the ballast pockets served to saturate the embankment.

For this embankment the repair was effected by placing sand on the surface of the embankment to a depth of 1.5-2m, as shown in Fig. 10.

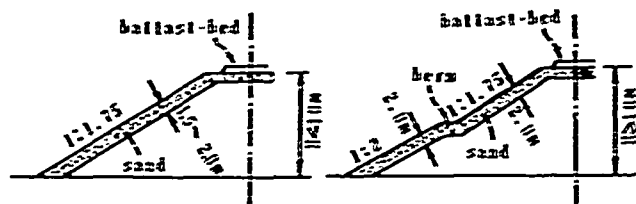


Fig. 10

1. The sand layer was designed to be 1.5m in thickness where the embankment was less than 10m high, and 2m in thickness for a higher embankment section. Under the ballast, sand was 1m thick.

2. Where there were deep ballast ruts or pockets, transverse stone-drains were constructed.

3. The slope gradient was changed so that the upper 10m of the embankment had 1v:1.75 slopes, and below this 1v:2h. A berm of 1.5-2m in width was constructed where the slope gradient changed 10m below the top of the embankment.

4. Naturally occurring grass was planted for protection on the slope.

It has been well over ten years since the embankment was repaired in 1975. The



embankment has been completely serviceable during this time. The sand of the shoulder at the crest and along the slope surface has slipped somewhat, but not sufficiently to warrant concern or repair.

#### THE XIANG-YU RAILWAY K309+636 TO K309+701

This 65m long section of 30m maximum height is part of a long embankment across a valley. As with the other cases cited, the upper slope was 1v:1.5h with a 2.5m wide berm and a lower slope of 1v:1.75h. On the berm a ditch was built. There was no other slope protection. The embankment material was again an expansive clay with the following properties:

LL = 43.6%, PL = 18.5%, PI = 25.1%,  
 SL = 11.0%,  
 $X_5 = 57.0\%$ ,  $X_{20} = 32.5\%$ ,  
 $FS = 57.0\%$ ,  $\delta_m = 26.5\%$ ,  $p_s = 100$  KPa.

The shear strength parameters of the compacted soil ( $W = W_{op}$ ,  $\gamma_d = \gamma_{dmax}$ ):  
 undrained shear test:  $c = 63.5$  KPa,  $\phi = 14.1^\circ$   
 saturation undrained shear test:  
 $c = 28.6$  KPa,  $\phi = 7.5^\circ$ .

Three railway lines were placed on the embankment. The project was completed in 1973.

Three shallow layer slides occurred on the slopes in the rainy season of 1981. A large amount of surface water had seeped into the slope. Makeshift measures were taken to effect a quick repair; timber piles were driven through the slide and straw bags packed with soil were placed to be a counterweight for the slide. Each of the three shallow layer slides began to migrate upwards, so that the slide body became about 30m wide, 1.5-2m thick with slide scarps about 1.5m high. Fig. 11 depicts this.

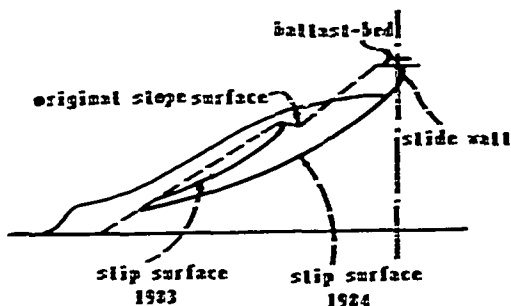


Figure 11

In September 1984, as the slide was being repaired, it rained almost continually for 20 days. A large slide about 60m wide, 4-5m thick with a slide scarp 3m high occurred from the top of the embankment, resulting in loss of support and suspension of 20m of rail.

The causes of the slide appeared to be:

1. The design slope was too steep. Using the saturated undrained shear strength of the embankment soil, a stability analysis showed that the factor of safety was less than 1.
2. Neither drainage ditches on the embankment surfaces nor slope protection was provided. Large ballast pockets had formed under the track and surface water had seeped into the slope from the pockets.

Fig. 12 shows the remedial measures taken to repair the slope.

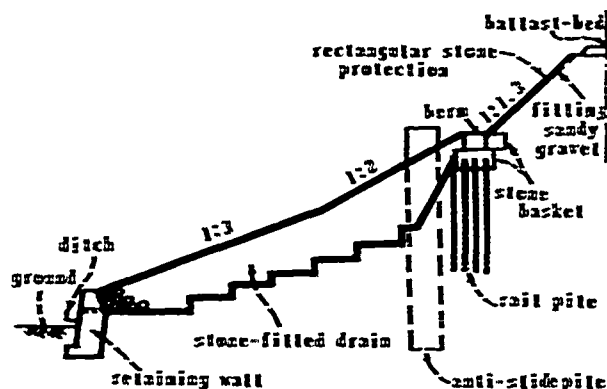


Fig. 12

1. The slope gradient was reduced. The upper 9m was 1v:1.3h, from 9 to 18m below the crest of the embankment, the slopes were 1v:2h, and all embankment below 18m was made with a 1v:3h slope. At the nine meter level a berm 2m wide was constructed. Two hundred twelve rail piles 12.5m long, at 1m spacing were driven below the berm. Reinforced stone baskets were placed on them. Just below the piles and stone basket on the slope were placed four large reinforced concrete anti-slide piles of 3.7m by 2.5m section 25m long.
2. After removal of the slide material, on the top 1:1.3 portion of the slope sandy gravel was placed on the surface with loose rectangular stone as surface protection.
3. From the level of the berm down, nine transverse stone-filled drains were built at 8m spacing, 3m wide, extending below the sliding surface. Between the drains the slope surface was placed a 1m thick layer of soil mixed with 30% sand and rammed in place. False Indigo was also planted on the slope.
4. A retaining wall 5m high with a 3m wide base was built at the base of the slope.

The repairs were made in the first half of 1986. Since then it has been subjected to two rainy seasons. Performance has been excellent.

## CONCLUSIONS

1. There are two basic types of slope failures in embankments constructed of expansive clay, normal slides and shallow layer slides. The former is large in scale and quite severe. Shallow layer slides, the more common, must be promptly repaired or they, too, will become severe.

2. In expansive soils shear strength rapidly decreases after the soil swells upon saturation with water. The effects of this shear strength decrease have not been considered in design and construction in the past. The immediate causes of failure are too steep a slope, improper slope protection, poor drainage, formation of ballast pockets and their saturation, rutting of the ballast, poor compaction and improper maintenance.

3. Provided that proper measures are taken in the design and construction, it is possible to ensure the slope stability of an expansive soil embankment. It is not impossible to construct a proper embankment of expansive soil. Restraining the use of expansive soils in embankments results in higher costs.

4. The most important consideration in the design of such an embankment on expansive soil is to use the proper saturated shear strength of the soil, to perfect the slope protection and drainage system, to treat the bedding for the ballast to prevent rutting and ballast pockets, and to ensure proper compaction during the construction.

## ACKNOWLEDGMENT

I should like to express my gratitude to Professor Norbert O. Schmidt who reviewed the paper and offered constructive criticism and to Allison Moldaway for typing the paper within the required format.

Zeng Lian and Zhou Genyuan supplied a lot of information for this paper. I'm thankful to them for all this help.

## SYMBOLS AND NOTATIONS LIST

FS Free Swell  
LL Liquid Limit  
PL Plastic Limit  
PI Plasticity Index  
SL Shrinkage Limit  
C Cohesion (KPa)  
 $\gamma_d$  Dry Unit Weight ( $\text{KN/m}^3$ )  
 $\gamma_{dmax}$  Maximum Dry Unit Weight ( $\text{KN/m}^3$ )  
 $P_s$  Swelling Pressure (KPa)  
W Water Content  
 $W_{op}$  Optimum Water Content  
 $X_2$  2 Soil Particle Content  
 $X_5$  5 Soil Particle Content  
 $\delta_m$  Percent of Volume Change from Saturation to Air-Dry  
 $\phi$  Angle of Internal Friction

## Performance Evaluation of Rarem Dam

M.C. Goel

Superintending Engineer, Investigation and Planning Circle (WB),  
Roorkee, India

Djoko Mudjihardjo

Institute of Hydraulics Engg., Bandung, Indonesia

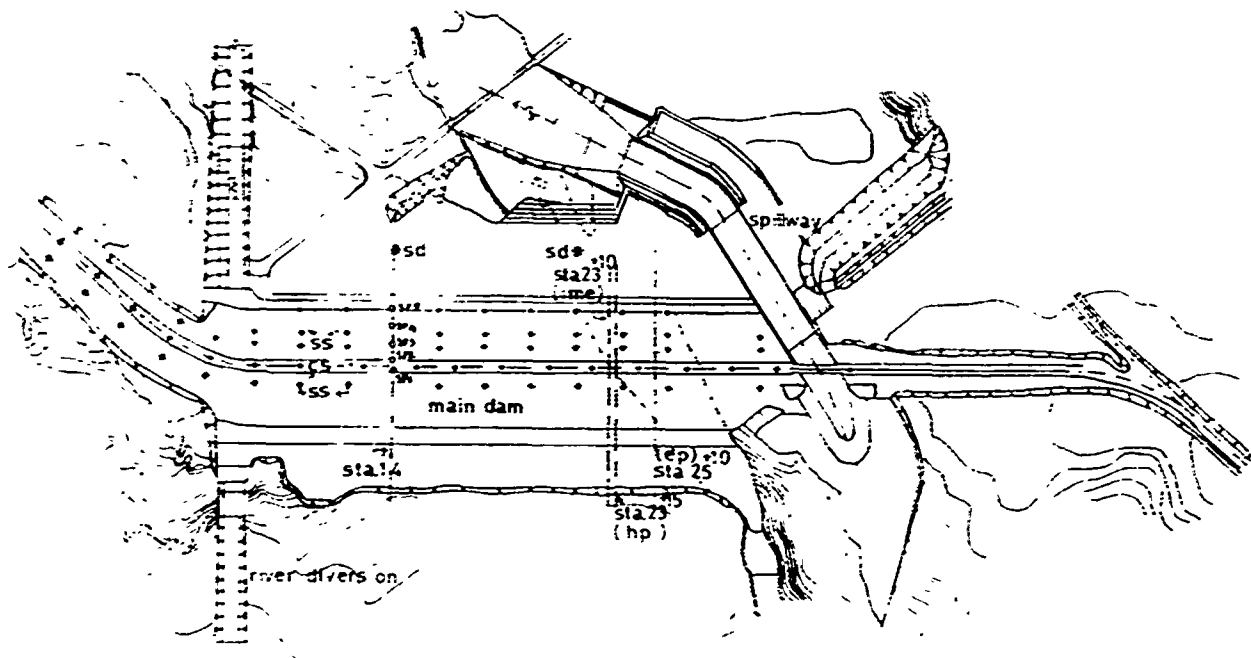
**SYNOPSIS** - 25.0 m high zoned Rarem dam in Indonesia was instrumented with hydraulic piezometers, electrical Carlson type piezometers, Cassagrande type vertical stand pipe piezometers, inclinometers, and surface settlement points. The analysis of observational data has indicated that settlement took place almost simultaneously with construction of dam and reservoir filling. Very low construction pore pressures were observed and phreatic line developed almost simultaneously with reservoir filling. The results of efficiency of flow curtain based on electrical analogy model studies are also discussed in the paper.

### INTRODUCTION

With a view to irrigate 22,600 ha area in North Lamoung, Sumatra, in Indonesia, 62 Million Cum reservoir capacity has been created by constructing 25.0 m high and 1550 m long zoned earthen dam section at Pekurum located about twenty five kilometers south-west of town Kotabumi. The construction of dam embankment was started in November 1981 and completed in early October 1983. Impounding of water into the reservoir started two weeks after completion of dam. The reservoir filling was complete by mid January 1984. The layout of works together with instrumentation plan is shown in Fig. 1. The project area

is covered by young sediments of andesite tuff formation - a product of quaternary volcanic activities. The andesite tuff (sed rock) is a complex of various layers varying in thickness less than 1.0 m to 10.0 m comprising of braccia, conglomerate tuff, tuffaceous sandstone and tuffaceous clay store. Geological profile along dam axis is shown in Fig. 2.

Vertical central clay core of Rarem dam section having upstream and downstream slopes as 0.2H:1V is protected by suitable filter transition zone. The shells are of rockfill having upstream and downstream slopes as 3H:1V and 2H:1V respectively. Typical cross-section of dam along with instrumentation details is shown



sp : Stand pipe piezometer

ep : Electric piezometer

hp : Hydraulic piezometer

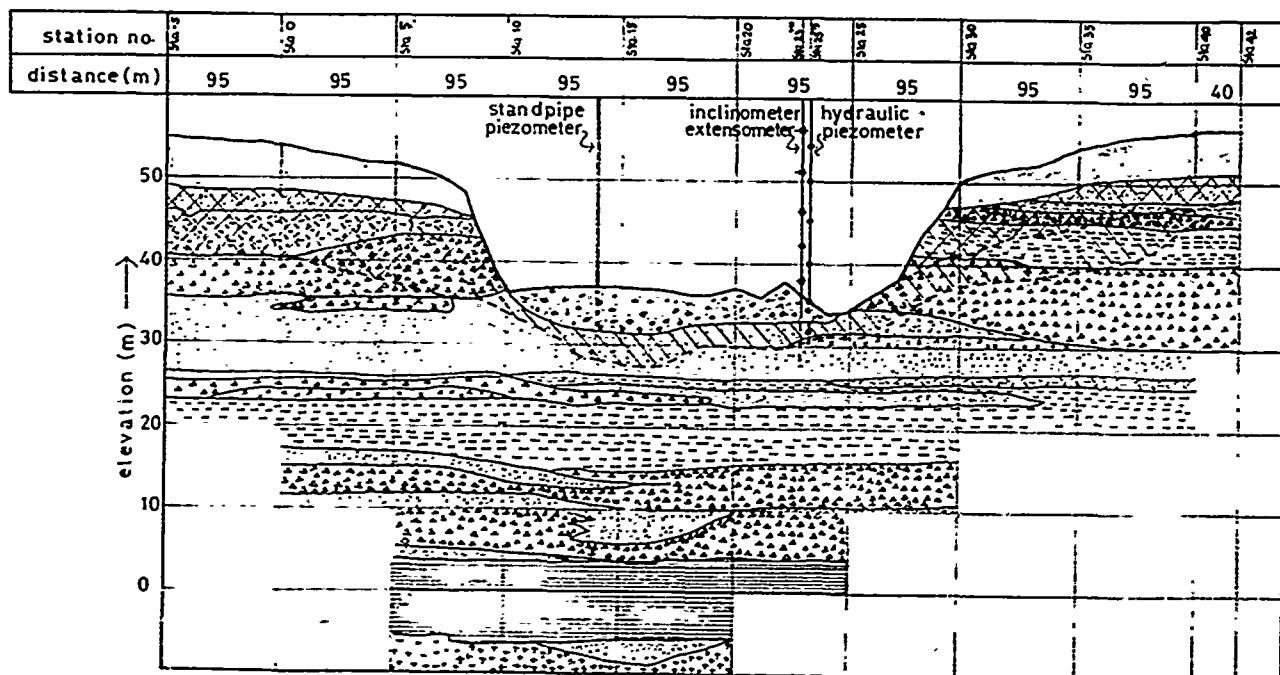
cs : Crest measuring point

ime : Inclinometer/magnetic extensometer

sd : Seepage discharge

sr : Surface measuring point

Fig. 1 : Plan of Instrumentation Installation at Rarem Dam



#### Legend:

|                                   |                                     |                             |                      |
|-----------------------------------|-------------------------------------|-----------------------------|----------------------|
| top soil & residual soil          | Sand & gravel river alluvium        | Intensively weathered       | moderately weathered |
| tuffaceous silt stone & claystone | tuffaceous sandstone and sandy tuff | silty tuff                  | tuff                 |
| diorite                           | tuff breccia                        | boundary of weathered zones |                      |

Fig. 2 : Geological Profile Along Dam Axis

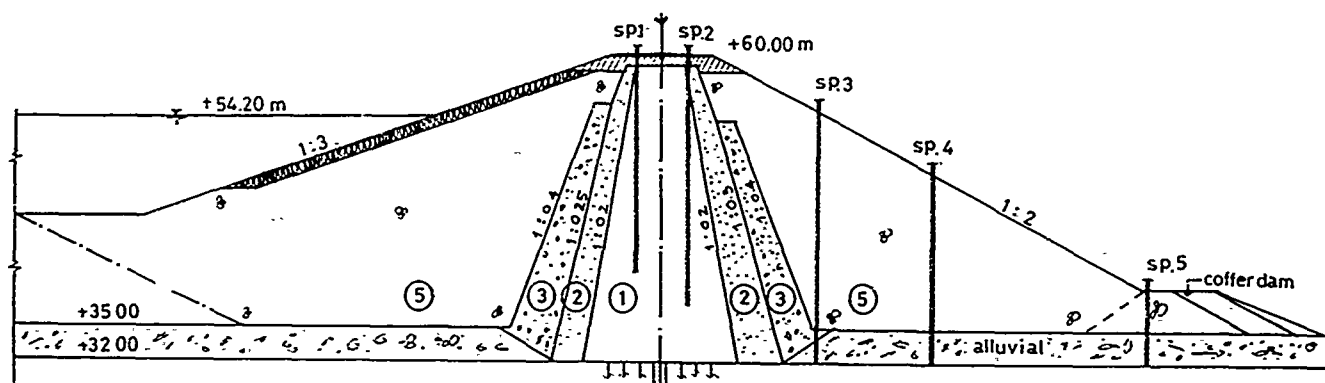
Table - 1 Properties of Material

| Zone               | Gradation   |                   |         | Atterberg limit (%) |    |      | Compaction                      |          | Shear strength               |          | Permeability<br>cm/sec |
|--------------------|-------------|-------------------|---------|---------------------|----|------|---------------------------------|----------|------------------------------|----------|------------------------|
|                    | Soil type   | Particle size(mm) | % finer | LL                  | PL | PI   | Dry density<br>t/m <sup>3</sup> | OmC<br>% | Cohesion<br>t/m <sup>2</sup> | $\phi^0$ |                        |
| Clay core zone(1)  | Clay        | $\leq .002$       | 29      |                     |    |      | 1.10                            | 48.60    |                              |          |                        |
|                    | Silt        | .002-.075         | 64.91   | 96.4                | 48 | 48.9 | to                              | to       | 1.0                          | 28       | $5.9 \times 10^{-6}$   |
|                    | Fine sand   | .075-0.45         | 7-9     |                     |    |      | 1.12                            | 50.50    |                              |          |                        |
| Filter zone(2)     | Fine sand   | .075-0.45         | 20-40   |                     |    |      |                                 |          |                              |          |                        |
|                    | Medium sand | .45-2.0           | 50-48   |                     |    |      | 1.987                           | 9.64     | 0                            | 36       | $1 \times 10^{-3}$     |
|                    | Coarse sand | 2.0-4.75          | 12-14   |                     |    |      |                                 |          |                              |          |                        |
| Transition zone(3) | Sand        | $\leq 4.75$       | 18-25   |                     |    |      |                                 |          |                              |          |                        |
|                    | Gravel      | 4.75-75.0         | 67-62   |                     |    |      | 2.192                           | 7.25     | 0                            | 38       |                        |
|                    | Cobbles     | 75-150            | 38      |                     |    |      |                                 |          |                              |          |                        |
| Rockfill zone(5)   |             | 0.3-3.50          |         |                     |    |      | 2.0                             |          | 0                            | 40       |                        |

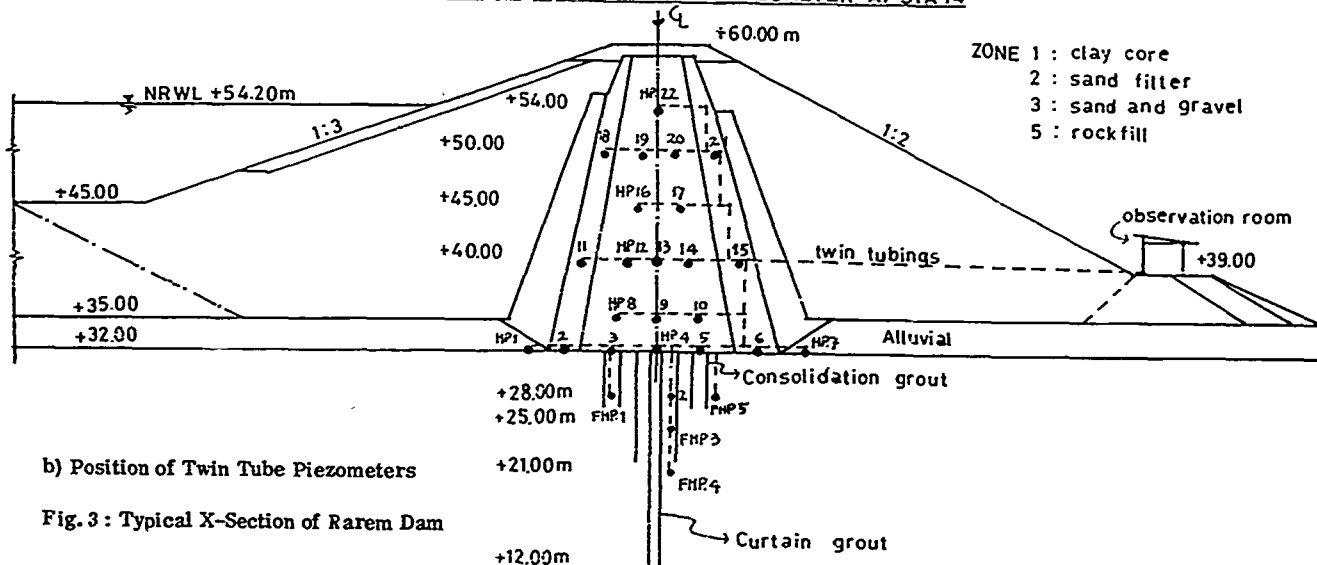
in Fig. 3. Material for clay core comprises reddish brown clay dominated by Kaolinite with high plasticity belonging to CH classification of soil. Material for sand filter and sand gravel transition zone was borrowed from Rarem river deposit whereas rockfill was quarried from andesite bed from a distance of about 6 km from dam site. The properties of material

used in the dam are given in Table-1.

Foundation treatment comprises curtain grout as well as consolidation grouting. Curtain grouting was done along dam areas in two rows, each 1.0 m apart in staggered position and spacing of the holes on each line was 1.5 m with depth ranging from 5



a) ARRANGEMENT OF STANDPIPE PIEZOMETER AT STA 14



b) Position of Twin Tube Piezometers

Fig. 3 : Typical X-Section of Rarem Dam

to 20 m. Consolidation and blanket grouting was done in upstream and downstream sides of curtain grout at the bottom of cut off trench for sections between Station 1 and Sta. 28. The grout holes were arranged at 3m interval on six parallel lines, 1.5 m apart from each other. The holes were drilled upto 10m depth on the lines adjacent to the grout curtain and 5 m on other lines. Consolidation and blanket grouting was done prior to curtain grout.

## 2.0 INSTRUMENTATION

Rarem dam has been instrumented with the following instruments:

- Electrical resistance Carlson type 27 piezometers at Sta. 25 + 10 to measure pore pressures.
- Bishop type hydraulic piezometers 27 numbers embedded at Sta. 23 + 15.
- Cassagrande type vertical stand pipe 5 piezometers, installed at Sta. 14, about 180 m away from the section of Bishop's type hydraulic piezometers.

Out of 27 nos. electrical piezometers, 7 were damaged during calibration stage and out of remaining 20 nos. 14 nos. became out of order during construction period. The readings obtained by these six Carlson type piezometers, were erratic and unreliable. The causes of damage were suspected as under:

- The wire gauges were broken due to vibrations or sudden shocking or hitting during transportation from manufacturer to the site.

- After embedment, the seal might have leaked thus allowing the water entry into the cell causing short circuiting in the system.

Hydraulic tips were embedded both in embankment fill and in foundation of dam. Tips in foundation were installed in drilled holes while in embankment, were placed at specified locations as fill progressed. Tips were carefully saturated with deaired water and taken to the site under water. The connecting tubes which were also deaired from the observation room by flushing with deaired water, were connected to the tip under water. The location of tips in dam section is shown in Fig. 3(b).

From this figure, it can be seen that five foundation tips have been installed in tuff rock foundation. Piezometers FHP 1, 2 & 5 have been embedded at El. + 28.0 where as FHP 3 is at El. +25.0 and FHP 4 at El. + 21.0. In all 22 piezometers have been installed in embankment in 6 tiers viz. 7 nos. (HP 1 to HP 7) in first tier (El. + 32.0 m), 3 nos. (HP 8 to HP 10) in second tier (El. + 35.0), 5 nos. (HP 11 to HP 15) in third tier (El. + 40.0), 2 nos. (HP 16 & HP 17) in fourth tier (El. + 45.0), 4 nos. (HP 18 to HP 21) in fifth tier (El. + 50.0) and one piezometer HP 22 in sixth tier at El. + 54.0. Piezometers HP 1 & HP 7 are installed in alluvium, HP 11, HP 15 HP 18 and HP 21 are in sand filter zone and balance are in clay core. Though the construction of dam started in November 1981 but the installation of foundation type piezometers could be started in July 1982 after completion of grouting. By that time, the fill attained the elevation of + 37.0 m.

Stand pipe piezometers were installed by drilling holes SP1 and SP2 at the crest in core zone, SP3 and SP4 on downstream slope of rock zone and SP5 on crest of downstream coffer dam. The location of these tips is shown in Fig. 3(a). These piezometers were installed in January 1984.

#### Inclinometers

One set of uniaxial inclinometer/extensometer was installed at Sta 23+10 vertically on the centre line of core zone. The instrument consisted of access tubes of aluminium with grooves in four directions perpendicular to each other, magnetic settlement plates surrounding the access tube, a torpedo with electric cable and a digital read out unit. By lowering the probe into the access tube, it can show the inclination of the access tube on the read out digital unit and the signals from magnetic plate would show the settlement. The installation was completed during 20th July 1982 to 20th March 1983.

#### Surface Settlement Points

For monitoring the displacement at the surface of dam, 37 points at crest and 61 points on slope of dam (24 on upstream slope and 37 on downstream slope) were provided. These points were made of suitably embedded 2.0 m long galvanized steel pipe of 100 mm and 150 mm diameter for crest and slope surface measurement respectively. On slope, these points were located in rows at approximately 40 m spacing on lines parallel to the centre line of dam at elevation + 55.0 for upstream and at El.53

and 39.00 for downstream slope.

Because of non-availability of reliable observational data (magnitude of movement being within the limit of error of the measuring method), no further analysis was done for surface movement points.

#### Monitoring

For observation of instruments, three periods have been specified viz. (i) loading, (ii) stabilization and (iii) maintenance. Loading test means one month prior to impounding to one year after filling the reservoir. Stabilization period follows upto four years after filling whereas maintenance period is after stabilization. The recommended frequency of observations is shown in Table-2.

Table - 2 Frequency of Observation

| Measuring device  | Frequency      |                      |                    |
|-------------------|----------------|----------------------|--------------------|
|                   | Loading period | Stabilization period | Maintenance period |
| Piezometers       | twice a week   | once a week          | once a month       |
| Inclinometer      | once a week    | once a month         | twice a year       |
| Surface monuments | twice a month  | once a month         | twice a year       |

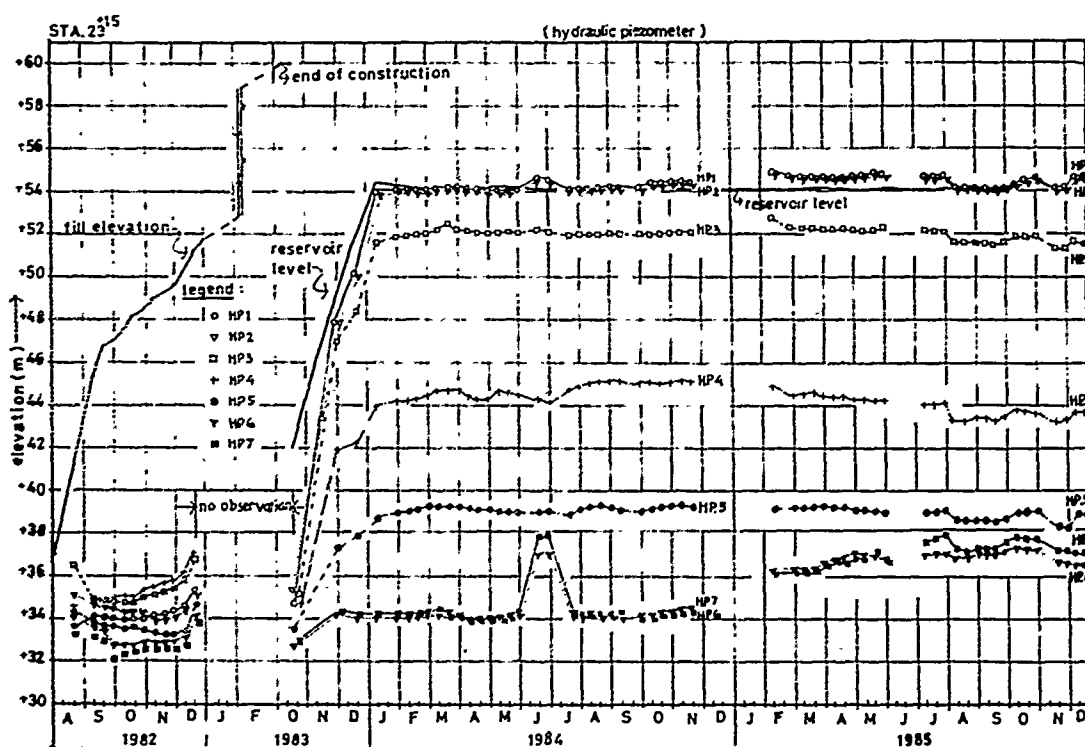


Fig. 4 : Pore Pressure Observations in First Tier

The observations on Bishop's type hydraulic piezometers were taken from August 1982 and continued upto December 1985 except a gap from January to October 1983. Readings on vertical stand pipe piezometers were started from January 1984.

#### ANALYSIS OF OBSERVATIONAL DATA

##### Construction Pore Pressures

Observed pore pressures from August 82 to December 1982 and from mid October 1983 to December 1985 for embankment piezometers HP1 to HP7 are shown in Fig. 4. A study of pore pressures recorded from August 82 to December 1982, indicates that tips no. HP1 and HP2 embedded in river alluvium and filter zone respectively upstream of clay core at El. +32.0m, have recorded almost constant pore pressures of the order of 2 to 2.5m of water head. Since the water level in the river, was at El. +34.0m, obviously these tips recorded pressures corresponding to river water level. Pore pressures recorded by tips No. HP6 and HP7 buried downstream of core in filter zone and alluvium respectively, are of the order of 0 to 1 m and are thus lesser than those recorded by tips located upstream of clay core in similar type of strata. Pore pressures measured by HP3 and HP4 embedded in the clay core show that their values tend to follow the increasing trend as height of embankment fill increases. Their values vary from El. 35.0 to 37.0 m i.e. pore pressure head of 3 to 5 m of water head. At 5m pore pressure head, corresponding dam height is 19m indicating thereby development of pore pressures of the order of 0.4H only. Other tips viz. HP8 to 10, HP12 to 14

and HP16 & 17 located in clay core at different elevations have recorded nil or very insignificant construction pore pressures.

The core material consists of high plasticity reddish clay belonging to CH group having PI about 48% indicating thereby that clay core should be highly compressible and high construction pore pressures should have developed but observed data has shown low pore pressures. Had the observations continued till March 1983, the period during which the dam height was raised further by 8m, more positive conclusions could have been drawn.

Theoretical analysis by Hilf's approach(1948) using one dimensional consolidation test data, has shown that corresponding to dam height of 19m, without any drainage, the pore pressures should have been of the order of 12.5m whereas maximum observed value is about 5.0m. This shows the dissipation of construction pore pressure by 60%. Since core material consists of high plastic clay, this dissipation factor value seems to be too high specially when time duration for dissipation was only 4 months and the rate of construction was considerably high(3.25m/month). Development of low construction pore pressures may be due to fill placement on dry side of OMC (-1.5%), low placement densities( $\gamma_d=1.12 \text{ t/m}^3$ ), nearness of filter zones and possibility of arching action because of lesser thickness of core and dam being of low height.

##### Pore Pressures in Foundation

Pore pressure observations in FHP1 to 5 alongwith reservoir

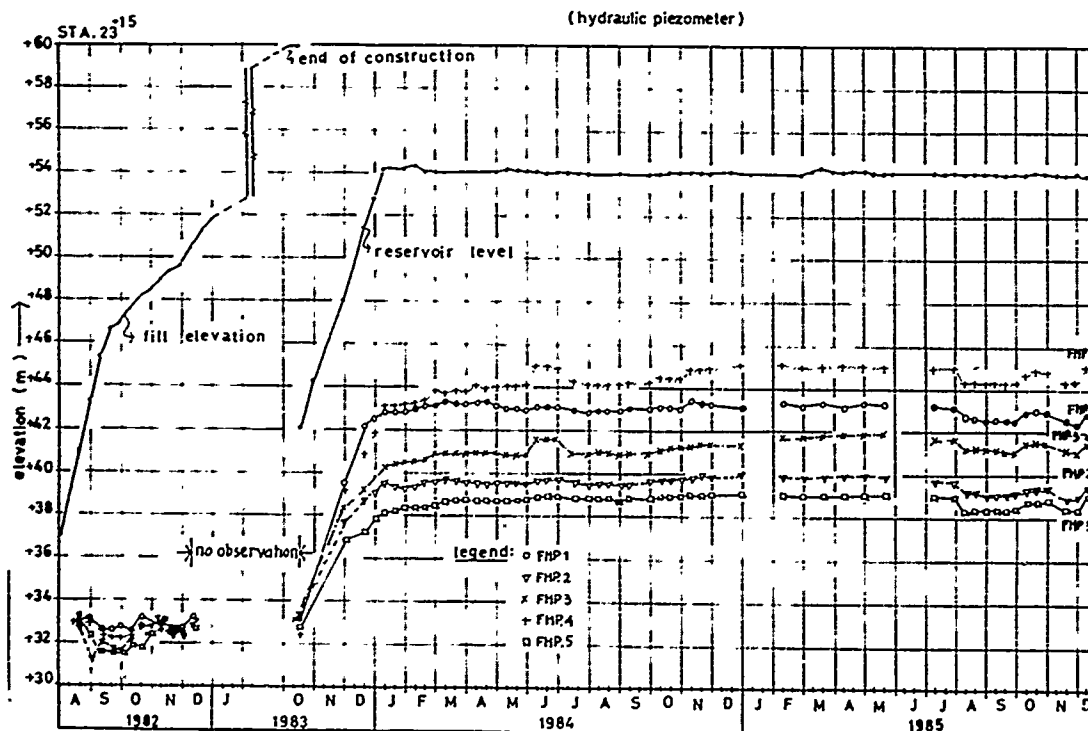


Fig. 5 : Pore Pressure Observations in Foundation

filling pattern are shown in Fig. 5. During reservoir filling period (October to December 1983), these tips have recorded increase in pore pressures following the pattern of reservoir level raising almost simultaneously. Since the reservoir level has remained almost constant from January 1984 onward, the pore pressures recorded by these five foundation tips are also almost constant during this period and the variation of the order of  $\pm 1.0$  m of water head may be due to inherent limitation of the instrumentation. Observations during and after reservoir filling indicate that for FHP1, 2 & 5 located at El.+27.0m, the pore pressures reduce from tip no. 1 to 5 indicating thereby the effect of consolidation grouting done upto El.+27.0. The pore pressures at tips Nos. FHP1 & 5 are of the order of 16m and 12m. respectively against reservoir head of 28.0 m. Tip no. FHP4 located downstream of grout curtain and at lowest level (El.+21.0m) has recorded highest pore pressures which are higher by about 2m head of water from those recorded by FHP1. Similarly tip no. FHP3 also located downstream of grout curtain at El.+25.0m, has also recorded higher pore pressures by about 2.0m as compared to tip no. FHP2. Recording of higher pore pressures by tips no. FHP3 & 4, is contrary to the expectations.

#### Effectiveness of Grout Curtain

The effectiveness of grout curtain is judged by the reduction of seepage discharge (Cassagrande 1961). In the absence of any data regarding seepage quantity, the efficiency of grout curtain was determined from decrease in pressure heads (Hari Krishna and Goel, 1978) using following formula -

$$\text{Efficiency} = \left( \frac{P_1 - P_2}{P} \right) \times 100 \text{ (in \%)} \quad (1)$$

where

$P_1$  &  $P_2$  are the pressure heads upstream and downstream of grout curtain respectively.

$P$  is effective reservoir head.

The efficiency of grout curtain has been calculated by taking total head corresponding to observed piezometer head in tip no. FHP1 and tail water level as recorded in a stand pipe (SP5) embedded at toe of dam at Sta. 14, which is about 180 m from the section of these piezometers. The recorded tail water level is at El.+32.50m and recorded pore pressure in FHP1 is at El. +43.30m. Based on this approach, the results of calculations of grout curtain efficiency are shown in Table-3.

Table 3 - Grout Curtain Efficiency Based on Observed Data

| Elevation | Tip No. | Obs. pore pressure (m) | $P_1 - P_2$ at El. 28.0 | Efficiency (%) |
|-----------|---------|------------------------|-------------------------|----------------|
| +28       | FHP1    | 15.3                   | 0                       | 0              |
| +28       | FHP2    | 11.5                   | 3.8                     | 35.19          |
| +28       | FHP5    | 10.5                   | 4.8                     | 44.45          |
| +25       | FHP3    | 15.7                   | 2.6                     | 24.07          |
| +21       | FHP4    | 23.2                   | -0.9                    | -8.33          |

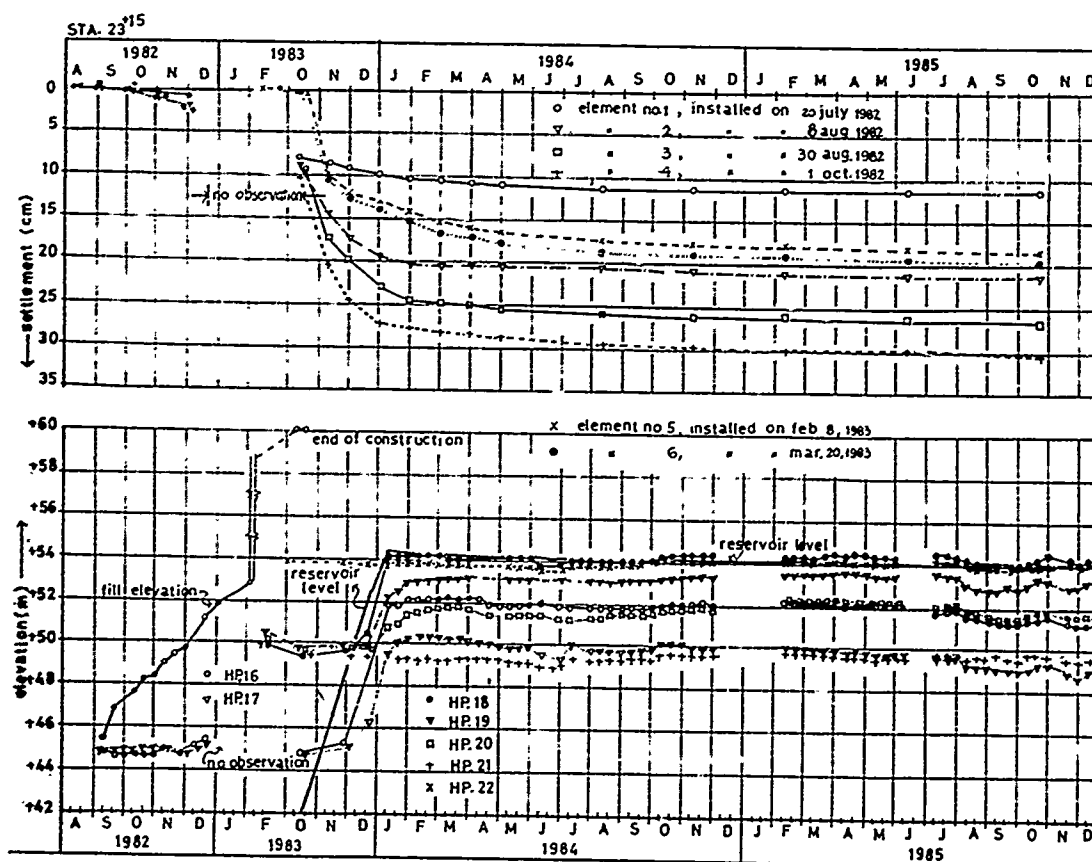


Fig. 6 : Pore Pressure and Settlement Observations



Since the base of core has been provided with consolidation grouting and thus, it is a case of multiple permeabilities in zoned dam section and foundations, and the excess recording of pore pressures by FHP3 & 4 is not explained, electrical analogy experiments to simulate the anisotropy in permeability, were conducted.

#### Steady Seepage Pore Pressures

A study of pore pressures recorded by tips nos. HP1 & HP2 located in upstream sand filter at El. +32.0m shown in Fig. 4 & that of tip no. HP18 again located in upstream sand filter at El. +50.0m (Fig. 6) indicates that the pore pressures are rising with reservoir filling with no time lag. This indicates that upstream filter is working satisfactorily. Recording of negative pore pressures by tip no. HP21 situated downstream of core in filter chimney at El. +50.0m (Fig. 6) and that of tip no. HP15 at El. +40, confirms that downstream filter chimney has been able to lower the phreatic line within core of the dam. Pore pressures recorded for tips no. HP6 and HP7 located downstream of core in filter are of the order of +2.0m (El. +34.0m) upto November 1984 but thereafter the pressures have further increased by 2 to 3 m and by end of December 1985, the excess pore pressures are of the order of 5m.

A study of pore pressures recorded by piezometers no. HP3, HP4 and HP5 (Fig. 4) located at tier no. 1 at El. +32.0m, HP8, HP9 and HP10 at tier no. 2 at El. +35.0m, HP12, HP13 and HP14 at tier no. 3 (El. +40.0m) (plot not shown in this paper), HP16 and 17 at tier no. 4 at El. +45.0m and HP19 and HP20 at tier no. 5 at El. +50.0m (Fig. 6), embedded in clay core, reveals that during water impounding period, pore pressure increased simultaneously with reservoir filling with practically no time lag. A close look of the pore pressures recorded by these tips indicate that from January 1984 onward when the reservoir has been filled upto El. +54.2, the readings of pore pressures of all the tips are almost constant and the steady seepage pore pressures developed follow the flownet pore pressure pattern.

As expected, vertical stand pipe piezometers SP3 to SP5 located in downstream shell of dam section, have not recorded any pore pressures thus indicating that downstream shell is dry and chimney filter is working satisfactorily. Piezometer SP2 located in clay core at El. +37.0 has recorded pore pressures of the order of 7.0m (El. +44.0m). Hydraulic piezometer tip no. HP10 located at El. +35.0m and almost at the location of SP2, has also recorded pore pressures of the same order (El. +44.0m). Thus, the observational data of hydraulic twin tube Bishop's type piezometers is confirmed by the observational data of Cassagrande type porous tube vertical stand pipe piezometers. Tip no. SP1 has been reported to be choked and hence no reliable data is available from this tip.

Equipore pressure contours for readings taken after fifteen months of reservoir filling (March 1985) are shown in Fig. 7. A study of this figure would indicate that the effect of anisotropy in the permeabilities of clay core, foundation treated by consolidation grouting and that of untreated foundation, is noticeable.

Free surface line as obtained from observations of twin tube hydraulic piezometers and that obtained by vertical stand pipe piezometers no. SP2 is shown in Fig. 7. From this, it can be seen that free surface line obtained by twin tube piezometers is higher as compared to that given by vertical stand pipe no. SP2. Free surface line has also been drawn by L. Cassagrande's approach presuming foundations to be impervious. Free surface line with this method lies in between the two observed free surfaces. Free surface line has also been drawn by electrical

analogy method taking permeability of clay core, consolidated grouted foundation zone and ungrouted foundations as  $6 \times 10^{-6}$ ,  $6 \times 10^{-4}$  and  $1 \times 10^{-3}$  cm/sec. respectively and the same is also shown in Fig. 7. It is seen that the free surface obtained by electrical analogy, coincides fairly well with the free surface obtained by twin tube piezometers. Thus the observational data of Bishop's type piezometer can be treated as reliable.

#### Vertical Movement

A study of Fig. 6 showing settlement data, indicates that during construction period (August to December 1982), the settlement recorded, varied from 0.5 cm to 2.5 cm, the smallest value was recorded by settlement plate no. 1 embedded at bottom most level at 32.773 and highest by plate no. 4 at El. +46.736 m. No significant settlement was recorded by plates no. 5 & 6 from their installation in February and March 1983 until October 1983 when reservoir filling started. At the end of construction in October 1983, the settlement of the order of 8 cm to 10.5 cm was recorded by plates no. 1, 2, 3 and 4.

During reservoir filling from October to December 1983, a steep rise in settlement is recorded by almost all plates. In case of plate no. 4, the settlement increased from 10 cm to 27 cm. For plate nos. 5 & 6 (El. 50.90 and 56.41m), increase in settlement was of the order of 12-13 cm by end of December 1983. Plates no. 1, 2 (El. 37.439) and no. 3 (El. 41.924), indicated rise during this period from 8.5 to 10 cm, 9 cm to 20 cm and 10 to 23 cm. respectively. This shows that depending upon the location of plate, maximum settlement has been recorded during reservoir filling which is of the order of 13 to 17 cm for plates located in

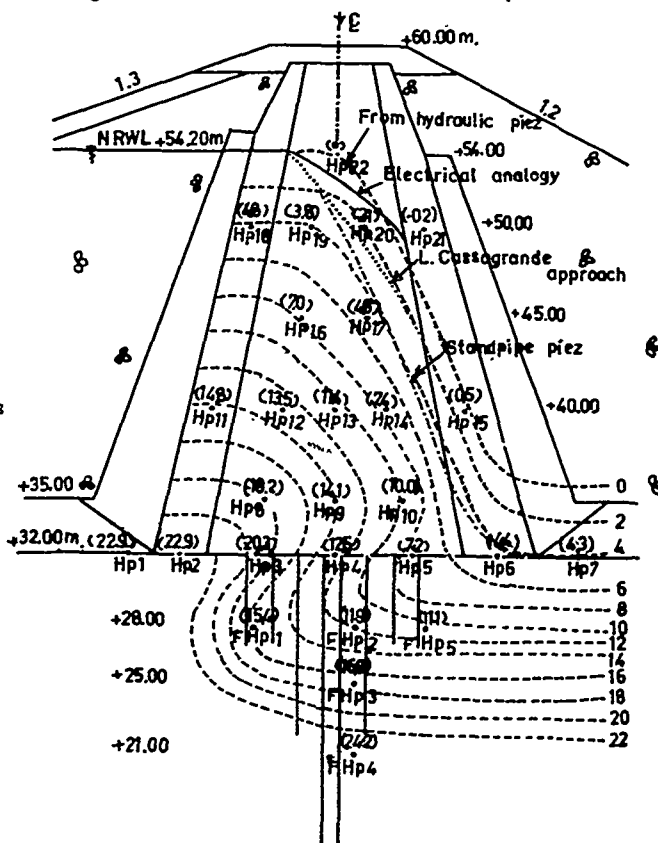


Fig. 7 : Equipore Pressure Contours and Phreatic Surface

upper height of dam. Non recording of settlement by top plates nos. 5 and 6 during construction period (March, September 1983) may be due to some arching action of core by adjoining shell zones which might have reduced during reservoir filling because of lubrication due to saturation and thus during reservoir filling, settlement is recorded by these plates as well. It is interesting to note that for plates no. 1 to 4, settlement after completion of filling (December 1983 upto October 1985) has increased only by about 2 to 3 cm whereas in case of plates no. 5 & 6, the settlement recorded in post filling period is of the order of 5 to 6 cm. This shows that from the date of starting reservoir filling, the total settlement recorded by plates nos. 4, 5 & 6 is of the same order i.e. about 19-20 cm. It may further be noted that beyond April 1984, settlement recorded is practically negligible and thus the settlements are also taking place almost simultaneously or with little time lag.

Theoretical settlement calculations based on Terzaghi's one-dimensional consolidation theory were also done taking coefficient of consolidation  $c_v$  value as  $6 \times 10^{-3} \text{ cm}^2/\text{sec}$ , initial void ratio  $e_0$  as 1.407 and compression index  $c_c$  as 0.118 determined from laboratory tests. The analysis has indicated that for 90% consolidation, total settlement of 53 cm is anticipated in a period of 18 years where as for 50 percent consolidation 29 cm shall take 4 years period. The total observed settlement is of the order of 30 cm which is almost 50 percent of estimated total settlement. This has been attributed to possible deficiencies in experimental results and quick settlement is due to, two dimensional effect in the prototype.

#### Horizontal Movement

Horizontal movement was measured by a torpedo moving in four mutually perpendicular grooves in alluminium casing of inclinometer. Two grooves are aligned in upstream and downstream direction and the other two in diversion canal and spillway direction. Fig. 8 shows a plot in between observed displacement and depth measured initially on 16th November 1982 on the completion of dam and continued until 25th Sept. 1985. During reservoir filling period at El. 54.20, maximum displacement of 4.1 cm (5.7-1.6) in diversion canal direction at about 14 m depth, was recorded on 25th Sept. 1985 and 6 cm (4+2) deformation in downstream of dam direction at about 17 m depth was also measured on 29th October 1984 and 27th March 1985. This shows that displacement of dam is taking place both along the dam axis as well as in upstream downstream direction.

A close look of Fig. 8 indicates that height wise, there are three distinct regions so far as horizontal movement is concerned. One is from top of dam to 4 m depth, second is 4 m to 10 m depth and third is 10 m depth to bottom most anchor point in foundation. In second zone, there is practically no movement either along the axis or perpendicular to it. In first region (top 4.0 m), downward movement of about 1.5 cm is recorded after 4 months of reservoir filling but it has returned to normal position by Sept. 1985 confirming that there is no downward movement. Similar is the trend for movement along dam axis in this region. However, in region 3 (10 m from top until foundation), maximum downward movement of the order of 4 cm from normal has been recorded after 10 months of filling (29th October 1984) which has subsequently reduced to 2.0 cm after one year (29th Sept. 1985). The movement towards diversion canal is increasing with time and has attained deflection of the order of 6.0 cm.

Normally no lateral movement should be expected and the behaviour of inclinometer readings in third zone needs further investigations.

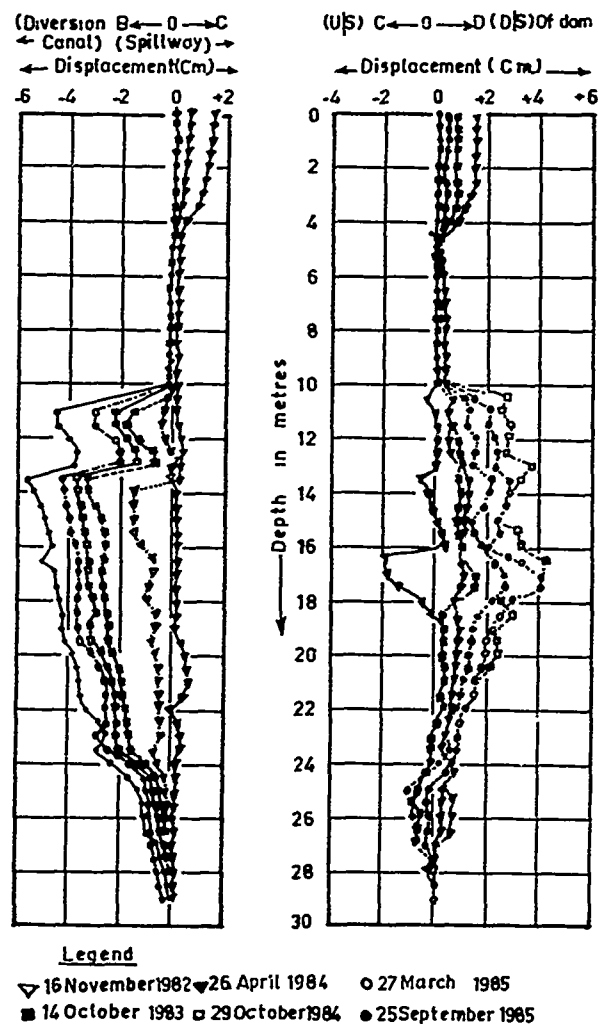


Fig. 8 : Observational Data for Horizontal Movement  
ELECTRICAL ANALOGY EXPERIMENTAL RESULTS

#### Experimental Set Up

With a view to find answer for the fallacy in the observational data of foundation piezometers FHP1 to FHP5 and to determine the efficacy of grouting, electrical analogy experiments using conductive tray were performed. The conductivities of four different electrolytes representing four different permeabilities in four zones (Table-4) were obtained by mixing sodium chloride in distilled water or tap water depending upon the range of conductivity. It was observed that maximum change in the conductivity of electrolyte for clay core prepared in distilled water, was 7.4% during experimentation and thus electrolyte can be said to have remained stable even though the range of maximum conductivity was 300 times that of minimum tested conductivity.

The tests were conducted for six conditions of grout curtain efficiencies viz. (i) 100% effective, (ii) 75% effective, (iii) 50% effective, (iv) 25% effective, (v) grout curtain completely ineffective and (vi) grout curtain as well as consolidation grout completely ineffective. First case was represented by using perspex sheet showing grout line whereas for fifth and sixth case, no perspex sheets were used. For other cases, corresponding percent area of perspex sheet was perforated to

Table 4 - Permeabilities and Conductivities of Different Zones

| Zone                   | Permeability(k)<br>(cm/sec) | Relative<br>K | Conductivity<br>micro mho |
|------------------------|-----------------------------|---------------|---------------------------|
| Clay core              | $6 \times 10^{-6}$          | 1 K           | $5.0 \times 10^2$         |
| Consolidation grouting | $5.6 \times 10^{-4}$        | 100K          | $5.0 \times 10^4$         |
| Foundation             | $1 \times 10^{-3}$          | 200K          | $10.0 \times 10^4$        |
| Downstream filter      | $1.8 \times 10^{-3}$        | 300K          | $15.0 \times 10^4$        |

Table 6 - Model Test Results with Variable Permeabilities in Consolidation Grouting Zone

| Tip No. | El. | Pore pressure of Relative Permeability of consolidation grout zone(%) |     |      |      | Observed pore pressure (%) |
|---------|-----|---|-----|------|------|----------------------------|
|         |     | 10K   | 50K | 100K | 200K |                            |
| FHP1    | +28 | 91  | 91  | 90   | 87   | 51                         |
| FHP2    | +28 | 50  | 54  | 55   | 50   | 35                         |
| FHP5    | +28 | 14  | 14  | 15   | 13   | 30                         |
| FHP3    | +25 | 37  | 42  | 45   | 39   | 43                         |
| FHP4    | +21 | 36  | 38  | 46   | 35   | 53                         |

Table 5 - Percent Grout Efficiency and Percent Observed Pore Pressures for Foundation Tips FHP to 1 FHP5

| Tip No. | Elevation | Observed Pore Pressure March 1985 |     | % Pore Pressures from Model Experiments Efficiency |     |     |     |            |                              |
|---------|-----------|-----------------------------------|-----|--|-----|-----|-----|------------|------------------------------|
|         |           | (m)                               | (%) | 100%   | 75% | 50% | 25% | No curtain | No curtain, No consolidation |
| FHP1    | +28       | 15.6                              | 51  | 90   | 89  | 90  | 90  | 88         | 89                           |
| FHP2    | +28       | 12.0                              | 35  | 55   | 58  | 60  | 70  | 74         | 79                           |
| FHP5    | +28       | 11.0                              | 30  | 15   | 17  | 20  | 25  | 36         | 65                           |
| FHP3    | +25       | 16.8                              | 43  | 45   | 62  | 65  | 70  | 76         | 80                           |
| FHP4    | +21       | 24.0                              | 53  | 46   | 58  | 60  | 70  | 80         | 82                           |

represent the efficacy of grout curtain. For example for case (ii), to represent 75% effectiveness of grout curtain, 25% area of perspex sheet was punctured by equi-spaced small holes.

#### Analysis and Comparison of Experimental Data

Electric potentials of grid points were obtained using wheat stone bridge for all the six cases and equipotential lines were drawn(not shown here because of paucity of space). From these equipotentials, percent potentials at location of piezometers FHP1 to FHP5 were determined for all six cases of grout efficiency. Using observational data on prototype of these piezometers, the relationship of percent grout efficiency and percent pore pressures are worked out in Table-5 and plotted in Fig.9. The model test results shown in Table-5, are for relative permeabilities of clay core, consolidation grout zone and foundation zone as K, 100K and 200K respectively.

From Table 5, it is seen that percent pore pressures of FHP1 from model studies are almost constant for various cases of grout efficiencies and are of the order of 90% irrespective of the fact that even if the grout curtain as well as consolidation grout is fully ineffective where as observed pore pressure in field is only 51%. This observed value seems to be too low and is not explainable even by model test results. Recording of low observed values may be either due to malfunctioning of tip or due to creation of some what impervious zone due to grouting around the tip. Observed pore pressure of FHP2 located downstream of grout curtain, is of the order of 35% whereas those observed on model, vary from 55% to 79%. The pore pressures as observed in the model are increasing as the efficiency of grout curtain is increasing. Reasons for low observed pore pressures recorded by tip no. FHP2 may be the same as for FHP1. Perhaps consolidation grout is very effective below dam core. Observed pore pressure of piezometer no. FHP5 located at same elevation as that of tip no. FHP1 and FHP2 (+28.0m) is of the order of 30% whereas those observed on model, vary from 15% to 65%. If it is presumed that actual field observation is correct, it may be concluded that grout curtain is efficient only to the extent of 21%

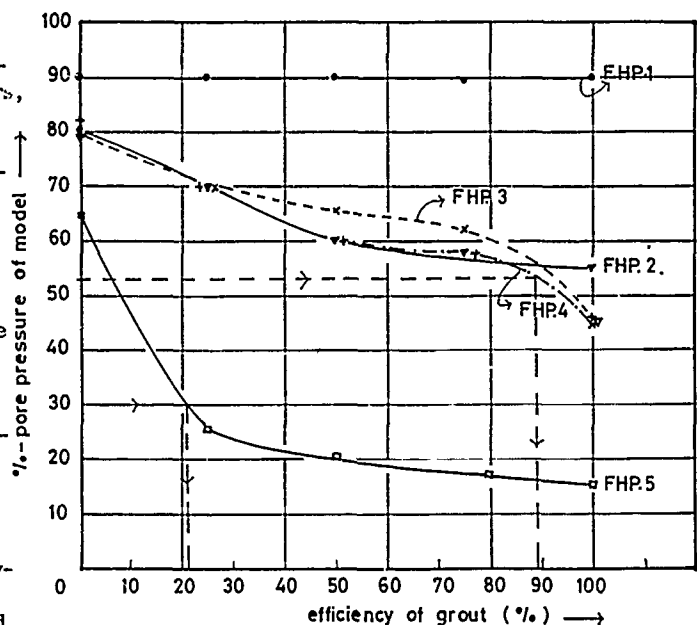


Fig.9 : Grout Efficiency vs Percent Pore Pressure

(Fig. 9). Reason for higher observed pore pressures in this tip, may be poor quality of consolidation grouting in this region. Permeability of foundation varies from  $7 \times 10^{-5}$  cm/sec. to  $0.84 \times 10^{-3}$  cm/sec and the assumption of average permeability of consolidated area as  $6 \times 10^{-4}$  cm/sec (100K) uniformly throughout, may not be correct.

To explore this matter further, model studies were extended with relative permeability of 10K, 50K, 100K and 200K in consolidation grout zone and 100% grout curtain efficiency and the results of these studies are shown in Table-6.

From Table 6, it can be seen that percent pore pressures from test data for all the tips are practically of the same order for different permeabilities in consolidation grout zone indicating thereby that if permeability in consolidation zone is taken uniform, by and large, there is no significant change in pore pressures recorded by foundation piezometers.

Percent pore pressures measured by piezometer tip no. FHP3 from model increases from 45 to 80% as the grout curtain efficiency decreases (Table-5) whereas observed pore pressure is 43%. Thus it can be said that efficiency of grout curtain is almost 100%. Similarly percentage of pore pressure measured by FHP4 (located also in the downstream of grout curtain at El. +21.0) from model studies, increases from 46 to 82% with decreasing efficiency of grout curtain. Observed pore pressure is 53% which corresponds to 89% efficiency of grout curtain (Fig. 9).

Keeping in view the readings recorded by tips in foundation, it can be said that both grouting viz. consolidation as well as curtain, are by and large successful at Rarem Dam.

## CONCLUSIONS

Based on the observational data of instrumented Rarem dam and the electrical analogy model studies, following conclusions are drawn:

- i) Bishop's type twin tube hydraulic piezometers are more sturdy and reliable as compared to Carlson type electrical resistance and strain gauge type piezometers.
- ii) At Rarem dam, the recorded construction pore pressures are of very low magnitude even though the core comprises of highly plastic clay.
- iii) The steady seepage pore pressures have developed almost simultaneously with reservoir filling with practically no time lag.
- iv) Major settlement has coincided with construction of dam and reservoir filling. Total settlement of 30 cm has taken place which is 50% of anticipated settlement. No further settlement is expected in future.
- v) There is no movement in direction perpendicular to dam axis. Whatever initial movement was there during initial reservoir filling, the same has been recovered back. However, there is some evidence of little movement along dam axis towards diversion canal side.
- vi) Electrical analogy model studies coupled with observational data of piezometers in foundation, have indicated that grouting done at Rarem dam is effective.

## REFERENCES

- Cassagrande, A. (1961), 'Control of Seepage Through Foundation and Abutments of Dam' First Rankine Lecture, Geotechnique, Vol. X. No. 3.
- Hari Krishna & Goel, M.C. (1978), 'Pore Pressure Observation and Efficiency of cut-off Walls at Obra Dam', IGJ Vol. 8, No. 3, July 1978.
- Hill, J.W. (1948), 'Estimating Construction Pore Pressure in Rolled Earth Dams' II ICSMFE Vol. III, pp. 234-240.
- Mudjihardjo, Djoko (1986), 'Analysis of Pore Pressure and Soil Movement Observational Data of Rarem Dam, North Lampung, Indonesia', M.E. Dissertation, WRDTC, UOR, Roorkee, Nov. 1986.

# Colbond Drains for Rapid Consolidation at Manggar Besar Dam

**M.C. Goel**  
Superintending Engineer, Investigation and Planning Circle (WB),  
Roorkee, India

**J.L. Surabaya**  
Malang, Indonesia

**Achmad Zainiko**  
Malang, Indonesia

**SYNOPSIS:** 7.3 m high and 280 m long Manggar Besar homogeneous earthen dam resting on 12.0 m thick soft silty clay, is under construction to supply water to the city of Balikpapan in Kalimantan island of Indonesia. To accelerate the anticipated 1.6 m settlement of dam, 30 cm wide strip type drains (Colbond CX 1000) using polyester non-woven fabric are being used 3 m centre to centre. It is expected that 70 percent consolidation shall take place within thirteen months of construction by these drains.

## INTRODUCTION

The drinking water requirement for Balikpapan city located in east Kalimantan island of Indonesia is forecasted for 2000 AD based on 1980 census (1,09,900 persons) with a growth rate of 5.3 percent per year assuming that each house and yard connection would serve one family of eight persons. Water consumption for each house and yard is expected to increase from 145 to 160 and 60 to 90 litres per day respectively during 1985-2000. Water requirement for industrial purposes and for other public purposes such as schools, hospitals, offices etc., has been assumed to be 20 percent of total domestic water consumption. Due to limited availability of water, 60 percent of population would be served by Balikpapan water supply project, 30 percent by Pertamina water supply project and balance 10 percent by shallow wells.

Balikpapan water supply system comprises, (i) a storage dam on Manggar Besar river to supply raw water throughout the year, (ii) raw water intake stations on Klandasan and Manggar Besar rivers, (iii) a treatment plant with a nominal design capacity of 400 lps, and (iv) distribution system. The catchment area of Manggar Besar reservoir is 48.5 sq. km. with an average rainfall of 230 mm/month.

Manggar Besar homogeneous earth dam is 7.3 m high and 280 m long requiring 100,000 m<sup>3</sup> of fill material to bridge the valley. 4.0 m high, 600 m long dyke requiring 10,000 m<sup>3</sup> of fill material is also constructed on the left bank of river.

## GEOLOGY AND SOIL INVESTIGATIONS

### Foundation

Based on subsoil investigations conducted from December 1978 to October 1982, geological formation in foundation along dam axis is shown in Fig. 1. From this figure it can be seen that foundation comprises the following three layers:

- i) A soft silty clay stratum of 12 m in the centre of flood plain and of 5.0 m on the hill sides (called soil type A).
- ii) A stiff clay layer (called soil type B) below soil type A with a thickness of 4.0 m in the centre of flood plain

and of 2 to 3 m on hill side.

- iii) A very stiff clay or dense silty sand (soil type C) below soil type B.

It implies that main dam is founded on very compressible soft silty clay. After construction of dam overall settlement in foundation is expected to be 1.75 m in a period of 270 years out of which 1.6 m is expected to take place in first 27 years.

### Fill Material

There are two borrow areas for embankment fill material. Borrow area I situated 500 m away from dam site comprises hard and stiff silty clay with some sand and gravel. Optimum water content for proper compaction (95 percent of Proctor's density) has been assessed at 25 percent on an average giving dry density of 1440 kg/m<sup>3</sup> and permeability of the order of  $6 \times 10^{-8}$  cm/sec. Borrow area II is situated just adjacent to dam site comprising silty clay layer (18,000 m<sup>3</sup>) similar to borrow area I. Clayey sand (55,000 m<sup>3</sup>) is also available at this site.

## DESIGN CONSIDERATIONS FOR DAM SECTION

The elevation of the valley at dam alignment is 0.5 mMP and the height of dam is 7.3 m. Dam has been designed at full supply level of 4.0 mMP (FSL I) during the period when subsoil is not yet sufficiently consolidated to withstand the higher water level. This will last for about 5 years after completion of works. After this, spillway gates will become operational and full supply level will be maintained at 5.8 mMP (FSL II). The top of the dam would be constructed at 9.4 mMP after taking into account settlement of 1.6 m (0.5 mMP + 7.30 m + 1.6 m).

To speed up the consolidation process, vertical drains have been provided in the foundation. The top width of dam is 4.5 m and the design side slopes are 3 H : 1 V but during the construction stage when consolidation has not yet been completed, side slopes would be 2.4 H : 1 V. Two berms each of 5.0 m width have been provided at ultimate design elevation of 4.9 mMP. As natural stone for rip rap is not available in Balikpapan area at reasonable cost, upstream slope is being protected by sand cement bags consisting of gunny bags filled

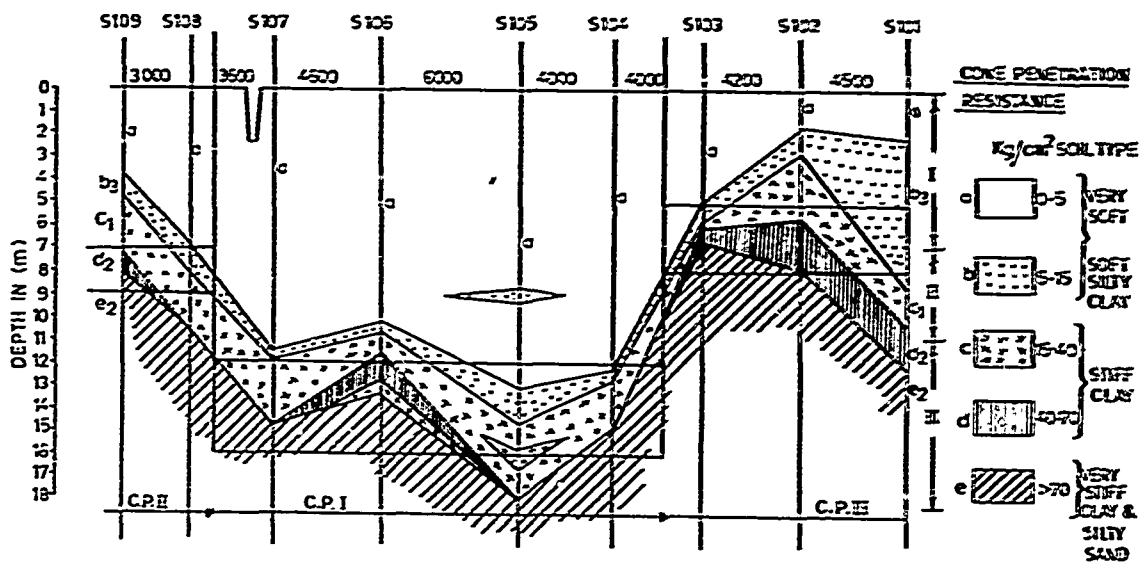


FIG. 1. GEOLOGICAL FORMATION DETAILS IN FOUNDATION ALONG AXIS OF MANGGAR BESAR DAM

with one volume of cement with six volumes of sand. A typical cross-section of dam is shown in Fig. 2.

Three stages are considered for stability analysis of embankment. Stage I refers to end of construction stage when embankment is constructed upto top (9.4 mMP) with no consolidation, no earthquake and no drawdown. The aimed factor of safety against sliding is 1.0 for this stage. Stage 2 refers to one year after completion when 70 percent consolidation has taken place and dam top is at 8.5 mMP. At this stage, factor of safety of 1.5 is required for normal steady seepage condition (FSL I at 4.0 mMP). With earthquake (0.1 g) or rapid drawdown, factor of safety of 1 was aimed at. Stage 3 is the final condition when 100 percent consolidation has taken place attaining crest level of 7.80 mMP and full supply level at 5.80 mMP (FSL II). The desired factors of safety in this stage, are the same as for stage 2.

#### DESIGN OF VERTICAL DRAINS

##### Various Alternatives

For structures resting on compressible soils with large foundations, such as dams, the usual practice is to consolidate the soft foundation strata in the minimum possible time by providing suitable drainage, as piles, wells and casons are uneconomical. Earlier practice was to form sand columns by filling sunken lost head casing with coarse sand and subsequently withdrawing the casing. Lost head driven casing was replaced by jetting because the former has adverse effect on horizontal flow of excess pore water towards drain due to densification and remoulding of soil around driven casing.

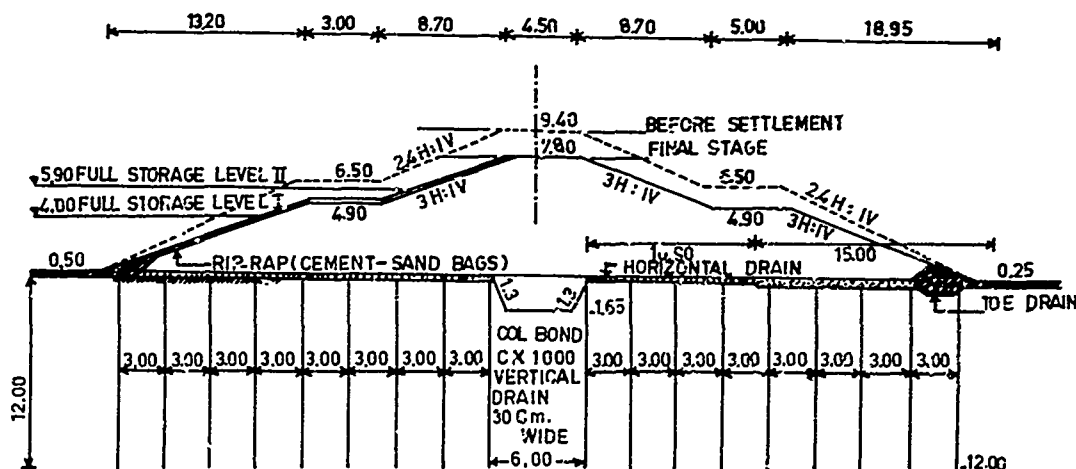


FIG. 2 TYPICAL CROSS SECTION OF MANGGAR BESAR DAM

Parallel to the development of sand drain, Bjellman (1951) developed strip type of cardboard vertical drain of size 4x140 mm. Bjellman method is based on the assumption that the drains are placed in a regular pattern and that each drain serves a cylindrical soil column of exactly the same length as the drain. It is assumed that (i) the increase in vertical load is evenly distributed over the consolidation area, (ii) horizontal layers remain horizontal throughout the consolidation process, (iii) permeability of cohesive soil, remains unchanged throughout consolidation process, and (iv) internal resistance of drain is negligible. The formula for design of strip drains is as under:

$$t = \frac{D^2}{8C_h} \times \log_e \left( \frac{1}{1-U_h} \right) \quad (1)$$

where,

$t$  = consolidation period in years

$D$  = diameter of drained soil cylinder (m)

= 1.05  $S$  for triangular grid spacing of drains (1a)

= 1.125  $S$  for square grid spacing of drains (1b)

$S$  = centre to centre spacing of drains

$C_h$  = horizontal consolidation coefficient ( $m^2/year$ )

$$\alpha = \frac{n^2}{n^2-1} \left[ \log_e(n) - \frac{3}{4} + \frac{1}{n^2} \left( 1 - \frac{1}{n^2} \right) \right] \quad (1c)$$

$n = D/d$

$d$  = equivalent diameter of drain (m)

For prefabricated drain installations, usually  $D/d > 5$  and the term  $n^2/(n^2-1)$  and  $\frac{1}{n^2} \left( 1 - \frac{1}{n^2} \right)$  in Eq. (1c), approaches 1 and 0 respectively and hence Eq. (1) reduces to

$$t = \frac{D^2}{8C_h} \left[ \log_e(D/d) - 3/4 \right] \cdot \log_e \left( \frac{1}{1-U_h} \right) \quad (2)$$

For the purpose of calculations, of equivalent drain diameter, the drain is assumed cylindrical. For strip type drain, the draining effect depends upon absorbent surface i.e. the periphery. The effective periphery of strip type drain is  $2 \times \text{width} \times f$ , where 'f' is correction factor allowing for (i) less favourable inflow of water to the drain because of rectangular section, and (ii) a possible disturbance due to densification and remoulding of the soil when installing the drain.

Based on the theoretical approach discussed above, design monograms for 10, 15 and 30 cm wide Colbond drains are given in Fig. 3.

#### Strip Drains for Manggar Besar Project

Tests under semifield conditions were carried out by Royal Adrain Walker Group Akzo Research under supervision of Delft Laboratory of Soil Mechanics, Netherland to decide the best design of drains for Manggar Besar project. Hence the drainage effect of 30 cm wide Colbond drain was compared with that of traditional sand drains under 3 m layer of sand with base area of  $20 \times 80 m^2$ . The area was split up into four sections of equal sizes, three of which were provided with Colbond drains at different spacings and fourth for conventional sand drains. From measurements of 40 settlement plates and piezometer readings taken for 600 days, it was concluded that Colbond drains accelerated consolidation process at least as much as that from traditional sand drains. Tests conducted on 4 mm thick KP 650

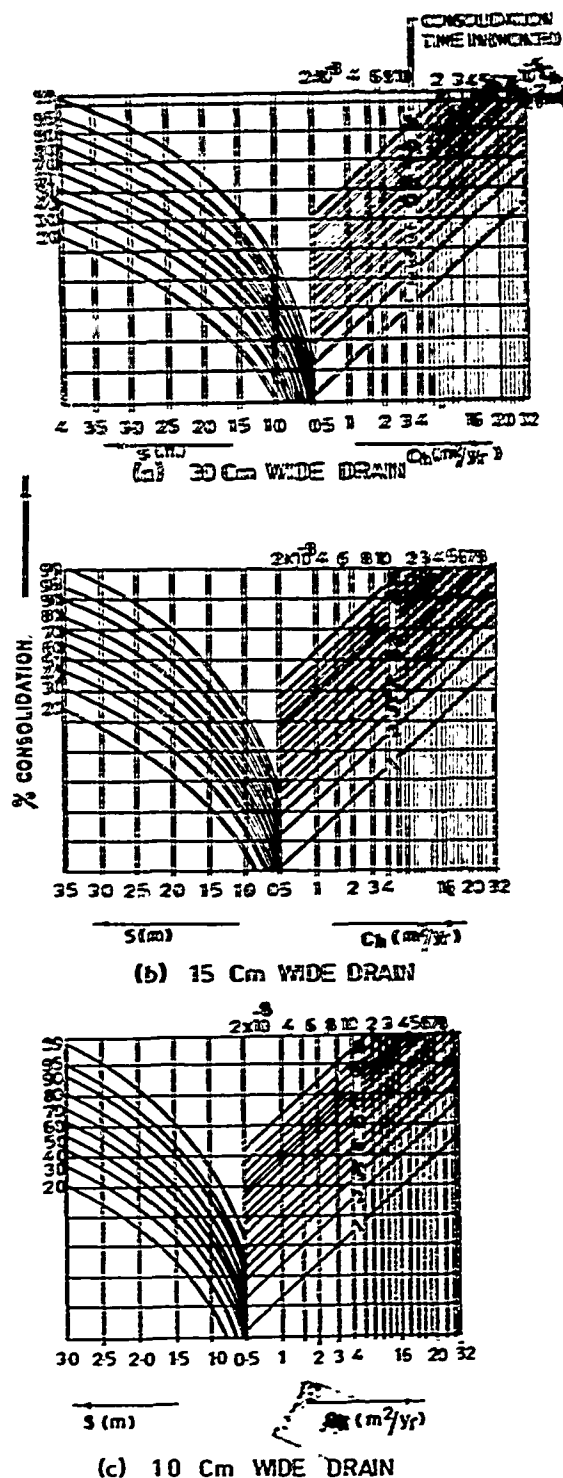


FIG. 3. DESIGN MONOGRAMS FOR COLBOND DRAIN

Colbond drains (polyester non-woven fabric) indicated some problem of reduction in drainage capacity in case of thick deposits of compressible layers. To produce a drain suitable for use in thick deposits, the drain was modified by (i) increasing the thickness to 5 mm, (ii) making core more coarser and (iii) improving its rigidity. This modified drain is named as CX1000 and retains 80 percent of its original volume under 3 kg/cm<sup>2</sup> pressure.

Laboratory tests on soft silty clay in foundation of Manggar Besar project has shown that on an average the value of horizontal coefficient of consolidation ( $C_h$ ) is 2.4 m<sup>2</sup>/year. The total base area of dam is 18725 m<sup>2</sup> and 70 percent consolidation is to be attained in 13 months period after construction of dam. Using design monograms given in Fig. 3, it was found that for 10, 15 and 30 cm wide CX1000 Colbond drains, the spacing required is 2.527, 2.673 and 2.989 m respectively and the corresponding number of drains are 2932, 2621 and 2096 respectively. This shows that number of 10 cm drains would be 1.4 times that for 30 cm wide drains. For Manggar Besar dam, Colbond CX1000, 30 cm wide drains at 3m centre to centre spacing were adopted.

#### CONSTRUCTION OF COLBOND DRAINS

##### Preparation of Area

Temporary cofferings were provided on left and right side of the river by making 1.5 m high dykes with side slopes of 1H:1V and area dewatered by six pumps. Then top soil was removed and the material dumped in spoil dump area located at 1.5 km downstream of dam. This was backfilled by stiff clay and work was done by machines. Horizontal trenches (100 x 100 mm) were excavated, along the path of vertical drains manually. For preparation of area, following equipment was used:

|              |                    |         |
|--------------|--------------------|---------|
| Bulldozer    | 15t                | 1 unit  |
| Swamp dozer  | 13t                | 1 unit  |
| Wheel loader | 1.3 m <sup>3</sup> | 1 unit  |
| Backhoe      | 0.7 m <sup>3</sup> | 1 unit  |
| Dump trucks  | 8t                 | 6 units |

##### Choice of Equipment and Installation of Drains

After taking into account relative merits and demerits of different construction equipment, it was decided that Colbond CX1000 30 cm vertical drains be installed by vibrations using light dragline and mandrel. For this, the following equipment was required.

|   |         |        |
|---|---------|--------|
| Dragline and attachment (drawler crane) | 30t     | 1 unit |
| Vibrohammer                             | 4.8t    | 1 unit |
| Mandrel                                 | 13.5m   | 1 unit |
| Generator set                           | 250 KVA | 1 unit |

For easier movement, generator set required for vibrohammer was fitted with crawler crane unit. Rolls of Colbond CX1000 were fitted to the front of crawler crane. Mandrel was prepared at job site and its details are shown in Fig. 4. Colbond drain was fitted to the shoe of mandrel to be left in situ after pushing the drain upto required depth of vibrations and then mandrel was withdrawn. After installation of vertical drain, it was cut off about 20-30 cm above ground surface level of horizontal drain and the trench of the same was filled manually by sand of suitable grade.

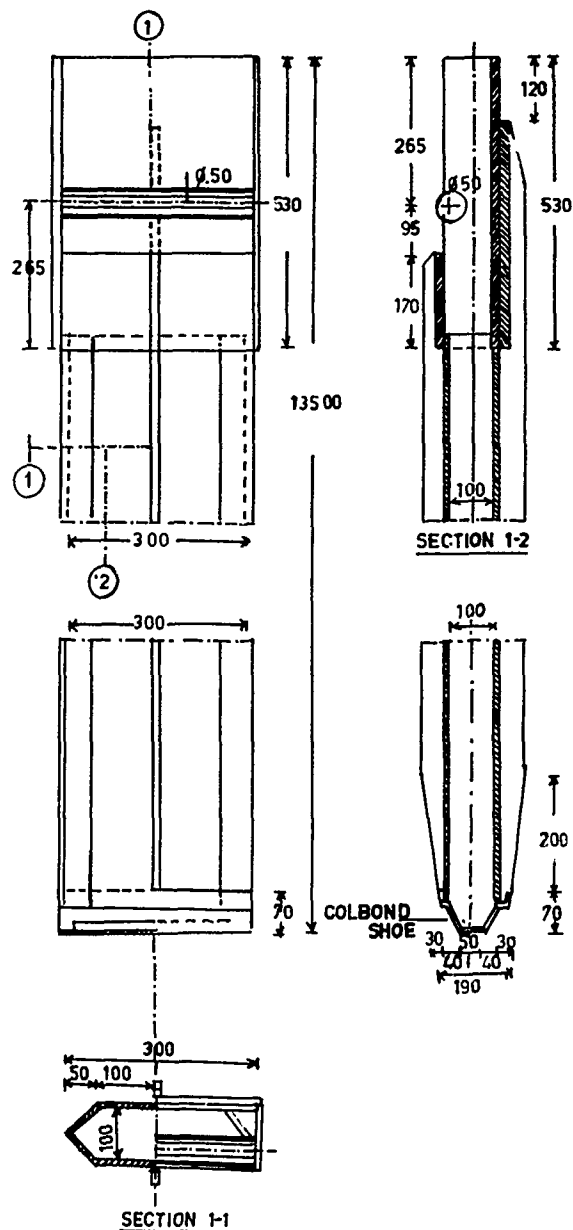


FIG.-4 MANDREL DETAILS

#### CONCLUSION

To accelerate the consolidation process of 12.0m thick soft silty clay foundation layer of 7.3m high Manggar Besar dam, Colbond CX1000-30 cmx5mm polyester non-woven fabric, 2096 nos. vertical drains have been provided which are 3m centre to centre spaced in square grid. These drains have been installed by light weight crawler crane using vibro hammer and mandrel.

#### REFERENCES

- ACHMAD ZAINIKO(1986) - Report on Social Problem 'Vertical Drains of Manggar Besar Dam Project', M.E. WRDTC, 1986.
- Kjellman, W. (1948), 'Accelerating Consolidation of Fine Grained Soils by Means of Card Wicks' 2nd ICSMFE, Rotterdam.



# Problems and Behaviour of a Dam Founded on a Weak Zone

**K.V. Rupchard**

Executive Engineer/Civil, Tamil Nadu Electricity Board, Madurai,  
India

**SYNOPSIS :** Any fault in the foundation of a dam presents a problem which has to be tackled in the proper way considering many aspects. This paper deals with such a foundation problem faced at Upper Aliyar Dam in South India in the shape of a weak zone. Several alternatives were thought of for tackling the weak zone. Ultimately a simple concrete plug with cut-offs was adopted considering the limited working season available and the fairly good in-situ compressive strength of the weak material. This was in preference to a raft foundation or a massive arch.

The methods adopted for tackling the problem have been elaborated. The performance of the dam during the past more than 20 years has been quite satisfactory considering that no leakage or settlement has occurred after the treatment of weak zone. The conclusions reached at the end provide significant points in the field of geotechnical engineering.

## INTRODUCTION

### General

Dams to impound water and use it for generation of electricity are the most important structures in Hydro Electric Projects. The criteria for fixing the locations of dams are storages required and Geological aspects. But, due to other considerations, dams are located at places not so ideal. Very often, numerous foundation problems are encountered while building dams at such locations. Faults at dam sites present the most difficult problems. This paper deals with the foundation problem faced at Upper Aliyar Dam in South India, the methods adopted for tackling the problem and the behaviour of the dam after construction.

### The Project

The Parambikulam-Aliyar Project in South India is a multipurpose project for development of irrigation and power. This composite project consists of several dams, tunnels and hydro-electric power houses. The project works were started in 1962 and completed in 1972. The project lies at about longitude 77° and latitude 10°. One of the key structures for this complex project is the Upper Aliyar Dam. This dam is the head-works of the Aliyar Power House (60 MW).

The Upper Aliyar Dam of this project has been integrated with the Kadamparai Hydro Electric Project under construction now. The Kadamparai Project is a mammoth pumped hydro electric project (400 MW) with reversible turbines, the first of its kind in Asia. Hence, the Upper Aliyar Dam is a very crucial component catering to two projects.

### Upper Aliyar Dam

Upper Aliyar Dam is 300 m long, 80 m high

and was constructed from 1962 to 1969. This dam is of solid gravity type and is built of random rubble masonry totalling 280,000 m<sup>3</sup>. It intercepts a catchment area of 105 km<sup>2</sup>. The spillway provided in the dam is designed for a maximum flood discharge of 1540 m<sup>3</sup>/sec.

The dam was located at the present site considering the storage required and geological aspects based on the preliminary investigations.

## FOUNDATION FOR DAM

### Geology

The rock types exposed in and around the dam site are hornblende biotite gneisses and charnockites belonging to the Archaeans of South India. The gneisses are pink in colour and medium grained. The foliation trend is N 60 W-S 60 E, the dip being 27° in S 30° W. The rocks are generally fresh but jointed. Close fracturing is also noticed in the pink granite gneisses of the left flank. The joint patterns in gneisses observed at the dam sites are as in Table 1.

**TABLE 1. Joint Pattern in Gneisses**

| Sl. No. | Trend             | Direction | Remarks                         |
|---------|-------------------|-----------|---------------------------------|
| 1.      | East-West         | Vertical  | ---                             |
| 2.      | N 60° W - S 60° E | -do-      | Almost parallel to river course |
| 3.      | N 10° W - S 10° E | -do-      | ---                             |

Outcrops of granite gneisses were exposed in the right flank as well as in the river section.

The left flank was covered with soil. The straight course along which the river flows in the vicinity of the dam site possibly indicated that the deep channel might lie along the weak zone.

#### Exploratory Drilling

A number of bore holes were drilled in the river bed on the left flank. This established the existence of a 30 m wide shear zone close to the left flank. The trend of the shear zone is parallel to the foliation in the gneisses. The shear zone was more than 30 m in the middle reaches and gradually decreased to 12-15 m on either side. The sheared material comprised of pink granite gneisses and pegmatite in the top portion and schistose material at depth. It was indicated that this reach containing weak zone was not suitable for construction of a masonry dam, the core recoveries from the bore holes being poor, ranging from 0% to 15%.

#### Weak Zone

The longitudinal section across the weak zone is shown in Fig.1.

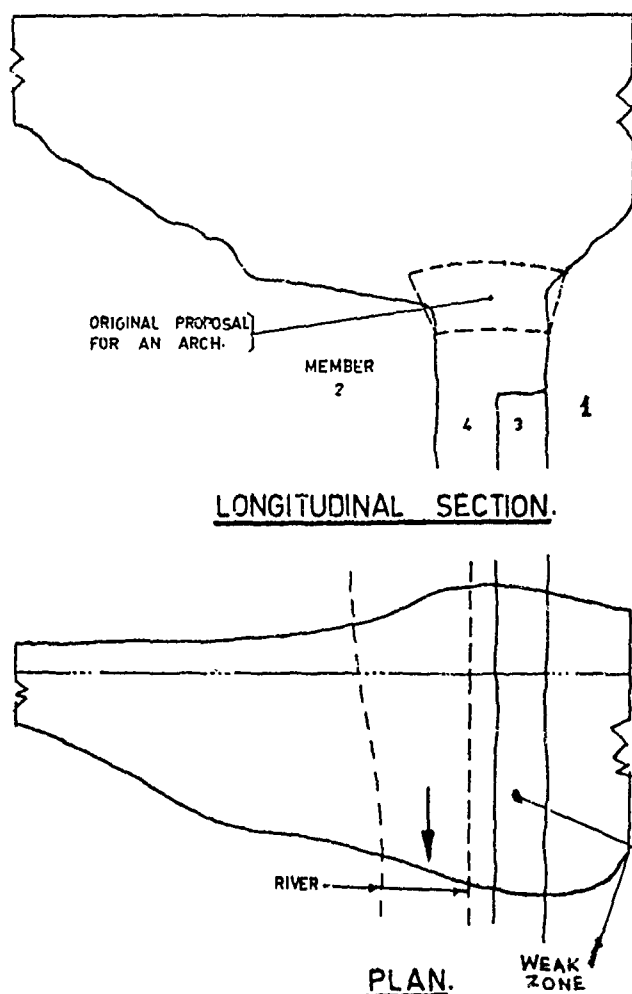


Fig.1  
UPPER ALIYAR DAM

For easy recognition of the different types of strata met with, the sections were indicated as Member 1,2 etc. The numbering of the members is in the descending order of their apparent strength. Member 1 was the strongest and Member 4 the weakest.

Member 1 and 2 on either side of the weak zone were sufficiently strong and solid. There was a sub-fault inside the major fault. Member 3 represents the base of the wider fault and is of fractured rock. Member 4 was the weakest, consisted of crushed pegmatite and appeared to extend very deep. The bearing capacities of Members 3 and 4 were quite adequate to found the dam. But the geological opinion necessitated the study of the percolation before proceeding further.

#### TREATMENT

##### Influencing Factors

The weak zone was located in the river bed and was excavated upto 24 m below the river bed. The water diversion arrangements during the work consisted of coffer dam which could be designed only for moderate floods. Hence, during flash floods, there was the threat of the river water spilling over the coffer dam and inundating the entire weak zone area. Such sudden flooding was dangerous to the safety of the men working. In addition, such a flooding brought forth in its wake, thousands of tonnes of debris and slush which had to be removed all over again after the flood subsided.

Also, Member 1 on left flank was over-hanging by as much as 9 m at some places, threatening to collapse due to exposure.

In view of all these reasons, any treatment to be given to the weak zone had to be done with utmost expedition. The dam area was prone to monsoon floods and the working season was restricted to about 6 to 8 months only in a year. Hence the method of treatment had to be evolved considering these restrictive factors.

##### Initial Proposals

One of the alternatives suggested was a reinforced concrete raft to spread the superimposed load for limiting stresses to about  $0.7 \text{ t/m}^2$ . But this idea was dropped considering the actual disposition of the various members in the weak zone.

The second alternative was to span the weak zone with a massive reinforced concrete arch to transfer the weight of the dam to the sides. This alternative was also considered not suitable due to the following reasons:

- Time required for such a treatment was more than the working season available to avoid flooding of the weak zone and consequent loss of time and money.
- Portion of the arch had to rest on the jointed rock Member 3. Heavy cutting to the extent of 5 m was required and this could not be done by the normal method of blasting, but only by chipping and wedging (requiring considerable time).

- c. The arch would require blasting of Members 1 and 2, thereby shattering the foundation rock.
  - d. Even the arch would require a concrete fill to prevent percolation.
  - e. The materials of Members 3 and 4 were strong in-situ requiring only confinement.
- Hence, the idea of arch was dropped.

#### Further Approach

It was found that the bearing capacity of the weak zone Member No.4 was a significant factor while deciding the exact course of treatment to be given to the weak zone. Hence, load-bearing tests were conducted at site. It was found that the weak zone Member 4 was capable of taking a load of more than  $260 \text{ t/m}^2$ , in-situ.

Another important factor was the permeability of Member No.4. Field tests were conducted and it was found that the permeability factor was within reasonable limits and was not large enough to cause any anxiety.

#### Final Decision

After the conclusive evidence of favourable values of bearing capacity and permeability of Member No.4, it was decided to merely plug the weak zone with concrete just as any other fault. The final decision was arrived at based on the opinion of several senior engineers. It was considered that the mass of concrete fill can be expected to act together as flat arch and distribute the load properly.

#### Precautions

Having decided to merely plug the weak zone with concrete, the following precautions were taken:

##### a. Construction Joints

It is the practice to provide construction joints at about 30 m intervals to take care of settlement etc., in dams built of random rubble masonry.

Originally, it was decided to locate one of the construction joints in a portion over the weak zone. It was considered that it is advisable to have construction joints on either side of the weak zone so that a single block of masonry would rest monolithically over the weak zone and any settlement of weak zone would not affect the adjacent blocks later. The normal spacing of construction joints was 30 m. In this case, this was increased to about 40 m so that a separate block of masonry exists over the weak zone.

##### b. Clay Blanket

A clay blanket for a length of about 30 m was provided on the upstream side of the dam in order to increase the percolation path.

##### c. Cut-offs

Deep cut-offs were provided both on the upstream and downstream side of the weak zone. These served the twin purposes of increasing the percolation path and also of confining the weaker material.

##### d. Gallery

A transverse drainage gallery was provided in such a way that it would run along the weak zone so that drilling of bore holes and grouting for consolidation can be done easily. Also, the rate of leakage (percolation) could be gauged later.

##### e. Shear Reinforcement

It can be seen from the Fig.1 that Members 1 and 3 were overhanging and it was difficult to provide for the normal jagged features required for the foundation of a dam. Hence, there was necessity to increase the shear or sliding resistance of the concrete over rock. This was achieved by provision of reinforcement in many shapes and sizes covering the surface of the weak zone members and also properly anchoring the reinforcement mat and propping from suitable places. The design of reinforcement was empirical. Incidentally, the props considerably reduced the fear of collapse of the overhanging ledge rocks on either side of the weak zone.

##### f. Grouting

The block containing the weak zone was grouted extensively. The grout curtain at the heel of the dam consisted of 40 holes in 3 rows, 18 to 30 m deep. The consolidation holes from the axis to toe of dam (numbering 90) were 6 to 18 m deep. The entire grouting operation was done extensively and meticulously after elaborate air and water tests.

#### PERFORMANCE

The Upper Aliyar Dam and its various components are being examined periodically according to a schedule of maintenance. The observation of leakage from drainage gallery is one of the aspects observed. The construction joints are also examined visually. It has been observed that the condition of the dam is quite stable, particularly in the weak zone area. The dam is in service for the past 20 years and there has been no untoward development. Hence, the treatment given to the weak zone must be considered satisfactory and adequate.

It has been the practice to plug the weak zones with mere concrete at most of the sites. This treatment was found quite satisfactory. But, in the instant case of Upper Aliyar Dam, the major difference in the situations is the enormous width of the weak zone which caused doubts about the efficacy of treating it with mere concrete plug, to serve as a flat arch.

#### DISCUSSION

##### Investigation

The admissible extent of investigations depends in part on the magnitude of the project and in part on how obvious the sub-surface conditions are. Considering the successful treatment of the weak zone, the investigations done at Upper Aliyar Dam can be reckoned as adequate.

### Treatment of Faults

Creager et al. state that "most unweathered cemented rocks possess sufficient strength to support dams of usual height. However, special consideration should be given to rocks in which seams or faults and weathered or crushed zones have resulted in separated or partly separated foundation blocks which might move slightly as a whole under the load of the dam.

"Narrow seams and faults frequently can be washed out and grouted. For wide seams the gouge, weathered or broken rock, or other material which fills them, can be excavated and the seams refilled with concrete".

"For low dams, small areas of relatively weak rock are sometimes left in place on the assumption that the dam will span over them. In several cases, vertical transverse faults of considerable size have been cleared out and filled with concrete for a depth only sufficient to provide an arch to span the opening, care being taken, of course, that the excavating or grouting extends far enough to obtain a tight cut-off at the upstream side".

### Faults in Seismic Areas

While treating the subject of design of dams for faults with reference to earth quakes, Creager et al. state that "a dam built across a fault on which slippage occurs may be subjected to an immeasurable force, and disruption can be avoided only by providing sufficient flexibility to absorb the motion without damage. Dam foundation crossed by active faults should be avoided. Fault movement is not necessarily confined by the fault on which the earth quake originates, but secondary movements may occur on any active fault in the disturbed area. It is not possible to insure that any prominent fault, although apparently dead, may not be subjected to some movement during an earth quake. However, secondary fractures bearing no evidence of movement in recent geological times, involve with danger. Slight movements are not necessarily disastrous".

The design of Upper Aliyar Dam was not made considering any forces due to earth quakes as the region is classified as non-seismic. However, the seiches during the sudden on-rush of waters into the reservoir during flash floods would cause effects similar to an earth quake but their magnitude would be quite small.

It is pertinent to note that it is now statutory to provide for earth quake forces also at 0.1 g in the designs of all major engineering structures in projects. Hence, the treatment of a weak zone shall bear all these aspects in mind.

### Interface Problems

There are several instances of the foundation problems containing weak zones being treated as an interface problem. Various additional factors like sliding resistance and stability are considered before taking a decision. But, these expositions are all of recent origin. The treatments have been simple.

Casinader (1974) has described the foundation problems faced at Sugarloaf Rockfill Dam, Australia as consisting of several seams of

clay occurring in a highly weathered zone. A concrete plinth had to be founded on this doubtful foundation at an acceptable depth. Clearly, total removal of the entire weathered stuff was not adopted.

Logani (1979) describes the techniques during foundation treatment of the Ullum Dam, Argentina. The dam 67 m high is founded on a foundation of slaking and expansive type sedimentary rock that consists of compaction type claystone and siltstone, sandstone with clay and silt matrix, and loosely cemented conglomerate. The treatment consisted of laying a concrete slab, cut-offs and grouting.

Pong Nai-Gouan (1979) has described the treatment of a broad fractured zone in the foundation rock under the concrete dam of Tanchangkou Project, China. The 110 m high dam had several fractured zones, 20 to 30 m wide. Part of the weak bed rock was excavated and back-filled with concrete to form a plug. A shallow cut-off wall with chemical grouting curtain was adopted. The behaviour of the dam was found normal after being in service for several years.

### Rock Parameters

A revised 'state of art' paper on rock parameters has been described by Bhawani Singh (1985). Attention has been focussed on usefulness of quantitative rock mass classification systems in assessing various characteristics of rock mass eg. standup time, modulus reduction factor, cohesion angle, angle of internal friction, allowable bearing pressure, slope of rock cut and grout intake. Bieniawski's and Barton's classification systems are considered practicable in India. However, these findings are of recent origin and were not available at the time when Upper Aliyar Dam was constructed. It will be quite interesting to apply the various norms to the different rock masses met with in the weak zone of Upper Aliyar Dam and strive for their proper classification. This would constitute a separate study by itself. Albeit, the treatment to be given for weak zones will remain a speciality and cannot be stereo typed.

### Critical Factors

It can be safely assumed that crushed rock need not cause any worry for founding a structure as long as it has adequate bearing capacity and low permeability. The instant case of weak zone in the Upper Aliyar Dam and the experience gained thereon can be extrapolated to other medium and minor structures as well. For example, instances of meeting soils of varying degree along the foundation of the walls of a building are too common. Normally, it is the practice to completely excavate such doubtful soils and provide a uniformly deep foundation. It will be worthwhile to experiment by providing shallow foundations that would provide for proper confinement of the doubtful soil which might be otherwise strong for founding a structure.

### Alternative Solutions

It would be also worthwhile to try for providing piles spread over such doubtful locations in the dam sites to take care of the

major problems of bearing capacity. There are several methods available for tackling the other problem viz. reducing percolation.

### CONCLUSION

- a. Simple concrete plugs are adequate for treating weak zones at dam sites.
- b. The in-situ bearing capacity of the weak material is the criterion for design rather than its unconfined compressive strength.
- c. Confinement of weak material prevents percolation resulting in a foundation which is adequate.
- d. It is preferable to isolate the portion of dam over weak zone by having construction joints on either side.
- e. It is necessary to have an observation gallery right over the top of weak zone.
- f. It is preferable to instal sensitive instruments for monitoring the performance of the weak zone.
- g. Random rubble masonry appears to be a more reliable material for construction of dam as it affords some sort of flexibility during settlement etc. however minor they may be. Solid concrete dams are more rigid.

### ACKNOWLEDGEMENT

Grateful thanks are due to the Member (Distribution) and Chairman of Tamil Nadu Electricity Board for their kind encouragement and approval in the preparation of this paper.

### REFERENCES

- Bhawani Singh, (1985), "Geotechnical Investigations for Rock Structures on the Basis of Classification Systems", Proc., Third Symposium on Rock Mechanics, Roorkee, India, Vol.1, II-38-61.
- Casinader R.J. and Stapledon D.H., (1979), "The Effect of Geology on the treatment of the dam foundation Interface of Sugarloaf Dam", Trans. of the 13th International Congress on Large Dams, New Delhi, Vol.1, 591.
- Creager, Justin and Hinds, (1968), "Engineering for Dams", Wiley Eastern, New Delhi, 1, 46, 47, 285.
- Logani K.L. and Hector M., (1979), "Techniques developed during foundation treatment of the Ullum Dam Constructed of Dispersive Soils", Trans. of the 13th International Congress on Large Dams, New Delhi, Vol.1, 729.
- Pong Nai-Gouan., (1979), "The treatment of Broad fractures zone in the foundation rocks under the Concrete dam of Tanchangkou Project", Trans. of the 13th International Congress on Large Dams, New Delhi, Vol.1, 1047.
- Tamil Nadu Electricity Board, (1970), "Technical Completion Report for Upper Aliyar Dam".

## Performance of a Harbor Embankment

D.G. Anderson

Senior Geotechnical Engineer, CH2M HILL, Bellevue, Washington

J.G. Dehner

Project Geotechnical Engineer, CH2M HILL, Bellevue, Washington

T.B. King

Manager, Civil Engineering, CH2M HILL, Bellevue, Washington

### SYNOPSIS

An instrumentation program to monitor deformations and pore pressures in foundation soils during construction of a container wharf and backlands fill at the Port of Los Angeles is described in this paper. Inclinedometers, vertical settlement systems, and pneumatic pore-pressure transducers were used to monitor the performance of a silty clay during various phases of container wharf and backlands construction. Results of the monitoring program and their impacts on wharf construction are presented and discussed. Instrumentation program refinements that were required during data gathering and interpretation are also noted.

### INTRODUCTION

A geotechnical instrumentation program was carried out in 1986 and 1987 for the Port of Los Angeles (POLA) as part of a container wharf and backlands improvement project. The program involved placing instrumentation in and beneath a quarry-run dike that had been constructed across a berth in Los Angeles Harbor. This instrumentation was used to monitor soil settlement, lateral soil displacement, and excess pore water pressures as a function of time after dike and backlands construction.

Information collected during this program was used to decide whether or not sufficient settlement and lateral movement had taken place in fine-grained soil to allow installation of production piles through the quarry-run dike. Information from the instrumentation program also was used to evaluate whether or not vertical and lateral movement of the pile-dike system was within anticipated and tolerable magnitudes following the installation of production piles.

This paper describes procedures used to instrument the dike and soil and presents instrumentation data collected through October 1987. Effects of dike and backlands construction, production pile installation, and the 1987 Whittier Narrows earthquake on soil response are discussed.

### BACKGROUND

The POLA project involved expansion of an existing marine terminal located along the main channel of Los Angeles Harbor. Improvements to the terminal included constructing a 600-foot-long quarry-run (rockfill) dike across the front of a 40-foot-deep berth and filling the berth behind the dike with approximately 450,000 cubic yards of sand fill. Over 500 twenty-four-inch octagonal, prestressed concrete piles were installed through the quarry-run dike to support a new concrete deck.

Field explorations and laboratory testing of soil during the design phase of the project revealed that foundation soil beneath the quarry-run dike is composed of nearly 60 feet of low plasticity silty clay and clayey silt over a very dense sand (Erickson, et al., 1986). The fine-grained soil is moderately over-consolidated with undrained shearing strengths typically greater than 1000 psf. The underlying sand is very dense, with blow counts from the Standard Penetration Test (SPT) typically greater than 100 blows per foot (bpf) and friction angles in excess of 35 degrees.

In the berth area, construction of the dike and filling of the backlands resulted in the addition of nearly 60 feet of soil and rock. The change in stress from the backlands fill material and the quarry-run dike was predicted to cause up to 27 inches of vertical movement and 13 inches of horizontal movement in the fine-grained soil over the 50-year design life of the structure. Approximately 70 percent of this movement was estimated to occur during primary consolidation. Ninety percent of the primary consolidation was expected to occur within 60 days of placing the quarry-run dike and backlands fill.

The magnitude of predicted horizontal movement created a significant design issue. If piles were driven before this horizontal movement occurred, they would be subjected to lateral loads from the displacing soil. Lateral pile load analyses using COM624 (Reese and Sullivan, 1980) revealed that allowable bending stresses in the piles might be exceeded because of the soil loading.

In view of the potential effects of lateral soil movement, it was decided that the quarry-run dike should be built and the backlands filled before the piles for the wharf were installed. Furthermore, it was decided that the amount and rate of vertical soil movement,

lateral soil movement, and pore water pressure dissipation should be monitored to assure that at least 70 percent of the primary consolidation and associated lateral movement had occurred before production piles were driven. Lateral soil movement occurring after 70 percent primary consolidation would result in stresses within the piles, but those stresses were predicted to be within allowable levels.

#### INSTRUMENTATION

Four clusters of instruments were installed in the quarry-run dike (Figure 1). Each cluster included one inclinometer casing, one Sondex system, one surface settlement plate, and two pneumatic piezometers. Instrumentation was manufactured by the Slope Indicator Company (SINCO).

The casing used in the inclinometer installation extended from the top of the dike (elevation +6 mllw) through the fine-grained soil into the dense sand, ending at approximately elevation -125 feet. Figure 2 shows a cross section of the soil profile and inclinometer locations.

The Sondex system extended from the top of the dike to elevation -105 feet. The Sondex system consists of a corrugated plastic tube fitted with stainless steel sensing rings. Sensing rings were attached to the tubing at approxi-

mately 2.5- and 5-foot intervals through the fine-grained material zone. As the soil settles, the corrugated tubing collapses in proportion to the soil settlement, causing the sensing rings to move together. The change in position of the sensing rings is measured by lowering a sensing probe down the tubing. Settlement is determined by measuring the relative distance between rings located in the fine-grained soil and a bottom "anchor" ring which is located (fixed) in the lower dense sand.

Settlement monuments were used to record settlement caused by densification of the dike material and settlement caused by consolidation of the underlying fine-grained soil. During the field monitoring phase of the program, survey elevations were also taken on top of 6-inch-diameter steel casings that were installed to protect the instrumentation systems within the quarry-run dike.

Pore water pressure was monitored using pneumatic push-in pore pressure transducers. These were conventional SINCO pneumatic transducers that were fitted with a pushing mandrel and a stainless steel push tip.

#### INSTALLATION

The instruments were installed through 6-inch-diameter steel casings that were driven through

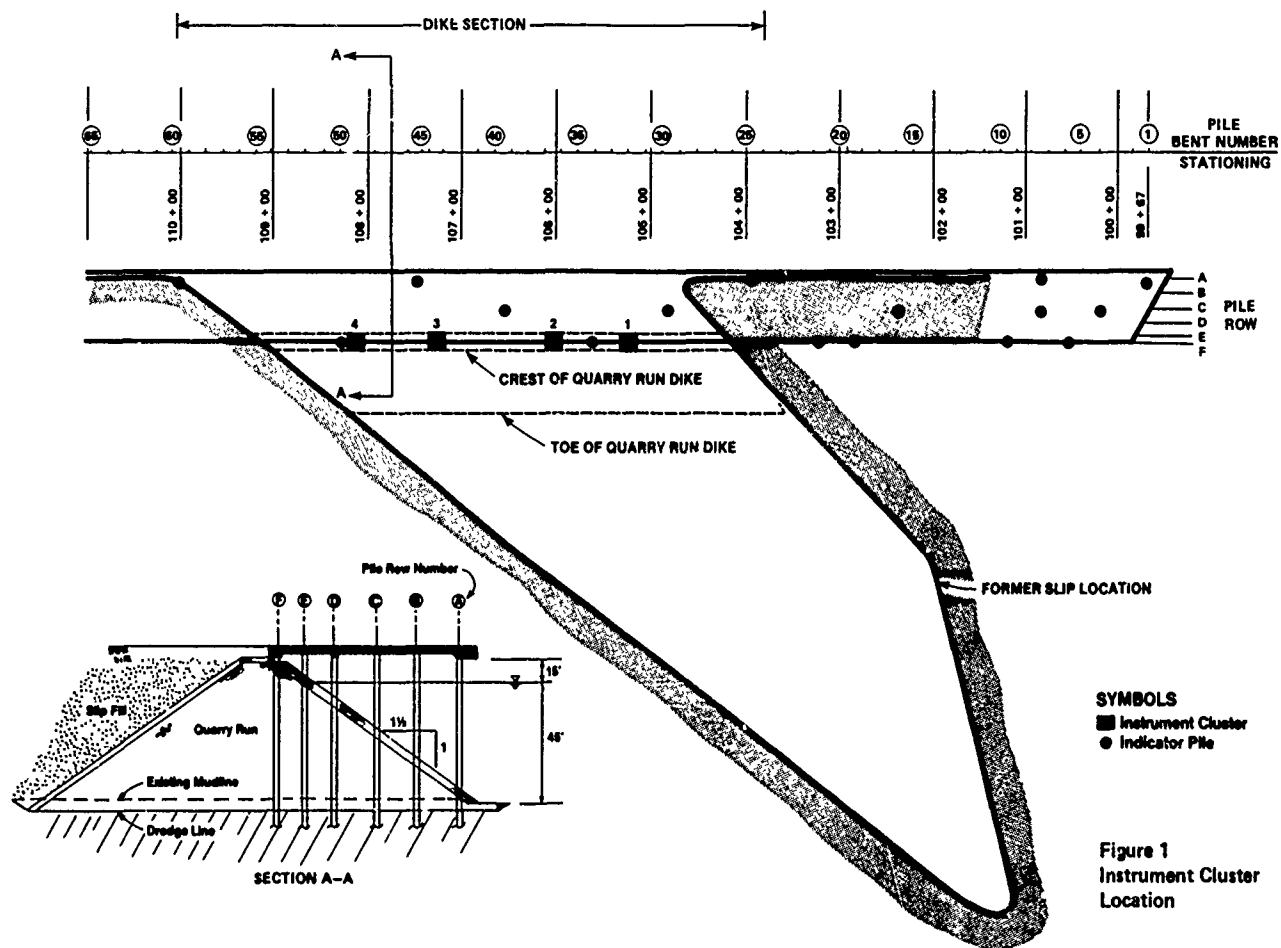


Figure 1  
Instrument Cluster  
Location

the quarry-run material. The purpose of the casing was to protect the instrumentation through the quarry-run dike and provide a cased hole through which a rotary mud drill rig could be used to drill in the soil beneath the quarry-run material.

For each cluster of instrumentation, the borehole for the inclinometer/Sondex system was drilled and sampled first since this was the deepest borehole of a cluster, extending through the fine-grained soil into the lower dense sand. The inclinometer casing was placed inside the Sondex tubing and the two were installed as a single unit. This combined installation isolated the inclinometer casing from downdrag caused by soil settlement, eliminated the need for telescoping couplings in the inclinometer system, and reduced the number of boreholes, thus allowing data to be gathered at an earlier date. The accuracy of the Sondex sensing probe was not affected by the inclinometer casing.

The anchor point for the inclinometer casing was approximately 20 feet into the lower dense sand layer. A Sondex ring was mounted on the inclinometer casing below the bottom of the Sondex tubing and just above the bottom of the hole. Since the inclinometer casing is relatively rigid from top to bottom, any changes measured in this distance represented Sondex cable stretch. The outside of the Sondex tubing was grouted-in using a low strength grout mix.

The pore pressure transducers were installed in boreholes that were drilled to approximately 24 inches above the desired depth of the transducer. The soil profile revealed during drilling for the inclinometer/Sondex system was used as a basis for selecting the installation depth. Once the borehole was drilled to the appropriate depth, the transducer was tied to a push mandrel that was mounted on a section of drill rod, lowered to the bottom of the borehole, and pushed into the soil. Prior to installation, the porous stone for the transducer was saturated for 24 hours. The transducer assembly was sealed in a thin, water-filled plastic bag to protect it from drilling mud and to maintain tip saturation. After installation the borehole was filled to the surface with a bentonite-cement grout.

#### DATA MONITORING AND INTERPRETATION

Data from each instrumentation system were recorded immediately after installation and at regular intervals thereafter. Initially, the recording intervals were relatively close, i.e., weekly to biweekly. The interval was increased to monthly and later every 3 months when the change in data indicated that settlement, pore pressure change, and lateral movement were relatively slow.

The inclinometer data were interpreted using the computer program PC-SLIN. The PC-SLIN program is a proprietary program developed by

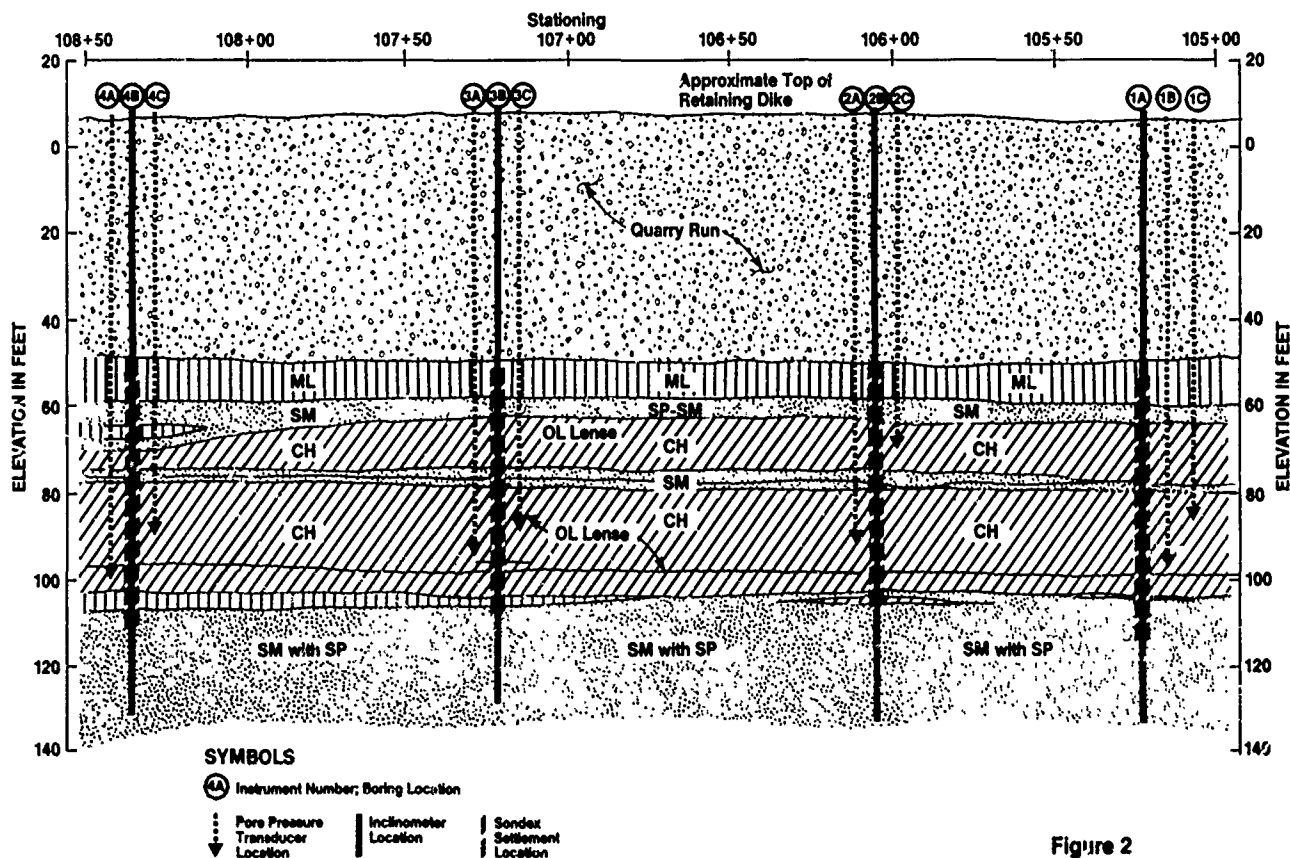


Figure 2  
Generalized Soil Profile  
and Instrument Location



Geo-Slope Programming Ltd. of Calgary, Alberta. This program is written so that the accuracy of input data can be checked, the performance of the inclinometer probe can be evaluated, and a variety of data sets can be obtained and plotted.

The Sondex data were interpreted by determining the distance between the anchor ring and the reference rings. In November 1986 it was realized that the instrument cable used to record the depths of the Sondex rings was undergoing "negative stretch." Apparently as the cable aged some of its elastomers evaporated, making the cable stiffer and hence shorter under the same sensor probe weight. This problem was corrected by using a steel measuring tape to lower and measure the location of the Sondex probe.

The total pore water pressure was recorded by each piezometer. To evaluate the percentage of settlement that had occurred, it was necessary to determine the excess pore water pressure. This involved subtracting the hydrostatic component of pore pressure from the total pore pressure reading after applying a tidal correction. The tidal correction factor was determined by monitoring the pressure change over a tidal cycle on two occasions.

## RESULTS

The instrumentation system has been monitored for over 400 days, as of mid-October 1987. During this period, the backlands area was filled, test piles were driven, and production piles were installed. Table 1 summarizes key events, dates, and elapsed time during the monitoring period.

Inclinometer profile plots for clusters 1, 2, and 3 at five different times after installation are shown in Figure 3. Two of the five profiles for each inclinometer show measurements before production piles were driven, and

three show measurements after production piles were driven. These plots summarize the change in horizontal location of the inclinometer casing relative to initial installation. Movement to the right (positive values) indicates movement towards the main channel; i.e., outward from the axis of the dike. The depths shown on these plots are the distances below elevation +6 feet, which was the top of the dike at the time of installation.

Settlements for each cluster recorded during the Sondex program and during level surveys are summarized as a function of time since installation in Figure 4. Figure 5 shows the change in excess pore water pressure with time.

Table 1  
KEY EVENTS DURING MONITORING PERIOD

| Event                      | Date                 | Elapsed Time |            |
|----------------------------|----------------------|--------------|------------|
|                            |                      | Dike         | Instrument |
| Start of dike construction | 6/13/86              | 0            | --         |
| Dike at elevation +6 feet  | 7/20/86              | 37           | --         |
| Instrumentation installed  | 8/12/86 to 8/28/86   | 60-76        | 0          |
| Test piles driven          | 10/01/86 to 10/27/86 | 110          | 34-50      |
|                            |                      | 136          | 60-76      |
| Production piles driven    | 12/19/86 to 4/15/87  | 189          | 113-129    |
|                            |                      | 307          | 231-247    |
| Whittier Narrows EQ        | 10/01/87             | 476          | 400-416    |
| Last data set              | 10/14/87             | 490          | 414-430    |

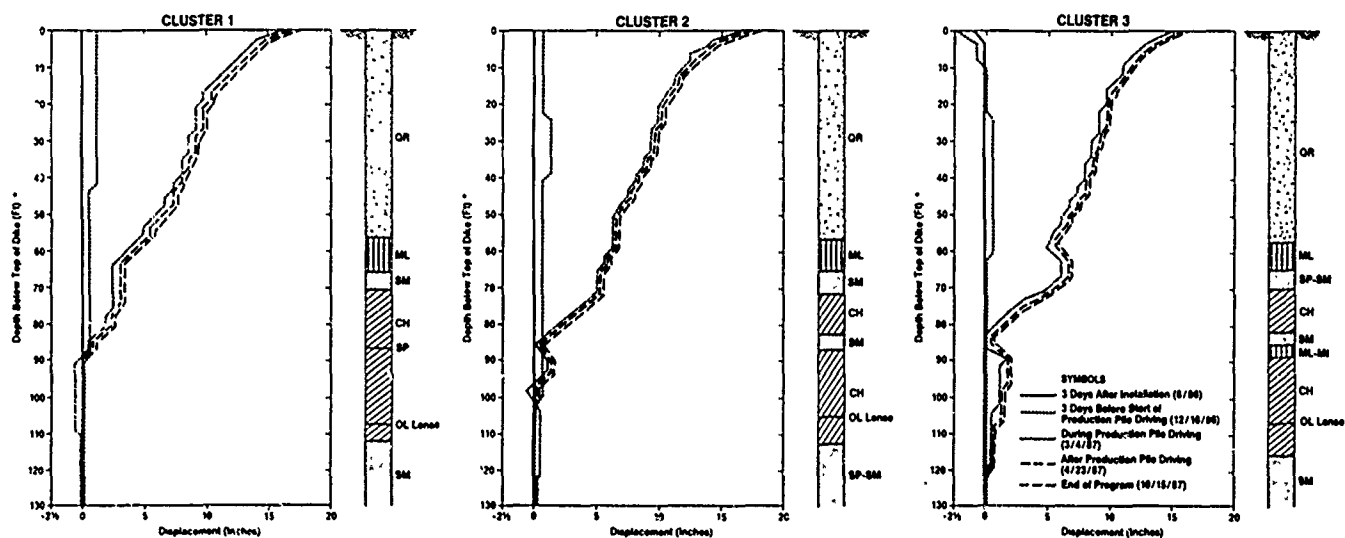
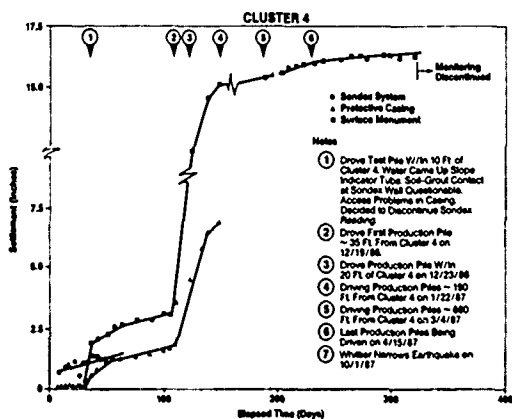
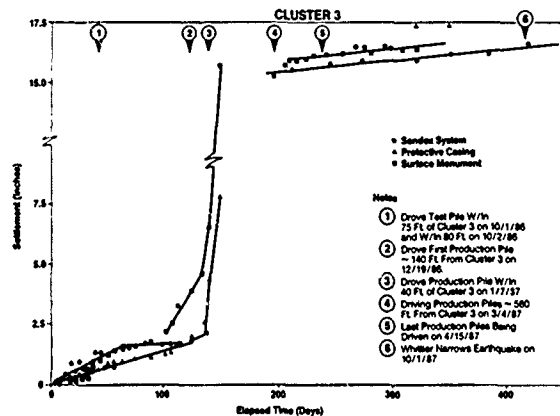
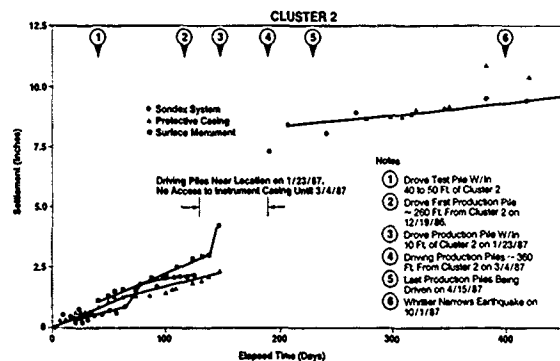
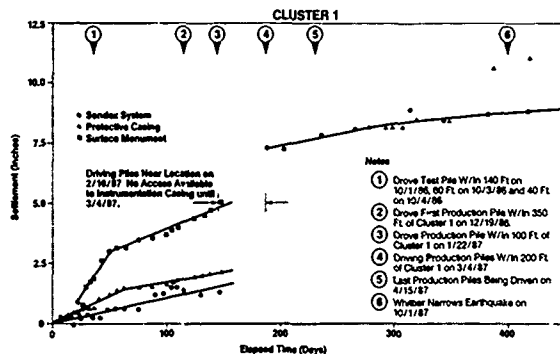
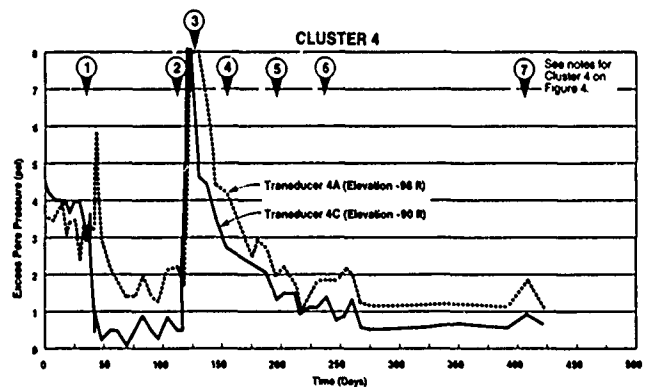
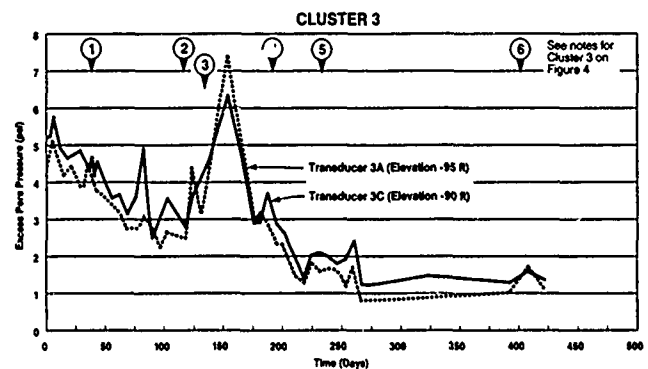
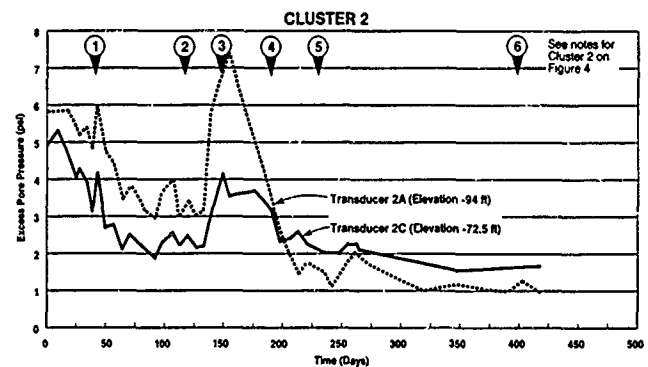
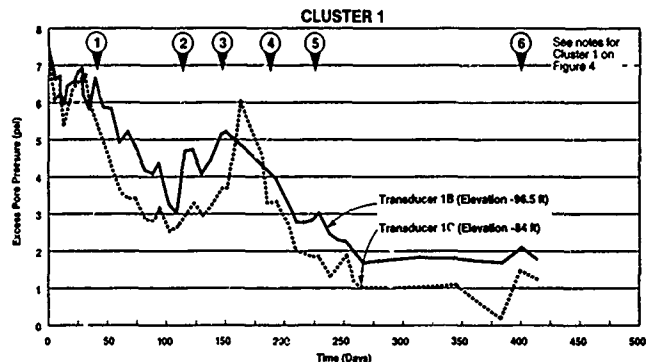


Figure 3  
Inclinometer Profile  
Plots for Instrument  
Clusters



**Figure 4**  
Settlement  
Results



**Figure 5**  
Excess Pore Pressure  
as a Function of Time

## DATA REVIEW

The monitoring period was broken into four time periods for the purpose of data review. These periods include initial (baseline) conditions, before and after test pile installation, before and after production pile installation, and post construction.

### Baseline Conditions

A set of data was collected for each instrument immediately after all instruments within the cluster had been installed. The baseline data represented conditions on the day that each cluster of instruments was read and, therefore, served as initial conditions for subsequent readings.

The baseline data did not represent initial conditions at the end of dike construction, since they were first monitored approximately 3 to 5 weeks after the dike reached an elevation of +6 feet. One of the objectives of the instrumentation program was to decide whether or not sufficient settlement and horizontal movement had taken place to install the production piles; therefore, it was necessary to estimate what the settlement and excess pore pressure would have been if the instrumentation had been installed before construction. This information was then used to decide how much additional pore pressure dissipation, settlement, and horizontal movement would have to occur before production piles could be driven.

Based on the ratio of measured excess pore pressure to the estimated value of initial excess pore pressure, the average degree of consolidation was estimated to range from 60 to 70 percent at the time of baseline monitoring. This suggested that 6 to 8 inches of settlement had probably occurred before the instrumentation system had been installed.

### Test Pile Installation

Test piles were installed during October of 1986, approximately 35 to 75 days after instrument installation. The rate of soil settlement before test pile installation was fairly small. Typically 1/2 inch or less of soil settlement was recorded by the Sondex system. This is consistent with pore pressure data, which suggested that much of the excess pore pressure had dissipated before the instrumentation was placed.

Typically, the test piles were driven 40 feet or more from the nearest instrument cluster (Figure 2). A test pile was driven approximately 10 feet from cluster 4 on October 2, 1986. During installation of the test pile, water from the pile jetting operation was observed to spout from the top of the inclinometer casing. Later when an attempt was made to obtain inclinometer readings in cluster 4, sediment was found to be accumulating in the casing. The cluster 4 location was subsequently abandoned.

The effects of test pile driving included increased settlement and excess pore water pressure. The amount of settlement ranged from less than 1/2 inch to more than 2 inches; excess pore pressures increased by several pounds per square inch (psi). The settlement was most

pronounced for the surface monuments. Very little settlement was recorded by the Sondex system. This suggests that most settlement resulted from densification of the quarry run material. No visible effects occurred in the inclinometer readings.

It was concluded from these measurements that test pile driving caused localized increases in pore pressure in the fine-grained soil and localized settlement of the quarry-run material, but no permanent horizontal movement or noticeable increases in fine-grained soil settlement.

### Production Pile Driving

Production pile driving began on December 19, 1986, and concluded in mid-April of 1987. During this period over 500 piles were driven. Driving was initiated approximately 25 feet south of cluster 4 and continued north along the dike section passing cluster 3 on approximately January 12, 1987; cluster 2 on approximately January 23, 1987; and cluster 1 on February 10, 1987.

By the start of production pile driving approximately 1.5 to 2.5 inches of settlement had been recorded by the Sondex settlement system and by taking elevations on the top of the protective casing. This meant that total settlement from the start of dike construction was roughly 8 to 11 inches. The required amount of settlement before pile driving could begin was estimated to be 9 to 10 inches; hence the settlement data suggested that production pile driving could begin with minimum risk. Excess pore water pressure data indicated that excess pore pressures were less than 3 psi by December 19, 1986. This corresponded to an average consolidation of 80 percent, which was greater than the 70 percent required for production pile driving to start. Inclinometer data suggested that horizontal movement of the soil between installation and the last recording date before production pile driving varied from 1/2 to 3/4 inch in the fine-grained soil. An additional 1/2 to 1 inch of horizontal movement apparently occurred in the quarry-run material.

Production pile driving had significant effects on all of the instrumentation. Settlement data indicate that 5 to 15 inches of soil settlement occurred as a result of production pile driving. Settlement at clusters 1 and 2 was approximately 5 inches, whereas settlement at clusters 3 and 4 was nearly 15 inches. Survey data for the surface monument and the instrumentation casing clearly showed that settlement increased as pile driving approached.

Excess pore pressures increased dramatically during production pile driving. At cluster 4 the excess pore pressure was 35 psi immediately after driving. A maximum pore pressure in excess of 30 psi was also recorded at cluster 3. These levels of pore pressure nearly exceed the effective overburden stress at the transducer elevations. Dissipation times for the excess pore pressures were greater than 2 months.

The inclinometer data show that 13 to 15 inches of movement occurred at the top of the quarry-run dike during production pile driving. This movement decreased somewhat linearly with depth, with no appreciable movement occurring

below elevation -80 feet. Closer inspection of the inclinometer data suggests that the steel protective casing in the quarry-run material rotated approximately 1 degree during production pile installation and that the soil beneath the quarry-run material displaced approximately 4 to 5 inches.

#### Post Construction

The last production pile was driven on approximately April 15, 1987. Since that date numerous construction activities have taken place at the project site, but none of these involved subsurface work such as pile driving or the addition of appreciable foundation loads. With the exception of the Whittier-Narrows earthquake on October 1, 1987, the foundation soil was subjected to constant stresses from the dike and backland fills during this post-construction period.

Pore pressure values from mid-April to mid-October of 1987 continue to decrease slightly or are relatively constant. The magnitude of the excess pore pressures as of October 14 was typically 1.5 psi or less. This represents roughly 90 percent consolidation or more. At least a portion of the remaining excess pore pressure could be attributed to uncertainties in correcting for tidal pressure effects. One excursion occurred consistently on all records approximately 400 days after the start of monitoring. This slight increase of approximately 0.5 psi was measured at about 2:45 p.m. on October 1, 1987, approximately 7 hours after the Whittier-Narrows earthquake. The epicenter for this earthquake was over 20 miles from the project. These excess pore pressures returned to levels recorded before October 1, 1987, by the next data recording period, which was 2 weeks later.

Results of Sondex measurements suggest that approximately 1 inch of settlement has occurred in the soil since the end of production pile driving. The rate of Sondex settlement appears to be decreasing with elapsed time, consistent with the normal consolidation and secondary compression processes. Settlements from the protective casing are generally consistent with the Sondex data. Significant jumps in the protective casing data in September are thought to be caused by construction activities. No increases in settlement were noted after the Whittier-Narrows earthquake.

Inclinometer data suggest that approximately 1 inch of outward movement has occurred at the top of the dike since mid-April. Less than 3/4 inch of outward movement has been recorded in the fine-grained soil (below elevation -60 feet) during the same period. No horizontal movement was detected during the earthquake.

#### DISCUSSION OF RESULTS

Results of the instrumentation program were relatively consistent with settlement predictions for dike and backlands loads. These predictions were based on results of laboratory consolidation tests and three-dimensional elastic stress estimates. The computer program FEADAM84 (Duncan et al., 1984) was also used to estimate stresses for different stages of construction. The magnitude of settlements and

lateral soil movement during production pile driving was, however, much greater than anticipated. This observation, along with the observed pore pressure increase during the Whittier-Narrows earthquake warrants additional comment.

#### Production Pile Driving

It was clear from the recorded data that production pile driving caused very large increases in pore pressure. These increases were attributed to the combined effects of soil displacement during driving and the large jetting pressures that were used to assist in pile installation. While both conditions can logically result in pore pressure increase, the magnitude of increase was surprising. It was originally postulated that the vent channel associated with jetting would minimize the cavity expansion component of pore pressure increase. This vent channel was also expected to dissipate most excess pore pressures immediately after the end of pile driving. Pore pressure data indicate that excess pressures did not immediately dissipate. Rather, they dissipated in much the same manner as was recorded for dike loading. This suggests that the entire area underwent a pore pressure increase.

A substantial amount of settlement was also recorded as a result of pile installation. Changes in pore pressure in the soil do not appear to explain the magnitude of these settlements. It is believed that at least some settlement could be due to remolding and actual loss of soil during the pile jetting sequence.

Up to 13 inches of movement in the quarry run material were recorded. Movement of the steel casing probably resulted from a combination of (1) densification of the quarry-run material, (2) lateral stresses from the fill material on the shoreward side of the dike, and (3) pore-pressure-related losses in bearing support beneath the channel side of the dike. Movement of the soil in excess of an inch starts approximately at elevation -80 feet. This indicates that the lower clay layer was being stressed sufficiently to deform. Movement seems to increase in the upper clay layer that exists between elevation -65 and -75 feet. It is postulated that immediately after pile driving shearing forces induced by the sand fill behind the dike temporarily exceeded the strength of this clay layer. This would require that a loss in soil strength occurred somewhere along the shearing plane during pile driving, possibly at the toe of the embankment where overburden stresses were low and high pore pressures had developed. This loss in soil strength could have resulted from a combination of liquefaction within the sand layer, high pore pressures within the clay layer, and material loss during jetting. Figure 6 illustrates this concept.

#### Whittier-Narrows Earthquake

The Whittier-Narrows earthquake appears to have caused an increase in pore pressures within the fine-grained soil of approximately 0.5 psi. The magnitude of this increase is somewhat surprising, given the distance from the epicenter and the magnitude of the earthquake ( $M=5.9$ ).

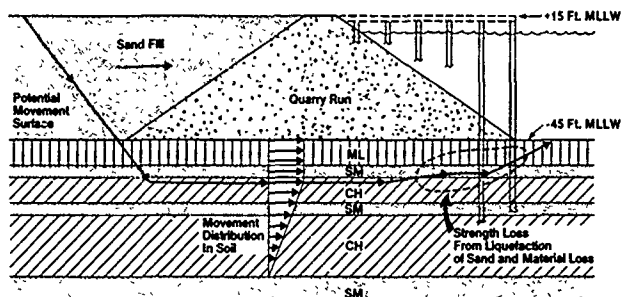


Figure 6  
Potential Mechanism  
for Dike Movement

It was estimated that accelerations at the top of the dense sand layer, nearly 100 feet below the ground surface, would be less than 0.05 g. The shearing strain in the fine-grained soil was estimated to be as high as 0.05 percent. This level of shearing strain was apparently high enough to result in residual excess pore pressures. The level of pore pressure increase was small enough that no horizontal or vertical movements were recorded with the Sondex settlement system and the inclinometer system.

#### CONCLUSIONS

Results of the instrumentation program were used to decide that production piles could be driven beginning in mid-December of 1986. Instrumentation data collected before and after production pile driving indicated that ground movements occurring during production pile driving were within tolerable levels in terms of pile capacity. Data also suggested that the wharf-dike system should continue to perform satisfactorily in the future.

The following additional specific conclusions were reached during this instrumentation program.

- o The instrumentation proved to be relatively easy to install and very reliable from the standpoint of operation. The only change in monitoring procedure involved using a steel measuring tape rather than the Sondex instrument cable to measure depths.
- o Baseline measurements taken approximately 3 to 5 weeks after completion of the dike to an elevation of +6 feet indicated that 60 to 70 percent of the excess pore pressure had dissipated in the various fine-grained soil layers beneath the dike by the start of the monitoring period and that 6 to 8 inches of settlement had occurred. Pore pressure readings determined that excess pore pressures were from 4 to 8 psi, representing 60 to 70 percent consolidation.
- o Test pile driving caused localized buildups in excess pore pressures. These pore pressures dissipated quickly. Settlement also occurred. Most of the settlement appeared to be within the quarry-run material.

- o Production pile driving caused large increases in pore pressure, significant settlement, and lateral movement. The amount of pore pressure increase was as high as 35 psi. Nearly 10 inches of settlement occurred at some cluster locations. Inclinometer data showed that approximately 12 inches of lateral movement occurred at the top of the dike and from 4 to 5 inches in the soil beneath the dike.

- o Very little settlement or horizontal movement has taken place since the end of production pile driving. Settlements have typically been less than 2 inches; lateral movement has been less than an inch. Excess pore pressures are generally less than 2 psi. Secondary compression of the soil appears to be under way.

The instrumentation program was a significant benefit to the Berths 225-229 project. For future projects involving the same design issues, consideration should be given to installing a similar instrumentation array to monitor soil behavior. If feasible, instrumentation used in any future array should be installed before dike construction.

#### ACKNOWLEDGMENTS

The instrumentation program described in this paper was performed for the Port of Los Angeles Harbor Department. Mr. Richard C. Wittkop served as the Project Manager for the Port of Los Angeles. His interest, as well as the excellent cooperation of General Construction Company, the contractor on the project, contributed significantly to the success of the project. Other CH2M HILL participants included Mr. Bradley P. Erickson, overall project manager; Dr. David Nyby, geotechnical engineer during design; and Mr. Art O'Brien, geotechnical engineer for instrumentation planning.

#### REFERENCES

- Reese, L. C., and W. R. Sullivan (1980), "Documentation of Computer Program COM624," Geotechnical Engineering Center. Department of Civil Engineering. The University of Texas at Austin.
- Duncan, J. M., R. B. Seed, K. S. Wong, and Y. Ozawa (1984), "FEADAM84: A Computer Program For Finite Element Analysis of Dams," Geotechnical Engineering. Department of Civil Engineering. Virginia Polytechnic Institute and State University.
- Erickson, B. P., T. B. King, D. W. Nyby, and D. C. Wittkop (1986), "Marginal Wharf and Embankments--Seismic Design," Ports 86. American Society of Civil Engineers.

## Cracking Studies at Sand H Basin by the Finite Element Method

Trevor Smith

Associate Professor of Civil Engineering, Portland State University,  
Portland, Oregon

Clifton E. Deal

Soil Mechanics Engineer, Soil Conservation Service, West National  
Technical Center, Portland, Oregon

**ABSTRACT:** An existing 30 feet high debris basin embankment has been found to be severely cracked longitudinally. Few investigations or analysis of longitudinal cracking are reported. This paper presents the results of a finite element analysis using in situ properties of the soils and gives recommendations for future use of the FEM for cracking studies at existing dams.

### INTRODUCTION

Cracking has been a problem for earth dams in many locations of the southwestern United States. Generally, the cracking causing most concern has been transverse to the center line of the dam and has been felt to be the result of desiccation or differential settlement. Little investigation or analysis has been done when longitudinal cracking is the major problem and the foundation materials are coarse grained and moisture sensitive.

Sand H Debris Basin, Monroe, Utah, typifies an earthen dam experiencing significant longitudinal cracking on the downstream slope with minor cracking on the upstream slope. The evaluation of the safety of this dam, using a conventional  $c$  and  $\phi$  approach, has not been satisfactory. It can not correctly predict the stresses and strains associated with cracked zones in the embankment together with the kinematics of displacement and modeling of these zones when using  $c$  and  $\phi$  parameters in the model. This paper presents the results of a finite element (FEM) evaluation of this site using quality in situ data directly in the FEM model.

### LOCAL GEOLOGY AND EMBANKMENT HISTORY

The site is located at the eastern edge of the Basin and Range Province in the Colorado Plateau-Sevier Plateau physiographic area of Utah. The embankment is constructed on fan debris flow deposits in the upper area of an alluvial fan developed at the confluence of Sand Canyon and H Canyon ephemeral streams. A commercially operated hot spring is located north and upstream of the structure in the proximity of the Sevier Fault which is about 1,000 feet upstream of the center line and is considered to be an active fault.

The materials comprising the foundation are stratified gravels, sands, and silts. The gravels contain less than 15 percent silt-size particles with 12-inch maximum size. The sands contain approximately 30 percent silt-size particles with 3-inch maximum size and the silt has a low plastic consistency with some clay-size particles. The classification of these materials using the Unified Soil Classification classifies the gravels as GP-GC and GM, the sands as SP-SM, SM-SC, and SM and the silts as ML-CL and ML.

The debris basin was designed in 1969, and constructed in 1971, as a zoned embankment with a 14-foot top width, 2H

to 1V downstream slope, 3H to 1V upstream slope and had a maximum height at the center line of 30 feet. The central zone (Zone I), consisted of a uniformly blended, well-graded mixture of small cobbles, gravels, sands, and silts with a minimum of 15 percent passing the No. 200 sieve. The shell zones (Zone III), consisted of a uniformly blended mixture of cobbles, gravels, sands, and silts containing a maximum rock size of twenty-four (24) inches. A vertical and horizontal drainage zone (Zone II), downstream of the center line of the embankment consisted of a graded gravel filter containing no more than 3 percent passing the No. 200 sieve, 85 to 55 percent passing the 1½ inch, and 10 to 30 percent passing the No. 20.

In 1984, it was reported that significant cracking was observed on the downstream slope of the embankment between the two outlet channels for the two principal spillways. In addition to the cracking on the embankment, several depressions were found on a football practice field, constructed in 1979, and on the reservoir floor. The major depression on the practice field and the reservoir floor are located downstream and upstream in the general area of the major cracking on the embankment. These features are located on a line that is approximately perpendicular with the center line of the structure.

The cracking consists of three (3) major longitudinal cracks at approximately 10 feet, 12.5 feet, and 17 feet, vertically, above the downstream toe. The crack traces are generally parallel to the center line but are wavy and splintered in some places with all of the cracks converging into one major crack which curves down across the left principal spillway berm. Since discovery in 1984, the cracks have enlarged to a total displacement of 12-inches wide, with a depth of 54 inches. Additionally, a new crack was found on the upstream slope of the embankment. This illustrates the kinematics of the situation.

### FEM "FEADAM" MODELING

The program used throughout this study was an IBM PC version of a computer program written by Duncan et al. (1980a) and is titled Finite Element Analysis of Dams (FEADAM). The output includes information on tension zones and shear failure zones which is of particular interest for the Sand H Basin study, but represents only an analysis during ( . as a result of), the construction sequence. However, valuable qualitative information can be gained on a number of the Sand H Basin characteris-

tics, including sinkhole development, downstream toe removal, and the potential for crack development.

The finite element code FEADAM assumes that no cracking is present and continuity of the soil mass is maintained. In addition, and compounding the problem, FEADAM cannot model post-construction dam behavior due to changes in soil properties. FEADAM only permits post-construction loading (both positive and negative) to take place. Therefore, the application of FEADAM to Sand H Debris Basin represents the limit of our existing technology when using accepted available computer codes designed for geotechnical application. Highly specialized codes do exist for cracking studies which have been adapted for geotechnical use. The theoretical development of the governing constitutive relationships is still in its infancy, however.

#### Soil Properties from In Situ Testing

Due to the nature and grain size of both the embankment and foundation soils, no triaxial tests could be performed at the debris basin site. However, a total of 41 pressuremeter tests were successfully completed and yielded data of equal quality to guide selection on the nine non-linear soil parameters (including Mohr Coulomb parameters) required in the Duncan and Chang (1970) and Duncan et al. (1980b) soil models.

Both Mechanical Friction Sleeve Cones and prebored pressuremeter testing were completed during the summer of 1986. Pressuremeter testing proved extremely valuable with testing in collapsed and uncollapsed zones using prebored and slotted tube techniques.

Many different theories and correlations exist to calculate cohesion  $c$  and friction angle  $\phi$  from both pressuremeter testing and cone testing. In general, the methods proposed by Menard (Baguelin et al. 1979) for pressuremeter testing in sands, together with recommendations from Robertson and Campanella for the cone, have been used. By direct analogy between the hyperbolic soil model, relating confining pressure, and Initial Tangent stiffness to that relating Pressuremeter Menard Modulus ( $E_m$ ) with effective overburden pressure (vertical confinement), guidance on the hyperbolic parameters can be obtained. Based on this approach, and the recommendations given by Duncan et al. (1980) the hyperbolic parameters used are given in table 1.

Table 1. Summary of FEH Hyperbolic Parameters

| Zone or Condition | Mat'l No. | Unit Wt. | Mod. No. |     |          | Failure Ratio | Bulk Mod. No. | Bulk Mod. Exp. | Cohesion Intercept | Friction Angle Parameter |          | Lateral Stress Ratio |
|-------------------|-----------|----------|----------|-----|----------|---------------|---------------|----------------|--------------------|--------------------------|----------|----------------------|
|                   |           |          | $E$      | $K$ | $K_{ur}$ |               |               |                |                    | $\phi$                   | $\theta$ |                      |
| Embankment        | 1         | 0.12     | 600      | 600 | 0.10     | 0.70          | 200           | 0.20           | 0                  | 42                       | 0.0      | 0.33                 |
| D Foundation      | 2         | 0.12     | 350      | 350 | 0.60     | 0.70          | 80            | 0.20           | 0                  | 36                       | 5.0      | 0.41                 |
| C Foundation      | 3         | 0.12     | 52       | 52  | 0.80     | 0.70          | 50            | 0.20           | 0                  | 22                       | 0.0      | 0.47                 |
| PC Foundation     | 4         | 0.12     | 250      | 250 | 0.70     | 0.70          | 65            | 0.20           | 0                  | 34                       | 2.5      | 0.44                 |
| Drain             | 5         | 0.12     | 200      | 200 | 0.4      | 0.7           | 50            | 0.20           | 0                  | 33                       | 3.0      | 0.45                 |
| Air               | 6         | U.S.     | 1        | 1   | 1.0      | 0.0           | 20            | 0.20           | 1.0                | 0                        | 0.0      | 0.10                 |

D Foundation - Dry  
C Foundation - Collapsed  
PC Foundation - Post-Collapsed

#### Parametric Study on Material Properties

One of the stated goals of this study is the attempt to predict, analytically, the observed cracking and other distress features on the dam. The evaluation and selection of material properties in FEADAM gives a wide range of valid parameters. To determine the sensitivity of the predicted stresses and possible tension zones (output), a material parametric study was conducted on the unit weight, the modulus number, the modulus exponent and the cohesion for dam and foundation materials.

Of particular relevance was the determination of the amount of non-linearity the dam exhibited until the onset of tension zones were predicted. Both cone and pressuremeter testing showed the dam material to be of very high stiffness with very little change in properties with depth, i.e., at the present time it's behaving elastically, up to yield.

All of the parametric studies used a model consisting of a non-linear dam on a non-linear soft foundation growing horizontally as a realistic scenario. The parametric study of the dam properties consisted of reducing the unit weight to 90 lb/cu ft, increasing the modulus exponent to  $n = 0.4$ , introducing a small cohesion ( $c = 200$  lb/sq ft) and using friction angles of 36 and 45 degrees. The foundation properties evaluated consisted of reducing the unit weight from 120 lb/cu ft to 90 lb/cu ft, using a modulus exponent of  $n = 0.4$  and reducing the modulus number to  $K = 200$ . The soft zone properties studied consisted of reducing the modulus exponent to 0.0 and leaving  $K$  as is, using a modulus number of  $K = 86$  and  $n = 0.0$  and reducing the modulus number to  $K = 22$  and  $n = 0.0$ .

Reduction of the dam unit weight initiates extensive shallow slope failure consistent with an infinite slope analysis. This zone of shear failure extends approximately 1- to 2-foot thick on the D/S face but up to 8-foot thick on the U/S face. Little change in the amount of shear and tension failure within the dam and foundation is observed. Therefore, the distress feature results within the areas of interest show no significant change. Increases in the modulus exponent  $n$  shows the most sensitive response from all model studies. By increasing  $n$  from 0.1 to 0.4, thus, strengthening the link between confining pressure and modulus causes low stressed elements to quickly undergo tension failure. Over 50 percent of the U/S face now shows tension failure in a single zone. This appears to verify that field measured modulus values (from the Pressuremeter) are important. Increasing the cohesion from zero to only 200 psf immediately produces a more "comfortable" dam, better able to maintain the profile without any distress features. It follows then that the models employing  $c = 0$  are worse case studies. Increasing  $\phi$  gives a very different response, but a reduction in  $\phi$  shows extensive U/S shear failure and D/S shear failure as conditions approach "infinite slope" failure.

Revisions were made to the "wet", during collapse properties. If it is speculated that the amount of collapse increases with higher overburden pressures, it follows the equivalent non-linear soil model stiffness may have to decrease with depth (or decrease with confining pressure)! To uncouple stiffness from confining pressure in all models the modulus exponent is taken as zero.

The parametric study of the collapsed properties produced LESS settlement since the soil stiffness is fixed in elastic behavior with modulus values HIGHER than the model

with horizontal soft zones (since the low stresses in elements, representing post collapsed properties are now not used in the analysis for soil stiffness). The increase in K by 50 percent in the model again shows no settlement change but most of the U/S face suffers tension failure. This supports the conclusion that there is a strong relationship between the D/S toe foundation soils and U/S face.

#### MESHERS AND MODELS

A series of models were assembled to study a variety of realistic scenarios, these included removal of the downstream toe, vertical and horizontal sinkhole development, and elasticity closed solution checks. A mesh was also designed to indicate the confidence with which displacement magnitudes could be assessed and confirmed that pressuremeter soil parameters are appropriate. Observed field surface displacements are of the order of 2 feet. Cumulative addition of the surface depression settlements from this model, for a three stage development of a 10-foot wide sinkhole, reached a total of approximately 1 foot. This settlement results from the incremental depression when the dam weight is added as a post construction surcharge of a 30-foot width. It may be stated then that the general order of movements may be reasonable and the pressuremeter estimate of this phenomenon is acceptable as an approximation. The most significant models, using the mesh shown in figure 1, are then summarized below.

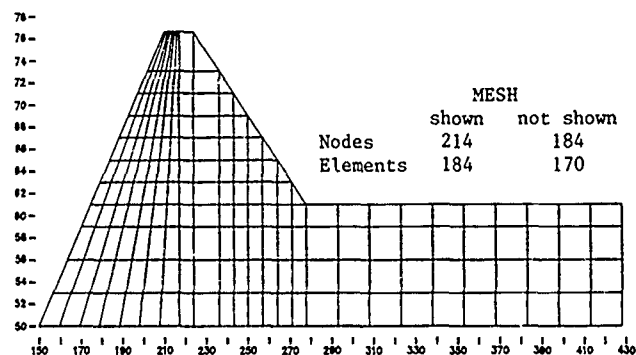


Figure 1. Basic Mesh (FEM)

#### Dam Behavior With Fixed Foundation

This model was used to perform elasticity checks to the solutions provided by Poulos and Davis (1974) and to give the reference settlements of the dam with a rigid foundation only. This provided a series of nodal displacements and stress states to be used as a datum in checking the effects studied in the other models.

Using a comparable closed form model and the same elastic parameters used in the FEM model, maximum center line deflections were calculated at 13 feet and 19 feet. From the base level, these settlements were 0.01375 and 0.0101 feet, respectively. The side slopes for Sand H Debris Basin Dam were comparable with the closed form model (16.6 degrees upstream and 24.4 degrees downstream).

The elastic models, construction in four layers and eleven construction layers, respectively, showed FEM settlement predictions 8 percent low and 17 percent high,

and 7.6 percent high and 17 percent high, when compared to the closed form model at 13 feet and 19 feet, respectively. These comparisons are perfectly satisfactory when the difference in dam profile is recognized.

Non-linear behavior models with two materials using four (4) construction layers and eleven (11) construction layers, respectively, were compared. Very significant differences in displacements, strains, stresses, and element modulus values resulted, particularly in the top eight feet. The model with eleven (11) construction layers, represents the datum model for evaluation of all other effects in later models. However, the general pattern of displacements and stresses is similar except on the side slopes. Local shear failure is predicted in six elements due, in all cases, to low confining pressures.

#### Non-Linear Behavior With Sinkhole in Foundation

This model introduced a foundation 50-feet deep (below the downstream toe), and was primarily used to study sinkhole growth in vertical and horizontal directions. This type of study reports what settlements and stresses would be, had the dam been constructed on collapsing soils. It should be recalled that the actual chronology of events is somewhat different. The actual observed behavior of the dam, over time, is probably the result of two time dependent phenomena (which may be coupled)--the spread of moisture initiating collapse and the rate of collapse. However, it is expected that an indication of tension and shear failure locations would be found.

The model incorporated soft zones (sinkhole), growing both horizontally and vertically, to simulate the progressive collapsing foundation in what is considered the most realistic locations. A simple sand "box" 50-feet square was developed to correlate material three (3) properties with the observed approximate 2-foot settlement in the downstream sinkhole. Both elastic and non-linear dam on non-linear dry foundation control analyses were made for comparison purposes. The elastic behavior highlights the tension zone development. For a linear elastic material tension stresses are permitted and no ultimate strength is assigned, hence, the development of tension zones represent potential crack zones in the embankment. It should be recalled that construction practice on the embankment has produced a stiff, brittle, soil type which may well exhibit strong elastic characteristics up to yield. Elastic embankment stiffness for this model is an order of magnitude higher than unaltered foundation soil type.

The output showed a dramatic increase in horizontal displacements throughout the model sinkhole zone, this clearly is the result of the "during construction" modeling. The dam foundation undergoes local shear failure in the soft zones and the material is, in effect, being "squeezed" out from between the dam above and the stiff foundation below.

A node at the downstream toe shows ten times more horizontal movement compared to vertical movement while a node at the upstream toe shows five times the vertical movement compared to horizontal movement. In fact the attempt to reproduce a vertical soft zone (sinkhole) resulted in the soft zone being "squeezed" out. Nevertheless, stresses, critical zones, and movements away from the soft zone area may show valid effects from the development of a soft zone (sinkhole).



The 50-foot wide sinkhole, which undercuts the toe by 20 feet, appears to contain all observed features and shows significant onset of tension failure. If settlements at the crests are approximately the same magnitude as the dam/foundation interface, this model suggests movements of the order 9 to 12 inches. In addition, the output shows that when the soft zone horizontal propagation approaches the center line of the dam the number of elements with low confining pressure and shear failure doubles. In effect, this shows the extent of the soft zone at its most critical position.

It may be concluded that vertical sinkhole development phenomena is less likely to cause the dam cracks to continue. Horizontal sinkhole development is expected to propagate continuing cracks at the same section. The almost vertical cracking exhibited on the D/S face produces isolated blocks due to the lack of tensile strength for the in place embankment.

#### Downstream Toe Removal

The only post construction boundary condition change permitted by the FEADAM program are applied nodal forces or element boundary pressures. The recent removal of material from the toe of the downstream slope (during regrading for construction of the football practice field) is felt by the dam as a removal of pressure. This scenario represents one that can be modeled by FEADAM. However, changes in the mesh to show the new ground surface profile after toe removal cannot take place during a program execution.

To accommodate this model the mesh was locally revised so that the boundary to elements in the area of the embankment that was removed represents the final ground profile, shown in figure 2. Overburden removal of the toe is then accomplished by applying a release of stress from the nodes representing the removed area. The magnitude and direction of these stresses must be those to give zero stress along the above stated boundary. Stresses too high result in tensile loading (or suction) applied to the toe.

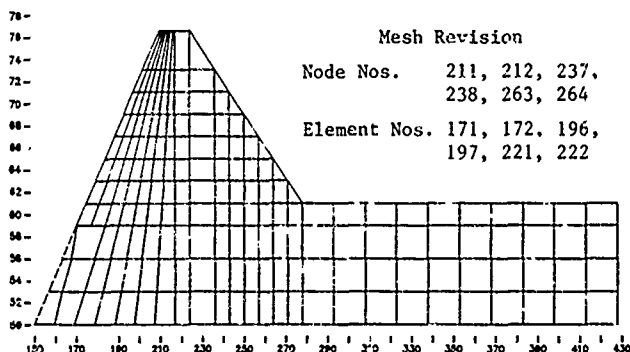


Figure 2. Revised Mesh (Toe Removal)

Therefore, the stress relief applied must be equal to the internal stresses in the dam along that boundary at the time of toe removal. These can be approximated by the FEADAM program by assuming the end of construction stresses still exist. Since the end of construction stresses represent part of the output, some calculations (based on given principal stresses), and manipulations

take place between executions to refine the input. The effects of toe removal are shown from the incremental results of the post-construction stress application.

The runs made were (1) revised mesh to establish the stress state to be removed by post-construction loads, (2) using stress relief calculated from post-construction load removal trial, and (3) final run with further refinement of input and vertical overburden relief along the boundary.

The output clearly has shown that horizontal stresses around the downstream toe are well above a simple  $K_0$  condition. The stress relief applied in the final run is believed to be within 10 percent of that from construction (it should be recognized that element stresses appear on the output at element centers, not at the boundaries). Dramatic distress is caused to the dam by regrading the toe back to a 1:1 slope. A significant increase in the extent of the zones in shear failure, tension failure, and those with low confining pressure occurred. At the present time, this toe removal represents the single most critical activity which is most likely to initiate and propagate further cracking, based on the FEADAM modeling.

#### Existing Conditions

The best estimate of all known conditions to model the construction with the exception of the cutoff was used. The 1:1 D/S toe slope was accommodated by using extremely soft properties (i.e., close to air) in the wedge to ensure no load would be taken by this zone (not by applying the post-construction forces). The output differences between this model and the previous are dramatic. If the extra zoning is ignored (not considered significant), the output shows the dam displays far less distress features when the construction to the 1986 profile is modeled. Removal of this downstream wedge, and hence the loss of horizontal support after construction was complete, IS HIGHLY SIGNIFICANT. A comparison of stresses between this and the previous model is shown in figure 3.

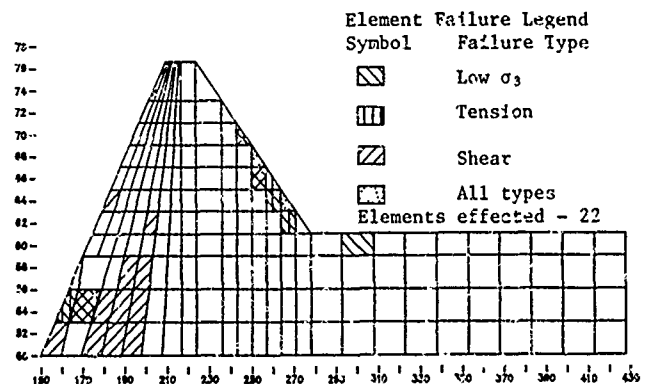


Figure 3. Increase in Distress Zones When Stress Relief is Considered.

Both models clearly demonstrate that CONSTRUCTION OF THE DAM IN ITS PRESENT CONDITION AND PROFILE WOULD QUICKLY RESULT IN SIMILAR DISTRESS FEATURES BEING CREATED. This would occur despite the more conservative approach of using 'air' properties in the D/S toe.

## CONCLUSIONS

Based on the extensive FEM modeling undertaken on the Sand H Debris Basin Dam study, the following conclusions may be drawn:

1. The use of in situ tools has enormous potential for measuring high quality, small and large strain data for use in FEM analysis.
2. Recording pre- and post-collapse properties using a variety of pressuremeter techniques gives settlement prediction of the correct order of magnitude.
3. It is of vital importance that the limitations of FEM codes are understood and not violated. In applying the method, a full geologic investigation, description, and interpretation must be available and applied to model realistic, geologic, and chronologic scenarios (where possible).
4. The existing Duncan and Chang Hyperbolic soil models has only a limited ability to represent the actual collapse phenomenon. It is anticipated that routine use of such codes by unskilled or unexperienced users will lead to erroneous results. Research studies should be initiated to develop an appropriate soil model (hence, a new code), to analytically model the moisture sensitive collapse phenomenon as it relates to dam distress after construction.

## REFERENCES

- Baguelin, F., J. F. Jezequel, and D. H. Shields (1978), The Pressuremeter and Foundation Engineering, Trans Tech Publications, Rockport, Mass.
- Duncan, M., K. S. Wong, and Y. Ozawa (1982a), "FEADAM: A Computer Program for Finite Element Analysis of Dams," Report No. UCB/GT/80-02, University of California, Berkeley, December.
- Duncan, M., P. Byre, K. S. Wong, and P. Mabry (1980), "Strength, Stress-Strain, and Bulk Modulus Parameters for Finite Element Analyses of Stresses and Movements in Soil Masses," Report No. UCD/GT/80-01, University of California, Berkeley, August.
- Duncan, M., and C. Y. Chang (1970), "Non-Linear Analysis of Stress and Strain in Soils," Journal of Soil Mechanics and Foundation Div., ASCE, Vol. 96, September.
- Kulhawy, F. H., J. M. Duncan, and H. B. Seed (1969), "Finite Element Analysis of Stresses and Movements in Embankments During Construction," Geotechnical Engineering Research Report No. TE-69-4, Department of Civil Engineering, University of California, Berkeley, California, November.
- Ozawa, Y. and J. M. Duncan (1973), "ISBILD: A Computer Program for Analysis of Static Stresses and Movements in Embankments," Report No. TE-73-4, University of California, Berkeley, California, December.
- Poulos, H. G., and E. H. Davies (1974), Elastic Solutions in Soil and Rock Mechanics, John Wiley and Sons, New York.
- Robertson, P. K. and R. G. Campanella (1984), Guidelines for the Use and Interpretation of the Electric Cone Penetration Test, Hogentogler and Company, Inc., 2nd Ed., September.
- Wilson, E. L. (1971), "Solid SAP, A Static Analysis Program for Three Dimensional Solid Structures," SESM Report 71-19, Structural Engineering Laboratory, University of California, Berkeley, September.
- Wilson, E. L., R. L. Taylor, W. P. Doherty, and J. Ghaboussai (1971), "Incompatible Displacement Modes," Proceedings of Office of Naval Research Symposium, University of Illinois, Urbana, Illinois, pp. 43-57.

## Failure of Railway Embankment

J. Christodoulis

Geotechnical Engineer, Soil Research Lab, Athens, Greece

H. Giannaros

Geotechnical Engineer, Soil Research Lab, Athens, Greece

**SYNOPSIS:** This article deals with the failure of a railway embankment in North Peloponese. The geotechnical investigation that followed aimed to specify the causes of the failure. The results of the above investigation are presented, an evaluation of the causes of failure is discussed and the remedial measures which have been taken are thoroughly described.

### INTRODUCTION

In the north part of Peloponese (Greece), 20 Km after the city of Corinthos, a road rail junction was constructed. The junction was consisted of the railway embankment and a concrete fly - over. The reasons for this structure were first to eliminate further collisions and second to reduce the distance by 3Km. The rail embankment project begun in 1983 and by October 1985 was completed, having max height 18m and length 350 m. The borrow pit area, situated one mile north to the rail line, consisted of two horizontal layers, one with well graded clay-gravel and one with red clay. Consequently it was necessary to mix the material from the two layers into one, in place. The excavation was carried out by bulldozer and then a shovel tyred tractor loaded the material directly in trucks, passing under a metal screen to separate the boulders. The fill was hauled to the embankment's site, spread by a bulldozer D7 in layers 50 cm thick along the axis and subsequently compacted with a vibratory half tyred roller, to the 90-95 percent Mod AASHTO density.

Next summer (1986) on the top of the embankment, longitudinal cracks appeared, along the axis, having length 2-3m and width varying from mm to 3cm (Fig 1). After this occurrence and before the lining of the rail steel bars, Public Works Research Laboratory-Soil Division, was asked by the inspector supervising the works, to proceed a geotechnical investigation, in order to identify the causes of the failure and propose measures to restore the embankment.

### THE GEOLOGY OF THE NEAR BY AREA

The surrounding the project area is mainly consisted of brackish to lacustrine deposits, containing clay and clayey gravel, yellowish to white Mails, intercalations and lenses of loose or dense conglomerates, coarse sandstone and marly limestones, having Pliocenic age.

The embankment was lodged on a conglomerate lens as it was identified after visual inspection and two shafts made as deep as possible, by a mechanical digger. No borehole logging investigation was done.

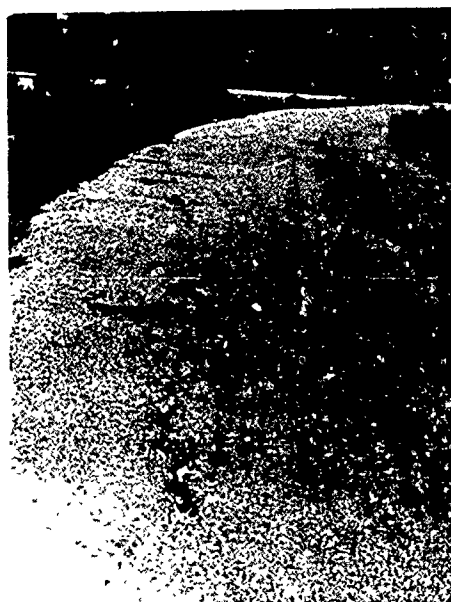


Fig. 1. Longitudinal cracks on the embankment.

### LABORATORY INVESTIGATION

A laboratory testing program was initiated to identify the problem and design remedial measures. Soil samples were obtained from the embankment and tested for :

- classification
- linear shrinkage
- swell potential
- mineralogy by x-ray diffraction
- shear strength tests

#### Classification Test

Particle size, liquid limit, plastic limit, plasticity index, were determined in accordance with ASTM test procedure. The coarse fraction passing US 3/8 sieve ranges between 32-56 percent. The

fine material passing US 200 sieve varies between 21-92 percent. The liquid limit ranges between 32-43 percent. The plasticity index varies between 18-27 percent. The colloidal content (minus 2 micron) varies between 16-34 percent. So the soil samples were identified as GC, SC, CL material, by the Unified Soil Classification System (AUSCS).

#### Linear Shrinkage

Eight bar linear shrinkage tests were carried out according to BS.1377. For this semi spherical soil bars were prepared in moulds, out of the liquid limit test. The obtained values were :

10.3 14.2 11.4 12.4  
10.7 12.3 8.5 14.3

According to Altmeyer (1955) and Chen (1975) all the above values (> 8) are in the critical stage of potential volume change.

#### Swell Potential

Load expansion swell tests were performed on remoulded soil samples, taken out of Proctor tests. The moisture contents were the optimum and above optimum. Half inch thick samples were placed between air dry porous stones of a 2.5 inch diameter consolidometer. The samples were subjected to loaded and Expanded test.

Loaded tests : Initial dial reading was recorded after applying a small load of 0.0703 Kg / cm<sup>2</sup> (1 psi). The specimen was saturated under zero swelling condition by applying small increments of load, until the full swelling pressure was developed.

Expanded test : Initial dial reading was recorded after applying a load of 0.0703 Kg/cm<sup>2</sup>. The specimen was saturated and expanded, until the expansion was completed under full swell conditions. The results of swell potential are illustrated on table I.

TABLE I. Range of Engineering Parameters

| W.C.<br>% | D.Density<br>KN/m <sup>3</sup> | Swell Press.<br>Kg/cm <sup>2</sup> | Swell<br>% |
|-----------|--------------------------------|------------------------------------|------------|
| 11.5      | 19.0                           | 2.25                               | -          |
| 14.3      | 18.6                           | -                                  | 7.0        |
| 14.0      | 18.7                           | -                                  | 7.5        |
| 15.8      | 17.9                           | 2.38                               | -          |
| 16.0      | 17.9                           | 1.80                               | -          |
| 16.1      | 18.0                           | -                                  | 3.5        |

#### X - Ray Diffraction test

The mineralogical composition of the fine particles was determined by x-ray diffraction analysis, as described by Brown (1980). The sample was allowed to air dry, powdered, saturated with glycerin, heated to 550°C to decompose carbonates and tested by Cuka radiation. The following minerals were identified by their characteristic x-ray peaks :

Quartz 30 %  
Calcite 30 %  
Montmorillonite 15 %  
Illite 15 %  
Chlorite 10 %

#### Shear Strength Tests

The material of the embankment contained a large proportion of coarse grained fraction (gravel and cobbles), which made the use of conventional tri-axial and direct shear box testing apparatuses extremely difficult or even impossible. In order to overcome this problem and model the actual field conditions, as closely as possible, it was decided that the large shear box apparatus, (300mm square by 160 mm thick), mainly used for testing aggregates, offered a great advantage.

Two series of tests were performed on prepared specimens with different water content and densities ( $\gamma_b = 18.5 \text{ KN/m}^3$ ,  $\gamma_b = 20.5 \text{ KN/m}^3$ ). Field densities and water content were previously determined in situ at different points and depths. The results from these shear tests are shown in figure 2.

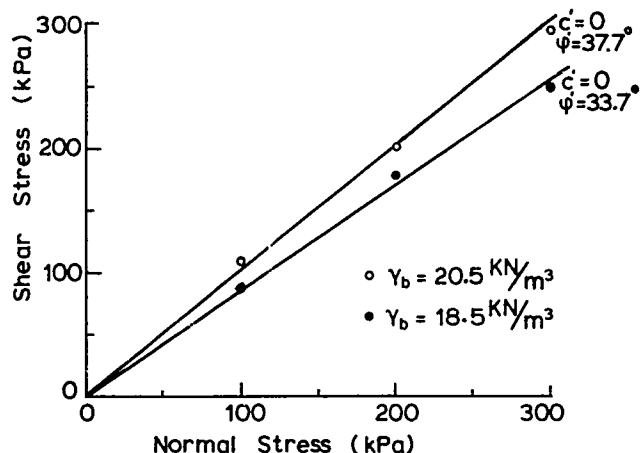


Fig. 2. Shear Strength Envelopes of fill material

#### SLOPE STABILITY ANALYSES

Slope stability analyses were performed on a typical cross section of the embankment, using as shear stress parameters the results of the large shear box tests. In the analyses we considered circular failure surfaces. The slope stability analyses were carried out for sixty-four possible centers of rotation and various slip circles. Different radius for each center were used. Factors of safety in excess of 3.0 were computed, indicating adequate factor of safety against slope stability failure.

#### CAUSES OF FAILURE

The above mentioned investigation showed that there was no problem of slope stability failure because :

- i. No signs of slope slides were observed and
- ii. Slope stability analyses carried out using as shear strength characteristics the results of shear box tests on prepared soil samples, indicated adequate factors of safety (> 3). The densities and water content of the samples were previously determined in situ, by the sand-cone replacement method.

From the linear shrinkage, the x-ray diffraction, the swelling percent and the swelling pressure tests, was revealed that the fine portion of the fill material contained swelling clay minerals. In this area there are remarkable sequences of wet and dry seasons (Fig.3). After the impregnation of the embankment during the wet season, intense shrinkage of the material followed, during the dry period, caused the appearance of cracks (Fig.1). In order to avoid the rainwater percolation, through the cracks and fissures, which would cause the material to swell and slake, the following remedial measures have been taken.

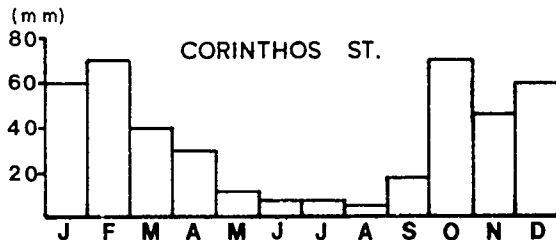


Fig. 3. Average Rainfall of Decade 1970-80

#### REMEDIAL WORKS

The top three meters of fill material were removed by a bulldozer D8 and carried away by trucks loaded by a tyred shovel tractor. For the next layer, the first 25cm were removed and kept in place. The other 25cm were scarified by a grader ripper and mixed with five percent lime (Fig.4).



Fig. 4. Soil-Lime Mixing by Grader

To obtain uniform mixture a disc harrow pulled by a tractor was used in eight passes. After the first pass, it was noticed that an amount of lime was taken away by the wind. So it was decided to stop the mixing and wet the layer up to optimum. Dry unit weight of the material plus lime was  $19 \text{ KN/m}^3$ , optimum moisture content 13 percent. For this, six water tanks per layer were used and then the mixing by the disc harrow ought to

be continued. Afterwards each layer was turned over by a grader Cat 14. For this, each layer was separated longitudinally in two strips, starting from the middle towards the edges. In order to succeed good mixing, thirty five passes of grader were necessary per layer. During the mixing several plasticity index tests were carried out in our project laboratory, until the material had achieved a non-plastic index.

Each layer was compacted by a roller Galion(14T) and one vibrating roller Hamm-Asdag (35T). In order to achieve hundred percent Mod AASHTO density, fifteen passes per layer were necessary. The ASTM sand-cone method was used to test the compaction of each layer. The rest of the fill, up to the top, was substituted with selected crushed gravel, having dry unit weight  $22-23 \text{ KN/m}^3$ , optimum moisture content 6-7 percent, and fine material passing US N200 sieve 5-7 percent. The material was hauled by trucks, spread by a grader to layers 30cm thick, wetted to optimum, scarified for better mixture, with water and compacted by six passes of the vibrating roller, to hundred percent of Mod AASHTO density (Fig.5).

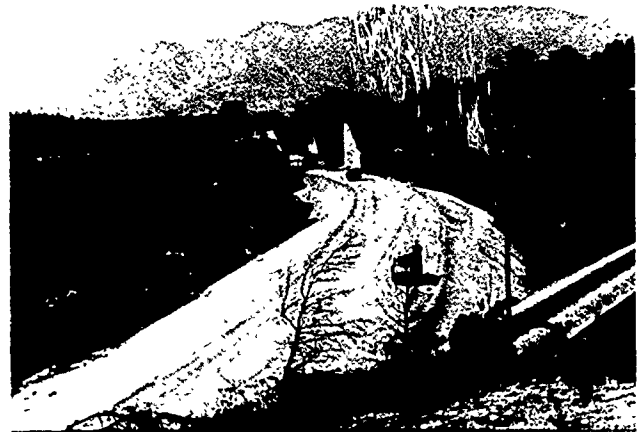


Fig. 5. Final Leveling of Embankment with Selected Crushed Material

After the final level was reached, the full length of the embankment was protected from water percolation and moisture changes. For this, the surface was covered by a membrane of hot petrol emulsion ( $3.5 \text{ lit per m}^2$ ) and then an asphalt membrane was applied by a man-carried springler ( $7 \text{ Kg per m}^2$ ). Finally because the whole structure was too dark in colour, a thin layer of crushed stone ( $0.0-5.0 \text{ mm}$ ) was spread and stuck on top of the asphalt membrane. The above remedial measures are outlined in figure 6.

The works were completed by December 1986. Until August 1987 no complementary works have been carried out, that is placing ballast and rail-steel bars, in order to attend the behaviour of the embankment. No cracks or any other signs of failure have been noticed since then.

#### CONCLUSIONS

The absence of investigation for expansive soils during the design of embankments might have unfavorable consequences concerning the behaviour of the project.

The existence of expansive soils in relation to the peculiar climatological conditions in Greece (certain dry months are followed by periods of heavy rain and vice versa) Have as result to activate the destructive action of the clay minerals.

A proper geotechnical investigation should contain all the relevant laboratory tests in order to identify the existence of swelling soils.

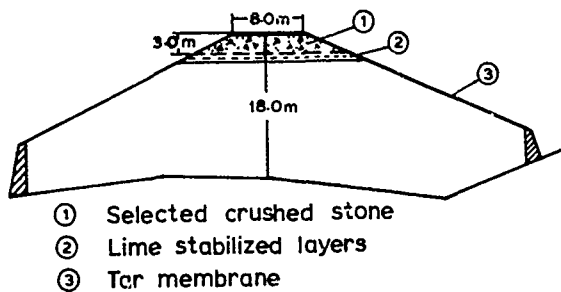


Fig. 6. Cross Section of Embankment after Remedial Works.

#### REFERENCES

- AASHTO, Washington D.C. (1974), Standard Specification for Transportation Material and Methods of Sampling and Testing, Part 2.
- Altmeyer, T.W. (1957), Discussion on "Engineering Properties of Expansive Clays" by Holtz & Gibbs, ASCE Transactions, Vol. 121.
- Brindley, G.W. & G. Brown (1980), Crystal Structure of Clay Minerals and their X-Ray Identification, London, 411-438.
- Chen, F.H. (1975), Foundation on Expansive Soils, Elsevier, Amsterdam.
- Holtz, W.G. & H.J. Gibbs (1957), "Engineering Properties of Expansive Clays", Proc. ASCE Transactions, Vol. 121, 641-677.
- Logani, K.L. (1980), "Construction on Expansive Rock", 4th International Conference on Expansive Soils, Vol. 1, ASCE, Snethen, NY.
- Weston, D.J. (1980), "Expansive Roadbed Treatment for Southern Africa", 4th International Conference on Expansive Soils, Vol. 1, ASCE, Snethen, NY.

## Construction Problems with an Earth and Rockfill Dam

Hasan Hejazi

Associate Professor of Civil Engineering, Tennessee Technological  
University, Cookeville, Tennessee

**SYNOPSIS:** Earth and rockfill dams became popular in the 1960's primarily because of increased heights of dams, poor foundation conditions that rule out concrete dams, and vast improvements in excavation and vibratory compaction equipment. Such equipment made excavation and processing of rock and placement of rockfill much more economical than in the past.

Due to the unique composition and the critical zone construction of earth and rockfill dams, they are subject to different types of problems. Some problems may be discovered and corrected during construction. Such problems cause changes in contract documents and delays in work, as in the case of Bay Springs Dam on the Tennessee-Tombigbee Waterway. Other serious problems may cause complete failure of the embankment, as in the case of Teton Dam in Idaho which failed in 1976.

This paper presents a case history of problems that were experienced during the construction of Bay Springs Lock and Dam, Figure 1.

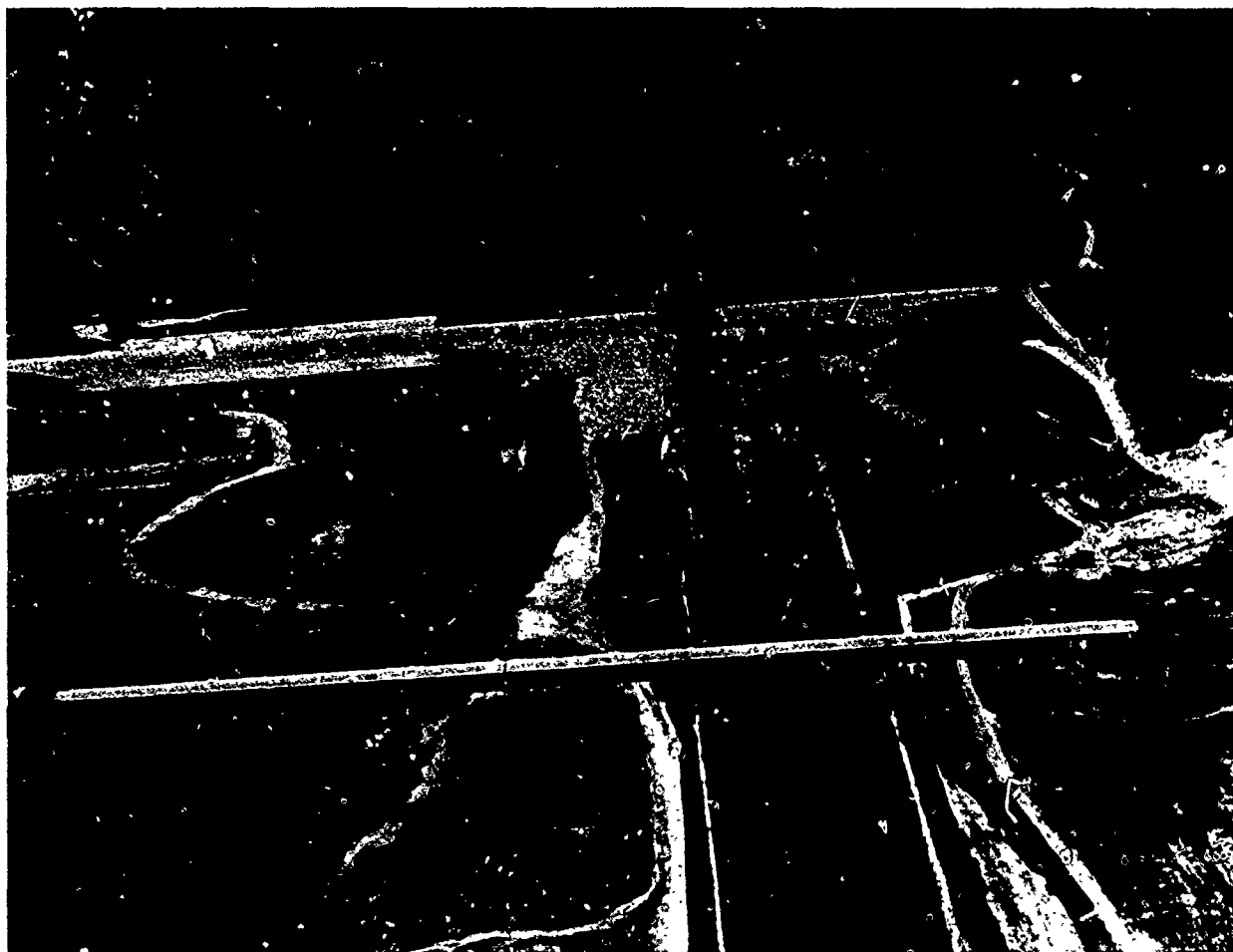


Figure 1. Aerial View of Bay Springs Lock and Dam.

## INTRODUCTION

Earth and rockfill embankments are by necessity constructed of different sizes and types of materials; each must be compacted by equipment compatible with the type of material involved to obtain the optimum density to limit settlement and meet design assumptions.

The embankment consists of zones: the core, the filters, and the shell. The core is the internal zone. It consists of impervious material and provides the water retention capability of the dam. The core is relatively thin and must function as an impermeable barrier to the passage of water. The transition zones or filters are located on both sides of the core. They are designed as graded filters, composed of rock materials changing gradually from fine on the side of core, to coarse on the side of shell. Their function is to retain the core material and to provide internal drainage control. Properly designed and constructed filters will act to heal the core if internal cracking should occur. The shells are the exterior zones adjacent to the filters. They slope outward forming the upstream and downstream slopes of the embankment. The shells retain the interior zones and give the dam bulk and stability.

Because of the critical function of each zone, as outlined above, it is essential that the embankment be designed and constructed properly to prevent failure through erosion and piping. Therefore, special care and attention should be given to the selection, gradation, placement, and compaction of the construction materials.

## DAM LOCATION

Bay Springs Lock and Dam is located on the Tennessee-Tombigbee Waterway which connects the north-flowing Tennessee River, at Pickwick Lake, to the south-flowing Black Warrior-Tombigbee Waterway at Demopolis, Alabama, Figure 2. The Waterway runs south from Pickwick Lake across the Tennessee Valley Divide in a deep cut, south down Mackey's Creek to the Tombigbee River, and down the Tombigbee River to Demopolis. Then, the existing Black Warrior-Tombigbee Waterway runs south 217 miles from Demopolis to Mobile. The distance from Pickwick Lake to Demopolis is 232 miles which makes the total length of the waterway, from the Tennessee River to Mobile 449 miles. It provides a continuous navigation route from the Tennessee, Upper Mississippi, and Ohio River Valleys to Mobile, Alabama, on the Gulf of Mexico. The Waterway provides savings of 829 miles in navigation distance from the Tennessee River to Mobile, as it reduces the distance from 1278 miles via the Mississippi River to 449 miles via the Waterway. The Tennessee-Tombigbee Waterway was designed and constructed by the U.S. Army Corps of Engineers. The channel width varies from 280 to 300 feet. Construction commenced in 1972 and it was completed in 1984, at a cost of about 2 billion dollars.

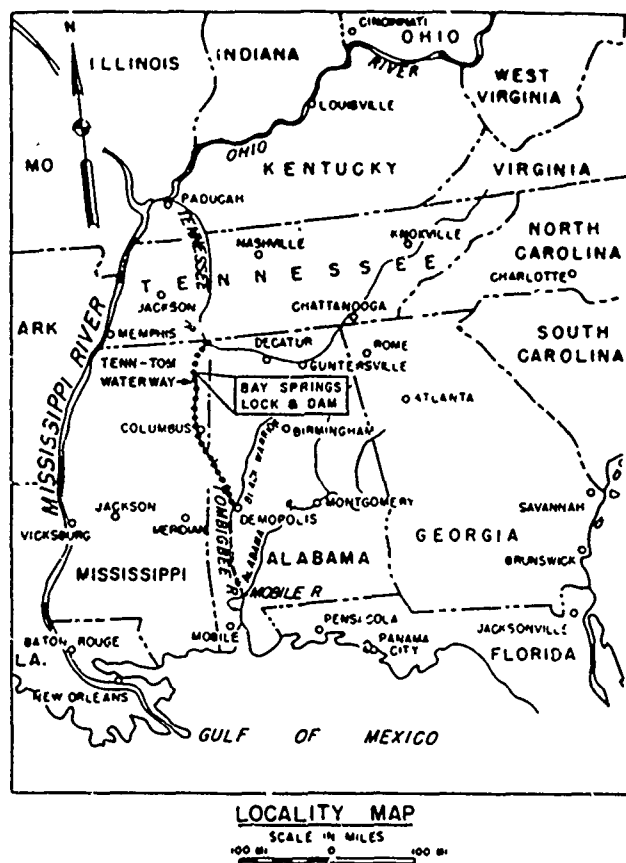


Figure 2. Tennessee-Tombigbee Waterway Locality Map.

The water level difference between the Black Warrior-Tombigbee Waterway at Demopolis and the Tennessee River, just above Pickwick Lock and Dam, is 341 feet. Bay Springs is the tenth and last Lock and Dam on the Waterway above Demopolis. The dam has a 600-foot long by 110-foot wide lock with a normal lift of 84 feet to provide navigation through the Divide Cut. The dam is located, on Mackey's Creek, in the Southwest corner of Tishomingo County, Mississippi. Construction of Bay Springs Dam commenced in 1979 and it was completed in 1983.

## GEOLOGY

General information on the geology of the area was obtained from the U.S. Geological Survey, Tennessee State Geological Survey, Mississippi Geological Survey, Alabama Geological Survey, and Tennessee Valley Authority. Additional data were obtained from exploratory drilling at the dam site conducted by the Mobile and Nashville Districts of the U.S. Army Corps of Engineers.

To supplement the drilling, an electric logging device was used in a number of the early Nashville District borings, prior to 1952, and downhole geophysical equipment was used in 77 borings drilled in the second phase of Nashville District Exploration which started in 1973.



The dam is located in the extreme eastern part of the Mississippi Embayment, a synclinal structure which is part of the Gulf Coastal Plain. This embayment has been divided into a number of physiographic districts. The dam site is located in the Fall Line Hills District which occupies the periphery of the embayment from Alabama to southern Tennessee. In this district, outcrops of Mississippian, Cretaceous, and Quaternary sediments are exposed. Most of the Mississippian rocks are overlain by Cretaceous and Quaternary clays, silts, sands, and gravels. The Mississippian rocks crop out only along the valleys, and like the Cretaceous and Quaternary sediments, have a westwardly regional dip toward the axis of the syncline.

The valley floor at the dam site is approximately 2,000 feet wide at Elevation 385 feet, with Mackey's Creek occupying approximately 35 feet of the flood plain and flowing on bedrock. In general, bedrock is covered by 15 feet of overburden except in the abutment areas of the dam where the average thickness is about 40 feet. Vertical cliffs of sandstone, rising approximately 50 feet above stream level, are common in the area upstream from the dam axis.

#### OVERBURDEN

Materials overlying the Mississippian rocks at the dam site consist of clays, silts, sands, and gravel of Cretaceous age as well as alluvial sands and gravels of Quaternary age. Immediately and unconformably overlying the Mississippian rocks are unconsolidated sediments of the Gordo formation (Tuscaloosa Group). This formation is thin in the site area, averaging 20 feet in thickness. These varicolored sands, gravels, and clays are overlain by interbedded and interlaminated

micaceous clays and glauconitic sands of the McShan formation that averages 40 feet in thickness. Overlying the McShan formation are approximately 30 feet of slightly glauconitic and micaceous sands and dark gray clays of the Eutaw formation. Also present along the valley slopes of Mackey's Creek are thin and intermittent terrace deposits which are not easily distinguished from the underlying sediments. Materials overlying the valley section along the axis of the dam are alluvial deposits of mostly sands, clays and some gravel. These deposits were mostly derived from the Eutaw formation, and partly from the McShan, Gordo, and Mississippian formations. In addition, large detached blocks of Mississippian sandstone have separated along joint and bedding planes and are common along the base of the bluffs.

#### EMBANKMENT DESCRIPTION

Bay Springs Dam has a zoned earth and rockfill embankment consisting of a central core, transition filters, select rockfill shells, and a cutoff trench, Figures 3 and 4.

The core has a top width of 10 feet with 4V on 1H side slopes. It consists of low plasticity clay compacted in a nine-inch loose lift by tamping or sheepfoot roller. The filters, fine and coarse, are eight feet wide with the fine filter No. 2, adjacent to the core, placed in 12-inch lifts compacted by a vibratory roller and having a gradation ranging from a No. 4 to a No. 100 standard sieve size. The coarse filter No. 1, between the shell and the fine filter is placed in 12-inch lifts compacted by a vibratory roller, and ranges in size from four inch to No. 4. The shells are placed in 24-inch lifts compacted by a vibratory roller and ranging in size from a maximum size of 16 inches to not more than 5% passing the 3-inch screen.

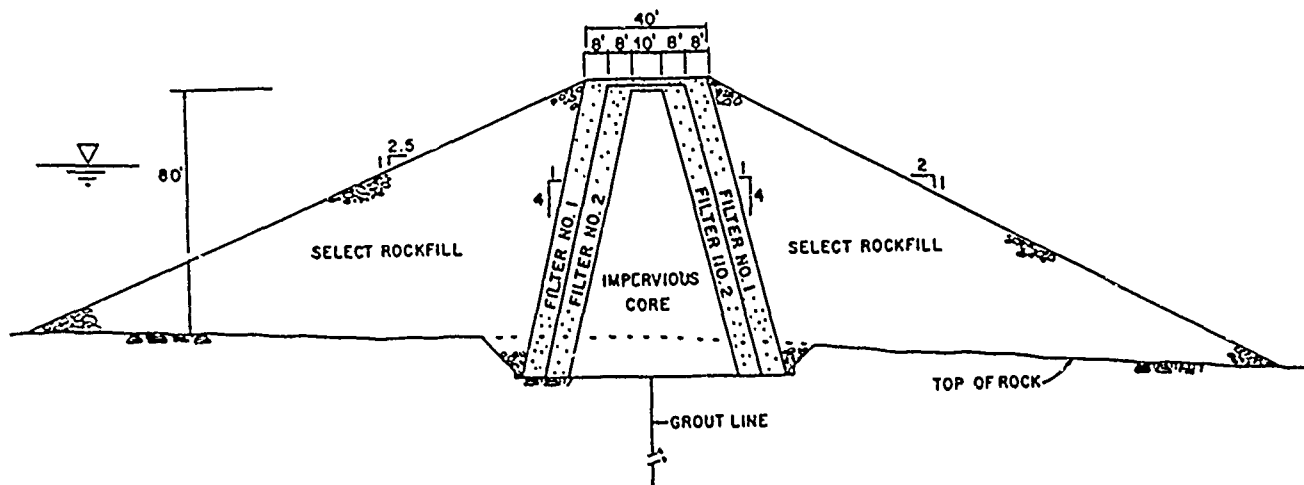


Figure 3. Section on Rock.

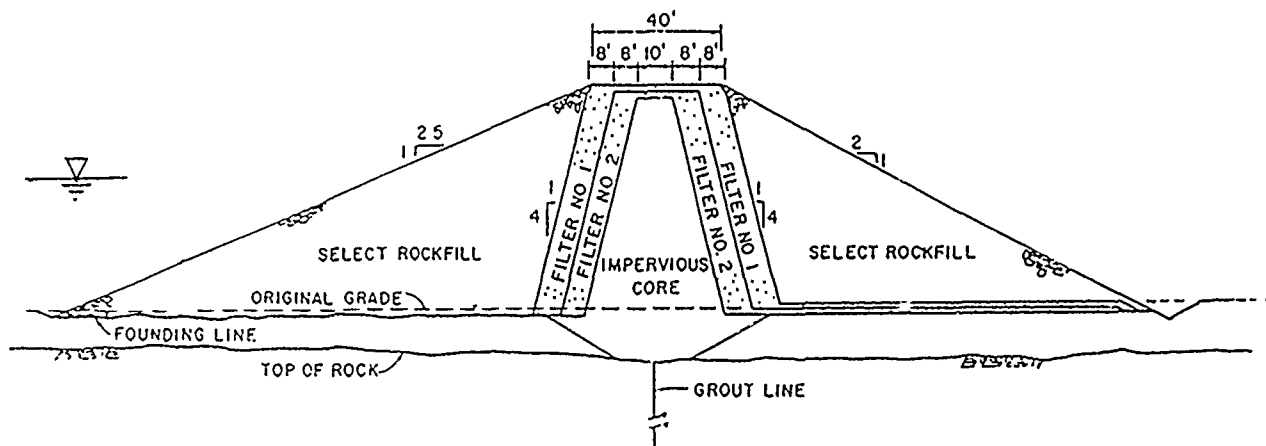


Figure 4. Section on Overburden.

A cutoff trench extends to rock in locations where the dam is founded on overburden. A grout curtain is provided to reduce seepage through the foundation. Measures were taken to dewater the area around the cutoff trench to reduce seepage during grouting and foundation preparation.

The embankment is 2750 feet long with a crest width of 40 feet. Upstream and downstream slopes are 1V on 2.5H and 1V on 2H, respectively. The embankment is approximately 80 feet high throughout most of its length, with a maximum height, located in the Mackey's Creek valley, of approximately 120 feet.

#### CONTRACT REQUIREMENTS

Some of the contract requirements that pertain to the problems discussed in this paper are as follows:

a. Filters No. 1 and 2 are each to be 8 feet wide (measured horizontally) with the following gradations:

| Filter No. 1 |           | Filter No. 2 |           |
|--------------|-----------|--------------|-----------|
| Sieve No.    | % Passing | Sieve No.    | % passing |
| 4"           | 100       | No. 4        | 92-100    |
| 3"           | 85-95     | No. 8        | 75- 95    |
| 1 1/2"       | 60-90     | No. 16       | 35-85     |
| 3/4"         | 35-60     | No. 30       | 10-63     |
| 2/8"         | 7-32      | No. 50       | 5-45      |
| No. 4        | 0- 7      | No. 100      | 0-15      |

b. Select rockfill material is required to be sound sandstone which is reasonably well graded from a maximum dimension of 16 inches to not more than 5 percent passing a 3-inch screen. This gradation requirement is to be met prior to placing select rockfill in the embankment.

c. The rockfill portions (select, random, and filters) of the embankment are required to be constructed of processed sound sandstone, dumped, and pushed into place in specified lifts. Rockfill is to be placed in such a manner as to produce a reasonably well-graded mass, with the smaller stones adjacent to the contacts with the internal zones of the dam. The larger size material is to be dispersed within the mass of the rockfill. The resulting embankment should have no pockets of small stones or clusters of larger stones. The placing shall be supplemented by whatever hand methods required to obtain even surfaces. A tolerance of plus or minus 6 inches from the slope and grade lines shown on the drawings is required at the boundaries of the internal zones of the embankment.

d. The lift thicknesses of the embankment materials before compaction are required to be not more than 12 inches for the filters, and not more than 24 inches for the select and random rockfill materials.

e. Minimum compaction for filters, select-, and random-rockfill materials requires 6 complete passes of a vibratory roller weighing 10-12 tons, operating at a maximum speed of 3 mph having a drum vibration frequency between 1,100-1,500 frequencies per minute.

f. Unless otherwise directed, the embankment is required to be maintained at approximately the same level throughout its construction, regardless of the number of types of materials being placed.

#### THE PROBLEMS

The problems encountered in this project fall under two categories: rock gradation and zone construction.

## ROCK GRADATION

Soils and rock fragments, minus 6 to 3 inches, are usually graded by the sieve size which is the size of a square opening.

The contractor obtained his rocks by blasting from a designated area near the dam, where he set up a grizzly operation for rock processing. The grizzly is a rugged machine or platform with sloping rails and bars that are set at the desired spacing. The specifications for the shell material called for a maximum size of 16 inches. The contractor interpreted maximum size as the size of his grizzly spacing. As a result of the fast grizzly operations, the contractor was stockpiling flat and long oversize rocks that did not meet gradation specifications. Work was stopped to discuss the specifications and to establish the meaning of the term maximum size. After lengthy discussions and checking the specifications of other organizations, it was established that larger rock fragments have been graded in several ways, including size and weight. The terms maximum size and maximum dimension have been used interchangeably, and they are intended to mean the size of a square opening; a terminology borrowed from soils gradation. However, the terms may be taken literally to mean the maximum dimension in any direction.

After about two months of work delay, a compromise was reached. The contractor was allowed to use any piece of rock that fits into the 2-foot lift thickness, provided that its maximum dimension is not greater than three times any other dimension.

## ZONE CONSTRUCTION

Placement of material in the zones became the most critical factor in the construction of

the embankment. Placement must be done in a manner to minimize segregation. The core and filters should always lead the outer shell rockfill, but not far enough to cause spilling of the leading zones over those lagging.

The contractor rockfill placement proceeded faster than the core and filter placements due to weather conditions. Site visits during early construction indicated that there were larger rock clusters adjacent to the filters. Areas of concern were:

a. The filters did not appear to be the full width, and they appeared to extend into each other.

b. The shell appeared to contain zones of segregation and numerous oversize rocks.

Further discussions led to questions concerning the integrity of the embankment. In order to determine the extent of the problem, work was stopped to conduct the investigations. Test pit excavations were made, at randomly selected locations at the shell and coarse filter contact. Excavations extended from the surface of the in-place embankment fill down to the top of the drainage blanket. Trenches were then extended from some of the pits, through the two filters, into the impervious core. Results of the test pit excavations revealed the following:

a. The filter zones were not constructed to specified lines and grades.

b. The shell rockfill was badly segregated and it contained up to 12% of oversize (+16 inch) rock.

c. The select rockfill was not as dense as would be expected for rockfill placed as specified.

d. The filter zones and the core were intermingled and overlapping as shown in Figures 5 and 6.

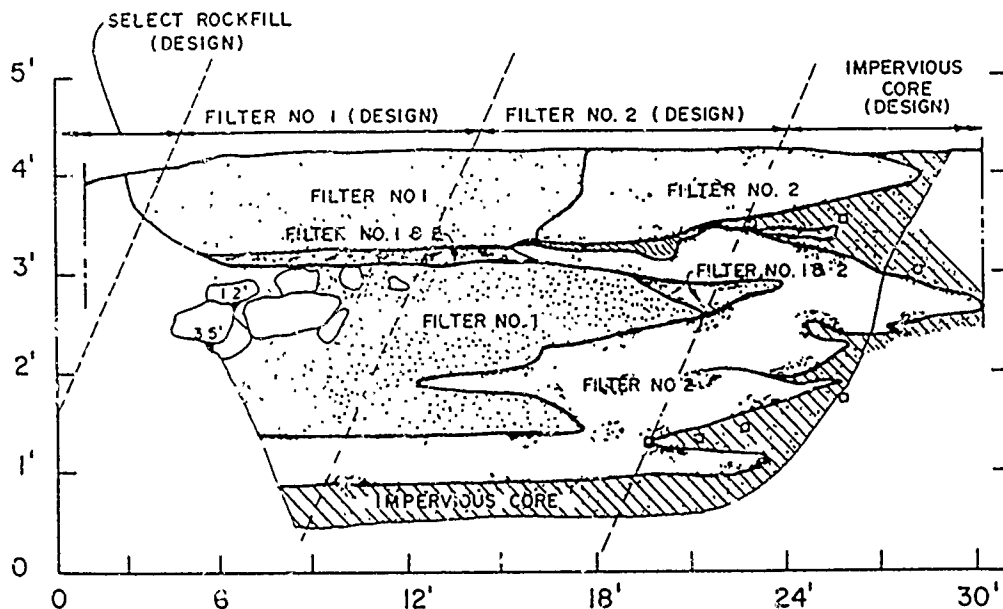


Figure 5. Overlapping Zones on Upstream Side of Embankment.

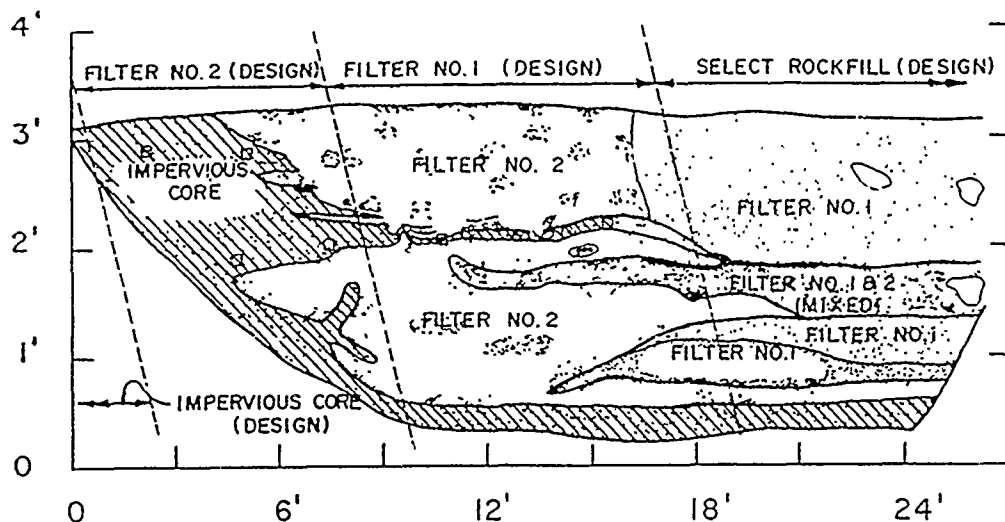


Figure 6. Overlapping Zones on Downstream Side of Embankment.

## CONCLUSIONS

The findings of the investigation rendered portions of the embankment in place unacceptable. The contractor was directed to proceed with the remedial work. He removed the unacceptable portions and replaced them according to specifications under rigid control. For the continued construction, the zones were constructed as near level as possible. Continuous monitoring of the proper location for the zones was maintained.

Periodic inspection reports indicate that the embankment condition and performance have been satisfactory. No problems have been detected since the dam was completed in 1983.

The embankment construction problems could have resulted in the ultimate failure of the structure, if they had not been discovered early and corrected properly. This incident illustrates a very important geotechnical engineering fact. It shows that critical design parameters, including shear strength, compressibility, and permeability come under the control of the Resident Engineer and his inspection team, once construction has begun.

Finally, very important lessons can be learned from this valuable experience:

1. Specifications must be followed.
2. Close attention must be paid to details, because many details that can become critical can easily be overlooked.
3. Inspectors must be qualified, experienced, and they must maintain a watchful presence in the field.
4. Quality assurance inspection must be thorough to insure that all details are being met.

## ACKNOWLEDGEMENTS

This paper is part of a research project sponsored by the Faculty Research Program at Tennessee Technological University. I am

grateful to Dr. Rafael B. Bustamante, Chairman, Department of Civil Engineering and to Dr. Dean V. Adams, Director, Center for the Management, Protection and Utilization of Water Resources, for their support. Thanks to Mr. Frank B. Couch, Chief, Geotechnical Branch, and Mr. James E. Paris, Chief, Soils and Embankment Design Sections, U.S. Army Corps of Engineers, Nashville District, who provided me with some data and with whom I had the pleasure of working on the Tennessee Tombigbee Waterway, during the summers of 1975 through 1983.

## REFERENCES

- Jansen, R.B. (1967), "Evaluation of Dam Safety in California", Journal of Soil Mechanics and Foundation Division, ASCE, Vol. 93.
- Leps, T.M. (1968) "Recent Experience with Earth and Rockfill Dams", Conference on Recent Developments in Design and Construction of Earth and Rockfill Dams, University of California, Berkeley.
- Sherard, J.L. (1963), "Earth and Earth Rock Dams", John Wiley and Sons, Inc., New York, New York.
- Terzaghi, Karl and Peck, R.B. (1967), "Soil Mechanics in Engineering Practice", John Wiley and Sons, Inc., New York, New York.
- U.S. Army Corps of Engineers, Nashville District (1986), "Embankment Criteria and Performance Report, Bay Springs Lock and Dam", Tennessee-Tombigbee Waterway, Nashville, Tennessee.
- U.S. Department of the Interior (1976), "Summary and Conclusions on Failure of Teton Dam", from report by Independent Panel to review cause of Teton Dam Failure, Washington, D.C.

# Peñitas Dam—In Situ Stress-Strain Characteristics of Materials

Jesús Alberro

Instituto de Ingeniería, UNAM, Mexico

Gabriel Macedo

Comision Federal de Electricidad Col., Nochebuena, Mexico

Luis Montañez

Comision Federal de Electricidad Col., Nochebuena, Mexico

Francisco González-Valencia

Comision Federal de Electricidad Col., Nochebuena, Mexico

**SYNOPSIS:** The deformability properties of all the materials of Peñitas Dam (43-m high) are estimated based upon the measurement of total stresses, pore pressures and strains by means of the instrumentation placed inside the embankment. The results of these measurements indicate that all the materials show octahedral stress-octahedral strain cuasilinear relationships as if they were elastic. The values of the deformability moduli  $E$  and the Poisson's ratios  $\nu$  computed from these relationships are compared with the moduli  $E$  obtained by means of confined plate bearing tests made in situ during construction of the dam, and are also used to feed a bidimensional finite element model analysis by which the states of stress and strain within the dam are computed and compared with the real stresses and strains measured.

## INTRODUCTION

Peñitas Dam was built by the Federal Commission of Electricity on the Grijalva River in the southeast of Mexico and is part of the most important hydroelectric system in the country. A detailed description of the project may be found in Montañez and Castilla (1985).

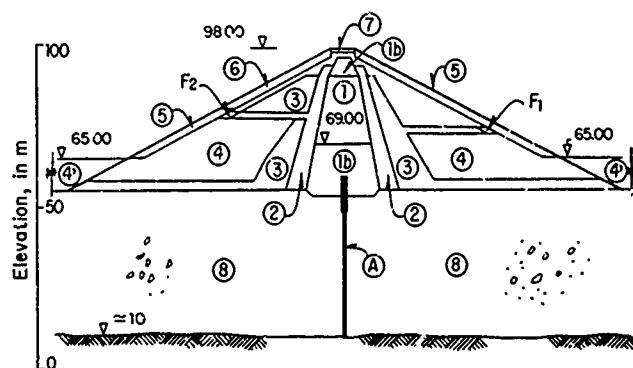
Many attempts have been made to determine stress-strain properties of the compacted materials of dams by means of laboratory and field tests of all kinds with different conditions and methods of compaction, different stress paths, with various rates of loading or deformation, etc. In Mexico, ever since the mid-sixties, we have been working with instrumentation placed in the dams in order to check the criteria used in the design of new dams, control their behaviour and try to determine the stress and strain conditions in the different materials of the dam, Marsal (1982).

This paper presents the results of the instrumental measurements to evaluate the behaviour of Peñitas dam during its construction.

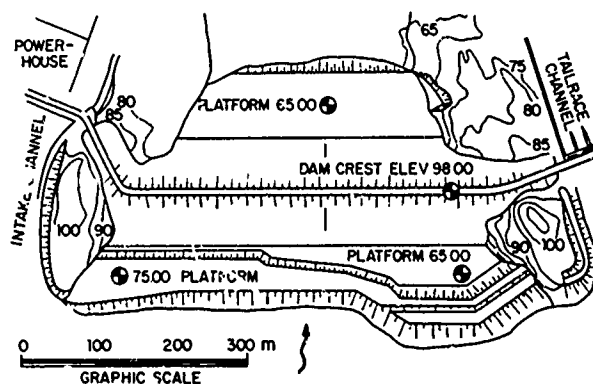
Furthermore, emphasis is put on the estimation of the deformability characteristics of the dam materials based on the total stresses, pore pressures and strains measured. The results allowed the determination of cuasilinear octahedral stress-octahedral strain relations for all the dam materials, from which the modulus,  $E$ , and Poisson's ratio,  $\nu$ , are obtained. These values are compared to those found by means of confined plate-bearing tests (CPBT) made during the construction of the embankment and are used to feed a bidimensional finite element model. Finally, these results are compared to the stresses and strains measured, thus allowing very interesting conclusions.

## DESCRIPTION OF THE DAM AND ITS FOUNDATION

Peñitas Dam is a 43-m high earth and rockfill embankment with a central core of compacted residual clay, fig 1. The volume of materials



a) Maximum cross section of dam



b) Plan view

- |                            |                                 |
|----------------------------|---------------------------------|
| ① Red silty clay           | ⑤ Dumped rockfill               |
| ①b Pinkish brown clay      | ⑥ Riprap                        |
| ② Filter                   | ⑦ Flexible pavement materials   |
| ③ Transition               | ⑧ Alluvial deposit              |
| ④ Compacted rockfill       | ⑨ Plastic-concrete cut-off wall |
| ④' Waste rockfill material |                                 |

Fig. 1 General layout of Peñitas Hydroelectric Project

is  $2.76 \times 10^6 \text{ m}^3$ , its crest is 750 m long and it is founded on alluvial deposits up to 56 m thick. It has a plastic-concrete cut-off wall cutting the alluvium and embedded in the basal rock, fig 1; the first 12 m of the alluvial material were densified by dynamic compaction, Montañez and Castilla (1985). Two platforms made of waste rockfill material link the main dam with the upstream and downstream cofferdams.

#### CHARACTERISTICS OF THE DAM MATERIALS AND OF THE CUT-OFF WALL

##### Dam

The properties of all the materials of the dam are:

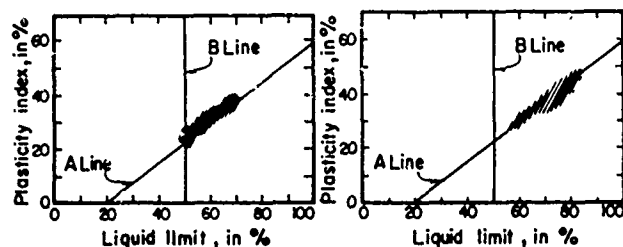
**Impervious core (materials 1b and 1).** In this part of the dam two different kinds of clay were used, fig 1. Between the foundation and elev 69, as well as between elevs 90.5 and 95.5 and in two 5 m wide strips in contact with the banks all way up the dam, a brown plastic clay was placed, whose properties are shown in table 1 and in figs 2 and 3a (material 1b). Most of the core is made of residual silty red clay (MH and CH), whose characteristics are also shown in table 1 and in figs 2 and 3b (material 1). Both clays were compacted with water content 1-3% above the optimum.

**Filters (material 2).** The mean index properties of this material are shown on table 2. Up to elev 85, a sand and gravel natural mixture dredged from the riverbed was used, fig 4a; between elevs 85 and 94 a uniform sand obtained by crushing alluvial material was placed, fig 4b.

**Transitions (material 3).** The sandy gravel used in the transitions was also obtained by dredging the riverbed; its gradation characteristics and index properties are shown in table 2 and in fig 4c.

**Rockfill (material 4)** or rather sandy shells are the product of the compaction of soft sandstones coming from the open pit excavations for the powerhouse (left bank) and for the spillway (right bank). Their physical characteristics can be found in table 2 and in fig 4d.

**Dumped rockfill (material 5) and Riprap (material 6).** Both also come from the rock excavations in both banks and were placed by pushing the bigger particles of material 4 to the outer slopes.



a) Plastic brown clay      b) Red silty clay

Fig. 2 Plasticity of the core materials

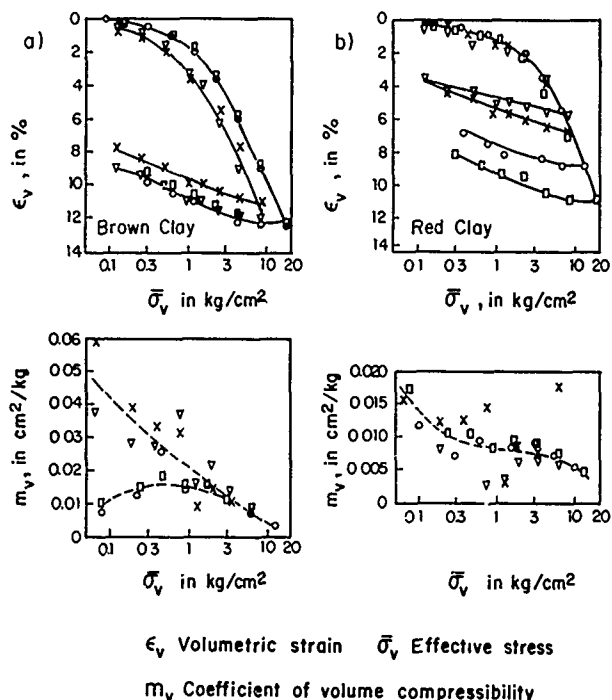


Fig. 3 Compressibility of the core materials

TABLE 1. PROPERTIES OF THE CORE MATERIALS

|            | Brown plastic clay |           |          | Silty red clay |           |          |
|------------|--------------------|-----------|----------|----------------|-----------|----------|
|            | N                  | $\bar{x}$ | $\sigma$ | N              | $\bar{x}$ | $\sigma$ |
| $\gamma_d$ | 550                | 1535      | 51       | 725            | 1388      | 149      |
| $\omega_t$ | 550                | 27.1      | 2.7      | 725            | 33.1      | 4.5      |
| $\gamma_p$ | 200                | 1554      | 187      | 547            | 1427      | 86       |
| $E_c$      | 270                | 98.2      | 2.9      | 725            | 97.5      | 8.1      |
| $q_u$      | 221                | 1.88      | 0.46     | 686            | 2.74      | 0.88     |
| $M_i$      | 221                | 33.7      | 29.1     | 686            | 129.1     | 103.2    |
| $\omega_L$ | 472                | 56.5      | 5.6      | 547            | 73.4      | 15.5     |
| $\omega_p$ | 472                | 27.4      | 2.1      | 547            | 34.7      | 4.2      |
| $s_s$      | 481                | 2.66      | 0.23     | 553            | 2.67      | 0.24     |
| $e$        | 481                | 0.75      | 0.08     | 725            | 0.93      | 0.13     |
| $S_r$      | 550                | 96.1      | 8.00     | 725            | 95.6      | 6.1      |
| $S_r$      | 477                | 14.3      | 5.3      | 549            | 20.2      | 5.5      |
| F          | 477                | 85.7      | 6.8      | 549            | 79.8      | 5.5      |

##### NOTATION

- $\gamma_d$  Field dry unit weight, in  $\text{kg/m}^3$
- $\omega_t$  Field water content, in %
- $\gamma_p$  Dry unit weight in Proctor test corresponding with  $\omega_t$ , in  $\text{kg/m}^3$
- $E_c$  Compaction efficiency ( $\gamma_d/\gamma_p$ ), in %
- $q_u$  Unconfined compression, in  $\text{kg/cm}^2$
- $M_i$  Initial deformation modulus in  $q_u$  test, in  $\text{kg/cm}^2$
- $\omega_L$  Liquid limit, in %
- $\omega_p$  Plastic limit, in %
- $s_s$  Specific gravity
- $e$  Void ratio
- $S_r$  Saturation ratio, in %
- $S_r$  Sand content, in %
- F Fines content (passing #200 sieve), in %
- N Number of determinations
- $\bar{x}$  Mean value
- $\sigma$  Standard deviation

TABLE 2. PROPERTIES OF THE GRANULAR MATERIALS

|                | Filters (2) |                      | Transitions (3) |                      | Rockfill (4) |                      |
|----------------|-------------|----------------------|-----------------|----------------------|--------------|----------------------|
|                | N           | $\bar{x}$            | N               | $\bar{x}$            | N            | $\bar{x}$            |
| Y <sub>d</sub> | 161         | 1863                 | 92              | 2009                 | 41           | 1826                 |
| w <sub>t</sub> | 161         | 6.7                  | 92              | 6.5                  | 41           | 11.1                 |
| s <sub>s</sub> | 161         | 2.72                 | 92              | 2.66                 | 41           | 2.65                 |
| e              | 161         | 0.47                 | 92              | 0.39                 | 41           | 0.45                 |
| >3"            | ---         | ---                  | 92              | 2.2                  | 41           | 36.6                 |
| G              | 161         | 25.7                 | 92              | 52.8                 | 41           | 34.1                 |
| S              | 161         | 71.0                 | 92              | 42.0                 | 41           | 22.7                 |
| F              | 161         | 3.3                  | 92              | 3.0                  | 41           | 6.7                  |
| k              | 4           | $3.2 \times 10^{-3}$ | 2               | $1.5 \times 10^{-3}$ | 3            | $2.1 \times 10^{-4}$ |

## NOTATION

G Gravel content, in %  
 >3" Percent of particles bigger than 3 in  
 k Coefficient of permeability, in cm/s  
 All other symbols defined under Table 1

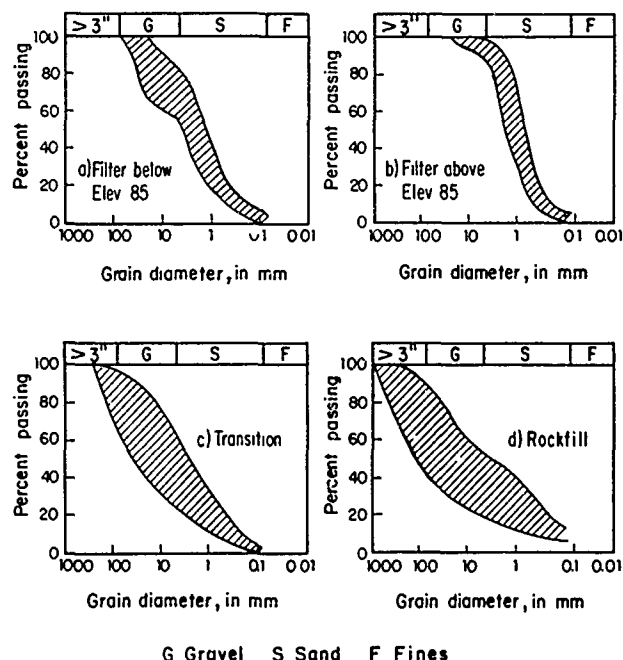


Fig. 4 Gradation of materials 2, 3 and 4

Besides the mentioned materials, the embankment includes: two filters (F1 and F2) between the drainage strips of both shells and the dumped rockfill, fig 1, and a flexible pavement layer on the upper 2.5 m (material 7).

The compaction data of all these materials are condensed in table 3.

Plastic cut-off wall

The cut-off wall built through the alluvial materials was made of plastic concrete so as to give it deformation characteristics similar to those of the alluvium and to make it flexible enough to avoid its penetration in the impervious core of the dam. The concrete mix properties are shown in table 4. During the pouring of the concrete into the trench, samples were

taken in cylindrical moulds. The average results of more than 600 samples tested under unconfined compression at the age of 28 days are also shown in table 4. To verify the quality of the cut-off wall in situ, water absorption tests were also carried out in two boreholes that crossed vertically the whole wall; the coefficient of permeability varies between  $3 \times 10^{-7}$  and  $3 \times 10^{-5}$  cm/s.

TABLE 3. COMPACTION CHARACTERISTICS OF THE DAM MATERIALS

| Material | Layer thickness (cm) | No. of passes | Compaction equipment* | Weight (ton) |
|----------|----------------------|---------------|-----------------------|--------------|
| 1        | 25                   | 6             | 1                     | 7.7          |
| 2        | 30                   | 2             | 2                     | 7.3          |
| 3        | 40                   | 4             | 2                     | 7.3          |
| 4        | 80                   | 4             | 2                     | 7.3          |
| 5        | N.C.                 | -             | 3                     | ---          |
| 6        | N.C.                 | -             | 3                     | ---          |
| F1       | 30                   | 2             | 2                     | 7.3          |
| F2       | 30                   | 2             | 2                     | 7.3          |
| 7        | 40                   | 6             | 2                     | 7.3          |

## NOTATION

\* 1 Sheepsfoot roller  
 2 Vibratory smooth-drum roller  
 3 Tractor  
 N.C. Not compacted

TABLE 4. CUT-OFF WALL CHARACTERISTICS

| Dosage                          |                         |
|---------------------------------|-------------------------|
| Cement                          | 150 kg/m <sup>3</sup>   |
| Gravel ( $\phi_{\max} = 19$ mm) | 375 kg/m <sup>3</sup>   |
| Sand ( $\phi_{\max} = 6$ mm)    | 975 kg/m <sup>3</sup>   |
| Bentonite slurry                | 300 l/m <sup>3</sup>    |
| Properties                      |                         |
| $q_u =$                         | 9.8 kg/cm <sup>2</sup>  |
| $M_i =$                         | 4055 kg/cm <sup>2</sup> |

## NOTATION

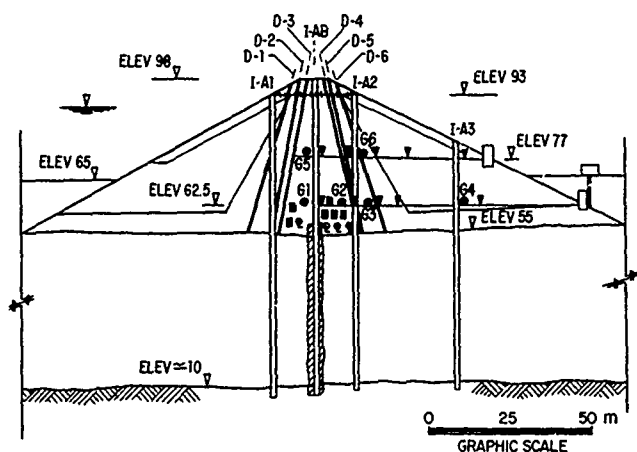
$q_u$  Unconfined compression strength  
 $M_i$  Initial modulus of deformation in  $q_u$

## INSTRUMENTATION

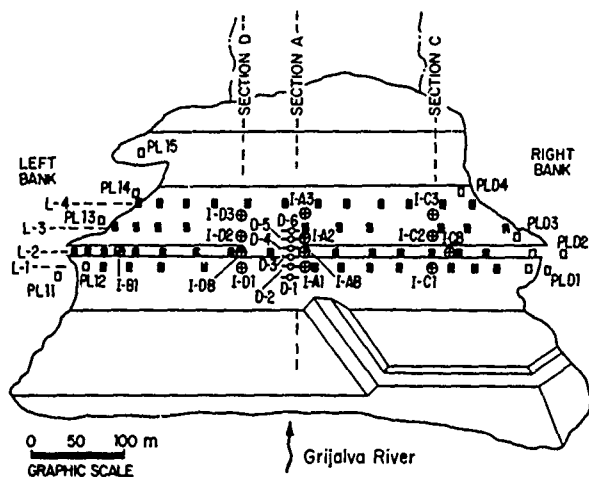
The instrumentation of the dam was designed keeping in mind: 1) the seismic activity of the zone, 2) the geometry of the damsite, 3) the properties of the rock and alluvium foundation, 4) the location of oil fields and important cities downstream of the damsite, and 5) the valuable information which is obtained from the instrumental measurements to improve both the design criteria and the analytical models used in the computation of stresses and strains in earth and rockfill dams.

The dam is instrumented in three transversal sections A, C and D, fig 5. Each section contains four inclinometers, six clusters of instruments to measure stresses and strains, and hydraulic leveling devices at two elevations;

section A is also equipped with six cross-arms. Besides, a few pressure cells and pneumatic piezometers were also installed at certain points of the dam, and several lines of extensometers are found near the crest. On the slopes of the dam several surface reference points at rows were installed for the topographic control of the crest and slopes movements, fig 5.



a) Cross Section A



b) Plan view

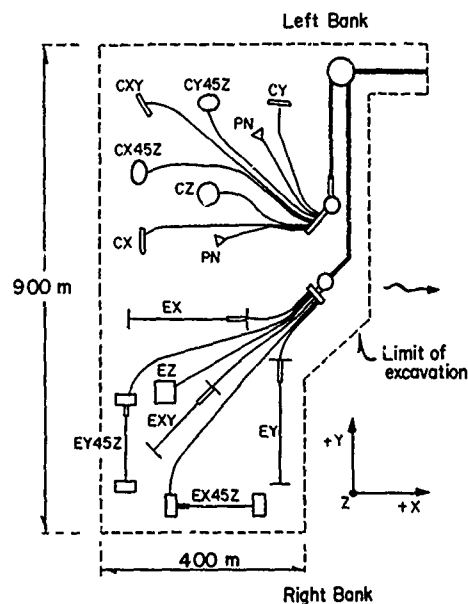
- Casagrande-type piezometers PLDi, PLII
- Instrument house
- Hydraulic leveling devices
- || ⊙ Inclinometers I-i
- Surface reference points at rows L-i
- Cross-arms D-i
- Cluster of instruments Gi
- ⊙ Pressure cells
- Pneumatic piezometers
- Extensometers

Fig. 5 Instrumentation of Peñitas Dam

Besides the instrumentation of the dam, several instruments were placed in both abutments, in the alluvial foundation, in/on the powerhouse and in/on the spillway for monitoring piezometric levels, water flow, vertical and horizontal movements and seismic activity.

In order to be able to make the analysis of the states of stress and strain, at least six pres-

sure cells and six extensometers per cluster of instruments must be placed in different directions, provided that any two directions are linearly independent. The analysis can be made in terms of effective stresses if the pore pressure is measured by means of piezometers too. Thus, each cluster of instruments installed in Peñitas dam is formed by 6 total pressure cells, 6 electric extensometers and 2 pneumatic piezometers (one redundant), placed as shown in fig 6; the characteristics of these instruments can be found in González-Valencia (1985) and Alberro and Borbón (1985).



| PRESSURE CELL | EXTENSOMETER | DIRECTOR COSINES |               |              |
|---------------|--------------|------------------|---------------|--------------|
|               |              | $\alpha$         | $\beta$       | $\gamma$     |
| CX            | EX           | 1                | 0             | 0            |
| CY            | EY           | 0                | 1             | 0            |
| CZ            | EZ           | 0                | 0             | 1            |
| CX45Z         | EX45Z        | $1/\sqrt{2}$     | 0             | $1/\sqrt{2}$ |
| CY45Z         | EY45Z        | 0                | $-1/\sqrt{2}$ | $1/\sqrt{2}$ |
| CXY           | EXY          | $1/\sqrt{2}$     | $-1/\sqrt{2}$ | 0            |

Fig. 6 Schematic layout of a cluster of instruments

## MEASURED STRESSES AND STRAINS

### Introduction

The analysis of the states of stress and strain based on the instrumental measurements is made in order to: 1) obtain the stress-strain relationships of the dam materials during the construction period, 2) verify the properties of the materials used in the Finite Element Method (FEM) computations, and 3) predict the future behaviour of the structure.

In each measuring direction  $i$  in space, defined by its direction cosines  $(\alpha_i, \beta_i, \gamma_i)$  with respect to a general coordinate system, the linear strain  $e_i$  is expressed by:



$$e_i = e_1 \alpha_i^2 + e_2 \beta_i^2 + e_3 \gamma_i^2 + 2g_1 \beta_i \gamma_i + 2g_2 \alpha_i \gamma_i + 2g_3 \alpha_i \beta_i \quad (1)$$

taking into account that

$$\bar{D} = \begin{bmatrix} e_1 & g_3 & g_2 \\ g_3 & e_2 & g_1 \\ g_2 & g_1 & e_3 \end{bmatrix} \quad (2)$$

is the strain tensor at the point of measurement.

The knowledge of the six  $e_i$  values in six different directions leads to the establishment of a system of six linear independent equations with the help of equation (1). The solution of this system gives the values of the six strains  $e_1, e_2, e_3, g_1, g_2$  and  $g_3$  which define the strain tensor  $\bar{D}$ . In the same way the stress tensor  $\bar{E}$  can be established:

$$\bar{E} = \begin{bmatrix} n_1 & t_3 & t_2 \\ t_3 & n_2 & t_1 \\ t_2 & t_1 & n_3 \end{bmatrix} \quad (3)$$

The knowledge of  $\bar{D}$  and  $\bar{E}$  tensors with respect to a general coordinate system allows the determination of the magnitude and direction of the principal strains and stresses ( $\epsilon_1, \epsilon_2, \epsilon_3$  and  $\sigma_1, \sigma_2, \sigma_3$ ).

The octahedral stresses and strains are defined as:

$$\begin{aligned} \bar{\sigma}_{oct} &= \frac{1}{3}(\bar{\sigma}_1 + \bar{\sigma}_2 + \bar{\sigma}_3) \\ \epsilon_{oct} &= \frac{1}{3}(\epsilon_1 + \epsilon_2 + \epsilon_3) \\ \tau_{oct} &= \frac{1}{3}[(\bar{\sigma}_1 - \bar{\sigma}_2)^2 + (\bar{\sigma}_1 - \bar{\sigma}_3)^2 + (\bar{\sigma}_2 - \bar{\sigma}_3)^2]^{1/2} \\ \gamma_{oct} &= \frac{1}{3}[(\epsilon_1 - \epsilon_2)^2 + (\epsilon_1 - \epsilon_3)^2 + (\epsilon_2 - \epsilon_3)^2]^{1/2} \end{aligned} \quad (4)$$

where  $\bar{\sigma}_1, \bar{\sigma}_2$  and  $\bar{\sigma}_3$  are the principal effective stresses and  $\epsilon_1, \epsilon_2$  and  $\epsilon_3$  are the principal strains.

With these values one can draw the variations of  $\epsilon_{oct}$  with respect to  $\bar{\sigma}_{oct}$ ,  $\gamma_{oct}$  with respect to  $\tau_{oct}$  and also the variation of  $\bar{\sigma}_1$  in regard to  $\bar{\sigma}_3$ .

#### Instrumental measurements

It is once again verified, Marsal (1976), that during the construction period the relationship  $\bar{\sigma}_1/\bar{\sigma}_3$  remains constant. Figs 7 to 12 show the octahedral stress-strain relationships for each cluster of instruments. These values of  $\bar{\sigma}_{oct}$ ,  $\epsilon_{oct}$ ,  $\tau_{oct}$  and  $\gamma_{oct}$  are determined via the measurement of: 1) total stresses (total pressure cells), 2) strains (electric extensometers), and 3) pore pressures (pneumatic piezometers).

The tendency of linearity in all the curves drawn up to the end of the construction period

(figs 7 to 12) is observed, except in the case of the  $\epsilon_{oct}$  vs  $\tau_{oct}$  curve of the 1C cluster; here the extensometer EX (in the river direction) was exposed to strong elongation because it was partly on the cut-off wall and partly beyond it, which altered the real value of the strain in that direction due to penetration of the cut-off wall in the clay core.

Considering the results shown in the preceding figures, it can be written for each material (or cluster in this case):

$$\begin{aligned} \bar{\sigma}_{oct} &= K \epsilon_{oct} \\ \tau_{oct} &= G \gamma_{oct} \end{aligned} \quad (5)$$

where K represents the bulk modulus and G is the shear modulus of the material. These relations are identical with those of the Theory of Elasticity in which

$$K = \frac{E}{1-2\nu} \text{ and } G = \frac{E}{2(1+\nu)}$$

where E is the Young's modulus and  $\nu$  is the Poisson's ratio.

Thus, based on the  $\bar{\sigma}_{oct}$  vs  $\epsilon_{oct}$  and  $\tau_{oct}$  vs  $\gamma_{oct}$  curves it is possible to find the values of E and  $\nu$  corresponding to the material which surrounds each cluster of instruments.

Using this method, the values of E and  $\nu$  were calculated for the different materials and the results can be found in table 5.

It is important to indicate that the values of E and  $\nu$  of the core material probably concern only the silty red clay (material 1) because this clay is enveloping clusters 1 and 2 in sections A and C with a 4 m thick layer. Only clusters 1 and 2 of section D are surrounded by plastic brown clay (material 1b) but unfortunately in these clusters some of the pressure cells failed shortly after having been placed.

The results presented in this section should be compared with those found by means of the confined plate bearing tests made during the construction as well as with the mechanical parameters of the clays obtained by means of laboratory consolidation tests, fig 3.

#### CONFINED PLATE BEARING TESTS AND CONSOLIDATION TESTS

##### Confined plate bearing tests (CPBT)

###### Description

A CPBT is actually a conventional plate bearing test; the difference lies in the fact that by means of an annular plate a confining stress is applied to the material being tested, Montañez *et al* (1979). Both plates are made of steel: the annular one has a 0.8 m inner diameter and 2.4 m outer diameter and the central plate has a diameter of 0.8 m.

The loads are transmitted to the plates by using hydraulic jacks which react against a metal platform onto which a loaded truck weighing 80 ton is driven, fig 13. The settlements

of the central plate are measured with three micrometers.

#### Test procedure

Initially, a 1 kg/cm<sup>2</sup> stress is applied to both plates. The settlement of the central one with respect to a fixed level is measured during a preestablished period of time and then a 1 kg/cm<sup>2</sup> load increment is applied to the central plate while the annular one is kept with the original load. The displacement of the central plate continues to be read and when the rate of settlement slows down to a fixed limit the next 1 kg/cm<sup>2</sup> load increment is applied. The test continues in a similar way until the pressure in the central plate reaches 4 kg/cm<sup>2</sup>. Afterwards, the plate is unloaded with load decrements of 1 kg/cm<sup>2</sup>.

#### Test interpretation

In order to calculate the modulus of deforma-

tion for each load increment, the next expression derived from the Theory of Elasticity is used:

$$E = \frac{1-\nu^2}{2a} \frac{\Delta p}{\Delta \delta} \quad (7)$$

where: E modulus of deformation  
 $\nu$  Poisson's ratio  
 $a$  inner plate radius  
 $\Delta p$  load increment on the plate  
 $\Delta \delta$  settlement caused by  $\Delta p$

The modulus of deformation of an elastic material loaded superficially with a load P on a rigid circular plate of radius a can be computed using expression (7). Even though this is not precisely the case in a CPBT because of the additional load on the annular plate, the results obtained with equation (7) are considered to be pretty close to reality.

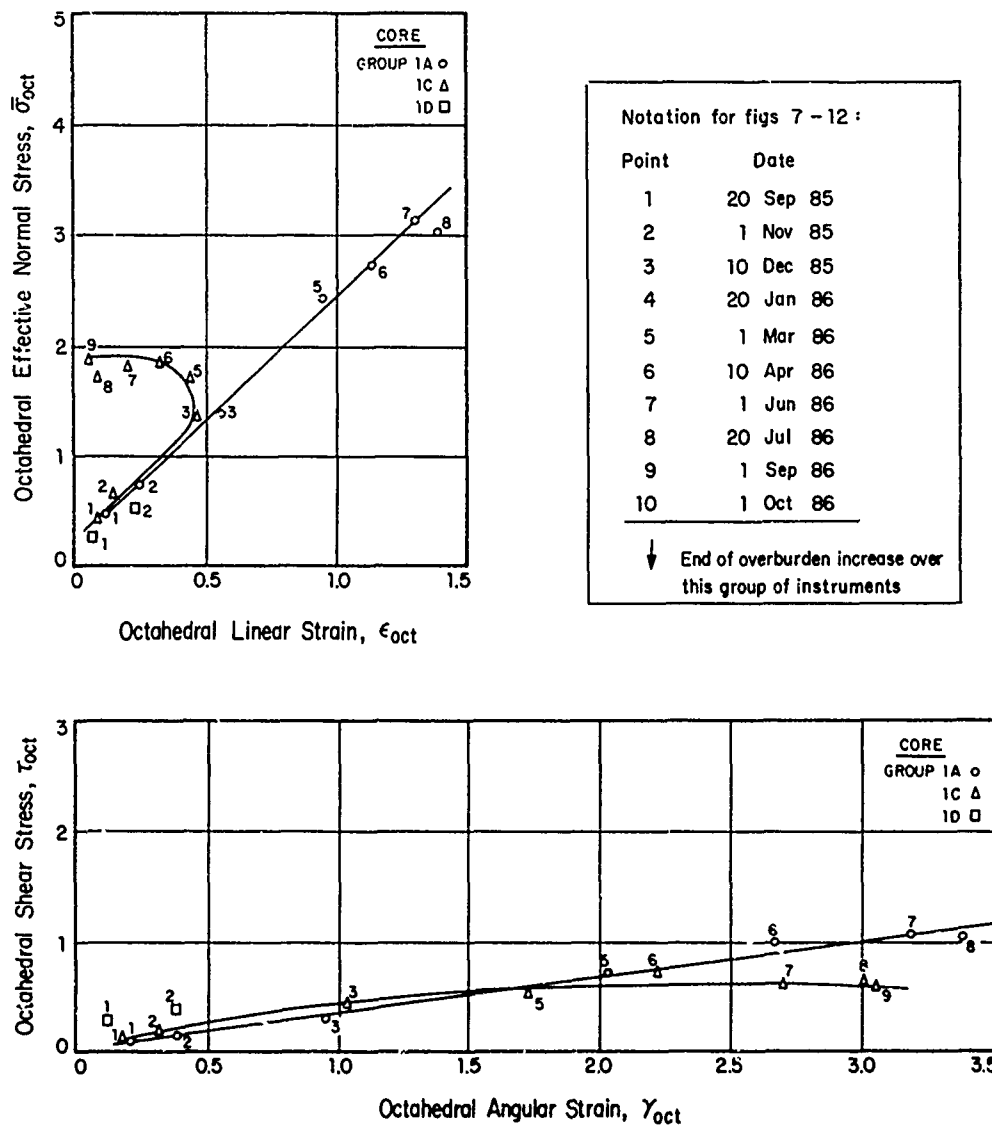


Fig. 7 Octahedral stress-strain curves for clusters No. 1 (core)

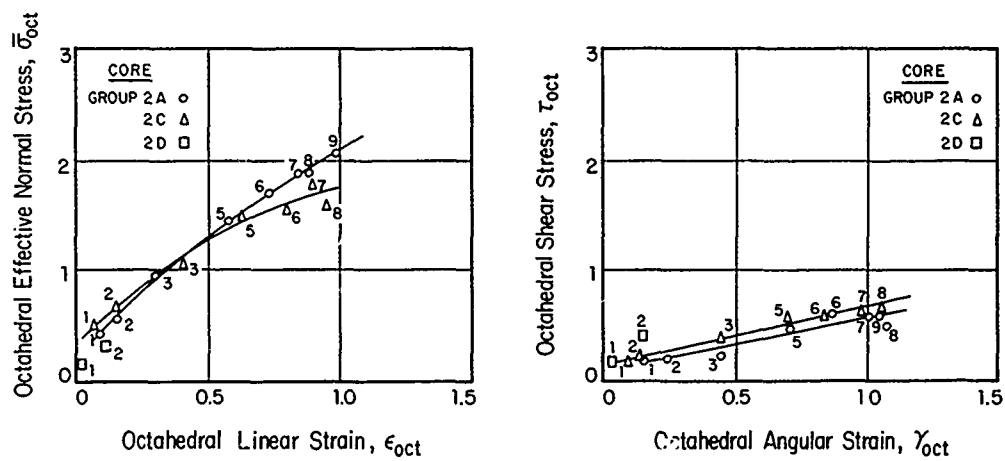


Fig. 8 Octahedral stress-strain curves for clusters No. 2 (core)

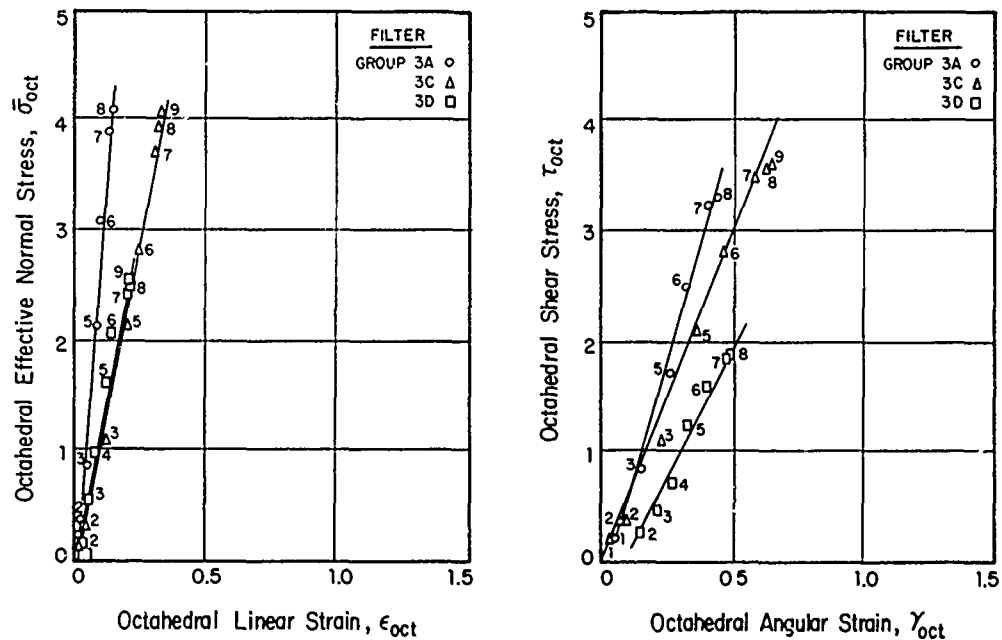


Fig. 9 Octahedral stress-strain curves for clusters No. 3 (Filter)

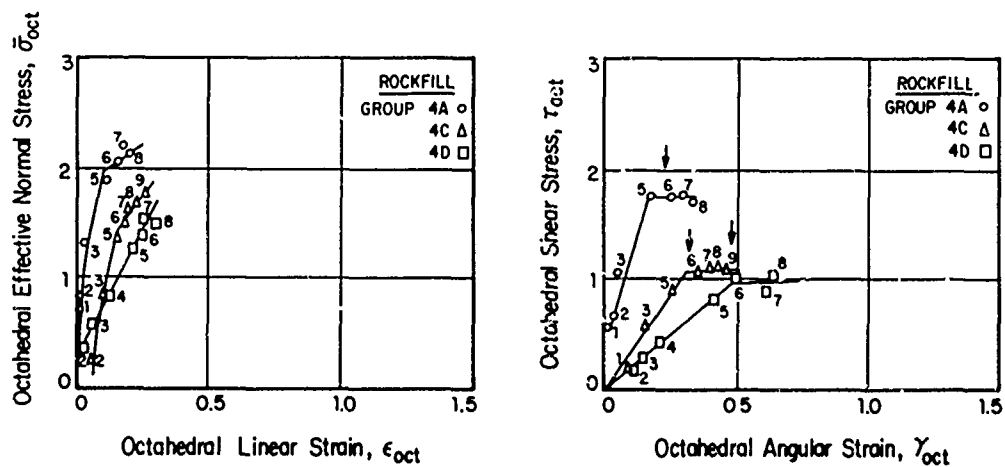


Fig. 10 Octahedral stress-strain curves for clusters No. 4 (Rockfill)

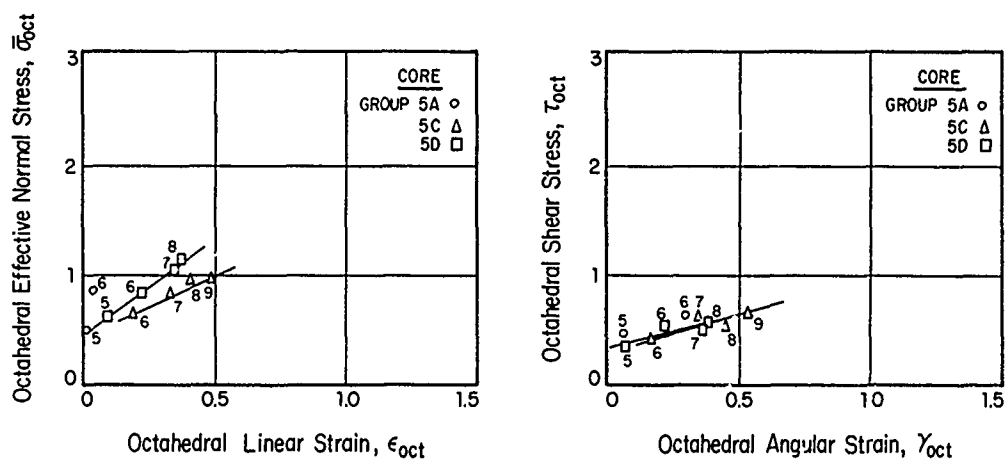


Fig. 11 Octahedral stress-strain curves for clusters No. 5 (Core)

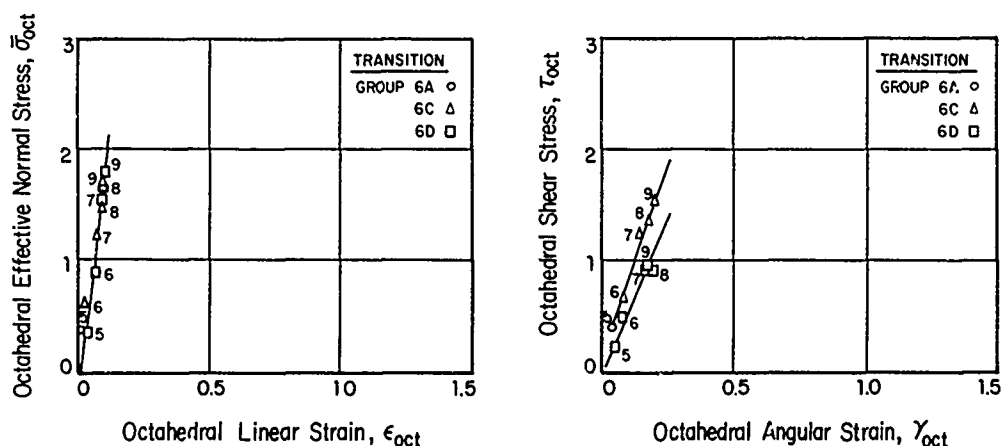


Fig. 12 Octahedral stress-strain curves for clusters No. 6 (Transition)

TABLE 5. ELASTIC PROPERTIES DETERMINED BY INSTRUMENTATION AND CPBT

| Material               | Instrumentation |      | CPBT             |
|------------------------|-----------------|------|------------------|
|                        | $\nu$           | E    | $E^b$            |
| Clay core <sup>a</sup> | 0.15            | 120  | 126              |
| Filters                | 0.15            | 1500 | 903 <sup>c</sup> |
| Transitions            | 0.15            | 1300 | 1295             |
| Rockfill               | 0.10            | 750  | 890              |

#### NOTATION

- a Silty red clay
- b Computed using  $\nu$  of the first column
- c Material placed above elev 85 (fig 4b)
- E. in  $\text{kg/cm}^2$

#### Results

In fig 14 the stress on the plate ( $\sigma_p$ ) versus settlement ( $\delta$ ) diagrams are shown for all materials tested; note that the unloading branches of the curves are not drawn for clarity. The average moduli E calculated with equation (7) considering the  $\nu$  values obtained by the instrumentation are shown in table 5. Comparing

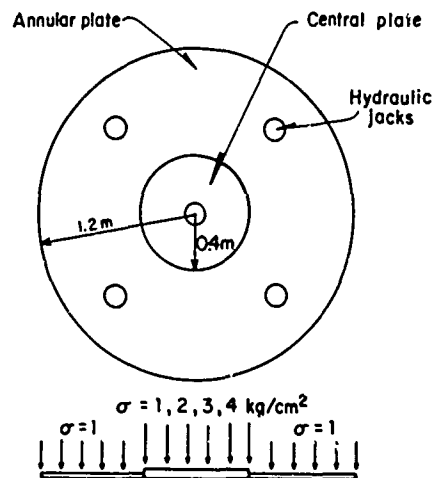


Fig. 13 Schematic layout of a CPBT

these values of E with those of the instrumentation an excellent correlation is observed, except in regard to the filter. However, it should be taken into account that the CPBT were made in the filter above elev 85 and therefore

in the fine uniform material obtained by crushing the dredged alluvium, fig 4b; the volume of this material is very small in comparison to the rest of material 2, fig 4a.

It should be noted that we tried to make CPBT in the plastic brown clay but this material is so compressible that when applying the first load of 1 kg/cm<sup>2</sup> on both plates, the stroke of the hydraulic jacks was exhausted, and for this reason no results could be obtained.

#### Consolidation tests of the core clays

The variation of the coefficient of volumetric compressibility,  $m_v$ , of both core clays (materials 1b and 1) is shown in figs 3a and 3b. The inverse of  $m_v$  is equal to 70 and 120 kg/cm<sup>2</sup> for clays 1b and 1 respectively in the effective stress range of 1 to 3 kg/cm<sup>2</sup>. The latter value of  $1/m_v$  corresponding to the red clay is pretty similar to the values of  $E$  obtained by instrumentation and CPBT.

#### FINITE ELEMENT METHOD

##### General remarks

The analysis of the states of stress and strain

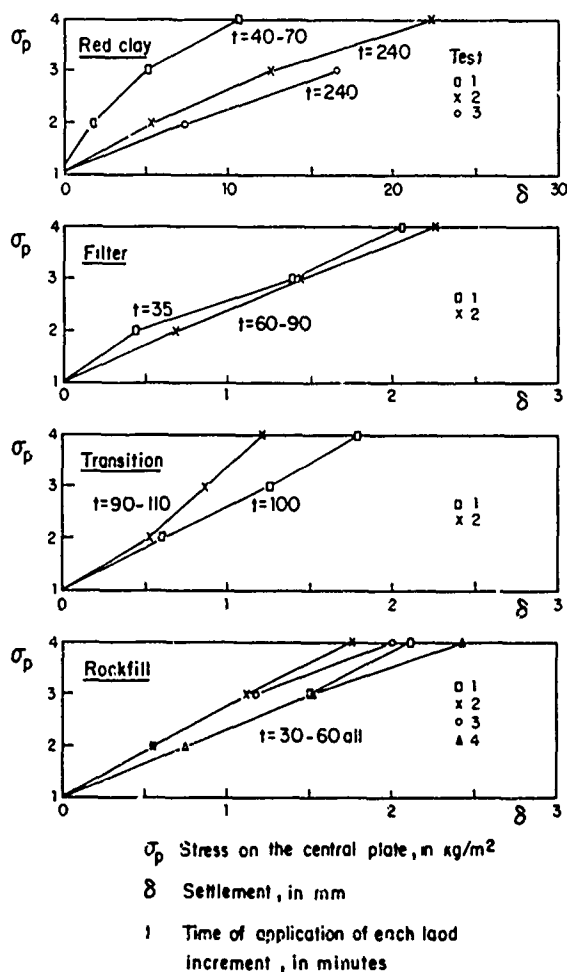


Fig. 14 Stress-settlement curves of the CPBT

by the Finite Element Method (FEM) was made taking into consideration a plane strain state in the maximum cross-section of the dam. The mesh used is shown in fig 15; the triangular elements are of such a kind that the strain is constant all through each element. To take account of the incremental construction, the FEM idealization was arranged in ten horizontal layers corresponding to construction lifts; the results presented below are the ones corresponding to the end of the construction.

#### Properties of the materials

The stress-strain properties used to feed the finite element program are the ones obtained by the instrumentation and are presented in table 6. The properties of the cut-off wall shown on the same table were obtained by the unconfined compression tests made in the course of its construction, table 4; the alluvium characteristics were estimated on the basis of in situ cross-hole tests made after the dynamic compaction (dynamic modulus  $E_d = 1100$  kg/cm<sup>2</sup>) and of the average properties which generally characterize these deposits.

Fig 16 shows the distribution of materials which were used for the numerical analysis. Note that the materials 4, 5, 6, F1 and F2 were assigned the properties of material 4. Besides, since no CPBT were made in the brown plastic clay and there is no instrumental information about this material, it was considered that the whole core is formed by the silty red clay (material 1).

One of the basic considerations for the FEM analysis was the constant values of  $E$  and  $\nu$  for each material during all the simulated construction of the dam. These constant values are a consequence of the already mentioned linearity of the  $\bar{\sigma}_{oct}$  vs  $c_{oct}$  and  $\tau_{oct}$  vs  $\gamma_{oct}$  curves.

#### Results

The resulting displacement vectors and vertical stress configuration are presented in figs 17 and 18, respectively. Note the tendency of the dam material to move towards its interior whereas the foundation material tends outwards, fig 17. In fig 18, three vertical stress concentrations stand out, one in the core above the cut-off wall and two others also in the clay near the filters, because of the interaction between the compressible core and the rigid diaphragm wall and the rigid filters.

#### Comparison with the instrumental measurements

The vertical effective stresses measured in several zones of the dam and the ones calculated by the FEM are presented in fig 19; the resemblance is clearly evident. The maximum differences occur in the clay core in the proximity of the filters in view of the reasons explained in the previous section.

In regard to the measured and calculated settlements, these are compared in fig 20, where the settlements measured with the central inclinometer I-AB and the settlements measured at elev 59 (crest of the cut-off wall) and elev 77 are shown. In this figure once again the

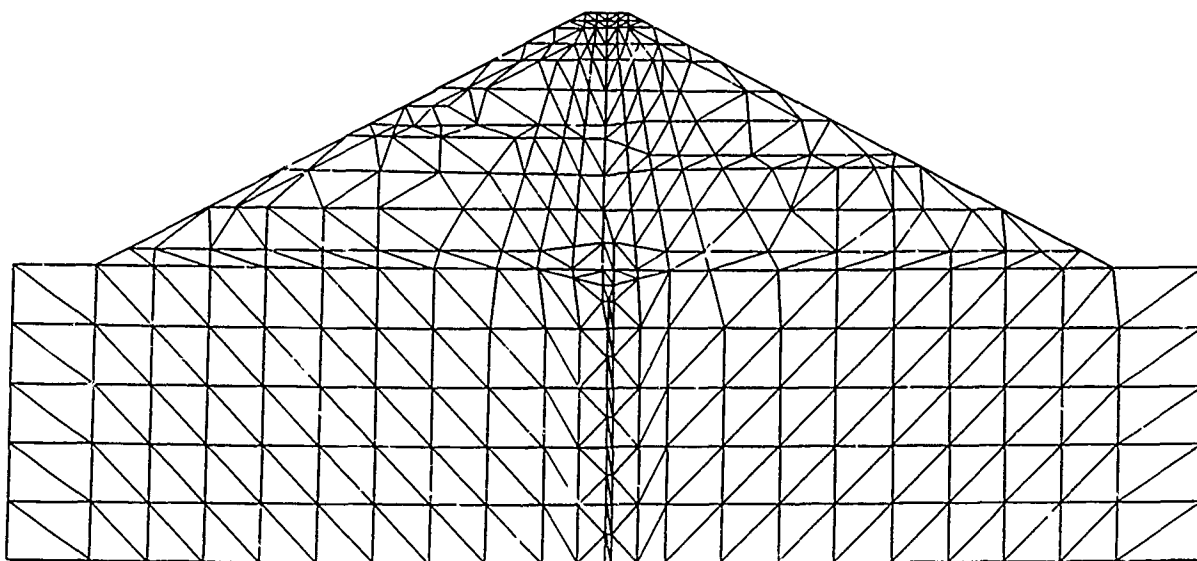
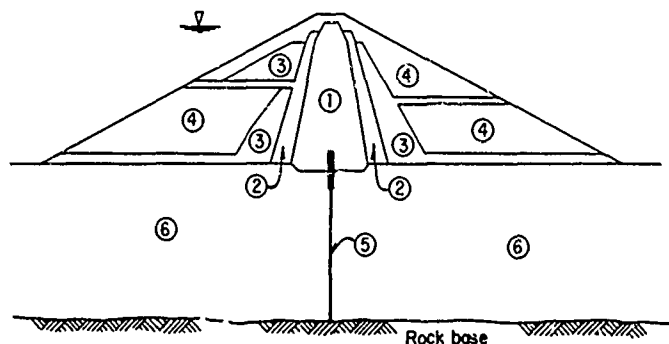


Fig. 15 Finite element mesh

TABLE 6. MATERIALS PROPERTIES USED IN THE FEM ANALYSIS

|   | Material     | $\nu$ | $E^*$ |
|---|--------------|-------|-------|
| 1 | Clay core    | 0.15  | 120   |
| 2 | Filters      | 0.15  | 1500  |
| 3 | Transitions  | 0.15  | 1300  |
| 4 | Rockfill     | 0.10  | 750   |
| 5 | Cut-off wall | 0.33  | 4055  |
| 6 | Alluvium     | 0.30  | 750   |

\* in kg/cm<sup>2</sup>



Notation in Table 6

Fig. 16 Materials used in the FEM analysis

great similarity of the measured and computed settlements can be seen, except at elev 59, where the computed ones are somewhat smaller perhaps because the plastic clay (material 1b), obviously more compressible than the red clay, fig 3, was not taken into consideration in the numerical model.

#### CONCLUSIONS

The determination of the stress-strain characteristics of the Peñitas dam materials by means

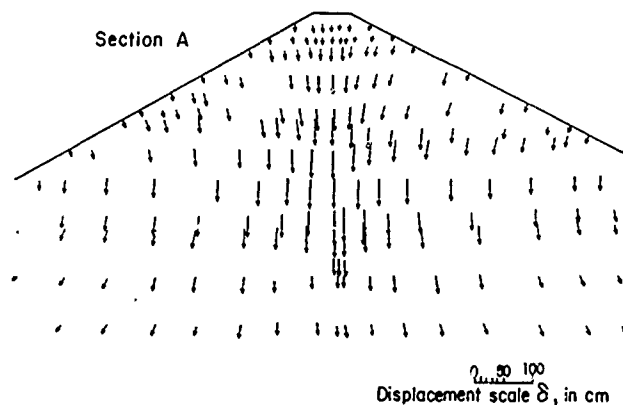


Fig. 17 Computed displacements at the end of construction

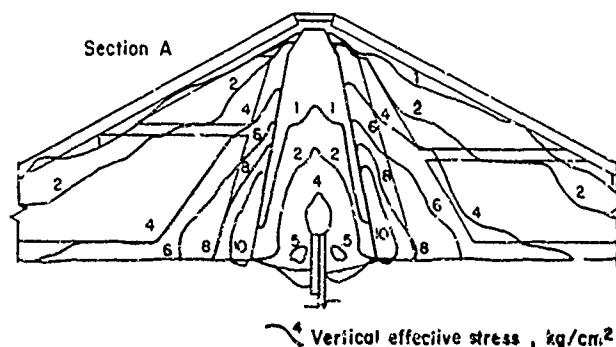


Fig. 18 Contours of equal vertical effective stresses

of the instrumental measurements leads to the following conclusions:

- As a consequence of the stress path followed during construction ( $\bar{\sigma}_1 / \bar{\sigma}_3 = \text{constant}$ ) the

materials behave as if they were linear elastic.

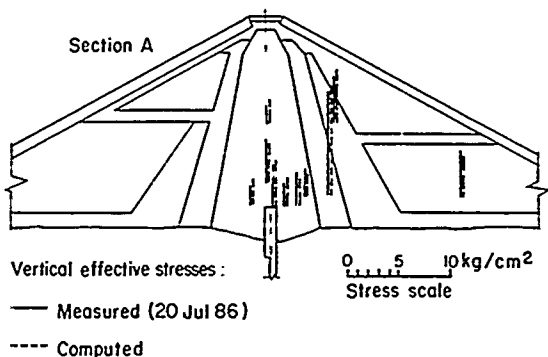


Fig. 19 Measured vs computed vertical effective stresses

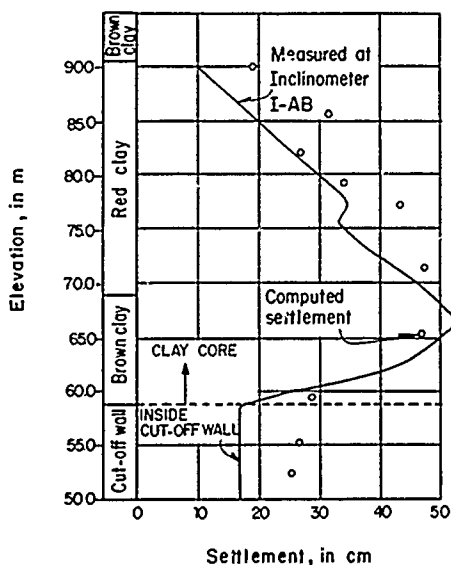
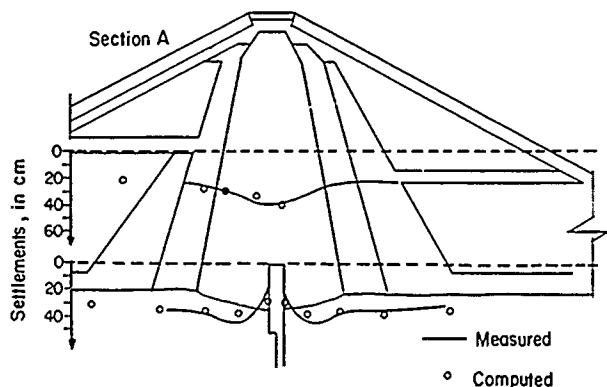


Fig. 20 Measured vs computed settlements

b) The computation of the states of stress and strain by means of the FEM is therefore simplified for the construction stage.

c) The confined plate bearing tests (CPBT), which also impose an approximately constant  $\bar{\sigma}_1/\bar{\sigma}_3$  path on the material, show values of the moduli  $E$  very similar to those obtained by instrumentation.

According to these conclusions and to the results of vertical stresses and strains obtained by the FEM, it is clear that one can design a structure in advance if the values of  $E$  are determined via CPBT made on test embankments, at least as far as granular materials are concerned. Besides, in the case of clayey materials the value of  $E$  determined in the field compares favourably with the inverse of the coefficient of volumetric compressibility,  $m_v$ , obtained by means of laboratory consolidation tests.

#### ACKNOWLEDGEMENT

The authors wish to express their gratitude to the Federal Commission of Electricity authorities for allowing the publication of the results presented in this paper.

#### REFERENCES

- Alberro, J. and J. Borbón, (1985), "Testing of Total Pressure Cells", in Behavior of Dams built in Mexico (1974-1984), Vol. II, Federal Commission of Electricity, 2.1-2.15.
- González-Valencia, F., (1985), "Statistics on the Behavior of Instruments", in Behavior of Dams built in Mexico (1974-1984), Vol. II, Federal Commission of Electricity, 1.1-1.16.
- Marsal, R. J., E. Moreno, A. Arenas, M. A. Guzmán and F. Saldaña, (1976), "La Angostura", in Behavior of Dams built in Mexico, Ministry of Hydraulic Resources, Federal Commission of Electricity and Institute of Engineering, UNAM, 313-391.
- Marsal, R. J., (1982), "Monitoring of Embankment Dam Behavior", Proc., Fourteenth Congress on Large Dams, Rio de Janeiro, Brasil, Vol. I, Q. 52, R. 84, 1441-1467.
- Montañez, L. and J. E. Castilla, (1985), "Peñitas, Chiapas", in Behavior of Dams built in Mexico (1974-1984), Vol. II, Federal Commission of Electricity, 8.1-8.23.
- Montañez, L., V. Ibarra and J. Alberro, (1979), "Pruebas de Placa Confinada en la Presa Chicoasén, México", Proc., VI Panamerican Conference on Soil Mechanics and Foundation Engineering, Lima, Peru, Vol. II, 449-457.

## Overview of Highland Valley Tailings Storage Facility

**M.D. Scott**

Superintendent, Technical Services, Highland Valley Copper, Logan Lake, British Columbia, Canada

**E.J. Klohn**

Chairman, Klohn Leonoff Ltd., Richmond, British Columbia, Canada

**R.C. Lo**

Associate, Klohn Leonoff Ltd., Richmond, British Columbia, Canada

**Ken K. Lum**

Geotechnical Engineer, Klohn Leonoff Ltd., Richmond, British Columbia, Canada

**SYNOPSIS:** This paper presents key features of the Highland Valley tailings storage facility comprising two tailings dams, a 107 m high H-H Dam and a 166 m high L-L Dam. The construction history to date including instrumentation observations is also reviewed. Although the tailings facility is situated in a low to moderate seismic area within the Interior Plateau of British Columbia, potential earthquake sources that might have an impact on the site have been carefully assessed. Both dams are designed to have adequate seismic resistance against design earthquakes appropriate for the site. The L-L Dam valley section, involving soft lacustrine deposits beneath the Starter Dam, has been buttressed by a compacted downstream berm founded on dense glacial till. As the geometry of the tailings storage and distribution facilities and waste dumps changes with time, the quantity and relative cost of various construction materials including natural borrow, cycloned sand and pit overburden also change. Ongoing construction is planned to maintain key earthquake and flood design criteria as well as to adjust the use and placement method of various materials to achieve an efficient and cost effective tailings storage operation. Inherent in the design of the two tailings dams, both constructed by the centerline method, is the flexibility which enables the storage capacity of the tailings facility to be increased beyond the present 1.8 billion tonnes if required at some future time.

### INTRODUCTION

Highland Valley Copper, a world-class mining company producing copper concentrate and molybdenum, was formed as a partnership of Lornex Mining Corporation and Cominco on July 1, 1986. The partnership combines the former Lornex and Cominco mining operations comprising the Lornex and Valley orebodies. The two ore bodies, which are only 4 km apart, are both low-grade porphyry copper deposits and are located in Highland Valley, British Columbia, about 200 km northeast of Vancouver (see Fig. 1). Development of the Lornex orebody commenced in 1972, and the Valley orebody in 1983. Since then, the operation has experienced a series of expansions. The latest expansion occurred in 1986-1987. It included the installation of two 1.5 m by 2.3 m semi-mobile in-pit crushers and 2 km long, twin 1.5 m conveyor belts capable of delivering a total of 12 000 tonnes of ore per hour from the Valley pit to the Lornex mill. In 1988 the average ore throughput reaches 120 000 tonnes per day and the operation ranks as the third largest open pit copper mine in the world with the second largest milling capacity (Hansen 1987).

Highland Valley Copper stores its tailings mainly in the Highland Valley tailings facility (ultimate capacity: 1.8 billion tonnes). Auxiliary storages are provided by the Trojan tailings facility (ultimate capacity: 85 million tonnes) and several abandoned pits and one abandoned tailings pond (combined ultimate capacity: 110 million tonnes). This paper describes only the design features of the main facility. As indicated in the general arrangement illustrated in Fig. 2, the facility includes three tailings dams: these are, going from east to west, the H-H, J-J and L-L Dams,

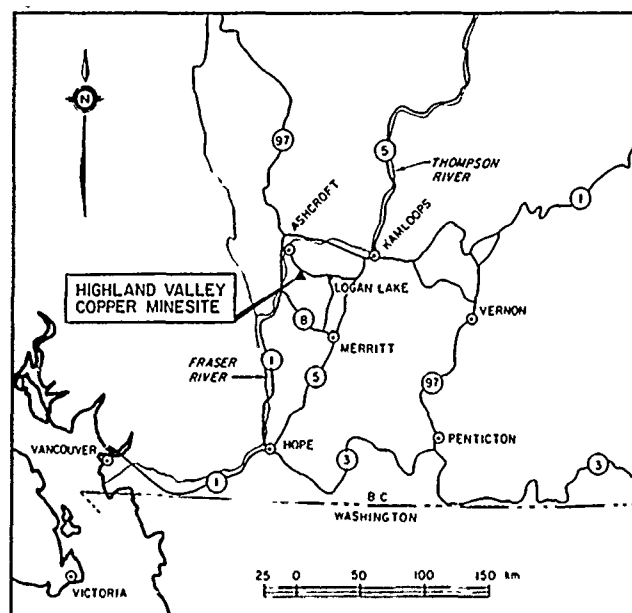


Fig. 1. Location of Highland Valley Copper Minesite

named after the alignment alternatives in the initial feasibility studies. A section through the Highland Valley from the Lornex mill to the L-L Dam is shown in Fig. 3. From 1970 to 1977 Canadian Bechtel Ltd. advised Lornex on tailings storage at the H-H and J-J Dams and the L-L Starter Dam. Since the completion of the L-L Starter Dam in 1977, Klohn Leonoff Ltd.



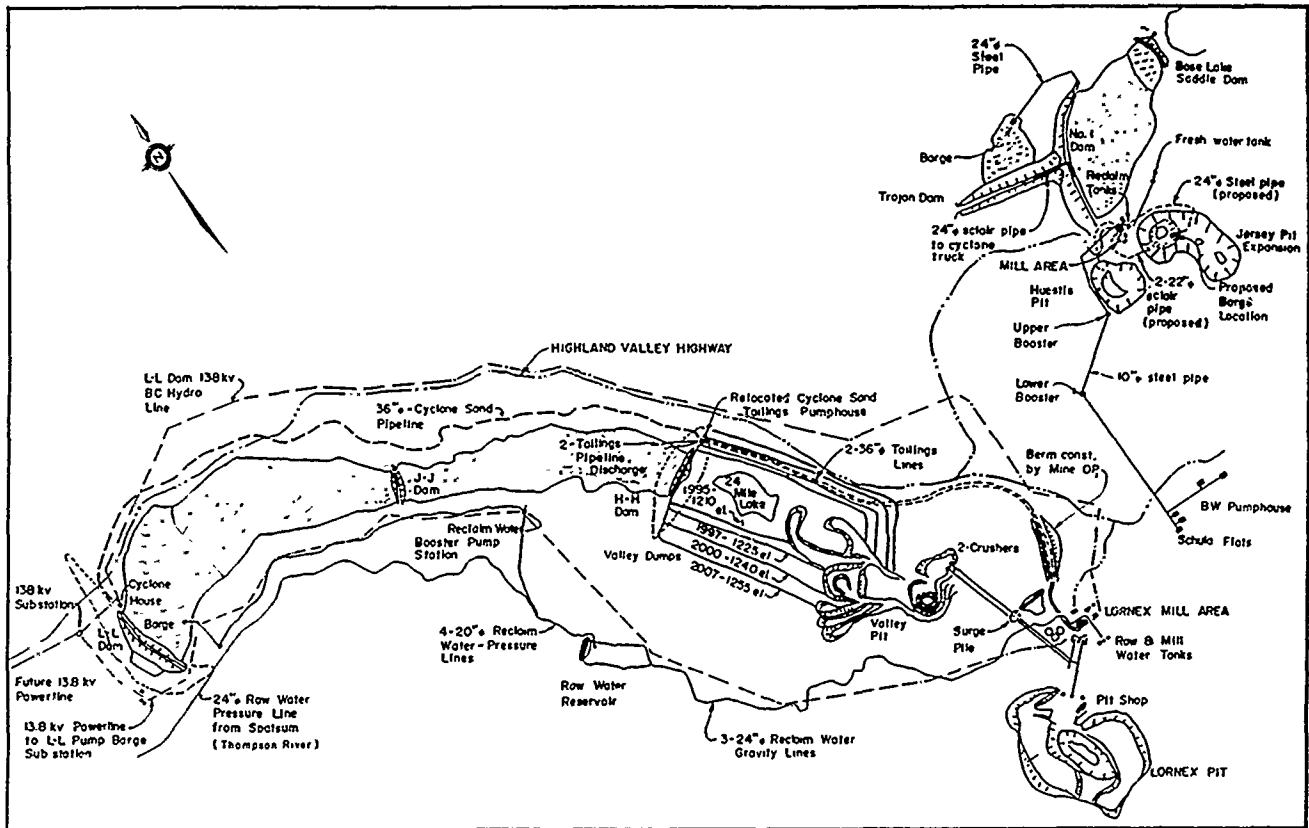


Fig. 2. General Arrangement of Highland Valley Tailings Facility

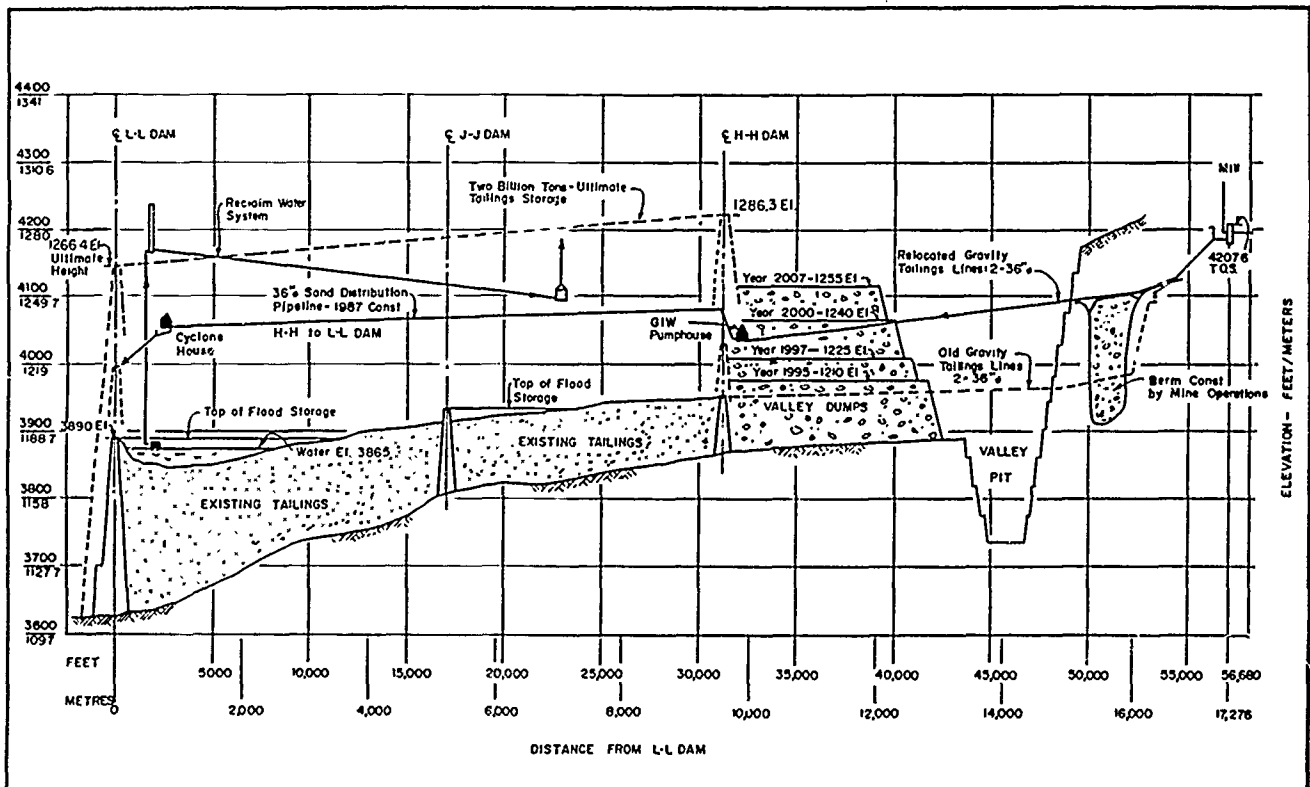


Fig. 3. Section Through Highland Valley Tailings Facility

has provided ongoing consultation and supervision of the raising of the L-L and the H-H Dams. The J-J Dam is scheduled to be buried by tailings in the near future.

This paper reviews key features of the tailings facility, the H-H Dam and the L-L Dam. The performance of the valley section of the L-L Dam, which is partly founded on lacustrine deposits, is also presented.

#### TAILINGS STORAGE FACILITY

The original Bechtel scheme envisaged the storage of 680 million tonnes of tailings initially in the Upper Pond bounded by the H-H and J-J Dams at a crest elevation of 1303 m. Thereafter, the remaining storage would be provided by the Lower Pond between the J-J and L-L Dams. The reason for adopting this scheme involving an ultimately redundant Middle (J-J) Dam was the lower initial capital cost of the scheme compared with the two-dam scheme involving the H-H and L-L Dams only. With the rapid rise of energy costs since 1973, the relative advantage of the three-dam scheme was eroded quickly. In 1975, Lornex decided to convert the tailings facility to the two-dam scheme.

The existing tailings storage facility is approximately 9.6 km long, and a pond is formed upstream of the L-L Dam. A portion of the tailings flows from the mill to the L-L Dam along a 914 mm diameter pipeline located on the north valley slope. Flow is mostly by gravity with some assistance by booster pumps located at the H-H Dam. Tailings delivered to the L-L Dam are cycloned at the north abutment to produce sand for dam construction. The remainder of the tailings is discharged via a 914 mm diameter pipeline into the tailings pond near the east abutment of the H-H Dam. Both the H-H and L-L Dams are to be raised annually from their respective present heights of 28 m and 93 m to ultimate heights of 107 m and 166 m to meet the ongoing tailings storage requirements of the mining operation.

#### Site Conditions

The Highland Valley is a broad, U-shaped valley located in the Interior Plateau of south central British Columbia. The Interior Plateau, a physiographic unit of the Canadian Cordillera, has a gently rolling topography with rounded glaciated hills rising to over 1850 m. The Highland Valley is bounded on the east by the broad, shallow Guichon Creek Valley and on the west by the deeply incised Thompson River Valley. There is a high point in the talweg (valley bottom) near the Valley Pit which creates a drainage divide at about 1220 m. From the divide, Pukaist Creek drains westward, directly into the Thompson River. Witches Brook drains eastward from the divide into the Thompson River via Guichon Creek and the Nicola River.

The Guichon Creek Batholith, a semi-concordant dome with an approximate width of 20 km, and

length of 65 km oriented with its long axis in the direction slightly west of north, is the predominant bedrock feature in the Highland Valley. Potassium-argon (K/Ar) dating of the Batholith indicates an age of  $200 \pm 8$  million years (Ma). The Batholith is one of several large plutons in the southern portion of the structural province known as the Intermontane Belt. The intrusive rock is associated and possibly comagmatic with Late Triassic volcanic rocks (McMillan 1985). The Highland Valley porphyry copper deposits occur near the center of the Batholith.

#### Seismo-tectonic Setting and Design Earthquake

The Canadian Cordillera appears to be an assemblage of terrains separated by major fault traces, ophiolite exposures and oceanic marginal basin stratigraphy. Dickinson (1976) links these terrains with the overall geodynamics of an active continental margin. The system was progressively broadened by tectonic accretion of oceanic elements to the edge of the continental block. Abandoned ocean margins, therefore, are located throughout British Columbia. Such a margin is characterized by the Cache Creek terrain and the related Passayten-Fraser-Yalakom Fault Systems. Many of the major structures in British Columbia are associated with these ancient continental margins.

Ewing (1980) postulated the following tectonic model for the North American Cordillera between  $40^\circ$  N and  $60^\circ$  N latitude. In Paleocene time, continuous subduction took place in this area. South of  $47^\circ$  N latitude, subduction continued without interruption since that time. However, north of  $47^\circ$  N latitude, a Pacific-North American transform boundary was formed at about 53 Ma due to the amalgamation of the Pacific, Kula and northern Farallon plates. Concurrently, transform motion was in part taken up on the Fraser-Tintina strike-slip system inland, cross-cutting the volcanism produced from the remnant of the subducted slab. At about 42 Ma, inland transform motion stopped, and all transform motion took place on the Queen Charlotte transform.

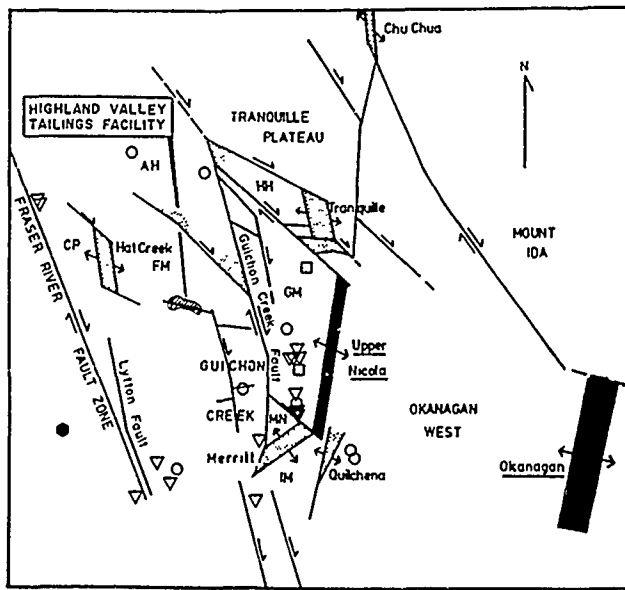
Present major tectonic activity in southern British Columbia is limited to major plate boundaries, such as transform faults off the west coast of Vancouver Island, and faulting associated with the thrusting of the Juan de Fuca Plate under southern Georgia Strait and the Puget Lowland. The northern limit of the subducting Juan de Fuca Plate is at approximately  $50^\circ$  N within Georgia Strait. To the south and to the north of this small subducting plate, strike-slip faulting is the prevalent displacement mode between the North American and Pacific plates.

Heaton and Hartzell (1987) outlined a potential seismic hazard related to large subduction earthquakes on the Cascadia subduction zone off the west coast of Vancouver Island. The Cascadia subduction zone shares many characteristics with those subduction zones in Southern Chile, Columbia and Southwestern Japan, where relatively young volcanic lithospheres are involved in the subduction. If the Cascadia subduction zone is storing elastic energy, either a series of several large earthquakes of

magnitude 8 ( $M_w = 8$ ) or a giant earthquake of magnitude 9.5 would be required to fill this 1200 km seismic gap. Because of the substantial distance of this earthquake source from the site (about 480 km), its impact on the site is not significant.

Evidence for most recent tectonic activity in central British Columbia is Tertiary plateau basalts. The basalts, commonly associated with a tensional stress field, were extruded at the same time as crustal extension began in the Basin and Range Provinces in the United States (Noble 1972). Present crustal stress conditions in the Highland Valley are unknown. However, stress levels are expected to be minor compared to stress levels near the continental margin.

Figure 4 (from Ewing 1981) shows an idealized sketch of major Eocene tectonic features in south central British Columbia. Superimposed on the figure are the Highland Valley tailings facility and epicentral locations of earthquakes with indicated magnitudes within an area bounded by  $50^\circ$  N and  $51^\circ$  N and  $120^\circ$  W and  $122^\circ$  W. The plotted seismic events from 1899 to 1984 are those which caused a Modified Mercalli intensity of II or greater at the site. On the other hand, all earthquakes from 1985 to March, 1987 within the area are plotted. Design earthquakes selected for the tailings facility are magnitude 6.5 earthquakes associated with the Guichon Creek Fault and the Lytton Fault. Since the Guichon Creek Fault is closer to the facility, 15 km to the H-H Dam, and 23 km to the L-L Dam, the earthquake associated with the Guichon Creek Fault governs the design of the tailings dams.



#### LEGEND

▽ M1 to 1.9    ○ M2 to 2.9    □ M3 to 3.9    △ M4 to 4.9    ● M5 to 5.9

Fig. 4. Epicenters and Major Eocene Tectonic Features in the Vicinity of Highland Valley (after Ewing 1981).

#### Surface Water

Highland Valley is located in the rain shadow of the Coast Mountain Range in an extension of the upper Sonora Desert of the United States. Most of the precipitation comes down as snow in the winter. Approximately 60% of the runoff in the creeks flowing in the vicinity of the mine occurs during spring runoff in May and June. Main sources of fresh make-up water used in the mill process come from runoffs collected from catchment areas around the mine and tailings pond and a pump installation in the Thompson River about 22 km from the mine. Groundwater tapped by deep wells near the mine provides the balance of the requirement. After sixteen years of operation, the total volume of freshwater in the tailings pond has not changed significantly, although it does undergo yearly fluctuation with runoff. Pumping from the Thompson River is minimized based on ongoing monitoring of freshwater volume in the pond in order to minimize power consumption.

The tailings pond is operated as a closed system, and is designed to store a design flood inflow volume of 40 600 dam<sup>3</sup> without release. This design flood is arrived at from two different criteria as follows: (1) the sum of the average annual runoff, the 100-year flood and the 24-hour probable maximum flood (PMF); and (2) the sum of the average annual snowmelt runoff and the runoff from a 120-hour probable maximum precipitation (PMP) assumed to occur during the snowmelt period. An additional freeboard of 1 m is added for preventing overtopping of the L-L Dam by waves, although the tailings beach formed in front of the dam tends to mitigate the wave action.

#### Reclamation and Mine Closure

Reclamation plans and techniques are being developed on an ongoing basis. Growth performance of grasses and legumes in test plots located on the tailings is monitored and evaluated for future reference in reclamation planning. Ultimate land uses for the long and gently sloped (0.3%) tailings pond include: seed production, enhanced grazing for cattle and wildlife, hay production, tree farming and public recreation.

It is envisioned that creeks flowing into the tailings pond, which is sloping from the H-H Dam toward the L-L Dam, will naturally irrigate the reclaimed pond area and form a shallow lake located about 200 m upstream of the L-L Dam. A permanent spillway system will be located on one of the abutments of the L-L Dam. The spillway will consist of an approach channel, a control structure located in a rock cut and an outlet channel. Its location will be determined prior to mine closure upon detailed investigation. The spillway control structure may consist of concrete culverts embedded in a concrete free overflow crest structure. The culverts would pass normal flows, and most flood flows due to the attenuating function of

surcharge storage provided by the L-L Dam above the invert elevation of the culverts. The overflow structure would generally not pass water unless the culverts became blocked or inflow rates approached those of a design PMP event.

In the event of a prolonged shutdown of mining operation prior to mine closure, a temporary spillway or other facilities will be provided to release flood water and protect the L-L Dam from overtopping.

Highland Valley Copper may consider developing the available water storage in the tailings pond for downstream irrigation usage and/or power generation after mine closure. This could entail provision of regulating gates on the culverts or stoplogs at the spillway to allow controlled release of stored water during the summer months. Water surplus to local irrigation requirements could be fed through the existing Thompson River pipeline to a hydroelectric plant installed in the Thompson River pumphouse.

#### H-H DAM

The H-H Dam, which forms the eastern limit of the tailings facility, is situated on Pukaist Creek, approximately 6.5 km northwest of the Lornex millsite. Figure 5 shows a typical section through the dam. The elevation of the valley floor at the damsite is about 1180 m with the valley walls gently sloping upward to a maximum elevation of 1820 m.

Results from several field investigation programs covering the foundation and abutments reveal the following subsoil profile at the damsite:

- medium dense surficial glaciofluvial sands and gravels, 2 to 18 m thick;
- very dense, well graded glacial till, 6 to 23 m thick;
- very dense interglacial sands and gravels and underlying inter-layered deposits, 0 to 135 m thick.

Depth to bedrock is in excess of 169 m near the center of the valley and decreases to about 5 m on the abutments near the ultimate crest elevation.

The Starter Dam, completed in 1972, is a zoned, earthfill structure with a 15.2 m wide central impervious core of glacial till and more pervious shells. A drainage zone is included in the downstream shell to control seepage through the dam. A cutoff trench was excavated at the center of the base of the impervious core to tie into the dense glacial till foundation. The trench was backfilled with impervious glacial till. Across the stream channel in the valley section, the cutoff trench was shifted upstream in order to reduce the amount of excavation and backfill required. Following the completion of the Starter Dam, the ongoing raising of the H-H Dam consists of the following major fill zones:

- (1) central impervious core extending above the core of the Starter Dam;
- (2) downstream shell composed of structural fill;
- (3) downstream pervious fill underlying the downstream shell;
- (4) upstream shell of random fill;
- (5) upstream zone of tailings.

The Starter Dam, the impervious glacial till core and the downstream shell materials are compacted to a minimum of 97% standard Proctor density. Upstream of the central core, the random fill is lightly compacted by routing construction equipment over the area during fill placement.

The future raising of the H-H Dam will continue the current practice of using natural borrow material for the central core and downstream zones. However, the relative cost of using cycloned sand and/or stripped overburden materials from the Valley Pit as fill materials for the downstream zone will be investigated to check their economic viability. Table 1 indicates required embankment volumes for the H-H Dam per unit of tailings storage. The ratio of embankment volume to tailings storage is quite small, in the range of 3 to 5 m<sup>3</sup>/1000 m<sup>3</sup> after 1988. Because of this low ratio, it is not justified to install a very sophisticated cyclone sand facility at the H-H Dam. Moreover, as the western limit of Valley Pit waste dumps progresses towards the H-H Dam, the incremental cost of hauling pit overburden from the waste dumps to the dam will decrease. Thus, the source of downstream fill for the H-H Dam may shift from natural borrow materials to mine waste. After 1995 the waste dumps will abut against the H-H Dam and act as an enormous downstream buttress.

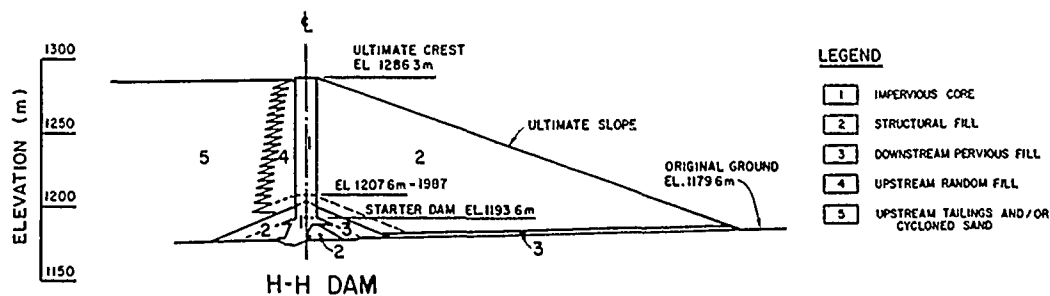


Fig. 5. Typical H-H Dam Section

**TABLE 1**  
**REQUIRED H-H DAM EMBANKMENT**  
**VOLUME PER UNIT OF TAILINGS STORAGE**

| YEAR      | DESCRIPTION OF<br>TAILINGS FACILITY           | REQUIRED<br>EMBANKMENT<br>VOLUME<br>PER UNIT OF<br>STORAGE<br>M <sup>3</sup> /1000 M <sup>3</sup> |
|-----------|---|---|
| 1976-1986 | Storage Between J-J<br>and L-L Dams           |   |
| 1987      | H-H Dam Raised Using<br>Natural Borrow        | 10.60   |
| 1988      | H-H Dam Raised Using<br>Natural Borrow        | 3.33  |
| 1989-1994 | H-H Dam Raised Using<br>Mine Waste as Option  | 5.33  |
| 1995-1996 | First Waste Dump Lift<br>Buttressing H-H Dam  | 4.65  |
| 1997      | Second Waste Dump Lift<br>Buttressing H-H Dam | 3.69  |

#### L-L DAM

The L-L Dam forms the western limit of the tailings facility. The L-L Dam is located on Pukaist Creek near the junction of the Highland Valley and the Thompson River Valley. The valley at the L-L Damsite is roughly U-shaped with a relatively flat floor at about elevation 1100 m and valley walls gently sloping to a maximum elevation of about 1829 m. Pukaist Creek meanders across the damsite and then cuts through a moraine of glacial till and starts its rapid descent to the Thompson River about 2.5 km downstream of the L-L Dam. Field investigation programs, carried out in stages covering the foundation and abutments, reveal the following subsoil profile:

- very soft to firm, sensitive swamp and lacustrine deposits involving volcanic silt-clay, varved clay, silt and silt-sand, up to 15.5 m thick in the valley section;
- up to 2.5 m of dense ablation till overlying very dense basal till of varying thickness;
- very dense, clean interglacial sands, up to 40 m thick in the valley section.

The depth of surficial soils overlying bedrock varies substantially along the centerline of the dam. On the south abutment, the overburden depth varies from about 1 m to 15 m. The soil thickens to about 75 m at the center of the valley. On the north valley slope, the soil layer tapers out to negligible thickness at elevation 1230 m on a volcanic knoll then thickens to 29 m or greater near the ultimate crest elevation of the dam.

The L-L Starter Dam is a zoned earthfill structure, with a central till core and an

upstream cutoff trench, constructed with locally borrowed soil over the soft swamp and lacustrine deposits (see Figs. 6 and 7). A system of vertical geo-drains and a horizontal sand and gravel blanket were used to accelerate the consolidation rate of the lacustrine deposits. The construction of the Starter Dam was also staged over two years: a 12.2 m high fill placed in 1976; and 30.5 m of fill placed in 1977. In addition, the foundation of the Starter Dam was extensively instrumented. Salient features of the design and construction of the Starter Dam were summarized by Burke and Smucha (1979).

The L-L Dam, which comprises a central till core, a downstream shell and upstream sluiced cycloned sand and tailings, is being raised using the centerline construction method (see Fig. 6). Two measures were taken to improve the foundation stability of the L-L Dam valley section (see Fig. 7) for both static and dynamic loadings and to allow the construction rate of the dam to accelerate according to the tailings storage need of the mining operation. These were:

- (1) excavating the soft swamp and lacustrine deposits from beneath downstream construction stages of the dam and replacing them with compacted granular fill, and
- (2) constructing a large buttress berm downstream of that portion of the Starter Dam founded on the soft deposits (Klohn, Lo and Olsen 1982).

Upon completion of the Starter Dam, a large portion of the tailings pumped to the L-L Dam was used to fill the void at the bottom of the valley immediately upstream of the dam. The filling involved on-dam cycloning, uniform spigotting, and end discharge from large pipes. From 1978 to 1979 all fill placed in the downstream zone of the dam came from natural borrow. Since 1980, the amount of cycloned sand used in the downstream zone has been steadily increased. By 1982, downstream fill came almost exclusively from cycloned sand. Cost-effective and efficient construction techniques involving direct hydraulic placement and mechanical compaction by bulldozers for handling and placing the sand have been developed since 1982 (Scott and Lo 1984). Table 2 shows required embankment volumes for the L-L Dam per unit of tailings storage since 1976. The ratio of embankment volume to tailings storage is quite large, in the range of 20 to 37 m<sup>3</sup>/1000 m<sup>3</sup>. The ratio was even higher during the Starter Dam construction in 1976 to 1978, and again during accelerated construction in 1987 to make up flood storage lost with the burial of the J-J Dam. With the exception of above two periods, the ratio steadily drops from 37 in 1979 to 20 in 1992. Therefore, the cycloned sand delivery system designed for earlier years will develop excess capacity in later years. With greater volumes of cycloned sand available for dam construction in the future, techniques with potential to further reduce construction cost will be studied.

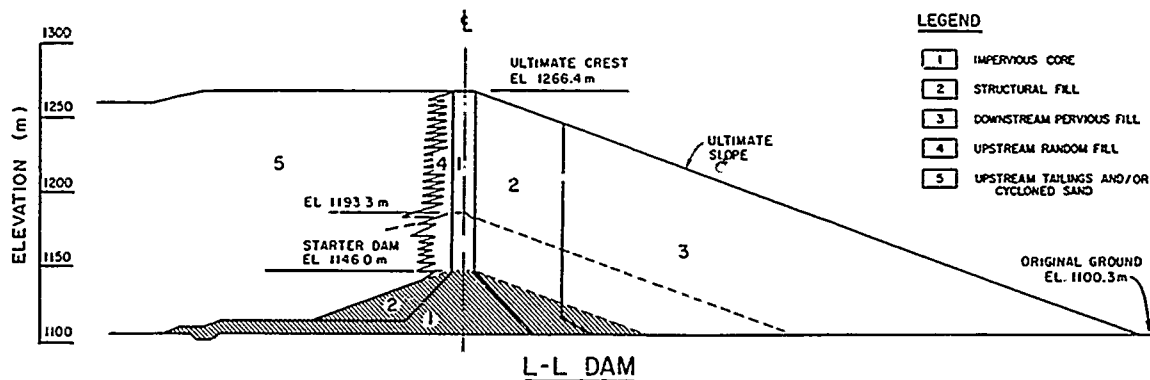


Fig. 6. Typical L-L Dam section

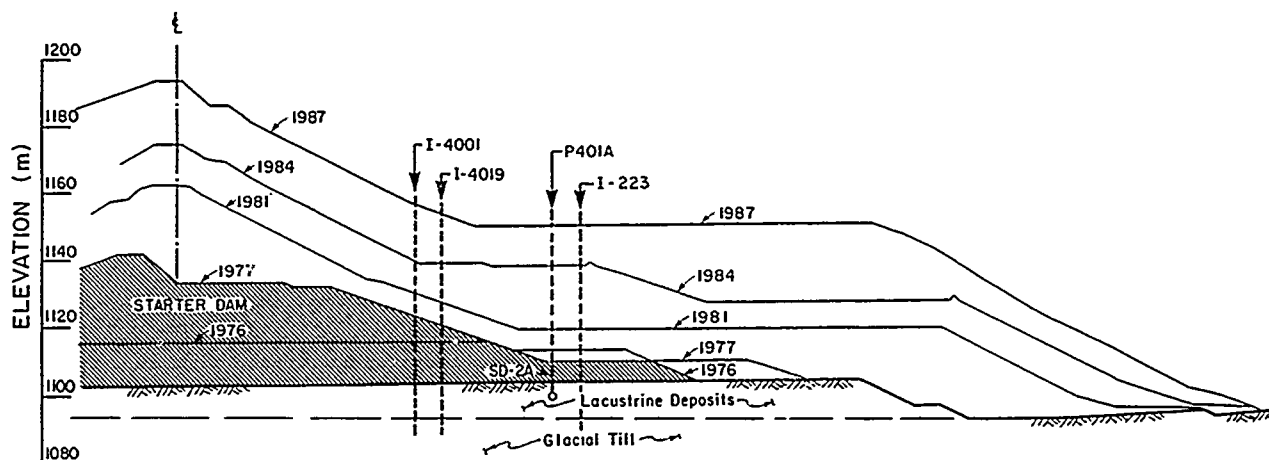


Fig. 7. L-L Dam Valley Section Over Lacustrine Deposits

TABLE 2  
REQUIRED L-L DAM EMBANKMENT VOLUMES  
PER UNIT OF TAILINGS STORAGE

| YEAR         | DESCRIPTION OF TAILINGS FACILITY               | REQUIRED EMBANKMENT VOLUME PER UNIT OF STORAGE M <sup>3</sup> /1000 M <sup>3</sup> |
|--------------|--|--|
| 1976-1978    | Starter Dam Construction                       | 142.54   |
| 1979-1986    | Storage Between J-J and L-L Dam                | 37.05  |
| 1987         | Accelerated Dam Construction for Flood Storage | 44.59  |
| 1988-1991    | Initial Storage Between H-H and L-L Dam        | 26.92  |
| 1992 Onwards | Ongoing Storage Between H-H and L-L Dam        | 19.83  |

The current L-L Dam design includes an alternative to incorporate a substantial zone of hydraulically placed, uncompacted sandfill in the downstream section above the saturation zone without compromising the resistance of the dam to seismic loadings. Techniques considered to place cycloned sand in this uncompacted zone include:

- (1) cell construction technique involving discharge of underflow through pipeline as used at Brenda Mines and the upstream section of the L-L Dam in 1987;
- (2) mobile, on-dam cyclone technique involving direct discharge of underflow from cyclone apexes as used at the Trojan Dam; and
- (3) fixed, on-dam cyclone technique involving direct discharge of underflow from cyclone apexes as used at Gibraltar Mines.

In the evaluation of various techniques, the cost of delivering and cycloning the sand has to be weighed with the cost of placing the sand in the embankment.

#### Instrumentation Observations and Back Analysis

Comprehensive instrumentation installed for monitoring the foundation performance of the Starter Dam consists of shallow pneumatic and standpipe (Geonor and Casagrande) piezometers, deep standpipe piezometers and observation wells, inclinometers, and pneumatic settlement gauges. Figure 7 shows the location of some instrumentation to be discussed later. This instrumentation has been maintained and expanded to include standpipe piezometers monitoring the saturation level in the dam fill. Piezometers located in the downstream pervious fills continue to show low saturation levels. Readings from shallow foundation piezometers located in the lacustrine deposits reflect the usual pattern of pore pressure rise during fill placement and its gradual dissipation with time. Shallow foundation piezometers located in the glacial till beneath the Starter Dam and abutment sections show little influence of seepage from the tailings pond. Deep foundation piezometer and observation wells indicate little to minor change of groundwater regime at depth since water impoundment in the tailings pond in 1976. To date total foundation settlements for the Starter Dam range from 1 to 3 m. These settlements reflect the consolidation of the lacustrine deposits in response to the increasing embankment loading. Downstream horizontal foundation movements within the Starter Dam range from 100 mm to 500 mm. These movements reflect the ongoing foundation adjustments to the embankment loading under partially drained condition.

Piezometric (P401A) and settlement (SD-2A) data from the lacustrine deposits beneath the Starter Dam are shown on Figs. 8(b) and (c). Solid lines represent continuous observation data, while long dashed lines represent extrapolated data based on other operating instruments. A one-dimensional consolidation finite-difference computer program (Wong and Duncan 1985) was used to back analyze the ongoing consolidation in response to fill loading in the berm area (see Fig. 8a). The computed pore pressure and settlement are also shown in Figs. 8(b) and 8(c) as short dashed lines. Table 3 summarizes laboratory test data and the back-analyzed field observation data. For the compression index,  $C_c$ , the field values are about one-half of the laboratory values possibly due to sample disturbance involved in laboratory tests. For the coefficient of consolidation,  $C_v$ , the field values are about four times the laboratory values. Horizontal stratification and the presence of vertical geo-drains in field deposits are considered as additional contributing factors to this difference between field and laboratory values.

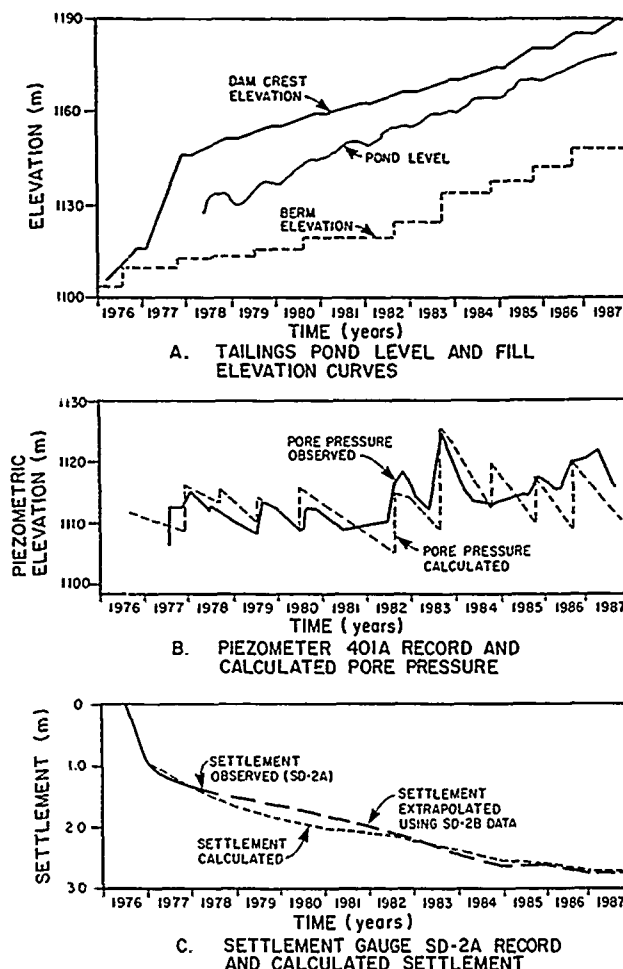


Fig. 8. Observed and Back Analyzed Pore Pressure and Settlement Data

Inclinometer (I-223) data in the mid-valley section showed horizontal displacements of about 200 mm from 1976 to 1977. In 1978, Inclinometer I-4001 was installed as a replacement for I-223. The inclinometer data for I-4001 is shown in Fig. 9 as displacement profiles and accumulated displacement-time plots for a reference point at the foundation level. Solid lines represent continuous observation data, while dashed lines represent extrapolated data based on an adjacent inclinometer (I-4019) installed in 1986 as a replacement for I-4001. The majority of movement is confined to the upper silt-clay/varved clay horizons. Inferred average field shear strains based on the initial thickness of these horizons are also shown in Fig. 9. Using the decreased thickness obtained from recorded settlements, the shear strain would be about 30% larger than that shown in Fig. 9 at the end of 1987.

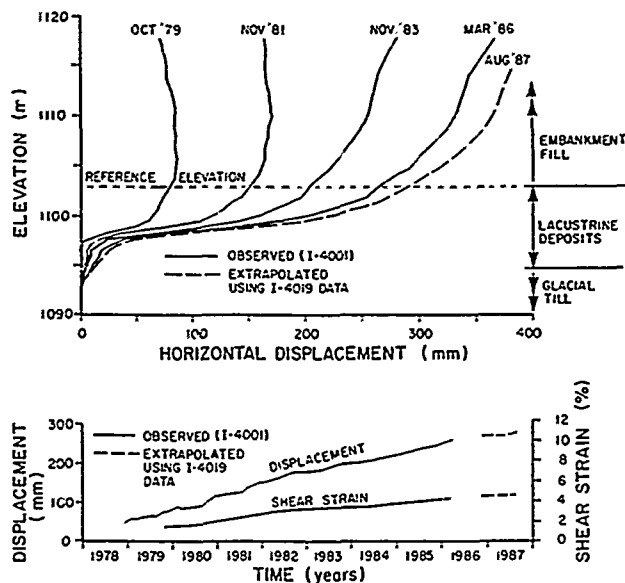
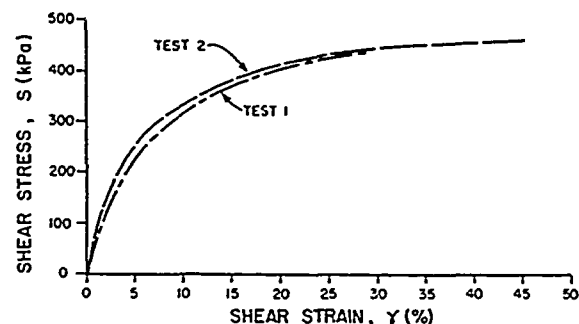
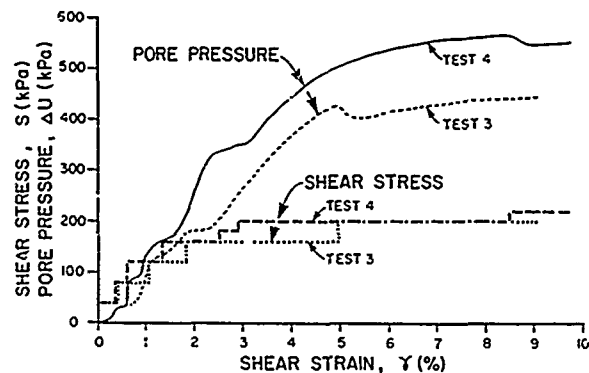


Fig. 9. Observed Inclinator Data

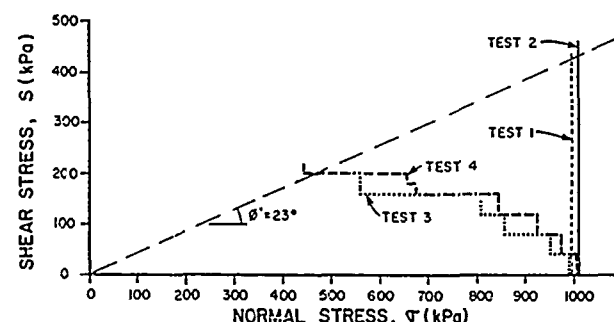
The embankment loading induced foundation deformation of relatively soft lacustrine deposits between more rigid foundation soils at depth and compacted fill above can be closely simulated by laboratory simple shear tests. Four simple shear tests: two consolidated-drained (Tests 1 and 2) and two consolidated-undrained (constant volume Tests 3 and 4) were carried out at the University of British Columbia. Results of these tests are shown in Fig. 10. Under drained condition, large shear strains (in the order of 25%) are associated with the ultimate shear strength whereas under undrained condition the corresponding strains are much smaller (in the order of 2%). The accumulated field shear strain in the region of shown inclinometers, including that inferred from Fig. 9 and that occurred earlier, is in the order of 8% representing foundation deformation under partially drained condition.



A. CONSOLIDATED-DRAINED TESTS



B. CONSOLIDATED-UNDRAINED (CONSTANT VOLUME) TESTS



C. EFFECTIVE STRESS PATHS ON HORIZONTAL PLANE

Fig. 10. Summary of Simple Shear Test Results

TABLE 3

CONSOLIDATION PARAMETERS FROM LABORATORY TESTS AND BACK-ANALYZED FIELD DATA

| LACUSTRINE<br>DEPOSITS | THICKNESS<br><br>(m) | OEDOMETER TESTS     |     |  |      |  |    | BACK-ANALYZED FIELD DATA |   |  |  |
|------------------------|----------------------|---------------------|-----|--|------|--|----|--------------------------|---|--|--|
|                        |                      | VOID RATIO<br>$e_o$ |     | COEFFICIENT OF<br>COMPRESSION<br>$C_c$ |      | COEFFICIENT OF<br>CONSOLIDATION<br>$C_v$<br>( $\times 10^{-4}$ cm <sup>2</sup> /s) |    | VOID<br>RATIO<br>$e_o$   | PORE PRESSURE<br>PARAMETER<br>$r_u$<br>( $=\Delta u/\Delta\sigma_v$ ) | COEFFICIENT OF<br>COMPRESSION<br>$C_c$ | COEFFICIENT OF<br>CONSOLIDATION<br>$C_v$<br>( $\times 10^{-4}$ cm <sup>2</sup> /s) |
|                        |                      |                     |     |  |      |  |    |                          |   |  |  |
|                        |                      |                     |     |  |      |  |    |                          |   |  |  |
|                        |                      |                     |     |  |      |  |    |                          |   |  |  |
| clay-silt              | 5.2                  | 4.7-4.9             | 4.9 | 2.7-3.3                                | 3.3  | 0.3-2.0  | 2  | 4.9                      | 0.8   | 1.15                                   | 8  |
| varved clay            | 4.0                  | 0.8-2.1             | 1.4 | 0.10-1.07                              | 0.65 | 4-700  | 10 | 1.4                      | 0.8   | 0.28                                   | 40   |



## SUMMARY

Since its initial impoundment in 1972, the Highland Valley tailings storage facility has continued to serve the need of the mining operation to store its tailings at an ever increasing rate. Throughout its development, the geometry of the tailings storage and distribution facilities and waste dumps undergoes continued changes. Ongoing construction of the storage facility is planned to maintain key earthquake and flood design criteria as well as to adjust the use and placement method of various construction materials including natural borrow, tailings sand and mine waste as they become available. Various construction techniques are explored to develop an efficient and cost effective tailings storage operation. Satisfactory performance of the H-H and L-L Dams are experienced to date. Back analysis of the instrumented L-L Dam valley section founded partially on the lacustrine deposits provides valuable information for planning ongoing construction activities. The flexibility inherent in the design of the two dams constructed by the centerline method allows the storage capacity of the facility to be expanded even beyond the current design of 1.8 billion tonnes, if required in the future. The facility will eventually be reclaimed in an orderly fashion to allow for multiple uses of the reclaimed land as well as the stored water. A permanent spillway system will be installed at the L-L Dam to ensure the safe passage of flood water through the storage facility back into the natural course of the Pukaist Creek downstream.

## ACKNOWLEDGEMENTS

The authors are grateful to Highland Valley Copper for their permission to allow the publication of this paper, and to their colleagues for their collective efforts in the ongoing development of the project as well as their assistance in the preparation of the paper.

## REFERENCES

- Burke, H.H. and Smucha, S.S. (1979), "Lornex Tailings Dam on a Soft Foundation", Proc. of 6th Pan-American Conf. on Soil Mech. and Fdn. Engrg., Lima, Vol. I, pp. 305-316.
- Dickinson, W.R. (1976), "Sedimentary Basins Developed During Evolution of Mesozoic - Cenozoic Arc-Trench System in Western North America", Can. J. Earth Sci., Vol. 13, No. 9, September, pp. 1268-1287.
- Ewing, T.E. (1980), "Paleogene Tectonic Evolution of the Pacific Northwest", J. of Geology, Vol. 88, No. 6, pp. 619-638.
- Ewing, T.E. (1981), "Regional Stratigraphy and Structural Setting of the Kamloops Group, South-Central British Columbia", Can. J. Earth Sci. Vol. 18, No. 9, pp. 1464-1477.
- Hansen, P. (1987), "Highland Valley Copper: A Strategy for Increased Productivity", The Canadian Mining and Metallurgical Bulletin, Vol. 80, No. 904, pp. 42-45.
- Heaton, T.H., and Hartzell, S.H. (1987), "Earthquake Hazards on the Cascadia Subduction Zone", Science, Vol. 236, April 10, pp. 162-168.
- Klohn, E.J., Lo, R.C., and Olsen, M.T. (1982), "Stability of a Tailings Dam on Sensitive Clay", Trans. of 14th Int'l Cong. on Large Dams, Rio de Janeiro, pp. 199-217.
- McMillan, W.J. (1985), "Geology and Ore Deposits of the Highland Valley Camp", Geological Association of Canada.
- Noble, D.C. (1972), "Some Observations on the Cenozoic Volcano - Tectonic Evolution of the Great Basin, Western United States", Earth Planet, Sec. 17, pp. 142-150.
- Scott, M.D. and Lo, R.C. (1984), "Evolution of Design and Construction of Lornex L-L Tailings Dam", Proc. of the Case Histories in Geotechnical Engineering Conference, St. Louis, Vol. III, pp. 1083-1088.
- Wong, K.S. and Duncan, J.M. (1985), "CONSOL: A Computer Program For 1-D Consolidation Analysis of Layered Soil Masses", Virginia Tech, Blacksburg.

## Excessive Seepage Losses at Westwood Lake Dam

### B. Bailey

Senior Project Manager, Southwestern Laboratories, Inc., Dallas, Texas

### E. Bloom

Head, Engineering Design Staff, Soil Conservation Service, Indianapolis, Indiana

### T.R. West

Department of Geosciences, Purdue University, West Lafayette, Indiana

### J.A. Mundell

Department of Civil Engineering, University of Notre Dame, Notre Dame, Indiana

**SYNOPSIS:** Excessive seepage losses at Westwood Lake Dam in east-central Indiana were apparent in 1974 during first filling of the lake when seepage areas developed downstream of the dam and abutments. Several remedial studies were performed which included additional test borings, field and laboratory tests, installation of observation wells, and a review of the site geology and hydrology. Data and observations from these studies were used to develop semi-quantitative assessments of seepage loss rates as related to lake levels. These analyses served as a basis for design of a major repair which consisted of blanketing a significant portion of the lake bottom with on-site, low-plasticity clays and clayey silts. The blanketing was completed in 1984 and post-repair filling required about two years. Subsequent monitoring and observations indicate that the lake level is holding at or within 1.5 ft of the original design normal pool.

Judgments and decisions regarding seepage control are among the most difficult faced by dam designers. Where granular soils or permeable rock strata are encountered in foundations or abutments, design decisions include considerations of cutoffs, upstream blanketing, drains, or other measures to help ensure a safe structure and hold seepage losses to within tolerable limits. However, in complex geologic conditions, especially for dams of small to intermediate size, it is often not possible to determine accurately the in-situ permeability of granular materials, the continuity of these deposits, the effect of weathering on exposed clays, and combinations of these factors. Under these circumstances, quantitative seepage analyses with flow nets or by other means typically do not sufficiently represent the actual conditions. Several of these factors came into focus during analyses and investigations for Westwood Lake Dam as described in this case history.

### BACKGROUND

Westwood Lake Dam was constructed in Henry County, Indiana as one of several similar earth dams on tributaries of the Big Blue River for flood control, water supply, and recreational purposes. The homogenous embankment dam is 1,200 ft long and 60 ft high. The drainage area encompasses almost four sq miles and the normal pool lake surface covers 173 acres. The dam crest is at Elevation 1023.6 (ft,MSL) and the normal pool is controlled by the principal spillway intake riser at Elevation 1015.2. An earth channel emergency spillway is located in the left abutment. A total of 300,000 cu yd of compacted fill was placed for the original embankment construction.

Initial geologic and geotechnical studies disclosed the presence of granular soils in the dam foundation and abutments. Seepage control measures for the original embankment construction in 1973 to 1974 included a cutoff trench to impervious foundation soils at a depth of about 10 feet in the recent alluvium. Also, blanketing with compacted impervious soils was placed over limited areas of exposed granular soils in the vicinity of the upstream abutments.

Early concerns with seepage losses were indicated in November, 1974, when the lake level reached Elevation 984 on first filling. Three seepage areas developed downstream of the dam and early remedial steps included installation of shallow trench drains to "dry up" the surface and restore these areas to their original use. Flows from these seepage areas were monitored with a flume device placed in the stream channel downstream of the dam.

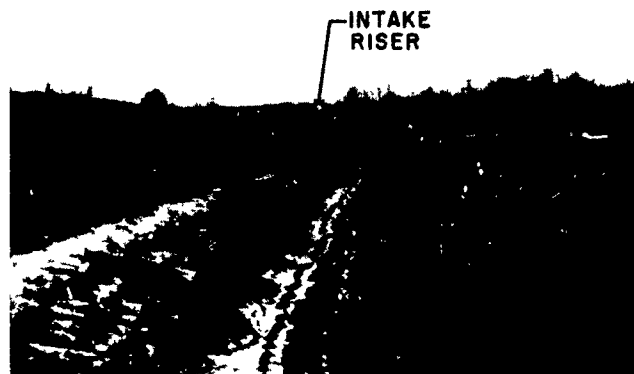


Figure 1. Pre-Repair Lake Below Intake Riser (Normal Pool) Control on Upstream Slope of Dam

Several series of post-construction test borings were drilled and groundwater observation wells were installed at intervals between 1975 and 1980. Records of lake elevations also have been maintained since 1975. Lake levels have fluctuated between Elevation 994 in October, 1977 and near the design normal pool (Elevation 1015.2) for a brief period in September, 1979. The typical lake level was well below the intake riser control level as shown in Figure 1.

Based on the remedial studies, a major repair consisting of draining the reservoir and blanketing of about half of the lake area was completed in 1984. This included a total of 416,000 cu yd of compacted blanket fill. The reservoir filled to the design normal pool within about two years and since has remained at or near that level.

#### GEOLOGY

According to published geologic information (Schneider and Gray, 1966), Silurian limestone is approximately 200 ft below the existing ground surface. The overburden soils were deposited by Kansan, Illinoian, and Wisconsin ice sheets (Wayne, 1965). The maximum extent of glaciation in Indiana during the Wisconsin Age is shown in Figure 2 (Wayne, 1966). The site is located between two former sublobes of the Wisconsin ice sheet along a mapped stagnation front north of the maximum glacial extent. The stagnation front developed approximately 20,000 years before present (BP). Meltwater discharge from both sublobes likely occurred at this location during the stagnation period. This flow then would have continued into an outwash channel, containing the present-day Big Blue River, with flow to the southwest. It is hypothesized that the granular soils beneath the dam and in the abutments were deposited in an "esker-like" manner with flow through ice-walled channels or tunnels. Esker deposits are often typified by a wide range for gradation of granular soils as found at this site.

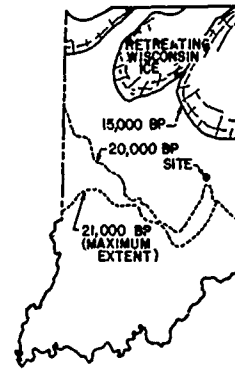


Figure 2. Wisconsin Glacial Stages in Indiana

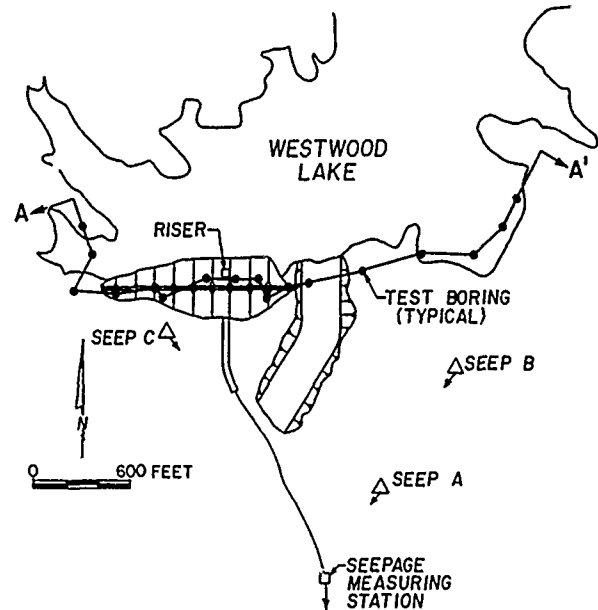


Figure 3. Locations of Site Features

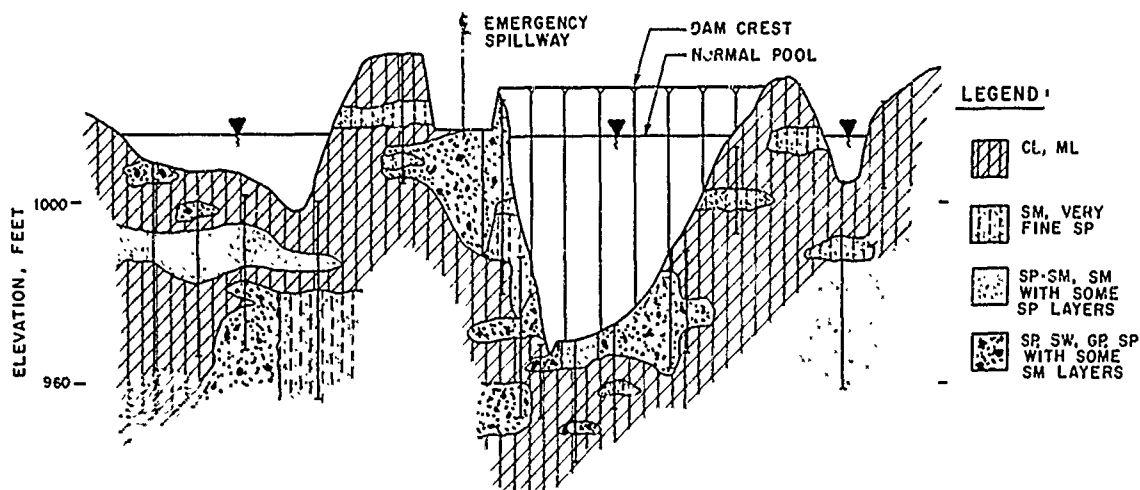


Figure 4. Subsurface Profile Beneath Dam (Section A-A', Figure 3)

These geologic considerations and test boring data suggested a southerly orientation to the granular deposits in the vicinity of the dam and abutments. The locations of several of the pre- and post-construction test borings in the vicinity of the dam are shown in Figure 3. The three seepage areas (Seeps A, B, and C) also are shown along with the seepage flow measuring station.

A subsurface profile (east-west Section A-A') developed from these borings is shown in Figure 4. This profile illustrates the extremely complex distribution of soils with widely varying permeabilities. Within the relatively impermeable glacial till are numerous deposits or channels of granular soils. Gradations for these granular soils varied over a wide range from poorly graded coarse gravel to silty fine sands. Many of the Unified Soil Classification System groups were represented in this profile.

#### HYDROLOGY

An average annual rainfall of 39 in. and an annual lake evaporation of 33 in. are estimated for this site. Several hydrologic analyses of the Westwood Lake watershed were performed based on more detailed seasonal runoff data. Among these was a determination of the theoretical time to fill the lake versus seepage loss rates at the normal pool elevation based on water balance calculations, shown in Figure 5. From this figure, it can be seen that for a total seepage loss rate on the order of 4.0 cfs, the lake will not fill. For the major blanketing repair, it was decided to use a maximum seepage loss rate of 2.0 cfs as a design criterion.

From the records of lake elevation maintained after the original construction, it was possible to estimate total seepage loss rates based on the relationship between reservoir storage versus time, prior to repair, shown in Figure 6. The stream inflow was determined to be approximately equal to the evaporation loss rates during these periods.

#### SEEPAGE

Results of the observed flow at the downstream seepage measuring station are summarized in Figure 7. It can be seen that the pre-repair points (solid circles) essentially form a linear relationship with the lake elevation. The pre-repair data were also utilized to estimate the portion of the "total lake seepage" (TLS) that exited the lake through granular deposits in the foundation and abutments and was monitored downstream of the dam. This is hereafter referred to as "front end seepage" (FES). At the normal pool Elevation 1015, an FES seepage rate of 2.8 cfs was measured. A limited number of post-repair data points also are shown in Figure 7 as open circles.

To develop a working hypothesis for the blanketing repair, these seepage relationships and the previously-described hydrologic observations are combined in Table 1. This

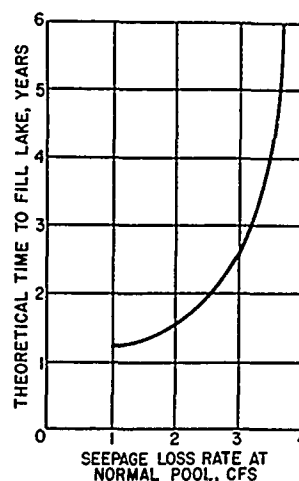


Figure 5. Theoretical Lake Filling Times

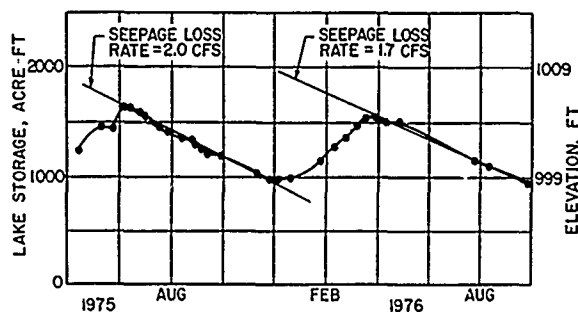


Figure 6. Total Lake Seepage (TLS) From Lake Elevation Records

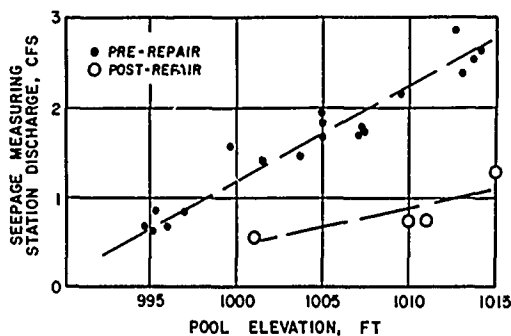


Figure 7. Measured Front End Seepage (FES), vs. Lake Elevation

table was developed by estimating a TLS rate of 2.0 cfs at lake Elevation 1002 from Figure 6 and a FES rate of 1.4 cfs from Figure 7. At lake Elevation 1015 (normal pool), the FES rate is 2.8 cfs, also from Figure 7. If it is assumed that the ratio between the FES and TLS rates remains constant with pool elevation, then the TLS rate would be about 4.0 cfs at the normal pool level.

Table 1. Summary of Lake Seepage Observations

| Lake Elevation<br>ft | Front End<br>Seepage (FES)<br>cfs | Total Lake<br>Seepage (TLS)<br>cfs |
|----------------------|-----------------------------------|------------------------------------|
| 1002                 | 1.4                               | 2.0                                |
| 1015                 | 2.8                               | 4.0                                |

This TLS rate is consistent with Figure 5, in which the lake theoretically would not fill at a seepage loss rate of 4.0 cfs and the observation that the lake did not fill after the original construction (prior to the repair). To achieve a maximum normal pool TLS rate of 2.0 cfs (determined to be acceptable from Figure 5), it was decided to attempt to reduce the normal pool FES rate from 2.8 to 0.8 cfs, taken as a blanketing repair criterion.

#### BLANKETING

The blanketing repair was indicated by the complex soils and the great depth to bedrock. Low plasticity silty and sandy clays and clayey silts (Unified Soil Classifications: CL, CL-ML, ML, liquid limit: 15 to 20, plastic limit: 3 to 9) were available in borrow areas adjacent to the lake. A design coefficient of permeability of  $1 \times 10^{-6}$  cm/sec was selected based on laboratory tests tempered with judgment regarding the anticipated ratio of field to laboratory permeabilities (Olson and Daniel, 1981).

The blanket thickness was determined using the idealized model shown in Figure 8 and the ensuing theoretical Equation (1) derived from Darcy's Law. This model assumes complete head loss through the blanket and is generally conservative for most locations in the lake area as compared to a more comprehensive analysis that assumes head loss through the blanket and underlying natural soils.

$$T = \frac{kH'}{q_a - k} \quad (1)$$

in which

- T = required blanket thickness
- k = coefficient of permeability for blanket
- H' = height of water over blanket
- $q_a$  = allowable leakage per unit area

The value for  $q_a$  was determined by dividing the allowable normal pool FES seepage criterion of 0.8 cfs, as established in the preceding section, by the estimated contributory area to the FES. Design relationships between the parameters in this equation are shown in Figure 9 illustrating the sensitivity to the design k-value. It can be seen that if the field k-value is on the order of  $10^{-7}$  cm/sec, then the blanket thicknesses based on  $k = 1 \times 10^{-6}$  cm/sec are very conservative. On the other hand, if k

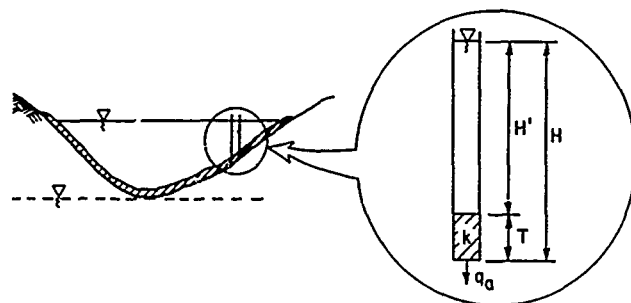


Figure 8. Idealized Seepage Model for Blanket

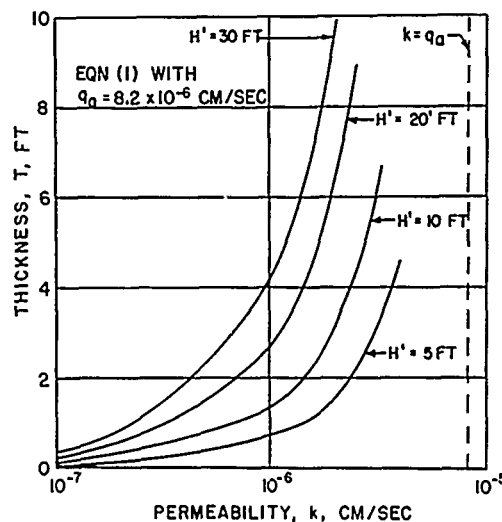


Figure 9. Blanket Thickness vs. Permeability

approaches  $10^{-5}$  cm/sec, the blanket is pervious and would serve no useful purpose.

Field permeability testing of natural exposed soils around the lake perimeter and results of test borings within the lake area were used to delineate areas where natural clays were present at the lake bottom. The design blanket thicknesses ranged from two ft (determined to be a practical minimum) to four ft in deeper lake areas. The blanketing fill was placed and compacted in lifts to 95 percent of the Standard Proctor value at moisture contents above two percent below the optimum moisture. Compaction near or above the optimum moisture level is important to achieve a high degree of imperviousness for fine-grained soils (Mundell and Bailey, 1985).

The extent of the contributory area to FES seepage was estimated based on the locations of Seeps A, B, and C, measured groundwater levels in observation wells, regional topography, and water well data. Although regional flow nets were judged to be only marginally applicable to such a heterogeneous soil deposit, probable flow directions were determined from the pre-repair groundwater contours as shown in Figure 10. Possible maximum and minimum FES contributory areas were estimated from these analyses. The possibility of extremely permeable coarse granular strata extending well

upstream of the dam, suggested by the downstream location of Seep A and as depicted in Figure 11, led to the decision to extend the blanketing to a point about midway in the lake, as shown in Figure 10. This also provided a margin of safety considered appropriate in light of the very approximate nature of the above analyses.

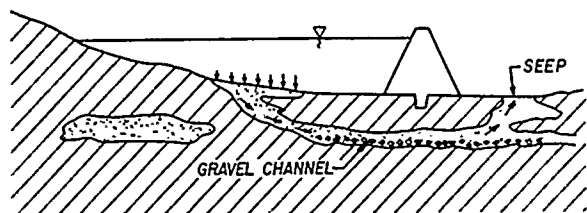


Figure 11. Possible Seepage Flow Path

#### PERFORMANCE

After the blanketing repair was completed in late 1983, the lake refilled to its design normal pool level in about two years under relatively normal rainfall conditions. In the summer of 1986, the water level dropped slightly to about one foot below normal pool level, but raised again after the fall rains. This closely matched the performance predicted for a final TLS rate of 2.0 cfs. However, in 1987, during a period of significantly below-normal rainfall, the lake level dropped to 1.5 ft below normal pool.

During refilling, the seepage flow re-emerged, at a low rate, at Seep B. The available post-repair seepage flow measurements as shown in Figure 7 indicate that the FES level was reduced from its original normal pool rate of 2.8 to 1.2 cfs, but not to the intended design level of 0.8 cfs.

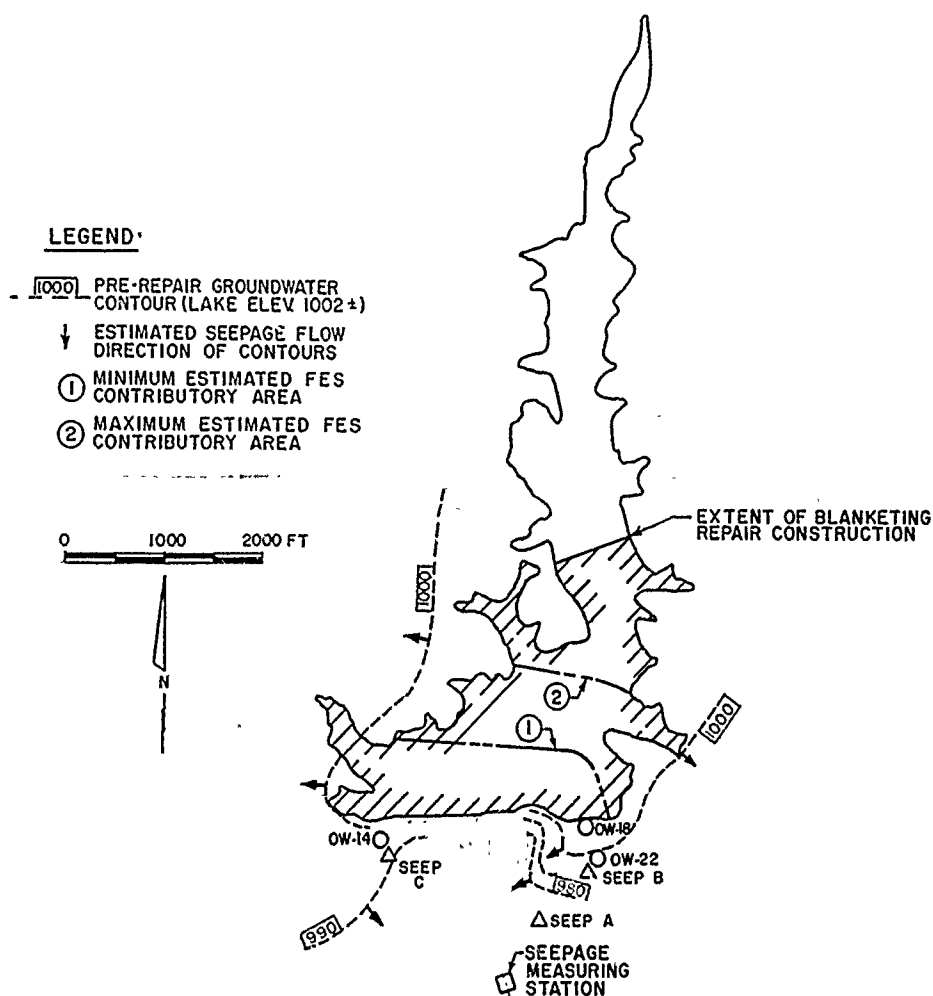


Figure 10. Estimated FES Contributory Areas and Extent of Blanketing

In general, the observation well readings were erratic, as would be expected for these conditions. However, some insight to the blanket performance is indicated by the readings in three typical groundwater observation wells, OW-14, OW-18, and OW-22, judged to be responsive to the lake levels before and after the blanketing repair, at locations shown in Figure 10. These readings are plotted in Figure 12. The before and after readings for OW-14 and OW-18 indicate an increased head loss or degree of separation between the lake and groundwater after the repair. The same holds true for OW-22 for lake levels above Elevation 1000.

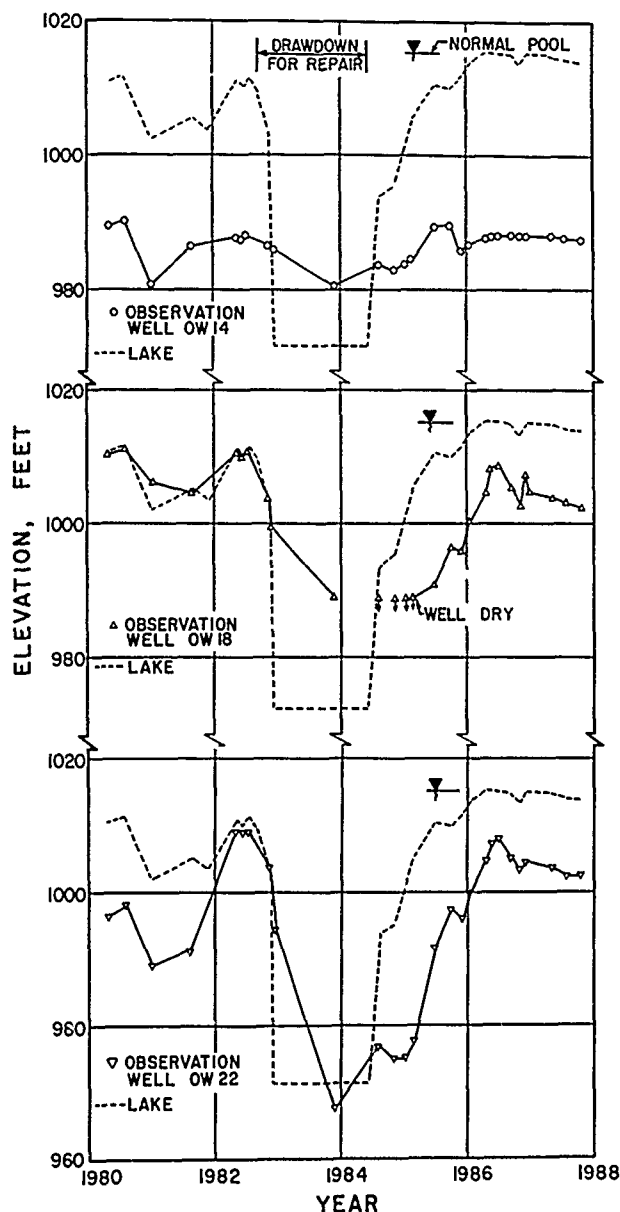


Figure 12. Measured Pre- and Post-Repair Groundwater Levels in Three Observation Wells

## CONCLUSIONS

Based on these analyses and observations, the following "lessons learned" or conclusions were developed:

1. The unusually large amount of information collected for this size project over this period of time permitted several different types of analyses to be made. However, because of the extremely complex geology, even this amount of information was not adequate to completely determine the seepage loss mechanisms and quantities.
2. The blanketing repair ultimately selected at this site required more volume of compacted fill than the embankment itself. This is due, in part, to the marginal permeabilities of the available on-site blanket soils. The repair generally appears to be functioning satisfactorily. However, what might have been regarded as a conservative repair still was not adequate to maintain the normal pool level during periods of significantly below-normal rainfall.
3. An early and complete understanding and appreciation of the site geologic conditions relative to seepage potential are often difficult to achieve. This requires the exercise of considerable engineering judgment and close coordination among the geotechnical engineer, engineering geologist, and hydrologist.

## REFERENCES

- Mundell, J.A., and Bailey, B., (1985), "The Design and Testing of a Compacted Clay Barrier to Limit Percolation Through Landfill Covers," *Hydraulic Barriers in Soil and Rock*, ASTM STP 874, A.I. Johnson, R.K. Frobel, N.J. Cavalli, and C.B. Pettersson, Eds., 246-262.
- Olson, R. E. and Daniel, D. E., (1981), "Measurement of the Hydraulic Conductivity of Fine-Grained Soils," *Permeability and Groundwater Contaminant Transport*, ASTM STP 746, T. F. Zimmie and C. O. Riggs, Eds., 18-64.
- Schneider, A.F. and Gray, H.H., (1966), "Geology of The Upper East Fork Drainage Basin, Indiana," *Department of National Resources, Geological Survey Special Report 3*, 55 pp.
- Wayne, W.J., (1965), "The Crawfordsville and Knightstown Moraines in Indiana," *Indiana Geological Survey Report of Progress 28*, 15 pp.
- Wayne, W.J., (1966), "Ice and Land," *Indiana Sesquicentennial Volume, Natural Features of Indiana*, Indiana Academy of Science, 33 pp.

## Testing of the Homestake Mine Tailings Deposit

Donald R. East

Managing Partner, Knight Piesold and Co., Denver, Colorado

John W. Ransone

Manager—Design & Construction, Homestake Mining Company,  
Golden, Colorado

William A. Cincilla

Project Engineer, Knight Piesold and Co., Denver, Colorado

**SYNOPSIS:** This paper discusses the geotechnical investigation of a large gold tailings facility which has been in operation since December 1977. The very thorough test program included 670 m (2200 ft.) of piezocone probing, 65 self-boring pressuremeter tests down to a maximum of 35 m (118 ft.), 60 SPT's and 9 laboratory triaxial tests as well as a well pump test. The study included a detailed geological and seismic study to determine earthquake design parameters and to assess the liquefaction potential of the deposit. Test results were utilized to determine the stability of an upstream constructed embankment employing the sub-aerial method of tailings deposition together with a comprehensive underdrainage system. The study indicates that liquefaction of the deposit is highly unlikely to occur and that the embankment has an acceptable factor of safety under sub-aerial conditions.

### INTRODUCTION

The Grizzly Gulch tailings dam, which is owned and operated by Homestake Mining Company, is located approximately 3.2 km (2 miles) southeast of the Town of Lead, in central Lawrence County, South Dakota. The area forms a part of the northern Black Hills which has been a center of precious metal mining activity for over a century. The locality of the site is shown in Figure 1.

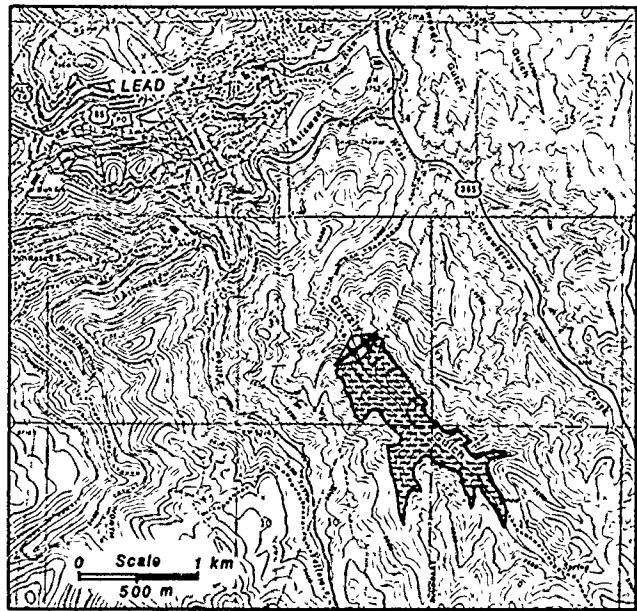


Figure 1 - Locality Map

As part of a study into an alternative construction method for raising Homestake Mining Company's 90 m (285 ft.) high Grizzly Gulch tailings embankment above its 1986 elevation of 5400 ft., a detailed geotechnical study was undertaken during the fall of 1986 into the properties of the existing tailings beach deposit.

The alternative upstream construction design incorporated an extensive blanket drain extending 100 m (305 ft.) out from the existing earth/rockfill embankment combined with a modification of the single-point tailings discharge to the sub-aerial method of tailings deposition (Knight and Haile 1983). This change would result in the formation of a fully-drained tailings beach capable of supporting and maintaining stability of the upstream phase-constructed raises in 3 to 5 m (10 to 15 ft.) lifts to elevation 5500 ft.

Testing mainly took place from preconstructed roadways onto the tailings beach using a track-mounted drill rig.

The detailed geotechnical investigation, which incorporated extensive piezocone, self-boring pressuremeter, SPT and laboratory testing of undisturbed samples, had the following objectives:

- To obtain a detailed three-dimensional picture of the variation of coarse and fine tailings within the deposit.
- To utilize sophisticated in situ testing techniques which could assure testing of cohesionless saturated deposits for strength and permeability.
- To obtain relatively undisturbed samples of tailings, identified by the piezocone profiling, for laboratory testing.
- To assess the liquefaction potential of the existing tailings deposit.

### DAM GEOLOGY AND REGIONAL SEISMICITY

The three rock units in the vicinity of the dam site in ascending order are: Precambrian metamorphic units of the Grizzly and Flagrock Formations, Cambrian sedimentary beds of the Deadwood Formation, and Tertiary igneous dikes and sills. A geologic cross-section for the area is presented in Figure 2.



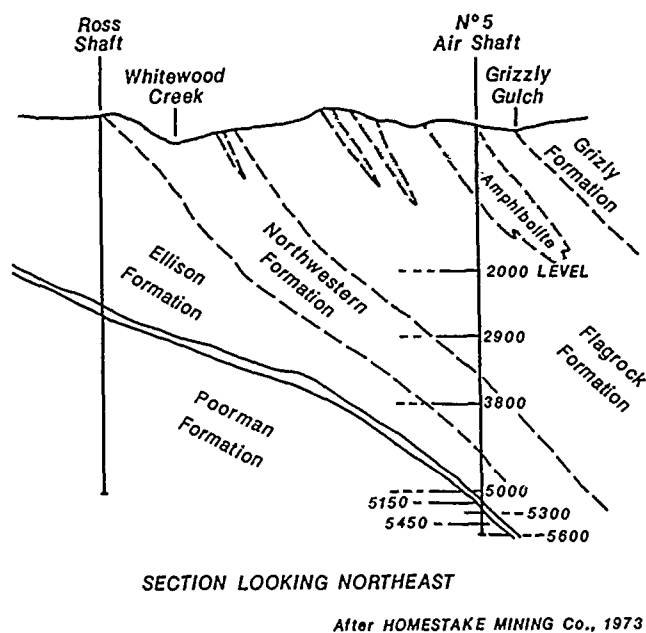


Figure 2 - Geologic Cross-Section of Grizzly Gulch

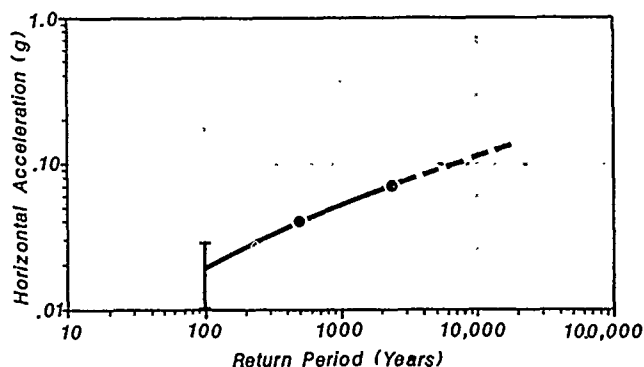
The valley floor and valley slopes, up to about elevation 5600, are generally underlain by the metamorphic beds of the Grizzly and Flagrock Formations which consist of micaceous schists, phyllites and slates, locally intruded by amphibolite dikes which are strongly foliated striking north and dipping about 40 to 80 degrees to the east. Some local shear zones were exposed during investigations in 1981 for the first raise of the embankment from elevation 5350 to elevation 5400, but it is considered that the most recent activity is pre-Tertiary.

A careful review of all available earthquake data indicates that very few, if any, earthquakes of felt intensity VI, or body wave magnitudes greater than 4.5, have occurred in the general vicinity of Grizzly Gulch tailings dam. On this basis, the dam site can be classified as an area of very low seismicity.

Because of the absence of faulting in the region and relatively low rates of activities, most investigators have divided regions of the west-central United States into source zones based on rates and magnitudes of historic earthquakes and broad geologic characteristics. Based on the historical seismicity of the region and on data developed for the central Mississippi Valley, Nuttli and Hermann (1978) developed a cumulative magnitude-recurrence curve for the South Dakota region and determined that the "maximum magnitude" earthquake with a return period of 1000 years corresponded to a body wave magnitude  $m_b = 6.0$ . Similar studies by Algermissen and Others (1982) arrived at a maximum local magnitude  $M_L = 6.1$ , which, for midplate earthquakes, may be

considered to be equal to magnitudes based on body waves.

Based on the work of Algermissen, probabilistic estimates of maximum horizontal acceleration in rock for exposure times of 10, 50 and 250 years at the 90% probability level of non-exceedence were established for the Grizzly Gulch site. The data is plotted in Figure 3, and it can be seen that for a return period of 10,000 years, an acceleration of 0.10 g is obtained. For a 250-year project life (return period greater than 2000 years), this corresponds to a 97.5% probability of non-exceedence and is a reasonable estimate of the maximum level of ground shaking to be expected within the bedrock surface at the dam site.



After ALMERGISSEN et al., 1982

Figure 3 - Horizontal Acceleration vs. Return Period

#### SITE INVESTIGATION

##### a) Piezometric Cone Testing

The investigation involved an initial appraisal of the tailings deposit by use of a Fugro piezometric cone which provided detailed continuous site profiles, thus allowing critical zones to be identified. Tip resistance, sleeve friction and porewater pressure data were recorded every 2 cm and stored on a microcomputer disk. Visual display of all data was shown graphically on the computer screen during the test. Classification charts produced by Robertson and Campanella (1983) based on cone bearing and friction ratio, and by Jones and van Zyl (1981) based on cone bearing ratio and excess pore pressure were used to identify the coarser silty sands from the finer silts. In all cases, the excess pore pressures generated in the silts clearly identified these finer layers. A section line extending 185 m (600 ft.) onto the tailings is shown in Figure 4. It will be noticed that the material behaves as a typical hydraulically placed material with the coarser tailings (silty sands) generating high cone bearings and no excess pore pressures, while the finer tailings (silts) generally have low cone bearings and excess pore pressures. It will be seen from Figure 4 that the tailings mainly consist of coarser deposits with some minor layering of silts, and that the profile clearly shows the depositional history.

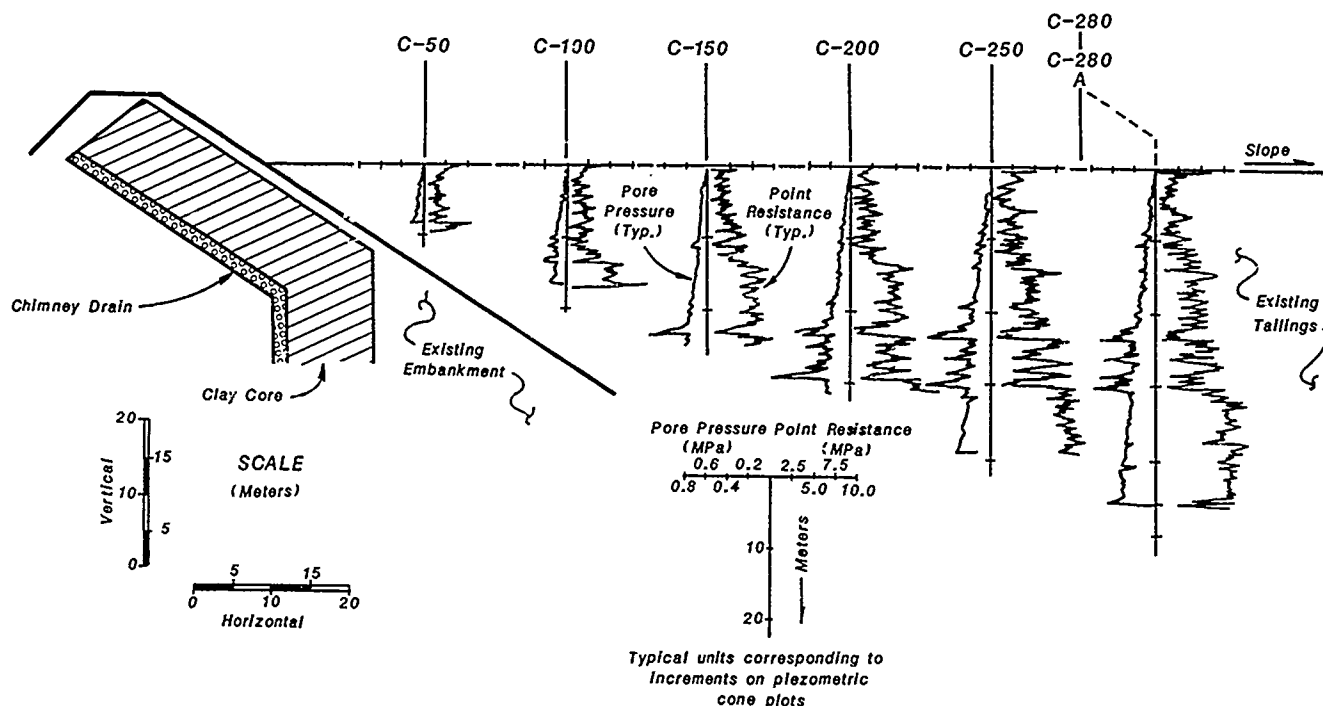


Figure 4 - Cross-Section of Tailings Deposit

For example, the tailings deposited at 22 m (72 ft.) at 26 m (87 ft.) represent a rapid deposition period under water. Above 22 m (72 ft.) the depositional environment is relatively uniform, with the rapid variations in tip load reflecting the meandering of the outflow streams down the beach.

An interesting aspect of the pore pressure trace is that, although it appears to be following a normal increase with depth according to the hydrostatic pressure, the values are in fact 22% below hydrostatic. This is not due to high dynamic negative pressures induced during penetration of the coarser sands as evidenced by the pore pressure dissipation test, but by the fact that a downward hydraulic gradient exists. This is confirmed by standpipe piezometers installed at different depths within the tailings.

The drained shear strength parameters of cohesionless, normally consolidated, moderately incompressible quartz sands have been determined in calibration chamber studies. The proposed correlation of Robertson and Campanella (1983), Figure 5, has been used to determine the effective friction angle for the free draining deposit. A comparison of some of these results with laboratory and pressuremeter tests is provided in Table 1.

The piezometric cone provided valuable information for selecting testing depths for the self-boring pressuremeter and undisturbed Shelby tube sampling points. A total of 670 m (2200 ft.) of probing was undertaken for this project.

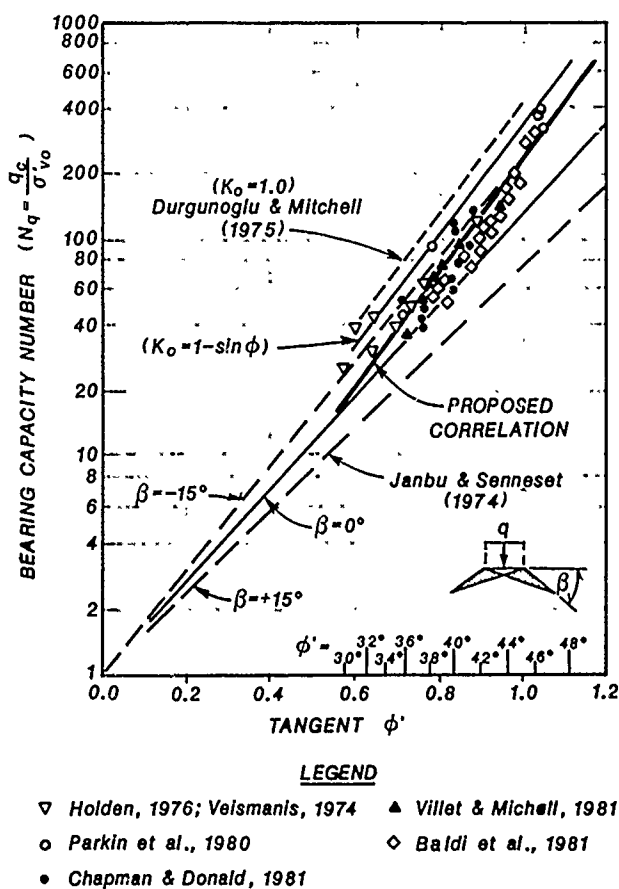


Figure 5 - Piezocone Correlation Chart

## b) Self-Boring Pressuremeter

The self-boring pressuremeter as developed by Hughes et al (1977) proved to be an ideal instrument for determining the friction angle at selected depths and to gain to some understanding of the likely dilation that would result on shearing. The instrument has a jetting tool recessed inside the cutting edge and tailings are removed with assistance of drilling fluids up the drill string without any disturbance of the surrounding material. The pressuremeter membrane is approximately 450 mm (18 in.) long with a diameter of 76 mm (3 in.). When in position at the required depth, the membrane is inflated slowly in increments until a radial displacement of 4 to 5% is reached and a reload cycle performed. The test is terminated at 15% radial strain.

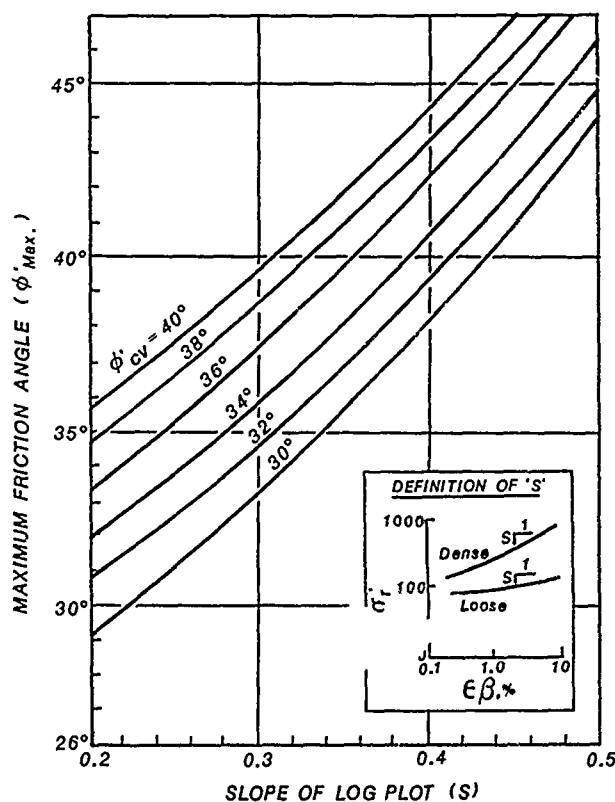
Since testing with the self-boring pressuremeter involves well-defined boundary conditions, it is possible to determine the friction angle of dense cohesionless materials using the methods of Hughes et al (1977) and Robertson and Hughes (1986). In this method, the standard plot of applied pressure against radial displacement is drawn to a log-log scale. If the slope of the straight line portion of the log-log plot is designated  $S$ , then the angle of friction,  $\phi'$ , is given by:

$$\sin \phi' = \frac{S(k+1)}{S(k-1)+2}$$

where  $k = \tan^2 (45 + \phi'_{cv}/2)$

and  $\phi'_{cv}$  = friction angle at constant volume

This method has been shown to be accurate for dense sands. For medium dense to loose sands, a correction which takes into account the dilation of the material is applied as shown in Figure 6. A summary of some of the comparative test results is shown in Table 1.



After ROBINSON and HUGHES, 1986

Figure 6 - Self-Boring Pressuremeter Calibration Graph

Table 1 - Selection of Some Comparative Results

| Boring No. | Depth (m) | $\gamma_D$<br>t/m <sup>3</sup> | M.C.<br>% | Effective Friction Angle $\phi'$ |          |               | Description of Tailings |
|------------|-----------|--------------------------------|-----------|----------------------------------|----------|---------------|-------------------------|
|            |           |                                |           | Triaxial                         | Piezcone | Pressuremeter |                         |
| B150       | 5.68      | 1.69                           | 23.0      | 41                               | 31       |               | Sandy Silt              |
| B150       | 16.89     | 1.58                           | 29.1      | 42                               | 20       |               | Sandy Silt              |
| B200       | 5.70      | 1.34                           | 41.4      | 37                               | 33       | 30            | Sandy Silt              |
| C100       | 7.77      | 1.73                           | 22.1      | 39                               | 34       |               | Silty Sand              |
| C200       | 13.34     | 1.70                           | 23.3      | 39                               | 34       | 30            | Silty Sand              |
| C280       | 4.21      | 1.67                           | 23.4      | 40                               | 29       |               | Silty Sand              |
| D200       | 4.57      | 1.71                           | 23.4      | 42                               | 33       | 35            | Silty Sand              |
| G200       | 19.93     | 1.47                           | 33.5      | 42                               | 24       | 40            | Silt                    |
| G200       | 20.94     | 1.62                           | 27.9      | 40                               | 23       | 40            | Silt                    |

### c) Standard Penetration Tests

In addition to the in situ testing, a number of boreholes were drilled into the tailings and standard penetration tests conducted at 1.5 m (5 ft.) intervals. The measured SPT values generally averaged a minimum value of 5 at a depth of 3 m, increasing to an average of 30 at depths of 25 m. Thin wall 71 mm (2.8 in.) Shelby tube samples were recovered using special sampling techniques for laboratory tests.

### d) Laboratory Tests

Apart from gradation tests on all split spoon and Shelby tube samples, specific gravity, moisture content and isotropically consolidated undrained triaxial shear tests were carried out. Considerable care was necessary to extrude the samples and to prepare for testing. Saturation normally took on the order of 1 to 3 days to obtain a B value greater than 0.95. The first stage of consolidation was reached by increasing the confining pressure in 35 kPa (5 psi) increments. Consolidation was completed within a period of 2 to 24 hours. The first two stages were each taken to 5% axial strain or until a peak value of the effective principal stress ratio was obtained. The third stage was taken up to 15% strain or failure.

The results of some of the triaxial tests are given in Table 1. The relatively high shear strengths are based on the dilatant behavior of the material and highly angular particle shape which was confirmed by microscopic examination of the tailings particles.

### e) Permeability Tests

An estimate of the permeability of the tailings can be obtained from pore pressure dissipation tests which are performed during the piezometric cone probing. This can only be done in materials which produce excess pore pressures during cone penetration. From these results, the average permeability varied in the range  $1 \times 10^{-5}$  cm/sec to  $3 \times 10^{-6}$  cm/sec.

A screened well was installed to a depth of 40 m (131 ft.) and piezometers installed along two axes at different radial distances. Up to four piezometers were installed in the same hole at different depths. Due to the fact that the drawdown cone around the well was affected by the highly variable deposit and that steady state conditions through the full depth of the deposit could not be reached within the 3-week pumping period, the results will tend to be biased towards the more free-draining tailings material where the piezometer response was the greatest. Depending on whether the analysis assumed a water table aquifer condition or a confined aquifer condition, the permeability obtained from this test is in the range  $3 \times 10^{-4}$  cm/sec to  $4.6 \times 10^{-4}$  cm/sec.

### LIQUEFACTION POTENTIAL

The basic cause of liquefaction or cyclic mobility in a saturated cohesionless material during an earthquake is the result of a build-up of excess hydrostatic pressure due to the

application of cyclic shear stresses induced by earthquake ground motions. In the ultimate state, the porewater pressure within the material becomes equal to the effective confining stress.

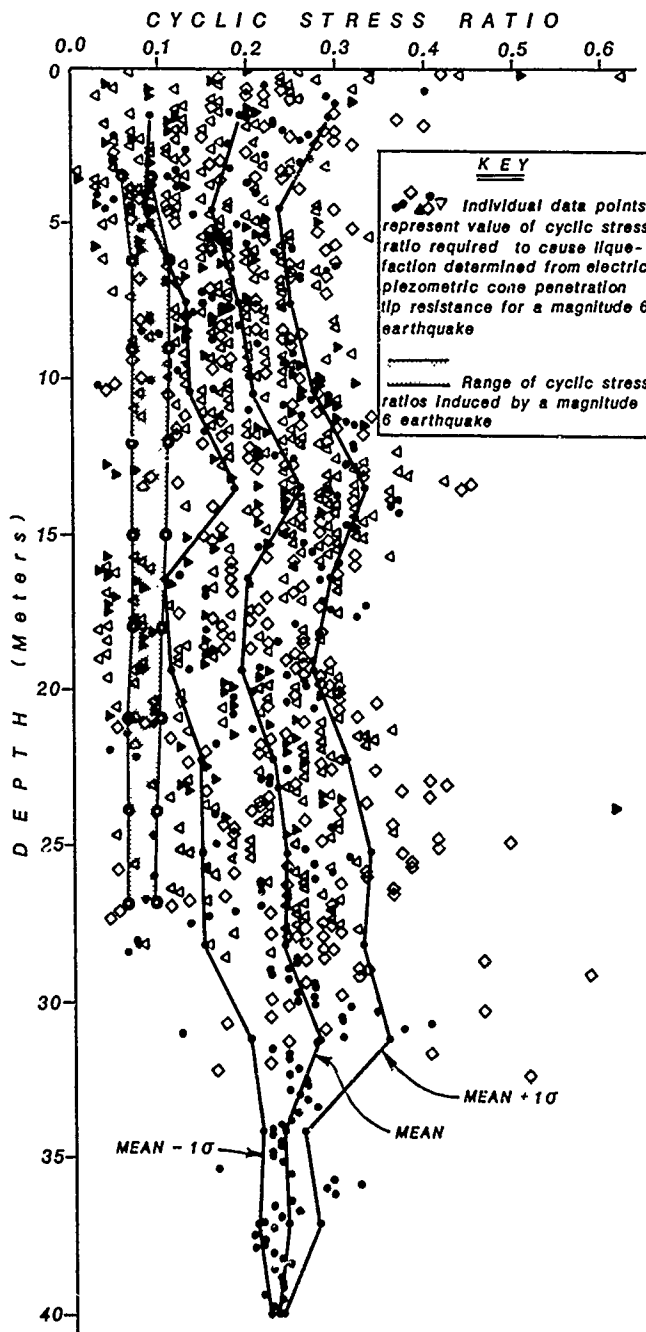


Figure 7 - CPT Cyclic Stress Ratios

The liquefaction potential was evaluated using both SPT and CPT data and the approach used in each case consisted of the following steps:

- i) Measured SPT blow count (or CPT tip resistance) data were corrected to account for effective overburden pressure.

ii) Corrected SPT (or CPT) data, along with empirical relationships (Seed et al, 1983, for SPT and Robertson and Campanella, 1983, 1984; Seed and De Alba, 1986, for CPT) used to estimate the cyclic stress ratios required to cause liquefaction with limited shear strain potential for the postulated maximum earthquake (Magnitude = 6).

iii) Cyclic stress ratios induced by the postulated maximum earthquake ground motions at various depths within the tailings deposits were calculated for peak ground surface accelerations between 0.10g and 0.15g.

The result of this analysis for the CPT data is shown in Figure 7, with the mean and mean plus and minus one standard deviation. It can be seen that the range of induced cyclic stresses falls to the left of the mean minus one standard deviation and on this basis liquefaction or limited straining of the tailings material during the postulated earthquake is highly unlikely.

In support of this conclusion, the results of laboratory triaxial shear tests on undisturbed samples have indicated a strongly dilatant behavior with little or no decrease in strength with increasing strain level. Various investigators (Casagrande, 1975; Castro, 1975; Poulos et al, 1985) have shown that materials which exhibit these characteristics cannot liquefy and/or undergo large deformations at low values of residual strength.

#### STATIC AND PSEUDOSTATIC STABILITY

A detailed water balance study was undertaken to determine the maximum elevation of the pond under the maximum design precipitation event, which for this study was the Possible Maximum Flood (PMF) plus 100-yr. storm effectively occurring back to back. The proposed sub-aerial deposition technique produces a highly anisotropic permeability condition as well as ensuring that the coarser sands are deposited close to the discharge on the embankment. The upstream design calls for an extensive horizontal drainage blanket to drain the sub-aerially deposited tailings beneath the embankment. A finite element seepage analysis for anisotropic tailings was carried out to determine the highest level of the phreatic surface under the maximum design precipitation. Figure 8 indicates a section through the tailings facility and the phreatic surfaces which were used for stability analysis.

Both circular and non-circular stability analyses were undertaken. For pseudostatic conditions, a horizontal earthquake coefficient of 0.1g was used. In all the many cases investigated involving the upstream construction, the lowest factors of safety were for a deep failure extending through the existing embankment with a F.O.S. of 1.5 as shown in Figure 9.

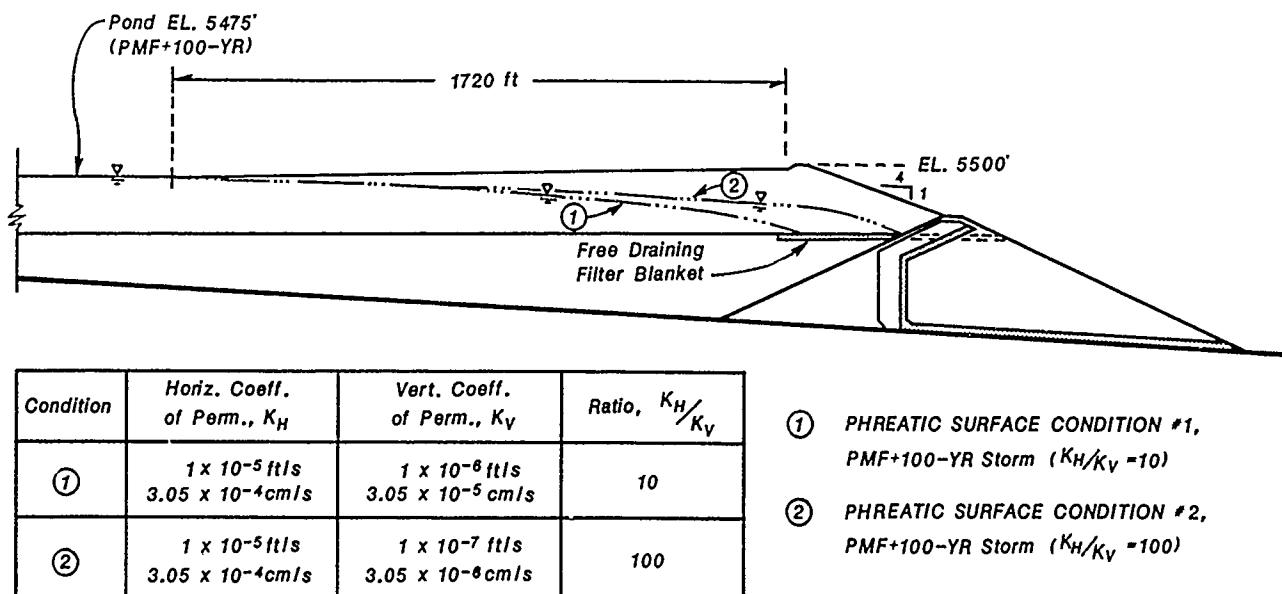


Figure 8 - Finite Element Determination of Phreatic Surface

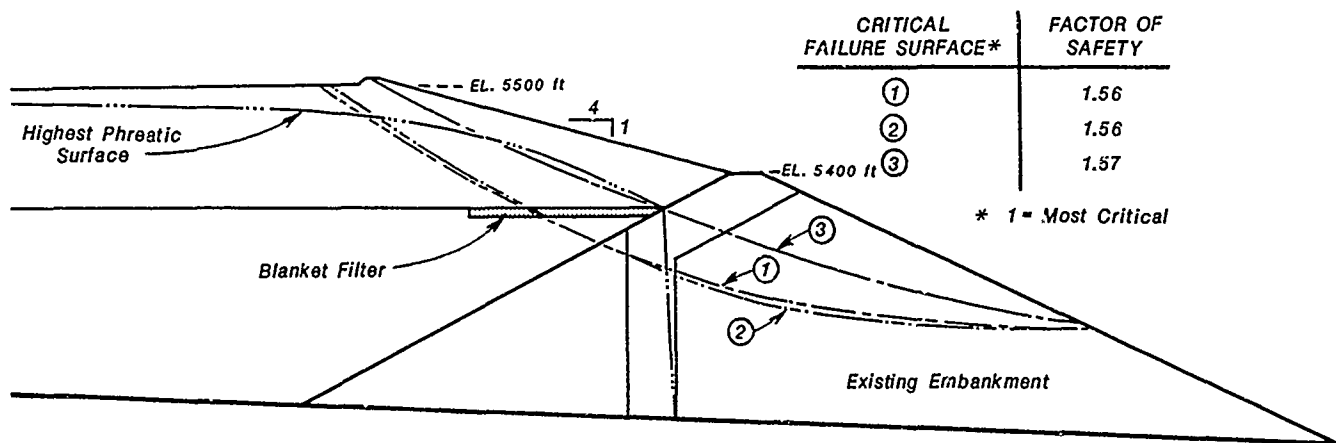


Figure 9 - Pseudo-static Stability Analysis for 0.1g Acceleration

As will be seen from Table 1, the laboratory shear strengths of the tailings under drained conditions are between 37° and 42°, with the pressuremeter giving effective friction angles between 30° and 40°. The piezocone values are also presented and, for the correlation used in the analysis (Figure 5) show results which are relatively close to the laboratory and pressuremeter values for the silty sands and sandy silts, but very low for the silts. This is most probably as a result of the fact that excess pore pressures were generated in the silts and this would reduce the effective stress of the tailings under virtually undrained conditions. For the free-draining tailings, an effective friction angle of 35° was considered reasonable for the stability analyses.

The layers which exhibit large excess pore pressures will behave as an undrained cohesive material. The evaluation of the cohesive property is in general determined in an empirical manner, with an equation of the form

$$c = (q - \sigma_v) / N$$

If N is taken in the range of 9 to 12, then the ratio of the shear strength to the effective vertical stress will lie in the region of 0.15 to 0.20, probably a reasonable lower bound for this "normally consolidated" material.

#### CONCLUSIONS

- The detailed piezometric cone profiling indicates that the tailings are mainly silty sands and sandy silts with only minor layers of silty tailings which, in themselves, are not continuous over large areas.
- The tailings exhibit dilatant behavior under shear and relatively high friction strength due to the highly angular particle shape.
- Partial or even a moderate degree of liquefaction of the tailings under a magnitude 6 seismic event is considered highly unlikely.

- The overall embankment configuration with sub-aerial upstream construction is stable under both static and pseudo-static loading and worst-case high phreatic surface.

#### ACKNOWLEDGMENTS

The authors wish to acknowledge the assistance given to them by the Homestake Mining Company in helping them complete the field studies and in allowing this paper to be published.

#### REFERENCES

- Algermissen, S.T., O.M. Perkins, P.C. Thenhaus, S.L. Hanson, and B.L. Bender (1982), "Probabilistic Estimates of Maximum Acceleration and Velocity in Rock in the Contiguous United States", U.S. Geological Survey Open File Report 82-1033.
- Casagrande, A. (1975), "Liquefaction and Cyclic Deformation of Sands, A Critical Review", Proc., 5th Pan-American Conference on Soil Mechanics and Foundation Engineering, Buenos Aires, Argentina.
- Castro, G. (1975), "Liquefaction and Cyclic Mobility of Saturated Sands", Journal of the Geotechnical Engineering Division, ASCE, Vol. 101, No. 6, 551-569.
- East, D.R., J.M.O. Hughes, W.A. Cincilla, and J. Benoit (1988), "The Use of the Electric Piezocone for Mine Tailings Deposits", First International Symposium on Penetration Testing, Orlando, Florida. (To be held March 20-24, 1988).
- Homestake Mining Company (1986), "Report on Geotechnical Investigation of Grizzly Gulch Tailings Deposit", Knight Piesold and Co., Denver, Colorado.
- Hughes, J.M.O., C.P. Wroth and D. Windle (1977), "Pressuremeter Tests in Sands", Geotechnique Vol 27, No. 4, 455-477.

- Jones, G.A. and D.J.A. van Zyl (1981), "The Piezometric Probe - A Useful Investigation Tool", Proc. 10th International Conference on Soil Mechanics and Foundation Engineering, Stockholm, Sweden.
- Knight, R.B. and J.P. Haile (1983), "Sub-Aerial Tailings Deposition", 7th Pan-American Conference on Soil Mechanics and Foundation Engineering, Vancouver, B.C., Canada.
- Nuttli, O.W. and R.B. Hermann (1978), "Credible Earthquakes for the Central United States", U.S. Army Waterways Experiment Station, Miscellaneous Paper S-73-I, Report 12.
- Poulos, S.J., G. Castro and J.W. France (1985), "Liquefaction Evaluation Procedure", Journal of the Geotechnical Engineering Division, ASCE, Vol. 111, No. 6.
- Robertson, P.K. and R.G. Campanella (1983), "Interpretation of Cone Penetration Tests, Part 1: Sand", Canadian Geotechnical Journal, Vol. 20.
- Robertson, P.K. and R.G. Campanella (1983), "Liquefaction Potential of Sands Using the CPT", Journal of the Geotechnical Engineering Division - ASCE, Vol. 111, No. 3.
- Robertson, P.K. and J.M.O. Hughes (1986), "Determination of the Properties of Sand from Self-Boring Pressuremeter Tests", The Pressuremeter and Its Marine Applications, 2nd International Symposium, ASTM, STP 950.
- Seed, H.B. and P. De Alba (1986), "Use of SPT and CPT Tests for Evaluating Liquefaction Resistance of Sands", Use of Insitu Tests in Geotechnical Engineering, Virginia Tech., Blacksburg, Geotechnical Special Publication No. 6.

## The Great Salt Lake Causeway—A Calculated Risk Revisited

James R. Lambrechts

Senior Engineer, Haley & Aldrich, Inc., Cambridge, Massachusetts

Edward B. Kinner

Senior Vice President, Haley & Aldrich, Inc., Cambridge, Massachusetts

**SYNOPSIS:** The construction of the Great Salt Lake Causeway involved several calculated risks. Original design assumptions on lake level and consolidation settlement were not realized, creating a unique situation where the critical time for stability of this embankment was not necessarily at the end-of-construction. Along more than half of the Causeway's 12-1/2 mile length, consolidation and strength gain has apparently been inhibited by a layer of salt. Because it was anticipated that calculated Factors of Safety for current conditions would be close to the 1.0 originally used, a comparative approach to stability evaluations was adopted. In this approach, Factors of Safety calculated for known, past stable conditions were compared with those predicted for future conditions. Judgements of future Causeway stability were made by comparing Factors of Safety with time. The presence of a salt layer in the foundation of a portion of the Causeway's length renders exact solution of stability intractable to usual analytical procedures.

### INTRODUCTION

In his 1964 Terzaghi Lecture, Casagrande (1965) described the design and construction of this 12-1/2 mile long embankment across the deepest portion of the Great Salt Lake, location indicated in Figure 1, as an outstanding example of a calculated risk. Completion of the Causeway in 1959 required the application

of considerable engineering judgement as the original design of the embankment underwent several empirical modifications based on the results of test fills and on actual construction failures. Initial "assumed" risks included;

1. Use of a design Factor of Safety close to 1.0, for expected greater economy of a less conservative design, but accepting the increased risk of failures.
2. Selection of crest elevation 4212<sup>1</sup>, based on lake levels over the previous 30 years and the anticipation that there was a general downward trend to the level of this terminal lake, see Figure 2. This crest elevation was more than 6 ft. lower than the rails on the 55 year old timber trestle that it was to replace.
3. The expectation that consolidation of the soft foundation clays would be on the order of 4 to 8 ft., and that this would occur within several years of construction, thus yielding a steady increase in stability.

However, the level of the Great Salt Lake, a lake with no natural outlet, has fluctuated nearly 20 ft. since 1959, see Figure 2. Recent historically high lake levels and continuing Causeway settlement due to foundation clay consolidation, also illustrated in Figure 2, have forced Southern

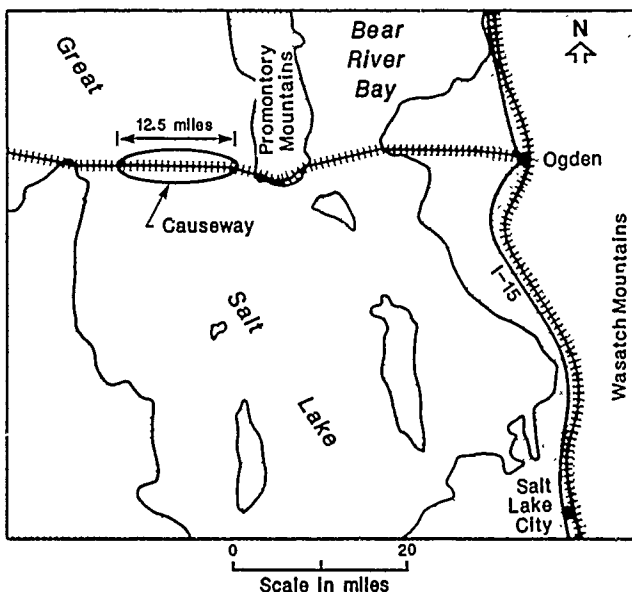


Figure 1. Location of the Great Salt Lake Causeway.

<sup>1</sup> All Elevations refer to Southern Pacific's Hood's Datum, and are therefore 3.4 ft. above elevations based on USGS datum.



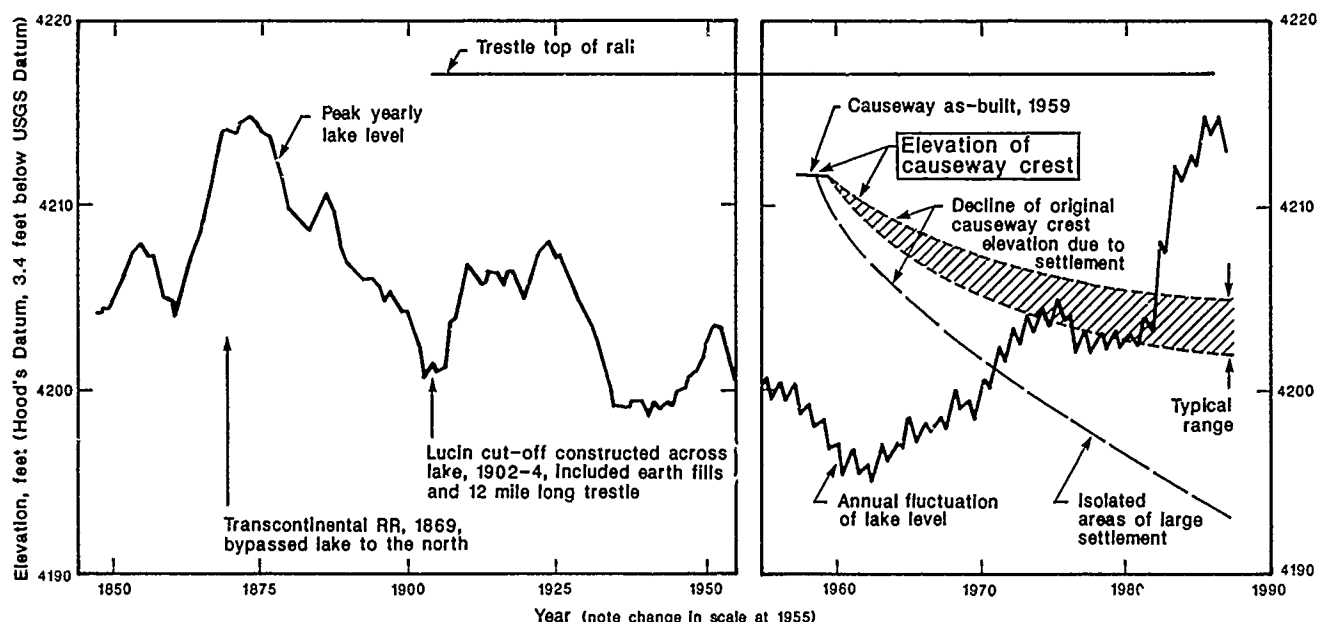


Figure 2. Levels of the Great Salt Lake and Causeway Crest.

Pacific railroad to add significant amounts of fill to the crest to maintain adequate freeboard. Filling has increased stresses on the foundation clays and necessitated re-assessment of Causeway stability. Studies have shown that a unique situation has developed wherein the end-of-construction condition was not necessarily the critical time for stability.

A comparative approach to stability assessments was adopted in which the Factors of Safety were calculated at selected cross-sections for differing conditions that existed at various times since construction. Changes in Factor of Safety from those calculated for past, stable conditions were then evaluated to assess present and future stability.

Although stability was found to have improved where the Causeway is directly founded on a clay foundation, the presence of a brittle salt layer beneath much of the Causeway's length renders stability calculation by "usual" procedures intractable. Assessment of stability in these areas still requires engineering judgement, thus continuing the calculated risks.

#### SUBSURFACE CONDITIONS ALONG THE CAUSEWAY

Although the Great Salt Lake basin has in places over 7,000 feet of sediment, only those strata within 150 to 200 feet of the present mudline were of consequence to Causeway stability. Below that level, stiff desiccated clay from an evaporative lake cycle is present. The overlying sediments are predominantly soft, plastic organic clays that exhibit brittle behavior in compression tests,

Casagrande (1959). Fine sand partings are found in deeper strata of the soft clays.

Of particular importance to Causeway stability is a stratum of Glauber's Salt. It is present in the deeper lake areas and is buried under about 25 ft. of the very soft sediments. This hydrated sodium sulfate was deposited during the evaporative aftermath of Lake Bonneville. The stratum contains a wide variety of salt compositions, each separated from the next by clay seams, as described by Eardley (1962). The Glauber's Salt increases in thickness from west to the east, being less than 1 ft. thick along the western 2-1/2 miles of the Causeway, up to 20 ft. beneath the central 6 miles, and as much as 45 ft. thick near the east side.

To evaluate soil shear strengths required for the recent stability studies, an extensive program of soil sampling and laboratory testing was undertaken in 1984. Borings were made at five different locations both through the centerline of the embankment and over-water through the counter-weight berms. Because SHANSEP procedures (Ladd and Foott, 1974) were used to assess clay shear strength, over 100 consolidation tests were performed to determine profiles of maximum past pressure.

The stress profiles shown in Figure 3 indicate that far less consolidation has occurred in clay overlain by the salt. This was an important discovery, because shear strength increase would be similarly less than where the salt is present. The Glauber's Salt stratum has apparently inhibited drainage from the underlying foundation clays. Thus less than 35 percent of the eventual consolidation has occurred in most salt areas.

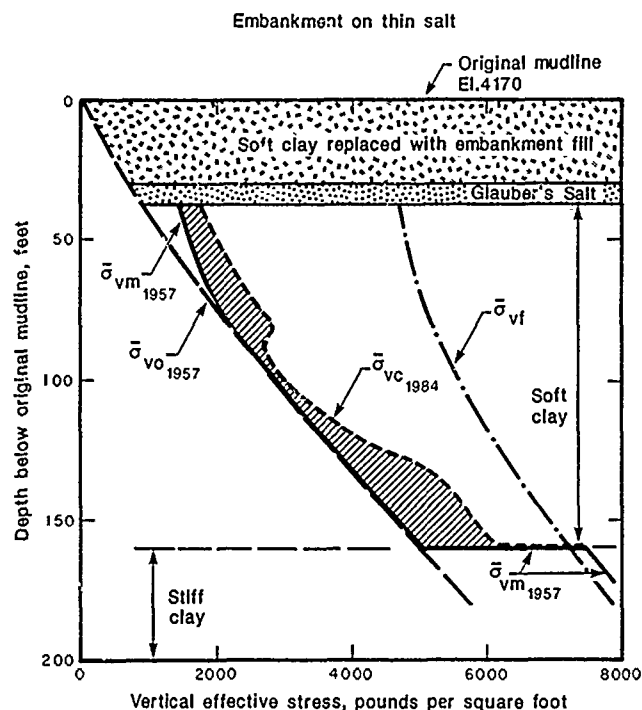
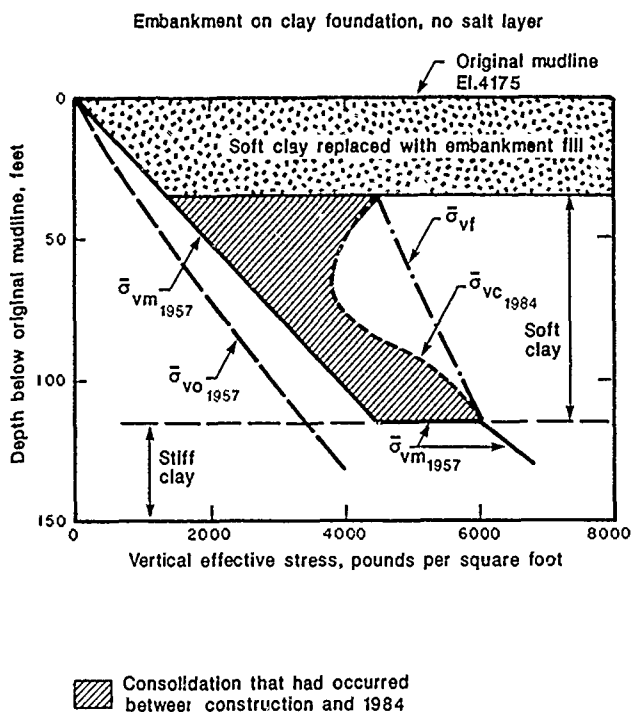


Figure 3. Stress Profiles Indicating Consolidation Since Causeway Construction.

where:  $\bar{\sigma}_{vo} 1957$  = preconstruction vertical effective stress

$\bar{\sigma}_{vm} 1957$  = preconstruction maximum past pressure based on consolidation tests

$\bar{\sigma}_{vc} 1984$  = vertical effective stress in 1984 (equals  $\bar{\sigma}_{vm} 1984$  where  $\bar{\sigma}_{vc} 1984$  is greater than  $\bar{\sigma}_{vm} 1957$ )

$\bar{\sigma}_{vf}$  = final vertical effective stress under Causeway centerline at full consolidation

#### ORIGINAL CONSTRUCTION

A plan of the completed Causeway circa 1959, a profile showing fill and salt thickness, and two typical cross-sections are shown in Figure 4.

Casagrande (1959 and 1965) and Newby (1980) describe the design and construction. In brief, the embankment was generally constructed to a 60 ft. wide crest that was 12 ft. above the average lake level. Side slopes of the earth and rock fill embankment were 2 horiz. to 1 vert. A key design element was the removal by dredging of 20 to 25 ft. of the softest lake bottom sediments from beneath the main body of the fill. Along much of its length, the main fill was placed on the

Glauber's Salt. Counter-weight berms were placed adjacent to most sections of the main fill. The depth and width of the dredged trench, and berm width and locations are shown in Figure 4.

During construction, test fills were constructed in each of the different foundation areas to provide insight on performance and to verify the design sections used because the design Factor of Safety was close to 1.0. Unexpected construction failures that occurred emphasized the fact that as-constructed stability was marginal. These failures resulted in several design revisions which became largely empirical, Casagrande (1965).

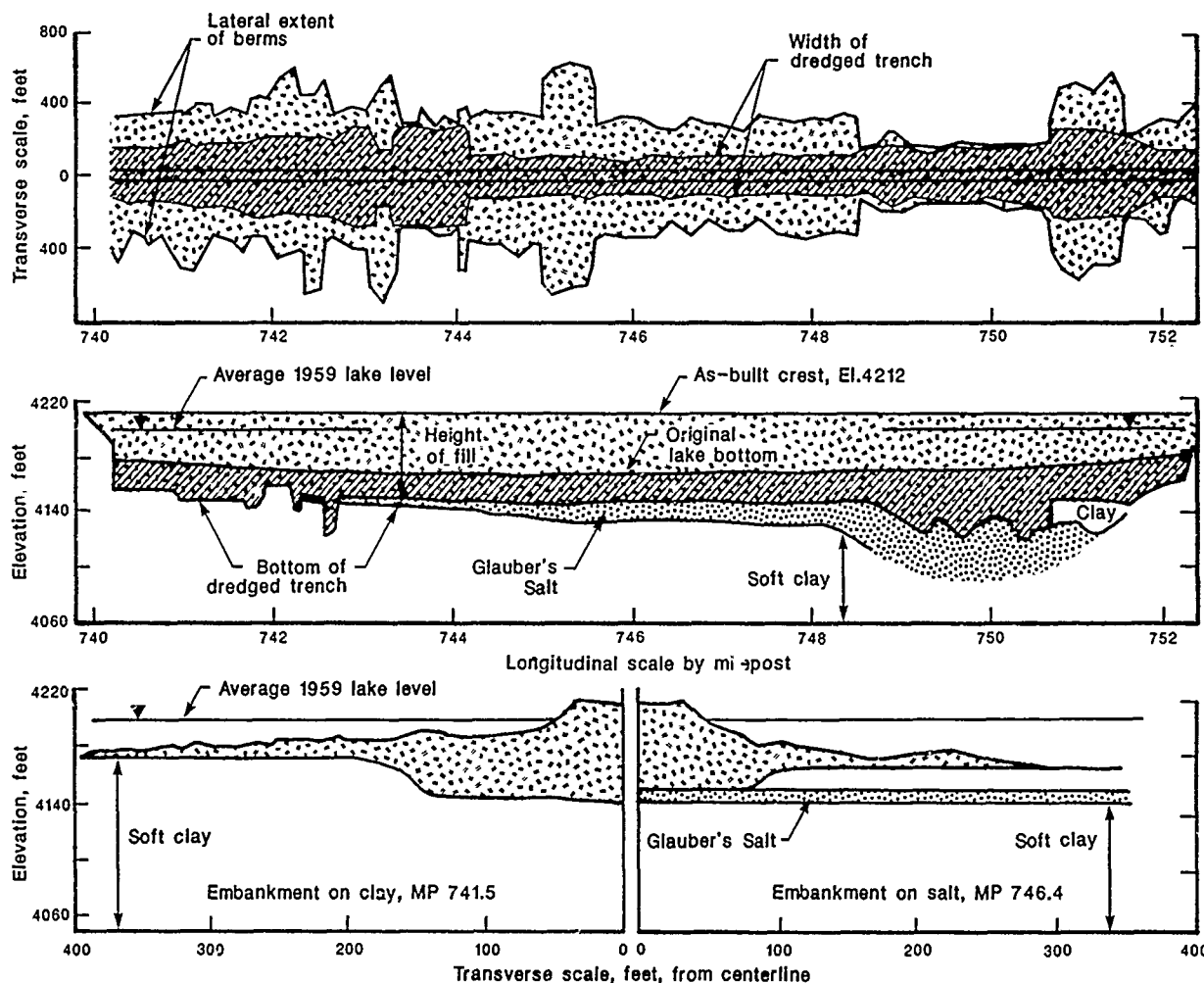


Figure 4. Plan, Profile, and Typical Cross-Sections of Causeway.

#### COMPARATIVE APPROACH TO STABILITY ASSESSMENTS

Unlike most embankments on soft ground, the critical time for Causeway stability was not necessarily at the end of construction. Falling and rising lake levels and the 12 to 25 ft. of fill added to the crest to accommodate settlement and rising lake level have caused changes in effective stresses on the foundation clays. Shear strength of the foundation clays has been very slow to increase in some areas.

In light of the above risks, a comparative approach was adopted for assessment of current and future stability. The Factors of Safety at the end of construction and other selected times since construction were calculated and compared. Judgements concerning stability were then made by comparing Factors of Safety for current and future conditions with those for past times when stable conditions were known to exist.

A few sections representative of the various constructed geometries along the 12-1/2 mile long Causeway were selected for detailed stability analysis. Stability analyses were made primarily for the West Side areas where the Causeway is solely on a clay foundation. These results and limited other analyses were used to temper judgements and assessments of instability risk where the stiff salt layer is present.

Stability analyses were made for the varying Causeway geometries, lake levels and shear strength profiles that were applicable to the past and present conditions at each section. Several possible future conditions were also analyzed to provide insight for the assessment of future risks of instability. The major changing conditions that were evaluated are listed in Table I.

The geometry of the Causeway surface was taken from cross-sections made at the end of

TABLE I. Changing Conditions Evaluated in Comparative Stability Analyses

| YEAR   | LAKE ELEVATION         | ACCUMULATED SETTLEMENT | BASIS FOR CLAY STRENGTH (feet)            | CAUSEWAY CONDITIONS/CHANGES  |
|--------|------------------------|------------------------|---|--|
| 1959   | 4200                   | 0                      | $\bar{\sigma}_{vm1957}$                   | END OF CONSTRUCTION  |
| 1963   | 4195                   | 2                      | $\bar{\sigma}_{vm1957}$                   | MINOR SETTLEMENT   |
| 1969   | 4198                   | 4                      | $\bar{\sigma}_{vm1969}$<br>(INTERPOLATED) | FILL ADDED TO RAISE SUBGRADE BACK TO AS-BUILT (EL.4212), SOME BERM EROSION |
| 1984   | 4210                   | 7                      | $\bar{\sigma}_{vm1984}$                   | FILL ADDED TO RAISE SUBGRADE TO EL.4214, BERM EROSION / ACCRETION          |
| FUTURE | VARIED<br>4213 TO 4190 | 7                      | $\bar{\sigma}_{vm1984}$                   | FILL ADDED TO RAISE SUBGRADE TO EL.4217                                    |

construction, and in 1966 and 1984. Settlement was distributed through the cross-section by assuming; 1. full settlement under the main body of the embankment, 2. no settlement under the berms, 3. linear variation in between. For perspective on the impact of "other factors" on instability risk, analyses were made for possible future lower and higher lake levels, addition or removal of fill from the crest, and berm thickness changes (field studies have indicated that erosion and accretion may have occurred).

Stability analyses were made using the Modified Bishop method for circular surfaces and Janbu method for non-circular surfaces, as available in the computer program STABLE, Boutrup (1977). A limited number of Morgenstern-Price analyses (ICES-LEASE) were performed which indicated Janbu to be approximately 10 percent conservative.

The shear strength of the foundation clays, both with depth and laterally from the main body of the fill, were determined by SHANSEP procedures for end-of-construction and later times. A stress ratio,  $s_u/\bar{\sigma}_{vm}$ , of 0.225 was established on the basis of laboratory undrained triaxial compression and extension tests and direct simple shear tests. The in-situ strength ratio was also estimated by back-analysis of two construction failures, which indicated somewhat lower values. A strength ratio of 0.20 was finally selected.

#### STABILITY OF EMBANKMENT ON CLAY

The section at MP 741.5 was evaluated because it is typical of "normal" West Side conditions where there is only clay in the foundation strata and did not experience a construction failure. The Factors of Safety calculated for this cross-section are summarized in Table II, as are the results of limited analyses for a cross-section at MP 747.6 where the salt layer is present.

The Factors of Safety calculated for conditions at the end of construction and four years later, when the Great Salt Lake was about 6 ft. lower, are essentially the same, and just slightly above unity. This agrees with design reports that the original design Factor of Safety was close to 1.0. The 1963 Factor of Safety was perhaps slightly higher than that calculated because some slight clay strength increase likely occurred, but was not considered in these analyses.

TABLE II. Calculated Changes in Factor of Safety with Time

| YEAR       | CALCULATED MINIMUM FACTOR OF SAFETY JANBU (NONCIRCULAR) |                                |
|------------|---|--------------------------------|
|            | NON-SALT (MP 741.5)                                     | SALT FOUNDATION (3) (MP 747.7) |
| 1959       | 1.06  | 1.37                           |
| 1963       | 1.04  | (4)                            |
| 1969       | 1.24  | (4)                            |
| 1984       | 1.25  | (4)                            |
| FUTURE (1) | 1.15  | 1.33                           |
| FUTURE (2) | 1.25  | 1.37                           |

1. SAME LAKE LEVEL AS 1984 CONDITIONS, CREST EL.4217.
2. LAKE LEVEL 3 FEET ABOVE 1984, CREST EL.4217.
3. SALT LAYER THICKNESS = 12 FEET, ASSUMED SALT SHEAR STRENGTH = 3600 psf.
4. NOT CALCULATED

The Factor of Safety calculated for 1969 conditions was 20 percent greater than original, a substantial improvement. This increased stability was primarily a consequence of increased shear strength in the foundation clay which more than offset the affect of the fill that was added to the crest in 1969 to compensate for 4 ft. of settlement that had occurred. The 1969 lake level was 2 ft. below 1959 level.

Calculations for 1984 conditions showed that the cumulative effects of continued foundation clay strength increase and lake level 10 ft. above the as-built level counteracted the destabilizing effects of the weight of an additional 6 to 7 ft. of fill placed on the crest in 1984 and the apparent erosion of about 2 ft. of material from the berms. The Factor of Safety was about the same as in 1969, about 20 percent greater than the as-built condition.

The effect of future changes in lake level, elevation of the crest, and erosion of the berms on Factor of Safety for Sta. 3550 were evaluated in a series of parameter studies. The results are shown on Figure 5 as change in Factor of Safety for each variable alone, the others being held constant at the 1984 conditions.

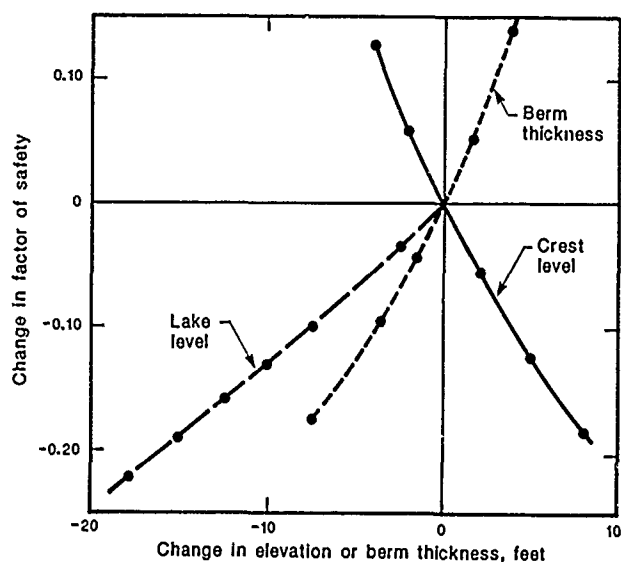


Figure 5. Effect of Various Parameters on Calculated Factor of Safety.

Changes in lake level were found to have about half of the effect on Factor of Safety as changes in either crest elevation or berm thickness. The direction of each effect is obvious. The Factors of Safety for two of the future conditions are included in Table II.

Based on these results, it was concluded that where there is only soft clay in the foundation, present and near-term, future Causeway stability would be greater than the as-built conditions. However, if lake levels recede below Elev. 4205, 5 ft. above the 1959 level, the calculated Factor of Safety would decrease to near the marginally stable values calculated for 1959 conditions.

#### PROBLEMS OF SALT OVER SOFT CLAY FOUNDATION

Stability calculations indicated that a working shear strength of the salt layer of between 10 and 25 times that of the clay at the same level was necessary for stability, i.e. Factor of Safety greater than 1.0. But it was not considered possible to make a meaningful analysis of Factor of Safety for the Causeway where the fill is on stiff salt over the soft foundation clays for the following reasons:

1. The salt is extremely heterogeneous, the spacing and frequency of clay seams varies with elevation and location.
2. The overall behavior of the salt is not understood, but is probably not adequately represented by laboratory compression tests on core samples.
3. The salt has probably experienced bending stresses due to differences in settlement between zones under the main body of the fill and beneath the lightly loaded berms, and compression due to the weight of the fill, but the effect of these changes on stratum strength is unknown.
4. There is strain incompatibility between the stiff, brittle salt and the soft clays below, although salt can typically accommodate large creep strains.

Limited comparative stability analyses were performed for insight on the magnitude of changes in Factor of Safety. The results of some of these analyses, presented in Table II, indicate little change in stability from as-built conditions. This is due primarily to the small gains in foundation clay shear strength. Assessments of present and future stability were therefore based substantially on judgement. Raising the crest to maintain freeboard was still considered a calculated risk that was necessarily taken to continue rail traffic over the Causeway.

Caution and continual monitoring of embankment performance were recommended, and contingency plans for adding fill to the berms were developed in case settlement rates became excessive.

In two areas, each about 1/2 mile long, settlement rates have recently been on the order of 1 to 1-1/2 ft. per year which is 2 to 4 times the "normal". Both areas have been identified as probably having a locally weaker

salt stratum. Inclinoimeters recently installed offshore have shown there to be significant, ongoing, lateral displacements of soft clay below the salt, nearly 30 years after construction. The question of the future performance of these areas and the possible development of other similar areas remains a calculated risk.

#### CONTINUING CALCULATED RISKS

Today, many uncertainties and limitations still exist which make assessments of Causeway stability, a continued calculated risk.

Principal contributing factors are:

1. Likely variations in foundation strata conditions from those assumed based on the limited number of borings made along the 12-1/2 mile long embankment.
2. The presence of the Glauber's Salt brittle yet ductile material, that is heterogeneous with depth and lateral extent. Its strength may change with time due to deformation from consolidation of the underlying clays.
3. Very slow consolidation and strength gain in the clays below the Glauber's Salt.
4. Lack of precision in the Factor of Safety calculation due to inaccuracy in determining soil parameters and soil and fill stratification.
5. Inability to adequately accommodate the salt layer in current stability analyses due to its strain incompatibility with the fill and foundation clays.
6. Inability to analyze more than a few representative cross-sections along the 12-1/2 mile long embankment due to cost and time constraints.

#### CONCLUSIONS

Original design expectations on lake levels and consolidation of the foundation clays below the salt stratum have not come to fruition. Consequently, the recent rise of the Great Salt Lake to historic levels and the need to add fill to the Causeway crest have created a unique situation wherein the end-of-construction was not necessarily the critical time for stability.

It was anticipated that Factors of Safety would again be close to the 1.0 adopted in design. The comparative approach to stability assessments, adopted for evaluations of current conditions and recent elevated lake levels, indicated 10 to 20 percent greater stability than at the end-of-construction where the Causeway is founded on soft clay.

However, embankment stability remains an intractable problem for more than half its length where the Causeway is founded on interbedded salt above soft clays, due to problems of salt/clay strain incompatibility and salt stratum heterogeneity and probable changes since construction. Therefore, the results of analyses made for the no-salt West Side were used for insight in stability considerations. However, the substantial amount of engineering judgement required in assessing stability continue to make such evaluations calculated risks.

#### REFERENCES

- Boutrup, E. (1977) "Computerized Slope Stability Analysis for Indiana Highways", Purdue University and the Indiana State Highway Commission, Joint Highway Research Project, JHRP-77-25, Vol. 1, pp. 1-210.
- Casagrande, A. (1959) "An Unsolved Problem of Embankment Stability on Soft Ground", Proceedings of the First Panamerican Conference on Soil Mechanics and Foundation Engineering, Vol. II, pp. 721-746.
- Casagrande, A. (1965) "Role of the 'Calculated Risk' in Earthwork and Foundation Engineering", Journal of the Soil Mechanics and Foundation Division, ASCE, Vol. 91, No. SM4, July, pp. 1-40.
- Eardley, A.J. (1962) "Glauber's Salt Bed West of Promontory Point, Great Salt Lake", Utah Geological and Mineralogical Survey, Special Studies 1, 12 pp.
- Ladd, C.C. and Foott, R. (1974) "New Design Procedure for Stability of Soft Clays", Journal of the Geotechnical Engineering Division, ASCE, Vol. 100, No. GT7, July, pp. 763-786.
- Newby, J.E. (1980) "Great Salt Lake Railroad Crossing", Utah Geological and Mineral Survey Bulletin 116, pp. 393-400.

#### ACKNOWLEDGEMENTS

The stability studies reported herein were undertaken for Southern Pacific Transportation Co. whose assistance and support is gratefully acknowledged. Also contributing significantly to this study were Board of Consultants members C.C.Ladd, T.Leps, and E.S.Smith.

# Wadi Qattarah Dams Case History

Jean Binquet

Chief Engineer, Coyne et Bellier, Consulting Engineers, Paris, France

Ugo Zappi

Chief Engineer, Coyne et Bellier, Consulting Engineers, Paris, France

## SUMMARY

Two earthfill dams were constructed on the Wadi Qattarah in Libya between 1969 and 1972 but the filling was never achieved for both dams. After a partial filling well below normal water level, Secondary Dam failed in December 1977. Several weaknesses may be found in the features of both dams and have been analyzed by the authors on the basis of dam instrumentation results, measurements and observations of the Secondary Dam failure. Several possible causes of failure of this dam are presented. No one can however be taken as certain. The series of events as reported by eye witnesses appear to point out a typical phenomenon of piping, but the responsible mechanism can be attributed to various causes.

## 1. HISTORICAL INTRODUCTION

The protection of Benghazi, the chief town of Cyrenaica and second largest city in Libya, and the surrounding plain against flooding by Wadi Qattarah has long been a subject of studies which materialized in 1965-67 with the issuing the Wadi Qattarah Project (Fig. 1).

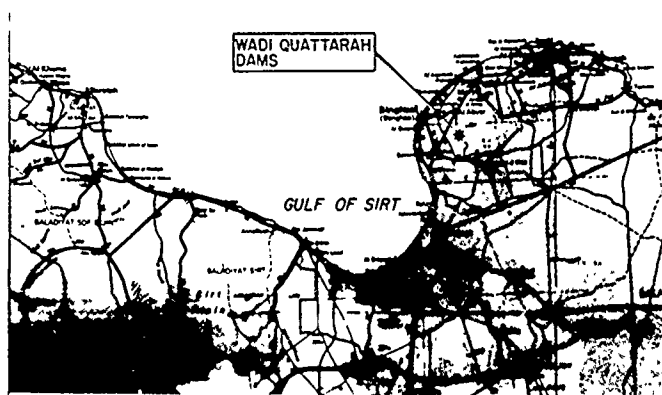


Fig. 1 - General Location of the Project

The upstream portion of the Project was formed mainly by the Main Dam and the Secondary Dam some 10 km farther downstream which were built from 1969 to 1972. The first filling started in May 1972 but the reservoir levels very seldom exceeded a third of the head and never reached the normal water level (NWL) at either dam. On 21 December 1977, the Secondary Dam failed with a water level well below NWL but fortunately major damage was avoided by a rather slow rate of retrogressive erosion of the embankment (about 6 hours) and by the relatively moderated volume of water stored, some  $3.5 \times 10^6 \text{ m}^3$  (Fig. 2).

Main Dam embankment was continuously monitored and two series of geotechnical investigations were carried out in 1978 and 1979 to ascertain that conditions similar to those at Secondary Dam did not develop.

In this paper the authors will describe the main geological and geotechnical features of both dams and report the observations made during the Secondary Dam Failure. On the basis of these features, observations and dams instrumentation results and measurements, they will present what are in their opinion the main weaknesses of these structures and they will analyze the



Fig. 2 - View of Secondary Dam after Failure

possible causes of failure of Secondary Dam pointing out the most likely ones.

The design work for rehabilitation of the Wadi Qattarah scheme including the strengthening of the existing structures and the reconstruction of the Secondary Dam has been presented elsewhere in a paper by El Turki et al (1985).

## 2. LOCAL CONDITIONS

### 2.1. General

Wadi Qattarah catchment upstream of the dams is located East of Benghazi on the escarpment zone, at elevations between 150 and 650 ; areas are  $1,224 \text{ km}^2$  and  $1,285 \text{ km}^2$  at Main Dam and Secondary respectively.

Climate is typical semi-arid zone but the nearness of the Mediterranean assures an average yearly rainfall of some 230 mm from October to March mainly.

The geological set-up is a rather regular Miocene series featuring near-horizontal beds of dolomitic limestones alternating with some more chalky and marly strata. Dissolution certainly exists in the area but probably not at a large scale as was evidenced by the various investigation boreholes which encountered voids only occasionally. Infiltration is however highly developed through the discontinuity system of horizontal bedding connected by subvertical fracturing. Rock mass

permeability is moderate (around  $10^{-3}$  m/s). The aquifer is some 150 m and 120 m below ground level at Main Dam and at Secondary Dam site respectively.

Infiltration data are largely scattered depending upon the year, for low water levels a progressive decrease is evident with time but for high water levels data and direct observations are too fragmentary to draw conclusions.

## 2.2. Main features of both Dams

Both dams are homogeneous embankments with similar design characteristics and similar appurtenant works. Fig. 3 and 4 show the plan view of both dams.

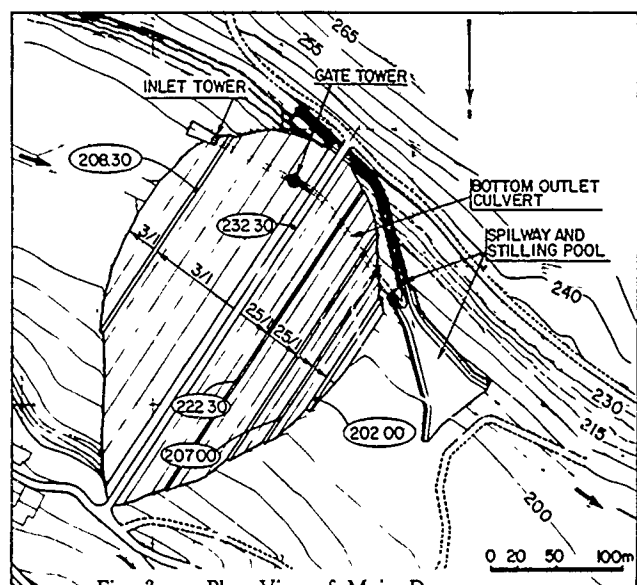


Fig. 3 - Plan View of Main Dam

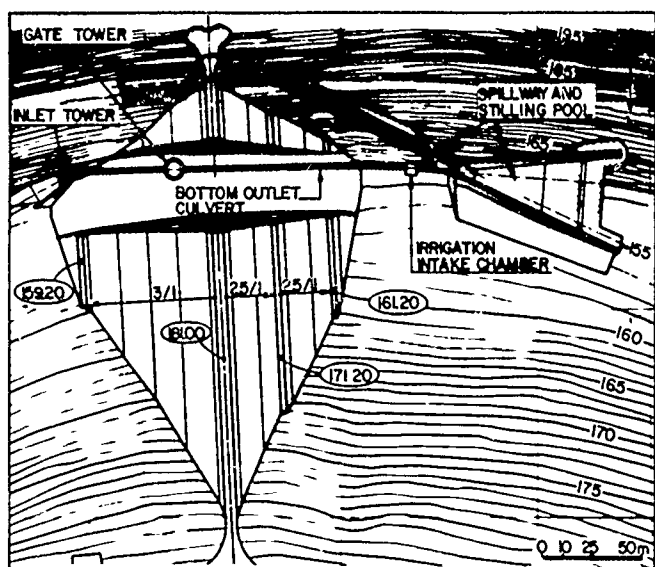


Fig. 4 - Plan View of Secondary Dam after Failure

### 2.2.1. Description of Main Dam Embankment

The maximum height of the embankment is 33.0 m and its crest length is 305 m. Fig. 5 shows the typical cross section of the embankment. The upstream slope of the embankment is 3.0 horizontal for 1.0 vertical (3.1). A 3-metre wide berm is located at El. 208.00, it was the crest of the upstream cofferdam. With this berm, the mean upstream slope becomes

3.1 horizontal for 1.0 vertical (3.1.1). The mean downstream slope of the embankment is 2.7 horizontal for 1.0 vertical (2.7:1) including the three 2-m wide berms.

This embankment is an homogenous earthfill whose design includes an inside drainage network in the downstream portion of the embankment.

- A chimney drain including successively from upstream to downstream a fine filter layer 0.40 m thick, a coarse filter layer 0.40 m thick and a drain layer.
- This chimney drain is connected at its base with a horizontal drainage system generally resting on the foundation under the downstream portion of the fill. This horizontal drainage system includes a continuous layer of the fine filter material, 0.40 m thick, and six finger drains approximately 30 m apart, forming the horizontal outlets from the chimney drain. The core of these finger drains (area 1.40 m<sup>2</sup> each) is made of the drain material wrapped in the coarse filter material 0.40 m thick without any fine filter between the coarse filter and the earthfill.
- The horizontal drainage system is connected downstream to a rock-fill drain founded at variable levels below the foundation level of the embankment. A fine filter layer 0.40 m thick has been placed underneath this rock fill toe drain in contact with the foundation. This drain collects the flow from the horizontal drains and also from surface runoff.

A rough estimate of the maximum drainage capacity of this downstream drainage system indicates a value of the order of 5 l/s for a hydraulic gradient of 0.3 and permeability coefficients of  $10^{-3}$  m/s and  $10^{-4}$  m/s for the drain and fine filter respectively. The main limitation of the drainage capacity is due to the small area of the finger drains in the horizontal drainage system.

The embankment is partly founded on the limestone which outcrops on the left and right banks, representing 2/3rds of the area of the foundation surface, and partly on alluvial deposits in the lower part of the valley. This alluvial deposit rests on the limestone foundation some 17 m below at the lowest point. In order to provide a watertight link between the grout curtain in the limestone foundation and the embankment, a key trench filled with silty clay material has been excavated in the alluvial deposit. The key trench, 12 m average width at its base, has near-vertical walls on the upstream and downstream sides (4 in 1 slope). The longitudinal axis of the key trench coincides with the axis of the dam. A small narrow trench has been dug along the axis of the key trench in the limestone formation in order to install the concrete cut-off wall on top of the grout curtain. Like the key trench, this narrow trench has almost vertical sides (4 in 1 slope). The top of the cut-off wall, which is 4 m high and 1.50 m wide, is located generally a few metres underneath the rock line level.

Concerning the preparation of the rock foundation before placing the earthfill, it must be pointed out that no mention of preparation of the surface by sealing fissures and holes with grout or cement mortar has been found in the construction records. The Technical Specifications in the Tender Documents require treatment of the fissures and holes in the bedrock foundation underneath the earthfill by filling them with a clayey backfill.

The condition of placing earthfill around the bottom outlet culvert has also to be mentioned. Both faces of the excavated trench in which the conduit lies are only 1 m from the concrete, which does not allow proper compaction of the backfill even by small hand-operated machines. This applies to the downstream portion of Main Dam culvert (Fig. 6).

In addition no particular drainage was provided around the downstream portion of the culvert. The filter blanket, part of the drainage system, appears to be located 1 m or 2 m above



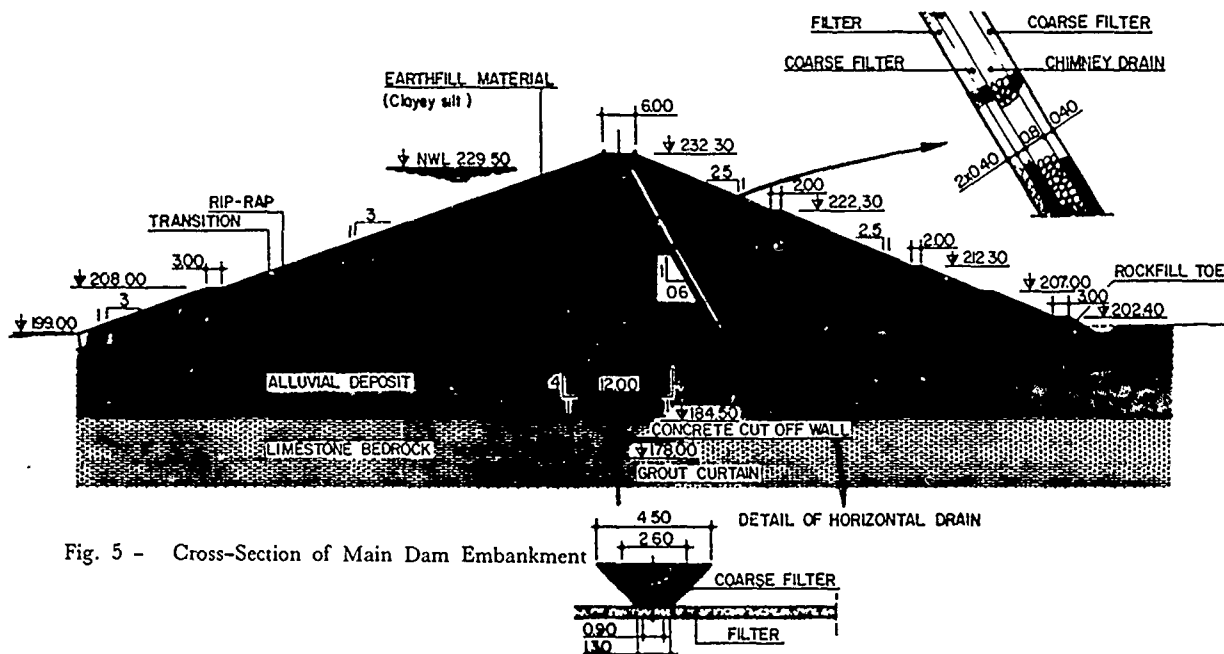


Fig. 5 - Cross-Section of Main Dam Embankment

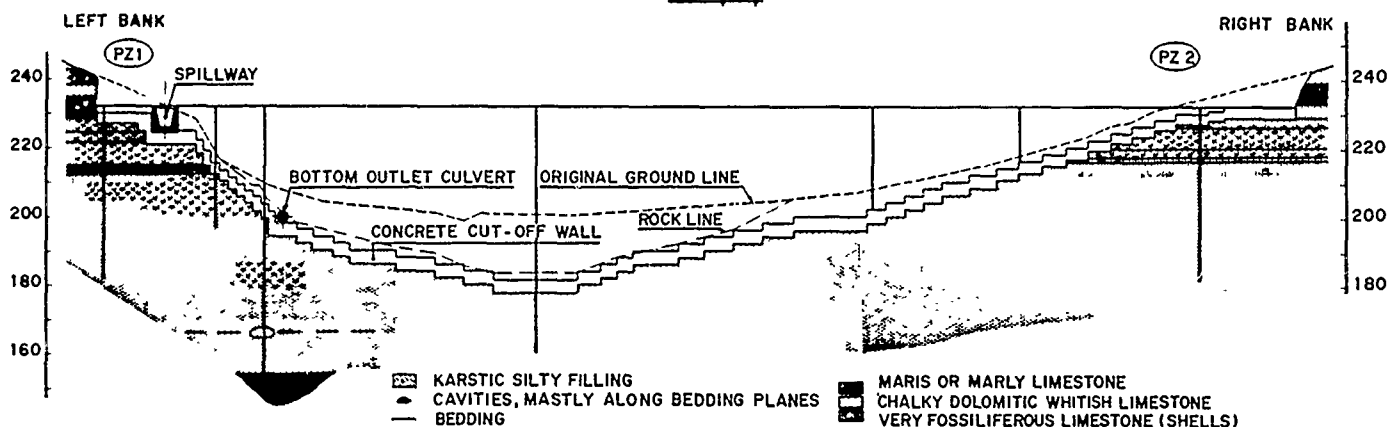


Fig. 6 - Longitudinal Cross-Section of Main Dam

the outlet culvert as well as the rockfill toe drain, whose base is about 3 m above the culvert.

Another feature of the design of this outlet culvert must be mentioned. The upstream part of the culvert from the intake structure to the gate tower is founded on alluvium through concrete piers. Consolidation of alluvium between the piers may have induced differential settlement of the alluvium and hence possibly allowed a seepage path to develop underneath the culvert.

## 2.2.2 Description of Secondary Dam Embankment

The design of Secondary Dam is very similar to that of Main Dam. The crest length of the embankment is about 217 m and the maximum height is 28.6 m. Fig. 7 shows the typical cross section of the embankment.

The upstream and downstream slopes are the same as at Main Dam. Secondary Dam was constructed simultaneously with Main Dam. In this case too, the embankment is an homogeneous earthfill whose design includes features identical to those described previously for Main Dam, except that in this case the alluvial deposit has a maximum depth of 9 m.

## 2.3. Geotechnical Properties of Embankment Materials

With regard to the assessment of the safety of Main Dam and the causes of the failure of Secondary Dam, the significant

embankment materials are the earthfill, filter and drain materials. The construction records indicate that both embankments were built with materials taken from the same borrow areas, and therefore no distinction will be made for their presentation below.

### 2.3.1. Description and identification material

The borrow area for earthfill is located about 2 km downstream of Main Dam site. The material was excavated from alluvial deposits. It is a clayey silt (classified CL2 in the USCS classification system) which has been identified as follows .

- The percentage of particle sizes smaller than 0.1 mm ranges from 75% to 95%.
- The percentage of particle sizes smaller than 2 microns ranges from 8% to 30%.
- The mean value of the specific gravity is 2.66 with a standard deviation of 0.03 (20 samples).
- The liquid limit WL ranges from 29% to 38%. The mean value is 33% with a standard deviation of 3% (80 samples).
- The plastic index PI ranges from 10% to 19%. The mean value is 14% with a standard deviation of 2% (80 samples).
- The shrinkage limit SL ranges from 10% to 14.5%. The mean value is 12%.

The natural water content generally increases with depth in the borrow areas. The average values ranges from 6% at 1 m to

12% at 5 m depth. Almost all the material was excavated from a depth less than 6 m.

According to the standard Proctor compaction tests (compaction energy  $600 \text{ kJ/m}^3$ ), the optimum moisture content  $W_{opt}$  ranges from 15% to 21% (mean value 18.1% with 1% standard deviation for 60 samples) and the maximum dry density  $D_d$  ranges from  $16.7$  to  $17.9 \text{ kN/m}^3$  (mean value  $17.3 \text{ kN/m}^3$  with  $0.3 \text{ kN/m}^3$  standard deviation for 60 samples).

Mineralogical and chemical analyses were performed on 5 samples of the embankment material from Main Dam. The minerals were predominantly clayey with 20% to 30% kaolinite, 25% to 35% illite, 25% to 35% illite-smectite, 5% to 15% smectite and some (less than 5%) attapulgite. The chemical analyses show predominantly  $\text{Fe}_2\text{O}_3$  and  $\text{Al}_2\text{O}_3$  ( $50\% \pm$  and  $110\% \pm$  respectively), some ( $30\% \pm$ )  $\text{CaCO}_3$  and traces of monoxides and dioxides ( $\text{CaO}$ ,  $\text{MgO}$ ,  $\text{Na}_2\text{O}$ ,  $\text{K}_2\text{O}$ ).

Eight pin hole tests were performed on samples compacted at dry density and water content close to the optimum values from the standard Proctor tests. All show non dispersive properties for this material (class ND1). Nevertheless, the authors visited the borrow areas and observed, in some locations, typical erosion patterns (see Fig. 8) as if the material was dispersive. Khan (1983) reported results of chemical analysis carried out on 25 samples which indicated a high  $\text{Na}^+/\text{Ca}^{++}$  ratio. All 25 samples fall in zone C indicating the soil to be moderately dispersive according to Sherard et al (1976). The crumb test also gave similar results (Grade III), but no critical shear stress test as recommended by Arulanandan and Perry (1983) was made.

The clayey silt material has been placed dry generally. From the construction records of Main Dam, it was reported that the water content of the compacted soil ranged from 13.6% to 21.1% with a mean value of 16.4%, which is almost 2% less than the main value of the optimum water content from the standard Proctor compaction tests. The dry densities of the compacted soil ranged from  $17.1$  to  $18.7 \text{ kN/m}^3$  with a mean value of  $17.9 \text{ kN/m}^3$ , which is 103% of the mean maximum dry density from the standard Proctor tests.

Regarding Secondary Dam, the water content of the compacted soil ranged from 15.2% to 17.6% with a mean value of 16.3% and the dry density ranged between  $17.1$  and  $19.0 \text{ kN/m}^3$  with a mean value of  $17.9 \text{ kN/m}^3$ .

### 2.3.2. Description of filter and drain material

The filter and drain materials were made by crushing limestone. This limestone presents rather good engineering properties (low porosity and high compressive strength). The main features of the grain size curves of the fine filter material are the following :

- $D_{max}$  ranging from 6 to 10 mm
- $D_{85}$  ranging from 3 to 7 mm
- $D_{50}$  ranging from 0.5 to 1.5 mm
- $D_{15}$  ranging from 0.15 to 0.5 mm

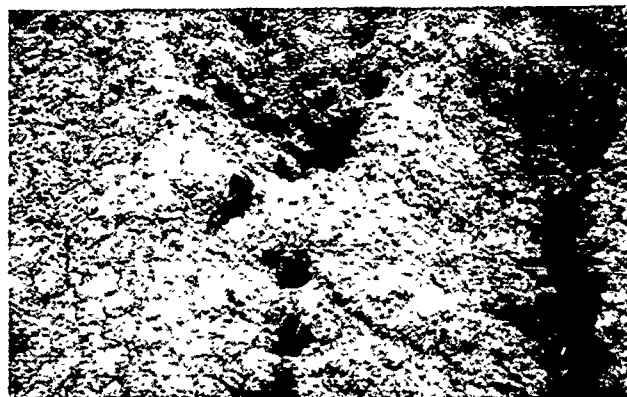


Fig. 8 - Erosion patterns observed in the borrow material areas

- Percentage of fines (below 80 microns) : generally 0%
- Uniformity coefficient  $D_{60}/D_{10}$  : values ranging from 6.0 to 15.0.

The main features of the grain size curves of the coarse Lfilter and drain materials (apparently no distinction is mentioned between these two materials in the construction records) are the following :

- $D_{max}$  ranging from 50 to 150 mm
- $D_{50}$  ranging from 12 to 50 mm
- $D_{15}$  ranging from 8 to 20 mm (generally ranging from 10 to 15 mm)
- Percentage of fines (below 80 microns) : 0%

These results show that the coarse filter has a very good permeability and satisfies the current filter criterion ( $D_{15}/d_{85} \leq 5$ ) with respect to the fine filter. The fine filter also satisfies the filter criterion ( $D_{15} < 0.5 \text{ mm}$ ) as recommended by Sherard et al (1984) since the  $d_{85}$  of the base material is 0.06 mm. According to Sherard et al (1984), such a fine filter is also acceptable for a dispersive clay.

### 2.4. Geotechnical properties of foundation materials

Underneath the alluvial deposits, the bedrock formation includes several kinds of more or less marly limestones. In the immediate vicinity underneath both embankments, the limestone has been termed as a dolomitic soft desintegrated porous limestone. Some unconfined compressive strength tests have been carried out on rock samples taken from boreholes in 1978 and 1979 through the main embankment. The results show a considerable scatter, with values ranging from 0.28 to 45.2 MPa for samples taken at similar elevations. This scatter may be due to the clay content (or marl content) of the samples. For samples exhibiting the lower values (0.28 to 1.14 MPa), undrained deformation modulus, if measured, would be of the same order of magnitude than that of the stiffer portions of the earthfill above. As the total vertical stresses applied to the limestone by this earthfill reach 0.9 to 1.0 MPa, the top portion of the foundation certainly behaves as a compressible medium.

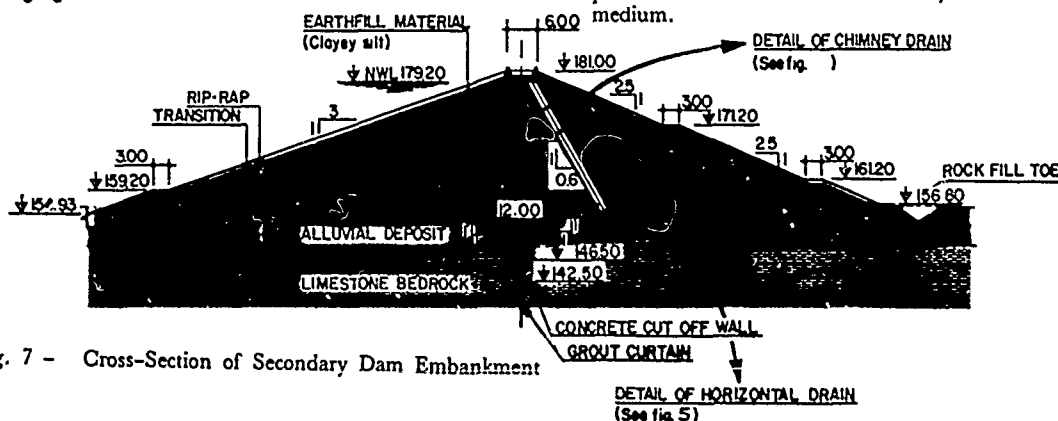


Fig. 7 - Cross-Section of Secondary Dam Embankment

Regarding the alluvial deposit, this material is described as clayey alluvium (silty clays, clayey silts, including gravelly layers and some blocks of weathered limestone). The field records mention that total loss of water was observed when drilling through the deposit. Due to the similar deposition conditions at Main and Secondary dam sites and borrow areas, the geotechnical properties of the alluvium deposit are very likely to be the same in the three zones. The identification characteristics and mechanical properties of the clayey silt from borrow areas have been reported in previous sections. The only additional information of interest is the in situ unit weight and water content of this material. These data obtained for superficial samples are the following :

- dry unit weight of undisturbed soil samples ranged from 14.4 to 16.5 kN/m<sup>3</sup> with a mean value of 15.3 kN/m<sup>3</sup> (38 samples),
- natural water content ranged from 7 to 12% with a mean value of 9.6%.

Unfortunately, data from deeper samples are not available. The above results indicate that the superficial part of the clayey silt deposit is in a dry and relatively loose state with respect to the optimum conditions of the Standard Proctor Compaction Test.

## 2.5. Observational Data on Main Dam Embankment

The observational data concern the following parameters

- water level in reservoir,
- water levels in piezometers,
- settlements of embankment layers using cross arms monitoring system,
- total stress in embankment using total stress cells (during construction only)
- movements of crest and slopes of embankment using topographic monuments (or bench marks).

### 2.5.1. Water level in piezometers

The provisions for piezometric measurements consist essentially of :

- a row of nine vertical standpipes, numbered PI through PIX with their tops opening on the downstream berm at El. 207 and pressure inlet in the filter blanket,
- two vertical standpipes in the bottom part of the valley, P2 and P6, 5 and 100 metres from the downstream toe of the dam, respectively. The pressure inlet of P5 seems to be set in the alluvial clayey deposit, and that of P2 in the underlying limestone,
- an isolated standpipe, PZ2, at the right bank end of the dam axis, with top opening at El. 232.30 and pressure inlet at El. 182.30 in the dolomitic limestone bedrock.

Piezometric levels in these standpipes have been recorded almost continuously since December 1977.

Some of the piezometers stay constantly dry (or with a few centimetres of water at the bottom) even with high water levels in the reservoir. At all other standpipes (PIII, PIV, PV, PVI, PVII, PVIII, PIX, P2 and PZ2, a rise in the reservoir level produced a significant rise in the piezometer level as follows :

- changes in the reservoir level below El. 211.00 do not produce any change in piezometric levels,
- when the water level in the reservoir rises from El. 211.00 to 216.00, piezometric level increases are between a few centimetres and about 20 cm.
- from El. 216.00 to 219.00 the reservoir fluctuation produces a significant change in piezometric levels, between 15 and 55 cm at sandpipes located on the downstream berm and up to 200 cm at PZ2 on the right bank.

- the changes in piezometric levels occur soon after the corresponding changes in the reservoir elevation, as the time lag appears generally less than one day. This quick response is not at all usual, the compacted clay should normally feature a coefficient of isotropic permeability  $K$  not higher than  $10^{-7}$  m/s, with which time lags must be considerably longer.

The abnormally fast response of some piezometers prompts the fear that seepage has worked preferential paths. These paths may be entirely contained in the limestone bedrock and thus by-pass the grout curtain laterally. However, the typical cross-section suggests that more direct paths may have also developed after hydrofracturation of the thin fill in the narrow trench immediately above the concrete cut-off.

### 2.5.2. Total stresses in embankment

Thirteen total stress cells were also installed in the embankment during construction. One of these total stress cells (No. 10) is located in the fill just above the concrete cut-off (El. 183.70). Another cell (No. 9) is located at El. 199 on the top of the backfill of the key trench, just above Cell No. 10. Readings of total stresses during construction show that :

- for almost all cells, except Nos. 9 and 10, the total stress measured is equal or slightly larger than the computed vertical stress (using the actual bulk density of the earthfill).
- cells Nos. 9 and 10 show a very different trend. The measured stress is 65% (cell No. 10) to 71% (No. 9) of the computed total vertical stress.

### 2.5.3. Settlements of embankment monitored with cross-arms

Five cross-arms vertical elements have been installed. Three of them are located on dam crest (CSI, II and III) and the other two on the upstream and downstream slopes (CSV and CSIV respectively). They are of the USBR type with steel pipes 2 and 1.5 inches in diameter, spacing between crosses nearly 3 m. The installation of the cross-arm elements progressed along with the placing of the fill and measurements of vertical deformations were taken during the construction.

The vertical deformation curves at the end of the construction are roughly parabolic with the maximum settlement at mid-height (including the key trench backfill). This is the usual settlement distribution in an earth dam. It is worthwhile mentioned that the settlement at CSII at end of construction and at the junction with the concrete cut-off wall is more than 3 cm which confirms the compressibility of the bedrock. From the distribution and magnitude of the settlements observed 8 and 9 years after the completion of the dam, the following remarks can be drawn :

- at the end of the 9-year period, the magnitude of the total post-construction settlement of the backfill in the key trench is 14 cm at CSI, 22 cm at CSII, 9.8 cm at CSIII and a few centimetres only in the alluvial deposit (according to the results of CSIV and V).
- the magnitude of the total post-construction settlement for all levels at CSV is about twice that at CSIV. The increase in soil saturation and the water load on the upstream portion of the dam may well explain the difference.
- the total settlement observed between February 1980 and February 1981 (1 year) represents an important fraction of the total settlement observed since the end of construction (9 years before) : 16% for CSI, 11% for CSII, 16% for CSIII, 14% for CSIV and 9.5% for CSV.

Thus, considerable settlement of the embankment is still developing, 9 years after the completion of the project.

### 2.5.3. Horizontal displacements of crest and slopes of the embankment

From the horizontal displacements of the crest and slopes taken from the bench mark measurements performed in 1980. It can be seen that the upstream slope has generally moved upstreamwards, with maximum displacements of 132 mm and the downstream slope downstreamwards with a maximum displacement of 70 mm.

The displacements of the crest are more erratic ; the right and central stretches have moved downstreamwards and towards the left bank ; the left stretch towards the right bank with an upstream component at Bench Marks No. 1 and 3, and, surprisingly enough, a large downstream component (50 mm) at Bench Mark No. 2.

The important displacement towards the right bank of the downstream slope near the left abutment (Bench Marks No. 1, 11 and 21) must be underscored. In places, the corresponding extension strain with reference to the nearest fixed point on the rocky edge may well exceed 0.5%. The development of significant extension strains in the area is confirmed by visual observation of the concrete parapet of the crest, between the spillway and the gate tower. The individual elements, 8 m long each making up this parapet, have separated or broken ; present openings are as follows : 25 mm between spillway right hand side wall and Element No. 1, 10 mm at a crack near the middle of Element No. 1, 12 mm between Elements No. 1 and 2 and 4 mm between Elements Nos. 2 and 3.

The above displacements reflect high extension strains (0.2 to 0.3%). Thus the presence of an extension zone in the earthfill near the contact with the steepest part of the left abutment (above El. 215.00) can be expected.

### 3. CHRONOLOGY OF SECONDARY DAM FAILURE

The following is a summary of the information gathered by the authors from the main witness, a technician in charge of the operation and maintenance of the electrical and mechanical equipment of the Wadi Qattarah Dams. According to the operation data, Secondary Dam had never impounded water until November 1977. Between December 13 to December 21, the reservoir level raised as follows :

| Date              | Reservoir Level                            |
|-------------------|--|
| Dec. 13           | 164.65                                     |
| Dec. 18           | 170.67                                     |
| Dec. 19, 6.00hrs  | 176.00                                     |
| Dec. 20, 7.00 hrs | 175.62                                     |
| Dec. 20, 9.30 hrs | 175.48                                     |
| Dec. 21, 9.30 hrs | 175.24 (rain, check of the gates as usual) |

Upon leaving the gate tower, on December 21, the technician went down the embankment slope along the spillway chute and over the outlet of the bottom conduit, on his way to the car, noting that no water was flowing out of the said conduit, an indication that the fixed-wheel gates had been properly closed. It was 10 a.m. approximately when he left the Secondary Dam area. At around 12 noon, a staff member informed the technician that he had just noticed muddy water flooding the toe of Secondary Dam above the bottom outlet (see Fig. 9). This observation had been made at 11.30 a.m., whereas the place was seen dry half an hour earlier.

Shortly after, the technician was back at Secondary Dam. A large discharge of water was flowing above the conduit in the area between the toe of the fill and the 1-meter diameter valve room. Soon the downstream slope started eroding, with blocks from the surface rip-rap raveling down. Water under pressure spat from a hole in the slope above the conduit. Then, the retrogressive erosion ate up progressively the downstream half of the embankment (see Fig. 10).

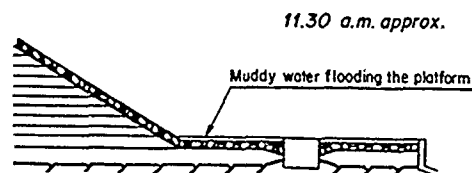


Fig. 9 - Sequence of Failure at Secondary Dam (11.30 a.m.)

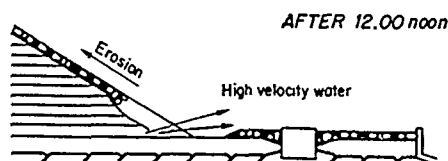


Fig 10 - Sequence of Failure at Secondary Dam (after 12.00 noon)

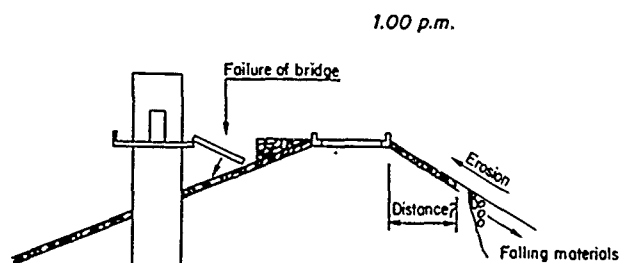


Fig.11 - Sequence of failure at Secondary Dam (1.00 p.m.)

At about 1 p.m., the service bridge between the crest of the dam and the gate tower fell down (see Fig. 11) and ten minutes later the retrogressive erosion broke through this crest, opening a breach to the reservoir; It took until 17 hours for the complete emptying, while the breach was widening and deepening; at no time, vortices or eddies were observed on the water surface in the reservoir.

### 4. MAIN WEAKNESSES OF THE DAMS AND POSSIBLE CAUSES OF FAILURE OF SECONDARY DAMS

The sequence of events in failure of the secondary dams as described above is typical of the phenomenon of piping.

As Post and Guerber (1973), Sherard (1986), and others stress, internal erosion results from dangerous seepage of water of diverse origins :

- cracking due to differential settlement, as was the case at the Stockton Creek dams in California in 1950, and at Wister Dam in Oklahoma in 1949 ;
- leakage either through the foundation/core contact plane, as at Hills Creek in 1970, or through one of the abutments, as at Fontenelle in 1965 ;
- horizontal cracking due to load transfer and hydraulic fracturing of slightly compressed zones, as at Hyttejuvet in Norway in 1966, at Balderhead in England in 1967, horizontal cracking causing wet seams in the cores of Manicouagan 3 in Canada, Yard's Creek in New Jersey, and El Guapo in Venezuela.

- iv) differential settlement near a fault or near an especially easily eroded, compressible foundation such as that at Baldwin Hills dam in the United States (1963) ;
- v) low internal stress due to drying out and shrinkage during and after construction, especially in low dams in arid climates such as La Escondida dam in 1972.

The characteristics of the two Wadi Qattarah dams and the instrumentation results outlined above give reason to think that at least 4 of the above-mentioned causes of seepage (i, ii, iii and v) could well have been present : cracking due to differential settlement, as shown by cross-arm measurement and monitoring of stretching at the crest and face on the left-bank side ; leakage along preferential passages in the foundation, as demonstrated by the rapid response of piezometers to reservoir level rise , horizontal cracking due to load transfer in the key trench fill, as seen from total pressure cell readings, as well as in the fill between the concrete culvert and the almost vertical sides of the trench through the rock ; and low internal stress due to drying out and shrinkage of the slightly to moderately plastic clay fill placed on the dry side of the Proctor optimum in a semi-arid climatic zone. To this can be added the drainage system which, although comprising filters and drains of satisfactory grain sizes, is very inadequate and badly situated.

As to how piping occurred at the Secondary Dam, several mechanisms are conceivable, but so far none of them can be retained definitely as the one responsible for failure. Two of the mechanisms seem almost equally probable :

- 1) Piping developed entirely through the compacted fill around the bottom outlet culvert and directly from the reservoir. This is supported by the conviction that the backfill around the culvert was poorly compacted and the arching could have developed, thus leading to hydraulic fracturing of the fill.
- 2) Piping developed through the downstream portion of the compacted fill around the bottom outlet culvert. The mechanism would be the same as (1) above but with the water head triggering the hydraulic fracturing initially applied at a point on the rock-fill interface intermediate between the cut-off wall and the downstream toe. The most conceivable path for bringing the full reservoir head to the said point is a solution channel in the limestone foundation.

In the opinion of the authors the second mechanism is the most likely.

## 5. CONCLUSIONS

Examination of the sequence of events leading to failure of the Secondary Dam would indicate that failure was brought about by internal regressive erosion of the clay fill, starting at above the bottom outlet culvert.

Examination of the characteristics of the Main and Secondary Dams, together with Main Dam monitoring results, would indicate that there are several possible causes of water infiltration :

- i) cracking of fill due to excessive differential settlement ;
- ii) cracking of fill (or low internal stress) due to excessive drying out and shrinkage ;
- iv) water flow along preferential passages in the limestone foundation (solution ducts).

From examination of the possible causes of Secondary Dam failure, it can be thought that the most probable mechanism for internal erosion resulted from a combination of flow in foundation solution ducts and hydraulic fracturing in fill around the downstream end of the bottom outlet culvert. This explanation does not exclude the involvement of other factors (cracking due to differential settlement or shrinkage) in facilitating the triggering of the mechanism.

Furthermore, the lack of adequately dimensioned filters and drains in the right places means that the phenomenon, once started, could not be efficiently combatted to prevent failure.

## REFERENCES

- Arulanandan, K , and E.B. Perry, (1983), "Erosion in relation to Filter Design Criteria in Earth Dams", Proc. ASCE, Journal of Geotechnical Engineering, Vol. 109, No. 5, May, pp. 682-698.
- Craft, C D., and R.G. Acciardi, (1984), "Failure of Pore-water Analyses for Dispersion", Proc. ASCE, Journal of Geotechnical Engineering, Vol. 110, No. 4, April, pp. 459-472.
- El Turki, M., U. Zappi, J. Binquet, and H. Garros, (1985), "The Rehabilitation Project of the Wadi Qattarah Dams", 15th International Congress on Large Dams, Lausanne, C.10, pp. 1207-1224.
- Khan, I.H., (1983), "Failure of an Earth Dam : A Case Study", Proc. ASCE, Journal of Geotechnical Engineering, Vol. 109, No. 2, Feb., pp. 244-259.
- Post G , and P. Guerber, (1973), "Conception du drainage dans les barrages en terre", La Houille Blanche, No. 5/6, pp. 467-476.
- Sherard, J L , L.P. Dunnigan, and R.S. Decker, (1976), "Identification and Nature of Dispersive Soils", Proc. ASCE, Journal of Geotechnical Engineering, Vol. 102, No. 4, April, pp. 287-301.
- Sherard, J.L., L.P. Dunnigan, R.S. Decker, and E.F. Steel, (1976), "Pin-hole test for Identifying Dispersive Soils", Proc. ASCE, Journal of Geotechnical Engineering, Vol. 102, No. 1, January, pp. 69-85.
- Sherard, J L , L.P. Dunnigan, and J.R. Talbot, (1984), "Filters for Silts and Clays", Proc. ASCE, Journal of Geotechnical Engineering, Vol. 110, No. 6, June, pp. 701-718.
- Sherard, J.L., (1986), "Hydraulic Fracturing in Embankment Dams", Proc. ASCE, Journal of Geotechnical Engineering, Vol. 112, No. 10, October, pp. 905-927.

## Comprehensive Seepage Assessment: Beaver Dam, Arkansas

J.L. Llopis

U.S. Army Engineers Waterways Experiment Station, Vicksburg,  
Mississippi

C.M. Deaver

U.S. Army Engineers District, Little Rock, Arkansas

D.K. Butler

U.S. Army Engineers Waterways Experiment Station, Vicksburg,  
Mississippi

S.C. Hartung

U.S. Army Engineers District, Little Rock, Arkansas

**SYNOPSIS:** A general philosophy of the role of engineering geology and engineering geophysics in seepage assessment is presented. Practical application of this philosophy is illustrated by a case history. A large dike continues to have anomalous seepage in spite of pre-construction and post-construction grouting. The dike is founded over a graben of cavernous limestone with about a 200-ft. vertical offset along the bounding fault zones, which are horizontally separated by about 1000 ft. Objectives of the seepage assessment program were to define the geological and hydrological conditions beneath the dike in sufficient detail to allow rational remedial planning.

Integration of results of a geophysical investigation with the overall assessment program is emphasized: preliminary interpretation of the geophysical results is used to site new piezometers; detailed analysis of the geophysical results is used to site exploratory borings; feedback from exploratory borings and new piezometers is used to refine geophysical interpretation.

### INTRODUCTION

#### Background

Earth dams and dikes are expected to seep, and their designs include drainage systems to collect and discharge seepage water into the downstream channel. Sometimes, however, seepage occurs in an unplanned manner, exceeding the capacity of the drainage system or along a path not considered in the seepage design. Excessive unplanned seepage may be just unsightly (though possibly disconcerting to the public), or it may threaten the integrity of the embankment. In these cases it may be necessary to conduct a seepage assessment program to detect and map seepage paths in order to more rationally plan remedial measures.

Dike 1, at Beaver Dam has been experiencing a general increase in seepage rates since initial reservoir filling in 1966. Recently however, the proliferation of seepage exits along the toe of Dike 1 has prompted the Little Rock District, U.S. Army Corps of Engineers (SWL) to undertake a comprehensive seepage assessment program. This program consisted of examining the project history, mapping and topographic surveying, surface geophysical testing, extending the piezometer network (including drilling, sampling and testing), exploratory drilling, seepage flow measurements, planning for and installing an automated piezometer and flow measurement data acquisition system, and remedial measure analysis. In support of this effort the U.S. Army Engineer Waterways Experiment Station (WES) was requested to perform a detailed geophysical investigation of the dike and its foundation.

#### Purpose

The purpose of this paper is to present the general philosophy of a seepage assessment program conducted at Beaver Dam, Arkansas. Described are the various phases of the program and how they are integrated to allow for a more rational approach to remedial planning.

#### Site Location and Description

Beaver Dam is located on the White River at river mile 609.0 in Carroll County, Arkansas, approximately 6 miles northwest of Eureka Springs, Arkansas. Beaver Dam is a straight, gravity-type, concrete structure flanked to the north by an earth embankment and three saddle dikes. The location of Dike 1 relative to the concrete dam and main embankment is shown in Figure 1. The reservoir (Beaver Lake) is used for flood control, power generation, and water supply. Construction of the dam was started in November 1960 and ended in June 1966. Dike 1 is approximately 1,000 ft in length and 30 ft high. The top of the conservation pool is elevation 1,120 ft while the top of the dike is elevation 1,142 ft. Dike 1 is founded on severely weathered limestone and is experiencing seepage from various exits.

### GEOLOGY

#### General Geology

Beaver Dam and reservoir area are located in an area known as the Ozark uplift, a region consisting of flat-lying sedimentary rocks composed chiefly of limestone and dolomitic limestone. The strata are nearly horizontal over the greater part of the area but are locally deformed by simple dislocations along southwest-northeast trending normal faults and shallow basins that in places are of considerable magnitude.

#### Physiography

The upland area around the dam is a part of the Springfield Plateau, the surface of which is developed at approximate elevation 1500 ft the cherty limestone of the Boone Formation. In the dam and reservoir area, the White River has cut a channel approximately 600 ft in depth. This

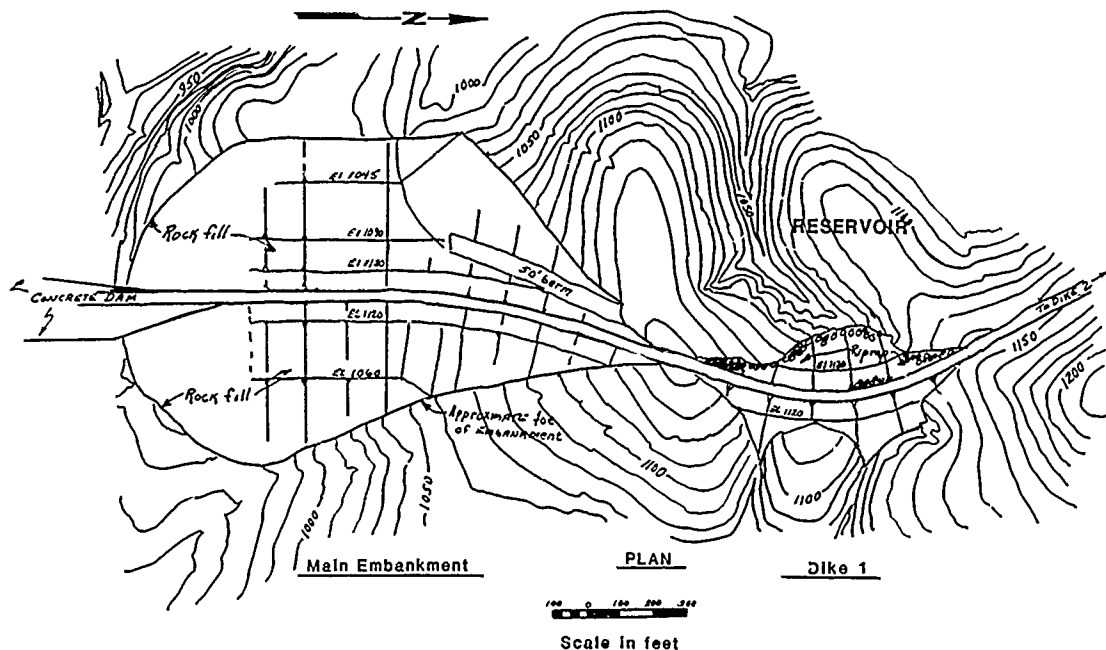


Figure 1. Location of Dike 1 relative to concrete dam and main embankment

incision into the Plateau surface has resulted in a deeply and intricately dissected type of topography. The entrenched river follows a meandering course across the area.

#### stratigraphy

Five formations are exposed at the dam site. They are (moving upsection) the Powell Formation, the Cotter and the Jefferson City Formations of the Jefferson City Group which is of Ordovician age, the Chattanooga Formation of Devonian age, and the Boone Formation of Mississippian age. The Chattanooga and the Boone Formations are generally above reservoir level except in the vicinity of the left abutment of the dam and Dike 1 where the units are downfaulted. In the vicinity of the dam site, the Boone Formation caps the higher ridges and forms the sides of the valley down to approximate elevation 1200 ft. Beneath this lies the Chattanooga Shale member (Chattanooga Formation), which in turn is underlain by its Sylamore Sandstone member. Beneath these and forming the valley walls below elevation 1180 ft and underlying the greater part of the valley bottom are limestones and dolomitic limestones of the Jefferson City Group (Design Memorandum No. 5, 1959).

#### Structural geology

The general structural geology of the region is that of flat lying rocks which are locally deformed by simple dislocations along southwest-northeast trending normal faults that extend for considerable distances, and by monoclines, low domes, and shallow basins. The Beaver Dam site lies near the northeast end of a very gentle, shallow, elongate, northeast-southwest trending structural basin known as the Price Mountain syncline. This basin is often faulted in areas where the downfolding is most pronounced. In the greater part of the lower end of the reservoir,

Ordovician strata underlie the valley floor and extend up the sides of the valley to about elevation 1,180 ft. Overlying these and almost everywhere above pool level are formations of Devonian and Mississippian age. In localized areas, these units have been downfaulted to form a part of the foundation under the most topographically desirable dam sites in the valley. This is the case at Dike 1.

#### Dike 1 Foundation Materials

Figure 2 shows the foundation materials underlying Dike 1. Dike 1 is founded on a downfaulted block of the Boone formation. This downfaulted block (graben) extends approximately between station 63+00 at the northern end to approximate station 75+00 at the southern end, a total distance of approximately 1,200 ft. The graben is bounded by steeply dipping normal faults on either side trending roughly in a northeast-southwest direction. The vertical displacement of these faults is approximately 200 ft. Cores of the rock adjacent to the northern fault zone show evidence of fracturing; however, the fractures appear to be filled or cemented and sound. Boring information from the southern fault zone area indicates the presence of many clay-filled cavities. The southern fault gouge does not appear to have the same degree of soundness as the northern fault zone. The Boone Chert which makes up the foundation of Dike 1 can be divided into two distinct sub-units. The upper sub-unit of the Boone Chert (estimated thickness, 100 ft) is composed of calcium carbonate and chert which upon weathering has resulted in the removal of calcium carbonate and left a spongy, vuggy, residual material that is predominately chert. The lower sub-unit of the Boone Chert (estimated thickness, 60 ft) is also composed of calcium carbonate and silica; however, this sub-unit is characterized as being slightly weathered to unweathered and contains more crystalline calcium

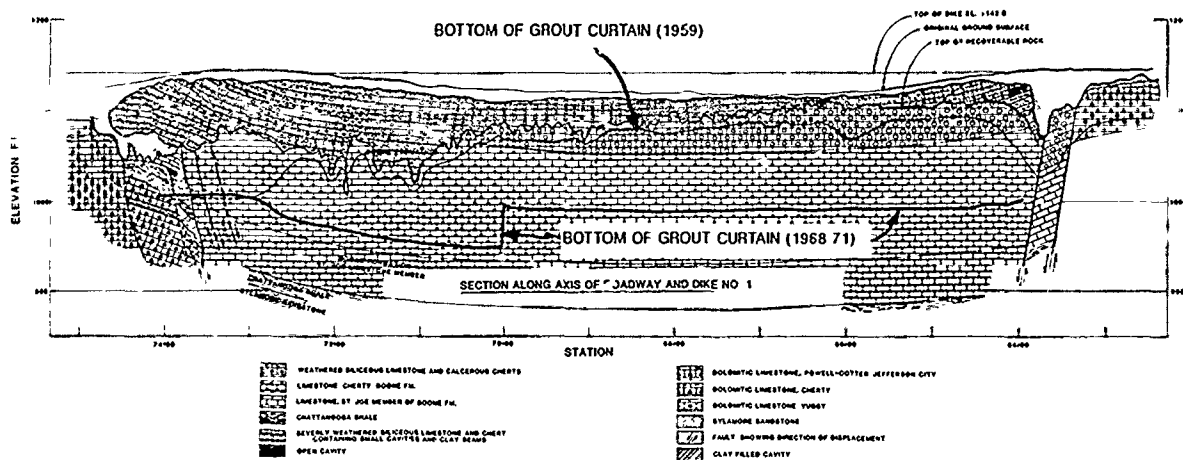


Figure 2. Foundation materials underlying Dike 1

carbonate. The lower sub-unit is moderately to closely jointed and this jointing has allowed the passage of water which has led to the dissolution of calcium carbonate and in turn has resulted in open channels and cavities.

Underlying the Boone Chert Unit is the St. Joe Limestone, described as non-cherty, gray to green-gray, crystalline, very fossiliferous, and containing numerous thin shale seams and partings. Underlying the St. Joe Limestone is the Chattanooga Shale described as black, firm, and fissile. The shale is considered to be an effective barrier to any downward movement of ground water.

#### SEEPAGE HISTORY OF DIKE 1

##### Pre-Construction Grout Curtain

The foundation materials of Dike 1 were recognized as being susceptible to seepage during the early phases of the site selection. In June 1959 it was decided that an economical solution to prevent a potential seepage problem was to install a grout curtain. The grout curtain consisted of two lines of holes spaced 5 ft apart with 10-ft hole spacings which extended to a depth of 5 ft below the top of sound or unweathered rock at all locations except between stations 72+70 and 74+70, where the grout curtain was extended deeper (16 to 65 ft) into sound rock (Figure 2). A total of 284 holes (24,200 linear ft) were drilled in this grouting program. The grout (31,000 cu. ft) was placed by gravity flow (Reconnaissance Report, Beaver Dam, 1984).

During initial filling of the reservoir (April 1966) seepage was detected in a small valley downstream of Dike 1. The reservoir pool elevation at this point was 1,102+ ft and the seep was flowing at a rate of 150-200 gpm. By June 1966 the reservoir elevation was 1114 ft and eight additional seeps were detected with a combined flow rate of approximately 400 gpm. By the time remedial grouting operations were initiated in 1968, the combined flow rate of these seeps

had risen to approximately 800 gpm. Conclusions from studies conducted at Dike 1, including flow measurements and dye tracing, indicated seepage was coming from the lake through two possible passages, either beneath the grout curtain through open cavities in the foundation rock, or along the top of rock or both. Seepage was occurring along the entire length of Dike 1 with the most concentrated flow occurring in the vicinity of station 71+00 near the southern portion of the dike (Reconnaissance Report, 1984).

Several possible explanations why the pre-construction grout curtain did not perform satisfactorily are as follows:

- Grout holes were not drilled deep enough to sound rock to intercept open joints.
- Since grout was placed by gravity flow, it is possible many small cavities and joints were not filled.
- Grout was too thick to enter some of the cavities and joints.
- Since drilling was performed with tricone roller bits using compressed air to remove cuttings, the cuttings could have plugged some of the cavities preventing them from being grouted.
- Many cavities and joints could have been missed altogether because of the grout hole spacing.

##### Early Seepage Flow Studies

Flow measurements, exploratory drilling, pressure tests, and dye and temperature tests were conducted from the time of leakage (1966) until 1968 to determine the extent and routes of seepage through and beneath the dike and to formulate possible remedial measures. These measurements were accomplished by installing two weirs, a Parshall flume, and twenty-seven piezometers. The data suggested that the leakage was issuing both through cavities below the original grout curtain and along the top of



crystalline/weathered rock interface. It was concluded that seepage occurred along the entire length of Dike 1 and to the fault zone beneath the main embankment at station 73+00, with the greatest seepage occurring along the shortest flow path in the vicinity of station 71+00.

#### Remedial Grout Curtain

During the period July 1968 to December 1971 an extensive grouting program was conducted in an effort to abate the seepage occurring at the dike. The program consisted of 30,040 linear ft being drilled in 228 holes. Also, 38,900 cubic ft of grout solids were pressure injected into these holes with the heaviest grout takes occurring in an area between stations 70+50 and 72+00 (Figure 2). Problems encountered during the grouting operations were collapsing boring walls (cave-in), insufficient seating of casing, and incapability of grout pump to grout some large cavities to refusal.

As a result of the remedial grouting program, seepage was reduced to approximately 450 to 500 gpm for mid-pool elevations (1120-1130 ft), a decrease in flow of 30 to 35 percent. During the period 1971 through 1984 piezometers were manually read approximately twice a year by SWL personnel while the Parshall flume was read on a monthly basis by project personnel. During a periodic inspection in 1980, a new seepage area was located on the downstream right abutment of the dike. This prompted SWL personnel to undertake an effort to locate, inspect, and describe all known seepage exits.

#### Dam Safety Assurance Program

When the U.S. Army Engineer Southwest Division's (SWD) Division-wide Master Plan for the Dam Safety Assurance Program was submitted in 1983, Beaver Dam was listed as requiring studies for a Reconnaissance Report under designated priorities of spillway adequacy and major seepage. The Reconnaissance Report (May 1984) concluded that seepage at Dike 1 would increase to near pre-grouting flows (800+ gpm.) during a Spillway Design Flood (Probable Maximum Flood, pool elevation 1,139.9 ft) and continue flowing at this rate even after the flood receded due to expansion of existing cavities. This conclusion was proven to be valid on 23 December 1984 when a Pool of Record (el 1,130.4 ft) occurred. During the emergency flood procedure inspection on that date the project superintendent observed a new seepage exit 500 feet downstream from Dike 1 with a flow rate of approximately 25 gpm. The alarming factor at the newly discovered exit however, was the large amounts of detrital material (sediment), ranging from clay- to gravel-size being discharged in the flow, i.e. muddy water. Another new seep was discovered on 2 January 1985 near the left dike/abutment contact at approximate elevation 1,106 ft (Figure 3). Water from this new seep was described as jetting vertically with a flow rate of approximately 7 gpm. at pool elevation 1,125.1 ft (Feature Design Memorandum, 1987). The 1984 Reconnaissance Report recommended that a seepage investigation be undertaken to determine the location and extent of seepage and develop remedial measures to control seepage at Dike 1.

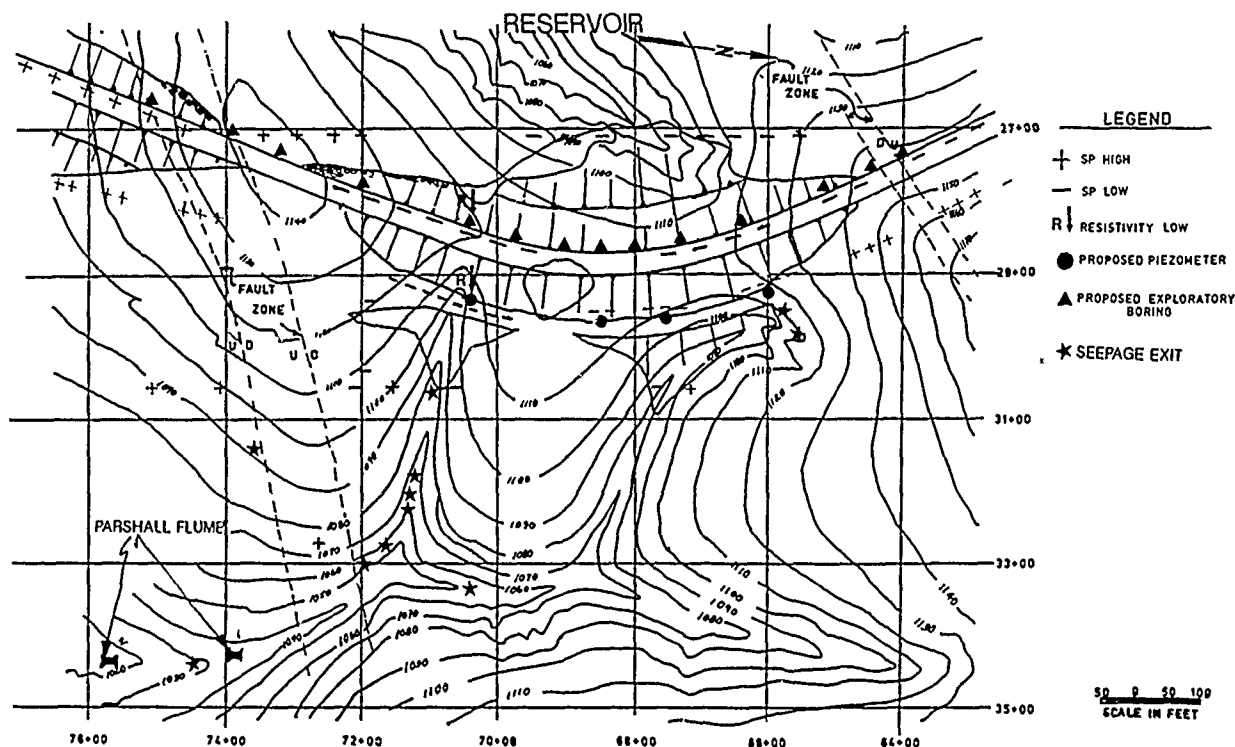


Figure 3. Location of seepage exits and proposed piezometer and exploratory borings.

A combined SWD/SWL/WES meeting was held at Beaver Dam on 14-16 January 1985 to discuss the proposed seepage investigations, which were initiated in February 1985.

## SEEPAGE INVESTIGATIONS

### General

The new muddy seepage exit below Dike 1 discovered during a pool-of-record (1,130.4 ft) in December 1984 not only substantiated the need for seepage investigations, but also added an element of urgency and a necessity to expedite the investigations, and recommendations of measures to control seepage. In 1985 the monitoring /inspection of instrumentation and seepage was revised to more frequent scheduling, especially for pool levels above elevation 1,128 ft. The action having the greatest impact on project operations, due to severe seepage, is the request and approval for a deviation (loss) of the authorized flood storage pool in Beaver Lake from elevation 1,130 to 1,128 ft until the seepage the seepage problem is resolved. The major elements of the seepage investigation are described below.

### Geophysical Investigations

In March 1985 WES personnel conducted a geophysical investigation at Dike 1. Several geophysical methods were used for this study including self-potential (SP), electrical resistivity, electromagnetic induction (EM), seismic refraction, magnetic profiling, and borehole water conductivity/temperature measurements. The objectives of the geophysical investigation were to (a) detect, map, and monitor seepage through the foundation of Dike 1, (b) delineate geologic structure beneath and immediately adjacent to Dike 1, and (c) provide input to the planning of remedial measures.

The geophysical methods necessary for a seepage analysis are not difficult to use. However, a geophysical survey program must be planned based, to the maximum extent possible on knowledge of the (1) surface geometry of the dam and associated features, (2) design and construction details of the structure, and (3) the geology of the foundation and abutments (Butler, 1985).

The primary, long-term geophysical method was the self-potential (SP) method, which was monitored throughout the duration of the investigation. SP data were obtained during various pool levels to determine relationships of seepage flows and pool levels. The SP arrays were installed by SWL personnel in February 1985. Initial SP readings were made by WES in March 1985. Subsequent readings, during various pool levels, were taken by SWL personnel and forwarded to WES for interpretation. Detailed results of the geophysical studies pertaining to the seepage investigation are presented in Supplement No. 1 of the Reconnaissance Report, 1986.

Additional geophysical studies were conducted at Beaver Dam in conjunction with the Corps of Engineers' Repair, Evaluation, Maintenance, and Rehabilitation Program (REMR). These REMR spon-

sored geophysical tests included high-resolution seismic reflection, ground-penetrating radar, microgravimetry, and additional SP investigations. The ground-penetrating radar survey was conducted in September 1985 with an additional survey being conducted in February 1986. In August 1986 a high-resolution seismic reflection and a "low pool level" SP survey was conducted. Detailed results of these geophysical surveys are presented in the Feature Design Memorandum, 1987.

The geophysical investigation was successful in delineating the fault zones bounding Dike 1, which are believed to act as channels for lake water to exit downstream, as well as identifying other faults which were not previously known to exist. The tests also identified fractured and saturated zones as well as determining the vertical extent of the weathered Boone Chert. The tests also indicated that seepage is occurring along the entire length of the dike. The geophysical tests suggest that both axial and transverse seepage flows are occurring along the south fault zone, but that the north fault zone is relatively tight (impermeable) to those flows. Based on results of the geophysical tests an integrated seepage map was produced showing that seepage flows are moving primarily in an east-southeasterly direction with the greatest flows occurring between stations 69+00 and 73+00, and along the south fault zone (Figure 4).

### Exploratory Borings

Twenty-five exploratory borings were drilled along the upstream crest of Dike 1 and its abutments during the period April 1986 to August 1987. The primary purpose of these borings was to delineate the limits and geologic characteristics of the downthrown faulted block of the Boone Formation beneath Dike 1 and the North and South fracture zones that bound the Dike. Originally, the boring locations were selected based on areas that had experienced high grout takes during the previous grouting program. However, locations for the borings were later changed to take advantage of information obtained from geophysical testing. Based on results of the SP, resistivity, and other geophysical testing and also considering previous grout takes, fault locations, and piezometer data, WES submitted a list of proposed locations for exploratory borings to SWL for approval. Figure 3 shows the WES suggested exploratory boring locations.

Extensive investigations were conducted on each of the borings, typically included soil sampling, diamond core drilling, detailed descriptive logging of rock core, dye testing at zones of drill fluid loss, pressure testing of rock, downhole geophysical logging, inspection with downhole video equipment, and laboratory testing of rock core samples.

The investigations conducted in the exploratory borings determined that the northern fault zone has a vertical offset of 230 ft while the southern fault zone's vertical displacement measures approximately 146 ft. The unsound nature of the fault zones was evidenced during drilling by noting the complete loss of drill fluid and large core losses. This condition was substantiated by SWD laboratory personnel while

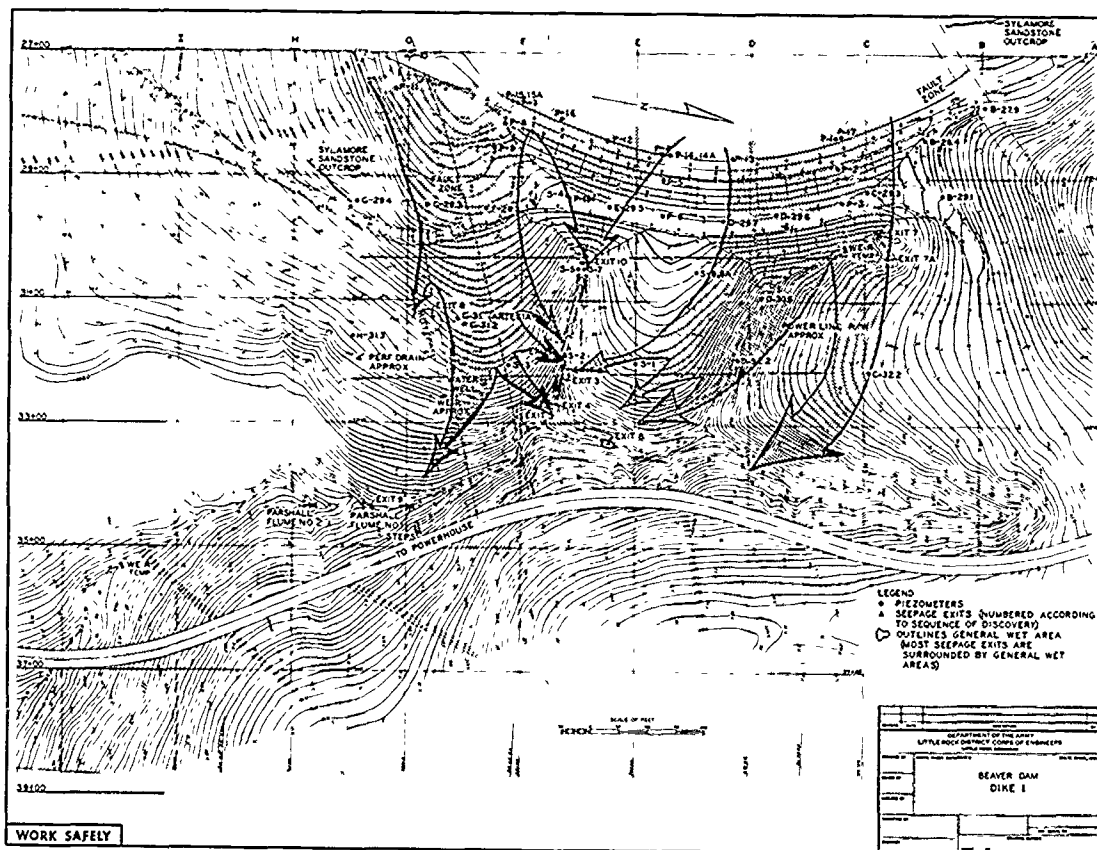


Figure 4. Integrated seepage map

performing "down-looking" and "side-wall looking" observations with a down-hole video camera. Numerous open cavities, channels, joints, and intensely fractured zones were encountered in the the fault zones as well as in the upper cherty Boone Formation. Subsurface flows through channels in rock were apparent in several borings where normally suspended fines could be seen moving rapidly.

#### Piezometers

There were 26 open (well point) piezometers at Dike 1 prior to the seepage investigation. A review and analysis of locations and depths of the existing piezometers was made to determine key areas (and depths) where piezometric data was inadequate for analyzing the overall groundwater (seepage) flow network beneath Dike 1. The new piezometers were located in a directional alignment pattern (grid) with existing piezometers to facilitate preparation of cross sections through the piezometers, both parallel and perpendicular to the dike. Piezometers were also located to give broader coverage (north/south) of the fault zones and downstream seepage areas (east/west). The new piezometers were dual-tipped and were designed such that the lower tip was placed at or near elevation 1040 ft, which is within the zone between known seepage exits and Parshall flumes located further downstream, and the upper tip placed within the upper weathered Boone Formation, at an average depth of 11 feet below top-of-rock.

Four of the new piezometer sites were relocated in May 1985 based on results of SP and resistivity geophysical tests conducted by WES. Figure 3 shows the WES proposed piezometer locations. Thirty piezometers were installed at Dike 1 between the period May and September 1985, giving a total of 56 piezometers at the structure.

The piezometer borings drilled in 1985 at Dike 1 were sampled and tested to determine subsurface conditions prior to installing the piezometers. A common difficulty was heavy loss of drilling (circulation) fluid, with most borings having a total circulation loss at some point during drilling. A downhole camera lowered into several of the piezometers in August 1985 indicated rock characteristics and features which contribute to subsurface seepage such as open cavities, channels, intensive fracturing, and weathering.

#### Seepage Flow Measurements

Prior to the seepage investigation there was only one Parshall flume used for measuring seepage flow rates downstream of Dike 1. The frequency of the flow measurements were taken based on pool level. Measurements were made by reading the water level on a scaled gauge on the interior wall of the flume and converting the readings to gpm. In October 1985, a flow recorder was installed on the Parshall flume allowing the seepage to be monitored continuously. In November 1985, a second Parshall flume and

recorder were installed approximately 170 ft downstream of the first flume. The necessity for a flume at this second location came from the appearance of the new muddy seepage flow which bypassed the first flume.

#### Topographic Surveys and Mapping

Field control for the seepage investigations, boring locations, and geophysical surveys was established by installing a 200-foot survey point grid. Also, the topographic map of Dike 1 was updated by a new planetable survey, with a final plan on 2-foot contour lines.

#### Seepage Study Findings and Recommendations

In April 1986 SWL reported the findings of the seepage study in Supplement No. 1 of the Reconnaissance Report. The report concluded that the foundation beneath Dike 1 was in an advanced stage of deterioration, and that seepage could be generally described as pervasive. Also, the risk factor and potential existed during a high (flood) pool condition for one of the numerous seepage flows to seek a new and larger exit path, by removal of detrital material (cavity clays, etc.), and "blowout" through the overburden in the downstream area. Finally the report concluded that the element of time was both a critical and a debatable factor on a seepage problem such as this.

The report also investigated various alternatives for controlling seepage beneath the dike. The seepage control alternatives considered at Dike 1 were construction of an additional grout curtain, a cutoff wall, a downstream berm, placement of an upstream blanket, or do nothing and continue monitoring the seepage. The recommended remedial technique was a concrete diaphragm cutoff wall installed upstream of the centerline of the dike. The report concluded that this was the most feasible method to adequately provide a positive cutoff of the seepage. The other methods were considered to be only temporary measures to control seepage and inadequate for providing a positive cutoff, which was deemed necessary from seepage investigations.

#### Automated Piezometer System

During the period November 1986 through April 1987 an automated monitoring network was installed at Beaver Dam to read all (88) open well point piezometers at Dike 1 and the main embankment and Dike 3. The system transmits the piezometer information via telephone modem to the District Office (250 miles). Readings are routinely taken every 4 hours and can be read with a higher frequency if needed. Since the installation of the automated system a high degree of interconnection between piezometers has been detected. This was evidenced during periods of drilling or performing down-hole tests when piezometers were being monitored at intervals as short as 1 hour. The automated system should aid in constructing more accurate piezometric profiles of the site since short term piezometric head versus pool level can be determined.

#### PLAN FOR REHABILITATION

In September 1987 a Feature Design Memorandum was prepared by SWL. The report described the recommended design for a concrete diaphragm cutoff wall. The plan for the wall consists of constructing the wall through the embankment and permeable zone of the foundation rock. The wall will be a minimum of 1,400 feet long, 2 feet wide, and vary in depth from 130 to 205 feet. The estimated cost of constructing the cutoff wall is \$16,000,000.

A rock-mill type excavation system will be used to excavate the cutoff wall trench, using bentonite slurry to stabilize the trench during both excavation and concrete placement. The rock-mill was determined to be the most efficient and cost effective method to construct the proposed wall due to the amount and characteristics of rock that will be encountered. More detailed information on this excavation method is given by Hess, 1985.

Also included in the Feature Design Memorandum was a recommendation by WES to install and maintain an automated geophysical monitoring network to monitor seepage before, during, and after implementation of a remedial measure (such as a concrete cutoff wall). The result of the monitoring network analysis will be an assessment of the effectiveness of the remedial measure. The computer controlled network is envisioned as consisting of a permanently installed SP array and borehole resistivity probes with the capability of scanning the network at any desired time interval.

#### SUMMARY AND CONCLUSIONS

The results of the seepage investigation indicated that the foundation beneath Dike 1 was in an advanced stage of deterioration, and that seepage can be generally described as pervasive. Also, the risk factor and potential exists during a high (flood) pool condition for one of the numerous seepage flows to "blowout" through the overburden in the downstream area. Finally the report concluded that the element of time is both a critical and debatable factor on a seepage problem such as the one above.

The investigation also recommended that a concrete diaphragm wall be installed upstream of Dike 1 as a mean of controlling seepage.

By conducting a comprehensive seepage program such as the one performed at Beaver Dam it has been demonstrated that integration of results from various phases of the investigation has led to a more rational approach to remedial seepage planning. In a program of this magnitude it is very important to consider the geophysical surveys as an integral part of the seepage analysis. It is also important for the project engineer and the geophysicist to communicate with each other and share their knowledge of the project in order to make more meaningful interpretations of test data and to more efficiently plan any future testing.

## ACKNOWLEDGMENTS

The tests described and the resulting data presented herein, unless otherwise noted, were obtained from research conducted under the Dam Safety Assurance and Repair, Evaluation, Maintenance, and Rehabilitation programs of the U.S. Army Corps of Engineers by the U.S. Army Engineer District, Little Rock and the U.S. Army Engineer Waterways Experiment Station. Permission was granted by the Chief of Engineers to publish this information.

## REFERENCES

- Butler, D. K. (1985), "Geophysical Methods Applied to Detect and Map Seepage Paths at Clearwater Dam", The REMR Bulletin, Vol 2, No. 2, U.S. Army Engineer Waterways Experiment Station, Vicksburg, Miss.
- Hess, C. M. (1985), "French Drilling Machine Shows Advantages in Excavating for Concrete Cutoff Wall", The REMR Bulletin, Vol 2, No. 2, U.S. Army Engineer Waterways Experiment Station, Vicksburg, Miss.
- U.S. Army Engineer District, Little Rock, 1959. Design Memorandum No. 5, Geology and Soils, Little Rock, Ark.
- U.S. Army Engineer District, Little Rock, 1984. Reconnaissance Report, Little Rock, Ark.
- U.S. Army Engineer District, Little Rock, 1986. Reconnaissance Report Supplement No. 1, Beaver Dam, Little Rock, Ark.
- U.S. Army Engineer District, Little Rock, 1987. Feature Design Memorandum, Beaver Dam, Little Rock, Ark.

## Remedial Measures to Seepage and Instability Aspect of a Dam Near Bombay

R.K. Katti

Professor of Civil Engineering, Indian Institute of Technology, Bombay, India

Dinesh R. Katti

Former Junior Research Officer, CBIP, Indian Institute of Technology, Bombay, India

Anand R. Katti

Research Scholar, Indian Institute of Technology, Delhi, India

**SYNOPSIS:** The paper describes the distress caused to a minor earth dam constructed at a high elevation in a mountainous area to conserve water. The distress related to instability of the dam and also due to high percolation underneath the dam coupled with formation of piping. The remedial measures taken to rectify instability and reduce percolation are described in this paper.

### INTRODUCTION

In India western ghats, a mountain chain runs parallel to west coast of India, starting from a few kilometers north of Bombay and go right upto Cape Comerin, covering a distance of 1500 km to 2000 km. These mountain ranges have elevation ranging from 1000 m to 4000 m. The rainfall varies from 2000 mm to 4000 mm that too during monsoon season. The rock formations are mostly of basaltic origin locally known as deccan trap. The mountain ranges are highly folded, faulted and jointed. The joints are present right upto a depth of 20 m to 40 m.

There are a large number of locations in these mountain ranges which are ideal for storing water at high elevations.

During recent years a large number of human settlements are getting established in such locations. To provide water for such settlements, reservoirs having capacity of 200 TCM to 300 TCM are constructed.

To develop a social welfare centre a tank having a storage capacity of 227.53 TCM was constructed at Kune, in Poona district, in western ghats. The main gorge and the upstream storage area is formed due to the presence of around 3 to 4 hills. Water is collected from a catchment of around 0.75 sq.km through 2 to 3 streams which converge at the gorge and join the main valley, after a vertical drop of 100 m.

A zoned rolled filled earth dam of height 15.9 m. and length 77 m. was constructed to store water. A waste weir was constructed by blasting the weathered rock, and is located at a distance of around 7 m. from the dam on the right flank. It was unlined.

During the first filling of the dam in the year 1984, the authorities noticed heavy seepage on the down stream side of the dam. They also observed subsidence and heaving on a portion of the down stream part of the dam close to the right flank. The tank was getting depleted at

a rate of around 11 cm. perday.

The authorities approached the authors to study the causes of the distress and suggest the remedial measures to be adopted. A systematic study was conducted through visual observations when the reservoir was empty and also by conducting appropriate subsurface investigations. Based on these studies various remedial measures were adopted. The efficacy of the remedial measures adopted was evaluated during the subsequent fillings of the dam. The paper describes the above aspects.

### LOCATION

The tank is located at Kune, in the state of Maharashtra. The latitude and longitude of location are 19°46'0" north and 73°24'0" east respectively. Location at which the tank is constructed is on the top of western ghats surrounded by highly folded, weathered and jointed hills and mountain features. It may be observed from the countour map given in Fig.1, that the dippression is formed by folding of almost 3 to 4 hills. A small valley in between the two hills provides an outlet for the water to drain into the main valley through a steep vertical drop. The underlying rock mass is made up of various types of basaltic rocks. The heavily jointed terrain is subjected to high degree of hydro thermal weathering of rock mass. The top 2 m. to 5 m. of over burden consists of murrum containing various amount of boulders, gravel and fine grained material. This is a typical tropical soil. On the basis of vegetation one can expect highly weathered fractured rock interspersed with murrum of thickness 10 m. to 12 m. As this site is close to a mountain fall one can expect jointing to reach a depth almost of the order of 40 m. or more.

An examination of the countour map indicates that the jointing and fracturing may converge at the main gorge. This may lead to collection

## BROAD FEATURES OF THE SCHEME

|                            |                |
|----------------------------|----------------|
| Nature of the catchment    | : ghat type    |
| Catchment area             | : 0.75 sq.km.  |
| Average rainfall           | : 3587.35 mm.  |
| Total yield available      | : 2690.51 TCM  |
| Total storage capacity     | : 227.53 TCM   |
| Storage yield              | : 211.75 TCM   |
| Storage due to borrow area | : 15.78 TCM    |
| Levels of the dam          |                |
| Lowest base level          | : RL 530.01 m. |
| FSL                        | : RL 543.00 m. |
| HFL                        | : RL 544.50 m. |
| TBL                        | : 77.00 m.     |

The dam is a zoned rolled filled earth dam. The salient features of the dam are given below. See Fig.2 and 3.

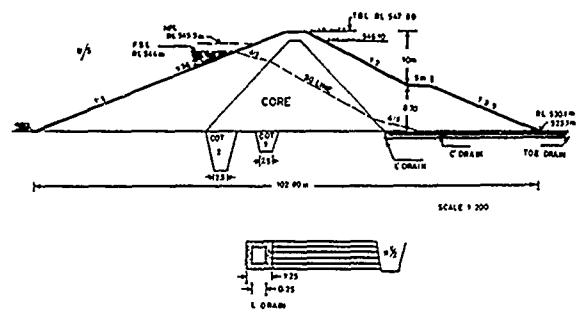


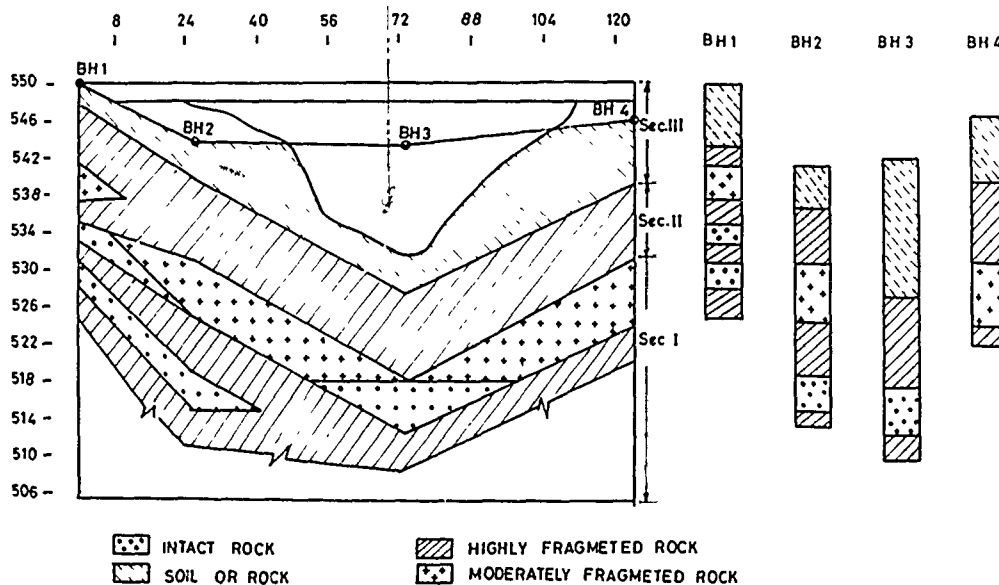
Fig. 3 Cross Section of the Zoned Dam.

The dam lies between : ch 36 and ch 113  
Deepest portion of the  
gorge lies between : ch 70 and ch 75  
Upstream slope : 1:3 upto RL 537.8; 1:2.5  
from RL 537.8 to TBL  
Down stream slope : 1:2.5 between RL 530.10  
and RL 537.8; 1:2 bet-  
ween RL 537.8 and  
RL 547.8

Berm of width 5 m. is provided on the down stream side at RL 537.8

Central core :  
 Top width of core : 2 m.  
 Slope of u/s and d/s side : 1:1

Cut off trench :  
Two cut off trenches are provided whose width is 2.6 m. and depth 3.6 m. Rock toe is provided on the d/s side.



**Fig. 2 Subsurface Section Along the Dam Axis**

#### Rip rap :

30 cm. to 40 cm. boulders are placed on upstream as well as down stream sides.

Density of hearting material : 1.29 gm/cc

Density of casing material : 1.80 gm/cc

#### Filter :

Longitudinal drain and cross drains are provided on the down stream side.

#### WASTE WEIR

The major portion of the waste weir passess through rocky strata. For construction in rocky strata blasting methods were adopted. The waste weir was left without lining and sides and bottom are highly jointed. The distance between the waste weir and the dam is around 5 m. to 7 m. The bottom of the waste weir is 10 m. wide corresponds to FSL (RL 544).

#### NATURE OF DISTRESS

During first filling of the dam two kinds of distresses were encountered. One related to stability aspect and the second related to the percolation aspect. The percolation aspect in turn may also be responsible for instability of the dam and the flanks. As a first step immediately after the whole water in the tank had got completely depleted, in the middle of February 1984, a thorough visual inspection of storage area, dam and the waste weir was conducted.

#### Reservoir Area

The whole area consisted of highly weathered soil mass followed by highly fractured and jointed basalt. See Fig.2. Such a condition of reservoir may give rise to high degree of subsurface percolation. It was also observed that a big piping had appeared close to the waste weir and was cutting across underneath the dam and was opening up down stream at RL 536. Further examination revealed that 2 to 3 streams which are passing through the reservoir area converge into goose neck and join the main valley. The location of the piping coincides with the course of the stream. It is presumed that the cut off trenches are above the bed of the streams which are filled up with sand and gravel. See Fig.5. It is also observed that considerable distress has taken place on the right flank due to blasting operation during the construction of waste weir. This can lead to heavy percolation through the right flank when the dam would be full.

#### Instability of Dam

The portion on the down stream of the dam enclosed between RL 538 and RL 542 and between chainage 40 and 68 showed subsidence and heave indicating potential possibility of slide. In addition a subsidence of around 30 cms was observed on the top of the dam towards d/s side between chainage 45 and 55.

The dam section used here is a standard section adopted in these regions for minor dam construction. These sections are stable when they are constructed by compacting the locally available

murrum to maximum standard proctor density with a variation of  $\pm 5\%$ .



Fig. 4 Nature of Basin.



Fig. 5 Stream Feeding the Reservoir.

#### Subsurface Investigation

To understand the causes of heavy seepage it was considered necessary to take around 4 boreholes along the dam axis. See Fig.2. With the help of 4 borehole logs a subsurface profile is developed to indicate the strata containing murrum, highly crushed fragmented rock and intact rock etc. It can be seen from the section that on the right flank murrum deposit is encountered upto RL 536 and at the centre of the dam it is upto RL 527.5. Near borehole 4 the murrum zone ends at RL 539. Below the murrum zone around 8 m. to 10 m. of thick fragmented crushed rock zone is encountered. On the left flank the rock strata encountered is moderately fragmented rock as shown in Fig.2. On the basis of subsurface section coupled with surface observations in the storage area it can be concluded that even after the dam is constructed almost all the water can percolate out at a high rate through the subsurface underneath the dam. The average thickness of crushed rock and murrum overburden would be around 18 m. Approximate computations show that the coefficient permeability K value would be  $2.2 \times 10^{-2}$  cm/sec. for average strata. However, the coefficient of permeability for fractured zone would be  $4 \times 10^{-1}$  cm/sec.



In the present case it is clear that the percolation is not only through the subsurface but also through the right flank.

#### Embedment

Inadequate embedment of right and left flanks of earth dam into the original natural ground has added to further seepage losses and also to instability of the dam itself. Weakening of the right flank due to construction activities in the waste weir has further contributed to high seepage and to instability to flanks and the dam. See Fig.4.

#### Steep Gorge

Because of narrow steep gorge 3 dimensional instability is induced into the earth dam. As such conventional analysis indicate that the dam should be stable under normal conditions.

#### Piping

In adequate cut off, untreated subsurface, and followed by storing of tank has resulted into high internal subsurface erosion and formation of pipes. See Fig.6.

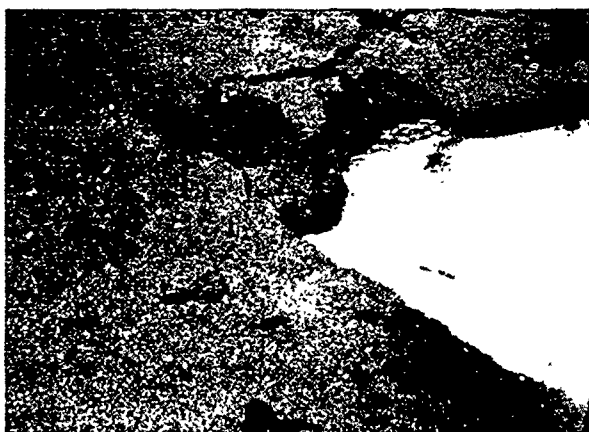


Fig.6 Piping

#### REMEDIAL MEASURES

Based on the visual observations of the reservoir area, dam, flanks, waste weir and the subsurface profiles, following remedial measures were adopted in stages to rectify the defects in stages as the time available for implementing the remedial measures was hardly 2 to 3 months. The remedial measures adopted for improving the stability of the dam and reducing the percolation are given below :

- i) Preventing the d/s slide with shear barriers using reinforcement
- ii) Adoption of curtain grouting
- iii) u/s dam protection
- iv) Treatment of reservoir area with impervious material
- v) Lining of the waste weir

#### Stability of d/s Side

Specially with respect to the stability of dam

on the d/s side, there was a need to take immediate rectification measures. The measures taken with respect to stability are described below. With the help of zone of subsidence and heave a probable circular potential plane of failure was adopted for analysis. The computed value of the activating force turns out to be 4 tonnes/m. width. It was considered prudent to provide shear connectors to take the whole activating force (4T/m. width) as the portion was already in the process of sliding. The method adopted consisted of providing 3 rows of shear connectors with the spacing as shown in Fig.7 and Fig.8.

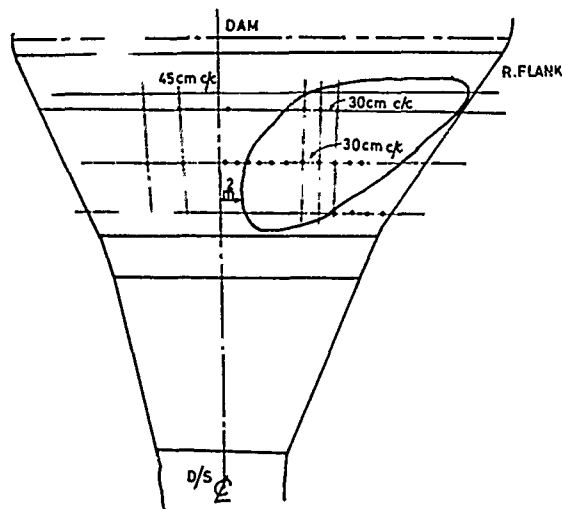


Fig. 7 d/s Face

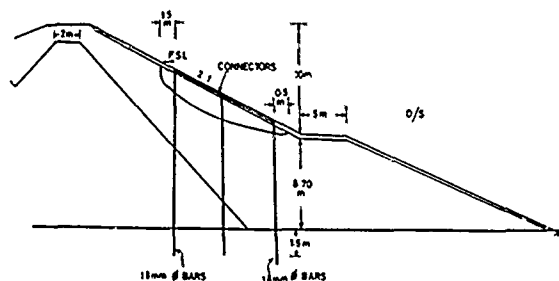


Fig. 8 d/s Section

#### Construction

Minimum number of rip rap stones were removed at the location where the shear reinforcement were to be inserted. Pneumatic drill was used to drill a 2.5 cm. diameter hole upto a depth of 1.5 m. into the original ground through the body of the dam. Care was taken to see that the surrounding rocks are not disturbed. After the drilling was completed 16 mm. diameter steel bars were inserted into the hole upto the desired depth. The remaining cavity of the whole was filled with cement slurry of 1 in 15 consistency. The 3 rows of bars were interconnected with 6 mm. diameter bars at the surface of the soil layer. Immediately after these rods are placed in position the rip rap

was reinstated.

### Grouting Procedure

As the pressure due to water is around  $1.5 \text{ kg/cm}^2$  it was necessary to use a thick mix 1:6 to 1:8. The cement bentonite ratio was 60%:40%. The grout mix was injected at  $2 \text{ kg/cm}^2$  and was raised up 4.5 to  $6 \text{ kg/cm}^2$  before termination between RL 505 and RL 520. See Fig.9.

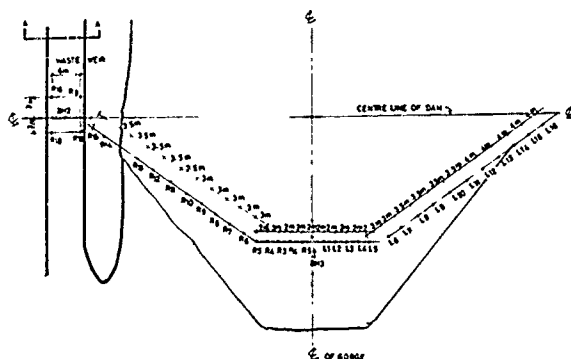


Fig. 9 Grouting Plan.

The second stage of grouting was between RL 525 and RL 520. The grout mix used was 1:8 to 1:9. The initial pressure was  $1.5 \text{ kg/cm}^2$  to  $2.5 \text{ kg/cm}^2$  and was raised to  $3.5 \text{ kg/cm}^2$  before termination.

The grouting in the weathered zone was done very carefully without increasing the pressure equal to the height of the dam.

The amount of grout consumption in terms of cement bags turned out to be more than 90 bags per hole between the waste weir and chainage 50 as compared to 2 to 5 bags per grout hole on the left flank. The above procedure was implemented only after the reservoir got emptied. The piping portion was plugged with cement concrete.

### u/s Face

To prevent heavy percolation through the upstream face the rip rap was completely removed. The whole area was covered with impervious, double ply polypropylene sheets passing over the top of the dam to around  $1/2 \text{ m.}$  on d/s face from the top. The rip rap was reinstated and was pointed with cement mortar. The same method was used in the inclined portion on either side of the dam.

### Basin

Asphaltic treatment was adopted to prevent seepage of water. The method consisted of scraping the area, placing 2 cm. to 3 cm. thick graded metal and lightly compacting it. 70-80 penetration asphalt was spread at the rate of 5% of the weight of the aggregate. Choke stone was spread and was lightly rolled. Subsequently a thin layer of asphalt was spread on the top and was covered with stone dust. Only some critical part of the basin could be treated before the rains during 1984. This helped

considerably in reducing the percolation as observed during the filling of the dam. See Fig.10. When the dam was completely filled suddenly a pipe appeared increasing the percolation. Subsequently it was observed that the pipe got started on the upper reaches of one of the stream. See Fig.10. With the help of asphaltic treatment and grouting the percolation was reduced to the extent of  $10^{-4}$  to  $10^{-5} \text{ cm/sec.}$  However, as the basin is small and the demand of water is high it was decided to adopt gunniting and sodium silicate treatment to treat the basin to prevent percolation. The streams were treated by gunniting to a considerable distance from the reservoir area.



Fig. 10 View Showing Basin Asphaltic Treatment and Grouting.

### Waste Weir

Waste weir was lined with bricks and was properly plastered. Polythene sheets were used below and around the brick lining to prevent water from percolating. The gap between the brick lining and undulated surface of the blasted waste weir wall was filled up with soil. See Fig. 11, Fig.12, Fig.13 and Fig.14.



Fig. 11 Waste Weir Prior to Lining.

### PERFORMANCE

#### Stability

During the last 2 fillings the dam has not shown

any distress and is stable. See Fig.15.

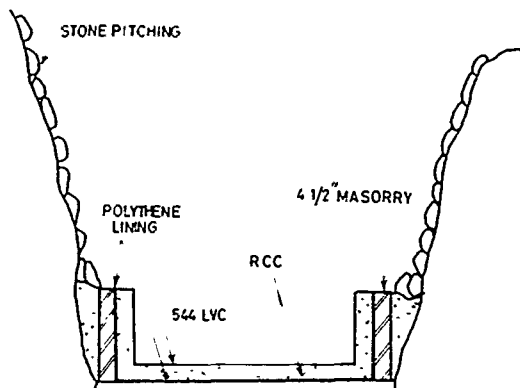


Fig. 12 Cross Section Showing Lining.



Fig. 13 View of Waste Weir After Lining.



Fig. 14 Pointing of the Dam Rip Rap and Gunniting.

#### Percolation

The treatment has reduced percolation to a reasonable degree. The problem of preventing the formation of piping has been done with treating the streams to a considerable distance from the reservoir area.



Fig. 15 Reservoir - Filledup

#### SUMMARY AND CONCLUSION

However, minor may be a dam it is necessary to construct it by adopting all well laid scientific and engineering procedures. Recification of a dam or a reservoir would add to considerable expenditure. The remedial measures adopted in the present case with respect to the stability of the dam are found to be quite satisfactory. The basin treatment with impervious material can be considered as a satisfactory solution to reduce percolation from the floor of the basin.

It is necessary to treat the streams to prevent percolation and formation of piping.

It is possible to develop cheaper basin treatment methods and also construction of stable minor dams to store water at higher elevation in mountainous area.

#### BACKUP LITERATURE

- Katti, R.K. et al. (1972), "Geotechnical Engineering Aspects of Twin City Area", Vol.1 and 2 (I.I.T. Bombay).
- Shearard, J.L.; Woodward, R.J.; Gizzienski, S.F. and Clevenger, W.A. (1963), "Earth and Earth-Rock Dams", John Wiley and Sons, Inc., Newyork, pp.1-725.
- Obert, L. and Duvall, W.I. (1967), "Rock Mechanics and the Design of Structures in Rock", John Wiley and Sons, Inc. New York, pp.1-650.

#### ACKNOWLEDGEMENT

The authors are thankful to authorities of IIT Bombay for constant encouragement.

The help rendered by Shri C.P. Chavan during preparation of the paper is appreciated.

Thanks are due to Miss Ajita T. Parab for typing this paper.

# The Probability of Failure of an in Stages Constructed Embankment on Soft Soil

R.J. Termaat  
Ministry of Public Works, The Netherlands

E.O.F. Calle  
Delft Geotechnics, The Netherlands

R.O. Petschl  
Delft Geotechnics, The Netherlands

**SYNOPSIS:** During construction of the first one of a twin dam in the Oosterschelde basin several instabilities occurred. Design of the construction plan of the dam was based on classical methods of analysis of stability and usually applied safety criteria. Back analysis of the failures consisted of a probabilistic analysis, indicating high overall probabilities of failure, and FEM analysis, indicating areas of large plastic deformation of the subsoil, caused by the steep setup of the sandfill in the initial construction stage, resulting in too concentrated surcharge. Based on these results, it was decided to apply these methods of analysis from the beginning in the design of the construction plan for the second dam. This plan has successfully been carried out.

## INTRODUCTION

In 1976 the Dutch government decided to build an open storm surge barrier in the Oosterschelde estuary, as final part of the Delta plan to protect the central and south west part of the Netherlands from flooding. This open barrier on the one hand will offer sufficient protection and on the other hand preserves the tidal regime in the estuary, which is desirable both from an economical and environmental point of view. Part of the plan was the construction of two separation dams, the Markiezaatskade and the Oesterdam (figure 1), in order to reduce the required number of salt intrusion and navigation locks in the economically important fairway, connecting Rotterdam and Antwerp.



Figure 1. Situation map, south-west part of the Netherlands.

During construction of the Markiezaatskade several instabilities of the soft subsoil occurred, though usually considered factors of safety had been applied in the design of the construction plan. Post analysis has been carried out, using probabilistic analysis of stability and finite element computations to investigate the causes of failure. These

analyses indicated the following conclusions:

- The designed relatively steep slopes of the sandfill caused areas of large plastic deformation in the subsoil, leading to unexpected large settlement of the dam.
- Due to relatively concentrated surcharge relatively small failure circles have been found to be critical, the effect of which is poor averaging of variations of shear strength, resulting in fairly high probabilities of failure (order 10 %).

It was therefore decided to follow a prudent approach in the design of the Oesterdam, and it was considered useful to apply these methods of analysis right from the start in the process of developing a construction plan.

## METHOD OF PROBABILISTIC STABILITY ANALYSIS

The computation model, used for probabilistic analysis of stability of the dam is based on the conceptual model discussed by Calle (1985). Basic components of this model are:

- a Gaussian homogeneous random field description of spatial fluctuations of shearing strength of the soil
- circular potential failure modes and a Bishop type of equilibrium analysis, however, adapted for second moment analysis of random variations of shearing strength.

As a consequence, the stability factor ( factor of safety)  $F$  is no longer a deterministic single valued quantity, but instead a Gaussian random function in the along slope direction specified by its statistics: expected mean value, standard deviation and autocorrelation function. From this, estimates of the probability of occurrence of a zone where  $F < 1$  somewhere along the slope axis and, if this occurs, an indication of the width of such zone, can be obtained.

Apart from spatial variability of shearing strength parameters, considerable uncertainty may be involved in the estimation of hydrostatic and excess pore water pressures in the subsoil stratum. The sources of uncertainty

are:

- Uncertainty about the extreme phreatic level which may occur in the course of time during the various construction stages. Development of the phreatic surface in the core of the dam is strongly related with tidal fluctuations and storm surge levels in the estuary and storm durations. Critical time instants, regarding geotechnical stability of the dam, occur at the moment of low tide following a high setup level during a storm. Estimates of critical phreatic levels have been determined, based on numerical groundwater-flow computations and electrical conductivity analogon experiments. Combined with statistical data on the occurrence of storms, statistical data on the occurrence of critical phreatic levels could be derived. The probability of geotechnical failure was estimated as the sum of conditional probabilities of failure, assuming specific phreatic levels, multiplied by the probabilities that these are extreme critical levels during the considered time span:

$$P_f = \sum_i P_{f|h_i} P(h_i)$$

where  $P_f$  denotes probability of failure,

$P_{f|h_i}$  conditional probability of failure,

given critical phreatic level  $h_i$ , and  $P(h_i)$

probability of  $h_i$  being the extreme level during the considered time span.

- During the construction stages due consideration must be given to excess pore water pressure development in the subsoil. Dissipation of excess pore water pressures, generated during the previous surcharge steps, is expressed in terms of consolidation rate factors, the factor zero denoting an undrained situation and the factor 1.0 complete consolidation. Estimates of these factors were based on numerical computations of the consolidation rate. Due account for uncertainties involved in these estimates was given in the probabilistic analysis of stability by considering a discrete number of sets of consolidation rate factors, symbolically denoted as  $\{A_j\}$  and its associated probabilities of occurrence  $P(A_j)$ , estimated on the basis of empirical data obtained during previous projects. The probability of failure may then be expressed as:

$$P_f = \sum_j P_{f|A_j} P(A_j)$$

or, in the case of uncertainty about the extreme phreatic level:

$$P_f = \sum_i \sum_j P_{f|h_i, A_j} P(A_j) P(h_i)$$

## RESULTS OF ANALYSES OF MARKIEZAATSKADE

During the construction of the Markiezaatsdam failures occurred when the crest level was raised up to MSL + 2.00 m. The geometry shortly before failure is given in fig. 2a. The dam failed by subsidence of the crest, whilst the adjacent sill slightly rose. Before failure

cracks developed at the surface of the sand sill, which widened after the failure. The cracks were parallel to the length axis of the dam. About 4 or 5 days after the first instability a dark strip of blue soft clay could be seen on the edge of the sand sill (fig. 2b).

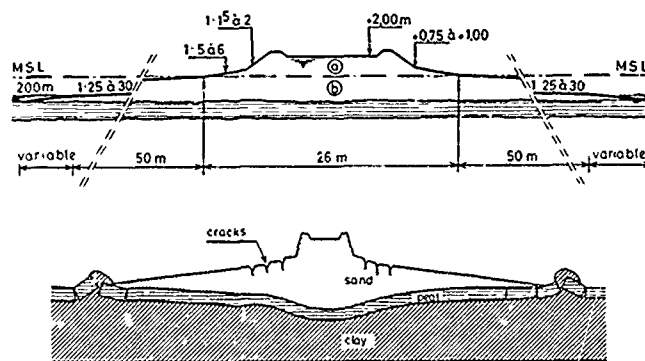


Figure 2. a. Designed cross section of the Markiezaatskade  
b. Observed deformations

The observed failures have been analysed applying a probabilistic stability approach and an elasto-plastic FEM analysis of deformations, i.e. the PLAXIS code (De Borst & Vermeer, 1984). The geometry and water levels applied in the calculations are given in figure 3. The soil properties are summarized in table I.

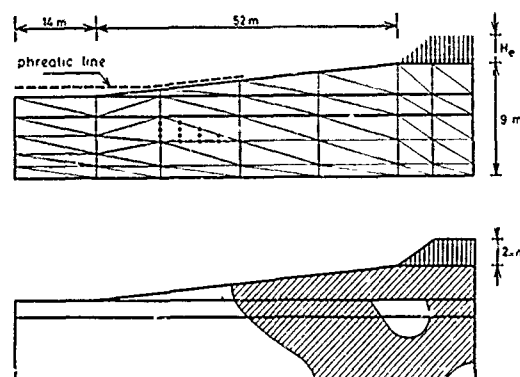


Figure 3. a. Geometry applied in probabilistic stability and FEM analyses

b. Plastic zone found in FEM analysis

Field observations indicated failure by large plastic deformation, resulting in settlement rates of the crest equal to or exceeding the surcharge rates. This could be reconstructed in the FEM calculations, provided that the shear modulus was adequately assessed. A good fit has been found for  $G = 40 C_u$  (fig. 4),  $C_u$  being the undrained shear strength, which corresponds very well with literature data (fig. 5)

TABLE I. Soil parameters Markiezaatskade

| depth<br>m+MSL | soil<br>type    | $\gamma$ | $\phi'$ |          | $c'$  |          | $A$   |          |
|----------------|-----------------|----------|---------|----------|-------|----------|-------|----------|
|                |                 |          | $\mu$   | $\sigma$ | $\mu$ | $\sigma$ | $\mu$ | $\sigma$ |
| -2.55          | peat            | 10       | 23      | 2.3      | 14    | 1.8      | 10    | 5        |
| -4.10          |                 |          |         |          |       |          |       |          |
| -8.60          | organic<br>clay | 15       | 21      | 2.2      | 4     | 0.5      | 45    | 2.5      |
|                | sand            | 20       | 30      | 2.9      | 0     | -        | 100   | -        |

$\gamma$  = unit weight ( $\text{kN/m}^3$ )

$\phi'$  = angle of internal friction ( $^\circ$ )

$c'$  = cohesion ( $\text{kN/m}^2$ )

$A$  = consolidation rate (%)

Plasticity index organic clay:  $88 \pm 22\%$

Statistical parameters:

$\mu$  = expected mean value

$\sigma$  = standard deviation

Correlation parameters  $D_h = 50$  m,  $D_v = 1$  m,

assumed autocorrelation model for shear strength variations:

$$\rho(\Delta x, \Delta z) = \exp(-\Delta x^2/D_h^2 - \Delta z^2/D_v^2)$$

$\Delta x$  being horizontal and  $\Delta z$  vertical lag

In the design an overall factor of safety against stability (Bishop analysis) of 1.15 had been applied, which is fairly low, but considered acceptable because:

- it was within our scope of experiences
- the strength data were based on Dutch cell tests and are generally conservative because in the test procedure limited the deformation rates are applied (Heynen & van Duren, 1979)
- we considered a construction stage in which slight failure would cause only limited damage.

The zone with critical slip circles corresponds with the plastic zone, found in the FEM analysis (Termaat et al, 1985)

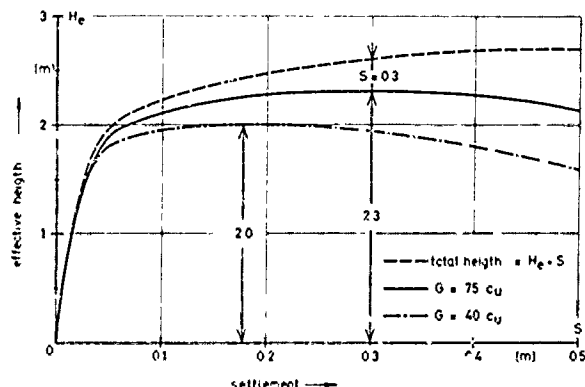


Figure 4. Effective surcharge height vs settlement

The probabilistic stability analyses resulted in a probability of failure of 0.08, which is fairly high. The main reason for it being the small perimeter of the critical slip circle, resulting in poor averaging of strength variations.

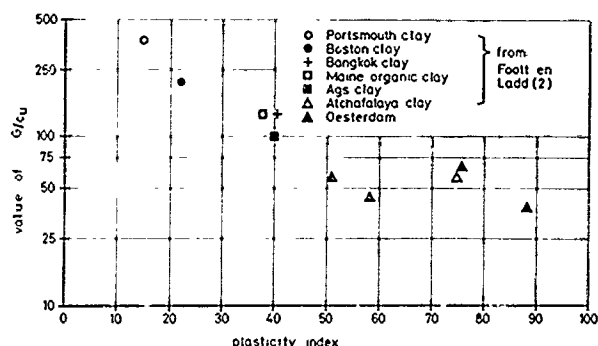


Figure 5. G/Cu ratio vs plasticity index

#### CONSTRUCTION PLAN FOR THE OESTERDAM

A three stage construction plan has been designed, roughly as indicated in figure 6. The stages will be referred to as the hydraulic sanfill stage (0-50 days), the intermediate preloading or consolidation stage (50-230 days) and the stage of final completion.

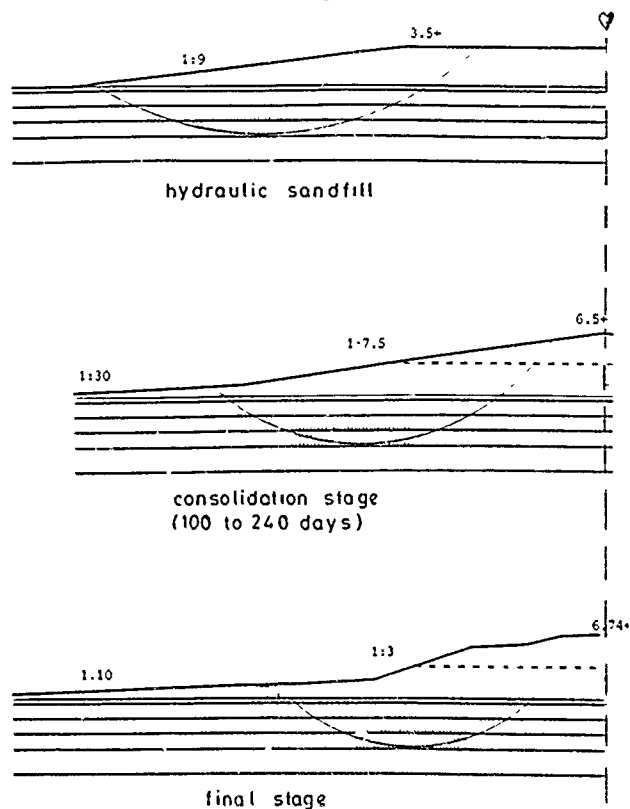


Figure 6. Envisaged construction stages of Oesterdam

The second stage, preloading during nearly one year, was planned to obtain both a sufficient reduction of the deformations and an adequate increase of stability. For each stage the probability of failure was determined with a probabilistic stability analysis for the characteristic section C2 of the dam (fig. 7). Based on this probabilistic approach safety factors for each stage had been determined and applied in the design of the other dam sections. The possibility of failure due to large

plastic deformations has been checked by elasto-plastic finite element analysis.

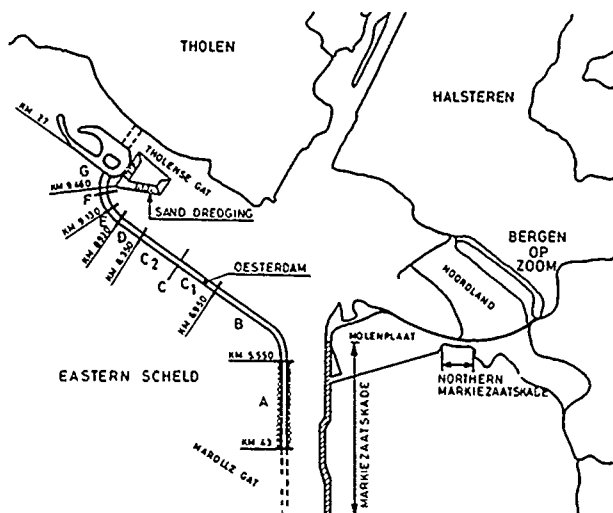


Figure 7. Situation of dam sections

#### SOIL PARAMETERS OESTERDAM

A great number of borings and static cone penetration tests (CPT) have been conducted in the stretch of the Oesterdam. Undisturbed samples were taken at five locations and subjected to compression tests (Dutch cell), oedometer tests and permeability tests. At damsection C2 additional investigation has been carried out, consisting of:

- One  $\phi$  29 mm Begemann type boring (continuous sampling), 1.6 to 9 m below MSL.
- One CPT with the Dutch cylindrical piezo-cone, 1.6 - 13 m below MSL, measuring cone resistance and excess pore water pressures generated at a penetration rate of 20 mm/s.
- Two sensitive CPT's (sensitivity five times as normal), 1.6 to 10 m below MSL.
- Vane tests at seven levels (unremoulded and remoulded).
- Mini-pressuremeter tests.
- Laboratory testing, including determination of sample unit weight, plasticity index of clay samples, and average unit weight per meter depth, determined from the continuous samples.

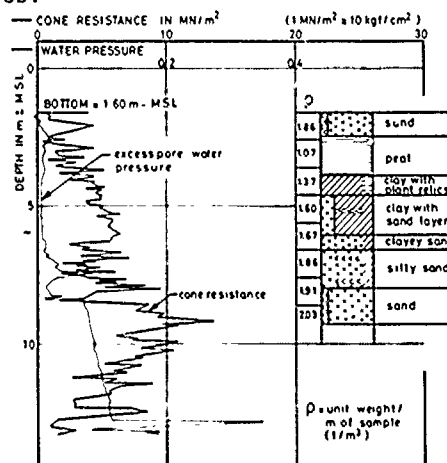


Figure 8. Results of piezo cone test and soil profile from continuous sampling.

A continuous sample profile is given in figure 8, together with the piezo cone measurement results. As can be seen excess pore water pressures indicate the impermeable layers. The results of the sensitive CPT's and the unremoulded shear strengths determined from the vane tests are given in figure 9. In the mini pressuremeter test, a  $\phi$  22 mm cell, mounted on a tube is pushed into the soil. The cell membrane consists of overlapping strips. The elastic shear modulus (G) of the soil is derived from the soil's reaction to volume increase of the cell. The results are summarized in table II. The average cone resistances have been included in this table for comparison.

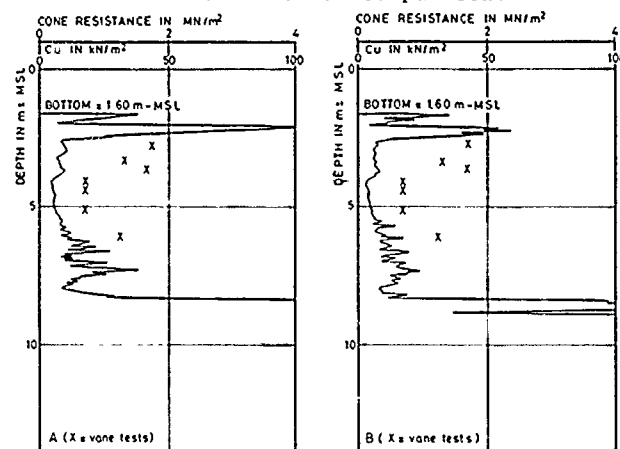


Figure 9. Results of sensitive CPT's and vane tests

TABLE II. Cone resistance and elastic shear modulus.

| depth<br>m - MSL | soil type              | average cone<br>resistance<br>kN/m <sup>2</sup> | G<br>kN/m <sup>2</sup> |
|------------------|------------------------|---|------------------------|
| 2.8              | peat                   | 300   | 550                    |
| 3.4              | peat                   | 250   | 378                    |
| 3.7              | peat                   | 300   | 484                    |
| 4.1              | organic clay           | 150   | 436                    |
| 4.4              | organic clay           | 200   | 392                    |
| 5.1              | silty clay + org. mat. | 200   | 313                    |
| 6.1              | sandy clay             | 400   | 716                    |

In the field vane tests only the unremoulded undrained shear strength was considered. Following Bjerrum (1972), the undrained shear strength has been reduced as function of the index of plasticity (figure 10). Unit weight ( $\gamma$ ), water content (WC), index of plasticity (PI) and results of vane tests ( $C_u$ ), with and without reduction have been given in table III.

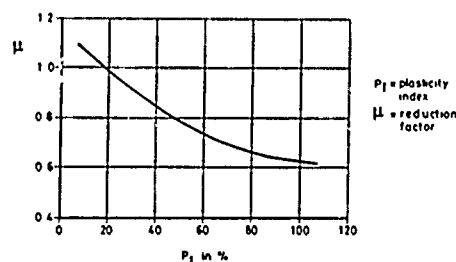


Figure 10. Reduction of undrained shear strength

TABLE III. Undrained shear strength

| Depth<br>m - NAP | $\gamma$<br>kN/m <sup>3</sup> | PI<br>% | WC<br>% | Cu<br>kN/m <sup>2</sup> | $\mu$ | Cu x $\mu$<br>kN/m <sup>2</sup> |
|------------------|-------------------------------|---------|---------|-------------------------|-------|---------------------------------|
| 2.8              | 10.7                          |         | 59      | 44                      |       |                                 |
| 3.35             | 10.5                          |         | 53      | 33                      |       |                                 |
| 3.7              | 10.8                          |         | 51      | 42                      |       |                                 |
| 4.1              | 14.3                          | 76      | 96      | 17                      | .7    | 12                              |
| 4.4              | 15.9                          | 52      | 78      | 17                      | .8    | 14                              |
| 5.1              | 16.5                          | 38      | 60      | 17                      | .9    | 15                              |
| 6                | 18.4                          | -       | 37      | 31                      |       |                                 |

The mean values for cohesion and angle of internal friction, as used in the stability analyses, are based on approximately 10 cell tests for each soil type. The standard deviations have been assessed on the basis of observed scatter in the test results and intuition. The values have been summarized in table IV. Results of the oedometer test are included in this table.

TABLE IV. Soil parameters used in the probabilistic stability analysis (sec. C2).

| top of<br>layer | $\gamma_s$ | $\mu_c$ | $\mu_\phi$ | $\sigma_c$ | $\sigma_\phi$ | $C_p$ | $C_s$ |
|-----------------|------------|---------|------------|------------|---------------|-------|-------|
| 1.5m-MSL        | 20         | 0       | 33         | 0          | 3.3           |       |       |
| 2.5             | 20         | 0       | 30         | 0          | 3             | 100   | 800   |
| 3.4             | 10         | 12.8    | 28         | 2.6        | 5.6           | 4     | 51    |
| 4.3             | 10.5       |         |            |            |               | 5     | 46    |
| 5.7             | 13.5       | 2       | 23         | 0.2        | 2.3           | 8     | 77    |
| 6.5             | 18.9       |         |            |            |               | 83    | 663   |
| 11.0            | 17.7       | 2.4     | 24         | 0.2        | 2.4           | 26    | 439   |
| 13.2            | 19.3       |         |            |            |               | 79    | 301   |

$\gamma_s$  = submerged unit weight (kN/m<sup>3</sup>)

$\mu_c, \mu_\phi$ , mean value of cohesion, friction angle

$\sigma_c, \sigma_\phi$ , standard deviations

$C_p, C_s$  compression constants

Autocorrelation parameters as indicated in table I.

probabilities of occurrence of the corresponding critical phreatic levels do not exactly coincide with the probabilities of occurrence of high tide levels. This has been done to take into account to effects, namely:

- Uncertainty involved in the determination of the phreatic level corresponding to some high tide level, which would cause the probability of occurrence of high phreatic levels to be underestimated.
- In many cases, the low tide level, following a storm, will still be influenced by the storm setup and not reach the normal low tide level. As a consequence the probability of occurrence of the combination of high phreatic level and normal low tide level would be overestimated.

The procedure to take these effects into account is as follows. The probability associated with some critical phreatic level is calculated as the weighed mean of the probabilities of occurrence of the corresponding high tide level, the next higher one and the next lower one, applying weight factors of 0.5, 0.25 and 0.25 respectively.

TABLE V. Water levels and probabilities

| High tide level<br>(including storm setup) |                      | Corresponding critical<br>phreatic level |                      |
|--|----------------------|--|----------------------|
| level                                      | probability          | level                                    | probability          |
|  | 4.3 10 <sup>-7</sup> |  | 2.1 10 <sup>-6</sup> |
| 6.21+MSL                                   | 7.0 10 <sup>-6</sup> | 4.03+MSL                                 | 2.6 10 <sup>-5</sup> |
| 5.36                                       | 8.9 10 <sup>-5</sup> | 3.48                                     | 3.5 10 <sup>-4</sup> |
| 4.51                                       | 1.1 10 <sup>-3</sup> | 2.93                                     | 7.1 10 <sup>-3</sup> |
| 3.66                                       | 2.6 10 <sup>-2</sup> | 2.38                                     | 1.5 10 <sup>-1</sup> |
| 2.82                                       | 5.6 10 <sup>-1</sup> | 1.83                                     | 3.9 10 <sup>-1</sup> |
| 1.97                                       | 4.1 10 <sup>-1</sup> | 1.28                                     | 4.5 10 <sup>-1</sup> |

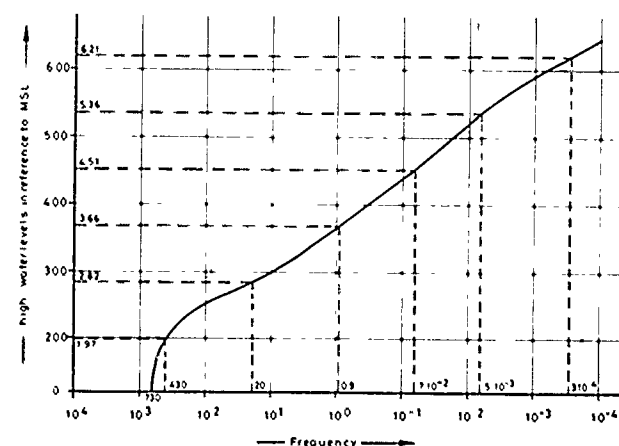


Figure 11. Observed frequencies of high tides

#### CRITICAL PHREATIC LEVELS, HYDRAULIC CONDITIONS

An important aspect of the analysis of stability of the dam concerns assessment of the phreatic water table in the dam. This level is highly influenced by tidal fluctuations and set up due to storms. Due to phreatic storage and limited draining capacity the water table response to tidal fluctuations involves phase shift, causing high phreatic levels at the critical time instants, i.e. at low tide in the estuary. Estimates of the critical phreatic levels have been determined on the basis of numerical calculations and experiments with an electrical conductivity analogon. In table V the determined phreatic levels as function of the corresponding high tide levels have been summarized. The probabilities of occurrence of these high tide levels have been indicated in this table. They have been derived from high tide level frequencies as observed during a number of years (figure 11) and extrapolation of the observed frequency curve. Note that the



The hydraulic conditions applied in the stability analysis, can be summarized as follows. During the hydraulic sandfill stage normal low tide level and completely saturated sandfill. During the consolidation stage and after completion of the dam normal low tide level and critical phreatic levels.

**EXCESS PORE WATER PRESSURES**

Dissipation of excess pore water pressures, induced by surcharging in the various construction stages, has been calculated on the basis of 1-D consolidation analysis. The governing soil properties are compression coefficients as function of effective soil stress (figure 12a) and permeability as function of effective soil stress (figure 12b).

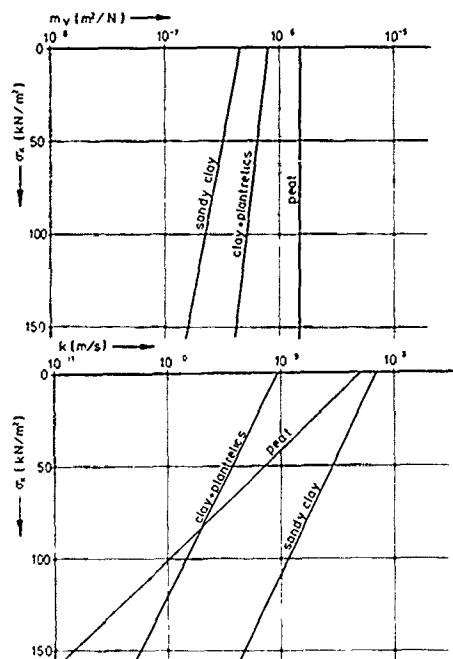


Figure 12. (a) Compression coefficients ( $m_v$ )  
(b) Permeability ( $k$ )

The results of the consolidation analyses, expressed in terms of expected consolidation rates, are summarized in table VI. Estimated standard deviations have been included.

TABLE VI. Expected consolidation rates and estimated standard deviations.

| stage:                      | sandfill | preloading | final   |
|-----------------------------|----------|------------|---------|
| top sandfill<br>(m + MSL):  | 3.5      | 6.5        | 6.0     |
| slope :                     | 1:9      | 1:7.5      | ≈1:4    |
| consolidation<br>rates (%): |          |            |         |
| peat                        | 15 (5)   | 30 (8)     | 40 (10) |
| org. clay                   | 3 (3)    | 10 (3)     | 20 (5)  |
| sandy clay                  | 3 (3)    | 10 (3)     | 30 (8)  |
| sand + clay                 | 5 (5)    | 25 (6)     | 55 (14) |

Parenthesized values indicate standard deviations.  
Predicted hydrodynamic period of preloading stage is 0.5 year.

The indicated consolidation rates reflect expected subsoil adaption at the start of each of the construction stages.

#### CALCULATED PROBABILITIES OF FAILURE

Computations have been carried out for the sandfill and preloading stages and for three subsequent periods of 100 days after completion of the dam. Results of computations for the hydraulic fill stage are summarized in table VII. As mentioned previously complete saturation has been assumed, so only uncertainty concerning the consolidation rates is involved. Weighed summation of conditional probabilities yields an estimate of the probability of failure in this stage of  $5 \cdot 10^{-3}$ . The expected failure width equals 20 - 30 m.

TABLE VII. Results of probabilistic computations for the hydraulic fill stage (Section C2).

| $A_i$           | F    | $P_{f A_i}$         | $P(A_i)$ | L    |
|-----------------|------|---------------------|----------|------|
| $\mu - 2\sigma$ |      | $3 \cdot 10^{-2}$ * | 0.066    |      |
| $\mu - \sigma$  | 1.15 | $8 \cdot 10^{-3}$   | 0.243    | 27 m |
| $\mu$           | 1.18 | $1.5 \cdot 10^{-3}$ | 0.382    | 23 m |
| $\mu + \sigma$  | 1.21 | $3 \cdot 10^{-4}$   | 0.309    | 21 m |

$\mu$  : expected consolidation rate  
 $\sigma$  : standard deviation of consolidation rate  
F : expected mean factor of safety  
 $P_{f|A_i}$  : conditional probability  
 $P(A_i)$  : probability of consolidation rate  $A_i$   
L : expected failure width  
\* extrapolated value

The results of computations for the consolidation stage are summarized in table VIII. In this stage both consolidation rate and extreme phreatic level are considered uncertain. The conditional probabilities, given a specific phreatic level in table VIII, have been determined accounting for uncertainty of consolidation rates similar to the procedure applied for the hydraulic fill stage. The intermediate results however have been omitted for reasons of space limitation. Weighed summation of failure probabilities yields an estimate of the probability of failure of  $8 \cdot 10^{-5}$  during the consolidation stage.

TABLE VIII. Probabilities of failure during the consolidation stage (Section C2).

| $h_p$      | F    | $P_{f h_p}$         | $P(h_p)$ | L       |
|------------|------|---------------------|----------|---------|
| 3.75 + MSL | 1.19 | $2.5 \cdot 10^{-3}$ | 0.001    | 20-35 m |
| 3.20       | 1.24 | $1.5 \cdot 10^{-4}$ | 0.015    | 20-30 m |
| 2.65       | 1.29 | $1.4 \cdot 10^{-6}$ | 0.813    | 15-20 m |
| 2.10       | 1.34 | $1.4 \cdot 10^{-7}$ | 0.023    | 10-15 m |
| 1.55       | 1.40 | $< 10^{-7}$         | -        | 10-15 m |

TABLE VIII. Continued

|            |   |
|------------|---|
| $h_p$      | = phreatic level (m + MSL).   |
| $P(f h_p)$ | = Conditional probability of failure.                                   |
| $P(h_p)$   | = Prob. that $h_p$ is the extreme level during the considered timespan. |
| $F$        | = Expected mean of factor of safety.                                    |

Similar computations have been carried out for the final stage, after completion of the dam. Three subsequent periods of 100 days have been analyzed. The intermediate results of the computation are omitted, the final results are given in table IX.

Table IX. Probabilities of failure after completion of the dam (section C2).

| Period         | F    | $P_f$             | L          |
|----------------|------|-------------------|------------|
| 0 - 100 days   | 1.20 | $5 \cdot 10^{-2}$ | 30 - 100 m |
| 100 - 200 days | 1.27 | $5 \cdot 10^{-3}$ |            |
| 200 - 300 days | 1.30 | $4 \cdot 10^{-4}$ |            |

## OBSERVED CONSOLIDATION RATES AND SETTLEMENTS

At five locations in the stretch of the dam Kistler type piezometers and settlement gauges have been installed, to monitor excess pore pressure dissipation and settlement. In the pilot section C2 seven piezometers, measuring pore water pressures in the sandfill, the deep sand and in the cohesive layers. Results of these measurements are plotted in figure 13.

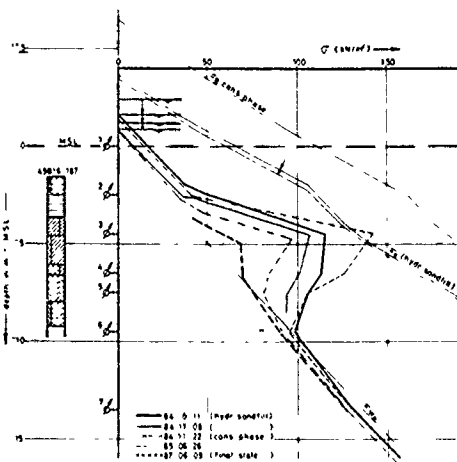


Figure 13. Observed pore water pressures in dam section 2.

From these measurements the consolidation rates have been determined, as indicated in figure 14. It is concluded that the dissipation rates were much greater than expected, and that the envisaged consolidation stage of 130 days was substantially more than actually required.

The settlements have also been measured and compared to the expected settlements, revealing a similar tendency, however no indication has

been found that the final settlements will substantially differ from the predicted ones.

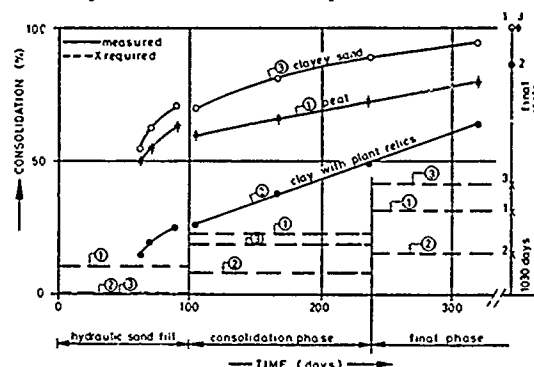


Figure 13. Observed consolidation rates.

The observed rapid development of excess pore pressure dissipation indicates that consolidation rates have been considerably underestimated. The actual consolidation rates even exceed the optimistic ( $\mu + \sigma$ ) levels. Based on this observation the following (posterior) adjustments of the probabilities of failure could be made: for the consolidation stage  $P(f) < 10^{-6}$  and for the first 100 day period after completion  $P(f) < 3 \cdot 10^{-6}$ , based on the conditional probabilities of failure assuming ( $\mu + \sigma$ ) consolidation rates.

## PLASTIC DEFORMATIONS

Figure 14 shows the development of zones of plastic shear when applying ultimate loading. Computed crest settlements versus surcharge are shown in figure 15, revealing an ultimate surcharge height of 7 m. The actually applied surcharge height was 4.5 m.

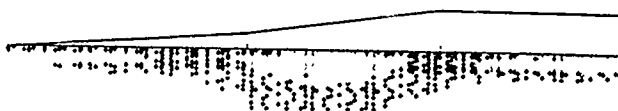


Figure 14. Zones of plastic shear as computed by FEM analysis.

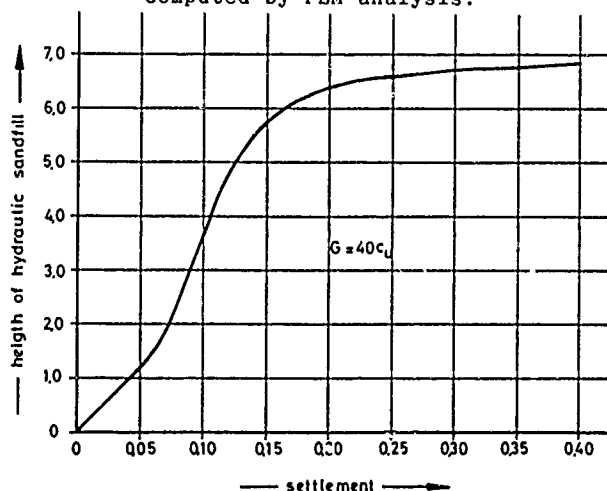


Figure 15. Height of sandfill vs settlement.

## OVERALL SAFETY FACTORS

The computed prior probabilities of failure were considered acceptable, at least as far as the first and second construction stage are concerned. Hence, the use of corresponding factors of safety was considered acceptable in the design for the other sections of the dam, since no substantially different subsoil strength and dissipation behaviour was expected. The applied factors of safety were 1.15 for the hydraulic fill stage and 1.20 for the consolidation stage.

## CONCLUSIONS

- Steep setup of the sandfill of the Markiezaatskade is considered the main cause of failure due to plastic deformation. This mechanism was found much less relevant for the Oesterdam, because of the flat slopes of the sandfill envisaged in the design.
- Identical factors of safety, applied in the design of both Markiezaatskade and Oesterdam, led to substantially different probabilities of failure. The reason for it being the smaller slip circle, in case of the Markiezaatskade, leading to poor averaging of strength variation and thus a high probability of failure.
- Based on the observed high consolidation rates, it would have been possible to reduce the envisaged preloading period. This adjustment of the design has not been considered.
- In the construction of embankments on soft soil with high plasticity index, attention should be paid to large plastic deformation.
- The factor of safety, as determined in classical stability analysis, is less decisive regarding safety as is generally assumed.

## ACKNOWLEDGEMENT

We would like to thank Dr P.A. Vermeer, Mr. R. J. Ernst and F. de Graaf, lecturer and students of the Delft University, who executed the FEM calculations, and Mr. G. Vergeer of the Dutch Ministry of Public Works for his contribution to this research.

## REFERENCES

- Bjerrum, L. (1972), "Embankments on soft Ground", Proceedings of Speciality Conference of Earth and Earth Supported Structures, Volume III.
- Borst, R. de & P.A. Vermeer (1984), "Possibilities and Limitations of Finite Elements for Limit Analysis", Geotechnique 34, no. 2.
- Calle, E.O.F. (1985), "Probabilistic analysis of stability of earth slopes", Proc. XIth ICSFME, San Francisco.
- Heynen, W.J. & F.J. van Duren (1979), "The Dutch Cell Test, Comparison of Results of Cell Tests and Triaxial Tests on Clay", Proc. VIIth ECSMFE, Brighton U.K., volume 2.
- Termaat, R.J., P.A. Vermeer & G. Vergeer (1985), "Failure by large plastic deformations", Proc. XIth ICSMFE, San Francisco.

## Dike Reconstruction Polder Oudendijk

J.A. van Herpen

Civil Engineer, Oranjewoud B.v., Oosterhout, The Netherlands

J. de Pee

Civil Engineer, Province of Friesland, Leeuwarden, The Netherlands

**SYNOPSIS:** Reconstruction of dikes on soft subsoil is a common practice in the Netherlands. However in recent years some slidings of innerslopes have occurred in the execution phase due to very large and rapidly placed replenishments. Therefore investigations have been made for new methods to determine the short term stability of the soil structures. This paper describes the problems experienced during the reconstruction of a polder dike in the western part of the Netherlands, based on which several new methods are tested.

### INTRODUCTION

The dike of the polder Oudendijk protects a low-lying area (polder) in the western part of the Netherlands. The water level inside the polder is approx. 4.5 m below the constant normal outside water level. In case of a breach the inundation depth will be 3 m. This will not only cause severe damage to economic activities in the polder (mainly farming and some small factories) but also endanger the lives of the 5000 people living in the village of Woubrugge.

Reconstruction of a section of appr. 3 km of the dike appeared to be necessary. Due to the constant settlement of the subsoil in the course of years the crest level had become too low. In some places it was even below the normal outside water level and flooding had to be prevented by a small bund placed on the crest. Furthermore, preliminary investigations also showed insufficient geotechnical stability of the inner-slopes (COW 1974). At the design outside water level, which lies 0.30 m above the normal level, the safety factor, calculated using a normal slip circle analysis, was 0.79. The lowest factor found at the normal outside water level was 1.10. Extensive seepage occurred. Vast parts of the innerslope were not even practicable, Figure 1.

### GEOTECHNICAL INVESTIGATIONS

Given the expected large replenishments of the innerslope and the soft subsoil conditions a vast geotechnical investigation was set up to achieve a firm basis for the reconstruction design.

First a visual inspection of the dike was carried out. Based on its results 12 locations (cross-sections) were selected for further investigation. This was done in two stages: a preliminary investigation to establish the quality of the existing dike, and an additional investigation to gather sufficient information for the actual reconstruction design. Soil borings (percussion method) and cone penetration tests were carried out to obtain information about the subsoil. To establish the phreatic line in the dike standpipes were placed. Totally 39 soil borings were executed varying in length



Fig. 1 Seepage at the innerslope

between 3.5 m (inner toe) and 11.5 m (crest) and 5 penetration tests (12 m). A number of 49 standpipes was placed.

In every cross-section at least 3 borings and 4 standpipes were considered to be necessary. From the borings undisturbed samples were taken which were used for laboratory-tests. From each sample the soil type, the unit weight (wet and dry), the water content and voids ratio were established. The friction properties of the soil under consolidated conditions (angle of internal friction and cohesion) were defined based on 35 compression tests and 28 direct shear tests. To investigate the consolidation properties 32

tests were performed. The permeability was tested for 15 samples.

On the basis of the results of the site investigation a geological profile along the dike section is composed (Oranjewoud 1987), Figure 2.  
At a depth of 11.20 - 12.20 m below the reference level N.A.P. sand formations formed during the late-pleistocene are present above which a thin layer of peat varying between 0.3 and 0.9 m is found.  
Besides a clay layer (holocene deposits) varying in thickness between 4 and 6 m on which a 3 - 5.5 m thick layer of peat can be found. The clay layer contains relatively a high quantity sand in the lower sections and vegetation remains in the upper sections.  
The upper layer, which is in fact the dike body, strongly varies in composition and thickness: besides peat, also sand, clay and debris are present. Human activities have strongly influenced this layer.

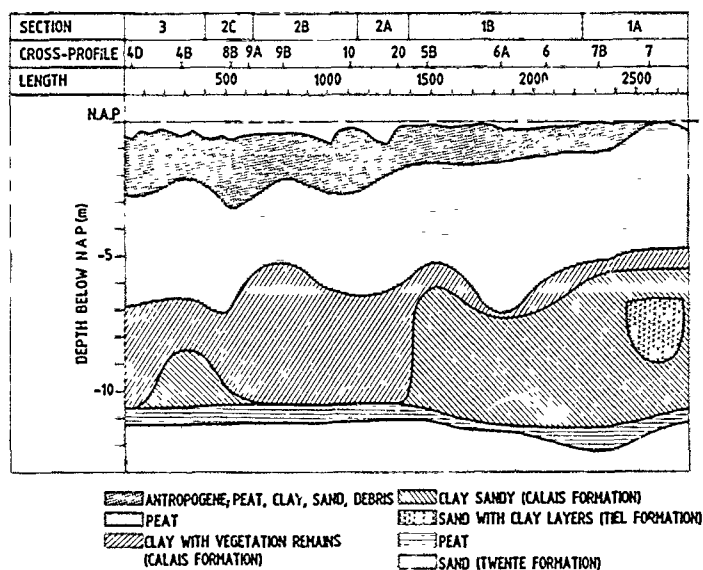


Fig. 2 Geological profile of the dike of polder Oudendijk

To give an indication of the soil properties in Table 1 the results of the laboratory tests carried out on the samples taken from the additional site investigation are shown.

TABLE 1 Results from laboratory tests (mean values)

| Soil type          | Volume weight (kN/m <sup>3</sup> ) | Angle of internal friction (dgr) | Cohesion (kN/m <sup>2</sup> ) | Compression modulus | Permeability (m/s)   |
|--------------------|------------------------------------|----------------------------------|-------------------------------|---------------------|----------------------|
| Antropogene        | 12,6                               | 20,7                             | 6,5                           | 8,8                 | $1,3 \cdot 10^{-7}$  |
| Peat               | 10,2                               | 20,8                             | 4,7                           | 4,2                 | $1,5 \cdot 10^{-6}$  |
| Clay, veg. remains | 13,9                               | 25,5                             | 2,6                           | 9,1                 | $2,9 \cdot 10^{-9}$  |
| Clay, sandy        | 16,8                               | 25,5                             | 1,9                           | 22,3                | $7,7 \cdot 10^{-10}$ |

Not only longitudinal variation in the geological stratification is found but also perpendicular to the axis of the dike.  
An example is given in Figure 3.

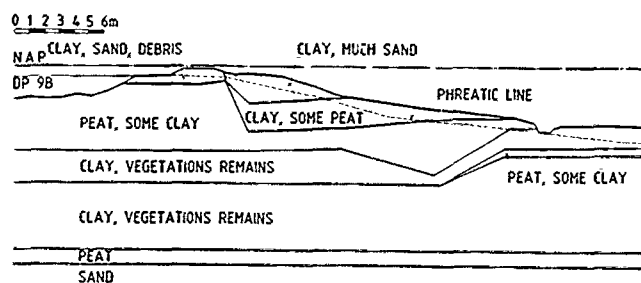


Fig. 3 Bottom schematization cross-section 9B

The geological investigation carried out was for Dutch circumstances very extensive, even for the type of dike considered in this paper, where the bottom profile varies within short ranges.  
However, as was experienced later on, it appeared to be insufficient.  
Local variations did occur which were not detected.

## RECONSTRUCTION DESIGN

### Design criteria

The design of the dike should meet to the following criteria:

- the dike should fulfill the criteria for a period of at least 20 years;
- the crest level should lie at least 0.50 m above the normal outside water level;
- the geo-technical stability has to be sufficient;
- seepage has to be reduced;
- if possible the highly-valued vegetation, that occurs on a 350 m long section of the innerslope should be preserved.

The stability of the dike can be improved and the seepage can be reduced by replenishments of the innerslope as well as by lowering the phreatic-line in the dike body. The latter can be obtained for example by an impermeable screen at the crest of the dike or a drainage system at the innerslope.

A significant reduction of the phreatic line however causes large additional settlements which on their turn lead to an extra crest-elevation.  
Since the crest has to be heightened anyway the method of innerslope-strengthening is chosen. The replenishments were carried out with sandy clay that is more permeable than the subsoil on which it is placed, is sufficient resistant to erosion and allows a good grass-growth.

### Crest-height

Settlement calculations were necessary to establish the crest height in such a way that in twenty years it would not become lower than the design level.

The calculation method applied was according to Terzaghi's formula:

$$z = \frac{h}{C} \ln \left( \frac{p_2}{p_1} \right) \quad (1)$$

In which:  $z$  = settlement (m)  
 $h$  = thickness of the soil-layer (m)  
 $C$  = coefficient of compressibility  
 $p_1$  = effective stress before loading (kN/m<sup>2</sup>)  
 $p_2$  = effective stress after loading (kN/m<sup>2</sup>)

For the peat layers use has been made of the adaption by Fokkens (Soudyn 1972):

$$z = \frac{h}{C + 1,5 \ln \left( \frac{p_2}{p_1} \right)} * \ln \left( \frac{p_2}{p_1} \right) \quad (2)$$

The existing cycle-track on the crest had to be replaced. The settlement calculations were carried out for several types of road construction varying in weight. The construction chosen was a top-layer of 0.08 m of asphaltic-concrete on a sub layer of 0.40 m of foam-slugs. Table 2 shows the results of the calculations for several cross-sections:

TABLE 2 Results of settlement-calculations  
 (\* = N.A.P. = the ordnance-datum)

| Cross-section<br>(no.) | Former crest-level<br>(m - N.A.P.)* | New crest-level<br>(m - N.A.P.)* | Expected settlement in<br>20 years<br>(m) | Percentage<br>of final<br>settlement |
|------------------------|-------------------------------------|----------------------------------|---|--------------------------------------|
| 8b                     | -0,60                               | +0,60                            | 0,70                                      | 93                                   |
| 9a                     | -0,49                               | +0,75                            | 0,85                                      | 96                                   |
| 9b                     | -0,42                               | +0,30                            | 0,40                                      | 87                                   |
| 10                     | -0,21                               | +0,40                            | 0,50                                      | 92                                   |
| 4b                     | -0,51                               | +0,20                            | 0,30                                      | 98                                   |
| 4d                     | -0,61                               | +0,40                            | 0,50                                      | 99                                   |

To increase settlements a temporary extra crest-elevation of 0.50 m was executed which after two years was excavated. This results in a decrease of rest-settlements.

### Stability

Under stability is meant the resistance against sliding of large parts of the dike body along a straight or a curved plane in which due to overloading no equilibrium of forces may be present (TAW 1985).

The method commonly used is based on a circular sliding surface where the potential failure mass is divided into slices.

The safety factor is defined by the ratio of the moment of shear along the failure plane and the moment of weight of the failure mass.

The objective is then to find the centre and radius of the circle with the lowest safety factor.

In this project use has been made of the simplified Bishop Method of Slices in which it is assumed that the resultant of the vertical forces acting on the sides of any slice is zero.

The shear force, needed to determine the moment of shear at a certain point of the slide-plane, is determined by:

$$\tau_{\max} = \frac{c' + \sigma_v' * \tan \phi'}{1 + \frac{\tan \phi' * \tan \alpha}{F}} \quad (3)$$

In which:  $\tau_{\max}$  = the maximum shear force (N/m<sup>2</sup>)  
 $\sigma_v'$  = the effective pressure acting on the slide plane (N/m<sup>2</sup>)  
 $\phi'$  = the angle of internal friction (dgr)  
 $c'$  = the cohesion (N/m<sup>2</sup>)  
 $F$  = safety factor  
 $\alpha^*$  =  $\alpha$  for  $\alpha > -\frac{1}{2}\pi + \frac{1}{2}\phi'$   
 $\alpha^*$  =  $-\frac{1}{2}\pi + \frac{1}{2}\phi'$  for  $\alpha \leq -\frac{1}{2}\pi + \frac{1}{2}\phi'$   
 $\alpha$  = the angle between the horizontal and the tangent of the slide-circle

The above mentioned conditions for  $\alpha$  prevent the shear force from obtaining extreme values in the passive zone ( $\alpha$  = negative in the passive zone).

The design dike profile is determined using the Bishop-method in which the shear stress is calculated under drained circumstances. The criteria is that the minimum safety factor is 1.3.

The calculations are carried out for 11 cross-sections. Figure 4 shows an example for one section.

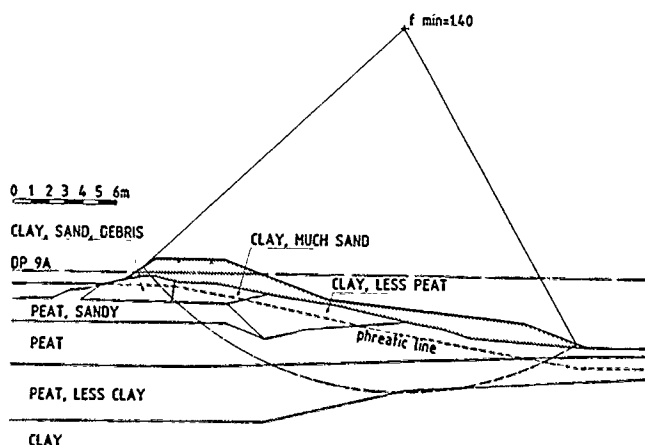


Fig. 4 Necessary replenishment and minimum slide-circle for cross-section 9a

Over a section of 1.3 km it was necessary to excavate a part of the toe of the dike and replace it by sand. Thus not only the stability was improved but also the seepage moved from the innerslope to the toe.

A distinction has to be made between the short and long term stability, or the design and execution stability. In case a rather impermeable subsoil (clay, peat) is present the placing of extensive innerslope replenishments may cause very high excess pore water pressures which will only slowly reduce and result in a proportional increase of the effective pressures. This means that in these cases the short term stability is generally decisive (De Pee, 1986).

To establish the execution-stability a common method in the Netherlands was to use the geotechnical parameters ( $\phi'$ ,  $c'$ ) under drained conditions. The short term effect is achieved by applying an extra hydraulic pressure for the less permeable subsoil layers similar to the weight of the replenishment. This means that the effective vertical stress used to determine the shear stress is equal to the effective vertical stress present just before the loading.

Although no criteria are present for the execution phase it was attempted to obtain a minimum safety factor of 1.2.

These calculations showed that the total replenishment could be carried out in one stage. However it was decided to strengthen first the innerslope and to heighten the crest afterwards.

## THE SLIDINGS

Nevertheless in the last phase of the work two slidings of the innerslope took place both appr. 24 hours after replenishing, Figure 5.

Immediately after detection security measurements were taken consisting of bringing extra soil, also from the crest, to the toe of the dike, placing a ship in front of the danger-zone and installing a drainage system to discharge the water in the dike body as quickly as possible.

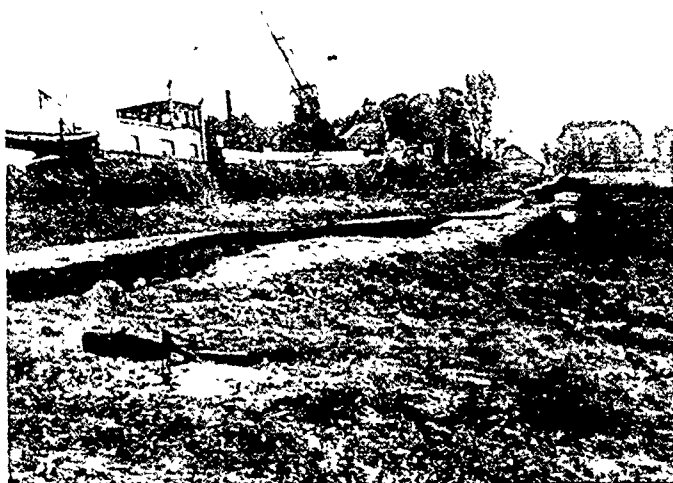


Fig. 5 Sliding of the innerslope of the dike

In order to detect the cause of the slidings additional soil borings, laboratory tests and stability calculations were carried out. With the help of visual interpretations, geological measurements and the borings the extent and shape of the slidings were estimated. The slide planes seemed to be rather circular. Also some horizontal displacements in the direction of the polder took place.

Two major causes for the slidings were derived:

1. compared to the geological profile extreme differences are detected, especially in the upper bottom layers. These mainly originate from human activities, such as former repairs of old slidings, old drainage tubes, etc.;
2. the calculation method did not correspond adequately to reality.

In order to elaborate the second cause, an alternative technique to establish the stability of soil structures in the execution phase was tested.

For this a team was formed consisting of members of the responsible water authority, the consultants, the Delft University of Technology and the Dutch Ministry of Public Works.

In this technique, named the  $c_u$ -method, which is already applied in many other countries, use is made of the undrained shear strength of the soil.

It is assumed that the poorly permeable subsoil-layers behave under undrained circumstances as frictionless material ( $\phi = 0$ ) with an apparent cohesion  $c_u$ . The value for  $c_u$  for normally consolidated soil is estimated with the help of the following derivation (Vermeer, 1983):

$$c_u = \frac{1}{2} (\sigma'_v + \sigma'_h)_0 * \sin \phi' + c' * \cos \phi' \quad (4)$$

In which:  $(\sigma'_v + \sigma'_h)_0$  = the sum of the vertical and horizontal effective stresses present just before loading

The horizontal effective stress can be estimated by:

$$\sigma'_h = (1 - \sin \phi') \sigma'_v \quad (5)$$

The  $c_u$ -value also can be found using (Termaat 1985):  
- the Skempton Formula:

$$c_u = (0.11 + 0.0037 * I_p) \sigma'_{v0}$$

in which:  $I_p$  = the plasticity index

- vane tests
- direct shear tests

Additional stability calculations are carried out using two methods based on this technique. The results are compared to those obtained from the previous described method in which drained conditions and  $\sigma'_v = \sigma'_{v0}$  are used. The first method is a normal slide-circle analysis according to Bishop in which  $\phi = 0$  and  $c = c_u$  are taken. In the second method the equilibrium of stresses in each element of the soil related to the highest possible loading is established. Owing to the static undetermined nature of the soil then also the deformation properties have to be taken into account.

Use has been made from the finite elements computerprogramme Plaxis that is based on an elasto-plastic behaviour of the soil. Failure is determined by a so-called flow-criterion derived from the Mohr-Coulomb stress-shear relation:

$$f = \tau^* - \sigma^* * \sin \phi' - c' * \cos \phi' \quad (6)$$

$$\tau^* = \left( \frac{1}{2} (\sigma'_{xx} - \sigma'_{yy})^2 + \sigma'^2_{xy} \right)^{\frac{1}{2}} \quad (7)$$

$$\sigma^* = \frac{1}{2} (\sigma'_{xx} + \sigma'_{yy}) \quad (8)$$

In which:  $f$  = flow-criterion  
if  $f = 0$ : plastic soil behaviour  
if  $f < 0$ : elastic soil behaviour

$\sigma'_{xx}$ ,  $\sigma'_{yy}$  = normal effective stresses  
 $\sigma'_{xy}$  = shear stress

The results of the stability calculations are given in Table 3.

TABLE 3 Results of stability calculations of failures

| Calculation method                                     | Safety factor |               |
|--|---------------|---------------|
|  | Sliding no. 1 | Sliding no. 2 |
| Slide circle drained<br>( $\sigma'_v = \sigma'_{v0}$ ) | 0,90          | 0,98          |
| Slide circle undrained                                 | 0,81          | 0,84          |
| Plaxis undrained                                       | 0,81          | 0,84          |

Figure 6 shows the slip-circles for the second sliding observed at the spot as well as found by means of calculations.

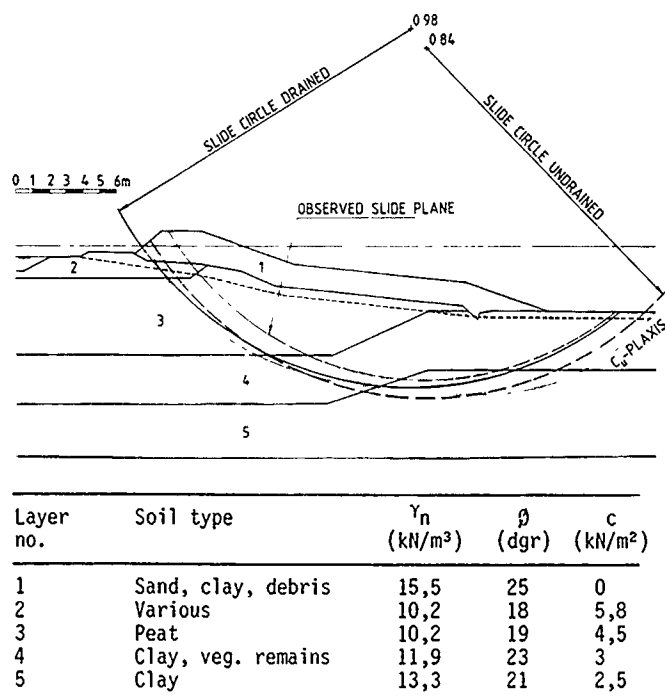


Fig. 6 Slide-circles for the second instability

Contradictory to the slide-plane methods the critical plane in Plaxis is found as result of the calculations. Figure 7 shows the displacement increments at failure. It has to be noted that not an exact circular slide plane is found.

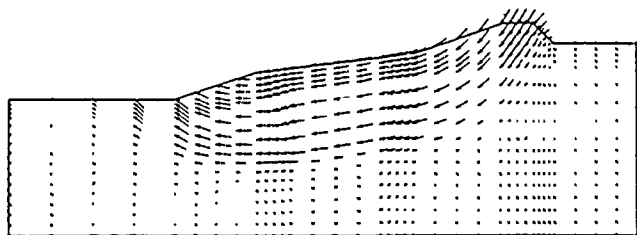


Fig. 7 Displacement increments for the second sliding

The calculated failure circles are rather comparable, Figure 6.

Also the safety factor determined with the  $c_u$ -method.

The safety factor established with the method in which drained soil parameters and hydrodynamical pressures are used gives much higher values. Especially at the passive section of the slide-plane (the toe of the dike) this method takes into account to favourable values for the shear strength. It is found that large groundwater pressures occur far beyond the dike profile which cannot be explained from a normal elastic theory.

In Figure 7 the results of measurements from waterpressuremeters in an other cross-section of the dike are given. It proved that the raise of the hydraulic pressure in the meters 1 and 2 passably corresponds with the weight of the loading; meter 3 however shows extensive pressures beyond the toe of the dike. The latter is taken into account by the  $c_u$ -method.

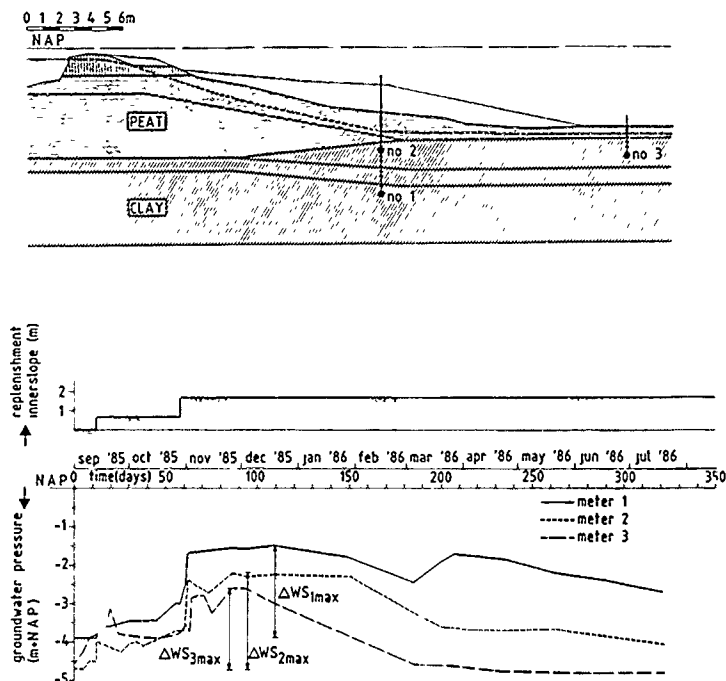


Fig. 8 Waterpressure measurements in cross-section 17a

## CONCLUSIONS

Since variations in the subsoil can occur within short distances not only along the dike-axis but also perpendicular to this it is for this kind of dikes very important that geotechnical investigations are carried out in such a manner that discontinuities can be detected adequately.

The short term stability (execution phase) is decisive. Using a slip circle analysis and taking into account drained soil properties and hydrodynamic pressures corresponding to the weight of the replenishment ( $\sigma'_v = \sigma'_{v0}$ ) results in high safety factors.

The method that applies to the apparent cohesion of the soil gives much lower values and has also a better theoretical background. Also the large pore water pressures occurring beyond the dike-toe are taken into account.

A slide-circle calculation according to the  $c_u$ -method can be carried out very easily and in case of circular slide



planes provides the same results as the more advanced finite element method.

#### ACKNOWLEDGEMENTS

The authors wish to thank Dr. Ir. P.A. Vermeer of the Delft University of Technology and Ing. R.J. Termaat of the Ministry of Public Works not only for their support to this paper but certainly also for their initiative to evaluate the slidings that occurred during the reconstruction of the dike by means of undrained stability theories.

#### REFERENCES

C.O.W. (1974), "Onderzoek naar de veiligheid van de boezemkade van de polder Oudendijk", Centrum voor Onderzoek Waterkeringen, The Hague, rep.no. A-74.008.

Oranjewoud (1987), "Kadeverbetering Polder Oudendijk", Oosterhout.

Soudijn, B.J.J. and R.A.J. de Kock (1972), "Compendium Geo-Tubomechanica", Provincie Zuid-Holland, The Hague.

TAW (1985), "Leidraad voor het ontwerpen van rivierdijken - deel 1 boven rivierengebied", Technical Committee on Waterdefences, The Hague.

Pee, J. de (1986), "Een Toetsing voor de Uitvoeringsstabiliteit", Section Geotechnique, Department of Civil Engineering, Delft University of Technology, nr. 269.

Vermeer, P.A. (1983), "Materiaalmodellen in de grondmechanica", Section Geotechnique, Department of Civil Engineering, Delft University of Technology, nr. b27.

Termaat, R.J., P.A. Vermeer and G.H.J. Vergeer (1985), "Failure by large plastic deformation", Proceedings of the 11th international conference on soil mechanics and foundation engineering.

# Evaluation of the Failure of an Important Dike in The Netherlands

J. Dekker

Senior Project Engineer, Delft Geotechnics, The Netherlands

**SYNOPSIS.** Flood embankments are extensively used in the lower Meuse-Rhine delta to contain the rivers & to protect the towns & the polders below mean sea level. Stability of these embankments is by their nature crucially important & has to be considered under a variety of conditions, from their staged construction or strengthening to their long term behaviour. In 1984 the landside slope of such a recently heightened & enlarged embankments constructed on a weak post-glacial peat & clay deposit, failed over a length of about 100m causing the demolition of 4 houses & necessitating extensive stabilization works. A precise analysis of the excess pore pressure monitored at its toe from the start of execution revealed unexplainably high pore pressures, which had been induced during a previous loading phase about 1 year before the failure. The measured increase of pore pressure was 2-3 times greater than indicated by elastic calculations. Stability analyses according to Bishop's simplified method could not give a satisfactory explanation for the failure. An extensive investigation on the causes of their failure has been carried out. The results of a back calculation of the induction & dissipation of the excess pore pressure using non-linear material models implemented in FEM codes will be compared with a classical approach, based on Bishop's circular slip method and linear elastic material models.

## 1. CONVENTIONAL STABILITY ANALYSIS

The design of an embankment reinforcement, based on various boundary conditions, always needs to be tested by criteria, which are directly related to the possible embankment failure mechanisms.

Besides the judgement of the long term stability of the embankment (fully consolidated situation), the stability during the various construction phases also needs to be analysed. The importance of these analysis is two-fold:

1. check whether the safety against an embankment failure is sufficiently satisfied.
2. check whether the envisaged embankment can be realized technically and economically within the available area.

In the Netherlands, stability analysis of staged constructions are performed with Bishop's simplified method in terms of effective stresses. The shear resistance is given by Coulomb's Law

$$\tau_u = c' + \sigma_n' \tan \phi' \quad (1)$$

in which  $c'$  and  $\phi'$  are the drained cohesion and friction angle evaluated from Dutch cell tests and  $\sigma_n'$  the effective normal stress. In Bishop's method, the effective normal stress and the ultimate shear resistance at the bottom of a slice are linear functions of the effective vertical stress  $\sigma_v$  (Bishop, 1955), which is given at any moment by

$$\sigma_v' = \sigma_{v0}' + \sum \Delta \sigma_{vi} \cdot U_{pi}(t) \quad (2)$$

The initial vertical stress ( $\sigma_{v0}'$ ) and the increase of the total vertical stress due to layer  $i$  ( $\Delta \sigma_{vi}$ ) follow directly from the weight of the slice above the chosen slip surface. The consolidation percentage  $U_{pi}(t)$  at time  $t$  after loading  $i$  follows from a one dimensional Terzaghi type consolidation analysis (in the case of prediction type design calculations) or from measured consolidation percentage with the piezometers (in the case of control calculation during construction or in the case of post diction type back calculations). In the design phase, the construction rate shown on fig. 2 has been established in order to ensure the required factor safety  $F_s = 1.2$  at any moment.

During construction excess pore water pressures are measured under or close to the embankment. The measurements are compared with the expected values, to investigate whether the consolidation process is in accordance with the design assumptions.

A method has been developed, which simply allows to control whether the measured excess pore pressures do not exceed the maximum allowable values during the various construction stages (the "red line").

The guidance of the construction using these "red lines" gives an impression of the stability during the various construction phases. The "red lines" are based on the equilibrium analysis as deduced from an elastic stress analysis for the various construction phases. The graphical presentation is such, that a relation is derived between the height of the embankment under construction and the maximum allowable excess pore pressures.

Moreover the maximum expected increase of the excess pore pressures due to the various loading steps is also presented graphically. Hence at any construction stage, it can be judged directly, whether it is justified to continue raising the embankment.

## 2. DIKE CROSS SECTION AND SEQUENCE OF EVENTS

The construction of the embankment reinforcement at Streefkerk (see figure 1) has started in August 1982.

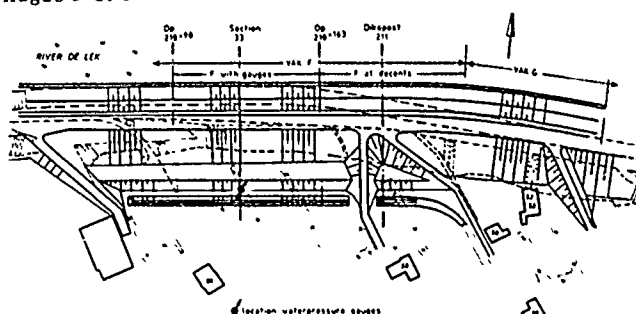


Fig. 1. Location of the embankment failure

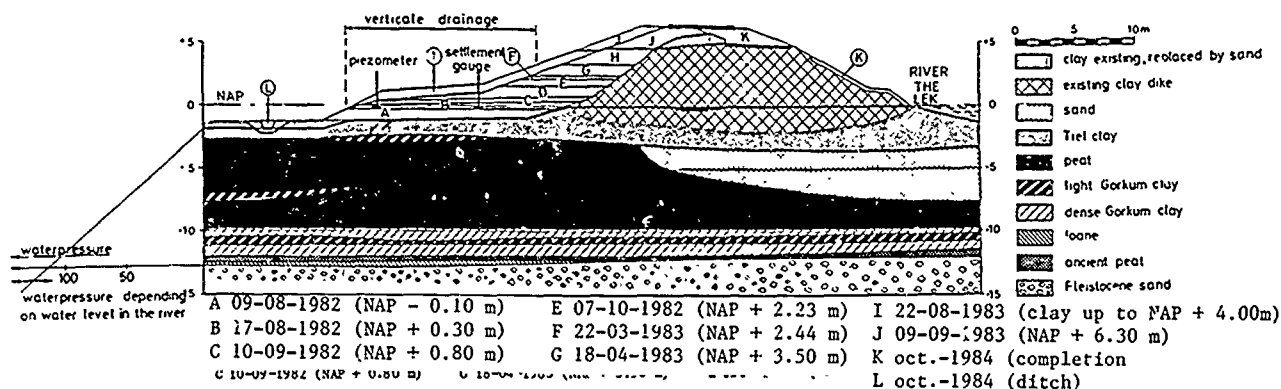


Figure 2. Geotechnical profile and fasing of the applied fill (heights related to NAP)

In order to shorten the consolidation period vertical drainage is applied under the berm. The type of the applied drains is Colbond KF 650 reaching up to approximately 1.5 m above the aquifer which is found at the level of NAP (New Amsterdam datum) -12.5 m. After the first working season the embankment reinforcement was raised up to NAP + 2.30 m. After the winter period the construction resumed in March 1983. In September 1983 the top level, NAP + 6.30 m, of the embankment was reached. The clay cover was brought up in August/September, 1983. The completion of the outer slope was carried out from August up to the end of September.

Broadening and deepening of the ditch at the toe of the inner slope would complete the construction (19th October). Shortly thereafter (21st October) instability symptoms appeared close to the descents at dike post (dp) 211.

The cross section of the existing dike and the various stages of the reinforcement, as well as their dates of execution and their levels are indicated on Figure 2.

Piezometers and settlement gauges were installed before construction to monitor the behaviour of the dike (see Figure 2). This is common practice in embankment constructions in the Netherlands.

### 3. SOIL PROFILE

The soil profile (see fig. 2) indicates a highly compressive post-glacial, normally or slightly overconsolidated clay and peat deposit, underlain by a stiff Pleistocene sand stratum. The stiff Pleistocene sand stratum at about NAP - 15 m is more or less in direct contact with the river. The potential head in this sand is determined by tidal and surge variations of the water level in the river. Some soil characteristics are shown in tabel 1. This soil profile is common in the Meuse Rhine delta. Soil investigation before construction and after the slope instability did not show significant differences.

### 4. THE SLIDING

"Sunday the 21th October 198 - 18.00 hrs". After a report from the police the dike administrator establishes crack formation over a

length of 80 m with height differences of approx. 5 cm in the vicinity of house Bergstoep 56. The polder side of the road has settled but shows no cracks. The other part of the road shows various cracks with a width of approx. 5 cm, which endanger the (bicycle) traffic.

Further the dike administrator reports:

- "close to Bergstoep 56 at a distance of approx. 40 m from the toe of the inner slope of the dike the wooden girder of a sheet piling perpendicular to the dike buckles, which indicates horizontal displacement.
- The last of a single row of tiles behind house Bergstoep 56 is pressed into in the hind lying soil (again horizontal displacements).
- The pile founded house Bergstoep 59 shows a crack of several metres in the flagstone floor of his dwelling, the crack has widened since this morning.

Early next morning (22 October) a maximum height difference of 20 cm was measured in the road surface (Figure 3). The settlement increased extensively during the day (approx. 3 cm per hour). The horizontal ground movements in the hindlying polder started to cause problems at the various houses. Around high tide the deformation/velocity seemed to be higher than at low tide.

Initially there weren't observed any uptrusts, but around noon it occurred that particularly the meadow between the houses 56 and 59 was forced up very smoothly. Remarkably the ditch visually didn't deform.



Fig. 3. Deformation of the road surface on 22 October at 10.00 hrs.

|                                 | $c'$<br>kN/m <sup>2</sup> | $\phi'$<br>° | G<br>kN/m <sup>2</sup> | K<br>kN/m <sup>2</sup> | $\nu'$<br>- | $\gamma$<br>kN/m <sup>3</sup> | n<br>% |
|---------------------------------|---------------------------|--------------|------------------------|------------------------|-------------|-------------------------------|--------|
| Dike material                   | 8                         | 23           | 450                    | 1335                   | 0.35        | 18                            | 50     |
| Tiel clay,<br>preloaded         | 10                        | 20           | 295                    | 765                    | 0.35        | 15                            | 60     |
| Tiel clay                       | 5                         | 22           | 255                    | 765                    | 0.35        | 15                            | 60     |
| Light Gorkum<br>clay            | 8                         | 17           | 240                    | 720                    | 0.40        | 11.5                          | 80     |
| Peat, preloaded                 | 18                        | 20           | 175                    | 235                    | 0.20        | 11                            | 80     |
| Peat                            | 5                         | 26           | 175                    | 235                    | 0.20        | 11                            | 80     |
| Dense Gorkum<br>clay, preloaded | 12                        | 21           | 320                    | 1500                   | 0.40        | 15                            | 60     |
| Dense Gorkum<br>clay            | 5                         | 21           | 320                    | 1500                   | 0.40        | 15                            | 60     |
| Sand                            | 0                         | 30           | 3800                   | 8300                   | 0.30        | 20                            | 40     |

Table 1. Material properties used for the calculations.

## 5. ANALYSIS

The total area, in which stability problems were encountered, lies between dp 210+ 90 m and dp 210+ 163 m.

As far as the analysis is concerned the following two parts can be distinguished:

- the central, most serious sliding in the vicinity of dp 211. Because of the variability of the cross-section (ascents and descents) of the dike analysing this part is very complex (Section "F at descents").
- the part west to the central sliding, situated between dp 210+ 90 m and dp 210+163m. Due to the availability of locally measured water pressures during construction an analysis of the causes was very well possible in this part (section "F with gauges").

The analysed cross section 33 was situated in section "F with gauges". The encountered damage is in the form of very serious deformations, more than to speak of a real sliding.

As first action was investigated in how far the actual construction rate was in accordance with starting points in the design phase. Further it was investigated whether the measured excess water pressures could have been an indication for the approaching clarity.

Just as figure 2, figure 4 indicates the times on which the various activities concerning ground work have been executed. These times are compared with the assumed loading rate in the design calculations.

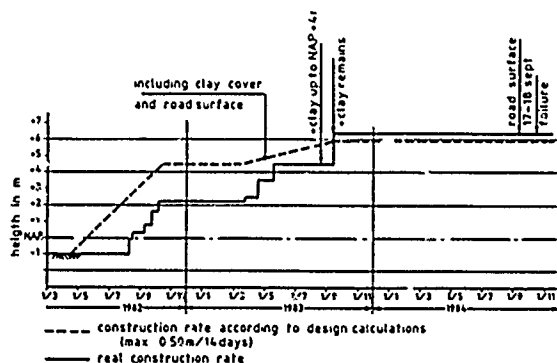


Fig. 4. Construction rate versus construction rate according to design calculations

Figure 5 indicates the measured excess pore pressures at the deepest (this has shown to be the most relevant) water pressure gauge. The water pressures are plotted as piezometric head with respect to NAP. In figure 6 the measured pressures are brought in relation with the earlier described "red line".

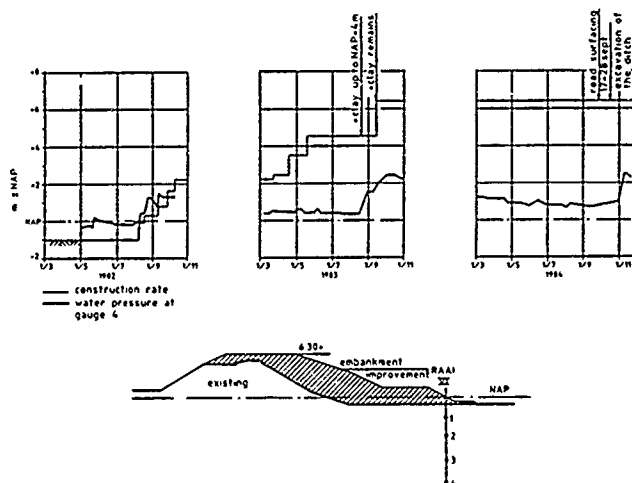


Fig. 5. Measured water pressures during construction

While studying the actual construction rate the following matters were noticed.

### 1982

At the end of the first working season the prescribed height of NAP + 4.50 m was not reached. This has to be imputed to the delayed start of the construction.

### 1983

Initially the embankment was raised at a substantial rate. By May three raising steps (totally about 2 m sand) were completed. The raisings, introduced none or hardly any increase of the water pressures (figure 5). According to the "red lines" (figure 6) no equilibrium problems were expected at this stage. After several months of rest great activity was employed around September (figure 4). In two weeks time a 0.70 m clay cover was positioned on the berm and the lower part of the slope, the sand body was raised from NAP + 4.50 m to NAP + 6.30 m and the upper part of the slope was covered with a 0.70 m clay layer. In fact this action meant the realization of the complete reinforcement with the exception of the finishing of the outer slope and the raising of a strip outside the reinforcement, directly above the former road. Consequently the loading stages through these last raisings in September the excess pressures increased much more than theoretically could be expected (see the "green line" in figure 6). The deepest gauge indicated even more than was allowed according to the "red line". High excess pressures and the end of working season implied the postponement of further activities.

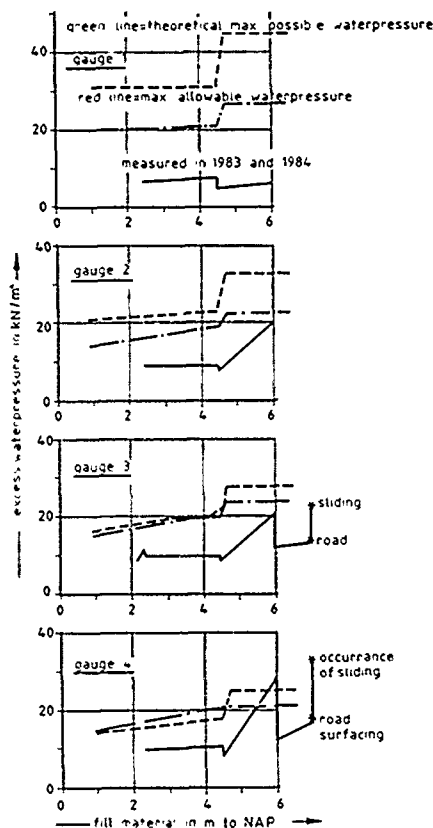


Fig. 6. Measured and allowable waterpressures 1984

At the start of the activities in 1984 the waterpressures had decreased significantly with respect to the measurements in November 1983 (figure 5 and 6).

The actual activities in this year were as follows (figure 2):

- In August and September activities were executed on the former outer slope.
- From 17 to 28 September the road foundation and surface were put in. (In the adjacent section besides the road foundation and surface also the descent was constructed).
- On the 19th October the trench at the inside slope was enlarged to form the final ditch. The excavated soil was deposited at the polderside of the ditch.

According to slipcircle analysis each of the above mentioned activities has only a limited influence on the stability of the embankment.

If the measured water pressures are brought in relation with the activities executed in 1984 it can be deduced that the activity on the outer slope didn't provoke an increase of the water pressures; the raising at the roadside, however, caused an increase of the water pressures. However, they did not reach the level at the end of 1983.

Construction of the road would provoke additional water pressures. However, figure 6 indicates that at that time the measured water pressures were sufficiently below the "red line" to allow the execution of these activities.

Within the scope of the analysis after events stability calculations were carried out with the same starting point as used for the design calculations, however using different water pressures.

The consolidation percentages  $U_{pi}(t)$  were determined from the measured increase of pore pressure due to loading  $i$  ( $\Delta u_i$ ) and the remaining pore pressure  $u_i(t)$  at time  $t$

$$U_{pi} = \frac{\Delta u_i - u_i(t)}{\Delta u_i} \quad (3)$$

Firstly calculations were carried out for the events in 1983. Herewith the situation just before and directly after the most extensive raising were investigated (about August and September respectively).

Further the effect of the raising in 1984 was analysed. The results of these calculation are resumed in table 2.

Table 2

|                            | $U_{pi}(\%)$ | $F_s$ |
|----------------------------|--------------|-------|
| August 83                  | 65           | 1.20  |
| September 83               | 65           | 1.03  |
| September 84 without ditch | 67           | 1.17  |
| September 84 with ditch    | -            | 1.15  |

Back analysis showed that the consolidation rate of the underlying soil strata was less than assumed during the design period. Whether this was due to the soil itself or the vertical drains could not be determined. The results show clearly among other things the great effect of the raising at the end of 1983. It is clear, that even loss of equilibrium at the end of 1983 would not have been impossible.

The calculated safety factor at the end of 1984 is greater than the one calculated at the end of 1983 (1.15 against 1.03 respectively). Nevertheless at the end of 1983 none and at the end of 1984 very serious deformation were observed.

Taking into account all possible unfavorable aspects still a factor of safety greater than 1.0 was calculated. The minimum calculated factor of safety appeared to be 1.04.

Concluding from these results, two main questions needed to be answered to get a better understanding of the failure mechanism and the embankment behaviour:

- Which are the reasons for the great differences between the measured and the predicted pore pressures up from August 1983, whilst a good accordance was found for earlier loading phases?
- For which reason did the small load step in October 1984 lead to failure, despite the important decrease of measured pore pressure and the higher value of  $F_s$  (calculated in terms of effective stresses with Bishop's method) at failure than in August 1983?

## 6. CALCULATION OF EXCESS PORE PRESSURE AT UNDRAINED LOADING

Because the classical method of predicting the pore pressure generation and dissipation was found to be unsatisfactory, these points are discussed from a more general point of view. For slightly overconsolidated or normally consolidated soils, the following distinction in pore water pressure development with increased loading and consolidation is made.

Initially, there is an elastic behaviour for  $OCR > 1$ . The increase of water pressure  $\Delta u^e$  is caused solely by an increased total isotropic stress. For plane strain and undrained behaviour (Poisson ratio  $\nu = 0.5$ ), this can be approximated by (effective stress path A'B and total stress path A'R on figure 7).

$$\Delta u^e = \beta \frac{\Delta \sigma_1 + \Delta \sigma_3}{2} = \beta \Delta p \quad (4)$$

wherein  $\beta$  is a pore pressure coefficient accounting for the presence of (dissolved) gas. In absence of dissolved gas,  $\beta = 1$ .  $\Delta \sigma_1$  and  $\Delta \sigma_3$  are the increase of major and minor total principal stresses.

After having developed a normally consolidated behaviour, either by consolidation (effective stress increase) or by shear stress increase, an increase of shear stress will also cause an increase of pore water pressure ( $\Delta u^s$ ). For plane strain conditions and undrained behaviour, this water pressure increase (which is a function of the increase of the octahedral shear stress  $\Delta \tau_{oct}$ ) can be written as (ESP B'-F' and TSP B-F on fig. 7).

$$\Delta u^s = \xi \left| \frac{\Delta \sigma_1 - \Delta \sigma_3}{2} \right| = \xi \Delta q \quad (5)$$

The magnitude ( $\xi$ ) of this stress increase depends on the actual effective stress and the location and the shape of the yield surface (Burland, 1971; fig. 7).

Indeed, when the effective stress path reaches the yield envelope, the excess pore pressure increments are related to the total stress so that the effective stress path remains practically on the yield envelope. The consolidation rate decreases considerably once the effective stress path has reached the yield envelope.

When the applied shear stress in the foundation layers somewhere equals the shear resistance, locally no further shear stress increase can occur (point F' and F on fig. 7). In this failed areas, local plastic flow will lead to a further increase of pore water pressure ( $\Delta u^p$ ) in comparison to the elastic solution. Indeed, at failure, the difference between the principal stresses  $\sigma_1$  and  $\sigma_3$  is equal to twice the undrained strength  $C_u$  at the moment of loading:

$$\sigma_1 - \sigma_3 = 2 C_u \quad (6)$$

With further loading (at unchanged  $C_u$ ) in the purely plastic area, the minor and major principal stresses will remain related by eq. 6, so that their increments will be equal:  $\Delta \sigma_1 = \Delta \sigma_3$ . Hence, local plastic flow leads to a higher excess pore pressure than can be derived from an elastic solution provided that the horizontal stress is smaller than the vertical stress (Hoeg, 1968; Burland, 1971; Law, 1979).

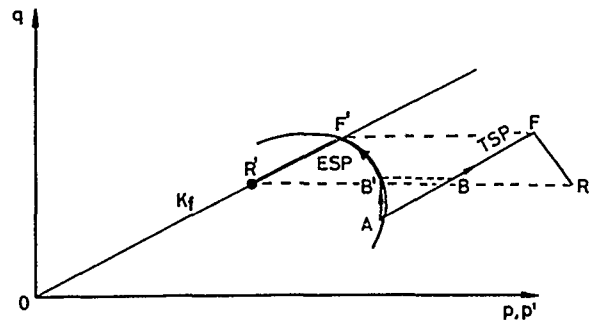


Fig. 7. Induction of excess pore pressure

Local plastic flow and the subsequent stress transfer in the plastic area, will affect the stress increases distribution in the nearby non-failed area (Bauduin, 1987), which become higher than resumed from an elastic solution. This phenomenon is comparable with the force redistribution in a hyperstatic steel beam when yielding is reached. Finite element calculations with elasto-plastic material behaviour enables the stress transfer to be calculated without restrictive assumptions. Sensitive clays show a sudden reduction in strength upon reaching the failure surface. As the effective stress path has to remain on the failure surface (Tavenas, 1977), this will cause a sudden increase of pore water pressure (ESP F'-R' and TSP F-R on fig. 7).

## 7. PORE PRESSURE DISSIPATION

The increase of effective stress during the consolidation phase governs the increase of the shear resistance and hence has to be evaluated as a function of time. The phenomena of pore pressure dissipation and consolidation settlements can be described by the Biot theory (Biot, 1941). The initial Biot theory is based on the assumption of elastic behaviour of the soil; it means that the initial pore water pressure distribution is given by eq. 3. Creep effects are not taken into account in Biot's initial theory, although there is some evidence that constant effective normal stresses as well as shear stresses can influence the consolidation process by apparently lowering the rate of dissipation of pore pressure (Magnan, 1979; Mesri, 1974; Garlangier, 1972). Biot's theory - in opposite of less rigorous theories - demonstrates that consolidation may also be responsible for some changes in the elastic stress distribution, which influences the pore water pressure (Mandel, 1953; Cryer, 1963; Schiffman, 1969).

## 8. SEQUENCE OF CALCULATIONS

During construction of the embankment, relatively short loading stages are followed by more or less longer periods of drainage in sequence. The analysis of pore pressure development, involves therefore a sequence of calculations of pore pressure generation during the loading stages and calculations of dissipation of excess pore pressure during the intermittent drainage periods. Two different finite element codes have been used to carry out these calculations, namely:

- the computercode SPONS, which is based on Biot's initial consolidation theory and allows to calculate the dissipation during the draining periods

- the computercode DIEKA, which is suitable for simulation of effective or total stress analyses of an instantaneous loading step, applying nonlinear stress strain behaviour. In the calculations, an elastic perfectly plastic stress strain behaviour has been used, assuming a Mohr-Coulomb type stress envelope in the case of an effective stress analysis and a Tresca type stress envelope in the case of a total stress analysis.

The process of pore pressure generation and dissipation in between two loading steps, say at time instants  $t_1$  and  $t_2$ , has been simulated as follows:

1. Assuming that the initial effective stress distribution  $\sigma'(t_1^-)$  and the pore pressure distribution  $u(t_1^-)$  at  $t_1^-$  (just before loading at  $t_1$ ) are known, the undrained shear strength can be calculated as:

$$S_u(t_1^-) = S_u(t_1) = c' \cos \phi' + p'(t_1) \sin \phi' \quad (7)$$

wherein  $p'(t_1)$  denotes the effective isotropic stress at failure, as derived from the actual effective isotropic stress, properly accounting for the effect of the yield envelope on the effective stress path during loading.

2. A total stress analysis using the DIEKA code is carried out, applying the total load, including the load step at  $t_1$ . The shear resistance is given by  $S_u(t_1)$ .

3. The generated pore pressures during the loading step due to increase of the normal stresses, including the effects of plastic yielding and global stress transfer equals

$$\Delta u^e(t_1) + \Delta u^p(t_1) = p(t_1^+) - p'(t_1^-) \quad (8)$$

in which  $p(t_1^+)$  denotes the isotropic total stress just after loading.  $\Delta u^e$  takes into account the stress redistribution in the non failed area due to stress transfer in the failed area.

4. The generated pore pressure during loading due to the increase of shear stresses  $\Delta u^s$  are calculated using the difference between the deviatorics after  $(q(t_1^+))$  and before  $(q(t_1^-))$  loading and the yield envelope

$$\Delta u^s(t_1) = \xi [q(t_1^+) - q(t_1^-)] \quad (9)$$

5. The total increase of excess pore pressure due to the loading step at  $t_1$  is given by:

$$\Delta u(t_1) = \Delta u^e(t_1) + \Delta u^p(t_1) + \Delta u^s(t_1) \quad (10)$$

The total excess pore pressure distribution just after loading  $u(t_1^+)$  given by:

$$u(t_1^+) = u(t_1^-) + \Delta u(t_1) \quad (11)$$

These pore pressures represent the initial conditions for the computation of dissipation during the period from  $t_1^+$  until  $t_1^-$ , using the SPONS code. The result of this calculation is the new pore pressure distribution  $u(t_2^-)$  and the increase of effective stresses  $\Delta \sigma'$ .

6. In order to determine the new effective stress field  $\sigma'(t_2^-)$  just before the loading step at  $t_2$ , a DIEKA effective stress analysis is carried out, starting from the effective stress field  $\sigma'(t_1^-)$  and applying the

effective stress increments  $\Delta \sigma'$ . This analysis completes the sequence of calculations for one loading consolidation cycle.

The complete sequence of calculations and their relation to in situ events has been summarized in table 3.

| Date of actual loading | Date designation                         | Number of days after 10 loading | Calculation method   | Program                 | Result  |
|------------------------|--|---------------------------------|--|-------------------------|---|
| see fig. 2             | $t_0$                                    | -                               | Drained EP stress  | DIEKA                   | Initial effective stresses $\sigma'_p(t_0)$   |
| B<br>C<br>D<br>E<br>F  | $t_0^+$                                  | 0-24<br>38<br>51<br>217         | Elastic pore pressure generation and dissipation between $t_0^+$ and $t_1^-$   | SPONS                   | Time-dependent excess pore pressure from $t_0^+$ to $t_1^-$ : $u_e(t)$<br>Elastic increase of effective stress at $t_1^-$ :   |
| G<br>H                 | $t_1^-$<br>$t_1^-$                       | 244<br>275<br>380<br>380        | Drained EP stress analysis<br>Shear resistance at $t_1^-$  | DIEKA<br>SHEAR          | $\Delta \sigma'_e(t_1^-)$<br>Elastic displacements from $t_0^+$ until $t_1^-$ : $d_e(t)$<br>Effective stresses at $t_1^-$ : $\sigma'_p(t_1^-)$<br>Undrained shear resistance at $t_1^-$ : $c_u(t_1^-) = c_u(t_1)$                                     |
| I, J                   | $t_1$<br>$t_1$<br>$t_1$                  | 380<br>380<br>380               | Total EP stress<br>Shear stress induced excess pore pressure<br>Excess pore pressure induced at $t_1$                | DIEKA<br>SHEAR<br>PORE  | Total stresses at $t_1^+$ : $\sigma_p(t_1^+)$<br>Shear stress induced excess pore pressure $\Delta u_s(t_1^+)$<br>Total excess pore pressure  |
|                        | $t_1^+$<br>$t_2^-$<br>$t_2^-$<br>$t_2^-$ | 581<br>770<br>770<br>770        | Elastic pore pressure<br>Dissipation between $t_1^+$ and $t_2^-$<br>Drained EP stress<br>Shear resistance at $t_2^-$ | SPONS<br>DIEKA<br>SHEAR | Time dependent excess pore pressure<br>Elastic increase of effective stress between $t_1^+$ and $t_2^-$ : $\sigma'_e(t_2^-)$<br>Effective stresses at $t_2^-$ : $\sigma'_p(t_2^-)$<br>Undrained shear resistance at $t_2^-$ : $c_u(t_2^-) = c_u(t_2)$ |
| K, L                   | $t_2$                                    | 771                             | Total EP stress  | DIEKA                   |   |

Table 3: Summary of loading and calculation sequence.

## 9. MATERIAL MODELLING

The calculation parameters have been evaluated from laboratory and in situ tests (see fig. 8 and table 1).

The shear stress parameters  $c'$  and  $\phi'$  were determined by Dutch cell tests and isotropically consolidated, drained triaxial compression (active failure zone) and extension (passive failure zone) tests for the peat. Probably due to some preconsolidation, the soil under the old dike has a lower friction angle and a higher cohesion than the virgin soil in the polder. The elastic parameters as used in the elastic-plastic and consolidation analyses are also given in table 1 in terms of average tangent modulus between initial and approximated final effective stress states. They have been determined in situ using pocket pressuremeters in the laboratory using C/D triaxial tests (peat only) and oedometer tests. The laboratory tests gave lower values than the pressuremeter tests and showed stress dependency.

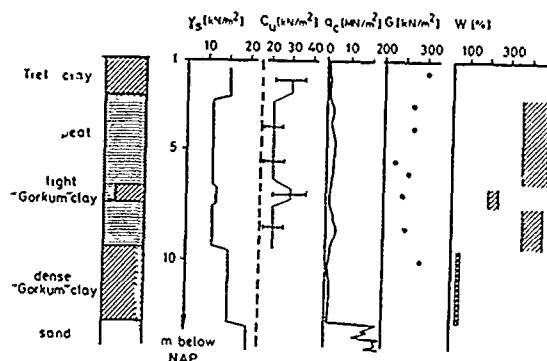


Fig. 8. Bore log and results of in situ soil investigation at the toe of the dike

A much simplified pore pressure induction model was used to simulate the yield surface (see figure 9). The choice of this model is based on the results of earlier CIU and CAU triaxial tests on young peat and soft clay in the Netherlands (Beetstra, 1978) and the YLIGHT model presented by Tavenas (1978). The permeability of the soil layers in vertical ( $k_v$ ) and horizontal ( $k_h$ ) directions were measured by laboratory tests. They appeared to be stress and direction dependent the results for the peat showed scatter. The coefficient of horizontal stress at rest ( $k_0$ ) has been taken approximately 0.6 for the clay and 0.5 for the peat.

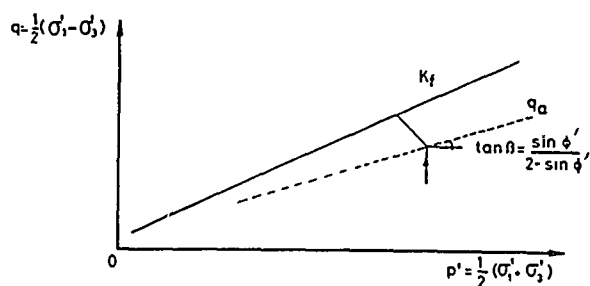


Fig. 9. Simplified material model as used for the calculations

## 10. EVALUATION OF THE CALCULATIONS AND MEASUREMENTS

The effective stress analysis of the initial situation at  $t = t_0$  showed only a little zone of maximal mobilized resistance under the existing old dike (see fig. 10a). As indicated in table 1, pore pressure development between  $t_0$  and  $t_1$  have been analysed using the elastic code SPONS only. The measured and calculated excess pore pressures are in good agreement (see fig. 11). In order to introduce some stress dependency on the values of the permeability coefficients, the calculation has been interrupted at  $t = 200$  days and restarted with lower values.

The elastic-plastic effective stress analysis at  $t = t_1$  shows a small increase of the zone of maximal mobilized shear strength (see fig. 10b).

The calculated settlement with the Biot theory are in reasonable agreement with the measurements.

From  $t_1^-$  until  $t_1^+$ , the dike was raised from NAP + 4.50 m to NAP + 6.30 m, including a 0.7 m thick clay layer covering the whole slope. This loading stage has been simulated using the analysis described in section 7. The calculated increase of  $\Delta u$ , compared to commonly used elastic predictions, has been summarized in table 4.

| loading phase  | measured $\Delta u$ (kN/m <sup>2</sup> )<br>piezometer |    |    | elastic $\Delta u$ (kN/m <sup>2</sup> )<br>piezometer |    |    | $\Delta u^e + \Delta u^p + \Delta u^s$ (kN/m <sup>2</sup> )<br>piezometer |    |    |
|----------------|--|----|----|---|----|----|---|----|----|
|                | 4  | 3  | 2  | 4   | 3  | 2  | 4   | 3  | 2  |
| September 1982 | 18   | 17 | 17 | 18  | 17 | 17 | 18  | 17 | 17 |
| August 1983    | 22   | 12 | 13 | 6   | 6  | 6  | 9   | 12 | 9  |
| October 1984   |  |    |    |   |    |    |   |    |    |

Table 4. Values of measured and calculated pore pressures

With the added effects of plastic flow and shear stress, a better correspondence between calculated and measured pore pressure is obtained. However, for the deepest piezometer, the measured value remains higher. Reasons for this can be an underestimate of the effects of a shear stress increment, strain softening or lack of accuracy in measurement or calculation. The measured time for  $\Delta u$  does not appear clearly from the calculations and could be a consequence of a delay in plastic stress transfer. Figure 11c show the area of maximal mobilized shear strength. The extend of this area, as well as the results of a sensitivity analysis of the undrained shear strength at  $t_1$ , indicated an almost complete loss of strength reserve during this loading stage.

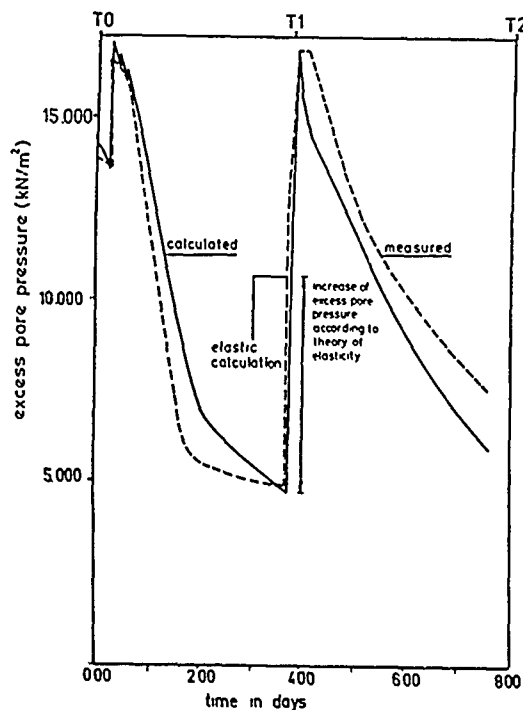
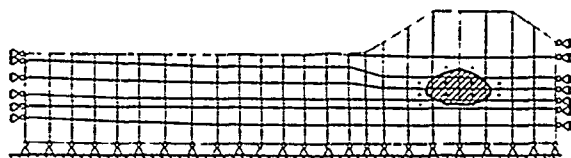
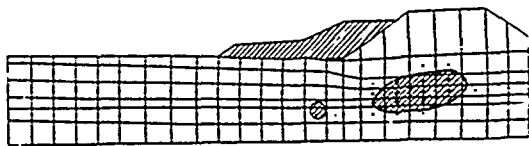


Fig. 11. Measured and calculated excess pore pressure at the toe of the dike (8.1 m below NAP) gauge 3.

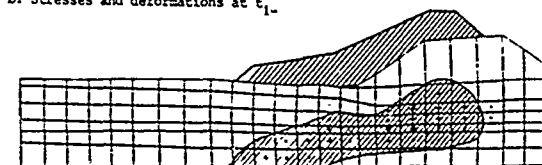




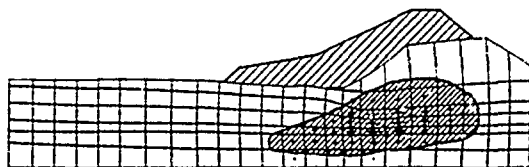
a. Initial stresses



b. Stresses and deformations at  $t_{1-}$



c. Stresses and deformations at  $t_1$



d. Stresses and deformations at  $t_{2-}$

Fig. 10. Stress distribution and deformations (shaded area: area of maximal mobilized shear stress)

Adding the settlements from the DIEKA analysis at  $t_1$  to the consolidation settlement at  $t_1$  gives a good agreement between measured and calculated settlement. This does not hold if elastic settlements at  $t_1$  only are added to the consolidation settlement.

During the subsequent drainage period, there is a substantial drop of excess pore pressures. The dissipation rate, however, was lower than in 1982. This could be a consequence of a lowered consolidation coefficient due to reduced soil permeability and/or stiffness, a less effective functioning of the vertical drains and increasing importance of creep effect. A good agreement between the measured and calculated dissipation percentage could be found when the  $k$ -values of the soil have been lowered up from  $t_1$ .

According to the method outlined in section 7, an effective stress analysis has been performed at  $t_{2-}$ , just before completion of the construction. This DIEKA analysis indicated an insignificant decrease of the plastic zone (see figure 10d). This leads to the conclusion that the embankment stability was critical throughout the loading stage at  $t_1$  and the subsequent drainage period, until the moment that the actual failure started, triggered by some additional minor cause (completion of dike). Dike failure was calculated for the applied loading at  $t_2$ .

In spite of some shortcomings, the FEM calculations showed that:

- Excess pore pressure in the peat can be estimated reasonably well by taking the effects of shear strain and stress transfer into account; they are somewhat underestimated in the Dense Gorkum clay. More accurate material modelling is needed in this case.
- The severe load increase at  $t_1$  led to a highly extended area of maximal mobilized shear strength and the embankment stability was critical throughout the whole period following this load increase.
- At high shear stress levels, the effects of shear stress and local plastic flow cannot be ignored. They play an important role in the development of the mechanism of failure. In the classical approach, these effects are not taken into account.
- An area of maximal mobilized shear strength is present during the whole construction period. At severe loading steps, its extent increases, firstly towards the crest and later on towards the toe.

### Conclusions

The analysis of the pore pressures based on an elastic soil behaviour and circular slip surface calculations in terms of effective stresses could not give a satisfactory explanation to the failure of the landside slope of a dike, just after completion. Detailed FE analyses, however, which followed the complete history of the elevation helped to understand the actual cause. A major aspect of the failure has been shown to be the generation of significant pore pressure in the zone with severe plastic deformations near the toe due to a severe loading step. In the future, this pore pressure generation should be predicted more accurately than using purely elastic theories. The understanding of the shear strength mobilization during staged loading near failure has been increased by the use of FE code. The learnings about the pore pressure generation and strength mobilization have led to an observational method of embankment stability (Bauduin and Moes, 1987).

## Coastal Bluff Retreat at Big Lagoon, California

R.C. Chaney

Professor of Environmental Resources Engineering, Humboldt State University, Arcata, California

D.C. Tuttle

Environmental Services Manager, Humboldt County Department of Public Works, Eureka, California

**SYNOPSIS:** Big Lagoon, located 30 miles north of Eureka, California is formed behind a bay barrier built across the mouth of a drowned river valley. To the south of the bay the beach follows rising wave cut slightly cemented sand and gravel sea cliffs and terminates at the south end of Agate Beach. The retreat of these sea cliffs and its effect on property development along the top of the cliff is the focus of the paper. Measurements of bluff retreat in this area have been documented extensively from November 1941 to March 1986 through ground surveys and air photos. Review of the data indicates that the retreat rate is not constant along the cliff but has either been decreasing or remaining the same over the last 45 years. Using information on the rate of retreat, a method is developed to predict the cliff erosion in the future.

### INTRODUCTION

As far back as geological records can be traced, there is evidence that the shorelines of the world are dynamic, subject to rises and falls in sea level, and elevations and depressions in land masses. Looking eastward from the town of Trinidad, California marine terraces and old beach lines can be seen rising step by step to an elevation of 1400 ft. There is clear evidence of the successive elevations in land masses along this coast. Coupled with these two geological phenomena is the fluctuating sea level, which has been rising since the beginning of the last ice age. Presently the sea level is rising along the north coast (Russell, 1957). The result of the rise of sea level with respect to the land is coastal erosion.

Big Lagoon, located 30 miles north of Eureka, California and 7 miles north of Trinidad, California is formed behind a bay barrier built across the mouth of a drowned river valley. The bay barrier is part of a sandy-beach section of coastline that extends from a cliffed headland at the north end of the lagoon to a low sandy bluff at the southern end. This beach then follows rising wave-cut sea cliffs and terminates at the south end of Agate Beach (Martinez, 1978). The sea cliffs are composed of a slightly cemented sand and gravel that form a soft sandstone. This sandstone is presently tilted downward to the north. Some of the layered structure extends along the floor of the lagoon until at the north end of the lagoon, it abruptly stops where it meets a rocky bluff. This change from a soft sandstone to rocky bluff marks a line of a fault. The erosion of the soft sandstone sea cliffs will be the focus of this study. A map of the area is shown in Figure 1. Also shown in Fig. 1 are numbered section lines which will be utilized to discuss historic erosion.

The bathymetry along the coast at this location does not exhibit any substantial change. There is a headland immediately south of the study area which does result in a focusing of waves.

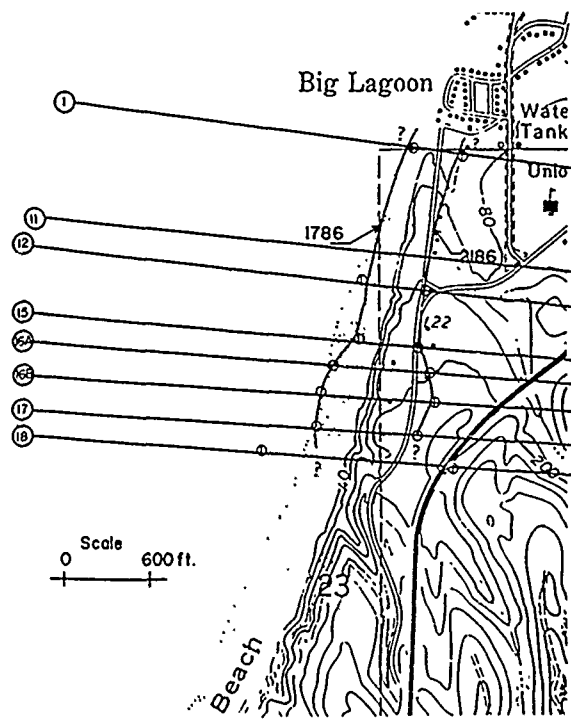


Fig. 1 Location of Coastal Bluffs at Big Lagoon

The erosion potential of a coast varies greatly from point to point and is dependent on a number of factors which may be listed as follows: (Adapted from King, 1959) (1) exposure of coastline to wave attack, (2) tide, (3) coastal type, (4) type of geologic material comprising coast, (5) offshore relief, (6) effect of man-made structures, (7) longshore movement of beach material, (8) tectonic changes, and (9) proximity of rivers carrying sediment to the ocean. The basic premise is that if the beaches below a coastal bluff are subject to sand depletion due to a lack of material transport by the longshore current then wave action will be able to actively attack the

coastal bluffs. Conversely, if the beaches are aggraded, then the wave action will not effect the coastal bluff.

#### WAVE AND TIDES

Incoming wave power is distributed among three recognizable "families" of waves, each with a particular season of effect and average angle of approach (Johnson et al., 1971; Scripps Institution of Oceanography, 1947). From April to November, the dominant wave energy component at the study area is the "prevailing swell". These waves are generated by storms in the north-central and north eastern Pacific. These waves are low energy wave forms, generally not higher than 9.8 ft. and averaging under 3.3 ft. high, and dominate the total wave power as a result of their long season of effect. The winter months, November through March, are characterized by very high energy "seas" which arrive from the south. These southerly waves average about 9.8 ft. high and range over 26 ft. high. They are associated with storm fronts passing through the study area during winter. A third group of waves arriving at the study area are seas generated by NNW winds which occur most strongly in the months of May to August. This family of waves has an average deep water approach direction of NW to NNW and an average height of 3.2 ft. to 6.4 ft. with a maximum height of 16.4 ft. Southward drift during the late spring and summer months is a result of the arrival of this group of waves. The total wave-power of this northerly group is about equal to the total wave-power of the winter southerly waves.

Tides in the study area are mixed semi-diurnal, with a mean tide range of about 5 ft., and a maximum tide range of about 11.2 ft. (N.O.A.A., 1980).

#### HISTORIC EROSION

Measurements from the centerline of Roundhouse Creek Drive/ Ocean View Drive to the top of the coastal bluffs are presented in Table 1 for the period of time from November 1941 to March 1986. Plots of cumulative time versus distance from the top of coastal bluffs to center of the road is presented in Figure 2. An inspection of Figure 2 shows that along a number of section lines a substantially linear relationship exists between coastal bluff erosion and time. An interpretation of this phenomenon would be that the rate of coastal bluff retreat has been fairly constant over the period of time that measurements have been taken. An implication of a relatively constant rate (ER) of coastal bluff erosion is that a constant amount of sediment is being transported along the coast by the littoral current.

#### EVALUATION OF EROSION RATE

The erosion rate (ER) is defined as the change in distance from a known point to the edge of the coastal bluffs as a function of time as shown in Figure 3 and as given in equation 1.

$$ER = \frac{D_1 - D_2}{Y_2} \quad (1)$$

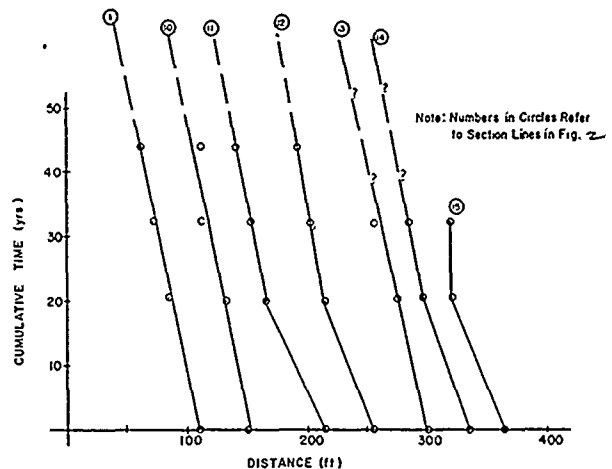


Fig. 2a Distance From Fixed Point To Coastal Bluff Versus Time

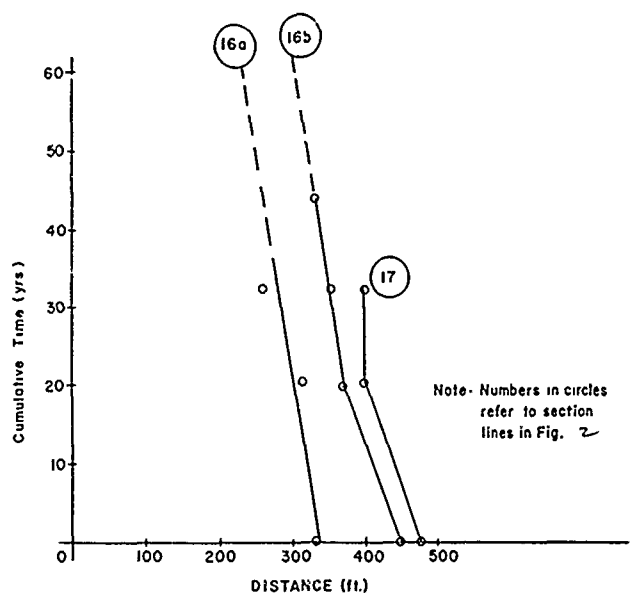


Fig. 2b Distance From Fixed Point To Coastal Bluff Versus Time

where: ER - Erosion Rate (ft./yr.)  
 $D_1$  - Initial distance from edge of coastal bluff to reference point (ft.)  
 $D_2$  - Distance from edge of coastal bluff to reference point at time  $T_2$  (ft.)  
 $Y$  - Number of years that have occurred since initial measurement

Plotting the calculated erosion rate versus time in years for section 11 and 16b are shown in Figures 4 and 5. A review of these figures indicates that the erosion rate (ER) has been decreasing from 1941 to the present (1986) for these specific location in contrast to other sections where the erosion rate is relatively constant.

| Line | Distance From Centerline of Ocean View Drive (feet) |           |           |            | Retreat (feet) |           |           | Average Erosion Rate (ft./yr.) |
|------|---|-----------|-----------|------------|----------------|-----------|-----------|--------------------------------|
|      | Nov. 1941   | Aug. 1962 | Aug. 1974 | March 1986 | 1941-1962      | 1941-1974 | 1941-1986 |                                |
| 1    | 110   | 85        | 72        | 62.5       | 25             | 38        | 47.5      | 1.06                           |
| 10   | 150   | 132       | 113       | 112.5      | 18             | 37        | 37.5      | 0.83                           |
| 11   | 215   | 165       | 153       | 140        | 50             | 62        | 75        | 1.67                           |
| 12   | 255   | 215       | 202       | 192        | 40             | 53        | 63        | 1.40                           |
| 13   | 300   | 275       | 255       | --         | 25             | 45        | --        | 1.36                           |
| 14   | 335   | 295       | 285       | --         | 40             | 50        | --        | 1.52                           |
| 15   | 365   | 320       | 320       | --         | 45             | 45        | --        | 1.36                           |
| 16a  | 330   | 315       | 260       | --         | 15             | 70        | --        | 2.12                           |
| 16b  | 445   | 385       | 355       | 330        | 60             | 90        | 115       | 2.56                           |
| 17   | 476   | 400       | 400       | --         | 76             | 76        | --        | 2.30                           |
| 18   | 467   | --        | 315       | --         | --             | 152       | --        | 4.61 <sup>(1)</sup>            |

Note: (1) Site of drainage culvert.

Table 1 Measurements From Centerline of Ocean View Drive To Top of Coastal Bluffs at Big Lagoon Subdivision (Adopted from Tuttle, 1981)

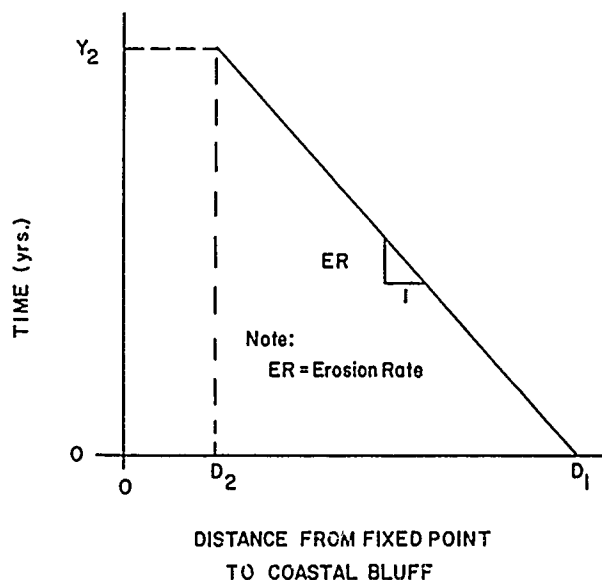


Fig. 3 Schematic Illustration of Distance from Fixed Point to Coastal Bluff Versus Time

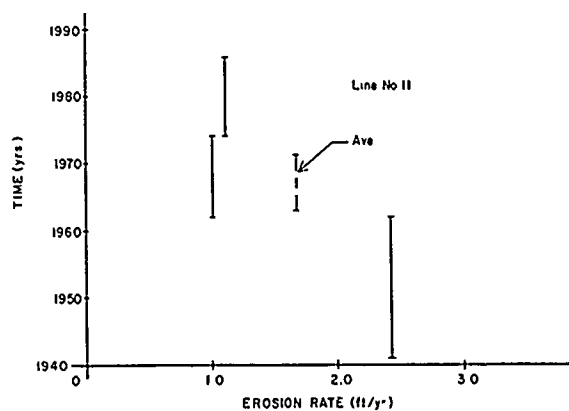


Fig. 4 Erosion Rate Versus Time, Line No. 11

#### HINDCASTING AND FORECASTING COASTAL BLUFF LOCATIONS

The coastal bluff location in the past or in the future can be estimated by rearranging equation 1 as follows:

$$D_2 = D_1 - (ER) Y_2 \quad (2)$$

Using equation 2 and assuming an average ER of 2 ft./yr. the location of the coastal bluff in 1786 and 2186 was estimated as shown in Figure 1. A review of the estimated coastal bluff locations as shown in Figure 1 indicates that a larger

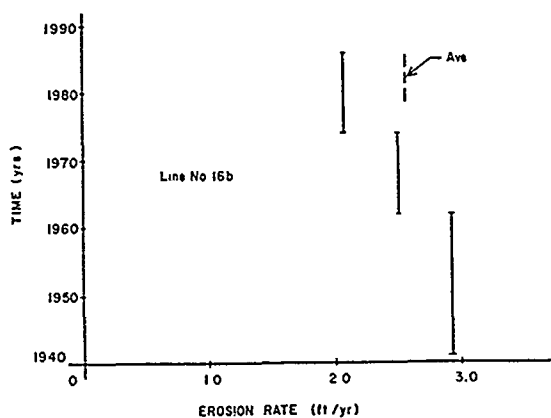


Fig. 5 Erosion Rate Versus Time, Line No. 16b

amount of movement occurs in the southern portion of the cliffs as opposed to the north.

#### CONCLUSIONS

(1) The coastal bluff erosion rate along each line has been relatively uniform over the last 45 years as shown by linear time versus distance plots.

(2) Erosion rates vary from 0.8 to 2.6 ft./yr. along the section investigated. Line 18 indicated an erosion rate of 4.6 ft./yr. but was probably influenced by the presence of a drainage culvert.

(3) Erosion rates seem to be decreasing with time along specific section lines. Reason for this decrease is unknown at the present time.

(4) Hindcasting and forecasting coastal bluff retreats based on average erosion rates indicates that the bluff has retreated from 170 to 500 ft. in the last 200 years and will probably experience an equal amount in the next 200 years.

#### REFERENCES

Johnson, J.W., J.T. Moore, and E.B. Orret (1971), "Summary of Annual Wave Power for Ten Deep Water Stations Along the California, Oregon, and Washington Coasts," University of California Hydraulics Engineering Laboratory, Technical Report HEL-24-9, College of Engineering, University of California-Berkeley.

King, C.A.M. (1959), Beaches and Coasts, Arnold, London.

Martinez, J. (1978), "Sedimentation of Big Lagoon Humboldt County California," Senior Thesis as partial fulfillment of requirements towards a Baccalaureate Degree in Geology, Humboldt State University, Arcata, California.

N.O.A.A. (1980), United States Coast Pilot 7, 16th ed., National Ocean Survey, Washington, D.C.

Russell, R. J. (1957), "Instability of Sea Level," American Scientist, Vol. 45, 5:414-430.

Scripps Institution of Oceanography (1947), "A Statistical Study of Wave Conditions at Five Open Sea Locations Along The California Coast," University of California, Wave Report No. 68, July, Stations A and B.

Tuttle, D.C. (1981), "Investigation of Methods for Determining Coastal Bluff Erosion - Historical Section," Humboldt County Department of Public Works, Eureka, California.

# Investigation of Settlements of a Trunk Road Embankment in Hong Kong

P.L.R. Pang

Civil Engineering Services Department, Geotechnical Control Office,  
Hong Kong

Y.C. Chan

Civil Engineering Services Department, Geotechnical Control Office,  
Hong Kong

**SYNOPSIS :** A 25 m high fill embankment was constructed as part of a Trunk Road scheme in Hong Kong. In June 1985, large settlements of the order of 250 mm were observed in the embankment. This was followed by a local slippage of surface material from the downstream slope face. To meet the schedule for opening the trunk road in late September, a number of emergency measures costing about HK\$1 M (US\$0.13 M) were implemented to stabilize the embankment. An investigation was subsequently carried out to assess the cause of the movement and the long term stability of the embankment.

This paper summarizes the sequence of events leading to the settlements and outlines the investigation carried out. The proposed hydrocompaction mechanism and the effects of grouting on the embankment are discussed.

## INTRODUCTION

In 1982, the Government of Hong Kong started the construction of a dual three-lane highway in the north of the Territory. The road was formed by cutting into headlands, filling valleys and building bridges. One of the embankments, which was 25 m high, was completed in 1983. This embankment settled and deformed in 1985. The Geotechnical Control Office was requested to look into the causes of the deformation and to advise on the long term stability of the embankment within five months.

By analysing monitoring records and ground investigation data, the authors used the method

of elimination and found that hydrocompaction might have initiated the settlements while later deformation was caused by redistribution of soil water. The hydrocompaction hypothesis was subsequently tested by a mathematical model.

## BACKGROUND

### The Site

The embankment is located in the northern part of the Hong Kong New Territories. It has been formed by filling over a valley, with the existing stream course diverted through a 2.5 m square box culvert underneath. The maximum thickness of filling is about 25 m, and the side slopes are at 1 vertical to 1.5 horizontal.

The foundation rock is a highly fractured (RQD = 0 to 25%) sedimentary siltstone of Upper Jurassic age, the fracturing being due to faulting. The top layer of rock has been completely decomposed to a well-graded clayey sandy silt. The rock mass is fairly permeable ( $k = 10^{-5}$  to  $10^{-6}$  m/s) compared with the residual decomposed rock ( $k = 10^{-7}$  m/s). The groundwater table is situated well down in rock. Though bouldery colluvium exists up-stream of the embankment, no colluvium was found under the fill. Figure 1 depicts a cross section through the trunk road showing the geological and groundwater conditions.

### Construction History

Excavation for the box culvert commenced in early 1983. Because of the low groundwater table, no drainage layer was placed underneath the embankment. Filling of the embankment commenced in November 1983 after completion of the box culvert. The fill was borrowed from the adjacent slope and compacted in 300 mm layers

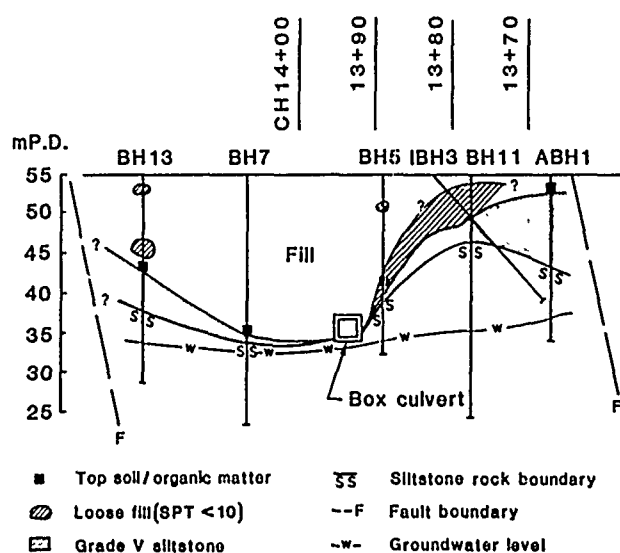


Figure 1 - Cross section through trunk road showing the geological and groundwater conditions

using vibratory rollers. Filling completed at the end of 1983.

The northbound carriageway was then used for aggregate stockpiling from January to October 1984. During this period, distress was observed at the surface channels on the slope after heavy rain. The defective channels were repaired in November, and the stormwater drains and gullies adjacent to the centre-line of the road were constructed. Road surfacing was completed in May 1985.

## SETTLEMENTS

In early June 1985, after a few days of rain, settlements were observed at the central divider of the road near Chainage 13+82. Monitoring of the settlements commenced on 6th June. Figure 2 shows the area of monitoring. The embankment was then test loaded to 20 kPa.

In early July, a defective gully close to point r (Figure 2) was found - the base of the gully had settled 20 mm relative to its side walls. The slope surface was observed to be wet. Cracks were also evident at the surface channels and catchpits on the slope. By late July, settlement at point r had reached 250 mm. The gully and a length of cracked stormwater drain were subsequently replaced. However settlement monitoring in late August indicated that the road was still settling.

In September, a series of grouting were carried out, both within the embankment body and at the interface of the fill and the insitu ground. Altogether 86 grout holes were formed and about 300 m<sup>3</sup> of cement were used. During drilling for the grout holes on 6th September, the insitu ground/fill interface was found to be 'saturated'. On the morning of 7th September, a shallow slip, involving a 1 m deep layer, occurred at the downstream slope face (Figure 2).

Reinstatement of the road surface was carried out after grouting, for road opening on 24th September. During the works, a small crack was observed in the gully previously replaced. The 3 gullies and a manhole on the embankment were subsequently blanked off.

The settlement histories of points r and s are shown in Figure 3.

## INVESTIGATION

### Site Investigation

Though the emergency grouting works had stabilised the embankment, the cause of the settlements was unknown and it was felt prudent to carry out a full investigation. The investigation had to be completed within a period of about five months so that any necessary remedial works could be implemented before the rainy season arrived.

Desk study and ground investigation therefore went hand in hand. Records including design and construction records, settlement monitoring

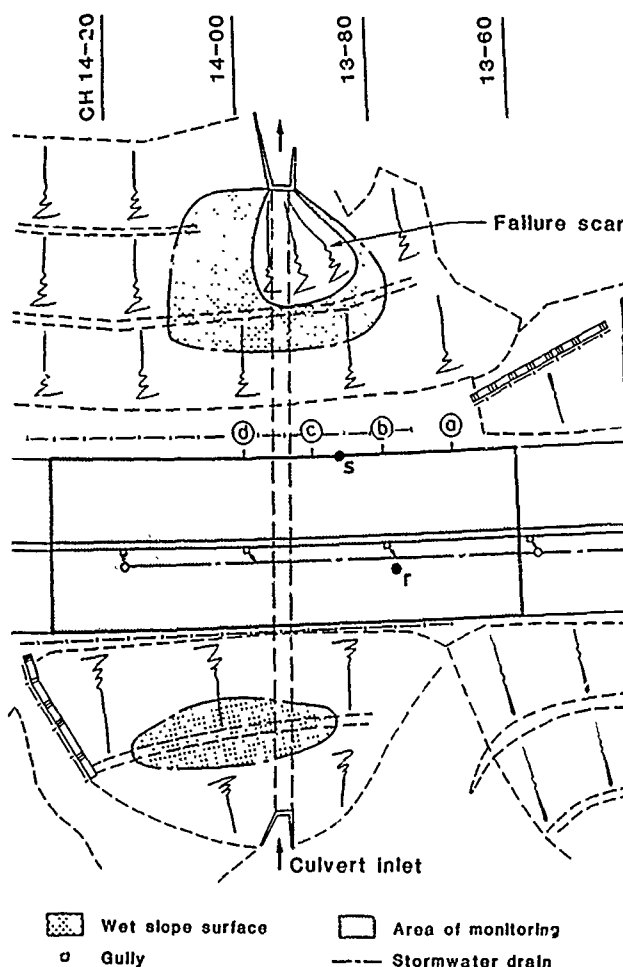


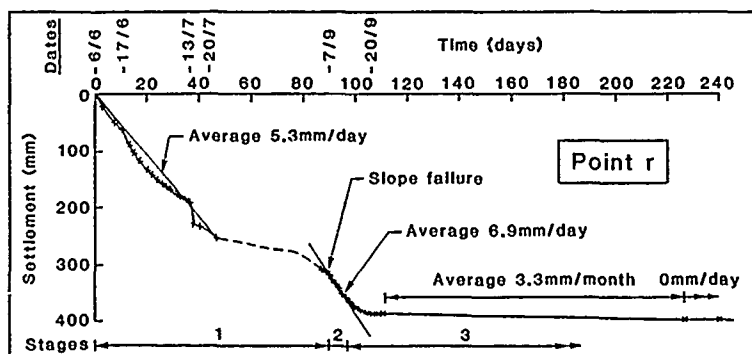
Figure 2 - Plan showing area of road surface monitored

data and records of emergency measures were scrutinised. Aerial photograph interpretation and field geological mapping were carried out. Trial pits, inspection trenches, GCO probings (GCO, 1987), drillholes and piezometers were ordered to assess the geological and ground-water conditions and the density of the fill. Air foam was used as the flushing medium for the drillholes that were sunk through the embankment body, to minimize the possibility of any adverse effects on the stability of the side slopes (Phillipson & Chipp, 1981; 1982). Drilling was closely supervised. Standard penetration tests carried out in the drillholes revealed the presence of a patch of loose material above the eastern valley face (Figure 1).

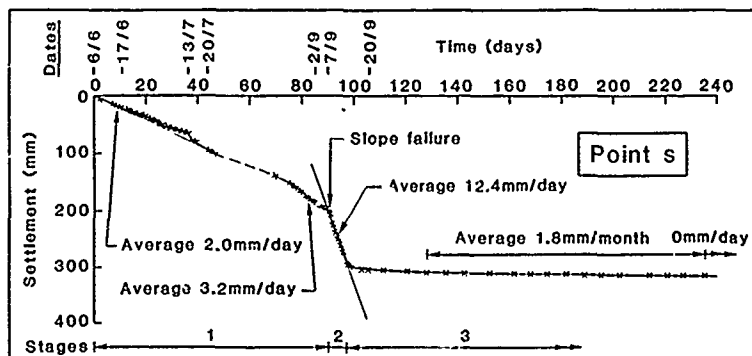
### Laboratory Testing

A series of laboratory tests were carried out on the fill materials. Apart from classification and compaction tests, shear box tests (using 100 mm square direct shear box on test specimens remolded to a range of densities) and dispersion tests, including double hydrometer tests (Decker & Dunnigan, 1977), crumb tests (Standards Association of Australia, 1980), and the determination of Exchangeable Sodium Percentage (Flanagan & Holmgren, 1977; Sherard et al, 1976) were carried out. The latter tests showed that

| Dates                        | Events   |
|------------------------------|--|
| 6/6/85                       | Monitoring started.  |
| 17/6                         | Test load of 20 kPa applied.   |
| 13/7                         | Leaking gully at Ch. 13+78 found.<br>Testing revealed leaking<br>stormwater drain.   |
| 20/7                         | Removal of test load.  |
| Late July<br>to<br>Late Aug. | Replacement of defective gully<br>and cracked stormwater drain.<br>Road reinstatement.                                       |
| 6/9                          | Grout hole drilling commenced.   |
| 7/9                          | Part of downstream slope failed.<br>Slope fully saturated.   |
| 10/9                         | Carriageway grouting started.<br>Seepage from slope face<br>during grouting.   |
| 16/9                         | Grouting completed.  |
| 19/9                         | Road surface reinstatement started.<br>Crack observed in repaired gully.<br>Three gullies and a manhole were<br>blanked off. |



(a) Settlement-time Relationship for Point r



(b) Settlement-time Relationship for Point s

Figure 3 - Settlement histories of points r and s with summary of events

the fill is non-dispersive.

A series of oedometer tests were also performed to investigate the compressibility characteristics and collapse potential of the fill. The test specimens, which were 75 mm diameter by 19 mm thick, were prepared from samples remolded at optimum moisture content. Two types of tests were carried out :

(a) Double oedometer tests (loading sequence of 25, 50, 100, 200 and 400 kPa)

| Condition of Specimen          | Density of Specimen |         |
|--------------------------------|---------------------|---------|
|                                | 80% MDD*            | 95% MDD |
| Unsoaked (air-drained)         | ✓                   | ✓       |
| Soaked (double-sided drainage) | ✓                   | ✓       |

\* MDD = Maximum dry density

(b) Wetting tests (soaking of compressed samples)

| Total stress applied (kPa) | Density of Specimen |         |
|----------------------------|---------------------|---------|
|                            | 80% MDD             | 95% MDD |
| 25                         | ✓                   | ✓       |
| 100                        | ✓                   | ✓       |
| 400                        | ✓                   | ✓       |

The results of these tests are summarized in Figure 4. It can be seen that there are two components of settlement, viz compression of the unsaturated material, and collapse due to wetting.

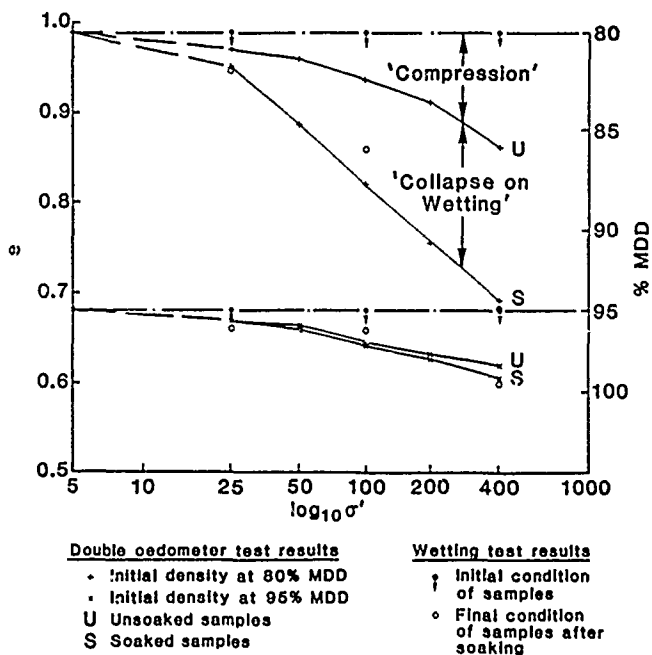


Figure 4 - Results of oedometer tests






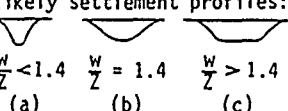


|                                      | No.  | Cause   | Expected Settlement Profile  | Expected Settlement/Time   | Supplementary Identifiers  |
|--------------------------------------|------|---|--|--|--|
|                                      |      |   |  |  |  |
| Foundation Problems                  | IA   | Foundation failure (in soil or in rock) due to embankment loading and surcharge   |   | Takes relatively short time to complete and sudden.  | Foundation condition.<br>Bearing capacity of foundation.   |
|                                      | IB   | Settlement of compressible layers (e.g. colluvium and top soil) due to embankment loading and surcharge                                   |   | Starts from the moment of loading. Settlement $s \propto \sqrt{t}$ (primary) or $s \propto \log t$ (secondary).  | Presence of compressible layers.   |
|                                      | IC   | Collapse of cavities (e.g. solution cavities, structural cavities or voids in bouldery colluvium) due to embankment loading and surcharge |  <p>Types of cavities :<br/>           (a) Sub-critical<br/>           (b) Critical (Gaussian)<br/>           (c) Super-critical</p> <p>Likely settlement profiles:</p>  <p><math>\frac{W}{Z} &lt; 1.4</math> (a)    <math>\frac{W}{Z} = 1.4</math> (b)    <math>\frac{W}{Z} &gt; 1.4</math> (c)</p> | Starts when the critical load of the cavities is reached and completes within a relatively short time. May be related to groundwater flow.   | Mineralogy of rock. Groundwater chemistry. Cavities detected from drilling.<br>Fracture state indices and nature of infill of rock joints.<br>Effect of stress relief on joint opening.<br>Presence of bouldery colluvium and rapid groundwater flow.<br>Maximum settlement up to 90% of cavity size only.<br>Volume of settlement trough less than cavity volume. |
| Problems with Fill - Embankment Body | IIA  | Collapse of deteriorating soil material (e.g. soil containing gypsum or other soluble salt) due to embankment loading and surcharge       | Erratic. Depends on rain or groundwater movement. If fill is totally saturated, then settlement $\propto$ fill thickness. If local solution, then profile resembles cavity-type settlement profile.  | Starts when critical void ratio is reached or shear strength reduces to limiting value. Can be gradual or stick-slip. Depends on rain or groundwater flow.   | Mineralogy of parent rock. Groundwater chemistry. Sulphate and carbonate content of soil. Evidence of water flowing through fill.  |
|                                      | IIB  | (a) Consolidation and creep of fill<br>(b) Settlement due to test loading   | Settlement $\propto$ fill thickness.   | Starts immediately after construction and application of test load. Consolidation $\propto \sqrt{t}$ , and creep $\propto \log t$ .  | Estimate of rate of primary consolidation and order of consolidation and creep. Estimate of settlement due to test loading. Construction/compaction records.   |
|                                      | IIC  | Internal erosion (due to fast flowing water or dispersive soil) and subsequent settlement due to embankment loading and surcharge         |   | Starts when critical void ratio is reached. Erratic and long term. Fluctuates with groundwater flow or rainfall.   | Evidence of water flowing through fill. If fast flowing, water will spring out of slope face and adjacent hillside. Dispersion potential of fill. Presence of loose zones in fill and structureless materials in rock joints.  |
|                                      | IID  | Slope failure (or creep) due to groundwater flow, infiltration or additional loading  |   | May be associated with rainfall. Can be rapid or slow.   | Laboratory tests on shear strength of fill. Presence of perched water table. Factor of safety of side slopes.  |
|                                      | IIIE | Hydrocompaction (i.e. collapse of unstable soil structure, e.g. loose fill or fill compacted dry of optimum moisture content)             | Depends on form of wetting. If totally saturated, then settlement $\propto$ fill thickness. If locally saturated, then profile resembles cavity-type settlement profile (see IC above).  | Completes soon after first saturation but soil may take some time to be completely saturated, particularly if water is from a local source. If caused by infiltration, side slopes will gradually subside. | Estimate of collapse settlements of loose fill (oedometer wetting tests). Assessment of ground conditions for perching. Identification of source of water for hydrocompaction. Estimate of quantity of water required for saturation. Construction/compaction records. Assessment of fill density (SPT's and GCO prebings).  |

Table 1 - Summary of the range of possible causes and their associated mechanisms

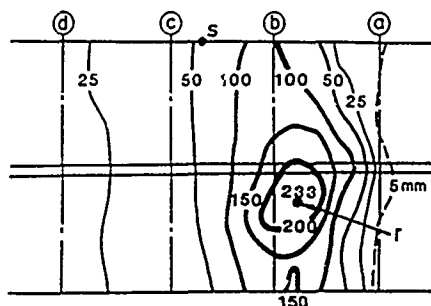
## POSSIBLE CAUSES

Possible causes of the settlements can be divided into two categories, viz causes which arise from the foundation and causes which arise from the fill embankment body. Table 1 summarizes the range of possible causes and their associated mechanisms. Each of the causes was systematically evaluated in the investigation.

As the settlement monitoring records are the most valuable information available, the settlement contours and settlement-time relationship were used as primary identifiers of the causes. These were supplemented by results of the site investigation and laboratory testings.

Analysis of settlement data revealed that the settlements can be separated into three stages :

- (a) Stage 1 settlements had a dish-shape and appeared to have resulted from a point disturbance around point r (Figure 5). They had a stick-slip relationship with time (Figure 3a), i.e. a 'collapse' type of settlement. Calculations indicated that the 20 kPa test load could have induced up to about 10% of the total settlements in this stage.



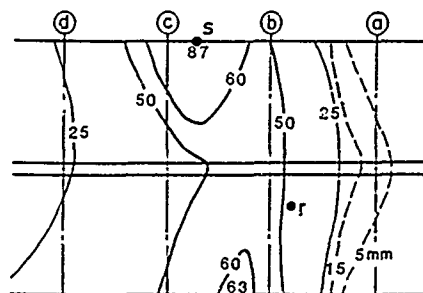
Prior to the removal of test load on 20/7

6/6 to 17/7

Figure 5 - Settlement contours for stage 1

- (b) Stage 2 settlements were much more rapid (Figure 3b) and were likely to be related to slope instability (Figure 6). Stability analyses of the side slopes assuming 'dry' condition, i.e. zero pore pressures, gave factors of safety in excess of 1.2. However, measurements taken in the grout holes after drilling indicated high water levels in the holes. In one of the holes, water was found to be only 5 m below the road surface. Further stability calculations using the measured 'phreatic surface' revealed factors of safety close to unity. There was heavy rainfall between 4th and 6th September. The rain could have had some effects on the slope, but it could not be the main cause of failure as the slope had survived previously harsher rainstorms.

- (c) Stage 3 settlements ranged from 1.8 to 3.3 mm per month. They could be due to effects of the previous stages or creep, which could give rise to a similar order of settlements.



Inclined holes grouting completed on 11/9

2/9 to 12/9

Figure 6 - Settlement contours for stage 2

## HYDROCOMPACTION

Systematic assessment of the range of causes in Table 1 revealed that hydrocompaction is the most likely cause of Stage 1 settlements.

Hydrocompaction is defined as the collapse of an unstable soil structure upon wetting, a phenomenon which has been recognized for many years (Holtz, 1948; Hilf, 1975; Clayton & Simons, 1981). An unstable soil structure may result when the fill is loose or when compaction has been carried out at too dry a placement moisture content. The amount of collapse is dependent upon the density of the soil, the placement moisture content, the consolidation characteristics of the soil and the loading conditions.

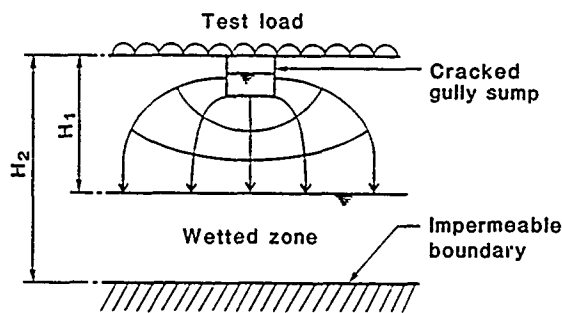
During the ground investigation, a patch of loose fill was detected. It was not possible to identify the source of the loose fill, except that all the mechanisms for which the fill could be loosened subsequent to compaction had proved to be impossible. For hydrocompaction to have occurred, the following needs to be answered :

- What is the source of water entering the fill?
- Do the geological conditions at the site permit it to occur?
- Can the order of settlements be explained?
- Can the source of water provide sufficient quantities for hydrocompaction to occur?

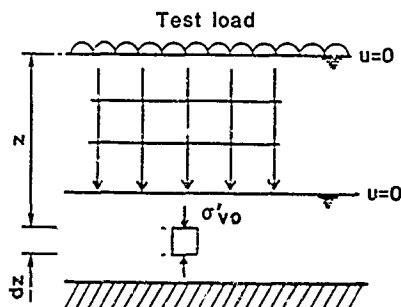
Various sources of water have been examined during the investigation. The cracked gully was identified to be the main possible source. Its location is remarkably close to point r, where maximum settlement had taken place (Figure 2).

The fill was found to be resting on top of a relatively impermeable layer of decomposed silt-

stone, with some top soil and organic matter at the base of the fill. This fill/insitu ground interface would allow any descending water from the gully to perch on, thus permitting the formation of a wetted zone that can advance upwards to initiate hydrocompaction of the loose patch of fill (Figure 7). An idealised 1-D model was used to compute the order of settlement, using the oedometer test results. The following summarizes the analytical approach adopted.



(a) Field Condition



(b) Idealised 1-D Model

Figure 7 - Proposed hydrocompaction mechanism for collapse of loose fill

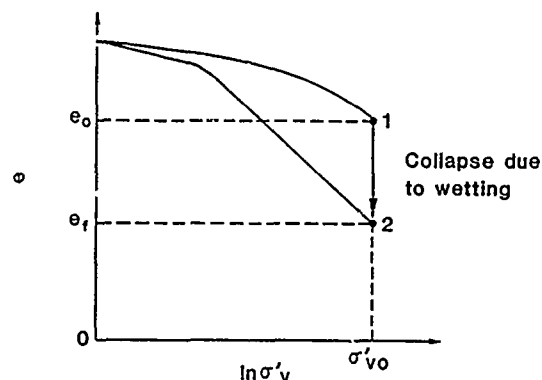
Figure 8a shows a typical set of wetting test results. A soil element denoted by point 1, upon wetting, will collapse to a denser state denoted by point 2. In the field, this will occur when the wetting front has advanced beyond the soil element at depth  $z$  (Figure 7b). The compression,  $ds$ , of the element is given by :

$$ds = \epsilon dz \quad (1)$$

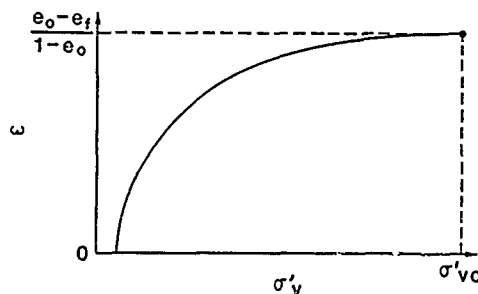
where  $\epsilon = (e_0 - e_f) / (1 + e_0)$  is the strain due to collapse,  $e_0$  and  $e_f$  are the initial and final void ratio of the soil element respectively. From the results of wetting tests, a relationship between strain  $\epsilon$  and vertical effective stress  $\sigma'_v$  can be derived (Figure 8b).

For 1-D condition, the total settlement at ground surface,  $s$ , is given by :

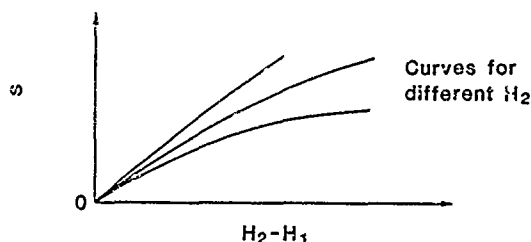
$$s = \int_{H_1}^{H_2} \epsilon dz \quad (2)$$



(a) Typical Wetting Test Results



(b) Strain versus Vertical Effective Stress



(c) Settlement as Function of  $H_1$  &  $H_2$

Figure 8 - Interpretation of oedometer test results

Using the above equations, a series of base curves were produced (Figure 8c) and these curves were used to evaluate the wetted depth  $H_1$  at each settlement monitoring point.

The quantity of water,  $Q$ , required for hydrocompaction can be shown to be given by :

$$Q = \int_{vol.} (m_f \rho_{df} - m_o \rho_{do}) dv \quad (3)$$

where  $m_o$ ,  $m_f$  are the initial and final moisture contents,  $\rho_{do}$ ,  $\rho_{df}$  are the initial and final bulk densities, and  $dv$  is the unit volume of the soil element.

Integration was carried out over a volume of the ground above which settlements had occurred. Because the initial moisture content of the loose material is unknown, a range of likely values ( $m = 20\%$  to  $26\%$ ) were used to derive a corresponding range of  $Q$  values.

The next step in the analysis involved calculation of the quantities of leakage water from the cracked gully. This water came from the rain

that fell onto the road carriageway during the period of settlements. The permeability of the soil is unknown but considered to be of the order of  $10^{-4}$  to  $10^{-5}$  m/s, based on the nature of the fill material. The total amount of leakage was estimated for this range of permeabilities, and the results were found to agree with the range of Q values calculated previously.

## GROUTING

Drilling and grouting in September 1985 had some effect on the slope but it eventually stabilized the embankment.

Because of the low permeability of the fill, the cement grout could not penetrate the fill mass. The grouting pressures imposed horizontal stresses which fractured the fill and allowed stiff columns and sheets of grout to be formed within the embankment body. These pressures momentarily increased the pore pressures, forcing water within the embankment towards the slope surface. Some of the free water in the grout had also leached into the fill mass before it had time to hydrate with the cement. The drainage of this water together with the water driven off by hydrocompaction of the fill are considered to have caused the rapid movements of the slope shoulders.

The water from the grout gradually spreaded to other parts of the embankment body, causing collapse of any loose pockets it encountered. This redistribution and downward migration of water had caused the post-grouting movements, which became stabilized after the grout had hardened.

## CONCLUSIONS

A rigorous investigation was carried out for a fill embankment which settled and showed signs of distress. A range of causes was considered, and, by a process of elimination, it was found that hydrocompaction, i.e. collapse of an unstable soil structure upon wetting, could have caused the early stage of settlements. A model was proposed for hydrocompaction of the loose fill. This model, together with the results of site investigation, lends support to the suggested cause.

Drilling and grouting was considered to have contributed to the slope movements. As the grout hardened, stability of the side slopes was restored.

As a result of the investigation, no major remedial works were considered necessary. Some minor works were recommended to deal with the loose fill and improve the stability of the downstream slope surface.

## ACKNOWLEDGEMENTS

This paper is published with the permission of the Director of Civil Engineering Services, Hong Kong Government.

## REFERENCES

- Clayton, C.R.I. & Simons, N.E. (1981). "The Collapse of Slabs on a Compacted Hoggin Fill" Ground Movements and Structures, Pentech Press, London, pp 655-670.
- Decker, R.S. & Dunnigan, L.P. (1977), "Development and use of the Soil Conservation Service dispersion test", Dispersive Clays, Related Piping, and Erosion in Geotechnical Projects, American Society for Testing and Materials, Special Technical Publication no. 623, pp 94-109.
- Flanagan, C.P. & Holmgren, G.G.S. (1977), "Field methods for determination of soluble salts and percent sodium from extract for identifying dispersive clay soils", Dispersive Clays, Related Piping, and Erosion in Geotechnical Projects, American Society for Testing and Materials, Special Technical Publication no. 623, pp 121-134.
- GCO (1987), Guide to Site Investigation (Geoguide 2), Geotechnical Control Office, Hong Kong, 362 p.
- Hilf, J.W. (1975). "Compacted Fill", Foundation Engineering Handbook, Van Nostrand Reinhold Company, New York, pp 244-311.
- Holtz, W.G. (1948), "The Determination of Limits for the Control of Placement Moisture in High Rolled Earth Dams", Proceedings of the American Society for the Testing of Materials, Philadelphia, pp 1240-1248.
- Phillipson, H.B. & Chipp, P.N. (1981), "High Quality Core Sampling - Recent Developments in Hong Kong", Hong Kong Engineer, vol. 9, no. 4, pp 9-15.
- Phillipson, H.B. & Chipp, P.N. (1982), "Air Foam Sampling of Residual Soils in Hong Kong", Proceedings of the Specialty Conference on Engineering and Construction in Tropical and Residual Soils, Honolulu, pp 339-356.
- Sherard, J.L., Dunningan, L.P. and Decker, R.S. (1976), "Identification and Nature of Dispersive Soils", Journal of the Geotechnical Engineering Division, American Society of Civil Engineers, vol. 102, pp 287-301.
- Standards Association of Australia (1980), "Determination of the Emerson Class Number of a Soil", Australian Standard Methods of Testing Soils for Engineering Purposes, no. AS 1289, C8.1-1980. Standards Association of Australia, Sydney, 3 p.

## Kerrville Ponding Dam, Guadalupe River, Texas

W.R. Stroman

Civil Engineer, Rone Engineers, Dallas, Texas

P.D. Thornhill

Civil Engineer, Espey, Huston & Associates, Austin, Texas

R.R.W. Beene

Consulting Civil Engineer, Fairfax, Virginia

**SYNOPSIS:** Kerrville Ponding Dam is a relatively small channel dam in the Guadalupe River in Kerrville, Texas. The dam is 22 feet (6.7M) high and 600 feet (183M) long and provides a water supply for the City of Kerrville. The dam was constructed during 1979-1980. Seepage problems in the abutments were observed during the initial filling of the reservoir. Some minor corrections to the problems were made at that time. In June 1981, after a moderate flood flow passed over the dam, additional seepage problems occurred. The downstream slope protection was displaced to the extent that cracks appeared in the concrete. This damage led to a more significant amount of repair. On December 31, 1984 the dam was overtopped by a flood to a depth of 10.5 feet (3.2M) above the spillway elevation. The dam suffered severe damage including loss of a portion of the concrete cap and significant erosion of the clay core over approximately one-third of the length of the dam, and seepage related damage at both the abutment areas. Figure 1 shows the conditions of the structure in January 1985. The dam suffered a "Type 1 Accident" as defined according to International Commission on Large Dams (ICOLD).

### INTRODUCTION

Kerrville Ponding Dam is owned and operated by the Upper Guadalupe River Authority, a functional entity of the State of Texas. The dam forms a lake having an area of 105 acres with a storage capacity of 840 acre-feet at normal pool elevation. The damaged Kerrville Ponding Dam consisted of a rolled clay core with 8-inch thick concrete upstream and downstream facing. The service spillway is 21 feet (6.4M) high and approximately 200 feet (60.9M) long. The overflow spillway is 22 feet (6.7M) high and 400 feet (121.9M) long. A centerline profile, looking upstream, is shown in Figure 2. At the abutments the embankment rises on 3 horizontal to 1 vertical slopes to elevation 1635 msl. Cast-in-place concrete cut-off walls extend from the clay core for a distance of 128 feet (39M) into the north abutment and 183 feet (56M) into the south abutment. It was intended that these cut-off walls would bottom a few inches in the sound rock and extend to the bottom of the impervious clay fill.

### SUBSURFACE CONDITIONS

A typical subsurface profile along the axis of the dam, showing the riverbed formation, the natural abutment materials and the rolled filled embankment is depicted in Figure 2. Kerrville Ponding Dam is built almost entirely within the Guadalupe River channel. The river bed exposes a marly clay shale (argillaceous limestone) of the Glen Rose formation, Cretaceous System. The fresh, unweathered limestone is dark bluish-gray in color, is intact, and contains no fissures or fractures. The rock rises approximately 10 feet (3M) above the incised river channel. In the north abutment the upper 5 feet (1.5M) of the limestone is less marly, more earthy, and is highly fissured and jointed with the fissures and joints principally oriented parallel to the



Fig. 1 Kerrville Ponding Dam, Jan. 1985

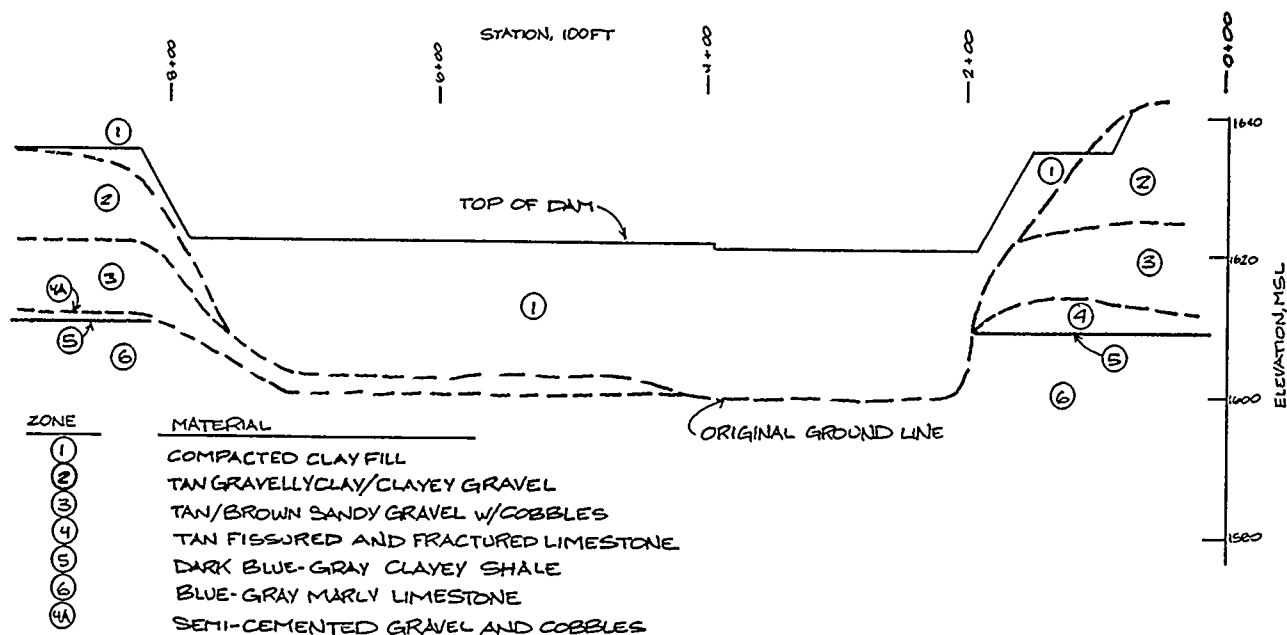


Fig. 2 Subsurface Profile

river flow. These fissures and joints are as much as 3 inches (76mm) wide and extend entirely through the upper limestone bed. On the south abutment, the sound marly limestone is overlain by a poorly cemented, highly vuggy and porous, gravelly and cobbly conglomerate which varies in thickness from 1 to 3 feet (0.3 to 0.9M). A thin bed of high plasticity clay, varying in thickness from 3 to 6 inches (25 to 150mm), lies between the sound rock and fissured rock in the north abutment and between the sound rock and the conglomerate in the south abutment.

On both abutments and the fissured limestone and conglomerate overlain by a loosely compacted silty and/or sandy gravel containing particles up to cobble size. This bed is approximately 10 feet (3.0M) in thickness and becomes more gravelly with depth. Overlying the gravel bed is an approximate 10-foot (3.0M) thick bed of clayey gravel/gravelly clay containing fines of moderate plasticity characteristics.

#### ORIGINAL PROJECT

Typical embankment sections are shown in Figure 3. The earth embankment consisted of moderate plasticity clay having liquid limit values ranging from 50 to 60. The clay was compacted to not less than 95% Standard Proctor density.

A 12-inch thick layer of filter drainage material was placed both beneath the bottom of the embankment, between the embankment and rock surface, and on top of the embankment, between the embankment and the concrete slope paving. The filter materials were obtained from natural sandy gravel deposits upstream of the dam. These deposits were continuations of the gravel bed shown on the subsurface profile, Figure 2. The upper filter blanket extended from the toe of the dam to the upstream edge of the crest beam as shown in Figure 3. In the river bed section the lower filter blanket extended from the toe to the centerline of the embankment. At the abutments the lower filter blanket extended

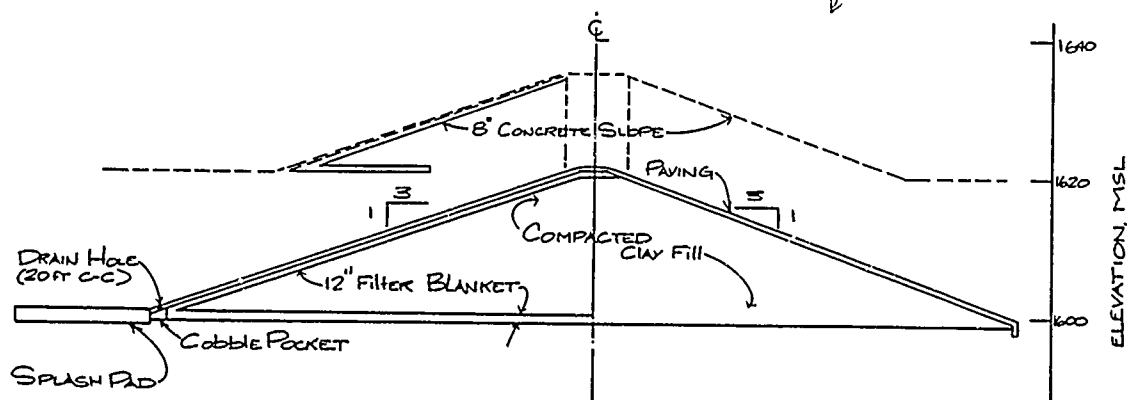


Fig. 3 Typical Embankment Section

from the toe to a point one-third the base of the embankment. The embankment was protected from erosion and scour by a lightly reinforced 8-inch thick concrete slab. A 2-foot thick by 20 feet wide concrete splash pad was placed along the downstream toe. The concrete slope paving was dowelled into the splash pad. Ten-foot high training walls were placed adjacent the steep river banks downstream of the embankment and extended approximately half-way into the downstream slope.

Four-inch diameter weep holes were placed on 20-foot (6.1M) centers at the juncture of the downstream slope protection and the splash pad and along the downstream training walls. To prevent loss of filter materials through the weep holes, one cubic foot pockets of cobbles ranging in size from 4 to 12 inches were placed between the filter zone and the weep holes.

Slope paving extended up the abutments to the crest of the non-overflow section as shown by the dashed-line embankment in Figure 3. A crest width of 10 feet (3M) was established for the non-overflow section. Slope paving was extended land-ward until its elevation of 1635 msl met natural ground surface. The cast-in-place concrete cut-off was constructed in open ditches excavated with a back-hoe through the cohesive and non-cohesive abutment materials.

Construction of the dam began in the Fall of 1979 and was essentially complete in the Fall of 1980. Impoundment began in Aug. 1980 and the reservoir was essentially full by October 1980.

#### EARLY DEFICIENCIES

During construction of the north abutment in the spring of 1980 it was discovered that the concrete cut-off wall had been bottomed on top of the fissured and fractured limestone. When excavations were being made for the left downstream training wall, water was observed flowing from the fissures. An additional cut-off wall upstream and adjacent the initial wall and bottoming a minimum of 1 foot (300mm) into the sound rock was installed. The top of this additional wall abutted and overlapped the bottom of the initial wall for a distance of 1 foot (300mm).

In September 1980, when the reservoir was first filling, excess seepage was observed in the south (right) abutment area. Significant seepage was observed coming through construction joints in the downstream slope paving slab. At one location a stream of water was observed jetting approximately 8 inches (200mm) above the slope paving at a point some 9 feet (2.7M) below the then existing reservoir elevation. A portion of the slope paving adjacent the right downstream training wall was removed and a 2-foot by 2-foot (500 x 500mm) aggregate filter surrounding a 4-inch (100mm) perforated pipe was installed. The concrete slope paving was then replaced. The exit point for the pipe was established at the downstream end of the right training wall.

Kerrville Ponding Dam was dedicated in June 1981. During the Spring and Summer of 1981 additional problems related to performance of

the embankment structure appeared. A storm had produced a flow 5.6 feet (1.7M) passing over the spillway. After the flow had subsided, a "rooster-tail", i.e. a fan-like spray of water, appeared on the downstream slope. This "rooster-tail" was actually produced by a crack in the concrete slope paving with an attendant 3/8-inch (9.5mm) vertical displacement. When the flow had further receded and the downstream slope paving could be more closely examined, several cracks in the slope paving could be seen. Most notable of these cracks was a continuous crack approximately mid-way down the downstream slope that extended from abutment to abutment. The condition beneath the concrete slope paving was investigated by coring 4-inch (100mm) holes through the concrete. It was found that a void space having a depth of as much as 3-inches in thickness (75mm) had formed beneath the slope paving. The surface area defining the lateral extent of the void covered a large percentage of the northern one-third of the embankment. This condition was "repaired" by drilling several holes through the concrete paving into which a mixture of concrete sand, water and "Revert" (TM) was placed; mostly by gravity flow but in some instances by pumping. Although no surveys were made to establish relative elevation of the slab, observers seem to think that the slab was in a "bowed" position at this time. The holes drilled through the concrete were filled with concrete and cracks in the slab were sealed with an elastomeric compound.

#### FAILURE OF DAM

During the night of December 31, 1984 the dam was overtopped by a flood to a depth of approximately 10.5 feet (3.2M) over the spillway section. The dam suffered extreme damage, including complete destruction of the downstream concrete slope protection. Approximately one-half of the concrete was completely removed from the left spillway section. The clay core eroded in some places as far as 10 feet (3.0M) beneath the remaining concrete paving slab on the left one-third of the dam. The concrete paving slab adjacent the south (right) abutment was cracked and displaced upwards as much as 1 foot (300mm). A significant amount of filter material was eroded from beneath the slab for a distance of 60 feet (18M) from the south abutment. A photograph showing the scope of damages is shown in Figure 1. The dam was not breached, so the incident could be classed as an ICOLD TYPE 1(1A) Accident. The reservoir was drawn down to elevation 1613 msl to alleviate further damage and yet maintain a water supply source for the City of Kerrville and, except for occasional rises of the river during the investigation and repair phase, was maintained at that level until repairs to the structure were completed.

#### INVESTIGATION OF FAILURE, FINDINGS

Several theories as to the cause of the damage were propounded by various personalities. Among the causes put forth was the effect of strong eddy currents and turbulence developing negative pressures against the concrete cover. Another cause considered was the beating and pounding action of logs and other debris caught in the roller waves downstream of the dam. However, careful observations of the condition of the dam

and its abutments, review of pre-construction geotechnical investigations together with construction quality control records, the incidences of seepage during construction and first filling and the remedial procedures used to mitigate these conditions, coupled with results of a fairly extensive subsurface investigation made after the failure gave strong indications that the basic problem dealt with the design of the dam; its internal hydrostatic control and drainage system and the communication established between the drainage system and the naturally occurring pervious materials found in the abutments.

Samples of the undisturbed filter materials used in constructing the dam were obtained for testing. Grain size analyses showed percent fines (-No. 200 sieve) varying from 5 to 18 percent. Atterberg limits tests indicated plasticity index values on the order of 8 to 15. A typical grain size curve for the filter material is shown in Figure 4.

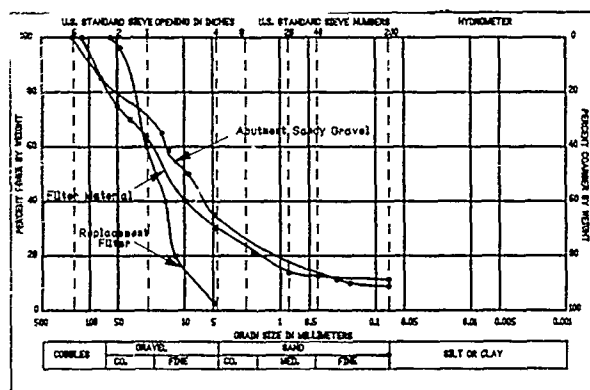


Fig. 4 Grain-Size Curves, Natural and Filter Materials

Bulk samples of the natural gravel stratum were obtained from large diameter test holes dug into the abutments both upstream and downstream of the embankment. Grain size analyses typical of the materials are also shown in Figure 4. It is obvious that these materials have very similar grain size characteristics. Analyses of grain size curves indicate that the materials are of a suffusion character. The  $D_{60}/D_{10}$  ratio are well in excess of 20 which according to U.S. Army Engineer Waterways Experiment Station Report "Design and Construction of Granular Filters for Embankment Dams" by Edward B. Perry, indicate the materials are internally unstable and susceptible to internal migration and possible loss of the finer particles.

Trenches were excavated into both abutments at locations where the cut-off trench could be exposed for inspection. On the south (right) abutment it was found that the concrete cut-off bottomed some 4 to 8 inches (100 to 200mm) above the sound rock. Very loose coarse gravel was found in the void between the concrete cut-off and the rock. In the north (left) abutment a void ranging from 2 to 6 inches (51 to 152mm) was found between the concrete and the fissured rock. Additionally, it was found that the concrete had been cast in three separate sections with coarse gravel intruding into the

Joints in the concrete. The triangular joint in the center of the two right pieces of wall is about 6x8 inches (152-203mm) in size. This condition is depicted in Figure 5. A 36-inch (0.9M) boring was made upstream of the cut-off to inspect the juncture between the original cut-off and the extended cut-off. It was found that an approximate 2-inch (51mm) vertical gap existed between the two walls. The gap was filled with loose coarse gravel and tree roots up to 1-1/2 inches (38mm) in diameter.



Fig. 5 Defects in North Cut-off Wall

#### BASIC CAUSE OF FAILURE

Based on visual observation, exploratory borings, and laboratory testing it was concluded that the distress to the dam was the result of three basic flaws:

1. The defects in the cut-off walls provided direct access of significant quantities of water under excess head from the reservoir into the filter materials in the area downstream of the crest of the dam. The sum of areas providing relief for the water flows was significantly less than the sum of inlet areas. Consequently the filter materials became overloaded, high hydrostatic pressures developed beneath the paving slabs, thereby lifting and disrupting the slab. Once the slabs were displaced and broken, the rush of water over the crest completed the destruction shown in Figure 1.
2. It is noted that the so-called filter material violated several of the recognized filter criteria when using the gravel as the base material. It can be said that the structure did not have a filtration or pressure reducing system in-so-far-as the more permeable base materials were concerned. Also, the filter materials were quite variable as to percent fines. This produced a great variation in filter permeability. Much of the filter contained significantly more fines than are usually permitted in a well designed filter material.



3. The "cobble pockets" at each of the weep holes were without any direct control as to particle size or size of voids produced. The size of the drain hole with respect to the size of the cobbles were such that one cobble could completely block a drain hole. Close examination indicated that perhaps only 4 of the 20 drain holes in the dam that remained after the accident were actually working.

#### REPLACEMENT DAM

Constraints placed on repair to the dam included that the repair structure should fit within the footprint of the original dam. Also, the reservoir remaining behind the damaged structure could not be lowered more than 10 feet (3.0M) without adversely impacting the City of Kerrville's water supply. Six basic options were considered: (1) remove the existing dam and replace it; (2) repair and replace the damaged portion in accordance with original plans; (3) construct a vertical concrete buttress dam; (4) replace the clay core dam with one having a much thicker concrete cap; (5) move the dam to a new location; and (6) replace the dam with a roller compacted concrete (RCC) dam.

Whatever of these solutions were adopted, it was considered imperative that the downstream pressure relief filter system would require replacement and that a new, continuous cut-off system would be necessary.

It was determined that a roller compacted concrete (RCC) dam offered several advantages to the other considerations. Not the least of these was the consideration that a RCC dam could withstand overtopping with a minimal damage to work in place.

Along the Guadalupe River and within easy haul distance of the dam site, several gravel bar deposits were being mined commercially to produce concrete, asphalt and base course aggregate. Generally, the sand and gravel is processed by washing and screening and/or crushing and blending to meet American Society of Testing Materials or Texas Highway Department specification requirements. Samples of the processed materials and pit-run materials were obtained from several of these pits to evaluate their potential use in producing roller

compacted concrete. Specification limits for grain size distribution were established as shown in Figure 6. Also shown are the average results of grain size analyses tests conducted on 52 samples taken from the mix plant during construction.

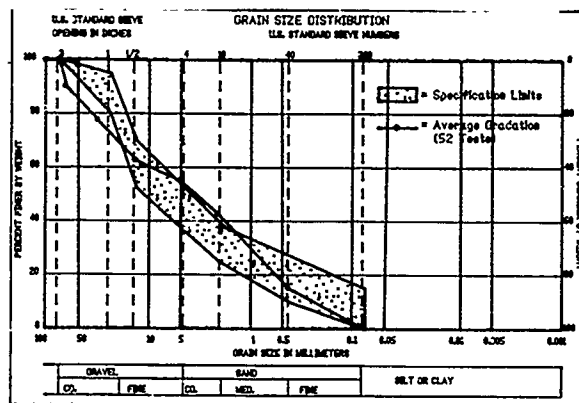


Fig. 6 Roller Compacted Concrete Gradation

Grain-size analyses of pit-run materials, and visual examination, showed that the various producers were all mining essentially the same materials. Grain-size distribution curves of materials "scalped" over a 3-inch screen were compared with curves reported by other RCC users and were found to conform quite well. Trial mixes showed that adequate strength, and durability could be obtained with moderate amounts of cement. Both Wetting-and-Drying and Freezing-and-Thawing (ASTM D559 and ASTM D560) on laboratory molded specimens showed losses ranging from 6 to 10 percent. Tests also indicated that the molded materials would develop compressive strength ranging from 1100 to 2000 psi at 28 days age on materials containing from 5 to 10 percent portland cement, by weight. The durability and quality of the aggregates themselves were well established by their use in numerous projects throughout the area.

The final embankment section for the RCC dam is shown in Figure 7. The RCC structure was designed to not only resist the forces generated by the reservoir but also to support the

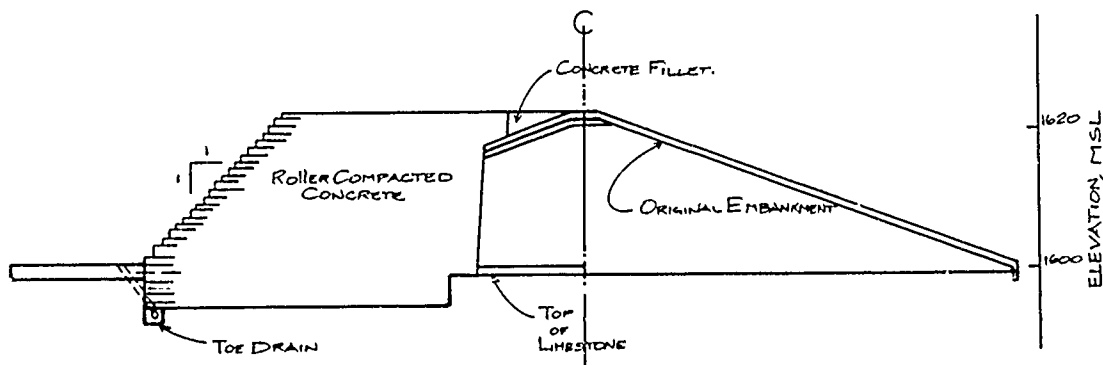


Fig. 7 Repaired Embankment Section

embankment that was to remain in place once the dam was completed. Based on Culman's method to determine the stability of near-vertical slopes composed of clay soils, it was decided that a vertical slope of 17 feet (5.2M) would be safe against failure for some reasonable period of time. Consequently, the original downstream slope was removed to a point some 16 feet (4.9M) downstream of the axis of the dam and a vertical slope established. The slope stood throughout the construction period of some four months with only minor sloughing even though it was overtopped by flood flows on two occasions. The portion identified as "original embankment" in

Figure 7 served to contain a reservoir during the construction period.

Roller compacted concrete was placed in 1-foot (300mm) thick lifts and rolled with a 10-ton vibratory steel wheel roller. It was decided that the bottom seven lifts and top five lifts of RCC would contain 10 percent portland cement by weight and that the interior lifts would contain 5 percent cement. This decision was based on the desire to provide a higher strength material in the base of the dam where tensile forces would be greatest and to provide more erosion resistance at the top of the dam.

Moisture and density control were conducted on a daily basis. Additionally, laboratory molded specimens were made from the materials being placed. Results of strength tests of laboratory molded specimens are shown in Figure 8. After the dam was completed both 6-inch (152mm) and 10-inch (250mm) specimens of in-place RCC were obtained with a diamond core barrel. Strength tests were conducted on specimens of the core. Results of these tests are shown in Figure 8 for comparison with laboratory molded specimens. Down-hole permeability tests were conducted in the core holes. Permeability values obtained from these tests ranged from  $1 \times 10^{-5}$  to  $1 \times 10^{-7}$  cm/sec.

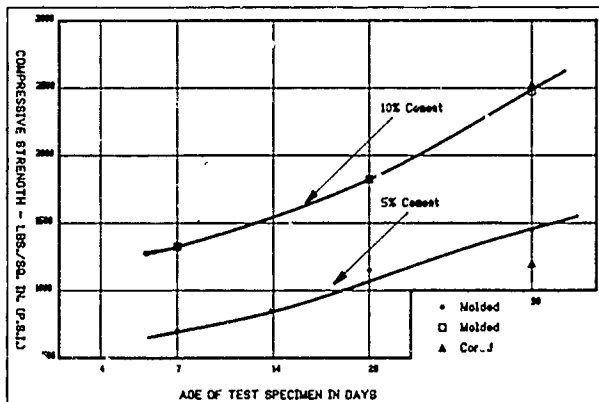


Fig. 8 Strength of RCC

The seepage through the abutments was controlled by constructing overlapping drilled cassions to distances of 130 feet (39.6M) into the abutments. The shafts extended from top of dam surface to at least 3 feet (0.9M) into the unweathered rock. The drilled shaft cut-off wall consisted of two rows of shafts. Shafts

forming the downstream row were 36 inches (914mm) in diameter spaced on 48-inch centers. Approximately 3 days after the concrete was cast in these shafts an 18-inch (460mm) shaft was drilled in the intervening space. Construction of the shafts were closely monitored to insure vertical continuity. The performance of the cut-off walls, when the embankment was overtopped near the end of construction, indicated perfect performance of this control feature.

The downstream pressure relief system (filter material) was redesigned using ASTM Standard Concrete Aggregate, 2-inch to 3/4-inch size. Estimated permeability of this material is quoted to be greater than 50 feet per minute (25 cm/sec). Surfaces of the gravel stratum in the abutments were carefully cleaned and this filter material was placed adjacent the gravel. The filter was carried along the interior of the downstream training walls and terminated at a concrete encased mass of cobbles similar to a gabion. A minimum cross-sectional area equal to 75 square feet (7 square meters) drainage area was provided. It is estimated that a gradient of less than 1/100 would develop in the filter system under maximum reservoir head. construction of the embankment began in the latter part of June 1985 and, except for downstream slope paving, was complete on September 29, 1985.

#### SERVICE HISTORY OF REPLACEMENT DAM

On October 19, 1985 after the embankment, cut-off walls and abutment pavement were complete but before the slope paving above the downstream training walls was complete, the Guadalupe River experienced a flood which overtopped the spillway by 13.4 feet (4.1M). No damage was experienced by the embankment structure. Parts of the downstream face of the drilled shaft cut-off walls were exposed but there was no evidence of through-seepage. Partially completed downstream filter zones and some of the concrete paving above the training walls were washed away. After the floodwaters receded no unusual seepages were observed that could indicate that the dam and cut-off were not functioning satisfactorily. The minor damages were corrected, filter materials were replaced and slope paving above the downstream training walls were completed.

On July 17, 1987 the dam was overtopped to a depth of 17.2 feet (5.24M). This was reported to be the largest flood in the past 40 years in this reach of the Guadalupe River. At the dam the flood reached elevation 1638.2 msl or 3.2 feet (1.0M) above the paved abutment sections. No damage was experienced by the embankment nor its downstream training walls. The only damage suffered by any of the Upper Guadalupe River Authorities' facilities was erosion of soil above the slope paving on the north (left) abutment and the loss of a head-wall and one section storm drainage pipe downstream of the south (right) training wall. Photograph of the dam taken after the July 17, 1987 flood is shown in Figure 9.



Fig. 9 Completed Dam, July 1987

#### CONCLUSION

It is concluded that the accident was caused principally by inadequate cut-off and filter design and construction and substandard hydrostatic relief systems in the downstream portion of the dam and abutments.

Roller Compacted Concrete proved to be an excellent choice for the replacement. Although the work-in-progress was overtopped by river flows several times during construction, loss of work-in-progress was minimal and clean-up and restart of construction seldom required more than one day.

By using roller-compacted concrete to rehabilitate the facility it was possible to maintain a pool of water sufficient to satisfy the City of Kerrville's needs without rationing the use of water.

Design strengths for the RCC mix were achieved and exceeded.

The continuous flow of water plus several large floods have not produced any scour or deterioration of the compacted concrete mass.

#### BIBLIOGRAPHY

Cedergren, H.B., (1967), "Seepage, Drainage, and Flow Nets", John Wiley and Sons, Inc., New York, N.Y.

Department of the Navy, (1971), DM-7, "Soil Mechanics, Foundations, and Earth Structures, Alexandria, VA.

Kenney, T.C. and D. Lau, (1985), "Internal Stability of Granular Filters", University of Toronto, Toronto, Ont.

Lubochkov, Ye.A., (1969), "The Calculation of Suffosion Properties of Noncohesive Soils When Using the Non-Suffosion Analog", International Conference on Hydraulic Research, Brno, Czechoslovakia.

Perry, E.B., (1984, "Design and Construction of Granular Filters for Embankment Dams.", U.S. Army Corps of Engineers, W.E.S., Vicksburg, Mississippi.

# A Case Study of Success to Structures Founded on Expansive Soils

Zhang Shixuan

Senior Engineer, Director of Guangdong Provincial Society for Rock Mechanics and Engineering of the People's Republic of China

**SYNOPSIS:** Since 1979, in accordance with the design program given by the author, no more than 3 storied buildings with an area of more than 200,000 square metres have been built in the expansive soil area of Guangxi Zhuang Autonomous Region and Guangdong Province in South China. The different measures have been adopted according to specification of light, medium and heavy expansive soil. Through the test of special weather and the deformation observation for 3 to 7 years, it has been proved that the intact rate of the buildings has reached 90-98 percent.

This paper mainly expounds three cases and has summed up very effective treatment methods from the practice.

## INTRODUCTION

In China, the expansive soil is distributed broadly over almost every province except northwest area, and especially widespread in the provinces of Guangdong, Hubei, Hunan, Yunnan, Shichuan and Guangxi Zhuang Autonomous Region. Because of the natural geographical distribution, these areas are rich in rainfall with an annual average between 1,000 and 2,000mm, about 70 percent are concentrated in the two seasons of summer and autumn, i.e. from April to September. In these two seasons, there're many storms and heavy flow, and the monthly average temperature is from 20 to 25 degrees centigrade. It's the main typical characteristics to have frequent rain and high temperature in the same seasons, so as to reduce a lot of rainfall seeping into the ground.

In winter and spring, the monthly rainfall would be only 300mm or even less. But the monthly average temperature remains 10 to 20 degrees centigrade. Therefore, during this period, the foundation soil becomes drying shrinkage, and at the same time, most of the buildings and houses begin to sink and crack. According to the result of moisture content observation for long time in South China, the weather-influenced depth may reach 5m, but the serious influenced depth by weather is about 1.5 to 2.5m (Figure 1).



Fig. 1 Two Storied-Building Damaged in South Yunnan

Due to the transverse movement of the soil, usually, the crack with 1 to 10cm in width, 1 to 3m in depth and 30 to 300m in length would appear on the ground. When the ground crack goes through the buildings, the fracture or crack on the wall and floor would emerge.

As known to all, the swelling and contracting deformation of expansive soil comes from the change of the moisture content in the soil. The moisture shift of foundation soil is a rather complicated matter which may be expressed by the moisture balance formula as follows:

$$W = W_0 + [P(1-r) + L + e] - (E + I + u)$$

Where: W = The moisture content in a certain soil layer after the moisture migration

W<sub>0</sub> = The initial moisture content before the moisture migration

P = Precipitation

r = Coefficient of surface run-off

L = The moisture shifted up from the subsoil by capillary

e = The water condensed from water gas

E = Evaporation

I = The moisture transpired from plants

u = The moisture migrated or infiltrated down into the ground

According to the weather condition in China and the moisture balance formula as mentioned above, a program of the comprehensive protection measures has been put forward by the author for the

treatment of the foundation on expansive soil. Here, the program of the comprehensive protection and management doesn't mean that all the measures must be adopted all together. It's required that engineers should not only have a correct design for the houses, i.e. usually, the foundation soil and foundation management would be taken as the main, and the upper-structure's strengthening as the second, but also the treatment of the surroundings of the houses such as building retaining wall, slope protection, drainage, vegetation, and so on should be put into the detailed consideration of design, so as to keep the relative balance of the moisture content in foundation soil, only in this way can the deformation range be shortened. On the other hand, whether the design can be succeeded and whether the desired result of the management measures can be obtained, it's not only by the design unit itself, but also the close co-operation come from the person in charge of construction and the house management or house owner. In accordance with the characteristics of expansive soil such as that it would swell when the moisture increase and it would contract when the moisture decrease, therefore the protection and management work in all fields must be done well.

For recent 10 years, the buildings with an area of 200,000 square metres have been built up in the expansive area of Guangxi Zhuang Autonomous Region and Guangdong Province. The author has conducted observation on foundation soil and buildings for many years. Through the test of special weather, the building intact rate has reached 90-98 percent. Here are the three successful cases specified by light, medium and heavy grades.

#### CASES STUDY

##### Case 1 Medical Ward Building of a Hospital in North Guangdong

##### Basic Condition

This is a three storied-building with 102m long, which is divided into 3 sections by deformation joints, and observation post is in the middle section (Figure 2B).

Figure 2A means the observation poles to observe the deformation for different layers in foundation soil, their depths are specified by 0.5, 1.0, 1.5, 2.0, 3.0, 4.0m.

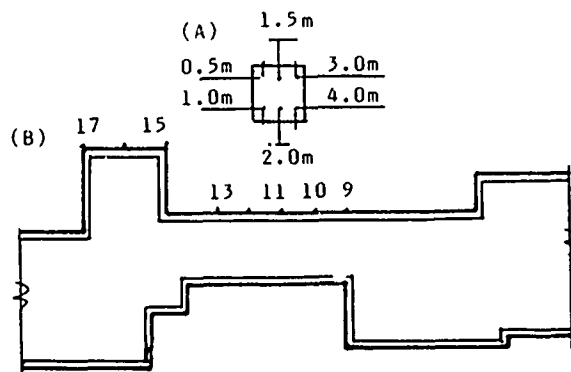


Fig. 2 Plan Figure of Experimental Site

In Figure 2B, the numbers of 9, 10, ..... 17 are observation posts of building deformation. The characteristics of the ground features of the observation field are eroded hilly land, and terrain is a slight slope. The depth of foundation soil layer is between 10 and 15m. Above 5m is residual clay by shale with brown and yellow colours as the main mixed up with light yellow and greyish stripes, hard to plasticity, soil test results shown as Table 1.

TABLE 1. Soil Test Results

| d (m)    | W(%) | WL(%) | Ip | D(%) | e(%)  | Ls(%) |
|----------|------|-------|----|------|-------|-------|
| 1.1-1.25 | 27   | 49    | 23 | 39   | 1.195 | 1.12  |
| 2.1-3.25 | 26   | 47    | 22 | 44   | 3.505 | 1.94  |
| 3.0-3.15 | 29   | 50    | 24 | 52   | 2.155 | 1.26  |
| 4.0-4.15 | 27   | 54    | 30 | 43   | 4.06  | 0.66  |
| 4.85-5.0 | 27   | 46    | 23 | 40   | 2.13  | 1.18  |

In Table 1: d = Embedded depth of soil sample  
W = Initial moisture content  
WL = Liquid limit  
Ip = Plasticity index  
D = <0.005mm grain composition  
e = Expansive rate  
Ls = Linear shrinkage

##### Management Measures

1. Strip foundation have been buried into 1m deep with sand cushion (Figure 3) and the two sides of foundation trough are filled with sand.

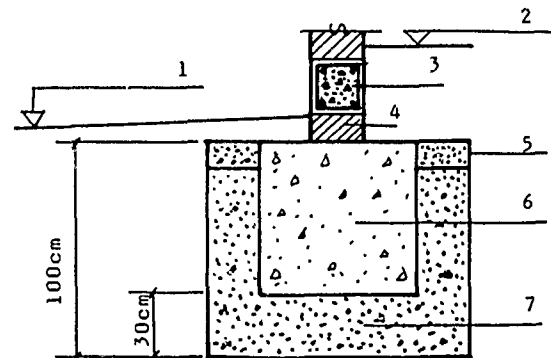


Fig. 3 Sand Cushion

In Figure 3: 1 = Outer ground surface

- 2 = Interior ground surface
- 3 = Periphery beam
- 4 = Brick wall
- 5 = Lime clay
- 6 = Footing
- 7 = Filled with sand

The sand diameter is from 0.25 to 0.5mm, and the moisture content is from 15 to 20 percent.

The unit weight is  $14\text{KN/m}^3$  about.

2. The pour-in-placed reinforced concrete floor and periphery beam.

3. The width of drainage slope is about 1.5-2.5m.

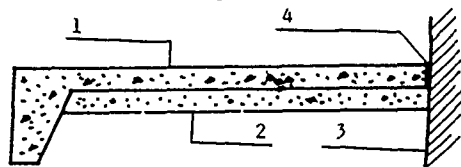


Fig. 4 Drainage Slope

In Figure 4: 1 = Concrete surface layer  
2 = Cushion by lime clay, etc.  
3 = Surface of outer wall  
4 = Expansion joint

The drainage slope around the building is divided by the expansion joint at intervals of 3 to 5m.

In order to prevent the crack of the concrete surface layer on the slope, the building-slope link should be divided by expansion joint, so as to prevent water infiltration into the ground.

The drainage slope's surface layer is made of concrete with its thickness of 80 to 100mm. And the cushion is made of native cement (lime, sand, broken stone), lime soil or sand-stone material.

#### 4. Surrounding Management

The slope hereby the building may be protected by building up the stone. At the foot of the slope, a retaining wall with 1 to 2m high should be built. At the middle of the slope, a drainage ditch should be excavated so as to complete the drainage system at the construction site.

The lower and easier trim away unwanted branches and twigs trees may be selected for scientific vegetation such as fruit and flower trees. It's prohibited to plant quick growing or heavy transpiring trees such as eucalyptus, poplar etc. The distance from trees to buildings should be about 5m. The spare ground should be covered by grass and bush as more as possible, but the irrigation must be controlled.

#### 5. The special requirements to the building construction.

To work out a construction plan is a special importance. The foundation must be laid quickly by continuous construction. The trough or pit should be prevented from heavy sunshine or soaked by water. In the construction site, used water must be controlled strictly and pay a good attention to the drainage of the construction site.

#### Results of Deformation Observation

Since September 1979 to May 1978, the author has conducted deformation observation of different layers of foundation soil with precise leveling instrument Wild N3.

The deformation curves are as Figure 5.

In Figure 5, it's clear to see that with the reopening of the foundation soil layer, the vertical deformation magnitude would be reduced gradually. It's very evident that they'll go up and come down in synchronism.

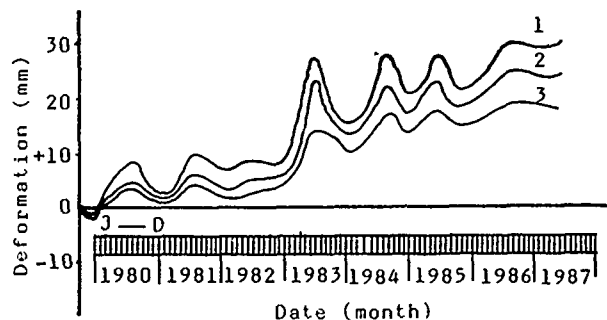


Fig. 5 Deformation Curves of Different Layers of Foundation Soil

In Figure 5: 1 = 0.5m Depth under ground  
2 = 1.5m Depth under ground  
3 = 3.0m Depth under ground

Besides it, the up and down deformation of the foundation soil coincides very much with the changes of the weather at the building area. In rainy season, the foundation soil rises up, and in dry season, it would subside. In 1983, it was a rain-rich year, the rising magnitude was beyond 20mm.

The comparison of the deformation curve of the foundation soil in 1m deep with the deformation curve of building observation post 11 shown in Figure 6.

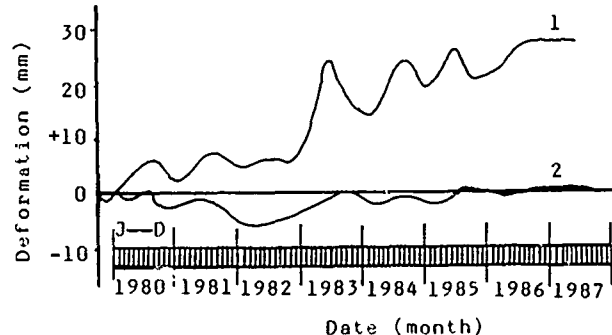


Fig. 6 Comparison of the Foundation Soil Deformation with the Building Deformation

In Fig. 6: 1 = Deformation curve of the foundation soil  
2 = Deformation curve of the building

It's clear in Figure 6:

1. In the same depth, the building deformation range is only the 23 percent of the foundation soil deformation range.
2. In the spring of 1984, the foundation soil was subsided 11mm, but the building was subsided only 2.5mm.

#### Analysis of Management Results

The building was used and observed for deformation for 8 years. Through the test of the very special weather in the summer of 1983 and the spring of 1984, the building remained well. It shows that the management was successful.

The sand cushion for the foundation soil management is different from the function of the exchange of soil by sand cushion on normal foundation soil. Here it's a part of the buffer area between the foundation soil and footing, and plays role together with upper-structure for the adjustment of the uneven swelling and contracting deformation of the foundation soil. On the basis of scale-down test and abundant observation data, it improves that on unit-weight about  $14\text{KN/m}^3$  condition, the sand cushion layer is in a state of medium density, which has an evident feature of elastic deformation. This feature can adjust or redistribute internal force transmitted by the deformation of foundation soil. The adjustable value is the 2 percent of the sand cushion thickness, or 5 to 10mm. The two flanks of foundation trough are filled with sand in moderate and fine size, which may prevent crevice and shift of the foundation and wall caused by ground crack when it goes through the buildings. This function has been improved by broad investigation.

The function of drainage slope may reduce the influence of the moisture content of the foundation soil caused by weather elements such as rainfall, temperature of atmosphere and earth's interior, and evaporation. So as to make the covering condition of both outside and inside building similar and reduce the deformation difference from inner and outer walls. Through the test and observation, it's improved that with the increasing of the width of the drainage slope, the deformation range of the foundation soil would be reduced evidently (Figure 7).

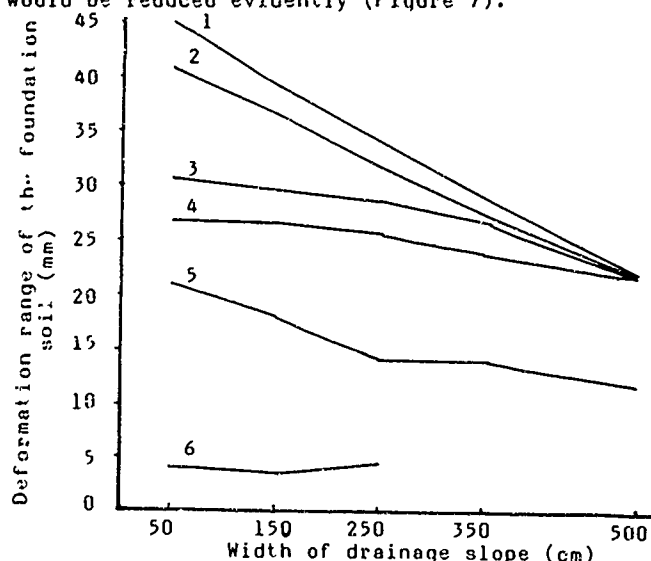


Fig. 7 Deformation Range Under Drainage Slope

In Figure 7:

- Curve 1 = Deformation of the foundation soil 0.5m under the ground surface
- Curve 2 = Deformation of the foundation soil 1.0m under the ground surface
- Curve 3 = 1.5m deep
- Curve 4 = 2.0m deep
- Curve 5 = 3.0m deep
- Curve 6 = 4.0m deep

In Figure 7, it shows that it's obvious to reduce the deformation range of the foundation soil between 1 to 2m under the ground surface by drainage slopes. Thereafter, the buried depth of the foundation can be reduced by widening the drain-

age slope.

The results of the other measures couldn't be introduced and analysed detailedly because of the limited paper space.

#### Case 2 A Hospital Dispensary in South Guangxi Zhuang Autonomous Region

##### Basic Condition

This is the two-storied building with a floor space of 282 square metres built on slight slope. Nereby the building, there're some originally built buildings which have cracked and damaged already.

The overburden soil stratum on the building construction site is the residual clay with thickness of 4 to 5m. The colour of soil is greyish mixed with light red and grey-green stripes. The bedrock is weathering mudstone.

The results of soil test shown as Table 2.

Table 2. Soil test Results

| d (m) | W(%) | WL(%) | Ip | D(%) | e(%) | Ls(%) |
|-------|------|-------|----|------|------|-------|
| 1     | 30   | 48    | 19 | 49   | 3.22 | 5.03  |
| 2     | 30   | 58    | 26 | 64   | 3.93 | 3.83  |
| 3     | 26   | 44    | 16 | 58   | 1.30 | 6.35  |
| 4     | 27   | 57    | 29 | /    | 3.37 | 3.65  |

The means of the symbols: d, W, ..... as Table 1

##### The Following Measures Taken for the Buildings:

1. Strip foundation laid in 1.5m deep with sand cushion in 50cm thick.
2. The pour-in-placed reinforced concrete floor and periphery beam.
3. Width of drainage slope is 2.5m.
4. Reinforced concrete column constructed in the four corners of the outer wall.
5. The surrounding management is the same as Case 1.

##### Management Results

Since the end of 1981, the author had begun to conduct deformation observation untill March 1987. Figure 8 shows the comparison of the deformation of managed and damaged old buildings.

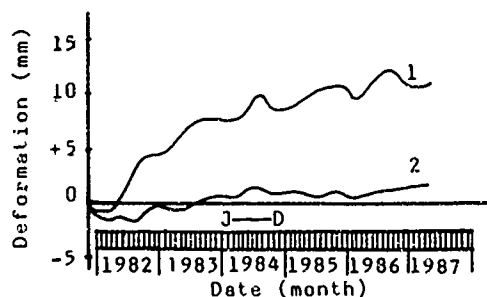


Fig. 8 Comparison of the Deformation

In Fig. 8:

Curve 1 = Damaged buildings with deformation range of 13mm.

Curve 2 = Managed dispensary with deformation range of 3.4mm.

In the rainy season of 1986 (from April to September), the rainfall was 22 percent higher than that of the annual average rainfall. The river was in flood, but the newly built dispensary was still in good condition, which stood up to the tests in special weathers.

### Case 3 A Dormitory Building in South Guangxi Zhuang Autonomous Region

#### Basic Condition

The building covers an area of 150 square metres, which is a single-storied house and built on the middle section of the slope covered by hard-to-plasticity clay with a thickness of 3 to 4m. The colour of soil is grey-green and yellowish white. The bed-rock is mudstone. The results of soil test shown as Table 3.

Table 3. Soil Test Results

| d (m) | W(%) | WL(%) | Ip | D(%) | e(%)  | Ls(%) |
|-------|------|-------|----|------|-------|-------|
| 1     | 25   | 56    | 24 | /    | 12.16 | 6.275 |
| 2     | 26   | 52    | 20 | 59   | 8.87  | 6.15  |
| 3     | 22   | 52    | 18 | /    | 2.94  | 7.725 |
| 4.5   | 23   | 56    | 29 | /    | /     | 6.68  |

The means of the symbols: d,W, ..... as Table 1

#### The Following Measures Taken for the Buildings

1. The pier foundation laid in 2.5m under the ground surface.
2. The width of drainage slope, 1.2m.
3. The pour-in-placed reinforced concrete roof-slab and periphery beam.
4. The surrounding management is the same as Case 1.

#### Management Results

The observation was begun in the January of 1984 and until the March of 1987, the maximum deformation range was 9.91mm and the building remains well (Figure 9).

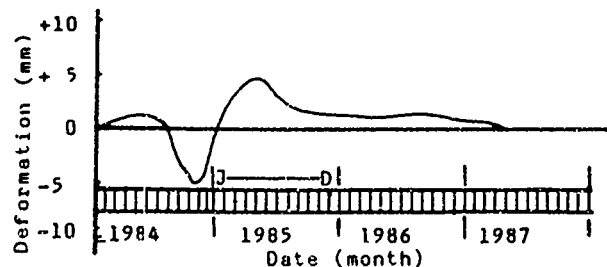


Fig. 9 Deformation Curve of the Building

#### CONCLUSION

The practice improves that in the management of the buildings on expansive soil, it's the only way to reach the previous result by comprehensive management with different measures according to

the condition of geology, terrain, weather, etc.

The observation data show that the swelling and contracting deformation of foundation soil is mainly influenced by weather elements such as rainfall, evaporation of atmosphere and earth's interior temperature. The influenced depth of 2m is usually most obvious in South China. Therefore, the foundation's embeded depth would be 1-1.5m in light expansive soil areas, 1.5-2m in medium expansive soil area, more than 2.0m in heavy expansive soil area. Besides it, the foundation soil must be managed with the measures such as sand cushion layer, replacement method, lime slurry injection process and so on. In architectural design, it's should be tried to reduce the corner of outer wall, because it's the severe-shifting area of moisture. When to determine the outdoor elevation, it should be tried to reduce the digging and filling, especially the measure to stabilize the slope must be taken for the buildings on hill-side field. The engineers must keep them in mind that: to manage slope should be stressed first, then follow after to build houses. In surrounding design, the stress should be laid to water drainage, scientific vegetation, so as to reduce the influence of foundation soil content caused by human element. In building construction, something must be stressed such as high-speed, soaking and sunshine prevention. During the usage of the buildings, it should be done to check whether the waterpipes, buildings and other facilities have been damaged, prune away unwanted branches and twigs in time, maintain the sod and so on.

#### REFERENCES

- Fu Hua Chen (1975), "Foundations on Expansive Soils", Eisevier Scientific Publishing Company Amsterdam-Oxford-New York.
- He Xinfang and Chen Lin (1984), Moisture Coefficient of Expansive Soil and its Application in Engineering Practice", Proceedings, Fifth International Conference on Expansive Soils, Adelaide, South Australia.
- Spangler and Handy (1973), "Soil Engineering", third edition, New York.
- I. I. Lougworth, A. Salam and B. Sunna (1984), "Correlation of Building Damage on Expansive Clay in Jordan with Geology, Local Environment and Type of Construction", Proceedings, Fifth International Conference on Expansive Soils, Adelaide, South Australia.

In the acknowledgement of the following gentlemen for their kind and great assistance in the research work:

Engineer Huan Guangxiang  
Engineer Xie Shiqi  
Engineer Wang Xianwen  
Engineer Wu Shupin

(END)



## Behaviour of Inginimitiya Embankment Dam

T. Sivapatham

Deputy Director, Irrigation Department, Sri Lanka

### SYNOPSIS

The prominent component of the Inginimitiya Reservoir Project is the Inginimitiya Dam. This dam with a maximum height of 58 ft. is essentially a homogeneous earthfill embankment except for the slope protection, filter and drainage arrangement. The cut-off for the foundation seepage and the provisions made in the design for seepage control are described in this paper.

The reservoir when partially impounded for the first time in 1983 "boiling" (bubbling with fines heaving up) was observed on the downstream at different locations close to the toe of the embankment between chainages 71 and 75. This reach when investigated revealed the presence of an impermeable residual soil layer on the ground surface. The material in the entire foundation of the dam upto bed rock is insitu weathered rock material which is heterogeneous in nature.

The analysis of the problem and the remedial measures adopted are discussed in detail. The performance of the embankment dam in 1984 and 1985 after the remedial measures were adopted is found to be satisfactory.

### 1. INTRODUCTION

The Inginimitiya Reservoir Project is situated in the North Western Province of Sri Lanka. The Embankment dam is the prominent component of the project. The dam is constructed across Mi-Oya and is 2 miles 4,690 ft long with a maximum height of 58 ft at the river.

Several dam sites were investigated and the present one was ultimately chosen as the most suitable site from considerations such as geology, storage capacity and the availability of foundation rock at the location of the spillway.

Water balance studies for irrigation of 6300 acres under the Project dictated the full supply level of 202 ft M.S.L. The dam top elevation was fixed at 212 ft M.S.L. allowing for the flood lift, wave height, wave ride up, etc.

In view of the availability of homogeneous and suitable embankment materials (all residual soils) in the vicinity of the dam site and the foundation conditions encountered along the dam axis, a homogeneous embankment dam was chosen to close this wide valley. This type of dam was found to be both economically feasible and technically sound.

### 2. DESIGN FEATURES OF DAM

The plan and longitudinal section of the dam axis are shown in Fig. 1. The typical design embankment section is shown in Fig. 2.

The width of the dam crest was chosen as 20 ft to facilitate vehicular traffic. The upstream and downstream slopes were chosen to be 1 on 2.5 and 1 on 2 respectively. The upstream slope was protected with rip-rap to prevent erosion by wave action. The downstream was provided with turf to prevent surface erosion by rain water. Sufficient freeboard was provided by keeping the dam top elevation at 212 ft M.S.L. to prevent overtopping of the embankment dam during floods. Due to the availability of a large quantity of decomposed rock materials from spill tail canal excavation it was decided to use this material on the downstream slope as shown in Fig. 2.

The average properties of the fill materials used for the construction of the embankment are shown in Table 1 (Nos. 1 & 2).

Since the foundation rock along the dam axis exists at greater depths (45 ft below bed level at the river) as shown in Fig. 1, only partial cut off was provided by taking the core trench to a depth of one-third the dam height. Generally the material encountered at the bottom of the core trench at this level was fairly

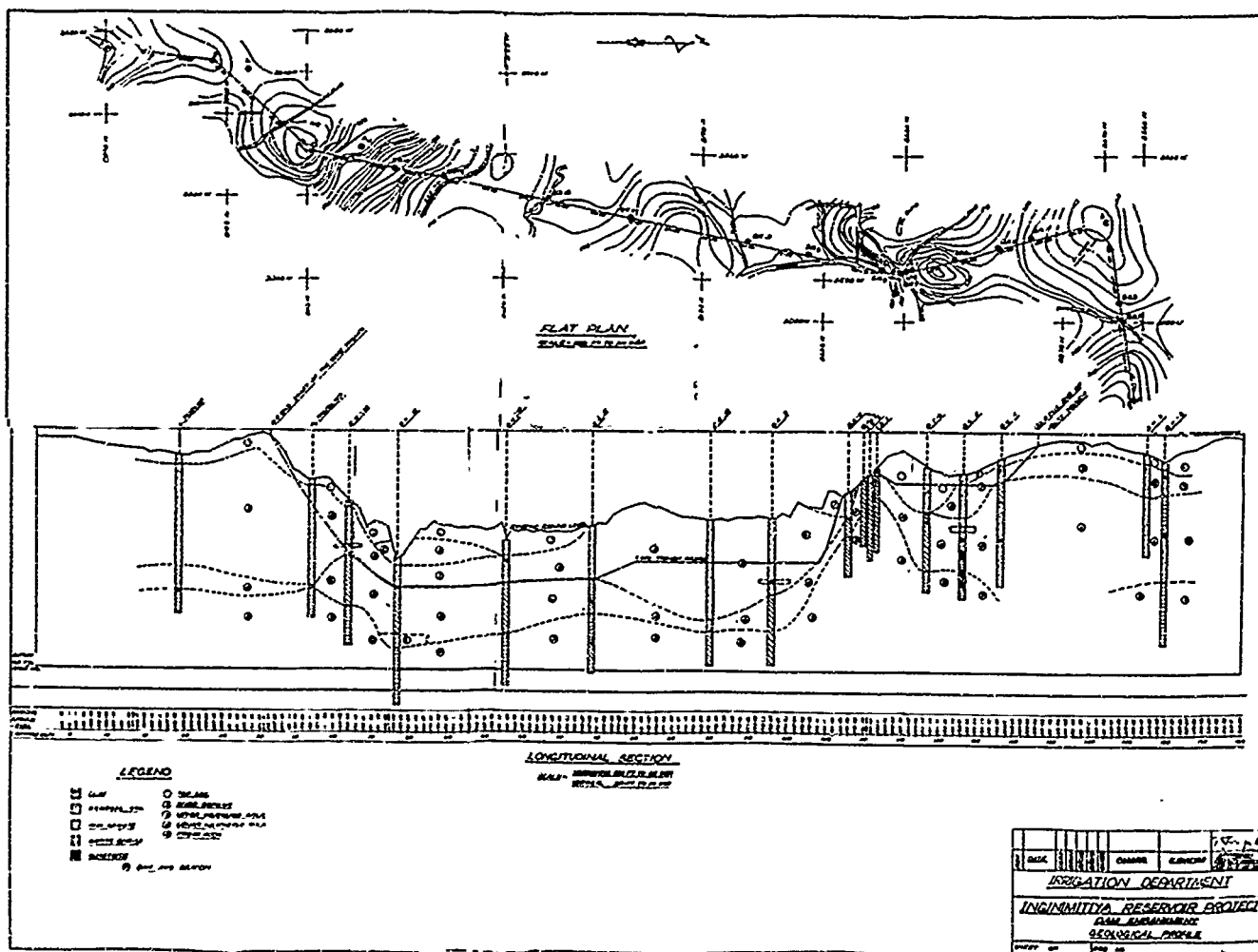


Fig. 1. - Plan and Longitudinal Section of Dam Axis

hard decomposed rock materials. Because of partial cut off, special attention was given to the downstream drainage arrangements during the design stage. The filters on the downstream included a horizontal sand blanket, a larger rock-toe filter and toe drain.

### 3. BEHAVIOUR OF THE DAM

The dam was completed in 1983 except for the construction of the toe drain in certain reaches and it was partially impounded in late 1983 by the help of a coffer dam across the spillway which was not completed at that time. After the water reached a maximum level of around 194. ft M.S.L. (full supply level being 202 ft M.S.L.) "boiling" (bubbling with fines heaving up) was observed on the downstream of the embankment close to the toe at many locations between chainages 71 and 75 and the downstream area in this reach was in a "quick condition". This "quick condition" or "boiling" was not observed anywhere outside this reach of the dam. The material that came out of the "boils" were very fine silty sand-clay mixture which was

decomposed rock materials. It is believed that the seepage path is below the bottom of the core trench which is about 26 ft below ground level. The dam height in this reach is around 42 ft.

Immediate remedial measures were attempted by reducing the water level by discharging water through the sluice and cutting a relief trench at the toe and filling with sand. Since the downstream area was in a "quick condition" the latter operation was found to be difficult. Fortunately the inflow into the reservoir reduced and the water level was gradually lowered. Hence there were no damages caused to the bund.

Sub-surface investigations were carried out in the reach from chainages 71 to 75 in the downstream toe area. Auger holes were dug and the soil samples were tested and classified. The material is basically a residual soil. The typical results of tests on samples in this reach are shown in Table 1 (Nos 3 & 4).

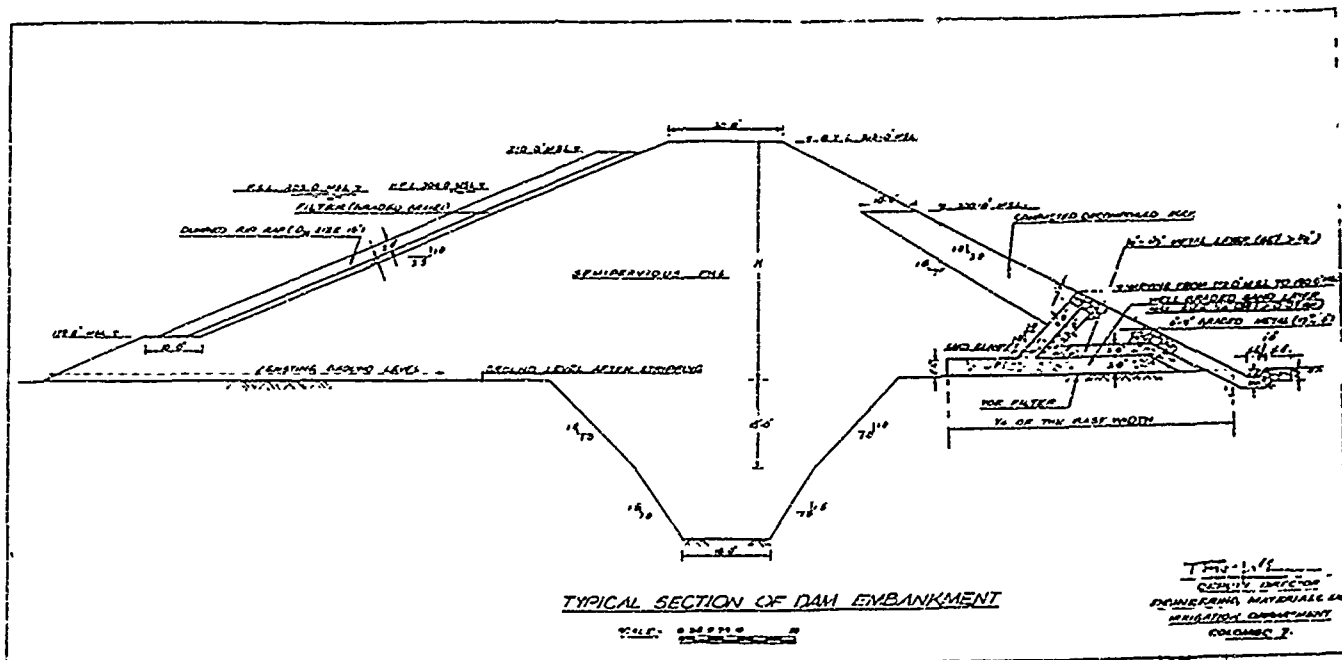


Fig. 2 - Design Embankment Section

#### 4. ANALYSIS OF THE PROBLEM

The investigations revealed the following:-

The seepage flow is confined only to this 16 ft between the bottom of the core trench and the bed rock.

- (i) The downstream area in the reach from chainage 71 to 75 was covered with a soil of very low coefficient of permeability.
- (ii) When the reservoir water level was at 181.6 ft M.S.L. the piezometric level at the downstream toe was at 170.0 ft M.S.L. which is the same as the average ground level in the reach from chainage 71 to 75
- (iii) The bed rock is 42 ft below ground level and 16 ft below bottom of the core trench in the reach from chainage 71 to 75.

The presence of impervious soil in the down-stream area was likely to have prevented free exit of seepage water with high exit gradients and thus exerted large seepage forces on the downstream which caused "boils" (bubbling with fines heaving up) at different locations in the downstream area.

The material below the foundation of the embankment is insitu weathered rock (residual soils) with bedding planes which characterise the parent rock. In this heterogeneous material

Table 1. - Average Results of Embankment materials and typical results on samples between chainages 71 and 75.

| No. | S A M P L E                                      | Unified Soil Classification | Liquid Limit | Plastic Limit | Plasticity Index | Specific Gravity | MECHANICAL ANALYSIS     |                      |                           |                           |                           |                         |                             |                   |                     |      | Optimum Moils: Content % | Maximum Dry density lb/ft <sup>3</sup> | C' lb/ft <sup>2</sup> | $\phi'$ degrees |
|-----|--|-----------------------------|--------------|---------------|------------------|------------------|-------------------------|----------------------|---------------------------|---------------------------|---------------------------|-------------------------|-----------------------------|-------------------|---------------------|------|--------------------------|--|-----------------------|-----------------|
|     |  |                             |              |               |                  |                  | % Clay $\leq 0.002$ mm. | % Silt 0.002-0.074mm | % Fine Sand 0.074-0.425mm | % Medium Sand 0.425-2.0mm | % Coarse Sand 2.0-4.75 mm | % Gravel $\geq 4.75$ mm | % Cobbles & Boulders $> 3"$ | % Pass No. 4 Mesh | % Pass No. 200 Mesh |      |                          |  |                       |                 |
|     |  |                             |              |               |                  |                  |                         |                      |                           |                           |                           |                         |                             |                   |                     |      |                          |  |                       |                 |
| 1.  | Fill Material                                    | SC                          | 51           | 21            | 30               | -                | 16                      | 22                   | 14                        | 14                        | 28                        | 06                      | -                           | 100               | 40                  | 14.2 | 112.5                    | 1150                                   | 22.5                  |                 |
| 2.  | Decomposed Rock Material                         | SC                          | 36           | 19            | 17               | -                | 12                      | 23                   | 22                        | 31                        | 08                        | 04                      | -                           | 96                | 35                  | -    | -                        | -                                      | -                     |                 |
| 3.  | Ground Surface on Downstream                     | SC                          | 25           | 17            | 8                | 2.60             | 08                      | 21                   | 35                        | 30                        | 04                        | 02                      | -                           | 98                | 29                  | -    | -                        | -                                      | -                     |                 |
| 4.  | Material From Locations where "boiling" occurred | SC                          | 87           | 17            | 70               | 2.64             | 16                      | 28                   | 32                        | 22                        | 02                        | -                       | -                           | 100               | 44                  | -    | -                        | -                                      | -                     |                 |

the locations of lines of least resistance against subsurface erosion and the hydraulic gradients required to produce a continuous channel along these lines depend only on geological details. This cannot be determined by any theoretical methods, Terzaghi & Peck (1968).

It is seen from Fig. 1 that in the reach from chainage 71 to 75 the distance between the bottom of the core trench and the bed rock is the smallest (16 ft) when compared to all other sections along the entire length of the embankment. Therefore, there would have been a concentration of seepage flow which probably would have produced continuous channels along lines of least resistance against internal erosion. The "boiling" observed may also be attributed to this internal erosion.

## 5. PERMANENT REMEDIAL MEASURES

A seepage analysis was carried out by sketching a flownet, Harr (1962), using the following conditions as applicable to the site.

- (i) The worst condition during floods with the reservoir water level at 204 ft MSL.
- (ii) The seepage through the foundation takes place within a 42 ft thick soil stratum which overlies bed rock with 16 ft thick soil stratum between the bottom of core trench and bed rock.
- (iii) 15 ft thick top impervious layer extending to a distance of 100 ft from downstream toe of dam.

From the flownet, the uplift pressures were calculated and the loads required to balance the uplift pressures with a factor of safety of 2.5 were computed.

Materials from the spill tail canal excavation which were in spoil dumps were used over a sand layer as stabilising fill to produce the loads required. As an additional safety measure a relief trench was excavated along the length of the dam close to the toe as possible and filled with sand. This sand was made continuous with the horizontal sand layer below the stabilising fill. Wrap-around toe drains and lead-away drains constituted the drainage for the area. The details of these arrangements are shown in Fig. 3.

Elsewhere along the downstream where this phenomenon of "boiling" was not observed and where the toe drain had not been constructed relief wells of 6 inch diameter filled with sand to a depth of about 10 ft at 10 ft intervals were provided below the bottom of the toe drain at locations where impervious material was encountered during the excavation for the construction of the toe drain. This is also shown in Fig. 3.

The remedial measures were completed in 1984. The reservoir was impounded in 1984 and in 1985 it was spilling with water level in the reservoir rising above 202 ft M.S.L. The "boiling" was not observed and the entire downstream area was safe with no visible signs of a "quick condition."

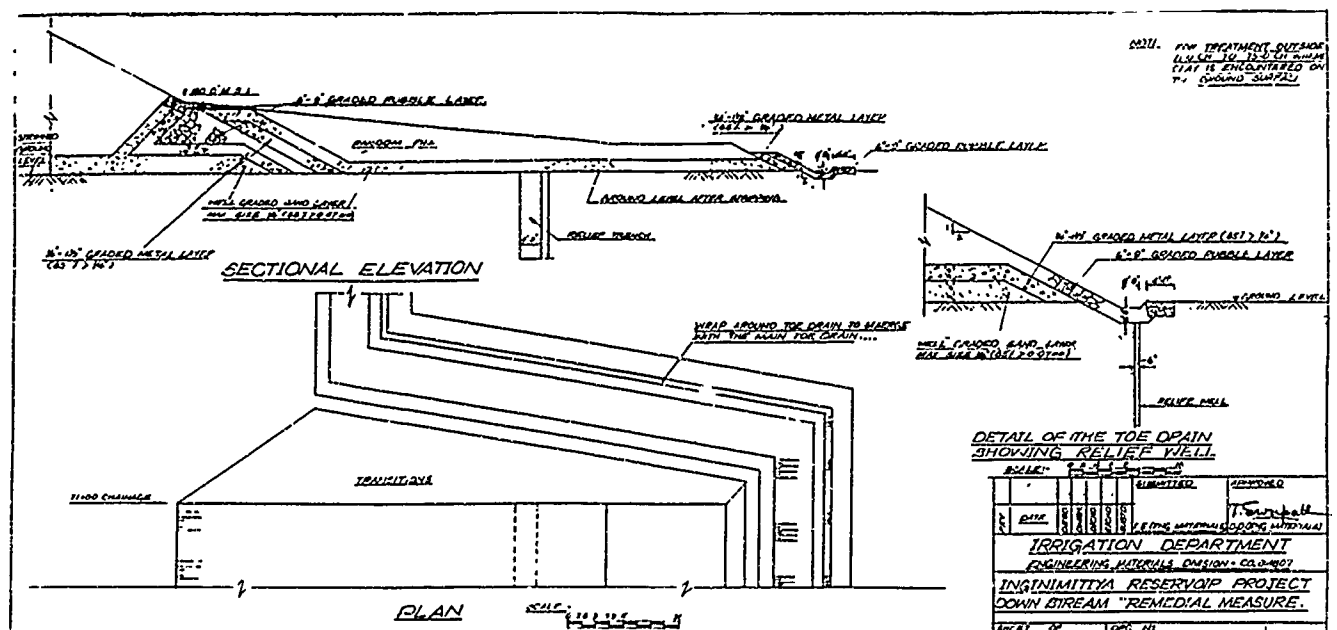


Fig. 3 - Downstream Remedial Measures

## 6. CONCLUSIONS

The causes for the occurrence of the 'boils' on the downstream portion of the embankment in the reach from chainage 71 to 75 may be attributed to the following:-

- (i) The presence of impervious soil in the downstream toe area which was subjected to high exit gradients.
- (ii) Concentration of seepage flow in the heterogeneous foundation material which produced continuous channels along lines of least resistance against internal erosion.

It is concluded that the remedial measures adopted are adequate for the satisfactory performance of the embankment.

## 7. ACKNOWLEDGEMENT

The author wishes to thank the Director of Irrigation, Sri Lanka for his permission to present this paper. The assistance and cooperation extended by the staff of the Engineering Materials Laboratory and the staff engaged in the construction of the Inginiyitiya Reservoir Project, all from the Department of Irrigation, Sri Lanka is gratefully acknowledged. Finally, thanks are due to Miss Vasantha Galappathi for the word-processing of this manuscript.

## 8. REFERENCES:

1. Harr, M.E. (1962), Groundwater and Seepage McGraw - Hill Book Company, New York.
2. Terzaghi, K and Peck, R.B. (1968), Soil Mechanics in Engineering Practice, John Wiley & Sons, Inc., New York.

## Performance of an Instrumented Earth Dam with Fat Clay Core

T.S. Mathur

USDA-forest Services, Eastern Region, USA

R.M. Willis

USDA-Forest Services, Mark Twain National Forest, USA

**SYNOPSIS:** Heavily instrumented dams are unusual in the midwestern United States. Council Bluff Dam, Missouri, USA has an imbankment that provides monitoring by piezometers, inclinometer, settlement plates, earth pressure cells, extensometers, tiltmeters, and datum plates. The collection, evaluation, and discussion of the data and instruments give insight into embankment performance. Emphasis has been placed on monitoring after construction.

### INTRODUCTION

This paper evaluates the performance of Council Bluff Dam embankment. The embankment height is 124 feet and represents the largest earthfill dam ever built by the USDA-Forest Service. Construction began in 1979 and was completed in 1981. The embankment is zoned with both a fat and lean clay zone and is anchored to steep abutment rock. The area of construction is a narrow rock canyon on the Big River in central Missouri.

Instrumentation was installed to monitor embankment performance due to the High hazard classification of the dam. Items being monitored: 1) Piping potential along the interface of the clay core and steep right abutment, 2) Piping potential around the conduit, 3) High stress around the top of the conduit, 4) Performance of all of the zones and chimney drain.

Woodward-Clyde Consultants of San Francisco, California designed the instrumentation and Shannon and Wilson, Inc. of St. Louis, Missouri installed and monitored the instruments during embankment construction. The Forest Service has done all monitoring since construction.

Instrumentation is composed of the following units: 21 piezometers, One inclinometer with settlement plates, Six sondex settlement devices, Six earth pressure cells, Six extensometers with tiltmeters, One mercury settlement device, and 22 surface monuments.

Monitoring of the instruments began immediately after installation and continues today. All of the instruments were in place by the fall of 1980. Reservoir filling began in 1981 with full pool achieved in 1984. Some instruments malfunctioned from the beginning, while others gave questionable readings, but most have performed well.

The dam has the following characteristics:

|                        |              |
|------------------------|--------------|
| Maximum Height         | 124 ft       |
| Crest Length           | 485 ft       |
| Zone Embankment        | 285,000 CY   |
| Dam Section -          |              |
| a) Fat Clay Core       |              |
| b) Lean Clay Core      |              |
| c) Lean Clay Blanket - |              |
| Upstream               |              |
| d) Chimney Drain       |              |
| e) Drain Blanket       |              |
| Full Pool Elevation    | 1087 ft      |
| Reservoir Surface Area | 440 Ac       |
| Full Pool Volume       | 12,640 Ac-ft |
| Construction Complete  | 1981         |
| Reservoir Filled       | 1984         |

### EMBANKMENT INSTRUMENTS

The instruments used to provide the needed information were designed as six different components. The following is a list of the components:

#### 1. Piezometers

Twenty-one piezometers were installed at locations shown in Table 2. These devices, model number P4KF10L or SINCO 51401, were supplied by Franz Gloetzl, D-7512 Rheinstatten, 4-Fo, West Germany. Their purpose was to monitor construction pore water pressure developed in the clay core and seepage conditions developed in the core and the foundation as the reservoir filled.

#### 2. Slope Indicator with Settlement Plates

A three-inch nominal diameter plastic casing was installed from the rock foundation to the top of the dam and aluminum settlement plates were placed every five feet up the

casing. The inclinometer (model Digitilt 50320) and other parts of the device were supplied by Slope Indicator Co., 3663 Albion Place N, Seattle, Washington 98103. This device is used to measure horizontal and vertical movements within the lean clay core during and after embankment construction.

### 3. Continuous Profile Settlement Device

This device, also called a Tube Profile Gauge, is installed to verify settlement and compressions in the embankment across and within the various zones. Two gauges are installed, one at elevation (EL) 1031.5 and another at EL 1067. At each elevation six datum plates are installed; one in the upstream random zone, one in the lean clay, and the remaining four in the fat clay core. The gauge was supplied by the Slope Indicator Company.

### 4. Extensometer and Tiltmeter Units

Four units were installed on the right abutment within the steep interface between the foundation and the fat clay core to measure relative movement of the core with respect to the abutment. Tilt sensor (model SINCO 50322) and parts of the unit were supplied by Slope Indicator Company. Two piezometers were installed immediately downstream of these units to monitor changes in seepage pressure which may accompany core movement.

### 5. Earth Pressure Cells

Two sets of cells were installed on the outside walls of the outlet conduit. Each set consists of three cells with one cell mounted on the top of the conduit and one cell mounted on each side of the conduit. The cells measure the total earth pressure on the conduit sections. The cells (model number E 15/25 KFA or SINCO S1482) were supplied by Franz Gloetzl. Four of the piezometers at elevation 1004 were located near the pressure cells on the side of the conduit to measure pore pressure and to detect seepage pressures near the conduit.

### 6. Surface Monuments

Thirteen surface monuments were installed along the crest of the dam and on the downstream berms to check horizontal and vertical movements after initial construction. In 1984, nine additional surface monuments were installed on the upstream side of the crest. The first monuments on the crest were located toward the downstream slope.

A variety of problems occurred during installation of the instruments. All of these problems required careful embankment construction of the areas around and adjacent to the instrument. Bloomsdale Construction, St. Louis, Missouri constructed the embankment and took the necessary care to protect the instruments.

## COLLECTION AND EVALUATION OF DATA

Data collection has been continuous since placement of the embankment began. During the construction phase, data collection was the responsibility of Woodward-Clyde, St. Louis, Missouri. Once the embankment was complete data collection and evaluation has been done by the Forest Service. The first four years after construction readings were taken every month except on the surface monuments, which were monitored twice each year. During 1984, it had become obvious that the structure was performing well, and the magnitude of the changes was not significant. In 1985, instruments were read quarterly and beginning in 1986 twice each year. Surface monuments have been surveyed once a year. The dam is visually inspected several times a year and is inspected for operation and maintenance annually. There is a surface water elevation monitor that records water levels daily and also initiates a response to a six-inch water elevation drop from full pool. This recorder transmits the data by radio signal to a receiver at a local office. The water level information will eventually be linked by data communication to several other office locations.

### Surface Monuments

Settlement of the embankment surface is well below the maximum anticipated and increases from the abutment interfaces toward the center of the embankment. The center 1/3 (horizontally) is experiencing the greatest amount of settlement. Maximum settlement at the surface is .44 feet, which is well below the anticipated 1.2 feet. It is also apparent that the upstream edge of the dam has settled more in the last two years than the downstream edge. Settlement varies from 0 - .12 downstream and .02 - .35 upstream. Initial movement of the monuments indicated a gradual migration upstream. The second set of monuments installed in 1984 now show a reverse of this trend and instead are moving slightly downstream. As the zones are loaded by reservoir water pressures it was anticipated that downstream movement would occur.

It was not anticipated that there would be an initial upstream movement of the embankment surface. It appears that this is a function of the differential settlement of various zones that compose the embankment. Most of these zones are upstream from the surface monuments that were initially installed. Associated with analysis of the crest settlement is the information on settlement of the two downstream berms where the instrument houses are located. Readings indicate that there is very little settlement in the downstream random zone. The upstream surface monuments (installed in 1984) have settled almost twice as much as the downstream monuments in the last two years with settlement over the last three years even greater. It is apparent that the upstream fat clay and

random zones have settled more than the downstream random zone and lean clay zone. It was expected that the fat clay zone would exhibit the greatest amount of settlement.

#### Settlement Plates

The lean clay zone experienced 68 percent of all settlement during construction. After construction, settlement has been greatest in the top 20 feet of the zone and the least in the bottom 20 feet. The zone is performing as anticipated with the middle 1/3 of the embankment experiencing the greatest settlement. Very little settlement has occurred in the lower section of the lean clay zone, while it has settled 1.24 feet in the upper area. Maximum settlement has been 2.5 feet with the maximum predicted settlement 1.2 feet. The prediction by Woodward-Clyde was based upon an analysis of five different dams with the observation stations normalized with respect to dam height. Actual settlement did exceed predicted settlement by 1.3 feet, but based upon the empirical methods used for prediction it is not a cause for concern. Seventy-nine percent of the settlement at the station that experienced the maximum occurred during construction.

#### Inclinometers

Information from the inclinometers indicates that minor deflections (less than .2 inches) occurred in both the downstream and upstream directions. The bottom 20 feet and top 15 feet of the lean clay zone have migrated a fraction of an inch downstream. The middle 80 feet of this zone has moved slightly upstream (maximum is about 1/2 inch). The upstream migration of most of the material in the zone is probably due to the increased settlement of the fat clay zone immediately upstream. It is more compressible and was expected to settle 2.5 times more than the lean clay zone. As the upstream face settles the lean clay core deflects slightly in the upstream direction. The very bottom of the zone has moved slightly downstream probably reflecting hydrostatic loading and is less affected by the upstream zones. The upper area is also less affected by the settlement of the upstream zones. This area is much closer to the downstream random zone and doesn't appear to be as significantly affected by upstream settlement. Once the phreatic surface reaches equilibrium most of this zone is expected to move slightly downstream. The question is whether or not all of the initial upstream movement will be overcome.

#### Piezometers

There are six piezometers that will never give equilibrium readings for the phreatic line. These piezometers were installed to measure pore pressures during construction and as precautions in the chimney drain and immediately downstream from the chimney drain. Two piezometers are no longer operating. It is obvious that the phreatic line has not reached equilibrium conditions. It appears that response of the foundation piezometers and the piezometers at elevation 1003 feet is good, but there is a substantial lag time in responding to actual water surface fluctuations. The piezometers at elevations 1031.0 and 1067.0 are much less

responsive. It took 2 years and 10 months after first filling to get a response in the first piezometer at 1031.0 and 3 years and one month to get a reading at elevation 1067. It is difficult to draw conclusions about the phreatic line in a pre-equilibrium state, but several things have become evident.

There is a substantial lag time for the piezometers to respond within the upstream random zone and fat clay zone. It would have been useful to have them located lower in the sections. It appears that it may take 10 years or more to reach equilibrium with the phreatic surface and there may never be any readings for some piezometers.

#### Extensometer and Tiltmeter Units

The extensometers placed on the right abutment interface with clay zone have moved very little since 1981. Maximum movements have been less than 1/4-inch during this period. Total movement of the four extensometers has varied from 10-1/2 inches to 1/3-inch with 83 percent of the movement occurring during construction. This interface has shown very little movement since construction and is performing well.

#### Earth Pressure Cells

The earth pressure cells along the conduit have not functioned very well. Two of the six cells are no longer working and another is giving questionable readings. There has been a dissipation of pore pressures on the top of the conduit since construction. It is difficult to establish the trend of the pore pressures on the sides of the conduit. The two surviving cells indicate that the pressures are reasonable, but one shows that the pressure has dissipated since construction while the other has increased. Pore pressures around the conduit are in the anticipated range and in general have dissipated since construction.

#### CONCLUSION

Analysis of the data on Council Bluff embankment indicates that most of the parameters are as predicted. The initial upstream movement of the fat and lean clay zones is not unusual and has occurred in other dams. Stanley D. Wilson noted a similar situation on the Muddy Run Embankment in an article for Dam Engineering in 1968. Equilibrium of the phreatic surface takes many years in this type of structure, and requires a long-term commitment to monitoring.

Data collection and interpretation is important. But it is also important to recognize what constitutes a problem and to have a plan in mind should a problem occur. The designer established anticipated maximum values for the parameters being monitored. This was a great assistance and serves as a guideline for evaluation. It is also important to provide more responsive systems to evaluate potential problems. The embankment devices require time to collect information and can only be monitored periodically. They are located in specific areas and provide information only for those areas. Together, all of the data gives a good



picture of how the embankment is performing. However, it is necessary to provide more responsive systems on some dams. Owners and managers of major dams need to consider these systems in view of their structure and downstream impacts.

Familiarity with instruments in a dam also identified information that would be valuable to collect but is not available. Surface movements on both the front and back crest of the embankment would have assisted evaluation from the beginning. It would also have been beneficial to locate some piezometers to better identify the pre-equilibrium phreatic surface.

#### LIST OF REFERENCES

- Fruco & Associates, St. Louis, Missouri, (May 1967), Design Report of Council Bluff Dam and Spillway for USDA-Forest Service, Milwaukee, Wisconsin. (Unpublished)
- Mead and Hunt, Inc., Madison Wisconsin, (May 1983), Evaluation of Emergency Potential for Emergency Action Plan for Council Bluff Dam, USDA-Forest Service, Mark Twain NF, Rolla, Missouri. (Unpublished)
- Shannon and Wilson, Inc., Geotechnical Consultants, St. Louis, Missouri, (March 1984), Instrumentation Evaluation of Council Bluff Dam for USDA-Forest Service, Milwaukee, Wisconsin. (Unpublished)
- R. Willis, USDA-Forest Service, (December 1984), Council Bluff Dam Instrumentation, University of Missouri-Rolla Special Problem in Graduate Study.
- Woodward-Clyde Consultants, San Francisco, California, (February 1978), Instrumentation Design Memorandum on Council Bluff Dam for USDA-Forest Service, Milwaukee, Wisconsin. (unpublished)

TABLE 1

#### DESIGN PROPERTIES OF EMBANKMENT MATERIALS

| PROPERTIES                   | LEAN CLAY | FAT CLAY |
|------------------------------|-----------|----------|
| Atterberg Limits             | 42        | 61       |
| Liquid Limit, %              | 18        | 25       |
| Plasticity Index             |           |          |
| Compaction Test (T-99)       |           |          |
| Max. Dry Density, PCF        | 109       | 100      |
| Optimum Moist. Content, %    | 16        | 22       |
| Shear Parameters             |           |          |
| Q-Test                       |           |          |
| Angle of Int. Friction, Deg. | 1         | 3        |
| Cohesion, TSF                | 0.8       | 0.6      |
| S-Test                       |           |          |
| Angle of Int. Friction, Deg. | 28        | 22       |
| Cohesion, TSF                | 0         | 0        |

Note: The angle of Internal Friction for  
Sand/Gravel = 30  
Rockfill = 36

#### Earth Pressure Cells Located on Conduit

| Pressure Cell | Max Anticipated (Psi) | Actual Readings (Psi) |      |      |      |
|---------------|-----------------------|-----------------------|------|------|------|
|               |                       | 1981                  | 1983 | 1985 | 1987 |
| North Side #1 | 39-62                 | 35                    | 30   | 35   | 43   |
| North Side #2 | 39-62                 | 34                    | 18   | 12   | 13   |
| Top #1        | 117-156               | 150                   | 107  | 51   | 46   |
| Top #2        | 117-156               | 131                   | 136  | 128  | 110  |
| South Side #1 | 39-62                 | 31                    | NW   | NW   | NW   |
| South Side #2 | 39-62                 | 36                    | 34   | NW   | NW   |

#### Extensometers Right Abutment

| Extensometer | Max (Ft) Anticipated | Actual Movement (Ft.) |      |      |      |
|--------------|----------------------|-----------------------|------|------|------|
|              |                      | 1981                  | 1983 | 1985 | 1987 |
| #1           | .97                  | .32                   | .36  | .36  | .36  |
| #2           | 1.11                 | .19                   | .23  | .23  | .23  |
| #3           | 1.25                 | .87                   | .88  | .88  | .88  |
| #4           | 1.39                 | .03                   | .05  | .05  | .05  |

TABLE 3

#### Piezometer Readings

| Piezometer | Est. Const. Pore Pres. | Est. Full Pool Pres. | Oct. 1981         | Oct. 1983     | Nov. 1985 | July 1987 |
|------------|------------------------|----------------------|-------------------|---------------|-----------|-----------|
| FP1        | -                      | 46                   | 11.1              | 31.1          | 37.1      | 38.7      |
| FP2        | -                      | 41                   | 23.5              | -not working- |           |           |
| FP3        | -                      | 23                   | 13.7              | 16.6          | 23.3      | 23.8      |
| FP4        | -                      | 7                    | 19.7              | 15.7          | 17.9      | 17.2      |
| P1A        | 78                     | 26                   | 0                 | 4.2           | 12.8      | 16.8      |
| P2A        | 78                     | 26                   | 0                 | x             | 24.8      | x         |
| P3A        | 77                     | 20                   | 0                 | 6.4           | 9.8       | 11.3      |
| P4A        | 77                     | 20                   | 0                 | 4.9           | 9.3       | 11.5      |
| P5A        | -                      | 0                    | 0                 | 0             | 0         | 0         |
| P1B        | -                      | 24                   | ---not working--- |               |           |           |
| P2B        | 50                     | 20                   | 0                 | 0             | 0         | 0         |
| P3B        | 50                     | 7                    | 0                 | 0             | 0         | 0         |
| P4B        | -                      | 0                    | 0                 | 0             | 0         | 0         |
| P5B        | -                      | 0                    | 0                 | 0             | 0         | 0         |
| P1C        | -                      | 5                    | 0                 | 2.8           | 7.7       | 8.8       |
| P2C        | 25                     | 0                    | 0                 | 0             | 0         | 0         |
| P3C        | 26                     | 0                    | 0                 | 0             | 0         | 0         |
| P4C        | -                      | 0                    | 0                 | 0             | 0         | 0         |
| PAP1       | 69                     | 25                   | 1.9               | 6.8           | 9.1       | 8.0       |
| PAP2       | 62                     | 25                   | 0                 | 6.9           | 8.7       | 8.3       |

## Settlement Plates

## Settlement

| Plate # | Initial<br>Elevation (FT) | Settlement (Feet) |      |      |      |
|---------|---------------------------|-------------------|------|------|------|
|         |                           | Cumulative        |      |      |      |
|         |                           | 1981              | 1983 | 1985 | 1987 |
| 1       | 995.53                    | .47               | .64  | .66  | .68  |
| 2       | 1000.91                   | .50               | .71  | .70  | .72  |
| 3       | 1006.39                   | .61               | .95  | .89  | .91  |
| 4       | 1011.90                   | .93               | 1.33 | 1.36 | 1.37 |
| 5       | 1017.32                   | 1.13              | 1.51 | 1.56 | 1.79 |
| 6       | 1022.78                   | 1.34              | 1.69 | 1.80 | 1.83 |
| 7       | 1028.17                   | 1.49              | 1.84 | 1.95 | 1.99 |
| 8       | 1033.55                   | 1.59              | 1.95 | 2.04 | 2.09 |
| 9       | 1038.95                   | 1.81              | 2.19 | 2.28 | 2.33 |
| 10      | 1044.29                   | 1.78              | 2.16 | 2.25 | 2.30 |
| 11      | 1049.70                   | 1.84              | 2.22 | 2.31 | 2.36 |
| 12      | 1055.08                   | 1.97              | 2.35 | 2.44 | 2.50 |
| 13      | 1059.99                   | 1.53              | 1.92 | 2.02 | 2.05 |
| 14      | 1065.38                   | 1.63              | 2.13 | 2.10 | 2.14 |
| 15      | 1070.47                   | 1.27              | 1.67 | 1.73 | 1.79 |
| 16      | 1075.83                   | 1.18              | 1.57 | -    | 1.84 |
| 17      | 1081.28                   | 1.16              | 1.56 | -    | 1.89 |
| 18      | 1086.48                   | 1.00              | 1.40 | -    | 1.92 |
| 19      | 1091.88                   | .95               | 1.52 | -    | 2.04 |
| 20      | 1096.84                   | .60               | 1.36 | -    | 1.84 |

| Monument # | Initial<br>Elevation | Settlement (Feet) |      |      |      |
|------------|----------------------|-------------------|------|------|------|
|            |                      | Cumulative (Feet) |      |      |      |
|            |                      | 1981              | 1983 | 1985 | 1987 |
| 1          | 1102.98              | .03               | .05  | .01  | .01  |
| 2          | 1103.22              | .06               | .25  | .34  | .41  |
| 3          | 1103.67              | .09               | .26  | .27  | .35  |
| 4          | 1103.87              | .10               | .14  | .32  | .44  |
| 5*         | 1103.75              | .11               | .19  | .33  | .43  |
| 6          | 1103.51              | .07               | .32  | .36  | .43  |
| 7          | 1103.53              | .04               | .03  | .03  | .08  |
| 8          | 1108.20              | .03               | .09  | .17  | .21  |
| 9          | 1103.08              | .01               | .02  | .02  | .01  |
| T-1*       | 1065.64              | +.02              | +.03 | .00  | .01  |
| T-2*       | 1031.48              | +.07              | +.12 | +.08 | .00  |
| 10**       | 1102.62              |                   |      | 0    | .04  |
| 11         | 1102.55              |                   |      | .06  | .11  |
| 12         | 1102.63              |                   |      | .08  | .26  |
| 13         | 1102.68              |                   |      | .13  | .34  |
| 14         | 1102.43              |                   |      | .13  | .35  |
| 15         | 1102.81              |                   |      | .10  | .28  |
| 16         | 1102.62              |                   |      | .08  | .24  |
| 17         | 1102.67              |                   |      | .03  | .07  |
| 18         | 1102.75              |                   |      | .00  | .03  |

\* Predicted maximum settlement at Station 5 is 1.20 feet, T-1 is .3 feet, and T-2 .5 feet.

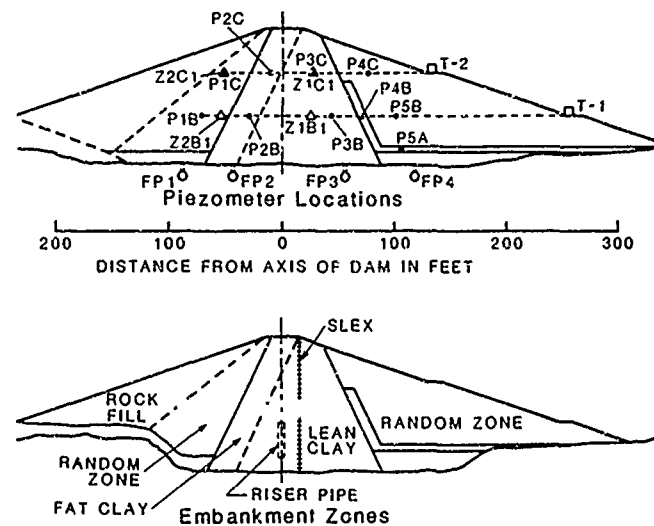
\*\*The initial elevations for Surface Monuments 10-18 were established in 1984.

TABLE 4

Surface Monument  
Horizontal Movement

| Monument # | 1982 | 1983 | 1984 | 1985 | 1986 | 1987 |
|------------|------|------|------|------|------|------|
| 1          | .06D | .06D |      | .03D | .04D | .03D |
| 2          | .02U | .01U |      | .0   | .01D | .00  |
| 3          | .03U | .02U |      | .01U | .0   | .01U |
| 4          | .04U | .04U |      | .04U | .05U | .06U |
| 5          | .04U | .04U |      | .05U | .06U | .06U |
| 6          | .03U | .03U |      | .04U | .04U | .05U |
| 7          | .02U | .02U |      | .03U | .02U | .04U |
| 8          | .00  | .01U |      | .00  | .01D | .00  |
| 9          | .00  | .00  |      | .00  | .01D | .01D |
| T-1        |      |      |      |      |      |      |
| T-2        |      |      |      |      |      |      |
| 10         |      |      |      | .02U | .0   | .03D |
| 11         |      |      |      | .03U | .03U | .00  |
| 12         |      |      |      | .04U | .03U | .03D |
| 13         |      |      |      | .07U | .05U | .00  |
| 14         |      |      |      | .06U | .02U | .03D |
| 15         |      |      |      | .05U | .04U | .00  |
| 16         |      |      |      | .04U | .01U | .03D |
| 17         |      |      |      | .01U | .0   | .04D |
| 18         |      |      |      | .01U | .02U | .00  |

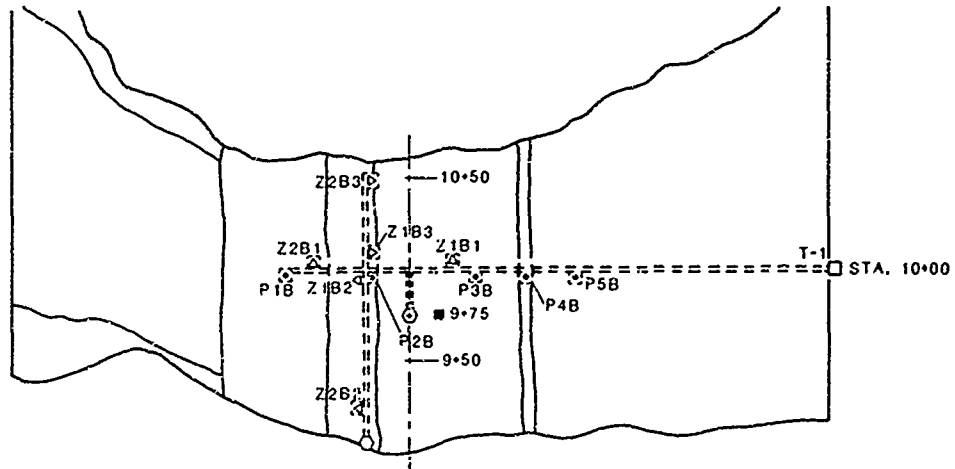
FIGURE 1: DAM SECTION STATION 10+00



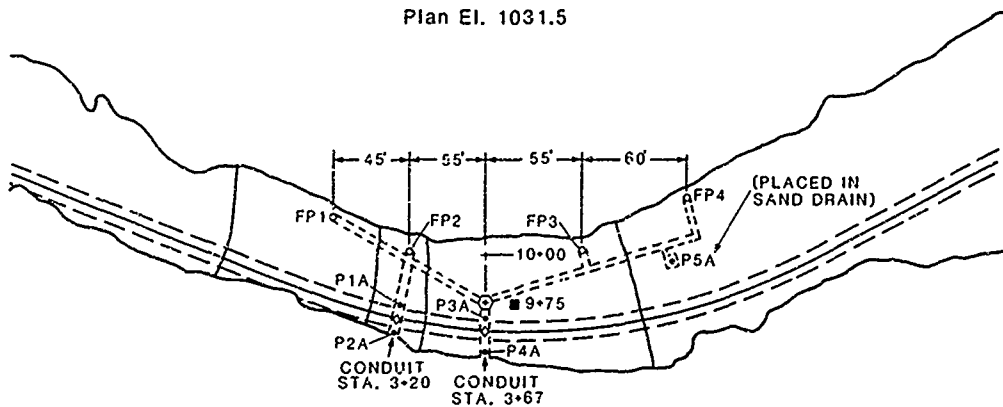
## Legend: (Figures One and Two)

- FOUNDATION PIEZOMETER (FP\_)
- EMBANKMENT PIEZOMETER (P\_)
- △ TUBE PROFILE GAGE DATUM PLATE (Z\_)
- SLOPE INDICATOR AND EXTENSOMETER (SLEX)
- ⊙ RISER PIPE
- ◇ SET OF THREE SOIL PRESSURE CELLS (SP\_)
- READOUT TERMINAL
- === INSTRUMENTATION TRENCH
- RIGHT ABUTMENT INSTRUMENT LEADS

FIGURE 2: FOUNDATION AND ELEVATION 1031.5 INSTRUMENTS

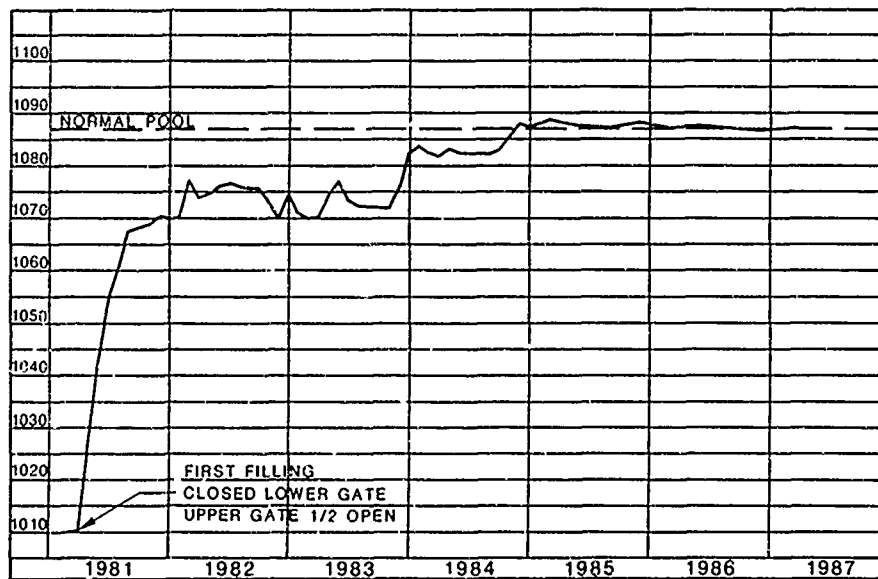


Plan El. 1031.5



Plan El. 1004

FIGURE 3: COUNCIL BLUFF LAKE - Water Elevation Vs. Time



## A Finite Element Analysis of the Utah "Thistle" Failure

Blaine D. Leonard  
President, LTR Associates, Salt Lake City, Utah

Joseph M. Olsen  
Chairman, Civil Engineering Department, University of South  
Alabama, Mobile, Alabama

**SYNOPSIS:** In the Spring of 1983, a large landslide occurred near the town of Thistle, Utah which blocked major transportation routes and impounded the Spanish Fork River, inundating the town with 200 feet of water. While much attention has been given to the slide and its impact, very little has been directed toward a quantitative understanding of its causes. An analysis was performed of the Thistle landslide using the SEEPSLOPE finite element system in order to evaluate the mechanisms, factors, and causes of the failure. An elastic, perfectly-plastic stress-strain curve was employed in the analysis to model the behavior of the overconsolidated clay soils. It is concluded that the landslide was a compound, progressive failure which initiated at the toe and progressed uphill. Seepage forces played a significant role in the failure.

### INTRODUCTION

Early in April 1983, motorists driving through Spanish Fork Canyon south of Provo, Utah, began noticing cracks in the road near the small town of Thistle. During the next few days, the cracks enlarged, the road began to heave, and the nearby railroad tracks began to be distorted. By the 14th of April, the Thistle landslide, a Quaternary earthflow deposit lying in a small canyon essentially perpendicular to the road, had moved sufficiently to lift the highway, sever the railroad, and block the Spanish Fork River. Within 30 days, this blockage had filled the canyon to a height of over 200 feet, buttressing against a large sandstone formation known locally as Billies Mountain. The small town of Thistle was buried with 62000 acre feet of water.

Property damage triggered a Presidential Disaster declaration. Opening a passageway for the Spanish Fork River and rebuilding transportation lines through the canyon subsequently cost local government and private entities in excess of 200 million dollars. The question of what to do with the slide mass is still unanswered. In addition, severe hardships were imposed on the displaced residents of the small town who as of early 1987 had not been compensated for the loss of their property.

This mass of overconsolidated clay, over a mile long and several hundred feet wide, has moved several times previously in geologic time, and has plagued the railroad lines for most of this century with occasional track movements due to creep. Deformation had been noted by some during the early Spring of 1983 which was attributed to the wet weather conditions. Precipitation during the winter of 1982-1983 had reached record levels, resulting in abnormally high antecedent moisture conditions. However, a movement of this magnitude had not been experienced in recorded time.

The geotechnical aspects of the Thistle landslide are complex and varied, and have been treated only qualitatively in previous studies.

This study was undertaken to quantitatively address the geotechnical mechanisms involved in the occurrence of the Thistle Landslide. The objective was to use a finite element stability analysis to draw conclusions about the physical causes and mode of the failure which occurred there. Evidence is presented which demonstrates that the slide was a progressive failure in overconsolidated clays which started at the toe of the slide and progressed uphill. High seepage forces played a significant role in the failure.

### BACKGROUND

The area of the slide is near the easternmost edge of the Middle Rocky Mountain Province which is characterized by generally high mountain ranges and plateaus transected by deeply incised erosional valleys. The toe of the slide in the bottom of the canyon was at an elevation of about 5030. The slide extended west approximately perpendicular to Spanish Fork Canyon a horizontal distance of 1200 feet, and then southwest another 4500 feet, reaching an elevation of about 5900 at the top. A twenty-foot scarp at the top is noticeable, and several related slides adjacent to the main slide mass are also evident. Total slide widths vary from about 850 feet at the top to 1200 feet just above the bend. Below the bend, widths are slightly less than 1000 feet (Duncan et al., 1985). The volume of landslide material in the canyon has been estimated to be between 3 and 6.5 million cubic yards (FEMA, 1983; Dames and Moore, 1985; Kaliser and Fleming, 1986). Total volumes involved in the landslide are generally considered to be about 25 to 30 million cubic yards.

Descriptions of the geology of the Thistle area are given by Witkind and Page (1983), Duncan, et al. (1985), and Kaliser and Fleming (1986). According to these sources, three formations underlie or are present as outcrops adjacent to the landslide. The Triassic Ankareh Formation, which is a weak, reddish, shaly siltstone and

sandstone underlies the Triassic-Jurassic Nugget sandstone, a strong, light colored sandstone which in turn underlies the Tertiary North Horn Formation, a weak, partly alluvial partly lacustrine deposit consisting of mudstone, claystone, sandstone, conglomerate, and limestone. The valley in which the Thistle landslide rests was cut from the Ankareh Formation which completely underlies the landslide and is exposed on the north boundary of the landslide. The Nugget Formation forms the prominent ridge that delineates the southeast flank of the landslide and underlies the landslide in the canyon bottom. Duncan, et al. (1985) concluded that "all movement of the Thistle landslide apparently was above this bedrock unit." The North Horn Formation is exposed along ridges on both the southeast and northwest borders of the landslide. The majority of the landslide is composed of debris and earthflow material derived from the North Horn Formation.

The Thistle landslide is an early Holocene (Kaliser and Fleming, 1986) landslide mass that has moved on several occasions in geologic time (Schroder, 1971 and Duncan, et al., 1985). However, Duncan, et al. (1985) argue that there was "no evidence that these older, deep-seated landslides, should they be present, were active during 1983 or later."

In approximately 115 years of historic records, there is no indication of massive movement of the Thistle slide, and no available written accounts of small movement (Kaliser and Fleming, 1986). However, the slide has caused repeated problems to the rail lines located at its toe (FEMA, 1983; Sumsion, 1983). The most recent report of troublesome movements dates to just two months before the catastrophic failure of 1983.

#### PHYSICAL DETAILS OF THE FAILURE

Opinions differ about when the 1983 movement of the Thistle Landslide began. Kaliser & Fleming, (1986) report that in January of 1983 an official of the Denver and Rio Grande Western Railroad reported cracks on the cut slope immediately west of the tracks which were "of size and depth far in excess of normal." These cracks apparently did not extend upslope of the cut slope. In early March (Kaliser and Fleming, 1986), an inspection revealed that a set of cracks had advanced upslope a distance of about 100 feet, but no material was noted on the inside track. Sumsion (1983, p. 12), showed a photograph taken April 2 of an active slump on the surface of the railroad cut at the toe of the landslide. Tension cracks parallel to and upslope from the railroad cut can be clearly seen in the photograph.

The earliest official records of the Thistle Landslide are dated April 13, 1983. At 7:30 a.m. on that day, Denver & Rio Grande Western Railroad personnel reported that their tracks were out of alignment (Sumsion, 1983; Duncan et al., 1985). As the tracks continued to heave, the railroad attempted to keep the tracks open. Late that evening, heave was noted along the road surface of U.S. Highway 6 and 89, which lay about 200 feet east of the tracks and across the Spanish Fork River. By the afternoon of

April 14, vertical deformation of the highway surface was so severe that the road was closed to traffic, and on the following day, the road had displaced approximately 10 vertical feet (Dames and Moore, 1985). On the evening of April 15, the last train used the tracks (Kaliser and Fleming, 1986).

From the first signs of movement considerable effort was applied to prevent the Spanish Fork River from being dammed and to keep the canyon open. By April 17, it was clear that these efforts were failing and the residents of Thistle were evacuated. At this time efforts had already turned to unloading what was thought to be the "head" of the slide, in the area immediately upslope from the railroad cut. Attention also turned to preventing overtopping of the dam by the new Lake Thistle, and evaluating new transportation routes. On April 22, Utah Governor Scott Matheson declared the area a state disaster area, and on April 30, President Ronald Reagan made the Thistle slide area Utah's first National Disaster Area.

Movement of the slide was measured by Railroad and county crews during the first crucial weeks of sliding. According to Duncan et al. (1985), the Railroad reported that the landslide was moving at about 0.75 feet per hour on April 14. This average rate increased to a maximum of 2.5 to 2.8 feet per hour during the period of April 17 to 19, and declined to 0.80 feet per hour by April 25. Total horizontal displacement for the bottom of the slide during this period is estimated to be about 500 feet. Vertical displacements of up to 1.5 feet per hour were noted (Dames and Moore, 1985). Peak sliding rates measured by Utah County were on the order of 6.6 feet per hour on April 19.

By the beginning of May, slide movement had largely halted because of the accumulation of slide debris in the valley and the buttressing effects of Billies Mountain.

#### ANALYSIS PROCEDURES

An analysis of the Thistle failure was performed using the SEEPSLOPE finite element system which consists of two component codes, CFLOW and WOODLUND. CFLOW is a code which calculates steady state flow through nonhomogeneous media (Taylor and Brown, 1967). WOODLUND is a stress analysis program for plane strain conditions originally developed to analyze underground openings in rock (Chang and Nair, 1973). It employs an elastic-perfectly plastic stress-strain formulation using a Drucker-Prager yield criterion.

These two programs were combined and enhanced by the Bureau of Mines (Corp, Schuster, and McDonald, 1975) to analyze mine tailing impoundments. SEEPSLOPE computations for the Thistle analysis were performed on a Gould 9080 minicomputer at the University of Utah College of Engineering. Details of the implementation of SEEPSLOPE are given by Leonard (1987).

An initial finite element mesh was fashioned which consisted of 1160 nodes and 1048 elements along an axis approximating the centerline of the slide. The mesh is 5800 feet long and relatively shallow, as is necessary to model the

actual failure. Thicknesses vary from 180 feet at the top to 265 feet at the middle, to 480 feet near the bottom. Topography is based on USGS Quadrangle maps and post-slide topographic maps prepared by the Utah County Engineer's Office.

Elements at the head of the slide were initially 100 feet long by about 30 feet high. Elements in the middle of the slide were reduced to 50 feet long and about 35 feet high. In the lower portion of the slide, elements were further reduced to 33 feet long by about 30 feet high. The majority of the elements are rectangular, although some triangular elements were included as needed to accommodate the physical boundaries and mesh transitions. The CFLOW program uses this initial mesh together with an estimate of the phreatic surface to perform seepage calculations. As CFLOW moves the nodes which lie on the phreatic surface to satisfy continuity of flow, the remainder of the mesh is distorted accordingly and element sizes vary.

The finite element mesh was divided into four soil types, representing the primary strata encountered on the site. Material parameters used in the analysis were based on data from investigations performed at the site of the slide under the direction of the Utah State Division of Water Rights and the Utah County Engineer (Duncan, et.al., 1985). While four principal soil types were identified for analysis purposes, there was significant spatial variability in the materials encountered at the site.

Very little is known about the precise pre-slide hydraulic conditions in the slide mass. Permeabilities were estimated from post-slide tests. Various inflow and outflow nodes were selected in the CFLOW analysis to model infiltration and known springs within the slide area. The SEEPSLOPE program calculated a phreatic surface location and computed the corresponding seepage forces.

For the stress analysis portion of the study, eight cases were developed, each with a slightly different set of soil parameters. The cases were designed to provide insight into the Thistle failure, since it was unlikely that any specific set of parameters would exactly model the actual conditions. Six of these cases used the full seepage forces computed by earlier portions of the SEEPSLOPE system. For the other two cases, seepage forces were reduced by one-half (J-1) or one-quarter (K-1) for all nodes within or above the zone of failure. This was done in an attempt to compensate for the assumptions of steady-state seepage and fully saturated conditions which the SEEPSLOPE system made. The transient conditions and partially saturated soil zones above the phreatic surface believed to exist prior to the slide would yield lower seepage forces than computed by the steady-state analysis performed by SEEPSLOPE.

The materials in the slide were predominantly stiff overconsolidated clays with many fissures and zones of high permeability. The strength of these materials also exhibited significant spatial variation. While there was undoubtedly some minor excess pore pressure buildup during the failure, the analysis was performed using effective stress methods and drained conditions

which are more appropriate for slopes in stiff fissured materials (Lambe & Whitman, 1969).

The strength parameters for the materials which participated in the slide are shown in Table 1. While there was considerable variation in the measured values of friction angle and cohesion (Leonard, 1987), there were data which suggested that the upper 50 feet was slightly weaker than the underlying materials. Accordingly, the top row of elements was designated as soil 1 while the remainder of the material above the claystone and sandstone bedrock was designated as soil 2.

TABLE 1. Soil Strength Parameters for Soils 1 and 2 for Each Case of WOODLUND Stress/Stability Analysis

|           | Soil 1       |            | Soil 2       |            |
|-----------|--------------|------------|--------------|------------|
|           | phi<br>(deg) | c<br>(psi) | phi<br>(deg) | c<br>(psi) |
| Case I-14 | 11.0         | 0.0        | 9.0          | 0.0        |
| Case I-15 | 27.4         | 0.0        | 27.4         | 0.0        |
| Case I-16 | 11.0         | 106.0      | 9.0          | 106.0      |
| Case I-17 | 11.0         | 122.0      | 9.0          | 122.0      |
| Case I-18 | 20.0         | 33.3       | 20.0         | 47.8       |
| Case I-19 | 20.0         | 122.0      | 20.0         | 122.0      |
| Case J-1  | 11.0         | 122.0      | 9.0          | 122.0      |
| Case K-1  | 11.0         | 122.0      | 9.0          | 122.0      |

The first two cases represent the pure residual shear strength condition. Duncan et al. (1985) theorized that "antecedent movements had probably reduced the strength along the sides and base of the slide to residual frictional values". In such a case, the stress strain curve would have no peak, but would level off at the residual value. In addition, the cohesion intercept would be zero. Case I-14 uses the lowest residual friction angle measured on Thistle samples in the laboratory. Case I-15 represents the highest angles measured.

Even in circumstances where residual shear strengths generally govern stress-strain behavior, small peak strengths are sometimes developed over time due to thixotropy. In addition, portions of a slide which do not contain previous failure surfaces will exhibit peak strengths before dropping to residual levels. In order to model these conditions the soil parameters used in case I-16 were modified to include a cohesion intercept. An unconfined compression test value of 106 psi was selected for use as a cohesion value, representing the second highest such value noted in the test data. A relatively high value was selected in order to insure stable results. Preliminary analyses had indicated that lower cohesion values would yield a totally unstable slide mass.

Case I-17 uses slightly higher cohesion values in an attempt to bracket the true failure conditions.

Case I-18 represents the average frictional and cohesion shear strength parameters from the laboratory data. Not a true residual strength

case, this set of data reflects a buildup of some peak strength due to thixotropy of unsheared soils with diagenetic bonding. The cohesion values are different for the two soils, reflecting the difference between the average unconfined compression values for soils shallower than 40 feet and deeper than 40 feet.

Case I-19 is intended to provide some comparative information relative to the other cases. This case uses the same cohesion intercept as I-17, but with a higher friction angle. It also uses the same friction angle as I-18, but with higher cohesions. The sensitivity of the stress analysis with respect to these two soil parameters can be evaluated using the results of this and the two previous cases. In addition, this combination of parameters forms an upper bound on the strength envelopes used for the analysis.

The last two cases use the same strength parameters as Case I-19, but with reduced seepage forces. For Case J-1, seepage forces above the assumed failure surface were reduced to one-half of their original values. For Case K-1, nodal seepage forces were reduced to one-quarter of their original levels for this case.

Each of the cases analyzed had some failed elements which led to redistribution of stresses during the calculations. These redistributions were successful in converging to a solution in all cases except I-14 and I-15. In these two cases computed stress levels were so high relative to soil strengths that nearly every element yielded in early load increments. In successive computer iterations, stresses were transferred back and forth between yielded elements and convergence toward a solution could not occur.

In all of the other cases a solution was produced with elements at or near failure clustered at or near the bottom of the slope. Only case I-18 with lower cohesion failed elements higher than approximately one-third of the way up the slope. In this case only the upper approximately one-fourth of the mesh was stable.

In order to better compare the various analyzed cases and more fully evaluate the stability computations for the Thistle Landslide, average factors of safety were computed for seven trial failure surfaces using data from each analysis case. The seven failure surfaces were selected specifically to aid in the understanding of the nature of the failure. Weighted average factors of safety were computed for each of the seven failure surfaces for each of the WOODLUND cases described above. Results of these computations are shown in Table 2. Although the total length of the landslide is known to be about 5700 feet, the depth and shape of the failure surface is still in question, and it is unclear whether the slide is made up of one long failure mass or many small compound failures.

Failure Surface 1 represents the full length failure, based on the theory that the slide was a long, shallow, continuous failure mass. Surface 2 also represents a relatively long, shallow landslide mass, but extends only one-third the length of the total slide, and does not completely cross the canyon floor. Failure Surface 3 is much shorter, and approaches the shape of a circular failure. Failure Surface 4 was developed to evaluate the validity of a deep failure. Some have postulated that the Thistle Landslide involved a deep failure which lifted the highway in the canyon floor. Surface 5 is a small, shallow, nearly circular failure. Surfaces 6 and 7 represent small, localized failures of the landslide. A small failure of this sort could be triggered by weather conditions or construction activity, and may lead to a larger, progressive failure event.

TABLE 2. Factors of Safety for Selected Failure Surfaces

| Case | Failure Surface Number |      |      |      |      |      |      |
|------|------------------------|------|------|------|------|------|------|
|      | 1                      | 2    | 3    | 4    | 5    | 6    | 7    |
| I-14 | 0.33                   | 0.22 | 0.55 | 0.84 | 0.72 | 0.67 | 0.57 |
| I-15 | 0.58                   | 0.62 | 1.05 | 0.96 | 1.42 | 1.89 | 1.88 |
| I-16 | 6.14                   | 7.87 | 1.57 | 1.71 | 1.09 | 1.63 | 1.33 |
| I-17 | 6.85                   | 8.95 | 1.74 | 1.89 | 1.30 | 1.80 | 1.39 |
| I-18 | 2.55                   | 0.73 | 0.81 | 1.05 | 1.05 | 1.27 | 1.31 |
| I-19 | 6.92                   | 9.16 | 1.95 | 2.09 | 1.46 | 1.98 | 1.63 |
| J-1  | 6.83                   | 7.20 | 4.24 | 3.57 | 2.07 | 1.87 | 1.45 |
| K-1  | 7.40                   | 9.24 | 2.78 | 2.50 | 1.70 | 1.91 | 1.44 |

#### DISCUSSION OF RESULTS

Sufficient data about the Thistle pre-slide groundwater conditions are not available to accurately model the variable transient conditions and resulting forces. In general, the phreatic surface computed by SEEPSLOPE seems realistic in its location and shape. Nodal seepage forces, however, are probably higher than they should be. Without the availability of more detailed information, arbitrarily reducing seepage forces above the failure surface is a simple method for approximating the transient conditions. Seepage forces were cut to one-half and one-quarter their original levels and the effects of those lowered forces studied in the stress analysis portion of this research. The effectiveness of this approach is demonstrated in two sets of relationships. First, it was evident in the distribution of failed elements in Cases I-19, J-1, and K-1 that the number of failed elements in the analyses with reduced forces is less than in I-19, particularly in the shallower elements. Since the seepage forces were reduced in these cases for elements above the proposed failure zone, this result is expected. Second, some trends can be seen in the factors of safety for the trial failure surfaces. Comparing Case J-1 with I-19, the decreased seepage forces yield higher or essentially equal factors of safety for five of the seven failure surfaces. The average increase in factor of safety is 27 percent. Comparing Case K-1 with J-1, higher or equivalent factors of safety are yielded for four of five surfaces. The factors of safety for Surfaces 6 and 7 remain roughly unchanged in all three cases. This would have relatively low seepage forces.

SEEPSLOPE was not able to compute realistic factors of safety for Cases I-14 and I-15 which did not converge. The specific results of these two cases must be generally disregarded, except as they relate to the overall failure parameters of the Thistle slide. The results of these two cases indicate that Thistle was not strictly a recurrence of an old slide along a previously failed surface. Element factors of safety were so uniformly low that transfer of excess stresses could not be accomplished. Even the high friction angle used in Case I-15 was not sufficient to bring about stability. Based on this information, it is likely that some peak strengths were involved in the failure.

All of the cases analyzed clearly indicate that the slide initiated at the toe. Even when large numbers of elements are yielded, as in Case I-18, factors of safety near the head are consistently greater than one. As the number of yielded elements decreases, they tend to be located primarily at the toe. This observation is strongly supported by the failure surface factors of safety. Disregarding cases I-14 and I-15, Failure Surfaces 1 and 2 never have the lowest factors of safety for a given case. In addi-

tion, in five of the six cases, the factors of safety for these two surfaces are considerable higher than those for the other surfaces.

Tension cracking noted in a photograph taken ten days before the slide began supports the argument that sliding began at the toe. It has been suggested (Duncan, et al., 1985) that it was unclear whether events at the toe or the head were more important in the initiation of sliding. Evidence from this study clearly indicates otherwise; the slide began at the toe.

With full seepage loads applied, the most stable result is yielded in Case I-19. The distribution of yielded elements clearly shows fewer yielded elements in this case than in the other cases using a full seepage load. The failure surface factor of safety results also support this observation. For any given failure surface, Case I-19 yields a higher factor of safety than the others.

Two observations can be drawn about the shape of the failure surface based on results of trial failure surface computations. First, the failure was not a deep seated circular failure. Among the six converging cases, the minimum factor of safety was associated with Failure Surface 5 in three of the cases and with Failure Surface 7 in two of the cases. Surface 5 is a very shallow, circular surface, and Surface 7 is a superficial sloughing failure of the toe. Failure Surface 4, the deep seated failure, never yields the lowest factor of safety. Second, the failure did not involve a long, continuous surface. Failure Surface 1 yields the highest aggregate factor of safety in each of the six cases.

Relatively high cohesion values were required to achieve convergence and stability in the various analyses. Cases involving low cohesion values, such as I-18, resulted in numerous yielded elements and low factors of safety on the trial failure surfaces. Four of the seven surfaces had factors of safety near or below one in Case I-18. None of the failure surfaces analyzed yielded factors of safety less than one in Cases I-17 and I-19. The cohesion value used in these two cases was 122 psi, representing the highest value obtained in the laboratory from unconfined compression tests. Since significant cohesion was required to achieve stability, it seems likely that soil strengths mobilized during the slide were higher than residual levels.

Only small increases in stability were obtained by increasing the friction angle. Comparison of Cases I-17 and I-19 demonstrates that for an 82 percent increase in friction angle, only a 9 percent increase in factor of safety resulted. The comparison of Cases I-16 and I-17 and Cases I-18 and I-19, however, demonstrate the sensitivity of the analysis to the cohesion parameter. Case I-17 used a 15 percent higher cohesion value than I-17, with a resulting increase in factor of safety of 11 percent. Case I-19 used a cohesion value averaging 310 percent higher than Case I-18, with a resulting increase in factor of safety of 340 percent.

Definite trends relating to the development of a compound failure surface are not evident in the results of this study. However, the observations that yielded elements are always concentrated at the toe of the slide, and long, continuous failure surfaces always have high factors of safety indicates that the failure as a compound progressive failure. Computed failure surfaces with low factors of safety are generally short, but the actual failure was quite long. It seems reasonable that small zones could fail near the toe of the slide, resulting in the removal of the resisting forces supporting higher elements, ultimately causing similar small failures of uphill areas. In this way, the failure would gradually

progress up the hill. For instance, in Case I-16, the minimum factor of safety is for the short, shallow Failure Surface 5. With a factor of safety of 1.09, this surface is near failure. Once this mass of elements fails and the support is removed from the mass above Failure Surface 3, it is likely that Surface 3 will approach instability. With the removal of elements near the canyon bottom, excess stresses would be passed to elements higher on the slide, and lower factors of safety would result. Such a scenario supports the compound failure theory.

#### CONCLUSIONS AND RECOMMENDATIONS

Several conclusions can be drawn from this study of the Thistle Landslide based on the results presented and considerations discussed. They are as follows.

1. The Thistle Slide was not a simple recurrence of a pre-existing slide acting solely at residual shear strength levels. It appears to be a compound progressive failure with peak strengths mobilizing in many of the soil zones. While ancient slides have occurred at this location and some of those failure surfaces may have been reactivated in 1983, the majority of the failure surface appears to have been in previously unfailed material. If this were not so, stability could be seen in those cases involving residual strength parameters.
2. Analyses performed in this study indicate that the slide started at the toe and progressed uphill.
3. The failure did not involve a deep-seated, circular failure surface or a long, continuous failure surface. It is more likely that relatively shallow masses of soil failed, progressively triggering failures in adjacent, uphill zones.
4. Seepage forces played a significant role in the failure at Thistle. As suggested by previous investigators of the Thistle Slide, water in the soil resulting from high precipitation levels was definitely a factor contributing to this failure.

#### REFERENCES

- Chang, C-Y., and K. Nair, (1973). Development and Applications of Theoretical Methods for Evaluating Stability of Openings in Rock, Final Report. Woodward-Lundgren & Assoc., U.S. Bureau of Mines Contract H0220038.
- Corp, E.L., R.L. Schuster, and M.M. McDonald, (1975). Elastic-Plastic Stability Analysis of Mine-Waste Embankments, Bureau of Mines Report of Investigation #8069.
- Dames and Moore, (1985). Engineering Geology and Geotechnical Engineering Studies: Thistle Landslide Alternatives Project, unpublished report.
- Duncan, J.M., R.W. Fleming, and F.D. Patton (1985). Report of the Thistle Slide Committee, unpublished report to the Utah State Engineer.
- FEMA, (1983). FEMA Hazard Mitigation Team Intergovernmental Hazard Report for the State of Utah in Response to the April 30, 1983 Disaster Declaration, FEMA report #FEMA-680-DR-UTAH.
- Kaliser, B. and R.W. Fleming, (1986). "The 1983 Landslide Dam at Thistle, Utah," Proc., ASCE Geotechnical Speciality Conference: Landslide Dams: Processes, Risk and Mitigation, p 59-83.



Leonard, B.D. (1987). A Finite Element Analysis of the Thistle Landslide, unpublished thesis presented to the graduate school of the University of Utah in partial fulfillment of the requirements for the degree of Master of Science.

Lambe, T.W. and R.V. Whitman, (1969). Soil Mechanics, John Wiley & Sons, New York, N.Y.

Schroder, J.F. (1971). "Landslides of Utah," Utah Geological and Mineralogical Survey, Bulletin 90.

Taylor, R.L. and C.B. Brown, (1967). "Darcy Flow Solutions with a Free Surface," ASCE Hydraulics Division Journal, vol 93, HY2, 25-33.

Witkind, I.J. and W.R. Page, (1963). "Geologic Map of the Thistle Area, Utah Co., Utah," Utah Geological and Mineral Survey, Map 69.

# Improvement of Mechanical Properties of Soft Soils by Use of a Pre-Loading Embankment

F. Colleselli

Istituto di Geotecnica, Facoltà di Ingegneria, Università di Padova, Italy

P. Simonini

Istituto di Geotecnica, Facoltà di Ingegneria, Università di Padova, Italy

M. Soranzo

Istituto di Geotecnica, Facoltà di Ingegneria, Università di Padova, Italy

**SYNOPSIS.** A preloading embankment, and its foundation soil, have been closely monitored in the Po river delta (Italy). After showing that the complete consolidation of the peaty and clayey soil has taken place, the shear strength increase measured with various tests has been considered and analyzed.

## PLANNING PROBLEMS AND SOIL CHARACTERISTICS

The new electric power station in Adria situated in the Po delta has been recently built in an area of about 70,000 m<sup>2</sup>, (210 x 315 m). This area is located in the surroundings of the navigable canal "Canal Bianco" and is distant about two kilometers from the Po river. Because of hydraulic protection problems against floods, due to the fact that the area was subject to a subsidence phenomenon in the past, the design of the final plan of the station provided for its being raised from ground level, situated at -1 - -2.5, to +1 a.s.l., by means of a large sand filling. Stratigraphy from the surface downwards was as follows:

- from 0 to -2m : over-consolidated silty clay of low plasticity; (Formation 1)
- from -2 to -5m: mainly peaty soil of high plasticity composed of not very fibrous peats mainly of amorphous and granular type (Amaryan et al. 1973) (unit weight  $10 \div 14$  kN/m<sup>3</sup>, liquid limit  $PI > 100$  and water content  $W > 120$ ); (Formation 2)
- from -5 to -8m: normally consolidated silty-clayey soils of medium plasticity; (Formation 3)
- from -8 to -14m: fine, sometimes silty, sands of medium density; (Formation 4)
- from -14 to -21m: alternating layers of fine sands and normally consolidated silty clay of medium and high plasticity; (Formation 5)
- from -21 to -30m: homogeneous medium fine grained sands of medium and high density; (Formation 6).

The foundation soils showed very poor characteristics of strength and high compressibility. Figure 1 shows a stratigraphic profile with some characteristics determined through a wide research survey in the laboratory and "in situ".

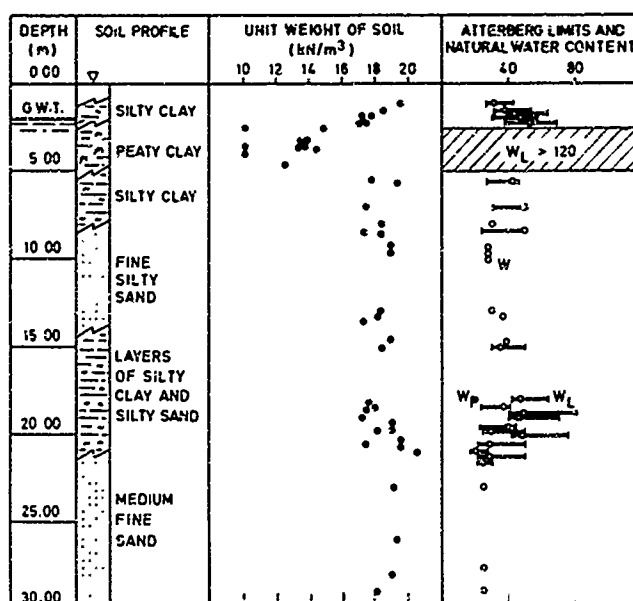


FIG. 1 - Some geotechnical properties of soil formations.

Therefore, the embankment foundation soil posed problems because of considerable settlements deferred in time due to the presence of plastic clay layers and organic soils. Organic soils of similar nature to the one found in this site have been studied by Colleselli et al. (1975).

It was decided to create a preloading embankment raising the design embankment of about 3 m (to level +4), which meant 5 ÷ 6.5 m in total height.

Figure 2 shows the general plan of the preloading embankment and figure 3 shows a cross section of the embankment side berm built in order to ensure the stability of the embankment itself.

The purpose of preloading was to reduce the compressibility and to improve the character-

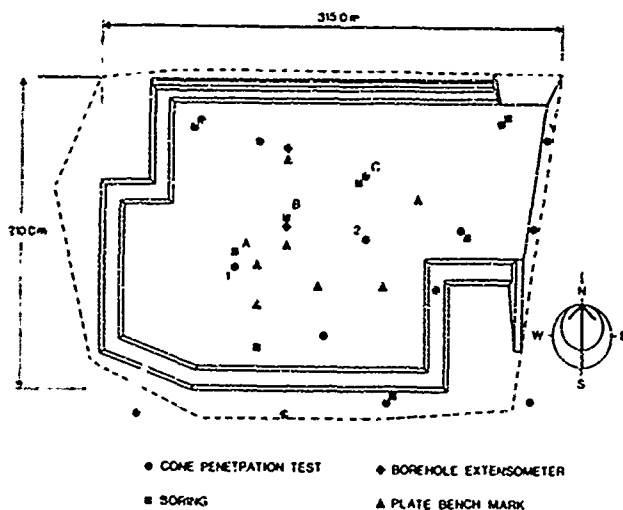


FIG. 2 - General plan of the preloading embankment.

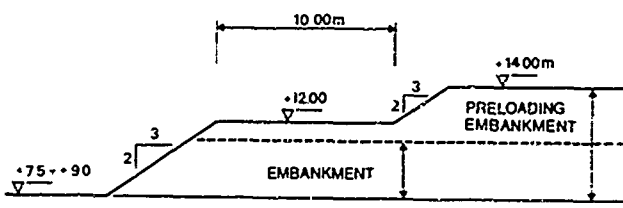


FIG. 3 - Cross section of the preloading embankment. Sea level has been taken as + 10.0 m.

istics of shear strength of the soil, thus allowing realization of buildings with shallow foundations.

The preloading design presented problems connected mainly with the prevision of settlement pattern in time and of the behaviour of peat soil layers under loading action.

Still during the planning stage, total settlements due to secondary compression in the order of 2 ÷ 3 cm per year were estimated in the various zones, they were related to the height of the embankment and to the thickness of the compressible layers.

Moreover, the preloading embankment was to be maintained for about 20 months assuming that 90 percent of primary consolidation would mature in roughly 500 days.

In order to control the foundation soil behaviour during all of the preloading phases, a remarkable geotechnical instrumentation consisting of plate bench marks, borehole extensometers and Casagrande and electro-pneumatic piezometers was incorporated in the design.

The whole sand embankment of about 500,000 m<sup>3</sup> in volume was built between July 1980 and January 1981 and was kept until the end of 1982.

The embankment was then removed to +1 (corresponding to +11 in figure 3), final design height, and the construction of the buildings of the electric power station began. It was completed at the end of 1983.

Before removing the preloading, a new research survey was carried out both in situ and in the laboratory in order to control the effects of the foundation soil improvement.

In this paper the increase of foundation soil mechanical properties due to the consolidation of the foundation soils themselves due to preloading is mainly considered.

## PRELOADING EMBANKMENT BEHAVIOUR

In order to calculate the preloading embankment settlements, the compressibility parameters ( $m_v$ ) of cohesive and peat formations have been obtained from oedometric consolidation tests.

Figure 4 shows the values of  $m_v$  as a function of effective stresses. The parameters for the settlement calculations have been chosen as function of geostatic stresses  $\sigma'_{v0}$  and of vertical stresses induced by overloading  $\sigma'_{v0} + \Delta\sigma'_v$  and calculation was carried out considering the hypothesis of monodimensional consolidations, which correspond to the geometry of the case examined.

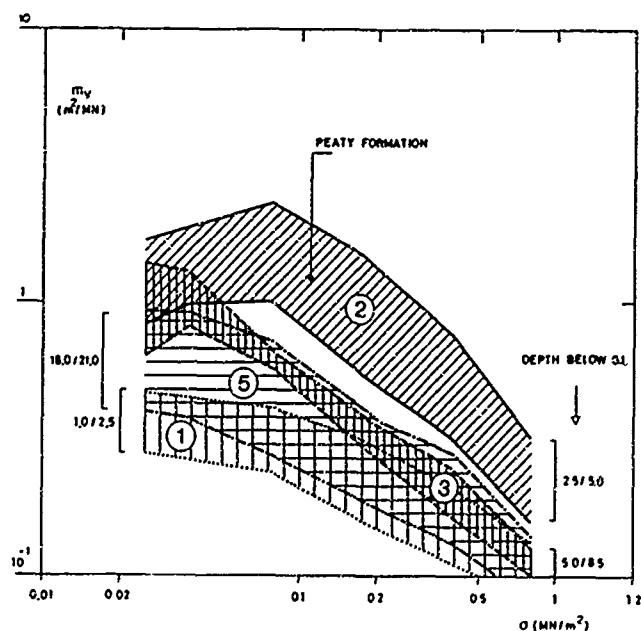


FIG. 4 - Trends of the  $m_v$  values of various formations vs. vertical effective stress.

The preloading embankment behaviour has been monitored with a considerable number of plate bench marks and borehole extensometers.

Figure 5, referring to a central point of

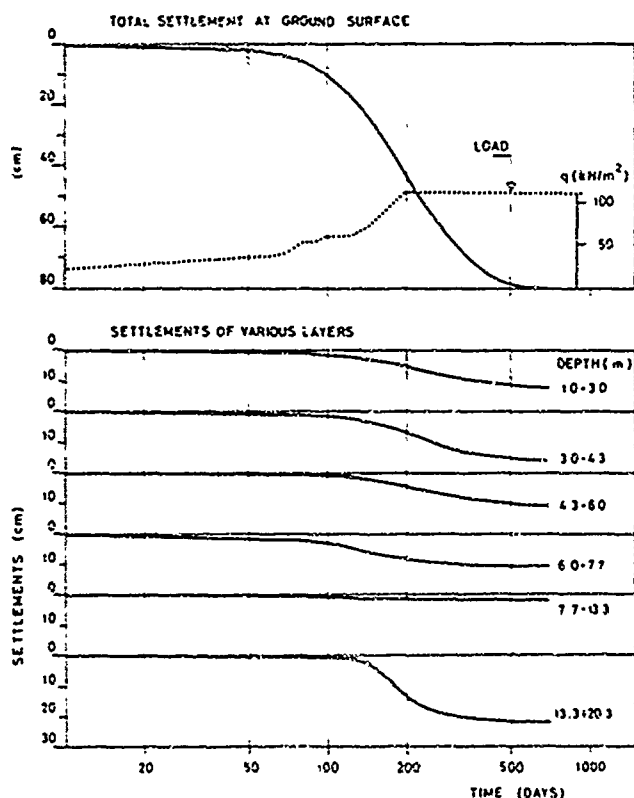


FIG. 5 - Trends of vertical settlements vs. consolidation time.

the embankment area, summarizes the settlement pattern in time of the foundation plan, and of the various layers, obtained through the difference measurements given by deep settlements gauges. The deep settlement gauges showed that soils at a depth greater than 30 m from ground level are responsible for a portion of the settlement equal to about 5 - 10 percent of total settlement.

From the diagrams it can be noticed that the settlement due to primary consolidation ended completely within 600 days from the beginning of the embankment realization.

From the examination and interpretation of figure 5 and of data from other deep settlement gauges, it was possible to estimate soil deformation moduli. In figure 6 the calculated moduli are compared with those established by laboratory tests: a substantial agreement between measurements in situ and in the laboratory with variations of  $\pm 25$  percent can be noticed.

At the end of the preloading permanence period, after about 20 months, settlements varying from 60 to 110 cm matured in the foundation soil.

Measurements of electropneumatic piezometers placed in clayey and peaty layers have given values of maximum pore pressures after construction of 20-30 kN/m<sup>2</sup>. These pressures dissipated in about 18 months.

Once the preloading was removed to +1, a 2 - 4 cm swell of foundation soil occurred. To date, after the completion of the construction

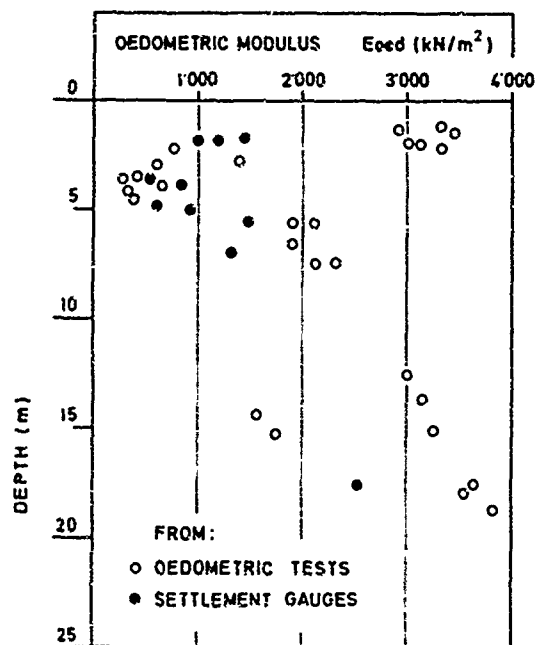


FIG. 6 - Comparison between in situ and in the laboratory constrained moduli.

of the buildings, which have a medium weight of 20 kN/m<sup>2</sup>, distributed on the embankment, a constant, and continuous, practically uniform, settlement of 1 - 2 cm/year occurred.

#### IMPROVEMENT OF THE MECHANICAL CHARACTERISTICS OF SOIL STRATA.

The complete primary consolidation of cohesive and peaty layers due to preloading embankment action was recorded with plate bench marks and borehole extensometers. The superficial pressure of the embankment, about 26 m high, turned out to be equal to 105 kN/m<sup>2</sup>. In the central part of the embankment this vertical stress is practically constant in the first 20 metres of soil which is the thickness our experimental research is concerned with.

As is well-known, the increase in vertical effective stresses causes a corresponding increase of shear strength in cohesive and granular materials. This strength increase was examined with routine laboratory tests (i.e. unconfined compression tests) and with routine in situ tests (i.e. CPT and Field Vane) carried out on specimens or on soil layers before and after the action of the preloading embankment.

In the cohesive soils examined the measured strength parameters are of the undrained type. The results of the different types of tests, will be examined separately.

#### UNCONFINED COMPRESSION STRENGTH

Unconfined compression tests have been carried

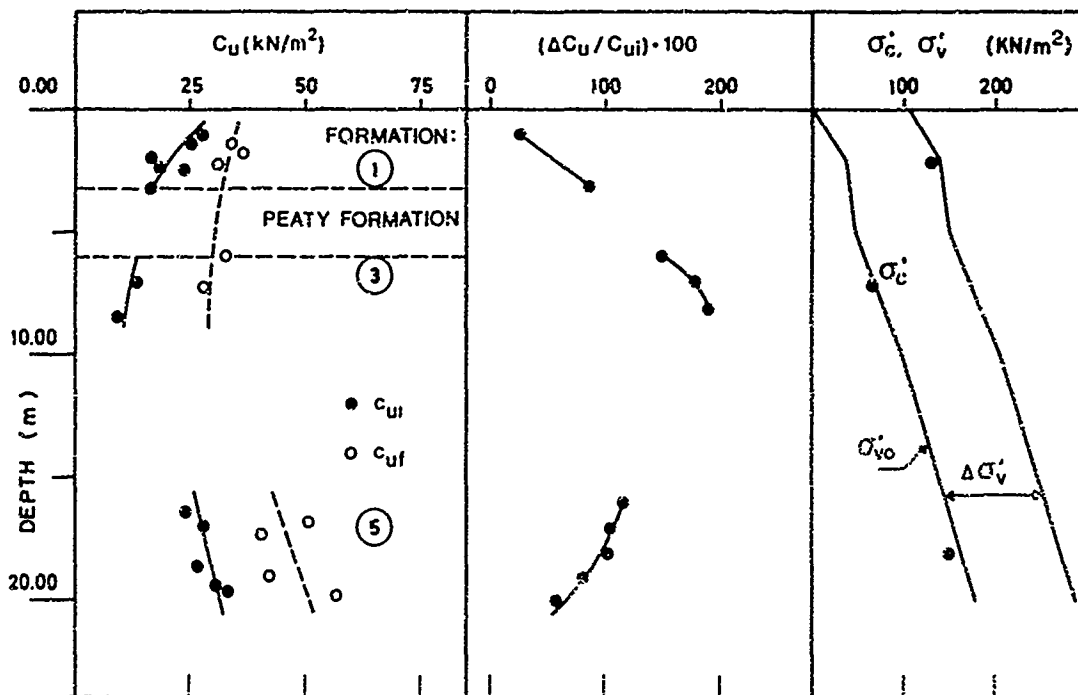


FIG. 7 - Variation of unconfined compression strength in clayey formations due to the increase in vertical effective stresses.

out, on specimens of the cohesive formations no. 1, 3 and 5, both before and after the preloading of the embankment.

The results of the performed tests have been summarized in fig. 7.  $C_{ui}$  are the values of the initial parameters while  $C_{uf}$  are the final ones. From these results the increase in shear strength is clearly visible and varies from 25 percent to almost 190 percent depending on the vertical effective overburden stresses and on the preconsolidation pressures acting at various depths as shown below.

From the research of Ladd e Foott (1974), Ladd et alii (1977) and Ladd (1982), the undrained shear strength can be expressed by the empirical relation :

$$c_u / \sigma'_{v0} = S (OCR)^m \quad (1)$$

where  $\sigma'_{v0}$  is the vertical effective stress,  $S = c_u / \sigma'_{v0}$  at  $OCR = 1$ ,  $OCR = \text{overconsolidation ratio} = \sigma'_c / \sigma'_{v0}$  and  $m = 0.8 \pm 0.05$  (empirical - experimental parameters as given in the above quoted references).

The well accepted Skempton equation (1957) has been utilized to express  $S$ , such as:

$$S = c_u / \sigma'_{v0} = (0.11 - 0.37 PI) \quad (2)$$

For plasticity indexes ranging from 20 to 35  $S$  can be taken as:

$$S = 0.21 \pm 0.03$$

and equation (1) can be rewritten as:

$$c_u = 0.21 \times \sigma'_{v0} \times OCR^{0.8} \quad (3)$$

so that the overconsolidation ratio of a soil specimen can be determined, if its  $c_u$  and the values of the vertical effective stresses are known, by the relation :

$$OCR = (c_u / (0.21 \times \sigma'_{v0}))^{1.25} \quad (4)$$

Relation (4) and the data of fig. 7 have been utilized to determine the OCR preconsolidation pressure ( $\sigma'_c$ ) for the specimens at the depth of 2, 7 and 18 m below ground level as reported in Table 1

| Depth (m) | $\sigma'_{v0}$ (kPa) | $c_{ui}$ (kPa) | OCR | $\sigma'_c$ (kPa) |
|-----------|----------------------|----------------|-----|-------------------|
| 2         | 36                   | 22             | 3.8 | 137               |
| 7         | 65                   | 13             | 1.0 | 65                |
| 18        | 160                  | 36             | 0.9 | 144               |

The values of the preconsolidation pressures have been plotted on fig. 7.

It can be seen that above the peaty formation the clay is well overconsolidated while below it results normally consolidated (NC).

In the other hand the final effective vertical stresses:  $\sigma'_f = \sigma'_{v0} + \Delta \sigma'_v$ , equal to the sum of the vertical effective and induced stresses

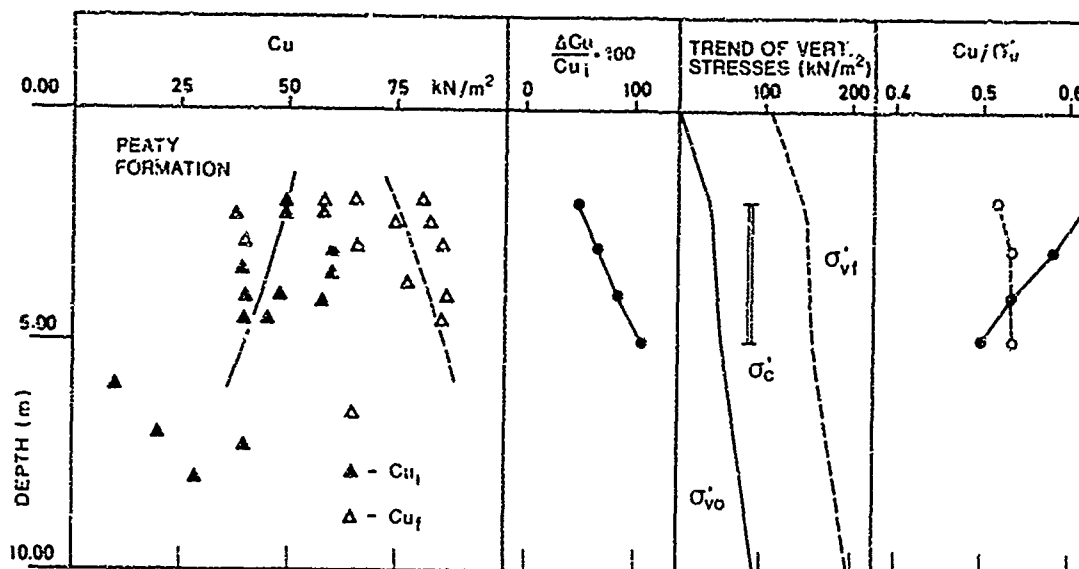


FIG. 8 - Variation of field vane strength in peaty formation as a consequence of increase in vertical effective stress.

are about equal to the preconsolidation pressure in formation 1. This explains the reason why the smallest increase in shear strength was measured at low depth.

With regard to NC soils, greater increases in percentage of strength were of course found where the ratio  $\Delta\sigma'_{vf}/\sigma'_{vo}$  was greater.

In this case a direct proportion of the type

$$\Delta c_u = (\Delta\sigma'_{vf}/\sigma'_{vo}) \times c_{u1} \quad (5)$$

can be used for NC soils to estimate the increase in shear strength and confirms the general validity of Skempton's equation (no.2 of this article).

#### FIELD VANE STRENGTH

The structure of the soil being formed predominantly of a peaty component did not allow execution on an undrained shear strength test in the laboratory. The comparison was therefore carried out through the use of field vane tests. In fig. 8 we can see the values for  $c_u(FV)$  as a function of depth. As it is possible to see, the undrained shear strength values before the application of the preload diminishes with depth going from values of 50 kN/m<sup>2</sup> to 40 kN/m<sup>2</sup>; after consolidation the situation changes with higher values being found equal to 85 kN/m<sup>2</sup> deep down, and lower values 75 kN/m<sup>2</sup> on the surface.

The average values of the consolidation pressure of the whole layer  $\sigma'_c$  was calculated with reference to the shape of the envelopes of the oedometric compressibility coefficients in fig. 4, interpreted according to the indications given by Ricciardi et al. (1985). That is, for soils with a PI greater than 50 the

$\sigma'_c$  can be determined from the change of slope in the diagram  $\log m_v$  vs.  $\log \sigma'_{vf}$ . This value resulted to be about 80 kN/m<sup>2</sup> and is reported together with the vertical effective stress values seen in the third column of fig. 8. The peaty formation resulted to be slightly overconsolidated with an average OCR value of about 1.8. The load application induces an increase of vertical effective stress to the point where it exceeds the pre-consolidation pressure value. The final condition reached is a normal-consolidated state that brings a percentage increase of the undrained shear strength that is variable in depth from 50 to 100%.

If the relation between the undrained shear strength value and the vertical effective stress  $c_u(FV)/\sigma'_{vf}$  is determined on the whole peaty formation, we obtain a pattern more or less constant with depth (fig.8, fourth column), with the exception of the first stretch, whose different slope can be presumably explained taking into account the clayey composition of the superficial layer that probably influenced the results of the field vane tests in some zones. The constant value of this relation is:

$$c_u(FV)/\sigma'_{vf} = 0.53 \quad (6)$$

and is fairly high. Nonetheless we need to remember that the ratio is related to the plasticity of the material. Taking into account the indications given by Bjerrum and Simons (1960) relative to the relationship between this same ratio and the plasticity index (PI) and extrapolating their considerations to higher plasticity, we obtain values that vary between 0.40 and 0.55 for plasticity indexes that range from 100 to 200, these later values being limiting values cha-

racteristic of the formation under examination. Thus, the calculated values correspond well with extrapolated values according to what was previously indicated. The pattern of the ratio  $c_{uf}/\sigma'_{vc}$  was introduced for comparison sake with the  $c_{uf}/\sigma'_{vf}$  ratio in fig. 8. The variation of the first with depth (i.e. the larger ratios are to be found closer to the surface) can be justified taking into account that the more superficial part of the peaty layer may have been subjected to a drying phenomenon that may have in this manner increased, in much the same manner that was seen for superficial clayey layers, the degree of consolidation. On the contrary the ratio was represented considering a uniform pre-consolidation pressure equal throughout the whole formation under examination.

#### THE CPT STRENGTH

The static cone penetration test (CPT) has also been utilized to estimate the increase in strength consequent to increase in vertical effective stress and other stresses correlated to it. The increase in strength has been directly measured and correlated to the soil nature as reported below: two typical CPT tests carried out in the same position before and after the preloading are shown in fig. 9.

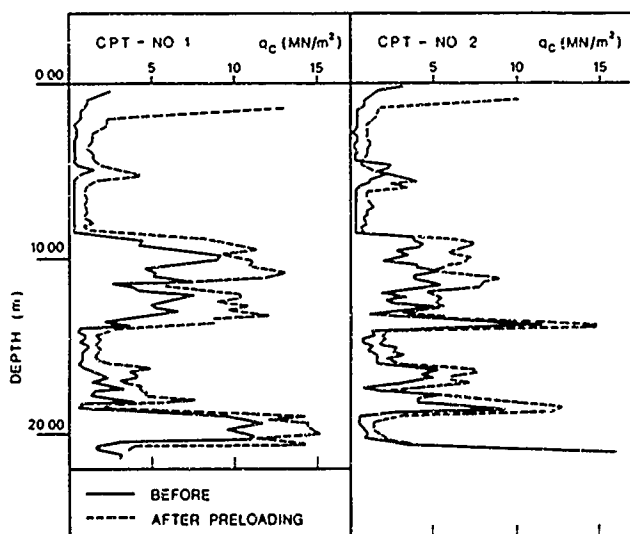


FIG. 9 - Results of two typical CPT tests before and after the preloading.

#### Cohesive soils

Clay and peaty clay are both considered cohesive. In this case the undrained shear strength is generally estimated by the expression

$$c_u = (q_c - \sigma'_{vo})/N \quad (7)$$

where  $q_c$  is the point resistance of the CPT and  $N$  is a bearing factor which due to the

same shape of the penetrating tip should substantially remain constant within each soil formation. Nevertheless, it has been seen from much experimental research (ESOPT I, II) that  $N$  may vary over a wide range depending on the soil plasticity (Baligh et al. 1980).

Equation (7) can be expressed as a function of  $N$ , such as:

$$N = (q_c - \sigma'_{vo})/c_u \quad (8)$$

The value of  $N$  has been determined referring the undrained shear strength parameter determined in unconfined compression tests (for clayey soil) and field vanes (for peaty soils). The results of these determinations are reported in table 2 and they refer to average  $c_u$  and  $q_c$  values.

TABLE 2

| Depth<br>(m)      | CPT<br>No. | PI   | $q_c$<br>(kN/m <sup>2</sup> ) | $c_u$ | N  |
|-------------------|------------|------|-------------------------------|-------|----|
| BEFORE PRELOADING |            |      |                               |       |    |
| Clayey formations |            |      |                               |       |    |
| 6.5               | (1)        | 20   | 300                           | 13    | 18 |
| 6.5               | (2)        |      | 300                           | 13    | 18 |
| 16.0              | (1)        | 30   | 800                           | 26    | 25 |
| 15.0              | (2)        |      | 900                           | 25    | 30 |
| Peaty formation   |            |      |                               |       |    |
| 3.5               | (1)        | >100 | 300                           | 45    | 6  |
| 3.5               | (2)        |      | 300                           | 45    | 6  |
| AFTER PRELOADING  |            |      |                               |       |    |
| Clayey formation  |            |      |                               |       |    |
| 6.5               | (1)        | 20   | 1000                          | 30    | 28 |
| 6.5               | (2)        |      | 900                           | 30    | 24 |
| 16.0              | (1)        | 30   | 1700                          | 44    | 32 |
| 15.0              | (2)        |      | 1800                          | 42    | 36 |
| Peaty formation   |            |      |                               |       |    |
| 3.5               | (1)        | >100 | 1400                          | 80    | 16 |
| 3.5               | (2)        |      | 1000                          | 80    | 11 |

These results indicate that notwithstanding a remarkable increase in both undrained shear strength and unit point resistance, the factor  $N$  does not remain constant with the strength increase in any specific formation.

Because of the limited number of tests and of the low values of the point resistance of the CPT no general comment can be made, except that  $N$  values are higher for cohesive soils ( $N = 18-30$ ) than for organic soils ( $N = 6-16$ ).

#### Granular soils

Sandy soils exhibited a substantial increase in the unit point resistance of the CPT ( $q_c$ ) as a consequence of the stress increase. So the normalized cone resistance, that is the  $q_c$ , divided by effective vertical stress  $\sigma'_{vo}$  should remain about constant. This linearity in the behaviour is not fully represented in nature as reported by Schmertmann (1976), Baldi et al. (1982). This effect has been seen analyzing the ratio

$$(q_c/\sigma'_{vo})_f / (q_c/\sigma'_{vo})_i = \alpha \quad (9)$$

In our case this ratio varies in CPT 1 and 2 from 0.83-0.85 in formation no. 4 and from 0.87-0.90 in formation no.6.  $\alpha$  values lower than 1.0 indicate a decrease of the normalized cone resistance with the increase of stresses. (This has been defined as scale effect).

## CONCLUSIONS

The findings presented in this paper are based on two well defined and controlled conditions:

- a consolidation process developed in uniaxial conditions due to the remarkable extension of the embankment compared to the analyzed depth;
- a stress variation in a particular site that induced a complete primary consolidation of the peaty and clayey strata.

Based upon the above conditions the shear strength increase has been considered analyzing the results of various types of tests: unconfined compression, field vane and cone penetration tests

It has been shown that each test must be considered separately and that it does not seem correct to generalize the use of empirical relations proposed in scientific literature. Each one needs to be verified on each site and on each formation before being used in the design.

In the laboratory only the clayey formations have been analyzed.

It has been shown that from the results of unconfined compression tests the OCR can be determined as well as the increase in the undrained shear strength.

The peaty formation has been studied with field vane (FV) tests.

The ratio  $c_u/\sigma'_v$  resulted to be in the order of 0.5 both before and after consolidation ( $\sigma'_v = \sigma'_c$  has been utilized before applying the preload); this apparently high value can be easily justified considering the very high plasticity of the peaty formation as pointed out by Bjerrum and Simons (1960). The CPT has shown that N values for cohesive and organic soil may vary considerably both due to the soil nature and to the stress level.

In granular soil a small scale effect has been clearly seen

## REFERENCES

- Amarayan, L.S., Sorokina, G.V., Oustronmova V., (1973), "Consolidation Laws and Mechanical-Structural Properties of Peaty Soils", Proc. of the 7th Int. Conf. on Soil Mech. Found. Eng. Moscow, Vol. 4/1, pp.1-6.
- Baldi, G., Bellotti, R., Ghionna, V., Jamiolkowski, M., Pasqualini, F. (1982), "Design Parameters for Sands from CPT", Proc. ESOPT II, Vol. 2, pp. 425-432.
- Bjerrum, L., Simons, N.E. (1960), "Comparison of Shear Strength Characteristic of Normally Consolidated Clays", Proc. ASCE, Res. Conf. on Shear Strength of Cohesive Soils, Boulder, Colorado, USA, pp. 711-726.

Colleselli, F., Errani, V., Previatello, P., (1975); "Sulle torbe della Pianura Veneta ed Emiliana", Le Strade, N. 6.

ESOPT I, (1974), Proc. of European Symp. on Penetration Testing, Naz. Swedish Build. Res., Stockholm.

ESOPT II, (1982), Proc. of the European Symp. on Penetration Testing, Balkema, Rotterdam.

Ladd, C.C. (1982), "Geotechnical Exploration in Clay Deposits with Emphasis on recent Advances in Laboratory and in Situ Testing and Analysis of Data Scatter", Special Lecture given at the National Taiwan University, pp. 1-69.

Ladd, C.C., Foott, R., (1974), "New Design Procedure for Stability of Soft Clays", JGED, ASCE, Vol. 100, N. GT7, pp. 763-786

Ladd, C.C., Foott, R., Ishihara, K., Schlosser, F., Poulos, H.G., (1977), "Stress-Deformation and Strength Characteristics", SOA Report Proc. 9th ICSMFE, Tokyo, Vol. 2, pp 421-494.

Ricceri, G., Favaretti, M., Mazzucato, A., Simonini, P., Soranzo, M. (1985), "Effects of Sampling on Artificially Reconstructed Cohesive Soils", proc. 11th ICSMFE, S. Francisco, pp. 1035-1040.

Schmertmann, J., (1976), "An updated Correlation between Relative Density  $D_r$  and Fugro Type Electric Cone Bearing  $q$ ", Waterways Experimental Station Contract Rep. DACW 39/76 M6646.

Skempton, A.W. (1957), "Discussion on the Planning of the New Hong Kong Airport", Proc. Inst. Civ. Eng. 7, p. 306.



## Deformation Response of Some Earth and Rock-fill Dams

T. Ramamurthy  
India

S.L. Jain  
India

**SYNOPSIS:** Vertical compressional data obtained from 10 earth and earth rock fill dams built in India has been analysed for during construction and post-construction response. The performance of these dams has been compared with some dams built in USA wherein the construction practices have been similar. The contributions of various factors, namely height of embankment, gradation and plasticity of soil, and placement conditions of moisture and density have been examined. A major portion of the total compression occurred by the end of construction. These compressions were found to be the functions of the height of the embankment. Both the compressions across and along the valley have been found to be small.

### INTRODUCTION

A large number of earth and earth rockfill dams have been constructed in India during the last four decades. It is believed that there are as many as 1600 large dams constructed in India. The highest earth structure constructed so far has been about 130 m height and the one with a height of 240 m is under construction and more such high earth structures are in the planning stage. The embankment dams which have already been constructed were designed safe against failure by rupture and were expected to undergo compressions of safe value without excessively distorting the structure and its function.. To check the performance of these dams, they were instrumented to measure compressions within the body of the dam and the foundation and also to measure and control the development of pore water pressures. The practices generally adopted by USBR have been followed in choosing and selecting soils for different zones of earth embankment dams, in laboratory and field testing, in controlling placement conditions of density and moisture content, in laying the thickness of layers for fine grained, coarse grained and rockfills and also in the technique of compacting the soils. The cross-arm devices installed were similar to those adopted by USBR. The construction periods were longer for the Indian dams. The performance of these dams was in no way different from those of USBR as far as the extent and nature of compressions are concerned.

This paper presents the case histories of 10 Indian dams built in different geological formations. Their performance in terms of embankment compression has been analysed and compared with a few dams of USA. These fifteen dams have indicated definite trends of vertical compression during construction and after construction with the height of the embankment. The influences of soil parameters like Atterberg limits, grain size distribution and placement conditions have also been examined.

### BEAS DAM

Beas dam is situated in the Himalayan foot hills 19.3 Km. south of Kangra. It is a central earth core-gravel shell type dam with a maximum height of 132.5m. above the deepest foundation level, as shown in Fig.1.

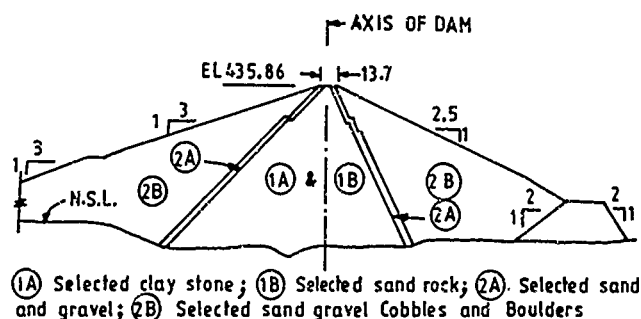


Fig.1 Cross-section of Beas Dam

### Geology

The Dam site is characterised by the presence of sedimentary rocks of alternative layers of sand rock and clay shale of the Upper Shivalik formation. A bed of boulders was located from 27 to 76 m. below the ground level. The clay shale is generally massive but includes silt and sand fractions. The sand rocks are coarse grained and showed considerable loss of strength upon soaking.

### Construction Material

The impervious core was made up of the clay stone and sand rocks. The material containing more than 50 per cent of clay shale was placed in zone 1(a) whereas the material containing more than 50 per cent sand rock in zone 1(b). The material of the zone 1(a) contains 70 per-

cent finer than 200 mesh and zone 1(b) contains 40 per cent. For the filter and the previous zone, hard quartzite with 22 to 31 per cent sand and 40 to 77 per cent gravel was used.

#### Design Properties

The properties of the soil for core adopted in the design of dam were as follows:

Bulk density : 2.08 g/c.c.  
Saturated density : 2.16 g/c.c.  
Specific gravity : 2.67  
Permeability :  $10^{-6}$  cm/sec.  
Angle of shearing :  $26.5^{\circ}$   
resistance  
Cohesion : 0.35 kg/sq. cm.

#### Fill Placement and Compaction

The fill placement for impervious zone was carried out in 20 cm. thick layers compacted to 15 cm. The specification allowed a minimum Proctor's density of 98 per cent and maximum 104 per cent. The laboratory Proctor's density was 1.96 g/c.c. The compaction moisture content specified varied from +1 per cent to -2 per cent of the optimum moisture content (i.e. 18 per cent).

#### Instrumentation

For the measurement of settlement of foundation and compression in the dam, seven USBR telescopic cross-arms were installed in the body of the dam. Three each at station 74 and 60 (at right abutment and central portion) and one at station 47 (on left abutment) were installed and labelled as A to G. To measure the cross valley deformation, six of the telescopic cross-arms were provided with internal horizontal movement devices at 30.5 m. vertical intervals. An Inclinator was installed at the deepest section through the impervious core. Surface movements to measure both settlement and horizontal alignment were set up on the upstream and downstream faces (Berry 1975, Char 1979).

#### Observations

The settlement of individual cross-arms against their elevation have been plotted as shown in Fig. 2. From the figure it is clear that the maximum settlement occurred at mid height of the dam.

Settlement of the individual cross-arm for each of the settlement devices has been plotted. It is observed that the maximum settlement have occurred in the device F which was embedded in the impervious core. During the early construction period compression was faster which slowed down with time. On an average 22.5 per cent of the total compression took place during the first one month after placement. Generally lower layers showed higher compression than the upper layers.

The total settlement has also been plotted as the percentage of the height of the embankment fill height for the period of the raising of the embankment as shown in Fig.3. From this

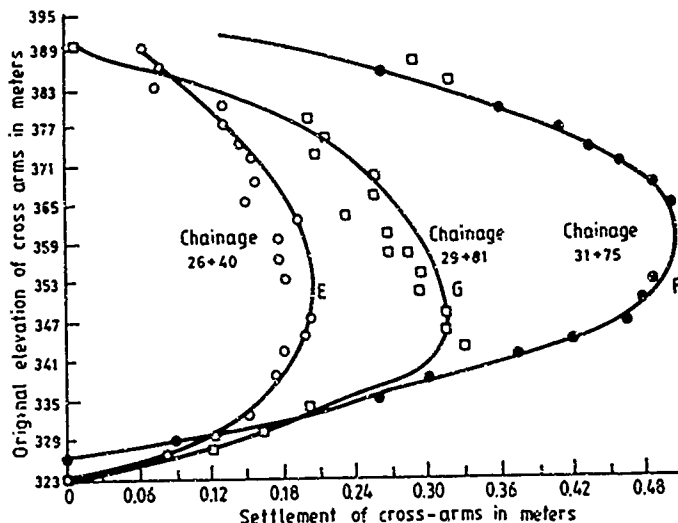


Fig.2. Settlements of Cross-arms in Beas Dam

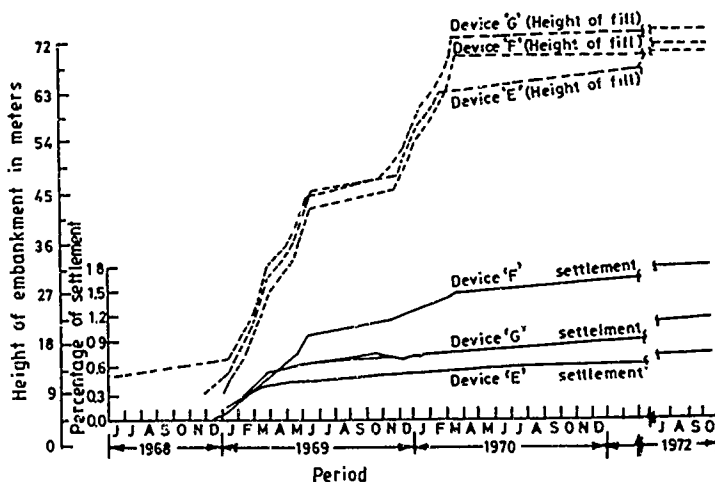


Fig.3. Settlement with Height of Fill in Beas Dam

plot, it is seen that the settlement curve largely follow the pattern of the fill placement curve with respect to time, (Ramamurthy 1984).

It is further observed that the maximum settlement took place in the settlement devices embedded in the impervious core. The highest percentage of settlement, 2.02 per cent, had taken place at the device C which was embedded in the core and where the height of fill was maximum.

## RAMGANGA DAM

The main earth and rockfill dam (127.5m high) constructed across Ramganga river at 3.2 Kms. upstream of Kalagarh in district Garhwal Fig.4.

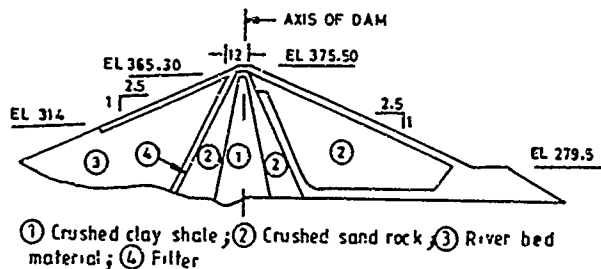


Fig.4. Cross-section of Ramganga Dam

The dam was located in the gorge portion between two right angled bends and the diversion tunnels and surplusing works located on the right flank together with the Power Houses.

### Geology

The dam rests on alternate bands of sand rocks and clay shale of middle Shivalik age. The general dip of the rock is towards upstream. The sand rock is massive, coarse jointed and poorly consolidated, whereas the clay shale layers vary from soft clays to silt stones. In the river bed the rock formations are covered by river bed deposits consisting mainly of sand, gravel and boulders. Percentage of fines being quite low.

### Construction Materials

The inner core consists of crushed clay shale and is encased on either side by crushed sand rock. Both these materials are impervious in nature. The permeability of the crushed clay shale and the crushed sand rock is of the order of  $0.8 \times 10^{-8}$  cm/sec. and  $0.1$  to  $2.6 \times 10^{-6}$  cm/sec. respectively.

The main source of pervious material for the shell of the dam is river bed deposit; on an average 50 per cent of the material is above 7.5 cm. in size, 17 per cent is sand and about 3 per cent is silt and clay.

### Design Properties

The properties of the soils adopted for the design of the dam were as follows:

| Properties                   | Impervious Material<br>Sand rock/<br>Clay shale | Pervious Material |
|------------------------------|---|-------------------|
| Bulk density g/c.c.          | 2.0/2.08  | 2.16              |
| Saturated density, g/c.c.    | 2.2/2.24  | 2.24              |
| Specific gravity             | 2.67  | 2.67              |
| Angle of shearing resistance | $22^{\circ}$                                    | $36.5^{\circ}$    |

### Fill Placement and Compaction

The clay stone was compacted by 12 to 14 passes on 15 cm. thick layers, for sandstone the number of passes varied from 17 to 21 on layers of 30 cm. thick. The river bed material was compacted by 2-3 passes of 10 tonne vibratory roller on 60 cm. thick layer. The specification allowed 90 per cent of proctor density. The laboratory proctor density was 1.76 g/c.c. The compaction moisture content was specified as -2 per cent of the optimum moisture content.

### Instrumentation

Six numbers of USBR cross-arm devices coupled with horizontal movement plates were installed at various sections and zones of the dam, to record settlements and horizontal movement in the body of the dam.

### Observations

The settlement of the individual cross-arm in each of the six devices were plotted against their original elevation. It is observed that the maximum settlement took place approximately at the mid-height of the embankment.

The settlement of individual cross-arm for the devices have been plotted in the form of contours of vertical settlement. It is observed from these contours that maximum settlement occurred at about the mid-height of the embankment.

The total settlements have been plotted as percentage of the height of the embankment for the period of raising of the embankment. It is observed that maximum settlements had taken place in the devices embedded in the impervious core and where fill heights are maximum (Verma and Raj 1978).

The total compression in the fill was about 1.8 per cent of the height of the dam. In the clay stone forming the core, the percentage compression at 10 Kg/sq. cm. was about 3.3 per cent and in the sandstone this value was 2.9 per cent.

### TAWA PROJECT

Tawa dam project is located across the river Tawa, a tributary of river Narmada in the district of Hoshangabad of Madhya Pradesh. The reservoir is created by constructing a 36.6 m. high earth dam with a masonry spillway in the river bed. Two saddles which exist on the left flank are also connected by the earth dam. The total length of the embankment is about 1.64 Km.

### Geology

The rocks met with at the dam site are Pachmarhi sandstones which are gritty in nature. Similar formation termed as the Bijori formation also exists, but with interbedded carbonaceous shales and coal seams with occasional layers of red clay stones. Both the formations have upstream dips.

### Construction Materials

The inner core consists of clay and is encased on either side by semi-impervious material. The permeability of the core material and the casing material is of the order  $12.2 \times 10^{-6}$  cm/sec. and  $42 \times 10^{-6}$  cm/sec. respectively. The properties adopted in the design are given below:

| Properties                   | Impervious | Semi-pervious | Foundation |
|------------------------------|------------|---------------|------------|
| Bulk density, g/c.c          | 2.0        | 2.17          | 2.06       |
| Saturated density, g/c.c     | 2.04       | 2.20          | 2.10       |
| Angle of shearing resistance | $19^\circ$ | $30^\circ$    | $25^\circ$ |
| Cohesion, kg/sq.cm           | 0.155      | 0.105         | 0.105      |

### Instrumentation

To measure compression within the embankment six USBR cross-arm devices coupled with horizontal movement plates were installed at three sections viz. 16.60, 36.35 and 44.10 as shown in Fig. 5.

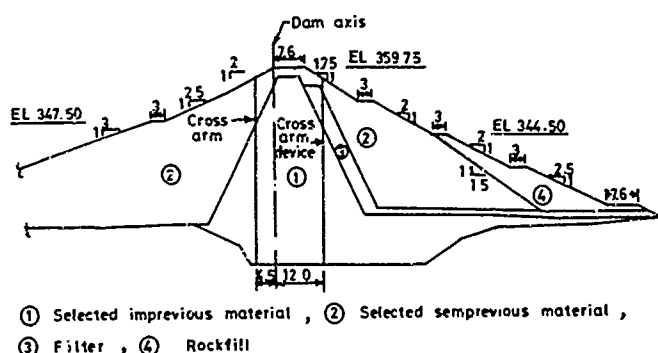


Fig.5. Cross-section of Tawa Dam

### Observations

The settlement of the individual cross-arm of all the settlement devices were plotted against their original elevation.

The settlement of individual cross-arm for the devices have been plotted in the form of contours of vertical settlement. It was observed that the maximum settlement occurred at about the mid height of dam. The embankment settlements were larger than those observed for other dams, (Ramamurthy, 1984).

### BUGGAVAGU DAM

A 31 meters high Buggavagu dam constructed across Buggavagu stream is situated on Nagarjuna Sagar Right Canal in Andhra Pradesh. The canal passes through Buggavagu streams in between 27.2 Km. and 33.0 Km. It is a rolled earth dam consisting of an impervious core zone with

semi-pervious shell and upstream and downstream rock toes.

### Geology

The foundation of the dam consists of Nepa and quartzite variety of rocks with a few widely spaced earth joints except in a length of 279 m. where it is soft conglomerate.

### Construction Materials

The average properties of soils for both core and shell zones of the dam are given below:

| Characteristics                        | Core zone | Shell zone |
|--|-----------|------------|
| Liquid Limit                           | 58%       | 31%        |
| Plasticity Index                       | 37%       | 23%        |
| Maximum Dry Density                    | 1.60      | 1.84       |
| Average Embankment Dry Density, g/c.c. | 1.66      | 1.92       |
| Optimum Water Content                  | 18%       | 10%        |
| Average Construction Water Content     | 17%       | 9%         |

### Instrumentation

The dam is provided with two sets of cross-arm (USBR) at 1.5 m. vertical interval for measuring settlement within the embankment. Settlement observations of various cross-arm showed that the maximum vertical movement of any individual cross-arm during construction period occurred near the mid height of the dam and equals to 34 cm.

The end of construction settlement at upstream installation of Buggavagu dam has been observed to be 1.49 per cent of the embankment height.

### BOR DAM

Bor dam is a rolled earthfill structure, 35.7 m. high above lowest river bed level across the Bor river, a tributary of Nardha river in Wardha district of Maharashtra.

### Geology

The dam lies in an area covered by rocks of the Deccan trap formation comprising of massive basalt.

### Construction Materials

The dam embankment comprises of a core zone of yellowish silty clay, mostly ML type with shell of murky soils reddish grey in colour (SC type).

### Properties

Properties of the soils used for the core shell are as follows:

| Characteristics          | core zone  | shell zone   |
|--------------------------|------------|--------------|
| Liquid Limit             | 38 to 52%  | 30 to 38%    |
| Plastic Limit            | 10 to 17%  | Non-plastic  |
| Dry Density              | 1.6 g/c.c. | 1.87 g/c.c.  |
| Optimum Moisture Content | 18 to 22%  | 11 to 19%    |
| Permeability cm/yr.      | 7.3 - 7.6  | 51.8 - 167.7 |
| Specific Gravity         | 2.67- 2.71 | 2.74 - 2.91  |

#### Instrumentation

The dam is provided with a USBR cross-arm installation in the core zone having 22 cross-arms at 1.5 m. interval.

#### Results

At the end of construction, the settlement has been on the lower side i.e. 0.8 per cent of the embankment height only. Post construction settlement during the following 2 years has been much higher i.e. 1.1 of embankment height. It has been observed that the maximum portion of settlement was recorded by the lower level cross-arm.

Settlement of embankment during construction though on lower side was still within the range of settlement observed on USBR dams of same soil classification i.e. ML soil (Gould, 1953,1954).

Lower placement moisture as compared to optimum moisture content seems to be mainly responsible for the lower settlement during construction. Substantial consolidation of soil due to rearrangement of soil gains after saturation of embankment seems to be mainly responsible for higher post construction settlements. It may be noted that although soil was compacted to 97.0 per cent of modified proctor maximum dry density but the value of average placement density was still substantially lower at 1.63 g/c.c. as against natural dry density of the soil which was found to be 1.68 to 1.71 g/c.c.

#### SETTLEMENT CORRELATIONS

Settlement of embankments at the end of construction versus height of embankment at cross-arm installations in respect of 15 earth and rockfill dams (5 of USA, Gould 1953, 1954) and 10 of Indians) has been plotted on log-log scale as shown in Fig.6. It is seen from this figure that at the end of construction, the compression is a power function of H, (i.e. the height of embankment). This data is included in Table 1. The best fit through the plot is given very closely by the relationship (Jain, 1985).

$$s_c = 0.007 H^{1.22} \quad (1)$$

where,

$s_c$  = settlement in metres

H = embankment height in meters

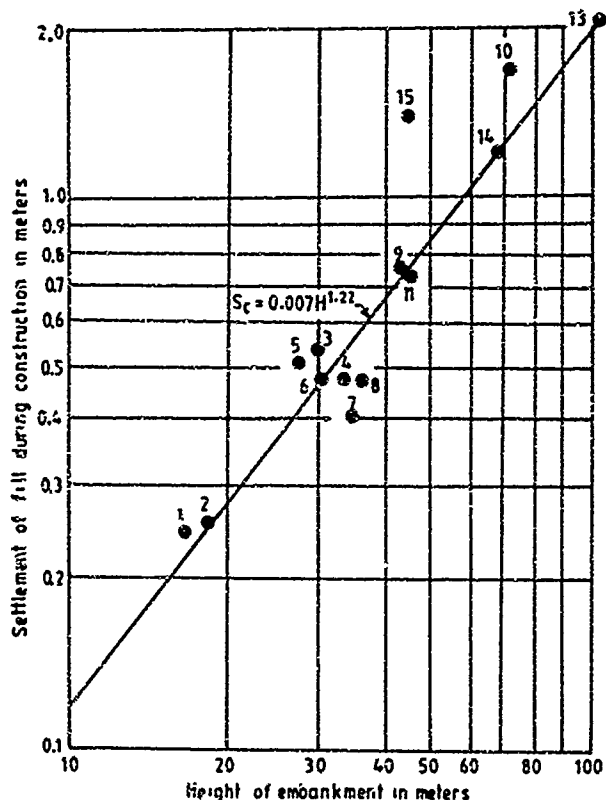


Fig.6. Settlement Variation during Construction with Fill Heights

Post-construction compression of the fill in respect of the dams has been plotted against height of the embankments on log-log scale. The points so obtained are very scattered and the plot does not indicate any definite correlation. It shows that the height of embankment of a rolled earth dam seem to have influence on the post construction settlements.

Figure 7 gives a plot between the height of embankment and the total compression on log-log scale. It indicates a best fit relationship to the data given by

$$s_t = 0.014 H^{1.1} \quad (2)$$

where,

$s_t$  = total settlement; end of construction and post-construction, m,

H = embankment height in meters.

Most of the dams referred above have indicated increasing post-construction compression with the increasing variation in the compaction moisture content allowed on the dry side of optimum moisture content. These dams have been compacted at moistures ranging from 0.2 to 4.0 per cent below optimum moisture content except for two dams which were compacted at 1.0 and 2.0 per cent above the optimum moisture content.

TABLE 1. Settlement Observational Data of some Embankment Dams

| Sl. No. | Name of Dam         | Soil in Core | Degree of compaction % | Max.height of cross-arm installation in meters | Settlement during construction in meters | Post-construction settlement in meters | Total Settlement in meters |
|---------|---------------------|--------------|------------------------|--|--|--|----------------------------|
| 1.      | Nanak Sagar, India  | CL           | 99.0                   | 16.36  | 0.247                                    | 0.148 in 5 1/2 yrs.                    | 0.395                      |
| 2.      | Baur, India         | CL           | 99.0                   | 18.59  | 0.262                                    | 0.061 in 3 yrs                         | 0.323                      |
| 3.      | Moosa Khand, India  | CL           | 101.2                  | 30.48  | 0.533                                    | 0.092 in 3 1/2 yrs.                    | 0.625                      |
| 4.      | MeJa, India         | CL           | 104.0                  | 34.30  | 0.469                                    | 0.131 in 3 1/2 yrs.                    | 0.600                      |
| 5.      | Jigro, India        | CL           | 101.5                  | 27.59  | 0.524                                    | 0.11 in 3 yrs.                         | 0.634                      |
| 6.      | Bhuggavagu, India   | CL           | 99.0                   | 31.1   | 0.463                                    | 0.143 in 2 1/2 yrs.                    | 0.607                      |
| 7.      | Box, India,         | CL           | 97.0                   | 36.3   | 0.289                                    | 0.400 in 2 1/2 yrs.                    | 0.689                      |
| 8.      | Hor-setooth, USA    | CL           | 98.8                   | 36.89  | 0.457                                    | 0.198 in 3 1/2 yrs.                    | 0.655                      |
| 9.      | Jackson Gulach, USA | CL           | 100.2                  | 44.20  | 0.762                                    | 0.244 in 3 1/2 yrs.                    | 1.006                      |
| 10.     | Granby, USA         | SC           | 98.8                   | 72.56  | 1.73                                     | 0.05 in 3 yrs                          | 1.78                       |
| 11.     | Deer Creek, USA     | CL-GC        | 99.4                   | 46.03  | 0.753                                    | 0.127 in 8 yrs                         | 0.88                       |
| 12.     | Fresno, USA         | ML-CL        | 99.8                   | 23.47  | 0.286                                    | 0.073 in 14 yrs                        | 0.359                      |
| 13.     | Beas, India         | CL           | 98-104                 | 110  | 2.32                                     | 0.39 in 3 yrs.                         | 2.71                       |
| 14.     | Ramganga, India     | CL           | 99.0                   | 67.0   | 1.24                                     | 0.106 in 3 yrs                         | 1.346                      |
| 15.     | Tawa, India         | CL           | 101.0                  | 44.0   | 1.458                                    | 0.022 in 3 yrs.                        | 1.480                      |

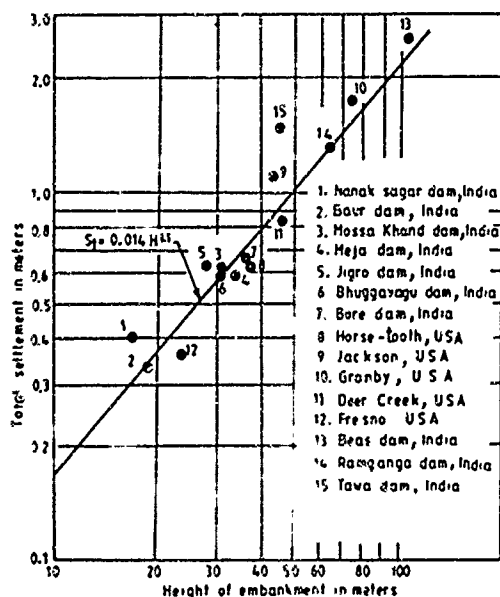


Fig.7. Variation of Total Settlement with Fill Height

Gould (1954) had established that under pressures greater than 7 kg/sq.cm, the compressibility of the embankment is mainly governed by the gradation of soil and plasticity of fines; the latter property has the predominant influence. For the cases of dams presented in this paper no influence of these factors was observed.

Post-construction compression of these dams increased near linearly with the increase of liquid limit which indirectly reflects on the magnitude of the higher compression index of the soils for having compacted on the drier side of the optimum moisture content.

When the data of the degree of compaction achieved has been compared with the total compression, a trend exists indicating lower compression with higher degree of compaction.

#### CONCLUSIONS

Based on the data collected from ten Indian earth and earth rockfill dams and some similar embankment dams of USA, the following broad conclusions are made on their compressional response:

1. A major portion of the total compression in earth and earth rockfill dams occurred by the end of construction.
2. Significantly large compression took place in the vertical direction in the central region of the core.
3. Compaction techniques and placement conditions similar to those adopted by USBR; the end of compression and total compression in these dams were found to be functions of the embankment height.
4. Both the compressions across and along a the valley have been small.
5. Larger compression was observed with larger deviations on dry side of the optimum moisture content.
6. No definite influence of mean particle size and plastic limit of soil was observed on the compression of the embankments. On the contrary, a definite influence of liquid limit on the compression was observed. Higher the liquid limit higher was the compression.
7. The degree of compaction achieved during the construction as related to Proctor's maximum dry density did effect the compressibility of the embankment; higher degree of compaction indicated reduced compression.
8. Although the bottom layers of embankments understandably undergo maximum vertical strain, the maximum vertical movement of any individual cross-arm occurred nearly at the mid-height of the embankment.

#### REFERENCES

- Berry, N.K. (1975), "Measurement of Displacements in Beas Dam Embankment", Indian Geotechnical Jnl., 5:3:151-168.
- Char, S.A. (1979), "Instrumentation and Behaviour of some Earth - Rockfill Dams", M. Tech. Thesis submitted to IIT Delhi, India.
- Gould, J.P. (1953), "The Compressibility of Rolled Fill Materials Determined from Field Observations", 3rd Int. Conf. Soil Mech. and Foundn. Engg., 2:239.
- Gould, J.P. (1954), "Compression Characteristics of Rolled Fill Materials in Earth Dams", Tech. Memorandum No. 648, Bureau of Reclamation, U.S. Deptt. of the Interior, Denver.
- Jain, S.K. (1985), "Settlement in Earth Dams", M. Tech. Thesis submitted to IIT Delhi, India.
- Ramamurthy, T. (1984), "Performance of Some Embankment Dams in India", Proc. Int. Conf. on Case Histories in Geotechnical Engineering, Roll, U.S.A., 3:1097 - 1102.
- Verma, R.K and B.B. Raj (1978), "Performance Analysis of Embankments - Case Studies", Proc. Geotechnical Conference, New Delhi, 1:114-119.

# History of Tehri Rockfill Dam Design

Bhagwat V.K. Lavanía

Professor of Earthquake Engineering, University of Roorkee,  
Roorkee, India

**SYNOPSIS :** A 260.5 m high rockfill dam is one of the main components of Tehri Dam Project which is under construction for the last over seventeen years. During this period detailed site investigations have been carried out and design of the dam is kept under constant review. A number of studies are conducted to provide feasible solutions to anticipated problems. The paper describes main design features of the dam, mentioning the changes necessitated time to time with regard to these.

## INTRODUCTION

The Tehri Project is an irrigation-power project of the State of Uttar Pradesh, in India, envisaging construction of: (1) A 260.5 m high rockfill dam across the Bhagirathi River to store 2,880,000 acre-ft of water; (2) underground power house, having installed capacity of 2000-2200 MW; and (3) spillway for design discharge capacity of 11,700 m<sup>3</sup>/s. The four diversion tunnels of 11.00 m diam each have already been constructed. The layout of project works is given in Fig. 1. The dam is to be placed at the site such that its

of tectonic deformations suffered by them, have been broadly graded as follows:

**Phyllites of Grade I** - This rock unit is predominantly arenaceous, massive in character, and distinctly jointed at phritiferous places that have lenticular elongated streaks of brown colored calcareous material.

**Phyllites of Grade II** - This rock is conspicuously banded due to the rapid alterations of arenaceous and argillaceous material. In physical quality and competence this unit is considered next to grade I phyllite.

**Phyllites of Grade III** - This unit is composed mainly of the argillaceous components with lesser amounts of arenaceous material. It carries quartz veins and is traversed by closely spaced foliation planes, cleavages, and joints. The unit is generally weathered. It is involved in minor folds and puckers.

**Sheared Phyllite** - The sheared phyllites constitute the weakest bedrock unit in the gorge and have resulted from crushing.

**Shear Zones** - A number of shear zones have been noticed at the dam site and its vicinity. Some of them are quite prominent. Shear zones are aligned mostly along the foliation direction and trending in N 40° W-S 40°E to N 70° W-S 70°E direction with dips of 30°-45° in the southwest direction, i.e. the downstream direction. These shear zones vary in thickness from fraction of centimeter to about half a meter. Apart from these, transverse shear zones, cross shear zones, and longitudinal shear zones (with respect to axis of dam) are also present.

1. **Transverse Shear Zones** - There are a number of transverse shear zones in the area. During initial investigations, a very prominent, about (10-m to 15-m thick) shear zones was interpreted from drill hole data in the river bed. It was therefore proposed (design of Dam, 1973) to construct an across the river tunnel to confirm its presence. However, the subsequent drilling and electrical logging did not indicate the presence of such a prominent feature, and the tunnel was not constructed. But, now, after a period of fourteen years, its construction has been started so as to leave no doubts about its presence before construction of the dam.

2. **Cross Shear Zones** - There are also a number of cross shear zones in the area. The most prominent of these is exposed in the vicinity of the dam. It has a strike

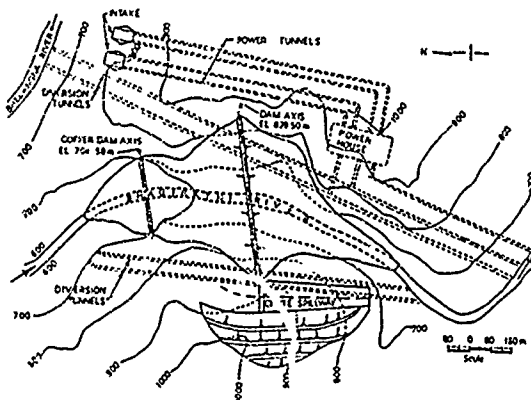


Fig. 1 - General Layout of the Project works

foundation will be highly jointed and sheared phyllitic rocks and its abutment contact slopes be steep. The area is also seismically active. The construction of the project was taken up in 1970. However, the activities did not move fast mainly because of the paucity of funds. But this provided the design engineers enough time to tackle the complex problems of this gigantic structure. The problems examined are: (1) The location of the dam axis; (2) the dam section (3) design of coffer dam; (4) the approach to slope stability analysis under static and dynamic conditions; and (5) the foundations treatment.

## GEOLOGY OF AREA

The rocks exposed in the area of the project site are phyllites of Chandpur-Series (Lavanía, 1975, Gupta et al., 1979). The rock bands are of variable thicknesses have dips of 45°-60° in the downstream direction, and strike almost east-west. The river flow in this reach is north-south. On the basis of their physical condition, the argillaceous and arenaceous materials present, and the varying magnitude



of N 85° W-S 85° E and dips at 55° in south-north direction. It appears at both banks of the river, as shown in Fig. 2, and its thickness in this area is about 4.0 m.

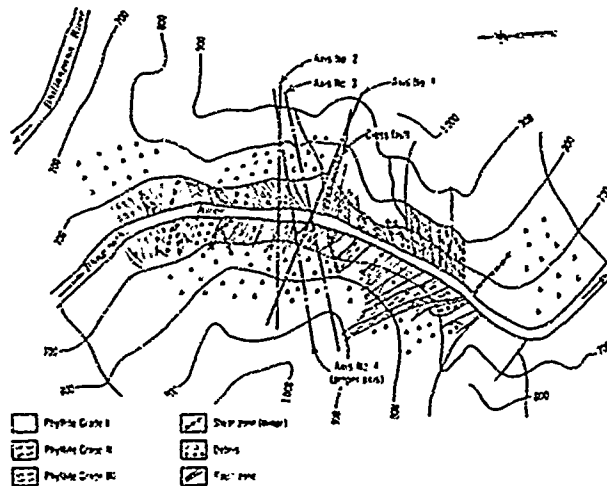


Fig. 2 - Geology of Dam Site

#### DAM AXIS

A number of alternative axes were considered for the dam. Initially dam axis No. 1, as shown in Fig. 2, was considered the suitable axis. It provided excellent seating for the dam. But with it, the major cross fault was coming under the core of the dam and therefore any movement along the fault due to earthquake or otherwise would have created some damage or even rupture of the core. The problem became more important in view of steep valley slopes. It was then proposed that the axis be shifted upstream of this abutment shear so that the dam core lies clear of it upstream. The shifted axis is shown as No. 2 axis in Fig. 2.

The investigations of the No. 2 axis pointed out that very heavy overburden, of the order of a 40-m depth, would most likely be met on the right abutment. Because of this, contact of the right abutment with the dam would have to be shifted further away into the hill, thereby shifting the spillway to the right, and thus involving increased excavation or a massive retaining wall about 50-m high, which would have to be constructed at the contact of the dam and spillway. This necessitated modification in the dam axis No. 2. Axis No. 3, which is on two spurs as shown in Fig. 2, was considered. However, this was also not agreed upon because of the valley divergence downstream of it. Finally, axis No. 4 was recommended for the axis of the dam. At this axis, the downstream convergence is available and the overburden on the right abutment is less compared to axis No. 2.

Curvature in the dam axis was proposed to give a little convexity to the dam axis upstream, with a view toward providing some sort of arch action in the dam which might help in reducing the tendency of transverse crack formation in the body of the dam.

#### DAM SECTION

**Available Fill Materials** - Phyllitic rocks are not suitable for use in the dam section where high pressures are expected to occur. Thus only grade I rocks, available from chute spillway excavation, will be utilized in the upper portions of the dam. The survey for construction materials for the dam indicated that the river terrace material containing silt, sand, gravel, and boulders can be utilized in pervious zones of the dam. Therefore, initially it was decided to have the core of the dam consist of two zones. As shown

in Fig. 3, zone A was proposed to consist of better clay, with a PI greater than 7% and zone B, enveloping zone A, was to consist of clay from other borrow areas.

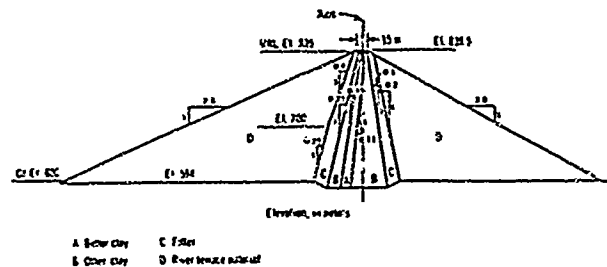


Fig. 3 - Initially Proposed Section

Further investigations for the dam fill materials suggested that in case the clay in the top layer of the river terraces is mixed with the underlying pervious material consisting of silt, sand, gravels, and boulders, a very good well-graded impervious material can be obtained for the core. The proposed gradation envelope of such a blended core material is given in Fig. 4. Such blended materials have already been used in the construction of the core of high dams like Nurek (309-m) in USSR, Mica (244 m) in Canada and Oroville (234 m) in the United States. In 1960 Bleifuss and Hawke recommended the use of a well-graded mixture of fine and coarse material for the core of the dam.

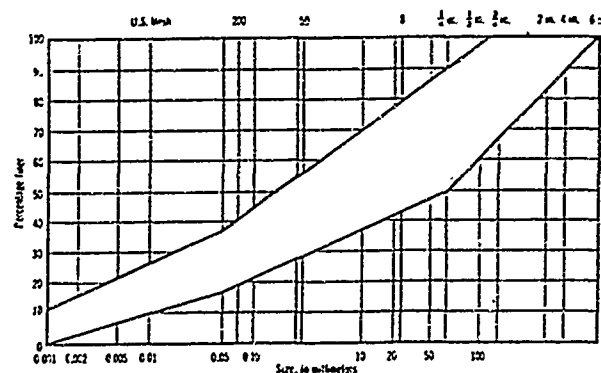


Fig. 4 - Proposed Gradation Envelope for Core Material

The project lies in the seismically active area of the country. Earthquakes with an 8-MM scale intensity have occurred on this seismic belt. Webster (1970), while describing the crack resistant measures taken at Mica Dam, mentions the use of blended material in the core as one of them. Hjeltness and Lavania (1980) have also found such material to be leakage, erosion and crack resistant. However, the practical difficulty of removing oversize boulders still persists. In case of Nurek Dam, it was achieved by rolling down the material on a hill slope.

**Zoning of Dam Section** - To be practical, all the materials used in the dam fill must be obtained from river terraces. The core material has to be obtained from the terraces where the thickness of upper clay layer is sufficient to impart the desired impermeability to the blended material-without adding fine material from other areas. The pervious material for upstream and downstream shell of the dam has to be obtained from terraces where the thickness of upper impervious material from it has good drainability; this must be done without screening off the fine material. The material for the filters between core and shells has to be obtained either from a river bed where clean gravels are available, or screened from the terrace material. Thus the zoning of the dam section became a very simple job.

The proposed dam section is shown in Fig. 5.

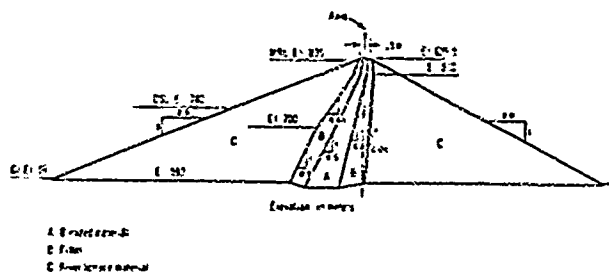


Fig. 5 - Proposed Section

**Shape of Core** - Both the vertical and inclined cores have been provided in high dams. The core of the Mica Dam is also moderately inclined with an upstream slope of 0.4:1 and a downstream slope (sloping towards upstream) of 0.1:1; the core of the Oroville Dam has an upstream slope of 0.9:1 and a downstream slope (sloping towards upstream) of 0.5:1; and the core of Nurek Dam is a central core, with both upstream and downstream slopes of 0.25:1. The model studies carried out at the University of California in 1958 and at University of Roorkee in 1962 have indicated that an inclined core is somewhat more earthquake resistant. A vertical clay core was initially proposed for the section shown in Fig. 3. It was thereafter proposed to have a moderately inclined core for the dam, as shown in Fig. 5.

**Thickness of Core** - Site investigations revealed the presence of sound rock in the river bed at EL 579 m. The core was therefore extended upto this level. Also, it was considered to have a seepage gradient of 0.5 and therefore the thickness of the core has been increased, as shown in Fig. 6, at the foundation contact level to 0.5H.

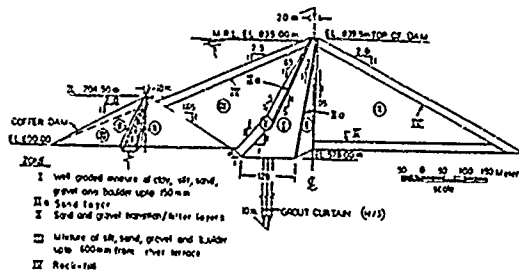


Fig. 6 - Main Dam and Cofferdam Section

**Design of Filters** - For high dams, specially in seismically active areas, well designed thick filter layers are preferred as compared to transition zones that roughly satisfy the filter criterion. However, it was not possible to design filter layer with respect to the proposed blended material for the core using Terzaghi or U.S.B.R. Criterion. Sherard (1979) provided solution to this problem of broadly graded coarse soils that are internally unstable and accordingly fine to medium sand layer has been provided on upstream and downstream faces of the core as shown in Fig. 6. The rest of filter layers on upstream and chimney drain on downstream have been designed with respect to this sand layer as the base layer.

#### DESIGN OF COFFER DAM

It was estimated that a 104.5 m high coffer dam would be needed to safe-guard against 1 in 1000 year frequency flood with a preceding flood of 1 in 25 year and 2.7 m freeboard. Fig. 6 shows the placement of the coffer dam as part of the main dam. Its upstream and downstream slopes are 2:1 and 1.85:1 respectively. There have been a number of exercises with various combinations of hydro-

logical parameters to determine the height of the coffer dam corresponding to 1 in 1000 year frequency flood and it has been found to vary between 85.0 m to 115.0 m. There have been discussions also regarding the design flood frequency and the decision has been in favour of 1 in 1000 year mainly because of not taking any risk for expected unprecedented flash flood in the absence of long-term hydrological data of the region. For the coffer dam section shown in Fig. 6, about 2.3 million  $m^3$  of fill is to be placed in one non-monsoon period of about six months in a very narrow gorge of the river. Corresponding to 1 in 100 year flood the fill quantities reduce to half. Alternate designs for placing the fill in two working seasons were worked out (upto et al., 1980). The sections were designed to withstand, (i) the overtopping (Fig. Nos. 7a and 7b) and, (ii) through flow and overflow simultaneously (Fig. Nos. 8a and 8b).

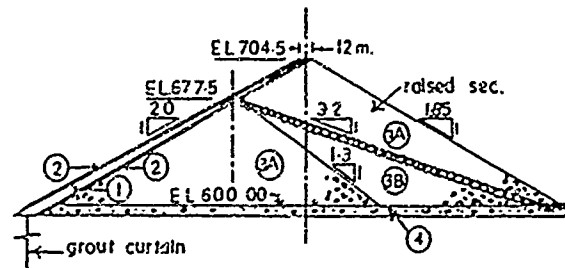


Fig. 7a - Overflow Section with u/s Blanket

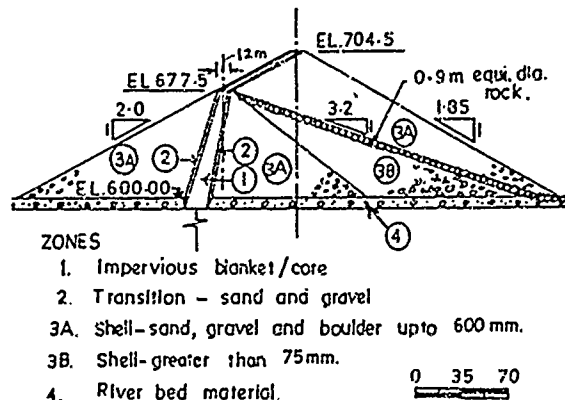


Fig. 7b - Overflow Section with Central Core

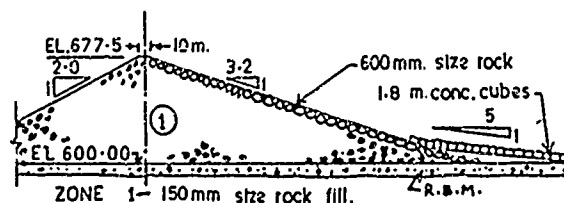


Fig. 8a - Through Flow Section

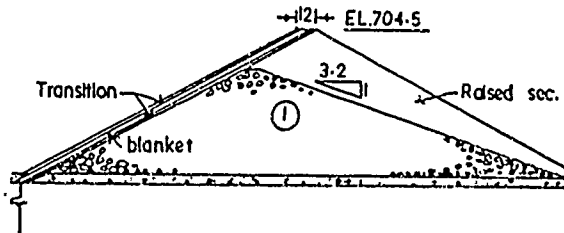


Fig. 8b - Through Flow Section with Raised Section and u/s Blanket.

There have been also suggestions for construction of concrete overflow section, below the core of the main dam, to serve as coffer dam or to reduce the fill quantities. There is yet another problem with the placing of coffer dam or the first stage dam as shown in Fig. 6. The axis of coffer dam, about 300 m upstream of the axis of main dam, would have all the problems anticipated for axis No. 2 of the dam as mentioned before.

Study to construct the first stage dam by directional blasting technique was also conducted in 1978. The inference drawn from the study was not in favour of adopting the technique mainly because of presence of very weak (sheared phyllites) rock bands, effect of heavy blasting on other structures of the project and, proximity of the site to the town.

#### STABILITY ANALYSIS OF DAM SLOPES

**Nonseismic Condition** - The outer slopes of the dam, have been fixed by carrying out the stability analyses by the Felinius method of slices (of circular slip surface) and by wedge method for the conditions of, (i) end of construction, (ii) steady seepage, (iii) sudden drawdown upto dead storage level and, (iv) sudden drawdown upto partial pool levels.

For determining the properties of fill materials, extensive sampling and testing has been done. In the borrow area for shell material (Dobata), 53 number of pits having depth of 9-10 metres were excavated (Gupta, et al., 1979). The gradation envelope of the material as in the borrow area is shown in Fig. 9. Initially the shear parameters of this material were determined by 30 cm x 30 cm size direct shear box. The maximum size of rock particle which could be used in the test apparatus was 25 mm only. The gradation curve for the specimen material was made in such a way that the curve for the coarser 70% of the material is parallel to that of borrow material as shown in Fig. 10. In order to find out the effect of particle size, plot was obtained for maximum particle size tested versus angle of friction value, as shown in Fig. 11. Extrapolation of this curve can

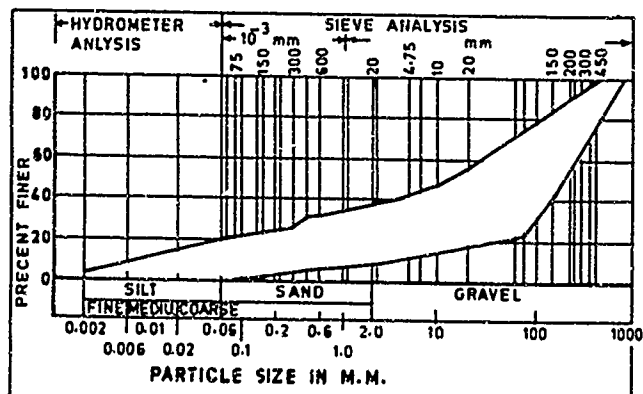


Fig. 9 - Gradation Envelope of Dobata Material

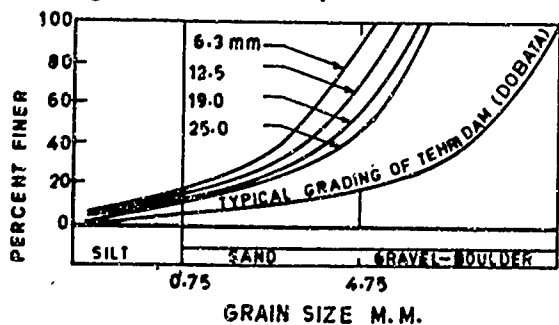


Fig. 10 - Gradation curves for Parallel Gradation Modelling Technique

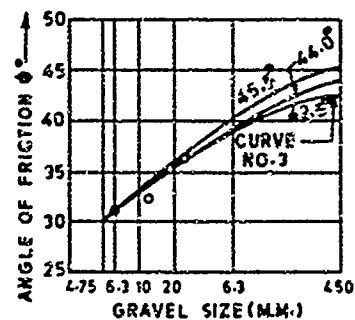


Fig. 11 - Extrapolation of Values Against Maximum Particle Size (I.R.I. 1977)

be done for higher sizes of materials along any of the three indicated paths. The lower most curve (No. 3) indicates angle of internal friction as 42.5°. The effect of confinement was later studied by conducting tests on 38 cm. dia size samples in the triaxial apparatus for shell and core materials (Lavama 1982). The angle of internal friction for the shell material (Zone III) adopted for the design is 38°. For core material friction angle is 27° and Cohesion 10 kilonewtons per square metre. For transition zone or filter layers friction angle adopted is 32°.

**Seismic Condition** - The conventional pseudostatic analysis was also carried out along with nonseismic condition analysis and the outer slopes were fixed on the base of minimum safety factor of 1.5 and unity for nonseismic and seismic condition with seismic coefficient of 0.15. Thereafter, a number of studies were taken up for seismic stability of the dam. Design earthquake parameters were determined for the site (1983). Fig. 12 shows the normalised plot of the design time history for the site. The recommended values (max.) of design base earthquake (DBL) and maximum credible earthquake (MCE) are 0.125 g and 0.25 g respectively.

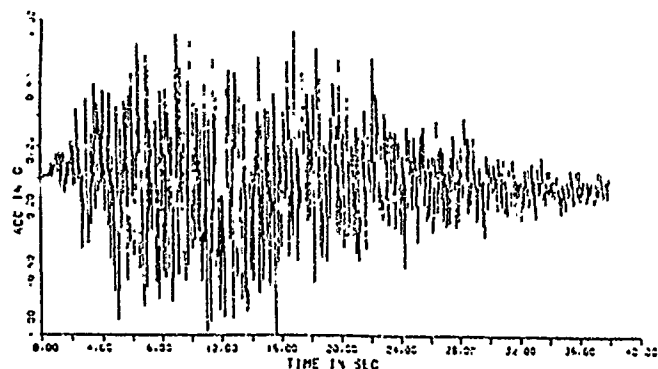


Fig. 12 - Artificial Earthquake for Tehri Site. Normalized to g.

Attempt has been made to estimate the non-recoverable deformations (1983) due to MCE, on the basis of evaluation of yield acceleration for rigid body movement of the sliding mass. As shown in the Fig. 13, only about 15.0 m and 10m depths of the upstream and downstream slopes are likely to be affected. Therefore, it has been proposed to place 20 m deep grade I rock (instead of gravel and boulder fill), which has angle of friction of about 45°. With this provision, as shown in Fig. 6, there is no likelihood of any slope deformation.

Tests were conducted at site on fill and foundation materials for determining the numerical values of dynamic shear modulus and damping coefficient. The plots of shear modulus versus strain level for the shell and core materials are

given in Figs. 14 and 15 (1983). The damping ratio of 10% has been adopted for these.

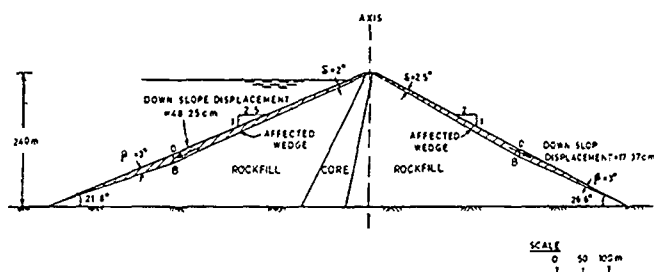


Fig. 13 - Affected Wedges of Dam

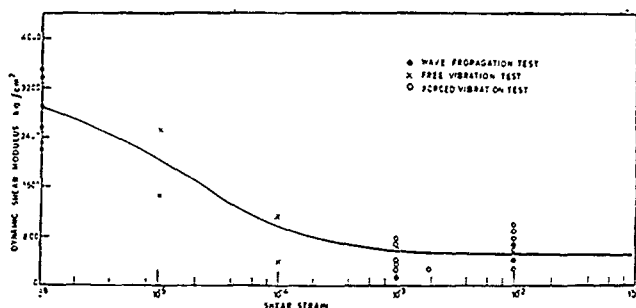


Fig. 14 - Dynamic Shear Modulus Versus Shear Strain (Dobata Material)

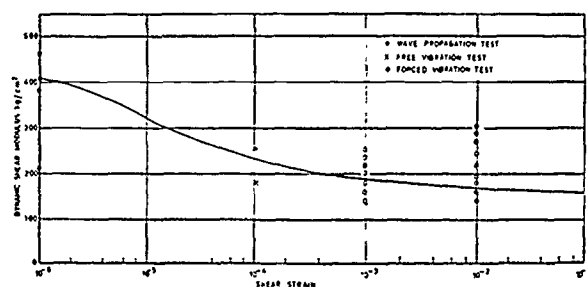


Fig. 15 - Dynamic Shear Mod. v/s Shear Strain, Core Material

The shell material as available in borrow areas has quite high percentage of silt and sand (Fig.9). Though it has been decided to restrict the silt size particles to 6% by selective borrowing but still the development of excess pore water pressure during earthquake could not be ruled out without tests on such a material. Similarly, there could be development of excess pore water pressures in the core. Therefore tests were conducted (1983) on shake table by placing the material in saturated condition with desired density and subjecting it to the sinusoidal cycles equivalent to the MCE design time history. It was observed from these tests that there would be no excess pore water pressure development (and thereby reduction in shear strength) for more than 70% R.D.

A number of finite element analyses have been carried out for the dam. Two dimensional linear and non-linear analyses do not show any sign of distress to the proposed dam section. There is, of course, slight concentration of stresses upstream of the core (in the shell) where it changes slope (from 0.5:1 to 1:1). But this does not seem to be of any consequence. The three dimensional analysis, which are in progress, are likely to present a more rational picture as the valley is very narrow and confinement effect would be substantial.

## FOUNDATION PROBLEMS

The foundation problems, which include abutment contact problems, are of the following two types: (1) Routine problems of earth dams; (2) special problems of the Tehri Dam arising out of the geological topographical conditions (Design Memo. 1973, Lavania 1975 and Gupta et al., 1979).

Routine problems that are characteristic to any earth dam generally relate to: (1) Seepage through foundation rock; (2) development and accumulation of water pressure in abutments; (3) removal of weathered or undesirable zones in foundation; (4) easing off the overhangs and local steep slopes in the area and; (5) treatment of local pockets of weak material, seams, and joints.

## PROPOSED REMEDIAL MEASURES

### Routine Foundation Problems

**Foundation Grouting** - For making the foundation sufficiently impervious so as to prevent excessive seepage, curtain grouting and blanket grouting in the core and transition filter contact was earlier proposed. In view of the highly jointed and sheared phyllitic rocks in the foundation, a three-line grout curtain was proposed. The depth of the primary holes at 12.0 m spacing would be 0.3 H, with a minimum of 25.0m at the crest. The secondary and tertiary holes would be about two-thirds and one-third the primary hole depth. This depth can be modified depending on the grout intakes.

Area grouting for the core contact area and downstream fine filter has been planned at 3.0 m spacing 10.0 m deep upstream of the curtain and 5.0 m deep downstream. The foundation grouting plan is given in Fig. 16.

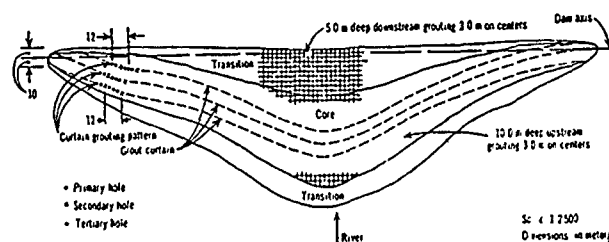


Fig. 16 - Foundation Grouting Plan

There has been lot of thinking on this aspect of foundation treatment during last about ten years and a number of alternative proposals have been studied. Though, the groutability tests conducted at the site have not shown any cause of concern; but the unprecedented height of the dam made some engineers to think for post construction grouting arrangements and accordingly the proposals of having foundation grouting tunnels as provided in Nurek Dam and Chicoasen Dam were prepared. Recently, proposals have been prepared that have grouting tunnel below the core either fully or partly (cut and cover) in the foundation rock and connected to shafts or abutment drainage tunnels on both the banks.

**Drainage Tunnels** - For preventing development and accumulation of pore-water pressures in the abutments, drainage tunnels are proposed at EL 700 m on both banks. A rock cover of 30.0 m (100 ft) minimum has been proposed over the tunnel below the dam fill.

**Foundation Stripping** - The ASCE Committee (1972) found, for the dams studied, that the overburden having depth of  $\pm 10.0$  ft (3.0 m) and less was removed from the entire area. In case of the Mica Dam, the overburden (called common material) was removed only below the core foundation; at Oroville Dam, the removal was done over the entire area; and at Bennet Dam it was in the area below

core and filters. The depth of overburden at the Tehri Dam area is not uniform. It has been proposed that in the area under upstream and downstream shells where overburden is met, stripping of a maximum 6.0 m (20.0 ft) be done. But the area under the dam core would be excavated upto sound rock level to provide an effective cut-off. The core foundation level and shell foundation level will be joined by excavation at a gentle slope not steeper than 1H:1V.

**Abutment Easing** - As shown in Fig. 17, the gorge section has slopes of right and left abutments as 1.1:1 and 0.95:1, respectively. Therefore, it is proposed that the local steep slopes and overhangs if any, be eased at a slope of 70° (0.36H:1V), as was done at the Mica Dam. However, the depth of silt, gravel, and boulder-fill in the river bed is expected to be of the order of 10-15 m. The gorge in this depth is likely to have almost vertical walls. Therefore, considerable excavation may have to be done. Keeping this in view, another proposal, as mentioned in the following section on "Special Treatment", is under consideration.

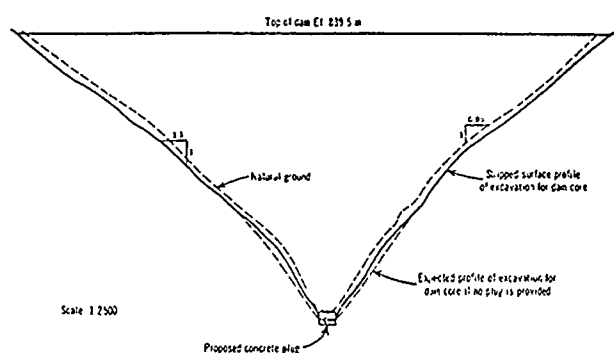


Fig. 17 - Proposal of Concrete Plug

**Treatment of Joints and Seams** - It is proposed that the foundation below core and filters be cleaned of loose and foreign materials, joints, faults, shear zones etc.; that it be cleaned upto a depth at least three times their width; and that it be back-filled with concrete or pneumatically applied mortar. Larger depressions would be backfilled with concrete.

Study has also been done to assess foundation settlements after the dam construction on the basis of plate load test data (Gupta et al., 1979).

#### Special Foundation Problems

**Concrete in River Section** - The abutments of the Tehri Dam are steeper than those of the Mica, Oroville, and Bennet Dams, and the water head is also greater than for these dams. However, the abutment slopes of the Nurek Dam (300 m) are of almost the same order, and the water head is also greater than that for the Tehri Dam. For the Tehri Dam, in case the excavation of abutments is done at the limiting slope of 70° from the core foundation level in the river bed, it would involve a huge excavation of the rocks and for a considerable height the abutment contact would be at a slope (70°) steeper than that available naturally from above the river water level. In the Nurek Dam, for a similar situation, it has been considered economically and technically sound to have the portion at the river bed filled with concrete (Odintov and Gladkov, 1971). This concrete block in the river bed, under the core contact area, is called a "concrete plug". It is 157 m long, 30 m-60 m wide, and accommodates three grouting galleries. Similar proposal (Fig. 17), with and without grouting galleries have been proposed for the Tehri Dam.

**Counterforts at Junction** - As the spillway is very close to the dam, a retaining wall of the order of about 25 m high is to be constructed at the junction of the two

structures. The main problem is to obtain a secure junction between the core of the dam and the retaining wall. This problem is likely to be of greater importance when the behaviour of this junction is visualized during an earthquake. At present, the wall of counterfort type is proposed.

#### **CONCLUSIONS**

The paper describes the design of main features of a 260.5m high Tehri rockfill dam with brief explanations as to what changes have been made time to time. This is to augment the rockfill dam technology and invite suggestions.

#### **REFERENCES**

- "Applicability of Directional Blasting Technique at Tehri Dam Site" (1978), Report, U.P. State Irrigation Design Organisation, Roorkee.
- Bleifuss, D.J. and Hawke J.P. (1960), "Rockfill Dam: Design and Construction Problems", Transaction, ASCE, Vol.125, Paper No. 3072, Part II, pp. 275-300.
- Clough R.W. and Pirtz D. (1958), "Earthquake Resistance of Sloping Core Dams", Transactions, ASCE, Vol. 123, Paper No. 2939, pp. 792-816.
- "Design of Dam" (1973), Design Memo. No. 3, Tehri Dam Project Designs, Roorkee.
- "Design Earthquake Parameters for Tehri Dam Site" (1983), Earthquake Engg. Studies, Report No. 83-04, Earthquake Engg. Deptt., University of Roorkee.
- "Dynamic Soil Parameters and other Studies for Tehri Dam" (1984) No.84-10, Earthquake Engg. Deptt. Uni. of Roorkee.
- "Foundation Treatment for Dam" (1973), Design Memo. No. 5, Tehri Dam Project Designs, Roorkee.
- "Foundation and Abutment Treatment for High Embankment Dams on Rock" (1972), Committee on Embankment and Slopes of Soil Mech. and Found. Dn., Proc. ASCE, Vol.98, SM5, paper 9269, pp. 1125-1128.
- Gupta, S.K., Lavania, B.V.K., Gupta, R.L. and Pathak, R.C. (1979), "Design on Dam Embankment and Foundation", Proc. Workshop on Tehri Dam Project, University of Roorkee, Vol. I, pp. 76-98.
- Gupta, S.K., Lavania, B.V.K. and Singh, N. (1980), "Coffer Dam at Tehri Dam Project", Proc. GEOTECH-80, Indian Institute of Technology, Bombay, Vol. I, pp. 132-137.
- Hjeidness E.I. and Lavania B.V.K. (1980), "Cracking, Leakage and Erosion of Earth Dam Materials". (1980), Proc. JGTD, ASCE, Vol. 106, GT2, pp. 117-135.
- Lavania B.V.K. (1975), "Tehri Rockfill Dam", Proc. JGTD, ASCE, Vol. 101, GT9, pp. 963-976.
- Lavania B.V.K. (1982), "Testing of Materials for use in High Earth and Rockfill Dams", Proc. 4th Int. Congress, Int. Assoc. of Engg. Geology, New Delhi, Vol. VI, pp. 243-251.
- Odintov A.K. and Gladkov B.F. (1971), "Construction of the Concrete Plug at the Base of Nurek Dam", Proc. Hydrotechnical Const. Jul., No. 1, pp. 31-35.
- Sherard J.L. (1979), "Sink-holes in Dams of Coarse Broadly Graded Soils", Trans. Thirteenth Int. Cong. on Large Dams, Vol. II, Q.No. 49, New Delhi, pp. 25-36.
- Webster J.L., (1970), "Mica Dam Designed with Special Attention to Control of Cracking", Trans. Tenth Int. Cong. on Large Dams, Vol. I, pp. 487-507.

## Treatment of Left Bank Slopes of Ichari Dam

Bhagwat V.K. Lavania

Professor of Earthquake Engineering, University of Roorkee,  
Roorkee, India

**SYNOPSIS :** The left bank of Ichari Diversion Dam was anticipated unstable because of toe submergence and drawdown effects after the construction of the dam, on the weak geological formations. Extensive laboratory and field investigations were carried out to determine the extent of stabilising measures needed. The proposals of providing pretensioned steel anchors or alternatively, reinforced concrete shaft anchors were considered in details to obviate the possibility of deep seated slides. The choice fell in favour of R.C. anchors mainly because there is no uncertainty about their in situ strength. These anchors were provided in two rows (one having vertical and other inclined anchors) at 9.0m spacing. The design of these anchors was done as continuous space frame with ultimate load theory. The two rows are connected at the top with a 6.0m thick concrete slab (monolith). A massive concrete retaining wall of 9.0m height rests on this slab with provision of shear keys. Above this elevation, concrete blocks and boulder pitching, with back filters, have been used to stabilise the slope at a gradient of 1.5:1 (H:V) in the hill wash material zone.

### INTRODUCTION

The works of Ichari, constructed during 1969-72 under Yamuna Hydroelectric Scheme stage II in State of Uttar Pradesh, India, comprise the diversion dam (55.0m high) and intake arrangements to divert the waters of river Tons into a 7.6m diameter and 6.3 km long head race tunnel for generation of hydro-power at Chibro underground power house. The elevation of top of the dam, above mean sea level, is 652.0m. and the river bed elevation before construction of the dam was about 610.0m. The preconstruction study of the geology of the left bank slopes of the river at the dam site revealed thick overburden of hill wash material and debris overlying a rock ledge which rises steeply behind it, at an approximate elevation of 636.0m. The underlying rock, consists of almost horizontal bands of quartzite, quartzite slate and thinly bedded slate, and has a number of shear zones and glid cracks dipping towards the river. On the basis of data from various drifts in the left abutment the formation, from the face, can be divided into the four zones, Fig. 1, viz, (i) hill wash material and debris (Zone-I), (ii) highly fragmented and weathered rock mass (Zone II), (iii) fresh but fractured and jointed rocks (Zone III) and, (iv) sound and fresh rock (Zone IV). The mantle of overburden extends to about more than 250 m in height above the river bed and about 140.0m upstream of the dam axis. On the downstream of the dam axis also, the over-burden material exists but to a lesser extent.

### THE PROBLEM

The existence of these geological features had created the problem of ensuring the stability of the left bank slopes and also of tying the dam securely to the left bank rocks. The solution of the first problem only is described in the paper. The slopes upstream of the dam axis, comprising of overburden material and the rock mass below it were found, by analysis, to be in a state of limiting equilibrium. The construction of the dam had to raise the water level from the general elevation level of about 612.0m to 644.75m (toe submergence). Also for peaking on the power houses daily there has to be drawdown in the reservoir from EL 644.75m to EL 636.0m, in a very short duration of about 4 hours. These situations had to bring down the stability of the hill mass. The condition of the slopes on the downstream of the axis did not materially change after the construction of the reservoir and therefore did not require as elaborate treatment as for upstream slopes.

### SHEAR PARAMETERS

The overburden material, consisting of mainly boulders and rock pieces, mixed with sand and small percentage of clay (GM, GP) was standing at an angle of about 37°. Any large scale removal of this material, which has maximum depth of over 30m at places, would have resulted in instability of the steep hill behind it that has number of secondary joints, cracks and shear zones. The insitu permeability of this material was found to vary from  $3 \times 10^{-5}$  cm/sec. to  $7 \times 10^{-5}$  cm/sec. and, therefore, it may be considered as semipervious to pervious. The cohesion and internal friction values obtained from laboratory tests were in the range of 0.07 to 0.27 kg/cm<sup>2</sup> and 34° to 36° respectively. The shear zone material samples were obtained from the three drifts in the left abutment at elevations 625.0m, 640.0m, 649.0m made to establish the extent of overburden and sound rock profile along the dam axis. These samples gave cohesion values of 0.29 kg/cm<sup>2</sup> to 0.35 kg/cm<sup>2</sup> and angle of internal friction values of 24° to 25°. The saturated unit weight of hill wash and the rock are 2.15 t/m<sup>3</sup> and 2.7 t/m<sup>3</sup> respectively. The pore water pressures in slope in the drawdown range were accounted for in the analysis by taking submerged weight of material for resisting forces and saturated weight for sliding forces. In the rock mass lying above the normal reservoir level, the pore water pressures due to rains, were not expected to be more than 25 % of the full saturation pressures due to perviousness of the overburden and existence of cracks and fishers in rocks.

### STABILITY ANALYSIS

For evaluation the stability of the slope a number of potential shear surfaces were considered (Fig.2). The stability of the overburden material was analysed by considering the two circular shear surfaces (case 1 & 2). The safety factors were calculated for each case with, (a) no pore water pressures and, (b) 25% pore water pressures and then combination of these conditions with earthquake loading (horizontal seismic coefficient - 0.1). For case 1, the existing slopes were just stable (safety factor 1.05) with no pore water pressures, no cohesion and no earthquake inertia force. Under drawdown conditions the safety factor reduced to 1.00 with no pore water pressures above EL 645.0m. In case 2, the stability had been tested with a small section of the earth, above EL 680.0m, removed with a provision of berm of 4.0m. The

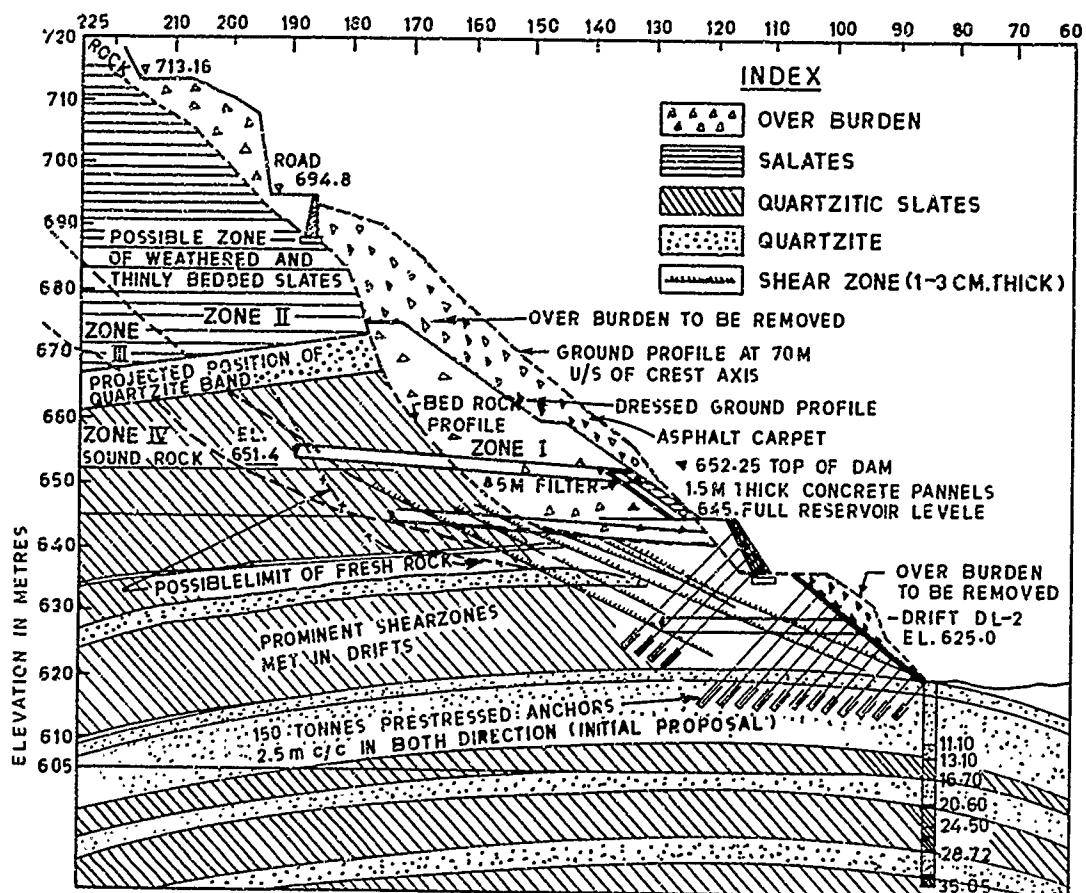


FIG. 1 - Geology at Section 70.m Upstream of Dam Axis (with Initial Proposal of Steel Anchors)

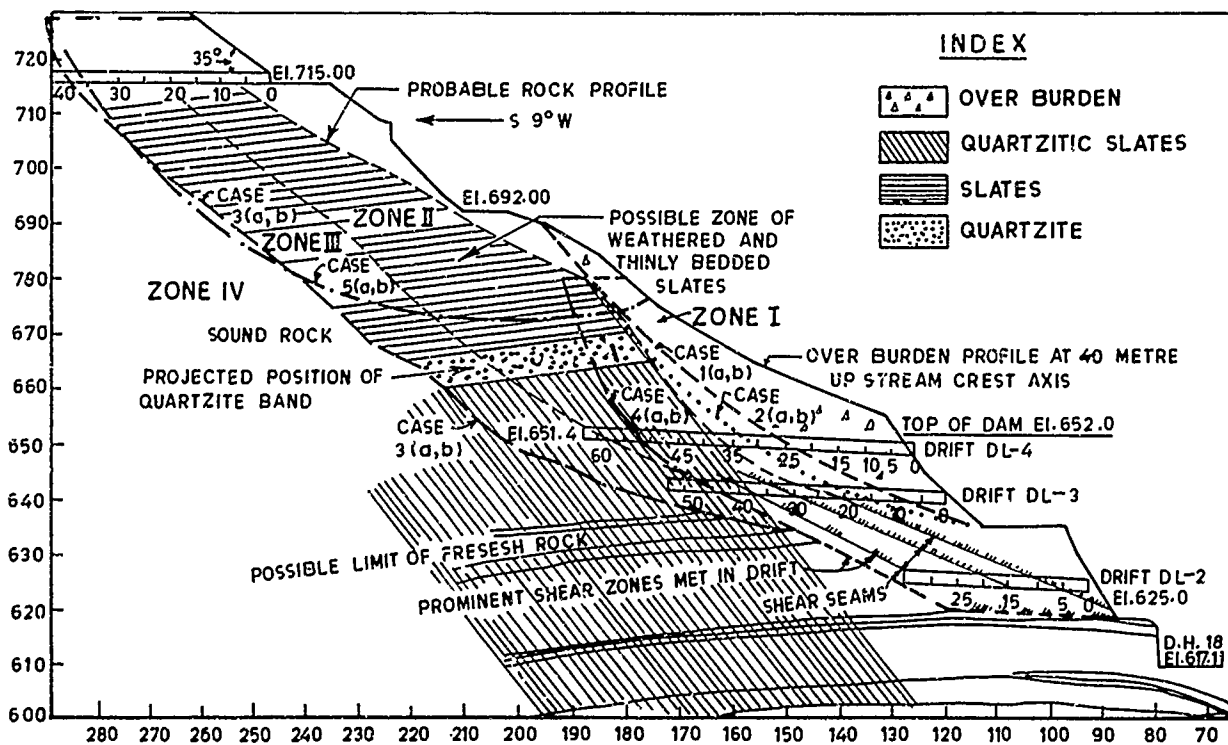


FIG. 2 - Location of Potential sliding Surfaces

remaining portion below EL 680.0m was assumed to have been dressed at an angle of  $34^\circ$  with berms at EL 660.0m and EL 645.0m. The safety factors for this slope worked out to be 1.1 with no pore pressures and 0.96 with 25% pore pressures. With earthquake effect these reduced to 0.89 and 0.77 respectively. For drawdown condition these safety factors were 1.06 with no pore pressures above drawdown level and 0.95 with 25% pore pressures. For dynamic condition these factors reduced to 0.84 and 0.75. The stability of the rock mass was analysed for three different potential shear surfaces (case 3, 4 and 5) having toe elevations 618.0m where lowest anticipated shear zone and crushed rock seam exist. The top elevations and hence the rock mass above the potential sliding circular surfaces vary in the three cases. In case 3, it was considered that the entire hill mass might slide down along the junction of zone III (fractured and jointed rocks) and zone IV (sound rock) and the shear zone at EL 618.0m. Neglecting the cohesion, all pore water pressures (dry condition) and the passive resistance to be offered by the eventual fill in the river bed, the safety factor worked out to 1.19. With cohesion above EL 644.75m and passive resistance of the fill, the safety factor was 1.26; with 25% pore pressures it reduced to 1.12. In case of earthquake with drawdown and no pore pressures above EL 644.75m, the safety factor was 0.89. This improved to 0.94 by taking into account the cohesion and passive resistance of the fill. In case 4, the stability of lower portion of the rock mass upto EL 690.0m and overburden dressed upto EL 680.0m was worked out, considering sliding along shear zone and crushed rock seam near EL 618.0m. The safety factors for this shear surface, as compared to that of the previous shear surface, were found to be lower. These were 0.85 against 1.19, 0.76 against 1.12, 0.61 against 0.89 and, 0.68 against 0.94. This indicated that there were more chances of failure occurring in the lower portion. In case 5, the stability of upper portion (above EL 670.0m) was worked out and the safety factors obtained were 0.94 in the existing condition without pore pressures and 0.84 with 25% pore pressures. With the earthquake effect, these reduced to 0.85 and 0.76 respectively. Hence it was considered necessary to take measures to stabilise this portion of the slope also.

#### STABILISING MEASURES

A number of measures were considered to stabilise the slopes. All these measure fall in two categories, namely, (i) reducing the actuating forces and, (ii) increasing the resisting forces. Under the first category, easing of the slopes, provision of drainage by drainage cum grouting galleries and, surface protection of the overburden material against water velocities during floods and also during drawdown were considered. It was decided that the overburden slopes be dressed to 1.5:1 (H:V) slopes ( $34^\circ$ ) with 5.0m berms at different levels above EL 645.0m. Pucca surface drains be provided along the berms and along the slopes. The drainage holes be drilled above EL 645.0m (reservoir elevation) and all joints and glide cracks be sealed by effective grouting. Also a thick filter layer (1.0m) and drainage holes with nonreturn flap valves be provided behind and in the toe wall in the drawdown range (EL 636.0m to 645.0m). The slope between elevations 645.0m to 652.0m (dam top elevation) was proposed to be protected by concrete blocks laid on boulder layer that was to be on a filter layer.

Under the second category, i.e., for increasing the resisting force the two proposals considered were: (1) Prestensioned steel anchors to hold down a R.C. toe wall constructed between EL 636.0m to EL 645.0m with varying thickness from 3.0m at bottom to 1.5m at the top, and provision of the steel anchors from EL 636.0m to EL 618.0 through the rock mass and butting against a R.C. membrane 300 mm thick on the rock face (Fig. 1). (2) Reinforced concrete anchors construction (in situ upto EL 608.0m) below a concrete gravity toe wall that is based on the rock ledge at EL 636.0m and varying in thickness from 7.0m at bottom and 3.0m at EL 645.0m (Fig. 3). Preliminary designs for the proposals were

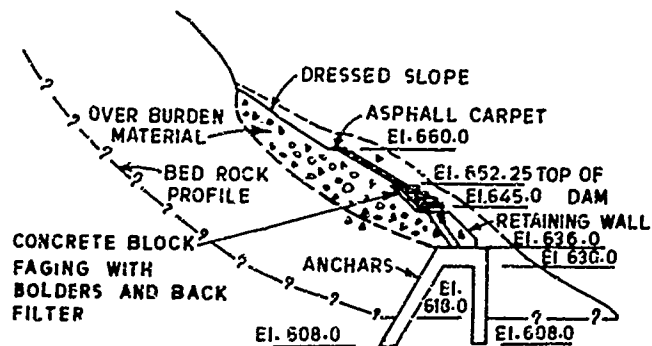


FIG. 3 - Stabilising Measures Provided

prepared and cost aspect was studied which revealed that provision of steel anchors would be slightly cheaper. The steel anchors find favour because, (i) a better solution lies in preventing the movement rather than catering for the support to the rock mass in which sliding tendency has been initiated, (ii) these anchors along with consolidation grouting would make a big chunk of rock mass at the toe to support the hill mass and, (iii) to obviate the necessity of blasting in a already sheared rock mass. However, this has disadvantages also mainly because of the problems of, (i) maintaining the prestress in the anchors in the rock over long periods and on occurrence of earthquakes due to existence of glide cracks, (ii) possibility of stress corrosion in the cables even after grouting and, (iii) reliability of maintenance of prestress in anchors passing through overburden material. On the other hand, the provision of concrete shaft anchors have the advantages that, (i) their strength is fully known and, (ii) know how for the construction was available at the site. The disadvantages of this proposal are, (i) the construction of shafts for the anchors would involve large scale but controlled blasting in already fractured and sheared rocks and, (ii) the concrete anchors would come in to play only after initiation of slide.

The decision was taken in favour of the second proposal mainly because the strength of R.C.C. anchors is fully known and there is no factor of uncertainty in the same. It was also decided that the shattered and laminated rock from EL 636.0m to 630.0m be replaced by concrete. Accordingly the rock loads (actuating force) for the design of the retaining wall and the concrete anchors were worked out on the basis of the stability analyses of the rock mass. Actual observations were made in bore holes for water table in the hill mass and it was found to be parallel to the rock profile at an approximate slope of 1.5:1. It was, therefore, assumed that after the rise in water level upstream of the dam to EL 644.75 m, the water table would also rise and readjust in a slope of approximately 1.5:1 above this elevation. In the zone above the hill mass water table, 25% of the full pore pressures were accounted for in the calculations. The vertical and inclined ( $30^\circ$  to vertical) concrete anchors in two rows were designed to be placed alternately at 9.0m centre to centre. The load per 9 metres under no earthquake condition, for safety factor of 1.25, worked out to be 11300 tons. With earthquake for safety factor of 1.0, it was 10660 tons. In the design the failure of the concrete anchors was considered in, (i) direct shear through the R.C.C. section, (ii) flexure through bending by cantilever action and, (iii) cracking due to diagonal shear. The design was thus governed by the minimum strength from these three considerations. Studies indicated that if these concrete anchors were considered acting separately and individually the deflections, bending moments and shear stresses were too high to enable worked out a safe design. Hence the design of these anchors was done as a continuous space frame (Fig. 4) consisting of the inclined and vertical anchors placed 9.0m c/c and connected through a series of horizontal members of 6.0m depth (from EL 630.0m





to EL 636.0m). The design was worked out for the four cases of the load distribution between the two legs of the frame, namely, (i) 100% load on inclined anchor, no direct load on vertical anchor, (ii) 75% load on inclined anchor 25% on vertical, (iii) 66% on inclined and 34% on vertical and (iv) 50% on inclined and 50% on vertical. The anchors were designed with ultimate load theory using tor (deformed) high strength steel bars.

## CONSTRUCTION

The vertical and inclined anchors were constructed (by shaft construction) and placed alternately at 9.0m centre to centre. Six metre thick concrete was laid from EL 630.0m to EL 636.0m to replace the weathered rock. The reinforced concrete retaining wall, held down by the anchors, was constructed from EL 636.0m to EL 645.0m to retain the slopes of overburden material. One drainage gallery was constructed at EL 636.5m at right angles to the dam axis inside the rock mass with cross galleries 15.0m apart and extending upto 15.0m inside the hill mass. These cross galleries have been provided with 8.0m deep 75 mm diameter drainage holes fanning out in all directions to intercept seepage. Another gallery was constructed at EL 652.0m. The retaining wall is 7.0m thick at base (EL 636.0m) and 3.0m thick at the top (EL 645.0m) with weep holes 75.0 mm diameter 3.0m centre to centre. The vertical anchor is 22.0m long and the inclined anchor is 26.0m long. The details are shown in Fig. 4.

## CONCLUSION

This treatment of the slope was completed with the construction of the dam in 1972. See-page discharge and other measurements are being taken regularly since then. The slope has not shown any sign of distress since last over fourteen years.

## REFERENCES

- Yamuna Valley Development, U.P.I.D. (1967), "Diversion Dam-Treatment of Flanks", Design Memorandum V A, Yamuna Hydroelectric Scheme Stage II, U.P., India.
- Central Design Directorate, U.P.I.D. (1968), "Ichari Dam, Treatment of Left Bank Hill Slopes and Tying of Dam Blocks to Left Bank Rock", Design Memo. 29.
- Central Design Directorate, U.P.I.D. (1969), "Ichari Dam, Treatment of Left Bank Slopes", Design Memo. 41.
- Central Design Directorate, U.P.I.D. (1970), "Ichari Dam, Treatment of Left Bank and Tying of Dam to Left Bank Rock", Design Memoranda 48 and 64.

## Design and Construction of Geocell Mattress as Embankment Foundation

Alistair J.T. Gilchrist

Area Civil Engineer, Netlon Limited, United Kingdom

**SYNOPSIS:** This paper describes the use of a high strength Geocell mattress as a new solution to the problem of the construction of embankments on soft foundations.

The paper deals in detail with the design of the Geocell mattress to support and distribute the imposed loading onto soft foundation. It considers the plastic condition of the soft clay to determine the factor of safety against foundation failure.

Two case studies will be examined to illustrate the construction techniques. Monitoring of settlement during construction of the Geocell and during embankment filling is compared with predicted values.

### INTRODUCTION

The A807 Auchenhowie Road runs to the north of the City of Glasgow, Strathclyde, Scotland and follows a very tortuous route with some very narrow right angled bends.

The general poor alignment and the sub standard condition of the road has contributed to a high accident record, thus the local Highway Authority embarked on a capital works scheme to re-align the road along a new route (Fig 1).

To the south of the existing road runs four large diameter water pipes which supply a large proportion of the population of Central Scotland with drinking water. Any disturbance of these pipes would have incurred a very heavy cost penalty (approximately £1.0 million).

This therefore pushed the realignment to the north into an area of marsh which once formed the southern part of the Dougalston Loch which had been drained many years before. This area was also very heavily wooded and to achieve the required vertical alignment and embankment, of some 4.5m in height, was required to be constructed across this marshland.

### SITE INVESTIGATION

In the area of the swamp (Fig 2) bore holes 103-105 penetrated between 31.1m and 3.95m of very soft deposits generally comprising of 1.3m to 1.5m of very soft brown organic silty clay interbanded with black peat and occasional lenses of fine sand and medium gravel. This was underlain by between 0.99m and 2.45m of very soft brown laminated silty clay interbanded with frequent partings of clayey silt.

The bore holes were terminated at approximately 4.0m depth in very weak highly weathered becoming weak friable grey mudstone.

Surprisingly the bore holes were generally dry with water only becoming apparent at the clay mudstone interface.

Hand bores number h.b. 101 to h.b. 104 again penetrated the very soft deposits to a depth of about 1.0m where they were terminated. Hand bores h.b. 105 and h.b. 106 went deeper but still remained within the soft laminated silty clay.

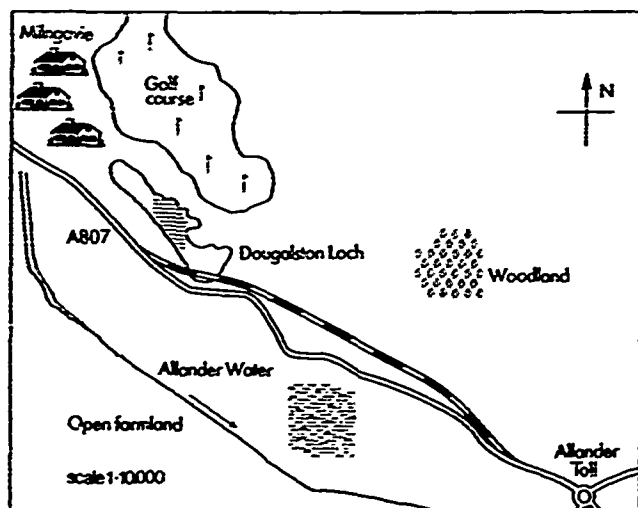


Figure 1

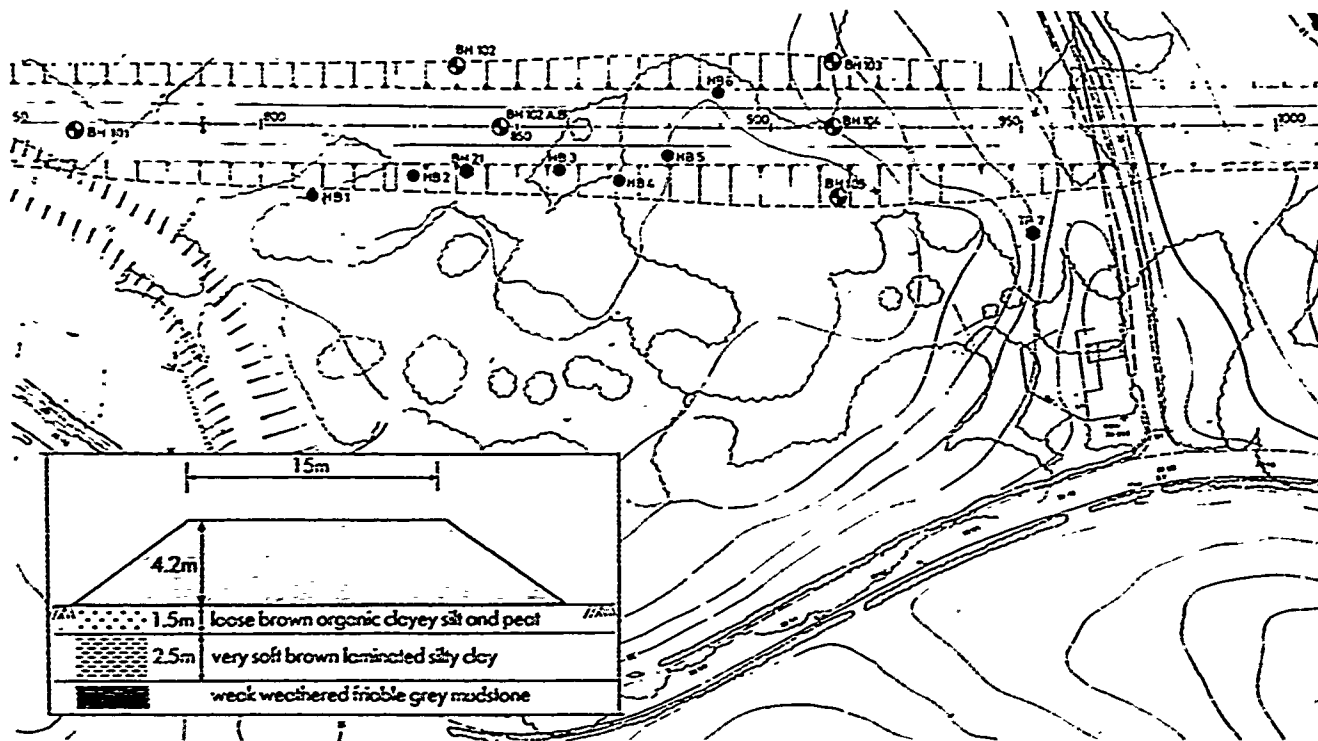


Figure 2

Bore hole number 101 was sunk into the bank of the loch and penetrated 2.2m of firm to stiff friable reddish brown very sandy clay underlain by 1.35m of dense to very dense, very clayey sand and gravel over decomposed mudstone.

Three bore holes sunk in the location of bore holes number 102 all terminated on obstructions.

#### Laboratory Results

Due to the poor nature of the underlying soils many undisturbed samples proved unsuitable for testing.

Where triaxial testing was possible, values of apparent cohesion of between 12 and 19 kN/sq m were recorded.

In bore holes 103, 104 and 105, moisture contents as high as 123% were recorded but average figures were in the order of 40% with average liquid limits of 50% and plasticity index of 24% (Fig 3).

To supplement the available information, laboratory vane shear tests were carried out on undisturbed samples from bore holes numbers 103, 104 and 105. These yielded undisturbed shear strengths of between 11 kN/sq m to 30 kN/sq m with an average value of 17.0 kN/sq m. The respective remoulded values varied from 3 kN/sq m to 8 kN/sq m with an average value of 5.0 kN/sq m.

The soft organic clay silt had an average organic content of 11.0%.

| Borehole 103   |  |  |  |  |  |  |  |  |  |
|----------------|--|--|--|--|--|--|--|--|--|
| Geological Log |  |  |  |  |  |  |  |  |  |
| Borehole 104   |  |  |  |  |  |  |  |  |  |
| Geological Log |  |  |  |  |  |  |  |  |  |
| Borehole 105   |  |  |  |  |  |  |  |  |  |
| Geological Log |  |  |  |  |  |  |  |  |  |
| Borehole 106   |  |  |  |  |  |  |  |  |  |
| Geological Log |  |  |  |  |  |  |  |  |  |
| Borehole 107   |  |  |  |  |  |  |  |  |  |
| Geological Log |  |  |  |  |  |  |  |  |  |
| Borehole 108   |  |  |  |  |  |  |  |  |  |
| Geological Log |  |  |  |  |  |  |  |  |  |
| Borehole 109   |  |  |  |  |  |  |  |  |  |
| Geological Log |  |  |  |  |  |  |  |  |  |
| Borehole 110   |  |  |  |  |  |  |  |  |  |
| Geological Log |  |  |  |  |  |  |  |  |  |
| Borehole 111   |  |  |  |  |  |  |  |  |  |
| Geological Log |  |  |  |  |  |  |  |  |  |
| Borehole 112   |  |  |  |  |  |  |  |  |  |
| Geological Log |  |  |  |  |  |  |  |  |  |
| Borehole 113   |  |  |  |  |  |  |  |  |  |
| Geological Log |  |  |  |  |  |  |  |  |  |
| Borehole 114   |  |  |  |  |  |  |  |  |  |
| Geological Log |  |  |  |  |  |  |  |  |  |
| Borehole 115   |  |  |  |  |  |  |  |  |  |
| Geological Log |  |  |  |  |  |  |  |  |  |
| Borehole 116   |  |  |  |  |  |  |  |  |  |
| Geological Log |  |  |  |  |  |  |  |  |  |
| Borehole 117   |  |  |  |  |  |  |  |  |  |
| Geological Log |  |  |  |  |  |  |  |  |  |
| Borehole 118   |  |  |  |  |  |  |  |  |  |
| Geological Log |  |  |  |  |  |  |  |  |  |
| Borehole 119   |  |  |  |  |  |  |  |  |  |
| Geological Log |  |  |  |  |  |  |  |  |  |
| Borehole 120   |  |  |  |  |  |  |  |  |  |
| Geological Log |  |  |  |  |  |  |  |  |  |
| Borehole 121   |  |  |  |  |  |  |  |  |  |
| Geological Log |  |  |  |  |  |  |  |  |  |
| Borehole 122   |  |  |  |  |  |  |  |  |  |
| Geological Log |  |  |  |  |  |  |  |  |  |
| Borehole 123   |  |  |  |  |  |  |  |  |  |
| Geological Log |  |  |  |  |  |  |  |  |  |
| Borehole 124   |  |  |  |  |  |  |  |  |  |
| Geological Log |  |  |  |  |  |  |  |  |  |
| Borehole 125   |  |  |  |  |  |  |  |  |  |
| Geological Log |  |  |  |  |  |  |  |  |  |
| Borehole 126   |  |  |  |  |  |  |  |  |  |
| Geological Log |  |  |  |  |  |  |  |  |  |
| Borehole 127   |  |  |  |  |  |  |  |  |  |
| Geological Log |  |  |  |  |  |  |  |  |  |
| Borehole 128   |  |  |  |  |  |  |  |  |  |
| Geological Log |  |  |  |  |  |  |  |  |  |
| Borehole 129   |  |  |  |  |  |  |  |  |  |
| Geological Log |  |  |  |  |  |  |  |  |  |
| Borehole 130   |  |  |  |  |  |  |  |  |  |
| Geological Log |  |  |  |  |  |  |  |  |  |
| Borehole 131   |  |  |  |  |  |  |  |  |  |
| Geological Log |  |  |  |  |  |  |  |  |  |
| Borehole 132   |  |  |  |  |  |  |  |  |  |
| Geological Log |  |  |  |  |  |  |  |  |  |
| Borehole 133   |  |  |  |  |  |  |  |  |  |
| Geological Log |  |  |  |  |  |  |  |  |  |
| Borehole 134   |  |  |  |  |  |  |  |  |  |
| Geological Log |  |  |  |  |  |  |  |  |  |
| Borehole 135   |  |  |  |  |  |  |  |  |  |
| Geological Log |  |  |  |  |  |  |  |  |  |
| Borehole 136   |  |  |  |  |  |  |  |  |  |
| Geological Log |  |  |  |  |  |  |  |  |  |
| Borehole 137   |  |  |  |  |  |  |  |  |  |
| Geological Log |  |  |  |  |  |  |  |  |  |
| Borehole 138   |  |  |  |  |  |  |  |  |  |
| Geological Log |  |  |  |  |  |  |  |  |  |
| Borehole 139   |  |  |  |  |  |  |  |  |  |
| Geological Log |  |  |  |  |  |  |  |  |  |
| Borehole 140   |  |  |  |  |  |  |  |  |  |
| Geological Log |  |  |  |  |  |  |  |  |  |
| Borehole 141   |  |  |  |  |  |  |  |  |  |
| Geological Log |  |  |  |  |  |  |  |  |  |
| Borehole 142   |  |  |  |  |  |  |  |  |  |
| Geological Log |  |  |  |  |  |  |  |  |  |
| Borehole 143   |  |  |  |  |  |  |  |  |  |
| Geological Log |  |  |  |  |  |  |  |  |  |
| Borehole 144   |  |  |  |  |  |  |  |  |  |
| Geological Log |  |  |  |  |  |  |  |  |  |
| Borehole 145   |  |  |  |  |  |  |  |  |  |
| Geological Log |  |  |  |  |  |  |  |  |  |
| Borehole 146   |  |  |  |  |  |  |  |  |  |
| Geological Log |  |  |  |  |  |  |  |  |  |
| Borehole 147   |  |  |  |  |  |  |  |  |  |
| Geological Log |  |  |  |  |  |  |  |  |  |
| Borehole 148   |  |  |  |  |  |  |  |  |  |
| Geological Log |  |  |  |  |  |  |  |  |  |
| Borehole 149   |  |  |  |  |  |  |  |  |  |
| Geological Log |  |  |  |  |  |  |  |  |  |
| Borehole 150   |  |  |  |  |  |  |  |  |  |
| Geological Log |  |  |  |  |  |  |  |  |  |
| Borehole 151   |  |  |  |  |  |  |  |  |  |
| Geological Log |  |  |  |  |  |  |  |  |  |
| Borehole 152   |  |  |  |  |  |  |  |  |  |
| Geological Log |  |  |  |  |  |  |  |  |  |
| Borehole 153   |  |  |  |  |  |  |  |  |  |
| Geological Log |  |  |  |  |  |  |  |  |  |
| Borehole 154   |  |  |  |  |  |  |  |  |  |
| Geological Log |  |  |  |  |  |  |  |  |  |
| Borehole 155   |  |  |  |  |  |  |  |  |  |
| Geological Log |  |  |  |  |  |  |  |  |  |
| Borehole 156   |  |  |  |  |  |  |  |  |  |
| Geological Log |  |  |  |  |  |  |  |  |  |
| Borehole 157   |  |  |  |  |  |  |  |  |  |
| Geological Log |  |  |  |  |  |  |  |  |  |
| Borehole 158   |  |  |  |  |  |  |  |  |  |
| Geological Log |  |  |  |  |  |  |  |  |  |
| Borehole 159   |  |  |  |  |  |  |  |  |  |
| Geological Log |  |  |  |  |  |  |  |  |  |
| Borehole 160   |  |  |  |  |  |  |  |  |  |
| Geological Log |  |  |  |  |  |  |  |  |  |
| Borehole 161   |  |  |  |  |  |  |  |  |  |
| Geological Log |  |  |  |  |  |  |  |  |  |
| Borehole 162   |  |  |  |  |  |  |  |  |  |
| Geological Log |  |  |  |  |  |  |  |  |  |
| Borehole 163   |  |  |  |  |  |  |  |  |  |
| Geological Log |  |  |  |  |  |  |  |  |  |
| Borehole 164   |  |  |  |  |  |  |  |  |  |
| Geological Log |  |  |  |  |  |  |  |  |  |
| Borehole 165   |  |  |  |  |  |  |  |  |  |
| Geological Log |  |  |  |  |  |  |  |  |  |
| Borehole 166   |  |  |  |  |  |  |  |  |  |
| Geological Log |  |  |  |  |  |  |  |  |  |
| Borehole 167   |  |  |  |  |  |  |  |  |  |
| Geological Log |  |  |  |  |  |  |  |  |  |
| Borehole 168   |  |  |  |  |  |  |  |  |  |
| Geological Log |  |  |  |  |  |  |  |  |  |
| Borehole 169   |  |  |  |  |  |  |  |  |  |
| Geological Log |  |  |  |  |  |  |  |  |  |
| Borehole 170   |  |  |  |  |  |  |  |  |  |
| Geological Log |  |  |  |  |  |  |  |  |  |
| Borehole 171   |  |  |  |  |  |  |  |  |  |
| Geological Log |  |  |  |  |  |  |  |  |  |
| Borehole 172   |  |  |  |  |  |  |  |  |  |
| Geological Log |  |  |  |  |  |  |  |  |  |
| Borehole 173   |  |  |  |  |  |  |  |  |  |
| Geological Log |  |  |  |  |  |  |  |  |  |
| Borehole 174   |  |  |  |  |  |  |  |  |  |
| Geological Log |  |  |  |  |  |  |  |  |  |
| Borehole 175   |  |  |  |  |  |  |  |  |  |
| Geological Log |  |  |  |  |  |  |  |  |  |
| Borehole 176   |  |  |  |  |  |  |  |  |  |
| Geological Log |  |  |  |  |  |  |  |  |  |
| Borehole 177   |  |  |  |  |  |  |  |  |  |
| Geological Log |  |  |  |  |  |  |  |  |  |
| Borehole 178   |  |  |  |  |  |  |  |  |  |
| Geological Log |  |  |  |  |  |  |  |  |  |
| Borehole 179   |  |  |  |  |  |  |  |  |  |
| Geological Log |  |  |  |  |  |  |  |  |  |
| Borehole 180   |  |  |  |  |  |  |  |  |  |
| Geological Log |  |  |  |  |  |  |  |  |  |
| Borehole 181   |  |  |  |  |  |  |  |  |  |
| Geological Log |  |  |  |  |  |  |  |  |  |
| Borehole 182   |  |  |  |  |  |  |  |  |  |
| Geological Log |  |  |  |  |  |  |  |  |  |
| Borehole 183   |  |  |  |  |  |  |  |  |  |
| Geological Log |  |  |  |  |  |  |  |  |  |
| Borehole 184   |  |  |  |  |  |  |  |  |  |
| Geological Log |  |  |  |  |  |  |  |  |  |
| Borehole 185   |  |  |  |  |  |  |  |  |  |
| Geological Log |  |  |  |  |  |  |  |  |  |
| Borehole 186   |  |  |  |  |  |  |  |  |  |
| Geological Log |  |  |  |  |  |  |  |  |  |
| Borehole 187   |  |  |  |  |  |  |  |  |  |
| Geological Log |  |  |  |  |  |  |  |  |  |
| Borehole 188   |  |  |  |  |  |  |  |  |  |
| Geological Log |  |  |  |  |  |  |  |  |  |
| Borehole 189   |  |  |  |  |  |  |  |  |  |
| Geological Log |  |  |  |  |  |  |  |  |  |
| Borehole 190   |  |  |  |  |  |  |  |  |  |
| Geological Log |  |  |  |  |  |  |  |  |  |
| Borehole 191   |  |  |  |  |  |  |  |  |  |
| Geological Log |  |  |  |  |  |  |  |  |  |
| Borehole 192   |  |  |  |  |  |  |  |  |  |
| Geological Log |  |  |  |  |  |  |  |  |  |
| Borehole 193   |  |  |  |  |  |  |  |  |  |
| Geological Log |  |  |  |  |  |  |  |  |  |
| Borehole 194   |  |  |  |  |  |  |  |  |  |
| Geological Log |  |  |  |  |  |  |  |  |  |
| Borehole 195   |  |  |  |  |  |  |  |  |  |
| Geological Log |  |  |  |  |  |  |  |  |  |
| Borehole 196   |  |  |  |  |  |  |  |  |  |
| Geological Log |  |  |  |  |  |  |  |  |  |
| Borehole 197   |  |  |  |  |  |  |  |  |  |
| Geological Log |  |  |  |  |  |  |  |  |  |
| Borehole 198   |  |  |  |  |  |  |  |  |  |
| Geological Log |  |  |  |  |  |  |  |  |  |
| Borehole 199   |  |  |  |  |  |  |  |  |  |
| Geological Log |  |  |  |  |  |  |  |  |  |
| Borehole 200   |  |  |  |  |  |  |  |  |  |
| Geological Log |  |  |  |  |  |  |  |  |  |

## SUMMARY OF GROUND CONDITIONS

From an inspection of the bore hole logs and from the available laboratory results obtained from site investigations the underlying strata beneath the proposed embankment is summarised as follows:

- (a) Peaty topsoil 0.4 m thick
- (b) Loose brown organic clayey silt and peat 1.50 m thick
- (c) Very soft brown laminated silty clay 2.50 m thick
- (d) Weak weathered friable grey mudstone

For design purposes the soft silty clay and peat area was taken to an average depth of 4.0m with an average undisturbed shear strength ( $C_u$ ) of 15.0 kN/sq m and = 0 degrees.

## EMBANKMENT FOUNDATIONS

Substituting these soil strengths into Terzaghi's equation:

$$q_u = C_u \times N_c + \gamma \times D \times N_q + (\gamma \times B/2) \times N_\gamma$$

taking  $D = 0$ ,  $N_q = 0$ ,  $N_c = (\pi + 2)$ , gave the following value

Ultimate bearing capacity - surface material

$$q_u = 77.1 \text{ kN/sq m}$$

Assuming a density of the imported material of 19.0 kN/ $C_u$  m and the height of the proposed embankment of 4.5m then:

$$\begin{aligned} \text{Imposed bearing pressure} &= 4.5 \times 19.0 \\ &= 85.5 \text{ kN/sq m} \end{aligned}$$

Therefore factor of safety against foundation failure = 0.9

## DESIGN CONSIDERATIONS

A number of design alternatives were looked at for the embankment, although only two are considered further by the author.

- (a) Removal of the soft layer of material and replacing with suitable rock fill. This method would have involved a considerable increase in traffic on and off the site. No rock cut was locally available on the site so all rock fill would have to be imported.

Owing to the high moisture content of the soft silts excavation and maintaining a dry site would have been difficult and weather dependent as would the removal and disposal of this highly fluid material off site. Due to the local environment this construction method would not be readily acceptable.

- (b) Construction of a high strength Geocell mattress directly onto the soft layer to form a foundation to the embankment.

This method of construction would require no significant increase in site traffic. It would also not be weather dependent and require no specialised site operations.

A straight cost comparison was made between these two options:

## Cost Comparisons

### Excavation and replacement

| Item                       | Quantity<br>cu m | Rate<br>£ | Total<br>cost £ |
|----------------------------|------------------|-----------|-----------------|
| Strip top soil             | 1840             | 1.00      | 1840.00         |
| Excavate U/s<br>(d = 3.5m) | 21460            | 0.50      | 10730.00        |
| Disposal off site          | 21460            | 3.00      | 64380.00        |
| Import suitable<br>fill    | 21460            | 3.50      | 75110.00        |

TOTAL = £152,060.00

### Construction of Geocell mattress

| Item                                    | Quantity  | Rate<br>£ | Total<br>cost £ |
|---|-----------|-----------|-----------------|
| Provide, assemble<br>and infill Geocell | 6132 sq m | 11.00     | 67452.00        |
| Free draining<br>infill                 | 6132 cu m | 8.00      | 49056.00        |

TOTAL = £116,508.00

|                                       |           |      |          |
|---------------------------------------|-----------|------|----------|
| Less cost of<br>10.m of<br>embankment | 6132 cu m | 2.00 | 12264.00 |
|---------------------------------------|-----------|------|----------|

Therefore effective  
cost of Geocell £104,244.00

This represents an estimated saving of approximately 31% or £48,000.00

This saving, by using the Geocell mattress, does not take into account the reduction in the environmental nuisance by cutting down off and on site traffic. It was therefore decided to proceed with the detailed design of the mattress.

## DESIGN OF FOUNDATION MATTRESS

Netlon Limited were approached in October 1984 by Strathclyde Regional Council Roads Department for advice on a suitable method of constructing an embankment over this soft material. At this time only approximate parameters for the soft clay were available and a preliminary design was prepared utilising a high strength Geocell mattress which had been successfully used on similar sites.

The main criteria for design was for an overall factor of safety of 1.5 to be achieved against foundation failure.

## DESIGN PHILOSOPHY

A Geocell mattress is a very stiff rigid foundation mattress designed to support an embankment over very soft ground. It is generally installed at existing ground level and with no soil strip (Fig 4).

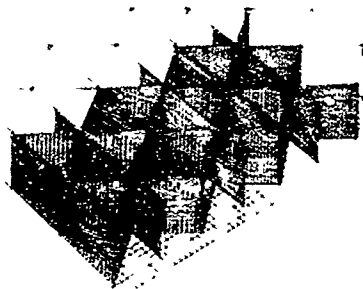
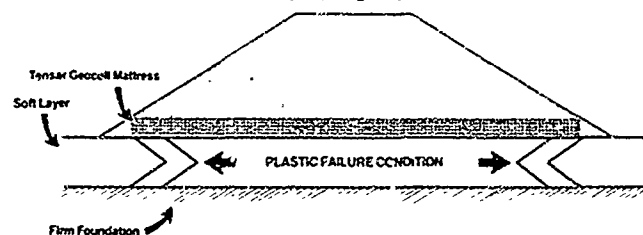


Figure 4

The mattress is constructed from high strength Tensor geogrids to form a cellular construction.

This rigid foundation mattress is assumed to alter the direction of the normal slip circle failure plane by forcing it to pass vertically through the mattress.

This has the effect of forcing the slip plane deeper into the underlying stiffer weathered mudstone.

Before this weathered mudstone can fail in shear, a plastic failure would be initiated within the softer silty clay beneath the embankment. The plastic failure condition or the soft silty clay is therefore considered in the design.

The foundation mattress is assumed to display the following properties:

- (1) Sufficient tensile strength to ensure that the full  $C_u$  value is mobilised on the base.
- (2) The mattress is rigid to ensure an even distribution of load onto the foundation material. This is provided by the high tensile strength of the Tensor SR2 diaphragms forming a triangular cellular construction.
- (3) The base of the mattress is rough to provide high frictional contact with the underlying soils. The base material is Tensor SS2 which allows partial penetration of the infill material through the apertures, creating a rough underside to the mattress.

The preliminary design was carried out prior to the site investigation being completed and was based on a depth of soft silty clay layer of 2.5m with an average  $C_u = 30\text{ kN/sq m}$  and  $\phi = 5$  degrees.

From the preliminary design the factor of safety against foundation failure was 3.51 and against failure of the mattress of 1.71.

The very high factor of safety reflected the under utilisation of the load carrying capacity of the Geocell mattress but compared with the alternative options available this still proved to be economical and the design was accepted by the Roads Department.

However, when more accurate soil parameters became available, a further design assessment was carried out.

The design parameters used in this final design were:

|                                |                             |
|--------------------------------|-----------------------------|
| Depth of soil silty clay layer | $d = 4.0\text{ m}$          |
| Average strength of layer      | $C_u = 15.0\text{ kN/sq m}$ |
| Height of embankment           | $n = 4.2\text{ m}$          |
| Width of embankment            | $l = 27.4\text{ m}$         |

From this design the minimum factor of safety against foundation was 1.58 and against mattress failure was 1.93.

The mattress required to be edge stiffened over the outer 6.0m. This was achieved by using 0.5m cells along the outer edges and conventional 1.0m cells within the remainder (Fig 5).

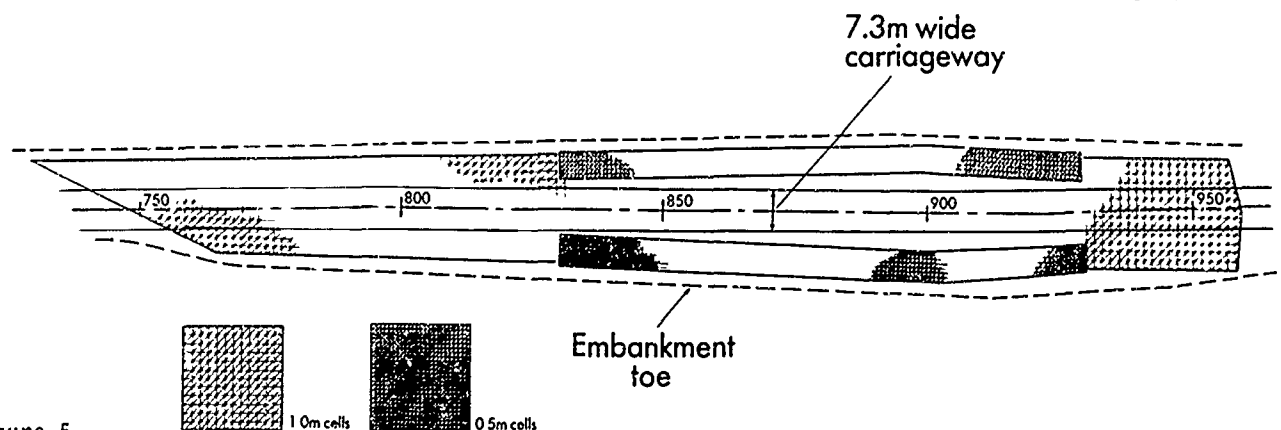


Figure 5

It was also shown that where the minimum value of  $C_u = 8.0 \text{ kN/sq m}$ , the minimum factor of safety remained greater than unity.

The Geocell now showed to be a very economical solution and was adopted for the contract.

The design procedure for the Geocell mattress is outlined in detail in Appendix 1.

## CONSTRUCTION

The Geocell foundation mattress was constructed insitu during January and February 1986. The dense vegetation of shrubs and trees was removed in order to gain access to the site. An island across the line of the mattress was partially levelled. Other than this no site preparation was required. The site was waterlogged and under standing water during the period of construction.

4.0m wide lengths of Tensar SS2 were rolled out along the line of the road to form the base of the mattress. These strips were lapped by 500mm. The main transverse diaphragms were Tensar SR2 and were installed at 1.0m centres across the mattress. The Tensar SR2 was stitched to the base material using HDPE braid (Fig 6).



Figure 6

After tensioning of the main diaphragms, the intermediate diaphragms, again Tensar SR2, were installed and fixed to the main diaphragms using steel bodkins. This forms 1.0m triangular cells. Over the areas where the edge stiffening was required, 0.5m triangular cells were constructed using short intermediate transverse diaphragms (Fig 7).

The cellular mattress was then infilled with imported free draining granular material. The filling procedure ensures that no cell is filled to more than half the height of the adjacent cell. This prevents excessive bulging of the cell walls (Ref 6).

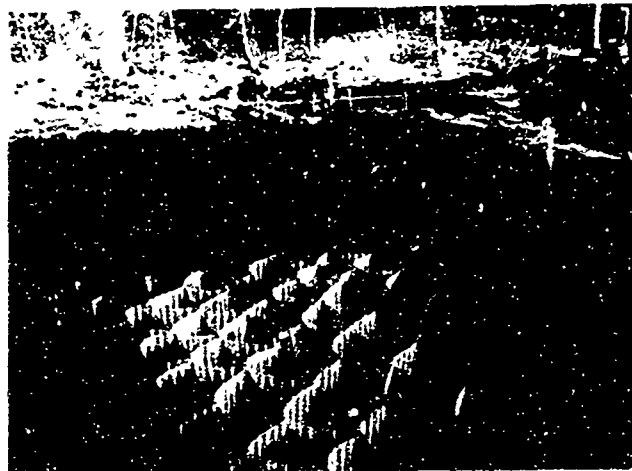


Figure 7

The infill material is not compacted and slight overfilling compensates for any slight settlement and also protects the top of the diaphragms from damage.

As the filled Geocell progresses the Contractor utilises it as a construction platform for infilling plant and the delivery of infill material. At no time does the Contractor's plant run on soft ground so delays from bogging down are eliminated (Fig 8).



Figure 8

This work was a new experience for the Contractor, Raynesway Construction Services Limited.

After the initial learning curve, outputs of completed, filled mattresses in excess of 350 sq m per shift were achieved. Weather conditions during the initial construction period were very poor.

The total time for construction was six and a half weeks and the actual installation cost was some £111,000.00 being £5,500.00 less than the original estimate.

The embankment was then constructed directly onto the Geocell mattress using conventional earthmoving plant. The embankment was raised to its full height rapidly and was completed in about 7 days (Fig 9).

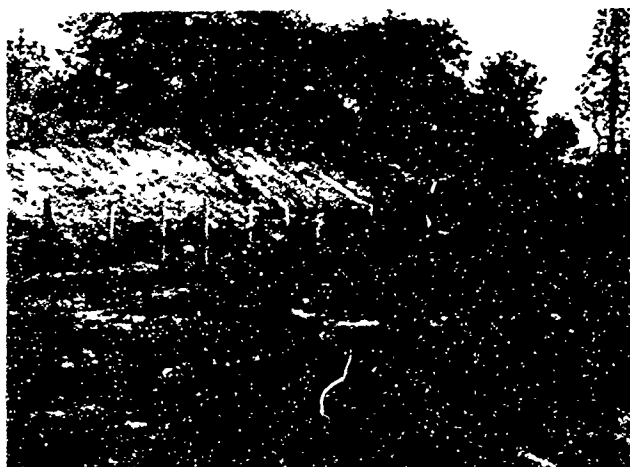


Figure 9

### SETTLEMENT

Using the information from the site investigation, the overall settlement of the completed embankment was expected to be in the order of 175mm over 1 year. The expected settlement during the 3 month construction period was expected to be 140mm.

Tubular settlement pins, welded to metal base plates, were placed onto the top of the completed Geocell base grid and supported by the infill material of the embankment. They were levelled every week as infilling and embankment construction progressed and the settlement recorded and plotted on a graph. An average initial settlement of approximately 90mm was recorded after the embankment was complete and before carriageway construction was started.

The settlement was noted to be even across the width of the embankment. No differential settlement has been monitored along the length of the completed road.

### CONCLUSIONS

1. By using the Geocell mattress there was no need to remove large quantities of unsuitable material from the site with the resulting problems of handling and disposal. There was also no appreciable increase in the off site traffic and environmental nuisance.
2. The factor of safety against foundation failure was significantly increased and embankment construction continued rapidly without having to incorporate rest periods into the construction programme to allow excess pore water pressures to dissipate.

3. The Contractor had a dry working platform on which to carry out Geocell filling operations and any subsequent drainage works if these were required. Wick drains can be installed through the mattress with no impairment. The mattress enables the Contractor to work continuously through bad weather with delivery vehicles running on the infilled Geocell.
4. The infill material to the Geocell provides a massive drainage blanket which aids consolidation of the completed embankment and reduces consolidation times.
5. The Geocell mattress showed considerable cost savings over alternative methods of construction.
6. No differential settlement had been evident after completion of the embankment. Settlement has been less than that protected for an unreinforced embankment. The Geocell mattress effectively spreads the load more evenly along the embankment foundation.

### APPENDIX 1

In this design, reference is made to "Engineering Plasticity" by W Johnson and P B Mellor, (Chapter 12.5: pages 392 to 401).

This considers the plastic failure of material compressed between two rough, rigid parallel platens being brought together. The platen widths exceed the soft material layer thickness (Fig 10).

The Geocell mattress represents the upper platen with the weathered mudstone representing the lower.

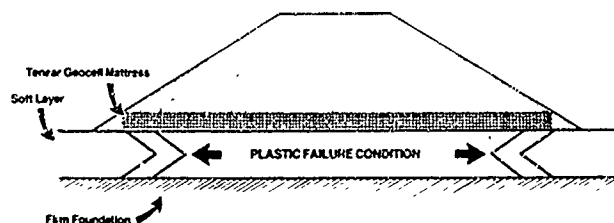


Figure 10

### DESIGN PARAMETERS

|                        |                              |
|------------------------|------------------------------|
| Weight of embankment   | $h = 4.2\text{m}$            |
| Embankment width       | $l = 27.4\text{m}$           |
| Depth of soft material | $d = 4.0\text{m}$            |
| Strength of soft layer | $C_u = 15.0 \text{ kN/sq m}$ |

The pressure diagram for half the embankment is evaluated. A value equal to twice the cohesion is added on to take into account the effect of passive pressure beyond the toe and neglecting the effect of upthrust within  $0.45 \times 2h$  of the toe.



Load distribution on the base is obtained from the equations given in the extract from "Engineering Plasticity" and from the 15 degree flow net (Fig 11).

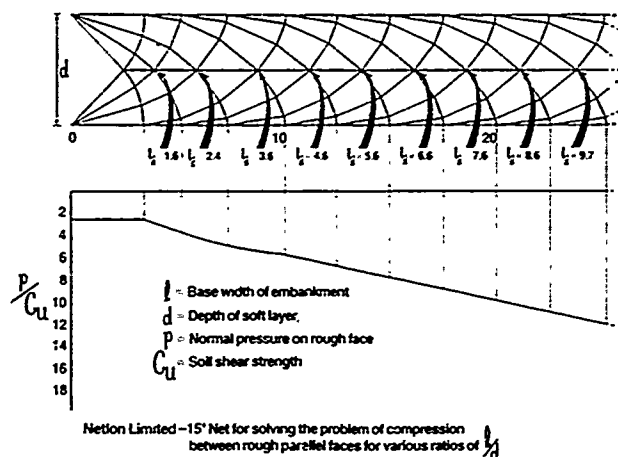


Figure 11

Calculation of the average base pressure over the rigid zone:-

|                               |                                   |       |       |                   |
|-------------------------------|-----------------------------------|-------|-------|-------------------|
| $\Delta X$                    | 1.966                             | 1.707 | 1.259 | $X = 4.932$       |
| $\Psi \text{ rad.}$           | 0.654                             | 0.393 | 0.131 | $h = 0.4\text{m}$ |
| $\Psi \times \Delta X$        | 1.286                             | 0.671 | 0.165 |                   |
| $\Sigma \Psi \times \Delta X$ | $= 2.122$                         |       |       |                   |
|                               | $p = 6.0 C_u + 2.0 C_u = 8.0 C_u$ |       |       |                   |

from eqn. 12.11

$$\frac{\bar{p}}{C_u} = 2 \left[ \frac{2 \cdot \Sigma \psi \cdot \Delta X + h}{2X} \right] + \frac{p}{C_u}$$

$$= 2 \left[ \frac{(2 \times 2.122) + 4.0}{2 \times 4.932} \right] + 8$$

$$\therefore \bar{p} = 9.67 C_u$$

Therefore, adopting an average cohesion of 15.0 kN/sq m for the soft layer, the load to failure for the half embankment is (Fig 12):-

$$2.8 \times 4.57 C_u = 190.40$$

$$5.8 (3.43/2 + 4.57) C_u = 545.20$$

$$5.0 \times 9.67 C_u = 725.25$$

Therefore load to failure = 1460.85 kN/m

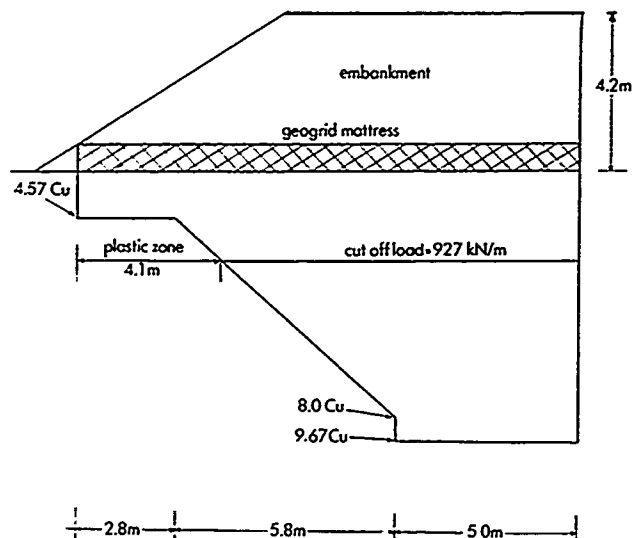


Figure 12

Imposed loading for half the embankment is:-

$$W = ((3.2 \times 7.15) + (1.0 \times 13.6) + (0.5 \times 3.2 \times 4.8)) \times 20.0 = 883.2$$

$$\text{Surcharge} = 3.65 \times 12.0 = 43.8$$

Therefore Total Imposed Load = 927.0 kN/m

Therefore factor of safety against foundation failure:-

$$\text{F.o.S} = 1.58$$

Consider load within the diaphragms of the Geocell.

For the factor of safety reduced to 1.0, at the centre of the embankment, the equivalent apparent cohesion for the soft layer would become:-

$$15.0 / 1.50 = 9.49 \text{ kN/sq m}$$

From a Mohr construction it can be shown that the horizontal load to be resisted by the Geocell mattress is:-

$$T_f = \frac{C_u}{\sin \phi}$$

Based on the infill material properties  $\phi = 30$  degrees. Therefore for a factor of safety of 1.0 the horizontal load is:-

$$T_{1.0} = \frac{9.49}{\sin 30^\circ} = 18.98 \text{ kN/m run}$$

This is the minimum condition and applies over the worst centre portion of the embankment.

At the edge of the embankment assume the worst condition where the factor of safety drops to 2.0.

i.e.  $C_u$  beneath embankment = 18.98 kN/sq m

The embankment load/foundation diagram is shown in Fig 12. The cut off line at support value of 927 kN/m shows the extent of the plastic zone.

Over this zone the horizontal force to be resisted by the mattress is:-

$$T_{2.0} = \frac{18.98}{\sin 30^\circ} = 37.96 \text{ kN/m run}$$

The diaphragms to the Geocell and Tensar SR2 geogrid.

Working load in the grid = 21.48 kN/m (Ref 5)

Therefore resistance of 1.0m cells is:-

$$T = 21.48 + \frac{21.48}{\sqrt{2}} = 36.76 \text{ kN/m run}$$

and resistance of 0.5m cells is:-

$$T = 2 \times 36.67 = 73.34 \text{ kN/m run}$$

Therefore factor of safety of Geocell against failure = 1.93

Therefore use 0.5m cells within 6.0m of the edge of the mattress and 1.0m in the remainder.

Where the embankment height is less than 3.0m high, 1.0m cells were used throughout.

## ACKNOWLEDGEMENTS

The author wishes to thank Mr W S McAlonan, MSc DipTg CEng, Director of Roads, Strathclyde Regional Council and Mr D L Hynd, CEng MICE, Divisional Engineer, Dumbarton, and to other members of the Roads Department for their help. The author would point out that the views and opinions expressed are his own and not necessarily those of the Regional Council.

Thanks are also due to Netlon Limited and Raynesway Construction Services Limited for their assistance.

## BIBLIOGRAPHY

Johnson, W. and Mellor, P.B., (VNR), Engineering Plasticity

Jones, C.J.F.P., Earth Reinforcement and Soil Structures

Netlon Limited, Design suggestions for the use of a High Strength Geocell mattress in the Construction of the Auchenhowie Embankment

Netlon Limited, Tensar Geocell Mattress

Netlon Limited, Test Methods and Physical Properties of Tensar Geogrids

Robertson, J. and Gilchrist, A.J.T., Design and Construction of a Reinforced Embankment Across Soft Lake Bed Deposits

Smith, G.N., Elements of Soil Mechanics for Civil and Mining Engineers

# Performance of an Earthdam and Cut-off Through Deep Alluvium

**N.H. Wade**

Assistant Chief Geotechnical Engineer, Monenco Consultants Ltd.,  
Canada

**L.F. Wei**

Supervising Geotechnical Engineer, Monenco Consultants Ltd.,  
Canada

**L.J. Courage**

Assistant Manager Hydro Resources, Monenco Consultants Ltd.,  
Canada

**R.A. Keys**

Manager Hydro Operations, TransAlta Utilities Corp., Canada

**SYNOPSIS:** The main dam at the Bighorn development consists of a zoned earthfill embankment with a concrete cut-off wall constructed through the river alluvium by the slurry trench technique. Upon first filling of the reservoir in 1972, erratic drops in piezometric heads in the alluvium upstream of the cut-off and significant downstream leakage prompted the construction of a weight berm at the downstream toe and implementation of a program of regular monitoring of all piezometers and seepage measuring facilities. Concern for the integrity of the structure was not allayed until completion of a dam safety evaluation in 1984. The paper summarizes the design and construction aspects of the main dam and concrete cut-off, documents the results of monitoring records of seepage and piezometric heads since reservoir filling and assesses the extent of reservoir siltation. Records and inspections demonstrate satisfactory performance of the structure.

## INTRODUCTION

The Bighorn hydroelectric development, located on the North Saskatchewan River in the frontal ranges of the Rocky Mountains about 100 miles northwest of the town of Banff, Alberta, was completed in 1972. The project consists of a 300 ft high main dam, a 100 ft high closure dam, an emergency spillway, and a gated intake structure for the 22.5 ft dia. power tunnel in the left abutment leading to the 120 megawatt powerhouse.

The main dam, consisting of a zoned earthfill embankment with a total crest length of 1700 ft, is founded on a 210 ft deep deposit of sand, gravel and boulders. To minimize seepage through the pervious foundation alluvium, a concrete diaphragm cut-off wall aligned along the dam axis was constructed through the alluvium to key into bedrock using slurry trench techniques. The layout of the dam and appurtenant facilities are shown on Figure 1, and a typical section through the dam is illustrated on Figure 2. The emergency spillway and closure dam are located at the entrance of a natural gully about 1.6 mi north of the damsite.

Bighorn dam impounds Lake Abraham which, with a storage capacity of 1,165,000 acre-feet, is the largest man-made lake in Alberta. The project, owned and operated by TransAlta Utilities Corp. of Calgary, serves as a storage and flood control facility while providing power generation benefits.

The control of seepage about the dam was of particular concern in view of the disturbed condition of the sedimentary rocks forming the abutments and the locally high permeabilities of the overburden deposits, particularly within the deep riverbed sediments. The countermeasures which were adopted comprised blanketing of the riverbed and certain abutment slopes upstream of the dam, the installation of shallow drains at the downstream toe and the downstream slope of the north abutment, and the construction of a concrete diaphragm cut-off wall to control seepage through the deep bed deposits. The performance of the main earthfill dam and the diaphragm wall forms the principal topic of this paper. A description of the development, previously reported by Gordon and Rutledge (1972) and Forbes et al (1973), is given in the following sections.

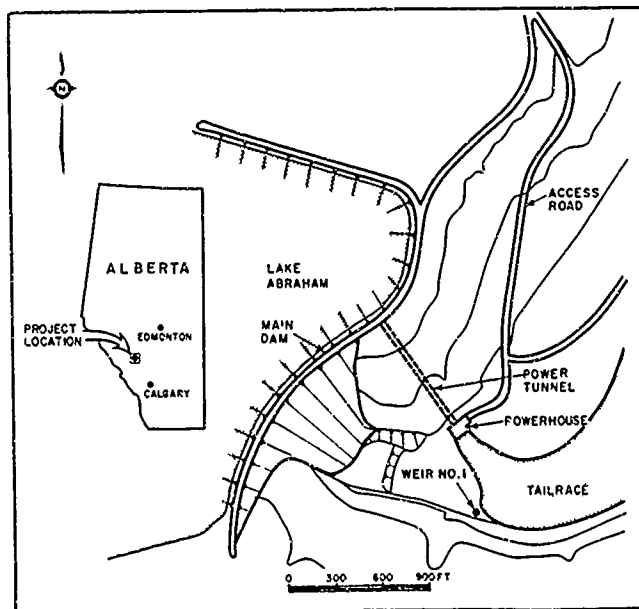
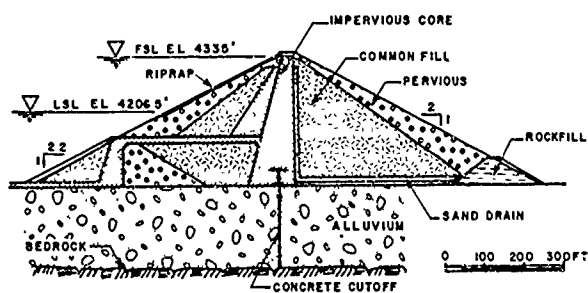


Fig. 1 Site layout



## SITE CONDITIONS

The topography of the region is well suited for hydro-electric development, with the broad glacial valley of the North Saskatchewan River providing a large reservoir capacity upstream from the narrow canyon in which the dam is sited. The geological conditions are, however, less favourable, with the disturbance arising from the tectonic upheavals during mountain building masked by subsequent glaciation and post-glacial downcutting.

The dominant rock formations in the region comprise thick strata of interbedded siltstones and sandstones of the Cretaceous period which were extensively faulted, folded and tilted with the building of the Rocky Mountains. A major regional strike fault of this period traverses the project site about 1000 ft upstream of the dam axis and has been estimated to have moved more than 1.5 mi in the northeast direction along its strike. The thrusting has produced a series of closely-spaced parallel step faults in the adjoining sediments, in which the slippage ranges from a few inches to several feet, while numerous shear planes or bedding faults are evident in the weaker strata.

In the area of the canyon, the upstream limb of the regional fault is formed, in ascending order, by the Luscar and Mountain Park Formations of Lower Cretaceous origin, while the downstream limb is formed by the Blackstone, Bighorn and Wapiabi Formations of Upper Cretaceous origin. The downstream formations form the western arm of a broad syncline through which the canyon was downcut by valley glaciers, glacial meltwaters and the present river. Siting of the dam within the canyon locates it wholly downstream from the regional fault with only the impervious blanket extending onto the upstream formations.

The Blackstone Formation forms the upstream segment of the canyon and descends downstream below riverbed level beneath the Bighorn Formation which predominates within the abutment areas of the dam as shown on Figure 3. The contact between the two formations dips conformably with

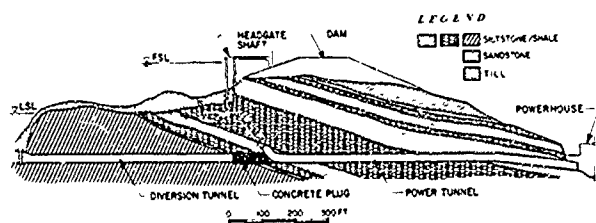


Fig. 3 Section through north abutment

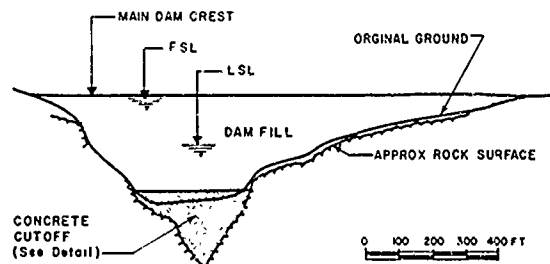
the bedding at about 14 degrees downstream and is estimated to lie at a depth of between 40 and 70 ft below the riverbed surface at the location of the cut-off wall. The Blackstone beds of dark, fissile, often ferruginous shales and dark grey siltstones extend to heights of up to 165 ft above the valley floor at their upstream limit where they daylight within the reservoir. The overlying Bighorn Formation embraces three principal fine-grained grey sandstone strata separated by relatively massive beds of siltstone, while some thin partings of carbonaceous shale and conglomerate were encountered. The blocky sandstones of this formation constitute the hardest rocks in the project area. The Wapiabi Formation, which overlies the Bighorn on the downstream flanks of the canyon, consists of highly friable siltstones in a fractured and weathered condition.

The permeability of the rock formations was given

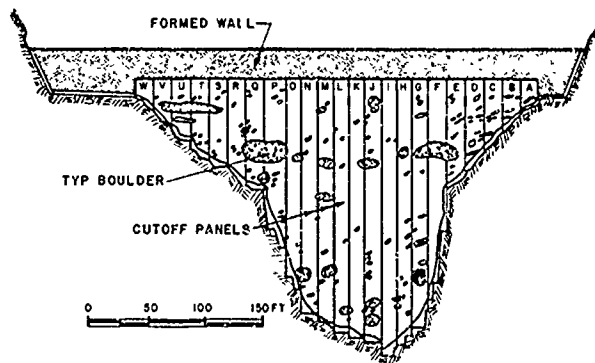
particular attention in view of the fractures and disturbance evident in outcrops. However, while drill water losses were often experienced in the investigation program, the packer permeability tests indicated generally tight conditions, even within the brecciated zones along the fault planes and in the Wapiabi Formation. Bedrock permeabilities measured in both abutments generally increased from about  $5 \times 10^{-4}$  cm/sec near the surface to about  $5 \times 10^{-5}$  cm/sec at 260 ft depth, while tests at shallow depths in the valley floor gave about  $1 \times 10^{-4}$  cm/sec. The highest values, exceeding  $1 \times 10^{-3}$  cm/sec, were obtained in the higher strata near the abutment slopes.

The rock formations outside the canyon are capped by glacial drift comprising clean sands and gravels, silts, gravelly fill and bouldery till. Though generally of shallow depth, the drift attains a depth of 165 ft on the north abutment within a linear depression in the bedrock surface. Seepage through this buried channel at higher reservoir levels was countered by blanketing the upstream exposure, constructing a series of shallow drains in the natural slopes downstream and installing three deep drainage wells collared at crest elevation.

The downcutting which formed the canyon extended through the cover of glacial drift, the Wapiabi and Bighorn Formations and into the Blackstone beds to a total depth of about 560 ft. Drilling in the valley floor indicated infill deposits extending to a maximum depth of 216 ft and consisting mainly of interbedded, river-sorted, silty to relatively clean sands and gravels in varying proportions, interspersed with bouldery talus from the canyon walls. It is noteworthy that the investigation of the bed was satisfactorily accomplished only with the advent of the Becker hammer drill, though it was difficult to appraise the consistency of the finer granular deposits and several lines of closely-spaced holes were needed to distinguish the massive boulders from the parent intact rock. The bedrock profile along the axis of the cut-off wall, and the boulders encountered, are shown on Figure 4.



(a) Longitudinal Section



(b) Cutoff Detail

Fig. 4 Concrete cut-off construction

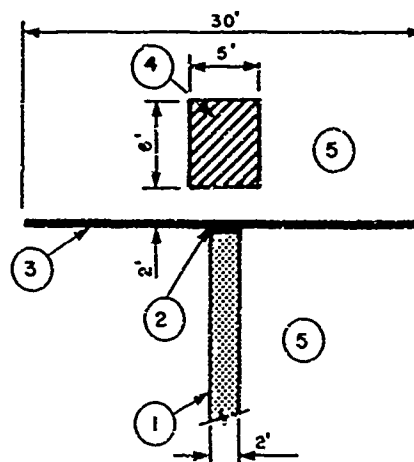
Extensive permeability testing in the riverbed deposits delineated three broad zones. In the uppermost zone, which comprises a 40 ft depth of silty sands and gravels, the horizontal permeability was found to be widely variable while the measured overall vertical permeability was  $1 \times 10^{-4}$  cm/sec. The underlying zone, which extends to 100 ft depth, consists mainly of uniform sands with some gravel and boulders. It was the most pervious zone within the depth tested, giving horizontal and vertical permeabilities of about  $2 \times 10^{-1}$  cm/sec and  $5 \times 10^{-2}$  cm/sec, respectively. The lowest zone extends to 140 ft depth and is composed of sand, coarse gravel and bouldery talus. The tests indicated overall permeabilities of roughly  $1 \times 10^{-1}$  cm/sec in the horizontal direction and  $4 \times 10^{-2}$  cm/sec in the vertical direction. The permeability of the bouldery deposits beyond 140 ft depth was not measured as a consequence of difficulties encountered in drilling through large boulders.

#### DAM DESIGN

The site was considered to be suitable for a zoned earthfill embankment structure founded on the riverbed deposits. The most critical factor in the design was the selection of the means of controlling seepage through the bed deposits, and detailed consideration was given to four alternatives, specifically, a grouted cut-off, an impervious upstream blanket, an excavated cut-off to bedrock and a concrete diaphragm wall keyed into bedrock. The use of a grouted cut-off was soon discarded due to uncertainties about its effectiveness and the high cost and time for implementation, while an upstream blanket was considered unsuitable in view of the limited space in the canyon for concurrent diversion of the river flows as well as the problems of ensuring an effective seal against the abutments. Although a core trench excavated to rock and backfilled with compacted impervious fill clearly constituted the most positive means to control seepage, its construction would have added at least six months to the construction schedule. Furthermore, its high direct cost would have been compounded by the added costs for related construction, such as a longer diversion tunnel, in comparison with a concrete diaphragm wall. The cost of dewatering alone was estimated to almost equal the cost of a diaphragm wall.

The relative advantages of a diaphragm wall were evident, particularly from a cost viewpoint. It could also be built during the winter, within a heated enclosure, and would not in consequence interfere with other construction activities or prolong the overall schedule. Nevertheless, the decision to adopt diaphragm wall construction was made only after extended deliberation of the possible adverse effects of anticipated settlements due to compression by the dam fill of loose zones in the foundation. There was concern that the settlements might be large enough to cause discontinuities in the wall sufficient to impair its effectiveness or within the impervious core as it settled downwards over the top of the wall. Another reason for hesitation was the limited precedent for the use of a concrete diaphragm cut-off wall under such high fill and hydraulic loadings.

The adoption of the diaphragm wall was based on the confidence expressed in its suitability by Dr. A. Casagrande who, together with Dr. R.M. Hardy, provided specialist geotechnical expertise to the project. To counter the effects of any disruption of the core arising from settlements relative to the wall, the wall was capped with a 30 ft wide galvanized steel plate surmounted by a 5 ft wide trench centred over the wall and filled with bentonite, as shown on Figure 5. As it was anticipated that differential heads across the wall exceeding 100 ft



1. CONCRETE CUT - OFF WALL
2. NEOPRENE
3. STEEL PLATE
4. BENTONITE FILL
5. IMPERVIOUS CORE

Fig. 5 Detail of cap at top of wall

would be sufficient to wash out the bentonite slurry bordering any imperfections or windows in the wall, the decision was taken to supplement the underseepage control by connecting the impervious core of the dam to the core of the integral upstream cofferdam, and to add a short upstream blanket.

Though the site offered an abundance of both impervious and pervious borrow, the zoning selected for the dam maximized use of the more readily available impervious glacial deposits within the core and inner shells, and limited the pervious materials, originating mostly from the riverbed, to the filters and thin outer shells. A filter of well-graded pit-run sand was provided between the core and the downstream common fill to protect against cracking the relatively brittle and low plasticity core material as a result of differential settlement. The dam was also arched upstream for the same reason.

#### DIAPHRAGM WALL CONSTRUCTION

The panel construction of the 2 ft thick cut-off wall is shown on Figure 4. Panel widths of 15 ft were used at the two ends of the wall where depth to bedrock did not exceed 120 ft and widths of 12.5 ft were used in the centre section where rock was deeper. The 15 ft wide panels were constructed in sequence, each being excavated through the bentonite slurry to bedrock by clamshell, and the excavation extended the requisite 2 ft into bedrock by percussion chisel. After clean-up a 2 ft diameter pipe was positioned vertically at the leading end of the excavation to prepare a concave interface for the next panel. The slurry was then displaced by tremie concrete with 3/4 in maximum size of aggregate and a mix designed for a 28 day strength of 4000 psi. The 12.5 ft wide panels, on the other hand, were constructed alternately. Guide holes were first drilled at the ends of an initial panel in order to maintain alignment, and the material between then excavated 2 ft into the bedrock as for the 15 ft wide panels. Concave interfaces were again left at the end of each panel.

Slurry losses within the more pervious deposits were reduced by the addition of sawdust and cellophane flakes. These additives proved insufficient in only one

of the earlier guide holes where hole sealing was accomplished by backfilling with weak concrete. The guidehole was re-established by percussion chisel once the concrete had partially cured. Sloughing of the bed deposits at the top of panels N and M (Figure 4) led to the formation of a large bulb of concrete which was subsequently line drilled and severed from the wall.

Numerous boulders up to 18 ft in size were encountered and were either broken up by percussion chisel or drilled and blasted. To ensure that the wall penetrated bedrock and not boulders, soundings were made at frequent intervals and the rock cuttings were closely observed. Excavation was terminated at the specified 2 ft embedment depth only when bedrock had been positively identified. To enhance water tightness at the periphery, grouting was performed through vertical pipes embedded in the wall at 5 ft intervals.

Reinforcing steel cages were installed in the top 20 ft of the slurry displaced wall, and dowels were left projecting above its surface for juncture with the 25 ft high wall of conventional concrete that was later superimposed to extend into the impervious core of the dam. To further increase the seepage path a galvanized steel sheet 30 ft wide was installed on top of the wall after the latter had first been ground smooth and a thick neoprene pad added with rubber cement bonding to both concrete and steel. This is shown on Figure 5. Also to protect the impervious core against cracking near its base due to either arching or differential settlement a plug of soft bentonite paste with a dry density of 35 pcf was added in a trench 5 ft wide and 8 ft deep immediately above the wall during subsequent construction.

During the initial placement of core fill against the wall, a flow of water emerged on the riverbed downstream at the juncture of panels R and Q (Figure 4). The flow, originating as seepage through the upstream cofferdam, was attributed to an imperfect interface between the panels or possibly a window in the vicinity of the large boulder overlying bedrock in that area. The joint was thoroughly grouted from holes extending to the boulder. The grouting was apparently successful, because later it proved necessary to provide temporary drainage for water ponding at the same location on the upstream side of the wall.

#### TUNNEL DESIGN

The diversion tunnel had a length of 1700 ft and passed through the siltstone and sandstone strata of the Bighorn and Blackstone Formations in the north abutment (Figure 3). It was lined throughout with concrete 12 in thick. Later it was plugged with concrete at an intermediate point, and converted to a power tunnel with an inclined shaft sloping up to a surface intake from the downstream side of the plug. About 690 ft of the original tunnel downstream of the plug was utilized in the conversion. When completed the power tunnel had a total length of approximately 1350 ft and a finished diameter of 22.5 ft. The upstream 60% of its length has a concrete lining 24 in thick, and the downstream 40% (or 560 ft to be exact), where internal pressure exceeds the overlying weight of rock, has a steel liner.

To prevent the buildup of excessive hydraulic pressure behind the lining when the tunnel is unwatered, radial drain holes were drilled into the rock at several sections along the tunnel alignment during construction. The discharge from these holes, as well as any leakage from the tunnel, is collected in header pipes behind the lining and conducted to the tailrace. On the way the flow is measured by a venturi meter.

#### INSTRUMENTATION

To monitor the post-construction performance of the embankment and the seepage control components incorporated into the structure, piezometers, settlement gauges and movement hubs were installed during construction. A total of 46 pneumatic and standpipe piezometers were placed in the embankment, foundation alluvium and abutment to monitor piezometric head variation. Four settlement gauges were installed to measure the settlement of the foundation, embankment fill and cut-off wall respectively. Movement hubs consisting of 2 in diameter galvanized pipe 8 ft long were installed at 50 ft intervals primarily along the upstream edge of the crest to monitor dam displacement and settlement as a result of reservoir operation and embankment weight.

Upon first filling of the reservoir, when erratic drops in head were observed in the foundation piezometers and seepage was reported at the downstream toe, additional piezometers and seepage measuring weirs were installed downstream of the dam. In 1984 as part of the dam safety evaluation, an inclinometer was installed in the north abutment to monitor potential downdip displacement of the rock above the powerhouse.

#### DAM PERFORMANCE

Seepage - As indicated by flow measurements from Weir 1, located between the downstream toe of the dam and the tailrace (Figure 1), the variation of seepage flows with reservoir elevation since first filling of the reservoir is reasonably consistent indicating no major increase in seepage with time. However, since a significant portion of the total dam and foundation seepage is flowing through the river bed alluvium under the weir, it is possible that reasonably large variations in total seepage may occur before a change in Weir 1 flows is observed. Maximum seepage flows as determined from stream gauge measurements taken in the river channel downstream of the powerhouse when the tunnel headgate is closed have reached 28 cfs (Figure 6) whereas the peak flows recorded at Weir 1 have been about 3.5 cfs. The flow values for different reservoir levels given on Figure 6 represent stream gauge readings taken at least 8 hr after headgate closure to minimize the effect of riverbed and abutment storage outflow at lower river levels. However, outflow from riverbed and abutment storage is a significant component of the measured flows as indicated by the 1981 reading taken 21 days after gate closure.

Since the stream gauging station is approximately 0.5 mi downstream of the powerhouse, it was recognized that the measured seepage flows at this location included not only seepage through the dam and foundation but also headgate leakage as well as seepage through the abutments. To increase confidence in the measured values an estimate of seepage through the cut-off wall, i.e. through construction joints, cracks, etc., was made utilizing measured piezometric levels in the alluvium downstream of the wall, permeability values from pump tests and, since the bedrock channel below the riverbed narrows in the tailrace to about 1/2 the width of that at the cut-off, an average area of flow equal to 75% of the cut-off wall area below the river bed. The calculated seepage flow through the wall was thus estimated to be between 8 cfs and 13 cfs when the reservoir is at full supply level (FSL). To this was added leakage past the headgate, estimated at 7 cfs based on depth of water in the tunnel and the velocity of a floating wood chip observed during a tunnel inspection in 1984. An assessment of abutment leakage was more difficult to perform in view of the conflicting evidence available. The steep faces of the canyon walls downstream of the dam are visibly jointed and faulted but exhibit insignificant seepage above the

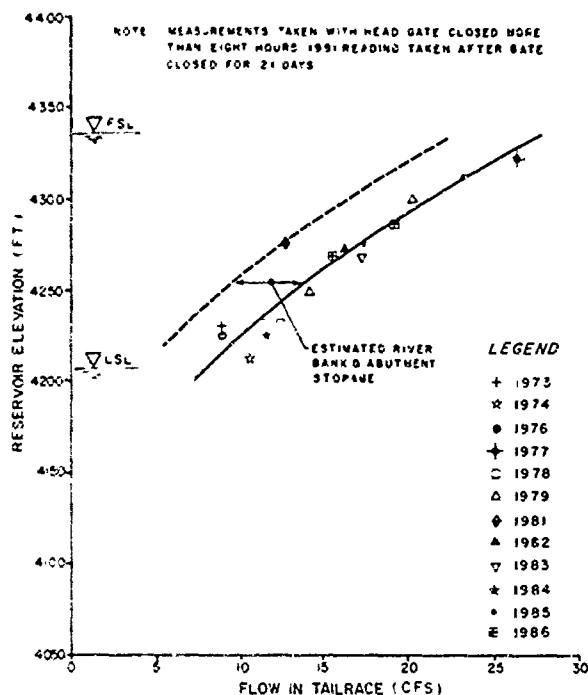


Fig. 6 Variation in seepage with reservoir level

river bed. Leakage from the diversion tunnel outlet in the north abutment rarely exceeds 0.5 cfs and piezometric heads within the left abutment rock remain well below FSL and are not significantly affected by changing reservoir levels. However, water losses were reported in a number of abutment drill holes and one hole required about 29 ft<sup>3</sup> of grout, bran, plaster of paris, calcium chloride and bentonite to seal the hole over a 100 ft interval. Allowing for random jointing, the total seepage through both abutments could be 2 to 3 times the quantity determined for intact strata and may be in the order of 6 cfs. Likewise an estimate of the leakage through bedrock below the cut-off contact was difficult to assess but, based on insitu pump tests, should be no greater than 1 cfs. It was concluded that the total calculated seepage from all sources when the generating units are not operating, the headgates are closed and the reservoir is at FSL was within the range of 18 to 27 cfs, which is comparable to measured flows in the tailrace after deducting the riverbed and abutment storage component.

**Piezometric Records** - Only five standpipe piezometers upstream of the cut-off have remained operational since 1972 to monitor piezometric heads in the river bed alluvium. Of these P25 is located 30 ft upstream of the wall and the tip is set approximately 60 ft below the original river bed (Figure 7). The other four, P45 through P48 inclusive, are collared on a berm on the upstream slope about 135 ft from the cut-off wall and are set just below the contact between the dam fill and the native gravels.

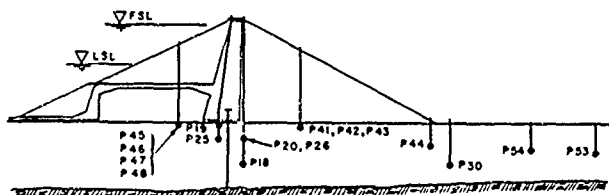


Fig. 7 Relative locations of foundation piezometers

Downstream of the cut-off eleven piezometers set in the alluvium are still functioning. Readings from P26, set closest to the wall and at about the same depth as P25, have been used, in conjunction with P25 readings, as an indication of the head drop across the cut-off.

As the reservoir was being filled in 1972, piezometric levels upstream of the concrete cut-off initially rose as expected in response to the rising reservoir level. When the reservoir reached a height about 150 ft above the river bed, however, P25 readings showed a sudden drop of 9 ft while P26 heads downstream of the cut-off rose about 3 ft. An additional drop of 15 ft in P25 and simultaneous increase of 4 ft in P26 occurred when the reservoir rose to 210 ft. At the same time, excessive seepage and sand boils were observed at the downstream toe of the embankment. The sudden drops in differential head were attributed at the time to "blow-outs" of the bentonite cake deposited in construction joints or other defects in the wall due to the high gradients across the wall. As a result of these observations and in accordance with the recommendations of the specialist consultants, a filter and buttressing berm 50 ft wide and 10 ft high was constructed along the downstream toe to enhance stability. Additional piezometers and a weir were installed adjacent to the downstream toe and a program of regular monitoring of all piezometers and seepage measuring facilities was instituted.

Over the years the piezometric levels in the alluvium immediately upstream of the cut-off gradually decreased until about 1982 when steady-state conditions were reached (Figure 8). Readings from piezometer P19,

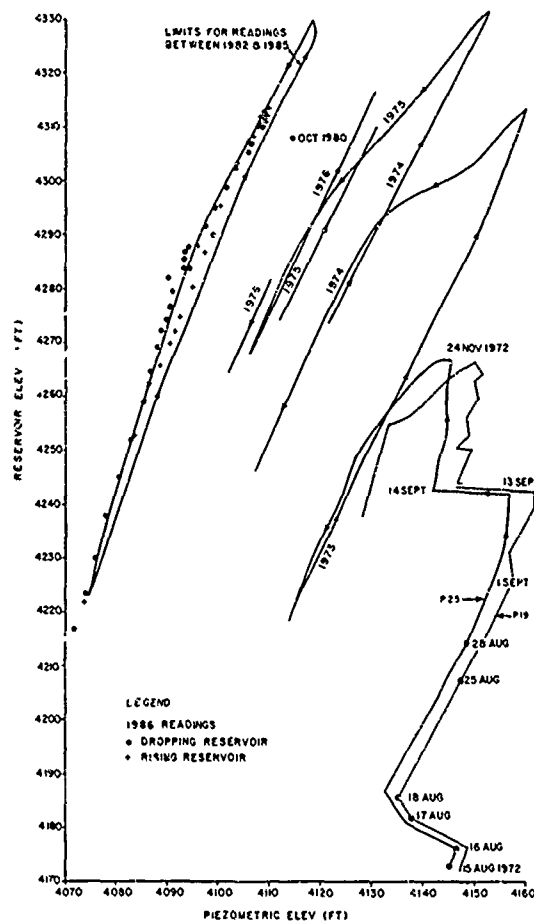


Fig. 8 Piezometric heads in P19 and P25

located about 30 ft upstream of the cut-off near the top of the river sediments about 100 ft south of P25, showed an almost identical variation in piezometric elevation as P25 until it became unserviceable in 1976. The records of these piezometers in the first few years of reservoir operation appear to confirm an abrupt and not insignificant reduction in the effectiveness of the concrete cut-off, resulting from either leaky construction joints in the panel wall, inadequate sealing of the wall at the bedrock contact or other imperfections in the concrete of unknown character.

Since about 1982, however, P25 readings have varied monotonously with reservoir level. This phenomenon is considered to be the result of either stabilized seepage conditions in the alluvium adjacent to wall apertures, or an increase in reservoir sedimentation or a combination of both effects. Records from piezometers P45, P46, P47 and P48, 100 ft farther upstream, are not particularly useful in explaining the current steady-state conditions across the wall. P46 readings indicate an hydraulic connection exists between this piezometer and P25, whereas piezometric levels in P45, P47 and P48 have remained relatively constant over the years (Figure 9). The linear relationship between P25 and P46 is not surprising as these piezometers appear from preconstruction river valley contours to lie in the main river channel. P45, P47 and P48, on the other hand, are located in the flood plain on either side of the main channel where less pervious sediments could be expected as a result of lensing and beaching effects.

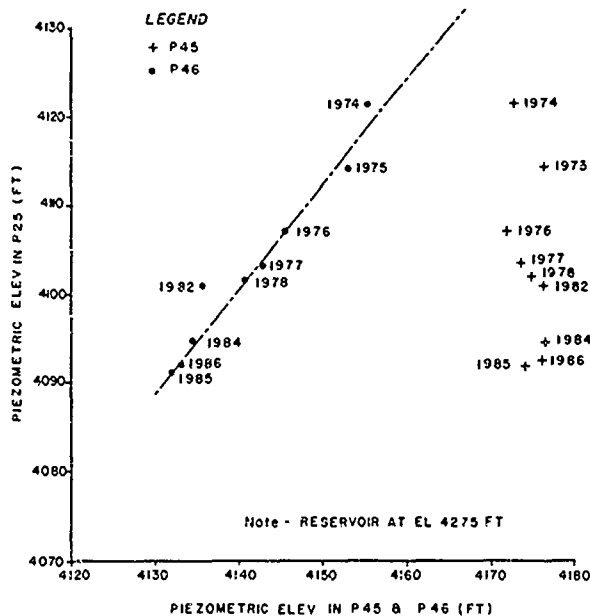


Fig. 9 Hydraulic connection between P46 and P25

An indication of the performance of the cut-off wall is illustrated on Figure 10. Except for erratic variations during the first few months following reservoir filling, the head drop across the wall has declined at a decreasing rate over the years until the early 1980's when conditions more or less stabilized (Figure 10a), varying only with reservoir elevation (Figure 10b). Downstream of the cut-off wall, the piezometric profile through the bottom of the chimney drain and underlying alluvium (Figure 11) indicates that hydrostatic conditions with heads 25 to 30 ft. higher than the tailrace level have prevailed in the alluvium since 1973. However, pneumatic piezometer G32, located in the chimney drain, denotes pressures in excess of hydrostatic suggesting the native sands and gravels are more pervious and acting as an

underdrain. Piezometers downstream of P26 exhibit an average gradient over a distance of approximately 1300 feet between the cut-off and the tailrace channel of about 0.02, a value which has decreased only marginally since reservoir filling.

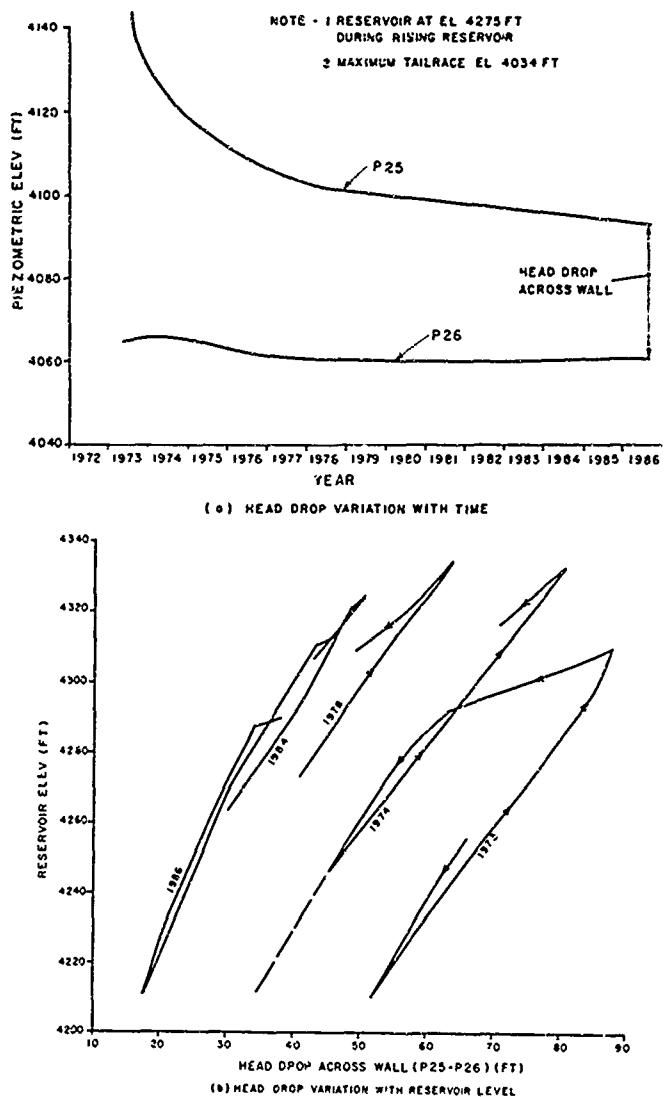


Fig. 10 Head drop across the cut-off

During initial reservoir filling, the impervious core of the main dam was not fully saturated and water from the pervious upstream shell and the foundation gradually seeped into the core as well as the common fill below the impervious blanket establishing a steady-state phreatic surface. Subsequent pressure reductions in the river gravel has allowed the foundation alluvium to act as an underdrain for the blanket and the impervious core (Figure 12). The hysteresis effects exhibited by pneumatic piezometer G37 also indicate the common fill under the upstream blanket is relatively impervious and the blanket is working satisfactorily (Figure 13).

**Displacements** - A survey carried out in 1984 on monuments installed along the dam crest indicated negligible downstream movement and a maximum settlement of 3.6 in. The crest profile remains from 6 to 12 in above design grade.

Settlement of the top of the cut-off wall, monitored with a settlement gauge installed during embankment construc-



tion, was reported to be 1.93 in at the end of construction (Gordon and Rutledge, 1972), with negligible settlement subsequently.

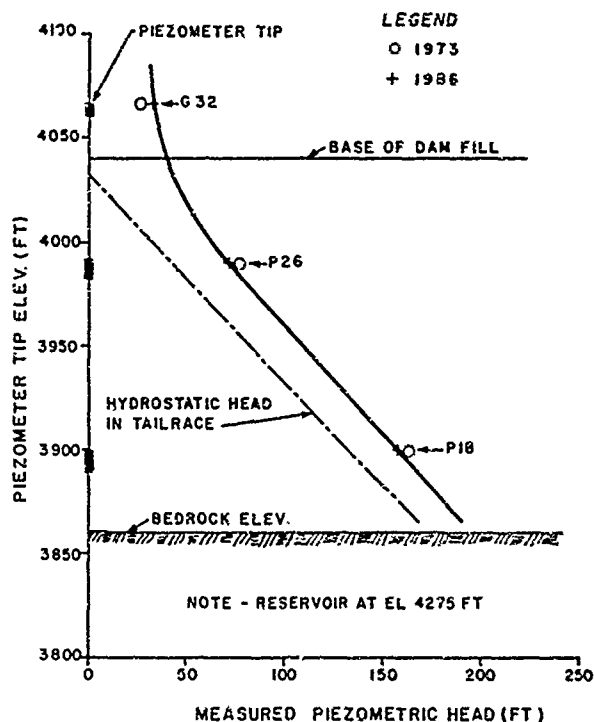


Fig. 11 Piezometric profile through alluvium downstream of cut-off

#### RESERVOIR SILTATION

To determine the extent of tightening of the lake bed upstream of the dam by siltation and thus ascertain whether the observed drop in piezometric heads in the alluvium upstream of the cut-off could result from reservoir siltation, an underwater survey was carried out by divers in the spring of 1986 at six locations in the reservoir below low supply level (LSL). The survey indicated that the accumulation of silt on the reservoir floor varied from 8 to 14 in with an average of about 12 in in the active reservoir area.

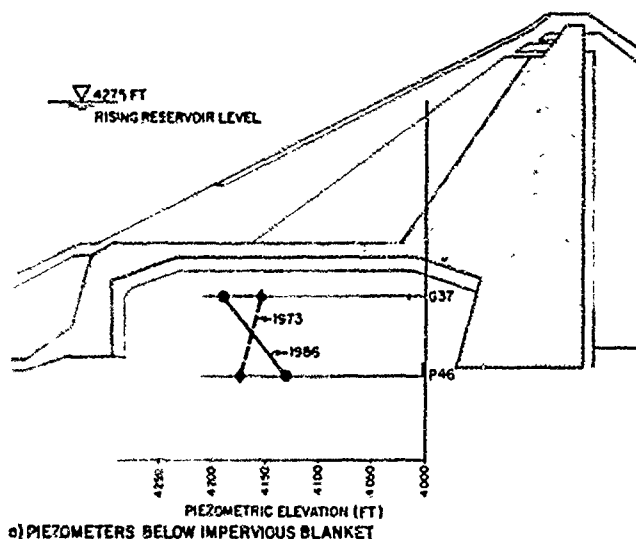
A rough estimate of the head loss through the silt blanket was made using D'Arcy's law as follows:

$$Q = kAi = kAh/t \quad (1)$$

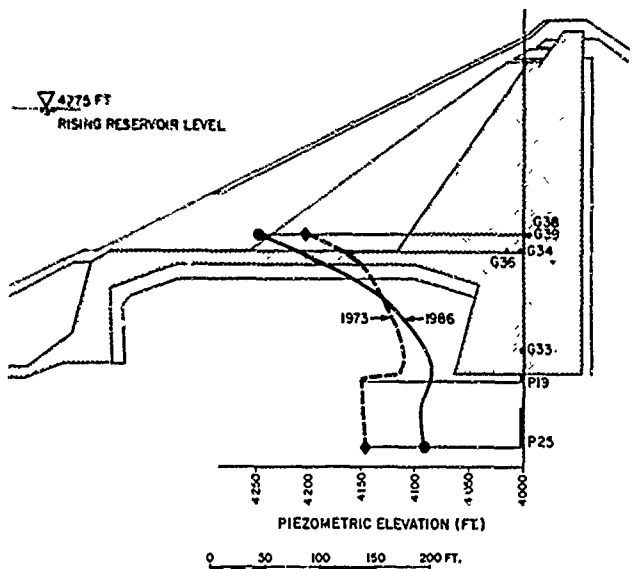
where:  $Q$  = Quantity of seepage through the silt  
 $k$  = Permeability coefficient for silt  
 $A$  = Effective area of silt blanket contributing to seepage  
 $i$  = Hydraulic gradient  
 $h$  = Head drop across silt  
 $t$  = Silt thickness

Assuming as a first approximation that the seepage through the alluvium and thus the silt layer varies as previously estimated from 8 to 13 cfs or about 10 cfs on average, the area of reservoir floor effectively contributing to seepage is, say, 1000 ft long by 400 ft wide, the permeability coefficient for the clayey silt is about  $5 \times 10^{-5}$  ft/min, and that the silt layer has a uniform thickness of 1 ft, the calculated head loss from Equation 1 is estimated to be about 30 ft when the reservoir is close to FSL. Although not a precise

analysis, the calculated head loss demonstrates the potential of reservoir siltation for reducing piezometric heads in the pervious foundation. Whether, in fact, the actual head reductions observed are due primarily to siltation, to an imperfect cut-off, or to a combination of both effects, is not certain. Nevertheless, it is considered that the silt deposition to date has been instrumental in stabilizing seepage losses through the foundation alluvium and compensating for some leakage through the concrete cut-off wall.



a) PIEZOMETERS BELOW IMPERVIOUS BLANKET



b) PIEZOMETERS IN DAM CORE

Fig. 12 Piezometric profile in embankment upstream of cut-off

#### TUNNEL PERFORMANCE

Periodic inspections of the tunnel when it is unwatered for routine plant maintenance indicate the steel lined section is in good condition. On the other hand some cracking of the concrete lining has occurred near the foot of the inclined section leading down from the head-gate. Three cracks, located in the 10 o'clock, noon and 2 o'clock positions, have been observed extending downstream for a distance of 120 ft. The maximum crack width was about 3/16 in. Measurements with a lead scribe installed across one of these cracks in 1986 indicate

that the annual variations in tunnel pressure (170 to 300 ft head change) and water temperature (range 32° to 55°F) are sufficient to cause the crack aperture to open and close by about 1/8 in from that observed when the tunnel is unwatered, giving a total movement of 1/4 in.

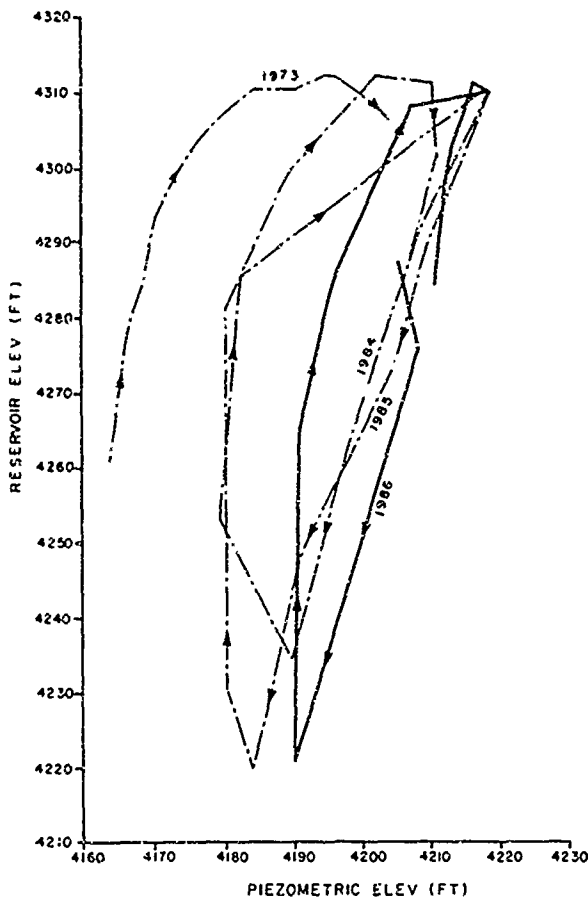


Fig. 13 Hysteresis effects in G37

Discharge from the tunnel drainage system when the tunnel is pressurized and the reservoir is at FSL is approximately 1800 Imperial gallons per minute. The discharge reduces to zero when the tunnel is drained signifying minor storage in the surrounding rock. In addition there appears to be no hydraulic connection between the tunnel drainage system and the river bed alluvium through faults and joints in the abutment rock. When the tunnel was unwatered in late 1972, the pressure head in the rock surrounding the tunnel dropped about 90 ft to Elev. 4095 ft as recorded in nearby piezometer P10 (Figure 14) whereas the piezometric heads in the river gravels remained within the range of Elev. 4148 (P19) to Elev. 4168 (P46).

#### DAM SAFETY EVALUATION

The safety evaluation of Bighorn dam was carried out in 1984 as part of a staged evaluation program for thirteen different projects comprising the hydroelectric generating system owned and operated by TransAlta Utilities Corp. (Wade et al, 1985). The evaluation was conducted in accordance with the Dam and Canal Safety Guidelines established by the Government of Alberta (1979). The guidelines designate, for new and existing dams, design floods ranging from full PMF for high hazard structures to 1 in 100 year floods for small storage

ponds. These guidelines are similar to those adopted by other regulatory agencies such as the U.S. Corps of Engineers (1979) and the British Institution of Civil Engineers (1978). Present day river basin use and the more stringent safety requirements have resulted in a situation where many existing dams and spillways no longer exhibit acceptable factors of safety when considering the PMF design requirements.

The safety evaluation procedures used at Bighorn consisted of the following (Monenno, 1986):

**Review Existing Data** - The object of the file search was to obtain the original information on construction materials, geological assessment of foundations, design calculations and notes, drawings and reports that were developed during construction. These records were then reviewed together with a summary of the maintenance history.

**Inspect Site** - Site inspections were carried out systematically using prepared check lists with emphasis on problems or specific areas of concern as established through the file search and discussion with owner's staff. Surveys and measurements were undertaken to obtain structural dimensions and verify information on the construction drawings.

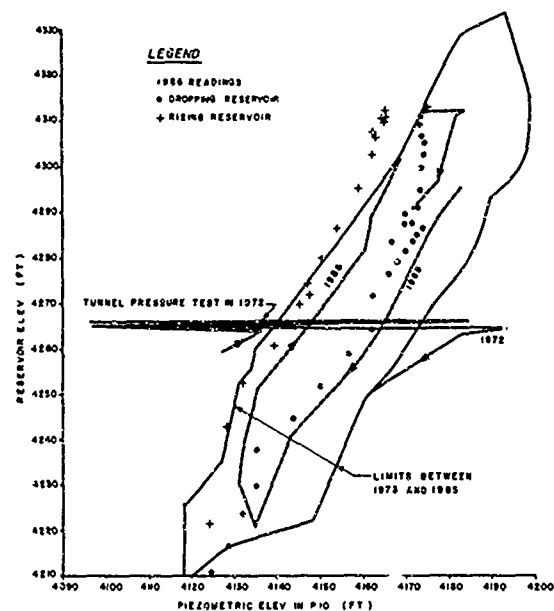


Fig. 14 Piezometric heads in north abutment

**Exploratory Drilling and Monitoring Installations** - The terms of reference established by the Safety Guidelines require that geotechnical properties and condition of embankment and foundation be verified by testing and instrumentation unless sufficient data exist to support the chosen parameters. Since considerable geotechnical information in the form of studies, reports, foundation investigations and construction records was available on file, drilling was limited to one hole in the north abutment for inclinometer installation and recovery of rock cores for strength testing. The objective in monitoring is to detect both gradual and rapid change of condition so that appropriate preventative action may be taken. Through the process of check lists, site inspections and evaluation of instrumentation records, long term performance was assessed. Leakage flows and piezometric levels, when plotted against corresponding reservoir levels, gave a good indication of the health of the dam.

Hydrology and Hydraulics Studies - Analyses of the river basin hydrology included a review of the reservoir operating criteria and available stream-flow records. Hazard potential for the project was assessed by carrying out routing studies for various floods up to the probable maximum flood (PMF) and by evaluating flood action plans.

Hydraulic studies were then made in conjunction with flood routing analyses to determine the capacity of the existing spillway structures. Using the spillway discharge rating curve, the head-discharge-load relationship for the turbines and the established operating procedures, it was found that the reservoir retaining structures would not be overtopped during the PMF.

Geotechnical and Structural Analyses - Stability analyses were carried out on each major structure considering records of seepage flows, piezometric and uplift pressures, geotechnical strength parameters and updated hydrologic criteria. Finally, an evaluation was made of the structural integrity of all concrete structures, including spillway gates, hoists and stoplogs to ensure each was sound and in satisfactory working condition.

Report - A dam safety evaluation report was prepared for the project that itemized the deficiencies found, recommended modifications or remedial work, revised operational practices, additional monitoring requirements and the frequency of future inspections. To ensure continued safety against unexpected failure and provide an early warning of deteriorating conditions in the future, critical monitoring procedures were outlined and "alarm" criteria established for piezometer levels and seepage flows.

#### CONCLUSIONS

As a result of the annual reviews of the piezometric and seepage data and the 1984 dam safety evaluation, it was concluded that the performance of the main dam and concrete cut-off-wall is satisfactory. Because of the magnitude of the seepage flows, however, it was recommended that readings of all monitoring installations be continued on a regular basis, that routine inspections of the facility be carried out by plant operating staff to ensure early detection of potential distress, and that a thorough inspection by professional engineers experienced in the design, construction and performance of earthfill and concrete dams be conducted every five years.

#### ACKNOWLEDGEMENTS

The authors would like to thank TransAlta Utilities Corporation, owner of the project, for permission to publish this paper. They also acknowledge and appreciate the critique of the draft paper provided by Mr. J.K. Sexton, Member of the Bighorn Review Board.

#### REFERENCES

- Forbes, D.J., J.L. Gordon and S.E. Rutledge (1973), "Concrete Diaphragm Wall, Bighorn Dam", Proc. ICOLD Conference, Madrid.
- Gordon, J.L. and S.E. Rutledge (1972), "The Bighorn Power Project", Engineering Journal, Vol. 55, Oct.
- Government of Alberta (1979) "Dam and Canal Safety Guidelines", Alberta Dept. of Environment, Dam Safety Branch, Pubi. No. D.S.3.
- Institution of Civil Engineers (1978), "Floods and Reservoir Safety - an Engineering Guide", Institution of Civil Engineers, London.
- Monenco (1986), "Dam Safety Evaluation for Bighorn Development", Report prepared for TransAlta Utilities Corp. by Monenco Consultants Ltd.
- U.S. Corps of Engineers (1979), "Engineering and Design, National Program for Inspection of Non-Federal Dams", Dept. of the Army, Office of the Chief of Engineers, Washington, D.C.
- Wade, N.H., L.R. Courage and M. Pildysh (1985), "Dam Safety Evaluation on a Number of Canadian Dams", Proc. ICOLD Conference, Lausanne, Switzerland.

# An Undrained Failure in the Foundation of an Earth Dam

K.B. Agarwal

Professor of Civil Engineering, University of Roorkee, Roorkee, India

**SYNOPSIS :** A short term slip occurred while excavating the foundation trench for an earth dam at Wraysbury in U.K. The slip took place three days after opening of the excavation. The clay present at the site was the Blue London Clay. The geometry of the slip surface was noted. When the slip was analysed taking conventionally accepted undrained strength of 38 mm x 76 mm. Triaxial samples, the factor of safety worked out to be much greater than one showing no failure condition.

Different factors and analyses responsible for reducing the undrained strength for factor of safety of 1.0 have been studied in this paper. It is found that the major role has been played by size of the sample, the anisotropy of undrained strength and the assumptions involved in stability analysis.

## INTRODUCTION

When a saturated non-fissured clay is brought to state of failure under condition of no water content change, it exhibits an angle of shearing resistance (with respect to applied total stresses) equal to zero. This fact forms the basis of the  $\phi = 0$  analysis of stability, when the most critical condition occurs immediately after the construction before the clay has had the opportunity to dissipate pore water pressure or to change its water content. Skempton and Sowa (1963) showed that the undrained strength of saturated clay is independent of the changes in total stresses acting on the clay provided the water content remains constant.

An earth dam was to be constructed in the estuary of river Thames at Wraysbury which is about 40 to 50 kms from London in U.K. When foundation trench for the construction of the earthdam was excavated, a slip occurred in the trench three days after opening of the excavation. The geometry of the slip surface was precisely surveyed and noted. An undisturbed Block sample of the clay was also taken from the site with the actual slip surface at about mid height in the sample, alongwith other undisturbed samples.

A large number of undrained shear tests were run on the clay both in the field and in the laboratory. The Blue London Clay is typically a highly over consolidated marine clay deposited before about 4000 years. It is a stiff clay which has microcracks developed called, the fissures. Fissures act as stress concentrators and tend to reduce the undrained strength. A general description of the clay and a discussion of the geological history are given elsewhere (Cooling & Skempton, 1942 & Glossop, 1948).

## EXCAVATIONS AND STRATA DESCRIPTION

Excavations were made so as to make a composite

slope with side slope of nearly 1:1 in gravel and 1 horiz : 2.2 Vert. in London Clay with a berm of about 2.13 m. As shown in Fig. 1, the upper strata is 6.06 m thick of gravel ( $\gamma = 2.083 \text{ Ton/m}^3$ ). Below this layer of gravel there is saturated clay ( $\gamma = 1.923 \text{ Ton/m}^3$ ) of sufficient depth to check the stability of the slope. The maximum depth of excavation in clay was 3.02 m.

## UNDRAINED SLIP

The short term slip occurred at chainage of 3684.9 m. The slip took place three days after opening of the complete excavation. The approximate shape of the slip has been shown in Fig. 1. The undrained strength mobilised along the slip surface was found by taking unit weights of gravel and clay as  $2.083 \text{ t/m}^3$  and  $1.923 \text{ t/m}^3$  respectively. The undrained strength mobilised in clay was  $3.082 \text{ t/m}^2$  without considering the strength of gravel. If the strength of gravel is considered, the mobilised strength in the clay would have been lower. The average water content of the mass of soil along slip surface in clay was 29.3 percent.

## UNDRAINED STRENGTH OF CLAY

One undisturbed block sample of clay with the slip surface at mid height was taken from the site. Two undisturbed samples of size 6 cm x 6 cm were prepared for direct shear box test with the slip surface at about mid height. The undrained shear tests were run on these samples causing shearing along the slip surface in the tests. The stress displacement curves are given in Fig. 2. The results of the tests are given in Table 1.

As can be seen from the Table, the average water content of the samples tested in the

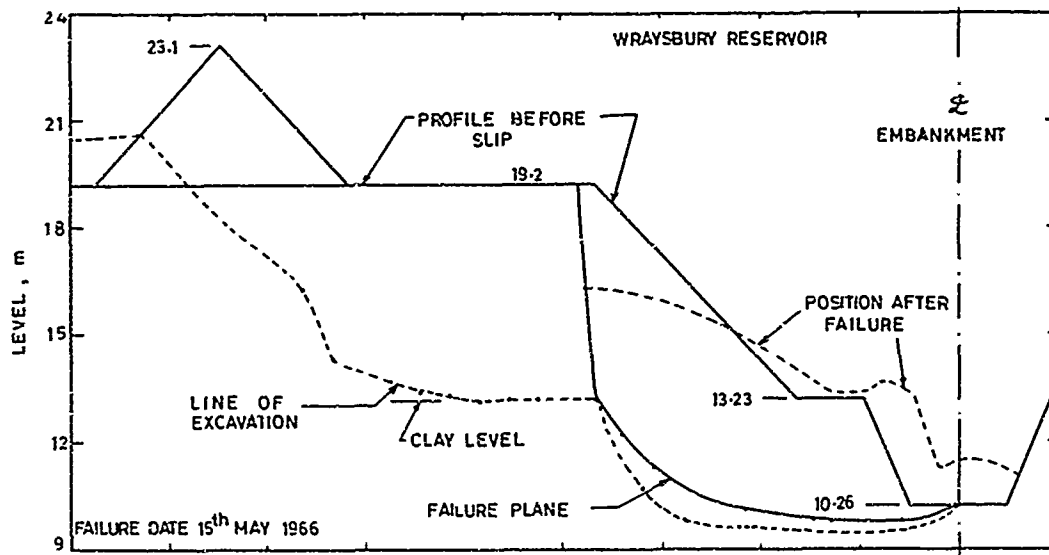


FIG. 1 - CROSS SECTION OF THE SLIP FAILURE AT 2 CHAINAGE 3684.9 m

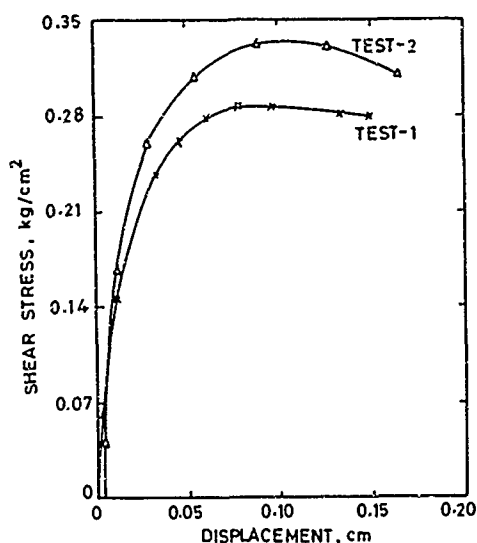
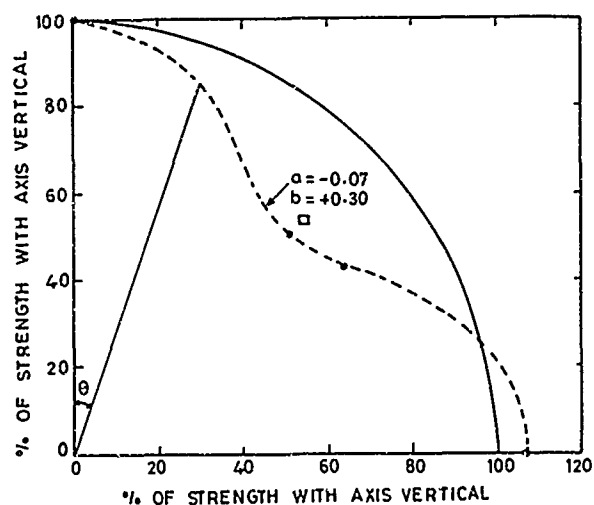


FIG. 2 - USB TESTS 6cm x 6cm SAMPLES WITH SHEARING ALONG FIELD SLIP SURFACE



FIG. 3 - ORIENTATION OF RUPTURE SURFACE



- U.U. TESTS 36x76 SAMPLES (BLOCK) (mm)
- U.U. TESTS 300x600 SAMPLES (BLOCK) (mm)

$$C_u = C_{u_{vrt.}} \times (1 - a \sin^2 \theta) (1 - b \sin^2 2\theta)$$

FITTED AT 0°, 45°, 90°

θ DENOTES INCLINATION OF MAJOR PRINCIPAL STRESS WITH RESPECT TO VERTICAL AXIS

FIG. 4 - POLAR DIAGRAM SHOWING VARIATION OF UNDRAINED STRENGTH WITH DIRECTION OF APPLIED STRESS

TABLE 1

| Test No. | Location      | W %  | $C_u$<br>$t/m^2$ | $t_f$<br>(min) | Displacement<br>(at failure)<br>(cm) |
|----------|---------------|------|------------------|----------------|--------------------------------------|
| 1.       | Block on slip | 30.9 | 2.874            | 3.5            | 0.08                                 |
| 2.       | Block on slip | 31.1 | 3.339            | 4.0            | 0.09                                 |
| Average  |               | 31.0 | 3.107            |                | 0.085                                |

laboratory was 1.7 percent higher than that in the field. This must be due to the fact that block sample was taken about 3 to 10 days after occurrence of the slip and there is a possibility that water must have migrated to the slip zone after failure.

Shear tests were also run on undisturbed samples of clay obtained by Block sampling or by U.4. tube from the site. A few 600mm x 600mm field shear box tests were also done at site. The triaxial shear tests were done on undisturbed block samples both on bigger sizes and conventional sizes i.e. 300mm x 600mm; 150mm x 300mm; 100mm x 200mm and 38mm x 76mm.

The results of the tests on different sized samples together with the strength mobilised in the slip are all summarised in Table 2.

the laboratory shear box samples with the shearing along the field slip surface was 8% higher than the mobilised strength.

#### ORIENTATION AND ANISOTROPY

In all  $\phi = 0$  analysis for short term loading, the undrained strength of the clay, except for the effects of sampling disturbance, generally seems to have been considered unique irrespective of the type of test (triaxial, vane or simple shear test) used to measure it and irrespective of the inclination or orientation of the slip surface implied in the problem.

In nature most soils are probably somewhat anisotropic, due to orientation and or sagrigation of particles during deposition and due to orientation arising from its subsequent stress history. Consequently the shear strength of some soils will vary with the direction of the failure surface. For instance consider a slope as giving in Fig. 3. AB is the potential surface of rupture, along which the failure of the slope is incipient. As can be seen from the figure, the orientation of the failure plane (sliding surface) is different at every point. If the angle between the failure plane and the plane on which major principal stress acted in the past (the horizontal plane) is called ' $\alpha$ ', then it can be seen from the figure that ' $\alpha$ ' varies from about  $56^\circ$  (assumed for London Clay) for a vertical sample to about  $-34^\circ$  for a horizontal sample. The undrained strength may

TABLE 2

| Test                         | W %  | $t_f$<br>min | Average $C_u$<br>$t/m^2$ | $C_u$ Corr.<br>w = 28%<br>$t/m^2$ | $C_u$ Corr.<br>w = 28% &<br>$t_f = 4000$ min<br>$t/m^2$ | Ratio w.r.t.<br>$C_u$ on slip |
|------------------------------|------|--------------|--------------------------|-----------------------------------|---|-------------------------------|
| Slip                         | 29.3 | 4000         | 3.092                    | 3.620                             | 3.620   | 1.00                          |
| 600mm x 600mm<br>Shear Box   | 28.1 | 71           | 4.907                    | 4.990                             | 4.500   | 1.24                          |
| 300mm x 600mm<br>TXL (Block) | 28.2 | 63           | 4.990                    | 5.185                             | 4.672   | 1.29                          |
| 38mm x 76mm<br>Block TXL     | 28.1 | 7            | 11.878                   | 11.985                            | 10.322  | 2.85                          |
| 38mm x 76mm<br>U.4. Tube     | 26.8 | 8            | 9.686                    | 8.267                             | 7.093   | 1.96                          |

All the undrained strength were corrected to a moisture content of 28 percent. The time for slip to occur was taken as 4000 minutes and hence the undrained strengths were further corrected to a time to failure of 4000 min. on the basis of La Rochellis work (1960). As can be seen from Table 2, the average undrained strengths from 300mm x 600mm vertical samples and 600mm x 600mm field shear box tests were 1.29 and 1.24 times the strength mobilised along the slip surface. The 38mm x 76mm samples from blocks and U.4 tubes measured 2.85 and 1.96 times the mobilised strength which shows that the conventional factor of safety of 1.5 on conventional undrained test results is rather inadequate. The measured strength on

be different at different points due to rotation of principal stresses and due to anisotropic structure and subsequent stress history of the soil.

The influence of orientation on undrained strength for the Blue London Clay from Wraybury was studied by taking the triaxial samples using undrained block sampling. The samples tested were 38mm x 76mm cut from block sample their axis vertical, horizontal and inclined at  $45^\circ$  and  $56^\circ$  to vertical. The tests were also done of 300mm x 600mm samples with their axis vertical and inclined at  $45^\circ$  to vertical.

The influence of orientation on undrained strength is studied by drawing a Polar diagram of strengths in terms of percentage of strength of vertical samples as shown in Fig. 4. which is given by the relation.

$$C_u = C_{u(vert)} (1 - a \sin^2 \theta) (1 - b \sin^2 2\theta)$$

where  $\theta$  is the angle with the vertical,  $C_{u(vert)}$  is the undrained strength of vertical sample. The values of parameters 'a' and 'b' were found to be -0.07 and +0.3 respectively.

It can be seen from Fig. 1 that the most of the field slip surface in the clay was nearly horizontal. This means that the most of the strength mobilised should correspond to the strength measured on samples tested with their axis at  $45^\circ$  and  $56^\circ$  to the vertical. The undrained strength along the slip surface before failure may not be constant along the length of the slip surface but may be dependent upon the orientation and the length of the rupture surface at any particular orientation.

#### ANALYSIS OF WRAYSBURY SLIP

Considering the failure surface to be circular, many possible slip circles were analysed at different tangent levels. The maximum mobilised shear stress is  $3.278 \text{ t/m}^2$  when the circle is tangent at 7.8 m level line. Whereas along the actual failure surface the shear stress is  $3.082 \text{ t/m}^2$ . This shows that the critical rupture surface obtained by the method is different from the actual surface.

The actual rupture surface is analysed by different methods. Janbu's method (1954) of non-circular analysis gives the undrained strength of  $3.368 \text{ t/m}^2$  whereas Nonveiller's method gives  $3.261 \text{ t/m}^2$ . Block analysis gives  $3.167 \text{ t/m}^2$ . The analysis clearly shows that the minimum mobilised undrained strength in the clay is  $3.082 \text{ t/m}^2$  without considering the strength of gravel. If the strength of gravel is considered, the mobilised strength will be further lowered.

The measured undrained strength of  $38\text{mm} \times 76\text{mm}$  Block samples of clay is 2.85 times the mobilised strength i.e.  $8.784 \text{ t/m}^2$ . The Blue London Clay is a fissured clay and therefore  $38\text{mm} \times 76\text{mm}$  size of sample may not include the representative soil structure and matrix. The  $300\text{mm} \times 600\text{mm}$  size Triaxial block sample gave the undrained strength of  $3.975 \text{ t/m}^2$  showing that there is significant sample size effect. However consideration of only sample size effect does not reduce the value of undrained strength to strength mobilised. This shows that effect of orientation and anisotropy of undrained strength is also there.

Based on the assumption that the angle made by failure plane with respect to horizontal in the triaxial sample is  $56^\circ$ , irrespective of the orientation of the sample, the actual rupture surface, Fig. 1, can probably be divided into three sections approximately of length of about 10 to 15% - Section I, about 75 to 85% - Section II and about 0 to 5% of

total length of slip surface as Section III. As can be seen from Fig. 1., the vertical strength may be taken as effective for Section I, the average inclined strength along Section II and the horizontal strength along Section III. If the sections I, II and III are taken as 10%, 85% and 5% respectively, the average undrained strength mobilised along the slip surface can be worked out, using Fig. 4, as 78.7% of that of vertical samples tested in triaxial machine, due to effect of orientation. If this ratio is applied to the undrained strength of  $300\text{mm} \times 600\text{mm}$  vertical samples, the ratio of measured strength to that mobilised along the slip surface becomes of the order of 1.015, showing only 1.5% difference. This clearly shows that only when we consider the influence of sample size, orientation and anisotropy on undrained strength of London Clay, the mobilised strength becomes nearly equal to measured strength making the failure along the actual rupture surface at Wraysbury possible.

#### CONCLUSION

The mobilised strength along the slip surface at Wraysbury was found to be  $3.082 \text{ t/m}^2$  without taking strength of gravel into consideration.

If the effect of orientation is taken into account, the average undrained strength mobilised along slip is 78.7% of that of vertical samples. Considering the orientation effect, the ratio of undrained strength of  $38\text{mm} \times 76\text{mm}$  vertical samples from blocks with respect to mobilised strength becomes 2.24, but if this factor is applied to undrained strength of  $300\text{mm} \times 600\text{mm}$ . Triaxial block samples, the ratio becomes equal to 1.015. It can be concluded that Wraysbury slip can be analysed only if the effects of sample size and the anisotropy of undrained strength, both are considered together.

#### REFERENCES

- Bishop, A.W., (1966), "The Strength of Soils as Engineering Materials", 6th Rankine Lecture, Geotechnique 16, 89-130.
- Bishop, A.W. and Henkel, D.J., (1962), "The Measurement of Soil Properties in the Triaxial Test", 2nd. Ed. Arnold, London.
- Brooms, B.B. and Casbarian, A.O. (1965), "Effects of Rotation of the Principal Stress Axis and of the Intermediate Principal Stress on the Shear Strength", Proc. 6th Int. Conf. Soil Mech. Toronto, Canada.
- Cooling, L.F. and Skempton, A.W. (1942), "A Laboratory Study of London Clay", Journ. Inst. Civ. Eng. 17:251-76.
- Glossop, R. (1948), "The London Clay Part I field and Laboratory Technique", Silicates Industriels 13:792-98.
- JANBU (1954), "Application of Composite Slip Surface for Stability Analysis", European Conference of Stability of Earth Slopes, Discussion, Vol. III, Stockholm, 1954.

La Rochelle, P. (1960), "The Short Term Stability of Slopes in London Clay", Ph.D. Thesis, University of London.

Lo, K.Y. (1965), "Stability of Slopes in Anisotropic Soils", Journ. Sm. and F. Dn., A.S.C.E., 91:4:85-106.

NONVEILLER (1965), "Stability of Noncircular Slopes", Proceedings of 6 th International Conference on Soil Mechanics and Foundation Engineering, Vol. II, pp. 522.

Skempton, A.W. (1948), "A Study of Immediate Triaxial Test on Cohesive Soils", Proc. 2nd. Int. Conf. Soil Mech., 1:192-96.

Skempton, A.W. and Sowa, V.A. (1963), "The Behaviour of Saturated Clays during Sampling and Testing", Geotechnique, 13:269-90.

Skempton, A.W. and LaRochelle, P. (1965), "The Bradwell Slip : A Short Term Failure in London Clay", Geotechnique 15:3:221-42.

Taylor, D.W. (1948), "Fundamentals of Soil Mechanics", John Wiley, New York and London.

Terzaghi and Peck (1967), "Soil Mechanics in Engineering Practice", John Wiley and Sons, Inc., Publication., N.Y.



## Design and Performance of Arena Dam

James R. Schneider

Senior Geotechnical Engineer, CH2M HILL, Denver, Colorado, USA

Roger W. Lindquist

Senior Geotechnical Engineer, CH2M HILL, Corvallis, Oregon, USA

George K. Sammy

Civil Engineer, Trinidad Engineering & Research, Ltd., Curepe, Trinidad

Formerly Civil Engineer, Trintoplan Consultants, Ltd., Tacarigua, Trinidad

**SYNOPSIS:** Arena Dam is located in north-central Trinidad, West Indies. The dam forms a 35,000-acre-foot reservoir, which serves as the main raw water storage facility for Trinidad. The 1.6-million-cubic-yard earthfill embankment has a crest elevation 80 feet above the original streambed. The upstream-sloping core is composed of dispersive clay. The shells are composed of compacted fine sand and silty fine sand. The dam is founded on deep, stiff, fissured clay deposits interbedded with sand. The project is located approximately 12 miles from the El Pilar Fault, a major Caribbean fault with seismic activity comparable to that of the San Andreas Fault in the United States. Important design concerns included the dispersive clay core, residual strength properties of the foundation, embankment and control structure settlement, and the seismic environment. This paper discusses the design criteria and approach, and field performance data from foundation and embankment piezometers and survey monuments in the outlet conduit.

### INTRODUCTION

Arena Dam is located on the Arena River in north-central Trinidad. Figures 1 through 4 show the location, plan view, and sections of the dam. The dam forms Arena Reservoir, which provides 35,000 acre-feet of storage to augment the dry season flow of the Caroni River. Water from the Arena River is impounded during the wet season (January through June) for release during the dry season (July through December). The Arena River provides about 40 percent of the water needed to fill the reservoir; the remainder is obtained from the adjacent Tumpuna River. A weir located downstream of the confluence of the Arena and Tumpuna Rivers backs water up the Arena River channel to the dam toe. During the wet season, a pump station at the base of the dam pumps water through the outlet works and into the reservoir. During the dry season, water is released through the outlet works and flows down the Arena and Tumpuna Rivers to the Caroni River, from which it is withdrawn for treatment. This system allows year-round production of 75 million U.S. gallons per day of treated drinking water, about half of the island's supply. The dam was designed from 1973 to 1975 and constructed from 1977 to 1983 for the Water and Sewerage Authority of the Government of Trinidad and Tobago.

### PHYSIOGRAPHY AND GEOLOGY

The main physiographic features of Trinidad are three mountain ranges and two intervening basins. The Northern Range mountains are the largest mountains on the island. They are oriented east-west, and form the northernmost portion of the land mass. The Southern Range lies along the south coast of the island, and is also oriented east-west. The Central Range forms much of the central portion of the land mass, and is oriented generally west-southwest to east-northeast. The Caroni River Basin lies between the Northern and Central Ranges, and drains to the west. The Arena River rises in

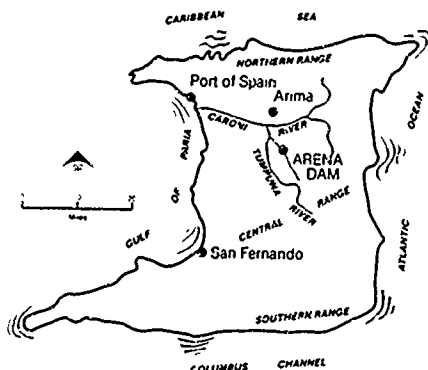


Fig. 1  
VICINITY MAP

the Central Range near the center of the island, and flows northerly to the Caroni River.

At the southern toe of the Northern Range, and 12 miles north of the dam, lies the El Pilar Fault Zone. This major fault is the contact between the South American tectonic plate from the Caribbean subplate. The fault turns northward to the east of Trinidad. To the west, it extends into northern Venezuela. From a seismicity standpoint, the El Pilar fault system is a major fault comparable to California's San Andreas Fault. Other regional faults are present, but none are as significant as the El Pilar Fault due to both its energy release potential and its proximity to the dam. A number of small faults in the vicinity of the dam are believed to have resulted from the same forces that created the major fault systems. Few earthquakes have occurred in Trinidad, based on over 300 years of historical data; seismic activity is centered in northern Venezuela, 55 to 95 miles west of the dam.

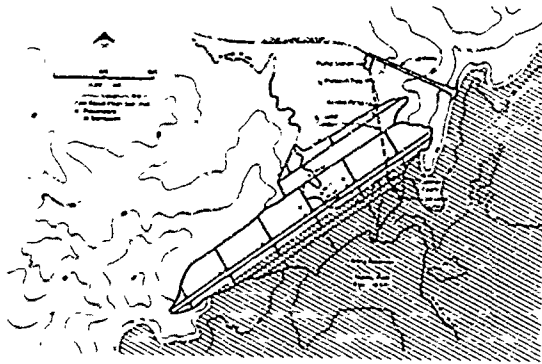


Fig. 2  
PLAN OF DAM

At the damsite, a flood plain approximately 800 feet wide lies at an elevation of approximately 73 feet above mean sea level. This flood plain is underlain by up to 50 feet of alluvium. Prior to dam construction, the Arena River flowed in a channel approximately 20 feet deep incised in the flood plain. The reservoir area consists of rolling hills with relief generally ranging from 150 to 200 feet.

The reservoir site is underlain by a thick sequence of poorly indurated sandstones and claystones, and by alluvium. The claystones, known geologically as the Upper Caparo Clay, consist of highly consolidated, stiff, fissured, fat clays. Based on the regional

geology and data from nearby oil wells, this clay is at least 800 feet thick at the dam. Approximately 2,400 feet of overlying material have been removed from the site by geologic forces.

#### SITE CONDITIONS

The Upper Caparo Clay contains frequent very thin sand partings; occasional thin layers of sand (up to 2 feet thick); interlayered sand, silt, and clay beds varying from a few inches to a few feet in thickness; and some varved sand/clay layers. Typical upper Caparo clay properties are given in Table 1. The recompression index was determined by conducting conventional consolidation tests with repeated loading and unloading at the stress levels expected to occur after dam construction. The average slope of the unloading and reloading curves was used as the recompression index. The plasticity characteristics of the clay are shown in Figure 5. The grain size distribution is shown in Figure 6.

The Upper Caparo Clay is typically highly plastic. Kaolinite predominates, followed by illite and montmorillonite. Measured clay mineral percentages (x-ray diffraction method) ranged from 40 to 65 percent for kaolinite, 19 to 34 percent for illite, and 16 to 28 percent for montmorillonite.

The alluvium consists of interbedded soft clays and loose sands up to 50 feet thick. Standard

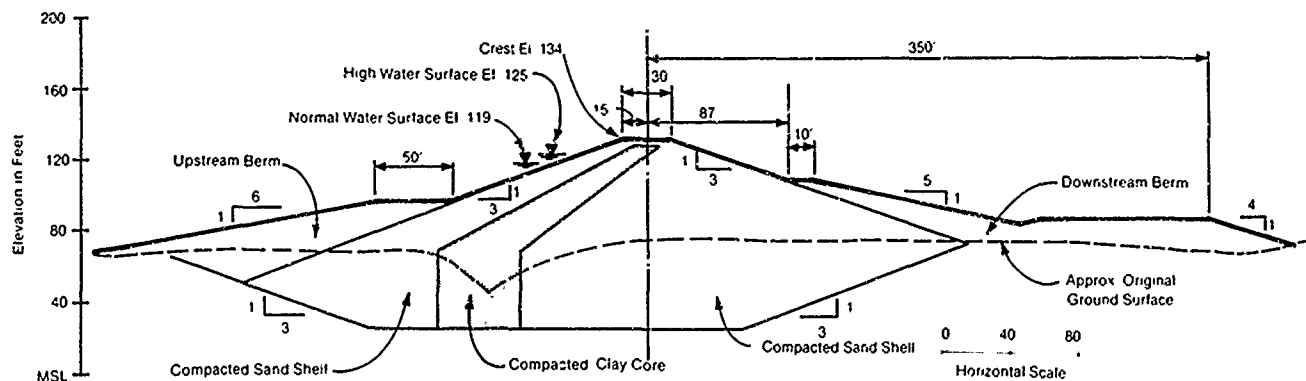


Fig. 3  
MAXIMUM DAM SECTION

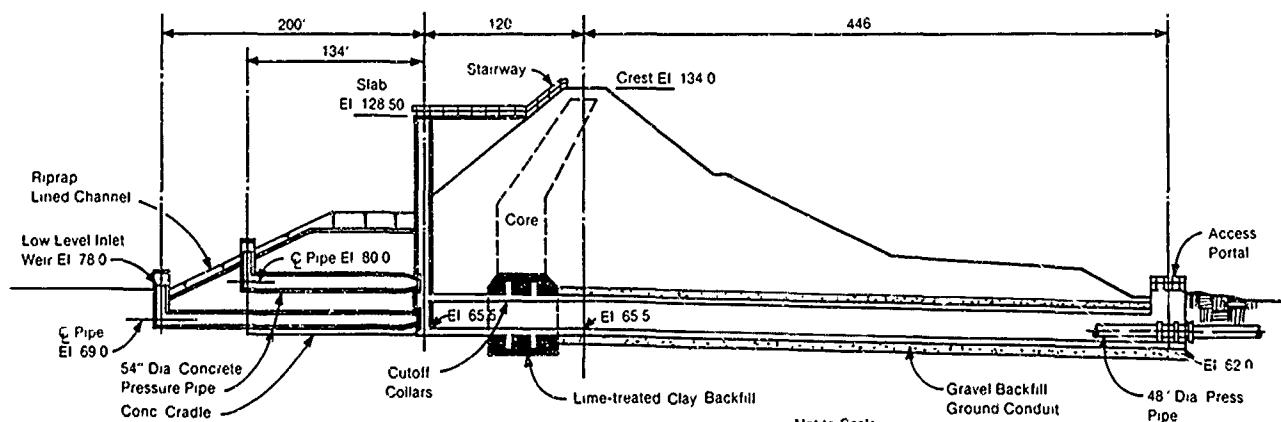


Fig. 4  
OUTLET CONDUIT PROFILE

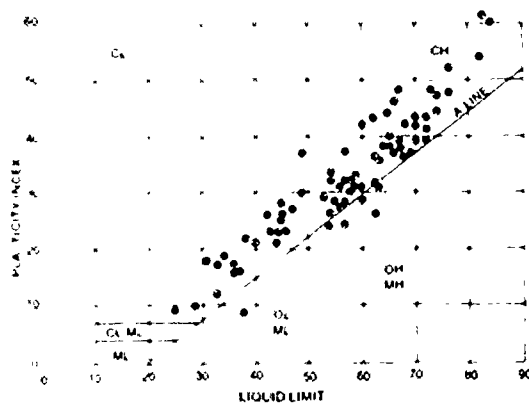


Fig. 5  
UPPER CAPARO CLAY PLASTICITY

TABLE 1. Typical Engineering Properties of the Upper Caparo Clay

| Parameter                  | Typical Values |
|----------------------------|----------------|
| Dry Unit Weight, pcf       | 85-110         |
| Moisture Content, percent  | 20-35          |
| Percent Passing #200 Sieve | 75-100         |
| In Situ Initial Void Ratio | 0.71-0.93      |
| Recompression Index        | 0.12           |

Penetration Test results in the alluvium ranged from 4 to 41. Most values were 20 or less; the higher values were generally associated with clayey sand lenses in the alluvium.

To the north of the damsite, the Mahaica or Arena Sand is exposed. This is a fine sand to fine silty sand. The grain size range is shown in Figure 6.

#### DESIGN PROPERTIES

Design properties were selected based on laboratory testing. The material properties chosen for design are presented in Table 2.

TABLE 2. Adopted Engineering Design Properties

| Material Type      | Total Unit Weight (pcf) | Effective Cohesion (psf) | Effective Friction Angle (degrees) |
|--------------------|-------------------------|--------------------------|------------------------------------|
| Remolded Borrow    | 120                     | 200                      | 19                                 |
| Upper Caparo Clay: |                         |                          |                                    |
| Peak strength      | 120                     | 850                      | 13                                 |
| Residual strength  | 120                     | 250                      | 7.5                                |
| In-situ Alluvium   | 120                     | 0                        | 23                                 |
| Arena Sand         | 125                     | 0                        | 28                                 |

#### MAJOR DESIGN CONCERNS

##### Seismicity

Because of the project's importance, its location upstream of major population centers, and its proximity to the El Pilar Fault Zone, a detailed study of the site's seismicity was undertaken by seismic consultants from the

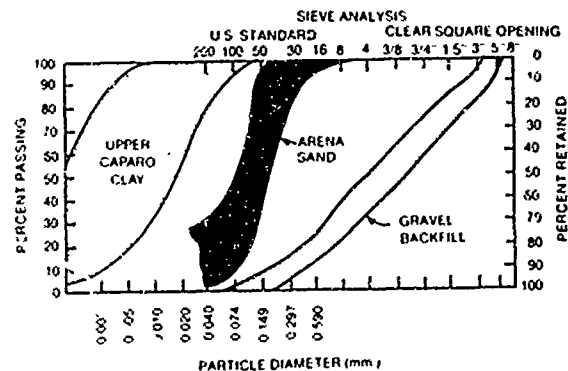


Fig. 6  
GRAIN SIZE DISTRIBUTIONS

University of the West Indies (Tomblin and Aspinall, 1973). The results of the seismicity study were used to develop three design earthquakes (Table 3). These three design earthquake levels were developed in the early 1970's, and differ from current practice.

TABLE 3. Design Earthquake Accelerations

| Acceleration Event | Hypocentral Distance (mi) | Maximum Horizontal (% of g) |
|--------------------|---------------------------|-----------------------------|
| MPE                | 94                        | 18                          |
| MRE                | 56                        | 60                          |
| MCE                | 12                        | 160                         |

The Maximum Probable Earthquake (MPE) was the greatest earthquake that was reasonably expected to occur during the project life. During the MPE, only minor damage would be tolerated, and all structures were designed to remain functional. Damages such as small cracks in concrete or minor surface slumps were considered to be acceptable.

The Maximum Credible Earthquake (MCE) was the greatest earthquake that could possibly be expected to occur if the greatest conceivable rupture were to occur at the closest possible location and at the shallowest possible depth, releasing the maximum conceivable amount of energy. This resulted in theoretical ground accelerations at the damsite that were so large that it was judged impractical to attempt to design a dam that could survive such an event.

Historic earthquakes had occurred 55 or more miles west of the damsite. Consequently, a third event, the Maximum Reasonable Earthquake (MRE) was defined as the earthquake that could be expected to occur if the greatest conceivable rupture were to occur 55 miles west of the site. The design goal for the MRE was to retain the reservoir, with the understanding that damage could occur at ancillary facilities such as the pump station or spillway.

##### Settlement

Foundation settlement calculations were made based on Terzaghi theory, except that the recompression index was used in place of the compression index. Stresses were assumed to be

distributed elastically in the foundation in accordance with the Boussinesq equations. The predicted total settlement was 6 to 8 feet at the centerline of the dam at its maximum section. This estimated settlement was reduced by a factor of two based on the observation of Terzaghi and Peck (1967) that Terzaghi consolidation theory overestimates settlement of highly preconsolidated soils by a factor of 2 to 5 or more. The resulting predicted consolidation settlement was 3 to 4 feet. Drainage conditions were complex beneath the dam, ranging from thin laminations of sand to widely spaced sand beds. It was estimated that approximately one-half of the consolidation settlement would occur during the dam construction period. Postconstruction foundation consolidation was thus estimated to be 1.5 to 2 feet. The embankment itself was expected to undergo 0.3 to 0.4 foot of postconstruction settlement based on the data collected by the U.S. Bureau of Reclamation and reported in Sherard et al. (1963). Thus, crest settlement of approximately 2 to 2.5 feet was anticipated after construction.

The same method was used at the outlet conduit. Settlement during embankment construction was included since the outlet conduit was constructed prior to the embankment. The maximum estimated settlement of the outlet conduit was approximately 3.5 feet at the dam centerline.

#### Base Spreading

Dam settlement was expected to cause spreading of the dam base, as described by Rutledge and Gould (1973). The principal concern was the outlet conduit. The maximum predicted extension was approximately 1/2 inch per 20 feet at the dam centerline. Predicted extensions decreased toward the dam toes. The outlet conduit had to be designed to tolerate this extension as well as the predicted settlement.

#### Dispersive Clay

During the dam design, dispersive clays were becoming widely recognized as a potential problem in dam design and construction (Sherard et al., 1972). Several of the preliminary identification tests (crumb test, SCS laboratory dispersion test, cation exchange capacity) were performed on samples of soil from the

dam area. When these tests suggested that dispersive clay could be present, a more definitive test (the pinhole test, as later described by Sherard et al., 1976) was performed on a variety of samples. The pinhole test results showed that most of the soils in the dam and reservoir area were dispersive. Thus, the design was required to provide defense against piping erosion of the dam and foundation materials.

#### Stiff, Fissured Clay Foundation

Laboratory testing of undisturbed and remolded specimens of the Upper Caparo Clay exhibited high peak strength at low strain followed by a rapid strength reduction until a constant value was reached. This suggested that residual strength analysis similar to that used in considering progressive failure (Bjerrum, 1967) should be used. Residual strengths were determined by slow direct shear tests and confirmed by a review of natural slopes.

Laboratory residual strength values were determined by conducting direct shear tests on 2.5-inch-diameter specimens with precut shear surfaces at approximately 0.0001 in/min. The results, shown in Table 2, were used for the stability analysis.

For the natural slope review, 66 slopes near the damsite were measured with tape and hand level. An additional 19 slopes were measured on topographic maps. The data were plotted as shown in Figure 7. A bounding curve was then drawn, representing the maximum observed slope for any given height. By assuming that the safety factor of these slopes was approximately one during saturated conditions, effective cohesion and friction angle values could be calculated using stability charts (Taylor, 1948). An effective cohesion of 200 pounds per square foot and an effective friction angle of 7.5 degrees produced a bounding curve that enveloped all but one of the observed points with a smooth curve, as shown.

#### DESIGN APPROACH

The above concerns required that special details be incorporated into the design of the dam and outlet conduit.

#### Stability Analysis

Because of the potential for progressive failure of the foundation, slope stability analysis for long-term conditions considered both peak and residual foundation strengths. The stability design criteria involved a long-term safety factor of not less than 1.5 using peak strengths, and not less than 1.1 using residual strengths. The calculated safety factor for the residual foundation strength case was 1.1, which controlled the design. The calculated safety factor was 2.0 using peak foundation strength parameters.

#### Dam Section

The dam section is shown in Figure 3. An upstream-sloping core was chosen to provide a large drained downstream shell for improved stability under earthquake conditions. The core was constructed of dispersive clay

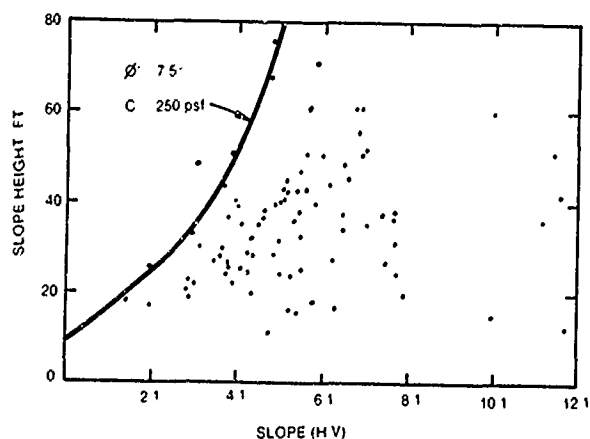


Fig. 7  
NATURAL SLOPES NEAR DAM

obtained from the reservoir area. The clay was compacted to not less than 95 percent of Standard Proctor density at a moisture content between 1 percentage point dry and 5 percentage points wet of optimum. This was provided a flexible, low permeability core. With the large settlements expected and the possibility of distortion due to earthquakes, the core was made more flexible and the dam crest was made wider and higher than it would have otherwise been.

The dam shells were constructed of fine Arena Sand. The specifications required a minimum of six complete coverages of each 6-inch-thick sand lift with a vibratory sheepsfoot roller having a dynamic energy of at least 25,000 pounds. The sand moisture content was not permitted to exceed 3 percentage points wet of Standard Proctor optimum. If, after six passes of the vibratory roller, a density less than 98 percent of Standard Proctor Density was obtained in any area, additional passes of the specified roller were paid for on an hourly basis. Densities generally exceeded 98 percent of Standard Proctor density with six passes.

A 20-foot-wide zone immediately downstream of the core was constructed of sand selected to provide sand with not more than 8 percent, by weight, passing the No. 200 sieve, washed basis. This zone serves as a downstream filter for the dispersive clay core and as a drain. Laboratory filter tests in both the pinhole apparatus and in 4-inch-diameter molds were used to confirm that the sand would filter the clay, even when preformed holes were made in the clay.

The upstream shell sand provides a supply of cohesionless material to flow into cracks that may develop in the core due to settlement, earthquake, or other causes.

#### Outlet Conduit

The outlet conduit (Figures 4 and 8) was designed as a reinforced concrete cut-and-cover dry tunnel with a 48-inch-diameter steel pressure pipe. This design was chosen to accommodate movement of the pressure pipe and to permit access for inspection and maintenance of the conduit.

The outlet conduit was constructed in 20-foot-long segments. Construction joints were provided on 20-foot centers so that the conduit would elongate in a controlled manner. Because of the area's seismicity and the expected dam base spreading, the longitudinal reinforcement was extended through the construction joints to provide continuous conduit reinforcement. A 3-foot-long plastic pipe sleeve was provided for each bar crossing each construction joint so that extension of the conduit would result in opening of the joints rather than cracking of the conduit segments. To provide for this extension, high-ductility steel was used for longitudinal reinforcing.

Each conduit construction joint was provided with a center-bulb waterstop to allow extension without leakage. The conduit was surrounded with a 2-foot-thick zone of 2-inch-minus, well-graded, sandy gravel (Figure 6). This gravel acts as a filter for the sand, and is

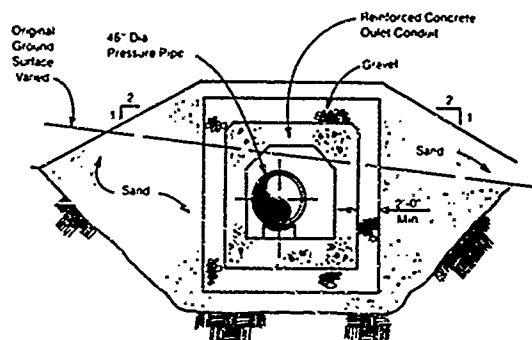


Fig. 8  
OUTLET CONDUIT SECTION

coarse enough to prevent piping into the predicted joint openings and other cracks that may develop. The gravel also provides drainage for the downstream shell near the conduit.

The 48-inch-diameter steel pressure pipeline was constructed in 40-foot lengths with thrust-restrained flexible couplings. The pipe joints were located at the conduit joints so the conduit and the pipe could move together.

At the core penetration, the clay core material within 5 feet of the outlet conduit in all directions was treated with hydrated lime  $[Ca(OH)_2]$ . Pinhole tests conducted on soil samples treated with lime showed that an application rate of 3 percent by dry weight of soil rendered the soil nondispersive. This reduced the potential for piping of the clay core into cracks or joints in the conduit.

#### Control Tower

The control tower was located in the upstream shell of the embankment (Figure 4) to improve the tower's seismic performance by reducing the height of the free-standing portion of the tower.

Because of the tower's location within the embankment, considerable settlement was anticipated. The estimated total settlement at the tower location was 2.5 to 3 feet. For this reason, the uppermost lift of the tower concrete was not placed until the dam was topped out in the area of the tower. This reduced the estimated postconstruction settlement of the tower top by eliminating the effects of elastic settlement and a portion of the consolidation settlement.

A small amount of tower tilting was also expected during and after construction because of the settlement and spreading of the dam. This tilting, together with movement during earthquakes, was expected to cause several inches of relative motion between the tower and the dam crest. To maintain access to the tower, the bridge was connected to the tower with a structural hinge, and was supported on the dam with a special bridge bearing that allows the bridge to move up to 18 inches toward or away from the dam crest.

#### EMBANKMENT PERFORMANCE

The embankment performance was satisfactory and similar to the design assumptions. Figure 9

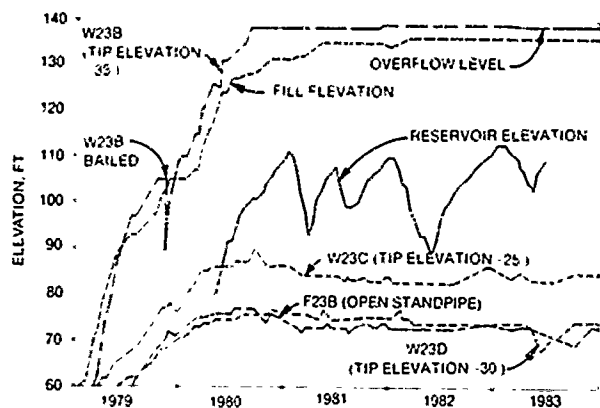


Fig. 9  
SELECTED EMBANKMENT PIEZOMETERS

shows the results of pore pressure monitoring at four instruments and the rate of embankment construction at the instruments. The instrument locations are shown in Figure 2.

The data shown are typical of 12 piezometers and 6 foundation settlement plates/standpipes. Only one piezometer showed unusual behavior: W23B. This piezometer was installed by drilling approximately 50 feet into the foundation from the bottom of the core trench prior to embankment construction. The riser was then protected and extended throughout embankment construction. At this piezometer, pore pressures rose as the dam was constructed. Eventually, the water level was above the dam crest. The riser pipe was extended above the crest, but overflow continued. Excess foundation pore pressure had been anticipated during design, but the dam stability in this area was reanalyzed during construction based on the results from piezometer W23B using a variety of conservative pore pressure assumptions. Safety factors remained acceptable, so construction was not slowed or stopped, and the design was not modified.

#### OUTLET CONDUIT PERFORMANCE

To monitor movement of the outlet conduit, monuments were installed inside the conduit and regularly surveyed. Figure 10 presents the settlement data for the outlet conduit. Despite the settlement, the outlet conduit continues to have positive drainage. The settlement at the dam centerline through December 1983 was approximately 1 foot, compared to the estimate of 3.5 feet.

#### CONCLUSIONS

Based on the performance of Arena Dam through 1983, the following conclusions are made:

1. Dispersive clay can be utilized in earth dams if proper precautions are taken.
2. The use of the recompression index in the terzaghi consolidation equations significantly overestimated settlement, even though predicted settlements had been halved to account for reported overestimates using the equations on preconsolidated clays.

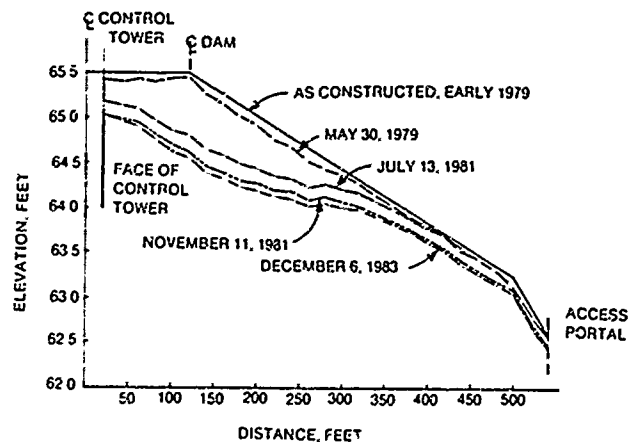


Fig. 10  
OUTLET CONDUIT SETTLEMENT

3. Residual strength analysis resulted in a design that has performed successfully to date and allowed construction on a difficult site.

#### REFERENCES

- Bjerrum, L. (1967), "Progressive Failure in Slopes of Overconsolidated Plastic Clay and Clay Shales," *Jour. Soil Mech. and Foundations Div. ASCE*, Vol. 93, No. SM5, September 1967, pp. 3-49. (Reprinted in Terzaghi Lectures, 1963-1972, ASCE, 1974.)
- Rutledge, P. C., and J. P. Gould (1973), "Movements of Articulated Conduits Under Earth Dams on Compressible Foundations," in *Embankment-Dam Engineering*, Casagrande Volume, R. C. Hirschfeld and S. J. Poulos, eds., John Wiley and Sons, New York, pp. 209-237.
- Sherard, J. L., R. S. Decker, and N. L. Ryker (1972), "Piping in Earth Dams of Dispersive Clay," *Proc. Spec. Conf. on Performance of Earth and Earth-Supported Structures*, ASCE, pp. 589-626.
- Sherard, J. L., L. P. Dunnigan, R. S. Decker, and E. F. Steele (1976), "Pinhole Test for Identifying Dispersive Soils," *Jour. Geot. Engrg. Div. ASCE*, Vol. 102, No. GT1, January 1976, pp. 69-85.
- Sherard, J. L., R. J. Woodward, S. F. Gizienski, and W. A. Clevenger (1963), *Earth and Earth-Rock Dams*, John Wiley and Sons, New York.
- Taylor, D. W. (1948), *Fundamentals of Soil Mechanics*, John Wiley and Sons, New York.
- Terzaghi, K., and R. B. Peck (1967), *Soil Mechanics in Engineering Practice*, Second Edition, John Wiley and Sons, New York.
- Tomblin, J. F., and W. P. Aspinall (1973), "Seismic Risk at the Arena Dam Site, Trinidad" (unpublished).

## Case History of a Partially Underground Power House

K.K. Kapoor

Deputy Chief Engineer (Civil), Mahi Hydel Project, R.S.E.B.,  
Banswara, India

S.C. Patodiya

Executive Engineer (Civil), R.S.E.B., Jaipur, India

**SYNOPSIS :** In the normal rock conditions, conventional type surface power houses have been built, whereas in structurally sound rock with sufficient rock cover, underground power houses have been attempted in India. The geological uncertainties plays major role in deciding the type of power house at a particular site. While in the surface type conventional power house huge excavation and concreting are involved, the access to the power house involves major work in the case of underground power house. There are very little examples when semi underground type of power houses have been attempted in India. The Mahi power house-II of Rajasthan is the sole attempt of shaft type of power house after the successful completion of small Giri power house in Himachal Pradesh. This paper presents the case study of this shaft type semi underground power house. Important features about its layout, design and construction have been discussed here.

### INTRODUCTION

Mahi Bajaj Sagar Project is a multi purpose river project providing irrigation facilities besides generation of power at two power houses. The power house-I is located at about 8 Km upstream of Mahi dam. The water released from this power house is discharged through balancing reservoir No.1 and thereafter through the canal and hydel channel to balancing reservoir No.2 which is the forebay of power house-II. The power house-II is having installed capacity of 3x45 MW. This power house was initially planned as a conventional type of surface power house involving nearly 3.75 lacs cum of excavation in 58 M deep open pit and 44,000 cum concreting. The huge quantities of excavation and concrete and availability of reasonably good rock strata made to re-think about the whole planning of this power house. By that time nearly 90,000 cum of rock excavation had been completed as per original layout. After examining all aspects about the geology and the type of treatment required, the power house layout was modified and the idea of shaft type power house was conceived.

### GEOLOGICAL FEATURES

The country rocks in the area are phyllites intercalated with amphibolites quartzite or quartzite bands of Aravali super group, later being in much lesser quantity. The foliation strikes from N 30°W - S 30°E to N 20°E-S20° W with 20° - 40° dips on either side. The values of 'c' and 'φ' obtained were 22.5 Kg/sq.cm. and 66° respectively.

### LAYOUT FEATURES

Since the excavation work as per the conventional type surface power house layout had already been taken up upto certain elevation, the revised layout was proposed on the follow-

ing lines.

(a) The power house has been excavated as an open pit upto the erection bay level i.e. El-147.5m. (NSL being 176.0m). The auxilliary space requirements have also been accommodated in the open pit excavation.

(b) The generating units have been placed in individual circular/vertical shafts of 16.3 m dia and 30.5 m depth. Rock ledge between unit 1&2 is only 6.0 m whereas between unit 2&3 it is 10.25 m as the unit 3 was taken up at a later stage when shafts for unit 1&2 had been excavated & protected by rock bolts & shotcrete.

(c) For the access to the various parts of generating units, the inter connecting tunnels have been provided at 3 levels at generator floor at El-139.80 m, turbine floor at El-136.15 m and draft tube inspection gallery level at El-126.10 m.

(d) Separate tunnels for penstock and draft tube have been provided with each shaft for entry and discharge of the water. For control/regulation of the downstream water levels, the draft tube gate shafts have been excavated in oblong shape.

(e) The approach to the power house is available only upto El-166.0 m and therefore, unloading bay has been provided at this level. Provision of lift alongwith staircase has been kept for access to the auxilliary floors, erection floor and generator floor.

(f) Various pipes, cables etc. from the generator level have been taken to the auxilliary floors through the niches excavated in the shafts to house their requirements.

(g) The excavation to the downstream of unit bays had been restricted to the level it was

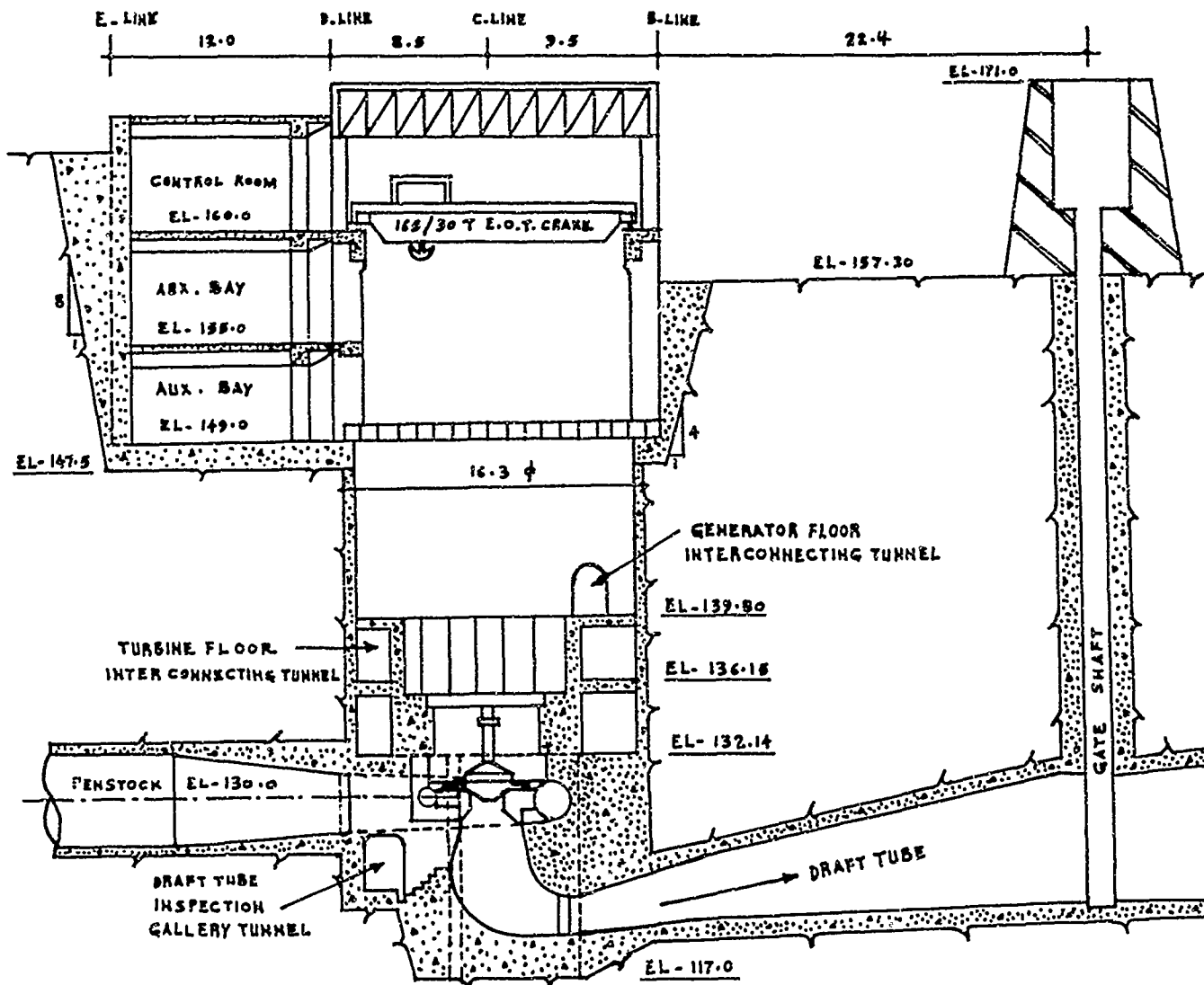


Fig.1 Cross section of power house

carried out till revision in the layout was made to save the height of protection wall. The protection wall of nearly 14 m height has been provided to protect the power house from the floods of river Anas flowing downstream of the power house.

#### DESIGN FEATURES

The shafts had been excavated after going for an open excavation upto the EL-147.5 m on upstream side and upto EL-157.0 m on downstream side. In open excavation stable slope of 1/4:1 had been adopted from top upto EL-157.0 m and of 1/8:1 below EL-157.0 m. The greatest risk involved in underground construction projects is the uncertainty in predicting ground conditions and assessing rock behaviour at the site. For stability of vertical rock surfaces in the shafts, surface treatment consisting of rock bolts and shotcreting have been adopted. Adequate drainage arrangements to drain rocks around the shafts have been made. Further,

R.C.C. lining has also been provided to help in resisting the hydro-static pressure from the rock.

#### Rock Bolting

Tensioned rock bolts with the slot and wedge type anchorage have been used as rock reinforcement to prevent the deformation or dilation of the rock, to mobilise the rock's natural competency to support itself with its inherent strength and to provide resistance to inward movement of rock. Rock bolts of 4 m length made from 25 mm dia for steel bars were installed in a regular pattern at a spacing of 1.75 m c/c. For a rock bolt adequate anchorage is very important. The effectiveness of the rock bolts was ensured through pull out tests. Fig.2 gives results of some of the such pull out tests. The rock bolts were further grouted pneumatically under a pressure of 3.5 kg/sq.cm. with neat cement paste to get full length bonding with the rock surface and to avoid the loss of



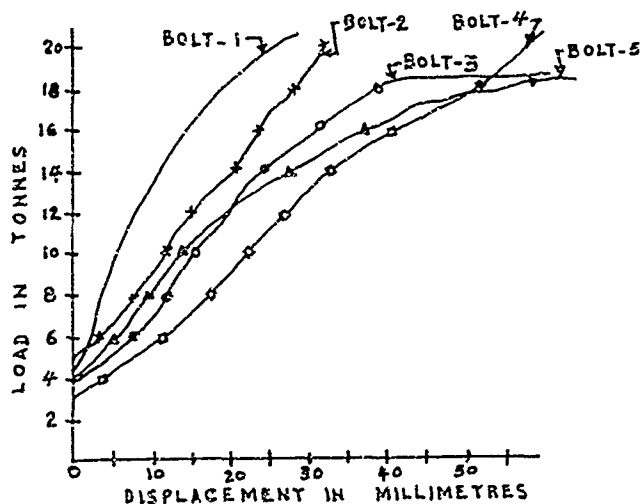


Fig.2 Rock bolt pull out test results

anchorage at a later stage. Ungrouted rock bolts were capable of taking 5 M.T. tensile load without any appreciable displacement.

### Shotcreting

To make the supporting system more effective, 75 mm thick shotcrete in 3 layers of 25 mm each reinforced with 10 gauge G.I. wire 50x50 mesh chain link fabric was applied on rock faces after rock bolting in shafts. The chain link fabric was fixed on the rock surface with the help of anchor bolts. Shotcrete mix was designed satisfying requirements such as shootability, self supporting without segging or sloughing early strength, durability, minimum rebound, economical etc.

Shotcrete was applied with dry mix technique at a pressure of 3.5 kg/sq.cm. Natural river gravel in maximum size 12.5 mm were used as coarse aggregates. The mix of the shotcrete finally selected was as below.

| Ingradients | Batch weight. | Percentage of total batch weight. |
|-------------|---------------|-----------------------------------|
| Cement      | 525 Kg.       | 23.16                             |
| Gravel      | 697 Kg.       | 30.74                             |
| Sand        | 1045 Kg.      | 46.10                             |
| Total       | 2267 Kg.      | 100.00                            |

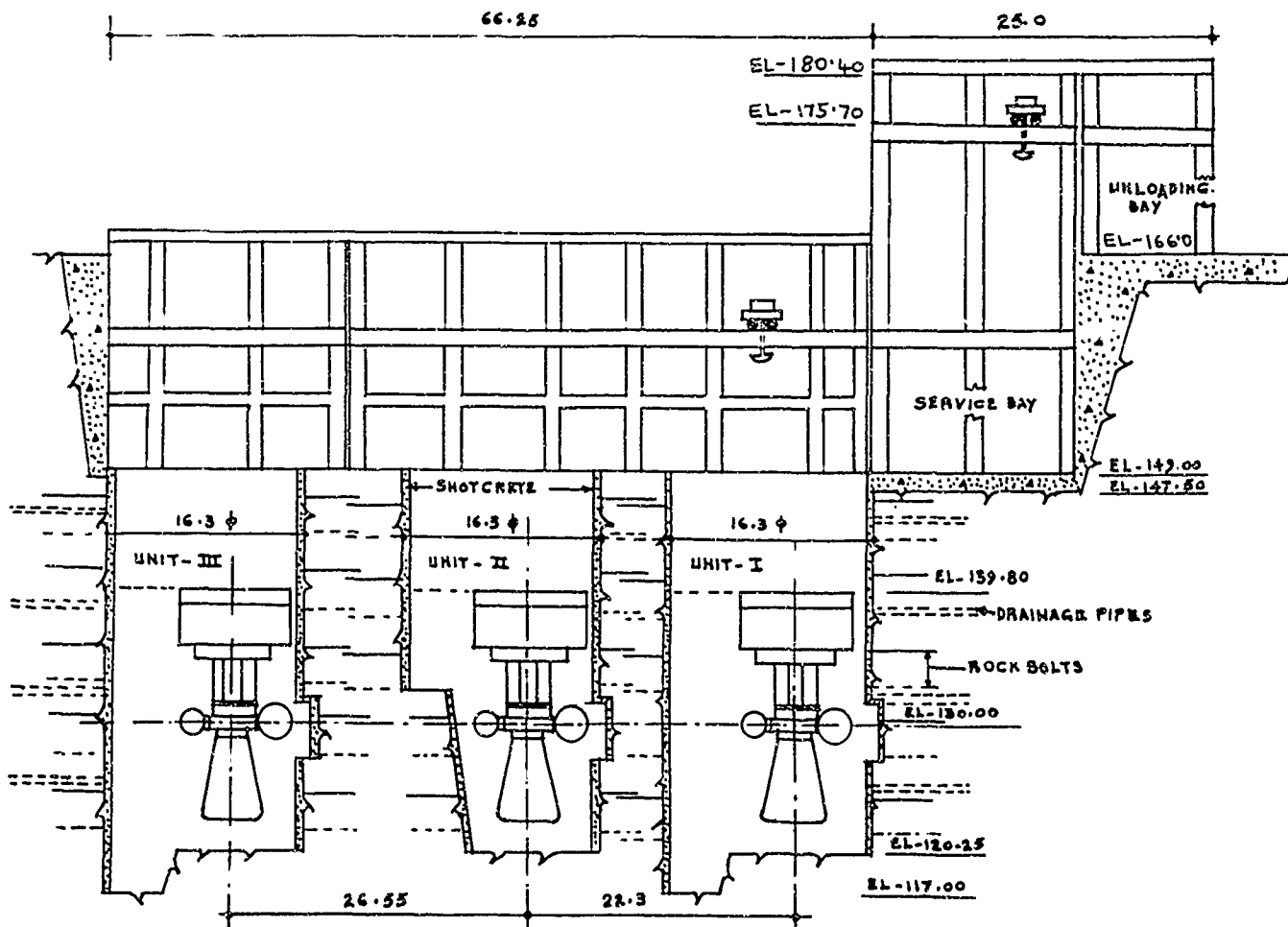


Fig. 3 Longitudinal section of power house.

The shotcrete with the above mix gave compressive strength of above 250 Kg/sq.cm. 2% sodium carbonate in dry powder form by weight of cement was used as set accelerator admixture for locations where rapid gain in early strength was required. With this mix, maximum rebound noticed was 30%.

#### Drainage Arrangement.

In order to release the pore pressure inside the rocks, drainage arrangements have been provided by inserting 4 m long, 75 mm dia. perforated pipes at a staggered spacing of 3 m c/c in the rocks. These perforated pipes allow seepage water from inside the rock to percolate into the drainage pit through a system of horizontal and vertical pipes. Apart from canalising the seepage water, arrangements have been made to divert surface water also. A drainage sump at the bottom most auxiliary floor at El-147.0 m has been provided to collect seepage water from the rock mass above shaft level through perforated pipes and porous drains. This seepage water collected into the sump is then pumped into the downstream river.

#### Structural Lining in the Shaft.

R.C.C. Lining 400 mm thick duly anchored to the rock surface has been provided in the shaft to resist the hydro-static pressure from the rock. Although arrangements for percolation of water have been made to reduce the hydro static pressure on the lining but due consideration has been given in the design of lining for this too. Residual in site pressure have also been accounted as function of overburden pressure. R.C.C. raft has been provided to transfer the load from crane columns to the rock masses. This arrangement has not only cut down the excavation further for the column foundations but also avoided any damage to the shafts due to concentration of stress as the columns are very close to the periphery of the shafts.

#### CONSTRUCTION FEATURES

The main features of construction are rock excavation, rock bolting, shotcreting, concreting and equipment erection work. Time lag in different operations such as excavation, rock bolting, shotcreting etc. is a very important parameter which largely depend upon quality of rock and site conditions. This time lag should be kept at minimum so that strains of inelastic nature are arrested early following excavation.

#### Excavation

Excavation for shaft has been carried out by controlled blasting and pre-splitting technique to safeguard against the damage to rock face and to keep the overbreak to the minimum. Rock ledge between shaft No. 1&2 is only 6m. and all precautions were taken to prevent any damage or overbreak in this rock ledge. Certain overbreaks were observed along the periphery at top in the initial stage for which special treatment had to be carried out as the column edges were falling on some overbreak portions.

#### Rock Bolting.

The strength of a rock bolt is determined by

its anchorage and adequate anchorage is very critical to the proper performance of the rock bolt. In a slot and wedge type rock bolt anchorage is obtained by inserting the wedge into the slotted end of the bolt and expanding the slot by driving the wedge against the end of the drill hole. Hence strict control over the length of drill hole has to be exercised. Further hammering cap was used to prevent damage to the threads of the bolt on hammering. Full expansion of slot by maximum insertion of wedge into it is to be ensured required tension of 5.0 M.T. in the rock bolt.

Although rock bolts were installed in regular pattern, additional bolts in localised areas of instability and weakness were also provided as spot reinforcement. All rock bolts were grouted under pressure of 3.5 kg/sq.cm. with neat cement slurry through a small key hole slot left in the bearing plate. The drill hole was 40 mm and the rock bolt was of 25 mm dia deformed bars therefore not much space was there between the hole and the rock bolt and so great care was required to ensure complete packing of the cavity.

#### Shotcreting

Dry process shotcrete was adopted for the shafts and tunnels applied in 3 layers of 25mm each



Fig. 4 Photo showing shafts

with chain link fabric as reinforcement. Highly experienced operator and nozzleman are required for good quality shotcrete work. Nozzleman alone controls main factors effecting quality of shotcrete work such as water-cement ratio, distance between nozzle and the surface, angle of the nozzle, stream & motion of the shotcrete etc. Uniform air and water pressure was ensured to prevent uneven flow of dry mix and to minimise pulsations in the delivery hose. Constant vigil over the pressure gauges was kept for controlling the shotcrete thickness steel pins were anchored in the rock. Reinforcement was located in the final layers of shotcrete to keep it near the outer fibers of shotcrete to make it more effective and useful in playing its important role of resisting bending moment which may develop in the rock. Chain link fabric due to its flexibility could be easily placed on undulated rock profile in the defined 75mm thickness of shotcrete. It is the work which requires close control and supervision at all levels.

#### Concreting.

The concreting in such power house carries significance specially in the shafts. Quantitatively it is small but it requires adequate arrangements. Since direct approach to the shafts for transportation of materials is not available, the concreting in shaft is possible only through a crane or any heavy handling equipment. The other important and little difficult item is the circular lining in the shafts. The lining is required to be anchored to the rock surface properly. The special features of the construction

is raising of this lining not from the bottom but from higher elevation i.e. from generator floor level in the shafts. Since the area in the shafts is quite limited and the erection of electrical parts may create problems due to the very little space available between the vertical face of the shaft and electrical parts, the lining in these portions has not been raised till the time the erection work is completed. This requirement of the erectors resulted in change in the pattern of construction and thus raising of lining from higher elevation. This arrangement involved additional anchoring and formation of a ring beam at this elevation. Great field problems have been experienced in raising the lining from higher elevation as it involved a massive scaffolding arrangement and the preparation of a platform for handling of materials. The thickness of concrete lining is only 400 mm and placement of reinforcement and maintaining its continuity becomes more difficult in such small section particularly where vertical header pipes for carrying the seepage water to the drainage pits have been encountered.

Such difficulties in concreting have resulted into more time consumption in placement of reinforcement and erection of shuttering. Difficulties for proper access to the shafts mainly in the gate shaft have also been felt during the construction.



Fig. 5 Photo showing power house complex.

## ERECTION FEATURES

Normally in the conventional type of power house, the erection is started when the E.O.T. crane is put to operation. A different approach has been adopted here. The erection of the draft tubes has been carried out with the help of a mobile crane. Similarly, speed ring has also been lowered with the help of mobile crane. The limited working space in the shaft poses many problems in the erection work.

## CONCLUSIONS

The power house shafts after rock bolting and shotcreting were left for more than 2 years without any construction activity because of some unavoidable circumstances. The supporting system has proved to be very effective and useful as the vertical surfaces of shafts faced all adverse effects of weather including rains successfully for 2 years and no adverse

effect or instability or deformation in any portion of shafts was observed.

The planning of a shaft type of power house is an important and interesting feature. It is definite that these power houses are quite economical both in respect of cost and time. However, judicious planning is required both for the layout and construction. Margins for the overbreaks and under cuts had to be made while deciding the location of columns, Nitches etc. Although the quantum of excavation and concreting gets reduced in shafts, but at the same time it requires more accuracy, it is costly and time consuming due to restricted space, areas and limitations of access. While deciding the layout of equipments, the erection space required for handling and erection of equipments requires due consideration.

## Iron Gates II: Design and Performance of Dams— Geotechnical Considerations

I.I. Corda  
Romania

**SYNOPSIS:** The first part of this paper briefly presents the concept of design and construction of the Iron Gates II dams. The paper will concentrate on the works performed by the author for geotechnical investigations concerning the foundation and embankment materials.

Based on the in situ investigations and large scale laboratory test data the numerical analysis for earth dam was carried out. In the second part, the observation and instrumented behaviour of foundations material were related to particular aspects: river leftbank instability and earth dam connection, foundation rebound during excavation for concrete structures; settlements, pore pressures and total pressures monitoring during construction, impounding, reservoir filling and for the first three operation years.

### INTRODUCTION

The Danube is the second of largest rivers of Europa with a catchment area of 817,000 km<sup>2</sup> and a length of 2,912 km. About 30% of the Danube catchment area is on the Romanian territory; an equal percentage of its length represents the Romanian south state border with Yugoslavia, Bulgaria and Soviet Union. About 40% of the total potential of the Danube i.e 15.8 milliards kWh/year is concentrated in the Romanian-Yugoslavian reach.

Taking into account the huge hydroelectric potential of the Danube in this reach the Governments of both countries agreed to the utilization of this potential in the interest of both Parts and have decided to found a Joint Commission for the management and coordination of the Project. The "Institute of Hydroelectrical Studies and Designs (ISPH)" - Bucharest, Romania and the "Energoprojekt"-Belgrad, Yugoslavia were chosen to elaborate the studies and designs for the Project.

By means of a detailed study of the morphological, hydrological and geological particularities of the Romanian-Yugoslavian reach of the Danube and by comparing the numerous alternatives it resulted that the best utilisation of the potential could be performed by the two hydroelectrical and navigation systems: the first "Iron Gates I" located at km D 943 and a second one "Iron Gates II" downstream, located at km D 863.

The Iron Gates I was put into operation at the designed full capacity in 1971; with an installed power of 2.10 millions kW and an average annual output of 11.6 billions kWh generates - one quarter of the capacity and output of the whole Danube capabilities (Spasic ed., 1972).

Having in mind those successes got in the Iron Gates I System implementation and operation, as well as the interest of both Parts in the subsequent utilisation of the Danube hydraulic potential, based on the following principles:

- equal participation in the investment effort and operating expenses;

- the right to equal part of the power capacity and output;

- exclusive property of each country on the constructions and installations located in their own territory, the Socialist Republic of Romania and the Socialist Federative Republic of Yugoslavia have decided in February 1977, to achieve the second common development - the "Iron Gates II" Hydroelectrical and Navigation System. The developed zone is located from km 860 + 800 to km 876 where the Ostrovul Mare Island divides the Danube into two forks of which the right branch is the main one (Fig.1)

The Iron Gates II scheme comprises the following main structures from the left to the right bank (Vasiliu and Scvorțov, 1976):

- On the secondary left river branch (Gogoșu) km D 875: the zoned earth dam (H max = 24.4 m, L = 286 m) the spillway structure (Romanian spillway dam) with 7 sector gates (21.0 x 14.5 m) designed to pass a maximum flow of 7,000 mc/sec, a secondary powerhouse equipped with 2 horizontal bulb turbine and generator units of 27 MW capacity each, and the right side earth embankment.

- On the Ostrovul Mare Island the 5,270 m long earthfill dam is located on lower level zone and makes the connection with the navigation facilities on the left side (the Romanian 310 x 34 m and 125 x 14 m locks, upstream and downstream layby bays).

- On the main Danube branch: the Romanian main powerhouse where 8 x 27 MW generators are installed, adjacent with Yugoslavia main powerhouse similar in design capacity (8 x 27 MW) and lower spillway structure with 7 sector gates (L = 21.0 m, H = 14.5 m) to discharge a maximum flow of 8,000 mc/sec. The earth dams (H = 24.0 m, L = 474 m) completes the retention front between the spillway, the Yugoslavian lock, the secondary (2 x 27 MW)

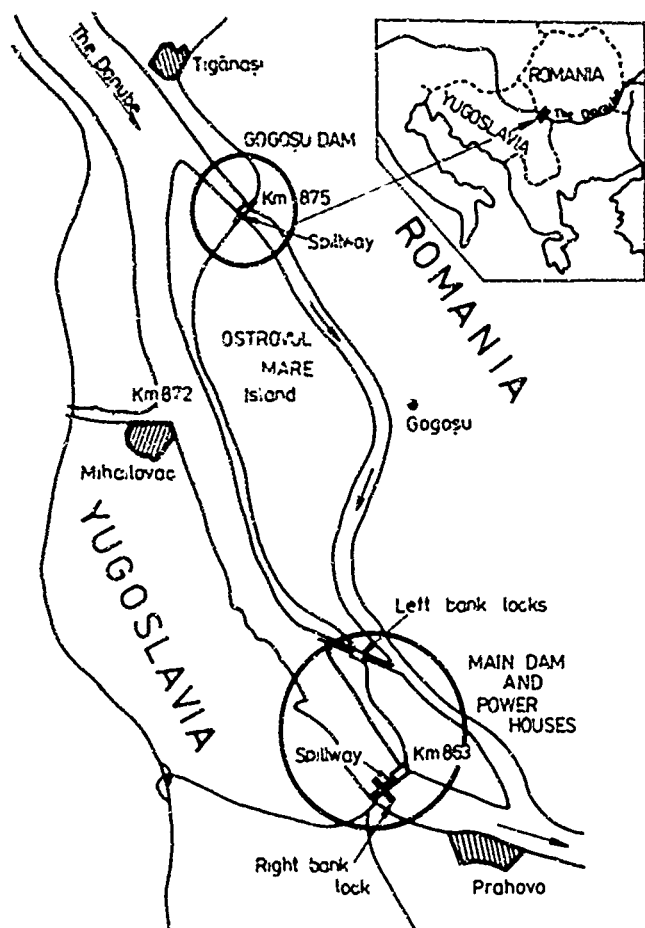


Fig.1. Site Location Map.

powerhouse and the right natural high bank (Figure 2).

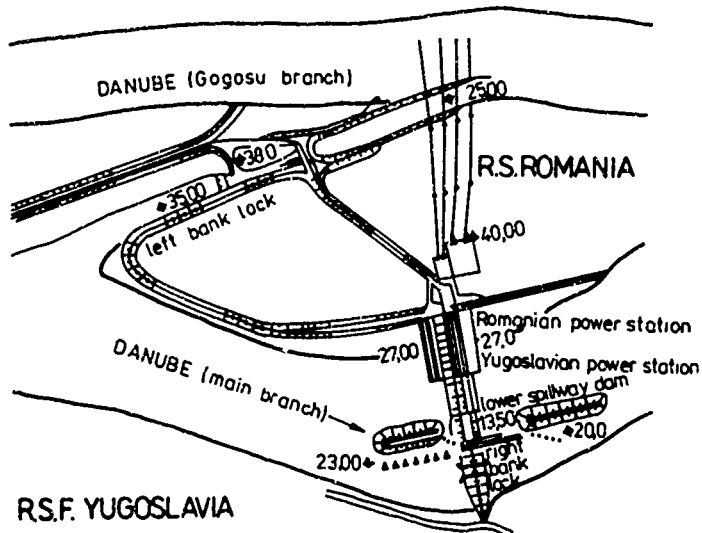


Fig.2. Iron Gates II - General Scheme.

The total volumes are: 15 mill. mc excavations, 2.1 mill. mc concretes, 11 mill. mc earthfill.

The water diversion necessary to carry out the main structures in dry conditions was achieved in two phases. In the first diversion phase the construction enclosures for spillways, earth dams and powerhouses were carried out.

In the second diversion phase, the construction of the Yugoslavian lock, secondary powerhouse and earth dams is progressing successfully and scheduled for completion in 1991. By river bed closing in Nov. 1984 the retention level is raised, the hydro-units are put into operation and the navigation is developing by the lock on the left bank.

#### GEOTECHNICAL INVESTIGATIONS

The damsite and the reservoir are situated in the southwestern part of the Romanian Plain area (Moesic Plateau). The bedrock, classified as stiff clays (marly-clays) - a sedimentary stratified rock of the Pliocene and Miocene ages is covered with the fluvial Quaternary deposits of variable thickness (from 0.5 m to 28 m) consists of: clayey silt, sand and gravel.

The aims of the geotechnical investigations were to: systematically identify those geological features; determine representative geomechanical properties of the foundation strata which are required for design and analyses of the structures; determine the suitability of materials got from excavations for use in permanent structures and facilities.

Table I gives a summary of the principal investigations carried out by the specialised division of ISPH Bucharest.

TABLE I. Summary of Geotechnical Investigations

|                      | No. | Length (m) |
|----------------------|-----|------------|
| Rotary core drilling | 314 | 9364       |
| Exploratory- shafts  | 16  | 220        |
| - galleries          | 2   | 150        |
| Seismic surveys      | 18  | 4200       |
| In situ tests:       |     |            |
| - deformability      | 11  |            |
| - direct shear       | 34  |            |
| - in situ shear box  | 142 |            |
| - permeability       | 10  | 187        |
| Laboratory tests:    |     |            |
| - direct shear       | 700 |            |
| - triaxial           | 80  |            |
| - uniaxial compr.    | 400 |            |

The main structures are founded on bedrock. The lightly over-consolidated clay possesses macro-structured features, such as fissures and joints that make them discontinuous. The clay is of marine origin containing numerous fine sand layers and considerable montmorillonite clay mineral throughout. The firm clay (marl) weathers rapidly when exposed in the air and breaks down completely on wetting and drying.

As space of the paper is limited, this report pays a special attention to the geotechnical characteristics only for earth and concrete dams.

At the dam site the exploration works led to the definition of the geologic structure, which is

from require excavations for the powerhouse and the spillway in order to use as core dam impervious material.

Figure 1 consists of two parts. Part (A) is a cross-section of the study area, showing a geological profile with various layers and features. The profile is labeled with 'e' at the top, 'd' for the shell layer, 'a' for the core, 'b' for the  $F_1$  layer, 'c' for the  $F_2$  layer, and 'f' for the bedrock. The profile is divided into sections with lengths of 41.00, 43.50, and 2.1. A scale bar indicates 0, 10, and 20m. Part (B) is a grain size distribution graph. The x-axis represents grain size in mm on a logarithmic scale, ranging from 0.0002 to 300. The y-axis represents percentage from 0 to 100. The graph is divided into five soil texture categories: COBB, GRAVEL, SAND, SILT, and CLAY. Several curves are plotted, labeled 'a' through 'e', representing different samples. The curves show the percentage of material finer than a given grain size. The legend indicates that the curves are labeled 'a' through 'e'.

In addition to the in situ tests, an important number of laboratory tests for obtaining information on compressibility, consolidation, shear strength and stress-strain relationships were carried out.

The initial design geotechnical characteristics for the specified three types of clayey layers are given in Table II.

TABLE II. Properties of Bedrock Adopted Design

| Property                  | Clayey horizon |                |                |
|---------------------------|----------------|----------------|----------------|
|                           | I<br>(Upper)   | II<br>(Inter.) | III<br>(Lower) |
| Deformation modulus (MPa) | 75...100       | 45 ... 60      | 75...100       |
| Poisson's ratio           | 0.35           | 0.35           | 0.35           |
| Apparent friction angle   | 17°            | 17°            | 17°            |
| Cohesion kPa              | 30             | -              | 50             |

In the first phase's dry foundation enclosures a typical cross-section of the earth dams shown in Figure 3 were chosen. The earth dam is a sandy-gravel embankment with slightly inclined central clay core protected upstream and downstream by filters, drains and rockfills (rip-rap). Gradation curves of materials used are also shown in Figure 3.

The material for shells was available in a sufficient amount along the Danube river in the form of natural sand and gravel from alluvial deposits, in the river bed, or in the terraces.

As regards finding core material a lot of researches were made, however the good-quality core material could not be found in the vicinity of dam site. Under these circumstances the Geotechnical Division of ISPH Bucharest made a decision to carry out an extensive testing program aiming to confirm the suitability of materials obtained

Fig.3. Earth Dam. Typical Section and Material.

This unconventional material presented in short elsewhere (Anagnosti, 1986), was in fact a highly plastic clay (CH) with a liquid limit fluctuating between 50% and 60%, a plasticity index ranging between 35% and 43% and a content of clay size (  $2 \mu$  ) particle between 30% and 42%.

Before starting the core placement, trial embankment tests were performed in order to prove if it is physically possible to construct a clay core with this material and to determine the suitable layer thickness of placement, moisture content, number of compaction passes and yield of the equipment to be employed.

The Proctor maximum dry density tested in laboratory has been a mean value of 1500 kg/mc with an optimum water content of 27%.

Before compaction, the residual clay material is spread in 150 mm layers in place by a bulldozer with a padded roller to give a good crushing and squeezing of the rock lumps into the clay matrix. Water was added on site by a spray tanker to counter evaporation. Compaction is carried out by six passes of a 30 t rubber-tired roller. The smooth surface was scarified to form a rough surface for a good binding between the existing and the newly compacted core material. This technique remoulded the stiff clay into a homogeneous core so that the product resembled a composite of small discrete chunks (up to 100 mm) within a soft matrix.

Quality control is performed by sampling and visually (including pits and trenches) to check for satisfactory texture. Undisturbed cubic block samples 30 cm side and core cutters of 100 mm

diameter were extracted at different levels to measure permeability, consolidation and determine deformability and shear strength parameters.

The average shear strength parameters in terms of effective stress from consolidated-drained triaxial test are about  $\phi' = 15^\circ$  and  $c' = 70$  kPa, with a yield strain above 10% and sometimes 20%. In the quick undrained condition such large strains were usual. The coefficient of volume change  $m_v$ , from oedometer tests was generally within the range  $0.057$  to  $0.013 \text{ m}^2/\text{MN}$  for pressures between 50 and 1000 kPa. Permeability values of  $1 \times 10^{-5}$  ...  $1 \times 10^{-7}$  cm/sec were obtained. The intact structured clay (marl) is highly resistant to erosion. Erodability pinhole tests have been conducted on clay core specimens. The resistance to erosion is decreased after remolding and reconsolidation, but laboratory tests indicated that reconsolidated clay in dam core (undisturbed block) have a surprising high resistance to erosion.

In place density tests were performed by relation weight-volume using rubber balloon method (ASTM D-2167-63 T). The core material was placed with an average dry density of 1550 kg/mc corresponding to 102% Proctor Standard. The moisture content as placed (determined by oven-drying method) varied between 23% and 29% with a mean value of about 1.2% wet of Proctor optimum. This placement wet of standard optimum was considered to give a "plastic" behaviour, better able to adjust to differential settlements not vulnerable to cracking although giving a slightly reduced density.

The design of filters has been made to protect the core on both downstream and upstream sides. The fine filter ( $F_1$ ) were located upstream of the core to serve as a crack-stopper and downstream side to prevent migration of impervious core soil particles. The coarse-grained filter ( $F_2$ ) were located to prevent fine sand material being washed into shell fills. Both good-quality filter materials were available to the batching plant were the aggregates (big fractions) for concrete have been obtained by screening. The finest parts of filters (0.1 ... 1 mm) were separated by means of hydrocyclones. Specifications require filter material an average 70% relative density. This relatively light compaction was based on the recognition to minimise the stiffness discontinuity of the core/filter interface and the risk of cracking.

The material used for the upstream and downstream shells was a mixture of rounded gravel particles and sand from the river bed deposits, that could also be classified as well graded sandy-gravel (GW). The average percentage of minus No. 4 (4.75 mm) fraction in the shell material was 50% and the average uniformity coefficient  $C_u = 32$ . The shell material was placed in 50 cm lifts and compacted by smooth drum vibratory rollers.

The average in place dry density was 2050 kg/mc which was equivalent to  $D_r = 0.80$ ; the maximum and minimum densities of the tested materials (maximum particle size: 50 mm) were determined in accordance with ASTM-D 2049-69. This mean density value was therefore adopted for simulating the "as built" condition for the preparation of laboratory samples.

Several comprehensive large scale tests were

performed, incorporating the triaxial isotropic consolidated drained and undrained tests (250 mm diameter specimen) and direct shear tests (1000 x 1000 mm and 400 x 400 mm shear-box) on modeled gradation and natural gravel-fill materials. From this information a drained angle of shearing resistance  $\phi = 32^\circ$  has been estimated as design value and parameters defining stress strain non-linear (hyperbolic) relationships. The vertical permeability of the modeled material (70 mm maximum particle size) determined from large scale (400 mm diameter samples) tests with surcharge pressure equivalent to the embankment load was  $2.4 \times 10^{-2}$  cm/sec.

#### NUMERICAL ANALYSIS OF THE EARTH DAM

The compacted sandy gravel fill used for the dam has a low compressibility, however it has also a comparatively low permeability which makes it susceptible to some strength loss due to pore pressure increases when it is subjected to earthquake loading in a saturated condition.

The Iron Gates II area is considered one of moderate seismicity. A Vrancea (Romania) maximum magnitude  $M = 7.2$  earthquake record of 1977, located approximately 370 km from the dam site was chosen for scaling and modeling design levels of earthquake shaking (Pascalov et al., 1979).

In the design phase a maximum seismic coefficient of 0.15 g was adopted for investigating the seismic stability of the structures by the conventional sliding method. However, considering the hypothetical greatest earthquake that could possibly occur at the site we cannot avail ourselves of "limit equilibrium" methods to predict the dam safety and extent of damage. We must push the investigation further to determine the extent of permanent deformation in the analysis incorporating pore pressure effects, using the recently ICOLD (Zienkiewicz et al., 1986) suggested procedures.

The computer program ISEILD (Ozawa and Duncan, 1975) were used to evaluate the stresses and deformation in the Iron Gates II earth dam prior the earthquake with simulating sequential construction and nonlinear (hyperbolic) finite element procedures.

In order to compute the distribution of accelerations, dynamic stresses and strains the suitable finite element computer programs FLUSH (Lysmer et al., 1975) and QUAD 4 (Idriss et al., 1973) were used. The strain-dependent values of shear modulus and damping ratio used were hypothetically assumed to be similar with curves obtained and used for Oroville dam (Banerjee et al., 1979) for the same general gravel particle sizes. A series of torsional resonant column and cyclic triaxial tests were conducted in ISPH Bucharest laboratory to evaluate the shear modulus and damping ratio for sand and clay samples under different confining pressures and shear strain.

Since the dam shells involve saturated materials with a vertical permeability coefficient of the order of 21 m/day it was considered to be of interest to investigate the pore pressures induced by earthquake shaking and degree of dissipation which might be expected to occur during and after the period of earthquake shaking. The computer program GADFLEA (Booker et al., 1976) has



## SAFETY FACTORS

|                           |     | up   | down  |
|---------------------------|-----|------|-------|
| NORMAL                    | (G) | 1,73 | 1,53  |
| PSEUDO<br>$\alpha = 0,15$ | (b) | 1,28 | 1,001 |
| PORE<br>PRESS             | (c) | 1,16 | 1,234 |

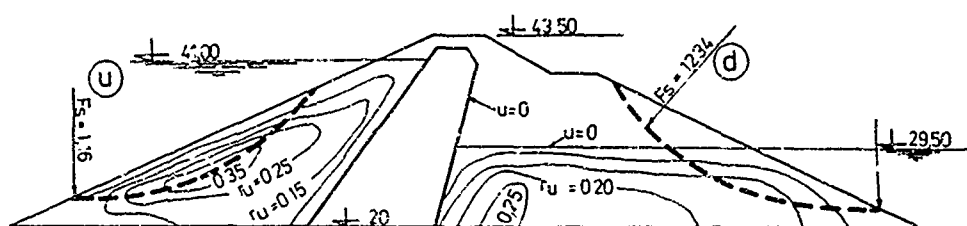


Fig.4. Pore Pressure Distribution After Earthquake and Stability Analysis.

used to evaluate pore water pressure ratios ( $ru$ ) distribution in both upstream and downstream shell. Pore water ratio distribution immediately after earthquake ( $M=7.2$ ) would have the approximate form shown in Figure 4. A stability computation using Bishop's modified method with residual porewater pressures (maximum values) when the shaking has stopped using an effective stress approach, indicates a minimum factor of  $Fs=1.16$  for critical circle upstream, compared with the minimum values of  $Fs=1.28$  from pseudo-static analysis ( $\alpha = 0.15$  g). It has been pointed out that most critical condition may not occur during the earthquake itself but sometime later when the pore water pressure attains its maximum value (Popovici et al., 1984). In downstream shell the pseudo-static analysis underestimates the stability. It may therefore be concluded that the dam is safe against the development of a major slide but the next step is to assess the magnitude of embankment deformations during the maximum possible earthquake.

This was accomplished by means of the strain potential concept using the nonlinear finite element program DEFORM (Serff et al., 1976).

The maximum estimated horizontal displacement was 0.18 m and settlement 0.30 m at the crest, which would seem to be tolerable for a dam of this size and for design connections to the concrete structures.

## OBSERVATIONS AND INSTRUMENTAL RECORDER BEHAVIOUR

The design of the earth Gogoşu dam in its left

zone was complicated by the presence of the riverbank landslides occurred during the spillway construction.

In the left riverbank zone between upstream and downstream cofferdams some settlement and cracking proved initially during the enclosure's dewatering.

Movement of the slides continued for several months until drainage reduces the pore pressure. The plots of deflection as a function of time (velocities) and composed direction for illustrative profiles are presented in Figure 5.

The slope indicator casings and piezometers were installed through the location of the failure area and a monitoring program instigated for further construction. The SINCO inclinometers are used to measure inclination of the drillhole. The shape of the slope indicator casing indicated that failure surface was at the boundary between bedrock and overlain formation consisting of a sequence of silty clays and silty fine sands as shown also in Figure 5.

A translational mode of failure is considered most likely to have occurred. Back analysis of instability shows that the slide movements are not determined only by materials characteristics, but also by the drawdown water level from dewatering and base erosion configuration. This specific case of drawdown failures also explained by piping of sand seams when groundwater flowing out of submerged river bank (piping holes and cavities in riverbank sandy strata have been observed).

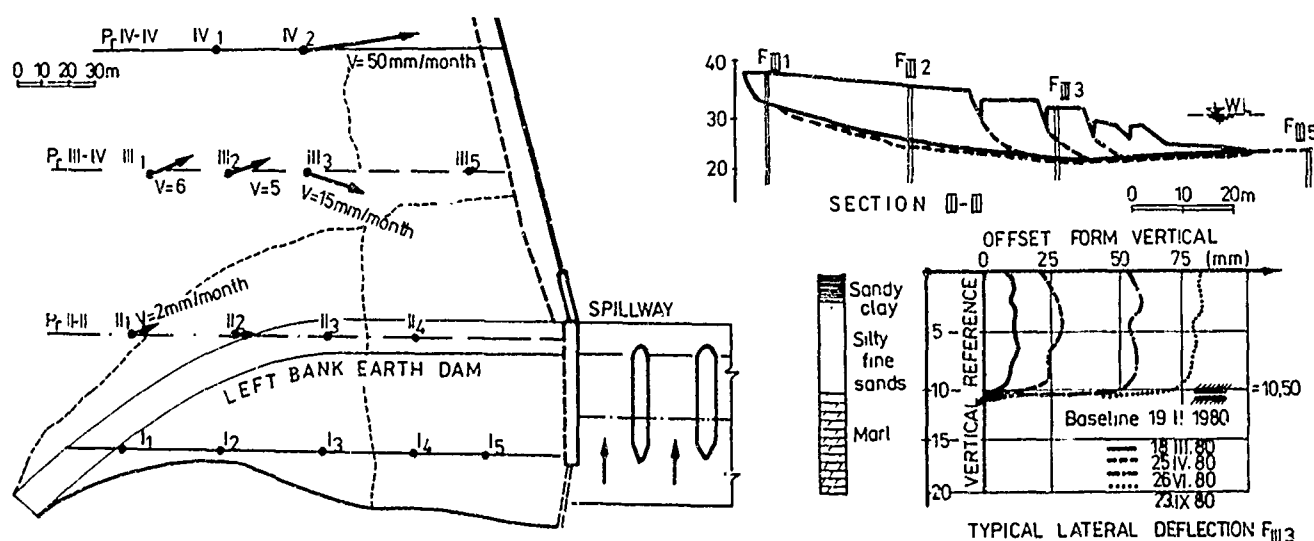


Fig.5. Left Riverbank Landslides Monitoring.

The axis of the earth dam was upstream curved to avoid decomposed zone and to solve foundation problem on the left side.

The left bank earthfill dam was designed for compatibility with the characteristics of the available foundation: part on bedrock (unweathered soft marl) rising to the surface, part on the riverbank alluvials with thickness from a few meter to more than 20 m. A typical profile within the dam on stiff bedrock differs from the ones within the left portion of dam overlying the riverbank deposits (Fig.6).

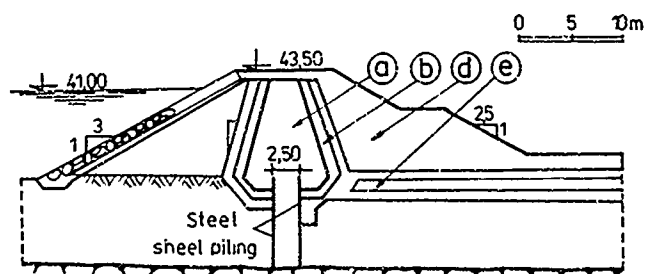


Fig.6. Earth Dam. Leftbank Connection.

The material affected by the slide was partially excavated from the dam foundation. Two parallel steel sheet piling walls were driven from the bottom of the excavated trench to the stiff clay (bedrock) to minimize seepage and to provide a cut-off beneath the dam.

In the riverbank zone downstream the dam, only a upper part of the terrace sagged and slipped was removed and the apparatuses (cracks) was backfilled. A new profil was reshaped by replacing the alluvial material with pervious blanket (drain between filters) connected with the earth drainage trench. In order to improve the riverbank stability the water-side embankment was protected by rockfill against flow over the spillway and waves.

No movement was noticed during the last three operation years in the reshaped and protected

riverbank. In order to measure the pore pressure of the earth dam clay core, electrical cells (vibrating wire) were placed in three sections. During construction, the pore pressure was close to zero (generally negative). This unusual pore pressure behaviour could be related to:

- placing the cells into unsaturated surrounding clay and enough time will remain before the water reservoir will saturate the core completely;

- properties of the core material (Beavan et al., 1977) and relatively low height of the embankment.

During the two years measurement period a rise of pore occurred but it do not follow the reservoir level exactly.

Measurement of the deformations during the operating period on the crest and faces by surveying and in depth of earth dam by means of electromagnetic torpedo in PVC vertical casings showed very small values (up to 50 mm). The dam suffered no damage during the 1986 Vrancea earthquake,  $M = 6.8$ , with strong attenuation at dam site ( $D = 370$  km).

The design and performance of powerhouse and spillway foundations are to a large extent governed by the evolution of deformation during excavation and construction processes.

A total of 26 heave gauges were installed in the proposed powerhouse and spillway excavations for field measurements of base rebound. In the main enclosure an excavation having a length of 540 m and a mean width of 125 m was at a depth between 38 m below existing level in left position and 8 m along the right border (Yugoslavian spillway position). For each gauge installation a 86 mm hole was first drilled and a telescopic plastic casing with metal rings around them (whose position is detected by magnetic torpedoes) was embedded at a predetermined depth.

Excavation base heave at various stages of excavation was measured. A maximum upward movement of

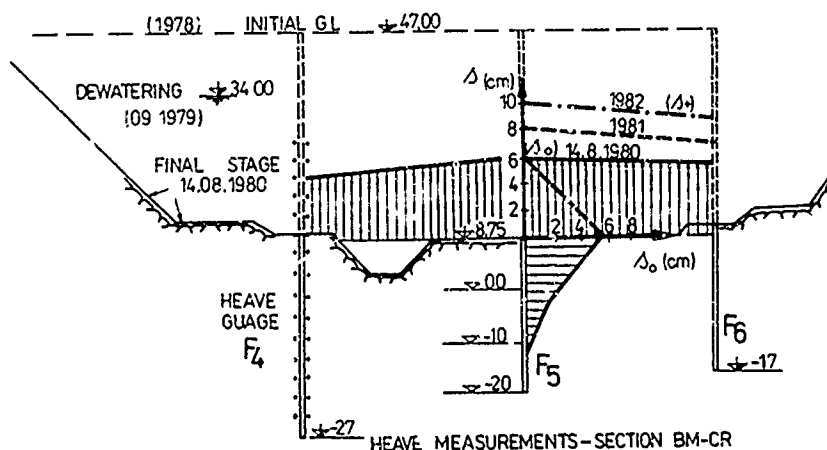
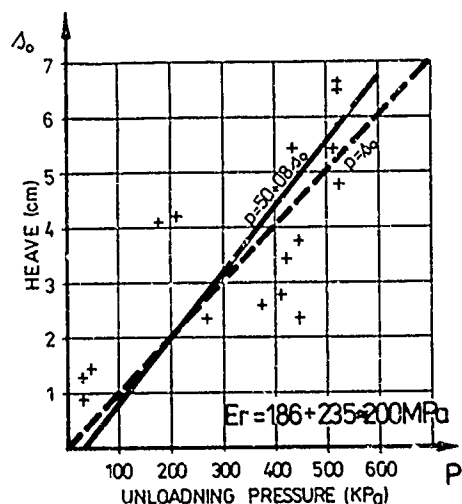


Fig.7. Field Measurements of Foundation Heave During Excavations.



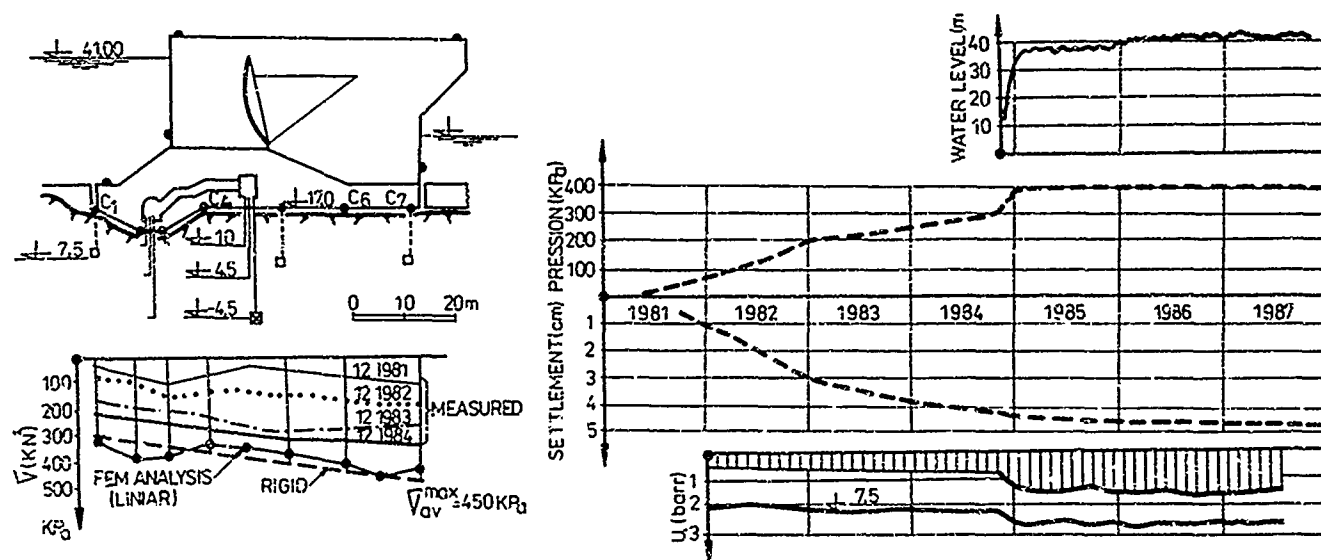


Fig.8. Spillway Dam Instrumentation Settlement and Total Pressure Recording.

10 cm was observed at gauge F 5 while the heave recorded in the spillway dam foundation was considerably less, being around of 0.5 cm. Plot of heave measurements versus pressures at various times are given in Figure 7 for profile with maximum depth of excavation (BM-R). A good correlation between the amount of the measured heave and the depth of excavation was observed, suggesting that the rebound was generally of a pseudo-elastic nature. An average field deformation modulus of 200 MPa was evaluated for the excavation stage. Factors such as the variation of rock properties across the site, and the "berm effect" (Klym et al., 1977) associated with excavated slopes were probably responsible for some discrepancies observed. The swelling process was also governed by the significant changes in pore pressures during dewatering and long time excavation schedules.

The behaviour of the foundations is monitored by: multiple rod extensometers to measure vertical movement and deformability of the bedrock; inverted pendulums for horizontal movement; water pressure cells within the rock and at the rock - concrete contact; total contact pressure cells, three orthogonal jointmeters installed in the exploratory and drainage galleries; survey target on concrete installed in galleries and at crest.

During construction a complementary system of survey targets on the upstream and downstream face of concrete block makes possible to get by direct levelling the value of vertical foundation displacement at various phases of construction. The spillway dam instrumentation scheme and foundation settlement versus load during concreting schedules, impounding, reservoir filling and the first operational years are presented in Figure 8.

The yield deformation modulus evaluated during construction is of 200 MPa for layer I (upper) and 250 MPa for intermediate stiff clay layer. There are presented recorded pressure on foundation base (level 12 mdm) and comparison between field measurements and calculated results.

## CONCLUSIONS

The second major Romanian - Yugoslavian projects "Iron Gate II" have been put into operation since 1985. The compressibility and shear strength properties were estimated by appropriate in situ tests.

An attempt has been made to a general description of the earth core material and construction procedure undertaken to place this material produced by way of foundation excavations.

The clay, sand and gravel characteristics developed from a comprehensive "in situ" and large scale laboratory tests were incorporated in static and dynamic analysis of earth dam, using the most current state of the art. According to the dynamic analysis, may be concluded that the stability analysis of earth dam using the pore pressure ratios developed after earthquake indicate the factor of safety within the acceptable limit. The maximum permanent deformation (horizontal 0.18 m and vertical 0.30 m) after an hypothetical earthquake of 7.2 magnitude can be considered acceptable without significant damage or any danger of release of water from reservoir.

The investigation of the river left bank instability has occurred during construction offered the ultimate opportunity to gain new insights and to improve the earth dam design process. The progress of foundation heave and settlement was measured during excavation and construction of concrete structures. The maximum heave recorded was about 10 cm. The movements were primarily of an elastic nature and correlated with the depth of the excavation. Rebound and compressibility moduli were computed and compared with the results of in situ loading plate tests and numerical computation.

After the first operation years the Iron Gates II structures foundations and earth dam performs successfully.

## ACKNOWLEDGMENTS

Several results presented in this paper were part of general studies carried out at the ISFH Bucharest, the firm to which the writer belongs to and has been in charge of feasibility studies, design and supervision of construction of the project. By its nature the geotechnical investigation for Iron Gates II is a team effort. The author wishes to acknowledge the collaboration of his office fellows from the Geotechnical Section and Yugoslavian geotechnical consultants. Appreciation is expressed to the Romanian Ministry of Electrical Energy and National Science and Technology Council for allowing to publish this paper.

## REFERENCES

- Anagnosti, P. (1986), "Use of Stiff Clay from Excavations of Iron Gates II Power Plant as Embankment Fill Material", Proc., 8 th Danube-European Conference on Soil Mechanics and Foundation Engineering, Nürnberg, Vol.1, 211-215.
- Banerjee, N.G., Seed, H.B. and Chan, C.K. (1979) "Cyclic Behavior of Dense Coarse - Grained Materials in Relation to the Seismic Stability of Dams", Report No.EERC 79-13, University of California, Berkeley, USA.
- Beavan, C.G., Colback, S.B. and Hodgson L.P., (1977), "Construction Pore Pressures in Clay Cores of Dams" Proc., 9 th International Conference on Soil Mechanics and Foundation Engineering, Tokio, Vol.2, 391-394.
- Booker, I.R., Rahman, M.S., Seed, H.B., (1976), "GADFEA-A computer Program for the Analysis of Pore Pressure Generation and Dissipation During Cyclic of Earthquake Loading", Report No. EERC 76-24, University of California, Berkeley USA.
- Idriss, I.M., Lysmer, J., Hwang, R., Seed, H.B., (1973), "QUAD 4 - A computer Program for Evaluating the Seismic Response of Soil Structures by Variable Damping Finite Element Procedures", Report No.EERC 73-16, University of California, Berkeley, USA.
- Klym, T.W., Lee, C.F., Debidin, F. (1977), "Heave Measurements within a Large Excavation", Proc., 9 th International Conference on Soil Mechanics and Foundation Engineering, Tokyo, Vol.2, 103-108.
- Lysmer, J., Udaka, T., Tsai, C.F., Seed, H.B., (1975), "FLUSH - A computer Program for Approximate 3-D Analysis of Soil - Structure Interaction Problems", Report No.EERC 75-30, University of California Berkeley, USA.
- Ozawa, Y., Duncan, J.M., (1973), "ISBILD - A Computer Program for Analysis of Static Stresses and Movements in Embankments, Report No. TE 73-4, University of California, Berkeley, USA.
- Pascalov, T., Milutinovici, Z., (1980), "Estimation of Seismic Parameters for Iron Gates II Dam Design" Report IZIS 80-97, Skoplje, Yugoslavia.
- Serff, N., Seed, H.B., Makdisi, F.I., Chang, C.Y. (1976), "Earthquake Induced Deformations of Earth Dams", Report No.EERC 76-4, University of California, Berkeley, USA.
- Spasici, A. (editor), (1972), "DERDEF Hydro - Energetical Navigational System (The Iron Gates)" - Export - Press, Beograd.
- Vasiliu, Al., Scvorțov, F., (1979), "The Iron Gates II - Hydroelectrical and Navigation System on Danube River", ISFH - Technical Scientific Papers, Vol.V, 74-64.
- Zienkiewicz, O.C., Clough, R.W., Seed, H.B., (1986), "Earthquake Analysis Procedures for Dams" - State of the Art - ICOLD Bulletin 52.

## Slope Stability Problems Related to a Semi-Bridge Construction

St. Christoulas

Public Works Research Center, Soils Division, Athens, Greece

E. Gassios

Public Works Research Center, Soils Division, Athens, Greece

N. Kaltefleiter

Public Works Research Center, Soils Division, Athens, Greece

G. Tsiambaos

Public Works Research Center, Soils Division, Athens, Greece

**SYNOPSIS:** In the area of "AKTEA", a summer-housing estate 36 Km away from the city of Athens, a great landslide affected the stability of a semi-bridge, constructed in 1980 for the widening of the nearby national road. Preliminary studies carried out before the semi-bridge construction and after the observed damage of most of the houses in the uphill area, favoured the existence of a very superficial creep affecting however the one or two storey buildings of the summer-housing estate.

After the semi-bridge construction, instability phenomena continued in an increasing rate and a more systematic geotechnical investigation revealed definite landslide movements (instead of a superficial creep) in a depth 2.5 to 4.0 metres below the foundation level of the piers of the semi-bridge and in a depth 6-8 m below the road level. This paper describes details of the above landslide, the investigations carried out and the remedial measures suggested.

### INTRODUCTION

The national road from Athens to Sounion, 68 Km long is of paramount importance since it is the main coastal road connecting the city of Athens (Greece) with the archeological site of Sounion passing through a series of coastal boroughs, and some of the most picturesque bays of Greece (inset to Figure 1). Serious slope instability problems have been observed between the 35 and 37 Km on this road. In particular the road and the nearby summer-housing estate of "AKTEA" located in the 36th Km have been affected by a major landslide. This housing estate was built in 1972-74 in a hilly region (40-60 meters above sea level) and in an average distance of about 160 metres from the nearby coast. The national road passes downhill from the housing estate of "AKTEA", in an elevation of about 25 metres, separating the above estate from the coastal area (Figure 1). The slope inclination varies between  $15^{\circ}$ -  $18^{\circ}$ , although locally much greater values can be observed. The slide has been active with intermittent movement for more than 30 years. It began to gather interest in the late 1960's as the summer-housing estate of Aktea was going to be founded and the old national road to be widened.

Before the estate was built a visual reconnaissance conducted by Kotzias and Stamatopoulos (1970) revealed some characteristic features of instability in the uphill region of the road, such as scarps on the ground and disturbed trees with obvious bends in their trunks. After the completion of the buildings construction some rather severe damages were noted (Figure 2) and another study was conducted by Muller (1976) which included borings (depth up to 40 metres), shafts (1.5 m diameter and up to 25 m deep) and a survey for levelling and measurement of horizontal displacements of slope surface. The results of this study led to the conclusion that the slope movement of "AKTEA" was a creep phenomenon (with a rate of displacement varying from 0.1 to 0.4 mm/day)

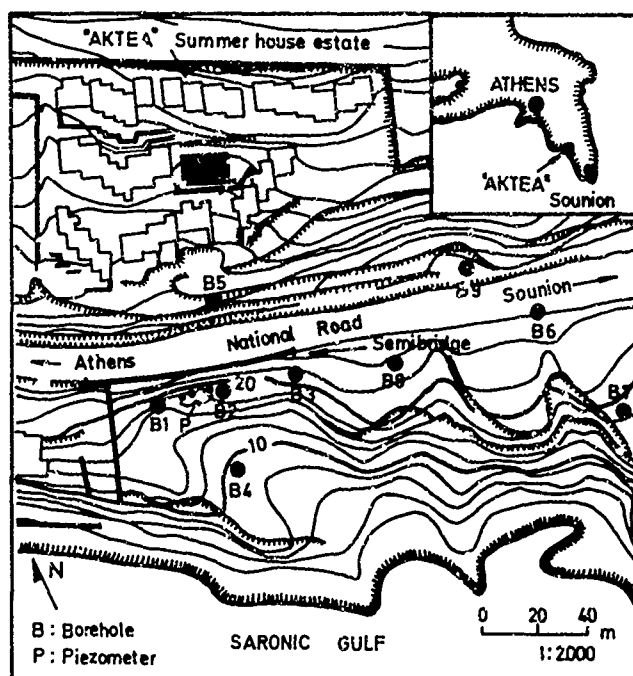


Fig. 1 Plan View of Slide Area

affecting the whole area of the estate which covers a surface of about 12000m<sup>2</sup>.

It must be noted that such sliding phenomena are easily noticeable in adjacent areas and very close to the national road as can be seen in Figure 3 where damaged and abandoned buildings due to landsliding are shown.

Later, in 1980, in order to widen the national road in this region and after taking into account



Fig. 2 Tilting of a Retaining Wall; inside the "AKTEA" Estate

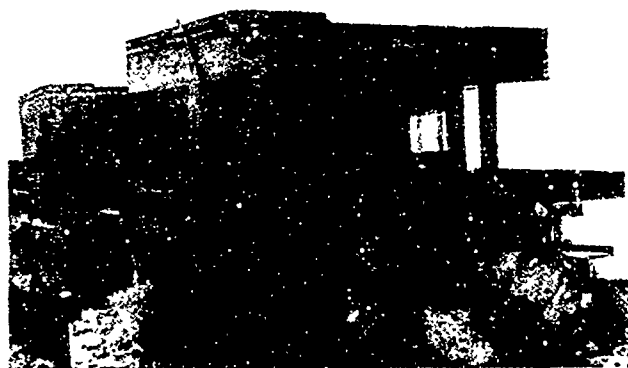


Fig. 3 Damaged Buildings due to Landsliding

the creep phenomena observed, it was decided that the best solution to the problem was by a semi-bridge construction. The piers of this bridge were founded on the sound rock and in a depth below the unstable superficial creep zone.

#### GEOLOGICAL SETTING

The broader area of "AKTEA" consists mainly of neogene lacustrine deposits, of a thickness more than 100 metres, overlying the bedrock of Triassic marble. These deposits include alternating layers of conglomerates and clayey or sandy marls with lenses or thin intercalations of sandstones. The conglomerates are well cemented and polymictic with a prominent joint set almost vertical to the bedding. The marls, brownish yellow or greyish coloured, are fissured and often laminated, and present characteristic polished surfaces with striations (slickensides). The intense microfolding and microfaulting of these marls result locally in a variation of the dip of the

strata which generally is opposite to the dip of the natural slope (dip direction of strata 10°-30°ENE).

The geological reconnaissance of some outcrops near the coast and of large excavations for building foundation close to the studied area, revealed characteristic features of synsedimentary faulting and slumping which disturbed the original structure of these deposits. Furthermore, a surficial zone of varying thickness (2 to more than 5 metres) was observed in which a rather great disturbance of rocks had taken place in the past probably due to a hillside instability which occurred during Pleistocene or even earlier. Interpretation of old aerial photographs taken before the "AKTEA" housing estate was built, showed typical characteristic features of active landslides such as scarps on the hillside and vegetation disturbance.

Finally, regarding the underground water conditions, the existence of a permanent water table is unlikely, since the water percolating the surficial zone flows through the strata of conglomerates and away from the slope. The percolation of underground water results, during wet seasons, in the moistening of the interlayers of the marls but probably without any pore pressure development.

#### PROBLEMS RELATED TO THE SEMI-BRIDGE CONSTRUCTION

The semi-bridge which was constructed for the road widening had a total length of about 60 metres and 12 spans with the sections of the roadway slab freely supported (Figures 4 and 5). During the excavation for the foundation construction the slope beside the working space was nearly vertical and without any temporary covering or support.

The rising piers have been backfilled to a new working level about three metres under the level of the existing road. The cross section of the rising piers was 0.8 X 0.8 square metres with a

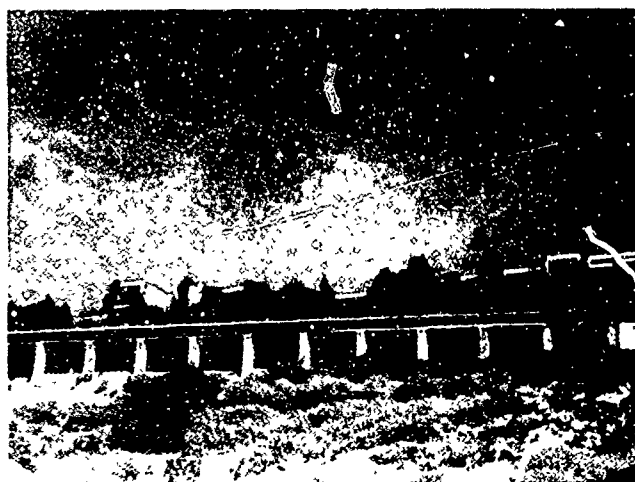


Fig. 4 View of the Semi-bridge and of "AKTEA" Summer-housing Estate

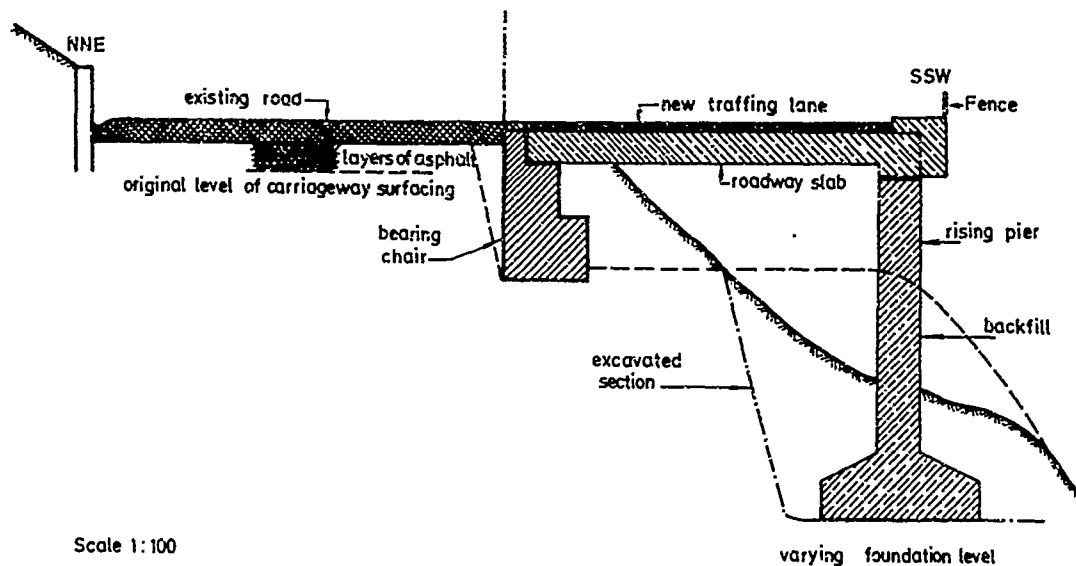


Fig. 5 Cross-section of the Semi-bridge and Details of Excavation and Backfilling

height of about seven metres. The construction of the piers was made in sections in order to avoid any risk of slope failure uphill from the semi-bridge. At that time the depth of the foundation level was considered to be satisfactory and in any case greater than the depth of the superficial creep.

A strip foundation (bearing chair) was constructed along the middle-line of the new road at an elevation of about three metres below the level of the existing road (Figure 5). The whole structure included also two wing-walls founded at about the same level as the piers.

However, two years after the completion of the semi-bridge construction some cracks appeared in the road-pavement and a rather large inclination of the wing-wall of the bridge was observed as it is illustrated in Figure 6. In addition a gradual loss of alignment of the piers and an offset increasing with time was observed as it

is clearly shown in Figure 7. These phenomena continued in an increasing rate and an extensive investigation program was planned and carried out



Fig. 7 Loss of Alignment of the Piers of the Semi-bridge

in order to have a better understanding of the cause of these movements and propose some remedial measures to solve the whole problem.

#### FIELD AND LABORATORY INVESTIGATIONS

In the narrow area of the semi-bridge, nine borings (Figure 1) were carried out in order to identify the subsurface geology, to obtain samples for laboratory testing and to install inclinometer tubes for determining the depth and shape of probable slides. Installation of four open standpipe piezometers at one single location for monitoring the underground water level was also considered necessary, even if the surface reconnaissance and previous investigations showed that



Fig. 6 Wing-Wall Tilting and Repaired Road Pavement

ground water table was almost at sea level.

Finally, a surface surveying was carried out to monitor movements of the ground surface, to determine the extent of landslide activity and the rate of movement. For this purpose the slope of "AKTEA" has been covered by benchmarks and transit stations located on stable ground and a net of hubs for which subsequent movements could be determined.

Drilling of boreholes and installation of inclinometers and piezometers was carried out in January - February of 1985 and monitoring started in March 1985 and ended in May 1987 because of the distortion of the tubes due to sliding. The surface surveying started in the summer of 1986 and is still in progress.

## RESULTS AND DISCUSSION

In Figure 8 a typical soil profile is shown based on the logging of borehole B2. As is shown in this Figure the narrow area of the semi-bridge consists of alternating layers of conglomerate, sandstone and marl, whereas the upper 1 - 2 metres consist of fill material. The thickness of the well cemented, polymictic conglomerate is about 3 metres. The sandstone is friable and marly or well cemented and its thickness varies from 3 to 4 metres. The marl is hard in greater depths and presents some slickensided surfaces. The SPT

values for the surficial layers of marl range between 10 and 30 whereas in greater depths these marls present a refuse to SPT sampler penetration.

Atterberg limit determinations on samples of marls obtained from borings, showed that most of material can be classified as CL (low to medium plasticity clays) or CH (high plasticity clays), whereas samples of friable sandstone or pockets of sand can be classified as SM (silty sand).

As it was impossible to take undisturbed samples of marl, because this was very hard and the use of thin wall samplers prohibitive, laboratory testing was restricted only to the estimation of its residual shear strength characteristics, by using the ring shear apparatus (Bromhead, 1979). The residual shear strength characteristics of marl, as found in this apparatus using remolded material with a water content approximately at the plastic limit, was  $c'_r = 0$  and  $\phi'_r = 14^\circ - 16^\circ$ . These values are very low considering other marls of various sites in Greece, (Tsiambaos, 1987), but this can be explained by the low calcium carbonate content of "AKTEA" marls ( $< 20\%$ ) as it was determined by chemical analyses.

Regarding the location of underground water level, the open standpipes showed no evidence of water above the sea level. It must be noted that for an accurate exploration of the underground water level the four standpipe piezometers were installed close, to each other and had different lengths. Their perforated sections were at different levels so that they covered totally a depth up to 25 metres. In this way any groundwater level (free or perched) could be easily detected.

The data from the inclinometers B1, B2, B3 demonstrated conclusively that slope failure was occurring along a surface 2.5 to 4.0 metres below the foundation level of the piers of the semi-bridge and in a depth 6 - 8 m below the road level. Analyses of the inclinometer B4 data installed downhill from the semi-bridge showed the existence of a slide in a depth of 8m while data from inclinometer B5 installed uphill from the semi-bridge (Figure 1) located the slide surface in a depth of approximately 5.8 m. The mean rate of movements (total horizontal displacements) was very low, locally varying between 0.6 and 2.0 cm/year, whereas the movement direction was  $N5^\circ W$  to  $N25^\circ E$ , towards the coast. The movement rate varied seasonally, being greatest in spring and early summer and least during fall and winter.

Figure 9 shows the angular variation and the resulted horizontal displacement for inclinometer B2 during the period 18.4.1985 and 19.2.1987, whereas in Figure 10 the total horizontal displacement ( $N6^\circ E$  direction) with time, is illustrated. The data from the inclinometers B6, B8 and B9, installed eastern from the semi-bridge (Figure 1) showed the same type of sliding as above in a depth of about 7.5 - 8.5 m below the surface of the new road. On the contrary, inclinometer B7 showed no evidence of sliding and so it could be considered that the location of this inclinometer is out of the limit of the observed landslide. Surface surveying which is still in progress showed a definite horizontal displacement of slope surface only in the narrow area of B6, B8 and B9 inclinometers and also a differential movement of the wing-walls of the semi-bridge.

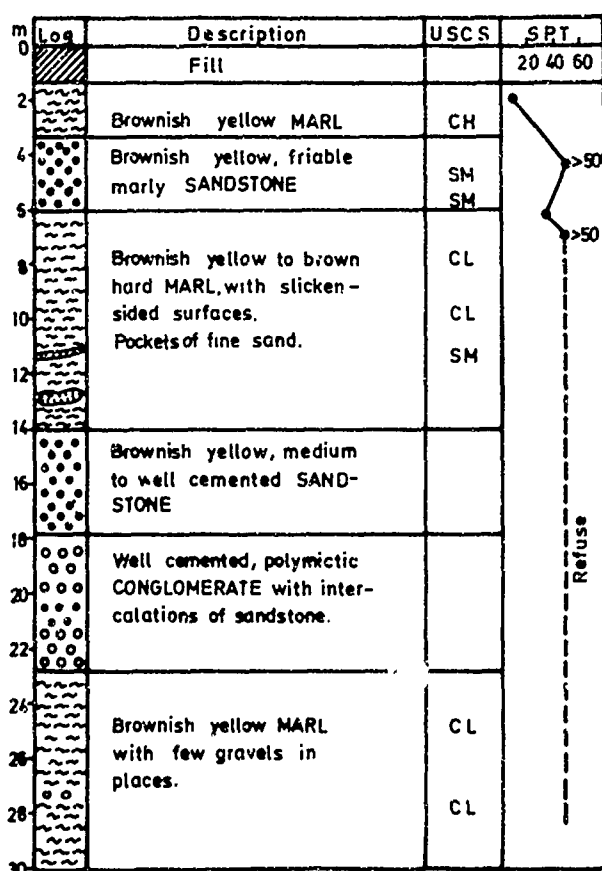


Fig. 8 Typical Soil Profile



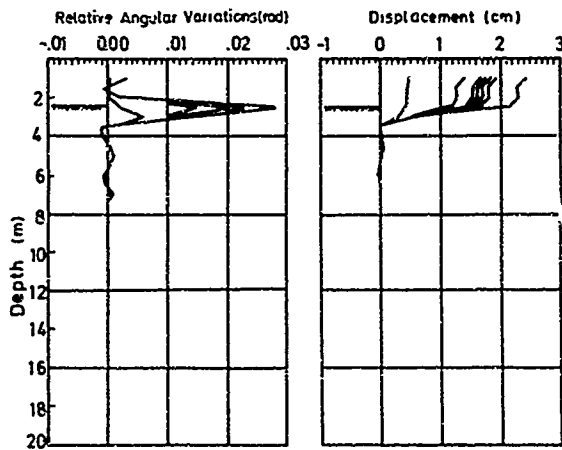


Fig. 9 Movement of Inclinator B2

On the basis of the geological data, the logs of boreholes and inclinometers data, the geological cross section across the inclinometers B5, B2 and B4, of a direction NNE to SSW, was able to be drawn as it is illustrated in Figure 11. As is shown in this Figure the slip surface is a rather undulating one which crosses the marl layers as well as the layers of conglomerates and sandstones. It must be noted that sliding takes place

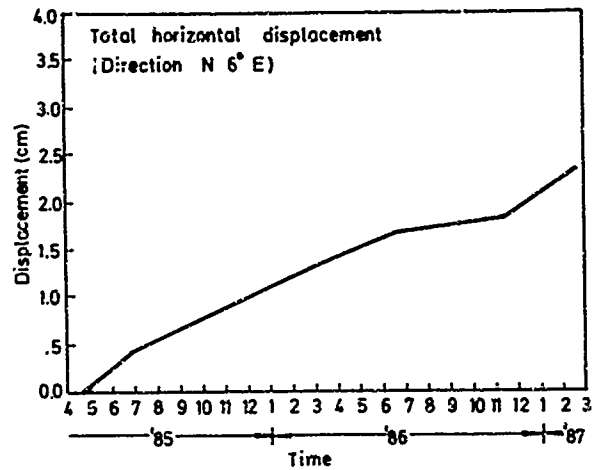


Fig. 10 Total Horizontal Displacement of Inclinator B2 with Time

through the mass of marls, but the sliding surface follows the joints and cracks of conglomerates and sandstones which are mainly subjected to extension and not to shearing. It is believed that the structure of the conglomerates and sandstones above the sliding surface has been disturbed due probably to an old landslide.

The landslide seems to extend under the bottom of

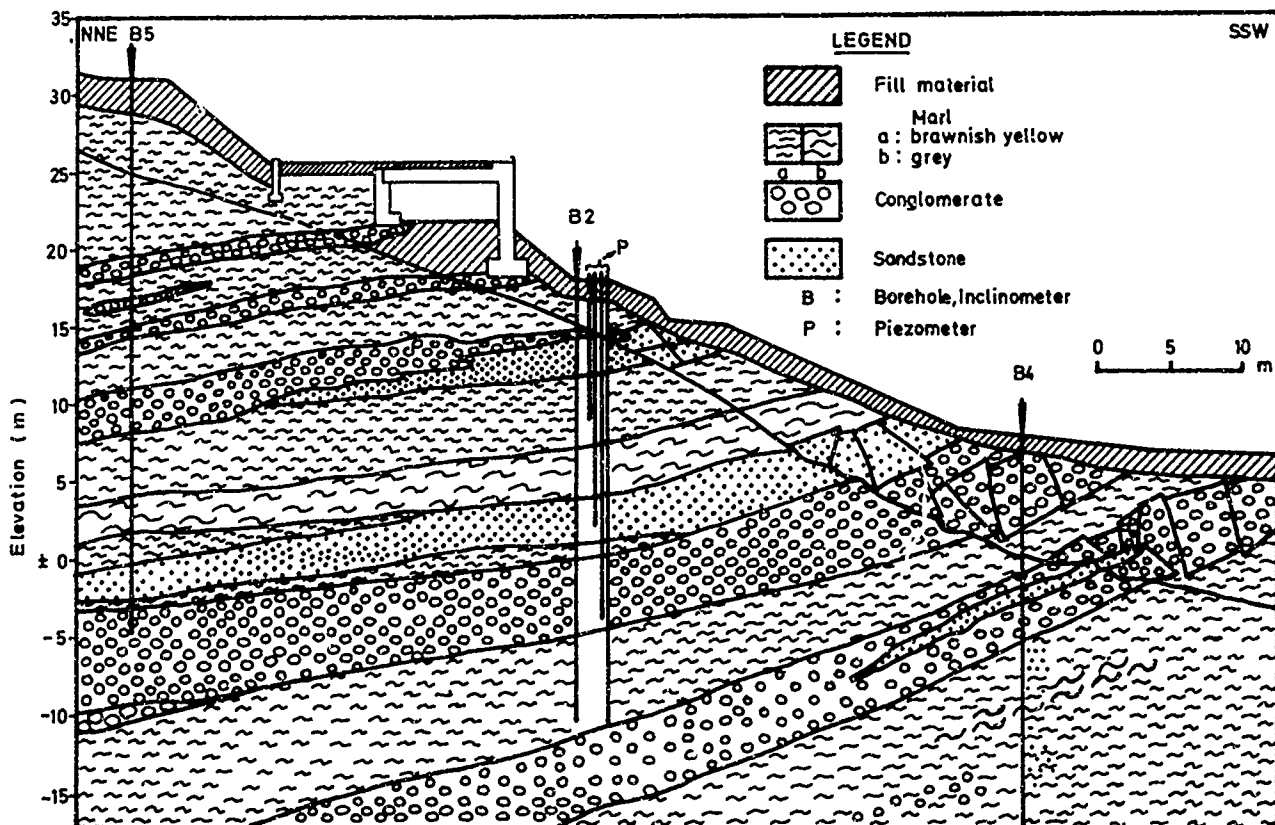


Fig. 11 Geological Cross Section and Location of Slip Surface

The landslide seems to extend under the bottom of the sea and in a remarkable distance from the coast line. Evidence to support this, are some characteristic geomorphological features on the bottom of the sea such as long open cracks and ridges which are easily observed under favorable weather conditions.

Janbu (1973) and Morgenstern and Price (1965) methods of slope stability analysis were used to analyze the slip surface assuming the sliding mass to be in a state of limiting equilibrium and a piezometric grade line coincident with the sea level. Drained strength parameters of  $\phi' = 14^\circ - 15^\circ$ ;  $c' = 0$  were backfigured as the average strength acting on the slip surface producing a safety factor of unity. It must be noted that the sections analyzed were slope configurations with : a) the crest of the landslide located in the uphill area (inside the housing estate) where the main scarps are easily noticeable, and the toe close to the semi-bridge and b) the same location for the crest of the landslide but with toe located at the sea bottom and at a distance from the coast line which is found following the curvature of the slip surface drawn in Figure 11.

The average soil strength parameters estimated from the above slope analyses were very close to the residual shear strength parameters of the marly soil confirming that : a) the landslide occurring in this area is an old one but still active and b) the major part of the length of the slip surface passes through the mass of the layers of marls.

It is well known that some actual or potential slides can be stabilized by means of piles (piers) driven or bored into stable underlying soil. In the case of the semi-bridge considered in this article, it is expected that a drilled cantilever pier wall downhill from the semi-bridge to stabilize the slope, has the advantage of being installed without significantly decreasing slope stability during its construction. In addition such a construction seems to be particularly advantageous in that it may be constructed with the minimum of excavation. It has been observed that, excavation downhill from the national road and adjacent to the area of the semi-bridge for foundation construction of a villa resulted in a large instability of the uphill region and in severe cracks of the national road pavement. Considering that, in urban areas such "AKTEA" the rights-of-way are restricted, the authors favoured and adopted the solution of a drilled cantilever pier wall suitably instrumented for future monitoring together with a series of subsidiary measures which are now under design.

## CONCLUSIONS

The conclusions that may be made from the case history concerning the behaviour and performance of the semi-bridge and analyses described in the article are as follows:

- the existence and implications of the old landslide in the area of "AKTEA" were not recognized almost 20 years ago when the works for building the summer-housing estate were designed and constructed.

- visual reconnaissance and incomplete field studies could not approach the real situation and the landslide was considered as a superficial creep.
- the monitoring of the mass movements showed definite but very slow landsliding in a depth of 6 - 8 m below the road level and 2.5 to 4.0 m below the foundation level of the piers affecting the overall stability of the semi-bridge.
- the residual shear strength parameters of marly soils obtained from laboratory testing were representative of the actual in situ mobilized strength of the soils involved and subjected to continuous landsliding.
- since, the national road from Athens to Sounion is of a great importance, the stabilization of the landslide in "AKTEA" area is an indispensable work to be done. The solution of the construction of a pier wall downhill from the semi-bridge seems to be attractive and together with some secondary remedial measures has been adopted and is now under design.

## ACKNOWLEDGEMENTS

Special thanks are due to Mr. D. Gerochristodoulou for his long hours and efforts during the field program, to Mrs. P. Florentzou for her help in editorial work and to Mrs. St. Lagoyanni who produced the typescript.

## REFERENCES

- Bromhead, E.N. (1979), "A Simple Ring Shear Apparatus", *Ground Engineering*, 12:40-44.
- Janbu, N. (1973), "Slope Stability Computations", In: *Embankment Dam Engineering*, Wiley, New York, 47-85.
- Kotzias, P.C. and A.C. Stamatopoulos (1970), "Geotechnical Reconnaissance for Buildings Foundation of "AKTEA" Summer-housing Estate", Interim Report to the Owners of "AKTEA" (unpublished).
- Morgenstern, N.R. and V.E. Price, (1965), "The Analysis of the Stability of General Slip Surfaces", *Geotechnique*, Vol. 15, 79-93.
- Müller, L. (1976), "Report on the Results of Investigation and Proposals for Measures to Retard the Slope Movements in "AKTEA" Summer-housing Estate", Interim Report (unpublished).
- Tsiambaos, G. (1987), "Engineering Geological Characteristics of Iraklion Marls", Ph.D. Thesis, University of Patras, Greece, 417 p.

# Monitoring of the Canales Dam and Its Control During Construction Period

Javier Andreu Posse

Civil Engineer, Geotechnical Division of EPTISA, Spain

Rafael Portilla Hermosilla

Civil Engineer, Geotechnical Division of EPTISA, Spain

J.M. Martínez Santamaría

Civil Engineer, Geotechnical Division of EPTISA, Spain

**SYNOPSIS:** This paper presents a study of the stress-deformation behaviour of the Canales Dam (Granada) during construction. The basis for this study has been the three dimensional (3D) finite elements method with hyperbolic material response. The analytical procedure used is presented and the study concludes with a comparative study of the results obtained from the calculation programme used and monitoring system's measurements.

## INTRODUCTION

The Canales Dam (Granada, Spain), the subject of this analysis, is an heterogeneous cross-section Dam which has limestone and slate rock fill shoulders, with a central core of clay. The transition materials are kakerite, a calcareous fragmented rock. The dam is a 155.5 metres high and the external slope is 1.7:1.

One of the main reasons for making a three dimensional model is the Dam's location in a shell offering longitudinal support on irregularly shaped di-symmetric and transversal slopes, Fig. 1.

Analysis was carried out in two stages, coinciding with the project's two technical phases: First technical phase (up to elevation 910) and second technical phase up to termination of the construction (elevation 965.5), Fig. 2.

The stress-deformation study was performed using two different but complementary methods. In the first case, a mathematical model was used by means of a three-dimensional finite elements programme simulating the process of construction of the Dam throughout successive phases of increasing loads per layer and, in the second case, the measurements taken by means of dam monitoring system equipment were analyzed. Prior adjustment of the model parameters was carried out in order to later establish a forecast of the behaviour of the Dam.

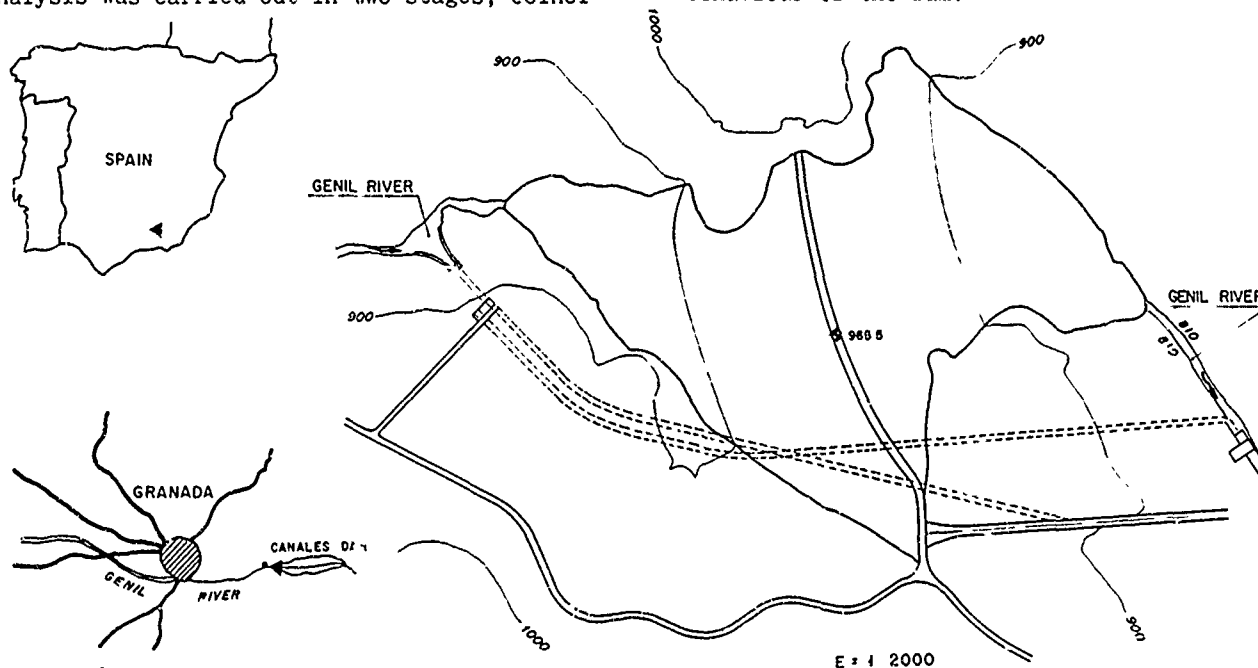


FIG.1 LOCATION MAP. PLANT OF THE DAM

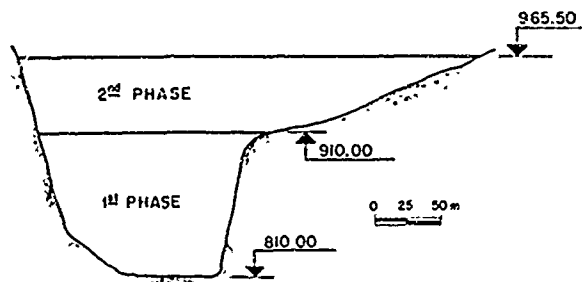


FIG.2 LONGITUDINAL PROFILE ALONG THE DAM AXIS

#### ANALYTICAL METHODOLOGY

The analytical methodology applied, is reflected in the following diagram, Fig. 3.

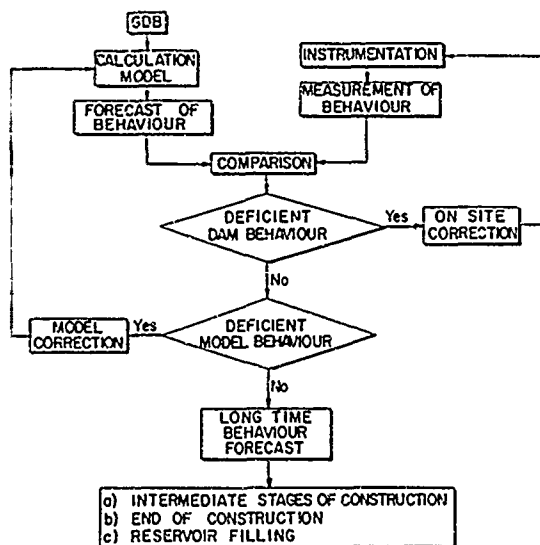


FIG.3 METHODOLOGY

#### Operation Method

The procedure has two independent inputs with a comparative phase:

1. The geotechnical data base (GDB) is used in order to obtain the calculation parameters for the mathematical model. In this respect, sampling campaigns are carried out in order to obtain the reference samples associated with each different material zone. The different tests necessary are performed under site conditions.
2. The monitoring process provides data serving as direct input to the comparison phase.
3. At the end of each of the stages foreseen in the control plan, an evaluation of the behaviour of the Dam up to that moment is performed, and the results obtained from the instrumentation are contrasted with those produced by the calculation method.

#### Calculation Model

a. Computer programme. For calculation of the stresses and movements within the body of the Dam, a mathematical model has been used via a computer programme called Fespon, which was developed at the University of Purdue by Rong-Her Chen (1981) and refined in a PRIME 2655 computer. This programme is based on application of the finite elements method to three dimensional calculation and has been designed fundamentally for use in studies of the stress-deformation behaviour of earth dams.

The programme allows the construction process of the Dam to be reproduced and simulates the incorporation of new layers of material by considering the successive layers of elements. Placing a new layer is simulated on the basis of the weight on those already existing.

When the final state of the dam calculation is finished, the effect of other external agents can be introduced, for example the effect of the water during the process of reservoir filling.

The deformability modules used by the programme are variable with the level of material deformation and confinement pressure. Specifically, the stress-deformation model proposed by Kodner and Zelasco (1963) and Duncan (1970) and better known as the "hyperbolic model" is used, Fig. 4.

Each increment in load is analyzed twice. At first, using the modules obtained from the stresses existing at the beginning of the incre-

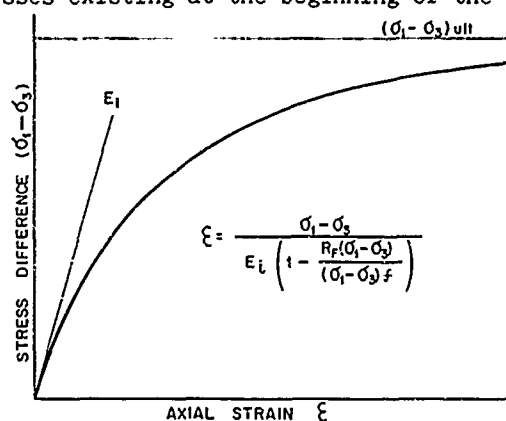


FIG.4 HYPERBOLIC MODEL

ment and then using the deformation modules obtained from the average stress values due to the initial increment analysis.

The changes occurring in stresses, deformation and movements with each increment are added to those already existing at the beginning of each new construction stage.

The Fespon programme uses incompatible isoparametric elements in calculation, i.e. elements using interpolation functions for relationships between displacements occurring within the elements and displacements of its nodes. This gives rise to excellent flexure behaviour on the part of the element, but also produces parabolic-type

incompatibilities at its limits. However, overall behaviour is better than that achieved using compatible isoparametric elements.

b. Finite element mesh. In order to carry out the study using the Fespon programme, the Dam was simulated by means of a three dimensional mesh made up of six and eight-node isoparametric elements placed such that the construction process could be reproduced by means of load increments. Simulation of the process was achieved by the placing of ten layers, recommended by Rong-Her Chen (1981), Schiffman (1977) and Marsall (1975), in order to obtain sufficient accuracy. The minimum thickness of these layers was ten metres and the maximum, 25 metres.

The remaining element magnitudes were adapted to the finite elements theory, which recommends the use of elements whose respective magnitudes are not excessively differentiated in order to achieve reliable results. In this respect, a valid ratio value should be between 1.5 and 2, transversal distribution with the Dam transversally distributed in 13 sections.

The number of elements into which the Dam was simulated was 556, with a total of 842 nodes, Fig. 5.

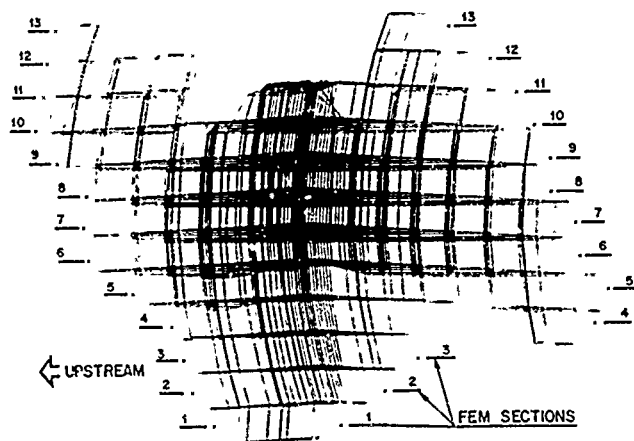


FIG. 5 DIAGRAM OF FINITE ELEMENTS MESH (FEM)

c. Materials characterization (Fig. 6). In order to determine the resistance and deformation parameters needed for calculation, the following process was used:

Study of materials characteristics based on laboratory and field tests, fundamentally tri-axial and shear tests respectively, during the first and second construction phases -estimation of basic calculation parameters- sensibility analysis of the values within the variation range, by means of the finite elements programme and comparison with the real measurements obtained from the instrumentation.

#### Monitoring System

In this study, the values obtained from the hy-

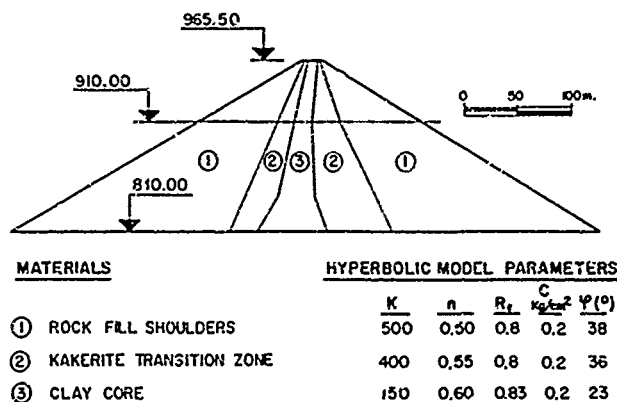
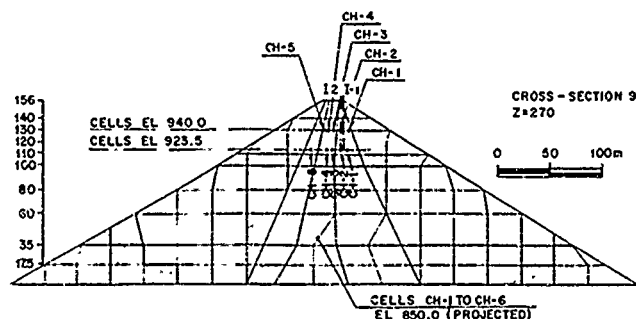


FIG. 6 TYPICAL DAM CROSS-SECTION

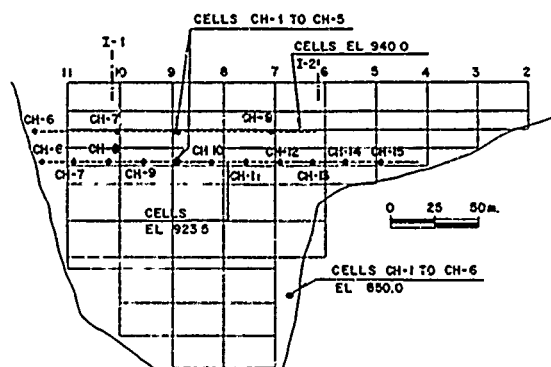
draulic settlement cells and horizontal displacement measuring inclinometers have been taken into account, Fig. 7.

The cells are located on three levels at elevations 850.0, 923.5 and 940.0

Inclinometers I1 and I2 are located in the vicinity of the left and right hand banks respectively.



a) TRANSVERSAL CROSS-SECTION



b) LONGITUDINAL SECTION

FIG. 7 LOCATION OF SETTLEMENT CELLS AND INCLINOMETERS

## RESULTS ANALYSIS

### General

Before analyzing the stress-deformation state results for the Dam, the following observations on the calculations carried out should be taken into account:

- The methodology used during discretization of the dam's body, involve some problems of accuracy, due to:

1. Sudden changes in geometry and typology of the elements, conditioned by the relative location of the materials, contact with the bed rock and outer slopes.

2. Contact in steps on the right hand bank and vertical contact on the left.

3. Size of the elements, especially in the bottom of the Dam.

- The Fespon program, after each incremental layer made nule displacements in the top nodes, wich simulate the fact that the end of construction has really happened at crown level.

- The non-deformability of the foundation in order to simplify the element mesh, leads to small errors given the high degree of relationship between the deformation modules of the rock and the materials used in the Dam.

- It should be pointed out that when comparing the readings from the instruments with the model, we have taken into account the fact that the measurements obtained from the cells corresponding to a given height of dam above the cell, including an initial and immediate settlement which occurs when the overload is increased, and a second long-time consolidation settlement process due to readjustment of the material particles, which is a function of the friction of the solid framework and the viscosity of the water surrounding the surfaces in contact. The rate of this last deformation reduces with time and finally reaches zero on termination of the phenomenon, wher a certain solidification of the material occurs.

The model calculates final deformations while the readings taken during construction do not reflect the total deferred consolidation. This means that in comparing the model and data from instruments, the deformations corresponding to settlement time curve asymptotic values must be considered. Given the shape of these curves, this has not meant increments above 10% with respect to previous readings recorded for a given elevation.

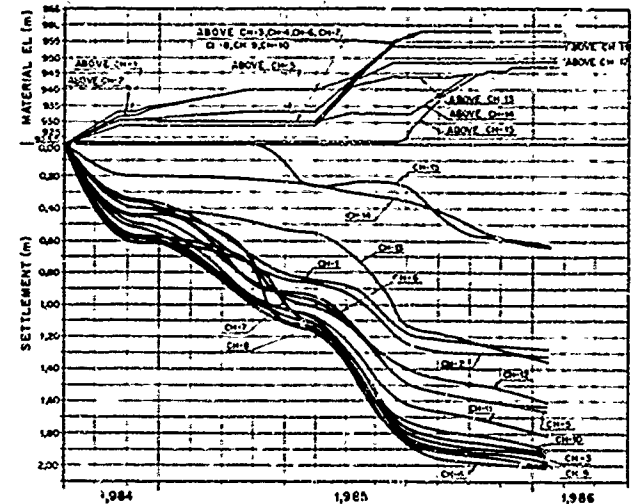
- A run was also performed without including the right hand part of the Dam above elevation 920, whose construction did not begin until the height of the central part of the Dam was at elevation 955. The results obtained have beer very similar to those corresponding to the overall Dam, with maximum deviations of 10% or less with respect both to displacements and stresses.

### Model Monitoring System Contrast. End of Construction

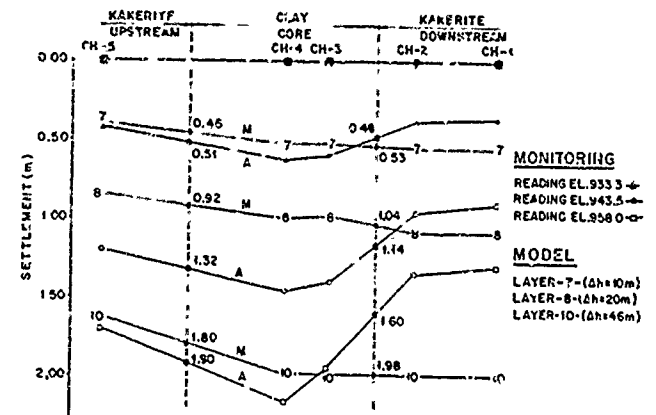
### a. Hidraulic cells.

Comparison between monitoring system and model adjustment were performed during the period between installation of the cells at elevation 923.5 (2nd October, 1984) and practically the end of the construction period with the Dam at elevation 958.0 on the 17th January, 1986.

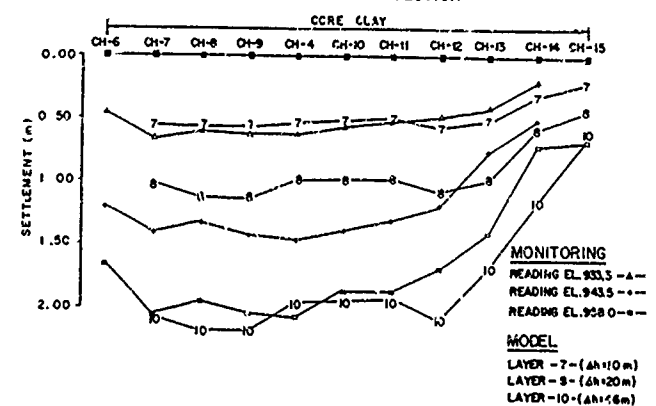
- Elevation 923.5, Fig. 8. Contrasts were carried



### a) READINGS FROM CELLS EL. 923.5



### b) CONTRAST IN TRANSVERSAL CROSS-SECTION



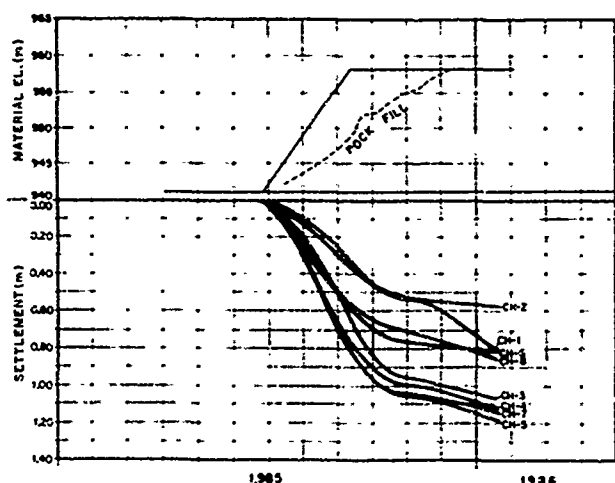
### c) CONTRAST IN LONGITUDINAL-SECTION

Fig. 8 CELLS EL. 923.5 MODEL-MONITORING SISTEM CONTRAST

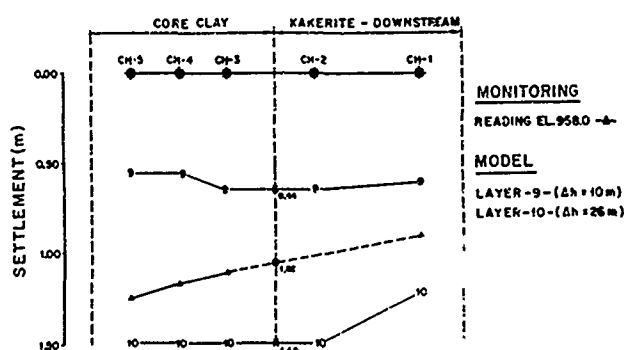
out in two directions perpendicular and parallel to the axis of the Dam by means of cells CH1 to CH5 and CH6 to CH15.

In the transversal cross-section, where the significant comparison values are those corresponding to the Dam core-kakerite contact points, the most significant points of contrast are the following:

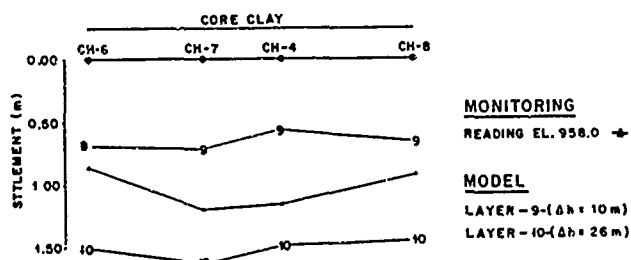
1. For an overload of 10m, contrast is good with deviations below 10%.
2. For an overload of 20m, the above values are maintained downstream, while upstream the deviation reaches 30%.



a) READINGS FROM CELLS EL. 940.0



b) CONTRAST IN TRANSVERSAL CROSS-SECTION



c) CONTRAST IN LONGITUDINAL-SECTION CORE CLAY

Fig. 9. CELLS EL. 940.0 MODEL-MONITORING SYSTEM CONTRAST

3. With regard to the final phase of reading, with a difference in overload ratio of 0.75, the direction of contrast established in point b. is inverted, giving a total maximum deviation of 24% which, following application of the above ratio, is reduced to 20%.

With respect to the longitudinal section the contrast is analogous to that established above, with a maximum deviation of 30% corresponding to an overload of 20m.

- Elevation 940, Fig. 9. Contrast was performed with the Dam at elevation 958, 18m above the cells.

On the basis of the results, it is estimated that on termination of construction of the Dam, the deviations with respect to the model will be below 20%.

#### b. Inclimometers

The readings recorded have given displacements for upstream and left hand-limit orientations on the order of 15 centimetres in both directions. The results obtained from the models, give values of around 10 cm upstream and practically nil in the perpendicular direction.

#### Deformations

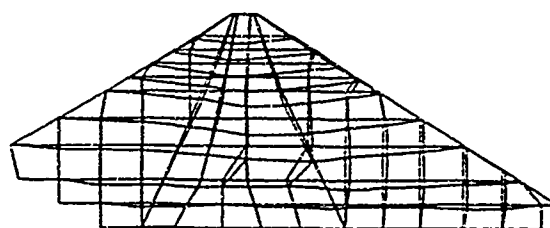
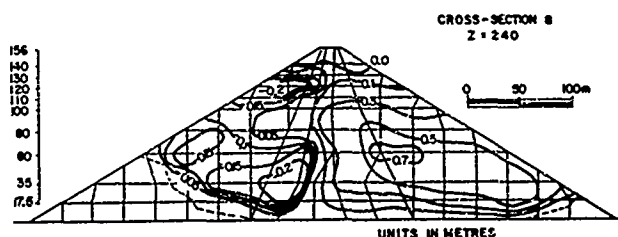
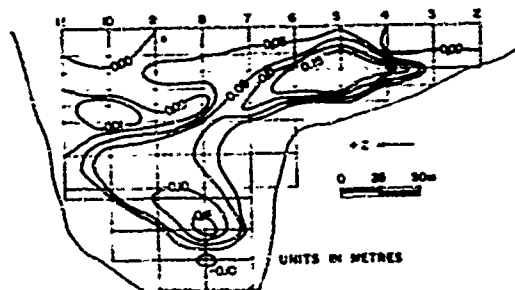


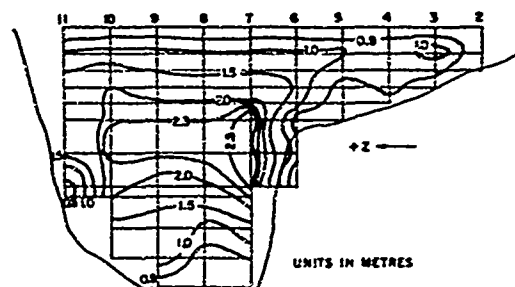
Fig. 10 DEFORMED TYPE TRANSVERSAL CROSS-SECTION



In order to obtain an overall idea of the behaviour of the Dam at the end of construction time, a deformation diagram of the central section of the Dam has been drawn, Fig. 10. along with the vertical and horizontal iso-displacements lines and a longitudinal cross-section along the axis of the core, Figs. 11 and 12.



a) ISO-LINES FOR HORIZONTAL MOVEMENTS Z



b) SETTLEMENT ISO-LINES

Fig. 12 LONGITUDINAL CROSS-SECTION.MOVEMENTS

### Stresses

In general terms, stresses tend to show a parallel orientation with respect to the slopes and material change surfaces.

The range of maximum stress has varied between 20 and 30 kg/cm<sup>2</sup> with the exception of certain elements at the contact points between the core and kakerite and Dam foundation in the higher sections and in others having singular geometries.

There are almost no elements in tension and only a small group of triangular elements and other elements located at the upstream point of contact between the rock fill and the kakerite have been plasticised, possibly due to excessive stresses arising as a result of the high degree of deformability of the clays in this area.

### CONCLUSIONS

The analysis carried out shows general deviations between the model and data measured of between 10 and 20% over absolute values of between 1 and 2 metres.

The maximum settlement is 2.45 metres, wich implies 1.6% of the total height of the Dam.

Horizontal movements maintain the tendency of

the Dam to open under its own weight, with values of 20 and 60 centimetres upstream and downstream respectively.

The normal range of maximum stresses is between 20 and 30 kp/cm<sup>2</sup> except in the case of certain elements in contact with the foundation and located below the maximum Dam heights.

### REFERENCES

Rong-Her Chen (1981) "Three-Dimensional Slope Stability Analysis", Purdue University, West Lafayette, Indiana.

Kondner and Zelasco (1963) "Hyperbolic Stress-Strain Formulation for Sands", Proceed. 2 nd Pan-American Conf. on Soil Mech. and Found Eng. Brazil.

Kondner R.L. (1963) "Hyperbolic Stress-Strain Response: Cohesive Soils" ASCESM-1, February.

Duncan, J.M. and Ching Yun Chang (1970) "Non-Linear Analysis of Stress and Strain in Soils", ASCESM-5, September.

Schiffman (1977) "Computer in Soil Mechanics Present and Future", 9th International Conf. on Soil Mech. and Foundation Eng., Tokyo.

Marsall, R.J. and Resendiz Nuñez, D. (1975) "Presas de Tierra y Enrocamiento", Ed. Limusa, Mexico.



## Performance of a Coal Refuse Embankment

David C. Cowherd

President and Chief Geotechnical Engineer, Bowser-Morner Associates, Inc., Dayton, Ohio

Vlad G. Perlea

Senior Engineer, Bowser-Morner Associates, Inc., Dayton, Ohio

Alvin Coulson

Civil Engineer, American Electric Power Service Corporation, Processing Engineering, Lancaster, Ohio

**SYNOPSIS** Continuous determinations of density, moisture content, and permeability through a 140-foot high coarse refuse embankment impounding slurry were made. The density determinations were made with nuclear moisture-density depth gauges continuously throughout 120-foot depth of the embankment. The permeability tests were made with a special packer permeability device and were conducted throughout the 120-foot depth of the embankment. Compaction density tests were made during compaction of the refuse. Comparisons were made to design, as-compacted, and in-place permeabilities, densities, and phreatic surface within the embankment. The study shows that coarse refuse embankments compacted in roughly 18-inch lifts with a special dozer and haulage equipment perform well in terms of comparisons of in-situ parameters to design parameters for seepage, density, and strength.

### INTRODUCTION

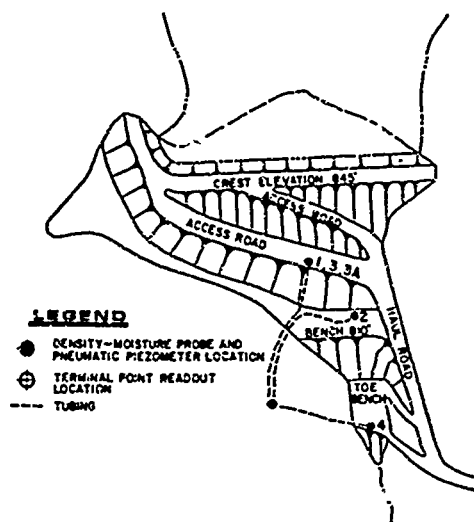
Two waste products are created by coal processing plants. The first is coarse refuse consisting of the non-coal material mined along with the coal, generally defined as being the +28 mesh sieve material. The second is fine refuse or slurry which is a by-product of the washing of the coal and is generally the -28 mesh material. The usual method of disposal of these two waste products is the construction of an embankment utilizing the coarse coal refuse and pumping of the slurry or fine coal refuse behind the embankment. The laboratory measured vertical coefficient of permeability of coarse coal refuse is usually on the order of  $10^{-4}$  cm/s and relatively large amounts of seepage from such an impoundment are generally calculated.

Typical design analyses of seepage from such an embankment usually assume the embankment impounds water and utilize the permeability of the coarse refuse to predict seepage. This procedure usually greatly over-estimates seepage as the fine coal refuse when settled generally has a coefficient of permeability on the order of  $10^{-5}$  to  $10^{-7}$  cm/s. In a normal disposal process the slurry is usually deposited near the face of the embankment creating a relatively low permeability material on the upstream face of the embankment and very little water is impounded on the slurry. The factor controlling seepage is, therefore, the permeability of the slurry and not that of the coarse refuse.

It is also generally thought that higher degrees of compaction of coarse refuse reduce the permeability and increase strength. Very little information relative to in-situ permeability and strength parameters for coarse refuse in actual embankments exists. This paper presents the data generated in an evaluation of the permeability, density, and strength of coarse refuse in an actual embankment. An embankment constructed of coarse refuse placed with standard in the industry compaction techniques, approximately 140 feet in height, was chosen for evaluation of the in-situ density, moisture content, and permeability.

The embankment chosen for study is a coarse refuse embankment with an earth starter dam. Construction on Stage I of the embankment was begun in 1979, with refuse placement beginning in January, 1982. At the time of this study, the embankment was approximately 140 feet high with a total of about 1.2 million cubic yards of refuse having been placed. The original specifications for the project required 90% of standard Proctor dry unit weight as a compaction specification. The method of placement of the refuse was a D-8 dozer tracking the refuse in roughly 18-inch lifts, and rubber tired scrapers hauling the refuse. No compaction equipment was used.

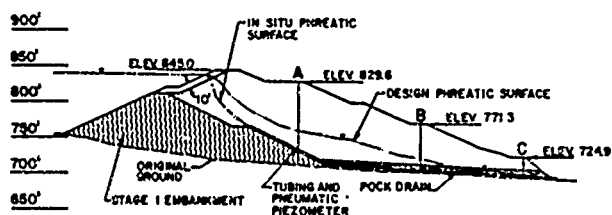
This evaluation was designed to compare design parameters to as-placed and in-situ parameters. Tests were performed on the coarse refuse as a part of the initial design. These tests included strength, permeability and other index testing. Subsequent to the design, the coarse refuse was placed and some 214 field density tests were performed during construction. A method was devised to determine in-situ density and moisture by nuclear depth-density and moisture gauges to obtain a continuous determination of density and moisture for about 120 feet of refuse. Moisture and density readings were made with the nuclear gauge at 1-foot intervals from elevation 829 feet to elevation 706 feet. In addition, bore hole permeability tests were performed with a special packer permeability device to obtain a continuous determination of permeability from elevation 829 feet to elevation 706 feet. Figure 1 shows the location of the test probes. In addition to this testing, conventional test borings were made and samples were obtained for triaxial and other index testing on the refuse. Pneumatic piezometers were installed to determine the in-situ phreatic surface for comparison with the design phreatic surface. This paper describes the results of the testing of the in-situ refuse and compares it to the design data and the as-compacted data.



**Fig. 1 Stage III Construction of the Embankment, at the Time of the Study**

### EMBANKMENT DESCRIPTION

The Muskingum refuse embankment for American Electric Power Service Corporation is located at Central Ohio Coal Company in Morgan County, Ohio. The project was initially designed and permitted in 1979 as a coarse refuse embankment impounding slurry. The starter embankment for the project was an earthfill embankment to elevation 805 feet. The starter embankment contained approximately 75,000 cubic yards and was completed in 1979. The remainder of the embankment is constructed of coarse refuse placed as downstream construction. The final planned embankment has several stages of coarse refuse with a top elevation of 885 feet. At the time of this study, the embankment was in Stage I11 with the configuration being approximately as shown on Figure 2. The top elevation of the embankment was about 845 feet and the embankment contained approximately 1.2 million cubic yards.



**Fig. 2 Cross-Section of the Embankment at the Time of the Study**

### INITIAL DESIGN DATA

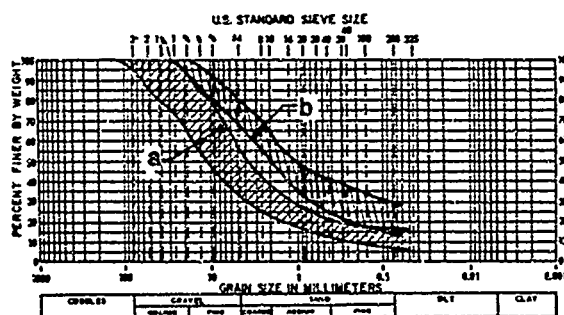
Samples of the various materials to be utilized in the embankment construction were obtained in an original exploration during 1979 and appropriate testing was performed. Samples of the coarse refuse from which the embankment would be constructed were obtained from the

preparation plant. Shear, permeability, and index testing were performed as a part of the design report. Table I details the initial design data.

Table 1. Initial Design Data for Coarse Refuse

| Parameter                                | Value                     |
|--|---------------------------|
| Classification                           | "GP-GM" to "GM"           |
| Maximum Standard Proctor Dry Unit Weight | 129.4 pcf                 |
| Optimum Moisture Content                 | 5.8%                      |
| Vertical Permeability                    | $1.1 \times 10^{-4}$ cm/s |
| Approximate Gradation                    |                           |
| Gravel                                   | 48% to 66%                |
| Sand                                     | 27% to 38%                |
| Silt and Clay                            | 7% to 14%                 |
| Specified Degree of Compaction           | 90%                       |
| $\phi'$ at 90% Compaction                | 36.4°                     |
| $C'$ at 90% Compaction                   | 0.0                       |

Figure 3 shows the gradation range (a) of the coarse refuse as initially tested.



**Fig. 3 Gradation Range for Refuse: a. Design; b. In-Situ**

A phreatic surface was calculated using a standard Casagrande construction. The phreatic surface for the design is as shown on Figure 2. An assumption was made in this calculation that the permeability of the coarse refuse was 100 times that of the slurry and that the horizontal permeability of the coarse refuse was equal to four times the vertical permeability. A 10-foot thick cohesive cover and a rock drain were designed to control seepage.

### PLACEMENT TECHNIQUE AND ORIGINAL COMPACTION DATA

It was decided to place the coarse refuse in approximate 18-inch to 2-foot lifts as experience had shown that equipment tracking the material could compact an 18-inch

lift to 90% of the maximum standard Proctor dry unit weight. The equipment hauling the refuse to the site was rubber tired scraper equipment. Compaction was accomplished by a D-8 dozer spreading and tracking the material and by the haulage equipment. This technique proved satisfactory to achieve greater than the required 90% standard Proctor dry unit weight and has been used throughout the placement of the refuse.

Approximately 214 density tests have been performed as a part of the inspection program to date. The average of those tests for each 5-foot lift of refuse are plotted on Figure 4.

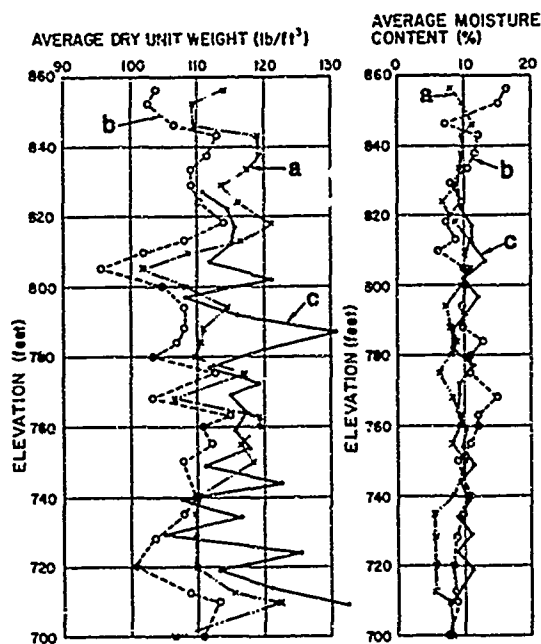


Fig. 4 Results of Measurements: a. Laboratory Standard Proctor; b. As-Compacted Values; c. In-Situ Measurements After Completion of the Embankment

As the refuse was being placed the character changed from time to time and standard Proctor tests were periodically performed to achieve proper control of the placement. A total of thirty-five standard Proctor tests have been performed. The average values for 5-foot lifts are shown in Figure 4.

The overall average degree of compaction of the refuse embankment from date of starting to the time of study was 95%. The construction specifications required 90%. Overall compaction moisture content varied between 6.2% and 16.4% with the average moisture content at compaction being 10.5%. The optimum moisture content of the coarse refuse from the various standard Proctor tests varied between 5.7% and 11.3%. A weighted average shows that the embankment was compacted at an average moisture content approximately 1.9% over the optimum moisture content as achieved by the standard Proctor tests. The original strength testing was performed at approximately 1% over optimum. Table II presents the average of the various parameters after compaction from 1982 through October of 1984, which represents some 1.2 million cubic yards of refuse placed.

## CONDITIONS AT THE TIME OF STUDY

A testing program was devised to determine the in-situ density, moisture content, permeability, gradation, strength, and phreatic surface. This program was designed to provide continuous determinations of density, moisture, and permeability throughout the depth of the embankment.

Table II. As Compacted Average Parameters

| Parameter                                     | Average Value |
|---|---------------|
| Average Percent Compaction                    | 95%           |
| Overall Average Dry Unit Weight of Embankment | 107.8 pcf     |
| Average Moisture Content of Embankment        | 10.5%         |
| Percentage Moisture Above Average Optimum     | 1.9%          |
| Average Standard Proctor Dry Unit Weight      | 113.4 pcf     |
| Average Optimum Moisture Content              | 8.6%          |

### 1) In-Situ Density and Moisture Content

The density and moisture content from elevation 829 feet down to elevation 705 feet were determined in 1-foot intervals utilizing depth nuclear gauge. The gauges used were Troxler depth-density and moisture gauges. The depth gauge is equipped with an 8 millicurie source of Cesium 137. The moisture gauge is equipped with a 3.5 AM-241/BE source. The density gauge works by emitting gamma rays into the soil. Some of these gamma rays are absorbed by the soil and some are reflected back to a detector. The denser the soil the more gamma rays are absorbed and the fewer are returned. It is possible to calibrate the gauge to density and this technique has been in use for determining density of materials since about 1950. The moisture gauge works on the principle of emitting fast neutrons into the soil. The fast neutrons are "slowed" by hydrogen atoms and counted as "slow" neutrons. The moisture content can, therefore, be determined from the nuclear readings. This technique has also been in use for about 35 years.

The density and moisture gauges were calibrated to the refuse. The purpose of calibrating the nuclear gauge is to establish a calibration curve relating nuclear gauge counts to total unit weight values. This calibration procedure was conducted in the field utilizing coal refuse from the site being studied by obtaining nuclear density readings at different density states. Coal refuse was collected in sufficient quantity to fill a calibrated barrel (approximately 8 cubic feet) and three density states were used. A metal tube was placed in the calibration barrel, the barrel was filled with coal refuse, and nuclear readings recorded. After each density state was evaluated in this manner the calibration curve was developed.

The nuclear moisture gauge calibration was made in conjunction with the density calibration. Nuclear moisture gauge readings were recorded for each density state. The moisture content was determined and the calibration curve developed.

The density and moisture content were determined with the nuclear gauge every foot throughout the embankment. A total of 120 density and moisture content determinations of the in-situ material were made during this study. Figure 4 shows the average density and moisture contents for each 5-foot increment throughout the depth of the embankment. The percentages for compaction shown in Figure 5 were calculated by utilizing appropriate standard Proctor curves for the various elevations of refuse from the initial inspection data. It can be calculated from Figure 5 that the following average conditions exist in the embankment to date (Table III).

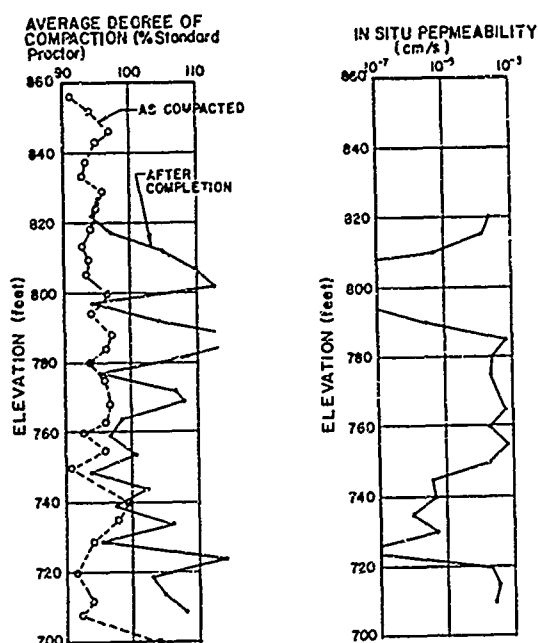


Fig. 5 Results of In-Situ Measurements

Table III. In-Situ Average Parameters

| Parameter                                     | Average Value |
|---|---------------|
| Average Percent Compaction                    | 102.2%        |
| Overall Average Dry Unit Weight of Embankment | 116.0 pcf     |
| Average Moisture Content of Embankment        | 10.1%         |
| Percentage Moisture Above Average Optimum     | 1.5%          |
| Average Standard Proctor Dry Unit Weight      | 113.4 pcf     |
| Average Optimum Moisture Content              | 8.6%          |

## 2) In-Situ Permeability Testing

Permeability testing was performed by a double end packer permeability device inserted below the casing as the casing for the nuclear density and moisture meters was being removed. The casing was removed in 5-foot increments and 5-feet of coarse refuse tested at one time. The flow of water through the 5-foot perforated packer pipe was calculated over a 10 minute period of time. Utilizing the flow, the area being tested at any given time, and the total head being applied, the permeability for each 5-foot section was calculated. The permeabilities are plotted on Figure 5. The above-referenced values obviously represent horizontal permeabilities. In most areas the horizontal permeability varies between about  $10^{-4}$  cm/s and  $10^{-6}$  cm/s. Some areas were found in which no water was taken indicating that there are zones in which the embankment is relatively impermeable. The overall average permeability of the embankment discarding those areas of zero permeability is  $2.31 \times 10^{-4}$  cm/s. The average horizontal permeability used in the design was  $1.6 \times 10^{-4}$  cm/s.

## 3) In-Situ Gradation

In addition to the above testing, samples were obtained for various parameter testing. The samples between elevations of different permeabilities were combined and an overall gradation test was performed on those samples. These areas were chosen to coincide with the higher and lower permeability zones. Table IV lists the pertinent factors relative to the grain size of the material in these zones.

Table IV. In-Situ Gradation Data

| Elevation Range (ft) | Classification | % Gravel | % Sand | % Silt & Clay | D <sub>30</sub> (mm) | D <sub>60</sub> (mm) |
|----------------------|----------------|----------|--------|---------------|----------------------|----------------------|
| 820.0-824.0          | SM             | 27       | 56     | 17            | 0.23                 | 2.52                 |
| 794.0-805.5          | SM             | 25       | 46     | 29            | 0.09                 | 2.00                 |
| 786.5-787.5          | SM             | 29       | 55     | 16            | 0.85                 | 3.59                 |
| 779.0-786.5          | SM             | 22       | 54     | 24            | 0.18                 | 2.15                 |
| 760.0-765.0          | SM             | 33       | 53     | 14            | 0.69                 | 3.74                 |
| 734.5-745.5          | SM             | 30       | 47     | 23            | 0.17                 | 2.79                 |

Figure 3 shows the gradation range (b) for the samples tested.

## 4) In-Situ Strength Parameters

Strength tests performed on undisturbed samples of the coarse refuse material yield the following values in comparison with design values.

Table V. Comparison of Design Strength to Actual Achieved Strength

| Samples                       | Type of Material  | Effective Strength Parameters     |                    | Avg. Dry Unit Weight (pcf) | Avg. Moisture Content (%) |
|-------------------------------|-------------------|-----------------------------------|--------------------|----------------------------|---------------------------|
|                               |                   | $\sigma' \text{ (}^\circ\text{)}$ | $c' \text{ (psi)}$ |                            |                           |
| Laboratory Compacted (Design) | Black Coal Refuse | 36.4                              | 0.0                | 117.8                      | 6.3                       |
| Undisturbed (Actual)          | Black Coal Refuse | 39.3                              | 0.0                | 102.1                      | 10.8                      |

Table V shows that the in-situ samples tested were at lower densities than the design tests (as well as the overall average for the embankment) and that the strength values are higher.

#### 5) In-Situ Phreatic Surface

In order to establish the current phreatic surface three pneumatic piezometers were installed. The piezometer works by applying pressure through a 3/16-inch polyethylene tubing to the piezometer point and reading the pressure which is equivalent to the head of water in the boring. These piezometers were installed at the junction of refuse and original soil. The depth and elevation of the three piezometers are shown in Figure 2.

After the piezometers were installed they were back-filled with 5 to 10 feet of sand to provide a filter around the piezometers. The boring was then closed off with 5 to 10 feet of bentonite pellets and the remainder of the hole filled with on-site material. The leads for the piezometers were buried in a trench and covered with refuse. They were then trenched into a manhole on the left abutment for a permanent installation. These piezometers were read at various times after the installation. Table VI shows the piezometer readings along with the elevations of the water level in each piezometer.

Table VI. In-Situ Phreatic Levels

| Piezometer | Elevation of Piezometer (ft) | Elevation of Water Surface (ft) |
|------------|------------------------------|---------------------------------|
| A          | 732.6                        | 733.5                           |
| B          | 707.4                        | 711.0                           |
| C          | 686.9                        | 690.0                           |

The above information was used to plot the actual phreatic surface in-situ. It can be seen from Figure 2 that the actual phreatic conditions within the embankment are much lower than those assumed during design. This is partially because the design conditions considered the embankment to be retaining water when in actual fact the embankment retains fine refuse which in itself has a relatively low permeability. There is very little water actually perched on top of the slurry and the actual flow conditions are considerably less than those calculated by assuming the embankment to be retaining water.

#### CONCLUSIONS

##### 1) Permeability and Seepage

Very little correlation between permeability and percent compaction within the coarse refuse embankment was noted. The permeabilities were performed continuously from top to bottom and coincided with various different densities. Figure 5 shows the plots of degree of compaction and permeability. It will be noted from Figure 5 that higher permeabilities do not necessarily coincide with lower densities, nor do lower permeabilities coincide with higher densities. The greater effect on permeability for coarse refuse is the grain size distribution, not the degree of compaction. Coarse refuse is basically a sand and gravel with a percentage of fines. The data shows percentage of fines in relationship to the percentage of the other size fractions within the total mix is what controls the permeability of the coarse refuse. Table VII shows the average permeability versus density and percentage of each fraction for each 5-foot level throughout the embankment.

Table VII. Comparison of Permeability to Percent Compaction and Grain Size

| Elevation Range (ft) | Permeability (cm/s)   | % Compaction | Average Dry Unit Weight (pcf) | % Gravel | % Sand | % Silt & Clay | D <sub>50</sub> (mm) |
|----------------------|-----------------------|--------------|-------------------------------|----------|--------|---------------|----------------------|
| 827.6-822.6          | 0                     | 95.3         | 110.7                         |          |        |               |                      |
| 822.6-817.6          | $2.46 \times 10^{-4}$ | 94.5         | 114.5                         | 26       | 57     | 17            | 0.23                 |
| 817.6-812.6          | $1.43 \times 10^{-4}$ | 97.3         | 115.6                         |          |        |               |                      |
| 812.6-807.6          | $4.83 \times 10^{-6}$ | 105.0        | 115.0                         |          |        |               |                      |
| 807.6-802.6          | 0                     | 109.8        | 111.9                         | 25       | 46     | 29            | 0.09                 |
| 802.6-797.6          | 0                     | 112.9        | 122.2                         | 25       | 46     | 29            | 0.09                 |
| 797.6-792.6          | 0                     | 94.4         | 108.2                         | 25       | 46     | 29            | 0.09                 |
| 792.6-787.6          | $2.90 \times 10^{-6}$ | 104.4        | 115.9                         | 29       | 55     | 16            | 0.85                 |
| 787.6-782.6          | $7.22 \times 10^{-4}$ | 118.2        | 130.7                         | 22       | 54     | 24            | 0.18                 |
| 782.6-777.6          | $2.59 \times 10^{-4}$ | 108.7        | 119.9                         | 22       | 54     | 24            | 0.18                 |
| 777.6-772.6          | $2.41 \times 10^{-4}$ | 95.5         | 111.7                         |          |        |               |                      |
| 768.4-763.4          | $4.38 \times 10^{-4}$ | 107.3        | 117.7                         | 33       | 53     | 14            | 0.69                 |
| 763.4-758.4          | $2.29 \times 10^{-4}$ | 96.9         | 115.6                         | 33       | 53     | 14            | 0.69                 |
| 758.4-753.4          | $7.54 \times 10^{-4}$ | 101.0        | 117.8                         |          |        |               |                      |
| 753.4-748.4          | $2.04 \times 10^{-4}$ | 94.1         | 111.3                         |          |        |               |                      |
| 748.4-743.4          | $3.87 \times 10^{-6}$ | 102.6        | 122.4                         | 30       | 47     | 23            | 0.17                 |
| 743.4-738.4          | $4.83 \times 10^{-6}$ | 97.7         | 107.7                         | 30       | 47     | 23            | 0.17                 |
| 738.4-733.4          | $9.67 \times 10^{-7}$ | 106.3        | 116.7                         | 30       | 47     | 23            | 0.17                 |
| 733.4-728.4          | $5.80 \times 10^{-6}$ | 95.6         | 105.0                         |          |        |               |                      |
| 728.4-723.4          | 0                     | 114.2        | 125.4                         |          |        |               |                      |
| 723.4-718.4          | $1.95 \times 10^{-4}$ | 103.2        | 113.3                         |          |        |               |                      |
| 718.4-713.4          | $3.84 \times 10^{-4}$ | 104.9        | 121.1                         |          |        |               |                      |
| 713.4-708.4          | $3.33 \times 10^{-4}$ | 108.2        | 132.5                         |          |        |               |                      |

It can be seen from Table VII that there is no correlation between percent compaction and permeability of the coarse refuse. The percent compaction for the  $10^{-4}$  cm/s permeability varied between 94.1% and 118.2%, while the percent compaction corresponding to the "zero" permeability material varied between 94.4% and 114.2%.

There is a rough correlation between  $D_{30}$  and permeability. The  $10^{-4}$  cm/s permeability refuse has a  $D_{30}$  ranging between about 0.18 mm and 0.85 mm. The "zero" permeability material has a  $D_{30}$  of 0.09 mm. The permeability of coarse refuse is, therefore, much more dependent on grain size, and in particular, the amount of fines than it is on percent compaction. The compaction of coarse refuse at 95% instead of 90% standard Proctor, therefore, has no appreciable effect on permeability or seepage. Specifying a higher degree of compaction for coarse refuse will not substantially decrease seepage through the embankment. Cohesive facings and subdrains should be used to control seepage through coarse refuse embankments as it is unproductive to try to control seepage by increased compaction of coarse refuse.

### 2) Density

Strad of placing coarse refuse in 18-inch to 2-foot lifts and tracking with a dozer and hauling equipment produces a well compacted fill that achieves the desired results. This method produced an average percentage of

compaction of 95% of the standard Proctor value with no additional compaction equipment being utilized. The embankment as it consolidated over a period of time increased in density. Thus, the density in coarse refuse embankments can be expected to increase somewhat with time as the embankment is consolidated under its own weight.

### 3) Stability

The in-situ stability was found to be greater than the design stability of the structure. The strength parameters in-situ were higher than the design strength parameters and the factor of safety comparably higher. This conclusion indicates that the design criteria for coarse refuse embankments are conservative and that a compaction specification of 90% standard Proctor is adequate to produce the required stability at slopes of 2.5:1.

### CONCLUSIONS

Design assumptions relative to permeability and seepage in coarse refuse embankments compare favorably with actual observed values. The design assumptions are shown to be conservative in this study. Coarse refuse can be compacted in 18-inch lifts by dozers and haulage equipment to provide a satisfactory embankment. Correlations of permeability to percent compaction indicate that it is not effective to try to reduce the permeability by increasing compaction for coarse refuse.

## Field Observation and Finite Element Analysis of a Subway Excavation

Roberto Azevedo

Assistant Professor, Pontifícia Universidade Católica do Rio de Janeiro, RJ, Brazil

Luis Anibal Santos

Universidade Federal da Bahia, BA, Brazil

**SYNOPSIS:** This paper analyzes a braced excavation executed during the construction of Rio de Janeiro City subway along a street (Catete Street) in which several old and historical buildings existed and should be preserved. The excavation had an average depth of 13 meters and was executed almost ten years ago in a subsoil in which the principal problems were caused by a 6 meters thick loose sand layer, underlain by a 4 meter thick silty organic clay layer. Several buildings were damaged and had to be repaired. The objective of this paper is to show that even using the incomplete laboratory and field testing data available at the time the design was made, some of this damage could be predicted and, therefore, possibly prevented. The paper firstly describes the excavation and the available information on the subsoil materials. Subsequently, a finite element analysis is made and the results are correlated to observed damage.

### INTRODUCTION

During the construction of the first line of Rio de Janeiro city subway, in Brazil, there was one part that passed below a street in which old and historical buildings were constructed, including one, Palácio do Catete (Catete Palace), that was the President's residence and office while Rio de Janeiro was the capital of the country (1763-1900).

The shallow foundations of these buildings were made at a time in which reinforced concrete was not available in the country and therefore they were made with large stones held together with a mixture of sand and cement.

The subway tunnel was built by a cut-and-cover procedure with retaining walls being used to avoid large ground deformations particularly because the excavation comprised almost all the street width thereby being very close to the building foundations. In spite of the retaining structure the movements caused by the excavation in the backfill cracked almost all the old buildings including the Catete Palace that had to be repaired over many years.

The objective of this paper is to show that even based on the little information available on the deformation characteristics of the subsoil materials, an analysis using the finite element method and considering the most important steps taken during the excavation construction, leads to differential settlements in the backfill that according to allowable settlement recommendations should be avoided in order to prevent cracking.

The paper firstly describes the excavation and the available information on the subsoil materials. Subsequently, this information is used to obtain deformability parameters for the different subsoil layers. Finally, an analysis

is made, its results are presented and conclusions are outlined.

### DESCRIPTION OF THE FIELD CASE

Part of the Rio de Janeiro city subway first line passes below Catete Street and joins Largo do Machado Station to Catete Station, in an area where several small streets and old buildings exist (Figure 1). A cross-section of this part is shown in Figure 2. The field and laboratory data available corresponding to the stretch between Ferreira Viana and Dois de Dezembro streets (Figure 1). In this region, borehole number S-505 was considered to be the most representative and its corresponding geotechnical profile is shown in Figure 3. As can be seen in this figure, the first layer is a fill that has an average thickness of 4 metres, an average blow-count number,  $N(SPT)$ , of 10 and liquid limit (LL) and plastic index (PI) equal to 20% and 10%, respectively. Underlying this fill, there is a 10 metre thick uniform, fine to medium sand layer in which the first 3 metres is in a dense state, relative density ( $D_r$ ) between 75% and 85%, and the last 7 metres are in a loose state ( $D_r$  between 25% and 35%). These relative density values were obtained correcting the  $N(SPT)$  according to the vertical effective pressure (Gibbs and Holtz, 1957 and Teng, 1972).

The organic silty clay layer has a granulometric distribution in which the percentage of particles passing through sieve number 200 varies from 40% to 65%. Average values of LL and PI are 43% and 27%, respectively. The value of  $N(SPT)$  varies from 2 to 3 and it has a soft to very soft consistency, with the natural moisture content observed in almost all the samples being greater than the liquid limit. The layer can be considered normally

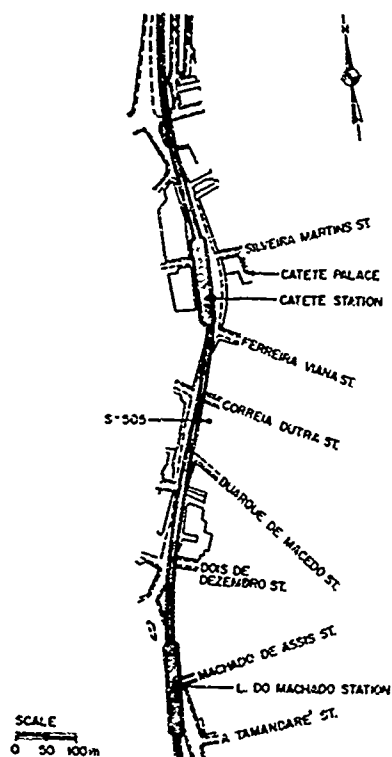


Fig. 1. Rio de Janeiro Subway General View at Catete Street

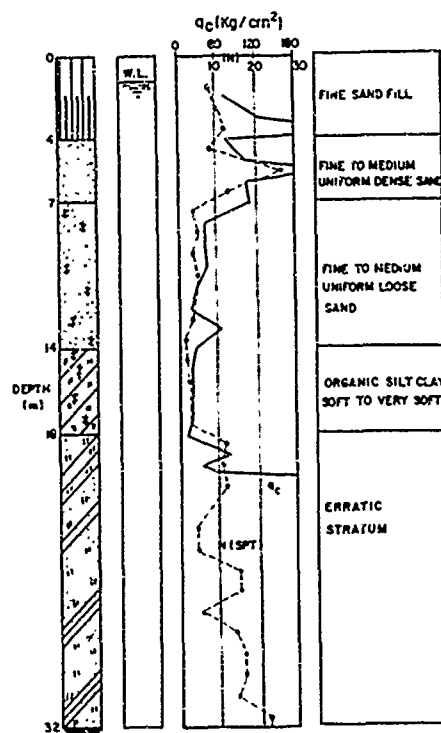


Fig. 3. Geotechnical Profile at Borehole S-505

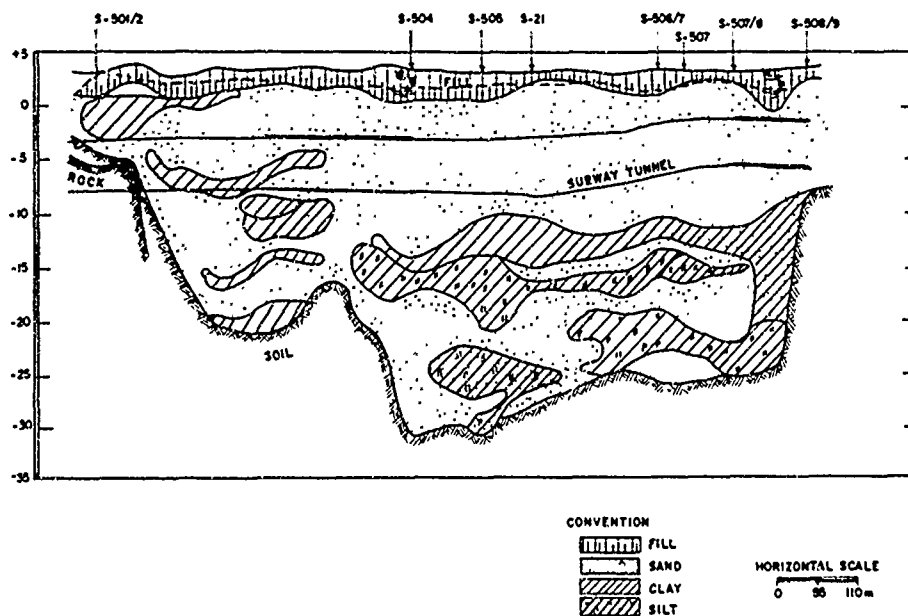


Fig. 2. Rio de Janeiro Subway Cross-Section at Catete Street



consolidated with OCR varying from 1 to 2, and sensitivity being approximately equal to 2. The permeability obtained with conventional oedometer test varied from  $10^{-7}$  to  $10^{-9}$  cm/sy.

The erratic stratum was characterized by having a much higher penetration resistance, average N(SPT) greater than 10. There is little information on this layer but its influence on the excavation behavior is considered to be negligible.

The retaining structure for the excavation slopes consisted of vertical walls supported laterally by three levels of struts that can be seen in Figure 4 where a cross-section and a top view of the retaining structure is presented. Slurry trench (diaphragm) walls incorporated to the final structure of the subway tunnel were used on these retaining structures (Xanthakos, 1979 and Hajnal et al., 1984).

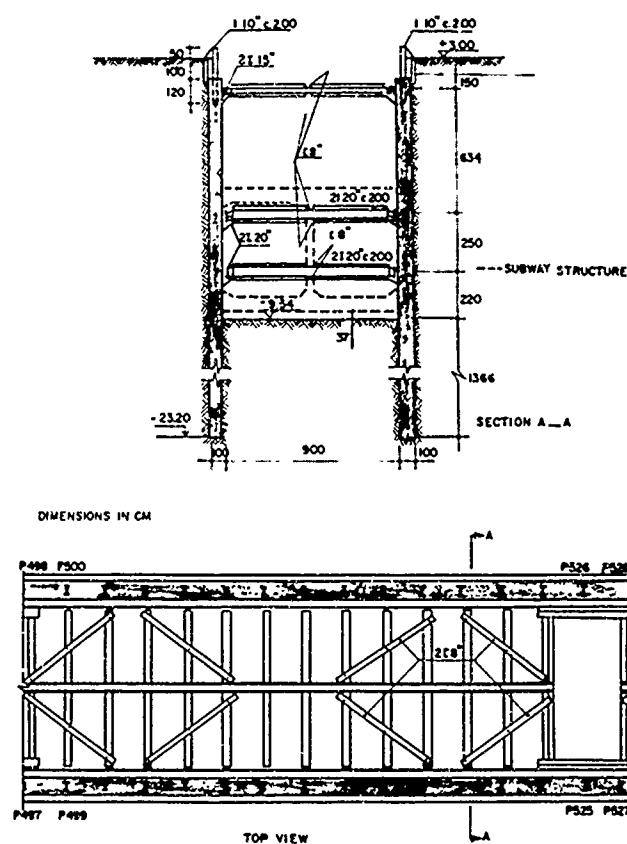


Fig. 4. Rio de Janeiro Subway Retaining Structure at Catete Street

The excavation was executed in four steps as shown in Figure 5. Steps 2, 3 and 4 consisted of first installing struts A, B and C, respectively, and then, excavating.

To control the building movements during excavation, settlement points were installed in most buildings. Figure 6 presents a top view of the location of some of these buildings as well as the observed settlement for different points

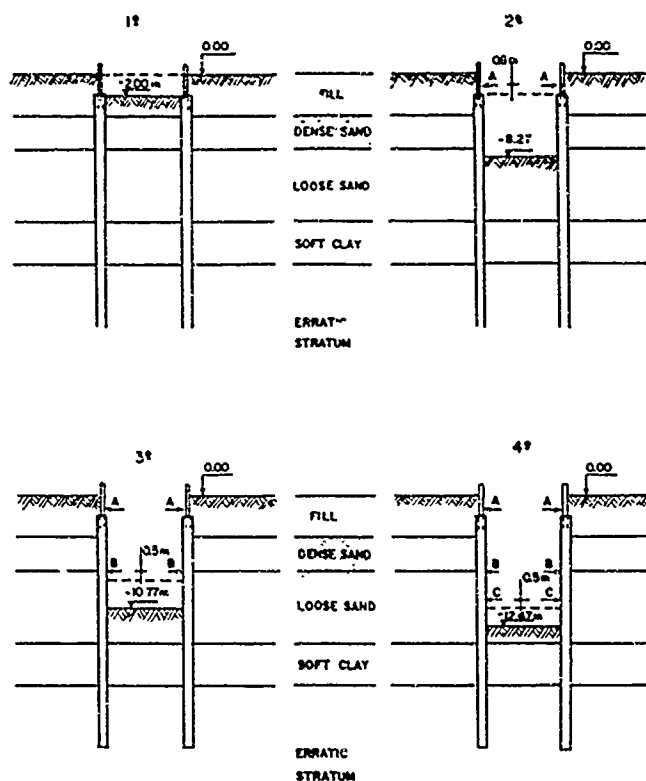


Fig. 5. Excavation Steps

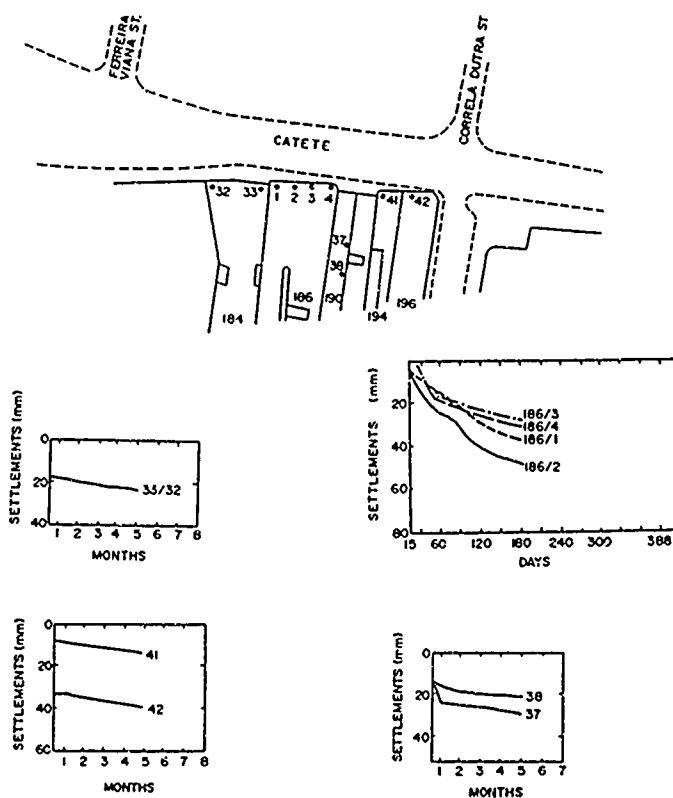


Fig. 6. Settlement of Points in Some Buildings

in each building. Only settlement of building 186 was measured from the beginning of excavation construction. The other points had already moved when the measuring started.

#### LABORATORY DATA

Besides field penetration tests, some laboratory tests were also performed. Conventional CU (consolidated-undrained) and UU (unconsolidated-undrained) triaxial tests were performed in Shelby samples of the organic silty clay layer as well as oedometer and direct shear tests. The sand layer was tested at different relative density with conventional direct shear tests and the erratic stratum was tested with conventional CU tests. No laboratory tests were available for the sand fill material.

Most of these tests did not have consistent results and were not sufficient to find parameters even for the hyperbolic non-linear elastic model (Duncan and Chang, 1970). Therefore they were used to estimate values of elasticity modulus only (Santos, 1980).

#### NUMERICAL ANALYSIS

The numerical analysis was performed using a finite element program, FENA-2D (Krishnayya, 1973), available at the time. The real problem was idealized as shown in Figure 7 and numerically solved using the mesh presented in Figure 8.

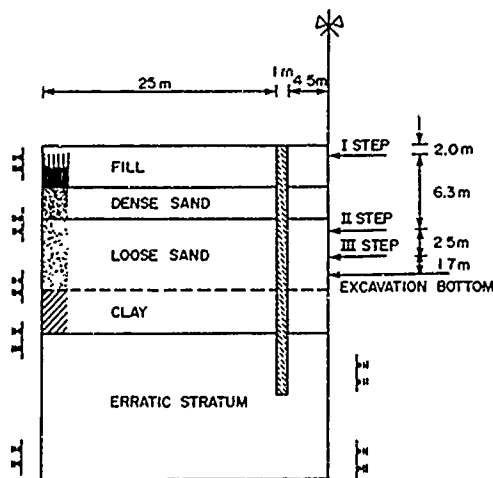


Fig. 7. Problem Idealization

The elasticity moduli ( $E$ ) used in the analysis were obtained for each layer averaging values obtained with different correlations with  $N(SPT)$  (Terzaghi and Peck, 1967; Webb, 1969; Parry, 1971 and Mello, 1971) and the laboratory test results (Figure 9).

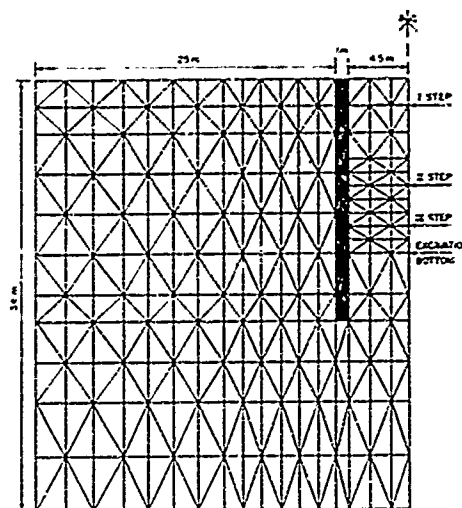


Fig. 8. Finite Element Mesh. 403 Elements and 233 Nodal Points

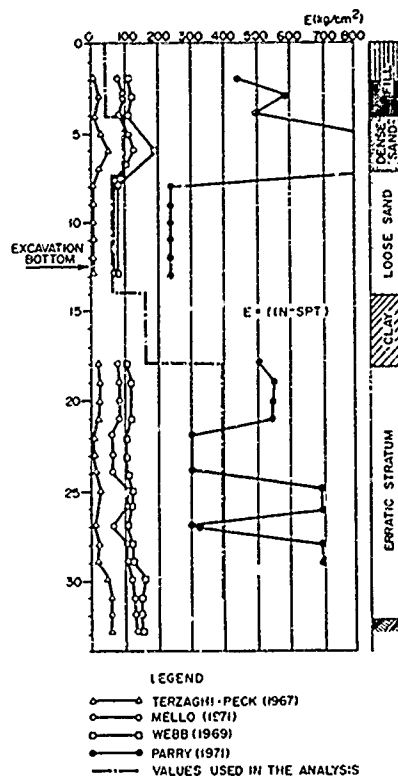


Fig. 9. Elasticity Modulus Correlation

Figure 10 shows vertical displacements of surface points near the excavation, together with the lateral movement of the diaphragm wall and the bottom heave, for each excavation step. As can be seen the vertical settlement was much smaller than the ones measured in building number 186 (Figure 6). There are many reasons to explain this difference. First, the use of linear elasticity disregards any decrease

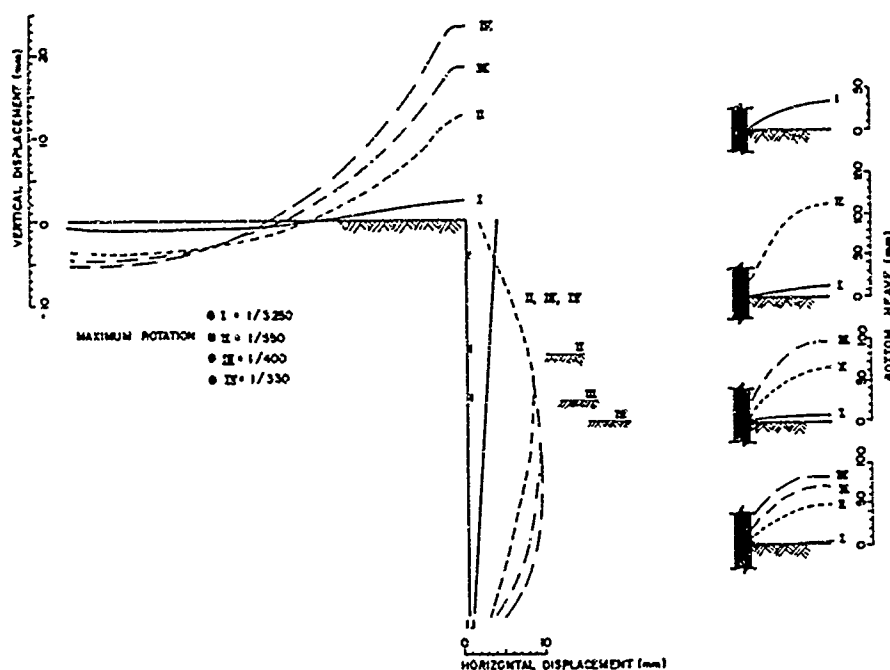


Fig. 10. Analytical (Numerical) Displacements

in the elasticity modulus during increasing shearing, underestimating the settlements. Second, movements caused by lowering the water table level were disregarded. Third, as already shown, the characterization of the subsoil deformability was not properly carried out which could probably lead to smaller settlements and, finally, some assumptions in the numerical model such as rigid struts, boundary and initial conditions might also have led to underestimation of the settlements.

Nevertheless the settlement profile obtained in the analysis gave rise to maximum rotation that may explain the damage which occurred. In fact, according to many authors in different countries (Skempton and MacDonald, 1956; Feld, 1965; Golder, 1971; Crant et al., 1974; Burland and Wroth, 1974; Vargas and Pacheco, 1976 and Novais, 1976) the maximum rotation has to be smaller than 1/300 to avoid wall cracking and to keep windows and doors smoothly functioning. Burland and Wroth (1974) point out that this limit value might be considerably smaller for old buildings and the value of 1/500 is usually used in practice. As is shown in Figure 10 this value is reached in the second excavation step, increasing thereafter. Therefore, these results justify the damage observed in most of the old buildings.

## CONCLUSIONS

In this paper an excavation field case associated with the construction of the Rio de Janeiro subway tunnel at Catete Street was reported.

As pointed out by Morgenstern and Eisenstein (1970) to accurately analyze excavations it is

necessary to have information on the geotechnical profile, the stress state in the ground prior to excavation, the deformability characteristics of the ground and the construction procedure (boundary conditions).

Unfortunately all this information was not available for the field case reported in this paper, especially with respect to the deformability characteristics of the subsoil. Although some laboratory and field data were available they were not sufficient to find parameters (calibration) for more adequate stress-strain constitutive models. Nevertheless, the paper aimed to use laboratory and field data normally encountered in engineering practice, together with a more accurate characterization of the geotechnical profile, the stress-state in the ground and the construction procedure, to investigate if some of the problems caused by the excavation could have been predicted and therefore possibly avoided.

It was shown that the movements obtained with the numerical analysis, although much smaller than that measured in the field, indeed gave rise to settlement profiles that justify the damage caused in the nearby buildings. Therefore an analysis such as the one presented in this paper would have helped to avoid the damage caused.

## REFERENCES

- Burland, J.B. and Wroth, C.P. (1974), "Settlement of Buildings and Associated Damage", Conf. on Settlement of Structures, Cambridge, U.K., Session 5, pp. 611-654.

- Duncan, J.M. and Chang, C.Y. (1970), "Non Linear Analysis of Stress and Strain in Soils", Journal of the Soil Mechanics and Foundation Engineering, ASCE, Vol. 96, SM5, pp. 1629-1653.
- Feld, J. (1965), "Tolerance of Structures to Settlement", Journal of the Soil Mechanics and Foundation Engineering, ASCE, Vol. 90, SM3, pp. 63-77.
- Gibbs, H.J. and Holtz, W.C. (1957), "Research on Determining the Density of Sand by Spoon Penetration Test", Proc. 4th Int. Conf. on Soil Mech. and Found. Eng., Vol. 1, pp. 35-39.
- Golder, H.O. (1971), "The Allowable Settlement of Structures", Proc. 4th Panamerican Conf. on Soil Mech. and Found. Eng., Puerto Rico, pp. 171-187.
- Grant, R., Christian, J.T. and Vanmarcke (1974), "Differential Settlement of Buildings", Journal of the Geotechnical Division, ASCE, Vol. 10, GT9, pp. 973-991.
- Hajnal, I., Marton, J. and Regele, Z. (1984), "Construction of Diaphragm Walls", John Wiley and Sons, pp. 399.
- Krishnayya, A. (1973), "Program FENA-2D Finite Element Non-Linear Analysis for Two Dimensional Problems", User's Manual, University of Alberta, Edmonton.
- Mello, V. (1971), "The Standard Penetration Test, Proc. 4th Panamerican Conf. on Soil Mech. and Found. Eng., Brazil, pps.
- Morgenstern, N.R. and Eisenstein, Z. (1970), "Methods of Estimating Lateral Loads and Deformations", Proc. ASCE Specialty Conference on Lateral Stresses and Retaining Structures, Cornell University, pp. 51-102.
- Novais, F.H. (1976a), "Allowable Settlements", in Portuguese, Geotecnia, Vol. 18, pp. 53-86.
- Novais, F.H. (1976b), "Allowable Settlements", in Portuguese, Geotecnia, Vol. 19, pp. 3-17.
- Parry, R.G. (1971), "A Direct Method of Estimating Settlements in Sands from SPT Values", Proc. Symp. Interaction of Structure and Foundation, Midland Soil Mech. and Found. Eng. Soc., Birmingham, pp. 29-37.
- Santos, L.A. (1980), "Procedure for the Analysis of Braced Excavations: the Example of Part 7 of the Subway of Rio de Janeiro (Catete Street)", in Portuguese, M.Sc. Thesis, Pontificia Universidade Catolica do Rio de Janeiro, Brazil, pps. 242.
- Skempton, A.W. and MacDonald, D.H. (1956), "Allowable Settlement of Buildings", Proc. of Institution of Civil Engineers, London, U.K., Vol. 5, Part 3, pp. 727-784.
- Teng, W.C. (1962), "Foundation Design", Prentice Hall, Englewood Cliffs, N.J., pp.
- Terzaghi, K. and Peck, R.B. (1967), "Soil Mechanics in Engineering Practice", John Wiley and Sons,
- Vargas, M. and Pacheco, F. (1976), "Settlement of Tall Buildings in Sao Paulo and Santos", Proc. on the Panamerican Regional Conf. on Tall Buildings, Porto Alegre, Brazil, pp.
- Webb, D.L. (1969), "Settlement of Structures on Deep Alluvial Sandy Sediments in Durban, South Africa", Conf. In-Situ Investigations in Soils and Rocks, British Geotechnical Society, London, pps. 181.
- Xanthakos, P.O. (1979), "Slurry Walls", McGraw-Hill Book Company, pps. 622.

# Failure of Flood Banks Due to Under Seepage

Arthur Marsland  
England

## SYNOPSIS:

Several failures of floodbanks caused by increases in water pressure and seepage in foundation soils during abnormal high floodwater conditions have been investigated. The particular type of failure which occurred depended upon the sequences of the foundation strata, the overall bank profile, and the height and duration of the floodwater. Both rotational and translational slides occurred in banks built on sands, peats and clays with underlying sandy gravels. Breaches occurred when the crest was sufficiently lowered to allow substantial overtopping or where gaps developed at the ends of the translational slides. Development of erosion pipes in multi-layered soils led to both partial collapse and breaching of banks. The need to anticipate possible failure mechanisms when evaluating the effectiveness of flood defences is emphasised.

## INTRODUCTION

Flood defence banks protecting low lying ground along rivers and coasts are of necessity constructed on alluvial deposits. These may comprise peats, soft clays, silts, sands and gravels. Wherever pervious strata outcrop on the foreshore or in river channels increases in groundwater pressures and flow gradients occur in the strata below the banks during high water conditions. As a result of these changes overall instability of the banks or the development of erosion pipes in unstable strata can occur. Rapid breaching and extensive flooding can result from both types of failure. The examples of failures described in the following sections have been chosen from the author's records in order to illustrate the various types of under seepage failures which occur in Britain. Studies of failure mechanisms and of conditions conducive to potentially dangerous under seepage form an essential requirement for the adequate assessment of the effectiveness of flood defences.

## FAILURE OF BANKS BUILT OF FINE SAND

Recent deposition under the tidal conditions occurring along the coastal and estuaries of Britain has resulted in soil profiles comprising a relatively thin layer of silty clay overlying fine sand. The thickness of the overlying silty clay present under the flood defence banks depends on the length of time deposition has occurred prior to construction of the banks. In the marshes along the east coast of Essex where a number of breaches occurred in the banks during the abnormally high tides in 1953 the silty clay is 1 to 2 metres thick. Fortunately most of the banks have extensive saltings on the seaward side and their blanket effect prevents large changes of pore water pressures occurring in the underlying sands. As a consequence most of the breaches followed the development of shallow slips in the fissured backslopes of the banks (Cooling and Marsland 1954, Marsland 1957, Marsland 1984) and were small or only partially

developed. However, a very large breach accounting for much of the flooding occurred along a stretch of bank flanking an outfall drain cut through the saltings. A cross-section through this bank is shown in Fig 1 (a). The presence of large lumps of clay from the bank more than 120 metres into the marsh indicated that the breach had developed rapidly.

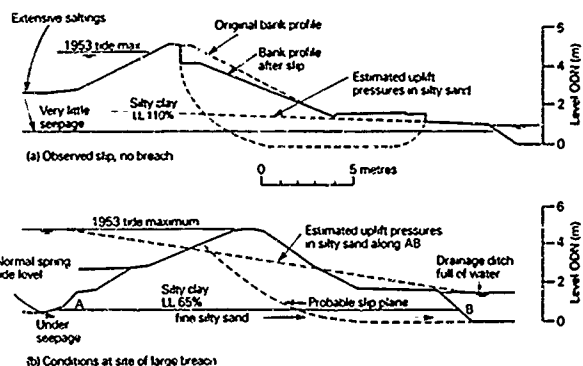


Fig 1 Uplift failures of banks built on fine sand in Essex.

Estimates of the likely pore water pressures which developed in the underlying sands during the 1953 tides were obtained by extrapolation of measurements made during subsequent spring tides. These indicated that equilibrium pressures corresponding to minimal seaward protection had probably occurred. When these pore water pressures were used in effective stress analyses incorporating a range of values of effective stress parameters determined from laboratory tests, factors of safety of between 0.75 and 1.0 were obtained. The available evidence suggested that most of the bank slid into the marsh as the tide reached this maximum level as shown in Fig 1a and this resulted in the formation of a deep wide breach in a very short time.

Further evidence of the critical nature of the stability of these banks during flood conditions was provided by a deep slip which occurred in an adjacent bank fronted by saltings. A section across this slip is shown in Fig 1b. Measurements of pore water pressures during subsequent high tides showed that changes at this location were much smaller than at the breach side. Changes in the level of the water in the landward ditch were quickly reflected as additional changes of pore water pressure in the sand under the bank. A combination of the pore water pressures caused by flooding of the landward ditches and the moderate increases due to under seepage were sufficient to cause the slip.

#### FAILURE OF BANKS BUILT ON LAMINATED DEPOSITS

Laminated silts, sands and clays are frequently formed in the less exposed inner regions within tidal estuaries. The author has no first hand experience of overall instability failures of banks built on these deposits due to under seepage. There is, however, a real possibility of their occurrence especially where the banks are subjected to high flood levels for prolonged periods. Banks built on laminated deposits are, however, prone to failure as a consequence of internal erosion. A serious breach and several other partial failures occurred during 1960 in banks along elevated drainage channels passing through the silt lands in the Norfolk Fens. A section through the bank at the site of the breach is shown in Fig 2a. The water level in the channel began to build up during 20 December and by midnight had reached + 3.4 m ODN. On 21 December the level gradually increased to a maximum of 3.85 m ODN at 1200 hours. Regular inspections were made of the banks and the drainage ditches on the marsh side until 1130 hours on 22 December when the flood levels had fallen by about 0.3 m. At this time there was only evidence of slight seepage along the side of the landward ditch. However, by 1400 hours silt laden water was observed pouring into the ditch and by 1430 hours a large breach had developed. The bank either side of the breach appeared to be undamaged. The formation of the breach removed all further evidence of the mode of development but erosion holes several feet across had been reported in banks in this area at positions A and B shown in Fig 2b during a comparable high water flood in 1947. A shaft approximately 2 metres across and 2.5 metres deep was also discovered in the crest of a bank along a parallel drainage channel (position C Fig 2b) at 1500 hours on 21 December 1960 when large quantities of silt laden water were seen pouring out into the marsh drainage ditch. Fortunately this did not lead to a complete breach and subsequent excavation revealed a horizontal pipe with a diameter of about 230 mm leading to the drainage ditch as shown in Fig 2b. Fortunately the horizontal pipes did not extend back to the main channel during the flood period. All the erosion pipes observed occurred in the laminated clay-silt-sand with the overlying clay and peat providing some roof support. Precise details of how the pipes developed is not known but grading curves on soil from individual lamina suggest that the washing of particles from finer into coarser lamina could have been a contributory factor.

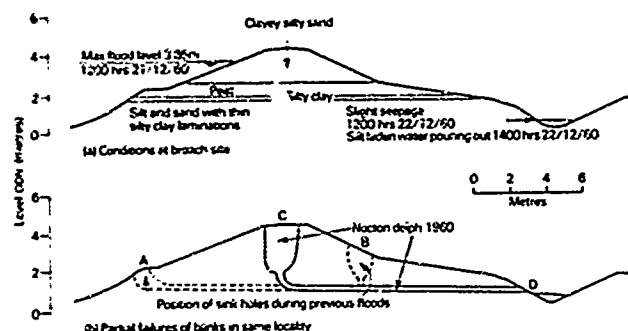


Fig 2 Underseepage failures of banks built on laminated clayey, silty, sandy deposits in the Lincolnshire Fens.

#### FAILURE OF BANKS BUILT ON PEAT

The gradual back-up of the inland water as the sea levels rose during the retreat of the ice following the last glaciation provided conditions favourable to the formation of peat deposits in shallow lagoons adjacent to many rivers and estuaries. The drainage of reclaimed peat lands has resulted in a considerable lowering of the surface levels due to consolidation, shrinkage, oxidation, and bacterial activity. As a consequence rivers now cross peat areas between banks with crests up to 6 metres above the surrounding ground. Many of these banks are subjected to high water levels for longer periods than coastal banks. Where the flood water has direct access to the peat layers near the banks, significant increases of pore water pressure can occur in the peats underlying the banks and adjacent marshes. Since peats are predominantly frictional soils this causes a reduction in strength and stability of the banks. A major breach in a bank protecting Bulcamp marshes on the south side of the river Blyth near Bythburgh, Suffolk, followed the development of a deep slip which occurred when the flood water was near its peak level. A photograph showing the temporary repairs to the bank is shown in Fig 3. A section showing the original and slipped profiles and the probable slip plane is shown in Fig 4. It is significant that the failure occurred during the most prolonged high tide to have occurred since the bank was reconstructed in 1954. Earlier breaches in other banks built on peat in the Fens (Johnson 1948 and Summers 1976) could also have developed in a similar way. It was also suggested by Summers 1975 that other breaches in the Fens may have been caused by banks being pushed landward by the pressure of the flood water. Unfortunately, no details of these failures were given. However, in 1976 the author inspected a breach alongside a drainage channel in the Somerset levels where this had occurred as shown in Fig 5. Peat extraction in the marsh had made the bank more vulnerable and both the bank and the strip of ground remaining at the rear of the bank moved as an intact unit towards the peat workings. Flooding of the marsh occurred through gaps between the ends of displaced length of bank and the adjacent stable bank.



Fig 3 Temporary repairs of a breach caused by uplift pressures in peat below bank. (Near Bythburgh, Suffolk).

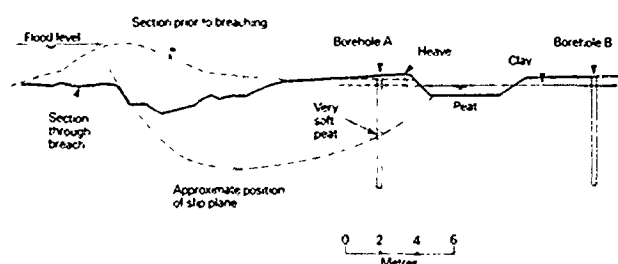


Fig 4 Section through centre line of breach shown in Fig 3.



Fig 5 Photograph of lateral displacement bank built on peat (Somerset Levels)

## FAILURE OF BANKS BUILT ON CLAYS AND PEATS OVERLYING SANDY GRAVEL

The flood plain deposits of the River Thames provide a good example of peat and clay sequences overlying sandy gravels (Marsland A 1986). These were deposited on late glacial sands and gravels which were deposited during the later stages of the last glaciation. The major channel of the present day river extends down into the gravels. Along the middle Thames pore water pressure changes equal to more than 50% of the twice daily tidal change (Spring tide range about 6 m) have been measured in the gravels below the marshes just landward of the flood banks. Detailed studies of these pore pressure changes (Marsland and Randolph 1978) have shown that the percentage response increases when tidal surges are superimposed on normal sinusoidal tides.

In the not too distant future, abnormal combinations of spring tides and tidal surges could cause uplift pressures in the gravels sufficient to float the existing layers of peats and clay (up to 7 metres thick) present in the marshes along parts of the Thames. The pore water pressure responses in the gravels along the tributaries of the Thames are much less but so are the thicknesses of the peats and clays. A 28 metre long breach occurred in the bank along the tributary of the Thames at Dartford during the abnormal tides of 31 January and 1 February 1953 (Marsland 1961).

The breach occurred at a locality where the thickness of the peat and clay was only 1.8 metres as shown in the section in Fig 6. Direct extrapolation of pore pressures measured in the gravel near the breach side over normal tides indicated that floatation of the peat and clay in the marsh had probably occurred before the bank failed. Effective stress analyses confirmed that the bank could have slipped into the marsh under these conditions as indicated in Fig 6. It should be noted that the pore water pressure response in the gravel near the bank was only about 25% of the tidal range in the river due to the presence of a 200 mm thick layer of mud which covered the bed.

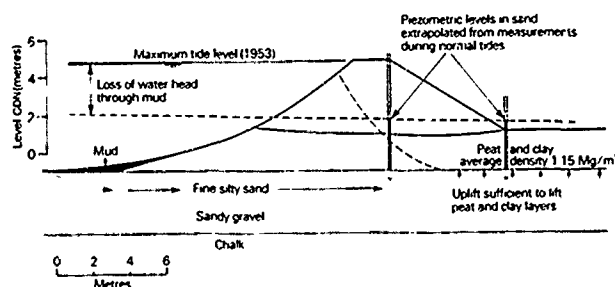


Fig 6 Section through breached bank near Dartford Lock, Kent.

## CONCLUSIONS

Under seepage through pervious and semi-pervious strata below flood banks can cause failures and serious breaching. The mechanism of failure at critical locations is mainly controlled by the nature of the underlying pervious strata and the overall profile of the banks. The length of time that the flood water remains near its peak level is almost as important as the maximum water levels reached.

## REFERENCES

1. Cooling, L F and Marsland, A (1954): Soil mechanics studies of failures in the sea defence banks of Essex and Kent. Proc Conf on the North Sea Floods 31 Jan/1 Feb 1953. Instn of Civil Engineers, London, pp 58-73.
2. Johnson, E A G (1948): 'Flooding in the Fens and remedial measures taken'. Maritime and Waterways Paper No 10 Institution of Civil Engineers, London April 1948.
3. Marsland, A (1957): The design and construction of earthen flood banks. Jnl Inst of Water Engineers, vol 11, pp 236-258.
4. Marsland, A (1961): A study of a breach in an earth embankment caused by uplift pressures. Proc 5th Int Conf Soil Mech & Found Eng, Paris 1961, vol 2, pp 663-668.
5. Marsland, A (1984): 'Controlled breaching of a full scale flood bank. International Conf on Case Histories in Geotechnical Engineering, St Louis Missouri, USA, vol 2 pp 645-653.
6. Marsland, A (1986): 'The Flood Plain Deposits of the Lower Thames' Quarterly Journal of Engineering Geology, London, vol 19 pp 223-247.
7. Marsland, A and Randolph, M F (1978): A study of the variation and effects of water pressures in the pervious strata underlying Crayford Marshes, Geotechnique, vol 28, No 4, pp 435-464.
8. Summers, D (1976): The Great Level: A history of drainage and land reclamation in the Fens. Published by David and Charles.



## Construction of Road Embankments over Very Soft Soils Using Band Drains and Preloading

John D. Nelson

Department Head, Civil Engineering Department, Colorado State University, Fort Collins, Colorado

Brian P. Wrench

Director, Steffen, Robertson and Kirsten, Inc., Johannesburg, South Africa

**SYNOPSIS:** As part of a new national road being constructed in South Africa an embankment was built over a deep deposit of very soft soil. To enhance stability the embankment was built in several stages and in order to reduce the time required for consolidation between stages, band drains were installed in the foundation soils. The soils were instrumented to monitor pore water pressure and settlement. The results of the monitoring phase showed that the band drains were effective and operated as designed.

This paper presents the results of the monitoring and discusses the prediction of degree of consolidation from settlement readings as opposed to pore water pressure along.

### INTRODUCTION

The National Transport Commission of South Africa is constructing a new national road between the towns of George and Knysna along the southern tip of Africa. The general area of the road is shown in Figure 1.

The road will traverse an alluvial flood plain in the area of the Goukamma River near Buffelsbaai, South Africa. The present alignment of the road was constructed close to a hillside on the edge of a flood plain so as to avoid the necessity for construction over deep soft foundation soils. The present construction calls for realignment of the road and construction of

embankments up to five metres high on deep deposits of soft organic clay and silt. Stability analyses indicated that for an embankment constructed to full height within a short period of time, the factor of safety for the most critical section would be less than unity. It was decided, therefore, to construct the embankment in several phases. To facilitate construction so as to reduce construction time, it was decided to utilize band drains for drainage of the foundation materials. During construction it was decided that an allowable factor of safety of 1.3 would be adequate providing that careful monitoring was conducted of excess pore water pressure and deformations.

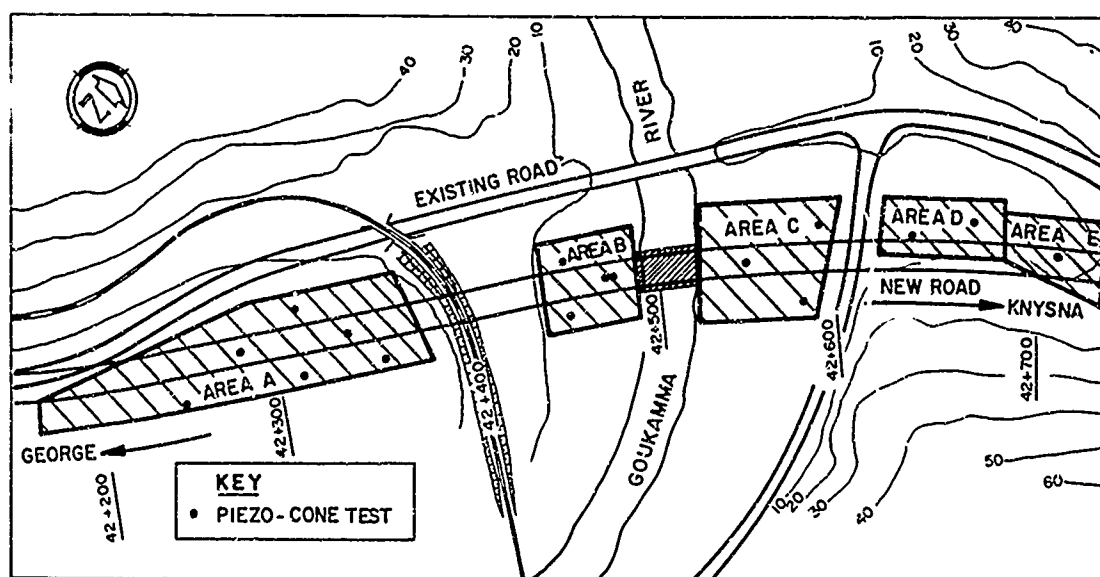


Fig. 1 Embankment Alignment Showing Test Hole Locations

This paper describes the general soil conditions and construction sequences. Results of pore water pressure response and consolidation as influenced by the band drains are presented. It was observed that the band drains operated as designed and were effective in enhancing the consolidation of each phase of construction.

## FIELD INVESTIGATION

### Site Description

The site is located on the alluvial flood plain of the Goukamma River approximately 10 km west of the town of Knysna along the southern coast of South Africa. The flood plain extends for approximately 700 m to the west of the river and 200 m to the east of the river. In general the site is flat and is used for pastureland and dairy cattle.

For purposes of site investigation and design the site was divided into five separate areas designated A through E. Figure 1 shows the general topography of the area and the alignment of the embankments.

### Soil Profile

The soil investigation initially comprised 23 piezocone tests at locations as shown on Figure 1. An additional four test holes were bored and samples were taken in the immediate vicinity of the Goukamma River. Figure 2 shows the soil profile through the centerline of the embankment alignment. As can be seen from Figure 1, the north side of the site rests up against a relatively steep hillside. This hill is primarily sand to a depth in excess of about 20 m overlying rock. The silt and clay strata shown on Figure 2 increase in depth from the north towards the south.

The silt and clay deposits were seen to include many thin lenses which exhibited rapid pore water pressure dissipation during the piezocone testing. From the samples taken in test holes near the river, it was seen that these lenses consisted of thin layers of highly organic soil and peat.

The soils were quite variable over the site. In general the soils were classified as being of low plasticity. The clayey silt exhibited values of liquid limit ranging from 31 to 42 with plasticity indices from 6 to 12. The silty clay had a liquid limit of about 60 with a plasticity index of 16. The soils all exhibited a high organic content.

A typical piezocone record from area C is shown in Figure 3. The existence of organic and/or sandy lenses can be seen from the pore water pressure record. From the point load data the value of undrained strength of the clayey silt was observed to generally be in the range of 10 to 15 kPa. The shear strength typically appeared to be uniform with depth.

The coefficient of consolidation was measured both from laboratory consolidation tests and from piezocone pore water pressure dissipation. The laboratory measured values were about  $0.8 \text{ m}^2/\text{yr}$ . The results from the

piezocone testing indicated values of  $1.5 \text{ m}^2/\text{yr}$  to  $6.5 \text{ m}^2/\text{yr}$  for areas A and E and 6 to  $20 \text{ m}^2/\text{yr}$  for areas B, C and D.

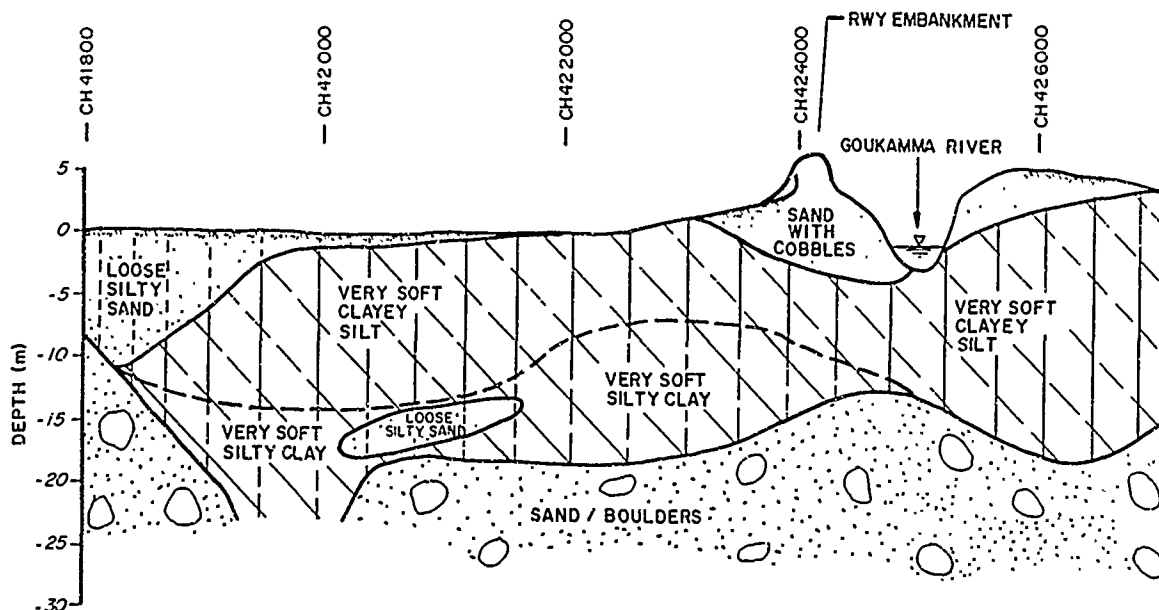


Fig. 2 Soil Profile Along Embankment Centerline

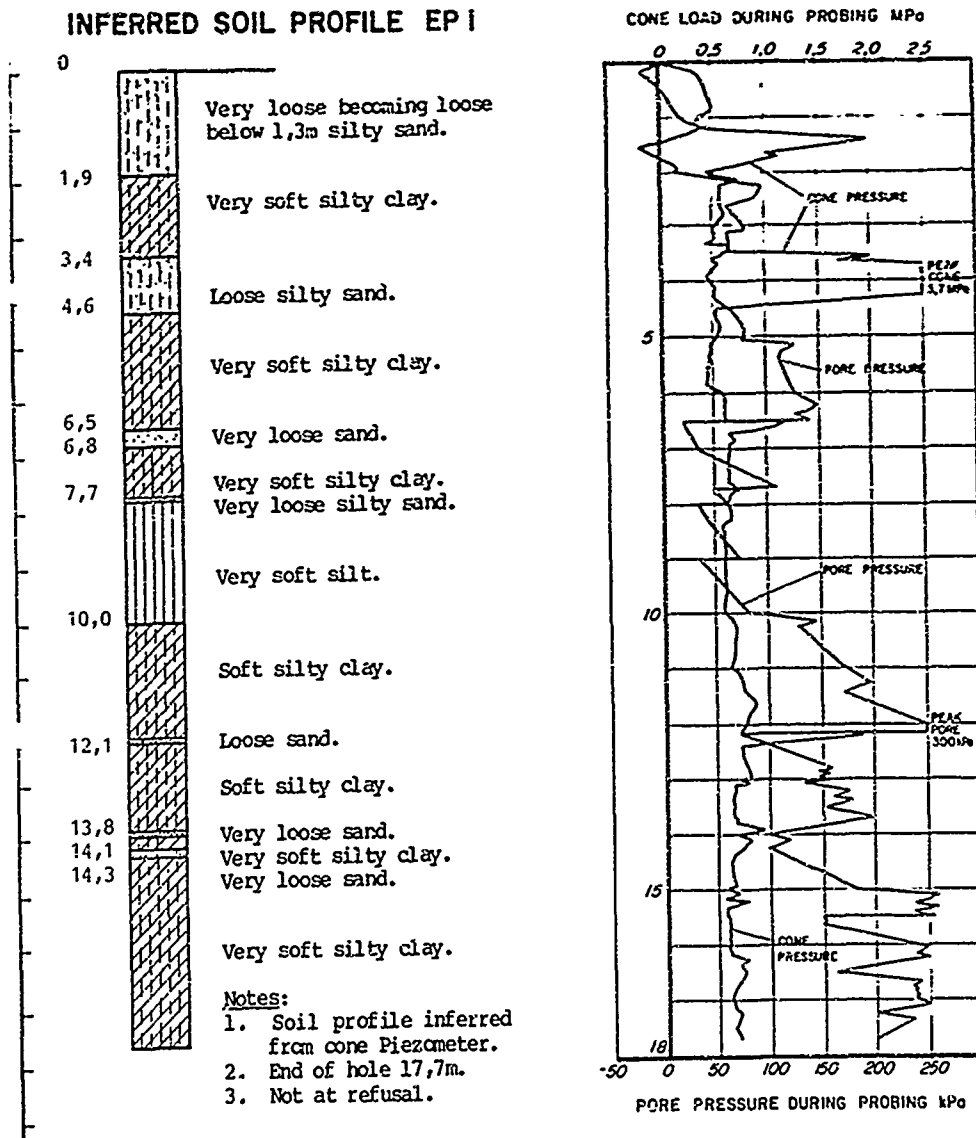


Fig. 3 Typical Piezocone Record - Area C

## EMBANKMENT STABILITY AND DESIGN

### General Considerations

The most critical time for stability of an embankment on soft soils of the nature encountered at this site is immediately after construction. Stability analyses utilizing undrained shear strength indicated that it would not be possible to construct the embankment to full height in one operation if time was not allowed for pore water pressure dissipation. It was decided therefore, to utilize staged construction allowing the pore water pressures to dissipate to 75 percent consolidation between lifts.

Even using the highest values of coefficient of consolidation (i.e., 6 and 20  $m^2/yr$ ) the times required

between lifts to achieve 75 percent consolidation would have been from about three to seven years. In order to shorten these times to values more consistent with allowable construction periods, it was decided to install band drains to enhance consolidation.

### Drain Design

It was desired to allow no more than six months between construction of each lift. The spacing of the drains was designed using the procedure developed by Hansbo (1979). The times required to achieve 75 percent dissipation as a function of wick or band drain spacing for various values of coefficient of consolidation are shown in Figure 4. The design drain spacings from different areas are shown in Table 1.

TABLE I. Design Drain Spacing

| Area | Drain Spacing | Chainage |       | Estimated Depth (m) |
|------|---------------|----------|-------|---------------------|
|      |               | From     | To    |                     |
| A    | 2,3           | 42165    | 42380 | 15                  |
| B    | 1,5           | 42450    | 42490 | 14                  |
| C    | 1,5           | 42520    | 42555 | 25                  |
| C    | 2,0           | 42555    | 42595 | 20                  |
| D    | 2,3           | 42615    | 42665 | 13                  |

Drains were driven on a square grid. A sand blanket 700 mm thick was placed on the surface to provide drainage. Finger drains were placed transverse to the centerline of the embankment at every fourth row of wick drains. The finger drains connected to a main collector drain along the edge of the embankment. The finger drains and collector drains consisted of 19 mm washed stone wrapped in geotextile filter fabric. The collector drain also contained a 100 mm diameter clay pipe.

#### Loading Procedure

The first lift of the embankment consisted of the drainage blanket. After 120 days a second lift was placed and a third lift was placed at about 300 days. The loading sequence is shown in Figures 6 and 7.

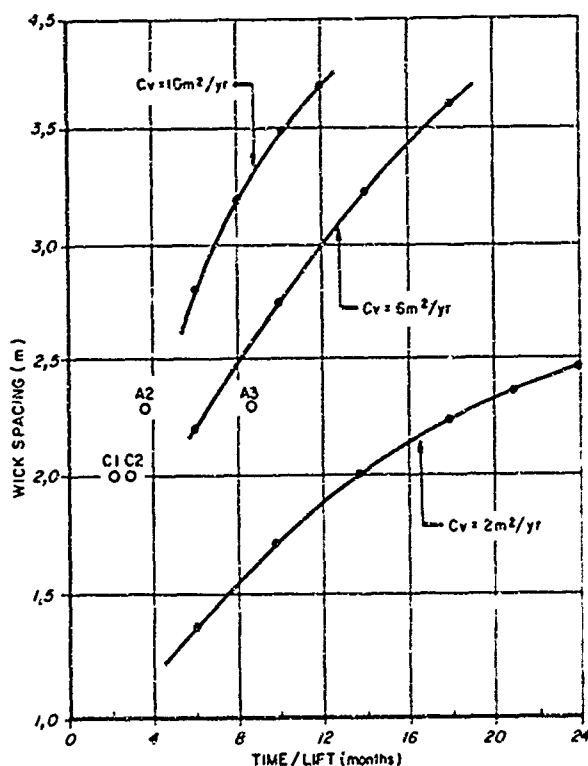


Fig. 4 Effect of Band Spacing on Times for Pore Pressure Dissipation

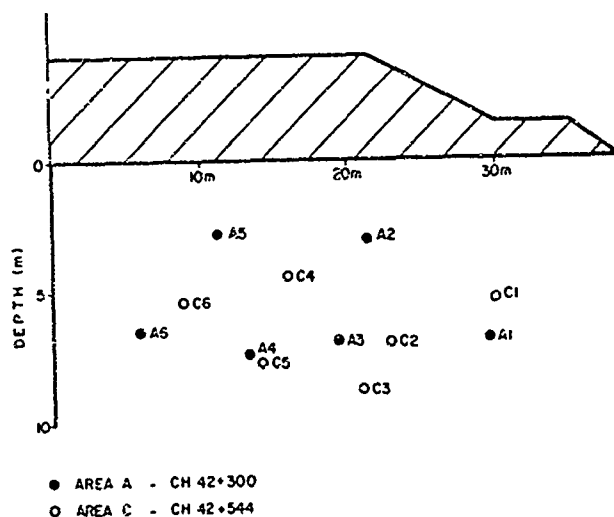


Fig. 5 Piezometer Locations

#### INSTRUMENTATION

Settlement plates and pneumatic piezometers were placed in areas A and C of the embankment. The settlement plates were installed at the centerline, at the shoulder of the embankment, and at the toe. The locations of the piezometers are shown on Figure 5. The piezometers were installed after placement of the drainage blanket (the first lift).

#### FIELD MEASUREMENTS

##### Piezometers

The loading history and the piezometer responses are shown on Figures 6 and 7. In area A the piezometer showed an almost immediate response of approximately 70 to 80 percent of the applied surface load. In area C the response was very close to 100 percent of the applied load.

Of particular interest is the fact the pore water pressure remained at a nearly constant level or even increased for several of the piezometers before it began to dissipate. Furthermore, the pore water pressure remained at a constant level higher than the hydrostatic level after the excess pore water pressure appeared to have dissipated. This phenomenon of delayed pore water pressure dissipation and the existence of a "trapped" pore water pressure after dissipation has also been observed by Hansko, Jamiolkowski, and Kok (1981). As they noted, it points out the difficulty of determining the degree of consolidation solely from piezometer data.

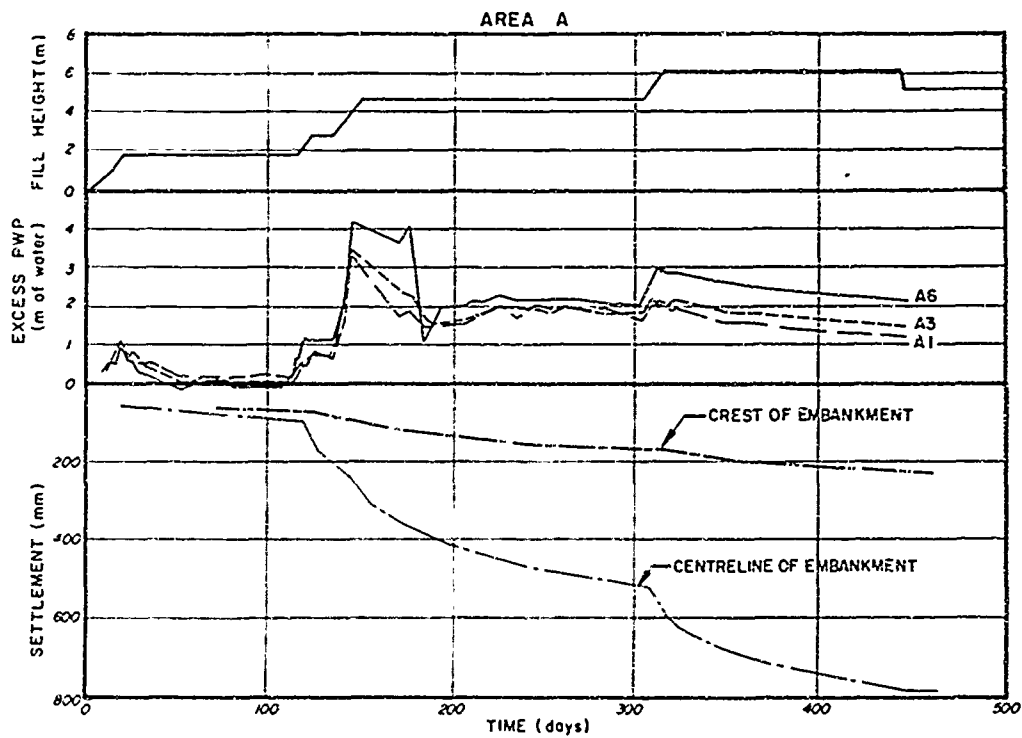


Fig. 6 Loading History, Piezometer Response and Settlement - Area A

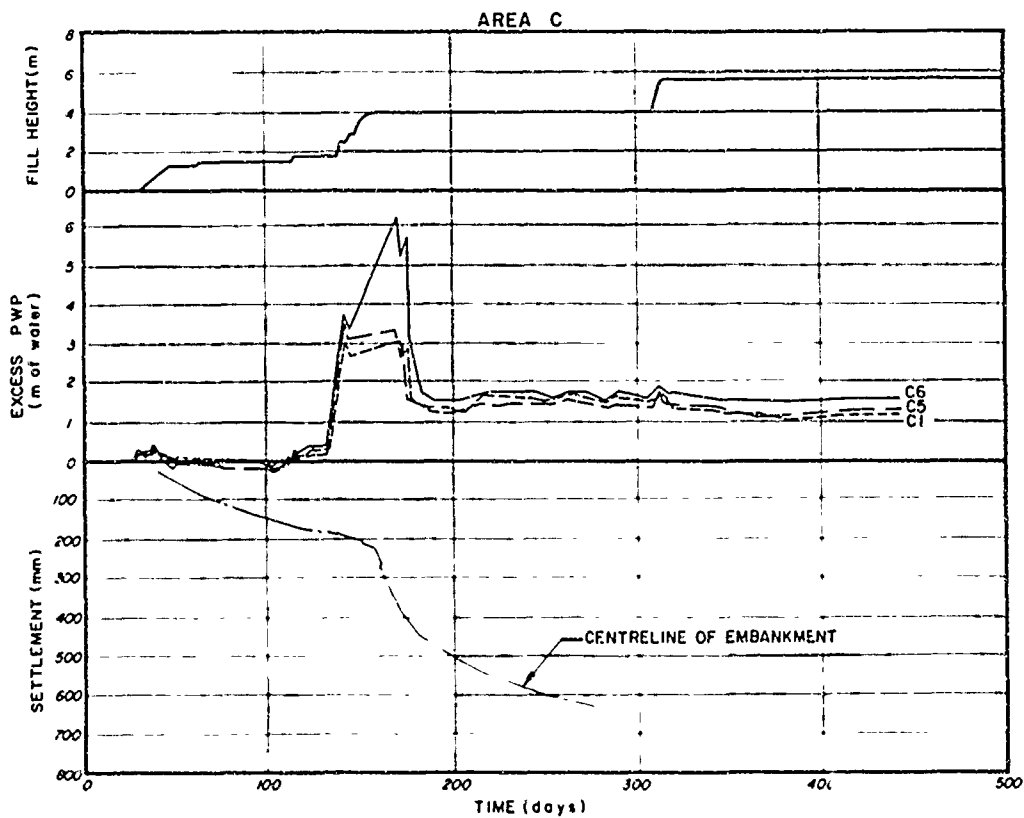


Fig. 7 Loading History, Piezometer Response and Settlement - Area C

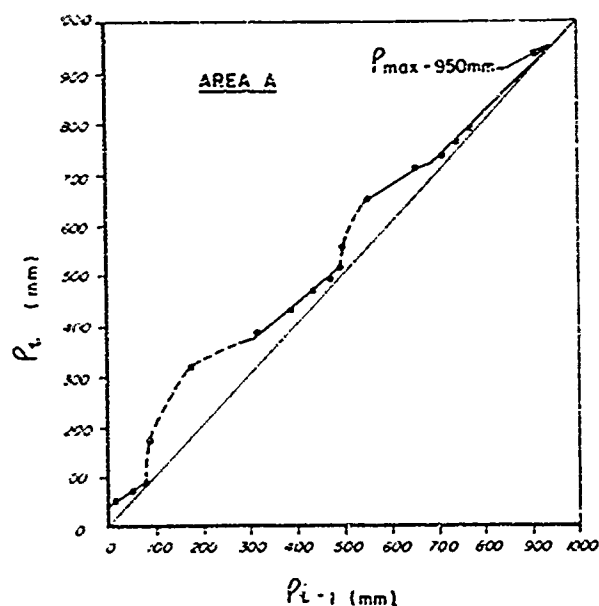


Fig. 8 Plot of Consolidation Data

It is of interest to note that piezometers A5, A6, C4, and C6 were located in areas of relatively high stress increase, which would have increased the breakdown of the soil structure. Also, the piezometers which exhibited the greatest delay in pore water pressure dissipation appeared to be in locations of relatively higher stress increase than those in which the pore water pressure dissipated more rapidly. It is believed that in this case the delayed pore water pressure dissipation and the increase in pore water pressure in the case of piezometers A5, A6, C4, and C6 is due to the collapse of the structure of the very soft soil. Until the soil structure can gain sufficient stiffness to begin to carry the effective stress, the pore water pressure carries the major part of the load. Because of the nonlinearity of the stress strain characteristics of the soft soil, a significant amount of water must be drained before the pore water pressure begins to dissipate. In the areas of lower applied stress level the soil structure was not broken down and it retained a greater initial stiffness.

#### Settlement

The settlement records are shown in Figures 6 and 7. These data were plotted in accordance with the procedures suggested by Asoaka (1978). This procedure consists of dividing the settlement-time curve into a

series of time increments and plotting  $\nu_i$  versus  $\nu_{i-1}$  where  $\nu_i$  is the increment of settlement in the time increment  $t_i$ . The point where this plot intersects a  $45^\circ$  line represents the point where  $\nu_i$  equals  $\nu_{i-1}$  or the point of 100 percent consolidation. The plots of the data for area A are shown in Figure 8.

The time required for 75 percent consolidation of the clay layer can then be determined as the time required for 75 percent of the projected 100 percent settlement to occur from Figures 6 and 7. These times are plotted on Figure 4. It can be seen that the times required for 75 percent consolidated are well within the general magnitudes predicted for the design wick spacings. The points fall within a range of values for coefficient of

consolidation of about  $6$  to  $10^2/\text{yr}$ , which are reasonable values determined on the basis of the piezocene data.

#### DISCUSSION AND CONCLUSIONS

It has been shown that the band drains were effective in increasing the rate of consolidation of the silty clay and clayey silt foundation soils under the embankments. It is of interest to note that for the points shown for both areas A and C on Figure 4, the time required for consolidation of subsequent loadings was greater than for the earlier loadings. One possible explanation for this is a decrease in the coefficient of consolidation for the foundation soils as consolidation takes place. This is very feasible at this site because of the existence of the lenses of inorganic material which would compress and also could become clogged by silt and clay being forced into the peaty material.

Another possibility for the increase in time of consolidation is the potential clogging of the wick drains by the piping of silt and clay through the outer geofabric covering. Either or both of these factors are a possibility.

It is evident that the band drains have been effective in increasing the rate of consolidation and that they have operated as designed.

#### ACKNOWLEDGMENTS

The authors wish to thank the National Transport Commission of South Africa and their consultants Messrs. Scott and de Waal for permission to publish the data presented in this paper. Many of the analyses were conducted by A. Pickles and the instrumentation was read and interpreted by J. D. Legge, while they were in the employ of Steffen, Robertson and Kirsten, Inc.

#### REFERENCES

- Hansbo, S., (1979), "Consolidation of Clay by Band Shaped Prefabricated Drains", *Ground Engineering*, Volume 12, No. 5, July, pp 16-25.
- Hansbo, S., Jamiolkowski, M. and Kok, L. (1981) "Consolidation by Vertical Drains", *Geotechnique*, Volume 31, No. 1, pp 45-66.
- Asoaka, A., (1978), "Observational Procedure of Settlement Prediction", *Soil and Foundations*, Vol. 18, No. 4, pp. 87-101.

## Seepage Problems and Remedies—Hub Dam

Izhar-ul-Haq

Director DMO, WAPDA, Lahore, Pakistan

**SYNOPSIS:** On the first impounding of Hub Dam, seepage problems started. The foundation piezometers showed rising pressures. The areas of concern were limestone, bed rock, jointed sandstone and gravel deposits at overburden-rock contact. Observational approach was followed. It was decided to fill the reservoir in stages. Various alternatives were considered to control the underseepage pressures. Relief Wells were installed which proved effective and economical to control the problem. A gravel shell was added on the downstream slope to enhance the stability of the homogeneous section in case of seepage through the body of the dam.

### GENERAL

Hub Dam Project located 55 KM North of Karachi on Hub River stores 0.86 million acre feet of water for municipal supply to the Karachi City and Irrigation purpose in Baluchistan province. The major project features consist of: Main Dam 15640 ft long, average height from river bed 152 ft; Saddle Dam 5740 ft long, average height 52 ft; Spillway a free overflow concrete gravity weir 6020 ft wide; the Intake Structure and the Canal. Fig.1 shows layout plan of Hub Dam Project. The construction of the project started in sixties and continued at a slow pace with intermittent stoppages and finally completed in 1979. The dam and the saddle are homogenous embankments of silty sand except for the river gorge portion where the embankment is zoned. The zoned embankment has silt in the core and clean

terrace gravel shoulders in the closure section, Fig. 2.

On the very first impounding, the piezometers installed at the downstream toe of the main embankment and saddle dam showed excessive pressure. Concern for dam safety led to investigations, extended instrumentation, review studies and some additional works. Observational approach was followed. Relief Wells were installed at the downstream toe of the dam which proved very effective in reducing the pressures at the toe. This paper describes the monitoring of the dam for the last 8 years, the problems faced and their remedies.

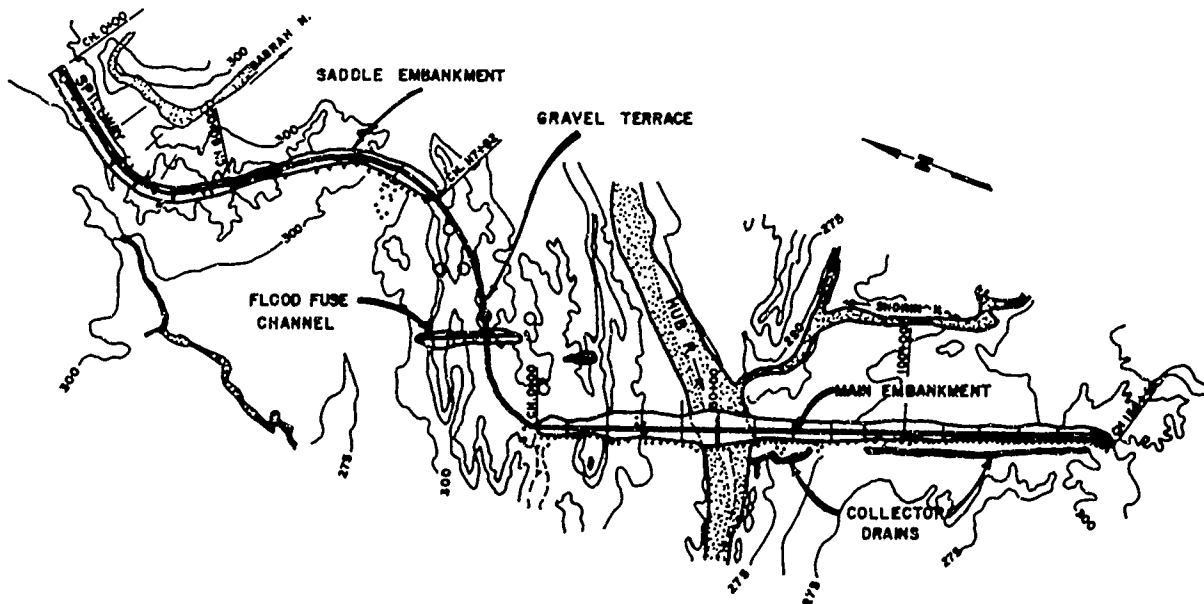


FIG.1 HUB DAM PROJECT - LAYOUT PLAN

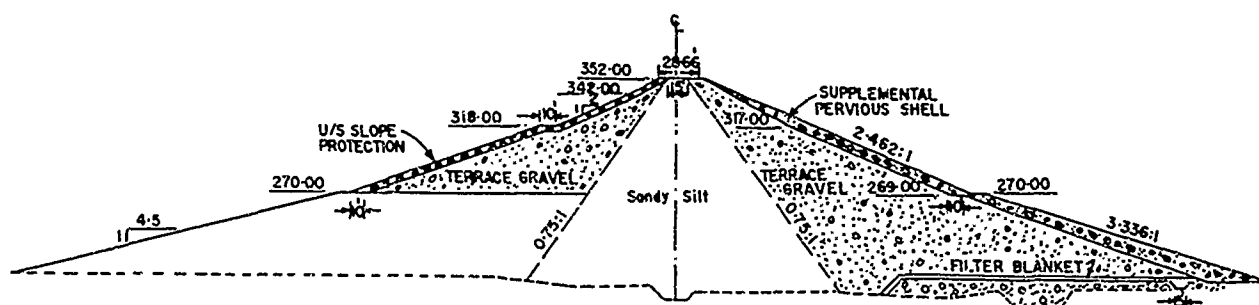


FIG. 2 HUB DAM - TYPICAL ZONED SECTION

## GEOLOGY AND FOUNDATION TREATMENT

The bed rocks along the main dam axis are mostly sandstone, siltstone and shale of middle Eocene age. A limestone bed about 15 ft thick 600 ft wide occurs in river section and is open jointed. The beds are nearly horizontal providing shortest path for seepage. Structurally the beds in the dam foundation do not show any folding or shearing and have a gentle dip. Bed-rocks dip across the river valley at inclinations of 6 to 10 degrees. The overburden is 5 to 20 ft deep on the left bank and upto 58 ft deep on the right bank. The former is silty sand with a thin layer of consolidated gravels over the bedrock. On the right bank it is mostly silty gravel in loose to cemented condition.

The Main Dam embankment is provided with a core trench which penetrates the bedrock by a minimum of 5 ft and is upto 25 ft deep in highly weathered or jointed rock strata. The shoulders of both the embankments are founded on stripped overburden. During excavation of core trench, seepage was encountered in limestone, certain reaches of jointed sandstone, siltstone mudstone and gypsiferous rock. These were treated by removal of open jointed rock, deepening and widening of core trench, limited cement grouting and filling of jointed areas by dental concreting. Piezometers were installed in such areas of concern to enable monitoring of foundation behaviour during reservoir impounding.

The Saddle Dam has a central core trench extending to bedrock except in a 770 ft stretch where it was terminated in silty sand. The bedrock in this reach, which is overlain by 10 to 50 ft deep alluvium, gradually rises in downstream direction and is found exposed about 2000 ft. downstream of the dam causing confinement of the overburden. Piezometers were installed in the dam foundation at rock overburden contact to monitor the pressures on impounding.

## UNDERSEEPAGE PROBLEM

The first summer impounding of September 1979 produced a rise of 29 ft in the reservoir surface level. The foundation instruments showed rising hydrostatic pressures mainly in three

areas i.e., limestone zone of Main Dam (Ch.67), jointed sandstone at Main Dam (Ch.78-79) and rock overburden contact in the partial cutoff reach of Saddle Dam (Ch.104). The piezometric surfaces at these places continued to rise over a month after the reservoir surface had remained static. The rise of piezometric levels at the Main Dam Toe ranged upto 60% of the reservoir rise while the response at the Saddle Dam toe exceeded 70%. The stabilized piezometric surfaces, however, remained well below the ground levels at the toe of the dams.

A 16 ft thick limestone bed at Ch.67 is sandwiched between relatively impervious beds of mudstone and siltstone. The prominent joints in limestone, filled with silt and clayey material are fairly tight except a few open ones. The joint at elevation 230 with iron-stains and weathered planes showed high water loss during drilling done for installation of piezometer. The sandstone at Ch.78-79 also has joints causing underseepage pressure. Review of piezometric observations after first impounding showed strikewise pressure gradient and influence of reservoir in causing underseepage at both the places.

Due to flat bedding planes and near horizontal prominent joints, horizontal permeability of the rock is higher than its vertical permeability. The general pattern of underseepage is characterised by hydrostatic pressure build-up resulting from confinement of alternating near horizontal beds having different permeabilities. The underseepage which finds its way to the dam foundation through thin overburden or exposed rock slopes in the reservoir remains confined due to flat beds and lack of natural drainage. The underseepage may be viewed as a confined flow in stratified soil with alternate impervious and pervious layers.

At the Saddle Dam the main problem was transmission of reservoir pressure to the downstream side through gravels in the overburden. High piezometric levels at the dam toe showed that the blanket of natural overburden was far from effective in lowering the underseepage pressures. Open-work conditions were not seen in the gravels sampled from the overburden; nevertheless control of hydrostatic pressures was



essential to prevent heaving or piping at the dam toe in the area of partial cutoff.

A programme of phased filling of the reservoir to El.305, 320 and 339 during the Observational Period was recommended. The reservoir rise was to be restricted, if need arose, by passing the higher inflows through a flood fuse channel excavated on the right bank gravel terrace. The first stage impounding level of El.305 was attained in August 1982 after three consecutive monsoon seasons of subnormal flows. In August 1983, when the reservoir level was approaching the second stage impounding level El.320, a decision was taken to allow the impounding to continue beyond this level. This was done after noting that the piezometric rise showed a lower response than the previous impoundings. The plug of the flood fuse channel was raised to El.352. The reservoir reached El.334.65 in the same month. Thus the reservoir rose in August 1983 not only to second stage impounding level (El.320) but also attained all but 5.35 ft of the third stage impounding level. The full impounding of stage-3 was attained in August 1984. The next monsoon produced the highest flood peak of the record period when the spillway overflowed with a surcharge of 5.3 ft over its crest. During this flood, the maximum reservoir rise of 21 ft (El.323.4 to El.344.3) took place in 3 days. The next summer impounding in 1985 produced a rise of 8 ft from El.329 to El.337.

#### REMEDIAL MEASURES

Various alternative measures were considered to control downstream underseepage pressures. These included weight berm, impervious blanket, grout curtain slurry trench and relief wells.

##### Weight Berm

A weight berm would merely transfer the point of upheaval or piping further downstream. Because of a flat piezometric gradient there would be no appreciable dissipation of hydrostatic pressures further downstream of the toe and the risk of failure would be shifted to the new toe. It was estimated that a weight berm of gravels underlain by filters built all along the Main Dam left flank would be too costly.

##### Blanket

An upstream blanket of impervious material increases the seepage path and decreases hydrostatic pressures in pervious foundation. However, a major area to be blanketed was already under water and laying of blanket on steep rock exposures of the river bank and hill slopes would be difficult. Also suitable clayey material was not available locally and cost of hauling over long distances would be prohibitive.

##### Grout Curtain

A grout curtain in the foundation conditions of Hub Dam would not be effective unless it had at least two rows and was accompanied by a drainage curtain downstream. Such a measure on a large-scale would be too expensive, besides involving the risk of drilling through the embankment fill. Also, previous experience at Hub Dam had shown that grout-take in thin-jointed rock (joints

generally 0.5 mm) was very poor. However, it was proposed that test grouting in selected reaches may be done after a few years when the material which filled the joints was expected to be flushed out by underseepage.

To evaluate the groutability of two typical foundation areas of concern i.e., limestone and gypsiferous sandstone, test grouting programme was implemented in 1982. Two reaches of 100 ft each, Ch.66+50 to Ch 67+50 and Ch 119 to Ch 120 were selected. Grout holes were located at split spacing with primary holes at 20 feet centres. Grouting of foundation rock under an existing embankment involved the precarious operation of drilling in about 100 feet of embankment fill and sealing the casing into rock to prevent the grout from entering the fill/rock contact zone under unacceptable pressures and in unacceptable quantities. Use of any drilling fluid was precluded to avoid the possibility of hydraulic fracturing in the embankment fill. Drilling in the embankment fill was done by augering. Watercement grout was injected by descending stage method. 58 holes were grouted in two reaches. There was no high grouttake zone in either of the two reaches. Most of the stages in limestone zone took less than 0.04 bags per ft. Exceptional takes in three stages were between 0.49 bags per ft and 0.74 bags per ft. The grout takes in gypsiferous zone were even poorer. Most of the stages in this zone either did not take any grout or accepted less than 0.04 bags per ft. No evidence of solution cavities was found. The tests demonstrated that the foundation rock at Hub Dam was not groutable by cementwater mix.

##### Slurry Trench

A slurry trench or a diaphragm wall would provide an effective barrier against underseepage. However, besides practical difficulties due to a partially filled reservoir, the cost of this solution would be prohibitive.

##### Relief Wells

The proposal of relief wells was found an effective and economical method of underseepage control in the given conditions. An important point was the depth of underseepage control depth equal to the reservoir head over upstream ground level was checked and found to give adequate factor of safety against heaving. Because of down-dip flows in the sedimentary rocks underseepage would be met even at great depths. Therefore, the deeper the proposed control, larger will be the reclaimed seepage. However, the estimated seepage quantity on the left flank being small (1.4 cfs), and the main objective being the control of hydrostatic pressures at the dam toe, the control depth fixed on the above criterion was considered adequate. The depth of drainage curtain so fixed worked out to an average of 56 ft on the left flank of Main Dam. The depth of wells varied with the ground level. Checked from drill hole data, all known open joints were intercepted by this control depth. Considering the irregular joint pattern and the foundation conditions of Hub Dam, a large number of wells with small capacity were required to drain the rock. Three inch internal dia wells with 4.5 inch shrouding material in 12 in dia drill holes were installed. The spacing was kept 25 ft in

more pervious rock zones and 50 ft in general. It was also stipulated that a second line of wells may be provided in selected reaches if pressure relief with single line of wells was not adequate. The wells were provided with slotted pipes in rock, penetrating to the control depth while the overburden portion was blinded. Filter material was selected mainly to check the material sizes which filled the joints. Relief wells costed only about 15% of the estimated cost of a two-row grout curtain. Wells of similar design were installed in selected reaches of Main Dam right flank where subsequent impoundings indicated the need of pressure relief.

About 300 relief wells were installed of which 270 were at the Main Dam and 30 at the Saddle Dam. Each relief well has an outflow pipe whose invert is generally 3 ft lower than the embankment filter drain level. The outflow pipes discharge into an open collector drain whose bed and sides are covered with filter material overlain by open-jointed stone pitching.

#### PIEZOMETRIC BEHAVIOUR

The behaviour of piezometers was closely monitored and evaluated during successive impoundings. Additional instruments were also installed midway between the relief wells at selected places to check the adequacy of their interspacing. Years 1980 and 1981 were very dry and the reservoir rise in these years was minor. In the summer impounding of 1982, the reservoir level gained by 18.28 ft. The instruments at the dam toe in limestone zone responded upto 10.4% of the reservoir rise in 1982 against 14% response during 1981 impounding. The toe instruments at Ch 78-79 responded by about the same percentage (19.6%) in 1981 and 1982.

The summer impounding of 1983 produced a reservoir rise of 34.25 ft when water level touched El 333.65 i.e., 5.35 ft short of full pool level El. 339. The response of the toe instruments in limestone zone was about the same as in 1982. The toe instruments at Ch 78-79 registered piezometric rise upto 14.94% against preceding year's 19.6%. Thus the rate of rise of hydrostatic pressures at the dam toe either decreased or generally remained the same, showing continued effectiveness of relief wells during successive reservoir fillings. Comparative gradients of hydrostatic pressures in the dam foundation in the above reach during different impoundings are shown in Fig.3.

The piezometers at the Saddle Dam toe Ch 104-105 responded by 65% to 69% of the reservoir rise in 1981 in spite of the relief wells. This was because the piezometric surface had just reached the invert levels of adjacent relief well outflow pipes. When the reservoir level and downstream piezometric surface rose further in 1982 impounding, the influence of relief wells was fully reflected in the response of piezometers which dropped to 35% from previous year's 69%. The relief wells at Saddle Dam, none of which was flowing before 1982 summer impounding, started discharging 472 lpm (0.28 cfs) after the said impounding. When the

reservoir rose by 34.25 ft in 1983, the same toe instruments at Ch 104-105 rose by only 14%. The total discharge of the flowing wells at the Saddle Dam rose to 885 lpm (0.52 cfs). Thus the rate of rise of piezometric surface at the dam toe decreased during successive impoundings while relief well discharges gained progressively, showing generally effective control of hydrostatic pressures at the well lines. Incipient boiling was noticed at a point in the collector drain after 1983 impounding. This place was covered with filter material and overlain with gravels and cobbles.

At two places in limestone zone and saddle area, the piezometers placed between 25 ft spaced wells showed higher piezometer readings than those in adjacent well line. Additional wells were installed at such places reducing the spacing to 12.5 ft.

#### SEEPAGE THROUGH THE DAM

The original design of the embankment envisaged a zoned section for major length of the Hub Dam. The proposed section comprised a central impervious core of sandy silt and shoulders of granular material, both abundantly available in the vicinity of the dam site. However, local construction constraints of early sixties led to the adoption of a homogeneous section of sandy silt material with downstream horizontal filter blanket.

Construction of Hub Dam spanned a number of years with several interruptions and involved widespread borrow areas. This inevitably resulted in numerous interfaces and in local variations of the embankment material. It was therefore considered possible that this lack of homogeneity could add to the normal degree of anisotropy present in any rolled fill to an extent that it could result in possible emergence of phreatic surface on the downstream slope of the embankment. In such an event the stability of the downstream slope calculated on the basis of the phreatic line discharging into the horizontal downstream drainage blanket provided in the dam would be jeopardised.

#### Gravel Shell

It was therefore decided to add a supplemental sand-gravel shell as shown in Fig.3 to enhance the stability of the downstream slope to acceptable limits under the particular conditions mentioned above. The shell was eventually constructed by selective borrowing of locally available river-run sand-gravel of required permeability without processing. The material, comprising upto 60% sand and rest gravel, was hauled by dumpers and trucks, placed and compacted to more than 70% relative density in lifts upto 18 inches using vibratory rollers. A protection layer of cobbles and boulders was provided over the shell slope.

#### CONCLUSIONS

The general pattern of underseepage is through joints and bedding planes below the core trench in the direction of strike. Hydrostatic

pressures build up results from confinement of underseepage by near-horizontal beds. At the Saddle Dam, the gravels at the overburden-rock contact provide a major path of underseepage.

Observational approach proved a successful method of evaluating the behaviour of dam during phased impoundings and taking remedial measures where necessary. An extensive network of 268 piezometers was the mainstay of a successful Observation Programme. The piezometers provided an important information in the problem areas.

The underseepage quantities are very small. The main problem is of relieving hydrostatic pressures downstream.

Drainage of the foundation rock by vertical wells provided an effective and economical method of relieving pressures. A control depth equal to the head of water above the dam heel proved satisfactory. A spacing of 25 ft centres was generally adequate in permeable rock zones.

Rolled fill homogeneous embankments built from widespread borrow areas are likely to have locally different permeabilities such that the phreatic line may emerge on the downstream face. A zoned section with pervious shoulders and an inclined chimney filter rather than a horizontal filter should be adopted in such conditions.

#### REFERENCES

Underseepage at Hub Dam left flank and its effective control, December 1979, by Associated Consulting Engineers.

Review of piezometric observations of the Hub Dam, October 1983 and September 1982 by Associated Consulting Engineers.

Instrumentation of Hub Dam by Dams Monitoring Organization, WAPDA.

Design of supplemental shell of Hub Dam by Associated Consulting Engineers.

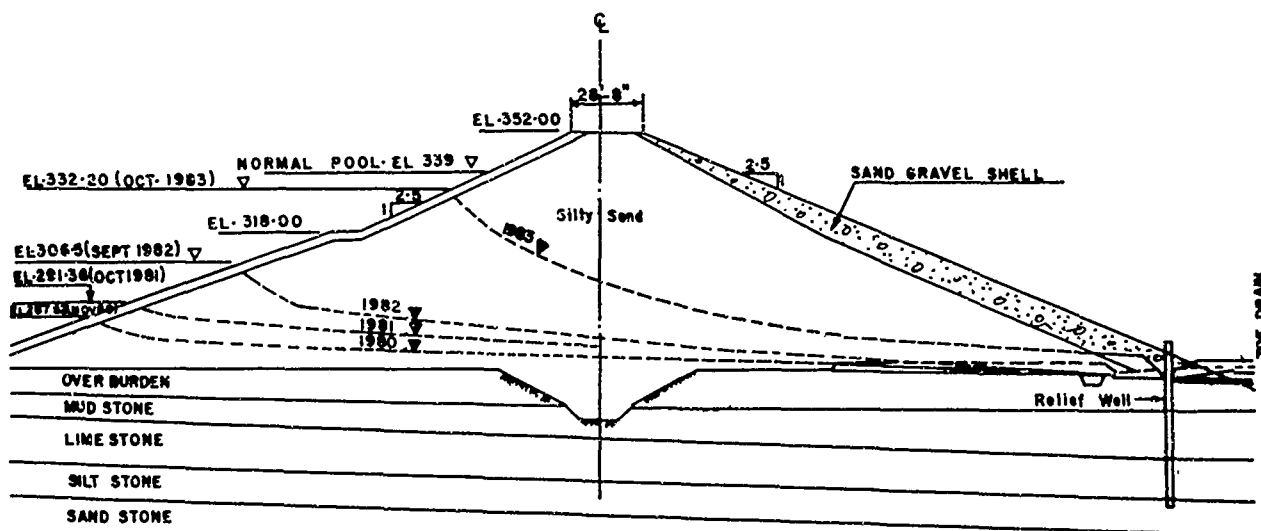


FIG.3 HYDRAULIC GRADIENTS AT DIFFERENT IMPOUNDINGS

## The Behaviour in Time of Ripa Albastra Dam Impervious Bentonitic Core

Aurel I. Hărsulescu

Supervisor Geological Engineer, Research and Design Institute for  
Water Resources Engineering, Bucharest, Romania

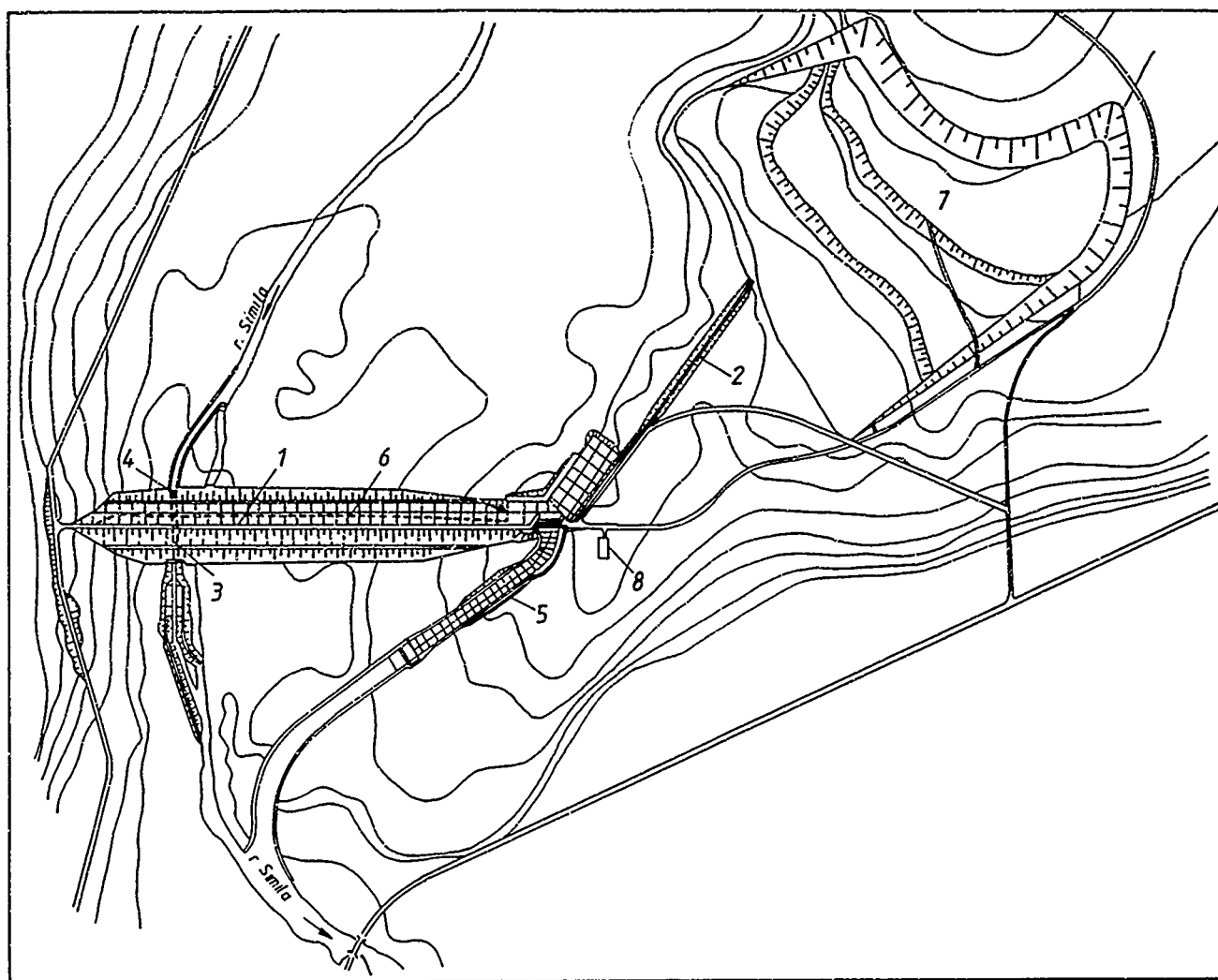


Fig. 1 Lay-out of Ripa Albastră Dam and Auxiliary Structures Location

|                 |                    |
|-----------------|--------------------|
| 1 Dam           | 5. Spillway        |
| 2 Lateral dyke  | 6 Cut-off wall     |
| 3 Bottom outlet | 7 Quarry           |
| 4 Water intake  | 8 Operator's cabin |

**SYNOPSIS:** The paper presents the results of laboratory and field research, the execution and behaviour under operation of the Rîpa Albaştră earth dam, the first Romanian dam with an impervious core achieved by the mechanical mixture of fine-medium sands and bentonite.

The dam structure and the geomorphological condition in the area are described.

further, the types of soils extracted from the dam quarry are described, together with their outstanding geotechnical characteristics in both natural and compacted state.

The paper continues by describing the physico-chemical properties of seven Romanian bentonites used in laboratory tests, as compared to some foreign bentonites of notoriety, as well as the physical properties of the mixture achieved between bentonites employed in varying percentage and the support material, with special considerations on their permeability.

After checking the results of laboratory research in the testing tracks preceding the execution, the paper presents the technology adopted for the achievement of the impervious core.

The paper concludes by analysing the results of observations conducted on the dam behaviour by means of piezometric boreholes drilled into the downstream prism, under the conditions of putting into operation the hydrotechnical scheme, with particular consideration for the recorded permeability.

## INTRODUCTION

Over the past twenty years, the Romanian scientists, engineers, designers, and hydrotechnical constructors made remarkable progress in the field of earth dams, materialized in the achievement of a great number of hydrotechnical development works on the rivers Lotru, Someş, Mureş, Olt, Sebeş, Siret, Argeş, Buzău, Dâmboviţa, Birlad, etc. The extremely high value of these investments entailed the search for and application of execution technologies allowing the achievement and operation under safety conditions of these structures, at the lowest possible costs. Such a technology was employed in the design and execution of the Rîpa Albaştră dam, whose impervious core was carried out by the mechanical mixture of sands and bentonite.

## THE RÎPA ALBĂȘTRĂ DAM

The Rîpa Albaştră reservoir was achieved over the period 1973-1975 within the general regulation plan of the Birlad hydrographic basin, with the main purpose of flood mitigation on the Simila river and water supply, and the subordinated purpose of irrigation and fish-farming.

The storage basin was carried out by an earth dam 18 m in maximum height, 1260 m crown length, and fill volume of about 650,000 cu.m. The ancillary structures of the dam consist in the water intake, bottom outlet, and spillway structure. The foundation ground screening was carried out by means of a concrete cast in place wall (SLSE), 1950 m long and 12 m in maximum height, Figure 1.

The Simila river has in the reservoir area a wide open "U"-Shaped Valley, the plain reaching heights of 800 - 1000 m. In the left slope of the dam site terrace deposits have been intercepted, 14 - 20 m. thick, and 200 - 400 m. wide.

The geological formation occurring in the dam location belong to the Neogene and Quaternary periods. The Neogene was intercepted at variable depths (2-5m. in the right slope and 3-12 m. in the plain and left slope), being represented by non-differentiated kersonian-moşian deposits

consisting of alternating grey-greenish finely stratified marley clays and yellowish-grey fine medium or clayey-silty sands. The Quaternary covers for the most part area, being represented by plain deposits, terrace and alluvial. The depth of ground water occurrence varied at the time of research between 1,30 and 4,70 m. in the plain, and 8-11 m. in the terrace.

Field and laboratory research revealed as the most favourable source of local materials for dam fillings, the fine-medium sands of the kersonian-moşian complex, occurring mainly in the left slope of the reservoir, exceeding 15 m. in thickness. From the quarry located about 1 km upstream of the dam site, covering a surface area of 3.3 ha, some 650,000 cu.m. fine-medium silty-sands were exploited, with natural water content values  $w = 7-10\%$ , degree of saturation  $S_r = 0.2-0.5$ , and natural volume weights of  $\gamma = 16-19.5$  kN/cu.m. Following laboratory compaction tests (PROCTOR), it was observed that sands compacted at natural water content with mechanical efforts  $E_f = 4-6$  dJ/cu.cm. can reach minimum dry volume weights of  $\gamma_d \geq 16.5$  kN/cu.m, shearing indices of  $I_p = 25-30\%$ ,  $c = 0.1-0.15$  daN/sq.cm, and permeability coefficients of  $k = 10^{-7} - 10^{-6}$  cm/sec. The relatively high values of permeability entailed the adoption of nonhomogeneous section dam, with an impervious core inclined towards the sandy supporting prisms, Figure 2

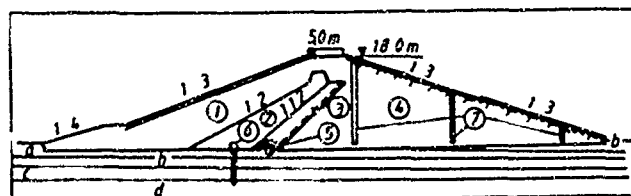


Fig. 2 Cross section of the Rîpa Albaştră Dam  
1 Upstream prism a Clayed sand  
2 Core (sand with bentonite) b Clay  
3 Filtering layer c Medium-fine sand with gravel

- 4 Downstream prism d Earley clay
- 5 Longitudinal drain
- 6 Cut-off wall
- 7 Piezometers

Investigations carried out in the reservoir area for borrowing clayey soil required for the impervious core, lead to the conclusion that their employment is not economical due to improper quality and quantity. Following extensive and in-depth research, the solution was adopted to achieve the impervious core or mixtures of fine-medium sands with bentonite.

#### THE SAND-BENTONITE MIXTURE

Researches carried out in the laboratory as well as in the field, in the experimental tracks laid in the dam location, was mainly set on determining the influence of treating fine-medium sands with bentonite on their permeability and shearing characteristics.

Bentonitic clays, complex Na, K, Mg or Fe aluminium silicates were formed from either igneous or sedimentary rocks under the action of chemical factors, the last genetic factor being in both cases the colloidal sediments formation.

Due to the occurrence of montmorillonite - the clayey mineral with the greatest adsorption capacity and overlapping crystal lattice in three layers which are not electrically neutral - bentonites are mainly characterized by an extreme swelling capacity. On the other hand,

it is known that so called alkaline bentonites (Na or K) have adsorption and swelling characteristics exceeding by for those of alkaline-earth bentonites (Mg or Fe). It is self-evident that in most cases they tend to use either alkaline bentonites, or alkaline - earth bentonites activated by various technologies such as  $\text{Na}_2\text{CO}_3$  treatment. In the laboratory experiments conducted for the dam core, seven types of Romanian bentonites have been tested:

- A - Breaza bentonitic clay, natural state (alkaline-earth);
- B - Ilovița bentonitic clay, (activated with  $\text{Na}_2\text{CO}_3$ );
- C - Ilovița bentonitic clay, natural state (alkaline-earth);
- D - Gura Sada bentonitic clay, (activated with  $\text{Na}_2\text{CO}_3$ );
- E - Gura Sada bentonitic clay, natural state (alkaline-earth);
- F - Valea Chioarului bentonite, natural state (soda);
- G - Craiul Nou bentonite, natural state (soda).

The mixture between fine-medium sands, sometimes with gravels, and the tested bentonites were achieved by adding powder bentonite in varying percentages (1-18% of the volume earth weight) and compacting them by the Proctor method at mechanical compaction efforts of  $\Delta p = 6-12$  dJ/cu.cm. The permeability tests on compacted mixtures (250 tests) were carried out with variable gradient ( $I_{\text{max}} = 10$ ), and the duration of an experiment was of about 72 hours. Experiments finished when the permeability became constant.

Table 1 presents the main characteristics of Romanian bentonites as compared to some foreign bentonites of notoriety.

Table 1 Physico-chemical Characteristics of the Bentonites used in the Experiments

| TYPE OF BENTONITES<br>PHYSICAL-<br>CHEMICAL CHARACTERISTICS | SYMBOL   | USA     | JAPAN  | ROMANIAN BENTONITES |             |             |             |             |             |             |
|---|--|---------|--------|---------------------|-------------|-------------|-------------|-------------|-------------|-------------|
|   |  | Aquagel | Telgel | A                   | B           | C           | D           | E           | F           | G           |
| SAND CONTENT  | S (%)  | 15      | 10     | 30                  | 12          | ~3          | -           | 6.0         | 6.4         | 2.4         |
| LIQUID LIMIT  | $W_L$ (%)                                      | -       | -      | 127.5-285           | 152.5-160.0 | 140.5-141.5 | 264.5-272.5 | 127.0-128.5 | 325.0-331.0 | 472.0-480.0 |
| ADSORPTION CAPACITY   | $C_A$ (%)                                      | -       | -      | 177.0               | 201.5       | 217.0       | 358.0       | 135.8       | 605.0       | 563.0       |
| SHRINKAGE LIMIT   | $W_S$ (%)                                      | -       | -      | 11.5-13.5           | 11.7-18.5   | 11.2-15.0   | 11.0-21.0   | 13.0-19.5   | 15.0-22.0   | 29.5-34.5   |
| UNCONFINED SWELLING   | $U_L$ (%)                                      | -       | -      | 215-240             | 210-240     | 250         | 260-290     | 170-190     | 390-420     | 575-530     |
| VOLUME SHRINKAGE  | $C_V$ (%)                                      | -       | -      | 96.0-116.0          | 97.0-130.5  | 131.0-145.0 | 149.5-167.0 | 75.0-77.5   | 237.0-249.0 | 258.0-278.0 |
| BEHAVIOUR OF 10 % SUSPENSION AFTER 24 HOUR HYDRATION        |  |         |        |                     |             |             |             |             |             |             |
| FILTRATION  | $F/t$ (cu.cm)                                  | 10.0    | 11.5   | 10.5                | 16.0        | -           | 10.5        | 24.0        | 11.0        | 12.0        |
| P H   | P H  | 6.0     | 6.5    | 7.5                 | 9.0         | 6.0         | 8.6         | 5.5         | 7.0         | 9.8         |
| CATION CHANGE CAPACITY                                      | $\frac{CCC}{(g \text{ coll } g \text{ clay})}$ | 0.2155  | 0.1796 | 0.1135              | 0.2066      | 0.1650      | 0.2089      | 0.2089      | 0.1971      | 0.1967      |
| EFFICIENCY  | $R$ (cu m/t)                                   | 15.0    | 13.4   | ~3.6                | 8.3         | 4.5         | 9.9         | 4.2         | 6.9         | 9.2         |

Figure 3 presents as an example the variation of the permeability coefficient of a fine-medium sand with gravel, compacted at 6 dj/cu.cm. efforts, with various percentages of A-G bentonite.

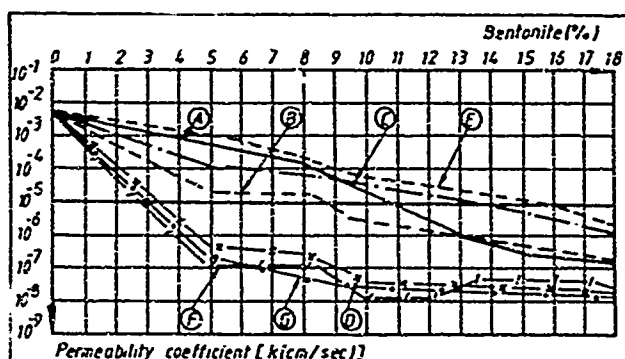


Fig. 3 The Variation of the Permeability Coefficient of Compacted fine-medium Sands with Gravel Depending on the Various Percentage of A-G Bentonites.

The results of laboratory analyses carried out on activated A and F type bentonite mixtures, revealed the following:

- the addition of 1-6% powder bentonite leads to a tenfold - ten thousands fold decrease in the permeability of the natural material;
- a mixture permeability of  $K < 1 \times 10^{-5}$  cm/sec is attained for a minimum addition of bentonite of 2 %;
- the treatment of sandy soils with 2 % bentonite should be associated with a rigorous compaction of the mixtures at the optimum compaction water content ( $W_{oc} = 13-14\%$ ) when a compaction effort of minimum  $E_p = 6$  dj/cu.cm. is used;
- the shearing strenght of compacted mixtures does not decrease significantly as compared to that of natural materials, up to bentonite additions of 5-6 %, Table 2;
- the mixtures between fine-medium sands and 5-6 % bentonite compacted in the laboratory did not reveal bentonite expulsion at gradients of  $I_{max} < 10$

Table 2 Physico-mechanical Characteristics of fine-medium sand<sup>a</sup> with 1-6 % Bentonite Addition.

| TYPE OF SOIL<br>GEOTECHNICAL CHARACTERISTICS     | SILTY FINE SAND | SILTY FINE SAND WITH 1% BENTONITE | SILTY FINE SAND WITH 6% BENTONITE |
|--|-----------------|-----------------------------------|-----------------------------------|
| PLASTICITY INDEX $I_p$ (%)                       | —               | —                                 | 23                                |
| SHRINKAGE LIMIT $W_s$ (%)                        | —               | —                                 | 22,5                              |
| UNCONFINED SWELLING $U_L$ (%)                    | —               | —                                 | 50                                |
| COMPACTING EFFORT $E(d)/cu.cm$                   | 6               | 6                                 | 6                                 |
| COMPACTING WATER CONTENT $W(\%)$                 | 8               | 8                                 | 8                                 |
| UNIT WEIGHT $\gamma' (kN/cu.m)$                  | 18,6-18,8       | 18,1-18,3                         | 19,4-19,6                         |
| POROSITY $n$ (%)                                 | 36,5-37,5       | 33-38                             | 36,5-37,0                         |
| ANGLE OF INTERNAL FRICTION $\phi_{int}$ (degree) | 28              | 30                                | 21                                |
| COHESION $c_{uu}$ (daN/cm <sup>2</sup> )         | 0,3             | 0                                 | 0                                 |

## THE EXECUTION OF THE BENTONITIC CORE

Following the experiments carried out during the execution of the dam lateral prisms with confirmed the conclusions of laboratory research and considering the contractors possibilities and equipment, the following technology has been adopted for achieving the impervious bentonitic core of the dam:

- spreading fine-medium sands in 15 cm. thick layers;
- adding the 2% powder bentonite in two stages from a special unit used for spreading chemical fertilizers fitted with a protection apron;
- homogenizing, the sands with the bentonite, by two passing of the 3.2 m. wide harrow after each stage of spreading powder bentonite;
- moistening of layers after the last homogenization by applying 2-5% b, means of a sprinkler unit;
- the compaction of each layer by 8 passing of the Hyster autocompactor, 40 t weight, Figure 4, followed by 2 passing of the transport facilities, thus ensuring a dry volume weight of the fillings of  $\gamma_d \geq 17.0$  kN/cu.m.;

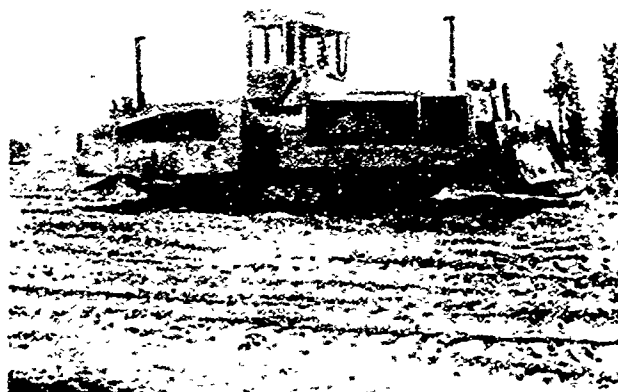


Fig. 4 Hyster Autocompactor 40 t. weight

The degree of core embankment compaction (about 72,000 cu.m.) was checked by the laboratory analysis of about 2,000 samples taken by the contractor from each layer and by 8" diameter control boreholes drilled in three different stages. The statistical processing of the dry volume weight values ( $\gamma_d$ ) obtained in the core, revealed the variation of this index according to the law of normal distribution, resulting in a mean square distortion of  $\sigma = 0.166$  and an average of  $\gamma_d = 18.045$  kN/cu.m. Under these circumstances the degree of compaction attained was 98 - 100%. The bentonitic core permeability compared to that of the sandy supporting prisms (upstream and downstream) was tenfold - hundredfold lower, the recorded values being  $6 \times 10^{-5}$  -  $7 \times 10^{-8}$  cm/sec, Figure 5.

The in operation dam behaviour has been continuously surveyed since the completion of the works (1975) and up to the present time by means of settlement markers, piezometric boreholes and cells, etc. The piezometric boreholes were located on the downstream face along three cross section profiles of the dam. On each profile three boreholes were drilled, in which the hydrostatic level of the seepage in the downstream prism is measured every ten days, thus obtaining an image of their evaluation in time depending on the

water level in the reservoir.

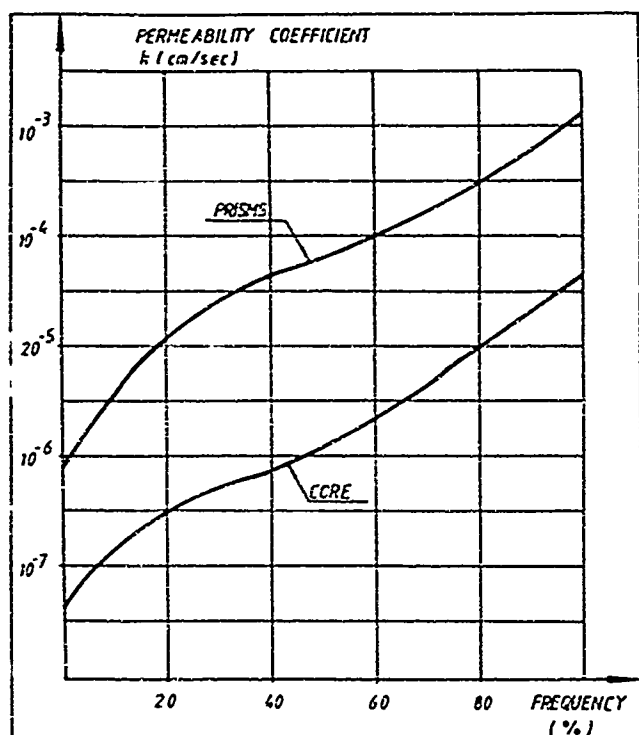


Fig. 5 The Variation of Core and Prisms Permeability of Rîpa Albastră Dam

Figure 6 presents as an example the diagram of the water levels in this prism, recorded in the central profile piezometer, during 1986.

The analysis of the hydrostatic levels measured in these boreholes reveal that the treatment of fine-medium sands in the core of the dam with 2% bentonite lead to the desired result, the compacted mixtures retaining their quasi-impervious character all over the period of measurement (12 years). Furthermore, during the first year after the reservoir filling, and therefore after the core flooding, a continuous decrease in its permeability was recorded, due to the gradual consumption of the bentonites swelling capacity. It should be mentioned that about two years after completion, on March, the 4<sup>th</sup>

1977, during the great earthquake affecting the dam area (intensity degree 7.2 Richter), neither the dam nor the bentonitic core revealed any sign of deterioration or instability.

Finally we underline that in selecting similar impermeabilization solutions of hydrotechnical structures embankments, it is desirable to take into special consideration the size of hydraulic gradients developing during operation as well as the types of earth and bentonite used, knowing that in exceeding critical hydraulic loads can lead to the expulsion of bentonite from the mixture pores.

#### REFERENCES

- Anon (1973), "Baroid's National for Sealing Reservoirs, Dams, Canals, Lakes, Swiches ... and other Porous Formation", Baroid Div National Lead Comp. Houston, (USA).
- Hârsulescu, A. Sima, N (1979) "The Use of Bentonites for Sealing Earth Dams", Engineering Geological Problems in Hydro-technical Construction - Tbilisi (USSR) p.222-226.
- Sarosi, L. Boha, I. Kélemen I. "Bentonit as Építőiparban Műszaki Könyvtár" Budapest (H).
- Sima, N. Hârsulescu, A. (1973) "Studiul Geotehnic privind Barajul Rîpa Albastră" ISPIF Bucureşti, (Romania).
- Stefănescu, D. (1975) "Studiu privind Folosirea Materialelor Bentonitice în Execuția Construcțiilor Hidrotehnice" (ICPGP Cîmpina, Romania).
- Zelenin, L. Sima, N. Hârsulescu, A. (1977) "Acumularea Rîpa Albastră" Hidrotehnica 22-6, p. 148-151.

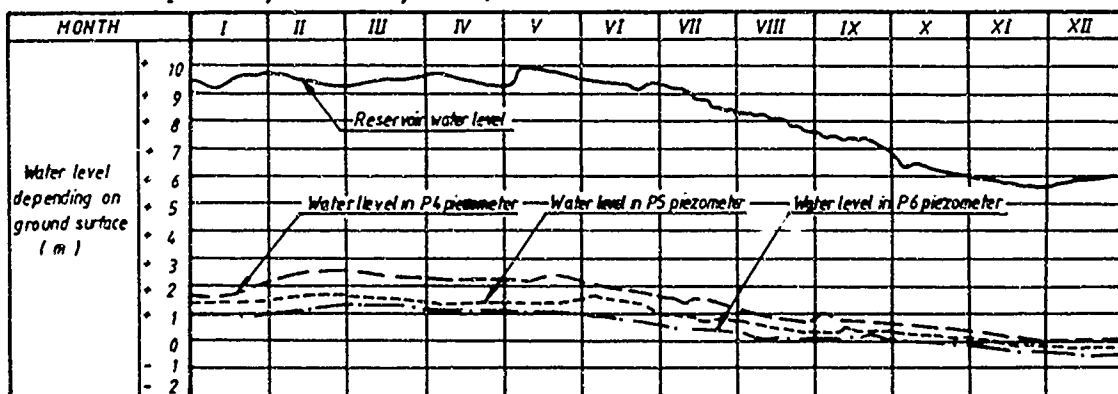


Fig. 6 The Diagram of the Downstream Hidrostatic Revels Recorded during 1986 Year.



## Horizontal and Vertical Movements of Red Clay Highway Embankments

F.J. Gichaga

Civil Engineering Department, University of Nairobi, Kenya

B.K. Sahu

Civil Engineering Department, University of Nairobi, Kenya

F.S. Atibu

Civil Engineering Department, University of Nairobi, Kenya

**SYNOPSIS:** The paper presents results of a study of horizontal and vertical movements of five highway embankments made up of red clay (red coffee soil). The highway embankments studied ranged from 4m to 15m in height.

The study also involved laboratory testing of the red soils which form these embankments.

Results of laboratory tests were used to compute cracking and collapse potentials of the embankments.

Results of field investigations showed embankments to suffer horizontal as well as vertical movements. It was further established that in the case of the embankments, whose bituminous pavements had showed severe longitudinal surface cracks, the cracking observed was not due to slope failure but due to moisture migration and differential settlements which resulted from low placement moisture and density conditions of the embankment during construction.

The red soils were found to be highly plastic, highly susceptible to cracking and were also very likely to collapse due to flooding.

### INTRODUCTION

The function of a highway embankment is basically to provide support for the pavement system constructed above it. The design of a highway embankment generally involves establishing the height, side slopes, type of construction material to be used, and specifying placement conditions of moisture content and density to be achieved. An embankment may fail due to a number of conditions including:-

- (i) presence of underground water which would undermine the embankment through seepage or lead to reduction in shear strength.
- (ii) poor foundation of low compressibility and consolidation characteristics leading to excessive settlements of the embankment.
- (iii) unsuitable material in the body of the embankment.
- (iv) poorly constructed embankment with insufficient compaction.

This paper presents results of a study of horizontal and vertical movements of five highway embankments of red clay. The paper also includes an analysis of the cause of longitudinal cracking of bituminous pavements constructed on red clay highway embankments.

### EXPERIMENTATION

The paper presents results of both field studies of the selected highway embankments as well as laboratory tests carried out on the materials used in the construction of the embankments (Atibu, 1986).

#### Field Studies

Field studies involved instrumentation of highway embankments on selected test sites and

monitoring the movements of the embankments.

#### Selected Test Sites

The following five test sites were selected for this study:-

##### (1) Test Site ES7 on Limuru-Uplands Road

This test site was selected on the Limuru-Uplands Road (on the Trans-African Highway) on a side hill red clay embankment whose height is about 6 metres at the road centre line gradually diminishing in height towards one side and increasing in height on the other side to about 13 metres at the bottom of the valley. The heavy duty bituminous pavement (asphaltic concrete) on this embankment showed severe longitudinal cracking on the road surface.

##### (2) Subsite ES7 at Kamirithu

This experimental site was selected on Limuru-Uplands Road adjacent to test-site ES7 at Kamirithu. It had a similar red clay embankment of 6m in height and the bituminous pavement had similar longitudinal cracking on the road surface to test site ES7.

##### (3) Test Site ES8 on Limuru-Uplands Road

This test site was selected on Limuru-Uplands Road about 4 kilometres from test site ES7 and the embankment at this test site was made of red clay and had almost similar geometry to ES7. The bituminous pavement on the embankment suffered from longitudinal cracking.

##### (4) Test Site ES9 on Thuchi Nkubu Road

This test site was selected about 7 kilometres from Nkubu towards Embu town. The embankment is about 15m high and is made up of red clay. There were no cracks on the bituminous pavement

surface (triple surface dressing).

#### (5) Test Site ES10 on Ruiru Nyanduma Road

This test site was selected about 30 kilometres from Ruiru on this low volume road. The embankment is about 4m high and constructed of red clay. There was no cracking on the road surface (single layer surface dressing).

#### Measurements of Horizontal Movements

Trenches were cut across the road pavement to a depth of 400mm. Then horizontal gauges were installed across the embankments as shown in figure 1. Backfilling of trenches was carefully done ensuring the backfilled material achieved same density as that of the original material. Periodic readings of the gauges were taken at the beginning and end of each season. Example of test results showing the movements observed for test site ES10 are shown in table 1.

#### Measurements of Vertical Movements

2m long vertical stakes were installed on the slopes of the embankments at 3m horizontal spacing whose levels were determined every three months (every month in the case of ES9) with a precise level to determine vertical movements of the embankments with time. Example of results of this study series for test site ES7 are shown in table 2.

#### Laboratory Studies

Various laboratory tests were carried out in accordance with BS 1377 (1975) on red clay samples taken from cut slopes on embankments along Limuru-Uplands Road and Ruiru Nyanduma Road. The laboratory tests programme included soil classification, mineralogical, compaction, CBR, shear strength, consolidation, unconfined compression strength, swelling pressure, suction and permeability tests. Some of the results obtained from the laboratory test series are shown in tables 3 to 8.

#### DISCUSSION OF RESULTS

As observed from table 1 the embankments studied suffered from horizontal movements both inwards and outwards depending on the amount of rainfall received during the period under consideration. The outward movement which occurred during the dry season was found to be more than the inward movement which occurred during the wet season. Table 2 shows that the embankments settled with time during the test period of about 16 months. The settlements observed from the field were higher than those computed from consolidation test results. The red clay showed that about 98% is finer than 0.075mm and plotted mainly below the A-line like silts of high plasticity. Mineralogical tests showed the red clay had about 56% metahalloysite in the case of Limuru-Uplands Road embankments and about 47% in the case of Ruiru Nyanduma Road embankment. Red clay specimens taken from Limuru Uplands embankments, compacted at 97% MDD on the dry side, showed collapse potential of about 12% which indicates that severe problem of collapse would be expected in respect of this red clay. Computations of cracking potential gave a value of about 31% which indicated the soil to be highly susceptible to cracking.

Results of particle size distribution, plastic limit, optimum moisture content and cracking potential suggest that the red clays (red coffee

soil) in the embankments investigated are likely to pose problems when compacted on the dry side of the optimum moisture content. This may partially explain the longitudinal cracking which had occurred along the Limuru-Uplands Road which has a heavy duty pavement (asphaltic concrete surfacing on bitumen macadam base laid on stabilized soft rock subbase on red clay subgrade) and developed longitudinal cracks within a year of opening the road to traffic. Investigations in the field showed that insitu moisture content in the embankments was as low as 80% of optimum and dry density was below the specified dry density (Atibu, 1986) at design stage. Due to these low placement moisture and density conditions of embankments there was moisture migration depending on the prevailing weather so that when it rains there will be tendency for moisture to migrate from the slopes towards the centre of the embankments and when dry the moisture would migrate in the opposite direction. This moisture migration in the body of the embankment resulted in the horizontal movements that were measured in the field. These horizontal movements introduced tensile strains in the body of the embankment when the movement was outwards (i.e. during the dry season). These tensile strains led to cracks developing in the embankment body and the same reflecting upwards causing longitudinal cracking of the bituminous pavement laid on the embankment. Slope stability analysis (Bishop, 1955; Janbu, 1973) of the embankments gave factors of safety of about 3 indicating that the embankments were not in danger of slope failure. This study suggests that longitudinal cracking observed in the bituminous pavement was not due to slope stability failure but due to moisture migration and consequent differential settlement in the embankment which resulted in tensile cracking of the embankment which reflected upwards causing similar cracking in the bituminous pavement.

#### CONCLUSIONS

The study on horizontal and vertical movements of Red Clay (Red Coffee Soil) embankments leads to the following conclusions:-

- (1) Highway embankments of red clay were found to move outwards during the dry season and inwards during the wet season.
- (2) Embankments of red clay were found to suffer from vertical deformations in the form of settlement with time.
- (3) The longitudinal cracking of the bituminous pavement on the embankments of red clay studied was found to be due to moisture migration and differential settlements resulting from low placement moisture content and density during the construction of the embankments.
- (4) The red clays (Red Coffee Soil) from the embankments studied were found to be highly plastic and plotted below the A-line.
- (5) The red clays from the embankments were found to be highly susceptible to cracking and also very likely to collapse due to flooding.
- (6) Mineralogical tests showed the red clays from the embankments studied to have between 47 and 66% metahalloysite.

Atibu, F.S. (1986) Evaluation and Analysis of Flexible Road Pavements and Red Clay Embankments in Kenya. M.SC. thesis, University of Nairobi.

Bishop, A.W. (1955) The use of the Slip Circle in the Stability Analysis of Slopes, Geotechnique, Vol. 5 No.1 pp 7-77.

British Standards Institution. BS1377 (1975). Methods of Test for Soils for Civil Engineering Purposes. London.

Janbu, N. (1973) Slope Stability Computations. Embankment Dam Engineering, R.C. Hirshfeld and S.J. Foulos (eds.) John Wiley and Sons, New York, pp.47-86.

Taylor, D.W. (1948) Fundamentals of Soil Mechanics. Wiley, New York.

Terzaghi, K. (1958) Design and Performance of the Sasumua Dam. Proc. Instn. Civ. Engrs. 9:pp 369-393.

DATE OF CONSTRUCTION : APRIL 1984

 $r = 0.657$

# COMPACTION TEST RESULTS

SOIL SOURCE: LIMUR (20) K.120 (30)  
SOIL TYPE: RED LOESSY SOIL

| INITIAL STATE                  | SAMPLE NO. | S S STANDARD COMPACTION |         |                         |         | HEAVY COMPACTION        |         |                         |         |
|--------------------------------|------------|-------------------------|---------|-------------------------|---------|-------------------------|---------|-------------------------|---------|
|                                |            | SEPARATE SAMPLES        |         | RE-USING SAMPLE         |         | SEPARATE SAMPLES        |         | RE-USING SAMPLE         |         |
|                                |            | MDD (GCM <sup>3</sup> ) | CMC (%) | MDD (GCM <sup>3</sup> ) | CMC (%) | MDD (GCM <sup>3</sup> ) | CMC (%) | MDD (GCM <sup>3</sup> ) | CMC (%) |
| NATURAL<br>MOISTURE<br>CONTENT | 12/1       | 12.52                   | 42      |                         |         |                         |         |                         |         |
|                                | 12/2       |                         |         |                         |         |                         |         | 14.80                   | 30      |
| AIR-DRY                        | 12/3       | 12.40                   | 41      | 12.30                   | 42      |                         |         |                         |         |
|                                | 12/4       | 12.75                   | 39      | 12.40                   | 41      |                         |         |                         |         |
|                                | 12/5       |                         |         | 13.15                   | 35      |                         |         |                         |         |
|                                | 12/6       |                         |         | 12.10                   | 54      | 11.23                   | 47      | 11.12                   | 49      |
|                                | 12/7       |                         |         | 12.83                   | 37      |                         |         |                         |         |
|                                | 12/8       | 13.55                   | 32      |                         |         |                         |         |                         |         |
| OVER-DRY                       | 12/9       | 12.95                   | 37      |                         |         |                         |         |                         |         |
|                                | 12/10      | 12.70                   | 47      | 10.80                   | 48      | 15.05                   | 22      | 15.00                   | 24      |

Table 7

Summary of properties of the soil used in the study

| S S COMPACTION          |         |                       |                       | C-B TEST              |                       |                       |                       | PROPERTIES OF SOIL    |                       |                       |                       |
|-------------------------|---------|-----------------------|-----------------------|-----------------------|-----------------------|-----------------------|-----------------------|-----------------------|-----------------------|-----------------------|-----------------------|
| MDD (GCM <sup>3</sup> ) | CMC (%) | W (GCM <sup>3</sup> ) | W (GCM <sup>3</sup> ) | W (GCM <sup>3</sup> ) | W (GCM <sup>3</sup> ) | W (GCM <sup>3</sup> ) | W (GCM <sup>3</sup> ) | W (GCM <sup>3</sup> ) | W (GCM <sup>3</sup> ) | W (GCM <sup>3</sup> ) | W (GCM <sup>3</sup> ) |
| 12.52                   | 42      | 133                   | 38                    | 12.52                 | 42                    | 133                   | 38                    | 12.52                 | 42                    | 133                   | 38                    |
| 12.40                   | 41      | 133                   | 38                    | 12.40                 | 41                    | 133                   | 38                    | 12.40                 | 41                    | 133                   | 38                    |
| 12.75                   | 39      | 133                   | 38                    | 12.75                 | 39                    | 133                   | 38                    | 12.75                 | 39                    | 133                   | 38                    |
| 12.30                   | 42      | 133                   | 38                    | 12.30                 | 42                    | 133                   | 38                    | 12.30                 | 42                    | 133                   | 38                    |
| 12.40                   | 41      | 133                   | 38                    | 12.40                 | 41                    | 133                   | 38                    | 12.40                 | 41                    | 133                   | 38                    |
| 13.15                   | 35      | 133                   | 38                    | 13.15                 | 35                    | 133                   | 38                    | 13.15                 | 35                    | 133                   | 38                    |
| 12.10                   | 54      | 133                   | 38                    | 12.10                 | 54                    | 133                   | 38                    | 12.10                 | 54                    | 133                   | 38                    |
| 12.83                   | 37      | 133                   | 38                    | 12.83                 | 37                    | 133                   | 38                    | 12.83                 | 37                    | 133                   | 38                    |
| 13.55                   | 32      | 133                   | 38                    | 13.55                 | 32                    | 133                   | 38                    | 13.55                 | 32                    | 133                   | 38                    |
| 12.95                   | 37      | 133                   | 38                    | 12.95                 | 37                    | 133                   | 38                    | 12.95                 | 37                    | 133                   | 38                    |
| 12.70                   | 47      | 133                   | 38                    | 12.70                 | 47                    | 133                   | 38                    | 12.70                 | 47                    | 133                   | 38                    |
| 10.80                   | 48      | 133                   | 38                    | 10.80                 | 48                    | 133                   | 38                    | 10.80                 | 48                    | 133                   | 38                    |
| 15.05                   | 22      | 133                   | 38                    | 15.05                 | 22                    | 133                   | 38                    | 15.05                 | 22                    | 133                   | 38                    |
| 15.00                   | 24      | 133                   | 38                    | 15.00                 | 24                    | 133                   | 38                    | 15.00                 | 24                    | 133                   | 38                    |

Measured at depth 10

| HEAVY COMPACTION        |         | LIGHTER COMPACTION      |         | SEVERE COMPACTION       |         |
|-------------------------|---------|-------------------------|---------|-------------------------|---------|
| MDD (GCM <sup>3</sup> ) | CMC (%) | MDD (GCM <sup>3</sup> ) | CMC (%) | MDD (GCM <sup>3</sup> ) | CMC (%) |
| 12.52                   | 42      | 12.40                   | 41      | 12.30                   | 42      |
| 12.75                   | 39      | 12.40                   | 41      | 12.40                   | 41      |
| 12.30                   | 42      | 12.40                   | 41      | 12.40                   | 41      |
| 12.40                   | 41      | 12.40                   | 41      | 12.40                   | 41      |
| 13.15                   | 35      | 12.40                   | 41      | 12.40                   | 41      |
| 12.10                   | 54      | 12.40                   | 41      | 12.40                   | 41      |
| 12.83                   | 37      | 12.40                   | 41      | 12.40                   | 41      |
| 13.55                   | 32      | 12.40                   | 41      | 12.40                   | 41      |
| 12.95                   | 37      | 12.40                   | 41      | 12.40                   | 41      |
| 12.70                   | 47      | 12.40                   | 41      | 12.40                   | 41      |
| 10.80                   | 48      | 12.40                   | 41      | 12.40                   | 41      |
| 15.05                   | 22      | 12.40                   | 41      | 12.40                   | 41      |
| 15.00                   | 24      | 12.40                   | 41      | 12.40                   | 41      |

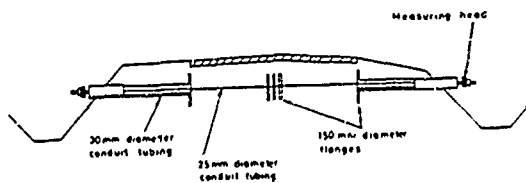


FIG 1. MEASUREMENT OF HORIZONTAL EDGE MOVEMENT OF THE ROAD SUB-GRADE RELATIVE TO THE ROAD CENTRE LINE

TABLE 8

| SAMPLE NO. | W (GCM <sup>3</sup> ) |                       | W (GCM <sup>3</sup> ) |                       | W (GCM <sup>3</sup> ) |                       | W (GCM <sup>3</sup> ) |                       |
|------------|-----------------------|-----------------------|-----------------------|-----------------------|-----------------------|-----------------------|-----------------------|-----------------------|
|            | W (GCM <sup>3</sup> ) | W (GCM <sup>3</sup> ) | W (GCM <sup>3</sup> ) | W (GCM <sup>3</sup> ) | W (GCM <sup>3</sup> ) | W (GCM <sup>3</sup> ) | W (GCM <sup>3</sup> ) | W (GCM <sup>3</sup> ) |
| 12/1       | 12.52                 | 42                    | 12.52                 | 42                    | 12.52                 | 42                    | 12.52                 | 42                    |
| 12/2       | 12.40                 | 41                    | 12.40                 | 41                    | 12.40                 | 41                    | 12.40                 | 41                    |
| 12/3       | 12.75                 | 39                    | 12.75                 | 39                    | 12.75                 | 39                    | 12.75                 | 39                    |
| 12/4       | 12.30                 | 42                    | 12.30                 | 42                    | 12.30                 | 42                    | 12.30                 | 42                    |
| 12/5       | 12.40                 | 41                    | 12.40                 | 41                    | 12.40                 | 41                    | 12.40                 | 41                    |
| 12/6       | 13.15                 | 35                    | 13.15                 | 35                    | 13.15                 | 35                    | 13.15                 | 35                    |
| 12/7       | 12.10                 | 54                    | 12.10                 | 54                    | 12.10                 | 54                    | 12.10                 | 54                    |
| 12/8       | 12.83                 | 37                    | 12.83                 | 37                    | 12.83                 | 37                    | 12.83                 | 37                    |
| 12/9       | 13.55                 | 32                    | 13.55                 | 32                    | 13.55                 | 32                    | 13.55                 | 32                    |
| 12/10      | 12.95                 | 37                    | 12.95                 | 37                    | 12.95                 | 37                    | 12.95                 | 37                    |
| 12/11      | 12.70                 | 47                    | 12.70                 | 47                    | 12.70                 | 47                    | 12.70                 | 47                    |
| 12/12      | 10.80                 | 48                    | 10.80                 | 48                    | 10.80                 | 48                    | 10.80                 | 48                    |
| 12/13      | 15.05                 | 22                    | 15.05                 | 22                    | 15.05                 | 22                    | 15.05                 | 22                    |
| 12/14      | 15.00                 | 24                    | 15.00                 | 24                    | 15.00                 | 24                    | 15.00                 | 24                    |

W (GCM<sup>3</sup>) = 1000 x W (GCM<sup>3</sup>)  
W (GCM<sup>3</sup>) = 1000 x W (GCM<sup>3</sup>)

TABLE 8

## SUMMARY OF COLLAPSE AND CRACKING CHARACTERISTICS OF LIMUR RED SOILS

|                    | DRY DENSITY (KN/M <sup>3</sup> ) | MOISTURE CONTENT (%) | COLLAPSE POTENTIAL (%) | CRACKING POTENTIAL (%) | SWELLING POTENTIAL (%) |
|--------------------|----------------------------------|----------------------|------------------------|------------------------|------------------------|
| 97% MDD (DRY SIDE) | 12.00                            | 34                   | 12                     |                        |                        |
| MDD                | 12.40                            | 41                   | 1                      | 31                     | 3.0                    |
| 97% MDD (WET SIDE) | 12.00                            | 44                   | 0.6                    |                        |                        |

## GUIDELINES ON COLLAPSE AND CRACKING POTENTIAL

| Collapse Potential Range (CP) | Severity of Collapse Problem |
|-------------------------------|------------------------------|
| 0 - 1%                        | No problem                   |
| 1 - 5%                        | Moderate problem expected    |
| 5 - 10%                       | Trouble expected             |
| 10 - 20%                      | Severe trouble expected      |
| > 20%                         | Very severe trouble expected |

| Cracking Potential Range | Susceptibility to Cracking |
|--------------------------|----------------------------|
| <10                      | No cracking expected       |
| 10 - 20                  | Moderate                   |
| >20                      | High                       |

**Session IV**  
**“Case Histories of Geotechnical Earthquake Engineering  
and Soil Dynamics”**

## Stability Analysis of Seismically Damaged Embankments

Yasuyuki Koga

Head, Soil Dynamics Division, Public Works Research Institute,  
Ministry of Construction, Japan

Osamu Matsuo

Senior Research Engineer, Soil Dynamics Division, Public Works  
Research Institute, Ministry of Construction, Japan

**Synopsis:** This paper describes a pseudo-static stability analysis of seismically damaged embankments during the 1983 Nihonkai-chubu earthquake (Japan). It places a great emphasis on the discussion of a dynamic shear strength of soils to be used in a seismic stability analysis of embankments.

Several existing concepts of a dynamic strength are reviewed, which vary from each other with respect to loading patterns, drainage conditions and strength criteria in soil element tests. The main part of this paper is to apply some of the dynamic soil strengths discussed above to seismic stability analyses of three embankment sections, laid on loose sandy deposits which were damaged by the 1983 Nihonkai-chubu earthquake in Japan, and to evaluate the applicability of those strengths. Dynamic response analyses and pseudo-static stability analyses were performed on the basis of field and laboratory soil test data, such as SPT, shear wave logging, CPT, VCPT (vibratory cone penetration test) and cyclic triaxial compression test. The safety factors obtained from the analyses were compared with the settlements of respective embankment sections which would have possibly occurred during the earthquake. It was concluded that the dynamic shear strength, which is defined as a sum of static and dynamic shear stresses that can produce a certain value of cumulative shear strain in a certain number of stress cycles, is the most reasonable of them.

### INTRODUCTION

It is widely recognized that the knowledge of a dynamic strength of soils is essential for a seismic stability analysis of slopes and embankments. They have been studied to date in a number of case studies and their concepts have already been described in some of the related design guidelines for practice.

However, the applicability of each concept of a soil strength for a seismic stability analysis has not yet been clearly discussed. This paper first reviews and discusses existing several types of soil strengths for seismic stability analyses and their premises as well.

Secondly three types of strengths of those above are applied to seismic stability analysis of three embankment sections which were damaged due to liquefied foundations in the 1983 Nihonkai-chubu earthquake in Japan. Then a rational soil strength for a seismic stability analysis is deduced on the basis of the comparison of the analyzed results and damage records in the field.

### CONSIDERATION ON A DYNAMIC SHEAR STRENGTH OF SOILS FOR SEISMIC STABILITY ANALYSIS

#### Failure of slopes and embankments due to earthquakes

Damages to slopes and embankments are often observed after a large earthquake. Such failure phenomena can be classified as follows from the viewpoint of a seismic motion and a time of failure occurrence.

- 1) Failure during an earthquake: this is most usually called a failure due to an earthquake and actually occurs most frequently.
- 2) Failure relatively soon after an earthquake ends: this sometimes occurs without such a change of an external load as rainfall after the load condition returns to a pre-earthquake condition. This requires a decrease of the resistance of embankment and ground, which is reduced to the change of an excess pore pressure distribution caused by a seismic load in the previous earthquake. This also belongs to the failure due to an earthquake and can be called as failure after an earthquake more

literally.

- 3) Some slopes where cracks have occurred during an earthquake fail fairly after an earthquake with the aid of rainfall and other causes. This may be included in the failure due to earthquake in a broad sense, however, this is generally excluded.

Such a classification plays an important role in a consideration of a load and a shear strength of soils for a seismic stability analysis.

#### Seismic stability analysis method

Though several analytical methods are available to investigate the stability of slopes, the simplest is a slip surface stability analysis based on a limit equilibrium method.

The effect of a seismic motion is considered as a static force through a seismic coefficient in a seismic stability analysis. Calculation formula for a slip surface analysis is given by

$$F_s = f(W, \tau_f, k) \quad (1)$$

where,  $F_s$  = a safety factor,  $f$  = a calculation equation of a safety factor,  $W$  = soil weight,  $\tau_f$  = strength of a soil and  $k$  = a seismic coefficient.

Eq. (1) shows a close interdependence of the factors. Therefore it is necessary to pursue a harmonized analysis method considering the interdependence of the factors. When a seismic effect is converted to a static force, seismic stability analysis equations can easily be obtained extending various static stability analysis equations.

#### Shear strength of soils for seismic stability analysis method

As is already described, slope failures due to earthquakes can be classified into failure during and after earthquakes respectively.

A shear strength of a soil is usually obtained by loading soil specimens in such a manner as will occur in the actual condition. Therefore each loading manner for the failure during and after an earthquake is as follows.

Failure during an earthquake : the strength  $\sigma_f$  is obtained from the condition for the strain to reach

failure strain  $\epsilon_f$  by changing the dynamic stress amplitude  $\sigma_d$  to correspond with a seismic inertia force.

Failure after an earthquake : As the load basically returns to an original one when an earthquake ends, the slope which did not fail during an earthquake, cannot fail, if its individual part behaves independently. Therefore the slope which actually failed should be reduced to the phenomenon in the overall slope such as a redistribution of the stress due to creep phenomenon and the pore pressure due to seepage. However, the residual strength  $\sigma_r$  against a static load after the soil was subjected to a static and a dynamic stress due to dead weight and a seismic motion may be used as a reference strength in this case.

The latter strength can also be used for a seismic stability analysis during an earthquake as follows. Consider a state of a slope which was subjected to  $N$  cycles of a dynamic stress to analyze a stability during an earthquake, then a safety factor can be obtained by comparing the dynamic stress of the next  $N + 1$  th cycle and the residual strength after  $N$  cycles of stress.

Table 1 is a summary of the above statement. Also is summarized in Table 2 various shear strengths of a soil for a seismic stability analysis. Here a saturated soil under undrained condition is considered. Figs. 1 and 2 show assumed loading patterns for respective strengths and stress paths to reach a failure. In Table 2 six types of strength are classified into static and dynamic ones.

Table 1 Loading patterns for respective types of failure

|                              |                                   |
|------------------------------|-----------------------------------|
| Failure during an earthquake | loading pattern: Fig. 1 or Fig. 2 |
| Failure after an earthquake  | loading pattern: Fig. 2           |

A static strength is mobilized under a monotonous loading as shown in Fig.1 (a) and used as an approximation of a dynamic strength for a seismic stability analysis. A dynamic strength assumes a repetitive loading as shown in Figs. 1 (b) (c). These are used for a stability analysis during and after an earthquake respectively. Moreover the latter dynamic strength can also be used for a stability analysis during an earthquake as stated previously. Among the six types of strengths, the features of three strengths (strength A, C, D) being frequently used in practice for a seismic stability analysis of embankments are as follows.

Table 2 Classification of strength

| Type                                 | Strength criteria   | Drainage condition  | Loading pattern | Stress path & strength | Time of strength mobilized                      | Corresponding loading condition                | Reference**)  |
|--------------------------------------|---|---|-----------------|------------------------|---|--|---|
| Static strength (Monotonous loading) | Mobilized maximum stress under a monotonous loading                                       | Drained   | a               | A                      | during earthquake (high permeability)           | Dead weight + seismic force                    | JNCOLD (1978)   |
|                                      |   | Undrained   | a               | B, B'                  | during earthquake (impulsive earthquake)        | do   | do  |
| Dynamic strength (Cyclic loading)    | Maximum stress of stress time history to cause a reference strain during a cyclic loading | Undrained   | b               | C                      | during earthquake                               | do   | Seed (1966)<br>Ishihara (1980)  |
|                                      | Maximum static strength after a cyclic loading  | Incompletely drained*) (Pore pressure during a cyclic loading remains constant) | c               | D                      | during earthquake<br>&<br>soon after earthquake | do<br><br>Dead weight                          | JNR (1972)<br>PWRI (1975)<br>HUDC (1984)<br>JMA (1980)                        |
|                                      |   | Undrained*)   | c               | E                      | during earthquake<br>&<br>soon after earthquake | Dead weight + Seismic force<br><br>Dead weight | Castro (1976)<br>Seed (1979)<br>Tokyo Metro. Govnt. (1983)<br><br>Seed (1979) |
|                                      |   | Drained*) (Pore pressure returns to initial pressure)                           | c               | F                      | long after earthquake                           | do   |   |

N.B. \*) This drainage condition refers to that for a static loading after a cyclic loading.  
An undrained condition is assumed during a cyclic loading.

Fig.3 shows the relation between above three strengths and number of cycles of seismic load for a saturated sand for which respective strengths differ very much. Here the strengths are expressed as follows.

$$\text{Strength A : } \tau_f = \sigma_{no}^- \cdot \tan \phi' \quad (2)$$

$$\text{Strength C : } \tau_f = \sigma_{no}^- \cdot \tan \phi_D = \sigma_{no}^- \cdot R_L(N) \quad (3)$$

$$\begin{aligned} \text{Strength D : } \tau_f &= (\sigma_{no}^- - u_e) \cdot \tan \phi' \\ &= \sigma_{no}^- \cdot (1 - u_e / \sigma_{no}^-) \cdot \tan \phi' \quad (4) \end{aligned}$$

where  $\tau_f$  = shear strength,  $\sigma_{no}^-$  = initial effective normal stress,  $\phi'$  = angle of static shearing resistance,  $\phi_D$  = angle of dynamic shearing resistance,  $R_L(N)$  = liquefaction strength ratio,  $u_e$  = excess pore pressure caused by a cyclic loading.

The strength A is a constant being independent of external load.

The strength C is determined if the equivalent number

of cycles  $N_{eq}$  of a seismic load and a failure strain  $\gamma_f$  are given.

The strength D depends on a stress  $\tau_d$  and number of cycles  $N_{eq}$  of a seismic load.

This indicates that the seismic effect up to a certain time has already been taken into account as an action to

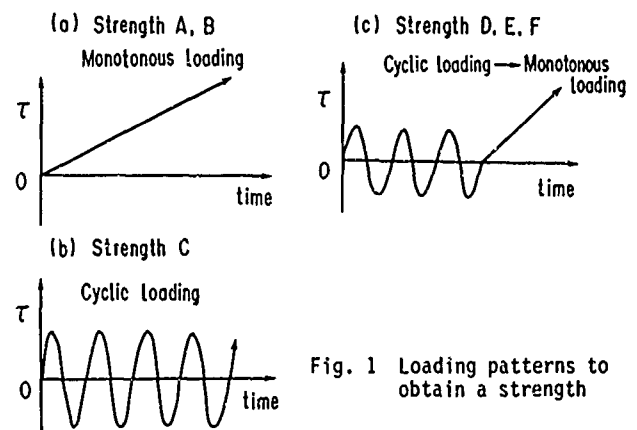


Fig. 1 Loading patterns to obtain a strength



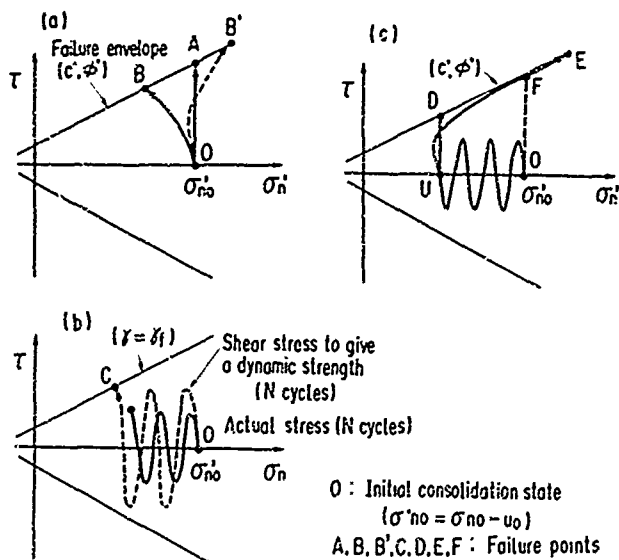


Fig. 2 Stress paths and strengths

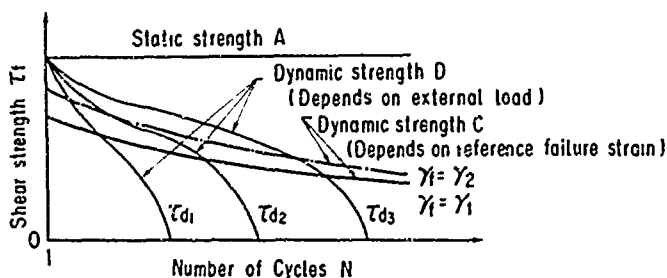


Fig. 3 Comparison of each strength

generate an excess pore pressure, therefore it is irrational if this strength is compared with the seismic load prior to that time to calculate a safety factor. Moreover it should be noted that the strength D is a post-earthquake strength under a special drain condition. Consequently these strengths can have a remarkable difference.

#### OUTLINE OF DAMAGED EMBANKMENTS

##### The 1983 Nihonkai-chubu Earthquake

The Nihonkai-chubu earthquake whose epicenter was in Japan Sea hit the northern part of Honshu-Island, Japan, on May 13, 1983 (Fig.4). Its magnitude was 7.7 in the Richter scale. The characteristics of the damage by this earthquake was the failure of many earth structures such as river dykes and road embankments which was mainly caused by the liquefaction of the sandy ground.

##### Outline of analyzed embankments

Among the damaged river dykes, Hachirogata reclamation

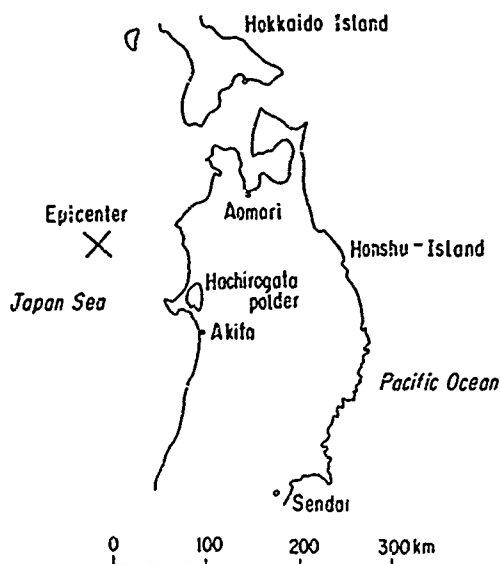


Fig. 4 Location of analyzed embankment sites

dyke which encloses a reclaimed land with the length of 100 km were damaged around 70 % of its total length. Three sections of this reclamation dyke which were located within 200 m were chosen for a detailed seismic analysis. These three sections showed a fairly different settlements as shown in Table 3 with a height of about 4.6 m. Because of such a difference, a rather detailed soil exploration and an analysis were conducted.

Table 3 Crest settlement of each section

|        |        |
|--------|--------|
| Site A | 19 cm  |
| Site B | 73 cm  |
| Site C | 133 cm |

##### Soil exploration

The conducted items of soil exploration are summarized in Table 4. Besides conventional soil test items, some dynamic soil exploration and tests were conducted as shown in the Table. The VCPT (Vibratory Cone Penetration Test) was developed at the PWRI to assess the liquefaction strength of sandy ground. Cyclic triaxial tests of undisturbed samples were performed to obtain conventional liquefaction strength  $R_L$  and dynamic strength under initial static shear stress based on a cumulative strain by use of isotropically consolidated and anisotropically consolidated specimens respectively. Fig. 5 shows the soil profiles obtained from above soil exploration. However, the number of undisturbed soil samples were not enough to conduct cyclic triaxial tests under all the required stress conditions. Therefore the effect of initial shear stress condition on a dynamic strength was

Table 4 Items of soil exploration

| Item                         | Site                                       | Akita port | A      | B      | C          |
|------------------------------|--|------------|--------|--------|------------|
| Soil exploration             | SPT (depth, m)                             | 50.0 m     | 24.4 m | 20.6 m | 30.5 m     |
|                              |  |            |        |        | 40.5       |
|                              |  |            |        |        | 35.5       |
|                              |  |            |        |        | 20.6       |
|                              |  |            |        |        |            |
|                              |  |            |        |        |            |
| Dynamic soil laboratory test | Dutch cone test (length, No. of points)    | —          | —      | —      | 32.2 m x 1 |
|                              |  |            |        |        | 19.0 ..    |
|                              |  |            |        |        | 33.0 ..    |
|                              |  |            |        |        |            |
|                              |  |            |        |        |            |
|                              |  |            |        |        |            |
| Dynamic soil laboratory test | VCPT* <sup>1</sup> (length, No. of points) | —          | 8.9 m  | 12.0 m | 12.0 m     |
|                              |  |            |        |        |            |
|                              |  |            |        |        |            |
|                              |  |            |        |        |            |
|                              |  |            |        |        |            |
|                              |  |            |        |        |            |
| Dynamic soil laboratory test | Ram sounding (length, No. of points)       | —          | —      | —      | 30.0 m x 3 |
|                              |  |            |        |        |            |
|                              |  |            |        |        |            |
|                              |  |            |        |        |            |
|                              |  |            |        |        |            |
|                              |  |            |        |        |            |
| Dynamic soil laboratory test | Seismic wave logging (length)              | 18 m       | —      | —      | 43 m       |
|                              |  |            |        |        |            |
|                              |  |            |        |        |            |
|                              |  |            |        |        |            |
|                              |  |            |        |        |            |
|                              |  |            |        |        |            |
| Dynamic soil laboratory test | Resonant column test (No. of specimens)    | —          | —      | —      | 1          |
|                              |  |            |        |        |            |
|                              |  |            |        |        |            |
|                              |  |            |        |        |            |
|                              |  |            |        |        |            |
|                              |  |            |        |        |            |
| Dynamic soil laboratory test | Cyclic triaxial test (No. of specimens)    | —          | —      | —      | 10         |
|                              |  |            |        |        |            |
|                              |  |            |        |        |            |
|                              |  |            |        |        |            |
|                              |  |            |        |        |            |
|                              |  |            |        |        |            |
| Dynamic soil laboratory test | Isotropic consolidation                    | —          | —      | —      | 8          |
|                              |  |            |        |        |            |
|                              |  |            |        |        |            |
|                              |  |            |        |        |            |
|                              |  |            |        |        |            |
|                              |  |            |        |        |            |
| Dynamic soil laboratory test | Anisotropic consolidation                  | —          | 4      | 7      | 8          |
|                              |  |            |        |        |            |
|                              |  |            |        |        |            |
|                              |  |            |        |        |            |
|                              |  |            |        |        |            |
|                              |  |            |        |        |            |

N.B. \*): Vibratory Cone Penetration Test, developed at PWRI to assess a liquefaction strength at the field.

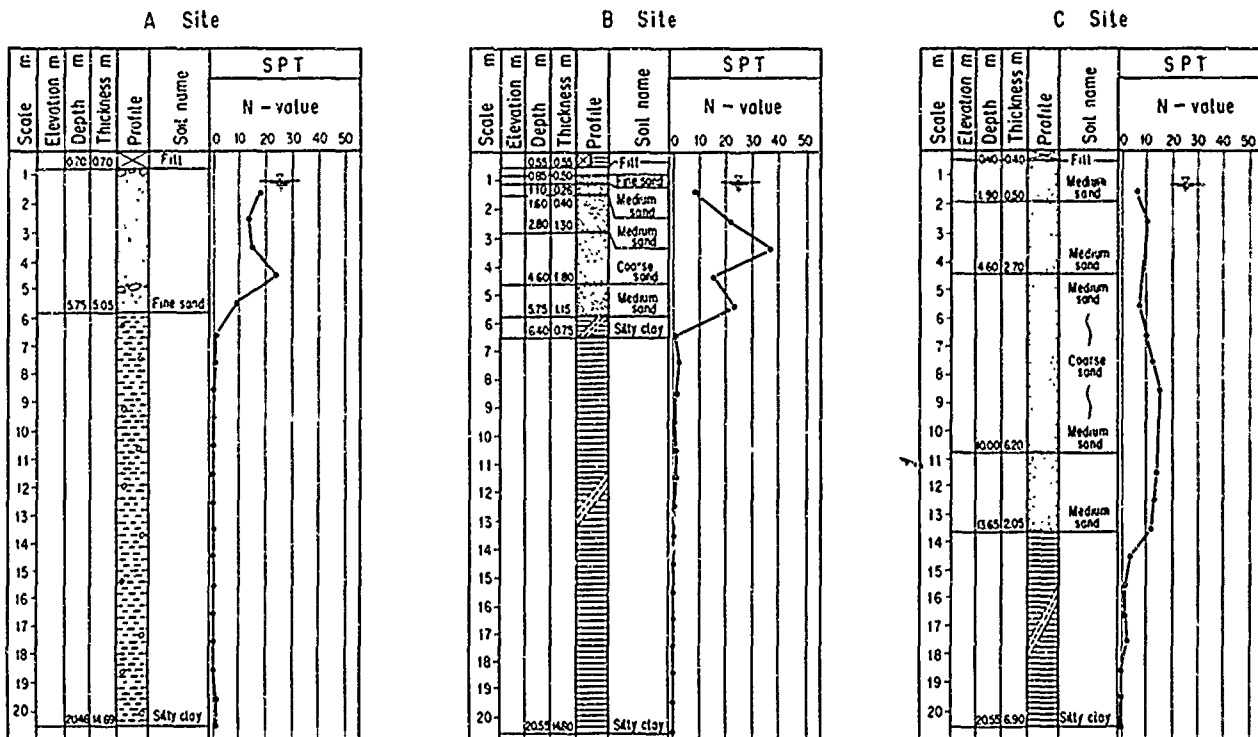


Fig. 5 Soil profile for each site

mainly assumed from existing data of another sand (Sengenyama sand) with similar gradation as this sand. Fig. 6 shows a main characteristic obtained in this manner. In this Figure, point A indicates a liquefaction

strength  $R_L$  without initial shear stress. The overall curve was vertically shifted to fit this point A to that of each site without changing the curve shape.

The characteristics of the excess pore pressure required to obtain a dynamic strength based on the excess pore pressure generated by a cyclic loading were obtained from cyclic triaxial tests of isotropically consolidated specimens. It is arranged as in Fig. 7.

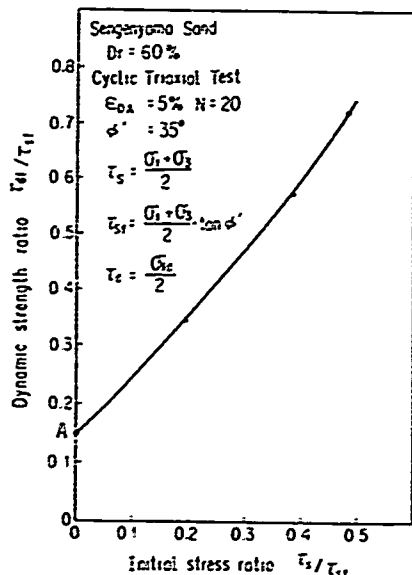


Fig. 6 Effect of initial shear stress on a dynamic strength

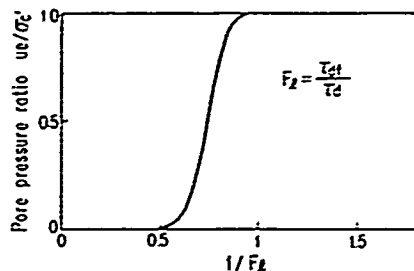


Fig. 7 Pore pressure generation characteristics

## SEISMIC STABILITY ANALYSIS

### Dynamic response analysis and seismic coefficient

The seismic coefficient for a seismic stability analysis was obtained following the procedure shown in Fig. 8.

A seismic record at the Akita port of around 17 km distance from the analyzed embankment sites were utilized. The program SHAKE was used for the multiple reflection analysis to consider the nonlinear characteristics of soil layers as the equivalent linear ones. The diluvial sandy gravel layer was assumed as a bedrock for the analysis. The seismic response of the embankments was analyzed by the 2 dimensional FEM program SADAP developed at the PWRI to consider the

nonlinear and hysteretic characteristics of soil layers by step-by-step numerical analysis. The equivalence coefficient  $C_r$  to convert a maximum acceleration response of the embankment  $a_{max}$  to a seismic coefficient  $K_h$  was calculated assuming the shear stress wave form is similar to that of the response acceleration and then

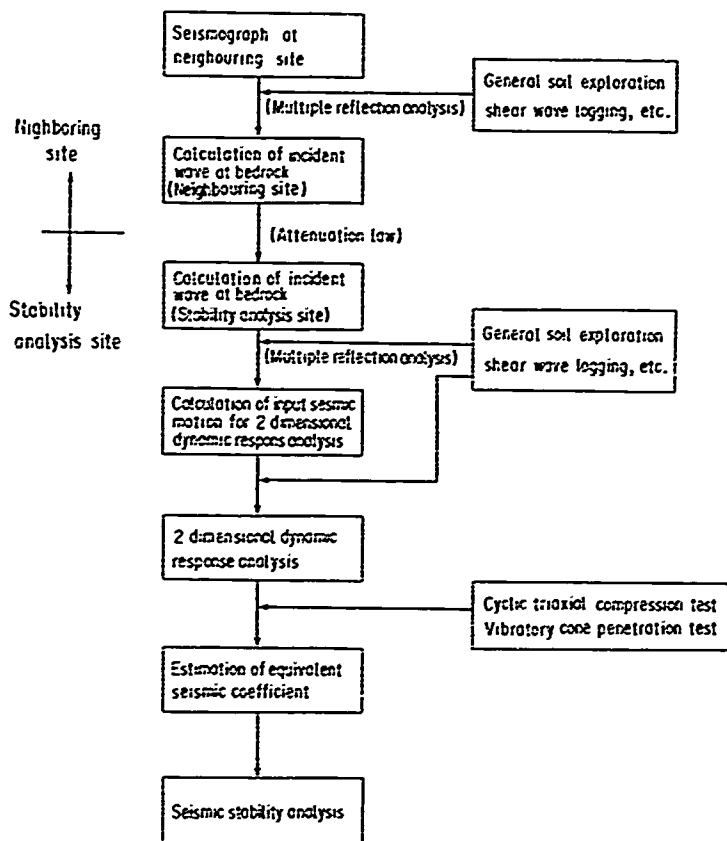


Fig. 8 Calculation of seismic coefficient

combining the cumulative damage concept and dynamic strength characteristics. Then an equivalent seismic coefficient  $K_h$  was calculated by the formula

$$K_h = C_r \times a_{max}/g \quad (5)$$

which was used for a seismic stability analysis described in the next section. It is noteworthy that  $C_r$  depends on the reference number of loading cycles  $N_{eq}$ . As  $N_{eq}$  increases,  $C_r$  decreases. Assuming  $N_{eq} = 20$ ,  $C_r$  was obtained for each site as follows:

$$\begin{aligned} \text{Site A: } C_r &= 0.678, & \text{Site B: } C_r &= 0.689, \\ \text{Site C: } C_r &= 0.689. \end{aligned}$$

### Seismic stability analysis method

The formula for a stability analysis was the following modified Fellenius method considering a simple circular slip surface (Fig. 9).

$$F_s = \frac{\Sigma(c' + (w-u-b)\cos\alpha \tan\phi')}{\Sigma(w-R\sin\alpha + k_h w \cdot y)} \quad (6)$$

$$= \frac{R\tau_{sf} \cdot l}{\Sigma(w-R\sin\alpha + k_h w \cdot y)} \quad (7)$$

where  $c$ ,  $\phi$ ,  $\tau_f$  : cohesion, angle of shearing resistance and strength of soils respectively,  $u$  : pore pressure, see Fig. 9 regarding other notations.

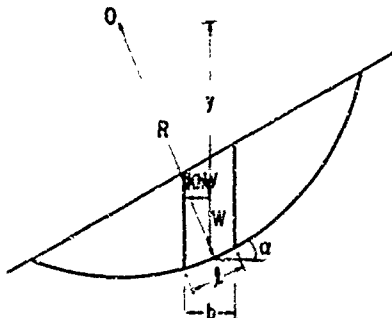


Fig. 9 Slip surface for seismic stability analysis

Three types of strengths described previously, that is, a static strength, a dynamic strength based on excess pore pressure during a cyclic loading and a dynamic strength based on a cumulative strain during a cyclic loading are considered. They are called as strength  $S_1$ ,  $S_2$ ,  $S_3$  in the following. The conducted analysis cases are summarized in Table 5.

The strength  $S_1$  was obtained assuming  $c' = 0.1 \text{ tf/m}^2$  and  $\phi' = 35^\circ$  in Eq. (6).

The strength  $S_2$  can be obtained as follows. Calculate the stress ratio in the ground using the equivalent seismic coefficient  $k_h$  corresponding to  $N_{eq} = 20$ . Then calculate excess pore pressure  $u_e$  through Fig. 7. The seismic stability analysis can be done substituting this  $u_e$  in Eq. (6). Considering that the maximum excess pore pressure may be generated during the seismic motion or

Table 5 Analysis Cases

| Case   | Strength parameters                            | Seismic coefficient | Pore pressure                   |
|--------|--|---------------------|---------------------------------|
| $S_1$  | $C' = 0.1 \text{ tf/m}^2$ , $\phi' = 35^\circ$ | With                | hydrostatic pressure            |
| $S_2$  | "  | With                | hydrostatic and excess pressure |
| $S_2'$ | "  | Without             | do                              |
| $S_3$  | $C_D$ , $\phi_D$ or $\tau_{fD}$                | With                | hydrostatic pressure            |

after it ends, two cases of stability analyses with a seismic coefficient  $k_h$  (Case  $S_2$ ) and without  $k_h$  (Case  $S_2'$ ) were conducted.

The strength  $S_3$  was incorporated in a seismic stability analysis by the method described by Ishihara (Ishihara, 1980) as follows.

First a static safety factor  $F_s$  was calculated using a static strength  $\tau_{sf}$  for a specified slip surface. Secondly, assuming the stress ratio is constant and equals to  $1/F_s$  along a slip surface, the dynamic strength  $\tau_{df}$  is obtained from Fig. 6.

#### Stability analysis results

Though the seismic coefficient at each site was already presumed, safety factors  $F_s$  for respective cases were calculated changing the seismic coefficient  $k_h$  0-0.3 in order to grasp the effect of  $k_h$  on  $F_s$ . The stability analysis results are shown in Fig. 10. Fig. 10 indicates the safety factor  $F_s$  depends much on the strength used. As regards both cases  $S_2$  and  $S_2'$ ,  $F_s$  decreases remarkably when  $k_h$  exceeds a certain value, which reflects that the excess pore pressure is very sensitive to the liquefaction resistance coefficient  $F_L$ .

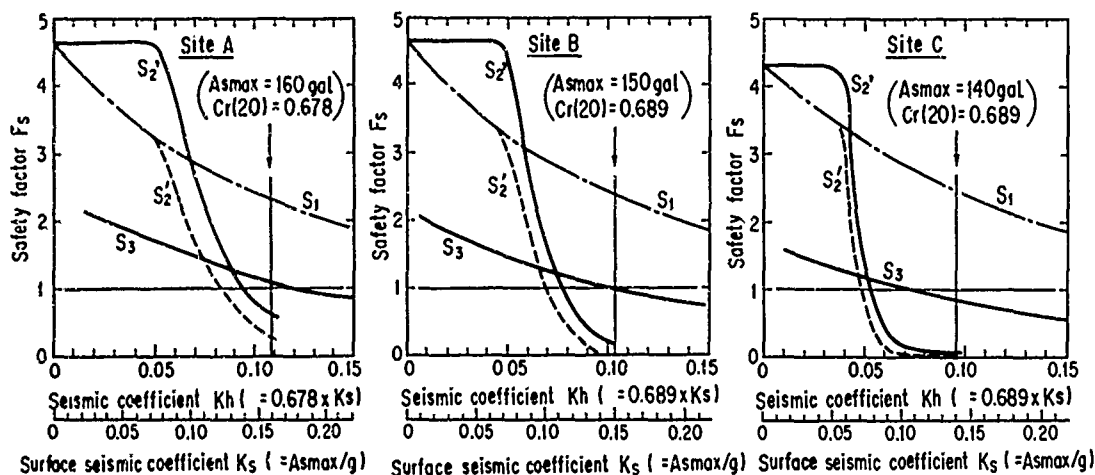


Fig. 10 Seismic coefficient vs. safety factor

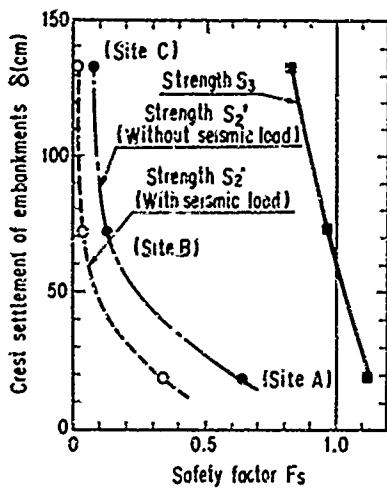


Fig. 11 Relation of safety factor vs. crest settlement

In the cases of  $S_1$  and  $S_3$ ,  $F_s$  changes depending only on the seismic coefficient  $k_h$  and its difference corresponds to the difference of the strength  $S_1$  and  $S_3$ . Moreover, the estimated seismic coefficients are indicated in Fig. 10. The figure shows that the safety factors by use of the strength  $S_1$  are fairly larger than unity, which contradicts the fact that each site was subjected to some damage. The relation between the safety factors using  $S_2$ ,  $S_2'$ ,  $S_3$  and the settlement of the embankments is plotted in Fig. 11. All the relations appear reasonable in that the settlement is large when  $F_s$  is small, however,  $F_s$  is too small in the cases where  $S_2$  and  $S_2'$  were used, considering the fact that some embankments in the neighborhood of these three were little damaged. Therefore these two strengths rather seem to lack rationality. On the other hand, in the case where  $S_3$  was used,  $F_s$  equals to approximately 1.2 when some damage occurs and  $F_s$  does not extremely decrease when the settlement is large. The corresponding relation between the settlement and  $F_s$  seems comparatively reasonable. This suggests that it is more rational to use a dynamic strength of a soil based on a cumulative strain for a seismic stability analysis (during an earthquake) than other strengths.

## CONCLUSIONS

Several dynamic shear strengths of a soil to be used for a seismic stability analysis were reviewed. In the adoption of respective strengths, the correspondence of the time when the failure occurs and the premise of the strength must be carefully noted. Three shear strengths of a soil frequently used in practice were compared on

the basis of the analysis of damaged river embankments at the Nihonkai-chubu earthquake. They are a static strength, a dynamic strength based on cumulative strain during a cyclic loading and a dynamic strength calculated through an excess pore pressure during a cyclic loading. The analysis results showed the dynamic shear strength based on a cumulative strain gives a reasonable relation to reported settlement. This proved rationality of using a dynamic strength based on a cumulative strain for a stability analysis during an earthquake.

## REFERENCE

- Castro, G. and Christian, J.T. (1976), "Shear Strength of Soils and Cyclic Loading", Journ. of GED, Proc. ASCE, Vol. 102, No. GT9.
- Housing & Urban Development Corporation, Urban Development Department (1984), "Technical Guideline for Earthquake Resistant Design of Housing Construction Site (draft)", (in Japanese).
- Ishihara, K. (1980), "Current Practice and Problems in the Earthquake Resistant Design of Earth Structures", Tsuchi-to-Kiso, JSSMFE, 28-8, (in Japanese).
- Japan Mining Association (1980), "Construction Standards for Tailings Dams", (in Japanese).
- Japanese National Committee on Large Dams (1978), "2nd Revised Standards for Dam Design", (in Japanese).
- Kusano, K. and Abe H. (1983), "Seismic Analysis of Embankment Considering Liquefaction Ground", Annual Report of Institute of Civil Engineering of Tokyo Metropolitan Government, (in Japanese).
- Kutara, K. and Koga, Y. (1975), "A Large Shaking Table Test of Model Embankment", Technical Memorandum of PWRI, NO. 1032, (in Japanese).
- Seed, H.B. (1966), "A Method for Earthquake Resistant Design of Earth Dams", Jour. of SMFD, Proc. ASCE, Vol. 92, No. SM1.
- Seed, H.B. (1979), "Considerations in the Earthquake Resistant Design of Earth and Rockfill Dams", Geotechnique 29, no. 3.
- Uezawa, H. et al (1972), "Experimental Study on Aseismicity of Embankment by Use of Large Shaking Table", Railway Technical Research Report, No. 822, Railway Technical Research Institute, Japanese National Railways, (in Japanese).

## Some Experiences from Damages of Embankments During Strong Earthquakes in China

Shen Chogang

Adviser, Senior Engineer, Institute of Water Conservancy and Hydroelectric Research (IWHR), Beijing, China

**SYNOPSIS:** This paper gives a series of case histories of earth dams which have been damaged by strong earthquakes in the past 25 years in China. These damages include slides, cracks, settlements, leakages and also some appurtenant structure failures. Experiences show it is necessary to stringently control the design and construction to resist earthquakes.

### INTRODUCTION

The practice of construction of embankment dams and their behavior during strong earthquakes are most important factors for understanding the nature force acting on these dams especially the dynamic forces. The understanding of the response of embankments will give some idea to build dams more reasonably. This is why engineers are paying attention and collecting them as good references.

### STRONG EARTHQUAKES IN THE LAST 7 YEARS IN CHINA

Since 1980 there were 2 earthquakes stronger than magnitude 7 and 36 earthquakes stronger than magnitude 6 in China.

There were 13 earthquakes with magnitude 6 in 1986. It was a rather active year even no earthquake stronger than 7 happened. During these earthquakes no damages were discovered except during two strong earthquakes, one in Yunnan Province and another in Xinjiang Uygur Autonomous Region in 1985.

### DAMAGE OF CHANGMAIDI EARTH DAM DURING 1985 LUQIEN AND QUENDIAN EARTHQUAKE IN YUNNAN PROVINCE

In April 18, 1985 the earthquake with magnitude 6.3 had a depth of epicenter only 5 km. The intensity of epicenter was 8 degree. Changmaidi earth dam is of homogeneous type with height 18m, crest length 105m. The nearest rim of reservoir is 6 km from epicenter, the local intensity was 6 degree. The reservoir storage capacity is 314000 m<sup>3</sup>. The upstream slope of this dam is 1:2.5, downstream slope is 1:1.9 without protection. No filter was provided in the downstream drainage. A culvert pipe was embedded in the dam body with an inclined gate (Fig. 1 and 2).

The reservoir was nearly full during earthquake. Water level was just 0.8 m below the crest of dam.

16 cracks were found on this dam after earthquake, mainly (12 cracks) along the abutments of dam (Fig. 1, 2 and 3). The width of cracks

was generally 1-3 cm, with maximum width of 18 cm. On the downstream slope the depth of cracks reached 2.5 m. 3 of 4 longitudinal cracks were on the crest, the longest one was 38 m. The fourth crack was on the downstream slope, the width of crack near the spillway channel was 10 cm, its depth was more than 1.2 m. Muddy water flowed through the culvert pipe about two hours after the earthquake.

### DAMAGES OF KASHI EARTH DAM DURING SEVERAL EARTHQUAKES IN XINJIANG UYGUR AUTONOMOUS REGION IN 1985

In 1985 from August 23 to September 12 there were a large number earthquakes in Uqia County of Xinjiang Uygur Autonomous Region. The magnitudes of two strong earthquakes were 7.4 with epicenter 21 km from the dam site, and 6.8 with epicenter 16 km from the dam site respectively. The intensity at the dam site was both 7 degree. This region is of high seismicity by records. There were 7 earthquakes with magnitude greater than 6, and 5 greater than 7 historically. After earthquakes there were rather serious damages on the earth dam.

The Kashi Hydroelectric Power Station has 3 sets generators each with 6500 kw capacity. The dam is with inclined core and sand gravel shells (Fig. 5 and 6); the height is 16 m and crest length is 480 m. The grain size distribution curves of shells and core are shown in Fig. 7.

There were some damages as sliding of upstream slope and settlements of dam during the first earthquake, but the power station was still in operation. While the repair work was going on, the second strong earthquake destroyed it and damaged it very seriously.

There were 6 longitudinal cracks, 2 of them were on the crest, 4 on the upstream slope (Fig. 8, 9). The horizontal displacements were 20-30 cm, the vertical displacements were 10-40 cm. 11 transverse cracks were discovered near abutments. The maximum width was 5 cm.

The slide of upstream slope 0+250 section show in Fig. 10, 11.

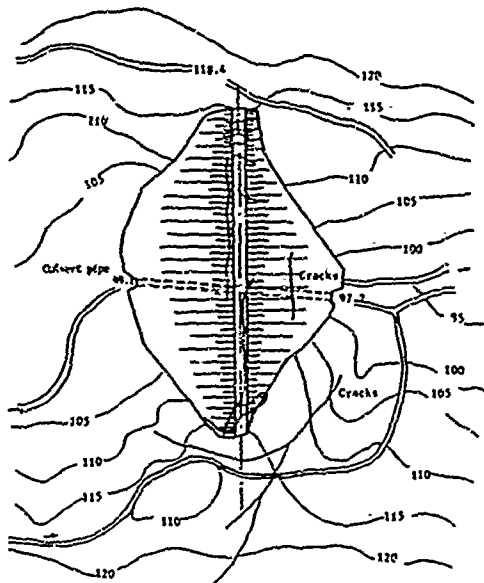


Fig. 1 Plan of Changmaidi earth dam



Fig. 2 Photograph of Changmaidi dam, transverse cracks on the dam.

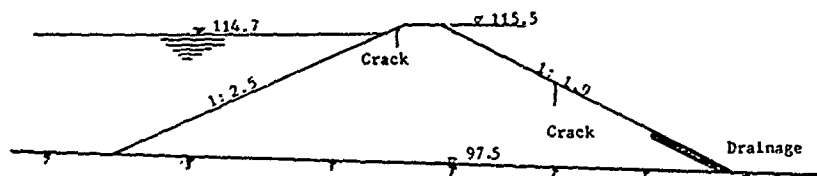


Fig. 3 Cross section of Changmaidi earth dam

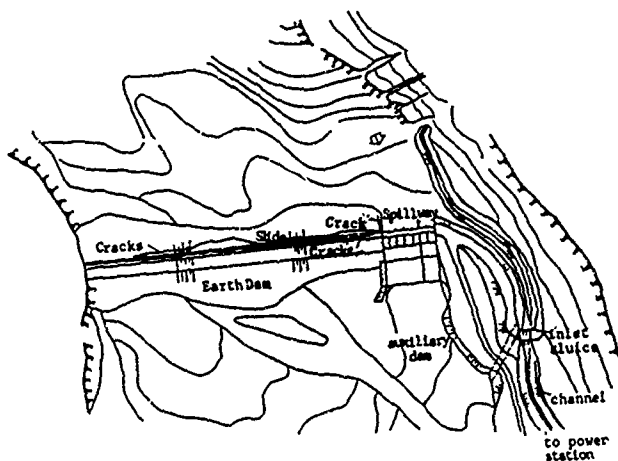


Fig. 4 Plan of Kashi hydroelectric power station



Fig. 5 Photograph of Kashi dam and spillway

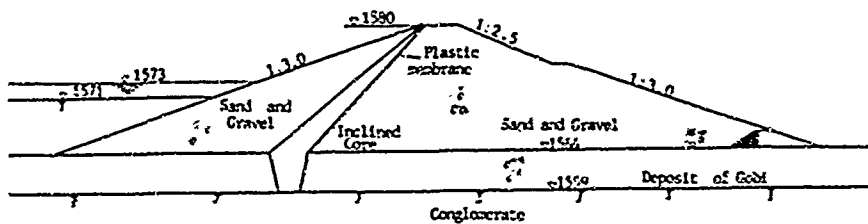


Fig. 6 Cross section of Kashi earth dam

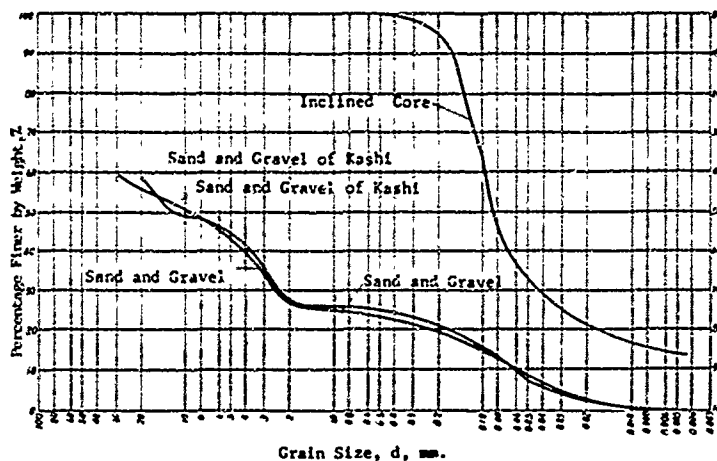


Fig. 7 Grain size distribution curves of Kashi earth dam



Fig. 8 Photograph of longitudinal cracks on the upstream slope of Kashi earth dam



Fig. 9 Photograph of longitudinal cracks on the upstream slope of Kashi earth dam



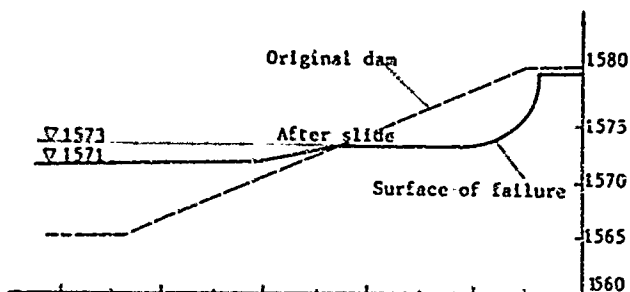


Fig. 10 Cross section of slide on the upstream slope of Kashi earth dam at 0+250 after earthquakes



Fig. 11 Photograph of the slide on the upstream slope of Kashi earth dam at 0+250

The settlement of dam crest was generally 20 cm during the first earthquake, and 60 cm after the second earthquake. The maximum settlement was 1.5 m near the middle of dam axis.

The masonry parapet on the crest of dam collapsed and fell onto the upstream slope mostly (Fig.12).

There is an auxiliary earth dam to the left of the spillway, 10 m high and 200 m long. This dam was protected by concret face slabs. Longitudinal and trasverse cracks were found with widths generally 10 cm.

Also the appurtenant structures had different damages. The power station had to stop operation.

#### RESULTS OF DIFFERENT DAMAGES DUE TO STRONG EARTHQUAKES AND THEIR ANALYSIS

Collection of different damages by earthquakes on earth dams in China from 1961 to 1986 is shown in the following table:

(See next page)



Fig. 12 Photograph of the failure of Parapet Wall on the crest of Kashi earth dam

From this table it is easy to find out:

- 1) In these strong earthquakes some damages of earth dams were very serious causing stoppages of normal operation but no one was collapsed.
- 2) In these 216 earth dams only 25 dams higher than 30 m, 4 dams higher than 40 m. The highest earth dam was Baihe dam in Miyun reservoir (H=66.2 m) and rockfill dam was Nangoudong in Henan Province (H=78 m).
- 3) The most common aspects of damage of earth dams were cracks. They took place about 78% of different types of damages in high and low intensities of earthquakes:
  - a) Transverse cracks appeared mostly along the abutments of dams by unequal settlements. Sometimes they were due to settlements of foundation overburdens.
  - b) Longitudinal cracks appeared on both slopes of dams. Some of them were curved in plan and may be the result of potential slides. Sometimes they may be due to the serious settlements of foundation, liquefaction of saturated silty soil or poor compaction during construction.
- 4) The slide of slope was more dangerous aspect of damages. Most slides appeared not only in high intensity of earthquakes like Douhe in Tangshan (degree 9) but in lower intensities (degree 5-6). The dominant factors are the types of embankments and the angle of friction of dam shells. For homogeneous earth dams filled by sluiced siltation method it is most critical. This type of damages is most typical for the downstream slope of many dams in the Heligeer Earthquake, even the intensity on the dam site was degree 6 only. Most upstream slope of saturated silty clay or fine sand and gravel during earthquake, as the slide of surface protection on the upstream slope of Baihe dam, which were investigated by many authors ten years ago.
- 5) Settlements appeared in many dams with accompanying cracks. Of course, earth dams always settle during earthquake, but sometimes the induced unequal settlement produced different types of cracks, as mentioned before. This problem was not so serious, because most of these earth dams were not so high.
- 6) The increase of leakage was a general aspect after earthquakes. Three different kinds of

# Different Types of Damages of Earth Dams by Strong Earthquakes from 1961 to 1986

(by Incomplete Statistics)

| Earthquakes                 |                    |                | Types of Damage                |                      |        |                           |                  |              |        |       |
|-----------------------------|--------------------|----------------|--------------------------------|----------------------|--------|---------------------------|------------------|--------------|--------|-------|
| Place                       | year, month        | Magni-<br>tude | Slide<br>of<br>Founda-<br>tion | Slide<br>of<br>slope | Cracks | Cracks<br>with<br>leakage | Settle-<br>ments | Leaka-<br>ge | Others | Total |
| Bachu(Xinjiang)             | 1961 Apr.          | 6.8            | 1                              |                      | 1      |                           | 1                |              |        | 1     |
| Urumqi(Xinjiang)            | 1965 Nov.          | 6.6            |                                |                      | 1      |                           |                  |              |        | 1     |
| Xingtai(Hebei)              | 1966 Mar.          | 6.8<br>7.2     |                                |                      | 4      |                           | 1                |              |        | 4     |
| Bohaiwan                    | 1969 Jul.          | 7.2            |                                | 3                    |        |                           |                  |              |        | 3     |
| Yangjiang(Guangdong)        | 1969 Jul.          | 6.4            |                                |                      | 5      |                           |                  |              |        | 5     |
| Tonhai(Yunnan)              | 1970 Jan.          | 7.7            |                                | 1                    | 41     |                           |                  |              |        | 41    |
| Liyang(Jiangsu)             | 1974 Apr.          | 5.5            |                                |                      | 6      |                           |                  |              |        | 6     |
| Zhaotong(Yunnan)            | 1974 May           | 7.1            |                                |                      | 1      |                           |                  | 1            |        | 2     |
| Haicheng(Liaoning)          | 1975 Feb.          | 7.3            |                                | 1                    | 26     |                           |                  | 11           |        | 35**  |
| Helingeer(Inner<br>Mongol.) | 1976 Apr.          | 6.3            |                                | 9                    | 17     |                           | 1                | 18           |        | 44    |
| Longling(Yunnan)            | 1976 May           | 7.5<br>7.6     |                                | 5                    | 19     | 1                         |                  |              |        | 21    |
| Tangshan(Hebei)             | 1976 Jul.          | 7.8<br>7.1     | 1                              | 2                    | 35     | 2                         | 2                | 9            | 1      | 39**  |
| Liyang(Jiangsu)             | 1979 Jul.          | 6.0            |                                |                      | 8      |                           |                  |              |        | 8     |
| Luqien<br>Quendian (Yunnan) | 1985 Apr.          | 6.3            |                                |                      | 5      | 2                         |                  |              |        | 5     |
| Kashi(Xinjiang)             | 1985 Aug.<br>Sept. | 7.4<br>6.8     |                                | 1                    | 1      |                           | 1                |              |        | 1     |
| Total                       | 15                 |                | 2                              | 17                   | 170    | 5                         | 69               | 39           | 1      | 216   |
| Percentage % *              |                    |                | 0.9                            | 7                    | 78     | 2                         | 2.7              | 18           | 0.4    | 100   |

\* The percentage will be higher than this figure, because some dams have two or three of damages.

\*\* Only dams with reservoir storage capacity greater than 1,000,000 m<sup>3</sup> are included.

leakage were discovered: The first was temporary increase after earthquake, sometimes with muddy water, and after a few hours stopped by self relief. The second was increase of leakage through the abutments or foundations due to damage of grout curtain. The third was opening new channels of leakage after earthquake mostly in karst regions.

7) Many parapet walls were destroyed during earthquake, because they stood on the crest of earth dams and there existed large horizontal acceleration force acting on them. Besides, the masonry structure had not enough tensile strength.

Another weak point of earth dam to resist earthquake was the interface between the embankment and concrete or masonry structures. The retaining walls of spillway and the culverts or pipes embedded in the dam body were always sources of trouble.

#### SOME EXPERIENCES

More than 200 examples of damages and 30 years of research works gave us some experiences, although some of them were well known already for many years.

##### 1) Improvement of Design

For some small earth dams located in the counties, their design had obvious defects without proper control. For instance, the Kashi earth dam is of inclined core (silty clay loam) with sand gravel shells, the designers wanted to have an impermeable barrier and they put on two layers of plastic membrane with thickness 0.2 mm not on the surface but on the bed (Fig. 2). It made the whole core under water saturated and decreased the friction angle from  $34^\circ$  to  $23^\circ$ . It undoubtedly was the reason of the surface slide (Fig. 6). This is also an example of liquefaction of the core and shell.

Some earth dams had too high phreatic lines and without drainage. Therefore the strength of soil decreased due to the increase of pore pressure during earthquakes. The correct design of drainage and filters are very important too. Some damages of earth dams were due to the defect of drainage.

##### 2) Improvements of Construction

Most of the damages like cracks, settlements and slides were caused by poor compaction. The low density of soil gives low strength and is vulnerable to liquefaction. For some small dams proper compaction equipments were not available. The self-consolidation needed a long time, so the dam was damaged even during minor earthquakes.

Damages also occurred due to bad foundation conditions. In some medium and small sized reservoirs the foundation treatment works of dams were too much simplified. Sometimes the grout curtain were not deep enough. Sometimes the saturated silt in the loose alluvium was not cleared away, causing liquefaction like in Kashi, mentioned above.

The quality control of materials (soil, rockfill

etc.) was not strict, causing damages as excessive settlements, leakage and displacements after completion of the dams.

##### 3) Adoption of Reasonable Safe Measures Against Earthquakes

For design of high earth dams the prediction of seismicity and research works were well done, the designers generally paid more attention to the careful choice of materials, therefore there were no problems during earthquakes of intensity less than degree 6. But for small dams it will be questionable to prove their safety at reasonable cost. The right approach is to make risk analysis and allow some damages but without failure. Some cracks may be considered allowable. In any case the possibility of immediate drawdown of reservoir water level with emergency spillway or bottom outlets was very necessary.

##### 4) Avoidance of High Structures of Parapet Wall on the Crest of Dams

High structures are always weak points during strong earthquakes, experience proved that, the masonry parapet walls on the crest of dams were quite often damaged due to whipping effect.

#### CONCLUSION

From the case histories of Chinese embankments damages by 15 strong earthquakes in the last 25 years, it can be concluded that:

1) Even 216 embankments were damaged, and some of them were very serious, but no one was collapsed.

2) Many serious damages of earth dams were caused by the defects of investigation and design, especially the inadequate drainage and the improper use of materials.

3) The poor compaction of earth dams in construction and unreasonable treatments of foundation were another main cause of damages, which must be avoided.

4) High structures or wave walls on the crest of dams should be avoided in any case.

Understanding the nature of seismic response of dams through practice is a direct and essential way. The analysis and research of data collected becomes the source of our knowledge. It is regretted that not sufficient data are available, because for many small dams there are almost no records. Therefore our research is a time consuming job. This paper is an attempt to solve this complex problem.

#### REFERENCES

- SHEN C. and CHEN H. (1980), "Thirty Years of Research Work on Earthquake Resistance of Hydraulic Structures in China", Proceedings of Conference on Dams and Earthquakes, Institution of Civil Engineering, London, 107-113.
- WANG Wenshao (1986), "Lessons from Earthquake Damages of Earth Dams in China", International Symposium on earthquakes and Dams, Vol. 1, May 20, 1987, Beijing, 243-257.
- LIU L, LI K. and BING D. (1980), "Earthquake Damage of Baihe Earth Dam and Liquefaction

Characteristics of Sand and Gravel Materials"  
Proceedings of the Seventh world Conference on  
Earthquake Engineering, Istanbul, Turkey, vol.  
3, 171-178.

WANG Zhongning (1985), "Report of Earth Dams  
During Luqien and Quendian Earthquakes in  
Yunnan Prov. " (in Chinese)

ZUO Xiuhong, LI Zuxin and ZHAO Dong (1985),  
"Report about Damages of Kashi Hydroelectric  
Power Station During Strong Earthquakes in  
Uqia County of Xinjiang Uygur Autonomous  
Region (in Chinese)

The Institute of Engineering Mechanics (1979)  
"The Damages by Haicheng Earthquakes" (in  
Chinese).

CHEN Lide, ZHAO Weicheng and others (1979)"The  
Damages by Longling Earthquake (in Chinese).

LIU Huixian and others (1986), "The Damages by  
Tangshan Earthquakes"Vol 3 (in Chinese).

# Vibration Response of Railway Bridge Piers to Nearby Pile Driving

I. Rosenthal

Senior Research Fellow, Building Research Station, Technion—Israel  
Institute of Technology, Haifa, Israel

M. Itskowitch

Research Engineer, Building Research Station, Technion—Israel  
Institute of Technology, Haifa, Israel

**SYNOPSIS:** In the development of a new highway system approaching Tel Aviv, Israel, long piles had to be driven very close to an existing railway bridge. In view of the danger of structural damage to the bridge, as a result of ground vibrations excited by the pile-driving work, field measurements were ordered.

Vibrations recorded at the bridge pier heads in the course of the driving operation were analyzed and compared with those excited by trains. Results showed that the former are generally lower than the latter, and neither one exceeds the limits prescribed by the codes.

## INTRODUCTION

The new highway system approaching Tel Aviv from the north, as part of the Ayalon project, will include several overpasses and intersections. The new construction will require piles to be driven very close to the Tel Aviv-Haifa railway bridge currently in use. In view of the danger of structural damage to the bridge as a result of ground vibrations excited by the pile-driving work, a program was carried out which included field measurements of the bridge piers while test piles were driven into the ground in various locations.

## THE SITE

The bridge, built in the fifties with its one-track railway and several spans, is a steel bridge supported on reinforced concrete piers, based on driven reinforced concrete piles. It is situated very close to the merging point of the Ayalon with the Yarkon River (Figs. 1 and 2).

Ground conditions, according to borehole investigations, were as follows: soft and medium strength clays on the south bank, as deep as 60m and similar clays on the north bank, interrupted by an intermediate 6m thick layer of compact sand between 16m and 22m deep. The water table is 2.5m below ground level.

These ground conditions required the use of prestressed concrete piles for the foundations of the new overpasses which will be built.

## TEST PROGRAM

The piles, 0.50m in diameter and 45m long, were composed of two equal shorter piles welded to one another after the first part has been driven into the ground. A special test pile differed from the others in that special metal devices were contained, to extend out of its faces, after the pile had been driven. The hammer in use was a Delmag-D44 with a rate of about one stroke per second.

Most of the vibration measurements (using 1Hz, nat. freq. seismometers) were carried out simultaneously at two different pier heads, and in each one - in both the longitudinal and transverse directions of the bridge. In some cases (Tests 1 and 2), the measurements were taken at the foot of the pier, on the ground, and at the same time at its head.

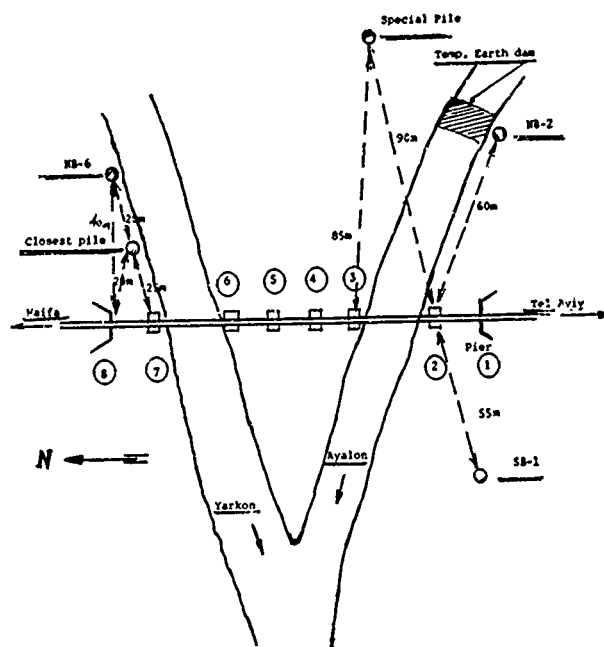


Fig. 1 - Layout of the railway bridge and location of the test piles.



Fig. 2 - Eastward view of pier 2.

The piers selected were always the closest ones to the driven pile, and the vibrations were measured at different pile depths. Vibrations were also measured during the passage of trains for comparison purposes.

## RESULTS

The detailed measurements appear in Table 1 with typical vibration records shown in Fig. 3 to 7. Velocity spectrum (third octave) were found for all tests, but only few of them are shown in Fig. 8 to 11. Results are also given in Table 2, including the computed maximum displacements of the vibrations.

Table 1 - Details of the measurements at various piers (see Fig. 1)

| Test | Pile    | Depth | Source of Vibration | Channel |     |     |     |
|------|---------|-------|---------------------|---------|-----|-----|-----|
|      |         |       |                     | 1       | 2   | 3   | 4   |
| 1    | SB-1    | 18m   | Hammer              | 2gt(*)  | 2gl | 2ht | 2hl |
| 2    |         | 18m   | Train               | "       | "   | "   | "   |
| 3    | NB-2    | 26m   | Hammer              | -       | -   | 2ht | 2hl |
| 4    |         | 32m   | "                   | -       | -   | "   | "   |
| 5    |         | 37m   | "                   | -       | -   | "   | "   |
| 6    | Special | 10m   | Hammer              | -       | 3nl | 2ht | 2hl |
| 7    | Pile    | 16m   | "                   | 3ht     | "   | "   | "   |
| 8    |         | 22m   | "                   | "       | "   | "   | "   |
| 9    |         | 28m   | "                   | "       | "   | "   | "   |
| 10   | Closest | 16m   | Rap. Train          | 8ht     | 8hl | 7ht | 7hl |
| 11   | to      | 16m   | Hammer              | "       | "   | "   | "   |
| 12   | pier 8  | 18.5  | "                   | "       | "   | "   | "   |
| 13   |         | 23m   | "                   | "       | "   | "   | "   |
| 14   |         | 30m   | "                   | "       | "   | "   | "   |
| 15   |         | 35m   | "                   | "       | "   | "   | "   |
| 16   |         | 38m   | "                   | "       | "   | "   | "   |
| 17   | NB-6    | 15m   | Hammer              | 8ht     | 8hl | 7ht | 7hl |
| 18   |         | 17m   | "                   | "       | "   | "   | "   |

(\*)The figure denotes = pier number;

gt,gl = ground measurements at the pier foot in the transverse, and longitudinal directions of the bridge;

ht,hl = pier head measurement in the transverse and longitudinal directions of the bridge.

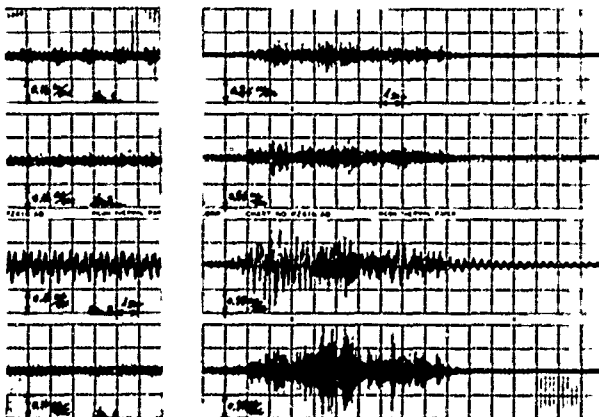


Fig. 3 - Vibration Measurements at pier 2:  
Test 1 (left); Test 2 (right).

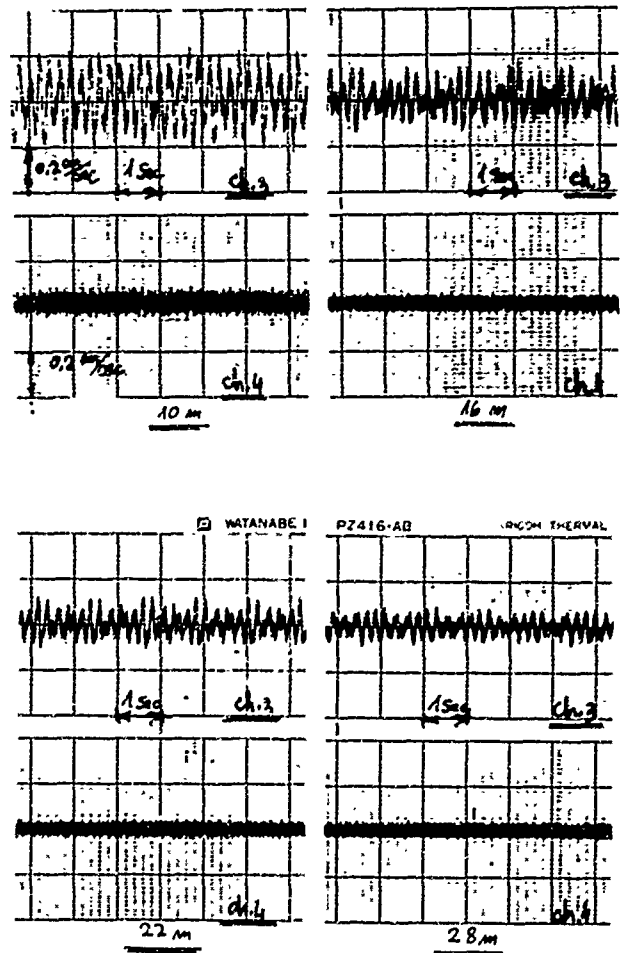


Fig. 4 - Vibration measurements at pier head 2, during driving of the special pile at various depths (Tests 6 to 9).

## DISCUSSION

It has been observed from all the measurements that the stiffness of the bridge is much greater in the longitudinal direction than in its transverse direction. The natural frequency and critical damping ratio of the bridge in that direction are 3 Hz and 1.5%, according to its free vibration after the passage of the train (Ch. 3, Fig. 3). As a result, the most significant quantities to be considered in the dynamic analysis of the bridge are therefore the transverse velocities or displacements.

It is interesting to note also, according to Tests 1 and 2, that the vibration at the pier head was amplified by a factor of two, as compared with the measurements at the foot of the same pier. This behaviour occurred during both hammer operation and train passage as well (Fig. 3). Vibrations at the pier heads 2 and 3 decreased with increasing depth of the driven pile, as can be seen in Fig. 4, mainly in the transverse direction. In the present case, the ground had a uniform composition in

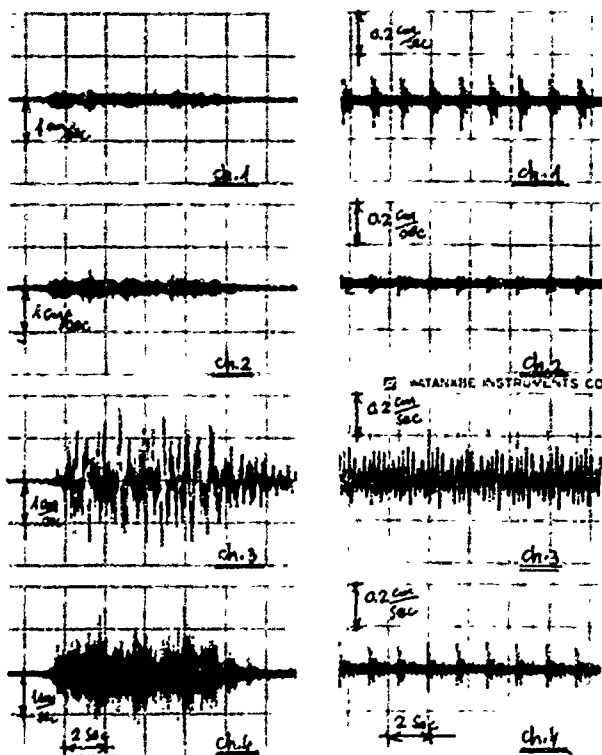


Fig. 5 - Measurements during passage of a rapid train (Test 10).

Fig. 6 - Measurements during driving of the closest pile (30m) (Test 14).

the south bank of soft and medium strength clays, as mentioned earlier. On the north bank, where there was a compact sand layer between 16m and 22m, the same phenomenon was observed again, as the vibration at the pier head No. 7 was drastically reduced when pile NB-6 was driven from 15m to 17m deep (Fig. 7). This reduction in the amplitude is due to the high strength of the compact sand layer.

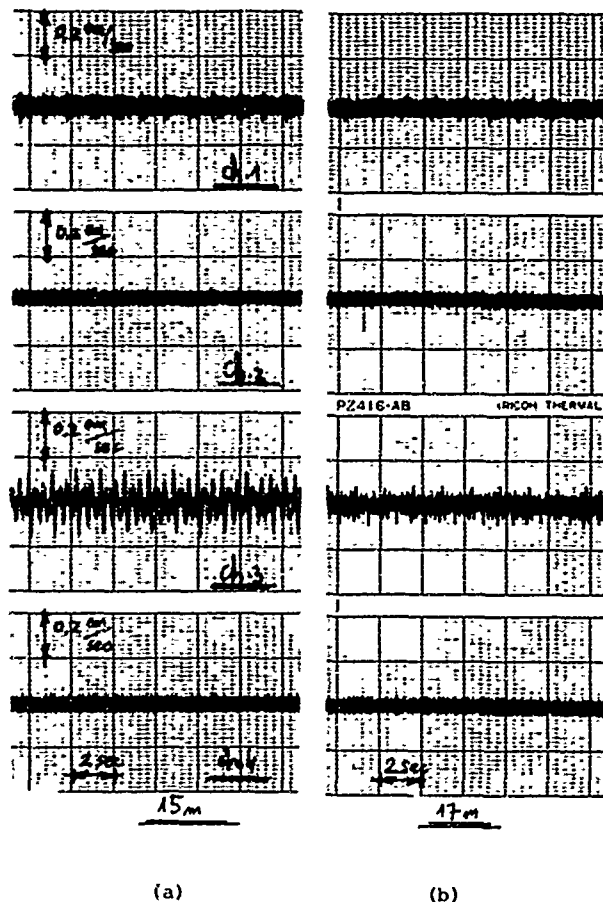


Fig. 7 - Vibration measurements during driving of pile NB-6: (a) Test 17 (15m); (b) Test 18 (17m).

Table 2 - Frequencies, peak velocities and displacements as obtained at the bridge piers

| Test | Channel | Pier | Frequency<br>Hz | Peak<br>Velocity<br>mm/sec | Maximum<br>Displacement<br>mm | Source of Vibration                  |
|------|---------|------|-----------------|----------------------------|-------------------------------|--------------------------------------|
| 1    | 3       | 2ht  | 4.4             | 0.66                       | 0.024                         | Hammer, pile SB-1 (18m)              |
| 2    | 3       | "    | 2.5             | 2.50                       | 0.159                         | Train                                |
| 2    | 4       | 2hl  | 50.0            | 1.50                       | 0.005                         | Train                                |
| 3    | 3       | 2ht  | 6.4             | 0.36                       | 0.009                         | Hammer, NB-2 (26m)                   |
| 4    | 3       | "    | 6.1             | 0.33                       | 0.009                         | " (32m)                              |
| 5    | 3       | "    | 4.5             | 0.39                       | 0.014                         | " (37m)                              |
| 6    | 3       | 2ht  | 4.3             | 1.20                       | 0.044                         | Hammer, Special pile (10m)           |
| 7    | 3       | "    | 4.8             | 0.75                       | 0.025                         | " (16m)                              |
| 8    | 3       | "    | 4.8             | 0.42                       | 0.014                         | " (22m)                              |
| 9    | 3       | "    | 4.8             | 0.33                       | 0.011                         | " (28m)                              |
| 10   | 1       | 8ht  | 80.0            | 1.20                       | 0.002                         | Rapid Train                          |
| 10   | 2       | 8hl  | 160.0           | 1.80                       | 0.002                         | "                                    |
| 10   | 3       | 7ht  | 4.0             | 5.40                       | 0.215                         | "                                    |
| 10   | (3)     | "    | (1.6)           | (4.20)                     | (0.418)(*)                    | "                                    |
| 10   | 4       | 7hl  | 56.0            | 8.40                       | 0.024                         | "                                    |
| 14   | 1       | 8ht  | 14.4            | 0.48                       | 0.005                         | Hammer, Pile closest to pier 8 (30m) |
| 14   | 3       | 7ht  | 4.2             | 0.75                       | 0.028                         | "                                    |

(\*) This maximum displacement is obtained according to a lower velocity (4.20mm/sec) than the maximum measured value (5.40mm/sec), and occurs at a frequency of 1.6 Hz.

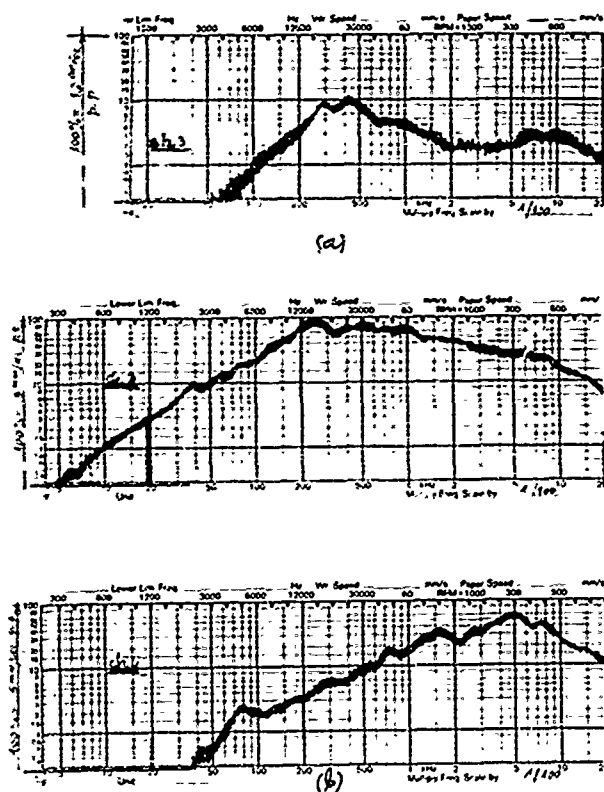


Fig. 8 - Velocity spectrum (third octave):  
a) Test 1, channel 3: driving of pile SB-1,  
b) Test 2, channels 3,4: passage of train.

Pier 8 was actually a retaining wall, and not a column type pier, like all other intermediate ones, and as a result its vibrations were always very low.

Spectrum analysis (third octave) of the measured velocities yielded the frequencies of the vibrations and permitted the calculation of the pier head displacement amplitudes (Table 2). In most cases the spectrum had only one peak velocity. However, that of Test 10, Channel 3 (Fig. 9), was rather a type of "plateau", and could be interpreted to show a peak at 4 Hz. In this particular case, a lower velocity, at a lower frequency of 1.6 Hz, yielded displacement of  $\pm 0.418\text{mm}$  instead of  $\pm 0.215\text{mm}$ , as computed from the peak velocity.

Analysis has shown that the peak transverse amplitude at pier head obtained during the passage of a rapid train were at least 10 times higher than during pile driving operation. Considering an amplification factor of 2 of the vibration at the pier head (see Fig. 3,a), the ground vibration at the pier foot should be half of it, or  $\pm 0.209\text{mm}$ . This result is in good agreement with amplitude limits of foundation block, which do not cause any damage to the structure, as mentioned in the British Code of Practice, i.e.  $\pm 0.200\text{mm}$ , up to 20 Hz. Other codes (e.g. DIN 4150), specify a limit velocity

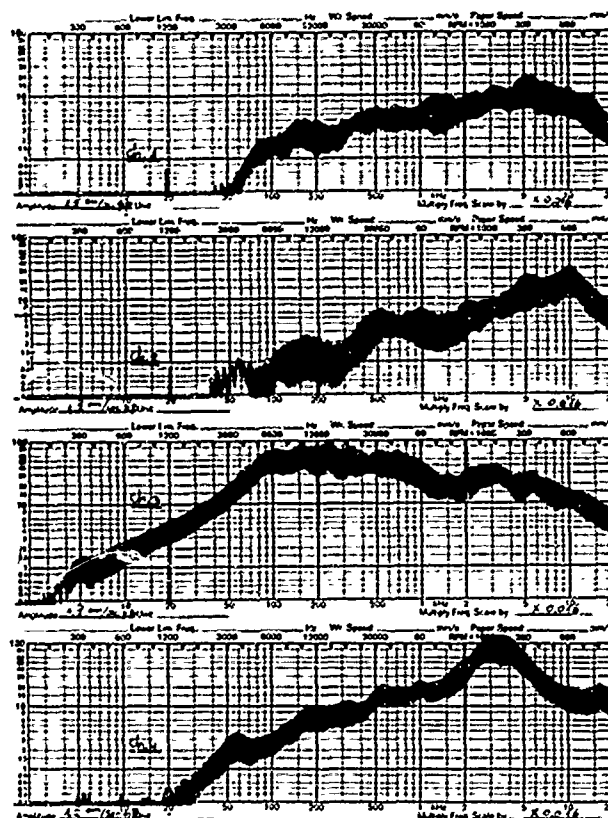


Fig. 9 - Velocity spectrum (third octave):  
Test 10, channels 1 to 4: passage  
of a rapid train.

of 20mm/sec up to 10 Hz, as one which generally does not produce any damage to a structure. The maximum velocity, as measured at pier head 7, was  $\pm 8.40\text{m/sec}$  or  $16.80\text{mm/sec}$  peak to peak, which does not yet endanger the bridge.

#### CONCLUSIONS

1. Vibrations recorded at pier heads during pile driving operation, were much higher in the lateral direction of the bridge than in its longitudinal direction, and pier head vibration was almost twice as large as that measured at the pier base. The natural frequency of the bridge in the transverse direction was 3 Hz, and the critical damping ratio of the system, about 1.5%.
2. Train passage caused lateral vibration at pier heads which was at least ten times bigger than the one caused by pile driving, namely  $\pm 0.418\text{mm}$ , or  $\pm 0.836\text{mm}$  peak to peak.
3. Neither velocity nor displacement obtained exceeded the limit values prescribed by the codes, thus indicating that no structural change is anticipated to the bridge during pile driving or even rapid train passage.



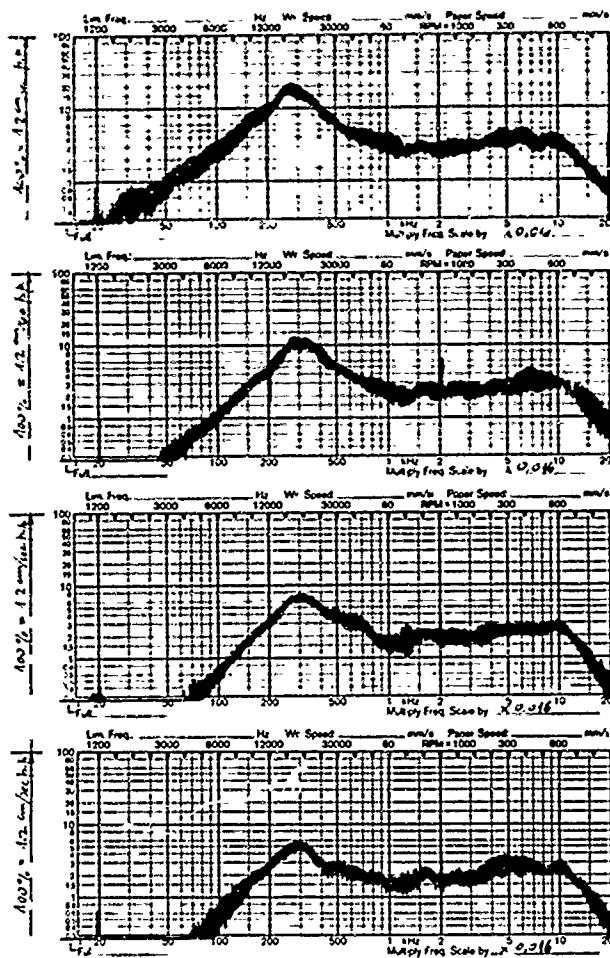


Fig. 10 - Velocity spectrum (third octave), Tests 6 to 9, channel 3: driving of special pile, at various depths.

4. Thanks to the field measurements, this stage of the Ayalon Project may be regarded safe, as far as causing damage to the existing bridge is concerned.

#### REFERENCES

- British Code of Practice - CP 2012, Part 1, 1974.  
Deutsche Norm - DIN 4150, Part 3, May 1986.

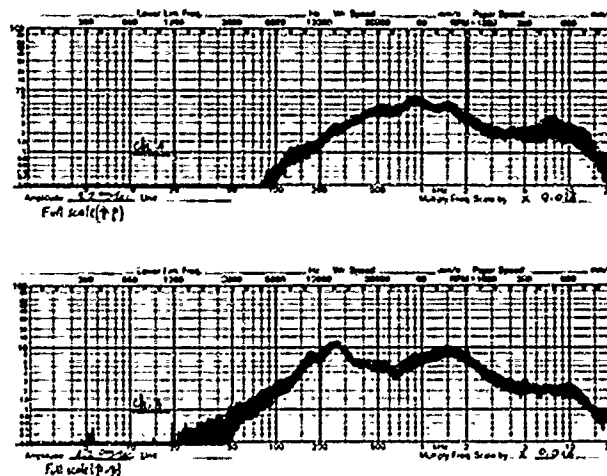


Fig. 11 - Velocity spectrum (third octave), Test 14, channels 1 and 3: driving of closest pile at 30m deep.

## Theory and Experiment of Hammer Foundation Vibration

Pan Fulan

Senior Engineer, Fifth Design and Research Institute, Beijing, China

**SYNOPSIS** The foundation of 1~16t hammer have been calculated with five calculation models and compared with the test data of the foundation and anvil for the hammer 1t, 2t, 3t, 5t, 10t and 16t built on the loess clayey loam stratum. The results show: (1) In the design of hammer foundation, calculation with model of two-degree-freedom and damped agrees rather better with the actual measurement. (2) The coefficient of subgrade compression rigidity increases with the increase of the depth of soil stratum. Both accurate calculations of the coefficient of subgrade compression rigidity and effected depth under the hammer foundation are most significant for designing a rational hammer foundation.

In this paper formulae are presented for calculating optimum ratios of anvil mass to hammer foundation mass and pad rigidity to subgrade rigidity according to different kinds of soil and different tonnages of the hammer.

### INTRODUCTION

Many forges have been built since 1960's and a tendency of using hammer with increasingly greater tonnage is seen as industry develops rapidly. From the investigation, a common problem has been found that most of these hammer foundations are oversized and embedded too deeply due to the impractical and improper selection of calculation models and values of subgrade rigidity.

In some countries at the present time, specifications for designing dynamic machinery foundations are based on the calculation model of one-degree-freedom and undamped with neglecting the influence of vibration frequency properties of anvil and pad on the whole system of the hammer foundation, thus resulting in greater calculation error. Furthermore the previous experiments are only conducted on hammer foundation itself, not also the anvil, with leads to an incomplete understanding of the dynamic properties of the hammer foundation system.

This paper intends to describe systematical tests of vibration frequency properties of foundations and anvils for the hammer 1t, 2t, 3t, 5t, 10t and 16t built on the loess clayey loam stratum and theoretical analysis with five calculation models. The results show that in the design of hammer foundation, calculation with model of two-degree-freedom and damped agrees rather better with the actual measured values.

Based on the fact that the coefficient of subgrade compression rigidity increases with the increase of the depth of soil stratum (Pan Fulan, 1982.), this paper defines the coefficient of subgrade compression rigidity within the effected depth under the hammer foundation, thus accurate calculation of the self-vibration properties of the hammer foundation can be obtained. In some countries' current specifications, the coefficient of compression rigidity is defined as a constant. This is not a proper definition parti-

cularly for the foundation with large base area and deeply embedded. Therefore, both accurate calculations of coefficient of subgrade compression rigidity and effected depth under the hammer foundation, as well as proper selection of calculation models, are most significant for designing a rational hammer foundation.

For the purpose of reducing hammer foundation vibration, in design a common practice is to increase subgrade rigidity (piling, enlarging base area, or deepening embedded depth of foundation) and foundation mass. Both theory and experiment have proved that it is necessary to have a certain foundation mass so as to reduce the vibration amplitude of hammer foundation. However this does not mean to have a foundation mass as greater as possible. This paper presents calculation formulae for selecting optimum ratios of anvil mass to hammer foundation mass, and pad rigidity to subgrade rigidity according to different kinds of soil and different tonnages of the hammer so as to obtain a more economical and reasonable design for the hammer foundation.

### THEORETICAL ANALYSIS OF HAMMER FOUNDATION VIBRATION

A hammer foundation mainly consists of falling part of hammer, hammer stand, anvil and foundation. The anvil and foundation are separated by a pad. All of the dynamic foundations, the hammer foundation is characterized by free vibration which is different from the others. This free vibration is an instantaneous vibration with damping. The instantaneous vibration is caused by two sources. One is an impulse, i.e. the action occurs at the instant when the falling hammer impacts the anvil. The other is a suddenly applied force, i.e. the force occurs as the impulse disappears. When the falling hammer is raising, the suddenly applied force disappears immediately, and then the impulsive force is formed. In general, the impulsive force is neglected, but the dynamic influence of the impulse is only con-

sidered in calculation of hammer foundation.  
(see Fig. 1)

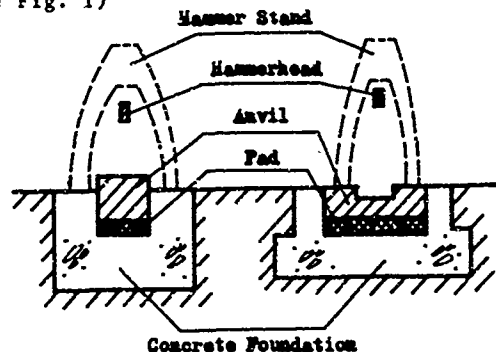


Fig. 1 Schematic of Free Forging and Die Forging

Based on Calculation Model for One-Degree-Freedom

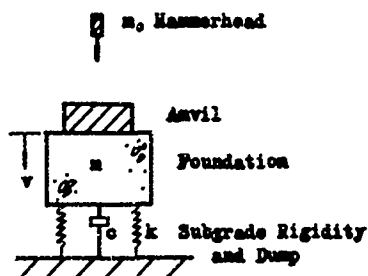


Fig. 2 Calculation Model for One-Degree-Freedom

Under the action of impact load, the amplitude of hammer foundation movement is

$$A_z = \frac{V}{\omega_n} e^{-\delta t} \sin \omega_n t \quad (1)$$

where:  $V = \frac{m_0 V_0 (1 - \psi)}{(m_1 + m_0)}$

$V$  = Initial speed of the hammer foundation movement (m/s);

$V_0$  = Max. speed of falling part of hammer (m/s);

$m_1$  = Mass of hammer frame, anvil and foundation ( $t \cdot s^2/m$ );

$m_0$  = Mass of falling part of hammer ( $t \cdot s^2/m$ );

$\psi$  = Influence coefficient of speed resilience in impact;

$\omega_z$  = Circular frequency of undamped free vibration of hammer foundation (1/s);

$$\omega_z^2 = \frac{K_z}{(m_1 + m_0)}$$

$K_z$  = Compression rigidity of natural subgrade ( $t/m$ );

$\omega_n$  = Circular frequency of damped free vibration of hammer foundation (1/s);

$$\omega_n = \omega_z \sqrt{1 - D^2}$$

$D$  = Damping ratio;

$$D = \frac{\delta}{\omega_z} \quad ; \quad \delta = \frac{C}{2m_1}$$

$C$  = Damping coefficient of natural subgrade ( $t \cdot s/m$ ).

Let  $\frac{dA_z}{dt} = 0$ , we obtain

$$e^{-\delta t} V \cos \omega_n t - \frac{V \delta}{\omega_n} e^{-\delta t} \sin \omega_n t = 0 \quad (2)$$

thus, Eq.(2) can be written as

$$t = \frac{\tan^{-1} \frac{\sqrt{1-D^2}}{D}}{\omega_n} \quad (3)$$

At this moment, the amplitude is the max. i.e.  $A = A_{zmax}$ . Substitute  $t$  into Eq.(1), the following equation can be obtained by simplifying.

$$A_{zmax} = \frac{V}{\omega_z \sqrt{1-D^2}} \exp\left(\frac{-D \omega_z \tan^{-1} \frac{\sqrt{1-D^2}}{D}}{\omega_z \sqrt{1-D^2}}\right) \sin \omega_n \frac{\tan^{-1} \frac{\sqrt{1-D^2}}{D}}{\omega_n}$$

$$= \frac{V_0 m_0 (1 + \psi)}{\sqrt{K_z (m_0 + m_1)}} \exp\left(\frac{-D}{\sqrt{1-D^2}} \tan^{-1} \frac{\sqrt{1-D^2}}{D}\right) \quad (4)$$

The max. amplitude when damping is not considered is:

$$A_{zmax} = \frac{V}{\omega_z} = \frac{V_0 m_0 (1 + \psi)}{\sqrt{K_z (m_0 + m_1)}} \quad (5)$$

According to the above analysis, the following conclusions can be drawn.

1. The calculated amplitude of hammer foundation of damped one-degree-freedom decreases with the increase of damping ratio.

2. The circular frequency of free vibration of hammer foundation decreases with the increase of damping ratio, too.

3. Time for the hammer foundation reaches its max. amplitude of vibration in dependent of damping ratio. The greater the damping ratio, the shorter the time required.

Based on Calculation Model for Two-Degree-Freedom

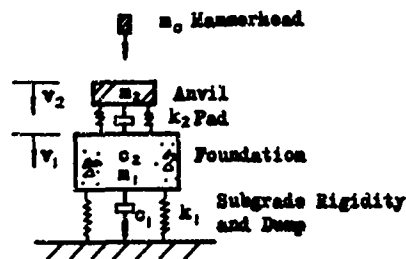


Fig. 3 Calculation Model for Two-Degree-Freedom

1. Equations of free vibration are

$$\left. \begin{aligned} m_2 \ddot{Z}_2 + K_2 (Z_2 - Z_1) &= 0 \\ m_1 \ddot{Z}_1 + K_1 Z_1 - K_2 (Z_2 - Z_1) &= 0 \end{aligned} \right\} \quad (6)$$

where:  $m_2$  = Mass of hammer frame and anvil ( $t \cdot s^2/m$ );

$m_1$  = Mass of hammer foundation ( $t \cdot s^2/m$ );

$k_2$  = Rigidity of pad beneath the anvil ( $t/m$ );

$k_1$  = Compression rigidity of natural subgrade ( $t/m$ ).

Two free vibration frequencies of Eq.(6) are:

$$\omega_{1,2}^2 = \frac{\alpha + C}{2} \mp \sqrt{\left(\frac{\alpha + C}{2}\right)^2 - bC} \quad (7)$$

where:

$$\alpha = \frac{K_1 + K_2}{m_1} \quad , \quad b = \frac{K_1}{m_1} \quad , \quad C = \frac{K_z}{m_2}$$

2. The motion equations of foundation and anvil when damping is not considered are:

$$\left. \begin{aligned} z_1 &= \frac{r_1 r_2 v}{(r_2 - r_1)} \left( \frac{\sin \omega_1 t}{\omega_1} - \frac{\sin \omega_2 t}{\omega_2} \right) \\ z_2 &= \frac{v}{(r_2 - r_1)} \left( \frac{r_2 \sin \omega_1 t}{\omega_1} - \frac{r_1 \sin \omega_2 t}{\omega_2} \right) \end{aligned} \right\} \quad (8)$$

When  $\omega_1 < \omega_2$ , coefficients of vibration mode are

$$r_1 = \frac{z_{11}}{z_{21}} = \frac{K_2}{K_1 + K_2 - m_1 \omega_1^2} = \frac{K_2 - m_2 \omega_1^2}{K_2}$$

--for 1st vibration mode

$$r_2 = \frac{z_{12}}{z_{22}} = \frac{K_2}{K_1 + K_2 - m_1 \omega_2^2} = \frac{K_2 - m_2 \omega_2^2}{K_2}$$

--for 2nd vibration mode

From Eq.(8), it can be known that the amplitude of each mass is the sum of the two vibration modes. Thus, the above equation can be written as

$$\begin{Bmatrix} z_1(t) \\ z_2(t) \end{Bmatrix} = \begin{Bmatrix} z_{11} \\ z_{21} \end{Bmatrix} \sin \omega_1 t + \begin{Bmatrix} z_{12} \\ z_{22} \end{Bmatrix} \sin \omega_2 t \quad (9)$$

Where the subscript stands for the amplitude of mass,  $m_1$  or  $m_2$ , the second subscript stands for the frequency and vibration mode in relation to the amplitude.

In Eq.(9),  $z_{11}$  and  $z_{12}$  represent the amplitude of mass  $m_1$  and  $m_2$  in the 1st and 2nd vibration mode respectively. The corresponding equations can be expressed as (Let  $\omega_a^2 = \frac{K_2}{m_2}$ ):

$$\left. \begin{aligned} z_{11} &= \frac{r_1 r_2 v}{(r_2 - r_1) \omega_1} = \frac{(\omega_a^2 - \omega_1^2)(\omega_a^2 - \omega_2^2) v}{(\omega_1^2 - \omega_2^2) \omega_1 \omega_a^2} \\ z_{12} &= \frac{-r_1 r_2 v}{(r_2 - r_1) \omega_2} = \frac{-(\omega_a^2 - \omega_1^2)(\omega_a^2 - \omega_2^2) v}{(\omega_1^2 - \omega_2^2) \omega_2 \omega_a^2} \\ z_{21} &= \frac{r_2 v}{(r_2 - r_1) \omega_1} = \frac{(\omega_a^2 - \omega_2^2) v}{(\omega_1^2 - \omega_2^2) \omega_1} \\ z_{22} &= \frac{-r_1 v}{(r_2 - r_1) \omega_2} = \frac{-(\omega_a^2 - \omega_1^2) v}{(\omega_1^2 - \omega_2^2) \omega_2} \end{aligned} \right\} \quad (10)$$

From the 1st formula in Eq.(8), let  $\frac{dz_1}{dt} = 0$ , we can obtain time  $t_1$  when  $z_1 = z_{\max}$  i.e.

$$\frac{r_1 r_2 v}{r_2 - r_1} (\cos \omega_1 t_1 - \cos \omega_2 t_1) = 0 \quad (11)$$

To develop it, we get

$$\left(1 - \frac{\omega_1^2 t_1^2}{2}\right) - \left(1 - \frac{\omega_2^2 t_1^2}{2}\right) = 0 \quad (12)$$

Therefore  $t_1 = 0$

From the 2nd formula in Eq.(8), let  $\frac{dz_2}{dt} = 0$ , we can obtain time  $t_2$  when  $z_2 = z_{\max}$  i.e.

$$\frac{v}{r_2 - r_1} (r_2 \cos \omega_1 t_2 - r_1 \cos \omega_2 t_2) = 0 \quad (13)$$

To develop it, we obtain

$$r_2 \left(1 - \frac{\omega_1^2 t_2^2}{2}\right) - r_1 \left(1 - \frac{\omega_2^2 t_2^2}{2}\right) = 0$$

Therefore

$$t_2 = \sqrt{\frac{2(r_2 - r_1)}{r_2 \omega_1^2 - r_1 \omega_2^2}} \quad (14)$$

3. The motion equation of foundation and anvil when damping is considered are

$$\left. \begin{aligned} z_1 &= e^{-\delta_1 t} \left[ \frac{r_1 r_2 v}{(r_2 - r_1) \omega_1} \sin \omega_1 t \right] - e^{-\delta_2 t} \left[ \frac{r_1 r_2 v}{(r_2 - r_1) \omega_2} \sin \omega_2 t \right] \\ z_2 &= e^{-\delta_1 t} \left[ \frac{r_2 v}{(r_2 - r_1) \omega_1} \sin \omega_1 t \right] - e^{-\delta_2 t} \left[ \frac{r_1 v}{(r_2 - r_1) \omega_2} \sin \omega_2 t \right] \end{aligned} \right\} \quad (15)$$

in which, damping is due to smaller, we can suppose that  $\omega_{n1} \approx \omega_1$  and  $\omega_{n2} \approx \omega_2$ . When  $\omega_1 < \omega_2$ , the coefficients of vibration mode are

$$r_1 = \frac{z_1}{z_2} = \frac{K_2 + C_2 \omega_1}{m_1 \omega_1^2 + K_1 + K_2 + (C_1 + C_2) \omega_1} = \frac{m_2 \omega_1^2 + C_2 \omega_1 + K_2}{C_2 \omega_1 + K_2}$$

--for 1st vibration mode

$$r_2 = \frac{z_1}{z_2} = \frac{K_2 + C_2 \omega_2}{m_1 \omega_2^2 + K_1 + K_2 + (C_1 + C_2) \omega_2} = \frac{m_2 \omega_2^2 + C_2 \omega_2 + K_2}{C_2 \omega_2 + K_2}$$

--for 2nd vibration mode

Because both amplitude of hammer foundation and amplitude of anvil are the sum of two vibration modes, the amplitudes of foundation and anvil when damping is considered at any instant are:

$$\begin{Bmatrix} z_1(t) \\ z_2(t) \end{Bmatrix} = \begin{Bmatrix} z_{11} \\ z_{21} \end{Bmatrix} e^{-\delta_1 \omega_1 t} \sin \omega_1 t + \begin{Bmatrix} z_{12} \\ z_{22} \end{Bmatrix} e^{-\delta_2 \omega_2 t} \sin \omega_2 t \quad (16)$$

in which,  $z_{11}$ ,  $z_{12}$ ,  $z_{21}$ ,  $z_{22}$  are the amplitudes of foundation and anvil of 1st 2nd vibration mode in Eq.(10) respectively.  $e^{-\delta \omega t}$  is the effect of damping ratio on the amplitude. This shows, the calculated amplitude (foundation and anvil included) in two-degree-freedom system decreases with the increase of damping ratio, too.

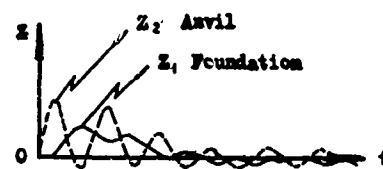


Fig. 4 Vibration Curves of Foundation and Anvil (in damped case)

#### 4. Damping ratio in two-degree-freedom system

From Fig.3, it can be seen that after the impact load acts on the hammer foundation the mass (i.e.  $m_1$ ,  $m_2$ ) cause a relative motion, and their relative amplitudes are

$$\left. \begin{aligned} \varepsilon_{1j} &= z_{1j} \\ \varepsilon_{2j} &= z_{2j} - z_{1j} \end{aligned} \right\} \quad (17)$$

The correspondent damping action are

$$\left. \begin{aligned} P(\epsilon_1) &= C_1 \dot{\epsilon}_{1j} = C_1 \epsilon_{1j} \omega_j \cos \omega_j t \\ P(\epsilon_2) &= C_2 \dot{\epsilon}_{2j} = C_2 \epsilon_{2j} \omega_j \cos \omega_j t \end{aligned} \right\} \quad (18)$$

The work done by damping action is

$$\begin{aligned} W &= \int_0^T \frac{2\pi}{\omega_j} P(\dot{\epsilon}) d\epsilon(t) \\ &= \pi \omega_j [C_2 (Z_{2j} - Z_{1j})^2 + C_1 Z_{1j}^2] \end{aligned} \quad (19)$$

The correspondent strain energy is

$$U = \frac{1}{2} (m_2 Z_{2j}^2 + m_1 Z_{1j}^2) \omega_j^2 \quad (20)$$

The work done by damping action is equal to the strain energy, therefore

$$D_j = \frac{W}{4\pi U} = \frac{C_2 (Z_{2j} - Z_{1j})^2 + C_1 Z_{1j}^2}{2(m_2 Z_{2j}^2 + m_1 Z_{1j}^2) \omega_j} \quad (21)$$

The damping ratio in the 1st vibration mode is:

$$\begin{aligned} D_1 &= \frac{C_2 (Z_{21} - Z_{11})^2 + C_1 Z_{11}^2}{2(m_2 Z_{21}^2 + m_1 Z_{11}^2) \omega_1} \\ &= \frac{C_2 m_2^2 \omega_1^4 + C_1 (K_2 - m_2 \omega_1^2)^2}{2\omega_1 [K_2^2 m_2 + m_1 (K_2 - m_2 \omega_1^2)^2]} \end{aligned} \quad (22)$$

The damping ratio in the 2nd vibration mode is

$$\begin{aligned} D_2 &= \frac{C_2 (Z_{22} - Z_{12})^2 + C_1 Z_{12}^2}{2(m_2 Z_{22}^2 + m_1 Z_{12}^2) \omega_2} \\ &= \frac{C_2 m_2^2 \omega_2^4 + C_1 (K_2 - m_2 \omega_2^2)^2}{2\omega_2 [m_2 K_2^2 + m_1 (K_2 - m_2 \omega_2^2)^2]} \end{aligned} \quad (23)$$

#### EXPERIMENT ON VIBRATION OF HAMMER FOUNDATION

##### Tests on the Amplitude, Frequency and Acceleration of Hammer Foundation and Anvil

In a factory nine forging hammers under production were selected for investigation. Among instruments used for measurements were oscillograph, amplifier and wave collector. A pre-prepared sheet steel plate with fixing screw was bound to the anvil and foundation by epoxy or by welding and then connected to wave collectors. Measurements of amplitude, frequency and acceleration of both anvil and foundation were taken when applying impact. Due to the variation of the height of falling hammer, temperature and shape of workpiece, the energy of impacts are different. For this reason, only average of several impacts was taken for amplitude of both hammer foundation and anvil. The measured values on die forging of 1t, 2t, 3t, 5t, 10t and 16t are shown as Table 1.

Table 1. Measured Values of Die Forging

| Ton- | Lo- | Fre.  | Log.   | Damp-  | Ampli- | Accel-  | Cz                  |
|------|-----|-------|--------|--------|--------|---------|---------------------|
| nage | ca- | tion  | Atten  | ing    | tude   | eration |                     |
|      |     | (Hz)  | Rate   | Ratio  | (μ)    | (g)     | (t/m <sup>3</sup> ) |
| 16t  | H   | 14.22 | 0.7652 | 0.1218 | 204    | 0.163   | 14400               |
|      | A   | 15.06 | 0.9681 | 0.1541 | 5320   | 4.800   |                     |
| 10t  | H   | 19.72 | 1.1370 | 0.1810 | 218    | 0.330   | 14400               |
|      | A   | 21.32 | 0.9356 | 0.1489 | 2874   | 4.857   |                     |
| 5t   | H   | 17.60 | 1.3901 | 0.2212 | 511    | 0.623   | 7173                |
|      | A   | 27.05 | 1.0000 | 0.1592 | 3798   | 10.960  |                     |
| 3t   | H   | 16.45 | 0.9658 | 0.1537 | 369    | 0.390   | 6221                |
|      | A   | 19.46 | 0.8518 | 0.1356 | 2344   | 3.500   |                     |
| 2t   | H   | 19.10 | 1.0433 | 0.1660 | 227    | 0.326   | 5760                |
|      | A   | 36.00 | 1.0435 | 0.1661 | 892    | 4.540   |                     |
| 1t   | H   |       |        |        |        |         | 5760                |

Note: H--Hammer foundation;

A--Anvil;

Cz--Compression rigidity (at foundation base).

##### Tests on Compression Rigidity Coefficient of Natural Subgrade

A trial pit is selected around the forging shop. The subsoil of it is same as that on the shop. Geological conditions of each layer are described as follows:

1. Top soil: -0.2~-0.3 m deep; loess clayer soil, slight wet, plastic;
2. Q3 loess: -1~-8 m deep, brown yellow; maximum moisture content is 20.8% at a depth of -4m, homogeneous soil, few snail shells are found, larger grain size at -8m around, with small amount of ginger nuts;
3. Pebble layer: -8 -11m deep, with its main composition of limestone, maxi grain size 10-15cm filled with 20% approx. of clay, hard with lenticular appearance;
4. Q2 Old clay: most hard, small compression coefficient around 0.003-0.004 cm<sup>2</sup>/kg, difficult to excavate, brown yellow, slightly moistured, containing some ginger nuts.

The trial pit was dug to a predetermined elevation (elevation of the hammer base). Concrete test block of square sizing 1.5X1.5X1 m<sup>3</sup> and round sizing d=0.845 m, h=1 m are placed into the pit respectively. Then, impact and forced vibration are applied onto them to get compression rigidity coefficient of subgrade of different hammer with different tonnages at different elevations. Their values are shown as Fig. 5.

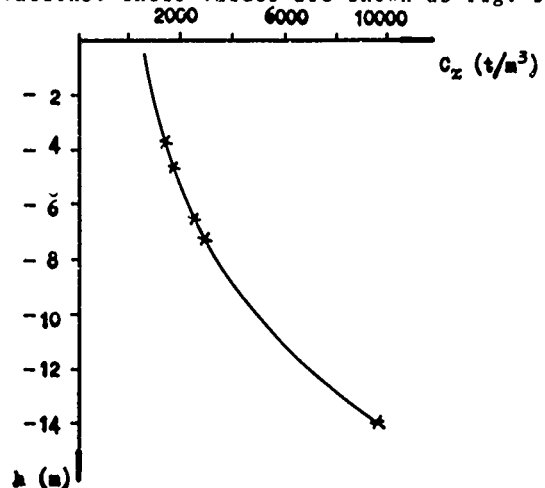


Fig. 5 Relationship between Cz and Depth

### Comparison of Theoretical Calculation and Measured Results

Calculations of six hammer foundations are carried out based respectively on "Design Specification of Dynamic Machinery Foundation", one-degree-freedom and two-degree-freedom and with results compared to the values measured on site. For detail refer to Table 2, 3 and 4. Both calculation values and measured values of the compression rigidity coefficient of subgrade are shown as Table 5.

Table 2. Calculations Based on "Design Specification of Dynamic Machinery Foundation"

| Tonnage                               | 16t  | 10t  | 5t   | 3t   | 2t   | 1t   |
|---------------------------------------|------|------|------|------|------|------|
| Coef. of Subgrade                     |      |      |      |      |      |      |
| Rig. $C_z(t/m^3)$                     | 4500 | 4500 | 3000 | 2000 | 2000 | 2000 |
| Ar. of Found.                         |      |      |      |      |      |      |
| Base F ( $m^2$ )                      | 180  | 120  | 71.8 | 48.8 | 38.5 | 20.0 |
| Wt of Hammer                          |      |      |      |      |      |      |
| Stand, Anvil, $W(t)$                  | 5609 | 3870 | 1204 | 824  | 427  | 200  |
| Found. & Soil                         |      |      |      |      |      |      |
| Spd of Falling                        |      |      |      |      |      |      |
| Part $V_0(m/s)$                       | 6.29 | 6.69 | 6.29 | 6.43 | 6.65 | 6.75 |
| Coef. of Resistance $\psi(s/m^{1/2})$ | 0.5  | 0.5  | 0.5  | 0.5  | 0.5  | 0.5  |
| Corr. $k_A$                           | 1.6  | 1.6  | 1.6  | 1.6  | 1.6  | 1.6  |
| Factor $k_A$                          | 0.6  | 0.6  | 0.6  | 0.6  | 0.6  | 0.6  |
| Frequency                             |      |      |      |      |      |      |
| Calc.                                 | 9.59 | 9.43 | 10.7 | 8.68 | 10.7 | 11.3 |
| of Found. Measd                       | 14.2 | 19.7 | 17.6 | 16.5 | 19.1 |      |
| f (Hz) Error (%)                      | 33   | 52   | 39   | 47   | 44   |      |
| Am. of Calc.                          | 429  | 435  | 574  | 691  | 618  | 679  |
| Found. Measd                          | 204  | 218  | 511  | 369  | 227  |      |
| Z ( $\mu$ ) Error (%)                 | 110  | 99.5 | 12.0 | 87   | 172  |      |

Note: Coefficient of subgrade rigidity based on the conversion of earth stamina [R].

Table 3. Calculations based on the Mode of One-Degree-Freedom

| Tonnage                               | 16t   | 10t   | 5t   | 3t   | 2t   | 1t   |
|---------------------------------------|-------|-------|------|------|------|------|
| Coef. of Subgrade                     |       |       |      |      |      |      |
| Rig. $C_z(t/m^3)$                     | 14400 | 14400 | 7173 | 6221 | 5760 | 5760 |
| Elev of Found.                        |       |       |      |      |      |      |
| Base h (m)                            | -14   | -14   | -7.3 | -6.5 | -4.6 | -3.7 |
| Ar. of Found.                         |       |       |      |      |      |      |
| Base F ( $m^2$ )                      | 180   | 120   | 71.8 | 48.8 | 38.5 | 20.0 |
| M. of Hammer                          |       |       |      |      |      |      |
| Stand, Anvil & Found. $m(t-s^2/m)$    | 386.4 | 218.9 | 88.1 | 68.4 | 39.7 | 18.2 |
| Spd of Falling                        | 6.29  | 6.69  | 6.29 | 6.43 | 6.65 | 6.75 |
| Part V ( $m/s$ )                      |       |       |      |      |      |      |
| Coef. of Resistance $\psi(s/m^{1/2})$ | 0.5   | 0.5   | 0.5  | 0.5  | 0.5  | 0.5  |
| Frequency                             |       |       |      |      |      |      |
| Calc.                                 | 13.0  | 12.5  | 12.2 | 10.6 | 11.9 | 12.7 |
| of Found. Measd                       | 14.2  | 19.7  | 17.6 | 16.5 | 19.1 |      |
| f (Hz) Error (%)                      | 8     | 37    | 31   | 36   | 38   |      |
| Am. of Calc.                          | 465   | 461   | 697  | 692  | 609  | 677  |
| Found. Measd                          | 204   | 218   | 511  | 369  | 227  |      |
| Z ( $\mu$ ) Error (%)                 | 128   | 111   | 36   | 87   | 168  |      |

Table 4. Calculations Based on the Mode of Two-Degree-Freedom

| Tonnage                     | 16t     | 10t    | 5t     | 3t    | 2t     | 1t     |
|-----------------------------|---------|--------|--------|-------|--------|--------|
| Elev of Found.              |         |        |        |       |        |        |
| Base h (m)                  | -14     | -14    | -7.3   | -6.5  | -4.6   | -3.7   |
| Pad Rig. $k_2(t/m)$         | 375000  | 319125 |        |       | 244800 |        |
| Subgrade                    | 2592000 | 514743 |        |       | 221760 |        |
| Rig. $k_1(t/m)$             | 1728000 |        | 303264 |       |        | 115200 |
| M. of Anvil                 | 43.4    | 32.1   | 16.1   | 8.0   | 5.9    | 3.3    |
| $m_2(t-s^2/m)$              |         |        |        |       |        |        |
| M. of Found. $m_1(t-s^2/m)$ | 341.4   | 248.9  | 71.5   | 60.1  | 33.6   | 14.8   |
| H. of Falling               |         |        |        |       |        |        |
| Hammer $m_0(t-s^2/m)$       | 1.56    | 1.01   | 0.50   | 0.33  | 0.18   | 0.10   |
| 1st Frequency               |         |        |        |       |        |        |
| $f_1(Hz)$                   | 11.9    | 12.1   | 11.8   | 10.5  | 11.8   | 12.5   |
| 2nd Frequency               |         |        |        |       |        |        |
| $f_2(Hz)$                   | 17.3    | 21.7   | 25.7   | 27.1  | 35.3   | 35.5   |
| Spd of Falling              |         |        |        |       |        |        |
| Part $V_0(m/s)$             | 6.29    | 6.72   | 6.28   | 6.43  | 6.65   | 6.75   |
| Spd of Found.               |         |        |        |       |        |        |
| Mov. V ( $m/s$ )            | 0.33    | 0.31   | 0.28   | 0.38  | 0.29   | 0.29   |
| Coef. of 1st                |         |        |        |       |        |        |
| Vib. Mode $r_1$             | 0.35    | 0.63   | 0.72   | 0.83  | 0.87   | 0.84   |
| Coef. of 2nd                | -0.36   |        | -0.31  |       | -0.19  |        |
| Vib. Mode $r_2$             |         | -0.21  |        | -0.16 |        | -0.27  |
| Calc.                       |         |        |        |       |        |        |
| Am. of Found. Measd         | 242     | 279    | 449    | 475   | 422    | 481    |
| $Z_1(\mu)$ Error (%)        | 19      | 28     | 12     | 28    | 85     |        |
| Calc.                       |         |        |        |       |        |        |
| Am. of Anvil Measd          | 3705    | 2701   | 2374   | 2800  | 1813   | 1855   |
| $Z_2(\mu)$ Error (%)        | 30      | 6      | 37     | 19    | 103    |        |

Table 5. Coefficients of Subgrade Compression Rigidity

| Soil Depth (m) | $C_z$ (found in DSDMF) ( $t/m^3$ ) | $C_z$ (measured) ( $t/m^3$ ) | Error (%) | Rate of $C_z$ Varying with Depth (1/m) |
|----------------|------------------------------------|------------------------------|-----------|--|
| -3.7           | 2000                               | 3452                         | 42        |  |
| -4.6           | 2000                               | 3836                         | 48        | 0.12                                   |
| -6.5           | 2000                               | 4503                         | 57        | 0.12                                   |
| -7.3           | 30000                              | 4910                         | 39        | 0.12                                   |
| -14.0          | 4500                               | 11600                        | 61        | 0.23                                   |

Note: DSDMF--"Design Specification of Dynamic Machinery Foundation"

From the comparison shown on above tables we can realized that the results obtained by calculations based on two-degree-freedom are closer to the measured values and this quite agreement with the practical working conditions of the hammer foundation. Of course, it is considered as a factor that the compression rigidity coefficient of subgrade increases with the increase of the soil depth in calculations, so that it makes the theory more agree with the practice, too.

### OPTIMUM DESIGN OF HAMMER FOUNDATION

From Eq.(16) can be seen that both the amplitude of hammer foundation and amplitude of anvil are the sum of two vibration modes. For simplifying the calculation, the 1st vibration mode is taken approximately, and then the ratio of am-

plitude of foundation to amplitude of anvil is

$$\frac{Z_{11}}{Z_{21}} = \frac{C_2 \omega_1 + K_2 - m_2 \omega_1^2}{C_2 \omega_1 + K_2} = 1 - \frac{m_2 \omega_1^2}{C_2 \omega_1 + K_2} \quad (24)$$

Let  $Z_{11}/Z_{21} = A$ ;  $k_1 = d k_2$ ;  $m_1 = \beta m_2$ , substitute them into Eq. (7). then

$$\omega_1^2 = \frac{K_2}{m_2} \left[ \frac{d+\beta+1}{2\beta} - \frac{1}{\beta} \sqrt{\frac{1}{4}(d+\beta+1)^2 - d\beta} \right]$$

Let

$$\frac{d+\beta+1}{2\beta} = I$$

$$\frac{1}{\beta} \sqrt{\frac{1}{4}(d+\beta+1)^2 - d\beta} = II$$

then

$$\omega_1^2 = \frac{K_2}{m_2} [I - II] \quad , \quad \omega_1 = \sqrt{\frac{K_2}{m_2} [I - II]}$$

Therefore, Eq. (24) can be written as

$$(1-A) C_2 \sqrt{\frac{K_2}{m_2} [I - II]} = K_2 [I - II] - (1-A) K_2$$

i.e.

$$[I - II] = (1-A) \left[ 1 + \frac{(1-A) C_2^2}{2 K_2 m_2} + \sqrt{\left[ 1 - \frac{(1-A) C_2^2}{2 K_2 m_2} \right]^2 - 1} \right] \quad (25)$$

And due to

$$I^2 - II^2 = \left( \frac{d+\beta+1}{2\beta} \right)^2 - \frac{1}{\beta^2} \left[ \frac{1}{4}(d+\beta+1)^2 - d\beta \right] = \frac{d}{\beta}$$

$$I + II = \left( \frac{d+\beta+1}{2\beta} \right) + \frac{1}{\beta} \sqrt{\frac{1}{4}(d+\beta+1)^2 - d\beta}$$

therefore

$$[I - II] \left[ \left( \frac{d+\beta+1}{2\beta} \right) + \frac{1}{\beta} \sqrt{\frac{1}{4}(d+\beta+1)^2 - d\beta} \right] = \frac{d}{\beta} \quad (26)$$

i.e.

$$\beta = \frac{d}{[I - II]} - \frac{1}{1 - [I - II]} \quad (27)$$

In design, if let both the amplitude of foundation and amplitude of anvil reach an allowable value at the same time and this is the most reasonable and economical,  $Z_{11}/Z_{21}$  would be equal to the allowable amplitude of foundation to the allowable amplitude of anvil. When the mass of anvil, rigidity and damp of pad are given,  $[I - II]$  can be obtained by Eq. (25). Substitute the value of  $[I - II]$  into Eq. (27), we can obtain the ratio  $\beta$  of foundation mass to anvil mass according to the ratio  $d$  of subgrade rigidity to pad rigidity.

## CONCLUSIONS

1. In the design of hammer foundation, it is an important factor to make the theory agree with the practice. It is proved by a lot of field measurements on hammer foundation that the results calculated by the mode of two-degree-freedom are closer in agreement with the practical working conditions of the hammer foundation.

2. A proper selection of the compression rigidity coefficient of foundation is another important factor. Because this coefficient increases with the depth of soil, particularly the foundation is embedded deeply, this factor must be considered sufficiently in design.

3. According to the condition that the amplitude of foundation and amplitude of anvil reach allowable values at the same time, we can calculate the optimum ratios of foundation mass to anvil mass when the rigidity ratios are different, this would help avoid the design foundation oversized and over embedded, and thus a more economical and reasonable design can be obtained.

## REFERENCES

- Pan Fulan (1982), "The Relation between Dynamic Elastic Parameters and Depth of Soil", Proceedings of the International Conference on Soil Dynamics and Earthquake Engineering, Southampton, UK.
- Pan Fulan (1984), "Study on Vibration in Site Selection for a Precision Instrument Factory", Proceedings of the International Conference on Case Histories in Geotechnical Engineering, Rolla, Missouri.

## Stress Field under a Reservoir and Its Induced Earthquake

Tao Zhen-yu

Professor of Rock Mechanics, Wuhan Institute of Hydraulic and Electric Engineering, Wuhan, China

Tang Fang-fu

Engineer, Wuhan Institute of Hydraulic and Electric Engineering, Wuhan, China

**SYNOPSIS:** This paper provides a conceptual model for the study of water-induced earthquake, from which a coupled analysis program of two-dimensional elasto-plastic media has been made. It analyzes the characteristics of the change of stress field and infiltration field under reservoir and studies the relationship between these characteristics and those of water-induced earthquake. At last, it gives out prediction results to a water-induced

### INTRODUCTION

Whether the water-induced earthquake takes place is mainly connected with the four factors of tectonics, rock properties, condition of geostress and the reservoir etc. That water induces the change of stress field, and then the breaking of rockmass and the sending out of energy is the mechanical explanation of water-induced earthquake. For the change of stress field of rockmass under reservoir, some scholars such as Gough (1969), Gough et al (1970) and Withers et al (1978) have done stimulating calculations in their own consideration. Each of them argues with the importance of water in water-induced earthquake. But all of them do not take into the main aspects connected with water-induced earthquake. However, Tao et al (1987) have made up for this shortcoming and have done some coupled analysis to this problem.

The final purpose of the studies to water-induced earthquake is to know whether a reservoir will induce earthquake or not, if it will, how about the three principal factors (time, position and earthquake magnitude), so as to provide data for dam design. General engineering geology method can not reach the quota accuracy, and only after the dam has been built, can the induced earthquake wave be got, so we try to use the conception of coupled analysis to set up a new conceptual model, calculating the stress field under reservoir and predicting the three prin-

cipal factors of water-induced earthquake.

### THE PRINCIPAL ASSUMPTIONS OF THE CONCEPTUAL MODEL

Water-induced earthquake is in connection with many factors. Different consideration to these factors makes models differ from each other. Almost all models presented are to special reservoirs and do not have widely fitation. Therefore we provide a new conceptual model, the principal assumptions of which are as follows:

- a) Neglecting secondary fracture, only taking into account big fault. The total area considered is divided into several parts, each of which is equal to a homogeneous and identical medium and has different mechanical data and porous ratio. The infiltration property of medium may be identical or unidentical in all directions.
- b) Rockmass are ideal elastic-plastic medium, the yielding function of which abides by Drucker prager rule or Mohr-Coulomb rule.
- c) The rockmass below certain depth under reservoir is unsaturated. The infiltration of underground water is saturated-unsaturated infiltrating fluid.
- d) Taking into account the dynamic and static force produced by infiltrating fluid and the softening effects of saturated rockmass.
- e) Taking into account the coupled actions between rockmass and underground water.
- f) As the depth increasing, the porosity of ro-



rockmass reduces down and the temperature rises up, so the porous pressure factor  $\gamma$  becomes lower and lower. Assume that  $\gamma$  is a linear function of depth  $h$ .

g) With the depth increasing, the infiltrating ability of rockmass becomes lower, which can be neglected below certain depth.

## SEVERAL PROBLEMS IN COUPLED ANALYSIS

### 1. The action of stress to fluid

The pumping test which has been done in fissured layer at different depth reveals that the formula

$$K = K_0 \exp(-\alpha \sigma_e) \quad (1)$$

$$\sigma_e = \gamma_t h - p \quad (2)$$

can express the change of infiltrating coefficient. In the formula:

$K_0$ : the infiltrating coefficient of top layer

$\gamma_t$ : the specific gravity of rockmass;

$h$ : the thickness of top layer;

$p$ : the compression force of water;

$\alpha$ : a coefficient

If layer contain no water, then:

$$K = K_0 \exp(-\alpha \gamma_t h) \quad (3)$$

When tectonic stress is considered, formula (3) can be revised as:

$$K = K_0 \beta(h, \sigma_x) \exp(-\alpha \gamma_t h) \quad (4)$$

$\beta(h, \sigma_x)$ : affecting coefficient of horizontal tectonic stress  $\sigma_x$ .

Therefore, the initial infiltrating coefficient  $K_{h0}$  at any depth can be given.  $K_{h0}$  has already take into account the influence of natural stress field. When the actions of water is considered, the stress field of rockmass will change, which will make the infiltrating coefficient change. But this change is too small to be neglected. However, if an element of rockmass breaks, the change of infiltrating coefficient of it has to be considered. We revise it as follows:

1) Broken by tension in one direction. Assume that  $\varphi$  is the angle between the direction of principal stress and X-axis, then:

$$K\varphi = K_{h0} \quad (5)$$

$$K\varphi + 90^\circ = K_{h0}\varphi + 90^\circ \quad (6)$$

2) Broken by tension in two directions:

$$K\varphi = \xi K_{h0}\varphi \quad (7)$$

$$K\varphi + 90^\circ = \xi K_{h0}\varphi + 90^\circ \quad (8)$$

3) Broken by yielding

$$K\varphi = K_{h0}\varphi \exp(-\alpha \sigma_1) \quad (9)$$

$$K\varphi + 90^\circ = K_{h0}\varphi + 90^\circ \exp(-\alpha \sigma_2) \quad (10)$$

The value of  $\xi$  may be gained through experiments.  $\alpha$  is a coefficient, the value of which may be a small number that get the infiltrating coefficient of that element approach to that of zones of fault.

### 2. The influence of fluid to stress field

The fluid in continuous media has force acting on media, the magnitude of which is:

$$F = -\text{grad} p \quad (11)$$

$$p = \gamma_w (\varphi - y) \quad (12)$$

$$\text{That is, } F = -\gamma_w \text{grad } \varphi + \gamma_w \text{grad } y \quad (13)$$

$A = \gamma_w \text{grad } y$  is static pressure, the effect of which is considered by means of effective stress.

$S = -\gamma_w \text{grad } \varphi = \gamma_w J$  is the dynamic force of water which is considered as external force at calculation.

3. The softening effects of saturated rockmass Using saturated-unsaturated infiltration method, we may affirm the forward surface of underground water at any time. Because the rockmass above the forward surface is saturated, the softening is considered in this area (P.A. Witherspoon et al, 1977). Assume the initial parameter matrix of rockmass as follows:

$$AMT(I, 8) = \begin{bmatrix} E_1 & \mu_1 & C_1 & \gamma_1 & C_1^f & \gamma_1^f & \gamma_1 & \sigma_{t1} \\ \vdots & \vdots & \vdots & \vdots & \vdots & \vdots & \vdots & \vdots \\ E_I & \mu_I & C_I & \gamma_I & C_I^f & \gamma_I^f & \gamma_I & \sigma_{tI} \end{bmatrix} \quad (14)$$

The softening matrix is as follows:

ckmass reduces down and the temperature rises up, so the porous pressure factor  $\gamma$  becomes lower and lower. Assume that  $\gamma$  is a linear function of depth  $h$ .

g) With the depth increasing, the infiltrating ability of rockmass becomes lower, which can be neglected below certain depth.

#### SEVERAL PROBLEMS IN COUPLED ANALYSIS

##### 1. The action of stress to fluid

The pumping test which has been done in fissured layer at different depth reveals that the formula

$$K = K_0 \exp(-\alpha \sigma_e) \quad (1)$$

$$\sigma_e = \gamma_t h - p \quad (2)$$

can express the change of infiltrating coefficient. In the formula:

$K_0$ : the infiltrating coefficient of top layer

$\gamma_t$ : the specific gravity of rockmass;

$h$ : the thickness of top layer;

$p$ : the compression force of water;

$\alpha$ : a coefficient

If layer contain no water, then:

$$K = K_0 \exp(-\alpha \gamma_t h) \quad (3)$$

When tectonic stress is considered, formula (3) can be revised as:

$$K = K_0 \beta(h, \sigma_x) \exp(-\alpha \gamma_t h) \quad (4)$$

$\beta(h, \sigma_x)$ : affecting coefficient of horizontal tectonic stress  $\sigma_x$ .

Therefore, the initial infiltrating coefficient  $K_{h0}$  at any depth can be given.  $K_{h0}$  has already take into account the influence of natural stress field. When the actions of water is considered, the stress field of rockmass will change, which will make the infiltrating coefficient change. But this change is too small to be neglected. However, if an element of rockmass breaks, the change of infiltrating coefficient of it has to be considered. We revise it as follows:

1) Broken by tension in one direction. Assume that  $\varphi$  is the angle between the direction of principal stress and X-axis, then:

$$K \varphi = K_{h0} \quad (5)$$

$$K \varphi + 90^\circ = K_{h0} \varphi + 90^\circ \quad (6)$$

2) Broken by tension in two directions:

$$K \varphi = \xi K_{h0} \varphi \quad (7)$$

$$K \varphi + 90^\circ = \xi K_{h0} \varphi + 90^\circ \quad (8)$$

3) Broken by yielding

$$K \varphi = K_{h0} \varphi \exp(-\alpha \sigma_1) \quad (9)$$

$$K \varphi + 90^\circ = K_{h0} \varphi + 90^\circ \exp(-\alpha \sigma_2) \quad (10)$$

The value of  $\xi$  may be gained through experiments.  $\alpha$  is a coefficient, the value of which may be a small number that get the infiltrating coefficient of that element approach to that of zones of fault.

##### 2. The influence of fluid to stress field

The fluid in continuous media has force acting on media, the magnitude of which is:

$$F = -\text{grad} p \quad (11)$$

$$p = \gamma_w (\varphi - y) \quad (12)$$

$$\text{That is, } F = -\gamma_w \text{grad } \varphi + \gamma_w \text{grad} y \quad (13)$$

$A = \gamma_w \text{grad} y$  is static pressure, the effect of which is considered by means of effective stress.

$S = -\gamma_w \text{grad } \varphi = \gamma_w J$  is the dynamic force of water which is considered as external force at calculation.

3. The softening effects of saturated rockmass Using saturated-unsaturated infiltration method, we may affirm the forward surface of underground water at any time. Because the rockmass above the forward surface is saturated, the softening is considered in this area (P.A. Witherspoon et al, 1977). Assume the initial parameter matrix of rockmass as follows:

$$\text{AMT}(I, 8) = \begin{bmatrix} E_1 & \mu_1 & C_1 & \gamma_1 & C_1^f & \gamma_1^f & \gamma_1 & \sigma_{t1} \\ \vdots & \vdots & \vdots & \vdots & \vdots & \vdots & \vdots & \vdots \\ E_I & \mu_I & C_I & \gamma_I & C_I^f & \gamma_I^f & \gamma_I & \sigma_{tI} \end{bmatrix} \quad (14)$$

The softening matrix is as follows:

When the forward surface reaches the depth of 6000 metres in 623<sup>th</sup> day, several rockmass elements in zone of fault begins to break, which sends out the energy of  $0.3186 \times 10^8$  t.m that equals to the earthquake magnitude of 4.1; With the underground water infiltrating furtherly, great readjustation of stress field takes place and the energy of  $0.6109 \times 10^8$  t.m. will be send out, which is equivalent to the earthquake magnitude of 4.2; When the forward surface reaches the depth of 9600 meters, the minor mainearthquake takes place., which sends out the energy of  $2.0868 \times 10^8$  t.m that is equicalent to the earthquake magnitude of 5; From this time, the stress field and infiltration field readjusts continuously and small earthquakes takes place frequently; The mainearthquake will take place in about 1300<sup>th</sup> day, the magnitude of which is 5.1. Fig.1 express the relationship between the energy and the time, the controlling point of which means the total energy sent out by all broken element in a period of time. Fig.2 shows the relationship between the earthquake magnitude and the time, which is corresponding to Fig.1. Because of the disconcentration of broken elements, the line connected through the controlling points may be regard as the maximum value line of earthquake sequence the energy sent out in any time will not surpass.

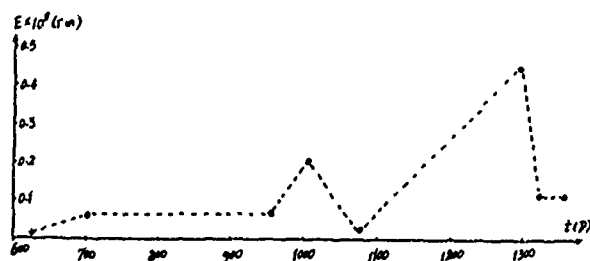


Fig.1 Energy-Time Relationship

From the change process of stress field and infiltration fluid field. We discover that water-induced earthquake is generally of the characteristics as follows: water-induced earthquake generally belongs to the type of preearthquake-mainearthquake-aftershock or earthquake clusters.



Fig.2 Earthquake Magnitude-Time Relationship

If the static water load can induce earthquake, the type of it will belong to that of mainearthquake-aftershock. In the long run, it will not belong to the type of isolated-earthquake. The broken rockmass elements appear firstly in the zone of fault and the area where rockmass property changes. The complication of the distribution of zone of fault and the constitution of the types of rockmass and the readjustation of coupled stress field have the earthquake epicentre of it be of the characteristics of disconcentration and jumpton.

#### CONCLUSION

The coupled action of rockmass and underground water reflects the mechanism of water-induced earthquake. Whether a reservoir induces earthquake or not is determined by the contradiction between the stress field and the strength of rockmass. The results from the analysis to infiltration fluid field principally reflects the general characteristics of water-induced earthquake, which shows the fitation of the conceptual model. The reliability of prediction results depends directly on the parameters used. Some of the parameters we used are obtained from experiments, but the others are obtained from comparison, so, the prediction results should be regard as reference.

#### REFERENCE

- Gough, D.I. (1969), "Incremental Stress under a Two-dimensional Artificial Lake", *Can.J. Sci.*, 6: 1067-1075 Earth

- Gough, D.I. and Gough, W.I. (1970) "Stress and Deflection in the Lithosphere near Lake Kariba", 1, Geophys.J.21:65-78.
- Withers, R.J. and Nyland, E. (1978), "Time Evaluation of Stress under an Artificial Lake and its Implication for Induced Seismicity," Can. J. Earth Sci, 15, No.9.
- Tao Zhen-yu and Shen Xiao-ying, (1987), "The Analysis of Coupled Stress of Reservoir-Induced Earthquake", Proc. of Intern. Symposium on Engineering Geological Environment in Mountainous Areas", Beijing, CHINA.
- Witherspoon, P.A. and Gale, J.E. (1977), Mechanical and Hydraulic Properties of Rocks Related to Induced Seismicity", Engineering Geology, 11, No.1, 23-25

# On Properties of Damping of Bases

Wang Xikang

Senior Engineer, Central Research Inst. of Building & Construction,  
Ministry of Metallurgical Ind., Beijing, China

**SYNOPSIS:** On the basis of many tests it has been proved that the damping properties of bases not only have bearing on magnitude of base area of foundation but also on weight of foundation and on mechanics model adopted. This paper puts forward the computation formulas of damping parameters to some soils.

## INTRODUCTION

In order to compute the vibration response of structures and foundations under machinery with satisfactory precision it is necessary to establish the damping properties of bases correctly. In recent years the problem above mentioned has been researched by the author and his colleagues under the conditions of field tests employing vertical forced vibration with smaller amplitude which were performed on foundation of different sizes and different soil conditions. When researching the damping properties of bases a new concept is cited, whereby the mass participating in foundation vibration includes not only mass of foundation but also soil mass. In consequence of considering the soil mass not only the damping parameters established agree with practice to a greater extent but also the precision of computation of vibration response acquires great improvement. In the following several main results of research are introduced in detail.

## 1. MECHANICS MODEL AND THEORETICAL FORMULAS FOR DAMPING COMPUTATION

Before researching the damping properties of bases the mechanics model of foundation vibration must be first developed because using the different mechanics model will obtain different dynamic parameters. When analysing the damping properties of bases, the model of Mass-Damping-Spring of linearity is adopted as shown in Fig.1 and the following assumptions are employed:

- 1) Base soils possess not only elasticity but also inertia effect.
- 2) The soil mass participating in vibration and vertical damping coefficient as well as vertical dynamic rigidity of bases are not varied within the range of exciting frequencies.

Because three dynamic parameters which are

dynamic rigidity, damping coefficient and soil mass must be determined the model may be referred to as three parameter model. The reasonableness of adopting three parameter model had been discussed in detail in the paper 2 and is not discussed herein.

Under the harmonic vertical exciting force with constant amplitude as shown in Fig.1 the equation of motion of foundation may be written as follows:

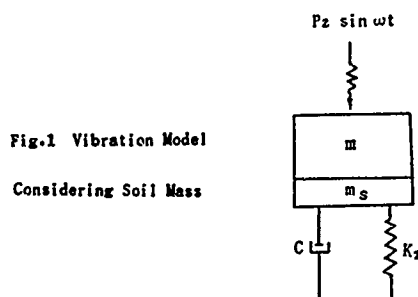


Fig.1 Vibration Model  
Considering Soil Mass

$$(m+m_s)\ddot{Z} + C\dot{Z} + K_z Z = P_z \sin \omega t \quad (1)$$

where:  $m$  and  $m_s$  = Mass of foundation and soil

$P_z$  and  $\omega$  = Maximum value and frequency of exciting force

$C$  = Vertical damping coefficient

$K_z$  = Dynamic rigidity of base

$Z$  = Vertical displacement of foundation

Limiting our discussion to forced vibration merely, we take the solution of the question in the form:

$$Z = A_z \sin(\omega t - \theta) \quad (2)$$

where:  $A_z$  = Amplitude of vibration

$\theta$  = Phase shift

In order to obtain three dynamic parameters we

may substitute the equation 2 into equation 1, and use three known conditions which are resonance frequency, resonance amplitude and amplitude of vibration or phase shift corresponding to a certain exciting frequency. In this paper the first three conditions are employed. When using the three conditions, we may obtain the computing formula for damping ratio  $D_z$  of bases as follows:

$$D_z = 0.707 \sqrt{1 - \sqrt{1 - d}} \quad (3)$$

where:

$$d = \frac{(1 - \alpha)^2}{\alpha^2 + \beta^2 - 2\alpha} \quad (4)$$

$$\alpha = \frac{\omega^2}{\bar{\lambda}_{zs}^2} \quad (5)$$

$$\beta = \frac{A_{z, \max}}{A_z} \quad (6)$$

$A_{z, \max}$  = Resonance amplitude

$A_z$  = Amplitude corresponding to a certain frequency

$\bar{\lambda}_{zs}$  = Resonance frequency

If the maximum value of exciting force is varied with exciting frequency, that is  $P_z = m_0 r \omega^2 \sin \omega t$  (where  $m_0$  is eccentric mass,  $r$  is eccentricity), then the damping ratio of base is determined as follows:

$$D_z = 0.707 \sqrt{1 - \sqrt{1 - \bar{d}}} \quad (7)$$

where:

$$\bar{d} = \frac{(1 - \alpha)^2}{\alpha^2 + \beta^2 - 2\alpha + 1} \quad (8)$$

It should be pointed out that the dynamic rigidity of base and soil mass participating in vibration can be immediately determined after obtaining the damping ratio [2].

In consideration of requirement of following discussion, the computation formula of damping ratio without considering the soil mass is written as follows [3]:

$$D_z = \frac{1 - \sqrt{1 - \xi_z}}{2} \quad (9)$$

where:

$$\xi_z = \frac{1}{1 + \beta z^2} \quad (10)$$

$$\beta_z = \frac{A_{z, \max}}{P_z} - m \bar{\lambda}_{zs}^2 \quad (11)$$

It should be pointed out that the formula 9 is derived according to following two conditions which are resonance amplitude and resonance frequency acquired. According to the above computation formulas of damping ratio the author analysed over 40 test data and obtained a several important phenomena as follows.

## 2. THE LAW OF DAMPING OF VIBRATION OF BASE

1) The obtained damping ratio according to three parameter model is significantly smaller than that according to two parameter model. To explain this point 8 analysed results are cited among many results. They are listed in Table I.

TABLE I, the Effect of Soil Mass Considered on Damping Ratio

| Number of Foundations | Ignoring Soil Mass |       | Considering Soil Mass  |       |
|-----------------------|--------------------|-------|------------------------|-------|
|                       | m (t)              | $D_z$ | m + m <sub>s</sub> (t) | $D_z$ |
| 1                     | 20.1               | 0.162 | 26.3                   | 0.122 |
| 2                     | 16.6               | 0.291 | 45.4                   | 0.119 |
| 3                     | 41.4               | 0.243 | 72.6                   | 0.417 |
| 4                     | 44.9               | 0.217 | 69.4                   | 0.145 |
| 5                     | 22.1               | 0.125 | 35.5                   | 0.079 |
| 6                     | 8.3                | 0.123 | 16.1                   | 0.065 |
| 7                     | 24.8               | 0.172 | 31.2                   | 0.137 |
| 8                     | 9.4                | 0.169 | 22.0                   | 0.074 |

It is clearly seen from the Table that the damping ratio taking into account the soil mass is 30 - 60% smaller than that without considering the soil mass. It is because the dynamic rigidity of bases having considered the soil mass has been markedly increased. Dynamic rigidity and soil mass participating in vibration are discussed in detail [2]. It should be pointed out that when computing these dynamic parameters it is necessary to use the frequencies beyond the range from 0.8 to 1.2. Because within this range the accuracy of amplitude of vibration obtained corresponding to a certain frequency is over-sensitive to dynamic parameters.

2) The vertical damping coefficient of bases is apparently related to the weight of foundation and the weight acting on the foundation. The important phenomena had been neglected in the past, e.g. the literature [4] showed that the damping coefficient of bases is related to rigidity of bases only and has nothing to do with the weight of foundation. Furthermore, the literature 4 gave the damping constants under different bases. Several American experts have not paid sufficient attention to the effect of foundation weight on damping coefficient as well. For simplification the experts F.E. Richart, Jr., and R.V. Whitman put forward the following equation of motion 12 to replace elastic semi-infinite body theory [5]:

$$m\ddot{z} + \frac{3.4}{1-\mu} r_0^2 \sqrt{G\rho} \dot{z} + \frac{4G\rho_0}{1-\mu} z = P_z \sin \omega t \quad (12)$$

where: m = Mass of foundation

$\mu$  = Poisson's ratio

$\rho$  = Density of soil

G = Elastic shear modulus of soil

$r_0$  = Equivalent radius,  $r_0 = (F/\pi)^{0.5}$

F = Base area of foundation

From expression 12 we obtain the damping coefficient C and damping ratio  $D_z$  as follows:

$$C = \frac{3.4}{1-\mu} r_0^2 \sqrt{G\rho} \quad (13)$$

$$D_z = \frac{C}{\bar{C}_c} = \frac{0.85}{(1-\mu)^{0.5}} \frac{1}{\sqrt{b_0}} \quad (14)$$

where  $b_0 = m/\rho r_0^3$  and  $\rho$  is the density of soil.

In this paper parameter b is used. The b is equal to  $0.18b_0$ .

It is seen from expressions 13 and 14 that the damping parameters have no bearing on weight of foundation. But lots of tests demonstrate that the damping of base is apparently related to the weight of foundation acting on the soil. The greater weight the greater damping of base. For instance, under the same base area of  $16\text{m}^2$  the damping coefficients increase from 2767 to 5136 kN.S/m corresponding to increase of foundation weight from 520 to 1000 kN. It may be seen from Table II.

TABLE II. Relationship between Damping Coefficient and Foundation Weight

| Foundation Weight (kN) | Base Area of Foundation ( $\text{m}^2$ ) | Damping Ratio (kN.s/m) |
|------------------------|--|------------------------|
| 130                    | 4.0                                      | 1213                   |
| 226                    |  | 1772                   |
| 322                    |  | 1700                   |
| 418                    |  | 1777                   |
| 292                    | 9.0                                      | 2038                   |
| 485                    |  | 2729                   |
| 677                    |  | 3206                   |

Of course, it is no doubt that the damping coefficients depend on the magnitude of base area of foundation, which agrees to basically theoretical results. It is shown in Table III. clearly.

3) The damping coefficients determined by three parameter model are much smaller than those by the expression 12 which corresponds to the elastic semi-infinite body theory under certain assumption as shown in Table II. Because the damping values determined by semi-infinite body theory are too large, the computing results of amplitude of vibration often do not coincide with the fact. This conclusion has been well proved by many researchers.

TABLE III. the Coefficient C Established by Two Mechanics Model

| Soil        | Equivalent Radius $r_0$ (m) | Damping coefficient of Base |                    |
|-------------|-----------------------------|-----------------------------|--------------------|
|             |                             | from three parameter Method | from Expression 13 |
| Grave-sand  | 0.902                       | 797                         | 1610               |
|             | 1.467                       | 2006                        | 4264               |
| Medium sand | 0.902                       | 562                         | 961                |
|             | 1.130                       | 1213                        | 1703               |
|             | 1.690                       | 2038                        | 3843               |
|             | 2.260                       | 5136                        | 6832               |

4) The damping ratio depends on the embedded depth  $h_m$  of foundation. The Larger the embedded depth the greater the damping ratio. This conclusion is drawn not only by the author but also by other experts. But the relationship of magnitude of  $D_z$  to embedded depth  $h_m$  has not

been established yet. The relationship of magnitude between  $D_z$  and  $h_m$  is shown in Fig.2 and expression 17. To clarify the effect of embedded depth of foundation on damping ratio 16 test foundations were built on clay loam and slight clay loam by the author and his colleagues.

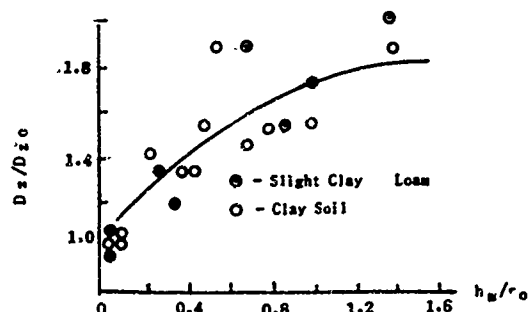


Fig.2 The Relationship between Relative Damping Ratio and Embedded Ratio of Foundation

In Fig.2 the parameters  $D_z$  and  $D_{z0}$  represent damping ratio corresponding to embedded depths  $h_m$  and zero respectively.

5) The tests reveal that the variation law of damping ratio  $D_z$  established by expression 12 with parameter  $b$  is markedly different from test results. Deviation of theory from practice is described in Fig.3. It should be noted that all these test results shown in Fig.3 were obtained under the condition of loessial clay loam with  $\mu = 0.33$ . In the figure the parameter  $b$  is equal to  $w/\gamma F 1.5$ , where  $W$  is weight of foundation,  $\gamma$  unit weight of base soil and  $F$  base area of foundation. Fig.3 shows that the damping ratio determined by expression 14 is not only too large but also its variation with  $b$  is oversharpe. From this we should understand that it is not suitable to use the mechanics model of homogeneous isotropic elastic semi-infinite body instead of practical nonhomogeneous isotropic body.

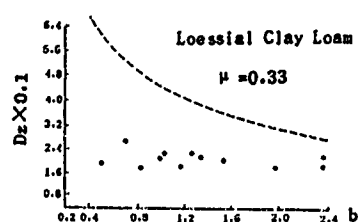


Fig.3 The Comparison of Theory with Test Results Under Different Value  $b$

### 3 EMPIRICAL FORMULAS OF COMPUTING DAMPING RATIO

All tests presented above demonstrate that the variation of damping ratio is very complicated because the parameter is strongly influenced by many factors such as the influences of stratification of base, level of ground water and so on. But on the basis of these tests it is possible to put forward an approximate computing formula under the condition of small strain according to three parameter model.

## 1) Exposed Foundation

The author altogether analysed 38 test data under various bases with Poisson's ratio ranging from 0.32 to 0.4 and shear modulus of elasticity from 39.2 Mpa to 176.4 Mpa. All of the test results are described in Fig.4.

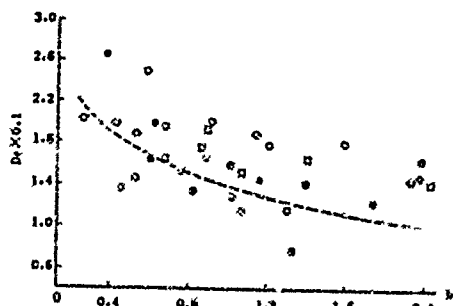


Fig.4 The Relationship between Damping Ratio and Value b under Different Soils

- Clay Soil
- Gravel Sand
- Clay Loam
- Medium Sand
- Loessial Clay Loam
- Residual Soil

According to these test data the damping ratio may be computed by the following formula:

$$D_{z0} = 0.16 / \sqrt{0.3 + b} \quad (15)$$

The formula 15 is basically suitable for these soils described in Fig.4. As for slight clay loam the damping is markedly smaller as compared with other soils as shown in Fig.5. The damping ratio may be approximately determined by expression 16

$$D_{z0} = \frac{0.11}{\sqrt{0.3 + b}} \quad (16)$$

It should be pointed out that the dashed line in Fig.4 represent computing results according to formula 15.

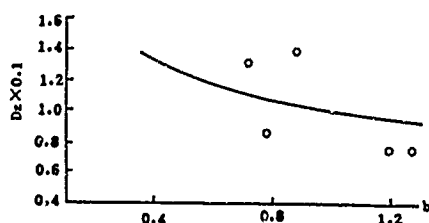


Fig.5 The Relationship between Slight Clay Loam and Value b

## 2) Embedded Foundations

Almost all of machine foundations and structures are embedded, hence the study of variation law of damping under this kind of condition has more practical meaning. The relative damping ratio for the soils described in Fig.2 may be written as follows:

$$\frac{D_z}{D_{z0}} = 1 + 0.7 \sqrt{hm/r_0} \quad (17)$$

The results of computation of the formula has

been represented by solid line in Fig.2.

## CONCLUSIONS

Through the analysis above a several major conclusions can be drawn as follows:

1) The magnitude of damping coefficient is related to mechanics model adopted. The value using three parameter model is smaller than that using two parameter model or semi-infinite body model.

2) The damping coefficient of bases is markedly related to the weight of foundation acting on base.

3) The magnitude and variation law of damping established by semi-infinite body theory deviates markedly from the test results.

4) In order to improve the properties of damping of vibration system it is an ideal way to use hollow deep foundations.

## REFERENCE

- R.V. Whitman and F.E. Richart, Design Procedures for Dynamically Loaded Foundations, Journal of the Soil Mechanics and Foundations Division, 1967, 11.
- Wang Xiang, Selected Works of Geotechnical Engineering, Special volume in Commemoration of the Golden Jubilee of ISSMFE, Chinese Society for Soil Mechanics and Foundation Engineering, 1985.
- Wang Xikang, On Analysis of Vibration of Embedded Footings Research Report 7925, Central Research Inst, of Building and Construction of Metallurgical Ind, 1979.
- O.A. Savinof, Foundations under Machinery (in Russian), 1955.
- F.E. Richart and R.V. Whitman, Comparison of Footing Vibration Tests with Theory, Journal of Soil Mechanics and Foundations Division, 1967, 11.



# On Propagation of Elastic Surface Wave in Soils

**Wang Xikang**

Senior Engineer, Central Research Inst. of Building & Construction of MMI, China

**Duan Shiwei**

Engineer, Central Research Inst. of Building & Construction of MMI, China

**Yang Xianjinan**

Senior Engineer, The Fourth Design Institute of Machinery Ministry, China

**SYNOPSIS:** It has been proved that the propagation law of elastic surface wave emanating from machinery foundations has bearing not only on distances from vibration source but also on frequencies and depth of vibration source and external pressure acting on soil surface of wave receivers. Based on plenty of tests the calculation formulas for elastic surface wave are put forward and the computation precision of which is satisfactory.

## INTRODUCTION

At present many researchers attach importance to the investigation of propagation law of elastic surface wave in soil because it has great significance to reasonably taking the area of factory zone, saving agriculture fields and arranging the precise instruments and devices. Especially, the environment request to persons is becoming more and more strict, which makes researchers pay more attention to the investigation of this discipline.

In the process of research of this discipline, the authors mainly adopted test method. It is because most of theoretical research is developed on the basis of the theory of elastic semi-infinite body, which does not coincide with fact because the bases are always formed of some strata of soils and the elastic properties of which, sometimes, are far from each other. Owing to the elastic constants of soils are related not only to normal stress acting on soil but also to initial stress existing in soil particles and other factors, then the relationship between stress and strain in soil disagrees with Hooke's law. All of these cases makes the propagation theory of elastic wave in soil based on elastic theory do not very well agree with practice [1]. Due to this case the authors try to put forward semi-empirical formula for computing the propagation law of elastic surface wave in soils by a number of tests. Therefore, on the ground of work carried out in the past the authors measured again lots of propagation law of elastic wave in recent years. The tested foundations involve in some special model foundations and actual machine foundations in operation. All tests are performed under the condition of stable exciting forces with frequencies changing from 5 to 400 Hz. The amplitudes of model foundations do not exceed 200  $\mu\text{m}$  and of actual machine foundations change from 300 to 600  $\mu\text{m}$ .

In order to make readers further understand the general cases tested the soil conditions and

sizes of these model foundations are listed in Table I.

**TAB. I.** The Magnitude of Foundations and Their Soil Conditions

| Sizes of Model Foundations (m) | Soil Conditions    |
|--------------------------------|--------------------|
| 3.5*3.5*1.5                    | Slight Clay Loam   |
| 2.0*3.0*1.5                    | Slight Clay Loam   |
| 1.6*1.6*2.2                    | Hard Clay Soil     |
| 1.6*1.6*0.7                    | Hard Clay Soil     |
| 1.0                            | Clay Soil          |
| 0.11                           | Loessial Clay Loam |

The actual foundations measured involve in five hammer foundations with weight of falling part 3 tons, two hammer foundations with weight of falling part 5 tons, four hammer foundations with 10 tons, 16 tons and two 1 ton and some foundations under compressors. These foundations are built on clay soil, clay loam, loessial clay loam, rock base and piles.

In the whole analysis, the authors employed the measured results performed in sixty times done by themself and lots of measured results done by some home and abroad experts. All together 149 measured curves of attenuation of amplitudes of vibration by forming of 1500 data are analysed in detail. From this the calculation formula of propagation of elastic surface wave in soils are put forward. The formula that shall be discussed in the following possesses following four main characteristics as comparison with the calculation formulas published at home and abroad:

- 1) The effect of frequencies is considered.
- 2) The effect of embedded depth of vibration sources is taken into account.

3) The influence of pressure acting on soil surface is considered.

4) And the effect of different distances is noted.

# I. The Effect of Frequencies of Vibration Sources

To this problem the famous professor B. Gorizin of Russian ever put forward following calculation formula of propagation of elastic surface wave:

$$Ar = Ao(r_o/r)^{0.5} \exp[-\alpha(r-r_o)] \quad (1)$$

Where:  $Ao$  = amplitude at distance  $ro$

$Ar$  = amplitude at distance  $r$

$ro$  = equivalent radius of foundation served as vibration source,

$ro = (F/\pi)^{0.5}$  (m)

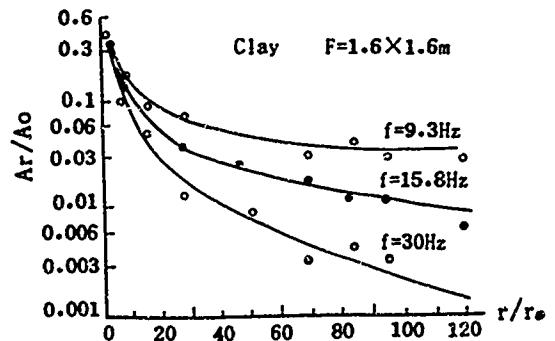
$F$  = base area of foundation ( $m^2$ )

$\alpha$  = coefficient of energy absorption ( $m^{-1}$ )

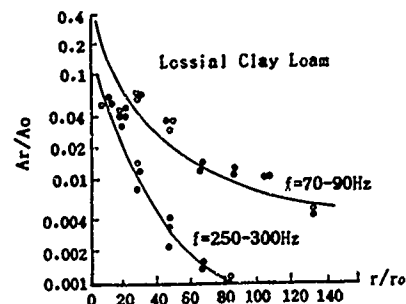
The coefficient  $\alpha$  changes from 0.04 to 0.12  $m^{-1}$  to different soils. So far the formula 1 is widely used in many countries.

It is seen from formula 1 that the propagation law of elastic wave in soils is only related to radius  $r$  and the coefficient of energy absorption, and has no bearing on frequencies of vibration source. It is worthy pointing out that up to now the effect of frequencies on propagation of wave has not been considered in many countries yet. However, it shows from experiments that not to consider the effect of frequencies is unreasonable because the soils are visco-elastic body, the dispersion of vibration energy of which is almost proportional to the vibration frequency. The tests done by the authors fully demonstrate that the propagation law of elastic surface wave has markedly bearing on the frequencies of vibration source. In order to show the phenomena the three typical test curves as shown in Fig. 1 are cited from many curves. It follows from Fig. 1 that the higher the frequencies, the faster the amplitude decreasing with distances. For example, it follows from Fig. 1a that at  $r/ro = 50$  the relative amplitudes of vibration  $Ar/Ao$  equal 0.045, 0.020 and 0.007 corresponding to exciting frequencies 9.3, 15.8 and 32 Hz. In the case of very high frequencies as shown in Fig. 1c the phenomenon is especially obvious. Here, it should be pointed out that the Fig. 1a-1b describe the relationship between exciting frequencies and the vertical components of vibration amplitudes under the vertical vibration source and the Fig. 1c describes the relation between exciting frequencies and horizontal amplitudes of vibration under the action of horizontal vibration source.

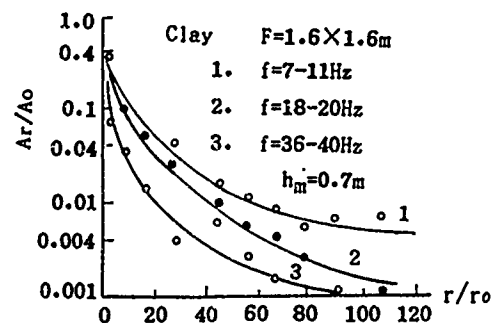
Owing to the influence of frequencies of vibration source is not taken into account by the formula 1, hence the computation results are often far from the measured results.



a) Attenuation of Vertical Wave under Vertical Vibration Source



b) Attenuation Law of High Exciting Frequency



c) Attenuation of Horizontal Wave under Horizontal Vibration Source

Fig.1 Effect of Frequency of Vibration Source on Propagation of Wave

## II. The Effect of Embedded Depth of Foundations on Propagation of Wave

Actual machinery foundations always possess a certain embedded depth. Therefore, researching the effect of embedded depth of foundations on propagation of elastic wave has much more actual meaning. However, the factor has not been taken into account so far. For instance, the design code of machinery foundations (CHM II 19-79) of USSR published in 1979 years put forward following calculation formula for propagation of

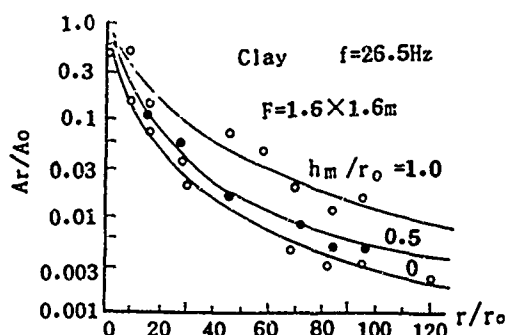
elastic surface wave:

$$A_r = A_0 \left\{ \frac{1}{\delta [1 + (\delta - 1)^2]} + \frac{\delta^2 - 1}{(\delta^2 + 1) \sqrt{3} \delta} \right\} \quad (2)$$

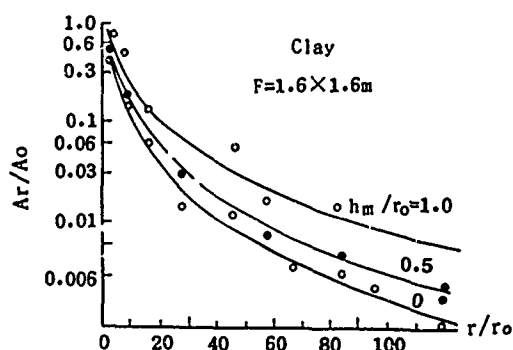
Where:

$$\delta = r/r_0$$

It shows from formula 2 that the attenuation of amplitudes of vibration with distances has only bearing on geometric parameter  $r/r_0$  and no bearing on embedded depth of foundations served as vibration source and other factors. However, the experiments show that the embedded depth of vibration source gives apparent influence to propagation of elastic wave. For instance, the figure 2a shows that at  $r/r_0 = 50$  and when  $h_m = 0, 0.5 r_0$  and  $1.0 r_0$  (  $h_m$  = embedded depth of foundation as vibration source ), then the measured relative amplitudes  $A_r/A_0$  equal 0.01, 0.018 and 0.40 respectively. Since the formula 2 does not consider the effect of embedded depth of vibration source on propagating wave and other factors, and then it makes the computation results do not coincide with measured results as shown in Table II.



a)



b)

Fig.2 Effect of Embedded Depth of Vibration Source on Propagation of Wave

TAB. II. The Comparison of Total Errors % of Amplitudes of Vibration ( According to 1500 test data )

| Calculation formula | For Model Foundations | For Actual Foundation |
|---------------------|-----------------------|-----------------------|
| By Expression 2     | 337                   | 321                   |
| By Code of China    | 65                    | 90                    |
| By Formulas 3 and 4 | 39                    | 41                    |

### III. The Effect of Pressure at Wave Receivers on Propagating Wave

In fact the persons take most care of the propagating law of wave under the action of external pressure at wave receivers because all foundations of structures and precise instruments, Without exception, give the base a certain pressure. Therefore, the research of effect of pressure on propagation law of elastic wave is especially important.

However, so far the effect of external pressure acting on the soil surface of wave receivers is scarcely researched. In order to clarify this problem a number of field tests is carried out by the authors. Experiments indicate that the amplitude under the action of pressure at wave receivers are much less than those of free soil surface as shown in Fig. 3.

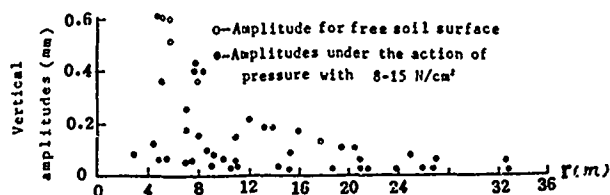


Fig.3 Effect of Pressure Acting on Soil Surface on Propagation of Wave

For example, at  $r=16$  m the amplitude equals 0.07 mm for free soil surface and only equals 0.02 mm for existing of pressure which equals 12 N/cm<sup>2</sup>, while the total acting force corresponding to pressure equals 1080 kN. Meanwhile, it follows from Fig. 3 that the ratio of vibration amplitudes under the action of external pressure to the amplitudes under free soil surface is different. Generally speaking, the shorter the distance from vibration source, the smaller the ratio. However, the ratios are not less than 0.4 within the range tested. The test results as shown in Fig. 3 are obtained under the action of pressure which equals 8-15 N/cm<sup>2</sup>, and which is induced by industrial factory building with one story. In the case of other pressures the ratio of amplitudes of vibration shall generate variation to some extent.

#### IV. The Effect of Different Soils

According to the propagation theory of elastic wave in absolutely isotropic homogeneous elastic body the attenuation law of amplitudes of vibration should be different for soils. In the period of research the authors ever paid attention to the effect of soils on propagating of wave and did to try to consider this factor. However, the practice does not coincide with expectation of authors. For instance, the figure 4 shows that the attenuation law of vibration amplitudes is different only in a

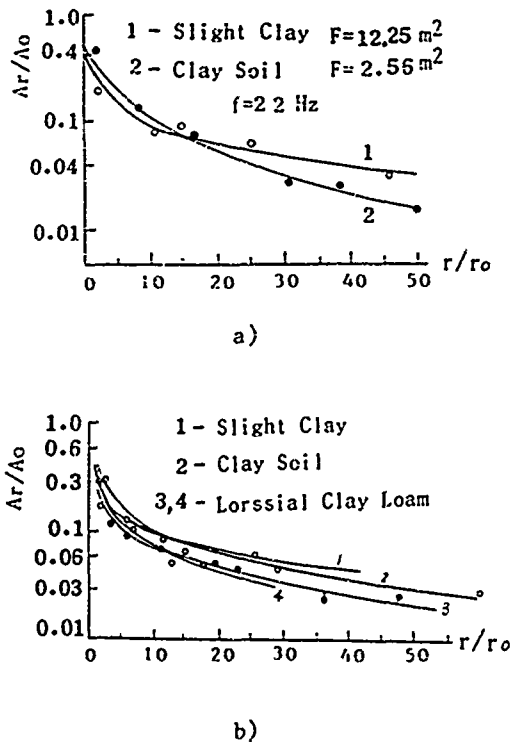


Fig.4 Effect of Different Soils on Propagation of Wave

small degree. Even, the inverse phenomenon is obtained in test results. For example, the attenuation of vibration amplitudes with distances for slight clay loam with smaller bearing capacity 15 N/cm² and smaller elasticity is more slow and moderate as compared with clay soil with larger bearing capacity 25 N/cm² and elasticity. The phenomenon like the kind of example above was ever introduced in literature [1], which points out that the coefficient of energy absorption for gray water-saturated sand with laminae of peat and organic silt equals 0.04 m⁻¹, while the coefficient for yellow water-saturated fine-grained sand with larger elasticity inversely equals 0.1 m⁻¹. On the ground of these cases we hold that the effect of soils on propagating of surface wave may be ignored to a first approximation under the soils tested. In this respect the treatment method of this paper is, in principle, is in agreement with the design code of machinery foundation (CHN II 19-79) of USSR.

#### V. The New Formula for Calculation of Propagation of Elastic Surface Wave

According to the discussion above we have known what factors should be considered. And then how to consider these factors becomes especially important problem. In the process of research the authors did try to adopt uniform computation formula for different distances and analyse five computation formulas. The analysed results show that the total errors on average are not satisfied when using uniform calculation formula. In order to decrease the errors, finally, two expressions are developed for short and long distances. The treatment method like this has theoretical ground. Because it is well known that the action of longitudinal and transverse waves is predominant near the source of vibration and the elastic surface wave is predominant under long distances. In order to establish the point distinguishing short from long distances the great computation work is carried out by virtue of elastic computer. It indicates from analysis that the distinguishing point should be adopted to equal 8 r₀. When r < 8 r₀, then the computation formula for short distance should be used, otherwise the formula for long distance should be used. Through the detail analysis the final calculation formulas of propagation of elastic surface wave may be written as follows:

for  $r < 8 r_0$

$$A_r = \xi A_0 \frac{r_0}{r} \frac{e^{-\alpha_1 f (r-r_0)}}{1 + \beta (1 - r_0/r)} \quad (3)$$

for  $r > 8 r_0$

$$A_r = \frac{2.83 \xi A_0}{8 + 7 \beta} e^{-7 \alpha_1 f r_0} \sqrt{\frac{r_0}{r}} e^{-\alpha_2 f (r-8 r_0)} \quad (4)$$

Where:  $\xi$  = correction coefficient of pressure acting, which may be adopted to equal 0.4

$f$  = frequencies of vibration source (Hz)

$\beta$  = coefficient of embedded depth of vibration source:

$$\beta = \frac{1}{2.0 + 0.5 h_m / r_0} \quad (5)$$

$h_m$  = embedded depth of foundation served as a source of wave (m)

$\alpha_1$  = attenuation coefficient of short distance, which may be adopted to equal 0.001 for soils studied

$\alpha_2$  = attenuation coefficient of long distance:

$$\alpha_2 = \frac{1}{600 + 4 r / r_0} \quad (6)$$

It should be indicated that the parameters in the coefficients  $\alpha_1$ ,  $\alpha_2$  and  $\beta$ , such as 0.001, 2.0, 0.5, 600 and 4, are obtained by virtue of analysis of elastic computer. In order to compare the errors computed by formulas 3 and 4, by formula 2 and by the design code of machinery foundations (GBJ 40-79) of china, a great computing is carried out. The precision of computation is determined by the errors as follows:

$$\varepsilon = \frac{1}{N} \sum_{i=1}^N \left| \left( 1 - \frac{A_{c,i}}{A_{m,i}} \right) \right| \cdot 100 \quad (7)$$

where:  $\varepsilon$  = total error on average

$N$  = total number of measured points

$A_{c,i}$  = computation amplitude of point  $i$

$A_{m,i}$  = measured amplitude of point  $i$

On the basis of analysis to 1500 data the total errors computed by three formulas are obtained as listed in Table II. It follows from Table II that the computation precision of formulas 3 and 4 is much better than those computed by formula 2 and by design code of China.

Finally, it should be pointed out again that the computation formulas 3 and 4 are put forward under these soils as mentioned above. In order to fully understand the reasonableness of formulas put forward by the authors the comparison of computation precision for other soils is performed and may be seen from Table III.

TAB. III. Comparison of Errors Computed by Three Formulas with Measured Results for Weak Soil, Rock Base And Pile Foundations

| Vibration Sources and Conditions | by Formula 2 | by Code of China | by Expression 3 and 4 |
|----------------------------------|--------------|------------------|-----------------------|
| 1                                | 67.7         | 32.2             | 30.3                  |
| 2                                | 81.5         | 61.4             | 31.2                  |
| 3                                | 65.5         | 45.9             | 17.9                  |
| 4                                | 123.0        | 70.0             | 51.0                  |
| 5                                | 545.0        | 67.0             | 49.0                  |
| 6                                | 622.0        | 65.0             | 56.0                  |

note: 1 includes following cases: hammer foundation with weight 5 tons, clay loam with silt, pile foundation and 9 points measured. 2: hammer with 2 tons, clay loam with silt, pile foundation and 7 points. 3: hammer with 3 tons, fine-grained base, pile foundation and 4 points. 4: hammer with 3 tons, silt base, pile foundation and 9 points, 5: hammer with 0.75 tons, rock base and 9 points. 6: hammer with 5 tons,

rock base and 6 points measured. It follows from Table III that the calculation precision computed by formulas 3 and 4 is also better than those computed by other formulas of computation.

## Conclusions

Through the detail analysis above some principal conclusions can be drawn as follows:

1) The propagation law of elastic surface wave emanating from machinery foundations is related not only to distances from vibration sources but also very markedly to frequency and embedded depth of vibration source and the magnitude of pressure acting on soil surface at wave receivers.

2) The computation precision of attenuation formulas for amplitudes of vibration put forward by the authors is much better than others above mentioned.

## References

- [1] D. D. Barkan, "Dynamics of Bases and Foundation", 1962
- [2] Wang Xikang, Liu Yaofu, "Some Problems in Design of Hammer Foundations", Selected Works of the First Conference on Soil Mechanics and Foundation Engineering, China Civil Engineering Society, 1964

# Influence of Pile Driving on Characteristics of Liquefiable Soils

Qiao Taiping

Deputy Chief Engineer, Basic Construction Office of CCP Shanxi Province, Taiyuan, China

Liu Huishan

Senior Engineer, Central Research Institute of Building and Construction, MMI, Beijing, China

**SYNOPSIS:** This paper offers a case of pile foundation supporting a 18-storied building rested on liquefiable sandy layers. The soil densities and the bearing capacities of piles both increased after pile driving. It is suggested that the influence of densification caused by pile driving should be considered in the case of dense spacing and large amount of piles. The formulas for sand piles are suggested for primary estimation of densification effect of pile driving.

## INTRODUCTION

The design method of pile foundation in liquefiable subsoils is still somewhat unclear. The key problem is that there is a lack of informations on practical engineering experiences accumulated in passed earthquakes. Authors had informed some experiences in this field got from Tangshan earthquake (1976), indicating that the most of pile foundations of buildings in liquefied layers during Tangshan earthquake survived after earthquake. Authors supposed that the following factors might play important roles: (1) Critical earthquake forces do not often simultaneously occur with critical situation of liquefaction; (2) Liquefied layers get shake-reducing character; (3) Densification of soils due to driving in the case of large amount of piles and dense pile spacing. To interpretate the third factor this paper offers a concret example showing the extent of soil densification due to pile driving.

## DESCRIPTION OF THE BUILDING

The construction site is located on the terrace of Fenhe River in Taiyuan, the capital city of Shanxi Province. The design earthquake intensity is 8 degree of corrected Mercalli. The building is 18-storied with a rigid box foundation supported by 825 precast piles. Fig. 1 and Fig. 2 show the building's plan and its pile distribution. The liquefiable sandy layers involved silty-fine sand, fine-medium sand and sandy loam at -3.5~-14.5m depth (Fig.1b and Table I).

TABLE I. Characteristics of Main Soil Layers

| Type of Soil       | Water Content<br>W, (%) | Unit Weight<br>r, (g/cm <sup>3</sup> ) | Void Ratio<br>(e) | Mean Thickness<br>(m) | d <sub>60</sub> /d <sub>10</sub> | d <sub>50</sub><br>(mm) | Remark      |
|--------------------|-------------------------|--|-------------------|-----------------------|----------------------------------|-------------------------|-------------|
| Loam               | 27.8                    | 1.83                                   | 0.866             | 3.0                   |                                  |                         |             |
| Silty-fine sand    | 24.9                    | 1.86                                   | 0.769             | 2.1                   | 7.2                              | 0.155                   | Liquefiable |
| Fine-medium sand   | 22.7                    | 1.92                                   | 0.701             | 12.0                  | 7.3                              | 0.200                   | "           |
| Medium-coarse sand | 22.4                    | 1.97                                   | 0.646             | 3.5                   | 11.9                             |                         | Nonliq.     |
| Loam               | 26.1                    | 1.98                                   | 0.710             | 2.8                   |                                  |                         | "           |

## Characteristics of the precast piles:

Length L = 19.5 m

Section d<sup>2</sup> = 400 x 400 mm<sup>2</sup>

Total number of piles n = 825

Spacing of piles = 3~4d (for most of the piles)  
7d (the max. spacing)

Weight of driving hammer 6t and 4.5t.

## DENSIFICATION EFFECT

The Fig. 3 pictures the plan of test site for pile load tests. The number of piles indicates also its turn during driving. The relative ratios of allowable bearing capacities are shown in the Table II.

TABLE II. Results of Pile Load Tests

| Section of Pile | Pile No. | Location of Pile | Allowable Bearing Capacity (t) | Relative Ratio of Allow. Bearing Capacities |
|-----------------|----------|------------------|--------------------------------|---|
| 350x350         | 5        | Border           | 93                             | 1.000                                       |
| "               | 6        | Centre           | 108                            | 1.161                                       |
| 400x400         | 2        | Border           | 110                            | 1.000                                       |
| "               | 3        | "                | 117                            | 1.064                                       |
| "               | 4        | "                | 122                            | 1.110                                       |
| "               | 7        | "                | 128                            | 1.163                                       |
| "               | 8        | Centre           | 131                            | 1.190                                       |

The piles at centre (piles No.6 and No.8) got such a bearing capacity that is as many as 1.161 and 1.190 times of the piles No.5 and No.2, respectively. In fact, during driving the soil had been so densified that about 2/3 of the total amount of piles could not been driven to reach their designed depth (-25m).

The blow counts per meter penetration of pile into ground showed that the later driven piles (No.4, No.8) needed more blow counts for their penetration. In order to compare the change of soil characteristics after driving a series of SPT and CPT had been conducted nearby the original bore holes (Fig. 1). The results of comparison of SPT are summarized in Fig. 5. The solid lines in Fig. 5 represent the critical SPT values for 8 intensity according to Chinese Code (TJ 11 - 78):

$$N' = \bar{N}(1 + 0.125(d_s - 3) - 0.05(d_w - 2)) \quad (1)$$

where:  $N'$  = SPT blow counts causing liquefaction, when depth of sand is  $d_s$ , and

underground water level is  $d_w$ ;

$\bar{N}$  =  $\bar{N}$  value when  $d_s = 3m$ ,  $d_w = 2m$ . For intensities 7, 8 and 9, the  $\bar{N}$  values are 6, 10 and 16 respectively;

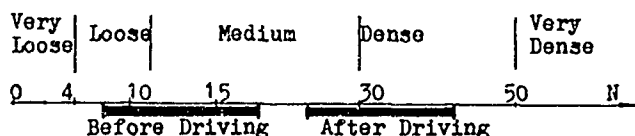
$d_s$  = Depth of saturated sand, m;

$d_w$  = Depth of underground water level below outdoor ground surface, m.

The dash lines in Fig. 5 represent the critical SPT values but according to Chinese Code (Draft, 1987):

$$N = \bar{N}(0.9 + 0.1(d_s - d_w)) \quad (2)$$

It can be seen from Fig. 5 that the SPT values after driving are much greater (from 70% to 130%) than those before driving and then the liquefiable sands become nonliquefiable. The SPT values after pile driving beneath the centre region of the building are even 3~4 times greater than before (Fig. 6) and shown as following:



The SPT values are greater than the critical values at the distance 3.0m out of the border of foundation and the liquefiable layers have lost their liquefiable character. But at distance 6.0m from the boundary of foundation only the soil layers at -12~-14m depth remain liquefiable (Fig. 7).

Fig. 8 and Fig. 9 picture the cone resistance  $q_c$  and  $f_c$  increased 150% and 30% 50% than before driving respectively.

The results of 15 load tests of piles, involved in pile group and reaching the depth 5m shallower than designed level showed that almost all allowable bearing capacities were between 111~153t, except one (104t). The average was 128t per pile, greater than the allowable bearing capacity of the isolated single test pile reaching -25m depth (110t, No.2 in Fig. 3) and also

67% greater than the allowable bearing capacity of the test pile reaching -20.0m depth.

Another remarkable phenomenon is subsidence of ground surface of the area occupied by piles. Total amount of the subsidence is 0.685m. According to the driving records every pile needed 1600~1800 blows for its entire penetration. For 6t driving hammer it meant 19200~21600t-m impact energy per pile. Such amount of energy was equivalent to the energy given by 400t-m dynamic consolidation in 50 times impacts. The compaction effect caused by driven piles involved two aspects: squeeze effect due to entrance of pile shafts into ground and shaking effect caused by driving. The first benefited to the deeper soil layers mainly and the second one benefited to the shallow and deep soil layers both.

A simple calculation has been made to clarify the influence of pile driving on soil density. Assume: the influenced area equals  $A_0$

$$A_0 = (A' + 6) \times (B' + 6) = 2415 \text{ m}^2$$

where  $A'$  and  $B'$  are length and width of the area occupied by piles respectively,

Average depth of pile penetration  $L = 22.4m$

Volum of influenced soil mass

$$V_0 = L A_0 = 54096 \text{ m}^3$$

Change of soil volum due to ground subsidence:

$$V_{st} = 0.685 A_0 = 1654.28 \text{ m}^3$$

Total volum of driven piles  $V_p = 2956.8 \text{ m}^3$

Virgin average void ratio of liquefiable soils

$$e_0 = 0.7211$$

Virgin volum of soil grains in mass  $V_s$ :

$$V_s = V_0 / (1 + e_0) = 31451.16 \text{ m}^3$$

Volum of pore after pile driving:

$$V_v' = e_0 V_0 / (1 + e_0) - V_{st} - V_p = 18033.76 \text{ m}^3$$

Void ratio after pile driving:

$$e' = V_v' / V_s = 18033.76 / 31451.16 = 0.5733$$

Since the average void ratio of liquefiable soil layers has been changed from  $e_0 = 0.7211$  into

$e' = 0.5733$  (dense state), it is easy to interpret that the soils are no longer liquefiable. On the other hand, since the volum of driven piles  $V_p$

is greater than the change of volum caused by subsidence of ground surface  $V_{st}$ , it can be said approximately that in our case the squeezing effect due to pile shafts is greater than shaking effect due to driving.

To estimate the densification effect of driving piles in preliminary design the formulas for sand piles can be used for rough guess and shaking effect due to driving is neglected on account of safety. In our case:

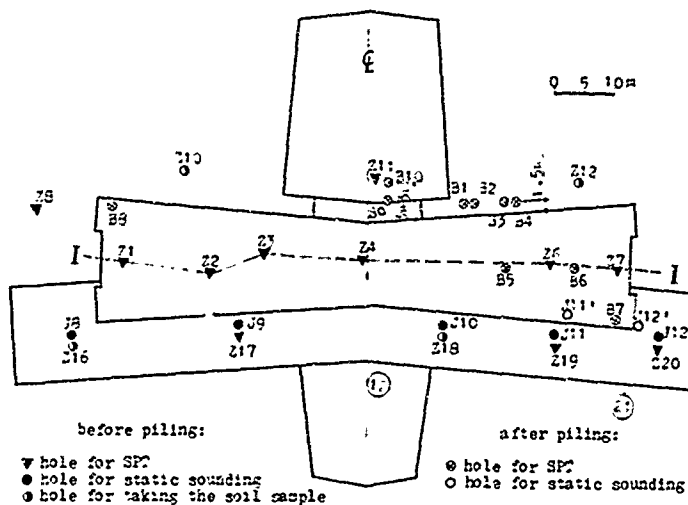
Area compacted by per pile  $A_p' = A_0 / n = 2.927 \text{ m}^2$

Change of void ratio due to squeezing effect:

$$\Delta e = (1 + e_0) d^2 / A_p' = 1.7211 \times 0.4^2 / 2.927 = 0.0941$$

Final void ratio:  $e_0 - \Delta e = 0.627$

Since the calculated final void ratio is 0.627; It means that the silty-fine-medium sands are in dense state and  $D_r < 0.7$ . Therefore the soils become nonliquefiable for area of 8 degree inten-



(a) Plan of bore holes and building

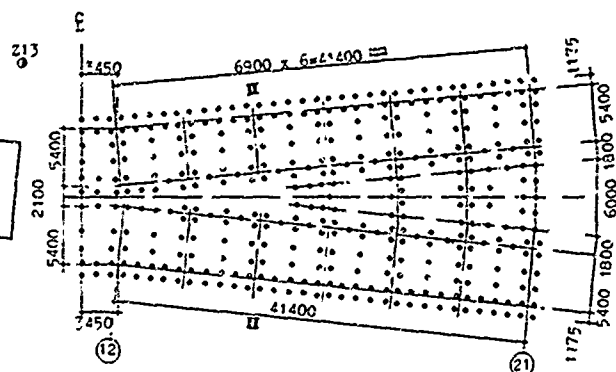
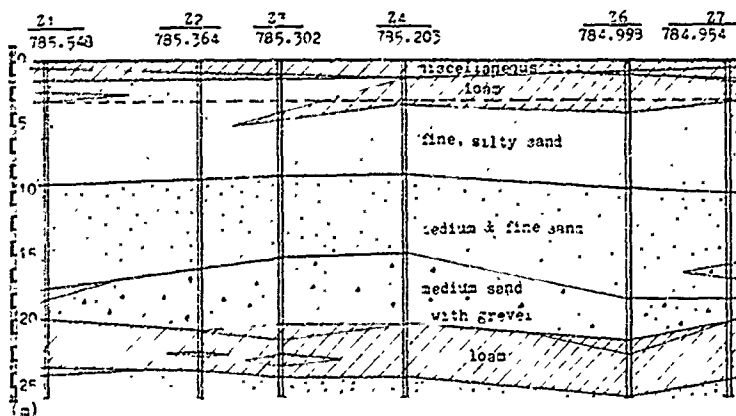
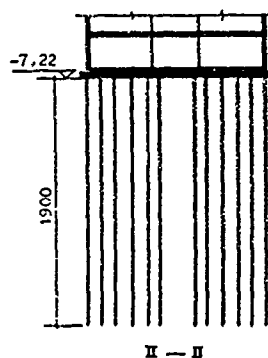


Fig. 2. Plan of pile distribution



(b) Soil profile I-I

Fig. 1. Plan of bore holes and soil layer profile



II - II

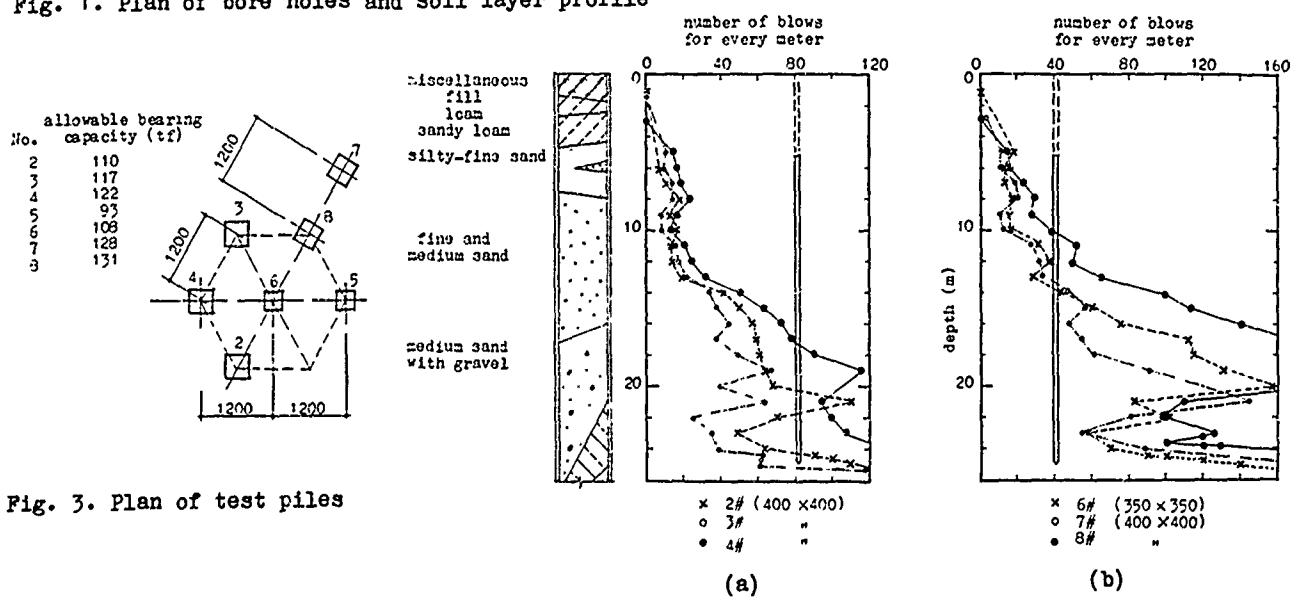


Fig. 3. Plan of test piles

Fig. 4. Driving records of test piles



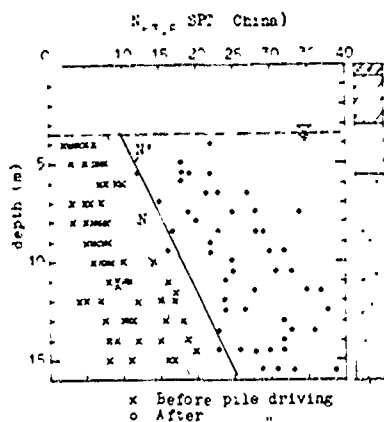


Fig. 5. Change of SPT values under whole area of pile foundation

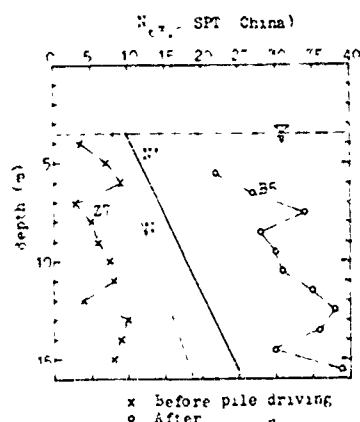


Fig. 6. Change of SPT values under the centre area of building

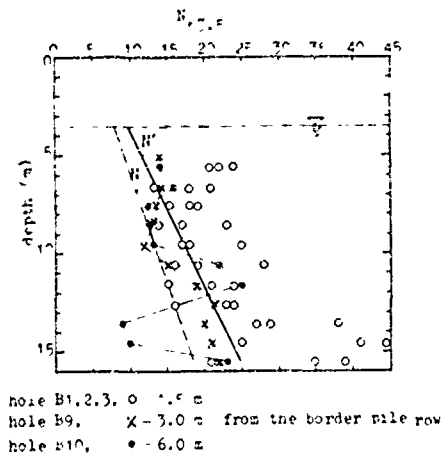
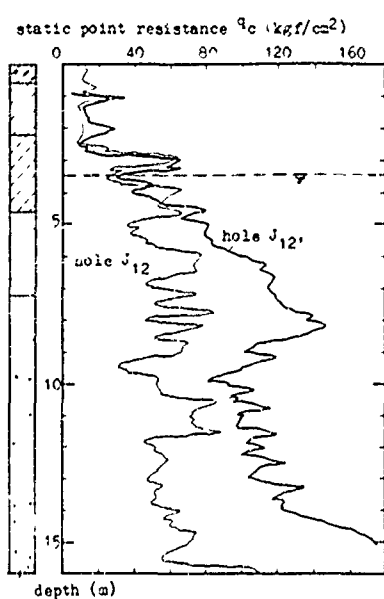
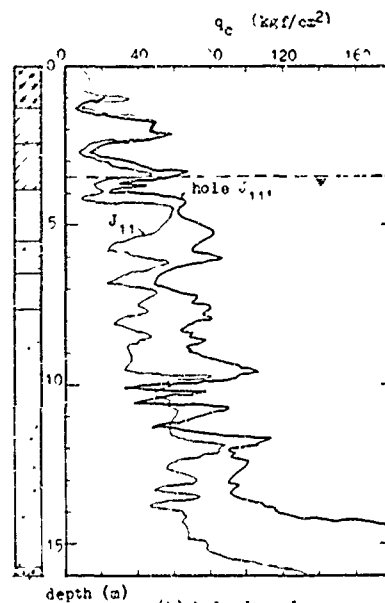


Fig. 7. SPT values for soils out of border pile row after driving



(a) hole J<sub>12</sub>, J<sub>12</sub>'



(b) hole J<sub>11</sub>, J<sub>11</sub>'

Fig. 8. Change of point resistance of CPT

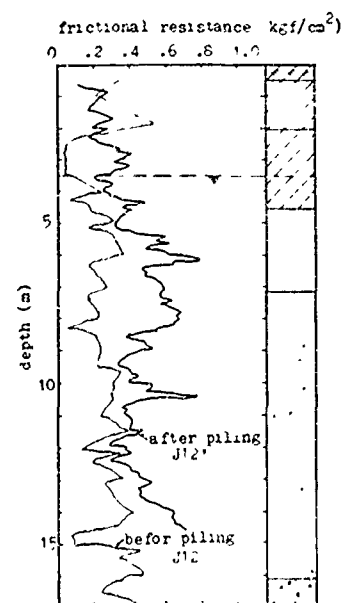


Fig. 9. Change of lateral friction of CPT

sity according to the Chinese Standard (1978).

#### SUGGESTIONS

The liquefiable subsoils under a building with many piles of spacing 3~7d would become nonliquefiable due to shaking and squeeze of pile driving, this should be considered during pile foundation design if the primary calculation shows the possibility. The testing pile driving should be conducted as a needed next step to identify the calculated situation. In case of positive results of calculation and tests both the following assumptions during pile foundation design are suggested:

1) Liquefiable subsoils located between piles can be treated as nonliquefiable and bearing capacity of single pile is taken as many

as in case of nonliquefiable subsoils.

2) Pile foundation is treated as a deep foundation but surrounded by liquefiable soils, so the frictional resistance along the lateral surface of such a foundation is neglected.

3) For primary estimation on densification effect of driven pile the formulas for sand pile design can be used.

#### REFERENCES

- Liu Huishan and Qiao Taiping (1984), "Pile Foundation under liquefiable soils", Intern. Conf. on case Histories in Geot. Eng. USA.
- M. Iyengar, (1981), "Improvement of Characteristics of a Liquefiable soil deposit by pile driving Operation" Intern. Conf. in Geot. Earth. Eng. and Soil Dynamics, USA.

## The Simplified Formulas for Predicting Seismic Liquefaction of Saturated Clayey Silt Site

Wang Yuqing

Senior Research Engineer, Central Research Institute Building and Construction of MMI, China

**SYNOPSIS:** In the reconstruction of old factories and in the small scale engineering, it is often taken place that the present methods for predicting liquefaction of clayey silt could be not used for lack of subsoil exploration data. Two simplified formulas which contain the coefficient of  $\alpha_p$  considering the effect of clay content  $P_c$  and the coefficient of  $\alpha_{lp}$  considering the effect of plasticity index  $I_p$  are presented for predicting seismic liquefaction of saturated clayey silt. Thus, the prediction of liquefaction of clayey silt could be effectively proceeded under the conditions lacking of analysing data of soil grain composition.

### INTRODUCTION

Clay silt refers to the low plastic soil, the plasticity index  $I_p$  of which changes from 3 to 10, and it may be also called fine-grained soil or silt. Recently, there is a rapid development in research for predicting seismic liquefaction of saturated clayey silt site at home and abroad, and several methods of solution have been put forward [1,2,3]. It should be indicated that the application of the present computation methods is always related to soil characteristic index. But in the reconstruction of old factories and in the small-scale engineering the lack of data of subsoil exploration is often met. For instance, in many engineering there are sometimes blow numbers of SPT and plasticity index  $I_p$  or only blow numbers of SPT  $N$ . And the data of stress ratio  $\tau_d/\sigma'_v$  of liquefaction, shear wave velocity  $V_s$ , static cone penetration value  $P_s$  and grain analysis data (clayey content  $P_s$  - grain diameter less than 0.005 mm, fine grain diameter content  $C$  - grain diameter less than 0.074 mm or average grain diameter  $D_{50}$ ) and so on are lacked. Thus, it is needed that to put forward a simplified computation formula for predicting liquefaction of saturated clayey silt with successful discrimination ratio.

Through research and analysis on the date of 299 groups, liquefied and non-liquefied, taken from the in situ investigation, the author has proposed two simplified formulas on predicting seismic liquefaction of saturated clayey silt, the formulas include the coefficient of  $\alpha_p$ , considering the effect of clay content  $P_c$  and the coefficient of  $\alpha_{lp}$ , considering the effect of plasticity index  $I_p$ . Further more, in this paper the successful discrimination ratio of two formulas are verified by using the 299 groups of data, and which is compared with the results derived from Xie Junfei's differentiation formula containing parameter  $P_c$  (1984) and with the differentiation formula put forward by the author (1980).

### THE PRESENT METHODS FOR PREDICTING LIQUEFACTION OF SOIL

The methods for predicting liquefaction of base soil may be divided into four classes:

#### 1. Standard Explosive Method

The method was presented by Florin and Ivanov [4], and some development was made by Prakash [5]. But the method is not yet widely used to predict sand liquefaction and to say nothing of saturated clayey silt.

#### 2. Simplified Analysis Method

The method was put forward by Seed and Idiss (1967) [6]. And it is widely used in the world. If the effect of fine grain in soil on the stress ratio of liquefaction is considered, the method may be used to evaluate liquefaction potential of low plastic soil. In this topic, Japan's Tatsueka et al (1980) and Ishihara et al (1981) proposed a expression, in which the stress ratio  $(\tau_d/\sigma'_v)_w$  of liquefaction was determined by average grain diameter  $D_{50}$  or fine grain content  $C$  or  $C$  and plasticity index [3], and thus the simplified analysis method may be used to predict liquefaction of low plastic soils very conveniently.

#### 3. Dynamic Response Analysis Method

The advantage of the method is that it may not only discriminate where there is liquefaction in layers and where no, but also predict the developing process and scale of liquefaction area. The method can also consider some soil properties, (for example, different characteristics of layer), boundary condition (stress condition and drainage condition) of liquefaction layer and so on [3,7]. Therefore, the method has a splendid future. But the method is more complex after all, and it requires more characteristic parameters of soil in analysing, now it is only used in a special important engineering.

#### 4. Empirical Method and Statistical Method Depending on Investigated Data

Lots of methods of this kind were put forward in the world. For instance, the discrimination chart of liquefaction which is put forward by Seed is one of the methods, later the author supplemented the proposition that the  $N_1$ -value should be revised based on fine grain content  $C$  [8], thus it may be used to predict the liquefaction of low plastic soil. In Japan, "The Structural Design Standard of Building Foundation" [1982] had also stipulated that the critical standard penetration numbers of liquefaction decrease with increase of fine grain content. Chinese researchers have done a lot of work in predicting liquefaction of saturated clayey silt since 1975. According to incompletely statistics, about 30 formulas mainly based on standard penetration value for predicting liquefaction of clayey silt have been presented ever since. The reference [2] had discussed these discriminants. Because of the length restriction of the paper, several differentiating formulas related to the paper are introduced as follows.

#### FORMULAS FOR PREREDICTING SEISMIC LIQUEFACTION OF SATURATED CLAYEY SILT

Two statistical formulas for predicting liquefaction of saturated clayey silt which contain 4 and 5 factors by using 231 groups of in-situ data of liquefaction and non-liquefaction derived from MMT Central Corporation for Engineering Exploration of CHINA and Tianjing Programming Bureau were built up by the author in 1980 [1]. And these two formulas were revised after deriving another 10 groups of liquefaction data and 5 groups of non-liquefaction data in the area of seismic intensity 7 from the First Machinery Ministry Exploration Corporation of CHINA. The revised calculation proceeded on statistical analysis by using of these three parts of data (246 groups as a whole). Through analysing, formulas for predicting liquefaction, which contain 4 and 5 factors, are given by means of critical penetration number  $N_{cri}$ , as follow:

$$N_{cri} = 46.25\alpha + 0.38ds - 0.32dw - 0.99Pc + C \quad (1)$$

$$N_{cri} = 44.74\alpha + 0.22ds - 1.05dw + C \quad (2)$$

Where:  $\alpha$  = the seismic coefficient (it equals to 0.1, 0.2 and 0.4 respectively when seismic intensity is 7, 8 or 9)

$ds$  = the depth of researched point (m)

$dw$  = the depth of groundwater level (m)

$Pc$  = the clay content in percent (%)

$C$  = constant related to discrimination ratio of liquefaction  $Pl$ . When  $Pc > 85\%$ ,  $C$  equals to 4.23 in formula (1) and  $C$  equals to 0.59 in formula (2).

Formula (2) has been recommended to predict liquefaction of low plastic soil under the conditions lacking of clay content by "Aseismic and Reinforce Technology Measure for Industrial & Public Building, CHINA" [10].

A formula for predicting liquefaction of clayey silt as well as sand from 299 groups of liquefaction and non-liquefaction data supplied by

reference [11] is derived by Xie [2] as follows:

$$N_{cri} = \bar{N} [1 + 0.125(ds-3) - 0.05(dw-2)] (3/Pc)^{0.5} \quad (3)$$

For sand  $Pc=3$ , thus the formula (3) changes into that for predicting liquefaction of sand in Chinese present code.

Two revisions were made by reference [12] for formula (3): 1) The coefficient of ground water level item was revised; 2) the other was adopting different value corresponding to distances of far earthquake and close earthquake to site. The formula is as follows:

$$N_{cri} = \bar{N} [0.9 + 0.1(ds-dw)] (3/Pc)^{0.5} \quad (4)$$

Formula (4) has been accepted by the revised edition of "Aseismic Design code for Industrial & public Building, CHINA", TJ 11-78.

#### SIMPLIFIED FORMULAS FOR PREDICTING SEISMIC LIQUEFACTION OF SATURATED CLAYEY SILT

The two formulas presented by the author are based on formula (4). They are stated one by one as follows:

##### 1. The Formula Containing 4 Factors with Revising Coefficient of Clay Content

In order to eliminate  $Pc$  in formula (4), by means of the results derived from studying the relationship of statistical formulas of 4 and 5 factors ahead, by virtue of original data of 299 groups, we calculated the average value  $Pc$  of clay content in 7, 8, 9 intensity area. The value  $Pc$  is 6.53, 7.51 and 9.60 respectively. Replacing these values into formula (4), the 4 factors formula containing is obtained as follows:

$$N_{cri} = \bar{N} [0.9 + 0.1(ds-dw)] \alpha_{pc} \quad (5)$$

Where:  $\alpha_{pc}$  = the revising coefficient considering the effect of clay content ( $d < 0.005$  mm). When seismic intensity is 7, 8 or 9, it equals to 0.68, 0.63 or 0.56 respectively.

##### 2. The Formula Containing 5 Factors with Revising Coefficient of Plasticity Index

The relationship  $I_p = f(Pc)$  can be obtained from original data above stated. It is shown in Fig.1.

Thus the formula (4) can be expressed as follows:

$$N_{cri} = \bar{N} [0.9 + 0.1(ds-dw)] \alpha_{ip} \quad (6)$$

where:  $\alpha_{ip}$  = the revising coefficient considering the effect of plasticity index  $I_p$ :

$$\alpha_{ip} = [1 + 0.657(I_p - 3)^{0.45}]^{-0.5} \quad (7)$$

##### 3. Inspection of Efficiency for Formula (5) and Formula (6)

The results of successful discrimination ratio, calculating with formula (4), (2), (5) and (6) are compared in List 1. For comparison all the presented original data of clayey silt mentioned above are used. It may be seen from these

Table 1 The Comparison of Calculating Results of Successful Ratio

|     |                  | Predicting Method |               |               |               |
|-----|------------------|-------------------|---------------|---------------|---------------|
|     |                  | Form.(4)          | Form.(2)      | Form.(5)      | Form.(6)      |
| 7   | Liquefaction     | 95                | 18/19<br>95   | 18/19<br>95   | *             |
|     | Non-liquefaction | 68                | 12/19<br>63   | 11/19<br>58   | 11/13<br>85   |
|     | Total            | 82                | 30/38<br>79   | 29/38<br>76   | 11/13<br>85   |
| 8   | Liquefaction     | 97                | 119/120<br>94 | 121/126<br>96 | 104/109<br>91 |
|     | Non-liquefaction | 79                | 81/96<br>84   | 70/90<br>73   | 69/87<br>79   |
|     | Total            | 88                | 200/222<br>90 | 191/222<br>86 | 173/196<br>88 |
| 9   | Liquefaction     | 100               | 27/27<br>100  | 27/27<br>100  | 9/9<br>100    |
|     | Non-liquefaction | 75                | 9/12<br>75    | 7/12<br>58    | 7/8<br>88     |
|     | Total            | 92                | 36/39<br>92   | 34/39<br>87   | 16/17<br>94   |
| 7-9 | Liquefaction     | 95                | 164/172<br>95 | 166/172<br>97 | 113/118<br>96 |
|     | Non-liquefaction | 77                | 102/127<br>80 | 88/127<br>69  | 76/95<br>80   |
|     | Total            | 86                | 266/299<br>89 | 254/299<br>85 | 139/213<br>89 |

\* No results because of lacking the value  $I_p$

results that formula (5) and (6) may replace formula (4) to predict liquefaction of saturated clayey silt.

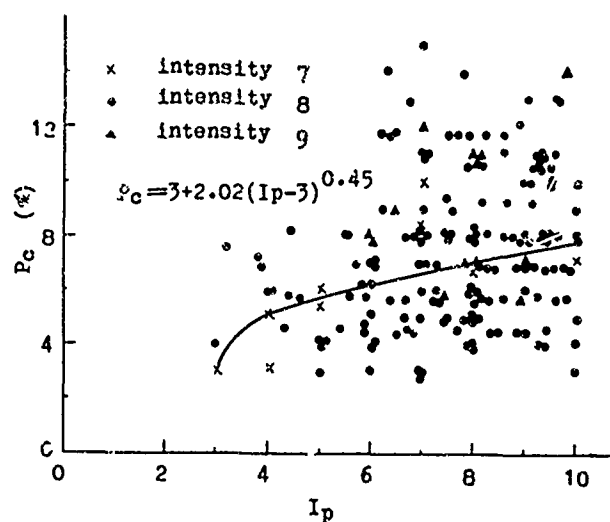
#### CONCLUSIONS

Under the conditions of lacking of exploration data, for bases of common building, formula (5) and (6) can also be used to predict liquefaction of saturated clayey silt besides formula (2). Certainly, the inspection of reliability for formula (5) and (6) in the paper is essential. With the accumulation of investigation data of liquefaction, the inspection of reliability for these two formula will be carried out by using new investigation data in the future.

#### REFERENCES

[1] Wang Yuqing, et al (1980), Formulae for Predicting Liquefaction Potential of Clayey Silt as Derived From a Statistical Method, Proc. 7th World Conference on Earthquake Engineering, Vol.3, pp 227-234.

[2] Shi Zhaoji, et al (1984), Prediction of Liquefaction Potential of Saturated Clayey Silt,

Fig.1 Plasticity Index  $I_p$  vs. Clay Content  $P_c$

Earthquake Engineering and Engineering Vibration, Vol.4, No.3, pp 71-82. (in chinese)

[3] Kenji Ishihara (1985), Stability of Natural Deposits During Earthquakes, Proc. 11th International Conference on Soil Mechanics and Foundation Engineering, Vol.I, pp321-376

[4] Ivanov P.L. et al (1977), Soil Liquefaction and Ground Stabilization, Proc. 9th International Conference on Soil Mech. and Found. Eng., Vol.2, pp265-268

[5] Shamsheer Prakash (1981), Soil Dynamics, McGraw-Hill Book Company.

[6] Seed H.B. et al (1967), Analysis of Soil Liquefaction, Niigata Earthquake, Proc. ASCE, SM3, pp63-108.

[7] Gu Weihua, Wang Yuqing (1985), The Liquefaction Inhibiting Effect of Gravel Drains and Surface Load, Chinese Journal of Geotechnical Engineering, Vol. 7 No. 4 pp34-44 (in chinese)

[8] Seed H.B. (1987), Design Problems in Soil Liquefaction, (to be Publish)

[9] Wang yuqing et al (1986), Evaluation of the liquefaction of saturated clayey, Proc. 4th. MMI conference on earthquake engineering, pp85-98 (in chinese)

[10] Aseismic and Reinforce Technology Measure for Industrial & Public Building, CHINA (1986), Earthquake Press, pp82, (in Chinese)

[11] Weng lunian (1983), Statement on Original Data Used in the Temporary Code of Evaluation of the liquefaction of Saturated Clayey Silt (in chinese)

[12] Xei Jinfei (1984), Some Comments on the Formula for Estimating the Liquefaction of Sand in Revised Aseismic Design Code, Earthquake Engineering and Engineering Vibration, Vol.4, No2 pp96-126 (in chinese)

# The Effect of Foundation Shape on Dynamic Parameter of Bases

Duan Shiwei

Engineer, Central Research Inst. of Building and Construction of Metallurgical Ind., Beijing, China

**SYNOPSIS:** It has been proved that the shape of foundation and its base side ratio affect the dynamic rigidity of sliding-rotation vibration of bases. Based on plenty of laboratory tests in a small sides the computing formulas of rigidity and damping of base considering the effect of base side ratio are put forward.

## INTRODUCTION

Up to now the research of the effect of foundation shape on dynamic parameter is far from enough. In order to correctly design dynamic machinery foundations and structures this problem has been researched by the author in recent years. All together 18 foundations with same base areas of  $0.5 \text{ m}^2$  and different height and base side ratio of foundations were tested under exposed and embedded conditions. All tests were performed under the action of harmonic exciting force. The 18 foundations tested were divided into four groups according to their base shape as follows:

1. The shape of foundations is rectangular, the base side ratios of which are 1:1, 1:2 and 1:3 corresponding to the first group, second group and third group.

2. The shape of the fourth group is circle with radius 0.28 m.

All tests were conducted under the condition of laboratory in which a sand pit was set. In the following a several main phenomena and conclusions are introduced.

### 1. Vertical Vibration

First all, it must be pointed out that the mechanics model of Mass-Damping-Spring within the range of linearity is adopted as shown in Fig.1. Meanwhile the following assumptions are used:

1. The foundations only possess inertia effect.
2. The base soils only possess the effect of elasticity
3. The damping of base coincides with the viscous damping theory.

According to the assumptions above, the equation of vertical motion of foundation may be

expressed as follows:

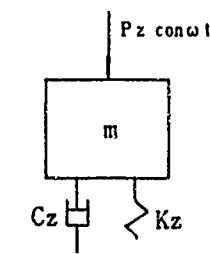


Fig.1 Mechanics Model of Foundation Vibration

$$m \ddot{Z} + C_z \dot{Z} + K_z Z = P_z \cos \omega t \quad (1)$$

Where:  $m$  = the total mass of foundation and machine

$P_z$  = maximum value of exciting force

$\omega$  = circle frequency of exciting force

$C_z$  = vertical damping coefficient

$K_z$  = vertical dynamic rigidity of base

$\dot{Z}, \ddot{Z}$  = the first and second derivalive of displacement  $Z$

It is well known that the amplitude  $A$  of vertical vibration corresponding to equation 1 is as follows:

$$A_z = \frac{P_z}{K_z \sqrt{\left(1 - \frac{\omega^2}{\lambda_z^2}\right)^2 + 4 D_z^2 \frac{\omega^2}{\lambda_z^2}}} \quad (2)$$

Where:

$$\lambda_z^2 = \frac{K_z}{m} \quad (3)$$

$$D_z = \frac{C_z}{2\sqrt{m K_z}} \quad (4)$$

The  $D_z$  is referred as to vertical damping ratio. When taking derivation of equation 2 to circle frequency and making it to be equal to zero, then the relation between resonance frequency and natural frequency is obtained:

$$\bar{\lambda}_z = \lambda_z \sqrt{1 - 2D_z^2} \quad (5)$$

The vertical damping ratio and rigidity of base may be expressed by the resonance frequency and amplitude obtained:

$$D_z = \frac{1 - \sqrt{1 - \frac{\bar{\lambda}_z^2}{\lambda_z^2}}}{2} \quad (6)$$

$$K_z = \frac{m \bar{\lambda}_z^2}{1 - 2D_z^2} \quad (7)$$

Where:

$$\bar{\lambda}_z = \frac{1}{1 + B_z^2} \quad (8)$$

$$B_z = \frac{A_z \cdot \max}{P_z} - m \bar{\lambda}_z^2 \quad (9)$$

By analysing the test data of vertical vibration of four group foundations, using the formulas above, the variation of damping and rigidity is obtained as listed in Table I.

In order to more clearly show the amplitude response in the whole range of exciting frequencies, herein the Amplitude-Frequency-Curve corresponding to the first group foundations is cited as shown in Fig. 2. For embedded foundations the curve corresponding to the first group foundations with height 1.08 m is described in Fig. 3. In these figures the parameter  $b = W/\gamma F^{1/2}$ , and  $\delta = h_m/\sqrt{F}$  (in which  $W$  = the total weight of foundation and machine,  $\gamma$  = unit weight of base soil,  $h_m$  = embedded depth of foundation and  $F$  = base area of foundation)

TABLE I. the Effect of Foundation Shape and Its Embedded Depth on Rigidity and Damping Ratio

| Num.of Group | Size of Foundation (m) |       |       | $h_m$ (m) | $D_z$ | $K_z$ (t/m) |
|--------------|------------------------|-------|-------|-----------|-------|-------------|
| 1            | 0.5                    | 0.5   | 0.135 | 0.00      | 0.55  | 880.5       |
| 2            | 0.5                    | 0.5   | 0.27  | 0.00      | 0.342 | 864.3       |
| 3            | 0.5                    | 0.5   | 0.54  | 0.00      | 0.185 | 1432.3      |
| 4            | 0.5                    | 0.5   | 0.81  | 0.00      | 0.098 | 1926.8      |
| 5            | 0.5                    | 0.5   | 1.08  | 0.00      | 0.059 | 2329.9      |
| 5            | 0.5                    | 0.5   | 1.08  | 0.27      | 0.130 | 2626.9      |
| 5            | 0.5                    | 0.5   | 1.08  | 0.54      | 0.218 | 3098.7      |
| 5            | 0.5                    | 0.5   | 1.08  | 0.81      | 0.229 | 3738.0      |
| 5            | 0.5                    | 0.5   | 1.08  | 1.08      | 0.473 | 5454.2      |
| 6            | 0.354                  | 0.707 | 0.135 | 0.00      | 0.531 | 842.3       |
| 7            | 0.354                  | 0.707 | 0.27  | 0.00      | 0.367 | 970.5       |
| 8            | 0.354                  | 0.707 | 0.54  | 0.00      | 0.192 | 1441.5      |
| 9            | 0.354                  | 0.707 | 0.81  | 0.00      | 0.090 | 1873.6      |
| 10           | 0.354                  | 0.707 | 1.08  | 0.00      | 0.070 | 2277.7      |
| 10           | 0.354                  | 0.707 | 1.08  | 0.27      | 0.122 | 2582.8      |
| 10           | 0.354                  | 0.707 | 1.08  | 0.54      | 0.195 | 2982.1      |
| 10           | 0.354                  | 0.707 | 1.08  | 0.81      | 0.323 | 3633.3      |
| 10           | 0.354                  | 0.707 | 1.08  | 1.08      | 0.410 | 4187.1      |
| 11           | 0.298                  | 0.868 | 0.135 | 0.00      | 0.513 | 749.5       |
| 12           | 0.289                  | 0.868 | 0.27  | 0.00      | 0.339 | 910.6       |
| 13           | 0.289                  | 0.868 | 0.54  | 0.00      | 0.190 | 1848.0      |
| 14           | 0.289                  | 0.868 | 0.81  | 0.00      | 0.104 | 1996.6      |
| 15           | 0.289                  | 0.868 | 1.08  | 0.00      | 0.067 | 2477.9      |
| 15           | 0.289                  | 0.868 | 1.08  | 0.27      | 0.144 | 2963.6      |
| 15           | 0.289                  | 0.868 | 1.08  | 0.54      | 0.231 | 3275.3      |
| 15           | 0.289                  | 0.868 | 1.08  | 0.81      | 0.382 | 4011.2      |
| 15           | 0.289                  | 0.868 | 1.08  | 0.81      | 0.382 | 4011.2      |
| 15           | 0.289                  | 0.868 | 1.08  | 1.08      | 0.455 | 4912.7      |
| 16           | R=0.28                 |       |       | 0.00      | 0.506 | 720.1       |
| 17           | R=0.28                 |       |       | 0.00      | 0.344 | 895.8       |
| 18           | R=0.28                 |       |       | 0.00      | 0.170 | 1372.7      |

It is clearly seen from Fig. 2 that the resonance frequencies are decreased with the increasing of parameter  $b$ . While the figure 3 shows that the resonance frequencies are increased with the increasing of embedded ratio of foundations. It should be shown that the resonance amplitudes are decreased with decreasing of  $b$  and increasing of  $\delta$ .

The variation law of damping and rigidity with parameter  $b$  may be seen from Fig. 4 and Fig. 5 for exposed foundations. Furthermore, the variation of damping ratio may be well expressed as follows:

$$D_z = 0.24/b \quad (10)$$

The expression 10 is represented in Fig. 4 by solid line.

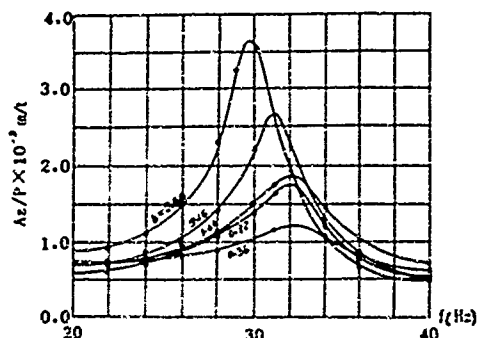


Fig.2 Amplitude-Frequency-Curve under Exposed Foundations and Vertical Vibration

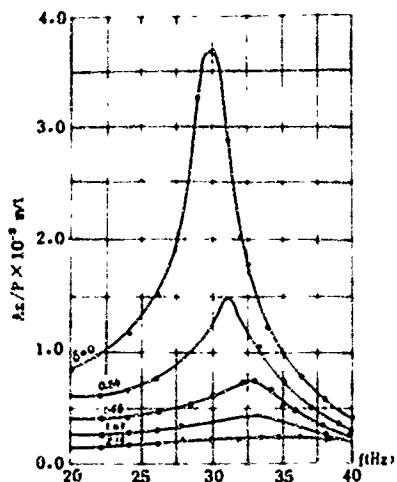


Fig.3 Amplitude-Frequency-Curve under Conditions of Embedded Foundation

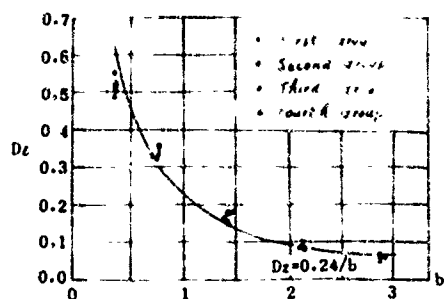


Fig.4 Relation between Vertical Damping Ratio and b under Exposed Foundation

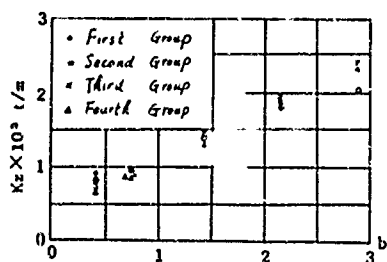


Fig.5 Relation between Vertical Rigidity and b under Exposed Foundation

In order to research the variation law of damping and rigidity of embedded foundation the following two parameters are adopted:

$$\alpha z = \frac{\lambda z}{\lambda z_0} \quad (11)$$

$$\beta z = \frac{Dz}{Dz_0} \quad (12)$$

Where:  $\lambda z_0, Dz_0$  = natural frequency, damping ratio corresponding to exposed foundations

$\lambda z, Dz$  = natural frequency, damping ratio corresponding to embedded foundations

It follows from 18 test foundations that the increasing coefficients of frequency, and damping ratio, are apparently increased with increasing of embedded ratio of foundations. These test results are well described in Fig.6 and Fig.7 and can be expressed by following two formulas:

$$\alpha z = 0.14 \delta^{0.4} + 1 \quad (13)$$

$$\beta z = 1.3 \delta^{1.5} + 1 \quad (14)$$

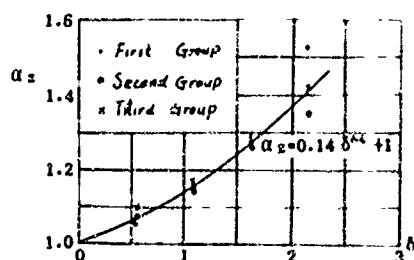


Fig.6 Relationship between Increasing Coefficient of Natural Frequency and Embedded Ratio of Foundation

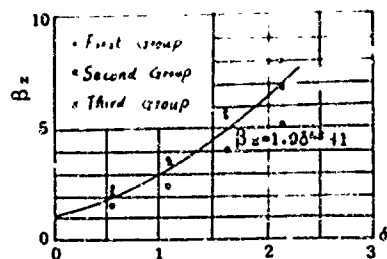


Fig.7 Varying Law of Increasing Coefficient of Vertical Damping Ratio with Parameter  $\delta$



By the analysing above mentioned, two main conclusions may be drawn:

1. The effect of mass ratio  $b$  on vertical rigidity and damping ratio of base should be considered.

2. When establishing the vertical rigidity, damping ratio, increasing coefficient of frequency and damping ratio, the base area of influence of base side ratio between length and width of foundation on these parameters may be ignored.

## II. Vibrations Accompanied by Simultaneous Rotation and Sliding

If vibrations are caused by an exciting moment and horizontal exciting force, the equation of forced vibration of foundation will be written as follows:

$$M\ddot{X} + \Phi S\dot{X} + SX = Px \sin \omega t$$

where:

$$M = \begin{pmatrix} m & 0 \\ 0 & J_m \end{pmatrix} \quad S = \begin{pmatrix} K_x & -h K_x \\ -h K_x & K + h K_x \end{pmatrix}$$

$$X = \begin{pmatrix} x \\ \varphi \end{pmatrix} \quad Px = \begin{pmatrix} Px \\ M \cdot Px \cdot h \end{pmatrix}$$

in which:  $J_m$  = moment of inertia of the foundation mass with respect to rotation axis

$K_x$  = horizontal rigidity of base,  $K_x = C_x F$

$K_\varphi$  = rotation rigidity of base,  $K_\varphi = C_\varphi I$

$C_x$  = coefficient of elastic uniform shear of base

$C_\varphi$  = coefficient of elastic nonuniform compression of base

$I$  = moment of inertia of contact base area of foundation with respect to rotation axis

$h_2$  = distance between the center of gravity of the mass of vibration system and foundation base

$h_3$  = distance from horizontal force to the center of mass

$\dot{x}, \ddot{x}$  = the first and second derivative of displacement  $x$

$\dot{\varphi}, \ddot{\varphi}$  = the first and second derivative of rotation angle  $\varphi$

$\Phi$  = proportion coefficient of damping

It is well known that the solution of forced vibration of equation 15 is summarised by the responses of the first and second vibration model. But in order to establish the dynamic parameters the effect of second vibration model on vibration response may be ignored because under the condition of smaller exciting frequency which does not exceed resonance frequency the influence of this model on amplitude of vibration is 5 % smaller than that

considering the model. Thus, the problem of two freedom degree may be simplified into one [1] and the equation of motion of vibration system may be written as follows:

$$J_1 \ddot{\phi} + C_1 \dot{\phi} + K_1 \phi = M_1 \sin \omega t \quad (16)$$

Where:

$$J_1 = J_m + m \rho_i^2$$

$$C_1 = \Phi [K_\varphi + K_x (\rho_1 - h_2)^2]$$

$$K_1 = K_\varphi + K_x (\rho_1 - h_2)^2$$

$$M_1 = M + P_x (h_3 + \rho_1)$$

$$\rho_i = \frac{h_2}{1 - \frac{\lambda_1^2}{\lambda_k^2}}$$

in which  $\lambda_1$  is the first natural frequency of vibration system and  $\rho_i$  is the rotation radius corresponding to the first vibration model. Thus, the solution of the equation 16 is entirely similar to the solution of equation 1 which is omitted herein. From equation 16 we may establish damping ratio  $D_{x\varphi}$  of sliding-rotation vibration and rigidities  $K_x$  and  $K_\varphi$ . It should be pointed out that the following results of analysing are obtained under the assumption of  $C_\varphi/C_x = 2.86$ . From this the rotation radius  $\rho_i$  will be easily established.

In order to research the effect of shape of foundation on sliding-rotation vibration the parameter  $K$  is adopted. The  $K$  is equal to  $b/a$ , in which  $a$  is the side parallel to horizontal force and  $b$  is perpendicular to horizontal force.

To embedded foundation the variation of rigidity and damping is expressed, in the same way, by the increasing coefficient of frequency and damping ratio, that is:

$$\alpha_{x\varphi} = \frac{\lambda_1}{\lambda_{1,0}} \quad (17)$$

$$\beta_{x\varphi} = \frac{D_{x\varphi}}{D_{x\varphi,0}} \quad (18)$$

Where:  $\lambda_{1,0}, \lambda_{x\varphi,0}$  = first natural frequency, damping ratio corresponding to  $h_m = 0$

$\lambda_1, \lambda_{x\varphi}$  = first natural frequency, damping ratio corresponding to  $h_m \neq 0$

In order to clarify the variation of amplitude of vibration with varying exciting frequency  $f$  (

in H ), the Fig. 8 and Fig.9 are cited. The Fig.8 describes the relation of amplitude to mass ratio  $b$  and exciting frequency under the condition of  $h_m = 0$ . It follows from Fig.8 that the greater the mass ratio  $b$ , the larger the response of amplitude. The Fig.9 describes the relation of amplitude to embedded ratio  $\delta$  of foundations and exciting frequencies  $f$ . It is seen from this figure that the greater the embedded ratio  $\delta$ , the smaller the response of amplitude of vibration.

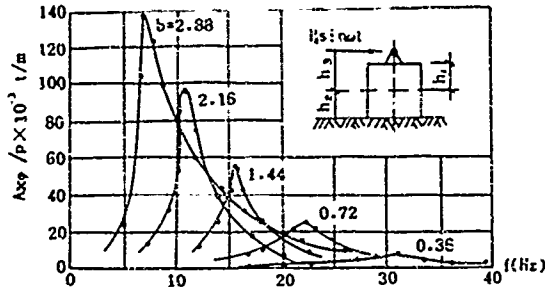


Fig.8 Horizontal Amplitude-Frequency-Curve under Different Value of  $b$

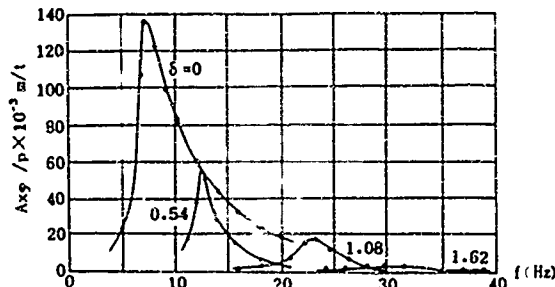


Fig.9 Horizontal Amplitude-Frequency-Curve under Different Value of  $\delta$

As for the variation of rigidity and damping with varying  $b$  under the condition of exposed foundations the Fig.10 and Fig.11 clearly describe it in detail.

Furthermore, the relationship between damping ratio  $D_{xg}$  and mass ratio  $b$  may be well expressed as follows:

$$D_x = 0.06/b \quad (19)$$

To embedded foundations the increasing coefficients of natural frequency and damping ratio are described in Fig.12 and Fig.13. Furthermore, these coefficients may be, with sufficient accuracy, expressed as follows:

$$\alpha_{xg} = \sqrt{K} \delta^{3/2} + 1 \quad (20)$$

$$\beta_x = 0.5\beta + 1 \quad (21)$$

These expressions are described in Fig.12 and Fig.13 in solid line.

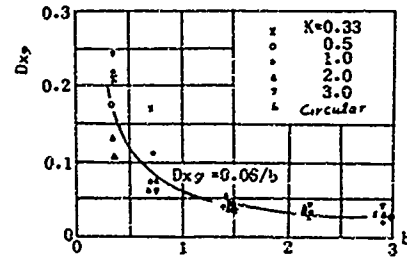


Fig.10 Relationship between Damping Ratio of Sliding-Rotation Vibration and Parameter  $b$  under Exposed Foundation

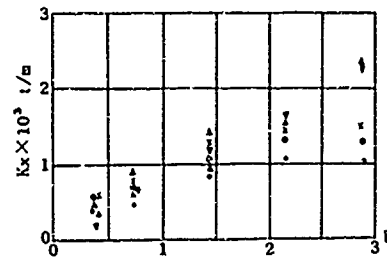


Fig.11 Relationship Between Horizontal Rigidity and Parameter  $b$

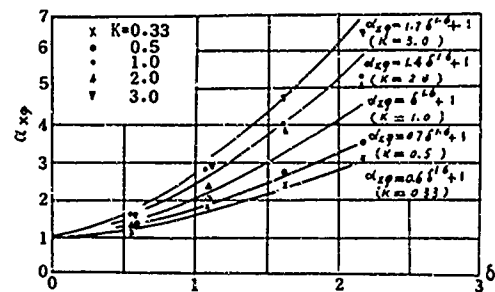


Fig.12 Variation of Increasing Coefficient of Natural Frequency with  $\delta$

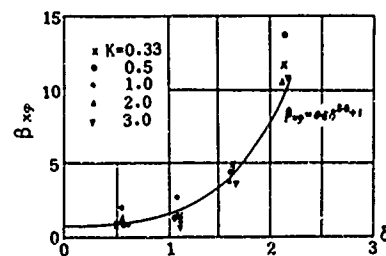


Fig.13 Variation of Increasing Coefficient of Damping Ratio with  $\delta$

## Conclusions

According to the discussion above the following conclusions may be drawn:

1. Under the condition of exposed foundations the horizontal rigidity  $K_x$ , rotation rigidity  $K_\theta$  and damping ratio  $D_{x\theta,0}$  are not related to the shape of foundation and its base side ratio basically.

2. Under the condition of embedded foundations the increasing coefficient of damping ratio is not related to the shape and its base side ratio of foundations in principle.

3. To the embedded foundations the increasing coefficient of natural frequency is apparently related to the foundation shape and its base side ratio. The greater the value  $K$ , the larger the increasing coefficient of natural frequency.

4. The horizontal and rotation rigidity of base are markedly related to mass ratio  $b$ . The greater the mass ratio  $b$ , the larger the rigidities.

## Reference

- [1] Wang Xikang, Wu Nanpeng, Jen Ton, and Wang Zongyin, on Analysis of Vibration of Embedded Footings, Research Report 7925, Central Research Inst. of Building and Construction of Metallurgical Ind., 1979

# Landslides in Rock Slopes during January 19, 1975, Kinnaur Earthquake in Himachal Pradesh, India

Lakshman Saran Srivastava

Professor, Department of Earthquake Engineering, University of Roorkee, Roorkee, India

**SYNOPSIS:** Ground failures in rugged terrain with more than 10,000ft (3000m) elevation above mean sea level in the epicentral tract of 19 January 1975 Kinnaur earthquake in Himachal Pradesh, India, indicate that most of the earthquake generated landslides occur in surficial cover. The collapse of such material on steep slopes often result in cascading rock avalanches obliterating roads and other constructions lying on its way. The accumulated debris during this earthquake dammed Parachu river creating a reservoir behind it. The dislodging, overturning and uplift of boulders on hill tops and scabing and slabbing of rocks along joints and other weak zones resulting in loosening, dilation and crumbling of frozen formations indicate that seismic waves incident on rock slope surface and near ground discontinuity surfaces filled with frozen ice on reflection as tensile stress waves shattered the ground. The study indicates the significance and desirability of detailed study of surficial cover on rock slopes in mountainous terrains for evaluation of stability of hill sides during earthquakes. In high altitude frozen ground and rock slopes, seismic stress waves play a significant role in shattering near surface rock mass.

## INTRODUCTION

An earthquake, causing severe ground motion in parts of Kinnaur and Lahaul-Spiti districts of Himachal Pradesh in Indian Himalayan Orogenic belt and Tibetan Plateau border region, occurred on January 19, 1975. Preliminary estimates of magnitude and focal depth of the main shock from macro-seismic data indicated the magnitude 6.7 and depth 25 km (Singh et al, 1975). The parameters of this event as reported by National Earthquake Information Service of USA are: origin time-08 h 02 m 02.55 (UTC), epicentre-32.45°N; 87.43°E, focal depth-normal, and magnitude-6.8. Figure 1 shows isoseismals of the earthquake in Himachal Pradesh (Singh et al, 1977). In addition to loss of life and damage to various constructions during this earthquake, extensive landslides, rock falls and avalanches in the snow bound and frozen ground in the rugged terrain of the area with more than 10,000ft (3000m) elevation above mean sea level, caused considerable damage to roads and structures. Fissures were developed in the ground. Greater damage to the ground and buildings was noted in north-south trending zone following Parachu and Spiti river valleys and the alignment of major fissures along this zone (Fig. 2) suggest genetic relation with a probable tectonic lineament named as Kaurik-Chango fault by Singh et al (1977). The earthquake provided an opportunity to observe rock slope failures in high altitude mountainous area and study their probable mechanisms.

## ROCK SLOPE STABILITY

Rock slopes with critical stability, when subjected to strong ground motion, can undergo irreversible displacements, which initiate movements leading to catastrophic landslides and slips. The rock mass movement during earthquakes depend on combination of factors governed by the properties and the structure of insitu rock mass and overlying surficial material, inclination and height of the slope, geohydrological conditions, climate and the stage of operative surface geological processes of erosion and denudation affecting their stability. Investigations for rock slope stability evaluation are directed to workout the general geological conditions with reference to spacial distribution of different rock formations and rock defects, assessment of their strength and deformation characteristics, monitoring of their behaviour in the prevailing geomorphological, geological and geohydrological environment, prediction of probable changes in physical and engineering properties as well as induced stress (pressure) conditions in the rock mass during earthquakes and extreme hydrometeorological conditions and workout the failure mecha-

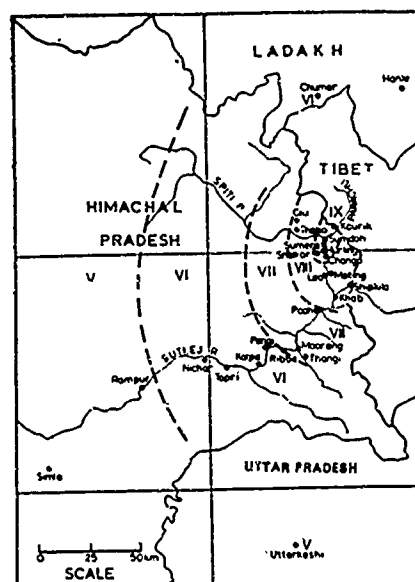


Fig. 1. Isoseismals (MM intensity) of 19 January 1975 Kinnaur Earthquake.

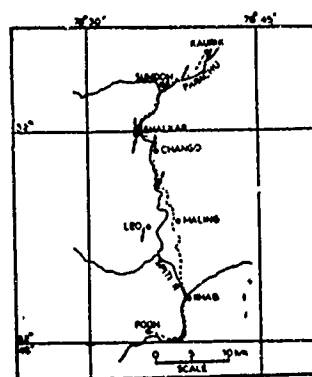


Fig. 2. General trend of ground fissures in area affected by 1975 Kinnaur earthquakes.

nism.

The geomechanical process leading to sudden failure of a rock slope consist of separation of volume of rock mass from the bulk of the relatively stable rock, and its outward and downward movement from the hillside. The separated mass may consist of intact rock or slowly (creep) deformed, ruptured, fragmented or dilated rockmass, or overlying sedimentary, glacial or weathered rock cover. Based on the topographic situation, in addition to sliding on the surface of separation (failure) the detached rock volume may undergo free fall, collapse, tumble down with leaps and bounces, run down slope or form a cascading avalanche. The causative mechanisms, resulting in loss of strength or development of stress, to produce rupture and sliding (and or detachment) of rock mass or tilting, overturning and movement of rock fragments, during earthquakes are effects of reflection and transmission of propagating seismic stress wave at major discontinuities separating intact rock from relatively loose rock mass, alluvial and glacial material or weathered rock cover (or rock-air boundary), and inertia forces induced in the rock mass volume on excitation through interaction of predominant periods of strong ground motion. It is difficult to account for all the possible factors due to scanty geological and geotechnical information. In many cases it is not possible to decipher all the parameters and to reach definite conclusions as the results of geognostic investigations are often open to various interpretations. Thus relative influence of various parameters can be considered in landslide studies. A geologists intuition and an engineering judgment is required in assessment of the probable kinematics of landslides in prevalent geological situations.

Study of stability of various segments of hillsides with high peaks and deep valleys, has to take into account the overall behaviour of the slopes from the top of the mountain to the valley base, as the operative static (and dynamic) forces differ at various elevations. In the upper reaches there is general splitting and loosening of rock along joints and other discontinuity surfaces during extreme climate, without any significant deformation and alteration of rock material. The loosened rock fragments cover the intact rock mass and in high attitude areas such material descend downwards with snow due to gravitational creep, avalanches, high velocity winds or snow storms forming bare rock peaks. The rock scree thus gradually thickens down slope and gets integrated with glacial and glacio-fluvial deposits in the valleys. In the lower parts of the slopes the rock below the scree and talus material and other surficial deposits, remain tightly wedged along discontinuity surfaces. However lateral strain under the vertical load of the mountain range results in outward movement of the rock mass. On being pushed out the rock mass undergoes dilation forming a loose stack of rock units (wedges) bounded by relief joints and openings. Thus even if the hillside is stable, in course of time rock mass may be pushed out to slide or tumble down, along with its overlying surface cover, if any. On exposure to earthquake hill side segments from the valley base to the top would undergo different movements resulting from effects of propagating stress wave and inertia forces induced in the rock mass due to variations in ground motion and characteristic impedance.

#### WAVE PROPAGATION

The force acting in the rockmass changes rapidly during stress wave propagation and the pressure acting for the particular duration of time at a point creates stress. For a one dimensional propagation in rockmass 'A' the force in the incident wave ( $P_i$ ) on the interface with another rockmass B, the force in the transmitted wave ( $P_t$ ) in rockmass B and force in the reflected wave ( $P_r$ ) in rock mass A can be evaluated from the following relation (Coats, 1987).

$$P_t = 2 P_i / (1+n) \quad (1a)$$

$$P_r = P_i (1-n)/(1+n) \quad (1b)$$

where  $n = (\rho_A E_A / \rho_B E_B)^{1/2}$  or  $(m_A K_A / m_B K_B)^{1/2}$ ,  $\rho$  is density and  $E$  is modulus of elasticity ( $m$  is mass per unit volume or length and  $K$  is stiffness) of rockmass A and B. Due to difference in wave velocity in the two rock masses the wave length of the incident and reflected waves are same. However the wave length of the transmitted wave is different. From equation (1) it is noted that when ratio  $n$  is greater than 1 wave will be tensile. The transmitted wave will always be compressive. When  $n$  is less than 1 the reflected wave will be compressive. When  $n$  equals infinity (rock-air boundary) the reflected wave equals the incident wave in magnitude and if the magnitude of the reflected tensile force is greater than about 10 percent of the compressive strength, it will cause tension fractures resulting in scabbing of rock. On such fractures the detached fragments would move in the direction of the incident wave with the velocity of the stress wave. In addition to longitudinal wave (P-waves), there are shear waves (S-waves) with particle motion transverse to the direction of the wave propagation that are transmitted through the rock mass during earthquakes. Besides the P and S waves (SV, SH Love waves), Rayleigh waves (R-wave) are transmitted along the ground surface in which particle vibrate in a plane parallel to the direction of the wave propagation and at right angles to the surface with an up and down and longitudinal motion similar to waves in water. The R-wave affect near surface ground, and the depth of influence can be calculated from their displacement amplitude and frequency records.

#### DAMAGE TO GROUND

Landslides, rock falls, avalanches, falling boulders and large rock fragments damaged and blocked roads, broke telegraph lines and completely disrupted means of transport and communications in Kinnaur and Lahaul-Spiti district during 1975 Kinnaur earthquake. Most of the affected area lie at an altitude above 10,000ft (3000m). The earthquake is reported to have caused damage across the Indian border in Tibet (China). Eye witnesses on the Indian side stated that they saw Tibetan hillocks crumbling with a deafening sound in heaps of debris. On the Indian side the severely affected zone extended for a distance of 25 miles (40km) from Kaurik towards south covering an approximate area of 300 sq miles (800 sq km) in Parachu and Spiti river valleys.

#### Fissures

Villages in the area have been located on hill slopes and flat lands over glacial till and moraine and river terrace



Fig. 3. Kaurik village located on glacial moraines which was completely destroyed large chunks were dislodged and slipped at the crest of upper terrace.

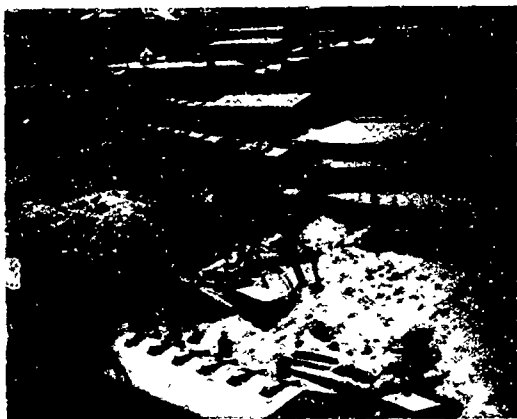


Fig. 4. Buildings constructed on stable ground in Kinnaur.

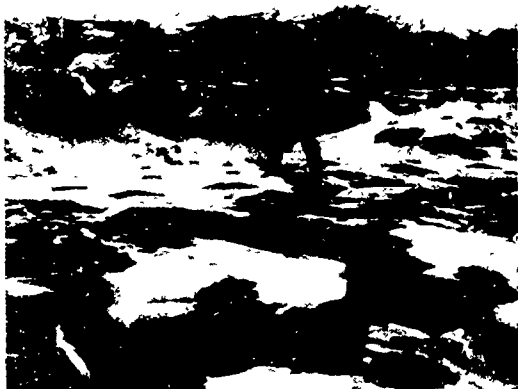


Fig. 5. Ground fissures which cut across Kaurik village.



Fig. 6. En echelon ground fissures (partly covered by subsequent snowfall) near Kaurik village.

(Fig. 3 and 4). Extensive fissures were developed in the frozen ground in glacial moraines overlying bed rock. Figure 5 show fissures passing through Kaurik village which was completely destroyed, and individual fissures extended to 50 ft to 100 ft (15-30m) in length trending  $N 335^\circ$  to  $N 35^\circ$  (Fig. 6). Width of openings varied from fraction of an inch to several feet (few cms to a metre) with down throw towards west. A fracture zone with opening of 4 to 6 in (10-15 cm) with individual en echelon fractures could be traced over 1100 yards (1 km) extending from the edge of the terrace south of Kaurik village, towards hill slopes north of the village. Fissures in the ground transverse to the ridge covered with frozen glacial moraines with openings from a fraction of an inch to 6 in (15 cm) developed between Sumdoh and Kaurik with their general trend along  $N 25^\circ$ .

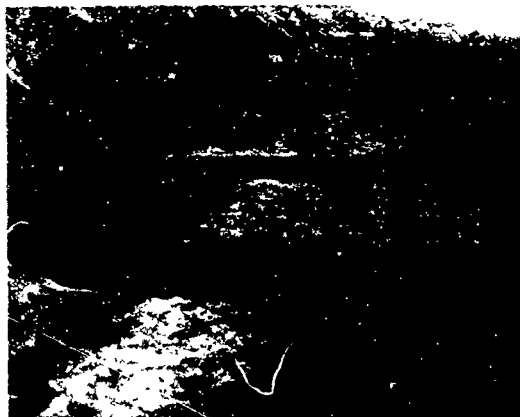


Fig. 7. Step faults across road between Sumdoh and Kaurik.

Figure 7 show step faults across India-Tibet road between Sumdoh and Kaurik with fractures trending along  $N 350^\circ$  and continuing towards hill side, with openings upto 2 ft (60 cm) width and extending to depths of 10 to 20ft (3 to 6m). At Sumdoh fissures overlapping each other were observed on top of river terrace with openings upto 2 in (5cm) in width extending over 55 yards (50m) length in  $N 40^\circ$  to  $N 60^\circ$  directions. Carbonaceous shales on left bank of spiti river near Shalkar developed fractures along preexisting north - south trending vertical joints. Similar vertical to steeply dipping fractures trending  $N 35^\circ$  to  $N 5^\circ$  were observed in lacustrine clay deposits with opening upto 6 in (15 cm) in width, and tabular slabs of clay were dislodged from vertical cliff transverse to such fractures. Similar fractures trending N-S, were observed in limestones at a distance of 2.5 miles (4km) from Shalkar.

Fig. 8 shows fracture trending  $N 20^\circ$  with down throw towards east in river bed of Spiti between chango and Mallang. Extensive fractures developed in glacial moraines forming flat ridge near Leo, and width of fissures varied upto 2.5 ft (75cm) with their trend towards  $N 345^\circ$ . Similar fractures were noted on hill slopes above Leo village with a trend towards  $N 10^\circ$ . Figure 2 show the general trend of ground fissures observed at various locations.

#### ROCK SLIDES

Innumerable instances of sliding and fall of blocks of frozen glacial moraines from the crest of the terraces (Fig. 3) were observed in the macroseismic tract. Major rock slides occurred along hill slopes, which continued for several days during moderate aftershocks. The badly affected regions were beyond Mallang, where in rock falls, landslides and rock avalanches damaged roads and disrupted traffic along India-Tibet road and at many locations the road was comp-



Fig. 8. Ground fissures in Spiti river bed.



Fig. 11. Stoppage of water flow in a spring in limestones near Shalkar village.



Fig. 9. Widening of pre-existing relief joints in hill slope cutting near Kah.



Fig. 12. Dislodging and overturning of boulders at the top of the ridge near Leo.



Fig. 10. Sliding of rock wedge in carbonaceous shales on India-Tibet road between Shalkar and Sumdoh.

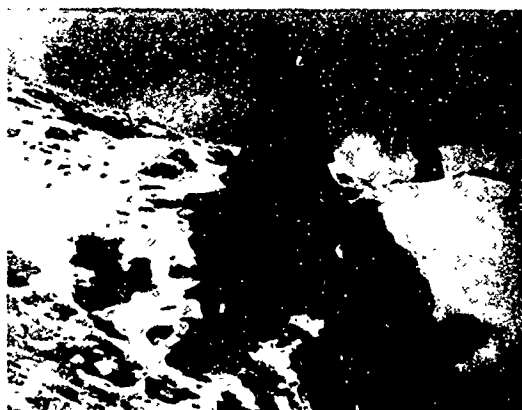


Fig. 13. Overturning and heaving up of large boulders at the crest of hill slope near Leo.



Fig. 14. Bending of telegraph pole resulting from impact of flying rock fragments.



Fig. 15. Large boulder fallen on road pavement between Mallang and Chango. Landslide in the back ground has obliterated the road.



Fig. 16. Collapse of check post at Shalkar on India-Tibet road. Big boulder rolling down from hill slope caused collapse of the building.

letely destroyed. Flat topped hill slopes in glacial moraines developed extensive cracks, indicating initiation of failure of slope towards the valleys. Similar fissures were observed parallel to road pavement on glacial moraines with wide openings upto 20m (50cm) in width. Loosening of rock mass along preexisting joints and fissures was noted on hill slopes. Figure 9 shows separation of rock mass along pre-existing discontinuity surfaces (bedding and joints) and sliding of a rock wedge in carbonaceous shales with rock debris fall at its bottom on India-Tibet road between Shalkar and Sumdoh. However such failure were of small size and very few in number and in general insitu rock mass remained stable during the earthquake. Widening of relief joints was observed in cuttings transverse to hill slopes. Figure 10 shows loosening of rock mass and widening of openings during the earthquake along relief joints in hill slope cutting near Kah between Khab and Mallang. Loosening and readjustment of rocks resulted in changing the seepage outlets in some of the surface springs in the area. Figure 11 shows the outlet of a spring in limestone near Shalkar village, which ceased to flow due to readjustment along joints. This spring has emerged due to opening of joints at a lower elevation after the earthquake.

Overtuning and sliding of boulders and rock blocks at the top of ridges (Fig. 12) and steep slopes took place by development of tension cracks. Seismic stress waves incident at the frozen ground surface on reflection as tensional stress wave shriveled and blighted the frozen ground and rockmass. The resulting scabbing and slabbing of rock mass along joints, partings and other weak planes caused loosening, dilation and crumbling of hill sides, often with deafening sounds in heap of debris. The reflected tensile stress wave caused separation along discontinuity surfaces filled with frozen ice and weathered material, frozen-glacial maraines and fluvio glacial deposits forming flat terraces and mounds along the river valleys developed similar tension fractures resulting in dislodging, overturning and heaving up of large boulders (Fig. 13) and chunks of rock mass. Boulders at hill tops were reported to toss up and down. Fragments from steep rock slopes on rupture flew off with seismic (P-wave) velocity and hit telegraph poles (fig. 14), trees and roof tops and some of the flying fragments pierced through telegraph poles. Large dislodged boulders and chunks of rock at many places fell on road (Fig. 15) disrupting and damaging hillside and roadside houses (fig. 16).

The fragmentation depending on nature and spacing and attitudes of preexisting discontinuity planes in insitu rock and thickness of frozen ice and ground composed of glacial and glaciofluvial material produced loose tabular



Fig. 17. Rock avalanche debris in quartzites along India-Tibet road between Chango and Shalkar.





Fig. 18. Catastrophic failure of slopes along India-Tibet road in weathered and jointed granitic gneisses.



Fig. 19. Landslide in thinly foliated phyllitic schist (covered by subsequent snow fall) on India-Tibet road between Chango and Shalkar.

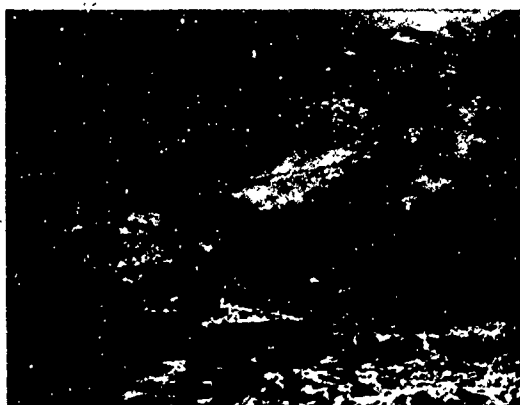


Fig. 20. Formation of debris dam across Parachu river between Sumdoh and Kaurik.

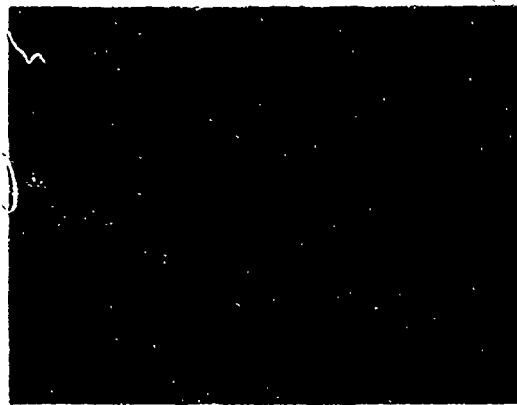


Fig. 21. The new path carved out by Parachu river on the left of its original course. Fissures are observed on the right hand side of the photograph.

and prismatic slabs of clay, carbonaceous shales, phyllites, quartzites, schists, gneisses, and unconsolidated materials, which cascaded along the hill slopes (fig. 17) obliterating the roads and other constructions lying on its way. Such surface runs and rock avalanches caused extensive damage to the India-Tibet road, which disrupted rescue and relief operations. There were catastrophic failures and landslides along a four kilometer stretch of the road on the right bank of Spiti river (fig. 18) and in some stretches the road was completely obliterated. Such slopes were composed of variety of thinly bedded carbonaceous shales with close spaced joining, quartzites, phyllitic schists, and granite gneisses. Fig. 19 shows landslide mass in thinly covered foliated phyllitic schists which entombed three ponies and a cow moving on the road which was completely destroyed.

Majority of catastrophic hill side failures were in steep rock slopes with surficial cover of scree material and loose fragmented aggregates, which in general had negligible soil and vegetal cover. Due to the dynamic amplification of ground motion at the hill tops, sliding, overturning and rolling of rock fragments initiated the slip at the higher elevations which gathered momentum in their descent hitting and dislodging other rock pieces and such bombardment gradually grew into a large mass hurling down slope with great speed forming huge rock debris in the valley base. Parachu valley was filled by such a debris from its right bank at a location between Sumdoh and Kaurik (fig. 20). The debris filled the valley upto a height of about 200 ft (60m) and blocked the flow of water creating a reservoir behind it. The debris dam of about 200 ft height and 500 ft (150m) in length was formed. The water started overflowing the debris in about six days and carved out a channel (fig. 21) shifting the course of Parachu by about 200 to 250ft (60-75m) from its original course towards its left bank within the flood plain of the valley. The newly created meander joined the original course of the river at a distance of about 1500ft (450m). Fissures forming linear scarps with up throw of 20-40m (50-100cm) were formed in the river bed (fig. 21).

#### CONCLUSIONS

Evaluation of rock slope stability during earthquakes is an essential exercise in implementation of development plans in active mountainous regions. Rock slopes carved out by geological processes in general have surficial cover of varying thickness. Steep slopes and narrow valleys with such loose rock overburden undergo mass movements causing extensive rock avalanches, rock falls and slides in which

the failure in general is restricted within surficial material and loose rock, and insitu rock forming the bulk of the hill mass remains stable during earthquakes. The nature and extent of such cover controls the loosening of slope material and its movement during earthquakes. In high altitude frozen ground or massive rock slope surface the incident seismic stress wave play a significant role in shattering the near surface rock mass and in detachment, overturning, uplifting, sliding or fall of boulders or chunks of rock from hill tops, higher reaches of rock slopes and crest of terraces.

#### ACKNOWLEDGEMENTS

The damage survey was carried out by Dr. S. Singh, Dr. A.K. Jain and Mr. P. Sinha.

#### REFERENCES

- Coates, D.F., (1967), Rock Mechanics Principles, Mines Branch Monograph 874 (Revised 1967), Dept. Energy, Mines and Resources, Government of Canada, Queen's Printer and Controller of Stationery, Ottawa, Canada.
- Singh, S., V.N. Singh, P. Sinha, A.K. Jain and L.S. Srivastava, (1975), A Preliminary Report on January 19, 1975 Kinnaur Earthquake, Bull. Ind. Soc. Earthq. Tech., Vol. 12, No.1.
- Singh, S., A.K. Jain, V.N. Singh and L.S. Srivastava, (1977), Damage During Kinnaur Earthquake of January 19, 1975 in Himachal Pradesh, India, Proc. 6th World Conf. Earthq. Engg., New Delhi, Jan. 1977, Vol. 1, Sarita Prakashan, Meerut, India.

## Probabilistic Analysis of Earthquake-Induced Pool Release

**T.F. Wolff**

Assistant Professor of Civil Engineering, Michigan State University,  
East Lansing, Michigan

**G.L. Hempen**

Geophysicist, Geotechnical Branch, St. Louis District, U.S. Army  
Corps of Engineers, St. Louis, Missouri

**M.M. Dimberger**

Civil Engineer, Geotechnical Branch, St. Louis District, U.S. Army  
Corps of Engineers, St. Louis, Missouri

**B.H. Moore**

Chief, Geotechnical Branch, St. Louis District, U.S. Army Corps of  
Engineers, St. Louis, Missouri

**SYNOPSIS:** Wappapello Dam was constructed in 1938 near the New Madrid seismic region. Loose sands in the dam foundation led to concern for liquefaction and embankment sliding if a large earthquake were to occur. However, it was also recognized that the operation of the dam for flood control results in relatively low reservoir levels the majority of the time, substantially reducing the risk of earthquake-induced flooding. Because of these factors, a probabilistic analysis was performed to assess the likelihood of the combination of required events leading to an earthquake-induced pool release. Results of such analyses provide better information on which to make both quantitative and qualitative judgements regarding remedial action.

### INTRODUCTION

Wappapello Dam is a flood control dam in southeastern Missouri, near the New Madrid seismic region. Its location is shown in Figure 1. The dam consists of a compacted earth embankment with a concrete outlet conduit and a concrete overflow spillway. The New Madrid series of earthquakes in 1811 - 1812 was among the largest and most prolonged sequence of seismic events on record. The dam was designed and constructed in the late 1930's, before the development of modern procedures both to analyze embankment stability during earthquakes and to consider defensive design alternatives. Nevertheless, some defensive measures were provided in the dam, such as flat embankment slopes and excess freeboard. A portion of the dam is underlain by loose sands for which liquefaction is a concern. Liquefaction of these sands could induce an embankment slide, in turn causing a pool release. Because of these concerns, the safety of Wappapello Dam during earthquakes was reviewed by its owner, the U.S. Army Corps of Engineers (CE), St. Louis District.

The risk of an earthquake-induced pool release at Wappapello is tempered by the fact that a combination of rare or unlikely events must first occur. The occurrence of an earthquake producing sufficient acceleration to cause liquefaction is itself a rare event. Secondly, a sufficiently high pool level is unlikely. The pool level is usually maintained as much as 60 feet (ft) below the dam crest to provide storage for flood control operations. Higher pool levels occur during extremely rainy periods, but even at spillway level the pool is 25 ft below the dam crest. Water has flowed over the spillway only once in the dam's 50 year history. Thirdly, if a liquefaction-induced slide did occur, the slide scarp elevation is uncertain. For a pool release to occur, a high pool level and a low upstream scarp elevation must occur simultaneously. If the remnant embankment was sufficiently higher than the pool, a pool release would not occur even though a slope failure occurred.

The likelihood of the combination of requisite rare events was assessed by a probabilistic analysis. The results of such an analysis provide an improved information base when deciding on the most appropriate and economic remedial action. The analysis considered uncertainty regarding earthquake magnitude, uncertainty regarding pool elevation at the time of earthquake, and uncertainty regarding the scarp elevation of a possible slide.

### SUBSURFACE INVESTIGATION

A typical embankment cross-section and generalized subsurface profile for Wappapello Dam are shown in Figure 2. The embankment materials are clayey sand and clayey gravel. Foundation materials consist of alluvial deposits from the St. Francis River overlying Ordovician dolomite and sandstone. Detailed subsurface cross-sections were constructed from the original and newly-obtained foundation information. Existing information included results from 63 borings made for design in the late 1930's, an extensive subsurface investigation made by the CE, Memphis District in the late 1970's, and geophysical investigations were conducted by the CE, Waterways Experiment Station in 1981 and St. Louis District in 1984. New investigations made for the present assessment included 20 standard penetration test (SPT) borings with hammer energy measurements and electrical borehole logging. Menard pressuremeter testing was performed in four of the borings. Geophysical investigations included electrical resistivity profiling and crosshole seismic studies. Laboratory investigations included classification testing, triaxial testing on cohesive materials, and cyclic triaxial tests on foundation sands with measurements of pore pressure response.

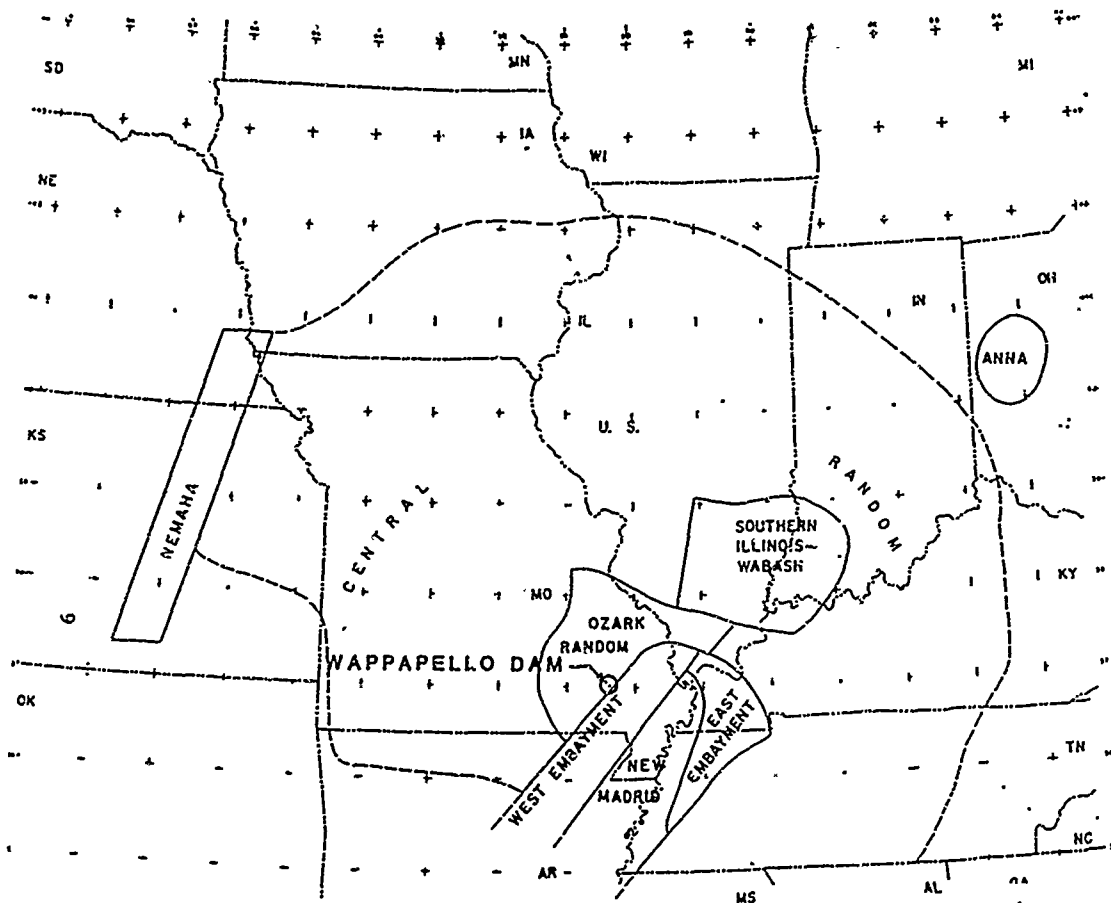


Figure 1. Location of Wappapello Dam and Adjacent Earthquake Source Zones.

## SEISMOLOGICAL STUDIES

A very detailed seismological investigation was conducted by the St. Louis District, which is only briefly summarized here. Several earthquake source zones have a potential effect on ground motion at Wappapello Dam, although the New Madrid zone is the most significant. Source zones in the region have been identified by USAED, 1981, and Hempen, et. al. 1981; the source zones are shown in Figure 1. Magnitude-recurrence relationships for these zones were previously developed by the St. Louis District (USAED, 1981). A probabilistic seismic analysis program (McGuire, 1976) was utilized that simultaneously considered randomness of earthquake size, randomness of the earthquake location within the zone, and distance from the dam to the earthquake location. Modified Mercalli Intensity, horizontal acceleration, and particle velocity at the site for specific probability values were determined with published recurrence formulas for intensity, acceleration, and velocity. Several attenuation relationships were considered in developing the expected site accelerations. The acceleration values assigned for the site are shown in Table 1.

The probabilistic ground motion evaluation estimates vibration parameters; it does not yield unique magnitude values at specific distances. Specific magnitude values, required for another

portion of the analysis, were developed from the inverse of the attenuation functions with the probabilistic ground motion data for an event 30 miles from the site. This distance is the closest approach of the New Madrid Fault to the dam site. The resulting equivalent magnitudes are also shown in Table 1. The earthquake magnitudes are more uniform in the body-wave scale, but appear to rise rapidly for great earthquakes in the Richter scale. Note that the increase in acceleration with longer return periods is systematic.

TABLE 1. Seismologic Recurrence Relationships.

| Return Period (yrs) | Annual Exceedance Risk | Peak Bedrock Acceleration (%g) | Equivalent Richter Magnitude, M, at 30 mi |
|---------------------|------------------------|--------------------------------|---|
| 50                  | 0.02                   | 11                             | 5.5                                       |
| 100                 | 0.01                   | 15                             | 6.0                                       |
| 250                 | 0.004                  | 20                             | 6.7                                       |
| 500                 | 0.002                  | 25                             | 6.9                                       |
| 800                 | 0.0013                 | 28                             | 7.3                                       |
| 1,000               | 0.0010                 | 30                             | 8.3                                       |

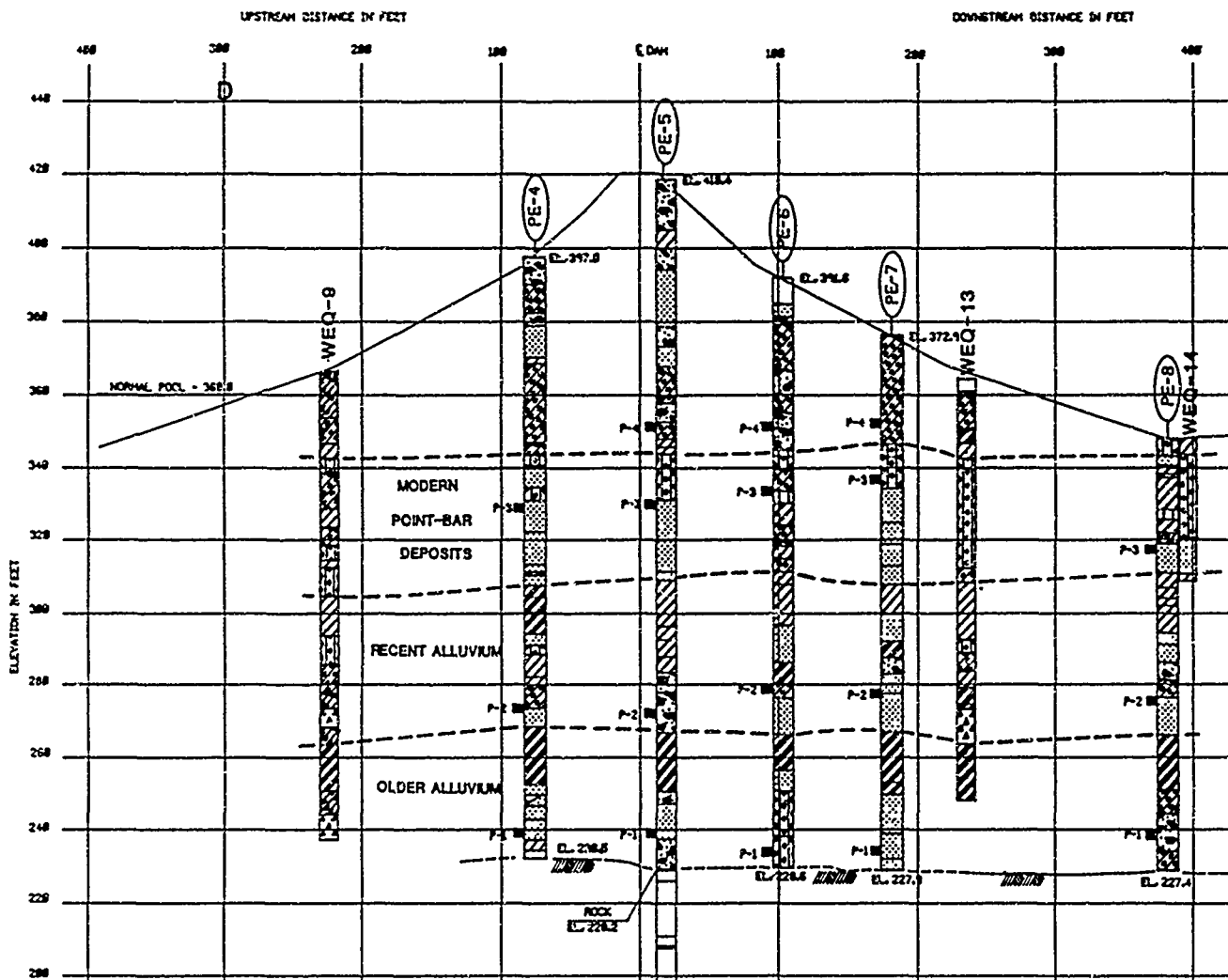


Figure 2. Generalized Cross Section of Embankment and Foundation.

#### LIQUEFACTION POTENTIAL

The most plausible potential failure mode was considered to be liquefaction of certain loose foundation sands. Liquefaction-induced settlement was of little concern as the maximum possible differential settlement, assuming a volume reduction to the minimum void ratio, was estimated to be less than a foot. Pool release caused by structural failure of the gated spillway or outlet conduit was not considered in the present analysis. Liquefaction could, however, trigger a slide through the embankment which could, in turn, result in an uncontrolled pool release. Thus, the potential for liquefaction to occur is the controlling embankment defect to be evaluated.

The Seed and Idriss (1981) method was used to assess liquefaction potential. This method requires a specific value for Richter magnitude,  $M$ . The required magnitude values were obtained from the probabilistic accelerations and the attenuation formulae for a causative event 30 miles from the site.

The liquefaction analysis also requires the standard penetration resistance or  $N$  value. Seed, et. al. (1985), recommended an energy ratio of 60% for standardization when interpreting  $N$  values for liquefaction assessments. On-site measurements of the energy delivered in the SPT indicated an average energy ratio of 54%. The energy correction for the test results at the site would then be:

$$N(60) = N \times (54/60) = 0.9 N \quad (1)$$

However, Seed et. al. (1985) also recommend a 10% increase in measured blowcount for the ASTM sampler used. Although this sampler has the standard 1-3/8 inch shoe, the barrel is enlarged to accept liners, which reduces the driving resistance. The two corrections nearly cancel, allowing  $N(60)$  to be taken as  $N$ . Corrections were also applied to the  $N$  values to account for overburden stress and the presence of fines in the sand.

Results of the liquefaction analyses indicated that Modern Point-Bar sands on the inside of the old river bend between dam stations 11+50 and 13+00 and above elevation 300 ft (National Geodetic Vertical Datum) would be susceptible to liquefaction under cyclic shear stresses generated by the 800 year earthquake.

#### EMBANKMENT STABILITY ANALYSES

The plausible modes of pool release induced by a significant earthquake are piping through the embankment and flow over the remnant embankment following an embankment slide. Piping through the cohesive embankment and undermining of the foundation materials is considered highly unlikely, because of the long path length required to produce a catastrophic water discharge. The embankment slope is so flat that inertial forces from the earthquake would not induce a slide on a stable foundation. A slide can be caused by liquefaction of the loose, Modern Point-Bar sands in the unmodified foundation of the dam.

A series of slope stability analyses were performed representing the range of possible earthquake events and failure arcs. The analyses utilized the Simplified Bishop method and considered the development of excess pore pressure in the Modern Point-Bar sands prior to liquefaction. The analyses used undrained strengths in the cohesive embankment and foundation materials and used drained strengths with specified pore pressures in the foundation sands. The presence of gravel in the embankment precluded conventional undisturbed sampling and laboratory testing. Based on the results of Menard pressuremeter testing, and undrained strength of 3000 pounds per square foot was used for analysis. The drained friction angle was taken as 28 degrees for the Modern Point Bar sands and 35 degrees for the underlying alluvial sands.

Bedrock motions for the 250, 500, and 800 year events were modeled using historic strong motion records from other sites with similar peak velocities. Minor scaling of the records was done to match peak acceleration values predicted from the seismologic analysis. The foundation and embankment motions were obtained from the bedrock motions using the computer program SHAKE (Seed, et. al., 1975). The SHAKE program was also used in conjunction with the cyclic triaxial testing to assess the pore pressure ratio,  $r_u$ , that would develop in the sand for various

events. To make such an assessment, the number of equivalent loading cycles,  $n_{eq}$ , for a par-

ticular shaking event (based on the induced shear stress predicted by SHAKE) was divided by the number of cycles to failure (initial liquefaction),  $n_1$ . The resulting ratio,  $n_{eq}/n_1$ ,

was then related to the pore pressure ratio,  $r_u$ , using the laboratory test data.

Relationships between factor of safety (FS) and scarp elevation were developed for each event from the stability analyses. For the 500 year event, the minimum FS obtained was 1.02, indicating a just stable imminent sliding condition. For the 800 year event, factors of safety as low

as 0.03 were obtained, and sliding is expected to occur. Therefore, the annual risk of a slide induced by liquefaction or high excess pore pressure is slightly less than 1 in 500.

#### INTEGRATED PROBABILISTIC ANALYSIS

The likelihood, or chance, of a pool release caused by an earthquake is the multiple of several events: all chances of a significant, nearby earthquake times the probability that particular earthquakes produce embankment defects times the likelihood of an embankment slide due to any earthquake-induced defect times the probability that the pool may be catastrophically released by the embankment slide. The critical defect that may be caused by a large earthquake is foundation liquefaction. An embankment slide, in turn, may be the outcome of a large liquefied volume within the foundation. Further, a substantial discharge is likely only for a pool level at, or exceeding, the remnant embankment following a slide. The remnant slide will be described as the upper elevation of the scarp plane contact with the remaining embankment slope face.

An earthquake-induced pool release for Wappapello Dam will occur only if an embankment slide is triggered by liquefaction and the reservoir pool elevation is at, or above, the resulting slide scarp. Lake Wappapello has an unusually large amount of freeboard, typically 60 ft, or 75% of the dam's total height. This results in a considerable likelihood that the pool would be retained, even if the embankment was unstable during larger earthquakes. The occurrence of a slide without a pool release is of significantly less concern than a pool release.

The probability of pool release can be mathematically expressed in a form similar to the previously expressed narrative.

$$\Pr(PR) =$$

$$\int_{\text{all } M} \Pr((PE \geq SE) | SL) \times \Pr(SL | M) \times \Pr(M) dM \quad (2)$$

where:

$\Pr(x)$  is the probability of event  $x$ ,  
 $PR$  is the event of a pool release,  
 $PE$  is the pool elevation,  
 $SE$  is the slide scarp elevation,  
 $SL$  is the event of an earthquake-induced slide,  
 $M$  is the earthquake event of magnitude  $M$ ,  
 and  $|$  is read "given."

The probability of a given earthquake magnitude,  $\Pr(M)$ , was determined by using the annual exceedance risk from Table 1 as a cumulative distribution function (cdf) for earthquake magnitude. Interval differences from this cdf were taken to develop an equivalent discrete probability distribution of shaking events. Each considered event may occur in a given year with the interval probability in Table 2.

TABLE 2. Probability of Discretized Earthquake Events.

| Return<br>Period<br>Interval<br>Midpoint(yrs) | Richter<br>Magnitude<br>M     | Interval<br>Limit<br>(yrs ) | Annual<br>Exceedance<br>Probability | Interval<br>Probability |
|---|-------------------------------|-----------------------------|-------------------------------------|-------------------------|
| all <350                                      |                               |                             |                                     | .993                    |
| 500   | 6.9                           | 350                         | .0029                               |                         |
| 300   | 7.3                           | 630                         | .00159                              | .0013                   |
| 1,000   | 8.3                           | 900                         | .00111                              | .00048                  |
| 2,000   | > 8.3 or<br>closer<br>to site | 1,400                       | .00071                              | .00040                  |
|   |                               | all > 1,400                 |                                     | .00071                  |

The probability of a slide occurring for a given level of shaking or magnitude,  $Pr(SL|M)$ , is:

$$Pr(SL|M) = Pr(SL|LQ) \times Pr(LQ|M) \quad (3)$$

where  $LQ$  is the occurrence of liquefaction.

The probability of liquefaction for a given magnitude,  $Pr(LQ|M)$ , is quite high, but not 100%, for events equal to and exceeding the 500 yr earthquake. This probability was assumed to be 0.95. This was a subjective assessment, but is conservative since distance of the event to the site is not considered: the distance to the epicenter could be great.

The probability of a slide given that liquefaction occurs,  $Pr(SL|LQ)$ , is likewise high and was assumed to be 0.90.

Given that a slide occurs, the probability of the pool elevation exceeding the scarp elevation is the convolution of the two respective probability density functions,  $f_x$ , with respect to

the scarp elevation, (SE). The mathematical expression is equivalent to that given by Ang and Tang (1984) and Frudenthal, et. al., (1966) for the probability of failure in the capacity-demand problem:

$$Pr((PE \geq SE)|SL) = \int_{SE_{min}}^{dam\ crest} [1 - f_{PE}(SE)] f_{SE}(SE) dSE \quad (4)$$

If discrete intervals are made from the set of possible scarp elevations each with probability  $Pr(SE|SL)$ , this becomes:

$$Pr((PE \geq SE)|SL) = \sum_{SE_{min}}^{dam\ crest} Pr(PE \geq SE) \times Pr(SE|SL) \quad (5)$$

The probability of a slide and the probability of the scarp elevation are functions of the earthquake magnitude. Thus, equation (2) was integrated over the range of possible earthquake magnitudes. To facilitate numerical integration, the range of earthquake magnitude or "size" was converted to discrete averages of 500, 800, 1,000, and 2,000 year events. These events are considered representative of the entire interval between their logarithmic averages as shown in Table 2. All events in the range of interest are treated as one of these discrete events. For events with return periods less than 350 years, liquefaction (and thus an embankment slide) is not expected to occur. For events with return periods larger than the table values, a discussion of the maximum credible earthquake and probability theory beyond the scope of this paper is necessary. The estimates for events of greater return periods do not affect the calculations. Equation (2) is then summed over the discrete set of possible events.

A conditional probability density function for the scarp elevation,  $f_{SE}$ , was developed:

obviously, given that a slide occurs. The construction of  $f_{SE}$  is dependent upon three elevations: the highest, lowest and the most likely scarp elevations. The highest and lowest scarp elevations were assumed to correspond to a low FS sliding condition,  $FS < 1.1$ , or the top of the dam. The most likely scarp elevation was assumed to occur at intersection of the failure arc for the lowest FS and the face of the embankment. A triangular probability density function was assumed. A different density function was constructed for each of the three earthquake magnitudes of Table 2 based on the results of the slope stability analyses.

The probability density function for the pool elevation relative to the slide scarp elevation,  $f_{PE}(SE)$ , was constructed from historical records

of the pool since impoundment. Seventy percent of the time the freeboard exceeds 60 ft. The freeboard exceeds 45 ft 90% of the time, and exceeds 36.5 ft 99% of the time. Taking differences between exceedance probabilities between two pool elevations gives the probability of the pool being in that respective range.

## Comparison of Probability Density Functions for Pool and Slide Scarp Elevations

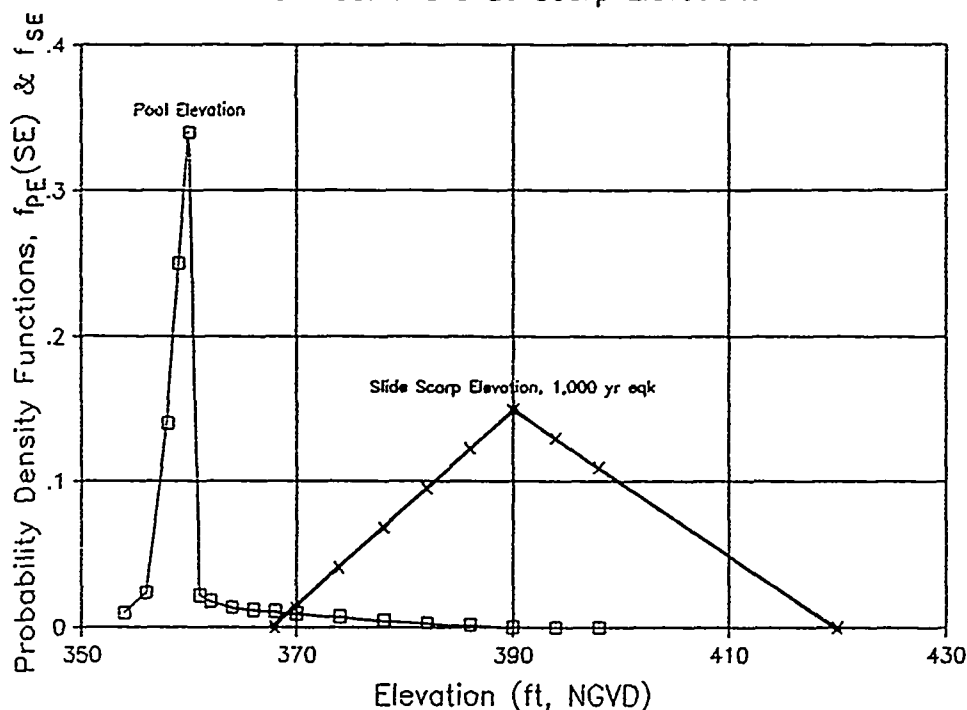


Figure 3. Comparison of Probability Density Functions for Slide Scarp and Pool Elevations.

The density functions for pool elevation,  $f_{PE}(SE)$ , and scarp elevation for the 1,000 year event,  $f_{SE}$ , are compared in Figure 3. The

shaded region of overlap between the two distributions is the region where the pool can exceed the scarp and pool release can occur. The convolution in Equation (4) is explained as follows: for any scarp elevation, the conditional probability of the pool elevation equalling or exceeding the scarp elevation is the area of the pool elevation density function above that scarp elevation. To obtain the total probability of the pool being at or above the aggregate scarp elevations, the conditional probabilities at each elevation possible are multiplied by the corresponding slide scarp probability, and the products integrated over the range of scarp elevations. This integration is performed numerically by treating the pool and scarp elevations as a series of discrete elevations, and summing the products.

The total annual risk of pool release is the combination of determined probabilities for all factors (Equations (3) and (5)), substituted in Equation (2) for each magnitude event. However, if annual interval probabilities were used, Equation (2) would yield the probability that the earthquake and high pool occur in the same year. It is assumed that the pool must be high on the same day that the earthquake occurs for pool to be released. Therefore, the interval probabilities are converted to daily probabilities. Equation (2) then yields the daily

probability of pool release. The daily probabilities are then converted to annual risks using the binomial distribution.

### RESULTS AND CONCLUSIONS

The annual risk of an "800 year earthquake" (1 in 800) is much larger than the risk of a pool release caused by such an event. The total annual risk of pool release due to all earthquake-caused embankment slides, was found to be on the order of 1 in 180,000.

The results of this probabilistic assessment can be used to assess the economics of structural remedies. A comparison of annualized damages from earthquake-induced flooding to the annualized cost of remedial measures was made for the Wappapello site and annualized construction cost was found to exceed annualized flooding damages.

The probability of reducing risk can also be considered. Rehabilitation of structures is not often considered on the basis of which of several structures has the greatest need, or which remediation system achieves the greatest reduction of hazard for a given expenditure. These controversial items can be discussed in terms of probability, but the decision to act or not act does not completely depend on quantitative factors.



The uncertainty associated with several elements of the analysis was not evaluated probabilistically. The probability of using correct strength and permeability values, for example, could be addressed. These items were not considered for two reasons: the choice to perform a probabilistic analysis developed after a deterministic assessment was made, thus significant reevaluation would be required to properly perform the assessment; and, many risks, other than earthquake-induced pool discharges, share the same elements of uncertainty when evaluated. Duplicative effort would be conducted for similar elements, if various risks were evaluated for comparison as single occurrence hazards.

There are two areas where additional studies might be considered. One such area would be the development of a statistically valid soil sampling and testing procedure. The second would be a more complete treatment of the uncertainty associated with pore pressure response during an earthquake. Recent advances in instrumentation have made it technically feasible to record pore pressure buildup in the field during a shaking event. The instrumentation of this or a similar structure has been recommended and is under consideration.

One important point requires emphasis. Probabilistic assessment only compares risk; it does not provide a basis for action. The repercussions of risk, including loss of life, require a qualitative evaluation leading to the decision to act or not to act. Even when cost factors are introduced and prevention costs exceed damage costs, as in this case, qualitative judgement is still required -- the event may or may not never occur.

## REFERENCES

- Ang, Alfredo H.-S., 1984, Probability Concepts in Engineering Planning and Design, Volume II: Decision, Risk, and Reliability, John Wiley and Sons, N.Y., 562 pp.
- Frudenthal, A. M., Garrelt, J. M., and Shinozuka, M., 1966, "The Analysis of Structural Safety," *Journal of the Structural Division, ASCE*, Vol. 92, No. ST1, Feb 66.
- Hempen, G. L., Klosterman, M. J., Moore, B. H., Rockaway, J. D., and Rupert, G. B., 1981, "Zonation of Central U. S. Earthquake Sources," *International Conference on Recent Advances in Geotechnical Earthquake Engineering and Soil Dynamics*, Vol. 1, pp. 541-544.
- McGuire, R. F., 1976, "FORTRAN Computer Program for Seismic Risk Analysis." USGS, Open File Rpt 76-67, Washington, DC, 90 pp.
- Schnabel, P. B., Lysmer, J., and Seed, H. B., 1972, "SHAKE: A Computer Program for Earthquake Response Analysis of Horizontally Layered Sites," *Earthquake Engineering Research Center, University of California, Berkeley, CA*, 88 pp.
- Seed, H. B., Tokimatsu, K., Harder, L. F., and Chung, R. M., 1985, "Influence of SPT Procedures in Soil Liquefaction Resistance Evaluations," *ASCE, Journal of Geotechnical Engineering*, Vol. 111, No. 12, pp. 1425-1445.
- Seed, H. B., and Idriss, 1981, "In-Situ Testing to Evaluate Liquefaction Susceptibility," *ASCE, Convention presentation, St. Louis, MO*, Preprint 81-544, 19 pp.
- U. S. Army Engineer District, St. Louis, (USAED), 1981, "Earthquake Potential of the St. Louis District," *St. Louis, MO*, 102 pp.

## Case History of Seismic Base Isolation of a Building— The Foothill Communities Law and Justice Center

Marshall Lew

Senior Engineer, LeRoy Crandall and Associates, USA

John C. Bowman, Jr.

County Geologist, County of San Bernardino, USA

**SYNOPSIS:** The Foothill Communities Law and Justice Center, located in seismically active Southern California, is the first building in the United States to be base isolated for seismic resistance. Natural rubber isolators with layers of steel plates were used to make the fundamental period of vibration of the base isolated building about twice as long as that for a comparable conventional fixed base building. Most earthquake energy is present in the shorter period ranges, and at longer periods, a building should be subjected to less earthquake input; this will allow buildings to be designed more economically and increase the likelihood of less damage, both structural and non-structural. The experience of the Law and Justice Center after three small earthquakes suggest that the concept is not only feasible, but may be the wave of the future for what would be relatively short period buildings.

### INTRODUCTION

The Foothill Communities Law and Justice Center (FCLJC) is the first building in the United States of America to utilize the principle of base isolation to resist strong earthquake ground motions. The principle of base isolation is completely opposite to the conventional technique of earthquake resistance in structures, which is to strengthen (stiffen) the structure. In adding stiffness to a structure, the structure will attract more force, making it more difficult to resist the earthquake forces and adding to the cost of the structure. Most low- to medium-rise buildings have fundamental periods of vibration in the range of periods where the earthquake energy is the greatest. If the fundamental period of the building can be shifted to a higher period where the earthquake energy is less, the building should be subjected to less induced forces. Base isolation introduces flexibility at the foundation level of a structure to limit the accelerations at the higher floors. Thus the superstructure will attract less force during an earthquake; this should make design simpler and the cost of the structure more economical. By reducing the forces in the structure, the likelihood of damage to non-structural elements of the structure (including contents) would be diminished. This could also reduce the hazard to human occupants.

### FCLJC BUILDING AND BASE ISOLATOR DESCRIPTION

The FCLJC building is four stories in height with a mechanical penthouse; the building also has a full basement and measures 417 feet by 110 feet in plan (Figure 1). The building is supported on 98 natural rubber isolators just above the foundations at a subbasement level. The basement of the building is actually a supported floor and required that there be two basement walls. There is an interior basement wall that is part of the base isolated building; there is also a separate retaining wall around the exterior of the building designed to

accommodate a possible 16 inch deflection of the building during a earthquake event. Traction elevators were needed because hydraulic-type elevators would have required shafts extending into the ground. Utilities providing services to the building were specially designed with extra loops or flexible joints to allow for the deflections of the building.

The building is mainly of steel construction with braced frames providing the lateral resistance (Way and Lew, 1986). At the basement level, the steel braced frames transfer lateral load to concrete shear walls which extend the full height of the basement; the basement of the building (from the basement floor to the ground floor) essentially acts as a large box girder to spread the lateral loads to the base isolators. A braced frame system was used instead of a moment frame to try to have rigid body motion of the building's superstructure.



Figure 1. Photograph of Foothill Communities Law and Justice Center.

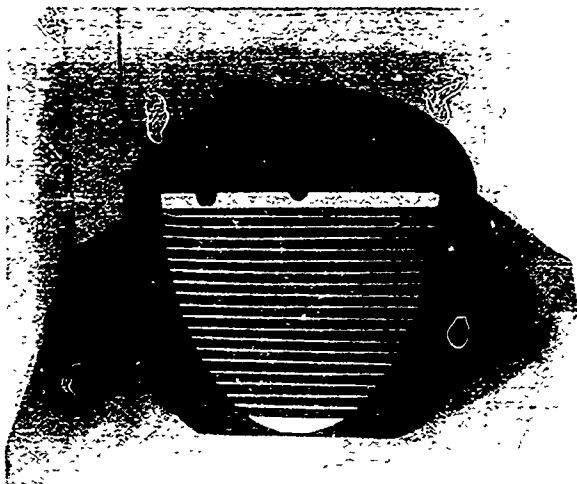


Figure 2. Cut-away view of natural rubber isolator used in the FCLJC Building.

The natural rubber base isolators selected for this project consisted of "high-damping" rubber isolators made up of alternating layers of rubber and steel plates (Figure 2). Although eight bearing types were actually utilized, all of the bearings had a diameter of 30 inches and height of 16 or 18 inches. During manufacture, additives were added to the natural rubber to improve ozone resistance, bond strength, tensile strength, stiffness, and damping. A description of the fabrication and quality assurance process for the bearings has been described by Tarics et al (1986).

#### GEOTECHNICAL SETTING

The FCLJC Building is located in seismically active southern California (Figure 3). The building is located about 40 miles east of downtown Los Angeles in the city of Rancho Cucamonga which is in the western part of the County of San Bernardino (Crandall, 1982). The site is within a region of large-scale crustal disturbance caused by faulting and is within the intersection of east-west trending Transverse Ranges Province, represented by the San Gabriel

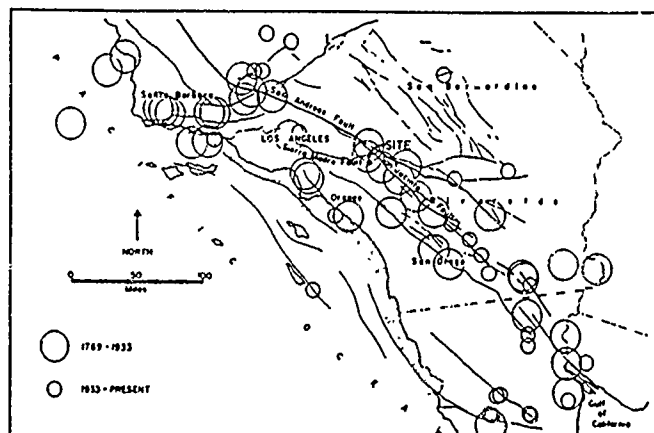


Figure 3. Location of Foothill Communities Law and Justice Center (After Lamar et al, 1973).

Mountains to the north, and the Peninsular Ranges Province, represented by the Puente Hills and Santa Ana Mountains to the south. The FCLJC building is located in the Chino Basin, which is an alluvium filled down-dropped fault block bounded by the San Jacinto fault zone on the east, the Chino-Elsinore fault zone on the west, and the Sierra Madre fault zone on the north. The famous San Andreas fault is located within 13.5 miles of the building; this is the portion of the fault that last ruptured in 1857 with about a Magnitude 8 earthquake and a similar event has been predicted by some seismologists and geologists within the next 30 to 50 years. Other major fault systems near the building are the San Jacinto, Elsinore, and Sierra Madre Faults which are located 11, 17, and 1.2 miles from the building location; these three fault systems are capable of up to Magnitude 7.5 events. An earthquake on any of these nearby faults or other of the numerous faults in southern California could produce significant ground motions at the building location.

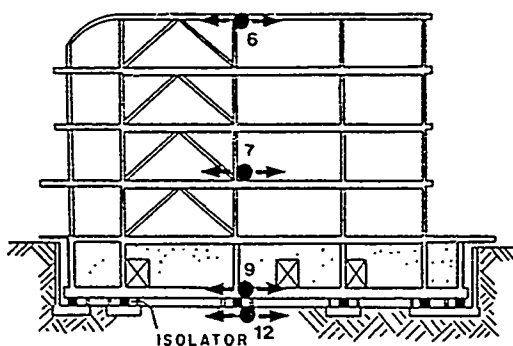
#### DESIGN CRITERIA AND EXPECTED RESPONSE

The FCLJC building was designed to remain essentially elastic under even the maximum credible earthquake events on the nearby faults; this criteria even exceeds the performance criteria that would be required for an essential facility designed by the Uniform Building Code. Under maximum credible earthquake conditions, a structure can not generally be designed to behave completely elastically; generally, it is only practical to design against collapse at these levels. With base isolation, it becomes practical to also protect the non-structural elements and the building contents as well as better protect the occupants.

By base isolation, the fundamental period of the FCLJC Building was made to be about 2.0 seconds; the fundamental period of an equivalent conventionally fixed-base building would be about 1.1 seconds. A thorough dynamic analysis of the base isolated building system was made to determine the expected response of the natural rubber isolators and the building superstructure to the seismic excitations from postulated earthquakes on the fault systems described earlier. With a base isolation system, the amplification of accelerations within the building from the base level to the roof level is expected to be nearly unity, implying rigid body motion above the base isolation level. The amplification factor for a fixed-base building would be expected to be about four times.

#### PERFORMANCE DURING SEVERAL SMALL EARTHQUAKES

The State of California Office of Strong Motion Studies has instrumented the FCLJC building with a total of 19 accelerometers as part of the California Strong Motion Instrumentation Program (Huang et al, 1986). Figure 4 shows a cross section through the center of the FCLJC building; also shown are the locations of four of the accelerometers which are oriented to record motions parallel to the minor axis of the building. Accelerometer No. 6 is located on the roof of the building, Accelerometer No. 7 is mounted on the second floor, Accelerometer No. 9 is located at the basement level (above the isolators), and Accelerometer No. 12 is mounted at the



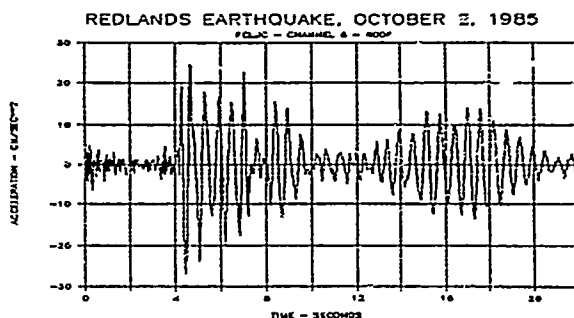
SOUTH/NORTH SECTION

Figure 4. Cross Section of the Minor Axis of the FCLJC and Locations of Accelerometers Nos. 6, 7, 9, and 12.

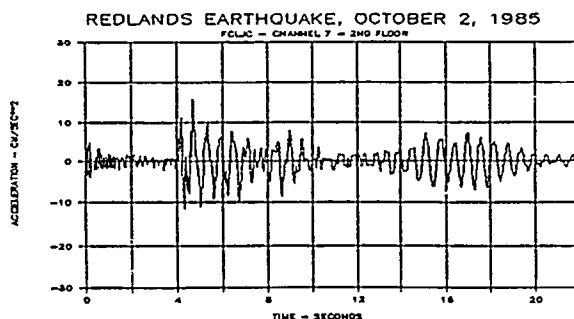
foundation level (within the subbasement and below the isolators).

Although only recently completed, ground and building motions caused by several small earthquakes have been recorded at the FCLJC building. The processed accelerograms for Accelerometer Nos. 6, 7, 9, and 12 recorded during the Redlands earthquake of October 2, 1985 (magnitude 4.8 ML) are shown in Figure 5; the epicenter of this event was about 30 kilometers from the building. It is obvious from a visual inspection of these four accelerograms that the high frequency horizontal motions present in the foundation recording have been filtered out by the isolators as these frequencies are not present in the records above the isolators; this can be clearly seen in the roof and second floor records and is even evident in the basement record. The maximum acceleration at the roof level was about the same as that recorded at the foundation level. The maximum acceleration levels in the basement and the second floor are less than that at the foundation level.

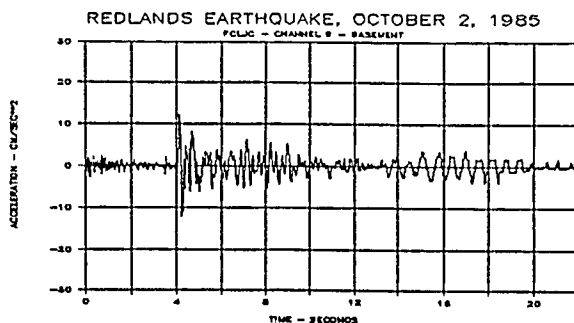
Processed accelerograms were also available from the Palm Springs earthquake of July 8, 1986 and the records from the same accelerometers are shown in Figure 6; the epicenter of this earthquake was about 100 kilometers from the building. As in the Redlands earthquake, the high frequency waveforms noted in the foundation level record are absent from the other three records. Unlike the Redlands earthquake, there is no reduction in the maximum acceleration level at the basement and there is some amplification of the maximum acceleration at the higher levels; the maximum acceleration at the roof level is about three times the maximum acceleration at the foundation level. Preliminary data from the recent Whittier Narrows earthquake of October 1, 1987 (magnitude 6.1 ML) indicate that a maximum acceleration of about 0.03g was measured at the foundation level and about 0.05g was measured at the roof level (Shakal, 1987); the epicenter was about 55 kilometers from the FCLJC building.



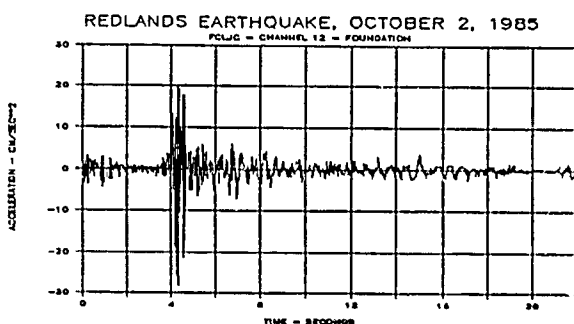
(a) Channel 6 - Roof



(b) Channel 7 - 2nd Floor

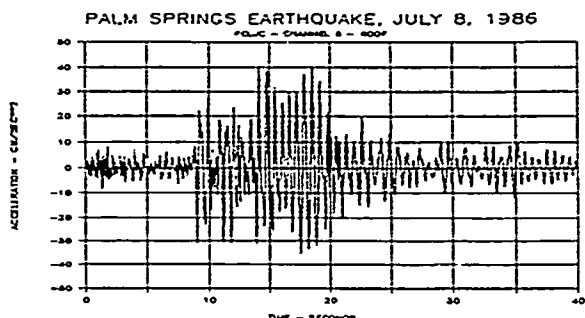


(c) Channel 9 - Basement

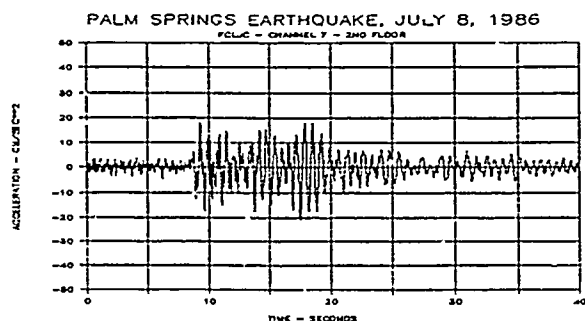


(d) Channel 12 - Foundation

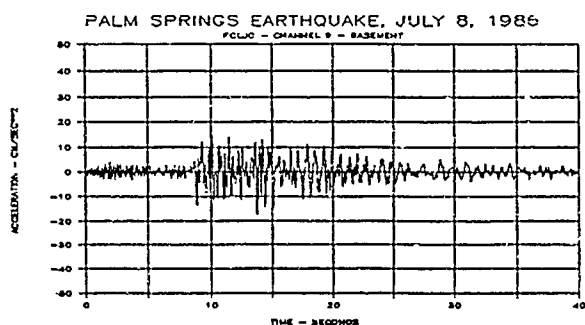
Figure 5. Acceleration-Time Histories Recorded During the Redlands earthquake of October 2, 1985.



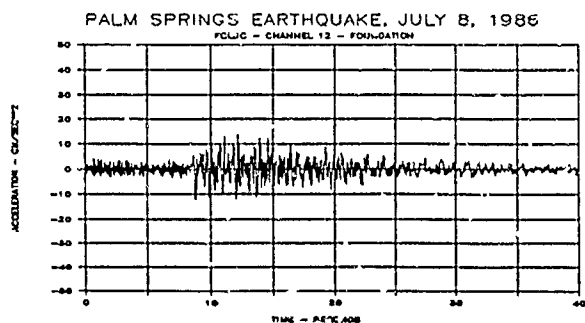
(a) Channel 6 - Roof



(b) Channel 7 - 2nd Floor



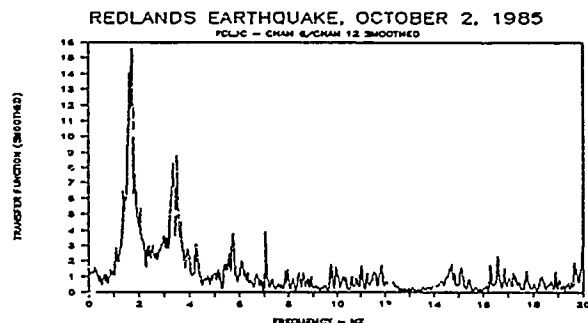
(c) Channel 9 - Basement



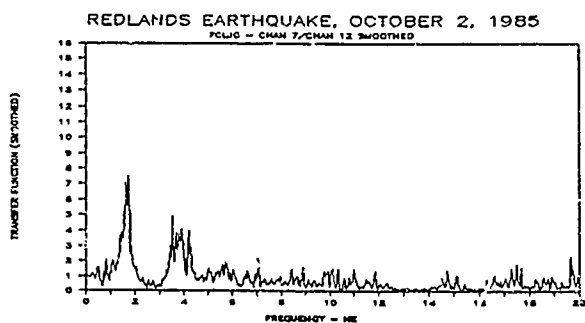
(d) Channel 12 - Foundation

Figure 6. Acceleration-Time Histories Recorded During the Palm Springs earthquake of July 8, 1986.

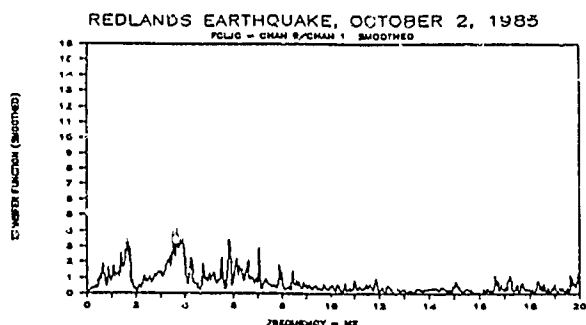
Spectral analyses were also performed for these accelerogram records from the two earthquakes. The Fast Fourier Transform (FFT) of each record was computed and smoothed once. Spectral ratios or transfer functions between the three upper building level records and the foundation level record were computed; the transfer functions are shown in Figures 7 and 8. The transfer functions from both earthquake events are very similar. High frequencies above about 10 Hertz are greatly deamplified above the isolators in the building. The fundamental



(a) Ch. 6 to Ch. 12 - Roof to Foundation



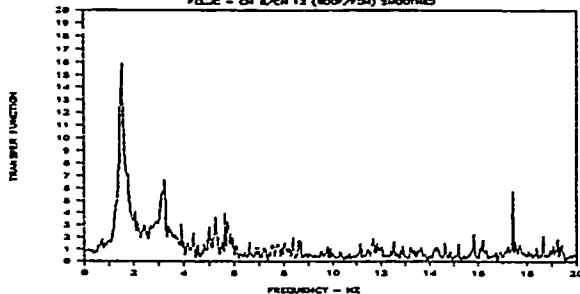
(b) Ch. 7 to Ch. 12 - 2nd Floor to Foundation



(c) Ch. 9 to Ch. 12 - Basement to Foundation

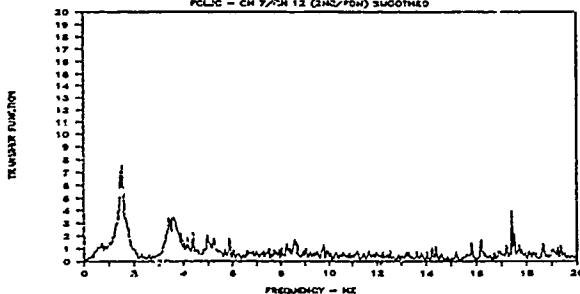
Figure 7. Fourier Transfer Functions - Redlands Earthquake.

PALM SPRINGS EARTHQUAKE - JULY 8, 1986  
FCLJC - CH 6/CH 12 (400/7734) SMOOTHED



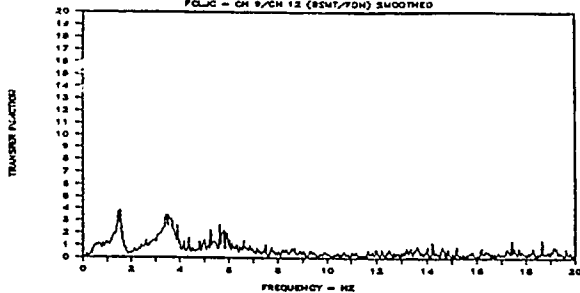
(a) Ch. 6 to Ch. 12 - Roof to Foundation

PALM SPRINGS EARTHQUAKE - JULY 8, 1986  
FCLJC - CH 7/CH 12 (2142/704) SMOOTHED



(b) Ch. 7 to Ch. 12 - 2nd Floor to Foundation

PALM SPRINGS EARTHQUAKE - JULY 8, 1986  
FCLJC - CH 9/CH 12 (8547/704) SMOOTHED



(c) Ch. 9 to Ch. 12 - Basement to Foundation

Figure 8. Fourier Transfer Functions - Palm Springs Earthquake.

period of vibration appears to have been about 0.6 seconds (corresponding to a frequency of 1.7 Hz) in the Redlands earthquake; it appears that the second period of vibration is about 0.3 seconds (3.5 Hz). For the Palm Springs earthquake, the fundamental period of vibration appears to be about 0.7 seconds (1.5 Hz) and second period of vibration is about 0.3 seconds (3.5 Hz).

#### CONCLUSIONS

The report card on the base isolation system for the Foothill Communities Law and Justice Center is still incomplete. The performance of the building during the Redlands and Palm Springs earthquakes is somewhat mixed. There was no amplification of acceleration in the building relative to the foundation level during the Redlands event; however, there was amplification during the Palm Springs event. There also seems to have been some amplification of the maximum accelerations in the Whittier Narrows earthquake. In the frequency domain, the transfer functions of the motions at the higher building levels compared to the foundation level are very similar for both the Redlands and Palm Springs events. The base isolators are very effective in filtering out the higher frequencies above 10 Hertz.

Of course, the measured responses of the building were in three distant and rather moderate earthquakes. With higher excitation levels, it would be expected that higher damping of the isolators would be developed. The observed filtering effect of the isolators for the higher frequencies is encouraging and at higher acceleration levels, it is hoped that the filtering effect would be observed at lower frequencies. In less than three years, three earthquakes have been recorded at the FCLJC building. There is no doubt that many more earthquake records will be available in the future that will help the engineering profession understand the behavior and performance of base isolation.

#### ACKNOWLEDGMENTS

Mr. Robert Rigney, former County Administrator of the County of San Bernardino, had the insight and courage to commit himself to building the first base isolated building in the United States of America. The design architects for the building were HMC Architects and Hellmuth, Obata & Kassabaum. The structural engineer was Taylor and Gaines and the base isolation consultant was Reid and Tarics.

Appreciation is extended to the Dr. Tony Shakal of the California Strong Motion Instrumentation Program (CSMIP) for providing earthquake time histories recorded at the FCLJC building.

## REFERENCES

- Crandall, LeRoy and Associates (1982), "Report of Geotechnical Investigation, Proposed West Valley Law and Justice Center, Foothill Boulevard near Haven Avenue, City of Rancho Cucamonga, for the County of San Bernardino".
- Huang, M. J., A. F. Shakal, D. L. Parke, J. T. Ragsdale and R. W. Sherburne (1986), "Processed Data from the Strong-Motion Record Obtained at a Base-Isolated Building in Rancho Cucamonga, California During the Redlands Earthquake of 2 October 1985", Report OSMS 86-01, Office of Strong Motion Studies, Calif. Div. of Mines and Geology, Sacramento, California.
- Lamar, D. L., P. M. Merifield, and R. J. Proctor (1973), "Earthquake Recurrence Intervals on Major Faults in Southern California", in Geology, Seismicity, and Environmental Impact, Association of Engineering Geologists Special Publication, pp. 265-276.
- Shakal, A. F. (1987), personal communication.
- Tarics, Alexander G., James Kelly, Douglas Way and Rodney Holland (1986), "Quality Assurance and Control of Fabrication For a High-Damping-Rubber Base Isolation System", Proceedings, Seminar and Workshop on Base Isolation and Passive Energy Dissipation, Applied Technology Council, San Francisco, pp. 455-464.
- Way, Douglas and Marshall Lew (1986), "Design and Analysis of a High-Damping Rubber Isolation System (Case History of the Foothill Communities Law and Justice Center)", Proceedings, Seminar and Workshop on Base Isolation and Passive Energy Dissipation, Applied Technology Council, San Francisco, pp. 83-92.

## Upgrading the Seismic Resistance of Stevens Creek Dam

**K.V. Rodda**

Manager, Earth and Rockfill Dams, Wahler Associates, Palo Alto, California

**C.W. Perry**

Vice President and Chief Engineer, Wahler Associates, Palo Alto, California

**R.E. Tepel**

Engineering Geologist, Santa Clara Valley Water District, San Jose, California

**SYNOPSIS:** Stevens Creek Dam is a rolled earthfill structure with a height of about 120 feet. A seismic safety evaluation in 1978 concluded that the dam would probably be severely damaged if subjected to a maximum credible earthquake originating on the nearby San Andreas fault. Normal reservoir operation was immediately restricted, pending decisions as to the fate of the project. Conceptual design studies were completed in 1982 to identify the most promising alternative remedial concepts. The most promising concepts were chosen and final design of modifications to the dam and its appurtenant hydraulic structures were completed in 1984. Modification of the dam was completed in 1986, involving the placement of massive buttresses on both the upstream and downstream slopes and installation of internal drains to control the phreatic line. This required extension of the existing outlet conduit and construction of new inlet and outlet control structures.

### INTRODUCTION

Stevens Creek Dam, owned by the Santa Clara Valley Water District, is located on the west side of the highly populated Silicon Valley in California (Fig. 1). The dam was designed and constructed in 1935, according to then-modern standards. It is located 2½ miles from the San Andreas fault, which is capable of a maximum credible earthquake (MCE) of Magnitude 8½. No major problems were reported over the 43 years following construction.

This paper describes site conditions, selected aspects of the 1978 seismic safety evaluation, alternative remedial design concepts that were evaluated, details of the final design that was ultimately selected, results of field, laboratory and engineering analyses on which the evaluations and the final design were based, and selected aspects of construction.

### SITE CONDITIONS

Stevens Creek Reservoir, with a capacity of about 3,500 acre-feet, impounds water for ground water recharge and also provides some flood control and recreation benefits. The dam is constructed of a gravelly, clayey sand, referred to as the Santa Clara formation, which underlies the dam and reservoir area. The dam section reportedly consists of an upstream "impervious" zone and a downstream "pervious" zone, separated by a contact inclined downward and upstream at 1:1 (horizontal to vertical) from about the midpoint of the crest. The foundation of the dam consists of Santa Clara Formation, overlain by up to 15 feet of alluvium and terrace deposits. A cutoff trench was excavated up to 40 feet to bedrock beneath the "impervious zone".

### SEISMIC SAFETY EVALUATION

A state-of-the-art seismic safety evaluation of Stevens Creek Dam was completed by Wahler Associates in 1978, as part of a comprehensive investigation of the Santa Clara Valley Water District's seven major dams.

#### Field and Laboratory Investigations

Because the cobbly materials in the embankment had defied previous, conventional "undisturbed" sampling (by others), an innovative

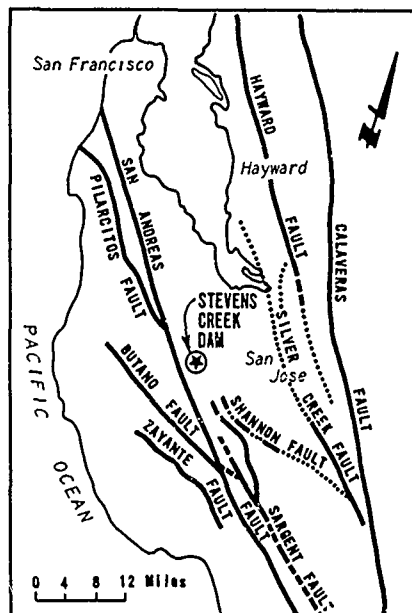


Fig. 1. Vicinity Map



technique was developed by Wahler Associates for taking relatively undisturbed samples from large-diameter bucket auger holes. A specially -designed bucket auger drilling machine was suspended from a 70-ton truck-mounted construction crane. Two holes were drilled, on the crest and the upstream face of the dam. Vertical samples were obtained by driving 6-inch-diameter heavy-walled sample tubes, with the kelly, at approximately 5-foot intervals as each hole was advanced, and the amount of energy required to advance the sampler was recorded for the purpose of estimating the equivalent penetration resistance of the materials. Six-inch-diameter horizontal push samples were also obtained from each of the drill holes, using a new horizontal sampling device, designed and fabricated by Wahler Associates. The new device uses a fixed-piston sampling technique to hydraulically push a relatively thin-walled tube. The sampler was mounted in a cage, designed to carry an operator, which was lowered into the 48-inch-diameter hole. The temporary casing that lined the hole had open "windows" along its length to permit selection of representative sampling locations within the dam. Several samples from each depth were obtained by rotating the casing to expose new sampling locations. Approximate in-place density determinations of the embankment materials were made in the 48-inch drill holes by weighing the entire cylinder of soil removed between known depths. Sand cone field density tests were conducted in exploratory trenches in the surficial foundation soils.

Laboratory testing included classification, density, permeability, static and dynamic strength and resonant column tests. Basic material properties determined from those tests are summarized in Table 1. It should be noted that only slight differences were found to exist in the gradations of the "impervious" and "pervious" materials.

Table 1 - Summary of Material Properties from 1978 Study

| Property                | Existing Dam       | Terrace Gravel | Alluvium |
|-------------------------|--------------------|----------------|----------|
| Ave. Unit Dry Wt. (pcf) | 120                | 131            | 106      |
| Ave. Gradation (%)      |                    |                |          |
| No. 4                   | 72                 | 53             | 30       |
| No. 200                 | 25                 | 8              | 14       |
| Liquid Limit (%)        | 25-30              | N.P.           | N.P.     |
| Plastic Index (%)       | 7-13               |                |          |
| Permeability (cm/sec)   |                    |                |          |
| Horiz.                  | $5 \times 10^{-6}$ | --             | --       |
| Vert.                   | $4 \times 10^{-7}$ | --             | --       |
| Strength                |                    |                |          |
| $\phi'$ (deg.)          | 37                 | --             | 36       |
| c' (ksf)                | 0.4                | --             | $\phi$   |

## Analyses and Results

A dynamic finite element analysis was performed on the maximum section of the dam. The finite element model was subjected to the expected motions from an MCE with a peak bedrock acceleration of 0.72 gravity and a duration of 100 seconds. The accelerogram and shear modulus values used in the analysis were adopted from previous studies by others (Woodward-Clyde Consultants, 1976). The results of the seismic stability evaluation indicated that strain potentials in most of the embankment would be much greater than 10 percent. However, meaningful quantitative estimates of deformation were not possible because the exact magnitude of the strain potentials in excess of 10 percent could not be determined (few of the laboratory cyclic triaxial tests could be carried out to cyclic strains greater than 10 percent). It was concluded that the dam had a high potential for lateral spreading and crest settlement, which could result in a reduction in freeboard below the reservoir level if the reservoir were full or nearly full.

## STUDY OF CONCEPTUAL ALTERNATIVES

In 1982, a study was completed (Wahler Associates, 1982), in which conceptual alternatives were evaluated and selected alternatives were detailed at the preliminary design level. Basic data was collected, from additional field geophysical surveys, limited cyclic triaxial and resonant column tests on samples taken from the upstream "impervious" zone of the embankment, and basic tests on potential borrow materials. Comparative, simplified dynamic analyses were performed on several trial embankment modification sections. The objectives of this study were to arrive at one or two basic remedial design concepts for restoring full reservoir capacity and to develop preliminary cost estimates for them. Two categories of remedial modification were initially considered: (1) improvement of seismic stability by the addition of buttresses; and (2) control of the phreatic line such as to minimize the areas of seismic concern. The second approach would depend entirely on the effectiveness of internal drains, which are not always reliable, and construction would be far more complicated and costly than the first approach. For those reasons, the second category was not pursued further.

## Field and Laboratory Investigations

A primary objective of the field investigation was to better define the shear moduli of both the existing and potential new fill materials. Geophysical surveys were conducted and a limited number of undisturbed samples taken at two, 3 hole arrays; from the crest and the upstream slope. Cross-hole measurements were made with a downhole shear wave hammer at 5-foot intervals. Measured shear modulus ( $K_{2max}$ ) values varied from 95 to 165 in the "pervious" zone of the dam and from 160 to 210 in the "impervious" zone. Shear modulus values in the "pervious" zone were found to be substantially lower than those measured in

1976. Although values of shear modulus from laboratory resonant column tests were found to consistently underestimate those from the field geophysical surveys, the differences were within the range normally attributed to sample disturbance and the differences in boundary conditions between the two types of test (Arango, et al., 1978, Drnevich, 1977). From laboratory resonant column tests, an average shear modulus value of 85 was calculated for new fill compacted to 95 percent relative compaction (ASTM D1557-78, modified to yield 20,000 ft.-lbs/ft<sup>3</sup> of compactive effort).

#### Conceptual Alternatives

A total of five conceptual modification alternatives were evaluated for the embankment section. The alternative modifications consisted of (1) upstream and downstream berms of various sizes to provide confinement; (2) partial excavation of the existing very stiff, overly-compacted upstream "impervious" zone and replacement with recompacted fill with a lower shear modulus; (3) similar to (2) above, but with a larger upstream zone; (4) similar to (3) above but including a wider dam crest to lower the phreatic line, and a small berm on the downstream slope to intercept seepage and provide confinement; and (5) similar to (4) above without excavation and replacement of the existing upstream "impervious" zone.

#### Analyses and Results

One-dimensional seismic response analyses, using the computer program SHAKE (Schnabel et al., 1972), were carried out on three or four selected soil columns for each section. In addition, simplified deformation analyses were performed on Modification No. 4 using the Makdisi-Seed (1978) method. The strain potential evaluation indicated that most of the embankment materials in all of the schemes would have strain potentials greater than 10 percent. However, the exact magnitudes of strain potentials could not be accurately determined, as had been the case in the 1978 study. On the positive side, the evaluation indicated a substantial reduction in seismically-induced stresses within the existing upstream "pervious" zone (compared to the 1978 study, and due primarily to the reduced shear modulus derived from the 1982 field geophysical survey) and also within the replaced embankment zone (modification alternatives 2 through 4 above). Because it was suspected that the dynamic strength of the upstream zone was probably being underestimated from the limited number of tests available, it appeared that additional laboratory triaxial tests should be carried out during final design before any further thought should be given to replacing this material with new fill. Based upon the above results, two remedial schemes were selected for preliminary design detailing and cost estimating (Fig. 2).

#### Selected Alternatives

The first scheme consisted of upstream and downstream buttresses, similar to modification alternative 5 above, with the objective of improving the dynamic stability of both the upstream and downstream slopes. Additional freeboard was also be provided to compensate

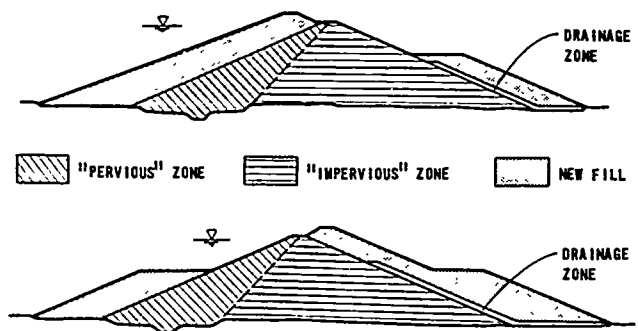


Fig. 2. Selected Design Concepts

for crest slumping, and a drainage zone was included between the existing downstream face and the new buttress to intercept seepage. The first scheme assumed no excavation and replacement of the existing upstream "impervious" zone. However, two optional sub-schemes were also evaluated: one involving partial excavation and replacement of existing upstream "impervious" material with lower density, new fill to reduce the shear moduli and thus improve the seismic resistance of the materials; and another utilizing high strength rockfill in the upstream berm to improve the seismic resistance of that slope.

The philosophy of the second scheme was entirely different from that of the first scheme. Instead of focusing on improving the dynamic stability of the upstream slope, the second approach was to provide additional mass and confinement downstream, to preclude catastrophic failure if there were severe damage to the upstream slope. A limited upstream buttress was, nevertheless, incorporated, to provide mass at the toe.

#### FINAL DESIGN

##### Field and Laboratory Investigations

Additional sampling of existing embankment and potential borrow materials was necessary for final design. Laboratory testing focused on better defining the cyclic and post-cyclic shear strength of the "impervious" and "pervious" materials in the dam, and the compaction, static, cyclic and post-cyclic strength, and shear modulus of potential fill materials. Selected cyclic strength data are presented on Figure 3. Post-cyclic strengths of existing and new fill was derived from samples strained to 6 to 10 percent under cyclic loading, then sheared, statically, to a post-cyclic level of 10 percent. The cyclic shear strength of borrow materials was interpreted from fabricated samples compacted to 95 percent relative compaction (ASTM D1557-78, modified to yield 20,000 ft.-lbs/ft<sup>3</sup> of compactive effort). Post-cyclic strength of new fill was derived from samples compacted to 98 percent relative compaction. The interpreted parameters were  $\phi' = 31^\circ$  and  $11.5^\circ$ , and  $c' = 0$  and 10.4 psi, respectively, for existing

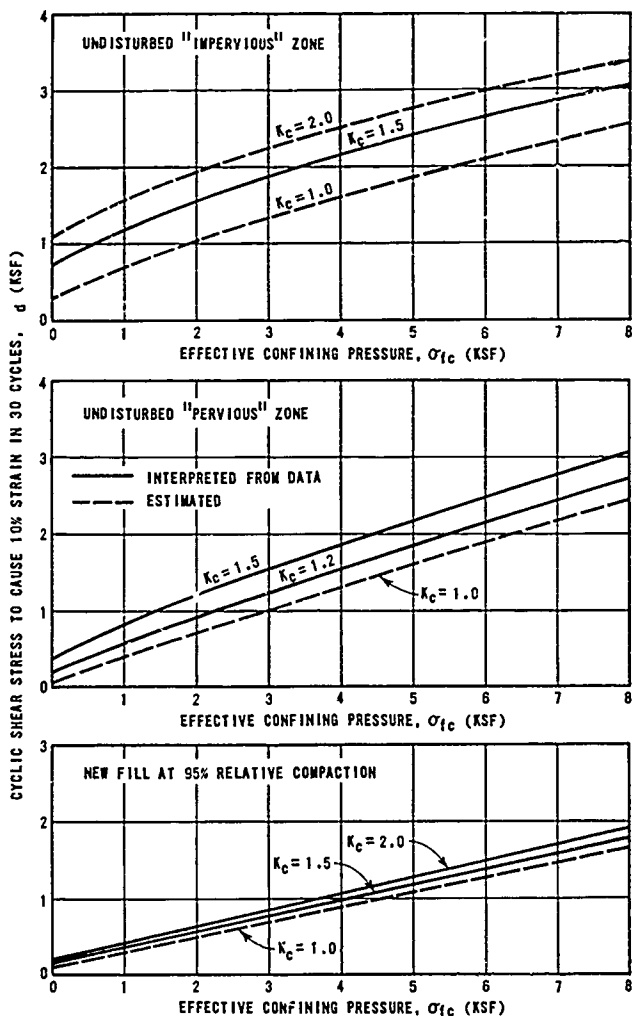


Fig. 3. Cyclic Shear Strengths

and new fill materials, plotted in terms of shear stress on the failure plane at failure vs. normal stress on the failure plane during consolidated.

#### Analysis of Alternatives

Final design analyses were carried out on the two selected preliminary design alternatives (Fig. 2), using static and dynamic finite element methods. The static non-linear finite element computer program FEADAM (Duncan, Wong and Ozawa, 1980) was used to simulate the embankment stresses and strains created by construction of the original dam and its alternative modifications. Seepage forces were then superimposed on the basis of flownets, assuming a ratio of horizontal to vertical permeabilities equal to 16. The dynamic response of the alternative modifications was analyzed for the same design earthquake as used in the 1978 study, using the non-linear finite element computer program QUAD-4 (Idriss, et al, 1973). The shear modulus values used in the analyses were the

same as developed in the 1982 study. A simple average of the curves for sand and clay (Seed and Idriss, 1970) was used to represent the modulus and damping attenuation characteristics of the existing and new embankment materials. The calculated maximum crest accelerations were 1.53 g and 1.25 g, respectively, for the two alternatives, indicating amplifications of 2.25 and 1.74 times the baserock acceleration. Fundamental periods were calculated to be 0.77 and 0.78 second, respectively. Stresses from the response analyses were converted to equivalent uniform cyclic shear stresses, using standard weighting curves (Seed, et al, 1975). Based on these curves, the irregular shear stress time histories in each element were represented by 30 cycles of uniform shear stress equal to two-thirds of the maximum induced shear stress. The strain potential for each element was calculated by comparing the stress required to cause specific strains, with the induced equivalent uniform cyclic shear stresses. The strain potential evaluation indicated that the strain potentials in the central and downstream portions of both remedial alternatives would be relatively low; however, the strain potentials in the entire upstream "impervious" zone of the existing embankment and the entire upstream buttress for both cases would be greater than 20 percent. These levels of strain potential indicated that the upstream materials in both alternatives would be subject to severe spreading and slumping during the MCE. The second alternative was considered to be more acceptable, because the more favorable downstream buttressing of the second alternative, and the fact that the first alternative considerably increased the load on the outlet conduit, which could result in an unsafe condition where the conduit crosses the existing core trench. A post-earthquake analysis was conducted on the second alternative, assuming that the upstream slope provided no support to the remaining embankment. This was a worst-case scenario, since the upstream buttress would, in fact, provide additional mass at a critical location, and the final upstream configuration would probably be merely slumped down from its original condition, on the order of, at worst, a few tens of feet. The results of that analysis indicated a minimum factor of safety of 1.3 for the upstream slope, calculated for a shallow circle that would not undermine the crest of the modified dam. Therefore, it was concluded that the modified embankment, while not necessarily remaining completely intact, would not fail catastrophically if subject to the MCE. In addition, a simplified estimate of permanent deformation was made, using the method of Makdisi and Seed (1978). The calculated total deformation was approximately 10 feet. The modified dam, with its increased normal freeboard (approximately 19 feet), is designed to retain sufficient residual freeboard, following the MCE, to prevent overtopping.

#### Details of the Final Design

A plan and section of the final design, as constructed, are shown on Figure 4. The dam section, as designed, was essentially the same as was analyzed, except that the bench at Elevation 490 on the downstream face was

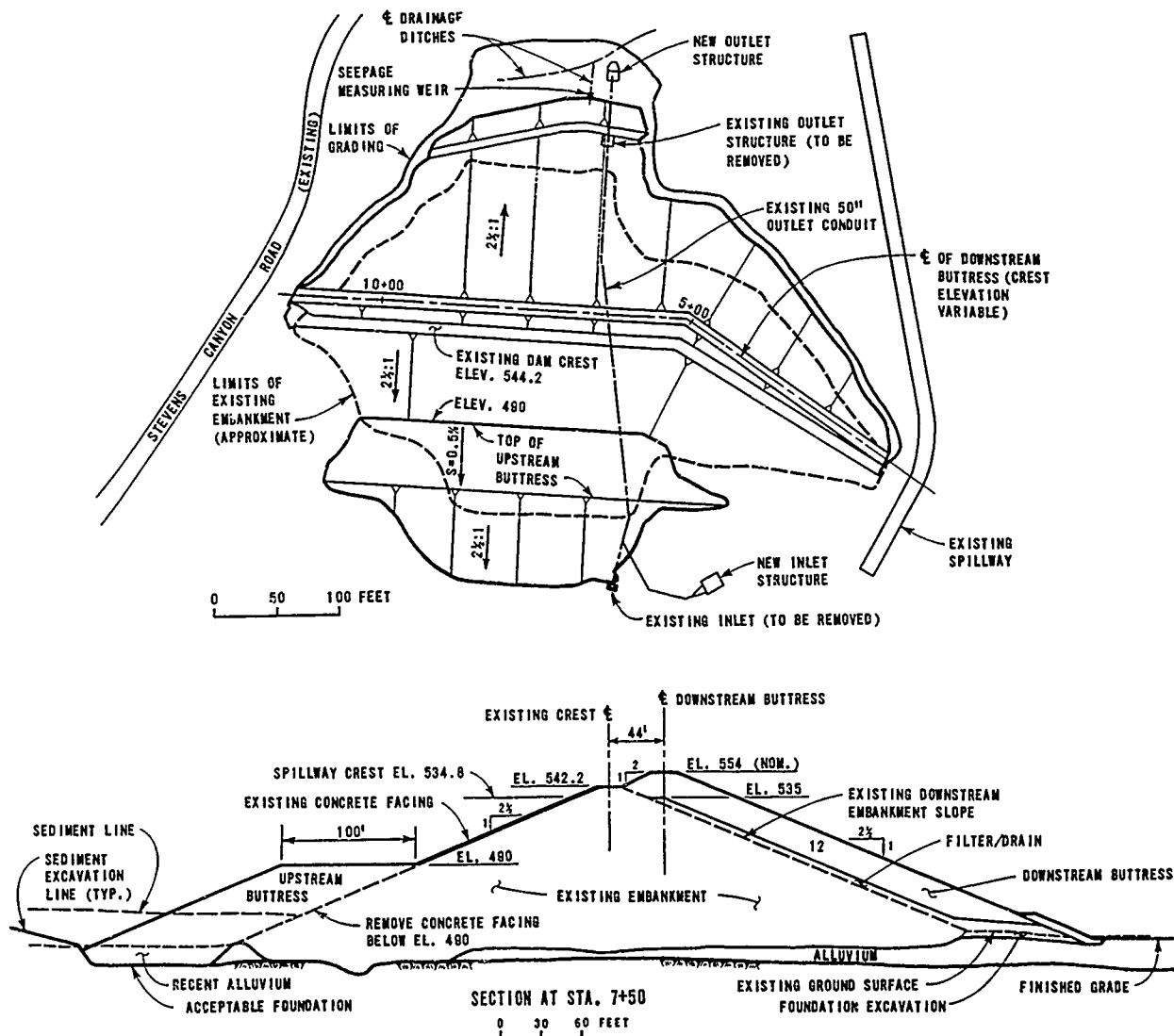


Fig. 4. Plan and Section of Modified Dam

deleted from the final design because it did little to improve the seismic performance of the dam. A 12-foot-thick, inclined chimney drain was incorporated at the interface of the existing downstream embankment face and overlying buttress, to prevent saturation of the buttress and to serve as a crack-stopping zone. The base of the chimney drain is in contact with a blanket drain in the channel, which terminates at an inverted filter at the toe of the dam.

The existing inlet and outlet structures were relocated by extending the 50-inch I.D. outlet conduit upstream and downstream. A new inclined inlet structure on the right abutment was designed to replace the former vertical weir. An inclined structure was chosen due to ease of maintenance and a lower susceptibility to damage from earthquake-induced deformations in the upstream part of the dam. The inlet consists of a wye inlet pipe, con-

trolled by two 42-inch diameter, hydraulically-operated sluice gates, located in a box structure with trashrack-covered ports on the top and sides. The new outlet structure consists of a valve chamber containing two 30-inch butterfly valves, immediately downstream of a wye branch, with dual energy dissipating chambers and stilling basins, and a common outlet apron with warped wing walls.

#### CONSTRUCTION AND OPERATION

Because of its extreme vulnerability to winter inflows, construction of the modifications took place in a single dry season "window", between June and December 1985. The only significant construction problem was the dewatering and removal of about 70,000 yd<sup>3</sup> of very soft sediment (silt) in the bottom of the reservoir, adjacent to the upstream toe of the

dam. Lacking definitive information on its depth (over 20 feet) and extent, the contractor relied on backhoe excavation of the silt, without subsurface dewatering. Most of the excavation was carried out under very wet conditions, because the silt was underlain by pervious stream deposits, which created high seepage gradients into the excavations and resulted in several large slides. Several alternative means of handling the wet silt were considered, such as deflocculation and pumping in slurry form, but were not implemented. After a lengthy delay, the silt was removed, leaving final excavation slopes that averaged somewhat steeper than 6:1 (horizontal to vertical). The remarkable steepness of those slopes was due primarily to the stabilizing effect of downward seepage gradients into the underlying pervious stream deposits.

The reservoir filled and spilled shortly after completion of the remedial construction. Data from piezometers installed during the modification work will be carefully monitored to verify the design assumptions regarding the phreatic line within the modified dam.

## CONCLUSIONS

The most significant conclusions drawn from the evaluation, remedial design and modification of Stevens Creek Dam were:

The excessive deformations that were predicted to occur in the existing dam in response to the MCE were due, principally, to its very close proximity to the San Andreas fault, the steep embankment slopes and the absence of effective internal drainage.

The very coarse materials in the existing dam required large diameter undisturbed samples for testing. The samples, however, limited the range of cyclic strains that could be induced in the laboratory and the consequent meaningfulness of predicted deformations.

The shear moduli of existing embankment materials could only be determined realistically from cross-hole geophysical tests. Resonant column test results significantly understated the shear moduli due to sample disturbance and other factors.

The response of the saturated upstream part of the existing dam could not be significantly improved by any practical scheme involving replacement of existing materials with more highly compacted materials, or placing buttresses on the upstream slope.

Due to the predicted excessive deformations within the saturated upstream slope of the dam, the most reliable solution was to place massive buttresses on the downstream slope and increase the available freeboard, in order to prevent catastrophic failure. Damage to the upstream part of the dam can be expected, but is not expected to undermine the crest.

Dewatering and excavation of reservoir sediments during construction were found to be the most difficult aspects of construction.

## REFERENCES

- Arango, I., Moriwaki, U., and Brown, F., (1978), "In-situ and Laboratory Shear Velocity and Modulus", Proc., Earthquake Engineering and Soil Dynamics Specialty Conference, ASCE, June, Pasadena, California.
- Drnevich, V.P., (1977), "Resonant Column Testing - Problems and Solutions", Symposium on Dynamic Geotechnical Testing, ASTM Special Technical Publication 654, June, Denver, Colorado.
- Duncan, J.M., Wong, and Ozawa, (1980), "FEADAM: A Computer Program for Finite Element Analysis of Dams", Report No. UCB/GT80-02, Dept. of Civil Eng., Univ. at California, Berkeley.
- Idriss, I.M., Lysmer, J., Hwang, R., and Seed, H.B., (1973), "QUAD-4, A Computer Program for Evaluating the Seismic Response of Soil Structures by Variable Damping Finite Element Procedures", EERC 73-6, Univ. of California, Berkeley.
- Makdisi, F.I., and Seed, H.B., (1978), "Simplified Procedure for Estimating Dam and Embankment Earthquake-Induced Deformations", Journ. Geotechnical Engineering Div., ASCE, Vol. 104, No. GT7 849-867.
- Schnabel, P.B., Lysmer, J., and Seed, H.B., (1972), "SHAKE, a Computer Program for Earthquake Response Analysis for Horizontally Layered Sites", EERC 72-12, Univ. of California, Berkeley.
- Seed, H.B., and Idriss, I.M., (1970), "Soil Moduli and Damping Factors for Dynamic Response Analysis", EERC, Univ. of California, Berkeley.
- Seed, H.B., and Idriss, I.M., Makdisi, F., and Banerjee, N., (1975), "Representation of Irregular Stress Time Histories by Equivalent Uniform Stress Series in Liquefaction Analyses", EERC 75-29, Univ. of California, Berkeley.
- Wahler Associates, (1978), "Seismic Safety Evaluation, Stevens Creek Dam", Report to Santa Clara Valley Water District.
- Wahler Associates, (1982), "Preliminary Remedial Design Investigation, Stevens Creek Dam, Report to Santa Clara Valley Water District.
- Wahler Associates, (1984), "Remedial Design Report, Stevens Creek Dam", Report to Santa Clara Valley Water District.
- Woodward-Clyde Consultants, (1976), "Part 1 - Geology and Seismicity - Seismic Stability Assessment of Four Dams", Report to the Santa Clara Valley Water District.

## Seismic Response Analysis of Forebay Structure for CW Pump House of a Nuclear Power Project

Malay Basu Ray

Project Engineer (Civil), Development Consultants Pvt. Ltd., Calcutta, India

Dhiman Kr. Ghosh

Dy. Chief Engineer (C&S), Development Consultants Pvt. Ltd., Calcutta, India

**SYNOPSIS:** The paper reviews the current state-of-the-art on the seismic response analysis of complex RCC structure like forebay which is usually connected with CW Pump House frame at its rear end for fulfilling circulating water requirement in power plant - nuclear or thermal. The need to include in such analysis and design effects of 3-Dimensional mathematical model and soil-structure interaction for studying overall behaviour of the structure are highlighted. The paper also discusses the usefulness, if any, of such rigorous analysis and identifies some problem areas in finalising realistic design data and adopting suitable models to represent the structural system.

### INTRODUCTION

From the basic requirement of process engineering of nuclear power plant, CWPB complex has its own importance in supplying the flow of water for APW and APCW point of view, for the safe functioning of the plant. The particular CWPB complex has been designed to provide process water to 2 x 235 MW capacity units. The entire complex has been divided into three separate structures from functional and other relevant aspects and the structures are basically RCC framed units and are partially buried into the subsoil. In front of two units of pump house structure, fan type forebay structures have been placed for controlling the flow of incoming water through the tunnels from the intake point before the water enters the pump house complex. For safety reasons detail seismic analysis of the aforesaid structures under both OBE & SSE conditions, have been carried out so that the safety regulation or such vital structures for the said nuclear power plant is fulfilled. Because of the unconventional shape of forebay structure unequal loadings arises out of various load combinations at the bottom of forebay raft. Hence a rigorous analysis for the said structure has been felt absolutely essential utilising FEM and considering soil-structure interaction. Since the design basis earthquake is of moderate intensity the corresponding ground strain level has been assumed to be  $10^{-2}$ . With respect to this strain level, the relevant soil dynamic parameters, i.e. low strain shear modulus of soil, 'G' and Poisson's ratio,  $\nu$  have been considered for the entire structure under SSE earthquake condition.

The soil part in soil-structure interaction has been done with frequency independent soil springs considering elastic half-space theory. The validity of such assumption can be amply justified due to the presence of more or less hard and compact ground condition. The 'Ground Response Spectra' and 'Accelerogram' for the particular site have been supplied by the Nuclear Power Board authorities after carrying out necessary tests and statistical data analysis.

This paper highlights synthesis of the present state-of-the-art in the analysis and design of such partially buried and predominantly rigid RCC fan-shaped type structure and the results are presented and briefly discussed hereunder.

### DESIGN CASE STUDY AND MODELLING OF IDEALISED SYSTEM

The dynamic seismic response analysis of the aforesaid forebay structure for CWPB complex have been carried out using 3-D analytical mathematical model as shown in Fig.4 comprising prismatic beam elements and boundary elements from the element library of the software package 'SAP VI' used in this case. The model consists of 232 nodes, 297 prismatic beam elements and 84 nos. of boundary elements, and the basic parameters considered in the analysis are as follows:

- (a) Dynamic modulus of elasticity of structural concrete of grade M-25 (as per IS Code) have been considered as  $3.0 \times 10^6 \text{ t/m}^2$  and for structural steel  $2.0 \times 10^7 \text{ t/m}^2$  respectively.
- (b) The overall viscous damping value for the entire mathematical model have been presumed as 10% of critical for SSE condition.
- (c) Poisson's ratio of structural concrete has been assumed as 0.20 and that for steel as 0.30 respectively.
- (d) Dynamic shear modulus of soil, 'G' have been assessed as  $1600 \text{ t/m}^2$  and Poisson's ratio,  $\nu$  has been considered as 0.40.

Fig.1 indicates the key plan of CWPB complex for the nuclear power plant showing relative position of cooling water pump house structures and the forebay structures and how these are inter-linked with each other. Fig.2 indicates typical sectional plans at two different elevations with relevant dimensions, while Fig.3 shows a typical sectional elevation of the forebay structure so that a clear idea of the actual structure may be obtained. The reader may correlate these

figures with Fig.4, i.e. mathematical model of the real structure. In order to show as many as many number of nodes as possible, the 3-D mathematical model have been shown in isometric view. The smoothend acceleration spectra for ground motion during safe shutdown earthquake for the typical plant site has been shown in Fig.5 using various percentages of damping, i.e. 2%, 5%, 10%, 20% etc.

The reason for considering a 3-D model with soil-structure interaction for the analysis and design of CWPB forebay structure may be attributed to its peculiar configurations from functional point of view and its rigidity also. Since it is basically rigid fan-shaped partially buried structure, by considering soil-structure interaction in the global analysis of the entire linear elastic system, the apparent rigid body motion of the entire structure as a whole during initial excitation due to ground movement could be well-recognised in the subsequent analytical results of eigen solution and corresponding response spectrum analysis part. The torsional deformity of the entire structure and also its individual members could only be computed by analysing the structure with 3-D FEM model. Thus the analytical result reveals the movement of structure as a whole and also the deformation of its various components within the structure during occurrence of the design basis earthquake. These aspects could not have been observed had the structure not been analysed using 3-D FEM model and also utilising soil-structure interaction concept. The above observations are particularly true for the forebay structure because this being a closed form RCC structure having criss-cross wall connections, the overall behaviour of the structure becomes very rigid, and in case of a fixed base model, the entire results of analysis would have been far from realistic.

TABLE 1. Eigen Values

| Mode No. | Circular Frequency (rad./sec.) | Frequency (Hertz) | Period (Sec.) |
|----------|--------------------------------|-------------------|---------------|
| 1        | 27.84                          | 4.431             | 0.2257        |
| 2        | 29.36                          | 4.673             | 0.2140        |
| 3        | 33.50                          | 5.332             | 0.1876        |
| 4        | 35.28                          | 5.615             | 0.1781        |
| 5        | 36.46                          | 5.803             | 0.1723        |
| 6        | 39.68                          | 6.315             | 0.1584        |

TABLE 2. Modal Participation Factors

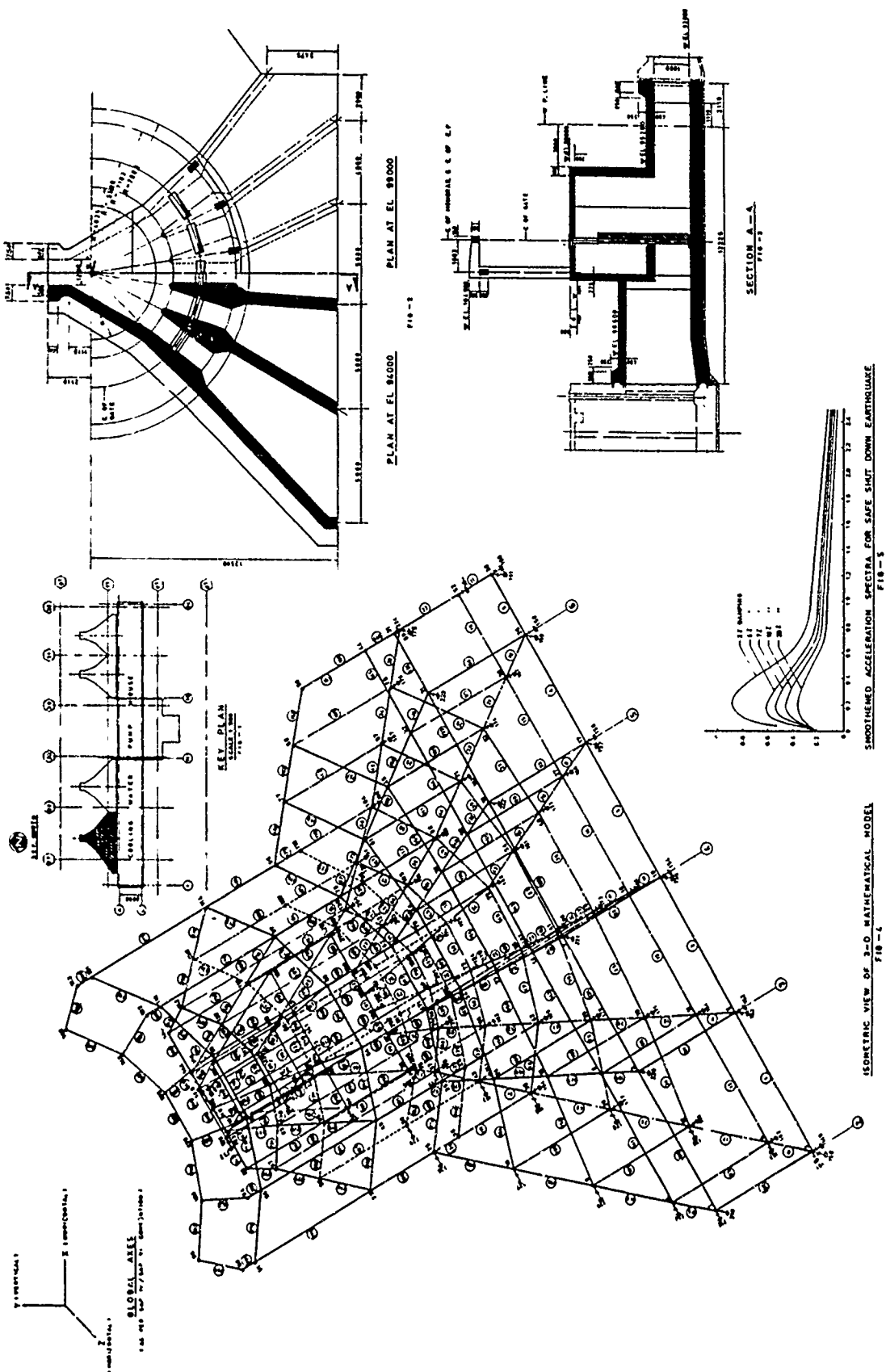
| Mode No. | X-direction | Y-direction | Z-direction |
|----------|-------------|-------------|-------------|
| 1        | 4.126       | 2.725       | -2.556      |
| 2        | -4.392      | 0.738       | -4.456      |
| 3        | 4.710       | -6.664      | -2.507      |
| 4        | -4.760      | -4.562      | -2.289      |
| 5        | 1.388       | 2.043       | -6.951      |
| 6        | -0.592      | 2.935       | -0.819      |

TABLE 3. Forces and Moments in Typical Structural Members

| Direction     | Axial Force (t) | Shear (t) | Shear (t) | Torsion (tm) | Moment (tm) | Moment (tm) |
|---------------|-----------------|-----------|-----------|--------------|-------------|-------------|
| Member (6):   |                 |           |           |              |             |             |
| X             | 15.80           | 3.17      | 5.37      | 0.36         | 12.23       | 4.29        |
| Y             | 9.57            | 1.51      | 3.56      | 0.15         | 7.81        | 2.07        |
| Z             | 26.27           | 2.43      | 4.83      | 0.31         | 11.61       | 3.35        |
| Member (148): |                 |           |           |              |             |             |
| X             | 10.37           | 1.50      | 6.92      | 0.10         | 13.42       | 0.86        |
| Y             | 3.73            | 0.71      | 4.02      | 0.05         | 7.85        | 0.31        |
| Z             | 11.23           | 1.17      | 5.18      | 0.08         | 9.92        | 0.73        |
| Member (215): |                 |           |           |              |             |             |
| X             | 4.40            | 2.16      | 2.39      | 0.22         | 2.91        | 1.28        |
| Y             | 2.33            | 1.07      | 1.31      | 0.11         | 1.67        | 0.64        |
| Z             | 8.93            | 1.73      | 1.58      | 0.20         | 3.06        | 1.04        |
| Member (272): |                 |           |           |              |             |             |
| X             | 0.58            | 1.85      | 2.82      | 0.22         | 11.21       | 4.14        |
| Y             | 0.38            | 1.32      | 1.42      | 0.28         | 5.81        | 0.03        |
| Z             | 0.43            | 1.53      | 3.66      | 0.38         | 14.69       | 3.46        |

TABLE 4. Deflections and Rotations at Typical Nodes

| Direction  | $\delta_x$ (mm) | $\delta_y$ (mm) | $\delta_z$ (mm) | $\theta_x \times 10^{-4}$ (rad.) | $\theta_y \times 10^{-5}$ (rad.) | $\theta_z \times 10^{-4}$ (rad.) |
|------------|-----------------|-----------------|-----------------|----------------------------------|----------------------------------|----------------------------------|
| Node (2):  |                 |                 |                 |                                  |                                  |                                  |
| X          | 2.40            | 5.48            | 1.56            | 3.33                             | 6.45                             | 3.71                             |
| Y          | 1.74            | 3.51            | 0.94            | 1.42                             | 4.60                             | 1.95                             |
| Z          | 1.50            | 3.30            | 2.50            | 3.21                             | 4.02                             | 2.60                             |
| Node (14): |                 |                 |                 |                                  |                                  |                                  |
| X          | 2.49            | 2.77            | 1.89            | 3.53                             | 7.96                             | 3.75                             |
| Y          | 1.29            | 1.89            | 0.72            | 1.47                             | 5.34                             | 1.99                             |
| Z          | 1.93            | 1.73            | 2.42            | 3.32                             | 5.14                             | 2.59                             |
| Node (49): |                 |                 |                 |                                  |                                  |                                  |
| X          | 3.07            | 2.32            | 2.90            | 4.98                             | 9.28                             | 4.87                             |
| Y          | 1.21            | 1.81            | 0.93            | 1.72                             | 6.54                             | 2.32                             |
| Z          | 2.47            | 1.49            | 3.06            | 4.67                             | 6.00                             | 3.36                             |
| Node (82): |                 |                 |                 |                                  |                                  |                                  |
| X          | 11.21           | 2.02            | 13.65           | 32.70                            | 49.00                            | 7.34                             |
| Y          | 6.15            | 1.62            | 5.64            | 15.90                            | 59.70                            | 4.14                             |
| Z          | 8.83            | 1.24            | 14.57           | 41.60                            | 77.20                            | 7.25                             |





## DISCUSSIONS ON RESULTS OF ANALYSIS

A close look at the computer response spectrum analysis output shown in very much abridged form in Table 1 thru' 4 shows that the entire structure has been basically low tuned and moved a bit as a whole along with the ground in its fundamental modes. Moreover, the resultant moment and forces in its various members due to inertial loading which have been generated with the corresponding response of the entire structure corresponding to ground excitation may be observed to be of considerably lower magnitude, thereby, confirming the basic fulfilment on the part of the designer to opt for such elaborate analysis at a relatively higher cost than going in for conventional 2-D fixed base quasistatic analysis under abovementioned earthquake. Table 1 gives a resume of eigen values in the first six fundamental modes; Table 2 indicates the modal participation factors along the three directions for the six fundamental modes, while Table 3 summarises typical values of forces and moments due to generation of inertial forces during earthquake in some of its important structural members. Table 4 indicates the deformations and rotations of corresponding nodes in which the abovementioned members are connected structurally. The forces and moments on the individual members due to ground motion have been found to be extremely low because the stiff forebay structure has a tendency of rigid body motion in the fundamental modes as stated earlier and corroborated subsequently by computer results.

During analysis, the main difficulties which had been faced by the analyst are realistic assessment of 'G' value for soil, corresponding to the particular strain level at which the response spectra of the ground motion have been considered for the analysis. It will be more useful if elaborate data on 'stress-strain' relationship for the subsoil at the location of the plant are available under various magnitude of ground motion and subsequent ground movement. Regarding structural modelling use of beam element or combination of beam and plate element should yield realistic results.

Assessment of appropriate damping parameter has also been uncertain because all the available standard software packages can only take care of an average value of overall viscous damping of the entire system comprising superstructure, substructure and soil in the form of Rayleigh damping parameter involving both mass and stiffness matrix only. Whereas in actual practice, there is considerable material damping from subsoil which cannot be simulated in exact manner in the abovementioned case. The structural part derives its damping parameter mainly from its geometry, mass and stiffness array. While carrying out the seismic response analysis under safe shutdown earthquake condition, dynamic modulus of elasticity for both structural concrete as well as subsoil have been utilised and the entire analysis have been done in linear elastic domain.

To facilitate initial strength design of various structural elements of the forebay structure, response spectrum analysis have been carried out first and subsequently, detail time history analysis have also been done to find out the spectral response at predetermined nodes which are

of interest to other mechanical and service installations of the said structure. The forebay structure as shown in Fig.1 between grid 16 and 24 is almost similar in configuration to that between grid 1 and 11. Considering the magnitude of seismic forces and moments it can be concluded that a separate analysis for the structure between grid 16 and 24 may not be warranted. The detailing may be done based on the analytical output for the part between grid 1 and 11.

## CONCLUSIONS

It can be emphasised that whatever may be the different load combinations and however unconventional may be the form of the structure, under seismic loading, systematic FEM analytical approach utilising soil-structure interaction concept may yield significant results which help the designer to understand the actual behaviour of the structure under complex dynamic loading; and it is felt in view of uncertainty of dynamic soil data pertaining to specific strain condition, a range analysis may be much more meaningful.

## REFERENCES

1. Clough, R.W. & Penzien, J. (1975), "Dynamics of Structures", McGraw-Hill.
2. Dowrick, D.J. (1977), "Earthquake Resistant Design", John Wiley & Sons.
3. Prakash, S. (1981), "Soil Dynamics", McGraw-Hill.
4. SAP VI User's Manual (1980), University of California, Berkeley.

## Characterization of Liquefaction Sites/Features in the Charleston, S.C. Area

Garry Maurath

Geologist, Earth Sciences Group, Ebasco Services, Incorporated,  
Greensboro, North Carolina

David Amick

Principal Geophysicist, Earth Sciences Group, Ebasco Services,  
Incorporated, Greensboro, North Carolina

**SYNOPSIS:** The Charleston, South Carolina earthquake of August 31, 1886 produced numerous liquefaction features. To date, over one hundred liquefaction sites have been identified. The characteristics of these sites were determined, and compared to those reported for worldwide cases of liquefaction. The findings of this investigation support the generally accepted models for the types of material and the hydrogeologic setting that are required for liquefaction to occur. However in contrast to some previous studies, these investigations identified relatively few liquefaction sites in Late Holocene sediments. Rather, most liquefaction sites identified in the Charleston area are located in deposits that are 100,000 to 200,000 years old. Finally, this study indicates that the depositional environment plays a key role in determining the type of liquefaction failure.

### INTRODUCTION

The Charleston, South Carolina earthquake of August 31, 1886 (MM intensity X, estimated body wave magnitude 6.6 to 7.1) is the largest seismic event to occur along the Atlantic Seaboard during historical times. The 1886 earthquake produced numerous seismically-induced liquefaction features over a 600 square mile area centered near Charleston.

Recently, investigators from the United States Geological Survey (USGS) and the University of South Carolina have conducted investigations of liquefaction features associated with the 1886 earthquake. During these investigations, liquefaction features caused by large prehistoric earthquakes of magnitudes similar to the 1886 event have also been discovered (Cox, 1984; Gohn and others, 1984; Obermeier and others, 1985; Talwani and Cox, 1985; Weems and others, 1986; and Obermeier and others, 1986). Age dating of these liquefaction features has shown the Charleston area has been the site of at least four large earthquakes during the past 7200 years. The estimated recurrence interval for events similar to the 1886 earthquake was found to be on the order of 1100 to 1800 years.

If the recurrence intervals for large earthquakes occurring at other locations along the Atlantic Seaboard are similar to those documented for the Charleston, S.C. source, the absence of a large damaging earthquake in these areas since colonization does not preclude the possibility of such an occurrence in the future. Consequently, the U.S. Nuclear Regulatory Commission is presently funding this research to determine if large prehistoric earthquakes have occurred elsewhere along the Atlantic Seaboard. Initial aspects of this investigation include the documentation of the characteristics of liquefaction sites and features located in the Charleston area, and identifying the criteria by which similar sites and features, which may be located outside the Charleston area, could be

identified. This paper presents the results of these initial characterization studies.

### CHARACTERIZATION OF LIQUEFACTION SITES

During these investigations, a total of 103 liquefaction sites have been identified in the Charleston, S.C. area. Of these, 63 were identified based on the authors evaluation of historical accounts of the 1886 earthquake (Dutton, 1889; Peters and Herrman, 1986), 28 were identified as a result of ongoing field studies conducted by the USGS (Gohn and others, 1984; Obermeier and others, 1986; and Obermeier, personal communication 1986), 4 were identified during past field studies carried out by investigators from the University of South Carolina (Cox, personal communication 1986; Talwani written communication, 1986) and 8 were identified by the authors during reconnaissance field studies conducted as part of these investigations.

Each of these 103 sites have been located on available geologic maps, county soil maps, and topographic maps. Primary sources of geologic data included Colquhoun (1969), and McCarten and others (1984). These data were augmented by a geomorphic evaluation of each site based on 1:20,000 topographic maps. In addition, field reconnaissance studies were conducted at about one third of the sites. This information was used to identify the age of liquefied materials, depositional environment, stratigraphic setting, soil type, hydrologic setting, and proximity to seismicity for each liquefaction site.

### Age of Host and Liquefied Materials

Age has a significant impact on the liquefaction susceptibility of sediments. With time natural diagenesis tends to compact sands, increasing

grain-to-grain contact, thus reducing liquefaction potential. Therefore, younger sediments are generally more susceptible to liquefaction than older sediments, given the same overall geologic, hydrologic and seismic setting. Further, most investigators also note that in general liquefaction potential decreases as the percentage of fines increase. Consequently, chemical weathering, which results in the alteration of feldspars to clay minerals, increases the percentage of fines within the sediment, thus reducing its liquefaction potential.

Based on published information, the age of the host and liquefied materials for each liquefaction site in the Charleston area was estimated. The distribution of liquefaction sites by the age of host materials is presented on Figure 1. As illustrated approximately 90% of the sites occur in materials that were deposited during Late Pleistocene or Holocene times. These deposits correspond to unit Q3 or younger materials as identified by McCarten and others (1984), and the Talbert Formation or younger formations of Coiquihoun (1969). As illustrated on Figure 1, the results of this study suggest that materials older than about 200,000 years appear to be significantly less susceptible to liquefaction than younger deposits. Further, none of the 103 SIL sites identified are located in materials older than about 700,000 years.

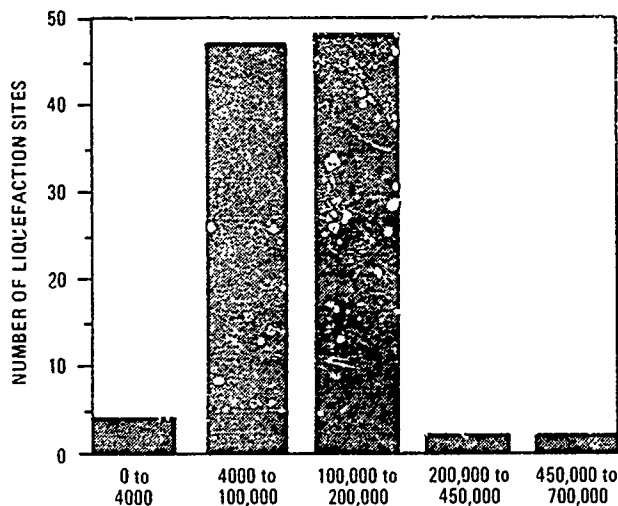


Fig. 1 Breakdown of Liquefaction Sites by Age (yrs).

These findings demonstrate that in the Charleston area sediments significantly older than Holocene are clearly liquefiable. This is in contrast to the results of some previous worldwide investigations that have found liquefaction to be restricted primarily to Holocene deposits. However, it should be noted that the sands that have experienced liquefaction in the Charleston area are composed of at least 95% silica. Consequently, the build-up of fines due to the weathering of feldspathic materials to form clays is very limited within these deposits. This may explain why these "older" sediments experience liquefaction.

### Geologic Setting

Previous investigations have found that in general, loose sands (i.e. those with relatively high void ratios) are more readily liquefied than dense compact sands. This observation suggests that, all other factors being equal, loose sands that are most often deposited in low to medium energy depositional environments (such as beach, lagoonal and river terrace settings) would be more prone to liquefy than compacted sands deposited in high energy settings (such as foreshore marine or river channel settings).

Based on published geologic data, field studies, and a geomorphological evaluation, the geologic setting of each of the 103 liquefaction sites was determined. The distribution of liquefaction sites by geologic setting is presented on Figure 2. As shown, virtually all of the liquefaction sites identified in the Charleston, S.C. area are located in one of three general types of geologic setting: 1) beach. 2) backbarrier, or 3) fluvial. As illustrated, approximately half of the sites occur in beach deposits. Most of the remaining sites are located in either back barrier (lagoonal) or fluvial (river) deposits. Very few (less than 4%) occur in other types of depositional environments. As noted by Weems and others (1986) and Obermeier (1986), liquefaction features within beach deposits in the Charleston area are most commonly found along the crests of Upper Pleistocene barrier island complexes.

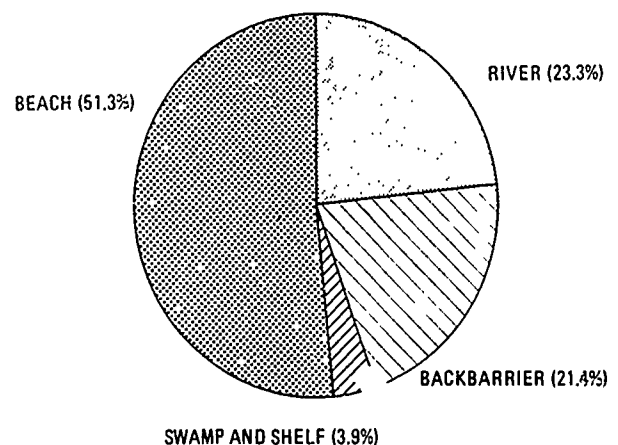


Fig. 2 Breakdown of Liquefaction Sites by Geologic Setting.

### Stratigraphic Setting

The locations of each of the liquefaction sites identified during this study were checked against the locations and logs for 2101 shallow auger holes and 540 water and test wells in the coastal plain of South Carolina. As a result, 26 boreholes or wells were identified that are located in relatively close proximity, (less than 1 mile) to the liquefaction sites identified during this study. The authors acknowledge that stratigraphy can vary widely over such a distance. However, for the purpose of this study it was felt that the extrapolation of available information, in the absence of site

specific subsurface data, could provide general information regarding stratigraphy in the vicinity of liquefaction sites.

Most investigators agree that liquefaction is almost exclusively restricted to sands or silty sands. Data from available boring logs are consistent with this model. All of the liquefaction sites identified during this study for which subsurface data is available were found to be underlain by fine to medium, well-sorted sand, or by interbedded sands, silts and clays. In all but one instance the total thickness of these deposits exceeds three meters. Where clay or silt beds are present they are generally thin (less than one to two meters thick). Conversely, the associated sand beds are typically over one to two meters thick. The depth of what have been interpreted as probable source sands is, in virtually every instance, less than six to seven meters below the ground surface.

A widely held misconception is that a non-liquefiable confining layer, such as clay, must be present over the source bed for liquefaction to occur. However, results of this study found less than 20% of the borings penetrated a clay confining layer above the probable source sand. A significant soil profile commonly referred to in boring logs as a "clayey sand" is present at about one fourth of the sites, while at more than half of the sites no confining layer is inferred from the available boring logs.

All sites are underlain at depth by an impermeable, calcareous, phosphatic clay (Cooper Marl Formation). This formation is present throughout most of the Southeastern Coastal Plain of S.C. The depth of this formation was found to vary between four to twenty meters, but was about nine meters below ground surface at most sites. In all cases the Cooper Marl is below the units that have been interpreted to have experienced liquefaction.

#### Soil Type

Soil maps were available for about 75% of the 103 SIL sites. Each of these sites were located on these maps and the host soil type was noted. As illustrated in Figure 3, over 60% of the SIL sites are located in soils that are described as sands or silty sands under the Unified Soil Classification System. If percentages are normalized to include only those sites for which soil information is available, almost 90% of the SIL features are located in sands or silty sands.

#### Hydrologic Setting

Previous investigations have documented the requirement of saturated conditions (i.e. shallow ground-water table) for liquefaction to occur. In keeping with these studies, the water table is relatively shallow at the great majority of liquefaction sites identified in the Charleston area. At almost all liquefaction sites the ground water table is less than one to three meters below ground surface and probable source sands are saturated.

NOT AVAILABLE (NA) (25.2%)

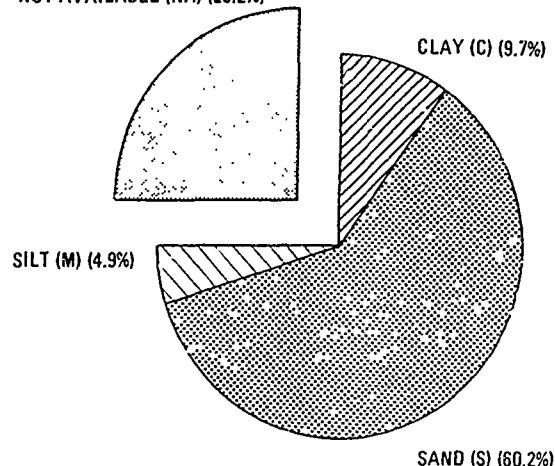


Fig. 3 Breakdown of Liquefaction Sites by USCS Soil Type.

#### Proximity to Seismicity

Each of the 103 liquefaction sites identified in the Charleston area have also been located with respect to the epicenters of the 1886 earthquake and recent, instrumentally located, magnitude 3+ seismicity. The liquefaction sites identified on the basis of historical accounts all lie within 40 km of previous seismicity. Most (over 80%) of the liquefaction sites identified by current investigators are also located within 40 kilometers of the epicentral area of the 1886 earthquake.

#### TYPES OF LIQUEFACTION FEATURES

In addition to identifying the characteristics of liquefaction sites located in the Charleston S.C. area, these investigations confirmed that the morphology of liquefaction features in the Charleston area varies significantly. Descriptions of liquefaction features reported by 19th century investigators of the 1886 earthquake, as well recent investigations by the USGS (Obermeier, 1986), and the results of this study confirm that two primary types of liquefaction features are present in the Charleston area. We refer to these features as sand-blow explosion craters and sand-vents/fissures.

#### Sand-Blow Explosion Craters

By far the most spectacular liquefaction features associated with the 1886 earthquake were sand-blow explosion craters. An example of this type of feature is shown in Figure 4. As described by Dutton (1889), typical sand-blow explosion craters associated with the 1886 earthquake were about 0.5 to 1.5 meters deep and 3 to 6 meters across. The largest craters reported were approximately 8 meters in diameter. An extensive ejection blanket of sand (up to 0.7 meters thick) extended for tens of

meters outward from many craters. At some sites ejected sands were found on tree limbs at heights up to 6 meters above the ground surface, attesting to the explosive nature of crater development (at least in some locales). However, at other locations reports suggest more passive crater development.



Fig. 4 Sand-Blow Explosion Crater associated with 1886 Earthquake (from Dutton, 1889).

Sand-blow explosion craters appear to form as a result of the explosive upward movement of liquefied sands, and are associated with a concave upwards bowl shaped "crater". They are roughly circular to elliptical in plan view. In cross section, the most distinctive features of sand-blow explosion craters are a central "feeder" vent and the occurrence of clasts of the "host" Bh soil horizon incorporated within the mobilized sands. As illustrated in Figure 5, two distinct well-sorted clast zones are commonly found: 1) a large-clast zone near the

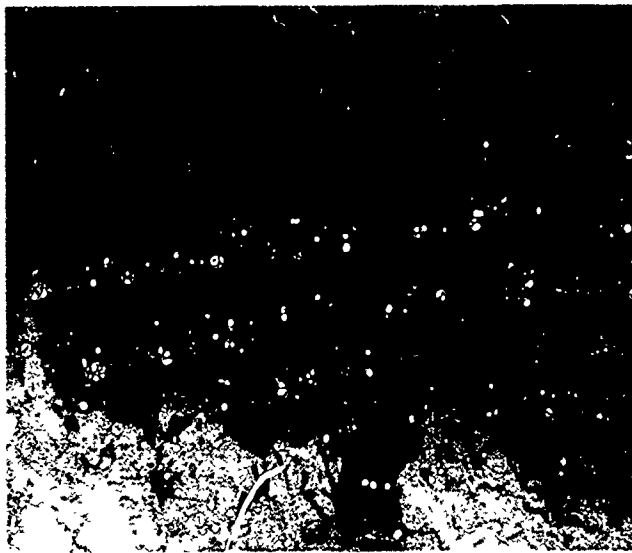


Fig. 5 "Classic" Sand-Blow Explosion Crater (from Obermeier and others, 1985).

base of the crater, and 2) a small-clast zone located near the top of the crater. Clasts within the large-clast zone, are generally cobble to boulder size, composed of Bh soil and are overlain by a zone of heterogeneous sand in which there are relatively few clasts and no distinctive flow structure. Above this heterogeneous layer is a small-clast zone composed of a horizontal layer of sand containing numerous small pebble sized clasts of Bh material. Above the small-clast zone, extending to the surface, are relatively horizontal thin layers of sand and silty sand (host Bh soil) deposited subsequent to formation of the sand blow. As noted by Obermeier (1985), small scale normal faults often cut crater infilling materials. These structures may result from compaction associated with dewatering.

Figure 5 (reproduced from Obermeier and others, 1985) provides a near perfect example of a sand-blow explosion crater. However, very rarely are all the features described above, and illustrated in this figure, preserved. For example, while a central "feeder" vent is shown in Figure 5, these features are small in cross sectional area when compared to the explosive crater. Consequently, they are only rarely exposed in near vertical excavations. Most commonly a bowl shaped section of the crater with the distinctive clast zones is all that can be viewed in trench walls. Further, in many pre-1886 sand-blow explosion craters bioturbation and weathering associated with soil development has masked or destroyed the uppermost features.

As illustrated in Figure 6, sand-blow explosion craters are found primarily in beach deposits, and are notably absent in fluvial settings.

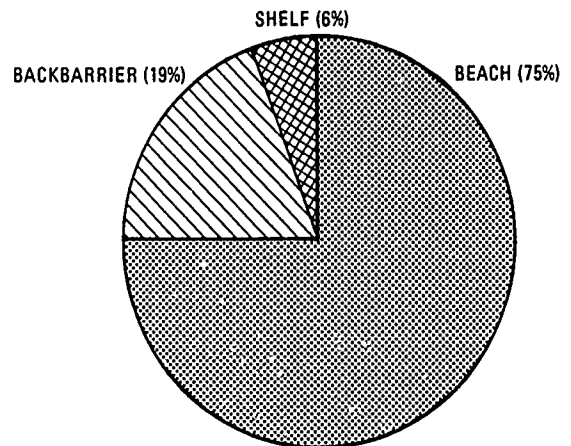


Fig. 6 Geologic Setting of Sand-Blow Explosion Craters.

Further, at many of the sand-blow explosion crater sites, especially beach locales, a confining layer of non-liquefiable material (other than a soil profile) is generally absent. Unsaturated sands overlying similar saturated material are the most common setting for "quick condition" mode liquefaction failure. However,

the explosive nature of the craters documented in the Charleston area is inconsistent with most quick condition failures. One explanation may be related to the depth of source sands in the Charleston area. As noted previously, source sands are almost always less than six to seven meters deep. Such a shallow source surely contributes to the observed explosive nature of many craters. Another factor that may contribute to the explosive nature of these features is the presence of an impermeable marl unit below the source bed. This unit represents a boundary condition that may tend to deflect or channel elevated pore-water pressures to the surface in an explosive manner.

#### Sand-Vents/Fissures

In addition to the sand-blow explosion craters, numerous fissures were also reported in the epicentral area of the 1886 earthquake. A photograph of a large dry fissure is presented in Figure 7. Some of these features generated by the 1886 earthquake were reported to be as much as 600 meters in length. Although the feature shown in Figure 7 was dry, many emitted large volumes of water laden with sediment. We refer to this type of liquefaction feature as a sand-vent/fissure. Historical accounts indicate that for the most part they were found along the banks of rivers and streams. Further, many of the accounts provided by historical investigators as well as the results of more recent investigations suggest that many of the sand-vents/fissures observed following the 1886 earthquake were the result of lateral spreading failures similar to those reported following the 1964 Alaskan earthquake (McCulloch and Bonilla, 1970) and the 1971 San Fernando earthquakes (Yould, 1973).



Fig. 7 Dry Fissure associated with the 1886 Earthquake (from Dutton, 1889).

At almost all locales where sand-vents/fissures have been found and excavated by 20th century investigators, a non-liquefiable confining layer or "cap" is present over the source bed of liquefied sands. At many sites the cap appears to have been transported short distances down slope due to a decrease in the friction along the boundary between the cap and the underlying sand, consistent with a lateral spreading model for formation. During transport, the cap apparently fails under laterally directed tension, resulting in the ejection of the underlying liquefied sands into the resulting tabular vent in the cap materials. The long axis of the sand-vents/fissures at these sites are generally oriented normal to the direction of lateral transport. Examples of this type of liquefaction feature are presented Figures 8, 9, and 10. When clasts occur within these vents,



Fig. 8 Example of Sand-Vent/Fissure

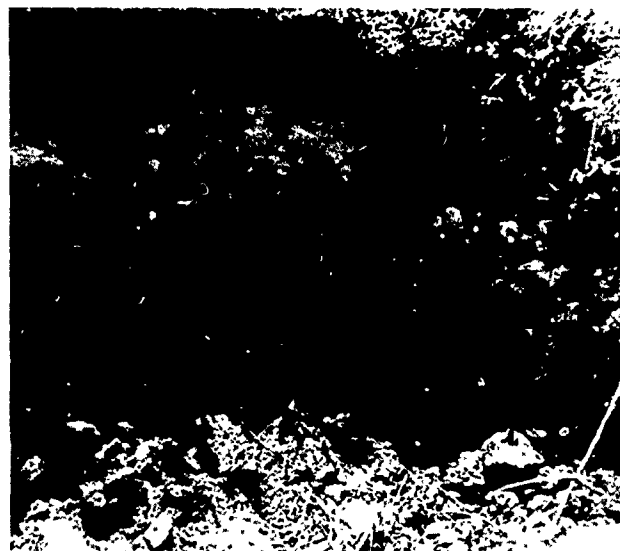


Fig. 9 Example of Sand-Vent/Fissure



Fig. 10 Example of 1886 Sand-Vent/Fissure  
(from Cox, 1984)

they are generally large, unsorted, and consist of the clay "cap" or "host" material. In contrast to sand-blow explosion craters, small clast and extensive flow structures are generally absent. In addition, small scale structures commonly observed in explosion craters and thought to result from compaction associated with dewatering are also generally absent.

As illustrated in Figure 11, at other

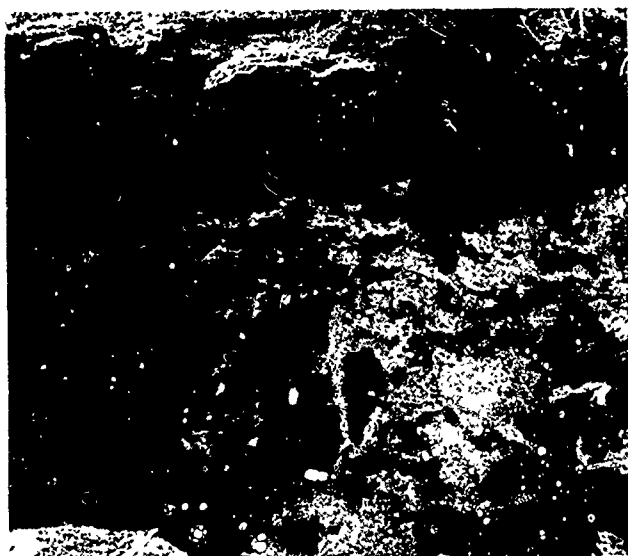


Fig. 11 Example of Sand-Vent/Fissure  
Note shattered character of cap.

sand-vent/fissure sites, the cap appears to have been shattered in place due to the forceable upward movement of underlying liquefied sands. At these sites the cap is often broken into polygons rather than along distinct tabular fissures. At other sand-vent/fissure sites the cap appears to have ruptured "under its own weight", perhaps due to the loss of bearing capacity of the underlying liquefied sands. At these sites, the mixing of cap and liquefied sands may be due to a density inversion. An example of this type of liquefaction feature is presented in Figure 12.

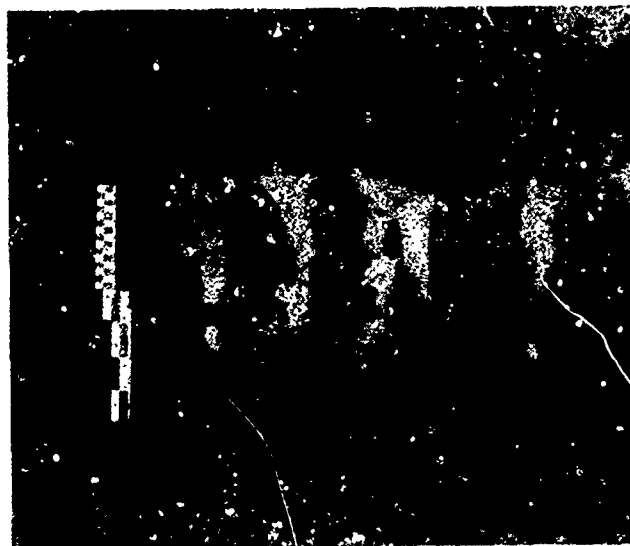


Fig. 12 Example of Sand-Vent/Fissure

Sand-vents/fissures are noted to occur almost exclusively where a confining unit lies above liquefiable sands. As illustrated in Figure 13, in the Charleston area this local stratigraphy is most commonly found within backbarrier marine sediments and in interbedded river terrace

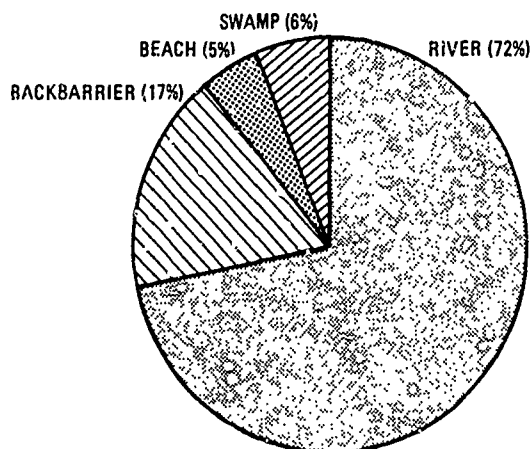


Fig. 13 Geologic Setting of Sand-Vent/Fissures

deposits. This type of feature is generally absent in beach settings, except where a thick soil profile or claypan has developed on the parent sand.

#### SUMMARY AND CONCLUSIONS

The magnitude 6.7 to 7.1 Charleston, South Carolina earthquake of August 31, 1886 produced numerous liquefaction features in the Southeastern Coastal Plain of South Carolina. The United States Nuclear Regulatory Commission is presently funding studies to characterize the liquefaction features associated with this significant historical earthquake.

During this study, a total of 103 liquefaction sites were identified in the Charleston area. Each of these 103 sites were located on available geologic maps, county soil maps, and topographic maps. In addition, a geomorphic assessment was carried out for each site. Field investigations were also conducted at about one third of the 103 sites. These data were used to determine the characteristics of liquefaction sites in the Charleston S.C. area, and to compare these characteristics to those reported in the literature.

The great majority of seismically-induced liquefaction sites located in the vicinity of the 1886 Charleston, S.C. earthquake occur in deposits that are either Late Pleistocene or Holocene in age (4,000 to about 200,000 years old). Materials older than about 200,000 years were found to be significantly less susceptible to liquefaction than these younger deposits. None of the liquefaction sites identified were found in materials older than about 700,000 years. Further, seismically-induced liquefaction features in the Charleston area occur almost exclusively in either beach backbarrier, or fluvial deposits. Among the three, beach settings are the most favorable depositional environment for the generation and preservation of seismically-induced liquefaction features.

Virtually all liquefaction sites for which local stratigraphic information is available are underlain at least three meters of sand, or by at least three meters of alternating sand, silt, and clay beds. The sands are generally fine to medium grained, well-sorted and have silica contents in excess of 95%. The depth to the probable source beds at these liquefaction sites is in almost every case less than six to seven meters and the ground-water table is characteristically less than one to three meters below the present ground surface. Finally, all of the liquefaction sites identified on the basis of historical accounts of the 1886 earthquake and most of the liquefaction sites associated with prehistoric earthquakes are located within 40 kilometers of previous seismicity.

The characteristics of liquefaction sites identified during this study are in general agreement with information previously published for liquefaction sites worldwide. A notable exception is that in the Charleston area sediments as old as about 200,000 years appear

to highly susceptible to liquefaction. This is in contrast with much of the information published that suggests Late Pleistocene age deposits are in general much less susceptible to liquefaction than Holocene age materials. Because the alteration of feldspars to clay minerals increases the percentage of fines, thus reducing the liquefaction potential of a material, feldspathic sands would tend to develop more fines during weathering than clean high silica sands of the same age. Consequently it should not be unusual to find liquefaction in "older" high silica sands such as those present in the Charleston area while "younger" feldspathic sands in other areas remain stable under similar levels of seismic loading.

In addition to identifying the characteristics of liquefaction sites located in the Charleston S.C. area, these investigations confirmed that the morphology of liquefaction features in the Charleston area varies significantly. While many factors must play a part in determining the morphology of a particular liquefaction feature, local stratigraphy appears to play the dominant role. Field observations suggest that the presence or absence of a non-liquefiable unit of the material overlying the source bed of liquified sands and the thickness and clay content of this unit controls to a great degree what type of liquefaction feature forms.

The two most common seismically-induced liquefaction features observed during this study were sand-blow explosion craters and sand-vents/fissures. Sand-blow explosion craters form as a result of the explosive upward movement of liquified materials and are associated with a concave upwards bowl shaped "crater". This type of liquefaction feature occurs almost exclusively where no significant confining layer, other than a soil profile, is present over liquefiable sands. In the Charleston area this local stratigraphic setting is most commonly found in old beach and near-shore marine depositional environments. Significantly, this type of seismically-induced liquefaction feature is virtually absent in fluvial sites, where interbedded silts, sands, and clays are common.

In addition to the sand-blow explosion craters, sand-vents/fissures were also found in the Charleston area. While the actual mechanism responsible for the generation of this type of liquefaction feature varies from site to site, at many locales the mode of failure appears to be one of lateral spreading. At these sites an overlying non-liquefiable cap material appears to have been transported short distances down slope due to a decrease in friction along the boundary between the cap and the underlying liquified sands. In the Charleston area, the local stratigraphic setting most commonly associated with sand-vents/fissures are interbedded river terrace or backbarrier deposits.

In summary, these investigations support the generally accepted models for the types of material and the hydrogeologic setting that are required for liquefaction to take place as a result of seismic loading. However in contrast to some previous investigations, these studies found relatively few liquefaction sites in Late Holocene materials. Rather, most liquefaction



sites identified in this study are located in materials 100,000 to 200,000 years old. Finally, this study indicates that the depositional environment may play a key role in determining the type of liquefaction failure.

Yould, T. Leslie, 1973, Liquefaction, flow and associated ground failure: USGS, Cir. 688, 12 p.

#### REFERENCES

- Colquhoun, D.J., 1969, Geomorphology of the Lower Coastal Plain of South Carolina, MS-15, Div. of Geology, State Development Board, Columbia, SC, 36 p.
- Cox, J.M., 1986, personal communication.
- Dutton, C.E., 1889, The Charleston earthquake of August 31, 1886: U.S. Geological Survey Annual Report of 1887-1888, p. 203-528.
- Gohn, Gregory S., Weems, R.E., Obermeier, S.F., and Gelinas, R.L., 1984, Field studies of earthquake-induced, liquefaction-flowage features in the Charleston, South Carolina, area--preliminary report: USGS OFR 84-670, 26 p.
- McCartan, L., Lemon, E.M., and Weems, R.E., 1984, Geologic map of the area between Charleston and Orangeburg, South Carolina: U.S. Geological Survey Misc. Invest. Map I-1472, 1:250,000, 2 sheets.
- McCulloch, D.S. and Bonilla, M.G., 1970, Effects of the earthquake of March 27, 1964, on the Alaska Railroad: USGS Prof. Paper 545-D, 161 p.
- Obermeier, Stephen F., Gohn, G.S., Weems, R.E., Gelinas, R.L., and Rubin, M., 1985, Geologic evidence for recurrent moderate to large earthquakes near Charleston, South Carolina: Science v. 227, p. 408-411.
- Obermeier, S.F., Jacobsen, R.B., Powers, D.S., Weems, R.E., Hallbick, D.C., Gohn, G.S., and Markenwich, H.W., 1986, Holocene and Late Pleistocene (?) earthquake-induced sand blows in coastal South Carolina, in: Third U.S. national conference on earthquake engineering--Charleston, South Carolina, v. I, p. 197-208.
- Peters, Kenneth E. and Herrman, Robert B., 1986, First-hand observations of the Charleston earthquake of August 31, 1886, and other earthquake materials: South Carolina Geol. Survey Bull. 41, 116 p.
- Talwani, Pradeep, and Cox, John, 1985, Paleoseismic evidence for recurrence of earthquakes near Charleston, South Carolina: Science, v. 229, p. 379-381.
- Weems, Robert E., Obermeier, S.F., Pavich, M.J., Gohn, G.S., Rubin, M., Phipps, R.L., and Jacobson, R.B., 1986, Evidence for three moderate to large prehistoric Holocene earthquakes near Charleston, S.C., in: Third U.S. national conference on earthquake engineering, Charleston, South Carolina, v. I, p. 3-13.

## Analysis and Measurement of Foundation Vibrations at Two Compressor Stations in Yugoslavia

**Predrag Kvasnička**

Research Assistant, Faculty of Civil Engineering, University of Zagreb, Yugoslavia

**Tomislav Ivšić**

Research Assistant, Faculty of Civil Engineering, University of Zagreb, Yugoslavia

**Aleksandar Kiričenko**

Professor of Civil Engineering, Faculty of Civil Engineering, University of Zagreb, Yugoslavia

**SYNOPSIS:** The design procedure and the measurements of foundation vibrations at two compressor stations are presented. Simple methods and models were used to predict machine foundation behavior and it is shown that they were effective in estimating the expected range of amplitudes through simple parameter variation.

In attempt to lower vibrations amplitudes, spreading of gravel layer under machine foundation was suggested, the effect of which is discussed in the paper.

### INTRODUCTION

The basic goal in the machine foundation design is to keep its motion in the limits which will enable the satisfactory operation of the machine without disturbing the people in the immediate vicinity. Thus, to achieve this goal, it is expected from the designer to correctly predict the machine foundation motion. As shown in figure 1, the prediction of machine foundation vibrations is a system which involves (1) the determination of machine loads and selection or first guess of the shape and mass of foundation (if it is not predefined due to other reasons), (2) the evaluation of soil profile and soil properties, (3) the selection and application of adequate method of analysis. The design procedure requires additional step: establishment of acceptance criteria. If the predicted motion do not meet these criteria (and all other steps are properly done), it would usually require the change in geometry and mass of the proposed foundation, or, in some cases, improving the soil properties.

According to Gazetas (1983), the post construction observation of foundation performance is also "an additional and often overlooked step in machine foundation design". The measured response of foundation on dynamic machine loads serves as a reliable source of information for verification of the whole design procedure:

- a) comparison of real performance with established criteria
- b) data for numerical comparison of measured and predicted vibrations.

Since it is not easy to separate the influences of all relevant factors needed for prediction of motion, the measured vibrations could be for instance used in (keeping other factors unchanged):

- verification of assumptions and models on which the method of analysis is based
- correlating the soil properties estimated from

ground investigations with those obtained from back analysis with particular method

- verification of proposed design measures for reducing amplitudes of vibrations.

The experience gained from such analyses impro-

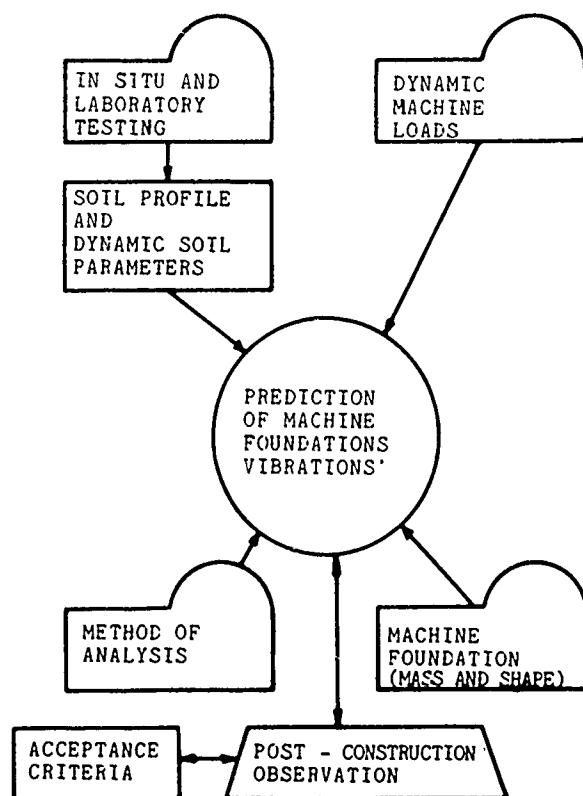


Figure 1. Machine foundation design procedure

ves the design procedure and understanding of the nature of the problem.

In this paper the design procedure and post construction observation of the compressor foundation in two compressor stations is presented.

The geometry and mass of compressor foundation in both cases came out satisfying other design requirements. Since the mass of the foundations was more than five times the weight of the supported machines, according to some "rules of thumb" no analysis of vibration would be necessary. The ground investigations on both sites showed that surface layers were of poor characteristics and it was decided to substitute them with densified gravel. Relatively simply-to-use-analysis according to Richart, Hall and Woods (1970) and Gazetas (1983), using only dominant loads, were performed "just to verify" additional costs.

Finally, post-construction measurements were undertaken to "everybody make sure".

#### COMPRESSOR STATION LEGRAD

Compressor station Legrad (c.s.Legrad) was settled in 1985. It consists of eleven compressors, eight compressors, type C-200, and three, type C-100.

Soil characteristics were determined by geotechnical investigations and geophysical measurements (Fig.2).

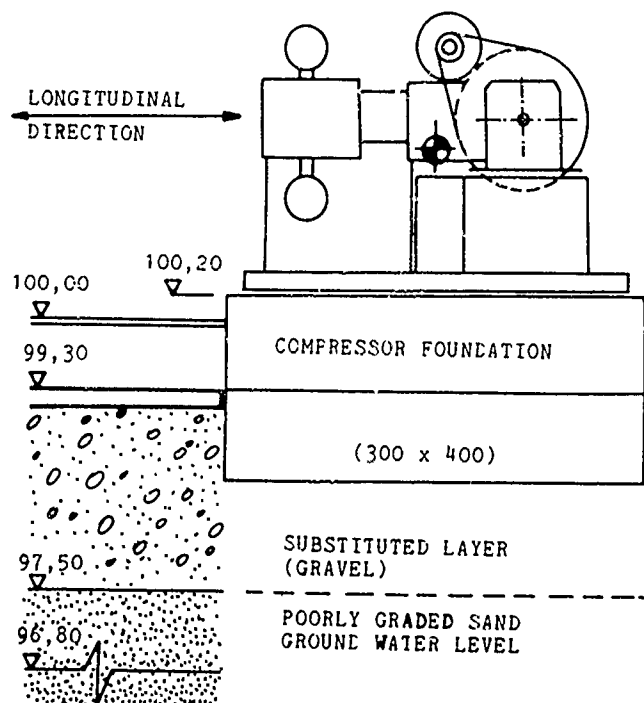


Figure 2. Cross-section of a foundation and soil in C.S.Legrad

Upper two meters of poor characteristics were substituted with gravel layer. Shear wave velocity ( $V_s$ ) of sand was measured by surface refraction method; range of  $V_s$  was from 220 to 250 m/s, what correspond to values of shear modulus of 100 MN/m<sup>2</sup>.

The shear modulus of gravel was estimated as 100 MN/m<sup>2</sup>.

Dominant unbalanced inertia forces act in longitudinal direction (Fig.2). According to the manufacturer of compressors the foundations must be designed to resist the following forces (dynamic loads):

| type  | maximum longitudinal primary force | maximum longitudinal secondary force | operating frequency |
|-------|------------------------------------|--------------------------------------|---------------------|
| C-200 | 11,8 kN                            | 3,40 kN                              | 294 c/min           |
| C-100 | 20,1 kN                            | 5,67 kN                              | 353 c/min           |

Compressor foundations were designed as massive concrete blocks (Fig.2) separated 1,0 m from each other. Mass of one compressor and foundation was 46,3 t. Schematic presentation of foundation layout is in the Fig.3.

Analyses were performed by two methods:

lumped parameter approximation (Richart et al, 1970) and dynamic impedance functions as described in Gazetas (1983). The acceptance criteria were adopted from Richart et al (1970).

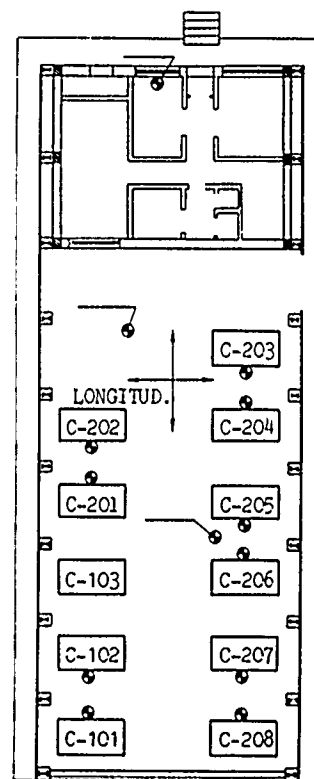


Figure 3. Layout of compressors in C.S.Legrad

Only the compressors of type C-100 using primary forces were analyzed on two models:

I foundation on the surface of elastic half-space  
 $G = 100 \text{ MN/m}^2$ ,  $\nu = 0.33$

II as I, but  $G = 50 \text{ MN/m}^2$

The first model was assumed to be "the real" one, and second "the worst" one, covering the neglected or unexpected influencing factors with variation of single parameter -  $G$ .

The results of the analyses are presented in Table I.

Table I Calculated values of amplitudes of longitudinal vibrations - C.S.Legrad

| Case | Richart et al<br>( $\mu\text{m}$ ) | Gazetas<br>( $\mu\text{m}$ ) |
|------|------------------------------------|------------------------------|
| I    | 19,8                               | 19,7                         |
| II   | 40,8                               | 38,2                         |

For cases analyzed, two methods correspond quite well.

The measurements were taken while nine of eleven compressors were simultaneously in operation (compressors C-103 and C-201 were not prepared). The measured amplitudes of vibrations are presented in Table II.

Table II Measured values of amplitudes of vibrations - C.S.Legrad

|       | D I R E C T I O N             |                              |                              | frequency<br>Hz |
|-------|-------------------------------|------------------------------|------------------------------|-----------------|
|       | Vertical<br>( $\mu\text{m}$ ) | Transv.<br>( $\mu\text{m}$ ) | Longit.<br>( $\mu\text{m}$ ) |                 |
| C-101 | 6                             | 2                            | 34                           | 6,2             |
| C-102 | 1                             | 2                            | 30                           | 6,2             |
| C-202 | 1                             | 2                            | 20                           | 5               |
| C-203 | 5                             | 4                            | 18                           | 5               |
| C-204 | 2                             | 2                            | 18                           | 5               |
| C-205 | 3                             | 1                            | 23                           | 5               |
| C-206 | 1                             | 1                            | 28                           | 5               |
| C-207 | 1,5                           | 1                            | 21                           | 5               |
| C-208 | 1                             | 2                            | 20                           | 5               |

Typical plot of measured vibrations is shown on Fig.4.

The intensity of amplitudes changed periodically showing low frequency "superior" influence. Anyhow, the average amplitude (cca  $20 \mu\text{m}$  for type C-100) corresponded well to predicted amplitudes using the model with best estimate of soil properties. The rest between 20 and  $30 \mu\text{m}$  is attributed to the influence of neighbouring compressors or unbalanced secondary forces.

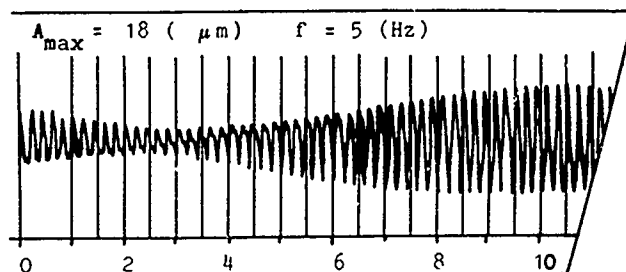


Figure 4. Longitudinal vibrations of compressor C-203

#### COMPRESSOR STATION BOKŠIĆ

Compressor station Bokšić was settled in 1986 and consists of eight compressors. The measurements were taken before the whole station was completed and only three compressors were in operation. The available results are presented.

Soil characteristics were determined by geotechnical investigations and geophysical measurements (Fig.5.).

Shear wave velocity of clay in upper three meters was between 140 and 160 m/s, so shear modulus of clay was supposed to be  $50,0 \text{ MN/m}^2$ . Shear wave velocity in sand ranged from 225 to 250 m/s and estimated shear modulus was  $100 \text{ MN/m}^2$ .

Dominant unbalanced inertia forces act as horizontal moments (torque). According to the manufacturer of compressors their amplitudes were:  
 maximum vertical moment 4,16 kNm  
 maximum horizontal primary moment 15,2 kNm.  
 operating frequency 740 c/min  
 Compressor foundations were designed as massive concrete blocks (Fig.5.) separated 3,0 m from each other. Mass of one compressor and foundation was 93,5 t.

Analysis was performed according to Gazetas (1983) and the soil profile was modelled as (clay) stratum-over-(sand) halfspace. It was difficult to estimate the positive influence of embedment with much confidence and it was conservatively neglected. The results are presented in Table III (case I).

Since the radial amplitudes were considered to be high and since there was not confidence in clay as direct foundation supporting soil, it was decided to substitute the clay above ground water level with one meter thick densified gravel layer. The gravel and the rest of the clay layer were separated with dense geotextile. The shear modulus of gravel was assumed as  $G = 100 \text{ MN/m}^2$ .

The analyses were performed in the same way as before using two models:

- foundation on halfspace with  $G = 100 \text{ MN/m}^2$  (thus, neglecting the clay sublayer) - case II in Table III.
- foundation stratum-over-halfspace with stratum having the "average" modulus  $G = 80 \text{ MN/m}^2$ , thickness  $H = 2 \text{ m}$  and halfspace with sand properties ( $G = 100 \text{ MN/m}^2$ ) - case III in Table III. The embedment effects were again neglected in analysis.

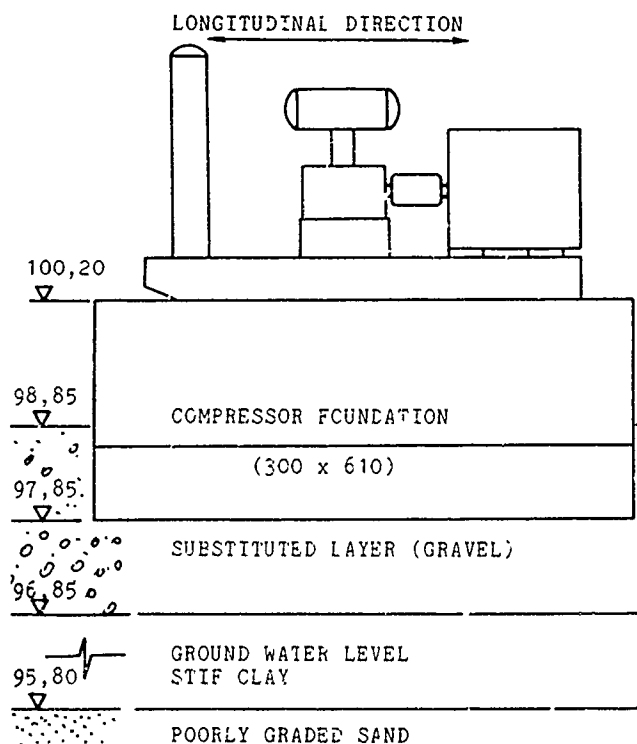


Figure 5. Cross-section of soil and foundation in C.S. Bokšić

Table III Calculated amplitudes of vibrations at corners of foundations - C.S. Bokšić

| case | longitudinal<br>( $\mu\text{m}$ ) | vertical<br>( $\mu\text{m}$ ) | radial<br>( $\mu\text{m}$ ) |
|------|-----------------------------------|-------------------------------|-----------------------------|
| I    | 1,1                               | 4,2                           | 23,2                        |
| II   | 0,6                               | 2,3                           | 5,9                         |
| III  | 0,8                               | 2,7                           | 11,3                        |

The measurements were taken in the middle (M) and at the corners (C) of the foundation edge for three foundations C1, C2 and C3 (table IV).

Table IV Measured values of amplitudes

|        | longitudinal<br>( $\mu\text{m}$ ) | vertical<br>( $\mu\text{m}$ ) | radial<br>( $\mu\text{m}$ ) |
|--------|-----------------------------------|-------------------------------|-----------------------------|
| C1 (M) | 0,4                               | 0,8                           | 1,08                        |
| (C)    | 0,4                               | 1,25                          | 1,33                        |
| C2 (M) | 0,9                               | 1,2                           | 2,19                        |
| (C)    | 0,9                               | 1,2                           | 2,5                         |
| C3 (M) | 1,2                               | 1,7                           | 2,5                         |

Comparing the results of estimated and observed vibrations it may be concluded that amplitudes were considerably lowered by putting the gravel layer under foundation.

The order of magnitude of vibrations is 1 mikron and it could not be felt (by humans) when the hand was put on the foundation.

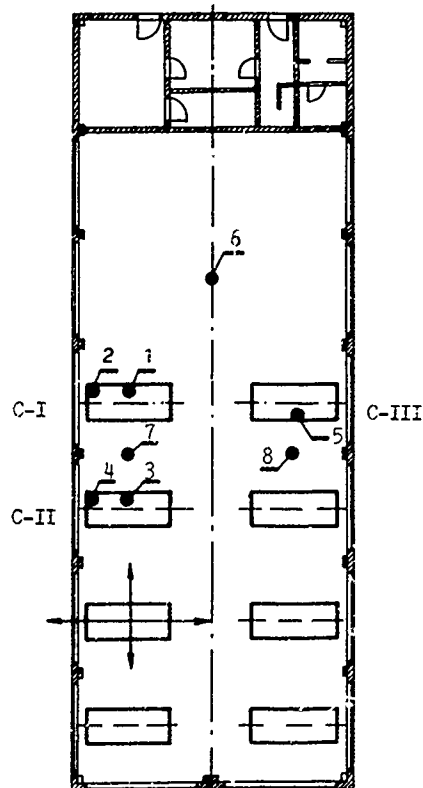


Figure 6. Layout of compressors in C.S. Bokšić

#### CONCLUSIONS

The design procedure and the results of measurements of foundation vibrations at two compressor stations are presented. The design procedure attempts to cover unfavourable conditions selected by engineering judgement and includes the best estimate of soil properties and relatively simple models and methods of analysis. During design, it was decided to improve the soil conditions by replacing the natural soil in shallow depths by densified gravel.

The observed performance supports the actions undertaken, showing that the measured amplitudes are in the range of predicted values.

It may be concluded that simple methods and models are effective in design practice allowing estimate of the expected range of amplitudes through simple parameter variations. Also spreading a relatively thick gravel layer under machine foundation is considered to be an effective low cost measure towards the lowering of the amplitudes of vibrations. This effect is primarily attributed to the increased stiffness of soil which directly supports the foundation.

#### ACKNOWLEDGMENTS

The work presented in this paper was supported by INA-Naftaplin, Zagreb. The authors wish to thank specially to Mr.D.Bobetko and Mr.Arbanas for valuable discussions and moral support.

#### REFERENCES

- Gazetas, G. (1983), Analysis of Machine Foundations: State of the art, Soil Dynamics and Earthquake Engineering, Vol. 2, No. 1, 2-42.
- Richart, F.E, Hall, J.R, Woods, R.D. (1970), Vibrations of Soils and Foundations, Prentice-Hall, Englewood Cliffs, New Jersey.

## Seismosedimentation and Lives of Reservoirs

Arun Bapat

Central Water and Power Research Station, Pune, India

**SYNOPSIS :** When moderate to major earthquakes, usually of magnitude more than or equal to 6.0 on Richter Scale, occur in catchment area of river, additional amount of geological materials is generated, which is called as Seismosediments and the process is known as Seismosedimentation. River flow mechanism carries it down to reservoir. This amount of seismosediment is quantified by a mathematical relation. A specific case of seismosedimentation with reference to sediments in Bhakra reservoir has been discussed. It is observed that seismosedimentation could reduce the economic life of reservoir and adversely affects the utility of reservoir. Re-examination of lives of large reservoirs in active seismic zones is recommended.

### INTRODUCTION

Construction of large reservoirs all over the world during last few decades had heralded an era of technological progress for various countries in the world. Water holds key to progress in agriculture, industries, power generation etc.. This is widely reflected in the prosperity achieved through various dams such as TVA dam in USA, Bhakra dam in India, Aswan dam in Egypt and Nurek dam in USSR and several other dams in the world. During the recent past a new group consisting of environmentalists, ecologists and nature conservationists is emerging and contesting construction of large reservoirs. The main objection of this group is the likely disturbing effects of these reservoirs on nature and geology. However it is felt that these effects are debatable. Each water reservoir has a finite life period and the benefits such as power generation and water for irrigation are projected over a finite length of time. Life of reservoir is primarily based on average annual rate of sedimentation. Like entropy, the available beneficiary potential of reservoir goes on decreasing with time. The main reason for this depleting power is reduction in effective volume of reservoir due to deposition of sediments in reservoir. There are several mathematical relationships and formulae for estimation of average annual rate of sedimentation. The values of coefficients in these relations vary with type of geology and river regime characteristics. Some of these have been tested with the help of physical models also. But presence of great degree of heterogeneity in river regime puts some constraints on these relationships. Despite these limitations, these relations offer a reasonable estimate of annual sediments.

Occurrence of earthquake in the vicinity of reservoir do affect the functioning of reservoir. This effect could be as small as causing a seiche in reservoir or collapse of the affected dam. During the present century about ten dams have collapsed due to seismic effect. The notable among these are failure of Sheffield dam during Santa Barbara Earthquake of June 29, 1925, slide in Lower San Fernando dam during San Fernando Earthquake of February 09, 1971, damage to Eklutna dam during Alaskan earthquake of March 1964, damage to Koyna dam during Koyna earthquake of December 10, 1967 and damage to 95 reservoirs due to Tokachi Offshore earthquake of May 1968 in Japan. In addition, the failure of 80 m high Baldwin Hill dam in the Western California was due to earth movement. The earth movement, due to subsidence manifested itself by opening and by offsetting at a fault, a plane of weakness. Failures of dams due to earthquake is not being considered in this paper. However, it is not known whether there were any reservoirs downstream of these failed dams. If so, then the entire sediment load from failed dam would have been deposited in the downstream reservoir.

Occurrence of medium to large earthquake in the vicinity of river regime generates additional amount of geological materials which in turn is collected as sediment by river flow mechanism. This effect was known to engineers and scientists for long but was not considered seriously. Bapat (1985) has described this as 'Seismosediments' and the process is called as 'Seismosedimentation'. Bapat (1981) had quantified seismosediments and has offered a mathematical relation for estimation of seismosediments in terms of average rate of

annual sedimentation, probability of occurrence of earthquake and estimated life of reservoir.

It proposed to discuss this effect for selected few cases in world, with a specific case from Bhakra reservoir in India.

## SEISMOSSEDIMENTATION

Bapat (1985) has given following definition of seismosediments and the process of seismosedimentation, "Geological materials which are crushed, fractured, loosened or displaced directly or indirectly as a result of earthquake induced processes such as landslides, landslips, slumps, mudflows, avalanches, liquefaction, rockfalls, rockslides etc. and which move under gravity in catchment area of river are defined as seismosediments and the process as Seismosedimentation". When an earthquake of moderate to major size, usually of magnitude 6.0 or more, occurs in the vicinity of catchment area of river, seismosediments are generated. This is illustrated with reference to the occurrence of an earthquake in the catchment area of river Sutlej in the Himalaya, on January 19, 1975. This earthquake has been described by Gosavi et al (1977). The epicenter of this earthquake was at about 32.5°N and 78.4°E with a magnitude of about 6.5 on Richter Scale. Geologically, the terrain consists of weathered loose formation such as Sivaliks, Krolls and glacial moraines. As a result of earthquake there was huge landslide near village Kaurick and the flow of river Parachu, a tributary of Sutlej, was temporarily blocked due to formation of natural dam. The height of this natural dam was about 20 m. This blockade breached between 27th - 28th January 1975 and a rise of about 50 cm in the water level of Sutlej was observed on 28th January 1975. The water was conspicuously turbid and the sediment load was very high. In addition, there were several landslides in Spiti valley. Bhakra reservoir and dam are constructed on river Sutlej and is located at about 200 km away from the epicenter of the earthquake on January 19, 1975. The sediment observation near the reservoir with reference to this earthquake has been described by Bapat (1980). He has further observed that as a result of earthquake the life of reservoir could be reduced by 15 - 30 percent of the estimated life. Normally, sediment load is high during the monsoon period of July-August-September and highest peak occurs during the month of August. Further, the sediment load during January-May is quite low. During the post-seismic period, there was sudden rise in sediments and it reached peak value of about 1100 hectre-metre in June 1975 and this was followed by the usual annual peak at about 687 hectre-metre in August 1975. The seismosediments are about 1.6 times that of the peak value. It is also possible that natural sediment at some distance from earthquake epicenter would flow alongwith seismosediments down to reservoir. Bapat (1981) has given following relation for quantification of seismosediments.

$$Q = RPTF \text{ (Tons)} \quad \dots(1)$$

where Q(Tons) is the amount of seismosediments during T(Years), R(Tons/Year) is the average annual rate of sedimentation, P is the probability of occurrence of earthquake in the vicinity of river regime and F is the fraction due to seismosediments. This relation has been further modified by Bapat (1988) to account for various magnitude ranges. It is also possible that earthquake epicenter may not be located within the limits of catchment area of river. Occurrence of earthquake at some distance from the limits of catchment area would also generate seismosediments. Table 1 gives the distribution of earthquake magnitude and effective distance range which could produce seismosediments. These distances are based on reports of several macroseismic observations during the post-seismic periods.

| Magnitude Range | (M)            | Distance upto which it may produce Seismosediments (km) |
|-----------------|----------------|---|
| 5.5 - 6.4       | M <sub>1</sub> | 30 - 50   |
| 6.5 - 7.4       | M <sub>2</sub> | 50 - 75   |
| M ≥ 7.5         | M <sub>3</sub> | upto 150 km or more                                     |

Table 1. Distribution of earthquake magnitude range and distance from the boundary of catchment area of earthquake epicenter which could produce seismosediments.

Considering the above distribution of magnitude range, relation (1) has been modified as

$$Q = RT (P_1 F_1 + P_2 F_2 + P_3 F_3) \quad \dots(2)$$

where P<sub>1</sub>, P<sub>2</sub> and P<sub>3</sub> are the corresponding probabilities of occurrences of earthquakes of magnitude ranges M<sub>1</sub>, M<sub>2</sub> and M<sub>3</sub> and F<sub>1</sub>, F<sub>2</sub> and F<sub>3</sub> are corresponding components of seismosediments. It is observed that the above relation, quantifying seismosediment is found useful in the case of Bhakra reservoir due to earthquake of magnitude 6.5 of January 1975.

## DISCUSSION

It is observed that seismic data for different countries are freely available. However monthly or yearly sedimentation data for various reservoirs located in active seismic



| No. | River      | Dam              | Type    | Height (m) | Location         | Country     |
|-----|------------|------------------|---------|------------|------------------|-------------|
| 1.  | Podda      | Oued             | Gravity | 100        | El-Asnam         | Algeria     |
| 2.  | Nechako    | Kenny            | Earth   | 104        | British Columbia | Canada      |
| 3.  | Sutlej     | Bhakra           | Gravity | 226        | Punjab           | India       |
| 4.  | Rangataiki | Matahina         | Earth   | 86         | Auckland         | New Zealand |
| 5.  | Tjitarun   | Djatiluhur       | Earth   | 103        | Jawa             | Indonesia   |
| 6.  | Cormor     | Alp Gera         | Gravity | 178        | Lombardia        | Italy       |
| 7.  | Balson     | El Infierillo    | Earth   | 148        | Michoacan        | Mexico      |
| 8.  | Indus      | Tarbela          | Earth   | 143        | Karipur          | Pakistan    |
| 9.  | Sakarya    | Sariyar          | Gravity | 108        | Ankara           | Turkey      |
| 10. | North Yuba | New Bullards Bar | Arch    | 194        | California       | USA         |
| 11. | Vakhsh     | Nurek            | Earth   | 317        | Tadjikistan      | USSR        |

Table 2. List of few selected large dams in active seismic parts of world.

regions are not available freely. At times these data are classified or it could not be made available. A few cases where the amount of seismosediments have been estimated during some post-seismic surveys of destructive earthquakes are available and these figures are quite informative. These estimates are grotesque and are observed during macro-seismic field investigations. But the figures speak about the massive effects of movement of geological materials. However there were no reservoirs downstream and the displaced mass has been estimated from field observation. Cluff (1970) has reported that the volume of displaced mass during the Peruvian earthquake of 1970 of magnitude 7.7 was about 50 - 80 million cubic meters. Adams (1981) has observed that during the 1929 Buller earthquake of New Zealand the displaced mass was about  $1 \times 10^{12}$  kg of sediments. The sediment load in the Karamea catchment area of Buller river, in the vicinity of earthquake epicenter, varies between  $0.3 \times 10^9$  kg/year to about  $1.2 \times 10^9$  kg/year. Taking these values, it is observed that the  $1 \times 10^{12}$  kg sediments generated during earthquake was equivalent to more than 800 years of 'normal' sediments. It is therefore much pertinent to examine this issue and make realistic assessment of lives of reservoirs in active seismic zones. As an illustration a few reservoirs from active seismic zones are listed in Table 2. The details are taken from World Register of Dams published by the International Commission on Large Dams.

It is seen that most of the dams mentioned in Table 2 are of more than 100 m height. All these dams are located in active seismic areas, which have experienced earthquakes of

magnitudes 6.0 and above and the effect of seismosedimentation must have been observed in the above listed or nearby reservoirs. Occurrence of medium to large earthquake during the estimated life of reservoir could be found out from available list of historical earthquakes and assuming statistical distribution of earthquake occurrence to be Poissonian by standard relation

$$P = 1 - e^{-\lambda T} \quad \dots(3)$$

where  $\lambda$  is the mean annual frequency of earthquakes and  $T$ (years) is the life of reservoir. If the statistical analysis indicates a finite ( $P \gg 0.6$ ) probability of occurrence of an earthquake, then the probable effects of earthquake involving area affected and likely volume of displaced mass could be worked out. It is not known just when earthquake of the size 7.0 or more, as seen in New Zealand, Peru or Alaska would re-occur in the catchment areas of rivers mentioned in Table 2 and similar other rivers. However these regions are believed to have experienced destructive earthquakes during historic periods. At some locations, the return periods of destructive earthquakes are of the order of several decades or centuries. It is possible that some reservoirs may escape this seismic contingency during their lifetime. In addition to large earthquakes, small magnitude earthquakes upto 5.0 also contribute in a small way to the process of seismosedimentation wherein small landslides occur over highly localised areas. The most important long term effects are that earthquakes make to surface rock weathering, as rock masses get loosened and make it more susceptible to erosion by wind and rain. Seismosediments are fresh and coarser and angular, which in turn cause more erosion of

banks and beds of river. This effect is highly exhibited in alluvial rivers.

Considering the present scenario at international levels it is felt that the hazardous effects of seismosediments in reducing the effective economic life of reservoir could be reasonably mitigated if there is useful interaction between hydrologists and seismologists. The designers could think of proper measures in design of dam crests and downstream alls to permit safe overtopping, the protection of abutments and provision of bottom openings sluiceways to flush accumulated seismosediments or provide construction of low height 'debris-dam' at upstream end of reservoir which could prevent flow of seismosediments to main reservoir. Several other measures could be provided to mitigate this seismic disaster.

#### CONCLUSION

It is observed that periodic occurrences of medium to major earthquakes in the vicinity of catchment area generates additional amount of geological materials, called seismosediments which adversely affect lives of reservoirs in active seismic zones. Estimated lives of existing reservoirs in active seismic zones should be re-examined so as to have a reasonable assessment of future lives. A mathematical relation provided in this paper would help in these calculations.

#### REFERENCES

Adams, John (1981), "Earthquakes, Landslides and Large Dams in New Zealand", Bulletin of the New Zealand National Society for Earthquake Engineering, 14(2). 93 - 95.

Bapat, Arun (1980), "Siltng of Reservoirs due to Earthquakes", Bulletin Indian Society of Earthquake Technology, 17(1). 29 - 32

Bapat, Arun (1981), "Generation of Silt due to Earthquakes", Proc. XIX Congress of International Association of Hydraulic Research, New Delhi, India, II, 43 - 48.

Bapat, Arun (1985), "The Phenomenon of Seismosedimentation", Proc. 2nd International Workshop on Alluvial River Problems, Dept. of Civil Engineering, Univ. of Roorkee, Roorkee, India, 47 - 52.

Bapat, Arun (1988), "Earthquakes and River Regimes", (to be published) Proc. International Conference on River Regimes, 18 - 20 May 1988, Hydraulic Research, Wallingford, U.K.

Cluff, Lloyd S. (1970), "Peru Earthquake of May 21, 1970, Engineering Geology Observations", Bull. Seismo. Soc. Am., 60 (5),

1561 - 1606.

Gosavi, P.D., A.V.Bapat and S.K.Guha (1977), "Macroseismic Studies of Four Recent Indian Earthquakes", Proc. 5th World Conference on Earthquake Engineering, New Delhi, India, I, 233 - 241.

International Commission on Large Dams (1973), World Register of Dams, Published by International Commission on Large Dams, Paris, France.

## Seismic Assessment of Syncrude Tailings Dyke

R.C. Lo

Associate, Kohn Leonoff, Richmond, British Columbia, Canada

W.G. Milne

Consultant, Victoria, British Columbia, Canada

Earle J. Kohn

Chairman, Kohn Leonoff, Richmond, British Columbia, Canada

G.T. Handford

Tailings Engineer, Section Head, Syncrude Canada, Fort McMurray, Alberta, Canada

**SYNOPSIS:** This paper describes the assessment of seismic risk at the Syncrude Site. It reviews the site physiographic and geologic setting and considers the site position relative to observed seismic events, strain release patterns, and main tectonic features in western Canada. Both deterministic and probabilistic approaches were employed in the seismic risk assessment. Data on seismic events that occurred between 1899 and 1985 were included in the evaluation. Of particular importance was determination of the impact on the site of a series of large earthquakes which occurred in the Nahanni area of the Northwest Territories during 1985. Hasegawa et al. (1981) attenuation relations were used for computing ground motion amplitudes at the site. The review confirmed that the seismic risk at the Syncrude Site remains low.

### SYNCRUDE OIL SAND PROJECT AND TAILINGS IMPOUNDMENT

Syncrude Canada Limited operates one of the largest open pit mining operations in the world. The mine and plantsite are located 40 km north of Fort McMurray in northeastern Alberta (see Fig. 1). Operating at design capacity, the mine produces 96 million tonnes of oil sand per year from an area which will eventually cover 24 km<sup>2</sup>. The mining operation results in the production of approximately 240 000 tonnes/day of tailings solids.

Approximately 475 million m<sup>3</sup> of sand, 400 million m<sup>3</sup> of thick sludge and 50 million m<sup>3</sup> of free water will require permanent storage within the Syncrude Tailings Pond. To accommodate these volumes, approximately 18 km of dyke ranging from 32 m to 90 m in final height will be constructed. At completion, the tailings pond will have a surface area of 17 km<sup>2</sup>. Present plans call for the completion of dyke construction by 1992.

The general layout of the tailings pond and perimeter dyke is illustrated in Fig. 2. Figure 3 illustrates a typical design section for the tailings dyke. The compacted shell is constructed by utilizing hydraulic construction techniques. This procedure involves sluicing of the tailings stream into construction cells orientated parallel to the dyke centerline. The tailings sand placed in the construction cells is spread and compacted by wide pad dozers during the sluicing operation. During the winter months when cell construction is not feasible, the tailings stream is discharged upstream of the compacted shell. The coarse sand fraction settles out to form a beach with a 2% to 3% slope. The water and sludge fractions of the tailings stream flow into the pond.

The downstream slope angles are largely dictated by the underlying geology and associated shear strength parameters as well as pore pressure

response and/or dissipation rates. In general, the foundation soils underlying the tailings disposal area consist of Pleistocene and

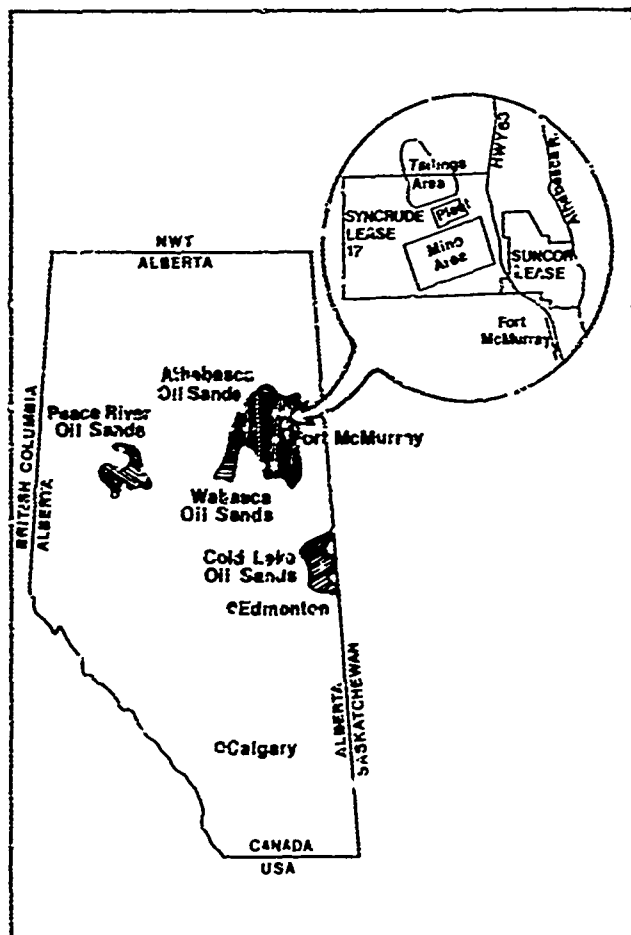


Fig. 1 Location of Syncrude Minesite and Tailings Area

Cretaceous overburden units which overlie the McMurray Formation (Km). The former Beaver Creek Channel defines an approximate boundary between two distinct foundation geology conditions (see Fig. 2). The portion of the dyke to the west of the creek valley is underlain by glacial till and the Clearwater Formation (Kc). The area to the east of the former creek channel is primarily underlain by Pleistocene fluvial sand and gravels (Pf) as well as glacial tills (Pg). The Clearwater Formation has been eroded in the eastern area with the exception of localized remnants of its basal units (Kcw and Kca).

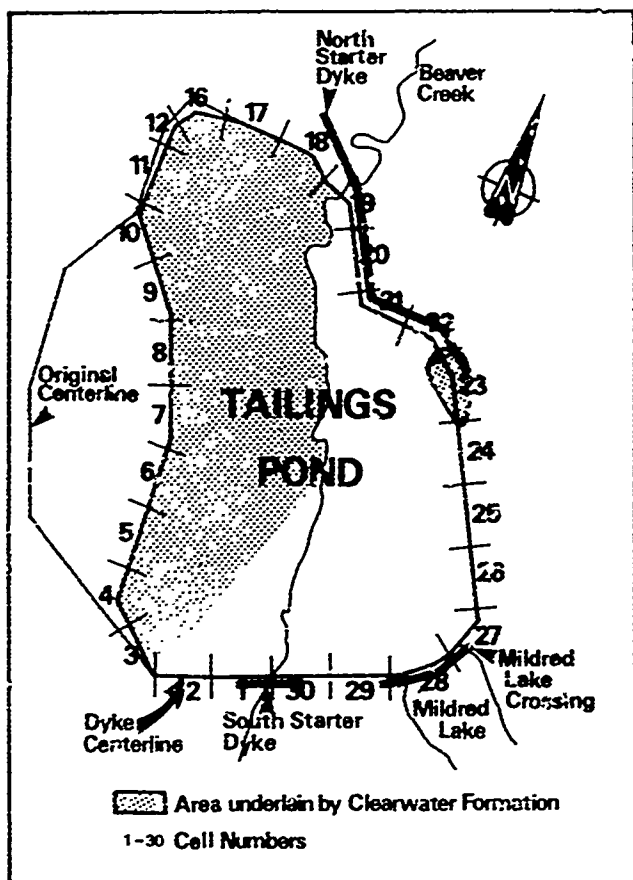


Fig. 2 Layout of Syncrude Tailings Disposal Area

#### SITE PHYSIOGRAPHIC AND GEOLOGIC SETTING

The Syncrude Site is located in the Alberta Plateau adjacent to the Saskatchewan Plain, both physiographic units belong to the Interior Plains Region (Bostock 1970). The Region, in turn, borders the Shield on the east and the mountains of the Cordilleran Region of the west (see Fig. 4). The Interior Plains are underlain by flat-lying Later Proterozoic, Paleozoic, and Tertiary strata. A smooth upland surface is the main feature of all the hills in the Alberta Plateau.

Locally, the Syncrude tailings pond is situated in the east-central part of a broad topographic lowland defined by the Muskeg Mountain and the Thickwood Hills to the east and south and the Birch Mountains to the west (Dean 1980). The

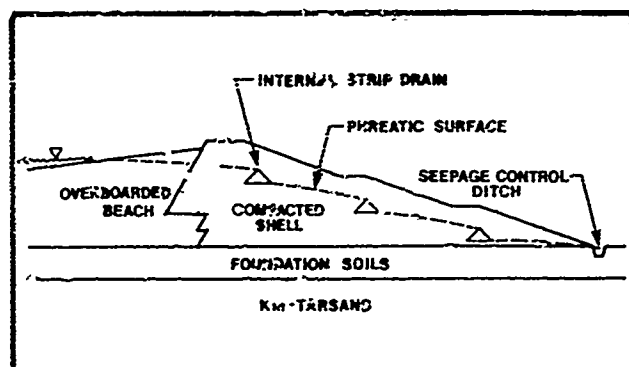


Fig. 3 Typical Design Section of Tailings Dyke

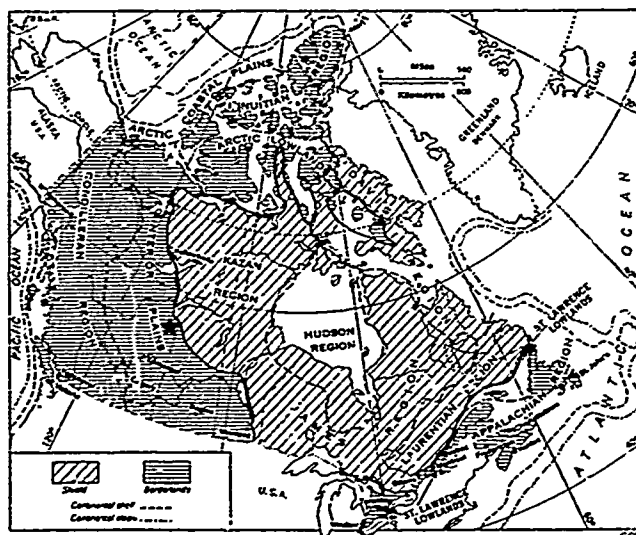


Fig. 4 Physiographic Regions of Canada (After Bostock 1970)

McKay and Athabasca Rivers flow through the central portions of this lowland produced by pedimentation.

Devonian highs of the Waterways Limestone Formation lie in the northwest and southwest areas of the tailings pond. An east-west trending broad trough-like structure lies between these highs. Cretaceous sediments of the McMurray and Clearwater Formations follow this basement configuration. Cretaceous sediments, in turn, are unconformably overlain by Pleistocene and Recent deposits over most of the tailings pond area.

Two faults affecting the Precambrian surface in the Athabasca Oil Sands Region were hypothesized by Hackbarth and Nastas (1979). The north-northwest trending Setetakun Fault follows approximately the Athabasca River north of Fort McMurray, while the other west-northwest

trending fault is located south of Fort McMurray. The Sewetakun Fault appears to have affected rock units as old as Devonian in age.

#### SEISMICITY AND TECTONICS

Data on seismic events affecting the Syncrude Site that occurred between 1899 and 1985 were obtained from the Pacific Geoscience Centre. Figure 5 (Milne et al. 1978) shows western Canada regional distribution of earthquakes with magnitude greater than or equal to three, updated to 1985 for the Syncrude Site. Figure 6 from the same paper, shows the pattern of strain release over the time period of 1899 to 1975 for western Canada. Strain release is calculated as the square root of the total observed seismic energy released during an earthquake. The strain release contours shown in the figure have been smoothed regionally and normalized to be the equivalent number of magnitude 5 earthquakes for an area of 100 km x 100 km and a time of 100 years.

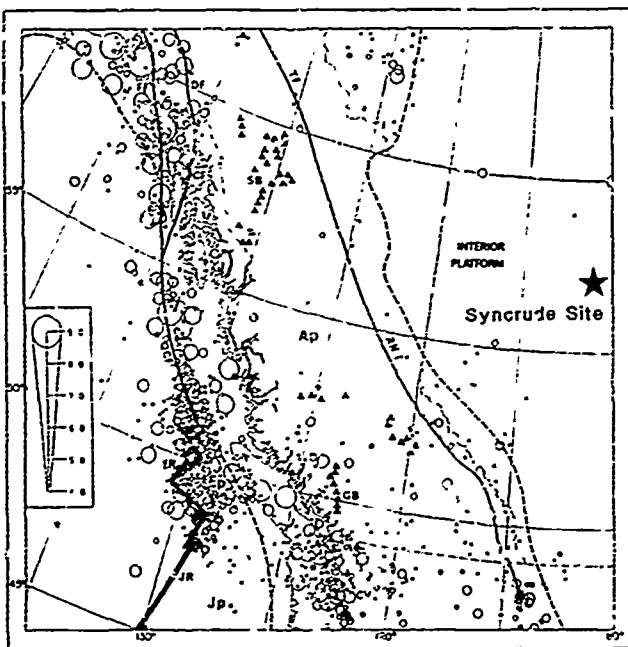


Fig. 5 Western Canada Seismicity Map and Tectonic Features (After Milne et al. 1978)

Figure 5 also shows the tectonic features of western Canada. As shown in the figure, the most active earthquake areas correspond, in general, to the boundaries between the major lithospheric plates. These plate boundaries include:

- (1) the Queen Charlotte (QCF) - Fairweather (FF) fault system (Pacific ( $P_p$ ) - America ( $A_p$ ) plates);
- (2) the offshore ridge-fracture zone system (Pacific - Juan de Fuca ( $J_p$ ) plates); and
- (3) the Vancouver Island - Puget Sound region (Juan de Fuca - America plates).

The Syncrude Site is plotted on Figs. 5 and 6 to indicate the site position relative to observed seismic events, strain release patterns, and main tectonic features in western Canada.

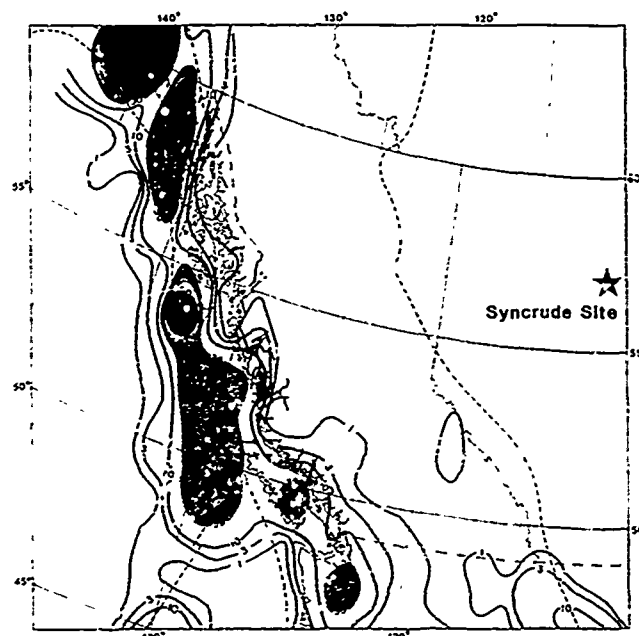


Fig. 6 Western Canada Strain Release Map (After Milne et al. 1978)

#### SEISMIC RISK ASSESSMENT

Seismic risk at the Syncrude Site was assessed using both deterministic and probabilistic approaches. The impact of a series of large earthquakes which occurred in the Nahanni area of the Northwest Territories during 1985 has been specifically addressed.

Both approaches used the same attenuation functions for computing ground motion amplitudes at specified distances from earthquakes of specified magnitudes. The amplitudes of acceleration (A) and velocity (V) are usually functions of (M) magnitude and (R) hypocentral distance. Hasegawa et al. (1981) defined the attenuation functions currently used in Canada for calculations for structures covered by the National Building Code of Canada (NBCC 1985). The attenuation functions for eastern and western Canada are presented in Table 1; both eastern and western relations are used in the National Building Code of Canada.

Based on the distribution of felt reports, earthquakes such as those in 1909, 1918 and others have shown that the area east of the Foothills has a low attenuation, such as the eastern function displays. Since the Syncrude Site is east of the Cordillera, the eastern type of attenuation function is used for this assessment. However, seismic waves do travel from the west to this site, so the attenuation function should be a combination of an east and west function. Hence, the usage of the eastern type of attenuation implicitly involves some degree of conservatism.

TABLE 1  
SUMMARY OF HASEGAWA ET AL. 1981  
ATTENUATION RELATIONS

|              |         |                             |
|--------------|---------|-----------------------------|
| Peak         | Western | $A_p (\%g) =$               |
| Horizontal   | Canada  | $1.02 e^{1.3M} R^{-1.5}$    |
| Ground       | Eastern | $A_p (\%g) =$               |
| Acceleration | Canada  | $0.35 e^{1.3M} R^{-1.1}$    |
| Peak         | Western | $V_p (cm/s) =$              |
| Horizontal   | Canada  | $0.00040 e^{2.3M} R^{-1.3}$ |
| Ground       | Eastern | $V_p (cm/s) =$              |
| Velocity     | Canada  | $0.00018 e^{2.3M} R^{-1.0}$ |

Where R = hypocentral distance in km  
M = earthquake magnitude

Seismic wave amplitudes are usually estimated for two general frequency ranges. For acceleration, the frequency extends from often very high values in the range of 50 Hz down to about 2.5 Hz. These high frequencies are considered to be characteristic of the type of ground motions one might expect from nearby earthquakes of a variety of magnitudes. One would not, on the basis of the historical record, expect to find these high frequency seismic waves present at the Syncrude Site. The range of frequencies which are typical of the velocity ground motions are from 2.5 Hz to 0.2 Hz. These corner frequencies are, however, not to be taken too rigidly, because there are no observations of strong-motion, seismic waves in the general region around the Syncrude Site.

#### Deterministic Assessment

No probabilities are stated or implied in this deterministic calculation of ground motion. Simply one places the largest historical earthquake, or the largest possible earthquake at a location as close as reasonably possible to the site. In this case, except where noted, the largest historical earthquake is used for the deterministic assessment.

There are three sources of seismic activity (see Table 2) which can contribute to measurable ground motion at this site. In addition, a fourth site has been chosen (see Table 2) to represent the possible location of a large earthquake east of the Cordillera, although the likelihood of such an event is very remote.

The first is the site of the largest earthquake in Canada, and this earthquake was generally felt over much of western Canada. Although the coast of Alaska also has large earthquakes and is perhaps somewhat closer to the site, the Queen Charlotte event is used. The motion at the Syncrude Site from the Alaska and Queen Charlotte seismic events would be comparable, and was probably of low frequency. The second seismic source is in the Nahanni area. Until the fall of 1985, there were no significant earthquakes in the region, but in 1985 one rather strong earthquake did occur in Nahanni, Northwest Territories along with several related events (Horner et al. 1985 and Wetmiller et al. 1986). A strong motion seismograph located near the epicentre did record some strong accelerations, in excess of 1 g (Weichert et al. 1986). The third seismic source is at the location of an earthquake known to have occurred in 1922, north of Lake Athabasca which was reported in the International Seismological Summary (ISS). The distribution of the seismic stations which recorded this earthquake is not ideal, and the epicentre of the event could easily be in the Nahanni region, or further north in the Richardson Mountains. For this report we accept the ISS epicentre as the site of an event of magnitude 5.5. For the fourth event, a site in the eastern Foothills is assumed, and the ground motions calculated to check the sensitivity of this assumption. This event is selected to cover the possibility that a large earthquake similar to that which occurred in Nahanni on December 23, 1985 could migrate along the Cordilleran Fold and Thrust Belt (Adams et al. 1986). Table 2 lists the results for these four events.

TABLE 2  
SUMMARY OF DETERMINISTIC ASSESSMENT OF PEAK GROUND  
MOTION PARAMETERS\* AT SYNCRUDE SITE

| EARTHQUAKE | EPICENTRE  | DATE    | MAGNITUDE        | EPICENTRAL<br>DISTANCE<br>(km) | PEAK<br>HORIZONTAL<br>GROUND<br>ACCELERATION<br>(% g) | PEAK<br>HORIZONTAL<br>GROUND<br>VELOCITY<br>(cm/sec) |
|------------|--|---------|------------------|--------------------------------|---|--|
| 1          | Queen Charlotte<br>Island                          | 1949    | 8.1 <sup>+</sup> | 1418                           | 0.99  | 3.9  |
| 2          | Nahanni  | 1985    | 6.9              | 890                            | 1.6   | 1.6  |
| 3          | North of Lake<br>Athabasca                         | 1922    | 5.5              | 340                            | 0.7   | 0.2  |
| 4          | Eastern Boundary<br>of Rocky Mountain<br>Foothills | Assumed | 7.0              | 527                            | 3.1   | 3.2  |

\* Focal depths of all earthquakes are assumed at 20 km.

+ For computation of Peak Ground Motion Parameters, M = 7.5 is used in Hasegawa et al. (1981) attenuation relations for all magnitudes greater than 7.5.

There have been no earthquakes near the Syncrude Site, so that a nearby event of any magnitude is not considered. In Alberta some small earthquakes have occurred near Cold Lake, Snipe Lake, Rocky Mountain House and west of Calgary. The Geophysics Department of the University of Alberta has been monitoring these areas for some time and reports no activity in the region of the Syncrude Site. In any event, the earthquakes reported at the above sites are often considered to be induced earthquakes associated with man-made activity.

Milne and Berry (1976) critically reviewed annual and cumulative catalogues of Canadian earthquakes prepared by Energy, Mines and Resources Canada to determine if they contain records of induced seismic events caused by human activities such as fluid injection in oil fields, impounding of water in large reservoirs and mining. They concluded that while there are many activities in Canada that have undoubtedly perturbed the ambient state of stress in the upper crust, there are comparatively few examples where this has resulted in seismic activity. Among these few examples, the magnitude of the induced earthquakes is generally lower than 5.0 with one exception. An earthquake with a body wave magnitude of 5.1 occurred within the Snipe Lake Oil Field, Alberta, where water injection was actively taking place. Since the epicentral distance from the Syncrude Site to the Snipe Lake earthquake is about 400 km, ground motions at the site caused by this earthquake would be less than that from the third seismic source included in Table 2.

### Probabilistic Assessment

For a site such as Syncrude, where there are no clearly defined areas of seismic activity which can make a significant contribution to the earthquake risk, the probabilistic method does provide a useful alternative method for estimating ground motions. Basham et al. (1982) gave details of such a probabilistic study for the 1985 National Building Code of Canada (NBCC). For the Syncrude study, we commenced with the NBCC assessment and then deviated from it by using solely the eastern type of attenuation functions and by modifying the NBCC seismogenic source model to test the sensitivity of the NBCC model to possible new events.

Seismic source zones used in the NBCC model are shown on Fig. 7. Table 3 lists those zones which could possibly make a contribution to the risk at the Syncrude Site. Within each source zone, seismic events can be fitted to a curve relating to the frequency of occurrence of an earthquake and its magnitude. Maximum magnitude is selected for each source zone, usually about 0.5 magnitudes larger than the strongest historical earthquake.

Table 4 lists the values for the acceleration and velocity amplitudes obtained from probabilistic evaluation using various models as described in the following:

#### NBCC 1985 Model:

Seismogenic model used for the National Building Code of Canada 1985, with the use of both western and eastern Canada attenuation relations.

TABLE 3

#### SUMMARY OF ZONAL PARAMETERS USED IN VARIOUS SEISMOGENIC ZONAL MODELS

| MODEL          | SEISMIC SOURCE ZONE | SOURCE ZONE AREA (km <sup>2</sup> ) | $\beta$ | $N_0$ PER ANNUM | MAXIMUM EARTHQUAKE $M_x$ | SOURCE ZONE CODE |
|----------------|---------------------|-------------------------------------|---------|-----------------|--------------------------|------------------|
| NBCC 1985      | McKenzie            | 697 616                             | 2.67    | 92 000          | 6.0                      | MKZ              |
| and            | Richardson          | 19 950                              | 1.76    | 1 560           | 7.0                      | RIC              |
| Model 1        | Northern B.C.       | 804 820                             | 2.28    | 1 830           | 5.0                      | NBC              |
|                | Sandspit            | 53 701                              | 1.87    | 1 240           | 7.0                      | SPT              |
|                | Queen Charlotte     | 426 026                             | 1.50    | 1 610           | 7.5                      | QCF              |
|                | Alaska Coast        | 124 086                             | 1.66    | 4 590           | 7.5                      | FWO              |
|                | Denali              | 109 840                             | 1.96    | 2 820           | 7.0                      | DSK              |
|                | Southern B.C.       | 255 000                             | 2.28    | 3 230           | 6.5                      | SBC              |
| Model 2        | McKenzie            | 697 616                             | 2.67    | 92 000          | 7.0                      | MKZ              |
| (NBCC 1985     | Northern B.C.       | 804 820                             | 2.28    | 1 830           | 7.0                      | NBC              |
| with these     | Southern B.C.       | 255 000                             | 2.28    | 3 230           | 7.0                      | ESC              |
| modifications) |                     |                                     |         |                 |                          |                  |
| Model 3        | New Nahanni         | 73 215                              | 1.76    | 2 189           | 7.0                      | LMK              |
| (NBCC 1985     | Source Zone         |                                     |         |                 |                          |                  |
| with these     |                     |                                     |         |                 |                          |                  |
| modifications) |                     |                                     |         |                 |                          |                  |
| Model 4        | Northern B.C.       | 804 820                             | 2.28    | 1 830           | 7.0                      | NBC              |
| (NBCC 1985     | Southern B.C.       | 255 000                             | 2.28    | 3 230           | 7.0                      | SBC              |
| with these     | Nahanni             | 73 215                              | 1.76    | 2 189           | 7.0                      | LMK              |
| modifications) |                     |                                     |         |                 |                          |                  |

Model 1:  
Same as that used for NBCC but with the use of eastern Canada attenuation relations only.

Model 2:  
The Nahanni (1985) event was of magnitude 6.9 and has occurred in the MKZ source zone. To accommodate this event, the maximum magnitude in the MKZ zone is raised to 7.0. If the Nahanni earthquake were to be repeated anywhere along the eastern MKZ region, and along the eastern Foothills of the mountains, then the equivalent to a Nahanni event should be extended all the way down to the United States border. To accomplish this, the maximum magnitudes in the NBC and SBC zones are also raised to 7.0.

Model 3:  
Since the Nahanni earthquake is a new real event, consideration must be given as to whether the above modification is the solution, or whether a new seismic source zone should be set in the southern part of the MKZ source zone. NBCC recognizes a small independent source zone in the region of the Richardson Mountain (RIC) towards the north central region of the MKZ. For this study, a source zone around the Nahanni area, with a maximum magnitude of 7.0 and an area larger than the RIC zone has been defined as LMK, for lower McKenzie.

Model 4:  
Finally a model is run with the new LMK zone and the changes in the NBC and SBC zones set out in Model 2.

From Table 4, one can obtain the levels of ground amplitude for a range of probabilities of exceedance. NBCC employs a 10% chance of exceedance in 50 years, or an annual probability of exceedance of  $1/475 = 0.0021$ . Results in

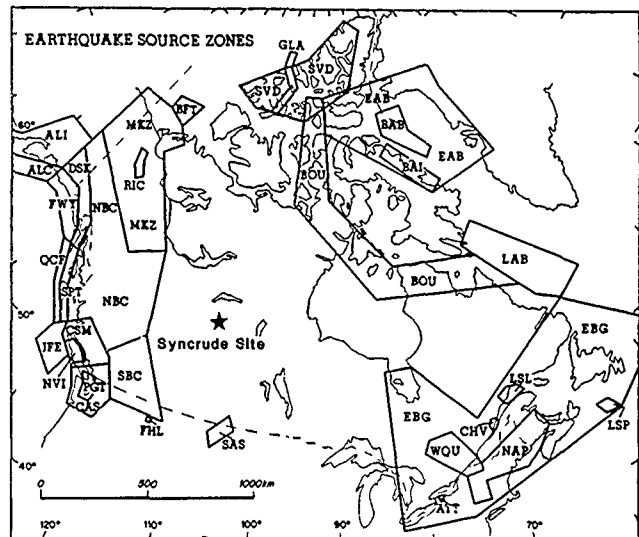


Fig. 7 Seismogenic Zones of Canada  
(After Basham et al. 1985)

this study are listed for an even lower probability down to an annual probability of 1/1000. Other lower values can be calculated, but the reliability of extending the computations to these low numbers is questionable. In the evaluation of the ground motion, a stochastic factor is employed to allow for the scatter of the data used for the calculation of the attenuation functions. For the NBCC computations, a value of this factor was set at 0.7. The use of this value increases the end result by a factor just under two. This procedure has been followed for the Syncrude study. Thus, another layer of conservatism has been added.

TABLE 4  
SUMMARY OF PROBABILISTIC ASSESSMENT OF  
PEAK HORIZONTAL GROUND ACCELERATION (PGA) AND VELOCITY (PGV)  
AT SYNCRUDE SITE

| Probability of Exceedance per Annum   |              | 0.01 | 0.005 | 0.0021 | 0.001 | Remarks on Model  |
|---------------------------------------|--------------|------|-------|--------|-------|---|
| Probability of Exceedance in 50 years |              | 40%  | 22%   | 10%    | 5%    |   |
| NBCC 1985                             | PGA (% g)    | 0.9  | 1.1   | 1.4    | 1.6   | National Building Code of Canada 1985                                       |
|                                       | PGV (cm/sec) | 2.5  | 3.2   | 3.9    | 4.7   |   |
| Model 1                               | PGA (% g)    | 2.3  | -     | 3.9    | 4.9   | Eastern Attenuations  |
|                                       | PGV (cm/sec) | 3.0  | -     | 6.0    | 7.7   |   |
| Model 2                               | PGA (% g)    | 2.3  | -     | 4.0    | 5.1   | Eastern Attenuations and Modification of Zones MKZ, NBC and SBC             |
|                                       | PGV (cm/sec) | 3.1  | -     | 6.0    | 7.8   |   |
| Model 3                               | PGA (% g)    | 2.5  | -     | 4.1    | 5.2   | Eastern Attenuations and New Zone LMK                                       |
|                                       | PGV (cm/sec) | 3.1  | -     | 6.1    | 7.8   |   |
| Model 4                               | PGA (%g)     | 2.5  | -     | 4.2    | 5.3   | Eastern Attenuations and New Zone LMK and Modification of Zones NBC and SBC |
|                                       | PGV (cm/sec) | 3.2  | -     | 6.1    | 7.9   |   |



## SUMMARY

The Syncrude Site is situated in the Alberta Plateau with a smooth upland surface and underlain by flat-lying Cretaceous sediments. There are some evidences suggesting nearby fault activities may have affected rock units as old as Devonian in age. Historically, the Site is positioned at considerable distances from seismic events observed over the last nine decades, main areas of strain release, and major tectonic features in western Canada. Our assessment summarized in Table 5 demonstrates that the large earthquakes in the Nahanni area

which occurred in 1985 do not increase significantly the seismicity of the Syncrude Site. Therefore, our review confirms the assumption of low seismicity at the Syncrude Site.

## ACKNOWLEDGEMENTS

The authors are grateful to Syncrude Canada Ltd. for their permission to allow the publication of this study, and to Drs. J. Adams and D.H. Weichert of Geologic Survey of Canada for their helpful discussion and assistance.

TABLE 5  
SUMMARY OF SEISMIC ASSESSMENT OF  
PEAK GROUND MOTION PARAMETERS  
AT SYNCRUDE SITE

| ASSESSMENT<br>APPROACH | PROBABILITY OF<br>EXCEEDANCE PER ANNUM | PEAK HORIZONTAL GROUND<br>ACCELERATION<br>% g | PEAK HORIZONTAL GROUND<br>VELOCITY<br>(cm/sec) |
|------------------------|--|---|--|
| Deterministic          | -                                      | 0.7 to 3.1                                    | 0.2 to 3.9                                     |
| Probabilistic          | 0.01                                   | 0.9 to 2.5                                    | 2.5 to 3.2                                     |
|                        | 0.0021                                 | 1.4* to 4.2                                   | 3.9* to 6.1                                    |
|                        | 0.001                                  | 1.6 to 5.3                                    | 4.7 to 7.9                                     |

\* These values correspond to NBCC 1985 code, which does not include the consideration of 1985 Nahanni earthquakes.

## REFERENCES

- Adams, J., Wetmiller, R.J., Horner, R.B. and Lamontagne, M.L., 1986. "Earthquakes and Seismic Hazard in the Eastern Cordillera Fold Belt, Canada - Implications from the 1985 Nahanni Earthquakes", Abstract, American Geophysical Union.
- Basham, P.W., Weichert, D.H., Anglin, F.M. and Berry, M.J., 1985. "New Probabilistic Strong Seismic Ground Motion Maps of Canada", Bull. Seism. Soc. Am., Vol. 75, No. 2, pp. 563-596.
- Bostock, H.S., 1970. "Physiographic Subdivisions of Canada", Geology and Economic Minerals of Canada edited by Douglas, R.J.W., Department of Energy, Mines and Resources Canada.
- Dean, R., 1980. "Surficial Geology of the Syncrude Tailings Pond", Geology Dept., Mine Engineering Division, Syncrude Canada Ltd., Jan., 21 pp.
- Hackbarth, D.A. and Nastasa, N., 1979. "The Hydrogeology of the Athabasca Oil Sands Area, Alberta", Alberta Research Council, Bull. 38.
- Hasegawa, H.S., Basham, P.W. and Bery, M.J., 1981. "Attenuation Relations for Strong Seismic Ground Motion in Canada", Bull. Seism. Soc. Am., Vol. 71, No. 6, December, pp. 1943-1962.
- Horner, R.B., Rigters, G.C., Weichert, D.H., Wetmiller, R.J., Lamontagne, M., North, R.G., Hasegawa, H.S., Basham, P.W., Adams, J., and Aitkins, J., 1985. "The Nahanni Earthquake, Northwest Territories, Canada: A Large Magnitude, Low Probability Event in the Northeastern Canadian Cordillera", Abstract, American Geophysical Union.
- Milne, W.G. and Berry, M.J., 1976. "Induced Seismicity in Canada", Engineering Geology, Vol. 10, No. 2-4, December, pp. 219-253.
- Milne, W.G., Rogers, G.C., Riddihough, R.P., McMechan, G.A., and Hyndman, R.D., 1978. "Seismicity of Western Canada", Can. J. Earth Sci., Vol. 15, No. 7, pp. 1170-1190.
- NBCC, 1985. "National Building Code of Canada", National Research Council of Canada.
- Weichert, D.H., Wetmiller, R.J. and Munro, P., 1986. "Vertical Earthquake Acceleration Exceeding 2g? - The Case of the Missing Peak", Bull. Seism. Soc. Am., Vol. 76, No. 5, pp. 1473-1478, Oct.
- Wetmiller, R.J., Horner, R.G., Lamontagne, M., Weichert, D.H., North, R.G., Hasegawa, H.S. and Adams, J., 1986. "The 1985 Nahanni Earthquakes, Northwest Territories, Canada: A Pair of Large Magnitude Events in the Northeastern Canadian Cordillera", Abstract, Canadian Geophysical Union.

# Reliability of the Wave Equation Analysis in the Estimation of Static Bearing Capacity of Vertical Pile—A Case Study

S. Bandyopadhyay

Earthquake Engineering Department, University of Roorkee,  
Roorkee, India

M.K. Gupta

Earthquake Engineering Department, University of Roorkee,  
Roorkee, India

A.S. Arya

Earthquake Engineering Department, University of Roorkee,  
Roorkee, India

**SYNOPSIS:** Application of wave equation, in the analysis of pile behavior, under dynamic loading has started with Smith [9]. This paper presents a modified explicit numerical scheme, based on Smith's approach, which retains the simplicity and minimum storage requirement of Smith's scheme but offers a faster and more accurate solution near critical time step. Bearing capacity of pile is estimated through Poulos [8] scheme, after evaluating dynamic properties of soil from set value through this modified scheme. Observed load test results establish a good promise for this analysis.

## INTRODUCTION

Estimation of static bearing capacity of a single vertical pile is very essential for foundation engineer. Fieldpile load-testing directly speaks for its bearing capacity but the large amount of cost involved in each testing puts a limitation on its number. Theoretical formulas [4], dynamic driving formulas [10] with their individual simplified idealization, do come handy to the field engineer for the assessment of this highly complicated problem. The use of the theory of one dimensional wave propagation [3,7] has now found increased application for the analysis of the driving behavior of piles and for predicting their static bearing capacity. Since pile driving causes failure of the soil, the idea of correlating the measurement made during pile driving to estimate the pile capacity seems apparently logical. Though the dynamic nature of penetration deviates from the static response of soil, considerable effort has been devoted to find suitable correlation. In this study, the actual field observed bearing capacity of piles has been compared with numerically predicted value, based on a modified Smith's approach of wave equation analysis.

## GEOTECHNICAL CONDITIONS

A detailed soil investigation of the particular site was conducted and it was found that the stratification is very uniform in nature. A typical soil profile is shown in Fig. 1. The sand layer which is main feature of this deposit is poorly graded uniform, mixed with fine sand or silt. Top 2m is covered with greyish brown silty clay (SPT  $N=5$ ). Below this layer the  $N$  value of clayey silt layer increases from 12 to 30 upto a depth of 20m from ground surface. Deeper strata offers  $N$  value as high as 60 to 80. Water table was found 2m below ground level. Engineering properties of the soil are given below:

|                          |        |
|--------------------------|--------|
| Specific gravity of soil | 2.52   |
| Mean grain size          | 0.18mm |
| Maximum void ratio       | 0.91   |
| Minimum void ratio       | 0.46   |

The deposit in the site is in medium to loose state upto a depth of 10m, below which higher  $N$  value indicate dense state.

## TEST PROGRAM

Test piles were of 450mm diameter, cast-in-situ concrete piles. Steel casing tubes, Length 24m, Outside diameter 450mm,

Youngs Modulus= $2.2 \times 10^6$  kg/cm<sup>2</sup>, were driven by 3.5t hammer. The hammer was dropped from a height of 1.3m by the usual method of releasing the clutch of the driving machine. There might be some possibility of slight variation in the height of fall but a close watch was always kept to maintain the uniformity. Number of blows needed for the penetration of each meter of depth was noted throughout. Set value was obtained from the time-transient displacement curve, in last few blows, on the driven casing tube. Depth of embedment, verticality of the casing tube, leakage through bottom shoe etc. were noted. After driving the casing tube, upto the required depth, reinforcement cage was inserted and concrete was poured in three stages. Casing tube was lifted slowly with short fall of hammer. Actual volume of concrete consumed was compared with the calculated volume required, to check against the formation of necking.

The piles were test loaded upto failure, about 45 days after casting. Cyclic load tests (Fig.2) were carried out on these piles by putting load with Hydraulic jack on finished pile head at cut-off level. Reaction was obtained from loads placed on steel girders. Movement of pile head under the application of each loading and subsequent unloading, were noted by 4 diagonally placed dial gauges on pile head. Load tests were conducted as per IS: 2911, Part 1 [11].

A typical load-settlement behavior for test pile TP 5 is shown in Fig. 3 and the results has been presented in Table 1. It may be observed that the average load carrying capacity of Pile is 160t with 60% skin friction and 40% point bearing, with 6mm elastic settlement (gross-net) at 160t.

## NUMERICAL WAVE EQUATION ANALYSIS

Smith's [9] proposed approach to the wave equation was the discrete idealization of pile body as an assemblage of (Fig. 4) lumped, concentrated weights  $W(1)$  through  $W(p)$ , which are connected by weightless spring  $K(1)$  through  $K(p-1)$ , representing pile stiffness. Resistance offered by soil was considered to be visco-elasto-plastic. Time was also discretised into small intervals. In general, the system is considered to be composed of: (i) A ram, (ii) A cap block, as cushioning material, (iii) A pile cap, (iv) A pile and (v) The supporting medium or soil.

The numerical scheme, developed by Smith [9] in its finite difference form is as follows:

$$\begin{aligned} D(m,t) &= D(m,t-1) + V(m,t-1) \\ C(m,t) &= D(m,t) - D(m+1,t) \\ F(m,t) &= C(m,t) \cdot KP(m) \\ R(m,t) &= [D(m,t) - D'(m,t)] \cdot KS \cdot [1 + J(m) \cdot V(m,t-1)] \\ V(m,t) &= V(m,t-1) + [F(m-1,t) - F(m,t) - R(m,t)] \cdot g \cdot dt / W(m) \end{aligned}$$

where  $D, C, F, R, V$  are displacement, compression of internal spring, force in internal spring, total soil resistance and velocity respectively of  $m$  pile element at time  $t$ .  $KP$  and  $KS$  are pile and soil stiffness modulus.  $J$  is the damping coefficient and  $dt$  is the time increment.

Numerical scheme [i] sweeps over time from the known impact velocity of the first element and with initial at-rest condition of all other pile and soil elements. The iteration of the Smith's scheme terminates when either of the following conditions is satisfied:

1. Pile tip, after penetrating to some maximum downward value starts rebounding upward.
2. Velocities of all the elements are negative or zero. Set is defined as the maximum tip displacement minus the plastic yielding Quake factor 'q'.

Smith's scheme is a spatially discrete model which is integrated forward in time to generate a transient dynamic response. This scheme solves one dimensional wave equation,  $C_p^2 \cdot d_{xx}^2 d_{tt} = f(x,t)$ , which characterizes dynamic axial load in pile body. Here  $d$  denotes the time dependent displacement of pile at a distance  $x$  and at time  $t$ , and the suffix denotes the respective partial differentiation. The constant  $C_p$  is propagation velocity of elastic wave through pile material.

The present study is based on Smith's scheme with following modifications:

- (i)  $R(m,t) = [D(m,t) - D'(m,t)] \cdot KS + q \cdot KS \cdot J(m) \cdot V(m,t-1)$
- (ii) Displacement and velocities are found out at the end of full time interval  $(n) \cdot dt$ ,  $(n+1) \cdot dt$  etc., but forces and accelerations are obtained at half time intervals  $(n+1/2) \cdot dt$ ,  $(n+3/2) \cdot dt$  etc.
- (iii) Iteration continues till the oscillations of all elements become negligibly small
- (iv) Set is defined as permanent downward movement of the pile.
- (v) Total static part of the dynamic resistance offered by soils considered as the maximum of  $[D(m,t) - D'(m,t)] \cdot KS$ , over all soil elements at each instant of time.
- (vi) Tip soil is a tension free element

The finite difference form of the semidiscrete wave equation can be represented as  $M \cdot d'' + KP \cdot d = F$ , where  $d$  is the displacement vector representing nodal degrees of freedom,  $d''$  is the nodal acceleration vector,  $M$  is the diagonal mass matrix for this lumped parameter model and  $KP$  is the linear stiffness matrix. The non homogeneous term  $F$ , which represents the soil resistance on the pile motion, is the vector of nodal 'loads'. At any instant,  $n \cdot dt$  of the discrete time domain, it should always satisfy the dynamic equilibrium equation:  $M \cdot d''(n) + KP \cdot d(n) = F(n)$ , where the term in the bracket indicates the vector at  $n$  instant of time. In this modified scheme, first a central difference expressions are introduced for the acceleration  $d''$  in terms of the velocity  $d'$  and then this velocity is expressed by central difference expression over displacement.

$$\begin{aligned} M \cdot d''(n) &= F(n) - KP \cdot d(n) \\ [d'(n+1/2) - d'(n-1/2)] / dt &= M^{-1} \cdot [F(n) - KP \cdot d(n)] \\ d'(n+1/2) &= d'(n-1/2) + M^{-1} \cdot [F(n) - KP \cdot d(n)] \cdot dt \\ d(n+1) &= d(n) + dt \cdot d'(n+1/2) \end{aligned}$$

Here the term  $F$  represent instantaneous soil resistance, which brings non-linearity in the partial differential wave equation. In original Smith's scheme the viscous part of it was expressed as product of the displacement and velocity. The present scheme considers the viscous part as velocity dependent only. Moreover, the modified scheme retains the simplicity of Smith's assumption that the total soil resistance may be considered as time independent constant during the travel of the wave through any pile element from the beginning

to the end of discrete time interval  $dt$ . The change in the soil resistance is evaluated at the end of each interval. Within the frame of these assumptions the term  $f(x,t)$  of the one dimensional wave equation has been considered as a constant  $F$  in the semidiscrete wave equation  $M \cdot d'' + KP \cdot d = F$ . To evaluate  $d(n+1)$  of any instant this explicit scheme utilizes one just previous value of  $d(n)$  and one just previous value of  $d'(n-1/2)$ . The velocities  $d'(n-1/2)$  are carried out at half time point. The diagonal nature of the mass matrix  $M$ , in this lumped parameter model, offers advantage of the speed of computer calculation and explicit nature of the scheme reduces the computer storage requirement.

## STABILITY OF THE MODIFIED SCHEME

The homogeneous part of the discrete scheme [6] may be written as  $d'(n+1/2) = d'(n-1/2) - dt \cdot M^{-1} \cdot KP \cdot d(n)$ , which when substituted in the central difference expression of velocity,  $d(n+1) = d(n) + dt \cdot d'(n+1/2)$  offers:

$$\begin{aligned} d(n+1) &= d(n) + dt \cdot [d'(n-1/2) - dt \cdot M^{-1} \cdot KP \cdot d(n)] \\ &= d(n) + dt \cdot d'(n-1/2) - (dt)^2 \cdot M^{-1} \cdot KP \cdot d(n) \end{aligned}$$

Since,  $d(n) = d(n-1) + dt \cdot d'(n-1/2)$ , this offers:

$$d(n+1) = d(n) + [d(n) - d(n-1)] \cdot (dt) \cdot M^{-1} \cdot KP \cdot d(n)$$

implies,  $d(n+1) - 2d(n) + d(n-1) + (dt)^2 \cdot M^{-1} \cdot KP \cdot d(n) = 0$

The solution is sought as  $d(n) = (\text{del}) \cdot \exp[p \cdot n \cdot dt]$ , where,  $\text{del}$  = arbitrary displacement vector,  $p$  is undetermined. Considering for any real physical system there exist a separate and distinct non-zero delta for each eigenvalue-eigenvector, this expression offers:  $\exp(p \cdot dt) - 2 + \exp(-p \cdot dt) + (dt)^2 \cdot M^{-1} \cdot KP = 0$

For any eigenvalue  $L$  of  $M^{-1} \cdot KP$  the characteristic equation for 'del' becomes:  $\exp(p \cdot dt) - 2 + \exp(-p \cdot dt) + (dt)^2 \cdot L = 0$

To check against the growth of original error, with increasing  $t$ , in the solution of wave equation, which is bounded for all time  $t$ , it is necessary and sufficient that  $1 - \exp(p \cdot dt) \leq 1$

This imposes a strict condition that  $(dt)^2 \cdot L \leq 4$ , i.e.,  $(dt)^2 \leq 4/L_{\max}$ , where  $L_{\max}$  is the maximum of all the eigenvalues of  $M^{-1} \cdot KP$ , which is  $L_{\max} = 4 \cdot C_p^2 / (dx)^2$  for lumped mass idealisation of discretised linear wave equation with uniform mesh discretisation 'dx'. Under this condition critical time step,  $t_{cr} = dx/C_p$ . So long the time step of integration is kept lower or equal to  $t_{cr}$  the numerical solution should converge to true solution. The space-time finite difference nodes of one dimensional wave equation fall exactly on the characteristic curve when the time step of integration  $dt$  is  $dx/C_p = \sqrt{W(m)/(KP(m) \cdot g)}$  and should offer exact solution.

## COMPARISON OF TWO SCHEMES

To compare the efficiency of these two schemes following problem was identified;

The pile consists of 24 elements of same mass and same stiffness and 3 elements for anvil, cap and capblock. Soil stiffness  $KS$  is set to zero. Initial displacements are 0 for all elements and for the first 10 pile elements initial velocity is set to unity. Remaining 10 pile element velocity is set to zero. The solution of this uniaxial deformation of a linearly elastic material is the propagation of one-half of the impact velocity into the stationary material and a reduction by same magnitude into the impacting material. Fig 5 compares the velocity wave front obtained from these two schemes. As the error in energy balance of the modified scheme is small it does not contain saw-tooth wave pulses of Smith's original scheme. The approximation brought in the partial differential wave equation by different idealisations, drifts the numerical solution away from its true behaviour. The original frequency content  $\omega$  gets distorted, either upward or downward into an approximated  $\omega'$  depending on the nature of mass and time discretisation. In the present problem, one is interested to know the history of stress wave propagation, through the pile body, because of the impact offered on the pile head by the falling hammer. The entire frequency content, needed to represent the shock wave propagation, is of prime importance. Lumped parameter mass idealisation of spatial discretisation [5,2] depresses the approximate frequency but the

central difference operator shifts it upward. Thus the combination of these approximation, adopted in the present modified scheme, tries to compensate each other. This scheme retains the simplicity of Smith's scheme along with a more accurate solution near the critical time step. Fig 6 compares the time displacement behaviour of the pile element just above ground through these two schemes.

Smith's scheme while assessing the stiffness of the soil modulus the total load carrying capacity of the pile  $R_u$  was assumed and it was distributed between side skin friction  $R_f$  and point bearing  $R_p$  ( $R_u = R_f + R_p$ ) from the knowledge of the sharing, obtained from cyclic load test results. Soil stiffness of the peripheral and tip soil  $K_S$  and  $K_B$  were obtained as  $K_S = R_f/q$  and  $K_B = R_p/q$ . Set values, obtained from this distribution of soil resistance were related with assumed total resistance  $R_u$ . It is implicit in this assumption that all the soil elements at some instant, will simultaneously undergo a deformation which is greater or equal to the quake factor, thus generating full capacity of resistance in each element, simultaneously, whose summation is the assumed load carrying capacity. In reality, static part of the total dynamic resistance offered by soil is the summation of the product of the instantaneous displacement of soil and its stiffness, over all the soil elements. Fig 7 shows that the mobilisation of maximum soil resistance is not instantaneous. As the depth increases, phase lag increases and the tip soil offers intermittent beat type resistance on the pile motion.

#### ANALYSIS OF THE TEST RESULT

Test results have been analysed as follows:

Step1. Modified scheme was used to generate Set-Dynamic shear stiffness curve, with quake factor  $1.25\text{mm} \& J = 0.002\text{sec/mm}$  Shear stiffness associated with the free length of the casing tube, above ground, was set to zero. Number of blows for the last meter of penetration for TP-8 was 330, which indicate final set value as  $3.0\text{mm}$ . When this set value is entered through Fig. 8 offers dynamic shear resistance of soil as  $990\text{t/m}$  which corresponds to soil shear modulus  $G = 1500\text{t/m}^2$ .  
Step2. Poulos [8] has offered the estimation of elastic settlement of pile under the application of vertical load. The load required to produce  $6\text{mm}$  elastic settlement for TP-5 (Length  $= 17\text{m}$ , Dia  $= 0.45\text{m}$ ,  $E = 2.1 \times 10^6\text{t/m}^2$ ,  $E_s = 2.0(1+25) = 3250\text{t/m}^2$ ) was found out as  $183\text{t}$ . Observed load from cyclic load test results have been presented in Table 1.

#### DISCUSSION AND CONCLUSION

Table 1 shows that the numerical prediction of the load carrying capacity of pile is in good agreement for TP-8, TP-5 and TP-10. But for the short length pile TP-7 this scheme under estimates by 44%. This may be because of the variation in local geological condition which has helped to increase the pile capacity by soil set-up.

This may be concluded from this study:

- i) Modified Smith's approach is numerically more stable
- ii) All peripheral soil element do not offer their individual maximum resistance simultaneously.
- iii) Defining Set as permanent downward displacement of pile under last blow, the modified scheme correlates well this set with the dynamic shear stiffness property of the peripheral soil.
- iv) Evaluating soil static modulus, from this dynamic shear stiffness, Poulos approach may very well predict the load carrying capacity at a given elastic settlement of pile.
- v) Proper consideration should be given to the development of soil strength because of compaction of soil through driving of the casing tube and thixotropic increase in soil shear strength.

TABLE 1. LOAD CARRYING CAPACITY OF PILE

| No.      | Pile Length (m) | Observed Load (t) | Set (mm) | Calculated Load (t) |
|----------|-----------------|-------------------|----------|---------------------|
| 1. TP-8  | 21              | 160               | 3.0      | 163                 |
| 2. TP-5  | 17              | 160               | 3.8      | 158                 |
| 3. TP-4  | 17              | 180               | 4.0      | 153                 |
| 4. TP-7  | 13              | 96                | 6.7      | 53                  |
| 5. TP-10 | 21              | 160               | 3.2      | 163                 |

#### REFERENCES

1. Bowles, J.E. (1977) Foundation Analysis and Design, 2nd Ed, New York. McGraw-Hill.
2. Clough, R.W. and Penzien, J. (1985). Dynamic of Structure, McGraw-Hill Inc.,
3. Forehand, P.W. & Reese, J.L. (1964) "Prediction of Pile Capacity by the Wave Equation". J.S.M.F.D., ASCE, Vol. 90, SM2: 1-25.
4. Fuller, F.M., (1979) Symposium on Deep Foundations, ASCE, New York.
5. Hurty, W.C. and Rubinstein, M.F. (1964). Dynamics of Structure, Prentice-Hall, Englewood Cliffs, N.J.
6. Leech, J.W., HSU, P.T. and Mack, E.W. (1965). "Stability of a finite-difference method for solving matrix equation, AI AA JI, Vol 3, No 11: 2172-2173.
7. McClelland, B. 1974, "Design of Deep Penetration Piles for Ocean Structure", Jnl. Geot. Eng. Div., ASCE, Vol. 100, no. GT7: 705-747.
8. Poulos, H.G. & Davis, E.H. (1968). "The settlement Behaviour of Single Axially-Loaded Incompressible Piles and Piers". Geot. Vol 18: 351-371.
9. Smith, E.A.L. (1960), "Pile driving Analysis by the Wave Equation", J.S.M.F.D., ASCE, Vol. 86 SM4: 35-61.
10. Young, F.E. (1981) Piles and Foundation, Thomas Telford Ltd., London, 121-133.
11. Indian Standard code of practice for Design and Construction of Pile Foundation. IS: 2511 (Part I)-1964 Manak Bhavan, New Delhi, India.

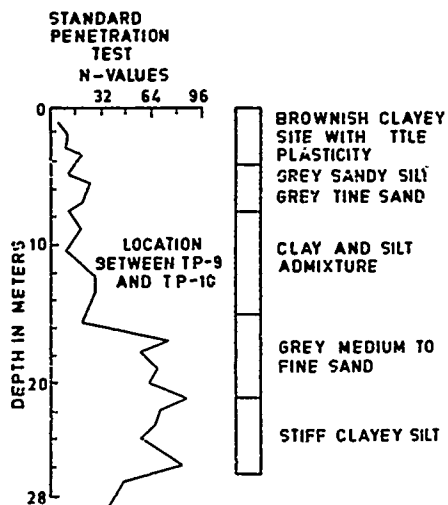


FIG.1 - GEOTECHNICAL PROFILE

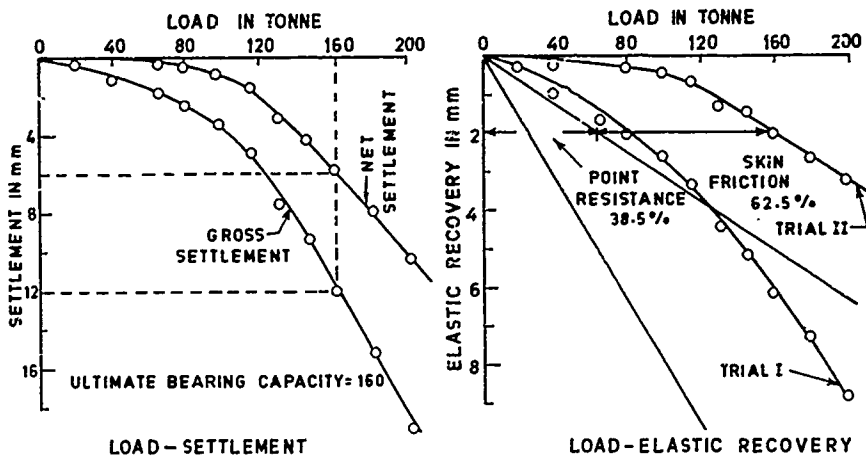


FIG.3 - CYCLIC LOAD TEST RESULT FOR TP-5

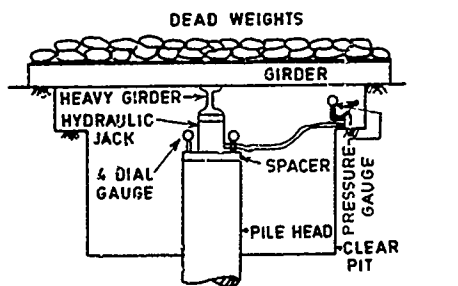


FIG.2 - PILE LOAD TEST ARRANGEMENT

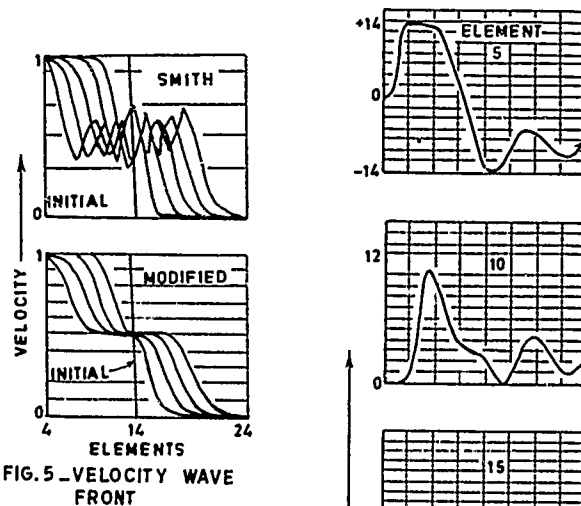
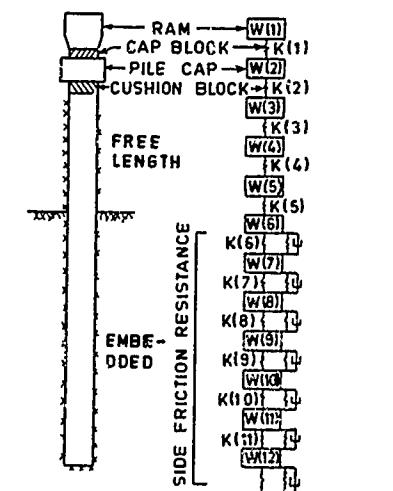


FIG.5 - VELOCITY WAVE FRONT



(a) ACTUAL PILE (b) IDEALIZED PILE  
FIG.4 - LUMPED MASS MODEL

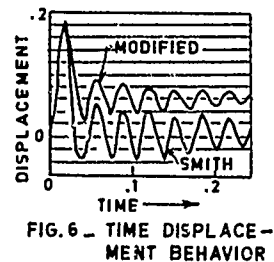


FIG.6 - TIME DISPLACEMENT BEHAVIOR

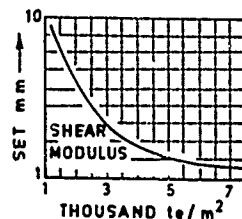


FIG.8 - SET VS SOIL RESISTANCE

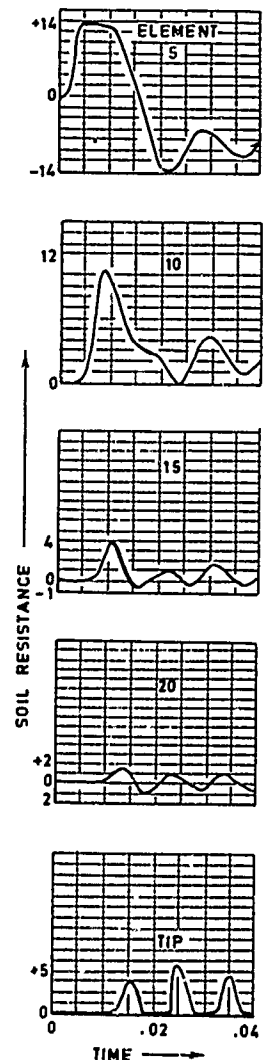


FIG.7 - MOBILISATION OF SOIL RESISTANCE

## The Observed Seismic Behavior of the Matahina Dam

M.D. Gillon

Senior Design Engineer, Ministry of Works and Development,  
Wellington, New Zealand

**SYNOPSIS:** On 2 March 1987 the 86 m high Matahina earth dam in the Eastern Bay of Plenty region of New Zealand was shaken by a nearby magnitude 6.3 earthquake. The dam response was recorded by five strong motion accelerometers and a maximum crest level acceleration of 0.42 g was measured. The crest level rockfill settled about 100 mm and moved downstream 250 mm during the earthquake. No major leakage has resulted from the earthquake.

The results of the damage investigations are described. A condition probably requiring remedial work has been identified on the left abutment.

### INTRODUCTION

At 1.42pm on 2 March 1987 a shallow magnitude 6.3 earthquake occurred near the town of Edgecumbe in the eastern Bay of Plenty region of New Zealand (Figure 1). There were no fatalities, possibly because failure of electric power supply in a large foreshock forced many people outdoors. There was extensive damage to several major industrial installations and moderate damage to housing.

The Matahina earth dam and power station near Edgecumbe is owned and operated by the Electricity Corporation of New Zealand. The civil works were designed and built by the New Zealand Ministry of Works and Development who remain as consultants to the owners. The dam is located on the Rangitaiki river about 23 km south of the main shock epicentre and 11 km from the main surface faulting. The intensity of shaking at the power station in the main shock was MM VII. Although initial observations did not indicate severe damage, the Matahina lake was drawn down 2.5 m as a precaution. The drawdown river flows were interpreted by residents downstream with alarm and the area was unofficially evacuated.

This paper describes the damage investigations carried out at the power station since the earthquake. These showed that crest level rockfill settlements of up to 100 mm together with a downstream movement of 250 mm had occurred during the earthquake. Crest level accelerations of 0.42 g were measured during the main shock. There has been no evidence of major leakage as a result of the earthquake. A condition probably requiring remedial work has been identified on the left abutment.

Further study of the dynamic behaviour of the dam is proposed.

### REGIONAL GEOLOGY

The Matahina power station is located on the eastern margin of the Central Volcanic Region of New Zealand (Staff NZ DSIR 1987). Spreading associated with the active convergent Pacific and Australian plate boundary which lies to the east of the North Island occurs within this region. Faulting is normal and trends NE-SW. The Central Volcanic Region is a zone of young igneous rocks mainly rhyolitic and andesitic in composition. It contains recent active volcanoes and geothermal areas.

A feature of the Central Volcanic Region is extensive sheets of rhyolitic and andesitic ignimbrite. These often extend up to 50-100 km from their source with total volumes up to 200 cubic kilometres covering several thousand square kilometres (Soons and Selby 1982). The welded portion of the Matahina ignimbrite sheet forms vertical cliffs along the canyon of the Rangitaiki River in the area of the dam and lake. At the damsite it is a hard columnar jointed welded tuff.

The earthquake occurred in the extreme north east of the Central Volcanic Region under the lowlying alluvial flood plain of the Rangitaiki River (Figure 1).

To the east of the damsite and the Central Volcanic Region lie the Jurassic greywacke rocks of the Raungaehe Range (Figure 2). Several major active faults occur in this area. These faults trend N-S and are associated with the major transcurrent movements occurring within New Zealand. One of these faults, the Waiohau fault, traverses the western edge of the damsite.

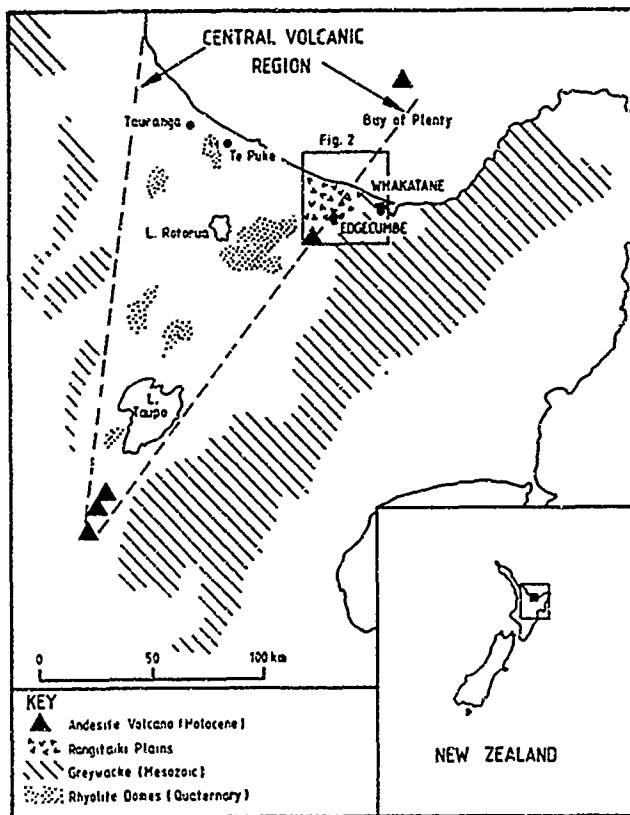


Figure 1. Location (Staff NZ DSIR, 1987)

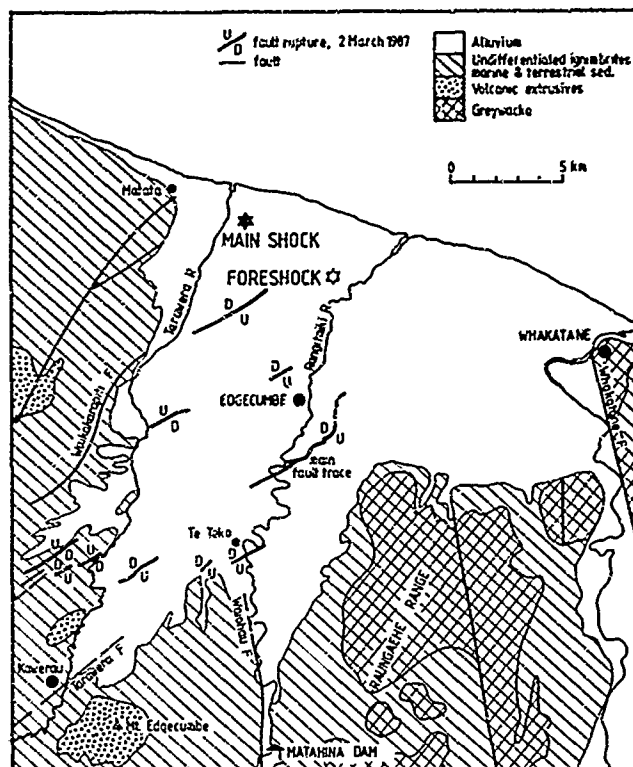


Figure 2. Geology, Epicentres, and Fault locations  
(Adapted from Staff NZ DSIR, 1987)

#### THE EDGECLUMBE EARTHQUAKE

In the two weeks preceding the main event there were earthquake swarms in the region (Staff NZ DSIR 1987). These culminated in the main shock at 01h 42m 34s on 2 March 1987 UT. The epicentre location was 8 km NNW of Edgecumbe (Figure 2) and the focal depth was estimated to be 12 km. The magnitude ( $M_L$ ) of the main shock was 6.3. A foreshock and four aftershocks had magnitudes of over 5.0 with epicentres within a few kilometres of the main shock.

The main surface rupture (Figure 2) occurred south of Edgecumbe and had a maximum of 2 m vertical displacement. Surface rupture and instrument records suggest normal faulting.

The accelerometer at the base of the dam recorded the  $M_L$  5.2 foreshock, the  $M_L$  6.3 main shock and the largest aftershock, the  $M_L$  5.5 event 8½ minutes after the main shock. The transverse (upstream-downstream) acceleration, velocity and displacement record from the base of the dam and the 5% damped acceleration response spectra are shown in Figure 3. The El Centro 1940 (N-S) response spectra is shown for comparison.

#### DESCRIPTION OF DAM

At the damsite the river has cut a gorge through an extensive ignimbrite sheet into compact gravels, sands and silty clays of Tertiary age. The dam abutments are therefore hard rock underlain by compact alluvial materials at lower levels. The Waiohau fault traverses the rock of the left abutment approximately 500 m from the dam and splinter faults from this occur within the dam foundation.

The diversion and dewatering tunnels, the spillway, the penstocks and powerhouse are founded on a prominent rock spur which forms the left abutment (Figure 4). There is a grout curtain forming a partial cutoff within the spur supplemented by two drainage drives. Seepage flows and groundwater levels are monitored.

The dam (Figure 5) stands 86 m high above foundation level and has a crest length of 400 m. It has an upstream sloping core of moderate width. The core material is weathered greywacke with a low plasticity gravelly clay grading. The dam shoulders are of hard ignimbrite rockfill compacted by heavy tractor track rolling. The transition zones between the core and shoulders comprise the fines and softer strippings from the ignimbrite rockfill quarry.

# A87085D2 MATAHINA DAM D (BOTTOM CENTRE) COMPONENT N07W

EARTHQUAKE 1987 MARCH 02 0142 UT  
 BAND-PASS FILTER TRANSITION BANDS ARE 0.100-0.250 HZ AND 24.5-25.5 HZ  
 @ Peak values: acceleration 2361 mm/s/s, velocity -216.5 mm/s, displacement -90.56 mm

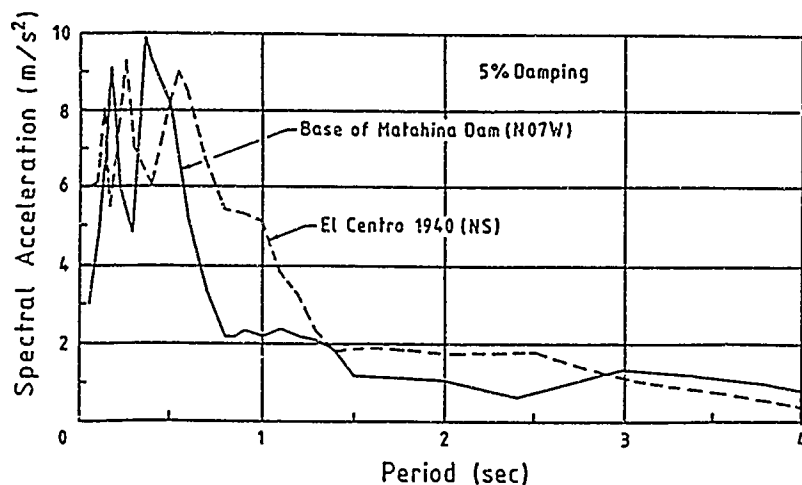
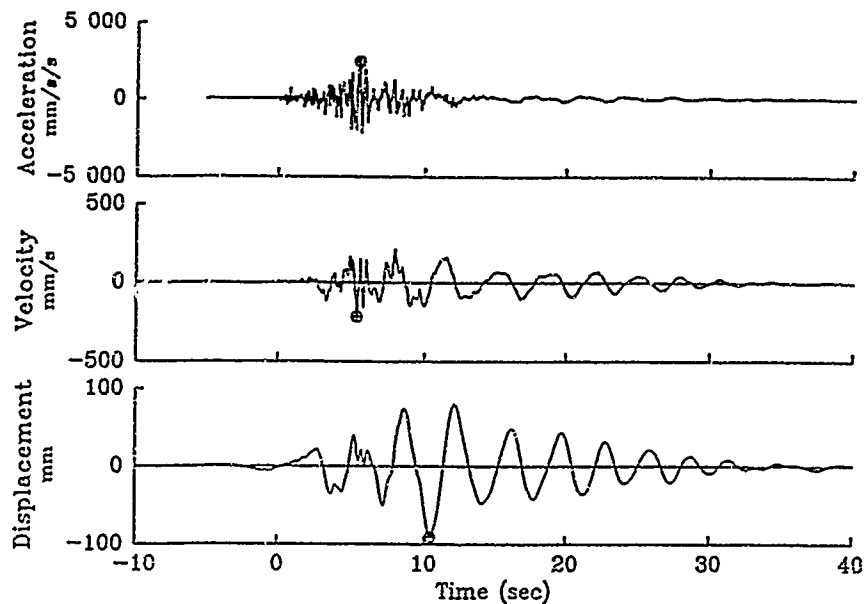


Figure 3. Acceleration, velocity and displacement at the base of the Matahina Dam and comparison of the 5% damped acceleration response spectra there with El Centro 1940 (NS).





Figure 4. Matahina Dam (D.L. Homer DSIR)

Underseepage is controlled by a shallow cutoff below the core and a 30 m deep curtain of drain holes which discharge into an extensive drainage blanket. Flow from the drainage blanket is monitored by a weir located in the old river channel downstream of the dam.

The dam instruments include five strong motion accelerometers from which records of the fore-shock and main shock were obtained. The extensive surface monument network had been resurveyed three weeks prior to the earthquake.

During lakefilling in 1967, core cracking, leakage and internal erosion occurred above a step in the right abutment (Galloway, 1967). High turbid leakage flows were observed at the drainage blanket monitoring weir. An erosion cavity was subsequently located downstream of the core. Repairs comprised a plastic concrete patch on the downstream side of the core backed by granular filter zones. The core was grouted with a cement bentonite mix and the lake refilled without further incident.

Settlement and downstream movement of the dam have continued since lake filling. The movements are consistent with the observed performance of similar dams.

## POST EARTHQUAKE INSPECTION

Detailed inspection following the earthquake showed surface cracking and minor local settlements near the abutments, a turbid and increased drainage flow from the left abutment spur, a minor increase in flow at the drainage blanket weir, settlement and downstream displacement of the crest and large settlements in the upstream rockfill shoulder. The lake was drawdown to near minimum operating level as a precaution. Generation was resumed 14 hours after the earthquake.

## DAMAGE INVESTIGATIONS

In view of the 1967 leakage incident, the presence of surface cracking and the considerable earthquake deformations which had occurred, the abutment areas were investigated using geophysical methods, surface trenching and air flushed drill holes.

Trenching showed the cracks to be shallow and not continuous through the core. It also revealed a large cavity beneath the roading basecourse upstream of the core on the right abutment. The location of the cavity directly upstream of the 1967 leak repair and the lack of large leakage flows at the drainage blanket weir strongly suggested that the cavity was related to the 1967 incident. It is considered that the earthquake compacted loose materials above the leakage area creating the void which was found.

As a result of surface deformation above the 1967 leakage repair two shafts were drilled to check the integrity of the repair. On the left abutment drilling showed high water inflows and this investigation was extended. Survey showed that continuing settlement of the dam and left abutment spur was occurring several weeks after the earthquakes.

During the investigations detailed monitoring was maintained. This included repeated precise level measurements, readings of selected permanent instrumentation, visual inspection and monitoring of additional investigation piezometers. The monitoring schedules were revised

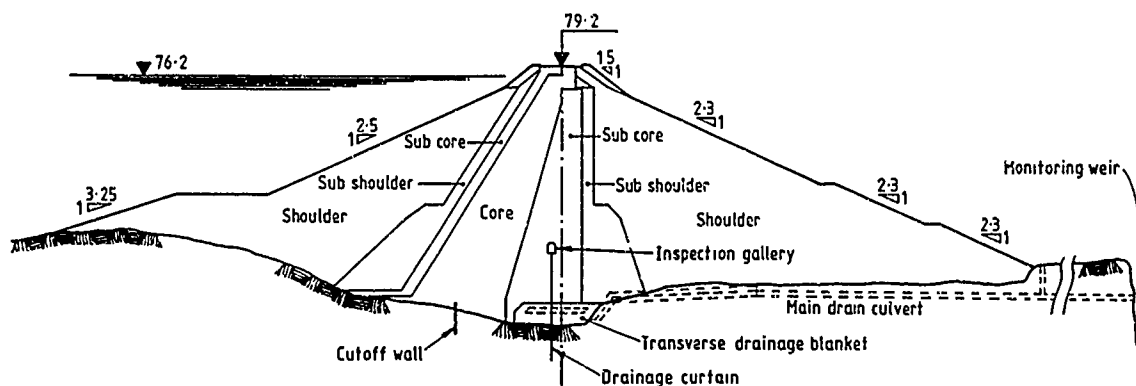


Figure 5. Cross section of the Matahina Dam.

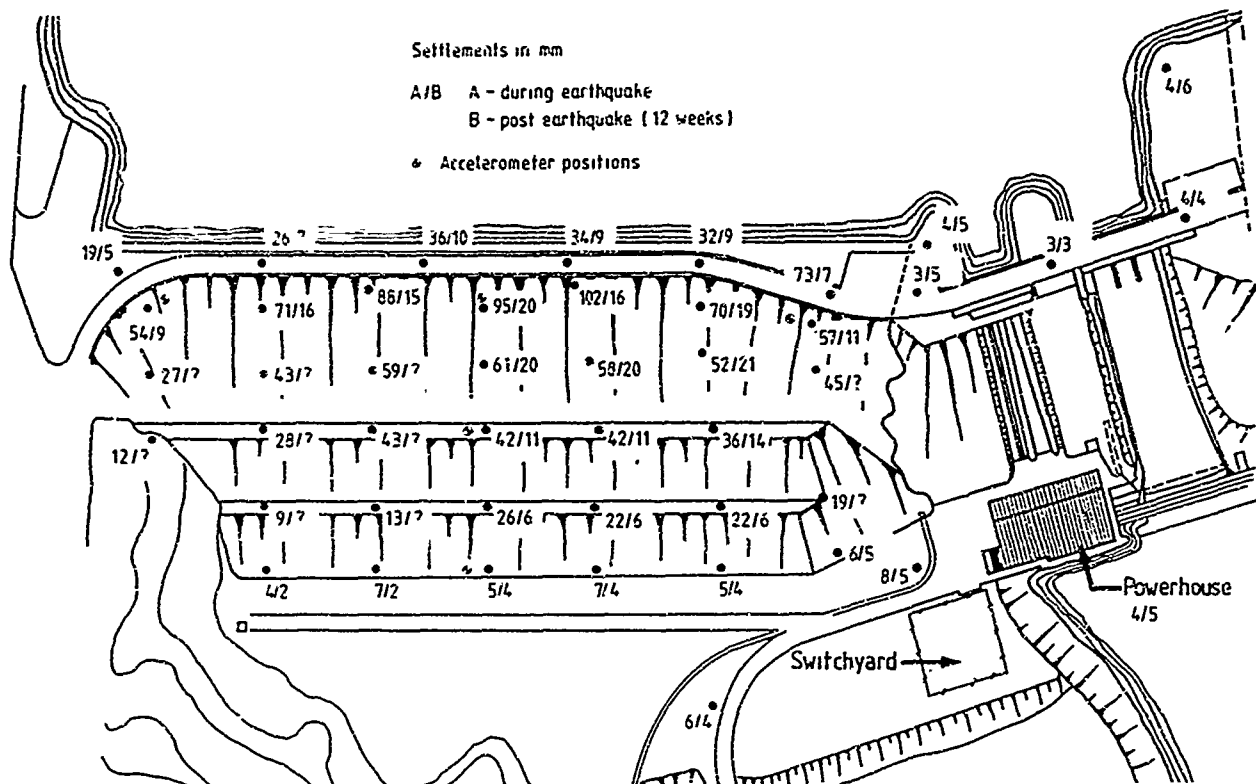


Figure 6. Settlements resulting from earthquake.

several times when conditions with possible safety implications were found. Currently the lake is held near minimum operating level with daily monitoring of selected instruments.

An alarm has been installed on the earth dam drainage blanket weir to detect abnormal flows.

## INVESTIGATION RESULTS

### Seepage

During the period of lake drawdown following the earthquake flow from the drainage blanket weir increased from 70 l/min to 630 l/min. Four days after the earthquake flow from the weir ceased and it has flowed only intermittently since then.

In order to interpret these observations, weir flow records were analysed with respect to lake level, tailwater level and local rainfall. While flows were clearly influenced by tailwater level and rainfall, the scatter of results inhibited interpretation. Flows of up to 350 l/min were injected into the drainage blanket without any discernible response.

The conclusions drawn from this work were that in periods of low tailwater level flow from the drainage blanket leaks into the groundwater system downstream of the dam; that the increase in flow after the earthquake was probably due to the increased tailwater level during drawdown; that increased leakage up to 2000 l/min

may not be detected during periods of zero weir flow, and that no major dam leakage has occurred as a result of the earthquake.

It is proposed to undertake tracer tests in the drainage blanket when weir flow is re-established. This would assist in the estimation of total drainage flows and losses.

Seepage flow from the left abutment rock spur which rose to four times normal flow after the earthquake has continued to slowly rise after initially decreasing. This trend is being closely monitored eight months after the earthquake.

### Settlements

Measured settlements of survey points are shown in Figure 6 (Currie, 1987). These show the very small settlements of the left abutment spur and the much larger settlement of the dam immediately after the earthquake. Given the level of shaking the settlements are not considered excessive but they were viewed with concern because of the core cracking and erosion associated with lake filling.

Settlement of the dam continued for several weeks. During this time the crest settlements were less than the rockfill settlements as would be expected. Measurements from the inspection gallery do not suggest significant foundation settlement (Figure 7).

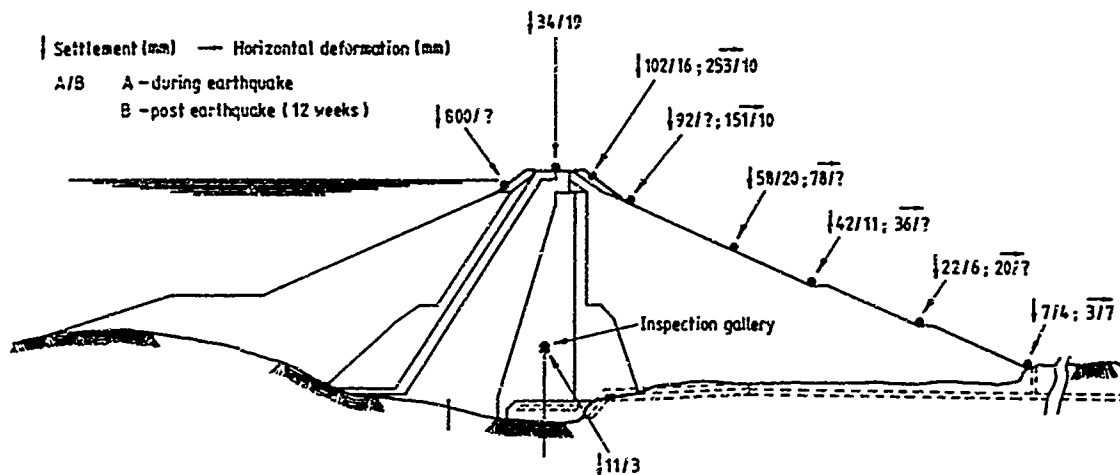


Figure 7. Deformations at centre of dam

The long term settlement of the left abutment spur was unexpected (Figure 6). The results indicate a fairly uniform settlement without tilting. The settlement caused increased leakage into the powerhouse. Initially it was suspected that the spur settlements may have been tectonic in origin but level traverses across the Waiohau fault did not support this. It is possible that the silt which is inferred to underlie the ignimbrite sheet compacted, developing excess pore pressures which took some weeks to dissipate.

The upstream shoulder settlements were estimated by levelling the colour change in the rip rap along the dam. (Normal lake level is marked by a distinct colour change). Settlements of 800 mm were typical. Subsurface sonar was used to check for evidence of underwater slope failure. There were no detectable scarps and it is considered that the settlements are simply the result of earthquake induced compaction of the rockfill.

#### Displacement

The displacement of the downstream rockfill shoulder is shown in Figure 7. The maximum displacement of 253 mm compares with about 220 mm during the lake filling period. The ratio of long term crest displacement/settlement (typically 2.5) is similar to that observed during the earthquake.

#### Right abutment leak repair area

Road seal cracking and settlement above the 1967 leak repair area was observed some weeks after the earthquake. The cracking was located above and along the step in the abutment where core erosion had occurred. SPT soundings in the repair zone and trenching observations showed that the sand filter was in a very loose state. Because of the uncertainty of leak detection from the drainage blanket weir and the possibility that the settlement and the low densities were due to leakage and material loss from the base of the repair, two cased shafts were drilled into it. These showed that the repair had not leaked significantly during the earthquake but that it had leaked soon after lake

filling in 1967. The loose nature of the sand filter was satisfactorily explained by checking the construction methods with the field staff who had supervised construction.

The fact of prior leakage was established when seams of eroded core material were found in the sand filter downstream of the plastic concrete patch. The seams had formed on the surface of the jute sand bags which were used as formwork for placing the plastic concrete. This established the timing as prior to the rotting of the jute. The location of the seams suggested that leakage had occurred around rather than through the plastic concrete. The sedimentary structure within the seams was indicative of smallish rather than large leaks.

The continued presence of core defects in which erosion has occurred indicates that the remedial core grouting carried out with the repair was probably not effective. Drilling and piezometer measurements from the current investigations support this view.

It was concluded that leakage defects still exist in the repair and that they are filled with eroded core material held in place by the sand filter in the repair zone.

#### Left abutment area

Four inclined drill holes were drilled using air flushing. High water inflows were encountered downstream of the core. Caving areas were found in two holes. Twelve piezometers were installed and anomalously high pore pressures measured. Permeabilities measured from falling head tests in the piezometers are at least 1000 times higher than expected.

The results indicate that core cracking and erosion had occurred similar to that observed in 1967 on the right abutment. It is not known whether the defects predate or postdate the earthquake. Intensive monitoring indicates that they are stable at present. Remedial measures are proposed. The lake is being held close to minimum operating level.

## DYNAMIC BEHAVIOUR

A summary of the maximum accelerations measured on the transverse dam centreline is given in Table 1. The accelerometer locations on the downstream rockfill shoulder are shown in Figure 6.

| Component      | Acceleration (mm/sec <sup>2</sup> ) |           |       |
|----------------|-------------------------------------|-----------|-------|
|                | Base                                | Midheight | Crest |
| Vertical       | 1378                                | 2012      | 2824  |
| Horizontal     |                                     |           |       |
| - maximum      | 3247                                | 4580      | 4155  |
| - transverse   | 2361                                | 4366      | 3427  |
| - longitudinal | 2774                                | 3209      | 2766  |

Table 1. Maximum main shock accelerations recorded on the dam centreline (McVerry, 1987)

The vertical base acceleration is amplified by a factor of over two at crest level. The horizontal crest components are amplified more in the transverse direction than in the longitudinal direction. An unexpected result is that the highest horizontal accelerations (0.43g) are measured on the rockfill shoulder at the mid-height of the dam. This aspect will be investigated further.

Analysis of the 2 March 1987 accelerograms is still in the initial stages. Fourier spectra analysis estimates (McVerry, 1987) of the transverse and longitudinal dam crest first mode period in the 2 March foreshock and main shock are given in Table 2 together with results for a small earthquake in 1977. As expected the results show a lengthening of the effective fundamental periods in the main shock compared with the two other smaller events.

| Event          | Maximum horizontal crest acceleration | First mode period (sec) |              |
|----------------|---------------------------------------|-------------------------|--------------|
|                |                                       | Transverse              | Longitudinal |
| 1977           | 0.045g                                | 0.79                    | 0.83         |
| 1987 Foreshock | 0.054g                                | 0.80                    | 0.89         |
| 1987 Mainshock | 0.42g                                 | 1.14                    | 1.12         |

Table 2. First Mode Periods from Fourier Spectra Peaks of Dam Crest Accelerograms

Some results are available from a preliminary analysis of the dam response in the mainshock using a linear modal approach (McVerry, 1987). A systematic identification technique was used to obtain the parameters of the first few modes of the dam in the transverse and longitudinal directions which provided the best least squares fit of the recorded crest response when subjected to the recorded base acceleration in the same direction.

The non linear behaviour of the dam in the course of the mainshock made it difficult to reproduce the recorded response with a single time-invariant linear model. Excellent matches of portions of the response were obtained by analysing segments of the recorded motions.

The results for the transverse crest response (Figure 8) show that the first mode period lengthens from about 0.80 seconds in the foreshock to 1.36 seconds during the time of strong response. The period drops to about 0.92 seconds in the decay portion of the record. First mode damping reached about 25% of critical in the largest amplitude motion dropping to about 7% in the decaying portion of the response.

The matching of response in the longitudinal direction was more difficult. First mode periods between 0.86 and 1.02 seconds were obtained for various segments. First mode damping was generally in the range of 12 to 14% of critical with one segment reaching 23%.

The results of the analysis to date show evidence of mainly hysteretic behaviour. The recovery in the decay portion of the transverse crest record (Figure 8) is reassuring but shows evidence of softening. The lack of mid crest accelerograms in the aftershocks prevents direct determination of the post earthquake first mode period. It is hoped that analysis of aftershock records from the other accelerometers will provide information on the post earthquake properties of the dam.

## CONCLUSIONS

The Matahina dam experienced significant shaking in a nearby magnitude 6.3 earthquake. The downstream rockfill shoulder settled 100 mm and was displaced up to 250 mm downstream in the earthquake. The upstream rockfill shoulder settled by about 800 mm. No major leakage has been observed. Conditions requiring remedial work have been located on the left abutment but it is not known if these result from the earthquake.

The highest acceleration on the dam body during the mainshock was 0.48g measured at the midheight. The maximum crest level acceleration was 0.42g. Fourier spectral analysis of foreshock and main shock records showed a significant lengthening of the first mode period in the mainshock. A preliminary linear modal analysis of segments of the main shock transverse accelerations showed a lengthening of the first mode period during the most intense shaking with partial recovery of stiffness in the decay part of the record.

## ACKNOWLEDGEMENT

The work described in this paper has been carried out for the Electricity Corporation of New Zealand by staff of the Ministry of Works and Development assisted by Department of Scientific and Industrial Research staff.

The permission of the Group Manager, Electricity Corporation of New Zealand to publish this paper is gratefully acknowledged.

#### REFERENCES

Currie, S.A. (1987), An Interim Report of Matahina Dam Deformation Surveys following the 2 March Earthquake, Ministry of Works and Development, Wairakei, New Zealand.

Galloway, J.H.H. (1967), "Installed Instruments in Matahina Earth Dam", 5th Australia-New Zealand Conference on Soil Mechanics and Foundation Engineering, pp 147-152 and 165-168.

McVerry, G.H. (1987), "Linear Modal Analysis of the Response of Matahina Dam in the Edgecumbe Earthquake". A report prepared for the Major Projects Branch, Ministry of Works and Development, Wellington, New Zealand.

Soons, J.M. and Selby, M.J., editors (1982), Landforms of New Zealand, Longman Paul Limited, Auckland, New Zealand.

Staff, New Zealand Department of Scientific and Industrial Research, Wellington, New Zealand (1987), "The 1987 March 2 Earthquake near Edgecumbe, North Island, New Zealand". Accepted for publication in EOS, Transactions American Geophysical Union.

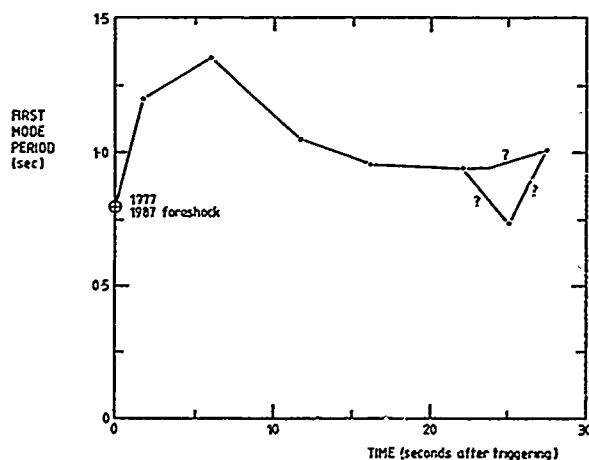


Figure 8. Variation of transverse first mode period during the mainshock (McVerry, 1987)

# Soil Liquefaction Potential of a Highway Bridge Foundation

Pedro S. Sêco e Pinto

Principal Research Engineer, Laboratório Nacional de Engenharia Civil, Portugal

**SYNOPSIS:** Dynamic properties of a highway bridge foundation were determined through extensive field and laboratory tests. The liquefaction potential of alluvia materials consisting of sand material with 10 m depth was evaluated by using field data obtained from standard penetration and cone penetration tests, as well as seismic tests by measuring longitudinal and shear waves velocities. In addition the laboratory testing program has included classification tests, cyclic triaxial and cyclic simple shear test.

The analyses have showed that comparable factors of safety may be obtained from both field and laboratory tests.

## INTRODUCTION

A liquefaction potential evaluation of Guadiana bridge foundation is performed. This bridge is located in the South of Portugal, within zone A of the Seismic Risk Map. Subsurface conditions were determined using informations obtained from drilling, laboratory tests and field tests. This paper presents the case studies involved in a liquefaction evaluation and shows how these procedures can be used in order to determine the assessment of liquefaction potential of the bridge foundation. The countermeasures adopted are also referred.

## GENERAL DESCRIPTION OF BRIDGE AND FOUNDATION

Guadiana bridge is a cable-stayed bridge with a total length of 842 m and has two towers that are 324 m apart. The deck structure consists of a triangulated box-girder with two inclined webs and interior stiffening provided by inclined struts. Each section of the towers is founded on a group of piles more than 1.5 m in diameter crossing the alluvia material and penetrating in the shale grawackes formations (Fig. 1).

The old Guadiana valley is filled by alluvia material that in some places reach a thickness of 80 m. Taking into account the information given by in situ tests (boring tests, geophysical tests, SPT and CPT tests and wave tests) and laboratory tests (classification tests) three complexes were considered LNEC (1976, 1978, 1985 a) which principal characteristics are described in Table 1.

The liquefaction evaluation of sandy material with a thickness of 10 m and located under the left tower is discussed in the following sections.

## EVALUATION OF LIQUEFACTION POTENTIAL

### Introduction

To express the ability of a soil element to resist liquefaction, the liquefaction resistance factor  $F_L$  is defined as

$$F_L = \frac{R}{L} \quad (1)$$

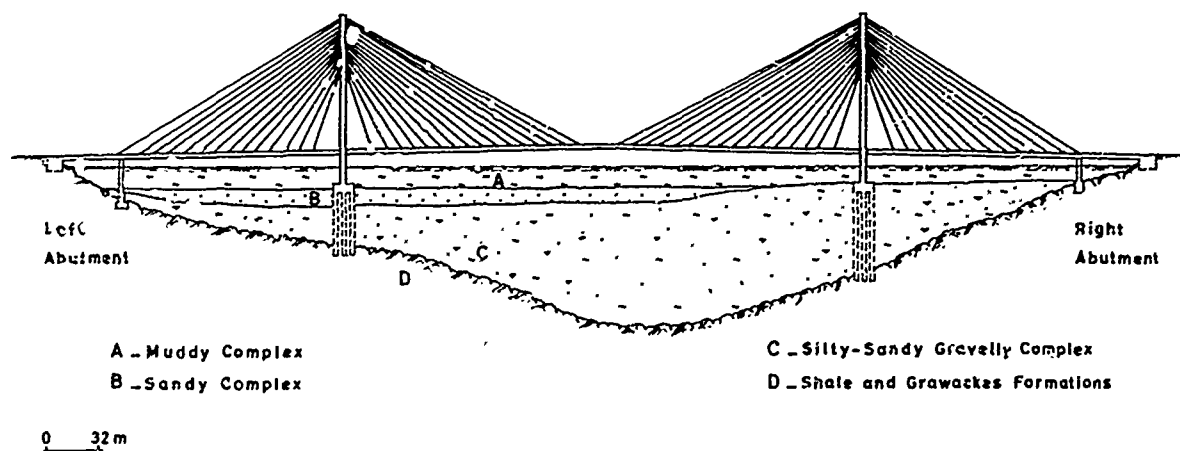


Fig. 1 General View and Foundation Section

TABLE I. - Summary of the Principal Geotechnical Characteristics of Alluvia Material

| Type                            | SPT<br>(N) |         | CPT<br>(Kpa) |         | P wave velocity<br>(m/s) |         | S wave velocity<br>(m/s) |         |
|---------------------------------|------------|---------|--------------|---------|--------------------------|---------|--------------------------|---------|
|                                 | Range      | Average | Range        | Average | Range                    | Average | Range                    | Average |
| Muddy Complex                   | 1-5        | 2       | 300- 1000    | 600     | 1300-1600                | 1400    | 60-230                   | 110     |
| Sandy Complex                   | 3-20       | 10-15   | 1000- 5000   | 2500    | 1000-1500                | 1300    | 105-360                  | 170     |
| Silty-sandy<br>gravelly complex | 6-60       | 20-40   | 2000-20000   | 10000   | 1500-1800                | 1600    | 115-400                  | 260     |

where R is the resistance of the soil element to an earth quake loading and L is the earthquake load induced by a seismic motion.

The estimation of cyclic shear strength can be determined by field performance correlated with a variety of soil index parameters, such as standard penetration resistance, cone penetration resistance, shear wave resistance or by an analysis of stress or strain conditions using laboratory testing procedures. In the evaluation of the liquefaction potential of Guadiana bridge foundation both methods were used.

#### Determination of Stresses Induced by Design Earthquakes

In the specifications for Earthquake Resistance Design of Highway Bridges issued by the Japan Road Association (1980) the value of L is defined by the following equation:

$$L = r_d K_s \frac{G_v}{G_v} \quad (2)$$

$$r_d = 1.0 - 0.015 Z \quad (3)$$

where: Z = Depth from the ground surface (m)

$K_s$  = Seismic coefficient for evaluation of liquefaction and can be determined by

$$K_s = v_1 \times v_2 \times v_3 \times K_{so} \quad (4)$$

$v_1$  = Seismic zone factor

$v_2$  = Ground condition factor

$v_3$  = Importance factor of the bridge

$K_{so}$  = Design seismic coefficient

$G_v$  = Total overburden pressure

$G'_v$  = Effective overburden pressure

As Guadiana bridge is located in an active seismic zone (Oliveira, 1977) from the seismic studies have resulted for the near earthquake a magnitude equal 6.5 and for this stress-time history 20 cycles was selected as the appropriate number. From equation (4) results  $K_s = 0.175$  and consequently  $L = 0.36$ .

#### Laboratory Testing

##### Identification Tests

A typical grain size distribution curve for the sandy materials is shown in Fig. 2.

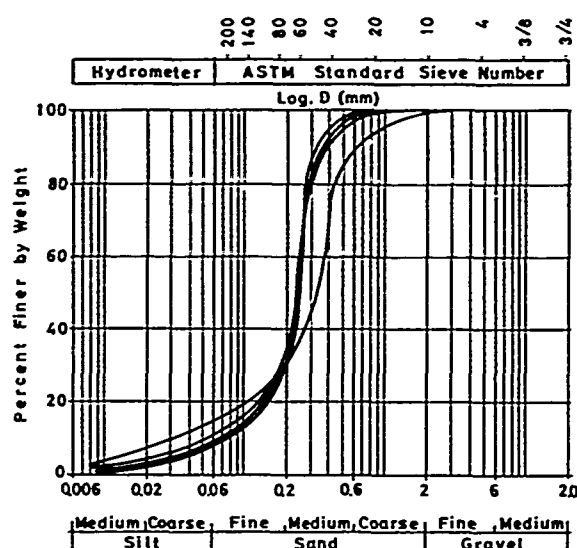


Fig. 2 Ranges of Grain Size Distribution Curves

#### Cyclic Triaxial Tests

After knowing the triaxial cyclic shear strength ( $R_1$ ) in situ cyclic shear strength (R) can be obtained by the following equation (Iwasaki, 1986):

$$R = C_1 \times C_2 \times C_3 \times C_4 \times C_5 \times R_1 \quad (5)$$

where:  $C_1$  is the correction factor because the cyclic triaxial test does not adequately reproduce the in situ stress conditions present during an earthquake and for alluvial deposits  $C_1 = 2/3$  (Ishihara and Li, 1972);  $C_2$  is the correction factor accounting for the difference be-

tween the in situ random loading pattern and the sinusoidal loading pattern used in the triaxial, an average value  $C_2 = 1.65$  is recommended by Ishihara and Yasuda (1975);  $C_3$  is the correction factor for the effects of soil disturbances during sampling;  $C_4$  is the correction factor for the effects of densification in the process of sampling and handling;  $C_5$  is the correction factor accounting for multi-direction shaking and Seed (1976) has proposed the value 0.9.

Considering that the two effects  $C_3$  and  $C_4$  may cancel out equation (5) becomes:

$$R = \frac{2}{3} \times 1.6 \times 1 \times 0.9 R_1 = R_1 \quad (6)$$

Cyclic triaxial tests were performed in representative samples to observe the stresses and strains to cause liquefaction (LNEC, 1978; 1985 b). The initial effective confining pressure was varied from 30 to 100 KPa and the samples were submitted to 120 cycles, and a value of 5 percent double amplitude strain was selected to avoid inconvenient deformations for the structure. Fig. 3 shows tests results plotted as the log of the number of cycles to 5 percent double amplitude strain versus the applied cyclic shear stress ratio  $\sigma_d/2\sigma'_3$ , where:

$\sigma_d$  = cyclic deviator stress and  $\sigma'_3$  = initial effective confining pressure. Since the induced stress ratio by earthquake exceeds the cyclic shear stress it can be concluded that the sand is likely to liquefy.

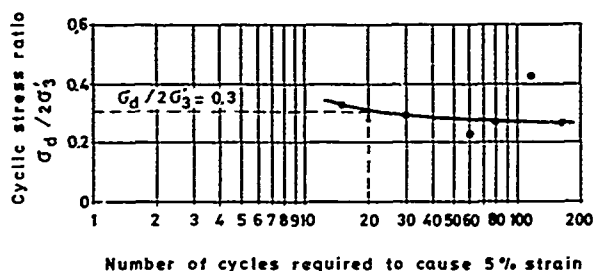


Fig. 3 Cyclic Triaxial Tests Results

#### Cyclic simple shear

The simple shear principle appeared to many investigators to be an appropriate way of reproducing in the laboratory the stresses experienced by an element of soil subject to the ideal earthquake loading.

The initial effective vertical confining pressures were chosen in order to duplicate the field conditions and failure was defined as 5 percent double amplitude strain. Test results plotted as the log of the number of cycles to 5 percent double amplitude strain versus the applied cyclic shear stress ratio  $\tau/\sigma'_v$  are shown in Fig. 4, where:  $\tau$  = cyclic horizontal stress and  $\sigma'_v$  = initial effective vertical confining pressure.

Since the stress ratio developed by the earthquakes exceeds the cyclic shear stress ratio the sand can liquefy.

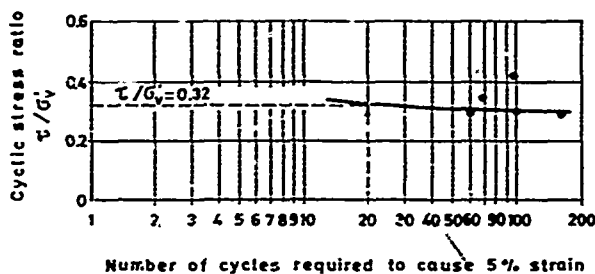


Fig. 4 Cycle Simple Shear Tests Results

#### Field Tests

##### SPT Tests

Since Alaska and Niigata earthquakes of 1964, geotechnical engineers search to determine the relationship between field values of cyclic stress ratio  $\tau_h/\sigma'_o$  (in which  $\tau_h$  = the average horizontal shear stress induced by an earthquake, and  $\sigma'_o$  = the initial effective overburden pressure on the soil layer involved) and the relative density of the sand, as determined from the standard penetration resistance.

Seed et al (1983) have correlate the standard penetration resistance with the effective overburden pressure by the relationship:

$$N_1 = C_N \cdot N \quad (7)$$

where  $C_N$  = a function of the effective overburden pressure at the depth where the penetration test was conducted. The values of  $C_N$  are shown in Fig. 5.

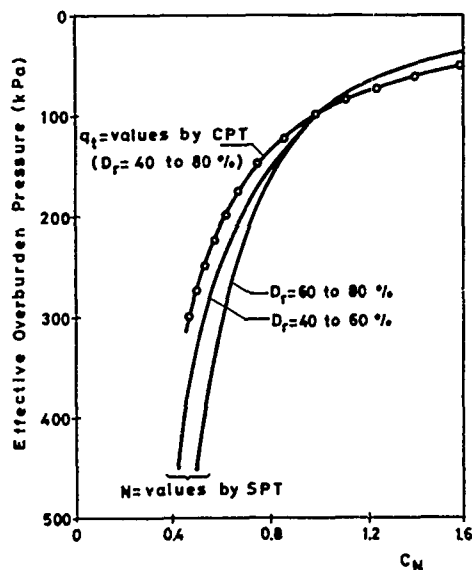


Fig. 5 Recommended Curves for Determination of  $C_N$  (after Seed et al., 1983)



From liquefaction studies performed from data of sites located in China, Guatemala, Argentina, Japan and U.S.A. Seed et al. (1985) have proposed a boundary line (or zone) separating sites known to have liquefied from sites which have apparently not liquefied in earthquakes of magnitude about 7 - 1/2 for sands and silty sands (Fig. 6). These results are also extended to other magnitude events (Seed et al., 1983).

Considering a standard penetration resistance value of about 12 at a depth of 10 m, for  $\sigma'_0$  (effective overburden pressure) = 75 Kpa,  $C_N = 1.1$  and  $N_1 = 13.2$ . For the SPT tests a safety hammer with 2 wraps of a rope around a pulley was used. From Fig. 6 it may be concluded that under an induced earthquake load of 0.36 with a correction factor 1.2 for  $M = 6.5$  and taking into account a fines content of 15% (Fig. 2) the soil will liquefy.

Tatsuoka et al. (1978) have proposed the following equations to obtain the value of  $R$

$$R = 0.0882 \sqrt{\frac{N}{\sigma'_v + 0.7}} + 0.225 \log_{10} \frac{0.35}{D_{50}} \quad (8)$$

(for  $0.02 \leq D_{50} \leq 0.60$  mm)

$$R = 0.0882 \sqrt{\frac{N}{\sigma'_v + 0.7}} - 0.05 \quad (9)$$

(for  $0.6 \leq D_{50} \leq 2.0$  mm)

where  $\sigma'_v$  is the effective overburden pressure and  $N$  is the SPT value.

Considering this proposition a value  $R = 0.27$  was obtained. As this value is smaller than  $L$  liquefaction can occur.

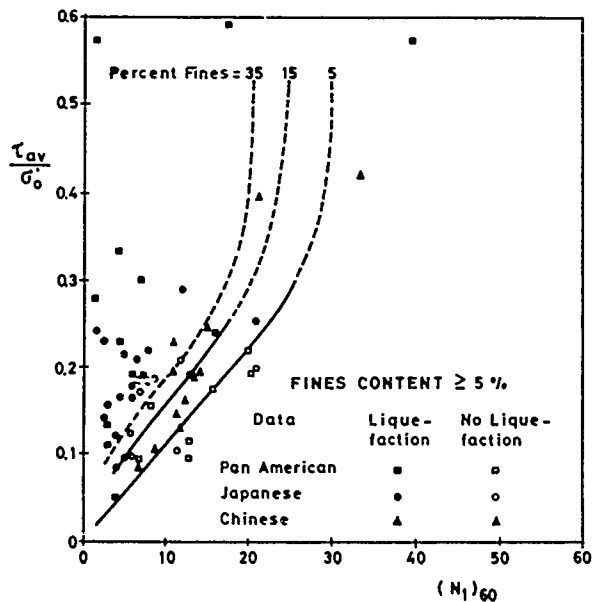


Fig. 6 Relationship between Stress Ratios Causing Liquefaction and  $N_1$  - Values for Silty Sands for  $M = 7, 1/2$  Earthquakes (after Seed et al., 1985)

## CPT tests

The main advantages of CPT test are that it provides data much more rapidly than does the SPT, it provides a continuous record of penetration resistance in any borehole, and it is less vulnerable to operator error than the SPT. The main disadvantage of the test, from the point of view of predicting the liquefaction resistance of a site, is that it has a very limited data base to provide a correlation between soil liquefaction characteristics and CPT values.

Using the relationships  $q_{c1}$  (Kpa) = 400 to 500  $N_1$  for clean sands and  $q_{c1}$  (Kpa) = 350 to 450  $N_1$  for silty sands proposed by Schmertmann (1976) the plots relating values of cyclic stress ratio causing liquefaction with  $q_{c1}$  values are shown in Fig. 7 (Seed et al., 1983).

Considering an average value of CPT = 2500 Kpa, from Fig. 7 it may be concluded that soil liquefaction can occur.

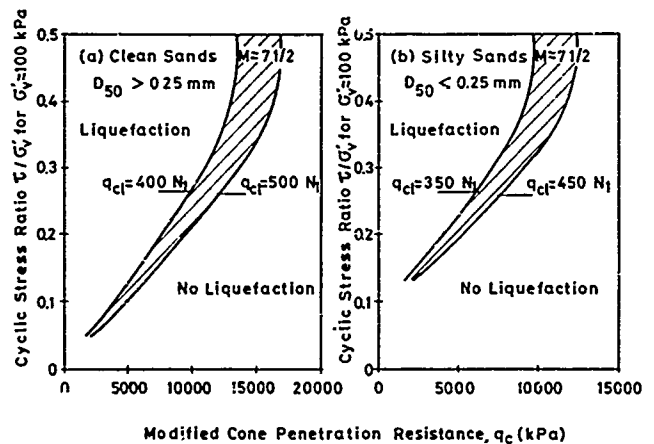


Fig. 7 Proposed Correlation between Liquefaction Resistance of Sands for Level Ground Conditions and Cone Penetration Resistance (adopted from Seed et al., 1983)

To evaluate liquefaction potential of sand Zhou (1981) has proposed the following expression:

$$P_{scr} = P_{so} [1 - 0.055 (H_w - 2)] [1 - 0.05 (H_o - 2)] \quad (10)$$

where  $P_{scr}$  is the critical cone resistance,  $H_w$  is the water level,  $H_o$  is the thickness of overburden layer and  $P_{so}$  is a factor depending the intensity of the earthquake.

The increase of fines content in sand will lead to a great drop in cone resistance, and meanwhile increases the cyclic shearing strength of the soil. The following equation has been proposed (Zhou, 1981):

$$P_s = 584 (\sigma'_v + 0.7) \Delta R_L^2 \quad (11)$$

where  $\sigma'_v$  is the overburden stress and  $\Delta R_L$  depends of the content of particles less than 0.074 mm.

From equation (10) the critical cone resistance  $P_{scr} = 7600$  Kpa. Considering an average point resistance value  $R_p = 2500$  Kpa and with the correction related with fines content in sand results  $R_p + P_s = 4200$  Kpa. As  $R_p + P_s < P_{scr}$  liquefaction can occur.

#### Seismic tests

In soil containing a significant proportion of gravel particles the shear wave velocity ( $v_s$ ) may provide a more suitable means for assessment of liquefaction potential. Seed et al. (1983) have proposed the equation

$$v_s = \frac{55 \sqrt{N_1}}{0.9} \approx 60 \sqrt{N_1} \quad (12)$$

for depths up to about 15 m. This relationship is shown in Fig. 8.

As the average shear wave velocity  $v_s = 170$  m/s is less than 366 m/s soil liquefaction can occur.

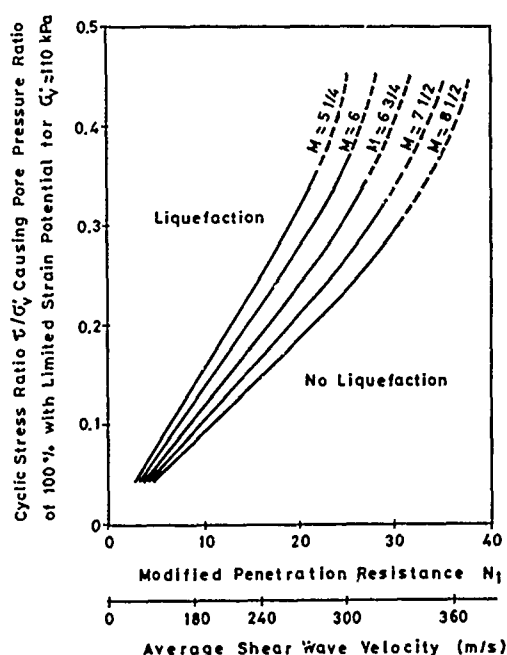


Fig. 8 Proposed Correlation between Liquefaction Resistance of Soils containing Gravels for Different Magnitude Earthquakes and Average Shear Wave Velocity (adopted from Seed et al., 1983)

In summary: Analyses were performed to determine the liquefaction potential of sandy materials. The analyses were done by comparison of induced stress conditions from earthquakes and stress conditions causing liquefaction in cyclic laboratory tests. In addition factors of safety against liquefaction in accordance with empirical methods based on the observation of performance of sand deposits during previous earthquakes using field tests were determined. Nevertheless these two approaches are quite dif-

ferent the computed factors of safety against liquefaction were in good agreement and pointed out that liquefaction could occur.

#### MEASURES AGAINST SOIL LIQUEFACTION

In designing an important civil engineering structure on soils vulnerable to liquefaction during earthquakes, it seems inevitable to consider the effects of soil liquefaction on the seismic stability of the structure. In Guadiana bridge soil improvement by vibroflotation and long pile foundations were jointly employed in order to upgrade the soil liquefaction vulnerability.

#### CONCLUSIONS

The advantageous and limitations of laboratory testing procedures and field tests were combined to assess the liquefaction potential of Guadiana bridge foundations. A good agreement was found between the several methods adopted reaching all of them the same conclusion.

As soil liquefaction could occur countermeasures were adopted related with soil improvement by vibroflotation and the use of long pile foundations.

#### ACKNOWLEDGMENTS

The writer has benefited greatly from talks with Dr. José Folque. Thanks are also due to JAE (Portuguese Road Board) for its permission to publish these results.

#### REFERENCES

- Ishihara, K. and Li, S. (1972), "Liquefaction of Saturated Sand in Triaxial Torsion Shear Test", Soils and Foundations, Japanese Society of Soil Mechanics and Foundation Engineering, 12, no. 2, 19-39.
- Ishihara, K. and Yasuda, S. (1975), "Sand Liquefaction in Hollow Cylinder Torsion under Irregular Excitation", Soils and Foundations, Japan Society of Soil Mechanics and Foundation Engineering, 15, no.1, 29-45.
- Iwasaki, T. (1986), "Soil Liquefaction Studies in Japan: State-of-the-Art", Soil Dynamics and Earthquake Engineering, Vol. 5, no. 1, 2-68.
- Japan Road Association (1980), "Specifications for Highway Bridges. Part V. Earthquake - Resistant Design", SPA.
- LNEC (National Laboratory of Civil Engineer) (1976), "International Guadiana Bridge - Preliminary Geotechnical Studies", Geotechnical Department, Report.
- LNEC (National Laboratory of Civil Engineer) (1978), "International Guadiana Bridge - Complementary Geotechnical Studies", Geotechnical Department, Report.
- LNEC (National Laboratory of Civil Engineer) (1985 a) "Seismic Tests for Guadiana Bridge Foundation". Geotechnical Department, Report.
- LNEC (National Laboratory of Civil Engineer) (1985 b) "International Guadiana Bridge. Laboratory Tests". Geotechnical Department, Report.

Oliveira, C. S. (1977), "Sismology, Seismicity and Seismic Risk. Applications for Portugal". LNEC, Structures Department, Report.

Schmertmann, J. H. (1976), "Predicting the  $q_c/N$  Ratio - Interpreting the Dynamics of the Standard Penetration Test", University of Florida, Report to the Department of Transportation.

Seed, H. B. (1976), "Evaluation of Soil Liquefaction Effects on Level Ground during Earthquakes", State of the Art Report Preprint of ASCE Annual Convention and Exposition on Liquefaction Problems in Geotechnical Engineering, Philadelphia, 1-104.

Seed, H. B., Idriss, I. M. and Arango, I. (1983), "Evaluation of Liquefaction Potential using Field Performance Data", Journal of Geotechnical Engineering Vol. 109, No 3, 458-482.

Seed, H. B., Tokimatsu, K., Harder, L. F. and Chung, R. M. (1985), "Influence of SPT Procedures in Soil Liquefaction Resistance Evaluations", Journal of Geotechnical Engineering, Vol. 111, No 12, 1425-1445.

Tatsuoka, F., Iwasaki, T., Tokida, K., Yasuda, S., Hirose, M., Imai, T. and Konono, M. (1978), "A Method for Estimating Undrained Cyclic Strength of Sandy Soils using Standard Penetration Resistances", Soils and Foundations, Japan Society of Soil Mechanics and Foundation Engineering 18, no. 3, 43-58.

Zhou, S. G. (1981), "Influence of Fines on Evaluating Liquefaction of Sand by CPT", International Conference on Recent Advances in Geotechnical Earthquakes Engineering and Soil Dynamics, Vol. 1, 167-172.

## A Study of Dynamic Pile-Soil Interaction

**P. Srinivasulu**

Assistant Director, Structural Research Center, Madras, India

**N. Lakshmanan**

Scientist, Structural Research Center, Madras, India

**K. Muthumani**

Scientist, Structural Research Center, Madras, India

**B. Sivarama Sarma**

Scientist, Structural Research Center, Madras, India

**SYNOPSIS:** The paper discusses briefly the state of art on the subject of pile dynamics including consideration of soil-pile interaction. An analytical model which gives the response of a single pile buried in a layered soil medium considering variation in soil properties in the radial direction in each layer is illustrated. The paper also presents an experimental study on a full size test pile 40 cm dia and 7 m long driven into a five layered soil stratum. The results of the analytical and experimental studies are compared and suggestions for further work are given.

### INTRODUCTION

Pile foundations are being used to support machinery and structures which experience dynamic forces. Examples are machinery foundations, off-shore installations, nuclear power plant structures, chimneys, etc. The dynamic forces involved may be of steady state type, as in the case of rotating machinery or of a random nature, as in the case of wind, seismic or wave actions. The subject of pile dynamics has been engaging the attention of researchers for more than a decade now. Yet, the modelling of piles for dynamic analysis incorporating the composite action of the pile and the surrounding soil in a realistic manner is far from satisfactory. Analytical solutions suggested in literature are not often corroborated by experimental results to justify the theoretical assumptions, some of which are too idealistic in nature. Keeping this in view, the authors undertook a study of the dynamic behaviour of a full sized test pile, 40 cm dia and 7 m long, driven through a five layered soil stratum at the CSIR Campus site at Madras, India (Srinivasulu et.al., 1986). The object of this paper is to present salient details of this study and discuss the results obtained therefrom.

### REVIEW OF THE STATE OF ART

A review of the current practices for the design of pile foundations experiencing dynamic loads suggests that while some of the methods (Barkan, 1962, Richart et.al., 1970) ignore pile-soil interaction altogether, some others deal with it in an empirical way. Among the latter, the method suggested by Singh et.al. (1977) is worth mentioning. This method suggests equivalent effective length of the pile for vertical vibrations and an equivalent bending length for horizontal vibrations under different site conditions. However, the method fails to represent a layered soil medium often encountered in practice.

Among the continuum-methods, Novak's plane strain model using complex soil reactions acting on discrete pile elements is popular (Novak, et.al., 1974, 1978). Plane strain approximation has been assumed in deriving modes of vibration. The original version of "PILAY" (SACDA, 1977) developed on this basis did not take

into account the contact effects due to imperfect bond, slippage etc., near the periphery of the pile. Some improvements were effected by Novak himself in a subsequent model (Novak & Sheta, 1980) which considers an inner massless ring of visco-elastic medium having lower shear modulus and higher damping than the far field soil medium. The size of the inner ring has, however, not been suggested. Lakshmanan and Minai (1981) suggested what they called a non-homogeneous soil model to represent the reduced shear modulus in the soil region close to the pile boundary. This method will be further discussed in the next section.

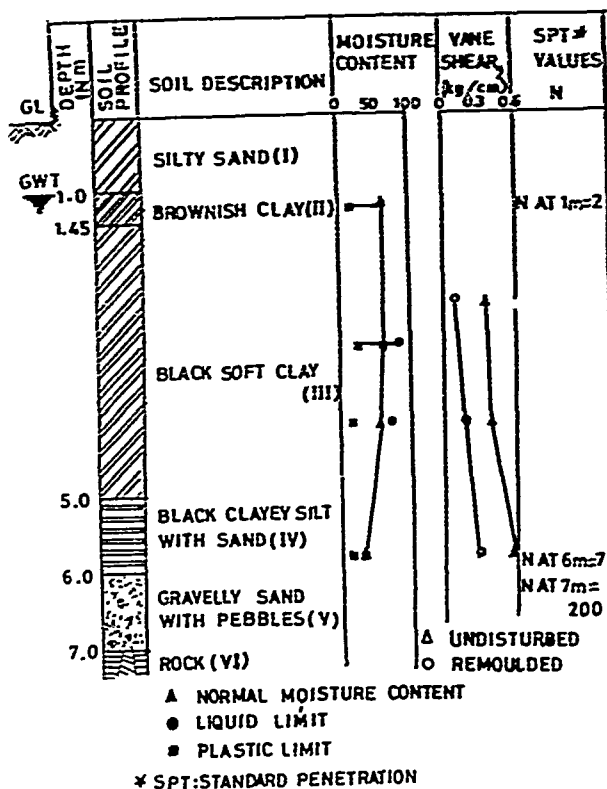
Among the classical finite element models, those involving axisymmetric elements to represent the pile and viscous energy absorbing boundaries to model the infinite boundaries in the soil medium (Kuhlemeyer, 1979) may be mentioned. These methods however, involve high computational costs and are not usually preferred, except for very special applications.

Among the experimental studies reported, those of Novak and Grigg (1976), Hall (1984) et.al., may be mentioned. Reported observations from experimental studies on full sized piles under actual field conditions are, however, still meagre. This paper aims to fulfil this need.

### AUTHOR'S STUDY

#### Analytical Work

For the rigorous analysis of a single pile buried in a layered soil stratum, the non-homogeneous model (Lakshmanan et.al., 1981) which assumes a linear variation of the shear modulus in a certain region of soil surrounding the pile will be considered. The analytical work done to define the non-homogeneous model in all respects will be illustrated with particular reference to a case study example of a full size test pile shown in Fig.1. The pile has a circular cross-section with a diameter of 40 cm and a total height of 7.0 m. The surrounding soil has five distinct layers, the properties of which are separately evaluated. This data is given in Table 1.



Soil-Profile at Test Site

TABLE-1 SOIL PROPERTIES

| Layer No. | Thick-ness (m) | Shear wave velocity ( $v_s$ ) m/sec | Density ( $\gamma$ ) $t/m^3$ | Young's modulus ( $E_s$ ) $t/m^2$ |
|-----------|----------------|-------------------------------------|------------------------------|-----------------------------------|
| I         | 1.00           | 175                                 | 1.68                         | 14400                             |
| II        | 0.45           | 150                                 | 1.68                         | 14400                             |
| III       | 3.55           | 85                                  | 1.68                         | 3400                              |
| IV        | 1.00           | 150                                 | 1.94                         | 22000                             |
| V         | 1.00           | 200                                 | 1.94                         | 22000                             |

Fig.2 shows the two analytical models involved in the dynamic analysis based on the continuum approach:- (a) a plane strain model assuming a homogeneous variation of shear modulus in the radial direction, and (b) the non-homogeneous model earlier referred to. In the latter, the shear modulus of soil is assumed to vary linearly from a value of  $C.G_0$  (where  $C < 1$ ) at the pile-soil interface to a value  $G_0$  at a distance of  $d/2C$  where  $d$  is the diameter of the pile and  $G_0$  is maximum shear modulus in the far field. The reduced shear modulus of soil is attributed to the high shear stresses in this region, the lowest value occurring at the pile-soil boundary. This model, therefore, divides the soil stratum in the radial direction into an inner ring having variable shear modulus of the above description and the outer medium which extends to infinity and possesses uniform visco-elastic soil properties.

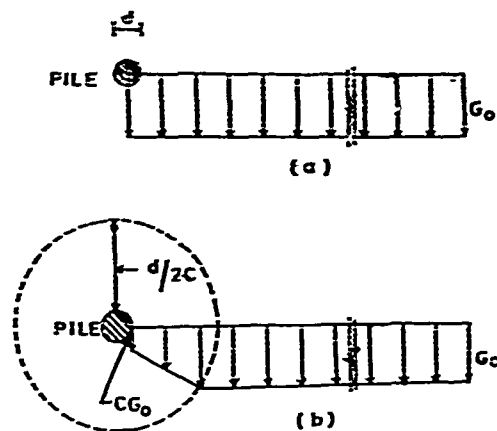


Fig.2 (a) Homogeneous Model  
(b) Non-Homogeneous Model

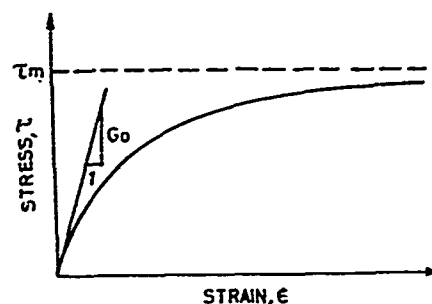


Fig.3 Typical Stress-Strain Variation in Soils

#### Response Under Static Vertical Loads

The general variation of shear stress with strain in soils is shown in Fig.3. According to the Ramberg-Osgood model, the shear modulus at any given shear stress  $\tau$  is given by:

$$G_{\tau} = G_0 \left[ \frac{1}{1 + 3 \left( \frac{\tau}{c_1 \tau_m} \right)^2} \right] \quad (1)$$

where  $C_1$  is a constant equal to 0.8 for sands and 0.4 for clays.  $G_0$  is the initial tangent modulus which represents the highest value of  $G$  uniformly present in the far field of the non-homogeneous model of the pile-soil system.

"G" can be expressed in the form "CG" where

$$C = \left[ \frac{1}{1 + 3 \left( \frac{\tau}{c_1 \tau_m} \right)^2} \right] \quad (2)$$

It is possible to obtain  $C$  for each soil layer from the above equation, once the induced shear stresses ( $\tau$ ) in each layer under a given axial load on the pile are evaluated. To evaluate " $C$ " by computation, the pile is discretised into finite elements, such that the boundaries between two adjacent soil layers coincide with the node points on the pile. To obtain the stiffness matrix of a pile element axially loaded at top and embedded in a homogeneous soil stratum, it is proposed to utilise the data provided by Poulos (1974) for an end bearing pile in the form of curves (Fig. 4 & 5) to yield the deflections at top and reactions at the tip of the pile respectively. If  $P$  is the load at the top of the element, then the deflection  $\delta_t$  at top is given by:

$$\delta_t = I \left( \frac{PL}{E_p A_p} \right) \quad (3)$$

where  $I$  is a reduction factor less than Unity.  $A_p$  and  $E_p$  are respectively the area of cross section and modulus of elasticity of the pile. Likewise, the tip reaction can be expressed in the form  $n.P$  where  $n$  is less than 1.0. The stiffness matrix of a pile element corresponding to the vertical deformations at its top and bottom can be written as:

$$[k] = \frac{E_p A_p}{IL} \begin{bmatrix} 1.0 & -n \\ -n & 1.0 \end{bmatrix} \quad (4)$$

The variation of  $I$  for the case of  $l/d$  equal to 10.0 is chosen as the representative curve. A second order equation is fitted to the above curve as given below:

$$I = 0.0613x^2 + 0.5413x - 0.118 \quad (5)$$

where  $x = \log K$  and  $K = E_p/E_s$ .

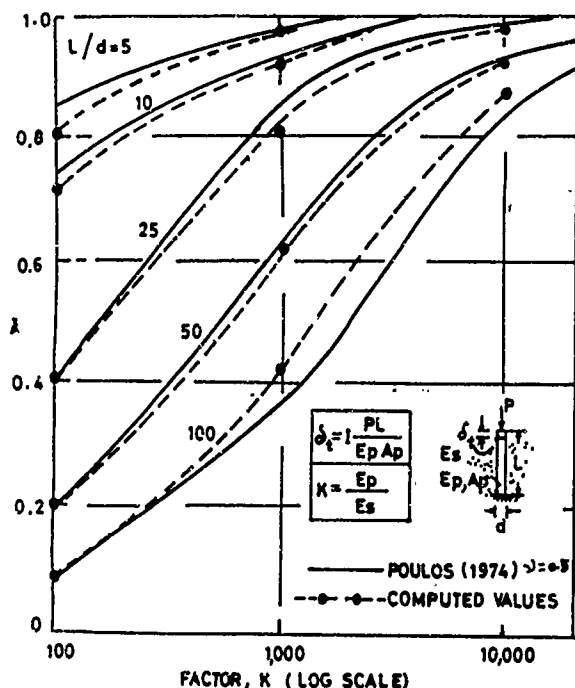


Fig. 4 Top Deformations for a Bearing Pile

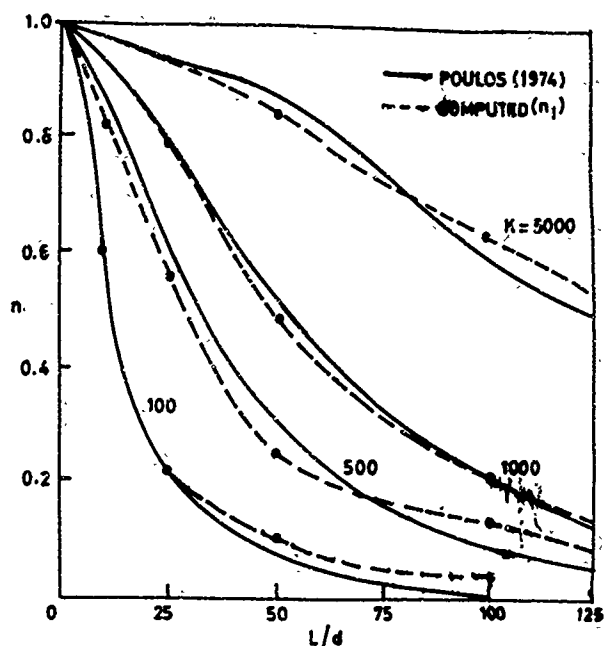


Fig.5 Tip Reactions for a Bearing Pile

Assuming linear variation of the load acting along the pile element as shown in Fig.6, the deflection  $\delta_t$  can be written as:

$$\delta_t = \left( \frac{P + nP}{2} \right) \frac{L}{E_p A_p} \quad (6)$$

From equations (3 & 6), the following relation is obtained:

$$n = (2I - 1.0) \quad (7)$$

A pile element having a longer length of embedment in a uniform soil medium greater than  $10d$  can be discretised into smaller segments each having a length of  $10d$  and a last embedment of length  $(l_1)$  less than  $10d$  (Fig.7). Equations (5) & (7) together may be used to define the load variation on the pile element as shown in this figure. The ordinate of

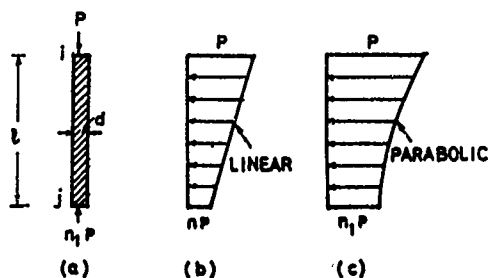


Fig.6 Load Variation on a Typical Pile Element in Uniform Soil

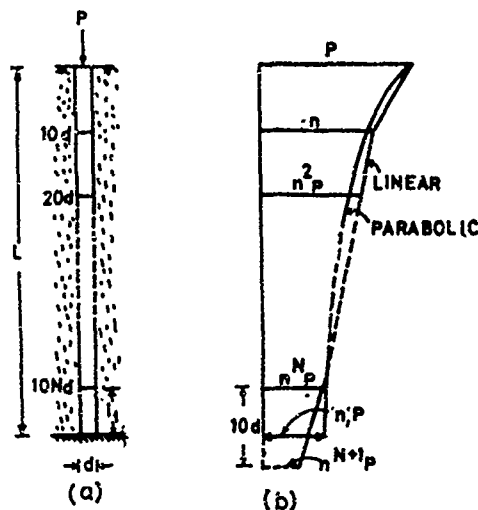


Fig. 7 Load Variation on a Long Pile Element in Uniform Soil

the load distribution diagram at the bottom of the pile element can be evaluated assuming a linear variation of the load in the last fictitious segment of length  $10d$  of which, the last component of length  $10d$  is a part. The deflection at the top of the pile element can now be computed using the load distribution diagram thus obtained and the given geometry of the pile. Fig.4 shows that the computed values of  $I$  agree reasonably well with the Poulos curves. It was however seen that the computed values of tip reaction (coefficient  $n$ ) did not agree well with the Poulos' curves given in Fig.5 for various values of  $1/d$  and  $K$ . In order to get a closer agreement with the curves shown in Fig.5, a parabolic load variation is tried along the pile element (Fig.6c) in such a way that the resulting deflection at the top of the pile remain unchanged. This gave the modified relation for tip reaction coefficient  $n_1$  in the form

$$n_1 = 3/2(1 - 1/3) \quad (8)$$

With the known value of  $I$  earlier evaluated,  $n_1$  now represents the modified tip reaction coefficient. The minimum value of  $n_1$  is taken as 0.51. Fig.5 shows good agreement between the values computed on this basis and the Poulos' curves for all the values of  $1/d$  and  $K$ . Replacing  $n$  by  $n_1$  in eq.(4), the stiffness matrices of successive pile elements can be formulated. The assembled stiffness matrix of the pile as a whole in a layered soil stratum is then obtained using the normal assembling procedures. Knowing the applied load at the top of the pile, it is now possible to evaluate the deformations at all the node points as well as stress resultants in the pile elements. If  $P_t$  and  $P_b$  are the force resultants acting at top and bottom of a pile element, the shear stress in the soil layer surrounding that element is given by  $(P_t - P_b)/\pi d \cdot l$ . The value of  $C$  which represents the reduction factor in shear modulus for any particular load on the pile is then deduced using eq.(2). When the computed shear stress in any soil layer exceeds the specified ultimate shear stress for that layer, the value of  $n_1$  in the stiffness matrix (eq.4) of the particular element which is in contact with that layer of soil shall be replaced by unity.

In the theoretical formulation above explained, it is possible to include consideration of the elasticity of the bedrock at the pile tip which can be expressed in the form

$$k_b = \left[ \pi \lambda E_b / 2(1 - \nu_b^2) \right] \quad (9)$$

where  $d$  is the diameter of pile;  $E_b$  and  $\nu_b$  are modulus of elasticity and Poisson's ratio respectively of the bedrock below the pile tip.

The above analytical procedure has been programmed in Fortran IV on Prime 750 computer and is available in the name of "PILSTAT" at the Structural Engineering Research Centre, Madras (India).

#### Application to a Dynamic Environment

The discussion in the preceding section is applicable only to statically applied vertical loads on the pile. It is, however, believed that the results of the analysis used for deducing values of shear moduli under static loads can also be used in dynamic computations. This is better justified for applications in machine foundations, where the dynamic strains are relatively smaller than the static values.

#### Dynamic Soil Reactions

The complex soil reactions acting on unit length of the pile and for unit deformation under various modes of vibration, using the non-homogeneous soil model earlier defined can now be evaluated (Lakshmanan, et.al., 1981). These can be expressed as follows:

$$\text{Vertical : } K_v = C_0 (S w_1 + i S w_2) \quad (10)$$

$$\text{Horizontal : } K_h = G_0 (S h_1 + i S h_2) \quad (11)$$

The real part of the above equations represents the soil stiffness while the imaginary part denotes the damping offered by the soil. Figs.8 & 9 show the variation of the non-dimensional stiffness parameters  $S w_1$ ,  $S w_2$  and  $S h_1$ ,  $S h_2$  respectively for the vertical and horizontal vibrations of the pile-soil system shown in Fig.1. The above stiffness and damping parameters of soil are also functions of the reduced shear modulus coefficients ( $C$ ) of each soil layer, its material damping value (DR), and the excitation frequency ( $f$ ). A value of  $DR = 0.1$  is assumed uniformly in this example. Figs.8 & 9 also show the variation of the stiffness and damping coefficients of soil for the case of homogeneous soil model assumed in the PILAY program. Considerable deviations are seen in the two sets of values which show the importance of the non-homogeneous soil model in dynamic computations.

#### Stiffness and Damping of the Pile-Soil System

The modified values of  $S w_1$ ,  $S w_2$  etc., are now used in place of the corresponding values derived from the PILAY program (SACDA, 1981) which is applicable for the plane strain case in a homogeneous soil medium. The PILAY program then yields the net stiffness and damping values of the pile-soil system for the non-homogeneous soil model earlier referred to.

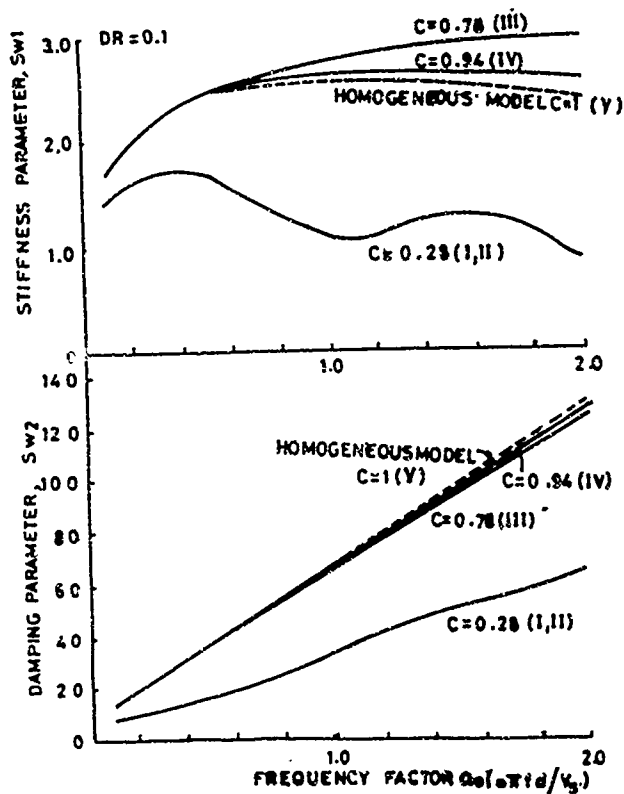


Fig. 9 Variation of  $Sw_1$  &  $Sw_2$  with  $a_0$   
(Non-Homogeneous Model)

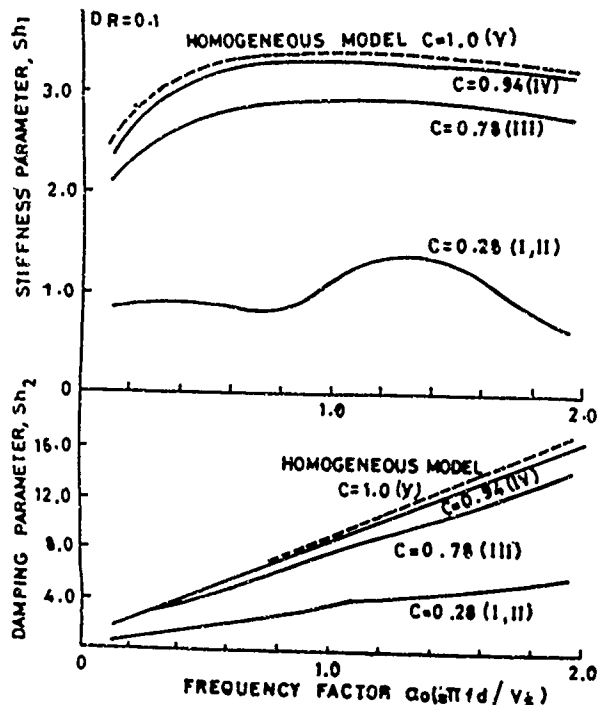


Fig. 9 Variation of  $Sh_1$  &  $Sh_2$  with  $a_0$   
(Non-Homogeneous Model)

## EXPERIMENTAL STUDY

### Static Tests

Fig.10 shows the static test set up used for loading the pile in the range of 0 to 100 tonnes. The load is incremented in stages and the average elastic deflection recorded by the dial gauges is noted after successive loading and unloading cycles. Fig.11 shows the variation of elastic deflection with the applied load as computed and as measured from the experiments. The agreement between the two sets of values is seen to be quite good, thus verifying the validity of the analytical model earlier explained.



Fig. 10 Close View of the Static Test Set-up

### Dynamic Tests

The purpose of this test programme was to verify under dynamic conditions, the validity of the radial non-homogeneous model earlier explained, using the values of  $C$  obtained from the static analysis. Vertical and horizontal dynamic tests have been conducted separately on the test pile by attaching at its top a mechanical oscillator coupled with a DC motor which induces steady state oscillations in the pile. Figs.12 & 13 show the test set up showing the pile under vertical and horizontal vibrations respectively.

The method of mounting the mechanical oscillator differs with the mode of vibration to be generated viz., vertical or horizontal. Provision exists in this oscillator to vary the eccentricity of unbalanced masses. The superimposed load on the test pile and exciting force level have been varied in the test programme.  $\omega$  is the mass ratio defined as the applied load normalised by the weight of the pile and  $R$  is



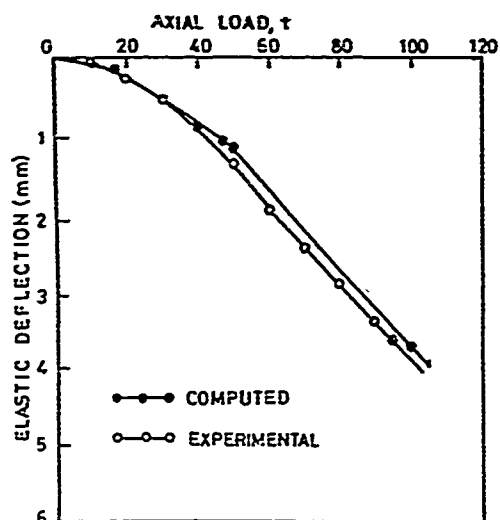


Fig. 11 Elastic Deflection Vs. Axial Load on the Test Pile

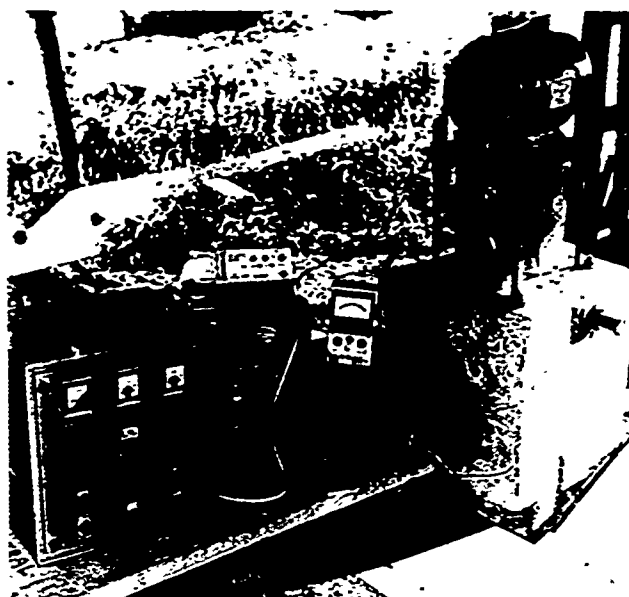


Fig. 13 Set-up for Horizontal Dynamic Test



Fig. 12 Set-up for Vertical Dynamic Test

a parameter which defines the dynamic force ( $F_d$ ) given by the relation  $F_d = Rf^2$ ,  $f$  being the frequency of excitation. Fig.14 & 15 show typical response plots obtained from the dynamic tests corresponding to one value of  $\alpha = 4.53$  and for varying values of  $R$ . The resonant frequencies are identified by the peaks of the response curves. Tables 2 & 3 show comparison of natural frequencies deduced from the theoretical models and experimental data. It is seen from Table 2 that there is no significant difference in the analytically deduced vertical frequencies using  $C = 1$  (homogeneous mode I) and using variable values of  $C$  (non-homogeneous model) obtained from the static analysis. This may be attributed to the marginal contribution of the soil layers having low values of  $C$ . However, in Table 3 which shows the horizontal frequencies, the experimental values agree more closely with the non-homogeneous model than the homogeneous model assumed in the PILAY program.

Fig. 14 Typical Pile Response (Vertical Dynamic Test)

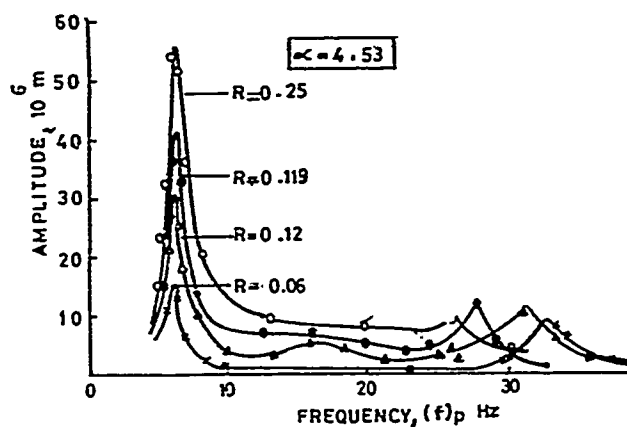


Fig. 15 Typical Pile Response (Horizontal Dynamic Test)

TABLE-2 COMPARISON OF FREQUENCIES UNDER VERTICAL EXCITATION

| Mass Ratio<br>$\alpha$ | Resonant Frequencies from tests (Hz) | Computed Frequencies (Hz) using |                       |
|------------------------|--------------------------------------|---------------------------------|-----------------------|
|                        |                                      | Homogeneous model (C=1)         | Non-homogeneous model |
| 0.35                   | 111.3                                | 97.24                           | 90.45                 |
| 0.67                   | 79.2                                 | 76.80                           | 74.48                 |
| 0.99                   | 49.0                                 | 67.87                           | 64.09                 |
| 1.30                   | 43.3                                 | 59.20                           | 57.88                 |
| 2.56                   | 43.0                                 | 43.60                           | 43.05                 |
| 4.53                   | 32.0                                 | 33.11                           | 32.64                 |
| 6.89                   | 27.0                                 | 26.84                           | 26.78                 |

TABLE-3 COMPARISON OF FREQUENCIES UNDER HORIZONTAL EXCITATION

| Mass Ratio<br>$\alpha$ | Resonant frequencies from tests (Hz) | Computed Frequencies (Hz) using |                       |
|------------------------|--------------------------------------|---------------------------------|-----------------------|
|                        |                                      | Homogeneous model (C=1)         | Non-homogeneous model |
| 0.35                   | 22                                   | 27.33                           | 25.87                 |
| 0.67                   | 15                                   | 19.73                           | 19.15                 |
| 0.99                   | 13                                   | 16.22                           | 15.89                 |
| 1.30                   | 11                                   | 14.15                           | 13.95                 |
| 2.56                   | 9                                    | 10.08                           | 9.63                  |
| 4.53                   | 6.25                                 | 7.58                            | 6.50                  |
| 6.89                   | 4.1                                  | 6.14                            | 4.40                  |

TABLE 4 COMPARISON OF DAMPING VALUES UNDER VERTICAL VIBRATIONS

| Mass Ratio<br>$\alpha$ | Damping constant from tests | Computed damping value (t.sec/m) using |                       |
|------------------------|-----------------------------|--|-----------------------|
|                        |                             | Homogeneous model C=1                  | Non-homogeneous model |
| 0.35                   | 3.1                         | 5.2                                    | 4.8                   |
| 0.67                   | 3.1                         | 5.2                                    | 4.9                   |
| 0.99                   | 4.1                         | 5.2                                    | 5.0                   |
| 1.30                   | 2.4                         | 5.2                                    | 5.0                   |
| 2.56                   | 6.2                         | 5.2                                    | 4.6                   |
| 4.53                   | 4.9                         | 5.2                                    | 3.5                   |
| 6.89                   | 3.8                         | 5.2                                    | 3.3                   |

It may be seen that the agreement between the theoretical and experimental values is closer for higher values of  $\alpha$ . Table 4 shows the damping values deduced from the theory of vertical vibrations using the two models aforementioned and the vertical vibration tests. The values given for the non-homogeneous model are seen to agree more closely with the experimental values.

#### CONCLUSIONS

The validity of the analytical model which considers the radial non-homogeneity of the soil, assuming a linearly varying shear modulus in a defined region of soil surrounding the pile has been verified. The reduction factor "C" for shear modulus at the pile-soil interface can be analytically deduced for each of the soil layers surrounding the pile, while it is carrying a certain axial load on its top. This procedure is illustrated in the paper on a full sized test pile. The values of C deduced from the static analysis can be used with confidence in dynamic computation as well. This is verified from the results of analysis and dynamic tests presented in the paper.

The agreement between the results of the analytical study using the non-homogeneous model and the experimental results is seen to be better at higher values of mass ratio. This shows the significance of the load carried by the pile in determining the influence of dynamic pile-soil interaction.

The results presented in the paper from an analytical model and the experimental study on a full sized test pile in the open field may serve as a useful reference data for the use of researchers engaged in this field. Further studies are however needed to study the effect of pile grouping and the interaction of the pile cap with the soil underneath it.

#### ACKNOWLEDGEMENT

This paper is published with the permission of the Director, Structural Engineering Research Centre, Madras (India).

## REFERENCES

- Barkan, D.D. (1962), Dynamics on Bases of Foundations", McGraw Hill Book Co., Inc., New York.
- John F. Hall (1984), "Forced Vibration and Earthquake Behaviour of an Actual Pile Foundation", International Journal of Structural Dynamics and Earthquake Engineering, Volume 3, No.2.
- Kuhlemeyer, R.L. (1979), "Vertical Vibration of Piles", J. Geotechnical Engineering Division, ASCE, 105.
- Kuhlemeyer, R.L. (1979), "Static and Dynamic Laterally Loaded Floating Piles", J. Geotechnical Engineering Division, ASCE, 105.
- Lakshmanan, N. and Minai, R. (1981), "Dynamic Soil Reactions in Radially Non-Homogeneous Soil Media", Bulletin of the Disaster Prevention Research Institute, Kyoto University, Volume 31.
- Novak, M. (1974), "Dynamic Stiffness and Damping of Piles", Canadian Geotechnical Journal, Vol.11, No.4.
- Novak, M. and Grigg, R.F. (1976), "Dynamic Experiments with Small Pile Foundations", Canadian Geotechnical Journal, Volume 13, No.4.
- Novak, M., Nogami, T., and Aboul Ella, F. (1978), "Dynamic Soil Reactions for Plane Strain Case", Journal of Engineering Mechanics Division, ASCE, Volume 104, No.EM4.
- Novak, M. and Aboul Ella, F. (1978), "Impedance Functions of Piles in Layered Media", Journal of the Engineering Mechanics Division, ASCE, Volume 104, No.EM6.
- Novak, M. and Sheta, M. (1980), "Approximate Approach to Contact Effects of Piles", Reprinted from "Dynamic Response of Pile Foundations" - Analytical Aspects, ASCE.
- Poulos, H.G., et.al. (1974), Elastic Solutions for Soil and Rock Mechanics", John Wiley & Sons Corporation, New York.
- Richart, F.E. Jr., Hall, J.R. Jr., and Woods, R.D. (1970), Vibration of Soils and Foundations", Prentice-Hall, Englewood Cliffs, New Jersey, U.S.A.
- SACDA (1977): "PILAY - A Computer Program for Calculation of Stiffness and Damping of Piles in Layered Media", University of Western Ontario, London (Canada).
- Singh, J.P., Donovan, N.C., and Jobnis, A.C. (1977), "Design Procedure for Dynamically Loaded Pile Supported Foundations", Journal of Geotechnical Engineering Division, ASCE, Volume 103, No.GT8.
- Srinivasulu, P., Lakshmanan, N., Muthumani, K., Sivarama Sarma, B., and Thandavamoorthy, T.S. (1986), "Study of the Effects of Pile-Soil Interaction under Dynamic Loads", Project Report, Structural Engineering Research Centre, Madras, India.

# Model Tests on Seismic Stability of an Approach Fill Embankment, Annacis Island Bridge Project, Vancouver, Canada

Peter M. Byrne

Department of Civil Engineering, University of British Columbia,  
Vancouver, British Columbia, Canada

Hans Vaziri

Golder Associates, Seattle, Washington, USA

Upul Atukorala

Golder Associates, Vancouver, British Columbia, Canada

Donald Fraser

Ministry of Highways, Province of British Columbia, Canada

**SYNOPSIS:** This paper describes a study performed to evaluate the seismic behaviour of a 10 m high bridge end sand fill placed upon soft organic foundation soils and supported on piles. Under static conditions the fill load is essentially carried by the piles by "arching action", and little deformation was observed to occur in the field. The results of both model tests and finite element analysis are in agreement with this finding. Concern arose as to the likely response of this structure under earthquake loading and a model sand embankment supported on 400 model piles was built and tested on the shake table. The model and testing procedures are described in some detail in the paper.

The results of the shaking table study indicate that during shaking the load is transferred from the piles onto the foundation resulting in large deformations of the fill. Analysis of the model tests based on this assumption gave deformations that were in good agreement with observed settlements. A similar analysis of the prototype indicates that seismic loading sufficient to cause such transfer would result in a settlement of the fill of about 0.4m, and that deformation would cease once the shaking stopped.

## INTRODUCTION

The purpose of the shaking table test series was to evaluate the seismic behaviour of proposed bridge end fills placed upon a soft foundation soil and supported by piles. The fills comprise of compacted sand 10 m high overlying about 15 m of soft organic soil. Because such soil could not support the weight of fill, piles which are driven through the soft soil and which project into the fill are used to transfer the load to a bearing layer beneath the organic soil. Experience indicates that under static conditions the fill load is carried by the piles by an arching mechanism within the sand so that little or no deformation occurs. However, under earthquake loading the concern is that such arching would break down causing the fill load to be transferred from the piles to the soft foundation soil resulting in large deformations. The prime purpose of the shaking table test was to investigate this concern.

The shaking table test was performed on a 1 to 65 scale model. The soft organic soil was modelled by a gelatin based solution while the embankment was modelled by a compact sand. The piles were modelled by lengths of 6.4 mm diameter aluminum tubing. The model was built within a perspex box which was bolted to the shaking table and subjected to a series of uniform cycles of acceleration simulating seismic excitation. The model was instrumented and videotaped allowing its response to be observed. This paper describes the model test, the test results and their implication for analysis and design of the prototype fills.

## DESCRIPTION OF TEST APPARATUS AND MODEL

The test was performed on a 1.2 m by a 2.7 m shaking table of welded aluminum and weighing

4.5 kN. It was supported by two v-slotted needle bearings and two flat bearings capable of moving in a horizontal direction. An MTS Earthquake Simulator console provided a controlled acceleration motion to the table. A reference accelerometer was located on the table.

The model was constructed in a plexiglass container bolted securely to the shaking table. The dimensions of the box were 1.84 m x 0.91 m x 0.6 m as indicated on Figures 1a and 1b. The soft organic foundation soil was modelled by a gelatin solution. The gelatin had a shear strength of 2.2 kPa. Such a shear strength was considered appropriate since it provided a

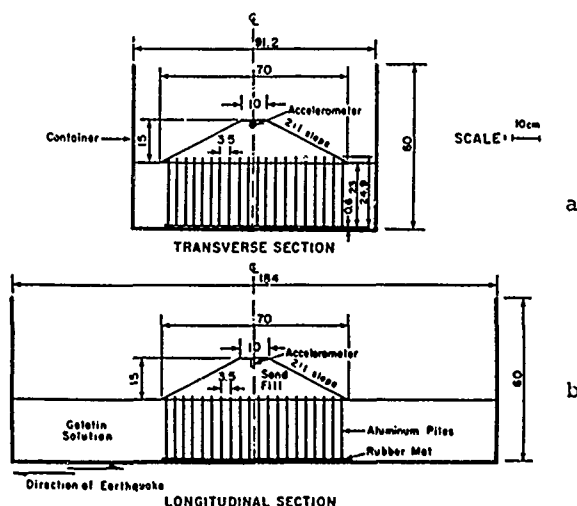


FIG. 1: Details of Model Set-Up.

reasonable factor of safety against a bearing capacity failure upon placement of the sand fill. The Young's modulus of the gelatin solution was approximately 10 kPa. Details of the type of gelatin and its preparation are outlined in Appendix A.

The test embankment was modelled by a uniformly graded fine to medium grained sand. The sand had a specific gravity of 2.7 and maximum and minimum void ratios of 0.9 and 0.5 respectively. When in place, the sand was estimated to have an average density of 16.2 kN/m<sup>3</sup>, a void ratio of 0.60 and a relative density of 75%.

A schematic representation of the fill cross-section and the location of the accelerometer are also shown on Figure 1. For the given size of the box, it was decided that a scaling factor of 1/65 would be the most appropriate since it places the fill at a reasonable distance from the end boundaries without reducing the model to an impractically small size.

The piled foundation proposed for the embankment was simulated by 400 piles held at the base by a fairly rigid rubber mat 0.6 cm thick. The piles were set out at 3.5 cm spacing over a mesh 70 cm x 70 cm. The piles comprised of 6.4 mm diameter, hollow aluminum tubes having a wall thickness of 0.9 mm, a bulk density of 16 kN/m<sup>3</sup> and a length of 25 cm.

#### Sequence of Construction

The rubber mat was positioned in the centre of the box and glued firmly to the base. The piles were placed into prebored holes in the mat which resulted in their being effectively held in a pin ended manner at the base. They were kept vertical during placement of the gel by means of a top plywood template through which locating nails were placed. This template was later removed when the gel had set. The gel was poured to 23.0 cm above the level of the rubber mat resulting in approximately 1.5 cm of the pile heads extending above the gel surface. The gelatin solution was then left for 5 days to allow it to fully set and attain its peak strength.

After this waiting period, the sand embankment was constructed on top of the gel by placing sand inside a pyramid shape former. The form was placed centrally over the piled area and sand was poured in four equal lifts, ensuring that each lift was uniformly placed with no visible gaps between the mold and the slopes. This necessitated compacting the sand as it was being pressed by hand into the corners of the forming mold. The form was then removed leaving a truncated pyramid shaped sand embankment with cross-sections as shown on Figure 1.

The surface of the sand was sprayed with a thin coat of black paint for the following reasons:

- (1) by binding the sand particles, the possibility of loose sand grains rolling down the slope was reduced;
- (2) zones of large movements could be detected from formation of cracks on the painted surface;

- (3) the thin crust provided a good surface for measuring the fill profile using a dial gauge;
- (4) the black surface produced a better photographic image of the fill.

#### Instrumentation

The principal instrumentation consisted of accelerometers mounted on the table and on the crest of the sand fill. A miniature piezo-electric accelerometer was used for the latter. The output of the accelerometers was filtered before being amplified and recorded on a oscilloscope. The filtering of high frequency noise levels was essential, particularly at low levels of excitation which would have otherwise been dominated by those higher frequencies. A cut-off frequency of 6 Hz and 20 DB noise cut out was used throughout the experiment.

The deformation of the test fill was measured by means of a dial gauge attached to the end of a graduated bar moving against a fixed vernier scale. This bar was then mounted on wheels over two parallel bars which in turn were fixed on wheels over two outer bars bolted firmly to the top of the container. Such an assembly enabled the dial gauge to be moved longitudinally and transversely over the fill. The profile was determined by lowering the dial gauge until it came into contact with the surface. Measurements were taken on a grid spacing of about 10 cm.

The surface movements were also monitored by video and movie cameras.

#### TESTING PROGRAM

The model was tested by subjecting it to a cumulative series of constant amplitude sinusoidal base acceleration motions. Each series comprised of about 15 cycles and the amplitude of acceleration was increased in each subsequent series. A total of 8 series were performed on the one model with base acceleration amplitudes of 2.5, 7.5, 10, 12.5, 15, 20 and 30 percent g.

A frequency of 3 Hz was used for all of the above test series. This frequency was selected based upon a preliminary low level amplitude shaking test. A base acceleration of 1% g was used for this low level preliminary test and the crest acceleration was monitored allowing the dynamic amplification factor, which is the ratio of the crest to base acceleration, to be computed. The results are shown in Table 1 and indicate the dynamic amplification factor increases from 1.4 at 1.0 Hz to 3 at 4.5 Hz. There were no dramatic changes in amplification with frequency and consequently a convenient testing frequency of 3 Hz was selected.

Vertical displacements at the surface of the embankment were taken over a grid spacing of approximately 10 cm, covering the entire geometry. Measurements were taken prior to shaking and after the termination of the test. Some measurements were also taken after the application of 10% g base acceleration. A complete list of the readings (Table B1) and the locations where measurements were taken (Figure B1) are presented in Appendix B.

Table 1.

Response of the sand embankment to a base acceleration of 1% g.

| Test Number | Applied Base Displacement (mm) | Frequency (Hz) | Induced Acceleration in the Fill (% g) | Amplification Factor |
|-------------|--------------------------------|----------------|--|----------------------|
| 1           | 3.61                           | 1.             | 1.4                                    | 1.4                  |
| 2           | 0.13                           | 1.6            | 1.4                                    | 1.4                  |
| 3           | 0.08                           | 2.0            | 1.5                                    | 1.5                  |
| 4           | 0.05                           | 2.6            | 1.6                                    | 1.6                  |
| 5           | 0.03                           | 3.0            | 1.7                                    | 1.7                  |
| 6           | 0.02                           | 3.4            | 1.8                                    | 1.3                  |
| 7           |                                | 4.0            | 2.0                                    | 2.0                  |
| 8           |                                | 4.5            | 3.0                                    | 3.0                  |

Table 2.

Values of the base excitation and the induced acceleration in the Fill.

| Frequency (Hz) | Number of Cycles | Applied Base Displacement cm | Applied Peak Base Acceleration | Peak Induced Acceleration in the Sand Fill | Amplification Factor = Fill Acceleration Base Acceleration |
|----------------|------------------|------------------------------|--------------------------------|--|--|
| 3              | 15               | 0.05                         | 0.02 g                         | 0.03 g                                     | 1.5  |
| 3              | 15               | 0.13                         | 0.05 g                         | 0.08 g                                     | 1.6  |
| 3              | 15               | 0.19                         | 0.075 g                        | 0.12 g                                     | 1.6  |
| 3              | 15               | 0.25                         | 0.10 g                         | 0.21 g                                     | 2.1  |
| 3              | 15               | 0.32                         | 0.125 g                        | 0.22 g                                     | 1.7  |
| 3              | 15               | 0.37                         | 0.15 g                         | 0.24 g                                     | 1.6  |
| 3              | 15               | 0.52                         | 0.20 g                         | 0.26 g                                     | 1.3  |
| 3              | 15               | 0.79                         | 0.30 g                         | 0.33 g                                     | 1.1  |

During the test series, it was observed that the movements were predominantly deep seated resulting from movements in the gel. However, some downslope movement of sand grains beneath the surface skin of paint also occurred. Movements began to manifest themselves at a base acceleration of 5% g and became significant at 10% g. At that point, the crest of the embankment had deformed approximately 2 cm, and the piles in the central region around the perimeter of the mesh had deflected outward by approximately 1 cm. The sand level at the toe of the fill increased. This could have resulted from either heave of the gel or from downslope movement of sand or a combination of the two effects. Increasing the amplitude of the base motion resulted in further movements in both vertical and lateral directions. Base excitation of 30% g led to large movements with crest deformation of over 5.5 cm and lateral spreading in the toe areas of approximately 10 cm in the direction of the applied motion. Lateral movements and spreading of the sand also occurred in the direction normal to the base motion and was approximately half the above magnitude.

From the post-failure examination of the embankment and upon its removal it was observed that significant deformations had occurred beneath the base of the fill. In addition, approximately 0.5 to 1 cm intrusion or penetration of the sand into the gel's surface had occurred. Such penetration is not likely to occur in the prototype foundation material. However, in

relation to the total amount of deformation (5.5 cm) this contributes not more than 20% of the total movement and so has only a minor effect on overall movements beneath the embankment. The deformation of the surface of the gel was not monitored during shaking. However, it appears that the major portion of the 5.5 cm of crest settlement was due to deformation of the gel rather than penetration of sand into the gel.

The sequence of movements of a section of the model prior to dynamic testing, after 10% base excitation and after 30% base excitation are depicted in Figure 2. These movements are based upon surface movement measurements, video and movie recordings, and visual observations during and after testing together with volume compatibility constraints. Details of the calculations involved are shown in Appendix C. Prior to dynamic testing, the piles at the toe of the embankment had moved outward about 1 cm due to construction of the fill. Such outward movement would induce downward movement of the sand-gel interface as shown. Crest deformation of 2 cm resulted after application of the 10% g base excitation motion. Additional outward movement of the toe piles together with movement of the gel surface occurred at the same time as shown in the Figure. The profile after 30% g is also shown in Figure 2 and indicates a crest movement in excess of 5 cm and lateral spreading of the fill of some 10 cm. The lateral movement of the pile heads at the toe of the slope was about 4.5 cm or about half the spreading movement of the

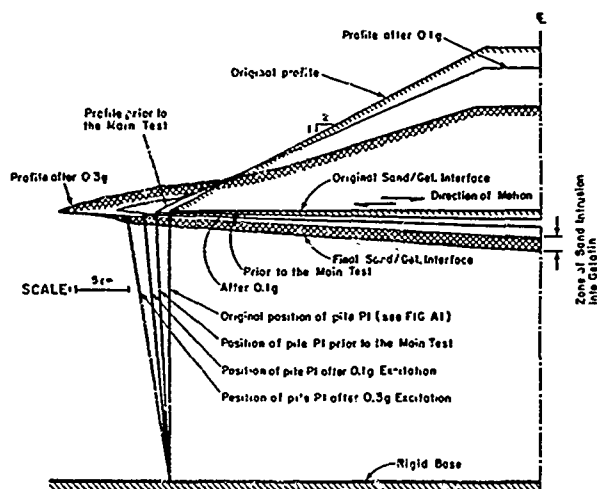


FIG. 2. Deformed Profiles at Various Stages of Shaking (Section 5-5, Fig. B1).

sand. The additional movement of the sand was caused by sand particles moving down the surface of the slope and rolling outward in the toe area.

#### APPLICATION TO PROTOTYPE FILLS

The base acceleration level of 10% g causes a crest acceleration of 21% g and corresponds approximately with the design earthquake. The model tests suggest a crest settlement of about 1.8 cm or 12% of the height of the model embankment for this level of excitation. For the prototype with an embankment height of 10 m, deformations corresponding to 12% of the height would result in a crest settlement of 1.2 m.

Prior to the shaking most of the weight of the embankment is carried by the piles as a result of an arching mechanism in the sand. The observed vertical movements recorded during the shaking table tests suggest that the arching is gradually lost with increasing levels of shaking. Thus during shaking the vertical load is gradually transferred from the piles to the soil foundation and results in large deformations.

Deformations of the foundation soils after the shaking ceases will be small because such movements will cause the load to be transferred back to the piles and thus deformations should essentially cease after the shaking ceases. The model test results are in agreement with this hypothesis.

Seismic deformations of the fill are therefore mainly due to deformations of the foundations caused by the transfer of vertical load from the piles to the foundation during the period of shaking. The maximum seismic deformations can be estimated for the prototype from a static finite element analysis in which all of the weight of the sand embankment is assumed to be transferred to the foundation soil during the shaking. Under these conditions the organic soil would behave in an undrained manner. Based on the soil profile and properties shown in Figure 3, a crest settlement of 0.4 m together with a horizontal longitudinal displacement of

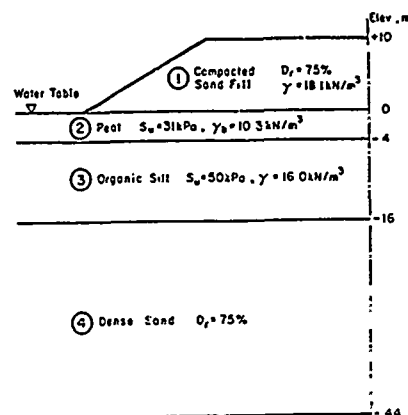


FIG. 3. Prototype Soil Profile.

0.4 m was predicted for the prototype fills. Details of the analysis are included in Appendix D.

Earthquake induced movements could be reduced by placing a reinforcing cloth horizontally above the pile tops. However, it would be prudent to assume that the same loss of arching would still occur with the vertical load being gradually transferred to the cloth and thence to the pile. In the limit, all of the weight of the soil would be carried by the cloth and the deflection of the cloth could be determined by analyzing a system comprised of a cloth blanket draped over the pile tops and subjected to a downward pressure equal to the weight of the soil above the blanket. The deflection of the cloth would lead to crest deformations and such deformations could be estimated from analysis. Results from finite element analyses of the above soil-structure interaction problem indicate that the placement of a reinforced cloth considerably reduces both vertical and horizontal deformations of the embankment (Brown (1986)). This is in accord with field observations on a prototype structure in which such a reinforcing cloth was incorporated (Brown (1986)).

Horizontal movements of the piles will induce shear forces and bending moments in the piles. These loads can be computed as outlined by Byrne et al. (1983).

#### CONCLUSIONS

The model tests indicate that horizontal base excitation comparable to the design earthquake will induce settlements of the order of 12% of the height of the embankment. Such deformations result from a transfer of vertical load from the piles to the foundation soil as a result of a loss in arching due to shaking. Finite element analyses indicate that such a transfer of load will cause a deformation of 0.4 m for the prototype fills. A reinforcing cloth placed above the pile tops would reduce such settlements.

The horizontal earthquake induced loads can be carried by the piles provided they can withstand the earthquake induced displacements. Such displacements can be computed as outlined by Byrne et al. (1983).

## ACKNOWLEDGEMENTS

Dr. R.G. Campanella's advice and comments on the model testing were most helpful. The figures were drawn by Mr. R. Brun and Mrs. K. Lamb typed the manuscript.

## REFERENCES

1. Byrne, P.M., Anderson, D.L. and Janzen, W. "Response of Piles and Casings to Horizontal Free-Field Soil Displacements", 36th Canadian Geotechnical Conference, Vancouver, June 1983.
2. Byrne, P.M. and Janzen, W. "SOILSTRESS: A Computer Program for Nonlinear Analysis of Stresses and Deformation in Soil", Soil Mechanics Series No. 52, Dept. of Civil Engineering, University of British Columbia, Vancouver, B.C., December 1981.
3. Byrne, P.M. and Eldridge, T.L. "A Three Parameter Dilatant Elastic Stress-Strain Model for Sand", International Symposium on Numerical Models in Geomechanics, Switzerland, September 1982.
4. Byrne, P.M. and Campanella, R.G. "A Report to Ministry of Transportation and Highways on Model Tests on Seismic Stability of the Approach Fill Embankments - Annacis Island Bridge Project", Department of Civil Engineering, University of British Columbia, Vancouver, B.C., May 1984.
5. Brown, P. "Queensborough Bridge Abutment: Predicting Deformations Using a Finite Element Computer Program - An Internal Report", Dept. of Civil Engineering, University of British Columbia, Vancouver, B.C., February 1986.

## APPENDIX A - PROPERTIES OF GELATIN

The gelatin used was a Bloom type 100. The Bloom unit is a measure of the force required to depress a prescribed area of the surface of a gelatin sample which is made up from a given concentration and according to a standard procedure, a set distance of 4 mm. It is simply a measure of the rigidity of the gel (1). The strength of the gel formed depends upon concentration and the intrinsic strength of the gelatin used which is a function both of structure and molecular weight. Commercially available gelatin range in Bloom between 100 to 275 and generally the higher the Bloom grade, the less gelatin will be required to produce the same strength. However, a minimum quantity of 3% gelatin is required to form a gel solution at room temperature and this largely dictates the choice of gel type if we are interested in developing solutions with low shear strength values. The gelatin solution used was made up of 6% gelatin crystals by weight. The solution was prepared at approximately 65°C which is the water temperature at which the gelatin crystals are dissolved quite readily and also result in the most stable composition. The graph showing

the change of strength with time for a gel prepared in this manner is shown on Figure A1. It can be observed that the peak strength is achieved after approximately 4 days, beyond which degradation occurs by bacteria and molds. The nature of the organisms which grow in gelatin solutions depend upon a number of factors. However, it was found that the rate of growth is significantly smaller for samples prepared at 65°C in comparison with other techniques of dissolving the gelatin crystals. Extreme care was exercised to ensure that the crystals were thoroughly dissolved before removing the foam and pouring the solution into the container. The solutions were prepared in 30 litre batches and the total amount (approximately 400 litres) was poured in place within 2.0 hours. Using a miniature vane device, the shear strength of the gel at the time of the experiment was measured to be 2.2 kPa. Such a shear strength was considered to be appropriate since it provided a reasonable factor of safety against a bearing capacity failure upon the placement of the sand fill as well as leaving some margin of safety for possible weakening of the gel peak strength prior to the experiment. The Young's modulus of the material was approximately 10 kPa and was determined by measuring the depression due to a uniform load applied to the gel's surface.

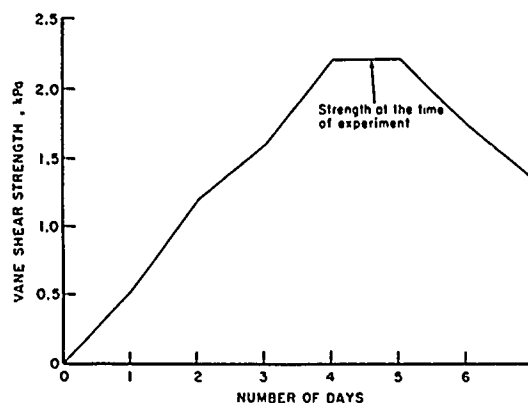


FIG. A1. Change of Shear Strength with Time for 6% Gelatin Solution Prepared at 65°C.

- 
- (1) Gelatin Manufacturers Institute of America, Inc., Standard Methods for Sampling and Testing of Gelatins, New York, 1964.

## APPENDIX B - RECORDED MOVEMENTS

The recorded vertical displacements after 0.1 g and 0.3 g base excitations are shown in Table B1. The recorded horizontal displacement are shown in Table B2. The locations of the recording points are shown in Figure B1.



Table B1. Deformation of the Points Shown on Fig. B1.

| Section | Cumulative Vertical Displacements<br>(Settlement + ve)/cm |             |
|---------|---|-------------|
|         | After 0.1 g   | After 0.3 g |
| B1      | -0.30   | -0.76       |
| B2      | 0.40  | 1.71        |
| B3      | 0.61  | 2.13        |
| B5      | 0.37  | 1.80        |
| B7      | 0.55  | 1.80        |
| B9      | 0.88  | 2.26        |
| C1      | -0.64   | -1.25       |
| C2      | 0.18  | 1.28        |
| C3      | 1.31  | 3.60        |
| C5      | 1.28  | 3.81        |
| C7      | 1.46  | 3.90        |
| C9      | 0.37  | 1.07        |
| D1      |   | -1.22       |
| D2      |   | 0.98        |
| D3      |   | x           |
| D4      |   | 5.73        |
| D5      |   | 5.57        |
| D6      |   | 5.36        |
| D7      |   | 3.57        |
| D8      |   | 2.23        |
| D9      |   | 0.88        |
| E1      |   | -0.76       |
| E2      |   | 0.91        |
| E3      |   | 3.17        |
| E4      |   | 5.64        |
| E6      |   | 5.55        |
| E7      |   | 3.57        |
| E9      |   | 1.07        |
| F1      | -0.37   | -0.88       |
| F2      | 0.0   | 0.91        |
| F3      | x   | x           |
| F4      | 2.01  | 5.52        |
| F5      | x   | 5.61        |
| F6      | 1.89  | 5.70        |
| F7      | 1.74  | 3.47        |
| F8      | x   | 2.44        |
| F9      | x   | 1.158       |
| G1      |   | 0.12        |
| G2      |   | 1.25        |
| G3      |   | 3.60        |
| G5      |   | 3.05        |
| G7      |   | 2.99        |
| G9      |   | 1.46        |
| H1      | -0.20   | 0.30        |
| H2      | 0.70  | 3.11        |
| H3      | 0.12  | 1.16        |
| H5      | 0.30  | 2.04        |
| H7      | x   | 2.38        |
| H9      | 0.12  | 1.92        |

Table B2. Movement of the piles shown on Figure A1.

| Cumulative Lateral Movement<br>of the Piles from the<br>Original Position |  |                     |                     | Lateral Move-<br>ment During<br>Each Phase |                           |
|---|--|---------------------|---------------------|--|---------------------------|
| Pile  | After<br>Embankment<br>Construct<br>cm | After<br>0.1g<br>cm | After<br>0.3g<br>cm | Up To<br>0.1g<br>cm                        | Between<br>0.1-0.3g<br>cm |
| P1  | 1.2                                    | 2.1                 | 3.5                 | 0.9  | 1.4                       |
| P2  | 1.7                                    | 2.6                 | 4.1                 | 0.9  | 1.5                       |

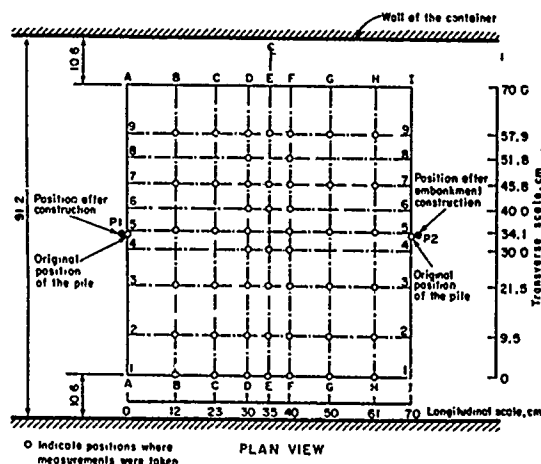


FIG. B1. Location of the Points Where Movements were Monitored.

#### APPENDIX C - BASE MOVEMENTS FROM VOLUME COMPATIBILITY

Based on observation and the measurements taken, the surface profile of the fill was determined. Knowing the deflection of the piles, and assuming that the piles and gelatin move together, the lateral component of the movements was obtained. If it is assumed that there is no change in the overall volume of the sand fill, analysis based on compatibility of volumes can be performed to establish the deformation profile at the base of the embankment. Such analysis require a trial and error balancing of areas. The estimated base profile at the end of the shaking (after 0.3 g) is shown in Figure C1. The areas involved were as follows:

- Zone 1) Settlement of the area below the surface of the fill + =  $93\text{cm}^2$
- Zone 2) Area involved in the lateral movement of the piles  $(2.3 \times 23.5/2) = 27\text{cm}^2$
- Zone 3) Area of the sluffed portion beyond the face of the slope =  $14\text{cm}^2$
- Zone 4) Area settled beneath the base of the fill  $(45.5 \times 1.6/2) = 37\text{cm}^2$

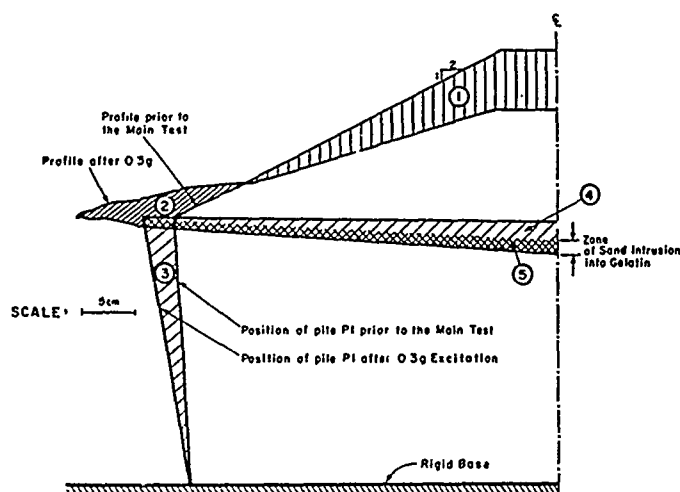


FIG. C1. Deformed Sand-Gel Interface Based on Volume Compatibility.

Zone 5) Area of sand intruded into the gel.  $A_5 = 1/2(1.0 \times 45.5) = 22.8 \text{ cm}^2$ . Because the sand pores in this area are now filled with gel, the actual area displaced  $= 1/1+e A_5 = 1/1.5 (22.8) = 15 \text{ cm}$

The summation of the zones 2,3,4 and 5 balance the downward movement given by zone 1.

#### APPENDIX D - ANALYSIS OF EARTHQUAKE INDUCED DISPLACEMENTS OF THE PROTOTYPE FILLS

The model studies indicate that the effect of seismic shaking is to break the arching effect by which the sand fill load is carried by the piles, with the result that the load is gradually transferred from the piles to the foundation soil as shaking proceeds. A worst case is to assume that all of the fill load must be taken by the foundation soil and that the piles carry no vertical load. This condition will exist during the shaking. After the shaking stops, the load will again revert to the piles as further settlement occurs either due to creep or settlement effects. Therefore the load transfer condition exists only for a short period of time and can be simulated assuming the fill must be carried by the foundation using undrained stress-strain relations for the organic soils.

A typical soil profile was shown in Figure (3) and the stress-strain parameters in Table D1. These parameters define a hyperbolic stress-strain curve that is now commonly used in practice and has been discussed by many researchers including Byrne and Janzen 1981. The parameters for the peat and organic clay were obtained from laboratory tests in which samples were first subjected to cyclic loading simulating earthquake loading and then tested in undrained shear to obtain their post cyclic stress-strain behaviour. The laboratory post-cyclic stress-strain curves are shown in Figure

D1. The stress-strain parameters for sand were based on Byrne and Eldridge, 1982.

The earthquake induced displacements were computed using the finite element method and assuming that all of the fill load must be carried by the foundation soil. The computer program SOILSTRESS (Byrne and Janzen, 1981) which performs an equivalent linear elastic analysis was used. The finite element mesh is shown in Figure D2. The computed displacement pattern is shown in Figure D3. It may be seen that the crest of the embankment settles about 0.4 m and also moves out horizontally about 0.4 m. Some heave is predicted to occur in the toe area.

Table D1

Hyperbolic Parameters Used in the Analysis.

| Parameter       | Material Number |       |        |       |
|-----------------|-----------------|-------|--------|-------|
|                 | 1               | 2     | 3      | 4     |
| $k_g$           | 356.0           | 5.0   | 23.0   | 356.0 |
| $n$             | 0.5             | 0.0   | 0.0    | 0.5   |
| $k_b$           | 334.0           | 500.0 | 2300.0 | 334.0 |
| $m$             | 0.5             | 0.0   | 0.0    | 0.5   |
| $\phi$          | 37.5°           | 0.0   | 0.0    | 37.5° |
| $\phi_{cv}$     | 33.0            | 0.0   | 0.0    | 33.0  |
| $\Delta\phi$    | 0.0             | 0.0   | 0.0    | 0.0   |
| $c(\text{kPa})$ | 0.0             | 31.0  | 50.0   | 0.0   |
| $R_F$           | .8              | .8    | .8     | .8    |

$$\text{Shear Modulus, } G = k_g P_a \left( \frac{\sigma_m}{P_a} \right)^n \left[ 1 - \frac{r R_F}{c + \sigma \tan \phi} \right]$$

$$\text{Bulk Modulus, } B = k_b P_a \left( \frac{\sigma_m}{P_a} \right)^m$$

where  $P_a$  = Atmospheric Pressure  
 $\sigma_m$  = the mean normal stress

See Byrne and Janzen (1981) for details.

| Material No. | Description  |
|--------------|--------------|
| 1            | Compact Sand |
| 2            | Peat         |
| 3            | Organic Silt |
| 4            | Compact Sand |

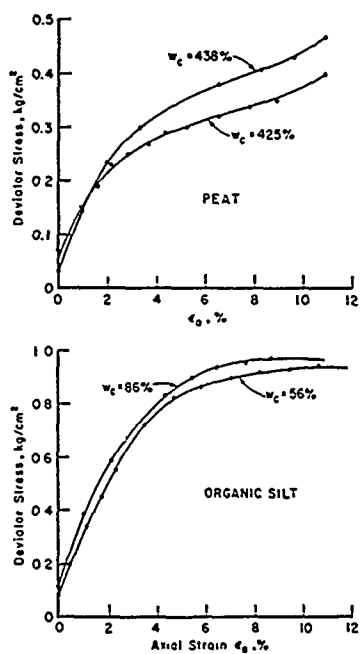


FIG. D1. Laboratory Post-Cyclic Stress-Strain Curves for Peat and Organic Silt.

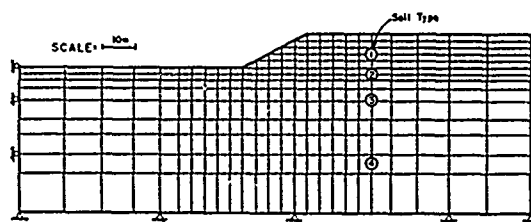


FIG. D2. Finite Element Mesh Used.

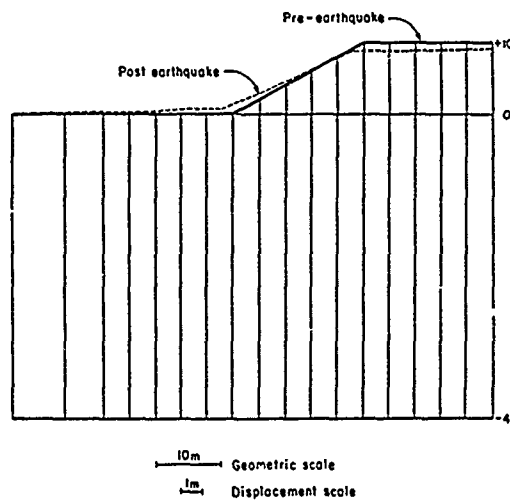


FIG. D3. Post Earthquake Deformation of Prototype.

# In-Situ Determination of Dynamic Properties of Soil for Foundation of a Turbo-Generator

V.D. Miglani

Professor of Civil Engineering, Regional Engineering College,  
Kurukshetra, Haryana, India

**SYNOPSIS:** The paper presents a case history of performance and analysis of results of vertical & horizontal resonance tests on a standard concrete block in a well, for in-situ determination of dynamic properties of soil required for design of a turbo-generator, under unusual conditions of high water table. Pumping from the two wells constructed for lowering the water level was not enough and pumping from within the main well had to be resorted to to bring down the water level to a little below the top surface of the model block. As expected, amplitude versus frequency curves for vertical resonance test showed two resonant peaks instead of one, indicating occurrence of two modes of vibration. A method for estimating dynamic co-efficients of soil, through derived curves for ratio of natural frequencies in horizontal and vertical modes versus effective area of base, has been suggested. A repeat test under good conditions confirmed the adequacy of the method.

## INTRODUCTION

Projects of progress have to be executed in a time bound frame. The author had an opportunity to carry out investigations for determining dynamic soil properties required for a 210 megawatt turbo-generator of such a thermal power project in India and was desired to make the recommendations within a limited time period.

The following dynamic properties of soil were required:

- (i) Co-efficient of Elastic uniform compression ( $C_u$ )
- (ii) Co-efficient of Elastic uniform shear ( $C_t$ )
- (iii) Co-efficient of Elastic Non-uniform compression ( $C_\phi$ )
- (iv) Co-efficient of Elastic Non-uniform shear ( $C_\psi$ )

The Indian Standard Code (IS: 5249-1977) prescribes size of pit (4.5 m x 2.75 m in plan, depth = depth of foundation) and size of block (1.5 m x 0.75 m x 0.7 m high) and also method of conduct of tests. Dynamic tests include resonance & wave propagation tests. On account of site conditions, departure from the provisions of the code had to be resorted to.

## SITE CONDITIONS & TEST ARRANGEMENT

The proposed depth foundation for the turbo-generator was 4.7 m below ground level (GL). The soil above and below was mainly sandy. Sub-soil water level (SSWL) was 2.5 m below GL. Because of these conditions, the resonance tests were planned to be conducted on a standard block 1.50 m x 0.75 m x 0.70 m of plain concrete

constructed in a brick well of 3.5 m internal diameter at the proposed foundation depth. Two side wells of 2 m internal diameter were also constructed (Fig. 1).

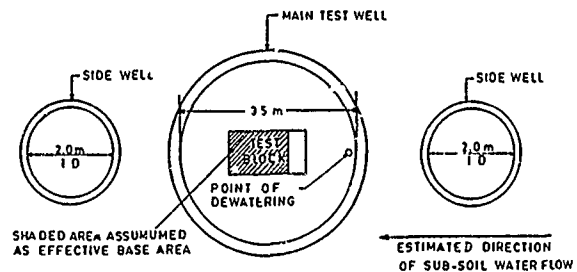


Fig. 1 - Plan of Test Arrangement

It was estimated that pumping out of water from the side wells would be enough to keep the water level in the main well below the surface of block during mounting of equipment & conduct of test. However, at the time of conduct of test, due to rise in SSWL, pumping out of water from the side wells was not enough to bring down the water level in the main well to desired extent. Water level in the test well remained at about 10 to 15 cm above the block. Although undesirable, pumping from within the main well had to be resorted to, on account of time bound programme of the project. The point chosen for this purpose was on the longer axis of the block, near the well boundary and as far as possible near the surface of water.

## BLOCK RESONANCE TESTS

The following resonance tests were conducted on the model block foundation:

1. Vertical resonance test
2. Horizontal resonance test

The wave propagation test was not possible on account of high water table.

The resonance tests were carried out by mounting a mechanical oscillator on top of the block. The oscillator was set to produce vertical or horizontal harmonic excitation. The oscillator was driven by a D.C. shunt motor, the speed of which was varied with an independent control unit. The vibrations of the model block were picked up by a velocity pick-up, the signals of which were integrated and amplified by means of a D.C. amplifier and observed on an amplitude meter. The line diagram of the set up of recording arrangement is shown in fig. 2.

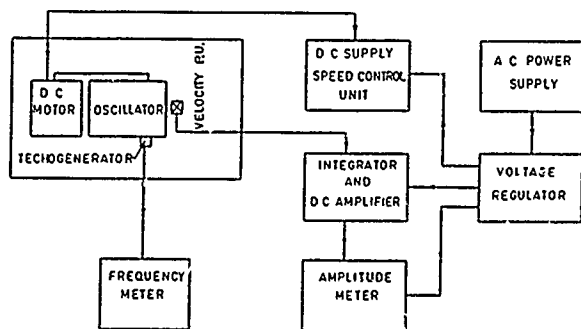


Fig. 2 - Line Diagram of Testing Equipment

### VERTICAL RESONANCE TEST

The oscillator was mounted centrally on the block such that it produced vertical harmonic exciting force and the line of action of such excitation passed through the centre of gravity of the block. On top of the block, the velocity pick-up was fixed with its sensing axis in the vertical direction. Amplitudes were observed on an amplitude meter and recorded for different frequencies and at angles of eccentricity of oscillator equal to  $72^\circ$ ,  $108^\circ$  and  $144^\circ$ . Frequency-amplitude curves at these eccentricities from these observations were drawn. A typical curve is shown in fig. 3.

The corresponding resonant frequencies are shown in Table 1. The co-efficient of elastic uniform compression ( $C_u$ ) is obtained by using the following expression:

$$C_u = \frac{4 \pi^2 \cdot f_{nz}^2 \cdot m}{A} \quad \dots(1)$$

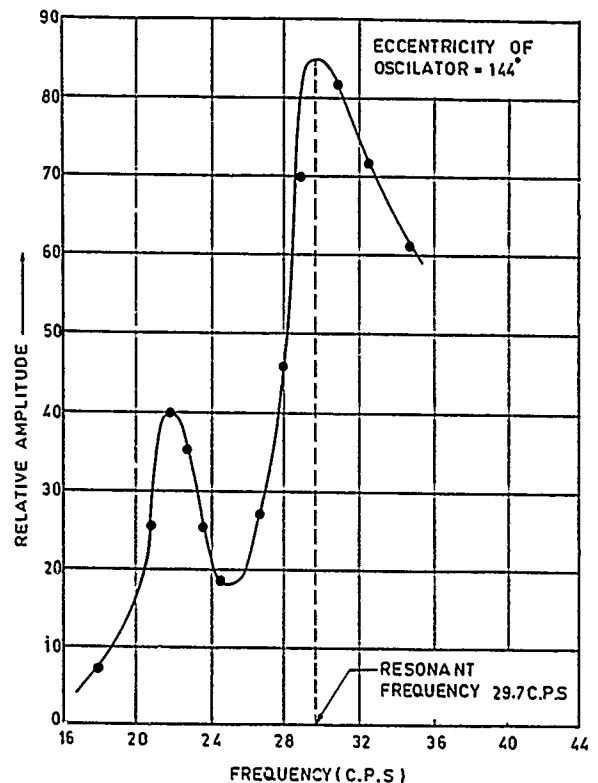


Fig. 3 - A Typical Amplitude v/s Frequency curve from Vertical Resonance Test

Where:-

$m$  = mass of the block plus that of the motor, oscillator and other mountings

$A$  = Base area of the block

=  $150 \text{ cm} \times 75 \text{ cm}$

$f_{nz}$  = Resonant frequency in the vertical mode

The values of the co-efficient of elastic uniform compression ( $C_u$ ) corresponding to base area of model block are listed in column 4 of Table-1 and the values of  $C_u$  corresponding to  $10 \text{ Sq m}$  area of foundation are tabulated in column 5 of the table. These were calculated by using relationship:

$$\frac{C_{u1}}{C_{u2}} = \sqrt{\frac{A_2}{A_1}} \quad \dots(2)$$

Where:

$C_{u1}$  and  $C_{u2}$  correspond to base areas  $A_1$  &  $A_2$

Such a relationship is valid for small areas upto about  $10 \text{ Sq m}$ . For base area greater than  $10 \text{ Sq m}$ , the value of  $C_u$  remains almost constant [Barkan (1962)].

TABLE - 1

Resonant Frequencies and Values of  $C_u$  from Vertical Resonance Test

| ANGLE OF<br>ECCENTRICITY<br>OF<br>OSCILLATOR | RESONANT<br>FREQUENCY<br>$f_{nx}$<br>(c.p.s.) | DYNAMIC<br>FORCE<br>(Kg) | $C_u$<br>(Kg/Cm <sup>2</sup> )<br>$A = 1.125 m^2$ | $C_u$<br>Kg/Cm <sup>2</sup><br>$A = 10 m^2$ |
|--|---|--------------------------|---|---|
| 1  | 2   | 3                        | 4   | 5   |
| 72°  | 31.0  | 120.3                    | 6.49  | 2.18  |
| 108°   | 30.2  | 157.2                    | 6.16  | 2.07  |
| 144°   | 29.7  | 178.7                    | 5.96  | 2.00  |

On account of dewatering from inside the main well, deviation from uniform reaction caused the block to vibrate in two modes:

- (i) rocking about a horizontal axis passing through the centre of the base area, and
- (ii) vertical.

Since the natural frequency ( and hence resonant frequency ) in the rocking mode is lower than that of the vertical mode, the first peaks appearing in amplitude v/s frequency curves have been ignored in computations.

It may be noted that the values of  $C_u$  in columns 4 & 5 need correction.

#### HORIZONTAL RESONANCE TEST

The mechanical oscillator was mounted on the block such that it generated horizontal harmonic excitation parallel to longitudinal axis of the block. The velocity pick-up was mounted on top of the block, with its sensing axis horizontal and parallel to the excitation. Horizontal amplitudes were recorded against different frequencies for different settings of angles of eccentricity of the oscillator.

Frequency v/s amplitude curves from the horizontal vibration test for angles of eccentricity of oscillator of 72°, 108° and 144° were drawn. A typical curve is shown in fig. 4.

The resonant frequencies obtained from these curves are listed in column 2 of the Table 2.

When an oscillator is mounted on the top of the block to produce horizontal excitation, such an excitation causes the block to vibrate in coupled translatory motion along the longitudinal axis and rocking motion about transverse axis of the block. Thus the system has two degrees of freedom and hence two natural frequencies and also two resonant frequencies. In order to determine whether the resonant frequency obtained is corresponding to first or second mode of vibration, the amplitudes were observed carefully for different frequencies of the oscillator which varied from 0 to about 30 c.p.s. in one case. It was observed that first resonance occurred near 12 c.p.s. The amplitudes were at the lowest at 24 c.p.s. and started

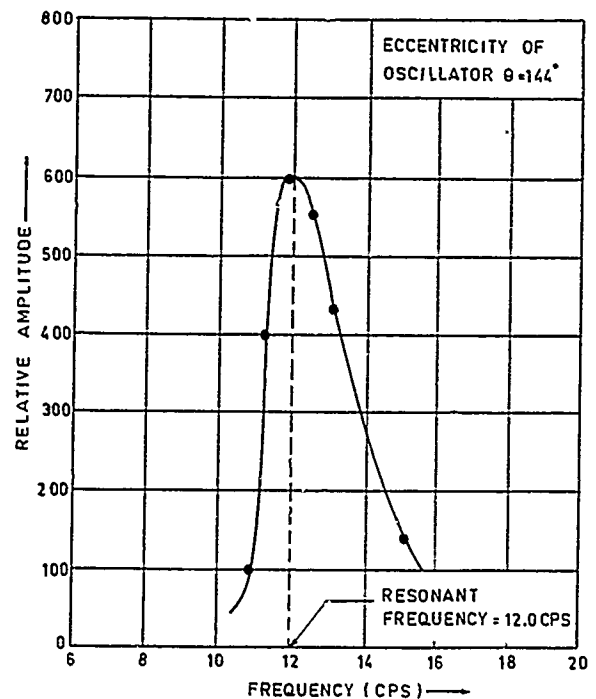


Fig. 4 - A Typical Amplitude v/s Frequency Curve from Horizontal Resonance Test

TABLE - 2

Resonant Frequencies and Values of  $C_t$  from Horizontal Resonance Test

| ANGLE OF<br>ECCENTRICITY<br>OF<br>OSCILLATOR | RESONANT<br>FREQUENCY<br>$f_{nx}$<br>(c.p.s.) | DYNAMIC<br>FORCE<br>(Kg) | $C_t$<br>(Kg/Cm <sup>2</sup> )<br>$A = 1.125 m^2$ | $C_t$<br>Kg/Cm <sup>2</sup><br>$A = 10 m^2$ |
|--|---|--------------------------|---|---|
| 1  | 2   | 3                        | 4   | 5   |
| 72°  | 12.8  | 215                      | 131   | 0.44  |
| 108°   | 12.4  | 285                      | 123   | 0.41  |
| 144°   | 12.0  | 292                      | 115   | 0.39  |

increasing beyond 24 c.p.s. thereby indicating second mode occurring beyond 30 c.p.s. The resonant frequencies listed in column 2 of the table 2 correspond to the first mode of vibration. After determining the mode of vibration, the co-efficient of elastic uniform shear  $C_t$  is obtained using the following relationship:

$$C_t = \frac{8 \times 10^6 r f_{nx}^2}{(A_o + I_o) \pm \sqrt{(A_o + I_o)^2 - 4 A_o I_o r}} \quad \dots (3)$$

where

$$r = M_m / M_{m0}$$

$f_{nx}$  = Resonant frequency obtained from horizontal vibration test

$A_0$  = A/m

$I_0$  =  $3.46 I/M_{mo}$

$M_m$  = Mass moment of inertia of block with mountings about the horizontal axis passing through centre of gravity of the block and perpendicular to the direction of vibration

$M_{mo}$  = Mass moment of inertia of block and mountings about the horizontal axis passing through centre of base area of the block and perpendicular to the direction of vibration

$I$  = Second moment of area of base of the block about the horizontal axis passing through the centre of gravity the area and perpendicular to the direction of vibration

Use the +ve sign for 2nd mode of vibration and -ve sign for the first mode of vibration.

For the size of the block used in this test and first resonant frequency, equation (3) reduces to:-

$$C_t = f_{nx}^2 / 125 \quad \dots(4)$$

Using the above relation, the co-efficient of elastic uniform shear for the base area of the block was calculated and these values are listed in column 4 of Table 2.

The value of  $C_t$  corresponding to 10 Sq m area were computed using the relationship:

$$\frac{C_{t1}}{C_{t2}} = \sqrt{\frac{A_2}{A_1}} \quad \dots(5)$$

where  $C_{t1}$  and  $C_{t2}$  correspond to areas  $A_1$  and  $A_2$  respectively. These values of  $C_t$  are recorded in column 5 of the Table 2.

As per Table - 1, the values of  $C_t$  in columns 4 & 5 of table 2 need correction.

CO-EFFICIENTS OF ELASTIC NON-UNIFORM COMPRESSION ( $C_\phi$ ) AND ELASTIC NON-UNIFORM SHEAR ( $C_\psi$ )

No direct field tests are available at present for determination of these properties of soil. The following relationship, as given in IS:5249-1977 may be used for these co-efficients:

$$C_\phi = 3.46 C_t \quad \dots(6)$$

$$C_\psi = 0.75 C_u \quad \dots(7)$$

## TEST RESULTS

The values of  $C_u$  corresponding to 10 Sq m base area as calculated from vertical resonance test conducted at different eccentricities of oscillator vary from 2.00 to 2.18 kg/cm<sup>3</sup> (Table 1).

The values of  $C_t$  corresponding to 10 Sq m base area as calculated from horizontal resonance test, similarly, vary from 0.39 to 0.44 kg/cm<sup>3</sup>, i.e., the values are of the order of one fifth of the values of  $C_u$  whereas actual values of  $C_t$  should be in the range of half to two third of values of  $C_u$ .

It is thus clear that the values of  $C_t$  have been affected considerably due to dewatering from inside the main well.

The values of  $C_u$  and  $C_t$  computed above, therefore, needed corrections.

## CORRECTIONS OF TEST RESULTS

An attempt was made to estimate correction factors to be applied to the values of soil parameters obtained in the tests by assuming that certain base area of the block near the point of dewatering was of no effect (see fig.1).

From equations (1) & (2), ratio of  $f_{nz}$  &  $f_{nx}$  (corresponding to first mode) can be written as:

$$\frac{f_{nz}}{f_{nx}} = \sqrt{\frac{C_u}{C_t} \cdot \frac{2A}{(D-E)}} \quad \dots(8)$$

where

$$D = A_0 + I_0$$

$$E = \sqrt{D^2 - 4 A_0 I_0}$$

Equation (8) reduces to:

$$\frac{f_{nz}}{f_{nx}} = \sqrt{\frac{C_u}{C_t} \cdot \frac{150}{d-e}} \quad \dots(9)$$

where

$$d = 121.1 + 223.9 p^2$$

$$e = \sqrt{d^2 - 70581 p^2}$$

$p$  = effective base area/total base area ratio

Using equation (9),  $f_{nz}/f_{nx}$  v/s per cent effective base area curve has been drawn in fig. 5. Correction factor v/s per cent effective base area has been derived using equation (2) and plotted in fig. 5.

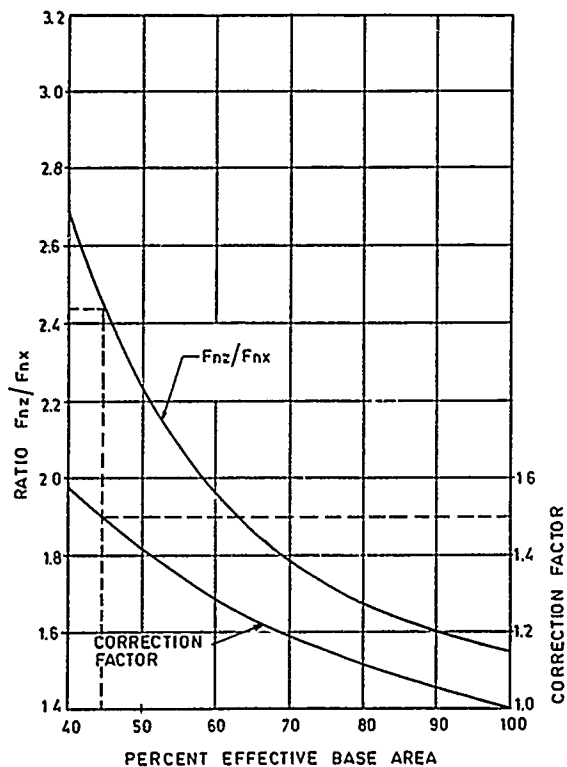


Fig. 5 - Ratio of Frequencies ( $f_{nz}/f_{nx}$ ) & Correction Factor v/s Effective Base Area Curves

Average  $f_{nz}$  = 30.3 c.p.s. (Table 1)

Average  $f_{nx}$  = 12.4 c.p.s. (Table 2)

Ratio: ( $f_{nz}/f_{nx}$ ) = 2.44

Per cent Effective area corresponding to this ratio on the curve is 44.9 (i.e.,  $p=.449$ ) and against this per cent effective area, correction factor is 1.5. Therefore, corrected values of  $C_u$  are equal to 3.0 to 3.3 kg/cm<sup>3</sup> and hence corrected values of  $C_t$  are equal to 1.5 to 1.7 kg/cm<sup>3</sup> for base areas of 10 Sq m.

These values could well serve the purpose of preliminary design of the foundation.

#### REPEAT TEST

The resonance tests were repeated after a lapse of about 4 months under very low draw-down conditions. The general water table was low on account of dewatering in the surrounding area. The level of water within the test well was further lowered by means of pumping out from the two side wells. Amplitudes observed were plotted against frequencies of the oscillator. In vertical resonance test, no second peak was observed indicating absence of rocking mode.

A typical amplitude v/s frequency curve from

vertical resonance test is shown in fig. 6. The results are shown in tables 3 & 4.

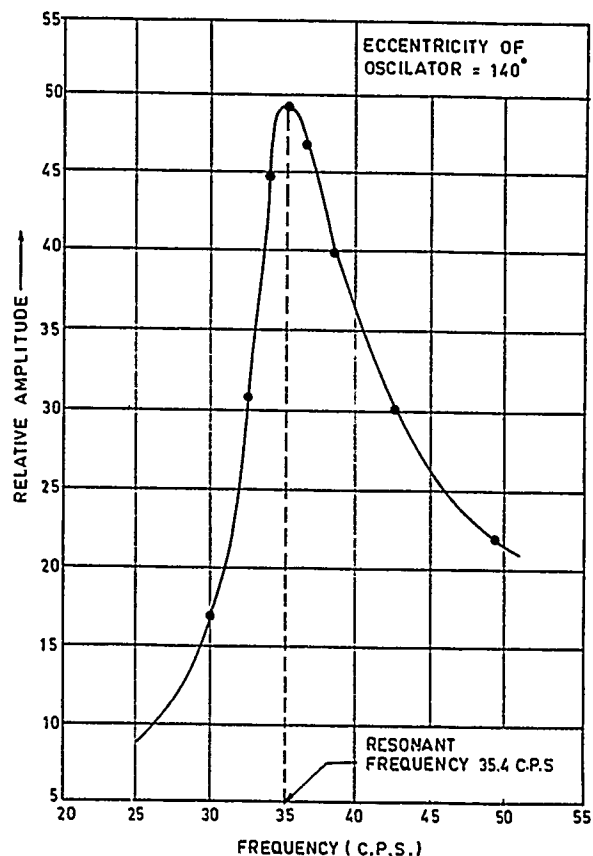


Fig. 6 - A Typical Amplitude v/s Frequency Curve from Vertical Resonance (Repeat) Test

TABLE - 3  
Resonance Frequencies and Values of  $C_u$   
from Vertical Resonance (Repeat) Test

| ANGLE OF<br>ECCENTRICITY<br>OF<br>OSCILLATOR | RESONANT<br>FREQUENCY<br>$f_{nz}$<br>(c.p.s) | DYNAMIC<br>FORCE<br>(Kg) | $C_u$<br>(Kg/Cm <sup>3</sup> )<br>A = 1.125m <sup>2</sup> | $C_u$<br>Kg/Cm <sup>3</sup><br>A = 10 m <sup>2</sup> |
|--|--|--------------------------|---|--|
| 1  | 2  | 3                        | 4   | 5  |
| 72°  | 36.0   | 163                      | 8.75  | 2.95   |
| 104°   | 35.4   | 211                      | 8.47  | 2.85   |
| 140°   | 34.8   | 254                      | 8.18  | 2.76   |



TABLE - 4

Resonant Frequencies and Values of  $C_t$   
from Horizontal Resonance (Repeat) Test

| ANGLE OF<br>ECCENTRICITY<br>OF<br>OSCILLATOR | RESONANT<br>FREQUENCY<br>$f_{nx}$<br>(c.p.s) | DYNAMIC<br>FORCE<br>(Kg) | $C_t$<br>(Kg/Cm <sup>2</sup> )<br>A = 1.125 m <sup>2</sup> | $C_t$<br>Kg/Cm <sup>2</sup><br>A = 10 m <sup>2</sup> |
|--|--|--------------------------|--|--|
| 1  | 2  | 3                        | 4  | 5  |
| 72°  | 28.5   | 102                      | 6.50   | 2.19   |
| 104°   | 25.5   | 110                      | 5.20   | 1.75   |
| 140°   | 25.0   | 127                      | 4.95   | 1.67   |

The other details of the tests are available elsewhere (Migiani - 1982).

#### CONCLUSION

Comparison of the results with corrected values of  $C_u$  &  $C_t$  indicates a reasonable prediction of design values of dynamic soil parameters and confirms the adequacy of the suggested method of correction.

#### REFERENCES

- Barkan, D.D. (1962), "Dynamics of Bases and Foundations", McGraw-Hill Book Co. Inc., New York.
- IS:5249-1977, "Indian Standard Method of Test for Determination of Dynamic Properties of Soil (First Revision)", Indian Standards Institution, New Delhi.
- Migiani, V.D. (1982), "Report on Dynamic Tests for Foundation of Turbogenerator at RTP, Ropar (C/GEOT/605)", Regional Engineering College, Kurukshetra.

## Geotechnical Services for a Bridge in a Seismic Area

Filippo Cluffi

Director of I.S.P.I.S. Geotechnical Division, Potenza, Italy

**SYNOPSIS:** The purpose of this paper is to describe the different stages and the final results of the geotechnical investigations and foundation design for a bridge in a seismic area, in the south of Italy. Particular attention is given to the procedure followed to study dynamic soil-pile interaction. Also described in summary fashion are a number of "borehole shear tests" carried out and their results.

### INTRODUCTION

The soil-pile interaction analysis for a bridge in a seismic area plays a very important role in the procedure for the foundations to withstand earthquake. In particular, the correct prediction of the bridge's piers displacements during earthquake ground motion has significant effects upon the stability of the whole bridge. The construction of a road between Forenza and Maschito, two small towns in southern Italy, has required the construction of a bridge on the Macchiarotonda gorge (Fig. 1).

Decribed in this paper are the different stages and the final results of the geotechnical investigations and foundations design for the bridge above mentioned. Particular stress is given to the procedure followed to design piles against earthquake.

The geotechnical consultancy services and the foundation design have been ordered by National Office for Extraordinary Works in Southern Italy.

### LOCATION OF BRIDGE AND GROUND CONDITIONS

The area under study is located approximately 2.5 km north of Forenza and 50 km north of Potenza, the regional chief city. The area, at the present time, is classified by italian law as a "seismic area". It is opportune to recall that Basilicata Region has been greatly damaged by the earthquake of 23rd No-

vember 1980.

The morfology is characterized by slope averaging 33% (right slope: 41%; left slope: 25%).

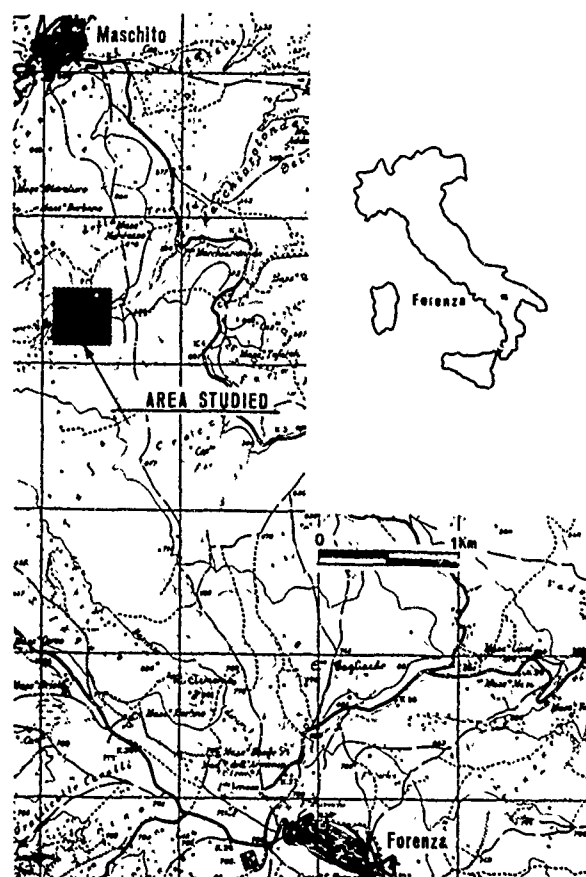


Fig.1. Location of the Site

As regards the geology, the soils are mostly belonging to the following formations: the so-called "Daunia Formation" (Miocene) and "Varicoloured Clays" (Oligo-Miocene). The first one is characterized by marly limestones. The second one is characterized by alternations of varicoloured clays (prevailing colours: red and green) and marly clays. At the bottom of the Macchiarotonda gorge, there are recent alluvial deposits.

#### PROCEDURE

The following procedure has been used.

- (i) First of all, the site has been studied on the basis of the analysis of aerial photographs.
- (ii) A detailed investigation has been carried out, in particular on the sites on which the bridge's piers will be located: on the right slope and on the left slope of Macchiarotonda gorge:
  - Cone Penetration Tests
  - Boring Tests
  - Borehole Shear Tests
  - Pore Pressure Measures
  - Laboratory Tests
- (iii) All data collected have been studied. Particular emphasis has been given to the interesting results of

Borehole Shear Tests. In fact, for the first time, Borehole Shear Tests have been performed in Italy.

- (iv) To summarize the results of the above mentioned analysis, a tridimensional soil profile map has been drawn to a scale of 1:200. The site conditions have suggested that bored cast in situ piles ( $\phi = 100$  cm) would be the appropriate choice.
- (v) The foundations design has been carried out by calculating both the ultimate capacity of the pile group and the soil-pile interaction under dynamic loads.

#### BOREHOLE SHEAR TESTS

Inasmuch as space is limited and we are unable to give due attention to all investigations made, we deem it opportune to limit ourselves to illustrating, at least with regard to basic essentials, a number of "borehole shear tests" carried out on representative points of the area under study. The "borehole shear test" measures shearing strength quickly and directly in situ in the sides of a 75 mm diameter borehole.

The tests described have all been carried out by the I.S.P.I.S. Geotechnical Division of Potenza (Italy).

Five "borehole shear tests" have been conducted on the sides on which the bridge's piers will be located (Fig. 2).

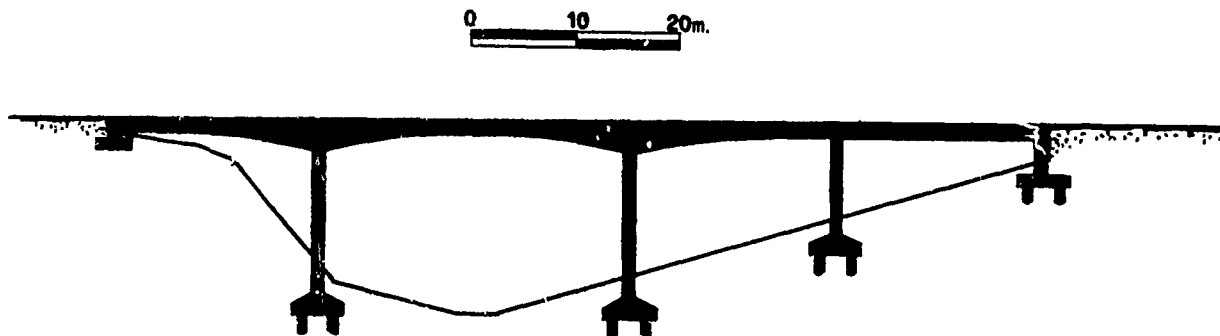


Fig. 2. Schematic Bridge's Section

For each point a series of tests with increasing applied normal stress ( $\sigma$ ) was performed, while the corresponding shear stress ( $\tau$ ) was measured. The consolidation time, before increasing normal stress, was evaluated by monitoring the dissipation of excess pore pressures generated after application of the normal stress. Shearing strength was then plotted versus normal stress to give a Mohr-Coulomb type failure envelope.

Test results are summarized in Table I.

| B.S.T.<br>(n.) | C<br>(p.s.i.) | $\phi$<br>(°) |          |
|----------------|---------------|---------------|----------|
| 1              | 4,2           | 17°7'         | left s.  |
| 1'             | 2,2           | 18°2'         | "        |
| 2              | 3,9           | 32°2'         | "        |
| 3              | 4,3           | 31°1'         | "        |
| 4              | 4,4           | 13°8'         | right s. |

Table I. B.S.T. Results

It can be seen from this table that the values of friction angles of the left slope are higher than that of the right slope. It may be of interest to note that, to evaluate the anisotropy, the B.S.T. 1' was performed, by rotating the apparatus 90°, in the same hole, at the same depth of B.S.T. 1. (Fig. 3).

#### SOIL-PILE INTERACTION ANALYSIS

The structural consultants indicated that the maximum load at the base of bridge's piers is expected to be about 1600 ton. The safe capacity of the pile group, calculated on the basis of "cone penetration resistance" (Meyerhof, 1976,1983), was estimated as 1756 ton. 10 m long pile on left slope and 14 m long pile on right slope were required.

It is important to emphasize that the geotechnical conditions of the left slope are decidedly better than those of the right slope.

#### BOREHOLE SHEAR TEST n° 1 X

| Normal Stress<br>(p.s.i.) | 14,5 | 17,0 | 19,6 | 22,2 | 24,7 |
|---------------------------|------|------|------|------|------|
| Cons. Time<br>(min)       | 15   | 12   | 10   | 8    | 8    |
| Shear Stress<br>(p.s.i.)  | 8,5  | 9,7  | 10,5 | 11,3 | 12,4 |

$$C = 4,25 \text{ p.s.i.} \quad \phi = 17^{\circ} 7'$$

#### BOREHOLE SHEAR TEST n° 1' X

| Normal Stress<br>(p.s.i.) | 24,7 | 27,3 | 32,4 |  |  |
|---------------------------|------|------|------|--|--|
| Cons. Time<br>(min)       | 15   | 11   | 10   |  |  |
| Shear Stress<br>(p.s.i.)  | 10,3 | 11,0 | 12,9 |  |  |

$$C = 2,2 \text{ p.s.i.} \quad \phi = 18^{\circ} 2'$$

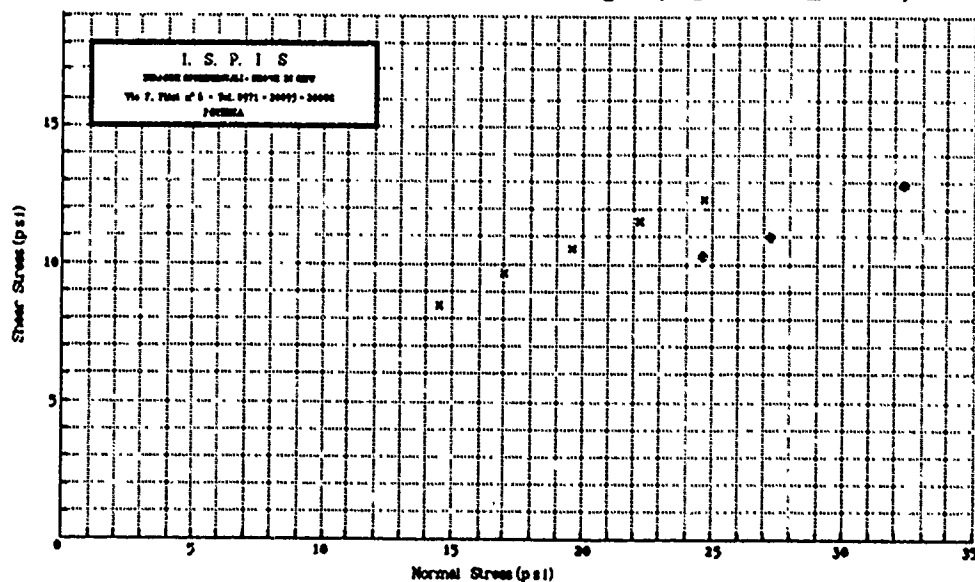


Fig. 3. B.S.T.'s 1 and 1'

Mostly to estimate the maximum displacement of the pile heads, the soil-pile interaction under dynamic loads has been studied, following the procedure proposed by Prakash and Chandrasekaran (Prakash and Chandrasekaran, 1980). This analysis is based on the following assumptions (Prakash, 1981):

- (i) The pile is divided into a convenient number of segments and mass of each segment is concentrated at its center point.
- (ii) The soil is assumed to act as a linear Winkler's spring. The soil reaction is separated into discrete parts at the center points of the masses. The soil modulus variation is considered both constant with depth and linearly varying with depth.
- (iii) The mass of the superstructure is concentrated at the pile top.
- (iv) The system is one-dimensional in its behavior.
- (v) The pile end conditions are either completely free to undergo translation and rotation or completely restrained against rotation but free to undergo translation.

The soil profile has been separated for both the slopes in two discrete parts A and B characterized by the following parameters (Table II).

|   | A                        | B                        |
|---|--------------------------|--------------------------|
| Young's modulus : $E$                               | 150 Kg cm <sup>-2</sup>  | 475 Kg cm <sup>-2</sup>  |
| Constant of horizontal subgrade reaction $\alpha_h$ | 1.03 Kg cm <sup>-3</sup> | 3.61 Kg cm <sup>-3</sup> |

Table II Soil Parameters for Dynamic Analysis

Note that the parts A and B are the same for both slopes, but while on left side the part A is 4.10 m long, on the right side its length is 9.10 m (Fig. 4). The dynamic analysis has been performed in the following steps:

- (i) The piles on the left slope have been studied. The maximum displacement of the pile head ( $S_{d \text{ left}}$ ), the maximum bending moment and the soil reaction have been computed.
- (ii) The lengths of the corresponding piles on right slope have been determined by imposing a value of maximum displacement of the pile head ( $S_{d \text{ right}}$ ) as follows:

$$S_{d \text{ right}} \leq 1.15 S_{d \text{ left}} \quad (1)$$

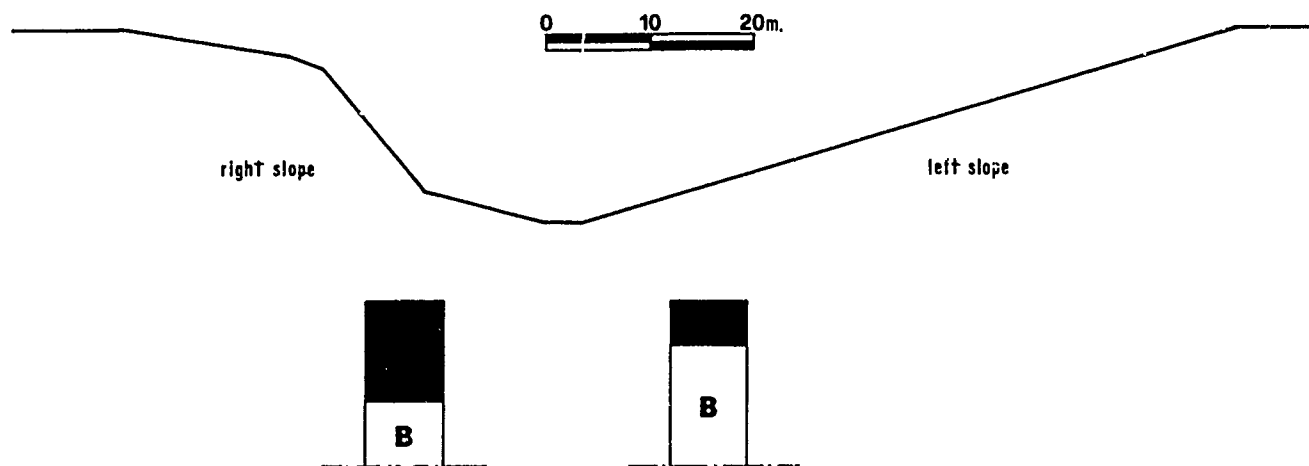


Fig.4. Soil Discrete Representation

The above described steps are illustrated in the Table III.

### KNOWN DATA UNKNOWN DATA

|                      |  |                      |  |
|----------------------|--|----------------------|--|
| SOIL CHARACTERISTICS | Young's Modulus $E$                            | DYNAMIC PARAMETERS   | Stiffness Factor $T$                   |
|                      | Constant of Horizontal Subgrade Reaction $n_h$ |                      | Max. Depth Factor $Z_{max}$            |
| PILE CHARACTERISTICS | Young's Modulus $E$                            |                      | Time Period $T_n$                      |
|                      | Diameter $D$                                   | DESIGNING PARAMETERS | Max. Displacement of the Pile Head $S$ |
|                      | Length $L$                                     |                      | Max Bending Moment $M$                 |
| MASS                 | Maximum Vertical Load $Q_{max}$                |                      | Soil Reaction $P_i$                    |

### PILES ON THE LEFT SLOPE

### KNOWN DATA UNKNOWN DATA

|                      |  |                    |                             |
|----------------------|--|--------------------|-----------------------------|
| SOIL CHARACTERISTICS | Young's Modulus $E$                            | DYNAMIC PARAMETERS | Stiffness Factor $T$        |
|                      | Constant of Horizontal Subgrade Reaction $n_h$ |                    | Max. Depth Factor $Z_{max}$ |
| PILE CHARACTERISTICS | Young's Modulus $E$                            |                    | Time Period $T_n$           |
|                      | Diameter $D$                                   | PILE CHAR.         | Length $L$                  |
| MASS                 | Maximum Vertical Load $Q_{max}$                |                    |                             |
| DESIGNING PARAMETERS | Max Displacement of the Pile Head $S$          |                    |                             |
|                      | Max Bending Moment $M$                         |                    |                             |
|                      | Soil Reaction $P_i$                            |                    |                             |

### PILES ON THE RIGHT SLOPE

Table III Piles Designing Procedure Representation

### CONCLUSIONS

The geotechnical consultancy services just illustrated have furnished, as was our intention, a number of indications extremely useful to structural consultants, in that they served as exact documentation for correctly designing the bird's structures against earthquake.

In particular, the soil-pile interaction under dynamic loads has been studied, mostly to predict the pile seismic performance. The lengths of piles have been calculated

to obtain, in different soils, the same maximum displacements (tolerance 15%) during earthquake ground motion.

#### REFERENCES

- Meyerhof, G.G., (1976), "Bearing capacity and settlement of pile foundations", J.G.E. D., ASCE, GT3, 197-228.
- Meyerhof, G.G., (1983), "Scale Effects of Ultimate Pile Capacity", J.G.E., ASCE, n° 6.
- Prakash, S., V. Chandrasekaran, (1980), "Analysis of Piles in Clay Against Earthquakes", Preprint n° 80-109, ASCE, Convention and Exposition, Portland, Ore.
- Prakash, S. (1981), "Soil Dynamics", McGraw Hill, New York, N.Y..

# Author's Index

|                         |            |                           |                  |
|-------------------------|------------|---------------------------|------------------|
| Aas, P.M. ....          | 1249       | Chonggang, S. ....        | 729              |
| Abdel-Salam, S. ....    | 1437       | Chouery-Curtis, V.E. .... | 1063             |
| Abolhassani, D. ....    | 347        | Chowdhary, G.R. ....      | 1133             |
| Abramson, L.W. ....     | 1191       | Christodoulis, J. ....    | 457              |
| Agarwal, K.B. ....      | 645        | Christopher, B.R. ....    | 1093, 1383       |
| Ahmad, S.A. ....        | 1343       | Christos, M. ....         | 337              |
| Alberro, J. ....        | 467        | Christoulas, St. ....     | 671              |
| Al-Yahyai, K.S. ....    | 1201       | Chua, K.M. ....           | 1417             |
| Amano, T. ....          | 1099       | Chugh, Y.P. ....          | 253              |
| Amick, D. ....          | 811        | Chukweze, H.O. ....       | 935, 1279        |
| Amin, D.P. ....         | 1165       | Chummar, A.V. ....        | 1271             |
| Anderson, D.G. ....     | 443        | Chung, K.Y.C. ....        | 1113             |
| Angeles, N.P. ....      | 1319       | Cincilla, W.A. ....       | 495              |
| Angelov, K. ....        | 299        | Ciuffi, F. ....           | 877              |
| Antes, D.A. ....        | 195        | Clough, G. Wayne ....     | 1597             |
| Arcangelii, E. ....     | 947        | Colleselli, F. ....       | 599              |
| Arya, A.S. ....         | 837        | Collins, S.A. ....        | 977              |
| Atibu, F.S. ....        | 717        | Consoli, M. ....          | 1465             |
| Atmatzidas, D.K. ....   | 1297, 1303 | Cooling, T.L. ....        | 1375             |
| Atukorala, U. ....      | 863        | Coons, L. ....            | 25               |
| Atwater, J. ....        | 55         | Corda, I.I. ....          | 663              |
| Aughenbaugh, N.V. ....  | 163        | Cordell, D.A. ....        | 35               |
| Azevedo, R. ....        | 689, 1465  | Coulson, A. ....          | 683              |
| Baer, G.R. ....         | 355        | Courage, L.R. ....        | 635              |
| Bahrami-Samani, F. .... | 347        | Cowherd, D.C. ....        | 683, 1471        |
| Bailey, B. ....         | 489        | Cramer, G.H. ....         | 71               |
| Baker Jr., C.N. ....    | 1383, 1389 | Curtis, R.L. ....         | 1063             |
| Baliga, B.D. ....       | 407        | Dailer, D. ....           | 1263             |
| Bandis, S.C. ....       | 107        | Daman, M.M. ....          | 1505             |
| Bandyopadhyay, S. ....  | 837        | Datye, K.R. ....          | 1075             |
| Bapat, A. ....          | 825        | Davie, J.R. ....          | 1019, 1309, 1395 |
| Barnes, G.E. ....       | 1229       | Deal, C.E. ....           | 451              |
| Bauer, L.T. ....        | 143        | Deaver, C.M. ....         | 519              |
| Beene, R.R.W. ....      | 567        | DeFour, S. ....           | 1001             |
| Berggren, B. ....       | 1169       | Dehner, J.G. ....         | 443              |
| Berry, R.M. ....        | 885        | Dekker, J. ....           | 547              |
| Betournay, M.C. ....    | 291        | Desai, C.S. ....          | 1551             |
| Bhandari, R.K. ....     | 245, 333   | Descour, J.M. ....        | 229              |
| Binquet, J. ....        | 511        | Dezfulian, H. ....        | 43               |
| Blendy, M.M. ....       | 1233       | Dhowian, A.W. ....        | 237, 1117        |
| Blight, G.E. ....       | 929        | Dirnberger, M.M. ....     | 787              |
| Bloom, E. ....          | 489        | Dominique, L.C. ....      | 941              |
| Borden, R.H. ....       | 1449       | Dong, J.G. ....           | 1501             |
| Borm, G. ....           | 953        | Doria, A.C. ....          | 1037             |
| Boscardin, M.D. ....    | 1029       | Dovnarovitch, S. ....     | 1245             |
| Bosscher, P.J. ....     | 63         | Dube, A.K. ....           | 211              |
| Bowman Jr., J.C. ....   | 795        | Dumas, J.C. ....          | 921              |
| Brenner, R.P. ....      | 347        | Duncan, J.M. ....         | 977              |
| Broms, B.B. ....        | 1515       | de Pee, J. ....           | 541              |
| Bruce, D.A. ....        | 1121       | Earley, K.H. ....         | 341              |
| Bucher, S.A. ....       | 1303       | East, D.R. ....           | 495              |
| Burgess, A.S. ....      | 81         | Edil, T.B. ....           | 63               |
| Butler, D.K. ....       | 519        | El-Sohby, M.A. ....       | 321              |
| Butts, R.L. ....        | 201        | Endicott, L.J. ....       | 123              |
| Syington, M.L. ....     | 1087       | Erol, A.O. ....           | 237              |
| Byrne, P.M. ....        | 863        | Erwin, J.W. ....          | 355              |
| Cabrera, J.G. ....      | 185        | Fang-Fu, T. ....          | 749              |
| Caldwell, J.A. ....     | 25         | Fan, W. ....              | 1047             |
| Calle, E.O.F. ....      | 533        | Farrel, E.R. ....         | 1145             |
| Cameron, R. ....        | 1209       | Fattohi, Z.R. ....        | 159              |
| Carr, C.A. ....         | 1209       | Fergusson, W.B. ....      | 1293             |
| Cazzuffi, D. ....       | 1137       | Ferrari, O.A. ....        | 941              |
| Celestino, T.B. ....    | 941        | Findlay, R.C. ....        | 401              |
| Chandrashekar, K. ....  | 253        | Finn, W.D.L. ....         | 1585             |
| Chandra, D. ....        | 361        | Finno, R.J. ....          | 1297             |
| Chaney, R.C. ....       | 555        | Fowler, J. ....           | 977              |
| Chang, Y.H. ....        | 417        | Fradkin, S.B. ....        | 221              |
| Chan, Y.C. ....         | 559        | Franks, L.W. ....         | 977              |
| Charles, R.D. ....      | 1069       | Fraser, D. ....           | 863              |
| Cheng, S.S.M. ....      | 1343       |                           |                  |



|                            |            |
|----------------------------|------------|
| Fulan, P. ....             | 743        |
| Gado, D.P. ....            | 1327       |
| Gallavresi, F. ....        | 1121       |
| Gambin, M. ....            | 969        |
| Garga, V.K. ....           | 1239       |
| Gassios, E. ....           | 671        |
| Gates, W.C.B. ....         | 1          |
| Gerber, F.A. ....          | 411        |
| Ghinelli, A. ....          | 1173       |
| Ghosh, D.K. ....           | 807        |
| Ghosh, N. ....             | 1055       |
| Giannaros, H. ....         | 457        |
| Gichaga, F.J. ....         | 717        |
| Gilchrist, A.J.T. ....     | 627        |
| Gillon, M.D. ....          | 841        |
| Glynn, E.F. ....           | 1293       |
| Goel, M.C. ....            | 423, 433   |
| Goel, R.K. ....            | 177        |
| Golder, M.H. ....          | 1107       |
| Gonzalez-Valencia, F. .... | 467        |
| Gouda, M.A. ....           | 1315       |
| Grainger, G.S. ....        | 201        |
| Grice, H. ....             | 885        |
| Grosch, J.J. ....          | 1201       |
| Gross, D.J. ....           | 143        |
| Guatterri, G. ....         | 1037       |
| Gupta, M.K. ....           | 837        |
| Gupta, V.K. ....           | 1509       |
| Gurevich, A.M. ....        | 89         |
| Handford, G.T. ....        | 829        |
| Hannink, G. ....           | 1403, 1409 |
| Hansbo, S. ....            | 1337       |
| Hansmire, W.H. ....        | 1191       |
| Hardin, D.J. ....          | 1087       |
| Harrel, H.C. ....          | 997        |
| Harsulescu, A.I. ....      | 711        |
| Hartung, S.C. ....         | 519        |
| Hasan, B. ....             | 271        |
| Hejazi, H. ....            | 461        |
| Hempen, G.L. ....          | 787        |
| Hepworth, R.C. ....        | 1349       |
| Hermosilla, R.P. ....      | 677        |
| Houssamy, I. ....          | 1505       |
| Hsieh, H.N. ....           | 7          |
| Huag, M.D. ....            | 55         |
| HuiShan, L. ....           | 765        |
| Hummert Jr., J.B. ....     | 1375       |
| Hurd, J.O. ....            | 1471       |
| Hu, G.A. ....              | 137        |
| Ilsley, R.C. ....          | 221        |
| Itskowitch, M. ....        | 737        |
| Ivanov, Y. ....            | 1245       |
| Ivsic, T. ....             | 819        |
| Izhar-ul-Haq ....          | 705        |
| Jain, J.K. ....            | 1289       |
| Jain, P.K. ....            | 1489       |
| Jain, S.L. ....            | 607        |
| Jethwa, J.L. ....          | 147, 177   |
| Jianyun, M. ....           | 167        |
| Jiayou, L. ....            | 167        |
| Johnson, L.D. ....         | 989        |
| Jokhyo, A.M. ....          | 279        |
| Jones, C.J.F.P. ....       | 1275       |
| Jones, D.L. ....           | 1107       |
| Judge, A.S. ....           | 1001       |
| Kalteziotis, N. ....       | 671        |
| Kapoor, K.K. ....          | 285, 657   |
| Karfakis, M.G. ....        | 173        |
| Katti, A.R. ....           | 527        |
| Katti, D.R. ....           | 527        |
| Katti, R.K. ....           | 527        |

|                           |                        |
|---------------------------|------------------------|
| Kauschinger, J.L. ....    | 1037                   |
| Kaushik, C.K. ....        | 1509                   |
| Keaveny, J.M. ....        | 1249                   |
| Keiley, G.P. ....         | 1327                   |
| Keys, R.A. ....           | 635                    |
| Ke, Z.J. ....             | 417                    |
| Khare, P.S. ....          | 207                    |
| Khare, R.K. ....          | 1289                   |
| Khera, R.P. ....          | 985                    |
| Kilkenny, W.M. ....       | 19                     |
| Kim, Y.S. ....            | 1443                   |
| King, T.B. ....           | 443                    |
| Kinner, E.B. ....         | 593                    |
| Kiricsenko, A. ....       | 819                    |
| Kiu, T.K. ....            | 1257                   |
| Klohn, E.J. ....          | 479, 829               |
| Knight, R.B. ....         | 55                     |
| Knuppel, L. ....          | 383                    |
| Koga, Y. ....             | 721                    |
| Kogure, K. ....           | 377                    |
| Kozicki, P. ....          | 55, 1149               |
| Kravits, S.J. ....        | 997                    |
| Krizek, R.J. ....         | 1303                   |
| Kropp, A. ....            | 1461                   |
| Kulkarni, S.G. ....       | 207                    |
| Kummerle, R.P. ....       | 921                    |
| Kvasnicka, P. ....        | 819                    |
| Kwong, J.K.P. ....        | 123                    |
| Lafleche, P. ....         | 1001                   |
| Laier, J.E. ....          | 993                    |
| Laird, G.S. ....          | 81, 89                 |
| Lakshmanan, N. ....       | 855                    |
| Lambrechts, J.R. ....     | 503                    |
| Lam, W. ....              | 1389                   |
| Lance, D.S. ....          | 911                    |
| Larson, J.A. ....         | 215                    |
| Lau, K.C. ....            | 291                    |
| Lavanaia, B.V.K. ....     | 615, 621               |
| Lengfelder, J. ....       | 1349                   |
| Leonard, B.D. ....        | 593                    |
| Leonard, M.S. ....        | 81                     |
| Lewis, M.R. ....          | 1019, 1233, 1309, 1395 |
| Lew, M. ....              | 795                    |
| Lien, W. ....             | 1449                   |
| Lifrieri, J.L. ....       | 195                    |
| Lindquist, R.W. ....      | 651                    |
| Lippincott, I.W. ....     | 1315                   |
| Lissey, A. ....           | 55                     |
| Li, J.C. ....             | 1421                   |
| Llopis, J.L. ....         | 519                    |
| Long, P.D. ....           | 1169                   |
| Lozier, W.B. ....         | 89                     |
| Lo, R.C. ....             | 479, 829               |
| Luan, D.Z. ....           | 1371                   |
| Lumsden, A.C. ....        | 123                    |
| Lum, K.K. ....            | 479                    |
| Luong, M.P. ....          | 1455                   |
| Lyman, T.J. ....          | 911                    |
| Macdonald, G.J. ....      | 1107                   |
| Macedo, G. ....           | 467                    |
| MacTavish, G.C. ....      | 369                    |
| Madhav, M.R. ....         | 1075                   |
| Marsland, A. ....         | 695                    |
| Martin III, James R. .... | 1597                   |
| Mashhour, M. ....         | 1437                   |
| Mastrantuono, C. ....     | 947                    |
| Mathur, T. ....           | 587                    |
| Matsui, T. ....           | 1099                   |
| Matsuo, K. ....           | 377                    |
| Matsuo, O. ....           | 721                    |
| Matthews, W.G. ....       | 369                    |
| Mattox, R.M. ....         | 993                    |
| Maurath, G. ....          | 811                    |
| Mazen, S.O. ....          | 321                    |

|                            |                  |
|----------------------------|------------------|
| McElroy, J.J.              | 1327             |
| McGrane, D.                | 13               |
| McLean, F.                 | 367              |
| Mehrotra, G.S.             | 245              |
| Meissner, H.               | 953              |
| Miglani, V.D.              | 871              |
| Miller, D.A.               | 1063             |
| Miller, R.J.               | 229              |
| Mills, D.E.                | 35               |
| Mills, S.V.                | 1087             |
| Milne, W.G.                | 829              |
| Mirza, C.                  | 291              |
| Missavage, R.              | 253              |
| Mithal, R.S.               | 311              |
| Mitsch, M.P.               | 1257             |
| Mitsuse, C.T.              | 941              |
| Modhwadia, K.E.            | 327              |
| Mokhashi, S.L.             | 207              |
| Montanez, L.               | 467              |
| Moore, B.H.                | 787              |
| Mosley, E.T.               | 885              |
| Mudjihardjo, D.            | 423              |
| Mundell, J.A.              | 489              |
| Murty, A.V.S.R.            | 361              |
| Muthumani, K.              | 855              |
| Nadim, F.                  | 1249             |
| Nainwa <sup>1</sup> , H.C. | 305              |
| Natarajan, T.K.            | 361, 365         |
| Nathan, S.V.               | 1483             |
| Nayak, G.C.                | 1489             |
| Nelson, J.D.               | 699              |
| Nerby, S.M.                | 1297             |
| Neyer, J.C.                | 1025             |
| Nhiem, T.V.                | 889              |
| Nicholson Jr., A.J.        | 1425             |
| Nowatzki, E.A.             | 1477             |
| Ohrli, M.L.                | 1133             |
| Olsen, J.M.                | 593              |
| Orr, T.L.L.                | 1145             |
| Otani, Y.                  | 1099             |
| Ou, C.Y.                   | 1183             |
| O'Donovan, T.              | 1145             |
| Pagotto, A.                | 1137             |
| Pancholi, D.M.             | 327              |
| Pang, P.L.R.               | 559              |
| Patel, N.M.                | 127              |
| Patodiya, S.C.             | 285, 657         |
| Paul, J.                   | 1127             |
| Perlea, V.G.               | 683, 1471        |
| Perry, C.W.                | 801              |
| Perry, E.B.                | 1037             |
| Peters, J.F.               | 977              |
| Petroff, L.J.              | 1417             |
| Petschl, R.O.              | 533              |
| Pitts, J.                  | 115              |
| Posse, J.A.                | 677              |
| Prabhakar, B.              | 147              |
| Prager, R.D.               | 201              |
| Prasad, C.                 | 305              |
| Price, H.R.                | 1025             |
| Qian, Y.P.                 | 1501             |
| Qiu, Y.                    | 1047             |
| Rager, R.E.                | 25               |
| Raghu, D.                  | 7, 51, 195, 1315 |
| Rahim, K.S.A.              | 1117             |
| Ramage, J.                 | 1577             |
| Ramamurthy, T.             | 263, 607         |
| Ranjan, G.                 | 1509             |
| Ransone, J.W.              | 495              |
| Rao, P.J.                  | 365              |
| Rapp, R.J.                 | 1495             |

|                      |                          |
|----------------------|--------------------------|
| Ray, M.B.            | 807                      |
| Reed, R.F.           | 1159                     |
| Richardson, T.L.     | 1011                     |
| Richards, D.P.       | 215                      |
| Riker, R.            | 1263                     |
| Rimoldi, P.          | 1137                     |
| Robison, M.J.        | 911                      |
| Rodda, K.V.          | 801                      |
| Rodriguez-Molina, C. | 151                      |
| Rodriguez-Perez, B.  | 151                      |
| Roodsari, A.         | 383                      |
| Rosenthal, I.        | 737                      |
| Rudenko, D.          | 341                      |
| Rupchang, K.V.       | 437                      |
| Sahu, B.K.           | 717                      |
| Samy, G.K.           | 651                      |
| Santamaria, J.M.M.   | 677                      |
| Santos, L.A.         | 689                      |
| San, K.C.            | 1099                     |
| Sarma, B.S.          | 855                      |
| Sarsby, R.V.         | 75                       |
| Schaefer, V.R.       | 977                      |
| Schneider, J.R.      | 651                      |
| Schubert, W.         | 1011                     |
| Schwenk, J.L.        | 1495                     |
| Scott, M.D.          | 479                      |
| Seco-e Pinto, P.S.   | 849                      |
| Seed, R.B.           | 1183                     |
| Shah, D.L.           | 1165                     |
| Sharma, D.           | 1365                     |
| Sharma, H.D.         | 1149                     |
| Sharma, V.M.         | 263                      |
| Sheng-sun, X.        | 1285                     |
| Shen, W.Y.           | 1501                     |
| Shiwei, D.           | 759, 773                 |
| Shixuan, Z.          | 575                      |
| Shi, L.P.            | 1421                     |
| Shi, M.              | 1047                     |
| Shorey, E.F.         | 221                      |
| Shroff, A.V.         | 1165                     |
| Shy, B.I.            | 1421                     |
| Simonini, P.         | 599                      |
| Singh, A.            | 1133                     |
| Singh, B.            | 147, 177, 211, 407, 1489 |
| Singh, V.K.          | 407                      |
| Sivapatham, T.       | 581                      |
| Smith, R.B.          | 395                      |
| Smith, T.            | 451                      |
| Solyman, Z.V.        | 369                      |
| Song, B.             | 969                      |
| Soranzo, M.          | 599                      |
| Sowers, G.F.         | 1567                     |
| Soydemir, C.         | 1257                     |
| Srinivasulu, P.      | 855                      |
| Srivastava, L.S.     | 779                      |
| Steinberg, S.B.      | 1389                     |
| Stipho, A.S.         | 1433                     |
| Stoll, U.W.          | 1319                     |
| Stroman, W.R.        | 567                      |
| Sullivan, W.J.       | 1449                     |
| Sundriya, Y.P.       | 305                      |
| Suprenant, B.A.      | 173                      |
| Surabaya, J.L.       | 433                      |
| Swaffar, K.M.        | 1025                     |
| Tabba, M.M.          | 1055                     |
| Taiping, Q.          | 765, 963                 |
| Tepel, R.E.          | 801                      |
| Termaat, R.J.        | 533                      |
| Testa, S.M.          | 97                       |
| Thompson, P.Y.       | 1443                     |
| Thornhill, P.D.      | 567                      |
| Thrasher, S.M.       | 1471                     |
| Tomolo, A.           | 947                      |
| Tsiambaos, G.        | 671                      |

|                           |           |
|---------------------------|-----------|
| Tsien, S.I. ....          | 1219      |
| Tucker, K.D. ....         | 1355      |
| Tuttle, D.C. ....         | 555       |
| Vaidya, P.H. ....         | 327       |
| Van Besien, A.C. ....     | 163       |
| Van Order, R.J. ....      | 51        |
| Van Quang, N. ....        | 1169      |
| Vannucchi, G. ....        | 1173      |
| Vaziri, H. ....           | 863       |
| Vazquez Castillo, A. .... | 151       |
| Vazquez Castillo, L. .... | 151       |
| Von M. Harwse, H.J. ....  | 411       |
| van Herpen, J.A. ....     | 541       |
| van Tol, A.F. ....        | 1409      |
| Wade, N.H. ....           | 635       |
| Wagner, A.B. ....         | 1093      |
| Wang, Z.Q. ....           | 131       |
| Weaver, C.L. ....         | 1395      |
| Weaver, K.D. ....         | 143       |
| Wei quen, Z. ....         | 963       |
| Wei, L.F. ....            | 635       |
| West, T.R. ....           | 489       |
| Wietek, B. ....           | 905       |
| Willis, R. ....           | 587       |
| Wolff, T.F. ....          | 787       |
| Wolosick, J.R. ....       | 1425      |
| Wrench, B.P. ....         | 699, 1477 |
| Wright, P. ....           | 1159      |
| Wu, A.H. ....             | 1179      |
| Xianjinan, Y. ....        | 759       |
| Xikang, W. ....           | 755, 759  |
| Yandell, W.O. ....        | 395       |
| Yao, H.L. ....            | 1421      |
| Yih, C.T. ....            | 985       |
| Yiji, W. ....             | 1225      |
| Yin, Y.A. ....            | 1501      |
| Yong, C.H. ....           | 417       |
| Young, L.W. ....          | 1019      |
| Yuqing, W. ....           | 769, 963  |
| Zainiko, A. ....          | 433       |
| Zappi, U. ....            | 511       |
| Zhang, R.X. ....          | 131       |
| Zhang, X.X. ....          | 1371      |
| Zhang, Z.S. ....          | 1371      |
| Zhao, X.H. ....           | 1501      |
| Zhen-Yu, T. ....          | 749       |